# *APPENDIX A*

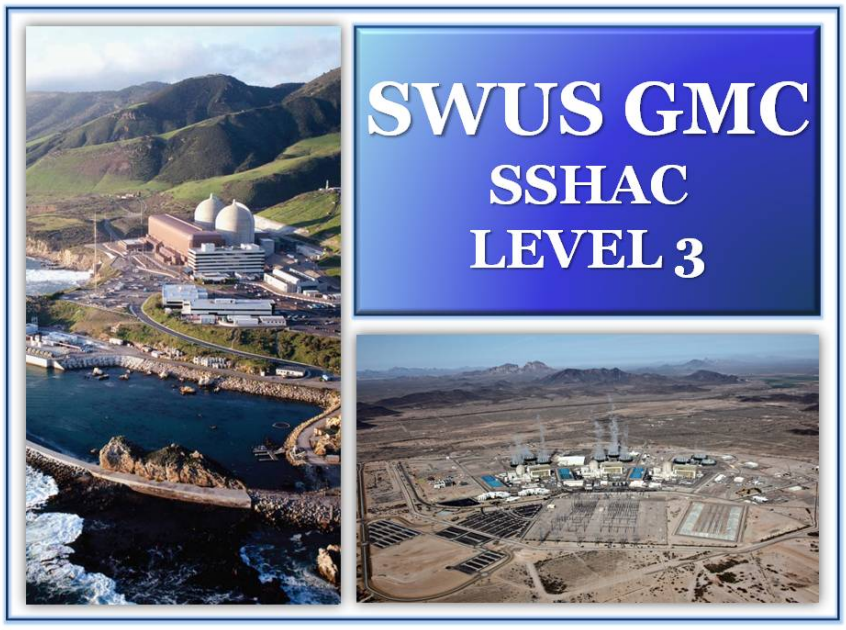
## PROJECT PLAN

# SOUTHWESTERN UNITED STATES GROUND MOTION CHARACTERIZATION SSHAC LEVEL 3

## Project Plan

Revision 3

April 16, 2014



# Southwestern U.S. Ground Motion Characterization

# Project Plan

**Prepared for:**


**Arizona Public Service Company**
Palo Verde Nuclear Generating Station
*Wandell, Christopher J.*
Senior Consulting "Chief" Civil Engineer
Phone: (623) 393-6741; E-mail: christopher.wandell@aps.com

**Pacific Gas and Electric Company**
Diablo Canyon Power Plant
*Klimczak, Richard*
Director Geosciences
Phone: (415) 973-2791; E-mail: RLK1@pge.com


**Prepared by:**


**GeoPentech, Inc.**

525 N. Cabrillo Park Drive, Suite 280
Santa Ana, CA 92701
Phone: 714-796-9100
Fax: 714-796-9191


## Version Control Information:

This project plan is a living document that will be used to communicate the project goals and activities to project participants and to the public. The following information is provided for tracking released versions.

| Version | Forwarding Date | Changes | Submitted by | Comments |
|---|---|---|---|---|
| Revision 3 | April 16, 2014 | Revision after Southern California Edison's withdrawal | | Main text of Project Plan has not been modified |

**TABLE OF CONTENTS**


Reason for Revision ..... iii
List of Acronyms ..... v
Introduction and Context of the Study ..... 1
Description of SSHAC Methodology ..... 2
Project Organization ..... 3
SWUS GMC Work Plan and Key Study Tasks ..... 6
Project Schedule ..... 15
Validation, Verification and Peer Review ..... 15
References ..... 15
Appendix A - Selection Criteria for Project Participants ..... A -1
Appendix B - PPRP Letter approving Project Plan ..... B -1

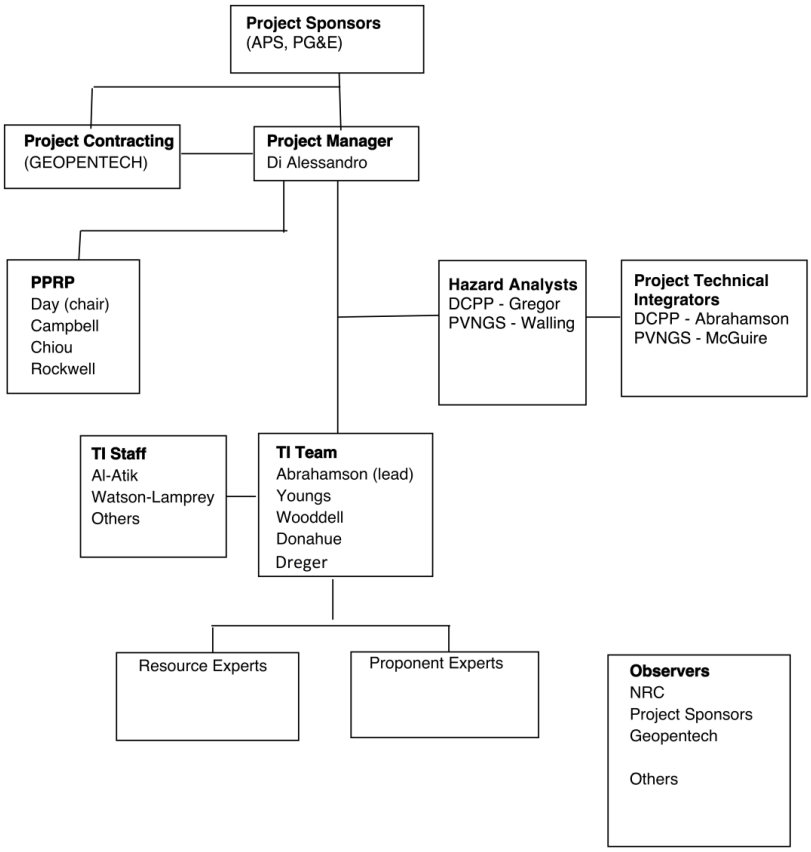

## REASON FOR REVISION

Effective October 1, 2013, a change in the Southwestern US Ground Motion Characterization (SWUS GMC) Senior Seismic Hazard Analysis Committee (SSHAC) Level 3 Project organization is undertaken to reflect Southern California Edison's (SCE) withdrawal from the project.

Under a Memorandum of Understanding (MOU) agreement among the former three project Sponsors Pacific Gas and Electric (PG&E), Arizona Public Service (APS) and SCE, SCE is released as a sponsor for the SWUS GMC SSHAC and all personnel devoted to providing ground motion characterization for the SONGS site are no longer part of this effort. As a result, the Project is now addressing ground motion characterization that will be used as input in PSHA studies for the DCPP and PVNGS sites.

In lieu of the former Project Organization Chart shown in Figure 1 of the Project Plan, the current Project Organization Chart is shown in the revised Figure 1 and is provided as follows:

Figure 1: Southwestern U.S. Ground Motion Characterization Project (Revised October 1, 2013)




Other than the changes to Figure 1, which modifies the Sponsors' list and removes the participation of personnel providing ground motion characterization for SONGS and the inclusion of the PPRP Project Plan Approval letter - Appendix B, the accompanying Project Plan remains unchanged.

**List of Acronyms**

| | |
|---|---|
| APS | Arizona Public Services |
| CBR | Center, Body, and Range |
| CEUS | Central and Eastern United States |
| CFR | Code of Federal Regulations |
| DCPP | Diablo Canyon Power Plant |
| EE | Evaluator Expert |
| EPRI | Electric Power Research Institute |
| GMC | Ground Motion Characterization |
| GMPE | Ground Motion Prediction Equation |
| HID | Hazard Input Document |
| ITC | Informed Technical Community |
| NGA | Next Generation Attenuation |
| NGA-west2 | Project name for the update of the 2008 NGA models |
| NRC | Nuclear Regulatory Commission |
| PE | Proponent Expert |
| PEER | Pacific Earthquake Engineering Research Center |
| PG&E | Pacific Gas & Electric |
| PM | Project Manager |
| PPRP | Participatory Peer Review Panel |
| PSHA | Probabilistic Seismic Hazard Analysis |
| PTI | Project Technical Integrator |
| PVNGS | Palo Verde Nuclear Generating Station |
| QA | Quality Assurance |
| RE | Resource Expert |
| RG | Regulatory Guide |
| SCE | Southern California Edison |
| SCEC | Southern California Earthquake Center |
| SONGS | San Onofre Nuclear Generation Station |
| SSC | Seismic Source Characterization |
| SSHAC | Senior Seismic Hazard Analysis Committee |
| SWUS | Southwestern United States |
| TDI | Technically Defensible Interpretation |
| TI | Technical Integrator |
| WUS | Western United States |

| | |
|---|---|
| USGS | United States Geological Survey |
| $V_{S30}$ | Shear Wave Velocity in the upper 30m |

## INTRODUCTION AND CONTEXT OF THE STUDY

In response to the March 2012 50.54(f) letter, an updated probabilistic seismic hazard analysis (PSHA) based on a Senior Seismic Hazard Analysis Committee (SSHAC) Level 3 process (Budnitz et al., 1997; NRC 2012, NUREG 2117) is required to be conducted for all operating nuclear power plants. A seismic hazard analysis requires a Seismic Source Characterization (SSC) and a Ground Motion Characterization (GMC).

Previous SSHAC level 3 studies for source characterization and ground motion characterization are available for the central and eastern United States (CEUS) (EPRI, 2004; CEUS, 2012), but SSHAC level 3 studies are not available for the western United States (WUS). The four WUS plant sites (DCPP, SONGS, PVNGS, and Columbia) have different seismic source issues that require separate SSC studies, but they have similar ground motion issues. The three plants in the southwestern US, DCPP, SONGS, and PVNGS, have joined together to sponsor a single GMC project for the southwestern United States (SWUS).

This Project Plan outlines the approach for conducting the SWUS GMC for application to the DCPP, SONGS, and PVNGS sites. As shown on the Project Organization Chart (Figure 1), the three utilities (PG&E, SCE, and APS) are the Project Sponsors and the project will be coordinated under the direction of a Project Manager, Dr. Carola Di Alessandro. The Project Schedule is shown on Figure 2, together with the schedule of the three SSC studies for the individual nuclear power plants. The project organization and schedule are described below.

A SSHAC Level 3 process is a formal, structured process for developing the SSC and GMC for use in PSHA. The SSHAC process provides guidelines for how the GMC study should be conducted, including: (a) identification of significant issues and data; (b) identification and solicitation of expert opinions and alternative models; (c) evaluation of the available data, expert opinions and alternative models; (d) integration of the information into GMC models that incorporate the range of technically defensible interpretations; (e) documentation of the model development; and (f) participatory peer review of the technical results and process. As described within the SSHAC guidelines (Budnitz et al, 1997; Hanks et al., 2009; Coppersmith et al., 2010; NRC, 2012), the goal of following a SSHAC process is to provide reasonable regulatory assurance that the center, body and range (CBR) of the technically defensible interpretations (TDI) in the GMC models have been adequately captured. The purpose of this Project Plan is to describe the SSHAC methodology, in general, and how the SSHAC Level 3 process will be applied to develop the GMC models for the SWUS region.

## DESCRIPTION OF SSHAC METHODOLOGY

In 1997, the Senior Seismic Hazard Analysis Committee published NUREG/CR-6372 (Budnitz et al., 1997) that detailed a methodology for capturing the epistemic uncertainty in input parameters for PSHAs. Factors motivating the development of this methodology were the observations that: (1) different PSHA studies (e.g., EPRI, 1988; Bernreuter et al., 1989) developed significantly different estimates of the mean seismic hazard for nuclear facilities; and (2) the primary reason for the difference in hazard estimates was that the SSCs and GMCs did not characterize the epistemic uncertainty within those characterizations in a consistent way. Recognizing the importance of characterizing epistemic uncertainty, the SSHAC spent approximately four years developing a methodology for characterizing epistemic uncertainties in SSC and GMC studies. Since publication of the original SSHAC methodology, there have been additional publications that have elaborated on the guidance and how it should be applied (e.g., Hanks et al., 2009; Coppersmith et al., 2010). These guidelines were finalized in NUREG 2117 (NRC, 2012). The following summary of the SSHAC methodology and the plan for the SWUS GMC study are consistent with these publications.

The stated goal of the SSHAC guidelines is to provide a methodology for developing SSC and GMC that "…represent the center, the body, and the range of technical interpretations that the larger informed technical community would have if they were to conduct the study" (Budnitz et al., 1997, p. 21). The terminology "center, body, and range" refers to the complete characterization of uncertainty. For simplicity, consider the single parameter of the maximum earthquake magnitude for a fault. In this case, "center" can be thought of as the average (i.e., median) maximum magnitude, "range" can be thought of as the extreme upper and lower estimates of the maximum magnitude limits, and "body" can be thought of as the shape of the distribution of potential maximum magnitudes within that range (e.g., symmetric or skewed distributions).

The use of the terminology "informed technical community" (ITC) also has an explicit meaning within the SSHAC guidance. This terminology is meant to communicate the hypothetical idea that if technical experts within the appropriate fields (e.g., GMC, SSC) (1) had detailed knowledge of the same data as those who developed the SSC and GMC, and (2) went through the same interactive process as the developers of the SSC and GMC, this ITC would develop characterizations that fit within the center, body, and range of those developed for the project. More recently, the NRC (2012, NUREG 2117) suggests replacing the term ITC with "technically defensible interpretations (TDI)" of the available data, models and methods to more clearly reflect the intent of the SSHAC process. They continue to emphasize that the careful evaluation of the larger technical community's viewpoints remains a vital part of the SSHAC process. By following the structured methodology of the SSHAC process, the intent is to provide reasonable regulatory assurance that the goal of representing the center, body, and range of the characterizations has been met, and thus provides the basis for developing seismic

hazard estimates that are reproducible, defensible, transparent, and stable (i.e., if someone else were to conduct a similar study they would not get significantly different results). For the remainder of this Project Plan, the term "technically defensible interpretations" (TDI) will be used rather than the earlier term "informed technical community" (ITC).

## PROJECT ORGANIZATION

The project organization is shown on Figure 1. As described by Budnitz et al. (1997) and Hanks et al. (2009), specific roles and responsibilities of individuals within a SSHAC process must be clearly defined because the guided interaction between the different roles allows for the center, body, and range of the SSC and GMC to be robustly characterized.

Members of the project team (TI Team and PPRP) were selected to provide a broad spectrum of (1) past experience on GMC models, (2) knowledge of data, methods and technical approaches relevant to ground motion in the WUS, and (3) prior SSHAC Level 3 experience. In addition, there was a goal to involve younger scientists on the TI team to help build up the number of people with experience with the SSHAC process for future projects. The basis for the selection of the PPRP and TI team members is given in Appendix A. The Project Plan provides for bringing all members of the project team to a common level of understanding of the technical data as well as explicit training in the SSHAC process. Specific roles of the SSHAC Project Team are described below.

Project Sponsor –The Project Sponsors provide financial support and "own" the results of the study in the sense of property ownership.

Project Manager (PM) – The PM is responsible for the scope, schedule, and budget and coordinates the execution of the project. In addition, the PM interacts with the Project Sponsors to keep them informed on the progress.

Project Technical Integrator (PTI) – The PTI is a technical expert with knowledge of the SSHAC process, both GMC and SSC studies, and the site-specific application for site response effects. The PTI is responsible for ensuring coordination and compatibility between the joint SWUS GMC study and the SSC studies being conducted separately by the three utilities. Each utility will assign a PTI who will be responsible for the coordination of the SWUS GMC, and plant-specific SSC, and site-specific site response.

Technical Integrator Team (TI Team) – The TI Team is a team of Evaluator Experts with PSHA experience that are responsible for conducting the evaluation and

integration process. The TI Team also will have a staff of Evaluator Experts that are not officially part of the TI Team but assist the team during the data evaluation part of the project. The TI Team will perform the integration and model-building part of the study and ultimately will "own" the results of the study with respect to intellectual responsibility for the results. As such, the TI Team is responsible for ensuring: (1) that the various data, models, and methods proposed by the larger technical community and relevant to the hazard analysis are considered in the evaluation; and (2) that the final GMC models represent the center, body and range of the TDI. Dr. Norman Abrahamson will be the TI Team Lead. Members of the TI Team are shown on Figure 1. The basis for the selection of the TI team members is given in Appendix A.

Evaluator Expert (EE) – An EE is an expert with PSHA experience capable of evaluating the relative credibility of multiple alternative hypotheses to explain observations. All members of the TI Team will be EEs. EEs use their professional judgment to objectively quantify epistemic uncertainty based on evaluations of the data, knowledge, and alternative models presented by the Resource and Proponent Experts. In addition, a support staff will assist the TI Team in their evaluation by conducting analyses of certain datasets and proponent models as directed by the TI team. Only the members of the TI Team will have intellectual ownership of the final logic tree and weights.

Resource Expert (RE) – A RE is an expert with a specialized knowledge of a particular data set, interpretation, or hypothesis who can present this information without a proponent bias. REs generally are invited to one or more Workshops and/or may be contacted outside of the Workshop environment by the TI Team to present and discuss their specialized knowledge regarding the strengths and weaknesses of alternative models and data sets. The REs will be identified as needed during the project. The REs provide their specialized knowledge to assist the TI team in the evaluation but they do not take ownership or endorse the final GMC models. For example, scientists from the U.S. Geological Survey may act as Resource Experts during the Workshops, but their participation does not imply that they support the GMC model developed by the TI team.

Proponent Expert (PE) – In contrast to the unbiased RE, a PE is an expert who advocates a particular hypothesis or technical position. The PE's opinion may range from mainstream to extreme (outlier) views. PEs generally are invited to one or more Workshops and/or may be contacted outside of the Workshop environment by the TI

Team to present and discuss their position. PEs will be identified as needed during the project, but are expected to mainly include model developers from PEER and SCEC.

Hazard Analyst – The Hazard Analyst is a PSHA expert responsible for performing the PSHA calculations. Hazard Analysts are incorporated into all phases of the study (e.g., evaluation, integration) because they can provide: (a) valuable insight into how to represent uncertainty within different parameters; and (b) sensitivity feedback with respect to what parameters have the most impact to the hazard calculations. Each utility will provide its own Hazard Analyst who is knowledgeable with the site-specific SSC so that the hazard feedback addresses the key issues at all three sites. The basis for the selection of the Hazard Analysts is given in Appendix A.

Participatory Peer Review Panel (PPRP) – The PPRP is a panel of experts with SSHAC methodology and/or PSHA experience that provide participatory peer review of the SSHAC methodology implementation process and technical judgments of the TI Team. The PPRP assures that the range of TDI is captured and documented through proper implementation of the SSHAC process. PPRP members should be highly regarded and recognized as experts in their respective technical fields. The members of the PPRP serve as individuals and not as an affiliate of any organization. Each member of the PPRP in the employ of any organization must ensure that it is understood that, as Panel members, they are not representing the position of their respective organizations, but rather, they are serving as recognized experts in their respective fields.

Members of the PPRP will attend all of the formal Workshops and are encouraged to participate in field reviews and selected working meetings of the TI Team. Opportunities to participate in working meetings will be identified by the PPRP and coordinated with the Project Manager.

The members of the PPRP are shown on Figure 1 and will consist of Dr. Steve Day (Chair), Dr. Ken Campbell, Dr. Brian Chiou, and Dr. Tom Rockwell. The composition of the PPRP includes individuals with prior SSHAC Level 3 experience (Campbell, and Chiou), as well as captures the breadth of technical requirements for the project including both empirical GMPEs and numerical simulations of ground motion. The basis for the selection of the PPRP members is given in Appendix A.

Outside Observers – Outside observers are not explicitly defined within the SSHAC guidance (Budnitz et al., 1997), but are discussed in the implementation guidelines (NRC, 2012; NUREG 2117). Observers may include sponsors, regulators, and other invited individuals that would benefit from observing the Workshops. Outside observers do not participate in any aspect of the SSHAC process (e.g., evaluation, integration, peer review, documentation), but they may be invited to observe some Workshops depending on the specific needs of the Project Sponsors. Time for observer comments will be accommodated at the end of each day of each Workshop.

## SWUS GMC WORK PLAN AND KEY STUDY TASKS

For the SWUS Project, the SSHAC Level 3 study will involve four components: (1) evaluation, (2) integration, (3) participatory peer review, and (4) documentation. Evaluation refers to the process of compiling and evaluating relevant data, alternative models/concepts, and alternative interpretations of the TDI. Integration refers to the assessment process where the various datasets, models, and interpretations are combined into a representation of the CBR of the TDI for the SSC and GMC. Participatory peer review refers to review of the evaluation and integration process by a peer review panel capable of providing feedback, during the project, on technical aspects of the project and whether the SSHAC Level 3 process was followed appropriately. By receiving feedback from the peer review panel during the project, the TI team can make necessary corrections before the project is complete. Documentation refers to the final reports produced by the project that document the technical results, the technical basis for the evaluation and assignment of weights on the logic tree, and how the SSHAC Level 3 process was implemented. The SSHAC Level 3 methodology formalizes the process of interaction between the technical community, the TI Teams, and the PPRP through a series of Workshops.

The process of evaluation, integration, peer review, and documentation will occur in a series of Workshops, Working Meetings, and internal work. These process components are described below.

Evaluation: The consideration of the complete set of data, models and methods proposed by the larger technical community that are relevant to the ground motion model's hazard at any of the three sites.

The process of evaluation includes, but is not limited to, the: (a) identification of hazard-significant issues; (b) compilation of relevant data and models; (c) evaluation of the data and models with respect to their impact on the GMC. The primary focus of the GMC evaluation process will be on (1) the applicability of the NGA-West2 empirical GMPE models and other candidate empirical GMPEs to the three SWUS

sites of interest, because each might require its own adjustment to the ground motion model(s), and (2) the applicability of the ground motions based on numerical simulations to the fault/site-specific geometries at each site. Through sensitivity analyses, those parts of the GMC Logic Tree that are most significant to hazard will be the focus for the discussions at the Workshops. Those parts of the GMC Logic Tree model that are not significant to hazard will be reviewed and updated to reflect the current state of scientific knowledge, as appropriate, but will not be the focus of detailed evaluation and further refinement.

The PPRP is involved in the evaluation process through attending Workshops, reviewing interim project documentation, and participating in Working Meetings of the TI Teams, as needed.

Integration: Representing the center, body and range of technically defensible interpretations in light of the evaluation process (i.e., informed by the assessment of existing data, models and methods).

Following the evaluation process, the TI Team will integrate the relevant data, models, and interpretations to develop a general GMC logic tree for the SWUS that captures the center, body, and range of the TDI. There will also be site-specific modifications of the GMC logic trees to address site-specific issues such as the reference $V_S$ for the ground motion model. The process of integration commonly includes: (a) development of a version of the GMC Logic Tree; (b) hazard sensitivity analyses to document the impact of model parameters on the seismic hazard; (c) feedback from the Resource Experts, Proponent Experts, and PPRP members on the logic tree models, and hazard sensitivity; and (d) the development of the next versions of the GMC logic tree. This process is iterated until final site-specific GMC logic trees are developed for each site.

The GMC TI Team will lead the integration process; the Hazard Analysts will conduct the iterative hazard sensitivity analyses. The REs and PEs will be less active in this process, but they can be called upon by the TI Teams as needed to provide clarification, resolve new issues, and provide feedback on the preliminary model. The majority of the integration process will occur through informal Working Meetings and internal work. The Workshops are designed to present the models and sensitivity results, and to collect feedback. The PPRP will be involved in the integration process

through attending Workshops, reviewing interim project documentation, and attending selected Working Meetings, as needed.

Peer Review – Participatory peer review is an integral component of a SSHAC Level 3 study. The overall goals of this review will be to ensure that the SSHAC process is adequately followed and that the technical results adequately characterize the CBR of the TDI. The review is participatory in that it will be a continuous process throughout the study, and not a singular review that occurs at the end of the study. As such, the PPRP will be kept abreast of project developments through a combination of attending Workshops, reviewing interim project documents, and attending selected field reviews and/or Working Meetings, as needed. The TI team will have the opportunity to address PPRP comments and make modifications during the project.

Documentation – Documentation also is an integral component of a SSHAC Level 3 study in that it provides a record of the final technical results, how they were reached, and how the SSHAC Level 3 process was implemented. In addition, the documentation provides the basis for review by any pertinent regulatory officials, if needed. Documentation for the study will include the Workshop summaries and presentations, PPRP letter reports and TI Team responses, GMC data tables showing how the different data sets and models were used, GMC logic trees, and the final report including the PPRP review of the final report.

The four process components of the SSHAC Level 3 study (evaluation, integration, peer review, and documentation) will be conducted using a series of formal Workshops, Working Meetings, and internal work. The following work plan summarizes the individual tasks that will be conducted for the SWUS GMC study. The major milestones of the work plan are shown on Figure 2.

## Databases

The GMC database will be the PEER NGA-west2 database with the addition of results from suites of numerical simulations computed using the SCEC broadband platform. The PEER NGA-west2 data will be stored at PEER which provides for public access to the data. If additional observed ground motion data are added to the PEER-NGA-west2 data set as part of the SWUS project, then these additional data will be provided to PEER for incorporation in the next version of the PEER ground motion database. It is expected that under the project a ground motion database for Arizona will be developed: it will include small magnitude recordings in the surrounding region of PVNGS and moderate to large magnitude recordings from California recorded in Arizona. The simulated ground motions developed specifically for the SWUS GMC will be archived at the Southern California

Earthquake Center (SCEC) and will be made available to the public after QA is completed. A project-specific website is being developed to maintain the project documents. The page is managed by SCE and has the format of a collaborative platform (cFolder). Full access will be warranted to Project Sponsor and participants, including PPRP members. We plan to provide specific limited access to REs and PEs. The platform will also include literature and other general information relevant to the three nuclear power plants. At the end of the project, final report, PPRP final letters, presentations from public Workshops, Workshop summaries minutes, Working Meetings material and reference documents will be made publicly available. The reference documents will include PEER reports describing the empirical ground motion studies and SCEC reports describing the simulation methods and the validation study. Project participants will have access to such repository throughout the project; critical reference material will be available prior to each Workshop to allow adequate time for PPRP review. If documentation for a specific model is not provided in a timely manner, the model might be downweighted in the subsequent evaluation process.

## General Tasks

### Task 1: Preparation of Project Plan and Kickoff Meeting

The Project Sponsors will prepare a letter that outlines sponsor expectations, required deliverables and schedule. The initial task for the SWUS GMC study will be to prepare the Project Plan and hold a Workshop 0 (the Kick-off Meeting). The kick-off meeting will involve the Project Sponsors, PPRP, TI team, Hazard Analyst from each utility, PTI from each utility, Project Manager, Project Contracting, and the representatives of the Project Sponsors. The purpose of the kick-off meeting is to review the project plan, discuss the roles of the project participants, and identify key interface issues (SSC, GMC, and site response) for the three sites. The PPRP will provide a letter documenting their review of the Project Plan after the Kick-off Meeting.

### Task 2: University Research to Develop Proponent Models

Two major ground motion projects are currently being conducted that are relevant to the hazard evaluation for the SWUS: PEER NGA-west2 and SCEC broadband platform validation. The PEER and SCEC studies are not part of the formal SSHAC process for the SWUS GMC study, but brief descriptions of these two studies are given below as they will be key inputs for the SWUS GMC study.

PEER is developing an updated ground motion database including key data from shallow crustal earthquakes in active regions around the world. This data set will increase the number of recordings above magnitude 5 by about a factor of 3 as compared to the original NGA data set (Chiou et al, 2008). PEER is using this expanded data set to develop new ground motion

prediction equations (GMPEs) that will be finalized in January 2013. It is expected that those models will include the traditional ergodic sigma (where the total variability is treated as a random variable that can be decomposed into between-events variability and within-event variability). Other studies are being conducted at PEER in coordination with the NGA-west 2 program that are focusing on other aspects relevant to the ground motion characterization such as single-station sigma (where there is an effort to remove the epistemic uncertainty from the total variability by recognizing systematic site effects not captured in the GMPEs – AlAtik et al., 2010), Kappa scaling, near fault fling effects; preliminary results from these additional studies should be available by March 2013 and their completion is expected by summer 2013. The PEER studies will result in a set of proponent models that will then be evaluated for their applicability to the three sites as part of the SWUS GMC study under the SSHAC process. The TI team evaluation will not be restricted to the NGA-west2 models. Other available GMPEs that may be applicable to the SWUS, such as GMPEs from Japan, Taiwan, Italy, Turkey, New Zealand, will also be considered.

SCEC is conducting a major systematic evaluation of the methods for numerical simulation of ground motion for engineering applications. They are developing a series of validation exercises that will be used to test the numerical simulation methods. These include two parts. The first part is a comparison of simulated motions with observations from past earthquakes using the optimized source parameters for each earthquake. This provides an evaluation of how well the simulation method works if the source is known. The second part is a comparison of the median simulation for future earthquakes (average of many realizations of the source) in the magnitude and distance range that are well constrained by the empirical data. This provides an evaluation of how well the method for generating source parameters for future earthquakes is working. To capture the CBR of the available simulation methods, SCEC will incorporate a range of different models with different approaches into the broadband platform for the validation. SCEC will provide a report describing the evaluation and recommending a set of simulations methods that pass the validation tests and represent proponent models for simulations. This set of proponent models will then be evaluated as part of the SWUS GMC study under the SSHAC process. The schedule of SCEC activities is set up so to expedite the validation and evaluation process. SCEC will hold several workshops that evaluate preliminary results to allow for early correction, reducing the risk of not meeting the SWUS schedule. In the event that SCEC cannot produce simulation methods that pass validation test in due time, the TI Team will consider the range of results from previous simulations along with the validation results and will likely need to increase the uncertainty of the GM appropriately.

Task 3: Workshop 1 (Significant Issues, Available Data and Data Needs)

The TI team and staff will develop the agenda for Workshop 1 (WS1), and identify the appropriate REs for WS1. The agenda and list of REs will be provided to the PPRP for their review. The PPRP may identify additional REs for consideration and/or significant issues or topics to be covered at the Workshop.

Workshop 1 will last for three days and be attended by the PTI, the TI team and staff, the PPRP, the Hazard Analysts, Resource Experts (REs), the Project Manager and support staff. The goals of WS1 are to (1) provide SSHAC training to the project participants, (2) discuss issues significant to hazard, and (3) identify available data to address the significant issues. REs will be asked to discuss specific data sets and to assist in identifying available data to address significant issues. Prior to the Workshop, letters will be sent to selected REs identifying directed topics and issues that they should be prepared to address at the meeting. The letters will help focus the Workshop discussion on key issues related to a particular data set, including quality of data, expected use of data, uncertainty or limitations in the data or interpretations, etc. The REs will be asked to present data and/or to participate in interactive discussion sessions with the TI staff and other related REs. This will inform the TI staff of the available data, and evaluations and interpretations of the data.

Key outcomes of Workshop 1 will include the definition of the scope of the numerical simulations to be conducted including the selection of the simulation methods to be implemented, and identification of the key ground motion data that can be used to check and/or constrain the GMPEs for application to the SWUS.

The PPRP will attend Workshop 1 mainly as observers, but in some cases, PPRP members may serve as a Resource Expert during the Workshop to take advantage of their specific technical knowledge on a topic. The PPRP may also ask clarification questions during the Workshop. The PPRP will provide verbal comments to the Project Manager and the TI team at the end of each day and at the conclusion of the Workshop. Following the three-day Workshop, a PPRP deliberation will take place to review the Workshop proceedings. PPRP will have the flexibility to complete its post-Workshop deliberations by teleconference and/or email. During this deliberation process, the PPRP will prepare verbal comments and feedback to the PTI and TI Teams. A written version of the PPRP comments will be provided at a later date so that they can be carefully edited and a consensus built and confirmed among the PPRP members. The PTI and TI Team Leads will provide written responses to the PPRP comments. Following the Workshop and PPRP deliberation, the proceedings of the Workshop will be documented in a brief Workshop summary for distribution to the Project

Sponsors and members of the PPRP, and the PPRP will submit a letter to the TI Team Leads documenting their observations of the Workshop. The Workshop summary and PPRP letter will become part of the final documentation of the SWUS GMC study.

Topics to be addressed at Workshop 1 will include the following:

- SSHAC training for project participants
- Summarize project overview and objectives
- Review SSHAC procedures and Workshop ground rules
- Identification of data needs or gaps
- Present sensitivity analysis to ground motion models for the three sites (GMC model V0)
- Review new data and GMPEs from PEER
- Review other GMPEs developed for extensional regimes
- Review simulation validation from SCEC
- Review available models for near fault effects including directivity, fling, hanging wall effects, splay faults for M6-M7.5 earthquakes at distances of 0 to 15 km (for DCPP and SONGS)
- Review available models for moderate (**M** 5.5—6.5) earthquakes at distances of 30-100 km from a site, for a variety of rupture mechanisms, including normal faulting (for PVNGS)
- Evaluate applicability of close scaling models and distant attenuation in Arizona for PVNGS
- Review base rock characteristics (e.g. $V_{S30}$) of available ground motion models, and select a representative reference $V_{S30}$ that is applicable to all three sites. Should a common $V_{S30}$ not be applicable for all sites and difficulties are found in this regard, then site-specific reference $V_{S30}$ can be selected.
- Interactive discussion with Resource Experts (selected presentations)
- Identify scenarios to be implemented in the numerical simulations

Task 4: Workshop 2 (proponent models)

Prior to Workshop 2, the TI Teams will identify all relevant proponent models for ground motions in the SWUS, develop version 1 of the GMC logic tree, and prepare the agenda for Workshop 2. A hazard sensitivity analysis will be conducted using the alternative proponent models to help focus the discussion of the proponent models on those features that are most important to the hazard at the three sites. The sensitivity analysis will be performed by the Hazard Analysts using version V1 of the GMC logic tree and the SSC models that are available at the time.

Prior to Workshop 2, REs and PEs will be identified and their names provided to the PPRP for their review. The PPRP may identify additional PEs and/or REs for consideration. The PEs and/or REs will be contacted prior to the Workshop and provided with a specific request for discussion topics.

Workshop 2 will last for three days and be attended by the PTI, the TI team and staff, the PPRP, the Project Manager, the Hazard Analyst, Resource Experts and Proponent Experts. The primary goal of WS2 will be to interactively use the PEs to evaluate the strengths and weakness of the candidate GMPEs and the data available for testing the models. The PEs may identify other alternative models or technical issues that are not currently captured in the V1 logic trees and that are needed to capture the CBR of the GMPEs. These alternative models or technical issues will be identified during the Workshop for evaluation by the TI Team and will be added to the GMC logic tree as appropriate.

The information gained from these interactions will form the basis for defining the CBR of the TDI and will then be used to develop the revised GMC model. The PPRP members will attend Workshop 2 as observers, but again, may also serve as Resource Experts when needed. The PPRP members will not serve as Proponent Experts for models. The PPRP will provide verbal comments at the end of each day and at the conclusion of the Workshop. Following the three-day Workshop, a PPRP deliberation will take place to review the Workshop proceedings. PPRP will have the flexibility to complete its post-Workshop deliberations by teleconference and/or email. During this deliberation process, the PPRP will prepare verbal comments and feedback to the PTI and TI Teams. A written version of the PPRP comments may be provided at a later date so that they can be carefully edited and a consensus built and confirmed among the PPRP members. The PTI and TI Team Leads will provide written responses to the PPRP comments. Following the Workshop and PPRP deliberation, the proceedings of the Workshop will be documented in a brief Workshop summary for distribution to the Project Sponsors and members of the PPRP, and the PPRP will submit a letter to the TI Team Leads documenting their observations of the Workshop. The Workshop summary and PPRP letter will become part of the final documentation of the SWUS GMC study.

<u>The topics to be addressed at Workshop 2 will include the following:</u>

- Review SSHAC procedures and Workshop ground rules
- Present hazard sensitivity analysis on the GMC V1 logic trees using available SSC models

- Present the proponent models and discuss their strengths and weaknesses through interactive discussion with Proponent Experts and Resource Experts
- Evaluate the proponent models with comparisons to data, as appropriate
- Identify model gaps, i.e. cases that don't appear to be covered by current models, and how to cover those gaps

Task 5: Workshop 3 (TI Evaluation)

Following Workshop 2, the TI Team will evaluate the proponent models and integrate the information into version V2 of the GMC logic tree based on the feedback from Workshop 2. Modeling gaps identified at Workshop 2 will be filled with modifications to existing models or development of new models. The Hazard Analysts will implement the new GMC model in the hazard code and conduct a hazard sensitivity analysis for each site to identify the key contributors to the uncertainty. The latest version of the SSC model will be implemented in the hazard sensitivity analysis. The latter will also be used to focus the discussion by the REs, PEs, and PPRP on the technical issues and parameters that have the greatest effect on the hazard at the three sites.

Workshop 3 will last for two days and be attended by the PTI, the TI teams and staff, the PPRP, the Project Manager, the Hazard Analysts, and selected REs and PEs that are identified by the TI Team, as needed. In contrast to Workshops 1 and 2, the PPRP will be active participants in Workshop 3 to fully query the model parameters, level of documentation, uncertainty, and rationale in developing the model. The focus of the PPRP review should be on the adequacy of the technical basis for the GMC model and not on the specific value of a particular weight on the logic tree. The primary focus of the Workshop 3 process will be for the TI Team to integrate information into models that represent the CBR of TDI.

The proceedings of Workshop 3 will be documented in a brief Workshop summary report for distribution to the Project Sponsors and members of the PPRP, and the PPRP will submit a letter to the TI Team Leads documenting their observations of the Workshop. The Workshop summary and PPRP letter will become part of the final documentation of the SWUS GMC study.

Task 6: Incorporation of PPRP Comments in GMC (V3) Models

Following Workshop 3, comments from the PPRP will be resolved and incorporated into the final GMC logic trees (V3), as needed.

Task 7: Documentation

The TI Team will develop the final documentation of the SWUS GMC study. An initial draft report will be prepared and submitted to the PPRP for review. It is expected that the main PPRP comments will have been addressed based on the PPRP comments in Workshop 3. The reporting will include complete documentation of the development of the GMC models and all of the parameters included within the models.

Upon completion of the PPRP review of the draft report, the TI Team will respond to PPRP comments and prepare a Final Report. The PPRP will review the response to comments and the Final Report, and provide a letter to the Project Sponsors and TI Team Leads documenting their evaluation of the SSHAC Level 3 process. This letter will be included in an appendix of the Final Report.

## PROJECT SCHEDULE

The schedule for completing the SWUS GMC Study is presented on Figure 2. The project will commence with Workshop 0 (Kickoff Meeting) in August 2012, and will be completed in mid 2014, a 2-year duration. Workshops are anticipated to be held at 6-month intervals every October and March during the study. As described above, the goal of following the SSHAC Level 3 methodology is to have reasonable assurance that epistemic uncertainties in the GMC logic trees have been adequately captured for use in a PSHA for DCPP, SONGS, and PVNGS.

## VALIDATION, VERIFICATION AND PEER REVIEW

Validation, verification and peer review provides the necessary quality assurance for development of the GMC models and is inherent in the SSHAC process itself and the participatory peer review. The participatory peer review is comparable to and, in many areas, much more thorough and comprehensive than the standard Independent Technical Review (ITR) of the QA procedures given in 10CFR50 Appendix B. Thus, following the guidelines in NUREG 2117, the SSHAC process will not be required to follow a formal 10CFR50 Appendix B QA procedure.

NOTE: The hazard calculations for the development of the GMRS are not part of this SWUS GMC project and are the responsibility of the Project Sponsors. QA of hazard codes is outside the scope of the project, however the translation of GMC models into PSHA inputs will be documented in Hazard Input Documents (HIDs) and the HIDs will be part of the QA documentation.

## REFERENCES


Al-Atik, L., N. Abrahamson, F. Cotton, F. Scherbaum, J. Bommer, and N. Kuehn , 2010, The variability of ground-motion prediction models and its components, *Seismological Research Letters* 81, no. 5, 794–801.

Bernreuter, D.L., Savy, J.B., Mensing, R.W., Chen, J.C., and Davis, B.C., 1989, Seismic hazard characterization of 69 nuclear plant sites east of the Rocky Mountains, NUREG/CR-5250, Volumes 1-8, U.S. Nuclear Regulatory Commission, Washington D.C.

Budnitz, R.J., Apostolakis, G., Boore, D.M., Cluff, L.S., Coppersmith, K.J., Cornell, C.A., and Morris, P.A., 1997, Recommendations for Probabilistic Seismic Hazard Analysis: Guidance on Uncertainty and Use of Experts: Washington, D.C., US Nuclear Regulatory Commission, NUREG/CR-6372, p. 278.

CEUS (2012). Central and Eastern United States Seismic Source Characterization for Nuclear Facilities, Report published by NRC Report **NUREG-2115**, DOE Report **NE-0140**, EPRI Report **1021097**, 6 Volumes.

Coppersmith, K.J., Bommer, J.J., Kammerer, A.M., and Ake, J., 2010, Implementation guidance for SSHAC Level 3 and 4 processes; 10th International Probabilistic Safety and Management Conference, Seattle, Washington, June 7-11, 2010.

Chiou, B., Darragh, R., Gregor, N., and Silva, W., 2008. NGA project strong motion database, *Earthquake Spectra,* 24, 23 - 44.

EPRI-SOG, 1988, Seismic hazard methodology for the central and eastern United States, EPRI NP-4726A, Revision 1, Volumes 1-11, Electric Power Research Institute, Palo Alto, California

EPRI, 2004. CEUS Ground motion project. Palo Alto, CA: Electric Power Research Institute, Final Report, EPRI Technical EPRI Report 1009684.

Hanks, T.C., Abrahamson, N.A., Boore, D.M., Coppersmith, K.J., and Knepprath, N.E., 2009, Implementation of the SSHAC Guidelines for Level 3 and 4 PSHAs—Experience Gained from Actual Applications, U.S. Geological Survey, Open File Report 2009-1093, p. 66.

NRC, 2007, Regulatory Guide 1.208: A Performance-Based Approach to Define the Site-Specific Earthquake Ground Motion, US Nuclear Regulatory Commission, p. 53.

NRC, 2012 Practical Implementation Guidelines for SSHAC Level 3 and 4 Hazard Studies: Washington D.C., US Nuclear Regulatory Commission, NUREG2117.

**Figure 1: Southwestern U.S. Ground Motion Characterization Project Organization**

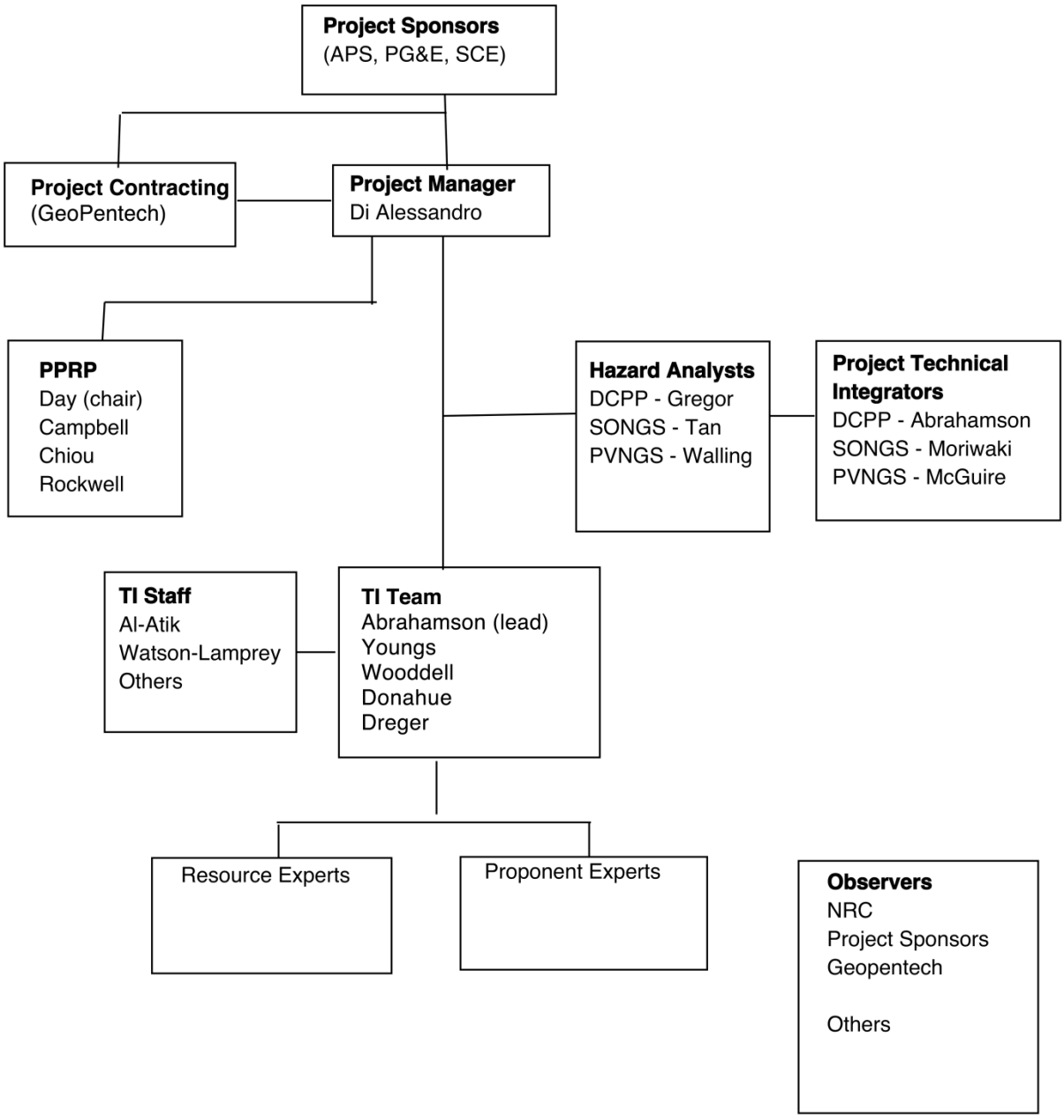
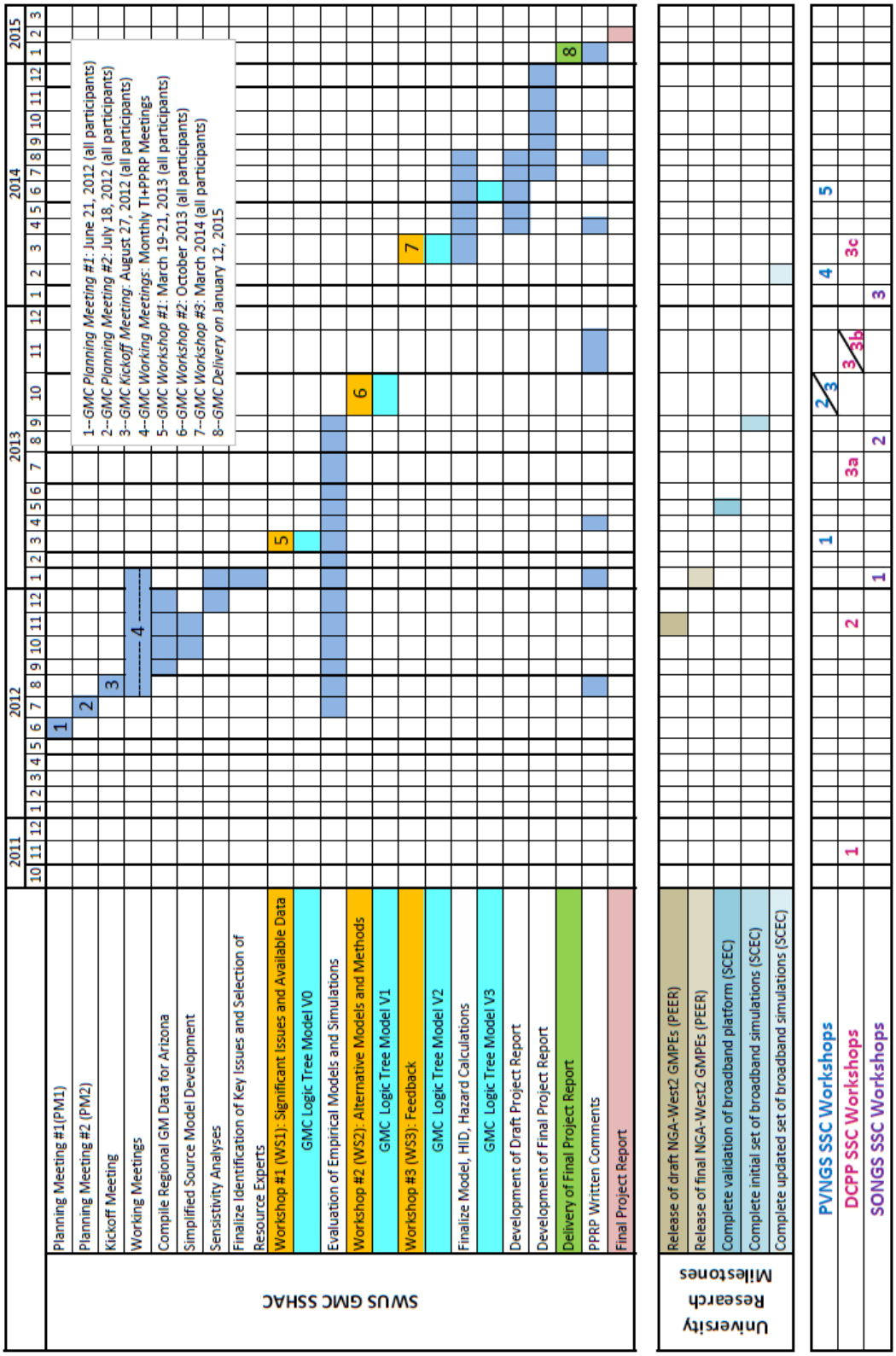


**Figure 2: SWUS GMC Schedule and Major Milestones**



## APPENDIX A – SELECTION CRITERIA FOR PROJECT PARTICIPANTS

This appendix describes the selection criteria for the selection of the TI team lead, TI team members, PPRP members, and Project Manager.

### 1. Technical Integrator (TI) Lead

The TI Lead is selected by the Project Sponsors. The TI team is selected by the TI Lead. The roles and responsibilities of the TI lead are given in Table 1A and the selection criteria are given in Table 1B.

The Project Sponsors selected Dr. Norm Abrahamson as the TI lead for the SWUS GMC. Dr. Abrahamson is an internationally recognized expert in field of ground motion with experience developing empirical GMPEs and using numerical simulations to develop GMPEs. He has also past experience with the SSHAC studies having served as the Technical Facilitator/Integrator for the 1996-1998 Yucca Mountain and 2001-2004 Swiss SSHAC level 4 GMCs. He has also served as the TI lead for the 2008-2011 BCHydro SSHAC level 3 GMC, as the TI co-lead for the ongoing NGA-east SSHAC level 3 GMC, and as TI team member for the Blue Castle SSHAC level 3 GMC.

| | **Table 1A. Roles and Responsibilities of TI Team Lead** |
|---|---|
| 1 | Preparation of Project Plan |
| 2 | Point of contact for all technical activities on the project |
| 3 | Selection of appropriate evaluator and integration experts for TI Team |
| 4 | Leading the evaluation and integration activities of the TI team, including the conduct of multiple working meetings |
| 5 | Finding and assuring participation of suitable Resource and Proponent Experts |
| 6 | Running Workshops and ensuring that the participants clearly understand the Workshop objectives, their individual roles, the required output from the Workshops, and the implication to hazard |
| 7 | Ensure that the project documentation is complete and comprehensive |

| | Table 1B. ATTRIBUTES / SELECTION CRITERIA for TI TEAM LEAD |
|---|---|
| 1 | A thorough understanding of the SSHAC goals and processes |
| 2 | Acknowledged technical expertise with particular emphasis in the GMC issues being addressed and in PSHA |
| 3 | Experience in conducting previous SSHAC Level 3 and 4 studies |
| 4 | Strong communication skills to work with the technical evaluators |
| 5 | Project management skills to ensure technical products are high-quality and delivered in a timely manner |
| 6 | Experience and familiarity with NRC regulations, quality assurance, and regulatory compliance |

**2. Technical Integrator (TI) Team**

The TI team members were selected with the goal of having a balance between senior members with extensive experience in SSHAC studies and younger members that have limited or no SSHAC experience. The purpose of including younger members is to build up the pool of ground motion experts with SSHAC experience.

Past experience has shown that a TI team of 3 to 5 people works well for GMC projects. A five person TI team was selected for this project with three senior people and two younger people.

Dr. Robert Youngs was selected as the second senior person (in addition to Dr. Abrahamson). Dr. Youngs has extensive experience with SSHAC studies for both GMC and SSC: 1998 Yucca Mountain SSC (SSHAC level 4), 2004 Swiss SSC (SSHAC level 4), 2004 EPRI GMC (SSHAC level 3), 2011 BCHydro GMC and SSC (SSHAC level 3), ongoing NGA-East GMC (SSHAC level 3), and ongoing Hanford GMC (SSHAC level 3). He is also a recognized ground motion expert and is an active participant in the PEER NGA studies for WUS ground motion models.

Prof. Douglas Dreger has been selected as a third senior evaluator expert with experience with numerical simulations. Through his well established academic career, Prof. Dreger is

knowledgeable with respect to the techniques employed in numerical simulation studies, as well as knowledgeable in the appropriate selection of model parameters for those studies.

Ms. Katie Wooddell was selected as a younger person on the TI team. Ms. Wooddell is an active participant in the PEER NGA-west2 empirical ground motion studies. She has also experience over the last three years testing and using the SCEC broadband simulation platform. She is currently participating in the SCEC broadband validation project. Having experience in both empirical GMPEs and numerical simulations gives Ms. Wooddell a good background for the SWUS GMC. Ms. Wooddell has some recent experience in SSHAC studies: she was on the TI team for the GMC for the initial work on the 2011 DCPP SSHAC level 3 study. She is also the Hazard Analyst for the ongoing DCPP SSC SSHAC level 3 study.

Dr. Jennifer Donahue was selected as the second younger member of the TI team. Dr. Donahue is an active participant in the NGA-west2 ground motion project with a focus on evaluation of hanging wall effects using both empirical data and numerical simulations. As hanging wall effects are likely to be an important issue for DCPP and SONGS, Dr. Donahue is well qualified to evaluate the alternative hanging wall models that will be part of the proponent models. Dr. Donahue has also some recent experience in SSHAC studies: she was on the TI team for the GMC for the initial work on the 2011 DCPP SSHAC level 3 study and she is providing project management support for the ongoing DCPP SSC SSHAC level 3 study.

**3. PPRP Members**

The PPRP members are selected by the TI lead, PM, and the Project Sponsors. The roles and responsibilities of the PPRP are given in Table 2A and the selection criteria are given in Table 2B. The PPRP members are selected so that, collectively, their experience and specialized technical knowledge meets the requirements given in Table 2B with a focus on experience in the SWUS region. For this project, an additional goal for the PPRP is to have a mixture of experience with the SSHAC process by including some members with limited SSHAC experience to help build up the available pool of people with SSHAC experience for future projects. Based on the criteria in Table 2B, the TI lead and the Project Sponsors selected the following members for the PPRP: Prof. Steve Day (Chair), Dr. Ken Campbell,

Dr. Brain Chiou, and Prof. Tom Rockwell. A brief description of the qualifications of each PPRP member is given below.

Prof. Steve Day is a recognized expert in ground motions with over 30 years experience with methods for the numerical simulation of ground motion. He has experience with both kinematic and dynamic approaches for simulation of ground motions and has participated in the SCEC ground motion simulation studies. He also has experience in simplifying results of numerical simulations into useable engineering models as part of the 2008 NGA project. Prof. Day has served on the NRC peer review panel for the 1985-1991 DCPP Long Term Seismic Program and also as a member of the seismic technical advisory board for both DCPP and SONGS. Prof. Day's experience with the SSHAC process is as a member of the PPRP for the ongoing DCPP SSC SSHAC level 3 study. He was selected as the PPRP chair because of the breath of his knowledge on ground motion, his strong communication skills, and his availability to commit the required time to work with the PPRP members to achieve a consensus and complete reporting on schedule.

Dr. Ken Campbell is a recognized expert in ground motion and seismic hazard. He has over 30 years experience in developing empirically based GMPEs. He was one of the GMPE developers in the 2008 NGA project and is a developer of updated GMPEs in the ongoing NGA-west2 project. Dr. Campbell has also extensive experience with the SSHAC process. He participated as an Expert Evaluator in the 1998 Yucca Mountain SSHAC level 4 GMC and is currently an Expert Evaluator in the ongoing SSHAC level 4 GMC for the PEGASOS refinement project and Chair of the PPRP in the ongoing SSHAC level 3 GMC study for the Hanford PSHA. In addition, Dr. Campbell has served as a PPRP member for the 2011 BCHydro SSHAC level 3 SSC and GMC studies, was a Resource Expert in the 2004 EPRI CEUS SSHAC level 3 GMC study, and was a Proponent Expert for the hybrid empirical method of modifying GMPEs for regional factors in the Blue Castle and Thyspunt SSHAC level 3 GMC studies.

Dr. Brian Chiou is a recognized expert in ground motion and seismic hazard. He was one of the GMPE developers in the 2008 NGA project and is a developer of updated GMPEs in the ongoing NGA-west2 project. For this project, his key expertise is in empirical data sets, empirical GMPEs, treatment of variability, and directivity effects. Dr. Chiou has previous experience with the SSHAC process having been a Resource Expert in the recently

completed BCHydro SSHAC level 3 GMC study and the ongoing Blue Castle SSHAC level 3 GMC study. He is currently serving as a PPRP member for the ongoing Hanford SSHAC level 3 SSC and GMC studies.

Prof. Tom Rockwell is a recognized expert in earthquake geology and characterization of active faults with experience in the SWUS and around the world. He is involved in the SCEC program for source characterization in southern California. Prof. Rockwell is relatively new to the SSHAC process with experience as a member of the PPRP for the ongoing DCPP SSC SSHAC level 3 study. Prof. Rockwell was selected as a PPRP member to provide a link between the GMC and the source characterization issues for the SWUS.

| | **Table 2A. Roles and responsibilities of the PPRP** |
|---|---|
| 1 | Provide a technical review of the TI team evaluation |
| 2 | Provide a process review of the SSHAC level 3 study |
| 3 | Attend all Workshops and selected working meetings |
| 4 | Review project plan |
| 4 | Review draft project report |
| 5 | Issue concurrence letter report (after review comments are adequately addressed) |

| | **Table 2B. ATTRIBUTES / SELECTION CRITERIA of the PPRP** |
|---|---|
| 1 | Technical expertise in empirical ground motion models for active crustal regions |
| 2 | Technical expertise in numerical simulations of ground motion models for active crustal regions |
| 3 | Technical expertise in source characterization in the SWUS (for interface issues between SSC and GMC models) |
| 4 | Working knowledge of PSHA |
| 5 | Past experience with SSHAC level 3 studies |

**4. Project Manager (PM)**

The PM is selected by the Project Sponsors. The roles and responsibilities of the Project Manager are given in Table 3A and the selection criteria are given in Table 3B.

The Project Sponsors selected Carola Di Alessandro as the PM. Dr. Di Alessandro has experience in engineering seismology and has also good organizational skills. She recently served as the coordinator for the Global Earthquake Model (GEM) ground motion characterization project conducted by PEER, coordinating a large number of ground motion experts. In the GEM project, she organized technical meetings and the preparation of technical reports that involved over 20 ground motion experts around the world.

| | **Table 3A. Roles and responsibilities** |
|---|---|
| 1 | With TI Lead, prepare Project Plan |
| 2 | Point of contact between Sponsors, TI Lead, PPRP, and QA |
| 3 | Responsible for development of and adherence to scope, schedule and budget |
| 4 | Responsible for establishing contracts and contractual compliance with all participants |
| 5 | Oversight of QA implementation Staff |
| 6 | Status reporting to Sponsors on schedule, scope, budget |
| 7 | Delivery of all technical products |

| | **Table 3B. ATTRIBUTES / SELECTION CRITERIA** |
|---|---|
| 1 | Familiarity with the SSHAC process, previous involvement in a SSHAC Level 3 or higher project |
| 2 | Proven ability to manage complex projects that involve multiple project roles, responsibilities, and participants |
| 3 | Technical background in seismic hazard |
| 4 | Experience and familiarity with NRC regulations, quality assurance, and regulatory compliance |
| 5 | Communication and management skills |
| 6 | Willingness to commit significant time to ensure timely delivery of all products |

**5. Hazard Analysts**

The Hazard Analysts are selected by each utility based on the selection criteria given in Table 4A. The roles and responsibilities of the Hazard Analysts are given in Table 4B. Based on the criteria in Table 4B, the Project Sponsors selected the following Hazard Analysts: Dr.

Nick Gregor for DCPP, Dr. Phalkun Tan and Andrew Dinsick for SONGS, and Dr. Melanie Walling for PVNGS. A brief description of the qualifications of each Hazard Analyst is given below.

Dr. Nick Gregor has over 20 years of experience in seismic hazard assessment. He was part of the Technical Support Staff for the Yucca Mountain project, being involved in the application of site-specific amplification factors using the PSHA hazard results. Recently Dr. Gregor was a TI Team member for the BCHydro GMC Level 3 study, where he assisted in the development of a new subduction earthquake ground motion prediction equation (GMPE) model based on world-wide data. In addition, he was part of the Technical Support Staff for the DCPP Shoreline Fault hazard study and is a Proponent Expert in the Hanford SSHAC level 3 project. During the last 15 plus years, Dr. Gregor has assisted Dr. Abrahamson in the modification and upgrade of his PSHA program. As part of this support, he was involved in producing the necessary QA validation documents for the hazard program used in the 2010 Shoreline report for PG&E. It is expected that for this project, the PSHA will again undergo modifications and Dr. Gregor will be the lead member for these expected changes.

Dr. Phalkun Tan is an Associate Engineer with GeoPentech and is heavily involved in the firm's geotechnical earthquake engineering practice. Dr. Tan has 24 years of experience in geotechnical earthquake engineering and numerical analysis. He was involved as Hazard Analyst in the ground motion evaluations for several important structures, such as the Vincent-Thomas Bridge in Long Beach, California, the Coronado Bay Bridge in San Diego, the Foothill Transportation Corridor alignment in Orange County, California, high rise commercial buildings in downtown Los Angeles and San Diego, earth dams and earth structures. He was also appointed the role of Hazard Analyst for the 2001 and 2010 SONGS PSHA studies. Additionally, he developed Woodward-Clyde and GeoPentech's computer program for probabilistic seismic hazard analysis. The GeoPentech computer code was one of the computer programs used in the PEER Verification of Probabilistic Seismic Hazard Analysis Computer Programs in 2009.

Dr. Melanie Walling has three years experience in seismic hazard and ground motion studies. She was one of the main people responsible for the QA of the LCI seismic hazard code. She is also part of the LCI team to compute the seismic hazard for many of the

Central and Eastern plants as part of their response to the NRC letter on Fukushima. She is working under the direction of Robin McGuire which will provide her additional support in seismic hazard as needed.

| | **Table 4A. Roles and responsibilities** |
|---|---|
| 1 | Responsible for hazard calculations and sensitivity analyses |
| 2 | Provide feedback to the TI Team and answer questions on the distributions used for the PSHA computation , identifying key contributors to uncertainty |

| | **Table 4B. ATTRIBUTES / SELECTION CRITERIA** |
|---|---|
| 1 | Technical expertise with hazard computation and analysis |
| 2 | Working knowledge of PSHA programs |
| 3 | Ability to perform hazard analysis under QA |

## APPENDIX B - PPRP LETTER APPROVING PROJECT PLAN

November 29, 2012

Carola Di Alessandro, Ph.D.
Project Manager for the SWUS GMC SSHAC
GeoPentech, Inc.
525 N. Cabrillo Park Drive, Suite 280
Santa Ana, CA 92701

Dear Dr. Di Alessandro:

The Participatory Peer Review Panel (PPRP) has reviewed the Project Plan (dated November 12, 2012) for the Southwestern U.S. Ground Motion Characterization (SWUS-GMC) SSHAC Level 3 study. The Project Plan document is well prepared, explains the SSHAC Level 3 guidelines well, and provides a framework for successful implementation of those guidelines. It is responsive to earlier PPRP's recommendations, as detailed in our memoranda dated September 17 and November 3, 2012, respectively. The Plan includes a Technical Integration (TI) team that brings the project an appropriate balance between experienced experts and more junior members, and includes high-level expertise in both empirical and simulation-based ground motion estimation.

The PPRP believes that the Project Plan has the elements required for meeting the SSHAC Level 3 objectives. We thank the project team for its efforts in developing the plan and look forward to its implementation.

Sincerely,

Steven M. Day
Chair, PPRP

Kenneth Campbell
Member, PPRP

Brian Chiou
Member, PPRP

Thomas Rockwell
Member, PPRP

# PPRP CLOSURE LETTER

March 10, 2015

Dr. Carola Di Alessandro
SWUS Project Manager
GeoPentech, Inc.
525 N. Cabrillo Park Drive, Suite 280
Santa Ana, CA 92701

Subject: Participatory Peer Review Panel Closure Letter, Southwest United States Ground Motion Characterization Level 3 SSHAC Project

Dear Dr. Di Alessandro:

The Participatory Peer Review Panel (PPRP, also referred to herein as the "Panel") for the Southwest United States (SWUS) Ground Motion Characterization (GMC) Project is pleased to issue this PPRP Closure Letter. Herein we describe our participation in the SWUS GMC SSHAC Level 3 project and present our findings. Pursuant to the guidelines for a SSHAC Level 3 study (NUREG/CR-6372; NUREG-2117), the PPRP was engaged at all stages of the project, including review of the final Project Plan, Workshop agendas and participant lists; the planning of the evaluation and model integration activities; and review of the project documentation. Throughout the project, the Panel reviewed and provided regular feedback on both the process followed, and the technical assessments made, by the Technical Integrator (TI) Team. By this letter the Panel documents the activities it has performed in the course of its review, its assessment of the process followed relative to SSHAC Level 3 expectations, and its assessment of the technical rationale underlying the GMC model.

The PPRP issued a previous letter dated February 24, 2015. In that letter, the Panel noted that there were limitations in the completeness and clarity of the project documentation. Those limitations were noted as exceptions to the Panel's finding that the project successfully met SSHAC Level 3 expectations. Since that time, the TI Team has produced a final report, designated Rev2, addressing the final set of comments from the Panel (PPRP Submittal No. 3, February 20, 2015). The Panel has reviewed Rev2 (including a short addendum supplied to the PPRP in draft form on March 9 which the TI Team has assured in writing will be incorporated in the final version) and finds that all material concerns have been adequately addressed and are now closed, apart from one remaining exception that will be described at the end of the SSHAC Process Review section below. Two GMC models were developed for application to Diablo Canyon Power Plant (DCPP) and Palo Verde Nuclear Generating Station (PVNGS), respectively. The exception applies only to the GMC model for DCPP, and is not relevant to the case of PVNGS.

**PPRP Activities in Support of the SWUS GMC Review**

In a SSHAC Level 3 study, the PPRP fulfills two roles. The first is that of technical review, in which the Panel ensures that the full range of data, models and methods are considered and that technical decisions and judgments are adequately justified and documented. The second is that of process review, under which the Panel ensures that the study maintains conformity with the SSHAC Level 3 guidelines. To fulfill these roles, the Panel requires adequate opportunities to gain understanding of the data being used, the analyses being performed, the TI Team's evaluations of data and models, and the technical justifications for the TI Team's model decisions. The table below summarizes the formal project activities in which the Panel participated. Fulfilling these roles also requires the Panel to provide regular feedback to the TI Team during the course of the project. In addition to verbal feedback during Working Meetings and Workshops, the Panel provided written comments and recommendations at key stages of the project. Those written submittals are also noted in the table.

| Date | PPRP Activity |
|---|---|
| June 21, 2012 | Working Meeting #1 (Planning). All PPRP members attended. |
| July 18, 2012 | Working Meeting #2 (Planning). All PPRP members attended. |
| August 27, 2012 | Kick-off Meeting. All PPRP members attended. |
| September 17, 2012 | PPRP submittal of written comments on the Project Plan. |
| October 8, 2012 | Working Meeting #3. PPRP representatives attended as observers. |
| November 3, 2012 | PPRP submittal of written comments on revised Project Plan. |
| November 29, 2012 | PPRP submittal of PPRP endorsement letter for Project Plan. |
| December 10, 2012 | Working Meeting #4. PPRP representatives attended as observers. |
| February 11, 2013 | Working Meeting #5. PPRP representatives attended as observers. |
| March 19-21, 2013 | Workshop #1: Critical issues and Data Needs. All PPRP members attended as observers. The PPRP provided verbal feedback to the TI Team at the end of each day of the Workshop |
| April 12, 2013 | Working Meeting #6. PPRP representatives attended as observers. |
| April 21, 2013 | PPRP submittal of written comments on Workshop #1. |
| May 23, 2013 | Working Meeting #7. PPRP representatives attended as observers. |
| June 24, 2013 | Working Meeting #8. PPRP representatives attended as observers. |
| July 16, 2013 | Working Meeting #9. PPRP representatives attended as observers. |
| August 21, 2013 | Working Meeting #10. PPRP representatives attended as observers. |
| October 2, 2013 | Working Meeting #11. PPRP representatives attended as observers. |
| October 15, 2013 | Working Meeting #12. PPRP representatives attended as observers. |
| October 22-24, 2013 | Workshop #2: Proponent Models and Alternative Interpretations. All PPRP members attended as observers. The PPRP provided verbal feedback to the TI Team at the end of each day of the Workshop. |
| November 26, 2013 | Working Meeting #13. PPRP representatives attended as observers. |
| December 3, 2013 | PPRP submittal of written comments on Workshop #2. |
| January 2, 2014 | Working Meeting #14. PPRP representatives attended as observers. |
| January 28-29, 2014 | Special Working Meeting. All PPRP members attended as observers. |
| March 3, 2014 | Working Meeting #15. PPRP representatives attended as observers. |
| March 10-12, 2014 | Workshop #3: Preliminary GMC Models and Hazard Feedback. All PPRP members attended as participants. The PPRP provided verbal feedback to the TI Team at the end of each day of the Workshop. |
| March 24, 2014 | Working Meeting #16. PPRP representatives attended as observers. |
| April 21, 2014 | PPRP submittal of written comments on Workshop #3. |

| | |
|---|---|
| May 14, 2014 | PPRP Closure Pre-Briefing. All PPRP members attended as participants. |
| July 17-18, 2014 | PPRP Closure Briefing. All PPRP members attended as participants. |
| December 13, 2014 | Submittal No. 1 of PPRP written review comments on SWUS GMC Report: Comments on SWUS GMC Report Rev.0, Chapters 7, 10, 11, 12, 13, and Appendices L, M, N, and R. |
| December 16, 2014 | Teleconference, PPRP and TI Team, to discuss the PPRP written review comments, Submittal No. 1. |
| January 5, 2015 | Submittal No. 2 of PPRP written review comments on SWUS GMC Report: Comments on SWUS GMC Report Rev.0, Chapters 6, 8, 9, 14, and Appendices H, I, J, K, O, and Q. |
| January 7, 2015 | Teleconference, PPRP and TI Team, to discuss the PPRP written review comments, Submittal No. 2. |
| January 26, 2015 | Teleconference, PPRP and TI Team, to discuss the main modifications introduced in SWUS GMC Report Draft Rev.1. |
| February 9, 2015 | Teleconference, PPRP and TI Team, to discuss observations from PPRP partial review of SWUS GMC Report Draft Rev.1. |
| February 16, 2015 | Teleconference, PPRP and Project Manager to discuss project completion schedule. |
| February 20, 2015 | Submittal No. 3 of PPRP written review comments on SWUS GMC Report: Comments on SWUS GMC Report Draft Rev.1. |
| February 24, 2015 | Submittal of Closure Letter based on Draft Rev.1 |

The PPRP finds that the level of ongoing review it was able to undertake, and the opportunities afforded the PPRP to provide feedback to the TI Team, met the expectations for a SSHAC Level 3 study. Interactions with the TI Team provided ample opportunity for the Panel to gain an understanding of the technical bases for the TI Team's evaluations. The Panel also was given adequate opportunity to query the TI Team, especially in Workshop #3 and in the Pre-Closure Briefing and Closure Briefing, to assess the justification provided for their model decisions. The TI Team provided written responses to each formal PPRP submittal, and in nearly every case the PPRP and TI Team subsequently discussed the comments and replies in a conference call or Working Meeting.

**SSHAC Process Review**

NUREG-2117 describes the goal of a SSHAC process as being "to carry out properly and document completely the activities of evaluation and integration, defined as:

> Evaluation: The consideration of the complete set of data, models and methods proposed by the larger technical community that are relevant to the hazard analysis.
> Integration: Representing the center, body, and range of technically defensible interpretations in light of the evaluation process (i.e., informed by the assessment of existing data, models, and methods)."

During the *Evaluation* activities, the TI Team considered new data, models and methods that have been introduced within the technical community since the previous seismic hazard studies were conducted for nuclear power plants in California and Arizona. The

Team evaluated newly available ground motion databases, ground motion prediction equations (GMPEs), and ground motion simulation techniques. Notably, the TI Team evaluated methods for the representation of non-Gaussian aleatory variability, as well as newly available methods for the visualization and characterization of epistemic uncertainty in ground motion prediction.

The PPRP finds that the TI Team's evaluation and the documentation thereof are consistent with the expectations for a SSHAC Level 3 study, apart from the specific reservation noted at the end of this section.

The *Integration* phase entails thoroughly documenting the technical bases for all elements of the GMC model, to provide assurance that the center, body and range of technically defensible interpretations have been captured. The TI Team used a new statistical technique to generate a suite of representative models for median ground motion prediction that collectively represent the epistemic uncertainty in ground motion more broadly than do the published GMPEs alone. This technique is combined with a new method to select and weight the predictions of the expanded suite of models. The TI Team's method for assigning weights is based on consideration of appropriate data sets and numerical simulations, with adequate justification. The TI Team's model for aleatory variability and weighting of alternative aleatory models is also adequately justified.

The PPRP finds that the TI Team's GMC model integration and the documentation thereof are consistent with the expectations of a SSHAC Level 3 project, apart from the specific reservation noted in the next paragraph.

The Panel finds that the TI Team's evaluation of directivity models has limitations. The TI Team make use of a simplified directivity model to save computational time, and the final report adequately describes that model, how it is used, and some of its limitations. However, because the simplified model is unpublished, it is also necessary for the TI Team to document that the simplified model is appropriate for the purpose for which it is applied, in the sense that it gives results that are essentially consistent with the published and peer-reviewed model that it is intended to approximate. The final report (in the March 9 addendum) documents the performance of the simplified model through comparison with results from a hazard calculation that uses the full, published directivity model. At hazard levels of $10^{-4}$ and above, the full model calculation confirms the conclusion obtained using the simplified model. At hazard levels below $10^{-4}$, however, the difference in calculated hazard between the full model and the simplified model increases with decreasing hazard level. This increasing trend has not been satisfactorily explained, has not been explored beyond the single fault case provided in the March 9 addendum, and has not been quantified in terms of impact on equal-hazard spectra at hazard levels of $10^{-5}$ and lower. Because the key rationale for the zero weighting of the directivity branch in the GMC model for periods longer than 0.5 s (the period range where the directivity effect applies) is the weak sensitivity of hazard to the directivity effect calculated using the simplified model, the PPRP finds that this weighting lacks sufficient technical justification.

**SSHAC Technical Review**

NUREG-2117 describes the PPRP's technical review role as follows:

> "The PPRP fulfills two parallel roles, the first being technical review. This means that the PPRP is charged with ensuring that the full range of data, models, and methods have been duly considered in the assessment and also that all technical decisions are adequately justified and documented.
>
> The responsibility of the PPRP is to provide clear and timely feedback to the TI/TFI and project manager to ensure that any technical or process deficiencies are identified at the earliest possible stage so that they can be corrected. More commonly, the PPRP provides its perspectives and advice regarding the manner in which ongoing activities can be improved or carried out more effectively. In terms of technical review, a key responsibility of the PPRP is to highlight any data, models or proponents that have not been considered. Beyond completeness, it is not within the remit of the PPRP to judge the weighting of the logic-trees in detail but rather to judge the justification provided for the models included or excluded, and for the weights applied to the logic-tree branches."

As summarized in the table above, the PPRP reviewed the TI Team's evaluations of data, models and methods on multiple occasions, and through various means, including written communications, in-person meetings, teleconferences, and review of the project report. The Panel was given adequate opportunity to question the TI Team concerning details of their analysis, and provided feedback verbally and in writing. The TI Team was responsive to the technical input from the Panel. The TI Team's responses included evaluating additional data sets suggested by the Panel, undertaking additional analyses to address specific Panel technical questions or concerns, and examining and assessing alternative technical approaches suggested by the Panel.

The PPRP therefore concludes that it has been afforded an adequate basis for technical assessment of the TI Team's evaluations and model integration. As noted above in the final paragraph of the SSHAC Process Review section, the evaluation of directivity effects has been inadequate and may constitute a technical limitation of the study. Apart from that reservation, the PPRP finds that the project meets technical expectations for a SSHAC Level 3 study.

**Conclusion**

On the basis of its review of the SWUS GMC project, the PPRP finds that the project meets, with respect to both process and technical standards, the expectations for a

SSHAC Level 3 study, with the reservation cited above. That reservation pertains specifically to application of the directivity component of the GMC model to the DCPP site.

Sincerely,

Steven M. Day
Chair, PPRP

Kenneth W. Campbell
Member, PPRP

Brian Chiou
Member, PPRP

Thomas K. Rockwell
Member, PPRP

# TI TEAM – PM RESPONSE TO PPRP CLOSURE LETTER

The PPRP letter identifies a limitation of the study due to the use of the Watson-Lamprey directivity model for the sensitivity studies that supported the TI Team judgment that directivity had only a small effect on the low-frequency ground-motion hazard at DCPP. The Watson-Lamprey model provides a simplified method to include the directivity in the CY14 model in a more efficient manner by randomizing over the hypocenter locations and developing site-specific adjustments to the median and standard deviation of the ground motion for the common-form models. The limitation is related to the differences in the computed hazard if the directivity model from CY14 is applied directly into the hazard rather than using the Watson-Lamprey implementation of the CY14 directivity scaling.

This limitation does not apply to PVNGS as there are no faults within 40 km of the site in the PVNGS SSC. The directivity model of CY14 reduces the directivity effects to zero for distances greater than 40 km, so there would be no directivity effects if the CY14 model was applied directly to the hazard calculations for the PVNGS site.

For DCPP, the differences between the directivity effects computed using the CY14 model directly and using the Watson-Lamprey model are discussed in Section 6.5 of this report. Including directivity for randomized hypocenter locations leads to additional variability of the low-frequency ground motion. This variability is combined with the total standard deviation. The key issue is if the standard deviation, developed from residuals from GMPEs that generally do not include directivity as a predictive parameter, should be reduced to account for the expected improved fit to the data if directivity parameters are included in the model. That is, should the additional aleatory variability be added to the standard deviation from the GMPEs or should it be added to a reduced standard deviation model that accounts for an improved fit if directivity parameters are included in the GMPE model.

The Watson-Lamprey model assumes that the standard deviations from the published GMPEs include the effects of variability due to directivity, and therefore, applies a reduction to standard deviation before adding the directivity effect on the standard deviation. If this reduction is not applied, then there will be an increase in the total standard deviation which leads to an increase in the hazard at low hazard levels. Section 6.5 shows examples of the effect on the hazard for these two alternatives. Developing a directivity model that is consistent with the median and standard deviation of the GMPEs remains an area of research.

The directivity sensitivity studies in this report that used the Watson-Lamprey model were for a period of 2 seconds. At this period, the reduction to the standard deviation in the Watson-Lamprey model is zero. Therefore, the conclusions from the hazard sensitivity for directivity are not affected by the approach of using a reduction to the standard deviation before adding the directivity effects. This

remains an issue for periods longer than 3 seconds, but the Watson-Lamprey model is not applied in the final GMC model.

At a period of 3 seconds, using either approach leads to a small effect on the hazard at the 1E-4 hazard level as shown in Section 6.5. The directivity effect is primarily a standard deviation effect. If the directivity effect is applied to the full standard deviation (without reduction), then there is a potential increase of 2% to 8% for the ground motion at the 1E-4 to 1E-6 hazard level for T = 3 seconds. This increase reflects the effect of the increased standard deviation. The range of total standard deviation models developed in Chapter 13 of this report for a period of T = 2 seconds leads to a broad range (15% to 25%) for 1E-4 to 1E-6, as shown in the hazard sensitivity results in Section 14. The same range of epistemic uncertainty will apply for T = 3 seconds. The TI Team agrees that implementation of directivity into ground-motion models needs further research and that there is uncertainty in the effect of directivity on the total standard deviation, but, given that the potential range of the directivity effects is well within the range captured by the epistemic uncertainty in the total sigma logic tree, the TI Team judges that total sigma logic tree adequately captures the potential range of the standard deviation including directivity effects. The limitation noted by the PPRP does not significantly affect the range of the standard deviation of the ground-motion model for application to DCPP.

# *APPENDIX C*

## FINAL SWUS GMC MODELS HAZARD INPUT DOCUMENTS (HIDS)

# PART I

## SWUS GMC MODELS HAZARD INPUT DOCUMENT (HID) FOR PVNGS

Revision 2

# 1. Notation

The notation in Table 1-1 is used for the ground motion models for PVNGS site.

**Table 1-1:** Notation used in HID, Part I: PVNGS.

| | |
|---|---|
| T | Period (sec) |
| M | Moment magnitude |
| NML | Normal sources (-120 ≤ rake ≤ -60) |
| REV | Reverse sources, including reverse-oblique (REV-OBL); (30 ≤ rake ≤ 150) |
| SS | Strike-slip sources, including normal-oblique; (-180 ≤ rake < -120, -60 < rake < 30, and 150 < rake ≤ 180) |
| $F_{NML}$ | Normal Style of faulting ($F_{NML}$=1 for NML, 0 otherwise) |
| $F_{RV}$ | Reverse Style of faulting ($F_{RV}$=1 for REV & REV-OBL, 0 otherwise) |
| $Z_{TOR}$ | Depth to top of rupture (km) |
| Dip | Fault dip (degrees) |
| W | Down-dip rupture width (km) |
| $R_{RUP}$ | Rupture distance (km) |
| $R_{JB}$ | Joyner-Boore distance (km) |
| $R_X$ | Horizontal distance from top of rupture measured perpendicular to strike (km) |
| $f_{HW}$ | Hanging-wall factor |
| $f$_ADD_Path | Additional epistemic uncertainty due to magnitude scaling when path effects are modelled |
| $f$_ADD_no_Path | Additional epistemic uncertainty due to magnitude scaling when path effects are not modelled |
| $\mu_{PATH}$ | Median path term |
| $\sigma_{SS}$ | Total sigma when path effects are not modelled |
| $\sigma_{SP-R}$ | Total sigma when path effects are modelled |

# 2. Median ground motion model for PVNGS: Greater Arizona Sources

## 2.1 Structure of the Logic Tree

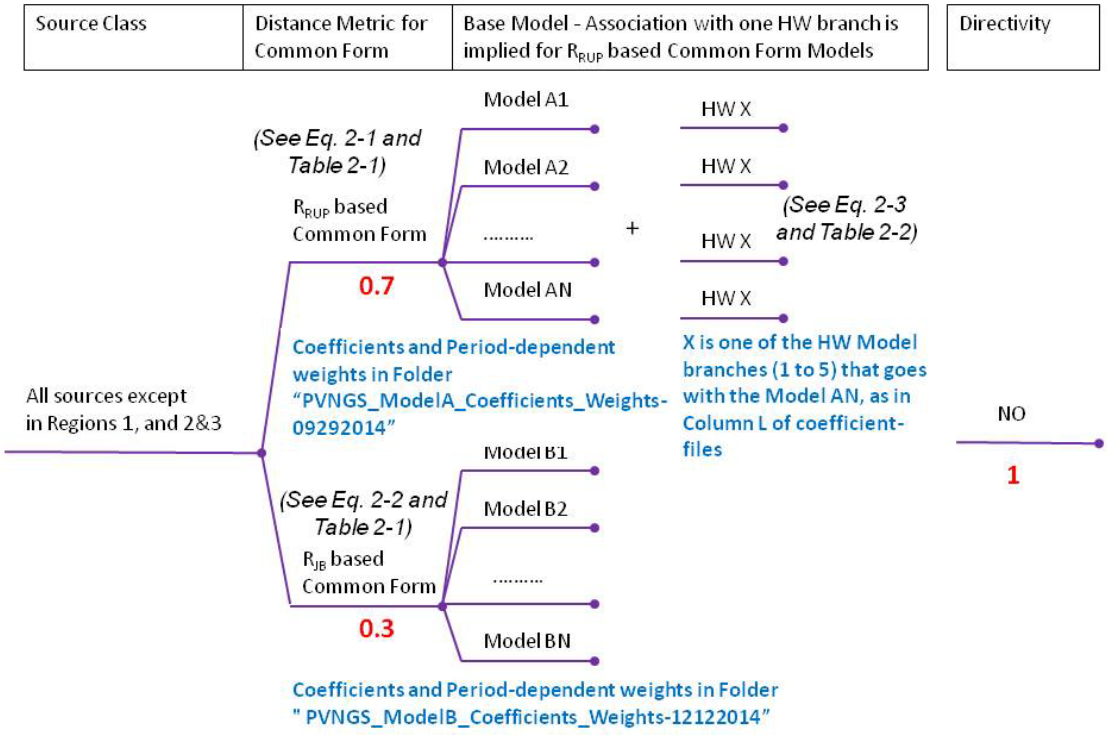



**Figure 2-1:** Logic Tree for Median at PVNGS (Greater Arizona Sources).

## 2.2 Common Functional Form for Base Model

There are two versions of the common functional form for the PVNGS GMPEs: the A Models based on the $R_{RUP}$ distance metric (Eq. 2-1) and the B Models based on the $R_{JB}$ distance metric (Eq. 2-2):

$$Ln\left(SA_A(M,R_{RUP},Z_{TOR},F,T)\right) = a_0(T) - a_7^2(T)R_{RUP} + a_8^2(T)Z_{TOR} - a_9^2(T)F_{NML} + \left(a_4(T) + a_5(T)(M-5)\right)\ln\left(\sqrt{R_{RUP}^2 + a_6^2(T)}\right) + a_{10}(T)F_{RV} + \begin{cases} -a_1(T) + a_2(T)(M-5.5) & for\ M < 5.5 \\ a_1(T)(M-6.5) & for\ 5.5 \le M \le 6.5 \\ a_3(T)(M-6.5) & for\ M > 6.5 \end{cases}$$

(Eq. 2-1)

$$Ln\left(SA_B(M,R_{JB},Z_{TOR},F,T)\right) = a_0(T) - a_7^2(T)R_{JB} + a_8^2(T)Z_{TOR} - a_9^2(T)F_{NML} + \left(a_4(T) + a_5(T)(M-5)\right)\ln\left(\sqrt{R_{JB}^2 + a_6^2(T)}\right) + a_{10}(T)F_{RV} + \begin{cases} -a_1(T) + a_2(T)(M-5.5) & for\ M < 5.5 \\ a_1(T)(M-6.5) & for\ 5.5 \le M \le 6.5 \\ a_3(T)(M-6.5) & for\ M > 6.5 \end{cases}$$

(Eq. 2-2)

The coefficients for 17 spectral periods and up to 31 models for the $R_{RUP}$-based models (A Models) are listed in the excel files named "Coefficients_Weights_PVNGS_ModelA_T*X*.csv", where *X* is the period, which are collected under the folder "PVNGS_ModelA_Coefficients_Weights-09292014". There may be less than 31 models for a specific period, so the User is invited to refer to the model ID information provided in the first column. The coefficients for the $R_{JB}$-based models (B Models) are listed in the excel files named "Coefficients_Weights_PVNGS_ModelB_T*X*.csv", where *X* is the period, which are collected under the folder "PVNGS_ModelB_Coefficients_Weights-12122014".

The weights for the models for each spectral period are also included in the same file as the coefficients. The list and characteristics of the files providing coefficients and weights are described in Section 6 of this document.

For the $R_{RUP}$-base models, there is a univocal association between each model ID and one of the five alternative HW adjustments branches (see Section 2.3), as specified in the column L of the coefficient files. The HW adjustment is not applied to the $R_{JB}$-based models.

The HW adjustments only apply to $R_X \geq 0$.

The model is applicable for SS, NML and REV earthquakes. For SS and NML earthquakes, $F_{RV}$ is zero. Period dependent $a_{10}$ coefficients for $F_{RV}$ are provided in Table 2-1. A single $a_{10}$ value is used at each period for all the common form models.

Validated tables showing predicted PSA for the $R_{RUP}$-based models (A Models) and for the $R_{JB}$-based models (B Models), for a range of magnitude, distance and other predictors are provided as an electronic attachment to the HID. List and details of the benchmarking tables are addressed in Section 7 of this document.

**Table 2-1:** Period dependent $a_{10}$ coefficients for $F_{RV}$.

| Period (sec) | $a_{10}$ |
|---|---|
| 0.01 | 0.070 |
| 0.02 | 0.070 |
| 0.03 | 0.070 |
| 0.05 | 0.070 |
| 0.075 | 0.070 |
| 0.1 | 0.070 |
| 0.15 | 0.070 |
| 0.2 | 0.070 |
| 0.25 | 0.070 |
| 0.3 | 0.070 |
| 0.4 | 0.070 |
| 0.5 | 0.058 |
| 0.75 | 0.049 |
| 1 | 0.039 |
| 1.5 | 0.030 |
| 2 | 0.020 |
| 3 | 0.000 |
| 4 | 0.000 |
| 5 | 0.000 |
| 7.5 | 0.000 |
| 10 | 0.000 |

## 2.3 Common Form for Hanging Wall Effects

The common form for the hanging wall effect is given in eq. 2-3a, 2-3b, and 2-3c:

$$f_{HW}(M, Dip, W, R_X, R_{JB}, R_{RUP}, Z_{TOR}) = C_1(T)\cos(dip)\left[C_2(T) + (1 - C_2(T))\tanh\left(\frac{C_3(T)R_X}{W\cos(dip)}\right)\right] \times \left(1 + C_4(T)(M-7)\right)T_{HW\_R}(R_{RUP}, R_{JB})T_{HW\_Z}(Z_{TOR})$$

(Eq. 2-3a)

where

$$T_{HW\_R}(R_{JB}, R_{RUP}) = 1 - \frac{R_{JB}}{R_{RUP} + 0.1} \quad \text{(Eq. 2-3 b)}$$

$$T_{HW\_Z}(Z_{TOR}) = \max\left\{0,\ \ 1 - \frac{Z_{TOR}}{12}\right\} \quad \text{(Eq. 2-3 c)}$$

The coefficients for the HW model are listed in Table 2-2 for the five alternative HW models. The C2, C3, and C4 terms are the same for all five models.

**Table 2-2:** Coefficients for HW Factor Model**.**

| Period (sec) | Model-dependent C1 Coefficients | | | | | Coefficients held Constant for all five models | | |
|---|---|---|---|---|---|---|---|---|
| | *Model HW1* | *Model HW 2* | *Model HW 3* | *Model HW 4* | *Model HW 5* | $C_2$ | $C_3$ | $C_4$ |
| 0.01 | 0.868 | 0.982 | 1.038 | 1.095 | 1.209 | 0.2160 | 2.0289 | 0.1675 |
| 0.02 | 0.867 | 0.987 | 1.046 | 1.106 | 1.226 | 0.2172 | 2.0260 | 0.1666 |
| 0.03 | 0.856 | 0.997 | 1.067 | 1.138 | 1.278 | 0.2178 | 2.0163 | 0.1670 |
| 0.05 | 0.840 | 1.027 | 1.121 | 1.215 | 1.402 | 0.2199 | 1.9870 | 0.1699 |
| 0.075 | 0.857 | 1.041 | 1.133 | 1.226 | 1.410 | 0.2218 | 1.9906 | 0.1817 |
| 0.1 | 0.848 | 1.040 | 1.135 | 1.231 | 1.422 | 0.2213 | 1.9974 | 0.1717 |
| 0.15 | 0.868 | 1.009 | 1.080 | 1.150 | 1.292 | 0.2169 | 2.0162 | 0.1814 |
| 0.2 | 0.850 | 1.005 | 1.082 | 1.160 | 1.315 | 0.2131 | 1.9746 | 0.1834 |
| 0.25 | 0.868 | 0.985 | 1.044 | 1.102 | 1.219 | 0.1988 | 1.9931 | 0.1767 |
| 0.3 | 0.839 | 0.974 | 1.041 | 1.108 | 1.242 | 0.2019 | 2.0179 | 0.1658 |
| 0.4 | 0.780 | 0.934 | 1.011 | 1.089 | 1.243 | 0.2090 | 2.0249 | 0.1624 |
| 0.5 | 0.741 | 0.902 | 0.982 | 1.063 | 1.223 | 0.2053 | 2.0041 | 0.1719 |
| 0.75 | 0.613 | 0.869 | 0.997 | 1.125 | 1.380 | 0.1713 | 1.8697 | 0.1866 |
| 1 | 0.621 | 0.788 | 0.872 | 0.955 | 1.123 | 0.1571 | 1.8526 | 0.3143 |
| 1.5 | 0.506 | 0.662 | 0.740 | 0.818 | 0.974 | 0.1559 | 1.8336 | 0.3195 |
| 2 | 0.391 | 0.537 | 0.609 | 0.682 | 0.828 | 0.1559 | 1.7996 | 0.3246 |
| 3 | 0.128 | 0.245 | 0.304 | 0.362 | 0.480 | 0.1616 | 1.6740 | 0.3314 |
| 4 | 0 | 0.034 | 0.088 | 0.138 | 0.231 | 0.1616 | 1.6740 | 0.3314 |
| 5 | 0 | 0 | 0 | 0 | 0.040 | 0.1616 | 1.6740 | 0.3314 |
| 7.5 | 0 | 0 | 0 | 0 | 0 | 0.1616 | 1.6740 | 0.3314 |
| 10 | 0 | 0 | 0 | 0 | 0 | 0.1616 | 1.6740 | 0.3314 |

## 2.4 PVNGS Ground Motion for the Median for Greater Arizona Sources

When $R_{RUP}$-based models are used, the PVNGS ground motion model for the median from sources in Greater Arizona is given by:

$$\ln(SA(g)) = Ln\left(SA_{BASE}(M, R_{RUP}, Z_{TOR}, F, T)\right) + f_{HW}(M, Dip, W, R_X, R_{JB}, R_{RUP}, Z_{TOR}) \quad \text{(Eq. 2-4)}$$

$f_{HW}$ only applies to $R_X \geq 0$.

When $R_{JB}$-based models are used, the PVNGS ground motion model for the median from sources in Greater Arizona is given by:

$$\ln(SA(g)) = Ln\left(SA_{BASE}(M, R_{JB}, Z_{TOR}, F, T)\right) \quad \text{(Eq. 2-5)}$$

# 3. Median Ground Motion Model for PVNGS: Sources in California and Mexico

## 3.1 Structure of the Logic Tree

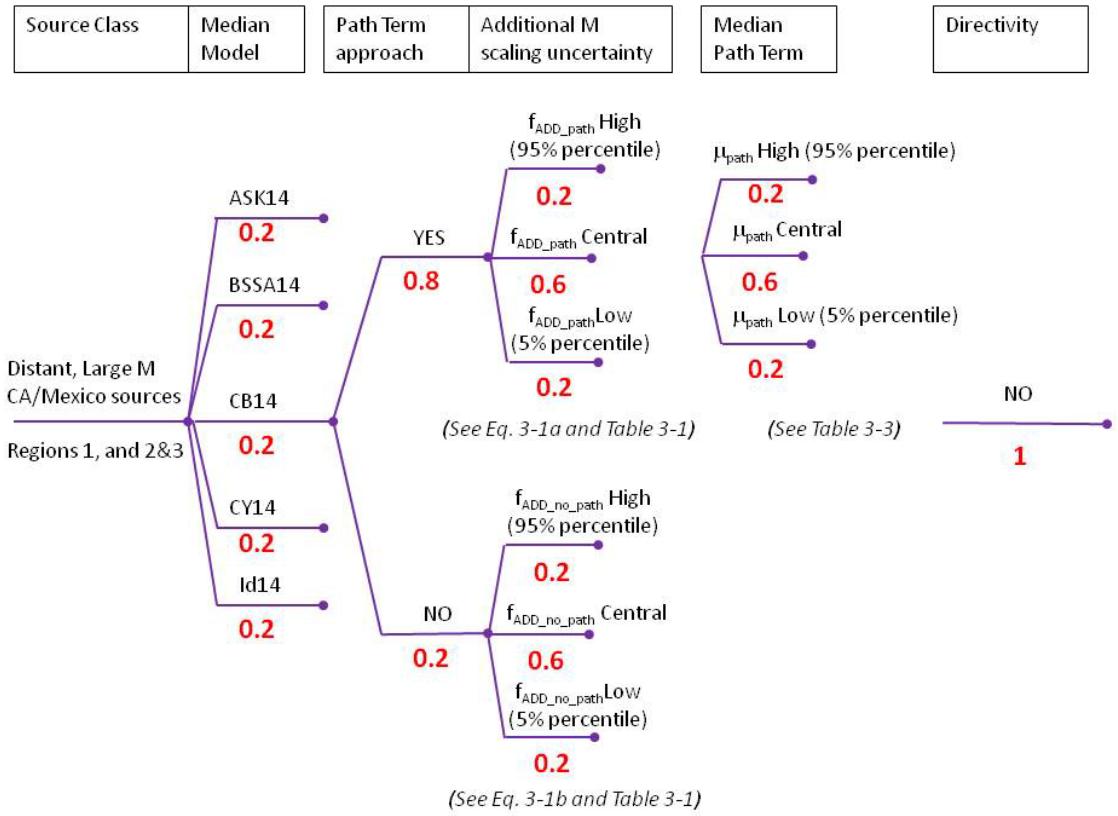



**Figure 3-1:** Logic Tree for Median at PVNGS (Sources in California and Mexico, i.e. Regions 1, 2&3).

The median base model is represented by the five NGA-West2 GMPEs (Abrahamson et al., 2014 – ASK14; Boore et al., 2014 – BSSA14; Campbell and Bozorgnia, 2014 – CB14; Chiou and Youngs, 2014 – CY14; and Idriss, 2014 – Id14) equally weighted.

## 3.2 Uncertainty for Large Magnitude Scaling

For the branch where the path effect is accounted for:

$$f_{ADD\_path}(M,T) = \begin{cases} 0 & \text{for } M \le 7 \\ c_1\sqrt{\left[0.083+0.056(M-7)\right]^2 - \left[0.083\right]^2} & \text{for } M > 7 \end{cases} \qquad \text{(Eq. 3-1a)}$$

For the branch where the path effect is not accounted for:

$$f_{ADD\_no\_path}(M,T) = c_1\left[0.083 + 0.056\max\{0, M-7\} + 0.0171\max\{0, \ln(T)\}\right] \quad \text{(Eq. 3-1b)}$$

**Table 3-1:** Coefficients for large magnitude scaling models

| Branch | $C_1$ |
|---|---|
| High | 1.6 |
| Central | 0.0 |
| Low | -1.6 |

## 3.3 Median Path Terms

Path terms, $\mu_{PATH}$, are given for two source regions: Region 1 and combined Regions 2&3. The boundaries of Region 1 and Regions 2&3 are shown in Figure 3-2. The geographical coordinates of the regions are provided in Tables 3-2a and 3-2b. Unambiguous association between ground motion regions (Region 1, Region 2&3, or other) and PVNGS sources is included in the PVNGS SSC HID documentation.

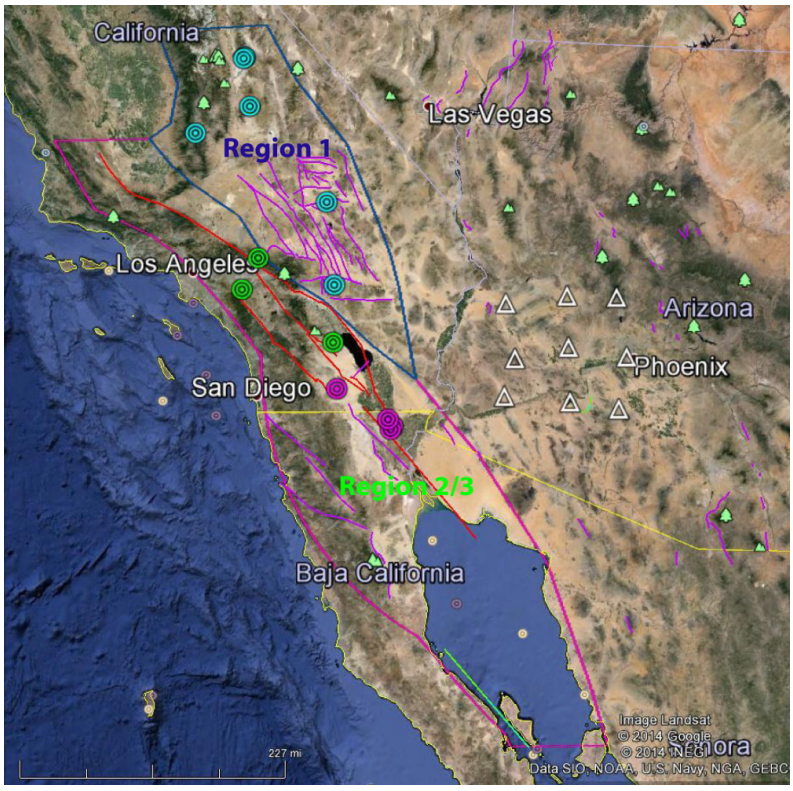



**Figure 3-2:** Geographical extension of Regions 1 and 2&3 for Path Effects Adjustment.

**Table 3-2a:** Geographic coordinates defining Region 1.

| Name | X | Y | ORDER |
|---|---|---|---|
| Region1 | -119.243 | 36.80123 | 0 |
| Region1 | -117.616 | 36.98277 | 1 |
| Region1 | -117.07 | 36.3597 | 2 |
| Region1 | -116.239 | 35.66656 | 3 |
| Region1 | -116.082 | 35.41244 | 4 |
| Region1 | -115.791 | 34.96007 | 5 |
| Region1 | -115.637 | 34.71788 | 6 |
| Region1 | -115.477 | 34.43189 | 7 |
| Region1 | -115.326 | 34.08243 | 8 |
| Region1 | -114.993 | 33.06271 | 9 |
| Region1 | -115.634 | 33.40997 | 10 |
| Region1 | -115.996 | 33.64553 | 11 |
| Region1 | -116.342 | 33.86293 | 12 |
| Region1 | -116.824 | 34.07176 | 13 |
| Region1 | -117.203 | 34.26695 | 14 |
| Region1 | -117.398 | 34.46703 | 15 |
| Region1 | -117.674 | 34.74249 | 16 |
| Region1 | -118.396 | 35.05972 | 17 |
| Region1 | -118.599 | 35.17647 | 18 |
| Region1 | -118.757 | 35.25629 | 19 |
| Region1 | -119.13 | 35.5388 | 20 |
| Region1 | -118.856 | 35.73904 | 21 |
| Region1 | -118.822 | 36.20548 | 22 |

**Table 3-2b:** Geographic coordinates defining combined Regions 2 and 3.

| Name | X | Y | ORDER |
|---|---|---|---|
| Region2&3 | -113.796 | 29.3302 | 0 |
| Region2&3 | -114.191 | 29.67062 | 1 |
| Region2&3 | -114.491 | 29.94781 | 2 |
| Region2&3 | -114.736 | 30.15802 | 3 |
| Region2&3 | -114.854 | 30.20975 | 4 |
| Region2&3 | -114.969 | 30.26373 | 5 |
| Region2&3 | -115.08 | 30.32048 | 6 |
| Region2&3 | -115.206 | 30.38903 | 7 |
| Region2&3 | -115.33 | 30.46132 | 8 |
| Region2&3 | -115.45 | 30.53726 | 9 |
| Region2&3 | -115.568 | 30.61677 | 10 |
| Region2&3 | -115.682 | 30.69976 | 11 |
| Region2&3 | -115.793 | 30.78611 | 12 |
| Region2&3 | -115.9 | 30.87574 | 13 |
| Region2&3 | -116.004 | 30.96854 | 14 |
| Region2&3 | -116.104 | 31.0644 | 15 |
| Region2&3 | -116.201 | 31.1632 | 16 |
| Region2&3 | -116.293 | 31.26483 | 17 |
| Region2&3 | -116.381 | 31.36916 | 18 |
| Region2&3 | -116.465 | 31.47608 | 19 |
| Region2&3 | -116.545 | 31.58544 | 20 |
| Region2&3 | -116.621 | 31.69714 | 21 |
| Region2&3 | -116.691 | 31.81102 | 22 |

The path terms are a constant added to the median prediction. The central, high, and low values of the path terms are listed in Table 3-3.

**Table 3-3:** Median Path Term**.**

| | Path Term - Region 1 | | | Path Term - Region 2&3 | | |
|---|---|---|---|---|---|---|
| Period (sec) | Central | High | Low | Central | High | Low |
| PGA | -0.119 | 0.1 | -0.338 | -0.626 | -0.387 | -0.866 |
| 0.02 | -0.119 | 0.1 | -0.338 | -0.626 | -0.387 | -0.866 |
| 0.03 | -0.119 | 0.1 | -0.338 | -0.626 | -0.387 | -0.866 |
| 0.05 | -0.119 | 0.1 | -0.338 | -0.626 | -0.387 | -0.866 |
| 0.075 | -0.119 | 0.1 | -0.338 | -0.626 | -0.387 | -0.866 |
| 0.1 | -0.119 | 0.1 | -0.338 | -0.626 | -0.387 | -0.866 |
| 0.15 | -0.119 | 0.1 | -0.338 | -0.626 | -0.387 | -0.866 |
| 0.2 | -0.119 | 0.1 | -0.338 | -0.626 | -0.387 | -0.866 |
| 0.25 | -0.119 | 0.1 | -0.338 | -0.626 | -0.387 | -0.866 |
| 0.3 | -0.119 | 0.1 | -0.338 | -0.626 | -0.387 | -0.866 |
| 0.4 | -0.119 | 0.1 | -0.338 | -0.626 | -0.387 | -0.866 |
| 0.5 | -0.119 | 0.1 | -0.338 | -0.626 | -0.387 | -0.866 |
| 0.75 | -0.119 | 0.1 | -0.338 | -0.626 | -0.387 | -0.866 |
| 1 | -0.119 | 0.1 | -0.338 | -0.626 | -0.387 | -0.866 |
| 1.5 | -0.119 | 0.131 | -0.369 | -0.626 | -0.331 | -0.921 |
| 2 | -0.119 | 0.163 | -0.401 | -0.626 | -0.276 | -0.977 |
| 3 | -0.119 | 0.184 | -0.421 | -0.626 | -0.256 | -0.996 |
| 4 | -0.119 | 0.198 | -0.436 | -0.626 | -0.229 | -1.023 |
| 5 | -0.119 | 0.209 | -0.447 | -0.626 | -0.210 | -1.042 |
| 7.5 | -0.119 | 0.23 | -0.468 | -0.626 | -0.195 | -1.057 |
| 10 | -0.119 | 0.245 | -0.483 | -0.626 | -0.168 | -1.084 |

## 3.4 PVNGS Ground Motion for the Median from California and Mexico Sources (Regions 1, and 2&3)

The ground motion models for the median at PVNGS (Sources in Regions 1, and 2&3) are valid for NML, SS and REV events. The median ground motion model is given by:

$$\ln\left(SA(g)\right)=\ln(ASK14)+f_{ADD\_MAG}(M,T)+\mu_{PATH}(T,Region) \quad \text{(Eq. 3-2a)}$$

$$\ln\left(SA(g)\right)=\ln(BSSA14)+f_{ADD\_MAG}(M,T)+\mu_{PATH}(T,Region) \quad \text{(Eq. 3-2b)}$$

$$\ln\left(SA(g)\right)=\ln(CB14)+f_{ADD\_MAG}(M,T)+\mu_{PATH}(T,Region) \quad \text{(Eq. 3-2c)}$$

$$\ln\left(SA(g)\right)=\ln(CY14)+f_{ADD\_MAG}(M,T)+\mu_{PATH}(T,Region) \quad \text{(Eq. 3-2d)}$$

$$\ln\left(SA(g)\right)=\ln(Id14)+f_{ADD\_MAG}(M,T)+\mu_{PATH}(T,Region) \quad \text{(Eq. 3-2e)}$$

Where $f_{ADD\_MAG}(M,T)$ is $f_{ADD\_\text{path}}(M,T)$ for the branch where the path effect is included, and is $f_{ADD\_\text{no\_path}}(M,T)$ for the branch where the path effect is excluded

For the branch without the path term, $\mu_{PATH}(T,Region)$ =0 in Eq. 3-2.

# 4. Total Sigma Model for PVNGS: Greater Arizona Sources

## 4.1 Structure of the Logic Tree

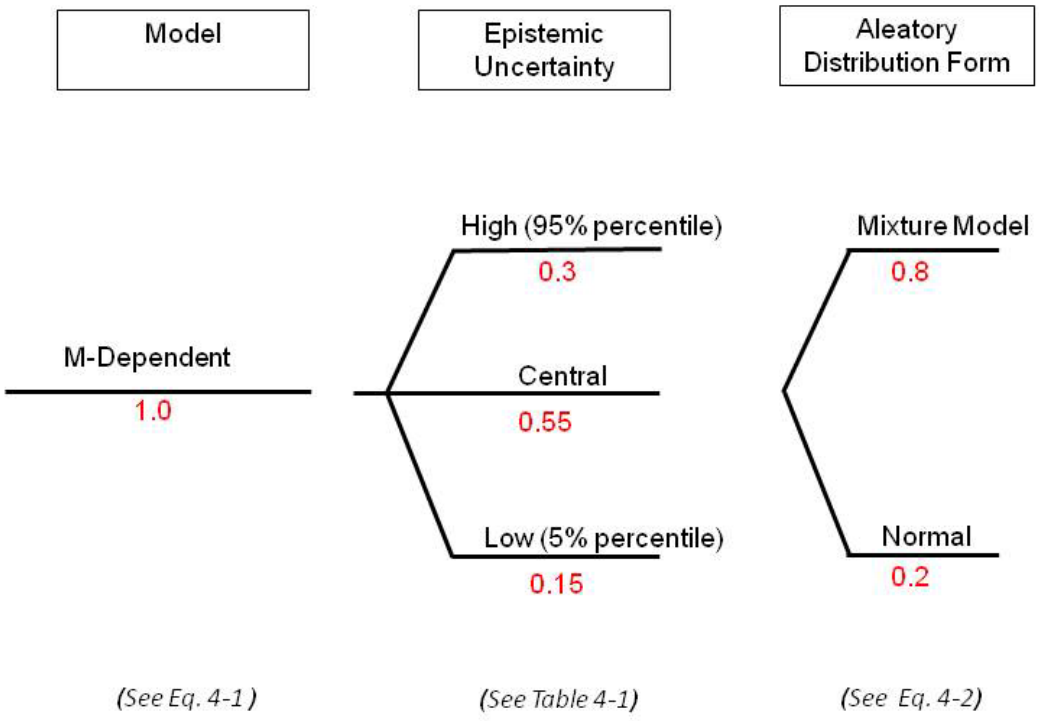



**Figure 4-1:** Logic Tree for Total Sigma at PVNGS (Greater Arizona Sources).

## 4.2 PVNGS Total Sigma Model for Sources in Greater Arizona

The model for σ is magnitude dependent and follows the formulation in Equation 4-1:

$$\sigma_{SS}(M) = \begin{cases} \sigma_1 + \frac{(M-5)}{2} * (\sigma_2 - \sigma_1) & for\ M < 7.0 \\ \sigma_2 & for\ M \geq 7.0 \end{cases} \quad \text{(Eq. 4-1)}$$

The resulting epistemic distribution and period-dependent values of $\sigma_1$ and $\sigma_2$ are listed in Table 4-1:

**Table 4-1:** Epistemic Distribution for $\sigma_{SS}$ for PVNGS – Greater Arizona Sources.

| Period (sec) | Low Branch | | Central Branch | | High Branch | |
|---|---|---|---|---|---|---|
| | $\sigma_1$ | $\sigma_2$ | $\sigma_1$ | $\sigma_2$ | $\sigma_1$ | $\sigma_2$ |
| 0.01 | 0.461 | 0.459 | 0.573 | 0.553 | 0.694 | 0.652 |
| 0.02 | 0.461 | 0.459 | 0.574 | 0.553 | 0.695 | 0.653 |
| 0.03 | 0.461 | 0.460 | 0.574 | 0.553 | 0.695 | 0.653 |
| 0.05 | 0.462 | 0.460 | 0.575 | 0.554 | 0.696 | 0.655 |
| 0.075 | 0.462 | 0.460 | 0.576 | 0.555 | 0.697 | 0.656 |
| 0.1 | 0.463 | 0.461 | 0.576 | 0.555 | 0.698 | 0.657 |
| 0.15 | 0.463 | 0.461 | 0.577 | 0.556 | 0.699 | 0.658 |
| 0.2 | 0.463 | 0.461 | 0.577 | 0.556 | 0.700 | 0.659 |
| 0.25 | 0.463 | 0.461 | 0.578 | 0.557 | 0.701 | 0.660 |
| 0.3 | 0.463 | 0.461 | 0.578 | 0.557 | 0.701 | 0.661 |
| 0.4 | 0.464 | 0.461 | 0.578 | 0.557 | 0.702 | 0.662 |
| 0.5 | 0.464 | 0.461 | 0.579 | 0.558 | 0.702 | 0.662 |
| 0.75 | 0.464 | 0.462 | 0.579 | 0.558 | 0.703 | 0.664 |
| 1 | 0.464 | 0.462 | 0.579 | 0.558 | 0.704 | 0.664 |
| 1.5 | 0.464 | 0.462 | 0.580 | 0.559 | 0.705 | 0.665 |
| 2 | 0.464 | 0.462 | 0.580 | 0.559 | 0.705 | 0.666 |
| 3 | 0.464 | 0.462 | 0.580 | 0.559 | 0.706 | 0.667 |
| 4 | 0.464 | 0.462 | 0.580 | 0.559 | 0.706 | 0.667 |
| 5 | 0.464 | 0.462 | 0.580 | 0.559 | 0.707 | 0.667 |
| 7.5 | 0.464 | 0.462 | 0.581 | 0.560 | 0.707 | 0.668 |
| 10 | 0.464 | 0.462 | 0.581 | 0.560 | 0.707 | 0.668 |

## 4.3 PVNGS Mixture Model

The mixture model is the sum of two equally weighted normal distributions with the standard deviation given by 0.8 and 1.2 times the total standard deviation. To implement the mixture model in the hazard calculation, the conditional probability of exceeding a ground motion value z is weighted average of the conditional probabilities computed for each of the standard deviation value separately (Eq. 4-2).

$$P_{MIX}(Sa > z \mid M, R, ..., \sigma_{SS}) = 0.5P(Sa > z \mid M, R, ..., 0.8\sigma_{SS}) + 0.5P(Sa > z \mid M, R, ..., 1.2\sigma_{SS})$$

(Eq. 4-2)

# 5. Total Sigma Model for PVNGS: Sources in California and Mexico

## 5.1. Structure of the Logic Tree

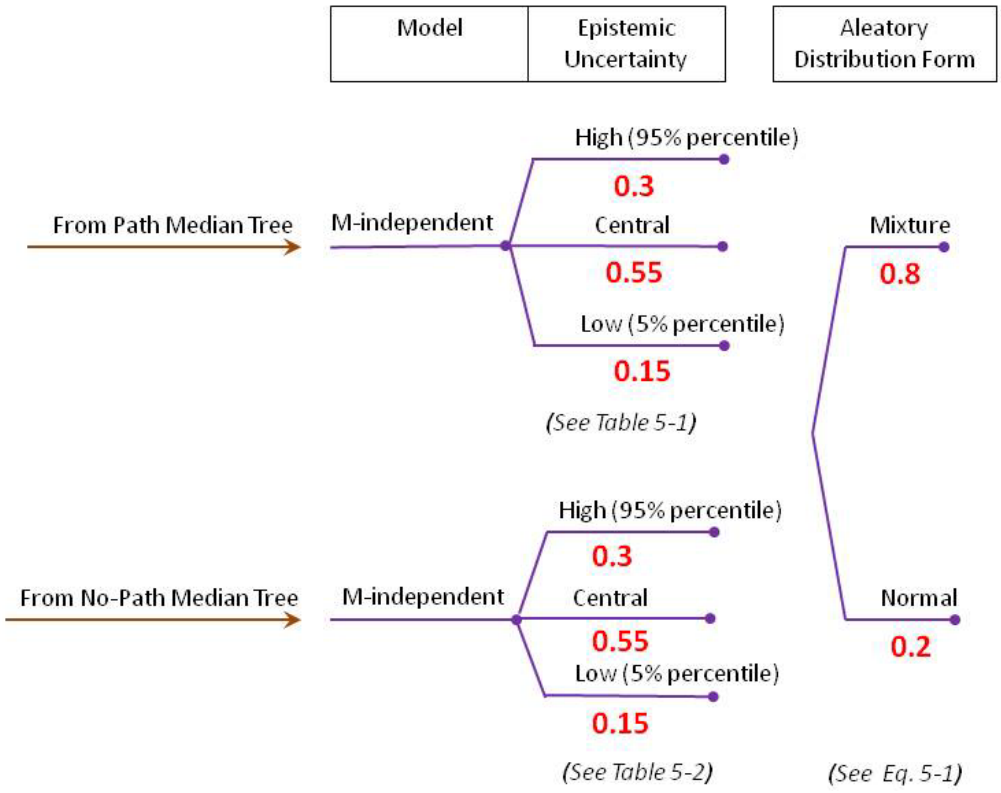



**Figure 5-1:** Logic Tree for Total Sigma at PVNGS (Sources in California and Mexico).

## 5.2. Structure of the Logic Tree PVNGS for Sources in California and Mexico

Two models are developed for σ for ground motions from the distant California/Mexico sources. One model is for the case when path specific adjustments are applied, designated $\sigma_{SP\text{-}R}$, and the second model is $\sigma_{SS}$ for the case when path adjustments are not applied. Both of these models are magnitude independent. The resulting values of σ are listed in Tables 5-1 and 5-2.

**Table 5-1:** Epistemic Distribution for $\sigma_{SP-R}$ for PVNGS – Distant California Sources, Path Effects Modelled Case.

| Period (sec) | Low Branch | Central Branch | High Branch |
|---|---|---|---|
| 0.01 | 0.354 | 0.449 | 0.552 |
| 0.02 | 0.354 | 0.449 | 0.552 |
| 0.03 | 0.354 | 0.449 | 0.552 |
| 0.05 | 0.354 | 0.449 | 0.552 |
| 0.075 | 0.354 | 0.449 | 0.552 |
| 0.1 | 0.354 | 0.449 | 0.552 |
| 0.15 | 0.354 | 0.449 | 0.552 |
| 0.2 | 0.354 | 0.449 | 0.552 |
| 0.25 | 0.354 | 0.449 | 0.552 |
| 0.3 | 0.354 | 0.449 | 0.552 |
| 0.4 | 0.354 | 0.449 | 0.552 |
| 0.5 | 0.354 | 0.449 | 0.552 |
| 0.75 | 0.375 | 0.473 | 0.579 |
| 1 | 0.390 | 0.491 | 0.600 |
| 1.5 | 0.410 | 0.517 | 0.631 |
| 2 | 0.425 | 0.535 | 0.655 |
| 3 | 0.425 | 0.535 | 0.655 |
| 4 | 0.425 | 0.535 | 0.655 |
| 5 | 0.425 | 0.535 | 0.655 |
| 7.5 | 0.425 | 0.535 | 0.655 |
| 10 | 0.425 | 0.535 | 0.655 |

**Table 5-2:** Epistemic Distribution for $\sigma_{SS}$ for PVNGS – Distant California Sources, Path Effects Not Modelled Case.

| Period (sec) | Low Branch | Central Branch | High Branch |
|---|---|---|---|
| 0.01 | 0.512 | 0.613 | 0.720 |
| 0.02 | 0.512 | 0.613 | 0.720 |
| 0.03 | 0.512 | 0.613 | 0.720 |
| 0.05 | 0.512 | 0.613 | 0.720 |
| 0.075 | 0.512 | 0.613 | 0.720 |
| 0.1 | 0.512 | 0.613 | 0.720 |
| 0.15 | 0.512 | 0.613 | 0.720 |
| 0.2 | 0.511 | 0.612 | 0.718 |
| 0.25 | 0.508 | 0.609 | 0.715 |
| 0.3 | 0.506 | 0.606 | 0.712 |
| 0.4 | 0.499 | 0.598 | 0.702 |
| 0.5 | 0.493 | 0.591 | 0.694 |
| 0.75 | 0.483 | 0.579 | 0.681 |
| 1 | 0.476 | 0.571 | 0.672 |
| 1.5 | 0.467 | 0.561 | 0.660 |
| 2 | 0.460 | 0.553 | 0.652 |
| 3 | 0.452 | 0.544 | 0.641 |
| 4 | 0.446 | 0.537 | 0.634 |
| 5 | 0.442 | 0.532 | 0.629 |
| 7.5 | 0.435 | 0.525 | 0.620 |
| 10 | 0.430 | 0.519 | 0.614 |

## 5.3. PVNGS Mixture Model

The mixture model is the sum of two equally weighted normal distributions with the standard deviation given by 0.8 and 1.2 times the total standard deviation. To implement the mixture model in the hazard calculation, the conditional probability of exceeding a ground motion value z is weighted average of the conditional probabilities computed for each of the standard deviation value separately (Eq. 5-1).

For the branch where Path effect is included:

$$P_{MIX}(Sa > z \mid M, R, ..., \sigma_{SS}) = 0.5P(Sa > z \mid M, R, ..., 0.8\sigma_{SS}) + 0.5P(Sa > z \mid M, R, ..., 1.2\sigma_{SS})$$
(Eq. 5-1a)

For the branch where Path effect is excluded:

$$P_{MIX}(Sa > z \mid M, R, ..., \sigma_{SP-R}) = 0.5P(Sa > z \mid M, R, ..., 0.8\sigma_{SP-R}) + 0.5P(Sa > z \mid M, R, ..., 1.2\sigma_{SP-R})$$
(Eq. 5-1b)

# 6. Coefficients and weights for the common-form ground motion models

The period-dependent coefficients and weights for the common-form ground motion models are provided in the electronic attachment to this HID document. The description of the material in the electronic attachment is provided below.

## 6.1. Coefficients and Weights for PVNGS

The period-dependent coefficients and weights for the common-form ground motion models for PVNGS are included in two zipped folders named "PVNGS_ModelA_Coefficients_Weights-09292014.zip" and "PVNGS_ModelB_Coefficients_Weights-12122014.zip". The A Models are based on $R_{RUP}$, whereas the B Models are based on $R_{JB}$.

The files included in the folders and their content's descriptions are provided in Tables 6-1 and 6-2 for the A Models and B Models, respectively. The structure of the file is the same for all the .csv files included in the zipped folders, and the structure specifications are provided in Tables 6-3 and 6-4 for the A Models and B Models, respectively.

**Table 6-1:** List and description of files included in electronic material "PVNGS_ModelA_Coefficients_Weights-09292014.zip".

| File Name | Description |
|---|---|
| Coefficients_Weights_PVNGS_ModelA_T001.csv | Coefficients and Weights for period T=0.01 sec |
| Coefficients_Weights_PVNGS_ModelA_T002.csv | Coefficients and Weights for period T=0.02 sec |
| Coefficients_Weights_PVNGS_ModelA_T003.csv | Coefficients and Weights for period T=0.02 sec |
| Coefficients_Weights_PVNGS_ModelA_T005.csv | Coefficients and Weights for period T=0.05 sec |
| Coefficients_Weights_PVNGS_ModelA_T0075.csv | Coefficients and Weights for period T=0.075 sec |
| Coefficients_Weights_PVNGS_ModelA_T01.csv | Coefficients and Weights for period T=0.1 sec |
| Coefficients_Weights_PVNGS_ModelA_T015.csv | Coefficients and Weights for period T=0.15 sec |
| Coefficients_Weights_PVNGS_ModelA_T02.csv | Coefficients and Weights for period T=0.2 sec |
| Coefficients_Weights_PVNGS_ModelA_T025.csv | Coefficients and Weights for period T=0.25 sec |
| Coefficients_Weights_PVNGS_ModelA_T03.csv | Coefficients and Weights for period T=0.3 sec |
| Coefficients_Weights_PVNGS_ModelA_T04.csv | Coefficients and Weights for period T=0.4 sec |
| Coefficients_Weights_PVNGS_ModelA_T05.csv | Coefficients and Weights for period T=0.5 sec |
| Coefficients_Weights_PVNGS_ModelA_T075.csv | Coefficients and Weights for period T=0.75 sec |
| Coefficients_Weights_PVNGS_ModelA_T1.csv | Coefficients and Weights for period T=1.0 sec |
| Coefficients_Weights_PVNGS_ModelA_T15.csv | Coefficients and Weights for period T=1.5 sec |
| Coefficients_Weights_PVNGS_ModelA_T2.csv | Coefficients and Weights for period T=2.0 sec |
| Coefficients_Weights_PVNGS_ModelA_T3.csv | Coefficients and Weights for period T=3.0 sec |
| Coefficients_Weights_PVNGS_ModelA_T4.csv | Coefficients and Weights for period T=4.0 sec |
| Coefficients_Weights_PVNGS_ModelA_T5.csv | Coefficients and Weights for period T=5.0 sec |
| Coefficients_Weights_PVNGS_ModelA_T75.csv | Coefficients and Weights for period T=7.5 sec |
| Coefficients_Weights_PVNGS_ModelA_T100.csv | Coefficients and Weights for period T=10.0 sec |

**Table 6-2:** List and description of files included in electronic material "PVNGS_ModelB_Coefficients_Weights-12122014.zip".

| File Name | Description |
|---|---|
| Coefficients_Weights_PVNGS_ModelB_T001.csv | Coefficients and Weights for period T=0.01 sec |
| Coefficients_Weights_PVNGS_ModelB_T002.csv | Coefficients and Weights for period T=0.02 sec |
| Coefficients_Weights_PVNGS_ModelB_T003.csv | Coefficients and Weights for period T=0.02 sec |
| Coefficients_Weights_PVNGS_ModelB_T005.csv | Coefficients and Weights for period T=0.05 sec |
| Coefficients_Weights_PVNGS_ModelB_T0075.csv | Coefficients and Weights for period T=0.075 sec |
| Coefficients_Weights_PVNGS_ModelB_T01.csv | Coefficients and Weights for period T=0.1 sec |
| Coefficients_Weights_PVNGS_ModelB_T015.csv | Coefficients and Weights for period T=0.15 sec |
| Coefficients_Weights_PVNGS_ModelB_T02.csv | Coefficients and Weights for period T=0.2 sec |
| Coefficients_Weights_PVNGS_ModelB_T025.csv | Coefficients and Weights for period T=0.25 sec |
| Coefficients_Weights_PVNGS_ModelB_T03.csv | Coefficients and Weights for period T=0.3 sec |
| Coefficients_Weights_PVNGS_ModelB_T04.csv | Coefficients and Weights for period T=0.4 sec |
| Coefficients_Weights_PVNGS_ModelB_T05.csv | Coefficients and Weights for period T=0.5 sec |
| Coefficients_Weights_PVNGS_ModelB_T075.csv | Coefficients and Weights for period T=0.75 sec |
| Coefficients_Weights_PVNGS_ModelB_T1.csv | Coefficients and Weights for period T=1.0 sec |
| Coefficients_Weights_PVNGS_ModelB_T15.csv | Coefficients and Weights for period T=1.5 sec |
| Coefficients_Weights_PVNGS_ModelB_T2.csv | Coefficients and Weights for period T=2.0 sec |
| Coefficients_Weights_PVNGS_ModelB_T3.csv | Coefficients and Weights for period T=3.0 sec |
| Coefficients_Weights_PVNGS_ModelB_T4.csv | Coefficients and Weights for period T=4.0 sec |
| Coefficients_Weights_PVNGS_ModelB_T5.csv | Coefficients and Weights for period T=5.0 sec |
| Coefficients_Weights_PVNGS_ModelB_T75.csv | Coefficients and Weights for period T=7.5 sec |
| Coefficients_Weights_PVNGS_ModelB_T100.csv | Coefficients and Weights for period T=10.0 sec |

**Table 6-3:** Structure of the files included in electronic material "PVNGS_ModelA_Coefficients_Weights-09292014.zip". The structure is common to all the files included in the zipped folder.

| Column | Description | Notes |
|---|---|---|
| Column A | Model ID | There may be less than 31 models for a specific period |
| Column B | Coefficient $a_0$ | Coefficients in Equation 2-1 |
| Column C | Coefficient $a_1$ | Coefficients in Equation 2-1 |
| Column D | Coefficient $a_2$ | Coefficients in Equation 2-1 |
| Column E | Coefficient $a_3$ | Coefficients in Equation 2-1 |
| Column F | Coefficient $a_4$ | Coefficients in Equation 2-1 |
| Column G | Coefficient $a_5$ | Coefficients in Equation 2-1 |
| Column H | Coefficient $a_6$ | Coefficients in Equation 2-1 |
| Column I | Coefficient $a_7$ | Coefficients in Equation 2-1 |
| Column J | Coefficient $a_8$ | Coefficients in Equation 2-1 |
| Column K | Coefficient $a_9$ | Coefficients in Equation 2-1 |
| Column L | Identifier of the HW branch which is associated to the specific Model ID | Coefficients for the 5 alternative HW adjustment models are provided in Table 2-2. The hanging-wall adjustment is to be applied only for the sites located in the hanging-wall side (i.e. with $R_X \geq 0$ km). |
| Column M | Total weights for the specific period | |
| Cell M34 | Sum of the total weights | Internal check that the weights sum to 1 |

**Table 6-4:** Structure of the files included in electronic material "PVNGS_ModelB_Coefficients_Weights-12122014.zip". The structure is common to all the files included in the zipped folder.

| Column | Description | Notes |
|---|---|---|
| Column A | Model ID | There may be less than 31 models for a specific period |
| Column B | Coefficient $a_0$ | Coefficients in Equation 2-2 |
| Column C | Coefficient $a_1$ | Coefficients in Equation 2-2 |
| Column D | Coefficient $a_2$ | Coefficients in Equation 2-2 |
| Column E | Coefficient $a_3$ | Coefficients in Equation 2-2 |
| Column F | Coefficient $a_4$ | Coefficients in Equation 2-2 |
| Column G | Coefficient $a_5$ | Coefficients in Equation 2-2 |
| Column H | Coefficient $a_6$ | Coefficients in Equation 2-2 |
| Column I | Coefficient $a_7$ | Coefficients in Equation 2-2 |
| Column J | Coefficient $a_8$ | Coefficients in Equation 2-2 |
| Column K | Coefficient $a_9$ | Coefficients in Equation 2-2 |
| Column L | Identifier of the HW branch which is associated to the specific Model ID | The identifier is 0 in all the cases because no HW adjustment is associated to B Models |
| Column M | Total weights for the specific period | |
| Cell M34 | Sum of the total weights | Internal check that the weights sum to 1 |

# 7. Benchmarking tables for common-form ground motion models

The following section includes example applications of the common-form ground motion models for PVNGS. The 5%-damping pseudo-spectral accelerations (PSA), using a range of predictors for periods up to 3 seconds, are provided in the electronic attachment to this HID document. The description of the material in the electronic attachment is provided below.

## 7.1. Benchmarking tables for PVNG

The benchmarking tables showing application of common-form ground motion models for PVNGS are included in the zipped folder named "PVNGS_Example_Predictions-09292014.zip" digitally attached to this HID. The zipped file consists of six sub-folders, one for each of the model type (A Models and B Models) and for each of the three sets of test cases.

### *7.1.1. Example 1 cases*

Two folders are associated to Example 1 test cases. They are named "Example1_ModelA" and Example1_ModelB", for the $R_{RUP}$- and $R_{JB}$-based models, respectively. The content of the two sub-folders is described in Tables 7-1 and 7-2 for the A Models and B Models, respectively.

The file structure and the range of predictors used in Example 1 are described in Tables 7-3 and 7-4 for the A Models and B Models, respectively.

In the Example 1 cases, a fault is assumed to dip 45 degrees, and the PSA values are provided for a site located on the foot-wall side of the fault.

**Table 7-1:** List and description of files included in electronic material "Example1_ModelA", included in directory "PVNGS_Example_Predictions-09292014.zip".

| File Name | Description |
|---|---|
| example1_PVNGS_ModelA_T001.csv | Example 1 benchmarking values for A Models, period T=0.01 sec |
| example1_PVNGS_ModelA_T002.csv | Example 1 benchmarking values for A Models, period T=0.02 sec |
| example1_PVNGS_ModelA_T003.csv | Example 1 benchmarking values for A Models, period T=0.02 sec |
| example1_PVNGS_ModelA_T005.csv | Example 1 benchmarking values for A Models, period T=0.05 sec |
| example1_PVNGS_ModelA_T0075.csv | Example 1 benchmarking values for A Models, period T=0.075 sec |
| example1_PVNGS_ModelA_T01.csv | Example 1 benchmarking values for A Models, period T=0.1 sec |
| example1_PVNGS_ModelA_T015.csv | Example 1 benchmarking values for A Models, period T=0.15 sec |
| example1_PVNGS_ModelA_T02.csv | Example 1 benchmarking values for A Models, period T=0.2 sec |
| example1_PVNGS_ModelA_T025.csv | Example 1 benchmarking values for A Models, period T=0.25 sec |
| example1_PVNGS_ModelA_T03.csv | Example 1 benchmarking values for A Models, period T=0.3 sec |
| example1_PVNGS_ModelA_T04.csv | Example 1 benchmarking values for A Models, period T=0.4 sec |
| example1_PVNGS_ModelA_T05.csv | Example 1 benchmarking values for A Models, period T=0.5 sec |
| example1_PVNGS_ModelA_T075.csv | Example 1 benchmarking values for A Models, period T=0.75 sec |
| example1_PVNGS_ModelA_T1.csv | Example 1 benchmarking values for A Models, period T=1.0 sec |
| example1_PVNGS_ModelA_T15.csv | Example 1 benchmarking values for A Models, period T=1.5 sec |
| example1_PVNGS_ModelA_T2.csv | Example 1 benchmarking values for A Models, period T=2.0 sec |
| example1_PVNGS_ModelA_T3.csv | Example 1 benchmarking values for A Models, period T=3.0 sec |

**Table C7-2:** List and description of files included in electronic material "Example1_ModelB", included in directory "PVNGS_Example_Predictions-09292014.zip".

| File Name | Description |
|---|---|
| example1_PVNGS_ModelB_T001.csv | Example 1 benchmarking values for B Models, period T=0.01 sec |
| example1_PVNGS_ModelB_T002.csv | Example 1 benchmarking values for B Models, period T=0.02 sec |
| example1_PVNGS_ModelB_T003.csv | Example 1 benchmarking values for B Models, period T=0.02 sec |
| example1_PVNGS_ModelB_T005.csv | Example 1 benchmarking values for B Models, period T=0.05 sec |
| example1_PVNGS_ModelB_T0075.csv | Example 1 benchmarking values for B Models, period T=0.075 sec |
| example1_PVNGS_ModelB_T01.csv | Example 1 benchmarking values for B Models, period T=0.1 sec |
| example1_PVNGS_ModelB_T015.csv | Example 1 benchmarking values for B Models, period T=0.15 sec |
| example1_PVNGS_ModelB_T02.csv | Example 1 benchmarking values for B Models, period T=0.2 sec |
| example1_PVNGS_ModelB_T025.csv | Example 1 benchmarking values for B Models, period T=0.25 sec |
| example1_PVNGS_ModelB_T03.csv | Example 1 benchmarking values for B Models, period T=0.3 sec |
| example1_PVNGS_ModelB_T04.csv | Example 1 benchmarking values for B Models, period T=0.4 sec |
| example1_PVNGS_ModelB_T05.csv | Example 1 benchmarking values for B Models, period T=0.5 sec |
| example1_PVNGS_ModelB_T075.csv | Example 1 benchmarking values for B Models, period T=0.75 sec |
| example1_PVNGS_ModelB_T1.csv | Example 1 benchmarking values for B Models, period T=1.0 sec |
| example1_PVNGS_ModelB_T15.csv | Example 1 benchmarking values for B Models, period T=1.5 sec |
| example1_PVNGS_ModelB_T2.csv | Example 1 benchmarking values for B Models, period T=2.0 sec |
| example1_PVNGS_ModelB_T3.csv | Example 1 benchmarking values for B Models, period T=3.0 sec |

**Table 7-3:** Structure of the files included in electronic material "Example1_ModelA", included in directory "PVNGS_Example_Predictions-09292014.zip".

| Column | Description | Notes |
|---|---|---|
| Column A | Progressive model identifier | This progressive number is not the Model ID. See column G for unique Model ID. |
| Column B | Moment Magnitude | **M** 5, 6.5 and 7.5 are used |
| Column C | $R_{RUP}$ distance in km | $R_{RUP}$ distances 1, 2, 5, 10, 50, 100 and 200 km are used |
| Column D | Depth to the top of rupture in km | 1 km is used in all cases |
| Column E | Style-of-faulting conditions | Normal fault mechanism is used in all cases |
| Column F | 5%-damped pseudo-spectral acceleration (PSA) | Values are provided in natural logarithm units |
| Column G | Model ID | Unique Model ID |

**Table 7-4:** Structure of the files included in electronic material "Example1_ModelB", included in directory "PVNGS_Example_Predictions-09292014.zip".

| Column | Description | Notes |
|---|---|---|
| Column A | Progressive model identifier | This progressive number is not the Model ID. See column G for unique Model ID. |
| Column B | Moment Magnitude | **M** 5, 6.5 and 7.5 are used |
| Column C | $R_{JB}$ distance in km | $R_{JB}$ distances 1, 2, 5, 10, 50, 100 and 200 km are used |
| Column D | Depth to the top of rupture in km | 1 km is used in all cases |
| Column E | Style-of-faulting conditions | Normal fault mechanism is used in all cases |
| Column F | 5%-damped pseudo-spectral acceleration (PSa) | Values are provided in natural logarithm units |
| Column G | Model ID | Unique Model ID |

### 7.1.2. *Example 2 cases*

Two folders are associated to Example 2 test cases. They are named "Example2_ModelA" and Example2_ModelB", for the $R_{RUP}$- and $R_{JB}$-based models, respectively. The content of the two sub-folders is described in Tables 7-5 and 7-6 for the A Models and B Models, respectively.

The file structure and the range of predictors used in Example 2 are described in Tables 7-7 and 7-8 for the A Models and B Models, respectively.

In the Example 2 cases, the PSA values are provided for a site located on the hanging-wall side of the fault.

**Table 7-5:** List and description of files included in electronic material "Example2_ModelA", included in directory "PVNGS_Example_Predictions-09292014.zip".

| File Name | Description |
|---|---|
| example2_PVNGS_ModelA_T001.csv | Example 2 benchmarking values for A Models, period T=0.01 sec |
| example2_PVNGS_ModelA_T002.csv | Example 2 benchmarking values for A Models, period T=0.02 sec |
| example2_PVNGS_ModelA_T003.csv | Example 2 benchmarking values for A Models, period T=0.02 sec |
| example2_PVNGS_ModelA_T005.csv | Example 2 benchmarking values for A Models, period T=0.05 sec |
| example2_PVNGS_ModelA_T0075.csv | Example 2 benchmarking values for A Models, period T=0.075 sec |
| example2_PVNGS_ModelA_T01.csv | Example 2 benchmarking values for A Models, period T=0.1 sec |
| example2_PVNGS_ModelA_T015.csv | Example 2 benchmarking values for A Models, period T=0.15 sec |
| example2_PVNGS_ModelA_T02.csv | Example 2 benchmarking values for A Models, period T=0.2 sec |
| example2_PVNGS_ModelA_T025.csv | Example 2 benchmarking values for A Models, period T=0.25 sec |
| example2_PVNGS_ModelA_T03.csv | Example 2 benchmarking values for A Models, period T=0.3 sec |
| example2_PVNGS_ModelA_T04.csv | Example 2 benchmarking values for A Models, period T=0.4 sec |
| example2_PVNGS_ModelA_T05.csv | Example 2 benchmarking values for A Models, period T=0.5 sec |
| example2_PVNGS_ModelA_T075.csv | Example 2 benchmarking values for Model A, period T=0.75 sec |
| example2_PVNGS_ModelA_T1.csv | Example 2 benchmarking values for Model A, period T=1.0 sec |
| example2_PVNGS_ModelA_T15.csv | Example 2 benchmarking values for Model A, period T=1.5 sec |
| example2_PVNGS_ModelA_T2.csv | Example 2 benchmarking values for Model A, period T=2.0 sec |
| example2_PVNGS_ModelA_T3.csv | Example 2 benchmarking values for Model A, period T=3.0 sec |

**Table 7-6:** List and description of files included in electronic material "Example2_ModelB", included in directory "PVNGS_Example_Predictions-09292014.zip".

| File Name | Description |
|---|---|
| example2_PVNGS_ModelB_T001.csv | Example 2 benchmarking values for B Models, period T=0.01 sec |
| example2_PVNGS_ModelB_T002.csv | Example 2 benchmarking values for B Models, period T=0.02 sec |
| example2_PVNGS_ModelB_T003.csv | Example 2 benchmarking values for B Models, period T=0.02 sec |
| example2_PVNGS_ModelB_T005.csv | Example 2 benchmarking values for B Models, period T=0.05 sec |
| example2_PVNGS_ModelB_T0075.csv | Example 2 benchmarking values for B Models, period T=0.075 sec |
| example2_PVNGS_ModelB_T01.csv | Example 2 benchmarking values for B Models, period T=0.1 sec |
| example2_PVNGS_ModelB_T015.csv | Example 2 benchmarking values for B Models, period T=0.15 sec |
| example2_PVNGS_ModelB_T02.csv | Example 2 benchmarking values for B Models, period T=0.2 sec |
| example2_PVNGS_ModelB_T025.csv | Example 2 benchmarking values for B Models, period T=0.25 sec |
| example2_PVNGS_ModelB_T03.csv | Example 2 benchmarking values for B Models, period T=0.3 sec |
| example2_PVNGS_ModelB_T04.csv | Example 2 benchmarking values for B Models, period T=0.4 sec |
| example2_PVNGS_ModelB_T05.csv | Example 2 benchmarking values for B Models, period T=0.5 sec |
| example2_PVNGS_ModelB_T075.csv | Example 2 benchmarking values for B Models, period T=0.75 sec |
| example2_PVNGS_ModelB_T1.csv | Example 2 benchmarking values for B Models, period T=1.0 sec |
| example2_PVNGS_ModelB_T15.csv | Example 2 benchmarking values for B Models, period T=1.5 sec |
| example2_PVNGS_ModelB_T2.csv | Example 2 benchmarking values for B Models, period T=2.0 sec |
| example2_PVNGS_ModelB_T3.csv | Example 2 benchmarking values for B Models, period T=3.0 sec |

**Table 7-7:** Structure of the files included in electronic material "Example2_ModelA", included in directory "PVNGS_Example_Predictions-09292014.zip".

| Column | Description | Notes |
|---|---|---|
| Column A | Progressive model identifier | This progressive number is not the Model ID. See column K for unique Model ID. |
| Column B | Moment Magnitude | **M** 6.5 is used in all the cases |
| Column C | $R_x$ distance in km | $R_x$ distances 0, 1, 2, 5, 10, and 20 km are used |
| Column D | $R_{JB}$ distance in km | |
| Column E | $R_{RUP}$ distance in km | |
| Column F | Depth to the top of rupture ($Z_{TOR}$) in km | $Z_{TOR}$ 1 and 5 km are used |
| Column G | Style-of-faulting conditions | Normal fault mechanism is used in all cases |
| Column H | Fault dip in degrees | Dips 45 and 60 deg. are used |
| Column I | Fault width in km | Although the fault width is not used as inputs in the common form models, the fault geometry information is used to compute compatible $R_X$, $R_{RUP}$ and $R_{JB}$ distances |
| Column J | 5%-damped pseudo-spectral acceleration (PSA) for the specific A Model | Values are provided in natural logarithm units |
| Column K | Model ID | Unique Model ID |

**Table 7-8:** Structure of the files included in electronic material "Example2_ModelB", included in directory "PVNGS_Example_Predictions-09292014.zip".

| Column | Description | Notes |
|---|---|---|
| Column A | Progressive model identifier | This progressive number is not the Model ID. See column K for unique Model ID. |
| Column B | Moment Magnitude | **M** 6.5 is used in all cases |
| Column C | $R_x$ distance in km | $R_x$ distances 0, 1, 2, 5, 10, and 20 km are used |
| Column D | $R_{JB}$ distance in km | |
| Column E | $R_{RUP}$ distance in km | |
| Column F | Depth to the top of rupture ($Z_{TOR}$) in km | $Z_{TOR}$ 1 and 5 km are used |
| Column G | Style-of-faulting conditions | Normal fault mechanism is used in all cases |
| Column H | Fault dip in degrees | Dips 45 and 60 deg. are used |
| Column I | Fault width in km | Although the fault width is not used as inputs in the common form models, the fault geometry information is used to compute compatible $R_X$, $R_{RUP}$ and $R_{JB}$ distances |
| Column J | 5%-damped pseudo-spectral acceleration (PSA) for the specific B Model | Values are provided in natural logarithm units |
| Column K | Model ID | Unique Model ID |

### *7.1.3. Example 3 cases*

Two folders are associated to Example 3 test cases. They are named "Example3_ModelA" and Example3_ModelB", for the $R_{RUP}$- and $R_{JB}$-based models, respectively. The content of the two sub-folders is described in Tables 7-9 and 7-10 for the A Models and B Models, respectively.

The file structure and the range of predictors used in Example 3 are described in Tables 7-11 and 7-12 for the A Models and B Models, respectively.

In the Example 3 cases, the PSA values are provided for a site located on the foot-wall side of the fault.

**Table 7-9:** List and description of files included in electronic material "Example3_ModelA", included in directory "PVNGS_Example_Predictions-09292014.zip".

| File Name | Description |
|---|---|
| example3_PVNGS_ModelA_T001.csv | Example 3 benchmarking values for A Models, period T=0.01 sec |
| example3_PVNGS_ModelA_T002.csv | Example 3 benchmarking values for A Models, period T=0.02 sec |
| example3_PVNGS_ModelA_T003.csv | Example 3 benchmarking values for A Models, period T=0.02 sec |
| example3_PVNGS_ModelA_T005.csv | Example 3 benchmarking values for A Models, period T=0.05 sec |
| example3_PVNGS_ModelA_T0075.csv | Example 3 benchmarking values for A Models, period T=0.075 sec |
| example3_PVNGS_ModelA_T01.csv | Example 3 benchmarking values for A Models, period T=0.1 sec |
| example3_PVNGS_ModelA_T015.csv | Example 3 benchmarking values for A Models, period T=0.15 sec |
| example3_PVNGS_ModelA_T02.csv | Example 3 benchmarking values for A Models, period T=0.2 sec |
| example3_PVNGS_ModelA_T025.csv | Example 3 benchmarking values for A Models, period T=0.25 sec |
| example3_PVNGS_ModelA_T03.csv | Example 3 benchmarking values for A Models, period T=0.3 sec |
| example3_PVNGS_ModelA_T04.csv | Example 3 benchmarking values for A Models, period T=0.4 sec |
| example3_PVNGS_ModelA_T05.csv | Example 3 benchmarking values for A Models, period T=0.5 sec |
| example3_PVNGS_ModelA_T075.csv | Example 3 benchmarking values for A Models, period T=0.75 sec |
| example3_PVNGS_ModelA_T1.csv | Example 3 benchmarking values for A Models, period T=1.0 sec |
| example3_PVNGS_ModelA_T15.csv | Example 3 benchmarking values for A Models, period T=1.5 sec |
| example3_PVNGS_ModelA_T2.csv | Example 3 benchmarking values for A Models, period T=2.0 sec |
| example3_PVNGS_ModelA_T3.csv | Example 3 benchmarking values for A Models, period T=3.0 sec |

**Table 7-10:** List and description of files included in electronic material "Example3_ModelB", included in directory "PVNGS_Example_Predictions-09292014.zip".

| File Name | Description |
|---|---|
| example3_PVNGS_ModelB_T001.csv | Example 3 benchmarking values for B Models, period T=0.01 sec |
| example3_PVNGS_ModelB_T002.csv | Example 3 benchmarking values for B Models, period T=0.02 sec |
| example3_PVNGS_ModelB_T003.csv | Example 3 benchmarking values for B Models, period T=0.02 sec |
| example3_PVNGS_ModelB_T005.csv | Example 3 benchmarking values for B Models, period T=0.05 sec |
| example3_PVNGS_ModelB_T0075.csv | Example 3 benchmarking values for B Models, period T=0.075 sec |
| example3_PVNGS_ModelB_T01.csv | Example 3 benchmarking values for B Models, period T=0.1 sec |
| example3_PVNGS_ModelB_T015.csv | Example 3 benchmarking values for B Models, period T=0.15 sec |
| example3_PVNGS_ModelB_T02.csv | Example 3 benchmarking values for B Models, period T=0.2 sec |
| example3_PVNGS_ModelB_T025.csv | Example 3 benchmarking values for B Models, period T=0.25 sec |
| example3_PVNGS_ModelB_T03.csv | Example 3 benchmarking values for B Models, period T=0.3 sec |
| example3_PVNGS_ModelB_T04.csv | Example 3 benchmarking values for B Models, period T=0.4 sec |
| example3_PVNGS_ModelB_T05.csv | Example 3 benchmarking values for B Models, period T=0.5 sec |
| example3_PVNGS_ModelB_T075.csv | Example 3 benchmarking values for B Models, period T=0.75 sec |
| example3_PVNGS_ModelB_T1.csv | Example 3 benchmarking values for B Models, period T=1.0 sec |
| example3_PVNGS_ModelB_T15.csv | Example 3 benchmarking values for B Models, period T=1.5 sec |
| example3_PVNGS_ModelB_T2.csv | Example 3 benchmarking values for B Models, period T=2.0 sec |
| example3_PVNGS_ModelB_T3.csv | Example 3 benchmarking values for B Models, period T=3.0 sec |

**Table 7-11:** Structure of the files included in electronic material "Example3_ModelA", included in directory "PVNGS_Example_Predictions-09292014.zip".

| Column | Description | Notes |
|---|---|---|
| Column A | Progressive model identifier | This progressive number is not the Model ID. See column G for unique Model ID. |
| Column B | Moment Magnitude | **M** 6 is used for all cases |
| Column c | $R_{RUP}$ distance in km | $R_{RUP}$ 10 km is used for all cases |
| Column D | Depth to the top of rupture ($Z_{TOR}$) in km | $Z_{TOR}$ 1 km is used for all cases |
| Column E | Style-of-faulting conditions | Strike-slip ($F_{NML}$ =0 and $F_{RV}$=0) and Reverse ($F_{NML}$ =0 and $F_{RV}$ =1) faults are used |
| Column F | 5%-damped pseudo-spectral acceleration (PSA) for the specific A Model | Values are provided in natural logarithm units |
| Column G | Model ID | Unique Model ID |

**Table 7-12:** Structure of the files included in electronic material "Example3_ModelB", included in directory "PVNGS_Example_Predictions-09292014.zip".

| Column | Description | Notes |
|---|---|---|
| Column A | Progressive model identifier | This progressive number is not the Model ID. See column G for unique Model ID. |
| Column B | Moment Magnitude | **M** 6 is used for all cases |
| Column c | $R_{JB}$ distance in km | $R_{JB}$ 10 km is used for all cases |
| Column D | Depth to the top of rupture ($Z_{TOR}$) in km | $Z_{TOR}$ 0 km is used for all cases |
| Column E | Style-of-faulting conditions | Strike-slip ($F_{NML}$ =0 and $F_{RV}$=0) and Reverse ($F_{NML}$ =0 and $F_{RV}$ =1) faults are used |
| Column F | 5%-damped pseudo-spectral acceleration (PSA) for the specific B Model | Values are provided in natural logarithm units |
| Column G | Model ID | Unique Model ID |

# 8. References

Abrahamson, N.A., Silva, W.J., and Kamai, R. (2014). Summary of the AKS14 Ground-Motion Relation for Active Crustal Regions, *Earthquake Spectra*, Vol. 30(3), 1025-1055, DOI: 10.1193/070913EQS198M.

Boore, D.M., Stewart, J.P., Seyhan, E., and Atkinson, G.M. (2014). NGA-West 2 Equations for Predicting PGA, PGV, and 5%-Damped PSA for Shallow Crustal Earthquakes, *Earthquake Spectra*, Vol. 30(3), 1057-1085, DOI: 10.1193/070113EQS184M.

Campbell, K.W., and Bozorgnia, Y. (2014). NGA-West2 Ground Motion Model for the Average Horizontal Components of PGA, PGV, and 5%-Damped Linear Acceleration Response Spectra, *Earthquake Spectra*, Vol. 30(3), 1087-1115, DOI: 10.1193/062913EQS175M.

Chiou, B.S.-J., and Youngs, R.R. (2014). Update of the Chiou and Youngs NGA Model for the Average Horizontal Component of Peak Ground Motion and Response Spectra, *Earthquake Spectra*, Vol. 30(3), 1117-1153, DOI: 10.1193/072813EQS219M.

Idriss, I.M. (2014). An NGA-West2 Empirical Model for Estimating the Horizontal Spectral Values Generated by Shallow Crustal Earthquakes, *Earthquake* Spectra, Vol. 30(3), 1155-1177, DOI: 10.1193/070613EQS195M.

# PART II

## SWUS GMC MODELS HAZARD INPUT DOCUMENTS (HID) FOR DCPP

Revision 2

# 1. Notation

The notation in Table 1-1 is used for the ground motion models for DCPP site

**Table 1-1:** Notation used in HID, Part II: DCPP.

| | |
|---|---|
| T | Period (seconds) |
| M | Moment magnitude |
| NML | Normal sources (-120 ≤ rake ≤ -60) |
| REV | Reverse sources, including Reverse-Oblique (REV-OBL); (30 ≤ rake ≤ 150) |
| SS | Strike-slip sources, including Normal-Oblique; (-180 ≤ rake < -120, -60 < rake < 30, and 150 < rake ≤ 180) |
| $F_{NML}$ | style of faulting ($F_{NML}$=1 for NML , 0 otherwise) |
| $F_{RV}$ | style of faulting ($F_{RV}$=1 for REV , 0 otherwise) |
| $Z_{TOR}$ | Depth to top of rupture (km) |
| Dip | Fault dip (degrees) |
| W | Down-dip rupture width (km) |
| L | Rupture length (km) |
| $R_{RUP}$ | Rupture distance (km) |
| $R_{JB}$ | Joyner-Boore distance (km) |
| $R_X$ | Horizontal distance from top of rupture measured perpendicular to strike (km) |
| $R_Y$ | Horizontal distance from center of rupture measured parallel to strike (km) |
| $f_{HW}$ | Hanging Wall factor |
| $\sigma_{SS}$ | Total sigma |

# 2. Median ground motion model for DCPP

The DCPP ground-motion models are separated into two sets: one set of models for the nearby faults and one set of models for the distant faults. The common-form models in Figure 1-1 are applicable to the following sources nearby DCPP:

- Hosgri Rupture Model
- Outward-Vergent Rupture Model
- Southwest-Vergent Rupture Model
- Northeast-Vergent Rupture Model
- Irish Hills-Estero Bay (IHEB) Source Zone

All of the other sources will use the logic tree in Figure 1-2. In that case, the median base model is represented by the five NGA-West2 GMPEs (Abrahamson et al., 2014 – ASK14; Boore et al., 2014 – BSSA14; Campbell and Bozorgnia, 2014 – CB14; Chiou and Youngs, 2014 – CY14; and Idriss, 2014 – ID14) equally weighted. The Al-Atik and Youngs (2014) epistemic uncertainty model for **M**>7 is applied everywhere for the distant sources case.

## 2.1 Structure of the Logic Tree

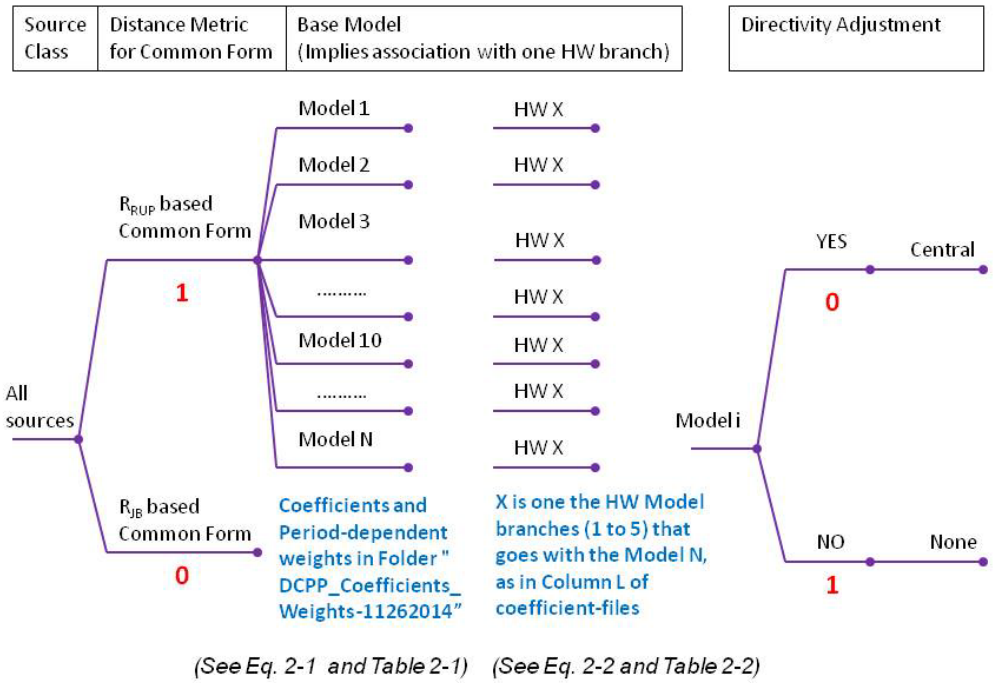



**Figure 1-1:** Logic Tree for Median at DCPP for the nearby faults.

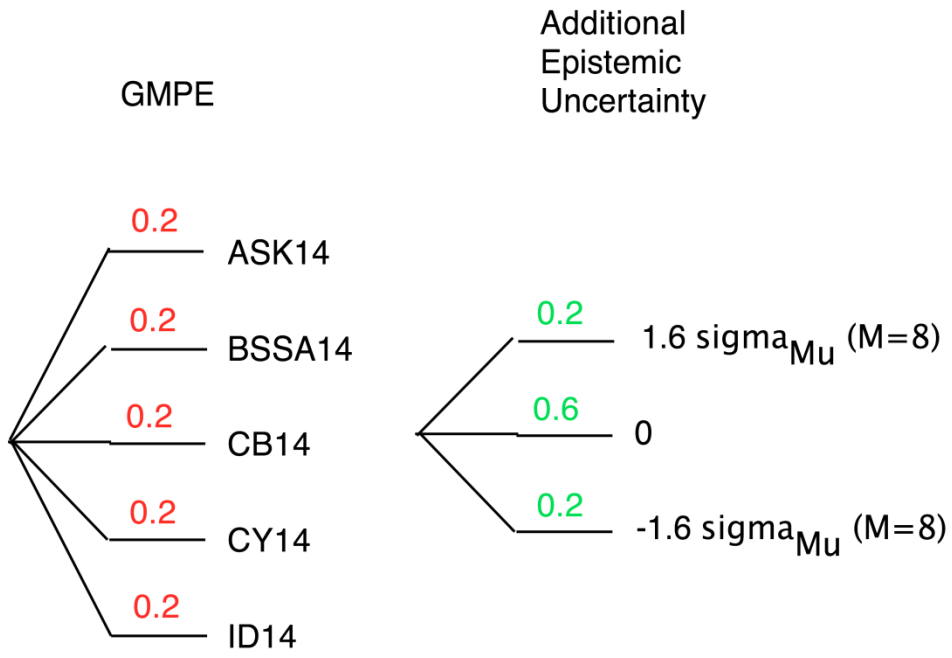



**Figure 1-2:** Logic Tree for Median at DCPP for the distant sources.

## 2.2 Common Functional Form for Base Model

The functional form of the DCPP base model GMPEs is given in Eq. 2-1:

$$Ln\left(SA_{BASE}(M,R_{RUP},Z_{TOR},F,T)\right) = a_0(T) - a_7^2(T)R_{RUP} + a_8^2(T)Z_{TOR} + a_{10}^2(T)F_{RV} + \left(a_4(T) + a_5(T)(M-5)\right)\ln\left(\sqrt{R_{RUP}^2 + a_6^2(T)}\right) - a_9(T)F_{NML} + \begin{cases} -a_1(T) + a_2(T)(M-5.5) & for\ M < 5.5 \\ a_1(T)(M-6.5) & for\ 5.5 \le M \le 6.5 \\ a_3(T)(M-6.5) & for\ M > 6.5 \end{cases}$$

(Eq. 2-1)

The coefficients for 17 spectral periods and up to 31 models are listed in excel files named "Coefficients_Weights_DCPP_T*X*.csv", where *X* is the period, which are collected under the folder "DCPP_Coefficients_Weights-11262014", which is provided as an electronic attachment to the HID. The list of the included excels files and their contents are described in Section 4 of this HID. There may be less than 31 models for a specific period, so the User is invited to refer to the model ID information provided in the first column.

There is a univocal association between each model ID and one of the five alternative HW adjustments branches (see Section 2.3), as specified in the column L of the coefficient files.

The weights for the models for each spectral period are also collected in the same zipped folder as the coefficients. The list of the files providing weights and their content is described in section 4.

The model is applicable for SS, REV and NML earthquakes. For SS and REV earthquakes, $F_{NML}$ is zero. Period dependent $a_9$ coefficients for $F_{NML}$ are provided in Table 2-1. A single $a_9$ value is used at each period for all the common form models.

The HW factor only applies to $R_X \geq 0$ km.

**Table 2-1:** Period dependent $a_9$ coefficients for $F_{NML}$.

| **Period (sec)** | **$a_9$** |
|---|---|
| 0.01 | 0.132 |
| 0.02 | 0.132 |
| 0.03 | 0.132 |
| 0.05 | 0.132 |
| 0.075 | 0.132 |
| 0.1 | 0.132 |
| 0.15 | 0.132 |
| 0.2 | 0.122 |
| 0.25 | 0.113 |
| 0.3 | 0.104 |
| 0.4 | 0.095 |
| 0.5 | 0.095 |
| 0.75 | 0.086 |
| 1 | 0.077 |
| 1.5 | 0.068 |
| 2 | 0.058 |
| 3 | 0.039 |
| 4 | 0.020 |
| 5 | 0.000 |
| 7.5 | 0.000 |
| 10 | 0.000 |

## 2.3 Common Form for Hanging Wall Effects

The common form for the hanging wall effect is given in Eq. 2-2a, 2-2b, and 2-2c:

$$f_{HW}(M, Dip, W, R_X, R_{JB}, R_{RUP}, Z_{TOR}) = C_1(T)\cos(dip)\left[C_2(T) + (1 - C_2(T))\tanh\left(\frac{C_3(T)R_X}{W\cos(dip)}\right)\right] \times \left(1 + C_4(T)(M-7)\right)T_{HW\_R}(R_{RUP}, R_{JB})T_{HW\_Z}(Z_{TOR})$$

(Eq. 2-2a)

where

$$T_{HW\_R}(R_{JB}, R_{RUP}) = 1 - \frac{R_{JB}}{R_{RUP} + 0.1}$$ (Eq. 2-2 b)

$$T_{HW\_Z}(Z_{TOR}) = \max\left\{0,\ \ 1 - \frac{Z_{TOR}}{12}\right\}$$ (Eq. 2-2 c)

The coefficients for the HW model are listed in Table 2-2 for the five alternative HW models. The C2, C3, and C4 terms are the same for all five models.

**Table 2-2:** Coefficients for HW Factor Model**.**

| Period (sec) | Model-dependent C1 Coefficients | | | | | Coefficients held Constant for all five models | | |
|---|---|---|---|---|---|---|---|---|
| | *Model HW1* | *Model HW 2* | *Model HW 3* | *Model HW 4* | *Model HW 5* | $C_2$ | $C_3$ | $C_4$ |
| 0.01 | 0.868 | 0.982 | 1.038 | 1.095 | 1.209 | 0.2160 | 2.0289 | 0.1675 |
| 0.02 | 0.867 | 0.987 | 1.046 | 1.106 | 1.226 | 0.2172 | 2.0260 | 0.1666 |
| 0.03 | 0.856 | 0.997 | 1.067 | 1.138 | 1.278 | 0.2178 | 2.0163 | 0.1670 |
| 0.05 | 0.840 | 1.027 | 1.121 | 1.215 | 1.402 | 0.2199 | 1.9870 | 0.1699 |
| 0.075 | 0.857 | 1.041 | 1.133 | 1.226 | 1.410 | 0.2218 | 1.9906 | 0.1817 |
| 0.1 | 0.848 | 1.040 | 1.135 | 1.231 | 1.422 | 0.2213 | 1.9974 | 0.1717 |
| 0.15 | 0.868 | 1.009 | 1.080 | 1.150 | 1.292 | 0.2169 | 2.0162 | 0.1814 |
| 0.2 | 0.850 | 1.005 | 1.082 | 1.160 | 1.315 | 0.2131 | 1.9746 | 0.1834 |
| 0.25 | 0.868 | 0.985 | 1.044 | 1.102 | 1.219 | 0.1988 | 1.9931 | 0.1767 |
| 0.3 | 0.839 | 0.974 | 1.041 | 1.108 | 1.242 | 0.2019 | 2.0179 | 0.1658 |
| 0.4 | 0.780 | 0.934 | 1.011 | 1.089 | 1.243 | 0.2090 | 2.0249 | 0.1624 |
| 0.5 | 0.741 | 0.902 | 0.982 | 1.063 | 1.223 | 0.2053 | 2.0041 | 0.1719 |
| 0.75 | 0.613 | 0.869 | 0.997 | 1.125 | 1.380 | 0.1713 | 1.8697 | 0.1866 |
| 1 | 0.621 | 0.788 | 0.872 | 0.955 | 1.123 | 0.1571 | 1.8526 | 0.3143 |
| 1.5 | 0.506 | 0.662 | 0.740 | 0.818 | 0.974 | 0.1559 | 1.8336 | 0.3195 |
| 2 | 0.391 | 0.537 | 0.609 | 0.682 | 0.828 | 0.1559 | 1.7996 | 0.3246 |
| 3 | 0.128 | 0.245 | 0.304 | 0.362 | 0.480 | 0.1616 | 1.6740 | 0.3314 |
| 4 | 0 | 0.034 | 0.088 | 0.138 | 0.231 | 0.1616 | 1.6740 | 0.3314 |
| 5 | 0 | 0 | 0 | 0 | 0.040 | 0.1616 | 1.6740 | 0.3314 |
| 7.5 | 0 | 0 | 0 | 0 | 0 | 0.1616 | 1.6740 | 0.3314 |
| 10 | 0 | 0 | 0 | 0 | 0 | 0.1616 | 1.6740 | 0.3314 |

## 2.4 Rule-based Approach for Complex and Splay Ruptures

For the purpose of ground motion computation, complex ruptures are defined as ruptures associated to changes in rake along strike, or significant changes in dip (greater than 15 degrees) within 20 km along strike. For these complex ruptures, the ground motion is given by the square root of the sum of the squares (SRSS) of the ground motions computed for each of the two sub-sources separately.

For the purpose of ground motion computation, splay ruptures are defined as overlapping ruptures of two sources. For splay ruptures, the ground motion is given by the SRSS of the ground motions computed for each of the two sub-sources separately.

## 2.5 DCPP Ground Motion for the Median

The DCPP ground motion model for the median from REV and SS sources is given by

$$\ln(SA(g)) = Ln\left(SA_{BASE}(M, R_{RUP}, Z_{TOR}, F, T)\right) + f_{HW}(M, Dip, W, R_X, R_{JB}, R_{RUP}, Z_{TOR}) + \begin{cases} f_{DIR\_SS}(M, R_{RUP}, R_x, R_y, L) & for\ SS\ events \\ f_{DIR\_RV}(M, R_{RUP}, R_x, R_y, W, L, Dip) & for\ REV\ events \end{cases} \quad \text{(Eq. 2-3)}$$

The DCPP ground motion model for the median from NML sources is given by

$$\ln(SA(g)) = Ln\left(SA_{BASE}(M, R_{RUP}, Z_{TOR}, F, T)\right) + f_{HW}(M, Dip, W, R_X, R_{JB}, R_{RUP}, Z_{TOR}) \quad \text{(Eq. 2-4)}$$

# 3. Total Sigma Model for DCPP

## 3.1 Structure of the Logic Tree

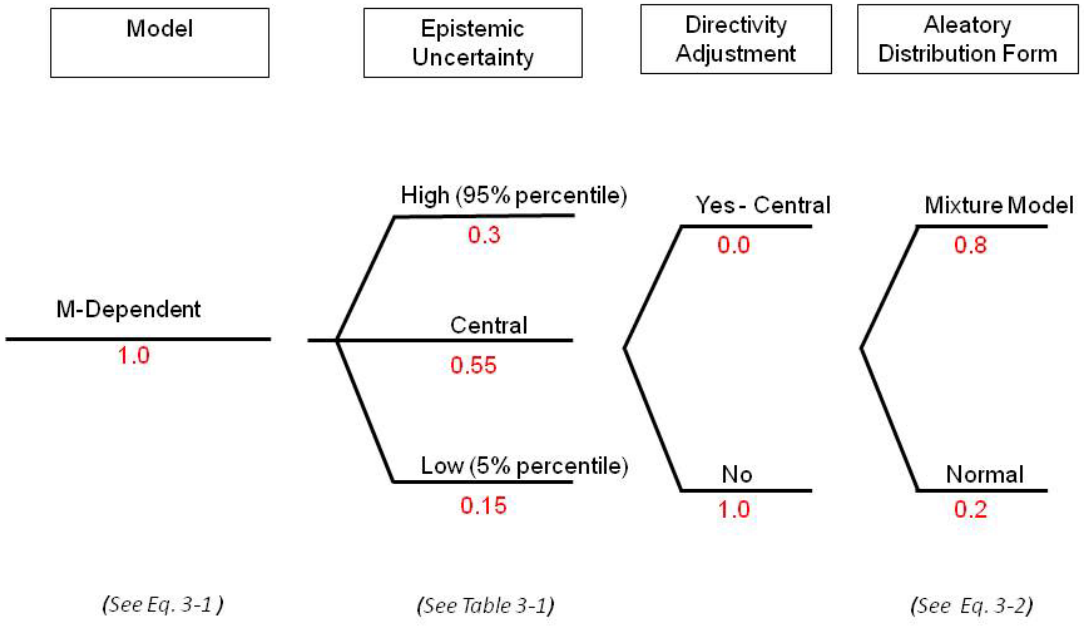



**Figure 3-1:** Logic Tree for Total Sigma at DCPP.

## 3.2 DCPP Total Sigma Model

The following values are provided obtain the total sigma as a function of Magnitude, $\sigma_{SS}(M)$, for hazard calculations using:

$$\sigma_{SS}(M) = \begin{cases} \sigma_1 + \frac{(M-5)}{2} * (\sigma_2 - \sigma_1) & for\ M < 7.0 \\ \sigma_2 & for\ M \geq 7.0 \end{cases} \quad \text{(Eq. 3-1)}$$

The period-dependent values of $\sigma_1$ and $\sigma_2$ are listed in Table 3-1:

**Table 3-1:** Epistemic Distribution for $\sigma_{SS}$ for DCPP.

| Period (sec) | Low Branch | | Central Branch | | High Branch | |
|---|---|---|---|---|---|---|
| | $\sigma_1$ | $\sigma_2$ | $\sigma_1$ | $\sigma_2$ | $\sigma_1$ | $\sigma_2$ |
| 0.01 | 0.456 | 0.390 | 0.576 | 0.495 | 0.699 | 0.614 |
| 0.02 | 0.457 | 0.394 | 0.577 | 0.498 | 0.699 | 0.614 |
| 0.03 | 0.458 | 0.396 | 0.577 | 0.499 | 0.700 | 0.615 |
| 0.05 | 0.460 | 0.402 | 0.578 | 0.504 | 0.700 | 0.616 |
| 0.075 | 0.461 | 0.407 | 0.578 | 0.507 | 0.701 | 0.617 |
| 0.1 | 0.462 | 0.411 | 0.579 | 0.510 | 0.702 | 0.618 |
| 0.15 | 0.464 | 0.416 | 0.580 | 0.514 | 0.703 | 0.620 |
| 0.2 | 0.465 | 0.419 | 0.581 | 0.517 | 0.703 | 0.621 |
| 0.25 | 0.465 | 0.422 | 0.581 | 0.519 | 0.704 | 0.622 |
| 0.3 | 0.466 | 0.424 | 0.581 | 0.520 | 0.704 | 0.623 |
| 0.4 | 0.466 | 0.427 | 0.582 | 0.522 | 0.704 | 0.625 |
| 0.5 | 0.467 | 0.429 | 0.582 | 0.524 | 0.705 | 0.626 |
| 0.75 | 0.468 | 0.432 | 0.583 | 0.527 | 0.705 | 0.628 |
| 1 | 0.468 | 0.434 | 0.583 | 0.529 | 0.706 | 0.629 |
| 1.5 | 0.469 | 0.437 | 0.584 | 0.531 | 0.706 | 0.631 |
| 2 | 0.469 | 0.439 | 0.584 | 0.532 | 0.707 | 0.632 |
| 3 | 0.470 | 0.441 | 0.585 | 0.534 | 0.707 | 0.633 |
| 4 | 0.470 | 0.441 | 0.585 | 0.534 | 0.707 | 0.634 |
| 5 | 0.470 | 0.441 | 0.585 | 0.535 | 0.707 | 0.634 |
| 7.5 | 0.471 | 0.442 | 0.585 | 0.535 | 0.708 | 0.635 |
| 10 | 0.471 | 0.442 | 0.586 | 0.536 | 0.708 | 0.635 |

### 3.3 DCPP Mixture Model

The mixture model is the sum of two equally weighted normal distributions with the standard deviation given by 0.8 and 1.2 times the total standard deviation. To implement the mixture model in the hazard calculation, the conditional probability of exceeding a ground motion value z is weighted average of the conditional probabilities computed for each of the standard deviation value separately (Eq. 3-2).

$$P_{MIX}(Sa > z \mid M, R, ..., \sigma_{SS}) = 0.5P(Sa > z \mid M, R, ..., 0.8\sigma_{SS}) + 0.5P(Sa > z \mid M, R, ..., 1.2\sigma_{SS})$$

(Eq. 3-2)

## 4. Coefficients and weights for the common-form ground motion models

The period-dependent coefficients and weights for the ground motion models based on common form are provided in the electronic attachment to this HID document. The description of the material in the electronic attachment is provided here below.

### 4.1 Coefficient and Weights for DCPP

The period-dependent coefficients and weights for the common form ground motion models for DCPP are included in the zipped folder named “DCPP_Coefficients_Weights-11262014.zip”.

The files included in the folder and their content’s description is provided in Table 4-1. The structure of the file is the same for all the .csv files included in the zipped folder, and the structure specifications are provided in Table 4-2.

**Table 4-1:** List and description of .csv files included in electronic material "DCPP_Coefficients_Weights-11262014.zip".

| File Name | Description |
|---|---|
| Coefficients_Weights_DCPP_T001.csv | Coefficients and Weights for period T=0.01 sec |
| Coefficients_Weights_DCPP_T002.csv | Coefficients and Weights for period T=0.02 sec |
| Coefficients_Weights_DCPP_T003.csv | Coefficients and Weights for period T=0.02 sec |
| Coefficients_Weights_DCPP_T005.csv | Coefficients and Weights for period T=0.05 sec |
| Coefficients_Weights_DCPP_T0075.csv | Coefficients and Weights for period T=0.075 sec |
| Coefficients_Weights_DCPP_T01.csv | Coefficients and Weights for period T=0.1 sec |
| Coefficients_Weights_DCPP_T015.csv | Coefficients and Weights for period T=0.15 sec |
| Coefficients_Weights_DCPP_T02.csv | Coefficients and Weights for period T=0.2 sec |
| Coefficients_Weights_DCPP_T025.csv | Coefficients and Weights for period T=0.25 sec |
| Coefficients_Weights_DCPP_T03.csv | Coefficients and Weights for period T=0.3 sec |
| Coefficients_Weights_DCPP_T04.csv | Coefficients and Weights for period T=0.4 sec |
| Coefficients_Weights_DCPP_T05.csv | Coefficients and Weights for period T=0.5 sec |
| Coefficients_Weights_DCPP_T075.csv | Coefficients and Weights for period T=0.75 sec |
| Coefficients_Weights_DCPP_T1.csv | Coefficients and Weights for period T=1.0 sec |
| Coefficients_Weights_DCPP_T15.csv | Coefficients and Weights for period T=1.5 sec |
| Coefficients_Weights_DCPP_T2.csv | Coefficients and Weights for period T=2.0 sec |
| Coefficients_Weights_DCPP_T3.csv | Coefficients and Weights for period T=3.0 sec |
| Coefficients_Weights_DCPP_T4.csv | Coefficients and Weights for period T=4.0 sec |
| Coefficients_Weights_DCPP_T5.csv | Coefficients and Weights for period T=5.0 sec |
| Coefficients_Weights_DCPP_T75.csv | Coefficients and Weights for period T=7.5 sec |
| Coefficients_Weights_DCPP_T100.csv | Coefficients and Weights for period T=10.0 sec |

**Table 4-2:** Structure of the files included in electronic material "DCPP_Coefficients_Weights-11262014.zip". The structure is common to all the files included in the zipped folder.

| Column | Description | Notes |
|---|---|---|
| Column A | Model ID | There may be less than 31 models for a specific period |
| Column B | Coefficient $a_0$ | Coefficients in Equation 2-1 |
| Column C | Coefficient $a_1$ | Coefficients in Equation 2-1 |
| Column D | Coefficient $a_2$ | Coefficients in Equation 2-1 |
| Column E | Coefficient $a_3$ | Coefficients in Equation 2-1 |
| Column F | Coefficient $a_4$ | Coefficients in Equation 2-1 |
| Column G | Coefficient $a_5$ | Coefficients in Equation 2-1 |
| Column H | Coefficient $a_6$ | Coefficients in Equation 2-1 |
| Column I | Coefficient $a_7$ | Coefficients in Equation 2-1 |
| Column J | Coefficient $a_8$ | Coefficients in Equation 2-1 |
| Column K | Coefficient $a_{10}$ | Coefficients in Equation 2-1 |
| Column L | Identifier of the HW branch which is associated to the specific Model ID | Coefficients for the 5 alternative HW adjustment models are provided in Table 2-2. The hanging wall adjustment is to be applied only for the sites located in the hanging wall side (i.e. with $R_X \geq 0$ km). |
| Column M | Total weights for the specific period | |
| Entry at M34 | Sum of the total weights | Internal check that the weights sum to 1 |

# 5. References

Abrahamson, N.A., Silva, W.J., and Kamai, R. (2014). Summary of the AKS14 Ground-Motion Relation for Active Crustal Regions, *Earthquake Spectra*, Vol. 30(3), 1025-1055, DOI: 10.1193/070913EQS198M.

Al Atik, L., and Youngs, R.R. (2014). Epistemic Uncertainty for NGA-West2 Models, *Earthquake Spectra*, Vol. 30(3), 1301-1318, DOI: 10.1193/062813EQS173M.

Boore, D.M., Stewart, J.P., Seyhan, E., and Atkinson, G.M. (2014). NGA-West 2 Equations for Predicting PGA, PGV, and 5%-Damped PSA for Shallow Crustal Earthquakes, *Earthquake Spectra*, Vol. 30(3), 1057-1085, DOI: 10.1193/070113EQS184M.

Campbell, K.W., and Bozorgnia, Y. (2014). NGA-West2 Ground Motion Model for the Average Horizontal Components of PGA, PGV, and 5%-Damped Linear Acceleration Response Spectra, *Earthquake Spectra*, Vol. 30(3), 1087-1115, DOI: 10.1193/062913EQS175M.

Chiou, B.S.-J., and Youngs, R.R. (2014). Update of the Chiou and Youngs NGA Model for the Average Horizontal Component of Peak Ground Motion and Response Spectra, *Earthquake Spectra*, Vol. 30(3), 1117-1153, DOI: 10.1193/072813EQS219M.

Idriss, I.M. (2014). An NGA-West2 Empirical Model for Estimating the Horizontal Spectral Values Generated by Shallow Crustal Earthquakes, *Earthquake* Spectra, Vol. 30(3), 1155-1177, DOI: 10.1193/070613EQS195M.

# APPENDIX D

# SIMPLIFIED SOURCE MODEL FOR GROUND-MOTION MODEL DEVELOPMENT

## D.1 Introduction

As part of the GM model development (see Chapter 6) simplified source models were developed for the DCPP and PVNGS sites. These simplified source models are intended to capture the broad features of the controlling seismic sources in terms of magnitude, distance and hanging wall contributions to the hazard. They are not intended to represent the actual hazard level for DCPP and PVNGS.

Using these simplified source models, the hazard is computed for each of the samples of the median ground-motion model based on common functional form GMPE models. The hazard results are used to weight the scenarios for the ground-motion model maps and to select representative models for each of the regions in the ground-motion model maps (see Chapter 6).

This Appendix describes the two simplified source models used in the study.

## D.2 DCPP Simplified Source Model

The hazard at the DCPP project site is controlled by the suite of faults that are closest to the plant site. Specifically, these are the Hosgri, Shoreline, Los Osos, and San Luis Bay faults with $R_X$ distances of about 5 km, 1 km, 10 km, and 2 km, respectively. Both the Hosgri and Shoreline faults are characterized as Strike-slip faults while the Los Osos and San Luis Bay faults are reverse mechanism sources. In addition, for these two reverse faults, the plant is located on the hanging wall of these faults.

The broad features that should be captured in the simplified source model are nearby strike-slip faults that can generate magnitudes in the **M**6 to **M**7.5 range and nearby reverse faults, with the site on the HW side, which can generate magnitudes in the range of **M**6 to **M**7.

To capture the broad features of the significant sources contributing to the hazard at DCPP, the simplified source model includes three parallel vertical strike-slip faults and three parallel 45 degree dipping reverse faults. To broaden the range of distances and hanging wall effects that may contribute to the hazard, for each of the two styles-of-faulting, the faults were placed at $R_X$ distances of 1, 5, and 10 km from the site. For the reverse cases, the site is located on the hanging wall side.

A map view of the three strike-slip faults and the site location is shown in Figure D.2-1a. The total length of these faults is 140 km and the mean characteristic maximum magnitude was set to be 6.5, 7.0, and 7.5 with associated weights of 0.2, 0.6, and 0.2. The Youngs and Coppersmith (1985) characteristic model was used for the magnitude density function with a b-value of 0.9. The specific fault parameters for these strike-slip faults are listed in Table D.2-1.

For the three reverse faults, the surface projection of the top edge of the fault plane is shown in Figure D.2-1b. These faults had a top of rupture of 0 km with a vertical thickness of 12 km. The length of these faults was 20 km with a dip of 45 degrees dipping to the east, which put the DCPP site on the hanging wall side of these faults. The maximum magnitudes assigned to these reverse faults were 6.5 and 7.0 with equal weights. The specific parameters for these reverse faults are listed in Table D.2-1.

Based on this simplified source model and using the center common functional form model for the GMPE, the hazard was computed and the resulting deaggregations are shown in Figures D.2-2a-d for spectral periods of 0.2 and 2.0 sec at annual hazard levels of $10^{-4}$ and $10^{-6}$. As expected, the controlling events are events within 10 km ($R_X$ distance metric) and with magnitudes in the range of about 6 - 7.5. The longer periods (2 sec) show greater contributions from larger magnitudes.

## D.3 PVNGS Simplified Source Model

The hazard at the PVNGS site is controlled by both the local host zones and also the more distance large magnitude sources located in the southern California region. For the development of the GM models, the simplified source model presented in this Appendix is based on a representation of the local host zone only because the objective is the selection of GMPEs for the greater Arizona sources. The more distant large magnitude sources located in Southern California are selected using a different approach (see Chapter 6). For the host zone, the simple source model is based on a suite of parallel dipping faults to represent the areal source zone in the region around the PVNGS site. This representation also captures the effects of hanging wall scaling on the hazard.

A map view of the suite of 41 dipping faults and the site location is shown in Figure D.3-1. These faults all dip 50 degrees to the east with a vertical thickness of 15 km and the top of the fault located at the surface. The length of each fault is 2 degrees in latitude (I.e., 222 km). Each of the 41 faults was assigned an activity rate of magnitude 5.0 and larger earthquakes of 1.8e-04 with an adopted b-value of 0.789. A range of maximum magnitude values was assigned ranging from 6.5 to 7.5 with associated weights. The mechanism for these faults was modeled as being 80% normal and 20% strike-slip. The specific values are all listed in Table D.3-1.

Based on this simplified source model and using the center common functional form GMPE defined as a function of rupture distance, an example deaggregation plot is shown in Figures D.3-2a-d for spectral periods of 0.2 and 2.0 sec at annual hazard levels of $10^{-4}$ and $10^{-6}$. For the $10^{-4}$ level, the contribution to the total hazard is broad spanning the $R_X$ range of about -75 to 75 km. The 0.2 sec case is controlled by slightly smaller magnitudes in the range of 5 – 7 whereas the long spectral period of 2 sec is controlled by slightly larger magnitude range of 5.5 – 7. For the $10^{-6}$ level the distribution on magnitude is similar to the $10^{-4}$ level but the distance contribution is more restrictive with the range being about -15 to 15 in $R_X$ distance.

## D.4 References

Youngs, R.R., and Coppersmith, K.J. (1985). Implications of fault slip rates and earthquake recurrence models to probabilistic seismic hazard estimates, *Bull. Seism. Soc. Am.*, Vol. 75(4), 939-964.

**Table D.2-1:** Fault Parameters for DCPP simplified source model.

| ***Strike-Slip Faults*** | | |
|---|---|---|
| *Parameter* | *Value* | *Weight* |
| Slip Rate | 1.0 mm/yr per fault | 1.0 |
| Dip | 90 | 1.0 |
| Top of Fault (km) | 0.0 | 1.0 |
| Bottom of Fault (km) | 12.0 | 1.0 |
| Maximum Magnitude | 6.5, 7.0, 7.5 | 0.2, 0.6, 0.2 |
| Mechanism | Strike-slip | 1.0 |
| ***Reverse Faults*** | | |
| *Parameter* | *Value* | *Weight* |
| Slip Rate | 0.5 mm/yr per fault | 1.0 |
| Dip | 45 (Dipping to the East) | 1.0 |
| Top of Fault (km) | 0 | 1.0 |
| Bottom of Fault (km) | 12.0 | 1.0 |
| Maximum Magnitude | 6.5, 7.0 | 0.5, 0.5 |
| Mechanism | Reverse | 1.0 |

**Table D.3-1:** Fault Parameters for PVNGS simplified source model.

| *Parameter* | *Value* | *Weight* |
|---|---|---|
| Activity Rate ($N \geq 5.0$) | 0.0738 eqk/yr for the region<br>(1.8e-04 eqk/yr per fault) | 1.0 |
| b-value | 0.79 | 1.0 |
| Dip | 50 (Dipping East) | 1.0 |
| Top of Rupture (km) | 0.0 | 1.0 |
| Vertical Thickness (km) | 15.0 | 1.0 |
| Maximum Magnitude | 6.5, 6.7, 6.9, 7.1, 7.3, 7.5 | 0.1, 0.1, 0.3, 0.3, 0.1, 0.1 |
| Mechanism | Normal (80%)<br>Strike-slip (20%) | 1.0 |

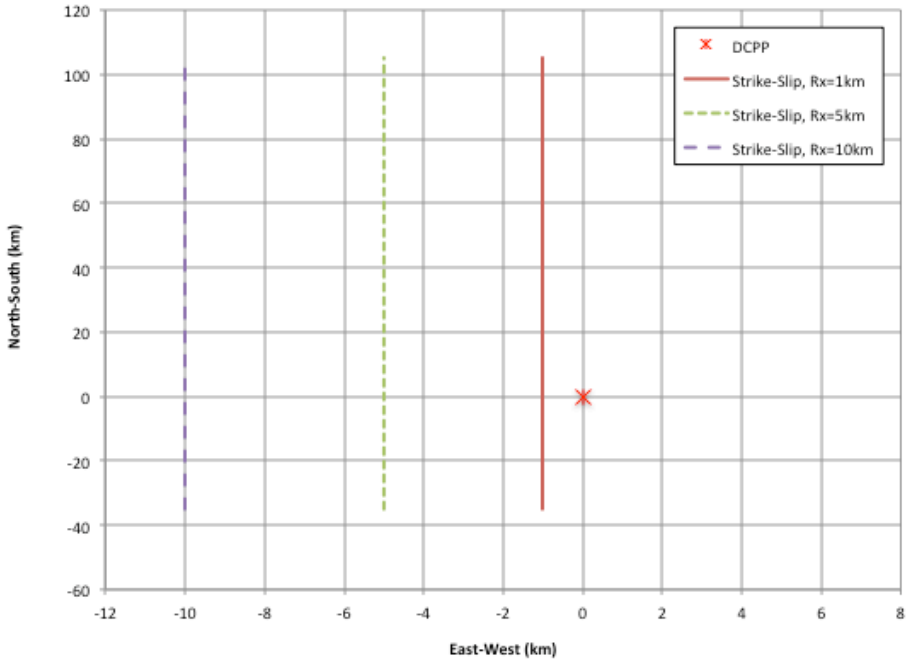



**Figure D.2-1a:** Map view showing the three vertical strike-slip faults at $R_X$ distances of 1, 5, and 10 km and the relative DCPP plant location.

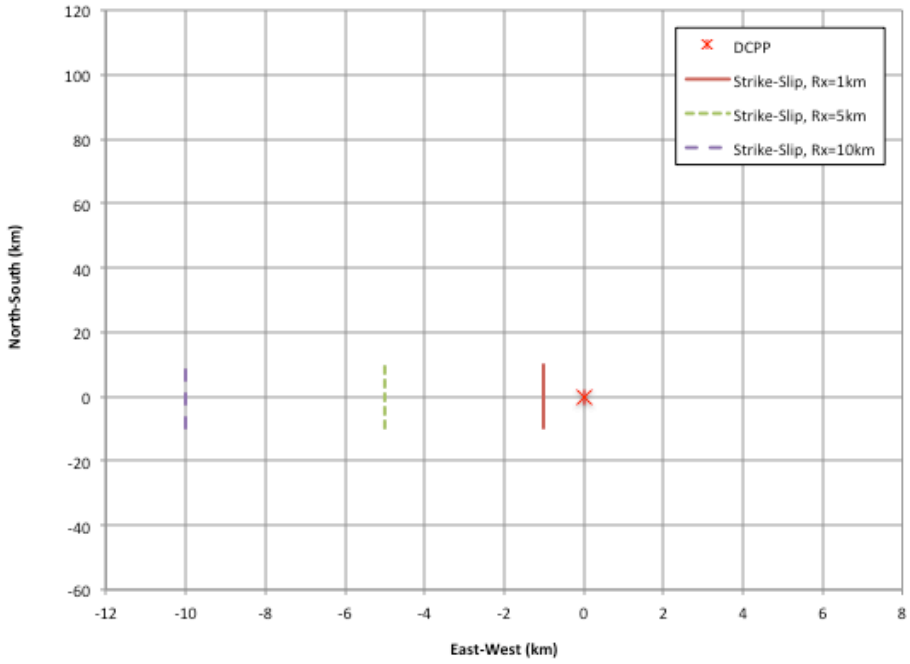



**Figure D.2-1b:** Map view showing the surface projection of the top of the three dipping reverse faults (dipping to the east at 45 degrees) at $R_X$ distances of 1, 5, and 10 km and the relative DCPP plant location.

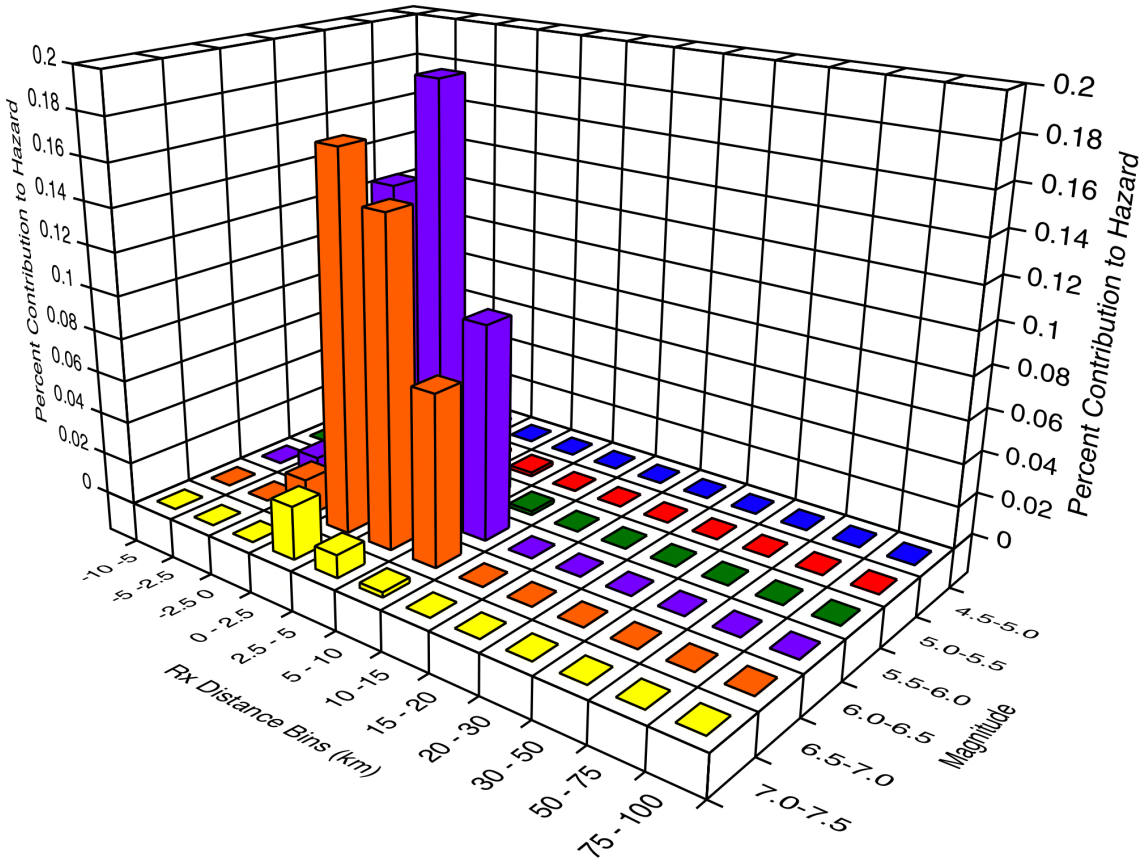



**Figure D.2-2a:** Deaggregation for 0.2 sec spectral period at the $10^{-4}$ annual frequency of exceedance level for the DCPP site based on the simplified source model and the central common functional form GMPE model.

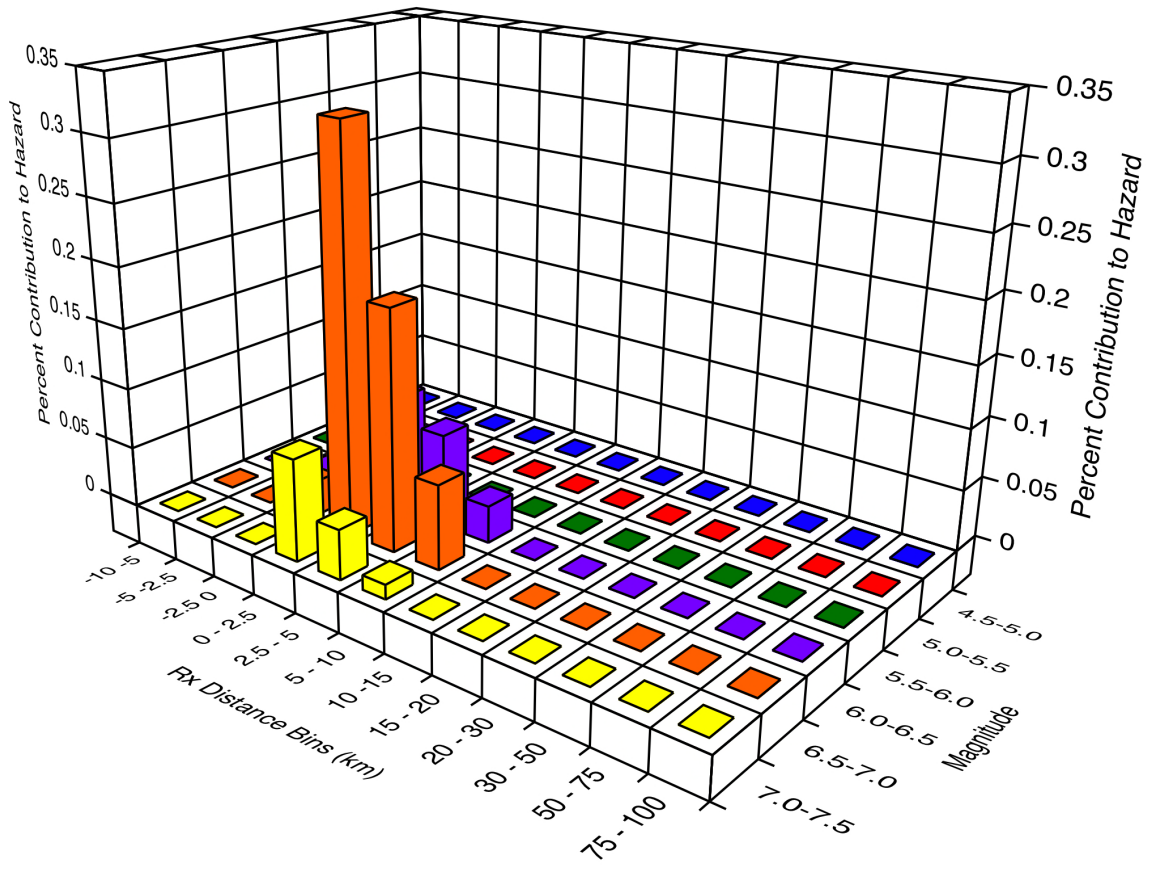



**Figure D.2-2b:** Deaggregation for 2 sec spectral period at the $10^{-4}$ annual frequency of exceedance level for the DCPP site based on the simplified source model and the central common functional form GMPE model.

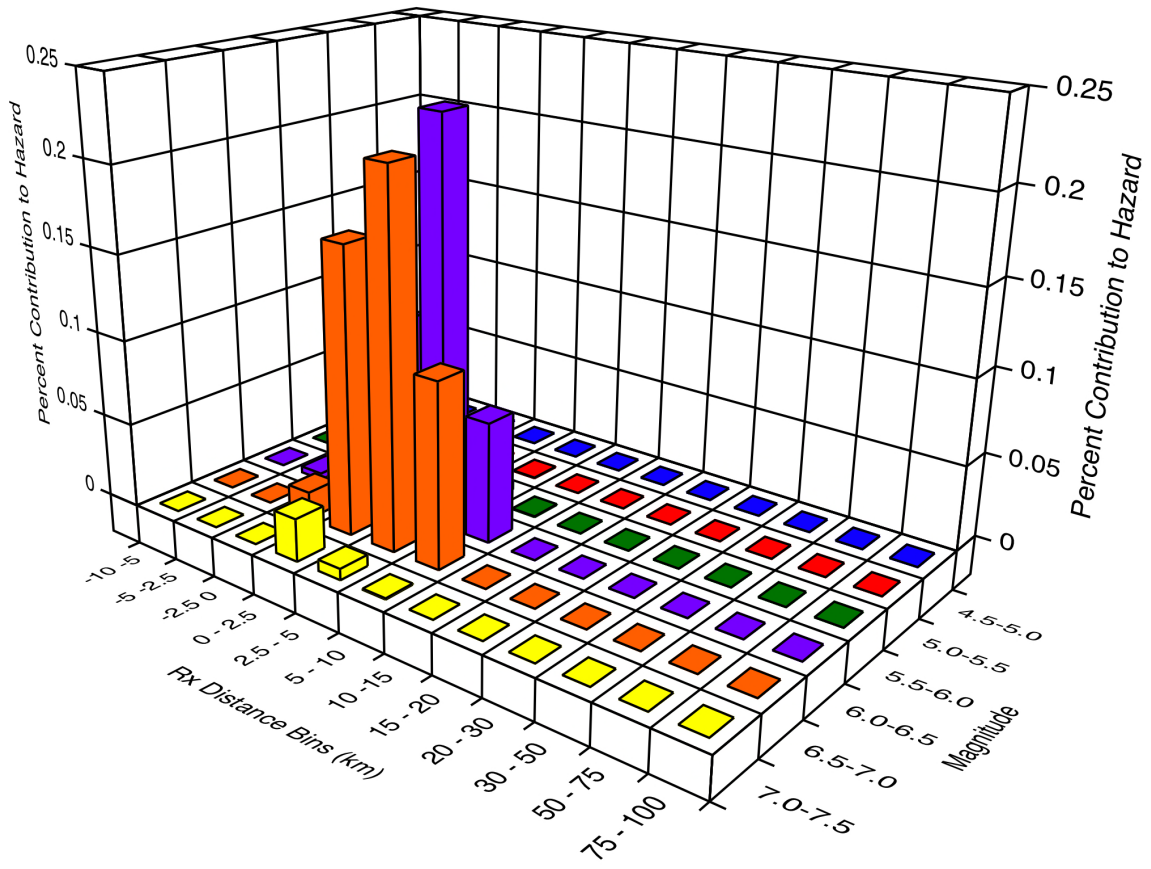



**Figure D.2-2c:** Deaggregation for 0.2 sec spectral period at the $10^{-6}$ annual frequency of exceedance level for the DCPP site based on the simplified source model and the central common functional form GMPE model.

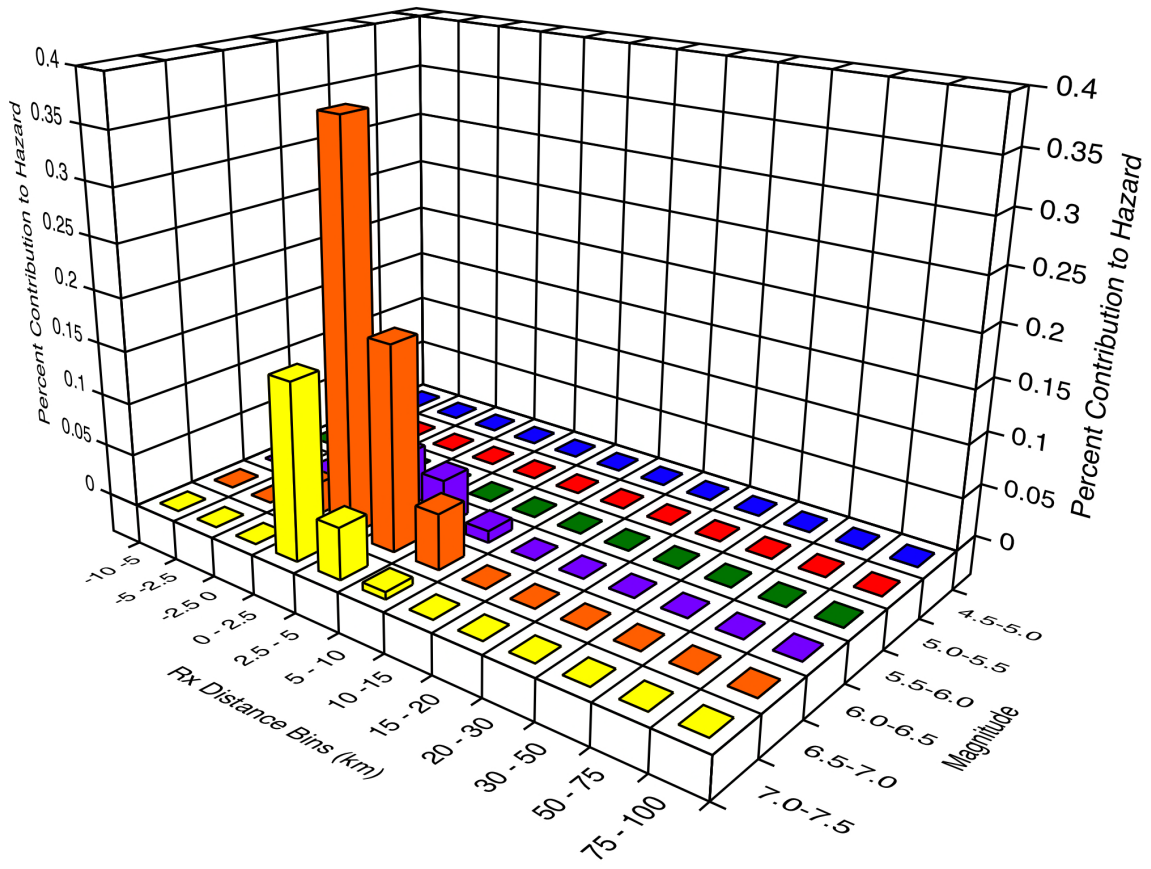



**Figure D.2-2d:** Deaggregation for 2 sec spectral period at the $10^{-6}$ annual frequency of exceedance level for the DCPP site based on the simplified source model and the central common functional form GMPE model.

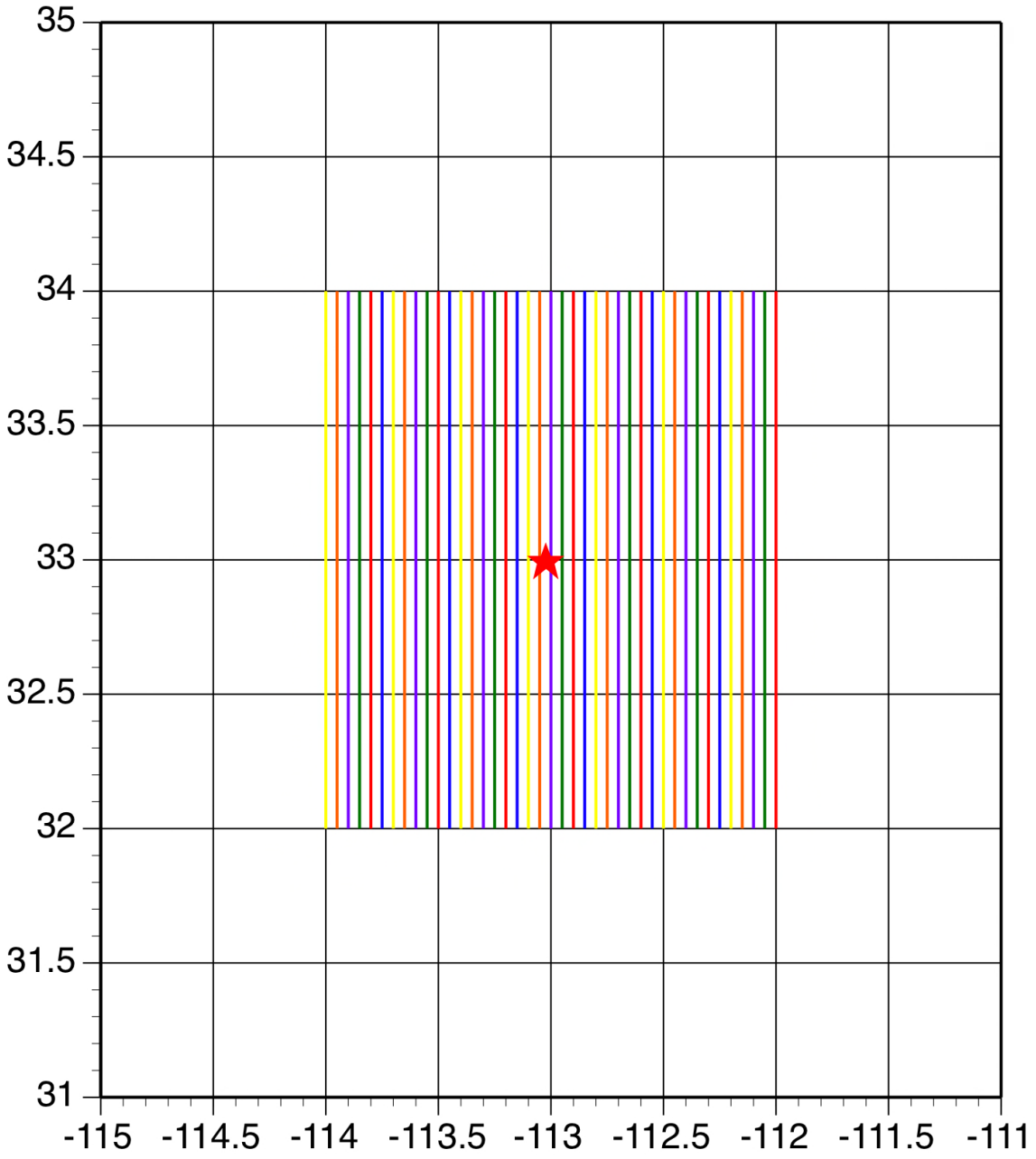



**Figure D.3-1:** Map view showing the surface projection of the top of the suite of dipping faults relative PVNGS plant location.

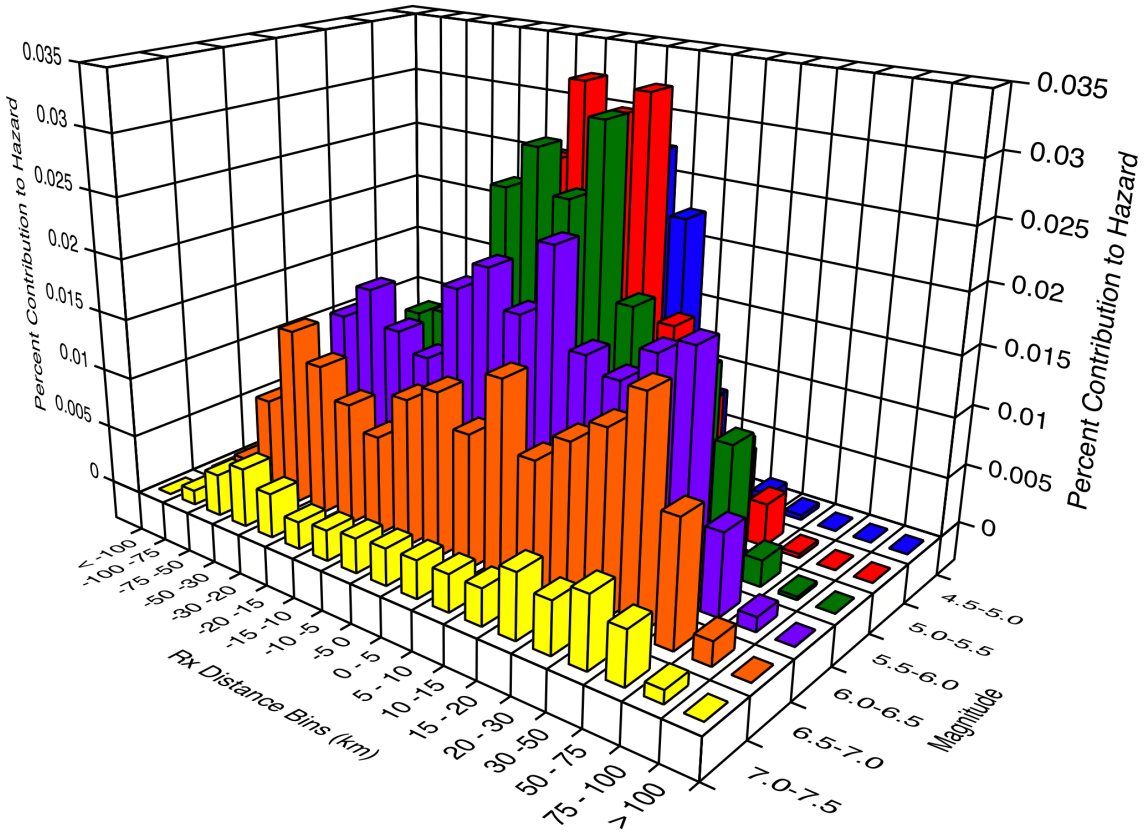



**Figure D.3-2a:** Deaggregation for 0.2 sec spectral period at the $10^{-4}$ annual frequency of exceedance level for the PVNGS site based on the simplified source model and the central common functional form GMPE model.

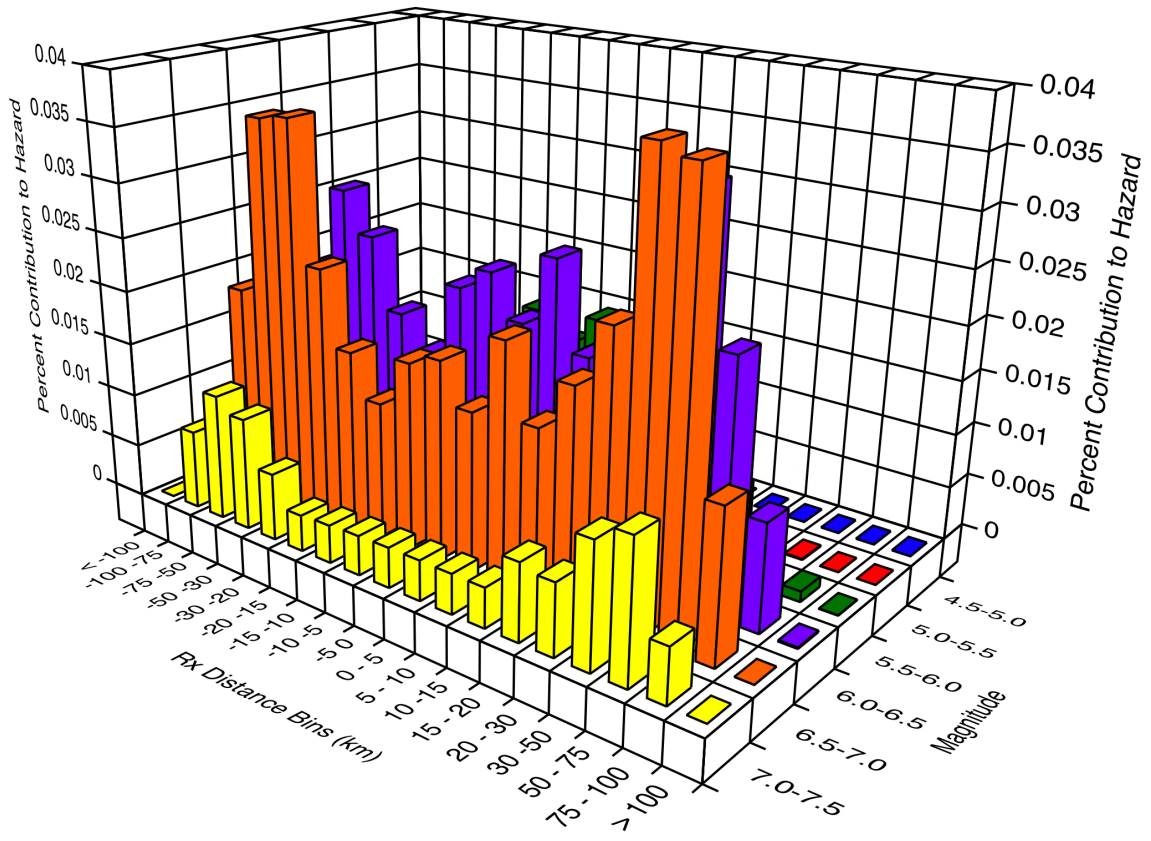



**Figure D.3-2b:** Deaggregation for 2 sec spectral period at the $10^{-4}$ annual frequency of exceedance level for the PVNGS site based on the simplified source model and the central common functional form GMPE model.

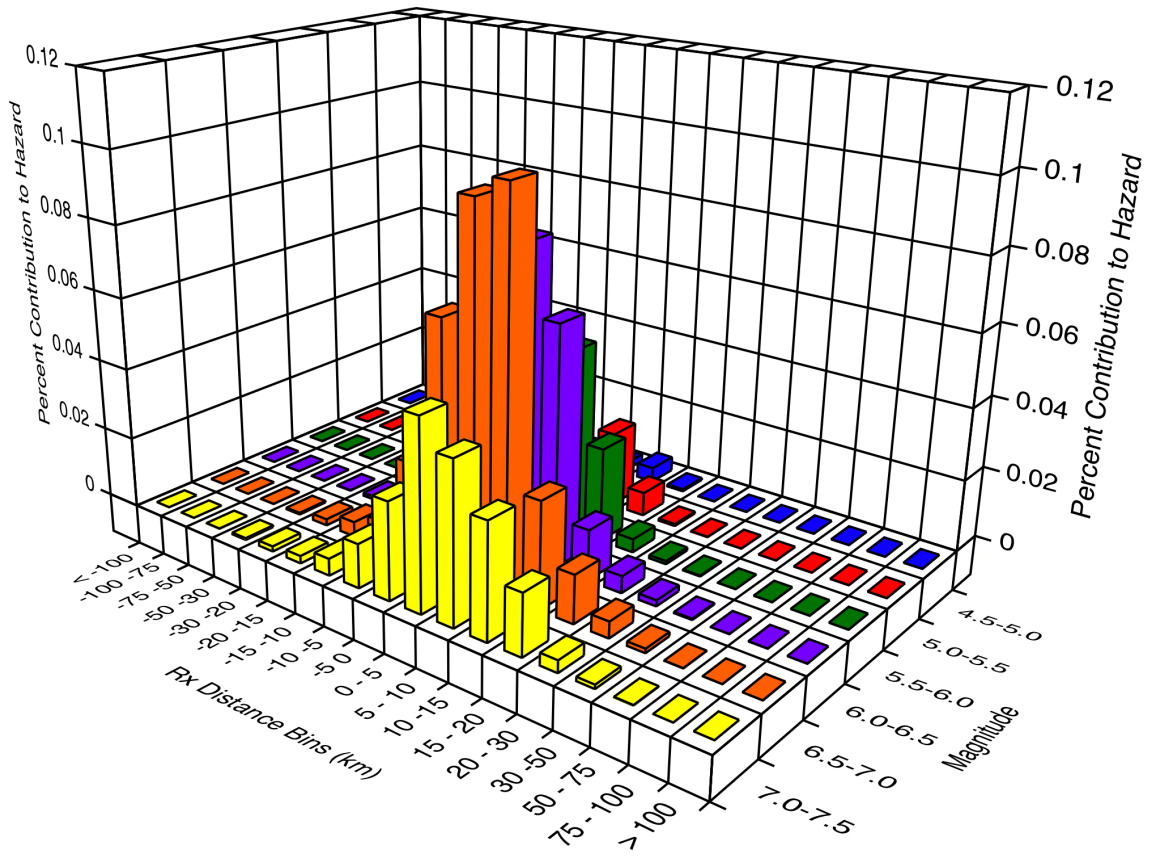



**Figure D.3-2c:** Deaggregation for 0.2 sec spectral period at the $10^{-6}$ annual frequency of exceedance level for the PVNGS site based on the simplified source model and the central common functional form GMPE model.

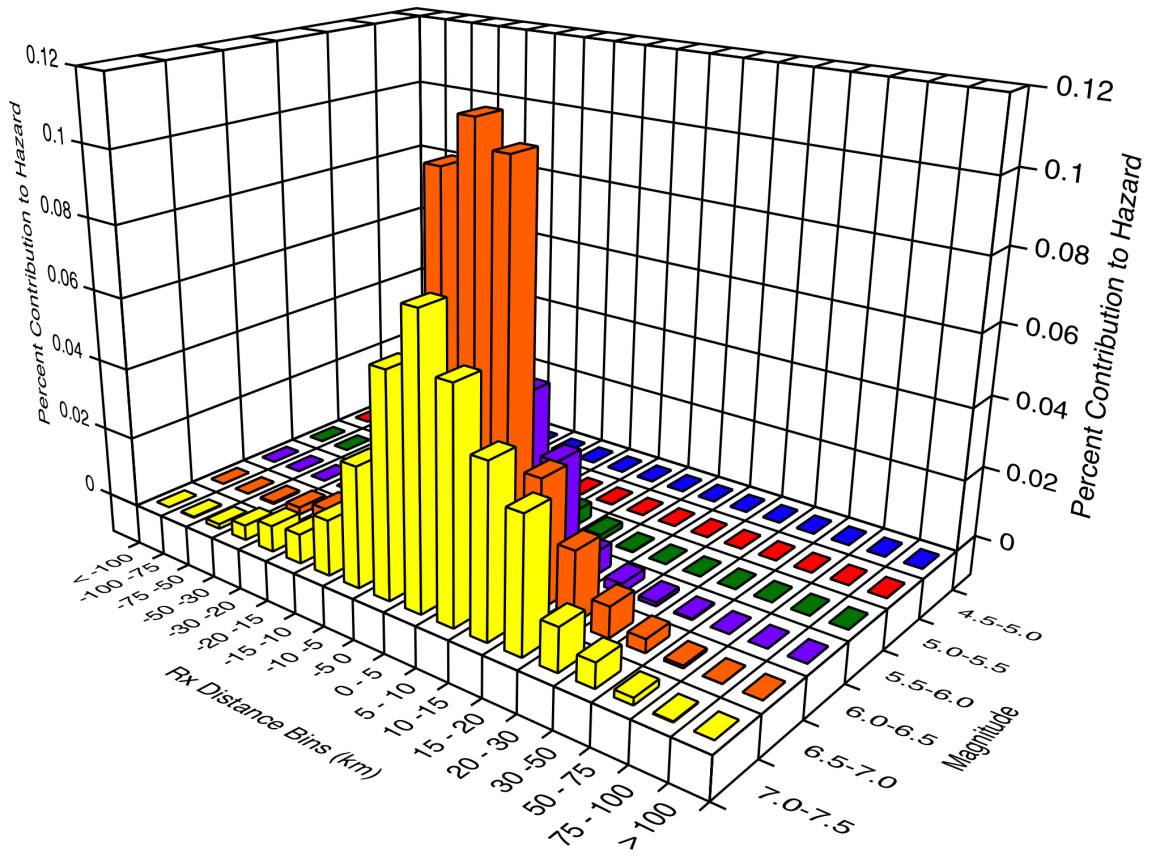



**Figure D.3-2d:** Deaggregation for 2 sec spectral period at the $10^{-6}$ annual frequency of exceedance level for the PVNGS site based on the simplified source model and the central common functional form GMPE model.

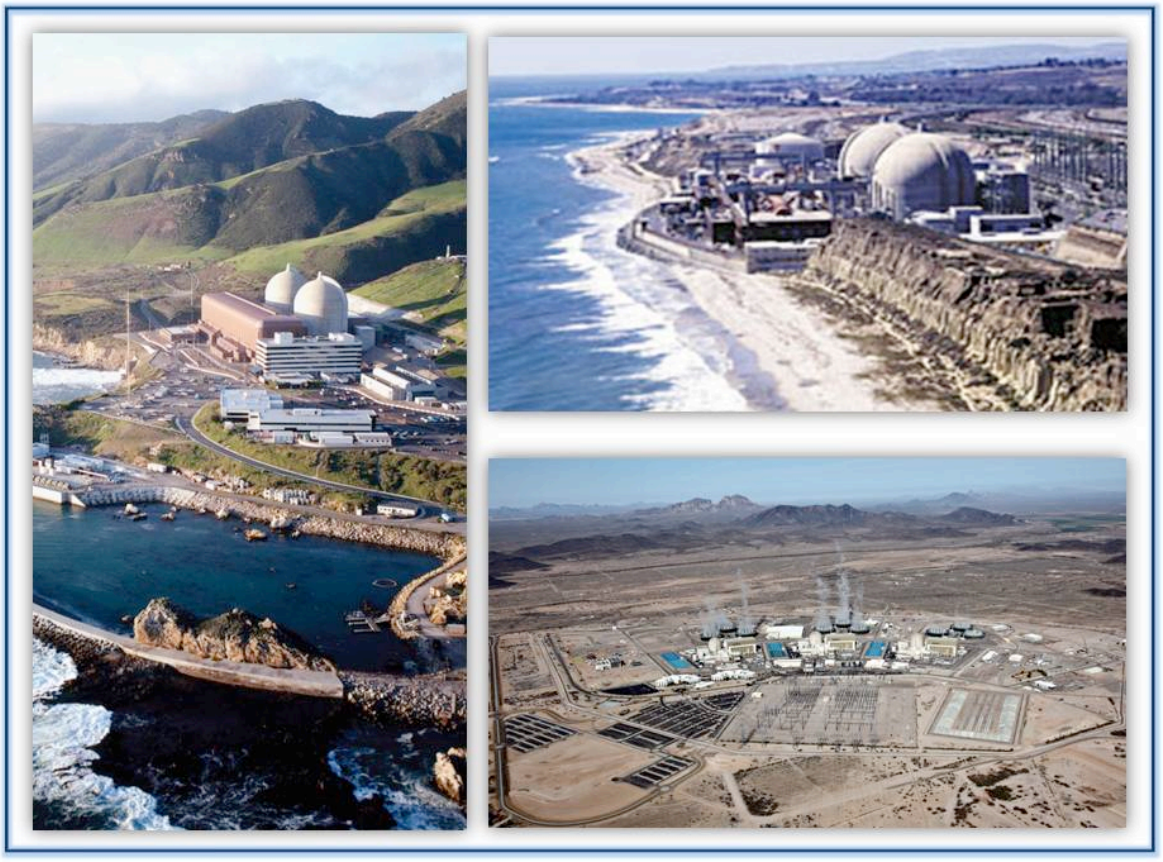
# *APPENDIX E*

## WORKSHOP #1 SUMMARY

# SOUTHWESTERN UNITED STATES GROUND MOTION CHARACTERIZATION SSHAC LEVEL 3

## Workshop #1 Proceedings

Version 1.2



aps PG&E SOUTHERN CALIFORNIA EDISON

GeoPentech
Geotechnical & Geoscience Consultants

# WORKSHOP #1 PROCEEDINGS:

# Critical Issues and Data Needs

## March 19-21, 2013

### Hilton Oakland Airport, California

**Prepared for:**

**Arizona Public Service Company**
Palo Verde Nuclear Generating Station
*Wandell, Christopher J.*
Senior Consulting "Chief" Civil Engineer
Phone: (623) 393-6741; E-mail: christopher.wandell@aps.com

**Pacific Gas and Electric Company**
Diablo Canyon Power Plant
*Klimczak, Richard*
Director Geosciences
Phone: (415) 973-2791; E-mail: RLK1@pge.com

**Southern California Edison Company**
San Onofre Nuclear Generating Station
*McAndrews, Caroline*
Director, Nuclear Strategic Projects
Phone: (949)368-3540; E-mail: Caroline.Mcandrews@sce.com

Version: 1.2
Date: August 7, 2014

## LIST OF ABBREVIATIONS and COMMON ACRONYMS

| | |
|---|---|
| ACR | Active Crustal Region |
| AFE | Annual Frequency of Exceedance |
| APS | Arizona Public Services |
| BBP | Broad Band Platform |
| CBR | Center, Body, and Range |
| CEA | California Earthquake Authority |
| CEC | California Energy Commission |
| CEUS | Central and Eastern United States |
| CFM | Community Fault Models |
| CFR | Code of Federal Regulations |
| CGS | California Geological Survey |
| CPUC | California Public Utilities Commission |
| DCPP | Diablo Canyon Power Plant |
| EE | Evaluator Expert |
| FGF | Fragile Geological Feature |
| FW | Foot Wall |
| GIS | Geographic Information System |
| GMC | Ground Motion Characterization |
| GMPE | Ground Motion Prediction Equation |
| GMRS | Ground Motion Response Spectrum |
| GPS | Global Positioning System |
| HID | Hazard Input Document |
| HC | Hazard Calculation |
| HW | Hanging Wall |
| Hz | Hertz |
| IPRG | Independent Peer Review Group |
| ITC | Informed Technical Community |
| LiDAR | Light Detection and Ranging |
| NGA | Next Generation Attenuation |
| NGA-West2 | Project name for the update of the 2008 NGA models |
| NI | Newport Inglewood |

| | |
|---|---|
| NI/RC | Newport Inglewood / Rose Canyon |
| NPP | Nuclear Power Plant |
| NSHM | National Seismic Hazard Mapping |
| PE | Proponent Expert |
| PEER | Pacific Earthquake Engineering Research Center |
| PGA | Peak Ground Acceleration |
| PG&E | Pacific Gas & Electric |
| OBT | Oceanside Blind Thrust |
| PM | Project Manager |
| PPRP | Participatory Peer Review Panel |
| PSHA | Probabilistic Seismic Hazard Analysis |
| PTI | Project Technical Integrator |
| PV | Palos Verdes |
| PVNGS | Palo Verde Nuclear Generating Station |
| QA | Quality Assurance |
| RC | Rose Canyon |
| RE | Resource Expert |
| RG | Regulatory Guide |
| SCE | Southern California Edison |
| SCEC | Southern California Earthquake Center |
| SCFM | Statewide Community Fault Model |
| SCSN | Southern California Seismic Network |
| SONGS | San Onofre Nuclear General Station |
| SSC | Seismic Source Characterization |
| SSHAC | Senior Seismic Hazard Analysis Committee |
| SWUS | Southwest United States |
| TA | Transportable Array |
| TDI | Technically Defensible Interpretation |
| TI | Technical Integrator |
| UCERF2 | Uniform California Earthquake Rupture Forecast, Version 2 |
| UCERF3 | Uniform California Earthquake Rupture Forecast, Version 3 |
| USGS | United States Geological Society |

| | |
|---|---|
| U.S.NRC | U.S. Nuclear Regulatory Commission |
| USR | Unified Structural Representation |
| $V_{S,30}$ | Shear Wave Velocity in the upper 30m |
| WGCEP | Working Group on California Earthquake Probabilities |
| WUS | Western United States |

# TABLE OF CONTENTS

Page

LIST OF ABBREVIATIONS and COMMON ACRONYMS ..... iii
TABLE OF CONTENTS ..... vii
WORKSHOP #1 INTRODUCTION ..... 1
Purpose: ..... 1
Approach: ..... 1
Workshop #1 Agenda ..... 3
Workshop #1 participants ..... 7
WORKSHOP #1 SUMMARY ..... 9
Project background ..... 9
General workshop summary ..... 9
Topic 1: Ground Motion Prediction Equations (GMPEs) ..... 10
Topic 2: Data to constrain GMPEs in Critical Ranges ..... 10
Topic 3: Use of Simulations for SWUS GMC ..... 11
Topic 4: Arizona Ground Motion Data and Issues ..... 12
Topic 5: California Ground Motion Data and Issues ..... 12
Topic 6: Fragile Geological Features ..... 13
Topic 7: Reference Conditions ..... 13
Topic 8: Addressing Sigma for SWUS GMC ..... 14
Focused questions submitted to Workshop #1 Presenters ..... 14
GROUND MOTION CHARACTERIZATION PRESENTATIONS ..... 22
TECHNICAL INTEGRATOR TEAM SUMMARIES and ACTIONS ..... 24
LETTER COMMENTARY FROM THE PARTICIPATORY PEER REVIEW PANEL ..... 45
TECHNICAL INTEGRATION TEAM LEAD RESPONSES TO PARTICIPATORY PEER REVIEW PANEL COMMENTS ..... 49
REFERENCES ..... 54

# WORKSHOP #1 INTRODUCTION

Pursuant to the Request for Information put forth on March 12, 2012 by the United States Nuclear Regulatory Commission in response to the Near-Term Task Force's (NTTF) evaluation of the Fukushima Dai-ichi accident, Pacific Gas and Electric Company (PG&E), Southern California Edison (SCE), and Arizona Public Service (APS) are co-sponsoring a joint Southwestern U.S. (SWUS) Ground Motion Characterization (GMC) SSHAC Level 3 study for the Diablo Canyon Power Plant (DCPP), the San Onofre Nuclear Generating Station (SONGS), and the Palo Verde Nuclear Generating Station (PVNGS).

This is the first out of three Workshops that will be conducted in accordance with the applicable SSHAC Level 3 guidelines.

## Purpose:

The specific goals of Workshop #1 are to:

1) Review the ground rules for the conduct of SSHAC workshops and expert roles within the project
2) Identify the technical issues of highest significance to the hazard analysis.
3) Review available data that will be considered for constructing the GMC model; this includes identification of data, information and/or additional work to be done on the continuing development of the project to address those issues. It will also address the evaluations to be performed in the period leading up to Workshop #2

## Approach:

The goals of the Workshop have been accomplished by a series of presentations and discussions designed to provide the Technical Integration (TI) team with information pertaining to: (1) assessment of the main ground motion and uncertainty contributors to the ground motion shaking hazard at the three sites of interest, and (2) discussion on the availability, applications, and limitations of the available data. Presentations are also to address the new data collection efforts currently underway and those that will be completed throughout the next two years to support this SSHAC project. All the presentations are part of the project record.

At this stage of the project, the focus is on identifying the data that are available to address the hazard-significant technical issues. Interpretation of the available data in terms of alternative models or implications to the seismic hazard at the site is to be avoided; this will be the focus of Workshop #2.

Speakers have been provided with detailed guidance by the TI Lead to ensure that the presentations are oriented to the goals of the project and Workshop. When inclusion of interpretations cannot be avoided, the speakers have been asked to identify biases or limitations in the interpretation process.

At the end of each day, Observers (including members of the PPRP and representatives of the Sponsors) have been provided with an opportunity to make comments and/or raise questions.

## Workshop #1 Agenda

| Session | Time | Topic | Duration (min.) | Speaker |
|---|---|---|---|---|
| Day 1 - AM | | 10:00 AM – 12:15 PM | | |
| WORKSHOP INTRODUCTION | 10:00 AM – 11:05 AM | Welcome and introduction | 10 | Di Alessandro |
| | | Sponsors' perspective | 15 | SWUS Utilities Representatives |
| | | Project overview and objectives | 20 | Abrahamson |
| | | Review SSHAC procedures and Workshop ground rules | 20 | Lettis |
| OVERVIEW of SEISMIC SOURCE CHARACTERIZATION | 11:05 AM - 12:15 PM | Diablo Canyon Power Plan (DCPP) | 20 | Thompson |
| | | San Onofre Nuclear Generating Station (SONGS) | 20 | Freeman |
| | | Palo Verde Nuclear Generating Station (PVNGS) | 20 | Lindvall |
| | | *Clarifications and questions* | 10 | Abrahamson leads; |
| 12:15 PM – 1:15 PM | | *Lunch* | | |
| Day 1 - PM | | 1:15 PM – 5:20 PM | | |
| GMC and SENSITIVITY ANALYSES | 1:15 PM - 2:55 PM | GMC Logic tree V0 | 30 | Wooddell |
| | | Hazard sensitivity analyses for DCPP | 20 | Gregor |
| | | Hazard sensitivity analyses for SONGS | 20 | Dinsick |
| | | Hazard sensitivity analyses for PVNGS | 20 | Walling |
| | | *Discussions: List of key Hazard sensitive GM issues* | 15 | Di Alessandro leads |
| 2:55 PM – 3:15 PM | | *Break* | | |
| GROUND MOTION PREDICTION EQUATIONs | 3:15 PM - 4:45 PM | GMPEs for active crustal regions: applicability for controlling sources | 30 | Stewart |
| | | NGA-West2 Database | 30 | Darragh |
| | | *Discussion: Are Hazard sensitive sources well constrained by GMPEs?* | 30 | Abrahamson leads; Additional REs: Boore, Bozorgnia, Kalkan, Baltay, Hanks, Silva |
| 4:45 PM – 5:05 PM | | Summary of GMC Day 1 | 20 | Donahue |
| 5:05 PM – 5:20 PM | | Observers (PPRP and Sponsors) comments | 15 | |
| Day 1 | | End of Formal Workshop Proceedings | | |
| Closed Meeting: PPRP, Sponsors, PM, TI Lead | | | | |

| Session | Time | Topic | Duration (min.) | Speaker |
|---|---|---|---|---|
| Day 2 - AM | | 8:00 AM – 11:50 AM | | |
| DATA to CONSTRAIN GMPEs in CRITICAL RANGES PART A | 8:00 AM - 10:00 AM | Directivity | 25 | Watson-Lamprey |
| | | Hanging Wall | 20 | Donahue |
| | | Fling | 15 | Kamai |
| | | *Discussion on data to constrain near-fault effects* | 30 | Wooddell leads; Additional REs: Somerville, Graves, Darragh, Baker |
| | | Multi-fault rupture | 30 | Donahue |
| 10:00 AM – 10:20 AM | | *Break* | | |
| DATA to CONSTRAIN GMPEs in CRITICAL RANGES PART B | 10:20 AM - 11:10 AM | Splays and linkage: dynamic rupture modeling | 25 | Harris |
| | | *Questions and Discussions on multi-fault ruptures* | 25 | Abrahamson leads; Additional REs: Somerville, Aagaard, Darragh |
| USE of SIMULATIONS for SWUS GMC PART A | 11:10 AM - 11:50 AM | Review on simulation validation from SCEC | 40 | Goulet |
| 11:50 AM – 12:50 PM | | *Lunch* | | |
| Day 2 - PM | | 12:50 PM – 4:45 PM | | |
| USE of SIMULATIONS for SWUS GMC PART B | 12:50 PM - 2:40 PM | *Discussion on simulation validation from SCEC* | 50 | Dreger leads; Additional REs: Olsen, Archuleta, Graves, Somerville, Bayless, Anderson, Jordan |
| | | *Discussions: Best uses of simulations (30 min) and Practical limitations (30 min)* Objectives: develop list of simulation cases to help constrain/establish uncertainty in GMPEs (Identify scenarios to be implemented in the numerical simulations) | 60 | Abrahamson leads; Additional REs: Somerville, Bayless, Graves, Jordan, Maechling, Silva, Bozorgnia, Boore, Aagaard, Heaton |
| 2:40 PM – 3:00 PM | | *Break* | | |
| ARIZONA GROUND MOTION DATA and ISSUES | 3:00 PM - 4:10 PM | Available GM data from Transportable Array in Arizona for both nearby earthquakes in Arizona and distant earthquakes in California | 25 | Watson-Lamprey |
| | | Additional GM data from Arizona from IRIS not part of the Transportable Array | 15 | Walling |
| | | *Discussions: Do we have sufficient data to resolve geometrical spreading, anelastic attenuation, kappa, and stress drop differences between California and Central Arizona?* | 30 | Youngs leads; Additional REs: Brumbaugh, Lindvall, Young, Silva, a CICESE representative (*) |

| Session (continued) | Time (cont.) | Topic (continued) | Duration (min. – cont.) | Speaker (continued) |
|---|---|---|---|---|
| 4:10 PM – 4:30 PM | | Summary of GMC Day 2 | 20 | Wooddell |
| 4:30 PM – 4:45 PM | | Observers (PPRP and Sponsors) comments | 15 | |
| Day 2 | | End of Formal Workshop Proceedings | | |
| Closed Meeting: PPRP, Sponsors, PM, TI Lead | | | | |

(*) Participation pending confirmation

| Session | Time | Topic | Duration (min.) | Speaker |
|---|---|---|---|---|
| Day 3 - AM | | 8:00 AM – 12:00 PM | | |
| CALIFORNIA GROUND MOTION DATA and ISSUES | 8:00 AM - 9:30 AM | Regional GM data for DCPP | 25 | Wooddell |
| | | Regional GM data for SONGS | 25 | Dinsick |
| | | CyberShake simulations for path effects near SONGS | 10 | Wang |
| | | *Discussions on data to derive path specific corrections to GMPEs* | 30 | Dreger leads; Additional REs: Helmberger, Heaton |
| FRAGILE GEOLOGIC FEATURES | 9:30 AM - 10:00 AM | *Discussions on fragile geologic features to constrain the hazard* | 30 | Youngs leads; Additional REs: Thompson, Dinsick, Lindvall |
| 10:00 AM – 10:20 AM | | *Break* | | |
| REFERENCE CONDITIONS | 10:20 AM - 11:15 AM | Review of reference rock conditions | 10 | Donahue |
| | | What is the kappa from the candidate GMPEs | 15 | Al-Atik |
| | | Kappa sensitivity for PVNGS | 10 | Silva |
| | | *Discussions on data to constrain kappa* | 20 | Donahue leads; Additional REs: Silva, Anderson, Ktenidou |
| ADDRESSING SIGMA FOR SWUS GMC PART A | 11:15 AM - 12:00 PM | SWUS plan for Sigma: ergodic vs. single station | 10 | Abrahamson |
| | | Review of available data for single station sigma models | 35 | Al-Atik |
| 12:00 PM – 1:00 PM | | *Lunch* | | |
| Day 3 - PM | | 1:00 PM – 3:35 PM | | |
| ADDRESSING SIGMA FOR SWUS GMC PART B | 1:00 PM - 2:30 PM | World wide data available for single-station sigma and $\Phi_{S2S}$ differences. | 30 | Rodriguez-Marek |
| | | *Discussions: Data needs and issues with single-station sigma* | 60 | Wooddell leads; Additional REs: Anderson, Rodriguez-Marek |
| 2:30 PM – 2:50 PM | | *Break* | | |
| 2:50 PM – 3:20 PM | | Summary of GMC Day 3 and Review of Day 1 and Day 2 | 30 | Abrahamson |
| 3:20 PM – 3:35 PM | | Observers (PPRP and Sponsors) comments | 15 | |
| Day 3 | | End of Formal Workshop Proceedings | | |
| Closed Meeting: PPRP, Sponsors, PM, TI Lead | | | | |

## Workshop #1 participants

| Group | Individual | Affiliation |
|---|---|---|
| PPRP | Day, Steven | San Diego State University |
| | Campbell, Kenneth | Ken Campbell Consulting |
| | Chiou, Brian | Brian Chiou Consulting |
| | Rockwell, Tom | San Diego State University |
| Project Management - GeoPentech | Barneich, John | GeoPentech, Inc. |
| | Di Alessandro, Carola | GeoPentech, Inc. |
| | Dinsick, Andrew | GeoPentech, Inc. |
| Project Management - Utilities | Arsene, Florin | Southern California Edison |
| | Horstman, William R. (*) | Pacific Gas and Electric Company |
| | Jahangir, Nozar | Pacific Gas and Electric Company |
| | Klimczak, Richard | Pacific Gas and Electric Company |
| | Malzahn, Mark | Southern California Edison |
| | Powell, Mike | Arizona Public Service |
| | Reidenbach, Nicholas | Arizona Public Service |
| | Wandell, Christopher | Arizona Public Service |
| Project Technical Integrator | Abrahamson, Norman A. | Pacific Gas and Electric Company |
| | McGuire, Robin | Lettis Consultants International, Inc. |
| | Moriwaki, Yoshi | GeoPentech, Inc. |
| Hazard Analysts | Dinsick, Andrew | GeoPentech, Inc. |
| | Gregor, Nick | Nick Gregor Consulting |
| | Walling, Melanie | Lettis Consultants International, Inc. |
| Technical Integrator Team | Abrahamson, Norman A. | Pacific Gas and Electric Company |
| | Donahue, Jennifer | Geosyntec Cons. |
| | Dreger, Doug | Univ. of California, Berkeley |
| | Wooddell, Katie | Pacific Gas and Electric Company |
| | Youngs, Bob | AMEC Geomatrix |
| Technical Integrator Support | Al-Atik, Linda | Linda Alatik Consulting |
| | Watson-Lamprey, Jennie | Watson-Lamprey Consulting |
| Resource and Proponent Experts | Aagaard, Brad (*) | U.S. Geological Survey, Menlo Park |
| | Anderson, John | Univ. of Nevada, Reno |
| | Archuleta, Ralph | Univ. of California, Santa Barbara |
| | Baker, Jack | Stanford University, Palo Alto |
| | Baltay, Annemarie | U.S. Geological Survey, Menlo Park |
| | Bayless, Jeff | URS |
| | Boore, David | U.S. Geological Survey, Menlo Park |
| | Bozorgnia, Yousef | Univ. of California, Berkeley |
| | Brumbaugh, David (*) | Northern Arizona University |
| | Castro Escamilla, Raul (*) | CICESE, Baja California |
| | Darragh, Robert | Pacific Engineering and Analysis |
| | Freeman, Tom | GeoPentech, Inc. |
| | Goulet, Christine | Univ. of California, Berkeley |
| | Graves, Robert (*) | U.S. Geological Survey, Pasadena |
| | Hanks, Tom | U.S. Geological Survey, Menlo Park |

| Group – Continued | Individual | Affiliation |
|---|---|---|
| Resource and Proponent Experts | Hardebeck, Jeanne (*) | U.S. Geological Survey, Menlo Park |
| | Harris, Ruth (*) | U.S. Geological Survey, Menlo Park |
| | Heaton, Thomas | California Institute of Technology |
| | Helmberger, Donald | California Institute of Technology |
| | Jordan, Tom | SCEC, Univ. of Southern California |
| | Kalkan, Erol | U.S. Geological Survey, Menlo Park |
| | Kamai, Ronnie | Univ. of California, Berkeley |
| | Ktenidou, Olga-Joan | ISTerre, France |
| | Lettis, William | Lettis Consultants International, Inc. |
| | Lindvall, Scott | Lettis Consultants International, Inc. |
| | Maechling, Phil | SCEC, Univ. of Southern California |
| | Olsen, Kim | San Diego State University |
| | Rodriguez-Marek, Adrian | Virginia Tech |
| | Silva, Walt (*) | Pacific Engineering and Analysis |
| | Somerville, Paul | URS |
| | Stewart, Jonathan | Univ. of California, Los Angeles |
| | Thompson, Steve | Lettis Consultants International, Inc. |
| | Wang, Feng | SCEC, Univ. of Southern California |
| | Youngs, Jeri | Arizona Geological Survey |
| Regulatory Observers | Anderson, Robert | California Seismic Safety Commission |
| | Chen, Rui | California Geological Survey |
| | Gibson, Bruce (*) | San Luis Obispo County |
| | Graizer, Vladimir | US Nuclear Regulatory Commission |
| | Hale, Christie | US Nuclear Regulatory Commission - Region IV |
| | Johnsson, Mark J. | California Coastal Commission |
| | Kammerer, Annie (*) | US Nuclear Regulatory Commission |
| | Stamatakos, John | Center for Nuclear Waste |
| | Stirewalt, Gerry (*) | US Nuclear Regulatory Commission |
| | Walter, Joan | California Energy Commission |
| | Weaver, Casey | California Energy Commission |
| | Williams, Megan | US Nuclear Regulatory Commission - Region IV |
| | Wills, Chris J. | California Geological Survey |
| Other Observers | Carlton, Brian | Univ. of California, Berkeley |
| | Dabaghi, Mayssa | Univ. of California, Berkeley |
| | El Menchawi, Osman | Fugro Consultants, Inc. |
| | Hollenback, Justin | Univ. of California, Berkeley |
| | Lisle, Greg A. | Columbia Project - Energy Northwest |
| | Nigbor, Robert L. | Univ. of California, Los Angeles |
| | Pitarka, Arben | Lawrence Livermore National Laboratory |
| | Retson, Thomas P. | Blue Castle Project - EnergyPath Corporation |
| | Sewell, Rob | R.T. Sewell Associates |
| | Skarlatoudis, Andreas | URS |

(*) Remote attendance

# WORKSHOP #1 SUMMARY

## Project background

Pursuant to the Request for Information put forth on March 12, 2012 by the United States Nuclear Regulatory Commission in response to the Near-Term Task Force's (NTTF) evaluation of the Fukushima Dai-ichi accident, Pacific Gas and Electric Company (PG&E), Southern California Edison (SCE), and Arizona Public Service (APS) are co-sponsoring a joint Southwestern U.S. (SWUS) Ground Motion Characterization (GMC) SSHAC Level 3 study for the Diablo Canyon Power Plant (DCPP), the San Onofre Nuclear Generating Station (SONGS), and the Palo Verde Nuclear Generating Station (PVNGS). The ultimate deliverable for this study will be a ground motion model developed following the guidelines of the SSHAC Level 3 process (Budnitz et al., 1997; NRC, 2012).

## General workshop summary

The first workshop of SWUS SSHAC was held at the Hilton Oakland Airport from March 19 to March 21, 2013. The introductory presentation delivered by the Project Manager, Dr. Carola Di Alessandro, served to highlight the focus of the workshop, i.e. to address the GMC data needs, with data defined as both raw data (e.g. seismicity, ground motion records, etc.) as well as outputs from ground motion simulations, and the critical GMC issues. Specific workshop goals included the identification of the technical issues of the highest significance to the hazard analysis and the review of available data that will be considered for constructing the GMC model. This includes the identification of data, information and/or additional work to be done on the continuing development of the project to address those issues. Evaluations to be performed prior to the second workshop were also identified and addressed.

Following the presentation about the Sponsors' Perspective, the TI Team Lead, Dr. Norman Abrahamson, presented an overview of the project schedule and scope, which includes derivation of ground motion logic trees and associated Hazard Input Documents (HIDs). The ground motion models need to be applicable to all of the relevant cases for the SSC for any of the three Nuclear Power Plants (NPPs). He also presented an overview of ground motion research being performed at the University level by Pacific Earthquake Engineering Research Center (PEER) and Southern California Earthquake Center (SCEC). The critical interface with the other PSHA-related tasks being conducted by the three Utilities was briefly addressed.

The workshop introduction on March 19 included a training session to review the SSHAC procedures, the Workshop 1 ground rules, and a representative from each of the respective Utilities presented an overview of their Seismic Source Characterization (SSC) model. This was followed by a presentation of the GMC Version 0 (V0) logic tree and the ground motion sensitivity analyses presented by each Utility's designated

hazard analyst. For both DCPP and SONGS, the controlling sources are near-fault (less than 15 km) sources. DCPP hazard is controlled by two strike-slip faults (the Hosgri and Shoreline faults) and two reverse faults (Los Osos and San Louis Bay). SONGS is controlled by a combination of the Newport-Inglewood/Rose Canyon (NI/RC) fault and the Oceanside Blind Thrust (OBT) faults. For both DCPP and SONGS, multi-segment ruptures including splay fault and HW effects may be important. In contrast, the hazard at PVNGS is controlled by large magnitude events at great distances (e.g. greater than 200 km) and by moderate magnitude (e.g., M6-M6.5) normal and strike-slip events within 20 km.

The focus for the remainder of Workshop 1 was on the GMC data needs and critical issues. A summary of these technical presentations and discussions follows.

### *Topic 1: Ground Motion Prediction Equations (GMPEs)*

Ground Motions Prediction Equations (GMPEs) are the empirical models used to calculate ground motion attenuation given earthquake magnitude, fault geometry, distance from the earthquake rupture to the site of interest, and site conditions ($V_{S,30}$). The standard practice in the western United States is to use the 2008 Next Generation Attenuation (NGA) models, however many alternative models exist and will be evaluated in addition to the 2008 NGA models as part of the SSHAC process.

Ground motion prediction equations are applicable to specific tectonic regions, and Dr. Jonathan Stewart presented a review of 15 GMPEs that are applicable in active crustal regions (or ACRs) such as the Southwestern U.S.; the set of models included both global models and regional models. The review focused on the parameterizations of the GMPEs and their ability to model the controlling fault sources for each Utility (DCPP, SONGS, and PVNGS) and the datasets from which they were derived. Dr. Robert Darragh presented the suite of earthquakes available in the NGA-West2 database to identify potential data gaps in regions critical for constraining the GMC hazard as identified by the sensitivity studies. His presentation highlighted the paucity of ground motions from normal-faulting events.

As part of these discussions, earthquakes that can provide additional constraints in the GMC hazard sensitivities were identified. Most of the key data discussed are either currently in the NGA-West2 dataset or will be processed by PEER for completion by the end of the summer 2013. The key earthquakes in the Japanese models are already included and there is a need to check the dataset used by Bindi et al. (2009 and 2010) for moderate magnitude normal faulting events from Italy. Additionally, the Fukushima-Hamadori normal faulting earthquake sequence in Japan (M~6.7 – 7.0) and the Wells, Nevada normal earthquake (M5.9) can be considered to augment the available data. The topics of magnitude saturation, how large magnitudes scale at high frequency and short distance, were discussed. Dr. David Boore presented empirical data showing oversaturation (larger ground motion amplitudes recorded from smaller magnitude earthquakes at short distance) at high frequency, and Dr. Annemarie Baltay presented scaling models showing full saturation (no scaling on ground motion with magnitude at short distance), though her models did not allow for oversaturation. The issue of full saturation versus over-saturation cannot be resolved by data alone and will require finite-fault simulations.

Finally, Dr. Erol Kalkan discussed which data have been considered to constrain the amplification of PGA in the near-field for the Graizer and Kalkan (2011 and 2012) GMPE. This model has a different distance scaling at short distance which leads to a decrease in ground motion at the faults. The robustness of the scaling should be evaluated using additional near-fault earthquake data.

### *Topic 2: Data to constrain GMPEs in Critical Ranges*

A variety of topics were discussed in an attempt to identify data gaps in areas affecting specific terms of the GMPEs. Dr. Jennie Watson-Lamprey presented a summary of the available directivity models. Directivity describes the potential amplification of ground motions as rupture moves towards a site, which can significantly affect the low frequency ground motions at short distances. The key technical issue is whether the standard deviation of the GMPEs adequately captures the effects of directivity or not. This topic is being addressed as part of the PEER ground motion research.

Dr. Jennifer Donahue presented earthquakes that have been recorded on both the hanging wall (HW) and the footwall (FW) of earthquakes in the NGA-West2 database to help constrain the hanging wall term of the Ground Motion Prediction Equations. Data recorded on both the HW and FW in a single earthquake is sparse, and in particular M5.5 to M6.5 earthquakes, which may be significant for the hazard at DCPP and SONGS, are not well constrained by the NGA-West2 empirical data. The available finite fault simulations covered the magnitude range 6 to 7.8 but do not constrain the small magnitude scaling below M6.5 It was decided that simulations might help improve this constraint. Japanese data may also be useful if the metadata can be obtained.

Dr. Ronnie Kamai presented an analysis to determine what is the impact of standard processing in the NGA-West2 database, in particular focusing on the amount of static displacement (fling) preserved in the processed data. Her analysis showed that static displacements are preserved out to the 3 to 5 second range. As the aim of this SSHAC project is to provide results out to 5 seconds, it was determined that records in the 3 to 5 second range would be further evaluated.

Dr. Jennifer Donahue then presented available information on multi-fault ruptures either available within the NGA-West2 database or from other resources. There are very few multi-fault ruptures with near-fault data. Additional multi-fault ruptures cases were identified, mainly recent events such as Christchurch, Darfield, and El Mayor-Cucapah. Approaches for characterizing parameters for multi-fault ruptures were also discussed. Some of the cases shown included either pre-seismic or post-seismic slip/displacement which is not relevant for ground motions for multi-fault ruptures. The rupture models need to be revised to include only the coseismic displacement for splay faulting and multi-segment ruptures.

Dr. Ruth Harris presented the results of the branch faulting dynamic rupture code verification exercise, and it was shown that about 5 models are capable of producing results that are consistent with each other. The discussion of this topic included a suggestion to develop alternative distance metrics for complex faulting, such as general coordinates system 2 (GC2) proposed in the PEER directivity studies. The cases shown used a single rupture initiation point located on the main traces away from the juncture of the splay fault.

Additional cases were suggested to consider scenarios where the rupture initiates on the splay and moves onto the main fault, as well as scenarios that include heterogeneous stress on the rupture plane.

### *Topic 3: Use of Simulations for SWUS GMC*

Due to a lack of data in critical regions, broadband (BB) simulations can be used to develop constraint on the GMPEs. Dr. Christine Goulet provided a review of the SCEC BB Platform simulation validation exercise scheduled to be completed in 2013. A list of cases to run on the BB Platform was proposed in the discussion that followed the presentation. The purpose of these cases is to provide data in regions where empirical data does not exist or is deemed to be insufficient; the use of multiple methods in the ground motion simulations will account for epistemic uncertainty. The cases recommended for consideration are provided in the "Day 2 - Main Points" presentations available at the "Technical Integrator Team Summaries and actions" section (page 39).

Discussion involved ground motion from multi-fault ruptures, dependence on the location of hypocenters within and at junctures in fault models, definitions of GMPEs parameters (style of faulting, dip) for ruptures with variable slip direction, dip and strike. These features can be addressed through simulations.

Other uses of simulations are to constrain hanging wall scaling, splay faulting, slip partitioning, large magnitude scaling, low dip angle scaling, linked/multi-segment faulting, and large magnitude/long distance scaling.

Preparations for using simulation capability include documentation of methodology, fixed and optimized parameters and other user-required information, description of 1D velocity structures (including Q) for each region, and passing the part A and part B validations.

### *Topic 4: Arizona Ground Motion Data and Issues*

Two presentations were given for the available data for the Palo Verde Nuclear Generating Station (PVNGS). The first presentation was given by Dr. Jennie Watson-Lamprey who provided the available data from the Transportable Array (TA) and other sources. The TA Earthscope stations near PVNGS captured 16 events, 1 with M≥3, 7 with M≥2 and 8 with M≥1 which occurred within the Sonora Basin and Range zone and within 100 km of the site. During the course of the presentation, it was revealed that improved site conditions at the recording stations was needed, to which Dr. Jeri Young of the AZGS is to provide depth to bedrock values. Given the number of small magnitude (M< 1.5) events available, it was postulated that the estimation of kappa_ds (otherwise known as kappa_mini) may be a possibility. Next the NGA-West2 database was reviewed for events in California and Baja California within 100, 200 and 400 km of Arizona. 32 events meet these criteria with possibly 20 events recorded by the TA Earthscope stations. An additional highlight of the presentation was that the available empirical data for long distance attenuation may be adequate, but a review of the regionalization may be needed for path adjustments.

Dr. Melanie Walling gave the second presentation regarding the Arizona ground motion issues. Additional empirical data and catalogue events were presented, and two additional events close to the transition zone but still potentially within the Sonora Basin and Range zone were recommended for considerations. The

ground motions resulting from mine blasts may provide constrains on kappa and their applicability should be evaluated by reviewing previous studies.

In the general discussion, led by Dr. Robert Youngs, one of the topics was to compare the Little Skull Mtn. event with the NTS nuclear blast with the intent to look at kappa effects resulting from the shallow depth of the blasts and also mining related events. It was also suggested that historical intensities for Arizona should be reviewed and the catalogue may be made available by Prof. Brumbaugh. Additional data points for the El Mayor-Cucapah event may also be available at the Roosevelt Dam and the VA Hospital.

### *Topic 5: California Ground Motion Data and Issues*

In contrast to the sparse data available at PVNGS, the available data for DCPP and SONGS was discussed. Ms. Wooddell presented available data for DCPP to include the recently recorded small magnitude events collected as part of the AB1632 DCPP onshore 3-D seismic survey. During the geophysical studies, small ($0.6<M<1.7$) events were well recorded by the geophones and can be used to focus on path effects from nearby offshore and onshore earthquakes. The 3-D velocity model by Dr. J. Hardeback (2009) was presented. An alternative 3-D model is expected to be completed this summer as part of the AB1632 studies. These studies should be considered in the development of the 1-D crustal models for implementation in the finite-fault simulations.

The available ground motion data for SONGS was presented by Mr. Andrew Dinsick. There are at least 28 events with $M>3$ within 200 km, recorded on the broadband (BB) instruments at SONGS. This information will be very useful going forward. Path effects may be important to SONGS and should be analyzed for both the NI/RC and OBT faults. Prof. Don Helmberger remarked that path effect at SONGS should be compared with the available data from other Southern California BB stations to determine if there is an atypical attenuation in the SONGS region. The nearby $M<3$ earthquakes at short distances may provide reliable estimate of kappa. Finally, the SCEC 3-D velocity model of the Unified Structural Representation for Southern California was presented.

CyberShake simulations provide a suite of 3-D finite fault simulations for the greater Los Angeles (L.A.) region including the SONGS site, which lies near the edge of the SCEC parameterization of the L.A. Basin. Mr. Feng Wang described the alternative 3-D crustal models and the available scenarios. Two scenarios capture the offshore sources that dominate the hazard at SONGS. These simulations can be used to evaluate potential 3-D path effects at SONGS. The two alternative 3-D crustal models (H and S4) have significant differences in the SONGS region that need to be evaluated. These large differences will have an effect on the long period motion near SONGS.

### *Topic 6: Fragile Geological Features*

Fragile geologic features (FGFs), or precariously balanced rocks, are geologic structures that may be used to constrain probabilistic seismic hazard analysis. When properly dated, and mechanically analyzed for minimum toppling or damaging forces, these features can yield an estimate of the maximum level of ground shaking (with a given confidence level) that could have occurred at the site since the formation of the fragile

structure. In this respect, they place constrains on the hazard at the site. At DCPP, one fragile geologic feature has been identified and should be considered for age dating and analysis.

At SONGS, no FGFs have been identified, but some constraints might be postulated considering that the foundation of the plant consists of sandstones older than 125k years which shows no signs of damage or dilation due to shaking.

At PVNGS, no FGF has been found. However, there might be a FGFs for consideration about 80km away which may have been subjected to M7.6 1887 earthquake ground motions, though no features have tumbled.

### *Topic 7: Reference Conditions*

Reference conditions are parameters used in the SWUS logic tree, which will be considered for the Base Case. Each of the Utilities will then apply site-specific parameters to these reference conditions. The first reference condition considered was the $V_{S,30}$. Dr. Jennifer Donahue presented information regarding the use of 760 m/s as the reference rock condition. This is a commonly used value in the GMPEs and there is sufficient data in the NGA-West2 database to constrain the GMPEs at this velocity. However, it will be worth reconsidering a lower $V_{S,30}$ velocity, such as 500-600 m/s, since more empirical data is available within this range. The disadvantage of using a lower velocity is that a greater correction is required to scale the ground motion to hard-rock conditions.

Dr. Linda Al-Atik reviewed the kappas associated with the current GMPEs and the three available approaches for kappa adjustments: hybrid empirical, IRVT, and empirical. The kappa values associated with ACRs are in the range of 0.035 to 0.044 seconds for 760 m/s conditions

Next, Dr. Walt Silva presented his recent sensitivity analysis for kappa at PVNGS. He showed the effect of different values of the underling rock kappa combined with the soil column. The soil column contributed only a small additional kappa and he concluded that the high frequency ground motion was sensitive to the assumed kappa value. His analysis highlighted that the potential difference in kappa on rock between Arizona and California can lead to significant differences in the ground motion at PVNGS. From this discussion, it was determined that kappa will be key to ground motions for Arizona due to site response effects. Dr. Olga Ktenidou advised that when using $V_{S,30}$-kappa relationships, as many records per site are required to capture both the kappa at the site and the 'sigma' of (or variability in) the kappa.

As previously stated, small magnitude (M<1.5) events at all sites may be useful for estimating kappa for the PVNGS region. However, the stations located near PVNGS have a limited high frequency bandwidth (14 Hz) that will require careful consideration.

At DCPP, there are survey data with useable frequencies up to 300 – 350 Hz which can provide an excellent opportunity for estimating kappa from small magnitude events.

### *Topic 8: Addressing Sigma for SWUS GMC*

Dr. Linda Al-Atik began the discussion of single station sigma, $\sigma_{ss}$, by addressing the associated terminology and equations. She then reviewed the available data within the NGA-West2 database with preliminary

results based on magnitude dependence, distance dependence, magnitude and distance dependence, and $V_{S,30}$ dependence. Single station sigma models are being developed as part of the PEER research and will be available for Workshop 2.

Dr. Adrian Rodriquez-Marek then presented data available from sources outside of the NGA-West2 database to include Taiwan, Turkey, and Japan. He showed that for single station phi, $\phi_{ss}$, there appears to be consistency across all regions (California, Taiwan, etc.) with no strong regional dependency or dependency on $V_{S,30}$. However, dependencies were shown to exist on magnitude and distance parameters. Conversely, the site-to-site term, $\phi_{s2s}$, does vary between regions, and there may be a dependency on $V_{S,30}$. Within his presentation he included an additional term, $\phi_{ss,s}$ which is the single station standard deviation for estimates at only one station. This work is still developing through PEER and will be a topic for Workshop 2.

Finally, there was a discussion as to how site amplification would be estimated for each Utility site. At DCPP, the Utility plans to use empirical data, based on recordings at DCPP, but with the small number of recordings, the epistemic uncertainty may be large. At SONGS, an analytical approach will be used with a range of inputs that captures the uncertainties in the geotechnical parameters. If the site terms from nearby sites are consistent, this may aid in the development of the site term. PVNGS is in the process of evaluating how to integrate the site-specific terms.

## Focused questions submitted to Workshop #1 Presenters

The following Tables 1 through 10 show the focused question that Workshop #1 Presenters were asked to address, subdivided by topic.

**Table 1** Focused questions for Workshop #1 Presenters: Session "OVERVIEW of SEISMIC SOURCE CHARACTERIZATION"

| Topic | Speaker | Questions / Topics to be addressed at WS #1 |
|---|---|---|
| Diablo Canyon Power Plan (DCPP) | Thompson | Summarize tectonic setting.<br>What is the range of dip angles (min and max) and faulting styles?<br>What is the seismogenic thickness?<br>Are you including deep ruptures in the upper mantle (~30 km)?<br>What is the largest magnitude in your sources (due to linked faults)?<br>Do you have a complex multi-segment rupture with different rake/dip along strike?<br>Do you have splay faults or overlapping segments? |
| San Onofre Nuclear Generating Station (SONGS) | Freeman | Summarize tectonic setting.<br>What is the range of dip angles (min and max) and faulting styles?<br>What is the seismogenic thickness?<br>Are you including deep ruptures in the upper mantle (~30 km)?<br>What is the largest magnitude in your sources (due to linked faults)?<br>Do you have a complex multi-segment rupture with different rake/dip along strike?<br>Do you have splay faults or overlapping segments? |
| Palo Verde Nuclear Generating Station (PVNGS) | Lindvall | Summarize tectonic setting.<br>What is the range of dip angles (min and max) and faulting styles?<br>What is the seismogenic thickness?<br>Are you including deep ruptures in the upper mantle (~30 km)?<br>What is the largest magnitude in your sources (due to linked faults)?<br>Do you have a complex multi-segment rupture with different rake/dip along strike?<br>Do you have splay faults or overlapping segments? |

**Table 2** Focused questions for Workshop #1 Presenters: Session "GMC and SENSITIVITY ANALYSES"

| Topic | Speaker | Questions / Topics to be addressed at WS #1 |
|---|---|---|
| GMC Logic tree V0 | Wooddell | Describe the GMC V0 Logic Tree.<br>What are the limitations of the current V0 Logic Tree?<br>What potential ground motion characteristics are not captured in the current V0 Logic Tree? |
| Hazard sensitivity analyses for the three sites | Gregor for DCPP / Dinsick for SONGS / Walling for PVNGS | Summarize the ground motion models used in the most recent seismic hazard study for the NPP site.<br>What are uncertainties in the ground motion models that lead to the largest uncertainties in hazard at PGA, 20 Hz, 5 Hz and 0.5 Hz?<br>What is the relative contribution of standard deviation uncertainties versus median uncertainties?<br>For the median uncertainty, what type of faults (magnitude, distances, style of faulting etc…) or source parameters (dip, depth etc...) lead to the largest uncertainties? |

| | | |
|---|---|---|
| *Discussion: List of key Hazard sensitive GM Issues* | All | What are the limitations on existing ground motion models?<br>Have we captured all the relevant uncertainties? |

**Table 3** Focused questions for Workshop #1 Presenters: Session "GROUND MOTION PREDICTION EQUATIONs"

| Topic | Speaker | Questions / Topics to be addressed at WS #1 |
|---|---|---|
| GMPEs for active crustal regions: applicability for controlling sources | Stewart | What is the distribution of magnitude, distance, site conditions, style of faulting, period range for which the GMPEs are well constrained?<br>Do the data include class 2 (aftershock) earthquakes?<br>Summarize which model address HW effects and which do not?<br>Summarize the base for the large magnitude scaling in those models (data available, theoretical bases or statistical extrapolation?). |
| NGA-West2 Database | Darragh | What is the distribution of magnitude, distance, site conditions, style of faulting, period range, depth distribution (Ztor, hypocentral depth etc…), dip angles, class 1 and class 2 in the NGA-West 2 Database?<br>Show the correlations with magnitude and distance for the above parameters ( i.e. break it up in several plots) |
| *Discussion: Are Hazard sensitive sources well constrained by GMPEs?* | All | Which Hazard sensitive sources are well constrained by GMPEs?<br>Which are not well covered by the NGA-West2 Database? |
| | Boore | Is there adequate data to constrain oversaturation? |
| | Kalkan | Discuss the near-fault dataset (within 5 km) to constrain the median near-fault's behavior of your model (reduction at very short distance). |
| | Baltay / Hanks | Describe the use of stress drop scaling (from small to large magnitudes) to constrain magnitude scaling. Do you see evidence for non-self similar scaling (i.e. not constant stress drop)? |

**Table 4** Focused questions for Workshop #1 Presenters: Session "DATA to CONSTRAIN GMPEs in CRITICAL RANGES"

| Topic | Speaker | Questions / Topics to be addressed at WS #1 |
|---|---|---|
| Directivity | Watson-Lamprey | Summarize the alternative directivity parameters from the NGA-West2 project.<br>Describe the sampling of the directivity parameters with magnitude in the NGA-West2 Dataset.<br>Show the correlation of the directivity parameters with magnitude, distance and site condition ($V_{S,30}$) |
| Hanging Wall | Donahue | Show the distribution of HW/FW recordings within 30 km event by event (plots of the HW effect for the events) in the NGA-West2 Database.<br>What other HW data are available?<br>Describe the HW data from SCEC simulations. |
| Fling | Kamai | Describe the dataset of records with both static displacement and standard processing in the NGA-West2 Database.<br>Show the effect of standard processing on the response spectra for records with fling.<br>Describe the currently available finite fault simulation dataset for fling effects. |

| | | |
|---|---|---|
| *Discussion on data to constrain near-fault effects* | All | Are the available empirical recordings in NGA-West2 capturing the average directivity effect (centering)?<br>Are the simulations centered for directivity effects?<br>Are the static displacements data consistent with the finite-fault simulations in terms of permanent displacement? |
| | Graves | How was the range of source input parameters (distribution of hypocentral locations) for the simulations defined and what is the basis for it? |
| | Darragh | Be prepared to describe details of the static processed dataset if questions arise. |
| | Baker | Discuss the value of including the intermediate step of parameterizing the ground motion model in terms of magnitude, distance and pulse-period, rather than just parameterizing the ground motion model in terms of magnitude and distance. |
| Multi-fault rupture | Donahue | Summarize the complex multi-rupture events in the NGA-West2 Database in magnitude and distance space.<br>What additional multi-fault cases are available that were not considered by NGA-West2 or where simplified into a simple fault rupture?<br>Show plots of the stations and rupture geometry for each complex multi-fault rupture event (in NGA-West2 or other regions).<br>Describe how dip, rake and depth are measured for complex ruptures. |
| Splays and linkage: dynamic rupture modeling | Harris | Describe the dynamic rupture verification effort for complex multi-fault segments ruptures.<br>Are alternative methods leading to similar results?<br>What is the schedule for the completion of the verification effort?<br>What frequency bands are covered by the models? |
| *Questions and Discussions on multi-fault ruptures* | All | Are there additional complex multi-fault rupture cases with strong motion data that we have missed?<br>What is the applicability of kinematic finite-fault simulations for multi-fault ruptures?<br>Will the currently available simulation methods on the SCEC BBP work for complex multi-fault ruptures?<br>Are there adequate data to validate simulations of complex ruptures? |
| | Somerville | If multi-fault ruptures are constructed from single-fault BBP simulations, what data are available to constrain the time delay between segments |
| | *Continued* | |
| | Aagaard | If multi-fault ruptures are constructed from single-fault BBP simulations, what data are available to constrain the time delay between segments |
| | Darragh | Be prepared to talk about the complex-ruptures in the NGA-West2 Database |

**Table 5** Focused questions for Workshop #1 Presenters: Session "USE of SIMULATIONS for SWUS GMC"

| Topic | Speaker | Questions / Topics to be addressed at WS #1 |
|---|---|---|
| Review on simulation validation from SCEC | Goulet | Describe the SCEC BBP validation exercise.<br>Summarize (list-type) the methods being evaluated.<br>What features are common among the methods?<br>What features are unique among the methods?<br>What is required in terms of source specification for each method?<br>Provide examples of preliminary validation results.<br>Include what is the schedule and planned process for the evaluation. |
| *Discussion on simulation validation from SCEC* | All | What are the current difficulties/challenges for the validation exercise for each modeler? |
| *Discussions: Best uses of simulations (30 min) and Practical limitations (30 min)* | All | What cases can the simulations provide the most benefit for SWUS (i.e. fill in the cases that are not well constrained by empirical data).<br>What is the best use of numerical simulations (where do we trust simulation)?<br>Do 1-D simulations satisfy the need? |
| | Jordan/ Maechling | What is the volume of simulations that can be run in the two-month time frame (multiple two-month time periods might be needed, up to three)? |

**Table 6** Focused questions for Workshop #1 Presenters: Session "ARIZONA GROUND MOTION DATA and ISSUES"

| Topic | Speaker | Questions / Topics to be addressed at WS #1 |
|---|---|---|
| Available GM data from Transportable Array in Arizona for both nearby earthquakes in Arizona and distant earthquakes in California | Watson-Lamprey | Describe the available data (magnitude, distance distribution) from the Transportable Array for central/southern Arizona at distances less than 100 km.<br>Describe the available data (magnitude, distance distribution) from distant earthquakes in California and Mexico (at distances 200-300 km).<br>Are these events from NGA-West2 or different datasets?<br>Is site condition information available?<br>What is the available event metadata (magnitude type, mechanism and depth)?<br>What is the usable frequency band of the Arizona ground motions? |
| Additional GM data from Arizona from IRIS not part of the Transportable Array | Walling | Describe the available data (magnitude, distance distribution) from IRIS for central/southern Arizona, not part of the Transportable Array |
| *Discussions: Do we have sufficient data to resolve geometrical spreading, anelastic attenuation, kappa, and stress drop differences between California and Central Arizona?* | All | Do we have sufficient data to resolve geometrical spreading and stress drop differences between Arizona and California?<br>Are there data with high-enough frequency content to resolve kappa?<br>Do we have sufficient data to resolve anelastic attenuation differences in California and central Arizona? If not, are there any other sources of data?<br>Do we need to expand to other regions (N. Arizona, Utah, Mexico)? |
| | Brumbaugh / Young | Are there any other ground motion data in Central Arizona that we have not considered? |
| | Lindvall | What is the tectonic relevance of N. Arizona and Utah to Central Arizona? |

| | | |
|---|---|---|
| | Silva | Is there a point (or finite fault) source stochastic model developed for Arizona? If not, are the current data sufficient to derive one? |
| | A representative from CICESE | Discuss metadata (magnitude type, mechanism and depth) quality for earthquakes from Mexico recorded in Arizona.<br>Do local earthquakes in the extension of the Basin&Range province in Mexico have similar ground motions to the ones in Central Arizona? |

**Table 7** Focused questions for Workshop #1 Presenters: Session "CALIFORNIA GROUND MOTION DATA and ISSUES"

| Topic | Speaker | Questions / Topics to be addressed at WS #1 |
|---|---|---|
| Regional GM data for DCPP | Wooddell | What are the regional ground motion data within 50 km from DCPP with M ≥ 3?<br>Are there earthquakes with 5 and more recordings within 50 km?<br>Present the ground motion data from DCPP free field station.<br>What differences in the attenuation do you see with respect to the regional model?<br>What are the 3D velocity structure models available for the site region within 30 km? |
| Regional GM data for SONGS | Dinsick | What are the regional ground motion data within 50 km from SONGS with M ≥ 3?<br>Are there earthquakes with 5 and more recordings within 50 km?<br>Present the ground motion data from SONGS free field station.<br>What differences in the attenuation do you see with respect to the regional model?<br>What are the 3D velocity structure models available for the site region within 30 km? |
| *Continued* | | |
| CyberShake simulations for path effects near SONGS | Wang | Provide a summary of the CyberShake simulations, including employed rupture and velocity models for example.<br>Do the SCEC 3D simulations show significant effects in the regions? |
| *Discussions on data to derive path specific corrections to GMPEs* | All | Considering both ground motion data and velocity structure, are there sufficient data to derive path specific correction to the GMPEs? |
| | Helmberger | Provide information on detailed modeling of the events close (within 30 km) to the NPP sites |
| | Heaton | Provide information on regional variability of geometrical spreading and attenuation characteristics within 100 km of NPP sites. |

**Table 8** Focused questions for Workshop #1 Presenters: Session "FRAGILE GEOLOGIC FEATURES"

| Topic | Speaker | Questions / Topics to be addressed at WS #1 |
|---|---|---|
| *Discussions on fragile geologic features to constrain the hazard* | Thompson for DCPP / Dinsick for SONGS / Lindlvall for PVNGS | Are there fragile geologic features at any of the sites whose age and failure ground motion would constrain the hazard at 10 -3 to 10 -6?<br>Have there been surveys for FGF at or near any of the sites?<br>If any features have been identified, what is the approximate age and failure ground motion? |

**Table 9** Focused questions for Workshop #1 Presenters: Session "REFERENCE CONDITIONS"

| Topic | Speaker | Questions / Topics to be addressed at WS #1 |
|---|---|---|
| Review of reference rock conditions | Donahue | What is the basis for selection of reference conditions?<br>Cover the issues for using a common reference conditions at all three sites.<br>Mention the need to specify the approach for adjusting the reference condition ground motions. |
| What is the kappa from the candidate GMPEs | Al-Atik | Describe the methods for estimating kappa for the candidate GMPEs and summarize the resulting kappa for each candidate GMPE |
| Kappa sensitivity for PVNGS | Silva | What is the kappa sensitivity at PVNGS? |
| *Discussions on data to constrain kappa* | All | Do we correct GMPEs to a single kappa?<br>What data are available to constrain kappa?<br>What data are available to constrain the rock kappa values at the 3 NPP sites? |
| | Silva | Does the Silva's kappa-VS,30 relation apply to Central Arizona? |
| | Anderson | Should there be regional differences in kappa for hard-rock sites (Central Arizona vs EUS)? |
| | Ktenidou | What are the main difficulties in estimating kappa that you have found from datasets you have evaluated (not from Arizona)?<br>What is the variability in kappa estimates for a single site with recording from multiple earthquakes? |

**Table 10** Focused questions for Workshop #1 Presenters: Session "ADDRESSING SIGMA FOR SWUS GMC"

| Topic | Speaker | Questions / Topics to be addressed at WS #1 |
|---|---|---|
| SWUS plan for Sigma: ergodic vs. single station | Abrahamson | How will sigma be implemented at each of the sites? Ergodic or partially non-ergodic |
| Review of available data for single station sigma models | Al-Atik | What are the data available in the NGA-West2 Dataset for single station sigma?<br>What are the 3D simulation data available for single station sigma? |
| World wide data available for single-station sigma and $\Phi_{S2S}$ differences. | Rodriguez-Marek | What are the world-wide data (non NGA-West2) available for single station sigma?<br>What are the ranges for the Φ S2S values? |
| *Discussions: Data needs and issues with single-station sigma* | All | How would single station sigma be used at the 3 sites?<br>What data (empirical or analytical) is available to estimate the site term at each site? |

# GROUND MOTION CHARACTERIZATION PRESENTATIONS

**Day 1 Introduction**

- Welcome and Introduction to the SWUS GMC WS #1 – Carola Di Alessandro (*GeoPentech, Inc.*)
- Sponsors' Perspective – Richard Klimczak (*Pacific Gas and Electric Company*) and Christopher Wandell (*Arizona Public Service*) in behalf of the SWUS Utilities Representatives
- Project Overview and Objectives – Norman Abrahamson (*Pacific Gas and Electric Company*)
- SSHAC Level 3 Training – William Lettis (*Lettis Consultants International, Inc.)*

**Day 1 Resource Expert Presentations**

- Overview of Seismic Source Characterization for the Diablo Canyon Power Plant – Steve Thompson (*Lettis Consultants International, Inc.*)
- SONGS SSC – Tom Freeman (*GeoPentech, Inc.*)
- Overview of the Seismic Source Characterization for the Palo Verde nuclear Generating Stations – Scott Lindvall (*Lettis Consultants International, Inc.*)
- Where are GMPEs well constrained – David Boore (*U.S. Geological Survey, Menlo Park*)
- Understanding NGA-West GMPEs: Smaller(er) Magnitude Theory and Trends – Annemarie Baltay (*U.S. Geological Survey, Menlo Park*)
- GK Model for Amplification of PGA at Near Field – Erol Kalkan (*U.S. Geological Survey, Menlo Park*)
- Ground Motion Characterization (GMC) Logic Tree (V0) – Kathryn Wooddell (*Pacific Gas and Electric Company*)
- Diablo Canyon SSHAC Level 3 Study, Hazard Sensitivity Analyses for DCPP – Nick Gregor (*NG Consulting*)
- SONGS GMC Sensitivity Analyses – Andrew Dinsick (*GeoPentech, Inc.*)
- Hazard Sensitivity for Palo Verde Nuclear Generating Station performed for South-Western United Stated (SWUS) Ground Motion Workshop 1 – Melanie Walling (*Lettis Consultants International, Inc.)*
- GMPEs for Active Crustal Regions: Applicability for Controlling Sources – Jonathan Stewart (*Univ. of California, Los Angeles*); includes material added during Day 2
- PEER NGA-West2 Database and Hazard Sensitive Sources – Robert Darragh (*Pacific Engineering & Analysis*)
- Hazard Sensitive Sources – Robert Darragh (*Pacific Engineering & Analysis*); Updated discussion material added during Day 2

**Day 2 Resource Expert Presentations**

- Directivity Parameters in the NGA West2 Dataset – Jennie Watson-Lamprey (*JWL Consulting*)
- Data to Constrain GMPEs in Critical Ranges – Hanging Walls – Jennifer Donahue (*Geosyntec*)
- Are Fling Effects Captured in NGA Models? – Ronnie Kamai (*PEER Center - Univ. of California, Berkeley*)

- Resource material: Processing of the PEER NGA-West2 Database – Robert Darragh (*Pacific Engineering & Analysis*)
- Resource material: Static Displacement (Fling) in the NGA-West2 Data Set - Robert Darragh (*Pacific Engineering & Analysis*)
- Data to Constrain GMPEs in Critical Ranges – Multi-Fault Ruptures – Jennifer Donahue (*Geosyntec*)
- The SCEC/USGS Rupture Dynamics Code Comparison Exercise – Ruth Harris (*U.S. Geological Survey, Menlo Park*)
- SWUS SSHAC Workshop 1, Broadband Ground Motion Simulations – Christine Goulet (*PEER Center - Univ. of California, Berkeley*)
- Broadband Computer estimates – Phil Maechling (*SCEC - Univ. of Southern California*)
- SWUS PVNGS Data Collection - Jennie Watson-Lamprey (*JWL Consulting*)
- South Western US Ground Motion Project Meeting – Melanie Walling *(Lettis Consultants International, Inc.*)

**Day 3 Resource Expert Presentations**

- California Ground Motion Data and Issues - Kathryn Wooddell (*Pacific Gas and Electric Company*)
- SONGS Ground Motion Data and Issues – Andrew Dinsick (*GeoPentech, Inc.*)
- Cyber Shake Simulations for Path Effects near SONGS – Feng Wang (*SCEC - Univ. of Southern California*)
- California Ground Motion Data and Issue – Doug Dreger (*Univ. California, Berkeley*)
- The Geophysics of Near Fault Ground Motions – Doug Dreger (*Univ. California, Berkeley*)
- Potential Use of Fragile Geologic Features – Robert Youngs (*AMEC*)
- Fragile Geologic Features Near Diablo Canyon Power Plant – Steve Thompson (*Lettis Consultants International, Inc.*)
- Review of Reference Rock – Jennifer Donahue (*Geosyntec*)
- Kappa for Candidate GMPEs – Linda Al Atik (*Al Atik Consulting*)
- Kappa Sensitivity for the PVNGS – Walt Silva (*Pacific Engineering & Analysis*)
- Seismic Ground Motion Hazards – John Anderson (*Univ. of Nevada, Reno*)
- Discussion of k issues – Olga-Joan Ktenidou *( ISTerre and PEER Center – Univ. of California, Berkeley*)
- Single-Station Sigma Using NGA-West2 Data – Linda Al Atik (*Al Atik Consulting*)
- World-wide Data Available for Single-Station Sigma and Regional Variation in the $\phi_{s2s}$ Term – Adrian Rodriquez-Mark (*Virginia Tech*)
- Resource material: Imperial P-Wave – Tom Heaton (*CalTech*)

# TECHNICAL INTEGRATOR TEAM SUMMARIES and ACTIONS

# Day 1 Summary

| Speaker | Topic | Issue |
|---|---|---|
| Steve Thompson | DCPP Seismic Source Characterization | • Complex velocity model (3D vs. 1D)<br>• Uncertainty with blind or buried faults<br>• No technical basis to rule out splay faults<br>• Not considering deep ruptures<br>• Review deeper events, may have originated in slab (possible background source) |
| Tom Freeman | SONGS Seismic Source Characterization | • Inclusion of UCERF3 in the SSC may change rakes, dips, and seismic sources<br>• Uncertainty regarding distance to closest fault: OBT and Offshore NI/RC faults<br>• Splay faulting is coming up-dip<br>• Horizontal splay faulting to be investigated as well<br>• Not considering deep ruptures<br>• Variability along strike, and dip |
| Scott Lindvall | PVNGS Seismic Source Characterization | • Mainly low slip rates<br>• Background zones will dominate<br>• Distances considered out to 400 km<br>• Not considering deep ruptures<br>• Mainly normal events, large magnitudes (up to M7.5), dips of 35-65 |

| Speaker | Topic | Issue |
|---|---|---|
| Katie Wooddell | GMC Logic Tree V0 | • Work in progress<br>• Possible distance dependence of epistemic uncertainty |
| Nick Gregor | DCPP-Hazard Sensitivity analysis | • May need to include splay faults<br>• Will include site-specific amplifications and single station sigma<br>• Large range of current sigma models<br>• Constraint on large uncertainty of epistemic uncertainty<br>• Governed by faults within 10 km<br>• Need a pdf for simulations at long periods (log-normal distribution) |

| Speaker | Topic | Issue |
|---|---|---|
| Andrew Dinsick | SONGS-Seismic Source Characterization | • Complex geometry (intercepting faults?) how to model in GMPEs? We need rules for complex rupture with the GMPEs<br>• Review of simulation results for large magnitude, short distance, and long period<br>• Review large differences in hanging wall effects<br>• Will include directivity<br>• Strike slip dist = 10km and reverse events Rjb = 0<br>• Will include single station sigma |
| Melanie Walling | PVNGS-Seismic Source Characterization | • Need hazard code consistent approach to HW effects for areal sources<br>• Geometrical spreading, Regional Q<br>• Large distance attenuation is required<br>• Normal faulting events to M7 control hazard<br>• Buried ruptures may be of issue |

| Speaker | Topic | Issue |
|---|---|---|
| J. Stewart | GMPEs for active crustal regions | • Review Japanese normal faulting event<br>• Review Bindi Data for M>5 not captured in NGA-W2 dataset<br>• Summary page of M-R pairs for all GMPEs<br>• Mostly empirically based scaling for large magnitudes.<br>• Hanging wall is mostly modeled by Rjb distance metric<br>• About half of the datasets use aftershocks |
| B. Darragh | NGA-West2 Database | • Review Japanese M7.2 event (surface rupture, post-Tohoku)<br>• Review Wells, Nevada M5.9 event, based on TA data<br>• Remake graphs for M-R with $V_{s30}$ > 500 m/s<br>• For large magnitudes, there is not much improvement over NGA-W1 |
| N. Abrahamson | Hazard sensitivities well constrained? | • How does saturation associate with ZTOR? (Somerville)<br>• Data for near-fault bump for Imperial Valley, Northridge, Parkfield, Darfield<br>• Empirical data showing oversaturation/saturation in source models (Boore), Oversaturation was rejected (Baltay) |

# Day 2 Summary

| Speaker | Topic | Issue |
|---|---|---|
| Jennie Watson-Lamprey | Data to Constrain GMPEs in Critical Ranges: Directivity | • For simulations, use multiple methods (R. Graves)<br>• Compare 1D and 3D directivity effects from simulations (K. Olsen) – Use existing 3D and compare with (new) 1D calculations.<br>• Evaluate Wells EQ TQ array data for directionality (D. Dreger)<br>• Pulse period correlated with Magnitude and only weakly with distance and site.<br>• Directivity (un-normalized) strongly correlated with magnitude. Correlation needs to be addressed.<br>• No data for large strike-slip case. Simulation data exists but directivity parameters have not yet been calculated.<br>• Look at special cases, for example, normal/reverse events with significant slip along strike (D. Dreger) |

| Speaker | Topic | Issue |
|---|---|---|
| Jennifer Donahue | Data to Constrain GMPEs in Critical Ranges: Hanging Wall | • Graves ran strike-slip events with dip. We should evaluate the HW effects for dipping for strike-slip events from simulations (P. Somerville). Consider multiple simulation approaches.<br>• Need to address HW effects for M5.5 to M6.5 not currently addressed for Japanese events. Will prob. Need to get at this through simulation. (A. Rodriguez – Marek)<br>• Near source dynamic rupture is difficult to constrain. High uncertainty in this type of modeling (T. Heaton). |

| Speaker | Topic | Issue |
|---|---|---|
| Ronnie Kamai | Data to Constrain GMPEs in Critical ranges: Fling | • Missing data for large magnitudes at close distances<br>• About 75 records have been processed to preserve static displacement. These are being supplemented with broadband simulations.<br>• Many simulations available to supplement the data in the NGA database.<br>• Filtering is impacting our results beyond about ~3 - 5 sec. If we are looking below 3 sec, the processing is not affecting our results much. Need to address potential effects in 3 – 5 sec range. |

| Speaker | Topic | Issue |
|---|---|---|
| Jennifer Donahue | Data to Constrain GMPEs in Critical ranges: Multi-Fault Ruptures | • Additional multi-fault cases that are available that were not considered by NGA-West2 (or were simplified into a simple fault rupture): John Bevin Darfield Model is more complex (get reference from Ralph A.), Christchurch and Darfield (could use more work – Bob. D.)<br>• Need to update Superstition Hills (A&B) rupture model to remove non-mainshock slip.<br>• Regarding Darfield: Bevin's mode had additional thrust segments on either end (more complicated than the current case).<br>• Other approaches for parameterizing complex multi-fault ruptures: consider spatial variability in amplitude of the slip (not simple enough), RMS distance to segments (Brian suggests a different coordinate system GC2).<br>• Graves – concern with distinguishing between geodetic and coseismic models |

| Speaker | Topic | Issue |
|---|---|---|
| Ruth Harris | Splays and Linkage: Dynamic Rupture Modeling | • Run case where hypocenter starts on the Shoreline<br>• Run case where hypocenter is at junction between faults.<br>• Verification for branched benchmark can be considered complete (5 models? Pass).<br>• Run splay fault with heterogeneous stresses. This will require another benchmark.<br>• Vary regional stress field to estimate how likely it is for one fault to rupture onto another (does it occur, how do we estimate the GM and frequency of occurrence) |

| Speaker | Topic | Issue |
|---|---|---|
| Christine Goulet | Splays and Linkage: Broadband Ground Motion Simulations | • 1D validation on track to be completed in June.<br>• 3D effects will be considered in a broad sense in the uncertainties. Look at available 3D studies and augment with 1D<br>• Acceptance out to 3 sec is probably ok. Out at long periods, the simulations may be providing a more accurate result.<br>• Rupture generator reliable from M8 - M8.5? – large events from CyberShake. GM with very high Peak ground velocities (few rare events in CyberShake M8.4?). Check if rupture generators saturate. |

| Speaker | Topic | Issue |
|---|---|---|
| Doug Dreger | Discussion on Simulations: Summaries from Modeling Teams etc. | • Ralph Archuleta: Working out a frequency dependent Q is difficult. Every time you change kappa, you need a new greens function. Under-predicting spectral peak at 5 Hz (w.r.t. GMPE)<br>• Kim Olsen: Hybrid method combining long period deterministic with high freq. stochastic based on Zeng et al crustal scattering. Have not considered freq. higher than 10 Hz. High freq. spectral accelerations adapted using low frequency level. If greens functions up to 1 Hz are not accurate enough, this could be a problem. 1D approach throws off the spectral level at 1 Hz. Scattering functions need to be convolved with slip rate functions at high frequencies (there are some candidate models for this).<br>• John Anderson: Frequency dependent Q model is the current challenge. Kappa can be introduced in the end, but having a working Q model (that gives the right kappa) is preferable. Work on this is currently underway. |

| Speaker | Topic | Issue |
|---|---|---|
| Doug Dreger | Discussion on Simulations: Summaries from Modeling Teams | • Translating the Graves and Pitarka's src file into Irikura's asperity model with discrete asperities. Northridge and LP results don't seem very good using this approach. (P. Somerville).<br>• Graves and Pitarka method: specifing the appropriate 1D velocity, Q model is difficult as you move to different regions. NO changes to the model are expected in the near term (R. Graves).<br><br>• Kappa is a fixed parameter. With freq. dependent Q model, kappa0 will be calculated. Post processing will add the correction to kappa to get the effective kappa at the end that was specified. (R. Archuleta)<br>• Definition of kappa is the slope of the FAS. In this project, kappa is extrapolating the slope back to zero km. If it is defined by FAS, freq. indepentent Q, then kappa is going to increase with distance (J. Anderson).<br>• Japanese implementation of slip model is very deterministic.<br>• High frequency Q is not controlled by data.<br>• Multi-segment rupture is still not possible on BB Platform (lower priority). |

| Speaker | Topic | Issue |
|---|---|---|
| Abrahamson | Discussion: Best use of Simulations and Practical Limitations | • Look at data from 2 Japanese events (Kobe: M6.9 and Tottori: M6.6) – Zhao et al.<br>• Check M5+ at within 50 km – Bindi et al. |

| Speaker | Topic | Issue |
|---|---|---|
| Jennie Watson-Lamprey | Available GM data from Transportable Array in Az for both nearby Eqs in AZ and distant Eqs in CA | • Additional AZ Data to Collect: Y13A data (will process), need to collect June 2012 M2.5 recordings, Jeri Young will send depth to bedrock values for nearby TA stations<br>• Geometrical Spreading: good coverage for nearby stations (dist < 100 km)<br>• Kappa: estimating Kappa_ds(mini) from these data should be possible, but need site conditions<br>• Additional PVNGS Data to collect<br>• Sufficient data near stations from CA and Baja Calif. Eqs to determine if the attenuation through Arizona differs significantly from CA<br>• Need improved site characterization – geotechnical characterization (soil thickness and damping) |

| Speaker | Topic | Issue |
|---|---|---|
| Melanie Walling | Available GM data from Transportable Array in Az for both nearby Eqs in AZ and distant Eqs in CA | • Look into adding two additional events<br>• This includes events in addition to catalog events<br>• Are the additional events blasts or earthquakes: many mine blasts removed from the catalog (J. Young) |

| Speaker | Topic | Issue |
|---|---|---|
| Bob Youngs | Discussion | • Mine blasts may be useable data. Sue Hugh - Kappa from mine blasts in NV study (J. Anderson). Kappa higher because waves travel twice through highly attenuating zone rather than once. Not sure if mine blast will give 2*kappa<br>• EQ clusters can be useful to evaluate sigma of kappa<br>• Comparative study of little skull Mtn. and NTS Nuke (nearly co-located) could get at the kappa problem.<br>• Should the Salton Trough be treated differently – large distance attenuation for AZ may need to be source region specific.<br>• Importance of magnitude estimate in estimating kappa – should be simple, but there are alternative models. Involve the right people. (J. Anderson)<br>• Datasets not yet considered: Historical intensities available for AZ (D. Brumbaugh)<br>• One more potential datapoint: Rosevelt Dam & VA Hospital triggered on El Mayor – Cucapah (J. Young). |

# Day 3 Summary

# DCPP region ground motion data

- Data for DCPP specific site effects (relative to GMPEs)
  - Strong motion data from 3 eqk
  - Basin waves seen from San Simeon earthquake recorded at DCPP
- Data for kappa for DCPP rock conditions
  - Deer Canyon
  - Small (M0.6 to M1.7) recorded on geophysical arrays
    - 25 to 300 Hz
- Path-Specific Effects
  - Focus on the path effects from nearby (15 km) offshore and onshore earthquakes (between Hosgri and Los Osos)
  - Few ground motions for these paths
  - Larger set of data from other paths within 100 km
    - Can be used to compare regional attenuation with GMPEs
- 3-D velocity models
  - Hardeback (2009) model from location of earthquake
  - New 3-D models being developed from recent onshore and offshore geophysical surveys (work by Dan O'Connell)
  - Need to use these studies to develop representative 1D models for use with Finite-fault simulations
    - Hosgri to DCPP
    - Los Osos to DCPP

# SONGS Region ground motion data

- Data for SONGS specific site effects
  - Ground motions from distant earthquakes
  - At SONGS, about 1 km depth to $V_S$=3000 m/s
  - Broadband (BB) at SONGS:
    - 28 eqk M>3 within 200 km
    - Compare with other BB data in the southern California region
- Data for kappa for SONGS rock conditions
  - Look for M<3 events at short distance (< 30 km)
- Path-Specific Effects
  - Focus on the path effects from nearby (15 km) offshore earthquakes (out to Newport Inglewood) and directly below SONGS (OBT)
  - There is enough ground motion data from SoCal (Chino Hills) to check for regionalization of the attenuation (geometrical spreading) as compared to the GMPEs
- 3-D velocity models
  - SCEC 3-D model in SONGS region can be simplified to 1-D for this region

# Simulations for Path Effects at SONGS

- CyberShake simulations
  - Large difference in 3D velocity models (S4 – H) in the SONGS region
    - Leads to significant difference in long period ground motion
  - Need to check if these velocity models apply to SONGS (near the edge of the SCEC region)
    - Can the ground motion data in the region provide a test of these two models?
    - Also, check consistency with the SONGS site-specific data for velocities
    - Is the gradient in from 760 m/s (ref) to 3000 m/s at SONGS consistent with the typical profile from data in the GMPEs?
  - Is the distance scaling from NI earthquakes (218, 219) to SONGS in CyberShake significantly different from the distance scaling in the GMPEs?
    - Focus on the long periods.

# Other Data

- Look at OBS data to evaluate the distance scaling offshore in SONGS region (M. Kohler)
- Check the strong motion data sets for path differences in SONGS region
  - This data should be included in the NGA-west2 data set
- Theoretical modeling of the distance attenuation may be useful for understanding the short distance scaling of the GMPEs
  - Address this topic as part of Workshop 2

# Fragile Geologic Features

- Are any FGF known to exist at any of the three NPP sites?
- DCPP
  - One promising FGF, but it is not ideal as compared to Yucca Mtn case
  - Needs age dating and fragility, and sensitivity on impacts on hazard
- SONGS
  - None identified by others, but no specific effort to look for FGF
  - SONGS foundation is on sandstone (San Mateo) with no damage (or dilation) to the sandstone over 125K years
    - Levels of shaking to damage sandstones not evaluated yet
    - Jack Daeman (UNR) may have looked at this along San Andreas, but not published.
- PVNGS
  - Some information on FGF in Arizona about 150 km north of PVNGS (Arrowsmith) – getting into the transition zone
  - FGF about 80 km from 1887 earthquake. Many non-toppled rocks

# Reference Site Condition

- Consider a lower $V_{S30}$ below 760 m/s
  - There is more data (better constrained GMPEs) at lower $V_{S30}$ values (say 500-600 m/s)
- Kappa corrections are better constrained at high $V_{S30}$ values
  - There is less correlation with kappa and site amplification for high $V_{S30}$ sites
- What reference $V_{S30}$ is best to use with the 3 sites consistent with site response approaches?

# Kappa

- Potential differences in kappa on rock between Arizona and CA can lead to significant differences on the ground motion for PVNGS (Silva)
- Need to get an estimate of rock kappa for APS

# Kappa discussion

- Use of small (M1) earthquakes to estimate kappa
  - May be useful, but consider multiple source models if working at freq below the corner freq (Anderson)
- Kappa for hard rock (EUS vs Arizona)
  - Also check regional Q for effects in the top 5 km, using freq dependent Q (Anderson)
  - If using kappa –$V_{S30}$ relations:
    - Large scatter in kappa- $V_{S30}$ relations for high $V_{S30}$ values may reflect regional differences (Olga)
      - **Try to get a relation for the specific region (not mixing regions)**
    - Functional form may need lower limit at high $V_{S30}$ for a specified region
    - May also depend on depth to bedrock
    - Need for good knowledge of the site in order to: (a) get a good estimate of $V_{S30}$ (if $k_0$ - $V_{S30}$ correlations are used) ) and (b) be able to estimate/anticipate the 1D site amplification pattern, so as not to let resonant peaks distort the kappa estimate. (Olga)
  - Issues for site response effects on the kappa
    - Amplification peaks can distort the kappa estimate
    - Removing soil effects from surface motions to estimate (rock) kappa
  - Due to the large single-site variability shown for kappa, we need for as many records per site as possible to capture both the mean $k_0$ and the (possibly source-dependent) 'sigma' of the mean $k_0$ (Olga)

# Kappa from small Mag

- Kappa for PVNGS region
  - Past experience estimating kappa from small magnitude events (M1-M2), with a limit of 14 Hz?
    - UNR studies for Yucca Mtn compared kappa from M1 with kappa from M4
- Kappa for DCPP region
  - Past experience with estimating kappa from small magnitudes events 25-300Hz?
    - None so far, but worth trying this approach

# Data Needs and Issues for Single-Station Sigma

- Is there enough data to constrain PhiSS?
  - Data in NGA-West2
    - 364 eqk at 838 stations, dominated by CA data
    - Taiwan data in NGA-West2 is limited and may have a similar path effect
  - Data from world-wide data
    - Current paper: CA, Taiwan, Turkey, Japan
      - Data for distance dependent PhiSS
        - » Increase at short distances for small mag (M<5) only
      - Data for magnitude dependent PhiSS
        - » Best constrained by CA data set
    - New data set: Japanese data
      - M>4, about 30,000 records - data set will be complete at the end of summer 2013
      - Distances: Rrup for M>6.5, Rhypo for M<6.5
      - Will this lead to overestimation of PhiSS at short distances due to distance metric?

# Data Needs and Issues for Single-Station Sigma

- Issues
  - To use PhiSS, epistemic uncertainty in the median site term needs to be included
  - Inclusion of epistemic uncertainty of PhiSS,s (how much does PhiSS change from site to site?)
    - This is a part of the epistemic uncertainty that has not been included in standard PSHA methodology
    - There is adequate data to estimate this for the entire data set, but unclear on site-specific application
    - So far, no attempt to look at the high PhiSS,s sites and understand what is causing the larger variability
      - Looking at the seismograms that may reveal what is happening
      - Is there something in the subsurface structure that would explain the high variability
      - Low variability sites may be from many earthquakes from the same path
      - It may partly reflect non-linearity (separately included in site response, be sure to avoid double counting
    - Topic for Workshop 2

# How to Estimate Site Terms

- DCPP
  - Empirical, based on recordings at DCPP
  - Still small number of earthquakes, so large epistemic uncertainty
- SONGS
  - Analytical using uncertainty in the geotechnical parameters
  - May also have ground motion data at the SONGS site from new earthquakes from the new instrument
  - Are the site terms from nearby sites consistent? If so, they may help to inform site term at SONGS
- PVNGS
  - Plans to use a site specific site terms are being evaluated

# Day 1 – Main points

- Import sources (M,R,F) for each site identified from hazard sensitivity (using existing models)
- Data sets (M,R,F) from which current GMPEs are derived
- NGA-West2 data (M,R,F)
  - Identified additional key events
    - M7.0 (Mw6.7) normal faulting Japanese earthquake (Fukushima Hamadori)
      - Additional (up to 10), M>5 in this sequence
    - Wells, Nevada eqk (normal)
    - Moderate mag normal events in Italy (check if included in NGA-West2)
    - Data for near-fault bump (GK model looks at 4 well recorded eqk)
- Large magnitude scaling
  - Oversaturation seen in empirical data at high freq (Boore)
  - See Full saturation for simple modeling of scaling (Baltay) – oversaturation not considered
  - Check if this is seen in new (planned) simulations?

# Day 2 – Main Points

- HW
  - Include dipping Strike-Slip (some simulations exist)
  - HW effects for M5.5 to 6.5 not well constrained by NGA-West2 empirical data. Consider simulations. Japanese data may help, but need meta data
- Splay faulting
  - Still unclear what will be in source model
  - Consider alternative (distance) metrics for complex faulting
  - Review existing characterization of complex ruptures in NGA-West2
  - Implement dynamic rupture models,
    - Considering initiation of rupture on splay or down-strike on main fault
    - Add heterogeneous stresses

- Broadband simulations
  - Cases on spreadsheet (see next slide)
  - Care needed when using rupture generators for M>8

| Model # | Issue | Magnitude | Distance (km) | Surface/ Buried, ZTOR (km) | Freq Range (Hz) | Addt. Notes |
|---|---|---|---|---|---|---|
| 1 | HW Scaling | 5.5 | 0-15km | 0, 5, 10 | up to 10 Hz | Possibly only out to 10 km, and use dynamic ruptures |
| 2 | Splay Faulting | Main,7 Splay, 6-6.5 | 0-15km | | up to 10 Hz | Splay faults, key issue is timing between segments |
| 3 | Slip partitioning (T. Rockwell) | 6.5-7.5 | 0-15km | | up to 10 Hz | Specific for SONGS |
| 4 | Large mag scaling | 7-8 | 0-15km | | up to 10 Hz | Look at constraints at long periods, Wenchuan (low), ChiChi (high), oversaturation is at high frequencies |
| 5 | Low dip angle scaling (10 deg) | 5.5-6.5 | 0-15km | 5, 10 | up to 10 Hz | Below 30 degrees, not constrained empirically, need buried, need close in |
| 6 | Linked, multi-segment faults (short distances) | 8.5 | 0-15km | | up to 10 Hz | Are rupture generators valid for M>8?, but expensive (time), oversaturation? |
| 7 | Large mag, long distances | 7.5-8.5 | 400 km | | 1 | Specific for PVNGS |
| | PDF - Long period energy at short distances (covered by #4) | | | | | |

# Arizona GM data

- Kappa
  - Need site conditions for key sites
  - Methods for small mag events with limited high freq bandwidth (14 Hz)
- Long distance attenuation
  - Empirical data adequate, but review needed for regionalization for path adjustment
- Consider use of intensity data as a check on GMPEs
  - Also check for additional GM data

# LETTER COMMENTARY FROM THE PARTICIPATORY PEER REVIEW PANEL

April 21, 2013

Carola Di Alessandro, Ph.D.
Project Manager for the SWUS GMC SSHAC
GeoPentech, Inc.
525 N. Cabrillo Park Drive, Suite 280
Santa Ana, CA 92701

Dear Dr. Di Alessandro:

This letter provides comments from the Participatory Peer Review Panel (PPRP) on Workshop No. 1 (Significant Issues and Available Data) of the Southwestern U.S. Ground Motion Characterization (SWUS GMC) project. The PPRP wishes to thank the management team for the opportunity to participate in the workshop, which was held on March 19-21 in Oakland, California. The PPRP participated as observers, in order to be informed and to provide a review of both the process and the technical developments. All four members of the PPRP (K. Campbell, B. Chiou, S. Day, and T. Rockwell) attended, and the panel observed all aspects of the workshop. The workshop was organized in a very professional and effective manner, and we appreciate the hospitality shown to us by the project team.

**Summary Comments**

The technical program was organized and conducted with the highest level of professionalism. As appropriate for the first workshop of a SSHAC Level 3 study, the focus was on framing the hazard issues, identifying available data, and identifying key data needs. The workshop began with a summary of the project, including clear statements of its objectives and scope. The SWUS GMC project interfaces with the three separate Seismic Source Characterization (SSC) studies supported by the respective sponsoring utilities. A series of presentations on the first day of the workshop outlined the principal seismic source issues for each site, expressed in terms of hazard sensitivity. This introduction was very useful in setting the broader context for the GMC study and in enabling subsequent discussions to focus on data that are most relevant to hazard.

The resource-expert presentations that followed were well chosen, well structured, and comprehensive, and each included a list of references. All five members of the Technical Integration (TI) Team were fully engaged in the discussions of these presentations and each played a valuable role in interrogating the presenters. The PPRP is unaware of any relevant avenues that were not explored.

The TI Team did a commendable job of keeping the workshop focus on the data issues, as is appropriate for the first workshop of a SSHAC Level 3 study. Maintaining the right focus was challenging, because the line between data and interpretations or models is not a sharp one, but the team found the right balance. A clear separation of roles was

maintained. For example, when occasionally a TI or PPRP Team member was required to comment in the role of a resource expert, that role was always clearly stated.

In summary, with respect to process, as well as with respect to technical quality and completeness, the workshop met all standards for a SSHAC Level 3 data workshop. A good foundation has been set for the exploration of proponent models in Workshop No. 2.

Specific comments and recommendations are given below. Those specific comments, suggestions, or recommendations that require a written response are underlined.

**Recommendations**

*1. Site Kappa and Single-Station Sigma Terminology*. Several resource experts presented very interesting and insightful information on the data needed to estimate the site attenuation parameter kappa and the ground motion standard deviation parameter single-site sigma. However, this material is quite technical and some of it is quite new. Not all participants and observers seemed to have a shared understanding of the terminologies being employed or how the estimated quantities can be applied in a self-consistent manner at each of the nuclear power plant sites where they will be used. Our concern comes partly from the lack of probing questions of the kappa and single-site sigma resource experts from the TI Team, partly from a lack of significant questions from the audience, and partly from questions expressed by members of the PPRP. Therefore, the PPRP suggests that the TI Team write White Papers, i.e., authoritative technical notes, on site kappa and single-station sigma, respectively, that define the terms, indicate how they are going to be estimated, and how they are to be used in the seismic hazard analysis of each of the NPPs. These documents would provide a common language and reference frame for future discussions and help allay concerns about possible double counting or other inconsistencies in these two parameters.

*2. Splay Fault Modeling*. The workshop included some discussion of dynamic rupture modeling of splay faulting, especially models leading to possible concurrent rupture of the Hosgri and Shoreline faults. Our understanding is that SCEC has been tasked with performing such modeling. We are concerned that this effort may not be as well interfaced with the relevant SSHAC projects (the DCPP and SONGS SSC studies and the SWUS GMC study) as it could be. In particular, the occurrence and extent of concurrent rupture on a splay depends quite strongly on the orientation of the maximum principal stress direction. It is likely also to be sensitive to rupture velocity. The SCEC team tasked for this work has been principally focused on canonical test problems for the purpose of code verification; it should not simply be assumed that the SCEC group has sufficient expertise and experience in the specific rupture dynamics questions being posed by the SSHAC projects to operate independently. The presentation at the workshop did not suggest that the SCEC team recognizes the importance of the principal stress orientations, nor the importance of exploring conditions conducive to a range of rupture velocities. We recommend that the SWUS GMC project and the other relevant SSHAC projects devise a plan to provide ongoing guidance and feedback to the SCEC modeling team.

*3. DCPP-SSC interface issue: Slab Earthquakes*. During the workshop, the possibility of earthquakes within a relic subducted slab beneath DCPP was broached during the presentation overviewing the DCPP SSC project. To our knowledge, this possibility of slab sources had not been mentioned at previous DCPP SSC workshops, and from the discussion at the workshop, it was not clear which project takes responsibility for assessing its technical defensibility and implications. Slab earthquakes are known to excite ground motion with systematically distinct characteristics relative to crustal sources. We recommend that the two projects clarify the lines of responsibility and establish effective communication on this subject so that the TI Team is not taken by surprise if slab events are characterized in the DCPP SSC.

*4. DCPP-SSC and SONGS-SSC interface issue: Maximum depth of rupture in crustal earthquakes*. During the DCPP-SSC overview presented at the workshop, the possibility was raised of deep rupture penetration, i.e., rupture extending to greater than 15-20 km depth, on some crustal faults in California. The SWUS-GMC TI Team seemed unaware that this was a possibility in the DCPP SSC project and it was not clear to us which project takes responsibility for the technical assessment of deep rupture. Furthermore, although this issue was not raised in the SONGS-SSC overview, similar depth-of-rupture considerations may pertain to both California sites. We recommend that the SWUS-GMC project work with the DCPP-SSC and SONGS-SSC projects, respectively, to clarify ownership of the depth-of-rupture problem and begin to communicate effectively and regularly about the status and implications of those ideas.

*5. Path-Specific Attenuation for Palo Verde*. The attenuation of ground motion between distant earthquakes and PVNPS may be quite strongly dependent upon the source location and might not be well represented by a single function of distance. The TI Team clearly recognizes this likelihood and has taken it into consideration in their plan to empirically estimate attenuation from distant sources to PVNPS using existing recordings from relevant source regions. We consider this a sound approach. However, the PPRP would suggest that the empirical approach be carefully applied in the light of a geological understanding of both the source and path regions (for example, it might be observed that paths crossing the Salton Trough are highly attenuative and geologic understanding might dictate that the same empirical correction not be applied to nearby sources that do not cross that province).

*6. Hand-off to Site-Specific Site-Response Analysis Team*. The GMC TI Team is proposing to characterize ground motions for a common reference rock condition with $V_{S30}$ = 760 m/s and to adjust the base case GMC model to incorporate utility-specific differences in site characteristics and modeling approach. We understand that each utility will adjust the resulting rock hazards to the local site condition at each NPP site when deriving the Hazard-Consistent Ground Motion Response Spectra (GMRS). The TI Team have acknowledged the need for interaction between these two efforts and emphasized the importance of proper handoff of the GMC model to the team responsible for site-specific site-response analysis. Still, we want to further emphasize it here by cautioning that lack of clarity and precision in the communication between the GMC TI Team and

the site response analysis team may make both vulnerable to misunderstandings and claims of inconsistency or double counting of effects. We recommend that the TI Team and the individual site projects collaborate to generate as soon as possible a reference document that describes the respective adjustments and procedures to be used at each site, and that explains the technical rationale in each case. As with the documents on kappa and single-site sigma recommended in Item 1 above, such a document would serve to guide future discussions, prevent misunderstandings, and ensure that no relevant data or models are neglected due to uncertainties about which project is responsible.

Please feel free to contact us if you would like to discuss further our comments or recommendations.

Sincerely,

Steven M. Day
Chair, PPRP

Kenneth Campbell
Member, PPRP

Brian Chiou
Member, PPRP

Thomas Rockwell
Member, PPRP

# TECHNICAL INTEGRATION TEAM LEAD RESPONSES TO PARTICIPATORY PEER REVIEW PANEL COMMENTS

May 5, 2013

Steven M. Day
Chair, Participatory Peer Review Panel
Department of Geological Sciences
San Diego State University
5500 Campanile Drive
San Diego, California 92182

Dear Prof. Day:

The TI Team and PM appreciate the valuable comments and suggestions received from the Participatory Peer Review Panel (PPRP), both during the Workshop No. 1 execution and in their formal letter commentary dated April 21, 2013. The present document serves to provide written responses to specific comments, suggestions, or recommendations that the PPRP identified (by underlining).

1. *Site Kappa and Single-Station Sigma Terminology*
   Several resource experts presented very interesting and insightful information on the data needed to estimate the site attenuation parameter kappa and the ground motion standard deviation parameter single-site sigma. However, this material is quite technical and some of it is quite new. Not all participants and observers seemed to have a shared understanding of the terminologies being employed or how the estimated quantities can be applied in a self-consistent manner at each of the nuclear power plant sites where they will be used. Our concern comes partly from the lack of probing questions of the kappa and single-site sigma resource experts from the TI Team, partly from a lack of significant questions from the audience, and partly from questions expressed by members of the PPRP. Therefore, the PPRP suggests that the TI Team write White Papers, i.e., authoritative technical notes, on site kappa and single-station sigma, respectively, that define the terms, indicate how they are going to be estimated, and how they are to be used in the seismic hazard analysis of each of the NPPs. These documents would provide a common language and reference frame for

future discussions and help allay concerns about possible double counting or other inconsistencies in these two parameters.

We agree. Our plan is to coordinate the preparation of the requested White Papers with the effort already initiated by Dr. Linda Al-Atik (a member of the TI Team Support group) for the Hanford site SSHAC project. In this way, in addition to providing a common understanding of the issues and terminology for the SWUS GMC project, we will address consistency with the other ongoing SSHAC projects conducted in the Western US region.

2. *Splay Fault Modeling*

   The workshop included some discussion of dynamic rupture modeling of splay faulting, especially models leading to possible concurrent rupture of the Hosgri and Shoreline faults. Our understanding is that SCEC has been tasked with performing such modeling. We are concerned that this effort may not be as well interfaced with the relevant SSHAC projects (the DCPP and SONGS SSC studies and the SWUS GMC study) as it could be. In particular, the occurrence and extent of concurrent rupture on a splay depends quite strongly on the orientation of the maximum principal stress direction. It is likely also to be sensitive to rupture velocity. The SCEC team tasked for this work has been principally focused on canonical test problems for the purpose of code verification; it should not simply be assumed that the SCEC group has sufficient expertise and experience in the specific rupture dynamics questions being posed by the SSHAC projects to operate independently. The presentation at the workshop did not suggest that the SCEC team recognizes the importance of the principal stress orientations, nor the importance of exploring conditions conducive to a range of rupture velocities. <u>We recommend that the SWUS GMC project and the other relevant SSHAC projects devise a plan to provide ongoing guidance and feedback to the SCEC modeling team.</u>

We note that SCEC has not been tasked with conducting dynamic rupture calculation for splay faulting for SWUS GMC. The activities at SCEC have focused only on code verification (i.e. to make sure codes are working as intended) for splay fault geometries that are relevant to DCPP and SONGS. Based on the results of the verification, we will identify potential groups for conducting dynamic rupture simulations for SWUS GMC Project. However, the decision on the extent of use of dynamic rupture simulations has not yet been made.

Our plan is for the TI Team (in particular Prof. Doug Dreger) to work in close contact with the SCEC dynamic rupture verification coordinator (Dr. Ruth Harris of USGS) to understand the role played by stress orientation and rupture velocity in the validation exercise. In addition, we will recommend that representatives from the SSC Teams meet with Ruth Harris to discuss the use of dynamic ruptures for constraining characteristics and frequencies of splay fault ruptures. This information can be used to constrain the source characterization for splay faulting.

3. *DCPP-SSC interface issue: Slab Earthquakes*
   During the workshop, the possibility of earthquakes within a relic subducted slab beneath DCPP was broached during the presentation overviewing the DCPP SSC project. To our knowledge, this possibility of slab sources had not been mentioned at previous DCPP SSC workshops, and from the discussion at the workshop, it was not clear which project takes responsibility for assessing its technical defensibility and implications. Slab earthquakes are known to excite ground motion with systematically distinct characteristics relative to crustal sources. We recommend that the two projects clarify the lines of responsibility and establish effective communication on this subject so that the TI Team is not taken by surprise if slab events are characterized in the DCPP SSC.

We agree and will engage the DCPP SSC Project Team to address the potential for slab earthquakes in the DCPP region. The final decision for inclusion or exclusion of slab earthquakes lies with the SCC Team but information from ground motion experts that maybe relevant to the SSC Team evaluation will be provided by the SWUS GMC project.

4. *DCPP-SSC and SONGS-SSC interface issue: Maximum depth of rupture in crustal earthquakes*
   During the DCPP SSC overview presented at the workshop, the possibility was raised of deep crustal earthquakes, i.e., greater than 15-20 km deep, on some crustal faults in California. The SWUS GMC TI Team seemed unaware that this was a possibility in the DCPP SSC project and it was not clear to us which project takes responsibility for the technical assessment of deep crustal earthquake modeling. We recommend that the two projects clarify ownership of the depth-of-faulting problem and begin to communicate effectively and regularly about the status and implications of those ideas.

We agree. Information on the maximum depth of rupture may be available from source inversions commonly used in ground motion studies that are not yet being considered by the DCPP and SONGS SSC TI Teams. Ensuring that this interface issue is addressed is the responsibility of the Project Technical Integrators (PTIs) for the SSC and GMC efforts for each site. We will provide examples of ground motion inversion studies to demonstrate the range of depth-of-ruptures implied by these studies so that the SSC TI Teams are fully informed. The final decision for the distribution of rupture depths lies with the individual SSC Teams.

5. *Path-Specific Attenuation for Palo Verde*
   The attenuation of ground motion between distant earthquakes and PVNPS may be quite strongly dependent upon the source location and might not be well represented by a single function of

distance. The TI Team clearly recognizes this likelihood and has taken it into consideration in their plan to empirically estimate attenuation from distant sources to PVNPS using existing recordings from relevant source regions. We consider this a sound approach. However, the PPRP would suggest that the empirical approach be carefully applied in the light of a geological understanding of both the source and path regions (for example, it might be observed that paths crossing the Salton Trough are highly attenuative and geologic understanding might dictate that the same empirical correction not be applied to nearby sources that do not cross that province).

We agree. The SWUS GMC TI Team will consider different regions (one being the Salton Trough region) when evaluating the residuals to derive empirical correction factors applicable to PVNGS. In order to preserve the statistical robustness of the analysis, we are expanding our ground motion dataset so to include more earthquakes generated in central California (up to 400 km from the Arizona border) and recorded by stations in Arizona located up to 100 km away from PVNGS, but still within the Sonoran Basin and Range zone as prescribed/mapped by the associated SSC effort. These additional earthquakes will allow us to evaluate the need for different path effects through the Salton Trough versus other path effects.

6. *Hand-off to Site-Specific Site-Response Analysis Team*

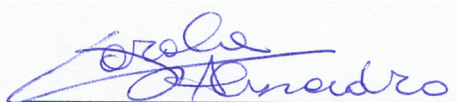
   The GMC TI Team is proposing to characterize ground motions for a common reference rock condition with $V_{S30}$ = 760 m/s and to adjust the base case GMC model to incorporate utility-specific differences in site characteristics and modeling approach. We understand that each utility will adjust the resulting rock hazards to the local site condition at each NPP site when deriving the Hazard-Consistent Ground Motion Response Spectra (GMRS). The TI Team have acknowledged need for interaction between these two efforts and emphasized the importance of proper handoff of the GMC model to the team responsible for site-specific site-response analysis. Still we want to further emphasize it here by cautioning that lack of clarity and precision in the communication between the GMC TI Team and the site response analysis team may make both vulnerable to misunderstandings and claims of inconsistency or double counting of effects. We recommend that the TI Team and the individual site projects collaborate to generate as soon as possible a reference document that describes the respective adjustments and procedures to be used at each site and that explains the technical rationale in each case. As with the documents on kappa and single-site sigma recommended in Item 1 above, such a document would serve to guide future discussions, prevent misunderstandings, and ensure that no relevant data or models are neglected due to uncertainties about which project is responsible.

We agree. Although site response is not part of the deliverable for SWUS GMC, the approaches being used for site response at the three NPP sites need to be understood and clearly documented to ensure a consistent interface between the base case ground motion and site response. The final decision on site response approaches lies with the individual NPP sites.

We plan on issuing a White Paper describing the site-response approaches being used at each of the three sites; this document will include the technical base for the selection of the reference rock conditions.

We hope this letter clarifies the questions and comments stated in the April 21, 2013 PPRP Commentary Letter. We wish to express our gratitude to the PPRP again for their efforts and cooperation, and for making this project a success.

Sincerely,





Carola Di Alessandro,
SWUS GMC Project Manager

Norman A. Abrahamson,
SWUS GMC TI Team Lead

CC: PPRP Panel, TI Team, PTIs

# REFERENCES

Abrahamson, N.A. (2012). DCPP SSC Workshop 2 presentation [available at http://www.pge.com/mybusiness/edusafety/systemworks/dcpp/SSHAC/workshops/ws2.shtml]

Abrahamson, N. A., and W. J. Silva (1997), Empirical Response Spectral Attenuation Relations for Shallow Crustal Earthquakes, *Seismological Research Letters*, Vol. 68(1), 94-127.

Abrahamson, N.A., and Silva, W. (2008). Summary of the Abrahamson & Silva NGA Ground-Motion Relations, *Earthquake Spectra*, Vol. 24(1), 67-97.

Abrahamson, N.A., and Silva, W.J. (2009). Errata for 'Summary of the Abrahamson & Silva NGA ground-motion relations' [available at http://peer.berkeley.edu/products/abrahamson-silva_nga_report_files/AS08_NGA_errata.pdf]

Abrahamson, N.A., Gregor, N., and Addo, K. (2012). BCHydro ground motion prediction equations for subduction earthquakes, *Earthquake Spectra* (in review).

Akkar, S. and Bommer, J.J. (2010). Empirical Equations for the Prediction of PGA, PGV, and Spectral Accelerations in Europe, the Mediterranean Region, and the Middle East, *Seism. Res. Letters*, Vol. 81, 195-206.

Akkar, S. and Çagnan, Z. (2010). A Local Ground-Motion Predictive Model for Turkey, and Its Comparison with Other Regional and Global Ground-Motion Models, *Bull. Seism. Soc. Am.*, Vol. 100(6), 2978-2995.

Al Atik, L., Abrahamson, N., Bommer, J., Scherbaum, F., Cotton, F., Kuehn, N. (2010). The variability of ground-motion prediction models and its components, *Seism. Res. Let*., 81(5), 794-801.

Al Atik, L. (2011). Summary of updated kappa-fpeak relationships, Report submitted to PEGASOS Refinement Project.

Al Atik, L. and Abrahamson, N. (2012). Kappa scaling using empirical ground motion data, Report prepared for the PEGASOS Refinement Project.

Al Atik, L., Kottke, A., Abrahamson, N., and Hollenback, J. (2013). Kappa scaling of ground motion prediction equations using IRVT approach, *Bull. Seism. Soc. Am.* (Submitted).

Allen, C. R., Silver, L.T., and Stehli, F.G. (1960). Agua Blanca fault – a major transverse structure of northern Baja California, Mexico, *Bull. Seism. Soc. Am.*, Vol. 71(4), 467-482.

Allen, T.I. and Wald, D.J. (2009). On the Use of High-Resolution Topographic Data as a Proxy for Seismic Site Conditions ($V_{S30}$), *Bull. Seism. Soc. Am*., Vol. 99(2A), 935-943

Ancheta, T.D., Darragh, R.B., Stewart, J.P., Seyhan, E., Silva, W.J., Chiou, B., Wooddell, K., Graves, R., Kottke, A., Boore, D.M., Kishida, T. and Donahue, J.L. (2013). PEER NGA-West2 Database, *PEER Report 2013/01*, Pacific Earthquake Engineering Research Center, University of California, Berkeley, CA.

Anderson, J.G., and Heaton, T.H. (1980). Aftershock accelerograms recorded on a temporary array in Johnson, C.E., Sharp, R., and Rohan, C., eds., The Imperial Valley Earthquake: *U.S. Geological Survey Professional Paper* No. 1254, pp 443-451.

Anderson, J. G., and Hough, S E. (1984). A model for the shape of the Fourier amplitude spectrum of acceleration at high frequencie, Bulletin of the Seismological Society of America, 74(5), 1969–1993.

Anderson, J.G. (1991). A preliminary descriptive model for the distance dependence of the spectral decay parameter in southern California, *Bull. Seism. Soc. Am.*, Vol. 81, 2186–2193.

Anderson, J.G., Wesnousky, S.G., and Stirling, M.W. (1996). Earthquake Size as a Function of Fault Slip Rate, *Bull. Seism. Soc. Am.*, Vol. 86(3), 683-690.

Anderson, J. G., and Brune, J. N. (1999). Probabilistic seismic hazard assessment without the ergodic assumption, *Seism. Res. Let*., Vol. 70, 19-28.

Anderson, J., Brune, J.N., Biasi, G., Anooshehpoor, A., and Purvance, M. (2011). Workshop Report: Application of Precarious Rocks and Related Fragile Geological Features to U.S. National Hazard Maps, *Seismological Research Letters*, Vol. 82, 431-441.

Anderson, J.G., and Uchiyama (2011). A Methodology to Improve Ground Motion Prediction Equations by Including Path Corrections, *Bull. Seism. Soc. Am.*, Vol. 101: 1822-1846

Arabasz, W. J., Pechmann, J. C., and Brown, E. D. (1987). Observational seismology and the evaluation of earthquake hazards and risk in the Wasatch Front area, Utah, in Gori, P. L., and Hays, W. W., eds., Assessment of regional earthquake hazards and risk along the Wasatch Front, Utah: *U. S. Geological Survey Open-File Report* 87-585, D1-D58.

Atkinson, G.M., and Boore, D.M. (2000). Reply to comment by R. A. W. Haddon on evaluation of models for earthquake source spectra in eastern North America by Gail M. Atkinson and David M. Boore, *Bull. Seism. Soc. Am.*, Vol. 90, 1339-1341.

Atkinson, G.M. (2006). Single-station sigma, *Bull. Seism. Soc. Am.,* Vol. 96, 446-455.

Atkinson, G.M., and Boore, D. M. (2006). Earthquake ground-motion prediction equations for eastern north America, *Bull. Seism. Soc. Am.*, Vol. 97(3), 2181- 2205.

Atkinson, G. M., Boore, D.M., Assatourians, K., Campbell K., and Motazedian, D. (2009). A guide to differences between stochastic point-source and stochastic finite-fault simulations, *Bull. Seism. Soc. Am.,* Vol. 99, 3192-3201.

Atwater, T.M. (1970). Implications of plate tectonics for the Cenozoic tectonic evolution of western North America, *Bull. Seism. Soc. Am.,* Vol. 81, 3513-3536.

Baltay, A.S., and Hanks, T.C. (2013). Magnitude Dependence of PGA and PGV in NGA-West2 Data: Parameterization of the Model for Use by NGA-Developers, Report provided to PEER

Baltay, A.S., and Hanks, T.C. (2013). Understanding the Magnitude Dependence of PGA and PGV in NGA-West2 Data, in preparation for submission to the Bulletin of the Seismological Society of America

Base Maps: PG&E Civil Site Facilities Layout Plan (modified 1994)

Bashir, L., Gao, S.S., Liu, K.H., and Mickus, K. (2011). Crustal structure and evolution beneath the Colorado Plateau and the southern Basin and Range Province: Results from receiver function and gravity studies, *Geochem. Geophys. Geosyst.*, Vol. 12, Q06008.

Bausch, D.B., and Brumbaugh, D.S. (1994). Seismic Hazards in Arizona: Arizona Ground Shaking Intensity and 100-year Acceleration Contour Maps, Prepared for Arizona Division of Emergency Management and FEMA by the Arizona Earthquake Information Center.

Bausch, D.B., and Brumbaugh, D.S. (1997). Flagstaff Community Earthquake Hazard Evaluation, Coconino County, Arizona. Flagstaff, AZ, *Northern Arizona University Arizona Earthquake Information Center*.

Bazzurro, P. and Cornell, C. A. (1999). Disaggregaion of seismic hazard, *Bull. Seism. Soc. Am.,* Vol. 89(2), 501-520.

Beard, L.S., Karlstrom, K.E., Young, R.A., and Billingsley, G.H., eds. (2011). CRevolution 2— Origin and evolution of the Colorado River system, workshop abstracts: *U.S. Geological Survey Open-File Report* 2011–1210, 300 p., [available at http://pubs.usgs.gov/of/2011/1210/]

Beavan, J., Samsonov, S., Motagh, M., Wallace, L., Ellis, S., and Palmer, N. (2010). The Darfield (Canterbury) earthquake: geodetic observations and preliminary source model, *Bulletin of the New Zealand Society for Earthquake Engineering*, Vol. 43 (4), 228-235

Beck, S., Linkimer, L., Zandt, G., and Holland, A. (2013). Focal Mechanisms and Preliminary Attenuation Measurements in Arizona, *Arizona Geological Survey Contributed Report* C-13, 21 p. [available at http://repository.azgs.az.gov/sites/default/files/dlio/files/nid1496/cr-13-c_az_seismic.pdf]

Bennett, R. A., Rodi, W., and Reilinger, R.E. (1996). Global Positioning System constraints on fault slip rates in southern California and northern Baja, Mexico, *Journal of Geophysical Research*, Vol. 101(B10), 21943–21960.

Beresnev, I., and Atkinson, G. (1998a). FINSIM: a FORTRAN program for simulating stochastic acceleration time histories from finite faults, *Seism. Res. Lett.*, Vol. 69, 27–32.

Berglund, H.T., Sheehan, A.F., Murray, M.H., Roy, M., Lowry, A.R., Nerem, R.S., and Blume, F. (2012). Distributed deformation across the Rio Grande Rift, Great Plains and Colorado Plateau, *Geology*, Vol. 40(1), 23-26.

Biasi, G.P., and Smith, K.D. (2001). Site effects for seismic monitoring stations in the vicinity of Yucca Mountain, Nevada, MOL20011204.0045, Report prepared for the US DOE/University and Community College System of Nevada (UCCSN) Cooperative Agreement.

Biasi, G., and Anderson, J.G. (2007). Measurement of the parameter kappa, and reealuation of kappa for small to moderate earthquakes at seismic stations in the vicinity of Yucca Mountain, Nevada, TR-07-007, Task ORD-FY04-006, Nevada System of Higher Education, Las Vegas.

Bindi, D., Luzi, L., Massa, M., and Pacor, F. (2009). Horizontal and Vertical ground motion prediction equations derived from the Italian Accelerometric Archive (ITACA), *Bull. Earthquake Eng*., Vol. 8(5), 1209-1230.

Bindi, D., Pacor, F., Luzi, L., Puglia, R., Massa, M., Ameri, G., Paolucci, R. (2011). Ground motion prediction equations derived from the Italian strong motion database, *Bull. Eqk Eng*., Vol. 9, 1899-1920.

Bird, P. (1998). Kinematic history of the Laramide orogeny in latitudes 35° -49° N, western United States, *Tectonics*, Vol. 17, 780-801.

Bird, P. (2003). An updated digital model of plate boundaries, *Geochemistry Geophysics Geosystems*, Vol. 4(3), 1027 p., doi:10.1029/2001GC000252.

Blackwell, D., Richards, M., Frone, Z., Batir, J., Ruzo, A., Williams, M., and Dingwall, R. (2011). Enhanced Geothermal Resources of the United States, *Geothermal Resources Council Transactions*, 35p.

Blank, H.R., Butler, W.C., and Saltus, R.W. (1998). Neogene Uplift and Radial Collapse of the Colorado Plateau--Regional Implications of Gravity and Aeromagnetic Data, in Friedman, J. D., and Huffman, A.C., Jr, eds., Laccolith Complexes of Southeastern Utah: Tectonic Control and Time of Emplacement - *Workshop Proceedings*: U.S. Geological Survey Bulletin 2158, 9-32.

Bommer, J. J., and Abrahamson, N. A. (2006). Why do modern probabilistic seismic-hazard analyses often lead to increased hazard estimates?, *Bull. Seism. Soc. Am.,* Vol. 96, 1967–1977.

Bommer, J.J. (2010). Sigma: What it is, why it matters and what we can do with it, *NGA-East workshop presentation*, February 10, 2010.

Boore, D.M. (2003). Simulation of ground motion using the stochastic method, *Pure and Applied Geophysics*, Vol. 160, 635-675.

Boore, D. M. (2005). SMSIM--Fortran Programs for Simulating Ground Motions from Earthquakes: Version 2.3--A Revision of OFR 96-80-A, *U.S. Geological Survey Open-File Report*

Boore, D.M. (2009). Comparing stochastic point-source and finite-source ground-motion simulations: SMSIM and EXSIM, *Bull. Seism. Soc. Am.*, Vol. 99, 3202-3216.

Boore, D.M., and Atkinson, G.M. (2008). Ground-Motion Prediction Equations for the Average Horizontal Component of PGA, PGV, and 5%-Damped PSA at Spectral Periods between 0.01s and 10.0s, *Earthquake Spectra*, Vol. 24(1), 99-138.

Boore, D.M., Azari, A., and Akkar, S. (2012). Using pad-stripped acausally filtered strong-motion data, *Bull. Seism. Soc. Am.* (Submitted).

Bradley, B.A. (2010). NZ-Specific Pseudo-Spectral Acceleration Ground Motion Prediction Equations Based on Foreign Modes, Department of Civil Engineering, University of Canterbury, Christchurch, New Zealand, Sept. 2010.

Brown, L.G. (1978). Recent fault scarps along the eastern escarpment of the Sierra San Pedro Martir, Baja California. *MS thesis*, San Diego State University, San Diego, California, 88 p.

Brumbaugh, D.S. (1987). A tectonic boundary for the southern Colorado Plateau, *Tectonophysics*, Vol. 136, 125–136.

Brumbaugh, D.S. (2008). Seismicity and tectonics of the Blue Ridge area of the Mogollon Plateau, Arizona, *Bull. Seism. Soc. Am.,* Vol. 98(3), 1527–1534

Brune, J. N. (1970). Tectonic stress and the spectra of seismic shear waves from earthquakes, *J. Geophys. Res*., Vol. 76, 4997–5009.

Brune, J.N. and Whitney, J.W. (2000). Precarious Rocks and Seismic Shaking at Yucca Mountain, Nevada: in Whitney, J.W. and Keefer, W.R., eds., Geologic and geophysical studies of Yucca mountain, Nevada, A potential high-level radioactive-waste repository, *USGS Digital Data Series 058*, Chapter M, 19 p.

Bull, W.B. and Pearthree, B.A. (1988). Frequency and size of Quaternary surface ruptures of the Pitaycachi fault, northeastern Sonora, Mexico, *Bull. Seism. Soc. Am.,* Vol. 78, 956-978.

Campbell, K.W. (2003). Prediction of strong ground motion using the hybrid empirical method and its use in the development of ground-motion (attenuation) relations in eastern North America, *Bull. Seism. Soc. Am.,* Vol. 93, 1012–1033.

Campbell, K.W. (2004). Erratum to Prediction of strong ground motion using the hybrid empirical method and its use in the development of ground-motion (attenuation) relations in Eastern North America, *Bull. Seism. Soc. Am.,* Vol. 94(6), 2418.

Campbell, K.W., and Bozorgnia, Y. (2008). NGA Ground Motion Model for the Geometric Mean Horizontal Component of PGA, PGV, PGD and 5% Damped Linear Elastic Response Spectra for Periods Ranging from 0.01 to 10 s, *Earthquake Spectra*, Vol. 24(1), 139-171.

Castro, R.R., Shearer P.M., Astiz L., Suter M., Jacques-Ayala, C. & Vernon F. (2010). The Long-Lasting Aftershock Series of the 3 May 1887 Mw 7.5 Sonora Earthquake in the Mexican Basin and Range Province, *Bull. Seism. Soc. Am.,* Vol. 100 (3), 1153–1164.

Castro, R.R., Acosta, J.G., Wong, V.M. (2011a). Location of Aftershocks of the 4 April 2010 Mw 7.2 El Mayor-Cucapah Earthquake of Baja California, Mexico, *Bull. Seism. Soc. Am.,* Vol. 101, 3072-3080.

Castro, R.R., Valdes-Gonzalez, C., Shearer, P., Wong, V., Astiz, L., Vernon, F., Perez-Vertti, A., and Mendoza, A. (2011b). The 3 August 2009 Mw 6.9 Canal de Ballenas region, Gulf of California, earthquake and its aftershocks, *Bull. Seism. Soc. Am.,* Vol. 101(3), 929-939.

Chandler, A.M., Lam, N.T.K., and Tsang, H.H. (2006). Near-surface attenuation modeling based on rock shear-wave velocity profile, *Soil Dyn. Earthq. Eng.,* Vol. 26, 1004–1014.

Chapman, M. C., and Godbee, R.W. (2012). Modeling Geometrical Spreading and the Relative Amplitudes of Vertical and Horizontal High-Frequency Ground Motions in Eastern North America, *Bull. Seism. Soc. Am.,* Vol. 102, 1957-1975, doi:10.1785/0120110081

Chen, Y-H., and Tsai, C-C.P. (2002). A new method for estimation of the attenuation relationship with variance components, *Bull. Seism. Soc. Am.,* Vol. 92, 1984-1991.

Chiou, B., Darragh, R., Gregor, N., and Silva, W. (2008). NGA project strong-motion database, *Earthquake Spectra*, Vol. 24(1), 23–44

Chiou, B.S-J and Youngs, R.R. (2008a). An NGA Model for the Average Horizontal Component of Peak Ground Motion and Response Spectra, *Earthquake Spectra*, 24(1), 173-215.

Chiou, B.S-J., and R.R. Youngs, (2008b). NGA model for average horizontal component of peak ground motion and response spectra, *PEER Report 2008/09*, Pacific Earthquake Engineering Research Center, University of California, Berkeley, CA.

Chiou, B.S-J., Youngs, R.R., Abrahamson, N.A., and Addo, K. (2010). Ground-motion attenuation model for small-to-moderate shallow crustal earthquakes in California and its implications on regionalization of ground-motion prediction models, *Earthquake Spectra,* Vol. 26(4), 907-926.

Community Fault Model (CFM), 2012, SCEC Community Fault Model version 4.0, accessed and downloaded January 2013, available at [http://structure.harvard.edu/cfm/modelaccess.html].

Community Velocity Model (CVM), 2012, SCEC Community Velocity Model version 4.0, accessed January 2013, available at [http://www.data.scec.org/research-tools/3dvelocity. html].

Community Velocity Model – Harvard (CVM-H), 2012, SCEC Community Velocity Model version 11.9.1, accessed January 2013, available at [http://www.data.scec.org/researchtools/3d-velocity.html].

Conrad, J. (2013). Personal communication to P. Umhoefer.

Conrad, J.E., Ryan, H.F., and Sliter, R.W. (2010). Tracing active faulting in the Inner Continental Borderland, Southern California, using new high-resolution seismic reflection and bathymetric data [abstract]: Seismological Society of America 2010 Annual Meeting, *Seismological Research Letters*, Vol. 81(2), 347.

DeCelles, P. G. (2004). Late Jurassic to Eocene Evolution of the Cordilleran, Thrust Belt and Foreland Basin Systems, Western U.S.A., *American Journal of Science*, Vol. 304, 105-168.

DeMets, C., and Dixon, T. (1999). New kinematic models for Pacific-North America motion from 3 Ma to present, I: Evidence for steady motion and biases in the NUVEL-1A model, *Geophysical Research Letters*, Vol. 26(13), doi: 1029/1999GL900405.

Demsey, K.A., and Pearthree, P.A. (1990). Late Quaternary Surface-Rupture History Of The Sand Tank Fault, And Associated Seismic Hazard For The Proposed Superconducting Super Collider Site, Maricopa County, Arizona, *Arizona Geological Survey, Open-File Report* 90-01, 46 p.

Dixon, T. H., Robaudo, S., Lee, J., and Reheis, M.C. (1995). Constraints on present-day Basin and Range deformation from space geodesy, *Tectonics*, Vol. 14(4), 755–772.

Dor, O., Ben-Zion, Y., Rockwell, T.K., and Brune, J.N. (2006a). Pulverized Rocks in the Mojave section of the San Andreas FZ, *Earth Planet. Sci. Lett*., Vol. 245, 642–654, doi:10.1016/j.epsl.2006.03.034.

Dor, O., Rockwell, T.K., and Ben-Zion, Y. (2006b). Geologic observations of damage asymmetry in the structure of the San Jacinto, San Andreas and Punchbowl faults in southern California: A possible indicator for preferred rupture propagation direction, *Pure Appl. Geophys*., Vol. 163, doi 10.1007/s00024-005-0023-9.

Dor, O., Yildirim, C., Rockwell, T.K., Ben-Zion, Y., Emre, O., Sisk, M., and Duman, T.Y. (2008). Geological and geomorphologic asymmetry across the rupture zones of the 1943 and 1944 earthquakes on the North Anatolian Fault: Possible signals for preferred earthquake propagation direction, *Geophys. J. Int*., Vol. 173, 483–504, doi:10.1111/j.1365-246X.2008.03709.x.

Dor, O., Chester, J.S., Ben-Zion, Y., Brune, J.N., and Rockwell, T.K. (2009). Characterization of damage in sandstones along the Mojave section of the San Andreas Fault: Implications for the shallow extent of damage generation, *Pure Appl. Geophys*., Vol. 166, 1747–1773, doi:10.1007/s00024-009-0516-z.

Dorsey, R. J. and Umhoefer, P. J. (2012). Influence of sediment input and plate motion obliquity on basin development along an active oblique-divergent plate boundary: Gulf of California and Salton Trough. In: Tectonics of Sedimentary Basins: Recent Advances (C. Busby and A. Azor, Editors), Blackwell Publishing, p. 209-225.

Douglas, J., Gehl, P., Bonilla, L.F., and Gelis, C. (2010). A kappa model for mainland France, *Pure Appl. Geophys*., Vol. 167, 1303–1315.

Douglas, J.P., and Boore, D.M. (2011). High-frequency filtering of strong-motion records, *Bulletin of Earthquake Engineering*, Vol. 9, 395-409.

Drouet S., Cotton F., and Gueguen, P. (2010). $v_{S30}$, κ, regional attenuation and Mw from accelerograms: application to magnitude 3–5 French earthquakes, *Geophys. J. Int*., Vol. 182, 880–898.

DuBois, S.M., Smith, AW., Nye, N.K., and Nowak, T.A, Jr. (1982). Arizona earthquakes, 1776-1980, *Arizona Bureau of Geology and Mineral Technology Bulletin* Vol. 193, 456 p., 1 sheet, scale 1:1,000,000.

Edwards, B., Faeh, D., and Giardini, D. (2011). Attenuation of seismic shear wave energy in Switzerland, *Geophys. J. Int*., Vol. 185, 967–984.

Electric Power Research Institute (1993). Guidelines for determining design basis ground motions, Palo Alto, California, Electric Power Research Institute, Vol. 1-5, EPRI TR-102293.

Euge, K.M., Schell, B.A., and Lam, I.P. (1992). Development of seismic acceleration maps for Arizona, *Arizona Department of Transportation Report* AZ92-344, 327 p., 5 sheets, scale1:1,000,000.

Faccioli, E., Bianchini, A., and Villani, M. 2010. New ground motion prediction equations for T > 1 s and their influence on seismic hazard assessment, *Proc. Univ. Tokyo Sym. on Long-Period Ground Motion and Urban Disaster Mitigation*, March 17-18, 2010

Fenton, C.R., Webb, R.H., Pearthree, P.A., Cerling, T.E., and Poreda, R.J. (2001). Displacement rates on the Toroweap and Hurricane faults--Implications for Quaternary downcutting in the Grand Canyon, Arizona, *Geology*, Vol. 29, 1035-1038.

Field, E. H., Jordan, T.H., and Cornell, C. A. (2003). OpenSHA: A developing community-modeling environment for seismic hazard analysis, *Seism. Res. Letters*, Vol. 74(4), 406-419.

Field, E., Dawson, T., Ellsworth, W., Felzer, V., Frankel, A., Gupta, V., Jordan, T., Parsons, T., Petersen, M., Stein, R., Weldon, R., and Wills, C. (2008). The Uniform California Earthquake Rupture Forecast, Version 2 (UCERF 2): U.S. Geological Survey Open-File Report and California Geological Survey Special Report Vol. 203, 97p.

Field, E. H., Dawson, T.E., Felzer, K.R., Frankel, A.D. Gupta, V., Jordan, T.H., Parsons, T., Petersen, M.D., Stein, R.S., Weldon R.J. II, and Wills C.J. (2009). Uniform California earthquake rupture forecast, version 2 (UCERF2.0). *Bull. Seism. Soc. Am*., Vol. 99, 2053-2107.

Fletcher, J.M. and Spelz, R.M. (2009). Patterns of Quaternary deformation and rupture propagation associated with an active low-angle normal fault, Laguna Salada, Mexico: Evidence of a rolling hinge?, *Geosphere*, Vol. 5, 385-407.

Frassetto, A., Gilbert, H., Zandt, G., Beck, S., and Fouch, M. (2006). Support of high elevation in the southern Basin and Range based on the composition and architecture of the crust in the Basin and Range and Colorado Plateau, *Earth and Planetary Science Letters,* Vol. 249(1-2), 62-73.

Fugro Consultants (2010). Initial assessment of precariously balanced rocks in the DCPP area (Ground Motion Task GM-3), draft letter report submitted to N. Abrahamson, PG&E, dated September 11, 2010. [Selected publications provided therein.]

Gastil, R. G. and Krummenacher, D. (1977). Reconnaissance geology of coastal Sonora between Puerto Lobos and Bahía Kino, *Geological Society of America Bulletin*, Vol. 88, 189-198.

GeoPentech, Inc. (2010). San Onofre Nuclear Generating Station Seismic Hazard Assessment Program: 2010 Seismic Hazard Analysis Report, prepared by GeoPentech, Inc. for Southern California Edison Co., 74 pp. plus appendices.

GeoPentech, Inc. (2013). San Onofre Nuclear Generating Station Long Term SONGS Seismic Setting Research Program: Site Characterization Report, prepared by GeoPentech, Inc. for Southern California Edison Co., Draft Report version October 2012, 53 pp. plus appendices.

Gibbard, P. L., Head, M. J., Walker, M. J. C., and the Subcommission on Quaternary Stratigraphy (2010). Formal ratification of the Quaternary System/Period and the Pleistocene Series/Epoch with a base at 2.58 Ma, *Journal of Quaternary Science*, Vol. 25, 96–102.

Gilbert, H., Velasco, A.A., and Zandt, G. (2007). Preservation of Proterozoic Terrane Boundaries Within the Colorado Plateau and Implications for Its Tectonic Evolution, *Earth and Planetary Science Letters*, Vol. 258, 237-248.

Gledhill, K., Ristau, J., Reyners, M., Fry, B, and Holden, C. (2011). The Darfield (Canterbury, New Zealand) Mw 7.1 Earthquake of September 2010: A Preliminary Seismological Report, *Seismological Research Letters*, Vol. 82(3), 378-386

Gonzales-Leon, C.M., Solari, L., Sole, J., Ducea, M.H., Lawton, T.F., Bernal, J.P., Becuar, E.G., Gray, F., Martinez, M.L., and Santacruz, R.L. (2011). Stratigraphy, geochronology, and geochemistry of the Laramide magmatic arc in north-central Sonora, Mexico, *Geosphere*, Vol. 7(6), 1392-1418.

Graizer, V. and Kalkan, E. (2011). Modular Filter-based Approach to Ground Motion Attenuation Modeling, *Seism. Res. Letters*, Vol. 82(1), 21 – 31.

Graizer, V. (2012), "Effects of low-pass filtering and re-sampling on spectral and peak ground acceleration in strong-motion records", *Proc. 15th World Conference of Earthquake Engineering*, Lisbon, Portugal, 24-28 Sep., 10 pp.

Graizer, V. (2012). Update to GMPE model, personal communication

Grant, L. B., and Rockwell, T.K. (2002). A northward-propagating earthquake sequence in coastal southern California, *Seismological Research Letters*, Vol. 73(4), 461–469.

Graves, R. (2012). Broadband Simulation Results for Footwall/Hanging Wall and Rupture Directivity Analysis – Deliverable in Subaward Agreement 000007598, Memorandum dated February 23 2012, submitted to Pacific Earthquake Engineering Research Center (PEER), University of California - Berkeley, CA, USA

Graves, R., Jordan, T.H., Callaghan, S., Deelman, E., Field, E.H., June, G., Kesselman, C., Maechling, P., Mehta, G., Okaya, D. , Small, P., and Vahi K. (2010). CyberShake: A Physics-Based Seismic Hazard Model for Southern California, *Pure Appl. Geophys*., Vol. 168(3-4), 367-381.

Graves, R. W. and Pitarka, A. (2010). Broadband Ground-Motion Simulation Using a Hybrid Approach, *Bull. Seism. Soc. Am*., Vol. 100 (5a), 2095-2123.

Gregor, N., Silva, W.J, and Darragh R. (2002). Development of attenuation relations for peak particle velocity and displacement" A PEARL Report to PG&E/CEC/Caltrans and available online at http://www.pacificengineering.org/rpts_page1.shtml.

Haddad, D.E., Zielke O, Arrowsmith, J.R., Purvance, M.D., Haddad, A.G., and Landgraf, A. (2012). Estimating two-dimensional static stabilities and geomorphic settings of precariously balanced rocks from unconstrained digital photographs, *Geosphere*, Vol. 8(5), 1042–1053; doi:10.1130/GES00788.1

Hall, C.A. Jr., Ernest, W.G., Prior, S.W., and Siese, J.W. (1979). Geologic map of the San Luis Obispo-San Simeon region, *U.S. Geological Survey Miscellaneous Investigation* I-1097.

Hall, C.A., Jr. (1973). Geologic map of the Morro Bay South and Port San Luis Quadrangles, San Luis Obispo County, California, U.S. Geological Survey

Hall, D.B. (1996). Modelling failure of natural rock columns, *Geomorphology*, Vol. 15, 123-134

Hardebeck in 2011 DCPP SSC Workshop 1 presentations [available at http://www.pge.com/mybusiness/edusafety/systemworks/dcpp/SSHAC/workshops/ws1.shtml]

Hardebeck, J.L. (2010). Seismotectonics and fault structure of the California central coast, *Bull. Seism. Soc. Am*., Vol. 100(1), 031-1050, and electronic supplement [available at: http://www.seismosoc.org/publications/BSSA_html/bssa_100-3/2009307-esupp/index.html]

Hardebeck, J. L. (2013). Geometry and Earthquake Potential of the Shoreline Fault, Central California, *Bull. Seism. Soc. Am.*, Vol. 103(1), 447-462, doi: 10.1785/0120120175

Harris, R.A., M. Barall, R. Archuleta, E. Dunham, B. Aagaard, J.P. Ampuero, H. Bhat, V. Cruz-Atienza, L. Dalguer, P. Dawson, S. Day, B. Duan, G. Ely, Y. Kaneko, Y. Kase, N. Lapusta, Y. Liu, S. Ma, D. Oglesby, K. Olsen, A. Pitarka, S. Song, E. Templeton (2009). The SCEC/USGS Dynamic Earthquake Rupture Code Verification Exercise, *Seism. Res. Lett.*, Vol. 80(1), 119-126, doi: 10.1785/gssrl.80.1.119.

Harris, R.A., M. Barall, D.J. Andrews, B. Duan, E.M. Dunham, S. Ma, A.-A. Gabriel, Y. Kaneko, Y. Kase, B. Aagaard, D. Oglesby, J.-P. Ampuero, T.C. Hanks, N. Abrahamson (2011). Verifying a computational method for predicting extreme ground motion, *Seism. Res. Lett*., Vol. 82(5), 638-644, doi: 10.1785/gssrl.82.5.638.

Hauksson, E. (2000). Crustal structure and seismicity distribution adjacent to the Pacific and North America plate boundary in southern California, *Journal of Geophysical Research*, Vol. 105, 13875-13903.

Hauksson, E., Stock, J., Hutton, K., Yang, W., Vidal-Villegas, J.A., and Kanamori, H. (2011).The 2010 Mw7.2 El Mayor-Cucapah earthquake sequence, Baja California, Mexico and southernmost California, USA; active seismotectonics along the Mexican Pacific margin, *Pure and Applied Geophysics*, Vol. 168, 1255–1279.

Hauksson, E., Yang, W., and Shearer, P.M. (2012). Waveform Relocated Earthquake Catalog for Southern California (1981 to June 2011), *Bull. Seism. Soc. Am*., Vol. 102(5), 2239-2244.

Hendricks, J. D., and Plescia, J.B. (1991). A Review of the Regional Geophysics of the Arizona Transition Zone, *Journal of Geophysical Research*, Vol. 96(B7), 12351–12373, DOI: 10.1029/90JB01781

Hirabayashi, C.K., Rockwell, T.K., Wesnowsky, S.G., Stirling, M.W., and Suárez, F. (1996). A neotectonic study of the San Miguel-Vallecitos Fault, Baja California, Mexico, *Bull. Seism. Soc. Am*., Vol. 86(6), 1770-1783.

Hirschberg, D.M., and Pitts, G.S. (2000). Digital geologic map of Arizona: a digital database derived from the 1983 printing of the Wilson, Moore, and Cooper 1:500,000-scale map: *U.S. Geological Survey Open-File Report* 00-409.

Hough, S.E., and Anderson, J.G. (1988). High-frequency spectra observed at Azna, California: Implications for Q structure, *Bull. Seism. Soc. Am*., Vol. 78, 692-707.

Hough, S.E., Anderson, J.G., Brune, J., Vernon, F., Berger, J., Fletcher, J., Haar, L., Hanks, T., and Baker, L. (1988). Attenuation near Anza, California, *Bull. Seism. Soc. Am*., Vol. 78, 672-691.

Idriss, I.M. (2008). An NGA Empirical Model for Estimating the Horizontal Spectral Values Generated By Shallow Crustal Earthquakes, *Earthquake Spectra*, Vol. 24(1), 217-242.

Irikura, K. and H. Miyake (2010). Recipe for Predicting Strong Ground Motion from Crustal Earthquake Scenarios, *Pure and Applied Geophysics*, Vol. 168, 85-104, DOI 10.1007/s00024-010-0150-9.

IRIS, DMC (March, 2013). Incorporated Research Institutions for Seismology Data Management Center. http://www.iris.edu/dms/dmc/.

Irwin, W.P. (1991). Geology and plate-tectonic development, in The San Andreas Fault System, California, Wallace, R.E. (Editor), *U.S. Geological Survey Professional Paper* 1515, 61-80.

Jackson, G.W. (1990). Tectonic geomorphology of the Toroweap fault, western Grand Canyon, Arizona: Implications for transgression of faulting on the Colorado Plateau, *Arizona Geological Survey Open-File Report* 90-4, 1–66.

Jennings, C.W., and Bryant, W.A. (2010), Fault activity map of California, California Geological Survey Geologic Data Map No. 6, map scale 1:750,000.

Kanno, T., Narita, A., Morikawa, N., Fujiwara, H. and Fukushima, Y. (2006) A New Attenuation Relation for Strong Ground Motion in Japan Based on Recorded Data, *Bull. Seism. Soc. Am*., Vol. 96, 879-897.

Kent, G. (2012). Personal communication to S. Duke.

Kilb D., Biasi, G., Anderson, J.G., Brune, J., Peng, Z., and Vernon F.L. (2012). A Comparison of Spectral Parameter Kappa from Small and Moderate Earthquakes Using Southern California ANZA Seismic Network Data, *Bull. Seism. Soc. Am*., Vol. 102, 284-300.

Kottke, A.R., and Rathje, E.M. (2008) Technical Manual for Strata. *PEER Report* 2008/10. University of California, Berkeley, California.

Krantz, R.W. (1989). Orthorhombic fault patterns: the odd axis model and slip vector orientations, *Tectonics*, Vol. 8, 483-495.

Kreemer, C., Blewitt, G., and Bennett, R. A. (2010). Present-day motion and deformation of the Colorado plateau, *Geophysical Research Letters*, Vol. 37(10), DOI: 10.1029/2010GL043374

Ktenidou O.-J., Drouet, S., Theodulidis, N., Chaljub, M., Arnaouti, S., and Cotton, F. (2012). Estimation of kappa (κ) for a sedimentary basin in Greece (EUROSEISTEST) - Correlation to site characterisation parameters, *Proc. 15th World Conference of Earthquake Engineering*, Lisbon, Portugal, 24-28 Sep., 10 pp.

Ktenidou O.-J., Gelis, C., Bonilla, F. (2013). A study on the variability of kappa in a borehole: implications of the computation process, *Bull. Seism. Soc. Am*., Vol. 103 (2A), 1048-1068, DOI: 10.1785/0120120093|hwp:resource-id:ssabull;103/2A/1048

Ktenidou, O.-J., Cotton, F. Abrahamson, N., and Anderson, J.G. (2013). Don't call it kappa: add a subscript!, *Seismological Research Letters* (in press).

Lettis, W. (2012). Diablo Canyon SSC Workshop 2 presentation [available at http:// www.pge.com/mybusiness/edusafety/systemworks/dcpp/SSHAC/workshops/ws2.shtml]

Levander, A., Niu, F., Miller, M.S. (2008). The Moho and the lithosphere-asthenosphere boundary under the western U.S. from USArray PdS receiver functions, Eos Transactions, American Geophysical Union, Vol. 89(53), Fall Meeting Supplemental, Abstract 231D-05, and supplemental information accessed 3/26/2012 at http://terra.rice.edu/department/faculty/levander/downloads.

Lewis, J. L., Day, S.M., Magistrale, H., Castro, R.R., Astiz, L., Rebollar, C., Eakins, J., Vernon, F.L., and Brune, J.N. (2001). Crustal thickness of the Peninsular Ranges and Gulf Extensional Province in the Californias, *Journal of Geophysical Research*, Vol. 106, 13,599–13,611.

Lin, G., Shearer, P.M., Hauksson, E., and Thurber, C.H. (2007). A three-dimensional crustal seismic velocity model for southern California from a composite event method, *J. Geophys. Res*., Vol. 112, B11306, doi:10.1029/2007JB004977

Lin, P-S., Chiou, B., Abrahamson, N., Walling, M., Lee, C-T, and Cheng, C-T (2011). Repeatable source, site, and path effects on the standard deviation for empirical ground-motion prediction models, Bulletin *Bull. Seism. Soc. Am*., Vol. 101(5), 2281-2295.

Liu, P., R. J. Archuleta and S. H. Hartzell (2006). Prediction of broadband ground-motion time histories: Hybrid low/high-frequency method with correlated random source parameters, *Bull. Seism. Soc. Am*., Vol. 96, 2118-2130, doi: 10.1785/0120060036.

Lockridge, J.S. (2011). *Arizona State University, Master's Thesis*, 112 p.

Lockridge, J., Fouch, M., and Arrowsmith, J.R. (2012). Seismicity within Arizona during the deployment of the EarthScope USArray Transportable Array, *Bull. Seism. Soc. Am*., Vol. 12(102), 1850-1863.

Lockridge, J.S., Fouch, M.J., Arrowsmith, J R., and Linkimer L. (2012). Analysis of seismic activity near Theodore Roosevelt Dam, Arizona, during the occupation of the EarthScope / USArray Transportable Array, *Seis. Res. Lett*., Vol. 83(6), 1014-1022, doi: 10.1785/0220120034.

Lund, W.R. (2005). Consensus preferred recurrence interval and vertical slip rate estimates - Review of Utah paleoseismic-trenching data by the Utah Quaternary Fault Parameters Working Group, *Utah Geological Survey Bulletin* Vol. 134.

Ma, S. (2008). A physical model for widespread near-surface and fault zone damage induced by earthquakes, *Geochemistry Geophysics Geosystems*, Vol. 9, 1-9.

Machette, M. N. (1998). Contrasts between short-term and long-term records of seismicity, in The Rıo Grande Rift: Important Implications for Seismic-Hazard Assessments in Areas of Slow Extension, Basin and Range Province Seismic-Hazards Summit, W. R. Lund (Editor), *Utah Geological Survey Misc. Publ*. Vol. 98(2), 84–95.

Magistrale, H., S. M. Day, R. W. Clayton, and R. W. Graves (2000). The SCEC Southern California reference three-dimensional seismic velocity model version 2, *Bull. Seism. Soc. Am*., Vol. 90(6B), S65-S76.

Mai, P., and Beroza, G. (2010). A spatial random field model to characterize complexity in earthquake slip, *J. Geophys. Res.*, Vol. 107(B11), doi:10.1029/2001JB000588.

Mai, P.M., Imperatori, W., Olsen, K.B. (2010), Hybrid Broadband Ground-Motion Simulations: Combining Long-Period Deterministic Synthetics with High-Frequency Multiple S-to-S Backscattering, *Bull. Seism. Soc. Am*., Vol. 100(5A), 2124-2142.

McGuire, R.K., Silva, W.J., and Costantino, C.J. (2001). Technical basis for revision of regulatory guidance on design ground motions: Hazard- and Risk- consistent ground motion spectra guidelines. *NUREG/CR-6728* Prepared for the U.S. NRC, Washington DC.

McVerry, G. H., Zhao, J. X., Abrahamson, N. A., Somerville, P. G. (2006). New Zealand acceleration response spectrum attenuation relations for crustal and subduction zone earthquakes, *Bulletin of the New Zealand Society for Earthquake Engineering*, Vol. 39, 1-58.

McLaren, M. (2011). DCPP SSC Workshop 1 presentation [available at http://www.pge.com/mybusiness/edusafety/systemworks/dcpp/SSHAC/workshops/ws1.shtml]

McLaren, M.K, Hardebeck, J.L, van der Elst, N., Unruh, J.R., Bawden, G.W., Blair, J.L. (2008). Complex Faulting Associated with the 22 December 2003 *M*w 6.5 San Simeon, California, Earthquake, Aftershocks, and Postseismic Surface Deformation, *Bull. Seism. Soc. Am*., Vol. 98(4), 1659-1680, doi: 10.1785/0120070088

McLaren, M.K, and Savage, W.U (2001). Seismicity of South-Central Coastal California: October 1987 through January 1997, *Bull. Seism. Soc. Am*., Vol. 91, 1629-1658, doi:10.1785/0119980192

Mena, B. and Mai, P. M., Olsen, K. B., Purvance, M. D. and Brune, J. N. (2010). Hybrid Broadband Ground-Motion Simulation Using Scattering Green's Functions: Application to Large-Magnitude Events, *Bull. Seism. Soc. Am*., Vol. 100, 2143-2162.

Menges, C.M., and Pearthree, P.A. (1989). Late Cenozoic tectonism in Arizona and its impact on regional landscape evolution. In Geologic Evolution of Arizona, edited by J.P. Jenney and S.J. Reynolds, pp. 649–680. Digest No. 17. Tucson, Arizona: Arizona Geological Society.

Miscellaneous Field Studies Map MF -511, scale 1:24,000.

Mooney, W. (2011). DCPP SSC Workshop 1 presentation [available at http://www.pge.com/mybusiness/edusafety/systemworks/dcpp/SSHAC/workshops/ws1.shtml]

Morikawa, N., Kanno, T., Narita, A., Fujiwara, H., Okumura, T., Fukushima, Y., and Guerpinar, A. (2008). Strong motion uncertainty determined from observed records by dense network in Japan, *J. Seism.,* Vol. 12(4), 529-546.

Motazedian, D., and G. M. Atkinson (2005). Stochastic finite-fault modeling based on a dynamic corner frequency, *Bull. Seism. Soc. Am*., Vol. 95, 995-1010.

Mueller, K.J. and Rockwell, T.K. (1991). Late Quaternary structural evolution of the western margin of the Sierra Cucapa, Baja California Norte, in The Gulf and Peninsular province of the Californias, Dauphin, J.P. and Simoneit, B.T. (Editors), *American Association of Petroleum Geologists, Memoir* 47, 249-260.

Mueller, K.J. and Rockwell, T.K. (1995). Late Quaternary activity of the Laguna Salada fault in northern Baja California, Mexico, *Geological Society of America Bulletin*, Vol. 107(1), 8-18.

Nagy, E.A., and Stock, J.M. (2000). Structural controls on the continent-ocean transition in the northern Gulf of California, *Journal of Geophysical Research*, Vol. 105(B7), 16251-16269.

Nazareth, J.J., and Hauksson, E. (2004). The seismogenic thickness of the southern California crust, *Bull. Seism. Soc. Am*., Vol. 94(3), 940-960.

Ness, G.E. and Lyle, M.W. (1991). A Seismo-Tectonic map of the Gulf and Peninsular Province of the Californias, Chapter 5: Part II Geological and Geophysical Maps, in *AAPG Special Volume* Book M47, pub ID A114

Oth, A., Bindi, D., Parolai, S., and Di Giacomo, D. (2011). Spectral Analysis of K-NET and KiK-net Data in Japan, Part II: On Attenuation Characteristics, Source Spectra, and Site Response of Borehole and Surface Stations, *Bull. Seism. Soc. Am*., Vol. 101, 667-687.

Pacheco, M., Martín-Barajas, A., Eldres, W., Espinosa-Cardeña, J.M., Belenes, J., and Segura, A. (2006). Stratigraphy and structure of the Altar basin of NW Sonora: implications for the history of the Colorado River delta and the Salton Trough, *Revista Mexicana de Ciencias Geológicas*, Vol. 23(1), 1–22.

Pacific Gas and Electric Company (2011). Shoreline Fault Report.

Pancha, A., Anderson, J.G., and Kreemer, C. (2006). Comparison of seismic and geodetic scalar moment rates across the Basin and Range Province, *Bull. Seism. Soc. Am*., Vol. 96, 11-32.

Pankow, K.L., and Pechmann, C. (2004). The SEA99 ground-motion predictive relations for extensional tectonic regimes: Revisions and a new peak ground velocity relation, *Bull. Seism. Soc. Am*., Vol. 94(1), 341-348.

Pearthree, P.A., compiler, (1998). Quaternary fault data and map for Arizona, *Arizona Geological Survey Open-File Report* 98-24, scale 1:750,000, 122 p.

Pearthree, P.A., Menges, C.M., and Mayer, L. (1983). Distribution, recurrence, and possible tectonic implications of late Quaternary faulting in Arizona, *Arizona Geological Survey Open-File Report* 83-20, 53 p.

Pearthree, P.A., Vincent, K.R., Brazier, R., and Hendricks, D.M. (1996). Pilo-Quaternary Faulting and Seismic Hazard in the Flagstaff Area, Northern Arizona, *Arizona Geological Survey, Bulletin* 200, 31p.

Pearthree, P. A., and Bausch, D. B. (1999). Earthquake hazards in Arizona. *Arizona Geological Survey*, Map 34, scale 1:1,000,000.

Pearthree, P.A., Amoroso, L., Fenton, C.R., and Stenner, H.D. (2002). Paleoseismology of the Hurricane fault zone in northwestern Arizona, *Geological Society of America Abstracts with Program*, Vol. 34(4), 4.

PEER GM Database (2011). Accessed and downloaded January 2013, available at [http://peer.berkeley.edu/peer_ground_motion_database/site].

PEER GM Processing. Resources available at [http://peer.berkeley.edu/smcat/process.html] and [http://www.cosmoseq.org/EVENTS/wkshop_records_processing/papers/Darragh_Silva_Gregor_Paper.pdf]

Persaud, P., Stock, J.M., Steckler, M.S., Martín-Barajas, A., Diebold, J.B., González-Fernández, A., and Mountain, G.S. (2003). Active deformation and shallow structure of the Wagner, Consag, and Delfín Basins, northern Gulf of California, Mexico, *Journal of Geophysical Research*, Vol. 108(B7), 2355.

Persaud, P., Perez-Campos, X., and Clayton, R. (2007). Crustal thickness variations in the margins of the Gulf of California from receiver functions, *Geophysical Journal International*, Vol. 170(2), 687-699.

Petersen, M.D., Frankel, A.D., Harmsen, S.C., Mueller, C.S., Haller, K.M., Wheeler, R.L., Wesson, R.L., Zeng, Y., Boyd, O.S., Perkins, D.M., Luco, N., Field, E.H., Wills, C.J., and Rukstales, K.S. (2008). Documentation for the 2008 Update of the United States National Seismic Hazard Maps, *U.S. Geological Survey Open-File Report* 2008–1128, 61 p.

Petersen, M.D., Dawson, T.E., Chen, R., Cao, T, Wills, C.J., Schwartz, D.P., Frankel, A.D (2011). Fault Displacement Hazard for Strike-Slip Faults, *Bull. Seism. Soc. Am*., Vol. 101(2), 805-825

Phillips, W.S., Mayeda, K M., and Malagnini, L. (2013). How to Invert a Multi-Band, Regional Phase Amplitudes for 2-D Attenuation and Source Parameters: Tests Using the USArray, Accepted *to PAGEOPH*

Plesch, A., Shaw J.H., Benson, C., Bryant, W.A., Carena, S., Cooke, M., Dolan, J., Fuis, G., Gath, E., Grant, L., Hauksson, E., Jordan, T., Kamerling, M., Legg, M., Lindvall, S., Magistrale, H., Nicholson, C., Niemi, N., Oskin, M., Perry, S., Planansky, G., Rockwell, T., Shearer, P., Sorlien, C., Süss, M.P., Suppe, J., Treiman, J., and Yeats, R. (2007). Community Fault Model (CFM) for Southern California, *Bull. Seism. Soc. Am*., Vol. 97, 1793-1820.

Purvance, M.D., and Anderson, J.G. (2003). A comprehensive study of the observed spectral decay in strong-motion accelerations recorded in Guerrero, Mexico, *Bull. Seism. Soc. Am*., Vol. 93, 600–611.

Replogle, C. T. (2011). Corestone and saprock development in a zone of precariously balanced rocks, Peninsular Ranges, southern California: Speculations on the effects of ground shaking during earthquakes, *M.S. thesis*, 67 pp., San Diego State Univ., San Diego, Calif.

Richard, S.M., Shipman, T.C., Greene, L.C., Harris, R.C. (2007). Estimated Depth to Bedrock in Arizona, *Digital Geologic Map Series* DGM-52, Version 1.0, prepared by Arizona Geological Survey

Rockwell, T.K., Schug, D.L., and Hatch, M.E. (1993). Late Quaternary slip rates along the Agua Blanca fault, Baja California, Mexico: in (P.L. Abbott, ed.) Geological Investigations of Baja California: South Coast Geological Society, Annual Field Trip Guidebook, 21, 53-92.

Rockwell, T., Sisk, M., Girty, G., Dor, O., Wechsler, N., and Ben-Zion, Y. (2009). Chemical and physical characteristics of pulverized Tejon Lookout Granite adjacent to the San Andreas and Garlock Faults: Implications for earthquake physics, *Pure Appl. Geophys*., Vol. 166, 1725–1746, doi: 10.1007/s00024-009-0514-1.

Rodriguez-Marek, A., and Cotton, F. (2011). Draft final report: single station sigma project, *Pegasos Refinement Project, report* EXT-TB-1058.

Rodriguez-Marek. A., Montalva, G.A., Cotton, F. and Bonilla, F. (2011). Analysis of Single-Station Standard Deviation Using the KiK-net Data, *Bull. Seism. Soc. Am*., Vol. 101 1242–1258.

Rodriguez-Marek, A., Cotton, F., Abrahamson, N., Akkar, S., Al Atik, L., Edwards, B., Montalva, G.A., and Dawood, H.M. (2013). A model for single-station standard deviation using data from various tectonic regions. Submitted to *Bull. Seism. Soc. Am*., February 2013.

Roy, M., Jordan, T.H., and Pederson, J. (2009). Colorado Plateau magmatism and uplift by warming of heterogeneous lithosphere, *Nature*, Vol. 459, 978-982.

Rymer, M.J., Treiman, J.A., Kendrick, K.J., Lienkaemper, J.J., Weldon, R.J., Bilham, R., Wei, M., Fielding, E.J., Hernandez, J.L., Olson, B.P.E., Irvine, P.J., Knepprath, N., Sickler, R.R., Tong, .X., and Siem, M.E. (2011). Triggered surface slips in southern California associated with the 2010 El Mayor-Cucapah, Baja California, Mexico, earthquake, *U.S. Geological Survey Open-File Report* 2010–1333 and California Geological Survey Special Report 221, 62 p.

Sandıkkaya, M. A., Yılmaz, M.T., Bakır, B.B., and Yılmaz, Ö. (2010). Site classification of Turkish national strong-motion stations, *Journal of Seismology*, Vol. 14, 543–563.

Scarborough, R.B., Menges, C.M., and Pearthree, P.A. (1986), Late Pliocene-Quaternary (post 4 m.y.) faults, folds, and volcanic rocks in Arizona, *Arizona Geological Survey*, Map 22, scale 1:1,000,000.

SCE (2001). San Onofre Nuclear Generating Station Units 2 and 3 Seismic Hazard Study of Postulated Blind Thrust Faults, prepared by Geomatrix Consultants, GeoPentech, and Southern California Edison for the Nuclear Regulatory Commission, 26 December 2001, 165 pp.

SCE (1995). Seismic Hazard at San Onofre Nuclear Generating Station, prepared by Risk Engineering, Inc. for Southern California Edison Co., 2244 Walnut Grove Avenue, Rosemead, California 91770, 25 August 1995, 340 pp.

SCEC Seismogram Transfer Program - STP (2007) accessed and downloaded January 2013, available at [http://www.data.scec.org/research-tools/stp-index.html].

SCEC (Southern California Earthquake Center), information accessed 4/13/2012 at http://www.data.scec.org/significant/cerroprieto.html.

SCEC wiki: http://scec.usc.edu/scecpedia/CyberShake, last accessed on March 17th, 2013.

Schellart, W.P., Stegman, D.R., Farrington, R.J., Freeman, J., and Moresi, L. (2010). Cenozoic tectonics of western North America controlled by evolving width of Farallon slab, *Science*, Vol. 329 (5989), 316-319.

Scherbaum F., Cotton, F., and Staedtke, H. (2006). The estimation of minimum-misfit stochastic models from empirical ground-motion prediction equations, *Bull. Seism. Soc. Am*., Vol. 96, 427–445.

Scherbaum F. (2010). Determination of Vs-k correction factors, *Report for PEGASUS Refinement Project (PRP*), TP2-TB-1036.

Schmedes J., Archuleta R.J. (2008). Near-source ground motion along strike-slip faults: insights into magnitude saturation of PGV and PGA, *Bull. Seism. Soc. Am*., Vol. 98, 2278-2290.

Schmedes, J., Archuleta, R.J., and Lavallée, D. (2010). Correlation of earthquake source parameters inferred from dynamic rupture simulations, *J. Geophys. Res*., Vol. 115, B03304, doi:10.1029/2009JB006689.

Schmedes, J., Archuleta, R.J., and Lavallée, D. (2010). Dependency of supershear transition and ground motion on the autocorrelation of initial stress, *Tectonophysics*, Vol. 493, 222-235, doi: 10.1016/j.tecto.2010.05.013

Schmedes, J., Archuleta, R.J., and Lavallée, D. (2013). A kinematic rupture model generator incorporating spatial interdependency of earthquake source parameters, *Geophys. J. Int*., Vol. 192(3), 1116-1131., doi: 10.1093/gji/ggs021

Seiler, C. (2009). Structural and thermal evolution of the Gulf Extensional Province in Baja California, Mexico: implications for Neogene rifting and opening of the Gulf of California, *PhD thesis*, Faculty of Science, Earth Sciences, The University of Melbourne.

Senior Seismic Hazard Analysis Committee (SSHAC) (1997). Recommendations for Probabilistic Seismic Hazard Analysis — Guidance on Uncertainty and Use of Experts, Prepared by SSHAC, NUREG/CR-6372.

Shaw, J.H., Plesch, A., Tape, C., Suess, M.P., Jordan, T., Hauksson, E., Tromp, J., Tanimoto, T., Maechling, P., Ely, G., Graves, R., Rivero, C., Lovely, P., Brankman, C., Munster, J. (2013). Unified Structural Representation of the southern California crust and upper mantle, EPSL (in prep).

Silva, W.J. and Darragh, R. (1995). Engineering characterization of earthquake strong ground motion recorded at rock sites, Palo Alto, Electric Power Research Institute, TR-102261.

Silva, W., Darragh, R.B., Gregor, N., Martin, G., Abrahamson, N., and Kircher, C. (1998). Reassessment of site coefficients and near-fault factors for building code provisions, Technical Report Program Element II: 98-HQ-GR-1010, Pacific Engineering and Analysis, El Cerrito, USA.

Silva, W. J. (2008). Site Response Simulations for the NGA project, Report prepared for the Pacific Earthquake Engineering Research Center, University of California, Berkeley, CA

Sleep, N. H. (2011). Seismically damaged regolith as self-organized fragile geological feature, *Geochem. Geophys. Geosyst*., Vol. 12, Q12013, doi:10.1029/2011GC003837.

Smith, R. B., and Sbar, M.L. (1974). Contemporary tectonics and seismicity of the western United States with emphasis on the intermountain seismic belt, *Geologic Society of American Bulletin*, Vol. 85, 1205-1218.

Somerville, P.G., Smith, N.F., Graves, R.W., and Abrahamson, N.A. (1997). Modification of empirical strong ground motion attenuation relations to include the amplitude and duration effects of rupture directivity, *Seismol. Res. Let.*, Vol. 68(1), 199-222.

Somerville, P. G., Callaghan, S., Maechling, P., Graves, R. W., Collins, N., Olsen, K. B., Imperatori, W., Jones, M., Archuleta, R., Schmedes, J., And Jordan, T.H. (2011). The SCEC Broadband Ground Motion Simulation Platform, *Seismol. Res. Let.*, Vol. 82(2), p. 275, 10.1785/gssrl.82.2.273.

Sonder, L.J., and Jones, C.H. (1999). Western United States extension: How the West was widened, *Annual Review of Earth and Planetary Sciences*, Vol. 27, 417-466.

Sorlien, C.C., Campbell, B.A., and Seeber, L., (2009b). Geometry, kinematics, and activity of a young mainland-dipping fold and thrust belt: Newport Beach to San Clemente, California, USDI/USGS Award No. 08HQGR0103 Final Technical Report, 25 pp.

Southwestern U.S. Ground Motion Characterization Project Plan, November 16, 2012 [available at www.swus-gmc.com/docs/SWUS_GMC_SSHAC_Plan.pdf]

Spelz, R.M., Fletcher, J.M., Owen, L.A., and Caffee, M.W. (2008). Quanternary alluvial-fan development, climate and morphologic dating of fault scarps in Laguna Salada, Baja California, Mexico, *Geomorphology*, Vol. 102, 578-594.

Spencer, J. E., and Reynolds, S. J. (1989). Middle Tertiary Tectonics of Arizona and Adjacent Areas, in Geologic Evolution of Arizona, edited by J. P. Jenney and S. J. Reynolds, *Arizona Geological Society Digest*, 17, 539-574.

Springer, A. (2010). Constraining basin geometry and fault kinematics on the Santo Tomás segment of the Agua Blanca Fault through a combined geophysical and structural study, *Theses and Dissertations*, Paper 1779.

Spudich, P., Joyner, W.B., Lindh, A.G., Boore, D.M., Margaris, B.M., and Fletcer, J.B. (1999). SEA99: A revised ground motion prediction relation for use in extensional tectonic regimes, *Bull. Seism. Soc. Am*., Vol. 89(5), 1156-1170.

Spudich, P., Watson-Lamprey, J., Somerville, P., Shahi, S., Rowshandel, B., Chiou, B.S.J., Bayless, J., Baker, J.W. (2013). Final Report of the NGA-West 2 Directivity Working Group, Draft *PEER Report*.

Stenner, H.D., Lund, W.R., Pearthree, P.A., and Everitt, B.L. (1999). Paleoseismic investigation of the Hurricane fault in northwestern Arizona and southwestern Utah, *Arizona Geological Survey, Open-File Report* 99-8, 137 p.

Stirling, M., Rhoades, D., and Berryman, K. (2002). Comparison of earthquake scaling relations derived from data of the instrumental and preinstrumental era, *Bull. Seism. Soc. Am*., Vol. 92(2), 812-830.

Stock, J. M. and Hodges, K. V. (1989). Pre-Pliocene extension around the Gulf of California and the transfer of Baja California to the Pacific Plate, *Tectonics*, Vol. 8, 99-115.

Stover, C.W., and Coffman, J.L. (1993). Seismicity of the United States, 1568-1989 (Revised), *U.S. Geological Survey Professional Paper* 1527, 418p.

Strasser, F.O., Abrahamson, N.A., and Bommer, J.J. (2009). Sigma: Issues, insights and challenges, *Seism. Res. Let*., Vol. 80(1), 40-54

Suarez, G., and Hough, S.E. (2008). Reevaluation of the macroseismic effects of the 1887 Sonora, Mexico earthquake and its magnitude estimation, accessed 9/14/2012 at http://usuarios.geofisica.unam.mx/cruz/Sismociones_Libres/Biblio_Sismocion/Sonora_v5.p df.

Suess, M.P., and Shaw, J.H. (2003). P-wave seismic velocity structure derived from sonic logs and industry reflection data in the Los Angeles basin, California, *J. Geoph. Res*., Vol. 108(B3), 2170, doi 10.1029/2001JB001628

Suter, M., and Contreras J. (2002). Active tectonics of northeastern Sonora, Mexico (Southern Basin and Range Province) and the 3 May 1887 Mw 7.4 Earthquake, *Bull. Seism. Soc. Am*., Vol. 92 (2), 581–589.

Suter, M. (2008a). Structural configuration of the Otates fault (southern Basin and Range Province) and its rupture in the 3 May 1887 Mw 7.5 Sonora, Mexico, earthquake, *Bull. Seism. Soc. Am*., Vol. 98, 2879–2893.

Suter, M. (2008b). Structural configuration of the Teras fault (southern Basin and Range Province) and its rupture in the 3 May 1887 Mw 7.5 Sonora, Mexico earthquake, *Revista Mexicana de Ciencias Geológicas*, Vol. 25, 179–195.

Sweeney, R.E., and Hill, P.L. (2001). Arizona aeromagnetic and gravity maps and data: A web site for distribution of data, *U.S. Geological Survey Open-File Report* 01-0081.

Thompson, G. A., and Zoback, M. L. (1979). Regional geophysics of the Colorado Plateau, *Tectonophysics*, Vol. 61, 149–181.

Thompson, S. (2012). DCPP SSC Workshop 2 presentation [available at http://www.pge.com/mybusiness/edusafety/systemworks/dcpp/SSHAC/workshops/ws2.shtml]

Till, C.B., Gans, P.B., Spera, F.J., MacMillan, I., and Blair, K.D. (2009). Perils of petrotectonic modeling: A view from southern Sonora, Mexico, *Journal of Volcanology and Geothermal Research*, Vol. 186, 160-168.

Topography from PG&E (1986 and later revisions). Plot plan drawing 471124

Toro, G.R. (2002). Modification of the Toro et al. (1997) attenuation equations for large magnitudes and short distances, *Technical Report*, Risk Engineering.

Toro, G.R. (2012). Characterization of Ground Motion Propagation for Palo Verde SSHAC Level 2 Probabilistic Seismic Hazard Assessment Report, Lettis Consultants International, Inc.

USGS (2009). Quaternary fault and fold database for the United States, accessed 25 October 2010, from USGS website, [http//earthquakes.usgs.gov/regional/qfaults/].

USGS (2008). Documentation for the 2008 update of the United States National Seismic Hazard Maps, prepared by Petersen, M. D., et al., *U.S. Geological Survey Open File Report* 2008-1128.

U.S.NRC (2012a). Near-Term Task Force, "Request For Information Pursuant To Title 10 Of The Code Of Federal Regulations 50.54(F) Regarding Recommendations 2.1,2.3, and 9.3, Of The Near-Term Task Force Review Of Insights From The Fukushima Dai-Ichi Accident."

U.S.NRC (2012b). Practical Implementation Guidelines for SSHAC Level 3 and 4 Hazard Studies, U.S.NRC NUREG-2117.

U.S.NRC (1997). Recommendations for probabilistic seismic hazard analysis: Guidance on uncertainty and use of experts, prepared by Senior Seismic Hazard Analysis Committee, Lawrence Livermore National Laboratory, Volume 1, Main Report, NUREG/CR-6372, UCRL-ID-122160, 280 pp.

Van Houtte, C., Drouet, S., and Cotton, F. (2011). Analysis of the origins of κ (kappa) to compute hard rock to rock adjustment factors for GMPEs, *Bull. Seism. Soc. Am*., Vol. 101, 2926-2941.

Vucetic, M., and Dobry, R. (1991). Effects of Soil Plasticity on Cyclic Response, *Journal of Geotechnical Engineering*, ASCE, Vol. 117(1), 89-107.

Wald, D.J., and Allen, T.I. (2007). Topographic slope as a proxy for seismic site conditions and amplification, *Bull. Seism. Soc. Am*., Vol. 97(5), 1379-1395.

Walker, J.D., and Geissman, J.W., compilers (2009). Geologic Time Scale, *Geological Society of America*, doi: 10.1130/2009.CTS004R2C.

Walling, M.A. (2009). Non-Ergodic Probabilistic Seismic Hazard Analysis and Simulation Spatial of Variation in Ground Motion, *PhD. Thesis*, University of California, Berkeley, Department of Civil and Environment Engineering.

Walling, M.A. (2012). PV profile, personal communication

Wdowinski, S. (2006). Current crustal movements across the southern San Andreas Fault and the southern Dead Sea Fault systems: A comparative study, MARGINS-RCL Workshop on "Lithospheric rupture in the Gulf of California – Salton Trough region", Ensenada, Mexico, Abstracts.

Wechsler, N., Rockwell, T.K., and Ben-Zion, Y. (2009). Application of high resolution DEM data to detect rock damage from geomorphic signals along the central San Jacinto Fault, *Geomorphology*, Vol. 113, 82–96, doi:10.1016/j.geomorph.2009.06.007.

Wei, M., Sandwell, D.T., Fialko, Y., and Bilham, R. (2011). Slip on faults in the Imperial Valley triggered by the 4 April 2010 Mw 7.2 El Mayor-Cucapah earthquake revealed by InSAR, *Geophysical Research Letters*, Vol. 38, L01308.

Wells, D. L. and Coppersmith, K.J. (1994). Analysis of Empirical Relationships among Magnitude, Rupture Length, Rupture Area, and Surface Displacement, *Bull. Seism. Soc. Am*., Vol. 84, 974-1002.

Wesnousky, S.G. (2005). The San Andreas and Walker Lane Fault systems, western North America: transpression, transtension, cumulative slip and the structural evolution of a major transform plate boundary, *Journal of Structural Geology*, Vol. 27, 1505-1512.

Wills, C.J., Weldon, R.J., II, and Bryant, W.A. (2008). California fault parameters for the National Seismic Hazard Maps and Working Group on California Earthquake Probabilities, Appendix A in The Uniform California Earthquake Rupture Forecast, version 2 (UCERF 2), *U.S. Geological Survey Open-File Report* 2007-1437A, and *California Geological Survey Special Report* 203A, 48 p.

Working Group on California Earthquake Probabilities - WGCEP (1995). Seismic hazards in southern California: probable earthquakes, 1994–2024, *Bull. Seism. Soc. Am*., Vol. 85, 379–439.

Working Group on California Earthquake Probabilities - WGCEP (2008). The Uniform California Earthquake Rupture Forecast, Version 2 (UCERF2), prepared by 2007 Working Group on California Earthquake Probabilities, *U.S. Geological Survey Open File Report* 2007-1437 and *California Geological Survey Special Report* 203.

Working Group on California Earthquake Probabilities - WGCEP (2012, in review). The Uniform California Earthquake Rupture Forecast, Version 3.1 (UCERF3.1), prepared by Working Group on California Earthquake Probabilities, accessed 5 February 2013 at [http://wgcep.org/UCERF3pt1].

Yan, Z., and R. W. Clayton (2007). Regional mapping of the crustal structure in southern California from receiver functions, *J. Geophys. Res*., Vol. 112, B05311, doi:10.1029/2006JB004622

Yang, W., Hauksson, E., and Shearer, P.M. (2012). Computing a Large Refined Catalog of Focal Mechanisms for Southern California (1981- 2010): Temporal Stability of the Style of Faulting, *Bull. Seism. Soc. Am*., Vol. 102(3), 1179-1194.

Youngs R.R. (2009). Epistemic uncertainty in the NGA models, Appendix D in Ground Motion Models for the Pacific Northwest, Report to B.C. Hydro, December 2010.

Youngs, R.R. (2011). Near Source Data from NGA (2008) and NGAW2 Datasets - Data Quantity and Implication for Uncertainty in GMPEs, DCPP Seismic Hazard Update, Workshop #1 (Nov. 29, 2011)

Youngs, R. R., and Coppersmith, K.J. (1985). Implications of fault slip rates and earthquake recurrence models to probabilistic seismic hazard estimates, *Bull. Seism. Soc. Am*., Vol. 58, 939–964.

Zeng, Y., J. G. Anderson and G. Yu (1994). A composite source model for computing realistic synthetic strong ground motions, *Geophysical Research Letters*, Vol. 21, 725-728.

Zhang, X., Paulssen, H., Lebedev, S., and Meier, T. (2007). Surface wave tomography of the Gulf of California, *Geophysical Research Letters*, Vol. 34(15), doi:10.1029/2007GL030631.

Zhao, J.X., Zhang, J., Asano, A., Ohno, Y., Oouchi, T., Takahashi, T., Ogawa, H., Irikura, K., Thio, H.K., Somerville, P.G., Fukushima, Y., and Fukushima, Y. (2006). Attenuation Relations of Strong Ground Motion in Japan Using Site Classification Based on Predominate Period, *Bull. Seism. Soc. Am*., Vol. 96, 898-913.

Zhao, J.X., Irikura, K., Zhang, J., Fukushima, Y., Somerville, P.G., Asano, A., Ohno, Y., Oouchi, T., Takahashi, T., and Ogawa, H. (2006). An empirical site-classification method for strong-motion stations in Japan using H/V response spectral ratio, *Bull. Seism. Soc. Am*., Vol. 96(3), 914-925.

Zhu, L. & Rivera, L. A. (2002) A note on the dynamic and static displacements from a point source in multilayered media, *Geophysical Journal International*, Vol. 148(3), 619-627.

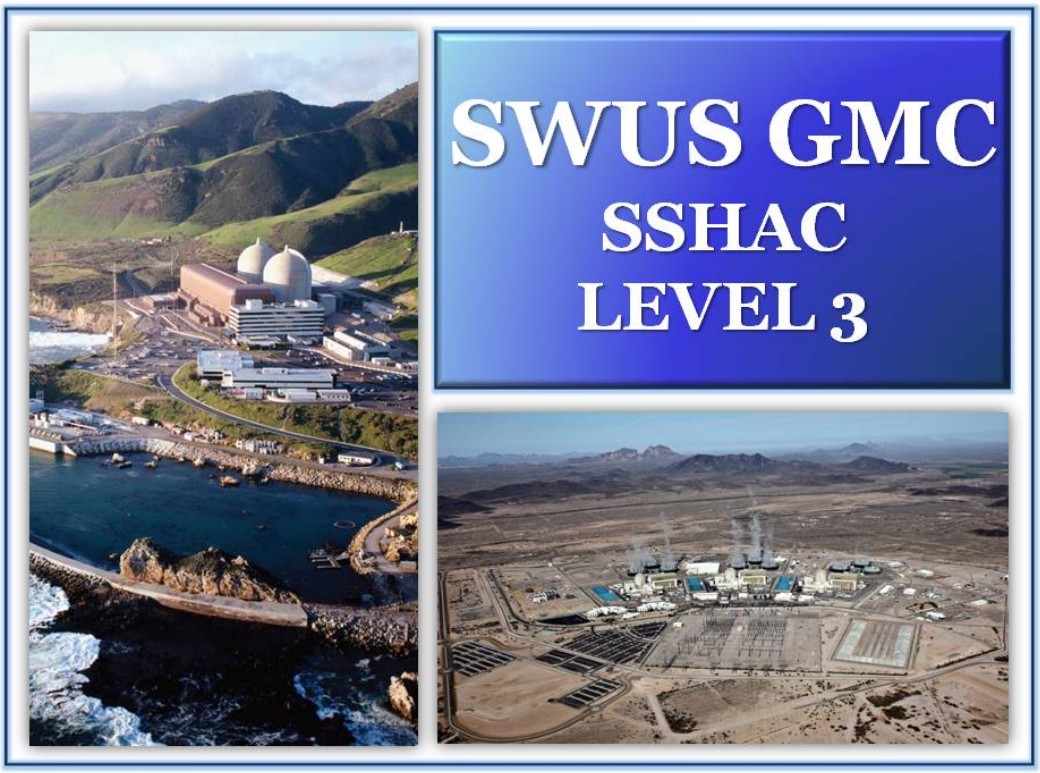
# *APPENDIX F*

## WORKSHOP #2 SUMMARY

# SOUTHWESTERN UNITED STATES GROUND MOTION CHARACTERIZATION SSHAC LEVEL 3

## Workshop #2 Proceedings

Version 1.3




aps PG&E

GeoPentech
Geotechnical & Geoscience Consultants

# WORKSHOP #2 PROCEEDINGS:

# Proponent Models and

# Alternative Interpretations

## October 22-24, 2013

### Hotel Shattuck Plaza, Berkeley, California

**Prepared for:**

**Arizona Public Service Company**
Palo Verde Nuclear Generating Station
*Wandell, Christopher J.*
Senior Consulting "Chief" Civil Engineer
Phone: (623) 393-6741; E-mail: christopher.wandell@aps.com

**Pacific Gas and Electric Company**
Diablo Canyon Power Plant
*Klimczak, Richard*
Director Geosciences
Phone: (415) 973-2791; E-mail: RLK1@pge.com

Version: 1.3
Date: August 7, 2014

## LIST OF ABBREVIATIONS and COMMON ACRONYMS

| | |
|---|---|
| ACR | Active Crustal Region |
| AFE | Annual Frequency of Exceedance |
| APS | Arizona Public Services |
| AZGS | Arizona Geological Survey |
| BBP | Broad Band Platform |
| CBR | Center, Body, and Range |
| CEA | California Earthquake Authority |
| CEC | California Energy Commission |
| CEUS | Central and Eastern United States |
| CFM | Community Fault Models |
| CFR | Code of Federal Regulations |
| CGS | California Geological Survey |
| CI | Closeness Index |
| CPUC | California Public Utilities Commission |
| DCPP | Diablo Canyon Power Plant |
| EE | Evaluator Expert |
| FFS | Finite Fault Simulations |
| FGF | Fragile Geological Feature |
| FW | Foot Wall |
| GIS | Geographic Information System |
| GM | Ground Motion |
| GMC | Ground Motion Characterization |
| GMPE | Ground Motion Prediction Equation |
| GMRS | Ground Motion Response Spectrum |
| GPS | Global Positioning System |
| HID | Hazard Input Document |
| HC | Hazard Calculation |
| HW | Hanging Wall |
| Hz | Hertz |
| IPRG | Independent Peer Review Group |
| ITC | Informed Technical Community |

| | |
|---|---|
| LiDAR | Light Detection and Ranging |
| MASW | Multi-channel Analysis of Surface Waves |
| NGA | Next Generation Attenuation |
| NGA-West2 | Project name for the update of the 2008 NGA models |
| NML | Normal (referred to normal faults) |
| NPP | Nuclear Power Plant |
| NSHM | National Seismic Hazard Mapping |
| PE | Proponent Expert |
| PEER | Pacific Earthquake Engineering Research Center |
| PGA | Peak Ground Acceleration |
| PG&E | Pacific Gas & Electric |
| PM | Project Manager |
| PPRP | Participatory Peer Review Panel |
| PSHA | Probabilistic Seismic Hazard Analysis |
| PTI | Project Technical Integrator |
| PV | Palos Verdes |
| PVNGS | Palo Verde Nuclear Generating Station |
| QA | Quality Assurance |
| RE | Resource Expert |
| RG | Regulatory Guide |
| $R_{JB}$ | Joyner and Boore Distance |
| $R_{RUP}$ | Rupture Distance |
| RV | Reverse (referred to reverse fault) |
| SASW | Spectral Analysis of Surface Waves |
| SCE | Southern California Edison |
| SCEC | Southern California Earthquake Center |
| SCFM | Statewide Community Fault Model |
| SCSN | Southern California Seismic Network |
| SONGS | San Onofre Nuclear General Station |
| SS | Strike Slip (referred to strike slip faults) |
| SSC | Seismic Source Characterization |
| SSHAC | Senior Seismic Hazard Analysis Committee |

| | |
|---|---|
| SSS | Single Station Sigma |
| SWUS | Southwest United States |
| TA | Transportable Array |
| TDI | Technically Defensible Interpretation |
| TI | Technical Integrator |
| UCERF2 | Uniform California Earthquake Rupture Forecast, Version 2 |
| UCERF3 | Uniform California Earthquake Rupture Forecast, Version 3 |
| USGS | United States Geological Society |
| U.S.NRC | U.S. Nuclear Regulatory Commission |
| USR | Unified Structural Representation |
| $V_{S,30}$ | Shear Wave Velocity in the upper 30m |
| WGCEP | Working Group on California Earthquake Probabilities |
| WUS | Western United States |

# TABLE OF CONTENTS

Page

LIST OF ABBREVIATIONS and COMMON ACRONYMS ..... 2
TABLE OF CONTENTS ..... 5
WORKSHOP #2 INTRODUCTION ..... 1
Purpose: ..... 1
Approach: ..... 1
Workshop #2 Agenda ..... 3
Workshop #2 participants ..... 7
WORKSHOP #2 SUMMARY ..... 10
Project background ..... 10
General workshop summary ..... 10
Topic 1: Introduction to GMC and Sensitivity Analyses ..... 10
Topic 2: Candidate Finite Fault Simulations (FFS) Methods: Results of SCEC BBP Validation Exercise ..... 11
Topic 3: Candidate Finite Fault Simulations (FFS) Methods: Initial Forward Simulations Results ..... 12
Topic 4: Epistemic Uncertainty - Introduction ..... 12
Topic 5: GMPEs Comparison and Identification of Issues ..... 12
Topic 6: Path Effects ..... 15
Topic 7: Candidate Models for Sigma ..... 16
Topic 8: Candidate Models of Adjustments to GMPEs: Changing Rake, Dip along Strike ..... 17
Topic 9: Kappa ..... 18
Topic 10: Candidate Models of Adjustments to GMPEs: Directivity ..... 19
Topic 11: Candidate Models of Adjustments to GMPEs: Splay Faulting / Branch Faulting ..... 19
Topic 12: Constraints from Fragile Geologic Features (FGFs) ..... 19
Focused questions submitted to Workshop #2 Presenters ..... 20
GROUND MOTION CHARACTERIZATION PRESENTATIONS ..... 27
TECHNICAL INTEGRATOR TEAM SUMMARIES and ACTIONS ..... 30
LETTER COMMENTARY FROM THE PARTICIPATORY PEER REVIEW PANEL ..... 45
TECHNICAL INTEGRATION TEAM LEAD RESPONSES TO PARTICIPATORY PEER REVIEW PANEL COMMENTS ..... 49
REFERENCES ..... 53

APPENDIX A Hand-out Material distributed during the Workshop #2 ..... A1
A.1 Data Needs from SWUS Workshop #1 ..... A1
A.2 SWUS Schedule ..... A2
A.3 Introduction to GMPEs Visualization Techniques (by N. Kuehn) ..... A3
A.3.1 Introduction ..... A3
APPENDIX B Memorandum received from Prof. Heaton after Workshop #2 ..... B1
B.1 Memorandum ..... B1

# WORKSHOP #2 INTRODUCTION

Pursuant to the Request for Information put forth on March 12, 2012 by the United States Nuclear Regulatory Commission in response to the Near-Term Task Force's (NTTF) evaluation of the Fukushima Dai-ichi accident, Pacific Gas and Electric (PG&E) and Arizona Public Service (APS) are co-sponsoring a joint Southwestern U.S. (SWUS) Ground Motion Characterization (GMC) SSHAC Level 3 study for the Diablo Canyon Power Plant (DCPP) and the Palo Verde Nuclear Generating Station (PVNGS).

This is the second of three Workshops that will be conducted in accordance with the applicable guidelines for performing a Senior Seismic Hazard Analysis Committee (SSHAC) Level 3 Probabilistic Seismic Hazard Analysis (PSHA) for the three sites in this study.

According to the SSHAC process, the Technical Integration (TI) team will make use of the Workshop #2 outcome to identify work to be addressed to complete the evaluation phase, which will be followed by the integration phase leading to the preliminary GMC model.

## Purpose:

The specific goals of Workshop #2 are to:

1) Review the ground rules for the conduct of SSHAC workshops and expert roles within the project;
2) Review the tasks that the Ground Motion Characterization (GMC) Technical Integration (TI) Teams are conducting as part of their ongoing evaluations;
3) Discuss the new data collection activities being performed after Workshop #1;
4) Present, discuss, and debate alternative models, methods, and viewpoints regarding key GMC technical issues of highest significance to the hazard analysis;
5) Identify the technical bases for the alternatives and discuss the associated uncertainties;
6) Provide a basis for the subsequent development of a preliminary GMC model that considers these alternatives;
7) Discuss the path forward for the SWUS GMC project;
8) Identify interface considerations between the SSC and GMC models, including the data pertinent to both models.

## Approach:

The goals of the Workshop have been accomplished by a series of presentations and discussions designed to provide the Technical Integration (TI) team with information to be evaluated, pertaining to: (1) qualities

of alternative models and methods as well as their associated uncertainties, and (2) updates on data collection to support this SSHAC project.

Presentations have been delivered by members of the TI Team as well as by invited Resource Experts (REs) and Proponent Experts (PEs). All the presentations are part of the project record.

Speakers have been provided with detailed guidance by the TI Lead to focus the presentations so that they are oriented to the goals of the project and Workshop. In particular, Proponent Experts have been asked to discuss the merits of specific methods, models or perspective regarding key issues of highest significance to the hazard at the two sites in the project. Also, Speakers have been requested to present strengths and limitations of the method or model they advocate, and to explain the underlying technical bases for applicability of the method or perspective. Whenever possible, discussions should be focused on the implications of the models to the hazard inputs, and not just to the scientific viability of the methods and viewpoints.

At the end of each day, the PPRP, Regulatory Observers and representatives of the Sponsors have been provided with an opportunity to make comments and/or raise questions.

## Workshop #2 Agenda

| Session | Time | Topic | Duration (minutes) | Speaker |
|---|---|---|---|---|
| Day 1 – AM | | 9:30 AM – 12:00 PM | | |
| WORKSHOP INTRODUCTION | 9:30 AM – 10:15 AM | Welcome and introduction | 10 | Di Alessandro |
| | | Short review of SSHAC procedures and Workshop ground rules | 10 | Di Alessandro |
| | | Project overview and objectives; Status of data needs identified at Workshop #1 | 25 | Abrahamson |
| INTRODUCTION to GMC and SENSITIVITY ANALYSES | 10:15 AM - 12:00 PM | Summary of the candidate GMPEs for ACRs | 15 | Gregor |
| | | Summary of current BBP results and parametric models | 15 | Donahue |
| | | GM Logic Tree V1 | 15 | Wooddell |
| | | Hazard feedback using the current GMPEs for DCPP | 15 | Gregor |
| | | Hazard feedback using the current GMPEs for PVNGS | 15 | Walling |
| | | *Clarifications and questions* | 30 | Abrahamson leads |
| 12:00 PM – 1:00 PM | | Lunch | | |
| Day 1 – PM | | 1:00 PM – 5:00 PM | | |
| CANDIDATE FFS METHODS: Results of SCEC BBP Validation Evaluation | 1:00 PM - 3:10 PM | Overview of the validation process – Part A and B | 30 | Goulet |
| | | SCEC Evaluation Committee findings | 30 | Dreger |
| | | Introduction to modelers questions | 10 | Dreger |
| | | Discussions: *Strength and weakness of simulations models; Technical bases for applicability of the methods.* | 60 | Dreger leads; Modellers' Panel |
| 3:10 PM – 3:30 PM | | *Break* | | |
| CANDIDATE FFS METHODS: Initial Forward Simulation Results | 3:30 PM - 4:20 PM | Comparisons of simulations and GMPEs for smaller magnitudes (M5.5-6.0) | 20 | Donahue |
| | | *Discussion* | 30 | Dreger leads; Modellers' Panel |
| Epistemic uncertainty tutorial | 4:20 PM – 4:50 PM | GMPEs visualization techniques: a methodology overview | 30 | Kuehn |
| 4:50 PM – 5:00 PM | | Observers (PPRP and Sponsors) comments | 10 | |
| Day 1 | | End of Formal Workshop Proceedings | | |
| Closed Meeting: PPRP, Sponsors, PM, TI Lead | | | | |
| Public Q/A session on DCPP science hosted by PG&E | | | | |

| Session | Time | Topic | Duration (minutes) | Speaker |
|---|---|---|---|---|
| Day 2 – AM | | 8:00 AM – 12:40 PM | | |
| 8:00 AM – 8:15 PM | | Summary of GMC Day 1 | 15 | Donahue |
| 8:15 AM – 8:25 AM | | Reminder of project objectives, rules of conduct and key sensitivity results | 10 | Abrahamson |
| APPLICABILITY of GM MODELS TO THE TWO SITES | 8:25 AM - 10:05 AM | GMPEs comparison and identification of issues | 30 | Gregor |
| | | NGA West 2 GMPEs (ASK13, CB13) | 30 minutes per model | Abrahamson, Bozorgnia |
| 10:05 AM – 10:30 AM | | *Break* | | |
| APPLICABILITY of GM MODELS TO THE TWO SITES | 10:30 AM - 12:40 PM | NGA West 2 GMPEs (BSSA13, CY13) | 30 minutes per model | Boore, Youngs |
| | | Graizer & Kalkan GMPE | 30 | Graizer and Kalkan |
| | | Akkar et al. GMPE | 20 | Akkar |
| | | Summary of other Pan-European GMPEs | 10 | Akkar |
| | | Update M scaling for Zhao's GMPE for large Magnitude crustal earthquakes | 10 | Abrahamson |
| 12:40 PM – 1:40 PM | | *Lunch* | | |
| Day 2 – PM | | 1:40 PM – 5:00 PM | | |
| APPLICABILITY of GM MODELS TO THE TWO SITES | 1:40 PM - 2:55 PM | Visualization of epistemic uncertainty to GMPEs | 30 | Kuehn |
| | | *Discussions: Do we have enough models to capture the CBR?* | 45 | Youngs leads |
| 2:55 PM – 3:25 PM | | *Break* | | |
| PATH EFFECTS | 3:25 PM - 4:30 PM | Additional Seismic Instrumentation at DCPP | 20 | McLaren |
| | | *Discussions: Path effects in Arizona and generic 1D vs 3D effects* | 45 | Walling leads; Toro, Mayeda, Pitarka |
| 4:30 PM – 4:50 PM | | Summary of GMC Day 2 | 20 | Youngs |
| 4:50 PM – 5:00 PM | | Observers (PPRP and Sponsors) comments | 10 | |
| Day 2 | | End of Formal Workshop Proceedings | | |
| Closed Meeting: PPRP, Sponsors, PM, TI Lead | | | | |
| Public Q/A session on DCPP science hosted by PG&E | | | | |

| Session | Time | Topic | Duration (minutes) | Speaker |
|---|---|---|---|---|
| Day 3 - AM | | 8:00 AM – 1:15 PM | | |
| 8:00 AM – 8:15 AM | | Reminder of project objectives, rules of conduct and hazard sensitive issues | 15 | Di Alessandro |
| CANDIDATE MODELS for SIGMA | 8:15 AM – 10:40 AM | Introduction of envisioned approaches for sigma at the two NPP sites | 10 | Abrahamson |
| | | Summary of traditional sigma from GMPEs models for reference rock conditions | 20 | Al-Atik |
| | | Proponent single station sigma (SSS) models from the PEER sigma group | 50 | Al-Atik |
| | | Proponent single-path sigma | 20 | Abrahamson |
| | | *Questions and Discussions on Sigma models* | 45 | Abrahamson leads; Rodriguez-Marek, Baker |
| 10:40 AM – 11:00 AM | | *Break* | | |
| CANDIDATE METHODS of ADJUSTEMTS to GMPEs: Changing Rake, Dip Along Strike | 11:00 AM – 11:50 AM | DCPP scenario for complex ruptures | 15 | Donahue |
| | | Proponent approach based on NGA West 2 residuals | 15 | Di Alessandro |
| | | *Discussions* | 20 | Donahue leads; GMPEs developers |
| CANDIDATE METHODS of ADJUSTEMTS to GMPEs: Directivity | 11:50 AM – 12:10 PM | *Discussions on directivity models* | 20 | Abrahamson leads; GMPEs modelers, Baker |
| KAPPA | 12:10 PM - 1:15 PM | DCPP *Values and effects* | 15 | Ktenidou |
| | | Plan on collecting $V_{S,30}$ for AZ recording stations sites | 10 | Di Alessandro |
| | | PVNGS *Update on AZ GM data* | 15 | Ktenidou |
| | | *Discussions* | 25 | Abrahamson leads; Bozorgnia |
| 1:15 PM – 2:00 PM | | *Lunch* | | |
| Day 3 - PM | | 2:00 PM – 5:00 PM | | |
| CANDIDATE METHODS of ADJUSTEMTS to GMPEs: Splay Faulting / Branch Faulting | 2:00 PM - 3:30 PM | Strike Slip Splay using dynamic rupture models | 40 | Lozos |
| | | Splay faulting adjustments factors using kinematic approach | 20 | Wooddell |
| | | *Discussions* | 30 | Wooddell leads; SCEC BBP modelers (selected subset) |
| CONSTRAINTS FROM FRAGILE GEOLOGIC FEATURES (FGF) | 3:30 PM – 4:00 PM | FGF near DCPP – Constraints on Hazard | 30 | Stirling |

*Continues on the next page*

| Session *(Continued from previous page)* | Time | Topic | Duration (minutes) | Speaker |
|---|---|---|---|---|
| 4:00 PM – 4:20 PM | | *Break* | | |
| 4:20 PM – 4:45 PM | | Summary of GMC Day 3 and Overview of Day 1 and Day 2 | 25 | Abrahamson |
| 4:45 PM – 4:55 PM | | Observers (PPRP and Sponsors) comments | 10 | |
| 4:55 PM – 5:00 PM | | Closure and adjourn | 5 | Di Alessandro |
| Day 3 | | End of Formal Workshop Proceedings | | |
| Closed Meeting: PPRP, Sponsors, PM, TI Lead | | | | |
| Public Q/A session on DCPP science hosted by PG&E | | | | |

## Workshop #2 participants

| Group | Individual | Affiliation |
|---|---|---|
| PPRP | Day, Steve | San Diego State University |
| | Campbell, Kenneth | Kenneth W Campbell Consulting |
| | Chiou, Brian | Brian Chiou Consulting |
| | Rockwell, Tom | San Diego State University |
| Project Management - GeoPentech | Barneich, John | GeoPentech, Inc. |
| | Di Alessandro, Carola | GeoPentech, Inc. |
| | Dinsick, Andrew | GeoPentech, Inc. |
| Project Management - Utilities | Klimczak, Richard | Pacific Gas and Electric Company |
| | Horstman, William R. (*) | Pacific Gas and Electric Company |
| | Jahangir, Nozar | Pacific Gas and Electric Company |
| | Wandell, Chris | Arizona Public Service |
| Project Technical Integrator | Abrahamson, Norman A. | Pacific Gas and Electric Company |
| | McGuire, Robin | Lettis Consultants International. Inc. |
| Hazard Analysts | Gregor, Nick | Bechtel Corporation |
| | Walling, Melanie | Lettis Consultants International, Inc. |
| Technical Integrator Team | Abrahamson, Norman A. | Pacific Gas and Electric Company |
| | Donahue, Jennifer | Geosyntec Cons. |
| | Dreger, Doug | Univ. of California, Berkeley |
| | Wooddell, Katie | Pacific Gas and Electric Company |
| | Youngs, Bob | AMEC Geomatrix |
| Technical Integrator Support | Al-Atik, Linda | Linda Alatik Consulting |
| Resource and Proponent Experts (Continues on following page) | Aagaard, Brad | U.S. Geological Survey, Menlo Park |
| | Akkar, Sinan | Middle East Technical University, Turkey |
| | Anderson, John (*) | Univ. of Nevada, Reno |
| | Archuleta, Ralph | Univ. of California, Santa Barbara |
| | Baker, Jack | Stanford University, Palo Alto |
| | Baltay, Annemarie (*) | U.S. Geological Survey, Menlo Park |
| | Bayless, Jeff | URS |
| | Boore, David | U.S. Geological Survey, Menlo Park |
| | Bozorgnia, Yousef | Univ. of California, Berkeley |
| | Goulet, Christine | Univ. of California, Berkeley |
| | Graves, Robert (*) | U.S. Geological Survey, Pasadena |
| | Hanks, Tom (*) | U.S. Geological Survey, Menlo Park |
| | Harris, Ruth (*) | U.S. Geological Survey, Menlo Park |
| | Heaton, Thomas | California Institute of Technology |
| | Kalkan, Erol | U.S. Geological Survey, Menlo Park |

| Group – Continued | Individual | Affiliation |
|---|---|---|
| **Resource and Proponent Experts (Continues from previous page)** | Ktenidou, Olga | ISTerre, France; Univ. of California, Berkeley |
| | Kuehn, Nicolas | Potsdam Univ, Germany; Univ. of California, Berkeley |
| | Lozos, Julian | Univ. of California, Berkeley |
| | Mayeda, Kevin | Univ. of California, Berkeley |
| | McLaren, Marcia | Pacific Gas and Electric Company |
| | Olsen, Kim | San Diego State University |
| | Pitarka, Arben | Lawrence Livermore National Laboratory |
| | Rodriguez-Marek, Adrian | Virginia Tech |
| | Somerville, Paul | URS |
| | Stewart, Jonathan | Univ. of California, Los Angeles |
| | Stirling, Mark | GNS Science, New Zealand |
| | Toro, Gabriel | Lettis Consultants International, Inc. |
| **Regulatory Observers** | Ake, Jon P. | US Nuclear Regulatory Commission |
| | Anderson, Robert | California Seismic Safety Commission |
| | Budnitz, Robert J. | Lawrence Livermore National Laboratory |
| | Chen, Rui | California Geological Survey |
| | Graizer, Vladimir | US Nuclear Regulatory Commission |
| | Hale, Christie | US Nuclear Regulatory Commission - Region IV |
| | Johnsson, Mark | California Coastal Commission |
| | McCarthy, Richard (*) | California Seismic Safety Commission |
| | Stamatakos, John | Center for Nuclear Waste |
| | Stirewalt, Gerry | US Nuclear Regulatory Commission |
| | Walter, Joan | California Energy Commission |
| | Weaver, Casey | California Energy Commission |
| | Wills, Chris J. | California Geological Survey |
| **Other Observers (Continues on following page)** | Abramson Ward, Hans | Lettis Consultants International. Inc. |
| | Ancheta, Timothy (*) | RMS |
| | Brumbaugh, David | Northern Arizona University |
| | Dabaghi, Mayssa | Univ. of California, Berkeley |
| | El Menchawi, Osman | Fugro Consultants, Inc. |
| | Ferre', Kent | Pacific Gas and Electric Company |
| | Geesman, John | A4NR |
| | Hamilton, Douglas | DHH Geoconsult |
| | Hardebeck, Jeanne (*) | U.S. Geological Survey, Menlo Park |
| | Kammerer, Annie | Bechtel Corporation |
| | Lettis, William (*) | Lettis Consultants International |
| | Lewis, Sherry | Mothers for Peace |

| Group – Continued | Individual | Affiliation |
|---|---|---|
| **Other Observers (Continues from previous page)** | Lin, Po-Shen | Sinotech, Taiwan |
| | Lisle, Greg A. | Columbia Project - Energy Northwest |
| | Liu, Hsun-Jen | Nat. Cent. for Res. on Earthq. Engin., Taiwan |
| | Renault, Philippe | PEGASOS Refinement Project - Swissnuclear |
| | Rowshandel, Badie | California Earthquake Authority |
| | Seyhan, Emel | Univ. of California, Berkeley |
| | Sewell, Rob | R.T. Sewell Associates |
| | Skarlatoudis, Andreas | URS |
| | Spudich, Paul (*) | U.S. Geological Survey, Menlo Park |
| | Thompson, Steve | Lettis Consultants International, Inc. |
| | Weisman, David | A4NR |
| | Wu, Chiun-lin | Nat. Cent. for Res. on Earthq. Engin., Taiwan |

(*) Remote attendance

# WORKSHOP #1 SUMMARY

## Project background

Pursuant to the Request for Information put forth on March 12, 2012 by the United States Nuclear Regulatory Commission in response to the Near-Term Task Force's (NTTF) evaluation of the Fukushima Dai-ichi accident, Pacific Gas and Electric Company (PG&E) and Arizona Public Service (APS) are co-sponsoring a joint Southwestern U.S. (SWUS) Ground Motion Characterization (GMC) SSHAC Level 3 study for the Diablo Canyon Power Plant (DCPP) and the Palo Verde Nuclear Generating Station (PVNGS). The ultimate deliverable for this study will be a ground motion model developed following the guidelines of the SSHAC Level 3 process (Budnitz et al., 1997; NRC, 2012).

## General workshop summary

The second workshop of the SWUS SSHAC was held at the Shattuck Plaza Hotel, Berkeley, California from October 22 to October 24, 2013. The introductory presentation delivered by the Project Manager, Dr. Carola Di Alessandro, served to highlight the focus of the workshop, which includes discussion of the new data collection activities performed after Workshop #1; presentation, discussion, and debate of alternative proponent models, methods, and viewpoints regarding key GMC technical issues; identifying the technical bases for alternatives; providing a basis for the subsequent development of the GMC model; and identifying interface considerations between the SSC and GMC models.

The workshop introduction on October 22 included a training session to review the SSHAC procedures, the Workshop #2 ground rules, also given by Dr. Carola Di Alessandro. Following this presentation, the TI Team Lead, Dr. Norman Abrahamson, presented an overview of the project schedule and objectives. This included addressing ground motions issues such as site response and time series selection, which are outside of the SWUS scope. Finally, he identified the nine data need categories identified during Workshop #1 and the progress taken on each.

### *Topic 1: Introduction to GMC and Sensitivity Analyses*

Ground Motions Prediction Equations (GMPEs) are the empirical models used to calculate ground motion attenuation given earthquake magnitude, fault geometry, and distance from the earthquake rupture to the site of interest, and site conditions (primarily characterized by $V_{S,30}$). The current state of practice in the western United States is to use the 2008 Next Generation Attenuation (NGA) models; however, alternative models such as the Graizer and Kalkan (2013), Zhao et al. (2006), Akkar et al. (2013), Bindi et al. (2011), as well as the 2013 NGA-West2 GMPEs will be evaluated as part of the SSHAC process. Dr. Gregor provided an

overview of the GMPEs, with several cases to show the variability in the median deterministic spectra and associated sigma models. Next, Dr. Donahue provided an update on the planned use of the broadband platform (BBP) simulations for hanging wall scenarios, splay faults, and complex ruptures. This was followed by a presentation of the GMC Version 1 (V1) logic tree, by Ms. Wooddell, and the ground motion sensitivity analyses presented by each Utility's designated hazard analyst (Dr. Gregor and Dr. Walling for DCPP and PVNGS, respectively). For DCPP, at short periods, the alternative models for the aleatory variability, parameterized by the standard deviation of ln(PSA), is the largest contributor to the uncertainty in the hazard. Second to this is the uncertainty in the strike-slip median models. At longer periods for DCPP, uncertainty in the GMPE medians for strike-slip earthquakes is the largest contributor to the uncertainty in hazard, followed by the uncertainty in the aleatory variability. For PVNGS, at short periods, the controlling sources are the distant faults at an AEF of $10^{-4}$ and the nearby (less than 15 km) source zones at an AEF of $10^{-6}$. At longer periods, the distant strike-slip faults are the major contributors to hazard at all AEF of interest. Uncertainty in the hazard from the nearby normal faulting sources is dominated by uncertainty in the median ground motions, which is controlled by the normal faulting factors among the GMPEs. Uncertainty in the hazard from the distant strike-slip faults is dominated by uncertainty in the median ground motion estimates. During the course of the discussion, it was recommended that the hazard feedback be extended to 5 seconds. It was also suggested by Dr. Budnitz to consider asymmetric distribution of epistemic uncertainty where warranted.

### *Topic 2: Candidate Finite Fault Simulations (FFS) Methods: Results of SCEC BBP Validation Exercise*

Where empirical data are lacking in critical prediction regions, broadband (BB) simulations can be used to develop constraints on the GMPEs. Dr. Christine Goulet provided a review of the SCEC BB Platform simulation validation exercise completed in the summer of 2013. Included in this discussion was a review of the selection of events, simulation methodologies, input parameters, and evaluation products. The evaluation process was clearly defined for the goodness of fit in respect to period range, magnitudes, and events for both the Part A (comparison with individual earthquakes) and part B (comparison with GMPEs) validations.

Dr. Doug Dreger then presented the results of the BBP Validation Exercise. Of the 5 methods that were evaluated, three methods were found to be suitable for simulation of spectral accelerations for the period range of 0.01 to 3 seconds over the distance range from 0 to 200 km within the validation magnitude range (Mw 5.9-7.2). These were the Graves and Pitarka (GP), San Diego State University (SDSU), and EXSIM methods. However, during the course of the evaluation, it was found that at periods between 1 and 3 seconds, there is increased bias.

Dr. Dreger then asked the modelling teams specific questions about their models. Both the GP and SDSU modellers stated that they believe the results of their models are consistent with their expectations, that they can be used for both buried and surface ruptures, that the models could be extrapolated as low as M5.5 and as high as M8. Proximity to the fault and incorporation of kappa were also discussed.

Further discussions of the FFS at long periods (T > 3 sec) lead to suggestions to summarize the surface slip distributions from the rupture generators (for different magnitudes) and check that the peak displacements, static displacements, and long-period spectral displacement of the simulations are consistent with the surface slip.

The FFS have not been validated for aleatory variability, but the variability of the FW sites can be compared to the HW sites to determine if there is a systematic increase in variability over the HW.

### *Topic 3: Candidate Finite Fault Simulations (FFS) Methods: Initial Forward Simulation Results*

Dr. Jennifer Donahue then presented how the three passing simulation methods compared to each other and to the GMPEs for HW effects. The constraints on magnitude scaling of the HW effect for representative cases, at both short periods and longer periods, were compared by showing the magnitude scaling of the spectral accelerations at a station located on the HW over the bottom edge of the fault. When comparing the magnitude scaling from the three FFS methods, the slope with magnitude is greatest for SDSU, while the slope for the GP method is the smallest and plateaus near M7.

Distance scaling of ground motion on FW and HW were compared for three FFS methods. During the discussion, it was suggested that the ground motion from the three FFS methods be normalized at a distance of 10-15 km for FW sites to remove differences in FW ground motion and to isolate the HW effect. Another topic of discussion was the influence of the radiation pattern at small magnitudes: does it become more deterministic at higher frequencies for smaller magnitudes, and does this affect the applicability of the FFS methods which do not include the radiation pattern at high frequencies?

### *Topic 4: Epistemic Uncertainty Visualization - Introduction*

The final presentation of the first day of Workshop #2 was an introductory tutorial for the GMPE visualization techniques. The Principal Component Analysis (PCA), Sammon's Maps, and Self-Organizing Maps (SOM) were explained and a simple example of each was given. Dr. Kuehn showed the effect of varying constant scale factors, magnitude scaling and distance scaling on the Sammon's map and SOM space.

### *Topic 5: GMPEs comparison and identification of issues*

Day 2 of Workshop #2 began with a presentation by Dr. Gregor on the comparison of the 14 GMPEs for representative deterministic scenarios. Each of the four controlling faults for DCPP, as well as nearby normal faults and large distance strike-slip faults for PVNGS were examined. Key features, such as magnitude scaling, distance scaling, hanging wall (HW) effects, soil response, and depth scaling, were evaluated.

The magnitude scaling from the 12 of the GMPEs is similar. The Bindi et al. (2011) model has much stronger magnitude scaling for magnitudes greater than 6.5; this is likely due to the lack of large magnitude data in the Bindi et al. dataset. The Zhao et al. (2006) model has stronger magnitude scaling above magnitude 7 but

Zhao and Lu (2011) has indicated that the data show no magnitude scaling for magnitude above 7, indicating the large magnitude scaling in Zhao et al. (2006) is not applicable.

The distance scaling for peak acceleration is similar for 13 of the GMPEs, with the exception being the Bindi et al. (2011) model at distances less than 10 km: again this is a distance range not well sampled in the Bindi et al. dataset. The distance scaling for 1 Hz is similar for distances greater than 20 km but shows large variability between the GMPEs at distances less than 5 km.

The HW scaling varies between the GMPEs depending if the model included the HW effects or not. Models that use $R_{JB}$ as a distance metric (Boore et al. NGA-West1 and NGA-West2 models, Akkar et al. 2013, Bindi et al. 2011) capture HW scaling consistent with GMPEs based on $R_{RUP}$ which also include a HW term (Chiou and Youngs NGA-West1 and NGA-West2 models, Abrahamson et al. NGA-West1 and NGA-West2 models, Campbell and Bozorgnia NGA-West1 and NGA-West2 models). Models based on $R_{RUP}$ which do not include HW term (Zhao et al. 2006, Idriss NGA-West1 and NGA-West2 models, Grazier and Kalkan 2013) have much lower ground motions for sites over the HW.

The depth scaling shows large difference between the GMPEs due to the model parameterization. Models based on $R_{JB}$ without depth scaling (Boore et al. NGA-West1 and NGA-West2 models, Akkar et al. 2013, Bindi et al. 2011) produce constant ground motions with varying depths. Models based on $R_{RUP}$ without a depth term (Zhao et al. 2006, Idriss NGA-West1 and NGA-West2 models, Grazier and Kalkan 2013) produce decreasing ground motion with increasing depths, and finally models based on $R_{RUP}$ with a depth term (Chiou and Youngs NGA-West1 and NGA-West2 models, Abrahamson et al. NGA-West1 and NGA-West2 models, Campbell and Bozorgnia NGA-West1 and NGA-West2 models) show increasing ground motion with increasing depth. (Note that the various PEER NGA-West2 developers assign dates of either 2013 or 2014 to their models. The project plans to utilize the final published versions of the NGA-West2 GMPE's, which will occur in 2014. Accordingly, all the NGA-West2 GMPEs are herein referred with the 2014 publication date.)

Heaton recommended that hazard for surface rupture of the nearby controlling faults be computed and compared to the long period ground motion hazard as a consistency check.

Next, the GMPE developers delivered their proponent model responses to the focused questions (Table 5).

Dr. Abrahamson introduced the Abrahamson, Silva, and Kamai '14 model (ASK14). He described the differences between the ASK14 and Abrahamson and Silva '08 (AS08) models, constrains on depth to top of rupture, magnitude scaling, style of faulting, and hanging wall effects. The large distance scaling is constrained by few California earthquakes, which show large variability in the associated distance scaling. The best recorded event (El Mayor-Cucapah) has the steepest scaling but the ASK14 model considered scaling by earthquake and not by number of recordings therefore the distance scaling is not as steep as other models. The TI Team asked for additional information on two topics: 1) Is the magnitude taper for HW effects too large for small magnitudes; 2) Does the inclusion of Class 2 events (aftershocks) have an effect of standard deviation model.

Dr. Bozorgnia introduced the Campbell and Bozorgnia updated model (CB14). Like the previous presentation, the key specific changes from CB08 to CB14 included adding small magnitude data, revised

hanging wall model, regionalization, additional range of applicability, and most notably, the change in source of depth scaling from Ztor to Zhyp. Dr Campbell noted that there is a shift in the peak of the response spectra to higher frequencies in their NGA-West2 GMPE compared to CB08 for sites with $V_{S,30}$ of 760 m/s and indicated that this shift is due to differences in $V_{S,30}$ scaling between the two models. The cause of the "bump" in tau at 10 Hz in their model was discussed. This increase in tau at 10 Hz was also present in the CB08 data and does not appear to be a result of including Japanese ground motion data. Dr. Bozorgnia did not have a conceptual model for the cause of the "bump" on tau but stated that it is observed in data and is an appropriate feature of their model which should, therefore, be preserved.

Dr. Boore introduced the Boore, Stewart, Seyhan, and Atkinson '14 (BSSA14) model and explained the change in approach from the BA08 model. Dr. Boore showed that the uncertainty in the normal faulting factors for T = 0.2 sec was ± 0.1, the TI Team requested him to tabulate the standard error of the normal faulting factors for the other periods. For the HW effects, the average residuals shown by Dr. Boore are unbiased, but the TI Team requested mean residuals for HW sites binned by dip and magnitudes for evaluating HW effects for low-dip angles and large magnitudes. The distance dependence of the standard deviation in the BSSA14 model is based in all data combined; a topic of discussion was the applicability of this distance dependence to western US as many of the large distance recordings are from Japanese events. The TI Team requested BSSA team to show the distance binned values of sigma for Japanese and non-Japanese events separately. Dr. Boore confirmed that the BSSA14 model includes the "bump" in tau at 10 Hz that they choose to retain as it is observed in data. Dr. Boore was asked to test his conceptual model suggesting that stress-drop variability was the cause of the "bump" in tau at 10 Hz. Preliminary analysis by Dr. Youngs showed that the stress-drop variability was unlikely to be the cause of the bump in tau but this result needs to be further investigates.

Dr. Youngs introduced the Chiou and Young '14 model (CY14). The main change from the CY14 model is the inclusion of regionalization and directivity. Dr Youngs noted that the normal faulting factors were retained from CY08 as there were limited normal faulting data in the dataset used for the update. The CY14 model also smoothed through the bump in tau at 10 Hz, as they believe the bump would represent a source effect. During the discussion regarding the 10 Hz bump in tau, the possible correlation of average kappa with the event term was discussed; if the average kappa changed from earthquake to earthquake, then site effects would be mapped into event terms which could explain this feature in tau. There is a need to find a way to remove this correlation from the estimates of tau for use in single station sigma models; PEER was asked to address this task. The TI Team requested Dr. Youngs to provide a table of the statistical uncertainty in phi and tau for periods of 0.01 to 10 sec to help with the evaluation of uncertainty of his aleatory variability.

Dr. Grazier presented the Grazier and Kalkan'13 model (GK13). The "bump" present in the GK13 model is of a different type that the "bump" in tau described above. For their model, the bump refers to a bump in the distance attenuation for sites close to a fault. Dr. Grazier described that there is no noticeable bias in the event terms with this distance bump included. To help with the evaluation of the GK model, the TI Team requested that additional plots of residuals be produced using the larger NGA-West2 dataset. The requested plots include: residuals for HW sites to compare the HW effects with the distance bump;

residuals for the event terms versus the hypocenter depths; and the estimates of phi and tau and not just the total sigma.

Dr. Akkar presented the major features of the model, its strength, assumptions and data constraints. He observed lack of magnitude-dependence both in phi and in tau indicating his sigma model in applicable for large magnitude events. The database is sparse for distances less than 10 km so the short distance scaling is not well constrained by data. Dr. Akkar was also asked to review the depth scaling of his model as there may be a trade-off between the magnitude scaling and hypocenter depth for small magnitude events. He was also asked to provide estimates of phi and tau and not just the total sigma for his model Akkar et al. '13 (ASB13). This evaluation should separate well versus poorly recorded earthquakes, and phi by distance bin and magnitude bin.

Dr. Akkar then presented a brief review of the GMPEs included in the RESORCE project. These included Akkar et al. 2013, Bindi et al. 2013, Derras et al. 2013, Hermkes et al. 2013, and Bora et al. 2013. Of the five RESORCE model, Bora et al, Derras et al., and Hermkes et al. are research models and not ready for engineering application. He also recommended replacing Bindi et al. '11 with Bindi et al. '13.

The next presentation was given by Dr. Abrahamson for Dr. Zhao. The Zhao and Lu 2011 (ZL11) model is a conceptual model and not a complete GMPE. The key concept is the lack of magnitude scaling for Mw>7. To implement this concept, the Zhao et al. (2006) model would be capped at Mw=7 for all events over Mw=7 with all other parts of the GMPEs unchanged. It was recommended by Dr. Olsen to look at the recent BBP simulations with plasticity effects to see if similar behaviour is witnessed for different magnitudes. Residuals for other models discussed in this section should also be examined for similar effects.

The final presentation of the session was given by Dr. Kuehn who applied the visualization techniques to the GMPEs. Sammon's maps, PCA maps, and SOMs were shown for the 14 GMPEs at periods of 0.2 sec, 1 sec, and 3 sec. Using these methods, several exploratory goals were introduced. The first is to explore implied GMPEs from cells in the SOM away from GMPE models to see if they are in the TDI, and conversely, explore gaps between the models to establish the Center, Body, and Range (CBR) of Technical Defensible Interpretations (TDI). The major issue becomes establishing the bounds within the SOM, PCA, or Sammon's maps that captures the CBR of the TDI. A related issue is which, if any, GMPEs fall outside of the range of the TDI. As part of the discussion, it was recommended to add the FF simulations to the SOM to see if they fall within the range currently spanned by the GMPEs. To make the visualization site specific, it was also recommended to use the magnitude-distance space from the hazard disaggregation to develop the visualization maps.

### *Topic 6: Path Effects*

Dr. Marcia McLaren reviewed the installation of the new seismic station at DCPP and the Ocean Bottom Seismometer (OBS) project. The OBS is designed to provide full waveform data for small earthquakes and on-scale acceleration recordings for larger earthquakes, which will be integrated into the onshore PG&E seismic network. Currently four temporary OBS units are in place with 4 long term OBS units planned. A

new temporary onshore station is also in place for the observation of path effects to DCPP; however, the recordings are noisy and a new station location is being looked into. Currently there is no adequate data available but as this will be revaluated in mid-Summer to compare with the GMPEs.

For PVNGS, two presentations were given for path effects. In the first by Dr. Toro, the NGA'08 and NGA-West2 GMPEs were compared with the NGA'08 GMPEs modified for high Q. Overall, the NGA-West2 GMPEs were consistent with the modified NGA'08. If possible, the GMPEs for use at PVNGS should be developed to allow adjustments for different Q by an explicit Q term in the functional form. The second presentation was delivered by Dr. Mayeda who reviewed the southwestern U.S. lateral variations in Q based on Lg waves. In the PVNGS region, there is a strong azimuthal dependence in Q with large differences between the Basin and Range to the north and the Salton Trough to the west. Mayeda noted that the digital version of their model can be used to integrate over 1/Q for specific paths for distant sources.

The final presentation in the session was given by Dr. Pitarka on 1D versus 3D wave propagation in the San Francisco Bay area. Using Loma Prieta as a validation event, he showed that both the 3D and 1D simulation motions are systemically lower than the recorded motion at periods greater than 3 seconds. However, the 3D modelling gives smaller bias at periods greater than 2 seconds than 1D modelling. Dr. Pitarka recommended using smooth 1D velocity profile to suppress artificial effect that can occur in 1D velocity models with sharp velocity contrasts extending over large distances. He also showed that adding topography does not result in improvements of ground motion estimations at low frequencies. Limitation of this comparison was that it was only for one earthquake and additional validation events are needed before this method can be applied.

### *Topic 7: Candidate Models for Sigma*

The first presentation of Day 3 of Workshop #2 was given by Dr. Abrahamson on the three approaches for applying sigma to the two NPP sites: traditional (ergodic), single-station sigma, and single-path sigma. The expected approach for DCPP will be to use single-station sigma with the site term (median and epistemic uncertainty) estimated by observed ground motions at DCPP and geotechnical modelling. For PVNGS, two approaches are expected to be taken. For the local, non-California sources, the single-station sigma approach with the site term (median and epistemic uncertainty) estimated by geotechnical modelling will be used. For distant California faults, a single-path sigma with path terms and site terms estimated from observed ground motions from California earthquakes recorded in Arizona and geotechnical modelling, respectively. When using geotechnical modelling, part of the site term is for the bedrock level, and, therefore, epistemic uncertainty of the bedrock site-term should be included.

Dr. Al Atik presented a summary of traditional (ergodic) sigma from the 14 GMPEs. Description of the development of sigma for each of the GMPEs was reviewed. Next, the sigmas for case studies for strike-slip, normal, and reverse events were compared. In most cases, the sigmas for the Pan-European models are higher than those for the NGA GMPEs. This difference may reflect metadata quality.

Dr. Al Atik then followed the previous presentation with a discussion of single-station phi ($\phi_{ss}$). Terminology and the approach taken to estimate $\phi_{ss}$ were discussed. It was found that there is a strong increase in $\phi_{ss}$ at the PGA for small magnitudes and short distances (M3 to M5 within 30 km) which is not seen in the higher magnitudes or longer periods. It was suggested this increase may be due to uncertainty in the hypocenter depth, but a quantitative evaluation is needed. Additionally, $\phi_{ss}$ does not appear to be region independent. For instance Taiwan and Italy have lower $\phi_{ss}$ when compared to California and Japan. Dr. Al Atik then introduced the method of using the Closeness Index (CI) for path effects.

Dr. Abrahamson then gave a presentation on proponent models for single-path sigma. In this presentation, the Lin et al 2011 and Villani and Abrahamson (VA) 2013 models were introduced and compared. While the VA 2013 model uses the NGA-West2 database and draws on more ground motions from global sources, only one spectral period (T=3 sec) is available. Conversely, while covering a wider range of spectral periods, the Lin 2011 is primarily taken from Taiwanese data. Because of this, the reduction in sigma may not be applicable to California and Arizona as site variability may differ by region. During the discussion session on the topic, when estimating the appropriate $\phi_{sp}$, it was recommended that the CI for the smallest data (approx. CI=0.05) be used and not extrapolated to CI=0.01 as was done in previous studies.

The discussion section featured two proponents for candidate models for sigma. The first was Dr. Rodriquez-Marek who primarily discussed his work with site-to-site variability. During the discussion session, the "bump" in sigma at 10Hz, was again discussed. Dr. Rodriquez-Marek noted that in review of the Japanese KiK-net data, the bump is seen at the surface and not in the borehole recordings indicating that this bump may be due to site terms. He also noted that there is a stronger regional dependency on $\phi_{s2s}$ when compared to $\phi_{ss}$ and that there may be a $V_{S,30}$ dependency in some datasets. Finally, he concluded with proponent models of the standard deviation of the $\phi_{ss,s}$.

Dr. Jack Baker gave the next proponent model for the influence of spatial correlation on sigma. In this ongoing study, the standard deviation can be correlated between a source, a location of interest, and a number of recording stations. The standard deviation in the empirical GMPEs may be underestimated due to this correlation. It was recommended that Dr. Baker utilize the NGA-West2 dataset to evaluate the potential underestimation in $\phi_{ss}$ due to this spatial correlation.

### *Topic 8: Candidate Methods of Adjustment to GMPEs: Changing rake, dip along strike*

Two presentations were given for complex ruptures. A complex rupture is defined by a significant change in the rake or dip of the rupture along strike. The first presentation on this topic was given by Dr. Jennifer Donahue for the case of complex ruptures at DCPP. First, three methods were discussed regarding how to compute ground motions for complex rupture parameters using the GMPEs. A single rake and dip are required. She then discussed how each of the GMPE developers would recommend determining the single rake and dip of complex ruptures for use with their GMPEs. Finally, she gave an overview of how the ground motions from possible complex faults near DCPP could be calculated and compared these results with their implications on hazard. While the potential impact on ground motion for a specific scenario can

be large, the expected impact on hazard is low due to the relatively low rate of occurrence of complex ruptures.

Dr. Carola Di Alessandro then followed the previous presentation with a comparison of the applicability of GMPEs for complex ruptures. First she described the events within the NGA-West2 database which are complex events, then analyzed proponent approaches for evaluating the effect of using either local or average fault geometry parameters in the ASK14 and CY14 models. The available ground motion data from complex ruptures are sparse. She found that using the closest segment parameters at short periods works best for ASK14, while there was no significant effect for either method using CY14.

During the discussion section, it was recommended that finite fault simulations (FFS) and dynamic simulations be used to help constrain predications of ground motions for complex ruptures. Ground motion from complex ruptures may be sensitive to the hypocentral locations, which has not been fully addressed in the current set of simulations. Another recommendation was to simulate the NGA-West2 complex events within the BBP using the known station locations as input parameters.

### *Topic 9: Kappa*

Dr. Olga Ktenidou gave the first presentation of the session on the preliminary estimation of kappa for DCPP. Based on three events recorded at DCPP, kappa was estimated using $k_{r\_AS}$ (or the high-frequency decay of the S-wave Fourier spectrum). She also computed kappa from these events recorded at other sites with $V_{S,30}$ > 500 m/s. The kappa values for DCPP were higher than typical for its $V_{S,30}$ range ($V_{S,30}$ > 900 m/s). During the discussion, it was recommended that, in addition to the 2012 vibroseis data which is now available, small magnitude earthquakes from the Central Coast Network also be reviewed to help constrain the estimation of kappa at DCPP.

Dr. Di Alessandro next presented the plans for collecting $V_{S,30}$ estimates for selected Arizona ground motion recording stations. Dr. Robert Kayen, from the USGS, will perform SASW at 9 selected locations. The testing should occur before the end of 2013 with a report on findings in June 2014. One issue that was raised during the discussion concerned the depth to which the SASW could accurately record the shear wave velocity and if this could capture the full soil profile. Also, it was recommended that Dr. Kayen provides a suite of alternative profiles that are compatible with the data, along with the uncertainty in the resulting profiles for each inversion approach.

Dr. Ktenidou then spoke of the kappa estimates for PVNGS. With the small useable bandwidth of 4-16 Hz for local recordings, the choice of the measurement method for kappa must be carefully considered. Due to the limited bandwidth and earthquake magnitude there are only a few proponent methods for modelling kappa that can be used. She then presented variations in determining kappa using a linear regression of Q or the “hockey stick” method, both of which are viable, but increased knowledge of the site effects from the SASW testing will provide better estimates. It was suggested that the Arizona Geological Survey may have additional records with better high frequency band width that should be considered.

The final presentation of this session was given by Dr. Yousef Bozorgnia on the high frequency rock issues currently being addressed by PEER. It is the intent of PEER to include kappa in GMPEs for both horizontal

and vertical components. Additionally, they are proposing to expand the range of applicability of GMPEs for hard rock sites by updating the $V_{S,30}$ scaling through a review of a collection of small magnitude recordings on hard rock and reviewing rock indices for better estimates.

### *Topic 10: Candidate Methods of Adjustment to GMPEs: Directivity*

The topic of directivity will be further discussed in Workshop #3; however, Dr. Jack Baker provided insight to adjusting sigma for directivity. The current Shahi and Baker model does not show an increase in sigma, but a change in the median could be incorporated in the sigma. Dr. Baker noted that their current model is being further evaluated and is not currently ready for application.

### *Topic 11: Candidate Methods of Adjustment to GMPEs: Splay Faulting/ Branch Faulting*

Two presentations were given on splay, or branching, faults which are defined as the rupture of two overlapping faults: a major fault with a secondary fault rupture. Dr. Julian Lozos described his current work of using dynamic rupture models to analyze the ground motions resulting from ruptures with strike-slip splay faults. First, he explained input parameters such as stress field, branch angles, and the velocity structure, then the proposed sensitivity study to be conducted. Ms. Wooddell recommended that splay ruptures for dipping faults also be addressed by the dynamic rupture modelling. It was discussed that the dynamic ruptures can also be used as a constraint for the source inputs for kinematic simulations.

Ms. Wooddell then gave the presentation on the current BBP kinematic simulations for splay faulting. She described the scenarios that have been implemented and how the time series for two ruptures, independently modelled, are combined into a single response spectrum. She then described the alternative methods for modelling complex ruptures using simple GMPEs and their implications on hazard. A discussion session followed regarding how splay faults should be modelled using the BBP with an emphasis on constraining for down-dip rupture width, combining time series, and partitioning seismic moment on fault segments.

### *Topic 12: Constraints from Fragile Geologic Features (FGFs)*

Fragile geologic features (or FGFs), or precariously balanced rocks, are geologic structures that may be used to constrain probabilistic seismic hazard analyses. When properly dated, these features can yield an estimate of the maximum level of ground shaking that has not occurred at the site since the formation of the fragile structure. In this respect, they place an upper bound on the ground motion value that has not occurred at the site during the age of the FGF. Previously, PG&E identified a couple of candidate FGFs near DCPP. Dr. Mark Stirling later toured DCPP, and identified three additional candidate FGFs that could be considered. If these features date to more than 1000 years, they may provide valuable constraints on the hazard. A review of the FGFs near PVNGS has been addressed in the PVNGS SSC SSHAC Workshop #1 and is still pending evaluation within this project.

## Focused questions submitted to Workshop #2 Presenters

The following Tables 1 through 12 show the focused question that Workshop #2 Presenters were asked to address, subdivided by topic.

**Table 1:** Focused questions for Workshop #2 Presenters: Session "INTRODUCTION to GMC and SENSITIVITY ANALYSES"

| Topic | Speaker | Questions / Topics to be addressed at WS #2 |
|---|---|---|
| Summary of the candidate GMPEs for ACRs | Gregor | Review of the candidate GMPE's US and International<br>Review of database used for each model<br>Presentation of databases used in the development of each model<br>Review magnitude and distance limitations for each model<br>Provide comparison of GMPE models for general deterministic scenarios |
| Summary of current BBP results and parametric models | Donahue | Summarize the planned use of simulations<br>Review of initial set of cases run |
| GM Logic Tree V1 | Wooddell | Present the GM Logic Tree Model V1 for hazard feedback:<br>– Base case;<br>– Form of the logic tree being considered. |
| Hazard feedback using the current GMPEs for DCPP | Gregor | Present sensitivity of hazard results using tornado plots for the following cases relative to the base case GMPEs:<br>– Individual GMPEs<br>– Individual GMPEs with fixed sigma=0.65<br>– Base case median GMPEs with individual GMPE sigma models<br>– Individual GMPEs with Phi sigma term adjusted<br>– Base case median GMPEs for strike-slip sources with individual GMPEs for reverse sources<br>– Base case median GMPEs for strike-slip sources with individual GMPEs for reverse sources all with fixed sigma=0.65<br>– Base case median GMPEs for reverse sources with individual GMPEs for strike-slip sources<br>– Base case median GMPEs for reverse sources with individual GMPEs for strike-slip sources all with fixed sigma=0.65 |
| Hazard feedback using the current GMPEs for PVNGS | Walling | Present sensitivity of hazard results using tornado plots for the following cases relative to the base case GMPEs:<br>– Individual GMPEs<br>– Individual GMPEs with fixed sigma=0.65<br>– Base case median GMPEs with individual GMPE sigma models<br>– Individual GMPEs with Phi sigma term adjusted<br>– Base case median GMPEs for strike-slip sources with individual GMPEs for normal sources<br>– Base case median GMPEs for strike-slip sources with individual GMPEs for normal sources all with fixed sigma=0.65<br>– Base case median GMPEs for normal sources with individual GMPEs for strike-slip sources<br>– Base case median GMPEs for normal sources with individual GMPEs for strike-slip sources all with fixed sigma=0.65 |

| | | |
|---|---|---|
| *Clarifications and questions* | | Which models are leading to the significant differences?<br>What are the limitations on existing ground motion models?<br>*Continued* |
| | | Have we captured all the relevant uncertainties? |

**Table 2:** Focused questions for Workshop #2 Presenters: Session "CANDIDATE FFS METHODS: Results of SCEC BBP Validation Evaluation"

| Topic | Speaker | Questions / Topics to be addressed at WS #2 |
|---|---|---|
| Overview of the validation process – Part A and B | Goulet | Summarize Part A and Part B of the validation effort (do not include the evaluation effort)<br>How were the acceptance criteria derived and are the acceptance criteria still consistent with the range of ACR GMPE's for California? |
| SCEC Evaluation Committee findings | Dreger | What models are ready for general application?<br>What were the uses of Part A and Part B evaluations for evaluating the models (which was most important?)?<br>Were any other relevant additional metrics considered? |
| Discussions:<br>*Strength and weakness of simulations models; Technical bases for applicability of the methods.* | All | Based on Sept 26 2013 SCEC meeting, is the output of the BBP consistent with the expectations from your method? Is there anything in the simulations that stand out as problematic?<br>Is there anything intrinsic to the method that would preclude using it to simulate very large magnitudes (M~8.0)?<br>– Are there constraints on the use of the magnitude-area relationship that you apply for your simulation method?<br>– Are there implications that arise from specifications of a minimum rupture width for large magnitudes?<br>Can the model be applied to both surface and buried ruptures?<br>– Are the Green's functions adequately sampling the shallow depth?<br>– How is the source modified in the top few kilometers of the crust (e.g. rise time, rupture velocity, etc…)?<br>Are there any limits in how close to the fault the ground motion simulations may be used?<br>How is kappa incorporated into the simulations? |

**Table 3:** Focused questions for Workshop #2 Presenters: Session "CANDIDATE FFS METHODS: Initial Forward Simulation Results"

| Topic | Speaker | Questions / Topics to be addressed at WS #2 |
|---|---|---|
| Comparisons of simulations and GMPEs for smaller magnitudes (M5.5-6.0) | Donahue | Discuss if the GMPEs' range captures the parameterization from simulation (focus on the median) for distances 1 to 25 km for a range of magnitudes for the cases that were run, i.e.:<br>– Are the HW effects for M 5.5- 6.5 (7.0) consistent with empirical GMPEs (1-25 km)? |
| *Discussion* | All | Is there anything intrinsic to the method that would preclude using it to simulate small magnitudes (M~5.5)?<br>– Is there a model resolution limit on the kinematic representations of the sub-faults?<br>– Given the specification of the sub-fault dimension, is there an effective bandwidth that we should be aware of?<br>Can the model be applied to both surface and buried ruptures?<br>– How is the source modified in the top few kilometers of the crust (e.g. rise time, rupture velocity, etc…)?<br>– If the prescribed rupture plane is mostly/fully contained in this shallow region, shallow fault dip cases, does the source modification still apply?<br>Are there any limits in how close to the fault the ground motion simulations may be used? |

**Table 4:** Focused questions for Workshop #2 Presenters: Session "Epistemic uncertainty tutorial"

| Topic | Speaker | Questions / Topics to be addressed at WS #2 |
|---|---|---|
| GMPEs visualization techniques: a methodology overview | Kuehn | Describe how the Sammon's maps and other visualization techniques show proximity of generic GMPEs.<br>What are the key assumptions needed to derive the visualization maps?<br>What are the limitations in these maps (strengths and weaknesses)? |

**Table 5:** Focused questions for Workshop #2 Presenters: Session "APPLICABILITY of GM MODELS TO THE TWO SITES"

| Topic | Speaker | Questions / Topics to be addressed at WS #2 |
|---|---|---|
| GMPEs comparison and identification of issues | Gregor | Summarize philosophy of scaling and main predictive variables for each GMPE.<br>Summarize the key differences between median and standard deviation of the candidate GMPEs for each of the two NPP sites for the controlling sources. |
| NGA West 2 GMPEs | All NGA-West2 Modellers | Basis for the changes in conceptual models/approaches from 2008 to 2013?<br>What is your estimate of the uncertainty on the normal fault factor?<br>What is your estimate of the uncertainty on the hanging wall factor?<br>What is your estimate of the uncertainty for M 8.0 at 5 km and 300 km?<br>What is your estimate of the uncertainty in the standard deviation? |
| ASK13/14 GMPE | Abrahamson | What is the constraint on the large distance scaling at long periods? (Why is the model so much higher than other developers, particularly in the long period range (>1 sec) at large distance? (PVNGS specific case))<br>What is the influence of aftershocks to phi and tau? |

| | | |
|---|---|---|
| CB13/14 GMPE | Bozorgnia | What is the basis for the shift in the peak of the spectrum towards higher frequencies as compared to the other NGA-w2 models?<br>Is the bump in the sigma at 10 Hz seen in the Calif. data or is it driven by Japanese data? What is a conceptual model for 10 Hz bump in tau? |
| | | *Continued* |
| BSSA13/14 GMPE | Boore | Is the $R_{JB}$ distance metric effective at capturing HW effects for dips < 30 degrees? (is there a limit of applicability for low angle dipping events and large magnitude events?);<br>What is the basis for no Ztor scaling? (show plots of event terms versus Ztor)<br>What is the uncertainty in their distance-dependence sigma for large distances? (PVNGS specific case);<br>Is the bump in the sigma at 10 Hz seen in the Calif. data or is it driven by Japanese data? What is a conceptual model for 10 Hz bump in tau? |
| Idriss 13/14 GMPE | Idriss (could not attend in person) | Is the shift in the peak for M6.8, Dip 45 (specific for Los Osos case) due to Vs-scaling?<br>What is the basis for the extrapolation to 1 km distance for SS faults at large magnitudes (M~7.0+) (specific for Shoreline);<br>What is the basis for no Ztor scaling? (show plots of event terms versus Ztor)<br>What is the basis for no HW scaling? (show plots of within event residuals versus distance on the HW) |
| CY13/14 GMPE | Youngs | What is the basis for ignoring the bump in tau at 10 Hz? |
| Graizer&Kalkan13 GMPE | Graizer and Kalkan | What is the process you used to estimate the standard deviation? In deriving sigma, was the correlation between residuals through the event terms accounted for?<br>What constraints were applied for magnitude scaling between M7-M8?<br>How many (and which percentage of the earthquakes) show the “bump” in the distance attenuation in the near-fault region?<br>How were the SoF factors derived, in particular for Normal Faults?<br>What is the basis for no Ztor scaling? (show plots of event terms versus Ztor);<br>What is the basis for no HW scaling? (show plots of within event residuals versus distance on the HW). |
| ASB13 GMPE; Summary of other Pan-European GMPEs | Akkar | Did you evaluate the magnitude dependence of the standard deviation? Is the standard deviation applicable to large magnitudes? Show the standard deviation for data with M >= 6;<br>What is the cause of the sharp reduction in sigma from 3 to 4 seconds?<br>Plot event terms residuals vs depth (any type, i.e. either hypo depth or Ztor);<br>Summarize the new set of pan European models being published on BEEE;<br>What are the Normal Faulting factors in the pan-European models?<br>Is a magnitude dependence of the Normal Faulting factors evaluated? |
| Update M scaling for Zhao’s GMPE for large Magnitude crustal earthquakes | Abrahamson | What is the current approach to implement Zhao and Lu (BSSA, 2011) magnitude adjustment? |
| Visualization of epistemic uncertainty to GMPEs | Kuehn | Show application of the epistemic uncertainty visualization for the candidate models. |

| | | |
|---|---|---|
| *Discussions: Do we have enough models to capture the CBR?* | All | Does the epistemic uncertainty in the candidate models capture the CBR of the TDI? Do we need to add to it?<br>Do the regional dataset provide improved constraints on specific aspects of the scaling such as Normal Faulting effects? |

**Table 6:** Focused questions for Workshop #2 Presenters: Session "PATH EFFECTS"

| Topic | Speaker | Questions / Topics to be addressed at WS #2 |
|---|---|---|
| Additional Seismic Instrumentation at DCPP | McLaren | Are there data to constraint path effects for offshore (from OBS) and onshore sources?<br>Installation of additional seismometers at DCPP to improve path effects. |
| *Discussions: Path effects in Arizona and generic 1D vs 3D effects* | All | What is the regional difference between Q in Arizona and in California for the same assumed geometrical spreading?<br>What is the impact of Q difference at distance 250-350 km? |
| | Toro | Comparison of 2010 PVNGS specific model with NGA West 2 GMPEs. |
| | Mayeda | Azimuths showing Q along "Salton trough" and "north of Salton trough" |
| | Pitarka | Show the average difference and the standard deviation of the difference obtained using a 3 D crustal velocity model for the simulations, as compared to the 1 D crustal velocity model.<br>– Do you see any correlation with the basin depths?<br>Show the bias plots of the simulations with respect of the empirical data using 1D and 3D crustal structure<br>– Do the 3D simulations fit the data better that the 1D simulations? If so, how much better?<br>– Are the 3D simulations systematically lower or higher?<br>Do the 3D simulations explain the apparent long period bias in the spectral acceleration? (Over-prediction of PSa at T>1 s - particularly >3s, wrt GMPEs and data). |

**Table 7:** Focused questions for Workshop #2 Presenters: Session "CANDIDATE MODELS for SIGMA"

| Topic | Speaker | Questions / Topics to be addressed at WS #2 |
|---|---|---|
| Summary of traditional sigma from GMPEs models for reference rock conditions | Al-Atik | Summarize the candidate GMPEs sigma models, discussing the need for magnitude and/or distance dependence. |
| Proponent single station sigma (SSS) models from the PEER sigma group | Al-Atik | Method used to derive NGA West 2 SSS models;<br>Comparison with other existing SSS models;<br>Discuss the site-to-site variability of the suite of models.<br>What are the ranges for the $\phi_{S2S}$ values?<br>What is the cause for the short-distance small magnitude increase for the SSS? Is it due to focal mechanism?<br>Uncertainty of SSS models. |
| Proponent single-path sigma | Abrahamson | What is the uncertainty on the single path sigma?<br>Are the AZ data consistent with the Calif. Single path sigma? |
| *Questions and Discussions on* | Rodriguez-Marek | Considering the Japanese data:<br>– Discuss the site-to-site variability of his models. |

| | | |
|---|---|---|
| *Sigma models* | Rodriguez-Marek | – What are the ranges for the $\phi_{S2S}$ value |
| | Baker | Show the standard deviation between sites as a function of closeness index in California |

**Table 8:** Focused questions for Workshop #2 Presenters: CANDIDATE METHODS of ADJUSTEMTS to GMPEs: Changing Rake, Dip Along Strike"

| Topic | Speaker | Questions / Topics to be addressed at WS #2 |
|---|---|---|
| DCPP scenario for complex ruptures | Donahue | What are the options for accounting variations of dip and rake along strike in GMPEs?<br>Show forward application for DCPP |
| Proponent approach based on NGA West 2 residuals | Di Alessandro | Summarize the available empirical data;<br>Is it sufficient to constraint the effect? |
| *Discussions* | GMPEs Modellers | What is the intended forward approach for your model for complex ruptures? |
| | Simulation Modellers | Alternative methods for modeling the slip on the secondary rupture?<br>Should we also consider a dynamic rupture simulation? |

**Table 9:** Focused questions for Workshop #2 Presenters: Session "CANDIDATE METHODS of ADJUSTEMTS to GMPEs: Directivity"

| Topic | Speaker | Questions / Topics to be addressed at WS #2 |
|---|---|---|
| *Discussions on directivity models* | GMPEs Modellers | For incorporating directivity, discuss the approach of the sigma/median adjustment versus the sigma only adjustment. |
| | Baker | Provide a status update of your Tp model.<br>Does it lead to a similar net-sigma change as the GMPE method?<br>Show impact on median and sigma. |

**Table 10:** Focused questions for Workshop #2 Presenters: Session "KAPPA"

| Topic | Speaker | Questions / Topics to be addressed at WS #2 |
|---|---|---|
| Kappa at DCPP: *Values and effects* | Ktenidou | What are the estimates and the uncertainties on the kappa values?<br>Plot kappa along the $V_{S,30}$ – kappa scaling plots. |
| Plan on collecting $V_{S,30}$ for AZ recording stations sites | Di Alessandro | Describe the envisioned scope of work and schedule for Rob Kayen to perform site characterization at selected recording sites |
| Kappa at PVNGS: *Update on AZ GM data* | Ktenidou | Provide an update on the ground motion data collected from selected Arizona stations |
| *Discussions* | All | Discussion on kappa estimates at DCPP |

**Table 11:** Focused questions for Workshop #2 Presenters: Session "CANDIDATE METHODS of ADJUSTEMTS to GMPEs: Splay Faulting / Branch Faulting"

| Topic | Speaker | Questions / Topics to be addressed at WS #2 |
|---|---|---|
| Strike Slip Splay using dynamic rupture models | Lozos | What is the envisioned approach to evaluate SS Splay using dynamic rupture models?<br>How does the connection point look like? Is there an agreement among the code validation community?<br>Based on preliminary results, what does the source look like on the splay fault? A separate earthquake? An evolution of a bigger one? |
| Splay faulting adjustments factors using kinematic approach | Wooddell | What are the options for accounting for splay faulting in GMPEs?<br>Describe kinematic simulation cases planned for splay rupturing;<br>Show preliminary results. |
| *Discussions* | All | |

**Table 12:** Focused questions for Workshop #2 Presenters: Session "CONSTRAINTS FROM FRAGILE GEOLOGIC FEATURES (FGF)"

| Topic | Speaker | Questions / Topics to be addressed at WS #2 |
|---|---|---|
| FGF near DCPP – Constraints on Hazard | Stirling | What FGF are available at DCPP to constraint hazard?<br>How fragile are these features?<br>Talk about initial estimates of fragility |

# GROUND MOTION CHARACTERIZATION PRESENTATIONS

**Day 1 Introduction**

- Welcome and Introduction to the SWUS GMC WS #2 – Carola Di Alessandro (*GeoPentech, Inc.*)
- SSHAC Procedures and Workshop rules– Carola Di Alessandro (*GeoPentech, Inc.*)
- Project Overview and Status of Data Needs – Norman Abrahamson (*Pacific Gas and Electric Company*)

**Day 1 Proponent/Resource Experts Presentations**

- Summary of the candidate GMPEs for ACRs – Nick Gregor (*NG Consulting*)
- Summary of current BBP results – Jennifer Donahue *(Geosyntec)*
- GM Logic Tree V1 - Kathryn Wooddell (*Pacific Gas and Electric Company*)
- Hazard feedback using the current GMPEs for DCPP- Nick Gregor (*NG Consulting*)
- Hazard feedback using the current GMPEs for PVNGS - Melanie Walling (*Lettis Consultants International, Inc.*)
- Overview of the validation process – Part A and B – Christine Goulet (*PEER Center - Univ. of California, Berkeley*)
- SCEC Evaluation Committee findings – Doug Dreger (*Univ. of California, Berkeley*)
- Introduction to Modelers' Panel Discussion on Finite Fault Simulations – Doug Dreger (*Univ. of California, Berkeley*)
- Graves & Pitarka Proponent Model – Robert Graves (*U.S. Geological Survey, Pasadena*)
- SDSU Proponent Model – Kim Olsen *(San Diego State University)*
- Comparison of simulations and GMPEs for smaller magnitudes (M5.5 and 6.0) - Jennifer Donahue *(Geosyntec)*
- GMPEs visualization techniques: a methodology overview – Nicolas Kuehn *(Potsdam Univ., Germany, and PEER Center - Univ. of California, Berkeley)*

**Day 2 Introduction**

- Reminder of project objectives, rules of conduct and key sensitivity results – Norman Abrahamson *(Pacific Gas and Electric Company)*

**Day 2 Proponent/Resource Experts Presentations**

- GMPEs comparison and identification of issues – Nick Gregor (*NG Consulting*)
- NGA West 2 GMPEs: Abrahamson et al. (ASK13/14) Proponent Model – Norman Abrahamson *(Pacific Gas and Electric Company)*

- NGA-West2 GMPEs: Campbell & Bozorgnia (CB13/14) Proponent Model – Yousef Bozorgnia (*PEER Center - Univ. of California, Berkeley)*
- NGA-West2 GMPEs: Boore et al. (BSSA13/14) Proponent Model – David Boore (*U.S. Geological Survey, Menlo Park*)
- NGA-West2 GMPEs: Chiou & Youngs (CY13/14) Proponent Model – Robert Youngs *(AMEC Geomatrix)*
- Graizer & Kalkan Proponent Model – Vladimir Grazier *(US NRC)* and Erol Kalkan (*U.S. Geological Survey, Menlo Park*)
- Akkar et al. (ASB13) Proponent Model – Sinan Akkar *(Middle Eastern Technical Univ.)*
- Summary of other Pan-European GMPEs – Sinan Akkar *(Middle Eastern Technical Univ.)*
- Proponent implementation of Zhao and Lu (2011) large Magnitude scaling for crustal earthquakes - Norman Abrahamson *(Pacific Gas and Electric Company)*
- Visualization of epistemic uncertainty to GMPEs – Nicolas Kuehn *(Potsdam Univ., Germany, and PEER Center - Univ. of California, Berkeley)*
- Discussion on the Center, Body and Range of the Technically Defensible Interpretations - Robert Youngs *(AMEC Geomatrix)*
- Additional Seismic Instrumentation at DCPP – Marcia McLaren *(Pacific Gas and Electric Company)*
- Discussion on Path Effects for Arizona: Southwestern Lateral Q Variations – Kevin Mayeda (*Univ. of California, Berkeley)*
- Discussion on Path Effects for Arizona: Path effects for PVNGS – Gabriel Toro (*Lettis Consultants International, Inc.*)
- Comparison of 3D and 1D wave propagation effects in the San Francisco Bay Area – Arben Pitarka *(Lawrence Livermore Natl. Laboratory)*

**Day 3 Proponent/Resource Experts Presentations**

- Introduction of envisioned approaches for sigma at the two NPP sites – Norman Abrahamson *(Pacific Gas and Electric Company)*
- Summary of traditional sigma from GMPE models for reference rock - Linda Al Atik *(Alatik Consulting)*
- Proponent single station sigma (SSS) models from the PEER sigma group - Linda Al Atik *(Alatik Consulting)*
- Proponent single-path sigma approach – Norman Abrahamson *(Pacific Gas and Electric Company)*
- Discussion on sigma models: Proponent single station sigma model – Adrian Rodriguez-Marek *(Virginia Tech)*
- Discussion on sigma models: Influence of Spatial Correlation to Sigma – Jack Baker *(Stanford Univ.)*
- DCPP scenario for complex ruptures – Jennifer Donahue *(Geosyntec)*
- Proponent approach for complex ruptures based on NGA West 2 residuals – Carola Di Alessandro *(Geopentech, Inc.)*

- Preliminary κ estimation for DCPP – Olga-Joan Ktenidou *( ISTerre and PEER Center – Univ. of California, Berkeley*)
- Plan on collecting $V_{S,30}$ for AZ recording stations sites – Carola Di Alessandro *(Geopentech, Inc.)*
- Issues in κ estimation for Arizona (PVNGS) – Olga-Joan Ktenidou *( ISTerre and PEER Center – Univ. of California, Berkeley*)
- High Frequency Rock Issues Being Addressed at PEER 2013-2015 - Yousef Bozorgnia (*Univ. of California, Berkeley)*
- Discussion on Directivity: Adjusting sigma to account for directivity – Jack Baker (*Stanford Univ.)*
- Strike Slip Splay using dynamic rupture models – Julian Lozos (*PEER Center – Univ. of California, Berkeley*)
- Splay faulting considerations using kinematic approach – Kathryn Wooddell *(Pacific Gas and Electric Company)*
- Fragile Geologic Features (FGF) near DCPP – Constraints on Hazard – Mark Stirling (GNS Science)

## TECHNICAL INTEGRATOR TEAM SUMMARIES and ACTIONS

# Day 1 Summary

- Is the set of candidate GM models broad enough to capture the full range?
  - Is there a credible method applicable to DCPP or PVNGS (TDI) that would give very different results that we are missing?
    - Slap down phase
- Extend hazard feedback to 5 sec
- Part B for small magnitude (M5.5) is there a elevated long period motions
- Check new CyberShake (M8) in long periods to compare with the 1D calculations
- Correct ASB plots (Donahue-HW)
- Check SDSU plots for CY'08 – M5.5 (HW)
- Consider asymmetric distributions of epistemic uncertainty – "body" of the uncertainty
  - Some aspects of models will be asymmetric
  - Avoid assuming symmetric distributions without a clear technical basis for the "body"
- Aleatory Variability for HW sites using FFS
  - To date, FFS have not been validated for the aleatory variability
  - Try using FFS to compare the variability for FW sites with the variability for HW sites

- FFS at long periods (T>3s)
  - Summarize the surface slip distributions from the rupture generators (for different magnitudes)
  - Check that the peak displacements of the simulations are consistent with the surface slip
- HW effects for different FFS methods
  - In addition to PSA values, compare normalized HW scaling (set to unity at Rx=-10 km) to compare with the empirical models
- HW effects for M5.5
  - If the radiation pattern becomes more deterministic at higher freq for smaller magnitudes, does this affect the applicability of the FFS down to M5.5 for freq near 5 Hz?

# Day 2 Summary

## NG – Comparisons of GMPEs for specific scenarios and M & R scaling

- Consistency check
  - Compare the hazard for surface slip with the hazard for long period ground motions

## ASK13

- HW for small magnitudes - is current magnitude taper too strong?
- Effect of aftershocks on sigma
  - Provide a table of the sigma with and without the aftershocks

# CB13

- Shift at high freq
  - May be due to differences in the VS30 scaling
    - Check the residuals against VS30 for all 5 NGA-west2 models
    - Does this explain the shift seen in CB13 compared to other NGA-west2 models?
  - Consider using a lower reference rock VS30 (e.g. 500 m/s)
    - Better constrained empirically
- Bump in tau at 10 Hz
  - Seen in data (not just Japan)
    - Check the tau by region for all NGA-west2 models
- Should there be smoothing of variance terms?

# BSSA13

- Uncertainty in the normal faulting factor
  - Tabulate the standard error of the mean of the normal faulting event terms (for the uncertainty in the NML faulting factor)
  - About ±0.1 for T=0.2 sec
- Ability of RJB to capture HW effects for low dips and large Mag
  - Possibly plot the mean HW residuals for short distances for dip&mag bins.
- For distance dependence of sigma
  - show the distance-binned values of sigma for Japan and non-Japan separately
- Bump in tau at 10 hz,
  - Check the conceptual model of bump being due to stress-drop variability using the point source model.
    - Youngs showed this is not seen in point source simulations
    - Check this

# CY13

- Uncertainty in sigma
  - Provide a table of the statistical uncertainty in phi and tau for periods of 0.01 to 10 sec
- Bump in tau at 10 Hz
  - Is kappa is mapped into event terms due to the correlation of kappa over the set recorded ground motion?
  - If so, then need to find a way to remove this from tau (PEER task) for use in single-station sigma
  - Evaluation of downhole data versus surface data may help to separate these effects

# GK13

- HW effects
  - Plot residuals for HW sites using NGA-west2 data
  - Compare tradeoff of HW effects with distance "bump"
- Hypo depth effects
  - Plot residuals of event terms versus hypo depth
- Sigma
  - Provide a table of phi and tau (not just total sigma)

# ASB13 & European Models

- Depth scaling
  - No depth scaling observed in event terms
  - Is there a trade-off between magnitude scaling hypo depth?
    - Plot event terms versus depth for a small mag range (e.g. M5-M6) to avoid correlations between depth and mag
- Sigma
  - Is the large difference between European and NGA sigma due to phi or tau?
    - Provide a table of the sigma separated into phi and tau for the ASB model
  - Also well versus poorly recorded (min number per eqk)
  - Phi by distance bin (e.g. < 70 km and > 70 km)
  - Separate by mag bin (e.g. M>5.5)
- Applicability to SWUS
  - ABS13 and Bindi13 are candidate models for SWUS
  - Other models are more research models that may have difficulties for applications

# Zhao and Lu (2011)

- No magnitude scaling above **M** 7
- Need to get response from Zhao on how to implement concept
- Check NGA/Other models for similar effects
- Are their instrumentation issues
- K. Olsen: recent BBP simulations with plasticity effects (near source) may indicate similar behavior, need to look at this for different magnitudes.

# Visualization of Epistemic Uncertainty Capturing the CBR of the TDI

- Explore implied GMPEs from cells of SOM away from models to see if they are in the TDI
- Include predictions from simulations in SOM/GMPE generators to check the "R" of the CBR
- Use the visualization approach as guidance along with "traditional" approaches iteratively to established CBR of the TDI
- Explore usage for smaller M/R space or use of hazard based weighting functions
- Possibly explore more formal use of Bayesian approaches

# DCPP – Additional Instrumentation

- Ocean bottom recordings – issues with ocean noise
  - Data may be available from some events, data needs to be retrieved and analyzed from temporary stations
  - Some data is currently available at USGS
- Onshore – some recordings, but noisy, looking for new site

# PVNGS

- Q variation maps
  - based on Lg
  - Strong azimuth variation
  - Can integrate 1/Q for specific paths from distant, active sources
- Range of NGAW2 at large distance generally consistent with previous adjustments
  - Need to check with data from Arizona
  - Need to build a model that will allow adjustments for different Q (translation between gamma and Q more explicit in model)
- 1D vs 3D path effects
  - Improvement in fits for Loma Prieta using 3D vs 1D for periods > 2 sec
  - Adding topography and statistic variation does result in further large improvements at low frequencies
  - Suggest using 1D with smooth velocity variations to approximate 3D effects – need to be careful to not over smooth
  - More cases need to be analyzed

# Day 3 Summary
# Sigma

- Application of single-station sigma using geotechnical modeling
  - Part of the site term is at the bedrock layer, so if the geotechnical modeling is used, it will only capture part of the site term.
    - Need to include the epistemic uncertainty in the bedrock layer GM
    - Consider period dependence
- Form of GM distribution
  - The standard approach assumes lognormal. This may not apply to highly non-linear cases and at long periods
    - Check distributions of slip from FFS rupture generators
    - Consider alternative to lognormal distribution
    - This may be a greater issue for the reduced PhiSS and PhiSP approaches
- Data collection for single-path sigma
  - Identify the optimal station coverage needed to support the collection of GM data for use in single-path sigma

- Increase at short dist for small Mag
  - Can this be explained by the uncertainty in the hypocenter depth?
- Estimation of PhiSP
  - Consider using the reduction at a closeness index of the smallest data (CI ~ 0.05), not extrapolated to shorter CI values
- Effect of spatial correlation on estimates of phiSSand tau
  - Evaluate bias in PhiSS due to spatial correlation (Baker)
    - Use NGA-west2 with site terms
- 10Hz bump in sigma
  - Seen at surface, but not borehole stations
  - Indicates this is a site term

# Complex & Splay Ruptures

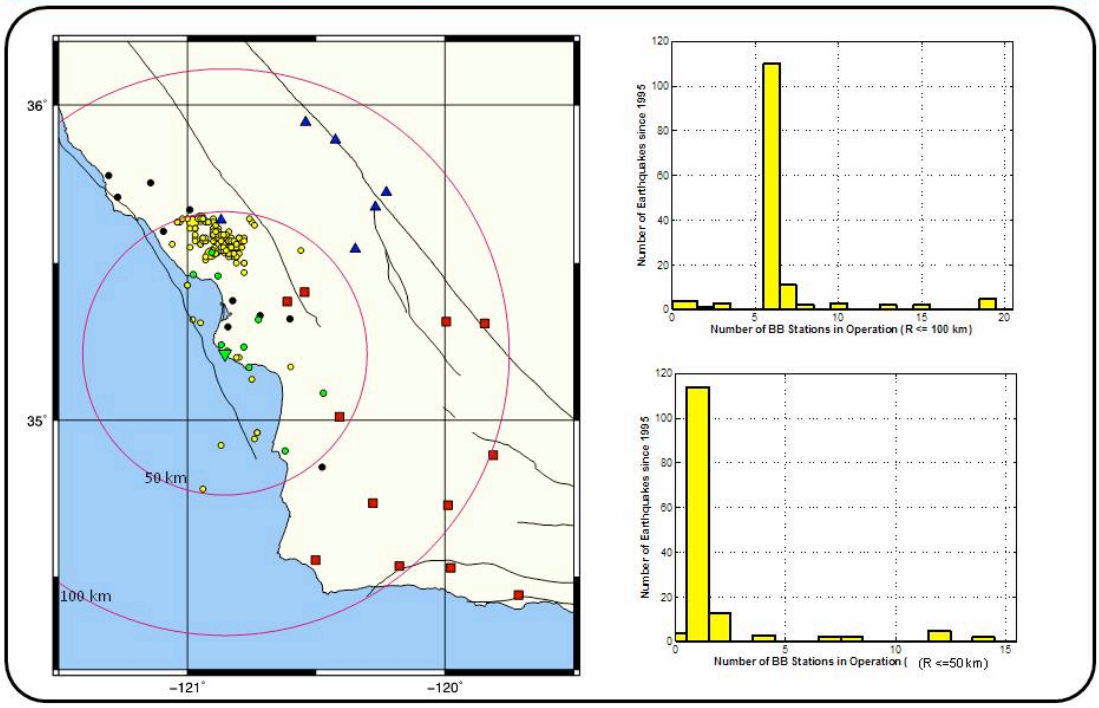
- Need simplified parameters to input into GMPEs
  - Includes rake (all sites) and dip (for HW sites)
  - Many complications, but can the FFS help inform the selection of a simplified method?
- Complex ruptures
  - Consider a broader range of hypocenter locations
  - Also use dynamic ruptures to guide secondary source
  - Consider using the nga-west2 complex FF inversions as inputs to a denser grid of stations

- Splay ruptures
  - Need to normalize the FFS based on the SA from the main rupture without the splay
  - Magnitude (total or separate sources ) is key for low frequencies
  - Hypocenter locations on the splay
    - For restraining branch, consider a jumping of the hypocenter
  - Rupture Generator for splay
    - Use the dynamic rupture runs to guide the relative amount of slip on the splay compared to the main rupture
      - And rupture tapering
    - Check geologic data for constraints
    - Rupture may start on the splay and go onto main fault
- Width of the rupture for large magnitudes
  - Needs to be addressed by SCEC BBP group

# Kappa

- DCPP
  - Add additional (less well recorded) small mag eqk recorded by the central coast network to the PEER data set
    - About 10 eqk with N>5 within 50 km of DCPP
- PVNGS
  - Correcting the AZ GM data for the site amplification is key
    - Interpretation of the SASW for site characterization should be extended to the maximum depth possible to try to capture as the full soil profile
    - Request uncertainties on the dispersion curve and inversion
  - Complete processing with QA
  - Check with AGS for other data that may have better high freq band width
  - High freq rock issues – longer term effort needed to expand range of applicability of gmpes

## Regional Ground Motion Data: CCSN Coverage Near DCPP



# Directivity

- Implementation of Shahi & Baker model
  - Current model shows no increase in sigma, but the change in the median (0.15 to 0.3) could be incorporated into the sigma
  - Model/method is being further evaluated to understand why the sigma did not increase
    - Not ready in current form
- Check with Spudich on his evaluation of the PEER working group directivity models.

# Dynamic Rupture Models

- Prioritize the best use of dynamic rupture model
  - Velocity model effects
    - Contrast across fault using 1-D models
    - Issues for this case in the code verification
  - Dip of splay fault
    - Consider a range of dips
  - Uses
    - Constraints on kinematic source inputs
  - Source characterization in terms of relative rates of splay fault ruptures
    - Dynamic rupture results may put limits on the complex or splay ruptures that are possible under the regional stress field

# Fragile Geologic Features

- Date samples taken for Double Rock East
  - If > 1000 yrs in the fragile position, then it could provide constraints on the hazard
- If ages are old enough, then develop 3-D models for Double rock and three other FGFs
- Check on the review of FGFs near PVNGS

# Overall Summary

- Data needs tasks
  - Some tasks not complete yet
    - Some new tasks identified in WS2
  - Need to complete by Feb 2013 or capture as increased uncertainty
- Candidate models
  - Median GMPEs:
    - Replace Bindi et al (2011) with Bindi et al (2013)
    - Add modified Zhao (2006) with Zhao and Lu (2011) mag scaling
  - Additional FFS scenarios
    - Median large Mag (M7 to M8) scaling
    - Complex and splay ruptures
  - Sigma models
    - Complete (and document) candidate single-station and single-path sigma models

- Epistemic model
  - Exploration using visualization tools
- Arizona data evaluation
  - Kappa
  - Path effects
- Directivity
  - Fold into sigma, but check with CY13 models
- March 2014 Workshop
  - Begin with a WS2 (proponent models) type workshop
    - Include the broad group of resource and proponent experts from Oct 2013 WS2
  - Follow with preliminary evaluation by TI team

# LETTER COMMENTARY FROM THE PARTICIPATORY PEER REVIEW PANEL

December 3, 2013

Carola Di Alessandro, Ph.D.
Project Manager for the SWUS GMC Project
GeoPentech, Inc.
525 N. Cabrillo Park Drive, Suite 280
Santa Ana, CA 92701

Dear Dr. Di Alessandro:

This letter comprises the comments of the Participatory Peer Review Panel (PPRP) on Workshop #2 (Proponent Models and Alternative Interpretations) of the Southwestern U.S. Ground Motion Characterization (SWUS GMC) project. Workshop #2 was held on October 22-24, 2013, in Berkeley, California. The PPRP participated as observers, to monitor the progress of the SWUS GMC project and provide a review of both the process and the technical developments. All four members of the PPRP (K. Campbell, B. Chiou, S. Day, and T. Rockwell) were present for the full workshop and observed all workshop sessions. The panel also met at regular intervals during the workshop to assess its effectiveness in probing the proponent models and in adhering to SSHAC Level 3 procedural guidelines.

The workshop was very well planned and conducted. We appreciate the organizational efforts of the Project Management team, and, in particular their hospitality and attention to our requirements as a review panel. The location and facilities were excellent, and most proponent and resource experts were able to participate for the full three days. The presence throughout the workshop of a critical mass of experts resulted in very focused and thorough discussion of proponent models, key technical issues, and progress on ongoing studies.

**Summary Comments**

The technical program was very well prepared by the Technical Integration (TI) team to address appropriate Workshop #2 goals in depth. Those goals are to present, discuss, and debate alternative technical viewpoints, identify alternative hypotheses and their uncertainties, and provide a basis for development of hazard models that consider the full range of alternative technically defensible interpretations. The team made this large task tractable within the confines of a three-day workshop through several devices that maintained focus without sacrificing depth and completeness of the discussions. First, the workshop began with a series of hazard sensitivity presentations that were well designed to provide workshop participants a shared understanding of the key issues. These presentations were very effective in directing subsequent discussions. Second, the TI team prepared well thought-out questions for each proponent expert and submitted these to the experts in advance. Those questions provided good direction to the presenters and guidance to the discussions. At the same time, the format was kept open enough to ensure that potentially relevant issues, concerns, and models not anticipated by the TI team could be proposed and explored, and several such examples received valuable discussion.

Each resource-expert or proponent-expert presentation was well chosen and each provided thorough coverage of a relevant study or model and included a list of references. The TI team interrogated all presenters effectively and led general discussions that successfully engaged the wider audience of ground motion experts. As we note in our recommendations below, most of the questioning during the first part of the workshop came from just a few of the TI team members. The PPRP encouraged all five members of the TI Team to bring their voices to bear in this process, and by the end of the workshop we were pleased to see progress toward a more balanced engagement of all team members. The overall process was successful in revealing the strengths, weaknesses, and uncertainties of the competing models, and, except as noted in the recommendations listed below, the PPRP is unaware of relevant issues that were not explored.

With respect to adherence to procedural guidelines, as well as with respect to technical quality, the workshop conformed well to standards for a SSHAC Level 3 workshop on alternative models and interpretations. There are some remaining issues of completeness that should be considered prior to Workshop #3, and these are noted, along with other issues to consider, in the comments and recommendations below. Those specific comments or recommendations that require a written response are underlined.

**Recommendations**

***1. Balanced participation by the TI team members.*** During the first two days of the workshop, a disproportionate amount of the interrogation of the proponent experts was done by the TI lead, with some contributions from other senior members of the team. Other members were not significantly engaged in the discussions on those days. This imbalance is a concern, because SSHAC guidelines for a Level 3 study explicitly call for TI team members to be prepared to voice independent views and technical challenges. The PPRP was pleased to see more balanced participation on the third day and recommends that the TI team take concrete steps to ensure that this progress continues during the remainder of the project. The importance of full TI team participation is emphasized in the NRC SSHAC guidance document (NUREG-2117), which states, for example (p. 36) "*membership in the TI team automatically implies sharing the ownership of the component models developed by that team,*" and (p. 38), while discussing the distinction of a Level 3 SSHAC study in contrast to lower level SSHAC studies, "*The TI must now be a team rather than an individual or small group, . . .at Level 3, this is essential both because no individual has the breadth of expertise required and because of the necessity for technical challenge and defense among the evaluators.*"

***2. Selection criteria and decision date for GMPEs.*** Some of the ground motion prediction equations (GMPEs) presented and discussed at the workshop appeared to the PPRP to be at a less mature stage of development than the others. For example, one has not yet been fully described and documented in a formal publication. We recommend that the TI team formulate and document, as soon as possible, clear criteria to be employed to determine which GMPEs will be used in hazard model development, and that documentation of the acceptance criteria include a justification, and that it specify a firm

cutoff date for achievement of the criteria, based on a realistic assessment of schedule requirements. The selection criteria should be applied on a consistent basis to all candidate GMPEs.

*3. Completeness of proponent-model analysis in Workshop #2.* The project team made a thorough effort to identify, select, and invite proponents of alternative interpretations. Not all invited proponents were able to attend the workshop. In the absence of a proponent to support the GMPE and magnitude-scaling recommendations of Dr. Zhao and his colleagues, their viewpoints on magnitude scaling of ground motion were solicited and presented by the TI Team; therefore an opportunity existed at the workshop to discuss and challenge them. This approach was fully consistent with guidance in the NRC SSHAC guidance document (NUREG-2117) (p. 70), which states, for example: "*Because not all proponents of alternative viewpoints may be able to attend the workshop, interpretations made by individuals who may not be present should be identified and discussed.*" On the other hand, Dr. Idriss (author of the Idriss NGA-West2 GMPE) and Drs. Atkinson and Assatourians (developers of the finite-fault stochastic simulation method, EXSIM) also were absent, yet no representatives were designated to represent their models. As a result, discussion and debate of the merits of these two models were largely incomplete. The PPRP recommends that the TI team make an additional effort to complete the evaluation of these two proponent models at a level equal to that of the other models being evaluated. It should take place before the development of preliminary hazard models, and in a setting consistent with NUREG 2117, which stipulates (p. 39) that in a Level 3 study, the interactions with proponent experts should be "*conducted openly in the presence of observers including the PPRP.*"

*4. Completion of Workshop #2 objectives*. The PPRP noted that there were many ongoing tasks that could not be evaluated in Workshop #2 because they were either incomplete or had just begun. The TI lead pointed out during the workshop that these tasks will need to be fully discussed and evaluated in order for the TI team to obtain feedback from the resource and proponent experts to factor into their evaluation. The PPRP agrees that there is the need for an additional meeting with resource and proponent experts, including the PPRP as observers, to cover these ongoing and incomplete tasks. The PPRP emphasizes, moreover, that sufficient time should be allowed between such a meeting and Workshop #3 to enable the TI Team to fully evaluate and discuss the feedback from the meeting and incorporate that feedback into the preliminary ground motion logic tree and the related sensitivity studies that will be presented and discussed in Workshop #3. This concept is embodied in the NRC SSHAC guidance document (NUREG-2117) that states (p. 67) "*Any new data collection activities should be identified early in the project, evaluated for their potential impact on the hazard results and associated uncertainties, and completed in a timely manner for use in the technical evaluations. Typically, this would mean that the activities should be completed prior to Workshop #3 on Feedback and certainly no later than the time that the models are finalized*; (p. 68) *Each workshop has a specific focus and goal, and each requires that particular work activities have been conducted prior to its occurrence and certain work activities will occur following*;" and (p. 73) "*Following Workshop #2 and prior to Workshop #3 Feedback, multiple working meetings will be necessary to develop a*

*preliminary model that can be used for purposes of sensitivity analyses to provide the necessary feedback to the TI Team.*" TI Team should consider scheduling this additional meeting such that there is sufficient time between it and Workshop #3 to prepare and revise the preliminary ground motion logic tree and to perform related sensitivity studies.

*5. Schedule and prioritization*. Over the course of the workshop, numerous technical issues that are currently under investigation were identified as requiring substantial further work before certain modeling procedures can be included in a hazard model. The PPRP is very pleased that the project has initiated important investigations that are likely to have a big impact over the longer term, and the fact that some will not reach full practical implementation during this project is understandable and inevitable in an effort such as this one. As the TI lead noted, in the short term, incomplete resolution of these technical issues can be accommodated in the hazard model through appropriate expansion of epistemic uncertainty estimates. The PPRP urges, however, that the TI team reach a prompt decision on which efforts to prioritize for inclusion in the hazard model. That decision should consider hazard sensitivities, and should be made early enough to realistically account for project schedule requirements. For example, by Workshop #3, which is scheduled for March 2014, a preliminary hazard model should have sufficient maturity that the PPRP and others can meaningfully probe its technical basis and understand the manner in which it incorporates the views of the larger technical community. We also note that a preliminary report is due for PPRP review within just a couple of months following Workshop #3.

Please feel free to contact us if you would like to discuss further our comments or recommendations.

Sincerely,

Steven M. Day
Chair, PPRP

Kenneth W. Campbell
Member, PPRP

Brian Chiou
Member, PPRP

Thomas Rockwell
Member, PPRP

# TECHNICAL INTEGRATION TEAM LEAD RESPONSES TO PARTICIPATORY PEER REVIEW PANEL COMMENTS

January 6, 2013

Steven M. Day
Chair, Participatory Peer Review Panel
Department of Geological Sciences
San Diego State University
5500 Campanile Drive
San Diego, California 92182

Dear Prof. Day:

The TI Team and PM appreciate the valuable comments and suggestions received from the Participatory Peer Review Panel (PPRP), both during the Workshop No. 2 execution and in their formal letter commentary dated December 3, 2013. The present document serves to provide written responses to specific comments, suggestions, or recommendations that the PPRP identified (by underlining).

1. ***Balanced participation by the TI team members.*** During the first two days of the workshop, a disproportionate amount of the interrogation of the proponent experts was done by the TI lead, with some contributions from other senior members of the team. Other members were not significantly engaged in the discussions on those days. This imbalance is a concern, because SSHAC guidelines for a Level 3 study explicitly call for TI team members to be prepared to voice independent views and technical challenges. <u>The PPRP was pleased to see more balanced participation on the third day and recommends that the TI team take concrete steps to ensure that this progress continues during the remainder of the project.</u> The importance of full TI team participation is emphasized in the NRC SSHAC guidance document (NUREG-2117), which states, for example (p. 36) *"membership in the TI team automatically implies sharing the ownership of the component models developed by that team"* and (p. 38), while discussing the distinction of a Level 3 SSHAC study in contrast to lower level SSHAC studies, "*The TI must now be a team rather than an individual or small group, . . .at Level 3, this is essential both because no individual has the breadth of expertise required and because of the necessity for technical challenge and defence among the evaluators."*

REPLY: We agree with the PPRP about the need of a full TI Team participation. The TI Lead will take responsibility to ensure that all members of the TI Team participate fully and, if necessary, actively asking each TI Team member to make comments or ask questions during the Workshops.

2. ***Selection criteria and decision date for GMPEs.*** Some of the ground motion prediction equations (GMPEs) presented and discussed at the workshop appeared to the PPRP to be at a less mature stage of development than the others. For example, one has not yet been fully described and documented in a formal publication. We recommend that the TI team formulate and document, as soon as possible, clear criteria to be employed to determine which GMPEs will be used in hazard model development, and that documentation of the acceptance criteria include a justification, and that it specify a firm cutoff date for achievement of the criteria, based on a realistic assessment of schedule requirements. The selection criteria should be applied on a consistent basis to all candidate GMPEs.

REPLY: Agree. We are currently planning on accepting GMPEs finalized (stable) and adequately documented by the end of 2013. GMPEs selection criteria will be clearly documented in the final project report, together with evaluation on applicability of the models for the project.

3. ***Completeness of proponent-model analysis in Workshop #2.*** The project team made a thorough effort to identify, select, and invite proponents of alternative interpretations. Not all invited proponents were able to attend the workshop. In the absence of a proponent to support the GMPE and magnitude-scaling recommendations of Dr. Zhao and his colleagues, their viewpoints on magnitude scaling of ground motion were solicited and presented by the TI Team; therefore an opportunity existed at the workshop to discuss and challenge them. This approach was fully consistent with guidance in the NRC SSHAC guidance document (NUREG-2117) (p. 70), which states, for example: *"Because not all proponents of alternative viewpoints may be able to attend the workshop, interpretations made by individuals who may not be present should be identified and discussed."* On the other hand, Dr. Idriss (author of the Idriss NGA-West2 GMPE) and Drs. Atkinson and Assatourians (developers of the finite-fault stochastic simulation method, EXSIM) also were absent, yet no representatives were designated to represent their models. As a result, discussion and debate of the merits of these two models were largely incomplete. The PPRP recommends that the TI team make an additional effort to complete the evaluation of these two proponent models at a level equal to that of the other models being evaluated. It should take place before the development of preliminary hazard models, and in a setting consistent with NUREG 2117, which stipulates (p. 39) that in a Level 3 study, the interactions with proponent experts should be *"conducted openly in the presence of observers including the PPRP."*

REPLY: Agree. We plan on evaluating the two aforementioned proponent models during a special working meeting (January 28 and 29, 2014) in the presence of PPRP, while also inviting relevant Proponent Experts and Resource Experts who attended the Workshop #2. Back up plans have also been discussed to make sure the TI Team has a chance to discuss the proponent model with the

experts if the authors cannot attend the meeting. These discussions will be summarized at the special working meeting.

4. ***Completion of Workshop #2 objectives.*** The PPRP noted that there were many ongoing tasks that could not be evaluated in Workshop #2 because they were either incomplete or had just begun. The TI lead pointed out during the workshop that these tasks will need to be fully discussed and evaluated in order for the TI team to obtain feedback from the resource and proponent experts to factor into their evaluation. The PPRP agrees that there is the need for an additional meeting with resource and proponent experts, including the PPRP as observers, to cover these ongoing and incomplete tasks. The PPRP emphasizes, moreover, that sufficient time should be allowed between such a meeting and Workshop #3 to enable the TI Team to fully evaluate and discuss the feedback from the meeting and incorporate that feedback into the preliminary ground motion logic tree and the related sensitivity studies that will be presented and discussed in Workshop #3. This concept is embodied in the NRC SSHAC guidance document (NUREG-2117) that states (p. 67) *"Any new data collection activities should be identified early in the project, evaluated for their potential impact on the hazard results and associated uncertainties, and completed in a timely manner for use in the technical evaluations. Typically, this would mean that the activities should be completed prior to Workshop #3 on Feedback and certainly no later than the time that the models are finalized;* (p. 68) *Each workshop has a specific focus and goal, and each requires that particular work activities have been conducted prior to its occurrence and certain work activities will occur following;"* and (p. 73) *"Following Workshop #2 and prior to Workshop #3 Feedback, multiple working meetings will be necessary to develop a preliminary model that can be used for purposes of sensitivity analyses to provide the necessary feedback to the TI Team."* TI Team should consider scheduling this additional meeting such that there is sufficient time between it and Workshop #3 to prepare and revise the preliminary ground motion logic tree and to perform related sensitivity studies.

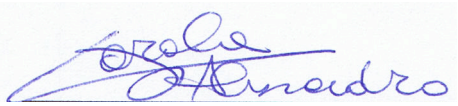
REPLY: Agree. The special working meeting planned at the end of January 2014. This provides adequate time for the TI Team to incorporate the information from the working meeting into the initial GM model to e presented at Workshop #3

5. ***Schedule and prioritization.*** Over the course of the workshop, numerous technical issues that are currently under investigation were identified as requiring substantial further work before certain modeling procedures can be included in a hazard model. The PPRP is very pleased that the project has initiated important investigations that are likely to have a big impact over the longer term, and the fact that some will not reach full practical implementation during this project is understandable and inevitable in an effort such as this one. As the TI lead noted, in the short term, incomplete resolution of these technical issues can be accommodated in the hazard model through appropriate expansion of epistemic uncertainty estimates. The PPRP urges, however, that the TI team reach a prompt decision on which efforts to prioritize for inclusion in the hazard model. That decision should consider hazard sensitivities, and should be made early enough to realistically account for project schedule requirements. For example, by Workshop #3, which is scheduled for March 2014, a preliminary hazard model should have sufficient maturity that the PPRP and others can

meaningfully probe its technical basis and understand the manner in which it incorporates the views of the larger technical community. We also note that a preliminary report is due for PPRP review within just a couple of months following Workshop #3.

REPLY: Agree. We are using hazard sensitivity to identify the critical technical issues.

Sincerely,





Carola Di Alessandro,
SWUS GMC Project Manager

Norman A. Abrahamson,
SWUS GMC TI Team Lead

CC: PPRP Panel, TI Team, PTIs

# REFERENCES

Abercrombie, R. E. (2000). Crustal attenuation and site effects at Parkfield, California. *J. Geophys. Res.*, Vol. 105 (B3), 6277-6286.

Abrahamson, N. A., and W. J. Silva (1997), Empirical Response Spectral Attenuation Relations for Shallow Crustal Earthquakes, *Seismological Research Letters*, Vol. 68(1), 94-127.

Abrahamson, N.A., and Silva, W. (2008). Summary of the Abrahamson & Silva NGA Ground-Motion Relations, *Earthquake Spectra*, Vol. 24(1), 67-97.

Abrahamson, N.A., Silva, W.J. and Kamai, R. (2014). Update of the AS08 Ground-Motion Prediction Equations Based on the NGA-West2 Data Set, *Earthquake Spectra*, (in press).

Akkar, S., Sandikkaya, M.A., and Bommer, J.J. (2013). Empirical ground-motion models for point- and extended-source crustal earthquake scenarios in Europe and the Middle East, *Bull. Earthquake Eng*., DOI 10.1007/s10518-013-9461-4

Akkar, S., Sandikkaya, M.A. and Bommer, J.J. (2013). Erratum to: Empirical ground-motion models for point- and extended-source crustal earthquake scenarios in Europe and the Middle East, *Bull. Earthquake Eng*, DOI 10.1007/s10518-013-9508-6

Akkar, S., Sandikayya, M., Senyurt, M., Azari Sisi, A., Ay, B., Traversa, P., Douglas, J., Cotton, F., Luzi, L., Hernandez, B., Godey, S. (2013). Reference database for seismic ground–motion in Europe (RESORCE), *Bull. Earthquake Eng*.

Al Atik, L., Abrahamson, N., Bommer, J., Scherbaum, F., Cotton, F., Kuehn, N. (2010). The variability of ground-motion prediction models and its components, *Seism. Res. Let*., 81(5), 794-801.

Al Atik, L., and Youngs, R. R. (2013). Epistemic Uncertainty for NGA-West2 Models, *PEER Report No. 2013/11*, Pacific Earthquake Engineering Research Center, University of California, Berkeley, CA, 59 pp.

Ancheta, T.D., Darragh, R.B., Stewart, J.P., Seyhan, E., Silva, W.J., Chiou, B.S.-J., Wooddell, K.E., Graves, R.W., Kottke, A.R., Boore, D.M., Kishida, T. and Donahue, J.L. (2014). PEER NGA-West2 Database, *Earthquake Spectra*, (in press).

Anderson, J.G., and Hough, S E. (1984). A model for the shape of the Fourier amplitude spectrum of acceleration at high frequencies, *Bull. Seism. Soc. Am*., Vol. 74(5), 1969–1993.

Anderson, J.G. (1991). A preliminary descriptive model for the distance dependence of the spectral decay parameter in southern California, *Bull. Seismol. Soc. Am*. Vol. 81, 2186–2193

Anderson, J.G., and Brune, J.N. (1999). Methodology for using precarious rocks in Nevada to test seismic hazard models, *Bull. Seism. Soc. Am.,* Vol. 89, 456-467.

Anderson, J.G., Brune, J., Biasi, G., Anooshehpoor, A., and Purvance, M., (2011). Workshop Report: Applications of Precarious Rocks and Related Fragile Geological Features to U.S. National Hazard Maps, *Seismological Research Letters*, Vol. 82(3), 431-441

Atkinson, G.M. (2006). Single-station sigma, *Bull. Seismol. Soc. Am*., Vol. 96, 446–455.

Atkinson, G.M., and Silva, W. (1997). An empirical study of earthquake source spectra for California earthquakes, *Bull. Seism. Soc. Am.,* Vol. 87, 97–113.

Atkinson, G.M., Boore, D.M., Assatourians, K., Campbell K., and Motazedian, D. (2009). A guide to differences between stochastic point-source and stochastic finite-fault simulations, *Bull. Seism. Soc. Am*., Vol. 99, 3192-3201.

Balco G., Purvance, M., Rood, D. (2011). Exposure dating of precariously balanced rocks, Quaternary Geochronology Vol. 6, 295-303

Barall, M. (2009). A grid-doubling technique for calculating dynamic three-dimensional spontaneous rupture on an earthquake fault, *Geophysical Journal International* Vol. 178, 845–859.

Barall, M. (2013). Branch fault benchmarks TPV24 and TPV25. Dynamic Rupture Code Validation Workshop, Menlo Park, CA. Conference presentation.

Bell, J.W., Brune, J.N., Liu, T., Zreda, M., and Yount, J.C. (1998). Dating precariously balanced rocks in seismically active parts of California and Nevada, *Geology,* Vol. 26, 495-498.

Beresnev, I., and Atkinson, G. (1998a). FINSIM: a FORTRAN program for simulating stochastic acceleration time histories from finite faults, *Seism. Res. Lett.*, Vol. 69, 27–32.

Biasi, G.P., and Smith, K.D. (2001). Site effects for seismic monitoring stations in the vicinity of Yucca Mountain, Nevada, *MOL20011204.0045*, a report prepared for the US DOE/University and Community College System of Nevada (UCCSN) Cooperative Agreement.

Bindi, D., Pacor, F., Luzi, L., Puglia, R., Massa, M., Ameri, G., and Paolucci, R. (2011). Ground motion prediction equations derived from the Italian strong motion database, *Bull Earthquake Eng*., Vol. 9, pp. 1899-1920.

Boore, D.M. (2005). SMSIM--Fortran Programs for Simulating Ground Motions from Earthquakes: Version 2.3--A Revision of OFR 96-80-A, *U.S. Geological Survey Open-File Report*

Boore, D.M. (2009). Comparing stochastic point-source and finite-source ground-motion simulations: SMSIM and EXSIM, *Bull. Seism. Soc. Am.*, Vol. 99, 3202-3216.

Boore, D.M., Watson-Lamprey, J., and Abrahamson, N. A. (2006). Orientation-independent measures of ground motion, *Bull. Seism. Soc. Am*., Vol. 96 (4A), 1502-1511.

Boore, D.M., and Atkinson, G.M. (2008). Ground-Motion Prediction Equations for the Average Horizontal Component of PGA, PGV, and 5%-Damped PSA at Spectral Periods between 0.01s and 10.0s, *Earthquake Spectra*, Vol. 24(1), 99-138.

Boore, D.M., Stewart, J.P., Seyhan, E., and Atkinson, G.M. (2013) "NGA-West2 Equations for Predicting Response Spectral Accelerations for Shallow Crustal Earthquakes," *Pacific Earthquake Engineering Research Center report* 2013/05.

Boore, D.M., Stewart, J.P., Seyhan, E., and Atkinson, G.M. (2014). NGA-West2 Equations for Predicting Response Spectral Accelerations for Shallow Crustal Earthquakes, *Earthquake Spectra*, (in press).

Bora, S.S., Scherbaum, F., Kuehn, N., and Stafford, P. (2013). Fourier spectral- and duration models for the generation of response spectra adjustable to different source-, propagation-, and site conditions, *Bulletin of Earthquake Engineering*, DOI 10.1007/s10518-013-9482-z

Boumediene, D., Bard, P.Y., and Cotton, F. (2013). Towards fully data driven ground-motion prediction models for Europe, *Bulletin of Earthquake Engineering*, DOI 10.1007/s10518-013-9481-0

Brune, J. N. (1970). Tectonic stress and the spectra of seismic shear waves from earthquakes, *J. Geophys. Res*., Vol. 76, 4997–5009.

Brune, J. N. (1971). Correction, *J. Geophys. Res.,* Vol. 76, 5002.

Brune, J.N. (1996). Precariously balanced rocks and ground motion maps for southern California, *Bull. Seism. Soc. Am.*, Vol. 86, 43-54.

Brune, J.N., Whitney, J.W. (1992). Precariously balanced rocks with rock varnish: paleoindicators of maximum ground acceleration? *Seism. Res. Lett*., Vol. 63, 1-21.

Campbell, K.W. (1997). Empirical near-source attenuation relations for horizontal and vertical components of peak ground acceleration, peak ground velocity, and pseudo-absolute acceleration response spectra, *Seismol. Res. Lett.*, Vol. 68, 154-179.

Campbell, K.W., and Bozorgnia, Y. (2008). NGA Ground Motion Model for the Geometric Mean Horizontal Component of PGA, PGV, PGD and 5% Damped Linear Elastic Response Spectra for Periods Ranging from 0.01 to 10 s, *Earthquake Spectra*, Vol. 24(1), 139-171.

Campbell, K.W., and Bozorgnia, Y. (2013). NGA-West2 Campbell-Bozorgnia Ground Motion Model for the Horizontal Components of PGA, PGV, and 5%-Damped Elastic Pseudo-Acceleration Response Spectra for Periods Ranging from 0.01 to 10 sec, *PEER Report 2013/06*.

Campbell, K.W., and Bozorgnia, Y. (2014). NGA-West2 Campbell-Bozorgnia Ground Motion Model for the Horizontal Components of PGA, PGV, and 5%-Damped Elastic Pseudo-Acceleration Response Spectra for Periods Ranging from 0.01 to 10 sec*, Earthquake Spectra*, (in press).

Chandler A.M., Lamb, N.T.K., Tsang, H.H. (2006). Near-surface attenuation modelling based on rock shear-wave velocity profile, *Soil Dyn. Earthq. Eng*., Vol. 26, 1004–1014.

Chapman, M.C., and Godbee, R.W. (2012). Modeling Geometrical Spreading and the Relative Amplitudes of Vertical and Horizontal High-Frequency Ground Motions in Eastern North America, *Bull. Seism. Soc. Am.,* Vol. 102, 1957-1975, doi:10.1785/0120110081

Chen, Y-H., and Tsai, C-C.P. (2002). A new method for estimation of the attenuation relationship with variance components, *Bull. Seism. Soc. Am*., Vol. 92, 1984-1991

Chiou, B.S.-J., Darragh, R., and Silva, W. (2008). An overview of the NGA database, *Earthquake Spectra,* Vol. 24, 23–44.

Chiou, B.S-J and Youngs, R.R. (2008). An NGA Model for the Average Horizontal Component of Peak Ground Motion and Response Spectra, *Earthquake Spectra*, 24(1), 173-215.

Chiou B.S.-J., Spudich P. (2013). The Chiou and Spudich NGA-West2 directivity predictor DPP, Chapter 6, *PEER Report 2013/09*, Pacific Earthquake Engineering Research Center, University of California, Berkeley, CA

Chiou, B.S-J. and Youngs, R.R. (2014). Update of the Chiou and Youngs NGA Ground Motion Model for Average Horizontal Component of Peak Ground Motion and Response Spectra, *Earthquake Spectra*, (in press).

Day, S.M., Graves, R., Bielak, J., Dreger, D., Larsen, S., Olsen, K. B., Pitarka, A. and Ramirez-Guzman, L. (2008). Model for basin effects on long-period response spectra in Southern California, *Earthquake Spectra*, Vol. 24 (1), 257-277.

Di Alessandro, C. and Abrahamson, A. (2013). Ground motion for complex multi-fracture, *Proceedings of IASPEI General Assembly*, Goteborg, July 2013 – Paper S201bS1.04

Donahue, J. (2013). Data to Constrain GMPEs in Critical Ranges –Multi-Fault Ruptures, Presentation to SWUS GMC Workshop #1.

Douglas, J., Gehl, P., Bonilla, L.F., and Gélis, C. (2010). A κ Model for Mainland France, *Pure Appl. Geophys*., Vol. 167, 1303-1315

Douglas, J., Akkar, S., Ameri, G., Bard. P-J, Bindi, D., Bommer, J.J, Bora, S.S., Cotton, F., Derras, B., Hermkes, M., Kuehn, N.M., Luzi, L., Massa, M., Pacor, F., Riggelsen, C., Sandıkkaya, M.A., Scherbaum, F., Stafford, P.J., Traversa, P. (2013). Comparisons among the five ground-motion models developed using RESORCE for the prediction of response spectral accelerations due to earthquakes in Europe and the Middle East, *Bulletin of Earthquake Engineering*, DOI 10.1007/s10518-013-9522-8

Dreger, D., Tinti, E., and Cirella, A. (2005). Slip velocity function parameterization for broadband ground motion simulation, *Seismol. Soc. Am. 2007 Annual Meeting*, Waikoloa, Hawaii, 11-13 April 2007.

Dreger, D.S., Beroza, G.C., Day, S.M., Goulet, C.A., Jordan, T. H., Spudich, P.A, and Stewart, J. P. (2013). Evaluation of SCEC Broadband Platform Phase 1 Ground Motion Simulation Results, 33 pp. plus Appendices, Report submitted to SCEC, Aug. 1 2013.

Drouet S., Cotton, F., and Gueguen, P. (2010). vS30, κ, regional attenuation and Mw from accelerograms: application to magnitude 3–5 French earthquakes, *Geophys. J. Int*., Vol. 182, 880–898.

Edwards B., Fah, D., and Giardini, D. (2011). Attenuation of seismic shear wave energy in Switzerland. *Geophys. J. Int.,* Vol. 185, 967–984

Erickson, D., McNamara, D.E., and Benz, H.M. (2004). Frequency-dependent Lg Q within the continental United States, *Bull. Seism. Soc. Am*., Vol. 94, 1630-1643.

Frankel, A., Carver, D., Cranswick, E., Bice, T., Sell, R., and Hanson, S. (2001). Observation of basin ground-motions from a dense seismic array in San Jose, California, *Bull. Seism. Soc. Am*., Vol. 91, 1-12.

GeoPentech, Inc. (2013). Southwester United States Ground Motion Characterization SSHAC Level 3 Workshop #1 Proceedings, prepared by GeoPentech, Inc. for Arizona Public Service Co., Pacific Gas and Electric Co. and Southern California Edison Co., 69 pp., [available at http://www.pge.com/includes/docs/pdfs/shared/edusafety/systemworks/dcpp/SSHAC/sugmworkshops/WS1_Proceedings.pdf].

Geusebroek, J., Burghouts, G., and Smeulders, A. (2005). The Amsterdam library of object images, *Int. J. Comput. Vision*, Vol. 61, 103-112.

Goda, K., and Hong, H. P. (2008). Spatial Correlation of Peak Ground Motions and Response Spectra *Bull. Seismol. Soc. Am.,* Vol. 98(1), 354–365.

Goldstein, P., Dodge, D., Firpo, M., and Minner, L. (2003). SAC2000: Signal processing and analysis tools for seismologists and engineers, *The IASPEI International Handbook of Earthquake and Engineering Seismology*, W.H.K. Lee, H. Kanamori, P.C. Jennings, C. Kisslinger (Editors), Academic Press, London.

Graizer, V. and Kalkan, E. (2007). Ground-motion Attenuation Model for Peak Horizontal Acceleration from Shallow Crustal Earthquakes, *Earthquake Spectra*, Vol. 23 (3), 585-613.

Graizer, V. and Kalkan, E. (2009). Prediction of response spectral acceleration ordinates based on PGA attenuation, *Earthquake Spectra*, Vol. 25 (1), 39-69.

Graizer, V. and Kalkan, E. (2011). Modular filter-based approach to ground-motion attenuation modeling, *Seism. Res. Lett.*, Vol. 82(1), 21-31.

Graizer, V., Shakal, A., Scrivner, C., Hauksson, E., Polet J., and Jones, L. (2002). TriNet strong-motion data from the M 7.1 Hector Mine, California, earthquake of 16 October 1999, *Bull. Seism. Soc. Am*., Vol. 92, 1525-1541.

Graizer, V., Kalkan, E., and Lin, K.W. (2013). Global ground-motion prediction equation for shallow crustal regions, *Earthquake Spectra*, Vol. 29 (3), 1-15.

Graizer, V. and Kalkan, E. (2014). Updated Graizer-Kalkan Ground-motion Prediction Equations for Western United States, 11 pp., *Proceedings for the 10th U.S. National Conference on Earthquake Engineering Frontiers of Earthquake Engineering*, July 21-25, 2014, Anchorage, Alaska.

Graves, R. (2012). Broadband Simulation Results for Footwall/Hanging Wall and Rupture Directivity Analysis – Deliverable in Subaward Agreement 000007598, Memorandum dated February 23 2012, submitted to Pacific Earthquake Engineering Research Center (PEER), University of California - Berkeley, CA, USA

Graves, R. W. and Pitarka, A. (2010). Broadband Ground-Motion Simulation Using a Hybrid Approach, *Bull. Seism. Soc. Am*., Vol. 100 (5a), 2095-2123.

Graves, R. W., Aagaard, B. T., and Hudnut, K. W. (2011). The ShakeOut earthquake source and ground motion simulations, *Earthquake Spectra*, Vol. 27(2), 273-291.

Gregor, N. (2013). Fortran implementation of the NGA-West 2 GMPEs.

Hanson, K., Wesling, J., Lettis, W., Kelson, K., and Mezger, L., (1994). Correlation, ages, and uplift rates of Quaternary marine terraces: South-central coastal California, in Alterman, I., McMullen, R., Cluff, L., and Slemmons, D., eds., Seismotectonics of the Central California Coast Ranges, *Geological Society of America Special Paper* 292, 45-71.

Hardebeck, J.L. (2010). Seismotectonics and fault structure of the California central coast, *Bull. Seismol. Soc. Am.* Vol. 92, 2264-2276.

Harris, R. (2013). Splays and linkage: dynamic rupture modeling. SWUS GMC Workshop #1, Oakland, CA. Conference presentation.

Hatayama, K. and Kalkan, E. (2012). Spatial Amplification of Long-Period (3 to 16 s) Ground Motions in and around the Los Angeles Basin during the 2010 M7.2 El Mayor-Cucapah Earthquake, *Proc. of the 15th World Conf. on Earthquake Engineering*, Lisbon, Portugal.

Hermkes, M., Kuehn, N.M., and Riggeslen, C. (2013). Simultaneous quantification of epistemic and aleatory uncertainty in GMPEs using Gaussian process regression, *Bulletin of Earthquake Engineering*, DOI 10.1007/s10518-013-9507-7

Hole, J.A. (1992). Non-linear high resolution three-dimensional seism travel time tomography, *J. Geophys. Res.,* Vol. 97, 6553-6562.

Hough, S.E., and Anderson, J.G. (1988). High-frequency spectra observed at Azna, California: Implications for Q structure, *Bull. Seismol. Soc. Am.,* Vol. 78, 692-707.

Hough, S.E., Anderson, J.G., Brune, J., Vernon, F., Berger, J., Fletcher, J., Haar, L., Hanks, T., and Baker, L. (1988). Attenuation near Anza, California, *Bull. Seismol. Soc. Am.*, Vol. 78, 672-691.

Hruby, C.E., and Beresnev, I.A. (2003). Empirical corrections for basin effect in stochastic ground-motion prediction, based on the Los Angeles basin analysis, *Bull. Seism. Soc. Am.,* Vol. 93, 1679-1690.

Idriss, I.M. (2008). An NGA Empirical Model for Estimating the Horizontal Spectral Values Generated By Shallow Crustal Earthquakes, *Earthquake Spectra*, Vol. 24(1), 217-242.

Idriss, I.M. (2014). NGA-West2 Model for Estimating Average Horizontal Values of Pseudo-Absolute Spectral Accelerations Generated by Crustal Earthquakes, *Earthquake Spectra*, in press.

Irikura, K. and Miyake, H. (2010). Recipe for Predicting Strong Ground Motion from Crustal Earthquake Scenarios, *Pure and Applied Geophysics*, Vol. 168, 85-104, DOI 10.1007/s00024-010-0150-9.

Jayaram, N., and Baker, J. W. (2009). Correlation model for spatially distributed ground-motion intensities. *Earthquake Engineering & Structural Dynamics*, Vol. 38(15), 1687–1708.

Joyner, W.B., and Boore, D.M. (1986). On simulating large earthquakes by Green's function addition of smaller earthquakes, in Earthquake Source Mechanics, *Geophysical Monograph* 37, Maurice Ewing Vol. 6, Eds S. Das, J. Boatwright, and C.H. Scholz.

Kame, N., Rice, J., and Dmowska, R. (2003). Effects of pre-stress state and rupture velocity on dynamic fault branching, *Journal of Geophysical Research* Vol. 108, 2265, doi: 10.1029/2002JB002189.

Kishida, T., Ktenidou, O.-J., Darragh, R., and Silva, W. (2013). Data processing for Fourier amplitude spectrum (FAS) estimation from NGA-West2 processed accelerations'. Pacific Earthquake Engineering Research Center, pp. 50 (in review).

Kohonen, T. (2001). Self-organizing maps, Springer 2001, 501 pages.

Ktenidou O.-J., Gelis, C., Bonilla, L.F. (2013). A study on the variability of kappa in a borehole: implications of the computation process, *Bull. Seism. Soc. Am.,* Vol. 103, 2A.

Ktenidou O.-J., Cotton, F., Abrahamson, N., Anderson, J.G. (2013b). Don't call it kappa: add a subscript!, *Seism. Res. Lett*. (in review).

Ktenidou O.-J., Drouet, S., Theodulidis, N., Chaljub, M., Arnaouti, S., Cotton, F. (2012). Estimation of kappa (κ) for a sedimentary basin in Greece (EUROSEISTEST) - Correlation to site characterisation parameters. *Proc. 15th World Conference of Earthquake Engineering*, Lisbon, Portugal, 24-28 Sep., 10 pp.

Lermo, J., and Chávez-García, F.-J. (1993). Site effect evaluation using spectral ratios with only one station, *Bull. Seism. Soc. Am.*, Vol. 83 1574-1594.

Loth, C., and Baker, J. W. (2013). A spatial cross-correlation model for ground motion spectral accelerations at multiple periods. *Earthquake Engineering & Structural Dynamics,* Vol. 42(3), 397–417.

LCI (2012). Characterization of Ground Motion Propagation for Palo Verde SSHAC Level 2 PSHA, Internal Project Report.

Lee, V. W., Trifunac, M. D., Todorovska, M. I. and Novikova, E. I. (1995). Empirical equations describing attenuation of peak of strong ground-motion, in terms of magnitude, distance, path effects and site conditions, *Report No. CE 95-02*. Los Angeles, California. 268 pp.

Leonard, M. (2010). Earthquake Fault Scaling: Self-Consistent Relating of Rupture Length, Width, Average Displacement, and Moment Release, *Bull. Seismol. Soc. Am.*, Vol. 100, 1971-1988.

Lin, P-S., Chiou, B., Abrahamson, N., Walling, M., Lee, C-T, and Cheng, C-T (2011). Repeatable source, site, and path effects on the standard deviation for empirical ground-motion prediction models, Bulletin *Bull. Seism. Soc. Am*., Vol. 101(5), 2281-2295.

Liu, P., Archuleta, R.J., and Hartzell, S.H. (2006). Prediction of broadband ground-motion time histories: Hybrid low/high-frequency method with correlated random source parameters, *Bull. Seism. Soc. Am*., Vol. 96, 2118-2130, doi: 10.1785/0120060036.

Lozos, J., Oglesby, D., Duan, B., and Wesnousky, S. (2011). The effects of double fault bends on rupture propagation: a geometrical parameter study, *Bull. Seism. Soc. Am*., Vol. 101, 385-398.

Lozos, J. (2013). Dynamic rupture and ground motion modeling on realistically complex strike-slip faults, *PhD dissertation*, University of California, Riverside.

Mai, P.M., and Beroza, G.C. (2003). A hybrid method for calculating near-source, broadband seismograms: Application to strong motion prediction, *Phys. Earth Planet. In.* Vol. 137(1-4), 183-199.

Mai, P.M., Imperatori, W., Olsen, K.B. (2010), Hybrid Broadband Ground-Motion Simulations: Combining Long-Period Deterministic Synthetics with High-Frequency Multiple S-to-S Backscattering, *Bull. Seism. Soc. Am*., Vol. 100(5A), 2124-2142.

Mena, B., Mai, P.M., Olsen, K.B., Purvance, M.D., and Brune, J.N. (2010). Hybrid Broadband Ground-Motion Simulation Using Scattering Green's Functions: Application to Large-Magnitude Events, *Bull. Seism. Soc. Am*., Vol. 100, 2143-2162.

Mitchell, B.J., and Hwang, H.J. (1987) Effect of low Q sediments and Crustal Q on Lg attenuation in the United States, *Bull. Seism. Soc. Am*., Vol. 77, 1197-1210.

Morikawa, N., Kanno, T., Narita, A., Fujiwara, H., Okumura, T., Fukushima, Y., and Guerpinar, A. (2008). Strong motion uncertainty determined from observed records by dense network in Japan. *J. Seismol.,* Vol. 12(4), 529–546.

Motazedian, D., and Atkinson, G.M. (2005). Stochastic finite-fault modeling based on a dynamic corner frequency, *Bull. Seism. Soc. Am*., Vol. 95, 995-1010.

NGA-West2 Flatfile (2013) [http://peer.berkeley.edu/ngawest2/databases/]

Olsen, K.B. (2000). Site amplification in the Los Angeles basin from three-dimensional modeling of ground motion. *Bull. Seism. Soc. Am*., Vol. 90(6B), S77-S94.

Oth, A., Bindi, D., Parolai, S., and Di Giacomo, D. (2011). Spectral Analysis of K-NET and KiK-net Data in Japan, Part II: On Attenuation Characteristics, Source Spectra, and Site Response of Borehole and Surface Stations, *Bull. Seismol. Soc. Am*., Vol. 101, 667-687

Parolai, S., and Bindi, D. (2004). Influence of soil-layer properties on k evaluation, *Bull. Seismol. Soc. Am*., Vol. 94, 349–356.

PG&E (2011). Report on the Analysis of the Shoreline Fault Zone, Central Coastal California, January 2011.

Phillips, W.S., Mayeda, K M., and Malagnini, L. (2013). How to Invert a Multi-Band, Regional Phase Amplitudes for 2-D Attenuation and Source Parameters: Tests Using the USArray, *PAGEOPH,* DOI 10.1007/s00024-013-0646-1.

Pitarka, A. (2009). Simulating forward and backward scattering in viscoelastic 3D media with random velocity variations and basin structure, *Tech. Rep., USGS, award number 06HQGR0042*.

Purvance, M.D., Anooshehpoor, A., and Brune, J.N. (2008). Freestanding block overturning fragilities: Numerical simulation and experimental validation, *Earthquake Eng & Struct. Dynamics*, Vol.37, 791-808.

Purvance, M. D., and Brune J.N. (2008). Fragile Geomorphic Features on Yucca Mountain, Nevada, *Seismol. Res. Lett.*, Vol. 79(2), 296

Rocscience (2005). Phase2, Elasto-plastic finite element stress analysis program for underground or surface excavations in rock or soil. Rocscience Inc., Toronto.

Rodriguez-Marek, A. (2012). Addendum to "Single Station Sigma", EXT-TN-1225 / prepared for PRP - Pegasos Refinement Project.

Rodriguez-Marek. A., Montalva, G.A., Cotton, F. and Bonilla, F. (2011). Analysis of Single-Station Standard Deviation Using the KiK-net Data, *Bull. Seism. Soc. Am*., Vol. 101, 1242–1258.

Rodriguez-Marek, A., Cotton, F., Abrahamson, N., Akkar, S., Al Atik, L., Edwards, B., Montalva, G.A., and Dawood, H.M. (2013). A model for single-station standard deviation using data from various tectonic regions, *Bull. Seism. Soc. Am*., Vol. 103(6), 3149-3163

Rodriguez-Marek, A., and Cotton, F. (2011). Final report: Single-station sigma project prepared for PEGASOS Refinement Project, *EXT-TB-1058*

Sadigh, K., Chang, C., Egan, J., Makdisi, F., and Youngs, R. (1997). Attenuation relationships for shallow crustal earthquakes based on California strong motion data, *Seism. Res. Lett*., Vol. 68, 180–189.

Sammon, J. (1969). A nonlinear mapping for data structure analysis, *IEEE Trans. Comput*. Vol. 524(C-18), 401–409.

Scherbaum, F., Kuehn, N., Koehler, A., and Ohrnberger, M. (2010). Exploring the Proximity of Ground-Motion Models Using High-Dimensional Visualization Techniques, *Earthquake Spectra,* Vol. 26, 1117–1138.

Schmedes, J., Archuleta, R.J., and Lavallée, D. (2010). Correlation of earthquake source parameters inferred from dynamic rupture simulations, *J. Geophys. Res*., Vol. 115, B03304, doi:10.1029/2009JB006689.

Schmedes, J., Archuleta, R.J., and Lavallée, D. (2010). Dependency of supershear transition and ground motion on the autocorrelation of initial stress, *Tectonophysics*, Vol. 493, 222-235, doi: 10.1016/j.tecto.2010.05.013

Schmedes, J., Archuleta, R.J., and Lavallée, D. (2013). A kinematic rupture model generator incorporating spatial interdependency of earthquake source parameters, *Geophys. J. Int*., Vol. 192(3), 1116-1131., doi: 10.1093/gji/ggs021

Shahi, S. K. (2013). A probabilistic framework to include the effects of near-fault directivity in seismic hazard assessment. *PhD Thesis*, Dept. of Civil and Environmental Engineering, Stanford University, Stanford, CA. http://purl.stanford.edu/hb804nv7861

Shi, B., Anooshehpoor, A., Zeng, Y., and Brune, J.N. (1996). Rocking and overturning of precariously balanced rocks by earthquakes, *Bull. Seism. Soc. Am*., Vol. 86, 1364–1371.

Silva, W., Darragh, R., Gregor, N., Martin, G., Abrahamson, N., and Kircher, C. (1998). Reassessment of site coefficients and near-fault factors for building code provisions, Technical Report Program Element II: *98-HQGR-1010*, Pacific Engineering and Analysis, El Cerrito, USA.

Silva, W.J., and Darragh, R. (1995). Engineering characterization of earthquake strong ground motion recorded at rock sites. Palo Alto, Calif: *Electric Power Research Institute, TR-102261*

Sjogreen, B., and Petersson, N.A. (2010). A fourth order accurate finite difference scheme for the elastic wave equation in second order formulation. *J. Sci. Comput*., Vol. 52, 17–48, 2012. DOI 10.1007/s10915-011-9531-1.

Somerville, P.G., Callaghan, S., Maechling, P., Graves, R.W., Collins, N., Olsen, K.B., Imperatori, W., Jones, M., Archuleta, R., Schmedes, J., and Jordan, T.H. (2011). The SCEC Broadband Ground Motion Simulation Platform, *Seismol. Res. Let.*, Vol. 82(2), p. 275, 10.1785/gssrl.82.2.273.

Stirling, M.W., and Anooshehpoor, R. (2006). Constraints on Probabilistic Seismic-Hazard Models from Unstable Landform Features in New Zealand, *Bull. Seism. Soc. Am.,* Vol. 96, 404-414.

Stirling, M.W., Ledgerwood, J., Liu, T., Apted, M. (2010). Age of unstable bedrock landforms southwest of Yucca Mountain, Nevada, and implications for past ground motions, *Bull. Seism. Soc. Am.,* Vol. 100(1), 74-86; doi: 10.1785/0120080359

Stirling, M.W. (2013). Diablo Canyon Power Plant: Field Reconnaissance of Fragile Geologic Features, August 2013. *GNS Science Letter Report 229LR*.

Trifunac, M.D. (1994). Q and high-frequency strong motion spectra, *Soil Dynamics and Earthquake Engineering*, Vol. 13, 149-161.

U.S.NRC (2012a). Near-Term Task Force, "Request For Information Pursuant To Title 10 Of The Code Of Federal Regulations 50.54(F) Regarding Recommendations 2.1,2.3, and 9.3, Of The Near-Term Task Force Review Of Insights From The Fukushima Dai-Ichi Accident."

U.S.NRC (2012b). Practical Implementation Guidelines for SSHAC Level 3 and 4 Hazard Studies, U.S.NRC NUREG-2117.

U.S.NRC (1997). Recommendations for probabilistic seismic hazard analysis: Guidance on uncertainty and use of experts, prepared by Senior Seismic Hazard Analysis Committee, Lawrence Livermore National Laboratory, Volume 1, Main Report, NUREG/CR-6372, UCRL-ID-122160, 280 pp.

Van Houtte, C., Drouet, S., and Cotton, F. (2011). Analysis of the origins of κ (Kappa) to compute hard rock to rock adjustment factors for GMPEs, *Bull. Seismol. Soc. Am*., Vol. 101, 2926-2941.

Villani, M., and Abrahamson, N. (2013). Repeatable site and path effects on the ground motion sigma based on empirical data from Southern California and simulated waveforms from the CyberShake platform. Poster at SCEC 2013 annual meeting and draft paper for Earthquake Spectra.

Walling, M. A. (2009). Non-Ergodic Probabilistic Seismic Hazard Analysis and Simulation Spatial of Variation in Ground Motion, *Ph.D. Thesis*, University of California, Berkeley, California.

Wessel, P., and Smith, W.H.F. (1998). New, improved version of the Generic Mapping Tools Released, *EOS Trans. AGU* Vol. 79, 579.

Youngs, R.R. (2009). Epistemic uncertainty in the NGA models, Appendix D in Ground Motion Models for the Pacific Northwest, *Report to B.C. Hydro*, December 2010.

Zeng, Y.H., Su, F., and Aki, K. (1991). Scattering wave energy propagation in a random isotropic scattering medium 1. Theory, *J. Geophys. Res.* Vol. 96 (B1), 607-619.

Zeng, Y.H., Aki, K., and Teng, T.L. (1993). Mapping of the high-frequency source radiation for the Loma Prieta earthquake, California, *J. Geophys. Res. Vol.* 98(B7), 11981-11993.

Zeng, Y., Anderson, J.G. and Yu, G. (1994). A composite source model for computing realistic synthetic strong ground motions, *Geophysical Research Letters*, Vol. 21, 725-728.

Zhao, J.X., Zhang, J., Asano, A., Ohno, Y., Oouchi, T., Takahashi, T., Ogawa, H., Irikura, K., Thio, H.K., Somerville, P.G., Fukushima, Y., and Fukushima, Y. (2006). Attenuation Relations of Strong Ground Motion in Japan Using Site Classification Based on Predominate Period, *Bull. Seism. Soc. Am*., Vol. 96, 898-913.

Zhao, J.X., and Lu, M. (2011). Magnitude-Scaling Rate in Ground-Motion Prediction Equations for Response Spectra from Large, Shallow Crustal Earthquakes, *Bull. Seism. Soc. Am*., Vol. 101, 2643-2661.

Zhu, L. and Rivera, L.A. (2002) A note on the dynamic and static displacements from a point source in multilayered media, *Geophysical Journal International*, Vol. 148(3), 619-627.

# APPENDIX A Hand-out Material distributed during the Workshop #2

Hand-out material that was distributed to Workshop #2 attendees is collected in Appendix A. It encompasses a table (Table A1) describing the status of the Data Needs identified at Workshop #1, an updated project schedule (Table A2), and some example application of the visualization techniques (Sammon's maps and Self-Organizing Maps) applied to the candidate GMPEs being evaluated under the project

## A.1 Data Needs from SWUS Workshop #1

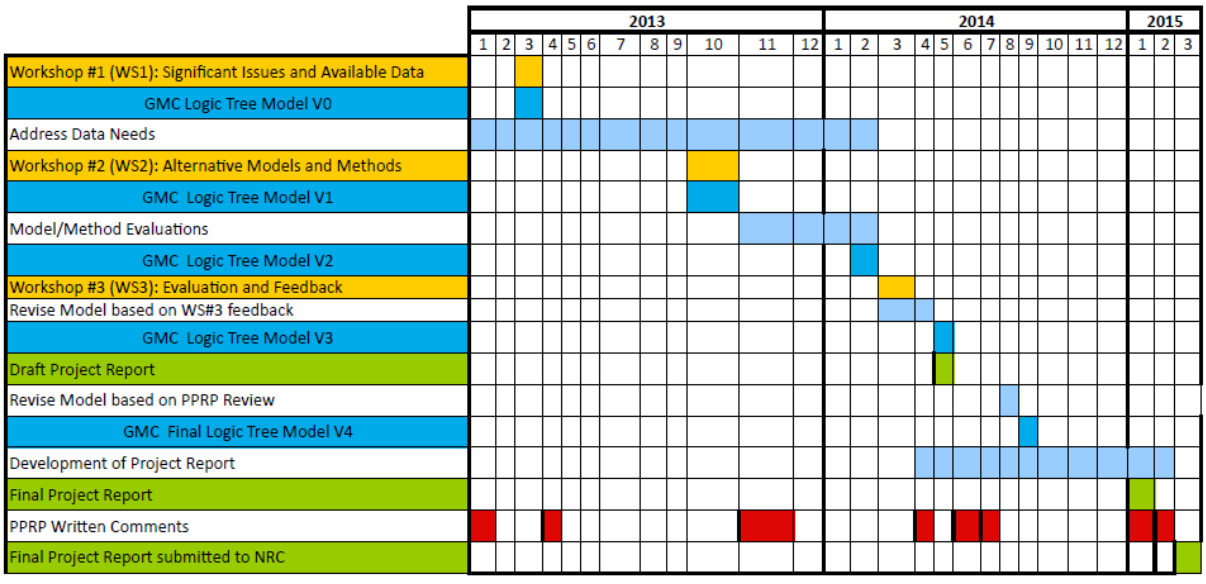
**Table A2:** Status of the Data Needs identified at SWUS GMC Workshop #1

| TASK # | TASK DESCRIPTION | STATUS |
|---|---|---|
| **1A** | Compute ground motions from Fukushima Hamadori earthquake (large Japanese normal faulting event) | In progress (PEER) |
| 1B | Review ground motion data from Wells, NV earthquake (Feb. 21, 2008) | Planned for WS#3 |
| 1C | Review Bindi Data for constraints on normal faulting factors | Completed |
| 1D | Review Source Data for Japanese Events for style-of-faulting | In progress for WS#3 |
| **2A** | Evaluate FFS for over-saturation at short distances | Planned for second set of simulations (for WS#3) |
| 2B | Evaluate what directivity is captured in the empirical models and standard deviation and what is missing | In progress |
| 2C | Review Static Offset (Fling) and check 3-5 sec | Completed |
| 2D | Review best use of Baker's model for directivity pulses | Presentation at WS#2 |
| **3A** | Review Japanese K-net and KiK-net data: Identify 4 or 5 candidate M5.5 to 6.5 HW events (events on both sides); If needed, perform source inversion of the best events | In progress, for WS#3 |
| 3B | Run FFS for M5.5 to M6.5 for HW | Completed |
| 3C | Run alternative FFS methods for HW effects | Completed for M7 |
| **4A** | Remove post-mainshock or pre-mainshock surface rupture from empirical data set (e.g. Superstition Hills) | Completed |
| 4B | Review multi-fault ruptures & simplifications in empirical data in NGA – West 2 | Presentation at WS#2 |
| 4C | Finite-fault simulations for complex ruptures | In progress, results at WS#3 |
| 4D | Finite-fault simulations for splay ruptures | In progress, initial results at WS#2 |
| 4E | Use dynamic ruptures to constraint source properties for splay ruptures | In progress |
| **5A** | Get a copy of Brumbaugh Intensity report | Completed |
| 5B | Add Roosevelt Dam and VA Hospital strong motion data from El Mayor-Cucapah earthquake to PEER database | Planned, for WS#3 |
| 5C | Compile and process local AZ data for kappa | Completed (PEER) |
| 5D | Compile AZ seismograms from distant CA earthquakes for path effects | Completed (PEER) |

| TASK # (cont.) | TASK DESCRIPTION (cont.) | STATUS (cont.) |
|---|---|---|
| **6A** | Identify key sites for kappa in Arizona | Completed |
| 6B | Identify key sites and conduct site characterization for Arizona stations | Scheduled: end of Oct. 2013 |
| 6C | Estimate kappa for Arizona stations | In progress |
| 6D | Review use of blasts for kappa in Arizona | Pending |
| 6E | Develop kappa estimates for small earthquakes recorded by the geophysical array at DCPP | Planned, for WS#3 |
| **7A** | Create a 1D velocity model for DCPP based on new seismic data for use in FFS | Pending. Will depend on schedule for simulations |
| 7B | Evaluate potential for missing important 3D effects at the 2 sites in the GM models using Loma Prieta. | In progress, discussion at WS#2 |
| 7C | Evaluate regional ground motion data near DCPP for path effects, focus on the onshore paths | Pending new data. New instrumentation presentations at WS#2 |
| 7D | Develop single-path sigma models based on CA data using NGA-West2 results | In progress, Presentation at WS#2 |
| **8A** | Develop single-station sigma models based on CA data using NGA-West2 results | In progress, Presentation at WS#2 |
| **9A** | Evaluate fragile geologic features near PVNGS | Completed |
| 9B | Evaluate fragile geologic features near DCPP | In progress, Presentation at WS#2 |

## A.2 SWUS Schedule

**Table A2:** Updated SWUS GMC SSHAC Level 3 Project Schedule



## A.3 Introduction to GMPEs Visualization Techniques (by N. Kuehn)

### *A.3.1 Introduction*

In this short document, results regarding the visualization of GMPEs using Sammon's and self-organizing maps (SOMs) are shown. The maps are based on distances in high-dimensional space, projected down to two dimensions. The high-dimensional vectors are based on a grid of 31 magnitudes (between 5 and 8) and 25 distances (between 1 km and 200 km, equally spaced logarithmically), resulting in. The style of faulting is strike slip, $V_{S,30}$ is 760m/s. There are maps for periods T = 0, 0.2, 1, 3 sec. Distances are calculated between the logarithms of the ground-motion values.

In the plots of the self-organizing maps, the color of each node denotes the average distance to the neighboring nodes, with darker colors indicating large distances and lighter colours indicating small distances. Black corresponds to a distance of d = 4, which corresponds to a scaling of 1.25. For comparison, the shortest distance between two models is $d_{min}$ = 3:8 between the models of Boore et al. (2013) and Chiou and Youngs (2013). The largest distance between two models is $d_{max}$ = 20:8 between the models of Bindi et al. (2011) and Graizer and Kalkan (2013).

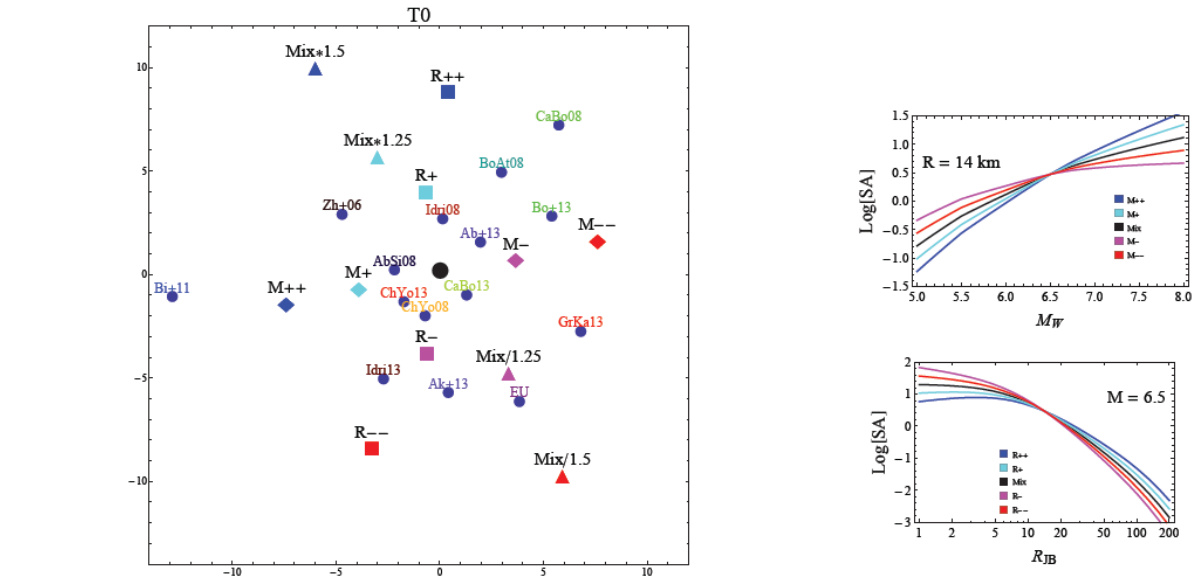



**Figure A1:** Left: Sammon's map of GMPEs for PGA, together with reference mixture and scaled mixture models. Right: Mixture model with adjusted magnitude and distance scaling for comparison.

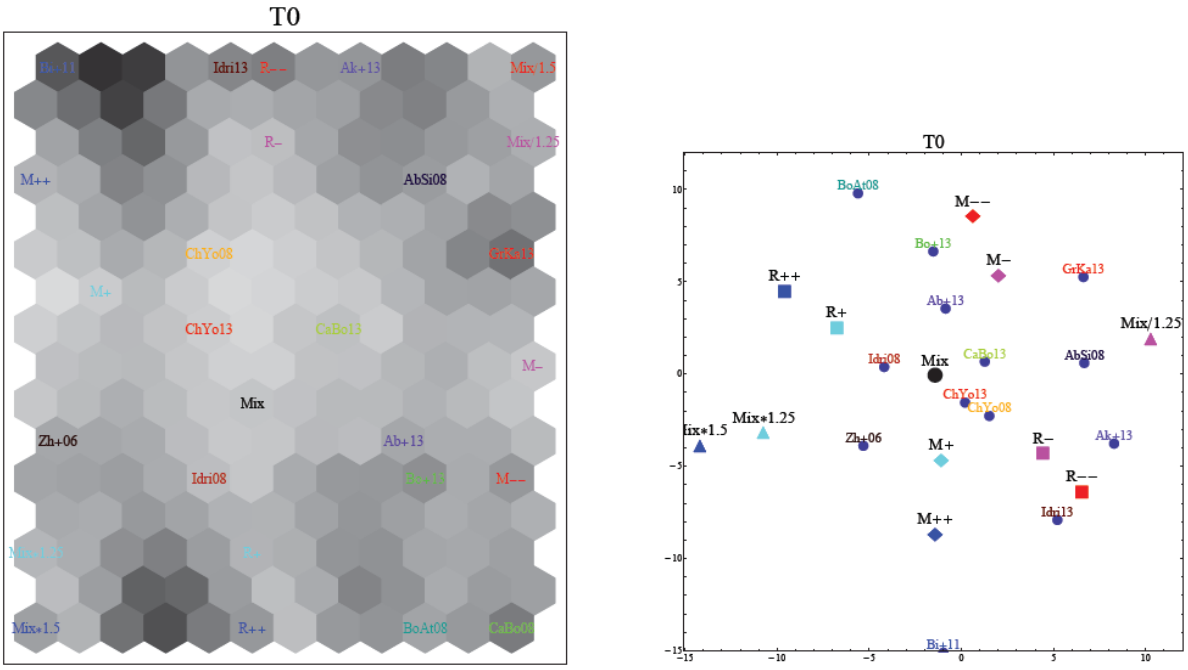



**Figure A2:** Left: U-Matrix of SOM for PGA, together with reference mixture and scaled mixture models. Right: Map based on shortest distances between models in the self-organizing **map.**

# T = 0.2s

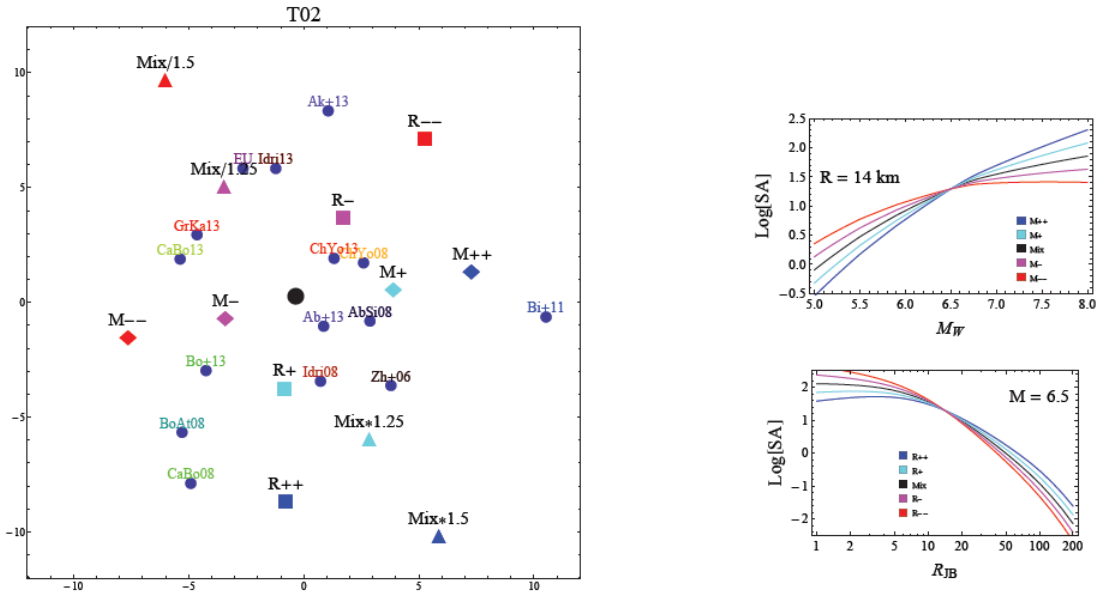



**Figure A3:** Left: Sammon's map of GMPEs for T = 0:2s, together with reference mixture and scaled mixture models. Right: Mixture model with adjusted magnitude and distance scaling for comparison.

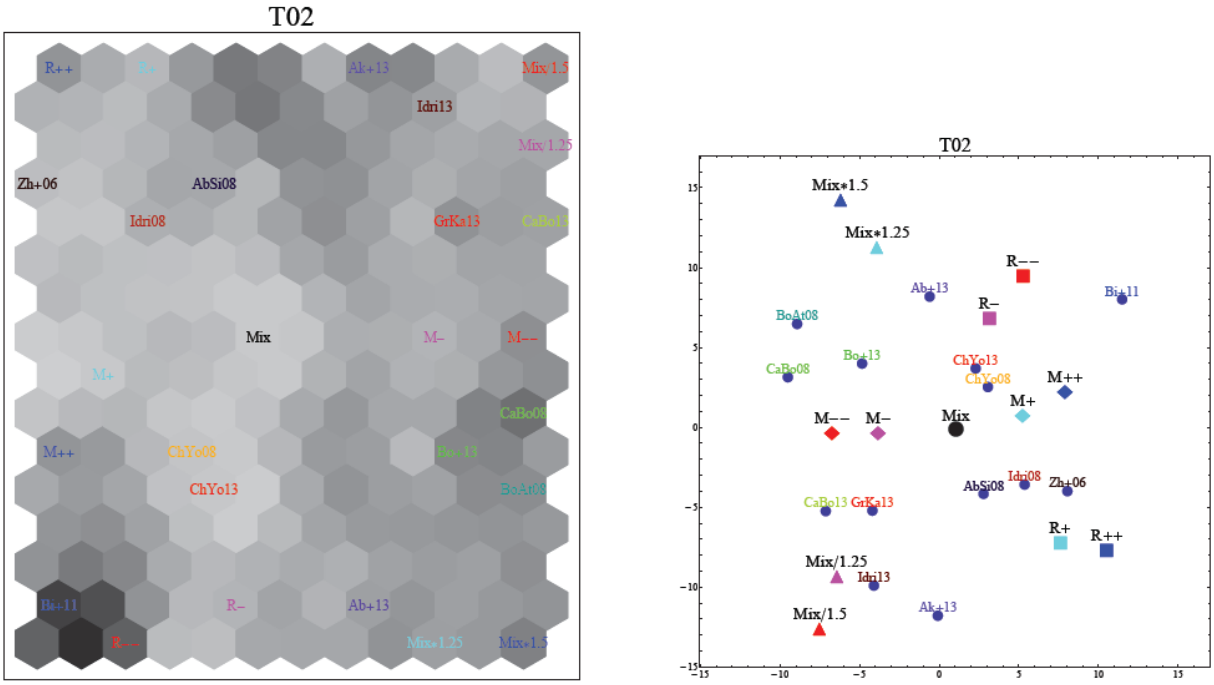



**Figure A4:** Left: U-Matrix of SOM for T = 0:2s, together with reference mixture and scaled mixture models. Right: Map based on shortest distances between models in the self-organizing map.

# T = 1s

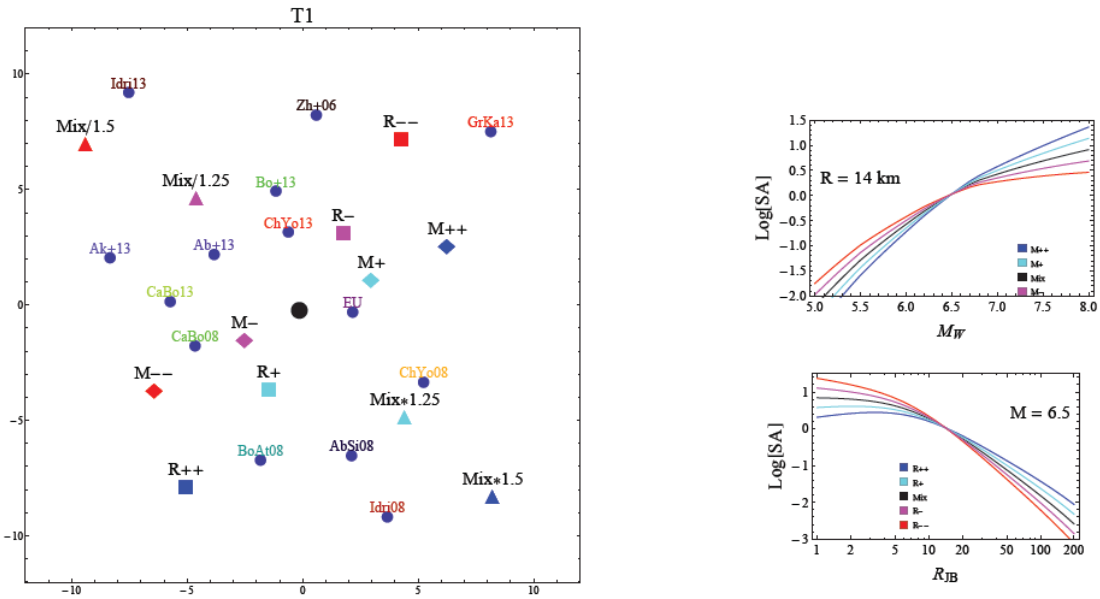



**Figure A5:** Left: Sammon's map of GMPEs for T = 1s, together with reference mixture and scaled mixture models. Right: Mixture model with adjusted magnitude and distance scaling for comparison.

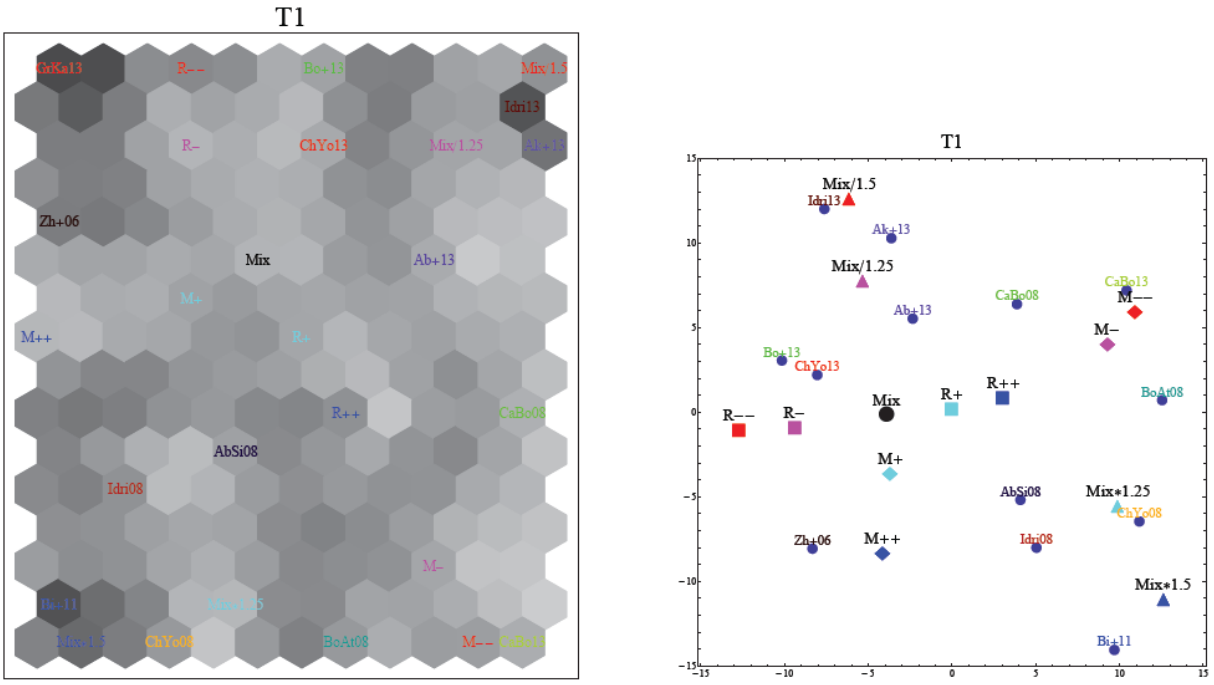



**Figure A6:** Left: U-Matrix of SOM for T = 0:2s, together with reference mixture and scaled mixture models. Right: Map based on shortest distances between models in the self-organizing map.

# T = 3s

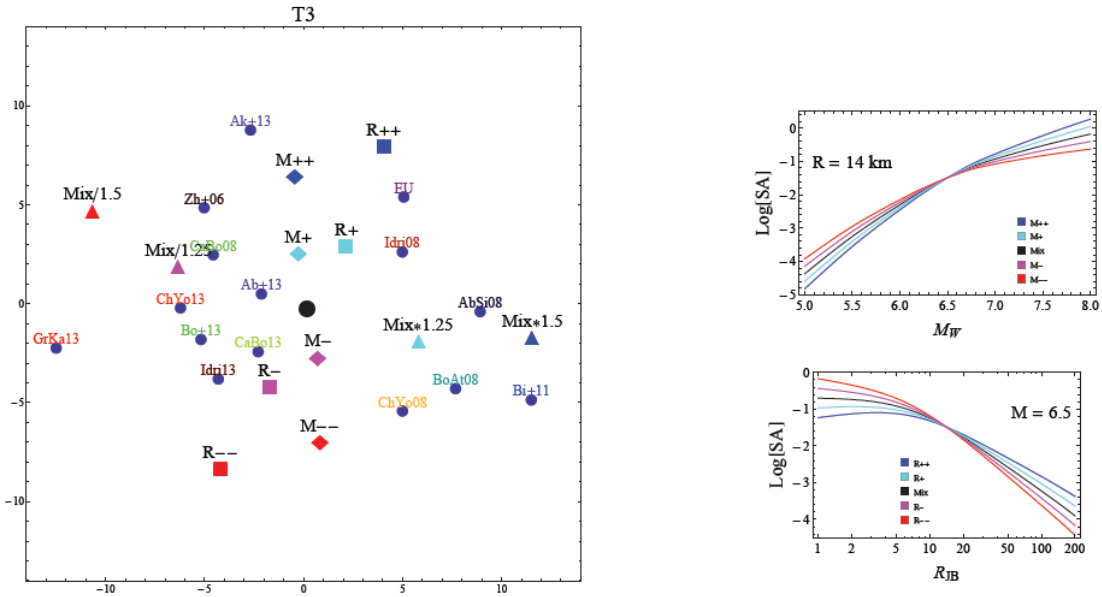



**Figure A7:** Left: Sammon's map of GMPEs for T = 3s, together with reference mixture and scaled mixture models. Right: Mixture model with adjusted magnitude and distance scaling for comparison.

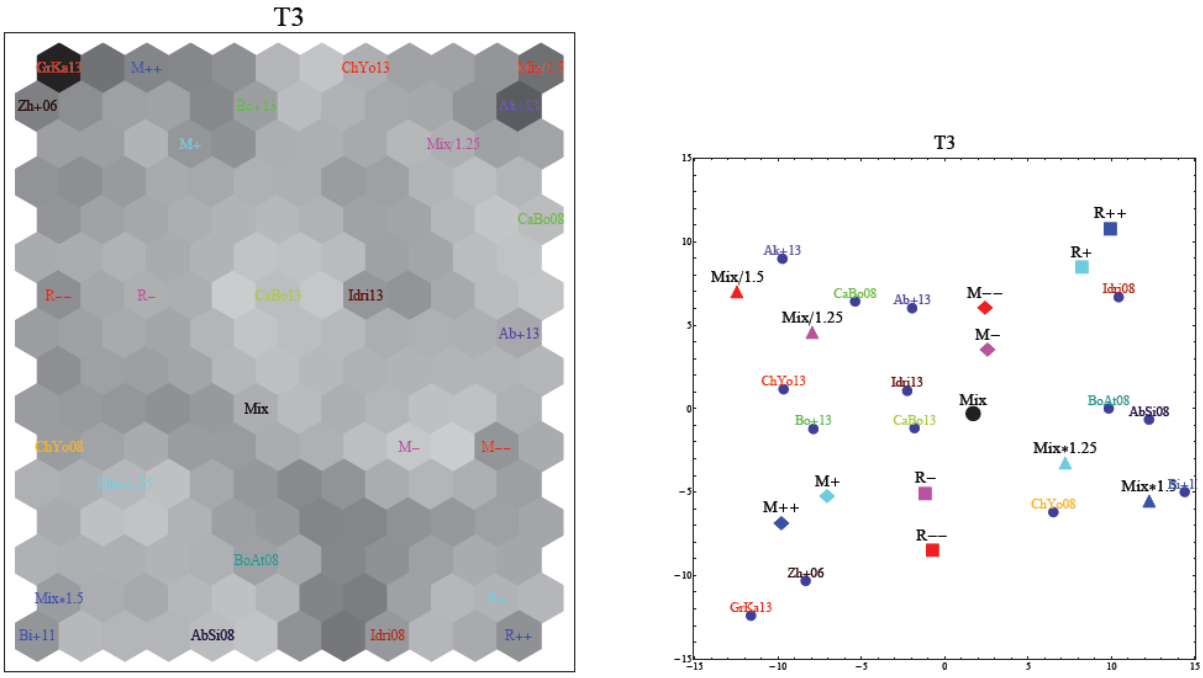



**Figure A8:** Left: U-Matrix of SOM for T = 0:2s, together with reference mixture and scaled mixture models. Right: Map based on shortest distances between models in the self-organizing map.

# APPENDIX B Memorandum received from Prof. Heaton after Workshop #2

Comments by Dr. Thomas Heaton (Caltech) on ground motion issues regarding probabilistic seismic hazards as applied to Diablo Canyon and Palo Verde Nuclear Generating Station.

## B.1 Memorandum

***From:*** Dr. Thomas Heaton

***To:*** Dr. Norman Abrahamson

***Subject:*** Comments on PSHA workshop of 22-24 October 2013

***Date:*** 5 November 2013

These are general comments on the probabilistic seismic hazard analyses (PSHA) of Diablo Canyon and Palo Verde nuclear power generating stations. These comments follow my participation at the Southwestern U.S. Ground Motion Characterization SSHAC Level 3 Workshop 2 – Proponent Models and Alternative Interpretations that I attended on October 22-24, 2013 at Shattuck Plaza Hotel, Berkeley, California.

In general the PSHA is making steady progress towards establishing a framework to characterize response spectral amplitudes (rsa's) as a function of earthquake magnitude, rake, JB distance, and site factor. Within the assumption that rsa's are log-normally distributed about a geometric mean that can be characterized by the chosen parameters, I think that the analysis is careful and rigorous. That said, I have some concerns that the current methodology may not characterize potentially important earthquake features that might be pertinent to nuclear power plant design.

1) If low frequency motions are a concern (sloshing of storage pools?), then whatever systems are affected are almost certainly not linear systems for very large motions. This means that modal analysis is not appropriate. It is important for the design engineers to directly communicate with scientists about what types of ground motion time histories are plausible. I would strongly discourage the use of "spectrum compatible motions" to simulate non-linear long-period dynamics.
2) The spatial distribution of slip is the key parameter that determines the nature of near-source long-period ground motion. For example, two earthquakes of identical magnitude can have very different average slips. Furthermore the maximum slip can be much larger than the average slip. However, when considering low-probability long-period motion, it's critically important to

characterize the statistical features of slip on segments of a fault that are close to the site. The current analysis does this problem by characterizing the source with moment magnitude, which is an averaging parameter for an earthquake. Variability is handled by assuming that long-period motions are log-normally distributed about the mean appropriate for the magnitude. However, I am not aware of any evidence that shows that the slip at a point is log-normally distributed about the mean. Instead, I would guess that we are looking at a power law distribution (Pareto). For a variety of reasons, I would argue that these slip distributions are approximately fractal in nature. Unfortunately, power law distributions are very hard to deal with when using standard statistical analysis. It may be more appropriate to simply say that PSHA is not well suited for this problem. The key issue is to design structures that are robust with respect to long-period ground motions. (Please see Yamada, M., A. Olsen, and T. Heaton 2009, Statistical features of short- and long-period near-source ground motions, Bull. Seism. Soc. Am., 99: 3264 - 3274)

3) When it comes to high-frequency near-source shaking, the evidence is good that observations are compatible with the hypothesis that pga's saturate with magnitude and that they are approximately log-normally distributed about ½ g with a standard deviation of a factor of about 2. You argue that this variability can be decomposed into separate site and source variabilities; this seems to be convincing and I fully support this approach. However, I am concerned about using a log-normal distribution to catch the tails of the distribution. In particular, I am concerned that we have now seen several examples of near-source peak accelerations whose time histories are asymmetric about their zero line (see Yamada, M., J. Mori, and T. Heaton, 2008, The slapdown phase in high acceleration records of large earthquakes, Seismological Research Letters; 80: 559 – 564). It has been hypothesized that this may be an example of 'slap down," a phenomenon that was well studied by the nuclear explosion test community. Slap down is clearly a nonlinear phenomenon and I would expect its statistics to be independent of the log-normal distribution that are used to characterize most of the data. It's very difficult to put an upper limit on slap down accelerations. There are many examples of objects that have been launched through the air in violent shaking from past earthquakes. Slap-down seems to be a plausible phenomenon in the near source of earthquakes.

4) While I know that it was not the function of this group to address the problem, I am concerned that moderate to large nearby earthquakes are excluded for the analysis of the Palo Verde plant. Simple examinations of Google Earth images (*Figure B1*) show clear lineations, one of which is within 13 km of the site. While the geologic investigation may indicate that these structures have not offset Pleistocene deposits, I feel that it is not justified to conclude that these structures are known to be incapable of future activity. At the very least, these structures should be considered in a logic tree. Based on our current capabilities to fully characterize these geologic structures, I suspect that we will obtain a finite probability on a logic tree. I suspect that this could significantly change the PSHA numbers for Palo Verde. The figure below is looking to the southwest from Phoenix, AZ, and it

shows remarkable lineations along the course of the lower Salt River (the lineation closest to the power station), and also along the course of the Gila River (the lineation that extends to California).




**Figure B1:** Google Earth image showing lineations around the PVNGS site

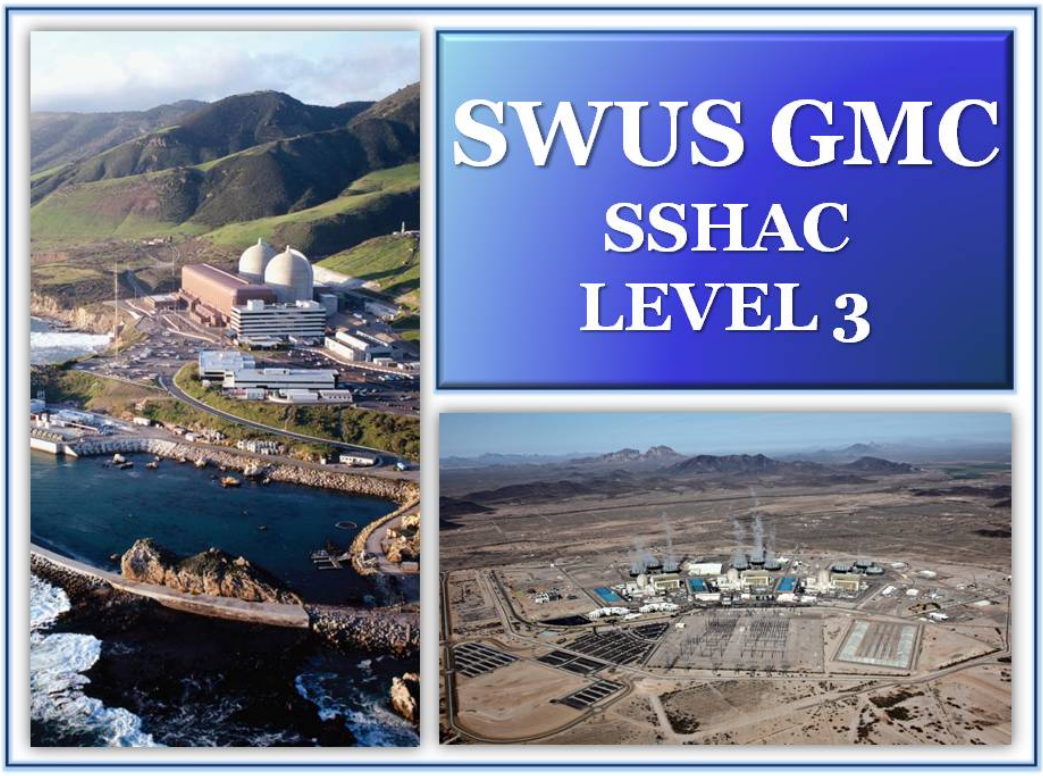
# *APPENDIX G*

## WORKSHOP #3 SUMMARY

# SOUTHWESTERN UNITED STATES GROUND MOTION CHARACTERIZATION SSHAC LEVEL 3

## Workshop #3 Proceedings

Version 1.1




aps PG&E

GeoPentech
Geotechnical & Geoscience Consultants

# WORKSHOP #3 PROCEEDINGS:

# Preliminary GMC Models and

# Hazard Feedback

## March 10-12, 2014

### International House, Berkeley, California

**Prepared for:**

**Arizona Public Service Company**
Palo Verde Nuclear Generating Station
*Wandell, Christopher J.*
Senior Consulting "Chief" Civil Engineer
Phone: (623) 393-6741; E-mail: christopher.wandell@aps.com

**Pacific Gas and Electric Company**
Diablo Canyon Power Plant
*Klimczak, Richard*
Director Geosciences
Phone: (415) 973-2791; E-mail: RLK1@pge.com

Version: 1.1
Date: June 4, 2014

## LIST OF ABBREVIATIONS and COMMON ACRONYMS

| | |
|---|---|
| ACR | Active Crustal Region |
| AFE | Annual Frequency of Exceedance |
| APS | Arizona Public Services |
| AZGS | Arizona Geological Survey |
| BBP | Broad Band Platform |
| CBR | Center, Body, and Range |
| CEA | California Earthquake Authority |
| CEC | California Energy Commission |
| CEUS | Central and Eastern United States |
| CFM | Community Fault Models |
| CFR | Code of Federal Regulations |
| CGS | California Geological Survey |
| CI | Closeness Index |
| CPUC | California Public Utilities Commission |
| DCPP | Diablo Canyon Power Plant |
| EE | Evaluator Expert |
| FAS | Fourier Amplitude Spectrum |
| FFS | Finite Fault Simulations |
| FGF | Fragile Geological Feature |
| FN | Fault Normal |
| FP | Fault Parallel |
| FW | Foot Wall |
| GIS | Geographic Information System |
| GM | Ground Motion |
| GMC | Ground Motion Characterization |
| GMPE | Ground Motion Prediction Equation |
| GMRS | Ground Motion Response Spectrum |
| GPS | Global Positioning System |
| HID | Hazard Input Document |
| HC | Hazard Calculation |
| HW | Hanging Wall |

| | |
|---|---|
| Hz | Hertz |
| IPRG | Independent Peer Review Group |
| ITC | Informed Technical Community |
| LiDAR | Light Detection and Ranging |
| MASW | Multi-channel Analysis of Surface Waves |
| NGA | Next Generation Attenuation |
| NGA-West2 | Project name for the update of the 2008 NGA models |
| NML | Normal (referred to normal faults) |
| NPP | Nuclear Power Plant |
| NSHM | National Seismic Hazard Mapping |
| PE | Proponent Expert |
| PEER | Pacific Earthquake Engineering Research Center |
| PGA | Peak Ground Acceleration |
| PG&E | Pacific Gas & Electric |
| PM | Project Manager |
| PPRP | Participatory Peer Review Panel |
| PSA | Pseudo-spectral acceleration |
| PSHA | Probabilistic Seismic Hazard Analysis |
| PTI | Project Technical Integrator |
| PV | Palos Verdes |
| PVNGS | Palo Verde Nuclear Generating Station |
| QA | Quality Assurance |
| RE | Resource Expert |
| RG | Regulatory Guide |
| $R_{JB}$ | Joyner and Boore Distance |
| $R_{RUP}$ | Rupture Distance |
| RV | Reverse (referred to reverse fault) |
| SASW | Spectral Analysis of Surface Waves |
| SCE | Southern California Edison |
| SCEC | Southern California Earthquake Center |
| SCFM | Statewide Community Fault Model |
| SCSN | Southern California Seismic Network |

| | |
|---|---|
| SONGS | San Onofre Nuclear General Station |
| SS | Strike Slip (referred to strike slip faults) |
| SSC | Seismic Source Characterization |
| SSHAC | Senior Seismic Hazard Analysis Committee |
| SSRS | Square Root of the Sum of the Squares |
| SSS | Single Station Sigma |
| SWUS | Southwest United States |
| TA | Transportable Array |
| TDI | Technically Defensible Interpretation |
| TI | Technical Integrator |
| UCERF2 | Uniform California Earthquake Rupture Forecast, Version 2 |
| UCERF3 | Uniform California Earthquake Rupture Forecast, Version 3 |
| USGS | United States Geological Society |
| U.S.NRC | U.S. Nuclear Regulatory Commission |
| USR | Unified Structural Representation |
| $V_{S,30}$ | Shear Wave Velocity in the upper 30m |
| WGCEP | Working Group on California Earthquake Probabilities |
| WNA | Western North America |
| WUS | Western United States |

# TABLE OF CONTENTS

Page

LIST OF ABBREVIATIONS and COMMON ACRONYMS ..... ii
TABLE OF CONTENTS ..... v
WORKSHOP #3 INTRODUCTION ..... 1
Purpose: ..... 1
Approach: ..... 2
Workshop #3 Agenda ..... 3
Workshop #3 participants ..... 6
Project background ..... 8
General workshop summary ..... 8
Topic 1: Post Workshop #2 Follow-up ..... 9
Topic 2: Proposed Approach for Median Models ..... 12
Topic 3: Finite Fault Simulations (FFS) ..... 14
Topic 4: PVNGS Hazard Feedback ..... 14
Topic 5: Evaluation of Candidate GM Models for PVNGS: Median for Arizona Sources ..... 15
Topic 6: Evaluation of Candidate GM Models for PVNGS: Median for California Sources ..... 15
Topic 7: DCPP Hazard Feedback ..... 16
Topic 8: Evaluation of Candidate GM Models for DCPP: Median for Strike-Slip Sources ..... 16
Topic 9: Evaluation of Candidate GM Models for DCPP: Median for Reverse Sources ..... 17
Topic 10: Other issues for DCPP ..... 17
Topic 11: Proposed Approach for Sigma Models ..... 18
Topic 12: Candidate GM Models and Logic Tree Structure for Sigma: Phi Models ..... 18
Topic 13: Candidate GM Models and Logic Tree Structure for Sigma: Tau Models ..... 19
Topic 14: Other Issues on Sigma ..... 20
Topic 15: Interface Issues and Other Topics ..... 21
GROUND MOTION CHARACTERIZATION PRESENTATIONS ..... 22
TECHNICAL INTEGRATOR TEAM SUMMARIES and PATH FORWARD ACTIONS ..... 24
LETTER COMMENTARY FROM THE PARTICIPATORY PEER REVIEW PANEL ..... 35
TECHNICAL INTEGRATION TEAM LEAD RESPONSES TO PARTICIPATORY PEER REVIEW PANEL COMMENTS ..... 40

REFERENCES.....44

# WORKSHOP #3 INTRODUCTION

Pursuant to the Request for Information put forth on March 12, 2012 by the United States Nuclear Regulatory Commission in response to the Near-Term Task Force's (NTTF) evaluation of the Fukushima Dai-ichi accident, Pacific Gas and Electric (PG&E) and Arizona Public Service (APS) are co-sponsoring a joint Southwestern U.S. (SWUS) Ground Motion Characterization (GMC) SSHAC Level 3 study for the Diablo Canyon Power Plant (DCPP) and the Palo Verde Nuclear Generating Station (PVNGS).

This is the last of three Workshops that will be conducted in accordance with the applicable guidelines for performing a Senior Seismic Hazard Analysis Committee (SSHAC) Level 3 Probabilistic Seismic Hazard Analysis (PSHA) for the two sites in this study.

According to the SSHAC process, following Workshop #2 "Proponent Models and Alternative Interpretations", the Technical Integration (TI) Team have developed an overall framework for the evaluations (often expressed as master logic-tree models) and the detailed evaluations of the relative weights on alternatives and uncertainties in associated parameters. The TI Team will make use of the feedback obtained during Workshop #3 to identify the bases for the finalization of the GMC models, while ensuring that no significant issues have been overlooked by considering the relative importance of the models, uncertainties, and assessments of weights.

## Purpose:

The specific goals of Workshop #3 are to:

1) Review the tasks that the Ground Motion Characterization (GMC) Technical Integration (TI) Team have conducted after Workshop #2 as part of their evaluations;
2) Present and discuss the preliminary GMC models and calculations in a forum that provides the opportunity for feedback to the evaluators;
3) Shed light on the most important technical issues through feedback given in the form of comments on hazard results and sensitivity analyses;
4) Obtain PPRP feedback; the PPRP are relieved of their observer status and expected to extensively question the preliminary GMC models;
5) Discuss the path forward towards the finalization of the GMC models in light of Workshop #3 feedback.

## Approach:

The goals of the Workshop will be accomplished by a series of presentations delivered by members of the TI Team as well as by invited Resource Experts (REs) and Proponent Experts (PEs). Presentations and video recordings will become part of the project record.

The workshop consists of two parts: (1) the evaluators presenting their preliminary models with particular emphasis on the manner in which alternative viewpoints and uncertainties have been incorporated, and (2) sensitivity analyses and hazard calculations that provide insight into the preliminary models. In the discussions of the preliminary models, the technical bases for the assessments and weights will be described to allow for a discussion of the implications and constraints provided by the available data.

The PPRP are relieved of their observer status and are expected to question and probe aspects of the preliminary model to understand the manner in which the views of the larger technical community have been considered and the range of technically defensible interpretations included.

Even if not formally requested to deliver presentations, Resource Experts (REs) and Proponent Experts (PEs) are encouraged to make comments during dedicated discussion breaks. Discussion will be focused on how the TI Team considered the views of the larger community and the manner in which their preliminary model represents current knowledge and uncertainties.

At the end of each day, the Observers will be provided with an opportunity to make comments and/or raise questions.

## Workshop #3 Agenda

| Session | Time | Topic | Duration (minutes) | Speaker |
|---|---|---|---|---|
| Day 1 – AM | | 8:30 AM – 12:00 PM | | |
| WORKSHOP INTRODUCTION | 8:30 AM – 9:00 AM | Welcome and introduction | 10 | Di Alessandro |
| | | Project overview and objectives; Status of data needs identified at Workshop #2 | 20 | Abrahamson |
| STATUS of TASK IDENTIFIED at WORKSHOP #2 | 9:00 AM - 10:15 AM | Feedback from REs/PEs after WS#2 | 60 | Youngs |
| | | *Discussions* | 15 | |
| 10:15 AM – 10:30 AM | | *Break* | | |
| STATUS of TASK IDENTIFIED at WORKSHOP #2 (Cont'd) | 10:30 AM - 11:20 AM | Summary of Working Meeting held on Jan. 28-29, 2014 | 40 | Abrahamson |
| | | *Discussions* | 10 | |
| PROPOSED APPROACH FOR MEDIAN MODELS | 11:20 AM - 12:00 PM | Overall approach for logic trees for median ground motion | 20 | Dreger |
| | | *Questions* | 20 | |
| 12:00 PM – 1:00 PM | | Lunch | | |
| Day 1 – PM | | 1:00 PM – 5:00 PM | | |
| UPDATES on VISUALIZATION TECHNIQUES | 1:00 PM - 2:45 PM | Visualizations and comparison with data sub-sets for constraining Center-Body-Range for median | 60 | Kuehn |
| | | *Discussions* | 45 | |
| 2:45 PM – 3:00 PM | | *Break* | | |
| FINITE FAULT SIMULATIONS | 3:00 PM - 4:35 PM | New set of forward finite-fault simulations to address splay ruptures | 15 | Bayless |
| | | Proponent rule for ground motions from splay ruptures | 15 | Wooddell |
| | | *Discussion* | 15 | |
| | | Consistency of long period displacement and fault slip for FFS | 30 | Dreger |
| | | *Discussion* | 20 | |
| 4:35 PM – 4:50 PM | | Summary of GMC Day 1 | 15 | Wooddell |
| 4:50 PM – 5:00 PM | | PPRP and Observers comments | 10 | |
| Day 1 | | End of Formal Workshop Proceedings | | |
| Closed Meeting: PPRP, Sponsors, PM, TI Lead | | | | |
| Public Q/A hosted by PG&E | | | | |

| Session | Time | Topic | Duration (minutes) | Speaker |
|---|---|---|---|---|
| Day 2 – AM | | 8:00 AM – 12:00 PM | | |
| PVNGS HAZARD FEEDBACK | 8:00 AM - 9:05 AM | Simplified source model for PVNGS | 10 | Walling |
| | | Logic Tree structure | 15 | Youngs |
| | | Hazard feedback and sensitivity results | 20 | Walling |
| | | *Discussion* | 20 | |
| EVALUATION of CANDIDATE GM MODELS for PVNGS: Median for AZ Host Sources | 9:05 AM - 10:30 AM | GM models for host AZ sources: median | 45 | Abrahamson |
| | | PPRP review, questions and comments | 20 | PPRP |
| | | REs questions and comments | 20 | Resource Experts |
| 10:30 AM – 10:45 AM | | *Break* | | |
| Follow up on Visualization Approach | 10:45 AM – 11:00 AM | Residuals for candidate GMPEs | 15 | Kuehn |
| EVALUATION of CANDIDATE GM MODELS for PVNGS: Approach for Median for Distant CA Sources | 11:00 AM - 12:00 PM | Approach for median for distant CA sources | 30 | Wooddell |
| | | PPRP review, questions and comments | 15 | PPRP |
| | | REs questions and comments | 15 | Resource Experts |
| 12:00 PM – 1:00 PM | | *Lunch* | | |
| Day 2 – PM | | 1:00 PM – 4:00 PM | | |
| CANDIDATE GM MODELS and LOGIC TREE STRUCTURE for SIGMA: Phi Models | 1:00 PM - 3:00 PM | Logic tree structure and models for Phi | 75 | Al-Atik |
| | | Other Issues for Sigma:<br>– Upper tail distribution using mixture model;<br>– Potential spatial correlation bias | 15 | Youngs |
| | | PPRP review, questions and comments | 20 | PPRP |
| | | REs questions and comments | 10 | Resource Experts |
| 3:00 PM | | *PM Snack served on site while continuing session* | | |
| CANDIDATE GM MODELS and LOGIC TREE STRUCTURE for SIGMA: Tau Models | 3:00 PM - 3:35 PM | Logic tree structure and models for Tau | 15 | Al-Atik |
| | | PPRP review, questions and comments | 10 | PPRP |
| | | REs questions and comments | 10 | Resource Experts |
| 3:35 PM – 3:50 PM | | Summary of GMC Day 2 | 15 | Dreger |
| 3:50 PM – 4:00 PM | | PPRP and Observers comments | 10 | |
| Day 2 | | End of Formal Workshop Proceedings | | |
| Closed Meeting: PPRP, Sponsors, PM, TI Lead | | | | |
| Public Q/A hosted by PG&E | | | | |

| Session | Time | Topic | Duration (minutes) | Speaker |
|---|---|---|---|---|
| Day 3 – AM | | 8:00 AM – 12:00 PM | | |
| DCPP HAZARD FEEDBACK | 8:00 AM - 9:05 AM | Simplified source model for DCPP | 10 | Gregor |
| | | Logic Tree structure | 15 | Youngs |
| | | Hazard feedback and sensitivity results | 20 | Gregor |
| | | *Discussion* | 20 | |
| Reminder on Visualization | 9:05 AM - 10:00 AM | Reminder on envisioned approach for Visualization Techniques | 30 | Kuehn |
| | | *Discussion* | 25 | |
| 10:00 AM – 10:15 AM | | *Break* | | |
| EVALUATION of CANDIDATE GM MODELS for DCPP: Median for Strike-Slip Sources | 10:15 AM - 12:00 PM | GM models for Strike-Slip earthquakes: median | 65 | Abrahamson |
| | | PPRP review, questions and comments | 20 | PPRP |
| | | REs questions and comments | 20 | Resource Experts |
| 12:00 PM – 1:00 PM | | *Lunch* | | |
| Day 3 – PM | | 1:00 PM – 5:00 PM | | |
| PROPONENT DIRECTIVITY MODEL | 1:00 AM - 1:50 PM | Directivity proponent model | 30 | Watson-Lamprey |
| | | *Discussions* | 20 | |
| EVALUATION of CANDIDATE GM MODELS for DCPP: Approach for Median for Reverse Sources | 1:50 PM - 3:20 PM | Availability of additional empirical data to constraint HW scaling for small magnitudes: Japanese data | 10 | Di Alessandro |
| | | Approach for median for reverse sources: | 40 | Youngs |
| | | PPRP review, questions and comments | 20 | PPRP |
| | | REs questions and comments | 20 | Resource Experts |
| 3:20 PM – 3:30 PM | | *Break* | | |
| EVALUATION of PATH EFFECTS for DCPP | 3:30 PM - 4:10 PM | Approach for Path effects evaluation at DCPP: PGV example | 20 | Abrahamson |
| | | *Discussion* | 20 | |
| PATH FORWARD and SUMMARY of GMC Workshop #3 | 4:10 PM – 4:50 PM | Summary of GMC Day 3 and Overview of Day 1 and Day 2; Path forward to finalize the GMC models | 40 | Abrahamson |
| 4:50 PM – 5:20 PM | | PPRP and Observers comments | 30 | |
| Day 3 | | End of Formal Workshop Proceedings | | |
| Closed Meeting: PPRP, Sponsors, PM, TI Lead | | | | |
| Public Q/A hosted by PG&E | | | | |

## Workshop #3 participants

| Group | Individual | Affiliation |
|---|---|---|
| **PPRP** | Day, Steven | San Diego State University |
| | Campbell, Kenneth | Ken Campbell Consulting |
| | Chiou, Brian | Brian Chiou Consulting |
| | Rockwell, Tom | San Diego State University |
| **Project Management - GeoPentech** | Barneich, John | GeoPentech, Inc. |
| | Di Alessandro, Carola | GeoPentech, Inc. |
| | Dinsick, Andrew | GeoPentech, Inc. |
| **Project Management - Utilities** | Klimczak, Richard | Pacific Gas and Electric Company |
| | Jahangir, Nozar | Pacific Gas and Electric Company |
| | Powell, Michael | Arizona Public Service |
| | Wandell, Christopher | Arizona Public Service |
| **Project Technical Integrator** | Abrahamson, Norman A. | Pacific Gas and Electric Company |
| | McGuire, Robin (*) | Lettis Consultants International. Inc. |
| **Hazard Analysts** | Gregor, Nick | NG Consulting |
| | Walling, Melanie | Lettis Consultants International, Inc. |
| **Technical Integrator Team** | Abrahamson, Norman A. | Pacific Gas and Electric Company |
| | Dreger, Doug | Univ. of California, Berkeley |
| | Wooddell, Katie | Pacific Gas and Electric Company |
| | Youngs, Bob | AMEC Environment and Infrastructure |
| **Technical Integrator Support** | Al-Atik, Linda | Linda Alatik Consulting |
| | Bayless, Jeff | URS Corporation |
| | Watson-Lamprey, Jennie | Watson-Lamprey Consulting |
| **Resource and Proponent Experts (continues on next page)** | Aagaard, Brad (*) | U.S. Geological Survey, Menlo Park |
| | Anderson, John (*) | Univ. of Nevada, Reno |
| | Archuleta, Ralph | Univ. of California, Santa Barbara |
| | Baker, Jack | Stanford University, Palo Alto |
| | Bozorgnia, Yousef | Univ. of California, Berkeley |
| | Goulet, Christine | Univ. of California, Berkeley |
| | Graves, Robert | U.S. Geological Survey, Pasadena |
| | Harris, Ruth (*) | U.S. Geological Survey, Menlo Park |
| | Heaton, Thomas | California Institute of Technology |
| | Idriss, IM | IM Idriss Consulting |
| | Kuehn, Nicolas | Univ. of California, Berkeley |
| | Lozos, Julian | Stanford Univ., Palo Alto |
| | Olsen, Kim | San Diego State University |
| | Pasyanos, Michael | Lawrence Livermore National Laboratory |
| | Pitarka, Arben | Lawrence Livermore National Laboratory |

| Group – Continued | Individual | Affiliation |
|---|---|---|
| **Resource and Proponent Experts (continued from previous page)** | Rodriguez-Marek, Adrian | Virginia Tech |
| | Somerville, Paul | URS Corporation |
| | Stewart, Jonathan | Univ. of California, Los Angeles |
| | Toro, Gabriel | Lettis Consultants International, Inc. |
| **Regulatory Observers** | Ake, Jon P. | US Nuclear Regulatory Commission |
| | Anderson, Robert | California Seismic Safety Commission |
| | Budnitz, Robert J. | Lawrence Livermore National Laboratory |
| | Chen, Rui | California Geological Survey |
| | Giacinto, Josef | US Nuclear Regulatory Commission |
| | Gibson, Bruce | San Luis Obispo County |
| | Graizer, Vladimir | US Nuclear Regulatory Commission |
| | Hale, Christie | US Nuclear Regulatory Commission - Region IV |
| | Johnsson, Mark | California Coastal Commission |
| | Stamatakos, John | Center for Nuclear Waste |
| | Walter, Joan | California Energy Commission |
| | Weaver, Casey | California Energy Commission |
| | Wills, Chris J. | California Geological Survey |
| **Other Observers** | AbramsonWard, Hans | Lettis Consultants International. Inc. |
| | Ancheta, Tim (*) | RMS |
| | Becker, Rochelle | A4NR |
| | Chao, Shu- Hsien | Nat. Cent. for Res. on Earthq. Engin., Taiwan |
| | Chang, Yu-Wen | Nat. Cent. for Res. on Earthq. Engin., Taiwan |
| | Ferre', Kent | Pacific Gas and Electric Company |
| | Geesman, John | A4NR |
| | Hamilton, Douglas | DHH Geoconsult |
| | Hardebeck, Jeanne (*) | U.S. Geological Survey, Menlo Park |
| | Hartleb, Ross | Lettis Consultants International |
| | Hollenback, Justin | Univ. of California, Berkeley |
| | Lewis, Sherry | Mothers for Peace |
| | Renault, Philippe | PEGASOS Refinement Project - Swissnuclear |
| | Silva, Fabio (*) | SCEC - Univ. of Southern California |
| | Thompson, Steve | Lettis Consultants International, Inc. |
| | Weisman, David | A4NR |

(*) Remote attendance

# WORKSHOP #3 SUMMARIES

## Project background

Pursuant to the Request for Information put forth on March 12, 2012 by the United States Nuclear Regulatory Commission in response to the Near-Term Task Force's (NTTF) evaluation of the Fukushima Dai-ichi accident, Pacific Gas and Electric Company (PG&E) and Arizona Public Service (APS) are co-sponsoring a joint Southwestern U.S. (SWUS) Ground Motion Characterization (GMC) SSHAC Level 3 study for the Diablo Canyon Power Plant (DCPP) and the Palo Verde Nuclear Generating Station (PVNGS). The ultimate deliverable for this study will be a ground motion model developed following the guidelines of the SSHAC Level 3 process (Budnitz et al., 1997; NRC, 2012).

## General workshop summary

The third and last workshop of the SWUS SSHAC was held at the International House, Berkeley, California from March 10 to March 12, 2014. The introductory presentation delivered by the Project Manager, Dr. Carola Di Alessandro, provided an overview on the primary purpose of Workshop #3, which is designed to (1) present, discuss, and debate preliminary Ground Motion Characterization (GMC) models for the two sites in the SWUS GMC SSHAC Level 3 study; (2) provide feedback to the Technical Integration (TI) Team regarding their proposed approach to develop models that represent the center, body, and range of technically defensible interpretations; (3) evaluate the hazard significance of various components of the GMC models; and (4) provide a basis for the subsequent development of final GMC hazard models.

The workshop introduction included also a review of the SSHAC procedures and the Workshop #3 ground rules, with particular emphasis to the role of the Participatory Peer Review Panel (PPRP), who were relieved of their observer status and were expected to extensively question the preliminary GMC models to ensure no significant issues have been overlooked by considering the relative importance of the models, uncertainties, and assessments of weights.

Following this presentation, the TI Team Lead, Dr. Norman Abrahamson, presented an overview of the project schedule and objectives. This included addressing interface with Seismic Source Characterization (SSC) and Site Response efforts, which are separate projects carried out by each Utility independently. Finally, he provided an overview of the progress achieved for the various data-need categories identified during Workshop #1 and #2, including a brief explanation on how they have been incorporated in the overall framework of the evaluation tasks conducted after Workshop #2.

### *Topic 1: Post Workshop #2 Follow-up*

During Workshop #2, some of the Proponent Experts' (PEs) and Resource Experts' (REs) had not addressed all of the focused questions addressed to their attention. In addition, there were several requests for additional information that resulted from the Workshop #2 discussion. These missing responses were presented at a Working Meeting in January 2014 (described below). Furthermore, at the time of Workshop #2, some proponent models (e.g. directivity, path adjustments, GM for complex and splay ruptures etc…) were not ready for discussion and evaluation. Lastly, two proponent models (Idriss NGA-West2 GMPE and the finite fault simulation method EXSIM) were not represented by their Proponent Experts (Prof. Idriss and Dr. Atkinson, respectively) due to their absence. In an effort to adequately capture the PEs and REs inputs, several communications occurred after Workshop #2 and many PEs and REs attended a Working Meeting held in Berkeley on January 28-29, 2014, designed to provide a framework for interaction between Experts and TI Team with the presence of the PPRP.

A summary of the additional information received from Experts (in alphabetical order) was provided by Dr. Robert Youngs, addressing the following topics:

- Abrahamson et al. (ASK14) GMPE (Dr. Norman Abrahamson): effect of removing Class 2 events on the aleatory variability terms tau and phi.
- Akkar et al. (ASK14) GMPE (Dr. Sinan Akkar): effect of earthquakes' depth and additional evaluation on the high aleatory variability as compared with the NGA-West2 models. The results highlighted that the high sigma is mainly controlled by large phi, which is not overly sensitive to the number of events/recordings used to compute it. Further evaluations are needed to assess whether the large phi is related to quality of metadata, non-uniform processing or larger site condition variability.
- Extreme ground motions (Dr. John Anderson): reference to papers and data addressing very large ground motions.
- EXSIM stochastic finite-fault simulation method (Dr. Gail Atkinson): summary of the principles behind the method, and responses to the focused questions addressed to the BBP modellers at Workshop #2. Particular emphasis was given to the issue of applicability of EXSIM to near fault conditions, where the model shows a numerical issue at distance 0 km and it leads to larger short-period ground motions at short distance (1 km) for M 6.5 as compared to the other FFS methods. Such difference decreases for larger magnitudes and is deemed to be a credible feature of the model according to Dr. Atkinson's Proponent input.
- Effect of spatial correlation on estimates of aleatory variability (Dr. Jack Baker): preliminary examples of spatial correlation in NGA-West2 residuals. When accounting for spatial correlation while fitting GMPEs, the within-event standard deviation can increase but the between-event standard deviations are smaller. A quantitative evaluation of the effect using NGA-West2 residuals and models is desirable while developing the finalized GM logic tree models.

- Bindi et al. (2014) Pan-European GMPE (Dr. Dino Bindi): the new GMPE is meant to update the 2011 GMPE for Italy. While the steep magnitude scaling above M 7 in the 2011 model is generally reduced in the 2014 update, such strong scaling is still present at 5 Hz.
- Effect of stress on "bump" in tau at 10 Hz (Dr. Dave Boore): series of stochastic point-source simulations for WNA with varying stress parameter (25 – 400 bars range) indicate that variation in stress is not the explanation for the peak in tau at short periods observed for all data expect California only. Presently, BSSA NGA-West2 GMPE retains the feature of the "bump" in tau.
- Boore et al. (BSSA14) GMPE (Dr. Dave Boore): standard error of the mean event terms for normal events, hanging wall residuals as function of dip and $R_{JB}$, regional variation of intra-event standard error.
- Relevant issues for developing SWUS GMC Model (Dr. Tom Heaton): addressing non-linearity of very large long period motion when performing structural analyses, importance of the statistical features (spatial distribution) of slip on segment close to the site, and evaluation of departure from log-normal assumption in the upper tail distribution.
- Idriss (ID14) GMPE (Prof. I.M. Idriss): summary of the method updates with respect of the 2008 version, and responses to the focused questions addressed to the GMPE modellers at Workshop #2. Particular emphasis was given to the issue of applicability of the model for short distances ($R \leq 1$ km) and to the lack of an explicit normal faulting factor and hanging wall factor.
- Phillips et al. (2013) gridded Q results (in terms of $Q_O$ and eta) provided by Dr. Kevin Mayeda.
- Fragile Geologic Feature investigation for PVNGS: recap on Resource Expert presentation provided by David Haddad (ASU) at PVNGS SSC SSHAC Workshop #1. No current feature is recognised around PVNGS.
- Chiou and Youngs (CY14) GMPE (Dr. Robert Youngs): uncertainty in tau and phi estimates, and analysis of CY14 residuals to evaluate peak in tau at high frequency. His conclusions indicate that the peak in tau represents site effects, i.e. differences in the average site effect for the set of stations recording each event.
- Update on Zhao and Lu (2011) magnitude scaling (Dr. John Zhao): using a combination of Japanese and NGA data, he found that at short periods magnitude scaling is nearly zero for $M > 7.1$ and tends to be negative at long periods (although he recommends setting it to zero in that case). Accordingly, a proponent implementation of Zhao and Lu (2011) magnitude scaling concept was presented by Dr. Youngs.

Additional salient outcomes of the January 2014 Working Meeting were presented by Dr. Norman Abrahamson, to include the following:

- Arizona Study (sponsored by PEER). Ground motion data recorded in Arizona has been collected and processed uniformly, and is publicly available through PEER's website. Eleven recording stations around PVNGS have been characterized in terms of $V_{S,30}$, NEHRP category, $V_S$ profiles and associated uncertainty through SASW analysis conducted by Dr. Rob Kayen (USGS). There are generally two

typical site types: deep alluvium (nine sites) and shallow soil over stiff rock (two sites). The distance attenuation for 14 NGA-West2 events recorded in Arizona has been studied by Dr. Jennie Watson-Lamprey in support of the path effect adjustment task for California sources contributing to PVNGS's hazard. Her results indicate that there is no significant difference between attenuation of the ground motion from California earthquakes recorded across southern California and Arizona, whether the ray paths cross the Salton Through extensional zone or not; accordingly, no modification to the NGA-West2 GMPEs' rate of attenuation is necessary. Although these results indicate that the Q difference between Arizona and California are not large enough, further analysis is needed to evaluate if there is a regional source effect causing differences in event terms for the various regions. Lastly, results of kappa analysis conducted by Dr. Olga Ktenidou for Arizona events recorded at the Arizona recording stations were summarized. Her "hockey stick" model leads to a $\kappa_O$ estimate slightly above 0.02±0.01 s, with reasonable distribution of model residuals versus $V_{S,30}$. A caveat for this analysis is that the site amplification and soil damping effect are not removed prior to estimating kappa. An updated analysis is needed to remove the site amplification to estimate rock kappa. Also, if characteristics of the data allows, it may be worth focusing on the two rock sites (Y16A and 113A).

- Hanging Wall effects: validation of finite-fault simulations for M5-M6 and HW effects at small magnitudes. A part B validation was conducted in winter 2013 for M5.5 reverse fault (dip = 45 deg, $Z_{TOR}$ = 6 km) scenario, using Leonard (2010) M-A scaling, on 30 stations in the FW at $R_{RUP}$ = 20 and 50 km, across the 3 FFS methods that passed the validation evaluation in June 2013 (EXSIM, Graves & Pitarka, and SDSU). Dr. Christine Goulet's results indicated that SDSU implementation needed a revision to pass the new Part B validation case; Dr. Kim Olsen subsequently provided the TI Team a simple rule for changing an input parameter for application to M < 6. Another topic covered in this session was the evaluation conducted by Dr. Douglas Dreger with regards to the persistence of the hanging wall characteristics at small magnitudes at short period, as shown by the FFS; according to his evaluation, the HW effect for M 5.5 seems to be associated to geometry effect, and might imply modifying the magnitude taper in the HW functions as implemented in the proponent NGA-West2 GMPEs.
- Shape of ground motion distribution: is there any deviation from log-normal assumption? Dr. Abrahamson analysed the distribution of upper tails from empirical data (ASK14 dataset) and simulations (Graves & Pitarka simulations for the validation of Landers earthquake). His results indicated that, for a subset of empirical data with M > 6 and R < 15 km, the within-event residuals show fatter tail above 2 epsilon, but a log-normal distribution cannot be rejected. A mixture model, as obtained by a weighted average of two log-normal distributions with the same mean but different values of the standard deviation, is worth being explored as an alternative distribution. The validation simulations for Landers do not deviate from the log-normal distribution, but such analysis should be repeated using all the methods and all the forward simulations; caution should be exerted however because the FFS have been validated for the median, and not for the variability (longer-term effort, not in SWUS timeline).

- Proponent models for addressing complex ruptures: adjustment factors derived from simulations results. Forward simulations for complex ruptures were analysed by Ms. Katie Wooddell to help constrain which input (rake, dip, and distance) to use into GMPEs when addressing complex ruptures (where rake and dip change along strike). Four proponent approaches on how to use the GMPEs to compute ground motions from complex ruptures were presented. The comparison with FFS simulations indicated that Method 1 (SRSS the response spectra from the two segments using each segment's dip, rake, distance and magnitude as inputs to the GMPEs) best approximates the FFS results directly which incorporated the complex geometry. Due to the low rate of occurrence of such complex events in the SSC, method 1 is recommended to be applied as a single rule, without epistemic uncertainty. The low rate of occurrence of such events needs to be confirmed with the draft DCPP SSC model as it becomes available. If the rate becomes high, that the need for epistemic uncertainty should be re-assessed.

Additional topics addressed during the January 2014 Working Meeting and being presented at the Workshop #3 are summarized in the respective sections.

### *Topic 2: Proposed Approach for Median Models*

The proposed approach to characterize median motion was introduced by Dr. Douglas Dreger. Candidate GMPEs selected for the various source classes (that can be captured by a common functional form) are re-parameterized using a common functional form and then a new set of 1000 models is generated by sampling the correlation structure of the coefficients. Visualization approach will generate Sammon's maps where the high-dimensional space (spectral accelerations for about 200 magnitude, distance, mechanism, $Z_{TOR}$, period etc… combinations) spanned by the 1000 models is projected into two-dimensions. The 1000 models broaden the GMPE space with respect to the published models. Appropriate data-subsets can be used to generate likelihood estimates and mean event terms for each of the 1000 models. Contour maps of the mean residuals and likelihood are superimposed on the Sammon's maps to help identifying the model-space which is not rejected by observations. Finite-fault simulations obtained from BBP can be used as well to evaluate the technically defensible space of the models. The credible space is partitioned into regions based on a concentric "spider net" pattern. A limited number of representative models will be extracted for each of the sub-groups. Weights can be developed considering the relevance of sampling density, likelihood, mean bias, etc… Subjective assessment on how the model distribution will be centered will rely on the TI Team's evaluation of the available information, including published GMPEs, simulations, alternative data-sets etc. The base model will consist of the representative new models, and by the candidate GMPEs that could not be re-sampled by common functional form. Adjustments for path effects, directivity effects, and rule-based approaches for splay and complex ruptures will be applied to the base model. Details of these adjustments are provided in subsequent topic sections.

Dr. Nicolas Kuehn provided a comprehensive presentation on the visualization approach and showed example comparison with data subsets to constrain the Center/Body/Range (CBR) for the strike-slip source

class at DCPP. A $R_{RUP}$-based functional form works generally well but leads to larger bias when fitting $R_{JB}$-based candidate GMPEs. During the discussion, a suggestion was made to use two forms (one based on $R_{RUP}$ and the other based on $R_{JB}$) to maintain the key features of the initial candidate GMPEs and to perform hazard sensitivity analyses on the impact of choosing one form versus the other. If hazard results are similar, then just one form can be retained, otherwise, maintain both forms and weight them. Another comment was to account for the misfit between the common form and the GMPEs and add this additional term to the aleatory variability if it is too large to be ignored (e.g. > 0.02 change (ln units) in the total sigma).

The choice of the common functional form was also discussed. It was suggested to adopt a better form that will result in fewer non-physical models (i.e. not acceptable magnitude and distance scaling rates). In addition, a mixed effects approach could be implemented using the individual GMPEs as a group factor so that their parameters associated to physical constraints are retained.

Several comments addressed the use of alternative subsets of data to compare with the Sammon's map: in particular, it was suggested to explore the subsets used by each GMPE developer, data from Class 1 events versus Class 2 and so forth. Furthermore, caution was recommended to not rely solely on goodness-of-fit to data for assessing model weights, because that would implicitly mean down-weighting the expert judgement that each GMPE developer exerted while deriving his/her model. A viable option would be to broaden the distribution of weights towards the data, so not to narrow the uncertainty but account for the average shift required to fit the data. As a last topic, Dr. Nicolas Kuehn showed that the within-model uncertainty as quantified by Al-Atik and Youngs PEER report on NGA-West2 epistemic uncertainty is much smaller than the resulting between-model epistemic uncertainty and is being captured by the overall range in the models being developed.

General comments on the use of Sammon's mapping included adding the GMPEs not used to develop the covariance matrix to the plots to provide further information for the centering evaluation. Also, it was suggested to insert magnitude and distance markers to provide a roadmap on how to read the distribution of models in the Sammon's space. The issue of how to interpret the Sammon's maps was further discussed throughout the Workshop: during Day 3, it was suggested to rotate the Sammon's plots so to have similar meaning (in terms of scaling) for a given direction, and also to add a metric to measure the ability of the 2-D projection to capture the separation distance in the higher dimensional space. As discussed during Day 3 (see "Topic 8: Evaluation of Candidate GM Models for DCPP: Median for Strike-Slip sources"), initial results show that sampling of representative models using a single Sammon's map that combined all periods does not sample the range that each period would have sampled individually. Accordingly, moving forward, the TI Team may need to consider period-dependent models and possibly apply period-dependent weights. Also, to achieve better information on the viable model space, if the likelihood plots are not bounded by the 1000 models, it was suggested to increase the range of the models by generating more than 1000 sampled models. Due to the innovative nature of the use of Sammon's map in hazard assessment, the method with examples needs to be properly documented, not only as a PEER Report, but also through journal papers. A tool for implementing the model should also be provided to other groups to use the model (i.e. BBP and USGS).

### *Topic 3: Finite Fault Simulations (FFS)*

Finite fault simulations (FFS) for splay faulting were addressed in the afternoon of Day 1. Mr. Jeff Bayless presented the scenarios that were run on the BBP to address the splay ruptures, how the waveforms were combined in the time domain, and how response spectra were computed to evaluate the ratio between the simulated ground motions from the combined primary and splay segments to simulated ground motions from the primary segment alone.

Ms. Katie Wooddell then addressed alternative proponent rules for ground motions for splay ruptures by comparing factors of combined to primary segment spectral amplitude from GMPEs using four different approaches with factors derived from the simulations. The comparison showed that factors using the GMPE SSRS method most closely resemble the period dependence of the factors computed from the simulations. One topic that requires follow up is that the SDSU factors showed a bump at 10 Hz which is not present for the other two FFS methods (i.e. Graves & Pitarka and EXSIM). The 10 Hz bump is more pronounced for the reverse splay simulations with respect to the strike-slip cases, and appears to result from a high frequency shift in the spectral peak for the larger magnitude splay rupture.

The last topic associated to finite fault simulations was the comparison of long-period motions and fault slip presented by Dr. Douglas Dreger. His evaluations showed that spectral displacements from GMPEs are generally consistent with the long-periods from the simulations, and that there is a correlation between static displacement, peak displacement, and long-periods displacement spectral amplitudes with spatially weighted averaged fault slip (where the weights of the faults slip are based on FP and FN radiation patterns with geometrical spreading).

### *Topic 4: PVNGS Hazard Feedback*

The morning of Day 2 started by addressing the Hazard Feedback at PVNGS site. First, Dr. Melanie Walling introduced a simplified source model consisting of the PVNGS SSHAC Level 2 (LCI, 2012) sources, to be used to evaluate the GMPE hazard sensitivity to the effect of local sources (0-200 km), distant sources (200-400 km) and path-specific effects.

She showed hazard sensitivity for following cases: 1) Host zone GMPEs (0-200 km); 2) Distant sources (200-400 km); 3) Sigma model; 4) Tail of distribution. The most important branch was the median model. The GMPE base case consisted of five equally weighted NGA-West1 GMPEs.

The TI Team suggested a revising the regionalization of the GM models, such that the distant sources from California are separated from the remaining distant sources (see “Topic 6: Evaluation of Candidate GM Models for PVNGS: Median for California Sources”). In addition, only the sources in California should be further divided into North and South paths using the northern tip of the Gulf of California background zone as a horizontal demarcation line. Future hazard sensitivities should isolate one branch of the logic tree at the time for creating the tornado plots, and should also change the GMPE base case to use selected

candidate models for each source class with equal weights. An outlier appearing at AFE $10^{-6}$ hazard for the epistemic uncertainty in the $\phi_{SS}$ branch, and lack of systematic reduction from the upper to median to lower $\phi_{SS}$ branches should be checked.

### *Topic 5: Evaluation of Candidate GM Models for PVNGS: Median for Arizona Sources*

The proposed approach for the GM logic trees for both median and sigma was discussed in the morning of Day 2 by Dr. Robert Youngs. In his overview, Dr. Youngs explained how the selection of candidate GMPEs has been further refined for each of the source classes for DCPP and PVNGS according to the appropriateness of data and assumptions on scaling adopted by the various modellers. He also presented a detailed overview of the preliminary draft GM Logic Trees Model structure for PVNGS, discussing the general framework for evaluation of the proponent models and approach to assign weight in the final GM model.

Following Dr. Robert Young's presentation on the general logic tree structure for PVNGS, Dr. Norman Abrahamson addressed the specific details for the Median GM Model for Arizona Host Source. He described the alternative data-sets to be used in the evaluation (NGA-West2 or European data, with M>5, R< 50 km and NML Style of Faulting (SOF), plus the subsets used by each candidate GMPE developer). The NGA-West2 database is largely driven by strike-slip and reverse data-sets, while the European datasets include more normal events but generally lacks reverse data. This results in large uncertainty in NML SOF factors for the candidate GMPEs. As part of the discussions, it was noted that the normal SOF of the NGA-West2 GMPEs were not all centered on the data due to the modellers' lack of confidence in factors obtained from sparse data. Accordingly, the PPRP asked that confidence intervals for the NML faulting factors be shown and that the evaluation on lack of centering for some NML earthquakes' event terms with respect to the GMPEs NML factors be document.

Because there are no known faults close to PVNGS, the seismic hazard is going to be modelled by randomly oriented faults with moderate magnitude events. The hanging wall (HW) effect for these events is proposed to be modelled using $R_{JB}$ parameterization in the common functional form for developing the models, which also works well for the FW cases. The PPRP challenged that proposed approach, asking the TI Team to demonstrate that the HW effects can be adequately captured through that approach.

Lastly, the PVNGS SSC SSHAC Level 3 Project Manager, Dr. Ross Hartleb, specified that the current PVNGS SSC draft preliminary model encompasses strike-slip sources in the host zone; therefore, this project needs to build a GM model for addressing strike-slip sources, but they are not likely to be the main contributors to the hazard due to the small fraction of strike-slip versus normal earthquakes.

### *Topic 6: Evaluation of Candidate GM Models for PVNGS: Median for California Sources*

Strike-slip and normal faults in Central and Southern California are important contributors to long period hazard at PVNGS. The approach for median GM for distant California sources was presented by Ms. Katie

Wooddell during the second half of the Day 2 morning. Candidate GMPEs to be used to generate the base model need to be valid for small magnitudes (M 4-5) to allow comparison with observed attenuation of events originated in California and Mexico and recorded in Arizona, and should also be applicable to large magnitudes (M 6.5-8.5) at large distances (200-400 km) for hazard application. Ms. Wooddell presented the GM logic tree structure for the California sources producing large magnitudes, and explained how path effects are accounted for sources whose paths travel north of the Mojave desert, or cross the Mojave/Salton Trough region. The median path term is a combination of path and source terms, and is evaluated for the nine TA stations around the PVNGS site, thus, making it a "source-to-region" path adjustment. During the discussion, some outlier event term residuals were seen for some specific GMPEs at specific periods which need to be checked by the GMPE developers. Also, Dr. Vladimir Graizer emphasize the importance of providing a scientific basis for the lack of change in distance attenuation (California to Arizona) needed in the NGA-West2 GMPEs, given that recent studies show that the Q structure is different among the two regions. Additionally, the PPRP suggested evaluating the average source terms for California sources with more attention, by including the event terms for all the NGA-West2 events associated to those sources, not just those recorded by the TA stations in Arizona. Finally, it was recommended to add a branch in the logic tree to account for no path effects. Moving forward towards the finalization of the GM model, care should be exerted in how to divide the north and south paths. There is also the plan to increase the epistemic uncertainty due to the limited (four) amount of candidate GMPEs, and their associated large magnitude scaling.

### *Topic 7: DCPP Hazard Feedback*

The morning of Day 3 started by addressing the Hazard Feedback at DCPP site. First, Dr. Nick Gregor introduced a simplified source model consisting of the four main faults sources contributing to the DCPP hazard and to be used to evaluate the GMPE hazard sensitivity to the effect of various branches in the logic tree. The four controlling faults are the Hosgri, Shoreline (both strike slip), Los Osos and San Luis Bay (both reverse, with the DCPP site located on the HW side). The GMPE base case consisted of five equally weighted NGA-West1 GMPEs. The TI Team suggested that future hazard sensitivities should isolate one branch of the logic tree at the time for creating the tornado plots, and should also change the GMPE base case to use selected candidate models for each source class with equal weights. Additionally, the sensitivity should also show the effect of the combined phi and tau models, not just phi and tau separately. The effect of directivity on the total sigma appears large and should be checked.

### *Topic 8: Evaluation of Candidate GM Models for DCPP: Median for Strike-Slip Sources*

Dr. Robert Youngs presented the GM logic tree structure for DCPP, for which two main source classes are accounted (i.e. nearby strike slip, and reverse sources on the HW side). As in the PVNGS's case, the base model will consist of representative GMPEs generated from sampling the covariance matrix, plus candidate GMPEs that cannot be fit by the selected common functional form.

Dr. Norman Abrahamson provided more details for the GM logic tree addressing strike-slip sources, starting by how the selection of the candidate GMPEs was further refined for the strike-slip/nearby source class case. Dr. Abrahamson reminded the audience about the proposed approach to implement the Zhao and Lu (2011) concept with reduced scaling for large magnitudes, and also discussed the plan to integrate the Graizer and Kalkan (GK13) model in the base model of the logic tree.

### *Topic 9: Evaluation of Candidate GM Models for DCPP: Median for Reverse Sources*

Dr. Robert Youngs presented the GM logic tree structure for DCPP associated to the reverse faulting earthquakes on the hanging wall side. The main rationale to develop a base model on the HW side is that DCPP is always on the HW position, and, by starting with candidate models which account for HW effects, it is possible to keep track of the correlation of the models' covariance matrix. The candidate GMPEs selection refinement retains only those candidate models which capture the HW effect, either explicitly through a dedicated function (ASK14, CB14 and CY14) or through the use of $R_{JB}$ distance metric (BSSA14, ASK13); GK13 is also retained because the peculiar near-source distance attenuation could mimic the HW effect, but it is not used to create the covariance matrix.

Issues to be considered while developing a common functional form is whether to use a $R_{RUP}$ or $R_{JB}$ based form, and how effective is the functional form in capturing: 1) variation with $R_X$ on the HW and just off the HW, and 2) effect of dip, depth and magnitudes on HW effects. HW effects are still not well constrained from empirical data and the magnitude tapering of the effect is worth more evaluation. Dr. Carola Di Alessandro, in her Resource Expert presentation, showed that the Japanese dataset by Prof. Adrian Rodriguez-Marek and collaborators (Dawood et al., 2014) does not provide additional cases for which ground motion is well recorded on both the FW and HW sides for moderate magnitude events. Therefore, the project should rely on FFS simulations to constraint the HW effects for moderate magnitude earthquakes.

### *Topic 10: Other issues for DCPP*

Both logic trees for the two source classes at DCPP include alternatives for treatment of directivity effects: one node specifically includes directivity and the other assumes directivity is captured in the aleatory variability of the GMPEs. The relative weights will be based on the evaluation of the CY14 residuals with and without directivity, and also in the assessment of the adjustment model maturity. With regards of this topic, Dr. Jennie Watson-Lamprey delivered a Proponent presentation about a directivity adjustment model that was developed in the framework of the NGA-West2 project. Her model provides the additional standard deviation term to be combined to the published GMPEs' sigmas, and also provides an adjustment for the median motion for locations around the rupture that can experience either positive or negative directivity effects based on rupture and source-to-site geometry. The current model addresses strike-slip and reverse faults separately, but does not encompass reverse-oblique sources explicitly. Sensitivity plots shown by Dr. Nick Gregor suggested that the directivity effect has a significant effect on the hazard, therefore, it was

recommended that the adjustment model be further refined so to: 1) include robust assessment of its epistemic uncertainty by giving consideration to the uncertainty associated to limited data, and 2) capture the range of directivity scaling from other published models (such as broadband directivity models, for instance). In order to evaluate the effect of other directivity models on different GMPEs consistently, such models need to be "centered" for given magnitudes and distances. The PPRP noted that the effect of the directivity model may be sensitive to the assumptions on the hypocentral distribution, and questioned whether the range of technically defensible hypocentral distributions has been given proper consideration.

During the discussions, Dr. Robin McGuire raised the issue of possible lack of correlation between base models for strike-slip and for reverse source classes if separate logic trees are used for each source class. This can affect the resulting fractiles of the hazard.

Current GM logic trees for DCPP do not include the effect of path terms explicitly. Dr. Norman Abrahamson presented a possible approach to address the issue of path term adjustment for DCPP, which conceptually resembles the method applied to PVNGS. There is a question of applicability of path factors developed for very small magnitude events (M 1.5-3) to larger magnitudes events; an associated issues is the compatibility of the scaling developed from Fourier Spectra (FAS) versus the one developed from response spectra (PSA). During the discussion, it was recommended to develop a consistent phi model if path effects adjustment is included, because $\phi_{SS}$ has a path term variability effect already included and one could risk double-counting that variability. Another issue worth additional consideration is the need to develop a GMPE applicable to very low magnitudes events (as low as M 1.5) if available data is to be used to assess path effects.

### *Topic 11: Proposed Approach for Sigma Models*

The proposed approach to model the aleatory variability was introduced by Dr. Robert Youngs while discussing the logic tree structure framework for PVNGS during Day 2. The proposed aleatory variability form includes both magnitude-dependent and magnitude-independent alternative models. The uncertainty range for the aleatory variability is based on the statistical estimates of the uncertainty. For application to hazard, the components of the variability (phi and tau) will be combined into the total sigma and the range will be captured by simplified three branches.

During the discussions, it was suggested to include both the standard log-normal and mixture model (heavy-tail) distributions of residuals as alternatives in the logic tree.

The details of the phi models, tau models, and associated logic trees were presented by Dr. Linda Al-Atik during the afternoon of Day 2 (see Topics 12 and 13).

### *Topic 12: Candidate GM Models and Logic Tree Structure for Sigma: Phi Models*

The presentation delivered by Dr. Al Atik addressed the phi ($\phi$) component of the ground motion variability. For this project, a partially non-ergodic approach is proposed. It requires the estimation of single-station phi ($\phi_{SS}$) and its epistemic uncertainty at a given station (SD[$\phi_{SS,S}$]). For sources in California affecting the hazard

at PVNGS, a single path-to-region phi component ($\phi_{SP-R}$) is introduced. As part of her presentation, Dr. Al-Atik reviewed the terminology and the approach to estimate $\phi_{SS}$ and $\phi_{SP-R}$ from the available datasets.

Evaluation of the $\phi_{SS}$ values versus various event and site parameters (magnitude, distance, SOF, $V_{S,30}$) showed magnitude dependence for Californian data, but no clear magnitude dependence for global dataset used in the evaluation. During the discussion, it was noted that there is an apparent correlation of $\phi_{SS}$ with $V_{S,30}$ (larger variability in rock sites) at short periods, which might be explained by variability of short-period spectral shape for rock sites. Further evaluations to understand this correlation are desirable.

Next, a summary of the central $\phi_{SS}$ models for DCPP and PVNGS was presented. For DCPP, there are three branches: one has a magnitude-dependent form based on the California dataset for M ≥ 5.5 and Dist ≤ 30 km; the other two branches have a magnitude-independent form, one based on the global data and the other based on the California data with M ≥ 5.5 and Dist ≤ 30 km. For PVNGS, separate $\phi_{SS}$ models are proposed for the local Arizona sources and distant California sources. For PVNGS (Arizona sources), only one central model is used. It has a magnitude-independent form, and is computed from appropriate global data with M ≥ 5.5 and Dist ≤ 50 km. Finally, for PVNGS (distant California source) there is one branch which has a constant form, and is computed from appropriate global data with M ≥ 5.5 and distance between 200 and 400 km. The proposed $\phi_{SS}$ models compare generally well with other $\phi_{SS}$ models (Pegasos Refinement Project, Hanford and Italian study by Luzi et al., 2014).

The epistemic uncertainty on $\phi_{SS}$ is estimated from its standard deviation at sites (SD[$\phi_{SS,S}$]) with several recordings. The estimated standard deviation of $\phi_{SS,S}$ is biased due to the small number of recordings per station. The proposed uncertainty of 0.1 units should be revised to address the small sample bias. During the discussion it was suggested to evaluate subsets of the data for limited magnitudes or $V_{S,30}$ ranges for constraining the epistemic uncertainty.

For PVNGS distant California sources, $\phi_{SP-R}$ was computed using data recorded at nine TA stations around PVNGS. Because the analysis used stations in the PVNGS region rather than a single station at PVNGS, the path effect is a region term. The path effects were evaluated for two sources regions (north and south), and two source-to-region $\phi_{SP-R}$ terms have been computed ($\phi_{SP-N}$ and $\phi_{SP-S}$). The results show an unusual increase in $\phi_{SP-S}$ as compared to $\phi_{SS}$. This unexpected trend should be checked. In addition, alternative boundaries for the south and north paths should be considered.

### *Topic 13: Candidate GM Models and Logic Tree Structure for Sigma: Tau Models*

The second presentation by Dr. Linda Al-Atik on Day 2 addressed the proposed tau (τ) model and its logic tree, which applies to both sites in the project (DCPP and PVNGS). The proposed model has a magnitude-dependent form and its central branch is derived from the ASK14, BSSA14, CB14, CY14 and Zhao et al. (2006) ergodic tau models. The proposed central model simplifies and smoothes through the different break points in the magnitude scaling of the proponent tau models During the discussions, it was recommended to apply magnitude breaks at M.5.5 (instead than M5.25) and at M7. Additionally, it was

noted that the period-independency of the tau model may be driven by including the Zhao et al. (2006) tau model; if Zhao et al. (2006) is excluded, there is an apparent period dependency. Accordingly, further evaluation is recommended on the applicability of the Zhao et al. (2006) tau model for large magnitudes and long periods. Also, there was a comment that the Zhao et al. (2006) model is not applicable to small magnitudes due to its underlying dataset. Therefore, it should not be used for constraining the magnitude dependence for tau. Another issue identified for the Zhao et al. (2006) model is that it uses a site classifications scheme not based on $V_{S,30}$.

The proposed tau model does not retain the 10 Hz "bump" in tau seen in some of the proponent tau models because the TI Team's evaluation is that the bump is related to regional site differences that are mapped into event terms (see "Topic 1: Post Workshop #2 Follow-up").

Following the approach used in the Hanford PSHA Project, the epistemic uncertainty in tau is based on the between-model variability of four NGA-West2 GMPEs (ASK14, BSSA14, CB14, and CY14), and on the within-model uncertainty informed by CY14 (estimation of the uncertainty in tau for CY14). The resulting epistemic uncertainty in tau is, on average, about 0.12. The range of the proposed tau branches adequately captures the range of the individual GMPE tau models.

### *Topic 14: Other Issues on Sigma*

Dr. Robert Youngs discussed other issues to be investigated in building aleatory variability models. The first issue addresses the shape of residual distribution in upper tail, and its deviation from the standard assumption of a lognormal distribution. The second issue addresses the effect of spatial correlation in ground motions on estimates of phi and tau.

Based on the observation that, for $M \geq 5$, the site corrected within-event residuals ($\delta W_{es}$) for ASK14 and CY14 have heavy tails for PGA and 1 Hz spectral acceleration, it is proposed to use a mixture model (weighted sum of two lognormal distributions with same median but different variances) to represent the heavy-tailed distribution. Initial exploration of an alternative upper tail distribution (power-law distribution – aka Pareto distribution) shows that the mixture model can reasonably capture the Pareto distribution at least up to four standard deviations. A positive comment received from Dr. Robert Budnitz was that the proposed mixture model approach finally allows fatter tails to be implemented in hazard analysis, even if the approach lacks a physical explanation. During the discussions, it was noted that the evaluation of the shape of the distribution should be extended to more spectral periods and GMPE models. In addition, a regional dependence on the mixture model could be examined.

Next, Dr. Youngs addressed preliminary results obtained by Dr. Shrey Shahi on the effect of spatial correlation in the sigma computation using the CY14 residuals. During Workshop #2 in October 2013, it was recommended that Dr. Baker utilize the NGA-West2 dataset to evaluate the potential underestimation in $\phi_{ss}$ due to the spatial correlation. The preliminary results obtained from Dr. Shahi indicate that the effect of spatial correlation has little effect at periods shorter than 0.3 seconds. There is a minor reduction in $\tau$ and minor increase in $\phi$ for small magnitudes (M 5) at longer periods, resulting in minor differences in the total

sigma for small magnitudes; however, there is a reduction in $\tau$ and increase in $\phi$ for large magnitudes ($M \geq 6.5$) at longer periods, resulting in a overall 10% to 20% increases in total sigma at large magnitudes. This analysis is preliminary and needs to be adequately documented and peer reviewed before including it in the logic tree.

### *Topic 15: Interface Issues and Other Topics*

During the discussion at Workshop #3, the topic of the interface between SWUS GMC and the SSC and site response efforts was addressed in several occasions. The comments emphasized the need for close interaction between the SWUS GMC group and site response groups for consistent treatment (interface) for kappa and site amplification. This project can benefit from Hanford PSHA's operational experience: the site response group wrote specifications for what they needed and addressed the interface issues between the GMC and site response through exchange of documents. A similar approach can be followed for PVNGS and DCPP. The need for frequent and effective interface discussion with the SSC groups was also emphasized, to make sure that all source types are adequately captured by the ground motion models.

In terms of documentation of the overall approach for the ground motion characterization effort, during the discussions it was argued that the term "logic tree" has specific meaning in PSHA, which may not be understood by the broader earthquake science community. It is recommended to document clearly the meaning of "logic tree" in the context of this project.

# GROUND MOTION CHARACTERIZATION PRESENTATIONS

**Day 1 Introduction**

- Welcome and Introduction (PDF, 1.1 MB) - Carola Di Alessandro (*GeoPentech, Inc.)*
- Project Overview and objectives; Status of Data Needs Tasks from Workshop #2 (PDF, 106 KB) - Norman Abrahamson (*Pacific Gas and Electric Company)*
- Additional feedback from Proponent and Resource Experts post Workshop #2 (PDF, 1.8 MB) - Robert Youngs (*AMEC Environment & Infrastructure)*
- Summary of conclusions from Jan. 28-29, 2014 Working Meeting(PDF, 4.9 MB) - Norman Abrahamson (*Pacific Gas and Electric Company)*

**Day 1 TI Team and Proponent Experts Presentations**

- Overall approach for logic trees for median ground motion (PDF, 933 KB)- Douglas Dreger (*Univ. of California, Berkeley)*
- Visualizations and comparison with data sub-sets for constraining Center-Body-Range for median (PDF, 21.3 MB) - Nicolas Kuehn (*Univ. of California, Berkeley)*
- New set of forward finite-fault simulations to address splay ruptures(PDF, 1.2 MB) - Jeff Bayless (*URS Corporation)*
- Proponent rule for ground motions from splay ruptures (PDF, 2.4 MB) - Katie Wooddell (*Pacific Gas and Electric Company)*
- Consistency of long period displacement and fault slip for FFS (PDF, 784 KB) - Douglas Dreger (*Univ. of California, Berkeley)*
- Summary of GMC Day 1 (PDF, 49 KB) - Katie Wooddell (*Pacific Gas and Electric Company)*

**Day 2 TI Team and Proponent Experts Presentations**

- Simplified source model for PVNGS (PDF, 1.5 MB) - Melanie Walling (*Lettis Consultants International, Inc.)*
- Logic Tree structure for PVNGS (PDF, 181 KB) - Robert Youngs (*AMEC Environment & Infrastructure)*
- Hazard feedback for PVNGS and sensitivity results (PDF, 2.4 MB) - Melanie Walling *(Lettis Consultants International, Inc.)*

- GM models for host AZ sources: median (PDF, 4.2 MB) - Norman Abrahamson (*Pacific Gas and Electric Company)*
- Follow up on visualization results – residuals for candidate GMPEs(PDF, 4 MB) - *Nicolas Kuehn (Univ. of California, Berkeley)*
- Approach for median for distant CA sources (PDF, 5.7 MB) - Katie Wooddell (*Pacific Gas and Electric Company)*
- Logic tree structure and models for Phi (PDF, 4.6 MB) - Linda Al-Atik (*Al-Atik Consulting)*
- Other Issues for Sigma (PDF, 190 KB) - Robert Youngs (*AMEC Environment & Infrastructure)*
- Logic tree structure and models for Tau (PDF, 225 KB) - Linda Al-Atik (*Al-Atik Consulting)*
- Summary of GMC Day 2 (PDF, 109 KB) - Douglas Dreger (*Univ. of California, Berkeley)*

**Day 3 TI Team and Proponent Experts Presentations**

- Simplified source model for DCPP (PDF, 0.9 MB) - Nick Gregor (*NG Consulting)*
- Logic Tree structure for DCPP (PDF, 96 KB) - Robert Youngs (*AMEC Environment & Infrastructure)*
- Hazard feedback for DCPP and sensitivity results (PDF, 1.7 MB) - Nick Gregor (*NG Consulting)*
- Reminder on visualization approach (PDF, 21.3 MB) - Nicolas Kuehn (*Univ. of California, Berkeley)*
- GM models for Strike-Slip earthquakes: median (PDF, 3.5 MB) - Norman Abrahamson (*Pacific Gas and Electric Company)*
- Directivity proponent model (PDF, 4.3 MB) - Jennie Watson-Lamprey *(Watson-Lamprey Consulting)*
- Availability of additional empirical data to constraint HW scaling for small magnitudes: Japanese data (PDF, 1.4 MB) - Carola Di Alessandro (*GeoPentech, Inc)*
- Approach for median for reverse sources (PDF, 280 KB) - Robert Youngs (*AMEC Environment & Infrastructure)*
- Approach for Path effects evaluation at DCPP: PGV example (PDF, 739 KB) - Norman Abrahamson *(Pacific Gas and Electric Company)*
- Summary of GMC Day 3 and Overview of Day 1 and Day 2 / Path forward (PDF, 81 KB) - Norman Abrahamson *(Pacific Gas and Electric Company)*

## TECHNICAL INTEGRATOR TEAM SUMMARIES and PATH FORWARD ACTIONS

# Day 1 Summary

- Higher Sigma for Akkar et al (2013)
  - Controlled by phi
  - It is not explained by number of recordings/eqk
  - Is it related to quality of meta-data?
  - Is it related to non-uniform processing of the data?
  - Is it related to larger variability in the site conditions (Similar to Japanese data)?
- Applicability of ExSim to near fault conditions
  - Numerical issues for 0 distance
  - FFS simulations show that ExSim leads to larger short-period ground motions at short distance (1 km) for M6.5, but less difference for larger magnitudes
    - Feature of the model. Atkinson considers this to be a credible model, but not clear why this is not seen at larger magnitude

- Simulations for splay faulting
  - Bump in 10 Hz factors for SDSU needs to be explained
  - Need close interaction between GMC group and site group for consistent treatment (interface) for kappa and site amplification
    - Hanford had the site response group write specifications for what they need
    - Prepare similar document for PVNGS and DCPP
  - Go back to the SSC groups to be sure that all source types are captured by the ground motion models

- Common functional form for GMPEs
  - Use two forms, one based on Rrup and one based on Rjb
    - Maintain the key features of the initial selected GMPEs
    - If similar in hazard, pick one. Otherwise maintain both and weight
  - If sigma of fit to GMPE values is large (e.g. > 0.2) then may need to add the sigmaFit to the aleatory variability
    - If less than 0.1, then can ignore it (< 0.02 ln units on total sigma)
- Generation of 1000 models
  - Develop a better functional form that will result in fewer non-physical models

- Computation of Covariance Matrix
  - Consider computing in a different way: run mixed effects model using individual GMPEs as the group factor
  - Issue of removing non-physical models from the realizations
    - Some parameters may have a physical meaning that requires limits (e.g. sign of a parameter may be constrained)
    - Add constraints to the sampling or the correlation structure
    - Transform to a variable that maintains the physics

- Use different subsets of data to compare with the Sammons maps (eg. Class 1, each developer DB, etc)
- Define limits of what the data will allow in terms of GMPEs
- Do not down weight expert judgment by considering only data. Use data as a guide (ex. broaden our distribution of weights towards the data).
  - Have other approaches been considered? (E.g. Directly sampling the covariance matrix)
  - Do not narrow uncertainty but take shift into account
  - Ensure that Linda & Bobs statistical uncertainty is covered

# Day 2 Summary

- Hazard sensitivity for PVNGS
  - Replot sensitivity isolating one branch of the logic tree at a time
  - Change the base-case to equal weight to the selected candidate models
  - Check/identify outlier for 1E-6 hazard
  - Check phiSS sensitivity – appears to go the wrong way

## Logic Tree structure

- Use of term “logic tree” can be confusing.
  - Document what we mean by the term
- Add branch for fat-tail (mixture models) or lognormal

# Host Zone - AZ

- Demonstrate that the Rjb-based common model captures the hanging wall effects.
- Show confidence intervals for NML style-of-faulting factors
- Document cases and justification for GMPEs not been centered for NML eqk
- Add models not used to develop the covariance matrix of coeff. to the Sammon's plots
- Need to address SS sources in host zone, not just NML, but host source zone likely to be dominated by NML
- Add road signs to the Sammon's plots to show direction of Mag, dist. scaling

# Distant AZ sources

- Comparison to Data
  - Check outliers:
    - Event 280 for CB14 at 1 Hz
    - Event 1017 for CY14 at 5 Hz
  - Provide the scientific basis for no change in distance attenuation (CA to AZ) but there is a change in Q
    - There could be a duration effect that is over ridding the Q
- Average source terms for the distant sources
  - Add event-terms from NGA-west2 eqk not recorded at AZ TA array station
- Logic tree
  - Add branch for zero path effect

# Sigma models - Phi

- Correlation of phiSS with VS30
  - Can this be explained by spectral shape variability for rock sites?
- Increase in phi_SP-R for southern sources compared to phi_SS.
  - Check this for a narrower path range
- Correct the uncertainty in Phi_SS for the bias due to small sample sizes

# Upper tail of Phi

- Mixture models captures broader tails
  - Can represent the power law distribution at least up to 4 standard deviations

# Sigma Models - Tau

- Magnitude break of proposed model
  - Apply magnitude break points of M5.5 and M7 to simplify and smooth through the different break points of the considered GMPE models
- Proposed central model
  - Evaluate need for period-dependent tau
    - Period-independence may be driven by including Zhao tau
    - Evaluate applicability of Zhao Tau at large magnitudes and long-periods
    - It is not applicable to small mag. due to data set

# Day 3 Summary

- Tornado plots
  - Change base case to all candidate models with equal weight
  - Isolate a single parameter (branch in logic tree) at a time
  - Add effect of the combined phi and tau models, not just phi and tau separately

# Sammon's Plots

- Issues for making the process easier to understand
  - Show that the common form gives an adequate fit of the published model
  - How to exclude non-physical models from the set of simulated values?
  - How to interpret the Sammons plots
  - Rotate Sammons plots to have similar meaning for a given direction
    - Such as make the x-axis the direction for change in median
  - Add a metric to measure the ability of the 2-D projection to capture the separation distance in the higher dimensional space

# Sammon's Plots

- Now that we all understand the Sammon's plots,
  - Use this method on the Broadband platform to help modelers evaluate/compare their results

# 1000 Median Models

- Correlation between SS and RV models
  - Find method to capture correlation for GM models used for hazard calculation
- Initial results show sampling (groups) using Sammon's maps for all periods does not sample the range for each period separately
  - Need to consider period-dependent weights
  - May have period-dependent models
  - If likelihood contours are not bounded , then increase the range of models

- Documentation
  - Peer report that describes the method with examples
  - More than just journal paper
  - Tool for implementation

# Directivity

- Sensitivity shows a significant effect
- Need to include epistemic uncertainty in this parameter
  - Uncertainty in derived model due to limited data
  - Capture range of directivity scaling from other models (such as broadband models) in this epistemic uncertainty

To use other directivity models, need to develop the centering of directivity for given mag. and dist.

Rev/obl will have a different directivity factor than REV

# REV model

- HW effects
  - HW still not well constrained from empirical data
  - Consider limitations of simulations in developing the models

* Spelling in the document corrected after Workshop #3

# DCPP Path

- If path term included, then need to develop consistent phi model
  - Phi-SS has path term variability effects included
- Check that response spectra factors for very small magnitudes are applicable for larger magnitudes
  - Issue of FAS scaling versus PSA scaling

# LETTER COMMENTARY FROM THE PARTICIPATORY PEER REVIEW PANEL

April 21, 2014

Carola Di Alessandro, Ph.D.
Project Manager for the SWUS GMC Project
GeoPentech, Inc.
525 N. Cabrillo Park Drive, Suite 280
Santa Ana, CA 92701

Dear Dr. Di Alessandro:

This letter comprises the comments of the Participatory Peer Review Panel (PPRP) for Workshop #3 of the Southwestern U.S. Ground Motion Characterization (SWUS GMC) project. Workshop #3 was held on March 10-12, 2014, in Berkeley, California. The PPRP observed both the process and the technical developments. Following the guidelines of NUREG-2117, the PPRP also actively participated in the discussion and questioning of the preliminary models. The four members of the PPRP (K. Campbell, B. Chiou, S. Day, and T. Rockwell) were present for the full workshop and observed all workshop sessions. The PPRP met at regular intervals during the workshop to assess its effectiveness in providing feedback to the model evaluators, as well as its adherence to SSHAC Level 3 procedural guidelines.

The PPRP congratulates the TI and Project Management teams for carrying out a very successful workshop in conformity with SSHAC Level 3 guidelines. The TI team organized the workshop format and presentations effectively, and we appreciate the efforts they and the Project Management team made to provide the PPRP with ample opportunity to interrogate the presenters.

**Summary Comments**

The goals of Workshop #3 are (1) to present the preliminary models, with emphasis on how alternative interpretations and uncertainties have been incorporated, (2) present sensitivity analyses and hazard calculations that provide insight into the preliminary models, and (3) address questions, including those from the PPRP, to provide an understanding of the technical bases for the model components and weights, and the manner in which the center, body and range (CBR) of technically defensible interpretations (TDI) have been included in the models. The TI team designed a set of presentations and discussions that was very successful in describing and exploring the overall structure for the GMC model. This enabled the PPRP to gain a good understanding of how the model is being framed. Several components of the model are very advanced and innovative. The use of Sammon mapping to visualize relationships among ground motion predictions (and to compare them with data and numerical simulations) is an especially noteworthy development. Also noteworthy is the exploration of possible non-Gaussian upper tails to ground motion distributions, and their incorporation into the characterization of aleatory uncertainty via a mixture of two Gaussian distributions. Likewise, non-ergodic aleatory uncertainty is being addressed with exceptional rigor in this project, and path-specific terms are being developed and applied where available data permit. We commend the TI team on their continuing efforts to bring these technical advances to fruition.

With respect to adherence to procedural guidelines, as well as with respect to technical quality, the workshop conformed well to standards for a SSHAC Level 3 workshop on model feedback. The entire TI team was fully engaged in presenting the model elements and addressing questions. The TI team and the project manager were attentive to the role of the PPRP. During the presentation and discussion of each model element, the TI team allocated sufficient time for the PPRP to ask detailed questions about the model formulation, its technical justifications, the basis for incorporation or rejection of alternative models, and the manner in which uncertainty is characterized. The TI lead, Project Manager, and in some cases the TI Team members met with the PPRP at the end of each day of the workshop to obtain immediate feedback. A number of requests for program adjustments were made at these meetings, and the TI team was fully responsive to all such requests. Parts of the model evaluation process are still in progress, and a complete preliminary model was not available at the time of the workshop. However, the presentations and discussions of the model framework and the key individual model elements were sufficient to enable the PPRP to provide substantial feedback to the TI team. In the comments and recommendations below, we endorse the TI team's plans to obtain further model feedback from the PPRP once a complete preliminary model is available.

**Comments and Recommendations (underlining indicates those requiring a written response)**

*1. Documentation.* As noted in the summary comments, the ground motion model contains a number of advanced elements aimed at providing improved confidence that the CBR of the TDI is being captured. The scientific development and validation of these advanced elements has been driven in large part by this project. The technical bases for these elements appear to be sound, and they represent significant advances in hazard assessment. However, because they are technically advanced and relatively complex, they will have to be carefully and fully documented in the project report. Careful and clear documentation of complex procedures and concepts (for example, the construction of a multidimensional GMPE space, its visualization via Sammon mapping, and its final characterization from representative points on that map, in light of disparate data sets and simulation results) may be critical to project success. The PPRP recommends that TI team members pay close attention to the documentation of these advanced model elements to ensure that the final report is not only complete and scientifically sound, but also as transparent and persuasive as possible to the PPRP and a broader technical audience.

*2. Site effects interface issue.* During the workshop, it became clear that the project had not yet produced a comprehensive reference document describing the adjustments and procedures to be used to modify the reference ground motions for use at each site (i.e., at PVNGS and DCPP). The PPRP previously recommended that such a document be developed in a letter to the Project Manager dated April 21, 2013 (Recommendation #6) following Workshop #1, and this recommendation is repeated here. As noted previously, any lack of clarity and precision in the communication between the TI team and a site response analysis team may make both vulnerable to misunderstandings and claims of inconsistency or double counting of effects. A comprehensive written document would serve to guide discussions, prevent misunderstandings, and ensure that no relevant data or models are neglected due to confusion about which project is responsible for which elements of the ground motion model.

*3. SSC interface issue.* The workshop revealed some apparent gaps in coordination between the TI team and the respective SSC TI teams for the DCPP and PVNGS SSHAC Level 3 projects. For example, the TI team appeared to be unaware of the inclusion of strike-slip sources in the local-source component of the SSC model for PVNGS, and only presented GMC models relevant to normal faulting. As a second example, the TI team discussed the PVNGS local-source component in terms of random fault orientations, whereas the PVNGS SSC TI team will provide preferred orientations in the final SSC model. A further concern is that the DCPP SSC model might include a large range of rakes on dipping faults, and some coordination between that project and the GMC project may be required to ensure that those sources are appropriately categorized for use in the GMC model (e.g., the treatment of oblique slip sources was not discussed by the TI team). The PPRP recommends that the TI team improve coordination with the TI teams of each of the SSC projects to ensure that the GMC approach is fully compatible with the respective SSC approaches, so that last-minute issues will not arise that could delay project completion.

*4. Feedback on a complete preliminary model.* The workshop provided a very good exposition of the conceptual framework of the ground motion logic trees to be employed, as well as their technical bases. In most cases, the specific branches were identified, and there was extensive technical questioning and discussion from the PPRP and other experts, meeting most of the workshop objectives. Nonetheless, the model feedback process was not quite completed at Workshop #3, because a complete preliminary model populated with weights was not available to be interrogated by the PPRP at that time. As noted in NUREG 2117 (p. 71), "In the discussions of the preliminary models, the technical bases for the assessments and weights should be described to allow for a discussion of the implications and constraints provided by the available data." The PPRP supports the TI team's preliminary decision to hold one or more briefing meetings to present a full preliminary model to the PPRP for feedback when it becomes available, in advance of their development of the final model.

*5. Geologic consistency of models for ground motion simulation.* The numerical simulation of specific sources at DCPP employed fault geometrical parameters (in particular, down-dip fault widths) that are not consistent with the SSC model. The PPRP recognizes that this may be largely an artifact of the way the numerical models are parameterized, together with the understandable project requirement to hold that parameterization fixed in the form it had when the numerical models were calibrated and validated. The PPRP also recognizes that the principal application of the simulations to date has been to test methods for combining empirical relationships so as to approximate special conditions not represented well in the database, such as the simultaneous rupture on a main fault and a secondary splay. In that type of application, the PPRP agrees that the results may be insensitive to the precise simulation geometry relative to the SSC model. However, the appearance of discordance between the simulation parameters and actual fault parameters developed by the DCPP SSC is a potential source of confusion. The PPRP recommends that project documentation give careful attention to any apparent inconsistency between the ground motion simulation parameters and the actual fault parameters developed by the DCPP SSC team. Where simulations are used only to test methods for applying empirical methods to special situations, the TI team might evaluate whether to simply treat the simulated faults as representatives of generic fault types, rather than associating them with specific faults from the SSC model. On the other hand, if simulated ground motions are

employed more directly, it will be necessary to document with care their actual relationship to the SSC model.

*6. Representation of CBR of hypocenter locations.* In the development of the model of additional standard deviation to account for rupture directivity, the TI team assumed a model of hypocenter locations in which strike-slip earthquake epicenters had a tendency to concentrate near the center of the rupture trace. The team cited empirical results of Mai and others in support of this assumption. However, other relevant data are available (e.g., global compilations such as that of McGuire et al. in BSSA, 2002, as well as data from detailed studies of individual earthquakes in California and elsewhere). If the form of the hypocenter distribution is significant to the conclusions of the directivity study, the PPRP recommends that the TI team further evaluate the hypocenter distribution model to ensure adoption of a final version that adequately captures the CBR of the TDI.

*7. Frequency shift of between-event standard deviation.* The TI team showed at the workshop that, if not removed by smoothing (as was done by some NGA-West2 developers), the between-event standard deviation tau has a so-called "bump" at short periods that is not as visible in the within-earthquake standard deviation phi. The TI team showed evidence from a simple stochastic analysis that this bump is likely due to systematic variability in site effects, presumably due to variability in kappa, that is being transferred to tau and should, therefore, be included as part of the within-earthquake variability. Based on this conclusion, the TI team has adopted as part of their logic tree a smoothed short-period tau model with no bump and instead is transferring this aleatory variability to the site-response model. One of the interesting features of the bump in tau, which is often described as being at 0.1 sec (10 Hz), is that it occurs at a shorter period for small earthquakes than for large earthquakes and has a pronounced dip near 0.3-0.5 sec, which also changes with magnitude. The PPRP recommends that the TI team seek an explanation of the apparent frequency shift of the bump and dip in tau with magnitude and assess whether it is consistent with the proposed hypothesis that these effects represent variability in site effects rather than source effects.

*8. Epistemic uncertainty in median prediction.* The epistemic uncertainty in predicted median ground motion includes two components – the within-GMPE uncertainty of estimated GMPE coefficients and the between-GMPE variability. At the workshop, the TI team's proposed approach for evaluating the latter component of uncertainty (via the construction of GMPE space) received substantial discussion and helpful feedback. There was, however, not as much discussion of the within-GMPE uncertainty. Since uncertainty in median motion is an important contributor to the uncertainty in calculated hazard, the PPRP recommends that both between-GMPE and within-GMPE components of epistemic uncertainty be evaluated with comparable rigor and that each be represented in the logic tree with an appropriate level of detail.

A potential means to capture within-GMPE uncertainty in a manner comparable to the treatment of between-GMPE uncertainty was noted by the TI lead during the workshop. The suggestion was that the within-GMPE covariance matrix of a training GMPE be used to generate more training GMPEs for the purpose of constructing GMPE space. The PPRP will be interested in any update of the TI team's views of this approach and any plans that they have to further evaluate it.

Please feel free to contact us if you would like to discuss further our comments or recommendations.

Sincerely,

Steven M. Day
Chair, PPRP

Kenneth W. Campbell
Member, PPRP

Brian Chiou
Member, PPRP

Thomas K. Rockwell
Member, PPR

# TECHNICAL INTEGRATION TEAM LEAD RESPONSES TO PARTICIPATORY PEER REVIEW PANEL COMMENTS

May 23, 2014

Steven M. Day
Chair, Participatory Peer Review Panel
Department of Geological Sciences
San Diego State University
5500 Campanile Drive
San Diego, California 92182

Dear Prof. Day:

The TI Team and PM appreciate the valuable comments and suggestions received from the Participatory Peer Review Panel (PPRP), both during the Workshop No. 3 execution and in their formal letter commentary dated April 21, 2014. The present document serves to provide written responses to specific comments, suggestions, or recommendations that the PPRP identified (by underlining).

1. ***Documentation.*** As noted in the summary comments, the ground motion model contains a number of advanced elements aimed at providing improved confidence that the CBR of the TDI is being captured. The scientific development and validation of these advanced elements has been driven in large part by this project. The technical bases for these elements appear to be sound, and they represent significant advances in hazard assessment. However, because they are technically advanced and relatively complex, they will have to be carefully and fully documented in the project report. Careful and clear documentation of complex procedures and concepts (for example, the construction of a multidimensional GMPE space, its visualization via Sammon mapping, and its final characterization from representative points on that map, in light of disparate data sets and simulation results) may be critical to project success. The PPRP recommends that TI team members pay close attention to the documentation of these advanced model elements to ensure that the final report is not only complete and scientifically sound, but also as transparent and persuasive as possible to the PPRP and a broader technical audience.

REPLY: We agree with the PPRP about the need of detailed documentation on the Sammon's map. A draft journal paper will be completed for the July 2014 PPRP Briefing Meeting.

2. ***Site effects interface issue.*** During the workshop, it became clear that the project had not yet produced a comprehensive reference document describing the adjustments and procedures to be used to modify the reference ground motions for use at each site (i.e., at PVNGS and DCPP). The PPRP previously recommended that such a document be developed in a letter to the Project Manager dated April 21, 2013 (Recommendation #6) following Workshop #1, and this recommendation is repeated here. As noted previously, any lack of clarity and precision in the communication between the TI team and a site response analysis team may make both vulnerable to misunderstandings and claims of inconsistency or double counting of effects. A comprehensive written document would serve to guide discussions, prevent misunderstandings, and ensure that no relevant data or models are neglected due to confusion about which project is responsible for which elements of the ground motion model.

REPLY: We agree. A white paper will be completed before the site response work is started.

3. ***SSC interface issue.*** The workshop revealed some apparent gaps in coordination between the TI team and the respective SSC TI teams for the DCPP and PVNGS SSHAC Level 3 projects. For example, the TI team appeared to be unaware of the inclusion of strike-slip sources in the local-source component of the SSC model for PVNGS, and only presented GMC models relevant to normal faulting. As a second example, the TI team discussed the PVNGS local-source component in terms of random fault orientations, whereas the PVNGS SSC TI team will provide preferred orientations in the final SSC model. A further concern is that the DCPP SSC model might include a large range of rakes on dipping faults, and some coordination between that project and the GMC project may be required to ensure that those sources are appropriately categorized for use in the GMC model (e.g., the treatment of oblique slip sources was not discussed by the TI team). The PPRP recommends that the TI team improve coordination with the TI teams of each of the SSC projects to ensure that the GMC approach is fully compatible with the respective SSC approaches, so that last-minute issues will not arise that could delay project completion.

REPLY: We agree. We have already improved the interaction with the SSC groups for both DCPP and PVNGS. We do not see any additional inconsistencies at this time.

4. ***Feedback on a complete preliminary model.*** The workshop provided a very good exposition of the conceptual framework of the ground motion logic trees to be employed, as well as their technical bases. In most cases, the specific branches were identified, and there was extensive technical questioning and discussion from the PPRP and other experts, meeting most of the workshop objectives. Nonetheless, the model feedback process was not quite completed at Workshop #3, because a complete preliminary model populated with weights was not available to be interrogated by the PPRP at that time. As noted in NUREG 2117 (p. 71), "In the discussions of the preliminary models, the technical bases for the assessments and weights should be described to allow for a discussion of the implications and constraints provided by the available data." The PPRP supports the TI team's preliminary decision to hold one or more briefing meetings to present a full preliminary model to the PPRP for feedback when it becomes available, in advance of their development of the final model.

REPLY: We agree. Two additional meetings have been scheduled with the PPRP: the first one on May 14, 2014 and the second one on July 17-18, 2014.

5. ***Geologic consistency of models for ground motion simulation.*** The numerical simulation of specific sources at DCPP employed fault geometrical parameters (in particular, down-dip fault widths) that are not consistent with the SSC model. The PPRP recognizes that this may be largely an artifact of the way the numerical models are parameterized, together with the understandable project requirement to hold that parameterization fixed in the form it had when the numerical models were calibrated and validated. The PPRP also recognizes that the principal application of the simulations to date has been to test methods for combining empirical relationships so as to approximate special conditions not represented well in the database, such as the simultaneous rupture on a main fault and a secondary splay. In that type of application, the PPRP agrees that the results may be insensitive to the precise simulation geometry relative to the SSC model. However, the appearance of discordance between the simulation parameters and actual fault parameters developed by the DCPP SSC is a potential source of confusion. The PPRP recommends that project documentation give careful attention to any apparent inconsistency between the ground motion simulation parameters and the actual fault parameters developed by the DCPP SSC team. Where simulations are used only to test methods for applying empirical methods to special situations, the TI team might evaluate whether to simply treat the simulated faults as representatives of generic fault types, rather than associating them with specific faults from the SSC model. On the other hand, if simulated ground motions are employed more directly, it will be necessary to document with care their actual relationship to the SSC model.

REPLY: We will document the limitations of the current capabilities of the Broad Band Platform (BBP) in terms of source characteristics, and explain the limitation of the applicability of the simulations to specific geometries obtained from the SSC teams.

6. ***Representation of CBR of hypocenter locations.*** In the development of the model of additional standard deviation to account for rupture directivity, the TI team assumed a model of hypocenter locations in which strike-slip earthquake epicenters had a tendency to concentrate near the center of the rupture trace. The team cited empirical results of Mai and others in support of this assumption. However, other relevant data are available (e.g., global compilations such as that of McGuire et al. in BSSA, 2002, as well as data from detailed studies of individual earthquakes in California and elsewhere). If the form of the hypocenter distribution is significant to the conclusions of the directivity study, the PPRP recommends that the TI team further evaluate the hypocenter distribution model to ensure adoption of a final version that adequately captures the CBR of the TDI.

REPLY: We agree. Alternative distributions for the hypocenters are being evaluated.

7. ***Frequency shift of between-event standard deviation.*** The TI team showed at the workshop that, if not removed by smoothing (as was done by some NGA-West2 developers), the between-event standard deviation tau has a so-called “bump” at short periods that is not as visible in the within-earthquake standard deviation phi. The TI team showed evidence from a simple stochastic analysis that this bump is likely due to systematic variability in site effects, presumably due to variability in kappa, that is being transferred to tau and should, therefore, be included as part of the within-earthquake variability. Based on this conclusion, the TI team has adopted as part of their logic tree a smoothed short-period tau model with no bump and instead is transferring this aleatory variability

to the site-response model. One of the interesting features of the bump in tau, which is often described as being at 0.1 sec (10 Hz), is that it occurs at a shorter period for small earthquakes than for large earthquakes and has a pronounced dip near 0.3-0.5 sec, which also changes with magnitude. The PPRP recommends that the TI team seek an explanation of the apparent frequency shift of the bump and dip in tau with magnitude and assess whether it is consistent with the proposed hypothesis that these effects represent variability in site effects rather than source effects.

REPLY: The apparent frequency shift of the bump and dip in tau with magnitude is likely a result of the different sampling of regions for small and large magnitudes. We will evaluate this issue by comparing the tau for small and large magnitudes from a restricted geographical region such as Southern California and see if the shift is no longer observed as we expect.

8. ***Epistemic uncertainty in median prediction.*** The epistemic uncertainty in predicted median ground motion includes two components - the within-GMPE uncertainty of estimated GMPE coefficients and the between-GMPE variability. At the workshop, the TI team's proposed approach for evaluating the latter component of uncertainty (via the construction of GMPE space) received substantial discussion and helpful feedback. There was, however, not as much discussion of the within-GMPE uncertainty. Since uncertainty in median motion is an important contributor to the uncertainty in calculated hazard, the PPRP recommends that both between-GMPE and within-GMPE components of epistemic uncertainty be evaluated with comparable rigor and that each be represented in the logic tree with an appropriate level of detail.

REPLY: As shown in the January 2014 Working Meeting by N. Kuehn, the within-model uncertainty as quantified by Al-Atik and Youngs PEER report on NGA-West2 epistemic uncertainty for is much smaller than the between-model epistemic uncertainty. Therefore there should not be comparable level of effort for these two uncertainties. We focus our evaluation on the between-GMPE uncertainty.

We hope this letter clarifies the questions and comments stated in the April 21, 2014 PPRP Commentary Letter. We wish to express our gratitude to the PPRP again for their insightful questions, and for their continuous review of this project.

Sincerely,





Norman A. Abrahamson,
SWUS GMC TI Team Lead

Carola Di Alessandro,
SWUS GMC Project Manager

CC: PPRP Panel, TI Team, PTIs

# REFERENCES

Abrahamson, N.A., and Silva, W. (2008). Summary of the Abrahamson & Silva NGA Ground-Motion Relations, *Earthquake Spectra*, Vol. 24(1), 67-97.

Abrahamson, N.A., Silva, W.J., and Kamai, R. (2014). Summary of the AKS14 Ground-Motion Relation for Active Crustal Regions, Earthquake Spectra, Vol. 30, DOI: 10.1193/070913EQS198M, (in press).

Akkar, S., Sandikkaya, M.A., and Bommer, J.J. (2013). Empirical ground-motion models for point- and extended-source crustal earthquake scenarios in Europe and the Middle East, *Bull. Earthquake Eng*., Vol. 12, 359–387, DOI 10.1007/s10518-013-9461-4

Akkar, S., Sandikkaya, M.A., and Bommer, J.J. (2013). Erratum to: Empirical ground-motion models for point- and extended-source crustal earthquake scenarios in Europe and the Middle East, *Bull. Earthquake Eng*, DOI 10.1007/s10518-013-9508-6

Akkar, S., Sandikayya, M., Senyurt, M., Azari Sisi, A., Ay, B., Traversa, P., Douglas, J., Cotton, F., Luzi, L., Hernandez, B., Godey, S. (2013). Reference database for seismic ground–motion in Europe (RESORCE), *Bull. Earthquake Eng*.

Al Atik, L., Abrahamson, N., Bommer, J., Scherbaum, F., Cotton, F., Kuehn, N. (2010). The variability of ground-motion prediction models and its components, *Seism. Res. Let*., 81(5), 794-801.

Al Atik, L., and Youngs, R.R. (2013). Epistemic Uncertainty for NGA-West2 Models, *PEER Report No. 2013/11*, Pacific Earthquake Engineering Research Center, University of California, Berkeley, CA, 59 pp.

Atik, L., and Youngs, R.R. (2014). Epistemic Uncertainty for NGA-West2 Models, *Earthquake Spectra*, Vol. 30, DOI: 10.1193/062813EQS173M, (in press).

Ancheta, T.D., Darragh, R.B., Stewart, J.P., Seyhan, E., Silva, W.J., Chiou, B.S.-J., Wooddell, K.E., Graves, R.W., Kottke, A.R., Boore, D.M., Kishida, T. and Donahue, J.L. (2014). PEER NGA-West2 Database, *Earthquake Spectra*, Vol. 30, DOI: 10.1193/070913EQS197M (in press).

Anderson, J.G., and Hough, S.E. (1984). A model for the shape of the Fourier amplitude spectrum of acceleration at high frequencies, *Bull. Seism. Soc. Am*., Vol. 74(5), 1969–1993.

Anderson, J. (2010). Source and site characteristics of earthquakes that have caused exceptional ground accelerations and velocities, *Bull. Seism. Soc. Am.,* Vol. 100, 1-36.

Anderson, J., Koketsu, K., and Miyake, H. (2013). Expanded Compilation and Statistics of Exceptional Ground Motions, USGS *External Grant G12AP20024 Final Technical Report*.

Aoi, S., Kunugi, T., and Fujiwara H. (2009). Trampoline effect in extreme ground motion, *Science*, Vol. 322, 727-730.

Arizona Database: ground motions processed at PEER (2014). [http://peer.berkeley.edu/ngawest2/wp-content/uploads/2010/09/Arizona_Database.zip]

Atkinson, G.M, and Assatourians, K. (2014). Implementation and validation of EXSIM (a stochastic finite-fault ground-motion simulation algorithm) on the SCEC broadband platform, *Seismol. Res. Letts* (in preparation)

Biasi, G.P., and Smith, K.D. (2001). Site effects for seismic monitoring stations in the vicinity of Yucca Mountain, Nevada, *MOL20011204.0045*, a report prepared for the US DOE/University and Community College System of Nevada (UCCSN) Cooperative Agreement.

Bindi, D., Pacor, F., Luzi, L., Puglia, R., Massa, M., Ameri, G., and Paolucci, R. (2011). Ground motion prediction equations derived from the Italian strong motion database, *Bull Earthquake Eng*., Vol. 9, 1899-1920.

Bindi D., Massa M., Luzi L., Ameri G., Pacor F., Puglia R., and Augliera, P. (2014). Pan-European Ground-Motion Prediction Equations for the Average Horizontal Component of PGA, PGV, and 5%-Damped PSA at Spectral Periods up to 3.0 s using the RESORCE dataset, *Bull Earthquake Eng*., Vol. 12, 391–430

Boore, D.M. (2005). SMSIM--Fortran Programs for Simulating Ground Motions from Earthquakes: Version 2.3--A Revision of OFR 96-80-A, *U.S. Geological Survey Open-File Report*

Boore, D.M., Watson-Lamprey, J., and Abrahamson, N.A. (2006). Orientation-independent measures of ground motion, *Bull. Seism. Soc. Am*., Vol. 96 (4A), 1502-1511.

Boore, D.M., and Atkinson, G.M. (2008). Ground-Motion Prediction Equations for the Average Horizontal Component of PGA, PGV, and 5%-Damped PSA at Spectral Periods between 0.01s and 10.0s, *Earthquake Spectra*, Vol. 24(1), 99-138.

Boore, D.M., Stewart, J.P., Seyhan, E., and Atkinson, G.M. (2013). NGA-West2 Equations for Predicting Response Spectral Accelerations for Shallow Crustal Earthquakes, *Pacific Earthquake Engineering Research Center report* 2013/05.

Boore, D.M., Stewart, J.P., Seyhan, E., and Atkinson, G.M. (2014). NGA-West 2 Equations for Predicting PGA, PGV, and 5%-Damped PSA for Shallow Crustal Earthquakes, *Earthquake Spectra*, DOI: 10.1193/070113EQS184M (in press).

Bozorgnia, Y., Abrahamson, N.A., Al Atik, L., Ancheta, T.D., Atkinson, G.M., Baker, J.W., Baltay, A., Boore, D.M., Campbell, K.W., Chiou, B.S.-J., Darragh, R., Day, S., Donahue, J., Graves, R. W., Gregor, N., Hanks, T. , Idriss, I.M., Kamai, R., Kishida, T., Kottke, A., Mahin, S.A., Rezaeian, S., Rowshandel, B., Seyhan, E., Shahi, S., Shantz, T., Silva, W., Spudich, P., Stewart, J.P., Watson-Lamprey, J., Wooddell, K., and Youngs, R. (2014). NGA-West2 Research Project, *Earthquake Spectra*, Vol. 30, DOI: 10.1193/072113EQS209M (in press).

Brune, J. N. (1970). Tectonic stress and the spectra of seismic shear waves from earthquakes, *J. Geophys. Res*., Vol. 76, 4997–5009.

Brune, J. N. (1971). Correction, *J. Geophys. Res.,* Vol. 76, 5002.

Campbell, K.W., and Bozorgnia, Y. (2008). NGA Ground Motion Model for the Geometric Mean Horizontal Component of PGA, PGV, PGD and 5% Damped Linear Elastic Response Spectra for Periods Ranging from 0.01 to 10 s, *Earthquake Spectra*, Vol. 24(1), 139-171.

Campbell, K.W., and Bozorgnia, Y. (2013). NGA-West2 Campbell-Bozorgnia Ground Motion Model for the Horizontal Components of PGA, PGV, and 5%-Damped Elastic Pseudo-Acceleration Response Spectra for Periods Ranging from 0.01 to 10 sec, *PEER Report* 2013/06.

Campbell, K.W., and Bozorgnia, Y. (2014). NGA-West2 Ground Motion Model for the Average Horizontal Components of PGA, PGV, and 5%-Damped Linear Acceleration Response Spectra, Earthquake Spectra, Vol. 30, DOI: 10.1193/062913EQS175M (in press).

Chiou, B.S.-J., Darragh, R., and Silva, W. (2008). An overview of the NGA database, *Earthquake Spectra,* Vol. 24, 23–44.

Chiou B.S.-J., Youngs R.R. (2008a). Appendix B in "NGA model for the average horizontal component of peak ground motion and response spectra", PEER Report 2008/09, Pacific Earthquake Engineering Research Center, University of California, Berkeley, CA

Chiou, B.S-J and Youngs, R.R. (2008b). An NGA Model for the Average Horizontal Component of Peak Ground Motion and Response Spectra, *Earthquake Spectra*, 24(1), 173-215.

Chiou, B.S.-J., Spudich P. (2013). The Chiou and Spudich NGA-West2 directivity predictor DPP, Chapter 6, *PEER Report 2013/09*, Pacific Earthquake Engineering Research Center, University of California, Berkeley, CA

Chiou, B.S-J. and Youngs, R.R. (2014). Update of the Chiou and Youngs NGA Model for the Average Horizontal Component of Peak Ground Motion and Response Spectra, *Earthquake Spectra*, Vol. 30, DOI: 10.1193/072813EQS219M (in press).

Darragh R.B., Silva W.J., Gregor N. (2004). Strong motion record processing procedures for the PEER center, *Proceedings of COSMOS Workshop on Strong-Motion Record Processing*, Richmond, California, pp. 1–12.

Dawood, H.M., Rodriguez-Marek, A., Bayless, J., Goulet, C., and Thompson E. (2014). Processing the Kik-Net strong ground motion database and compilation of metadata for GMPE development, *Earthquake Spectra* (in preparation)

DePolo, C.M., and LaPointe, D.D - Editors (2011). The 21 February 2008 Mw 6.0 Wells, Nevada Earthquake - A compendium of earthquake-related investigations prepared by the University of Nevada, Reno*, Nevada Bureau of Mines and Geology Special Publication* Vol. 36

Donahue, J., and Abrahamson, N.A. (2014). Simulation-based Hanging-Wall Effects, *Earthquake Spectra* (*accepted*)

Dreger, D.S., Beroza, G.C., Day, S.M., Goulet, C.A., Jordan, T. H., Spudich, P.A, and Stewart, J. P. (2013). Evaluation of SCEC Broadband Platform Phase 1 Ground Motion Simulation Results, 33 pp. plus Appendices, Report submitted to SCEC, Aug. 1 2013.

Fukushima ground motions processed at PEER (2014). [http://peer.berkeley.edu/ngawest2/wp-content/uploads/2010/09/Fukushima_Flatfile_RotD50_d050_04112014.zip]

Geusebroek, J., Burghouts, G., and Smeulders, A. (2005). The Amsterdam library of object images, *Int. J. Comput. Vision*, Vol. 61, 103-112.

Graizer, V. (2014). Updated Graizer-Kalkan Ground-motion Prediction Equations for Western United States, 11 pp., *Proceedings for the 10th U.S. National Conference on Earthquake Engineering Frontiers of Earthquake Engineering*, July 21-25, 2014, Anchorage, Alaska.

Graves, R. W. and Pitarka, A. (2010). Broadband Ground-Motion Simulation Using a Hybrid Approach, *Bull. Seism. Soc. Am*., Vol. 100 (5a), 2095-2123.

Graves, R. W. and Pitarka, A. (2014). Refinements of the Graves and Pitarka (2010) Broadband Ground-Motion Simulation Method, *Seismol. Res. Letts* (submitted)

Gregor, N. (2014). Fortran implementation of the NGA-West 2 GMPEs.

Haddad, D. (2013). Precariously balanced rocks near Palo Verde Nuclear Generating Station. Resource Expert presentation at PVNGS SSC SSHAC Level 3 Workshop #1.

Hough, S.E., and Anderson, J.G. (1988). High-frequency spectra observed at Anza, California: Implications for Q structure, *Bull. Seismol. Soc. Am.,* Vol. 78, 692-707.

Idriss, I.M. (2008). An NGA Empirical Model for Estimating the Horizontal Spectral Values Generated By Shallow Crustal Earthquakes, *Earthquake Spectra*, Vol. 24(1), 217-242.

Idriss, I.M. (2014). NGA-West2 Model for Estimating Average Horizontal Values of Pseudo-Absolute Spectral Accelerations Generated by Crustal Earthquakes, *Earthquake Spectra*, (in review).

Jayaram, N., and Baker, J.W. (2010). Considering spatial correlation in mixed-effects regression and the impact on ground-motion models, *Bull. Seism. Soc. Am.,* Vol. 100, 3295-3303.

Kishida, T., Ktenidou, O.-J., Darragh, R., and Silva, W. (2014). Data processing for Fourier amplitude spectrum (FAS) estimation from NGA-West2 processed accelerations, Chapter 7 in the PEER NGA-East Database Report Pacific Earthquake Engineering Research Center, pp. 50 (in review).

Kishida, T., Kayen, R.E., Ktenidou, O.-J., Silva, W., Darragh, R., and Watson-Lamprey, J. (2014). PEER Arizona Strong Motion Database and GMPEs Evaluation, Pacific Earthquake Engineering Research Center PEER Report, in preparation

Kohonen, T. (2001). Self-organizing maps, Springer 2001, 501 pages.

Ktenidou O.-J., Cotton, F., Abrahamson, N.A., and Anderson, J.G. (2014). Taxonomy of kappa: a review of definitions and estimation methods targeted to applications, *Seismol. Res. Letts*, Vol. 85(1), pp. 135-146.

LCI (2012). Characterization of Ground Motion Propagation for Palo Verde SSHAC Level 2 PSHA, Internal Project Report.

Leonard, M. (2010). Earthquake Fault Scaling: Self-Consistent Relating of Rupture Length, Width, Average Displacement, and Moment Release, *Bull. Seismol. Soc. Am.*, Vol. 100, 1971-1988.

Lin, P-S., Chiou, B., Abrahamson, N., Walling, M., Lee, C-T, and Cheng, C-T (2011). Repeatable source, site, and path effects on the standard deviation for empirical ground-motion prediction models, *Bull. Seism. Soc. Am*., Vol. 101(5), 2281-2295.

Luzi, L., Bindi, D., Puglia, R., Pacor, F. and Oth, A. (2014). Single-Station Sigma for Italian Strong-Motion Stations, *Bull. Seism. Soc. Am*., Vol. 104(1), 467-483.

Mayeda, K., and Malagnini, L. (2010). Source radiation invariant property of local and near-regional shear-wave coda: Application to source scaling for the Mw 5.9 Wells, Nevada sequence, *Geophysical Research Letters*, Vol. 37, L07306.

NGA-West2 Flatfile (2013). [http://peer.berkeley.edu/ngawest2/databases/]

Nodal Zland Earthquake Database ( 2011). [http://www.pge.com/mybusiness/edusafety/systemworks/dcpp/SSHAC/legacy_documents/datasets/index.shtml ]

Olsen, K. and Takedatsu, R. (2014). The SDSU Broadband Ground Motion Generation Module BBtoolbox Version 1.5, *Seismol. Res. Letts,* (in preparation)

Pasyanos, M.E. (2013). A lithospheric attenuation model of North America, *Bull. Seismol. Soc. Am.,* Vol. 103, 3321-3333.

PG&E (2011). Report on the Analysis of the Shoreline Fault Zone, Central Coastal California, January 2011.

Phillips, W.S., Mayeda, K.M., and Malagnini, L. (2013). How to Invert a Multi-Band, Regional Phase Amplitudes for 2-D Attenuation and Source Parameters: Tests Using the USArray, *PAGEOPH,* DOI 10.1007/s00024-013-0646-1.

Rodriguez-Marek, A. (2014). Crustal Sigma Model, SSHAC Level-3 Site-Wide PSHA for the Hanford Site, WA. TI Team Presentation.

Rodriguez-Marek, A., Cotton, F., Abrahamson, N., Akkar, S., Al Atik, L., Edwards, B., Montalva, G.A., and Dawood, H.M. (2013). A model for single-station standard deviation using data from various tectonic regions, *Bull. Seism. Soc. Am*., Vol. 103(6), 3149-3163

Rodriguez-Marek, A., and Cotton, F. (2011). Final report: Single-station sigma project prepared for PEGASOS Refinement Project, *EXT-TB-1058*

Sammon, J. (1969). A nonlinear mapping for data structure analysis, *IEEE Trans. Comput*. Vol. 524(C-18), 401–409.

Scherbaum, F., Kuehn, N., Koehler, A., and Ohrnberger, M. (2010). Exploring the Proximity of Ground-Motion Models Using High-Dimensional Visualization Techniques, *Earthquake Spectra,* Vol. 26, 1117–1138.

Somerville, P.G., Callaghan, S., Maechling, P., Graves, R.W., Collins, N., Olsen, K.B., Imperatori, W., Jones, M., Archuleta, R., Schmedes, J., and Jordan, T.H. (2011). The SCEC Broadband Ground Motion Simulation Platform, *Seismol. Res. Letts.*, Vol. 82(2), p. 275, 10.1785/gssrl.82.2.273.

Spudich, P., Bayless, J.R., Baker, J.W., Chiou, B.S-J., Rowshandel, B., Shay, S.K., and Somerville, P. (2013). Final Report of the NGA-West2 Directivity Working Group, *PEER Report 2013/09*, Pacific Earthquake Engineering Research Center, University of California, Berkeley, CA

US Array (2003). [http://www.usarray.org/researchers/obs/transportable] (Last accessed Dec. 15, 2013)

USGS (2009). Quaternary fault and fold database for the United States, accessed 25 October 2010, from USGS website, [http//earthquakes.usgs.gov/regional/qfaults/].

U.S.NRC (2012a). Near-Term Task Force, “Request For Information Pursuant To Title 10 Of The Code Of Federal Regulations 50.54(F) Regarding Recommendations 2.1,2.3, and 9.3, Of The Near-Term Task Force Review Of Insights From The Fukushima Dai-Ichi Accident.”

U.S.NRC (2012b). Practical Implementation Guidelines for SSHAC Level 3 and 4 Hazard Studies, U.S.NRC NUREG-2117.

U.S.NRC (1997). Recommendations for probabilistic seismic hazard analysis: Guidance on uncertainty and use of experts, prepared by Senior Seismic Hazard Analysis Committee, Lawrence Livermore National Laboratory, Volume 1, Main Report, NUREG/CR-6372, UCRL-ID-122160, 280 pp.

Villani, M., and Abrahamson, N. (2013). Repeatable site and path effects on the ground motion sigma based on empirical data from Southern California and simulated waveforms from the CyberShake platform. Poster at SCEC 2013 annual meeting and draft paper for Earthquake Spectra.

Walling, M. A. (2009). Non-Ergodic Probabilistic Seismic Hazard Analysis and Simulation Spatial of Variation in Ground Motion, *Ph.D. Thesis*, University of California, Berkeley, California.

Wooddell, K.E., and Abrahamson, N.A. (2012). New earthquake classification scheme for mainshocks and aftershocks in the NGA-West2 ground motion prediction equations, *Proceedings, 15th World Conference on Earthquake Engineering,* Lisbon, Portugal.

Yamada, M., K. Mori, and T. Heaton, 2009, Slapdown phase in high acceleration records of large earthquakes, *Seismol. Res. Letts*, Vol. 80, 559-564.

Yamada, M., Olsen, A., and Heaton, T. (2009). Statistical features of short- and long-period near-source ground motions, *Bull. Seism. Soc. Am*., Vol. 99, 3264 -3274.

Yoo, S.H., and Mayeda, K. (2013). Validation of non-self-similar source scaling using ground motions from the 2008 Wells, Nevada, earthquake sequence, *Bull. Seism. Soc. Am*., Vol. 103, 2508-2519.

Youngs, R.R. (2009). Epistemic uncertainty in the NGA models, Appendix D in Ground Motion Models for the Pacific Northwest, *Report to B.C. Hydro*, December 2010.

Zhao, J.X., Zhang, J., Asano, A., Ohno, Y., Oouchi, T., Takahashi, T., Ogawa, H., Irikura, K., Thio, H.K., Somerville, P.G., Fukushima, Y., and Fukushima, Y. (2006). Attenuation Relations of Strong Ground Motion in Japan Using Site Classification Based on Predominate Period, *Bull. Seism. Soc. Am*., Vol. 96, 898-913.

Zhao, J.X., and Lu, M. (2011). Magnitude-Scaling Rate in Ground-Motion Prediction Equations for Response Spectra from Large, Shallow Crustal Earthquakes, *Bull. Seism. Soc. Am*., Vol. 101, 2643-2661.

# *APPENDIX H*

## EVALUATION OF COMMON-FORM MODELS

# Contents

**Contents** i

**List of Figures** v

**1 Introduction** 1
1.1 Introduction on the Application of Visualization Tools to GMPE Distribution . . . 1
1.1.1 2D Visualization of GMPEs . . . 1
1.1.2 Sammon's Mapping . . . 3
Sammons Map Conceptual Examples . . . 3
1.1.3 Distances Between GMPEs . . . 3
1.1.4 Sammons Maps of GMPEs . . . 5
1.2 APPLICATION OF VISUALIZATION TOOLS TO THE SWUS GMC STUDY . . . 9
1.2.1 Explanation of Plots . . . 9

**2 DCPP – Model A** 11
2.1.2 Deaggregation . . . 11
GM-Level 2 . . . 11
GM-Level 8 . . . 20
2.1.3 Maps – Selection . . . 29
2.1.4 Maps – Voronoi Cells . . . 46
2.1.5 Hazard Curves . . . 63
2.1.6 CDF Plots . . . 69
T = 0.01s . . . 69
T = 0.2s . . . 76
T = 0.5s . . . 83
T = 1.s . . . 90
T = 3.s . . . 97
2.1.7 Quantile Plots vs. Distance . . . 104
T = 0.01s . . . 104
T = 0.2s . . . 107
T = 0.5s . . . 110
T = 1.s . . . 113
T = 3.s . . . 116
2.1.8 Quantile Plots vs. Distance with GMPEs . . . 119
T = 0.01s . . . 119
T = 0.2s . . . 122
T = 0.5s . . . 125
T = 1.s . . . 128
T = 3.s . . . 131
2.1.9 Quantile Plots vs. Magnitude . . . 134
T = 0.01s . . . 134
T = 0.2s . . . 141
T = 0.5s . . . 148
T = 1.s . . . 155
T = 3.s . . . 162
2.1.10 Quantile Plots vs. Period . . . 169
2.1.11 Quantile Ratios vs. Distance . . . 178
2.1.12 Magnitude Scaling with GMPEs . . . 187
T = 0.01s . . . 187

T = 0.2s . . . 190
T = 0.5s . . . 193
T = 1.s . . . 196
T = 3.s . . . 199
2.1.13 Distance Scaling with GMPEs . . . 202
T = 0.01s . . . 202
T = 0.2s . . . 205
T = 0.5s . . . 208
T = 1.s . . . 211
T = 3.s . . . 214
2.1.14 Quantile Plots vs. Magnitude with GMPEs . . . 217
T = 0.01s . . . 217
T = 0.2s . . . 220
T = 0.5s . . . 223
T = 1.s . . . 226
T = 3.s . . . 229
2.1.15 Quantile Plots vs. Period with GMPEs . . . 232
2.1.16 Median Residuals . . . 241

**3 PVNGS – Model A** **258**
3.1.1 Deaggregation . . . 258
GM-Level 2 . . . 258
GM-Level 8 . . . 267
3.1.2 Maps – Selection . . . 276
3.1.3 Maps – Voronoi Cells . . . 293
3.1.4 Hazard Curves . . . 310
3.1.5 CDF Plots . . . 319
T = 0.01s . . . 319
T = 0.2s . . . 337
T = 0.5s . . . 355
T = 1.s . . . 373
T = 3.s . . . 391
3.1.6 Quantile Plots vs. Distance . . . 409
T = 0.01s . . . 409
T = 0.2s . . . 412
T = 0.5s . . . 415
T = 1.s . . . 418
T = 3.s . . . 421
3.1.7 Quantile Plots vs. Distance with GMPEs . . . 424
T = 0.01s . . . 424
T = 0.2s . . . 427
T = 0.5s . . . 430
T = 1.s . . . 433
T = 3.s . . . 436
3.1.8 Quantile Plots vs. Magnitude . . . 439
T = 0.01s . . . 439
T = 0.2s . . . 444
T = 0.5s . . . 449
T = 1.s . . . 454
T = 3.s . . . 459
3.1.9 Quantile Plots vs. Period . . . 464
3.1.10 Quantile Ratios vs. Distance . . . 482
3.1.11 Magnitude Scaling with GMPEs . . . 485
T = 0.01s . . . 485
T = 0.2s . . . 491
T = 0.5s . . . 497
T = 1.s . . . 503
T = 3.s . . . 509
3.1.12 Distance Scaling with GMPEs . . . 515
T = 0.01s . . . 515
T = 0.2s . . . 518

T = 0.5s . . . 521
T = 1.s . . . 524
T = 3.s . . . 527
3.1.13 Quantile Plots vs. Magnitude with GMPEs . . . 530
T = 0.01s . . . 530
T = 0.2s . . . 536
T = 0.5s . . . 542
T = 1.s . . . 548
T = 3.s . . . 554
3.1.14 Quantile Plots vs. Period with GMPEs . . . 560
3.1.15 Median Residuals . . . 578

**4 PVNGS – Model B** **596**
4.1.1 Deaggregation . . . 596
GM-Level 2 . . . 596
GM-Level 8 . . . 605
4.1.2 Maps – Selection . . . 614
4.1.3 Maps – Voronoi Cells . . . 631
4.1.4 Hazard Curves . . . 648
4.1.5 CDF Plots . . . 657
T = 0.01s . . . 657
T = 0.2s . . . 675
T = 0.5s . . . 693
T = 1.s . . . 711
T = 3.s . . . 729
4.1.6 Quantile Plots vs. Distance . . . 747
T = 0.01s . . . 747
T = 0.2s . . . 750
T = 0.5s . . . 753
T = 1.s . . . 756
T = 3.s . . . 759
4.1.7 Quantile Plots vs. Distance with GMPEs . . . 762
T = 0.01s . . . 762
T = 0.2s . . . 765
T = 0.5s . . . 768
T = 1.s . . . 771
T = 3.s . . . 774
4.1.8 Quantile Plots vs. Magnitude . . . 777
T = 0.01s . . . 777
T = 0.2s . . . 782
T = 0.5s . . . 787
T = 1.s . . . 792
T = 3.s . . . 797
4.1.9 Quantile Plots vs. Period . . . 802
4.1.10 Quantile Ratios vs. Distance . . . 811
4.1.11 Magnitude Scaling with GMPEs . . . 814
T = 0.01s . . . 814
T = 0.2s . . . 820
T = 0.5s . . . 826
T = 1.s . . . 832
T = 3.s . . . 838
4.1.12 Distance Scaling with GMPEs . . . 844
T = 0.01s . . . 844
T = 0.2s . . . 847
T = 0.5s . . . 850
T = 1.s . . . 853
T = 3.s . . . 856
4.1.13 Quantile Plots vs. Magnitude with GMPEs . . . 859
T = 0.01s . . . 859
T = 0.2s . . . 865
T = 0.5s . . . 871

T = 1.s . . . 877
T = 3.s . . . 883
4.1.14 Quantile Plots vs. Period with GMPEs . . . 889
4.1.15 Median Residuals . . . 907

**5 PVNGS – Model AB** **925**
5.1.1 Combined Maps . . . 925
5.1.2 Combined Quantile Plots vs. Distance with GMPEs . . . 943
T = 0.01s . . . 943
T = 0.2s . . . 946
T = 0.5s . . . 949
T = 1.s . . . 952
T = 2.s . . . 955
T = 3.s . . . 958
5.1.3 Combined Quantile Plots vs. Magnitude with GMPEs . . . 961
T = 0.01s . . . 961
T = 0.2s . . . 979
T = 0.5s . . . 997
T = 1.s . . . 1015
T = 2.s . . . 1033
T = 3.s . . . 1051
5.1.4 Combined Quantile Plots vs. Period with GMPEs . . . 1069
5.1.5 Median Residuals . . . 1078

**Bibliography** **1096**

# List of Figures


1.1 Histogram of predictions of 11 GMPEs, for one scenario (left) and two scenarios (right). . . . . 2
1.2 Magnitude and distance scaling for 11 GMPEs used as example in the introduction to this Appendix. . . . 2
1.3 Pictures of rotated rubber ducks. . . . . 4
1.4 Left: Sammons map of rubber duck" space, with insets of pictures; Right: same map, but with rotation angle of each picture at the respective coordinate. . . . . 4
1.5 Differences between two GMPEs at different $R_{JB}$ -distance values, which go into the calculation of the (high-dimensional) distance $\overline{\Delta_{GMij}}$ between GMPEs $i$ and $j$ (BSSA14 and CB14 in this case). . . . . 5
1.6 Difference in scaling of reference models that help the interpretation of the Sammons maps. . . . . 6
1.7 Sammons map for 11 GMPEs, together with reference models. GMPE-distances in high dimensions are calculated using the $L_2$-distance. . . . . 7
1.8 Magnitude and distance scaling of three GMPEs, for a detailed interpretation of the relative differences as shown in the map (cf. Figure 1.7). . . . . 7
1.9 Top: Sammons map of GMPEs, based on L1 and L2-GMPE-distances. The reference models are plotted for the map based on the L2-map. Bottom: Sammons map of GMPEs, based on $L_2$ and $L_\infty$-distances. The reference models are plotted for the map based on the $L_\infty$-map. The black points are at the same coordinates as in the top map and in Figure 1.7. Note the different scale on the two maps. . . . . 8

2.1 DCPPv4: Deaggregation for a ground-motion level of 0.163g, calculated using a simple source model for DCPP4 and the center model of the ModelA distribution. For $T = 0.01$s. . . . . 11
2.2 DCPPv4: Deaggregation for a ground-motion level of 0.163g, calculated using a simple source model for DCPP4 and the center model of the ModelA distribution. For $T = 0.02$s. . . . . 12
2.3 DCPPv4: Deaggregation for a ground-motion level of 0.167g, calculated using a simple source model for DCPP4 and the center model of the ModelA distribution. For $T = 0.03$s. . . . . 12
2.4 DCPPv4: Deaggregation for a ground-motion level of 0.17g, calculated using a simple source model for DCPP4 and the center model of the ModelA distribution. For $T = 0.05$s. . . . . 13
2.5 DCPPv4: Deaggregation for a ground-motion level of 0.174g, calculated using a simple source model for DCPP4 and the center model of the ModelA distribution. For $T = 0.075$s. . . . . 13
2.6 DCPPv4: Deaggregation for a ground-motion level of 0.33g, calculated using a simple source model for DCPP4 and the center model of the ModelA distribution. For $T = 0.1$s. . . . . 14
2.7 DCPPv4: Deaggregation for a ground-motion level of 0.33g, calculated using a simple source model for DCPP4 and the center model of the ModelA distribution. For $T = 0.15$s. . . . . 14
2.8 DCPPv4: Deaggregation for a ground-motion level of 0.33g, calculated using a simple source model for DCPP4 and the center model of the ModelA distribution. For $T = 0.2$s. . . . . 15
2.9 DCPPv4: Deaggregation for a ground-motion level of 0.174g, calculated using a simple source model for DCPP4 and the center model of the ModelA distribution. For $T = 0.25$s. . . . . 15
2.10 DCPPv4: Deaggregation for a ground-motion level of 0.174g, calculated using a simple source model for DCPP4 and the center model of the ModelA distribution. For $T = 0.3$s. . . . . 16
2.11 DCPPv4: Deaggregation for a ground-motion level of 0.17g, calculated using a simple source model for DCPP4 and the center model of the ModelA distribution. For $T = 0.4$s. . . . . 16
2.12 DCPPv4: Deaggregation for a ground-motion level of 0.152g, calculated using a simple source model for DCPP4 and the center model of the ModelA distribution. For $T = 0.5$s. . . . . 17
2.13 DCPPv4: Deaggregation for a ground-motion level of 0.085g, calculated using a simple source model for DCPP4 and the center model of the ModelA distribution. For $T = 0.75$s. . . . . 17
2.14 DCPPv4: Deaggregation for a ground-motion level of 0.038g, calculated using a simple source model for DCPP4 and the center model of the ModelA distribution. For $T = 1$.s. . . . . 18
2.15 DCPPv4: Deaggregation for a ground-motion level of 0.019g, calculated using a simple source model for DCPP4 and the center model of the ModelA distribution. For $T = 1.5$s. . . . . 18
2.16 DCPPv4: Deaggregation for a ground-motion level of 0.017g, calculated using a simple source model for DCPP4 and the center model of the ModelA distribution. For $T = 2$.s. . . . . 19

2.17 DCPPv4: Deaggregation for a ground-motion level of 0.008g, calculated using a simple source model for DCPP4 and the center model of the ModelA distribution. For $T = 3$.s. . . . 19
2.18 DCPPv4: Deaggregation for a ground-motion level of 3.021g, calculated using a simple source model for DCPP4 and the center model of the ModelA distribution. For $T = 0.01$s. . . . 20
2.19 DCPPv4: Deaggregation for a ground-motion level of 3.021g, calculated using a simple source model for DCPP4 and the center model of the ModelA distribution. For $T = 0.02$s. . . . 20
2.20 DCPPv4: Deaggregation for a ground-motion level of 3.594g, calculated using a simple source model for DCPP4 and the center model of the ModelA distribution. For $T = 0.03$s. . . . 21
2.21 DCPPv4: Deaggregation for a ground-motion level of 4.141g, calculated using a simple source model for DCPP4 and the center model of the ModelA distribution. For $T = 0.05$s. . . . 21
2.22 DCPPv4: Deaggregation for a ground-motion level of 4.926g, calculated using a simple source model for DCPP4 and the center model of the ModelA distribution. For $T = 0.075$s. . . . 22
2.23 DCPPv4: Deaggregation for a ground-motion level of 6.622g, calculated using a simple source model for DCPP4 and the center model of the ModelA distribution. For $T = 0.1$s. . . . 22
2.24 DCPPv4: Deaggregation for a ground-motion level of 6.622g, calculated using a simple source model for DCPP4 and the center model of the ModelA distribution. For $T = 0.15$s. . . . 23
2.25 DCPPv4: Deaggregation for a ground-motion level of 6.622g, calculated using a simple source model for DCPP4 and the center model of the ModelA distribution. For $T = 0.2$s. . . . 23
2.26 DCPPv4: Deaggregation for a ground-motion level of 4.926g, calculated using a simple source model for DCPP4 and the center model of the ModelA distribution. For $T = 0.25$s. . . . 24
2.27 DCPPv4: Deaggregation for a ground-motion level of 4.926g, calculated using a simple source model for DCPP4 and the center model of the ModelA distribution. For $T = 0.3$s. . . . 24
2.28 DCPPv4: Deaggregation for a ground-motion level of 4.141g, calculated using a simple source model for DCPP4 and the center model of the ModelA distribution. For $T = 0.4$s. . . . 25
2.29 DCPPv4: Deaggregation for a ground-motion level of 3.511g, calculated using a simple source model for DCPP4 and the center model of the ModelA distribution. For $T = 0.5$s. . . . 25
2.30 DCPPv4: Deaggregation for a ground-motion level of 2.071g, calculated using a simple source model for DCPP4 and the center model of the ModelA distribution. For $T = 0.75$s. . . . 26
2.31 DCPPv4: Deaggregation for a ground-motion level of 1.689g, calculated using a simple source model for DCPP4 and the center model of the ModelA distribution. For $T = 1$.s. . . . 26
2.32 DCPPv4: Deaggregation for a ground-motion level of 1.056g, calculated using a simple source model for DCPP4 and the center model of the ModelA distribution. For $T = 1.5$s. . . . 27
2.33 DCPPv4: Deaggregation for a ground-motion level of 0.825g, calculated using a simple source model for DCPP4 and the center model of the ModelA distribution. For $T = 2$.s. . . . 27
2.34 DCPPv4: Deaggregation for a ground-motion level of 0.503g, calculated using a simple source model for DCPP4 and the center model of the ModelA distribution. For $T = 3$.s. . . . 28
2.35 DCPPv4: Contour Plots used for selection. For $T = 0.01$s. . . . 29
2.36 DCPPv4: Contour Plots used for selection. For $T = 0.02$s. . . . 30
2.37 DCPPv4: Contour Plots used for selection. For $T = 0.03$s. . . . 31
2.38 DCPPv4: Contour Plots used for selection. For $T = 0.05$s. . . . 32
2.39 DCPPv4: Contour Plots used for selection. For $T = 0.075$s. . . . 33
2.40 DCPPv4: Contour Plots used for selection. For $T = 0.1$s. . . . 34
2.41 DCPPv4: Contour Plots used for selection. For $T = 0.15$s. . . . 35
2.42 DCPPv4: Contour Plots used for selection. For $T = 0.2$s. . . . 36
2.43 DCPPv4: Contour Plots used for selection. For $T = 0.25$s. . . . 37
2.44 DCPPv4: Contour Plots used for selection. For $T = 0.3$s. . . . 38
2.45 DCPPv4: Contour Plots used for selection. For $T = 0.4$s. . . . 39
2.46 DCPPv4: Contour Plots used for selection. For $T = 0.5$s. . . . 40
2.47 DCPPv4: Contour Plots used for selection. For $T = 0.75$s. . . . 41
2.48 DCPPv4: Contour Plots used for selection. For $T = 1$.s. . . . 42
2.49 DCPPv4: Contour Plots used for selection. For $T = 1.5$s. . . . 43
2.50 DCPPv4: Contour Plots used for selection. For $T = 2$.s. . . . 44
2.51 DCPPv4: Contour Plots used for selection. For $T = 3$.s. . . . 45
2.52 DCPPv4: Contour Plots used for weighting. For $T = 0.01$s. . . . 46
2.53 DCPPv4: Contour Plots used for weighting. For $T = 0.02$s. . . . 47
2.54 DCPPv4: Contour Plots used for weighting. For $T = 0.03$s. . . . 48
2.55 DCPPv4: Contour Plots used for weighting. For $T = 0.05$s. . . . 49
2.56 DCPPv4: Contour Plots used for weighting. For $T = 0.075$s. . . . 50
2.57 DCPPv4: Contour Plots used for weighting. For $T = 0.1$s. . . . 51
2.58 DCPPv4: Contour Plots used for weighting. For $T = 0.15$s. . . . 52
2.59 DCPPv4: Contour Plots used for weighting. For $T = 0.2$s. . . . 53

2.60 DCPPv4: Contour Plots used for weighting. For $T = 0.25$s. . . . 54
2.61 DCPPv4: Contour Plots used for weighting. For $T = 0.3$s. . . . 55
2.62 DCPPv4: Contour Plots used for weighting. For $T = 0.4$s. . . . 56
2.63 DCPPv4: Contour Plots used for weighting. For $T = 0.5$s. . . . 57
2.64 DCPPv4: Contour Plots used for weighting. For $T = 0.75$s. . . . 58
2.65 DCPPv4: Contour Plots used for weighting. For $T = 1$.s. . . . 59
2.66 DCPPv4: Contour Plots used for weighting. For $T = 1.5$s. . . . 60
2.67 DCPPv4: Contour Plots used for weighting. For $T = 2$.s. . . . 61
2.68 DCPPv4: Contour Plots used for weighting. For $T = 3$.s. . . . 62
2.69 DCPPv4: hazard curves for $T = 0.01$ . . . 63
2.70 DCPPv4: hazard curves for $T = 0.02$ . . . 63
2.71 DCPPv4: hazard curves for $T = 0.03$ . . . 64
2.72 DCPPv4: hazard curves for $T = 0.05$ . . . 64
2.73 DCPPv4: hazard curves for $T = 0.075$ . . . 64
2.74 DCPPv4: hazard curves for $T = 0.1$ . . . 65
2.75 DCPPv4: hazard curves for $T = 0.15$ . . . 65
2.76 DCPPv4: hazard curves for $T = 0.2$ . . . 65
2.77 DCPPv4: hazard curves for $T = 0.25$ . . . 66
2.78 DCPPv4: hazard curves for $T = 0.3$ . . . 66
2.79 DCPPv4: hazard curves for $T = 0.4$ . . . 66
2.80 DCPPv4: hazard curves for $T = 0.5$ . . . 67
2.81 DCPPv4: hazard curves for $T = 0.75$ . . . 67
2.82 DCPPv4: hazard curves for $T = 1$. . . . 67
2.83 DCPPv4: hazard curves for $T = 1.5$ . . . 68
2.84 DCPPv4: hazard curves for $T = 2$. . . . 68
2.85 DCPPv4: hazard curves for $T = 3$. . . . 68
2.86 DCPPv4: CDF for $M = 5.5$, $R_x = -1$., $F = 0$, and $T = 0.01$ . . . 69
2.87 DCPPv4: CDF for $M = 5.5$, $R_x = -5$., $F = 0$, and $T = 0.01$ . . . 69
2.88 DCPPv4: CDF for $M = 5.5$, $R_x = -10$, $F = 0$, and $T = 0.01$ . . . 70
2.89 DCPPv4: CDF for $M = 6.5$, $R_x = -1$., $F = 0$, and $T = 0.01$ . . . 70
2.90 DCPPv4: CDF for $M = 6.5$, $R_x = -5$., $F = 0$, and $T = 0.01$ . . . 70
2.91 DCPPv4: CDF for $M = 6.5$, $R_x = -10$, $F = 0$, and $T = 0.01$ . . . 71
2.92 DCPPv4: CDF for $M = 7.5$, $R_x = -1$., $F = 0$, and $T = 0.01$ . . . 71
2.93 DCPPv4: CDF for $M = 7.5$, $R_x = -5$., $F = 0$, and $T = 0.01$ . . . 71
2.94 DCPPv4: CDF for $M = 7.5$, $R_x = -10$, $F = 0$, and $T = 0.01$ . . . 72
2.95 DCPPv4: CDF for $M = 5.5$, $R_x = -1$., $F = 1$, and $T = 0.01$ . . . 72
2.96 DCPPv4: CDF for $M = 5.5$, $R_x = -5$., $F = 1$, and $T = 0.01$ . . . 72
2.97 DCPPv4: CDF for $M = 5.5$, $R_x = -10$, $F = 1$, and $T = 0.01$ . . . 73
2.98 DCPPv4: CDF for $M = 6.5$, $R_x = -1$., $F = 1$, and $T = 0.01$ . . . 73
2.99 DCPPv4: CDF for $M = 6.5$, $R_x = -5$., $F = 1$, and $T = 0.01$ . . . 73
2.100 DCPPv4: CDF for $M = 6.5$, $R_x = -10$, $F = 1$, and $T = 0.01$ . . . 74
2.101 DCPPv4: CDF for $M = 7.5$, $R_x = -1$., $F = 1$, and $T = 0.01$ . . . 74
2.102 DCPPv4: CDF for $M = 7.5$, $R_x = -5$., $F = 1$, and $T = 0.01$ . . . 74
2.103 DCPPv4: CDF for $M = 7.5$, $R_x = -10$, $F = 1$, and $T = 0.01$ . . . 75
2.104 DCPPv4: CDF for $M = 5.5$, $R_x = -1$., $F = 0$, and $T = 0.2$ . . . 76
2.105 DCPPv4: CDF for $M = 5.5$, $R_x = -5$., $F = 0$, and $T = 0.2$ . . . 76
2.106 DCPPv4: CDF for $M = 5.5$, $R_x = -10$, $F = 0$, and $T = 0.2$ . . . 77
2.107 DCPPv4: CDF for $M = 6.5$, $R_x = -1$., $F = 0$, and $T = 0.2$ . . . 77
2.108 DCPPv4: CDF for $M = 6.5$, $R_x = -5$., $F = 0$, and $T = 0.2$ . . . 77
2.109 DCPPv4: CDF for $M = 6.5$, $R_x = -10$, $F = 0$, and $T = 0.2$ . . . 78
2.110 DCPPv4: CDF for $M = 7.5$, $R_x = -1$., $F = 0$, and $T = 0.2$ . . . 78
2.111 DCPPv4: CDF for $M = 7.5$, $R_x = -5$., $F = 0$, and $T = 0.2$ . . . 78
2.112 DCPPv4: CDF for $M = 7.5$, $R_x = -10$, $F = 0$, and $T = 0.2$ . . . 79
2.113 DCPPv4: CDF for $M = 5.5$, $R_x = -1$., $F = 1$, and $T = 0.2$ . . . 79
2.114 DCPPv4: CDF for $M = 5.5$, $R_x = -5$., $F = 1$, and $T = 0.2$ . . . 79
2.115 DCPPv4: CDF for $M = 5.5$, $R_x = -10$, $F = 1$, and $T = 0.2$ . . . 80
2.116 DCPPv4: CDF for $M = 6.5$, $R_x = -1$., $F = 1$, and $T = 0.2$ . . . 80
2.117 DCPPv4: CDF for $M = 6.5$, $R_x = -5$., $F = 1$, and $T = 0.2$ . . . 80
2.118 DCPPv4: CDF for $M = 6.5$, $R_x = -10$, $F = 1$, and $T = 0.2$ . . . 81
2.119 DCPPv4: CDF for $M = 7.5$, $R_x = -1$., $F = 1$, and $T = 0.2$ . . . 81
2.120 DCPPv4: CDF for $M = 7.5$, $R_x = -5$., $F = 1$, and $T = 0.2$ . . . 81

2.121DCPPv4: CDF for $M = 7.5$, $R_x = -10$, $F = 1$, and $T = 0.2$ . . . 82
2.122DCPPv4: CDF for $M = 5.5$, $R_x = -1.$, $F = 0$, and $T = 0.5$ . . . 83
2.123DCPPv4: CDF for $M = 5.5$, $R_x = -5.$, $F = 0$, and $T = 0.5$ . . . 83
2.124DCPPv4: CDF for $M = 5.5$, $R_x = -10$, $F = 0$, and $T = 0.5$ . . . 84
2.125DCPPv4: CDF for $M = 6.5$, $R_x = -1.$, $F = 0$, and $T = 0.5$ . . . 84
2.126DCPPv4: CDF for $M = 6.5$, $R_x = -5.$, $F = 0$, and $T = 0.5$ . . . 84
2.127DCPPv4: CDF for $M = 6.5$, $R_x = -10$, $F = 0$, and $T = 0.5$ . . . 85
2.128DCPPv4: CDF for $M = 7.5$, $R_x = -1.$, $F = 0$, and $T = 0.5$ . . . 85
2.129DCPPv4: CDF for $M = 7.5$, $R_x = -5.$, $F = 0$, and $T = 0.5$ . . . 85
2.130DCPPv4: CDF for $M = 7.5$, $R_x = -10$, $F = 0$, and $T = 0.5$ . . . 86
2.131DCPPv4: CDF for $M = 5.5$, $R_x = -1.$, $F = 1$, and $T = 0.5$ . . . 86
2.132DCPPv4: CDF for $M = 5.5$, $R_x = -5.$, $F = 1$, and $T = 0.5$ . . . 86
2.133DCPPv4: CDF for $M = 5.5$, $R_x = -10$, $F = 1$, and $T = 0.5$ . . . 87
2.134DCPPv4: CDF for $M = 6.5$, $R_x = -1.$, $F = 1$, and $T = 0.5$ . . . 87
2.135DCPPv4: CDF for $M = 6.5$, $R_x = -5.$, $F = 1$, and $T = 0.5$ . . . 87
2.136DCPPv4: CDF for $M = 6.5$, $R_x = -10$, $F = 1$, and $T = 0.5$ . . . 88
2.137DCPPv4: CDF for $M = 7.5$, $R_x = -1.$, $F = 1$, and $T = 0.5$ . . . 88
2.138DCPPv4: CDF for $M = 7.5$, $R_x = -5.$, $F = 1$, and $T = 0.5$ . . . 88
2.139DCPPv4: CDF for $M = 7.5$, $R_x = -10$, $F = 1$, and $T = 0.5$ . . . 89
2.140DCPPv4: CDF for $M = 5.5$, $R_x = -1.$, $F = 0$, and $T = 1.$ . . . 90
2.141DCPPv4: CDF for $M = 5.5$, $R_x = -5.$, $F = 0$, and $T = 1.$ . . . 90
2.142DCPPv4: CDF for $M = 5.5$, $R_x = -10$, $F = 0$, and $T = 1.$ . . . 91
2.143DCPPv4: CDF for $M = 6.5$, $R_x = -1.$, $F = 0$, and $T = 1.$ . . . 91
2.144DCPPv4: CDF for $M = 6.5$, $R_x = -5.$, $F = 0$, and $T = 1.$ . . . 91
2.145DCPPv4: CDF for $M = 6.5$, $R_x = -10$, $F = 0$, and $T = 1.$ . . . 92
2.146DCPPv4: CDF for $M = 7.5$, $R_x = -1.$, $F = 0$, and $T = 1.$ . . . 92
2.147DCPPv4: CDF for $M = 7.5$, $R_x = -5.$, $F = 0$, and $T = 1.$ . . . 92
2.148DCPPv4: CDF for $M = 7.5$, $R_x = -10$, $F = 0$, and $T = 1.$ . . . 93
2.149DCPPv4: CDF for $M = 5.5$, $R_x = -1.$, $F = 1$, and $T = 1.$ . . . 93
2.150DCPPv4: CDF for $M = 5.5$, $R_x = -5.$, $F = 1$, and $T = 1.$ . . . 93
2.151DCPPv4: CDF for $M = 5.5$, $R_x = -10$, $F = 1$, and $T = 1.$ . . . 94
2.152DCPPv4: CDF for $M = 6.5$, $R_x = -1.$, $F = 1$, and $T = 1.$ . . . 94
2.153DCPPv4: CDF for $M = 6.5$, $R_x = -5.$, $F = 1$, and $T = 1.$ . . . 94
2.154DCPPv4: CDF for $M = 6.5$, $R_x = -10$, $F = 1$, and $T = 1.$ . . . 95
2.155DCPPv4: CDF for $M = 7.5$, $R_x = -1.$, $F = 1$, and $T = 1.$ . . . 95
2.156DCPPv4: CDF for $M = 7.5$, $R_x = -5.$, $F = 1$, and $T = 1.$ . . . 95
2.157DCPPv4: CDF for $M = 7.5$, $R_x = -10$, $F = 1$, and $T = 1.$ . . . 96
2.158DCPPv4: CDF for $M = 5.5$, $R_x = -1.$, $F = 0$, and $T = 3.$ . . . 97
2.159DCPPv4: CDF for $M = 5.5$, $R_x = -5.$, $F = 0$, and $T = 3.$ . . . 97
2.160DCPPv4: CDF for $M = 5.5$, $R_x = -10$, $F = 0$, and $T = 3.$ . . . 98
2.161DCPPv4: CDF for $M = 6.5$, $R_x = -1.$, $F = 0$, and $T = 3.$ . . . 98
2.162DCPPv4: CDF for $M = 6.5$, $R_x = -5.$, $F = 0$, and $T = 3.$ . . . 98
2.163DCPPv4: CDF for $M = 6.5$, $R_x = -10$, $F = 0$, and $T = 3.$ . . . 99
2.164DCPPv4: CDF for $M = 7.5$, $R_x = -1.$, $F = 0$, and $T = 3.$ . . . 99
2.165DCPPv4: CDF for $M = 7.5$, $R_x = -5.$, $F = 0$, and $T = 3.$ . . . 99
2.166DCPPv4: CDF for $M = 7.5$, $R_x = -10$, $F = 0$, and $T = 3.$ . . . 100
2.167DCPPv4: CDF for $M = 5.5$, $R_x = -1.$, $F = 1$, and $T = 3.$ . . . 100
2.168DCPPv4: CDF for $M = 5.5$, $R_x = -5.$, $F = 1$, and $T = 3.$ . . . 100
2.169DCPPv4: CDF for $M = 5.5$, $R_x = -10$, $F = 1$, and $T = 3.$ . . . 101
2.170DCPPv4: CDF for $M = 6.5$, $R_x = -1.$, $F = 1$, and $T = 3.$ . . . 101
2.171DCPPv4: CDF for $M = 6.5$, $R_x = -5.$, $F = 1$, and $T = 3.$ . . . 101
2.172DCPPv4: CDF for $M = 6.5$, $R_x = -10$, $F = 1$, and $T = 3.$ . . . 102
2.173DCPPv4: CDF for $M = 7.5$, $R_x = -1.$, $F = 1$, and $T = 3.$ . . . 102
2.174DCPPv4: CDF for $M = 7.5$, $R_x = -5.$, $F = 1$, and $T = 3.$ . . . 102
2.175DCPPv4: CDF for $M = 7.5$, $R_x = -10$, $F = 1$, and $T = 3.$ . . . 103
2.176DCPPv4: Distance scaling for $M = 5.5$, $F = 0$, and $T = 0.01$ . . . 104
2.177DCPPv4: Distance scaling for $M = 6.5$, $F = 0$, and $T = 0.01$ . . . 104
2.178DCPPv4: Distance scaling for $M = 7.5$, $F = 0$, and $T = 0.01$ . . . 105
2.179DCPPv4: Distance scaling for $M = 5.5$, $F = 1$, and $T = 0.01$ . . . 105
2.180DCPPv4: Distance scaling for $M = 6.5$, $F = 1$, and $T = 0.01$ . . . 106
2.181DCPPv4: Distance scaling for $M = 7.5$, $F = 1$, and $T = 0.01$ . . . 106

2.182DCPPv4: Distance scaling for $M = 5.5$, $F = 0$, and $T = 0.2$ . . . 107
2.183DCPPv4: Distance scaling for $M = 6.5$, $F = 0$, and $T = 0.2$ . . . 107
2.184DCPPv4: Distance scaling for $M = 7.5$, $F = 0$, and $T = 0.2$ . . . 108
2.185DCPPv4: Distance scaling for $M = 5.5$, $F = 1$, and $T = 0.2$ . . . 108
2.186DCPPv4: Distance scaling for $M = 6.5$, $F = 1$, and $T = 0.2$ . . . 109
2.187DCPPv4: Distance scaling for $M = 7.5$, $F = 1$, and $T = 0.2$ . . . 109
2.188DCPPv4: Distance scaling for $M = 5.5$, $F = 0$, and $T = 0.5$ . . . 110
2.189DCPPv4: Distance scaling for $M = 6.5$, $F = 0$, and $T = 0.5$ . . . 110
2.190DCPPv4: Distance scaling for $M = 7.5$, $F = 0$, and $T = 0.5$ . . . 111
2.191DCPPv4: Distance scaling for $M = 5.5$, $F = 1$, and $T = 0.5$ . . . 111
2.192DCPPv4: Distance scaling for $M = 6.5$, $F = 1$, and $T = 0.5$ . . . 112
2.193DCPPv4: Distance scaling for $M = 7.5$, $F = 1$, and $T = 0.5$ . . . 112
2.194DCPPv4: Distance scaling for $M = 5.5$, $F = 0$, and $T = 1.$ . . . 113
2.195DCPPv4: Distance scaling for $M = 6.5$, $F = 0$, and $T = 1.$ . . . 113
2.196DCPPv4: Distance scaling for $M = 7.5$, $F = 0$, and $T = 1.$ . . . 114
2.197DCPPv4: Distance scaling for $M = 5.5$, $F = 1$, and $T = 1.$ . . . 114
2.198DCPPv4: Distance scaling for $M = 6.5$, $F = 1$, and $T = 1.$ . . . 115
2.199DCPPv4: Distance scaling for $M = 7.5$, $F = 1$, and $T = 1.$ . . . 115
2.200DCPPv4: Distance scaling for $M = 5.5$, $F = 0$, and $T = 3.$ . . . 116
2.201DCPPv4: Distance scaling for $M = 6.5$, $F = 0$, and $T = 3.$ . . . 116
2.202DCPPv4: Distance scaling for $M = 7.5$, $F = 0$, and $T = 3.$ . . . 117
2.203DCPPv4: Distance scaling for $M = 5.5$, $F = 1$, and $T = 3.$ . . . 117
2.204DCPPv4: Distance scaling for $M = 6.5$, $F = 1$, and $T = 3.$ . . . 118
2.205DCPPv4: Distance scaling for $M = 7.5$, $F = 1$, and $T = 3.$ . . . 118
2.206DCPPv4: Distance scaling of quantiles with GMPEs for $M = 5.5$, $F = 0$, and $T = 0.01$ . . . 119
2.207DCPPv4: Distance scaling of quantiles with GMPEs for $M = 6.5$, $F = 0$, and $T = 0.01$ . . . 119
2.208DCPPv4: Distance scaling of quantiles with GMPEs for $M = 7.5$, $F = 0$, and $T = 0.01$ . . . 120
2.209DCPPv4: Distance scaling of quantiles with GMPEs for $M = 5.5$, $F = 1$, and $T = 0.01$ . . . 120
2.210DCPPv4: Distance scaling of quantiles with GMPEs for $M = 6.5$, $F = 1$, and $T = 0.01$ . . . 121
2.211DCPPv4: Distance scaling of quantiles with GMPEs for $M = 7.5$, $F = 1$, and $T = 0.01$ . . . 121
2.212DCPPv4: Distance scaling of quantiles with GMPEs for $M = 5.5$, $F = 0$, and $T = 0.2$ . . . 122
2.213DCPPv4: Distance scaling of quantiles with GMPEs for $M = 6.5$, $F = 0$, and $T = 0.2$ . . . 122
2.214DCPPv4: Distance scaling of quantiles with GMPEs for $M = 7.5$, $F = 0$, and $T = 0.2$ . . . 123
2.215DCPPv4: Distance scaling of quantiles with GMPEs for $M = 5.5$, $F = 1$, and $T = 0.2$ . . . 123
2.216DCPPv4: Distance scaling of quantiles with GMPEs for $M = 6.5$, $F = 1$, and $T = 0.2$ . . . 124
2.217DCPPv4: Distance scaling of quantiles with GMPEs for $M = 7.5$, $F = 1$, and $T = 0.2$ . . . 124
2.218DCPPv4: Distance scaling of quantiles with GMPEs for $M = 5.5$, $F = 0$, and $T = 0.5$ . . . 125
2.219DCPPv4: Distance scaling of quantiles with GMPEs for $M = 6.5$, $F = 0$, and $T = 0.5$ . . . 125
2.220DCPPv4: Distance scaling of quantiles with GMPEs for $M = 7.5$, $F = 0$, and $T = 0.5$ . . . 126
2.221DCPPv4: Distance scaling of quantiles with GMPEs for $M = 5.5$, $F = 1$, and $T = 0.5$ . . . 126
2.222DCPPv4: Distance scaling of quantiles with GMPEs for $M = 6.5$, $F = 1$, and $T = 0.5$ . . . 127
2.223DCPPv4: Distance scaling of quantiles with GMPEs for $M = 7.5$, $F = 1$, and $T = 0.5$ . . . 127
2.224DCPPv4: Distance scaling of quantiles with GMPEs for $M = 5.5$, $F = 0$, and $T = 1.$ . . . 128
2.225DCPPv4: Distance scaling of quantiles with GMPEs for $M = 6.5$, $F = 0$, and $T = 1.$ . . . 128
2.226DCPPv4: Distance scaling of quantiles with GMPEs for $M = 7.5$, $F = 0$, and $T = 1.$ . . . 129
2.227DCPPv4: Distance scaling of quantiles with GMPEs for $M = 5.5$, $F = 1$, and $T = 1.$ . . . 129
2.228DCPPv4: Distance scaling of quantiles with GMPEs for $M = 6.5$, $F = 1$, and $T = 1.$ . . . 130
2.229DCPPv4: Distance scaling of quantiles with GMPEs for $M = 7.5$, $F = 1$, and $T = 1.$ . . . 130
2.230DCPPv4: Distance scaling of quantiles with GMPEs for $M = 5.5$, $F = 0$, and $T = 3.$ . . . 131
2.231DCPPv4: Distance scaling of quantiles with GMPEs for $M = 6.5$, $F = 0$, and $T = 3.$ . . . 131
2.232DCPPv4: Distance scaling of quantiles with GMPEs for $M = 7.5$, $F = 0$, and $T = 3.$ . . . 132
2.233DCPPv4: Distance scaling of quantiles with GMPEs for $M = 5.5$, $F = 1$, and $T = 3.$ . . . 132
2.234DCPPv4: Distance scaling of quantiles with GMPEs for $M = 6.5$, $F = 1$, and $T = 3.$ . . . 133
2.235DCPPv4: Distance scaling of quantiles with GMPEs for $M = 7.5$, $F = 1$, and $T = 3.$ . . . 133
2.236DCPPv4: Magnitude scaling for $R_x = -1.$, $F = 0$, and $T = 0.01$ . . . 134
2.237DCPPv4: Magnitude scaling for $R_x = -5.$, $F = 0$, and $T = 0.01$ . . . 134
2.238DCPPv4: Magnitude scaling for $R_x = -10$, $F = 0$, and $T = 0.01$ . . . 135
2.239DCPPv4: Magnitude scaling for $R_x = -1.$, $F = 0$, and $T = 0.01$ . . . 135
2.240DCPPv4: Magnitude scaling for $R_x = -5.$, $F = 0$, and $T = 0.01$ . . . 135
2.241DCPPv4: Magnitude scaling for $R_x = -10$, $F = 0$, and $T = 0.01$ . . . 136
2.242DCPPv4: Magnitude scaling for $R_x = -1.$, $F = 0$, and $T = 0.01$ . . . 136

2.243DCPPv4: Magnitude scaling for $R_x = -5.$, $F = 0$, and $T = 0.01$ . . . 136
2.244DCPPv4: Magnitude scaling for $R_x = -10$, $F = 0$, and $T = 0.01$ . . . 137
2.245DCPPv4: Magnitude scaling for $R_x = -1.$, $F = 1$, and $T = 0.01$ . . . 137
2.246DCPPv4: Magnitude scaling for $R_x = -5.$, $F = 1$, and $T = 0.01$ . . . 137
2.247DCPPv4: Magnitude scaling for $R_x = -10$, $F = 1$, and $T = 0.01$ . . . 138
2.248DCPPv4: Magnitude scaling for $R_x = -1.$, $F = 1$, and $T = 0.01$ . . . 138
2.249DCPPv4: Magnitude scaling for $R_x = -5.$, $F = 1$, and $T = 0.01$ . . . 138
2.250DCPPv4: Magnitude scaling for $R_x = -10$, $F = 1$, and $T = 0.01$ . . . 139
2.251DCPPv4: Magnitude scaling for $R_x = -1.$, $F = 1$, and $T = 0.01$ . . . 139
2.252DCPPv4: Magnitude scaling for $R_x = -5.$, $F = 1$, and $T = 0.01$ . . . 139
2.253DCPPv4: Magnitude scaling for $R_x = -10$, $F = 1$, and $T = 0.01$ . . . 140
2.254DCPPv4: Magnitude scaling for $R_x = -1.$, $F = 0$, and $T = 0.2$ . . . 141
2.255DCPPv4: Magnitude scaling for $R_x = -5.$, $F = 0$, and $T = 0.2$ . . . 141
2.256DCPPv4: Magnitude scaling for $R_x = -10$, $F = 0$, and $T = 0.2$ . . . 142
2.257DCPPv4: Magnitude scaling for $R_x = -1.$, $F = 0$, and $T = 0.2$ . . . 142
2.258DCPPv4: Magnitude scaling for $R_x = -5.$, $F = 0$, and $T = 0.2$ . . . 142
2.259DCPPv4: Magnitude scaling for $R_x = -10$, $F = 0$, and $T = 0.2$ . . . 143
2.260DCPPv4: Magnitude scaling for $R_x = -1.$, $F = 0$, and $T = 0.2$ . . . 143
2.261DCPPv4: Magnitude scaling for $R_x = -5.$, $F = 0$, and $T = 0.2$ . . . 143
2.262DCPPv4: Magnitude scaling for $R_x = -10$, $F = 0$, and $T = 0.2$ . . . 144
2.263DCPPv4: Magnitude scaling for $R_x = -1.$, $F = 1$, and $T = 0.2$ . . . 144
2.264DCPPv4: Magnitude scaling for $R_x = -5.$, $F = 1$, and $T = 0.2$ . . . 144
2.265DCPPv4: Magnitude scaling for $R_x = -10$, $F = 1$, and $T = 0.2$ . . . 145
2.266DCPPv4: Magnitude scaling for $R_x = -1.$, $F = 1$, and $T = 0.2$ . . . 145
2.267DCPPv4: Magnitude scaling for $R_x = -5.$, $F = 1$, and $T = 0.2$ . . . 145
2.268DCPPv4: Magnitude scaling for $R_x = -10$, $F = 1$, and $T = 0.2$ . . . 146
2.269DCPPv4: Magnitude scaling for $R_x = -1.$, $F = 1$, and $T = 0.2$ . . . 146
2.270DCPPv4: Magnitude scaling for $R_x = -5.$, $F = 1$, and $T = 0.2$ . . . 146
2.271DCPPv4: Magnitude scaling for $R_x = -10$, $F = 1$, and $T = 0.2$ . . . 147
2.272DCPPv4: Magnitude scaling for $R_x = -1.$, $F = 0$, and $T = 0.5$ . . . 148
2.273DCPPv4: Magnitude scaling for $R_x = -5.$, $F = 0$, and $T = 0.5$ . . . 148
2.274DCPPv4: Magnitude scaling for $R_x = -10$, $F = 0$, and $T = 0.5$ . . . 149
2.275DCPPv4: Magnitude scaling for $R_x = -1.$, $F = 0$, and $T = 0.5$ . . . 149
2.276DCPPv4: Magnitude scaling for $R_x = -5.$, $F = 0$, and $T = 0.5$ . . . 149
2.277DCPPv4: Magnitude scaling for $R_x = -10$, $F = 0$, and $T = 0.5$ . . . 150
2.278DCPPv4: Magnitude scaling for $R_x = -1.$, $F = 0$, and $T = 0.5$ . . . 150
2.279DCPPv4: Magnitude scaling for $R_x = -5.$, $F = 0$, and $T = 0.5$ . . . 150
2.280DCPPv4: Magnitude scaling for $R_x = -10$, $F = 0$, and $T = 0.5$ . . . 151
2.281DCPPv4: Magnitude scaling for $R_x = -1.$, $F = 1$, and $T = 0.5$ . . . 151
2.282DCPPv4: Magnitude scaling for $R_x = -5.$, $F = 1$, and $T = 0.5$ . . . 151
2.283DCPPv4: Magnitude scaling for $R_x = -10$, $F = 1$, and $T = 0.5$ . . . 152
2.284DCPPv4: Magnitude scaling for $R_x = -1.$, $F = 1$, and $T = 0.5$ . . . 152
2.285DCPPv4: Magnitude scaling for $R_x = -5.$, $F = 1$, and $T = 0.5$ . . . 152
2.286DCPPv4: Magnitude scaling for $R_x = -10$, $F = 1$, and $T = 0.5$ . . . 153
2.287DCPPv4: Magnitude scaling for $R_x = -1.$, $F = 1$, and $T = 0.5$ . . . 153
2.288DCPPv4: Magnitude scaling for $R_x = -5.$, $F = 1$, and $T = 0.5$ . . . 153
2.289DCPPv4: Magnitude scaling for $R_x = -10$, $F = 1$, and $T = 0.5$ . . . 154
2.290DCPPv4: Magnitude scaling for $R_x = -1.$, $F = 0$, and $T = 1.$ . . . 155
2.291DCPPv4: Magnitude scaling for $R_x = -5.$, $F = 0$, and $T = 1.$ . . . 155
2.292DCPPv4: Magnitude scaling for $R_x = -10$, $F = 0$, and $T = 1.$ . . . 156
2.293DCPPv4: Magnitude scaling for $R_x = -1.$, $F = 0$, and $T = 1.$ . . . 156
2.294DCPPv4: Magnitude scaling for $R_x = -5.$, $F = 0$, and $T = 1.$ . . . 156
2.295DCPPv4: Magnitude scaling for $R_x = -10$, $F = 0$, and $T = 1.$ . . . 157
2.296DCPPv4: Magnitude scaling for $R_x = -1.$, $F = 0$, and $T = 1.$ . . . 157
2.297DCPPv4: Magnitude scaling for $R_x = -5.$, $F = 0$, and $T = 1.$ . . . 157
2.298DCPPv4: Magnitude scaling for $R_x = -10$, $F = 0$, and $T = 1.$ . . . 158
2.299DCPPv4: Magnitude scaling for $R_x = -1.$, $F = 1$, and $T = 1.$ . . . 158
2.300DCPPv4: Magnitude scaling for $R_x = -5.$, $F = 1$, and $T = 1.$ . . . 158
2.301DCPPv4: Magnitude scaling for $R_x = -10$, $F = 1$, and $T = 1.$ . . . 159
2.302DCPPv4: Magnitude scaling for $R_x = -1.$, $F = 1$, and $T = 1.$ . . . 159
2.303DCPPv4: Magnitude scaling for $R_x = -5.$, $F = 1$, and $T = 1.$ . . . 159

2.304DCPPv4: Magnitude scaling for $R_x = -10$, $F = 1$, and $T = 1$. . . . . 160
2.305DCPPv4: Magnitude scaling for $R_x = -1.$, $F = 1$, and $T = 1$. . . . . 160
2.306DCPPv4: Magnitude scaling for $R_x = -5.$, $F = 1$, and $T = 1$. . . . . 160
2.307DCPPv4: Magnitude scaling for $R_x = -10$, $F = 1$, and $T = 1$. . . . . 161
2.308DCPPv4: Magnitude scaling for $R_x = -1.$, $F = 0$, and $T = 3$. . . . . 162
2.309DCPPv4: Magnitude scaling for $R_x = -5.$, $F = 0$, and $T = 3$. . . . . 162
2.310DCPPv4: Magnitude scaling for $R_x = -10$, $F = 0$, and $T = 3$. . . . . 163
2.311DCPPv4: Magnitude scaling for $R_x = -1.$, $F = 0$, and $T = 3$. . . . . 163
2.312DCPPv4: Magnitude scaling for $R_x = -5.$, $F = 0$, and $T = 3$. . . . . 163
2.313DCPPv4: Magnitude scaling for $R_x = -10$, $F = 0$, and $T = 3$. . . . . 164
2.314DCPPv4: Magnitude scaling for $R_x = -1.$, $F = 0$, and $T = 3$. . . . . 164
2.315DCPPv4: Magnitude scaling for $R_x = -5.$, $F = 0$, and $T = 3$. . . . . 164
2.316DCPPv4: Magnitude scaling for $R_x = -10$, $F = 0$, and $T = 3$. . . . . 165
2.317DCPPv4: Magnitude scaling for $R_x = -1.$, $F = 1$, and $T = 3$. . . . . 165
2.318DCPPv4: Magnitude scaling for $R_x = -5.$, $F = 1$, and $T = 3$. . . . . 165
2.319DCPPv4: Magnitude scaling for $R_x = -10$, $F = 1$, and $T = 3$. . . . . 166
2.320DCPPv4: Magnitude scaling for $R_x = -1.$, $F = 1$, and $T = 3$. . . . . 166
2.321DCPPv4: Magnitude scaling for $R_x = -5.$, $F = 1$, and $T = 3$. . . . . 166
2.322DCPPv4: Magnitude scaling for $R_x = -10$, $F = 1$, and $T = 3$. . . . . 167
2.323DCPPv4: Magnitude scaling for $R_x = -1.$, $F = 1$, and $T = 3$. . . . . 167
2.324DCPPv4: Magnitude scaling for $R_x = -5.$, $F = 1$, and $T = 3$. . . . . 167
2.325DCPPv4: Magnitude scaling for $R_x = -10$, $F = 1$, and $T = 3$. . . . . 168
2.326DCPPv4: Spectra for $M_W = 5.5$, $R_x = -1.$, $F = 0$ . . . . . 169
2.327DCPPv4: Spectra for $M_W = 5.5$, $R_x = -5.$, $F = 0$ . . . . . 169
2.328DCPPv4: Spectra for $M_W = 5.5$, $R_x = -10$, $F = 0$ . . . . . 170
2.329DCPPv4: Spectra for $M_W = 6.5$, $R_x = -1.$, $F = 0$ . . . . . 170
2.330DCPPv4: Spectra for $M_W = 6.5$, $R_x = -5.$, $F = 0$ . . . . . 171
2.331DCPPv4: Spectra for $M_W = 6.5$, $R_x = -10$, $F = 0$ . . . . . 171
2.332DCPPv4: Spectra for $M_W = 7.5$, $R_x = -1.$, $F = 0$ . . . . . 172
2.333DCPPv4: Spectra for $M_W = 7.5$, $R_x = -5.$, $F = 0$ . . . . . 172
2.334DCPPv4: Spectra for $M_W = 7.5$, $R_x = -10$, $F = 0$ . . . . . 173
2.335DCPPv4: Spectra for $M_W = 5.5$, $R_x = -1.$, $F = 1$ . . . . . 173
2.336DCPPv4: Spectra for $M_W = 5.5$, $R_x = -5.$, $F = 1$ . . . . . 174
2.337DCPPv4: Spectra for $M_W = 5.5$, $R_x = -10$, $F = 1$ . . . . . 174
2.338DCPPv4: Spectra for $M_W = 6.5$, $R_x = -1.$, $F = 1$ . . . . . 175
2.339DCPPv4: Spectra for $M_W = 6.5$, $R_x = -5.$, $F = 1$ . . . . . 175
2.340DCPPv4: Spectra for $M_W = 6.5$, $R_x = -10$, $F = 1$ . . . . . 176
2.341DCPPv4: Spectra for $M_W = 7.5$, $R_x = -1.$, $F = 1$ . . . . . 176
2.342DCPPv4: Spectra for $M_W = 7.5$, $R_x = -5.$, $F = 1$ . . . . . 177
2.343DCPPv4: Spectra for $M_W = 7.5$, $R_x = -10$, $F = 1$ . . . . . 177
2.344DCPPv4: Quantile ratio for $M = 5.5$, $F = 0$ and all periods . . . . . 178
2.345DCPPv4: Quantile ratio for $M = 5.5$, $F = 0$ and all periods . . . . . 178
2.346DCPPv4: Quantile ratio for $M = 5.5$, $F = 0$ and all periods . . . . . 179
2.347DCPPv4: Quantile ratio for $M = 6.5$, $F = 0$ and all periods . . . . . 179
2.348DCPPv4: Quantile ratio for $M = 6.5$, $F = 0$ and all periods . . . . . 180
2.349DCPPv4: Quantile ratio for $M = 6.5$, $F = 0$ and all periods . . . . . 180
2.350DCPPv4: Quantile ratio for $M = 7.5$, $F = 0$ and all periods . . . . . 181
2.351DCPPv4: Quantile ratio for $M = 7.5$, $F = 0$ and all periods . . . . . 181
2.352DCPPv4: Quantile ratio for $M = 7.5$, $F = 0$ and all periods . . . . . 182
2.353DCPPv4: Quantile ratio for $M = 5.5$, $F = 1$ and all periods . . . . . 182
2.354DCPPv4: Quantile ratio for $M = 5.5$, $F = 1$ and all periods . . . . . 183
2.355DCPPv4: Quantile ratio for $M = 5.5$, $F = 1$ and all periods . . . . . 183
2.356DCPPv4: Quantile ratio for $M = 6.5$, $F = 1$ and all periods . . . . . 184
2.357DCPPv4: Quantile ratio for $M = 6.5$, $F = 1$ and all periods . . . . . 184
2.358DCPPv4: Quantile ratio for $M = 6.5$, $F = 1$ and all periods . . . . . 185
2.359DCPPv4: Quantile ratio for $M = 7.5$, $F = 1$ and all periods . . . . . 185
2.360DCPPv4: Quantile ratio for $M = 7.5$, $F = 1$ and all periods . . . . . 186
2.361DCPPv4: Quantile ratio for $M = 7.5$, $F = 1$ and all periods . . . . . 186
2.362DCPPv4: Magnitude scaling for $R_X = -1.$, $F = 0$, and $T = 0.01$ . . . . . 187
2.363DCPPv4: Magnitude scaling for $R_X = -5.$, $F = 0$, and $T = 0.01$ . . . . . 187
2.364DCPPv4: Magnitude scaling for $R_X = -10$, $F = 0$, and $T = 0.01$ . . . . . 188

2.365DCPPv4: Magnitude scaling for $R_X = -1.$, $F = 1$, and $T = 0.01$ . . . 188
2.366DCPPv4: Magnitude scaling for $R_X = -5.$, $F = 1$, and $T = 0.01$ . . . 189
2.367DCPPv4: Magnitude scaling for $R_X = -10$, $F = 1$, and $T = 0.01$ . . . 189
2.368DCPPv4: Magnitude scaling for $R_X = -1.$, $F = 0$, and $T = 0.2$ . . . 190
2.369DCPPv4: Magnitude scaling for $R_X = -5.$, $F = 0$, and $T = 0.2$ . . . 190
2.370DCPPv4: Magnitude scaling for $R_X = -10$, $F = 0$, and $T = 0.2$ . . . 191
2.371DCPPv4: Magnitude scaling for $R_X = -1.$, $F = 1$, and $T = 0.2$ . . . 191
2.372DCPPv4: Magnitude scaling for $R_X = -5.$, $F = 1$, and $T = 0.2$ . . . 192
2.373DCPPv4: Magnitude scaling for $R_X = -10$, $F = 1$, and $T = 0.2$ . . . 192
2.374DCPPv4: Magnitude scaling for $R_X = -1.$, $F = 0$, and $T = 0.5$ . . . 193
2.375DCPPv4: Magnitude scaling for $R_X = -5.$, $F = 0$, and $T = 0.5$ . . . 193
2.376DCPPv4: Magnitude scaling for $R_X = -10$, $F = 0$, and $T = 0.5$ . . . 194
2.377DCPPv4: Magnitude scaling for $R_X = -1.$, $F = 1$, and $T = 0.5$ . . . 194
2.378DCPPv4: Magnitude scaling for $R_X = -5.$, $F = 1$, and $T = 0.5$ . . . 195
2.379DCPPv4: Magnitude scaling for $R_X = -10$, $F = 1$, and $T = 0.5$ . . . 195
2.380DCPPv4: Magnitude scaling for $R_X = -1.$, $F = 0$, and $T = 1.$ . . . 196
2.381DCPPv4: Magnitude scaling for $R_X = -5.$, $F = 0$, and $T = 1.$ . . . 196
2.382DCPPv4: Magnitude scaling for $R_X = -10$, $F = 0$, and $T = 1.$ . . . 197
2.383DCPPv4: Magnitude scaling for $R_X = -1.$, $F = 1$, and $T = 1.$ . . . 197
2.384DCPPv4: Magnitude scaling for $R_X = -5.$, $F = 1$, and $T = 1.$ . . . 198
2.385DCPPv4: Magnitude scaling for $R_X = -10$, $F = 1$, and $T = 1.$ . . . 198
2.386DCPPv4: Magnitude scaling for $R_X = -1.$, $F = 0$, and $T = 3.$ . . . 199
2.387DCPPv4: Magnitude scaling for $R_X = -5.$, $F = 0$, and $T = 3.$ . . . 199
2.388DCPPv4: Magnitude scaling for $R_X = -10$, $F = 0$, and $T = 3.$ . . . 200
2.389DCPPv4: Magnitude scaling for $R_X = -1.$, $F = 1$, and $T = 3.$ . . . 200
2.390DCPPv4: Magnitude scaling for $R_X = -5.$, $F = 1$, and $T = 3.$ . . . 201
2.391DCPPv4: Magnitude scaling for $R_X = -10$, $F = 1$, and $T = 3.$ . . . 201
2.392DCPPv4: Distance scaling of quantiles with GMPEs for $M = 5.5$, $F = 0$, and $T = 0.01$ . . . 202
2.393DCPPv4: Distance scaling of quantiles with GMPEs for $M = 6.5$, $F = 0$, and $T = 0.01$ . . . 202
2.394DCPPv4: Distance scaling of quantiles with GMPEs for $M = 7.5$, $F = 0$, and $T = 0.01$ . . . 203
2.395DCPPv4: Distance scaling of quantiles with GMPEs for $M = 5.5$, $F = 1$, and $T = 0.01$ . . . 203
2.396DCPPv4: Distance scaling of quantiles with GMPEs for $M = 6.5$, $F = 1$, and $T = 0.01$ . . . 204
2.397DCPPv4: Distance scaling of quantiles with GMPEs for $M = 7.5$, $F = 1$, and $T = 0.01$ . . . 204
2.398DCPPv4: Distance scaling of quantiles with GMPEs for $M = 5.5$, $F = 0$, and $T = 0.2$ . . . 205
2.399DCPPv4: Distance scaling of quantiles with GMPEs for $M = 6.5$, $F = 0$, and $T = 0.2$ . . . 205
2.400DCPPv4: Distance scaling of quantiles with GMPEs for $M = 7.5$, $F = 0$, and $T = 0.2$ . . . 206
2.401DCPPv4: Distance scaling of quantiles with GMPEs for $M = 5.5$, $F = 1$, and $T = 0.2$ . . . 206
2.402DCPPv4: Distance scaling of quantiles with GMPEs for $M = 6.5$, $F = 1$, and $T = 0.2$ . . . 207
2.403DCPPv4: Distance scaling of quantiles with GMPEs for $M = 7.5$, $F = 1$, and $T = 0.2$ . . . 207
2.404DCPPv4: Distance scaling of quantiles with GMPEs for $M = 5.5$, $F = 0$, and $T = 0.5$ . . . 208
2.405DCPPv4: Distance scaling of quantiles with GMPEs for $M = 6.5$, $F = 0$, and $T = 0.5$ . . . 208
2.406DCPPv4: Distance scaling of quantiles with GMPEs for $M = 7.5$, $F = 0$, and $T = 0.5$ . . . 209
2.407DCPPv4: Distance scaling of quantiles with GMPEs for $M = 5.5$, $F = 1$, and $T = 0.5$ . . . 209
2.408DCPPv4: Distance scaling of quantiles with GMPEs for $M = 6.5$, $F = 1$, and $T = 0.5$ . . . 210
2.409DCPPv4: Distance scaling of quantiles with GMPEs for $M = 7.5$, $F = 1$, and $T = 0.5$ . . . 210
2.410DCPPv4: Distance scaling of quantiles with GMPEs for $M = 5.5$, $F = 0$, and $T = 1.$ . . . 211
2.411DCPPv4: Distance scaling of quantiles with GMPEs for $M = 6.5$, $F = 0$, and $T = 1.$ . . . 211
2.412DCPPv4: Distance scaling of quantiles with GMPEs for $M = 7.5$, $F = 0$, and $T = 1.$ . . . 212
2.413DCPPv4: Distance scaling of quantiles with GMPEs for $M = 5.5$, $F = 1$, and $T = 1.$ . . . 212
2.414DCPPv4: Distance scaling of quantiles with GMPEs for $M = 6.5$, $F = 1$, and $T = 1.$ . . . 213
2.415DCPPv4: Distance scaling of quantiles with GMPEs for $M = 7.5$, $F = 1$, and $T = 1.$ . . . 213
2.416DCPPv4: Distance scaling of quantiles with GMPEs for $M = 5.5$, $F = 0$, and $T = 3.$ . . . 214
2.417DCPPv4: Distance scaling of quantiles with GMPEs for $M = 6.5$, $F = 0$, and $T = 3.$ . . . 214
2.418DCPPv4: Distance scaling of quantiles with GMPEs for $M = 7.5$, $F = 0$, and $T = 3.$ . . . 215
2.419DCPPv4: Distance scaling of quantiles with GMPEs for $M = 5.5$, $F = 1$, and $T = 3.$ . . . 215
2.420DCPPv4: Distance scaling of quantiles with GMPEs for $M = 6.5$, $F = 1$, and $T = 3.$ . . . 216
2.421DCPPv4: Distance scaling of quantiles with GMPEs for $M = 7.5$, $F = 1$, and $T = 3.$ . . . 216
2.422DCPPv4: Magnitude scaling for $R_x = -1.$, $F = 0$, and $T = 0.01$ . . . 217
2.423DCPPv4: Magnitude scaling for $R_x = -5.$, $F = 0$, and $T = 0.01$ . . . 217
2.424DCPPv4: Magnitude scaling for $R_x = -10$, $F = 0$, and $T = 0.01$ . . . 218
2.425DCPPv4: Magnitude scaling for $R_x = -1.$, $F = 1$, and $T = 0.01$ . . . 218

2.426DCPPv4: Magnitude scaling for $R_x = -5.$, $F = 1$, and $T = 0.01$ . . . 219
2.427DCPPv4: Magnitude scaling for $R_x = -10$, $F = 1$, and $T = 0.01$ . . . 219
2.428DCPPv4: Magnitude scaling for $R_x = -1.$, $F = 0$, and $T = 0.2$ . . . 220
2.429DCPPv4: Magnitude scaling for $R_x = -5.$, $F = 0$, and $T = 0.2$ . . . 220
2.430DCPPv4: Magnitude scaling for $R_x = -10$, $F = 0$, and $T = 0.2$ . . . 221
2.431DCPPv4: Magnitude scaling for $R_x = -1.$, $F = 1$, and $T = 0.2$ . . . 221
2.432DCPPv4: Magnitude scaling for $R_x = -5.$, $F = 1$, and $T = 0.2$ . . . 222
2.433DCPPv4: Magnitude scaling for $R_x = -10$, $F = 1$, and $T = 0.2$ . . . 222
2.434DCPPv4: Magnitude scaling for $R_x = -1.$, $F = 0$, and $T = 0.5$ . . . 223
2.435DCPPv4: Magnitude scaling for $R_x = -5.$, $F = 0$, and $T = 0.5$ . . . 223
2.436DCPPv4: Magnitude scaling for $R_x = -10$, $F = 0$, and $T = 0.5$ . . . 224
2.437DCPPv4: Magnitude scaling for $R_x = -1.$, $F = 1$, and $T = 0.5$ . . . 224
2.438DCPPv4: Magnitude scaling for $R_x = -5.$, $F = 1$, and $T = 0.5$ . . . 225
2.439DCPPv4: Magnitude scaling for $R_x = -10$, $F = 1$, and $T = 0.5$ . . . 225
2.440DCPPv4: Magnitude scaling for $R_x = -1.$, $F = 0$, and $T = 1.$ . . . 226
2.441DCPPv4: Magnitude scaling for $R_x = -5.$, $F = 0$, and $T = 1.$ . . . 226
2.442DCPPv4: Magnitude scaling for $R_x = -10$, $F = 0$, and $T = 1.$ . . . 227
2.443DCPPv4: Magnitude scaling for $R_x = -1.$, $F = 1$, and $T = 1.$ . . . 227
2.444DCPPv4: Magnitude scaling for $R_x = -5.$, $F = 1$, and $T = 1.$ . . . 228
2.445DCPPv4: Magnitude scaling for $R_x = -10$, $F = 1$, and $T = 1.$ . . . 228
2.446DCPPv4: Magnitude scaling for $R_x = -1.$, $F = 0$, and $T = 3.$ . . . 229
2.447DCPPv4: Magnitude scaling for $R_x = -5.$, $F = 0$, and $T = 3.$ . . . 229
2.448DCPPv4: Magnitude scaling for $R_x = -10$, $F = 0$, and $T = 3.$ . . . 230
2.449DCPPv4: Magnitude scaling for $R_x = -1.$, $F = 1$, and $T = 3.$ . . . 230
2.450DCPPv4: Magnitude scaling for $R_x = -5.$, $F = 1$, and $T = 3.$ . . . 231
2.451DCPPv4: Magnitude scaling for $R_x = -10$, $F = 1$, and $T = 3.$ . . . 231
2.452DCPPv4: Spectra for $M_W = 5.5$, $R_x = -1.$, $F = 0$ . . . 232
2.453DCPPv4: Spectra for $M_W = 5.5$, $R_x = -5.$, $F = 0$ . . . 232
2.454DCPPv4: Spectra for $M_W = 5.5$, $R_x = -10$, $F = 0$ . . . 233
2.455DCPPv4: Spectra for $M_W = 6.5$, $R_x = -1.$, $F = 0$ . . . 233
2.456DCPPv4: Spectra for $M_W = 6.5$, $R_x = -5.$, $F = 0$ . . . 234
2.457DCPPv4: Spectra for $M_W = 6.5$, $R_x = -10$, $F = 0$ . . . 234
2.458DCPPv4: Spectra for $M_W = 7.5$, $R_x = -1.$, $F = 0$ . . . 235
2.459DCPPv4: Spectra for $M_W = 7.5$, $R_x = -5.$, $F = 0$ . . . 235
2.460DCPPv4: Spectra for $M_W = 7.5$, $R_x = -10$, $F = 0$ . . . 236
2.461DCPPv4: Spectra for $M_W = 5.5$, $R_x = -1.$, $F = 1$ . . . 236
2.462DCPPv4: Spectra for $M_W = 5.5$, $R_x = -5.$, $F = 1$ . . . 237
2.463DCPPv4: Spectra for $M_W = 5.5$, $R_x = -10$, $F = 1$ . . . 237
2.464DCPPv4: Spectra for $M_W = 6.5$, $R_x = -1.$, $F = 1$ . . . 238
2.465DCPPv4: Spectra for $M_W = 6.5$, $R_x = -5.$, $F = 1$ . . . 238
2.466DCPPv4: Spectra for $M_W = 6.5$, $R_x = -10$, $F = 1$ . . . 239
2.467DCPPv4: Spectra for $M_W = 7.5$, $R_x = -1.$, $F = 1$ . . . 239
2.468DCPPv4: Spectra for $M_W = 7.5$, $R_x = -5.$, $F = 1$ . . . 240
2.469DCPPv4: Spectra for $M_W = 7.5$, $R_x = -10$, $F = 1$ . . . 240
2.470DCPPv4Histogram of differences for medians calculated with different weights to median calculated with total weights. Bottom row left shows differences between medians for the GMPE distribution to median calculated with total weights. Bottom row right shows differences between the original GMPEs (without uncertainty) to median calculated with total weights. For DCPP4, ModelA and $T = 0.01$s. . . . 241
2.471DCPPv4Histogram of differences for medians calculated with different weights to median calculated with total weights. Bottom row left shows differences between medians for the GMPE distribution to median calculated with total weights. Bottom row right shows differences between the original GMPEs (without uncertainty) to median calculated with total weights. For DCPP4, ModelA and $T = 0.02$s. . . . 242
2.472DCPPv4Histogram of differences for medians calculated with different weights to median calculated with total weights. Bottom row left shows differences between medians for the GMPE distribution to median calculated with total weights. Bottom row right shows differences between the original GMPEs (without uncertainty) to median calculated with total weights. For DCPP4, ModelA and $T = 0.03$s. . . . 243
2.473DCPPv4Histogram of differences for medians calculated with different weights to median calculated with total weights. Bottom row left shows differences between medians for the GMPE distribution to median calculated with total weights. Bottom row right shows differences between the original GMPEs (without uncertainty) to median calculated with total weights. For DCPP4, ModelA and $T = 0.05$s. . . . 244

2.474 DCPPv4 Histogram of differences for medians calculated with different weights to median calculated with total weights. Bottom row left shows differences between medians for the GMPE distribution to median calculated with total weights. Bottom row right shows differences between the original GMPEs (without uncertainty) to median calculated with total weights. For DCPP4, ModelA and $T = 0.075$s. . . . . 245
2.475 DCPPv4 Histogram of differences for medians calculated with different weights to median calculated with total weights. Bottom row left shows differences between medians for the GMPE distribution to median calculated with total weights. Bottom row right shows differences between the original GMPEs (without uncertainty) to median calculated with total weights. For DCPP4, ModelA and $T = 0.1$s. . . . . 246
2.476 DCPPv4 Histogram of differences for medians calculated with different weights to median calculated with total weights. Bottom row left shows differences between medians for the GMPE distribution to median calculated with total weights. Bottom row right shows differences between the original GMPEs (without uncertainty) to median calculated with total weights. For DCPP4, ModelA and $T = 0.15$s. . . . . 247
2.477 DCPPv4 Histogram of differences for medians calculated with different weights to median calculated with total weights. Bottom row left shows differences between medians for the GMPE distribution to median calculated with total weights. Bottom row right shows differences between the original GMPEs (without uncertainty) to median calculated with total weights. For DCPP4, ModelA and $T = 0.2$s. . . . . 248
2.478 DCPPv4 Histogram of differences for medians calculated with different weights to median calculated with total weights. Bottom row left shows differences between medians for the GMPE distribution to median calculated with total weights. Bottom row right shows differences between the original GMPEs (without uncertainty) to median calculated with total weights. For DCPP4, ModelA and $T = 0.25$s. . . . . 249
2.479 DCPPv4 Histogram of differences for medians calculated with different weights to median calculated with total weights. Bottom row left shows differences between medians for the GMPE distribution to median calculated with total weights. Bottom row right shows differences between the original GMPEs (without uncertainty) to median calculated with total weights. For DCPP4, ModelA and $T = 0.3$s. . . . . 250
2.480 DCPPv4 Histogram of differences for medians calculated with different weights to median calculated with total weights. Bottom row left shows differences between medians for the GMPE distribution to median calculated with total weights. Bottom row right shows differences between the original GMPEs (without uncertainty) to median calculated with total weights. For DCPP4, ModelA and $T = 0.4$s. . . . . 251
2.481 DCPPv4 Histogram of differences for medians calculated with different weights to median calculated with total weights. Bottom row left shows differences between medians for the GMPE distribution to median calculated with total weights. Bottom row right shows differences between the original GMPEs (without uncertainty) to median calculated with total weights. For DCPP4, ModelA and $T = 0.5$s. . . . . 252
2.482 DCPPv4 Histogram of differences for medians calculated with different weights to median calculated with total weights. Bottom row left shows differences between medians for the GMPE distribution to median calculated with total weights. Bottom row right shows differences between the original GMPEs (without uncertainty) to median calculated with total weights. For DCPP4, ModelA and $T = 0.75$s. . . . . 253
2.483 DCPPv4 Histogram of differences for medians calculated with different weights to median calculated with total weights. Bottom row left shows differences between medians for the GMPE distribution to median calculated with total weights. Bottom row right shows differences between the original GMPEs (without uncertainty) to median calculated with total weights. For DCPP4, ModelA and $T = 1$.s. . . . . 254
2.484 DCPPv4 Histogram of differences for medians calculated with different weights to median calculated with total weights. Bottom row left shows differences between medians for the GMPE distribution to median calculated with total weights. Bottom row right shows differences between the original GMPEs (without uncertainty) to median calculated with total weights. For DCPP4, ModelA and $T = 1.5$s. . . . . 255
2.485 DCPPv4 Histogram of differences for medians calculated with different weights to median calculated with total weights. Bottom row left shows differences between medians for the GMPE distribution to median calculated with total weights. Bottom row right shows differences between the original GMPEs (without uncertainty) to median calculated with total weights. For DCPP4, ModelA and $T = 2$.s. . . . . 256
2.486 DCPPv4 Histogram of differences for medians calculated with different weights to median calculated with total weights. Bottom row left shows differences between medians for the GMPE distribution to median calculated with total weights. Bottom row right shows differences between the original GMPEs (without uncertainty) to median calculated with total weights. For DCPP4, ModelA and $T = 3$.s. . . . . 257

3.1 PVNGSv2: Deaggregation for a ground-motion level of 0.001g, calculated using a simple source model for PVNGS2 and the center model of the ModelA distribution. For $T = 0.01$s. . . . . 258
3.2 PVNGSv2: Deaggregation for a ground-motion level of 0.001g, calculated using a simple source model for PVNGS2 and the center model of the ModelA distribution. For $T = 0.02$s. . . . . 259
3.3 PVNGSv2: Deaggregation for a ground-motion level of 0.001g, calculated using a simple source model for PVNGS2 and the center model of the ModelA distribution. For $T = 0.03$s. . . . . 259
3.4 PVNGSv2: Deaggregation for a ground-motion level of 0.001g, calculated using a simple source model for PVNGS2 and the center model of the ModelA distribution. For $T = 0.05$s. . . . . 260

3.5 PVNGSv2: Deaggregation for a ground-motion level of 0.001g, calculated using a simple source model for PVNGS2 and the center model of the ModelA distribution. For $T = 0.075$s. . . . . 260
3.6 PVNGSv2: Deaggregation for a ground-motion level of 0.001g, calculated using a simple source model for PVNGS2 and the center model of the ModelA distribution. For $T = 0.1$s. . . . . 261
3.7 PVNGSv2: Deaggregation for a ground-motion level of 0.001g, calculated using a simple source model for PVNGS2 and the center model of the ModelA distribution. For $T = 0.15$s. . . . . 261
3.8 PVNGSv2: Deaggregation for a ground-motion level of 0.001g, calculated using a simple source model for PVNGS2 and the center model of the ModelA distribution. For $T = 0.2$s. . . . . 262
3.9 PVNGSv2: Deaggregation for a ground-motion level of 0.001g, calculated using a simple source model for PVNGS2 and the center model of the ModelA distribution. For $T = 0.25$s. . . . . 262
3.10 PVNGSv2: Deaggregation for a ground-motion level of 0.001g, calculated using a simple source model for PVNGS2 and the center model of the ModelA distribution. For $T = 0.3$s. . . . . 263
3.11 PVNGSv2: Deaggregation for a ground-motion level of 0.001g, calculated using a simple source model for PVNGS2 and the center model of the ModelA distribution. For $T = 0.4$s. . . . . 263
3.12 PVNGSv2: Deaggregation for a ground-motion level of 0.001g, calculated using a simple source model for PVNGS2 and the center model of the ModelA distribution. For $T = 0.5$s. . . . . 264
3.13 PVNGSv2: Deaggregation for a ground-motion level of 0.001g, calculated using a simple source model for PVNGS2 and the center model of the ModelA distribution. For $T = 0.75$s. . . . . 264
3.14 PVNGSv2: Deaggregation for a ground-motion level of 0.g, calculated using a simple source model for PVNGS2 and the center model of the ModelA distribution. For $T = 1$.s. . . . . 265
3.15 PVNGSv2: Deaggregation for a ground-motion level of 0.g, calculated using a simple source model for PVNGS2 and the center model of the ModelA distribution. For $T = 1.5$s. . . . . 265
3.16 PVNGSv2: Deaggregation for a ground-motion level of 0.g, calculated using a simple source model for PVNGS2 and the center model of the ModelA distribution. For $T = 2$.s. . . . . 266
3.17 PVNGSv2: Deaggregation for a ground-motion level of 0.g, calculated using a simple source model for PVNGS2 and the center model of the ModelA distribution. For $T = 3$.s. . . . . 266
3.18 PVNGSv2: Deaggregation for a ground-motion level of 0.278g, calculated using a simple source model for PVNGS2 and the center model of the ModelA distribution. For $T = 0.01$s. . . . . 267
3.19 PVNGSv2: Deaggregation for a ground-motion level of 0.266g, calculated using a simple source model for PVNGS2 and the center model of the ModelA distribution. For $T = 0.02$s. . . . . 267
3.20 PVNGSv2: Deaggregation for a ground-motion level of 0.29g, calculated using a simple source model for PVNGS2 and the center model of the ModelA distribution. For $T = 0.03$s. . . . . 268
3.21 PVNGSv2: Deaggregation for a ground-motion level of 0.358g, calculated using a simple source model for PVNGS2 and the center model of the ModelA distribution. For $T = 0.05$s. . . . . 268
3.22 PVNGSv2: Deaggregation for a ground-motion level of 0.407g, calculated using a simple source model for PVNGS2 and the center model of the ModelA distribution. For $T = 0.075$s. . . . . 269
3.23 PVNGSv2: Deaggregation for a ground-motion level of 0.427g, calculated using a simple source model for PVNGS2 and the center model of the ModelA distribution. For $T = 0.1$s. . . . . 269
3.24 PVNGSv2: Deaggregation for a ground-motion level of 0.475g, calculated using a simple source model for PVNGS2 and the center model of the ModelA distribution. For $T = 0.15$s. . . . . 270
3.25 PVNGSv2: Deaggregation for a ground-motion level of 0.456g, calculated using a simple source model for PVNGS2 and the center model of the ModelA distribution. For $T = 0.2$s. . . . . 270
3.26 PVNGSv2: Deaggregation for a ground-motion level of 0.427g, calculated using a simple source model for PVNGS2 and the center model of the ModelA distribution. For $T = 0.25$s. . . . . 271
3.27 PVNGSv2: Deaggregation for a ground-motion level of 0.387g, calculated using a simple source model for PVNGS2 and the center model of the ModelA distribution. For $T = 0.3$s. . . . . 271
3.28 PVNGSv2: Deaggregation for a ground-motion level of 0.358g, calculated using a simple source model for PVNGS2 and the center model of the ModelA distribution. For $T = 0.4$s. . . . . 272
3.29 PVNGSv2: Deaggregation for a ground-motion level of 0.313g, calculated using a simple source model for PVNGS2 and the center model of the ModelA distribution. For $T = 0.5$s. . . . . 272
3.30 PVNGSv2: Deaggregation for a ground-motion level of 0.214g, calculated using a simple source model for PVNGS2 and the center model of the ModelA distribution. For $T = 0.75$s. . . . . 273
3.31 PVNGSv2: Deaggregation for a ground-motion level of 0.139g, calculated using a simple source model for PVNGS2 and the center model of the ModelA distribution. For $T = 1$.s. . . . . 273
3.32 PVNGSv2: Deaggregation for a ground-motion level of 0.098g, calculated using a simple source model for PVNGS2 and the center model of the ModelA distribution. For $T = 1.5$s. . . . . 274
3.33 PVNGSv2: Deaggregation for a ground-motion level of 0.075g, calculated using a simple source model for PVNGS2 and the center model of the ModelA distribution. For $T = 2$.s. . . . . 274
3.34 PVNGSv2: Deaggregation for a ground-motion level of 0.043g, calculated using a simple source model for PVNGS2 and the center model of the ModelA distribution. For $T = 3$.s. . . . . 275
3.35 PVNGSv2: Contour Plots used for selection. For $T = 0.01$s. . . . . 276

3.36 PVNGSv2: Contour Plots used for selection. For $T = 0.02$s. . . . 277
3.37 PVNGSv2: Contour Plots used for selection. For $T = 0.03$s. . . . 278
3.38 PVNGSv2: Contour Plots used for selection. For $T = 0.05$s. . . . 279
3.39 PVNGSv2: Contour Plots used for selection. For $T = 0.075$s. . . . 280
3.40 PVNGSv2: Contour Plots used for selection. For $T = 0.1$s. . . . 281
3.41 PVNGSv2: Contour Plots used for selection. For $T = 0.15$s. . . . 282
3.42 PVNGSv2: Contour Plots used for selection. For $T = 0.2$s. . . . 283
3.43 PVNGSv2: Contour Plots used for selection. For $T = 0.25$s. . . . 284
3.44 PVNGSv2: Contour Plots used for selection. For $T = 0.3$s. . . . 285
3.45 PVNGSv2: Contour Plots used for selection. For $T = 0.4$s. . . . 286
3.46 PVNGSv2: Contour Plots used for selection. For $T = 0.5$s. . . . 287
3.47 PVNGSv2: Contour Plots used for selection. For $T = 0.75$s. . . . 288
3.48 PVNGSv2: Contour Plots used for selection. For $T = 1.$s. . . . 289
3.49 PVNGSv2: Contour Plots used for selection. For $T = 1.5$s. . . . 290
3.50 PVNGSv2: Contour Plots used for selection. For $T = 2.$s. . . . 291
3.51 PVNGSv2: Contour Plots used for selection. For $T = 3.$s. . . . 292
3.52 PVNGSv2: Contour Plots used for weighting. For $T = 0.01, 0.02, 0.03, 0.05, 0.075, 0.1, 0.15, 0.2, 0.25, 0.3, 0.4, 0.5, 0.75, 1.,$
3.53 PVNGSv2: Contour Plots used for weighting. For $T = 0.01, 0.02, 0.03, 0.05, 0.075, 0.1, 0.15, 0.2, 0.25, 0.3, 0.4, 0.5, 0.75, 1.,$
3.54 PVNGSv2: Contour Plots used for weighting. For $T = 0.01, 0.02, 0.03, 0.05, 0.075, 0.1, 0.15, 0.2, 0.25, 0.3, 0.4, 0.5, 0.75, 1.,$
3.55 PVNGSv2: Contour Plots used for weighting. For $T = 0.01, 0.02, 0.03, 0.05, 0.075, 0.1, 0.15, 0.2, 0.25, 0.3, 0.4, 0.5, 0.75, 1.,$
3.56 PVNGSv2: Contour Plots used for weighting. For $T = 0.01, 0.02, 0.03, 0.05, 0.075, 0.1, 0.15, 0.2, 0.25, 0.3, 0.4, 0.5, 0.75, 1.,$
3.57 PVNGSv2: Contour Plots used for weighting. For $T = 0.01, 0.02, 0.03, 0.05, 0.075, 0.1, 0.15, 0.2, 0.25, 0.3, 0.4, 0.5, 0.75, 1.,$
3.58 PVNGSv2: Contour Plots used for weighting. For $T = 0.01, 0.02, 0.03, 0.05, 0.075, 0.1, 0.15, 0.2, 0.25, 0.3, 0.4, 0.5, 0.75, 1.,$
3.59 PVNGSv2: Contour Plots used for weighting. For $T = 0.01, 0.02, 0.03, 0.05, 0.075, 0.1, 0.15, 0.2, 0.25, 0.3, 0.4, 0.5, 0.75, 1.,$
3.60 PVNGSv2: Contour Plots used for weighting. For $T = 0.01, 0.02, 0.03, 0.05, 0.075, 0.1, 0.15, 0.2, 0.25, 0.3, 0.4, 0.5, 0.75, 1.,$
3.61 PVNGSv2: Contour Plots used for weighting. For $T = 0.01, 0.02, 0.03, 0.05, 0.075, 0.1, 0.15, 0.2, 0.25, 0.3, 0.4, 0.5, 0.75, 1.,$
3.62 PVNGSv2: Contour Plots used for weighting. For $T = 0.01, 0.02, 0.03, 0.05, 0.075, 0.1, 0.15, 0.2, 0.25, 0.3, 0.4, 0.5, 0.75, 1.,$
3.63 PVNGSv2: Contour Plots used for weighting. For $T = 0.01, 0.02, 0.03, 0.05, 0.075, 0.1, 0.15, 0.2, 0.25, 0.3, 0.4, 0.5, 0.75, 1.,$
3.64 PVNGSv2: Contour Plots used for weighting. For $T = 0.01, 0.02, 0.03, 0.05, 0.075, 0.1, 0.15, 0.2, 0.25, 0.3, 0.4, 0.5, 0.75, 1.,$
3.65 PVNGSv2: Contour Plots used for weighting. For $T = 0.01, 0.02, 0.03, 0.05, 0.075, 0.1, 0.15, 0.2, 0.25, 0.3, 0.4, 0.5, 0.75, 1.,$
3.66 PVNGSv2: Contour Plots used for weighting. For $T = 0.01, 0.02, 0.03, 0.05, 0.075, 0.1, 0.15, 0.2, 0.25, 0.3, 0.4, 0.5, 0.75, 1.,$
3.67 PVNGSv2: Contour Plots used for weighting. For $T = 0.01, 0.02, 0.03, 0.05, 0.075, 0.1, 0.15, 0.2, 0.25, 0.3, 0.4, 0.5, 0.75, 1.,$
3.68 PVNGSv2: Contour Plots used for weighting. For $T = 0.01, 0.02, 0.03, 0.05, 0.075, 0.1, 0.15, 0.2, 0.25, 0.3, 0.4, 0.5, 0.75, 1.,$
3.69 Hazard curves, calculated for a simple source model for PVNGS2. Left: 2000 hazard curves for all sampled A-models (gray) and the center model of the ModelA distribution (red); Right: hazard curves of selected models. For $T = 0.01$s. . . . 310
3.70 Hazard curves, calculated for a simple source model for PVNGS2. Left: 2000 hazard curves for all sampled A-models (gray) and the center model of the ModelA distribution (red); Right: hazard curves of selected models. For $T = 0.02$s. . . . 310
3.71 Hazard curves, calculated for a simple source model for PVNGS2. Left: 2000 hazard curves for all sampled A-models (gray) and the center model of the ModelA distribution (red); Right: hazard curves of selected models. For $T = 0.03$s. . . . 311
3.72 Hazard curves, calculated for a simple source model for PVNGS2. Left: 2000 hazard curves for all sampled A-models (gray) and the center model of the ModelA distribution (red); Right: hazard curves of selected models. For $T = 0.05$s. . . . 311
3.73 Hazard curves, calculated for a simple source model for PVNGS2. Left: 2000 hazard curves for all sampled A-models (gray) and the center model of the ModelA distribution (red); Right: hazard curves of selected models. For $T = 0.075$s. . . . 312
3.74 Hazard curves, calculated for a simple source model for PVNGS2. Left: 2000 hazard curves for all sampled A-models (gray) and the center model of the ModelA distribution (red); Right: hazard curves of selected models. For $T = 0.1$s. . . . 312
3.75 Hazard curves, calculated for a simple source model for PVNGS2. Left: 2000 hazard curves for all sampled A-models (gray) and the center model of the ModelA distribution (red); Right: hazard curves of selected models. For $T = 0.15$s. . . . 313
3.76 Hazard curves, calculated for a simple source model for PVNGS2. Left: 2000 hazard curves for all sampled A-models (gray) and the center model of the ModelA distribution (red); Right: hazard curves of selected models. For $T = 0.2$s. . . . 313
3.77 Hazard curves, calculated for a simple source model for PVNGS2. Left: 2000 hazard curves for all sampled A-models (gray) and the center model of the ModelA distribution (red); Right: hazard curves of selected models. For $T = 0.25$s. . . . 314

3.78 Hazard curves, calculated for a simple source model for PVNGS2. Left: 2000 hazard curves for all sampled A-models (gray) and the center model of the ModelA distribution (red); Right: hazard curves of selected models. For $T = 0.3$s. . . . 314
3.79 Hazard curves, calculated for a simple source model for PVNGS2. Left: 2000 hazard curves for all sampled A-models (gray) and the center model of the ModelA distribution (red); Right: hazard curves of selected models. For $T = 0.4$s. . . . 315
3.80 Hazard curves, calculated for a simple source model for PVNGS2. Left: 2000 hazard curves for all sampled A-models (gray) and the center model of the ModelA distribution (red); Right: hazard curves of selected models. For $T = 0.5$s. . . . 315
3.81 Hazard curves, calculated for a simple source model for PVNGS2. Left: 2000 hazard curves for all sampled A-models (gray) and the center model of the ModelA distribution (red); Right: hazard curves of selected models. For $T = 0.75$s. . . . 316
3.82 Hazard curves, calculated for a simple source model for PVNGS2. Left: 2000 hazard curves for all sampled A-models (gray) and the center model of the ModelA distribution (red); Right: hazard curves of selected models. For $T = 1$.s. . . . 316
3.83 Hazard curves, calculated for a simple source model for PVNGS2. Left: 2000 hazard curves for all sampled A-models (gray) and the center model of the ModelA distribution (red); Right: hazard curves of selected models. For $T = 1.5$s. . . . 317
3.84 Hazard curves, calculated for a simple source model for PVNGS2. Left: 2000 hazard curves for all sampled A-models (gray) and the center model of the ModelA distribution (red); Right: hazard curves of selected models. For $T = 2$.s. . . . 317
3.85 Hazard curves, calculated for a simple source model for PVNGS2. Left: 2000 hazard curves for all sampled A-models (gray) and the center model of the ModelA distribution (red); Right: hazard curves of selected models. For $T = 3$.s. . . . 318
3.86 PVNGSv2: CDF for $M = 5.$, $R_x = -50.$, $F = 0$, and $T = 0.01$ . . . 319
3.87 PVNGSv2: CDF for $M = 5.$, $R_x = -30.$, $F = 0$, and $T = 0.01$ . . . 319
3.88 PVNGSv2: CDF for $M = 5.$, $R_x = -15.$, $F = 0$, and $T = 0.01$ . . . 320
3.89 PVNGSv2: CDF for $M = 5.$, $R_x = -5.$, $F = 0$, and $T = 0.01$ . . . 320
3.90 PVNGSv2: CDF for $M = 5.$, $R_x = 5.$, $F = 0$, and $T = 0.01$ . . . 320
3.91 PVNGSv2: CDF for $M = 5.$, $R_x = 15.$, $F = 0$, and $T = 0.01$ . . . 321
3.92 PVNGSv2: CDF for $M = 6.$, $R_x = -50.$, $F = 0$, and $T = 0.01$ . . . 322
3.93 PVNGSv2: CDF for $M = 6.$, $R_x = -30.$, $F = 0$, and $T = 0.01$ . . . 322
3.94 PVNGSv2: CDF for $M = 6.$, $R_x = -15.$, $F = 0$, and $T = 0.01$ . . . 323
3.95 PVNGSv2: CDF for $M = 6.$, $R_x = -5.$, $F = 0$, and $T = 0.01$ . . . 323
3.96 PVNGSv2: CDF for $M = 6.$, $R_x = 5.$, $F = 0$, and $T = 0.01$ . . . 323
3.97 PVNGSv2: CDF for $M = 6.$, $R_x = 15.$, $F = 0$, and $T = 0.01$ . . . 324
3.98 PVNGSv2: CDF for $M = 7.$, $R_x = -50.$, $F = 0$, and $T = 0.01$ . . . 325
3.99 PVNGSv2: CDF for $M = 7.$, $R_x = -30.$, $F = 0$, and $T = 0.01$ . . . 325
3.100 PVNGSv2: CDF for $M = 7.$, $R_x = -15.$, $F = 0$, and $T = 0.01$ . . . 326
3.101 PVNGSv2: CDF for $M = 7.$, $R_x = -5.$, $F = 0$, and $T = 0.01$ . . . 326
3.102 PVNGSv2: CDF for $M = 7.$, $R_x = 5.$, $F = 0$, and $T = 0.01$ . . . 326
3.103 PVNGSv2: CDF for $M = 7.$, $R_x = 15.$, $F = 0$, and $T = 0.01$ . . . 327
3.104 PVNGSv2: CDF for $M = 5.$, $R_x = -50.$, $F = -1$, and $T = 0.01$ . . . 328
3.105 PVNGSv2: CDF for $M = 5.$, $R_x = -30.$, $F = -1$, and $T = 0.01$ . . . 328
3.106 PVNGSv2: CDF for $M = 5.$, $R_x = -15.$, $F = -1$, and $T = 0.01$ . . . 329
3.107 PVNGSv2: CDF for $M = 5.$, $R_x = -5.$, $F = -1$, and $T = 0.01$ . . . 329
3.108 PVNGSv2: CDF for $M = 5.$, $R_x = 5.$, $F = -1$, and $T = 0.01$ . . . 329
3.109 PVNGSv2: CDF for $M = 5.$, $R_x = 15.$, $F = -1$, and $T = 0.01$ . . . 330
3.110 PVNGSv2: CDF for $M = 6.$, $R_x = -50.$, $F = -1$, and $T = 0.01$ . . . 331
3.111 PVNGSv2: CDF for $M = 6.$, $R_x = -30.$, $F = -1$, and $T = 0.01$ . . . 331
3.112 PVNGSv2: CDF for $M = 6.$, $R_x = -15.$, $F = -1$, and $T = 0.01$ . . . 332
3.113 PVNGSv2: CDF for $M = 6.$, $R_x = -5.$, $F = -1$, and $T = 0.01$ . . . 332
3.114 PVNGSv2: CDF for $M = 6.$, $R_x = 5.$, $F = -1$, and $T = 0.01$ . . . 332
3.115 PVNGSv2: CDF for $M = 6.$, $R_x = 15.$, $F = -1$, and $T = 0.01$ . . . 333
3.116 PVNGSv2: CDF for $M = 7.$, $R_x = -50.$, $F = -1$, and $T = 0.01$ . . . 334
3.117 PVNGSv2: CDF for $M = 7.$, $R_x = -30.$, $F = -1$, and $T = 0.01$ . . . 334
3.118 PVNGSv2: CDF for $M = 7.$, $R_x = -15.$, $F = -1$, and $T = 0.01$ . . . 335
3.119 PVNGSv2: CDF for $M = 7.$, $R_x = -5.$, $F = -1$, and $T = 0.01$ . . . 335
3.120 PVNGSv2: CDF for $M = 7.$, $R_x = 5.$, $F = -1$, and $T = 0.01$ . . . 335
3.121 PVNGSv2: CDF for $M = 7.$, $R_x = 15.$, $F = -1$, and $T = 0.01$ . . . 336
3.122 PVNGSv2: CDF for $M = 5.$, $R_x = -50.$, $F = 0$, and $T = 0.2$ . . . 337

3.123PVNGSv2: CDF for $M = 5.$, $R_x = -30.$, $F = 0$, and $T = 0.2$ . . . 337
3.124PVNGSv2: CDF for $M = 5.$, $R_x = -15.$, $F = 0$, and $T = 0.2$ . . . 338
3.125PVNGSv2: CDF for $M = 5.$, $R_x = -5.$, $F = 0$, and $T = 0.2$ . . . 338
3.126PVNGSv2: CDF for $M = 5.$, $R_x = 5.$, $F = 0$, and $T = 0.2$ . . . 338
3.127PVNGSv2: CDF for $M = 5.$, $R_x = 15.$, $F = 0$, and $T = 0.2$ . . . 339
3.128PVNGSv2: CDF for $M = 6.$, $R_x = -50.$, $F = 0$, and $T = 0.2$ . . . 340
3.129PVNGSv2: CDF for $M = 6.$, $R_x = -30.$, $F = 0$, and $T = 0.2$ . . . 340
3.130PVNGSv2: CDF for $M = 6.$, $R_x = -15.$, $F = 0$, and $T = 0.2$ . . . 341
3.131PVNGSv2: CDF for $M = 6.$, $R_x = -5.$, $F = 0$, and $T = 0.2$ . . . 341
3.132PVNGSv2: CDF for $M = 6.$, $R_x = 5.$, $F = 0$, and $T = 0.2$ . . . 341
3.133PVNGSv2: CDF for $M = 6.$, $R_x = 15.$, $F = 0$, and $T = 0.2$ . . . 342
3.134PVNGSv2: CDF for $M = 7.$, $R_x = -50.$, $F = 0$, and $T = 0.2$ . . . 343
3.135PVNGSv2: CDF for $M = 7.$, $R_x = -30.$, $F = 0$, and $T = 0.2$ . . . 343
3.136PVNGSv2: CDF for $M = 7.$, $R_x = -15.$, $F = 0$, and $T = 0.2$ . . . 344
3.137PVNGSv2: CDF for $M = 7.$, $R_x = -5.$, $F = 0$, and $T = 0.2$ . . . 344
3.138PVNGSv2: CDF for $M = 7.$, $R_x = 5.$, $F = 0$, and $T = 0.2$ . . . 344
3.139PVNGSv2: CDF for $M = 7.$, $R_x = 15.$, $F = 0$, and $T = 0.2$ . . . 345
3.140PVNGSv2: CDF for $M = 5.$, $R_x = -50.$, $F = -1$, and $T = 0.2$ . . . 346
3.141PVNGSv2: CDF for $M = 5.$, $R_x = -30.$, $F = -1$, and $T = 0.2$ . . . 346
3.142PVNGSv2: CDF for $M = 5.$, $R_x = -15.$, $F = -1$, and $T = 0.2$ . . . 347
3.143PVNGSv2: CDF for $M = 5.$, $R_x = -5.$, $F = -1$, and $T = 0.2$ . . . 347
3.144PVNGSv2: CDF for $M = 5.$, $R_x = 5.$, $F = -1$, and $T = 0.2$ . . . 347
3.145PVNGSv2: CDF for $M = 5.$, $R_x = 15.$, $F = -1$, and $T = 0.2$ . . . 348
3.146PVNGSv2: CDF for $M = 6.$, $R_x = -50.$, $F = -1$, and $T = 0.2$ . . . 349
3.147PVNGSv2: CDF for $M = 6.$, $R_x = -30.$, $F = -1$, and $T = 0.2$ . . . 349
3.148PVNGSv2: CDF for $M = 6.$, $R_x = -15.$, $F = -1$, and $T = 0.2$ . . . 350
3.149PVNGSv2: CDF for $M = 6.$, $R_x = -5.$, $F = -1$, and $T = 0.2$ . . . 350
3.150PVNGSv2: CDF for $M = 6.$, $R_x = 5.$, $F = -1$, and $T = 0.2$ . . . 350
3.151PVNGSv2: CDF for $M = 6.$, $R_x = 15.$, $F = -1$, and $T = 0.2$ . . . 351
3.152PVNGSv2: CDF for $M = 7.$, $R_x = -50.$, $F = -1$, and $T = 0.2$ . . . 352
3.153PVNGSv2: CDF for $M = 7.$, $R_x = -30.$, $F = -1$, and $T = 0.2$ . . . 352
3.154PVNGSv2: CDF for $M = 7.$, $R_x = -15.$, $F = -1$, and $T = 0.2$ . . . 353
3.155PVNGSv2: CDF for $M = 7.$, $R_x = -5.$, $F = -1$, and $T = 0.2$ . . . 353
3.156PVNGSv2: CDF for $M = 7.$, $R_x = 5.$, $F = -1$, and $T = 0.2$ . . . 353
3.157PVNGSv2: CDF for $M = 7.$, $R_x = 15.$, $F = -1$, and $T = 0.2$ . . . 354
3.158PVNGSv2: CDF for $M = 5.$, $R_x = -50.$, $F = 0$, and $T = 0.5$ . . . 355
3.159PVNGSv2: CDF for $M = 5.$, $R_x = -30.$, $F = 0$, and $T = 0.5$ . . . 355
3.160PVNGSv2: CDF for $M = 5.$, $R_x = -15.$, $F = 0$, and $T = 0.5$ . . . 356
3.161PVNGSv2: CDF for $M = 5.$, $R_x = -5.$, $F = 0$, and $T = 0.5$ . . . 356
3.162PVNGSv2: CDF for $M = 5.$, $R_x = 5.$, $F = 0$, and $T = 0.5$ . . . 356
3.163PVNGSv2: CDF for $M = 5.$, $R_x = 15.$, $F = 0$, and $T = 0.5$ . . . 357
3.164PVNGSv2: CDF for $M = 6.$, $R_x = -50.$, $F = 0$, and $T = 0.5$ . . . 358
3.165PVNGSv2: CDF for $M = 6.$, $R_x = -30.$, $F = 0$, and $T = 0.5$ . . . 358
3.166PVNGSv2: CDF for $M = 6.$, $R_x = -15.$, $F = 0$, and $T = 0.5$ . . . 359
3.167PVNGSv2: CDF for $M = 6.$, $R_x = -5.$, $F = 0$, and $T = 0.5$ . . . 359
3.168PVNGSv2: CDF for $M = 6.$, $R_x = 5.$, $F = 0$, and $T = 0.5$ . . . 359
3.169PVNGSv2: CDF for $M = 6.$, $R_x = 15.$, $F = 0$, and $T = 0.5$ . . . 360
3.170PVNGSv2: CDF for $M = 7.$, $R_x = -50.$, $F = 0$, and $T = 0.5$ . . . 361
3.171PVNGSv2: CDF for $M = 7.$, $R_x = -30.$, $F = 0$, and $T = 0.5$ . . . 361
3.172PVNGSv2: CDF for $M = 7.$, $R_x = -15.$, $F = 0$, and $T = 0.5$ . . . 362
3.173PVNGSv2: CDF for $M = 7.$, $R_x = -5.$, $F = 0$, and $T = 0.5$ . . . 362
3.174PVNGSv2: CDF for $M = 7.$, $R_x = 5.$, $F = 0$, and $T = 0.5$ . . . 362
3.175PVNGSv2: CDF for $M = 7.$, $R_x = 15.$, $F = 0$, and $T = 0.5$ . . . 363
3.176PVNGSv2: CDF for $M = 5.$, $R_x = -50.$, $F = -1$, and $T = 0.5$ . . . 364
3.177PVNGSv2: CDF for $M = 5.$, $R_x = -30.$, $F = -1$, and $T = 0.5$ . . . 364
3.178PVNGSv2: CDF for $M = 5.$, $R_x = -15.$, $F = -1$, and $T = 0.5$ . . . 365
3.179PVNGSv2: CDF for $M = 5.$, $R_x = -5.$, $F = -1$, and $T = 0.5$ . . . 365
3.180PVNGSv2: CDF for $M = 5.$, $R_x = 5.$, $F = -1$, and $T = 0.5$ . . . 365
3.181PVNGSv2: CDF for $M = 5.$, $R_x = 15.$, $F = -1$, and $T = 0.5$ . . . 366
3.182PVNGSv2: CDF for $M = 6.$, $R_x = -50.$, $F = -1$, and $T = 0.5$ . . . 367
3.183PVNGSv2: CDF for $M = 6.$, $R_x = -30.$, $F = -1$, and $T = 0.5$ . . . 367

3.184PVNGSv2: CDF for $M = 6.$, $R_x = -15.$, $F = -1$, and $T = 0.5$ . . . 368
3.185PVNGSv2: CDF for $M = 6.$, $R_x = -5.$, $F = -1$, and $T = 0.5$ . . . 368
3.186PVNGSv2: CDF for $M = 6.$, $R_x = 5.$, $F = -1$, and $T = 0.5$ . . . 368
3.187PVNGSv2: CDF for $M = 6.$, $R_x = 15.$, $F = -1$, and $T = 0.5$ . . . 369
3.188PVNGSv2: CDF for $M = 7.$, $R_x = -50.$, $F = -1$, and $T = 0.5$ . . . 370
3.189PVNGSv2: CDF for $M = 7.$, $R_x = -30.$, $F = -1$, and $T = 0.5$ . . . 370
3.190PVNGSv2: CDF for $M = 7.$, $R_x = -15.$, $F = -1$, and $T = 0.5$ . . . 371
3.191PVNGSv2: CDF for $M = 7.$, $R_x = -5.$, $F = -1$, and $T = 0.5$ . . . 371
3.192PVNGSv2: CDF for $M = 7.$, $R_x = 5.$, $F = -1$, and $T = 0.5$ . . . 371
3.193PVNGSv2: CDF for $M = 7.$, $R_x = 15.$, $F = -1$, and $T = 0.5$ . . . 372
3.194PVNGSv2: CDF for $M = 5.$, $R_x = -50.$, $F = 0$, and $T = 1.$ . . . 373
3.195PVNGSv2: CDF for $M = 5.$, $R_x = -30.$, $F = 0$, and $T = 1.$ . . . 373
3.196PVNGSv2: CDF for $M = 5.$, $R_x = -15.$, $F = 0$, and $T = 1.$ . . . 374
3.197PVNGSv2: CDF for $M = 5.$, $R_x = -5.$, $F = 0$, and $T = 1.$ . . . 374
3.198PVNGSv2: CDF for $M = 5.$, $R_x = 5.$, $F = 0$, and $T = 1.$ . . . 374
3.199PVNGSv2: CDF for $M = 5.$, $R_x = 15.$, $F = 0$, and $T = 1.$ . . . 375
3.200PVNGSv2: CDF for $M = 6.$, $R_x = -50.$, $F = 0$, and $T = 1.$ . . . 376
3.201PVNGSv2: CDF for $M = 6.$, $R_x = -30.$, $F = 0$, and $T = 1.$ . . . 376
3.202PVNGSv2: CDF for $M = 6.$, $R_x = -15.$, $F = 0$, and $T = 1.$ . . . 377
3.203PVNGSv2: CDF for $M = 6.$, $R_x = -5.$, $F = 0$, and $T = 1.$ . . . 377
3.204PVNGSv2: CDF for $M = 6.$, $R_x = 5.$, $F = 0$, and $T = 1.$ . . . 377
3.205PVNGSv2: CDF for $M = 6.$, $R_x = 15.$, $F = 0$, and $T = 1.$ . . . 378
3.206PVNGSv2: CDF for $M = 7.$, $R_x = -50.$, $F = 0$, and $T = 1.$ . . . 379
3.207PVNGSv2: CDF for $M = 7.$, $R_x = -30.$, $F = 0$, and $T = 1.$ . . . 379
3.208PVNGSv2: CDF for $M = 7.$, $R_x = -15.$, $F = 0$, and $T = 1.$ . . . 380
3.209PVNGSv2: CDF for $M = 7.$, $R_x = -5.$, $F = 0$, and $T = 1.$ . . . 380
3.210PVNGSv2: CDF for $M = 7.$, $R_x = 5.$, $F = 0$, and $T = 1.$ . . . 380
3.211PVNGSv2: CDF for $M = 7.$, $R_x = 15.$, $F = 0$, and $T = 1.$ . . . 381
3.212PVNGSv2: CDF for $M = 5.$, $R_x = -50.$, $F = -1$, and $T = 1.$ . . . 382
3.213PVNGSv2: CDF for $M = 5.$, $R_x = -30.$, $F = -1$, and $T = 1.$ . . . 382
3.214PVNGSv2: CDF for $M = 5.$, $R_x = -15.$, $F = -1$, and $T = 1.$ . . . 383
3.215PVNGSv2: CDF for $M = 5.$, $R_x = -5.$, $F = -1$, and $T = 1.$ . . . 383
3.216PVNGSv2: CDF for $M = 5.$, $R_x = 5.$, $F = -1$, and $T = 1.$ . . . 383
3.217PVNGSv2: CDF for $M = 5.$, $R_x = 15.$, $F = -1$, and $T = 1.$ . . . 384
3.218PVNGSv2: CDF for $M = 6.$, $R_x = -50.$, $F = -1$, and $T = 1.$ . . . 385
3.219PVNGSv2: CDF for $M = 6.$, $R_x = -30.$, $F = -1$, and $T = 1.$ . . . 385
3.220PVNGSv2: CDF for $M = 6.$, $R_x = -15.$, $F = -1$, and $T = 1.$ . . . 386
3.221PVNGSv2: CDF for $M = 6.$, $R_x = -5.$, $F = -1$, and $T = 1.$ . . . 386
3.222PVNGSv2: CDF for $M = 6.$, $R_x = 5.$, $F = -1$, and $T = 1.$ . . . 386
3.223PVNGSv2: CDF for $M = 6.$, $R_x = 15.$, $F = -1$, and $T = 1.$ . . . 387
3.224PVNGSv2: CDF for $M = 7.$, $R_x = -50.$, $F = -1$, and $T = 1.$ . . . 388
3.225PVNGSv2: CDF for $M = 7.$, $R_x = -30.$, $F = -1$, and $T = 1.$ . . . 388
3.226PVNGSv2: CDF for $M = 7.$, $R_x = -15.$, $F = -1$, and $T = 1.$ . . . 389
3.227PVNGSv2: CDF for $M = 7.$, $R_x = -5.$, $F = -1$, and $T = 1.$ . . . 389
3.228PVNGSv2: CDF for $M = 7.$, $R_x = 5.$, $F = -1$, and $T = 1.$ . . . 389
3.229PVNGSv2: CDF for $M = 7.$, $R_x = 15.$, $F = -1$, and $T = 1.$ . . . 390
3.230PVNGSv2: CDF for $M = 5.$, $R_x = -50.$, $F = 0$, and $T = 3.$ . . . 391
3.231PVNGSv2: CDF for $M = 5.$, $R_x = -30.$, $F = 0$, and $T = 3.$ . . . 391
3.232PVNGSv2: CDF for $M = 5.$, $R_x = -15.$, $F = 0$, and $T = 3.$ . . . 392
3.233PVNGSv2: CDF for $M = 5.$, $R_x = -5.$, $F = 0$, and $T = 3.$ . . . 392
3.234PVNGSv2: CDF for $M = 5.$, $R_x = 5.$, $F = 0$, and $T = 3.$ . . . 392
3.235PVNGSv2: CDF for $M = 5.$, $R_x = 15.$, $F = 0$, and $T = 3.$ . . . 393
3.236PVNGSv2: CDF for $M = 6.$, $R_x = -50.$, $F = 0$, and $T = 3.$ . . . 394
3.237PVNGSv2: CDF for $M = 6.$, $R_x = -30.$, $F = 0$, and $T = 3.$ . . . 394
3.238PVNGSv2: CDF for $M = 6.$, $R_x = -15.$, $F = 0$, and $T = 3.$ . . . 395
3.239PVNGSv2: CDF for $M = 6.$, $R_x = -5.$, $F = 0$, and $T = 3.$ . . . 395
3.240PVNGSv2: CDF for $M = 6.$, $R_x = 5.$, $F = 0$, and $T = 3.$ . . . 395
3.241PVNGSv2: CDF for $M = 6.$, $R_x = 15.$, $F = 0$, and $T = 3.$ . . . 396
3.242PVNGSv2: CDF for $M = 7.$, $R_x = -50.$, $F = 0$, and $T = 3.$ . . . 397
3.243PVNGSv2: CDF for $M = 7.$, $R_x = -30.$, $F = 0$, and $T = 3.$ . . . 397
3.244PVNGSv2: CDF for $M = 7.$, $R_x = -15.$, $F = 0$, and $T = 3.$ . . . 398

3.245PVNGSv2: CDF for $M = 7.$, $R_x = -5.$, $F = 0$, and $T = 3.$ . . . 398
3.246PVNGSv2: CDF for $M = 7.$, $R_x = 5.$, $F = 0$, and $T = 3.$ . . . 398
3.247PVNGSv2: CDF for $M = 7.$, $R_x = 15.$, $F = 0$, and $T = 3.$ . . . 399
3.248PVNGSv2: CDF for $M = 5.$, $R_x = -50.$, $F = -1$, and $T = 3.$ . . . 400
3.249PVNGSv2: CDF for $M = 5.$, $R_x = -30.$, $F = -1$, and $T = 3.$ . . . 400
3.250PVNGSv2: CDF for $M = 5.$, $R_x = -15.$, $F = -1$, and $T = 3.$ . . . 401
3.251PVNGSv2: CDF for $M = 5.$, $R_x = -5.$, $F = -1$, and $T = 3.$ . . . 401
3.252PVNGSv2: CDF for $M = 5.$, $R_x = 5.$, $F = -1$, and $T = 3.$ . . . 401
3.253PVNGSv2: CDF for $M = 5.$, $R_x = 15.$, $F = -1$, and $T = 3.$ . . . 402
3.254PVNGSv2: CDF for $M = 6.$, $R_x = -50.$, $F = -1$, and $T = 3.$ . . . 403
3.255PVNGSv2: CDF for $M = 6.$, $R_x = -30.$, $F = -1$, and $T = 3.$ . . . 403
3.256PVNGSv2: CDF for $M = 6.$, $R_x = -15.$, $F = -1$, and $T = 3.$ . . . 404
3.257PVNGSv2: CDF for $M = 6.$, $R_x = -5.$, $F = -1$, and $T = 3.$ . . . 404
3.258PVNGSv2: CDF for $M = 6.$, $R_x = 5.$, $F = -1$, and $T = 3.$ . . . 404
3.259PVNGSv2: CDF for $M = 6.$, $R_x = 15.$, $F = -1$, and $T = 3.$ . . . 405
3.260PVNGSv2: CDF for $M = 7.$, $R_x = -50.$, $F = -1$, and $T = 3.$ . . . 406
3.261PVNGSv2: CDF for $M = 7.$, $R_x = -30.$, $F = -1$, and $T = 3.$ . . . 406
3.262PVNGSv2: CDF for $M = 7.$, $R_x = -15.$, $F = -1$, and $T = 3.$ . . . 407
3.263PVNGSv2: CDF for $M = 7.$, $R_x = -5.$, $F = -1$, and $T = 3.$ . . . 407
3.264PVNGSv2: CDF for $M = 7.$, $R_x = 5.$, $F = -1$, and $T = 3.$ . . . 407
3.265PVNGSv2: CDF for $M = 7.$, $R_x = 15.$, $F = -1$, and $T = 3.$ . . . 408
3.266Distance scaling for $M = 5.$, $F = -1$, and $T = 0.01$ . . . 409
3.267Distance scaling for $M = 5.$, $F = 0$, and $T = 0.01$ . . . 409
3.268Distance scaling for $M = 6.$, $F = -1$, and $T = 0.01$ . . . 410
3.269Distance scaling for $M = 6.$, $F = 0$, and $T = 0.01$ . . . 410
3.270Distance scaling for $M = 7.$, $F = -1$, and $T = 0.01$ . . . 410
3.271Distance scaling for $M = 7.$, $F = 0$, and $T = 0.01$ . . . 411
3.272Distance scaling for $M = 5.$, $F = -1$, and $T = 0.2$ . . . 412
3.273Distance scaling for $M = 5.$, $F = 0$, and $T = 0.2$ . . . 412
3.274Distance scaling for $M = 6.$, $F = -1$, and $T = 0.2$ . . . 413
3.275Distance scaling for $M = 6.$, $F = 0$, and $T = 0.2$ . . . 413
3.276Distance scaling for $M = 7.$, $F = -1$, and $T = 0.2$ . . . 413
3.277Distance scaling for $M = 7.$, $F = 0$, and $T = 0.2$ . . . 414
3.278Distance scaling for $M = 5.$, $F = -1$, and $T = 0.5$ . . . 415
3.279Distance scaling for $M = 5.$, $F = 0$, and $T = 0.5$ . . . 415
3.280Distance scaling for $M = 6.$, $F = -1$, and $T = 0.5$ . . . 416
3.281Distance scaling for $M = 6.$, $F = 0$, and $T = 0.5$ . . . 416
3.282Distance scaling for $M = 7.$, $F = -1$, and $T = 0.5$ . . . 416
3.283Distance scaling for $M = 7.$, $F = 0$, and $T = 0.5$ . . . 417
3.284Distance scaling for $M = 5.$, $F = -1$, and $T = 1.$ . . . 418
3.285Distance scaling for $M = 5.$, $F = 0$, and $T = 1.$ . . . 418
3.286Distance scaling for $M = 6.$, $F = -1$, and $T = 1.$ . . . 419
3.287Distance scaling for $M = 6.$, $F = 0$, and $T = 1.$ . . . 419
3.288Distance scaling for $M = 7.$, $F = -1$, and $T = 1.$ . . . 419
3.289Distance scaling for $M = 7.$, $F = 0$, and $T = 1.$ . . . 420
3.290Distance scaling for $M = 5.$, $F = -1$, and $T = 3.$ . . . 421
3.291Distance scaling for $M = 5.$, $F = 0$, and $T = 3.$ . . . 421
3.292Distance scaling for $M = 6.$, $F = -1$, and $T = 3.$ . . . 422
3.293Distance scaling for $M = 6.$, $F = 0$, and $T = 3.$ . . . 422
3.294Distance scaling for $M = 7.$, $F = -1$, and $T = 3.$ . . . 422
3.295Distance scaling for $M = 7.$, $F = 0$, and $T = 3.$ . . . 423
3.296PVNGSv2: Distance scaling of quantiles with GMPEs for $M = 5.$, $F = 0$, and $T = 0.01$ . . . 424
3.297PVNGSv2: Distance scaling of quantiles with GMPEs for $M = 6.$, $F = 0$, and $T = 0.01$ . . . 424
3.298PVNGSv2: Distance scaling of quantiles with GMPEs for $M = 7.$, $F = 0$, and $T = 0.01$ . . . 425
3.299PVNGSv2: Distance scaling of quantiles with GMPEs for $M = 5.$, $F = -1$, and $T = 0.01$ . . . 425
3.300PVNGSv2: Distance scaling of quantiles with GMPEs for $M = 6.$, $F = -1$, and $T = 0.01$ . . . 426
3.301PVNGSv2: Distance scaling of quantiles with GMPEs for $M = 7.$, $F = -1$, and $T = 0.01$ . . . 426
3.302PVNGSv2: Distance scaling of quantiles with GMPEs for $M = 5.$, $F = 0$, and $T = 0.2$ . . . 427
3.303PVNGSv2: Distance scaling of quantiles with GMPEs for $M = 6.$, $F = 0$, and $T = 0.2$ . . . 427
3.304PVNGSv2: Distance scaling of quantiles with GMPEs for $M = 7.$, $F = 0$, and $T = 0.2$ . . . 428
3.305PVNGSv2: Distance scaling of quantiles with GMPEs for $M = 5.$, $F = -1$, and $T = 0.2$ . . . 428

3.306PVNGSv2: Distance scaling of quantiles with GMPEs for $M = 6.$, $F = -1$, and $T = 0.2$ . . . . . 429
3.307PVNGSv2: Distance scaling of quantiles with GMPEs for $M = 7.$, $F = -1$, and $T = 0.2$ . . . . . 429
3.308PVNGSv2: Distance scaling of quantiles with GMPEs for $M = 5.$, $F = 0$, and $T = 0.5$ . . . . . 430
3.309PVNGSv2: Distance scaling of quantiles with GMPEs for $M = 6.$, $F = 0$, and $T = 0.5$ . . . . . 430
3.310PVNGSv2: Distance scaling of quantiles with GMPEs for $M = 7.$, $F = 0$, and $T = 0.5$ . . . . . 431
3.311PVNGSv2: Distance scaling of quantiles with GMPEs for $M = 5.$, $F = -1$, and $T = 0.5$ . . . . . 431
3.312PVNGSv2: Distance scaling of quantiles with GMPEs for $M = 6.$, $F = -1$, and $T = 0.5$ . . . . . 432
3.313PVNGSv2: Distance scaling of quantiles with GMPEs for $M = 7.$, $F = -1$, and $T = 0.5$ . . . . . 432
3.314PVNGSv2: Distance scaling of quantiles with GMPEs for $M = 5.$, $F = 0$, and $T = 1.$ . . . . . 433
3.315PVNGSv2: Distance scaling of quantiles with GMPEs for $M = 6.$, $F = 0$, and $T = 1.$ . . . . . 433
3.316PVNGSv2: Distance scaling of quantiles with GMPEs for $M = 7.$, $F = 0$, and $T = 1.$ . . . . . 434
3.317PVNGSv2: Distance scaling of quantiles with GMPEs for $M = 5.$, $F = -1$, and $T = 1.$ . . . . . 434
3.318PVNGSv2: Distance scaling of quantiles with GMPEs for $M = 6.$, $F = -1$, and $T = 1.$ . . . . . 435
3.319PVNGSv2: Distance scaling of quantiles with GMPEs for $M = 7.$, $F = -1$, and $T = 1.$ . . . . . 435
3.320PVNGSv2: Distance scaling of quantiles with GMPEs for $M = 5.$, $F = 0$, and $T = 3.$ . . . . . 436
3.321PVNGSv2: Distance scaling of quantiles with GMPEs for $M = 6.$, $F = 0$, and $T = 3.$ . . . . . 436
3.322PVNGSv2: Distance scaling of quantiles with GMPEs for $M = 7.$, $F = 0$, and $T = 3.$ . . . . . 437
3.323PVNGSv2: Distance scaling of quantiles with GMPEs for $M = 5.$, $F = -1$, and $T = 3.$ . . . . . 437
3.324PVNGSv2: Distance scaling of quantiles with GMPEs for $M = 6.$, $F = -1$, and $T = 3.$ . . . . . 438
3.325PVNGSv2: Distance scaling of quantiles with GMPEs for $M = 7.$, $F = -1$, and $T = 3.$ . . . . . 438
3.326Magnitude scaling for $R_x = -50.$, $F = -1$, and $T = 0.01$ . . . . . 439
3.327Magnitude scaling for $R_x = -50.$, $F = 0$, and $T = 0.01$ . . . . . 439
3.328Magnitude scaling for $R_x = -30.$, $F = -1$, and $T = 0.01$ . . . . . 440
3.329Magnitude scaling for $R_x = -30.$, $F = 0$, and $T = 0.01$ . . . . . 440
3.330Magnitude scaling for $R_x = -15.$, $F = -1$, and $T = 0.01$ . . . . . 440
3.331Magnitude scaling for $R_x = -15.$, $F = 0$, and $T = 0.01$ . . . . . 441
3.332Magnitude scaling for $R_x = -5.$, $F = -1$, and $T = 0.01$ . . . . . 441
3.333Magnitude scaling for $R_x = -5.$, $F = 0$, and $T = 0.01$ . . . . . 441
3.334Magnitude scaling for $R_x = 5.$, $F = -1$, and $T = 0.01$ . . . . . 442
3.335Magnitude scaling for $R_x = 5.$, $F = 0$, and $T = 0.01$ . . . . . 442
3.336Magnitude scaling for $R_x = 15.$, $F = -1$, and $T = 0.01$ . . . . . 442
3.337Magnitude scaling for $R_x = 15.$, $F = 0$, and $T = 0.01$ . . . . . 443
3.338Magnitude scaling for $R_x = -50.$, $F = -1$, and $T = 0.2$ . . . . . 444
3.339Magnitude scaling for $R_x = -50.$, $F = 0$, and $T = 0.2$ . . . . . 444
3.340Magnitude scaling for $R_x = -30.$, $F = -1$, and $T = 0.2$ . . . . . 445
3.341Magnitude scaling for $R_x = -30.$, $F = 0$, and $T = 0.2$ . . . . . 445
3.342Magnitude scaling for $R_x = -15.$, $F = -1$, and $T = 0.2$ . . . . . 445
3.343Magnitude scaling for $R_x = -15.$, $F = 0$, and $T = 0.2$ . . . . . 446
3.344Magnitude scaling for $R_x = -5.$, $F = -1$, and $T = 0.2$ . . . . . 446
3.345Magnitude scaling for $R_x = -5.$, $F = 0$, and $T = 0.2$ . . . . . 446
3.346Magnitude scaling for $R_x = 5.$, $F = -1$, and $T = 0.2$ . . . . . 447
3.347Magnitude scaling for $R_x = 5.$, $F = 0$, and $T = 0.2$ . . . . . 447
3.348Magnitude scaling for $R_x = 15.$, $F = -1$, and $T = 0.2$ . . . . . 447
3.349Magnitude scaling for $R_x = 15.$, $F = 0$, and $T = 0.2$ . . . . . 448
3.350Magnitude scaling for $R_x = -50.$, $F = -1$, and $T = 0.5$ . . . . . 449
3.351Magnitude scaling for $R_x = -50.$, $F = 0$, and $T = 0.5$ . . . . . 449
3.352Magnitude scaling for $R_x = -30.$, $F = -1$, and $T = 0.5$ . . . . . 450
3.353Magnitude scaling for $R_x = -30.$, $F = 0$, and $T = 0.5$ . . . . . 450
3.354Magnitude scaling for $R_x = -15.$, $F = -1$, and $T = 0.5$ . . . . . 450
3.355Magnitude scaling for $R_x = -15.$, $F = 0$, and $T = 0.5$ . . . . . 451
3.356Magnitude scaling for $R_x = -5.$, $F = -1$, and $T = 0.5$ . . . . . 451
3.357Magnitude scaling for $R_x = -5.$, $F = 0$, and $T = 0.5$ . . . . . 451
3.358Magnitude scaling for $R_x = 5.$, $F = -1$, and $T = 0.5$ . . . . . 452
3.359Magnitude scaling for $R_x = 5.$, $F = 0$, and $T = 0.5$ . . . . . 452
3.360Magnitude scaling for $R_x = 15.$, $F = -1$, and $T = 0.5$ . . . . . 452
3.361Magnitude scaling for $R_x = 15.$, $F = 0$, and $T = 0.5$ . . . . . 453
3.362Magnitude scaling for $R_x = -50.$, $F = -1$, and $T = 1.$ . . . . . 454
3.363Magnitude scaling for $R_x = -50.$, $F = 0$, and $T = 1.$ . . . . . 454
3.364Magnitude scaling for $R_x = -30.$, $F = -1$, and $T = 1.$ . . . . . 455
3.365Magnitude scaling for $R_x = -30.$, $F = 0$, and $T = 1.$ . . . . . 455
3.366Magnitude scaling for $R_x = -15.$, $F = -1$, and $T = 1.$ . . . . . 455

3.367Magnitude scaling for $R_x = -15.$, $F = 0$, and $T = 1$. . . . 456
3.368Magnitude scaling for $R_x = -5.$, $F = -1$, and $T = 1$. . . . 456
3.369Magnitude scaling for $R_x = -5.$, $F = 0$, and $T = 1$. . . . 456
3.370Magnitude scaling for $R_x = 5.$, $F = -1$, and $T = 1$. . . . 457
3.371Magnitude scaling for $R_x = 5.$, $F = 0$, and $T = 1$. . . . 457
3.372Magnitude scaling for $R_x = 15.$, $F = -1$, and $T = 1$. . . . 457
3.373Magnitude scaling for $R_x = 15.$, $F = 0$, and $T = 1$. . . . 458
3.374Magnitude scaling for $R_x = -50.$, $F = -1$, and $T = 3$. . . . 459
3.375Magnitude scaling for $R_x = -50.$, $F = 0$, and $T = 3$. . . . 459
3.376Magnitude scaling for $R_x = -30.$, $F = -1$, and $T = 3$. . . . 460
3.377Magnitude scaling for $R_x = -30.$, $F = 0$, and $T = 3$. . . . 460
3.378Magnitude scaling for $R_x = -15.$, $F = -1$, and $T = 3$. . . . 460
3.379Magnitude scaling for $R_x = -15.$, $F = 0$, and $T = 3$. . . . 461
3.380Magnitude scaling for $R_x = -5.$, $F = -1$, and $T = 3$. . . . 461
3.381Magnitude scaling for $R_x = -5.$, $F = 0$, and $T = 3$. . . . 461
3.382Magnitude scaling for $R_x = 5.$, $F = -1$, and $T = 3$. . . . 462
3.383Magnitude scaling for $R_x = 5.$, $F = 0$, and $T = 3$. . . . 462
3.384Magnitude scaling for $R_x = 15.$, $F = -1$, and $T = 3$. . . . 462
3.385Magnitude scaling for $R_x = 15.$, $F = 0$, and $T = 3$. . . . 463
3.386PVNGSv2: Spectra for $M_W = 5.$, $R_x = -50.$, $F = 0$ . . . . 464
3.387PVNGSv2: Spectra for $M_W = 5.$, $R_x = -30.$, $F = 0$ . . . . 464
3.388PVNGSv2: Spectra for $M_W = 5.$, $R_x = -15.$, $F = 0$ . . . . 465
3.389PVNGSv2: Spectra for $M_W = 5.$, $R_x = -5.$, $F = 0$ . . . . 465
3.390PVNGSv2: Spectra for $M_W = 5.$, $R_x = 5.$, $F = 0$ . . . . 466
3.391PVNGSv2: Spectra for $M_W = 5.$, $R_x = 15.$, $F = 0$ . . . . 466
3.392PVNGSv2: Spectra for $M_W = 6.$, $R_x = -50.$, $F = 0$ . . . . 467
3.393PVNGSv2: Spectra for $M_W = 6.$, $R_x = -30.$, $F = 0$ . . . . 467
3.394PVNGSv2: Spectra for $M_W = 6.$, $R_x = -15.$, $F = 0$ . . . . 468
3.395PVNGSv2: Spectra for $M_W = 6.$, $R_x = -5.$, $F = 0$ . . . . 468
3.396PVNGSv2: Spectra for $M_W = 6.$, $R_x = 5.$, $F = 0$ . . . . 469
3.397PVNGSv2: Spectra for $M_W = 6.$, $R_x = 15.$, $F = 0$ . . . . 469
3.398PVNGSv2: Spectra for $M_W = 7.$, $R_x = -50.$, $F = 0$ . . . . 470
3.399PVNGSv2: Spectra for $M_W = 7.$, $R_x = -30.$, $F = 0$ . . . . 470
3.400PVNGSv2: Spectra for $M_W = 7.$, $R_x = -15.$, $F = 0$ . . . . 471
3.401PVNGSv2: Spectra for $M_W = 7.$, $R_x = -5.$, $F = 0$ . . . . 471
3.402PVNGSv2: Spectra for $M_W = 7.$, $R_x = 5.$, $F = 0$ . . . . 472
3.403PVNGSv2: Spectra for $M_W = 7.$, $R_x = 15.$, $F = 0$ . . . . 472
3.404PVNGSv2: Spectra for $M_W = 5.$, $R_x = -50.$, $F = -1$ . . . . 473
3.405PVNGSv2: Spectra for $M_W = 5.$, $R_x = -30.$, $F = -1$ . . . . 473
3.406PVNGSv2: Spectra for $M_W = 5.$, $R_x = -15.$, $F = -1$ . . . . 474
3.407PVNGSv2: Spectra for $M_W = 5.$, $R_x = -5.$, $F = -1$ . . . . 474
3.408PVNGSv2: Spectra for $M_W = 5.$, $R_x = 5.$, $F = -1$ . . . . 475
3.409PVNGSv2: Spectra for $M_W = 5.$, $R_x = 15.$, $F = -1$ . . . . 475
3.410PVNGSv2: Spectra for $M_W = 6.$, $R_x = -50.$, $F = -1$ . . . . 476
3.411PVNGSv2: Spectra for $M_W = 6.$, $R_x = -30.$, $F = -1$ . . . . 476
3.412PVNGSv2: Spectra for $M_W = 6.$, $R_x = -15.$, $F = -1$ . . . . 477
3.413PVNGSv2: Spectra for $M_W = 6.$, $R_x = -5.$, $F = -1$ . . . . 477
3.414PVNGSv2: Spectra for $M_W = 6.$, $R_x = 5.$, $F = -1$ . . . . 478
3.415PVNGSv2: Spectra for $M_W = 6.$, $R_x = 15.$, $F = -1$ . . . . 478
3.416PVNGSv2: Spectra for $M_W = 7.$, $R_x = -50.$, $F = -1$ . . . . 479
3.417PVNGSv2: Spectra for $M_W = 7.$, $R_x = -30.$, $F = -1$ . . . . 479
3.418PVNGSv2: Spectra for $M_W = 7.$, $R_x = -15.$, $F = -1$ . . . . 480
3.419PVNGSv2: Spectra for $M_W = 7.$, $R_x = -5.$, $F = -1$ . . . . 480
3.420PVNGSv2: Spectra for $M_W = 7.$, $R_x = 5.$, $F = -1$ . . . . 481
3.421PVNGSv2: Spectra for $M_W = 7.$, $R_x = 15.$, $F = -1$ . . . . 481
3.422Quantile ratio for $M = 5.$, $F = -1$ and all periods . . . . 482
3.423Quantile ratio for $M = 5.$, $F = 0$ and all periods . . . . 482
3.424Quantile ratio for $M = 6.$, $F = -1$ and all periods . . . . 483
3.425Quantile ratio for $M = 6.$, $F = 0$ and all periods . . . . 483
3.426Quantile ratio for $M = 7.$, $F = -1$ and all periods . . . . 484
3.427Quantile ratio for $M = 7.$, $F = 0$ and all periods . . . . 484

3.428PVNGSv2: Magnitude scaling for $R_X = -50.$, $F = 0$, and $T = 0.01$ . . . 485
3.429PVNGSv2: Magnitude scaling for $R_X = -30.$, $F = 0$, and $T = 0.01$ . . . 485
3.430PVNGSv2: Magnitude scaling for $R_X = -15.$, $F = 0$, and $T = 0.01$ . . . 486
3.431PVNGSv2: Magnitude scaling for $R_X = -5.$, $F = 0$, and $T = 0.01$ . . . 486
3.432PVNGSv2: Magnitude scaling for $R_X = 5.$, $F = 0$, and $T = 0.01$ . . . 487
3.433PVNGSv2: Magnitude scaling for $R_X = 15.$, $F = 0$, and $T = 0.01$ . . . 487
3.434PVNGSv2: Magnitude scaling for $R_X = -50.$, $F = -1$, and $T = 0.01$ . . . 488
3.435PVNGSv2: Magnitude scaling for $R_X = -30.$, $F = -1$, and $T = 0.01$ . . . 488
3.436PVNGSv2: Magnitude scaling for $R_X = -15.$, $F = -1$, and $T = 0.01$ . . . 489
3.437PVNGSv2: Magnitude scaling for $R_X = -5.$, $F = -1$, and $T = 0.01$ . . . 489
3.438PVNGSv2: Magnitude scaling for $R_X = 5.$, $F = -1$, and $T = 0.01$ . . . 490
3.439PVNGSv2: Magnitude scaling for $R_X = 15.$, $F = -1$, and $T = 0.01$ . . . 490
3.440PVNGSv2: Magnitude scaling for $R_X = -50.$, $F = 0$, and $T = 0.2$ . . . 491
3.441PVNGSv2: Magnitude scaling for $R_X = -30.$, $F = 0$, and $T = 0.2$ . . . 491
3.442PVNGSv2: Magnitude scaling for $R_X = -15.$, $F = 0$, and $T = 0.2$ . . . 492
3.443PVNGSv2: Magnitude scaling for $R_X = -5.$, $F = 0$, and $T = 0.2$ . . . 492
3.444PVNGSv2: Magnitude scaling for $R_X = 5.$, $F = 0$, and $T = 0.2$ . . . 493
3.445PVNGSv2: Magnitude scaling for $R_X = 15.$, $F = 0$, and $T = 0.2$ . . . 493
3.446PVNGSv2: Magnitude scaling for $R_X = -50.$, $F = -1$, and $T = 0.2$ . . . 494
3.447PVNGSv2: Magnitude scaling for $R_X = -30.$, $F = -1$, and $T = 0.2$ . . . 494
3.448PVNGSv2: Magnitude scaling for $R_X = -15.$, $F = -1$, and $T = 0.2$ . . . 495
3.449PVNGSv2: Magnitude scaling for $R_X = -5.$, $F = -1$, and $T = 0.2$ . . . 495
3.450PVNGSv2: Magnitude scaling for $R_X = 5.$, $F = -1$, and $T = 0.2$ . . . 496
3.451PVNGSv2: Magnitude scaling for $R_X = 15.$, $F = -1$, and $T = 0.2$ . . . 496
3.452PVNGSv2: Magnitude scaling for $R_X = -50.$, $F = 0$, and $T = 0.5$ . . . 497
3.453PVNGSv2: Magnitude scaling for $R_X = -30.$, $F = 0$, and $T = 0.5$ . . . 497
3.454PVNGSv2: Magnitude scaling for $R_X = -15.$, $F = 0$, and $T = 0.5$ . . . 498
3.455PVNGSv2: Magnitude scaling for $R_X = -5.$, $F = 0$, and $T = 0.5$ . . . 498
3.456PVNGSv2: Magnitude scaling for $R_X = 5.$, $F = 0$, and $T = 0.5$ . . . 499
3.457PVNGSv2: Magnitude scaling for $R_X = 15.$, $F = 0$, and $T = 0.5$ . . . 499
3.458PVNGSv2: Magnitude scaling for $R_X = -50.$, $F = -1$, and $T = 0.5$ . . . 500
3.459PVNGSv2: Magnitude scaling for $R_X = -30.$, $F = -1$, and $T = 0.5$ . . . 500
3.460PVNGSv2: Magnitude scaling for $R_X = -15.$, $F = -1$, and $T = 0.5$ . . . 501
3.461PVNGSv2: Magnitude scaling for $R_X = -5.$, $F = -1$, and $T = 0.5$ . . . 501
3.462PVNGSv2: Magnitude scaling for $R_X = 5.$, $F = -1$, and $T = 0.5$ . . . 502
3.463PVNGSv2: Magnitude scaling for $R_X = 15.$, $F = -1$, and $T = 0.5$ . . . 502
3.464PVNGSv2: Magnitude scaling for $R_X = -50.$, $F = 0$, and $T = 1.$ . . . 503
3.465PVNGSv2: Magnitude scaling for $R_X = -30.$, $F = 0$, and $T = 1.$ . . . 503
3.466PVNGSv2: Magnitude scaling for $R_X = -15.$, $F = 0$, and $T = 1.$ . . . 504
3.467PVNGSv2: Magnitude scaling for $R_X = -5.$, $F = 0$, and $T = 1.$ . . . 504
3.468PVNGSv2: Magnitude scaling for $R_X = 5.$, $F = 0$, and $T = 1.$ . . . 505
3.469PVNGSv2: Magnitude scaling for $R_X = 15.$, $F = 0$, and $T = 1.$ . . . 505
3.470PVNGSv2: Magnitude scaling for $R_X = -50.$, $F = -1$, and $T = 1.$ . . . 506
3.471PVNGSv2: Magnitude scaling for $R_X = -30.$, $F = -1$, and $T = 1.$ . . . 506
3.472PVNGSv2: Magnitude scaling for $R_X = -15.$, $F = -1$, and $T = 1.$ . . . 507
3.473PVNGSv2: Magnitude scaling for $R_X = -5.$, $F = -1$, and $T = 1.$ . . . 507
3.474PVNGSv2: Magnitude scaling for $R_X = 5.$, $F = -1$, and $T = 1.$ . . . 508
3.475PVNGSv2: Magnitude scaling for $R_X = 15.$, $F = -1$, and $T = 1.$ . . . 508
3.476PVNGSv2: Magnitude scaling for $R_X = -50.$, $F = 0$, and $T = 3.$ . . . 509
3.477PVNGSv2: Magnitude scaling for $R_X = -30.$, $F = 0$, and $T = 3.$ . . . 509
3.478PVNGSv2: Magnitude scaling for $R_X = -15.$, $F = 0$, and $T = 3.$ . . . 510
3.479PVNGSv2: Magnitude scaling for $R_X = -5.$, $F = 0$, and $T = 3.$ . . . 510
3.480PVNGSv2: Magnitude scaling for $R_X = 5.$, $F = 0$, and $T = 3.$ . . . 511
3.481PVNGSv2: Magnitude scaling for $R_X = 15.$, $F = 0$, and $T = 3.$ . . . 511
3.482PVNGSv2: Magnitude scaling for $R_X = -50.$, $F = -1$, and $T = 3.$ . . . 512
3.483PVNGSv2: Magnitude scaling for $R_X = -30.$, $F = -1$, and $T = 3.$ . . . 512
3.484PVNGSv2: Magnitude scaling for $R_X = -15.$, $F = -1$, and $T = 3.$ . . . 513
3.485PVNGSv2: Magnitude scaling for $R_X = -5.$, $F = -1$, and $T = 3.$ . . . 513
3.486PVNGSv2: Magnitude scaling for $R_X = 5.$, $F = -1$, and $T = 3.$ . . . 514
3.487PVNGSv2: Magnitude scaling for $R_X = 15.$, $F = -1$, and $T = 3.$ . . . 514
3.488PVNGSv2: Distance scaling of quantiles with GMPEs for $M = 5.$, $F = 0$, and $T = 0.01$ . . . 515

3.489PVNGSv2: Distance scaling of quantiles with GMPEs for $M = 6.$, $F = 0$, and $T = 0.01$ . . . . . 515
3.490PVNGSv2: Distance scaling of quantiles with GMPEs for $M = 7.$, $F = 0$, and $T = 0.01$ . . . . . 516
3.491PVNGSv2: Distance scaling of quantiles with GMPEs for $M = 5.$, $F = -1$, and $T = 0.01$ . . . . . 516
3.492PVNGSv2: Distance scaling of quantiles with GMPEs for $M = 6.$, $F = -1$, and $T = 0.01$ . . . . . 516
3.493PVNGSv2: Distance scaling of quantiles with GMPEs for $M = 7.$, $F = -1$, and $T = 0.01$ . . . . . 517
3.494PVNGSv2: Distance scaling of quantiles with GMPEs for $M = 5.$, $F = 0$, and $T = 0.2$ . . . . . 518
3.495PVNGSv2: Distance scaling of quantiles with GMPEs for $M = 6.$, $F = 0$, and $T = 0.2$ . . . . . 518
3.496PVNGSv2: Distance scaling of quantiles with GMPEs for $M = 7.$, $F = 0$, and $T = 0.2$ . . . . . 519
3.497PVNGSv2: Distance scaling of quantiles with GMPEs for $M = 5.$, $F = -1$, and $T = 0.2$ . . . . . 519
3.498PVNGSv2: Distance scaling of quantiles with GMPEs for $M = 6.$, $F = -1$, and $T = 0.2$ . . . . . 519
3.499PVNGSv2: Distance scaling of quantiles with GMPEs for $M = 7.$, $F = -1$, and $T = 0.2$ . . . . . 520
3.500PVNGSv2: Distance scaling of quantiles with GMPEs for $M = 5.$, $F = 0$, and $T = 0.5$ . . . . . 521
3.501PVNGSv2: Distance scaling of quantiles with GMPEs for $M = 6.$, $F = 0$, and $T = 0.5$ . . . . . 521
3.502PVNGSv2: Distance scaling of quantiles with GMPEs for $M = 7.$, $F = 0$, and $T = 0.5$ . . . . . 522
3.503PVNGSv2: Distance scaling of quantiles with GMPEs for $M = 5.$, $F = -1$, and $T = 0.5$ . . . . . 522
3.504PVNGSv2: Distance scaling of quantiles with GMPEs for $M = 6.$, $F = -1$, and $T = 0.5$ . . . . . 522
3.505PVNGSv2: Distance scaling of quantiles with GMPEs for $M = 7.$, $F = -1$, and $T = 0.5$ . . . . . 523
3.506PVNGSv2: Distance scaling of quantiles with GMPEs for $M = 5.$, $F = 0$, and $T = 1.$ . . . . . 524
3.507PVNGSv2: Distance scaling of quantiles with GMPEs for $M = 6.$, $F = 0$, and $T = 1.$ . . . . . 524
3.508PVNGSv2: Distance scaling of quantiles with GMPEs for $M = 7.$, $F = 0$, and $T = 1.$ . . . . . 525
3.509PVNGSv2: Distance scaling of quantiles with GMPEs for $M = 5.$, $F = -1$, and $T = 1.$ . . . . . 525
3.510PVNGSv2: Distance scaling of quantiles with GMPEs for $M = 6.$, $F = -1$, and $T = 1.$ . . . . . 525
3.511PVNGSv2: Distance scaling of quantiles with GMPEs for $M = 7.$, $F = -1$, and $T = 1.$ . . . . . 526
3.512PVNGSv2: Distance scaling of quantiles with GMPEs for $M = 5.$, $F = 0$, and $T = 3.$ . . . . . 527
3.513PVNGSv2: Distance scaling of quantiles with GMPEs for $M = 6.$, $F = 0$, and $T = 3.$ . . . . . 527
3.514PVNGSv2: Distance scaling of quantiles with GMPEs for $M = 7.$, $F = 0$, and $T = 3.$ . . . . . 528
3.515PVNGSv2: Distance scaling of quantiles with GMPEs for $M = 5.$, $F = -1$, and $T = 3.$ . . . . . 528
3.516PVNGSv2: Distance scaling of quantiles with GMPEs for $M = 6.$, $F = -1$, and $T = 3.$ . . . . . 528
3.517PVNGSv2: Distance scaling of quantiles with GMPEs for $M = 7.$, $F = -1$, and $T = 3.$ . . . . . 529
3.518PVNGSv2: Magnitude scaling of quantiles with GMPEs for $R_X = -50.$, $F = 0$, and $T = 0.01$ . . . . . 530
3.519PVNGSv2: Magnitude scaling of quantiles with GMPEs for $R_X = -30.$, $F = 0$, and $T = 0.01$ . . . . . 530
3.520PVNGSv2: Magnitude scaling of quantiles with GMPEs for $R_X = -15.$, $F = 0$, and $T = 0.01$ . . . . . 531
3.521PVNGSv2: Magnitude scaling of quantiles with GMPEs for $R_X = -5.$, $F = 0$, and $T = 0.01$ . . . . . 531
3.522PVNGSv2: Magnitude scaling of quantiles with GMPEs for $R_X = 5.$, $F = 0$, and $T = 0.01$ . . . . . 532
3.523PVNGSv2: Magnitude scaling of quantiles with GMPEs for $R_X = 15.$, $F = 0$, and $T = 0.01$ . . . . . 532
3.524PVNGSv2: Magnitude scaling of quantiles with GMPEs for $R_X = -50.$, $F = -1$, and $T = 0.01$ . . . . . 533
3.525PVNGSv2: Magnitude scaling of quantiles with GMPEs for $R_X = -30.$, $F = -1$, and $T = 0.01$ . . . . . 533
3.526PVNGSv2: Magnitude scaling of quantiles with GMPEs for $R_X = -15.$, $F = -1$, and $T = 0.01$ . . . . . 534
3.527PVNGSv2: Magnitude scaling of quantiles with GMPEs for $R_X = -5.$, $F = -1$, and $T = 0.01$ . . . . . 534
3.528PVNGSv2: Magnitude scaling of quantiles with GMPEs for $R_X = 5.$, $F = -1$, and $T = 0.01$ . . . . . 535
3.529PVNGSv2: Magnitude scaling of quantiles with GMPEs for $R_X = 15.$, $F = -1$, and $T = 0.01$ . . . . . 535
3.530PVNGSv2: Magnitude scaling of quantiles with GMPEs for $R_X = -50.$, $F = 0$, and $T = 0.2$ . . . . . 536
3.531PVNGSv2: Magnitude scaling of quantiles with GMPEs for $R_X = -30.$, $F = 0$, and $T = 0.2$ . . . . . 536
3.532PVNGSv2: Magnitude scaling of quantiles with GMPEs for $R_X = -15.$, $F = 0$, and $T = 0.2$ . . . . . 537
3.533PVNGSv2: Magnitude scaling of quantiles with GMPEs for $R_X = -5.$, $F = 0$, and $T = 0.2$ . . . . . 537
3.534PVNGSv2: Magnitude scaling of quantiles with GMPEs for $R_X = 5.$, $F = 0$, and $T = 0.2$ . . . . . 538
3.535PVNGSv2: Magnitude scaling of quantiles with GMPEs for $R_X = 15.$, $F = 0$, and $T = 0.2$ . . . . . 538
3.536PVNGSv2: Magnitude scaling of quantiles with GMPEs for $R_X = -50.$, $F = -1$, and $T = 0.2$ . . . . . 539
3.537PVNGSv2: Magnitude scaling of quantiles with GMPEs for $R_X = -30.$, $F = -1$, and $T = 0.2$ . . . . . 539
3.538PVNGSv2: Magnitude scaling of quantiles with GMPEs for $R_X = -15.$, $F = -1$, and $T = 0.2$ . . . . . 540
3.539PVNGSv2: Magnitude scaling of quantiles with GMPEs for $R_X = -5.$, $F = -1$, and $T = 0.2$ . . . . . 540
3.540PVNGSv2: Magnitude scaling of quantiles with GMPEs for $R_X = 5.$, $F = -1$, and $T = 0.2$ . . . . . 541
3.541PVNGSv2: Magnitude scaling of quantiles with GMPEs for $R_X = 15.$, $F = -1$, and $T = 0.2$ . . . . . 541
3.542PVNGSv2: Magnitude scaling of quantiles with GMPEs for $R_X = -50.$, $F = 0$, and $T = 0.5$ . . . . . 542
3.543PVNGSv2: Magnitude scaling of quantiles with GMPEs for $R_X = -30.$, $F = 0$, and $T = 0.5$ . . . . . 542
3.544PVNGSv2: Magnitude scaling of quantiles with GMPEs for $R_X = -15.$, $F = 0$, and $T = 0.5$ . . . . . 543
3.545PVNGSv2: Magnitude scaling of quantiles with GMPEs for $R_X = -5.$, $F = 0$, and $T = 0.5$ . . . . . 543
3.546PVNGSv2: Magnitude scaling of quantiles with GMPEs for $R_X = 5.$, $F = 0$, and $T = 0.5$ . . . . . 544
3.547PVNGSv2: Magnitude scaling of quantiles with GMPEs for $R_X = 15.$, $F = 0$, and $T = 0.5$ . . . . . 544
3.548PVNGSv2: Magnitude scaling of quantiles with GMPEs for $R_X = -50.$, $F = -1$, and $T = 0.5$ . . . . . 545
3.549PVNGSv2: Magnitude scaling of quantiles with GMPEs for $R_X = -30.$, $F = -1$, and $T = 0.5$ . . . . . 545

3.550PVNGSv2: Magnitude scaling of quantiles with GMPEs for $R_X = -15.$, $F = -1$, and $T = 0.5$ . . . . . 546
3.551PVNGSv2: Magnitude scaling of quantiles with GMPEs for $R_X = -5.$, $F = -1$, and $T = 0.5$ . . . . . 546
3.552PVNGSv2: Magnitude scaling of quantiles with GMPEs for $R_X = 5.$, $F = -1$, and $T = 0.5$ . . . . . 547
3.553PVNGSv2: Magnitude scaling of quantiles with GMPEs for $R_X = 15.$, $F = -1$, and $T = 0.5$ . . . . . 547
3.554PVNGSv2: Magnitude scaling of quantiles with GMPEs for $R_X = -50.$, $F = 0$, and $T = 1.$ . . . . . 548
3.555PVNGSv2: Magnitude scaling of quantiles with GMPEs for $R_X = -30.$, $F = 0$, and $T = 1.$ . . . . . 548
3.556PVNGSv2: Magnitude scaling of quantiles with GMPEs for $R_X = -15.$, $F = 0$, and $T = 1.$ . . . . . 549
3.557PVNGSv2: Magnitude scaling of quantiles with GMPEs for $R_X = -5.$, $F = 0$, and $T = 1.$ . . . . . 549
3.558PVNGSv2: Magnitude scaling of quantiles with GMPEs for $R_X = 5.$, $F = 0$, and $T = 1.$ . . . . . 550
3.559PVNGSv2: Magnitude scaling of quantiles with GMPEs for $R_X = 15.$, $F = 0$, and $T = 1.$ . . . . . 550
3.560PVNGSv2: Magnitude scaling of quantiles with GMPEs for $R_X = -50.$, $F = -1$, and $T = 1.$ . . . . . 551
3.561PVNGSv2: Magnitude scaling of quantiles with GMPEs for $R_X = -30.$, $F = -1$, and $T = 1.$ . . . . . 551
3.562PVNGSv2: Magnitude scaling of quantiles with GMPEs for $R_X = -15.$, $F = -1$, and $T = 1.$ . . . . . 552
3.563PVNGSv2: Magnitude scaling of quantiles with GMPEs for $R_X = -5.$, $F = -1$, and $T = 1.$ . . . . . 552
3.564PVNGSv2: Magnitude scaling of quantiles with GMPEs for $R_X = 5.$, $F = -1$, and $T = 1.$ . . . . . 553
3.565PVNGSv2: Magnitude scaling of quantiles with GMPEs for $R_X = 15.$, $F = -1$, and $T = 1.$ . . . . . 553
3.566PVNGSv2: Magnitude scaling of quantiles with GMPEs for $R_X = -50.$, $F = 0$, and $T = 3.$ . . . . . 554
3.567PVNGSv2: Magnitude scaling of quantiles with GMPEs for $R_X = -30.$, $F = 0$, and $T = 3.$ . . . . . 554
3.568PVNGSv2: Magnitude scaling of quantiles with GMPEs for $R_X = -15.$, $F = 0$, and $T = 3.$ . . . . . 555
3.569PVNGSv2: Magnitude scaling of quantiles with GMPEs for $R_X = -5.$, $F = 0$, and $T = 3.$ . . . . . 555
3.570PVNGSv2: Magnitude scaling of quantiles with GMPEs for $R_X = 5.$, $F = 0$, and $T = 3.$ . . . . . 556
3.571PVNGSv2: Magnitude scaling of quantiles with GMPEs for $R_X = 15.$, $F = 0$, and $T = 3.$ . . . . . 556
3.572PVNGSv2: Magnitude scaling of quantiles with GMPEs for $R_X = -50.$, $F = -1$, and $T = 3.$ . . . . . 557
3.573PVNGSv2: Magnitude scaling of quantiles with GMPEs for $R_X = -30.$, $F = -1$, and $T = 3.$ . . . . . 557
3.574PVNGSv2: Magnitude scaling of quantiles with GMPEs for $R_X = -15.$, $F = -1$, and $T = 3.$ . . . . . 558
3.575PVNGSv2: Magnitude scaling of quantiles with GMPEs for $R_X = -5.$, $F = -1$, and $T = 3.$ . . . . . 558
3.576PVNGSv2: Magnitude scaling of quantiles with GMPEs for $R_X = 5.$, $F = -1$, and $T = 3.$ . . . . . 559
3.577PVNGSv2: Magnitude scaling of quantiles with GMPEs for $R_X = 15.$, $F = -1$, and $T = 3.$ . . . . . 559
3.578PVNGSv2: Spectra for $M_W = 5.$, $R_x = -50.$, $F = 0$ . . . . . 560
3.579PVNGSv2: Spectra for $M_W = 5.$, $R_x = -30.$, $F = 0$ . . . . . 560
3.580PVNGSv2: Spectra for $M_W = 5.$, $R_x = -15.$, $F = 0$ . . . . . 561
3.581PVNGSv2: Spectra for $M_W = 5.$, $R_x = -5.$, $F = 0$ . . . . . 561
3.582PVNGSv2: Spectra for $M_W = 5.$, $R_x = 5.$, $F = 0$ . . . . . 562
3.583PVNGSv2: Spectra for $M_W = 5.$, $R_x = 15.$, $F = 0$ . . . . . 562
3.584PVNGSv2: Spectra for $M_W = 6.$, $R_x = -50.$, $F = 0$ . . . . . 563
3.585PVNGSv2: Spectra for $M_W = 6.$, $R_x = -30.$, $F = 0$ . . . . . 563
3.586PVNGSv2: Spectra for $M_W = 6.$, $R_x = -15.$, $F = 0$ . . . . . 564
3.587PVNGSv2: Spectra for $M_W = 6.$, $R_x = -5.$, $F = 0$ . . . . . 564
3.588PVNGSv2: Spectra for $M_W = 6.$, $R_x = 5.$, $F = 0$ . . . . . 565
3.589PVNGSv2: Spectra for $M_W = 6.$, $R_x = 15.$, $F = 0$ . . . . . 565
3.590PVNGSv2: Spectra for $M_W = 7.$, $R_x = -50.$, $F = 0$ . . . . . 566
3.591PVNGSv2: Spectra for $M_W = 7.$, $R_x = -30.$, $F = 0$ . . . . . 566
3.592PVNGSv2: Spectra for $M_W = 7.$, $R_x = -15.$, $F = 0$ . . . . . 567
3.593PVNGSv2: Spectra for $M_W = 7.$, $R_x = -5.$, $F = 0$ . . . . . 567
3.594PVNGSv2: Spectra for $M_W = 7.$, $R_x = 5.$, $F = 0$ . . . . . 568
3.595PVNGSv2: Spectra for $M_W = 7.$, $R_x = 15.$, $F = 0$ . . . . . 568
3.596PVNGSv2: Spectra for $M_W = 5.$, $R_x = -50.$, $F = -1$ . . . . . 569
3.597PVNGSv2: Spectra for $M_W = 5.$, $R_x = -30.$, $F = -1$ . . . . . 569
3.598PVNGSv2: Spectra for $M_W = 5.$, $R_x = -15.$, $F = -1$ . . . . . 570
3.599PVNGSv2: Spectra for $M_W = 5.$, $R_x = -5.$, $F = -1$ . . . . . 570
3.600PVNGSv2: Spectra for $M_W = 5.$, $R_x = 5.$, $F = -1$ . . . . . 571
3.601PVNGSv2: Spectra for $M_W = 5.$, $R_x = 15.$, $F = -1$ . . . . . 571
3.602PVNGSv2: Spectra for $M_W = 6.$, $R_x = -50.$, $F = -1$ . . . . . 572
3.603PVNGSv2: Spectra for $M_W = 6.$, $R_x = -30.$, $F = -1$ . . . . . 572
3.604PVNGSv2: Spectra for $M_W = 6.$, $R_x = -15.$, $F = -1$ . . . . . 573
3.605PVNGSv2: Spectra for $M_W = 6.$, $R_x = -5.$, $F = -1$ . . . . . 573
3.606PVNGSv2: Spectra for $M_W = 6.$, $R_x = 5.$, $F = -1$ . . . . . 574
3.607PVNGSv2: Spectra for $M_W = 6.$, $R_x = 15.$, $F = -1$ . . . . . 574
3.608PVNGSv2: Spectra for $M_W = 7.$, $R_x = -50.$, $F = -1$ . . . . . 575
3.609PVNGSv2: Spectra for $M_W = 7.$, $R_x = -30.$, $F = -1$ . . . . . 575
3.610PVNGSv2: Spectra for $M_W = 7.$, $R_x = -15.$, $F = -1$ . . . . . 576

3.611PVNGSv2: Spectra for $M_W = 7.$, $R_x = -5.$, $F = -1$ . . . . . 576
3.612PVNGSv2: Spectra for $M_W = 7.$, $R_x = 5.$, $F = -1$ . . . . . 577
3.613PVNGSv2: Spectra for $M_W = 7.$, $R_x = 15.$, $F = -1$ . . . . . 577
3.614PVNGSv2: Histogram of differences for medians calculated with different weights to median calculated with total weights. Bottom row left shows differences between medians for the GMPE distribution to median calculated with total weights. Bottom row right shows differences between the original GMPEs (without uncertainty) to median calculated with total weights. For PVNGS2, ModelA and $T = 0.01$s. . . 579
3.615PVNGSv2: Histogram of differences for medians calculated with different weights to median calculated with total weights. Bottom row left shows differences between medians for the GMPE distribution to median calculated with total weights. Bottom row right shows differences between the original GMPEs (without uncertainty) to median calculated with total weights. For PVNGS2, ModelA and $T = 0.02$s. . . 580
3.616PVNGSv2: Histogram of differences for medians calculated with different weights to median calculated with total weights. Bottom row left shows differences between medians for the GMPE distribution to median calculated with total weights. Bottom row right shows differences between the original GMPEs (without uncertainty) to median calculated with total weights. For PVNGS2, ModelA and $T = 0.03$s. . . 581
3.617PVNGSv2: Histogram of differences for medians calculated with different weights to median calculated with total weights. Bottom row left shows differences between medians for the GMPE distribution to median calculated with total weights. Bottom row right shows differences between the original GMPEs (without uncertainty) to median calculated with total weights. For PVNGS2, ModelA and $T = 0.05$s. . . 582
3.618PVNGSv2: Histogram of differences for medians calculated with different weights to median calculated with total weights. Bottom row left shows differences between medians for the GMPE distribution to median calculated with total weights. Bottom row right shows differences between the original GMPEs (without uncertainty) to median calculated with total weights. For PVNGS2, ModelA and $T = 0.075$s. . . 583
3.619PVNGSv2: Histogram of differences for medians calculated with different weights to median calculated with total weights. Bottom row left shows differences between medians for the GMPE distribution to median calculated with total weights. Bottom row right shows differences between the original GMPEs (without uncertainty) to median calculated with total weights. For PVNGS2, ModelA and $T = 0.1$s. . . . 584
3.620PVNGSv2: Histogram of differences for medians calculated with different weights to median calculated with total weights. Bottom row left shows differences between medians for the GMPE distribution to median calculated with total weights. Bottom row right shows differences between the original GMPEs (without uncertainty) to median calculated with total weights. For PVNGS2, ModelA and $T = 0.15$s. . . 585
3.621PVNGSv2: Histogram of differences for medians calculated with different weights to median calculated with total weights. Bottom row left shows differences between medians for the GMPE distribution to median calculated with total weights. Bottom row right shows differences between the original GMPEs (without uncertainty) to median calculated with total weights. For PVNGS2, ModelA and $T = 0.2$s. . . . 586
3.622PVNGSv2: Histogram of differences for medians calculated with different weights to median calculated with total weights. Bottom row left shows differences between medians for the GMPE distribution to median calculated with total weights. Bottom row right shows differences between the original GMPEs (without uncertainty) to median calculated with total weights. For PVNGS2, ModelA and $T = 0.25$s. . . 587
3.623PVNGSv2: Histogram of differences for medians calculated with different weights to median calculated with total weights. Bottom row left shows differences between medians for the GMPE distribution to median calculated with total weights. Bottom row right shows differences between the original GMPEs (without uncertainty) to median calculated with total weights. For PVNGS2, ModelA and $T = 0.3$s. . . . 588
3.624PVNGSv2: Histogram of differences for medians calculated with different weights to median calculated with total weights. Bottom row left shows differences between medians for the GMPE distribution to median calculated with total weights. Bottom row right shows differences between the original GMPEs (without uncertainty) to median calculated with total weights. For PVNGS2, ModelA and $T = 0.4$s. . . . 589
3.625PVNGSv2: Histogram of differences for medians calculated with different weights to median calculated with total weights. Bottom row left shows differences between medians for the GMPE distribution to median calculated with total weights. Bottom row right shows differences between the original GMPEs (without uncertainty) to median calculated with total weights. For PVNGS2, ModelA and $T = 0.5$s. . . . 590
3.626PVNGSv2: Histogram of differences for medians calculated with different weights to median calculated with total weights. Bottom row left shows differences between medians for the GMPE distribution to median calculated with total weights. Bottom row right shows differences between the original GMPEs (without uncertainty) to median calculated with total weights. For PVNGS2, ModelA and $T = 0.75$s. . . 591
3.627PVNGSv2: Histogram of differences for medians calculated with different weights to median calculated with total weights. Bottom row left shows differences between medians for the GMPE distribution to median calculated with total weights. Bottom row right shows differences between the original GMPEs (without uncertainty) to median calculated with total weights. For PVNGS2, ModelA and $T = 1.$s. . . . . 592

3.628 PVNGSv2: Histogram of differences for medians calculated with different weights to median calculated with total weights. Bottom row left shows differences between medians for the GMPE distribution to median calculated with total weights. Bottom row right shows differences between the original GMPEs (without uncertainty) to median calculated with total weights. For PVNGS2, ModelA and $T = 1.5$s. . . . 593
3.629 PVNGSv2: Histogram of differences for medians calculated with different weights to median calculated with total weights. Bottom row left shows differences between medians for the GMPE distribution to median calculated with total weights. Bottom row right shows differences between the original GMPEs (without uncertainty) to median calculated with total weights. For PVNGS2, ModelA and $T = 2$.s. . . . . 594
3.630 PVNGSv2: Histogram of differences for medians calculated with different weights to median calculated with total weights. Bottom row left shows differences between medians for the GMPE distribution to median calculated with total weights. Bottom row right shows differences between the original GMPEs (without uncertainty) to median calculated with total weights. For PVNGS2, ModelA and $T = 3$.s. . . . . 595

4.1 PVNGSv2: Deaggregation for a ground-motion level of 0.001g, calculated using a simple source model for PVNGS2 and the center model of the ModelB distribution. For $T = 0.01$s. . . . . 596
4.2 PVNGSv2: Deaggregation for a ground-motion level of 0.001g, calculated using a simple source model for PVNGS2 and the center model of the ModelB distribution. For $T = 0.02$s. . . . . 597
4.3 PVNGSv2: Deaggregation for a ground-motion level of 0.001g, calculated using a simple source model for PVNGS2 and the center model of the ModelB distribution. For $T = 0.03$s. . . . . 597
4.4 PVNGSv2: Deaggregation for a ground-motion level of 0.001g, calculated using a simple source model for PVNGS2 and the center model of the ModelB distribution. For $T = 0.05$s. . . . . 598
4.5 PVNGSv2: Deaggregation for a ground-motion level of 0.001g, calculated using a simple source model for PVNGS2 and the center model of the ModelB distribution. For $T = 0.075$s. . . . . 598
4.6 PVNGSv2: Deaggregation for a ground-motion level of 0.001g, calculated using a simple source model for PVNGS2 and the center model of the ModelB distribution. For $T = 0.1$s. . . . . 599
4.7 PVNGSv2: Deaggregation for a ground-motion level of 0.001g, calculated using a simple source model for PVNGS2 and the center model of the ModelB distribution. For $T = 0.15$s. . . . . 599
4.8 PVNGSv2: Deaggregation for a ground-motion level of 0.001g, calculated using a simple source model for PVNGS2 and the center model of the ModelB distribution. For $T = 0.2$s. . . . . 600
4.9 PVNGSv2: Deaggregation for a ground-motion level of 0.001g, calculated using a simple source model for PVNGS2 and the center model of the ModelB distribution. For $T = 0.25$s. . . . . 600
4.10 PVNGSv2: Deaggregation for a ground-motion level of 0.001g, calculated using a simple source model for PVNGS2 and the center model of the ModelB distribution. For $T = 0.3$s. . . . . 601
4.11 PVNGSv2: Deaggregation for a ground-motion level of 0.001g, calculated using a simple source model for PVNGS2 and the center model of the ModelB distribution. For $T = 0.4$s. . . . . 601
4.12 PVNGSv2: Deaggregation for a ground-motion level of 0.001g, calculated using a simple source model for PVNGS2 and the center model of the ModelB distribution. For $T = 0.5$s. . . . . 602
4.13 PVNGSv2: Deaggregation for a ground-motion level of 0.001g, calculated using a simple source model for PVNGS2 and the center model of the ModelB distribution. For $T = 0.75$s. . . . . 602
4.14 PVNGSv2: Deaggregation for a ground-motion level of 0.g, calculated using a simple source model for PVNGS2 and the center model of the ModelB distribution. For $T = 1$.s. . . . . 603
4.15 PVNGSv2: Deaggregation for a ground-motion level of 0.g, calculated using a simple source model for PVNGS2 and the center model of the ModelB distribution. For $T = 1.5$s. . . . . 603
4.16 PVNGSv2: Deaggregation for a ground-motion level of 0.g, calculated using a simple source model for PVNGS2 and the center model of the ModelB distribution. For $T = 2$.s. . . . . 604
4.17 PVNGSv2: Deaggregation for a ground-motion level of 0.g, calculated using a simple source model for PVNGS2 and the center model of the ModelB distribution. For $T = 3$.s. . . . . 604
4.18 PVNGSv2: Deaggregation for a ground-motion level of 0.278g, calculated using a simple source model for PVNGS2 and the center model of the ModelB distribution. For $T = 0.01$s. . . . . 605
4.19 PVNGSv2: Deaggregation for a ground-motion level of 0.266g, calculated using a simple source model for PVNGS2 and the center model of the ModelB distribution. For $T = 0.02$s. . . . . 605
4.20 PVNGSv2: Deaggregation for a ground-motion level of 0.29g, calculated using a simple source model for PVNGS2 and the center model of the ModelB distribution. For $T = 0.03$s. . . . . 606
4.21 PVNGSv2: Deaggregation for a ground-motion level of 0.358g, calculated using a simple source model for PVNGS2 and the center model of the ModelB distribution. For $T = 0.05$s. . . . . 606
4.22 PVNGSv2: Deaggregation for a ground-motion level of 0.407g, calculated using a simple source model for PVNGS2 and the center model of the ModelB distribution. For $T = 0.075$s. . . . . 607
4.23 PVNGSv2: Deaggregation for a ground-motion level of 0.427g, calculated using a simple source model for PVNGS2 and the center model of the ModelB distribution. For $T = 0.1$s. . . . . 607
4.24 PVNGSv2: Deaggregation for a ground-motion level of 0.475g, calculated using a simple source model for PVNGS2 and the center model of the ModelB distribution. For $T = 0.15$s. . . . . 608

4.25 PVNGSv2: Deaggregation for a ground-motion level of 0.456g, calculated using a simple source model for PVNGS2 and the center model of the ModelB distribution. For $T = 0.2$s. . . . 608
4.26 PVNGSv2: Deaggregation for a ground-motion level of 0.427g, calculated using a simple source model for PVNGS2 and the center model of the ModelB distribution. For $T = 0.25$s. . . . 609
4.27 PVNGSv2: Deaggregation for a ground-motion level of 0.387g, calculated using a simple source model for PVNGS2 and the center model of the ModelB distribution. For $T = 0.3$s. . . . 609
4.28 PVNGSv2: Deaggregation for a ground-motion level of 0.358g, calculated using a simple source model for PVNGS2 and the center model of the ModelB distribution. For $T = 0.4$s. . . . 610
4.29 PVNGSv2: Deaggregation for a ground-motion level of 0.313g, calculated using a simple source model for PVNGS2 and the center model of the ModelB distribution. For $T = 0.5$s. . . . 610
4.30 PVNGSv2: Deaggregation for a ground-motion level of 0.214g, calculated using a simple source model for PVNGS2 and the center model of the ModelB distribution. For $T = 0.75$s. . . . 611
4.31 PVNGSv2: Deaggregation for a ground-motion level of 0.139g, calculated using a simple source model for PVNGS2 and the center model of the ModelB distribution. For $T = 1$.s. . . . 611
4.32 PVNGSv2: Deaggregation for a ground-motion level of 0.098g, calculated using a simple source model for PVNGS2 and the center model of the ModelB distribution. For $T = 1.5$s. . . . 612
4.33 PVNGSv2: Deaggregation for a ground-motion level of 0.075g, calculated using a simple source model for PVNGS2 and the center model of the ModelB distribution. For $T = 2$.s. . . . 612
4.34 PVNGSv2: Deaggregation for a ground-motion level of 0.043g, calculated using a simple source model for PVNGS2 and the center model of the ModelB distribution. For $T = 3$.s. . . . 613
4.35 PVNGSv2: Contour Plots used for selection. For $T = 0.01$s. . . . 614
4.36 PVNGSv2: Contour Plots used for selection. For $T = 0.02$s. . . . 615
4.37 PVNGSv2: Contour Plots used for selection. For $T = 0.03$s. . . . 616
4.38 PVNGSv2: Contour Plots used for selection. For $T = 0.05$s. . . . 617
4.39 PVNGSv2: Contour Plots used for selection. For $T = 0.075$s. . . . 618
4.40 PVNGSv2: Contour Plots used for selection. For $T = 0.1$s. . . . 619
4.41 PVNGSv2: Contour Plots used for selection. For $T = 0.15$s. . . . 620
4.42 PVNGSv2: Contour Plots used for selection. For $T = 0.2$s. . . . 621
4.43 PVNGSv2: Contour Plots used for selection. For $T = 0.25$s. . . . 622
4.44 PVNGSv2: Contour Plots used for selection. For $T = 0.3$s. . . . 623
4.45 PVNGSv2: Contour Plots used for selection. For $T = 0.4$s. . . . 624
4.46 PVNGSv2: Contour Plots used for selection. For $T = 0.5$s. . . . 625
4.47 PVNGSv2: Contour Plots used for selection. For $T = 0.75$s. . . . 626
4.48 PVNGSv2: Contour Plots used for selection. For $T = 1$.s. . . . 627
4.49 PVNGSv2: Contour Plots used for selection. For $T = 1.5$s. . . . 628
4.50 PVNGSv2: Contour Plots used for selection. For $T = 2$.s. . . . 629
4.51 PVNGSv2: Contour Plots used for selection. For $T = 3$.s. . . . 630
4.52 PVNGSv2: Contour Plots used for weighting. For $T = 0.01, 0.02, 0.03, 0.05, 0.075, 0.1, 0.15, 0.2, 0.25, 0.3, 0.4, 0.5, 0.75, 1.,$
4.53 PVNGSv2: Contour Plots used for weighting. For $T = 0.01, 0.02, 0.03, 0.05, 0.075, 0.1, 0.15, 0.2, 0.25, 0.3, 0.4, 0.5, 0.75, 1.,$
4.54 PVNGSv2: Contour Plots used for weighting. For $T = 0.01, 0.02, 0.03, 0.05, 0.075, 0.1, 0.15, 0.2, 0.25, 0.3, 0.4, 0.5, 0.75, 1.,$
4.55 PVNGSv2: Contour Plots used for weighting. For $T = 0.01, 0.02, 0.03, 0.05, 0.075, 0.1, 0.15, 0.2, 0.25, 0.3, 0.4, 0.5, 0.75, 1.,$
4.56 PVNGSv2: Contour Plots used for weighting. For $T = 0.01, 0.02, 0.03, 0.05, 0.075, 0.1, 0.15, 0.2, 0.25, 0.3, 0.4, 0.5, 0.75, 1.,$
4.57 PVNGSv2: Contour Plots used for weighting. For $T = 0.01, 0.02, 0.03, 0.05, 0.075, 0.1, 0.15, 0.2, 0.25, 0.3, 0.4, 0.5, 0.75, 1.,$
4.58 PVNGSv2: Contour Plots used for weighting. For $T = 0.01, 0.02, 0.03, 0.05, 0.075, 0.1, 0.15, 0.2, 0.25, 0.3, 0.4, 0.5, 0.75, 1.,$
4.59 PVNGSv2: Contour Plots used for weighting. For $T = 0.01, 0.02, 0.03, 0.05, 0.075, 0.1, 0.15, 0.2, 0.25, 0.3, 0.4, 0.5, 0.75, 1.,$
4.60 PVNGSv2: Contour Plots used for weighting. For $T = 0.01, 0.02, 0.03, 0.05, 0.075, 0.1, 0.15, 0.2, 0.25, 0.3, 0.4, 0.5, 0.75, 1.,$
4.61 PVNGSv2: Contour Plots used for weighting. For $T = 0.01, 0.02, 0.03, 0.05, 0.075, 0.1, 0.15, 0.2, 0.25, 0.3, 0.4, 0.5, 0.75, 1.,$
4.62 PVNGSv2: Contour Plots used for weighting. For $T = 0.01, 0.02, 0.03, 0.05, 0.075, 0.1, 0.15, 0.2, 0.25, 0.3, 0.4, 0.5, 0.75, 1.,$
4.63 PVNGSv2: Contour Plots used for weighting. For $T = 0.01, 0.02, 0.03, 0.05, 0.075, 0.1, 0.15, 0.2, 0.25, 0.3, 0.4, 0.5, 0.75, 1.,$
4.64 PVNGSv2: Contour Plots used for weighting. For $T = 0.01, 0.02, 0.03, 0.05, 0.075, 0.1, 0.15, 0.2, 0.25, 0.3, 0.4, 0.5, 0.75, 1.,$
4.65 PVNGSv2: Contour Plots used for weighting. For $T = 0.01, 0.02, 0.03, 0.05, 0.075, 0.1, 0.15, 0.2, 0.25, 0.3, 0.4, 0.5, 0.75, 1.,$
4.66 PVNGSv2: Contour Plots used for weighting. For $T = 0.01, 0.02, 0.03, 0.05, 0.075, 0.1, 0.15, 0.2, 0.25, 0.3, 0.4, 0.5, 0.75, 1.,$
4.67 PVNGSv2: Contour Plots used for weighting. For $T = 0.01, 0.02, 0.03, 0.05, 0.075, 0.1, 0.15, 0.2, 0.25, 0.3, 0.4, 0.5, 0.75, 1.,$
4.68 PVNGSv2: Contour Plots used for weighting. For $T = 0.01, 0.02, 0.03, 0.05, 0.075, 0.1, 0.15, 0.2, 0.25, 0.3, 0.4, 0.5, 0.75, 1.,$
4.69 Hazard curves, calculated for a simple source model for PVNGS2. Left: 2000 hazard curves for all sampled B-models (gray) and the center model of the ModelB distribution (red); Right: hazard curves of selected models. For $T = 0.01$s. . . . 648
4.70 Hazard curves, calculated for a simple source model for PVNGS2. Left: 2000 hazard curves for all sampled B-models (gray) and the center model of the ModelB distribution (red); Right: hazard curves of selected models. For $T = 0.02$s. . . . 648

4.71 Hazard curves, calculated for a simple source model for PVNGS2. Left: 2000 hazard curves for all sampled B-models (gray) and the center model of the ModelB distribution (red); Right: hazard curves of selected models. For $T = 0.03$s. . . . 649
4.72 Hazard curves, calculated for a simple source model for PVNGS2. Left: 2000 hazard curves for all sampled B-models (gray) and the center model of the ModelB distribution (red); Right: hazard curves of selected models. For $T = 0.05$s. . . . 649
4.73 Hazard curves, calculated for a simple source model for PVNGS2. Left: 2000 hazard curves for all sampled B-models (gray) and the center model of the ModelB distribution (red); Right: hazard curves of selected models. For $T = 0.075$s. . . . 650
4.74 Hazard curves, calculated for a simple source model for PVNGS2. Left: 2000 hazard curves for all sampled B-models (gray) and the center model of the ModelB distribution (red); Right: hazard curves of selected models. For $T = 0.1$s. . . . 650
4.75 Hazard curves, calculated for a simple source model for PVNGS2. Left: 2000 hazard curves for all sampled B-models (gray) and the center model of the ModelB distribution (red); Right: hazard curves of selected models. For $T = 0.15$s. . . . 651
4.76 Hazard curves, calculated for a simple source model for PVNGS2. Left: 2000 hazard curves for all sampled B-models (gray) and the center model of the ModelB distribution (red); Right: hazard curves of selected models. For $T = 0.2$s. . . . 651
4.77 Hazard curves, calculated for a simple source model for PVNGS2. Left: 2000 hazard curves for all sampled B-models (gray) and the center model of the ModelB distribution (red); Right: hazard curves of selected models. For $T = 0.25$s. . . . 652
4.78 Hazard curves, calculated for a simple source model for PVNGS2. Left: 2000 hazard curves for all sampled B-models (gray) and the center model of the ModelB distribution (red); Right: hazard curves of selected models. For $T = 0.3$s. . . . 652
4.79 Hazard curves, calculated for a simple source model for PVNGS2. Left: 2000 hazard curves for all sampled B-models (gray) and the center model of the ModelB distribution (red); Right: hazard curves of selected models. For $T = 0.4$s. . . . 653
4.80 Hazard curves, calculated for a simple source model for PVNGS2. Left: 2000 hazard curves for all sampled B-models (gray) and the center model of the ModelB distribution (red); Right: hazard curves of selected models. For $T = 0.5$s. . . . 653
4.81 Hazard curves, calculated for a simple source model for PVNGS2. Left: 2000 hazard curves for all sampled B-models (gray) and the center model of the ModelB distribution (red); Right: hazard curves of selected models. For $T = 0.75$s. . . . 654
4.82 Hazard curves, calculated for a simple source model for PVNGS2. Left: 2000 hazard curves for all sampled B-models (gray) and the center model of the ModelB distribution (red); Right: hazard curves of selected models. For $T = 1$.s. . . . 654
4.83 Hazard curves, calculated for a simple source model for PVNGS2. Left: 2000 hazard curves for all sampled B-models (gray) and the center model of the ModelB distribution (red); Right: hazard curves of selected models. For $T = 1.5$s. . . . 655
4.84 Hazard curves, calculated for a simple source model for PVNGS2. Left: 2000 hazard curves for all sampled B-models (gray) and the center model of the ModelB distribution (red); Right: hazard curves of selected models. For $T = 2$.s. . . . 655
4.85 Hazard curves, calculated for a simple source model for PVNGS2. Left: 2000 hazard curves for all sampled B-models (gray) and the center model of the ModelB distribution (red); Right: hazard curves of selected models. For $T = 3$.s. . . . 656
4.86 PVNGSv2: CDF for $M = 5.$, $R_x = -50.$, $F = 0$, and $T = 0.01$ . . . 657
4.87 PVNGSv2: CDF for $M = 5.$, $R_x = -30.$, $F = 0$, and $T = 0.01$ . . . 657
4.88 PVNGSv2: CDF for $M = 5.$, $R_x = -15.$, $F = 0$, and $T = 0.01$ . . . 658
4.89 PVNGSv2: CDF for $M = 5.$, $R_x = -5.$, $F = 0$, and $T = 0.01$ . . . 658
4.90 PVNGSv2: CDF for $M = 5.$, $R_x = 5.$, $F = 0$, and $T = 0.01$ . . . 658
4.91 PVNGSv2: CDF for $M = 5.$, $R_x = 15.$, $F = 0$, and $T = 0.01$ . . . 659
4.92 PVNGSv2: CDF for $M = 6.$, $R_x = -50.$, $F = 0$, and $T = 0.01$ . . . 660
4.93 PVNGSv2: CDF for $M = 6.$, $R_x = -30.$, $F = 0$, and $T = 0.01$ . . . 660
4.94 PVNGSv2: CDF for $M = 6.$, $R_x = -15.$, $F = 0$, and $T = 0.01$ . . . 661
4.95 PVNGSv2: CDF for $M = 6.$, $R_x = -5.$, $F = 0$, and $T = 0.01$ . . . 661
4.96 PVNGSv2: CDF for $M = 6.$, $R_x = 5.$, $F = 0$, and $T = 0.01$ . . . 661
4.97 PVNGSv2: CDF for $M = 6.$, $R_x = 15.$, $F = 0$, and $T = 0.01$ . . . 662
4.98 PVNGSv2: CDF for $M = 7.$, $R_x = -50.$, $F = 0$, and $T = 0.01$ . . . 663
4.99 PVNGSv2: CDF for $M = 7.$, $R_x = -30.$, $F = 0$, and $T = 0.01$ . . . 663
4.100 PVNGSv2: CDF for $M = 7.$, $R_x = -15.$, $F = 0$, and $T = 0.01$ . . . 664
4.101 PVNGSv2: CDF for $M = 7.$, $R_x = -5.$, $F = 0$, and $T = 0.01$ . . . 664

4.102PVNGSv2: CDF for $M = 7.$, $R_x = 5.$, $F = 0$, and $T = 0.01$ . . . 664
4.103PVNGSv2: CDF for $M = 7.$, $R_x = 15.$, $F = 0$, and $T = 0.01$ . . . 665
4.104PVNGSv2: CDF for $M = 5.$, $R_x = -50.$, $F = -1$, and $T = 0.01$ . . . 666
4.105PVNGSv2: CDF for $M = 5.$, $R_x = -30.$, $F = -1$, and $T = 0.01$ . . . 666
4.106PVNGSv2: CDF for $M = 5.$, $R_x = -15.$, $F = -1$, and $T = 0.01$ . . . 667
4.107PVNGSv2: CDF for $M = 5.$, $R_x = -5.$, $F = -1$, and $T = 0.01$ . . . 667
4.108PVNGSv2: CDF for $M = 5.$, $R_x = 5.$, $F = -1$, and $T = 0.01$ . . . 667
4.109PVNGSv2: CDF for $M = 5.$, $R_x = 15.$, $F = -1$, and $T = 0.01$ . . . 668
4.110PVNGSv2: CDF for $M = 6.$, $R_x = -50.$, $F = -1$, and $T = 0.01$ . . . 669
4.111PVNGSv2: CDF for $M = 6.$, $R_x = -30.$, $F = -1$, and $T = 0.01$ . . . 669
4.112PVNGSv2: CDF for $M = 6.$, $R_x = -15.$, $F = -1$, and $T = 0.01$ . . . 670
4.113PVNGSv2: CDF for $M = 6.$, $R_x = -5.$, $F = -1$, and $T = 0.01$ . . . 670
4.114PVNGSv2: CDF for $M = 6.$, $R_x = 5.$, $F = -1$, and $T = 0.01$ . . . 670
4.115PVNGSv2: CDF for $M = 6.$, $R_x = 15.$, $F = -1$, and $T = 0.01$ . . . 671
4.116PVNGSv2: CDF for $M = 7.$, $R_x = -50.$, $F = -1$, and $T = 0.01$ . . . 672
4.117PVNGSv2: CDF for $M = 7.$, $R_x = -30.$, $F = -1$, and $T = 0.01$ . . . 672
4.118PVNGSv2: CDF for $M = 7.$, $R_x = -15.$, $F = -1$, and $T = 0.01$ . . . 673
4.119PVNGSv2: CDF for $M = 7.$, $R_x = -5.$, $F = -1$, and $T = 0.01$ . . . 673
4.120PVNGSv2: CDF for $M = 7.$, $R_x = 5.$, $F = -1$, and $T = 0.01$ . . . 673
4.121PVNGSv2: CDF for $M = 7.$, $R_x = 15.$, $F = -1$, and $T = 0.01$ . . . 674
4.122PVNGSv2: CDF for $M = 5.$, $R_x = -50.$, $F = 0$, and $T = 0.2$ . . . 675
4.123PVNGSv2: CDF for $M = 5.$, $R_x = -30.$, $F = 0$, and $T = 0.2$ . . . 675
4.124PVNGSv2: CDF for $M = 5.$, $R_x = -15.$, $F = 0$, and $T = 0.2$ . . . 676
4.125PVNGSv2: CDF for $M = 5.$, $R_x = -5.$, $F = 0$, and $T = 0.2$ . . . 676
4.126PVNGSv2: CDF for $M = 5.$, $R_x = 5.$, $F = 0$, and $T = 0.2$ . . . 676
4.127PVNGSv2: CDF for $M = 5.$, $R_x = 15.$, $F = 0$, and $T = 0.2$ . . . 677
4.128PVNGSv2: CDF for $M = 6.$, $R_x = -50.$, $F = 0$, and $T = 0.2$ . . . 678
4.129PVNGSv2: CDF for $M = 6.$, $R_x = -30.$, $F = 0$, and $T = 0.2$ . . . 678
4.130PVNGSv2: CDF for $M = 6.$, $R_x = -15.$, $F = 0$, and $T = 0.2$ . . . 679
4.131PVNGSv2: CDF for $M = 6.$, $R_x = -5.$, $F = 0$, and $T = 0.2$ . . . 679
4.132PVNGSv2: CDF for $M = 6.$, $R_x = 5.$, $F = 0$, and $T = 0.2$ . . . 679
4.133PVNGSv2: CDF for $M = 6.$, $R_x = 15.$, $F = 0$, and $T = 0.2$ . . . 680
4.134PVNGSv2: CDF for $M = 7.$, $R_x = -50.$, $F = 0$, and $T = 0.2$ . . . 681
4.135PVNGSv2: CDF for $M = 7.$, $R_x = -30.$, $F = 0$, and $T = 0.2$ . . . 681
4.136PVNGSv2: CDF for $M = 7.$, $R_x = -15.$, $F = 0$, and $T = 0.2$ . . . 682
4.137PVNGSv2: CDF for $M = 7.$, $R_x = -5.$, $F = 0$, and $T = 0.2$ . . . 682
4.138PVNGSv2: CDF for $M = 7.$, $R_x = 5.$, $F = 0$, and $T = 0.2$ . . . 682
4.139PVNGSv2: CDF for $M = 7.$, $R_x = 15.$, $F = 0$, and $T = 0.2$ . . . 683
4.140PVNGSv2: CDF for $M = 5.$, $R_x = -50.$, $F = -1$, and $T = 0.2$ . . . 684
4.141PVNGSv2: CDF for $M = 5.$, $R_x = -30.$, $F = -1$, and $T = 0.2$ . . . 684
4.142PVNGSv2: CDF for $M = 5.$, $R_x = -15.$, $F = -1$, and $T = 0.2$ . . . 685
4.143PVNGSv2: CDF for $M = 5.$, $R_x = -5.$, $F = -1$, and $T = 0.2$ . . . 685
4.144PVNGSv2: CDF for $M = 5.$, $R_x = 5.$, $F = -1$, and $T = 0.2$ . . . 685
4.145PVNGSv2: CDF for $M = 5.$, $R_x = 15.$, $F = -1$, and $T = 0.2$ . . . 686
4.146PVNGSv2: CDF for $M = 6.$, $R_x = -50.$, $F = -1$, and $T = 0.2$ . . . 687
4.147PVNGSv2: CDF for $M = 6.$, $R_x = -30.$, $F = -1$, and $T = 0.2$ . . . 687
4.148PVNGSv2: CDF for $M = 6.$, $R_x = -15.$, $F = -1$, and $T = 0.2$ . . . 688
4.149PVNGSv2: CDF for $M = 6.$, $R_x = -5.$, $F = -1$, and $T = 0.2$ . . . 688
4.150PVNGSv2: CDF for $M = 6.$, $R_x = 5.$, $F = -1$, and $T = 0.2$ . . . 688
4.151PVNGSv2: CDF for $M = 6.$, $R_x = 15.$, $F = -1$, and $T = 0.2$ . . . 689
4.152PVNGSv2: CDF for $M = 7.$, $R_x = -50.$, $F = -1$, and $T = 0.2$ . . . 690
4.153PVNGSv2: CDF for $M = 7.$, $R_x = -30.$, $F = -1$, and $T = 0.2$ . . . 690
4.154PVNGSv2: CDF for $M = 7.$, $R_x = -15.$, $F = -1$, and $T = 0.2$ . . . 691
4.155PVNGSv2: CDF for $M = 7.$, $R_x = -5.$, $F = -1$, and $T = 0.2$ . . . 691
4.156PVNGSv2: CDF for $M = 7.$, $R_x = 5.$, $F = -1$, and $T = 0.2$ . . . 691
4.157PVNGSv2: CDF for $M = 7.$, $R_x = 15.$, $F = -1$, and $T = 0.2$ . . . 692
4.158PVNGSv2: CDF for $M = 5.$, $R_x = -50.$, $F = 0$, and $T = 0.5$ . . . 693
4.159PVNGSv2: CDF for $M = 5.$, $R_x = -30.$, $F = 0$, and $T = 0.5$ . . . 693
4.160PVNGSv2: CDF for $M = 5.$, $R_x = -15.$, $F = 0$, and $T = 0.5$ . . . 694
4.161PVNGSv2: CDF for $M = 5.$, $R_x = -5.$, $F = 0$, and $T = 0.5$ . . . 694
4.162PVNGSv2: CDF for $M = 5.$, $R_x = 5.$, $F = 0$, and $T = 0.5$ . . . 694

4.163PVNGSv2: CDF for $M = 5.$, $R_x = 15.$, $F = 0$, and $T = 0.5$ . . . 695
4.164PVNGSv2: CDF for $M = 6.$, $R_x = -50.$, $F = 0$, and $T = 0.5$ . . . 696
4.165PVNGSv2: CDF for $M = 6.$, $R_x = -30.$, $F = 0$, and $T = 0.5$ . . . 696
4.166PVNGSv2: CDF for $M = 6.$, $R_x = -15.$, $F = 0$, and $T = 0.5$ . . . 697
4.167PVNGSv2: CDF for $M = 6.$, $R_x = -5.$, $F = 0$, and $T = 0.5$ . . . 697
4.168PVNGSv2: CDF for $M = 6.$, $R_x = 5.$, $F = 0$, and $T = 0.5$ . . . 697
4.169PVNGSv2: CDF for $M = 6.$, $R_x = 15.$, $F = 0$, and $T = 0.5$ . . . 698
4.170PVNGSv2: CDF for $M = 7.$, $R_x = -50.$, $F = 0$, and $T = 0.5$ . . . 699
4.171PVNGSv2: CDF for $M = 7.$, $R_x = -30.$, $F = 0$, and $T = 0.5$ . . . 699
4.172PVNGSv2: CDF for $M = 7.$, $R_x = -15.$, $F = 0$, and $T = 0.5$ . . . 700
4.173PVNGSv2: CDF for $M = 7.$, $R_x = -5.$, $F = 0$, and $T = 0.5$ . . . 700
4.174PVNGSv2: CDF for $M = 7.$, $R_x = 5.$, $F = 0$, and $T = 0.5$ . . . 700
4.175PVNGSv2: CDF for $M = 7.$, $R_x = 15.$, $F = 0$, and $T = 0.5$ . . . 701
4.176PVNGSv2: CDF for $M = 5.$, $R_x = -50.$, $F = -1$, and $T = 0.5$ . . . 702
4.177PVNGSv2: CDF for $M = 5.$, $R_x = -30.$, $F = -1$, and $T = 0.5$ . . . 702
4.178PVNGSv2: CDF for $M = 5.$, $R_x = -15.$, $F = -1$, and $T = 0.5$ . . . 703
4.179PVNGSv2: CDF for $M = 5.$, $R_x = -5.$, $F = -1$, and $T = 0.5$ . . . 703
4.180PVNGSv2: CDF for $M = 5.$, $R_x = 5.$, $F = -1$, and $T = 0.5$ . . . 703
4.181PVNGSv2: CDF for $M = 5.$, $R_x = 15.$, $F = -1$, and $T = 0.5$ . . . 704
4.182PVNGSv2: CDF for $M = 6.$, $R_x = -50.$, $F = -1$, and $T = 0.5$ . . . 705
4.183PVNGSv2: CDF for $M = 6.$, $R_x = -30.$, $F = -1$, and $T = 0.5$ . . . 705
4.184PVNGSv2: CDF for $M = 6.$, $R_x = -15.$, $F = -1$, and $T = 0.5$ . . . 706
4.185PVNGSv2: CDF for $M = 6.$, $R_x = -5.$, $F = -1$, and $T = 0.5$ . . . 706
4.186PVNGSv2: CDF for $M = 6.$, $R_x = 5.$, $F = -1$, and $T = 0.5$ . . . 706
4.187PVNGSv2: CDF for $M = 6.$, $R_x = 15.$, $F = -1$, and $T = 0.5$ . . . 707
4.188PVNGSv2: CDF for $M = 7.$, $R_x = -50.$, $F = -1$, and $T = 0.5$ . . . 708
4.189PVNGSv2: CDF for $M = 7.$, $R_x = -30.$, $F = -1$, and $T = 0.5$ . . . 708
4.190PVNGSv2: CDF for $M = 7.$, $R_x = -15.$, $F = -1$, and $T = 0.5$ . . . 709
4.191PVNGSv2: CDF for $M = 7.$, $R_x = -5.$, $F = -1$, and $T = 0.5$ . . . 709
4.192PVNGSv2: CDF for $M = 7.$, $R_x = 5.$, $F = -1$, and $T = 0.5$ . . . 709
4.193PVNGSv2: CDF for $M = 7.$, $R_x = 15.$, $F = -1$, and $T = 0.5$ . . . 710
4.194PVNGSv2: CDF for $M = 5.$, $R_x = -50.$, $F = 0$, and $T = 1.$ . . . 711
4.195PVNGSv2: CDF for $M = 5.$, $R_x = -30.$, $F = 0$, and $T = 1.$ . . . 711
4.196PVNGSv2: CDF for $M = 5.$, $R_x = -15.$, $F = 0$, and $T = 1.$ . . . 712
4.197PVNGSv2: CDF for $M = 5.$, $R_x = -5.$, $F = 0$, and $T = 1.$ . . . 712
4.198PVNGSv2: CDF for $M = 5.$, $R_x = 5.$, $F = 0$, and $T = 1.$ . . . 712
4.199PVNGSv2: CDF for $M = 5.$, $R_x = 15.$, $F = 0$, and $T = 1.$ . . . 713
4.200PVNGSv2: CDF for $M = 6.$, $R_x = -50.$, $F = 0$, and $T = 1.$ . . . 714
4.201PVNGSv2: CDF for $M = 6.$, $R_x = -30.$, $F = 0$, and $T = 1.$ . . . 714
4.202PVNGSv2: CDF for $M = 6.$, $R_x = -15.$, $F = 0$, and $T = 1.$ . . . 715
4.203PVNGSv2: CDF for $M = 6.$, $R_x = -5.$, $F = 0$, and $T = 1.$ . . . 715
4.204PVNGSv2: CDF for $M = 6.$, $R_x = 5.$, $F = 0$, and $T = 1.$ . . . 715
4.205PVNGSv2: CDF for $M = 6.$, $R_x = 15.$, $F = 0$, and $T = 1.$ . . . 716
4.206PVNGSv2: CDF for $M = 7.$, $R_x = -50.$, $F = 0$, and $T = 1.$ . . . 717
4.207PVNGSv2: CDF for $M = 7.$, $R_x = -30.$, $F = 0$, and $T = 1.$ . . . 717
4.208PVNGSv2: CDF for $M = 7.$, $R_x = -15.$, $F = 0$, and $T = 1.$ . . . 718
4.209PVNGSv2: CDF for $M = 7.$, $R_x = -5.$, $F = 0$, and $T = 1.$ . . . 718
4.210PVNGSv2: CDF for $M = 7.$, $R_x = 5.$, $F = 0$, and $T = 1.$ . . . 718
4.211PVNGSv2: CDF for $M = 7.$, $R_x = 15.$, $F = 0$, and $T = 1.$ . . . 719
4.212PVNGSv2: CDF for $M = 5.$, $R_x = -50.$, $F = -1$, and $T = 1.$ . . . 720
4.213PVNGSv2: CDF for $M = 5.$, $R_x = -30.$, $F = -1$, and $T = 1.$ . . . 720
4.214PVNGSv2: CDF for $M = 5.$, $R_x = -15.$, $F = -1$, and $T = 1.$ . . . 721
4.215PVNGSv2: CDF for $M = 5.$, $R_x = -5.$, $F = -1$, and $T = 1.$ . . . 721
4.216PVNGSv2: CDF for $M = 5.$, $R_x = 5.$, $F = -1$, and $T = 1.$ . . . 721
4.217PVNGSv2: CDF for $M = 5.$, $R_x = 15.$, $F = -1$, and $T = 1.$ . . . 722
4.218PVNGSv2: CDF for $M = 6.$, $R_x = -50.$, $F = -1$, and $T = 1.$ . . . 723
4.219PVNGSv2: CDF for $M = 6.$, $R_x = -30.$, $F = -1$, and $T = 1.$ . . . 723
4.220PVNGSv2: CDF for $M = 6.$, $R_x = -15.$, $F = -1$, and $T = 1.$ . . . 724
4.221PVNGSv2: CDF for $M = 6.$, $R_x = -5.$, $F = -1$, and $T = 1.$ . . . 724
4.222PVNGSv2: CDF for $M = 6.$, $R_x = 5.$, $F = -1$, and $T = 1.$ . . . 724
4.223PVNGSv2: CDF for $M = 6.$, $R_x = 15.$, $F = -1$, and $T = 1.$ . . . 725

4.224PVNGSv2: CDF for $M = 7.$, $R_x = -50.$, $F = -1$, and $T = 1.$ . . . 726
4.225PVNGSv2: CDF for $M = 7.$, $R_x = -30.$, $F = -1$, and $T = 1.$ . . . 726
4.226PVNGSv2: CDF for $M = 7.$, $R_x = -15.$, $F = -1$, and $T = 1.$ . . . 727
4.227PVNGSv2: CDF for $M = 7.$, $R_x = -5.$, $F = -1$, and $T = 1.$ . . . 727
4.228PVNGSv2: CDF for $M = 7.$, $R_x = 5.$, $F = -1$, and $T = 1.$ . . . 727
4.229PVNGSv2: CDF for $M = 7.$, $R_x = 15.$, $F = -1$, and $T = 1.$ . . . 728
4.230PVNGSv2: CDF for $M = 5.$, $R_x = -50.$, $F = 0$, and $T = 3.$ . . . 729
4.231PVNGSv2: CDF for $M = 5.$, $R_x = -30.$, $F = 0$, and $T = 3.$ . . . 729
4.232PVNGSv2: CDF for $M = 5.$, $R_x = -15.$, $F = 0$, and $T = 3.$ . . . 730
4.233PVNGSv2: CDF for $M = 5.$, $R_x = -5.$, $F = 0$, and $T = 3.$ . . . 730
4.234PVNGSv2: CDF for $M = 5.$, $R_x = 5.$, $F = 0$, and $T = 3.$ . . . 730
4.235PVNGSv2: CDF for $M = 5.$, $R_x = 15.$, $F = 0$, and $T = 3.$ . . . 731
4.236PVNGSv2: CDF for $M = 6.$, $R_x = -50.$, $F = 0$, and $T = 3.$ . . . 732
4.237PVNGSv2: CDF for $M = 6.$, $R_x = -30.$, $F = 0$, and $T = 3.$ . . . 732
4.238PVNGSv2: CDF for $M = 6.$, $R_x = -15.$, $F = 0$, and $T = 3.$ . . . 733
4.239PVNGSv2: CDF for $M = 6.$, $R_x = -5.$, $F = 0$, and $T = 3.$ . . . 733
4.240PVNGSv2: CDF for $M = 6.$, $R_x = 5.$, $F = 0$, and $T = 3.$ . . . 733
4.241PVNGSv2: CDF for $M = 6.$, $R_x = 15.$, $F = 0$, and $T = 3.$ . . . 734
4.242PVNGSv2: CDF for $M = 7.$, $R_x = -50.$, $F = 0$, and $T = 3.$ . . . 735
4.243PVNGSv2: CDF for $M = 7.$, $R_x = -30.$, $F = 0$, and $T = 3.$ . . . 735
4.244PVNGSv2: CDF for $M = 7.$, $R_x = -15.$, $F = 0$, and $T = 3.$ . . . 736
4.245PVNGSv2: CDF for $M = 7.$, $R_x = -5.$, $F = 0$, and $T = 3.$ . . . 736
4.246PVNGSv2: CDF for $M = 7.$, $R_x = 5.$, $F = 0$, and $T = 3.$ . . . 736
4.247PVNGSv2: CDF for $M = 7.$, $R_x = 15.$, $F = 0$, and $T = 3.$ . . . 737
4.248PVNGSv2: CDF for $M = 5.$, $R_x = -50.$, $F = -1$, and $T = 3.$ . . . 738
4.249PVNGSv2: CDF for $M = 5.$, $R_x = -30.$, $F = -1$, and $T = 3.$ . . . 738
4.250PVNGSv2: CDF for $M = 5.$, $R_x = -15.$, $F = -1$, and $T = 3.$ . . . 739
4.251PVNGSv2: CDF for $M = 5.$, $R_x = -5.$, $F = -1$, and $T = 3.$ . . . 739
4.252PVNGSv2: CDF for $M = 5.$, $R_x = 5.$, $F = -1$, and $T = 3.$ . . . 739
4.253PVNGSv2: CDF for $M = 5.$, $R_x = 15.$, $F = -1$, and $T = 3.$ . . . 740
4.254PVNGSv2: CDF for $M = 6.$, $R_x = -50.$, $F = -1$, and $T = 3.$ . . . 741
4.255PVNGSv2: CDF for $M = 6.$, $R_x = -30.$, $F = -1$, and $T = 3.$ . . . 741
4.256PVNGSv2: CDF for $M = 6.$, $R_x = -15.$, $F = -1$, and $T = 3.$ . . . 742
4.257PVNGSv2: CDF for $M = 6.$, $R_x = -5.$, $F = -1$, and $T = 3.$ . . . 742
4.258PVNGSv2: CDF for $M = 6.$, $R_x = 5.$, $F = -1$, and $T = 3.$ . . . 742
4.259PVNGSv2: CDF for $M = 6.$, $R_x = 15.$, $F = -1$, and $T = 3.$ . . . 743
4.260PVNGSv2: CDF for $M = 7.$, $R_x = -50.$, $F = -1$, and $T = 3.$ . . . 744
4.261PVNGSv2: CDF for $M = 7.$, $R_x = -30.$, $F = -1$, and $T = 3.$ . . . 744
4.262PVNGSv2: CDF for $M = 7.$, $R_x = -15.$, $F = -1$, and $T = 3.$ . . . 745
4.263PVNGSv2: CDF for $M = 7.$, $R_x = -5.$, $F = -1$, and $T = 3.$ . . . 745
4.264PVNGSv2: CDF for $M = 7.$, $R_x = 5.$, $F = -1$, and $T = 3.$ . . . 745
4.265PVNGSv2: CDF for $M = 7.$, $R_x = 15.$, $F = -1$, and $T = 3.$ . . . 746
4.266Distance scaling for $M = 5.$, $F = -1$, and $T = 0.01$ . . . 747
4.267Distance scaling for $M = 5.$, $F = 0$, and $T = 0.01$ . . . 747
4.268Distance scaling for $M = 6.$, $F = -1$, and $T = 0.01$ . . . 748
4.269Distance scaling for $M = 6.$, $F = 0$, and $T = 0.01$ . . . 748
4.270Distance scaling for $M = 7.$, $F = -1$, and $T = 0.01$ . . . 748
4.271Distance scaling for $M = 7.$, $F = 0$, and $T = 0.01$ . . . 749
4.272Distance scaling for $M = 5.$, $F = -1$, and $T = 0.2$ . . . 750
4.273Distance scaling for $M = 5.$, $F = 0$, and $T = 0.2$ . . . 750
4.274Distance scaling for $M = 6.$, $F = -1$, and $T = 0.2$ . . . 751
4.275Distance scaling for $M = 6.$, $F = 0$, and $T = 0.2$ . . . 751
4.276Distance scaling for $M = 7.$, $F = -1$, and $T = 0.2$ . . . 751
4.277Distance scaling for $M = 7.$, $F = 0$, and $T = 0.2$ . . . 752
4.278Distance scaling for $M = 5.$, $F = -1$, and $T = 0.5$ . . . 753
4.279Distance scaling for $M = 5.$, $F = 0$, and $T = 0.5$ . . . 753
4.280Distance scaling for $M = 6.$, $F = -1$, and $T = 0.5$ . . . 754
4.281Distance scaling for $M = 6.$, $F = 0$, and $T = 0.5$ . . . 754
4.282Distance scaling for $M = 7.$, $F = -1$, and $T = 0.5$ . . . 754
4.283Distance scaling for $M = 7.$, $F = 0$, and $T = 0.5$ . . . 755
4.284Distance scaling for $M = 5.$, $F = -1$, and $T = 1.$ . . . 756

4.285Distance scaling for $M = 5.$, $F = 0$, and $T = 1.$ . . . 756
4.286Distance scaling for $M = 6.$, $F = -1$, and $T = 1.$ . . . 757
4.287Distance scaling for $M = 6.$, $F = 0$, and $T = 1.$ . . . 757
4.288Distance scaling for $M = 7.$, $F = -1$, and $T = 1.$ . . . 757
4.289Distance scaling for $M = 7.$, $F = 0$, and $T = 1.$ . . . 758
4.290Distance scaling for $M = 5.$, $F = -1$, and $T = 3.$ . . . 759
4.291Distance scaling for $M = 5.$, $F = 0$, and $T = 3.$ . . . 759
4.292Distance scaling for $M = 6.$, $F = -1$, and $T = 3.$ . . . 760
4.293Distance scaling for $M = 6.$, $F = 0$, and $T = 3.$ . . . 760
4.294Distance scaling for $M = 7.$, $F = -1$, and $T = 3.$ . . . 760
4.295Distance scaling for $M = 7.$, $F = 0$, and $T = 3.$ . . . 761
4.296PVNGSv2: Distance scaling of quantiles with GMPEs for $M = 5.$, $F = 0$, and $T = 0.01$ . . . 762
4.297PVNGSv2: Distance scaling of quantiles with GMPEs for $M = 6.$, $F = 0$, and $T = 0.01$ . . . 762
4.298PVNGSv2: Distance scaling of quantiles with GMPEs for $M = 7.$, $F = 0$, and $T = 0.01$ . . . 763
4.299PVNGSv2: Distance scaling of quantiles with GMPEs for $M = 5.$, $F = -1$, and $T = 0.01$ . . . 763
4.300PVNGSv2: Distance scaling of quantiles with GMPEs for $M = 6.$, $F = -1$, and $T = 0.01$ . . . 764
4.301PVNGSv2: Distance scaling of quantiles with GMPEs for $M = 7.$, $F = -1$, and $T = 0.01$ . . . 764
4.302PVNGSv2: Distance scaling of quantiles with GMPEs for $M = 5.$, $F = 0$, and $T = 0.2$ . . . 765
4.303PVNGSv2: Distance scaling of quantiles with GMPEs for $M = 6.$, $F = 0$, and $T = 0.2$ . . . 765
4.304PVNGSv2: Distance scaling of quantiles with GMPEs for $M = 7.$, $F = 0$, and $T = 0.2$ . . . 766
4.305PVNGSv2: Distance scaling of quantiles with GMPEs for $M = 5.$, $F = -1$, and $T = 0.2$ . . . 766
4.306PVNGSv2: Distance scaling of quantiles with GMPEs for $M = 6.$, $F = -1$, and $T = 0.2$ . . . 767
4.307PVNGSv2: Distance scaling of quantiles with GMPEs for $M = 7.$, $F = -1$, and $T = 0.2$ . . . 767
4.308PVNGSv2: Distance scaling of quantiles with GMPEs for $M = 5.$, $F = 0$, and $T = 0.5$ . . . 768
4.309PVNGSv2: Distance scaling of quantiles with GMPEs for $M = 6.$, $F = 0$, and $T = 0.5$ . . . 768
4.310PVNGSv2: Distance scaling of quantiles with GMPEs for $M = 7.$, $F = 0$, and $T = 0.5$ . . . 769
4.311PVNGSv2: Distance scaling of quantiles with GMPEs for $M = 5.$, $F = -1$, and $T = 0.5$ . . . 769
4.312PVNGSv2: Distance scaling of quantiles with GMPEs for $M = 6.$, $F = -1$, and $T = 0.5$ . . . 770
4.313PVNGSv2: Distance scaling of quantiles with GMPEs for $M = 7.$, $F = -1$, and $T = 0.5$ . . . 770
4.314PVNGSv2: Distance scaling of quantiles with GMPEs for $M = 5.$, $F = 0$, and $T = 1.$ . . . 771
4.315PVNGSv2: Distance scaling of quantiles with GMPEs for $M = 6.$, $F = 0$, and $T = 1.$ . . . 771
4.316PVNGSv2: Distance scaling of quantiles with GMPEs for $M = 7.$, $F = 0$, and $T = 1.$ . . . 772
4.317PVNGSv2: Distance scaling of quantiles with GMPEs for $M = 5.$, $F = -1$, and $T = 1.$ . . . 772
4.318PVNGSv2: Distance scaling of quantiles with GMPEs for $M = 6.$, $F = -1$, and $T = 1.$ . . . 773
4.319PVNGSv2: Distance scaling of quantiles with GMPEs for $M = 7.$, $F = -1$, and $T = 1.$ . . . 773
4.320PVNGSv2: Distance scaling of quantiles with GMPEs for $M = 5.$, $F = 0$, and $T = 3.$ . . . 774
4.321PVNGSv2: Distance scaling of quantiles with GMPEs for $M = 6.$, $F = 0$, and $T = 3.$ . . . 774
4.322PVNGSv2: Distance scaling of quantiles with GMPEs for $M = 7.$, $F = 0$, and $T = 3.$ . . . 775
4.323PVNGSv2: Distance scaling of quantiles with GMPEs for $M = 5.$, $F = -1$, and $T = 3.$ . . . 775
4.324PVNGSv2: Distance scaling of quantiles with GMPEs for $M = 6.$, $F = -1$, and $T = 3.$ . . . 776
4.325PVNGSv2: Distance scaling of quantiles with GMPEs for $M = 7.$, $F = -1$, and $T = 3.$ . . . 776
4.326Magnitude scaling for $R_x = -50.$, $F = -1$, and $T = 0.01$ . . . 777
4.327Magnitude scaling for $R_x = -50.$, $F = 0$, and $T = 0.01$ . . . 777
4.328Magnitude scaling for $R_x = -30.$, $F = -1$, and $T = 0.01$ . . . 778
4.329Magnitude scaling for $R_x = -30.$, $F = 0$, and $T = 0.01$ . . . 778
4.330Magnitude scaling for $R_x = -15.$, $F = -1$, and $T = 0.01$ . . . 778
4.331Magnitude scaling for $R_x = -15.$, $F = 0$, and $T = 0.01$ . . . 779
4.332Magnitude scaling for $R_x = -5.$, $F = -1$, and $T = 0.01$ . . . 779
4.333Magnitude scaling for $R_x = -5.$, $F = 0$, and $T = 0.01$ . . . 779
4.334Magnitude scaling for $R_x = 5.$, $F = -1$, and $T = 0.01$ . . . 780
4.335Magnitude scaling for $R_x = 5.$, $F = 0$, and $T = 0.01$ . . . 780
4.336Magnitude scaling for $R_x = 15.$, $F = -1$, and $T = 0.01$ . . . 780
4.337Magnitude scaling for $R_x = 15.$, $F = 0$, and $T = 0.01$ . . . 781
4.338Magnitude scaling for $R_x = -50.$, $F = -1$, and $T = 0.2$ . . . 782
4.339Magnitude scaling for $R_x = -50.$, $F = 0$, and $T = 0.2$ . . . 782
4.340Magnitude scaling for $R_x = -30.$, $F = -1$, and $T = 0.2$ . . . 783
4.341Magnitude scaling for $R_x = -30.$, $F = 0$, and $T = 0.2$ . . . 783
4.342Magnitude scaling for $R_x = -15.$, $F = -1$, and $T = 0.2$ . . . 783
4.343Magnitude scaling for $R_x = -15.$, $F = 0$, and $T = 0.2$ . . . 784
4.344Magnitude scaling for $R_x = -5.$, $F = -1$, and $T = 0.2$ . . . 784
4.345Magnitude scaling for $R_x = -5.$, $F = 0$, and $T = 0.2$ . . . 784

4.346Magnitude scaling for $R_x = 5.$, $F = -1$, and $T = 0.2$ . . . 785
4.347Magnitude scaling for $R_x = 5.$, $F = 0$, and $T = 0.2$ . . . 785
4.348Magnitude scaling for $R_x = 15.$, $F = -1$, and $T = 0.2$ . . . 785
4.349Magnitude scaling for $R_x = 15.$, $F = 0$, and $T = 0.2$ . . . 786
4.350Magnitude scaling for $R_x = -50.$, $F = -1$, and $T = 0.5$ . . . 787
4.351Magnitude scaling for $R_x = -50.$, $F = 0$, and $T = 0.5$ . . . 787
4.352Magnitude scaling for $R_x = -30.$, $F = -1$, and $T = 0.5$ . . . 788
4.353Magnitude scaling for $R_x = -30.$, $F = 0$, and $T = 0.5$ . . . 788
4.354Magnitude scaling for $R_x = -15.$, $F = -1$, and $T = 0.5$ . . . 788
4.355Magnitude scaling for $R_x = -15.$, $F = 0$, and $T = 0.5$ . . . 789
4.356Magnitude scaling for $R_x = -5.$, $F = -1$, and $T = 0.5$ . . . 789
4.357Magnitude scaling for $R_x = -5.$, $F = 0$, and $T = 0.5$ . . . 789
4.358Magnitude scaling for $R_x = 5.$, $F = -1$, and $T = 0.5$ . . . 790
4.359Magnitude scaling for $R_x = 5.$, $F = 0$, and $T = 0.5$ . . . 790
4.360Magnitude scaling for $R_x = 15.$, $F = -1$, and $T = 0.5$ . . . 790
4.361Magnitude scaling for $R_x = 15.$, $F = 0$, and $T = 0.5$ . . . 791
4.362Magnitude scaling for $R_x = -50.$, $F = -1$, and $T = 1.$ . . . 792
4.363Magnitude scaling for $R_x = -50.$, $F = 0$, and $T = 1.$ . . . 792
4.364Magnitude scaling for $R_x = -30.$, $F = -1$, and $T = 1.$ . . . 793
4.365Magnitude scaling for $R_x = -30.$, $F = 0$, and $T = 1.$ . . . 793
4.366Magnitude scaling for $R_x = -15.$, $F = -1$, and $T = 1.$ . . . 793
4.367Magnitude scaling for $R_x = -15.$, $F = 0$, and $T = 1.$ . . . 794
4.368Magnitude scaling for $R_x = -5.$, $F = -1$, and $T = 1.$ . . . 794
4.369Magnitude scaling for $R_x = -5.$, $F = 0$, and $T = 1.$ . . . 794
4.370Magnitude scaling for $R_x = 5.$, $F = -1$, and $T = 1.$ . . . 795
4.371Magnitude scaling for $R_x = 5.$, $F = 0$, and $T = 1.$ . . . 795
4.372Magnitude scaling for $R_x = 15.$, $F = -1$, and $T = 1.$ . . . 795
4.373Magnitude scaling for $R_x = 15.$, $F = 0$, and $T = 1.$ . . . 796
4.374Magnitude scaling for $R_x = -50.$, $F = -1$, and $T = 3.$ . . . 797
4.375Magnitude scaling for $R_x = -50.$, $F = 0$, and $T = 3.$ . . . 797
4.376Magnitude scaling for $R_x = -30.$, $F = -1$, and $T = 3.$ . . . 798
4.377Magnitude scaling for $R_x = -30.$, $F = 0$, and $T = 3.$ . . . 798
4.378Magnitude scaling for $R_x = -15.$, $F = -1$, and $T = 3.$ . . . 798
4.379Magnitude scaling for $R_x = -15.$, $F = 0$, and $T = 3.$ . . . 799
4.380Magnitude scaling for $R_x = -5.$, $F = -1$, and $T = 3.$ . . . 799
4.381Magnitude scaling for $R_x = -5.$, $F = 0$, and $T = 3.$ . . . 799
4.382Magnitude scaling for $R_x = 5.$, $F = -1$, and $T = 3.$ . . . 800
4.383Magnitude scaling for $R_x = 5.$, $F = 0$, and $T = 3.$ . . . 800
4.384Magnitude scaling for $R_x = 15.$, $F = -1$, and $T = 3.$ . . . 800
4.385Magnitude scaling for $R_x = 15.$, $F = 0$, and $T = 3.$ . . . 801
4.386PVNGSv2: Spectra for $M_W = 5.$, $R_x = -50.$, $F = 0$ . . . 802
4.387PVNGSv2: Spectra for $M_W = 5.$, $R_x = -15.$, $F = 0$ . . . 802
4.388PVNGSv2: Spectra for $M_W = 5.$, $R_x = 5.$, $F = 0$ . . . 803
4.389PVNGSv2: Spectra for $M_W = 6.$, $R_x = -50.$, $F = 0$ . . . 803
4.390PVNGSv2: Spectra for $M_W = 6.$, $R_x = -15.$, $F = 0$ . . . 804
4.391PVNGSv2: Spectra for $M_W = 6.$, $R_x = 5.$, $F = 0$ . . . 804
4.392PVNGSv2: Spectra for $M_W = 7.$, $R_x = -50.$, $F = 0$ . . . 805
4.393PVNGSv2: Spectra for $M_W = 7.$, $R_x = -15.$, $F = 0$ . . . 805
4.394PVNGSv2: Spectra for $M_W = 7.$, $R_x = 5.$, $F = 0$ . . . 806
4.395PVNGSv2: Spectra for $M_W = 5.$, $R_x = -50.$, $F = -1$ . . . 806
4.396PVNGSv2: Spectra for $M_W = 5.$, $R_x = -15.$, $F = -1$ . . . 807
4.397PVNGSv2: Spectra for $M_W = 5.$, $R_x = 5.$, $F = -1$ . . . 807
4.398PVNGSv2: Spectra for $M_W = 6.$, $R_x = -50.$, $F = -1$ . . . 808
4.399PVNGSv2: Spectra for $M_W = 6.$, $R_x = -15.$, $F = -1$ . . . 808
4.400PVNGSv2: Spectra for $M_W = 6.$, $R_x = 5.$, $F = -1$ . . . 809
4.401PVNGSv2: Spectra for $M_W = 7.$, $R_x = -50.$, $F = -1$ . . . 809
4.402PVNGSv2: Spectra for $M_W = 7.$, $R_x = -15.$, $F = -1$ . . . 810
4.403PVNGSv2: Spectra for $M_W = 7.$, $R_x = 5.$, $F = -1$ . . . 810
4.404Quantile ratio for $M = 5.$, $F = -1$ and all periods . . . 811
4.405Quantile ratio for $M = 5.$, $F = 0$ and all periods . . . 811
4.406Quantile ratio for $M = 6.$, $F = -1$ and all periods . . . 812

4.407Quantile ratio for $M = 6.$, $F = 0$ and all periods . . . 812
4.408Quantile ratio for $M = 7.$, $F = -1$ and all periods . . . 813
4.409Quantile ratio for $M = 7.$, $F = 0$ and all periods . . . 813
4.410PVNGSv2: Magnitude scaling for $R_X = -50.$, $F = 0$, and $T = 0.01$ . . . 814
4.411PVNGSv2: Magnitude scaling for $R_X = -30.$, $F = 0$, and $T = 0.01$ . . . 814
4.412PVNGSv2: Magnitude scaling for $R_X = -15.$, $F = 0$, and $T = 0.01$ . . . 815
4.413PVNGSv2: Magnitude scaling for $R_X = -5.$, $F = 0$, and $T = 0.01$ . . . 815
4.414PVNGSv2: Magnitude scaling for $R_X = 5.$, $F = 0$, and $T = 0.01$ . . . 816
4.415PVNGSv2: Magnitude scaling for $R_X = 15.$, $F = 0$, and $T = 0.01$ . . . 816
4.416PVNGSv2: Magnitude scaling for $R_X = -50.$, $F = -1$, and $T = 0.01$ . . . 817
4.417PVNGSv2: Magnitude scaling for $R_X = -30.$, $F = -1$, and $T = 0.01$ . . . 817
4.418PVNGSv2: Magnitude scaling for $R_X = -15.$, $F = -1$, and $T = 0.01$ . . . 818
4.419PVNGSv2: Magnitude scaling for $R_X = -5.$, $F = -1$, and $T = 0.01$ . . . 818
4.420PVNGSv2: Magnitude scaling for $R_X = 5.$, $F = -1$, and $T = 0.01$ . . . 819
4.421PVNGSv2: Magnitude scaling for $R_X = 15.$, $F = -1$, and $T = 0.01$ . . . 819
4.422PVNGSv2: Magnitude scaling for $R_X = -50.$, $F = 0$, and $T = 0.2$ . . . 820
4.423PVNGSv2: Magnitude scaling for $R_X = -30.$, $F = 0$, and $T = 0.2$ . . . 820
4.424PVNGSv2: Magnitude scaling for $R_X = -15.$, $F = 0$, and $T = 0.2$ . . . 821
4.425PVNGSv2: Magnitude scaling for $R_X = -5.$, $F = 0$, and $T = 0.2$ . . . 821
4.426PVNGSv2: Magnitude scaling for $R_X = 5.$, $F = 0$, and $T = 0.2$ . . . 822
4.427PVNGSv2: Magnitude scaling for $R_X = 15.$, $F = 0$, and $T = 0.2$ . . . 822
4.428PVNGSv2: Magnitude scaling for $R_X = -50.$, $F = -1$, and $T = 0.2$ . . . 823
4.429PVNGSv2: Magnitude scaling for $R_X = -30.$, $F = -1$, and $T = 0.2$ . . . 823
4.430PVNGSv2: Magnitude scaling for $R_X = -15.$, $F = -1$, and $T = 0.2$ . . . 824
4.431PVNGSv2: Magnitude scaling for $R_X = -5.$, $F = -1$, and $T = 0.2$ . . . 824
4.432PVNGSv2: Magnitude scaling for $R_X = 5.$, $F = -1$, and $T = 0.2$ . . . 825
4.433PVNGSv2: Magnitude scaling for $R_X = 15.$, $F = -1$, and $T = 0.2$ . . . 825
4.434PVNGSv2: Magnitude scaling for $R_X = -50.$, $F = 0$, and $T = 0.5$ . . . 826
4.435PVNGSv2: Magnitude scaling for $R_X = -30.$, $F = 0$, and $T = 0.5$ . . . 826
4.436PVNGSv2: Magnitude scaling for $R_X = -15.$, $F = 0$, and $T = 0.5$ . . . 827
4.437PVNGSv2: Magnitude scaling for $R_X = -5.$, $F = 0$, and $T = 0.5$ . . . 827
4.438PVNGSv2: Magnitude scaling for $R_X = 5.$, $F = 0$, and $T = 0.5$ . . . 828
4.439PVNGSv2: Magnitude scaling for $R_X = 15.$, $F = 0$, and $T = 0.5$ . . . 828
4.440PVNGSv2: Magnitude scaling for $R_X = -50.$, $F = -1$, and $T = 0.5$ . . . 829
4.441PVNGSv2: Magnitude scaling for $R_X = -30.$, $F = -1$, and $T = 0.5$ . . . 829
4.442PVNGSv2: Magnitude scaling for $R_X = -15.$, $F = -1$, and $T = 0.5$ . . . 830
4.443PVNGSv2: Magnitude scaling for $R_X = -5.$, $F = -1$, and $T = 0.5$ . . . 830
4.444PVNGSv2: Magnitude scaling for $R_X = 5.$, $F = -1$, and $T = 0.5$ . . . 831
4.445PVNGSv2: Magnitude scaling for $R_X = 15.$, $F = -1$, and $T = 0.5$ . . . 831
4.446PVNGSv2: Magnitude scaling for $R_X = -50.$, $F = 0$, and $T = 1.$ . . . 832
4.447PVNGSv2: Magnitude scaling for $R_X = -30.$, $F = 0$, and $T = 1.$ . . . 832
4.448PVNGSv2: Magnitude scaling for $R_X = -15.$, $F = 0$, and $T = 1.$ . . . 833
4.449PVNGSv2: Magnitude scaling for $R_X = -5.$, $F = 0$, and $T = 1.$ . . . 833
4.450PVNGSv2: Magnitude scaling for $R_X = 5.$, $F = 0$, and $T = 1.$ . . . 834
4.451PVNGSv2: Magnitude scaling for $R_X = 15.$, $F = 0$, and $T = 1.$ . . . 834
4.452PVNGSv2: Magnitude scaling for $R_X = -50.$, $F = -1$, and $T = 1.$ . . . 835
4.453PVNGSv2: Magnitude scaling for $R_X = -30.$, $F = -1$, and $T = 1.$ . . . 835
4.454PVNGSv2: Magnitude scaling for $R_X = -15.$, $F = -1$, and $T = 1.$ . . . 836
4.455PVNGSv2: Magnitude scaling for $R_X = -5.$, $F = -1$, and $T = 1.$ . . . 836
4.456PVNGSv2: Magnitude scaling for $R_X = 5.$, $F = -1$, and $T = 1.$ . . . 837
4.457PVNGSv2: Magnitude scaling for $R_X = 15.$, $F = -1$, and $T = 1.$ . . . 837
4.458PVNGSv2: Magnitude scaling for $R_X = -50.$, $F = 0$, and $T = 3.$ . . . 838
4.459PVNGSv2: Magnitude scaling for $R_X = -30.$, $F = 0$, and $T = 3.$ . . . 838
4.460PVNGSv2: Magnitude scaling for $R_X = -15.$, $F = 0$, and $T = 3.$ . . . 839
4.461PVNGSv2: Magnitude scaling for $R_X = -5.$, $F = 0$, and $T = 3.$ . . . 839
4.462PVNGSv2: Magnitude scaling for $R_X = 5.$, $F = 0$, and $T = 3.$ . . . 840
4.463PVNGSv2: Magnitude scaling for $R_X = 15.$, $F = 0$, and $T = 3.$ . . . 840
4.464PVNGSv2: Magnitude scaling for $R_X = -50.$, $F = -1$, and $T = 3.$ . . . 841
4.465PVNGSv2: Magnitude scaling for $R_X = -30.$, $F = -1$, and $T = 3.$ . . . 841
4.466PVNGSv2: Magnitude scaling for $R_X = -15.$, $F = -1$, and $T = 3.$ . . . 842
4.467PVNGSv2: Magnitude scaling for $R_X = -5.$, $F = -1$, and $T = 3.$ . . . 842

4.468PVNGSv2: Magnitude scaling for $R_X = 5.$, $F = -1$, and $T = 3.$ . . . 843
4.469PVNGSv2: Magnitude scaling for $R_X = 15.$, $F = -1$, and $T = 3.$ . . . 843
4.470PVNGSv2: Distance scaling of quantiles with GMPEs for $M = 5.$, $F = 0$, and $T = 0.01$ . . . 844
4.471PVNGSv2: Distance scaling of quantiles with GMPEs for $M = 6.$, $F = 0$, and $T = 0.01$ . . . 844
4.472PVNGSv2: Distance scaling of quantiles with GMPEs for $M = 7.$, $F = 0$, and $T = 0.01$ . . . 845
4.473PVNGSv2: Distance scaling of quantiles with GMPEs for $M = 5.$, $F = -1$, and $T = 0.01$ . . . 845
4.474PVNGSv2: Distance scaling of quantiles with GMPEs for $M = 6.$, $F = -1$, and $T = 0.01$ . . . 845
4.475PVNGSv2: Distance scaling of quantiles with GMPEs for $M = 7.$, $F = -1$, and $T = 0.01$ . . . 846
4.476PVNGSv2: Distance scaling of quantiles with GMPEs for $M = 5.$, $F = 0$, and $T = 0.2$ . . . 847
4.477PVNGSv2: Distance scaling of quantiles with GMPEs for $M = 6.$, $F = 0$, and $T = 0.2$ . . . 847
4.478PVNGSv2: Distance scaling of quantiles with GMPEs for $M = 7.$, $F = 0$, and $T = 0.2$ . . . 848
4.479PVNGSv2: Distance scaling of quantiles with GMPEs for $M = 5.$, $F = -1$, and $T = 0.2$ . . . 848
4.480PVNGSv2: Distance scaling of quantiles with GMPEs for $M = 6.$, $F = -1$, and $T = 0.2$ . . . 848
4.481PVNGSv2: Distance scaling of quantiles with GMPEs for $M = 7.$, $F = -1$, and $T = 0.2$ . . . 849
4.482PVNGSv2: Distance scaling of quantiles with GMPEs for $M = 5.$, $F = 0$, and $T = 0.5$ . . . 850
4.483PVNGSv2: Distance scaling of quantiles with GMPEs for $M = 6.$, $F = 0$, and $T = 0.5$ . . . 850
4.484PVNGSv2: Distance scaling of quantiles with GMPEs for $M = 7.$, $F = 0$, and $T = 0.5$ . . . 851
4.485PVNGSv2: Distance scaling of quantiles with GMPEs for $M = 5.$, $F = -1$, and $T = 0.5$ . . . 851
4.486PVNGSv2: Distance scaling of quantiles with GMPEs for $M = 6.$, $F = -1$, and $T = 0.5$ . . . 851
4.487PVNGSv2: Distance scaling of quantiles with GMPEs for $M = 7.$, $F = -1$, and $T = 0.5$ . . . 852
4.488PVNGSv2: Distance scaling of quantiles with GMPEs for $M = 5.$, $F = 0$, and $T = 1.$ . . . 853
4.489PVNGSv2: Distance scaling of quantiles with GMPEs for $M = 6.$, $F = 0$, and $T = 1.$ . . . 853
4.490PVNGSv2: Distance scaling of quantiles with GMPEs for $M = 7.$, $F = 0$, and $T = 1.$ . . . 854
4.491PVNGSv2: Distance scaling of quantiles with GMPEs for $M = 5.$, $F = -1$, and $T = 1.$ . . . 854
4.492PVNGSv2: Distance scaling of quantiles with GMPEs for $M = 6.$, $F = -1$, and $T = 1.$ . . . 854
4.493PVNGSv2: Distance scaling of quantiles with GMPEs for $M = 7.$, $F = -1$, and $T = 1.$ . . . 855
4.494PVNGSv2: Distance scaling of quantiles with GMPEs for $M = 5.$, $F = 0$, and $T = 3.$ . . . 856
4.495PVNGSv2: Distance scaling of quantiles with GMPEs for $M = 6.$, $F = 0$, and $T = 3.$ . . . 856
4.496PVNGSv2: Distance scaling of quantiles with GMPEs for $M = 7.$, $F = 0$, and $T = 3.$ . . . 857
4.497PVNGSv2: Distance scaling of quantiles with GMPEs for $M = 5.$, $F = -1$, and $T = 3.$ . . . 857
4.498PVNGSv2: Distance scaling of quantiles with GMPEs for $M = 6.$, $F = -1$, and $T = 3.$ . . . 857
4.499PVNGSv2: Distance scaling of quantiles with GMPEs for $M = 7.$, $F = -1$, and $T = 3.$ . . . 858
4.500PVNGSv2: Magnitude scaling of quantiles with GMPEs for $R_X = -50.$, $F = 0$, and $T = 0.01$ . . . 859
4.501PVNGSv2: Magnitude scaling of quantiles with GMPEs for $R_X = -30.$, $F = 0$, and $T = 0.01$ . . . 859
4.502PVNGSv2: Magnitude scaling of quantiles with GMPEs for $R_X = -15.$, $F = 0$, and $T = 0.01$ . . . 860
4.503PVNGSv2: Magnitude scaling of quantiles with GMPEs for $R_X = -5.$, $F = 0$, and $T = 0.01$ . . . 860
4.504PVNGSv2: Magnitude scaling of quantiles with GMPEs for $R_X = 5.$, $F = 0$, and $T = 0.01$ . . . 861
4.505PVNGSv2: Magnitude scaling of quantiles with GMPEs for $R_X = 15.$, $F = 0$, and $T = 0.01$ . . . 861
4.506PVNGSv2: Magnitude scaling of quantiles with GMPEs for $R_X = -50.$, $F = -1$, and $T = 0.01$ . . . 862
4.507PVNGSv2: Magnitude scaling of quantiles with GMPEs for $R_X = -30.$, $F = -1$, and $T = 0.01$ . . . 862
4.508PVNGSv2: Magnitude scaling of quantiles with GMPEs for $R_X = -15.$, $F = -1$, and $T = 0.01$ . . . 863
4.509PVNGSv2: Magnitude scaling of quantiles with GMPEs for $R_X = -5.$, $F = -1$, and $T = 0.01$ . . . 863
4.510PVNGSv2: Magnitude scaling of quantiles with GMPEs for $R_X = 5.$, $F = -1$, and $T = 0.01$ . . . 864
4.511PVNGSv2: Magnitude scaling of quantiles with GMPEs for $R_X = 15.$, $F = -1$, and $T = 0.01$ . . . 864
4.512PVNGSv2: Magnitude scaling of quantiles with GMPEs for $R_X = -50.$, $F = 0$, and $T = 0.2$ . . . 865
4.513PVNGSv2: Magnitude scaling of quantiles with GMPEs for $R_X = -30.$, $F = 0$, and $T = 0.2$ . . . 865
4.514PVNGSv2: Magnitude scaling of quantiles with GMPEs for $R_X = -15.$, $F = 0$, and $T = 0.2$ . . . 866
4.515PVNGSv2: Magnitude scaling of quantiles with GMPEs for $R_X = -5.$, $F = 0$, and $T = 0.2$ . . . 866
4.516PVNGSv2: Magnitude scaling of quantiles with GMPEs for $R_X = 5.$, $F = 0$, and $T = 0.2$ . . . 867
4.517PVNGSv2: Magnitude scaling of quantiles with GMPEs for $R_X = 15.$, $F = 0$, and $T = 0.2$ . . . 867
4.518PVNGSv2: Magnitude scaling of quantiles with GMPEs for $R_X = -50.$, $F = -1$, and $T = 0.2$ . . . 868
4.519PVNGSv2: Magnitude scaling of quantiles with GMPEs for $R_X = -30.$, $F = -1$, and $T = 0.2$ . . . 868
4.520PVNGSv2: Magnitude scaling of quantiles with GMPEs for $R_X = -15.$, $F = -1$, and $T = 0.2$ . . . 869
4.521PVNGSv2: Magnitude scaling of quantiles with GMPEs for $R_X = -5.$, $F = -1$, and $T = 0.2$ . . . 869
4.522PVNGSv2: Magnitude scaling of quantiles with GMPEs for $R_X = 5.$, $F = -1$, and $T = 0.2$ . . . 870
4.523PVNGSv2: Magnitude scaling of quantiles with GMPEs for $R_X = 15.$, $F = -1$, and $T = 0.2$ . . . 870
4.524PVNGSv2: Magnitude scaling of quantiles with GMPEs for $R_X = -50.$, $F = 0$, and $T = 0.5$ . . . 871
4.525PVNGSv2: Magnitude scaling of quantiles with GMPEs for $R_X = -30.$, $F = 0$, and $T = 0.5$ . . . 871
4.526PVNGSv2: Magnitude scaling of quantiles with GMPEs for $R_X = -15.$, $F = 0$, and $T = 0.5$ . . . 872
4.527PVNGSv2: Magnitude scaling of quantiles with GMPEs for $R_X = -5.$, $F = 0$, and $T = 0.5$ . . . 872
4.528PVNGSv2: Magnitude scaling of quantiles with GMPEs for $R_X = 5.$, $F = 0$, and $T = 0.5$ . . . 873

4.529PVNGSv2: Magnitude scaling of quantiles with GMPEs for $R_X = 15.$, $F = 0$, and $T = 0.5$ . . . . . 873
4.530PVNGSv2: Magnitude scaling of quantiles with GMPEs for $R_X = -50.$, $F = -1$, and $T = 0.5$ . . . . . 874
4.531PVNGSv2: Magnitude scaling of quantiles with GMPEs for $R_X = -30.$, $F = -1$, and $T = 0.5$ . . . . . 874
4.532PVNGSv2: Magnitude scaling of quantiles with GMPEs for $R_X = -15.$, $F = -1$, and $T = 0.5$ . . . . . 875
4.533PVNGSv2: Magnitude scaling of quantiles with GMPEs for $R_X = -5.$, $F = -1$, and $T = 0.5$ . . . . . 875
4.534PVNGSv2: Magnitude scaling of quantiles with GMPEs for $R_X = 5.$, $F = -1$, and $T = 0.5$ . . . . . 876
4.535PVNGSv2: Magnitude scaling of quantiles with GMPEs for $R_X = 15.$, $F = -1$, and $T = 0.5$ . . . . . 876
4.536PVNGSv2: Magnitude scaling of quantiles with GMPEs for $R_X = -50.$, $F = 0$, and $T = 1.$ . . . . . 877
4.537PVNGSv2: Magnitude scaling of quantiles with GMPEs for $R_X = -30.$, $F = 0$, and $T = 1.$ . . . . . 877
4.538PVNGSv2: Magnitude scaling of quantiles with GMPEs for $R_X = -15.$, $F = 0$, and $T = 1.$ . . . . . 878
4.539PVNGSv2: Magnitude scaling of quantiles with GMPEs for $R_X = -5.$, $F = 0$, and $T = 1.$ . . . . . 878
4.540PVNGSv2: Magnitude scaling of quantiles with GMPEs for $R_X = 5.$, $F = 0$, and $T = 1.$ . . . . . 879
4.541PVNGSv2: Magnitude scaling of quantiles with GMPEs for $R_X = 15.$, $F = 0$, and $T = 1.$ . . . . . 879
4.542PVNGSv2: Magnitude scaling of quantiles with GMPEs for $R_X = -50.$, $F = -1$, and $T = 1.$ . . . . . 880
4.543PVNGSv2: Magnitude scaling of quantiles with GMPEs for $R_X = -30.$, $F = -1$, and $T = 1.$ . . . . . 880
4.544PVNGSv2: Magnitude scaling of quantiles with GMPEs for $R_X = -15.$, $F = -1$, and $T = 1.$ . . . . . 881
4.545PVNGSv2: Magnitude scaling of quantiles with GMPEs for $R_X = -5.$, $F = -1$, and $T = 1.$ . . . . . 881
4.546PVNGSv2: Magnitude scaling of quantiles with GMPEs for $R_X = 5.$, $F = -1$, and $T = 1.$ . . . . . 882
4.547PVNGSv2: Magnitude scaling of quantiles with GMPEs for $R_X = 15.$, $F = -1$, and $T = 1.$ . . . . . 882
4.548PVNGSv2: Magnitude scaling of quantiles with GMPEs for $R_X = -50.$, $F = 0$, and $T = 3.$ . . . . . 883
4.549PVNGSv2: Magnitude scaling of quantiles with GMPEs for $R_X = -30.$, $F = 0$, and $T = 3.$ . . . . . 883
4.550PVNGSv2: Magnitude scaling of quantiles with GMPEs for $R_X = -15.$, $F = 0$, and $T = 3.$ . . . . . 884
4.551PVNGSv2: Magnitude scaling of quantiles with GMPEs for $R_X = -5.$, $F = 0$, and $T = 3.$ . . . . . 884
4.552PVNGSv2: Magnitude scaling of quantiles with GMPEs for $R_X = 5.$, $F = 0$, and $T = 3.$ . . . . . 885
4.553PVNGSv2: Magnitude scaling of quantiles with GMPEs for $R_X = 15.$, $F = 0$, and $T = 3.$ . . . . . 885
4.554PVNGSv2: Magnitude scaling of quantiles with GMPEs for $R_X = -50.$, $F = -1$, and $T = 3.$ . . . . . 886
4.555PVNGSv2: Magnitude scaling of quantiles with GMPEs for $R_X = -30.$, $F = -1$, and $T = 3.$ . . . . . 886
4.556PVNGSv2: Magnitude scaling of quantiles with GMPEs for $R_X = -15.$, $F = -1$, and $T = 3.$ . . . . . 887
4.557PVNGSv2: Magnitude scaling of quantiles with GMPEs for $R_X = -5.$, $F = -1$, and $T = 3.$ . . . . . 887
4.558PVNGSv2: Magnitude scaling of quantiles with GMPEs for $R_X = 5.$, $F = -1$, and $T = 3.$ . . . . . 888
4.559PVNGSv2: Magnitude scaling of quantiles with GMPEs for $R_X = 15.$, $F = -1$, and $T = 3.$ . . . . . 888
4.560PVNGSv2: Spectra for $M_W = 5.$, $R_x = -50.$, $F = 0$ . . . . . 889
4.561PVNGSv2: Spectra for $M_W = 5.$, $R_x = -30.$, $F = 0$ . . . . . 889
4.562PVNGSv2: Spectra for $M_W = 5.$, $R_x = -15.$, $F = 0$ . . . . . 890
4.563PVNGSv2: Spectra for $M_W = 5.$, $R_x = -5.$, $F = 0$ . . . . . 890
4.564PVNGSv2: Spectra for $M_W = 5.$, $R_x = 5.$, $F = 0$ . . . . . 891
4.565PVNGSv2: Spectra for $M_W = 5.$, $R_x = 15.$, $F = 0$ . . . . . 891
4.566PVNGSv2: Spectra for $M_W = 6.$, $R_x = -50.$, $F = 0$ . . . . . 892
4.567PVNGSv2: Spectra for $M_W = 6.$, $R_x = -30.$, $F = 0$ . . . . . 892
4.568PVNGSv2: Spectra for $M_W = 6.$, $R_x = -15.$, $F = 0$ . . . . . 893
4.569PVNGSv2: Spectra for $M_W = 6.$, $R_x = -5.$, $F = 0$ . . . . . 893
4.570PVNGSv2: Spectra for $M_W = 6.$, $R_x = 5.$, $F = 0$ . . . . . 894
4.571PVNGSv2: Spectra for $M_W = 6.$, $R_x = 15.$, $F = 0$ . . . . . 894
4.572PVNGSv2: Spectra for $M_W = 7.$, $R_x = -50.$, $F = 0$ . . . . . 895
4.573PVNGSv2: Spectra for $M_W = 7.$, $R_x = -30.$, $F = 0$ . . . . . 895
4.574PVNGSv2: Spectra for $M_W = 7.$, $R_x = -15.$, $F = 0$ . . . . . 896
4.575PVNGSv2: Spectra for $M_W = 7.$, $R_x = -5.$, $F = 0$ . . . . . 896
4.576PVNGSv2: Spectra for $M_W = 7.$, $R_x = 5.$, $F = 0$ . . . . . 897
4.577PVNGSv2: Spectra for $M_W = 7.$, $R_x = 15.$, $F = 0$ . . . . . 897
4.578PVNGSv2: Spectra for $M_W = 5.$, $R_x = -50.$, $F = -1$ . . . . . 898
4.579PVNGSv2: Spectra for $M_W = 5.$, $R_x = -30.$, $F = -1$ . . . . . 898
4.580PVNGSv2: Spectra for $M_W = 5.$, $R_x = -15.$, $F = -1$ . . . . . 899
4.581PVNGSv2: Spectra for $M_W = 5.$, $R_x = -5.$, $F = -1$ . . . . . 899
4.582PVNGSv2: Spectra for $M_W = 5.$, $R_x = 5.$, $F = -1$ . . . . . 900
4.583PVNGSv2: Spectra for $M_W = 5.$, $R_x = 15.$, $F = -1$ . . . . . 900
4.584PVNGSv2: Spectra for $M_W = 6.$, $R_x = -50.$, $F = -1$ . . . . . 901
4.585PVNGSv2: Spectra for $M_W = 6.$, $R_x = -30.$, $F = -1$ . . . . . 901
4.586PVNGSv2: Spectra for $M_W = 6.$, $R_x = -15.$, $F = -1$ . . . . . 902
4.587PVNGSv2: Spectra for $M_W = 6.$, $R_x = -5.$, $F = -1$ . . . . . 902
4.588PVNGSv2: Spectra for $M_W = 6.$, $R_x = 5.$, $F = -1$ . . . . . 903
4.589PVNGSv2: Spectra for $M_W = 6.$, $R_x = 15.$, $F = -1$ . . . . . 903

4.590PVNGSv2: Spectra for $M_W = 7.$, $R_x = -50.$, $F = -1$ . . . . . 904
4.591PVNGSv2: Spectra for $M_W = 7.$, $R_x = -30.$, $F = -1$ . . . . . 904
4.592PVNGSv2: Spectra for $M_W = 7.$, $R_x = -15.$, $F = -1$ . . . . . 905
4.593PVNGSv2: Spectra for $M_W = 7.$, $R_x = -5.$, $F = -1$ . . . . . 905
4.594PVNGSv2: Spectra for $M_W = 7.$, $R_x = 5.$, $F = -1$ . . . . . 906
4.595PVNGSv2: Spectra for $M_W = 7.$, $R_x = 15.$, $F = -1$ . . . . . 906
4.596PVNGSv2: Histogram of differences for medians calculated with different weights to median calculated with total weights. Bottom row left shows differences between medians for the GMPE distribution to median calculated with total weights. Bottom row right shows differences between the original GMPEs (without uncertainty) to median calculated with total weights. For PVNGS2, ModelB and $T = 0.01$s. . . 908
4.597PVNGSv2: Histogram of differences for medians calculated with different weights to median calculated with total weights. Bottom row left shows differences between medians for the GMPE distribution to median calculated with total weights. Bottom row right shows differences between the original GMPEs (without uncertainty) to median calculated with total weights. For PVNGS2, ModelB and $T = 0.02$s. . . 909
4.598PVNGSv2: Histogram of differences for medians calculated with different weights to median calculated with total weights. Bottom row left shows differences between medians for the GMPE distribution to median calculated with total weights. Bottom row right shows differences between the original GMPEs (without uncertainty) to median calculated with total weights. For PVNGS2, ModelB and $T = 0.03$s. . . 910
4.599PVNGSv2: Histogram of differences for medians calculated with different weights to median calculated with total weights. Bottom row left shows differences between medians for the GMPE distribution to median calculated with total weights. Bottom row right shows differences between the original GMPEs (without uncertainty) to median calculated with total weights. For PVNGS2, ModelB and $T = 0.05$s. . . 911
4.600PVNGSv2: Histogram of differences for medians calculated with different weights to median calculated with total weights. Bottom row left shows differences between medians for the GMPE distribution to median calculated with total weights. Bottom row right shows differences between the original GMPEs (without uncertainty) to median calculated with total weights. For PVNGS2, ModelB and $T = 0.075$s. . . 912
4.601PVNGSv2: Histogram of differences for medians calculated with different weights to median calculated with total weights. Bottom row left shows differences between medians for the GMPE distribution to median calculated with total weights. Bottom row right shows differences between the original GMPEs (without uncertainty) to median calculated with total weights. For PVNGS2, ModelB and $T = 0.1$s. . . . 913
4.602PVNGSv2: Histogram of differences for medians calculated with different weights to median calculated with total weights. Bottom row left shows differences between medians for the GMPE distribution to median calculated with total weights. Bottom row right shows differences between the original GMPEs (without uncertainty) to median calculated with total weights. For PVNGS2, ModelB and $T = 0.15$s. . . 914
4.603PVNGSv2: Histogram of differences for medians calculated with different weights to median calculated with total weights. Bottom row left shows differences between medians for the GMPE distribution to median calculated with total weights. Bottom row right shows differences between the original GMPEs (without uncertainty) to median calculated with total weights. For PVNGS2, ModelB and $T = 0.2$s. . . . 915
4.604PVNGSv2: Histogram of differences for medians calculated with different weights to median calculated with total weights. Bottom row left shows differences between medians for the GMPE distribution to median calculated with total weights. Bottom row right shows differences between the original GMPEs (without uncertainty) to median calculated with total weights. For PVNGS2, ModelB and $T = 0.25$s. . . 916
4.605PVNGSv2: Histogram of differences for medians calculated with different weights to median calculated with total weights. Bottom row left shows differences between medians for the GMPE distribution to median calculated with total weights. Bottom row right shows differences between the original GMPEs (without uncertainty) to median calculated with total weights. For PVNGS2, ModelB and $T = 0.3$s. . . . 917
4.606PVNGSv2: Histogram of differences for medians calculated with different weights to median calculated with total weights. Bottom row left shows differences between medians for the GMPE distribution to median calculated with total weights. Bottom row right shows differences between the original GMPEs (without uncertainty) to median calculated with total weights. For PVNGS2, ModelB and $T = 0.4$s. . . . 918
4.607PVNGSv2: Histogram of differences for medians calculated with different weights to median calculated with total weights. Bottom row left shows differences between medians for the GMPE distribution to median calculated with total weights. Bottom row right shows differences between the original GMPEs (without uncertainty) to median calculated with total weights. For PVNGS2, ModelB and $T = 0.5$s. . . . 919
4.608PVNGSv2: Histogram of differences for medians calculated with different weights to median calculated with total weights. Bottom row left shows differences between medians for the GMPE distribution to median calculated with total weights. Bottom row right shows differences between the original GMPEs (without uncertainty) to median calculated with total weights. For PVNGS2, ModelB and $T = 0.75$s. . . 920

4.609 PVNGSv2: Histogram of differences for medians calculated with different weights to median calculated with total weights. Bottom row left shows differences between medians for the GMPE distribution to median calculated with total weights. Bottom row right shows differences between the original GMPEs (without uncertainty) to median calculated with total weights. For PVNGS2, ModelB and $T = 1.$s. . . . . 921
4.610 PVNGSv2: Histogram of differences for medians calculated with different weights to median calculated with total weights. Bottom row left shows differences between medians for the GMPE distribution to median calculated with total weights. Bottom row right shows differences between the original GMPEs (without uncertainty) to median calculated with total weights. For PVNGS2, ModelB and $T = 1.5$s. . . . 922
4.611 PVNGSv2: Histogram of differences for medians calculated with different weights to median calculated with total weights. Bottom row left shows differences between medians for the GMPE distribution to median calculated with total weights. Bottom row right shows differences between the original GMPEs (without uncertainty) to median calculated with total weights. For PVNGS2, ModelB and $T = 2.$s. . . . . 923
4.612 PVNGSv2: Histogram of differences for medians calculated with different weights to median calculated with total weights. Bottom row left shows differences between medians for the GMPE distribution to median calculated with total weights. Bottom row right shows differences between the original GMPEs (without uncertainty) to median calculated with total weights. For PVNGS2, ModelB and $T = 3.$s. . . . . 924

5.1 PVNGSv2: Contour Plots used for weighting. For $T = 0.01$s. . . . . 926
5.2 PVNGSv2: Contour Plots used for weighting. For $T = 0.02$s. . . . . 927
5.3 PVNGSv2: Contour Plots used for weighting. For $T = 0.03$s. . . . . 928
5.4 PVNGSv2: Contour Plots used for weighting. For $T = 0.05$s. . . . . 929
5.5 PVNGSv2: Contour Plots used for weighting. For $T = 0.075$s. . . . . 930
5.6 PVNGSv2: Contour Plots used for weighting. For $T = 0.1$s. . . . . 931
5.7 PVNGSv2: Contour Plots used for weighting. For $T = 0.15$s. . . . . 932
5.8 PVNGSv2: Contour Plots used for weighting. For $T = 0.2$s. . . . . 933
5.9 PVNGSv2: Contour Plots used for weighting. For $T = 0.25$s. . . . . 934
5.10 PVNGSv2: Contour Plots used for weighting. For $T = 0.3$s. . . . . 935
5.11 PVNGSv2: Contour Plots used for weighting. For $T = 0.4$s. . . . . 936
5.12 PVNGSv2: Contour Plots used for weighting. For $T = 0.5$s. . . . . 937
5.13 PVNGSv2: Contour Plots used for weighting. For $T = 0.75$s. . . . . 938
5.14 PVNGSv2: Contour Plots used for weighting. For $T = 1.$s. . . . . 939
5.15 PVNGSv2: Contour Plots used for weighting. For $T = 1.5$s. . . . . 940
5.16 PVNGSv2: Contour Plots used for weighting. For $T = 2.$s. . . . . 941
5.17 PVNGSv2: Contour Plots used for weighting. For $T = 3.$s. . . . . 942
5.18 PVNGSv2: Distance scaling of quantiles with GMPEs for $M = 5.$, $F = -1$, and $T = 0.01$ . . . . . 943
5.19 PVNGSv2: Distance scaling of quantiles with GMPEs for $M = 5.$, $F = 0$, and $T = 0.01$ . . . . . 943
5.20 PVNGSv2: Distance scaling of quantiles with GMPEs for $M = 6.$, $F = -1$, and $T = 0.01$ . . . . . 944
5.21 PVNGSv2: Distance scaling of quantiles with GMPEs for $M = 6.$, $F = 0$, and $T = 0.01$ . . . . . 944
5.22 PVNGSv2: Distance scaling of quantiles with GMPEs for $M = 7.$, $F = -1$, and $T = 0.01$ . . . . . 945
5.23 PVNGSv2: Distance scaling of quantiles with GMPEs for $M = 7.$, $F = 0$, and $T = 0.01$ . . . . . 945
5.24 PVNGSv2: Distance scaling of quantiles with GMPEs for $M = 5.$, $F = -1$, and $T = 0.2$ . . . . . 946
5.25 PVNGSv2: Distance scaling of quantiles with GMPEs for $M = 5.$, $F = 0$, and $T = 0.2$ . . . . . 946
5.26 PVNGSv2: Distance scaling of quantiles with GMPEs for $M = 6.$, $F = -1$, and $T = 0.2$ . . . . . 947
5.27 PVNGSv2: Distance scaling of quantiles with GMPEs for $M = 6.$, $F = 0$, and $T = 0.2$ . . . . . 947
5.28 PVNGSv2: Distance scaling of quantiles with GMPEs for $M = 7.$, $F = -1$, and $T = 0.2$ . . . . . 948
5.29 PVNGSv2: Distance scaling of quantiles with GMPEs for $M = 7.$, $F = 0$, and $T = 0.2$ . . . . . 948
5.30 PVNGSv2: Distance scaling of quantiles with GMPEs for $M = 5.$, $F = -1$, and $T = 0.5$ . . . . . 949
5.31 PVNGSv2: Distance scaling of quantiles with GMPEs for $M = 5.$, $F = 0$, and $T = 0.5$ . . . . . 949
5.32 PVNGSv2: Distance scaling of quantiles with GMPEs for $M = 6.$, $F = -1$, and $T = 0.5$ . . . . . 950
5.33 PVNGSv2: Distance scaling of quantiles with GMPEs for $M = 6.$, $F = 0$, and $T = 0.5$ . . . . . 950
5.34 PVNGSv2: Distance scaling of quantiles with GMPEs for $M = 7.$, $F = -1$, and $T = 0.5$ . . . . . 951
5.35 PVNGSv2: Distance scaling of quantiles with GMPEs for $M = 7.$, $F = 0$, and $T = 0.5$ . . . . . 951
5.36 PVNGSv2: Distance scaling of quantiles with GMPEs for $M = 5.$, $F = -1$, and $T = 1.$ . . . . . 952
5.37 PVNGSv2: Distance scaling of quantiles with GMPEs for $M = 5.$, $F = 0$, and $T = 1.$ . . . . . 952
5.38 PVNGSv2: Distance scaling of quantiles with GMPEs for $M = 6.$, $F = -1$, and $T = 1.$ . . . . . 953
5.39 PVNGSv2: Distance scaling of quantiles with GMPEs for $M = 6.$, $F = 0$, and $T = 1.$ . . . . . 953
5.40 PVNGSv2: Distance scaling of quantiles with GMPEs for $M = 7.$, $F = -1$, and $T = 1.$ . . . . . 954
5.41 PVNGSv2: Distance scaling of quantiles with GMPEs for $M = 7.$, $F = 0$, and $T = 1.$ . . . . . 954
5.42 PVNGSv2: Distance scaling of quantiles with GMPEs for $M = 5.$, $F = -1$, and $T = 2.$ . . . . . 955
5.43 PVNGSv2: Distance scaling of quantiles with GMPEs for $M = 5.$, $F = 0$, and $T = 2.$ . . . . . 955
5.44 PVNGSv2: Distance scaling of quantiles with GMPEs for $M = 6.$, $F = -1$, and $T = 2.$ . . . . . 956

5.45 PVNGSv2: Distance scaling of quantiles with GMPEs for $M = 6.$, $F = 0$, and $T = 2.$ . . . . . 956
5.46 PVNGSv2: Distance scaling of quantiles with GMPEs for $M = 7.$, $F = -1$, and $T = 2.$ . . . . . 957
5.47 PVNGSv2: Distance scaling of quantiles with GMPEs for $M = 7.$, $F = 0$, and $T = 2.$ . . . . . 957
5.48 PVNGSv2: Distance scaling of quantiles with GMPEs for $M = 5.$, $F = -1$, and $T = 3.$ . . . . . 958
5.49 PVNGSv2: Distance scaling of quantiles with GMPEs for $M = 5.$, $F = 0$, and $T = 3.$ . . . . . 958
5.50 PVNGSv2: Distance scaling of quantiles with GMPEs for $M = 6.$, $F = -1$, and $T = 3.$ . . . . . 959
5.51 PVNGSv2: Distance scaling of quantiles with GMPEs for $M = 6.$, $F = 0$, and $T = 3.$ . . . . . 959
5.52 PVNGSv2: Distance scaling of quantiles with GMPEs for $M = 7.$, $F = -1$, and $T = 3.$ . . . . . 960
5.53 PVNGSv2: Distance scaling of quantiles with GMPEs for $M = 7.$, $F = 0$, and $T = 3.$ . . . . . 960
5.54 PVNGSv2: Magnitude scaling of quantiles with GMPEs for $R_X = -50.$, $F = -1$, and $T = 0.01$ . . . . 961
5.55 PVNGSv2: Magnitude scaling of quantiles with GMPEs for $R_X = -50.$, $F = 0$, and $T = 0.01$ . . . . . 961
5.56 PVNGSv2: Magnitude scaling of quantiles with GMPEs for $R_X = -30.$, $F = -1$, and $T = 0.01$ . . . . 962
5.57 PVNGSv2: Magnitude scaling of quantiles with GMPEs for $R_X = -30.$, $F = 0$, and $T = 0.01$ . . . . . 962
5.58 PVNGSv2: Magnitude scaling of quantiles with GMPEs for $R_X = -15.$, $F = -1$, and $T = 0.01$ . . . . 963
5.59 PVNGSv2: Magnitude scaling of quantiles with GMPEs for $R_X = -15.$, $F = 0$, and $T = 0.01$ . . . . . 963
5.60 PVNGSv2: Magnitude scaling of quantiles with GMPEs for $R_X = -5.$, $F = -1$, and $T = 0.01$ . . . . . 964
5.61 PVNGSv2: Magnitude scaling of quantiles with GMPEs for $R_X = -5.$, $F = 0$, and $T = 0.01$ . . . . . 964
5.62 PVNGSv2: Magnitude scaling of quantiles with GMPEs for $R_X = 5.$, $F = -1$, and $T = 0.01$ . . . . . 965
5.63 PVNGSv2: Magnitude scaling of quantiles with GMPEs for $R_X = 5.$, $F = 0$, and $T = 0.01$ . . . . . 965
5.64 PVNGSv2: Magnitude scaling of quantiles with GMPEs for $R_X = 15.$, $F = -1$, and $T = 0.01$ . . . . . 966
5.65 PVNGSv2: Magnitude scaling of quantiles with GMPEs for $R_X = 15.$, $F = 0$, and $T = 0.01$ . . . . . 966
5.66 PVNGSv2: Magnitude scaling of quantiles with GMPEs for $R_X = -50.$, $F = -1$, and $T = 0.01$ . . . . 967
5.67 PVNGSv2: Magnitude scaling of quantiles with GMPEs for $R_X = -50.$, $F = 0$, and $T = 0.01$ . . . . . 967
5.68 PVNGSv2: Magnitude scaling of quantiles with GMPEs for $R_X = -30.$, $F = -1$, and $T = 0.01$ . . . . 968
5.69 PVNGSv2: Magnitude scaling of quantiles with GMPEs for $R_X = -30.$, $F = 0$, and $T = 0.01$ . . . . . 968
5.70 PVNGSv2: Magnitude scaling of quantiles with GMPEs for $R_X = -15.$, $F = -1$, and $T = 0.01$ . . . . 969
5.71 PVNGSv2: Magnitude scaling of quantiles with GMPEs for $R_X = -15.$, $F = 0$, and $T = 0.01$ . . . . . 969
5.72 PVNGSv2: Magnitude scaling of quantiles with GMPEs for $R_X = -5.$, $F = -1$, and $T = 0.01$ . . . . . 970
5.73 PVNGSv2: Magnitude scaling of quantiles with GMPEs for $R_X = -5.$, $F = 0$, and $T = 0.01$ . . . . . 970
5.74 PVNGSv2: Magnitude scaling of quantiles with GMPEs for $R_X = 5.$, $F = -1$, and $T = 0.01$ . . . . . 971
5.75 PVNGSv2: Magnitude scaling of quantiles with GMPEs for $R_X = 5.$, $F = 0$, and $T = 0.01$ . . . . . 971
5.76 PVNGSv2: Magnitude scaling of quantiles with GMPEs for $R_X = 15.$, $F = -1$, and $T = 0.01$ . . . . . 972
5.77 PVNGSv2: Magnitude scaling of quantiles with GMPEs for $R_X = 15.$, $F = 0$, and $T = 0.01$ . . . . . 972
5.78 PVNGSv2: Magnitude scaling of quantiles with GMPEs for $R_X = -50.$, $F = -1$, and $T = 0.01$ . . . . 973
5.79 PVNGSv2: Magnitude scaling of quantiles with GMPEs for $R_X = -50.$, $F = 0$, and $T = 0.01$ . . . . . 973
5.80 PVNGSv2: Magnitude scaling of quantiles with GMPEs for $R_X = -30.$, $F = -1$, and $T = 0.01$ . . . . 974
5.81 PVNGSv2: Magnitude scaling of quantiles with GMPEs for $R_X = -30.$, $F = 0$, and $T = 0.01$ . . . . . 974
5.82 PVNGSv2: Magnitude scaling of quantiles with GMPEs for $R_X = -15.$, $F = -1$, and $T = 0.01$ . . . . 975
5.83 PVNGSv2: Magnitude scaling of quantiles with GMPEs for $R_X = -15.$, $F = 0$, and $T = 0.01$ . . . . . 975
5.84 PVNGSv2: Magnitude scaling of quantiles with GMPEs for $R_X = -5.$, $F = -1$, and $T = 0.01$ . . . . . 976
5.85 PVNGSv2: Magnitude scaling of quantiles with GMPEs for $R_X = -5.$, $F = 0$, and $T = 0.01$ . . . . . 976
5.86 PVNGSv2: Magnitude scaling of quantiles with GMPEs for $R_X = 5.$, $F = -1$, and $T = 0.01$ . . . . . 977
5.87 PVNGSv2: Magnitude scaling of quantiles with GMPEs for $R_X = 5.$, $F = 0$, and $T = 0.01$ . . . . . 977
5.88 PVNGSv2: Magnitude scaling of quantiles with GMPEs for $R_X = 15.$, $F = -1$, and $T = 0.01$ . . . . . 978
5.89 PVNGSv2: Magnitude scaling of quantiles with GMPEs for $R_X = 15.$, $F = 0$, and $T = 0.01$ . . . . . 978
5.90 PVNGSv2: Magnitude scaling of quantiles with GMPEs for $R_X = -50.$, $F = -1$, and $T = 0.2$ . . . . . 979
5.91 PVNGSv2: Magnitude scaling of quantiles with GMPEs for $R_X = -50.$, $F = 0$, and $T = 0.2$ . . . . . 979
5.92 PVNGSv2: Magnitude scaling of quantiles with GMPEs for $R_X = -30.$, $F = -1$, and $T = 0.2$ . . . . . 980
5.93 PVNGSv2: Magnitude scaling of quantiles with GMPEs for $R_X = -30.$, $F = 0$, and $T = 0.2$ . . . . . 980
5.94 PVNGSv2: Magnitude scaling of quantiles with GMPEs for $R_X = -15.$, $F = -1$, and $T = 0.2$ . . . . . 981
5.95 PVNGSv2: Magnitude scaling of quantiles with GMPEs for $R_X = -15.$, $F = 0$, and $T = 0.2$ . . . . . 981
5.96 PVNGSv2: Magnitude scaling of quantiles with GMPEs for $R_X = -5.$, $F = -1$, and $T = 0.2$ . . . . . 982
5.97 PVNGSv2: Magnitude scaling of quantiles with GMPEs for $R_X = -5.$, $F = 0$, and $T = 0.2$ . . . . . 982
5.98 PVNGSv2: Magnitude scaling of quantiles with GMPEs for $R_X = 5.$, $F = -1$, and $T = 0.2$ . . . . . 983
5.99 PVNGSv2: Magnitude scaling of quantiles with GMPEs for $R_X = 5.$, $F = 0$, and $T = 0.2$ . . . . . 983
5.100 PVNGSv2: Magnitude scaling of quantiles with GMPEs for $R_X = 15.$, $F = -1$, and $T = 0.2$ . . . . . 984
5.101 PVNGSv2: Magnitude scaling of quantiles with GMPEs for $R_X = 15.$, $F = 0$, and $T = 0.2$ . . . . . 984
5.102 PVNGSv2: Magnitude scaling of quantiles with GMPEs for $R_X = -50.$, $F = -1$, and $T = 0.2$ . . . . . 985
5.103 PVNGSv2: Magnitude scaling of quantiles with GMPEs for $R_X = -50.$, $F = 0$, and $T = 0.2$ . . . . . 985
5.104 PVNGSv2: Magnitude scaling of quantiles with GMPEs for $R_X = -30.$, $F = -1$, and $T = 0.2$ . . . . . 986
5.105 PVNGSv2: Magnitude scaling of quantiles with GMPEs for $R_X = -30.$, $F = 0$, and $T = 0.2$ . . . . . 986

5.106PVNGSv2: Magnitude scaling of quantiles with GMPEs for $R_X = -15.$, $F = -1$, and $T = 0.2$ . . . . . 987
5.107PVNGSv2: Magnitude scaling of quantiles with GMPEs for $R_X = -15.$, $F = 0$, and $T = 0.2$ . . . . . 987
5.108PVNGSv2: Magnitude scaling of quantiles with GMPEs for $R_X = -5.$, $F = -1$, and $T = 0.2$ . . . . . 988
5.109PVNGSv2: Magnitude scaling of quantiles with GMPEs for $R_X = -5.$, $F = 0$, and $T = 0.2$ . . . . . 988
5.110PVNGSv2: Magnitude scaling of quantiles with GMPEs for $R_X = 5.$, $F = -1$, and $T = 0.2$ . . . . . 989
5.111PVNGSv2: Magnitude scaling of quantiles with GMPEs for $R_X = 5.$, $F = 0$, and $T = 0.2$ . . . . . 989
5.112PVNGSv2: Magnitude scaling of quantiles with GMPEs for $R_X = 15.$, $F = -1$, and $T = 0.2$ . . . . . 990
5.113PVNGSv2: Magnitude scaling of quantiles with GMPEs for $R_X = 15.$, $F = 0$, and $T = 0.2$ . . . . . 990
5.114PVNGSv2: Magnitude scaling of quantiles with GMPEs for $R_X = -50.$, $F = -1$, and $T = 0.2$ . . . . . 991
5.115PVNGSv2: Magnitude scaling of quantiles with GMPEs for $R_X = -50.$, $F = 0$, and $T = 0.2$ . . . . . 991
5.116PVNGSv2: Magnitude scaling of quantiles with GMPEs for $R_X = -30.$, $F = -1$, and $T = 0.2$ . . . . . 992
5.117PVNGSv2: Magnitude scaling of quantiles with GMPEs for $R_X = -30.$, $F = 0$, and $T = 0.2$ . . . . . 992
5.118PVNGSv2: Magnitude scaling of quantiles with GMPEs for $R_X = -15.$, $F = -1$, and $T = 0.2$ . . . . . 993
5.119PVNGSv2: Magnitude scaling of quantiles with GMPEs for $R_X = -15.$, $F = 0$, and $T = 0.2$ . . . . . 993
5.120PVNGSv2: Magnitude scaling of quantiles with GMPEs for $R_X = -5.$, $F = -1$, and $T = 0.2$ . . . . . 994
5.121PVNGSv2: Magnitude scaling of quantiles with GMPEs for $R_X = -5.$, $F = 0$, and $T = 0.2$ . . . . . 994
5.122PVNGSv2: Magnitude scaling of quantiles with GMPEs for $R_X = 5.$, $F = -1$, and $T = 0.2$ . . . . . 995
5.123PVNGSv2: Magnitude scaling of quantiles with GMPEs for $R_X = 5.$, $F = 0$, and $T = 0.2$ . . . . . 995
5.124PVNGSv2: Magnitude scaling of quantiles with GMPEs for $R_X = 15.$, $F = -1$, and $T = 0.2$ . . . . . 996
5.125PVNGSv2: Magnitude scaling of quantiles with GMPEs for $R_X = 15.$, $F = 0$, and $T = 0.2$ . . . . . 996
5.126PVNGSv2: Magnitude scaling of quantiles with GMPEs for $R_X = -50.$, $F = -1$, and $T = 0.5$ . . . . . 997
5.127PVNGSv2: Magnitude scaling of quantiles with GMPEs for $R_X = -50.$, $F = 0$, and $T = 0.5$ . . . . . 997
5.128PVNGSv2: Magnitude scaling of quantiles with GMPEs for $R_X = -30.$, $F = -1$, and $T = 0.5$ . . . . . 998
5.129PVNGSv2: Magnitude scaling of quantiles with GMPEs for $R_X = -30.$, $F = 0$, and $T = 0.5$ . . . . . 998
5.130PVNGSv2: Magnitude scaling of quantiles with GMPEs for $R_X = -15.$, $F = -1$, and $T = 0.5$ . . . . . 999
5.131PVNGSv2: Magnitude scaling of quantiles with GMPEs for $R_X = -15.$, $F = 0$, and $T = 0.5$ . . . . . 999
5.132PVNGSv2: Magnitude scaling of quantiles with GMPEs for $R_X = -5.$, $F = -1$, and $T = 0.5$ . . . . . 1000
5.133PVNGSv2: Magnitude scaling of quantiles with GMPEs for $R_X = -5.$, $F = 0$, and $T = 0.5$ . . . . . 1000
5.134PVNGSv2: Magnitude scaling of quantiles with GMPEs for $R_X = 5.$, $F = -1$, and $T = 0.5$ . . . . . 1001
5.135PVNGSv2: Magnitude scaling of quantiles with GMPEs for $R_X = 5.$, $F = 0$, and $T = 0.5$ . . . . . 1001
5.136PVNGSv2: Magnitude scaling of quantiles with GMPEs for $R_X = 15.$, $F = -1$, and $T = 0.5$ . . . . . 1002
5.137PVNGSv2: Magnitude scaling of quantiles with GMPEs for $R_X = 15.$, $F = 0$, and $T = 0.5$ . . . . . 1002
5.138PVNGSv2: Magnitude scaling of quantiles with GMPEs for $R_X = -50.$, $F = -1$, and $T = 0.5$ . . . . . 1003
5.139PVNGSv2: Magnitude scaling of quantiles with GMPEs for $R_X = -50.$, $F = 0$, and $T = 0.5$ . . . . . 1003
5.140PVNGSv2: Magnitude scaling of quantiles with GMPEs for $R_X = -30.$, $F = -1$, and $T = 0.5$ . . . . . 1004
5.141PVNGSv2: Magnitude scaling of quantiles with GMPEs for $R_X = -30.$, $F = 0$, and $T = 0.5$ . . . . . 1004
5.142PVNGSv2: Magnitude scaling of quantiles with GMPEs for $R_X = -15.$, $F = -1$, and $T = 0.5$ . . . . . 1005
5.143PVNGSv2: Magnitude scaling of quantiles with GMPEs for $R_X = -15.$, $F = 0$, and $T = 0.5$ . . . . . 1005
5.144PVNGSv2: Magnitude scaling of quantiles with GMPEs for $R_X = -5.$, $F = -1$, and $T = 0.5$ . . . . . 1006
5.145PVNGSv2: Magnitude scaling of quantiles with GMPEs for $R_X = -5.$, $F = 0$, and $T = 0.5$ . . . . . 1006
5.146PVNGSv2: Magnitude scaling of quantiles with GMPEs for $R_X = 5.$, $F = -1$, and $T = 0.5$ . . . . . 1007
5.147PVNGSv2: Magnitude scaling of quantiles with GMPEs for $R_X = 5.$, $F = 0$, and $T = 0.5$ . . . . . 1007
5.148PVNGSv2: Magnitude scaling of quantiles with GMPEs for $R_X = 15.$, $F = -1$, and $T = 0.5$ . . . . . 1008
5.149PVNGSv2: Magnitude scaling of quantiles with GMPEs for $R_X = 15.$, $F = 0$, and $T = 0.5$ . . . . . 1008
5.150PVNGSv2: Magnitude scaling of quantiles with GMPEs for $R_X = -50.$, $F = -1$, and $T = 0.5$ . . . . . 1009
5.151PVNGSv2: Magnitude scaling of quantiles with GMPEs for $R_X = -50.$, $F = 0$, and $T = 0.5$ . . . . . 1009
5.152PVNGSv2: Magnitude scaling of quantiles with GMPEs for $R_X = -30.$, $F = -1$, and $T = 0.5$ . . . . . 1010
5.153PVNGSv2: Magnitude scaling of quantiles with GMPEs for $R_X = -30.$, $F = 0$, and $T = 0.5$ . . . . . 1010
5.154PVNGSv2: Magnitude scaling of quantiles with GMPEs for $R_X = -15.$, $F = -1$, and $T = 0.5$ . . . . . 1011
5.155PVNGSv2: Magnitude scaling of quantiles with GMPEs for $R_X = -15.$, $F = 0$, and $T = 0.5$ . . . . . 1011
5.156PVNGSv2: Magnitude scaling of quantiles with GMPEs for $R_X = -5.$, $F = -1$, and $T = 0.5$ . . . . . 1012
5.157PVNGSv2: Magnitude scaling of quantiles with GMPEs for $R_X = -5.$, $F = 0$, and $T = 0.5$ . . . . . 1012
5.158PVNGSv2: Magnitude scaling of quantiles with GMPEs for $R_X = 5.$, $F = -1$, and $T = 0.5$ . . . . . 1013
5.159PVNGSv2: Magnitude scaling of quantiles with GMPEs for $R_X = 5.$, $F = 0$, and $T = 0.5$ . . . . . 1013
5.160PVNGSv2: Magnitude scaling of quantiles with GMPEs for $R_X = 15.$, $F = -1$, and $T = 0.5$ . . . . . 1014
5.161PVNGSv2: Magnitude scaling of quantiles with GMPEs for $R_X = 15.$, $F = 0$, and $T = 0.5$ . . . . . 1014
5.162PVNGSv2: Magnitude scaling of quantiles with GMPEs for $R_X = -50.$, $F = -1$, and $T = 1.$ . . . . . 1015
5.163PVNGSv2: Magnitude scaling of quantiles with GMPEs for $R_X = -50.$, $F = 0$, and $T = 1.$ . . . . . 1015
5.164PVNGSv2: Magnitude scaling of quantiles with GMPEs for $R_X = -30.$, $F = -1$, and $T = 1.$ . . . . . 1016
5.165PVNGSv2: Magnitude scaling of quantiles with GMPEs for $R_X = -30.$, $F = 0$, and $T = 1.$ . . . . . 1016
5.166PVNGSv2: Magnitude scaling of quantiles with GMPEs for $R_X = -15.$, $F = -1$, and $T = 1.$ . . . . . 1017

5.167PVNGSv2: Magnitude scaling of quantiles with GMPEs for $R_X = -15.$, $F = 0$, and $T = 1.$ . . . . . 1017
5.168PVNGSv2: Magnitude scaling of quantiles with GMPEs for $R_X = -5.$, $F = -1$, and $T = 1.$ . . . . . 1018
5.169PVNGSv2: Magnitude scaling of quantiles with GMPEs for $R_X = -5.$, $F = 0$, and $T = 1.$ . . . . . 1018
5.170PVNGSv2: Magnitude scaling of quantiles with GMPEs for $R_X = 5.$, $F = -1$, and $T = 1.$ . . . . . 1019
5.171PVNGSv2: Magnitude scaling of quantiles with GMPEs for $R_X = 5.$, $F = 0$, and $T = 1.$ . . . . . 1019
5.172PVNGSv2: Magnitude scaling of quantiles with GMPEs for $R_X = 15.$, $F = -1$, and $T = 1.$ . . . . . 1020
5.173PVNGSv2: Magnitude scaling of quantiles with GMPEs for $R_X = 15.$, $F = 0$, and $T = 1.$ . . . . . 1020
5.174PVNGSv2: Magnitude scaling of quantiles with GMPEs for $R_X = -50.$, $F = -1$, and $T = 1.$ . . . . . 1021
5.175PVNGSv2: Magnitude scaling of quantiles with GMPEs for $R_X = -50.$, $F = 0$, and $T = 1.$ . . . . . 1021
5.176PVNGSv2: Magnitude scaling of quantiles with GMPEs for $R_X = -30.$, $F = -1$, and $T = 1.$ . . . . . 1022
5.177PVNGSv2: Magnitude scaling of quantiles with GMPEs for $R_X = -30.$, $F = 0$, and $T = 1.$ . . . . . 1022
5.178PVNGSv2: Magnitude scaling of quantiles with GMPEs for $R_X = -15.$, $F = -1$, and $T = 1.$ . . . . . 1023
5.179PVNGSv2: Magnitude scaling of quantiles with GMPEs for $R_X = -15.$, $F = 0$, and $T = 1.$ . . . . . 1023
5.180PVNGSv2: Magnitude scaling of quantiles with GMPEs for $R_X = -5.$, $F = -1$, and $T = 1.$ . . . . . 1024
5.181PVNGSv2: Magnitude scaling of quantiles with GMPEs for $R_X = -5.$, $F = 0$, and $T = 1.$ . . . . . 1024
5.182PVNGSv2: Magnitude scaling of quantiles with GMPEs for $R_X = 5.$, $F = -1$, and $T = 1.$ . . . . . 1025
5.183PVNGSv2: Magnitude scaling of quantiles with GMPEs for $R_X = 5.$, $F = 0$, and $T = 1.$ . . . . . 1025
5.184PVNGSv2: Magnitude scaling of quantiles with GMPEs for $R_X = 15.$, $F = -1$, and $T = 1.$ . . . . . 1026
5.185PVNGSv2: Magnitude scaling of quantiles with GMPEs for $R_X = 15.$, $F = 0$, and $T = 1.$ . . . . . 1026
5.186PVNGSv2: Magnitude scaling of quantiles with GMPEs for $R_X = -50.$, $F = -1$, and $T = 1.$ . . . . . 1027
5.187PVNGSv2: Magnitude scaling of quantiles with GMPEs for $R_X = -50.$, $F = 0$, and $T = 1.$ . . . . . 1027
5.188PVNGSv2: Magnitude scaling of quantiles with GMPEs for $R_X = -30.$, $F = -1$, and $T = 1.$ . . . . . 1028
5.189PVNGSv2: Magnitude scaling of quantiles with GMPEs for $R_X = -30.$, $F = 0$, and $T = 1.$ . . . . . 1028
5.190PVNGSv2: Magnitude scaling of quantiles with GMPEs for $R_X = -15.$, $F = -1$, and $T = 1.$ . . . . . 1029
5.191PVNGSv2: Magnitude scaling of quantiles with GMPEs for $R_X = -15.$, $F = 0$, and $T = 1.$ . . . . . 1029
5.192PVNGSv2: Magnitude scaling of quantiles with GMPEs for $R_X = -5.$, $F = -1$, and $T = 1.$ . . . . . 1030
5.193PVNGSv2: Magnitude scaling of quantiles with GMPEs for $R_X = -5.$, $F = 0$, and $T = 1.$ . . . . . 1030
5.194PVNGSv2: Magnitude scaling of quantiles with GMPEs for $R_X = 5.$, $F = -1$, and $T = 1.$ . . . . . 1031
5.195PVNGSv2: Magnitude scaling of quantiles with GMPEs for $R_X = 5.$, $F = 0$, and $T = 1.$ . . . . . 1031
5.196PVNGSv2: Magnitude scaling of quantiles with GMPEs for $R_X = 15.$, $F = -1$, and $T = 1.$ . . . . . 1032
5.197PVNGSv2: Magnitude scaling of quantiles with GMPEs for $R_X = 15.$, $F = 0$, and $T = 1.$ . . . . . 1032
5.198PVNGSv2: Magnitude scaling of quantiles with GMPEs for $R_X = -50.$, $F = -1$, and $T = 2.$ . . . . . 1033
5.199PVNGSv2: Magnitude scaling of quantiles with GMPEs for $R_X = -50.$, $F = 0$, and $T = 2.$ . . . . . 1033
5.200PVNGSv2: Magnitude scaling of quantiles with GMPEs for $R_X = -30.$, $F = -1$, and $T = 2.$ . . . . . 1034
5.201PVNGSv2: Magnitude scaling of quantiles with GMPEs for $R_X = -30.$, $F = 0$, and $T = 2.$ . . . . . 1034
5.202PVNGSv2: Magnitude scaling of quantiles with GMPEs for $R_X = -15.$, $F = -1$, and $T = 2.$ . . . . . 1035
5.203PVNGSv2: Magnitude scaling of quantiles with GMPEs for $R_X = -15.$, $F = 0$, and $T = 2.$ . . . . . 1035
5.204PVNGSv2: Magnitude scaling of quantiles with GMPEs for $R_X = -5.$, $F = -1$, and $T = 2.$ . . . . . 1036
5.205PVNGSv2: Magnitude scaling of quantiles with GMPEs for $R_X = -5.$, $F = 0$, and $T = 2.$ . . . . . 1036
5.206PVNGSv2: Magnitude scaling of quantiles with GMPEs for $R_X = 5.$, $F = -1$, and $T = 2.$ . . . . . 1037
5.207PVNGSv2: Magnitude scaling of quantiles with GMPEs for $R_X = 5.$, $F = 0$, and $T = 2.$ . . . . . 1037
5.208PVNGSv2: Magnitude scaling of quantiles with GMPEs for $R_X = 15.$, $F = -1$, and $T = 2.$ . . . . . 1038
5.209PVNGSv2: Magnitude scaling of quantiles with GMPEs for $R_X = 15.$, $F = 0$, and $T = 2.$ . . . . . 1038
5.210PVNGSv2: Magnitude scaling of quantiles with GMPEs for $R_X = -50.$, $F = -1$, and $T = 2.$ . . . . . 1039
5.211PVNGSv2: Magnitude scaling of quantiles with GMPEs for $R_X = -50.$, $F = 0$, and $T = 2.$ . . . . . 1039
5.212PVNGSv2: Magnitude scaling of quantiles with GMPEs for $R_X = -30.$, $F = -1$, and $T = 2.$ . . . . . 1040
5.213PVNGSv2: Magnitude scaling of quantiles with GMPEs for $R_X = -30.$, $F = 0$, and $T = 2.$ . . . . . 1040
5.214PVNGSv2: Magnitude scaling of quantiles with GMPEs for $R_X = -15.$, $F = -1$, and $T = 2.$ . . . . . 1041
5.215PVNGSv2: Magnitude scaling of quantiles with GMPEs for $R_X = -15.$, $F = 0$, and $T = 2.$ . . . . . 1041
5.216PVNGSv2: Magnitude scaling of quantiles with GMPEs for $R_X = -5.$, $F = -1$, and $T = 2.$ . . . . . 1042
5.217PVNGSv2: Magnitude scaling of quantiles with GMPEs for $R_X = -5.$, $F = 0$, and $T = 2.$ . . . . . 1042
5.218PVNGSv2: Magnitude scaling of quantiles with GMPEs for $R_X = 5.$, $F = -1$, and $T = 2.$ . . . . . 1043
5.219PVNGSv2: Magnitude scaling of quantiles with GMPEs for $R_X = 5.$, $F = 0$, and $T = 2.$ . . . . . 1043
5.220PVNGSv2: Magnitude scaling of quantiles with GMPEs for $R_X = 15.$, $F = -1$, and $T = 2.$ . . . . . 1044
5.221PVNGSv2: Magnitude scaling of quantiles with GMPEs for $R_X = 15.$, $F = 0$, and $T = 2.$ . . . . . 1044
5.222PVNGSv2: Magnitude scaling of quantiles with GMPEs for $R_X = -50.$, $F = -1$, and $T = 2.$ . . . . . 1045
5.223PVNGSv2: Magnitude scaling of quantiles with GMPEs for $R_X = -50.$, $F = 0$, and $T = 2.$ . . . . . 1045
5.224PVNGSv2: Magnitude scaling of quantiles with GMPEs for $R_X = -30.$, $F = -1$, and $T = 2.$ . . . . . 1046
5.225PVNGSv2: Magnitude scaling of quantiles with GMPEs for $R_X = -30.$, $F = 0$, and $T = 2.$ . . . . . 1046
5.226PVNGSv2: Magnitude scaling of quantiles with GMPEs for $R_X = -15.$, $F = -1$, and $T = 2.$ . . . . . 1047
5.227PVNGSv2: Magnitude scaling of quantiles with GMPEs for $R_X = -15.$, $F = 0$, and $T = 2.$ . . . . . 1047

5.228PVNGSv2: Magnitude scaling of quantiles with GMPEs for $R_X = -5.$, $F = -1$, and $T = 2.$ . . . . . 1048
5.229PVNGSv2: Magnitude scaling of quantiles with GMPEs for $R_X = -5.$, $F = 0$, and $T = 2.$ . . . . . 1048
5.230PVNGSv2: Magnitude scaling of quantiles with GMPEs for $R_X = 5.$, $F = -1$, and $T = 2.$ . . . . . 1049
5.231PVNGSv2: Magnitude scaling of quantiles with GMPEs for $R_X = 5.$, $F = 0$, and $T = 2.$ . . . . . 1049
5.232PVNGSv2: Magnitude scaling of quantiles with GMPEs for $R_X = 15.$, $F = -1$, and $T = 2.$ . . . . . 1050
5.233PVNGSv2: Magnitude scaling of quantiles with GMPEs for $R_X = 15.$, $F = 0$, and $T = 2.$ . . . . . 1050
5.234PVNGSv2: Magnitude scaling of quantiles with GMPEs for $R_X = -50.$, $F = -1$, and $T = 3.$ . . . . . 1051
5.235PVNGSv2: Magnitude scaling of quantiles with GMPEs for $R_X = -50.$, $F = 0$, and $T = 3.$ . . . . . 1051
5.236PVNGSv2: Magnitude scaling of quantiles with GMPEs for $R_X = -30.$, $F = -1$, and $T = 3.$ . . . . . 1052
5.237PVNGSv2: Magnitude scaling of quantiles with GMPEs for $R_X = -30.$, $F = 0$, and $T = 3.$ . . . . . 1052
5.238PVNGSv2: Magnitude scaling of quantiles with GMPEs for $R_X = -15.$, $F = -1$, and $T = 3.$ . . . . . 1053
5.239PVNGSv2: Magnitude scaling of quantiles with GMPEs for $R_X = -15.$, $F = 0$, and $T = 3.$ . . . . . 1053
5.240PVNGSv2: Magnitude scaling of quantiles with GMPEs for $R_X = -5.$, $F = -1$, and $T = 3.$ . . . . . 1054
5.241PVNGSv2: Magnitude scaling of quantiles with GMPEs for $R_X = -5.$, $F = 0$, and $T = 3.$ . . . . . 1054
5.242PVNGSv2: Magnitude scaling of quantiles with GMPEs for $R_X = 5.$, $F = -1$, and $T = 3.$ . . . . . 1055
5.243PVNGSv2: Magnitude scaling of quantiles with GMPEs for $R_X = 5.$, $F = 0$, and $T = 3.$ . . . . . 1055
5.244PVNGSv2: Magnitude scaling of quantiles with GMPEs for $R_X = 15.$, $F = -1$, and $T = 3.$ . . . . . 1056
5.245PVNGSv2: Magnitude scaling of quantiles with GMPEs for $R_X = 15.$, $F = 0$, and $T = 3.$ . . . . . 1056
5.246PVNGSv2: Magnitude scaling of quantiles with GMPEs for $R_X = -50.$, $F = -1$, and $T = 3.$ . . . . . 1057
5.247PVNGSv2: Magnitude scaling of quantiles with GMPEs for $R_X = -50.$, $F = 0$, and $T = 3.$ . . . . . 1057
5.248PVNGSv2: Magnitude scaling of quantiles with GMPEs for $R_X = -30.$, $F = -1$, and $T = 3.$ . . . . . 1058
5.249PVNGSv2: Magnitude scaling of quantiles with GMPEs for $R_X = -30.$, $F = 0$, and $T = 3.$ . . . . . 1058
5.250PVNGSv2: Magnitude scaling of quantiles with GMPEs for $R_X = -15.$, $F = -1$, and $T = 3.$ . . . . . 1059
5.251PVNGSv2: Magnitude scaling of quantiles with GMPEs for $R_X = -15.$, $F = 0$, and $T = 3.$ . . . . . 1059
5.252PVNGSv2: Magnitude scaling of quantiles with GMPEs for $R_X = -5.$, $F = -1$, and $T = 3.$ . . . . . 1060
5.253PVNGSv2: Magnitude scaling of quantiles with GMPEs for $R_X = -5.$, $F = 0$, and $T = 3.$ . . . . . 1060
5.254PVNGSv2: Magnitude scaling of quantiles with GMPEs for $R_X = 5.$, $F = -1$, and $T = 3.$ . . . . . 1061
5.255PVNGSv2: Magnitude scaling of quantiles with GMPEs for $R_X = 5.$, $F = 0$, and $T = 3.$ . . . . . 1061
5.256PVNGSv2: Magnitude scaling of quantiles with GMPEs for $R_X = 15.$, $F = -1$, and $T = 3.$ . . . . . 1062
5.257PVNGSv2: Magnitude scaling of quantiles with GMPEs for $R_X = 15.$, $F = 0$, and $T = 3.$ . . . . . 1062
5.258PVNGSv2: Magnitude scaling of quantiles with GMPEs for $R_X = -50.$, $F = -1$, and $T = 3.$ . . . . . 1063
5.259PVNGSv2: Magnitude scaling of quantiles with GMPEs for $R_X = -50.$, $F = 0$, and $T = 3.$ . . . . . 1063
5.260PVNGSv2: Magnitude scaling of quantiles with GMPEs for $R_X = -30.$, $F = -1$, and $T = 3.$ . . . . . 1064
5.261PVNGSv2: Magnitude scaling of quantiles with GMPEs for $R_X = -30.$, $F = 0$, and $T = 3.$ . . . . . 1064
5.262PVNGSv2: Magnitude scaling of quantiles with GMPEs for $R_X = -15.$, $F = -1$, and $T = 3.$ . . . . . 1065
5.263PVNGSv2: Magnitude scaling of quantiles with GMPEs for $R_X = -15.$, $F = 0$, and $T = 3.$ . . . . . 1065
5.264PVNGSv2: Magnitude scaling of quantiles with GMPEs for $R_X = -5.$, $F = -1$, and $T = 3.$ . . . . . 1066
5.265PVNGSv2: Magnitude scaling of quantiles with GMPEs for $R_X = -5.$, $F = 0$, and $T = 3.$ . . . . . 1066
5.266PVNGSv2: Magnitude scaling of quantiles with GMPEs for $R_X = 5.$, $F = -1$, and $T = 3.$ . . . . . 1067
5.267PVNGSv2: Magnitude scaling of quantiles with GMPEs for $R_X = 5.$, $F = 0$, and $T = 3.$ . . . . . 1067
5.268PVNGSv2: Magnitude scaling of quantiles with GMPEs for $R_X = 15.$, $F = -1$, and $T = 3.$ . . . . . 1068
5.269PVNGSv2: Magnitude scaling of quantiles with GMPEs for $R_X = 15.$, $F = 0$, and $T = 3.$ . . . . . 1068
5.270PVNGSv2: Spectra for $M_W = 5.$, $R_x = -50.$, $F = 0$ . . . . . 1069
5.271PVNGSv2: Spectra for $M_W = 5.$, $R_x = -15.$, $F = 0$ . . . . . 1069
5.272PVNGSv2: Spectra for $M_W = 5.$, $R_x = 5.$, $F = 0$ . . . . . 1070
5.273PVNGSv2: Spectra for $M_W = 6.$, $R_x = -50.$, $F = 0$ . . . . . 1070
5.274PVNGSv2: Spectra for $M_W = 6.$, $R_x = -15.$, $F = 0$ . . . . . 1071
5.275PVNGSv2: Spectra for $M_W = 6.$, $R_x = 5.$, $F = 0$ . . . . . 1071
5.276PVNGSv2: Spectra for $M_W = 7.$, $R_x = -50.$, $F = 0$ . . . . . 1072
5.277PVNGSv2: Spectra for $M_W = 7.$, $R_x = -15.$, $F = 0$ . . . . . 1072
5.278PVNGSv2: Spectra for $M_W = 7.$, $R_x = 5.$, $F = 0$ . . . . . 1073
5.279PVNGSv2: Spectra for $M_W = 5.$, $R_x = -50.$, $F = -1$ . . . . . 1073
5.280PVNGSv2: Spectra for $M_W = 5.$, $R_x = -15.$, $F = -1$ . . . . . 1074
5.281PVNGSv2: Spectra for $M_W = 5.$, $R_x = 5.$, $F = -1$ . . . . . 1074
5.282PVNGSv2: Spectra for $M_W = 6.$, $R_x = -50.$, $F = -1$ . . . . . 1075
5.283PVNGSv2: Spectra for $M_W = 6.$, $R_x = -15.$, $F = -1$ . . . . . 1075
5.284PVNGSv2: Spectra for $M_W = 6.$, $R_x = 5.$, $F = -1$ . . . . . 1076
5.285PVNGSv2: Spectra for $M_W = 7.$, $R_x = -50.$, $F = -1$ . . . . . 1076
5.286PVNGSv2: Spectra for $M_W = 7.$, $R_x = -15.$, $F = -1$ . . . . . 1077
5.287PVNGSv2: Spectra for $M_W = 7.$, $R_x = 5.$, $F = -1$ . . . . . 1077

5.288 PVNGSv2: Histogram of differences for medians calculated with different weights to median calculated with total weights. Bottom row left shows differences between medians for the GMPE distribution to median calculated with total weights. Bottom row right shows differences between the original GMPEs (without uncertainty) to median calculated with total weights. For PVNGS2, combined Model A and B and $T = 0.01$s. . . . . 1079
5.289 PVNGSv2: Histogram of differences for medians calculated with different weights to median calculated with total weights. Bottom row left shows differences between medians for the GMPE distribution to median calculated with total weights. Bottom row right shows differences between the original GMPEs (without uncertainty) to median calculated with total weights. For PVNGS2, combined Model A and B and $T = 0.02$s. . . . . 1080
5.290 PVNGSv2: Histogram of differences for medians calculated with different weights to median calculated with total weights. Bottom row left shows differences between medians for the GMPE distribution to median calculated with total weights. Bottom row right shows differences between the original GMPEs (without uncertainty) to median calculated with total weights. For PVNGS2, combined Model A and B and $T = 0.03$s. . . . . 1081
5.291 PVNGSv2: Histogram of differences for medians calculated with different weights to median calculated with total weights. Bottom row left shows differences between medians for the GMPE distribution to median calculated with total weights. Bottom row right shows differences between the original GMPEs (without uncertainty) to median calculated with total weights. For PVNGS2, combined Model A and B and $T = 0.05$s. . . . . 1082
5.292 PVNGSv2: Histogram of differences for medians calculated with different weights to median calculated with total weights. Bottom row left shows differences between medians for the GMPE distribution to median calculated with total weights. Bottom row right shows differences between the original GMPEs (without uncertainty) to median calculated with total weights. For PVNGS2, combined Model A and B and $T = 0.075$s. . . . . 1083
5.293 PVNGSv2: Histogram of differences for medians calculated with different weights to median calculated with total weights. Bottom row left shows differences between medians for the GMPE distribution to median calculated with total weights. Bottom row right shows differences between the original GMPEs (without uncertainty) to median calculated with total weights. For PVNGS2, combined Model A and B and $T = 0.1$s. . . . . 1084
5.294 PVNGSv2: Histogram of differences for medians calculated with different weights to median calculated with total weights. Bottom row left shows differences between medians for the GMPE distribution to median calculated with total weights. Bottom row right shows differences between the original GMPEs (without uncertainty) to median calculated with total weights. For PVNGS2, combined Model A and B and $T = 0.15$s. . . . . 1085
5.295 PVNGSv2: Histogram of differences for medians calculated with different weights to median calculated with total weights. Bottom row left shows differences between medians for the GMPE distribution to median calculated with total weights. Bottom row right shows differences between the original GMPEs (without uncertainty) to median calculated with total weights. For PVNGS2, combined Model A and B and $T = 0.2$s. . . . . 1086
5.296 PVNGSv2: Histogram of differences for medians calculated with different weights to median calculated with total weights. Bottom row left shows differences between medians for the GMPE distribution to median calculated with total weights. Bottom row right shows differences between the original GMPEs (without uncertainty) to median calculated with total weights. For PVNGS2, combined Model A and B and $T = 0.25$s. . . . . 1087
5.297 PVNGSv2: Histogram of differences for medians calculated with different weights to median calculated with total weights. Bottom row left shows differences between medians for the GMPE distribution to median calculated with total weights. Bottom row right shows differences between the original GMPEs (without uncertainty) to median calculated with total weights. For PVNGS2, combined Model A and B and $T = 0.3$s. . . . . 1088
5.298 PVNGSv2: Histogram of differences for medians calculated with different weights to median calculated with total weights. Bottom row left shows differences between medians for the GMPE distribution to median calculated with total weights. Bottom row right shows differences between the original GMPEs (without uncertainty) to median calculated with total weights. For PVNGS2, combined Model A and B and $T = 0.4$s. . . . . 1089
5.299 PVNGSv2: Histogram of differences for medians calculated with different weights to median calculated with total weights. Bottom row left shows differences between medians for the GMPE distribution to median calculated with total weights. Bottom row right shows differences between the original GMPEs (without uncertainty) to median calculated with total weights. For PVNGS2, combined Model A and B and $T = 0.5$s. . . . . 1090

5.300 PVNGSv2: Histogram of differences for medians calculated with different weights to median calculated with total weights. Bottom row left shows differences between medians for the GMPE distribution to median calculated with total weights. Bottom row right shows differences between the original GMPEs (without uncertainty) to median calculated with total weights. For PVNGS2, combined Model A and B and $T = 0.75$s. . . . . 1091
5.301 PVNGSv2: Histogram of differences for medians calculated with different weights to median calculated with total weights. Bottom row left shows differences between medians for the GMPE distribution to median calculated with total weights. Bottom row right shows differences between the original GMPEs (without uncertainty) to median calculated with total weights. For PVNGS2, combined Model A and B and $T = 1$.s. . . . . 1092
5.302 PVNGSv2: Histogram of differences for medians calculated with different weights to median calculated with total weights. Bottom row left shows differences between medians for the GMPE distribution to median calculated with total weights. Bottom row right shows differences between the original GMPEs (without uncertainty) to median calculated with total weights. For PVNGS2, combined Model A and B and $T = 1.5$s. . . . . 1093
5.303 PVNGSv2: Histogram of differences for medians calculated with different weights to median calculated with total weights. Bottom row left shows differences between medians for the GMPE distribution to median calculated with total weights. Bottom row right shows differences between the original GMPEs (without uncertainty) to median calculated with total weights. For PVNGS2, combined Model A and B and $T = 2$.s. . . . . 1094
5.304 PVNGSv2: Histogram of differences for medians calculated with different weights to median calculated with total weights. Bottom row left shows differences between medians for the GMPE distribution to median calculated with total weights. Bottom row right shows differences between the original GMPEs (without uncertainty) to median calculated with total weights. For PVNGS2, combined Model A and B and $T = 3$.s. . . . . 1095

# Chapter 1

# Introduction

## 1.1 Introduction on the Application of Visualization Tools to GMPE Distribution

Section 1.1 of this introductory Chapter is a shortened version of the PEER Report being prepared on the epistemic uncertainty using Sammons map. The purpose of the introductory Chapter in Appendix H is to review the use of GMPE mapping for PSHA as built upon the work of Scherbaum et al. (2010)[18] to use high-dimensional visualization techniques to represent epistemic uncertainty. Also, this Chapter describes how a metric to measure the distances between GMPEs (in a ground-motion sense) can be defined, and how these can be interpreted in a meaningful way. Distances in median GMPE predictions are addressed as a means of providing a full assessment of differences between GMPEs, noting that they should be treated as distributions. It has become common practice, however, to separate the two ingredients of GMPEs (median predictions and aleatory variability), and build a separate logic tree for both components. The methods presented herein can be used to assess the range of median GMPE predictions.

### 1.1.1 2D Visualization of GMPEs

High-dimensional visualization tools are a natural choice to compare different GMPEs. This is illustrated in Figure 1.1 and it is closely related to the use of an ensemble of GMPEs (Atkinson et al., 2014) [6]. In the left part of Figure 1.1, the predictions of 11 GMPEs for one particular scenario (M = 5.5, RJB = 10 km) are shown as a histogram. These 11 GMPEs are selected for the sake of example, and do not correspond to the candidate GMPEs selected for the SWUS GMC study, although they include the SWUS GMC candidate GMPEs. The 11 GMPEs selected as example for this introductory Chapter in Appendix H are listed as follows:

- Abrahamson et al. (2014) [1], hereafter ASK14
- Akkar and Cagnan (2010) [2], hereafter AC14
- Akkar et al. (2014,b) [3, 4], hereafter Ak14
- Bindi et al. (2014a,b) [7, 8], hereafter Bi14
- Boore et al. (2014) [9], hereafter BSSA14
- Bora et al. (2014) [10], hereafter Bora14
- Campbell and Bozorgnia (2014) [11], hereafter CB14
- Chiou and Youngs (2014), [12], hereafter CY14
- Graizer (2014) [14], hereafter GK13
- Idriss (2014) [16], hereafter I14
- Zhao et al. (2006) [19], hereafter Zhao06

Since there are 11 discrete GMPEs, there are 11 discrete median ground-motion predictions. However, because there should be a continuous distribution of predictions, the intermediate values are not impossible; there just is no (published) model that predicts them. For a single scenario (one dimension), one can fit a continuous distribution to the predictions (in Figure 1.1 the best fitting normal distribution is shown), and evaluate the predictions and the continuous model graphically. Going to two scenarios, this is still possible, as shown in the right part of Figure 1.1. For more than three scenarios, the

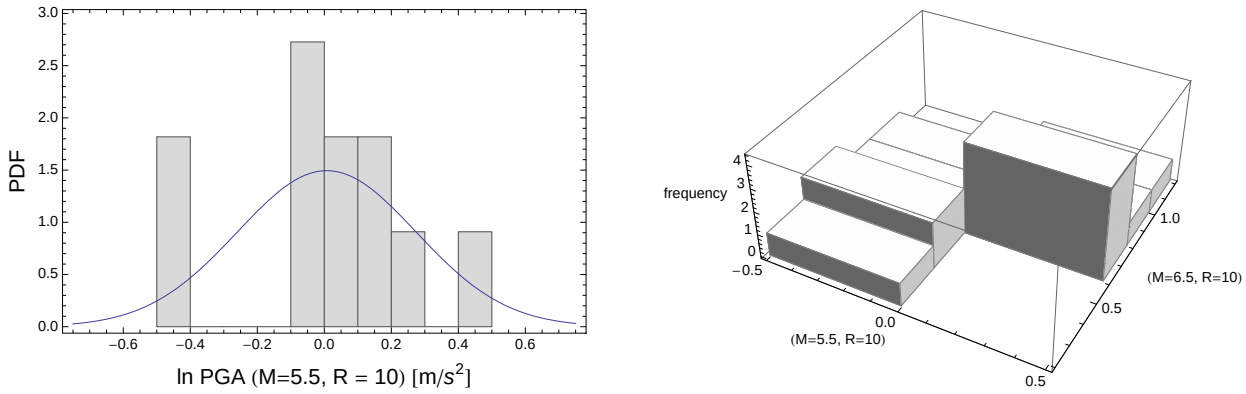



Figure 1.1: Histogram of predictions of 11 GMPEs, for one scenario (left) and two scenarios (right).

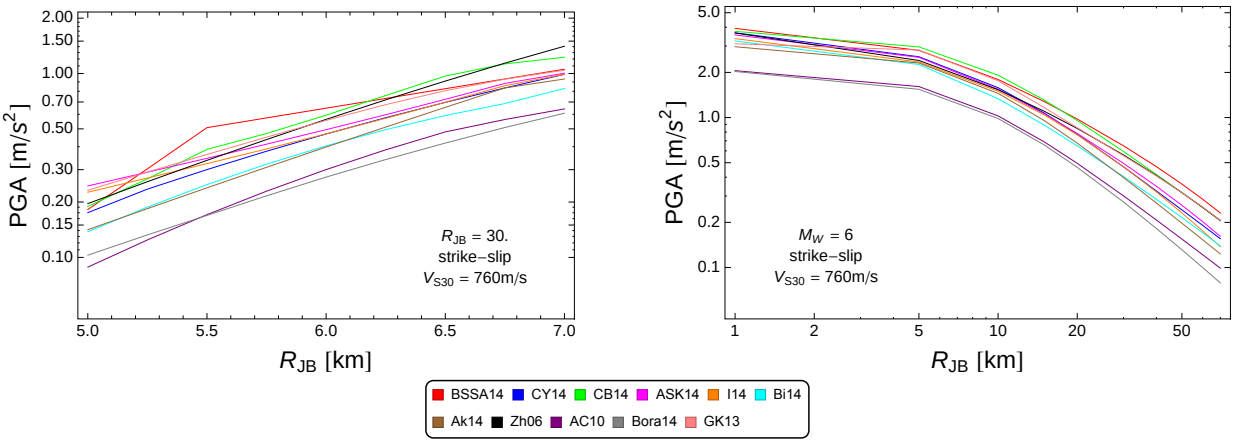



Figure 1.2: Magnitude and distance scaling for 11 GMPEs used as example in the introduction to this Appendix.

simultaneous (graphical) evaluation of different GMPEs becomes almost impossible. However, for purposes of assessing the models (and their corresponding continuous distribution) with respect to their application in PSHA, the models need to be evaluated for many different magnitude-distance scenarios.

For the single scenario case (one setting of the predictor variables such as magnitude-distance and so on), the problem is easy: the difference between the GMPEs is just the difference between their predictions. If one keeps all predictor variables fixed and changes only the distance, one can plot the ground motion predictions vs. distance; for just a few GMPEs, it is feasible to recognize trends, evaluate differences in distance scaling, and so forth. With an increasing number of GMPEs it becomes more difficult to assess similarities or differences between GMPEs. Figure 1.2, shows the magnitude and distance scaling of the 11 aforementioned GMPEs, as an example. In this case, it is difficult to evaluate differences between individual models. The only thing one can assess is the range covered by the models. If one were to plot all combinations of only two models out of those 11 GMPEs for one particular magnitude or distance, one would have 55 plots. To compare the models at other magnitudes and distances, even more plots are needed.

To capture the center, body, and range of median GMPE predictions, it is, however, necessary to assess the similarity of GMPEs over a wide range of magnitudes and distances that are relevant to the hazard at the site. Projecting the GMPEs into two dimensions is a good way to achieve that objective. Basically, the GMPEs are mapped, and thus they can be evaluated visually.

The basic idea is that GMPEs live in some abstract model space. This space can be thought of as (in the simplest case) the space of all functions of magnitude and distance. Most of these functions, however, are not physically realizable; there are decreasing functions with magnitude or functions with unrealistic slopes. Hence, GMPEs form a subspace of this function space. The basic assumption is that the GMPEs occupy a lower dimensional manifold in the larger model space. If this manifold is two-dimensional, it is possible to plot it on a map and is easy to visualize.

To assess the model space, the following are considered:

- The median prediction of a GMPE is a function.
- By evaluating the GMPE at certain values of its predictor variables (M,R-scenarios), it is discretized.

- If the GMPE is evaluated at N different values of its predictor variables, it can be represented as an N-dimensional vector of ground-motions, one entry for each M,R pair.
- Each GMPE is evaluated at the same N values of the predictor variables this means that each GMPE corresponds to a point in N-dimensional ground-motion space. This is an approximation of the GMPE model space.
- The N-dimensional space is projected to two dimensions.

In the next section, the estimation of Sammons maps is briefly described.

### 1.1.2 Sammon's Mapping

Sammons mapping (Sammon, 1969) [17] is a nonlinear dimensional reduction technique. In Sammons mapping, a configuration of points in two dimensions is sought that resembles the distance distribution in high dimensions. In this case, distance describes the difference between coordinates (i.e. between their median predictions), and is not a physical distance like $R_{JB}$ or $R_{RUP}$. Throughout this introductory Chapter to Appendix H, the term GMPE-distance, or $\overline{\Delta_{GM}}$ , will be used to describe differences between GMPEs in ground-motion space. The misfit function is the difference between the GMPE-distances in high dimensions and two dimensions:

$$E = \frac{1}{\sum_{i<j} \overline{\Delta_{GM}}_{ij}} \sum_{i<j} \frac{(\overline{\Delta_{GM}}_{ij} - \overline{\Delta_{map}}_{ij})^2}{\overline{\Delta_{GM}}_{ij}} \tag{1.1}$$

where $\overline{\Delta_{GM}}_{ij}$ is the GMPE-distance between GMPEs $i$ and $j$ in high-dimensions, and $\overline{\Delta_{map}}_{ij}$ is the corresponding shortest distance on the map (in two dimensions), respectively. $\overline{\Delta_{map}}$ is the shortest path between two points on the map, which is the Euclidean distance in two dimensions. E is called the Sammons stress. To produce a 2D-projection, E is minimized with respect to the positions in two dimensions through an iterative process (e.g. via gradient descent). As a starting configuration, a random set of points on the map can be used. Another common choice is to use the output of principal component analysis (PCA, described in Hotelling, 1933) [15] as a starting configuration.

From the description of Sammons mapping, only the relative positions of GMPEs on the map are important. The absolute coordinates depend on the starting configuration of the points on the map. On the other hand, relative positions and map GMPE-distances do have a meaning: they correspond to the relative positions in high dimensions. They can be rotated and/or mirrored without changing the $\overline{\Delta_{map}}_{ij}$.

#### Sammons Map Conceptual Examples

As a simple example of the relative position described above, a situation where the distance between three cities is known is considered. For example, the distance between San Francisco and Los Angeles is 552 km, the distance between San Francisco and Las Vegas is 662 km, and Los Angeles and Las Vegas are 377 km apart. This is sufficient information to infer the relative geometry of those three cities on a map. It does not, however, indicate which of the cities is the northernmost. For some applications, like estimating the cost of jet fuel, this can be all that is needed.

The following example is similar in spirit to the situation of comparing GMPEs, but the map can be evaluated intuitively. Example visualization is shown that exemplifies the power of high-dimensionalization tools. In Figure 1.3, 18 pictures of rubber ducks are shown as an intuitive example borrowed from Geusebroek et al. (2005) [13]. The rubber ducks in the 18 individual pictures show the same duck, each time rotated by 20°. Each of the pictures is a grid of 32x32 pixels, and each pixel is associated with a red, green and blue value. Hence, each picture can be represented by a 3072-dimensional vector, so each picture is a point in a 3072-dimensional "rubber duck"-space. The analog to the situation for a GMPE is that each pixel corresponds to a particular magnitude-distance scenario. In Figure 1.4, a Sammons map is shown as calculated for the 18 pictures of the ducks. The map is easily interpretable: pictures that are close (one rotation apart) are close on the map. Hence, Figure 1.4 shows the potential of using visualization techniques to reveal structure in a high-dimensional data set.

### 1.1.3 Distances Between GMPEs

In a Sammons map for GMPEs, the map distances correspond to high-dimensional GMPE-distances. As described before, the high-dimensional coordinates of a GMPE correspond to its predictions at different values of the predictor variables. Hence, GMPE-distances in high dimensions can be easily calculated from the differences in their predictions. There are, however, various GMPE-distance metrics that one can use. Three of these distances will be discussed in this Appendix, though theoretically any valid distance metric could be used.

Three naturally arising metrics are based on the L1, L2 and L norms. The GMPE-distances are then defined as

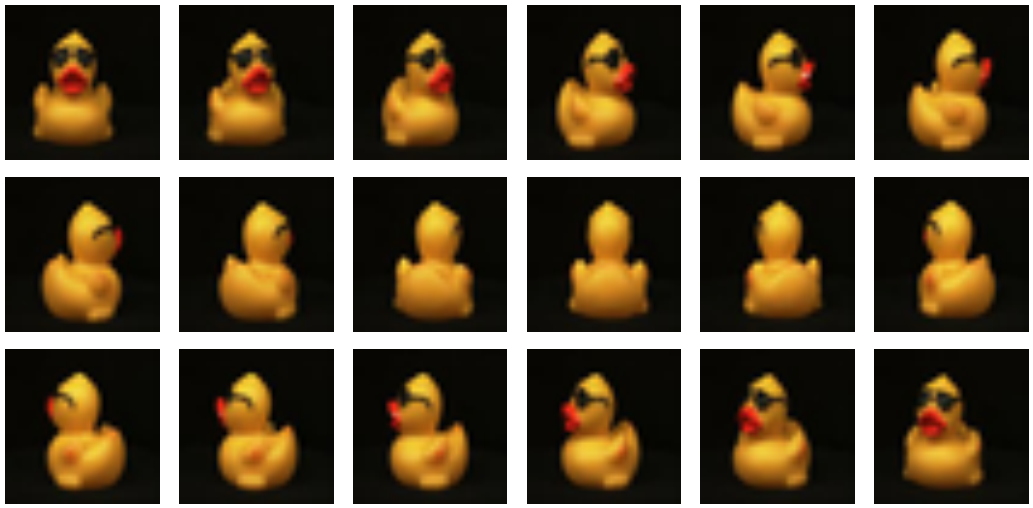


Figure 1.3: Pictures of rotated rubber ducks.

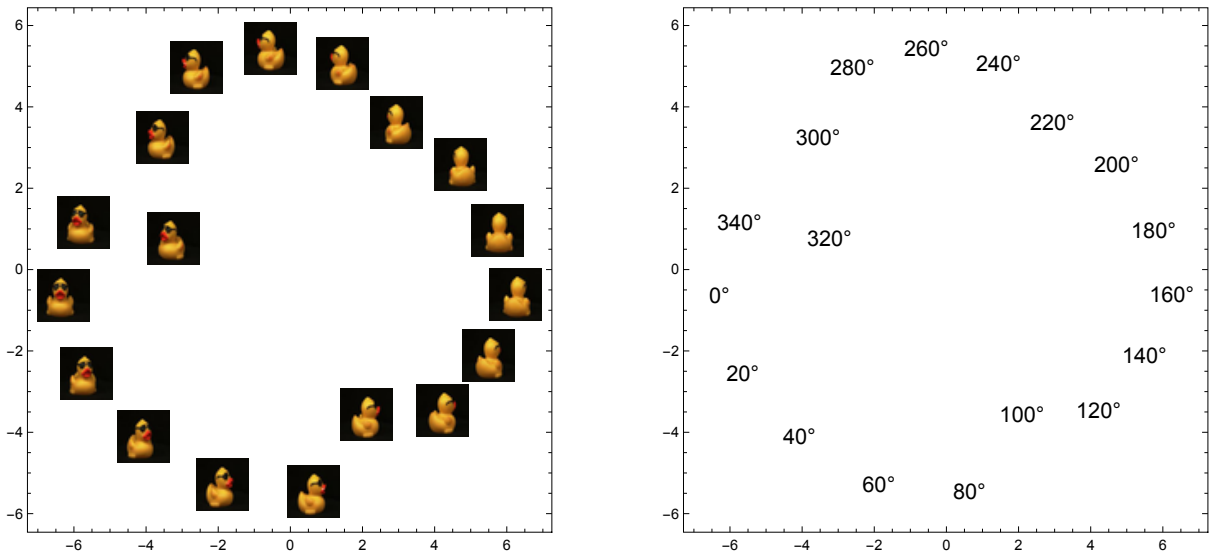



Figure 1.4: Left: Sammons map of rubber duck" space, with insets of pictures; Right: same map, but with rotation angle of each picture at the respective coordinate.

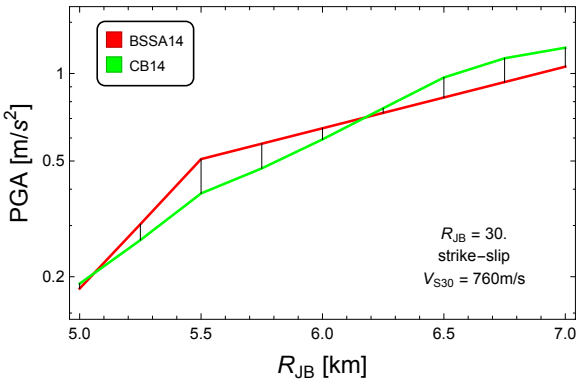



Figure 1.5: Differences between two GMPEs at different $R_{JB}$ -distance values, which go into the calculation of the (high-dimensional) distance $\overline{\Delta_{GM}}_{ij}$ between GMPEs $i$ and $j$ (BSSA14 and CB14 in this case).

$$\overline{\Delta_{GM}}_{ij}(L_1) = \frac{1}{N}\sum_{k}^{N} |\text{GMPE}_{ik} - \text{GMPE}_{jk}| \tag{1.2}$$

$$\overline{\Delta_{GM}}_{ij}(L_2) = \sqrt{\frac{1}{N}\sum_{k}^{N} (\text{GMPE}_{ik} - \text{GMPE}_{jk})^2} \tag{1.3}$$

$$\overline{\Delta_{GM}}_{ij}(L_\infty) = \max_{k} |\text{GMPE}_{ik} - \text{GMPE}_{jk}|, \tag{1.4}$$

where $k$ indexes the different values of the predictor variables, $N$ is the number of dimensions, $\overline{\Delta_{GM}}_{ij}(L_1)$ is the $L_n$-distance between GMPEs $i$ and $j$, and $\text{GMPE}_{ik}$ is the ground-motion prediction of the $i$th GMPE corresponding to the $k$th predictor variable combination. The difference $\text{GMPE}_{ik} - \text{GMPE}_{jk}$ between two GMPEs is illustrated in Figure 1.5. The factors $\frac{1}{N}$ and $\sqrt{\frac{1}{N}}$ in the definition of the $L_1$ and $L_2$-distances are there to normalize the GMPE-distances so that they have units of ground-motion and can easily be interpreted. Since $L_\infty$ is based on only one ground-motion-value, it is already in units of ground motion.

### 1.1.4 Sammons Maps of GMPEs

In this Section, Sammons maps are generated for the 11 different GMPEs, the same ones that are shown in Figures 1.1 and 1.2 .These models are selected to cover a relatively wide range of epistemic uncertainty, not with the intention to reflect any specific PSHA application.

The GMPEs are evaluated for PGA (or $T = 0.01$ sec), at moment magnitudes $\boldsymbol{M}$ = 5.0, 5.25,. . .,7.0 and $R_{JB}$ = 1, 5, 10, 15, 20, 30,. . ., 70 km. For each magnitude, a depth-to-the-top-of-the-rupture $Z_{TOR}$ is calculated, using the relation given in Chiou and Youngs (2014) [12]. The faulting style is assumed to be vertical strike-slip, so rupture distances can be easily calculated from $R_{JB}$ and $Z_{TOR}$. The site condition is set to $V_{S30} = 760$ m/s. All other predictor variables, such as the depth to a shear wave velocity horizon of 1000 m/s, are set to the default values for each GMPE. Hence, each GMPE is evaluated at 90 magnitude-distance pairs. Consequently, each GMPE can be represented as a point in a 90-dimensional ground-motion space, where each coordinate corresponds to the prediction for one particular magnitude-distance pair. The GMPEs, however, cannot reside anywhere in this 90-dimensional space. For example, the ground-motion prediction for a magnitude $M_1$ cannot not be smaller than that for a magnitude $M_2$ (at the same distance) if $M_1 > M_2$, in order to have a non-decreasing slope with magnitude (keeping possible oversaturation aside). In addition, the prediction for $M_1$ cannot be arbitrarily larger than the one for $M_2$, because there are physical restrictions on the slope. Hence, physically plausible GMPEs can only occupy a rather restricted part of the ground-motion space. Under the assumption that physically plausible GMPEs reside on a two-dimensional manifold (i.e. a surface that is locally flat), this manifold can be estimated using Sammons maps.

To facilitate interpretation of the map, reference models are added to the set of 11 GMPEs. These reference models are:

- the average of all models, hereafter called $mix$
- scaled versions of the average model: $mix + \ln\alpha$, with $\alpha = 0.67, 0.8, 1.25, 1.5$, called $S--$, $S-$, $S+$, $S++$
- the average model with changed magnitude scaling: $mix+\beta(M-6)$, with $\beta = -0.4, -0.2, 0.2, 0.4$, called $M--$, $M-$, $M+$, $M++$

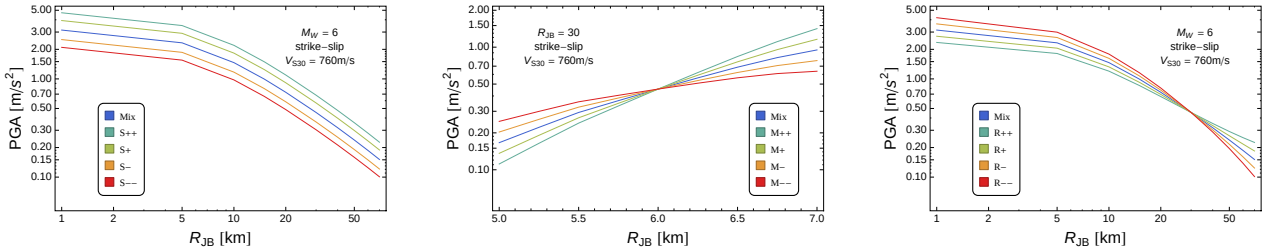



Figure 1.6: Difference in scaling of reference models that help the interpretation of the Sammons maps.

Table 1.1: High-dimensional GMPE-distances $\overline{\Delta_{GM}}$ and map distances $\overline{\Delta_{MAP}}$ for pairs of three GMPEs, calculated for maps based on the $L_1$, $L_2$ and $L_\infty$ distances. The map distances are always shortest distances on the map.

| GMPEs | $\overline{\Delta_{GM}}(L_2)$ | $\overline{\Delta_{MAP}}(L_2)$ | $\overline{\Delta_{GM}}(L_1)$ | $\overline{\Delta_{MAP}}(L_1)$ | $\overline{\Delta_{GM}}(L_\infty)$ | $\overline{\Delta_{MAP}}(L_\infty)$ |
|---|---|---|---|---|---|---|
| Zh06,Bora14 | 0.71 | 0.70 | 0.66 | 0.68 | 1.04 | 1.07 |
| Zh06,BSSA14 | 0.25 | 0.29 | 0.21 | 0.24 | 0.64 | 0.32 |
| BSSA14,Bora14 | 0.77 | 0.82 | 0.73 | 0.75 | 1.30 | 1.27 |

- the average model with changed distance scaling: $mix + \gamma(R - 30)$, with $\gamma = -0.01, -0.005, 0.005, 0.01$, called $R--$, $R-$, $R+$, $R++$

The scaling of these reference models is shown in Figure 1.6. The reference models can be used to orient the maps in a consistent way. First, the map is centered on the average model at the point $\{0, 0\}$. Then, the map is rotated so that the model $S++$ is to the right and the line from $S$ to $S++$ is approximately horizontal. In a last step, the map is mirrored such that the $M++$ model is in the upper half of the model.

The resulting Sammons map is shown in Figure 1.7 using the $L_2$-distance. A quick look at the map reveals that the models of Bora14 and AC10 are separated from the other models, which form a tighter cluster. Comparison with the reference models shows that the two models are close to the $S$ model, which is the average model down-scaled by 0.67. This can already be seen in Figure 1.2, where the Bora14 and AC10 models are consistently lower than the other models. In general, the reference models help the interpretation of directions in which GMPEs change in a systematic way. The different reference models (up/down-scaled, changed magnitude scaling, changed distance scaling) align in different directions. That allows one to quickly assess differences between GMPEs over a wide magnitude-distance range (the range that was used to generate the map) in a qualitative way.

To illustrate that the map is a viable representation of the GMPE model space, three GMPEs are given special consideration: BSSA14, Bora14 and Zh06. Their magnitude and distance scaling is repeated in Figure 1.8. Table 1.1 compiles the GMPE-distances ($L_1$, $L_2$ and $L_\infty$) between the three models, both for high dimensions and the map. The map distances are always the shortest path between the points corresponding to the GMPEs on the map (i.e. the Euclidean distance in 2D). The values of $\overline{\Delta_{GM}}$ are generally in good agreement, indicating that the maps can adequately represent the relative differences of the GMPEs over a wide magnitude/distance range. It should be checked, however, that the algorithm really has converged: for example, the $L_\infty$-distances between the Zh06 and BSSA14 models is not captured in two dimensions. The Zh06 and the Bora14 models are more or less parallel in both magnitude and distance scaling they are (approximately) up/down-scaled version of each other. That is why they align roughly in the same direction as the $S++$, $S$ reference models (cf. Figure 1.7). On the other hand, the Zh06 and BSSA14 models have a similar overall ground-motion level, but their magnitude scaling is very different. Hence, in Figure 1.7 they mainly differ in their y-coordinate, which corresponds to differences in magnitude scaling, as evidenced by the reference models.

Figure 1.9 shows the effect of using different GMPE-distance metrics in the high-dimensional space. The top part displays the two-dimensional configurations based on the high-dimensional $L_2$ and $L_1$-distance. Since the values of $\overline{\Delta_{GM}}$ are normalized, they can be shown in the same map. It should be noted, however, that these really are two maps, estimated separately. To avoid cluttering, only the reference models for the map based on the $L_2$-distance are shown. The difference between the two maps is small, with the models in the $L_1$-map being slightly closer together. This is expected, since in the $L_1$-distance larger differences have a smaller influence than in the $L_2$-distance. Overall, the maps based on the $L_1$ and $L_2$-distance metrics are similar, i.e. the relative positions of the individual GMPEs are similar. This means that the interpretation of their relative differences in scaling is unaffected by the specific GMPE-distance metric.

When using the $L_\infty$-distance, shown in the bottom part of Figure 1.9, the relative map distances between the GMPEs become larger. This is due the definition of the $L_\infty$-distance, which is equivalent to the maximum individual difference between the GMPE predictions over the whole magnitude-distance range. The interpretation for this GMPE-distance metric becomes difficult, as the maximum differences can occur at different magnitude-distance scenarios. This is reflected in the position of the reference models, which do not exhibit the same pattern as in the $L_2$-distance case. This is due to the fact that the $L_\infty$-distance cannot pick up differences in magnitude or distance scaling, since it is based on only one value.

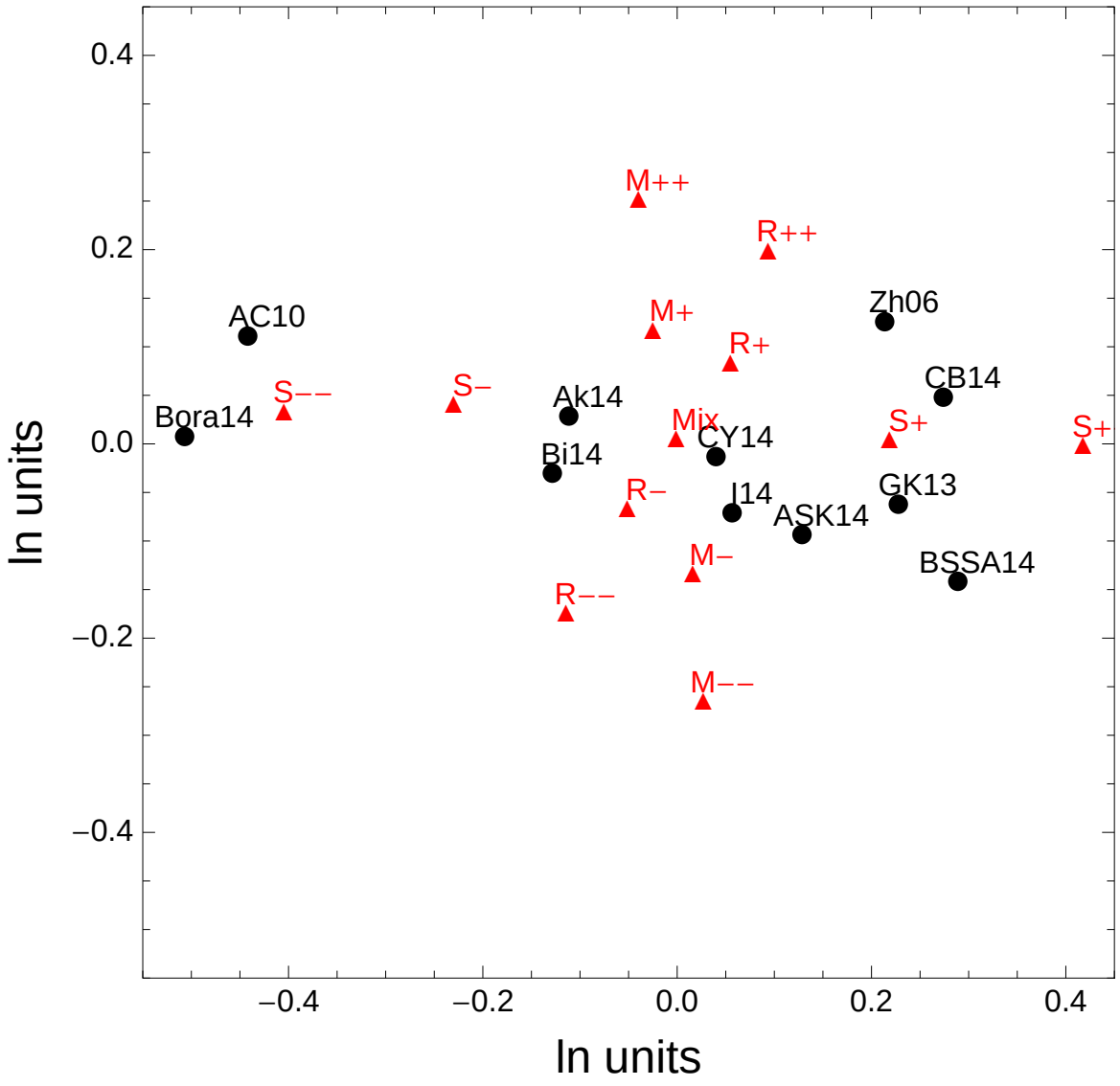



Figure 1.7: Sammons map for 11 GMPEs, together with reference models. GMPE-distances in high dimensions are calculated using the $L_2$-distance.

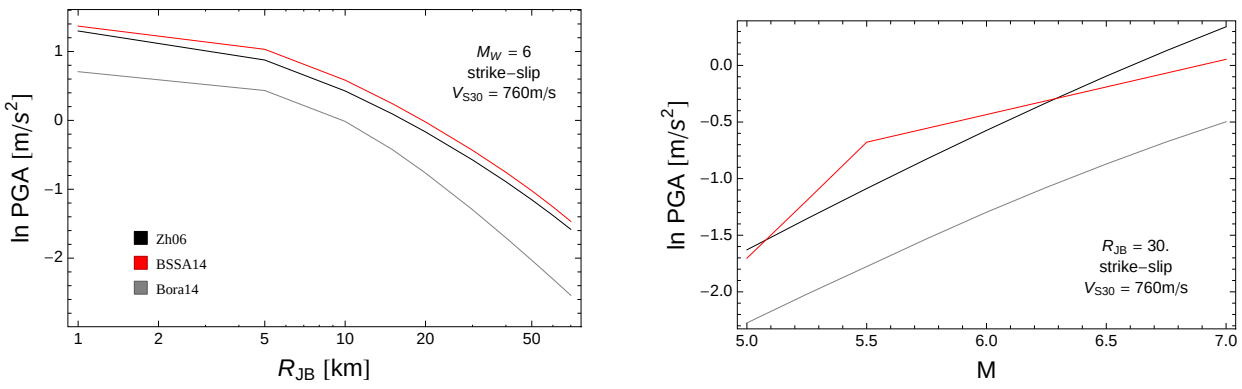



Figure 1.8: Magnitude and distance scaling of three GMPEs, for a detailed interpretation of the relative differences as shown in the map (cf. Figure 1.7).

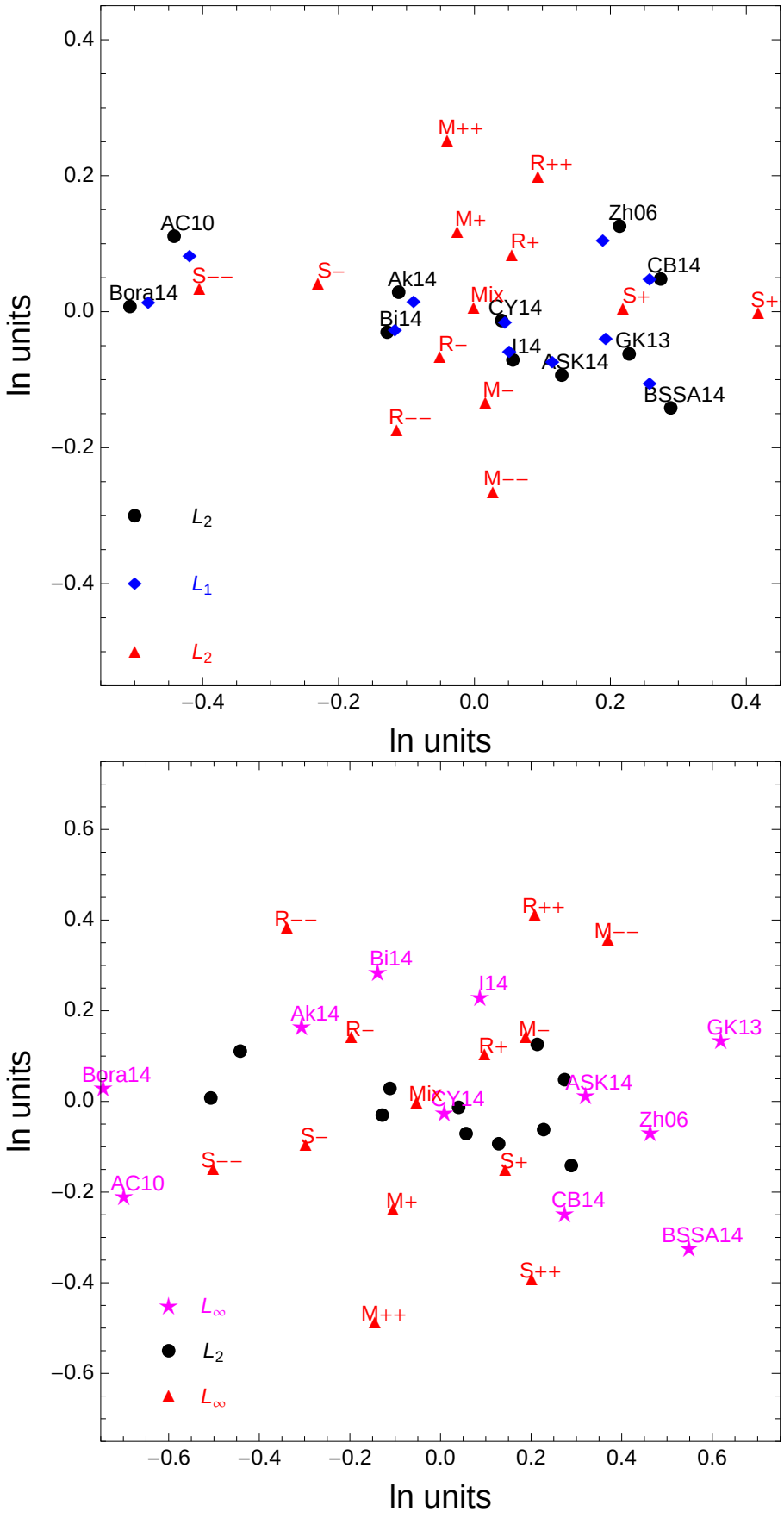



Figure 1.9: Top: Sammons map of GMPEs, based on L1 and L2-GMPE-distances. The reference models are plotted for the map based on the L2-map. Bottom: Sammons map of GMPEs, based on $L_2$ and $L_\infty$-distances. The reference models are plotted for the map based on the $L_\infty$-map. The black points are at the same coordinates as in the top map and in Figure 1.7. Note the different scale on the two maps.

Table 1.2: Ground-motion levels for PVNGS and Model A and Model B used in the calculation of hazard curves and deaggregation.

| T | $A_1$ | $A_2$ | $A_3$ | $A_4$ | $A_5$ | $A_6$ | $A_7$ | $A_8$ | $A_9$ | $A_{10}$ |
|---|---|---|---|---|---|---|---|---|---|---|
| 0.01 | 0.0004 | 0.001019 | 0.002593 | 0.006604 | 0.016816 | 0.042818 | 0.109027 | 0.277618 | 0.706903 | 1.8 |
| 0.02 | 0.0004 | 0.001012 | 0.002561 | 0.006479 | 0.016394 | 0.041479 | 0.104951 | 0.265546 | 0.671884 | 1.7 |
| 0.03 | 0.0004 | 0.001025 | 0.002625 | 0.006724 | 0.017224 | 0.044123 | 0.113029 | 0.289541 | 0.741706 | 1.9 |
| 0.05 | 0.0004 | 0.001056 | 0.00279 | 0.007368 | 0.019459 | 0.05139 | 0.135721 | 0.358436 | 0.94662 | 2.5 |
| 0.075 | 0.0003 | 0.000841 | 0.002356 | 0.006604 | 0.018508 | 0.05187 | 0.14537 | 0.407411 | 1.1418 | 3.2 |
| 0.1 | 0.0003 | 0.000846 | 0.002388 | 0.006739 | 0.019013 | 0.053647 | 0.151365 | 0.427081 | 1.20502 | 3.4 |
| 0.15 | 0.0003 | 0.000859 | 0.002462 | 0.007054 | 0.020209 | 0.057896 | 0.165863 | 0.475177 | 1.36132 | 3.9 |
| 0.2 | 0.0003 | 0.000854 | 0.002434 | 0.006931 | 0.019741 | 0.056227 | 0.160143 | 0.456113 | 1.29908 | 3.7 |
| 0.25 | 0.0003 | 0.000846 | 0.002388 | 0.006739 | 0.019013 | 0.053647 | 0.151365 | 0.427081 | 1.20502 | 3.4 |
| 0.3 | 0.0003 | 0.000835 | 0.002323 | 0.006463 | 0.017985 | 0.050043 | 0.139248 | 0.387465 | 1.07814 | 3. |
| 0.4 | 0.0004 | 0.001056 | 0.00279 | 0.007368 | 0.019459 | 0.05139 | 0.135721 | 0.358436 | 0.94662 | 2.5 |
| 0.5 | 0.0004 | 0.001036 | 0.002684 | 0.006952 | 0.018008 | 0.046646 | 0.120828 | 0.31298 | 0.810715 | 2.1 |
| 0.75 | 0.0003 | 0.000767 | 0.001961 | 0.005013 | 0.012817 | 0.032769 | 0.083777 | 0.214187 | 0.547596 | 1.4 |
| 1. | 0.0001 | 0.000281 | 0.000791 | 0.002224 | 0.006254 | 0.017588 | 0.049461 | 0.139093 | 0.391155 | 1.1 |
| 1.5 | 0.0001 | 0.000267 | 0.000715 | 0.001913 | 0.005116 | 0.013683 | 0.036593 | 0.097866 | 0.261737 | 0.7 |
| 2. | 0.0001 | 0.000258 | 0.000664 | 0.00171 | 0.004405 | 0.01135 | 0.02924 | 0.075332 | 0.194077 | 0.5 |
| 3. | 0.00005 | 0.000131 | 0.000346 | 0.000909 | 0.002389 | 0.00628 | 0.01651 | 0.043404 | 0.114111 | 0.3 |

## 1.2 APPLICATION OF VISUALIZATION TOOLS TO THE SWUS GMC STUDY

In this Appendix H, the selected ground-motion models, based on the common functional form (cf. Chapter 6), are evaluated. The selection and weighting procedure is described in Chapter 6. In the following, $R_{RUP}$-based models are called Model A, whereas $R_{JB}$-based models are called Model B. For each case (DCPP, PVNGS Model A and PVNGS Model B), different plots detailing the selection, weighting and evaluation are shown. The respective plots are in Chapters 2, 3 and 4 of this Appendix H. In addition, Chapter 5 in this Appendix H shows some plots evaluating the combined PVNGS Model A and B. First, deaggregation plots are shown, calculated using a simplified source model (cf Appendix D). The deaggregation is calculated at 10 ground-motion levels. These are listed in Tables 1.2 and 1.3. The plots show the deaggregation weights for 2nd and 8th ground-motion level. For the calculation of the weighted distances to be used in the calculation of the Sammons maps, the deaggregation weights are averaged over the 10 ground-motion levels. Then, Sammons maps are shown, with the relevant contours (residuals and likelihoods) overlain. These are shown detailing the selection as well as the weighting (i.e. the Voronoi cells). Hazard curves of the sampled 2000 models and the selected models are shown, using the same simplified source model as in the creation of the deaggregation plots. To evaluate the selected models, plots of the cumulative distribution function of the model distribution are shown. Quantile plots showing the 0.05, 0.5 and 0.95 quantiles are shown vs. distance, magnitude and period. Ratios of the quantiles for all periods are shown vs. distance. The scaling of the original GMPEs and the selected models vs. distance and magnitude are compared for several scenarios.

### 1.2.1 Explanation of Plots

Several plots are shown to assess the selected models and their weights, such as plots of the empirical cumulative distribution. These plots are produced for the following scenarios:

- DCPP
  - $M_W = 5.5, 6.5, 7.5$, $R_x = -1, -5, -10$km, strike-slip and reverse
- PVNGS
  - $M_W = 5., 6., 7.$, $R_x = -5, 5, -15, 15, -30, -50$km, strike-slip and normal

For both DCPP and PVNGS, the selected periods for the plots are $T = 0.01, 0.2, 0.5, 1., 3.$s. For DCPP, the scenarios are on the footwall, even though the selection process is done on the hanging wall and thus each selected model has a haning wall associated with it. The reason is that the models I14, ZL11 and Z06 are based on rupture distance, but do incorporate hanging wall effects. Therefore, they cannot be evaluated above the hanging wall.

As mentioned previously, weights are calculated using different statistics such as the mean between-event residual or the likelihood. To compare the impact of these different weights, plots of the resulting cumulative distribution function (CDF) are shown for several scenarios and periods. Therefore the ground-motion predictions from the different models

Table 1.3: Ground-motion levels for DCPP and ModelA used in the calculation of hazard curves and deaggregation.

| T | $A_1$ | $A_2$ | $A_3$ | $A_4$ | $A_5$ | $A_6$ | $A_7$ | $A_8$ | $A_9$ | $A_{10}$ |
|---|---|---|---|---|---|---|---|---|---|---|
| 0.01 | 0.1 | 0.162725 | 0.264794 | 0.430887 | 0.701161 | 1.14097 | 1.85664 | 3.02121 | 4.91627 | 8. |
| 0.02 | 0.1 | 0.162725 | 0.264794 | 0.430887 | 0.701161 | 1.14097 | 1.85664 | 3.02121 | 4.91627 | 8. |
| 0.03 | 0.1 | 0.16681 | 0.278256 | 0.464159 | 0.774264 | 1.29155 | 2.15444 | 3.59381 | 5.99484 | 10. |
| 0.05 | 0.1 | 0.170224 | 0.289761 | 0.493242 | 0.839616 | 1.42923 | 2.43288 | 4.14134 | 7.04955 | 12. |
| 0.075 | 0.1 | 0.174497 | 0.304492 | 0.531329 | 0.927154 | 1.61786 | 2.82311 | 4.92624 | 8.59614 | 15. |
| 0.1 | 0.2 | 0.329737 | 0.543633 | 0.896281 | 1.47769 | 2.43624 | 4.0166 | 6.62211 | 10.9178 | 18. |
| 0.15 | 0.2 | 0.329737 | 0.543633 | 0.896281 | 1.47769 | 2.43624 | 4.0166 | 6.62211 | 10.9178 | 18. |
| 0.2 | 0.2 | 0.329737 | 0.543633 | 0.896281 | 1.47769 | 2.43624 | 4.0166 | 6.62211 | 10.9178 | 18. |
| 0.25 | 0.1 | 0.174497 | 0.304492 | 0.531329 | 0.927154 | 1.61786 | 2.82311 | 4.92624 | 8.59614 | 15. |
| 0.3 | 0.1 | 0.174497 | 0.304492 | 0.531329 | 0.927154 | 1.61786 | 2.82311 | 4.92624 | 8.59614 | 15. |
| 0.4 | 0.1 | 0.170224 | 0.289761 | 0.493242 | 0.839616 | 1.42923 | 2.43288 | 4.14134 | 7.04955 | 12. |
| 0.5 | 0.09 | 0.151897 | 0.256363 | 0.432675 | 0.730244 | 1.23247 | 2.08008 | 3.51065 | 5.92507 | 10. |
| 0.75 | 0.05 | 0.085112 | 0.144881 | 0.246621 | 0.419808 | 0.714613 | 1.21644 | 2.07067 | 3.52477 | 6. |
| 1. | 0.02 | 0.037693 | 0.07104 | 0.133887 | 0.252332 | 0.475563 | 0.896281 | 1.6892 | 3.18358 | 6. |
| 1.5 | 0.01 | 0.019459 | 0.037865 | 0.073681 | 0.143374 | 0.27899 | 0.542884 | 1.05639 | 2.05562 | 4. |
| 2. | 0.009 | 0.017162 | 0.032725 | 0.062403 | 0.118993 | 0.226904 | 0.432675 | 0.825052 | 1.57326 | 3. |
| 3. | 0.004 | 0.007979 | 0.015916 | 0.031748 | 0.063329 | 0.126325 | 0.251984 | 0.502642 | 1.00264 | 2. |

are calculated, and the empirical ground-motion CDF is calculated by summing the weights of the models which give a prediction lower than a specified ground-motion value. For both cases (DCPP and PVNGS), only the CDFs based on the used set of weights are shown, together with the total weights. In addition, the GMPE distribution is shown. To calculate the CDF of the GMPEs, they are equally weighted, and the weight of an individual GMPE is partitioned 80%/10%/10% into its median and plus/minus uncertainty model (using two times the standard deviation of the uncertainty model of Al-Atik and Youngs, 2014) [5].

From the CDF of the ground-motion distribution based on the total weights, the 0.05,0.5 and 0.95 quantiles are calculated, as well as for the GMPE distribution. These are plotted versus distance and magnitude, for several magnitude distance values, respectively. This allows to compare the width/range of the distribution of the selected models and the original GMPEs. In addition, the 0.05,0.5,0.95 quantiles are plotted against periods, for several scenarios. In all these cases, the GMPEs are equally weighted (as described above), while the model distribution is based on the selected models and total weights.

To assess the width of the model distribution, the ratio of the 0.05/0.5 and 0.95/0.5 quantile are plotted against distance, for several magnitudes. This is an indicator of possible skewness of the model distribution. The model distribution (i.e. its 0.05,0.5 and 0.95 quantiles) are also plotted together with the original GMPEs. In this case, also the highest and lowest prediction of a selected model is shown.

To assess differences in the scaling of the selected models with magnitude and distance, the selected models are plotted against magnitude and distance, together with the original GMPEs (without the uncertainty model). For DCPP, in addition to the used GMPEs the model of Graizer (2014) [14] is shown.

For both DCPP and PVNGS, contour plots of the relevant mean residuals and the log-likelihood, plotted on top of the maps, are shown, together with the selected models and the areas used for the weights.

For DCPP and PVNGS (Model A and B), for each scenario the differences between the 0.5 quantile, calculated with all weights, and the 0.5 quantile calculated with total weights is calculated. These are then plotted as a histogram, to see which weights tend to produce median predictions that larger or smaller than the predictions based on total weights.

In chapter 5, the combined model A and B distribution for PVNGS is evaluated. Therefore, the quantiles (0.05,0.5 and 0.95) are calculated, based on weights of 0.7 for Model A and 0.3 for Model B. The quantiles are then plotted vs. magnitude, distance and period and compared with the original GMPEs. In addition, combined Sammon maps are calculated, with the 2000 individual models each. The mean between-event residuals and likelihoods, based on the weighted NGA dataset and the European dataset, are overlain, to show that even the combined models produce relatively smooth contours and thus the two distributions overlap. The dimensions of the map are the same as for the maps calculated solely for Model B. The Euclidean distances between the different GMPEs are not weighte according to the deaggregation, since it is different for Model A and B. Instead, the Euclidean distances are divided by $N$, the number of dimensions in the high-dimensional vector.

# Chapter 2

# DCPP – Model A

### 2.1.2 Deaggregation

**GM-Level 2**

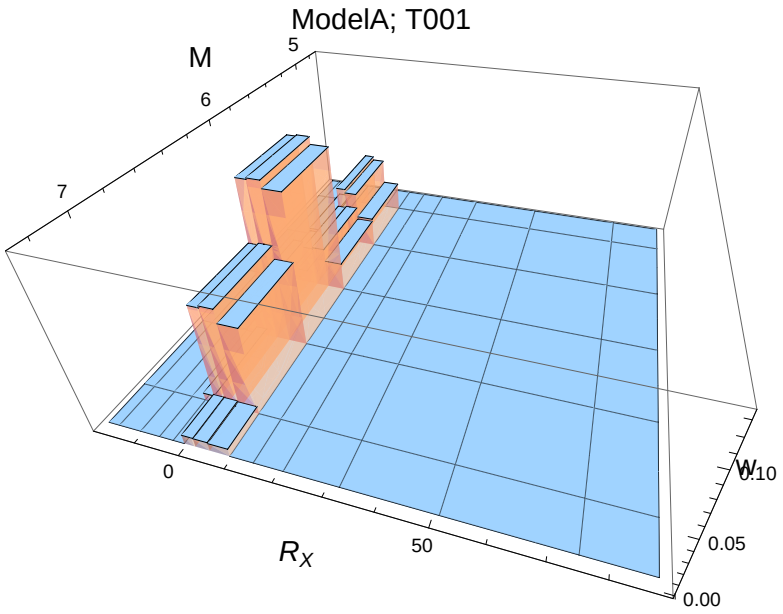



Figure 2.1: DCPPv4: Deaggregation for a ground-motion level of 0.163g, calculated using a simple source model for DCPP4 and the center model of the ModelA distribution. For $T = 0.01$s.

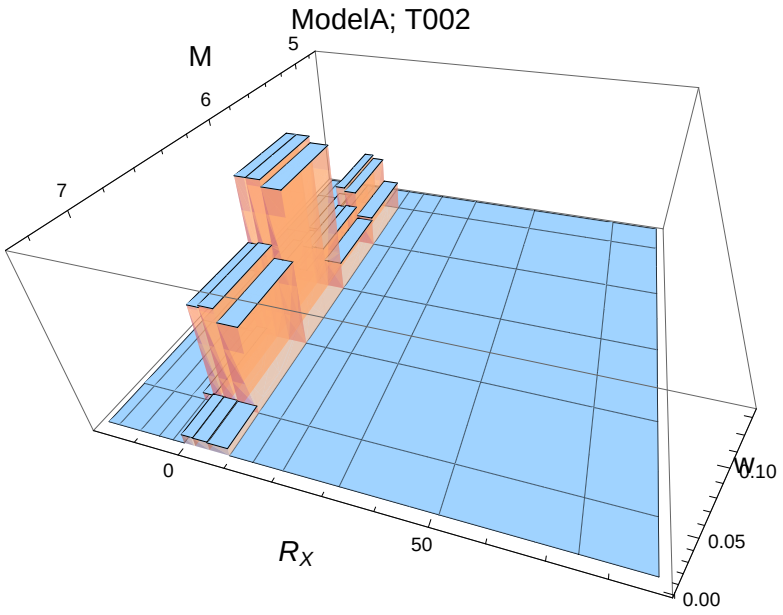



Figure 2.2: DCPPv4: Deaggregation for a ground-motion level of 0.163g, calculated using a simple source model for DCPP4 and the center model of the ModelA distribution. For $T = 0.02$s.

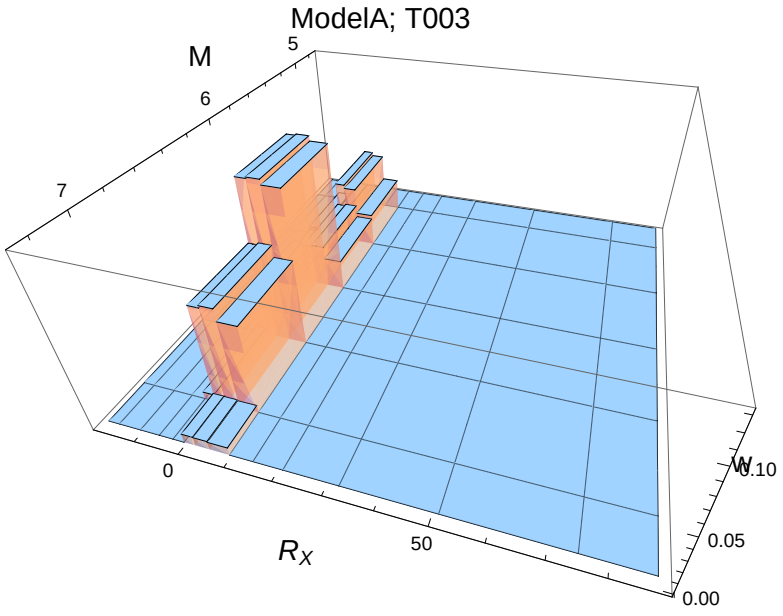



Figure 2.3: DCPPv4: Deaggregation for a ground-motion level of 0.167g, calculated using a simple source model for DCPP4 and the center model of the ModelA distribution. For $T = 0.03$s.

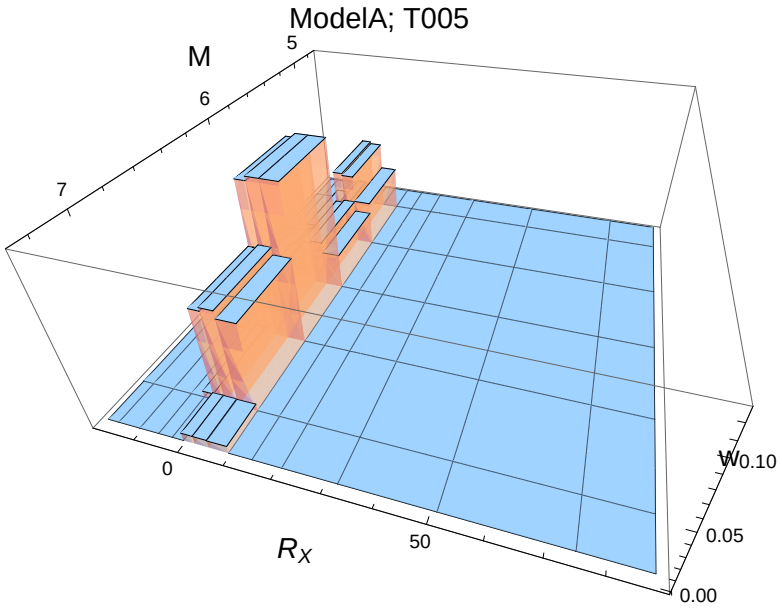



Figure 2.4: DCPPv4: Deaggregation for a ground-motion level of 0.17g, calculated using a simple source model for DCPP4 and the center model of the ModelA distribution. For $T = 0.05$s.

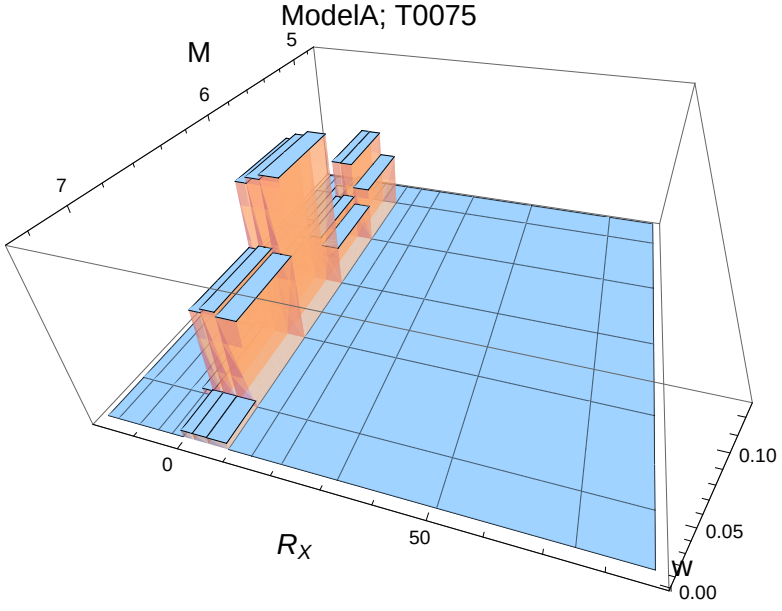



Figure 2.5: DCPPv4: Deaggregation for a ground-motion level of 0.174g, calculated using a simple source model for DCPP4 and the center model of the ModelA distribution. For $T = 0.075$s.

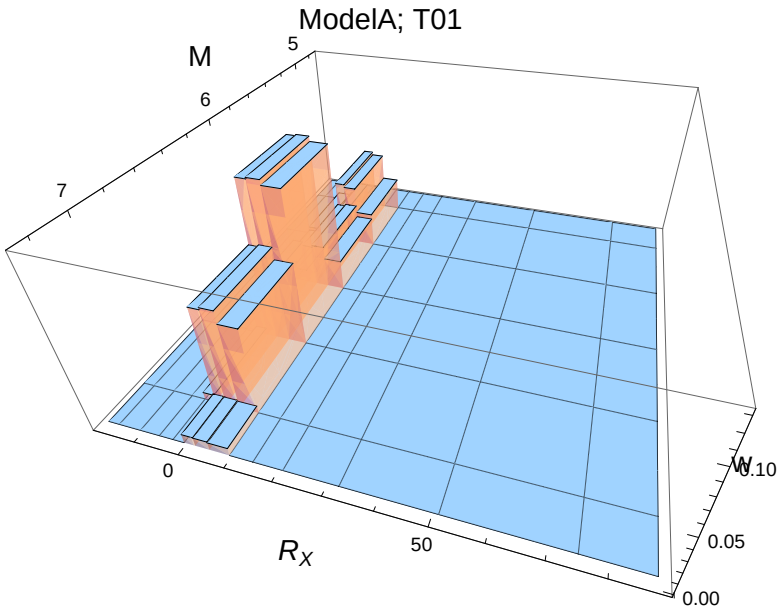



Figure 2.6: DCPPv4: Deaggregation for a ground-motion level of 0.33g, calculated using a simple source model for DCPP4 and the center model of the ModelA distribution. For $T = 0.1$s.

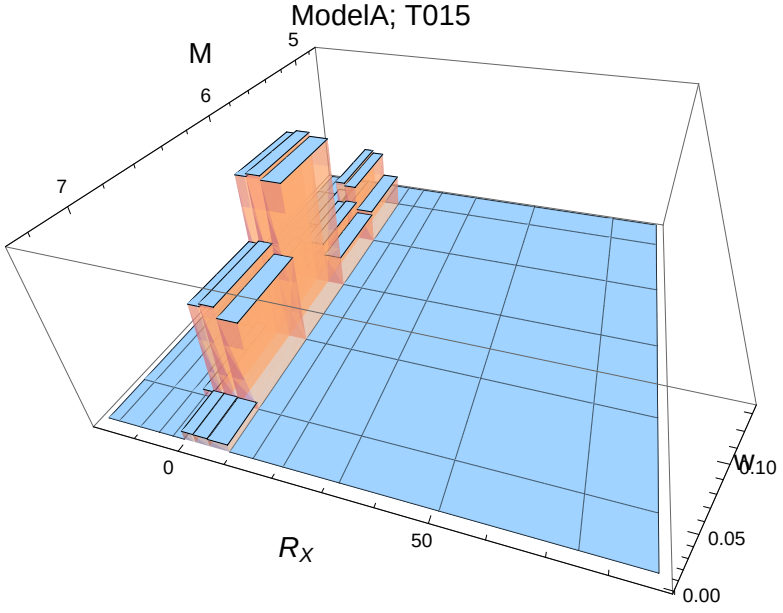



Figure 2.7: DCPPv4: Deaggregation for a ground-motion level of 0.33g, calculated using a simple source model for DCPP4 and the center model of the ModelA distribution. For $T = 0.15$s.

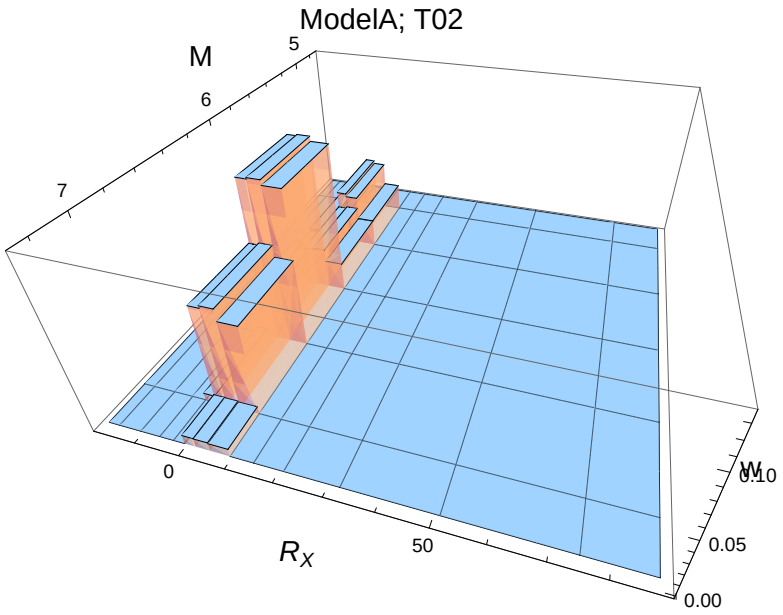



Figure 2.8: DCPPv4: Deaggregation for a ground-motion level of 0.33g, calculated using a simple source model for DCPP4 and the center model of the ModelA distribution. For $T = 0.2$s.

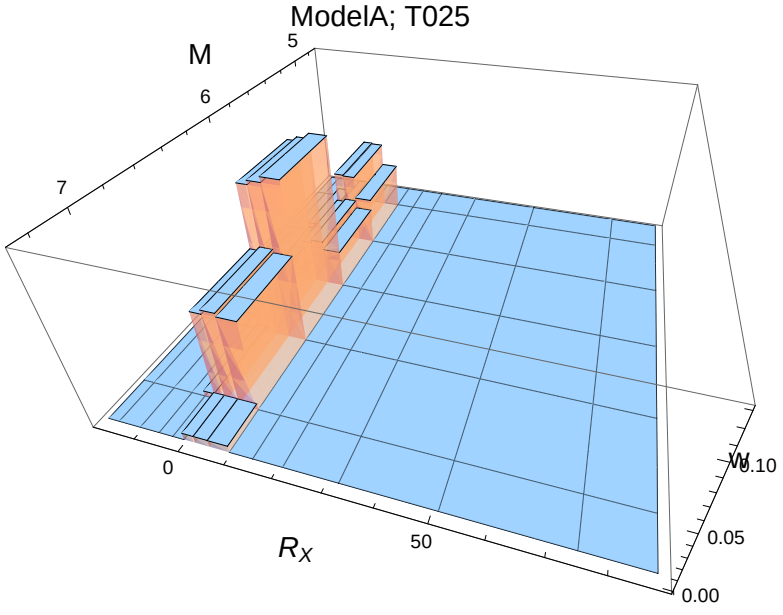



Figure 2.9: DCPPv4: Deaggregation for a ground-motion level of 0.174g, calculated using a simple source model for DCPP4 and the center model of the ModelA distribution. For $T = 0.25$s.

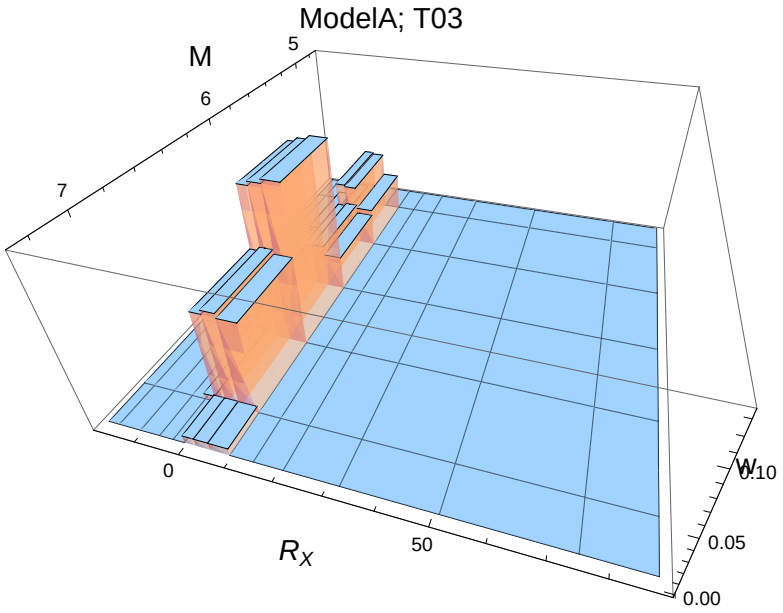



Figure 2.10: DCPPv4: Deaggregation for a ground-motion level of 0.174g, calculated using a simple source model for DCPP4 and the center model of the ModelA distribution. For $T = 0.3$s.

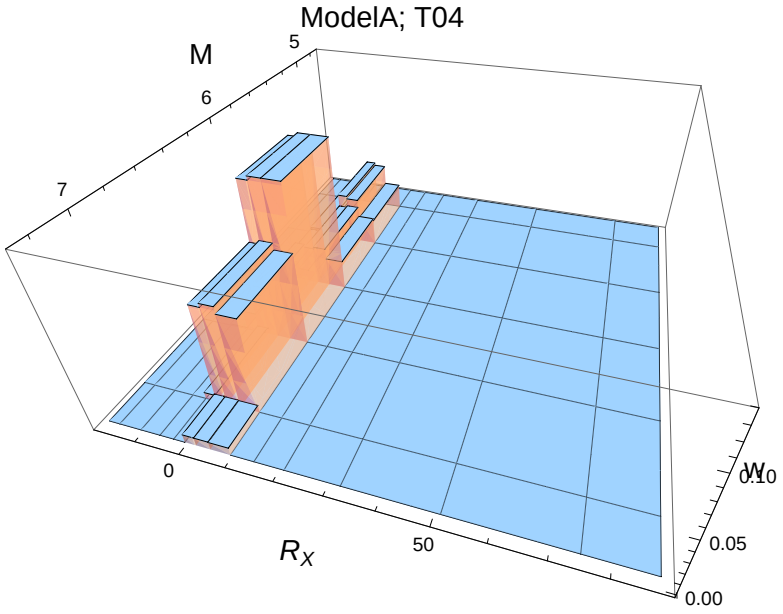



Figure 2.11: DCPPv4: Deaggregation for a ground-motion level of 0.17g, calculated using a simple source model for DCPP4 and the center model of the ModelA distribution. For $T = 0.4$s.

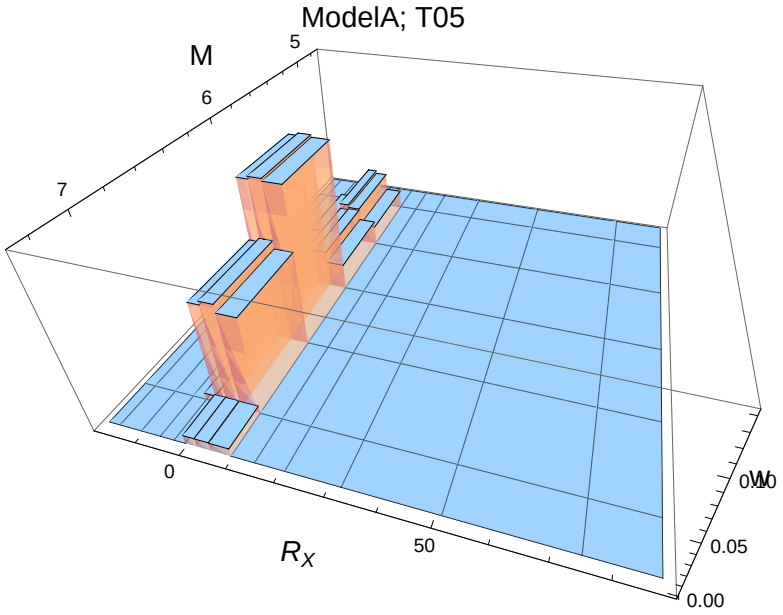



Figure 2.12: DCPPv4: Deaggregation for a ground-motion level of 0.152g, calculated using a simple source model for DCPP4 and the center model of the ModelA distribution. For $T = 0.5$s.

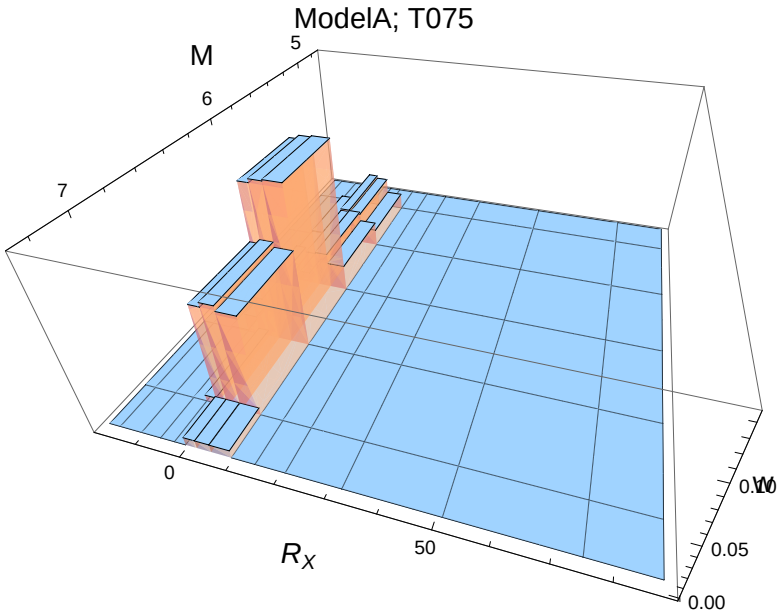



Figure 2.13: DCPPv4: Deaggregation for a ground-motion level of 0.085g, calculated using a simple source model for DCPP4 and the center model of the ModelA distribution. For $T = 0.75$s.

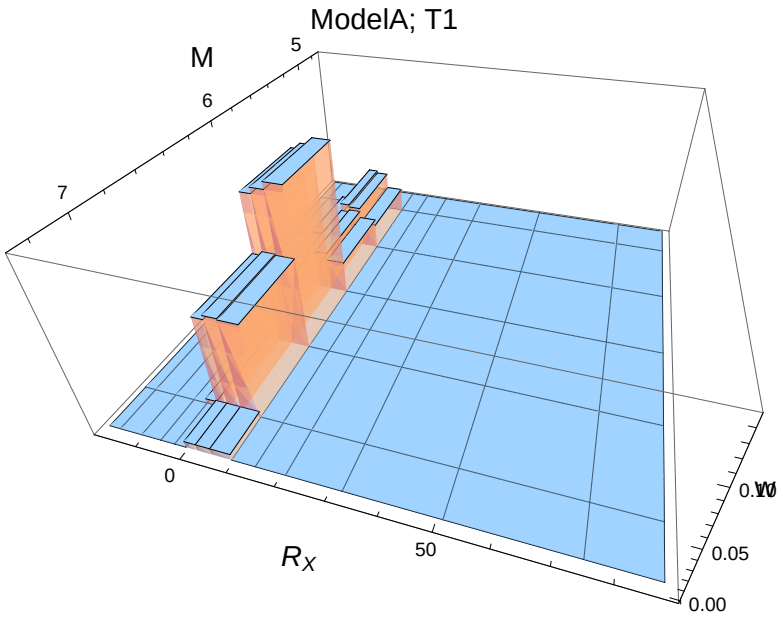



Figure 2.14: DCPPv4: Deaggregation for a ground-motion level of 0.038g, calculated using a simple source model for DCPP4 and the center model of the ModelA distribution. For $T = 1$.s.

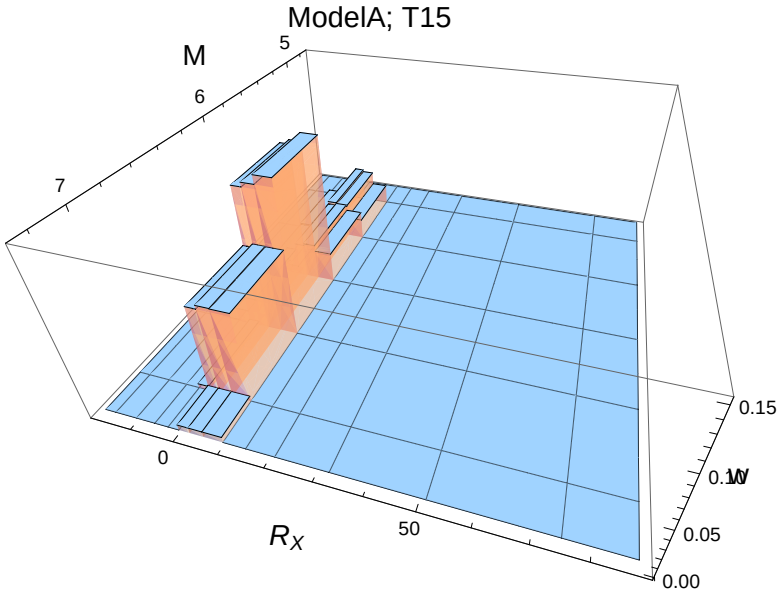



Figure 2.15: DCPPv4: Deaggregation for a ground-motion level of 0.019g, calculated using a simple source model for DCPP4 and the center model of the ModelA distribution. For $T = 1.5$s.

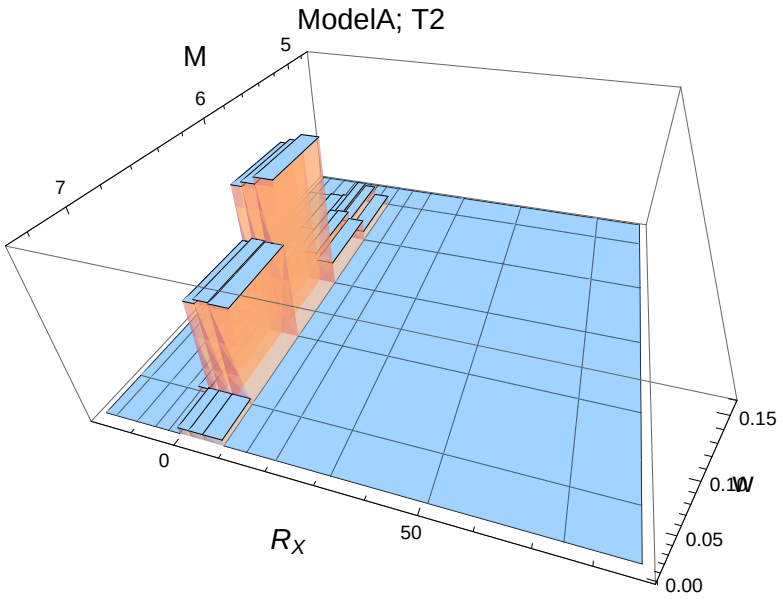



Figure 2.16: DCPPv4: Deaggregation for a ground-motion level of 0.017g, calculated using a simple source model for DCPP4 and the center model of the ModelA distribution. For $T = 2$.s.

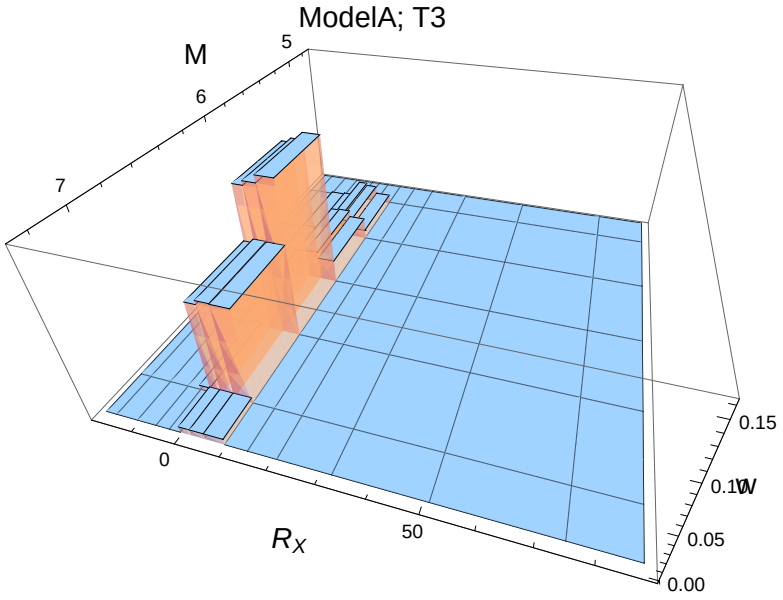



Figure 2.17: DCPPv4: Deaggregation for a ground-motion level of 0.008g, calculated using a simple source model for DCPP4 and the center model of the ModelA distribution. For $T = 3$.s.

**GM-Level 8**

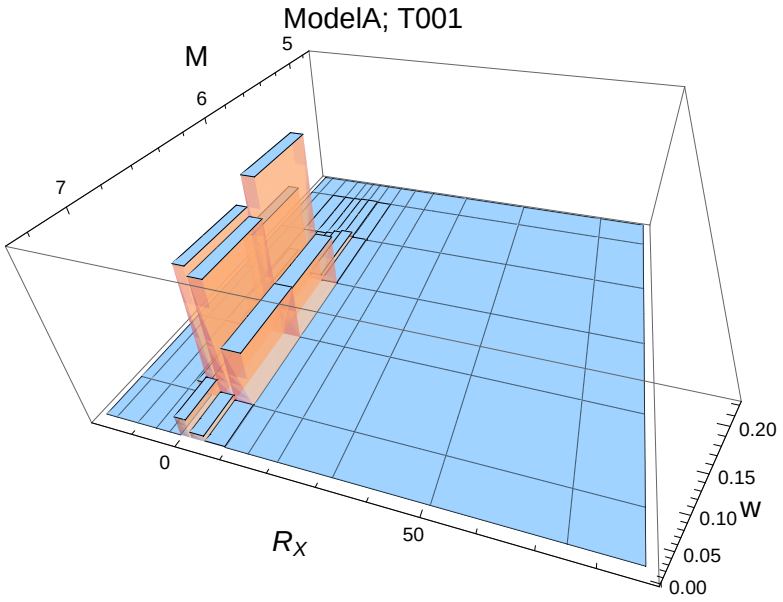



Figure 2.18: DCPPv4: Deaggregation for a ground-motion level of 3.021g, calculated using a simple source model for DCPP4 and the center model of the ModelA distribution. For $T = 0.01$s.

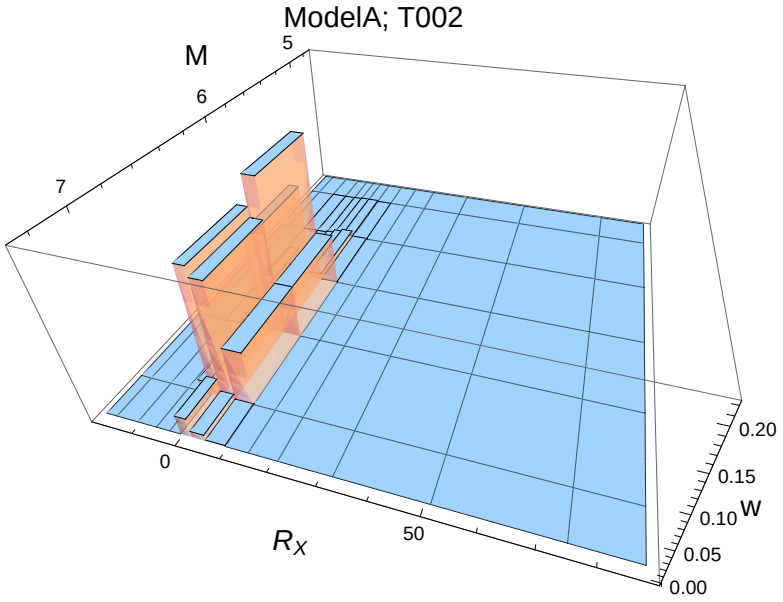



Figure 2.19: DCPPv4: Deaggregation for a ground-motion level of 3.021g, calculated using a simple source model for DCPP4 and the center model of the ModelA distribution. For $T = 0.02$s.

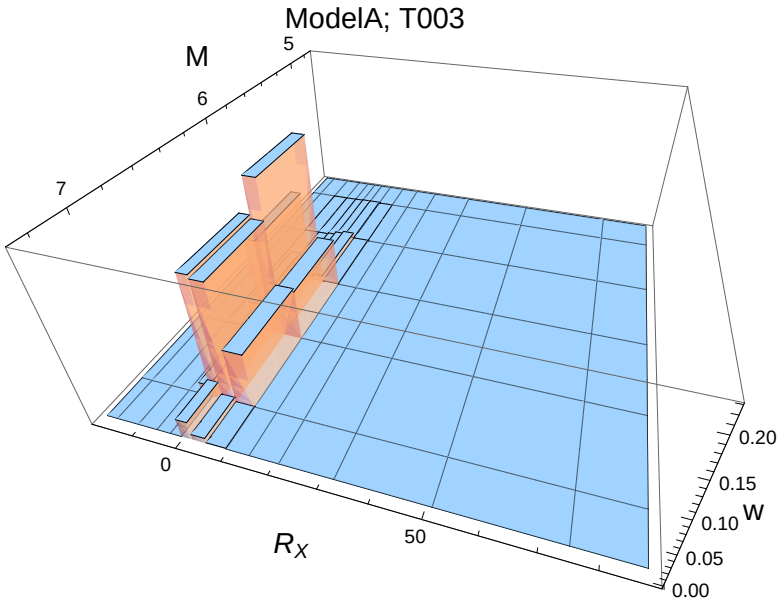



Figure 2.20: DCPPv4: Deaggregation for a ground-motion level of 3.594g, calculated using a simple source model for DCPP4 and the center model of the ModelA distribution. For $T = 0.03$s.

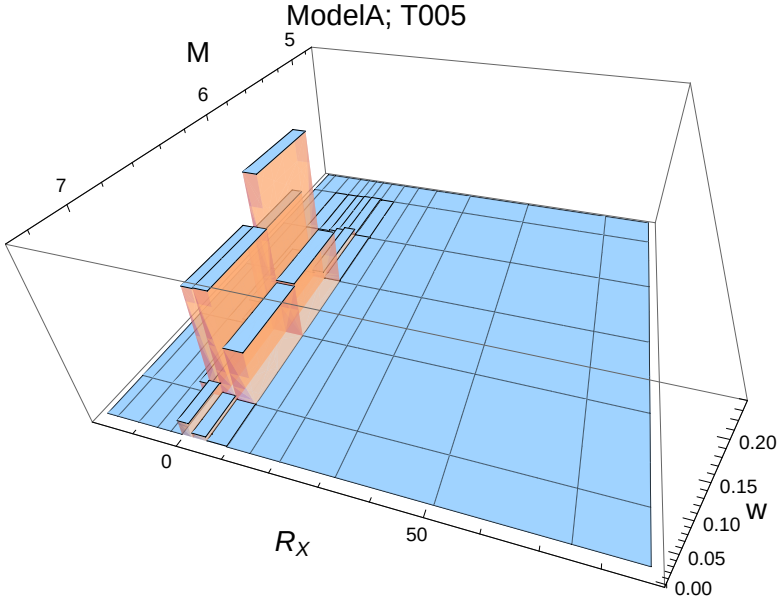



Figure 2.21: DCPPv4: Deaggregation for a ground-motion level of 4.141g, calculated using a simple source model for DCPP4 and the center model of the ModelA distribution. For $T = 0.05$s.

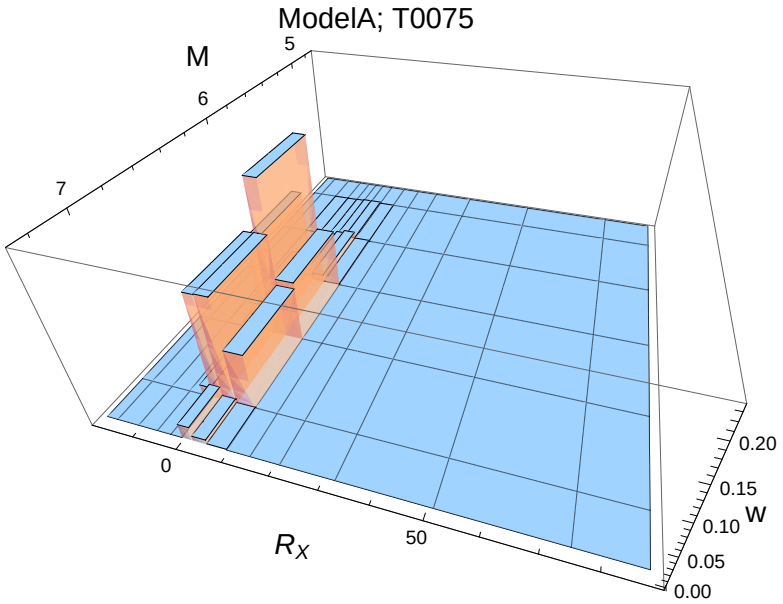



Figure 2.22: DCPPv4: Deaggregation for a ground-motion level of 4.926g, calculated using a simple source model for DCPP4 and the center model of the ModelA distribution. For $T = 0.075$s.

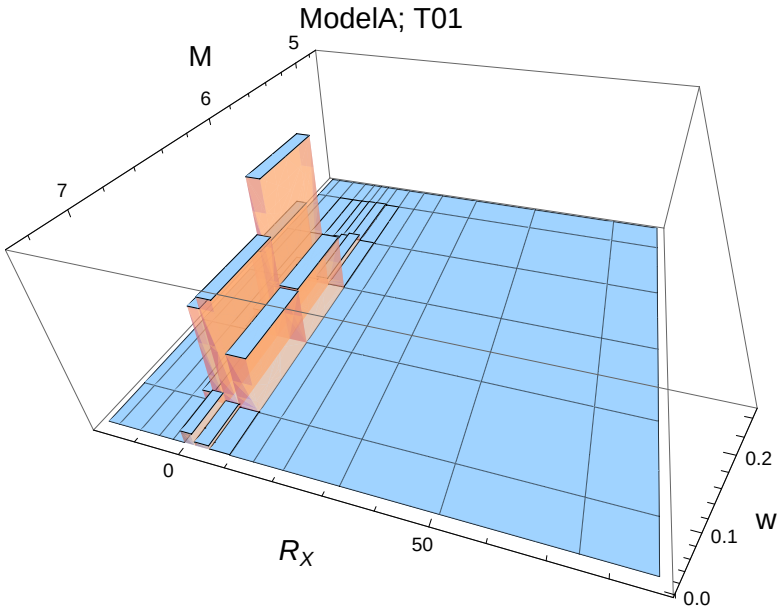



Figure 2.23: DCPPv4: Deaggregation for a ground-motion level of 6.622g, calculated using a simple source model for DCPP4 and the center model of the ModelA distribution. For $T = 0.1$s.

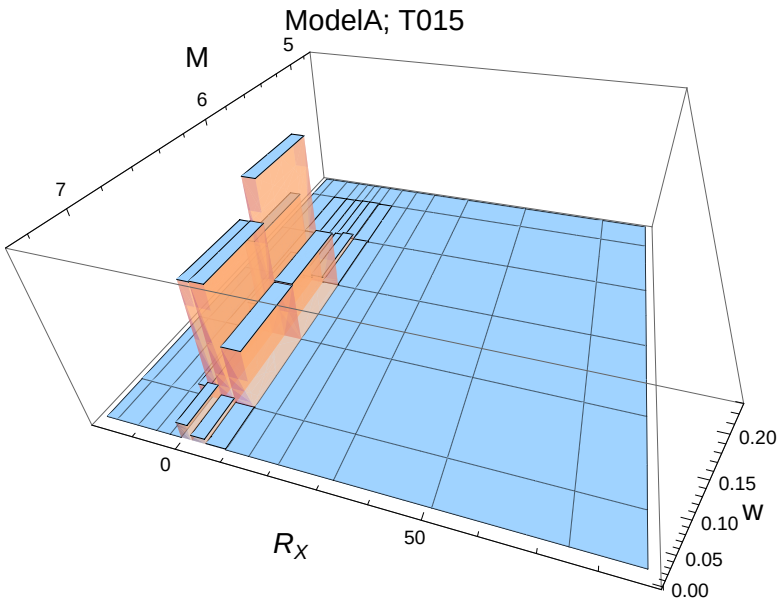



Figure 2.24: DCPPv4: Deaggregation for a ground-motion level of 6.622g, calculated using a simple source model for DCPP4 and the center model of the ModelA distribution. For $T = 0.15$s.

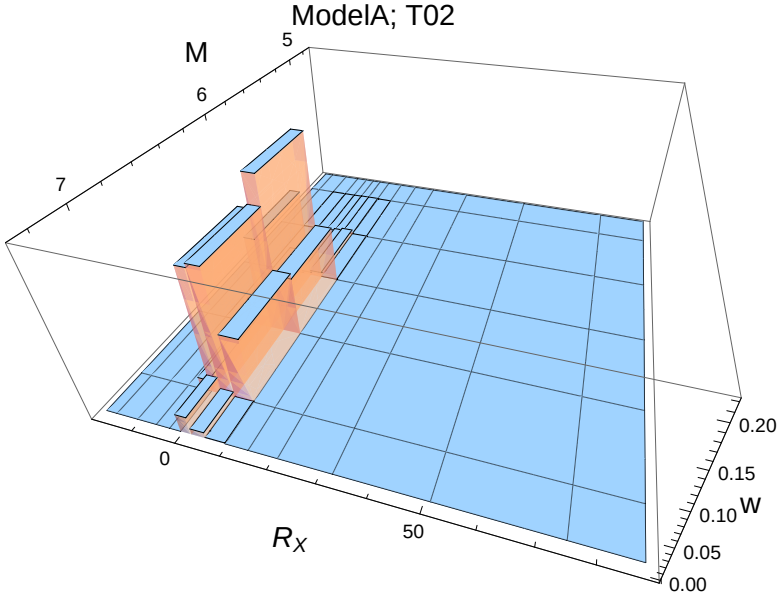



Figure 2.25: DCPPv4: Deaggregation for a ground-motion level of 6.622g, calculated using a simple source model for DCPP4 and the center model of the ModelA distribution. For $T = 0.2$s.

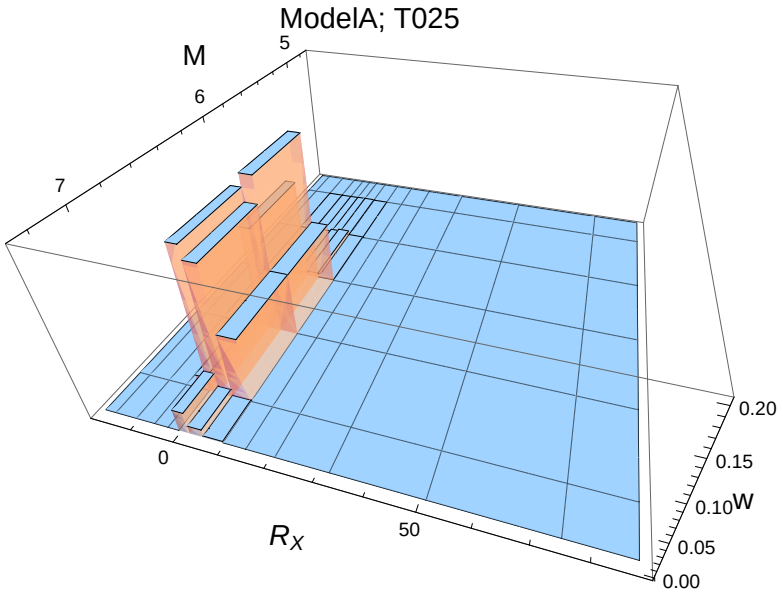



Figure 2.26: DCPPv4: Deaggregation for a ground-motion level of 4.926g, calculated using a simple source model for DCPP4 and the center model of the ModelA distribution. For $T = 0.25$s.

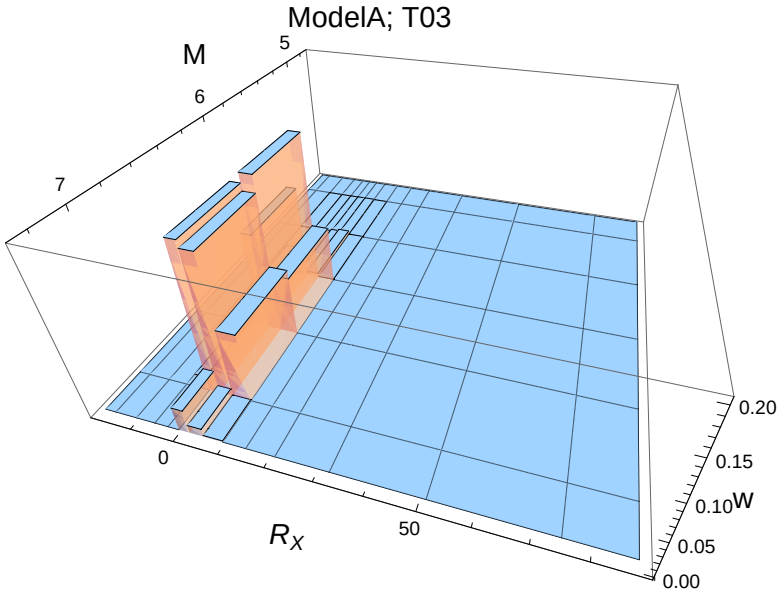



Figure 2.27: DCPPv4: Deaggregation for a ground-motion level of 4.926g, calculated using a simple source model for DCPP4 and the center model of the ModelA distribution. For $T = 0.3$s.

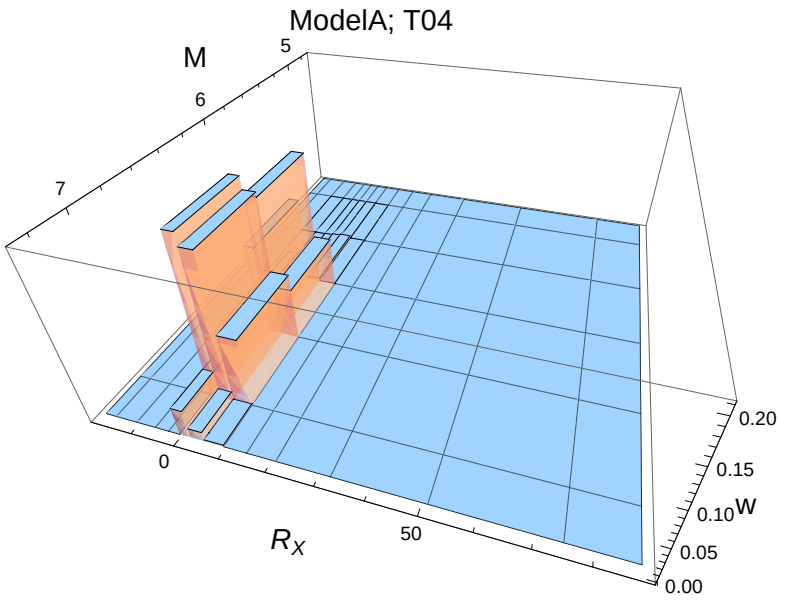



Figure 2.28: DCPPv4: Deaggregation for a ground-motion level of 4.141g, calculated using a simple source model for DCPP4 and the center model of the ModelA distribution. For $T = 0.4$s.

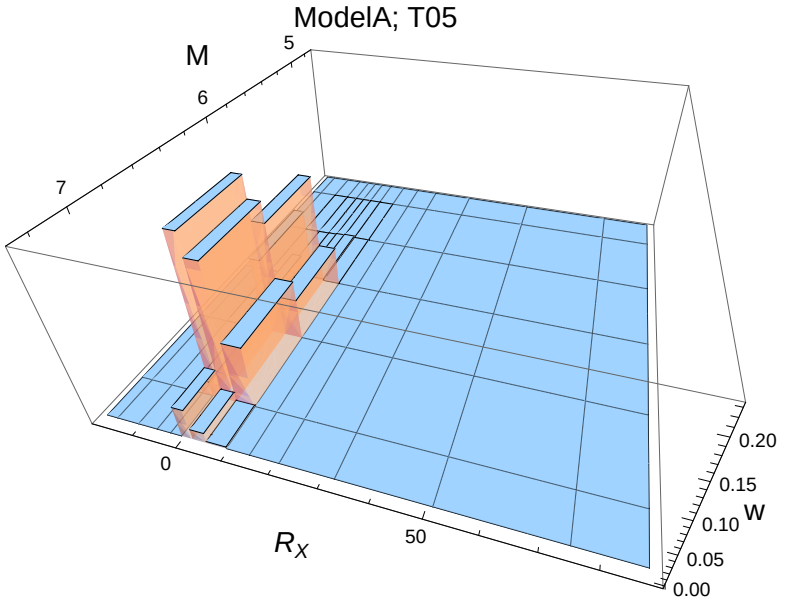



Figure 2.29: DCPPv4: Deaggregation for a ground-motion level of 3.511g, calculated using a simple source model for DCPP4 and the center model of the ModelA distribution. For $T = 0.5$s.

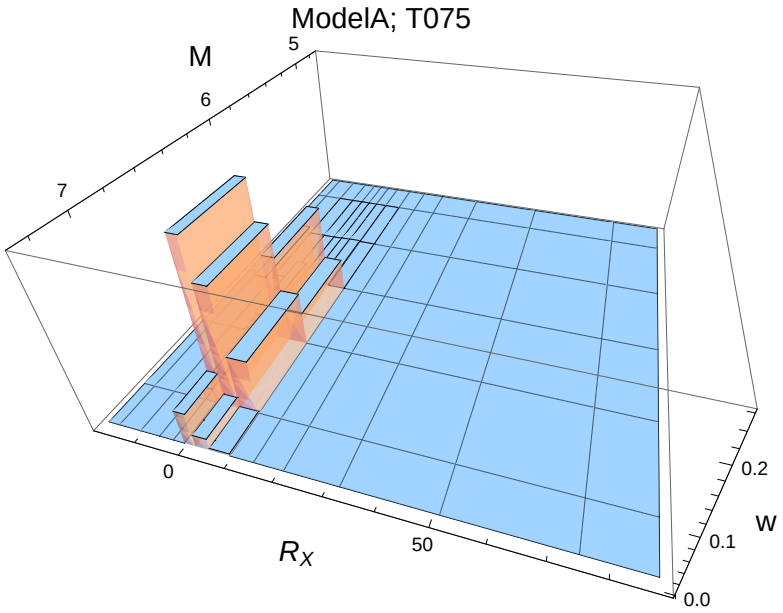



Figure 2.30: DCPPv4: Deaggregation for a ground-motion level of 2.071g, calculated using a simple source model for DCPP4 and the center model of the ModelA distribution. For $T = 0.75$s.

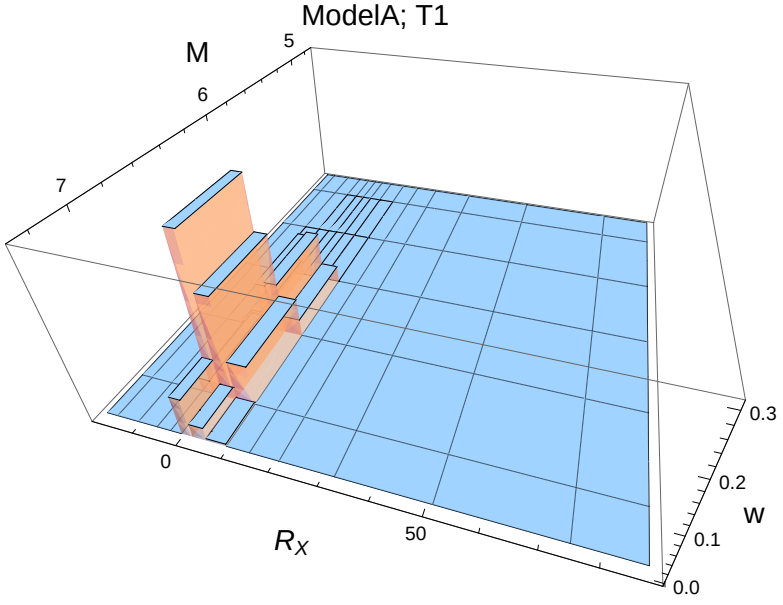



Figure 2.31: DCPPv4: Deaggregation for a ground-motion level of 1.689g, calculated using a simple source model for DCPP4 and the center model of the ModelA distribution. For $T = 1$.s.

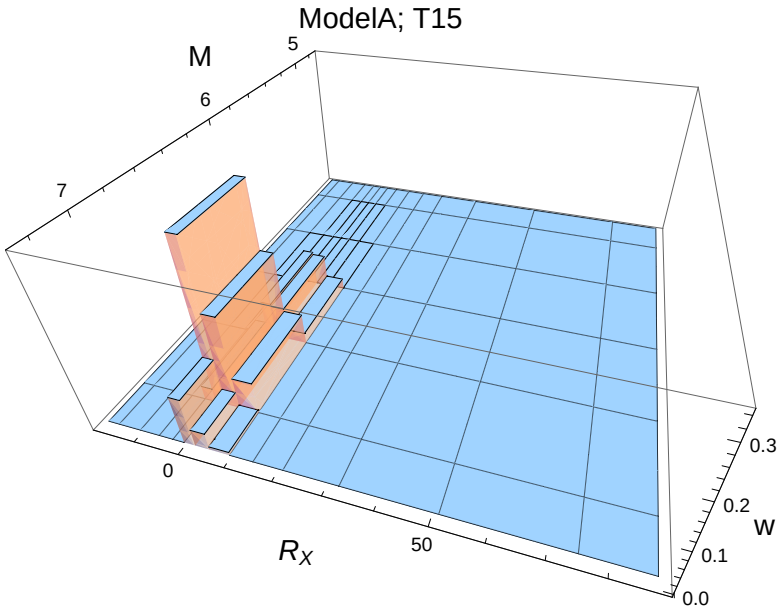



Figure 2.32: DCPPv4: Deaggregation for a ground-motion level of 1.056g, calculated using a simple source model for DCPP4 and the center model of the ModelA distribution. For $T = 1.5$s.

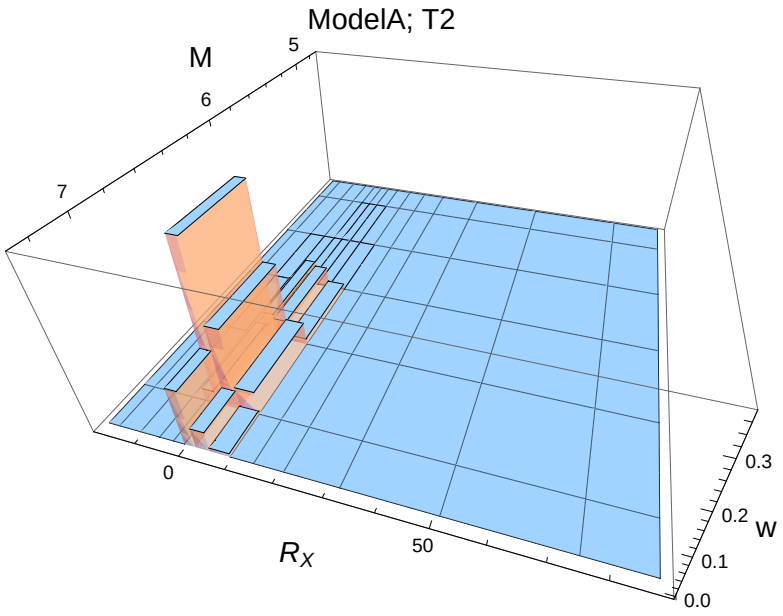



Figure 2.33: DCPPv4: Deaggregation for a ground-motion level of 0.825g, calculated using a simple source model for DCPP4 and the center model of the ModelA distribution. For $T = 2$.s.

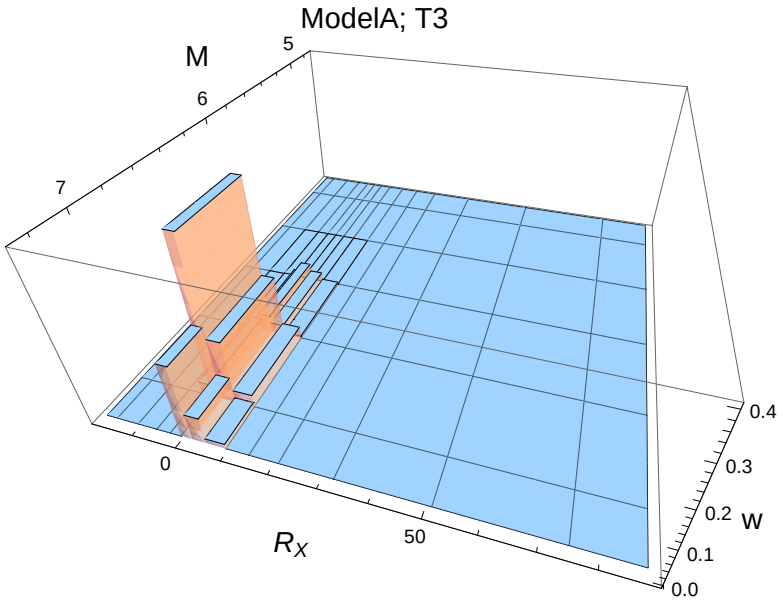



Figure 2.34: DCPPv4: Deaggregation for a ground-motion level of 0.503g, calculated using a simple source model for DCPP4 and the center model of the ModelA distribution. For $T = 3$.s.

### 2.1.3 Maps – Selection

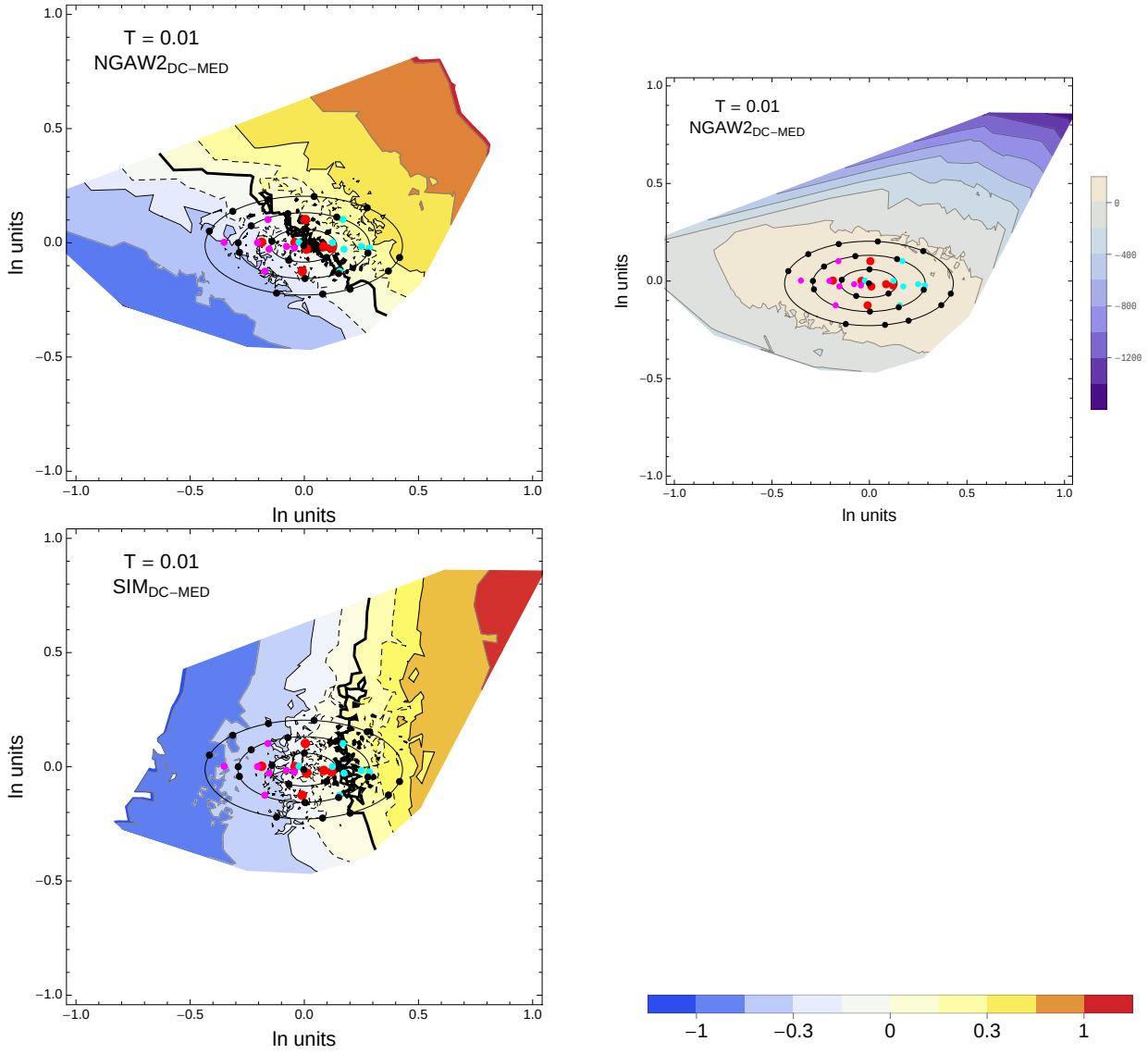



Figure 2.35: DCPPv4: Contour Plots of mean residuals (top left) and likelihood (top right) for the NGA$_{DC-MED}$ dataset, and mean residuals (bottom left) for the simulations (SIM$_{DC-MED}$). Reference points are black dots. The original GMPEs are red dots, plus/minus uncertainty are magenta/cyan dots. The contour for the zero residual is a thick black line, the -0.15/0.15 contours are dashed black lines and the -0.3/0.3 contours are thin black lines. For $T = 0.01$s.

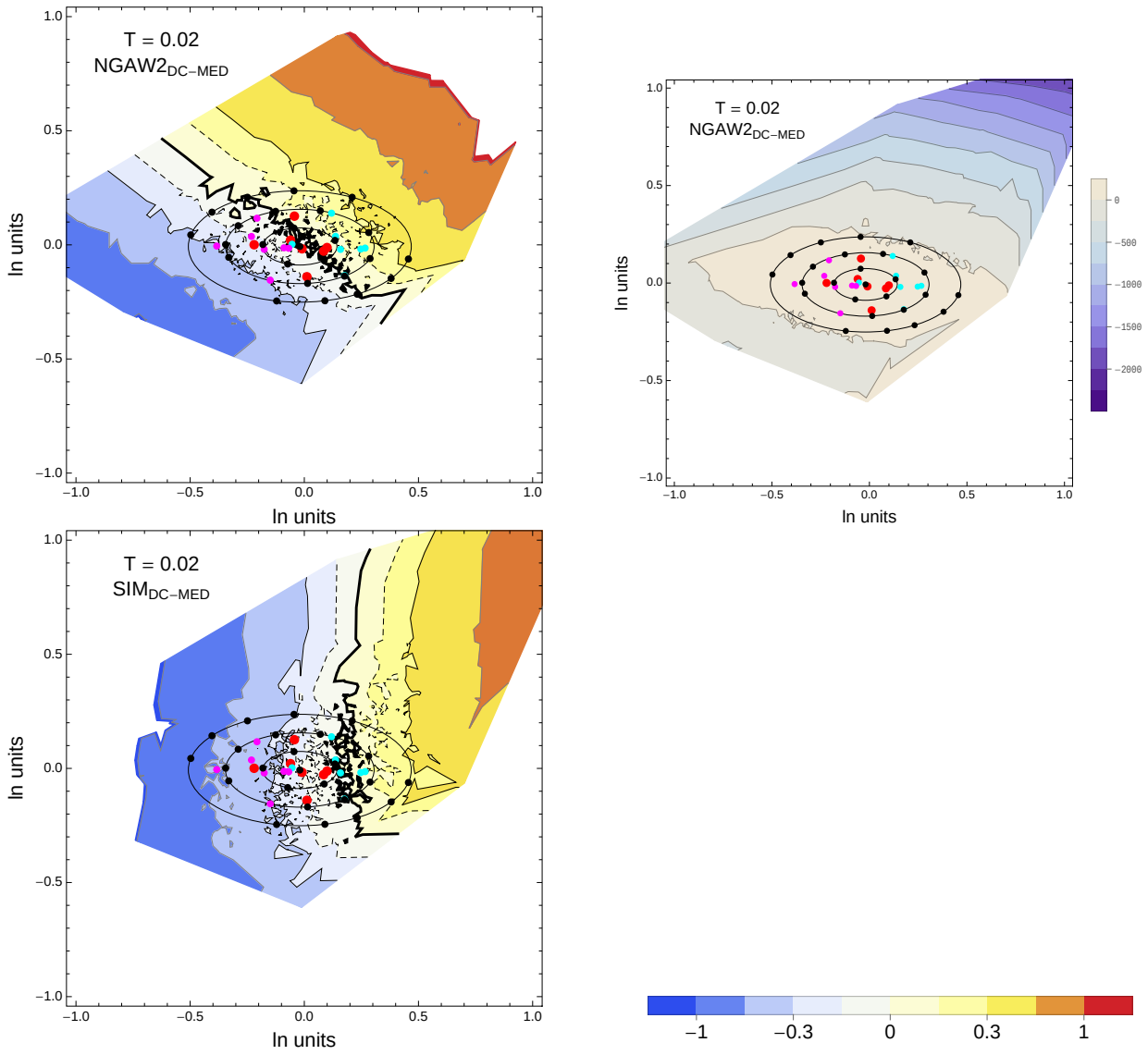



Figure 2.36: DCPPv4: Contour Plots of mean residuals (top left) and likelihood (top right) for the NGA$_{DC-MED}$ dataset, and mean residuals (bottom left) for the simulations (SIM$_{DC-MED}$). Reference points are black dots. The original GMPEs are red dots, plus/minus uncertainty are magenta/cyan dots. The contour for the zero residual is a thick black line, the -0.15/0.15 contours are dashed black lines and the -0.3/0.3 contours are thin black lines. For $T = 0.02$s.

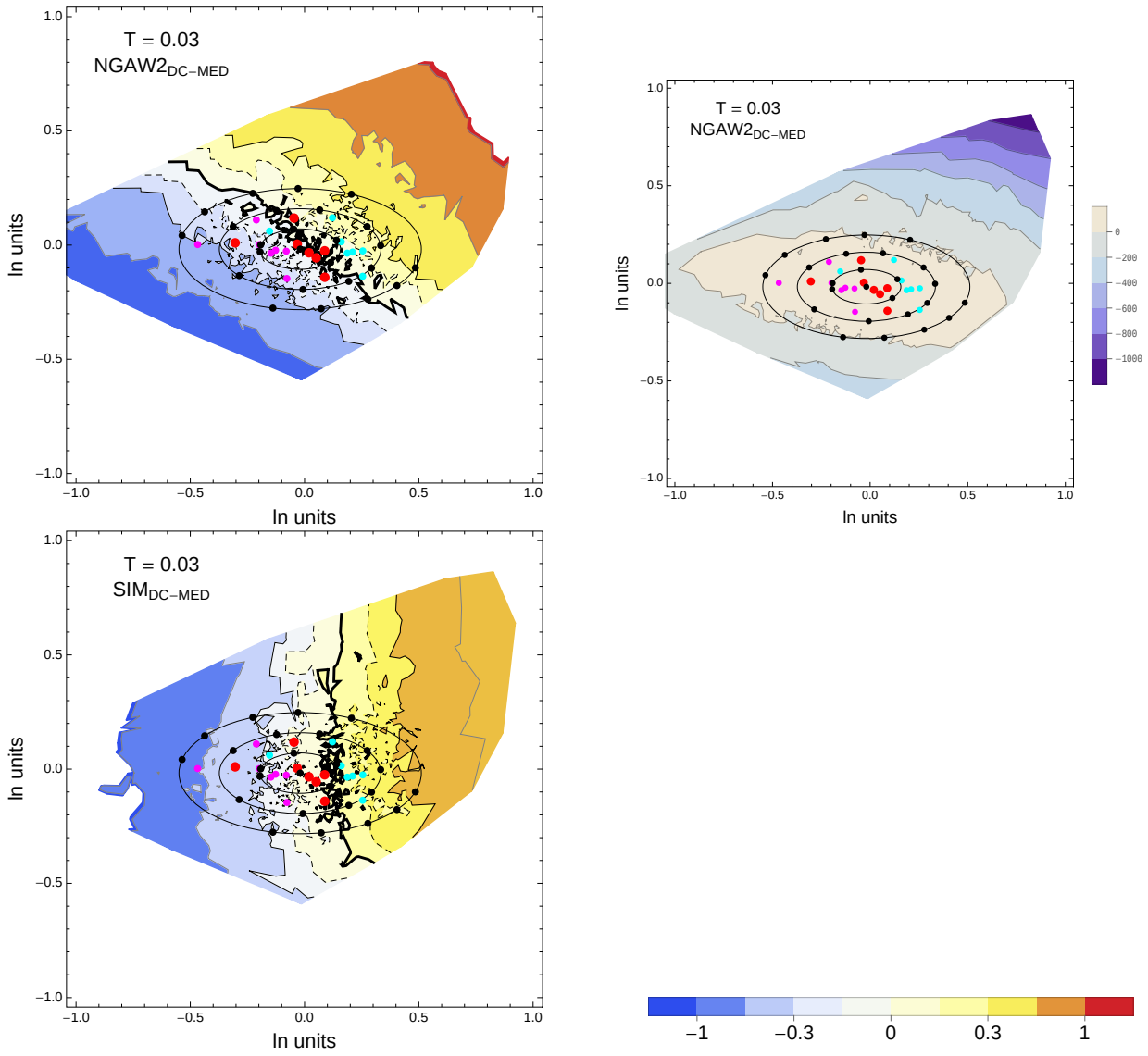



Figure 2.37: DCPPv4: Contour Plots of mean residuals (top left) and likelihood (top right) for the NGA$_{DC-MED}$ dataset, and mean residuals (bottom left) for the simulations (SIM$_{DC-MED}$). Reference points are black dots. The original GMPEs are red dots, plus/minus uncertainty are magenta/cyan dots. The contour for the zero residual is a thick black line, the -0.15/0.15 contours are dashed black lines and the -0.3/0.3 contours are thin black lines. For $T = 0.03$s.

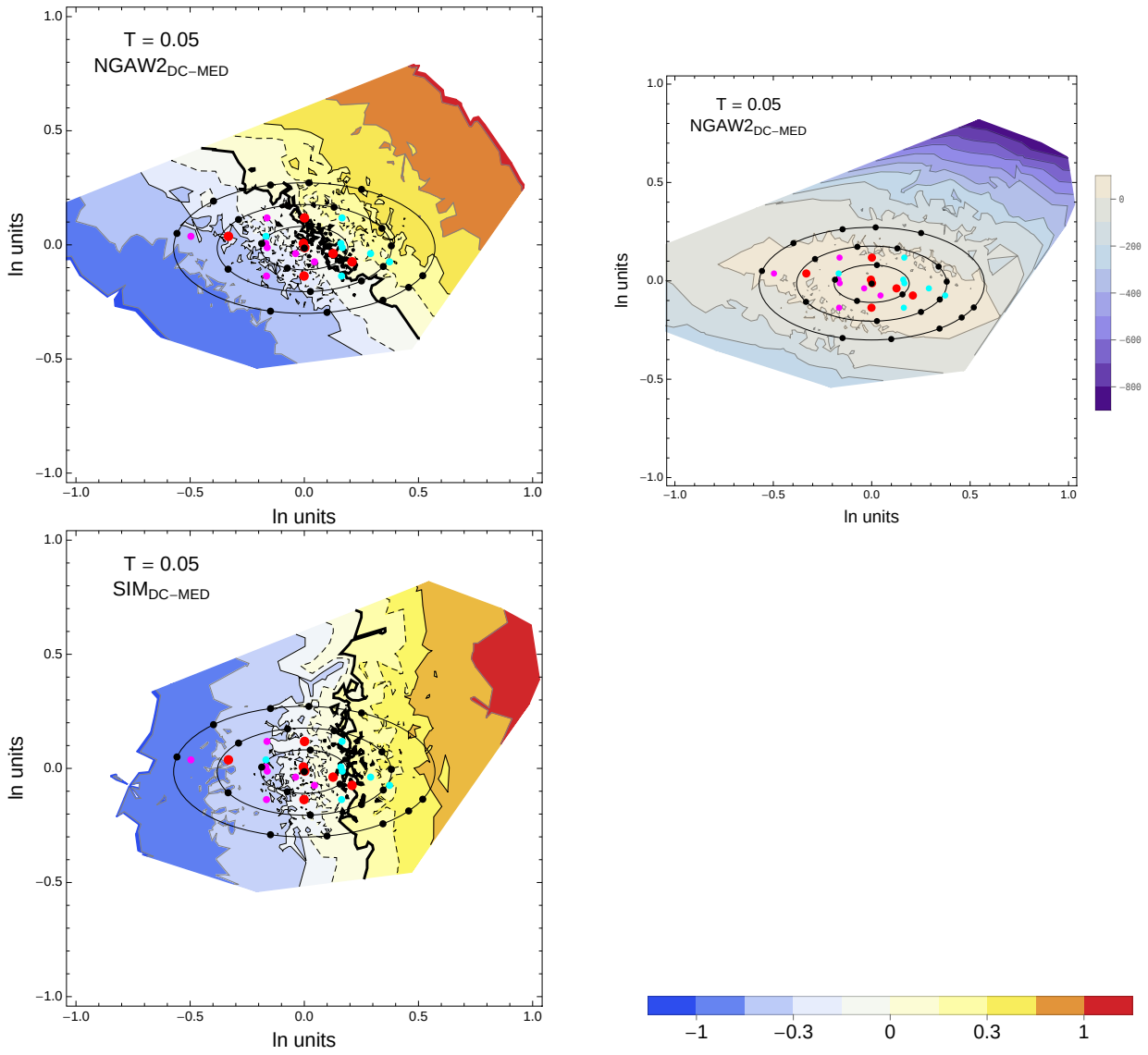



Figure 2.38: DCPPv4: Contour Plots of mean residuals (top left) and likelihood (top right) for the NGA$_{DC-MED}$ dataset, and mean residuals (bottom left) for the simulations (SIM$_{DC-MED}$). Reference points are black dots. The original GMPEs are red dots, plus/minus uncertainty are magenta/cyan dots. The contour for the zero residual is a thick black line, the -0.15/0.15 contours are dashed black lines and the -0.3/0.3 contours are thin black lines. For $T = 0.05$s.

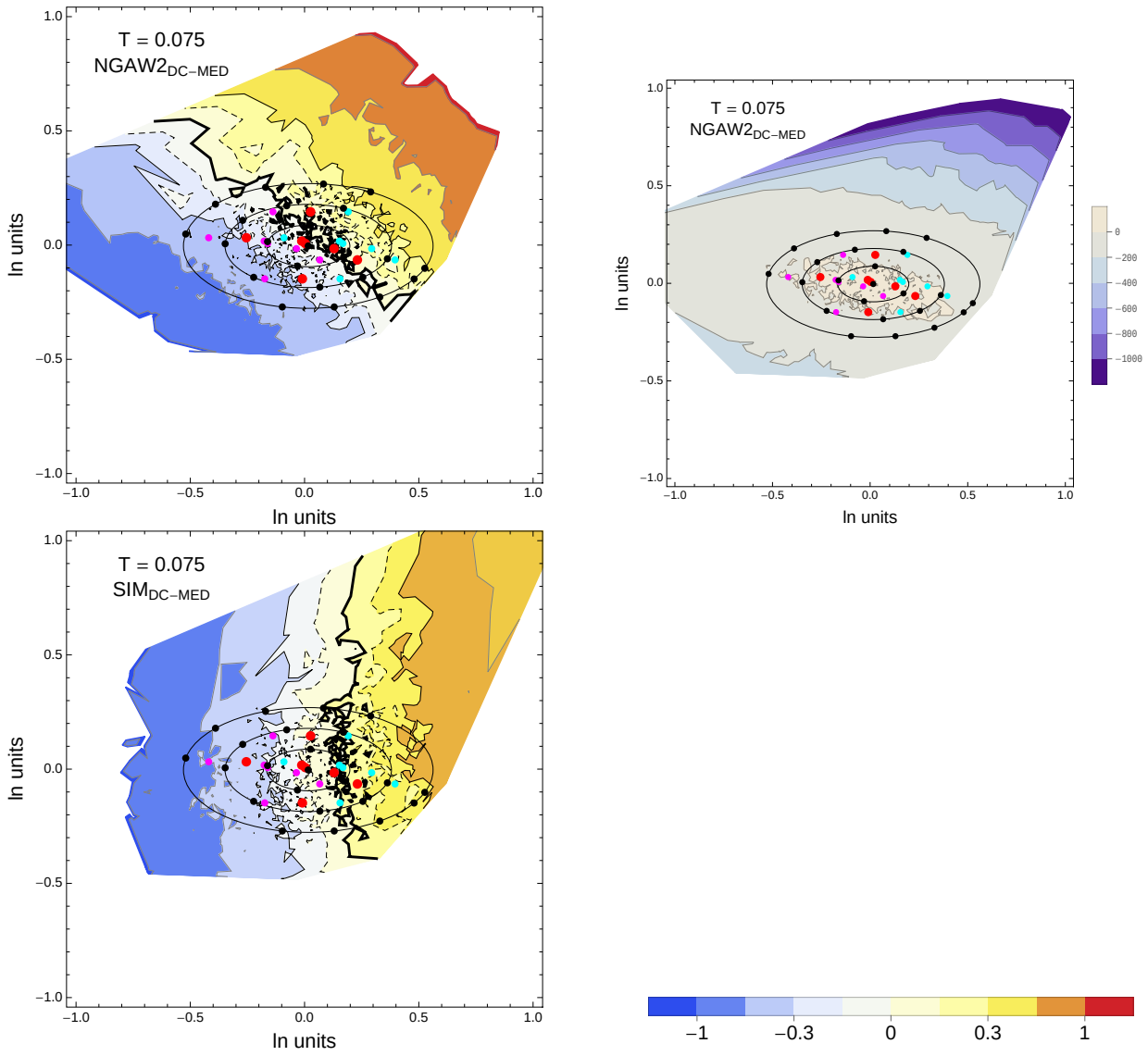



Figure 2.39: DCPPv4: Contour Plots of mean residuals (top left) and likelihood (top right) for the NGA$_{DC-MED}$ dataset, and mean residuals (bottom left) for the simulations (SIM$_{DC-MED}$). Reference points are black dots. The original GMPEs are red dots, plus/minus uncertainty are magenta/cyan dots. The contour for the zero residual is a thick black line, the -0.15/0.15 contours are dashed black lines and the -0.3/0.3 contours are thin black lines. For $T = 0.075$s.

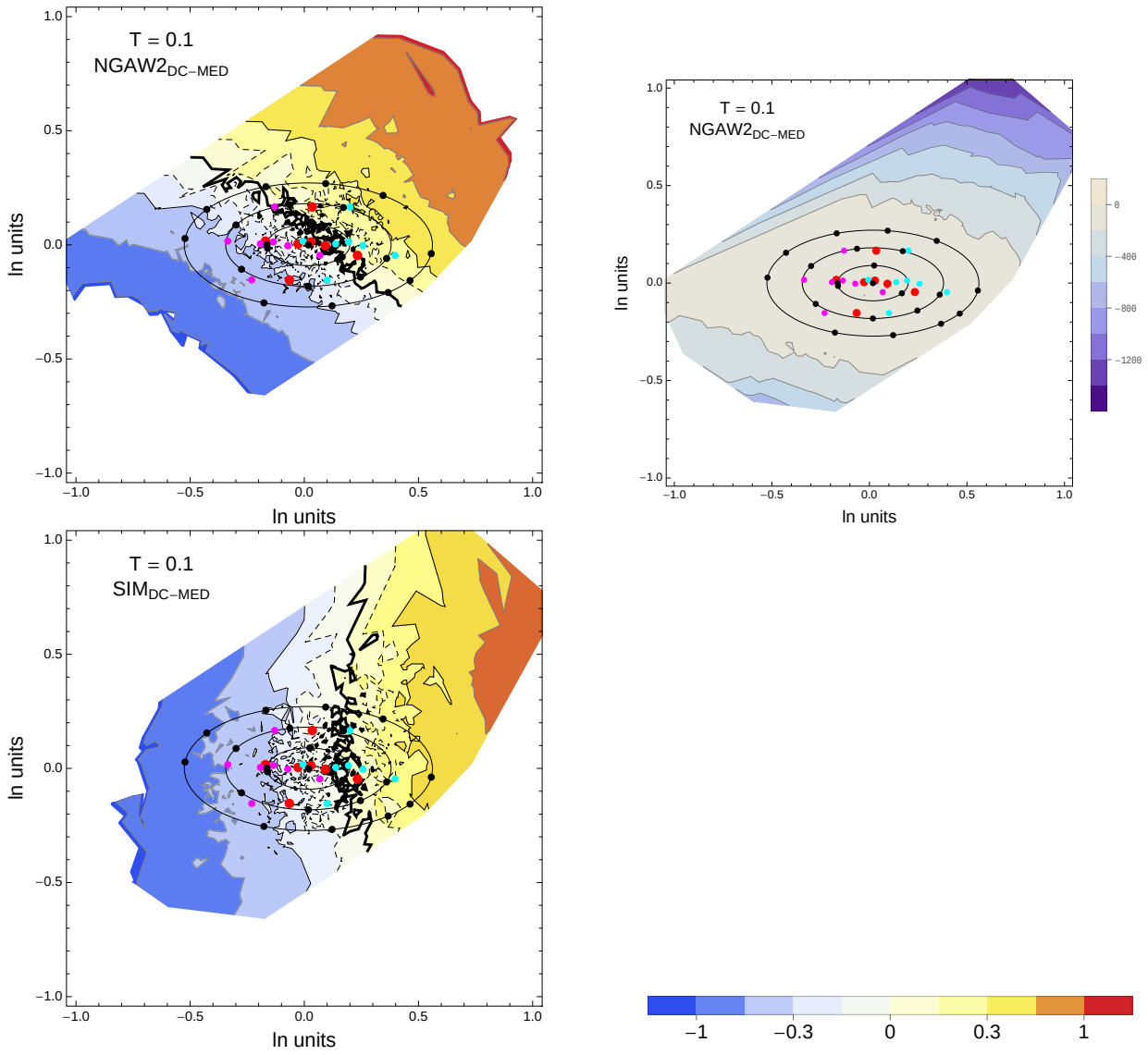



Figure 2.40: DCPPv4: Contour Plots of mean residuals (top left) and likelihood (top right) for the NGA$_{DC-MED}$ dataset, and mean residuals (bottom left) for the simulations (SIM$_{DC-MED}$). Reference points are black dots. The original GMPEs are red dots, plus/minus uncertainty are magenta/cyan dots. The contour for the zero residual is a thick black line, the -0.15/0.15 contours are dashed black lines and the -0.3/0.3 contours are thin black lines. For $T = 0.1$s.

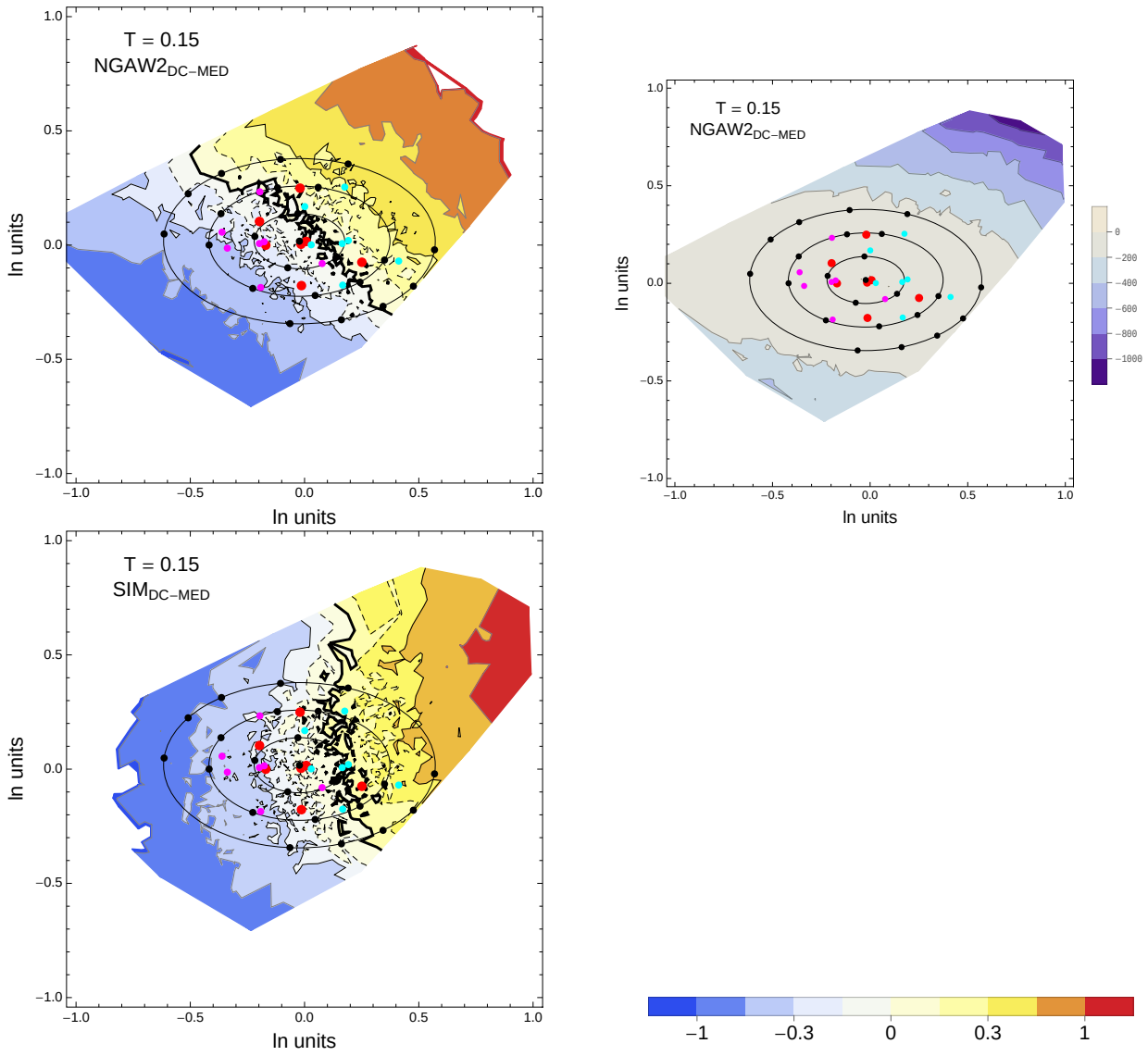



Figure 2.41: DCPPv4: Contour Plots of mean residuals (top left) and likelihood (top right) for the NGA$_{DC-MED}$ dataset, and mean residuals (bottom left) for the simulations (SIM$_{DC-MED}$). Reference points are black dots. The original GMPEs are red dots, plus/minus uncertainty are magenta/cyan dots. The contour for the zero residual is a thick black line, the -0.15/0.15 contours are dashed black lines and the -0.3/0.3 contours are thin black lines. For $T = 0.15$s.

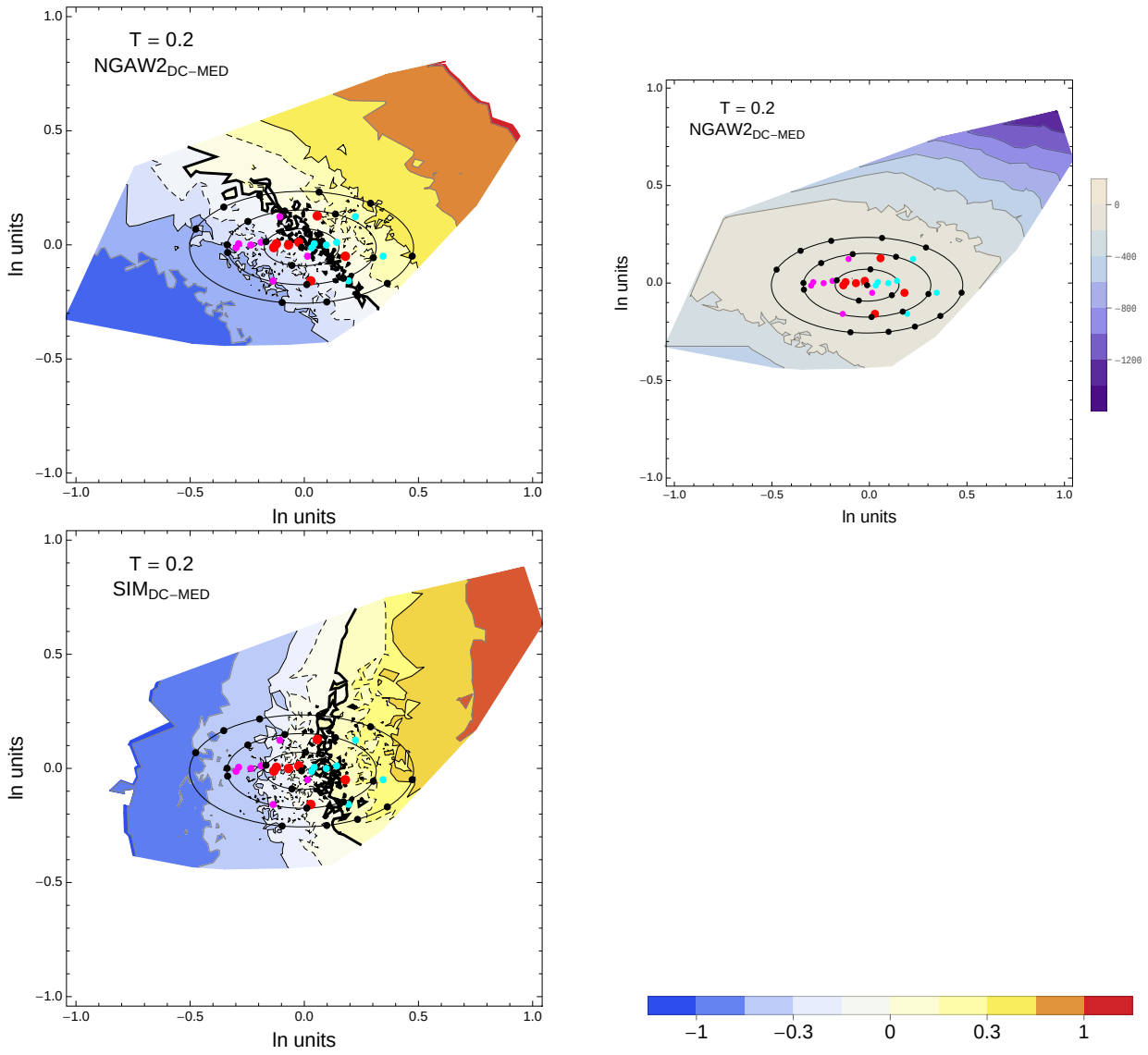



Figure 2.42: DCPPv4: Contour Plots of mean residuals (top left) and likelihood (top right) for the NGA$_{DC-MED}$ dataset, and mean residuals (bottom left) for the simulations (SIM$_{DC-MED}$). Reference points are black dots. The original GMPEs are red dots, plus/minus uncertainty are magenta/cyan dots. The contour for the zero residual is a thick black line, the -0.15/0.15 contours are dashed black lines and the -0.3/0.3 contours are thin black lines. For $T = 0.2$s.

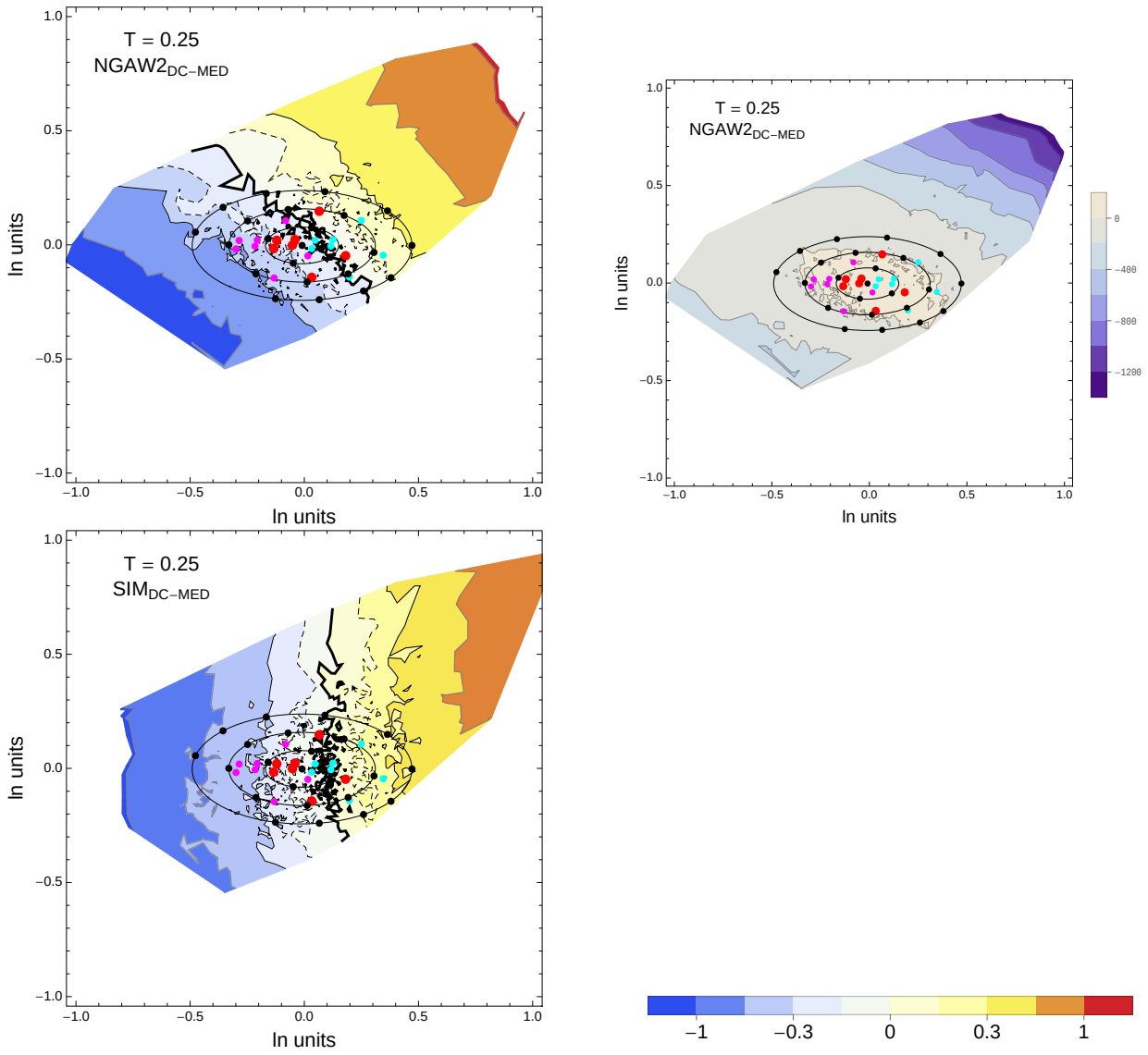



Figure 2.43: DCPPv4: Contour Plots of mean residuals (top left) and likelihood (top right) for the NGA$_{DC-MED}$ dataset, and mean residuals (bottom left) for the simulations (SIM$_{DC-MED}$). Reference points are black dots. The original GMPEs are red dots, plus/minus uncertainty are magenta/cyan dots. The contour for the zero residual is a thick black line, the -0.15/0.15 contours are dashed black lines and the -0.3/0.3 contours are thin black lines. For $T = 0.25$s.

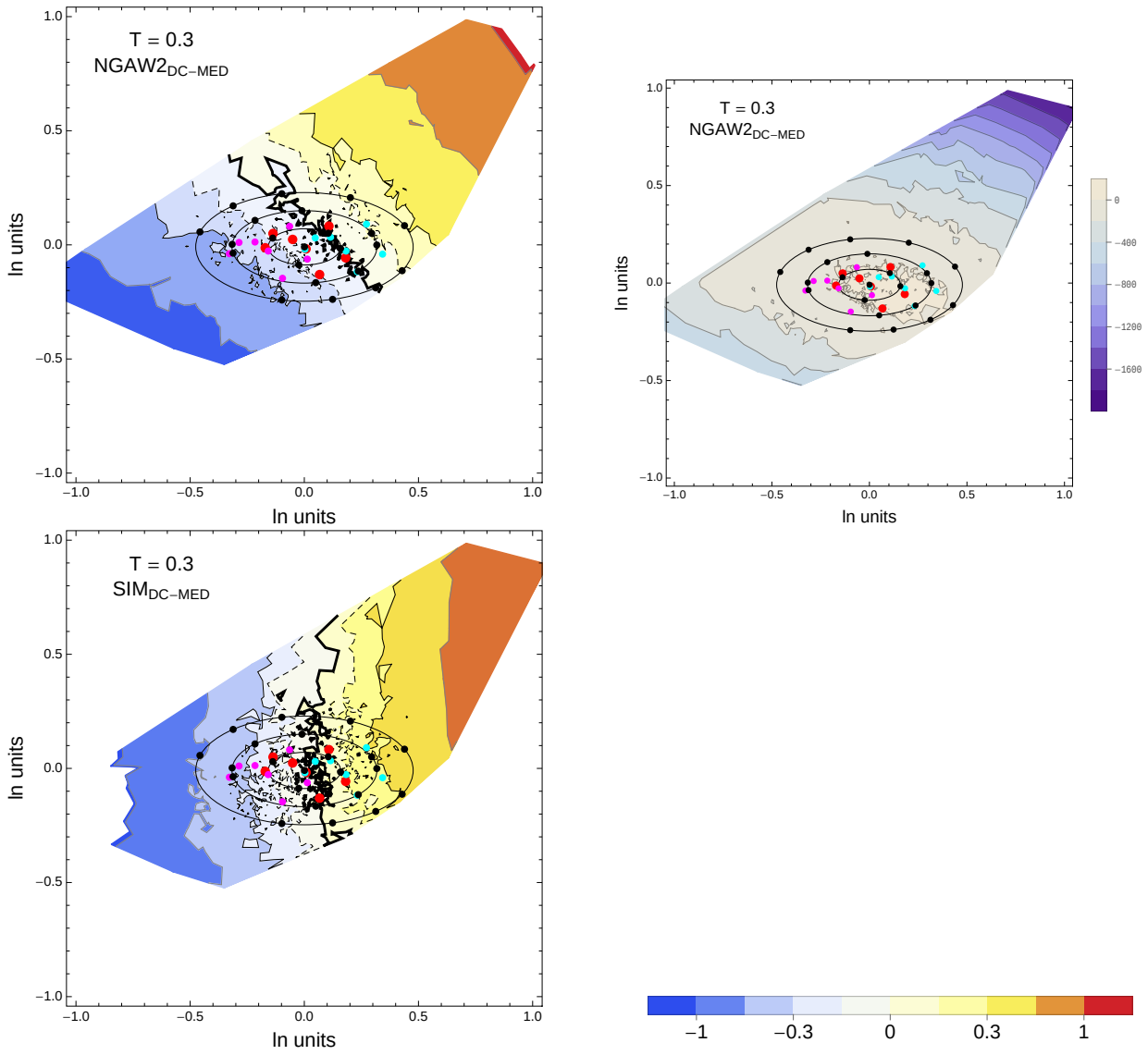



Figure 2.44: DCPPv4: Contour Plots of mean residuals (top left) and likelihood (top right) for the NGA$_{DC-MED}$ dataset, and mean residuals (bottom left) for the simulations (SIM$_{DC-MED}$). Reference points are black dots. The original GMPEs are red dots, plus/minus uncertainty are magenta/cyan dots. The contour for the zero residual is a thick black line, the -0.15/0.15 contours are dashed black lines and the -0.3/0.3 contours are thin black lines. For $T = 0.3$s.

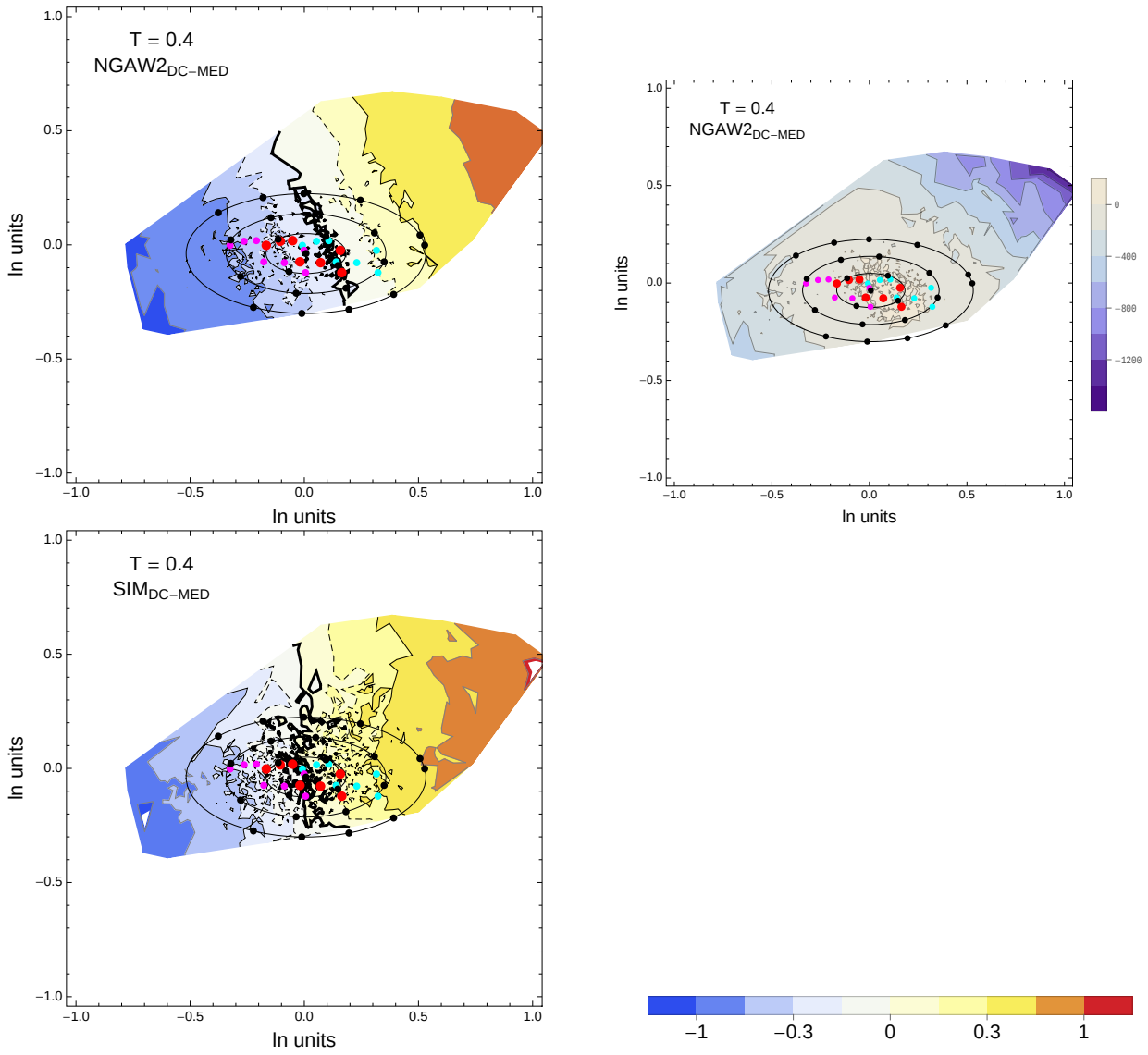



Figure 2.45: DCPPv4: Contour Plots of mean residuals (top left) and likelihood (top right) for the NGA$_{DC-MED}$ dataset, and mean residuals (bottom left) for the simulations (SIM$_{DC-MED}$). Reference points are black dots. The original GMPEs are red dots, plus/minus uncertainty are magenta/cyan dots. The contour for the zero residual is a thick black line, the -0.15/0.15 contours are dashed black lines and the -0.3/0.3 contours are thin black lines. For $T = 0.4$s.

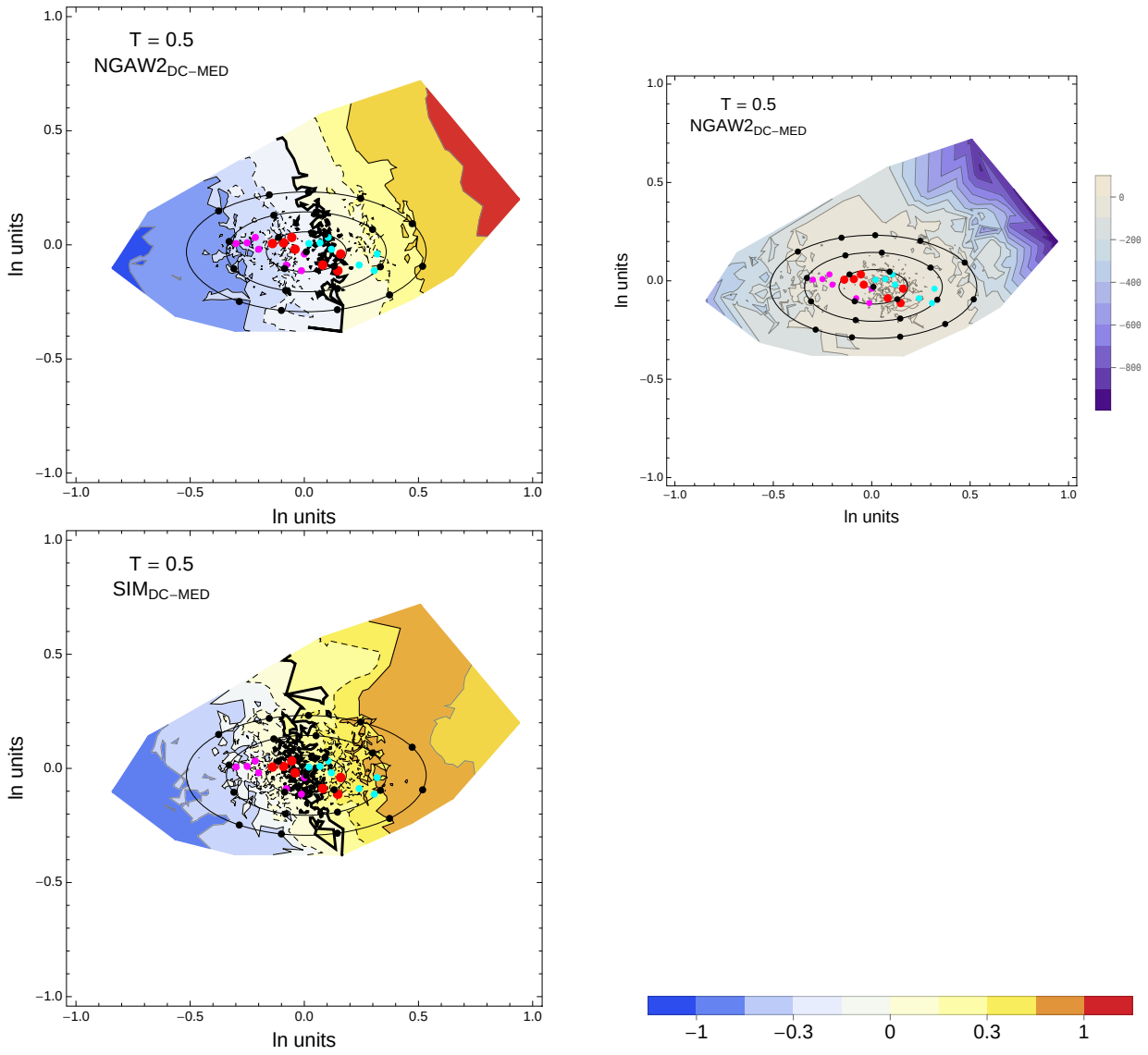



Figure 2.46: DCPPv4: Contour Plots of mean residuals (top left) and likelihood (top right) for the NGA$_{DC-MED}$ dataset, and mean residuals (bottom left) for the simulations (SIM$_{DC-MED}$). Reference points are black dots. The original GMPEs are red dots, plus/minus uncertainty are magenta/cyan dots. The contour for the zero residual is a thick black line, the -0.15/0.15 contours are dashed black lines and the -0.3/0.3 contours are thin black lines. For $T = 0.5$s.

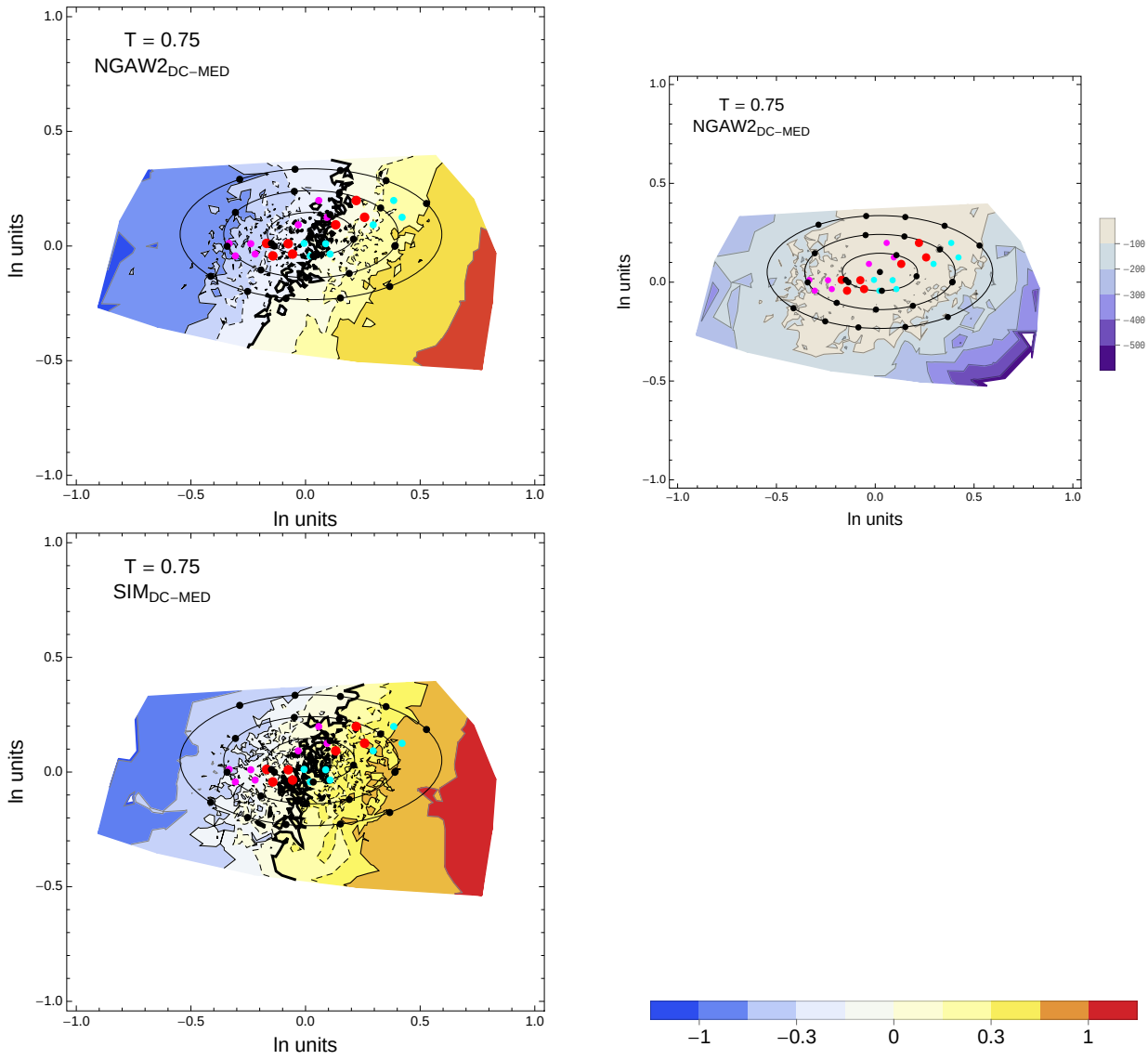



Figure 2.47: DCPPv4: Contour Plots of mean residuals (top left) and likelihood (top right) for the NGA$_{DC-MED}$ dataset, and mean residuals (bottom left) for the simulations (SIM$_{DC-MED}$). Reference points are black dots. The original GMPEs are red dots, plus/minus uncertainty are magenta/cyan dots. The contour for the zero residual is a thick black line, the -0.15/0.15 contours are dashed black lines and the -0.3/0.3 contours are thin black lines. For $T = 0.75$s.

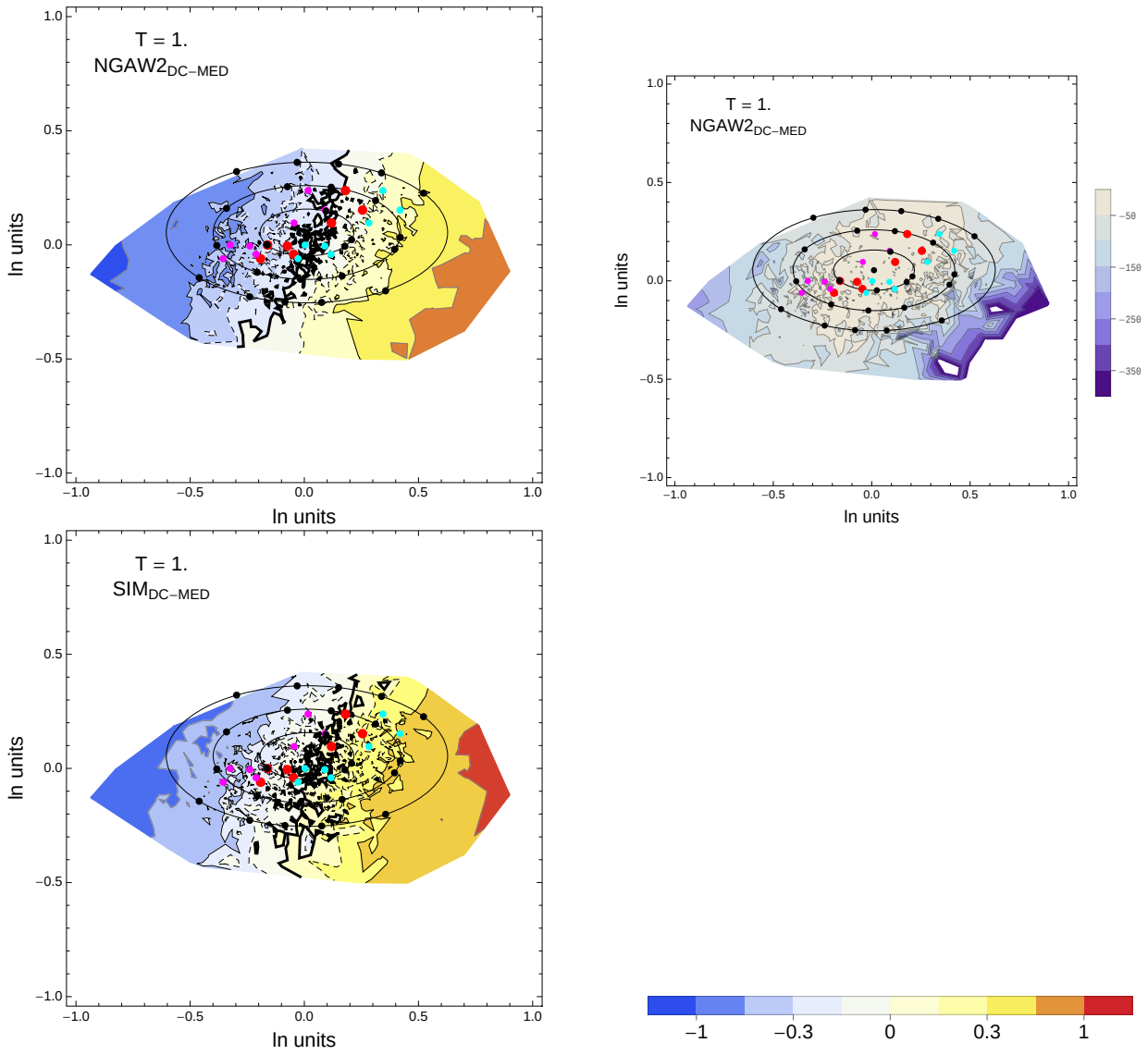



Figure 2.48: DCPPv4: Contour Plots of mean residuals (top left) and likelihood (top right) for the NGA$_{DC-MED}$ dataset, and mean residuals (bottom left) for the simulations (SIM$_{DC-MED}$). Reference points are black dots. The original GMPEs are red dots, plus/minus uncertainty are magenta/cyan dots. The contour for the zero residual is a thick black line, the -0.15/0.15 contours are dashed black lines and the -0.3/0.3 contours are thin black lines. For $T = 1$.s.

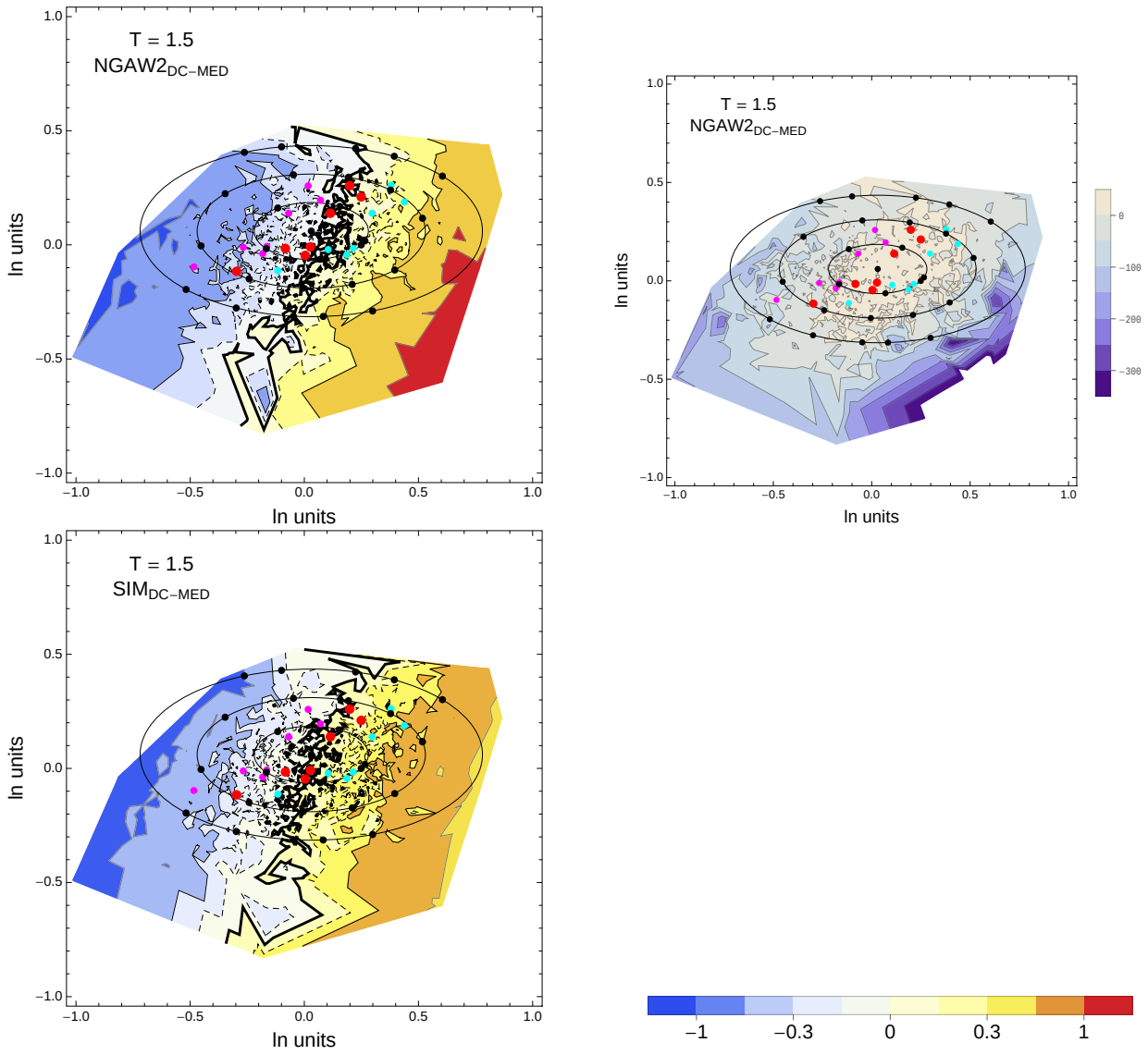



Figure 2.49: DCPPv4: Contour Plots of mean residuals (top left) and likelihood (top right) for the NGA$_{DC-MED}$ dataset, and mean residuals (bottom left) for the simulations (SIM$_{DC-MED}$). Reference points are black dots. The original GMPEs are red dots, plus/minus uncertainty are magenta/cyan dots. The contour for the zero residual is a thick black line, the -0.15/0.15 contours are dashed black lines and the -0.3/0.3 contours are thin black lines. For $T = 1.5$s.

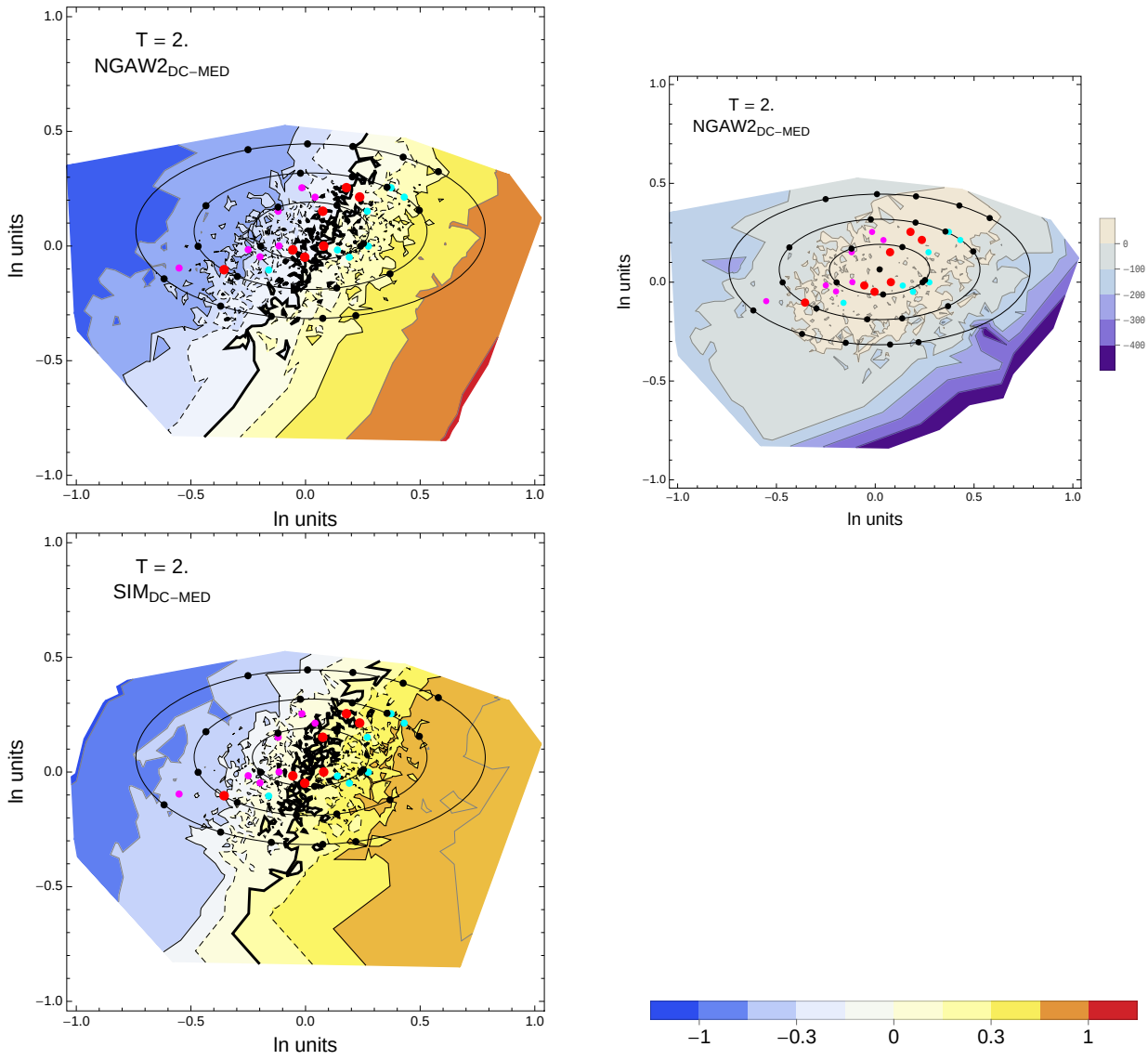



Figure 2.50: DCPPv4: Contour Plots of mean residuals (top left) and likelihood (top right) for the NGA$_{DC-MED}$ dataset, and mean residuals (bottom left) for the simulations (SIM$_{DC-MED}$). Reference points are black dots. The original GMPEs are red dots, plus/minus uncertainty are magenta/cyan dots. The contour for the zero residual is a thick black line, the -0.15/0.15 contours are dashed black lines and the -0.3/0.3 contours are thin black lines. For $T = 2$.s.

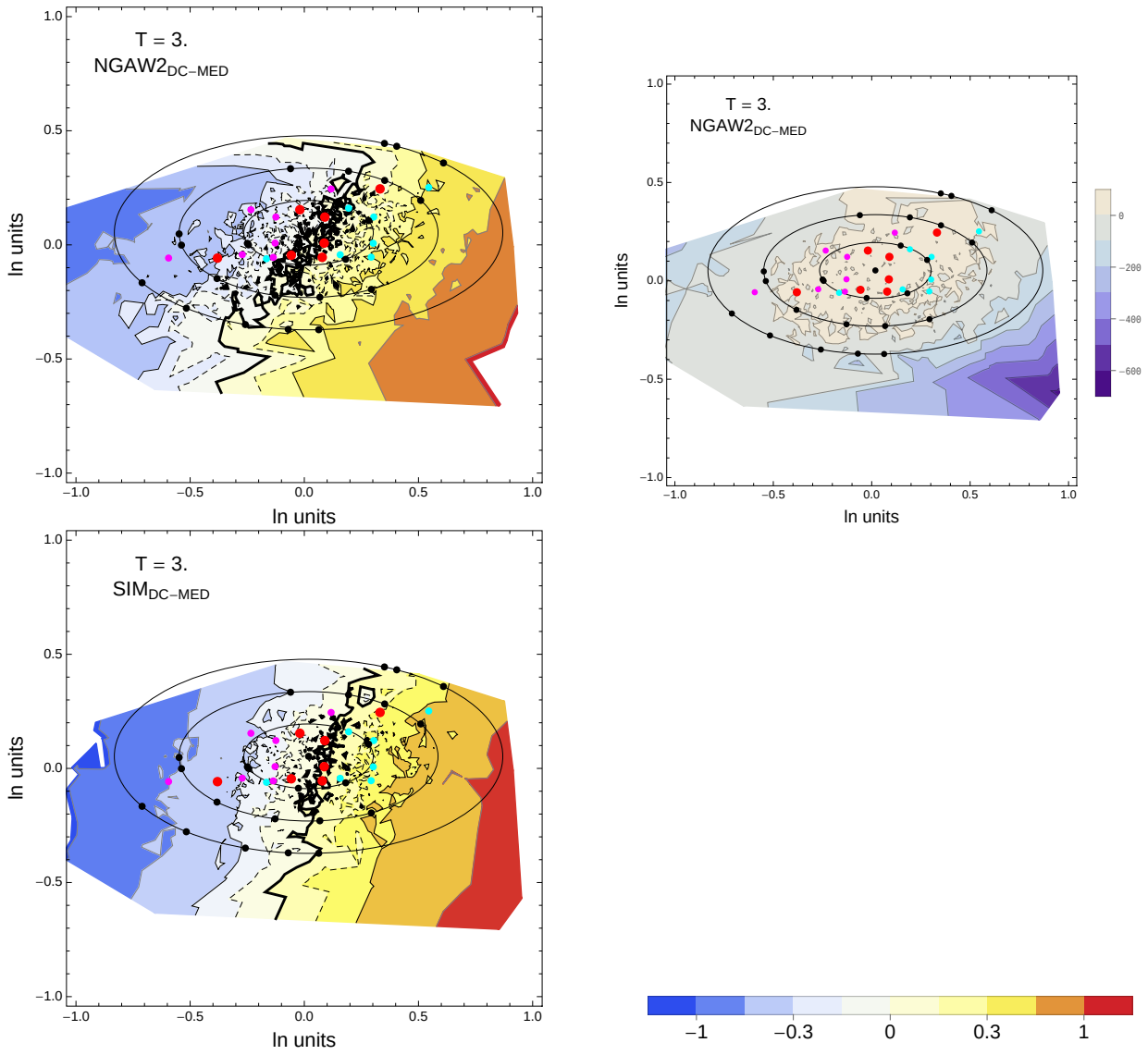



Figure 2.51: DCPPv4: Contour Plots of mean residuals (top left) and likelihood (top right) for the NGA$_{DC-MED}$ dataset, and mean residuals (bottom left) for the simulations (SIM$_{DC-MED}$). Reference points are black dots. The original GMPEs are red dots, plus/minus uncertainty are magenta/cyan dots. The contour for the zero residual is a thick black line, the -0.15/0.15 contours are dashed black lines and the -0.3/0.3 contours are thin black lines. For $T = 3$.s.

### 2.1.4 Maps – Voronoi Cells

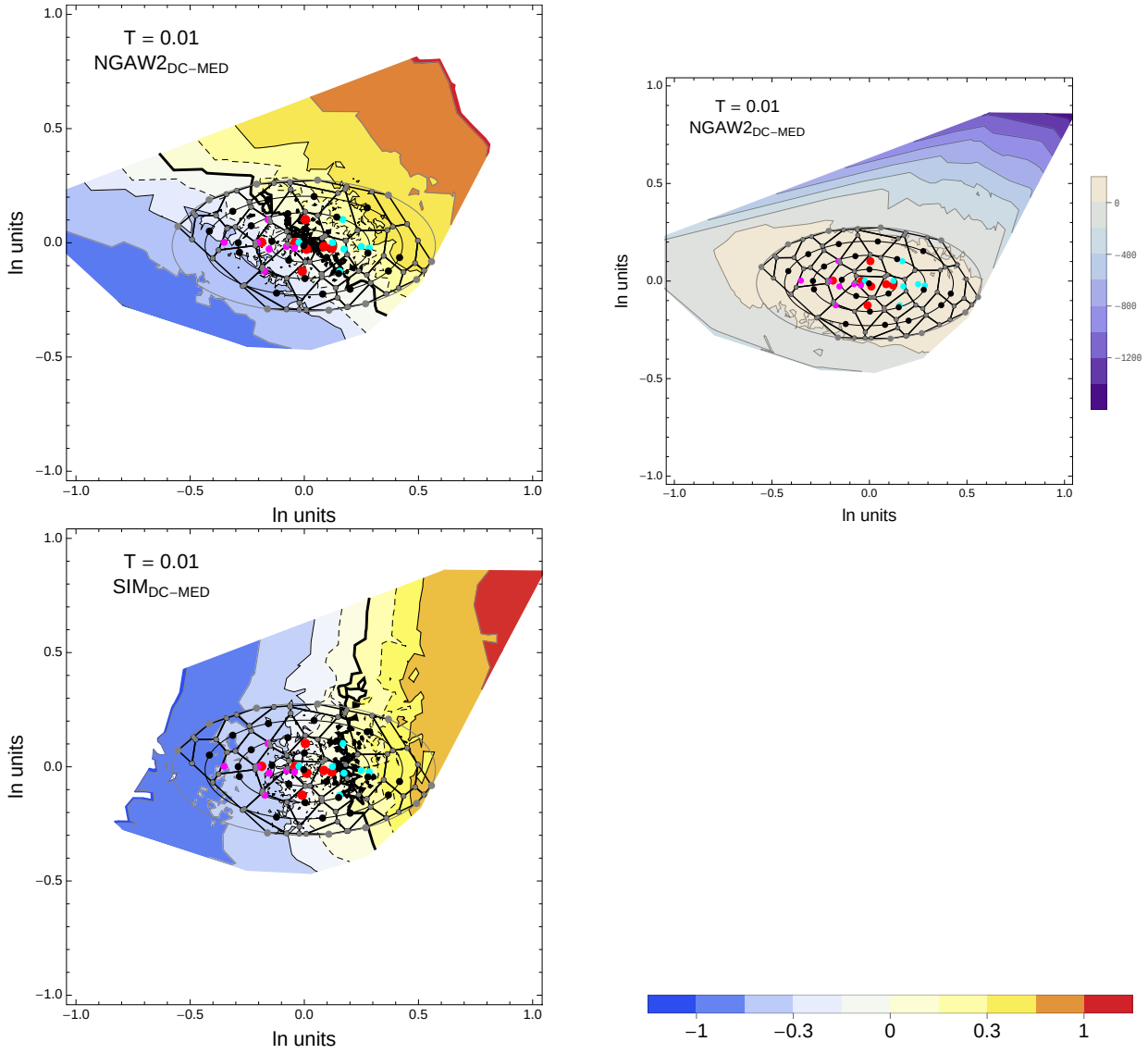



Figure 2.52: DCPPv4: Contour Plots of mean residuals (top left) and likelihood (top right) for the NGA$_{DC-MED}$ dataset, and mean residuals (bottom left) for the simulations (SIM$_{DC-MED}$). The Voronoi cells used for selecting and weighting models are shown as black lines. The original GMPEs are red dots,plus/minus uncertainty are magenta/cyan dots. The original GMPEs are red dots, plus/minus uncertainty are magenta/cyan dots. The contour for the zero residual is a thick black line, the -0.15/0.15 contours are dashed black lines and the -0.3/0.3 contours are thin black lines. For $T = 0.01$s.

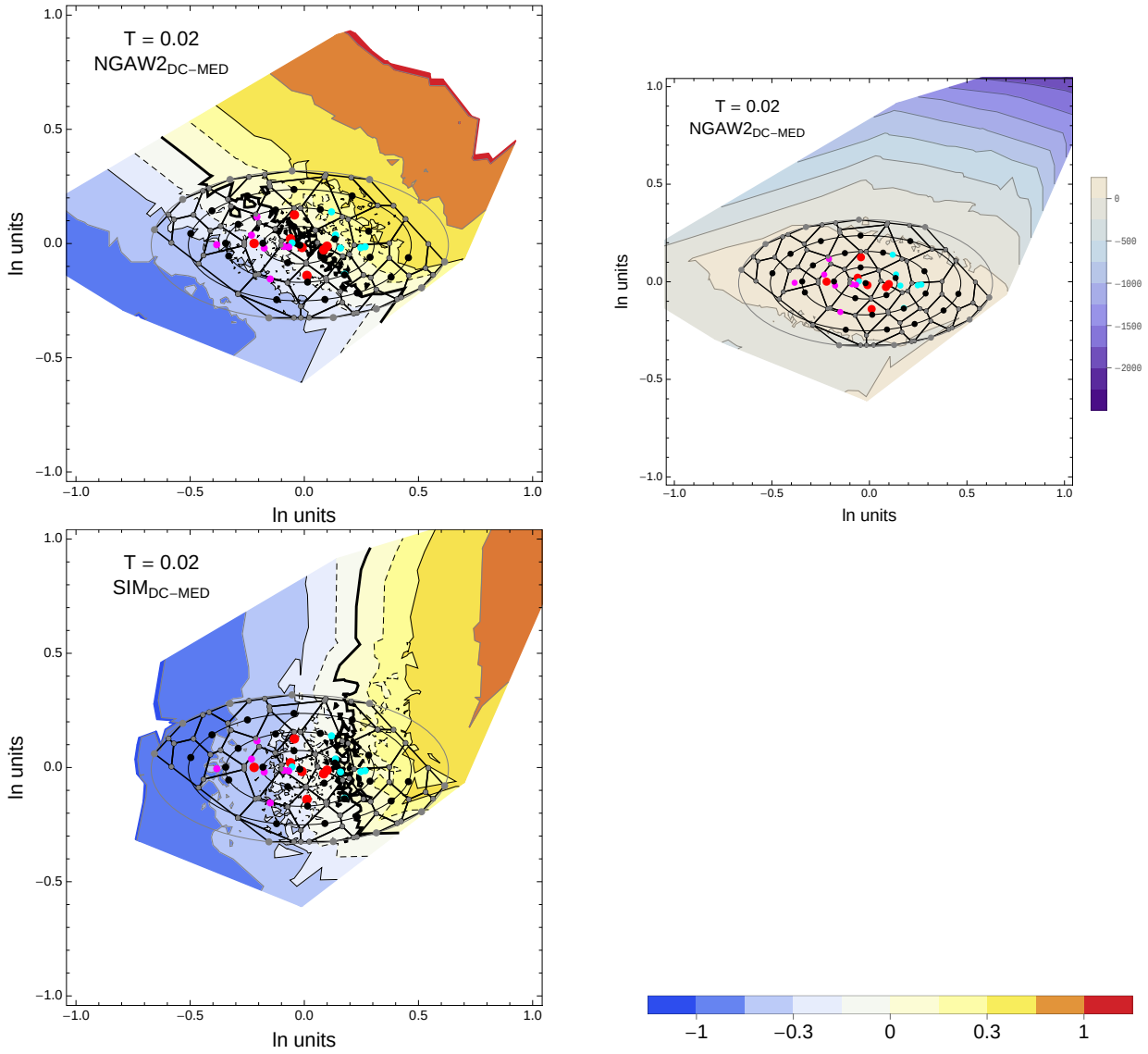



Figure 2.53: DCPPv4: Contour Plots of mean residuals (top left) and likelihood (top right) for the NGA$_{DC-MED}$ dataset, and mean residuals (bottom left) for the simulations (SIM$_{DC-MED}$). The Voronoi cells used for selecting and weighting models are shown as black lines. The original GMPEs are red dots,plus/minus uncertainty are magenta/cyan dots. The original GMPEs are red dots, plus/minus uncertainty are magenta/cyan dots. The contour for the zero residual is a thick black line, the -0.15/0.15 contours are dashed black lines and the -0.3/0.3 contours are thin black lines. For $T = 0.02$s.

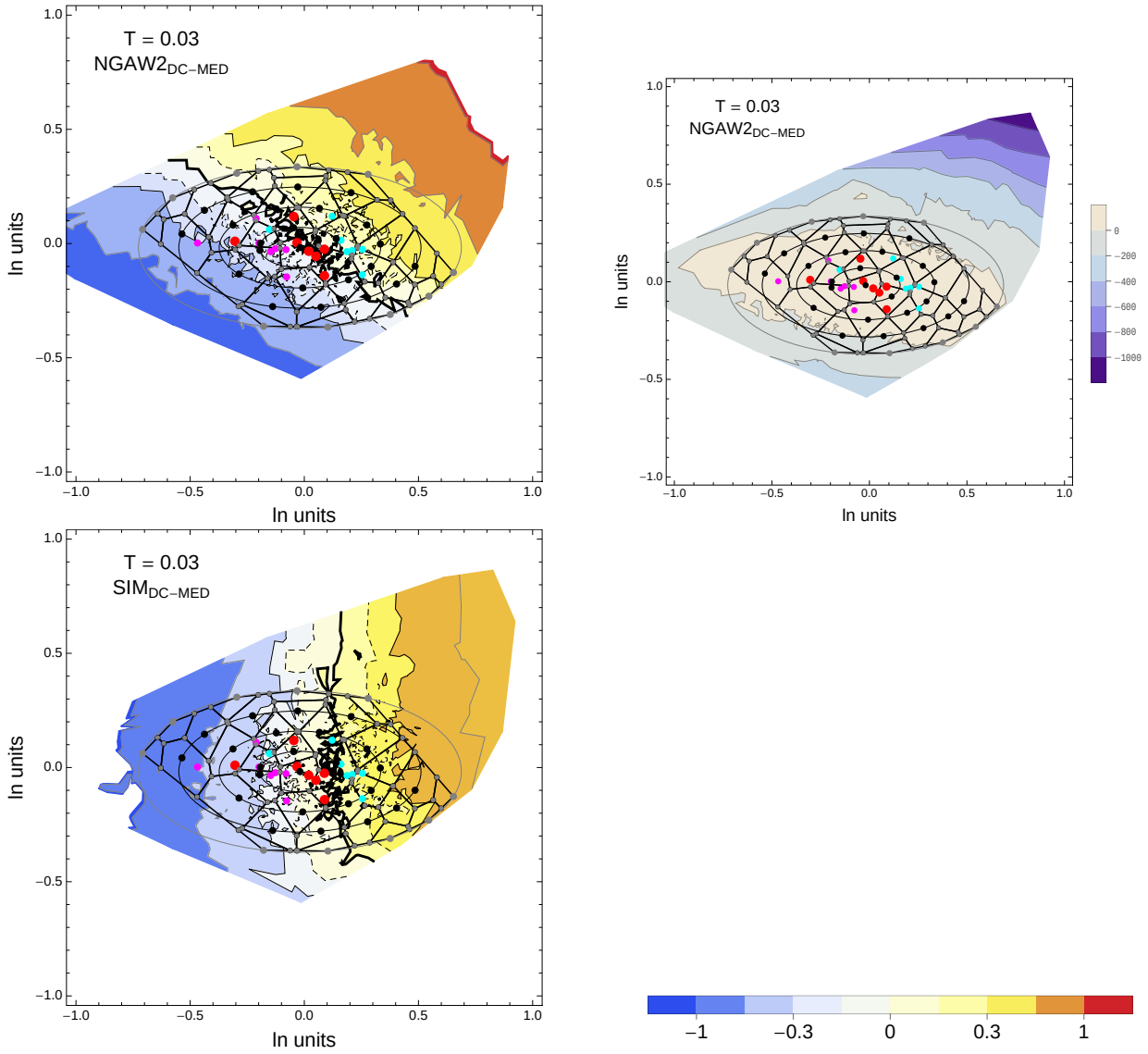



Figure 2.54: DCPPv4: Contour Plots of mean residuals (top left) and likelihood (top right) for the NGA$_{DC-MED}$ dataset, and mean residuals (bottom left) for the simulations (SIM$_{DC-MED}$). The Voronoi cells used for selecting and weighting models are shown as black lines. The original GMPEs are red dots,plus/minus uncertainty are magenta/cyan dots. The original GMPEs are red dots, plus/minus uncertainty are magenta/cyan dots. The contour for the zero residual is a thick black line, the -0.15/0.15 contours are dashed black lines and the -0.3/0.3 contours are thin black lines. For $T = 0.03$s.

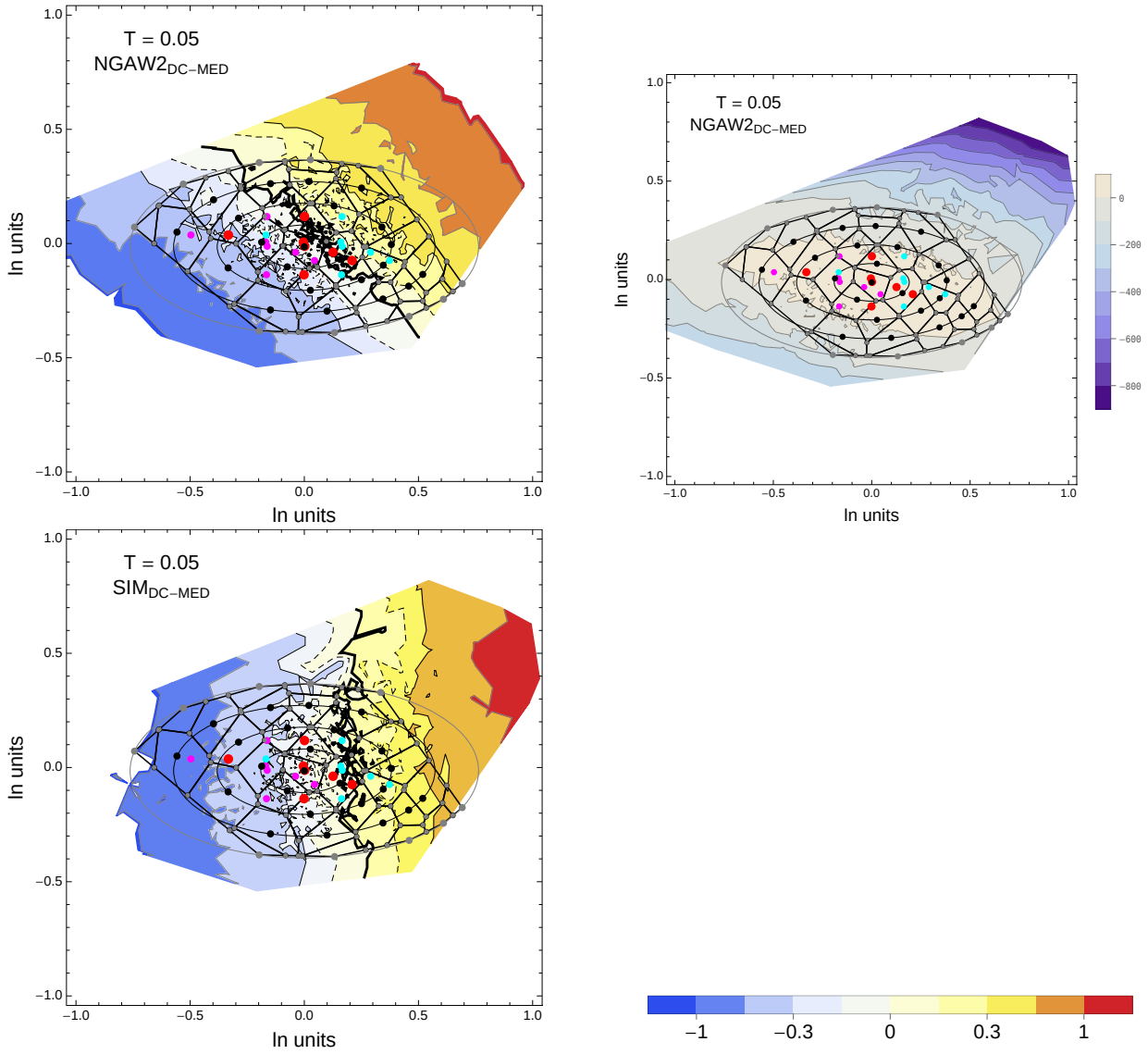



Figure 2.55: DCPPv4: Contour Plots of mean residuals (top left) and likelihood (top right) for the NGA$_{DC-MED}$ dataset, and mean residuals (bottom left) for the simulations (SIM$_{DC-MED}$). The Voronoi cells used for selecting and weighting models are shown as black lines. The original GMPEs are red dots,plus/minus uncertainty are magenta/cyan dots. The original GMPEs are red dots, plus/minus uncertainty are magenta/cyan dots. The contour for the zero residual is a thick black line, the -0.15/0.15 contours are dashed black lines and the -0.3/0.3 contours are thin black lines. For $T = 0.05$s.

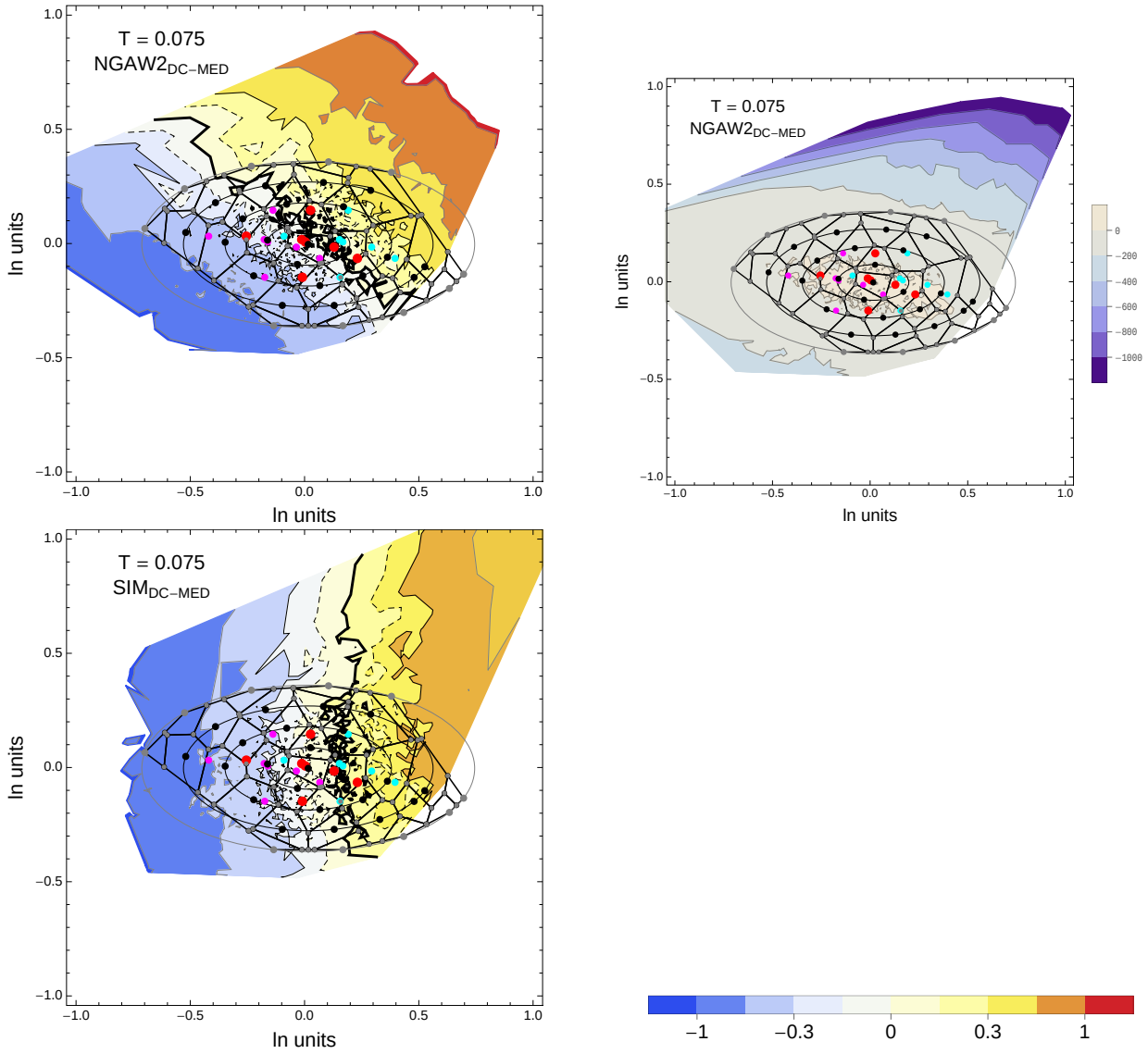



Figure 2.56: DCPPv4: Contour Plots of mean residuals (top left) and likelihood (top right) for the NGA$_{DC-MED}$ dataset, and mean residuals (bottom left) for the simulations (SIM$_{DC-MED}$). The Voronoi cells used for selecting and weighting models are shown as black lines. The original GMPEs are red dots,plus/minus uncertainty are magenta/cyan dots. The original GMPEs are red dots, plus/minus uncertainty are magenta/cyan dots. The contour for the zero residual is a thick black line, the -0.15/0.15 contours are dashed black lines and the -0.3/0.3 contours are thin black lines. For $T = 0.075$s.

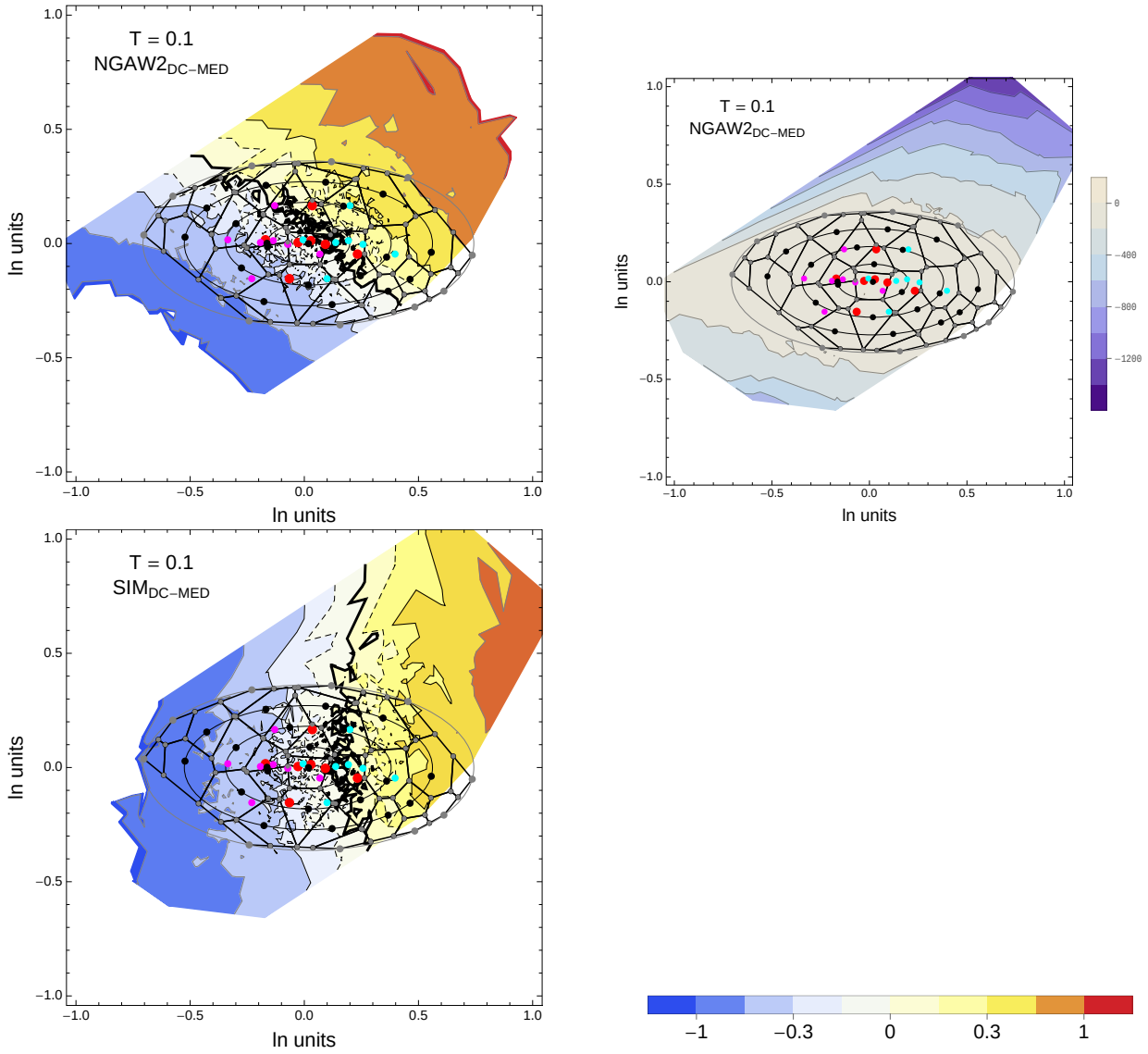



Figure 2.57: DCPPv4: Contour Plots of mean residuals (top left) and likelihood (top right) for the NGA$_{DC-MED}$ dataset, and mean residuals (bottom left) for the simulations (SIM$_{DC-MED}$). The Voronoi cells used for selecting and weighting models are shown as black lines. The original GMPEs are red dots,plus/minus uncertainty are magenta/cyan dots. The original GMPEs are red dots, plus/minus uncertainty are magenta/cyan dots. The contour for the zero residual is a thick black line, the -0.15/0.15 contours are dashed black lines and the -0.3/0.3 contours are thin black lines. For $T = 0.1$s.

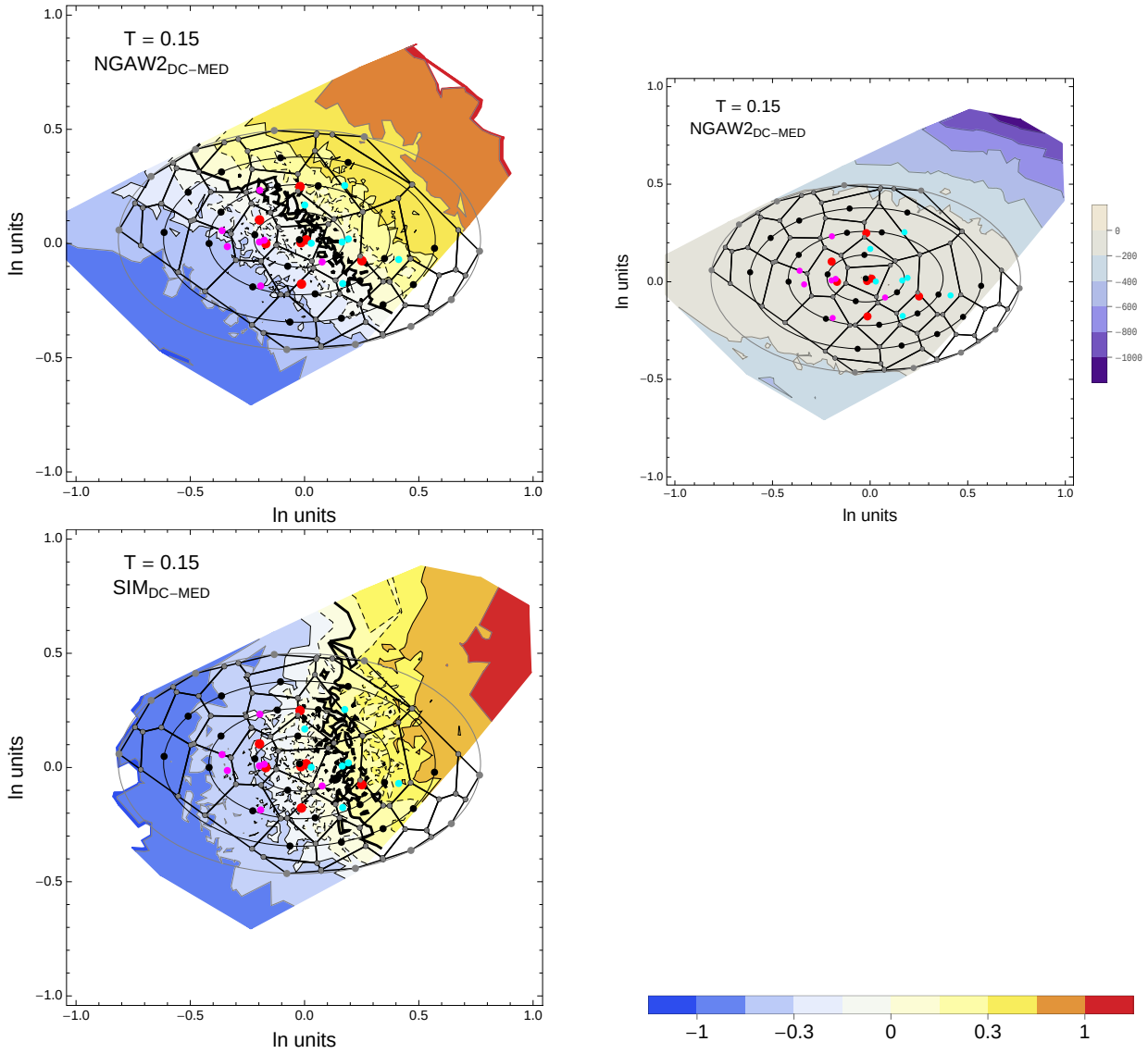



Figure 2.58: DCPPv4: Contour Plots of mean residuals (top left) and likelihood (top right) for the NGA$_{DC-MED}$ dataset, and mean residuals (bottom left) for the simulations (SIM$_{DC-MED}$). The Voronoi cells used for selecting and weighting models are shown as black lines. The original GMPEs are red dots,plus/minus uncertainty are magenta/cyan dots. The original GMPEs are red dots, plus/minus uncertainty are magenta/cyan dots. The contour for the zero residual is a thick black line, the -0.15/0.15 contours are dashed black lines and the -0.3/0.3 contours are thin black lines. For $T = 0.15$s.

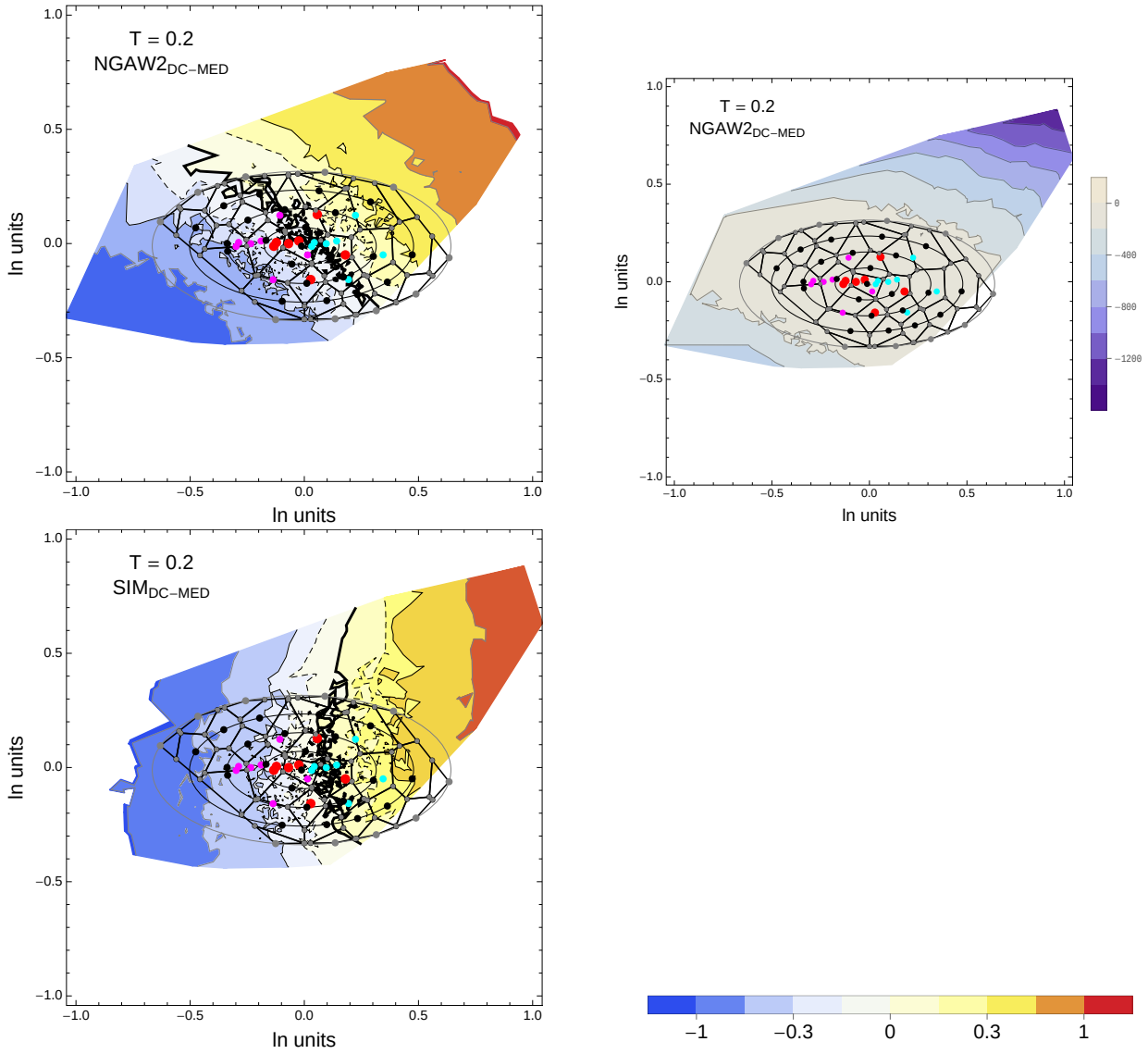



Figure 2.59: DCPPv4: Contour Plots of mean residuals (top left) and likelihood (top right) for the NGA$_{DC-MED}$ dataset, and mean residuals (bottom left) for the simulations (SIM$_{DC-MED}$). The Voronoi cells used for selecting and weighting models are shown as black lines. The original GMPEs are red dots,plus/minus uncertainty are magenta/cyan dots. The original GMPEs are red dots, plus/minus uncertainty are magenta/cyan dots. The contour for the zero residual is a thick black line, the -0.15/0.15 contours are dashed black lines and the -0.3/0.3 contours are thin black lines. For $T = 0.2$s.

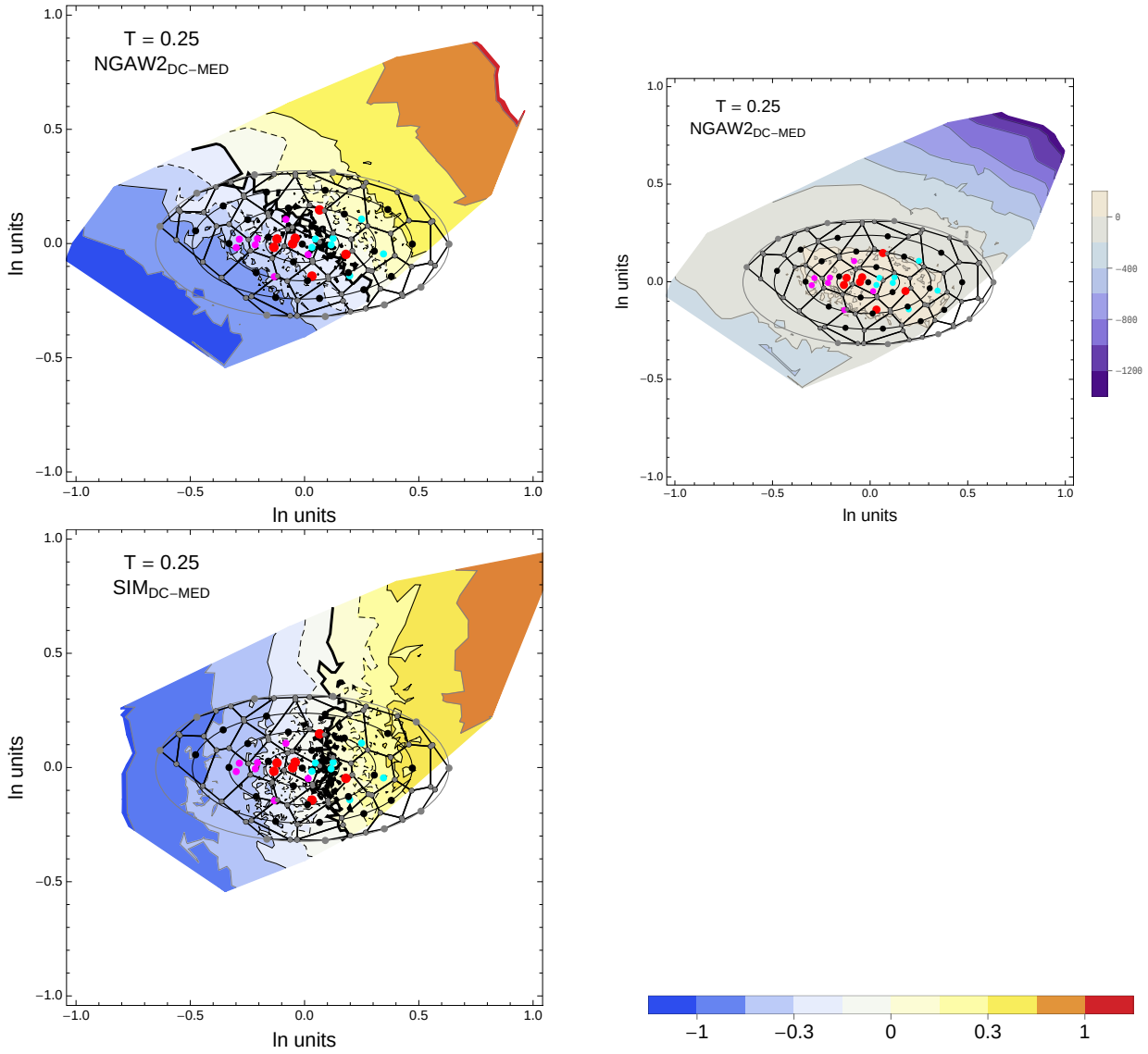



Figure 2.60: DCPPv4: Contour Plots of mean residuals (top left) and likelihood (top right) for the NGA$_{DC-MED}$ dataset, and mean residuals (bottom left) for the simulations (SIM$_{DC-MED}$). The Voronoi cells used for selecting and weighting models are shown as black lines. The original GMPEs are red dots,plus/minus uncertainty are magenta/cyan dots. The original GMPEs are red dots, plus/minus uncertainty are magenta/cyan dots. The contour for the zero residual is a thick black line, the -0.15/0.15 contours are dashed black lines and the -0.3/0.3 contours are thin black lines. For $T = 0.25$s.

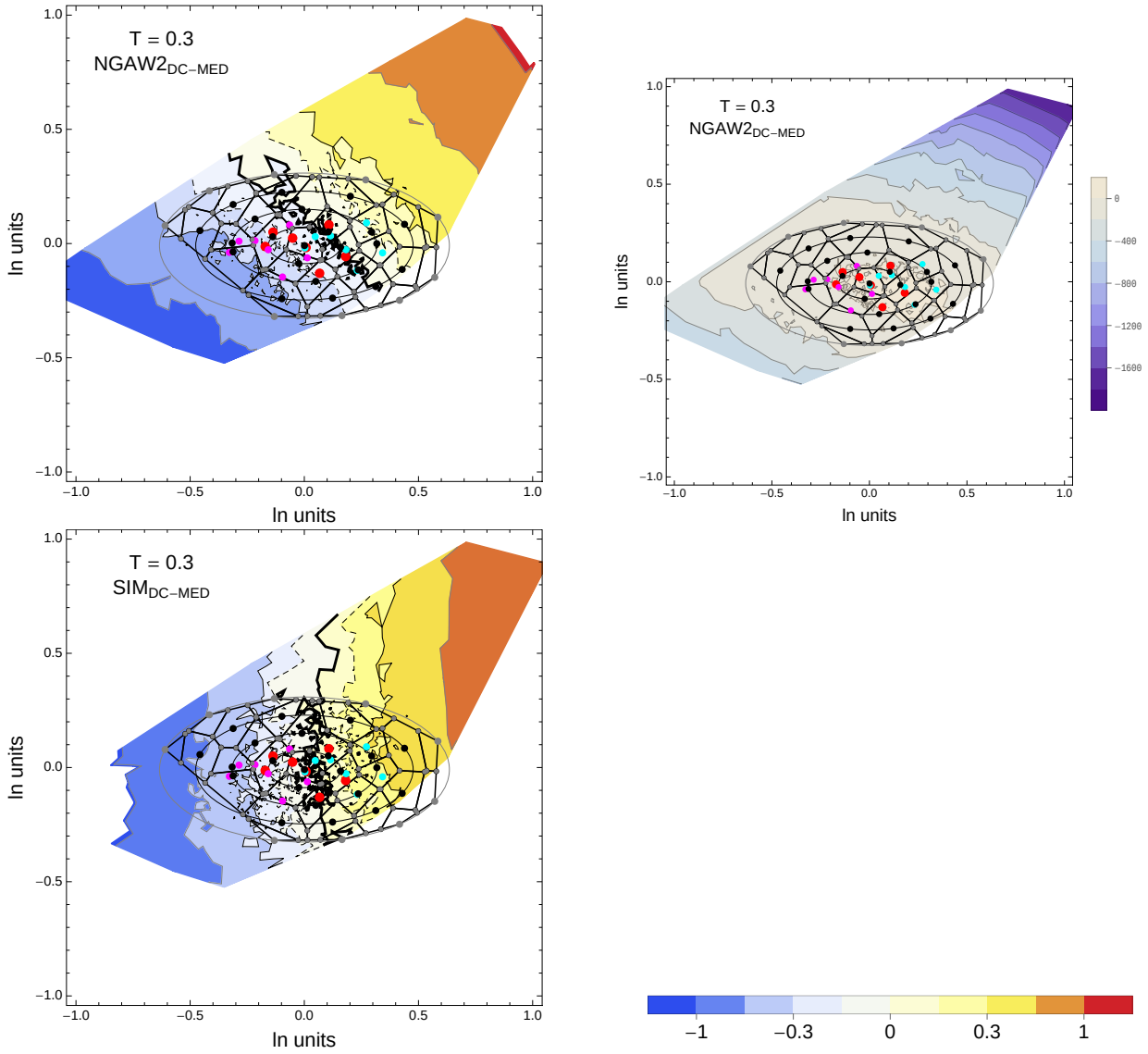



Figure 2.61: DCPPv4: Contour Plots of mean residuals (top left) and likelihood (top right) for the NGA$_{DC-MED}$ dataset, and mean residuals (bottom left) for the simulations (SIM$_{DC-MED}$). The Voronoi cells used for selecting and weighting models are shown as black lines. The original GMPEs are red dots,plus/minus uncertainty are magenta/cyan dots. The original GMPEs are red dots, plus/minus uncertainty are magenta/cyan dots. The contour for the zero residual is a thick black line, the -0.15/0.15 contours are dashed black lines and the -0.3/0.3 contours are thin black lines. For $T = 0.3$s.

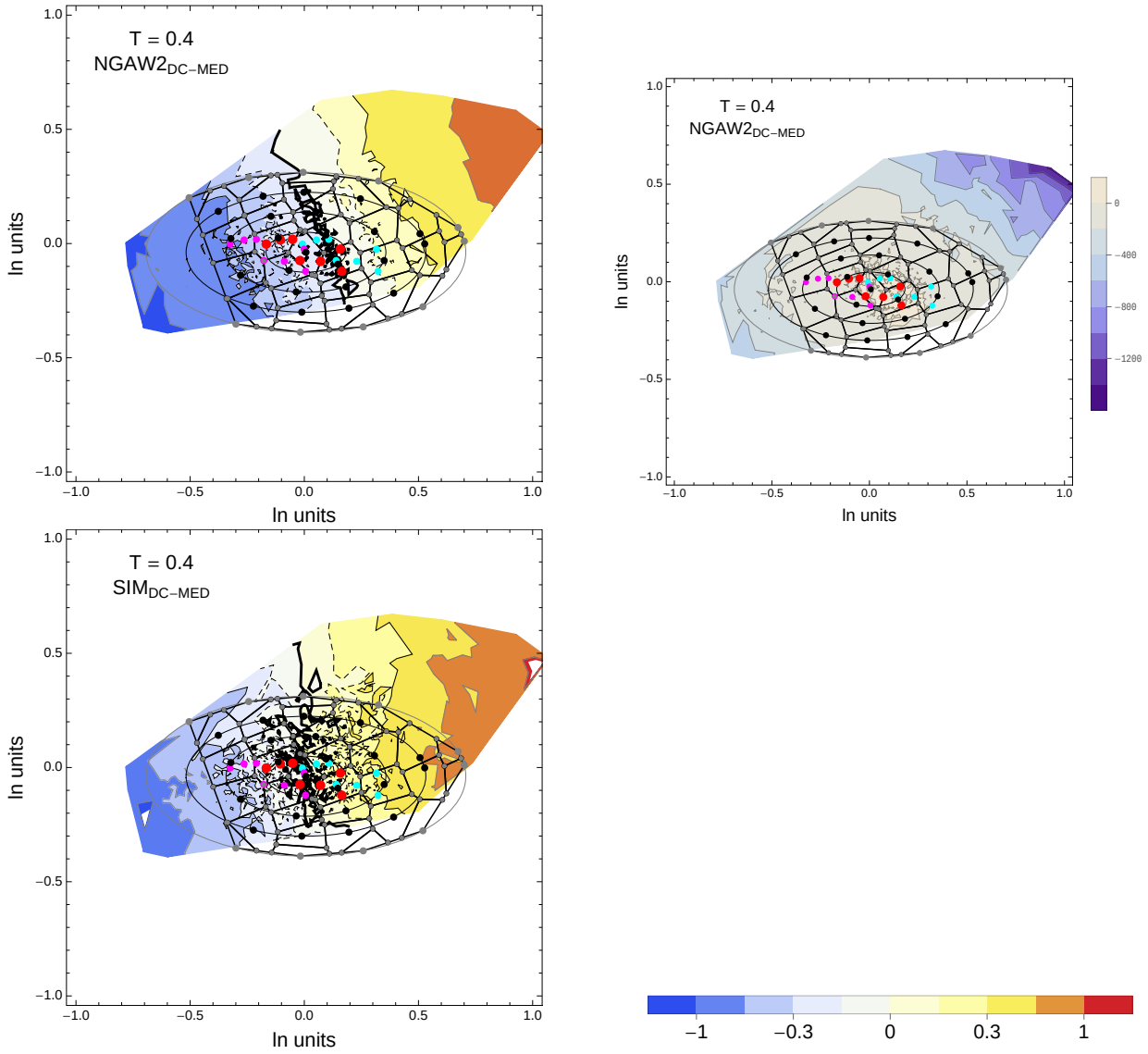



Figure 2.62: DCPPv4: Contour Plots of mean residuals (top left) and likelihood (top right) for the NGA$_{DC-MED}$ dataset, and mean residuals (bottom left) for the simulations (SIM$_{DC-MED}$). The Voronoi cells used for selecting and weighting models are shown as black lines. The original GMPEs are red dots,plus/minus uncertainty are magenta/cyan dots. The original GMPEs are red dots, plus/minus uncertainty are magenta/cyan dots. The contour for the zero residual is a thick black line, the -0.15/0.15 contours are dashed black lines and the -0.3/0.3 contours are thin black lines. For $T = 0.4$s.

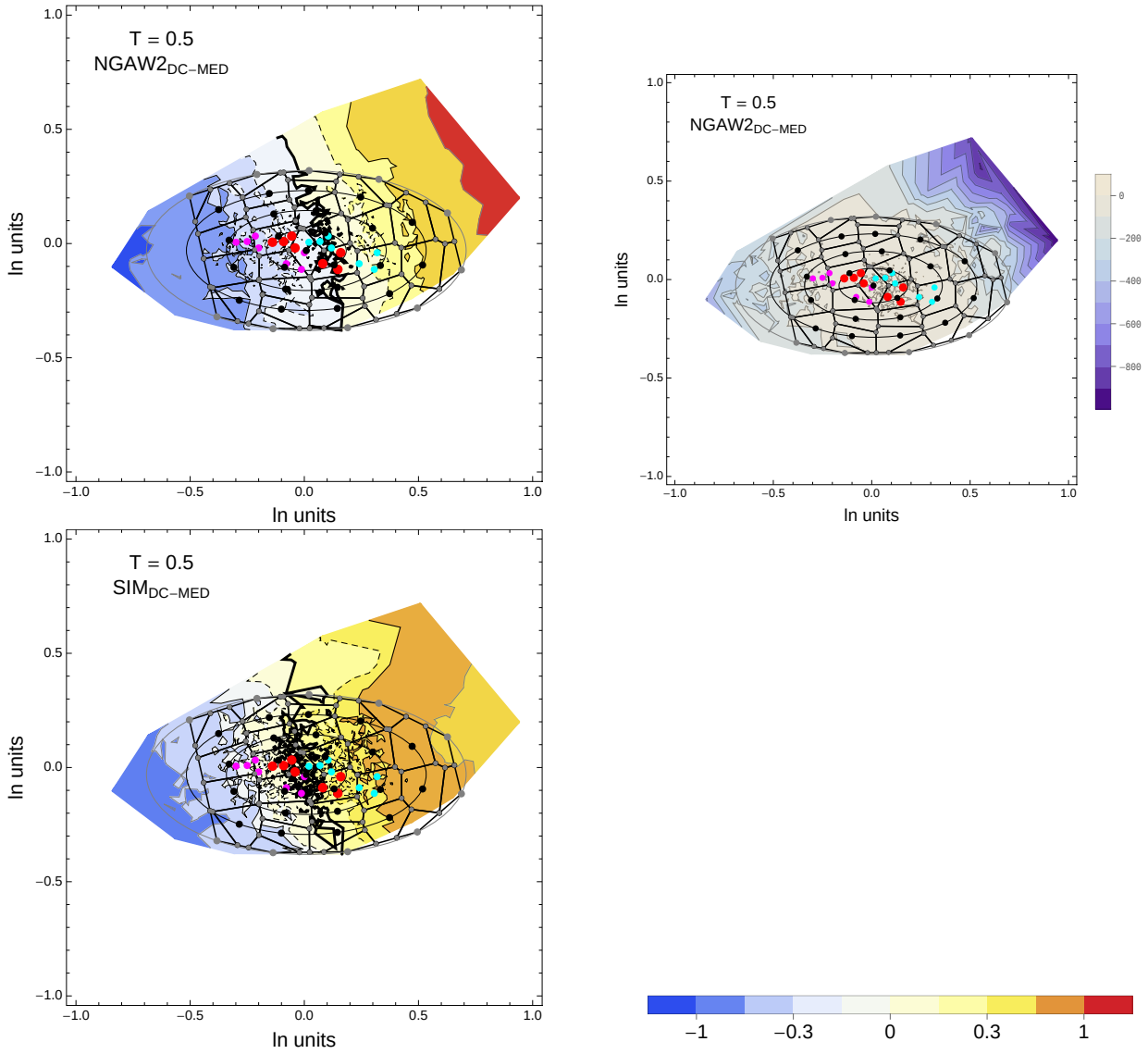



Figure 2.63: DCPPv4: Contour Plots of mean residuals (top left) and likelihood (top right) for the NGA$_{DC-MED}$ dataset, and mean residuals (bottom left) for the simulations (SIM$_{DC-MED}$). The Voronoi cells used for selecting and weighting models are shown as black lines. The original GMPEs are red dots,plus/minus uncertainty are magenta/cyan dots. The original GMPEs are red dots, plus/minus uncertainty are magenta/cyan dots. The contour for the zero residual is a thick black line, the -0.15/0.15 contours are dashed black lines and the -0.3/0.3 contours are thin black lines. For $T = 0.5$s.

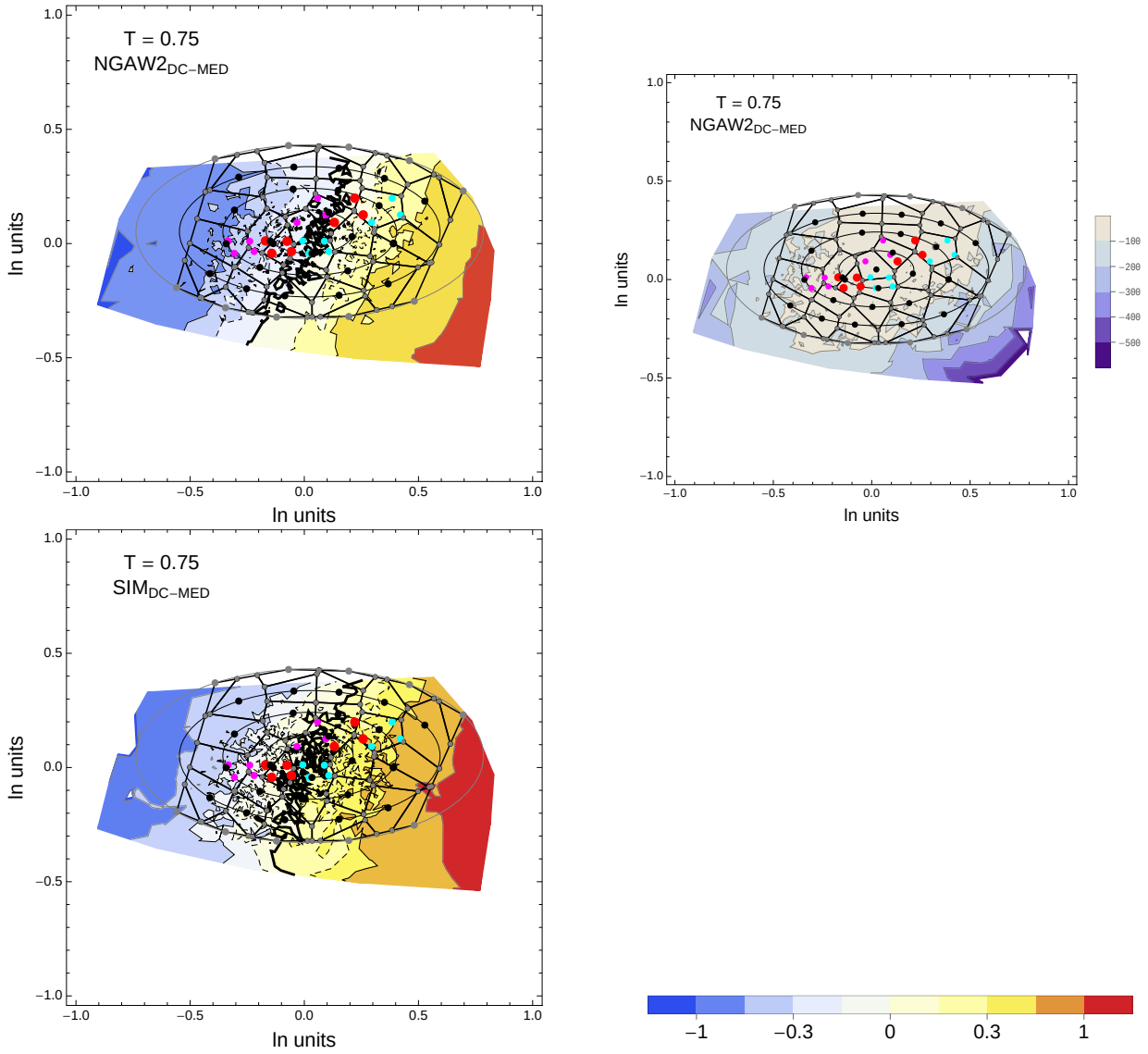



Figure 2.64: DCPPv4: Contour Plots of mean residuals (top left) and likelihood (top right) for the NGA$_{DC-MED}$ dataset, and mean residuals (bottom left) for the simulations (SIM$_{DC-MED}$). The Voronoi cells used for selecting and weighting models are shown as black lines. The original GMPEs are red dots,plus/minus uncertainty are magenta/cyan dots. The original GMPEs are red dots, plus/minus uncertainty are magenta/cyan dots. The contour for the zero residual is a thick black line, the -0.15/0.15 contours are dashed black lines and the -0.3/0.3 contours are thin black lines. For $T = 0.75$s.

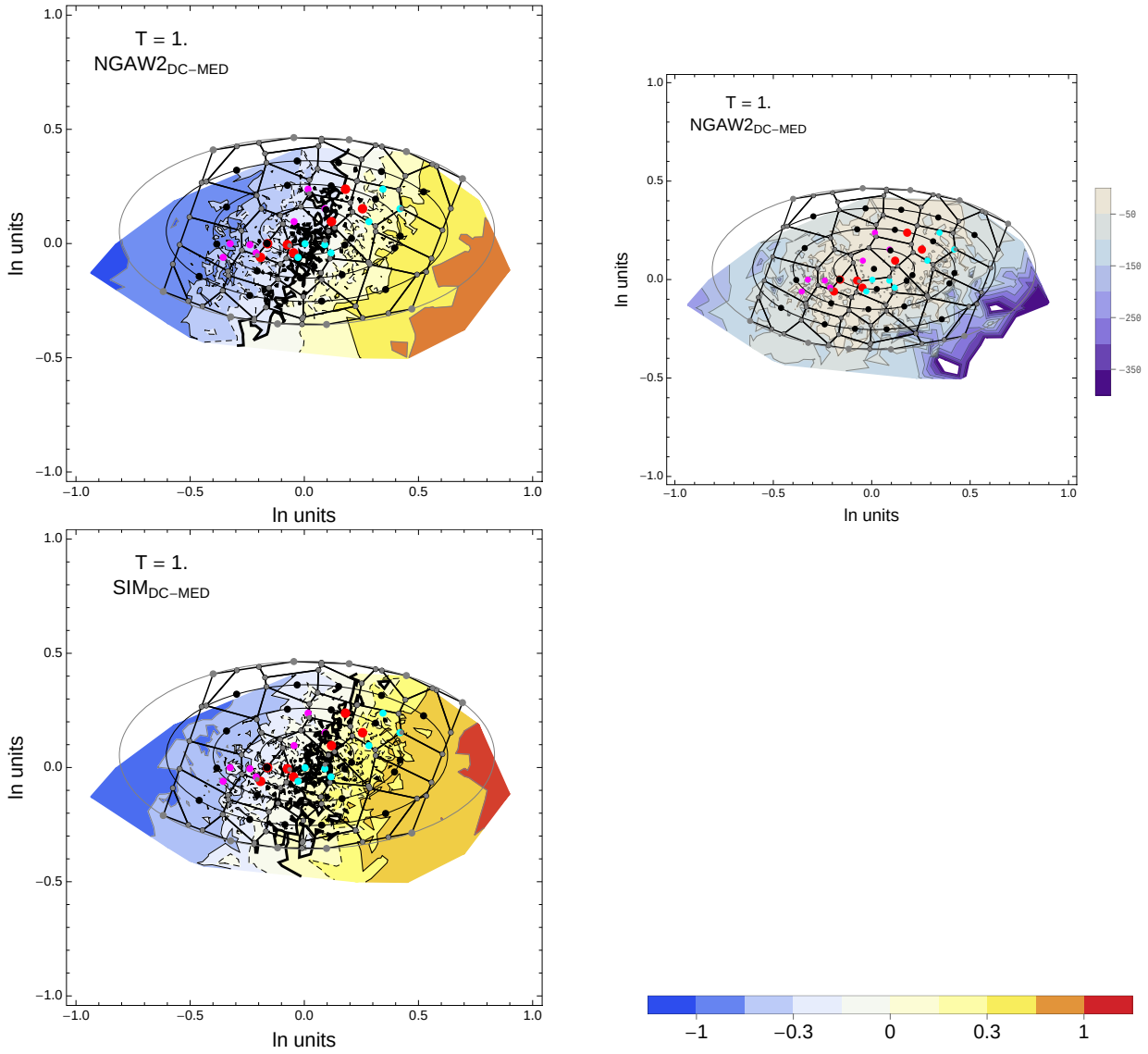



Figure 2.65: DCPPv4: Contour Plots of mean residuals (top left) and likelihood (top right) for the NGA$_{DC-MED}$ dataset, and mean residuals (bottom left) for the simulations (SIM$_{DC-MED}$). The Voronoi cells used for selecting and weighting models are shown as black lines. The original GMPEs are red dots,plus/minus uncertainty are magenta/cyan dots. The original GMPEs are red dots, plus/minus uncertainty are magenta/cyan dots. The contour for the zero residual is a thick black line, the -0.15/0.15 contours are dashed black lines and the -0.3/0.3 contours are thin black lines. For $T = 1$.s.

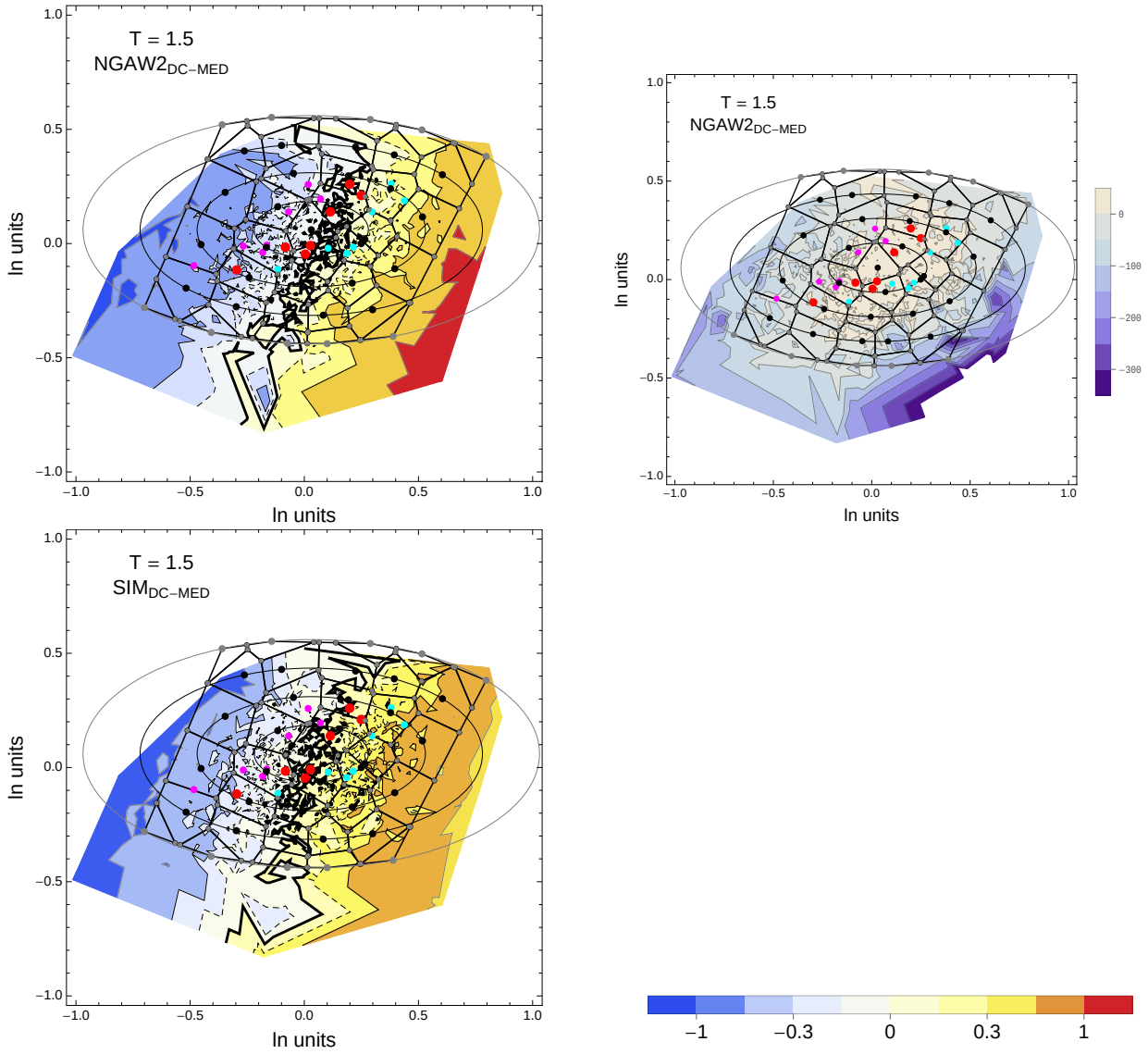



Figure 2.66: DCPPv4: Contour Plots of mean residuals (top left) and likelihood (top right) for the NGA$_{DC-MED}$ dataset, and mean residuals (bottom left) for the simulations (SIM$_{DC-MED}$). The Voronoi cells used for selecting and weighting models are shown as black lines. The original GMPEs are red dots,plus/minus uncertainty are magenta/cyan dots. The original GMPEs are red dots, plus/minus uncertainty are magenta/cyan dots. The contour for the zero residual is a thick black line, the -0.15/0.15 contours are dashed black lines and the -0.3/0.3 contours are thin black lines. For $T = 1.5$s.

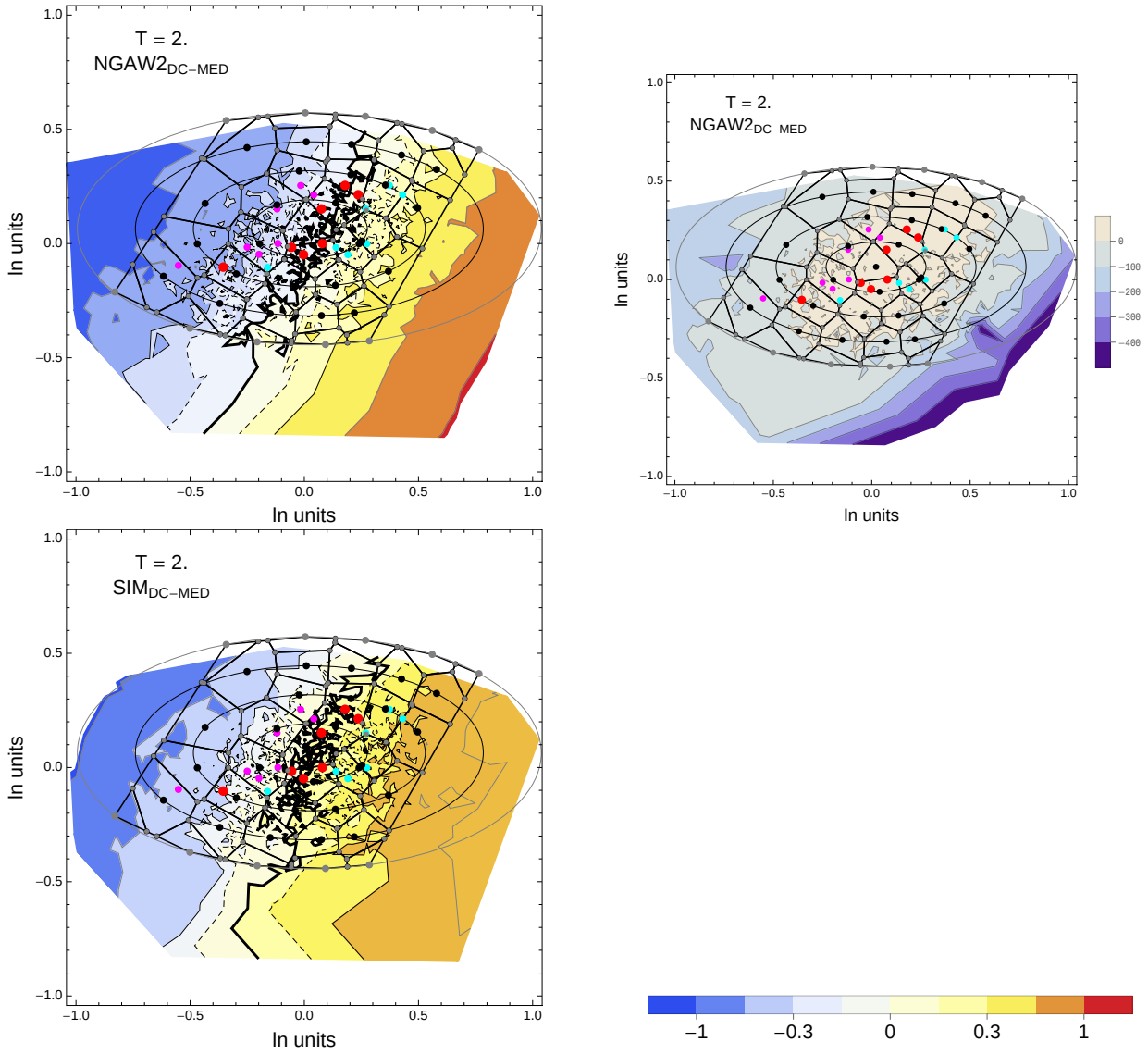



Figure 2.67: DCPPv4: Contour Plots of mean residuals (top left) and likelihood (top right) for the NGA$_{DC-MED}$ dataset, and mean residuals (bottom left) for the simulations (SIM$_{DC-MED}$). The Voronoi cells used for selecting and weighting models are shown as black lines. The original GMPEs are red dots,plus/minus uncertainty are magenta/cyan dots. The original GMPEs are red dots, plus/minus uncertainty are magenta/cyan dots. The contour for the zero residual is a thick black line, the -0.15/0.15 contours are dashed black lines and the -0.3/0.3 contours are thin black lines. For $T = 2$.s.

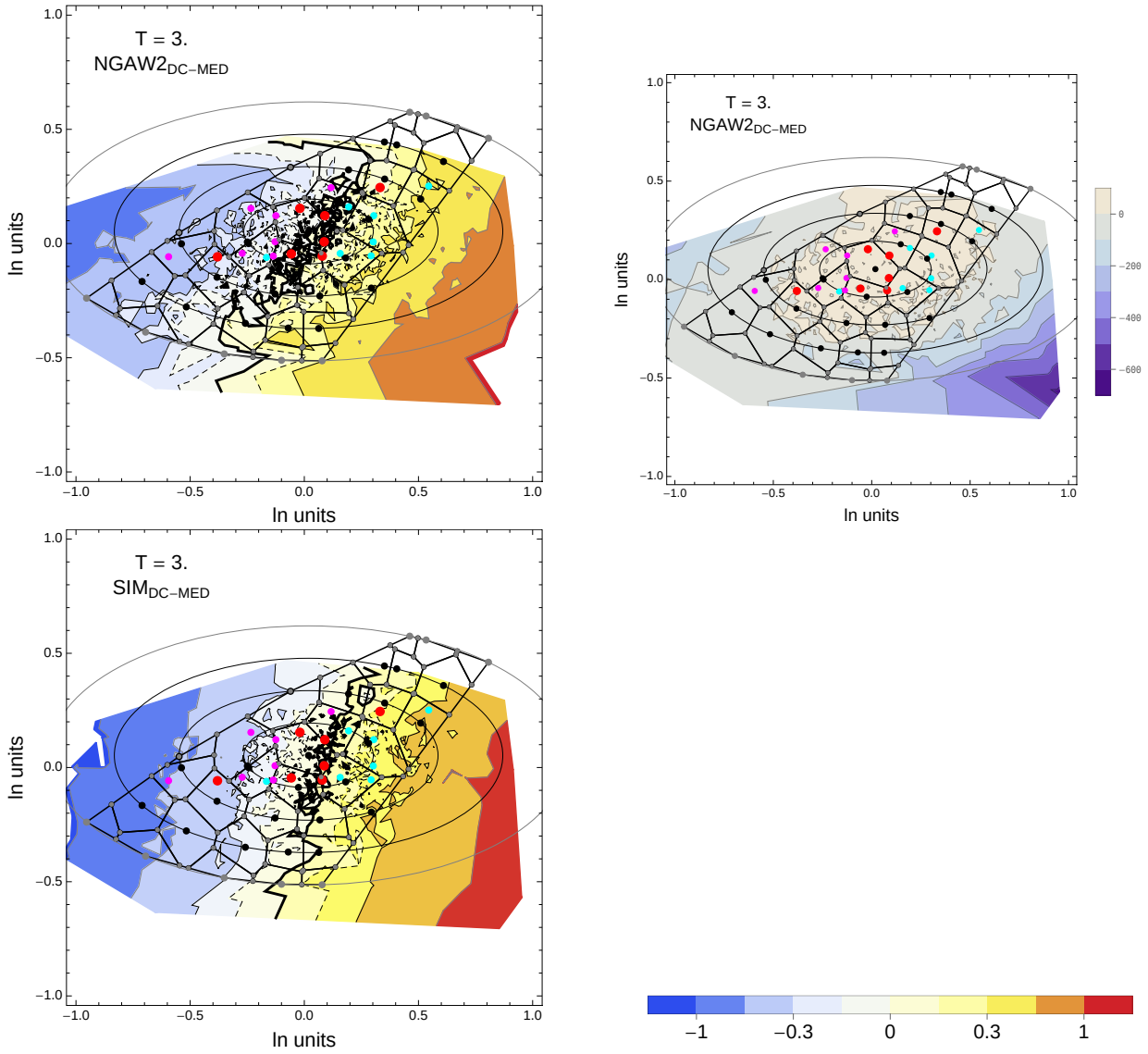



Figure 2.68: DCPPv4: Contour Plots of mean residuals (top left) and likelihood (top right) for the NGA$_{DC-MED}$ dataset, and mean residuals (bottom left) for the simulations (SIM$_{DC-MED}$). The Voronoi cells used for selecting and weighting models are shown as black lines. The original GMPEs are red dots,plus/minus uncertainty are magenta/cyan dots. The original GMPEs are red dots, plus/minus uncertainty are magenta/cyan dots. The contour for the zero residual is a thick black line, the -0.15/0.15 contours are dashed black lines and the -0.3/0.3 contours are thin black lines. For $T = 3$.s.

### 2.1.5 Hazard Curves

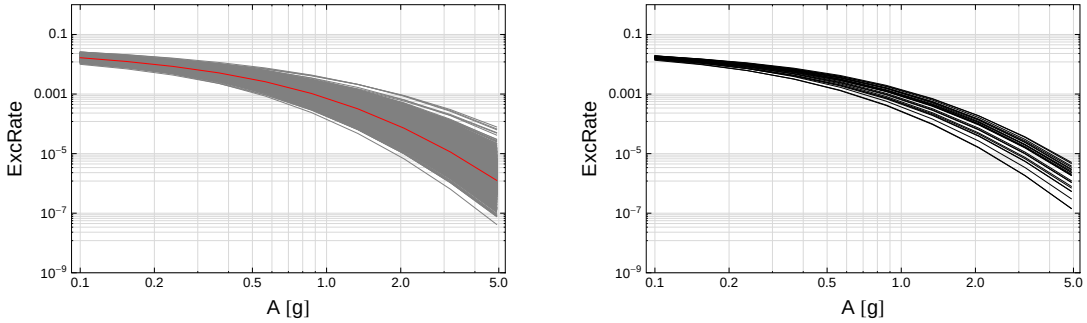



Figure 2.69: DCPPv4: Hazard curves, calculated for a simple source model for DCPP4. Left: 2000 hazard curves for all sampled models (gray) and the center model of the ModelA distribution (red); Right: hazard curves of selected models. For $T = 0.01$s.

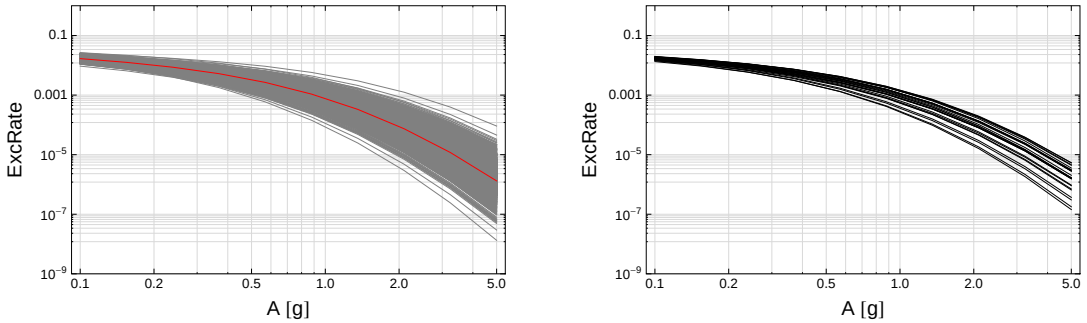



Figure 2.70: DCPPv4: Hazard curves, calculated for a simple source model for DCPP4. Left: 2000 hazard curves for all sampled models (gray) and the center model of the ModelA distribution (red); Right: hazard curves of selected models. For $T = 0.02$s.

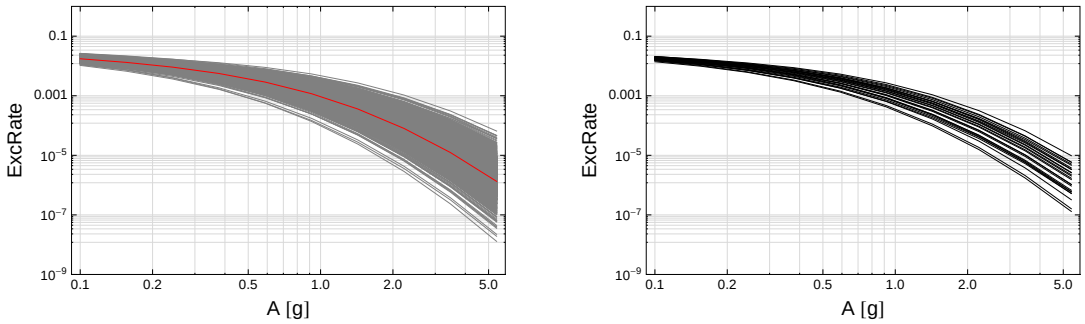



Figure 2.71: DCPPv4: Hazard curves, calculated for a simple source model for DCPP4. Left: 2000 hazard curves for all sampled models (gray) and the center model of the ModelA distribution (red); Right: hazard curves of selected models. For $T = 0.03$s.

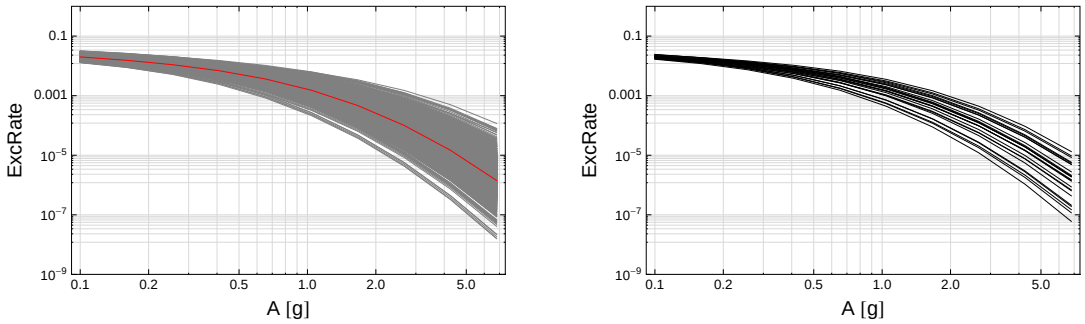



Figure 2.72: DCPPv4: Hazard curves, calculated for a simple source model for DCPP4. Left: 2000 hazard curves for all sampled models (gray) and the center model of the ModelA distribution (red); Right: hazard curves of selected models. For $T = 0.05$s.

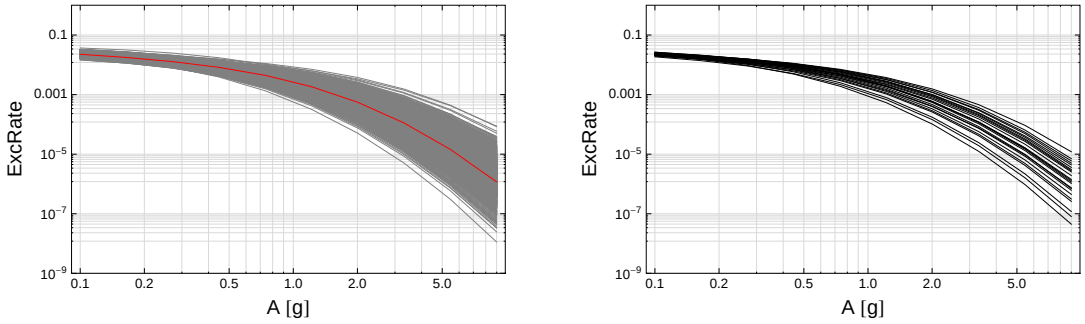



Figure 2.73: DCPPv4: Hazard curves, calculated for a simple source model for DCPP4. Left: 2000 hazard curves for all sampled models (gray) and the center model of the ModelA distribution (red); Right: hazard curves of selected models. For $T = 0.075$s.

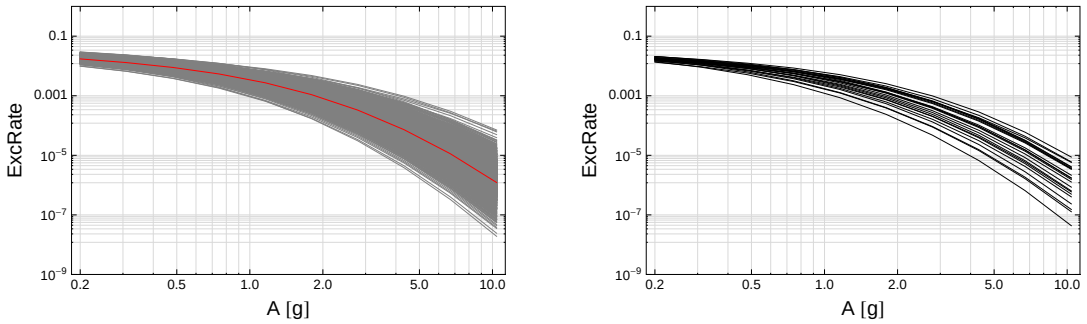



Figure 2.74: DCPPv4: Hazard curves, calculated for a simple source model for DCPP4. Left: 2000 hazard curves for all sampled models (gray) and the center model of the ModelA distribution (red); Right: hazard curves of selected models. For $T = 0.1$s.

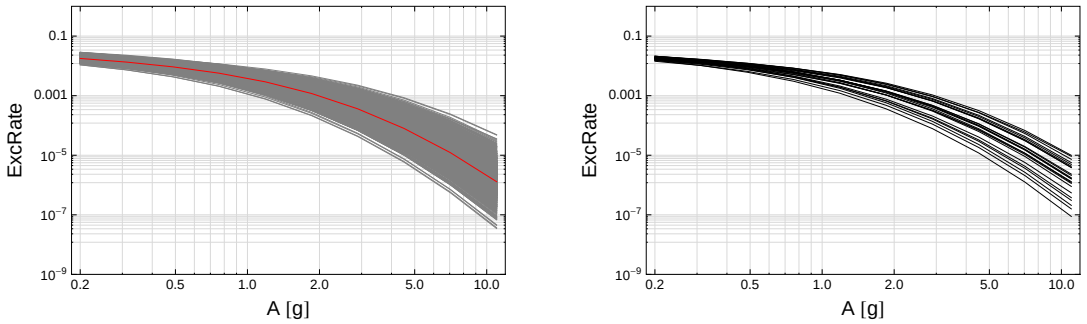



Figure 2.75: DCPPv4: Hazard curves, calculated for a simple source model for DCPP4. Left: 2000 hazard curves for all sampled models (gray) and the center model of the ModelA distribution (red); Right: hazard curves of selected models. For $T = 0.15$s.

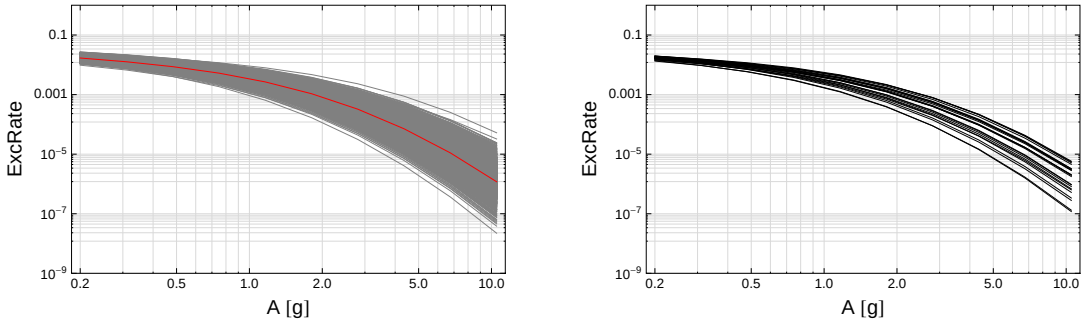



Figure 2.76: DCPPv4: Hazard curves, calculated for a simple source model for DCPP4. Left: 2000 hazard curves for all sampled models (gray) and the center model of the ModelA distribution (red); Right: hazard curves of selected models. For $T = 0.2$s.

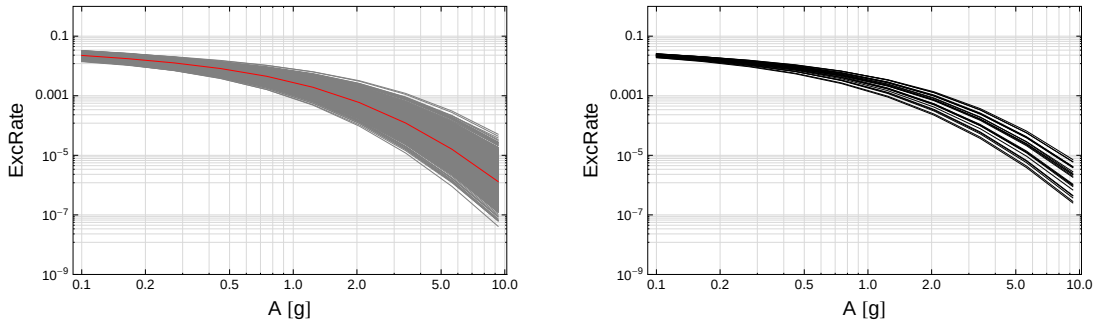



Figure 2.77: DCPPv4: Hazard curves, calculated for a simple source model for DCPP4. Left: 2000 hazard curves for all sampled models (gray) and the center model of the ModelA distribution (red); Right: hazard curves of selected models. For $T = 0.25$s.

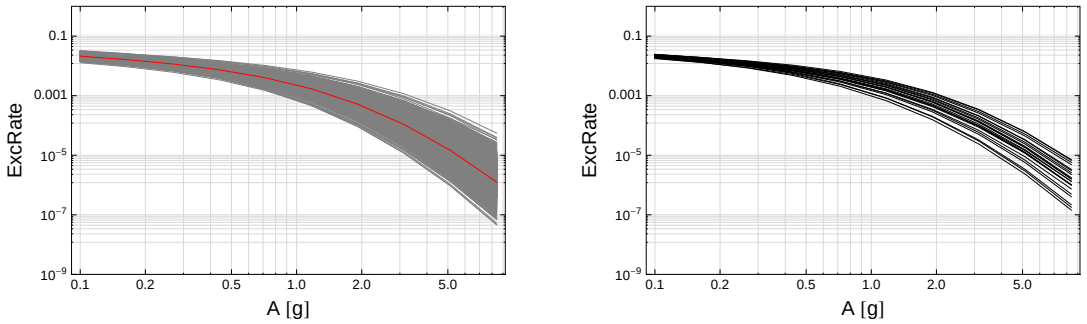



Figure 2.78: DCPPv4: Hazard curves, calculated for a simple source model for DCPP4. Left: 2000 hazard curves for all sampled models (gray) and the center model of the ModelA distribution (red); Right: hazard curves of selected models. For $T = 0.3$s.

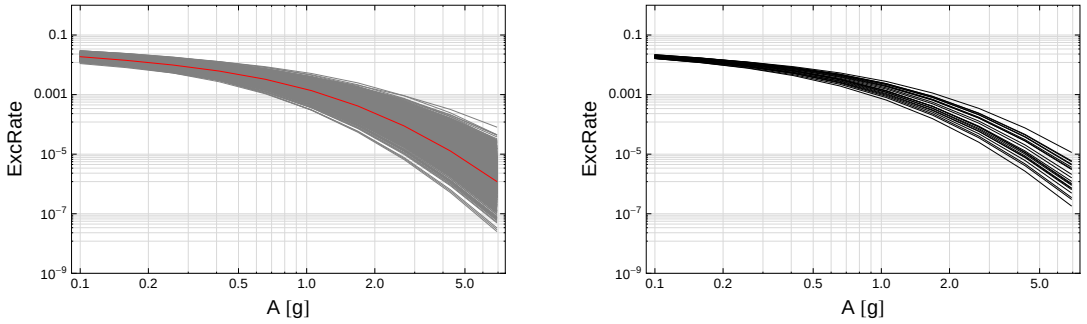



Figure 2.79: DCPPv4: Hazard curves, calculated for a simple source model for DCPP4. Left: 2000 hazard curves for all sampled models (gray) and the center model of the ModelA distribution (red); Right: hazard curves of selected models. For $T = 0.4$s.

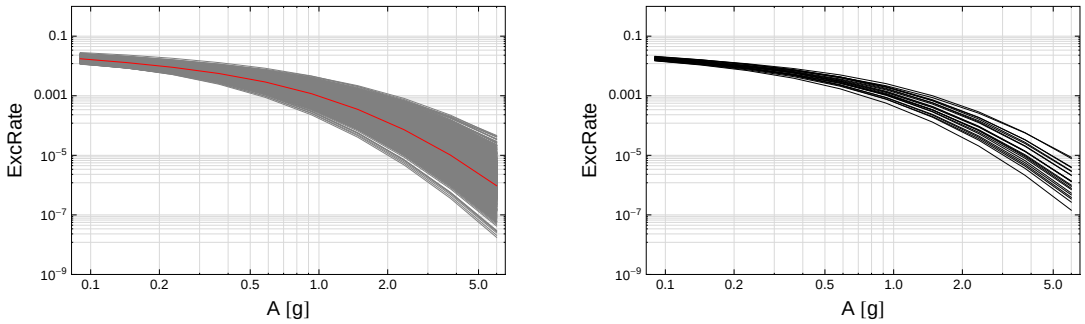



Figure 2.80: DCPPv4: Hazard curves, calculated for a simple source model for DCPP4. Left: 2000 hazard curves for all sampled models (gray) and the center model of the ModelA distribution (red); Right: hazard curves of selected models. For $T = 0.5$s.

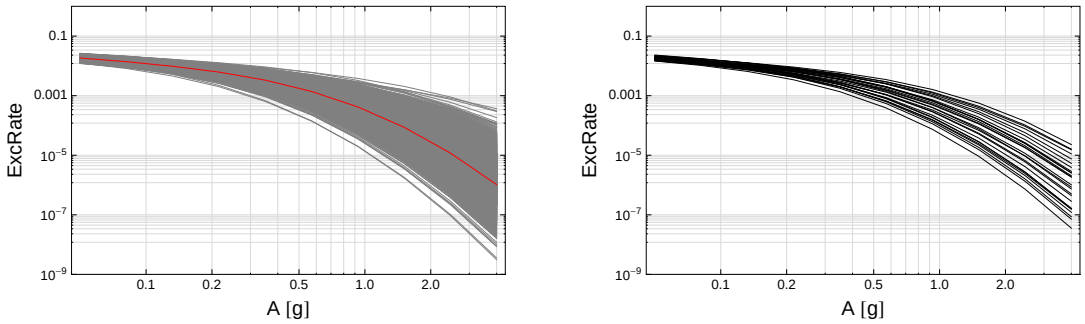



Figure 2.81: DCPPv4: Hazard curves, calculated for a simple source model for DCPP4. Left: 2000 hazard curves for all sampled models (gray) and the center model of the ModelA distribution (red); Right: hazard curves of selected models. For $T = 0.75$s.

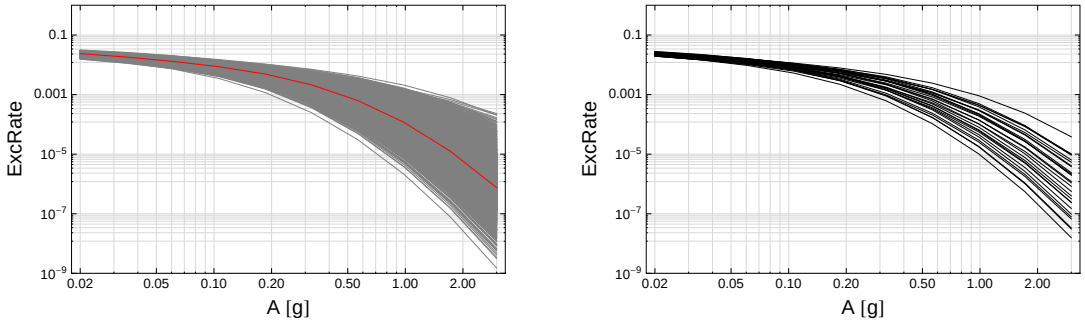



Figure 2.82: DCPPv4: Hazard curves, calculated for a simple source model for DCPP4. Left: 2000 hazard curves for all sampled models (gray) and the center model of the ModelA distribution (red); Right: hazard curves of selected models. For $T = 1$.s.

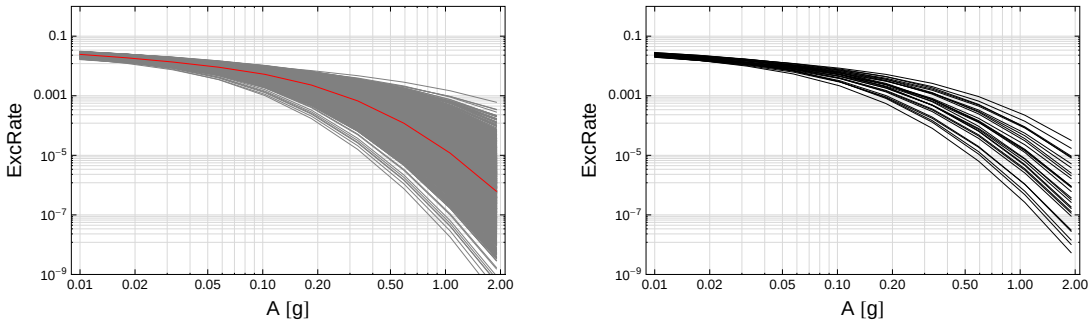



Figure 2.83: DCPPv4: Hazard curves, calculated for a simple source model for DCPP4. Left: 2000 hazard curves for all sampled models (gray) and the center model of the ModelA distribution (red); Right: hazard curves of selected models. For $T = 1.5$s.

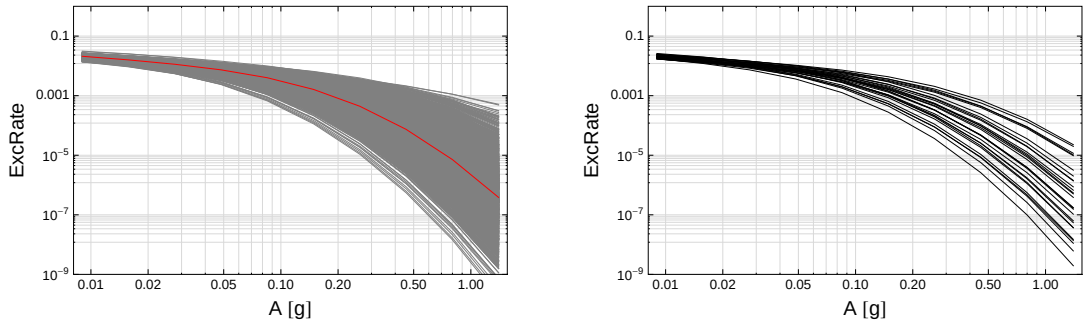



Figure 2.84: DCPPv4: Hazard curves, calculated for a simple source model for DCPP4. Left: 2000 hazard curves for all sampled models (gray) and the center model of the ModelA distribution (red); Right: hazard curves of selected models. For $T = 2$.s.

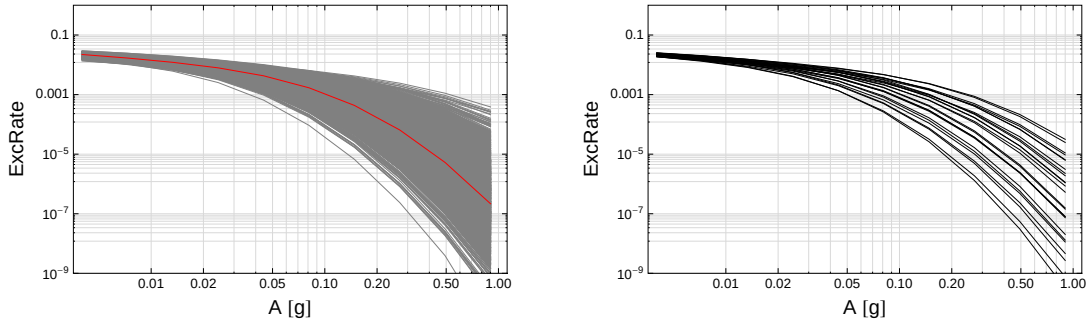



Figure 2.85: DCPPv4: Hazard curves, calculated for a simple source model for DCPP4. Left: 2000 hazard curves for all sampled models (gray) and the center model of the ModelA distribution (red); Right: hazard curves of selected models. For $T = 3$.s.

### 2.1.6 CDF Plots

In this section, the cumulative distribution function (CDF) of the original GMPEs and the selected models (based on the different sets of weights) is shown. The original GMPEs are equal weighted, their weight is split 0.8/0.1/0.1 for their original form and the two uncertainty models. The distributions for the selected common form models are based on the different weights: the weight based on residuals (wResidual) and likelihood (wLL) w.r.t. the $\text{NGA}_{DC-MED}$ dataset and the simulations $\text{SIM}_{DC-MED}$ dataset, and the weight based on the value of the PDF (wPrior).

**T = 0.01s**

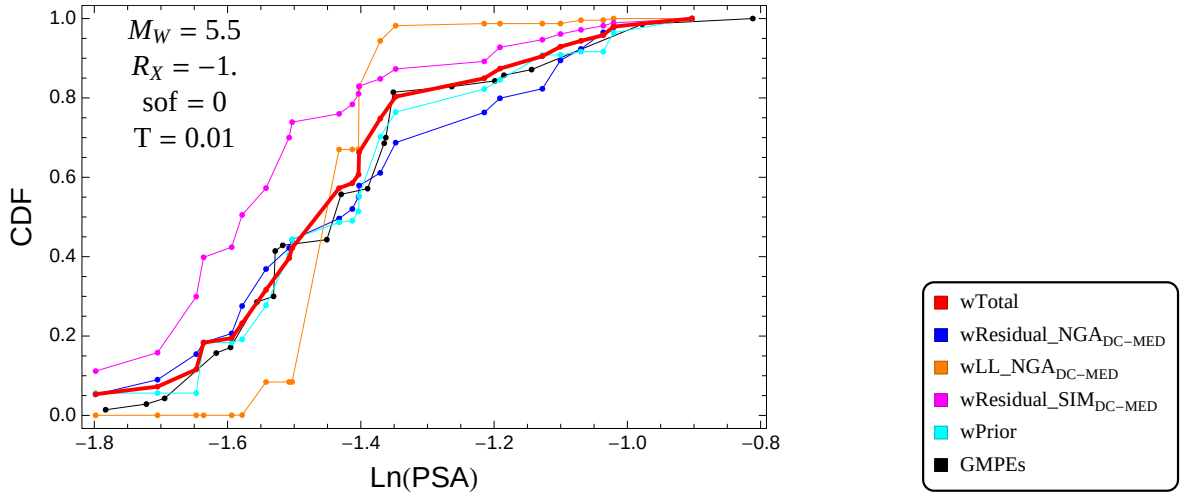



Figure 2.86: DCPPv4: Cumulative distribution function of GMPEs (black) and selected models, for different sets of weights, for a scenario with $M = 5.5$, $R_x = -1.$, $F = 0$, and $T = 0.01$s

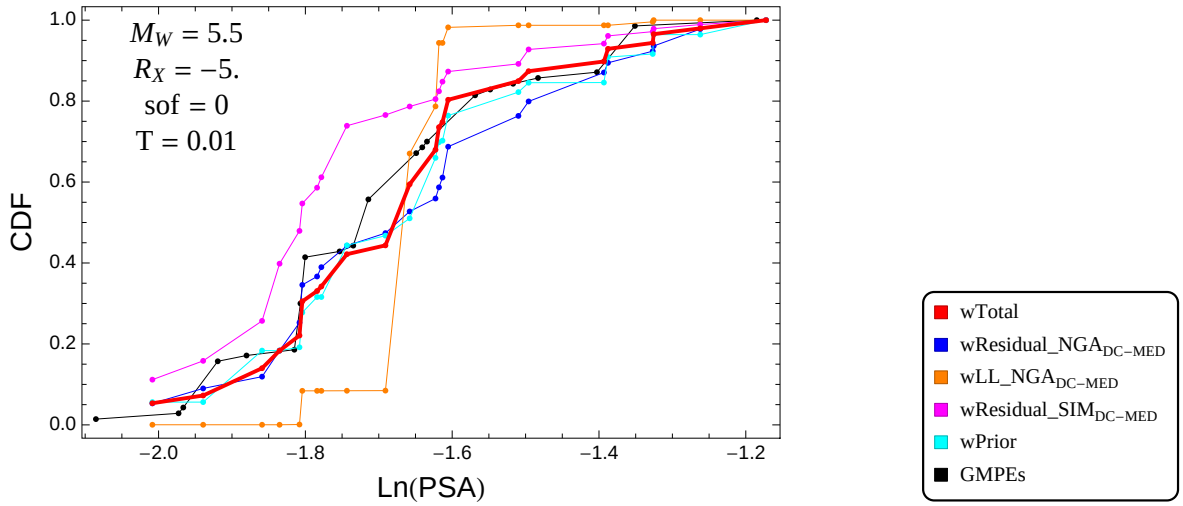



Figure 2.87: DCPPv4: Cumulative distribution function of GMPEs (black) and selected models, for different sets of weights, for a scenario with $M = 5.5$, $R_x = -5.$, $F = 0$, and $T = 0.01$s

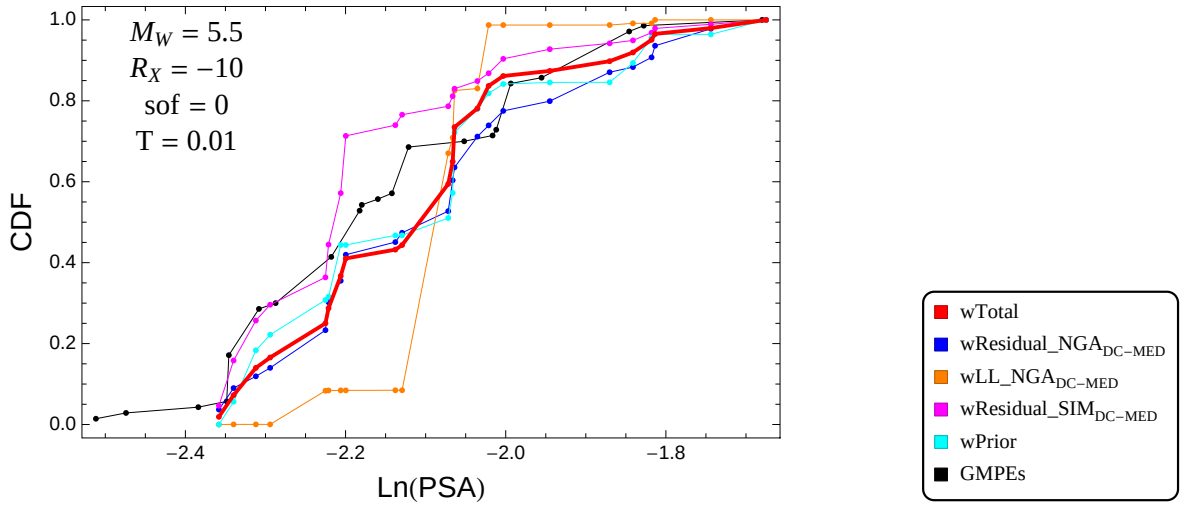



Figure 2.88: DCPPv4: Cumulative distribution function of GMPEs (black) and selected models, for different sets of weights, for a scenario with $M = 5.5$, $R_x = -10$, $F = 0$, and $T = 0.01$s

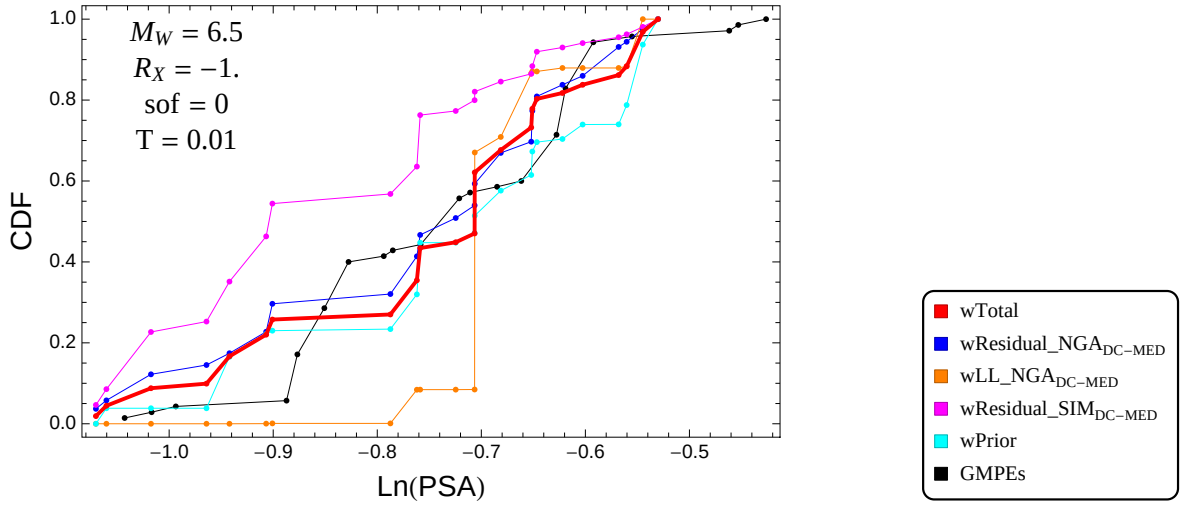



Figure 2.89: DCPPv4: Cumulative distribution function of GMPEs (black) and selected models, for different sets of weights, for a scenario with $M = 6.5$, $R_x = -1.$, $F = 0$, and $T = 0.01$s

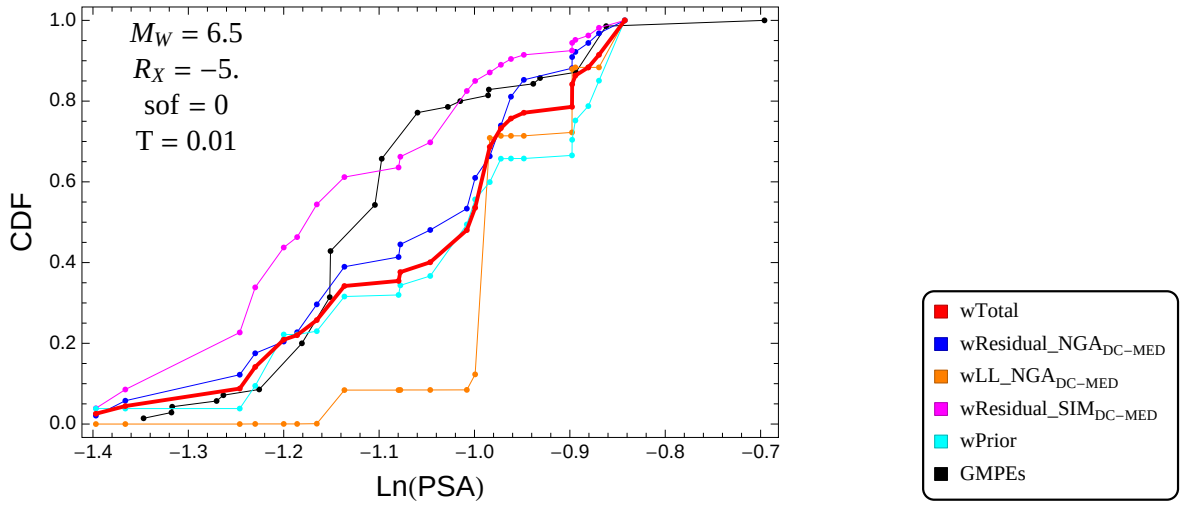



Figure 2.90: DCPPv4: Cumulative distribution function of GMPEs (black) and selected models, for different sets of weights, for a scenario with $M = 6.5$, $R_x = -5.$, $F = 0$, and $T = 0.01$s

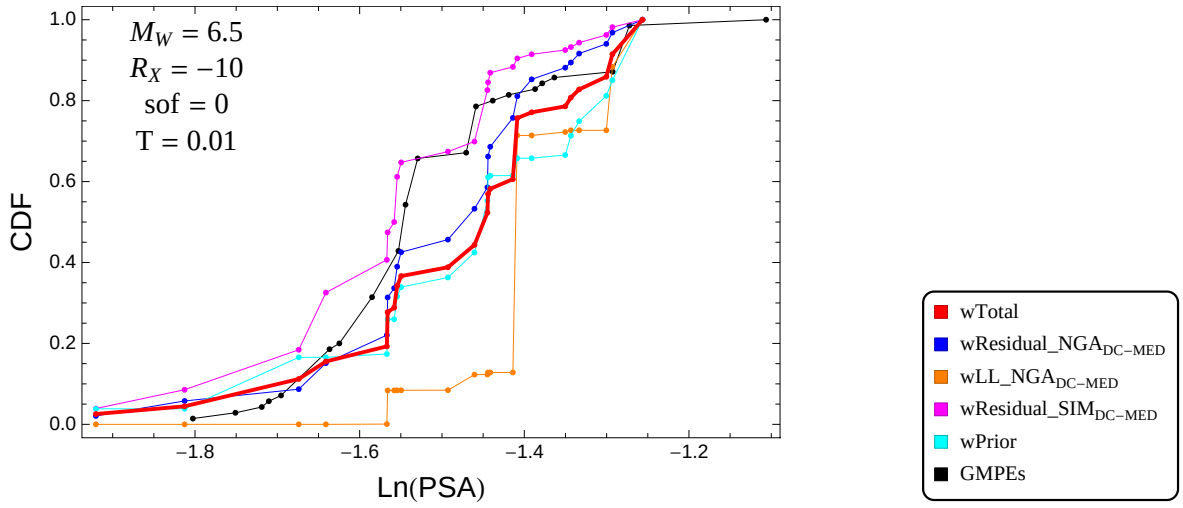



Figure 2.91: DCPPv4: Cumulative distribution function of GMPEs (black) and selected models, for different sets of weights, for a scenario with $M = 6.5$, $R_x = -10$, $F = 0$, and $T = 0.01$s

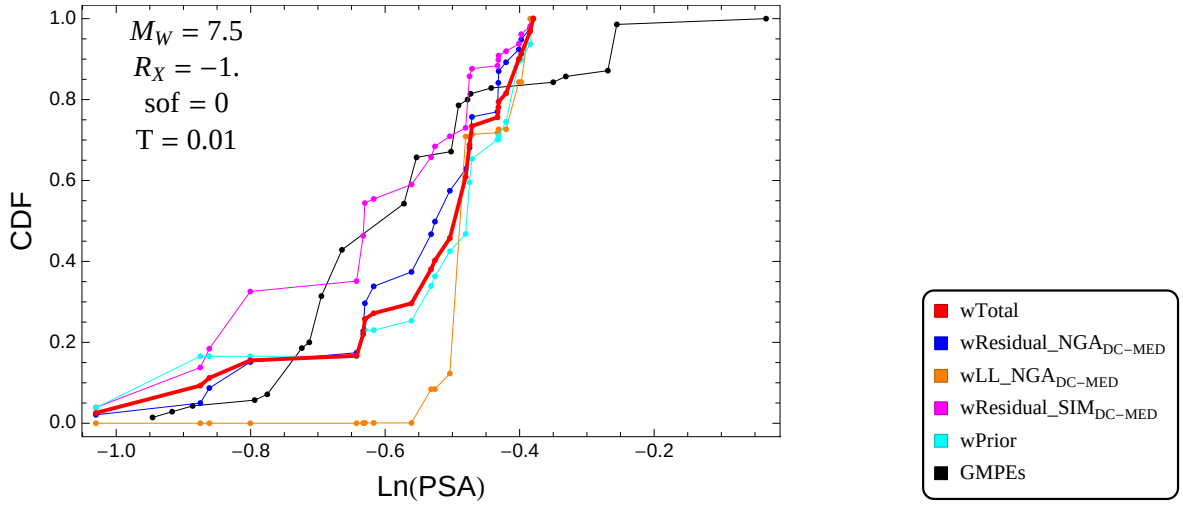



Figure 2.92: DCPPv4: Cumulative distribution function of GMPEs (black) and selected models, for different sets of weights, for a scenario with $M = 7.5$, $R_x = -1.$, $F = 0$, and $T = 0.01$s

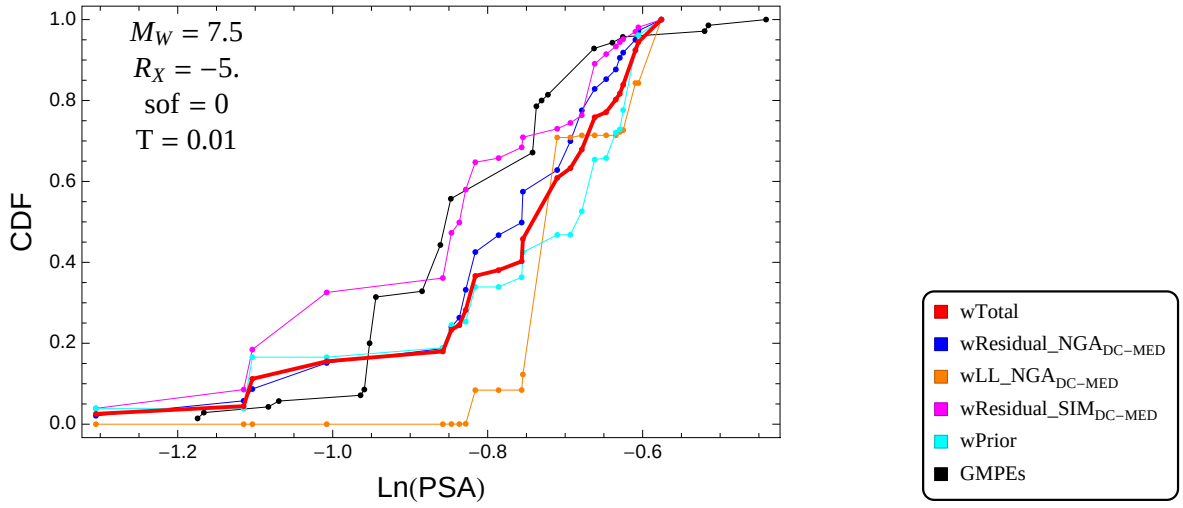



Figure 2.93: DCPPv4: Cumulative distribution function of GMPEs (black) and selected models, for different sets of weights, for a scenario with $M = 7.5$, $R_x = -5.$, $F = 0$, and $T = 0.01$s

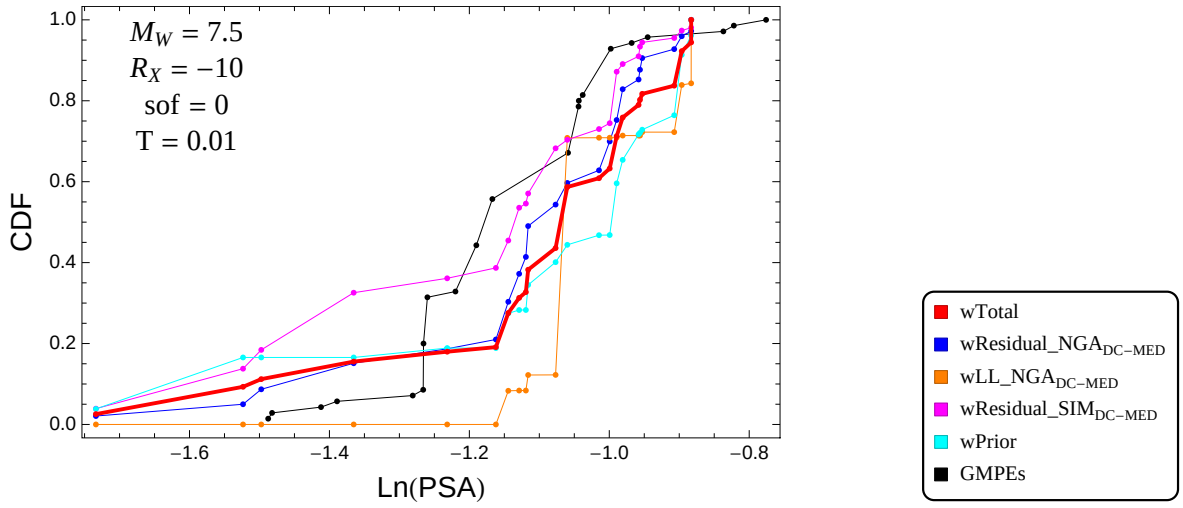



Figure 2.94: DCPPv4: Cumulative distribution function of GMPEs (black) and selected models, for different sets of weights, for a scenario with $M = 7.5$, $R_x = -10$, $F = 0$, and $T = 0.01$s

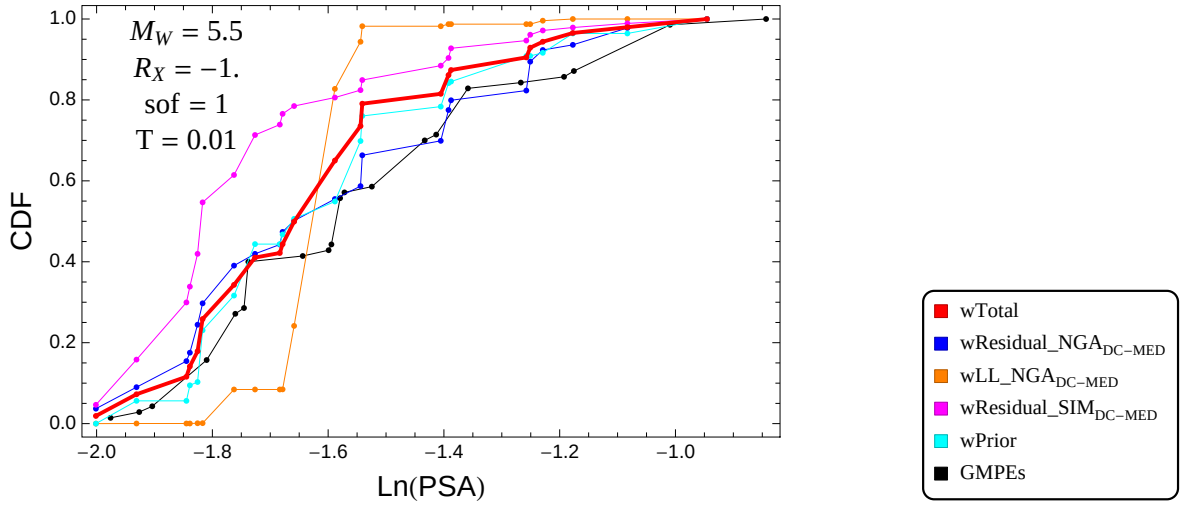



Figure 2.95: DCPPv4: Cumulative distribution function of GMPEs (black) and selected models, for different sets of weights, for a scenario with $M = 5.5$, $R_x = -1.$, $F = 1$, and $T = 0.01$s

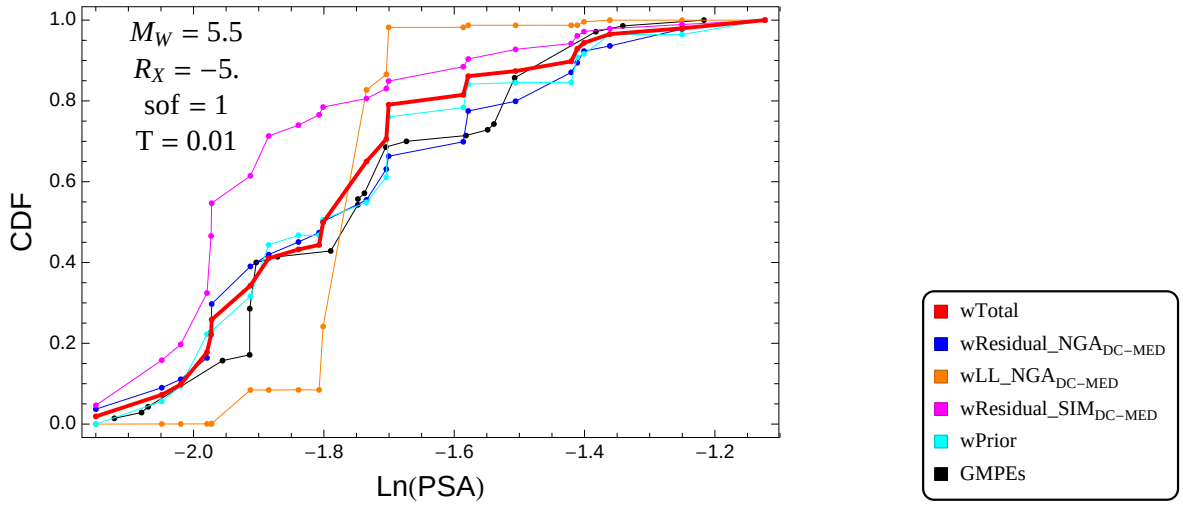



Figure 2.96: DCPPv4: Cumulative distribution function of GMPEs (black) and selected models, for different sets of weights, for a scenario with $M = 5.5$, $R_x = -5.$, $F = 1$, and $T = 0.01$s

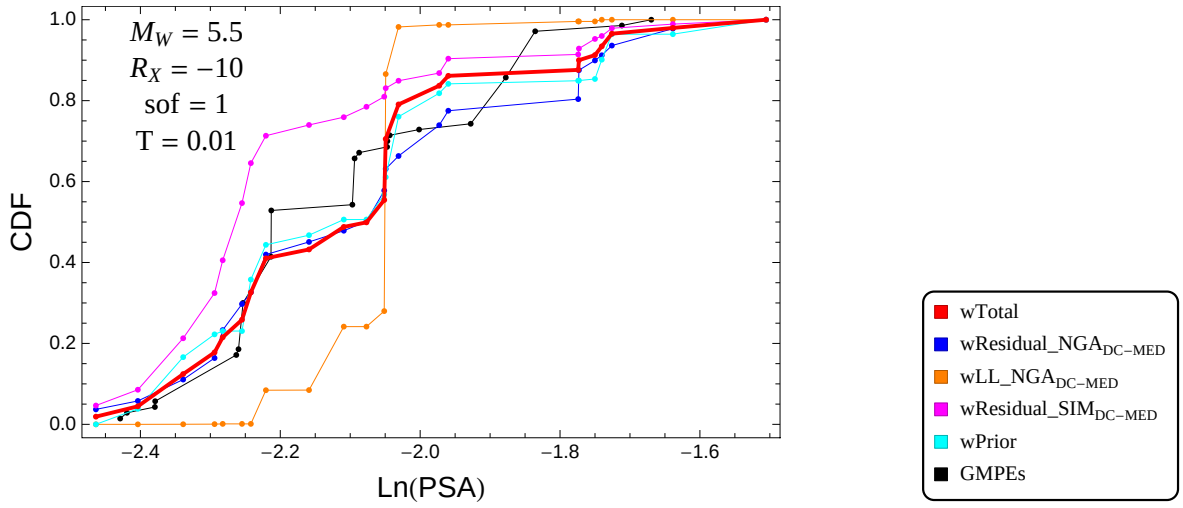



Figure 2.97: DCPPv4: Cumulative distribution function of GMPEs (black) and selected models, for different sets of weights, for a scenario with $M = 5.5$, $R_x = -10$, $F = 1$, and $T = 0.01$s

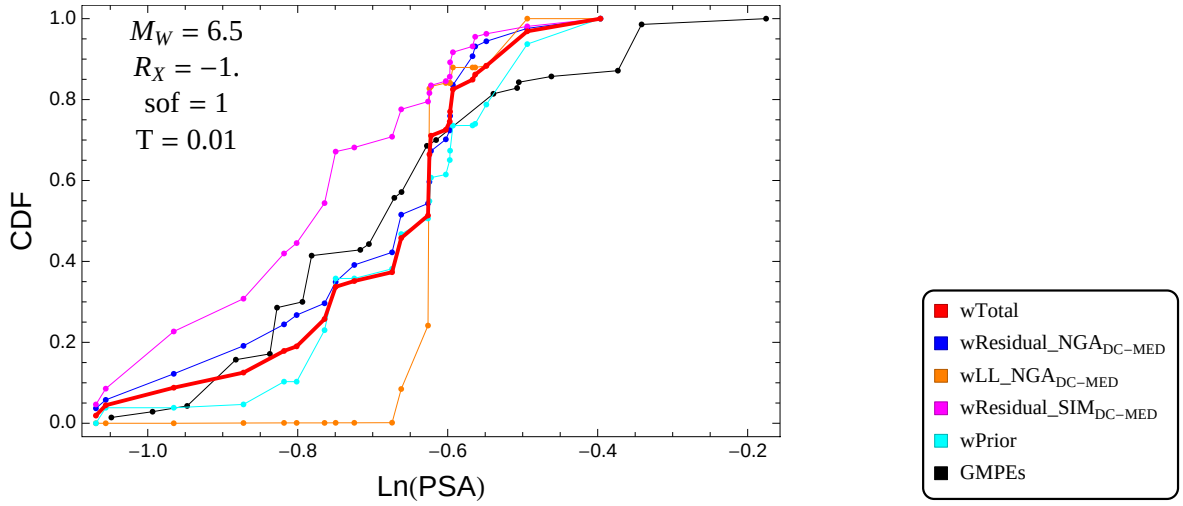



Figure 2.98: DCPPv4: Cumulative distribution function of GMPEs (black) and selected models, for different sets of weights, for a scenario with $M = 6.5$, $R_x = -1.$, $F = 1$, and $T = 0.01$s

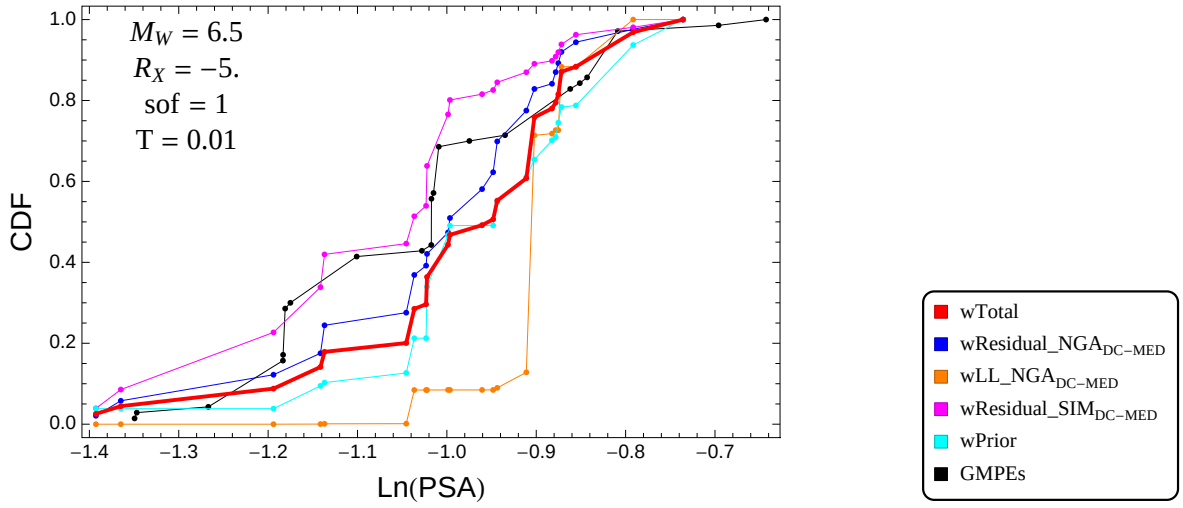



Figure 2.99: DCPPv4: Cumulative distribution function of GMPEs (black) and selected models, for different sets of weights, for a scenario with $M = 6.5$, $R_x = -5.$, $F = 1$, and $T = 0.01$s

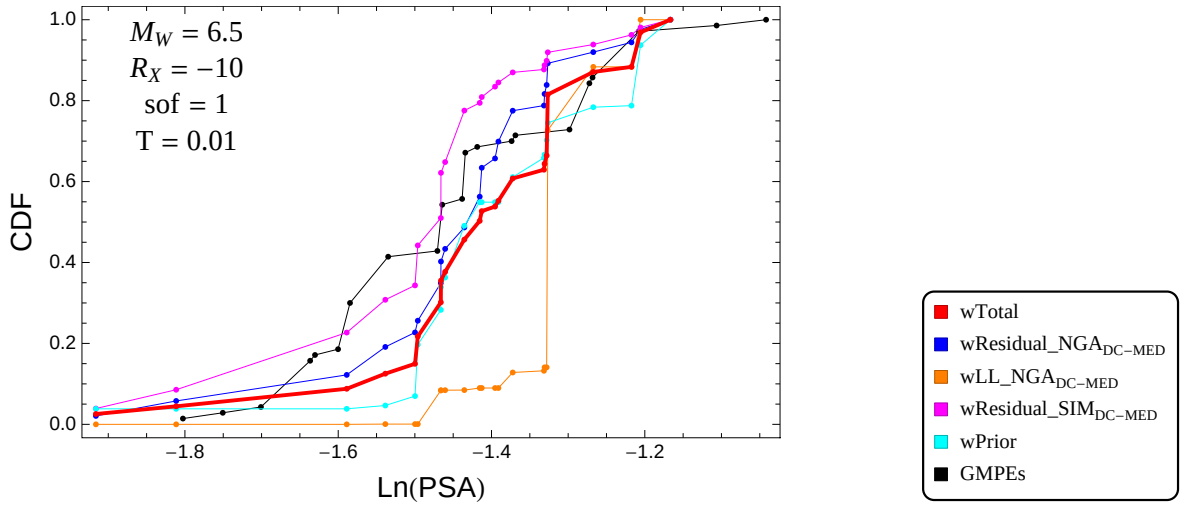



Figure 2.100: DCPPv4: Cumulative distribution function of GMPEs (black) and selected models, for different sets of weights, for a scenario with $M = 6.5$, $R_x = -10$, $F = 1$, and $T = 0.01$s

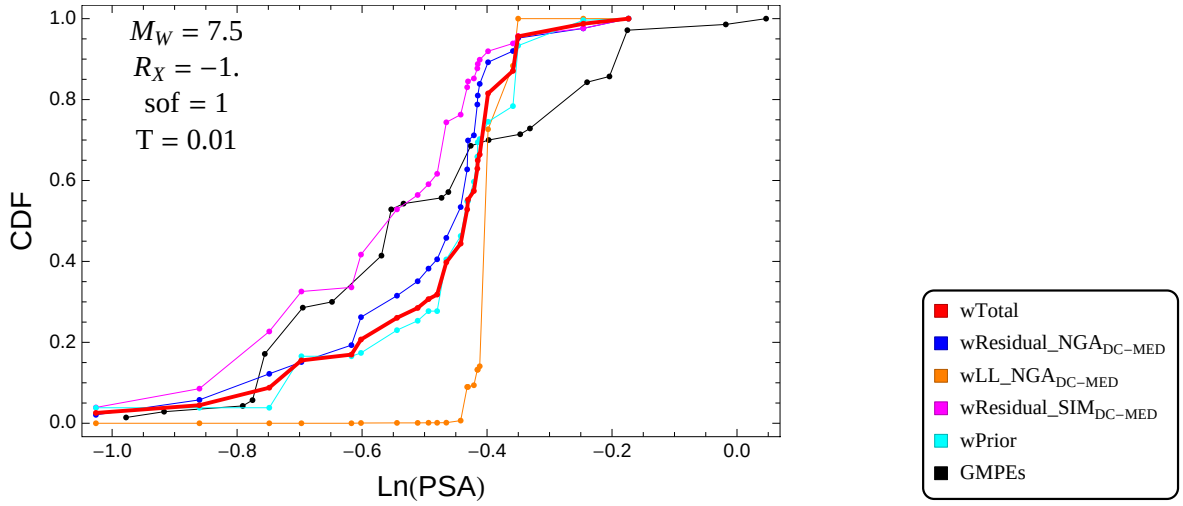



Figure 2.101: DCPPv4: Cumulative distribution function of GMPEs (black) and selected models, for different sets of weights, for a scenario with $M = 7.5$, $R_x = -1.$, $F = 1$, and $T = 0.01$s

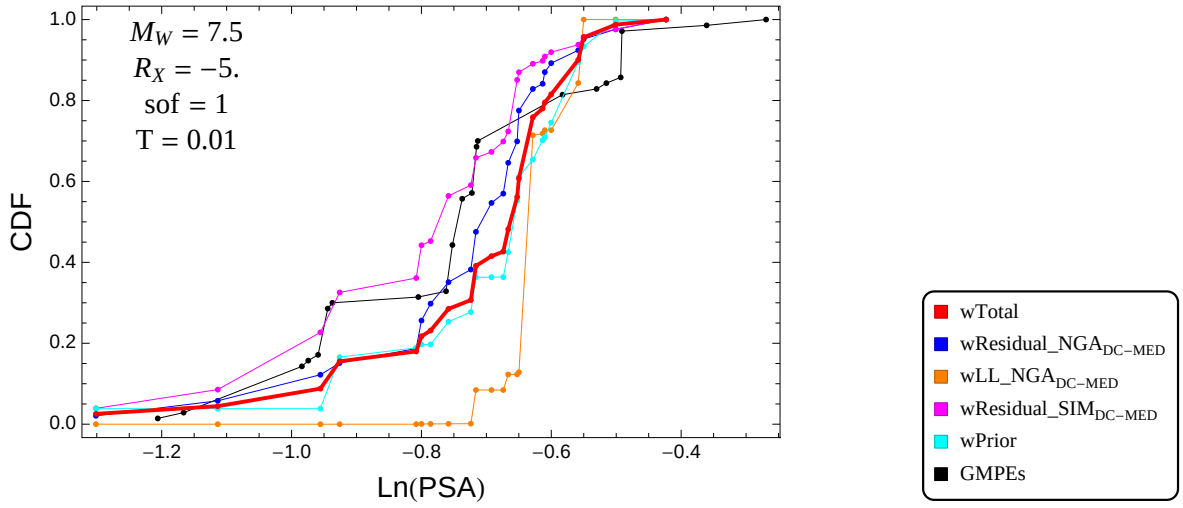



Figure 2.102: DCPPv4: Cumulative distribution function of GMPEs (black) and selected models, for different sets of weights, for a scenario with $M = 7.5$, $R_x = -5.$, $F = 1$, and $T = 0.01$s

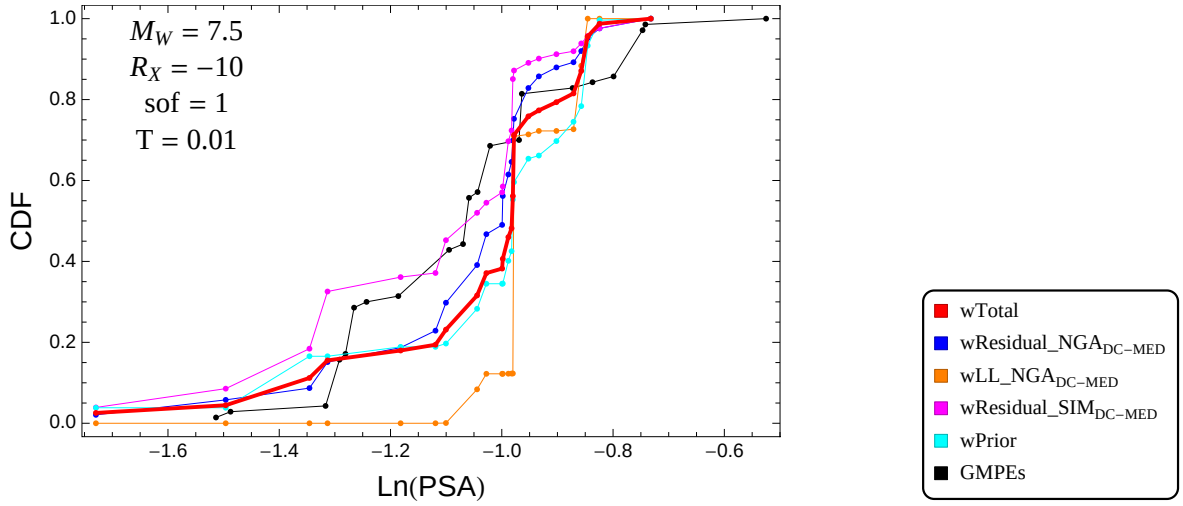



Figure 2.103: DCPPv4: Cumulative distribution function of GMPEs (black) and selected models, for different sets of weights, for a scenario with $M = 7.5$, $R_x = -10$, $F = 1$, and $T = 0.01$s

**T = 0.2s**

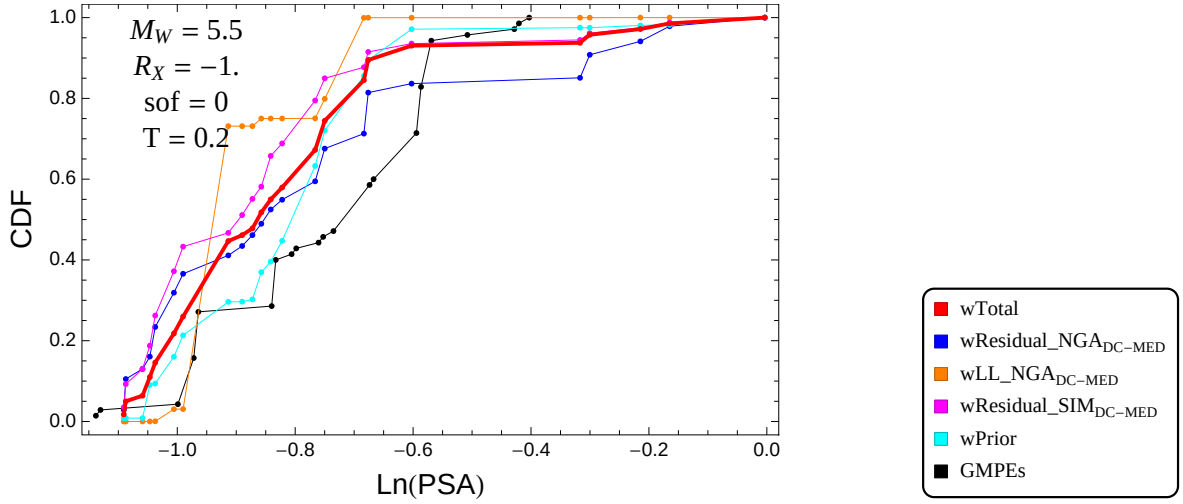



Figure 2.104: DCPPv4: Cumulative distribution function of GMPEs (black) and selected models, for different sets of weights, for a scenario with $M = 5.5$, $R_x = -1.$, $F = 0$, and $T = 0.2$s

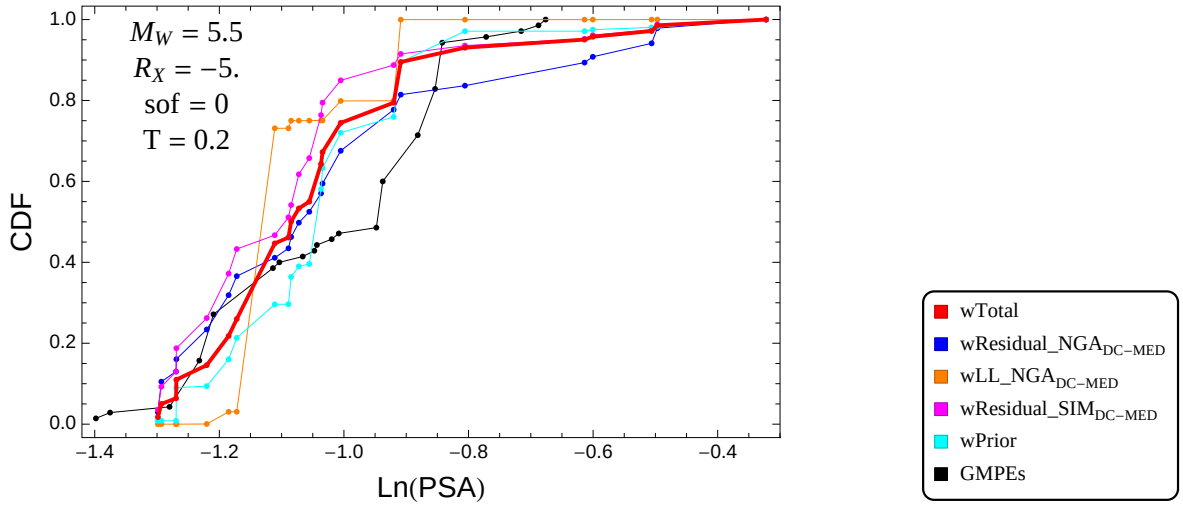



Figure 2.105: DCPPv4: Cumulative distribution function of GMPEs (black) and selected models, for different sets of weights, for a scenario with $M = 5.5$, $R_x = -5.$, $F = 0$, and $T = 0.2$s

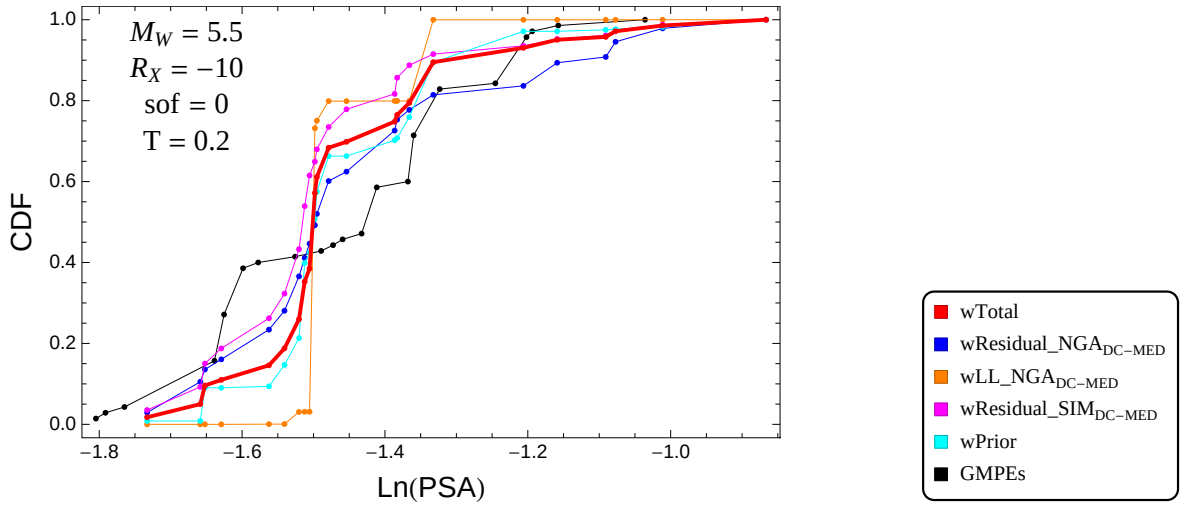



Figure 2.106: DCPPv4: Cumulative distribution function of GMPEs (black) and selected models, for different sets of weights, for a scenario with $M = 5.5$, $R_x = -10$, $F = 0$, and $T = 0.2$s

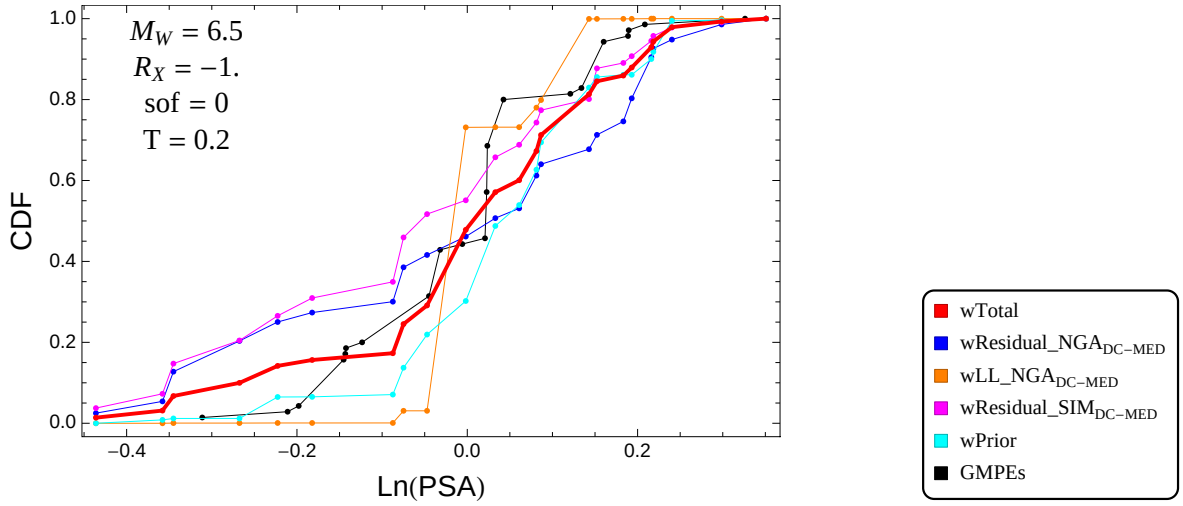



Figure 2.107: DCPPv4: Cumulative distribution function of GMPEs (black) and selected models, for different sets of weights, for a scenario with $M = 6.5$, $R_x = -1.$, $F = 0$, and $T = 0.2$s

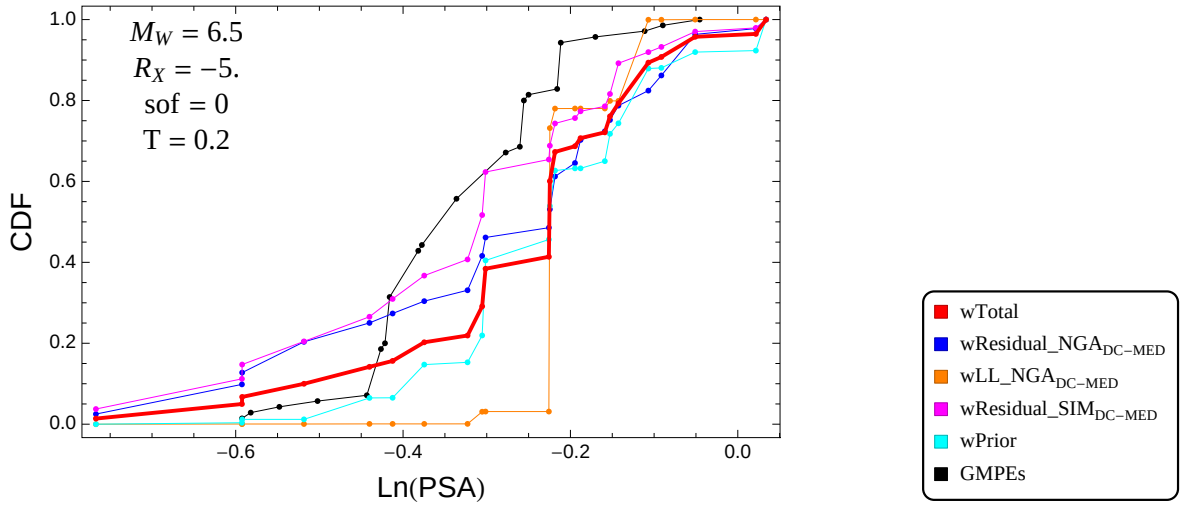



Figure 2.108: DCPPv4: Cumulative distribution function of GMPEs (black) and selected models, for different sets of weights, for a scenario with $M = 6.5$, $R_x = -5.$, $F = 0$, and $T = 0.2$s

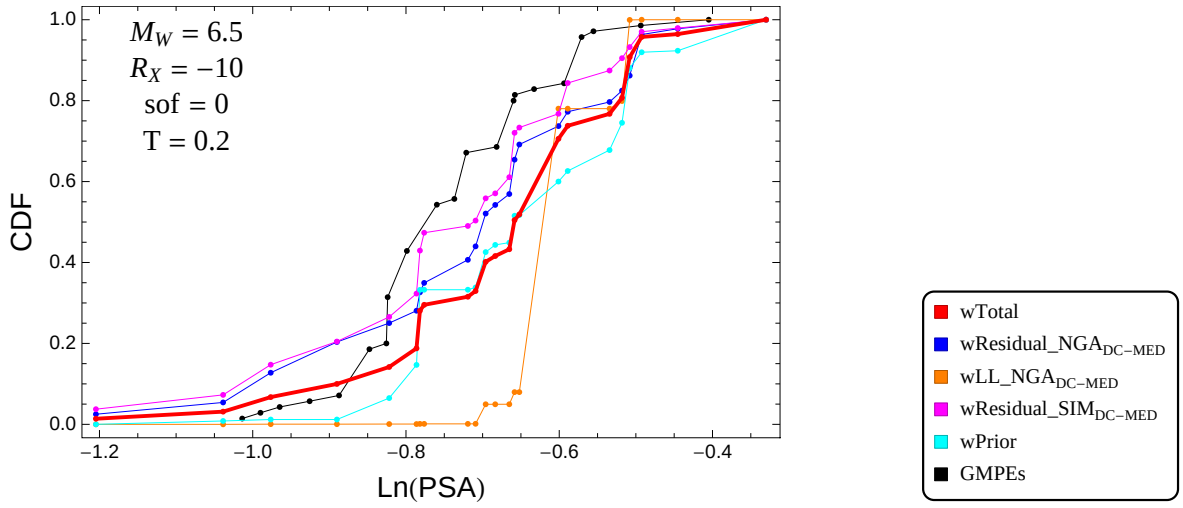



Figure 2.109: DCPPv4: Cumulative distribution function of GMPEs (black) and selected models, for different sets of weights, for a scenario with $M = 6.5$, $R_x = -10$, $F = 0$, and $T = 0.2$s

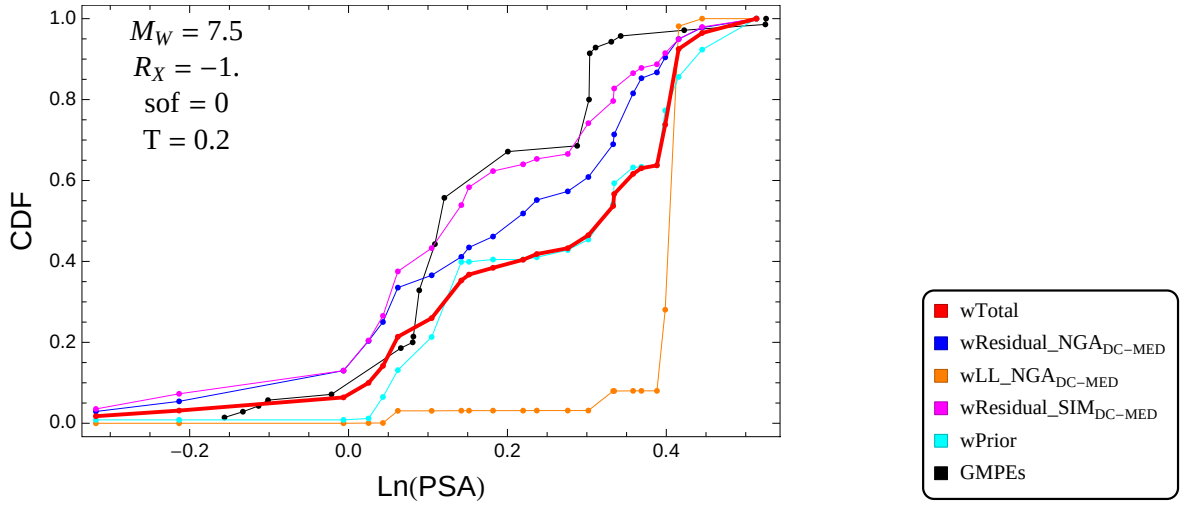



Figure 2.110: DCPPv4: Cumulative distribution function of GMPEs (black) and selected models, for different sets of weights, for a scenario with $M = 7.5$, $R_x = -1.$, $F = 0$, and $T = 0.2$s

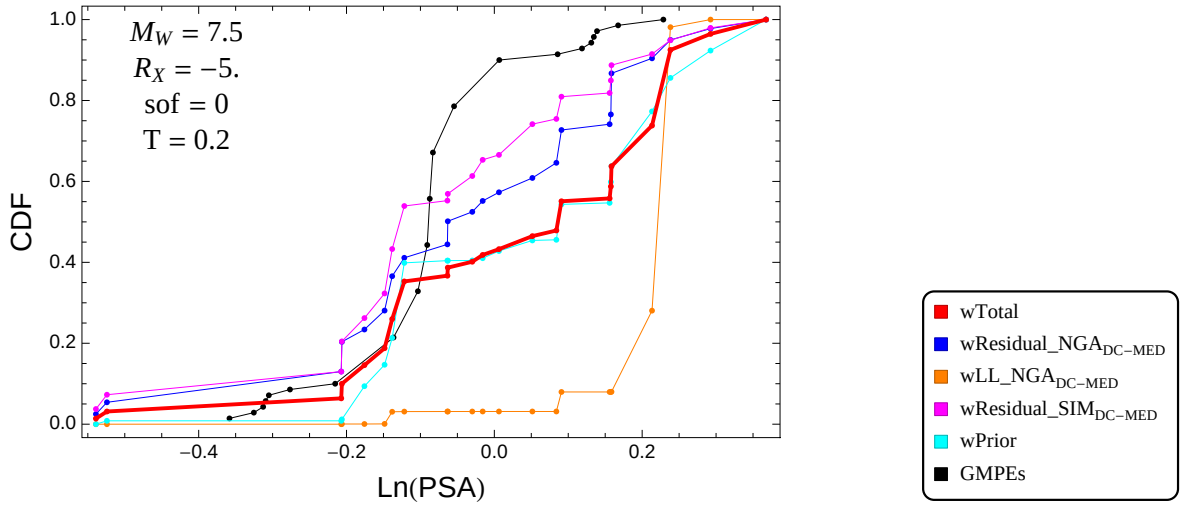



Figure 2.111: DCPPv4: Cumulative distribution function of GMPEs (black) and selected models, for different sets of weights, for a scenario with $M = 7.5$, $R_x = -5.$, $F = 0$, and $T = 0.2$s

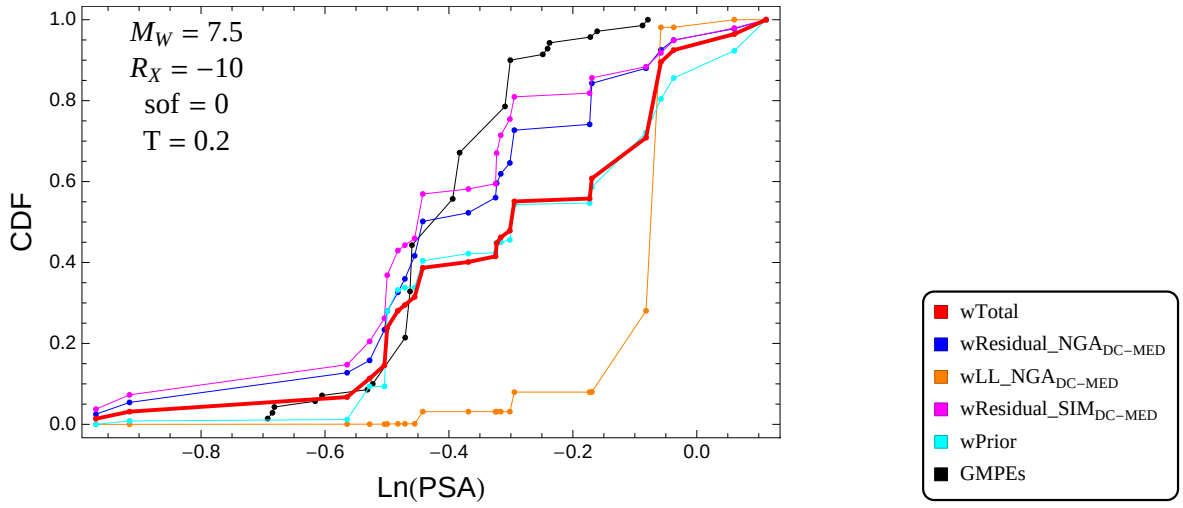



Figure 2.112: DCPPv4: Cumulative distribution function of GMPEs (black) and selected models, for different sets of weights, for a scenario with $M = 7.5$, $R_x = -10$, $F = 0$, and $T = 0.2$s

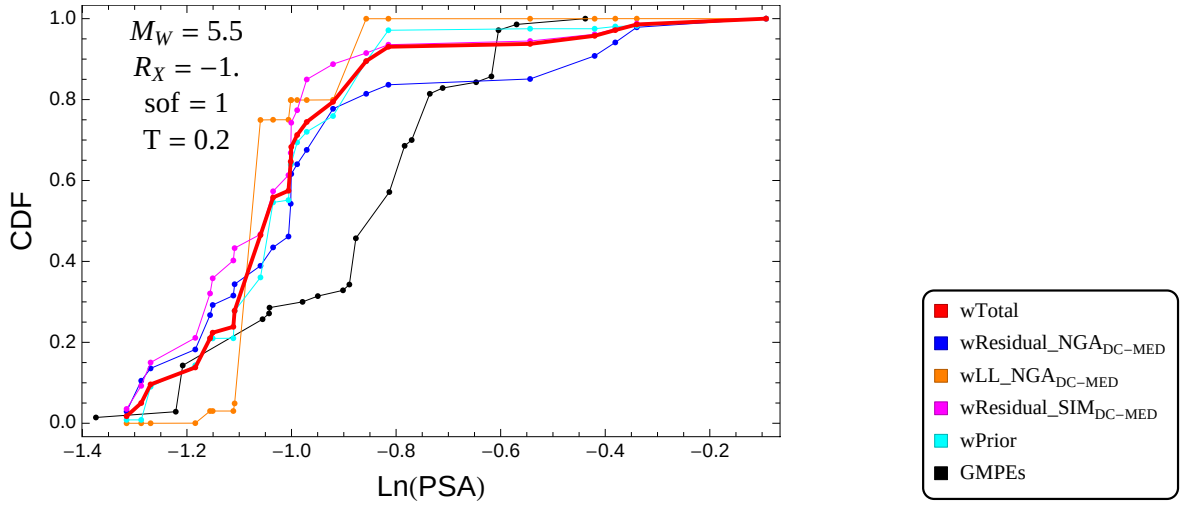



Figure 2.113: DCPPv4: Cumulative distribution function of GMPEs (black) and selected models, for different sets of weights, for a scenario with $M = 5.5$, $R_x = -1.$, $F = 1$, and $T = 0.2$s

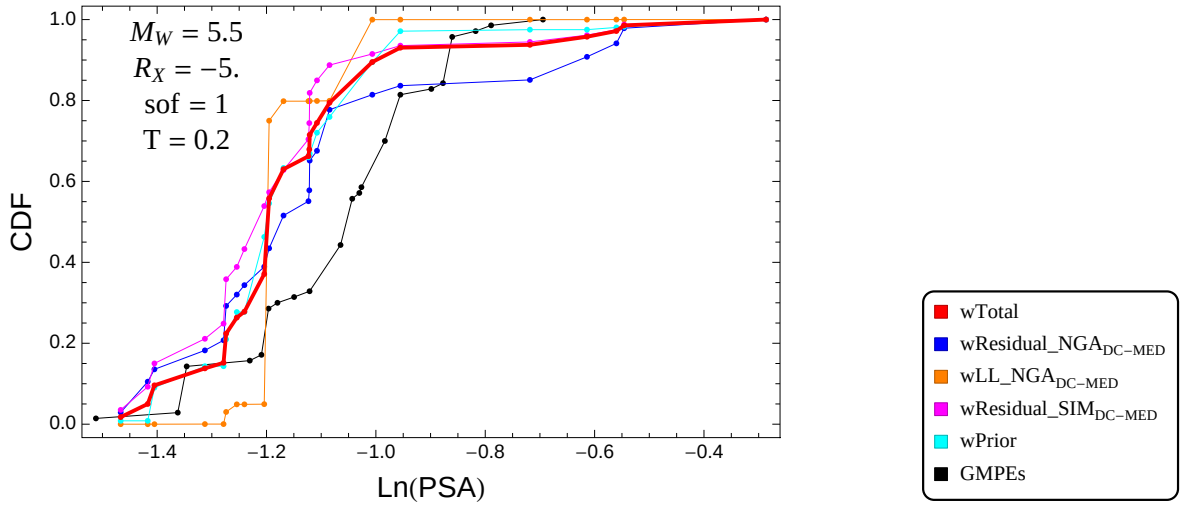



Figure 2.114: DCPPv4: Cumulative distribution function of GMPEs (black) and selected models, for different sets of weights, for a scenario with $M = 5.5$, $R_x = -5.$, $F = 1$, and $T = 0.2$s

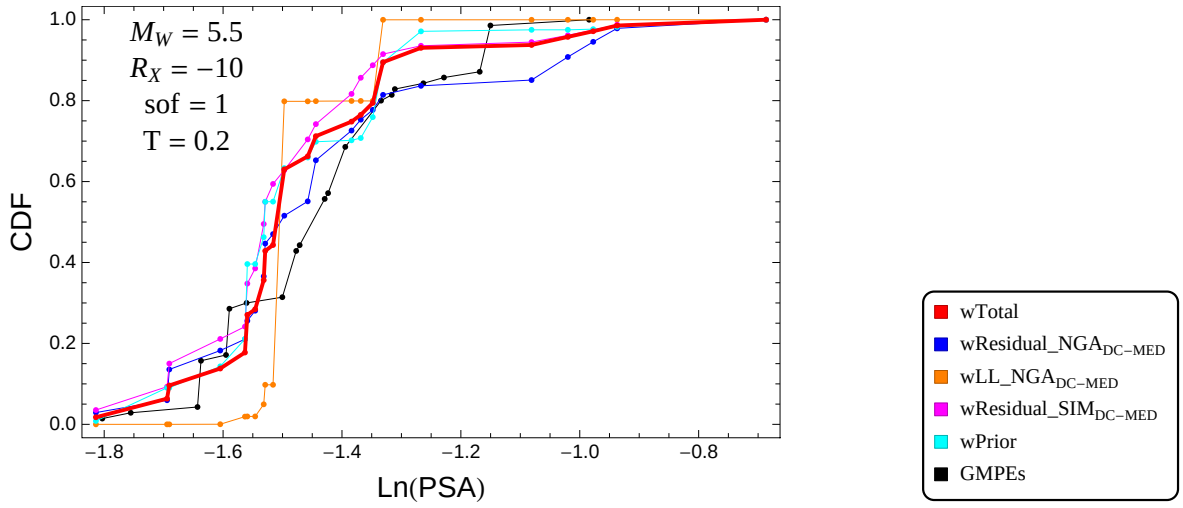



Figure 2.115: DCPPv4: Cumulative distribution function of GMPEs (black) and selected models, for different sets of weights, for a scenario with $M = 5.5$, $R_x = -10$, $F = 1$, and $T = 0.2$s

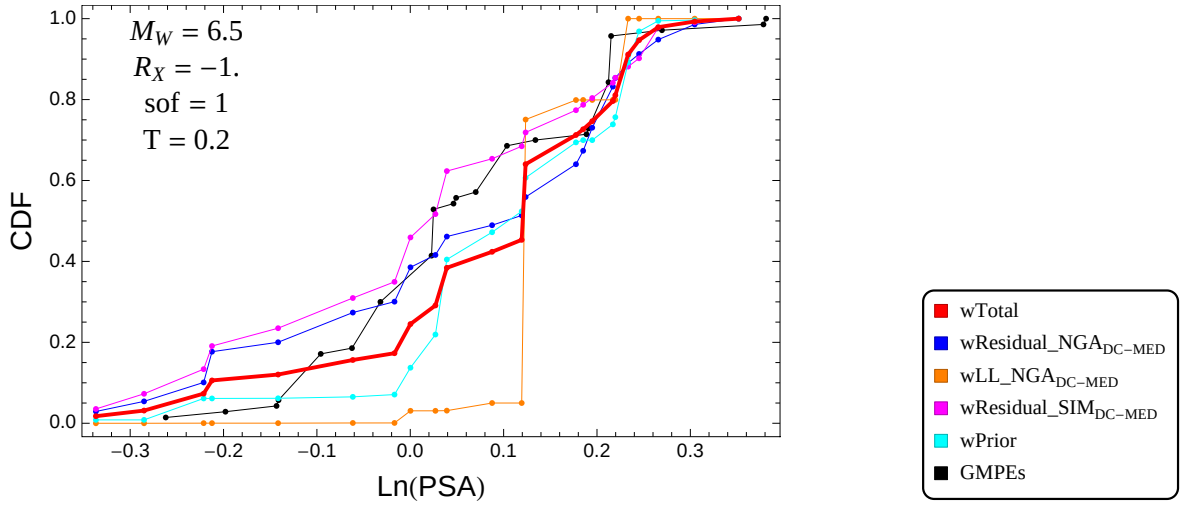



Figure 2.116: DCPPv4: Cumulative distribution function of GMPEs (black) and selected models, for different sets of weights, for a scenario with $M = 6.5$, $R_x = -1.$, $F = 1$, and $T = 0.2$s

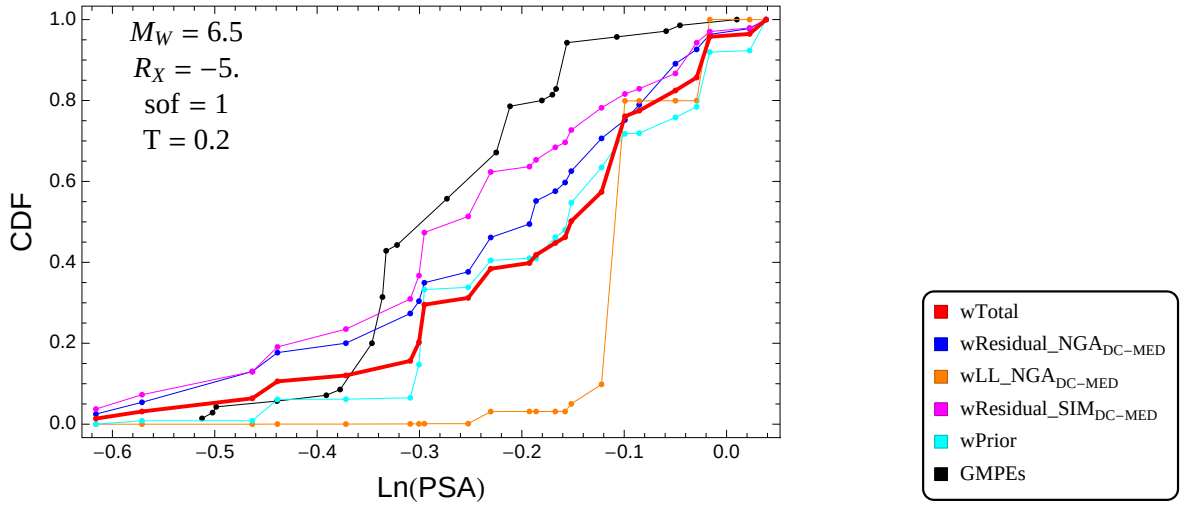



Figure 2.117: DCPPv4: Cumulative distribution function of GMPEs (black) and selected models, for different sets of weights, for a scenario with $M = 6.5$, $R_x = -5.$, $F = 1$, and $T = 0.2$s

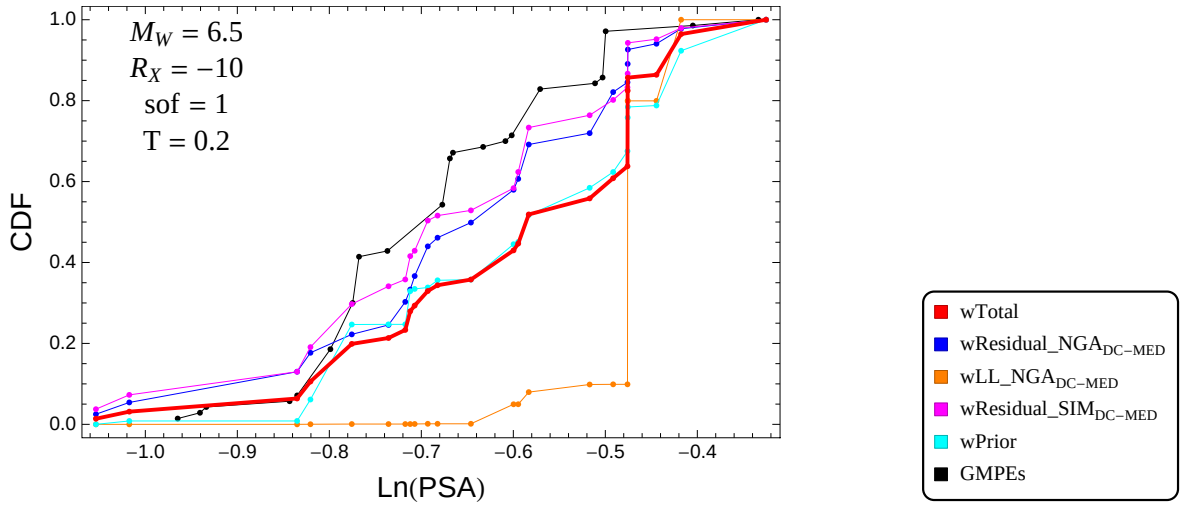



Figure 2.118: DCPPv4: Cumulative distribution function of GMPEs (black) and selected models, for different sets of weights, for a scenario with $M = 6.5$, $R_x = -10$, $F = 1$, and $T = 0.2$s

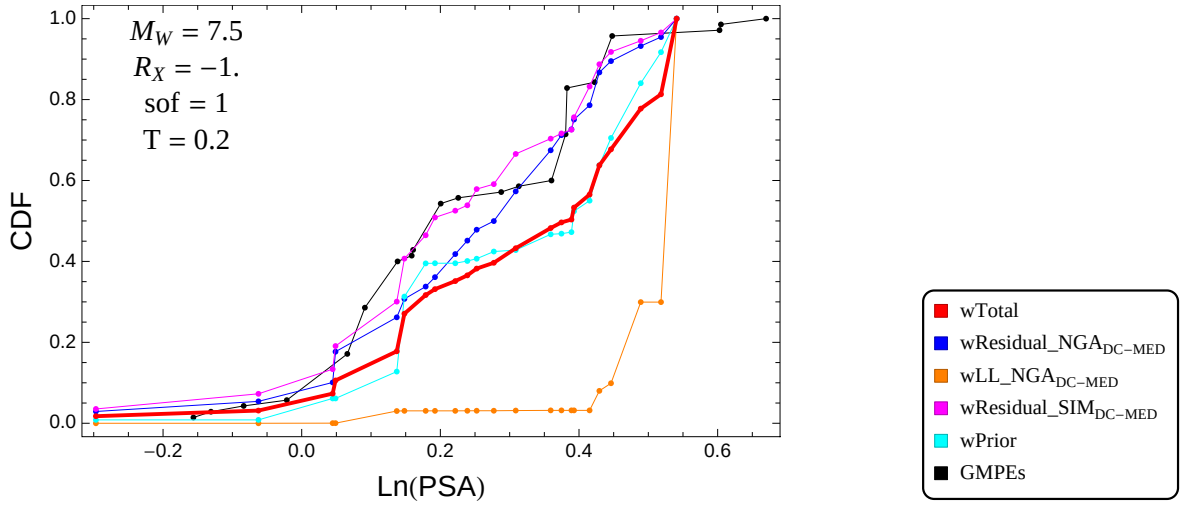



Figure 2.119: DCPPv4: Cumulative distribution function of GMPEs (black) and selected models, for different sets of weights, for a scenario with $M = 7.5$, $R_x = -1.$, $F = 1$, and $T = 0.2$s

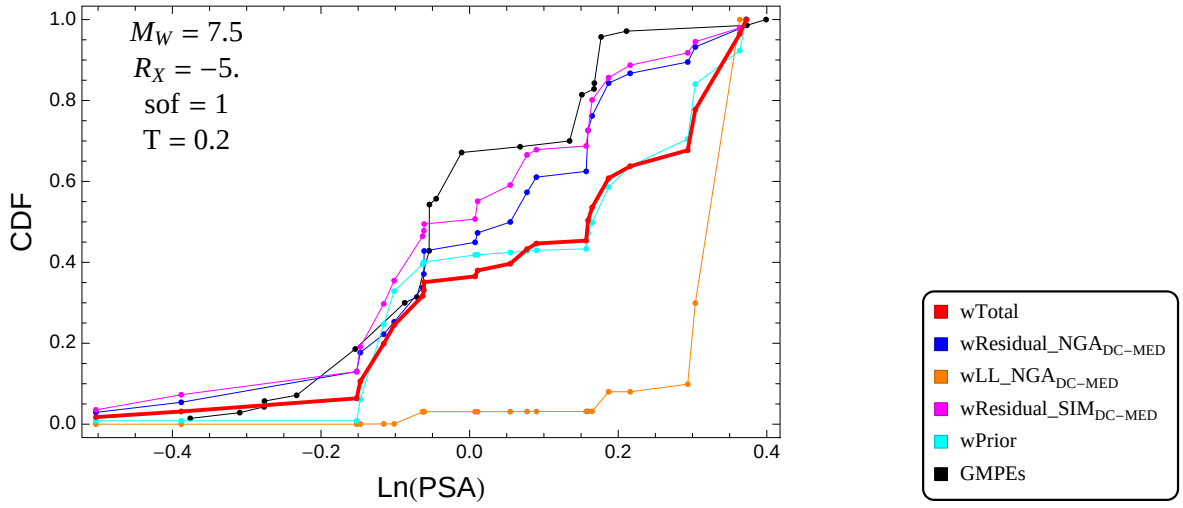



Figure 2.120: DCPPv4: Cumulative distribution function of GMPEs (black) and selected models, for different sets of weights, for a scenario with $M = 7.5$, $R_x = -5.$, $F = 1$, and $T = 0.2$s

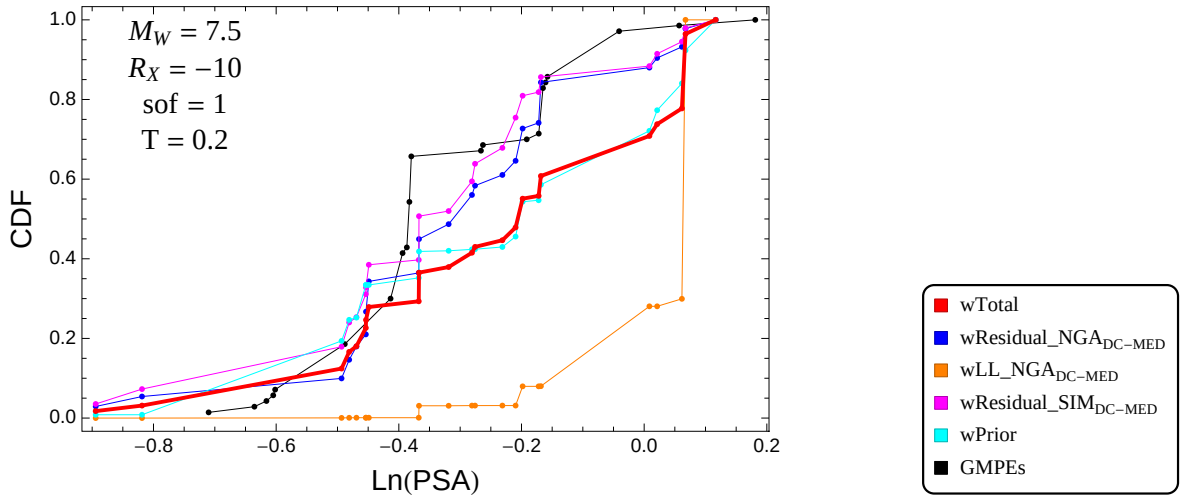



Figure 2.121: DCPPv4: Cumulative distribution function of GMPEs (black) and selected models, for different sets of weights, for a scenario with $M = 7.5$, $R_x = -10$, $F = 1$, and $T = 0.2$s

**T = 0.5s**

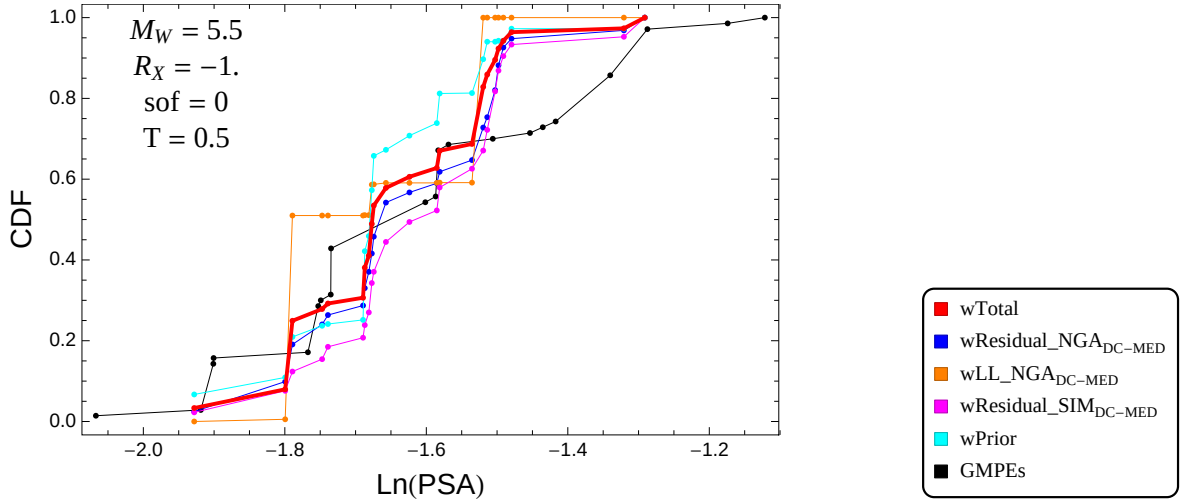



Figure 2.122: DCPPv4: Cumulative distribution function of GMPEs (black) and selected models, for different sets of weights, for a scenario with $M = 5.5$, $R_x = -1.$, $F = 0$, and $T = 0.5$s

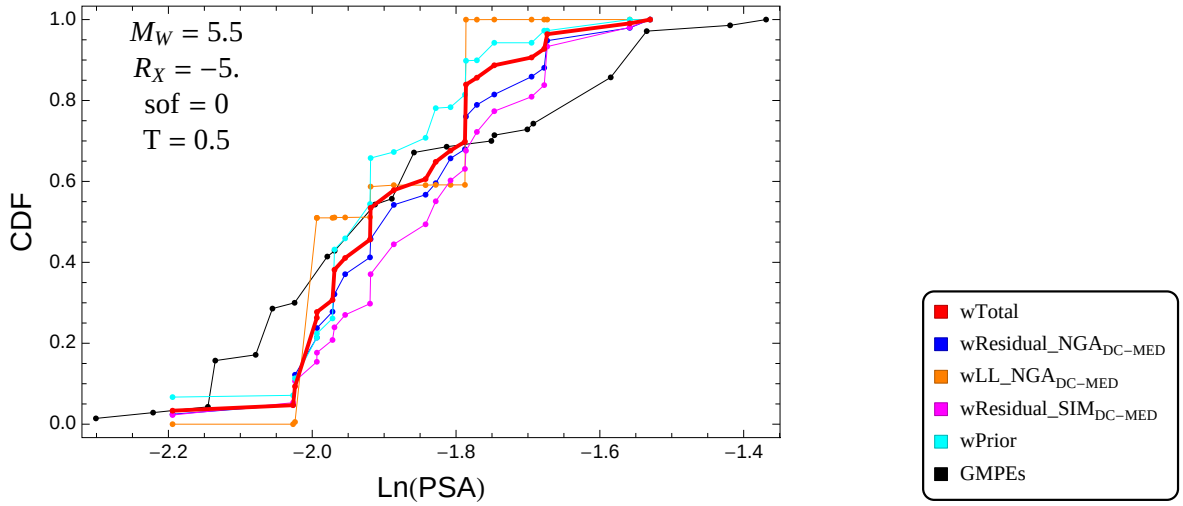



Figure 2.123: DCPPv4: Cumulative distribution function of GMPEs (black) and selected models, for different sets of weights, for a scenario with $M = 5.5$, $R_x = -5.$, $F = 0$, and $T = 0.5$s

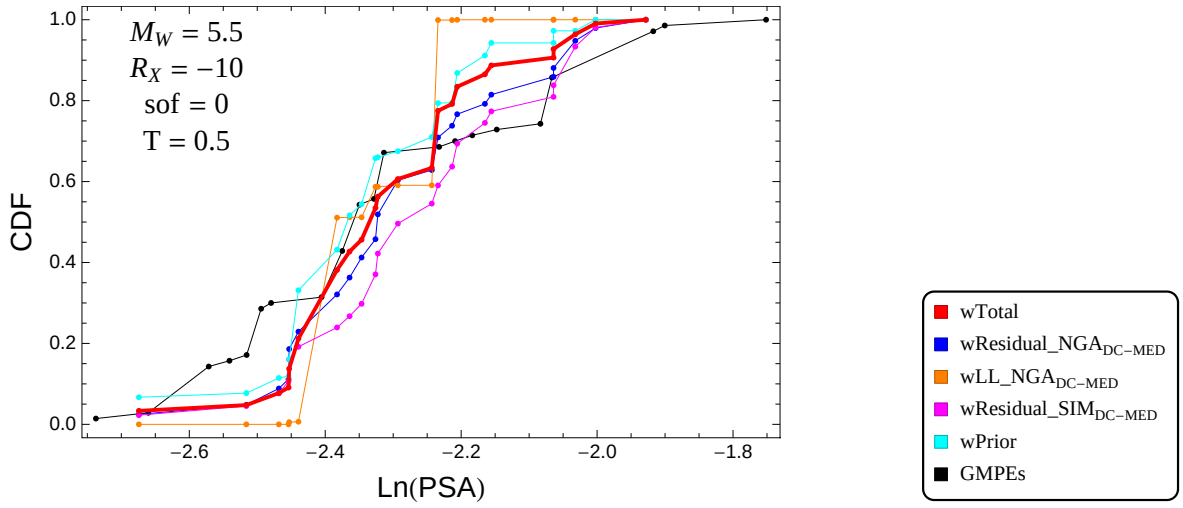



Figure 2.124: DCPPv4: Cumulative distribution function of GMPEs (black) and selected models, for different sets of weights, for a scenario with $M = 5.5$, $R_x = -10$, $F = 0$, and $T = 0.5$s

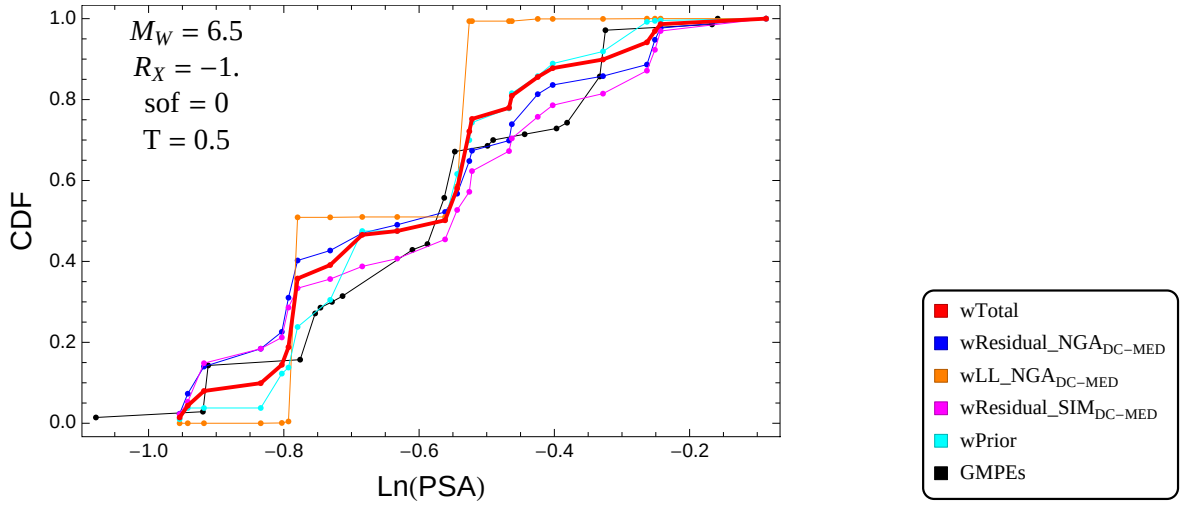



Figure 2.125: DCPPv4: Cumulative distribution function of GMPEs (black) and selected models, for different sets of weights, for a scenario with $M = 6.5$, $R_x = -1.$, $F = 0$, and $T = 0.5$s

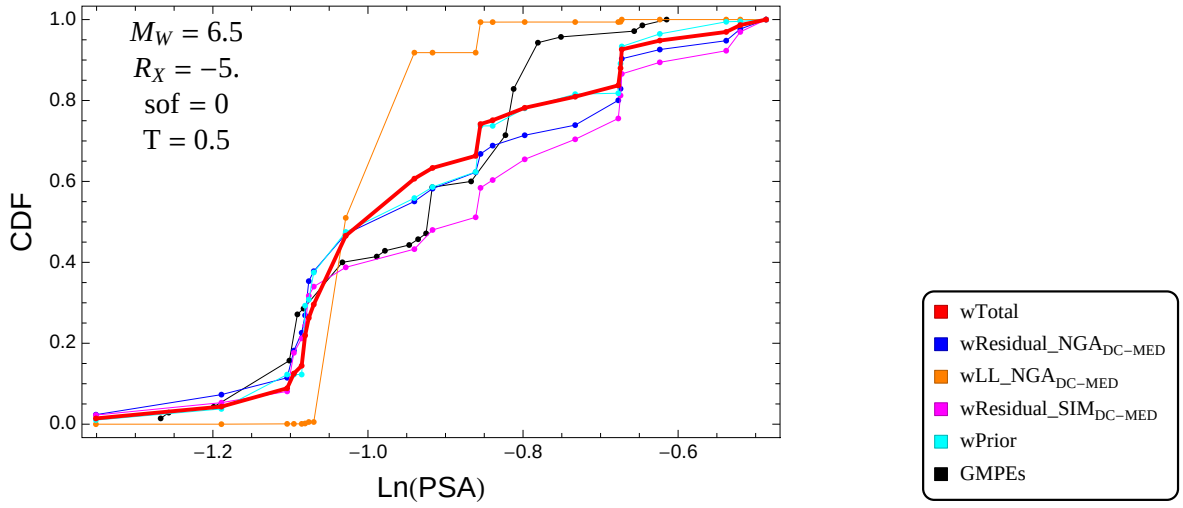



Figure 2.126: DCPPv4: Cumulative distribution function of GMPEs (black) and selected models, for different sets of weights, for a scenario with $M = 6.5$, $R_x = -5.$, $F = 0$, and $T = 0.5$s

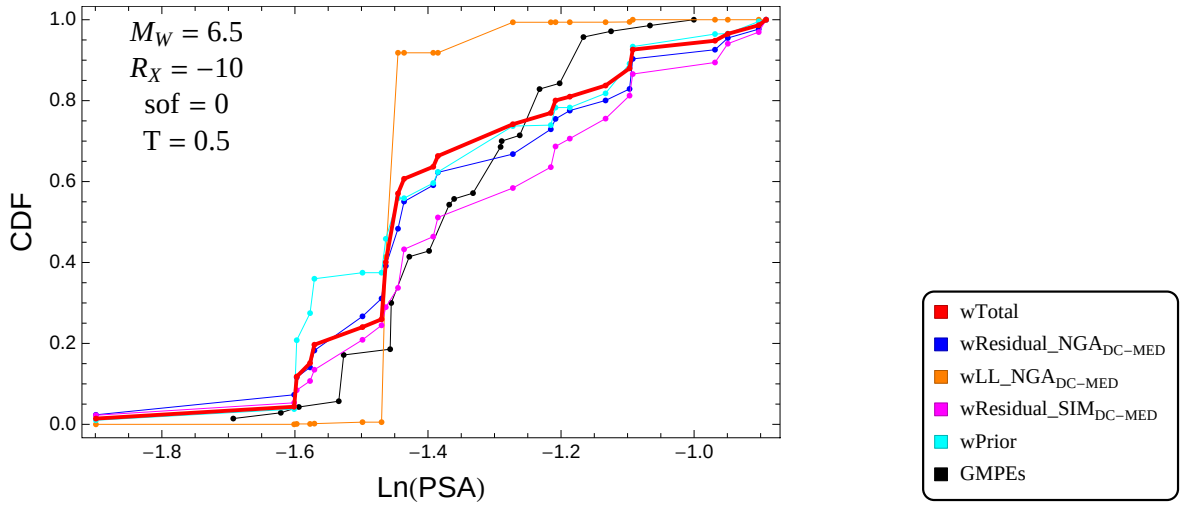



Figure 2.127: DCPPv4: Cumulative distribution function of GMPEs (black) and selected models, for different sets of weights, for a scenario with $M = 6.5$, $R_x = -10$, $F = 0$, and $T = 0.5$s

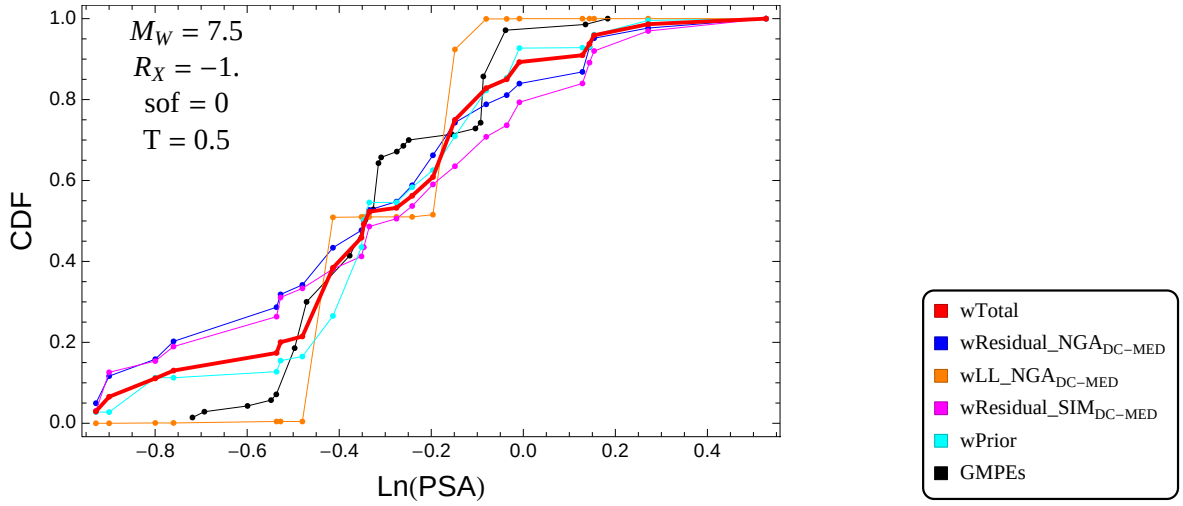



Figure 2.128: DCPPv4: Cumulative distribution function of GMPEs (black) and selected models, for different sets of weights, for a scenario with $M = 7.5$, $R_x = -1.$, $F = 0$, and $T = 0.5$s

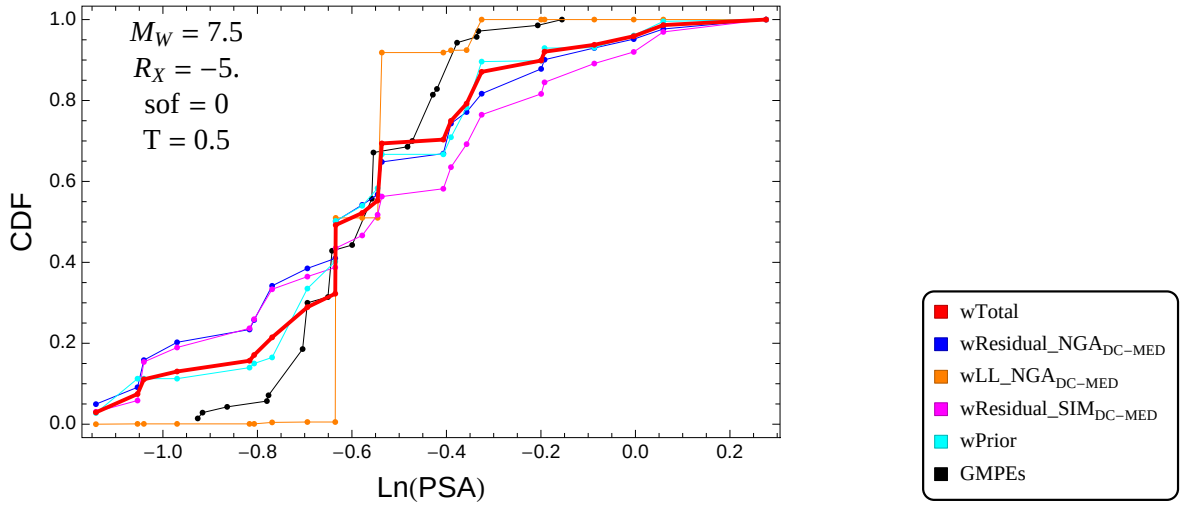



Figure 2.129: DCPPv4: Cumulative distribution function of GMPEs (black) and selected models, for different sets of weights, for a scenario with $M = 7.5$, $R_x = -5.$, $F = 0$, and $T = 0.5$s

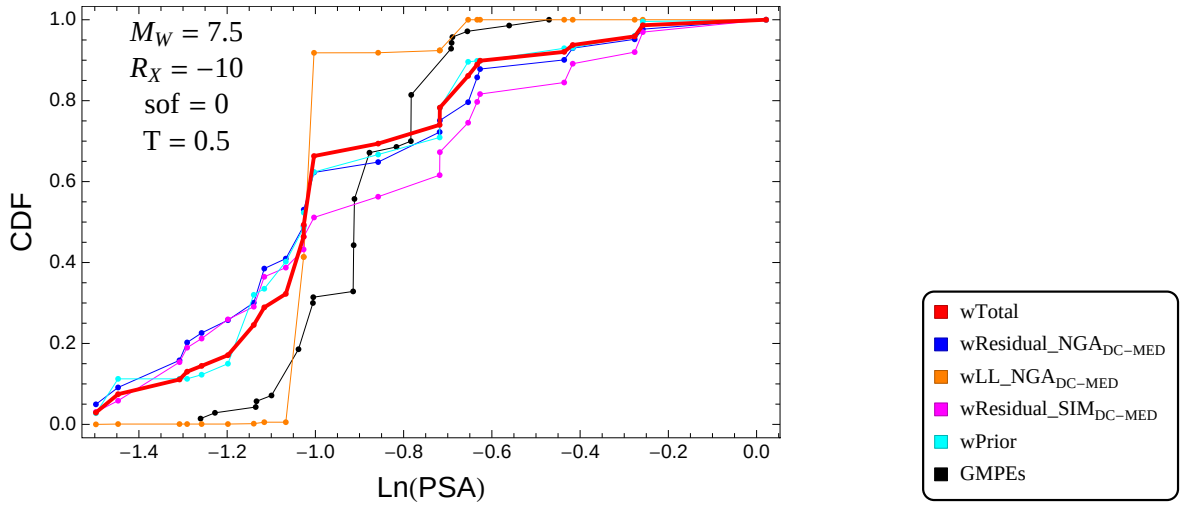



Figure 2.130: DCPPv4: Cumulative distribution function of GMPEs (black) and selected models, for different sets of weights, for a scenario with $M = 7.5$, $R_x = -10$, $F = 0$, and $T = 0.5$s

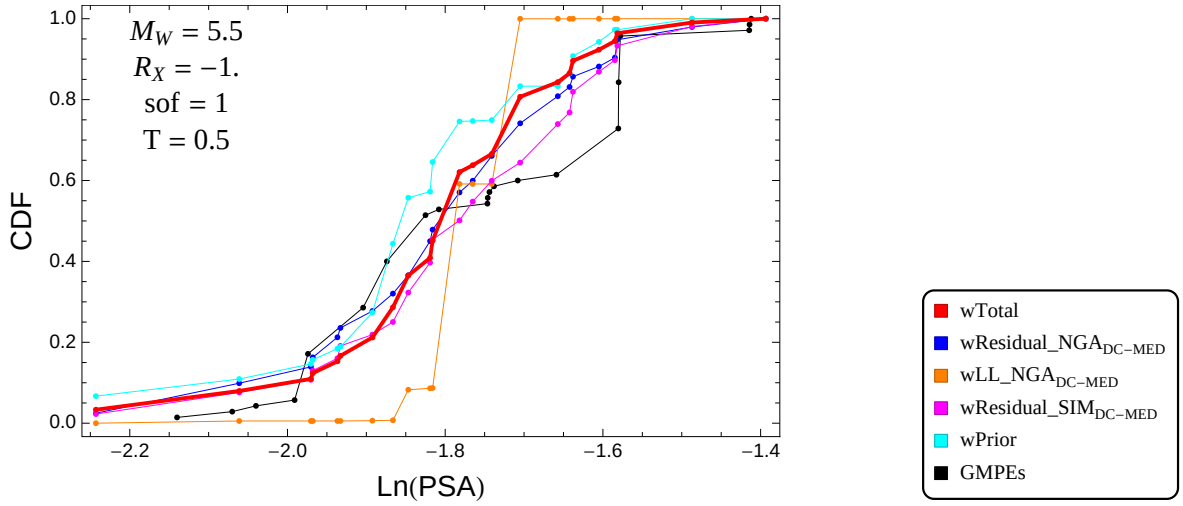



Figure 2.131: DCPPv4: Cumulative distribution function of GMPEs (black) and selected models, for different sets of weights, for a scenario with $M = 5.5$, $R_x = -1.$, $F = 1$, and $T = 0.5$s

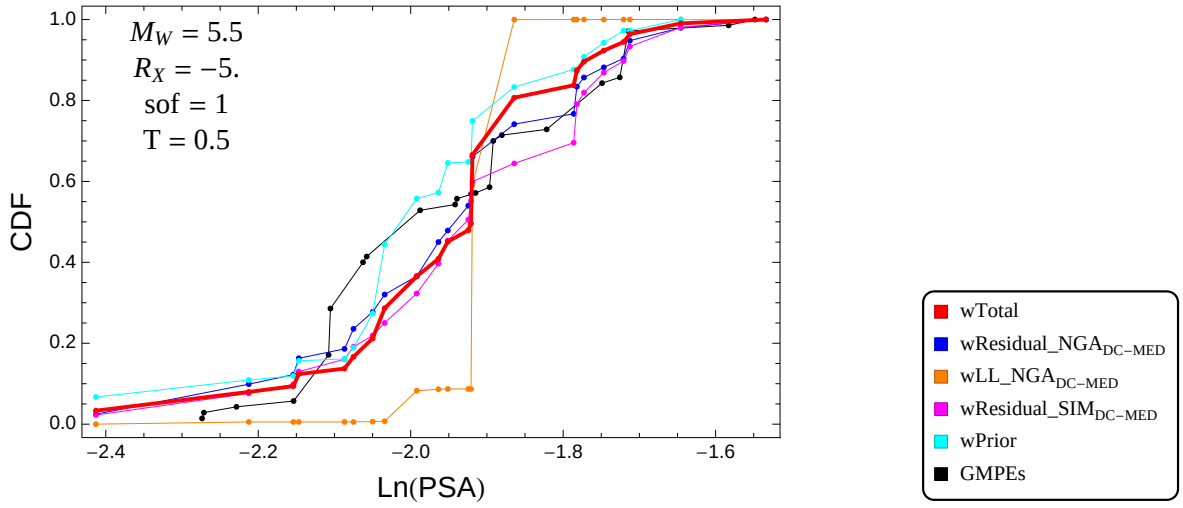



Figure 2.132: DCPPv4: Cumulative distribution function of GMPEs (black) and selected models, for different sets of weights, for a scenario with $M = 5.5$, $R_x = -5.$, $F = 1$, and $T = 0.5$s

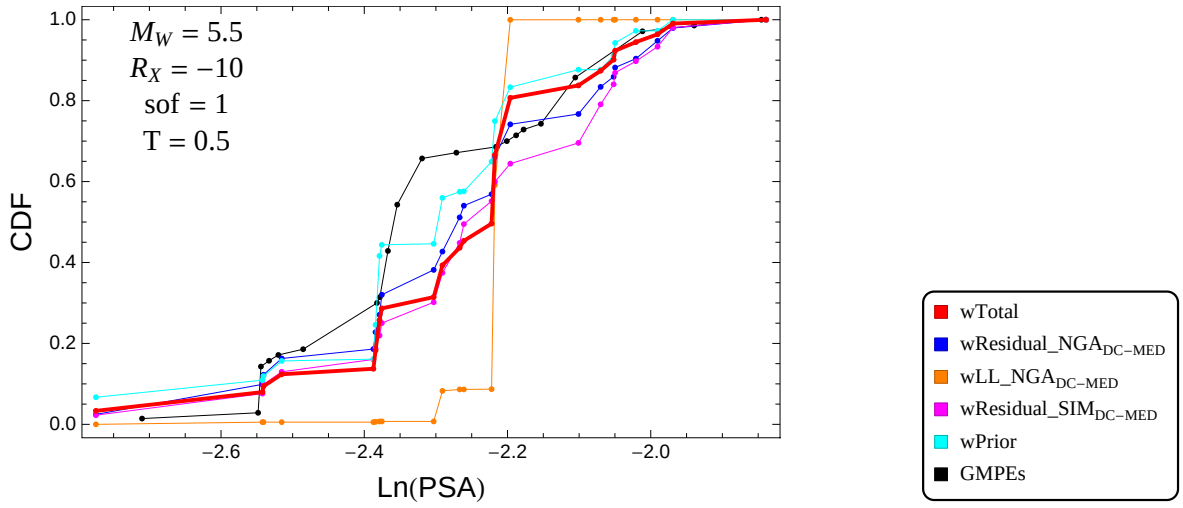



Figure 2.133: DCPPv4: Cumulative distribution function of GMPEs (black) and selected models, for different sets of weights, for a scenario with $M = 5.5$, $R_x = -10$, $F = 1$, and $T = 0.5$s

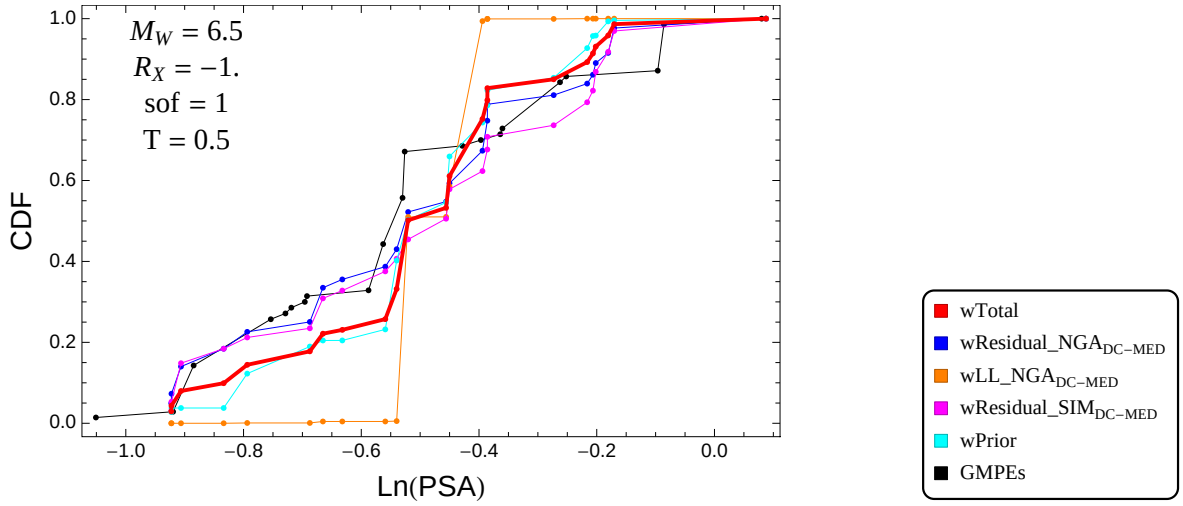



Figure 2.134: DCPPv4: Cumulative distribution function of GMPEs (black) and selected models, for different sets of weights, for a scenario with $M = 6.5$, $R_x = -1.$, $F = 1$, and $T = 0.5$s

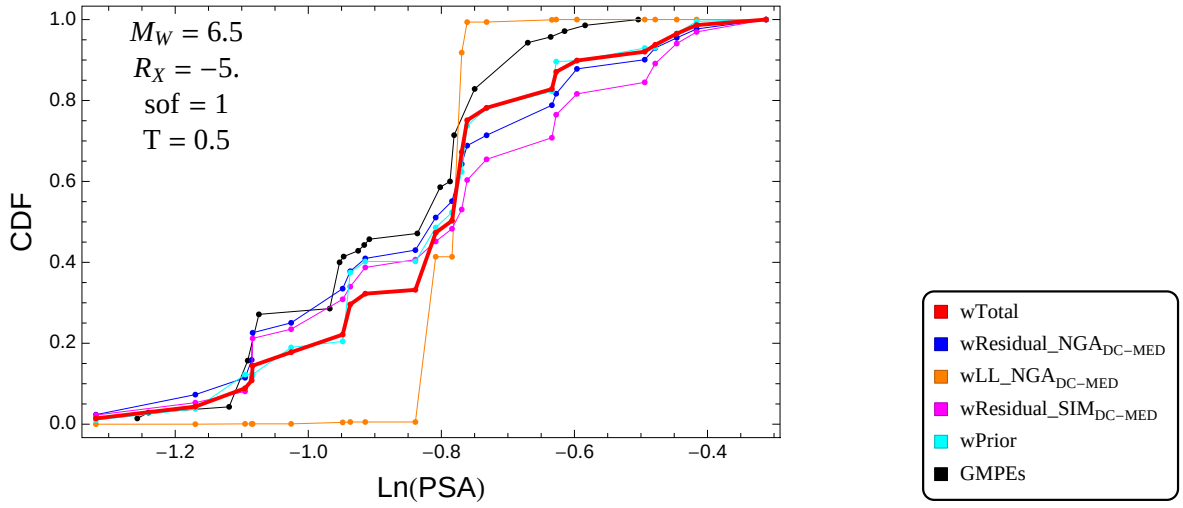



Figure 2.135: DCPPv4: Cumulative distribution function of GMPEs (black) and selected models, for different sets of weights, for a scenario with $M = 6.5$, $R_x = -5.$, $F = 1$, and $T = 0.5$s

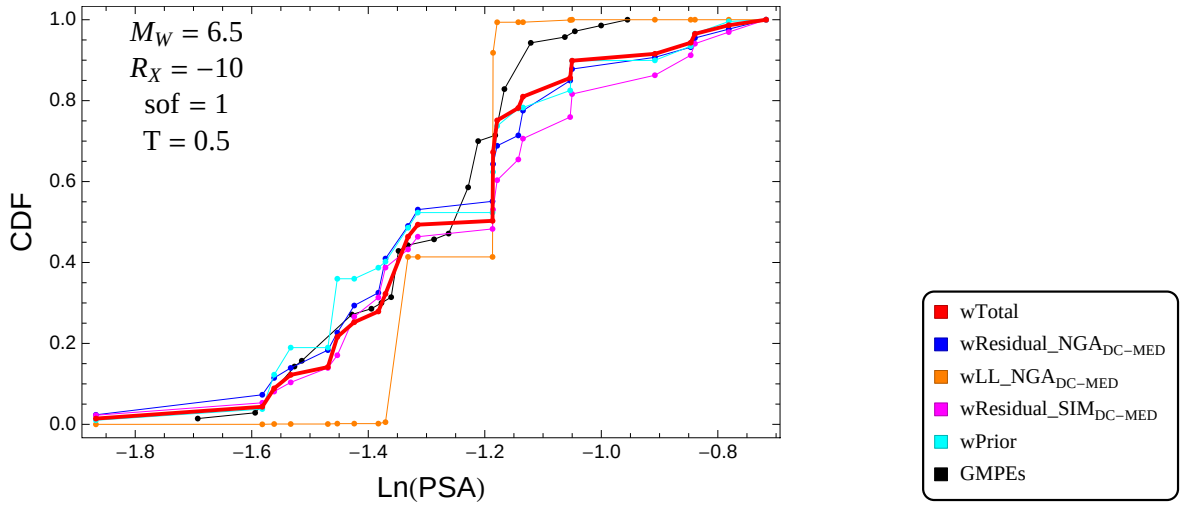



Figure 2.136: DCPPv4: Cumulative distribution function of GMPEs (black) and selected models, for different sets of weights, for a scenario with $M = 6.5$, $R_x = -10$, $F = 1$, and $T = 0.5$s

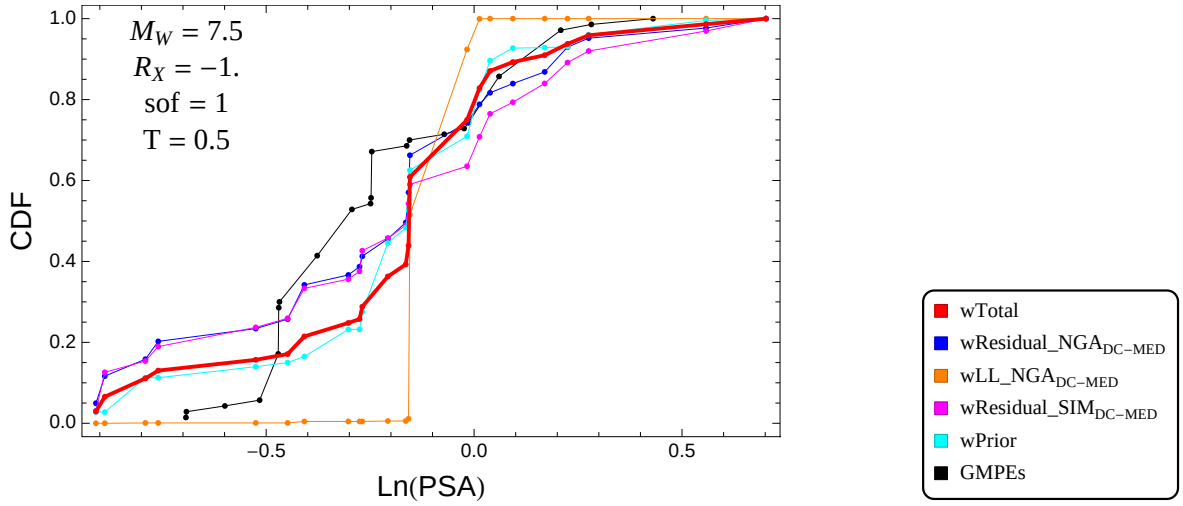



Figure 2.137: DCPPv4: Cumulative distribution function of GMPEs (black) and selected models, for different sets of weights, for a scenario with $M = 7.5$, $R_x = -1.$, $F = 1$, and $T = 0.5$s

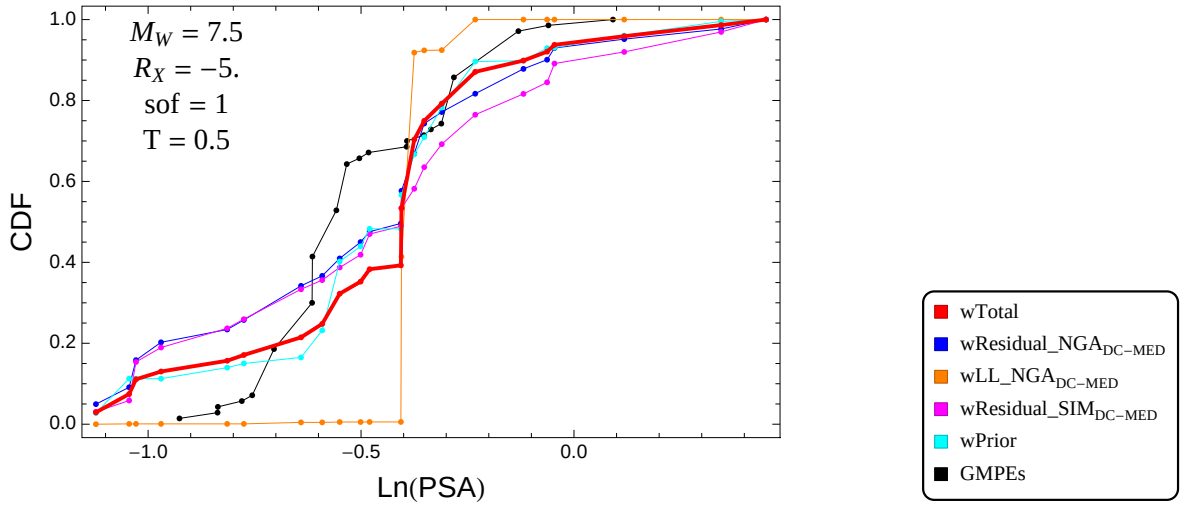



Figure 2.138: DCPPv4: Cumulative distribution function of GMPEs (black) and selected models, for different sets of weights, for a scenario with $M = 7.5$, $R_x = -5.$, $F = 1$, and $T = 0.5$s

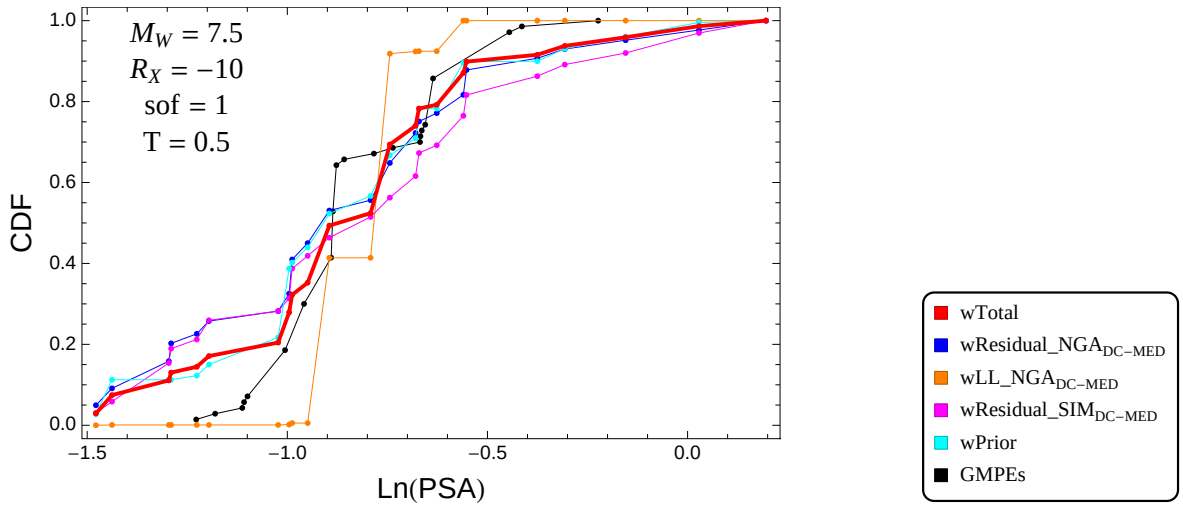



Figure 2.139: DCPPv4: Cumulative distribution function of GMPEs (black) and selected models, for different sets of weights, for a scenario with $M = 7.5$, $R_x = -10$, $F = 1$, and $T = 0.5$s

**T = 1.s**

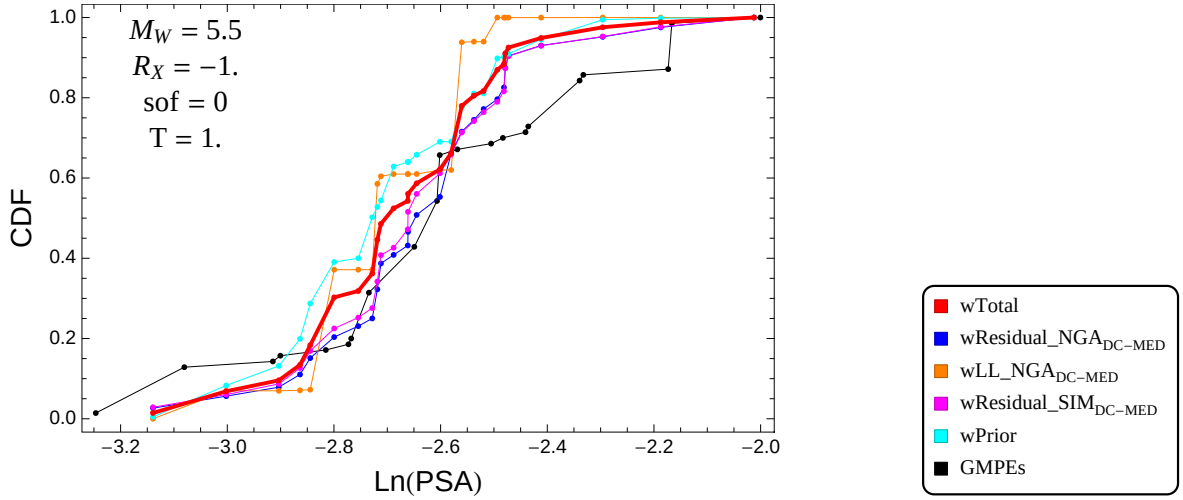



Figure 2.140: DCPPv4: Cumulative distribution function of GMPEs (black) and selected models, for different sets of weights, for a scenario with $M = 5.5$, $R_x = -1.$, $F = 0$, and $T = 1.$s

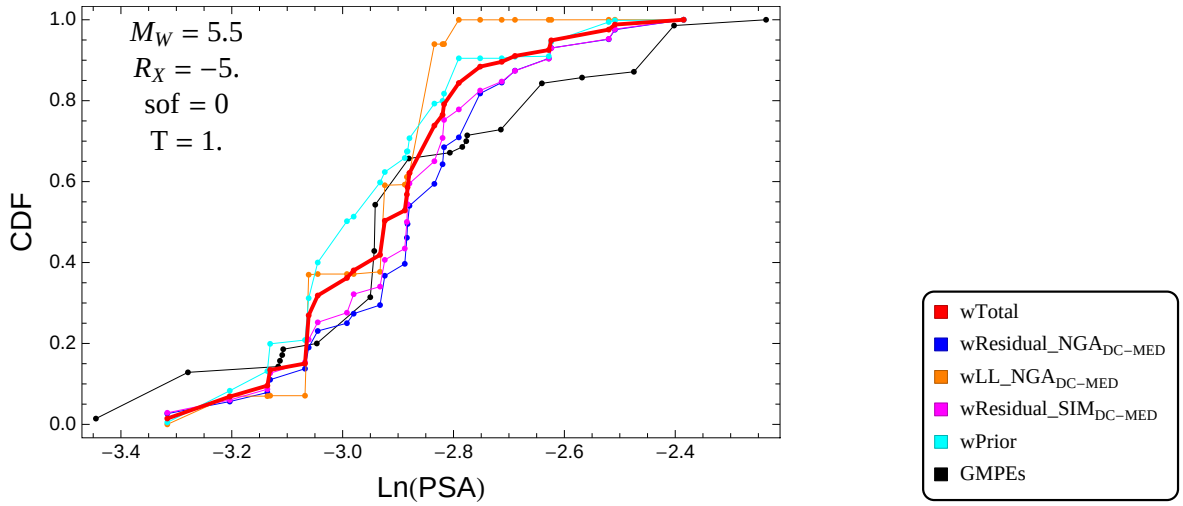



Figure 2.141: DCPPv4: Cumulative distribution function of GMPEs (black) and selected models, for different sets of weights, for a scenario with $M = 5.5$, $R_x = -5.$, $F = 0$, and $T = 1.$s

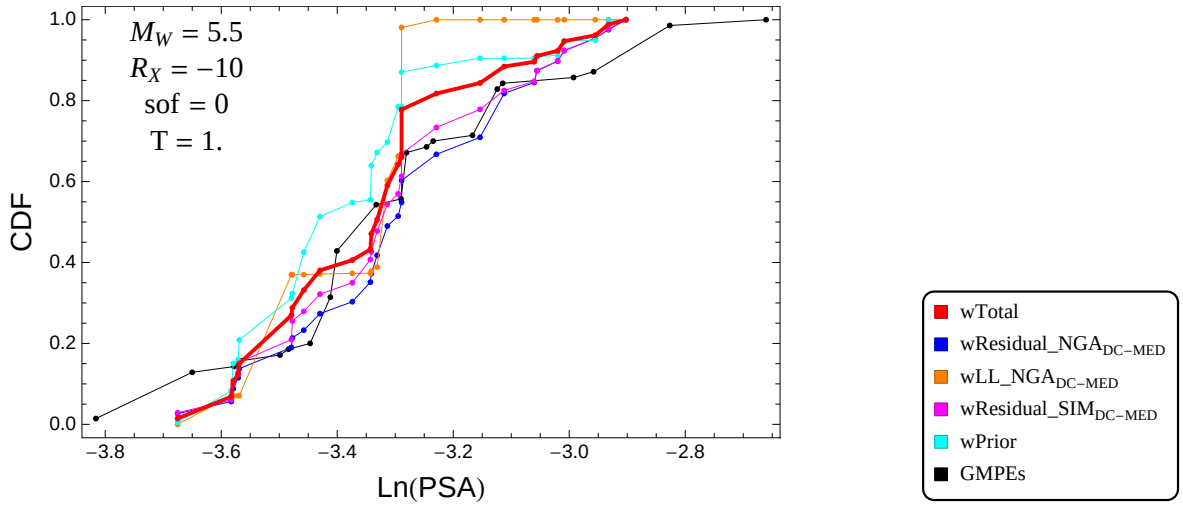



Figure 2.142: DCPPv4: Cumulative distribution function of GMPEs (black) and selected models, for different sets of weights, for a scenario with $M = 5.5$, $R_x = -10$, $F = 0$, and $T = 1.$s

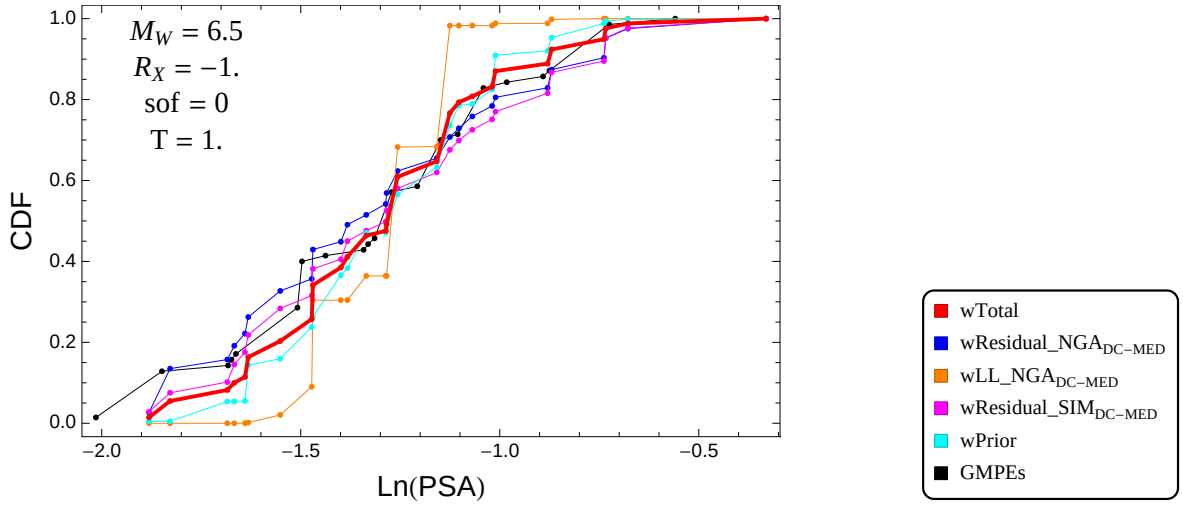



Figure 2.143: DCPPv4: Cumulative distribution function of GMPEs (black) and selected models, for different sets of weights, for a scenario with $M = 6.5$, $R_x = -1.$, $F = 0$, and $T = 1.$s

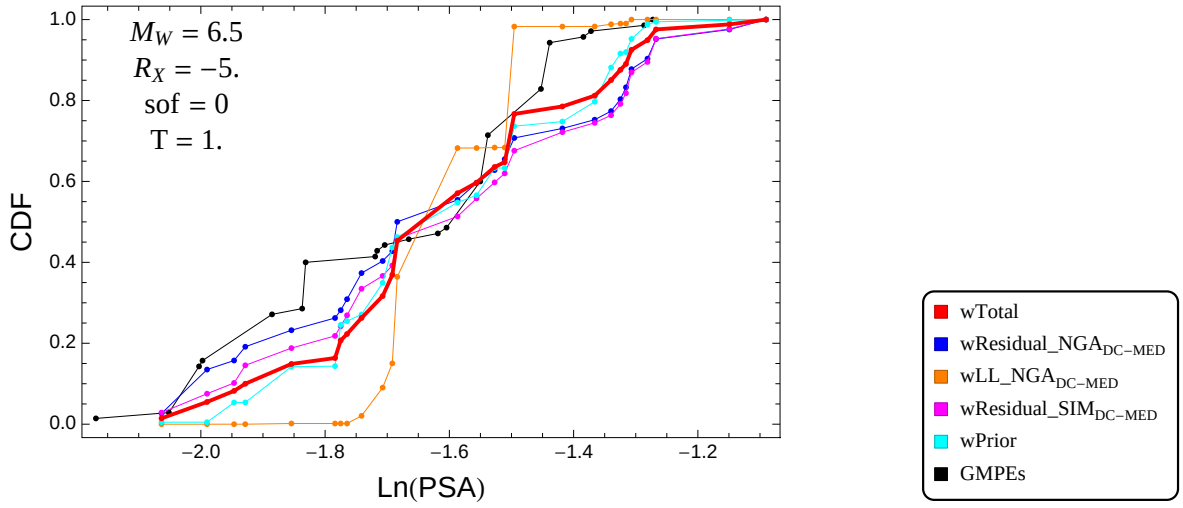



Figure 2.144: DCPPv4: Cumulative distribution function of GMPEs (black) and selected models, for different sets of weights, for a scenario with $M = 6.5$, $R_x = -5.$, $F = 0$, and $T = 1.$s

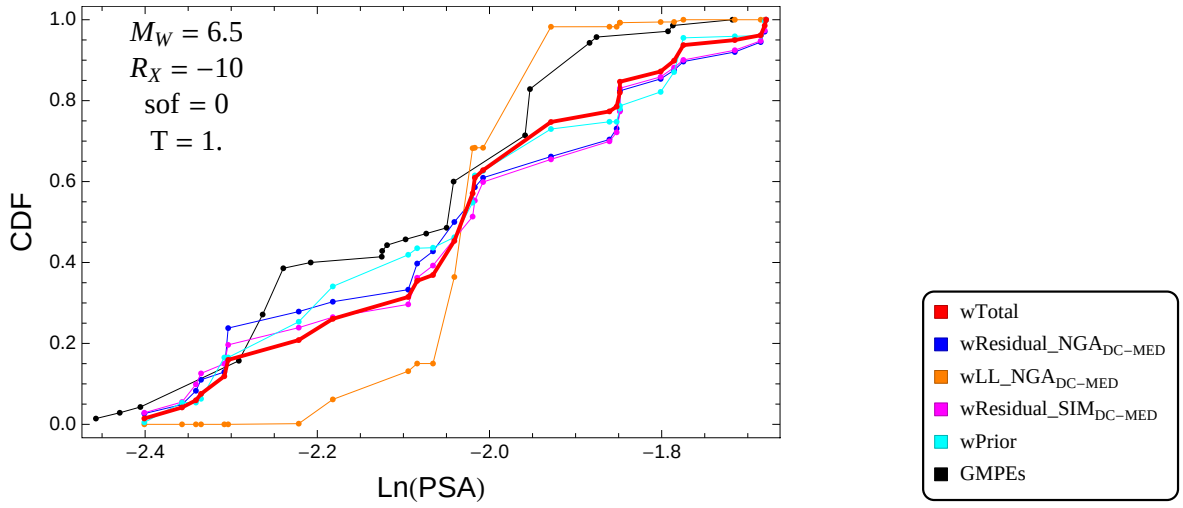



Figure 2.145: DCPPv4: Cumulative distribution function of GMPEs (black) and selected models, for different sets of weights, for a scenario with $M = 6.5$, $R_x = -10$, $F = 0$, and $T = 1.$s

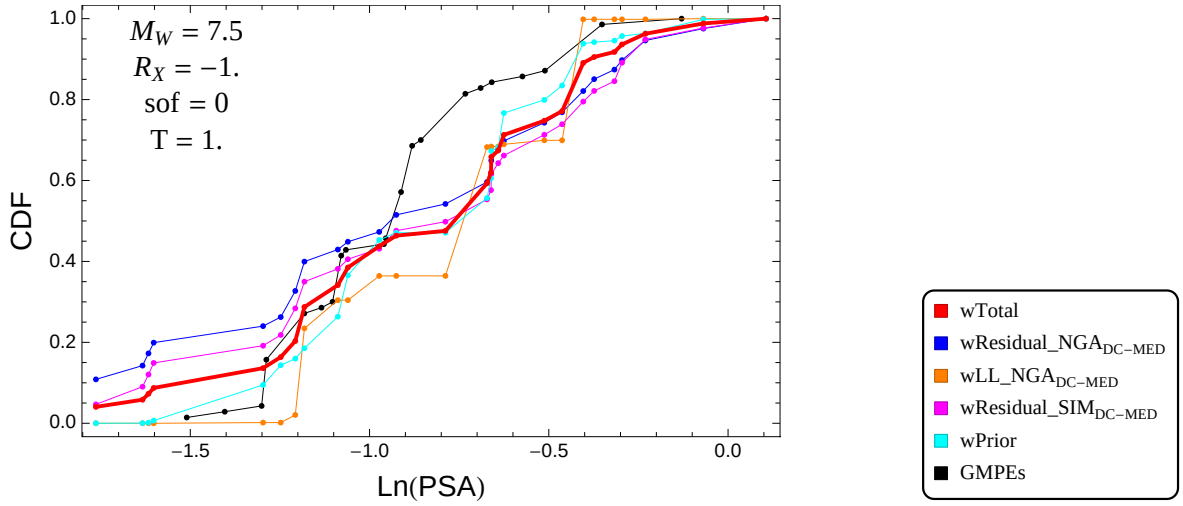



Figure 2.146: DCPPv4: Cumulative distribution function of GMPEs (black) and selected models, for different sets of weights, for a scenario with $M = 7.5$, $R_x = -1.$, $F = 0$, and $T = 1.$s

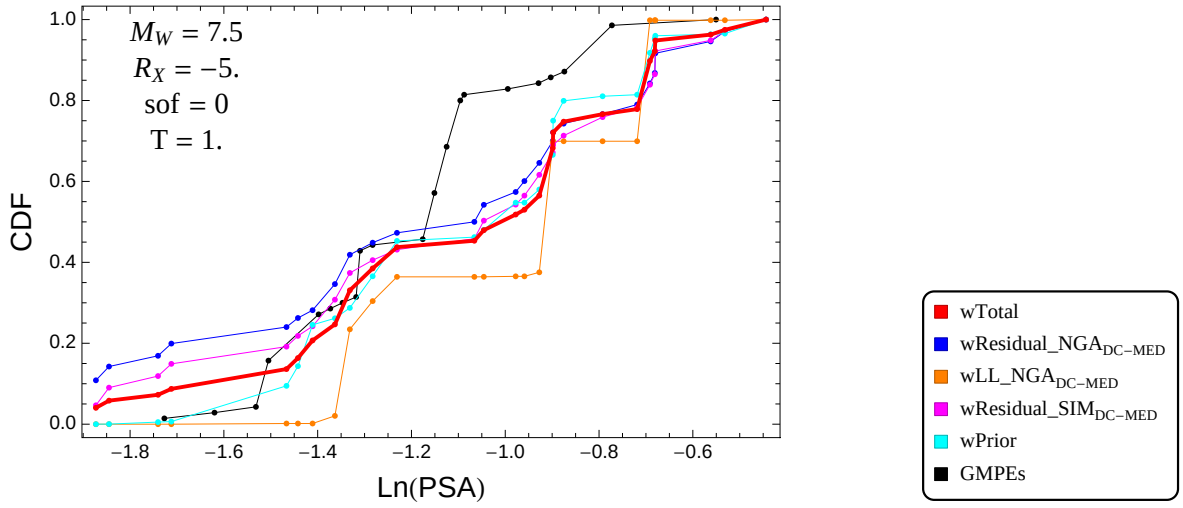



Figure 2.147: DCPPv4: Cumulative distribution function of GMPEs (black) and selected models, for different sets of weights, for a scenario with $M = 7.5$, $R_x = -5.$, $F = 0$, and $T = 1.$s

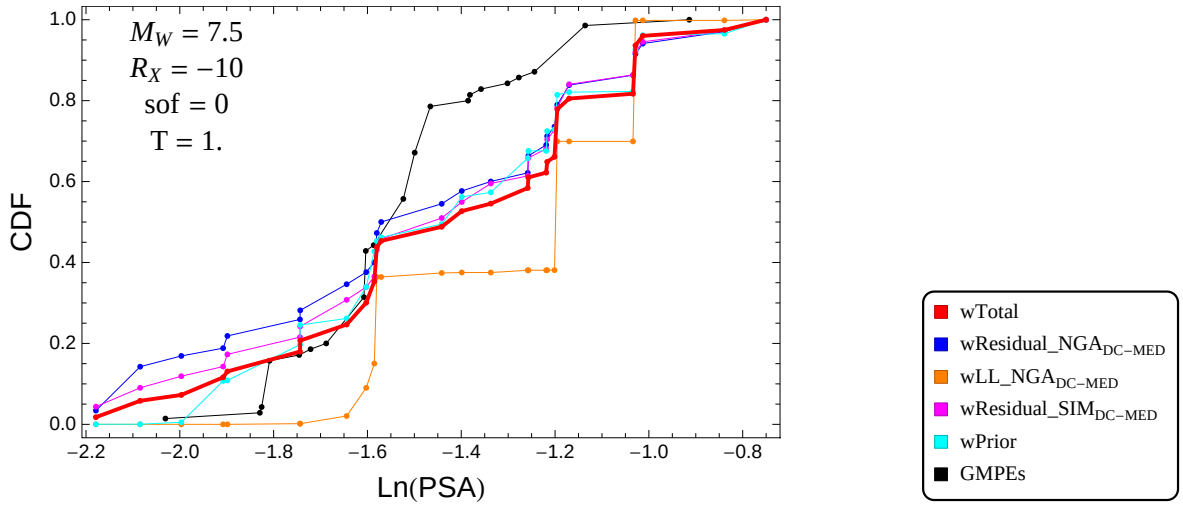



Figure 2.148: DCPPv4: Cumulative distribution function of GMPEs (black) and selected models, for different sets of weights, for a scenario with $M = 7.5$, $R_x = -10$, $F = 0$, and $T = 1$.s

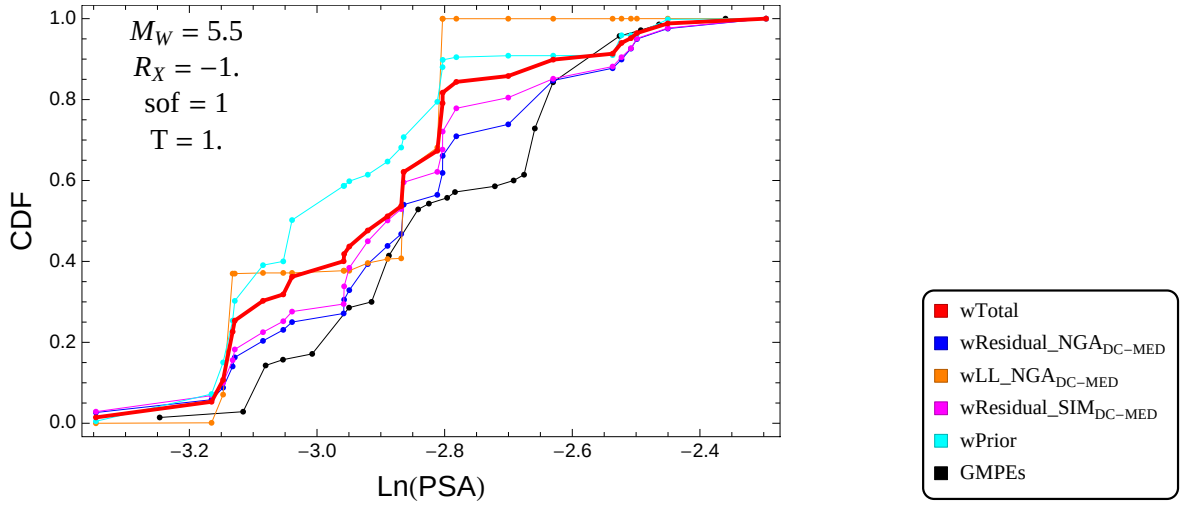



Figure 2.149: DCPPv4: Cumulative distribution function of GMPEs (black) and selected models, for different sets of weights, for a scenario with $M = 5.5$, $R_x = -1.$, $F = 1$, and $T = 1$.s

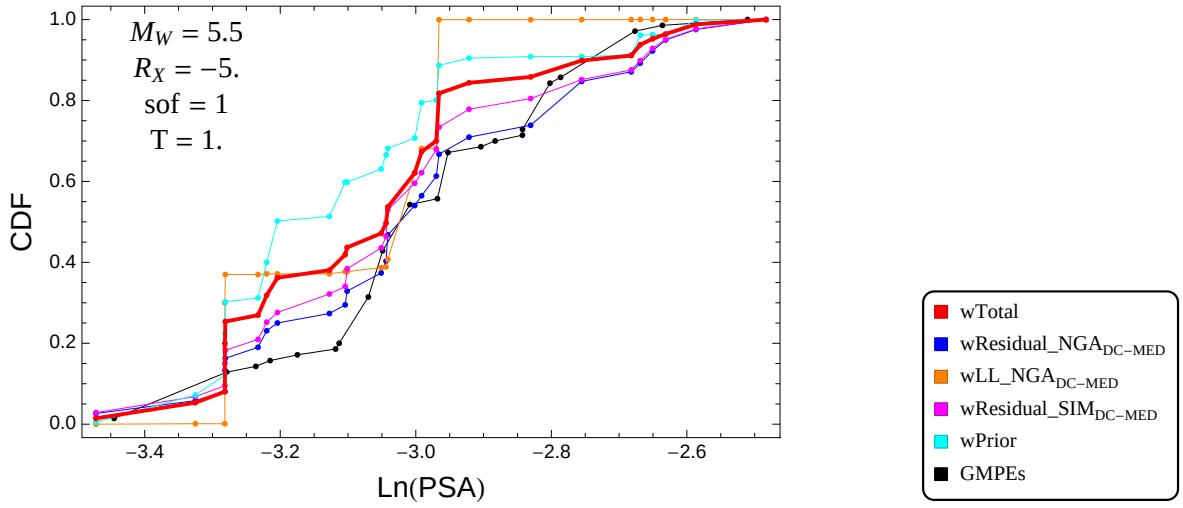



Figure 2.150: DCPPv4: Cumulative distribution function of GMPEs (black) and selected models, for different sets of weights, for a scenario with $M = 5.5$, $R_x = -5.$, $F = 1$, and $T = 1$.s

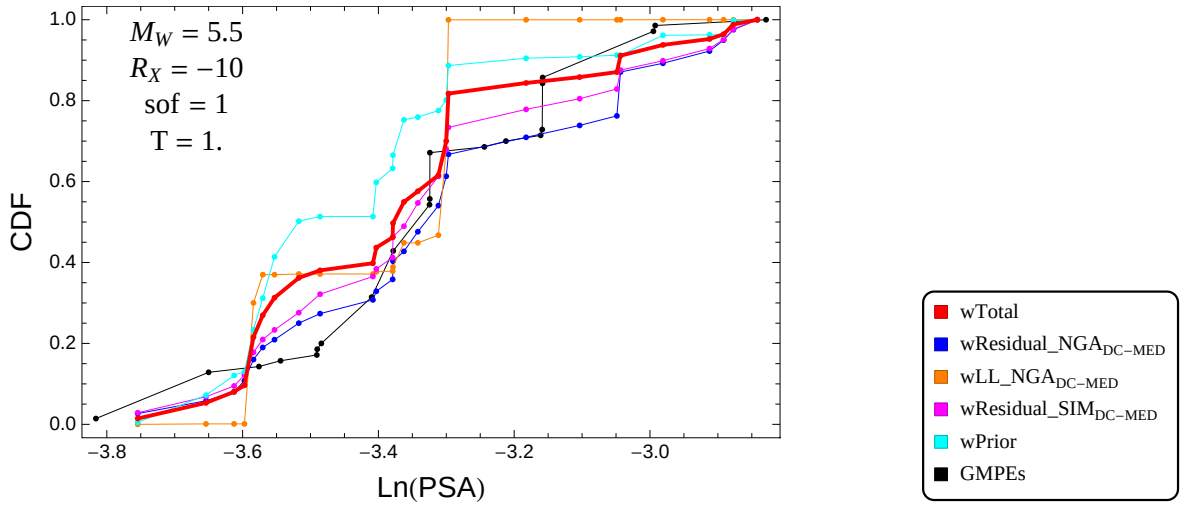



Figure 2.151: DCPPv4: Cumulative distribution function of GMPEs (black) and selected models, for different sets of weights, for a scenario with $M = 5.5$, $R_x = -10$, $F = 1$, and $T = 1$.s

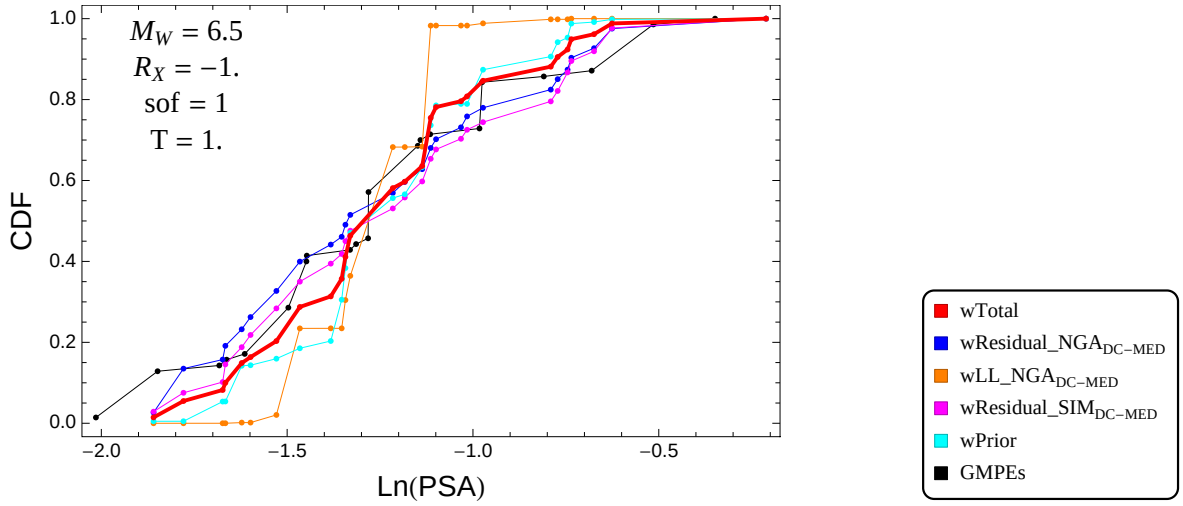



Figure 2.152: DCPPv4: Cumulative distribution function of GMPEs (black) and selected models, for different sets of weights, for a scenario with $M = 6.5$, $R_x = -1.$, $F = 1$, and $T = 1$.s

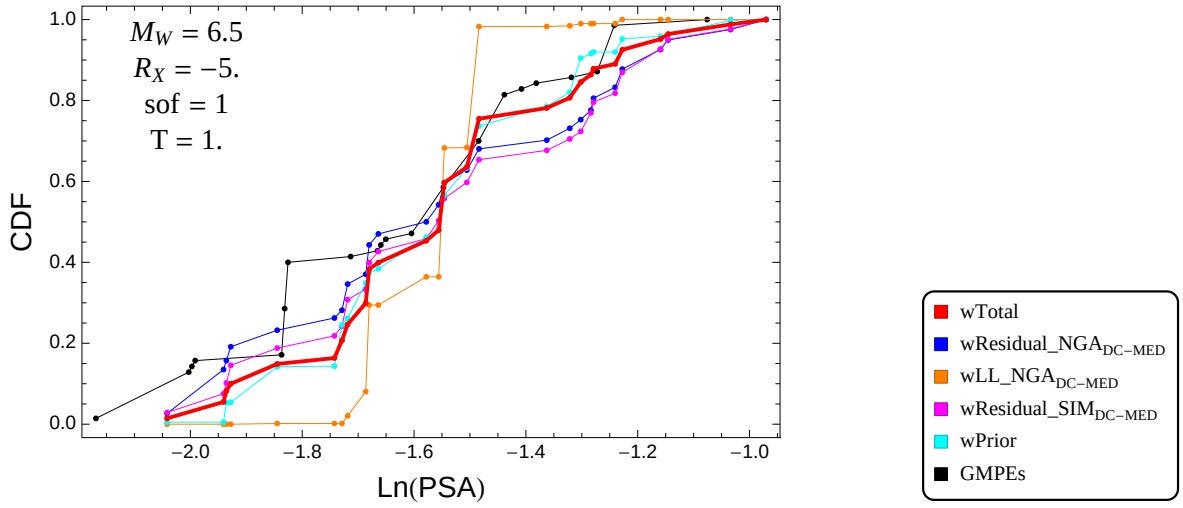



Figure 2.153: DCPPv4: Cumulative distribution function of GMPEs (black) and selected models, for different sets of weights, for a scenario with $M = 6.5$, $R_x = -5.$, $F = 1$, and $T = 1$.s

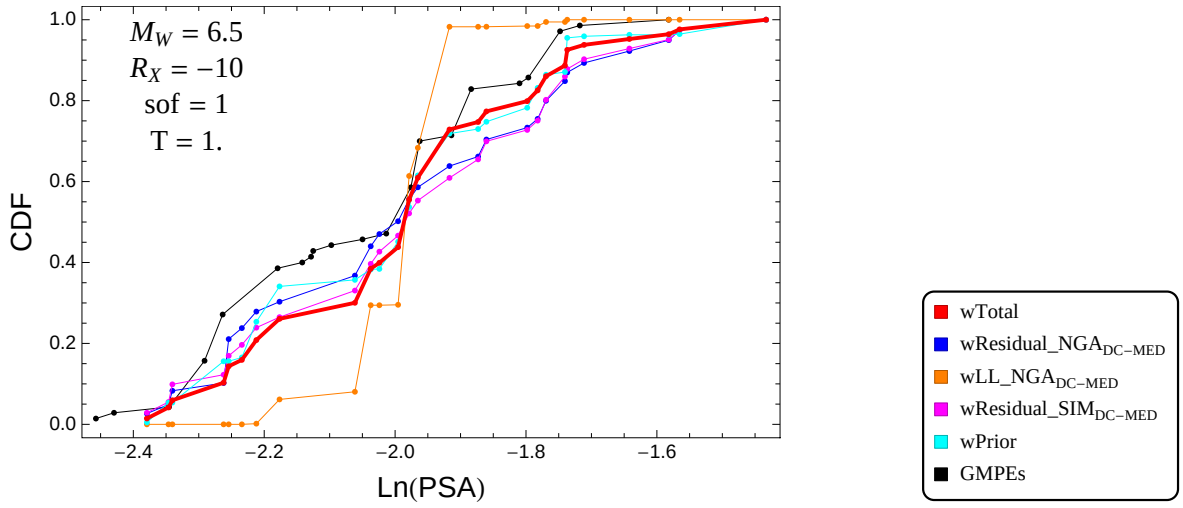



Figure 2.154: DCPPv4: Cumulative distribution function of GMPEs (black) and selected models, for different sets of weights, for a scenario with $M = 6.5$, $R_x = -10$, $F = 1$, and $T = 1.$s

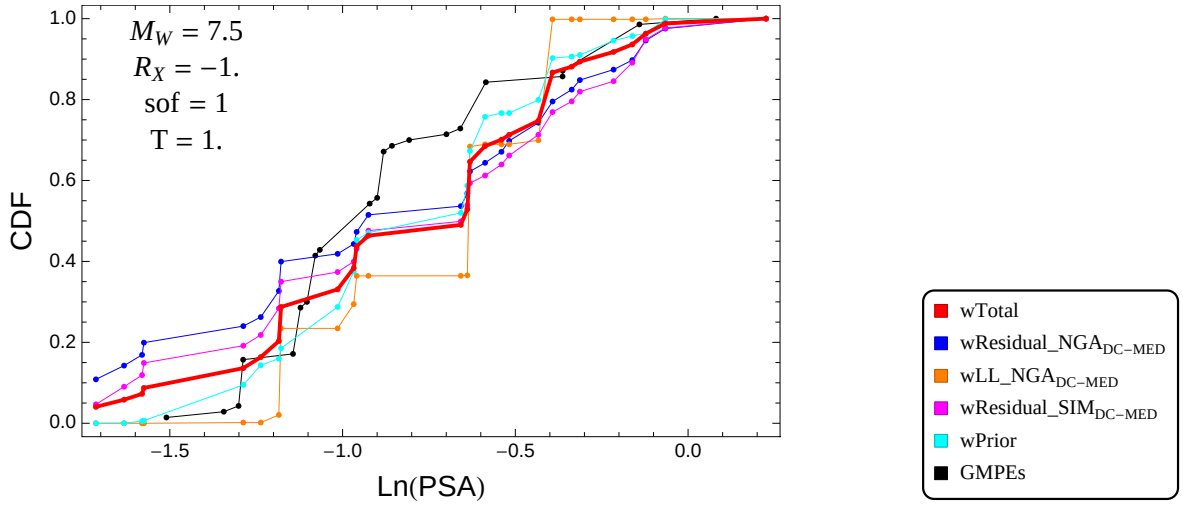



Figure 2.155: DCPPv4: Cumulative distribution function of GMPEs (black) and selected models, for different sets of weights, for a scenario with $M = 7.5$, $R_x = -1.$, $F = 1$, and $T = 1.$s

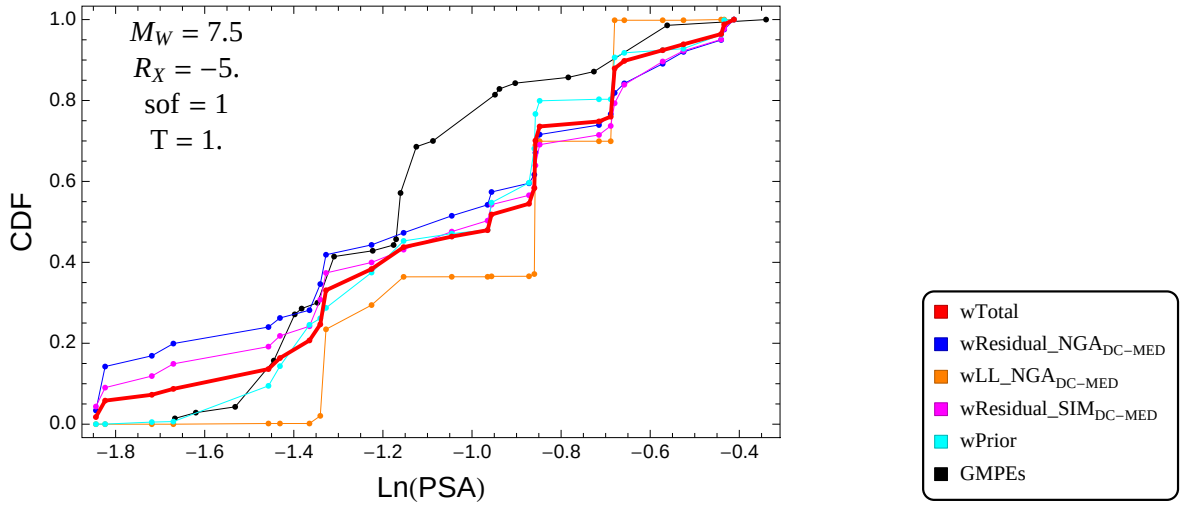



Figure 2.156: DCPPv4: Cumulative distribution function of GMPEs (black) and selected models, for different sets of weights, for a scenario with $M = 7.5$, $R_x = -5.$, $F = 1$, and $T = 1.$s

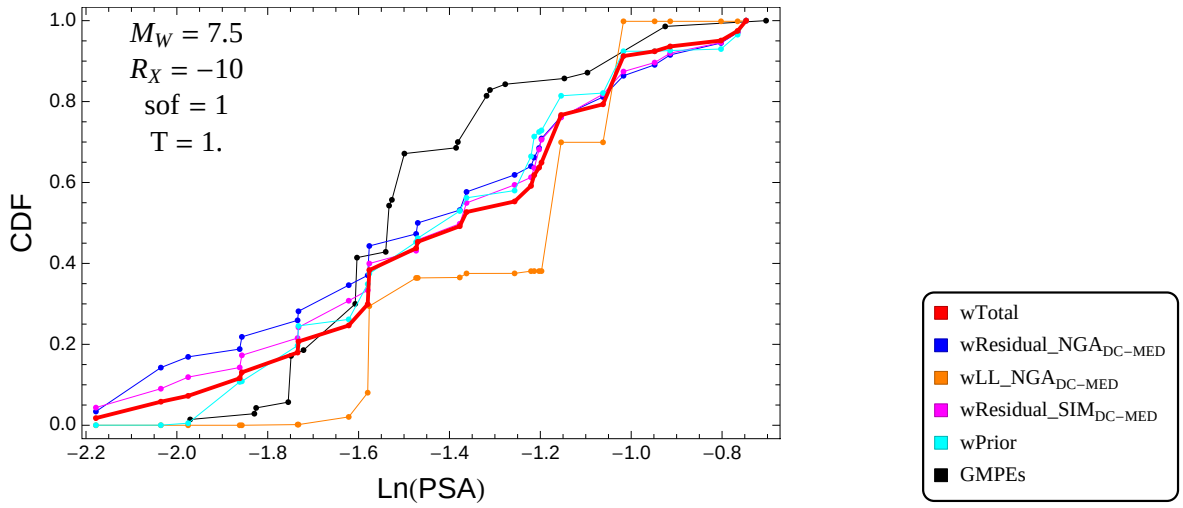



Figure 2.157: DCPPv4: Cumulative distribution function of GMPEs (black) and selected models, for different sets of weights, for a scenario with $M = 7.5$, $R_x = -10$, $F = 1$, and $T = 1$.s

**T = 3.s**

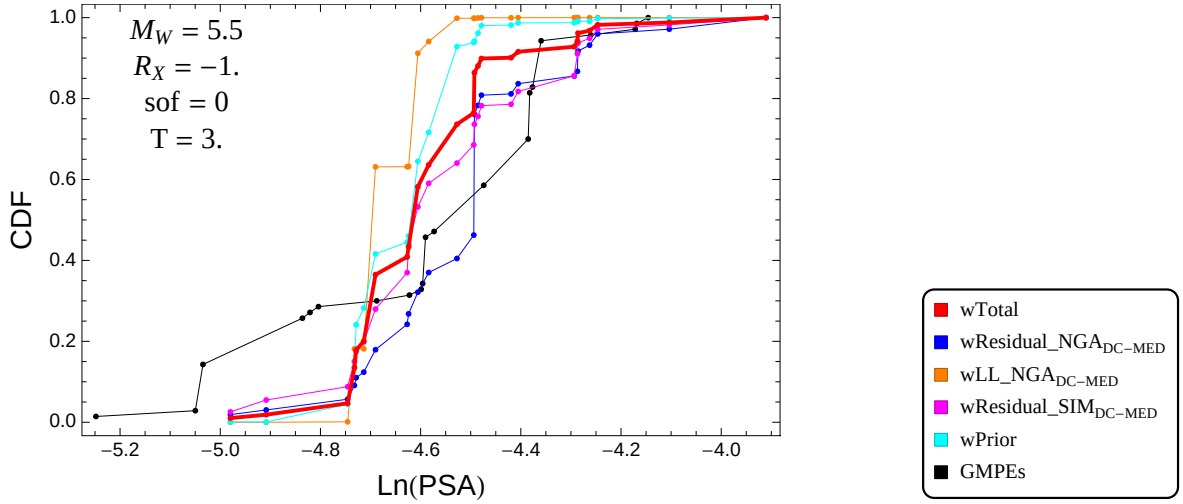



Figure 2.158: DCPPv4: Cumulative distribution function of GMPEs (black) and selected models, for different sets of weights, for a scenario with $M = 5.5$, $R_x = -1.$, $F = 0$, and $T = 3.$s

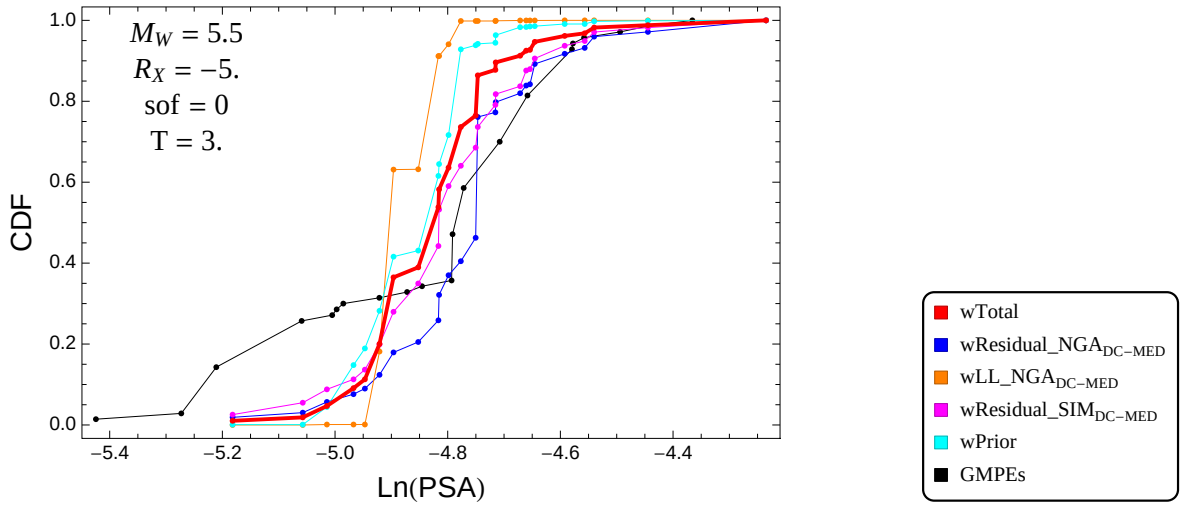



Figure 2.159: DCPPv4: Cumulative distribution function of GMPEs (black) and selected models, for different sets of weights, for a scenario with $M = 5.5$, $R_x = -5.$, $F = 0$, and $T = 3.$s

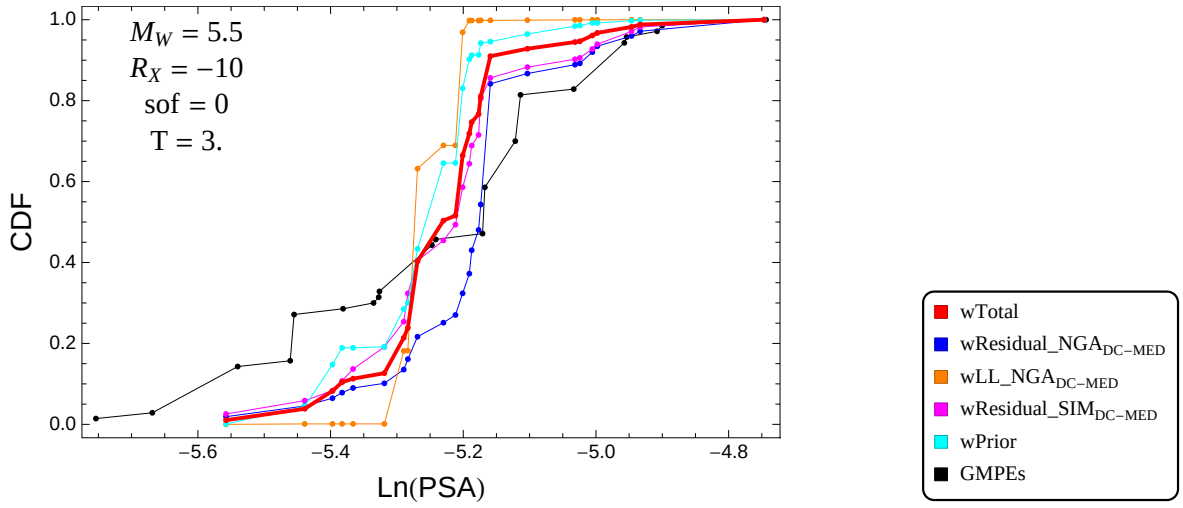



Figure 2.160: DCPPv4: Cumulative distribution function of GMPEs (black) and selected models, for different sets of weights, for a scenario with $M = 5.5$, $R_x = -10$, $F = 0$, and $T = 3.$s

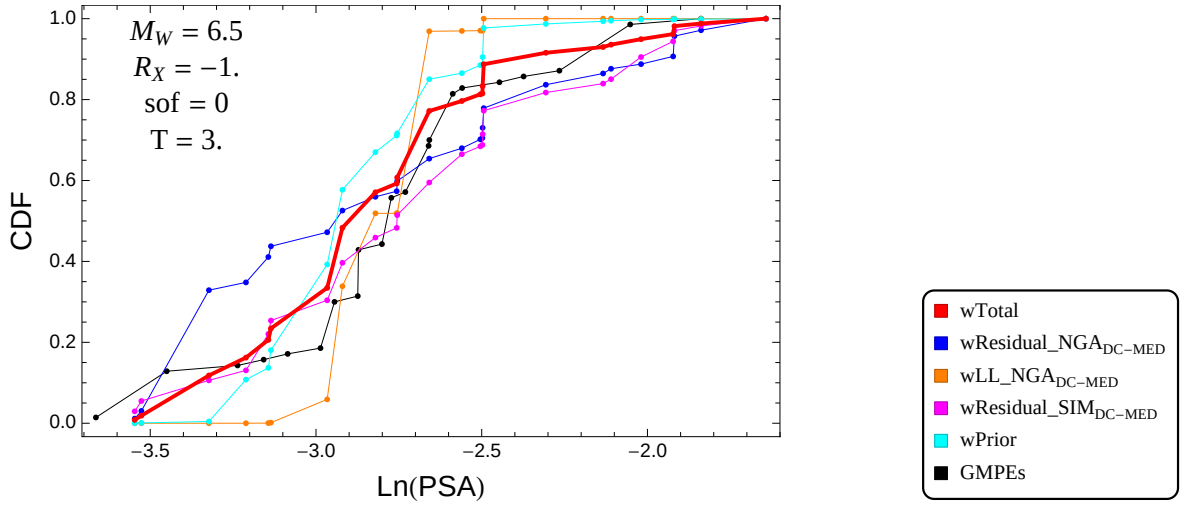



Figure 2.161: DCPPv4: Cumulative distribution function of GMPEs (black) and selected models, for different sets of weights, for a scenario with $M = 6.5$, $R_x = -1.$, $F = 0$, and $T = 3.$s

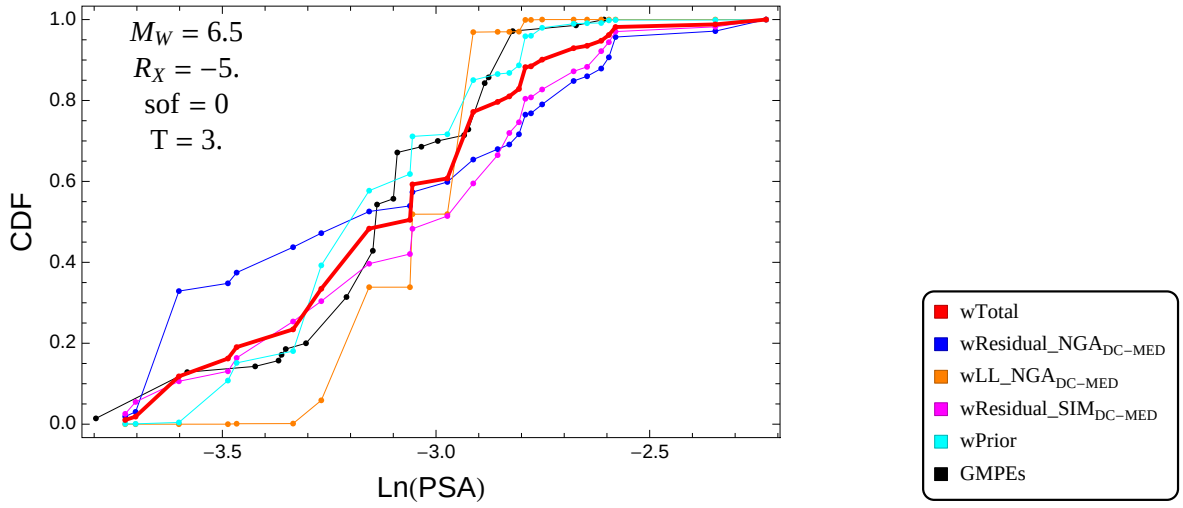



Figure 2.162: DCPPv4: Cumulative distribution function of GMPEs (black) and selected models, for different sets of weights, for a scenario with $M = 6.5$, $R_x = -5.$, $F = 0$, and $T = 3.$s

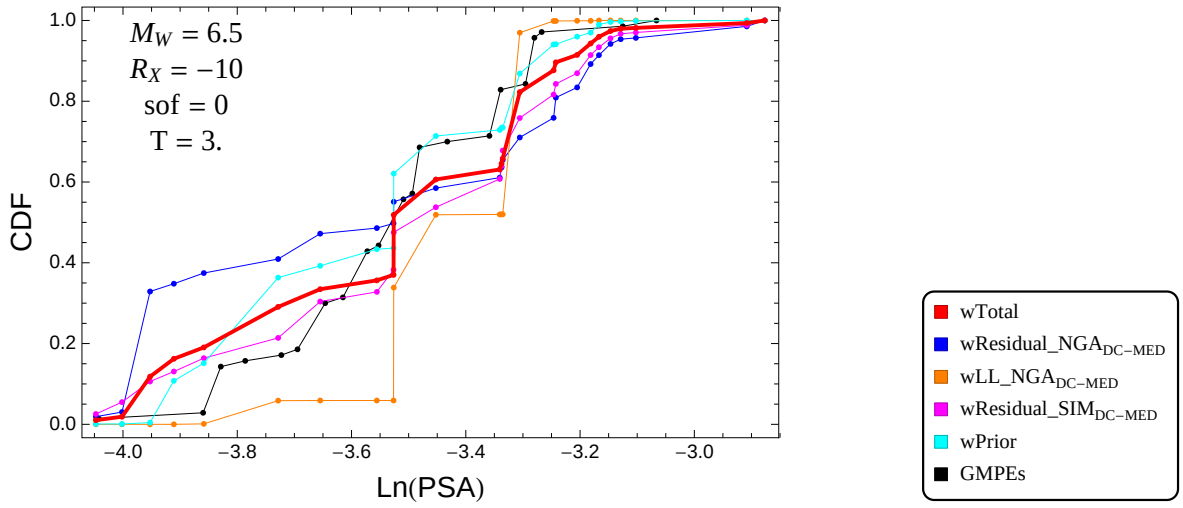



Figure 2.163: DCPPv4: Cumulative distribution function of GMPEs (black) and selected models, for different sets of weights, for a scenario with $M = 6.5$, $R_x = -10$, $F = 0$, and $T = 3.$s

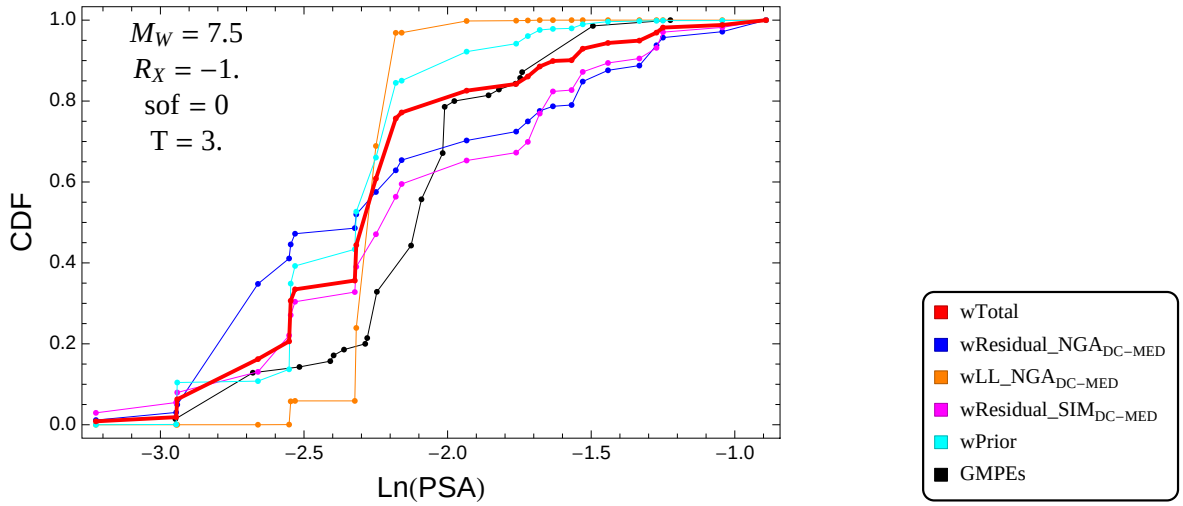



Figure 2.164: DCPPv4: Cumulative distribution function of GMPEs (black) and selected models, for different sets of weights, for a scenario with $M = 7.5$, $R_x = -1.$, $F = 0$, and $T = 3.$s

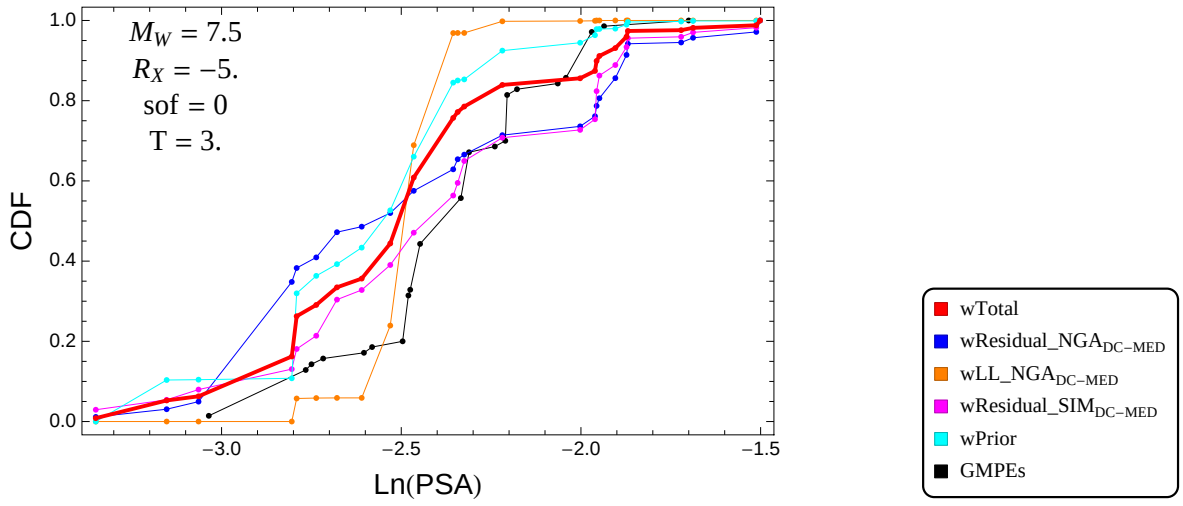



Figure 2.165: DCPPv4: Cumulative distribution function of GMPEs (black) and selected models, for different sets of weights, for a scenario with $M = 7.5$, $R_x = -5.$, $F = 0$, and $T = 3.$s

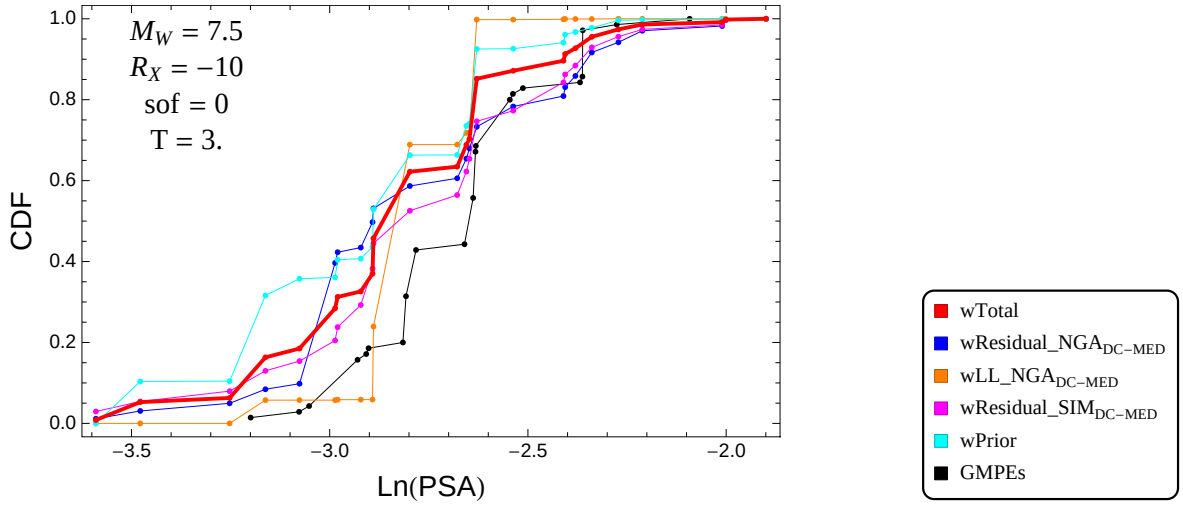



Figure 2.166: DCPPv4: Cumulative distribution function of GMPEs (black) and selected models, for different sets of weights, for a scenario with $M = 7.5$, $R_x = -10$, $F = 0$, and $T = 3.$s

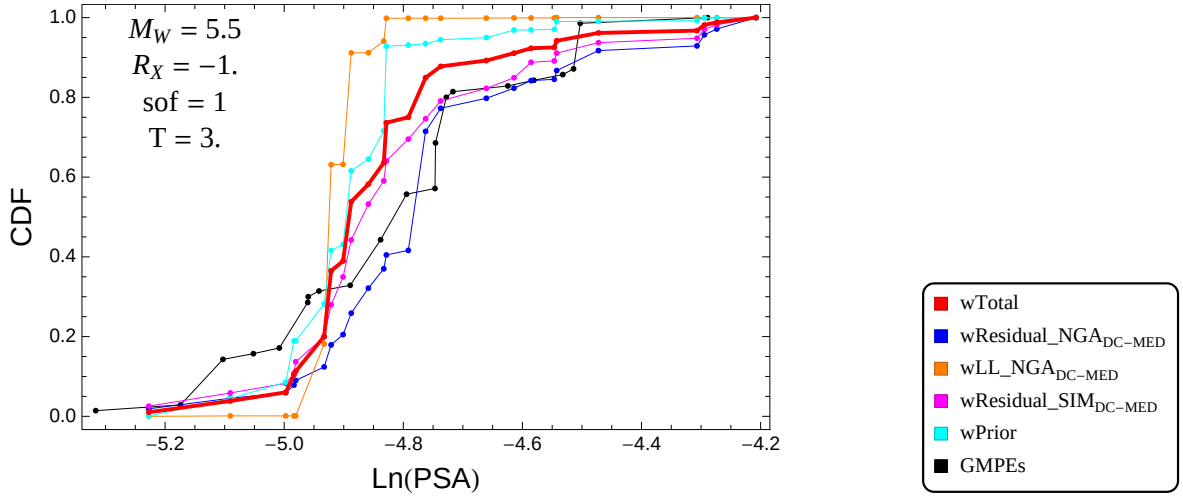



Figure 2.167: DCPPv4: Cumulative distribution function of GMPEs (black) and selected models, for different sets of weights, for a scenario with $M = 5.5$, $R_x = -1.$, $F = 1$, and $T = 3.$s

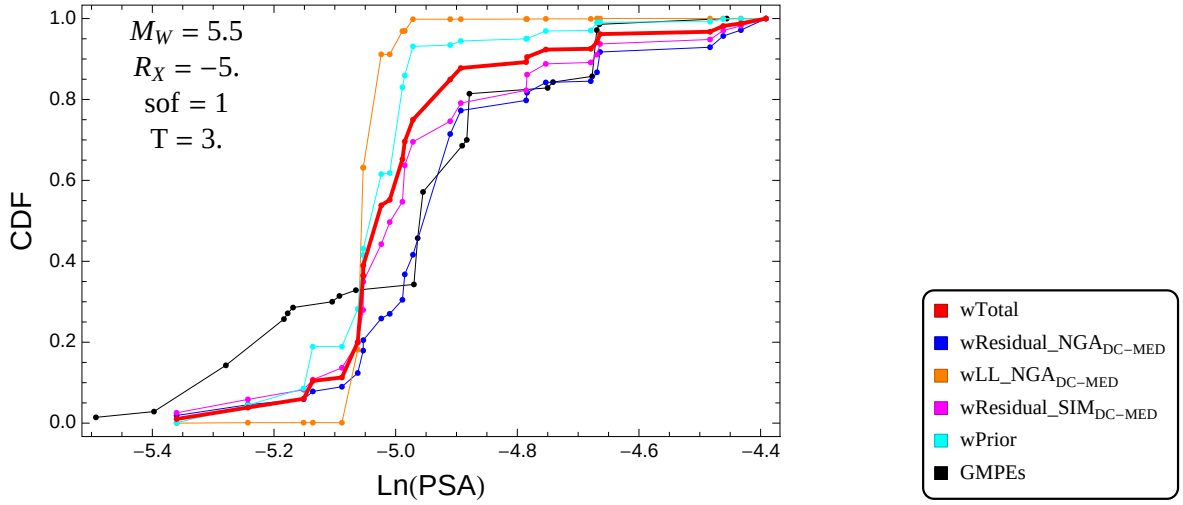



Figure 2.168: DCPPv4: Cumulative distribution function of GMPEs (black) and selected models, for different sets of weights, for a scenario with $M = 5.5$, $R_x = -5.$, $F = 1$, and $T = 3.$s

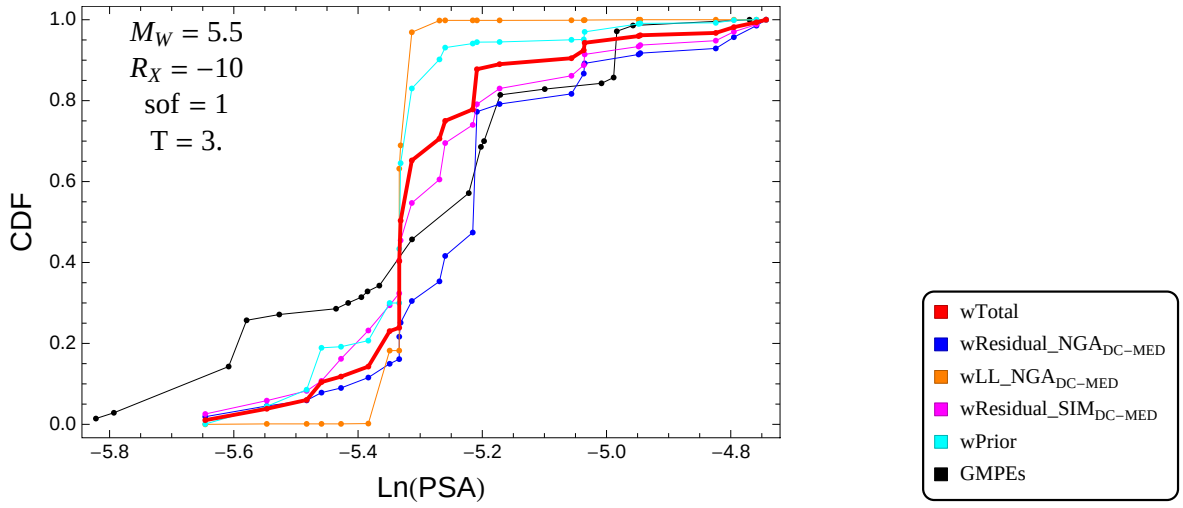



Figure 2.169: DCPPv4: Cumulative distribution function of GMPEs (black) and selected models, for different sets of weights, for a scenario with $M = 5.5$, $R_x = -10$, $F = 1$, and $T = 3.$s

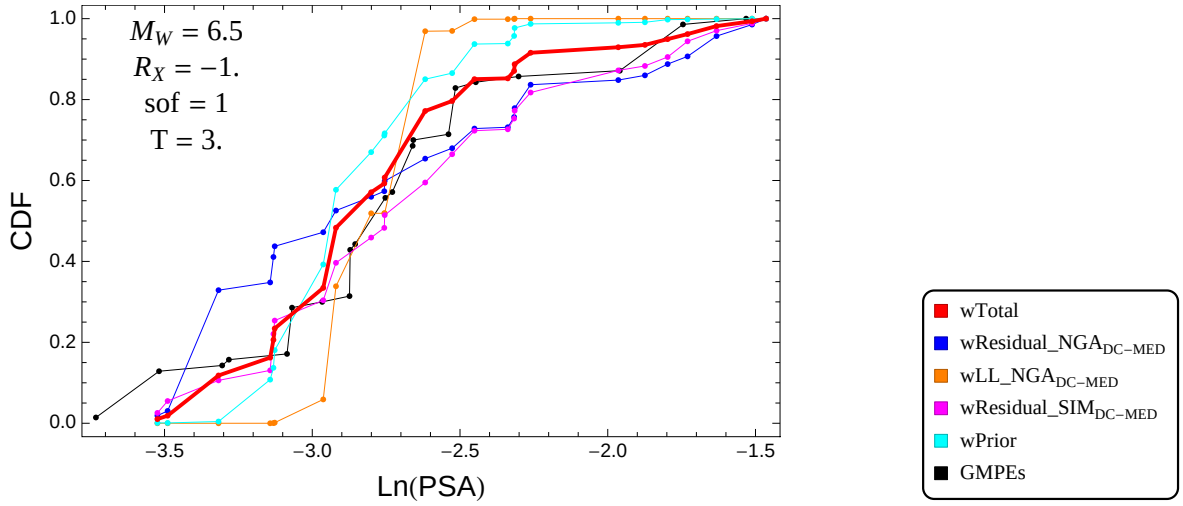



Figure 2.170: DCPPv4: Cumulative distribution function of GMPEs (black) and selected models, for different sets of weights, for a scenario with $M = 6.5$, $R_x = -1.$, $F = 1$, and $T = 3.$s

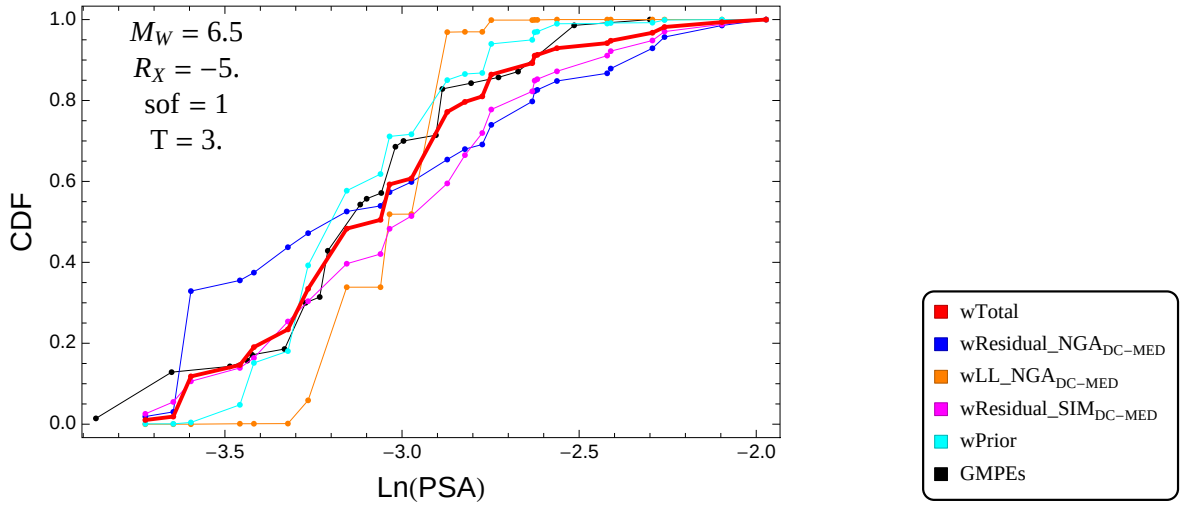



Figure 2.171: DCPPv4: Cumulative distribution function of GMPEs (black) and selected models, for different sets of weights, for a scenario with $M = 6.5$, $R_x = -5.$, $F = 1$, and $T = 3.$s

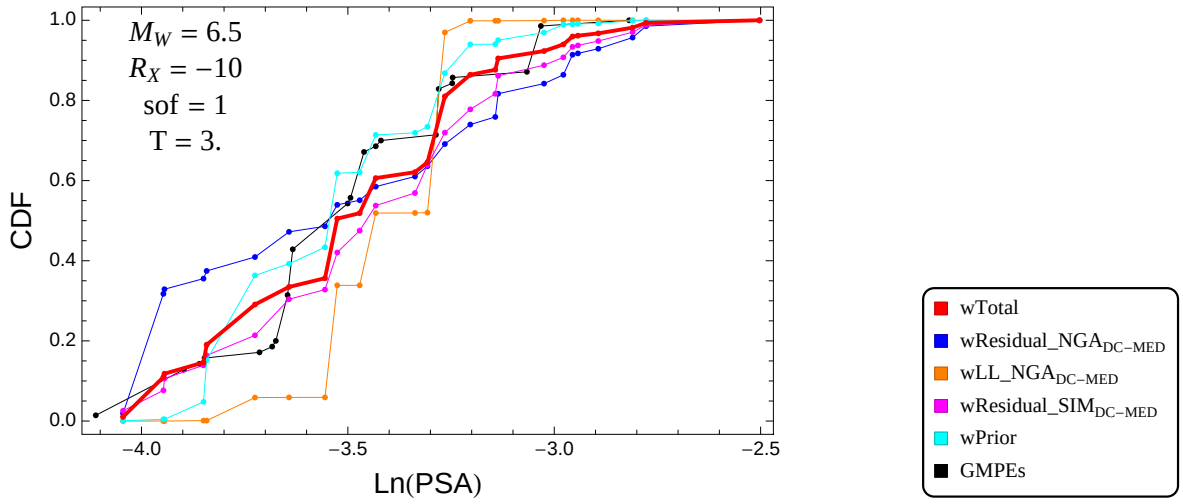



Figure 2.172: DCPPv4: Cumulative distribution function of GMPEs (black) and selected models, for different sets of weights, for a scenario with $M = 6.5$, $R_x = -10$, $F = 1$, and $T = 3.$s

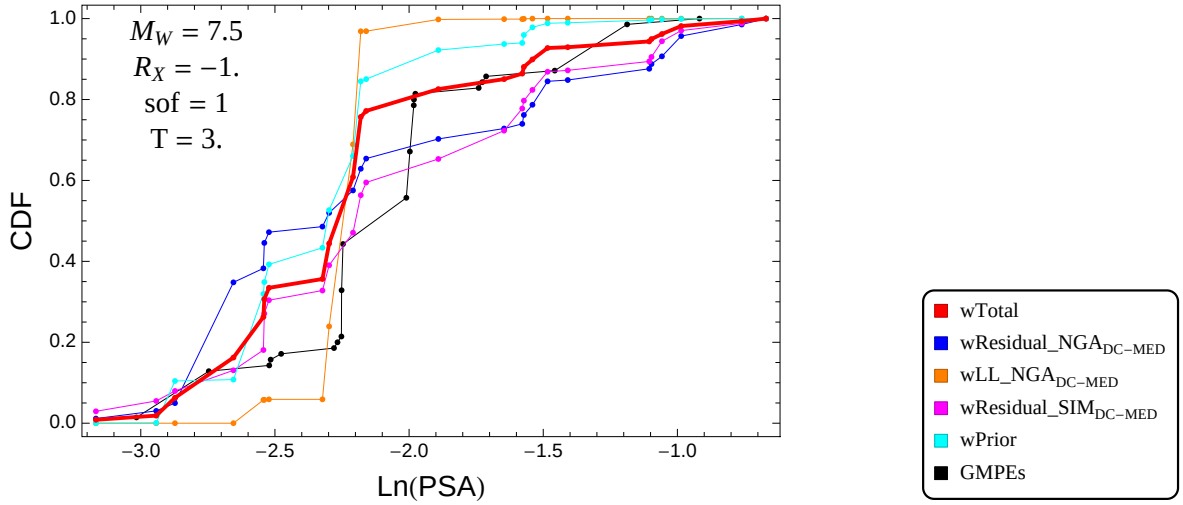



Figure 2.173: DCPPv4: Cumulative distribution function of GMPEs (black) and selected models, for different sets of weights, for a scenario with $M = 7.5$, $R_x = -1.$, $F = 1$, and $T = 3.$s

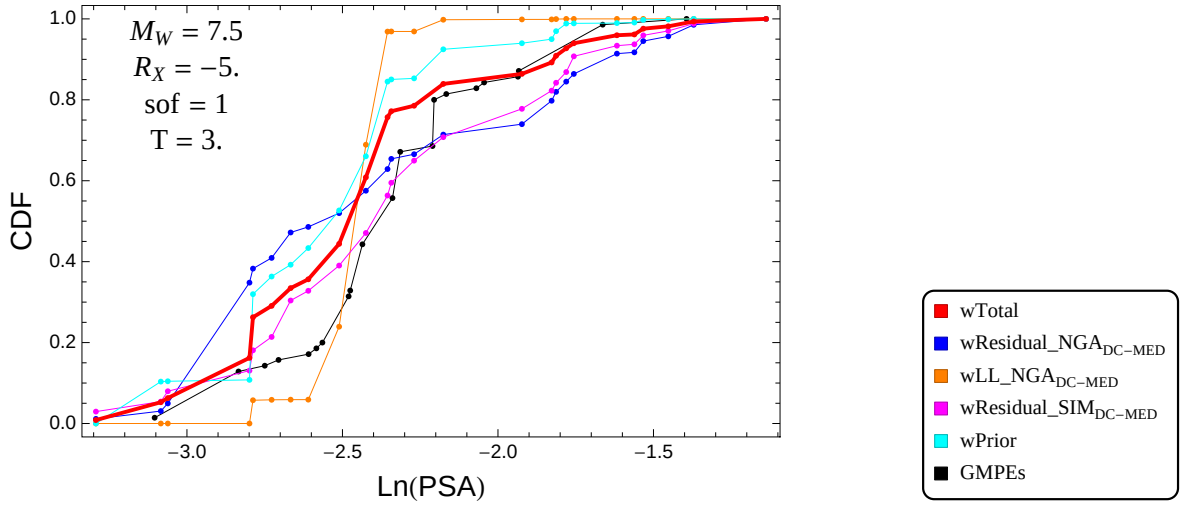



Figure 2.174: DCPPv4: Cumulative distribution function of GMPEs (black) and selected models, for different sets of weights, for a scenario with $M = 7.5$, $R_x = -5.$, $F = 1$, and $T = 3.$s

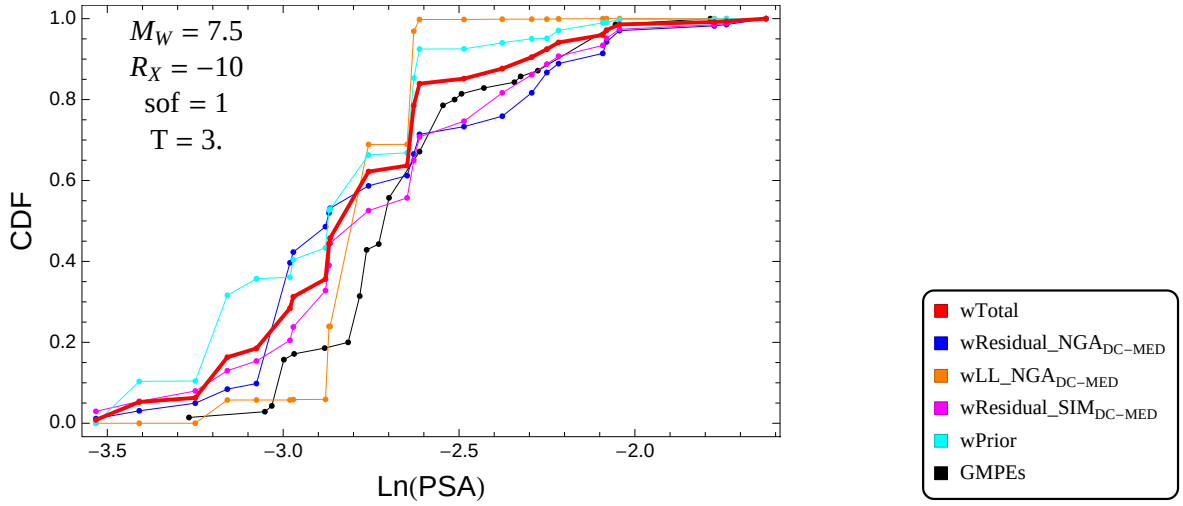



Figure 2.175: DCPPv4: Cumulative distribution function of GMPEs (black) and selected models, for different sets of weights, for a scenario with $M = 7.5$, $R_x = -10$, $F = 1$, and $T = 3$.s

### 2.1.7 Quantile Plots vs. Distance

**T = 0.01s**

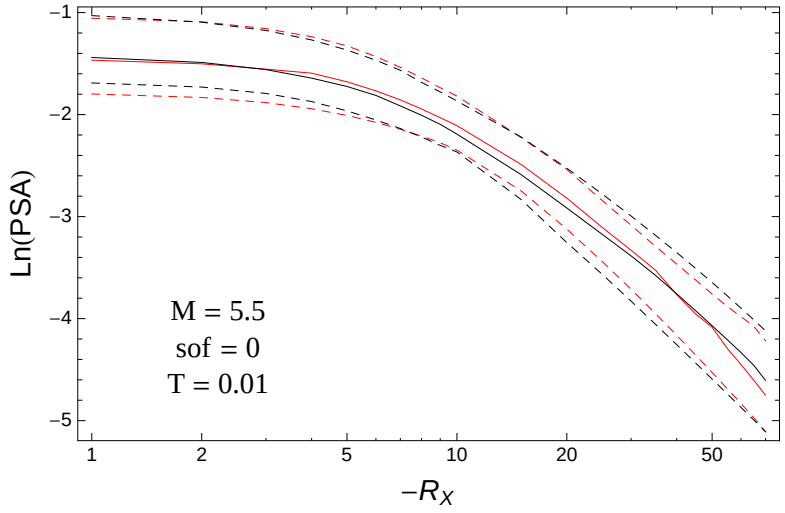



Figure 2.176: DCPPv4: Distance scaling of 0.05,0.5,0.95 quantile of the GMPE distribution (black) and the ModelA distribution (red) with total weights, for a scenario with $M = 5.5$, $F = 0$, and $T = 0.01$s.

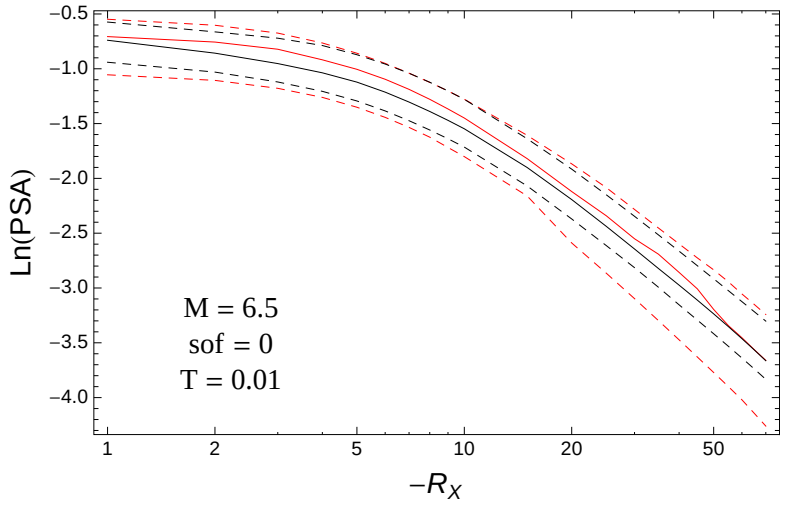



Figure 2.177: DCPPv4: Distance scaling of 0.05,0.5,0.95 quantile of the GMPE distribution (black) and the ModelA distribution (red) with total weights, for a scenario with $M = 6.5$, $F = 0$, and $T = 0.01$s.

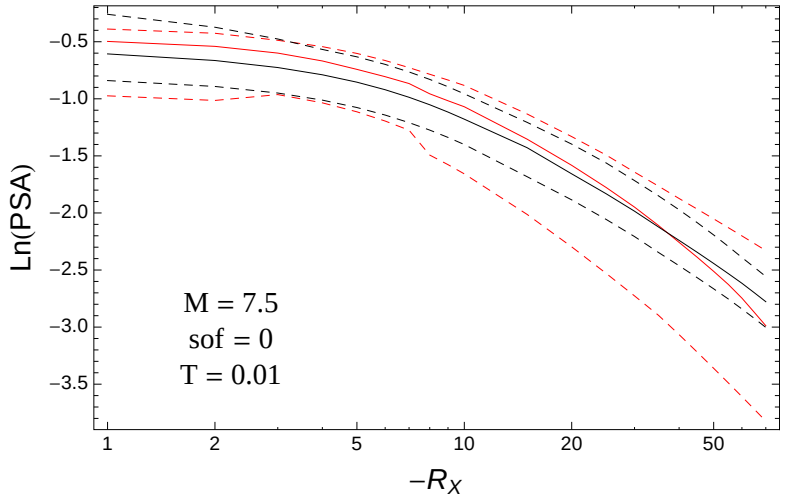



Figure 2.178: DCPPv4: Distance scaling of 0.05,0.5,0.95 quantile of the GMPE distribution (black) and the ModelA distribution (red) with total weights, for a scenario with $M = 7.5$, $F = 0$, and $T = 0.01$s.

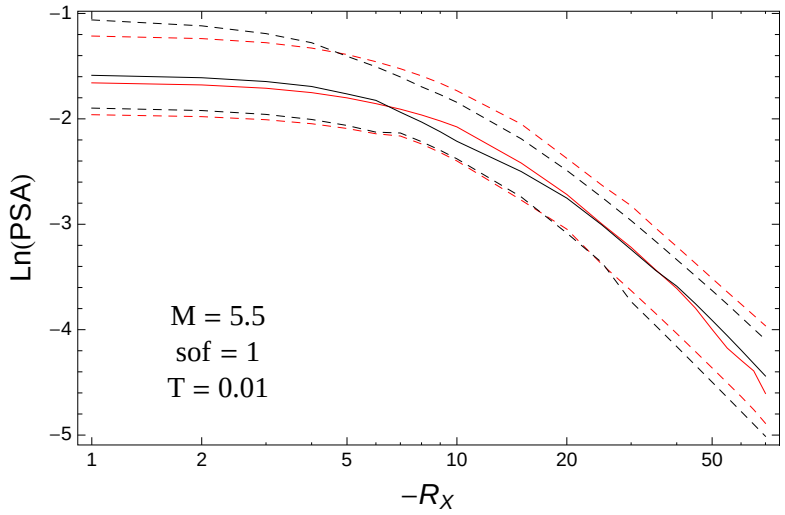



Figure 2.179: DCPPv4: Distance scaling of 0.05,0.5,0.95 quantile of the GMPE distribution (black) and the ModelA distribution (red) with total weights, for a scenario with $M = 5.5$, $F = 1$, and $T = 0.01$s.

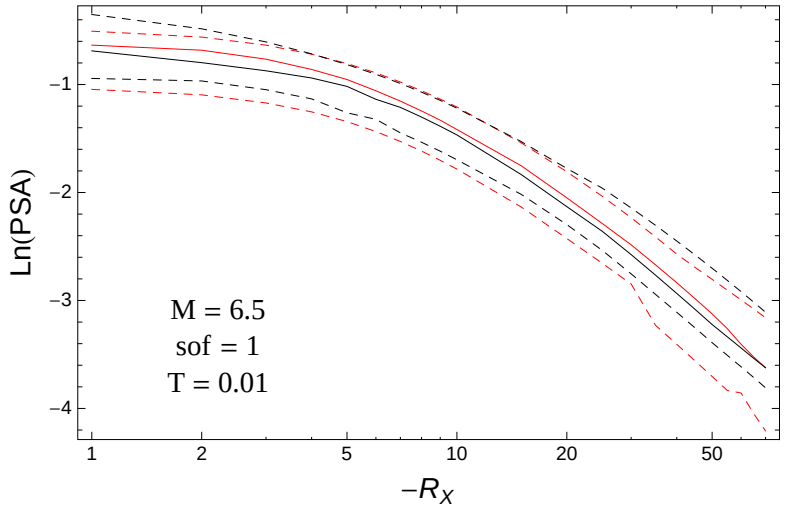



Figure 2.180: DCPPv4: Distance scaling of 0.05,0.5,0.95 quantile of the GMPE distribution (black) and the ModelA distribution (red) with total weights, for a scenario with $M = 6.5$, $F = 1$, and $T = 0.01$s.

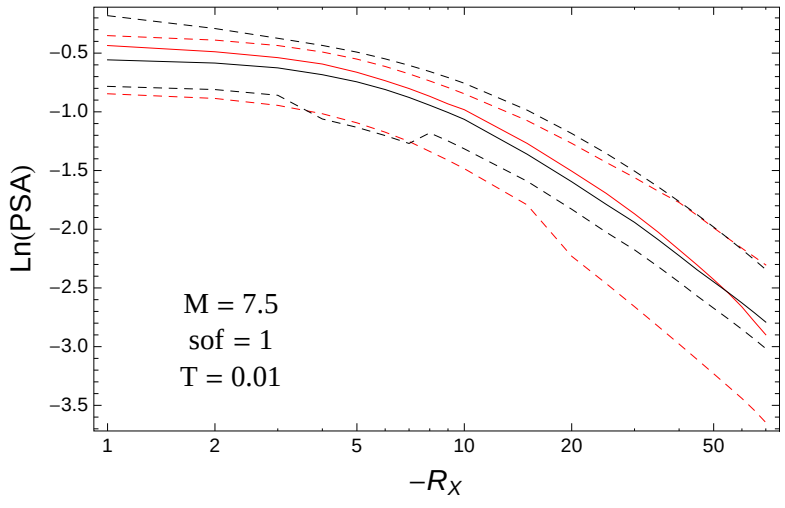



Figure 2.181: DCPPv4: Distance scaling of 0.05,0.5,0.95 quantile of the GMPE distribution (black) and the ModelA distribution (red) with total weights, for a scenario with $M = 7.5$, $F = 1$, and $T = 0.01$s.

**T = 0.2s**

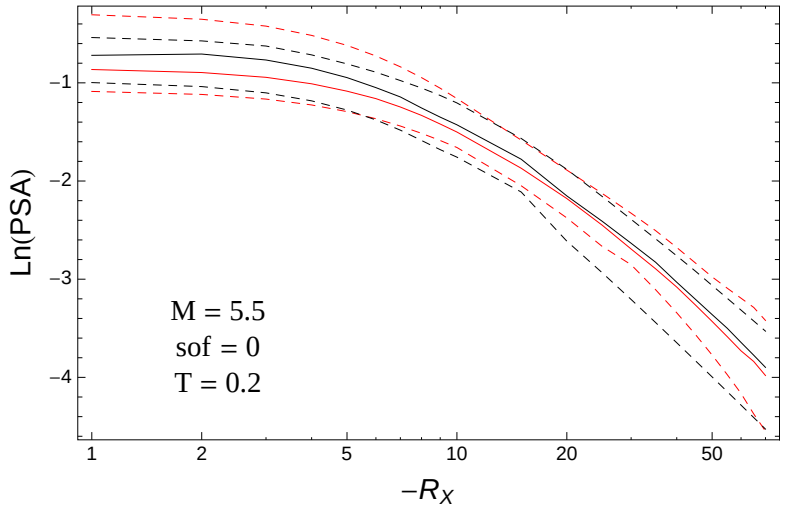



Figure 2.182: DCPPv4: Distance scaling of 0.05,0.5,0.95 quantile of the GMPE distribution (black) and the ModelA distribution (red) with total weights, for a scenario with $M = 5.5$, $F = 0$, and $T = 0.2$s.

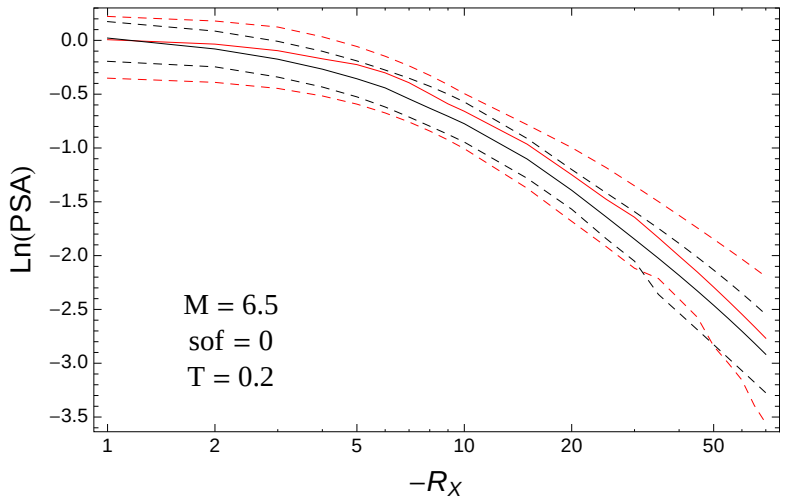



Figure 2.183: DCPPv4: Distance scaling of 0.05,0.5,0.95 quantile of the GMPE distribution (black) and the ModelA distribution (red) with total weights, for a scenario with $M = 6.5$, $F = 0$, and $T = 0.2$s.

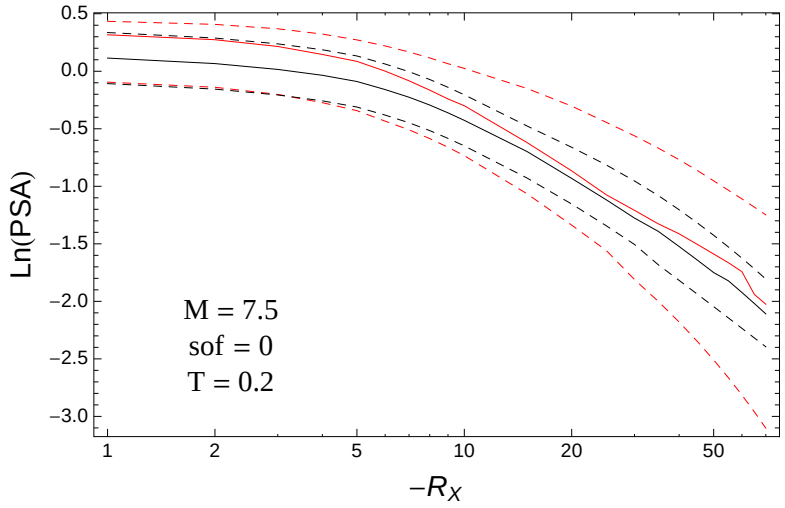



Figure 2.184: DCPPv4: Distance scaling of 0.05,0.5,0.95 quantile of the GMPE distribution (black) and the ModelA distribution (red) with total weights, for a scenario with $M = 7.5$, $F = 0$, and $T = 0.2$s.

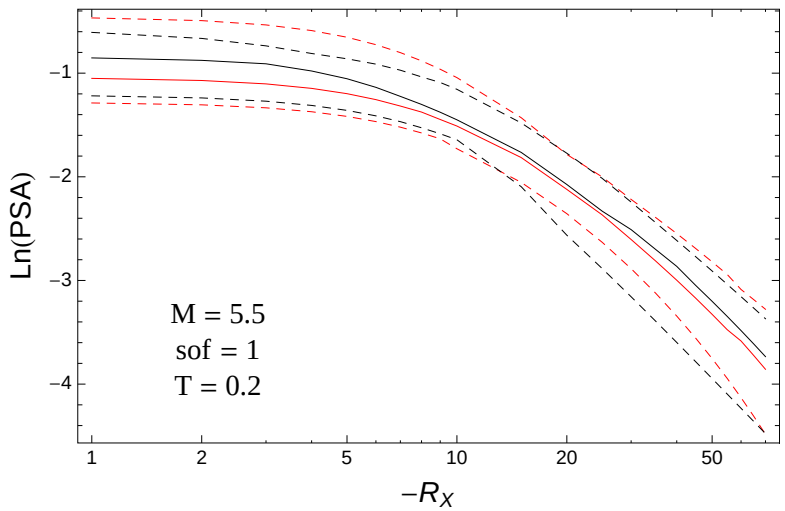



Figure 2.185: DCPPv4: Distance scaling of 0.05,0.5,0.95 quantile of the GMPE distribution (black) and the ModelA distribution (red) with total weights, for a scenario with $M = 5.5$, $F = 1$, and $T = 0.2$s.

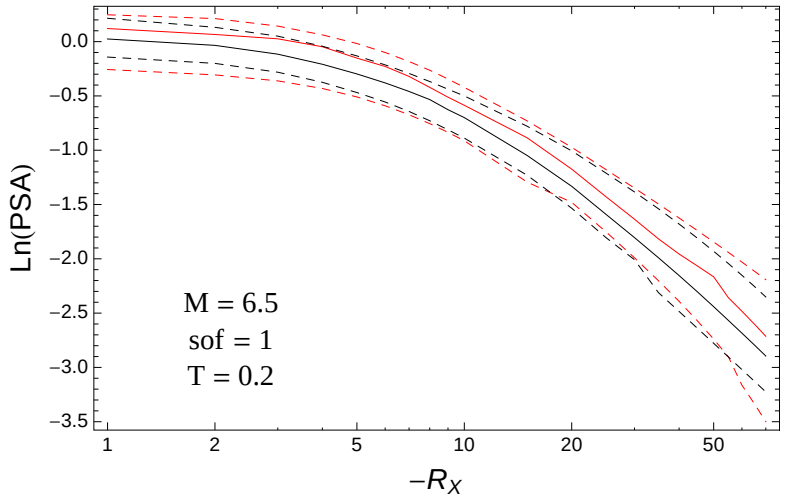



Figure 2.186: DCPPv4: Distance scaling of 0.05,0.5,0.95 quantile of the GMPE distribution (black) and the ModelA distribution (red) with total weights, for a scenario with $M = 6.5$, $F = 1$, and $T = 0.2$s.

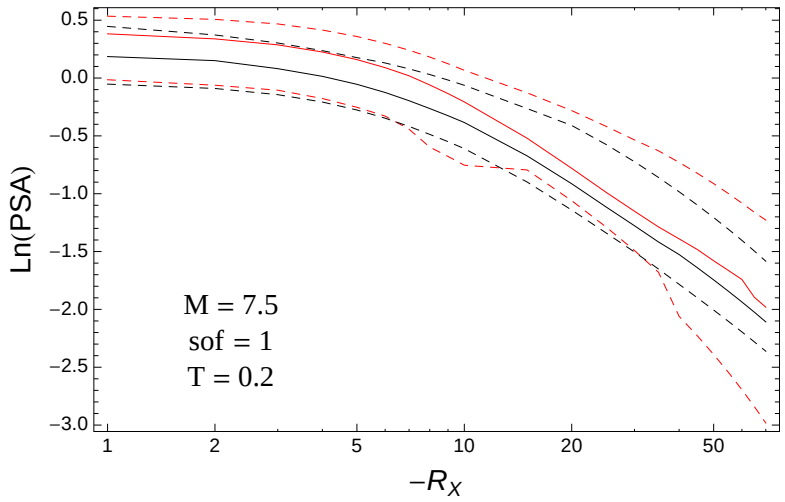



Figure 2.187: DCPPv4: Distance scaling of 0.05,0.5,0.95 quantile of the GMPE distribution (black) and the ModelA distribution (red) with total weights, for a scenario with $M = 7.5$, $F = 1$, and $T = 0.2$s.

**T = 0.5s**

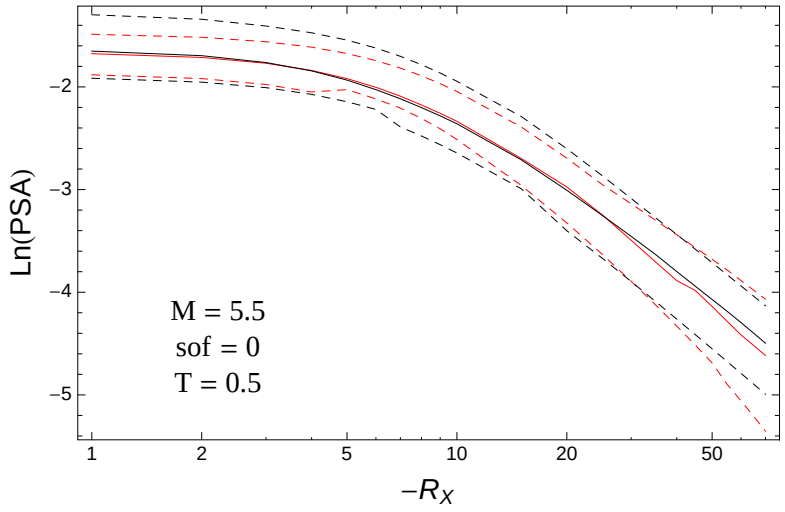



Figure 2.188: DCPPv4: Distance scaling of 0.05,0.5,0.95 quantile of the GMPE distribution (black) and the ModelA distribution (red) with total weights, for a scenario with $M = 5.5$, $F = 0$, and $T = 0.5$s.

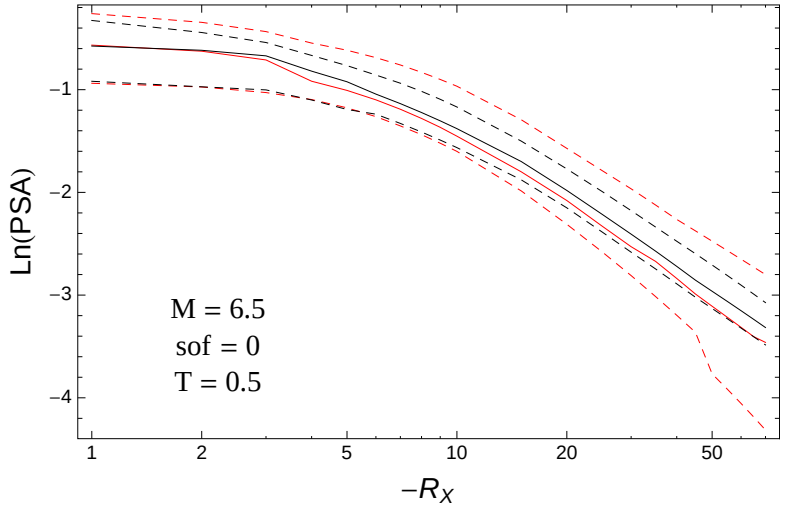



Figure 2.189: DCPPv4: Distance scaling of 0.05,0.5,0.95 quantile of the GMPE distribution (black) and the ModelA distribution (red) with total weights, for a scenario with $M = 6.5$, $F = 0$, and $T = 0.5$s.

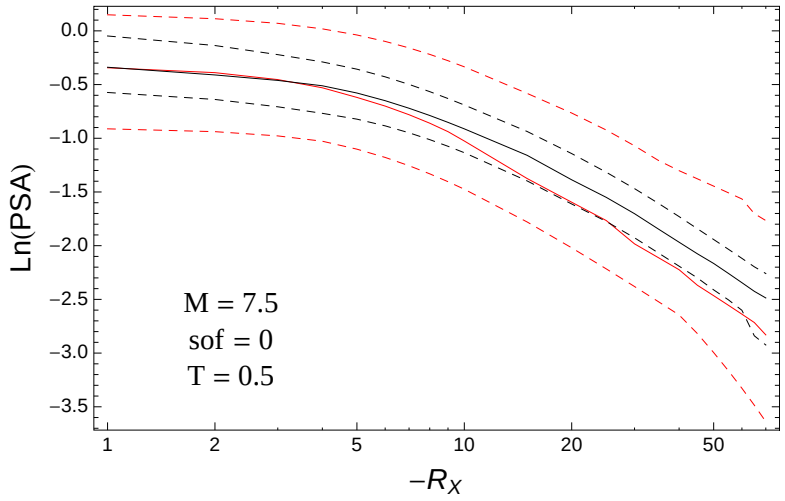



Figure 2.190: DCPPv4: Distance scaling of 0.05,0.5,0.95 quantile of the GMPE distribution (black) and the ModelA distribution (red) with total weights, for a scenario with $M = 7.5$, $F = 0$, and $T = 0.5$s.

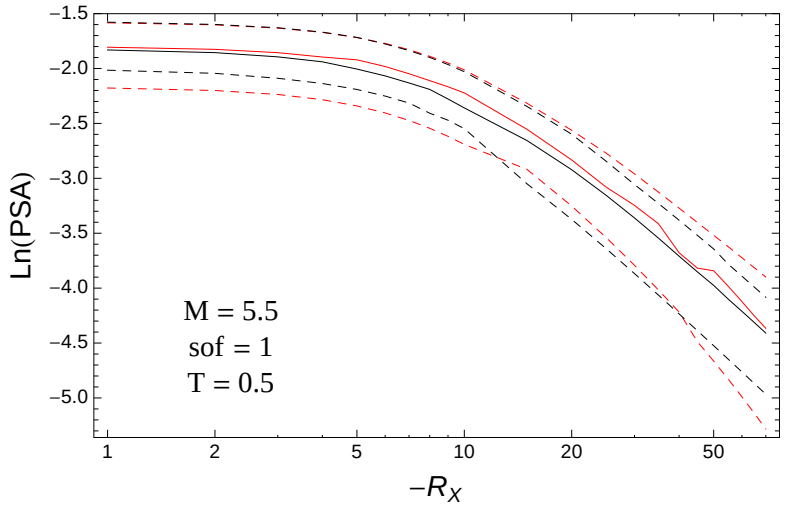



Figure 2.191: DCPPv4: Distance scaling of 0.05,0.5,0.95 quantile of the GMPE distribution (black) and the ModelA distribution (red) with total weights, for a scenario with $M = 5.5$, $F = 1$, and $T = 0.5$s.

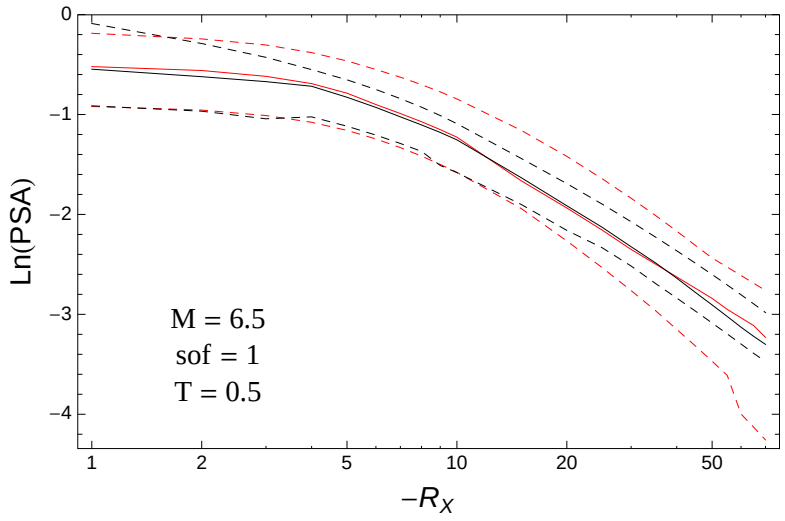



Figure 2.192: DCPPv4: Distance scaling of 0.05,0.5,0.95 quantile of the GMPE distribution (black) and the ModelA distribution (red) with total weights, for a scenario with $M = 6.5$, $F = 1$, and $T = 0.5$s.

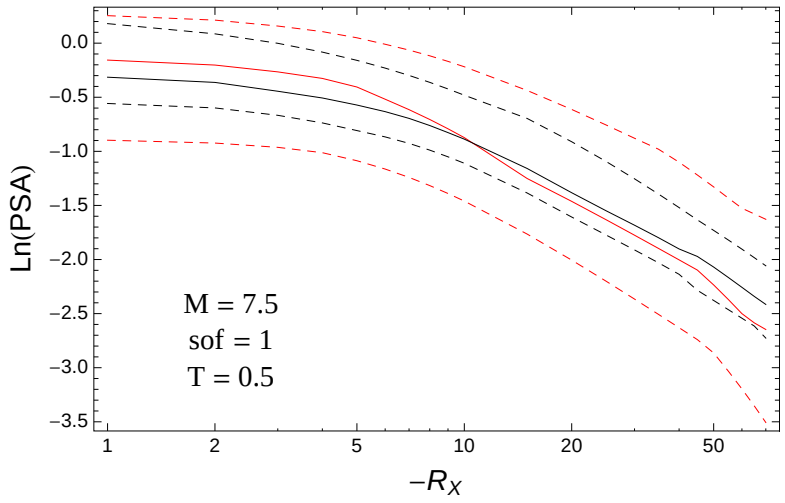



Figure 2.193: DCPPv4: Distance scaling of 0.05,0.5,0.95 quantile of the GMPE distribution (black) and the ModelA distribution (red) with total weights, for a scenario with $M = 7.5$, $F = 1$, and $T = 0.5$s.

**T = 1.s**

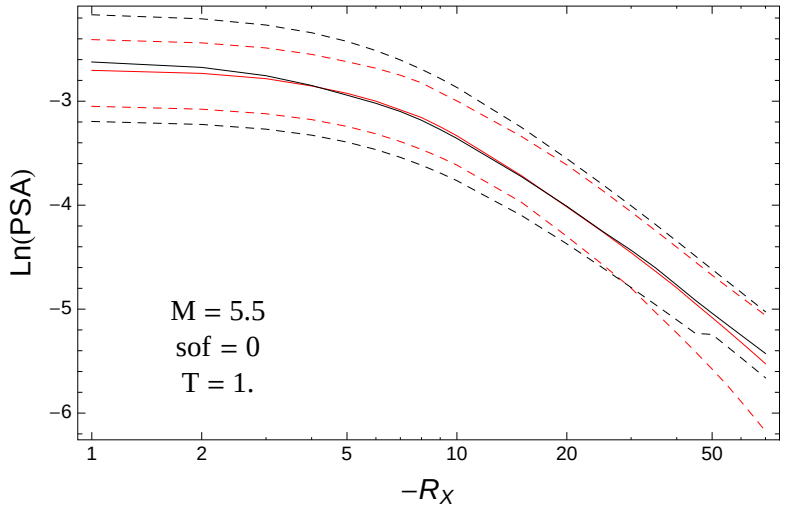



Figure 2.194: DCPPv4: Distance scaling of 0.05,0.5,0.95 quantile of the GMPE distribution (black) and the ModelA distribution (red) with total weights, for a scenario with $M = 5.5$, $F = 0$, and $T = 1.$s.

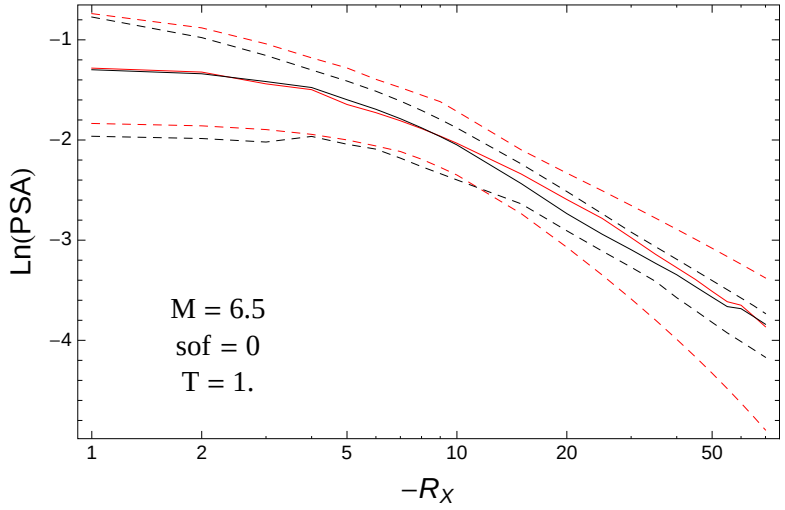



Figure 2.195: DCPPv4: Distance scaling of 0.05,0.5,0.95 quantile of the GMPE distribution (black) and the ModelA distribution (red) with total weights, for a scenario with $M = 6.5$, $F = 0$, and $T = 1.$s.

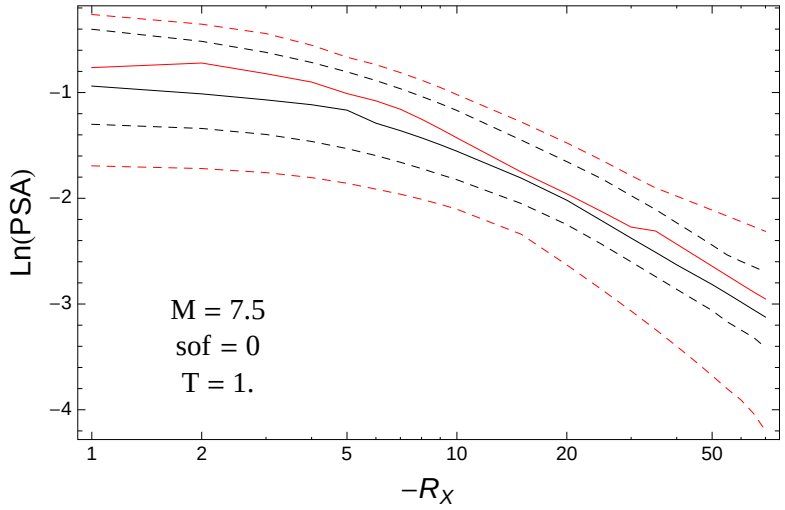



Figure 2.196: DCPPv4: Distance scaling of 0.05,0.5,0.95 quantile of the GMPE distribution (black) and the ModelA distribution (red) with total weights, for a scenario with $M = 7.5$, $F = 0$, and $T = 1$.s.

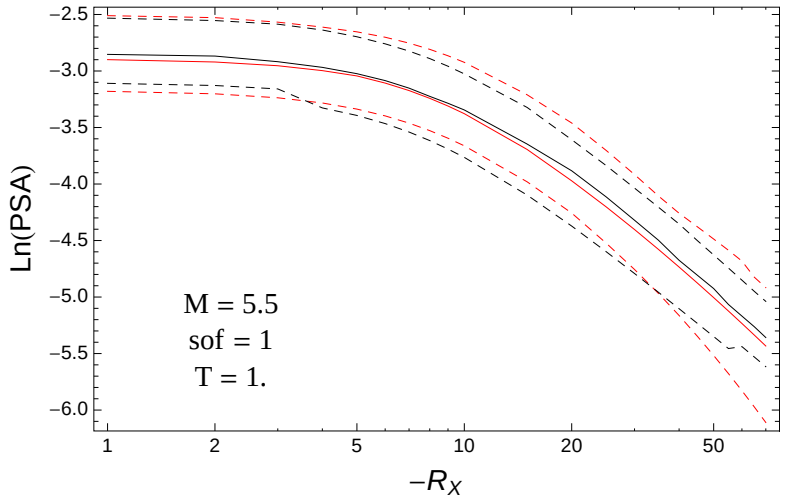



Figure 2.197: DCPPv4: Distance scaling of 0.05,0.5,0.95 quantile of the GMPE distribution (black) and the ModelA distribution (red) with total weights, for a scenario with $M = 5.5$, $F = 1$, and $T = 1$.s.

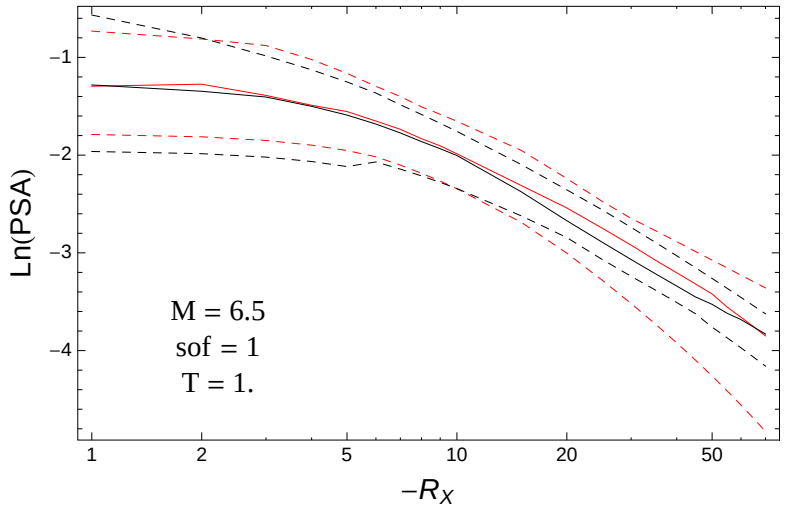



Figure 2.198: DCPPv4: Distance scaling of 0.05,0.5,0.95 quantile of the GMPE distribution (black) and the ModelA distribution (red) with total weights, for a scenario with $M = 6.5$, $F = 1$, and $T = 1$.s.

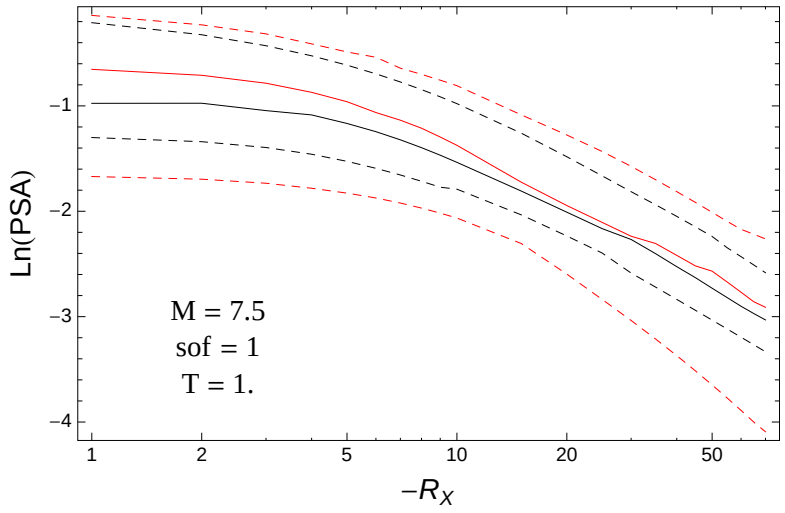



Figure 2.199: DCPPv4: Distance scaling of 0.05,0.5,0.95 quantile of the GMPE distribution (black) and the ModelA distribution (red) with total weights, for a scenario with $M = 7.5$, $F = 1$, and $T = 1$.s.

**T = 3.s**

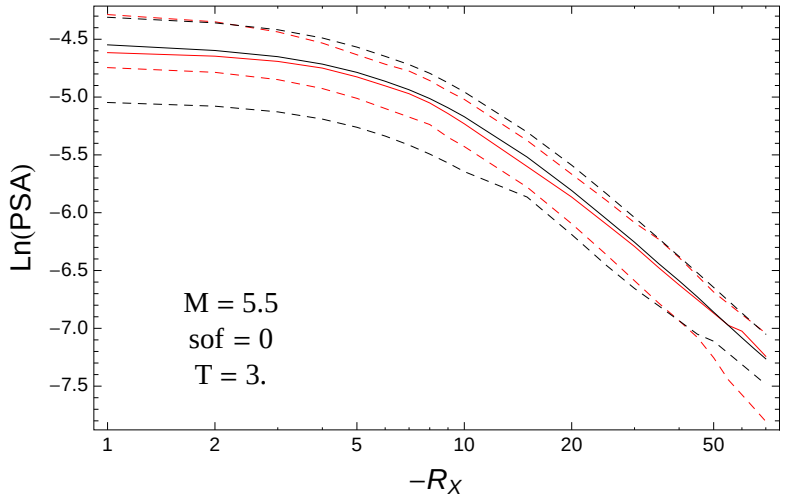



Figure 2.200: DCPPv4: Distance scaling of 0.05,0.5,0.95 quantile of the GMPE distribution (black) and the ModelA distribution (red) with total weights, for a scenario with $M = 5.5$, $F = 0$, and $T = 3$.s.

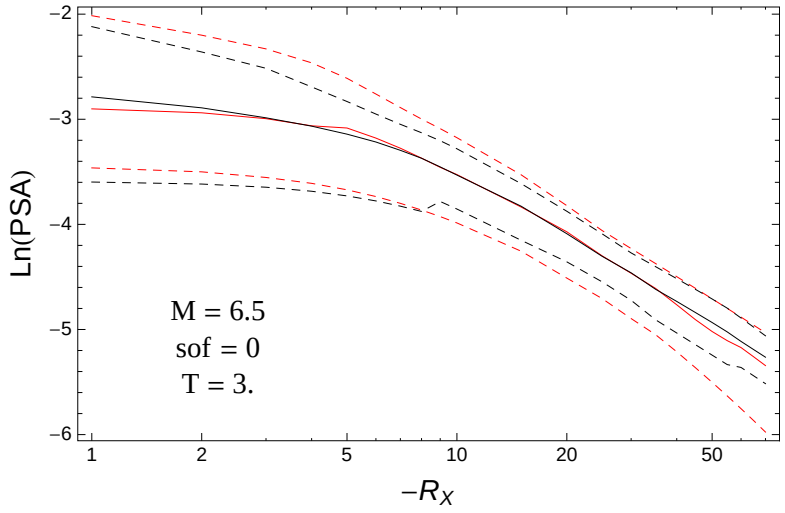



Figure 2.201: DCPPv4: Distance scaling of 0.05,0.5,0.95 quantile of the GMPE distribution (black) and the ModelA distribution (red) with total weights, for a scenario with $M = 6.5$, $F = 0$, and $T = 3$.s.

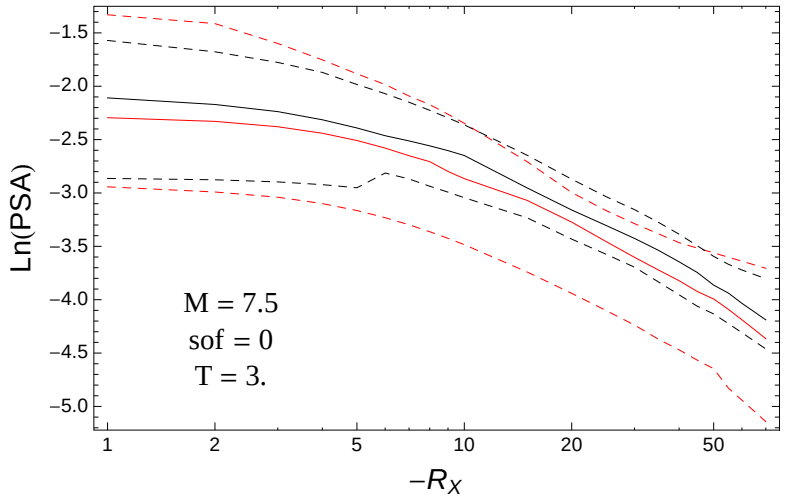



Figure 2.202: DCPPv4: Distance scaling of 0.05,0.5,0.95 quantile of the GMPE distribution (black) and the ModelA distribution (red) with total weights, for a scenario with $M = 7.5$, $F = 0$, and $T = 3$.s.

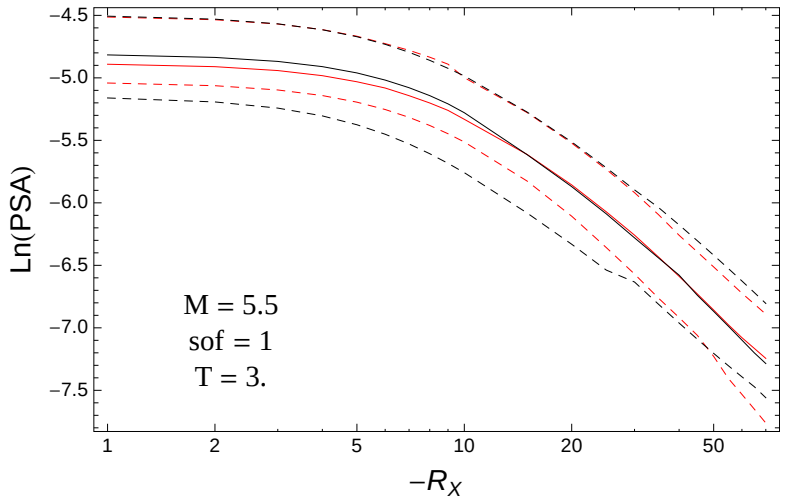



Figure 2.203: DCPPv4: Distance scaling of 0.05,0.5,0.95 quantile of the GMPE distribution (black) and the ModelA distribution (red) with total weights, for a scenario with $M = 5.5$, $F = 1$, and $T = 3$.s.

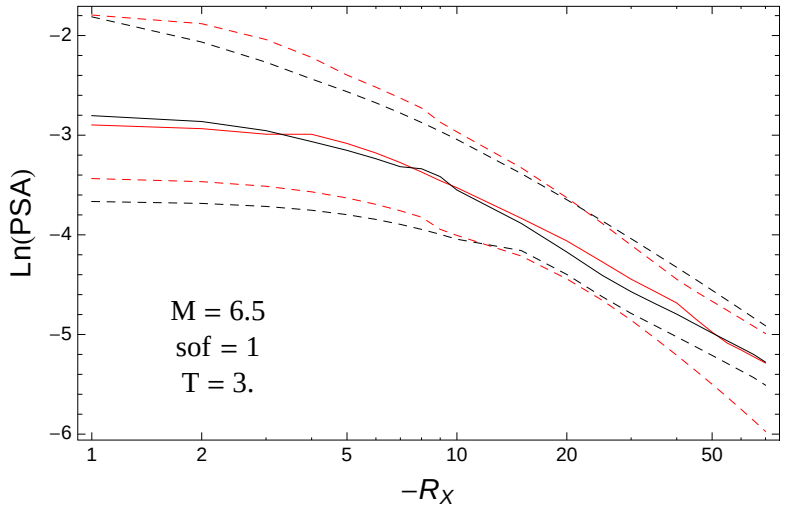



Figure 2.204: DCPPv4: Distance scaling of 0.05,0.5,0.95 quantile of the GMPE distribution (black) and the ModelA distribution (red) with total weights, for a scenario with $M = 6.5$, $F = 1$, and $T = 3$.s.

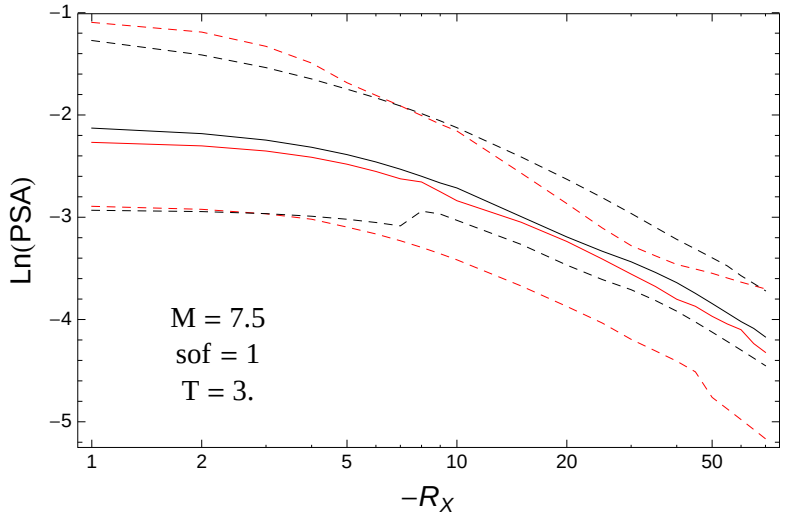



Figure 2.205: DCPPv4: Distance scaling of 0.05,0.5,0.95 quantile of the GMPE distribution (black) and the ModelA distribution (red) with total weights, for a scenario with $M = 7.5$, $F = 1$, and $T = 3$.s.

### 2.1.8 Quantile Plots vs. Distance with GMPEs

**T = 0.01s**

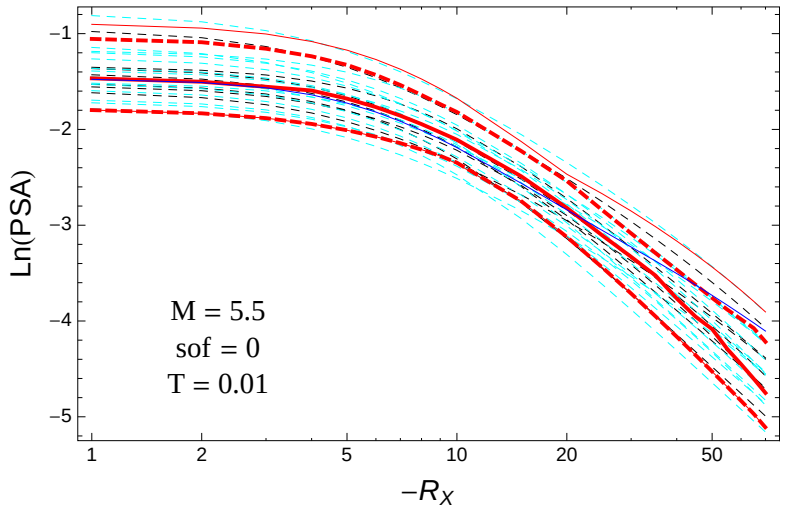



Figure 2.206: DCPPv4: Distance scaling of the original GMPEs (dashed black), the original GMPEs with the uncertainty model (dashed cyan) and 0.05,0.5,0.95 quantile of the ModelA distribution (red) with total weights and the model of Graizer (2014) (blue), for a scenario with $M = 5.5$, $F = 0$, and $T = 0.01$s.

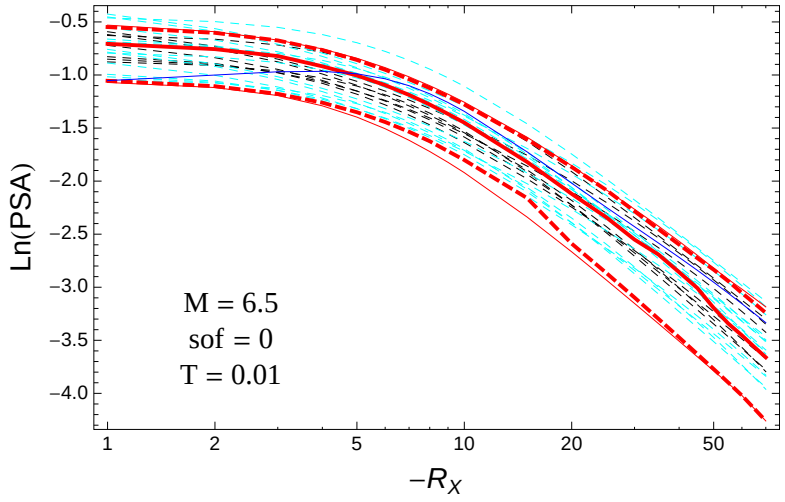



Figure 2.207: DCPPv4: Distance scaling of the original GMPEs (dashed black), the original GMPEs with the uncertainty model (dashed cyan) and 0.05,0.5,0.95 quantile of the ModelA distribution (red) with total weights and the model of Graizer (2014) (blue), for a scenario with $M = 6.5$, $F = 0$, and $T = 0.01$s.

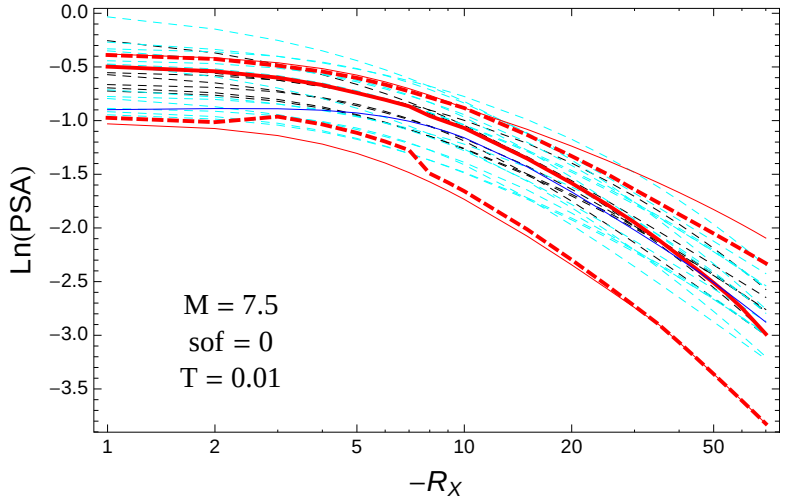



Figure 2.208: DCPPv4: Distance scaling of the original GMPEs (dashed black), the original GMPEs with the uncertainty model (dashed cyan) and 0.05,0.5,0.95 quantile of the ModelA distribution (red) with total weights and the model of Graizer (2014) (blue), for a scenario with $M = 7.5$, $F = 0$, and $T = 0.01$s.

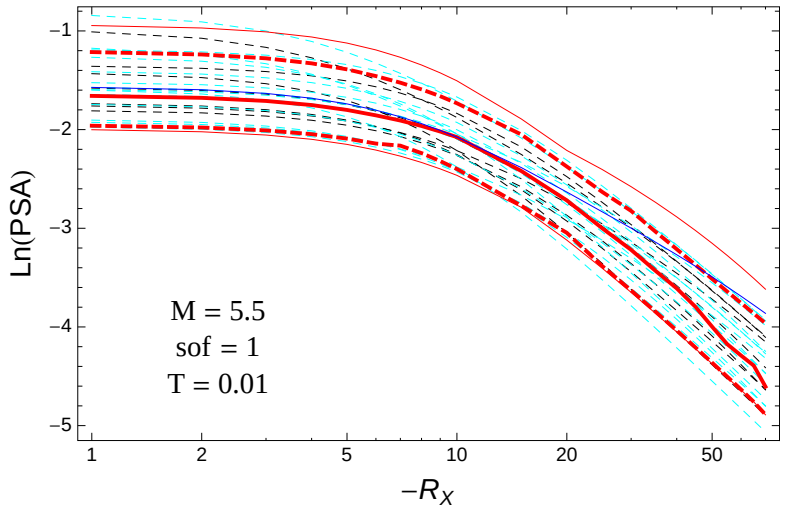



Figure 2.209: DCPPv4: Distance scaling of the original GMPEs (dashed black), the original GMPEs with the uncertainty model (dashed cyan) and 0.05,0.5,0.95 quantile of the ModelA distribution (red) with total weights and the model of Graizer (2014) (blue), for a scenario with $M = 5.5$, $F = 1$, and $T = 0.01$s.

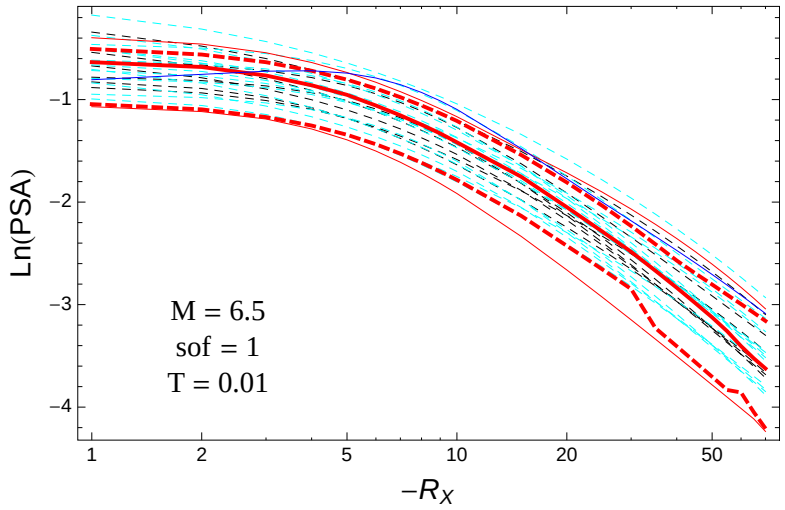



Figure 2.210: DCPPv4: Distance scaling of the original GMPEs (dashed black), the original GMPEs with the uncertainty model (dashed cyan) and 0.05,0.5,0.95 quantile of the ModelA distribution (red) with total weights and the model of Graizer (2014) (blue), for a scenario with $M = 6.5$, $F = 1$, and $T = 0.01$s.

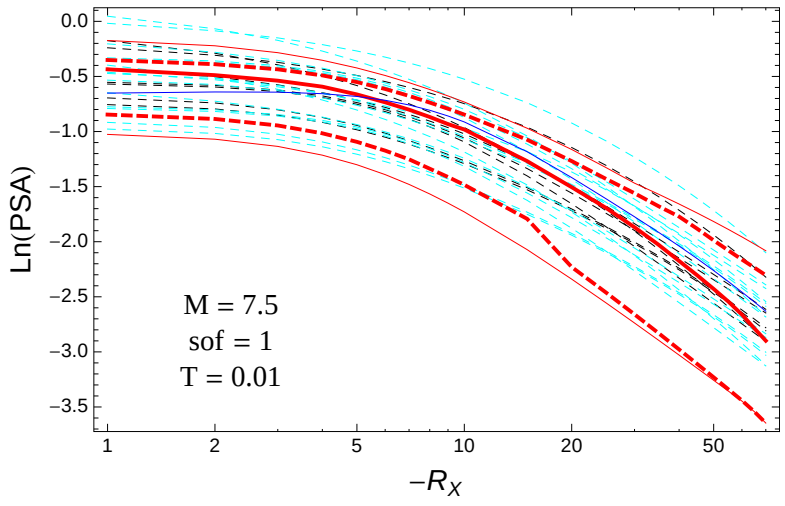



Figure 2.211: DCPPv4: Distance scaling of the original GMPEs (dashed black), the original GMPEs with the uncertainty model (dashed cyan) and 0.05,0.5,0.95 quantile of the ModelA distribution (red) with total weights and the model of Graizer (2014) (blue), for a scenario with $M = 7.5$, $F = 1$, and $T = 0.01$s.

**T = 0.2s**

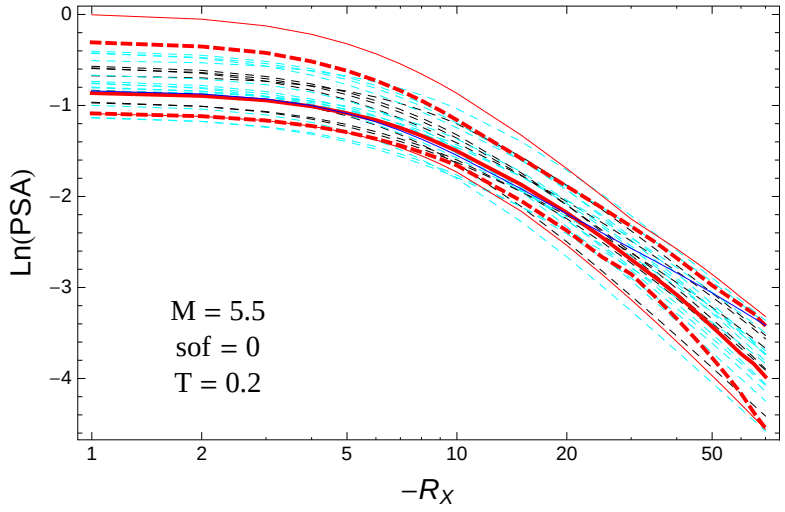



Figure 2.212: DCPPv4: Distance scaling of the original GMPEs (dashed black), the original GMPEs with the uncertainty model (dashed cyan) and 0.05,0.5,0.95 quantile of the ModelA distribution (red) with total weights and the model of Graizer (2014) (blue), for a scenario with $M = 5.5$, $F = 0$, and $T = 0.2$s.

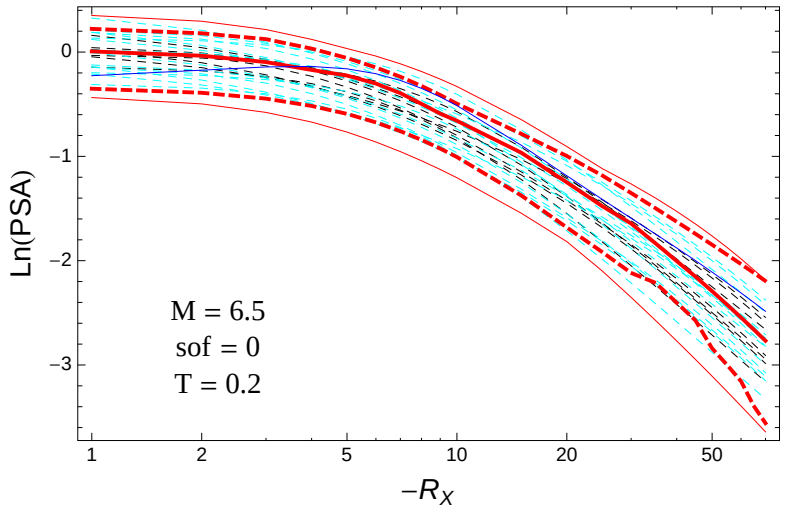



Figure 2.213: DCPPv4: Distance scaling of the original GMPEs (dashed black), the original GMPEs with the uncertainty model (dashed cyan) and 0.05,0.5,0.95 quantile of the ModelA distribution (red) with total weights and the model of Graizer (2014) (blue), for a scenario with $M = 6.5$, $F = 0$, and $T = 0.2$s.

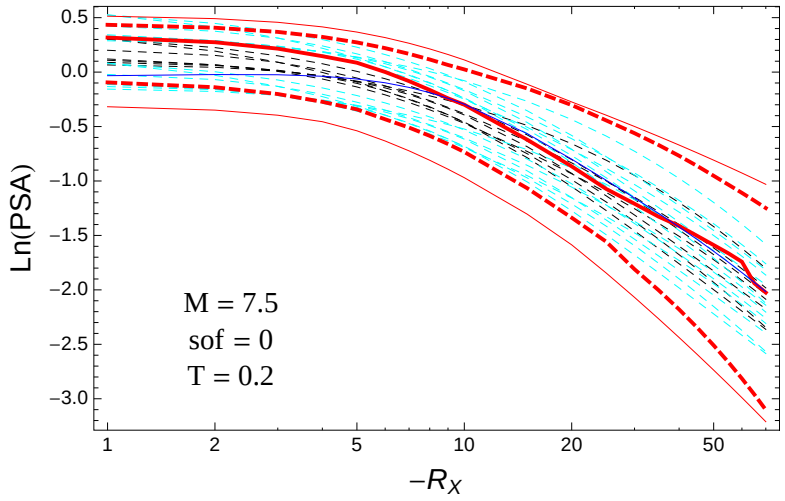



Figure 2.214: DCPPv4: Distance scaling of the original GMPEs (dashed black), the original GMPEs with the uncertainty model (dashed cyan) and 0.05,0.5,0.95 quantile of the ModelA distribution (red) with total weights and the model of Graizer (2014) (blue), for a scenario with $M = 7.5$, $F = 0$, and $T = 0.2$s.

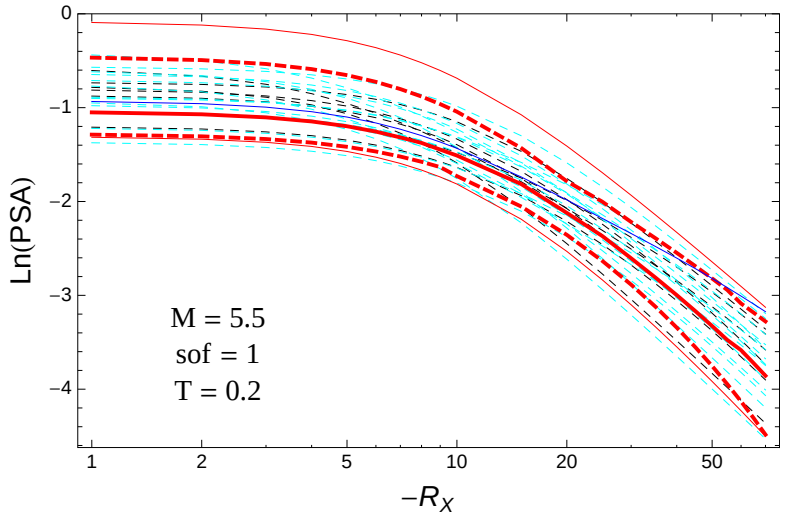



Figure 2.215: DCPPv4: Distance scaling of the original GMPEs (dashed black), the original GMPEs with the uncertainty model (dashed cyan) and 0.05,0.5,0.95 quantile of the ModelA distribution (red) with total weights and the model of Graizer (2014) (blue), for a scenario with $M = 5.5$, $F = 1$, and $T = 0.2$s.

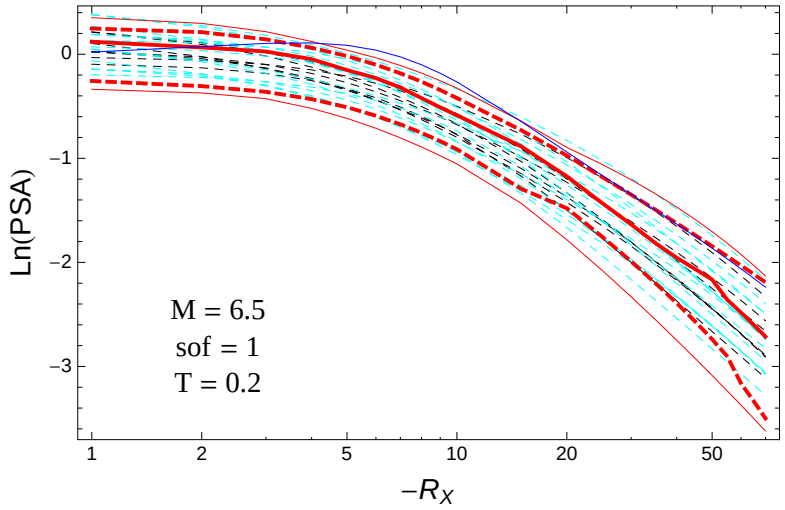



Figure 2.216: DCPPv4: Distance scaling of the original GMPEs (dashed black), the original GMPEs with the uncertainty model (dashed cyan) and 0.05,0.5,0.95 quantile of the ModelA distribution (red) with total weights and the model of Graizer (2014) (blue), for a scenario with $M = 6.5$, $F = 1$, and $T = 0.2$s.

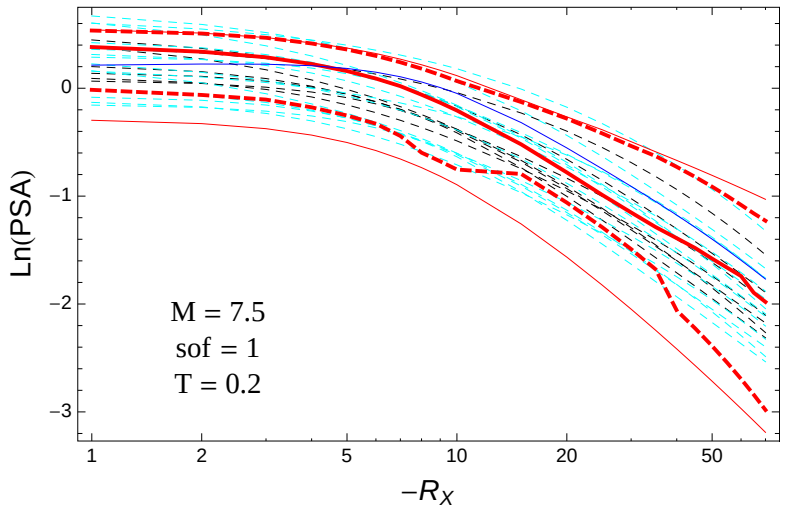



Figure 2.217: DCPPv4: Distance scaling of the original GMPEs (dashed black), the original GMPEs with the uncertainty model (dashed cyan) and 0.05,0.5,0.95 quantile of the ModelA distribution (red) with total weights and the model of Graizer (2014) (blue), for a scenario with $M = 7.5$, $F = 1$, and $T = 0.2$s.

**T = 0.5s**

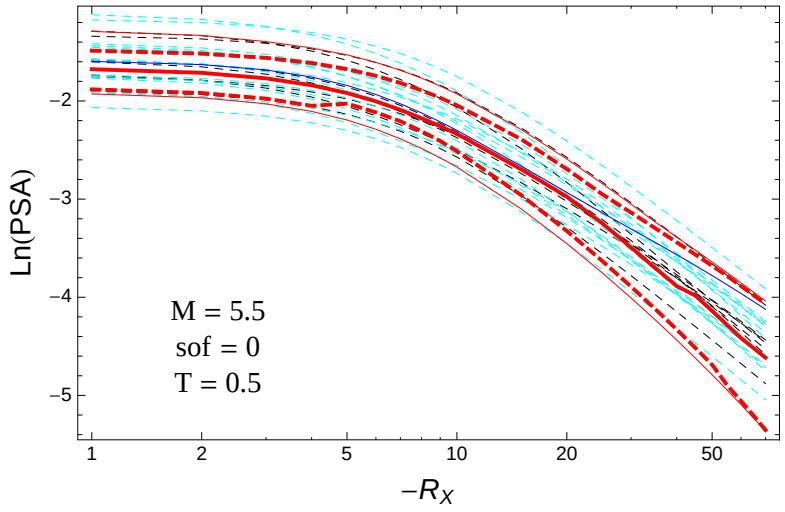



Figure 2.218: DCPPv4: Distance scaling of the original GMPEs (dashed black), the original GMPEs with the uncertainty model (dashed cyan) and 0.05,0.5,0.95 quantile of the ModelA distribution (red) with total weights and the model of Graizer (2014) (blue), for a scenario with $M = 5.5$, $F = 0$, and $T = 0.5$s.

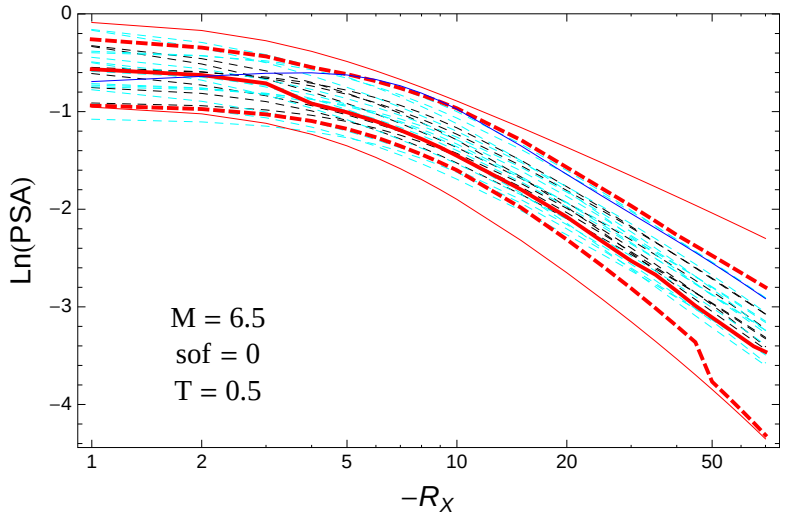



Figure 2.219: DCPPv4: Distance scaling of the original GMPEs (dashed black), the original GMPEs with the uncertainty model (dashed cyan) and 0.05,0.5,0.95 quantile of the ModelA distribution (red) with total weights and the model of Graizer (2014) (blue), for a scenario with $M = 6.5$, $F = 0$, and $T = 0.5$s.

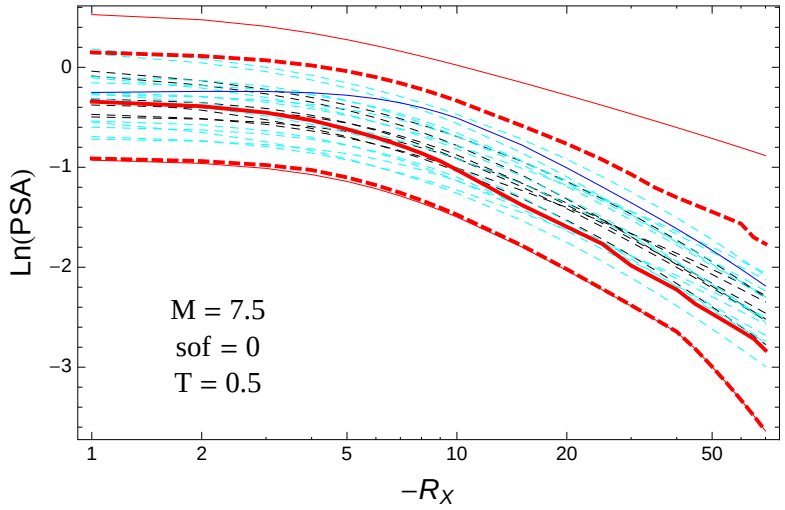



Figure 2.220: DCPPv4: Distance scaling of the original GMPEs (dashed black), the original GMPEs with the uncertainty model (dashed cyan) and 0.05,0.5,0.95 quantile of the ModelA distribution (red) with total weights and the model of Graizer (2014) (blue), for a scenario with $M = 7.5$, $F = 0$, and $T = 0.5$s.

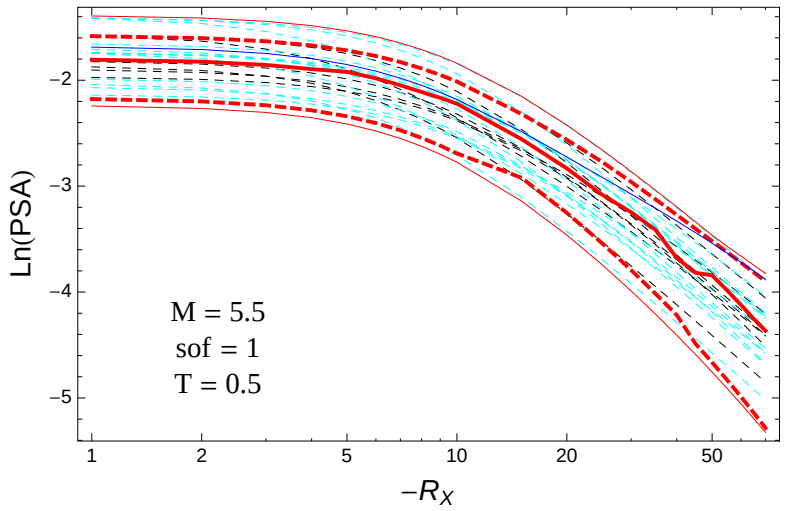



Figure 2.221: DCPPv4: Distance scaling of the original GMPEs (dashed black), the original GMPEs with the uncertainty model (dashed cyan) and 0.05,0.5,0.95 quantile of the ModelA distribution (red) with total weights and the model of Graizer (2014) (blue), for a scenario with $M = 5.5$, $F = 1$, and $T = 0.5$s.

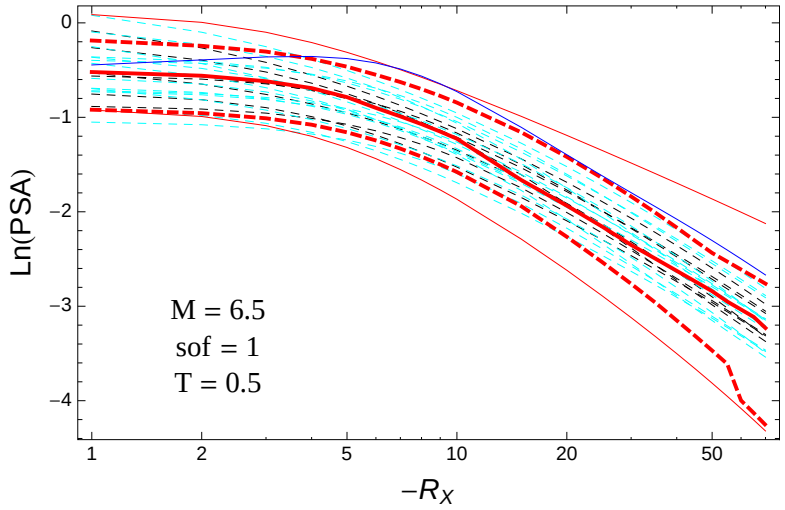



Figure 2.222: DCPPv4: Distance scaling of the original GMPEs (dashed black), the original GMPEs with the uncertainty model (dashed cyan) and 0.05,0.5,0.95 quantile of the ModelA distribution (red) with total weights and the model of Graizer (2014) (blue), for a scenario with $M = 6.5$, $F = 1$, and $T = 0.5$s.

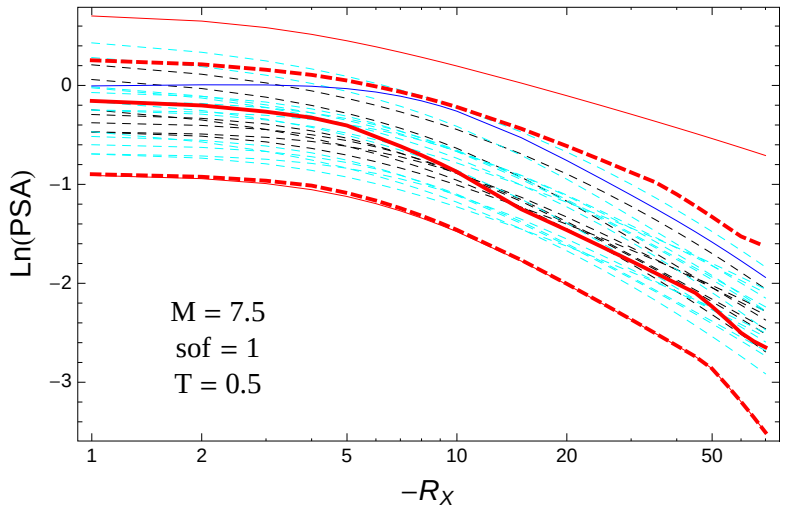



Figure 2.223: DCPPv4: Distance scaling of the original GMPEs (dashed black), the original GMPEs with the uncertainty model (dashed cyan) and 0.05,0.5,0.95 quantile of the ModelA distribution (red) with total weights and the model of Graizer (2014) (blue), for a scenario with $M = 7.5$, $F = 1$, and $T = 0.5$s.

**T = 1.s**

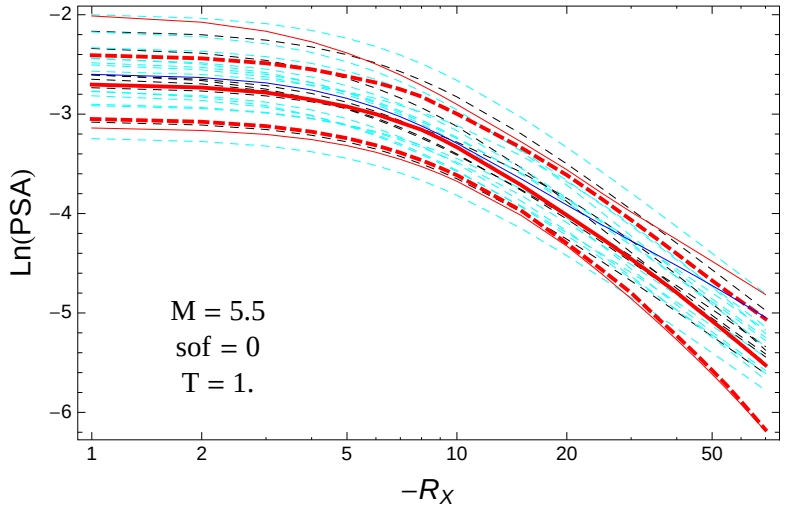



Figure 2.224: DCPPv4: Distance scaling of the original GMPEs (dashed black), the original GMPEs with the uncertainty model (dashed cyan) and 0.05,0.5,0.95 quantile of the ModelA distribution (red) with total weights and the model of Graizer (2014) (blue), for a scenario with $M = 5.5$, $F = 0$, and $T = 1$.s.

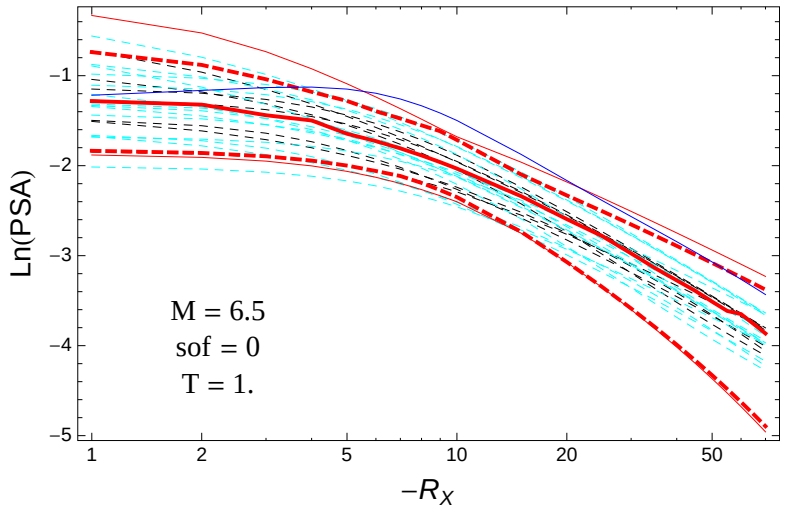



Figure 2.225: DCPPv4: Distance scaling of the original GMPEs (dashed black), the original GMPEs with the uncertainty model (dashed cyan) and 0.05,0.5,0.95 quantile of the ModelA distribution (red) with total weights and the model of Graizer (2014) (blue), for a scenario with $M = 6.5$, $F = 0$, and $T = 1$.s.

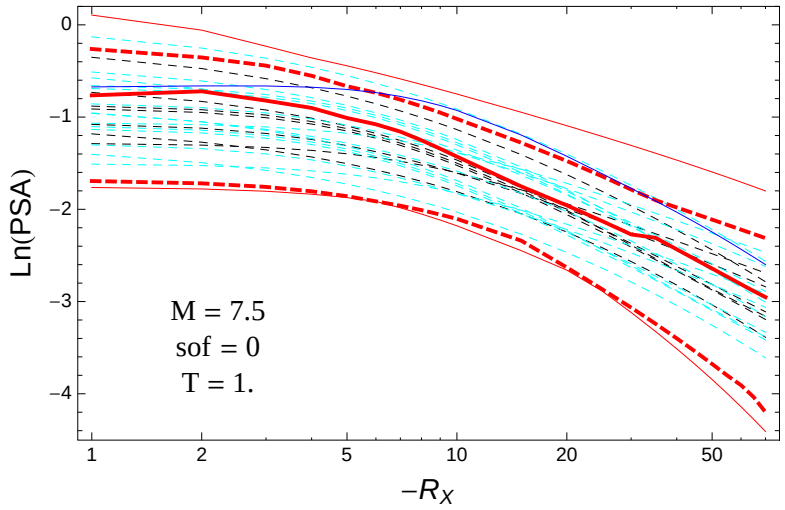



Figure 2.226: DCPPv4: Distance scaling of the original GMPEs (dashed black), the original GMPEs with the uncertainty model (dashed cyan) and 0.05,0.5,0.95 quantile of the ModelA distribution (red) with total weights and the model of Graizer (2014) (blue), for a scenario with $M = 7.5$, $F = 0$, and $T = 1$.s.

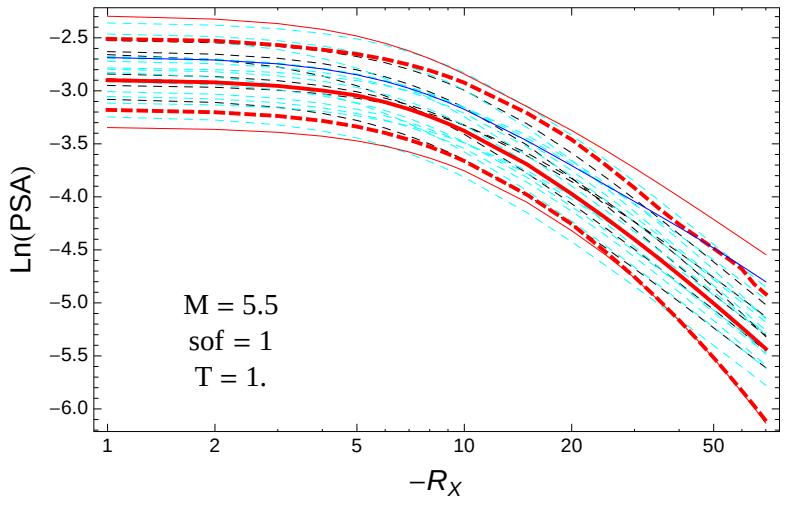



Figure 2.227: DCPPv4: Distance scaling of the original GMPEs (dashed black), the original GMPEs with the uncertainty model (dashed cyan) and 0.05,0.5,0.95 quantile of the ModelA distribution (red) with total weights and the model of Graizer (2014) (blue), for a scenario with $M = 5.5$, $F = 1$, and $T = 1$.s.

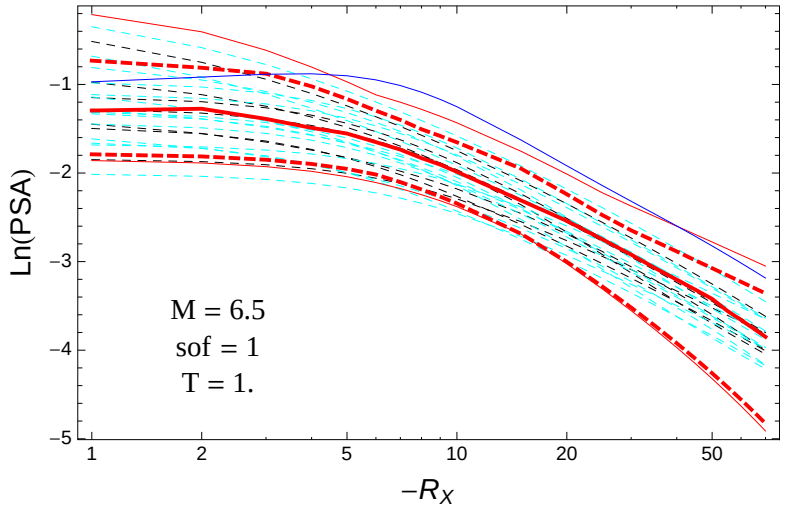



Figure 2.228: DCPPv4: Distance scaling of the original GMPEs (dashed black), the original GMPEs with the uncertainty model (dashed cyan) and 0.05,0.5,0.95 quantile of the ModelA distribution (red) with total weights and the model of Graizer (2014) (blue), for a scenario with $M = 6.5$, $F = 1$, and $T = 1$.s.

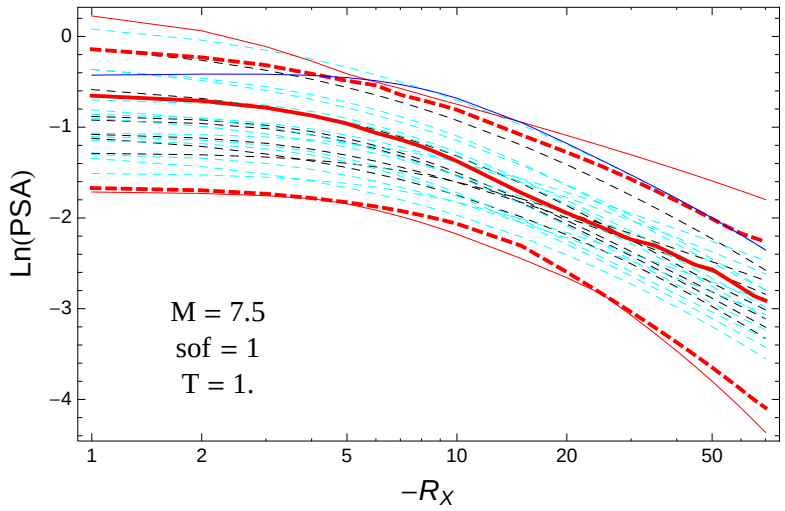



Figure 2.229: DCPPv4: Distance scaling of the original GMPEs (dashed black), the original GMPEs with the uncertainty model (dashed cyan) and 0.05,0.5,0.95 quantile of the ModelA distribution (red) with total weights and the model of Graizer (2014) (blue), for a scenario with $M = 7.5$, $F = 1$, and $T = 1$.s.

**T = 3.s**

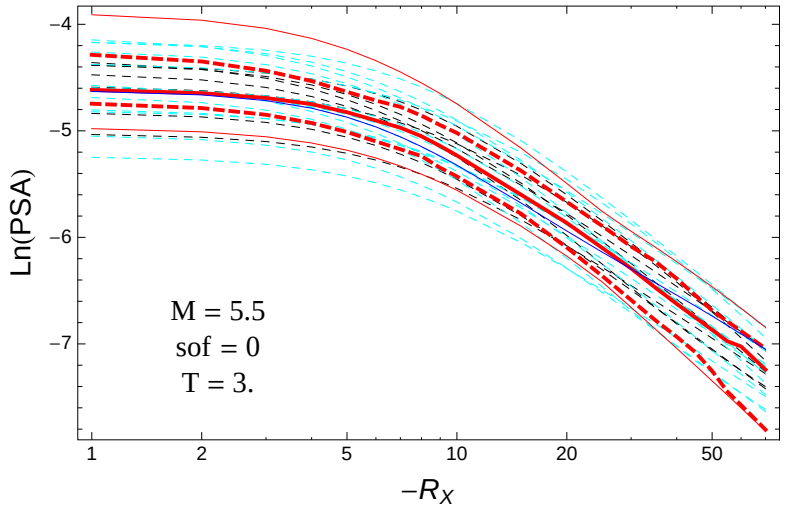



Figure 2.230: DCPPv4: Distance scaling of the original GMPEs (dashed black), the original GMPEs with the uncertainty model (dashed cyan) and 0.05,0.5,0.95 quantile of the ModelA distribution (red) with total weights and the model of Graizer (2014) (blue), for a scenario with $M = 5.5$, $F = 0$, and $T = 3$.s.

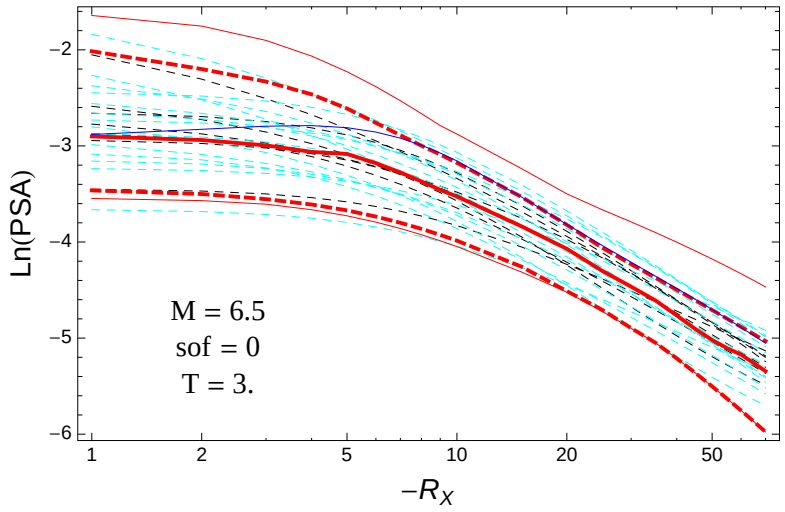



Figure 2.231: DCPPv4: Distance scaling of the original GMPEs (dashed black), the original GMPEs with the uncertainty model (dashed cyan) and 0.05,0.5,0.95 quantile of the ModelA distribution (red) with total weights and the model of Graizer (2014) (blue), for a scenario with $M = 6.5$, $F = 0$, and $T = 3$.s.

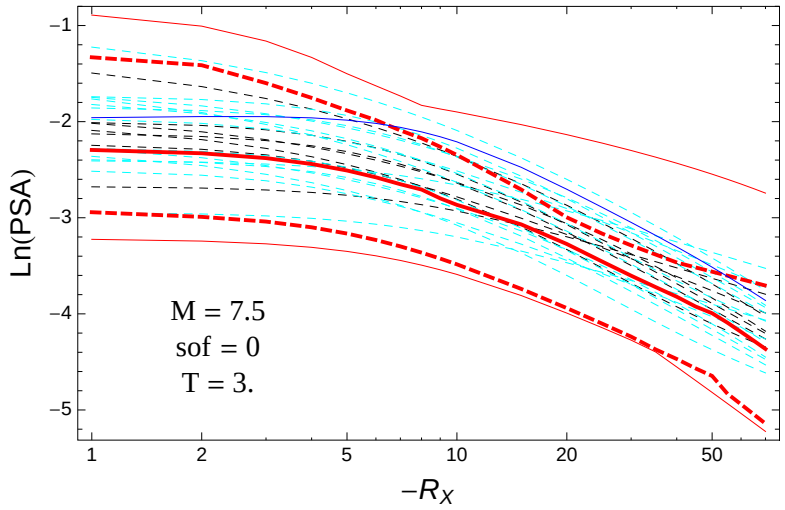



Figure 2.232: DCPPv4: Distance scaling of the original GMPEs (dashed black), the original GMPEs with the uncertainty model (dashed cyan) and 0.05,0.5,0.95 quantile of the ModelA distribution (red) with total weights and the model of Graizer (2014) (blue), for a scenario with $M = 7.5$, $F = 0$, and $T = 3$.s.

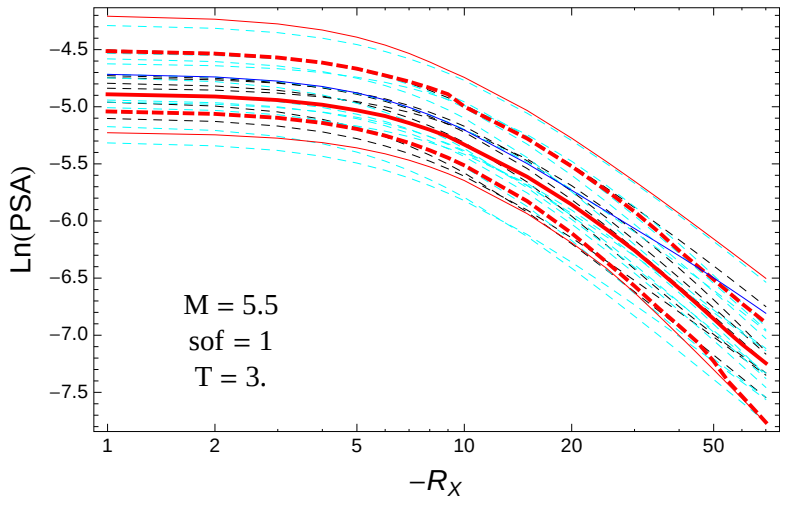



Figure 2.233: DCPPv4: Distance scaling of the original GMPEs (dashed black), the original GMPEs with the uncertainty model (dashed cyan) and 0.05,0.5,0.95 quantile of the ModelA distribution (red) with total weights and the model of Graizer (2014) (blue), for a scenario with $M = 5.5$, $F = 1$, and $T = 3$.s.

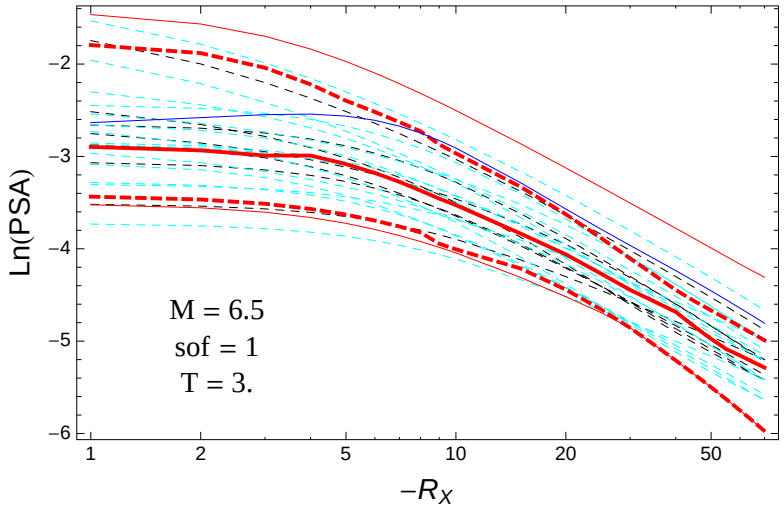



Figure 2.234: DCPPv4: Distance scaling of the original GMPEs (dashed black), the original GMPEs with the uncertainty model (dashed cyan) and 0.05,0.5,0.95 quantile of the ModelA distribution (red) with total weights and the model of Graizer (2014) (blue), for a scenario with $M = 6.5$, $F = 1$, and $T = 3$.s.

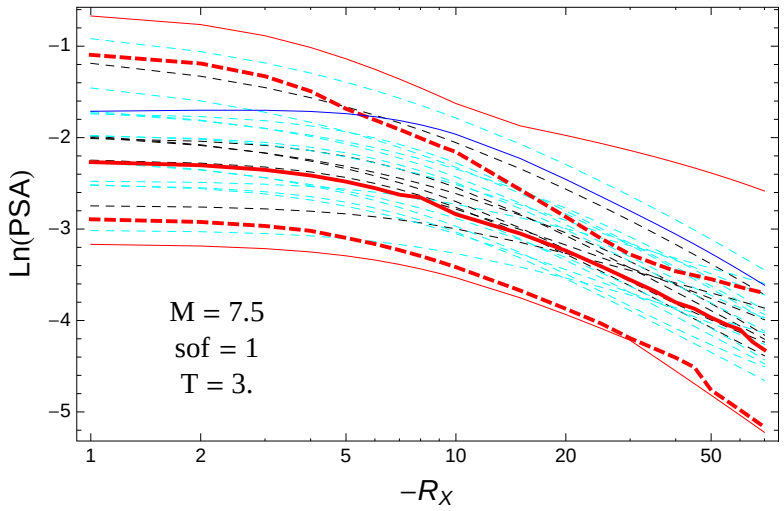



Figure 2.235: DCPPv4: Distance scaling of the original GMPEs (dashed black), the original GMPEs with the uncertainty model (dashed cyan) and 0.05,0.5,0.95 quantile of the ModelA distribution (red) with total weights and the model of Graizer (2014) (blue), for a scenario with $M = 7.5$, $F = 1$, and $T = 3$.s.

### 2.1.9 Quantile Plots vs. Magnitude

**T = 0.01s**

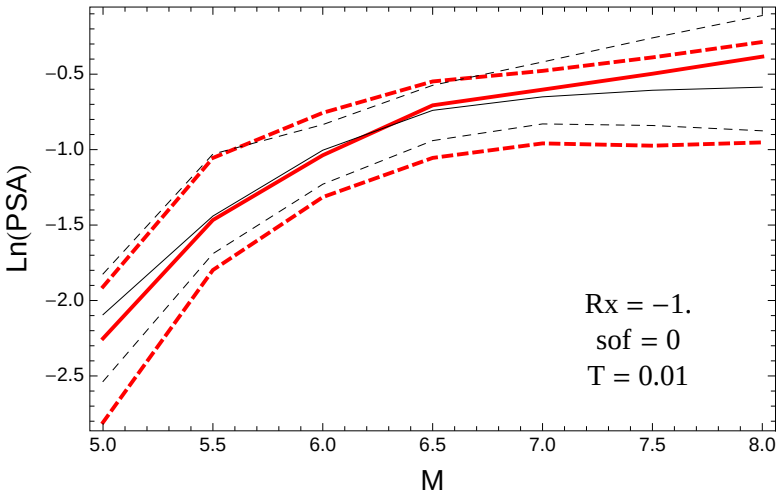



Figure 2.236: DCPPv4: Magnitude scaling of 0.05,0.5,0.95 quantile of the GMPE distribution (black) and the ModelA distribution (red) with total weights, for a scenario with $R_x = -1.$, $F = 0$, and $T = 0.01$s.

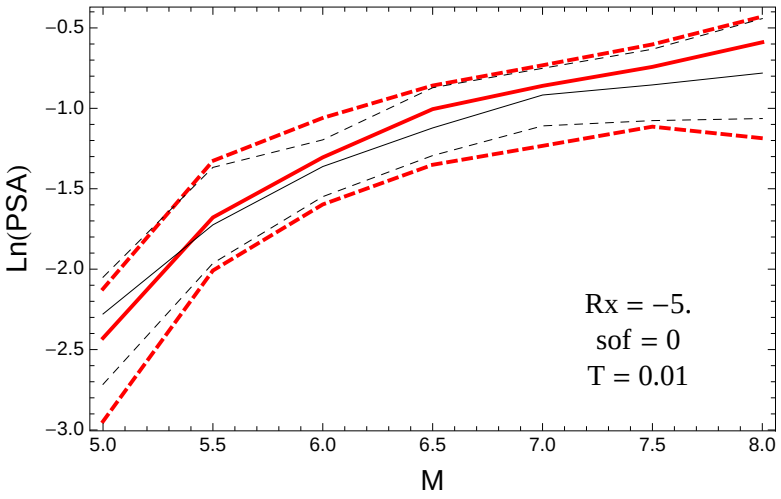



Figure 2.237: DCPPv4: Magnitude scaling of 0.05,0.5,0.95 quantile of the GMPE distribution (black) and the ModelA distribution (red) with total weights, for a scenario with $R_x = -5.$, $F = 0$, and $T = 0.01$s.

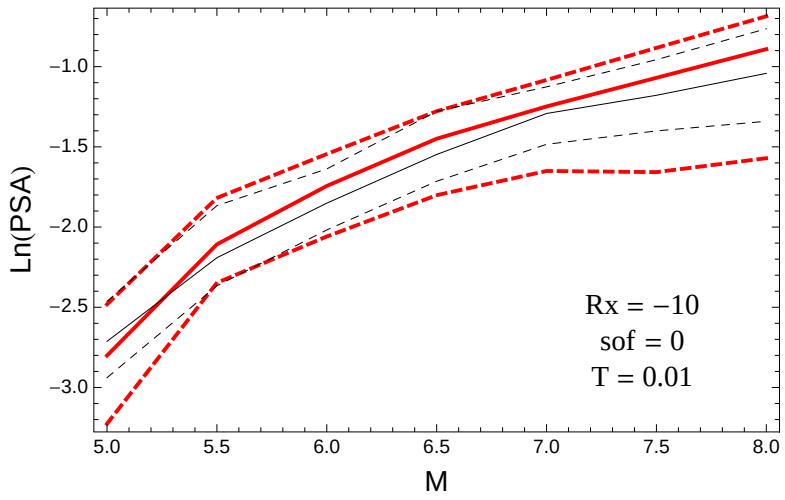



Figure 2.238: DCPPv4: Magnitude scaling of 0.05,0.5,0.95 quantile of the GMPE distribution (black) and the ModelA distribution (red) with total weights, for a scenario with $R_x = -10$, $F = 0$, and $T = 0.01$s.

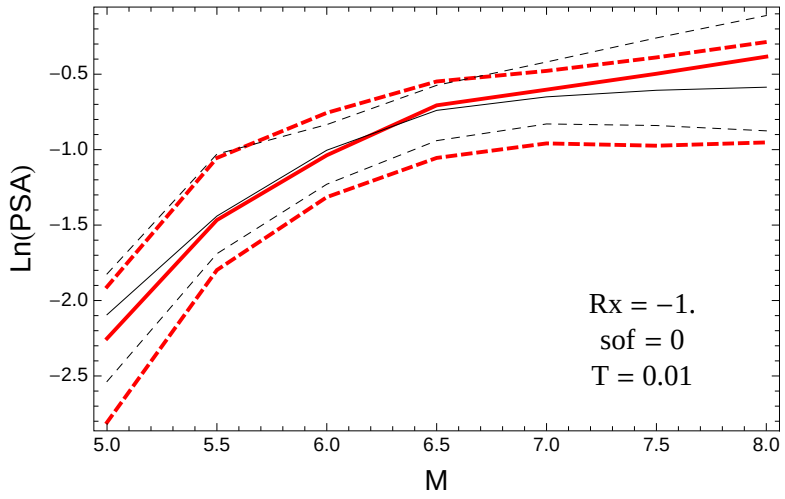



Figure 2.239: DCPPv4: Magnitude scaling of 0.05,0.5,0.95 quantile of the GMPE distribution (black) and the ModelA distribution (red) with total weights, for a scenario with $R_x = -1.$, $F = 0$, and $T = 0.01$s.

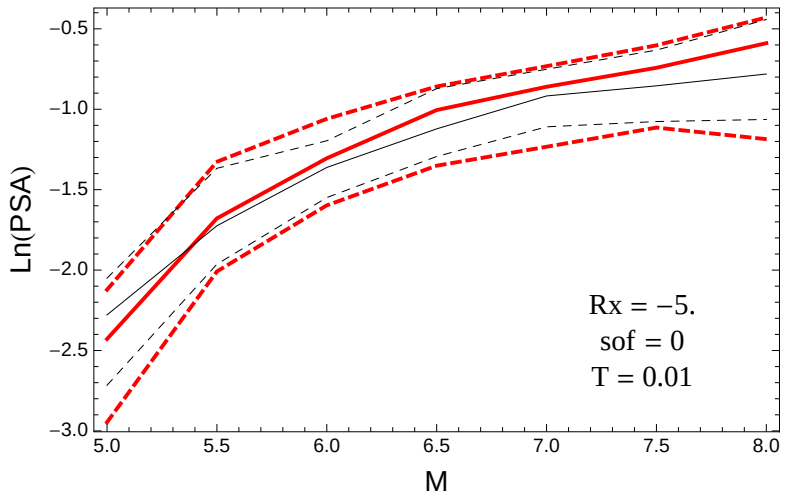



Figure 2.240: DCPPv4: Magnitude scaling of 0.05,0.5,0.95 quantile of the GMPE distribution (black) and the ModelA distribution (red) with total weights, for a scenario with $R_x = -5.$, $F = 0$, and $T = 0.01$s.

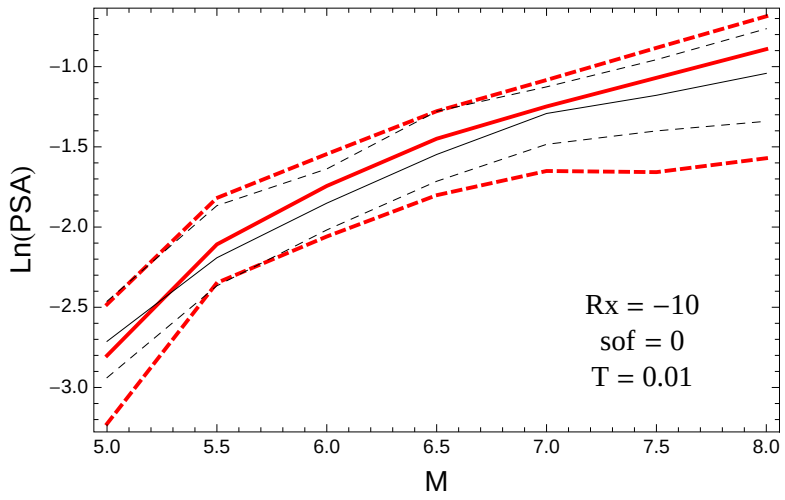



Figure 2.241: DCPPv4: Magnitude scaling of 0.05,0.5,0.95 quantile of the GMPE distribution (black) and the ModelA distribution (red) with total weights, for a scenario with $R_x = -10$, $F = 0$, and $T = 0.01$s.

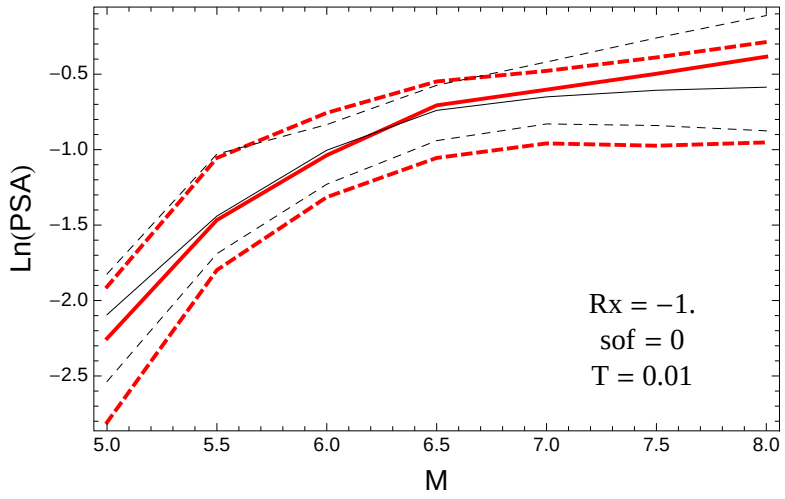



Figure 2.242: DCPPv4: Magnitude scaling of 0.05,0.5,0.95 quantile of the GMPE distribution (black) and the ModelA distribution (red) with total weights, for a scenario with $R_x = -1.$, $F = 0$, and $T = 0.01$s.

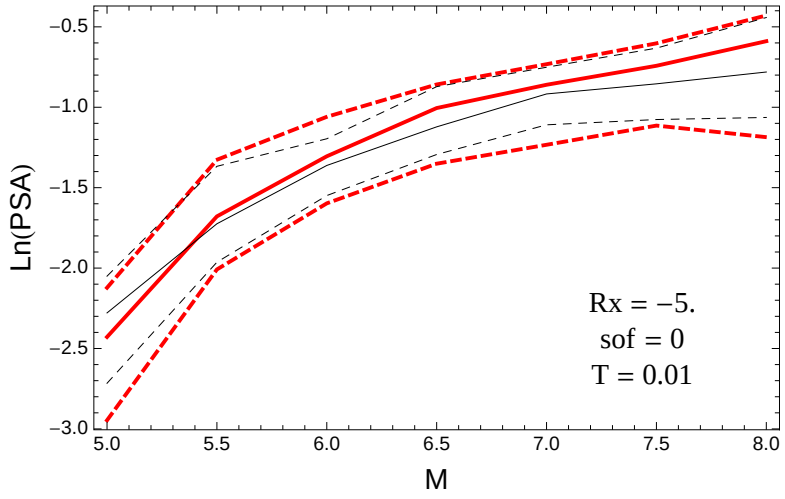



Figure 2.243: DCPPv4: Magnitude scaling of 0.05,0.5,0.95 quantile of the GMPE distribution (black) and the ModelA distribution (red) with total weights, for a scenario with $R_x = -5.$, $F = 0$, and $T = 0.01$s.

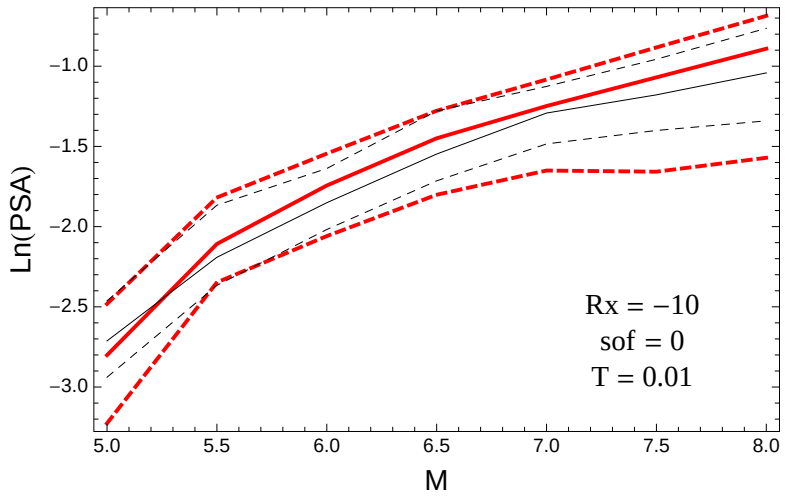



Figure 2.244: DCPPv4: Magnitude scaling of 0.05,0.5,0.95 quantile of the GMPE distribution (black) and the ModelA distribution (red) with total weights, for a scenario with $R_x = -10$, $F = 0$, and $T = 0.01$s.

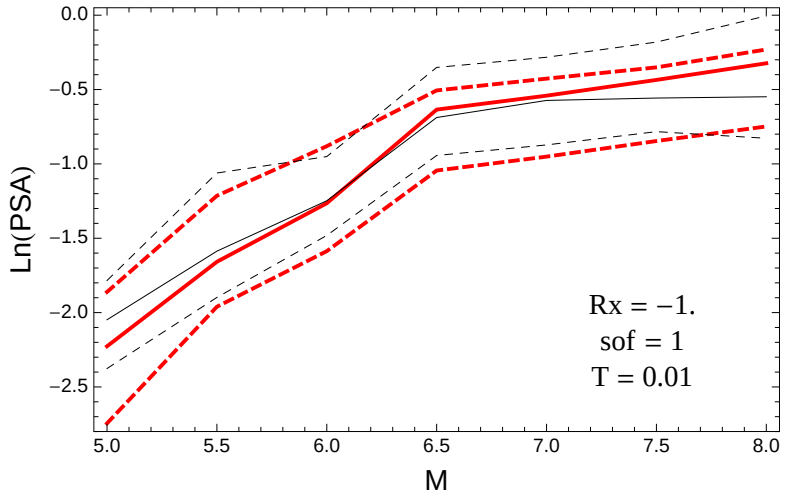



Figure 2.245: DCPPv4: Magnitude scaling of 0.05,0.5,0.95 quantile of the GMPE distribution (black) and the ModelA distribution (red) with total weights, for a scenario with $R_x = -1.$, $F = 1$, and $T = 0.01$s.

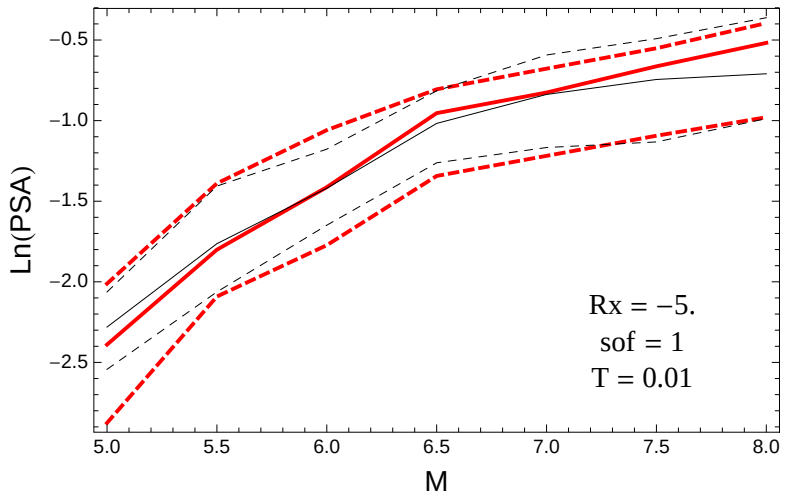



Figure 2.246: DCPPv4: Magnitude scaling of 0.05,0.5,0.95 quantile of the GMPE distribution (black) and the ModelA distribution (red) with total weights, for a scenario with $R_x = -5.$, $F = 1$, and $T = 0.01$s.

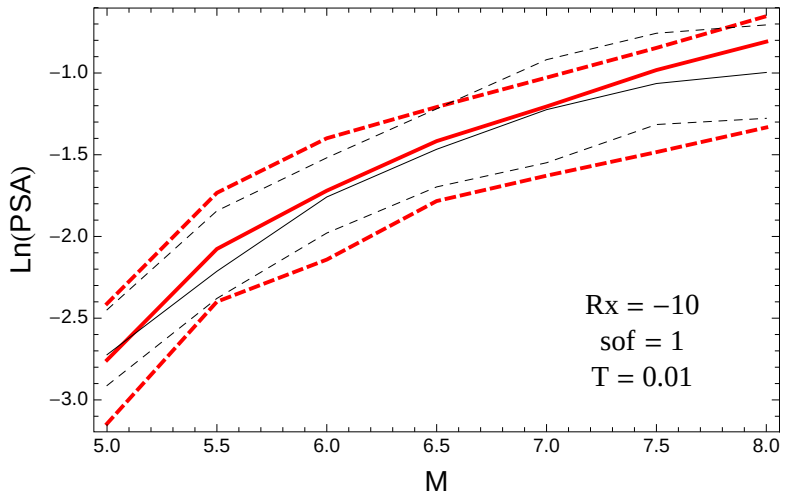



Figure 2.247: DCPPv4: Magnitude scaling of 0.05,0.5,0.95 quantile of the GMPE distribution (black) and the ModelA distribution (red) with total weights, for a scenario with $R_x = -10$, $F = 1$, and $T = 0.01$s.

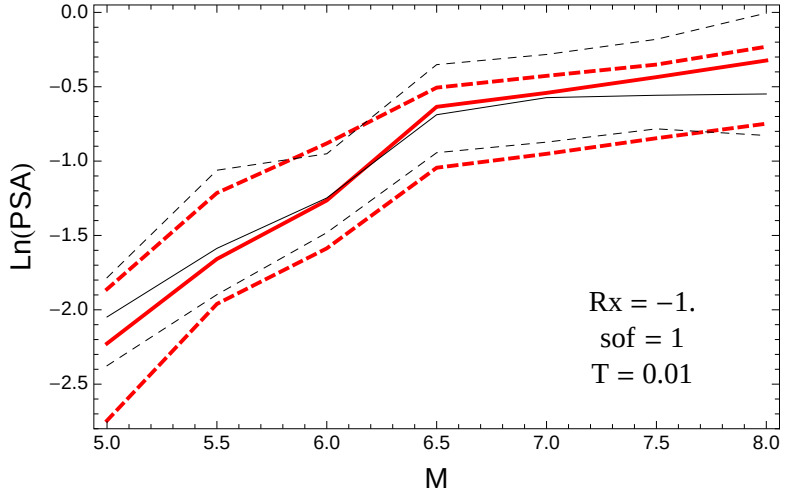



Figure 2.248: DCPPv4: Magnitude scaling of 0.05,0.5,0.95 quantile of the GMPE distribution (black) and the ModelA distribution (red) with total weights, for a scenario with $R_x = -1.$, $F = 1$, and $T = 0.01$s.

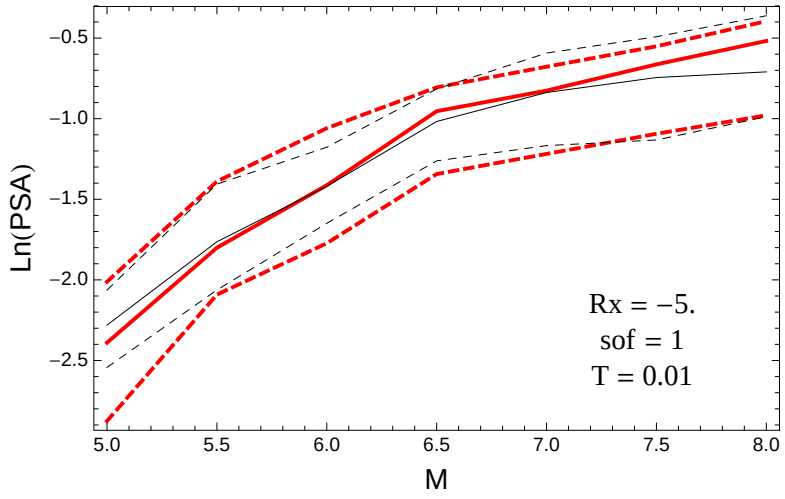



Figure 2.249: DCPPv4: Magnitude scaling of 0.05,0.5,0.95 quantile of the GMPE distribution (black) and the ModelA distribution (red) with total weights, for a scenario with $R_x = -5.$, $F = 1$, and $T = 0.01$s.

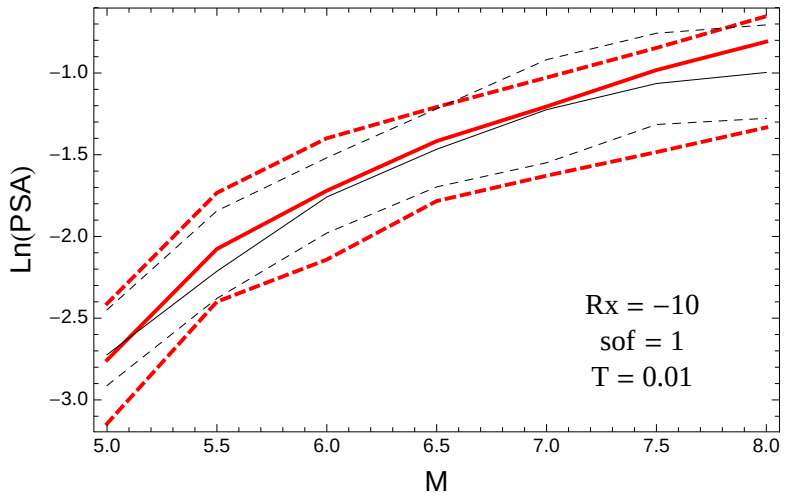



Figure 2.250: DCPPv4: Magnitude scaling of 0.05,0.5,0.95 quantile of the GMPE distribution (black) and the ModelA distribution (red) with total weights, for a scenario with $R_x = -10$, $F = 1$, and $T = 0.01$s.

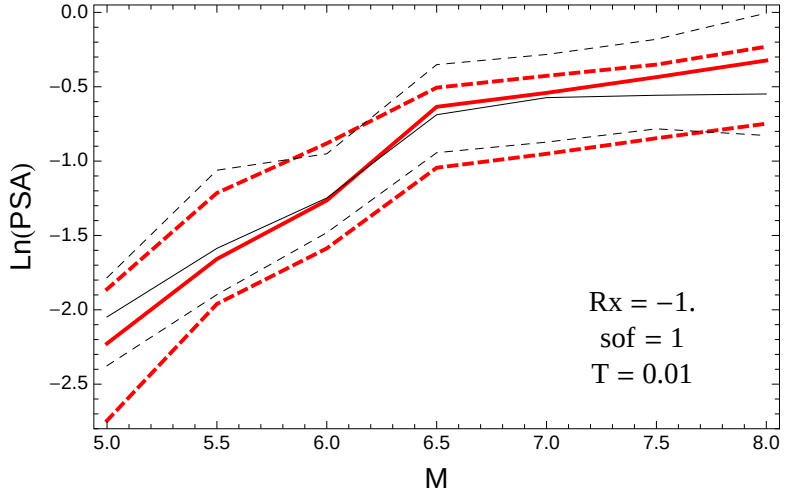



Figure 2.251: DCPPv4: Magnitude scaling of 0.05,0.5,0.95 quantile of the GMPE distribution (black) and the ModelA distribution (red) with total weights, for a scenario with $R_x = -1.$, $F = 1$, and $T = 0.01$s.

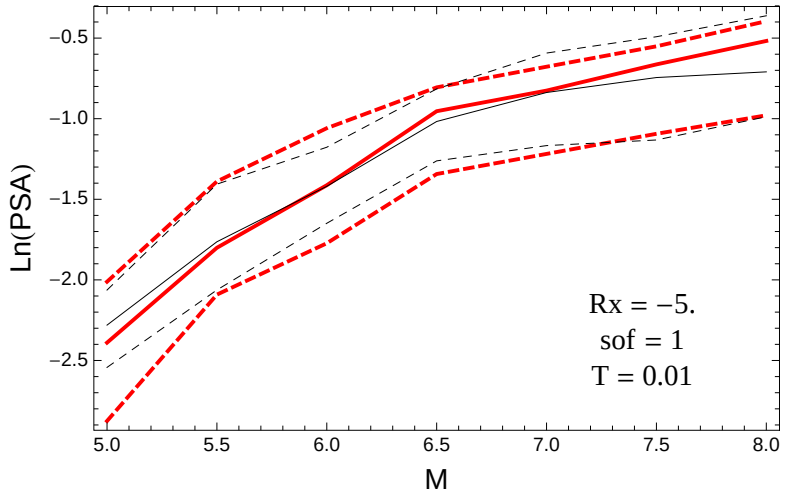



Figure 2.252: DCPPv4: Magnitude scaling of 0.05,0.5,0.95 quantile of the GMPE distribution (black) and the ModelA distribution (red) with total weights, for a scenario with $R_x = -5.$, $F = 1$, and $T = 0.01$s.

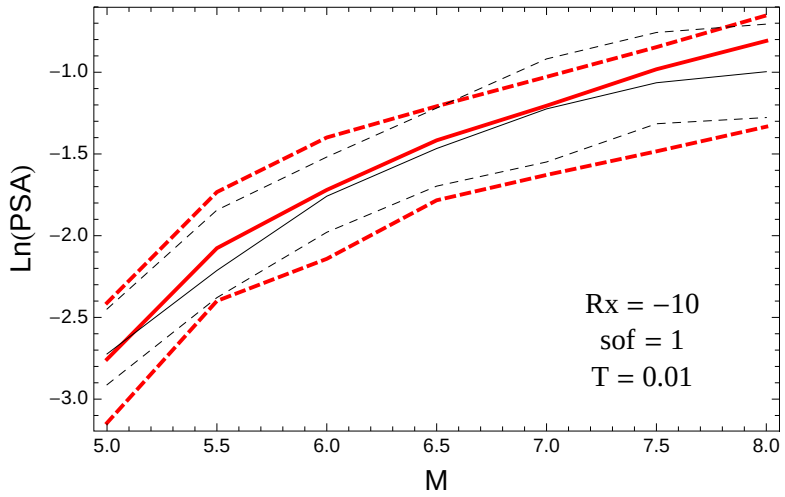



Figure 2.253: DCPPv4: Magnitude scaling of 0.05,0.5,0.95 quantile of the GMPE distribution (black) and the ModelA distribution (red) with total weights, for a scenario with $R_x = -10$, $F = 1$, and $T = 0.01$s.

**T = 0.2s**

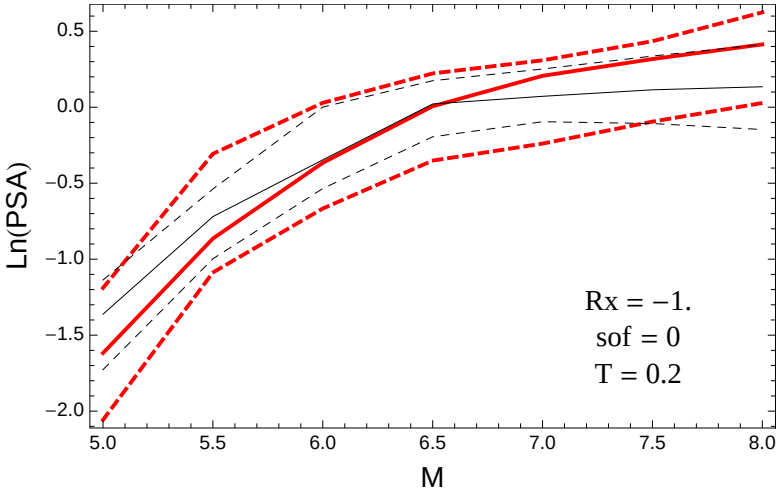



Figure 2.254: DCPPv4: Magnitude scaling of 0.05,0.5,0.95 quantile of the GMPE distribution (black) and the ModelA distribution (red) with total weights, for a scenario with $R_x = -1.$, $F = 0$, and $T = 0.2$s.

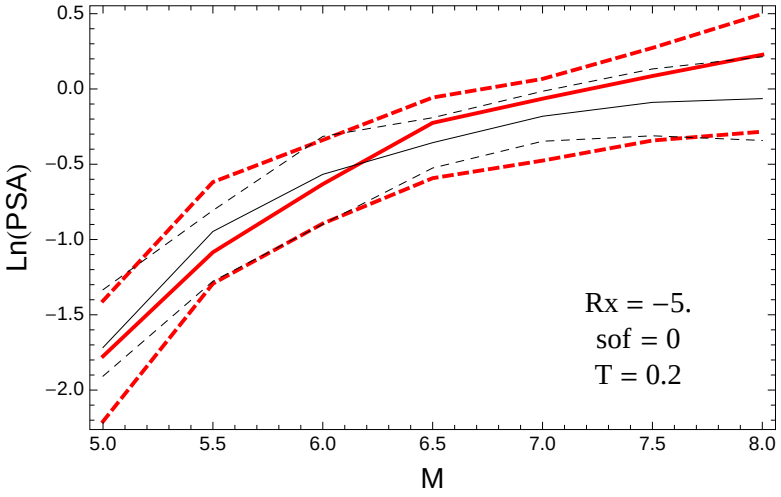



Figure 2.255: DCPPv4: Magnitude scaling of 0.05,0.5,0.95 quantile of the GMPE distribution (black) and the ModelA distribution (red) with total weights, for a scenario with $R_x = -5.$, $F = 0$, and $T = 0.2$s.

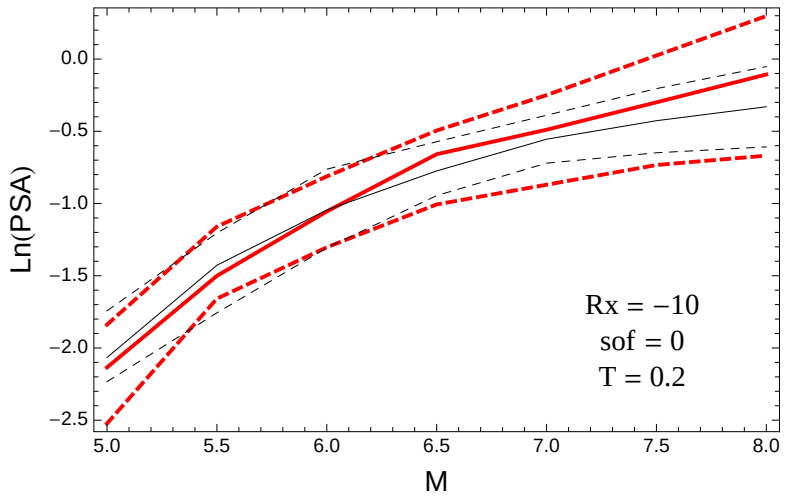



Figure 2.256: DCPPv4: Magnitude scaling of 0.05,0.5,0.95 quantile of the GMPE distribution (black) and the ModelA distribution (red) with total weights, for a scenario with $R_x = -10$, $F = 0$, and $T = 0.2$s.

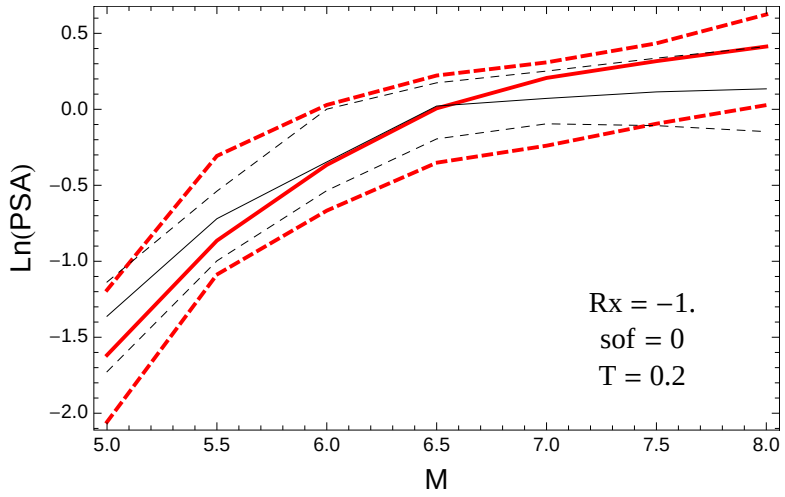



Figure 2.257: DCPPv4: Magnitude scaling of 0.05,0.5,0.95 quantile of the GMPE distribution (black) and the ModelA distribution (red) with total weights, for a scenario with $R_x = -1.$, $F = 0$, and $T = 0.2$s.

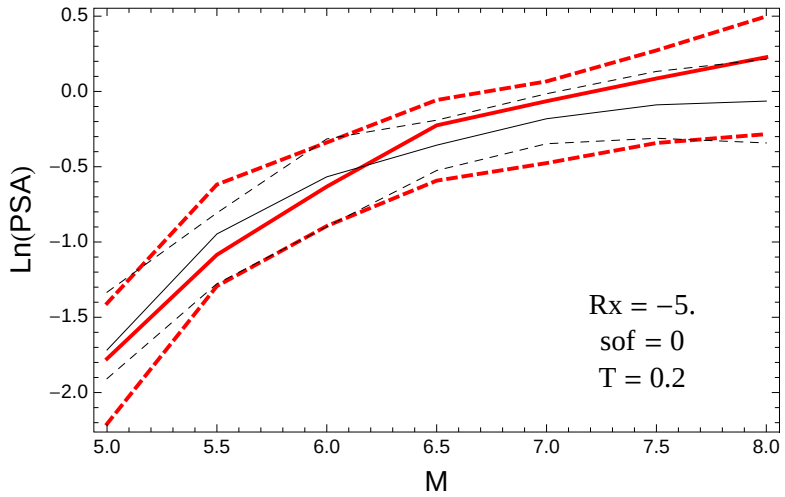



Figure 2.258: DCPPv4: Magnitude scaling of 0.05,0.5,0.95 quantile of the GMPE distribution (black) and the ModelA distribution (red) with total weights, for a scenario with $R_x = -5.$, $F = 0$, and $T = 0.2$s.

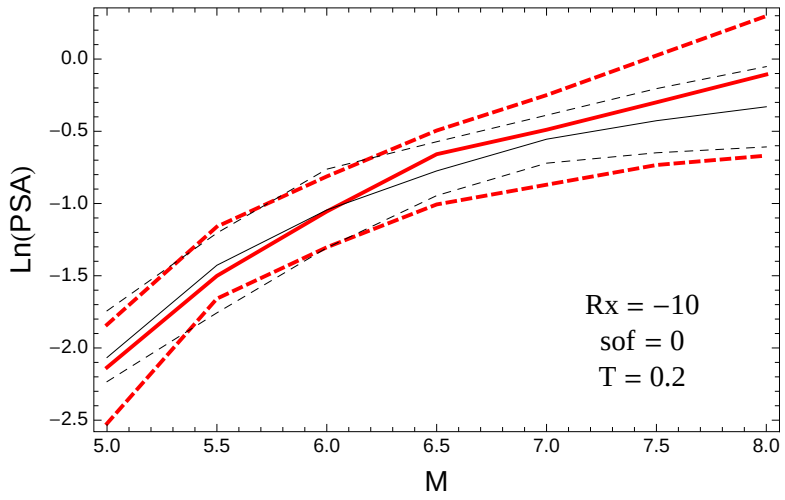



Figure 2.259: DCPPv4: Magnitude scaling of 0.05,0.5,0.95 quantile of the GMPE distribution (black) and the ModelA distribution (red) with total weights, for a scenario with $R_x = -10$, $F = 0$, and $T = 0.2$s.

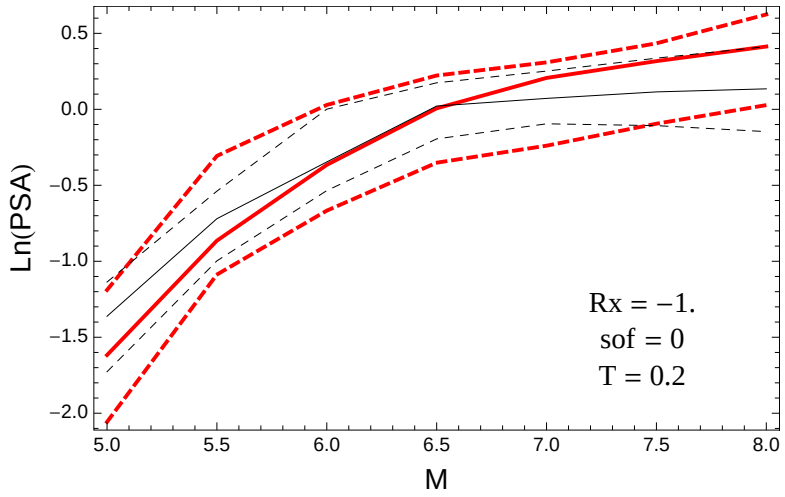



Figure 2.260: DCPPv4: Magnitude scaling of 0.05,0.5,0.95 quantile of the GMPE distribution (black) and the ModelA distribution (red) with total weights, for a scenario with $R_x = -1.$, $F = 0$, and $T = 0.2$s.

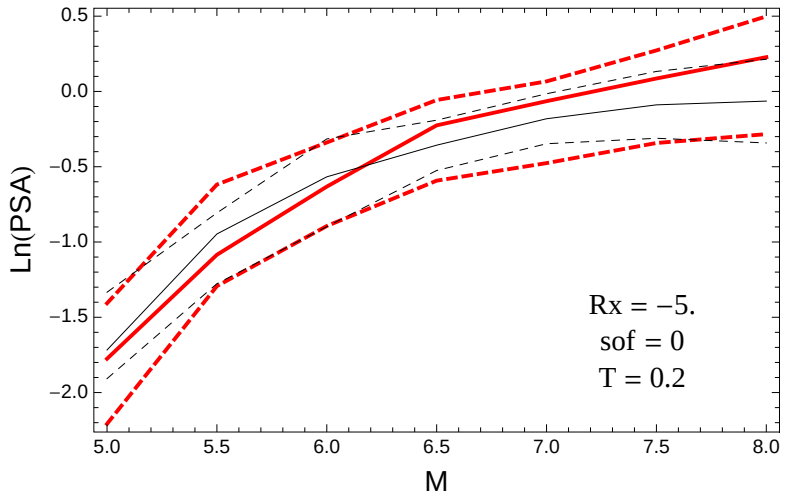



Figure 2.261: DCPPv4: Magnitude scaling of 0.05,0.5,0.95 quantile of the GMPE distribution (black) and the ModelA distribution (red) with total weights, for a scenario with $R_x = -5.$, $F = 0$, and $T = 0.2$s.

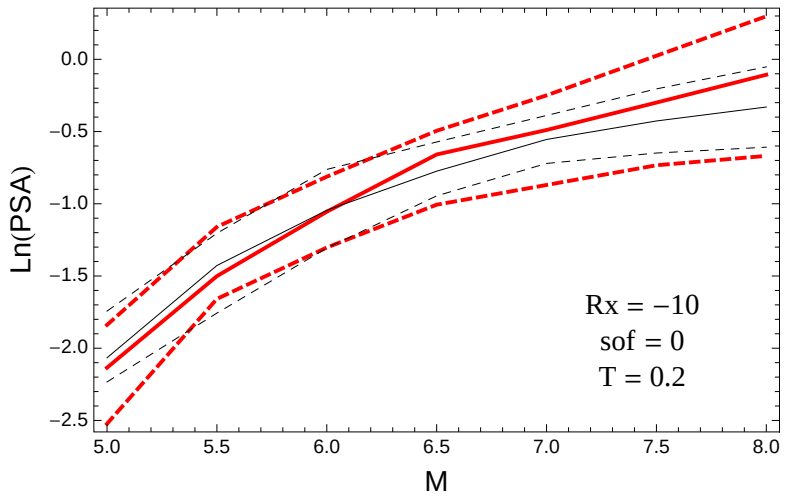



Figure 2.262: DCPPv4: Magnitude scaling of 0.05,0.5,0.95 quantile of the GMPE distribution (black) and the ModelA distribution (red) with total weights, for a scenario with $R_x = -10$, $F = 0$, and $T = 0.2$s.

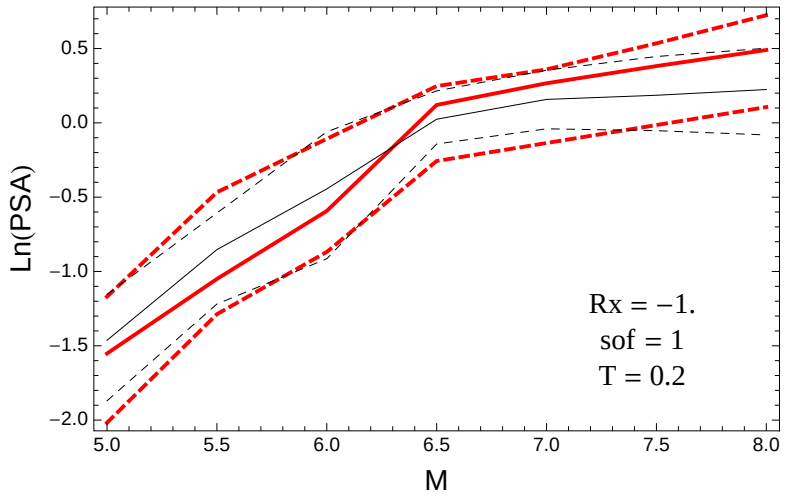



Figure 2.263: DCPPv4: Magnitude scaling of 0.05,0.5,0.95 quantile of the GMPE distribution (black) and the ModelA distribution (red) with total weights, for a scenario with $R_x = -1.$, $F = 1$, and $T = 0.2$s.

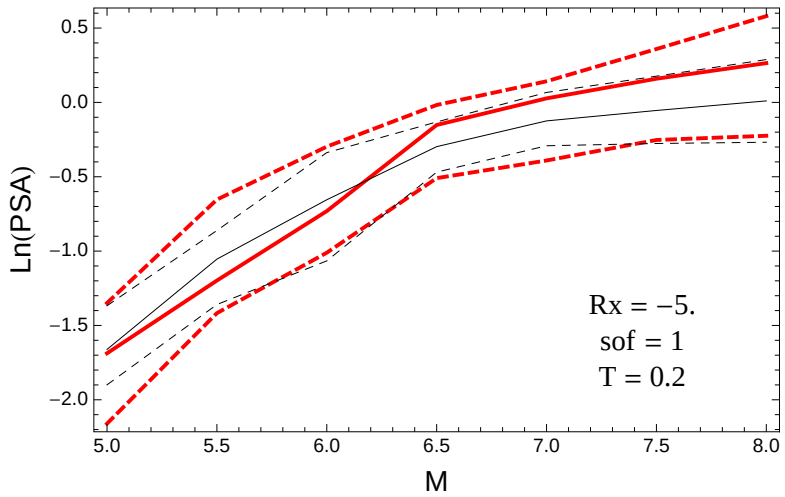



Figure 2.264: DCPPv4: Magnitude scaling of 0.05,0.5,0.95 quantile of the GMPE distribution (black) and the ModelA distribution (red) with total weights, for a scenario with $R_x = -5.$, $F = 1$, and $T = 0.2$s.

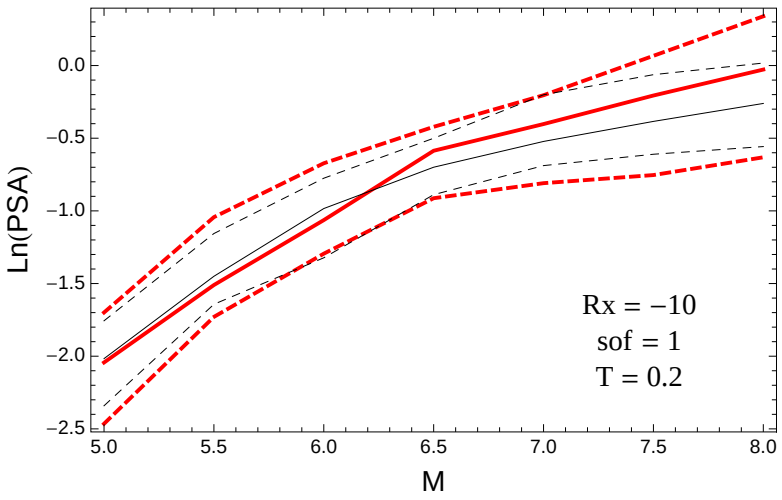



Figure 2.265: DCPPv4: Magnitude scaling of 0.05,0.5,0.95 quantile of the GMPE distribution (black) and the ModelA distribution (red) with total weights, for a scenario with $R_x = -10$, $F = 1$, and $T = 0.2$s.

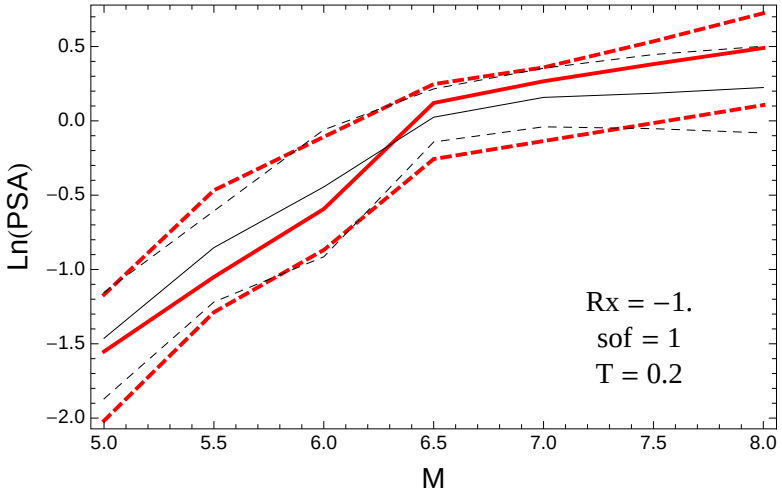



Figure 2.266: DCPPv4: Magnitude scaling of 0.05,0.5,0.95 quantile of the GMPE distribution (black) and the ModelA distribution (red) with total weights, for a scenario with $R_x = -1.$, $F = 1$, and $T = 0.2$s.

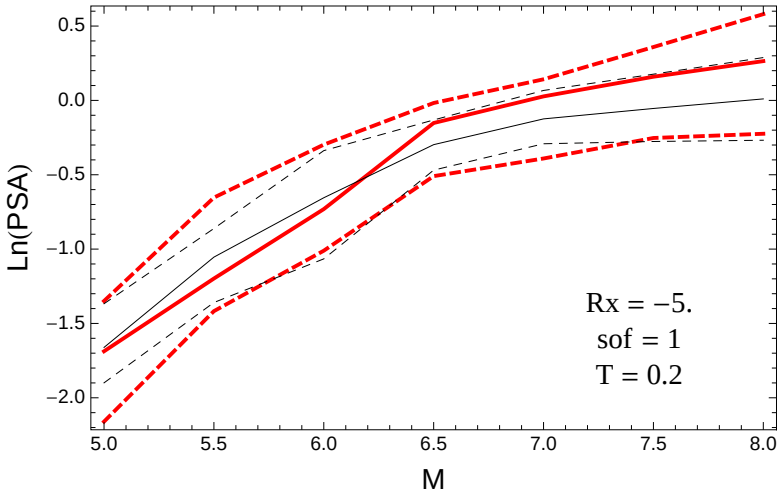



Figure 2.267: DCPPv4: Magnitude scaling of 0.05,0.5,0.95 quantile of the GMPE distribution (black) and the ModelA distribution (red) with total weights, for a scenario with $R_x = -5.$, $F = 1$, and $T = 0.2$s.

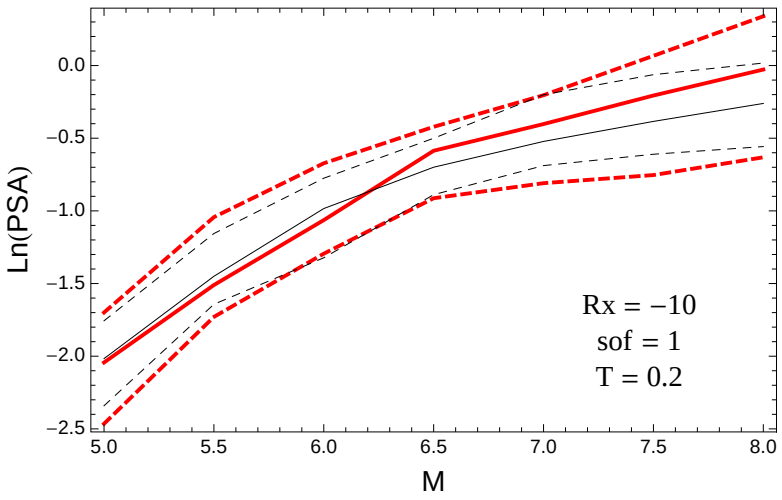



Figure 2.268: DCPPv4: Magnitude scaling of 0.05,0.5,0.95 quantile of the GMPE distribution (black) and the ModelA distribution (red) with total weights, for a scenario with $R_x = -10$, $F = 1$, and $T = 0.2$s.

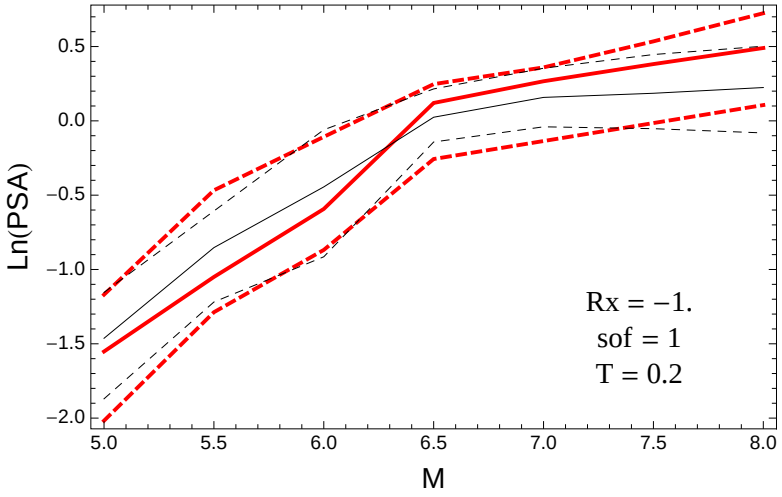



Figure 2.269: DCPPv4: Magnitude scaling of 0.05,0.5,0.95 quantile of the GMPE distribution (black) and the ModelA distribution (red) with total weights, for a scenario with $R_x = -1.$, $F = 1$, and $T = 0.2$s.

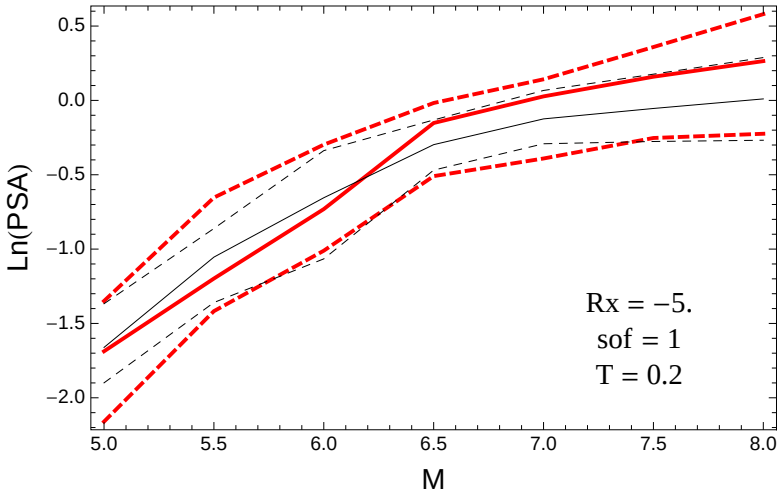



Figure 2.270: DCPPv4: Magnitude scaling of 0.05,0.5,0.95 quantile of the GMPE distribution (black) and the ModelA distribution (red) with total weights, for a scenario with $R_x = -5.$, $F = 1$, and $T = 0.2$s.

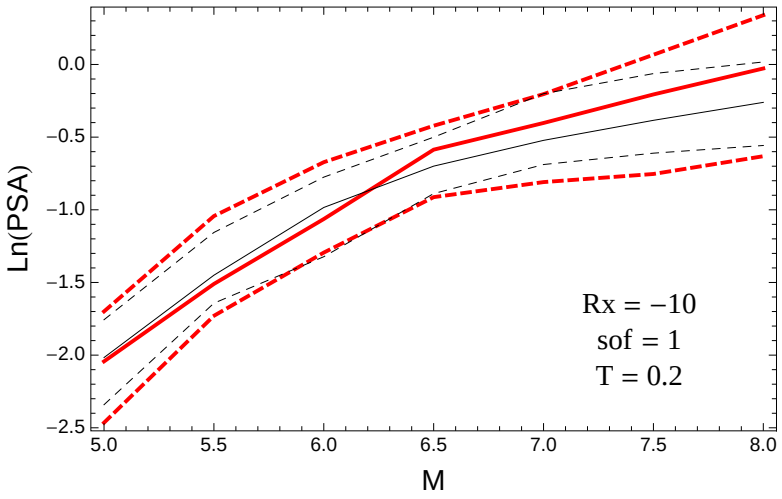



Figure 2.271: DCPPv4: Magnitude scaling of 0.05,0.5,0.95 quantile of the GMPE distribution (black) and the ModelA distribution (red) with total weights, for a scenario with $R_x = -10$, $F = 1$, and $T = 0.2$s.

**T = 0.5s**

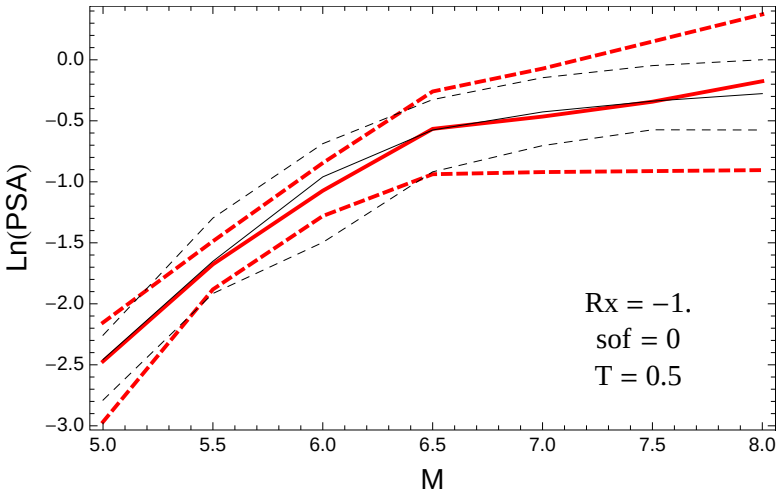



Figure 2.272: DCPPv4: Magnitude scaling of 0.05,0.5,0.95 quantile of the GMPE distribution (black) and the ModelA distribution (red) with total weights, for a scenario with $R_x = -1.$, $F = 0$, and $T = 0.5$s.

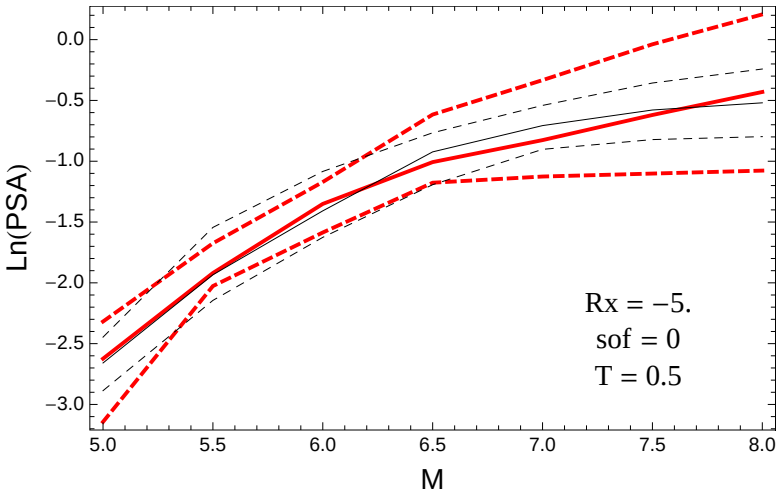



Figure 2.273: DCPPv4: Magnitude scaling of 0.05,0.5,0.95 quantile of the GMPE distribution (black) and the ModelA distribution (red) with total weights, for a scenario with $R_x = -5.$, $F = 0$, and $T = 0.5$s.

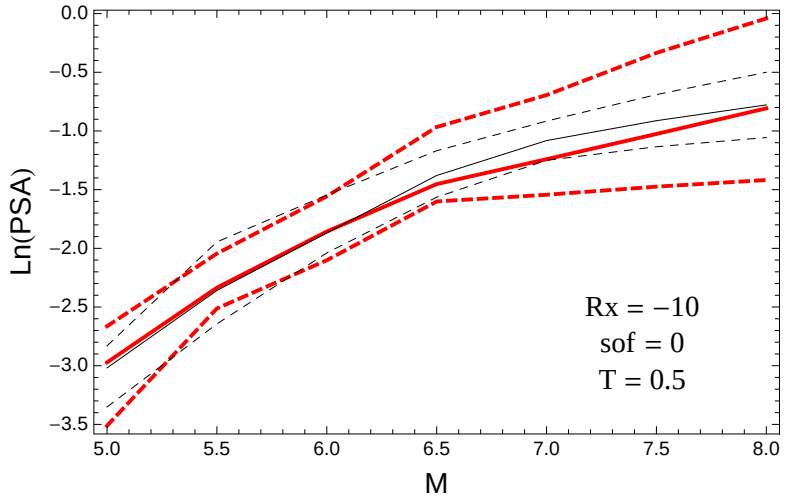



Figure 2.274: DCPPv4: Magnitude scaling of 0.05,0.5,0.95 quantile of the GMPE distribution (black) and the ModelA distribution (red) with total weights, for a scenario with $R_x = -10$, $F = 0$, and $T = 0.5$s.

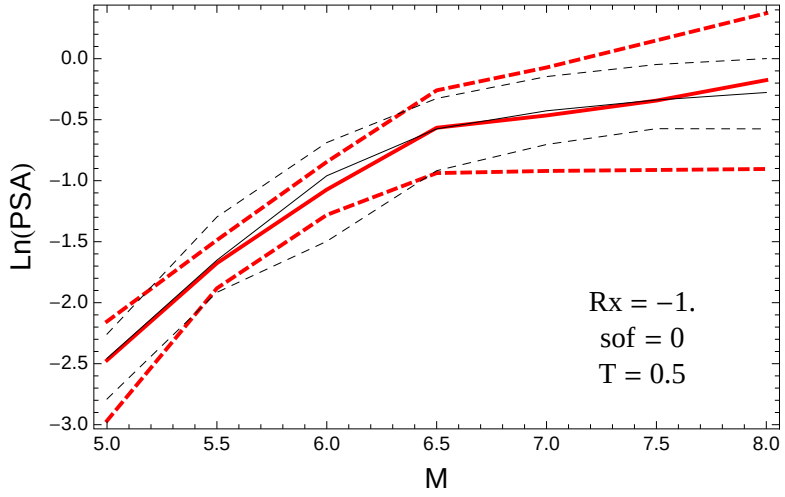



Figure 2.275: DCPPv4: Magnitude scaling of 0.05,0.5,0.95 quantile of the GMPE distribution (black) and the ModelA distribution (red) with total weights, for a scenario with $R_x = -1.$, $F = 0$, and $T = 0.5$s.

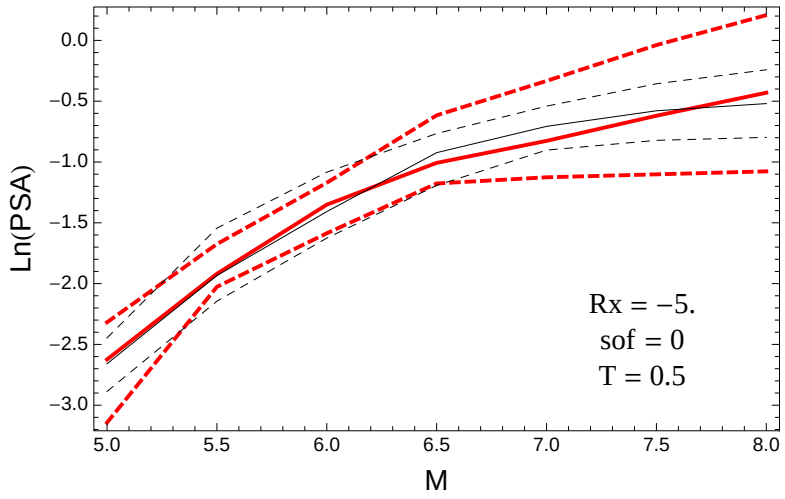



Figure 2.276: DCPPv4: Magnitude scaling of 0.05,0.5,0.95 quantile of the GMPE distribution (black) and the ModelA distribution (red) with total weights, for a scenario with $R_x = -5.$, $F = 0$, and $T = 0.5$s.

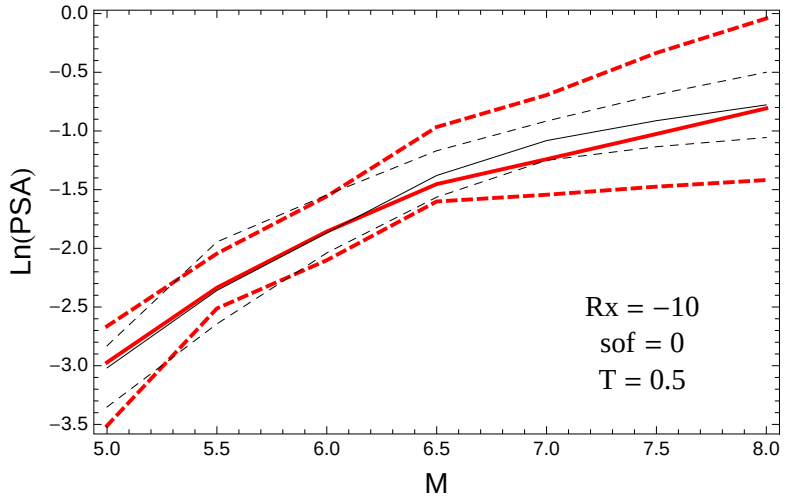



Figure 2.277: DCPPv4: Magnitude scaling of 0.05,0.5,0.95 quantile of the GMPE distribution (black) and the ModelA distribution (red) with total weights, for a scenario with $R_x = -10$, $F = 0$, and $T = 0.5$s.

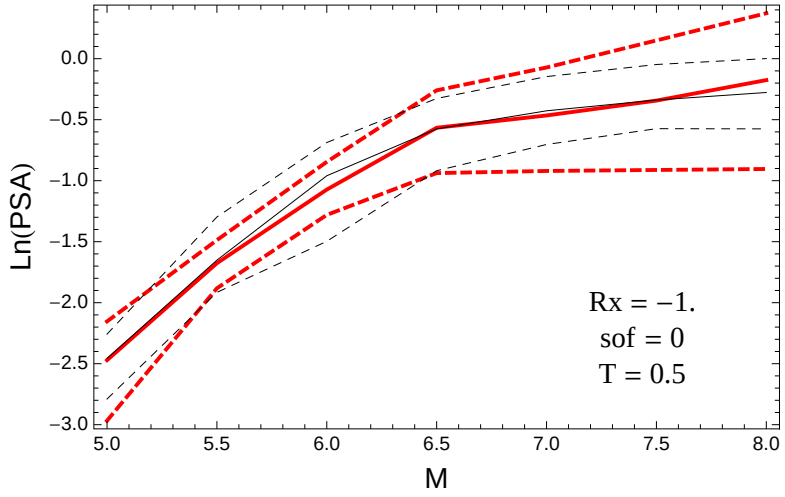



Figure 2.278: DCPPv4: Magnitude scaling of 0.05,0.5,0.95 quantile of the GMPE distribution (black) and the ModelA distribution (red) with total weights, for a scenario with $R_x = -1.$, $F = 0$, and $T = 0.5$s.

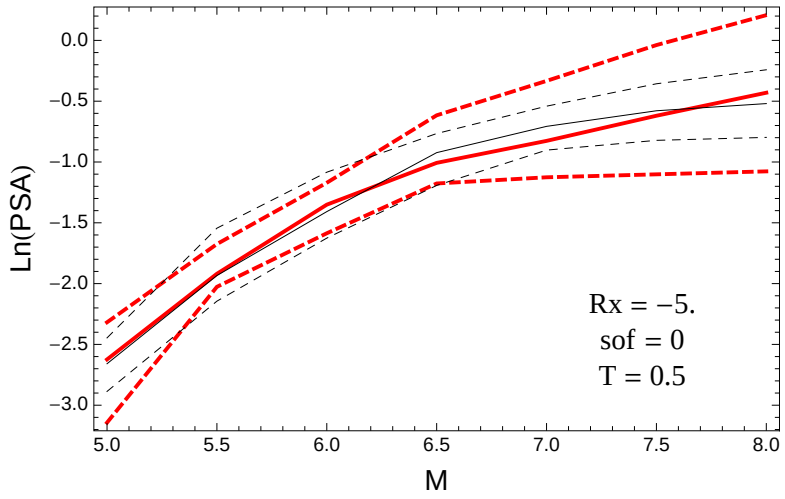



Figure 2.279: DCPPv4: Magnitude scaling of 0.05,0.5,0.95 quantile of the GMPE distribution (black) and the ModelA distribution (red) with total weights, for a scenario with $R_x = -5.$, $F = 0$, and $T = 0.5$s.

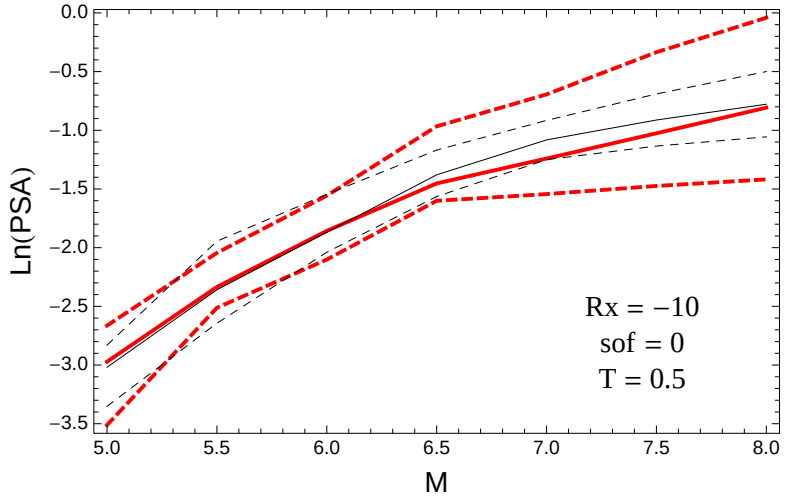



Figure 2.280: DCPPv4: Magnitude scaling of 0.05,0.5,0.95 quantile of the GMPE distribution (black) and the ModelA distribution (red) with total weights, for a scenario with $R_x = -10$, $F = 0$, and $T = 0.5$s.

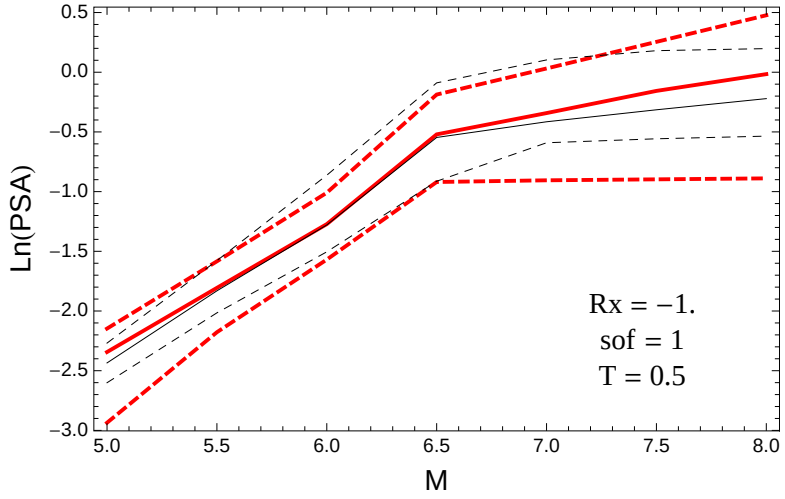



Figure 2.281: DCPPv4: Magnitude scaling of 0.05,0.5,0.95 quantile of the GMPE distribution (black) and the ModelA distribution (red) with total weights, for a scenario with $R_x = -1.$, $F = 1$, and $T = 0.5$s.

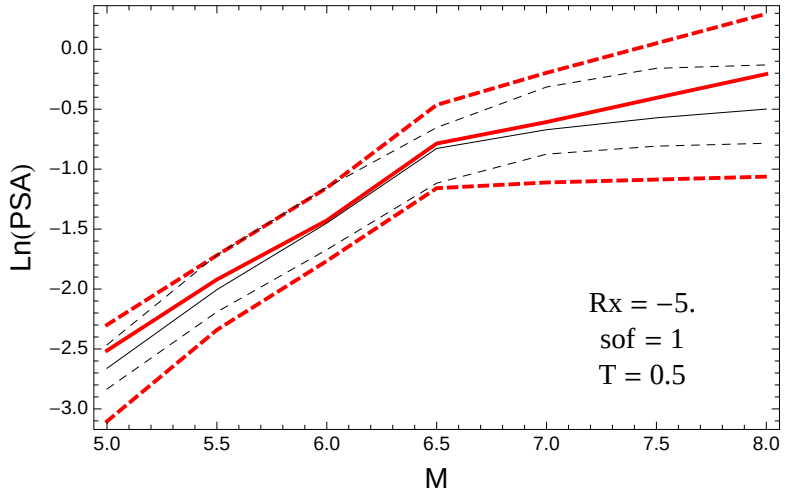



Figure 2.282: DCPPv4: Magnitude scaling of 0.05,0.5,0.95 quantile of the GMPE distribution (black) and the ModelA distribution (red) with total weights, for a scenario with $R_x = -5.$, $F = 1$, and $T = 0.5$s.

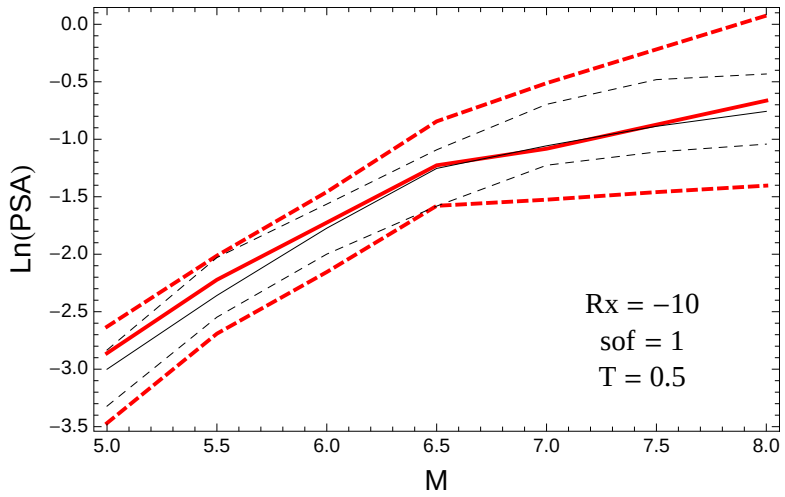



Figure 2.283: DCPPv4: Magnitude scaling of 0.05,0.5,0.95 quantile of the GMPE distribution (black) and the ModelA distribution (red) with total weights, for a scenario with $R_x = -10$, $F = 1$, and $T = 0.5$s.

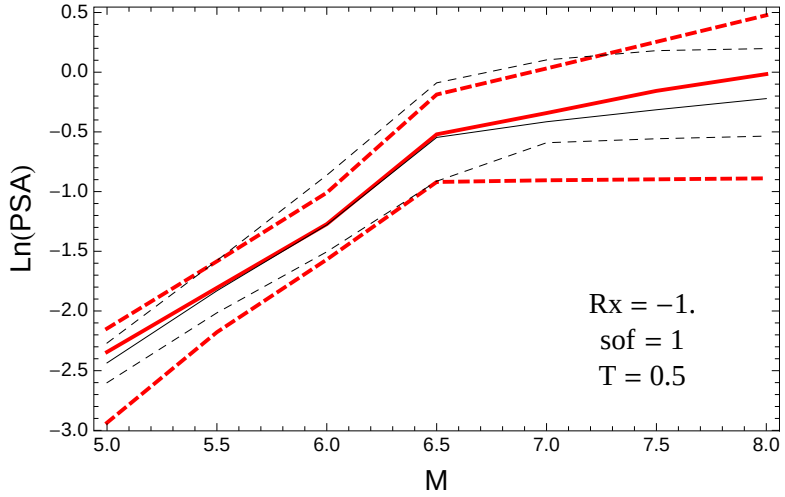



Figure 2.284: DCPPv4: Magnitude scaling of 0.05,0.5,0.95 quantile of the GMPE distribution (black) and the ModelA distribution (red) with total weights, for a scenario with $R_x = -1.$, $F = 1$, and $T = 0.5$s.

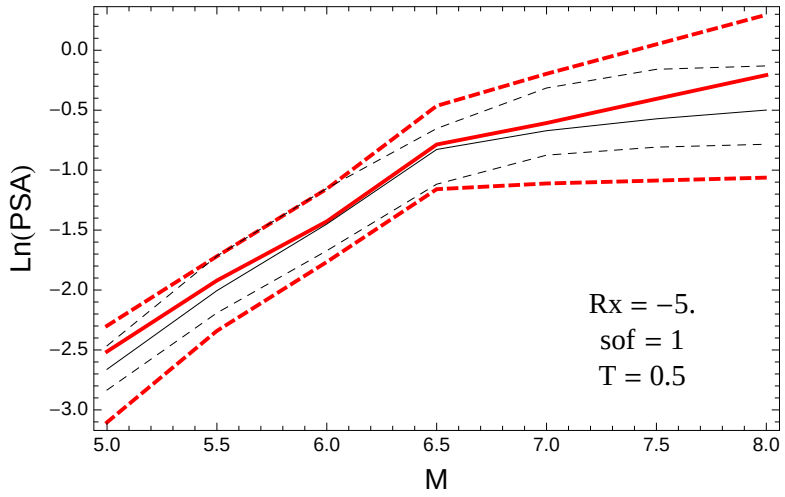



Figure 2.285: DCPPv4: Magnitude scaling of 0.05,0.5,0.95 quantile of the GMPE distribution (black) and the ModelA distribution (red) with total weights, for a scenario with $R_x = -5.$, $F = 1$, and $T = 0.5$s.

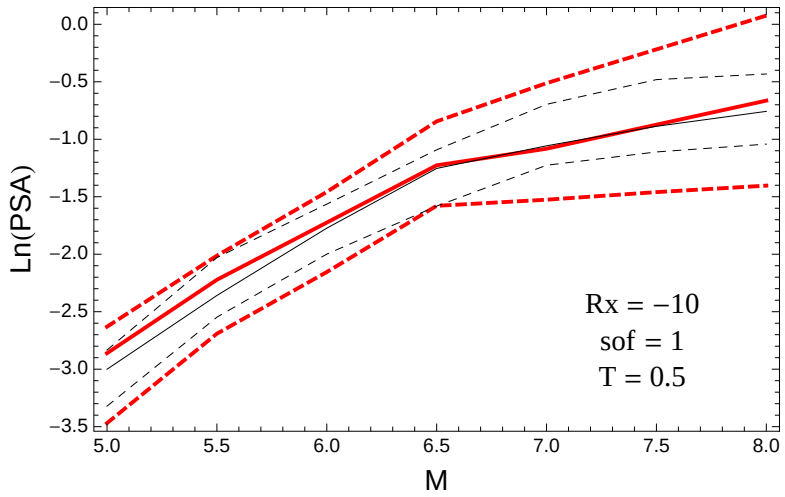



Figure 2.286: DCPPv4: Magnitude scaling of 0.05,0.5,0.95 quantile of the GMPE distribution (black) and the ModelA distribution (red) with total weights, for a scenario with $R_x = -10$, $F = 1$, and $T = 0.5$s.

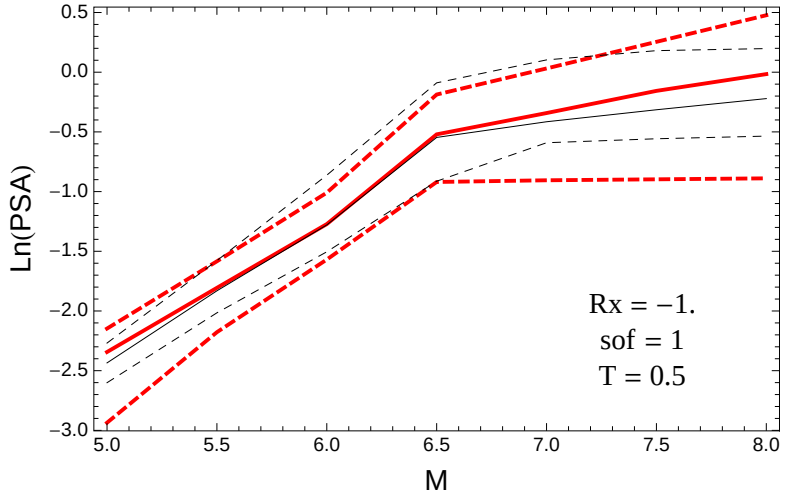



Figure 2.287: DCPPv4: Magnitude scaling of 0.05,0.5,0.95 quantile of the GMPE distribution (black) and the ModelA distribution (red) with total weights, for a scenario with $R_x = -1.$, $F = 1$, and $T = 0.5$s.

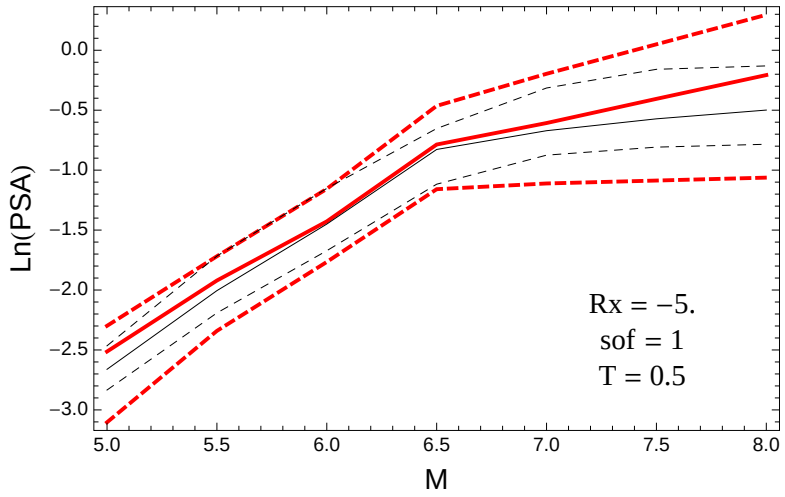



Figure 2.288: DCPPv4: Magnitude scaling of 0.05,0.5,0.95 quantile of the GMPE distribution (black) and the ModelA distribution (red) with total weights, for a scenario with $R_x = -5.$, $F = 1$, and $T = 0.5$s.

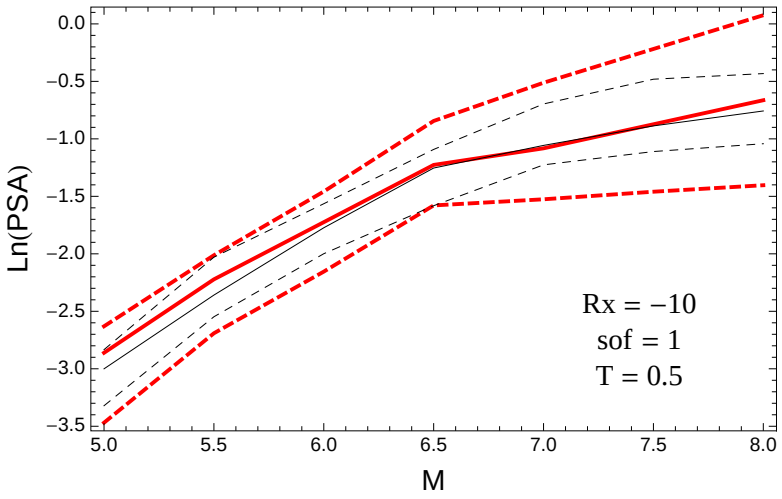



Figure 2.289: DCPPv4: Magnitude scaling of 0.05,0.5,0.95 quantile of the GMPE distribution (black) and the ModelA distribution (red) with total weights, for a scenario with $R_x = -10$, $F = 1$, and $T = 0.5$s.

**T = 1.s**

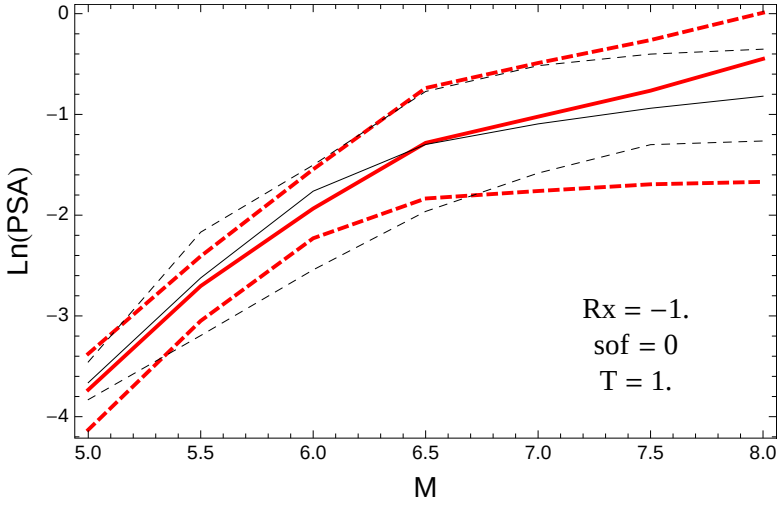



Figure 2.290: DCPPv4: Magnitude scaling of 0.05,0.5,0.95 quantile of the GMPE distribution (black) and the ModelA distribution (red) with total weights, for a scenario with $R_x = -1.$, $F = 0$, and $T = 1.$s.

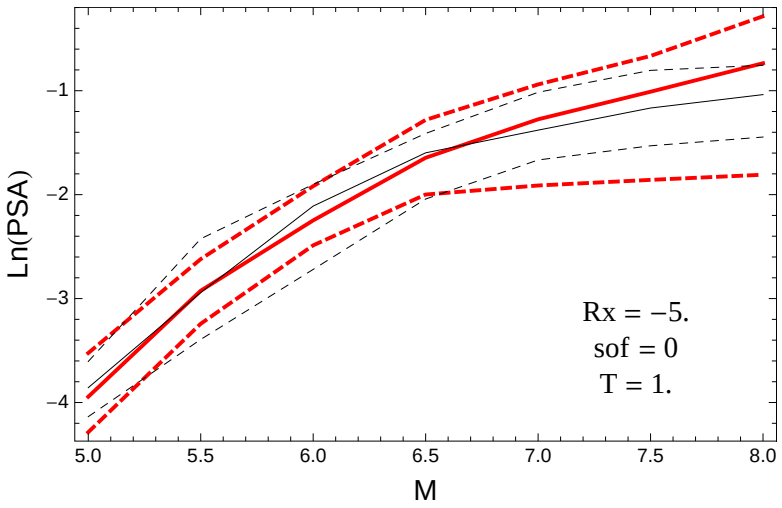



Figure 2.291: DCPPv4: Magnitude scaling of 0.05,0.5,0.95 quantile of the GMPE distribution (black) and the ModelA distribution (red) with total weights, for a scenario with $R_x = -5.$, $F = 0$, and $T = 1.$s.

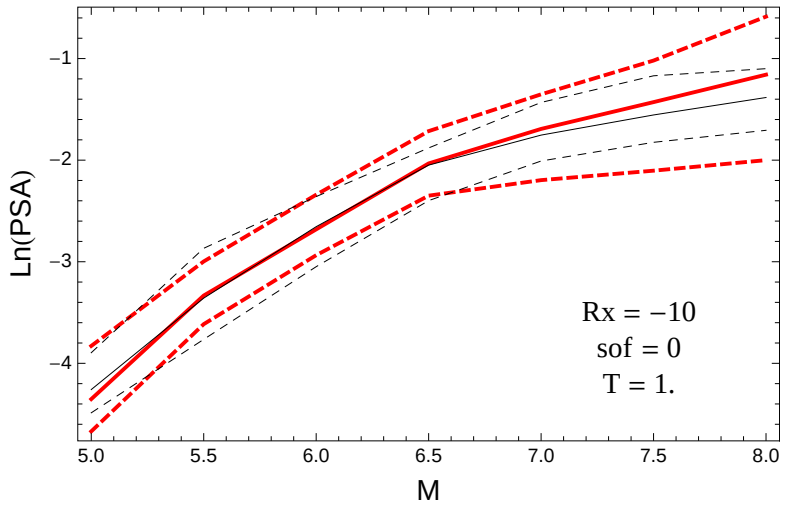



Figure 2.292: DCPPv4: Magnitude scaling of 0.05,0.5,0.95 quantile of the GMPE distribution (black) and the ModelA distribution (red) with total weights, for a scenario with $R_x = -10$, $F = 0$, and $T = 1$.s.

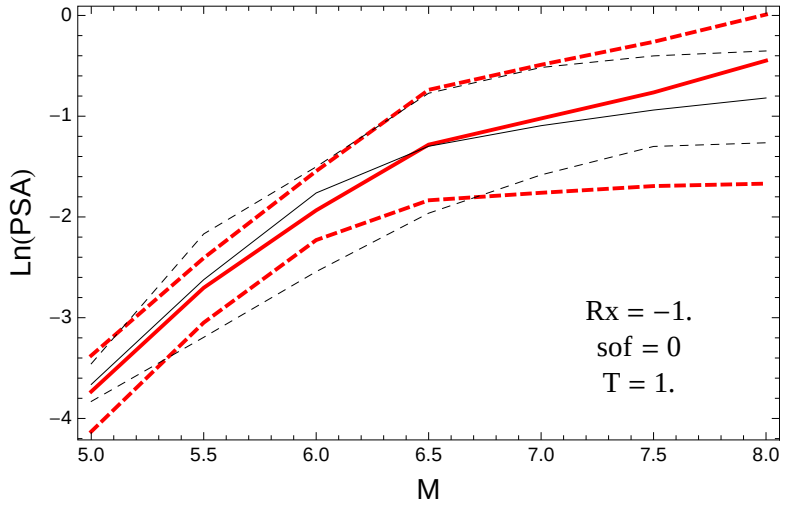



Figure 2.293: DCPPv4: Magnitude scaling of 0.05,0.5,0.95 quantile of the GMPE distribution (black) and the ModelA distribution (red) with total weights, for a scenario with $R_x = -1.$, $F = 0$, and $T = 1$.s.

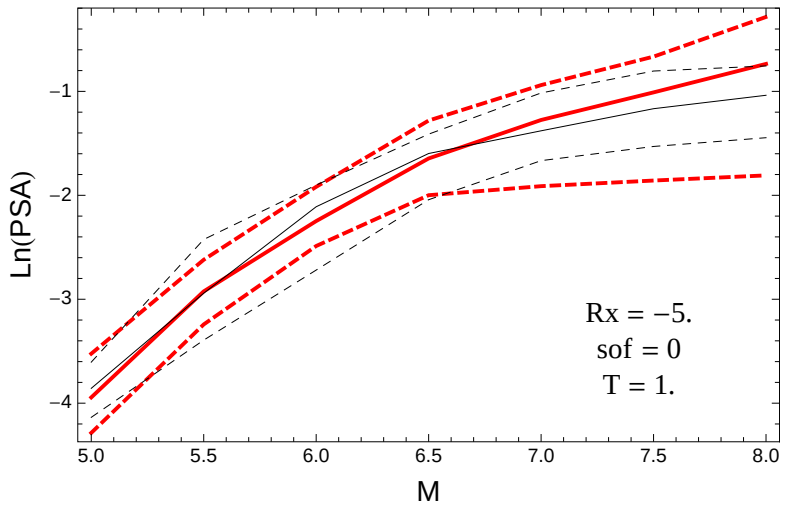



Figure 2.294: DCPPv4: Magnitude scaling of 0.05,0.5,0.95 quantile of the GMPE distribution (black) and the ModelA distribution (red) with total weights, for a scenario with $R_x = -5.$, $F = 0$, and $T = 1$.s.

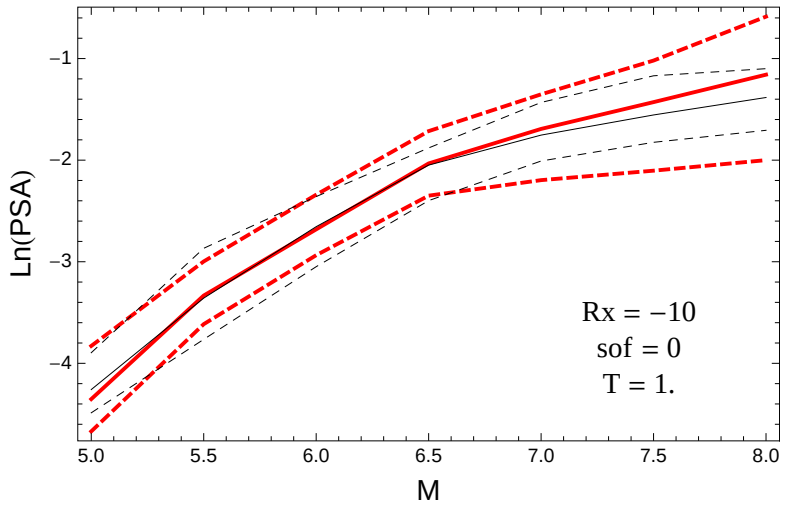



Figure 2.295: DCPPv4: Magnitude scaling of 0.05,0.5,0.95 quantile of the GMPE distribution (black) and the ModelA distribution (red) with total weights, for a scenario with $R_x = -10$, $F = 0$, and $T = 1$.s.

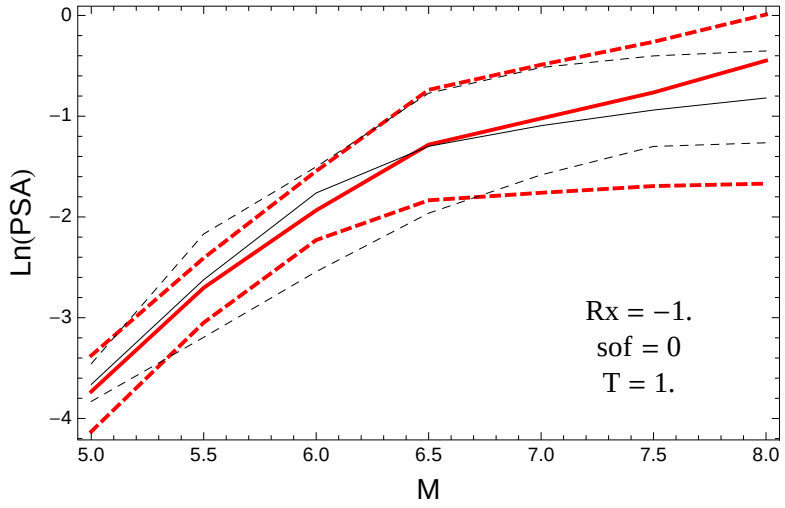



Figure 2.296: DCPPv4: Magnitude scaling of 0.05,0.5,0.95 quantile of the GMPE distribution (black) and the ModelA distribution (red) with total weights, for a scenario with $R_x = -1.$, $F = 0$, and $T = 1$.s.

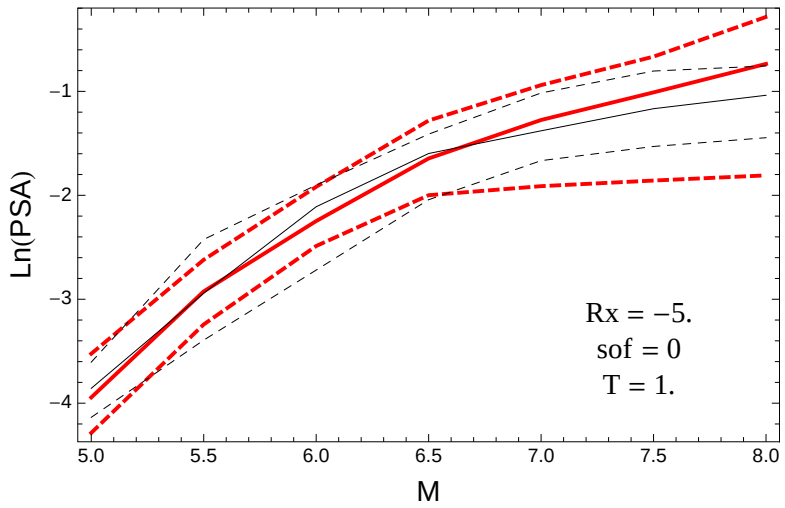



Figure 2.297: DCPPv4: Magnitude scaling of 0.05,0.5,0.95 quantile of the GMPE distribution (black) and the ModelA distribution (red) with total weights, for a scenario with $R_x = -5.$, $F = 0$, and $T = 1$.s.

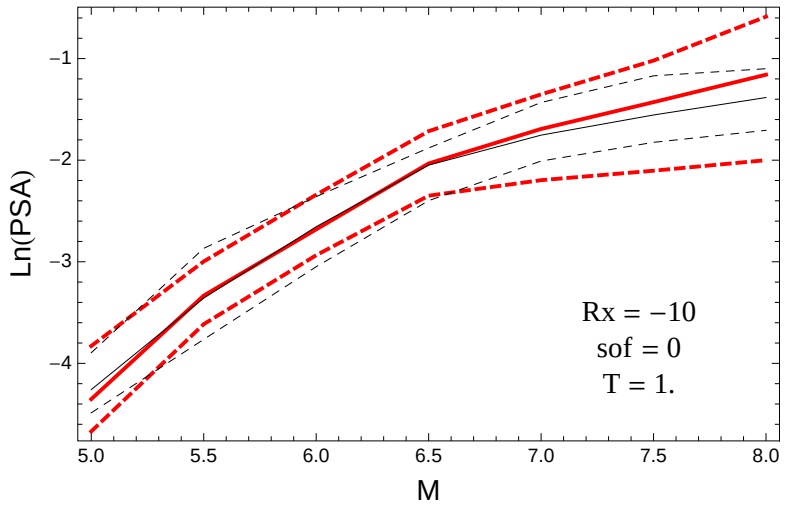



Figure 2.298: DCPPv4: Magnitude scaling of 0.05,0.5,0.95 quantile of the GMPE distribution (black) and the ModelA distribution (red) with total weights, for a scenario with $R_x = -10$, $F = 0$, and $T = 1$.s.

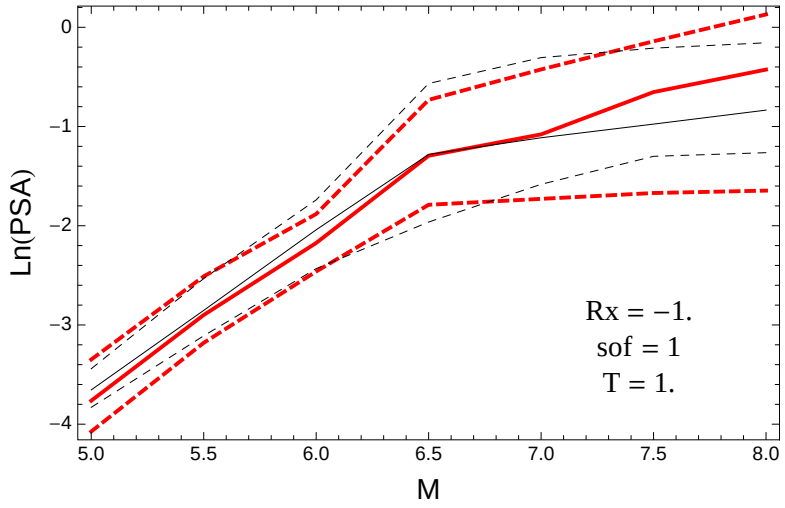



Figure 2.299: DCPPv4: Magnitude scaling of 0.05,0.5,0.95 quantile of the GMPE distribution (black) and the ModelA distribution (red) with total weights, for a scenario with $R_x = -1.$, $F = 1$, and $T = 1$.s.

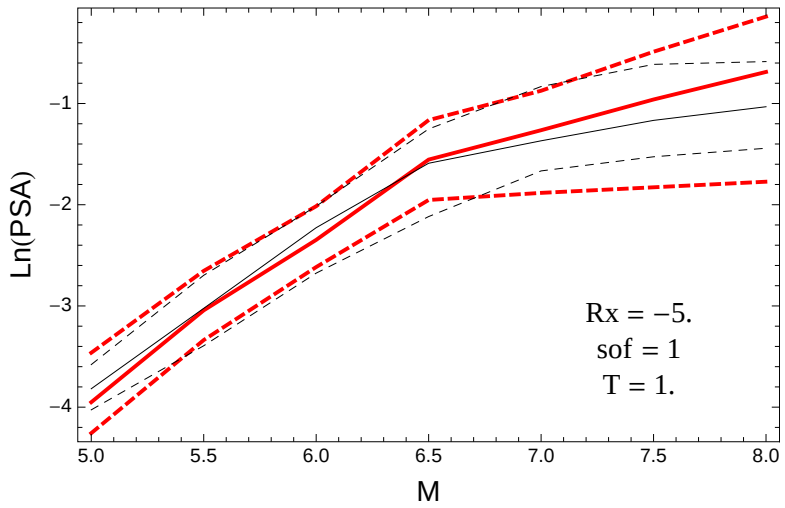



Figure 2.300: DCPPv4: Magnitude scaling of 0.05,0.5,0.95 quantile of the GMPE distribution (black) and the ModelA distribution (red) with total weights, for a scenario with $R_x = -5.$, $F = 1$, and $T = 1$.s.

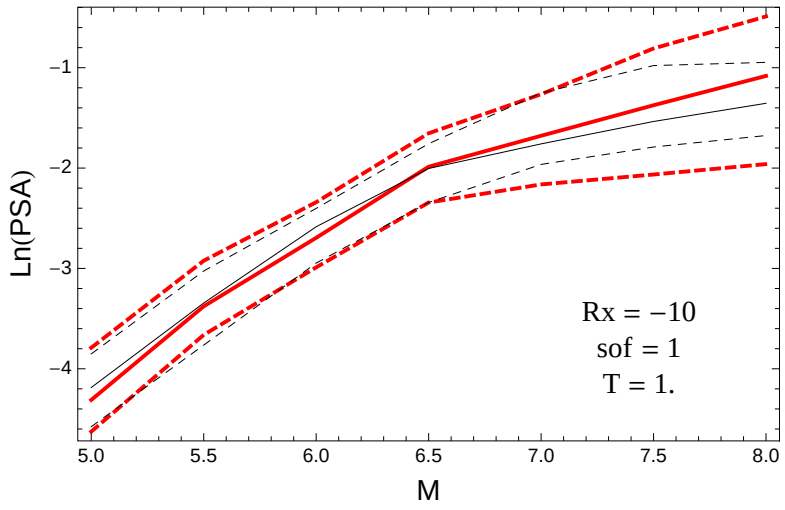



Figure 2.301: DCPPv4: Magnitude scaling of 0.05,0.5,0.95 quantile of the GMPE distribution (black) and the ModelA distribution (red) with total weights, for a scenario with $R_x = -10$, $F = 1$, and $T = 1$.s.

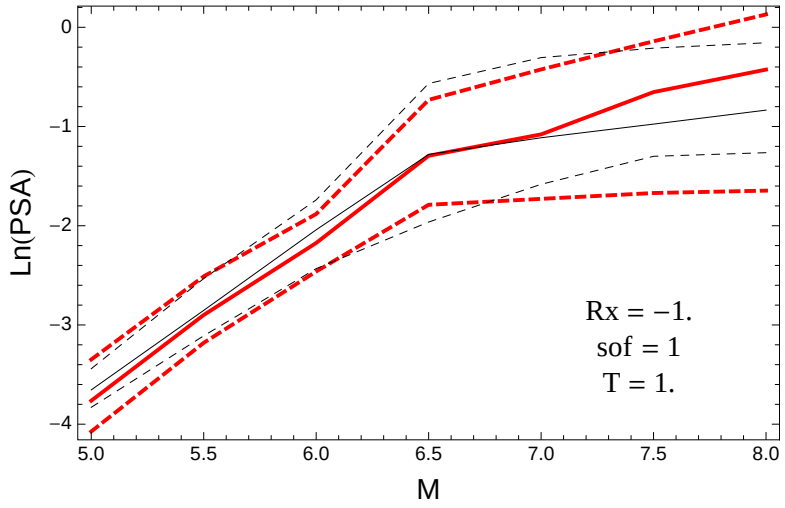



Figure 2.302: DCPPv4: Magnitude scaling of 0.05,0.5,0.95 quantile of the GMPE distribution (black) and the ModelA distribution (red) with total weights, for a scenario with $R_x = -1.$, $F = 1$, and $T = 1$.s.

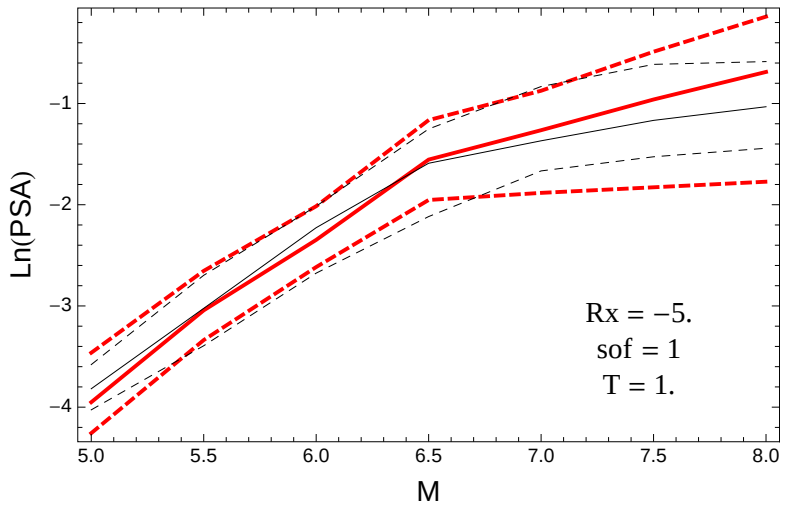



Figure 2.303: DCPPv4: Magnitude scaling of 0.05,0.5,0.95 quantile of the GMPE distribution (black) and the ModelA distribution (red) with total weights, for a scenario with $R_x = -5.$, $F = 1$, and $T = 1$.s.

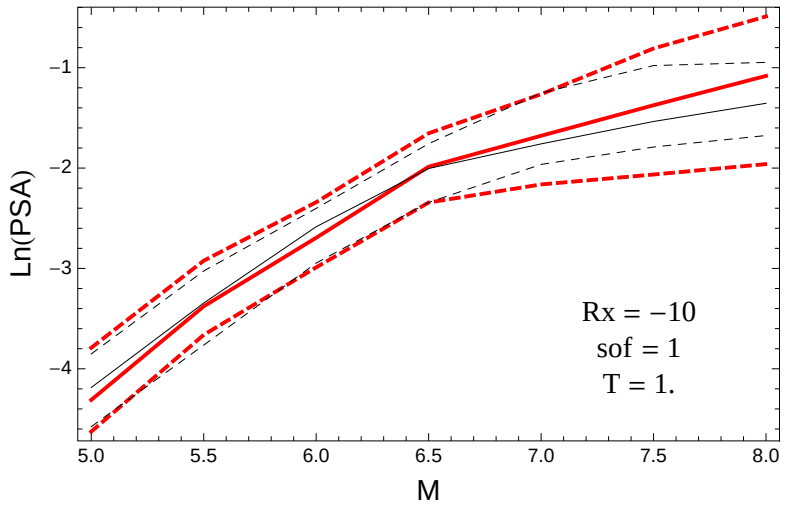



Figure 2.304: DCPPv4: Magnitude scaling of 0.05,0.5,0.95 quantile of the GMPE distribution (black) and the ModelA distribution (red) with total weights, for a scenario with $R_x = -10$, $F = 1$, and $T = 1$.s.

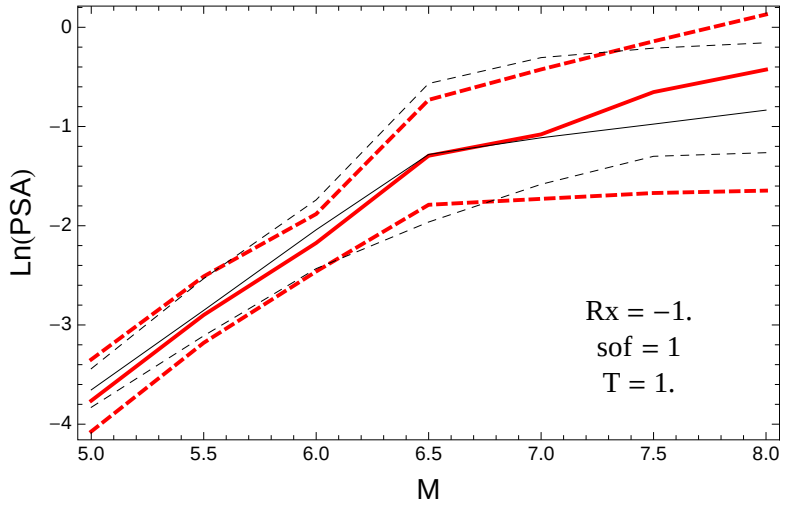



Figure 2.305: DCPPv4: Magnitude scaling of 0.05,0.5,0.95 quantile of the GMPE distribution (black) and the ModelA distribution (red) with total weights, for a scenario with $R_x = -1.$, $F = 1$, and $T = 1$.s.

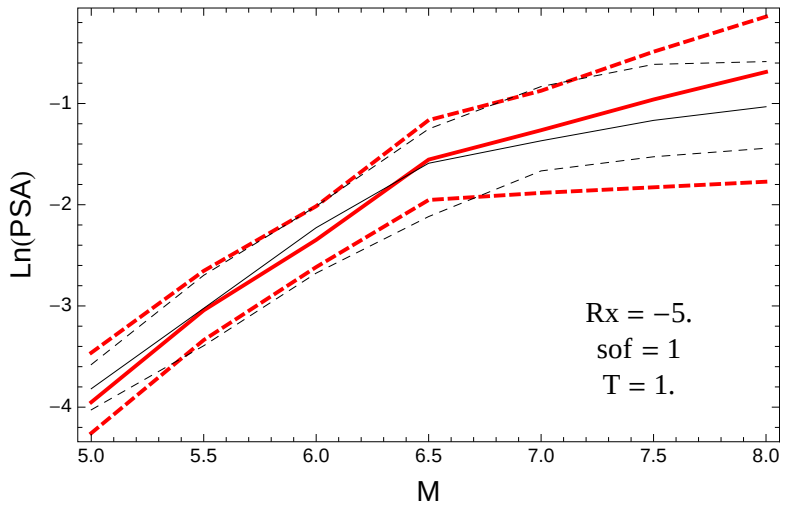



Figure 2.306: DCPPv4: Magnitude scaling of 0.05,0.5,0.95 quantile of the GMPE distribution (black) and the ModelA distribution (red) with total weights, for a scenario with $R_x = -5.$, $F = 1$, and $T = 1$.s.

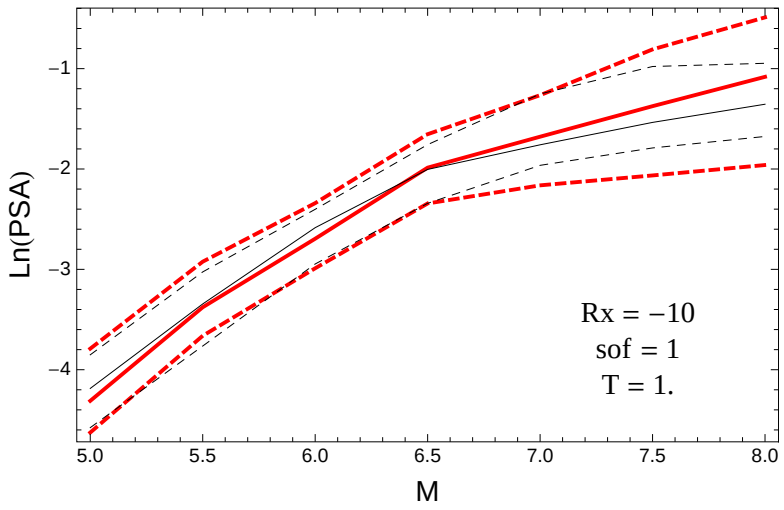



Figure 2.307: DCPPv4: Magnitude scaling of 0.05,0.5,0.95 quantile of the GMPE distribution (black) and the ModelA distribution (red) with total weights, for a scenario with $R_x = -10$, $F = 1$, and $T = 1$.s.

**T = 3.s**

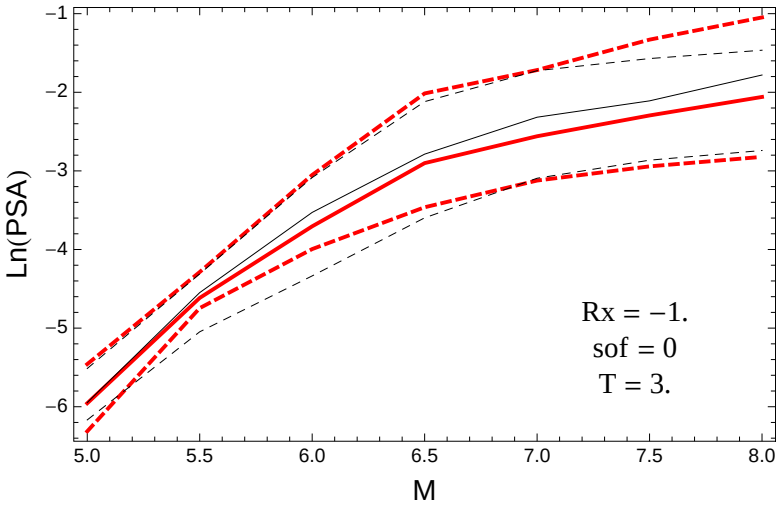



Figure 2.308: DCPPv4: Magnitude scaling of 0.05,0.5,0.95 quantile of the GMPE distribution (black) and the ModelA distribution (red) with total weights, for a scenario with $R_x = -1.$, $F = 0$, and $T = 3.$s.

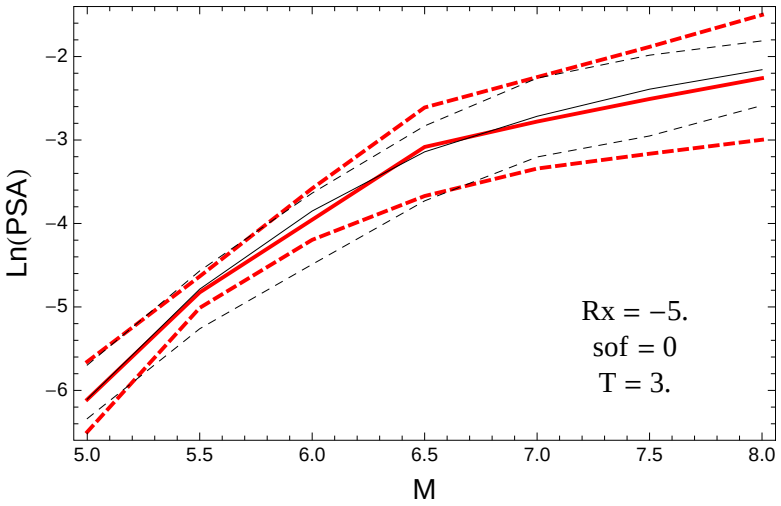



Figure 2.309: DCPPv4: Magnitude scaling of 0.05,0.5,0.95 quantile of the GMPE distribution (black) and the ModelA distribution (red) with total weights, for a scenario with $R_x = -5.$, $F = 0$, and $T = 3.$s.

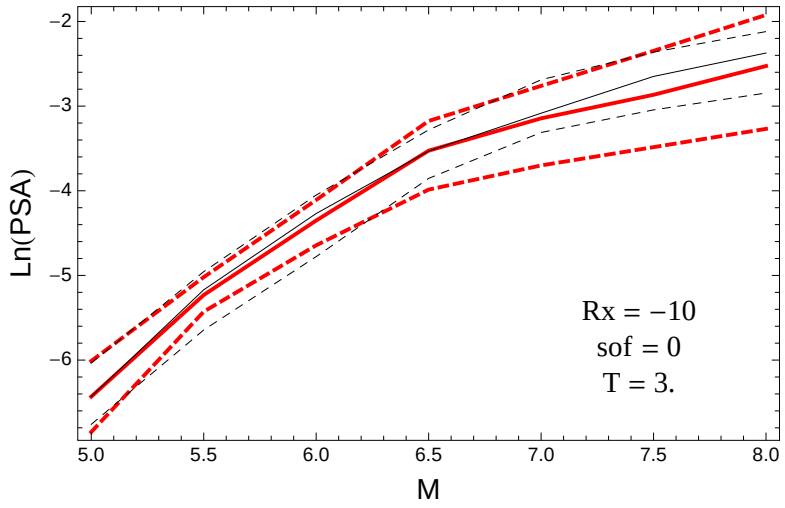



Figure 2.310: DCPPv4: Magnitude scaling of 0.05,0.5,0.95 quantile of the GMPE distribution (black) and the ModelA distribution (red) with total weights, for a scenario with $R_x = -10$, $F = 0$, and $T = 3$.s.

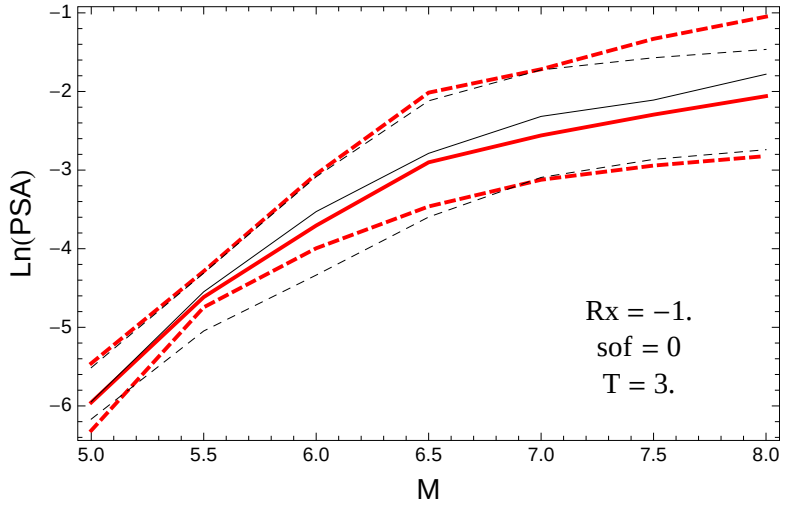



Figure 2.311: DCPPv4: Magnitude scaling of 0.05,0.5,0.95 quantile of the GMPE distribution (black) and the ModelA distribution (red) with total weights, for a scenario with $R_x = -1.$, $F = 0$, and $T = 3$.s.

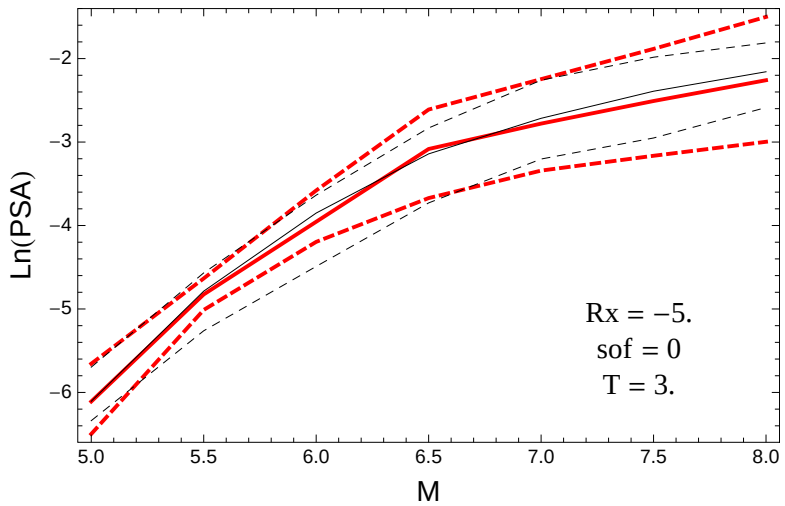



Figure 2.312: DCPPv4: Magnitude scaling of 0.05,0.5,0.95 quantile of the GMPE distribution (black) and the ModelA distribution (red) with total weights, for a scenario with $R_x = -5.$, $F = 0$, and $T = 3$.s.

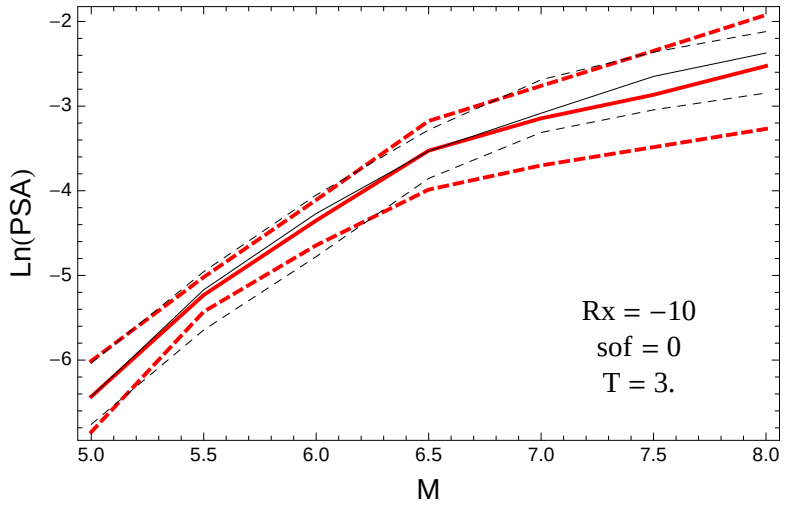



Figure 2.313: DCPPv4: Magnitude scaling of 0.05,0.5,0.95 quantile of the GMPE distribution (black) and the ModelA distribution (red) with total weights, for a scenario with $R_x = -10$, $F = 0$, and $T = 3$.s.

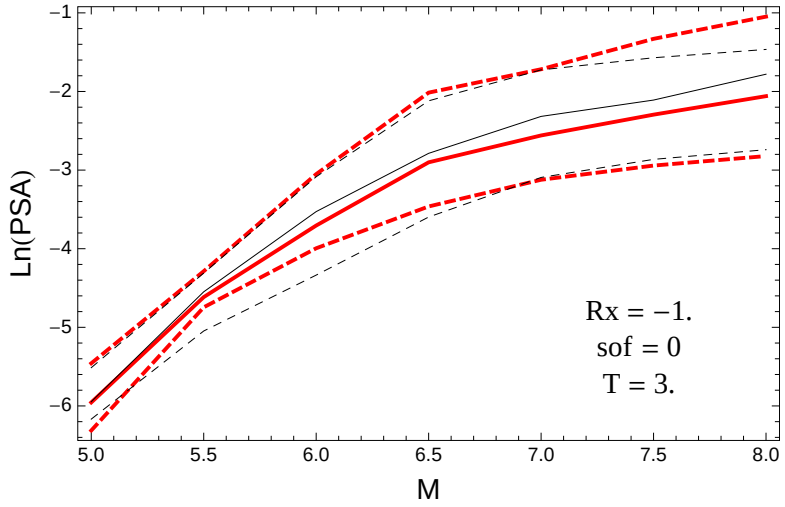



Figure 2.314: DCPPv4: Magnitude scaling of 0.05,0.5,0.95 quantile of the GMPE distribution (black) and the ModelA distribution (red) with total weights, for a scenario with $R_x = -1.$, $F = 0$, and $T = 3$.s.

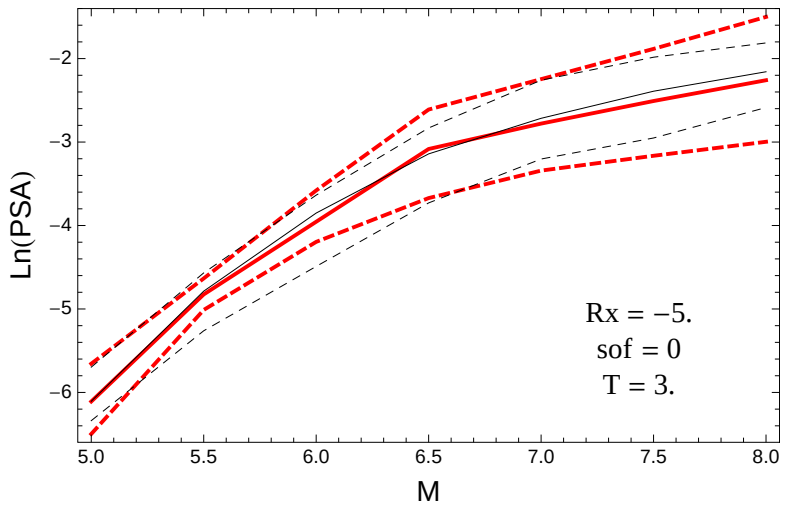



Figure 2.315: DCPPv4: Magnitude scaling of 0.05,0.5,0.95 quantile of the GMPE distribution (black) and the ModelA distribution (red) with total weights, for a scenario with $R_x = -5.$, $F = 0$, and $T = 3$.s.

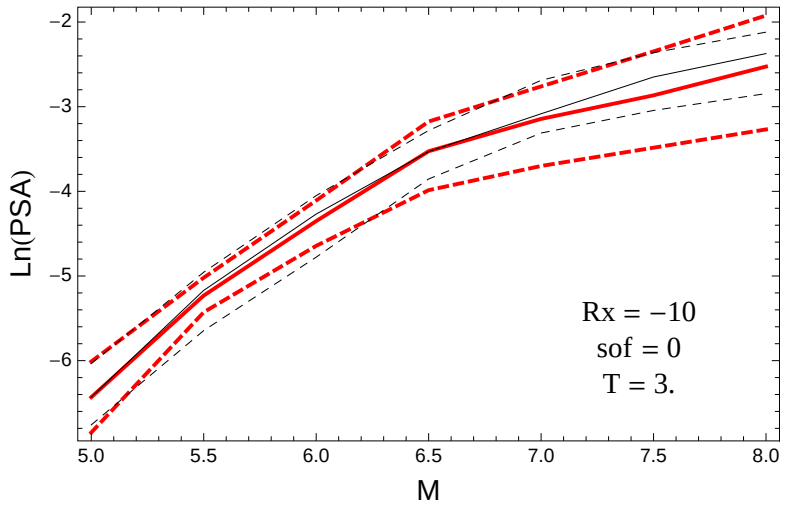



Figure 2.316: DCPPv4: Magnitude scaling of 0.05,0.5,0.95 quantile of the GMPE distribution (black) and the ModelA distribution (red) with total weights, for a scenario with $R_x = -10$, $F = 0$, and $T = 3$.s.

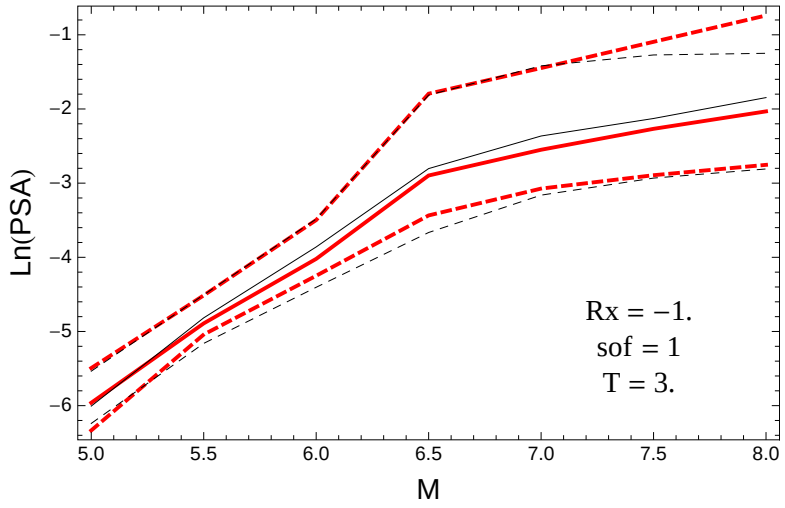



Figure 2.317: DCPPv4: Magnitude scaling of 0.05,0.5,0.95 quantile of the GMPE distribution (black) and the ModelA distribution (red) with total weights, for a scenario with $R_x = -1.$, $F = 1$, and $T = 3$.s.

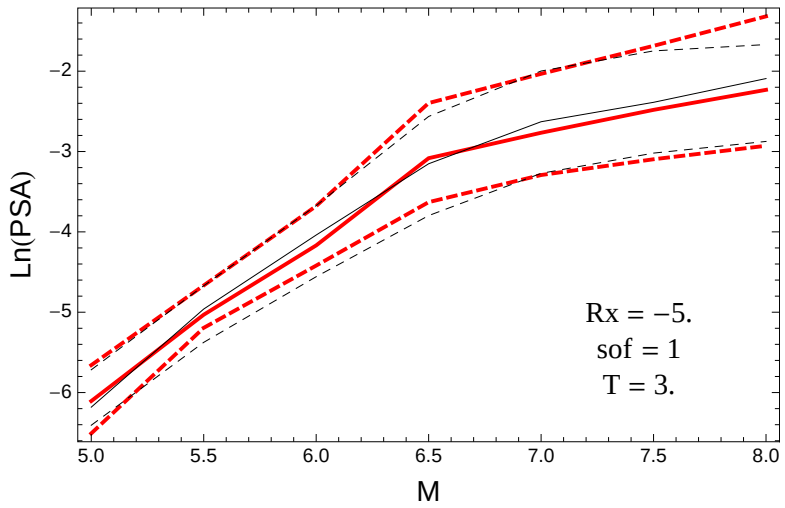



Figure 2.318: DCPPv4: Magnitude scaling of 0.05,0.5,0.95 quantile of the GMPE distribution (black) and the ModelA distribution (red) with total weights, for a scenario with $R_x = -5.$, $F = 1$, and $T = 3$.s.

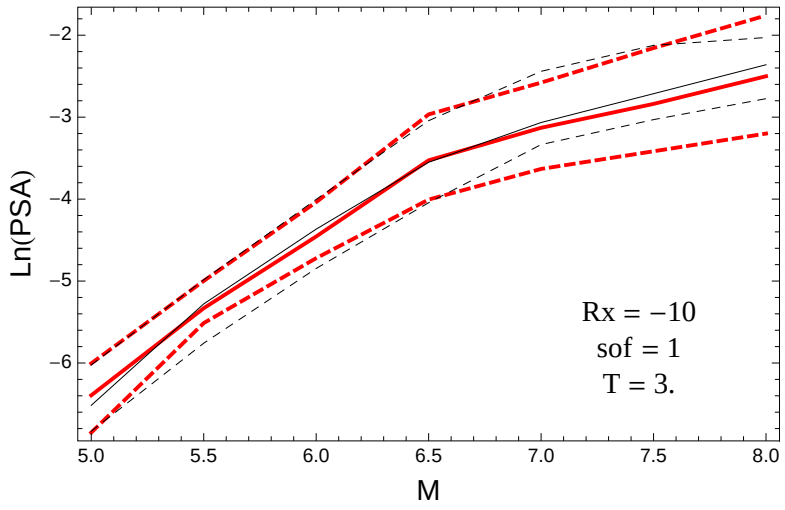



Figure 2.319: DCPPv4: Magnitude scaling of 0.05,0.5,0.95 quantile of the GMPE distribution (black) and the ModelA distribution (red) with total weights, for a scenario with $R_x = -10$, $F = 1$, and $T = 3$.s.

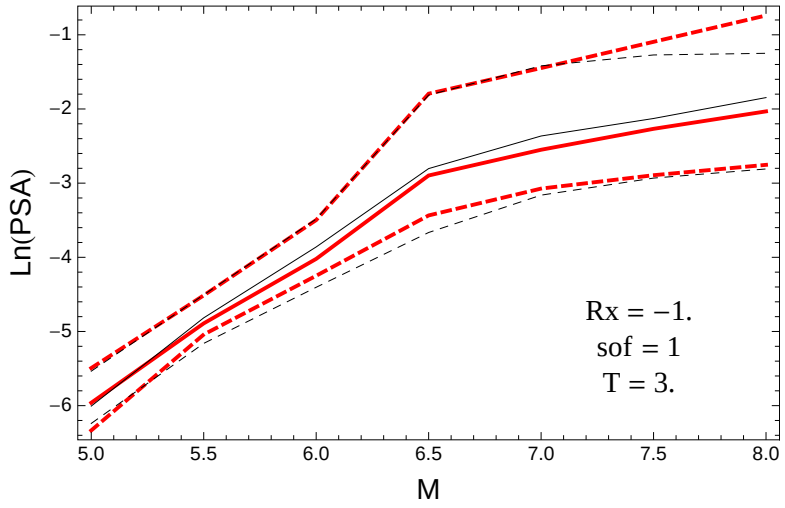



Figure 2.320: DCPPv4: Magnitude scaling of 0.05,0.5,0.95 quantile of the GMPE distribution (black) and the ModelA distribution (red) with total weights, for a scenario with $R_x = -1.$, $F = 1$, and $T = 3$.s.

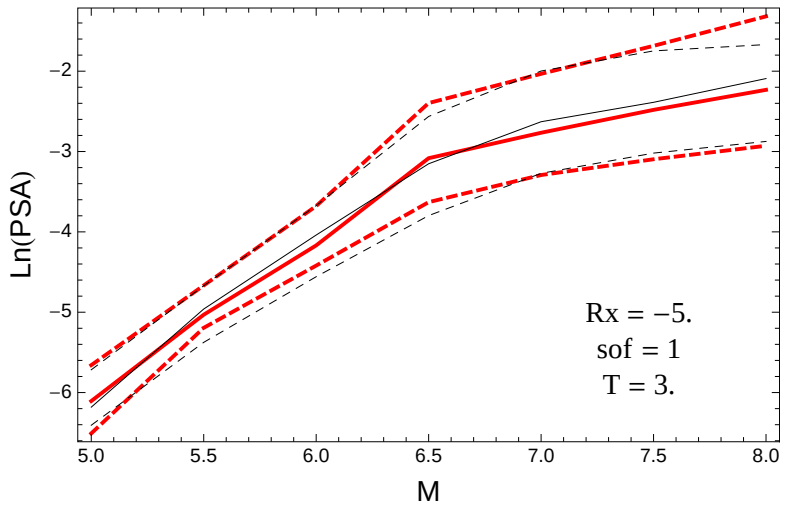



Figure 2.321: DCPPv4: Magnitude scaling of 0.05,0.5,0.95 quantile of the GMPE distribution (black) and the ModelA distribution (red) with total weights, for a scenario with $R_x = -5.$, $F = 1$, and $T = 3$.s.

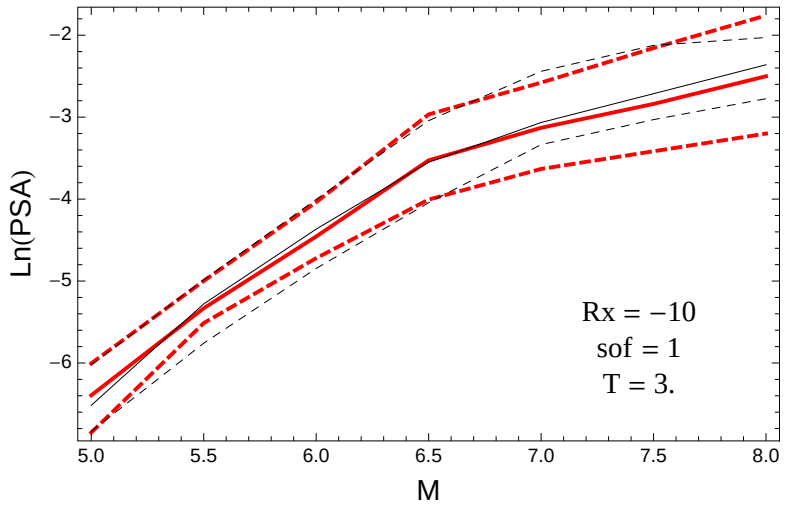



Figure 2.322: DCPPv4: Magnitude scaling of 0.05,0.5,0.95 quantile of the GMPE distribution (black) and the ModelA distribution (red) with total weights, for a scenario with $R_x = -10$, $F = 1$, and $T = 3$.s.

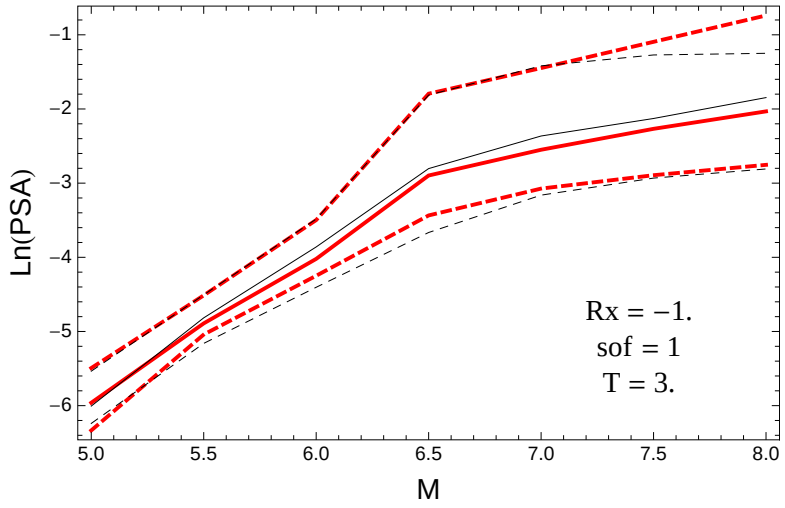



Figure 2.323: DCPPv4: Magnitude scaling of 0.05,0.5,0.95 quantile of the GMPE distribution (black) and the ModelA distribution (red) with total weights, for a scenario with $R_x = -1.$, $F = 1$, and $T = 3$.s.

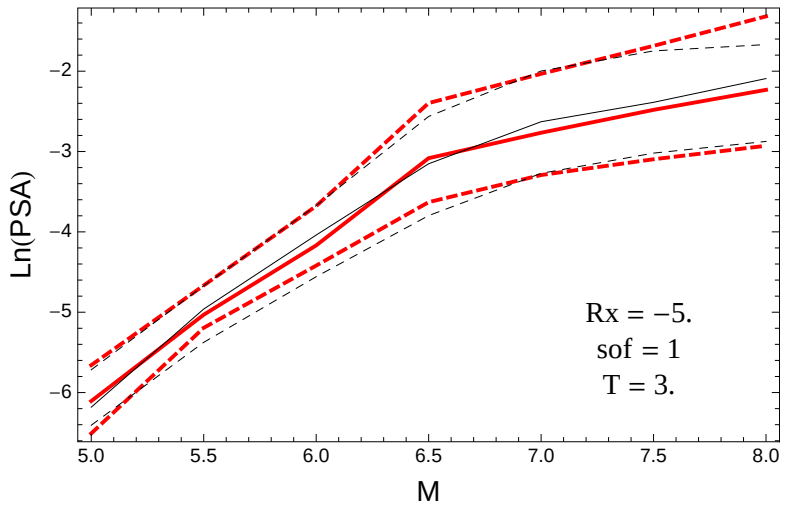



Figure 2.324: DCPPv4: Magnitude scaling of 0.05,0.5,0.95 quantile of the GMPE distribution (black) and the ModelA distribution (red) with total weights, for a scenario with $R_x = -5.$, $F = 1$, and $T = 3$.s.

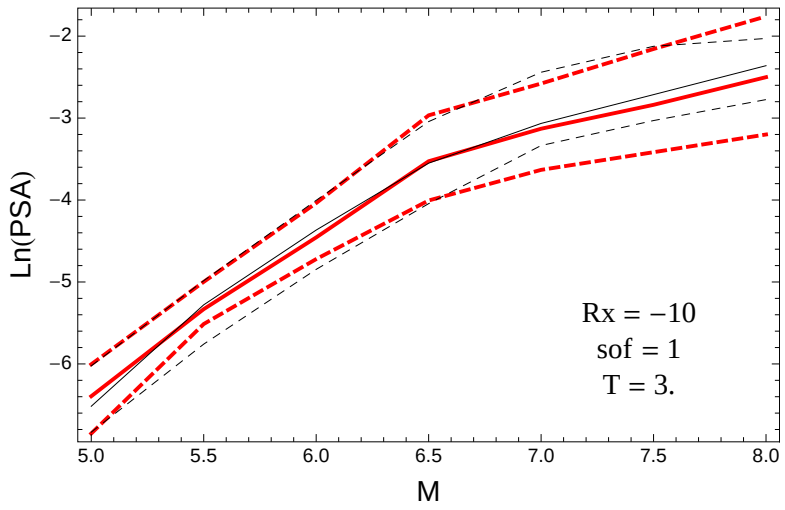



Figure 2.325: DCPPv4: Magnitude scaling of 0.05,0.5,0.95 quantile of the GMPE distribution (black) and the ModelA distribution (red) with total weights, for a scenario with $R_x = -10$, $F = 1$, and $T = 3$.s.

### 2.1.10 Quantile Plots vs. Period

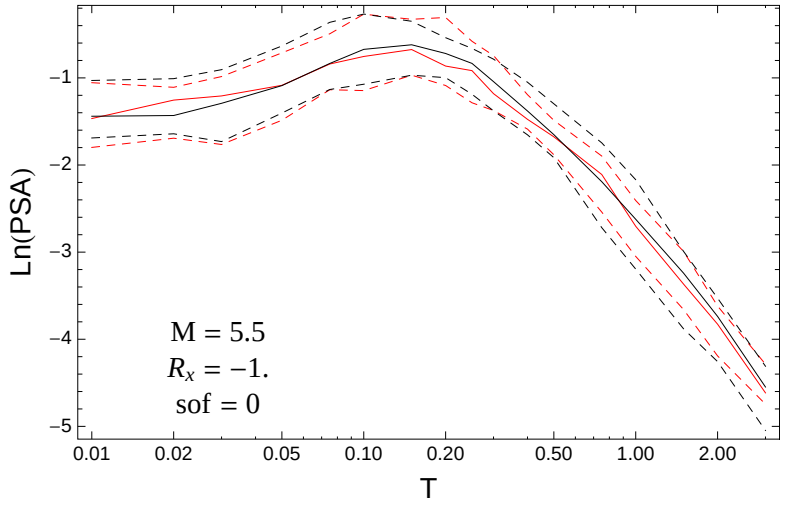



Figure 2.326: DCPPv4: Spectra of 0.05,0.5,0.95 quantile of the GMPE distribution (black) and the model distribution (red) with total weights, for a scenario with $M_W = 5.5$, $R_x = -1.$, $F = 0$.

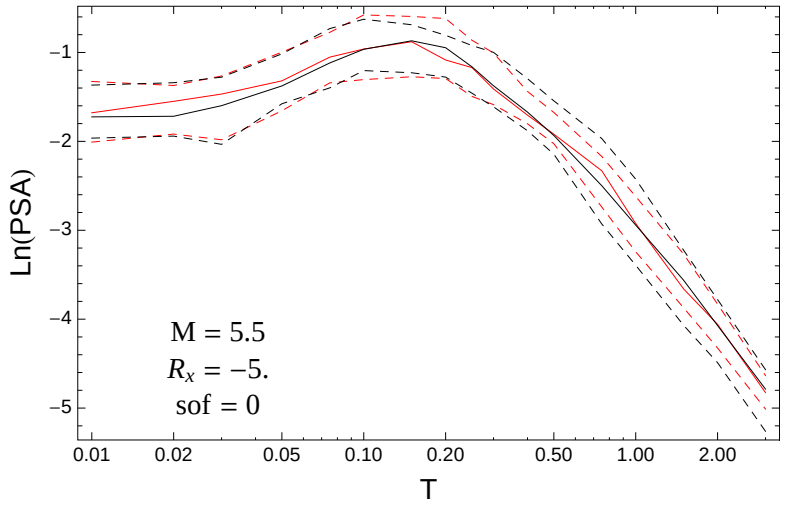



Figure 2.327: DCPPv4: Spectra of 0.05,0.5,0.95 quantile of the GMPE distribution (black) and the model distribution (red) with total weights, for a scenario with $M_W = 5.5$, $R_x = -5.$, $F = 0$.

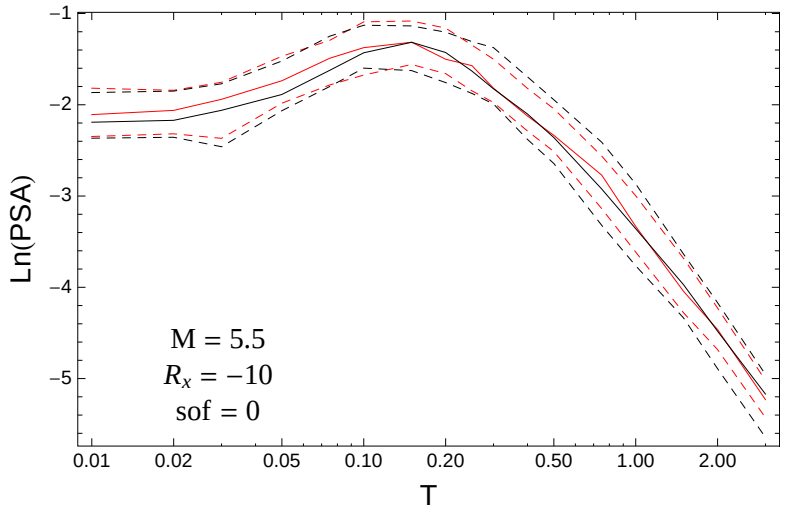



Figure 2.328: DCPPv4: Spectra of 0.05,0.5,0.95 quantile of the GMPE distribution (black) and the model distribution (red) with total weights, for a scenario with $M_W = 5.5$, $R_x = -10$, $F = 0$.

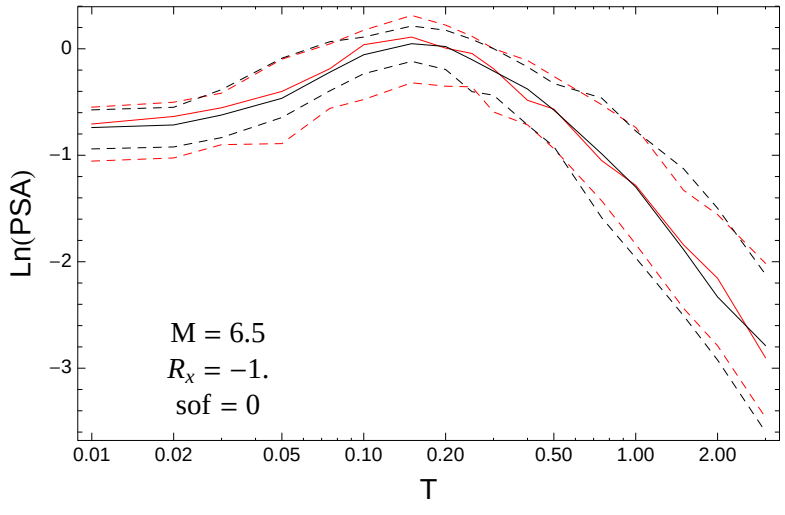



Figure 2.329: DCPPv4: Spectra of 0.05,0.5,0.95 quantile of the GMPE distribution (black) and the model distribution (red) with total weights, for a scenario with $M_W = 6.5$, $R_x = -1.$, $F = 0$.

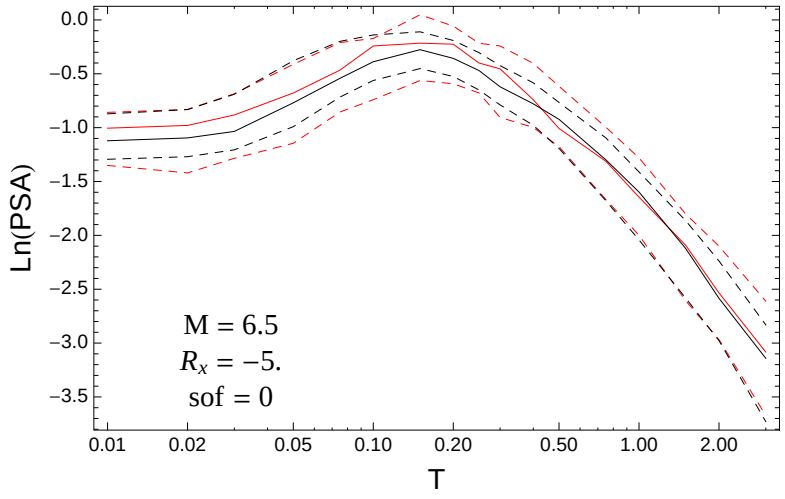



Figure 2.330: DCPPv4: Spectra of 0.05,0.5,0.95 quantile of the GMPE distribution (black) and the model distribution (red) with total weights, for a scenario with $M_W = 6.5$, $R_x = -5.$, $F = 0$.

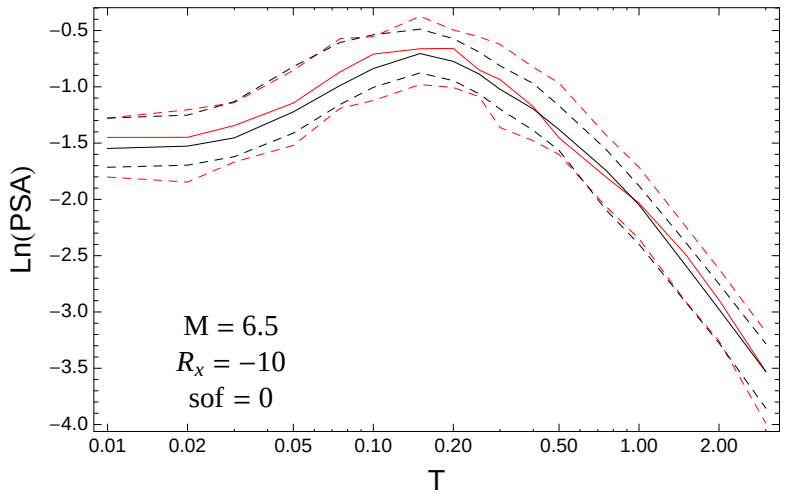



Figure 2.331: DCPPv4: Spectra of 0.05,0.5,0.95 quantile of the GMPE distribution (black) and the model distribution (red) with total weights, for a scenario with $M_W = 6.5$, $R_x = -10$, $F = 0$.

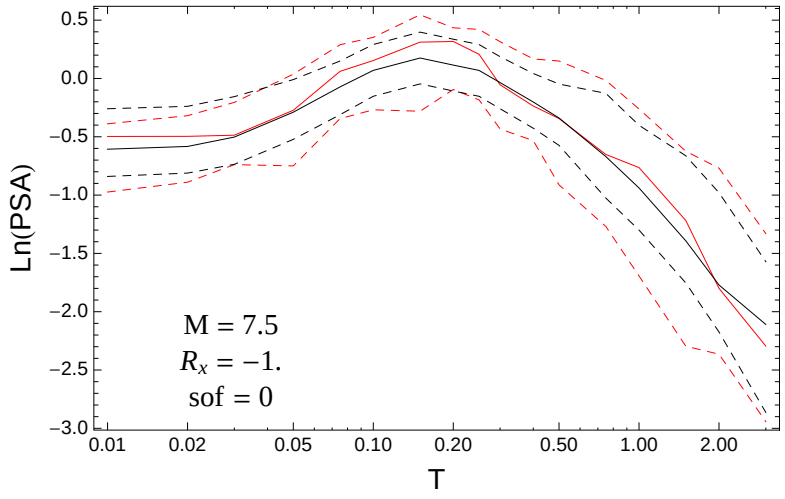



Figure 2.332: DCPPv4: Spectra of 0.05,0.5,0.95 quantile of the GMPE distribution (black) and the model distribution (red) with total weights, for a scenario with $M_W = 7.5$, $R_x = -1.$, $F = 0$.

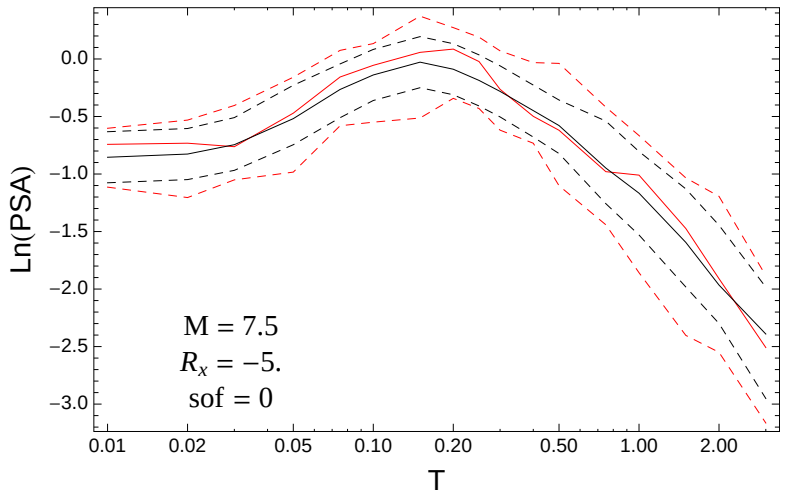



Figure 2.333: DCPPv4: Spectra of 0.05,0.5,0.95 quantile of the GMPE distribution (black) and the model distribution (red) with total weights, for a scenario with $M_W = 7.5$, $R_x = -5.$, $F = 0$.

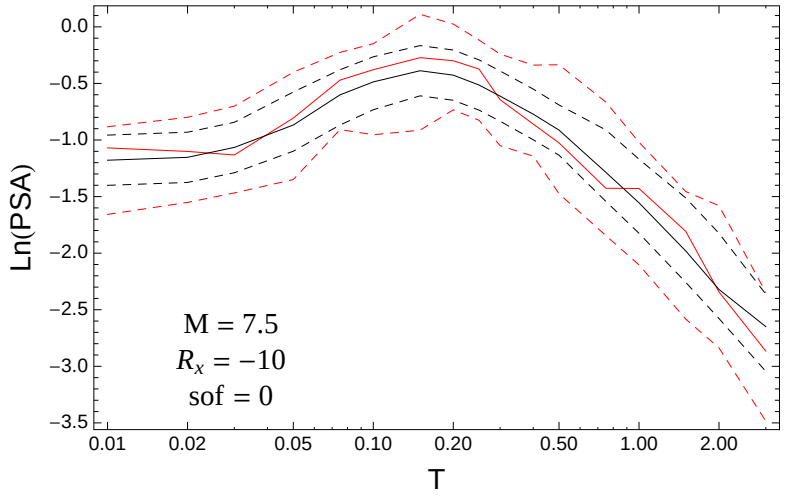



Figure 2.334: DCPPv4: Spectra of 0.05,0.5,0.95 quantile of the GMPE distribution (black) and the model distribution (red) with total weights, for a scenario with $M_W = 7.5$, $R_x = -10$, $F = 0$.

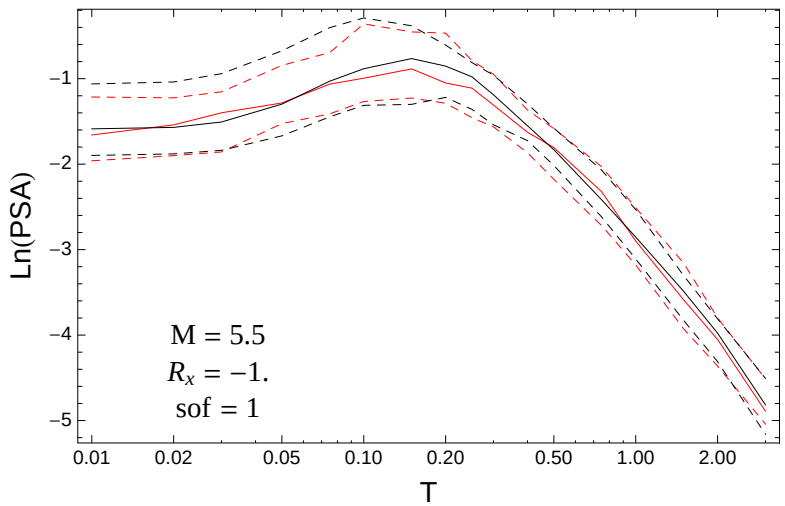



Figure 2.335: DCPPv4: Spectra of 0.05,0.5,0.95 quantile of the GMPE distribution (black) and the model distribution (red) with total weights, for a scenario with $M_W = 5.5$, $R_x = -1.$, $F = 1$.

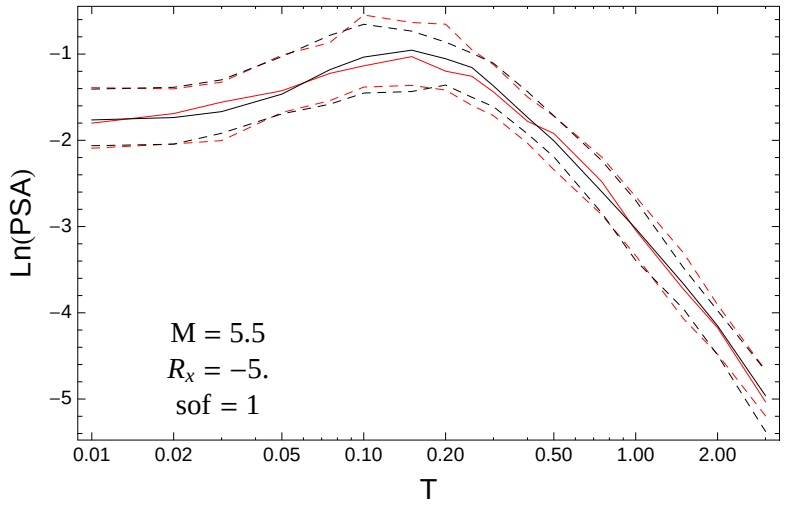



Figure 2.336: DCPPv4: Spectra of 0.05,0.5,0.95 quantile of the GMPE distribution (black) and the model distribution (red) with total weights, for a scenario with $M_W = 5.5$, $R_x = -5.$, $F = 1$.

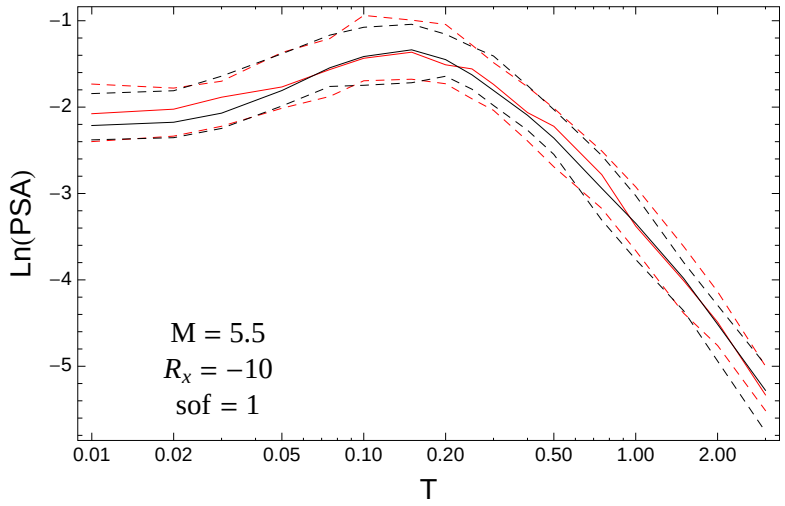



Figure 2.337: DCPPv4: Spectra of 0.05,0.5,0.95 quantile of the GMPE distribution (black) and the model distribution (red) with total weights, for a scenario with $M_W = 5.5$, $R_x = -10$, $F = 1$.

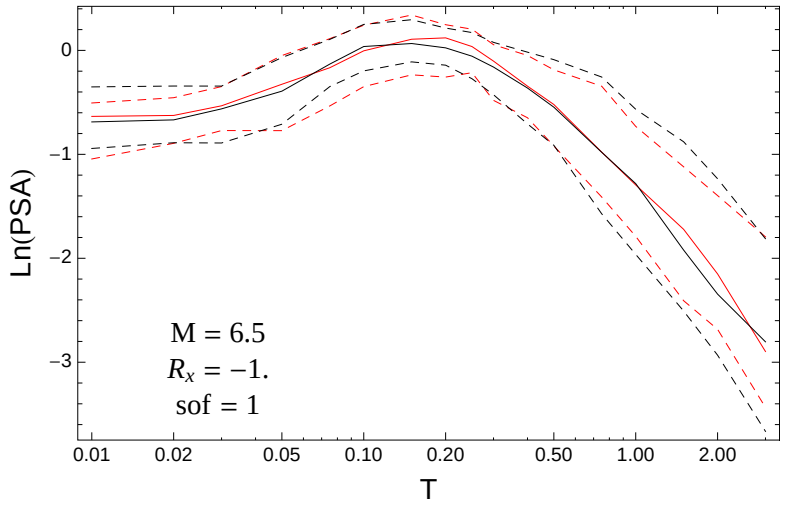



Figure 2.338: DCPPv4: Spectra of 0.05,0.5,0.95 quantile of the GMPE distribution (black) and the model distribution (red) with total weights, for a scenario with $M_W = 6.5$, $R_x = -1.$, $F = 1$.

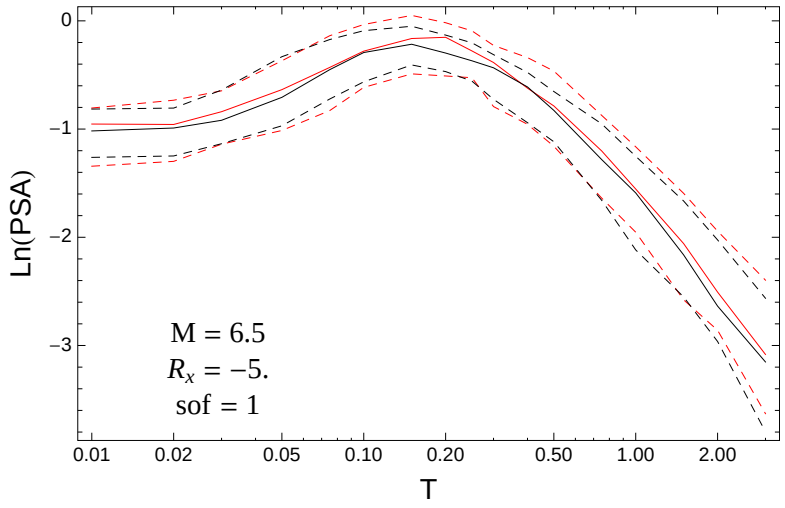



Figure 2.339: DCPPv4: Spectra of 0.05,0.5,0.95 quantile of the GMPE distribution (black) and the model distribution (red) with total weights, for a scenario with $M_W = 6.5$, $R_x = -5.$, $F = 1$.

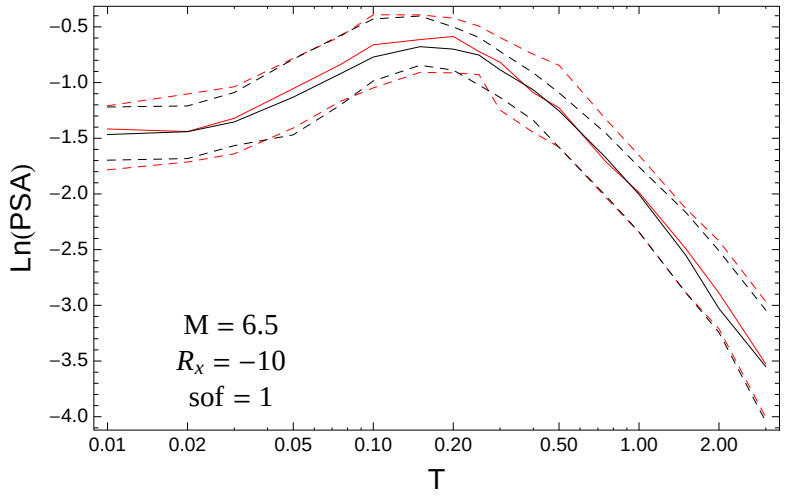



Figure 2.340: DCPPv4: Spectra of 0.05,0.5,0.95 quantile of the GMPE distribution (black) and the model distribution (red) with total weights, for a scenario with $M_W = 6.5$, $R_x = -10$, $F = 1$.

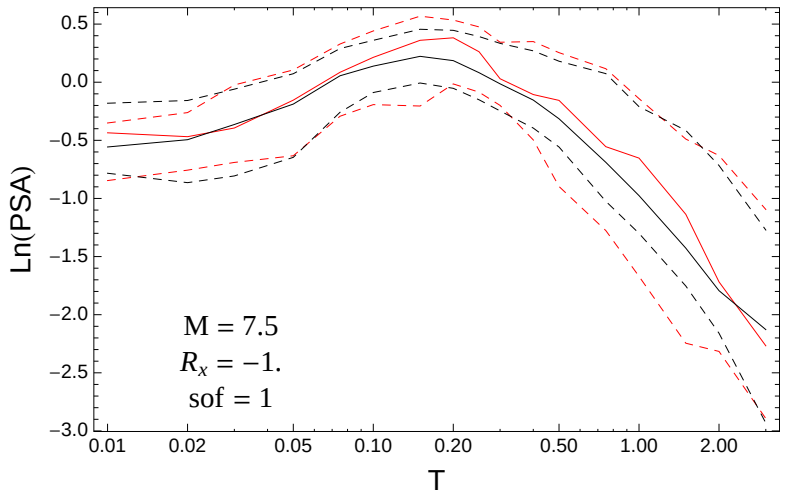



Figure 2.341: DCPPv4: Spectra of 0.05,0.5,0.95 quantile of the GMPE distribution (black) and the model distribution (red) with total weights, for a scenario with $M_W = 7.5$, $R_x = -1.$, $F = 1$.

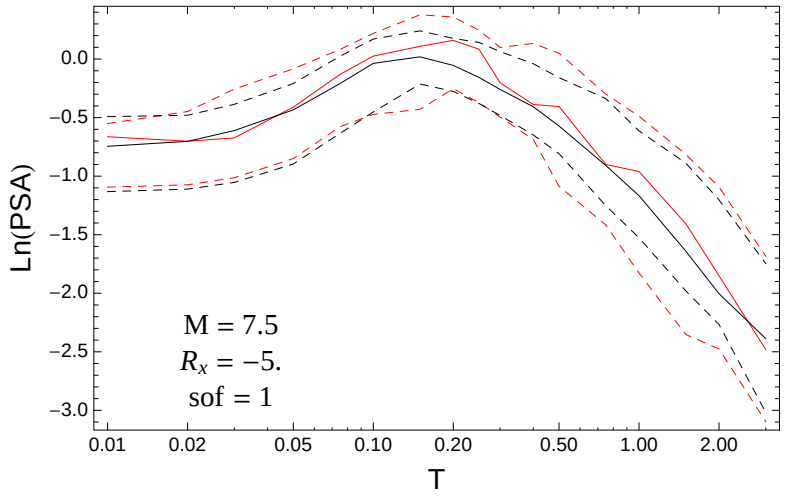



Figure 2.342: DCPPv4: Spectra of 0.05,0.5,0.95 quantile of the GMPE distribution (black) and the model distribution (red) with total weights, for a scenario with $M_W = 7.5$, $R_x = -5.$, $F = 1$.

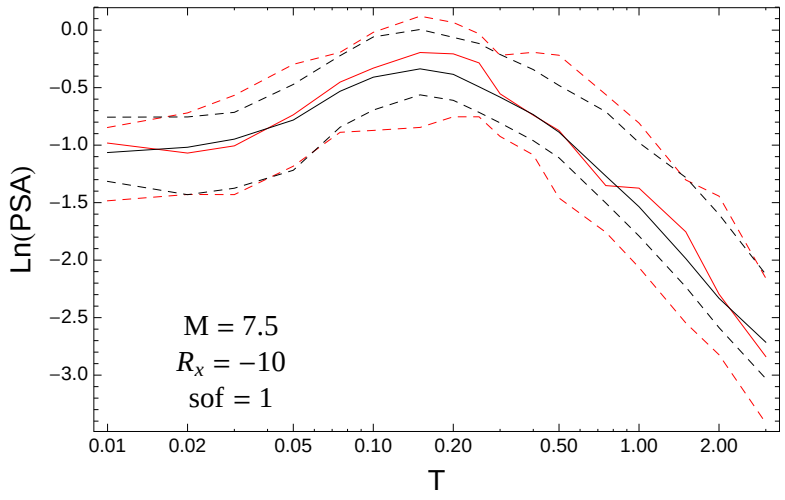



Figure 2.343: DCPPv4: Spectra of 0.05,0.5,0.95 quantile of the GMPE distribution (black) and the model distribution (red) with total weights, for a scenario with $M_W = 7.5$, $R_x = -10$, $F = 1$.

### 2.1.11 Quantile Ratios vs. Distance

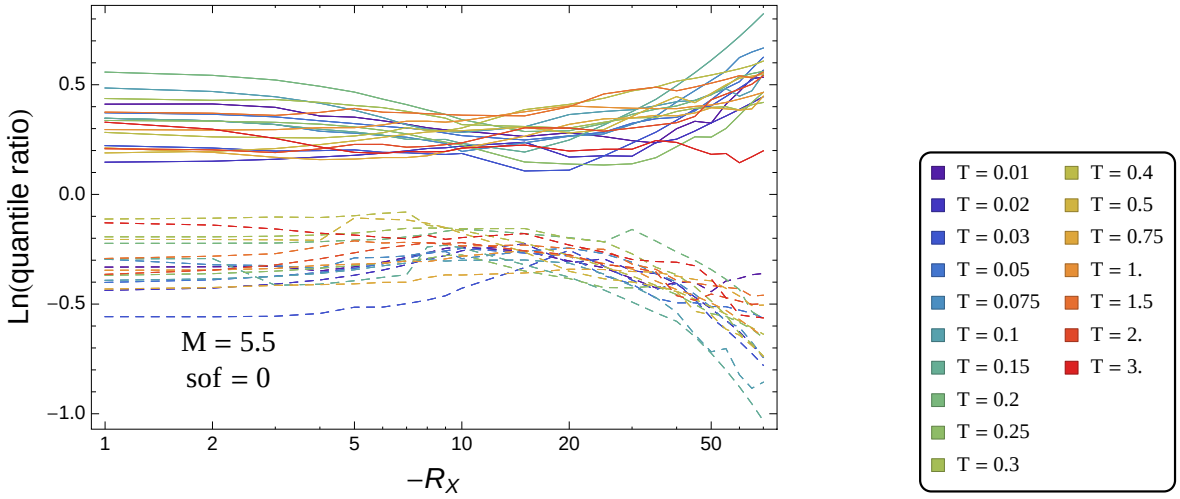



Figure 2.344: DCPPv4: Ratio of 0.05 to 0.5 (dashed) and ratio of 0.95 to 0.5 quantile (solid) of the ModelA distribution with total weights, for a scenario with $M = 5.5$, $F = 0$, and all periods.

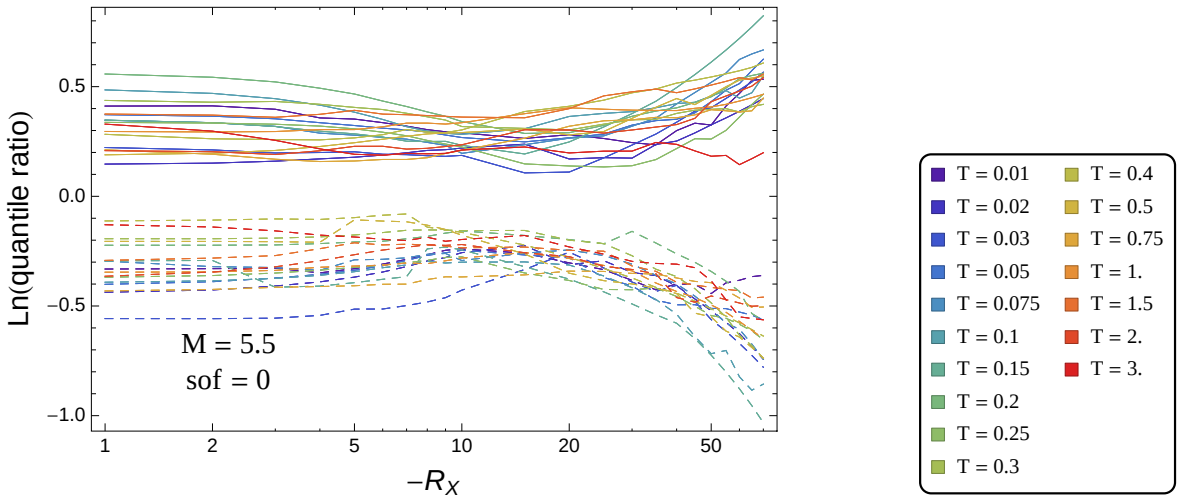



Figure 2.345: DCPPv4: Ratio of 0.05 to 0.5 (dashed) and ratio of 0.95 to 0.5 quantile (solid) of the ModelA distribution with total weights, for a scenario with $M = 5.5$, $F = 0$, and all periods.

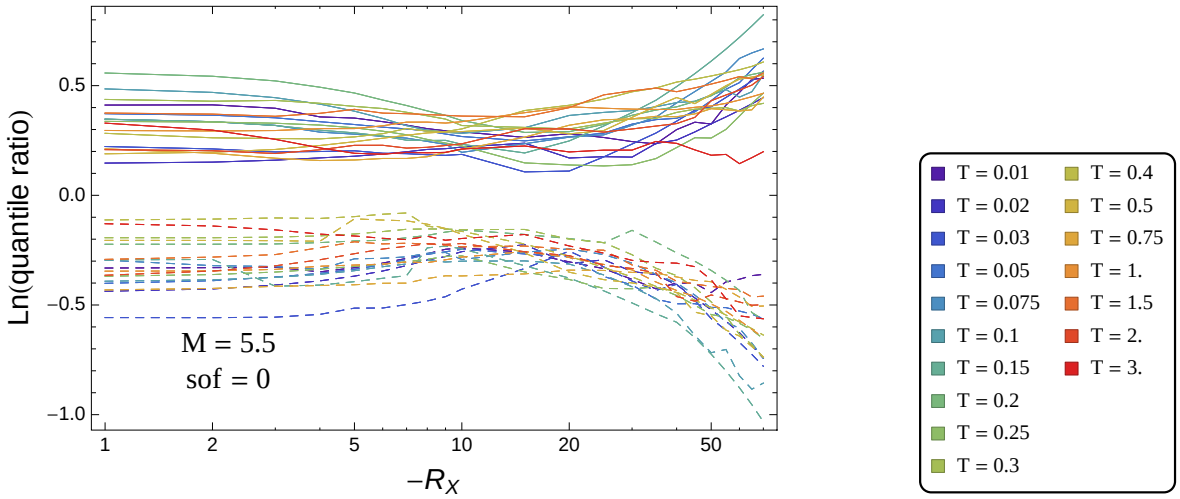



Figure 2.346: DCPPv4: Ratio of 0.05 to 0.5 (dashed) and ratio of 0.95 to 0.5 quantile (solid) of the ModelA distribution with total weights, for a scenario with $M = 5.5$, $F = 0$, and all periods.

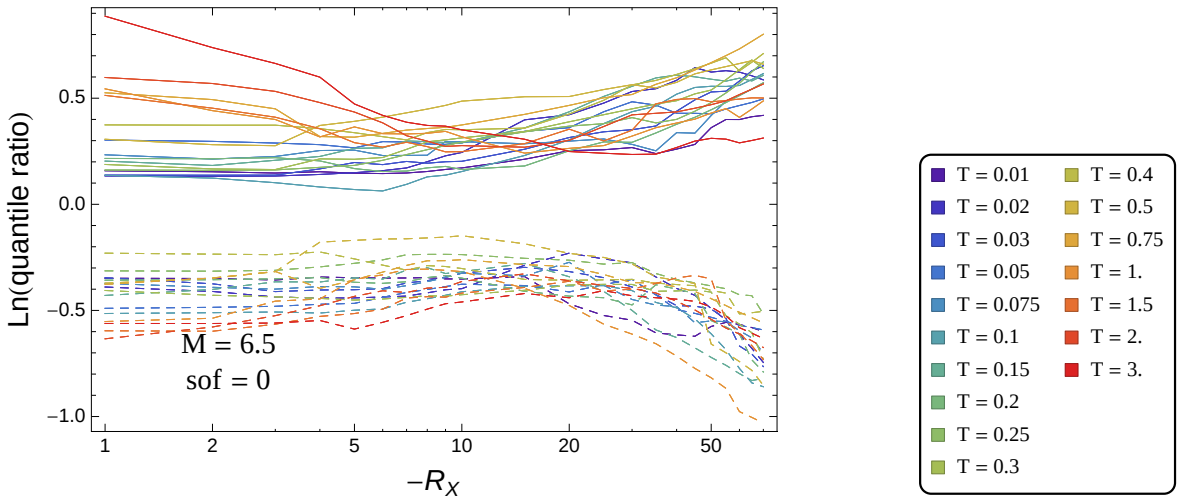



Figure 2.347: DCPPv4: Ratio of 0.05 to 0.5 (dashed) and ratio of 0.95 to 0.5 quantile (solid) of the ModelA distribution with total weights, for a scenario with $M = 6.5$, $F = 0$, and all periods.

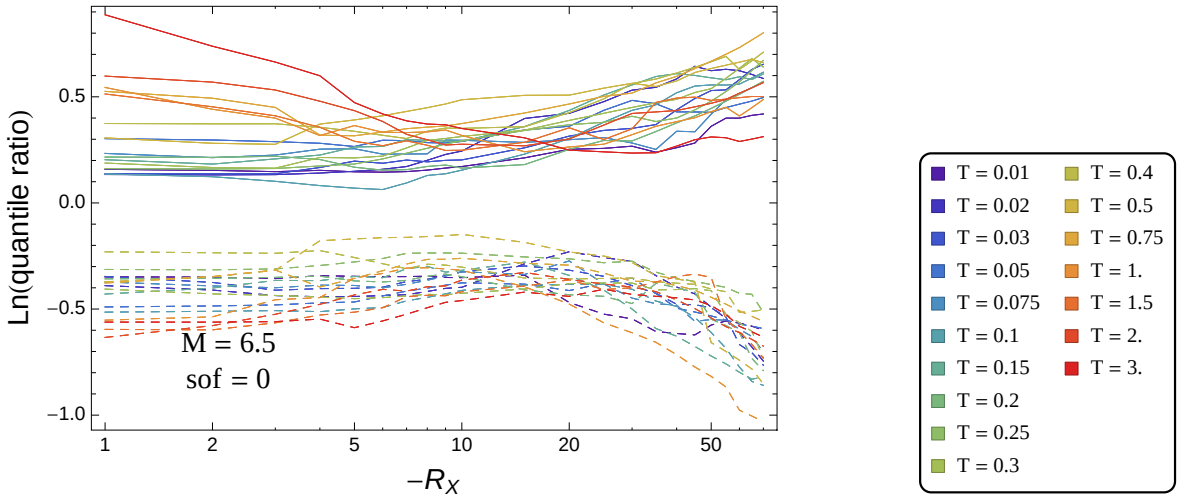



Figure 2.348: DCPPv4: Ratio of 0.05 to 0.5 (dashed) and ratio of 0.95 to 0.5 quantile (solid) of the ModelA distribution with total weights, for a scenario with $M = 6.5$, $F = 0$, and all periods.

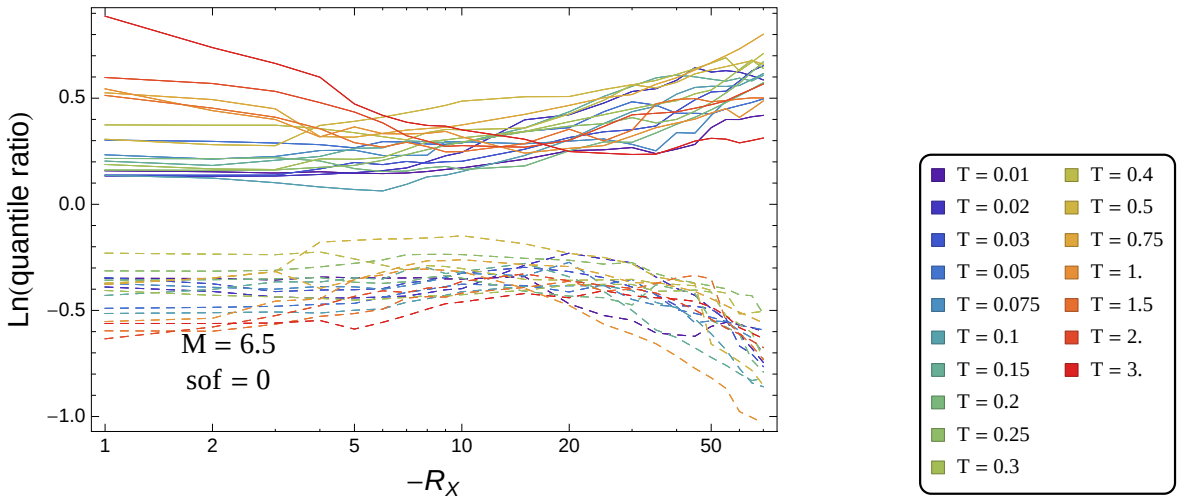



Figure 2.349: DCPPv4: Ratio of 0.05 to 0.5 (dashed) and ratio of 0.95 to 0.5 quantile (solid) of the ModelA distribution with total weights, for a scenario with $M = 6.5$, $F = 0$, and all periods.

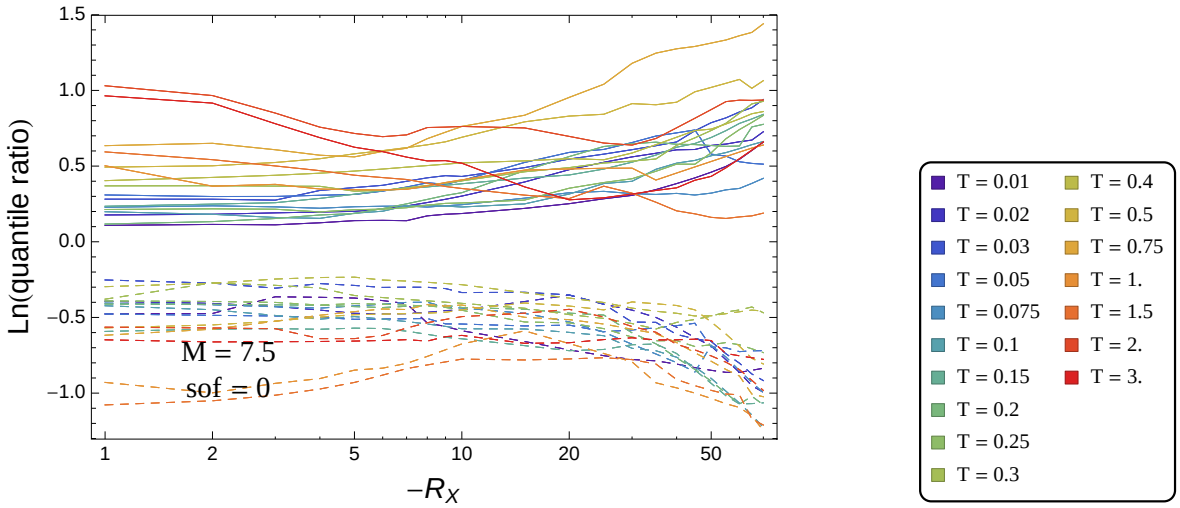



Figure 2.350: DCPPv4: Ratio of 0.05 to 0.5 (dashed) and ratio of 0.95 to 0.5 quantile (solid) of the ModelA distribution with total weights, for a scenario with $M = 7.5$, $F = 0$, and all periods.

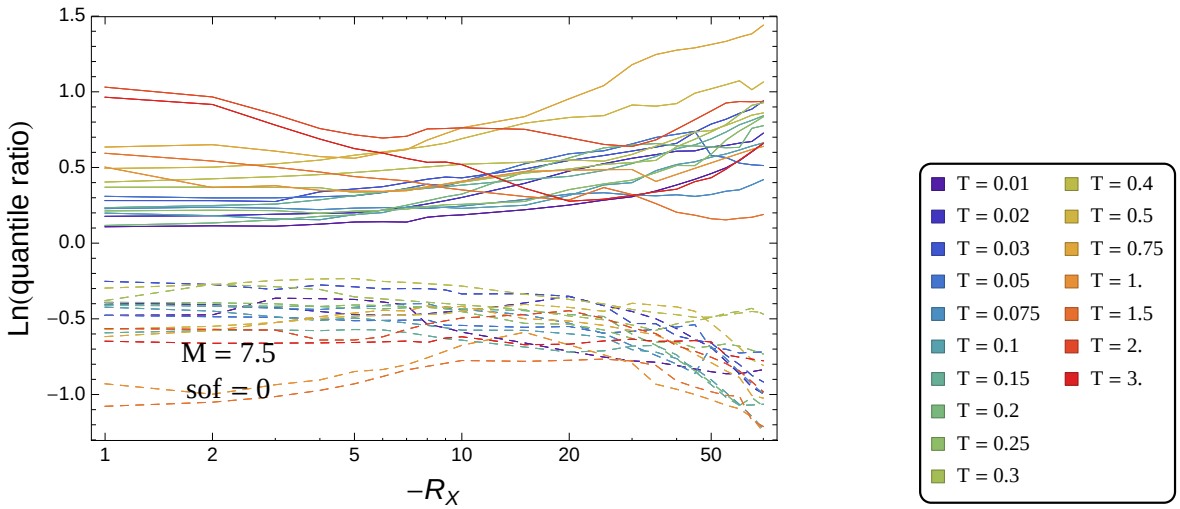



Figure 2.351: DCPPv4: Ratio of 0.05 to 0.5 (dashed) and ratio of 0.95 to 0.5 quantile (solid) of the ModelA distribution with total weights, for a scenario with $M = 7.5$, $F = 0$, and all periods.

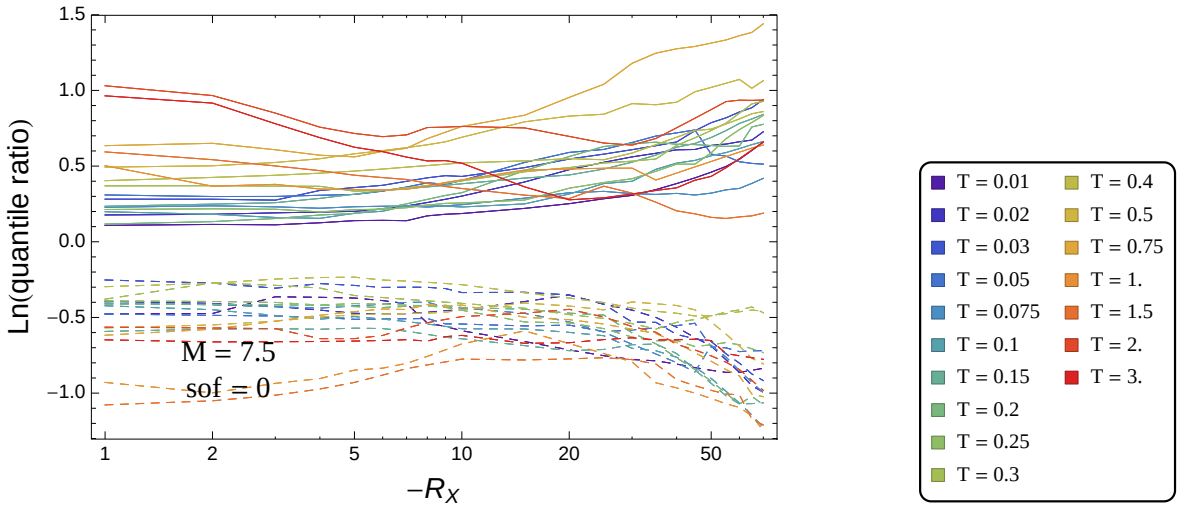



Figure 2.352: DCPPv4: Ratio of 0.05 to 0.5 (dashed) and ratio of 0.95 to 0.5 quantile (solid) of the ModelA distribution with total weights, for a scenario with $M = 7.5$, $F = 0$, and all periods.

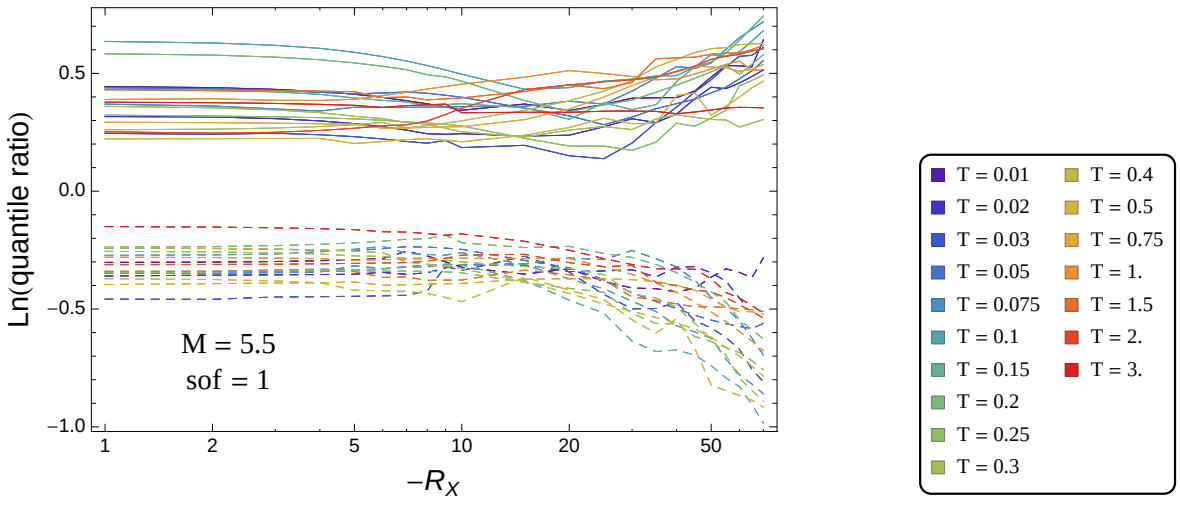



Figure 2.353: DCPPv4: Ratio of 0.05 to 0.5 (dashed) and ratio of 0.95 to 0.5 quantile (solid) of the ModelA distribution with total weights, for a scenario with $M = 5.5$, $F = 1$, and all periods.

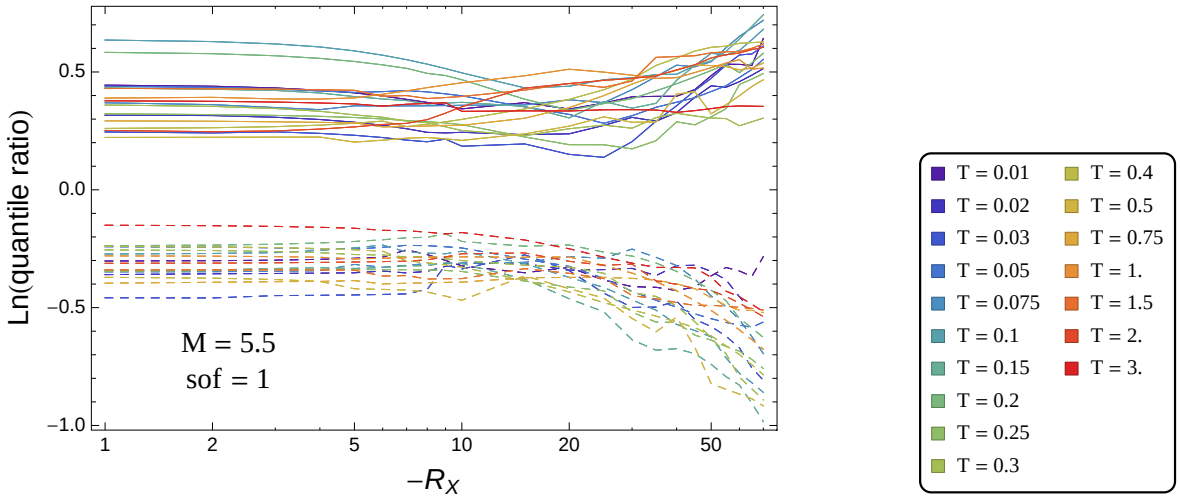



Figure 2.354: DCPPv4: Ratio of 0.05 to 0.5 (dashed) and ratio of 0.95 to 0.5 quantile (solid) of the ModelA distribution with total weights, for a scenario with $M = 5.5$, $F = 1$, and all periods.

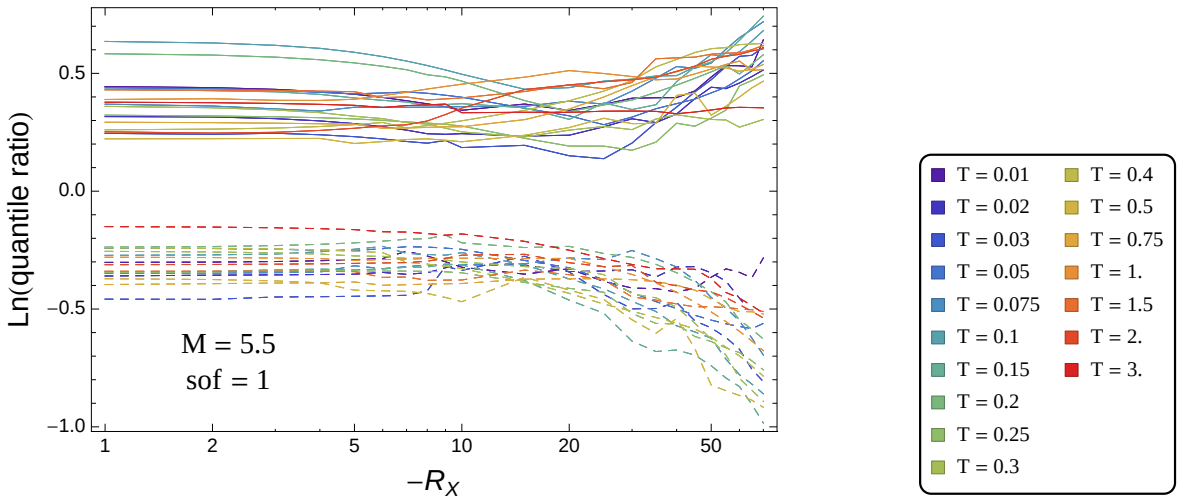



Figure 2.355: DCPPv4: Ratio of 0.05 to 0.5 (dashed) and ratio of 0.95 to 0.5 quantile (solid) of the ModelA distribution with total weights, for a scenario with $M = 5.5$, $F = 1$, and all periods.

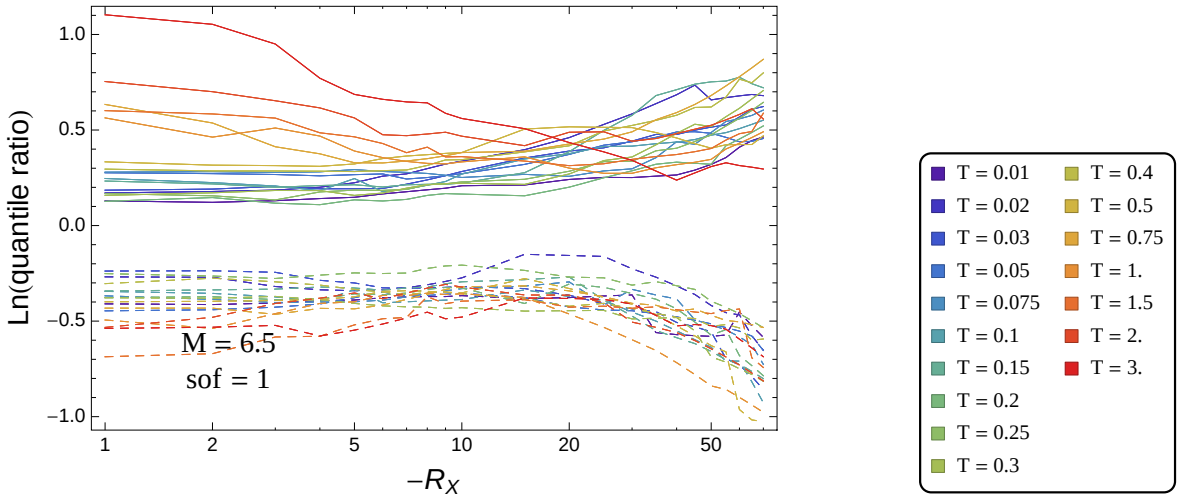



Figure 2.356: DCPPv4: Ratio of 0.05 to 0.5 (dashed) and ratio of 0.95 to 0.5 quantile (solid) of the ModelA distribution with total weights, for a scenario with $M = 6.5$, $F = 1$, and all periods.

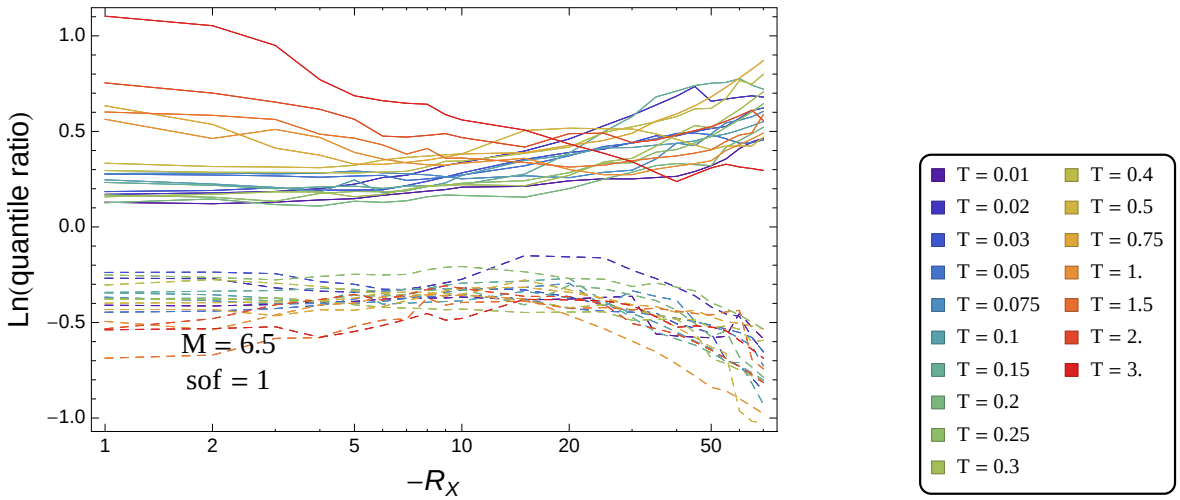



Figure 2.357: DCPPv4: Ratio of 0.05 to 0.5 (dashed) and ratio of 0.95 to 0.5 quantile (solid) of the ModelA distribution with total weights, for a scenario with $M = 6.5$, $F = 1$, and all periods.

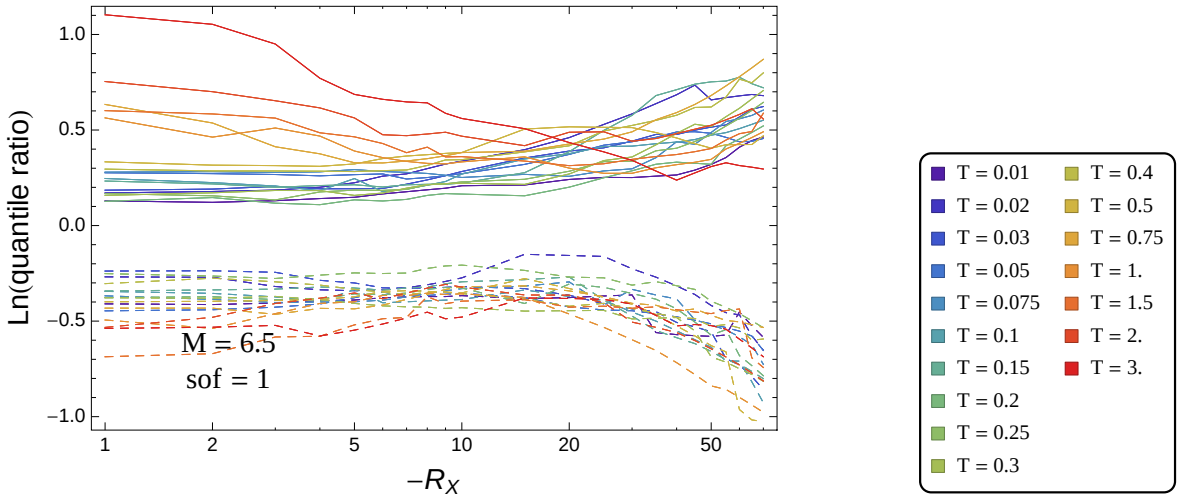



Figure 2.358: DCPPv4: Ratio of 0.05 to 0.5 (dashed) and ratio of 0.95 to 0.5 quantile (solid) of the ModelA distribution with total weights, for a scenario with $M = 6.5$, $F = 1$, and all periods.

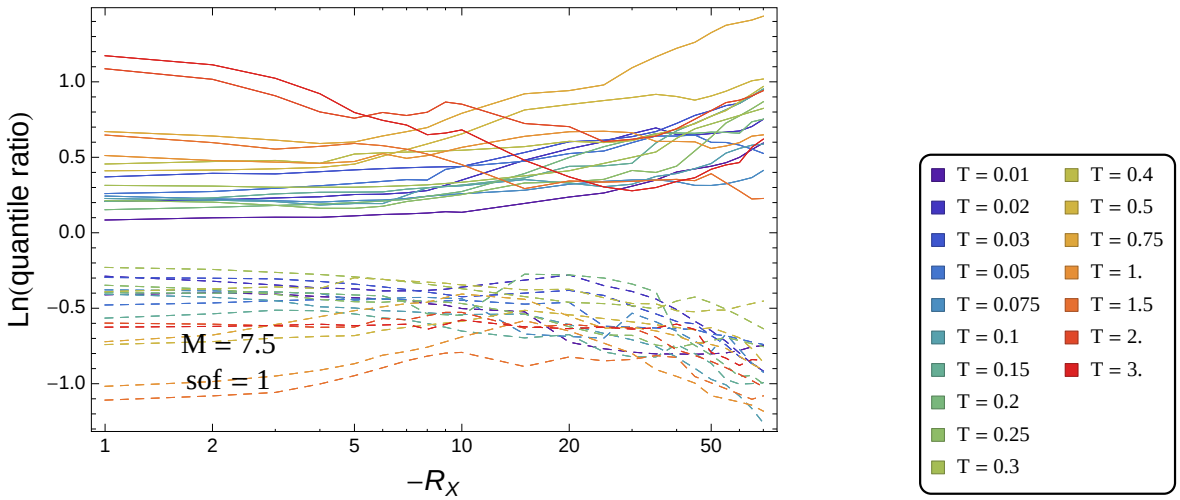



Figure 2.359: DCPPv4: Ratio of 0.05 to 0.5 (dashed) and ratio of 0.95 to 0.5 quantile (solid) of the ModelA distribution with total weights, for a scenario with $M = 7.5$, $F = 1$, and all periods.

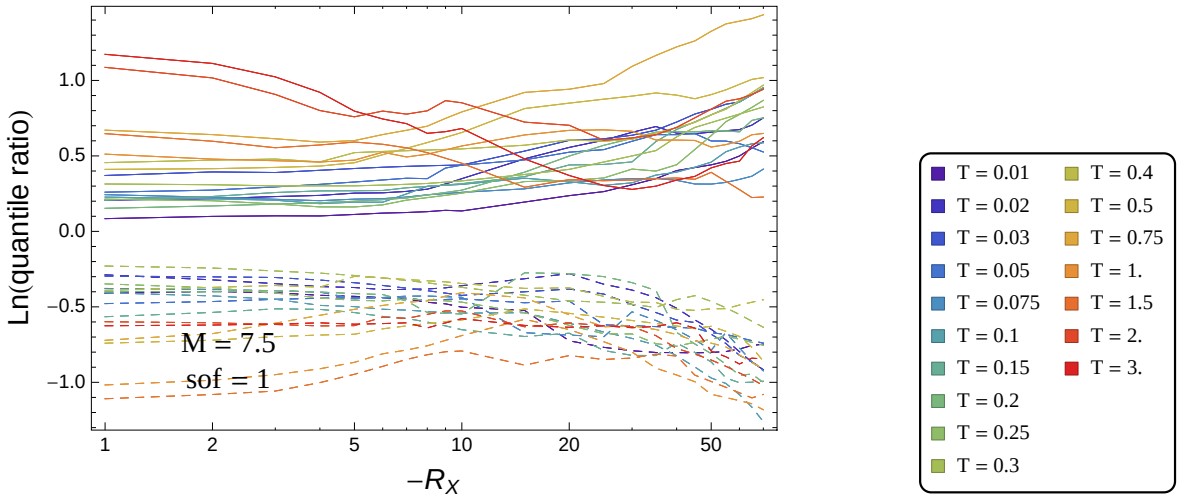



Figure 2.360: DCPPv4: Ratio of 0.05 to 0.5 (dashed) and ratio of 0.95 to 0.5 quantile (solid) of the ModelA distribution with total weights, for a scenario with $M = 7.5$, $F = 1$, and all periods.

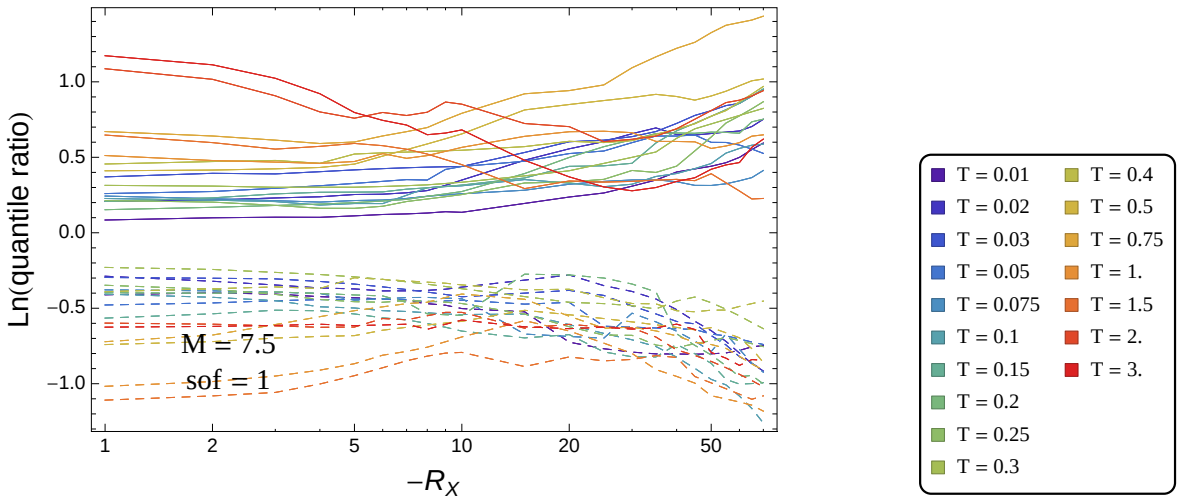



Figure 2.361: DCPPv4: Ratio of 0.05 to 0.5 (dashed) and ratio of 0.95 to 0.5 quantile (solid) of the ModelA distribution with total weights, for a scenario with $M = 7.5$, $F = 1$, and all periods.

### 2.1.12 Magnitude Scaling with GMPEs

**T = 0.01s**

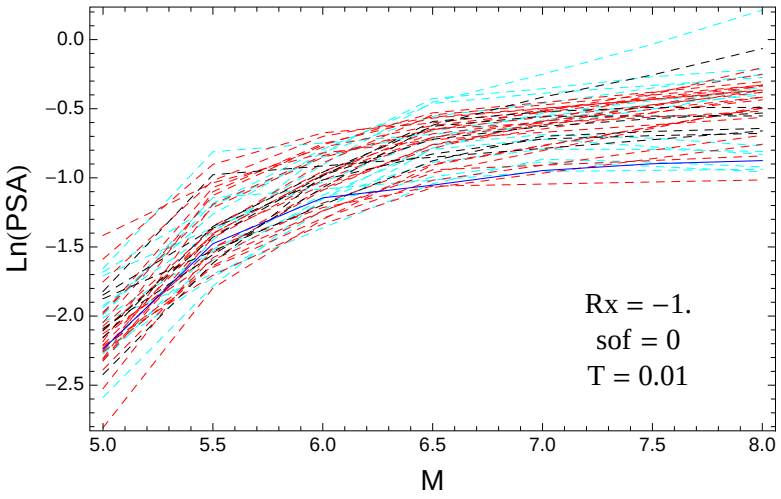



Figure 2.362: DCPPv4: Magnitude scaling of the original GMPEs (dashed black), the original GMPEs with uncertainty model (dashed cyan) and selected A models (dashed red) and the model of Graizer (2014), for a scenario with $R_X = -1.$, $F = 0$, and $T = 0.01$s.

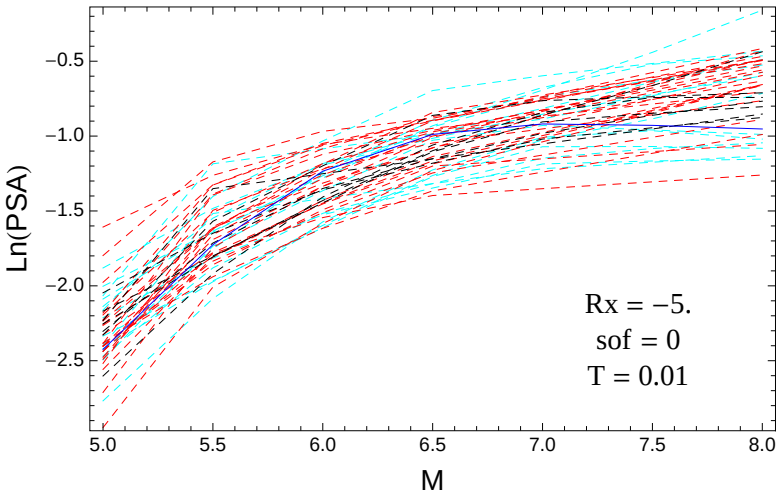



Figure 2.363: DCPPv4: Magnitude scaling of the original GMPEs (dashed black), the original GMPEs with uncertainty model (dashed cyan) and selected A models (dashed red) and the model of Graizer (2014), for a scenario with $R_X = -5.$, $F = 0$, and $T = 0.01$s.

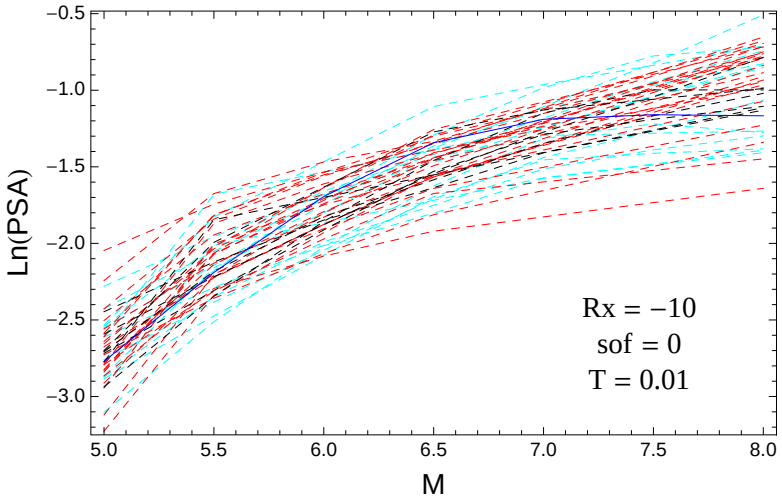



Figure 2.364: DCPPv4: Magnitude scaling of the original GMPEs (dashed black), the original GMPEs with uncertainty model (dashed cyan) and selected A models (dashed red) and the model of Graizer (2014), for a scenario with $R_X = -10$, $F = 0$, and $T = 0.01$s.

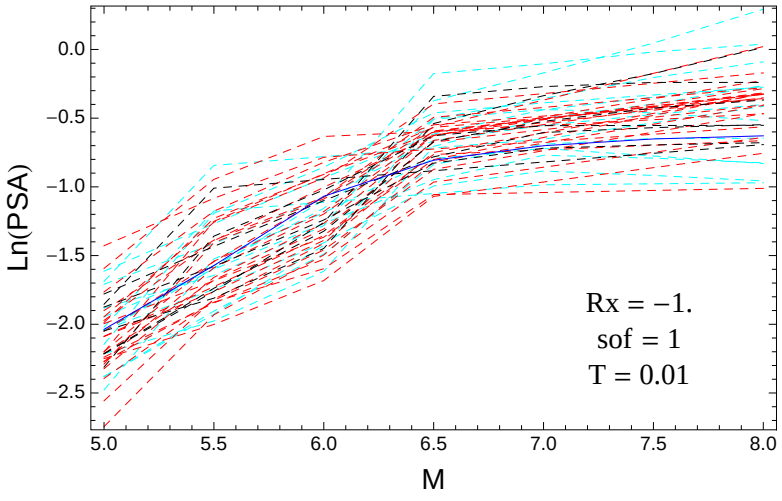



Figure 2.365: DCPPv4: Magnitude scaling of the original GMPEs (dashed black), the original GMPEs with uncertainty model (dashed cyan) and selected A models (dashed red) and the model of Graizer (2014), for a scenario with $R_X = -1.$, $F = 1$, and $T = 0.01$s.

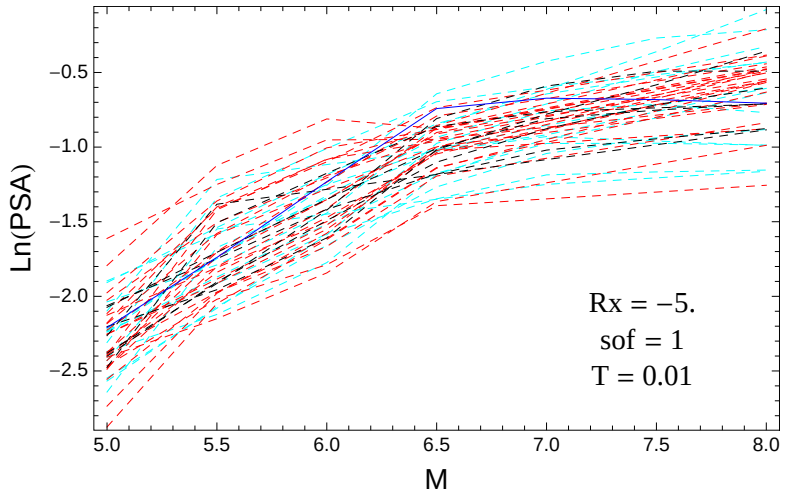



Figure 2.366: DCPPv4: Magnitude scaling of the original GMPEs (dashed black), the original GMPEs with uncertainty model (dashed cyan) and selected A models (dashed red) and the model of Graizer (2014), for a scenario with $R_X = -5.$, $F = 1$, and $T = 0.01$s.

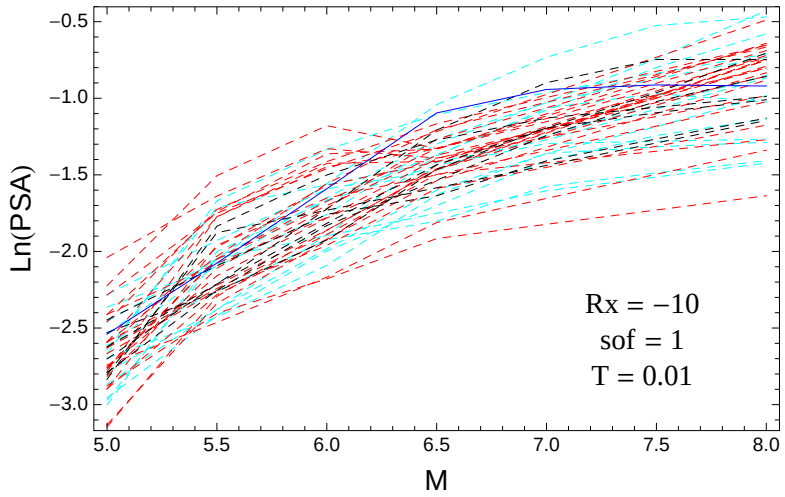



Figure 2.367: DCPPv4: Magnitude scaling of the original GMPEs (dashed black), the original GMPEs with uncertainty model (dashed cyan) and selected A models (dashed red) and the model of Graizer (2014), for a scenario with $R_X = -10$, $F = 1$, and $T = 0.01$s.

**T = 0.2s**

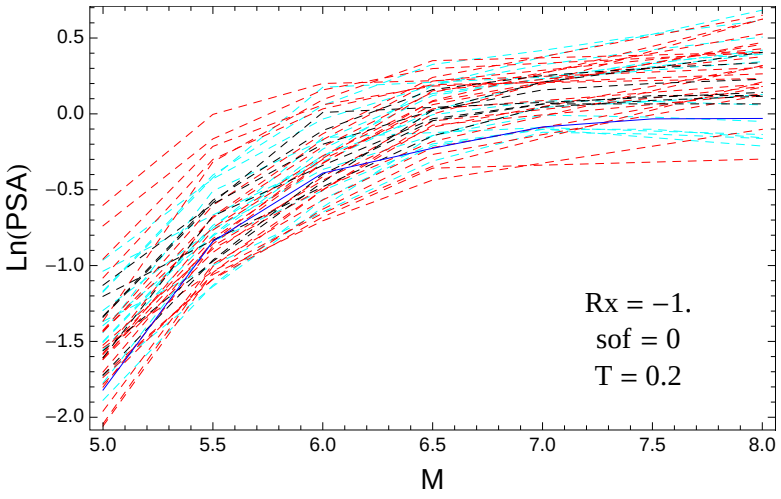



Figure 2.368: DCPPv4: Magnitude scaling of the original GMPEs (dashed black), the original GMPEs with uncertainty model (dashed cyan) and selected A models (dashed red) and the model of Graizer (2014), for a scenario with $R_X = -1.$, $F = 0$, and $T = 0.2$s.

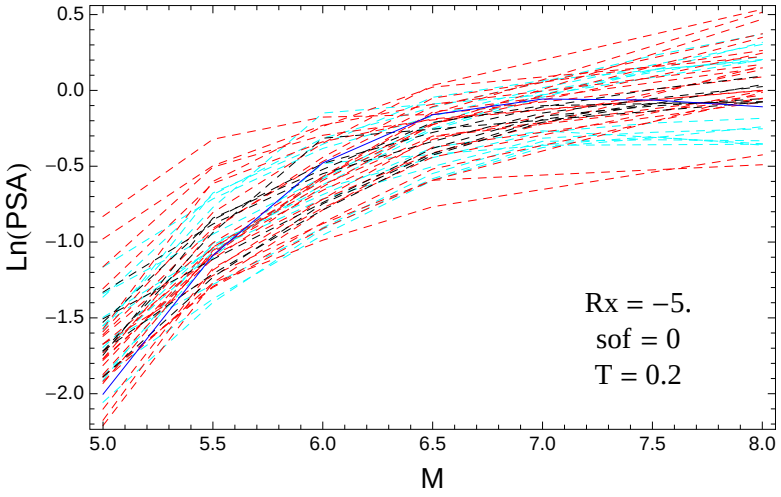



Figure 2.369: DCPPv4: Magnitude scaling of the original GMPEs (dashed black), the original GMPEs with uncertainty model (dashed cyan) and selected A models (dashed red) and the model of Graizer (2014), for a scenario with $R_X = -5.$, $F = 0$, and $T = 0.2$s.

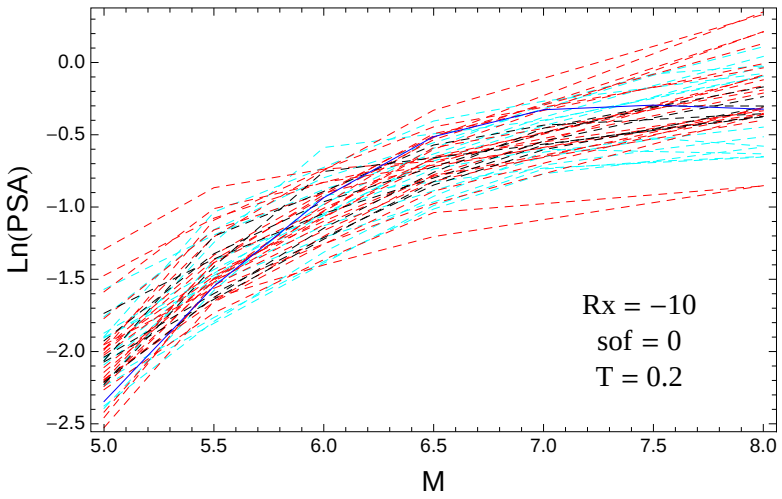



Figure 2.370: DCPPv4: Magnitude scaling of the original GMPEs (dashed black), the original GMPEs with uncertainty model (dashed cyan) and selected A models (dashed red) and the model of Graizer (2014), for a scenario with $R_X = -10$, $F = 0$, and $T = 0.2$s.

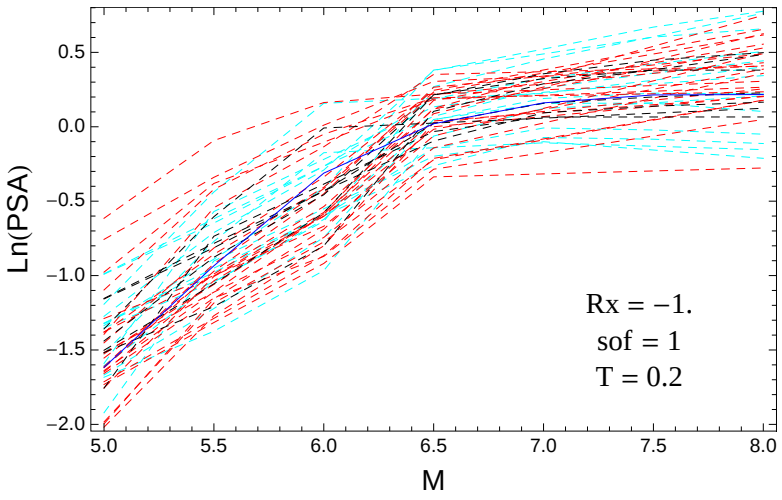



Figure 2.371: DCPPv4: Magnitude scaling of the original GMPEs (dashed black), the original GMPEs with uncertainty model (dashed cyan) and selected A models (dashed red) and the model of Graizer (2014), for a scenario with $R_X = -1.$, $F = 1$, and $T = 0.2$s.

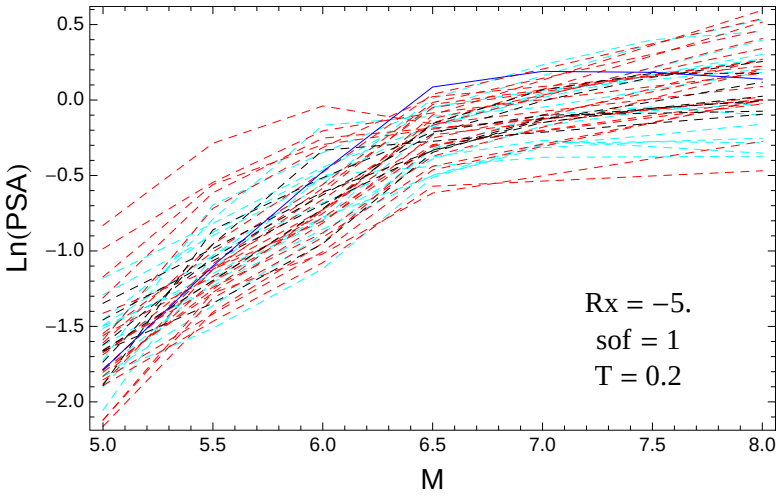



Figure 2.372: DCPPv4: Magnitude scaling of the original GMPEs (dashed black), the original GMPEs with uncertainty model (dashed cyan) and selected A models (dashed red) and the model of Graizer (2014), for a scenario with $R_X = -5.$, $F = 1$, and $T = 0.2$s.

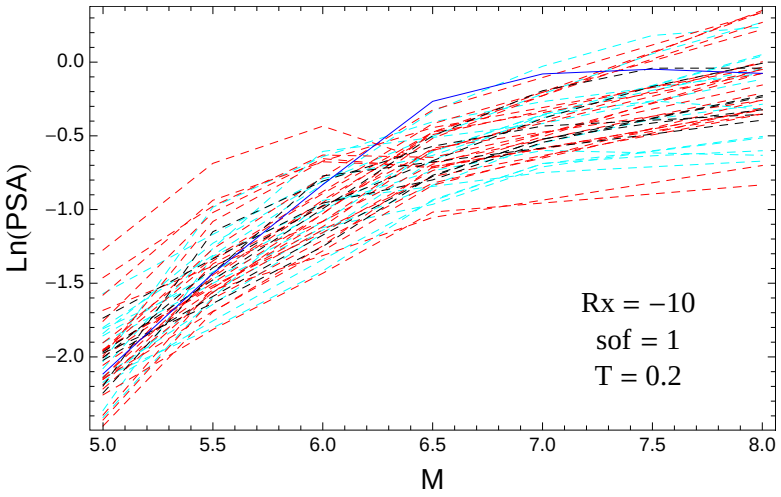



Figure 2.373: DCPPv4: Magnitude scaling of the original GMPEs (dashed black), the original GMPEs with uncertainty model (dashed cyan) and selected A models (dashed red) and the model of Graizer (2014), for a scenario with $R_X = -10$, $F = 1$, and $T = 0.2$s.

**T = 0.5s**

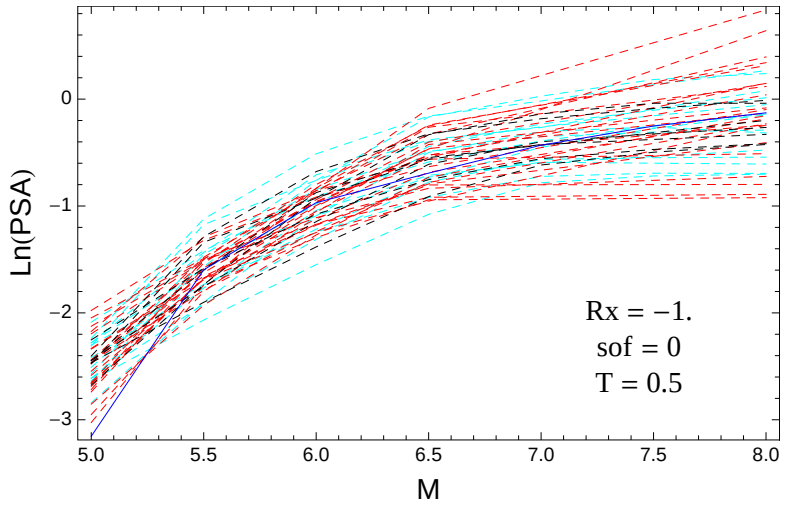



Figure 2.374: DCPPv4: Magnitude scaling of the original GMPEs (dashed black), the original GMPEs with uncertainty model (dashed cyan) and selected A models (dashed red) and the model of Graizer (2014), for a scenario with $R_X = -1.$, $F = 0$, and $T = 0.5$s.

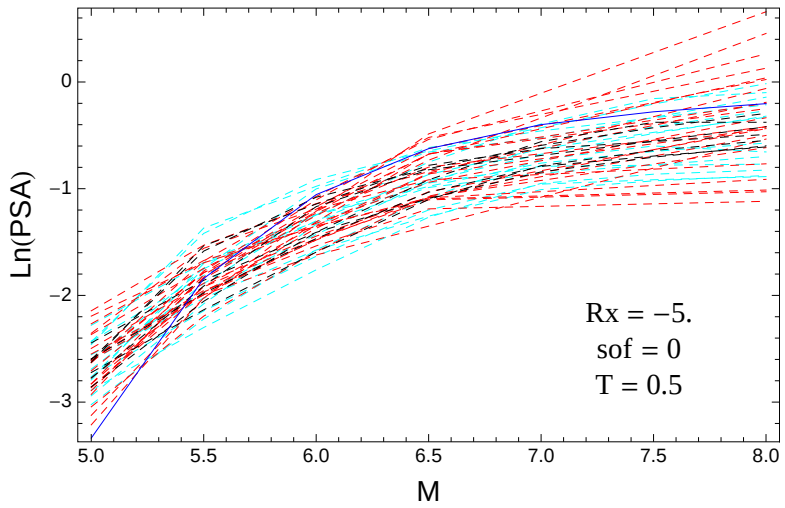



Figure 2.375: DCPPv4: Magnitude scaling of the original GMPEs (dashed black), the original GMPEs with uncertainty model (dashed cyan) and selected A models (dashed red) and the model of Graizer (2014), for a scenario with $R_X = -5.$, $F = 0$, and $T = 0.5$s.

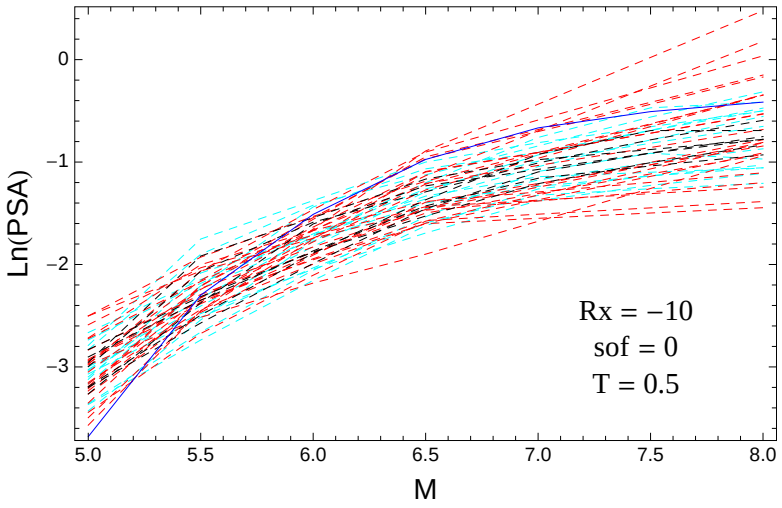



Figure 2.376: DCPPv4: Magnitude scaling of the original GMPEs (dashed black), the original GMPEs with uncertainty model (dashed cyan) and selected A models (dashed red) and the model of Graizer (2014), for a scenario with $R_X = -10$, $F = 0$, and $T = 0.5$s.

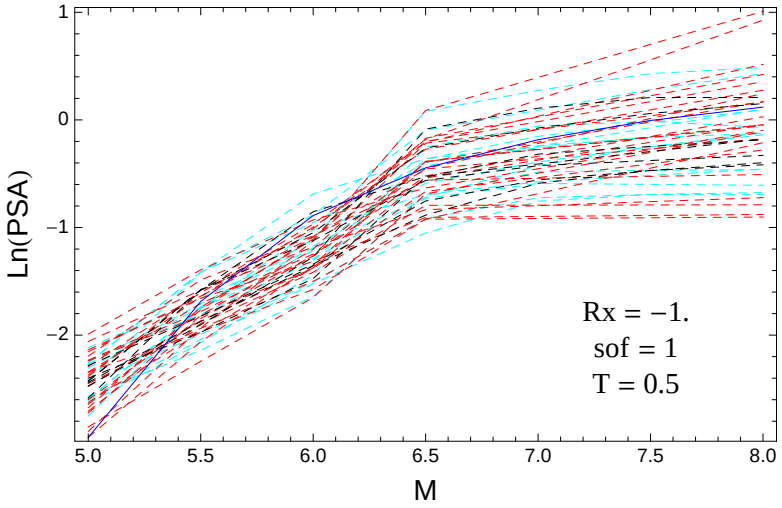



Figure 2.377: DCPPv4: Magnitude scaling of the original GMPEs (dashed black), the original GMPEs with uncertainty model (dashed cyan) and selected A models (dashed red) and the model of Graizer (2014), for a scenario with $R_X = -1.$, $F = 1$, and $T = 0.5$s.

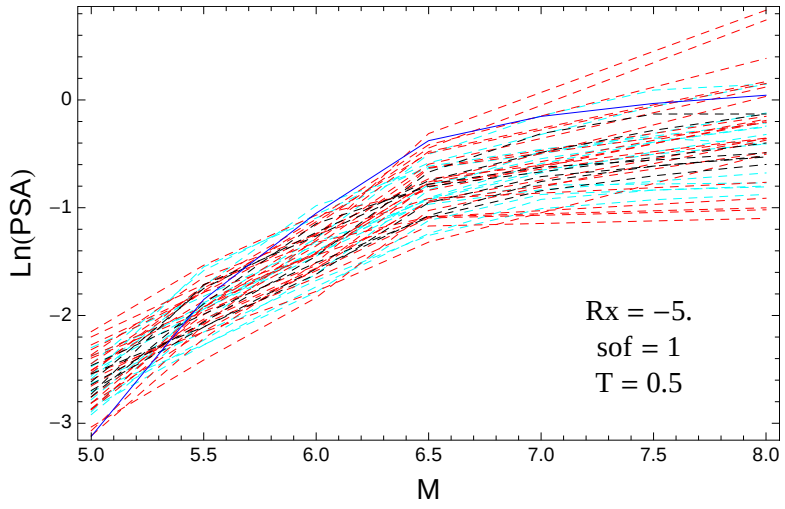



Figure 2.378: DCPPv4: Magnitude scaling of the original GMPEs (dashed black), the original GMPEs with uncertainty model (dashed cyan) and selected A models (dashed red) and the model of Graizer (2014), for a scenario with $R_X = -5.$, $F = 1$, and $T = 0.5$s.

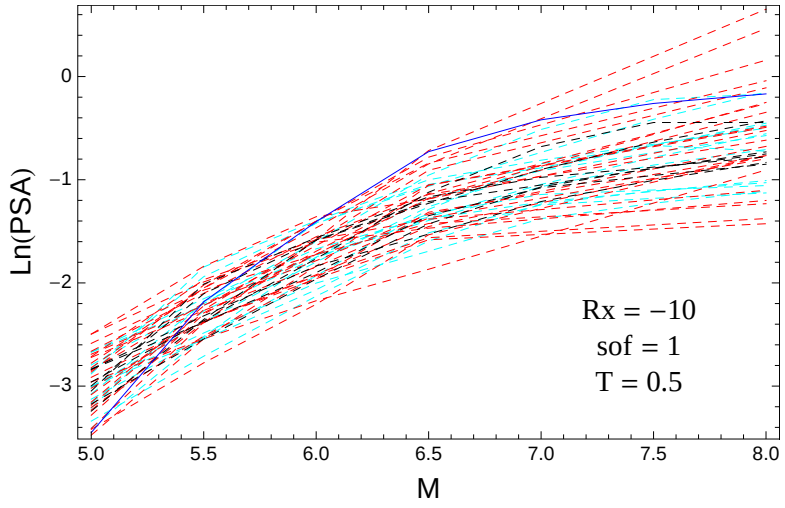



Figure 2.379: DCPPv4: Magnitude scaling of the original GMPEs (dashed black), the original GMPEs with uncertainty model (dashed cyan) and selected A models (dashed red) and the model of Graizer (2014), for a scenario with $R_X = -10$, $F = 1$, and $T = 0.5$s.

**T = 1.s**

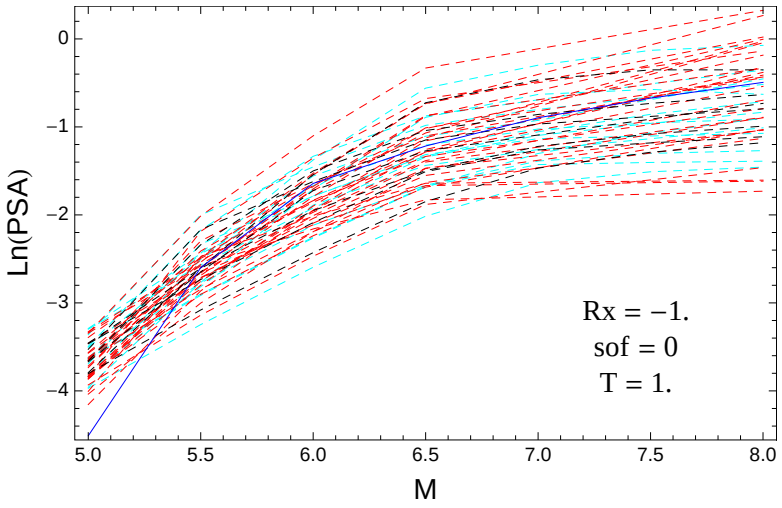



Figure 2.380: DCPPv4: Magnitude scaling of the original GMPEs (dashed black), the original GMPEs with uncertainty model (dashed cyan) and selected A models (dashed red) and the model of Graizer (2014), for a scenario with $R_X = -1.$, $F = 0$, and $T = 1.$s.

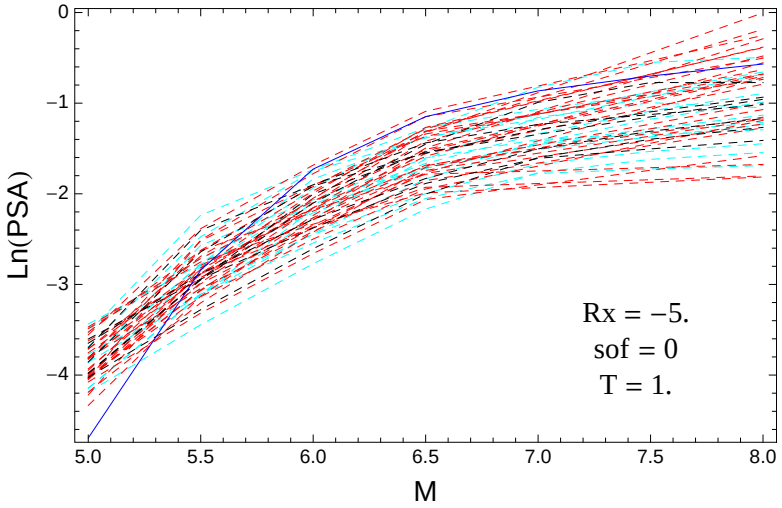



Figure 2.381: DCPPv4: Magnitude scaling of the original GMPEs (dashed black), the original GMPEs with uncertainty model (dashed cyan) and selected A models (dashed red) and the model of Graizer (2014), for a scenario with $R_X = -5.$, $F = 0$, and $T = 1.$s.

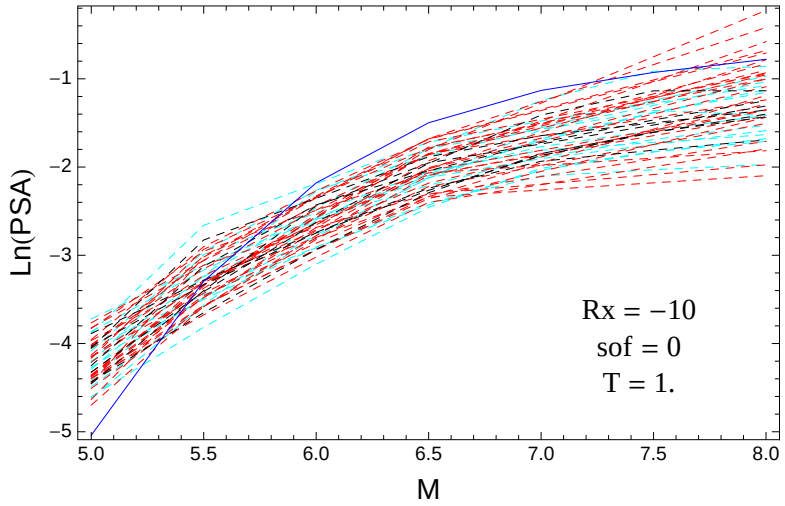



Figure 2.382: DCPPv4: Magnitude scaling of the original GMPEs (dashed black), the original GMPEs with uncertainty model (dashed cyan) and selected A models (dashed red) and the model of Graizer (2014), for a scenario with $R_X = -10$, $F = 0$, and $T = 1$.s.

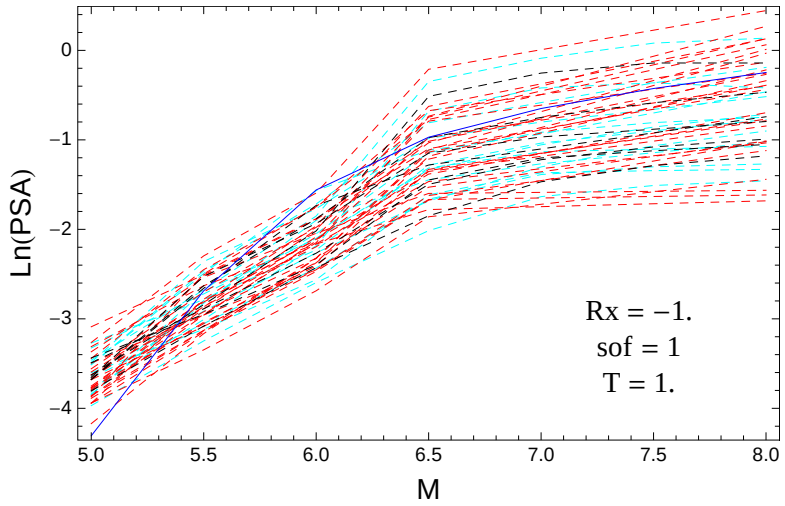



Figure 2.383: DCPPv4: Magnitude scaling of the original GMPEs (dashed black), the original GMPEs with uncertainty model (dashed cyan) and selected A models (dashed red) and the model of Graizer (2014), for a scenario with $R_X = -1.$, $F = 1$, and $T = 1$.s.

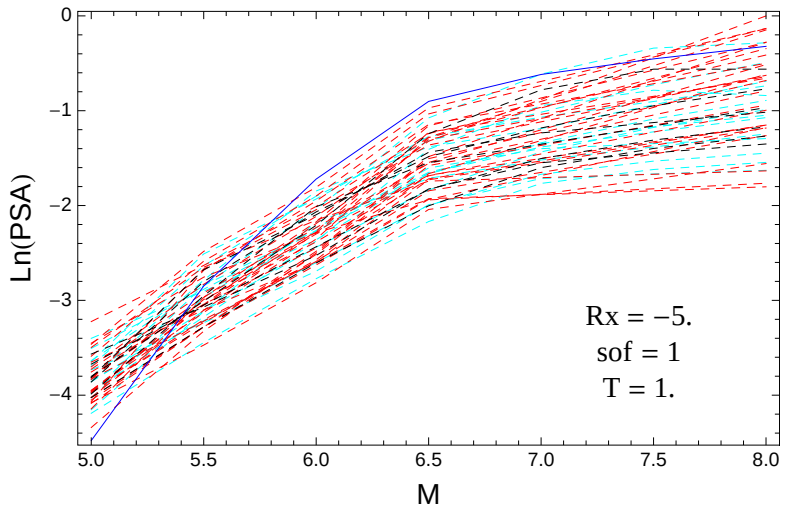



Figure 2.384: DCPPv4: Magnitude scaling of the original GMPEs (dashed black), the original GMPEs with uncertainty model (dashed cyan) and selected A models (dashed red) and the model of Graizer (2014), for a scenario with $R_X = -5.$, $F = 1$, and $T = 1$.s.

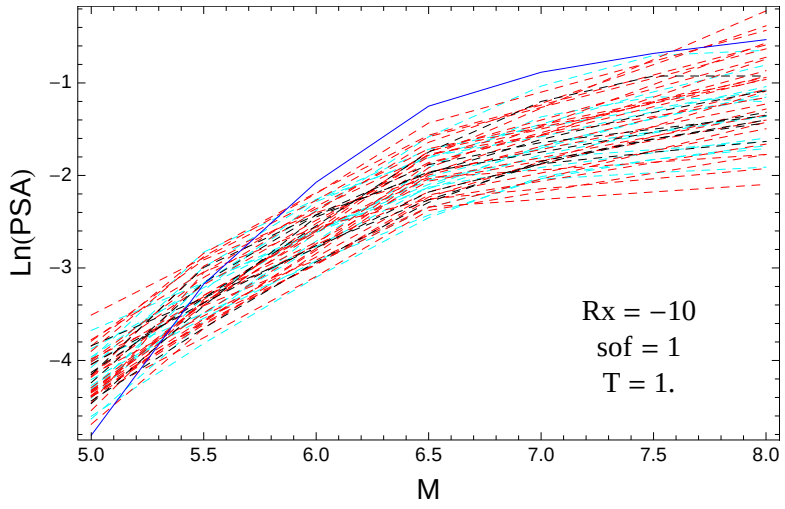



Figure 2.385: DCPPv4: Magnitude scaling of the original GMPEs (dashed black), the original GMPEs with uncertainty model (dashed cyan) and selected A models (dashed red) and the model of Graizer (2014), for a scenario with $R_X = -10$, $F = 1$, and $T = 1$.s.

**T = 3.s**

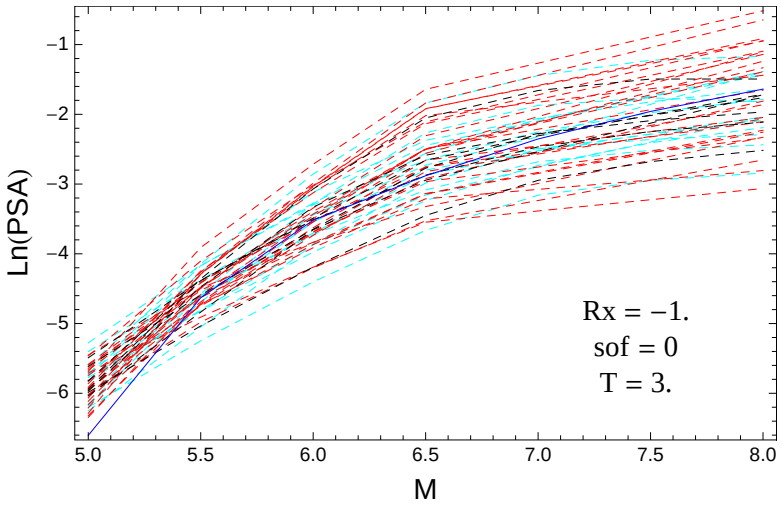



Figure 2.386: DCPPv4: Magnitude scaling of the original GMPEs (dashed black), the original GMPEs with uncertainty model (dashed cyan) and selected A models (dashed red) and the model of Graizer (2014), for a scenario with $R_X = -1.$, $F = 0$, and $T = 3.$s.

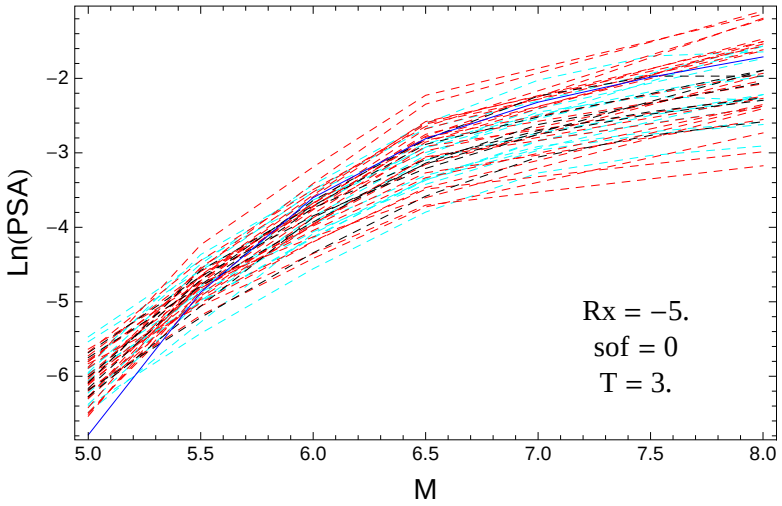



Figure 2.387: DCPPv4: Magnitude scaling of the original GMPEs (dashed black), the original GMPEs with uncertainty model (dashed cyan) and selected A models (dashed red) and the model of Graizer (2014), for a scenario with $R_X = -5.$, $F = 0$, and $T = 3.$s.

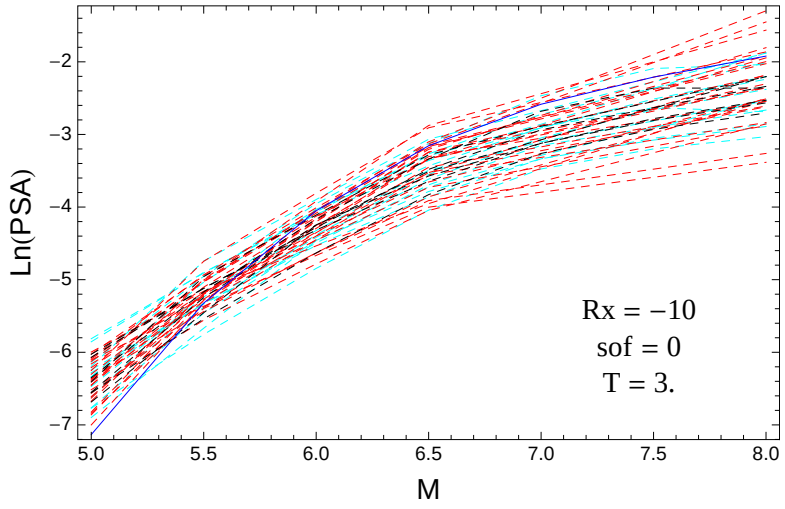



Figure 2.388: DCPPv4: Magnitude scaling of the original GMPEs (dashed black), the original GMPEs with uncertainty model (dashed cyan) and selected A models (dashed red) and the model of Graizer (2014), for a scenario with $R_X = -10$, $F = 0$, and $T = 3$.s.

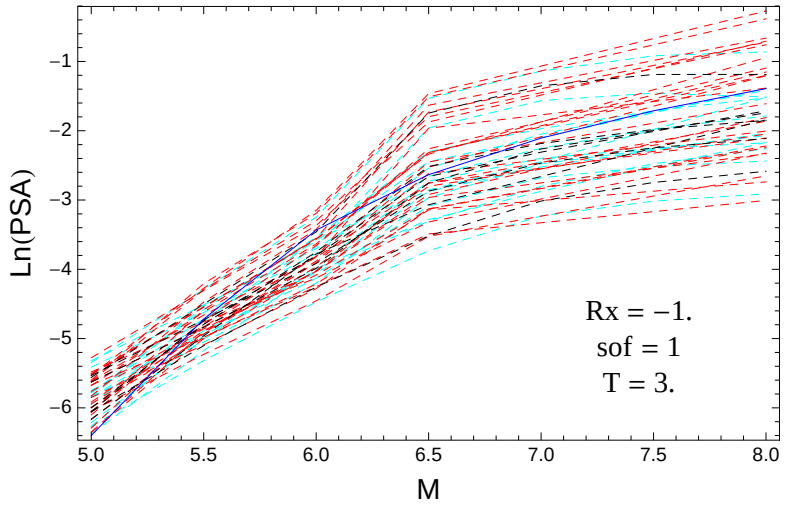



Figure 2.389: DCPPv4: Magnitude scaling of the original GMPEs (dashed black), the original GMPEs with uncertainty model (dashed cyan) and selected A models (dashed red) and the model of Graizer (2014), for a scenario with $R_X = -1.$, $F = 1$, and $T = 3$.s.

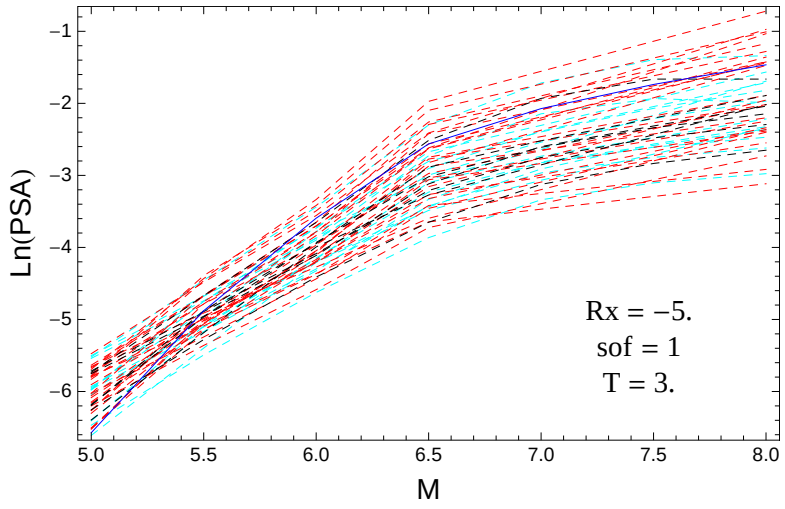



Figure 2.390: DCPPv4: Magnitude scaling of the original GMPEs (dashed black), the original GMPEs with uncertainty model (dashed cyan) and selected A models (dashed red) and the model of Graizer (2014), for a scenario with $R_X = -5.$, $F = 1$, and $T = 3.$s.

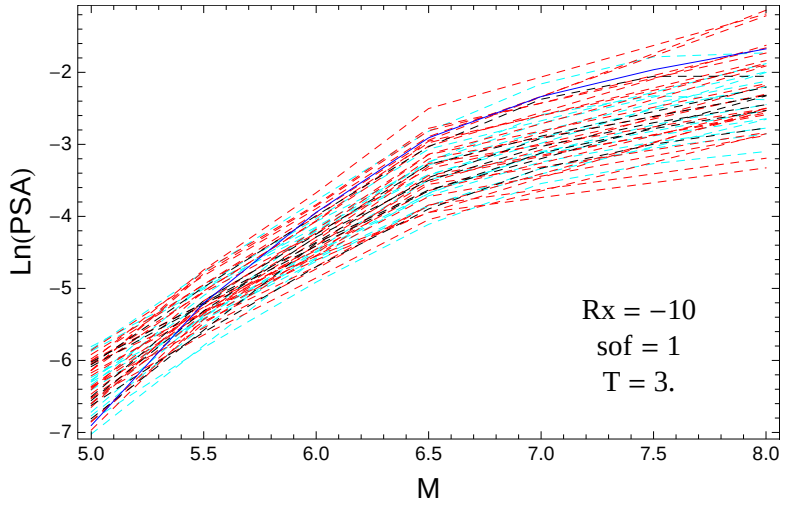



Figure 2.391: DCPPv4: Magnitude scaling of the original GMPEs (dashed black), the original GMPEs with uncertainty model (dashed cyan) and selected A models (dashed red) and the model of Graizer (2014), for a scenario with $R_X = -10$, $F = 1$, and $T = 3.$s.

### 2.1.13 Distance Scaling with GMPEs

**T = 0.01s**

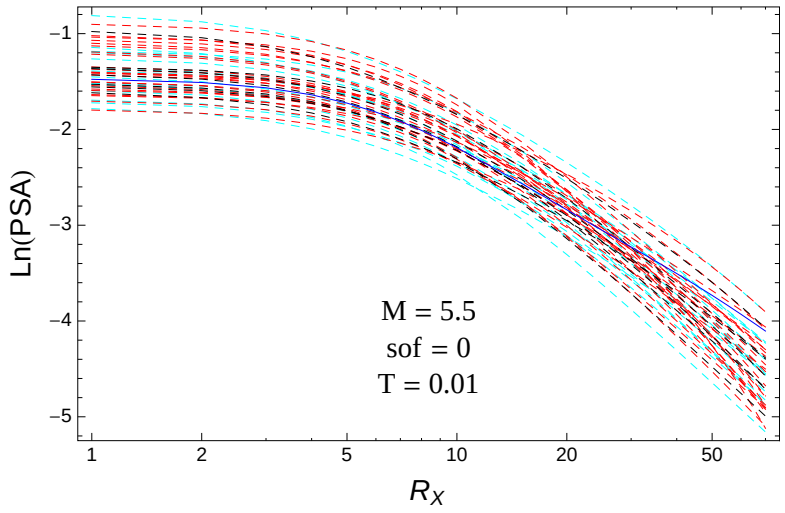



Figure 2.392: DCPPv4: Distance scaling of the original GMPEs (dashed black), the original GMPEs with uncertainty model (dashed cyan) and selected A models (dashed red) and the model of Graizer (2014) (blue), for a scenario with $M = 5.5$, $F = 0$, and $T = 0.01$s.

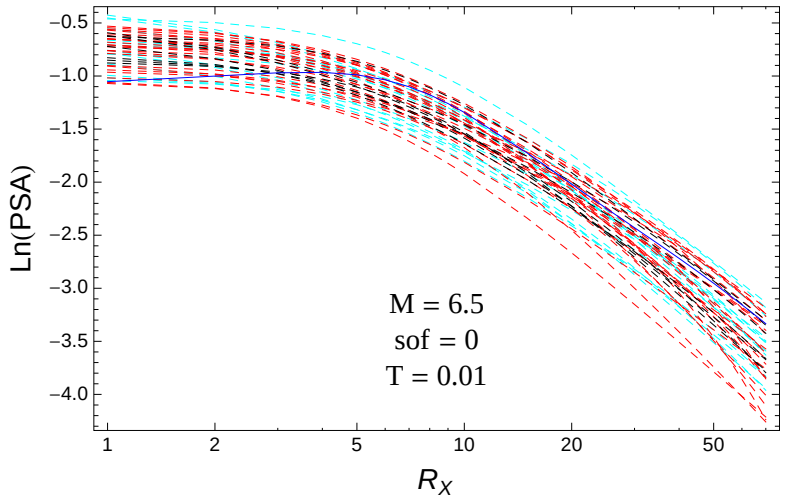



Figure 2.393: DCPPv4: Distance scaling of the original GMPEs (dashed black), the original GMPEs with uncertainty model (dashed cyan) and selected A models (dashed red) and the model of Graizer (2014) (blue), for a scenario with $M = 6.5$, $F = 0$, and $T = 0.01$s.

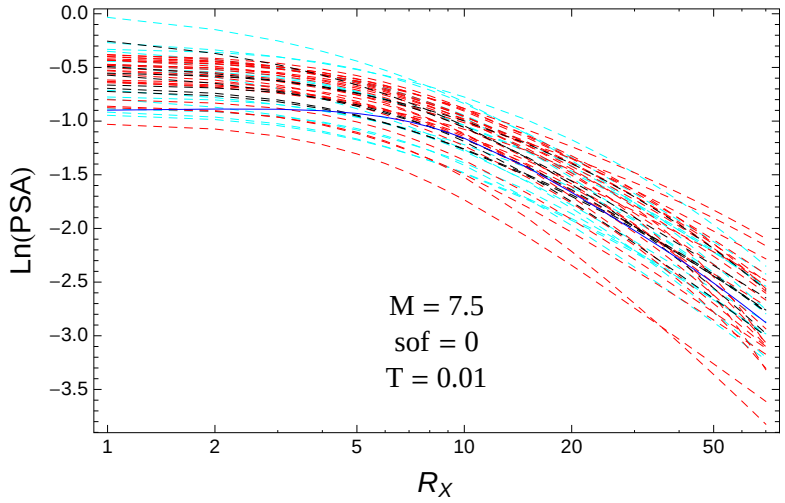



Figure 2.394: DCPPv4: Distance scaling of the original GMPEs (dashed black), the original GMPEs with uncertainty model (dashed cyan) and selected A models (dashed red) and the model of Graizer (2014) (blue), for a scenario with $M = 7.5$, $F = 0$, and $T = 0.01$s.

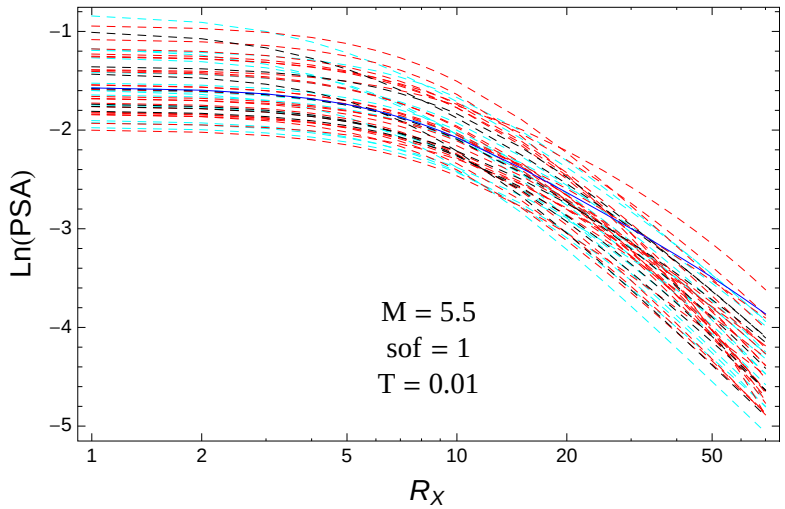



Figure 2.395: DCPPv4: Distance scaling of the original GMPEs (dashed black), the original GMPEs with uncertainty model (dashed cyan) and selected A models (dashed red) and the model of Graizer (2014) (blue), for a scenario with $M = 5.5$, $F = 1$, and $T = 0.01$s.

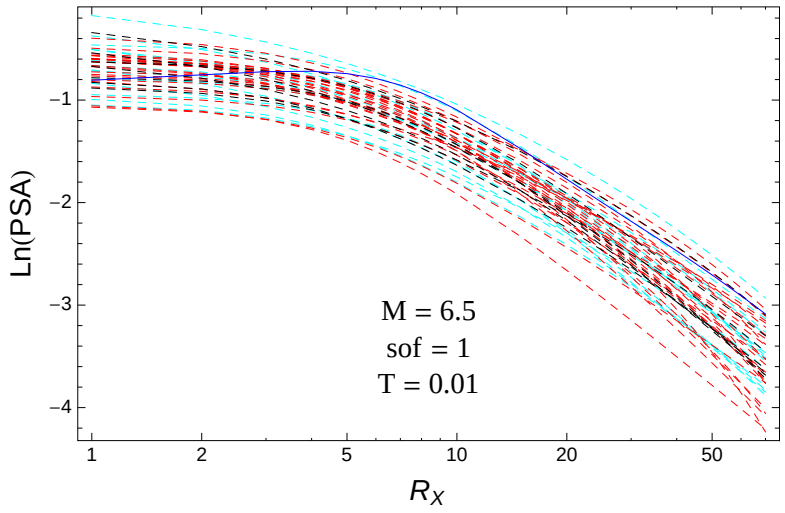



Figure 2.396: DCPPv4: Distance scaling of the original GMPEs (dashed black), the original GMPEs with uncertainty model (dashed cyan) and selected A models (dashed red) and the model of Graizer (2014) (blue), for a scenario with $M = 6.5$, $F = 1$, and $T = 0.01$s.

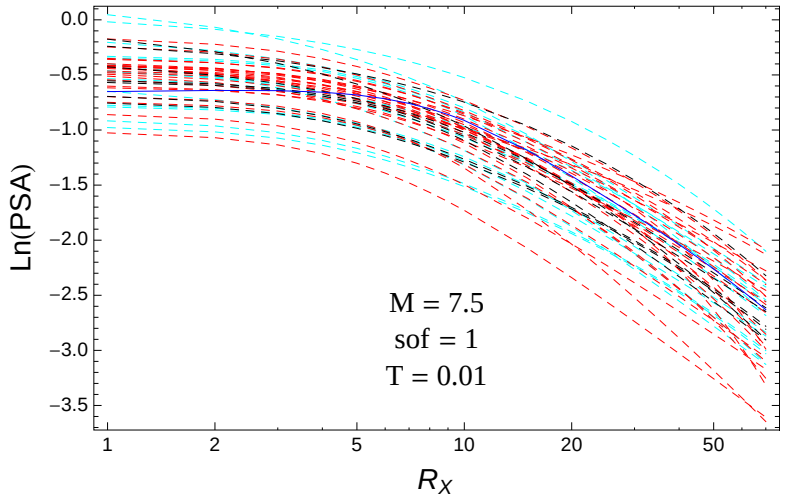



Figure 2.397: DCPPv4: Distance scaling of the original GMPEs (dashed black), the original GMPEs with uncertainty model (dashed cyan) and selected A models (dashed red) and the model of Graizer (2014) (blue), for a scenario with $M = 7.5$, $F = 1$, and $T = 0.01$s.

**T = 0.2s**

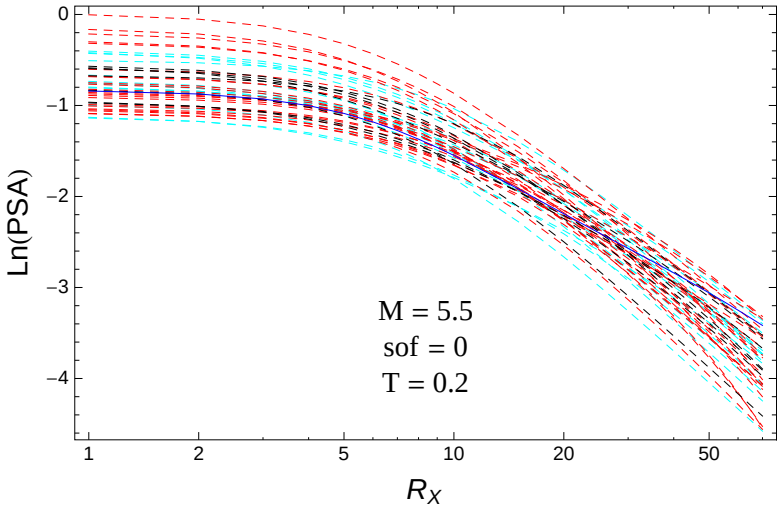



Figure 2.398: DCPPv4: Distance scaling of the original GMPEs (dashed black), the original GMPEs with uncertainty model (dashed cyan) and selected A models (dashed red) and the model of Graizer (2014) (blue), for a scenario with $M = 5.5$, $F = 0$, and $T = 0.2$s.

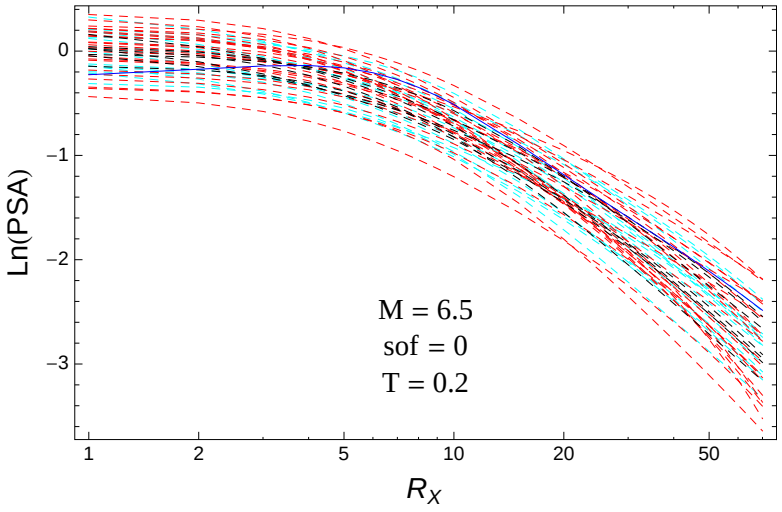



Figure 2.399: DCPPv4: Distance scaling of the original GMPEs (dashed black), the original GMPEs with uncertainty model (dashed cyan) and selected A models (dashed red) and the model of Graizer (2014) (blue), for a scenario with $M = 6.5$, $F = 0$, and $T = 0.2$s.

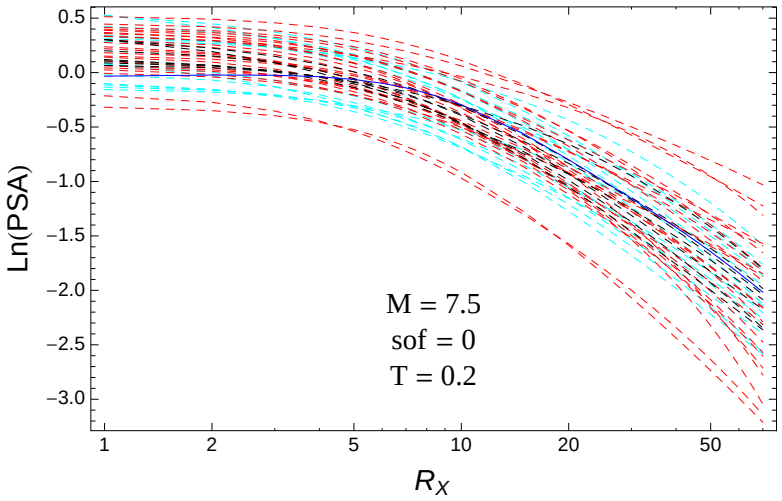



Figure 2.400: DCPPv4: Distance scaling of the original GMPEs (dashed black), the original GMPEs with uncertainty model (dashed cyan) and selected A models (dashed red) and the model of Graizer (2014) (blue), for a scenario with $M = 7.5$, $F = 0$, and $T = 0.2$s.

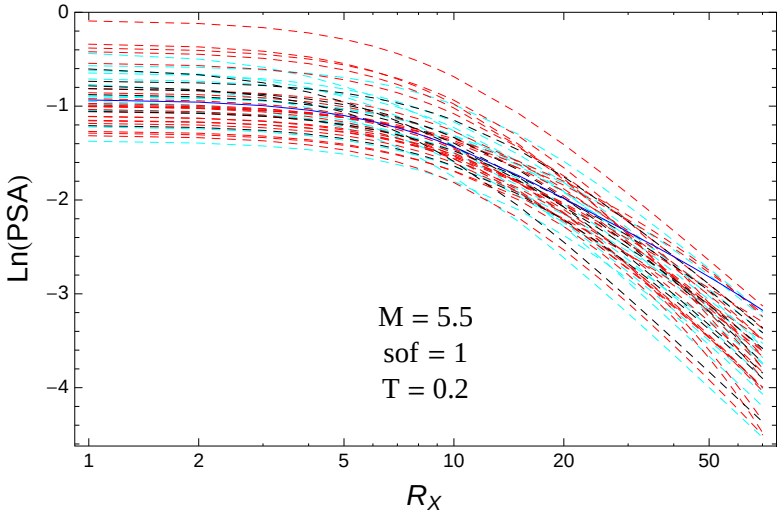



Figure 2.401: DCPPv4: Distance scaling of the original GMPEs (dashed black), the original GMPEs with uncertainty model (dashed cyan) and selected A models (dashed red) and the model of Graizer (2014) (blue), for a scenario with $M = 5.5$, $F = 1$, and $T = 0.2$s.

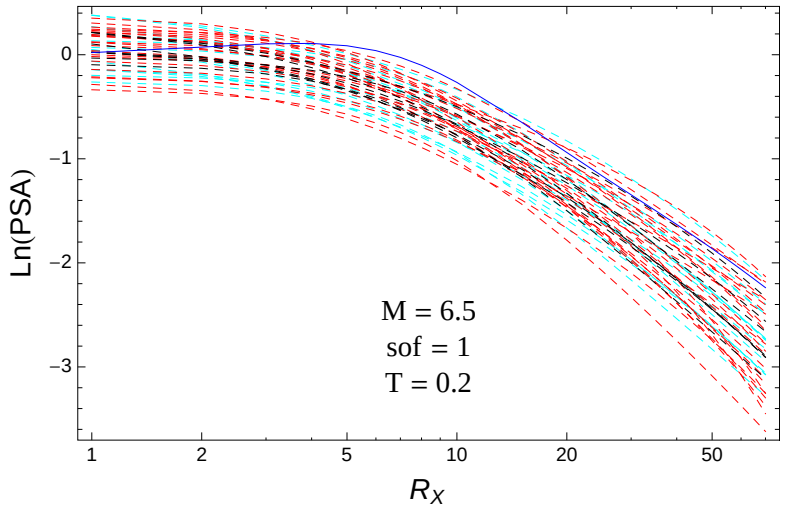



Figure 2.402: DCPPv4: Distance scaling of the original GMPEs (dashed black), the original GMPEs with uncertainty model (dashed cyan) and selected A models (dashed red) and the model of Graizer (2014) (blue), for a scenario with $M = 6.5$, $F = 1$, and $T = 0.2$s.

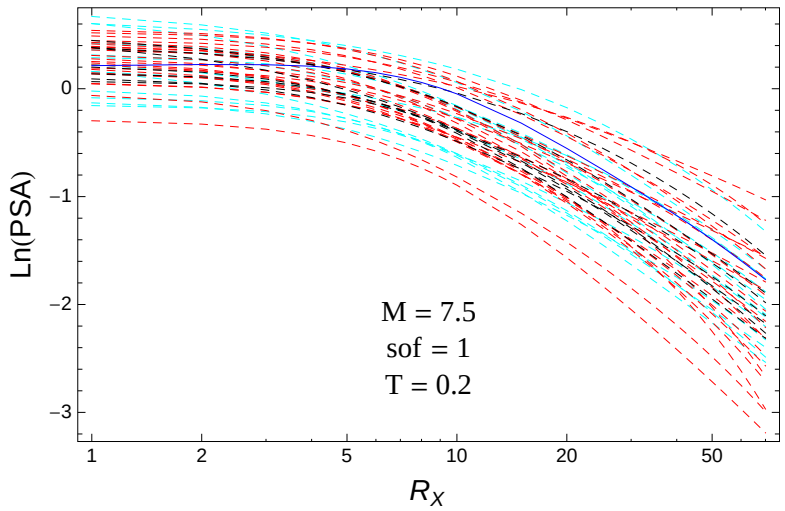



Figure 2.403: DCPPv4: Distance scaling of the original GMPEs (dashed black), the original GMPEs with uncertainty model (dashed cyan) and selected A models (dashed red) and the model of Graizer (2014) (blue), for a scenario with $M = 7.5$, $F = 1$, and $T = 0.2$s.

**T = 0.5s**

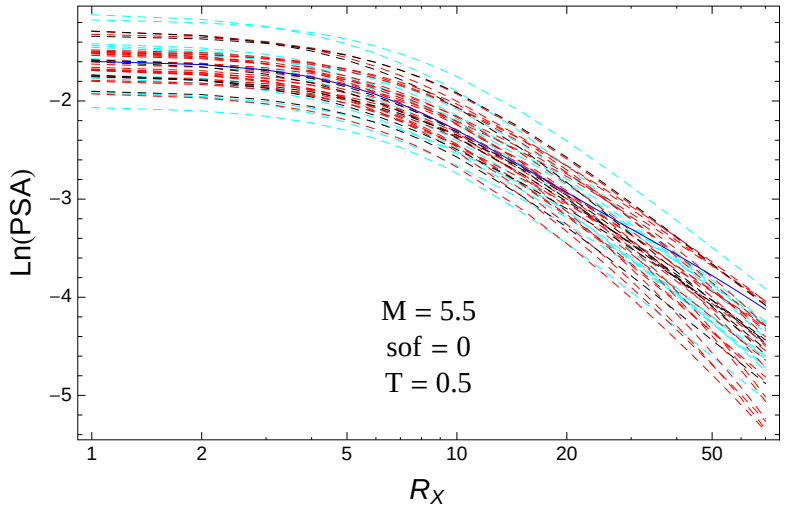



Figure 2.404: DCPPv4: Distance scaling of the original GMPEs (dashed black), the original GMPEs with uncertainty model (dashed cyan) and selected A models (dashed red) and the model of Graizer (2014) (blue), for a scenario with $M = 5.5$, $F = 0$, and $T = 0.5$s.

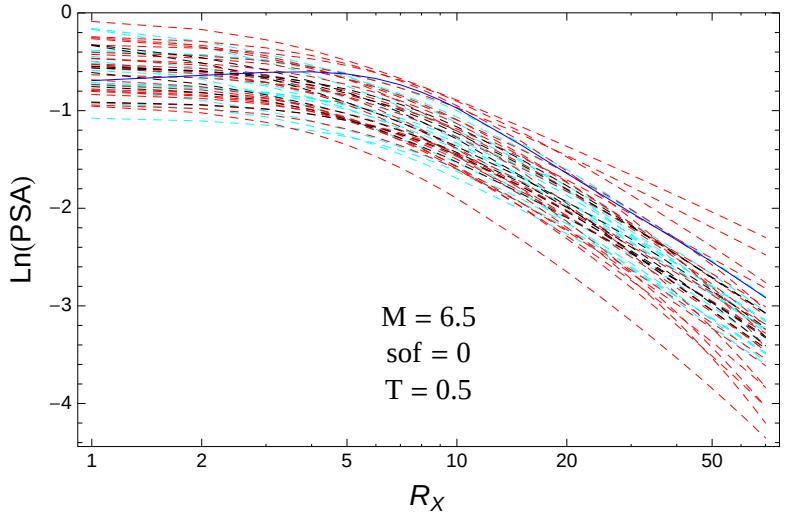



Figure 2.405: DCPPv4: Distance scaling of the original GMPEs (dashed black), the original GMPEs with uncertainty model (dashed cyan) and selected A models (dashed red) and the model of Graizer (2014) (blue), for a scenario with $M = 6.5$, $F = 0$, and $T = 0.5$s.

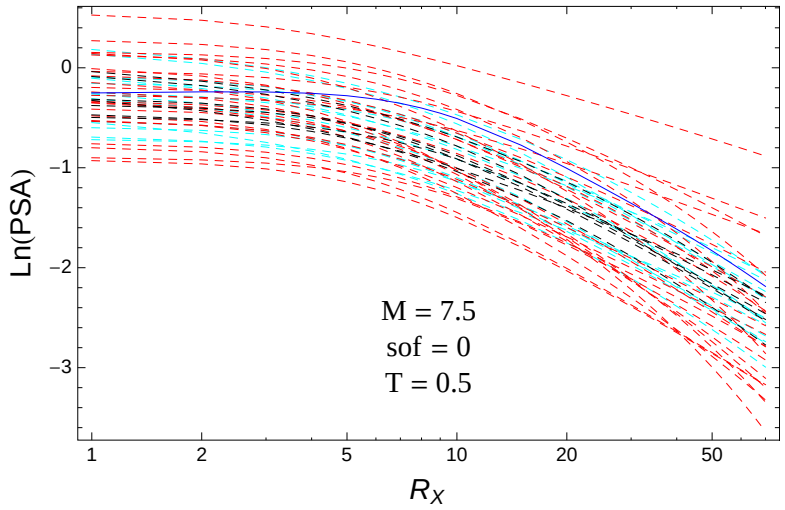



Figure 2.406: DCPPv4: Distance scaling of the original GMPEs (dashed black), the original GMPEs with uncertainty model (dashed cyan) and selected A models (dashed red) and the model of Graizer (2014) (blue), for a scenario with $M = 7.5$, $F = 0$, and $T = 0.5$s.

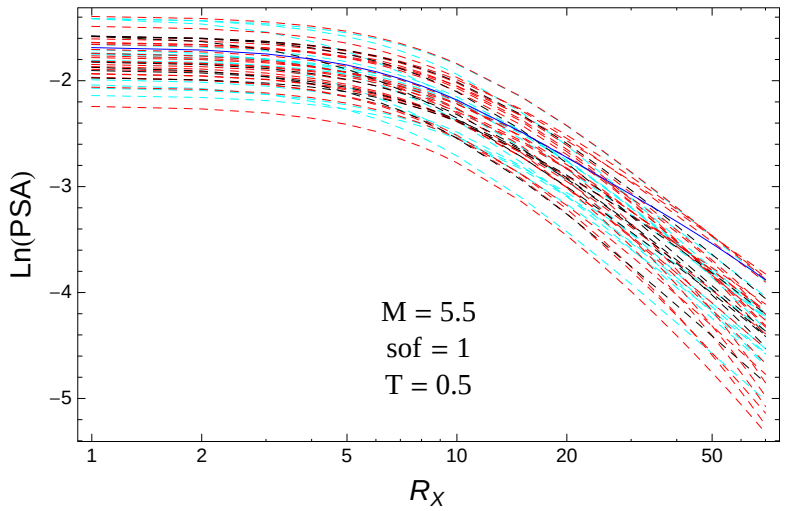



Figure 2.407: DCPPv4: Distance scaling of the original GMPEs (dashed black), the original GMPEs with uncertainty model (dashed cyan) and selected A models (dashed red) and the model of Graizer (2014) (blue), for a scenario with $M = 5.5$, $F = 1$, and $T = 0.5$s.

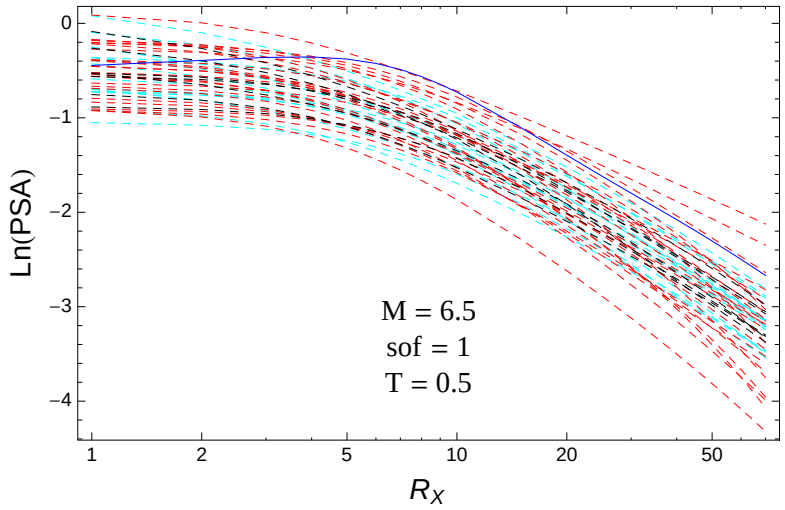



Figure 2.408: DCPPv4: Distance scaling of the original GMPEs (dashed black), the original GMPEs with uncertainty model (dashed cyan) and selected A models (dashed red) and the model of Graizer (2014) (blue), for a scenario with $M = 6.5$, $F = 1$, and $T = 0.5$s.

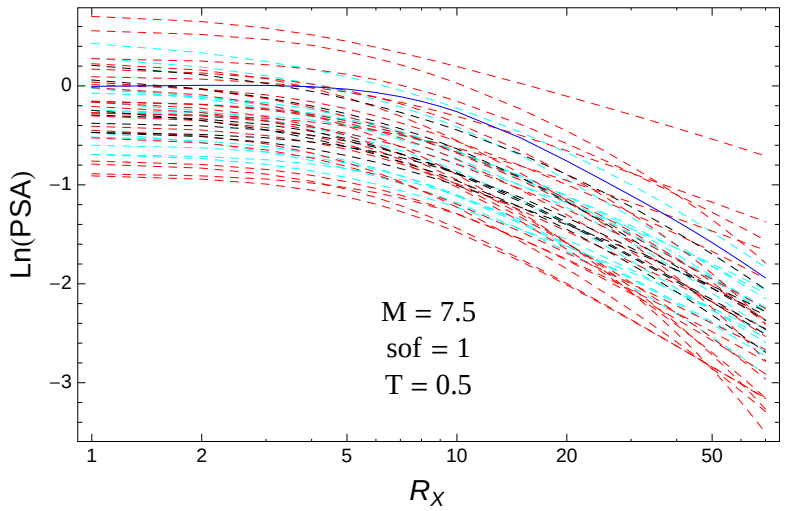



Figure 2.409: DCPPv4: Distance scaling of the original GMPEs (dashed black), the original GMPEs with uncertainty model (dashed cyan) and selected A models (dashed red) and the model of Graizer (2014) (blue), for a scenario with $M = 7.5$, $F = 1$, and $T = 0.5$s.

**T = 1.s**

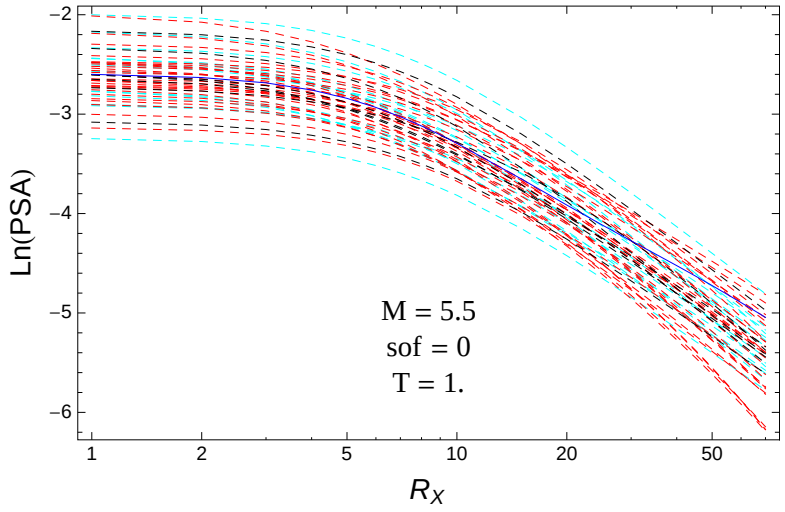



Figure 2.410: DCPPv4: Distance scaling of the original GMPEs (dashed black), the original GMPEs with uncertainty model (dashed cyan) and selected A models (dashed red) and the model of Graizer (2014) (blue), for a scenario with $M = 5.5$, $F = 0$, and $T = 1$.s.

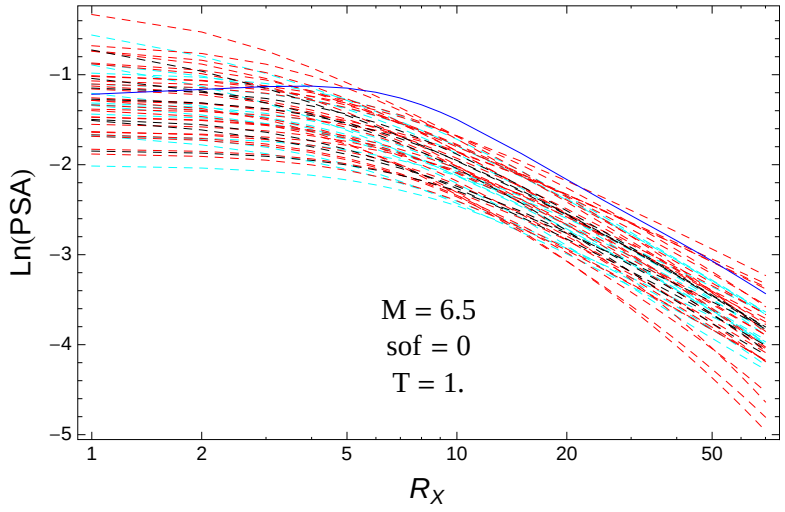



Figure 2.411: DCPPv4: Distance scaling of the original GMPEs (dashed black), the original GMPEs with uncertainty model (dashed cyan) and selected A models (dashed red) and the model of Graizer (2014) (blue), for a scenario with $M = 6.5$, $F = 0$, and $T = 1$.s.

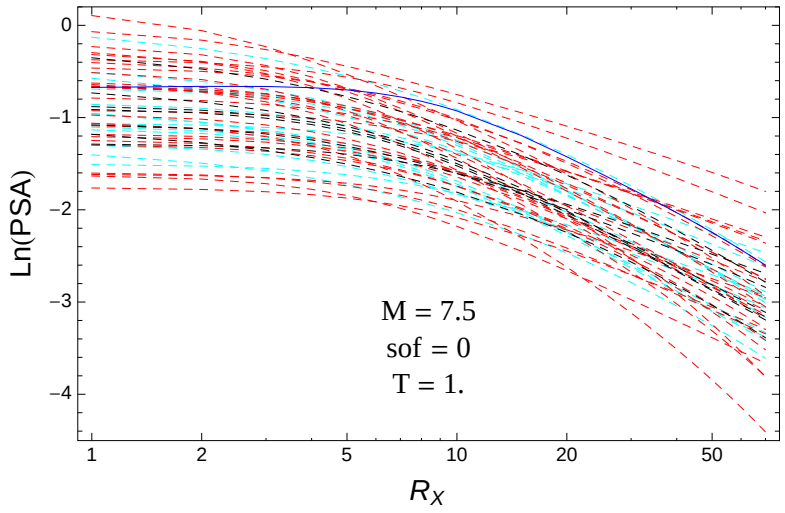



Figure 2.412: DCPPv4: Distance scaling of the original GMPEs (dashed black), the original GMPEs with uncertainty model (dashed cyan) and selected A models (dashed red) and the model of Graizer (2014) (blue), for a scenario with $M = 7.5$, $F = 0$, and $T = 1$.s.

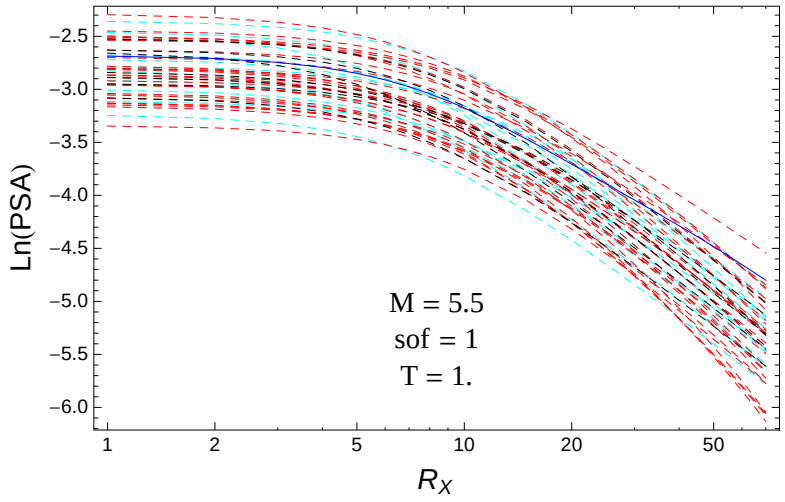



Figure 2.413: DCPPv4: Distance scaling of the original GMPEs (dashed black), the original GMPEs with uncertainty model (dashed cyan) and selected A models (dashed red) and the model of Graizer (2014) (blue), for a scenario with $M = 5.5$, $F = 1$, and $T = 1$.s.

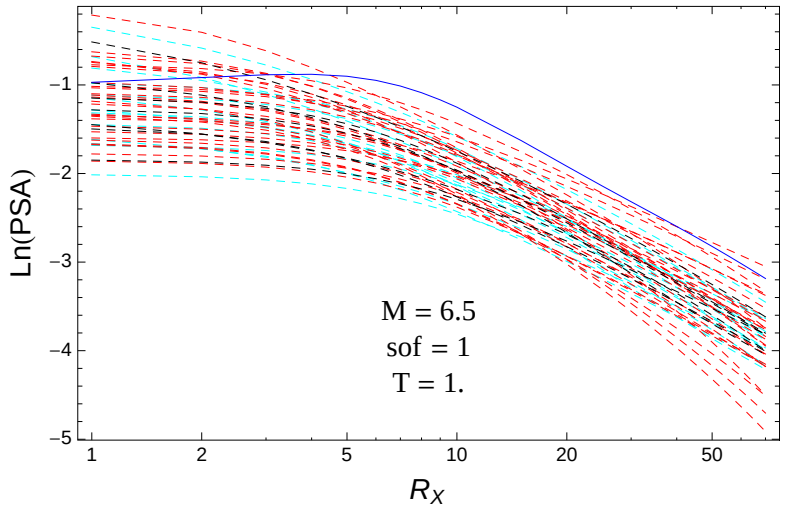



Figure 2.414: DCPPv4: Distance scaling of the original GMPEs (dashed black), the original GMPEs with uncertainty model (dashed cyan) and selected A models (dashed red) and the model of Graizer (2014) (blue), for a scenario with $M = 6.5$, $F = 1$, and $T = 1$.s.

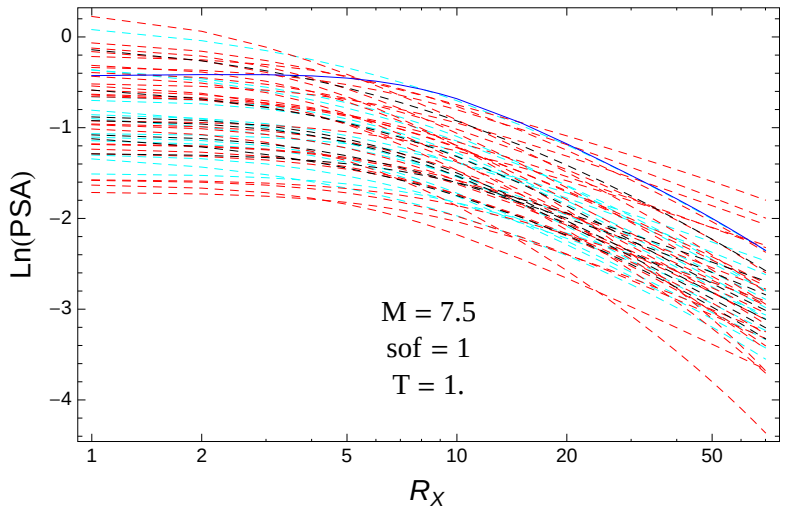



Figure 2.415: DCPPv4: Distance scaling of the original GMPEs (dashed black), the original GMPEs with uncertainty model (dashed cyan) and selected A models (dashed red) and the model of Graizer (2014) (blue), for a scenario with $M = 7.5$, $F = 1$, and $T = 1$.s.

**T = 3.s**

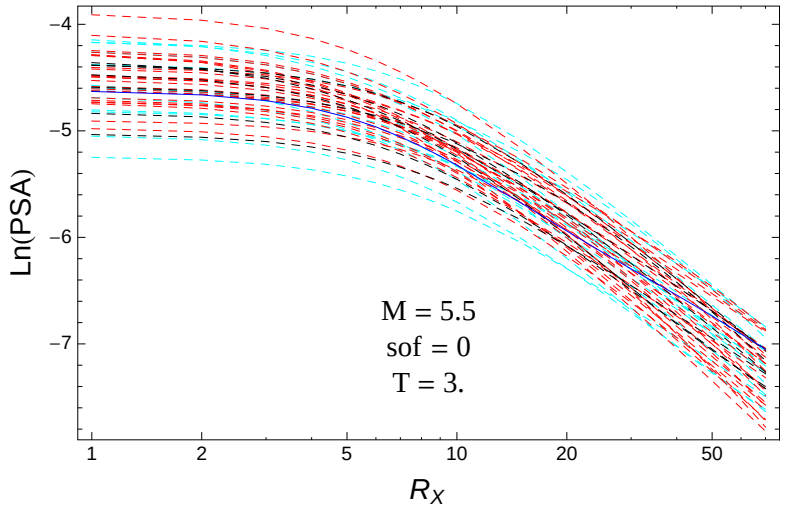



Figure 2.416: DCPPv4: Distance scaling of the original GMPEs (dashed black), the original GMPEs with uncertainty model (dashed cyan) and selected A models (dashed red) and the model of Graizer (2014) (blue), for a scenario with $M = 5.5$, $F = 0$, and $T = 3$.s.

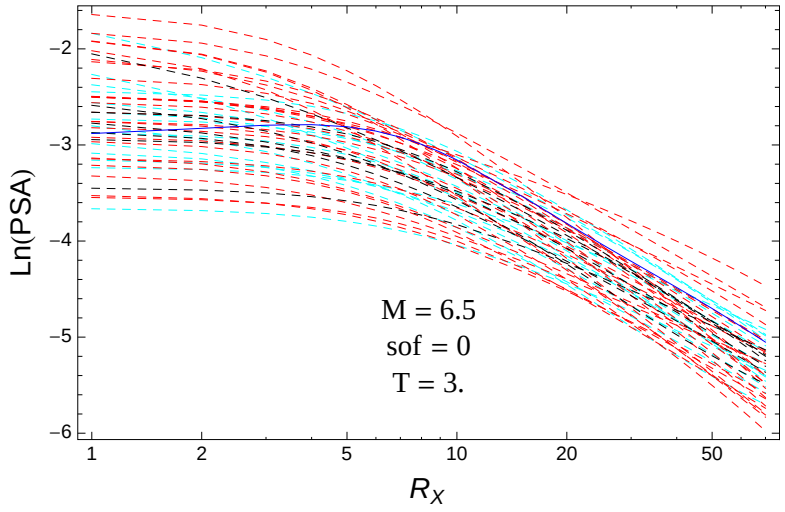



Figure 2.417: DCPPv4: Distance scaling of the original GMPEs (dashed black), the original GMPEs with uncertainty model (dashed cyan) and selected A models (dashed red) and the model of Graizer (2014) (blue), for a scenario with $M = 6.5$, $F = 0$, and $T = 3$.s.

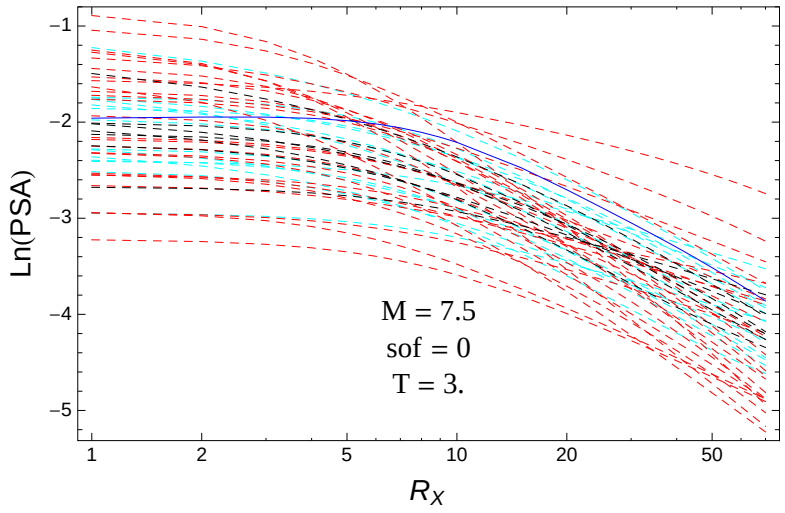



Figure 2.418: DCPPv4: Distance scaling of the original GMPEs (dashed black), the original GMPEs with uncertainty model (dashed cyan) and selected A models (dashed red) and the model of Graizer (2014) (blue), for a scenario with $M = 7.5$, $F = 0$, and $T = 3$.s.

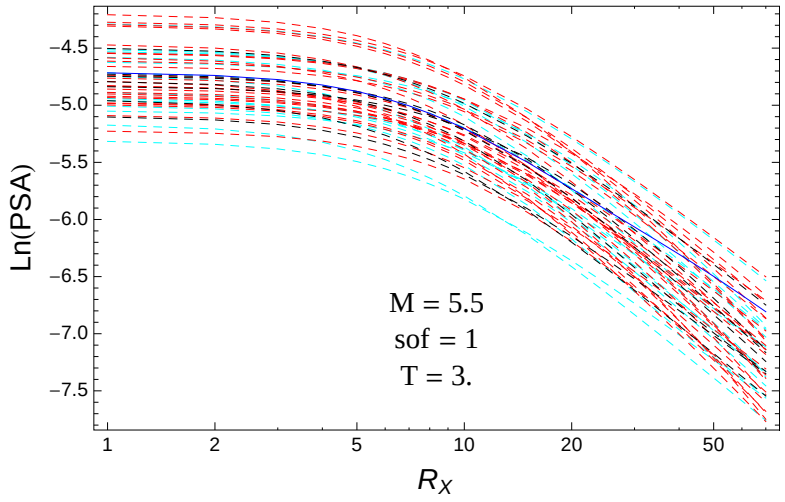



Figure 2.419: DCPPv4: Distance scaling of the original GMPEs (dashed black), the original GMPEs with uncertainty model (dashed cyan) and selected A models (dashed red) and the model of Graizer (2014) (blue), for a scenario with $M = 5.5$, $F = 1$, and $T = 3$.s.

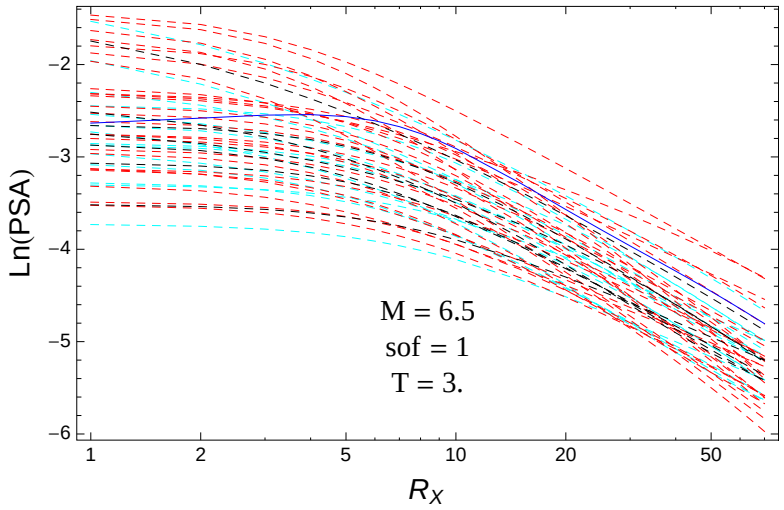



Figure 2.420: DCPPv4: Distance scaling of the original GMPEs (dashed black), the original GMPEs with uncertainty model (dashed cyan) and selected A models (dashed red) and the model of Graizer (2014) (blue), for a scenario with $M = 6.5$, $F = 1$, and $T = 3$.s.

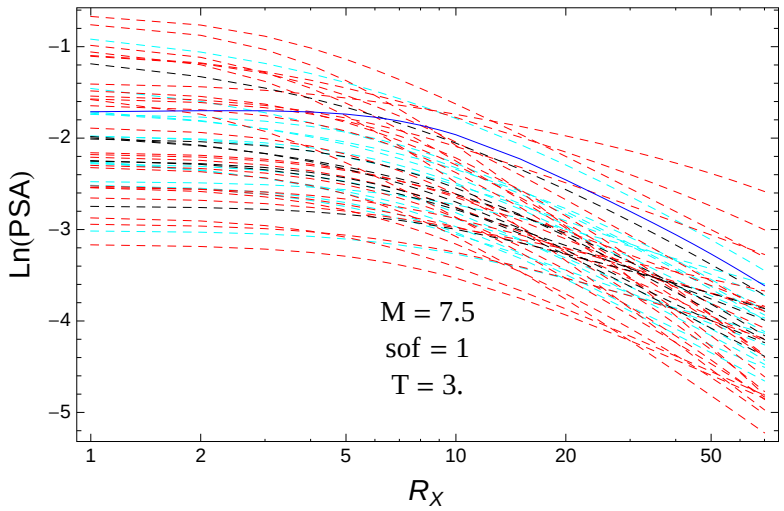



Figure 2.421: DCPPv4: Distance scaling of the original GMPEs (dashed black), the original GMPEs with uncertainty model (dashed cyan) and selected A models (dashed red) and the model of Graizer (2014) (blue), for a scenario with $M = 7.5$, $F = 1$, and $T = 3$.s.

### 2.1.14 Quantile Plots vs. Magnitude with GMPEs

**T = 0.01s**

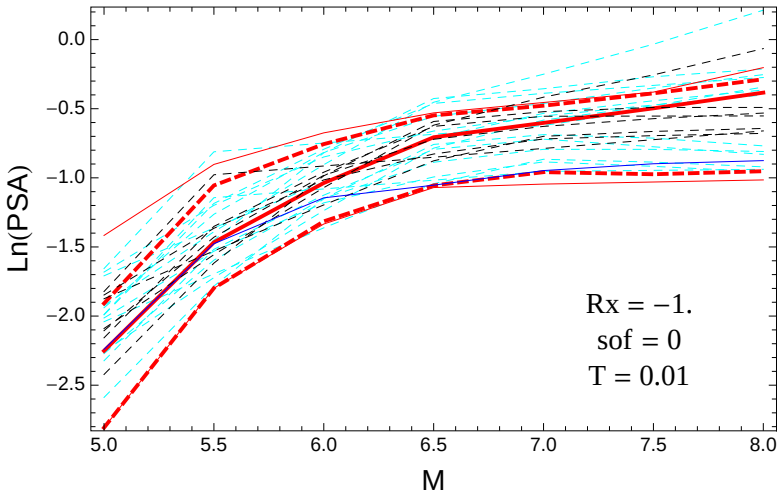



Figure 2.422: DCPPv4: Magnitude scaling of 0.05,0.5,0.95 quantile and the ModelA distribution (red) with total weights, original GMPEs (dashed black), original GMPEs with uncertainty model (dashed cyan) and the model of Graizer (2014) (blue), for a scenario with $R_x = -1.$, $F = 0$, and $T = 0.01$s.

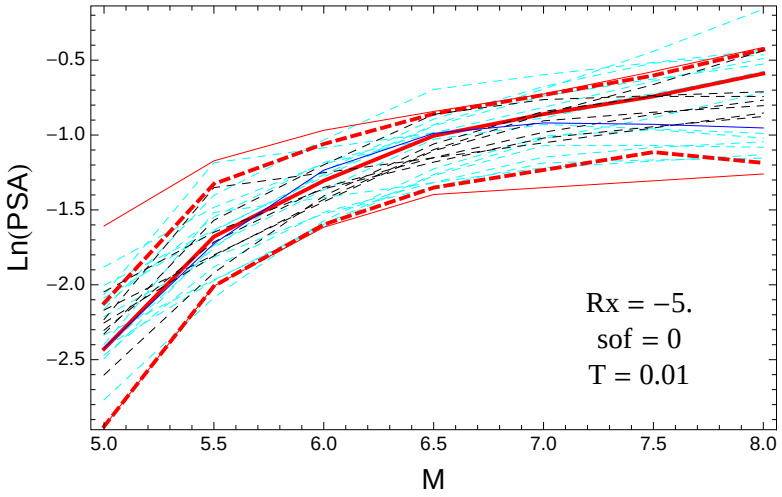



Figure 2.423: DCPPv4: Magnitude scaling of 0.05,0.5,0.95 quantile and the ModelA distribution (red) with total weights, original GMPEs (dashed black), original GMPEs with uncertainty model (dashed cyan) and the model of Graizer (2014) (blue), for a scenario with $R_x = -5.$, $F = 0$, and $T = 0.01$s.

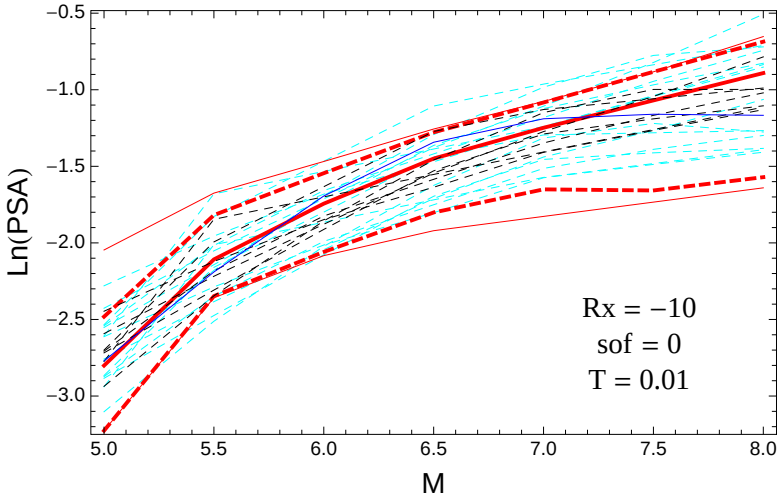



Figure 2.424: DCPPv4: Magnitude scaling of 0.05,0.5,0.95 quantile and the ModelA distribution (red) with total weights, original GMPEs (dashed black), original GMPEs with uncertainty model (dashed cyan) and the model of Graizer (2014) (blue), for a scenario with $R_x = -10$, $F = 0$, and $T = 0.01$s.

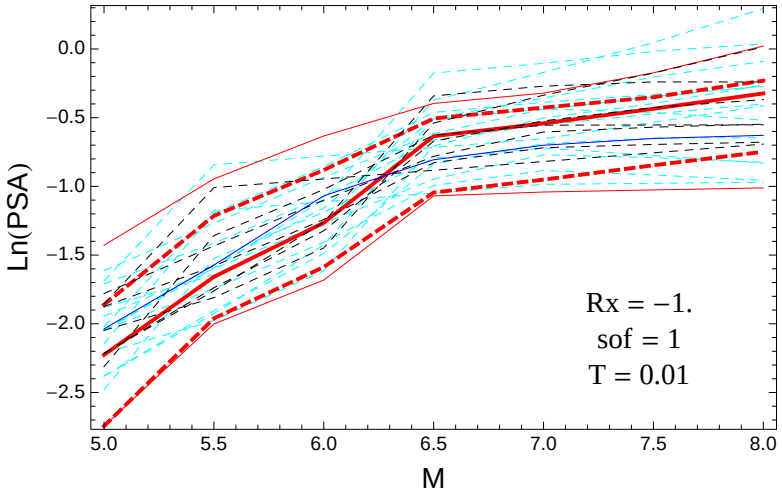



Figure 2.425: DCPPv4: Magnitude scaling of 0.05,0.5,0.95 quantile and the ModelA distribution (red) with total weights, original GMPEs (dashed black), original GMPEs with uncertainty model (dashed cyan) and the model of Graizer (2014) (blue), for a scenario with $R_x = -1.$, $F = 1$, and $T = 0.01$s.

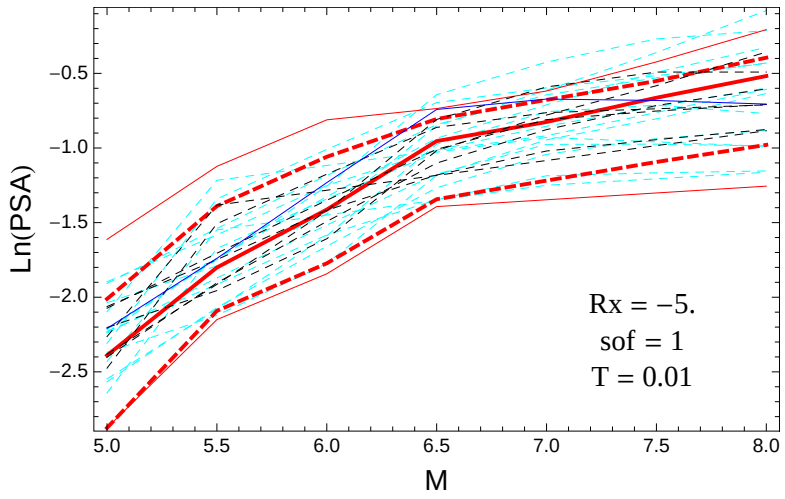



Figure 2.426: DCPPv4: Magnitude scaling of 0.05,0.5,0.95 quantile and the ModelA distribution (red) with total weights, original GMPEs (dashed black), original GMPEs with uncertainty model (dashed cyan) and the model of Graizer (2014) (blue), for a scenario with $R_x = -5.$, $F = 1$, and $T = 0.01$s.

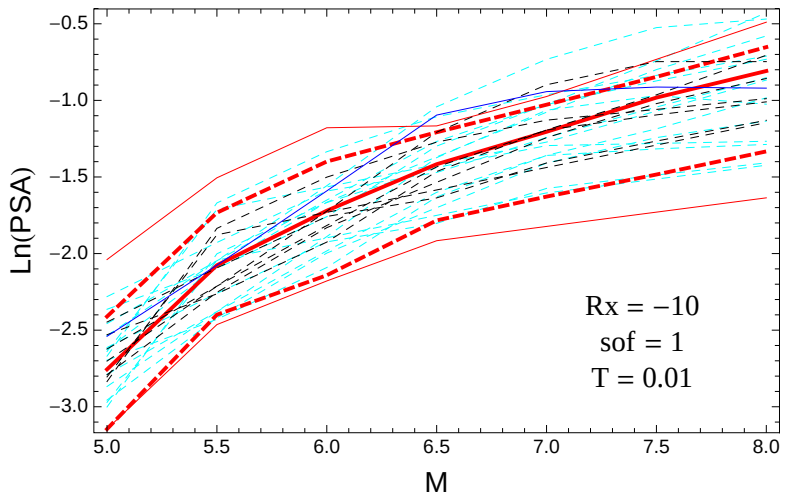



Figure 2.427: DCPPv4: Magnitude scaling of 0.05,0.5,0.95 quantile and the ModelA distribution (red) with total weights, original GMPEs (dashed black), original GMPEs with uncertainty model (dashed cyan) and the model of Graizer (2014) (blue), for a scenario with $R_x = -10$, $F = 1$, and $T = 0.01$s.

**T = 0.2s**

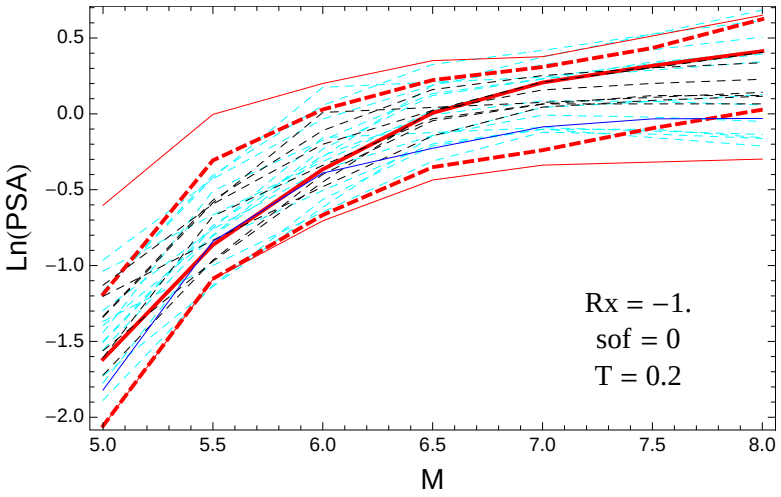



Figure 2.428: DCPPv4: Magnitude scaling of 0.05,0.5,0.95 quantile and the ModelA distribution (red) with total weights, original GMPEs (dashed black), original GMPEs with uncertainty model (dashed cyan) and the model of Graizer (2014) (blue), for a scenario with $R_x = -1.$, $F = 0$, and $T = 0.2$s.

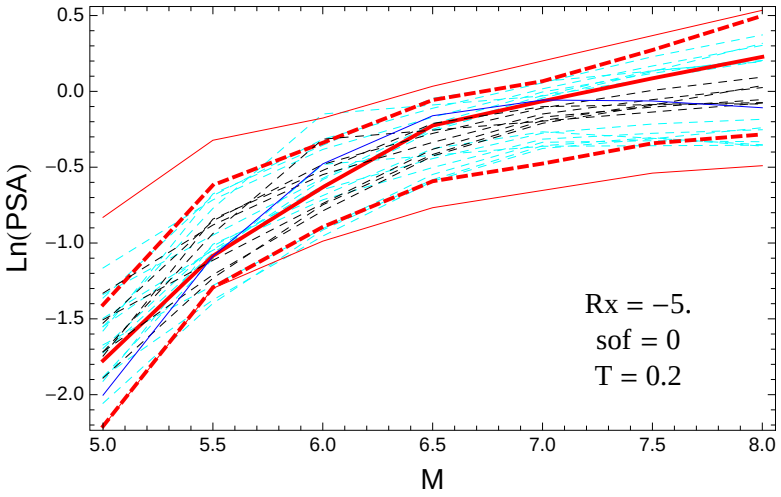



Figure 2.429: DCPPv4: Magnitude scaling of 0.05,0.5,0.95 quantile and the ModelA distribution (red) with total weights, original GMPEs (dashed black), original GMPEs with uncertainty model (dashed cyan) and the model of Graizer (2014) (blue), for a scenario with $R_x = -5.$, $F = 0$, and $T = 0.2$s.

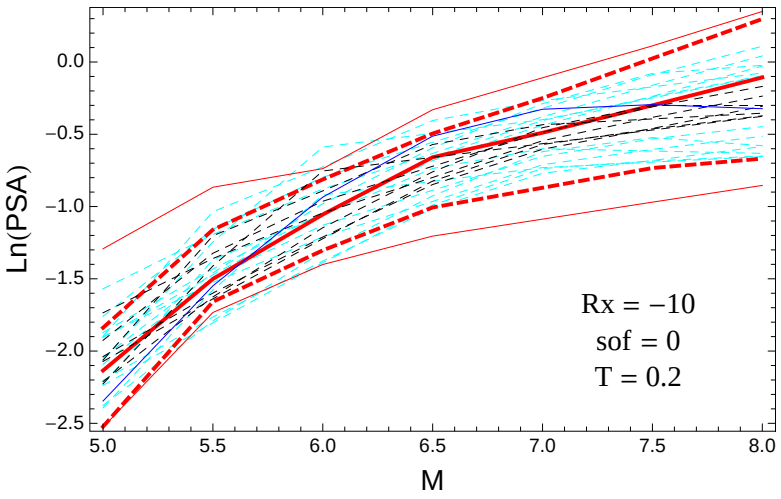



Figure 2.430: DCPPv4: Magnitude scaling of 0.05,0.5,0.95 quantile and the ModelA distribution (red) with total weights, original GMPEs (dashed black), original GMPEs with uncertainty model (dashed cyan) and the model of Graizer (2014) (blue), for a scenario with $R_x = -10$, $F = 0$, and $T = 0.2$s.

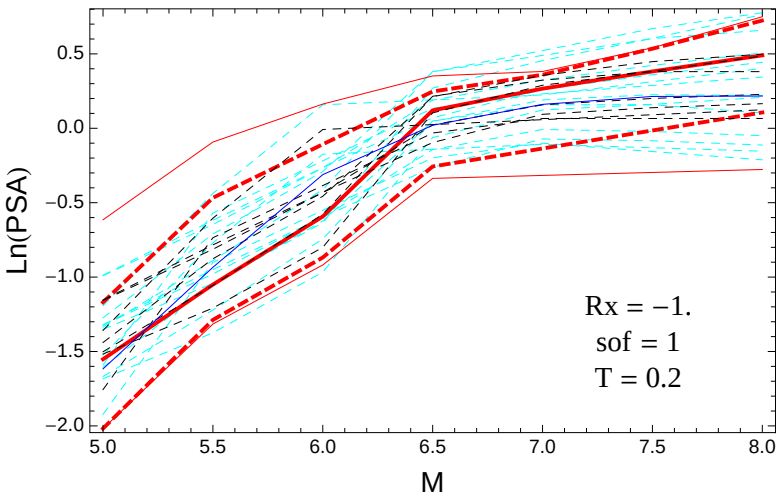



Figure 2.431: DCPPv4: Magnitude scaling of 0.05,0.5,0.95 quantile and the ModelA distribution (red) with total weights, original GMPEs (dashed black), original GMPEs with uncertainty model (dashed cyan) and the model of Graizer (2014) (blue), for a scenario with $R_x = -1.$, $F = 1$, and $T = 0.2$s.

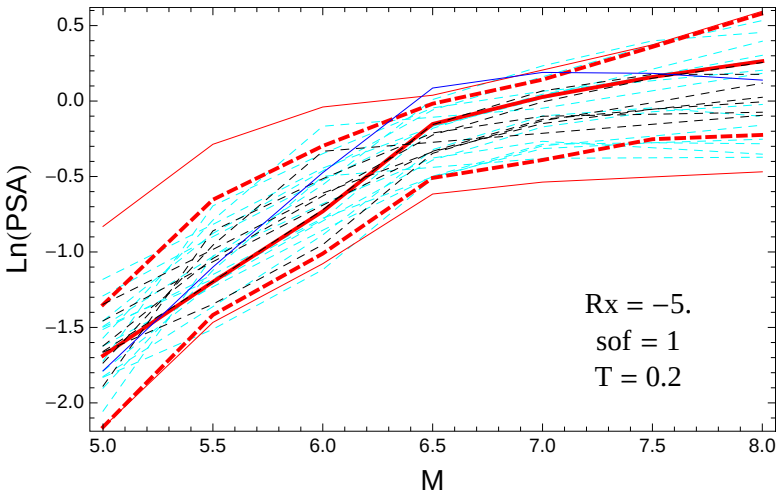



Figure 2.432: DCPPv4: Magnitude scaling of 0.05,0.5,0.95 quantile and the ModelA distribution (red) with total weights, original GMPEs (dashed black), original GMPEs with uncertainty model (dashed cyan) and the model of Graizer (2014) (blue), for a scenario with $R_x = -5.$, $F = 1$, and $T = 0.2$s.

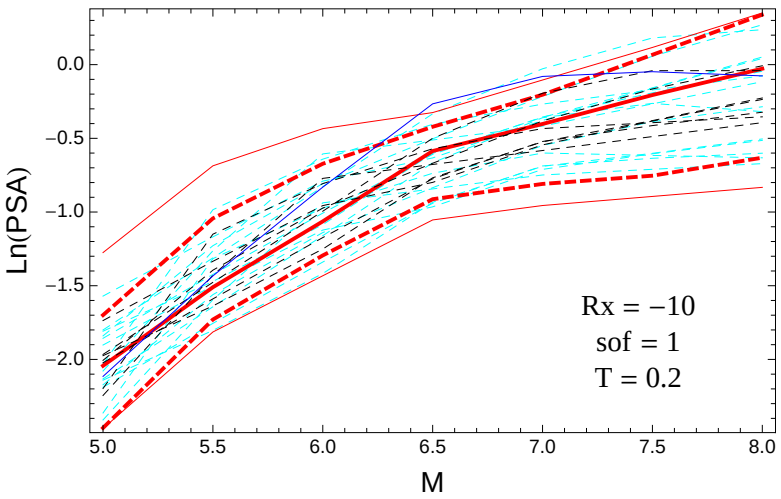



Figure 2.433: DCPPv4: Magnitude scaling of 0.05,0.5,0.95 quantile and the ModelA distribution (red) with total weights, original GMPEs (dashed black), original GMPEs with uncertainty model (dashed cyan) and the model of Graizer (2014) (blue), for a scenario with $R_x = -10$, $F = 1$, and $T = 0.2$s.

**T = 0.5s**

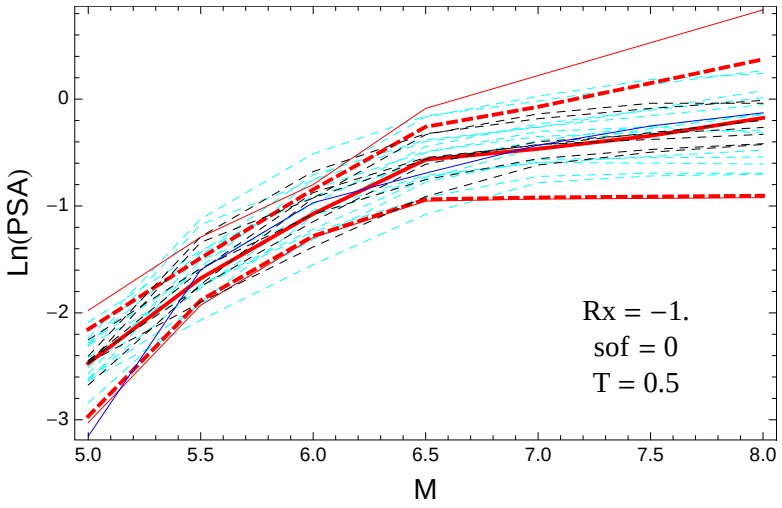



Figure 2.434: DCPPv4: Magnitude scaling of 0.05,0.5,0.95 quantile and the ModelA distribution (red) with total weights, original GMPEs (dashed black), original GMPEs with uncertainty model (dashed cyan) and the model of Graizer (2014) (blue), for a scenario with $R_x = -1.$, $F = 0$, and $T = 0.5$s.

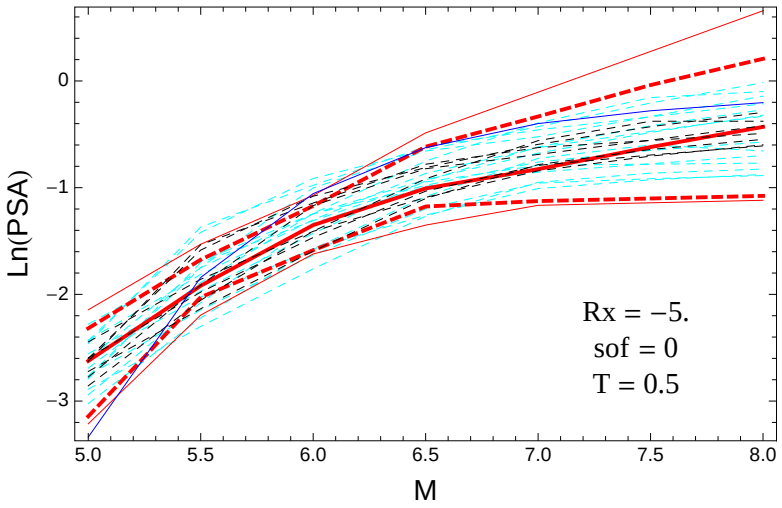



Figure 2.435: DCPPv4: Magnitude scaling of 0.05,0.5,0.95 quantile and the ModelA distribution (red) with total weights, original GMPEs (dashed black), original GMPEs with uncertainty model (dashed cyan) and the model of Graizer (2014) (blue), for a scenario with $R_x = -5.$, $F = 0$, and $T = 0.5$s.

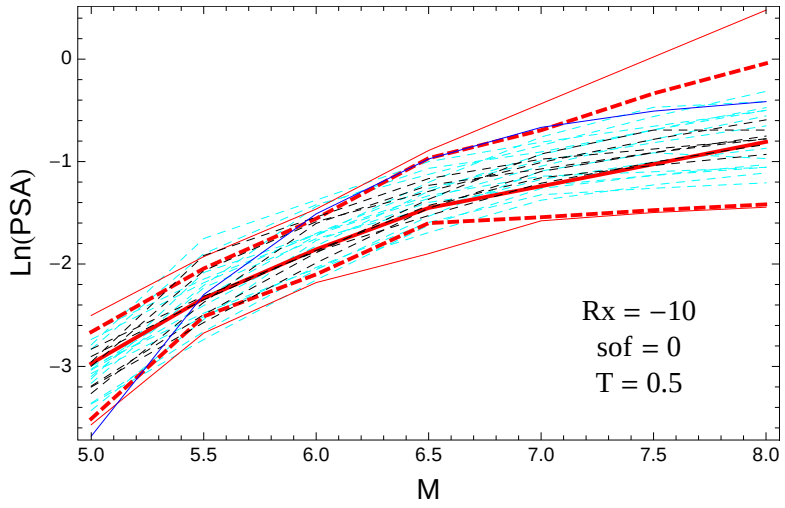



Figure 2.436: DCPPv4: Magnitude scaling of 0.05,0.5,0.95 quantile and the ModelA distribution (red) with total weights, original GMPEs (dashed black), original GMPEs with uncertainty model (dashed cyan) and the model of Graizer (2014) (blue), for a scenario with $R_x = -10$, $F = 0$, and $T = 0.5$s.

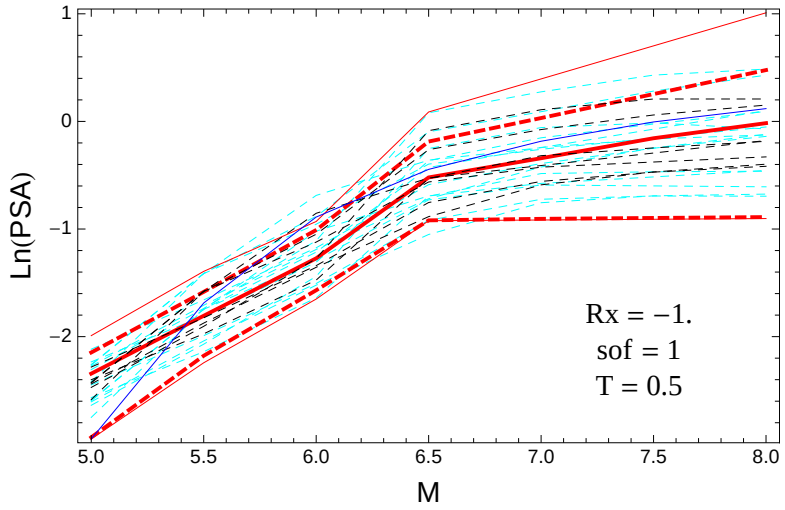



Figure 2.437: DCPPv4: Magnitude scaling of 0.05,0.5,0.95 quantile and the ModelA distribution (red) with total weights, original GMPEs (dashed black), original GMPEs with uncertainty model (dashed cyan) and the model of Graizer (2014) (blue), for a scenario with $R_x = -1.$, $F = 1$, and $T = 0.5$s.

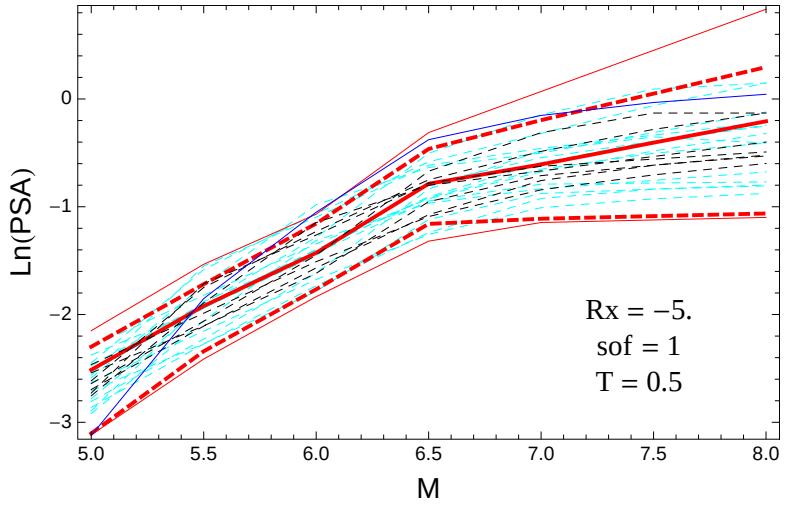



Figure 2.438: DCPPv4: Magnitude scaling of 0.05,0.5,0.95 quantile and the ModelA distribution (red) with total weights, original GMPEs (dashed black), original GMPEs with uncertainty model (dashed cyan) and the model of Graizer (2014) (blue), for a scenario with $R_x = -5.$, $F = 1$, and $T = 0.5$s.

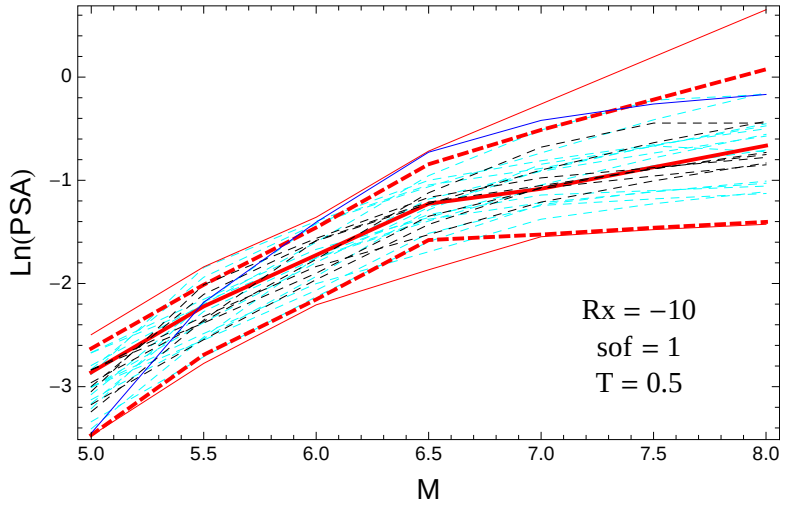



Figure 2.439: DCPPv4: Magnitude scaling of 0.05,0.5,0.95 quantile and the ModelA distribution (red) with total weights, original GMPEs (dashed black), original GMPEs with uncertainty model (dashed cyan) and the model of Graizer (2014) (blue), for a scenario with $R_x = -10$, $F = 1$, and $T = 0.5$s.

**T = 1.s**

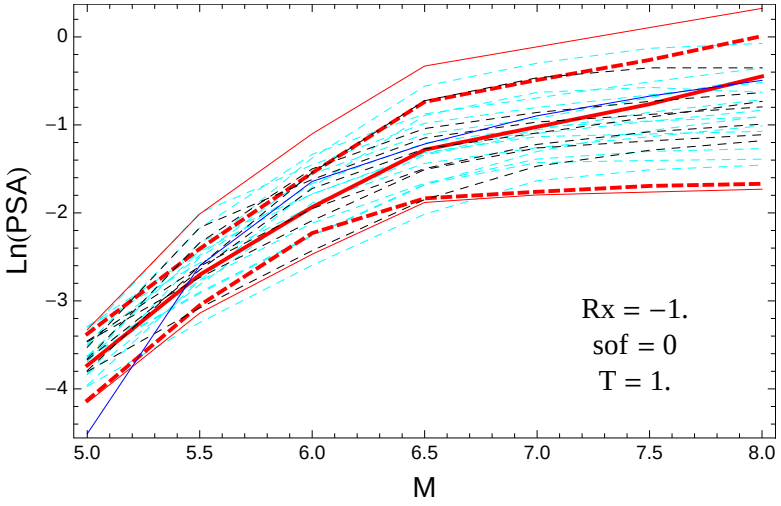



Figure 2.440: DCPPv4: Magnitude scaling of 0.05,0.5,0.95 quantile and the ModelA distribution (red) with total weights, original GMPEs (dashed black), original GMPEs with uncertainty model (dashed cyan) and the model of Graizer (2014) (blue), for a scenario with $R_x = -1.$, $F = 0$, and $T = 1.$s.

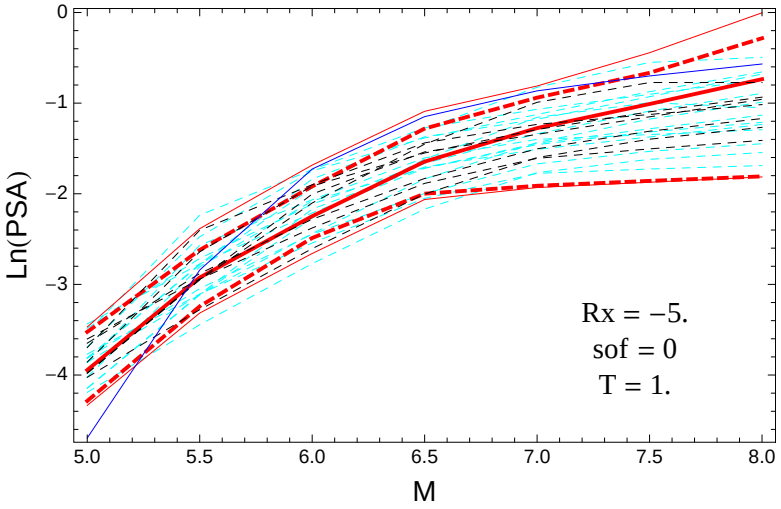



Figure 2.441: DCPPv4: Magnitude scaling of 0.05,0.5,0.95 quantile and the ModelA distribution (red) with total weights, original GMPEs (dashed black), original GMPEs with uncertainty model (dashed cyan) and the model of Graizer (2014) (blue), for a scenario with $R_x = -5.$, $F = 0$, and $T = 1.$s.

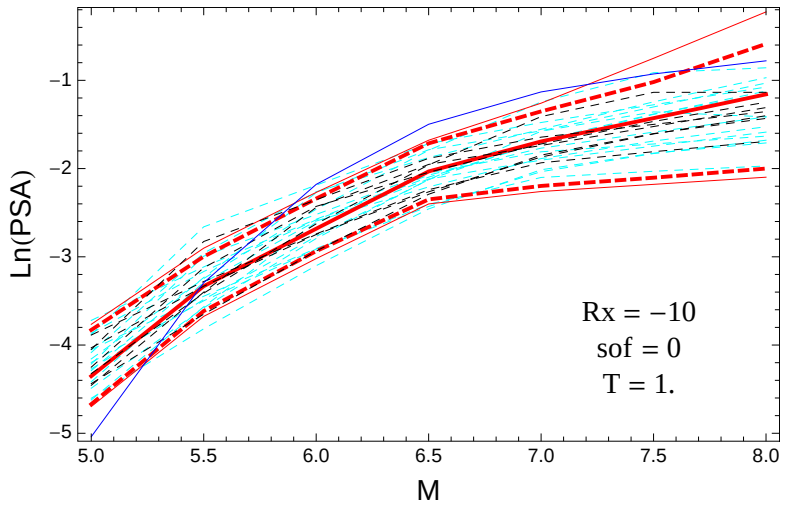



Figure 2.442: DCPPv4: Magnitude scaling of 0.05,0.5,0.95 quantile and the ModelA distribution (red) with total weights, original GMPEs (dashed black), original GMPEs with uncertainty model (dashed cyan) and the model of Graizer (2014) (blue), for a scenario with $R_x = -10$, $F = 0$, and $T = 1$.s.

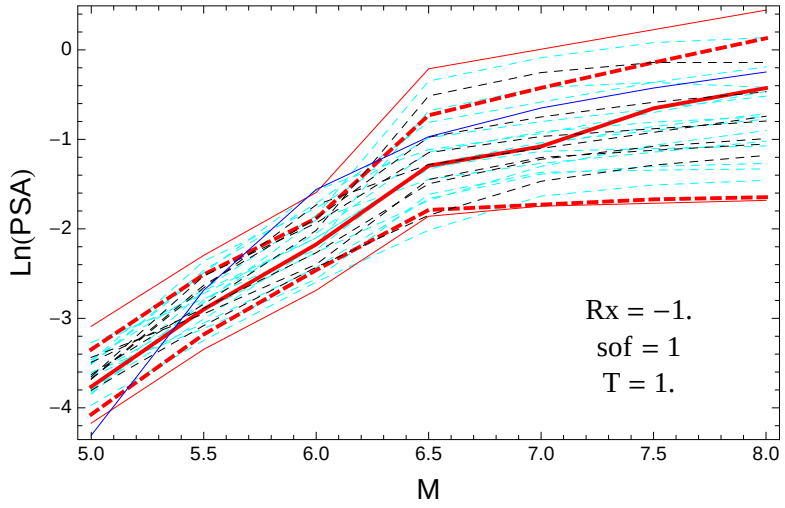



Figure 2.443: DCPPv4: Magnitude scaling of 0.05,0.5,0.95 quantile and the ModelA distribution (red) with total weights, original GMPEs (dashed black), original GMPEs with uncertainty model (dashed cyan) and the model of Graizer (2014) (blue), for a scenario with $R_x = -1.$, $F = 1$, and $T = 1$.s.

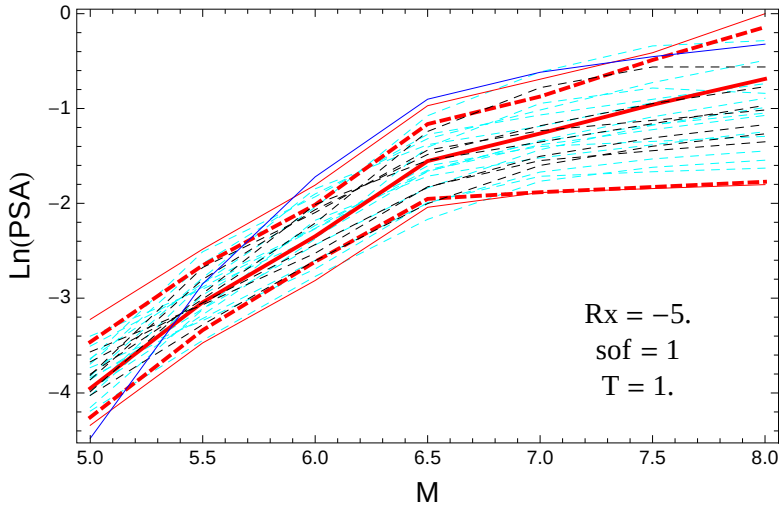



Figure 2.444: DCPPv4: Magnitude scaling of 0.05,0.5,0.95 quantile and the ModelA distribution (red) with total weights, original GMPEs (dashed black), original GMPEs with uncertainty model (dashed cyan) and the model of Graizer (2014) (blue), for a scenario with $R_x = -5.$, $F = 1$, and $T = 1.$s.

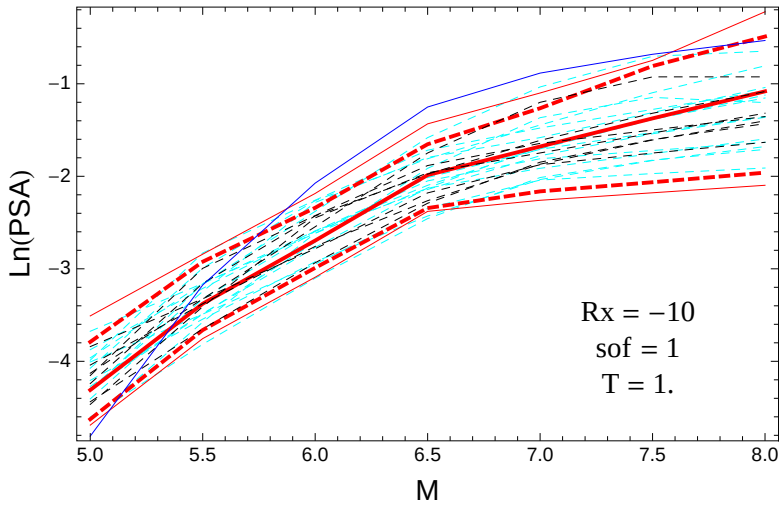



Figure 2.445: DCPPv4: Magnitude scaling of 0.05,0.5,0.95 quantile and the ModelA distribution (red) with total weights, original GMPEs (dashed black), original GMPEs with uncertainty model (dashed cyan) and the model of Graizer (2014) (blue), for a scenario with $R_x = -10$, $F = 1$, and $T = 1.$s.

**T = 3.s**

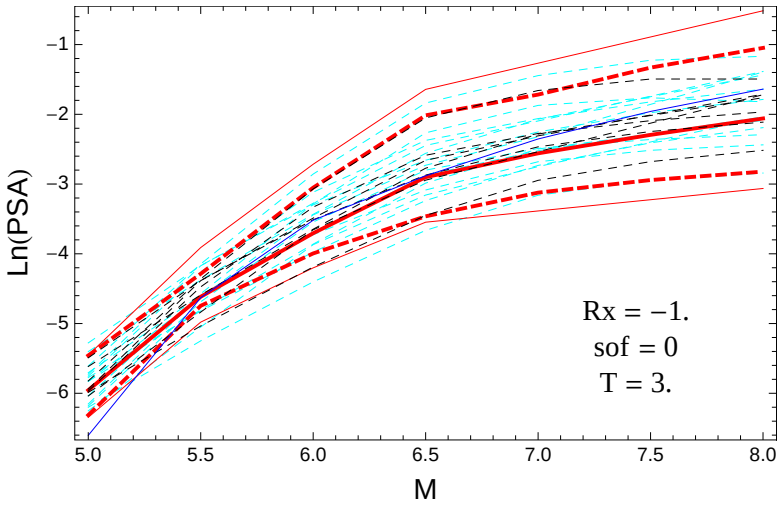



Figure 2.446: DCPPv4: Magnitude scaling of 0.05,0.5,0.95 quantile and the ModelA distribution (red) with total weights, original GMPEs (dashed black), original GMPEs with uncertainty model (dashed cyan) and the model of Graizer (2014) (blue), for a scenario with $R_x = -1.$, $F = 0$, and $T = 3.$s.

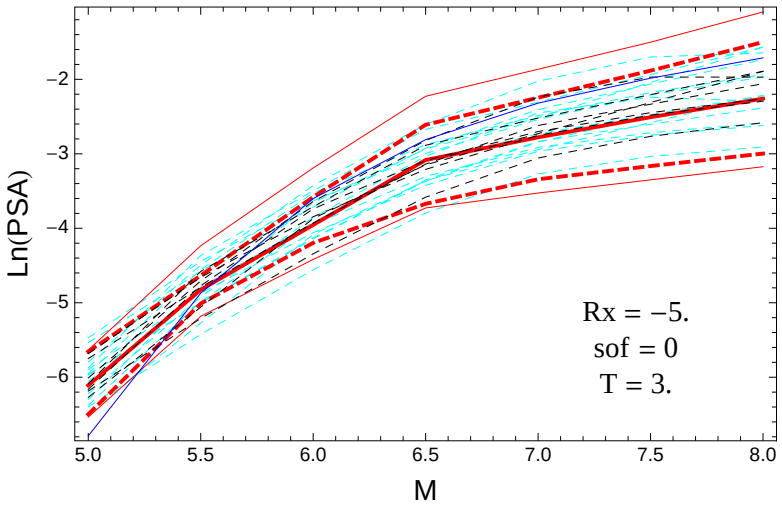



Figure 2.447: DCPPv4: Magnitude scaling of 0.05,0.5,0.95 quantile and the ModelA distribution (red) with total weights, original GMPEs (dashed black), original GMPEs with uncertainty model (dashed cyan) and the model of Graizer (2014) (blue), for a scenario with $R_x = -5.$, $F = 0$, and $T = 3.$s.

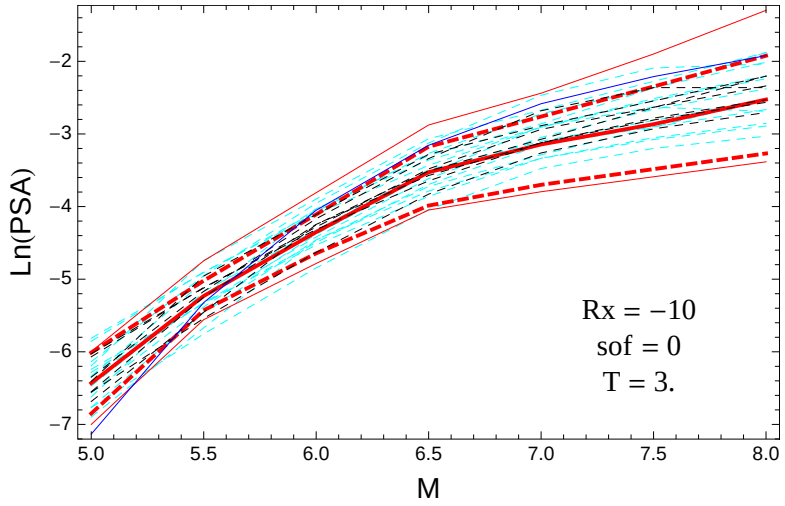



Figure 2.448: DCPPv4: Magnitude scaling of 0.05,0.5,0.95 quantile and the ModelA distribution (red) with total weights, original GMPEs (dashed black), original GMPEs with uncertainty model (dashed cyan) and the model of Graizer (2014) (blue), for a scenario with $R_x = -10$, $F = 0$, and $T = 3$.s.

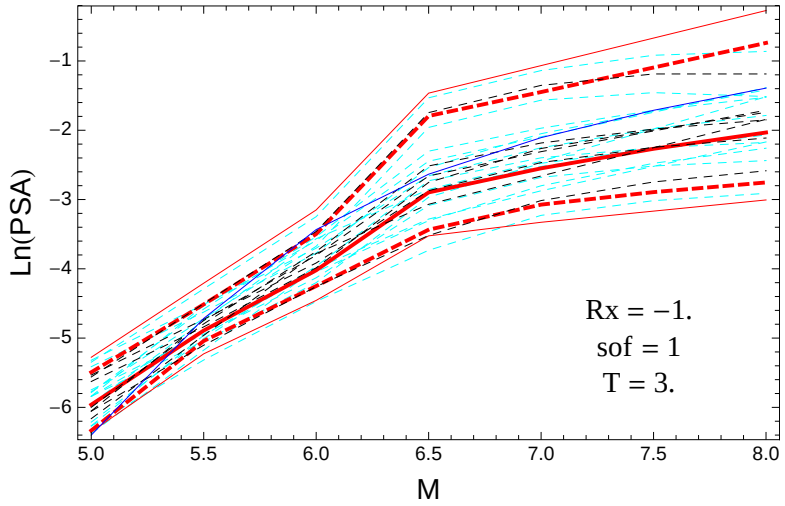



Figure 2.449: DCPPv4: Magnitude scaling of 0.05,0.5,0.95 quantile and the ModelA distribution (red) with total weights, original GMPEs (dashed black), original GMPEs with uncertainty model (dashed cyan) and the model of Graizer (2014) (blue), for a scenario with $R_x = -1.$, $F = 1$, and $T = 3$.s.

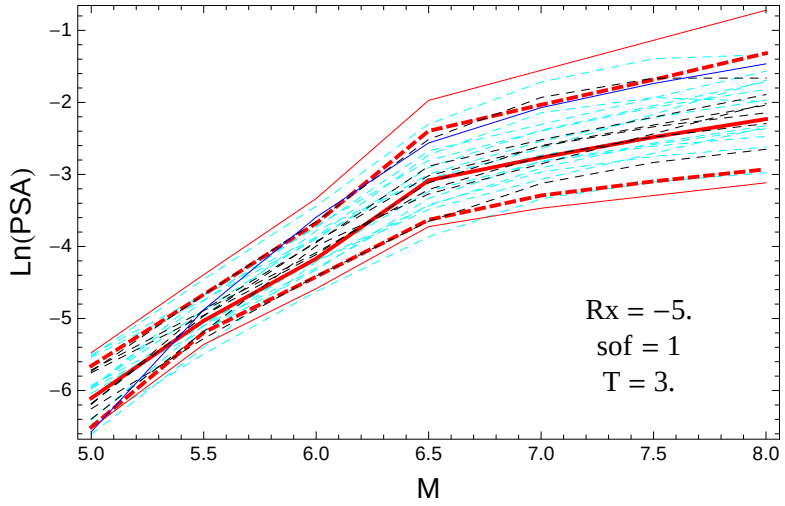



Figure 2.450: DCPPv4: Magnitude scaling of 0.05,0.5,0.95 quantile and the ModelA distribution (red) with total weights, original GMPEs (dashed black), original GMPEs with uncertainty model (dashed cyan) and the model of Graizer (2014) (blue), for a scenario with $R_x = -5.$, $F = 1$, and $T = 3.$s.

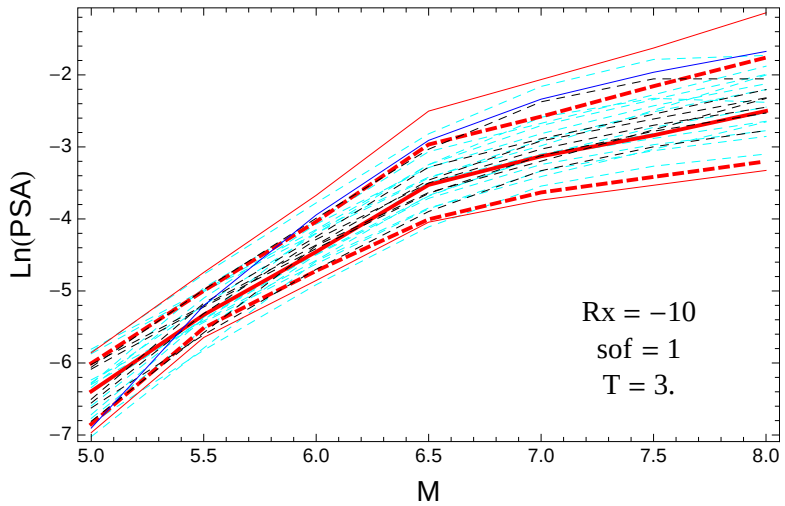



Figure 2.451: DCPPv4: Magnitude scaling of 0.05,0.5,0.95 quantile and the ModelA distribution (red) with total weights, original GMPEs (dashed black), original GMPEs with uncertainty model (dashed cyan) and the model of Graizer (2014) (blue), for a scenario with $R_x = -10$, $F = 1$, and $T = 3.$s.

### 2.1.15 Quantile Plots vs. Period with GMPEs

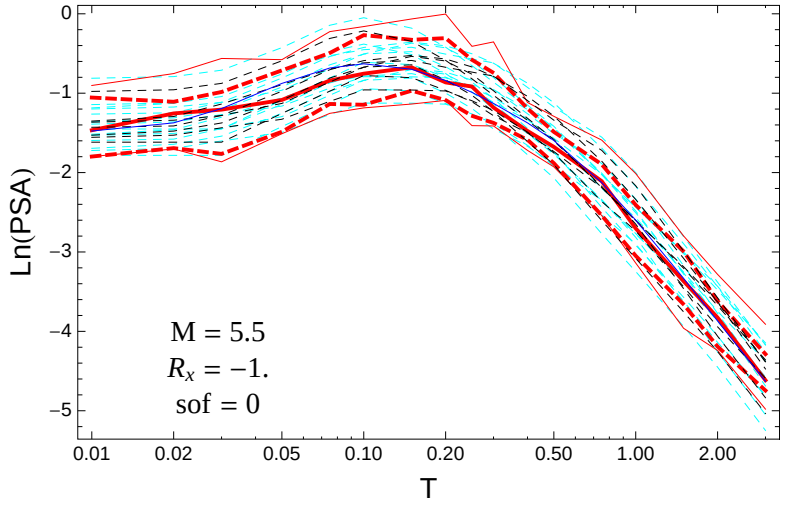



Figure 2.452: DCPPv4: Spectra of 0.05,0.5,0.95 quantile of the model distribution (red) with total weights, the original GMPEs (dashed black), original GMPEs with uncertainty model (dashed cyan) and the model of Graizer (2014) (blue), for a scenario with $M_W = 5.5$, $R_x = -1.$, $F = 0$.

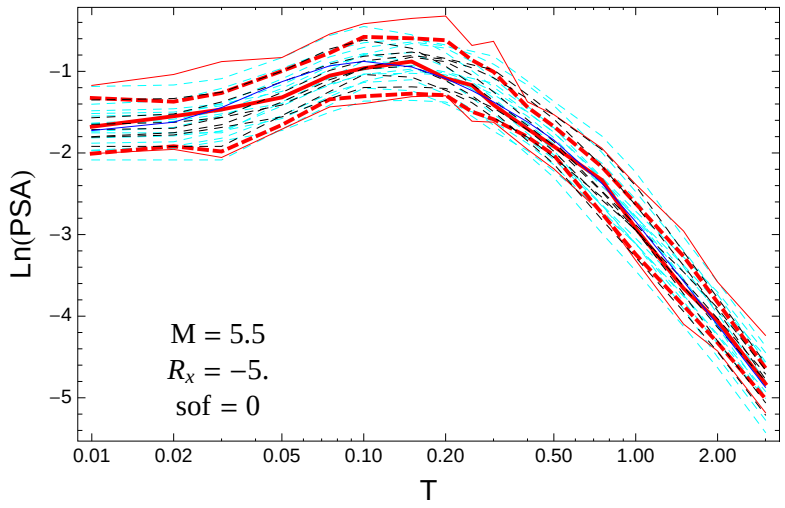



Figure 2.453: DCPPv4: Spectra of 0.05,0.5,0.95 quantile of the model distribution (red) with total weights, the original GMPEs (dashed black), original GMPEs with uncertainty model (dashed cyan) and the model of Graizer (2014) (blue), for a scenario with $M_W = 5.5$, $R_x = -5.$, $F = 0$.

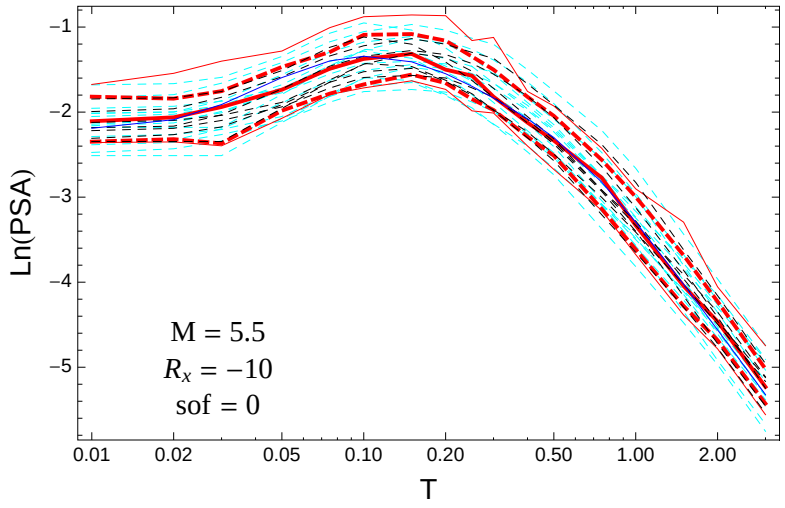



Figure 2.454: DCPPv4: Spectra of 0.05,0.5,0.95 quantile of the model distribution (red) with total weights, the original GMPEs (dashed black), original GMPEs with uncertainty model (dashed cyan) and the model of Graizer (2014) (blue), for a scenario with $M_W = 5.5$, $R_x = -10$, $F = 0$.

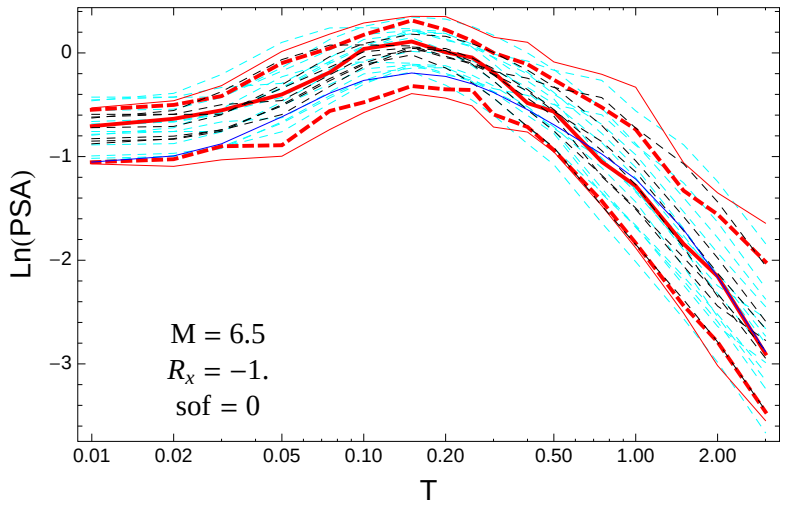



Figure 2.455: DCPPv4: Spectra of 0.05,0.5,0.95 quantile of the model distribution (red) with total weights, the original GMPEs (dashed black), original GMPEs with uncertainty model (dashed cyan) and the model of Graizer (2014) (blue), for a scenario with $M_W = 6.5$, $R_x = -1.$, $F = 0$.

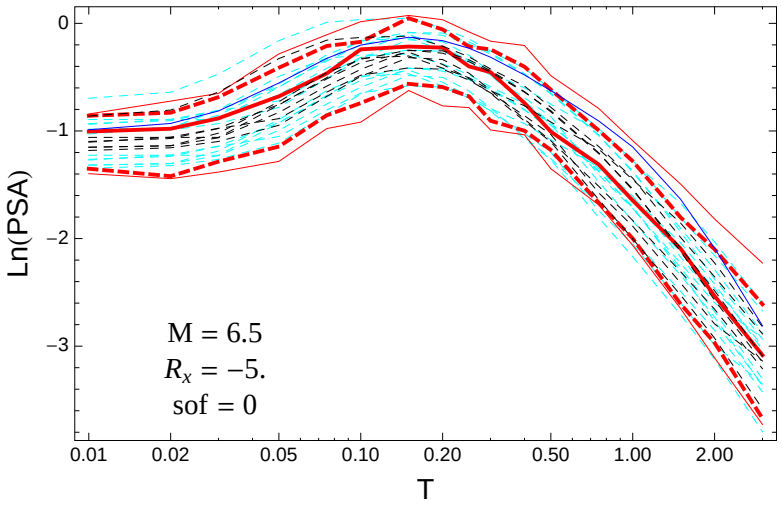



Figure 2.456: DCPPv4: Spectra of 0.05,0.5,0.95 quantile of the model distribution (red) with total weights, the original GMPEs (dashed black), original GMPEs with uncertainty model (dashed cyan) and the model of Graizer (2014) (blue), for a scenario with $M_W = 6.5$, $R_x = -5.$, $F = 0$.

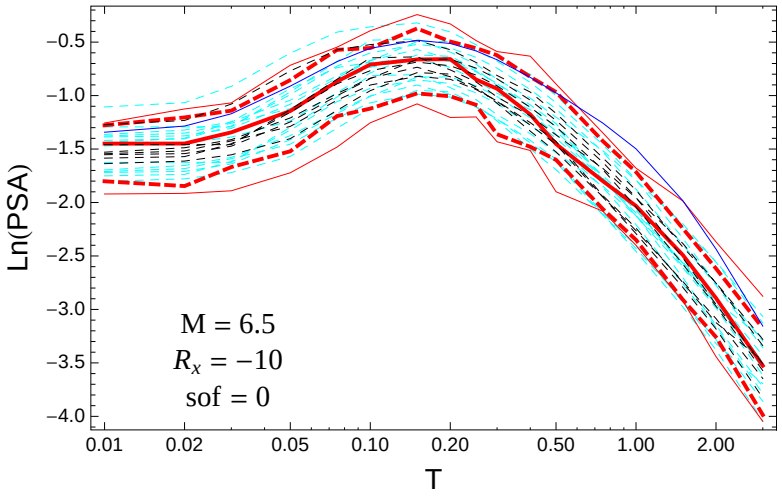



Figure 2.457: DCPPv4: Spectra of 0.05,0.5,0.95 quantile of the model distribution (red) with total weights, the original GMPEs (dashed black), original GMPEs with uncertainty model (dashed cyan) and the model of Graizer (2014) (blue), for a scenario with $M_W = 6.5$, $R_x = -10$, $F = 0$.

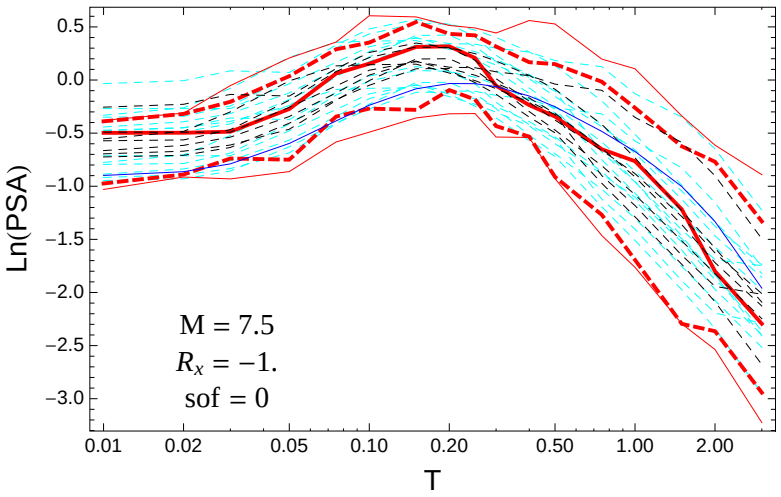



Figure 2.458: DCPPv4: Spectra of 0.05,0.5,0.95 quantile of the model distribution (red) with total weights, the original GMPEs (dashed black), original GMPEs with uncertainty model (dashed cyan) and the model of Graizer (2014) (blue), for a scenario with $M_W = 7.5$, $R_x = -1.$, $F = 0$.

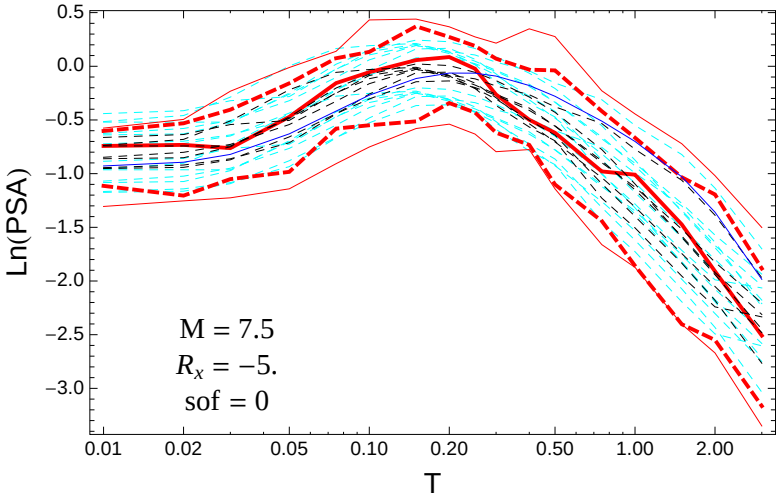



Figure 2.459: DCPPv4: Spectra of 0.05,0.5,0.95 quantile of the model distribution (red) with total weights, the original GMPEs (dashed black), original GMPEs with uncertainty model (dashed cyan) and the model of Graizer (2014) (blue), for a scenario with $M_W = 7.5$, $R_x = -5.$, $F = 0$.

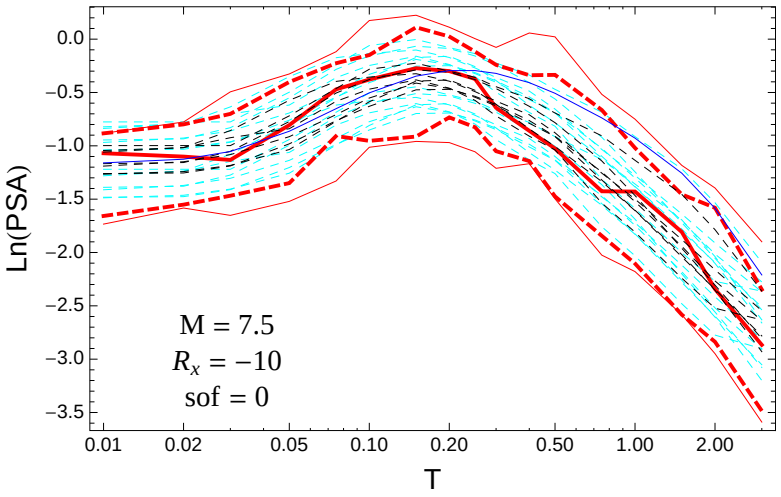



Figure 2.460: DCPPv4: Spectra of 0.05,0.5,0.95 quantile of the model distribution (red) with total weights, the original GMPEs (dashed black), original GMPEs with uncertainty model (dashed cyan) and the model of Graizer (2014) (blue), for a scenario with $M_W = 7.5$, $R_x = -10$, $F = 0$.

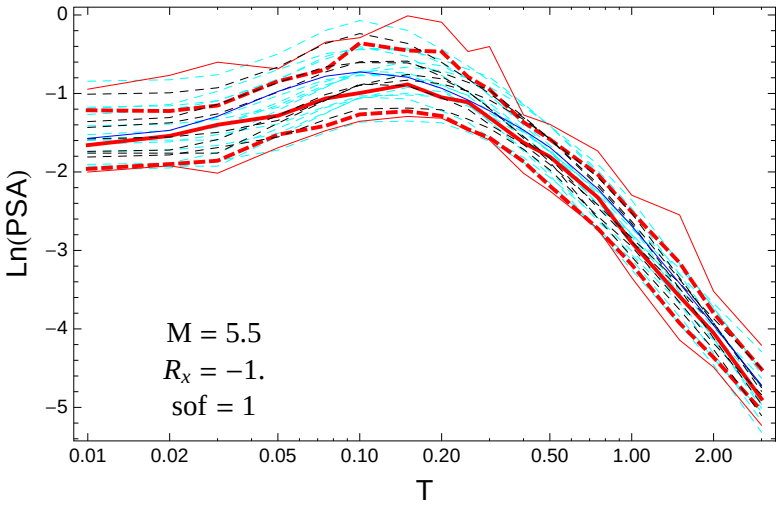



Figure 2.461: DCPPv4: Spectra of 0.05,0.5,0.95 quantile of the model distribution (red) with total weights, the original GMPEs (dashed black), original GMPEs with uncertainty model (dashed cyan) and the model of Graizer (2014) (blue), for a scenario with $M_W = 5.5$, $R_x = -1.$, $F = 1$.

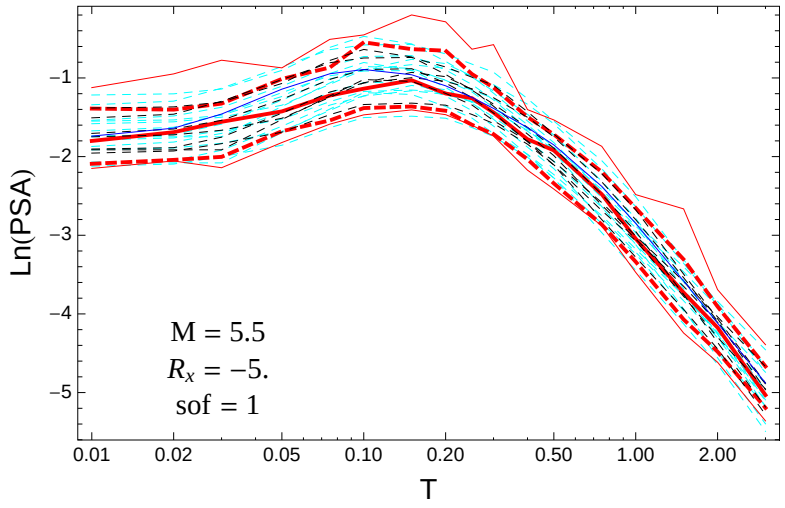



Figure 2.462: DCPPv4: Spectra of 0.05,0.5,0.95 quantile of the model distribution (red) with total weights, the original GMPEs (dashed black), original GMPEs with uncertainty model (dashed cyan) and the model of Graizer (2014) (blue), for a scenario with $M_W = 5.5$, $R_x = -5.$, $F = 1$.

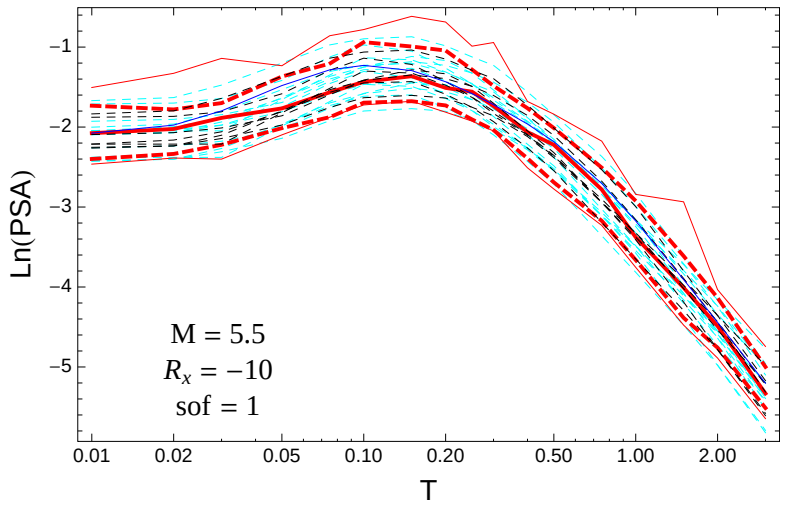



Figure 2.463: DCPPv4: Spectra of 0.05,0.5,0.95 quantile of the model distribution (red) with total weights, the original GMPEs (dashed black), original GMPEs with uncertainty model (dashed cyan) and the model of Graizer (2014) (blue), for a scenario with $M_W = 5.5$, $R_x = -10$, $F = 1$.

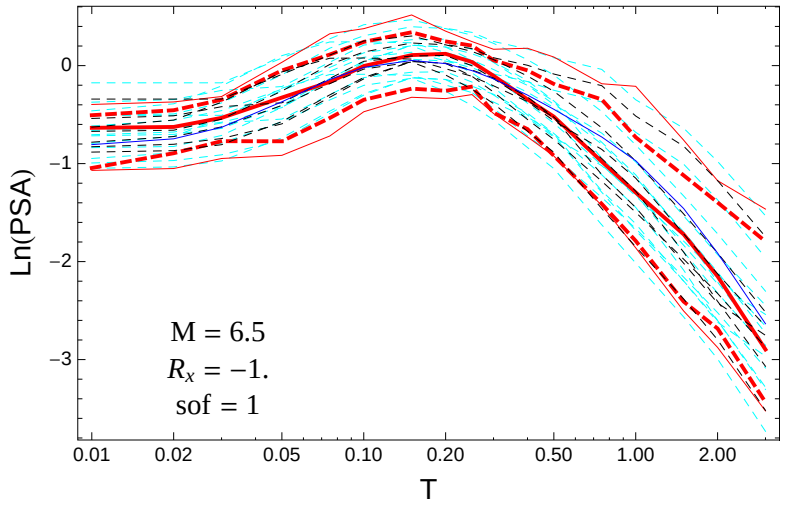



Figure 2.464: DCPPv4: Spectra of 0.05,0.5,0.95 quantile of the model distribution (red) with total weights, the original GMPEs (dashed black), original GMPEs with uncertainty model (dashed cyan) and the model of Graizer (2014) (blue), for a scenario with $M_W = 6.5$, $R_x = -1.$, $F = 1$.

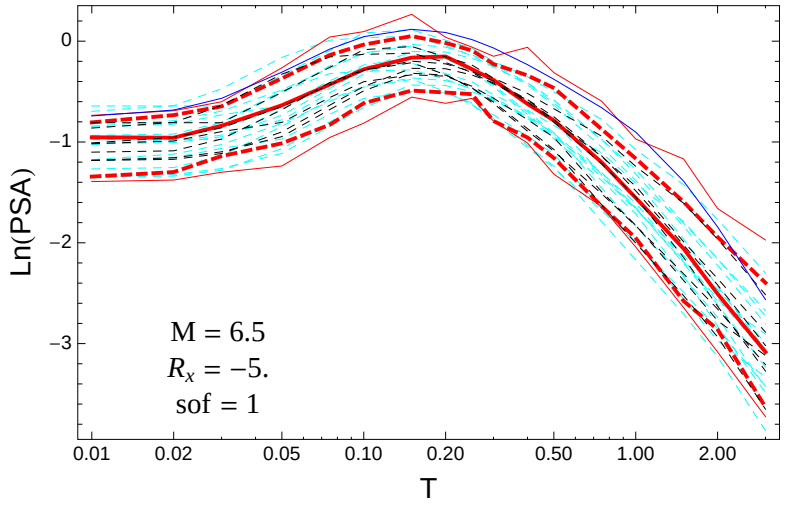



Figure 2.465: DCPPv4: Spectra of 0.05,0.5,0.95 quantile of the model distribution (red) with total weights, the original GMPEs (dashed black), original GMPEs with uncertainty model (dashed cyan) and the model of Graizer (2014) (blue), for a scenario with $M_W = 6.5$, $R_x = -5.$, $F = 1$.

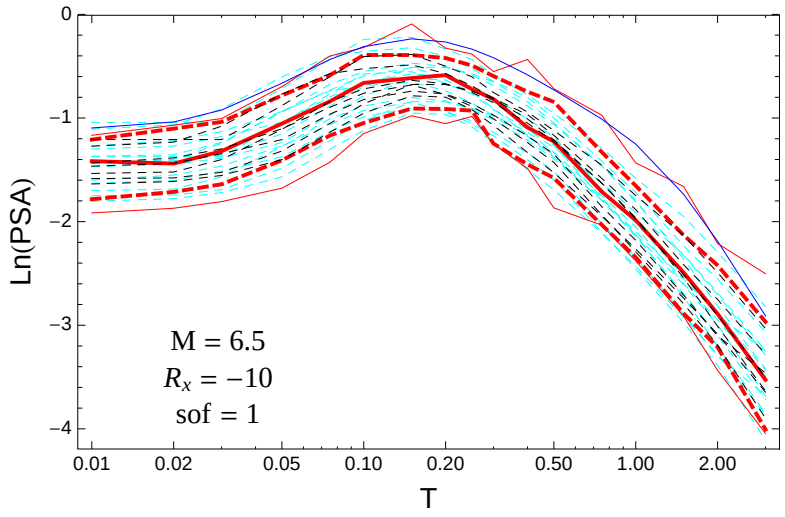



Figure 2.466: DCPPv4: Spectra of 0.05,0.5,0.95 quantile of the model distribution (red) with total weights, the original GMPEs (dashed black), original GMPEs with uncertainty model (dashed cyan) and the model of Graizer (2014) (blue), for a scenario with $M_W = 6.5$, $R_x = -10$, $F = 1$.

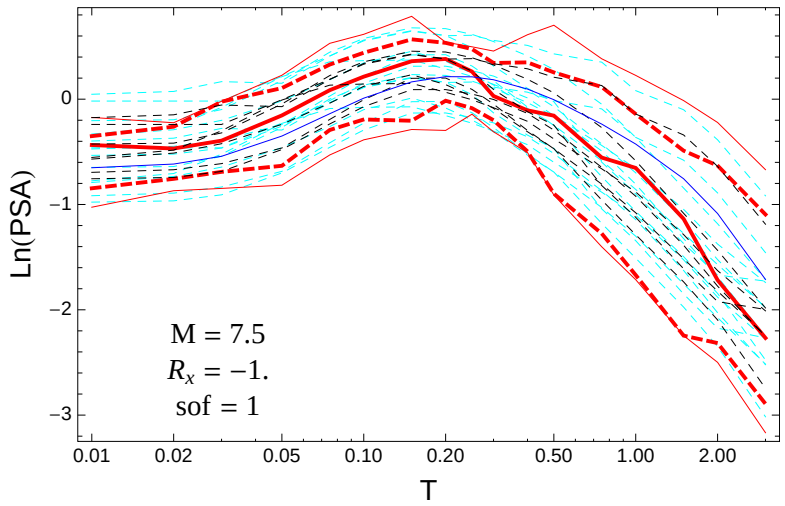



Figure 2.467: DCPPv4: Spectra of 0.05,0.5,0.95 quantile of the model distribution (red) with total weights, the original GMPEs (dashed black), original GMPEs with uncertainty model (dashed cyan) and the model of Graizer (2014) (blue), for a scenario with $M_W = 7.5$, $R_x = -1.$, $F = 1$.

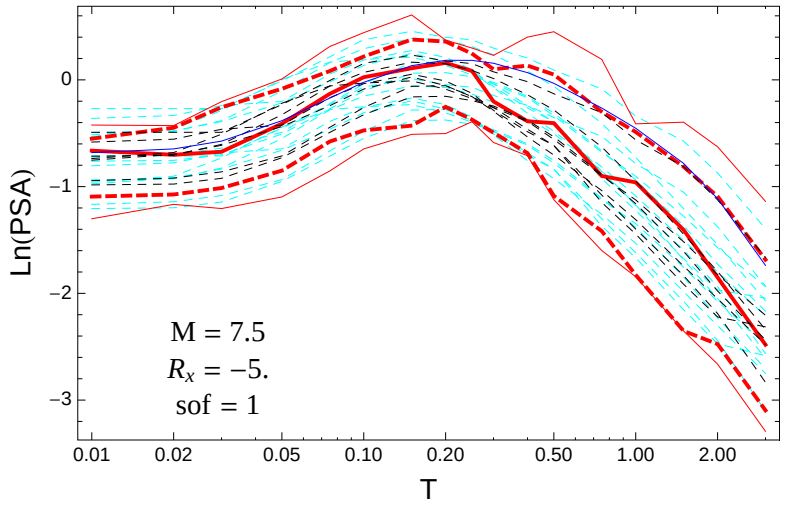



Figure 2.468: DCPPv4: Spectra of 0.05,0.5,0.95 quantile of the model distribution (red) with total weights, the original GMPEs (dashed black), original GMPEs with uncertainty model (dashed cyan) and the model of Graizer (2014) (blue), for a scenario with $M_W = 7.5$, $R_x = -5.$, $F = 1$.

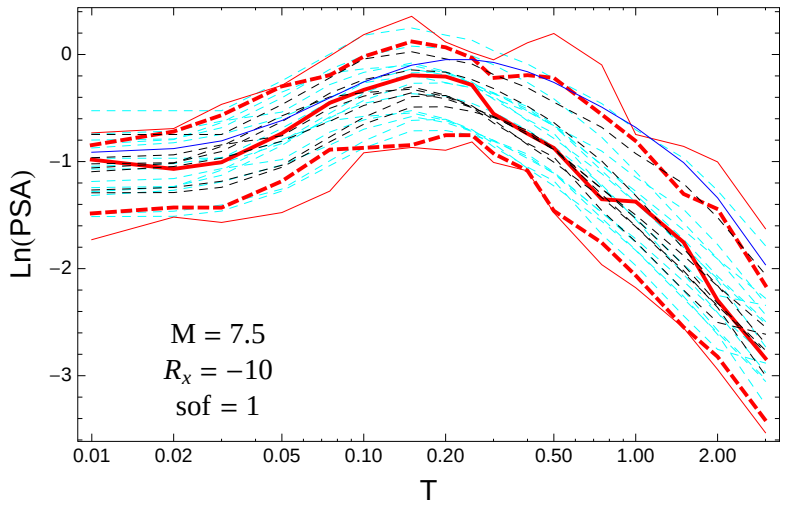



Figure 2.469: DCPPv4: Spectra of 0.05,0.5,0.95 quantile of the model distribution (red) with total weights, the original GMPEs (dashed black), original GMPEs with uncertainty model (dashed cyan) and the model of Graizer (2014) (blue), for a scenario with $M_W = 7.5$, $R_x = -10$, $F = 1$.

### 2.1.16 Median Residuals

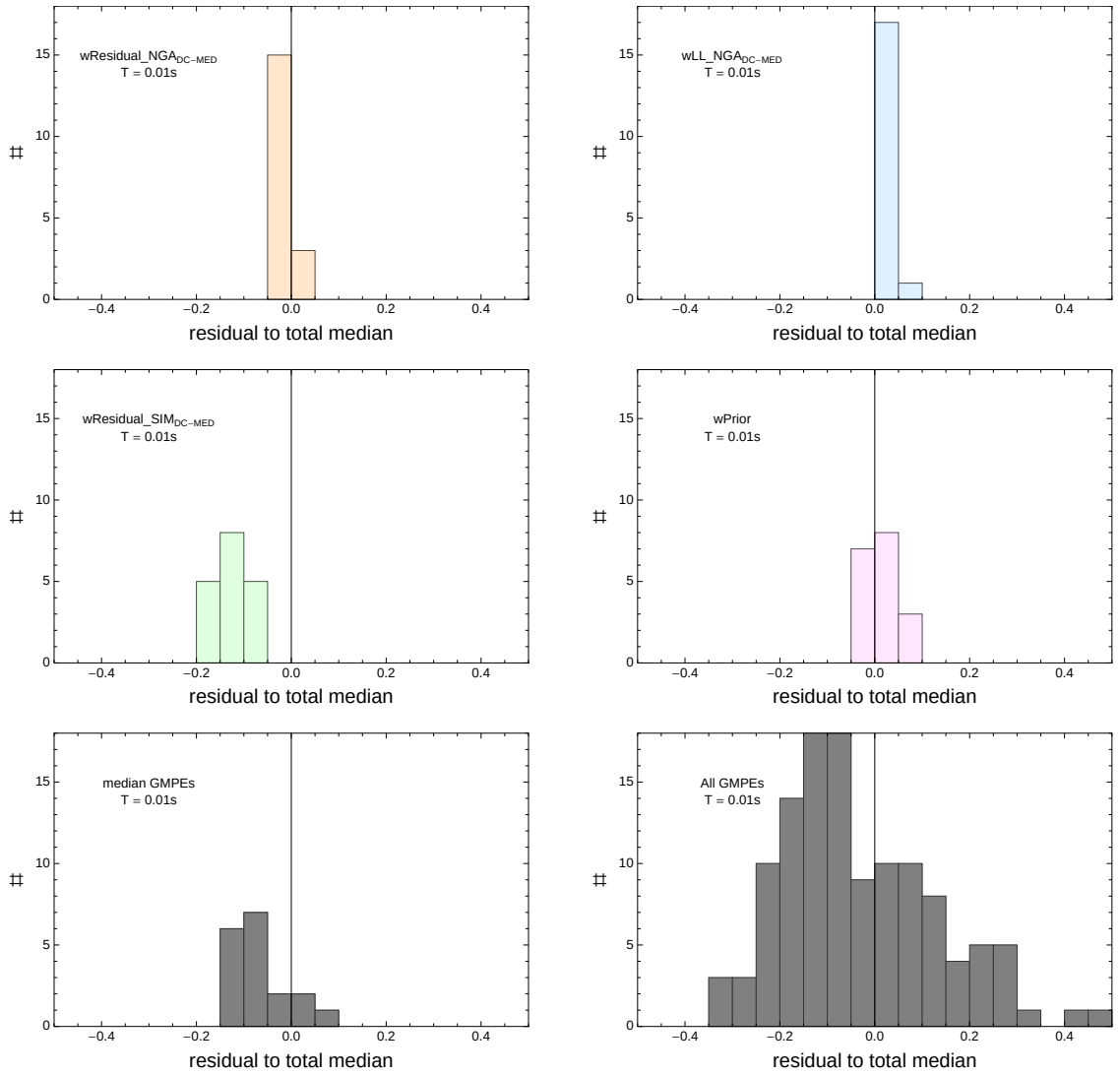



Figure 2.470: DCPPv4Histogram of differences for medians calculated with different weights to median calculated with total weights. Bottom row left shows differences between medians for the GMPE distribution to median calculated with total weights. Bottom row right shows differences between the original GMPEs (without uncertainty) to median calculated with total weights. For DCPP4, ModelA and $T = 0.01$s.

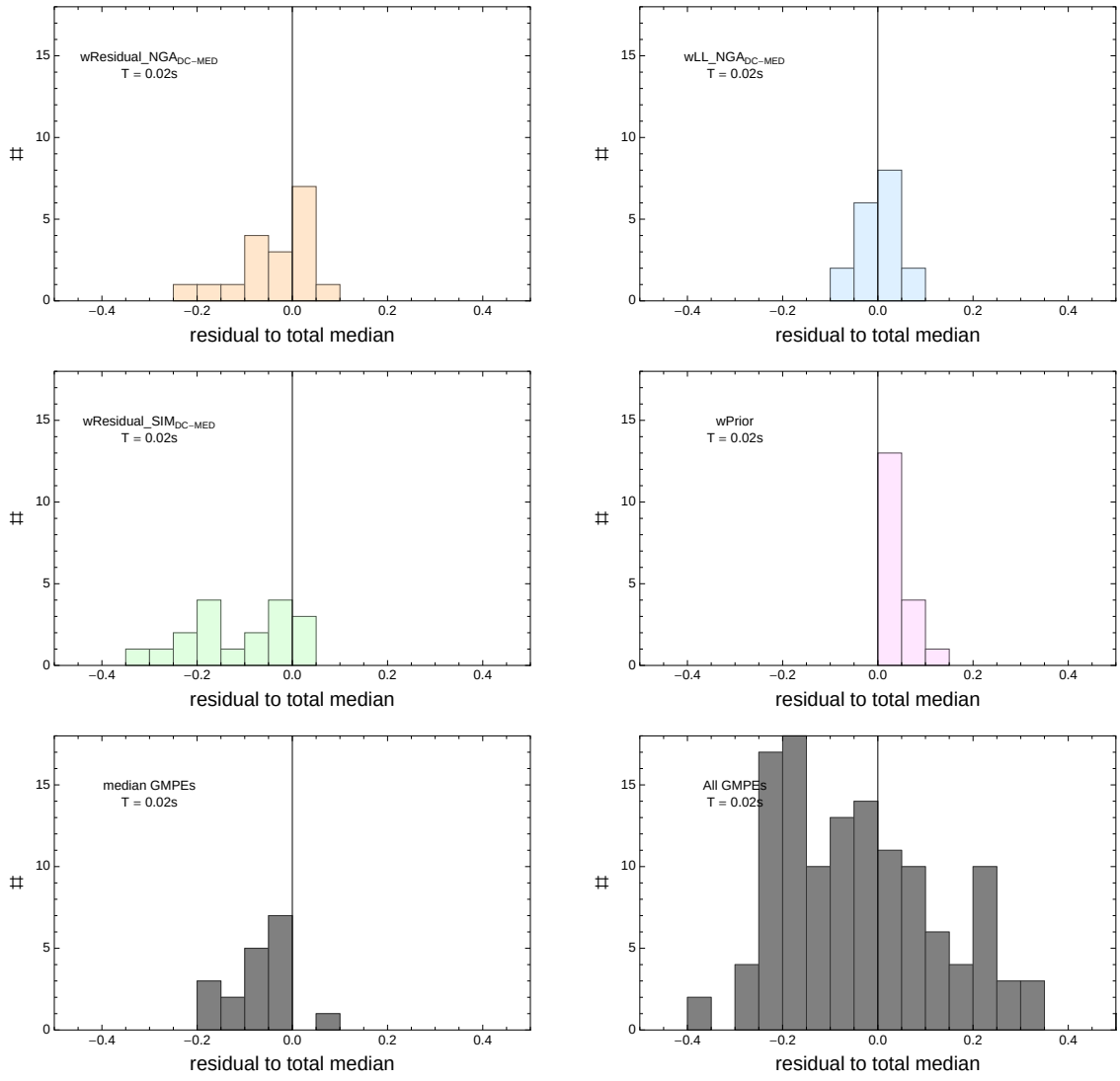



Figure 2.471: DCPPv4Histogram of differences for medians calculated with different weights to median calculated with total weights. Bottom row left shows differences between medians for the GMPE distribution to median calculated with total weights. Bottom row right shows differences between the original GMPEs (without uncertainty) to median calculated with total weights. For DCPP4, ModelA and $T = 0.02$s.

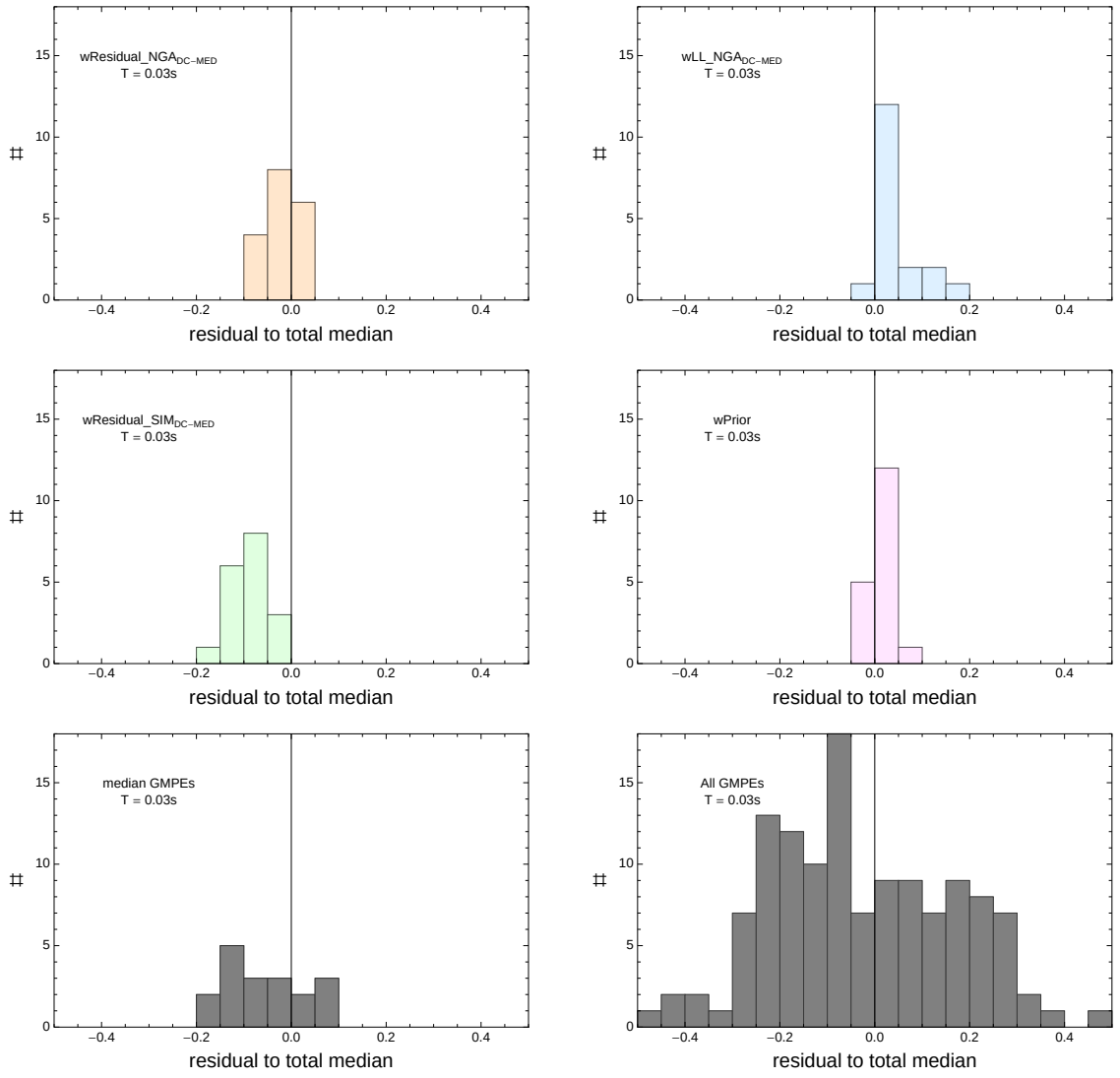



Figure 2.472: DCPPv4Histogram of differences for medians calculated with different weights to median calculated with total weights. Bottom row left shows differences between medians for the GMPE distribution to median calculated with total weights. Bottom row right shows differences between the original GMPEs (without uncertainty) to median calculated with total weights. For DCPP4, ModelA and $T = 0.03$s.

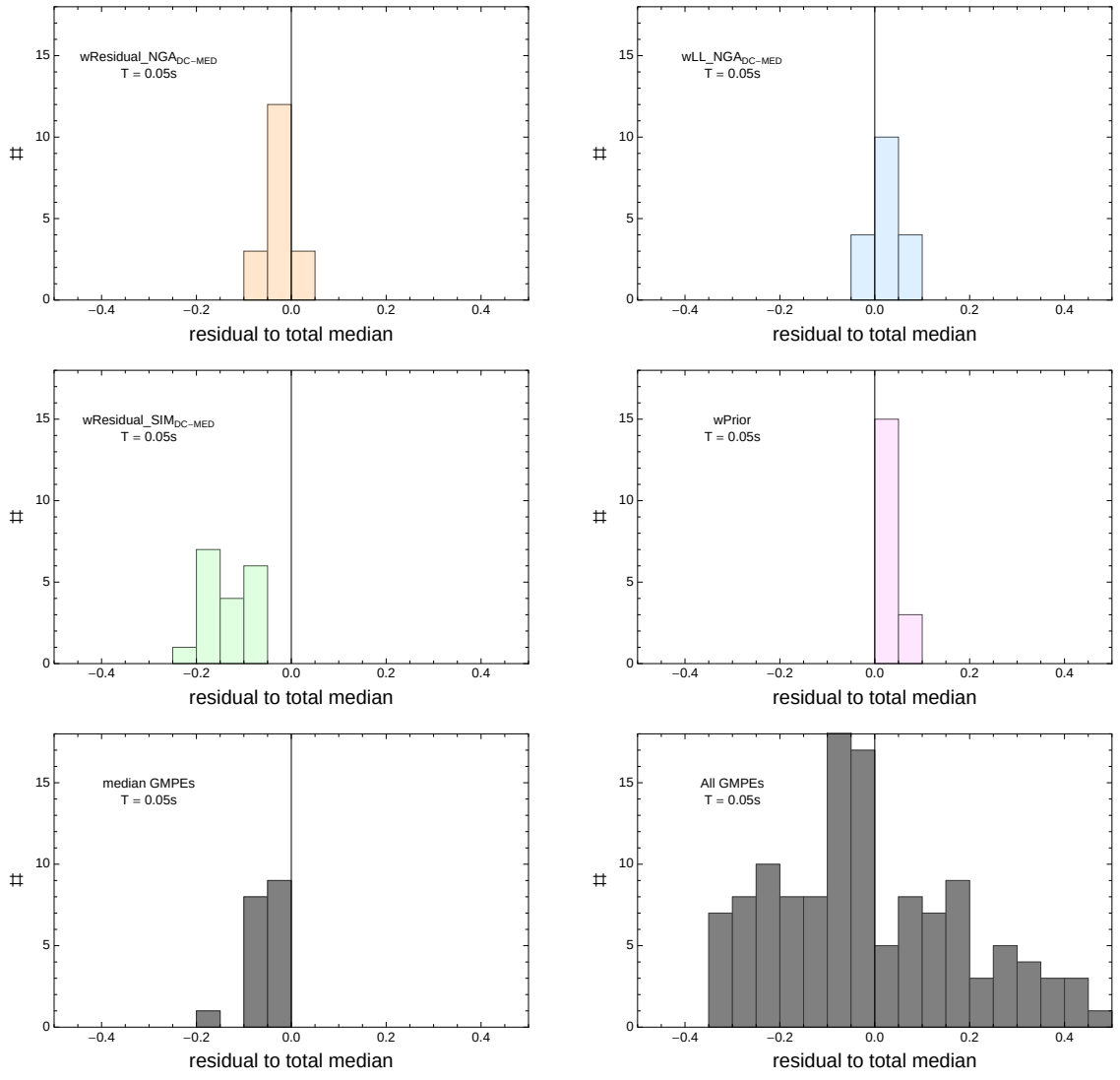



Figure 2.473: DCPPv4Histogram of differences for medians calculated with different weights to median calculated with total weights. Bottom row left shows differences between medians for the GMPE distribution to median calculated with total weights. Bottom row right shows differences between the original GMPEs (without uncertainty) to median calculated with total weights. For DCPP4, ModelA and $T = 0.05$s.

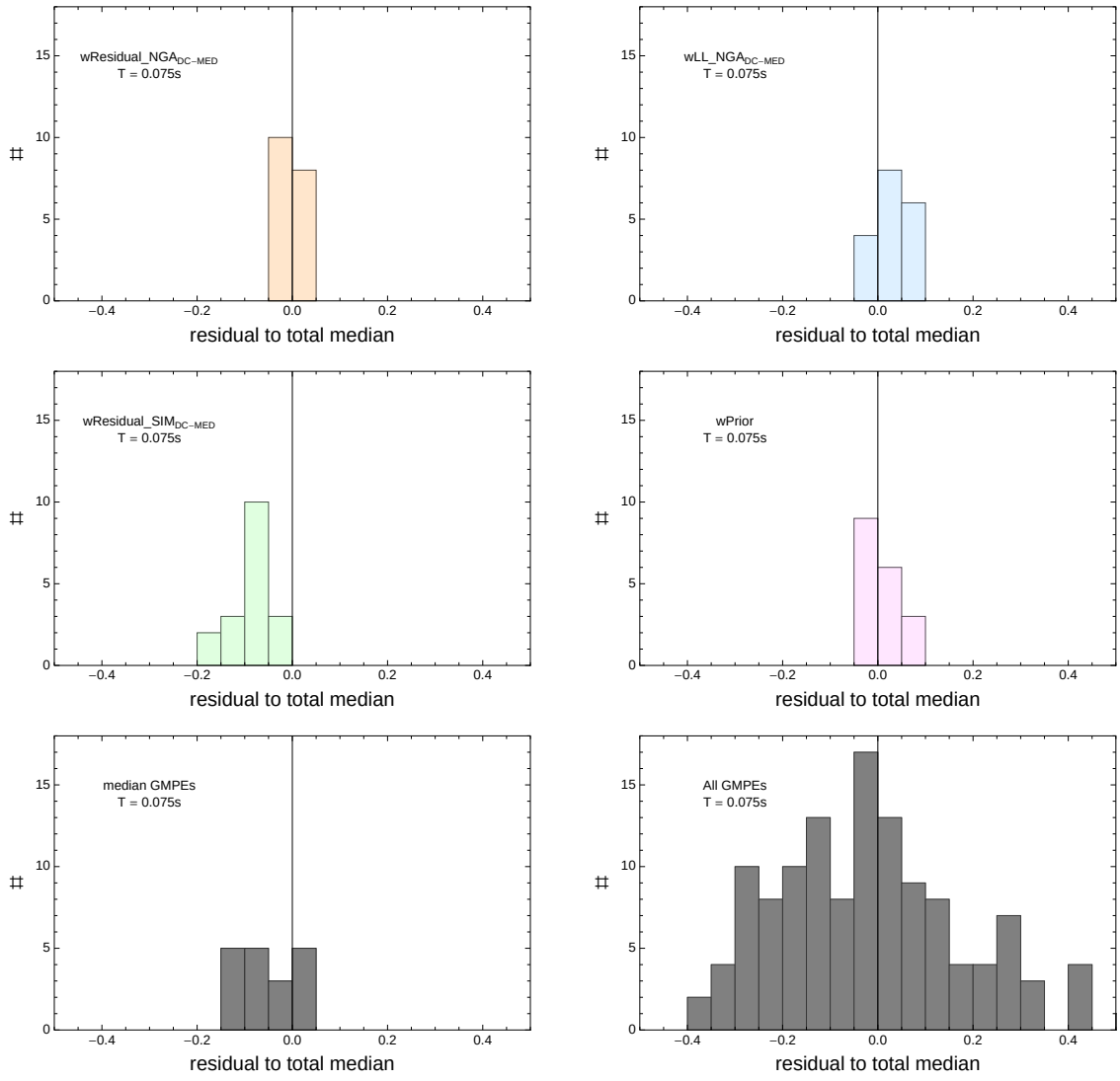



Figure 2.474: DCPPv4Histogram of differences for medians calculated with different weights to median calculated with total weights. Bottom row left shows differences between medians for the GMPE distribution to median calculated with total weights. Bottom row right shows differences between the original GMPEs (without uncertainty) to median calculated with total weights. For DCPP4, ModelA and $T = 0.075$s.

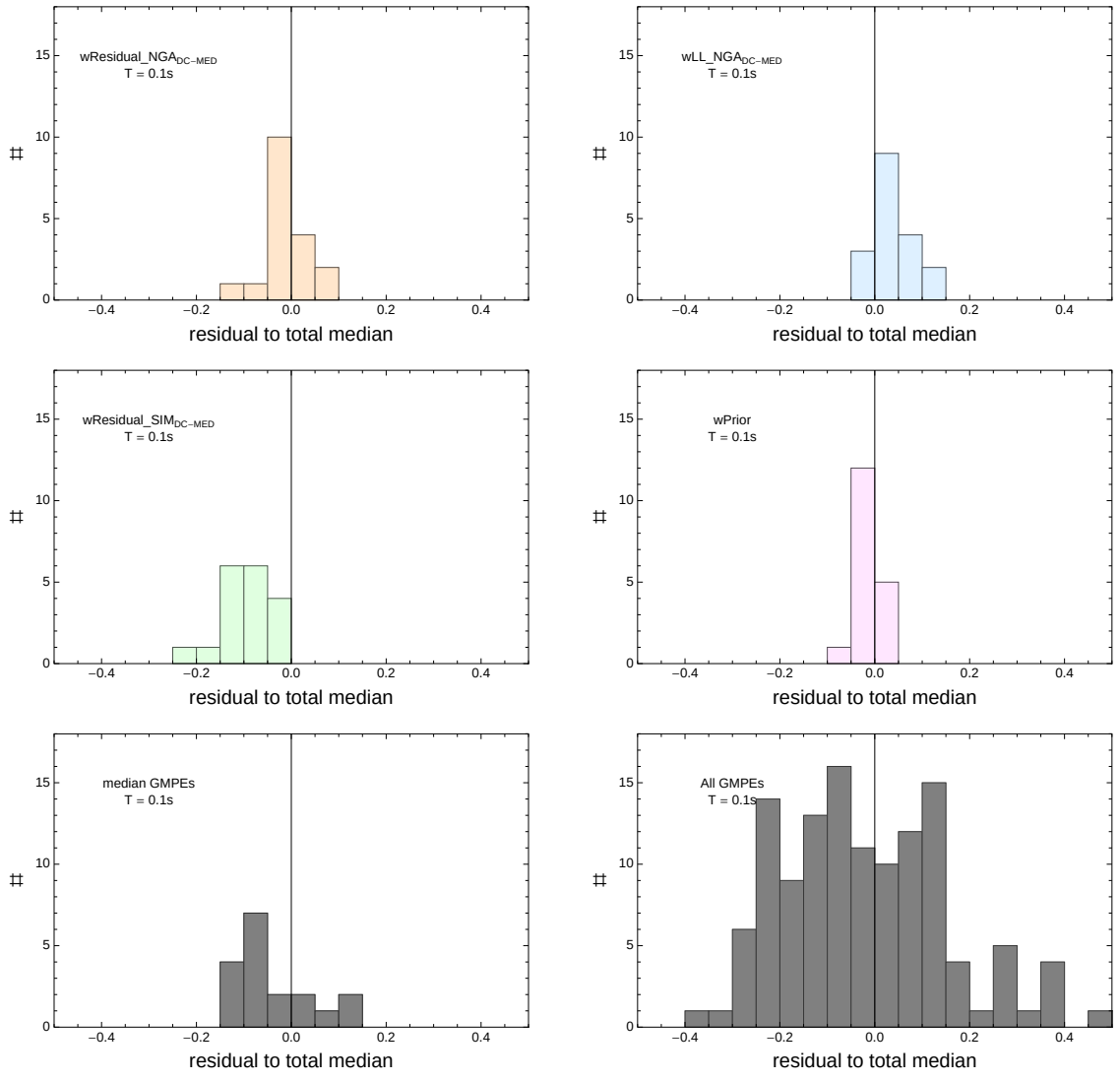



Figure 2.475: DCPPv4Histogram of differences for medians calculated with different weights to median calculated with total weights. Bottom row left shows differences between medians for the GMPE distribution to median calculated with total weights. Bottom row right shows differences between the original GMPEs (without uncertainty) to median calculated with total weights. For DCPP4, ModelA and $T = 0.1$s.

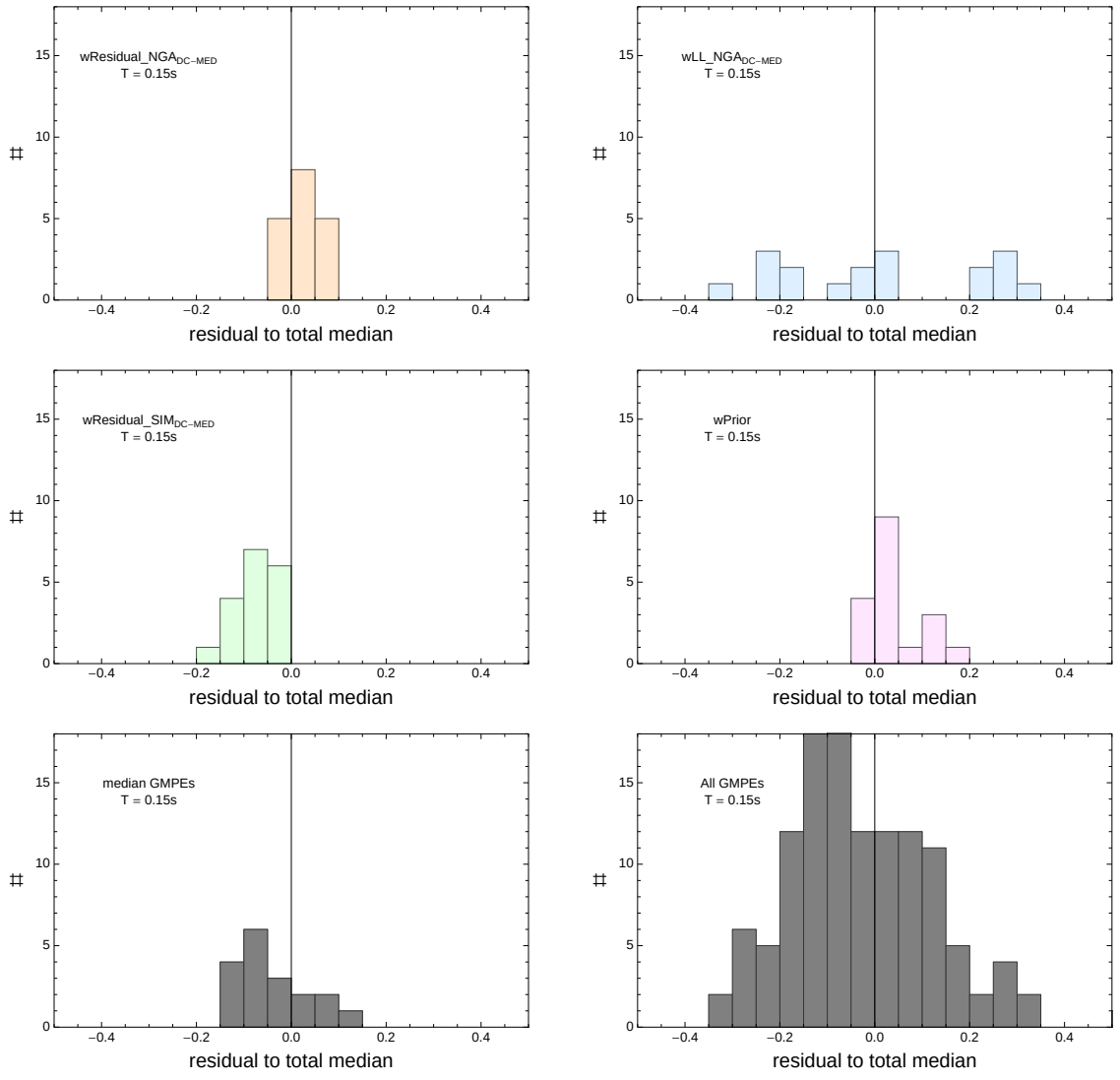



Figure 2.476: DCPPv4Histogram of differences for medians calculated with different weights to median calculated with total weights. Bottom row left shows differences between medians for the GMPE distribution to median calculated with total weights. Bottom row right shows differences between the original GMPEs (without uncertainty) to median calculated with total weights. For DCPP4, ModelA and $T = 0.15$s.

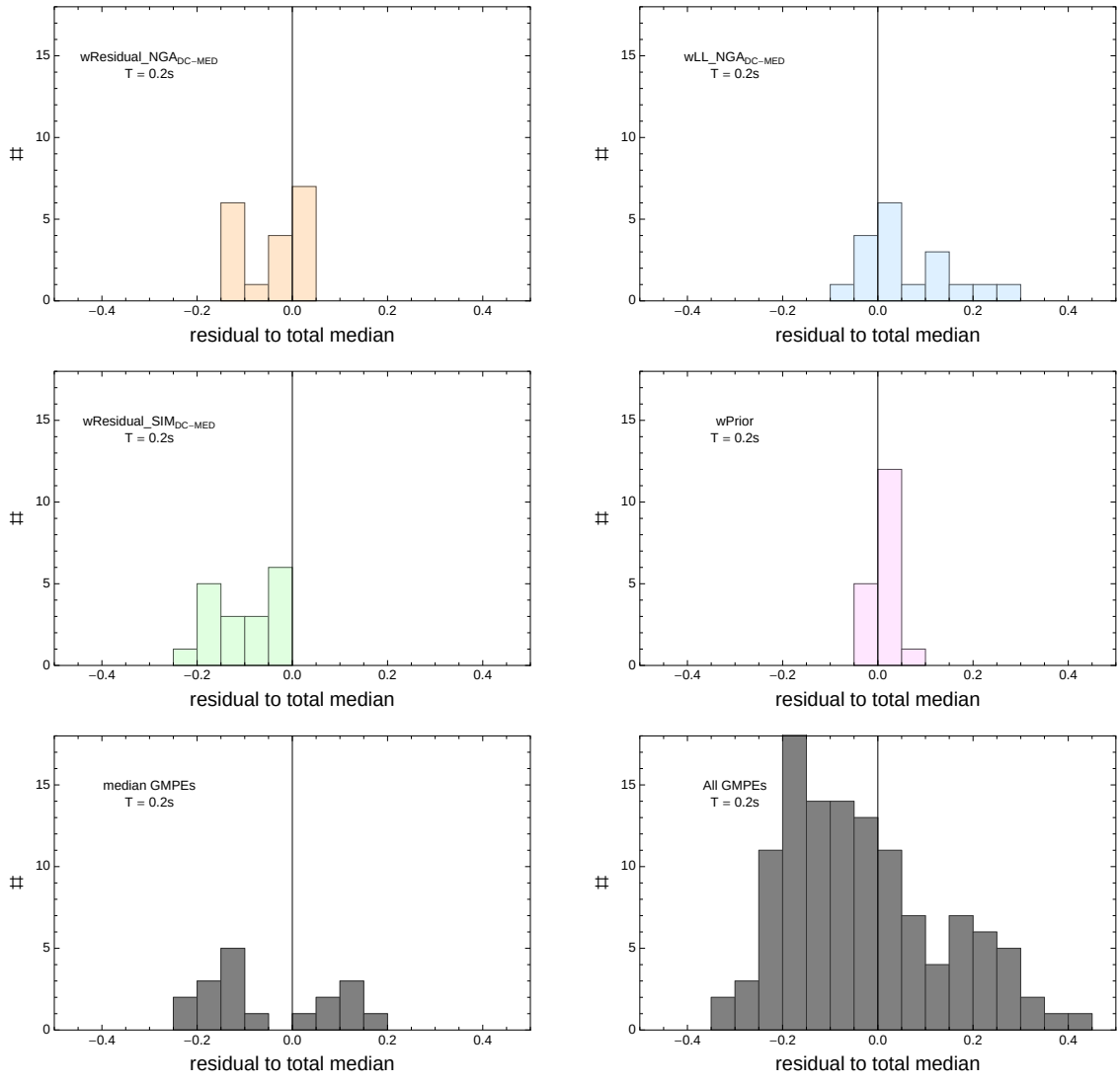



Figure 2.477: DCPPv4Histogram of differences for medians calculated with different weights to median calculated with total weights. Bottom row left shows differences between medians for the GMPE distribution to median calculated with total weights. Bottom row right shows differences between the original GMPEs (without uncertainty) to median calculated with total weights. For DCPP4, ModelA and $T = 0.2$s.

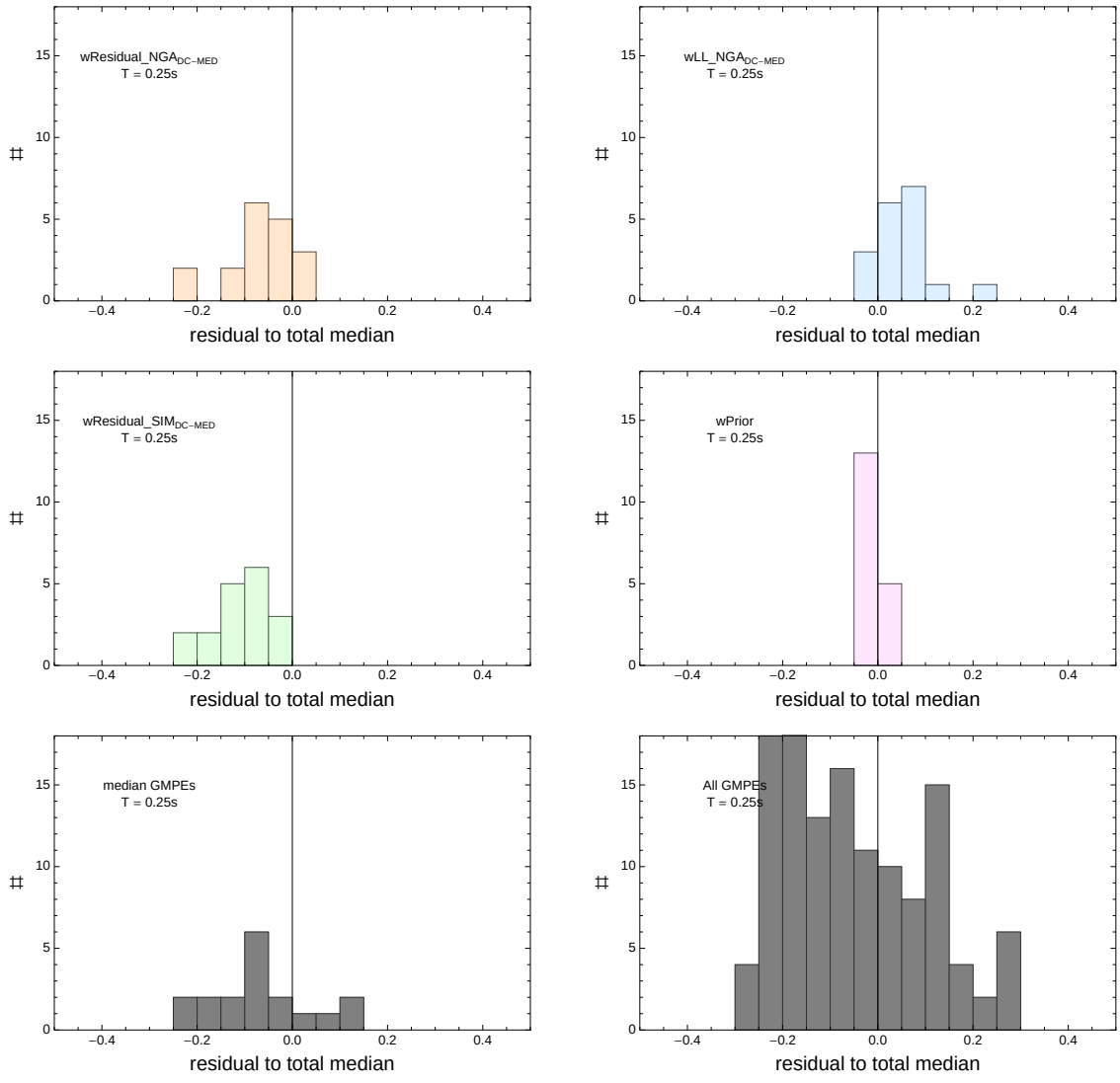



Figure 2.478: DCPPv4Histogram of differences for medians calculated with different weights to median calculated with total weights. Bottom row left shows differences between medians for the GMPE distribution to median calculated with total weights. Bottom row right shows differences between the original GMPEs (without uncertainty) to median calculated with total weights. For DCPP4, ModelA and $T = 0.25$s.

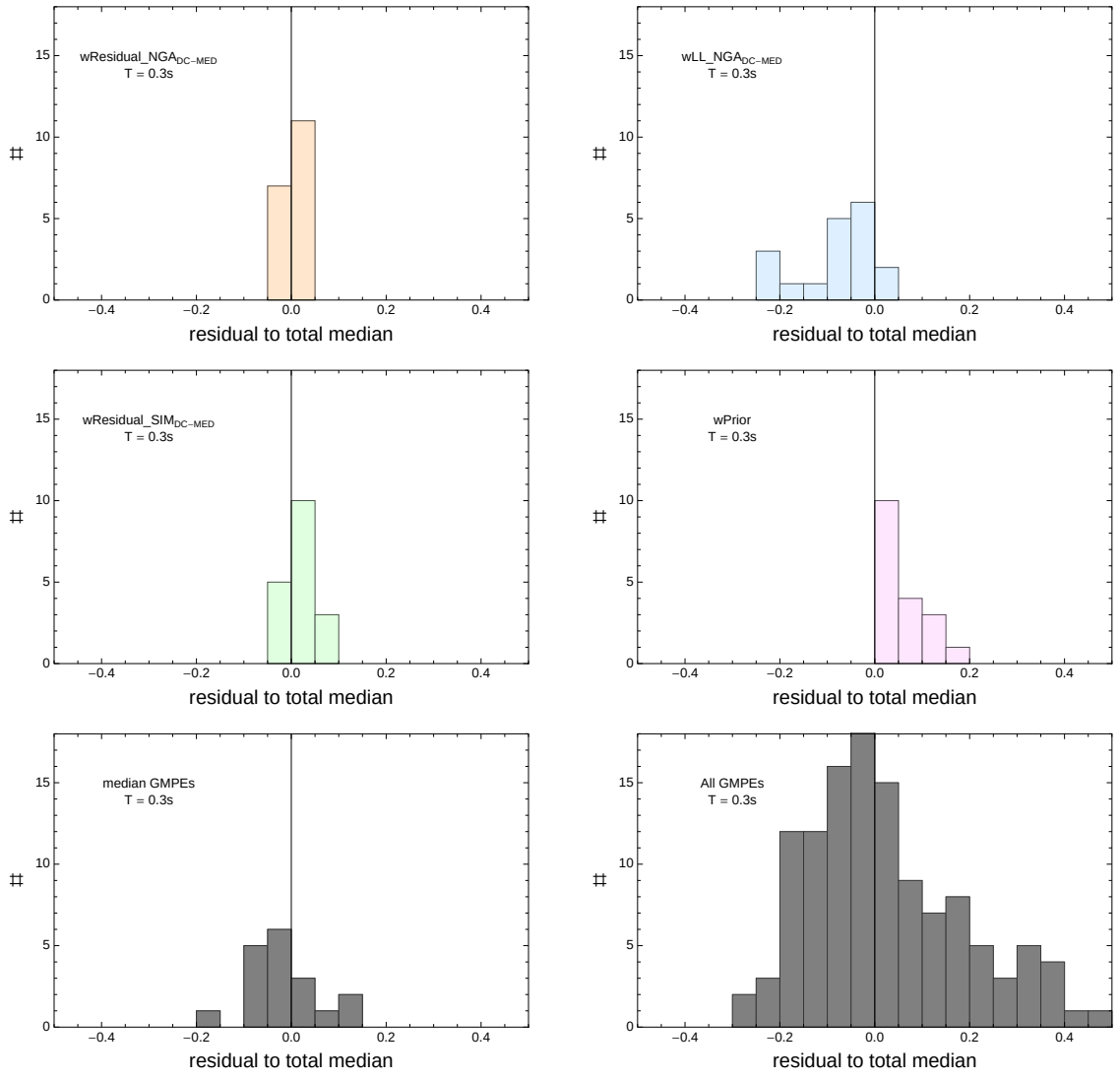



Figure 2.479: DCPPv4Histogram of differences for medians calculated with different weights to median calculated with total weights. Bottom row left shows differences between medians for the GMPE distribution to median calculated with total weights. Bottom row right shows differences between the original GMPEs (without uncertainty) to median calculated with total weights. For DCPP4, ModelA and $T = 0.3$s.

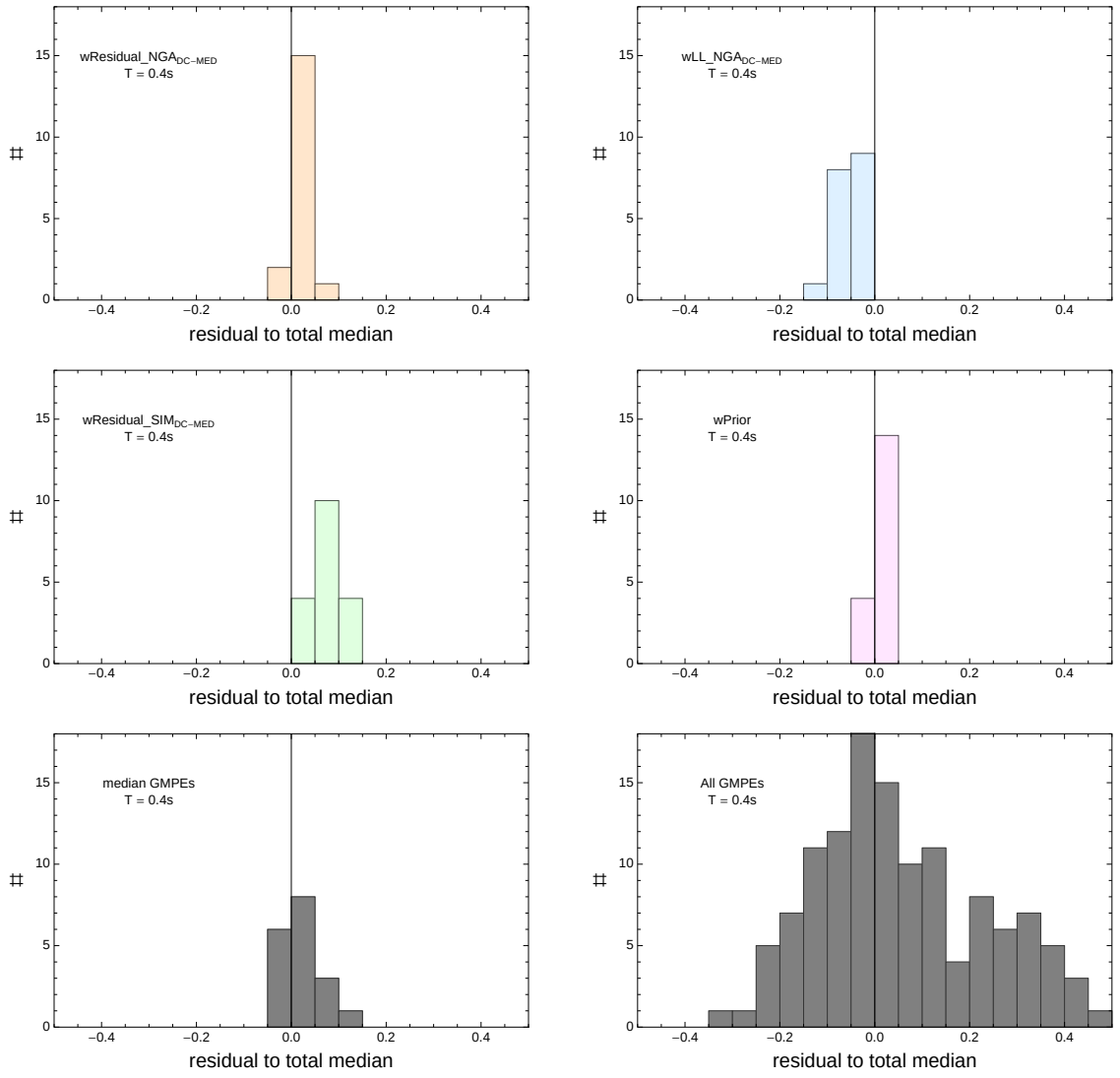



Figure 2.480: DCPPv4Histogram of differences for medians calculated with different weights to median calculated with total weights. Bottom row left shows differences between medians for the GMPE distribution to median calculated with total weights. Bottom row right shows differences between the original GMPEs (without uncertainty) to median calculated with total weights. For DCPP4, ModelA and $T = 0.4$s.

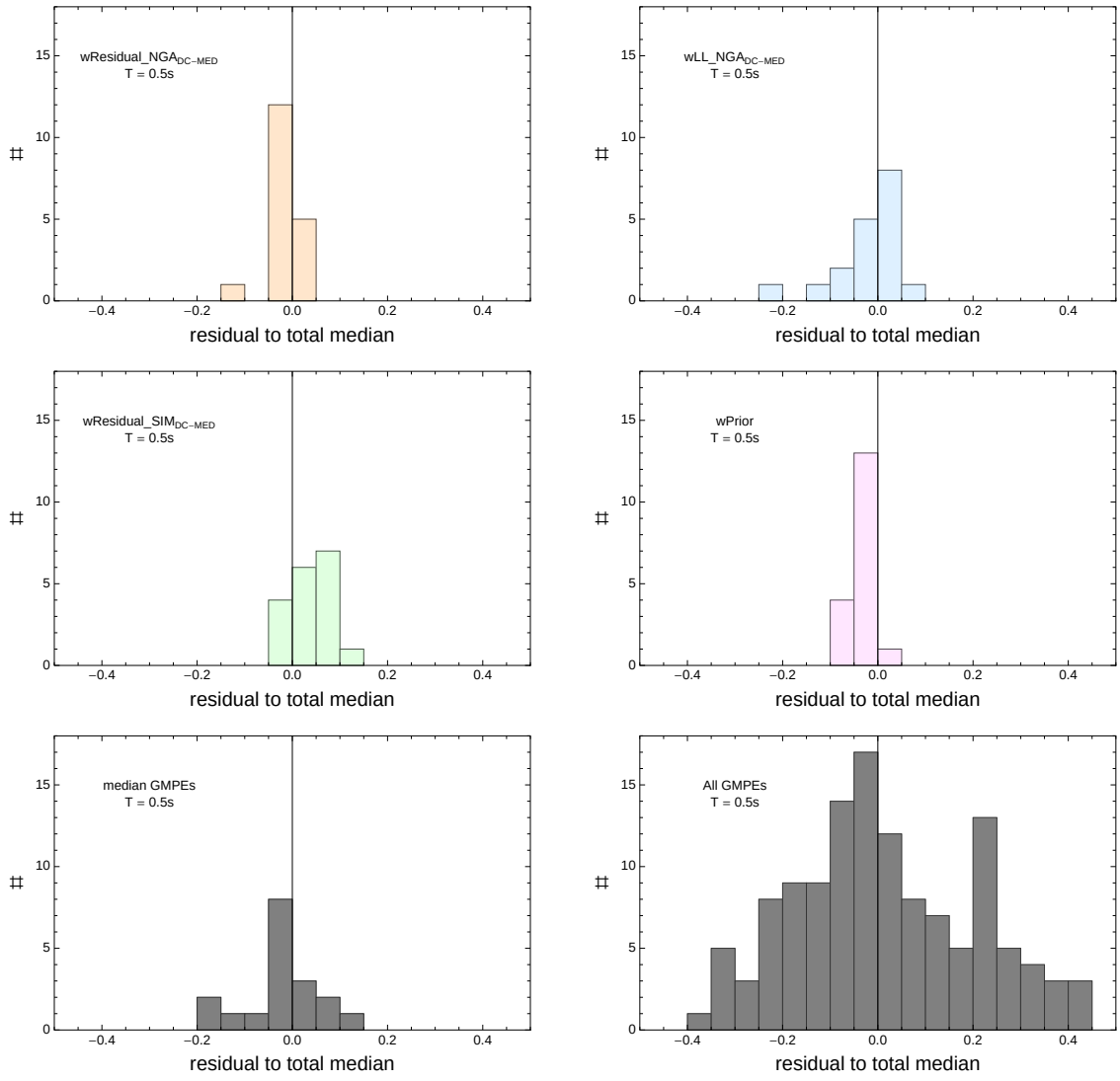



Figure 2.481: DCPPv4Histogram of differences for medians calculated with different weights to median calculated with total weights. Bottom row left shows differences between medians for the GMPE distribution to median calculated with total weights. Bottom row right shows differences between the original GMPEs (without uncertainty) to median calculated with total weights. For DCPP4, ModelA and $T = 0.5$s.

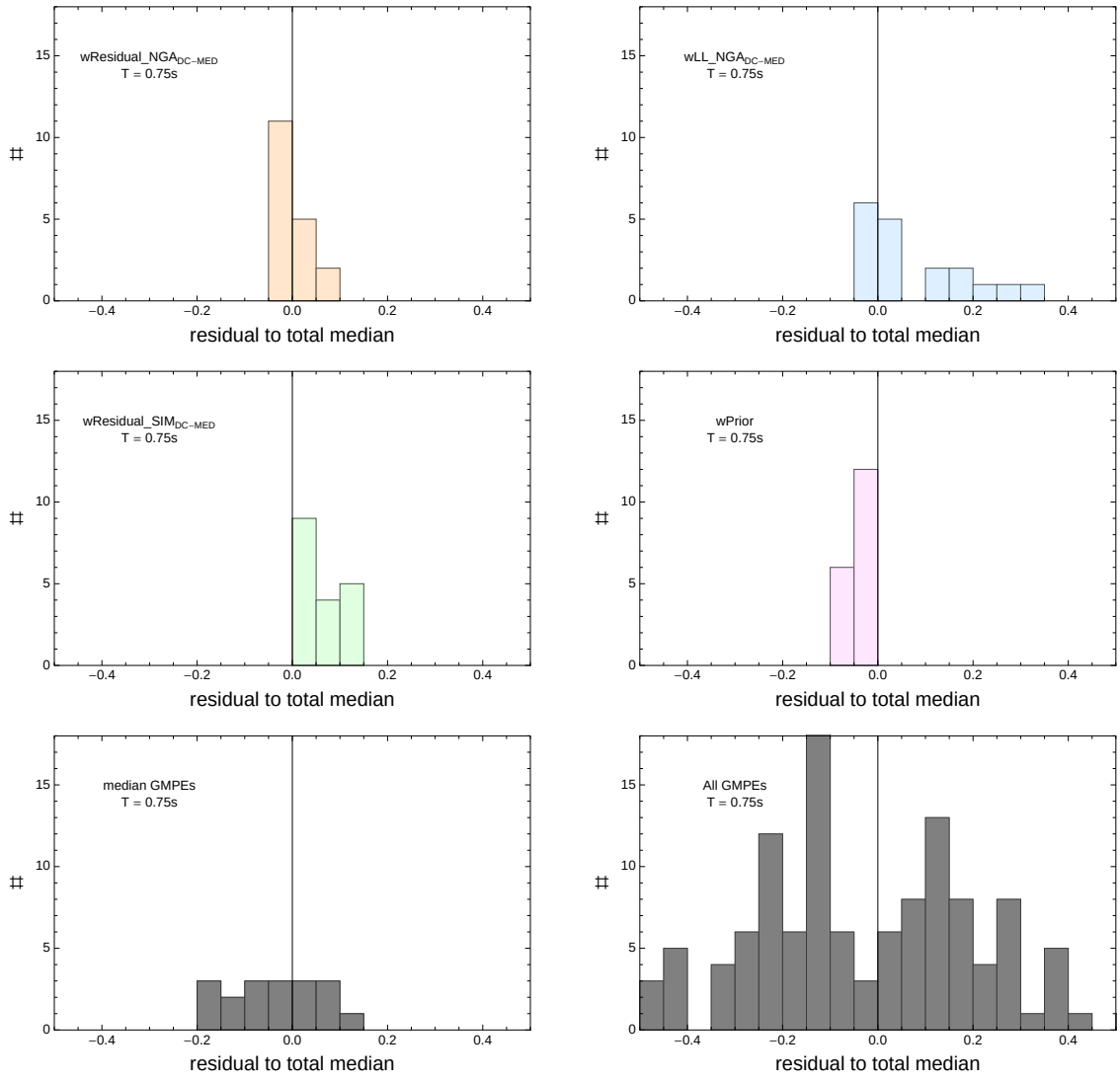



Figure 2.482: DCPPv4Histogram of differences for medians calculated with different weights to median calculated with total weights. Bottom row left shows differences between medians for the GMPE distribution to median calculated with total weights. Bottom row right shows differences between the original GMPEs (without uncertainty) to median calculated with total weights. For DCPP4, ModelA and $T = 0.75$s.

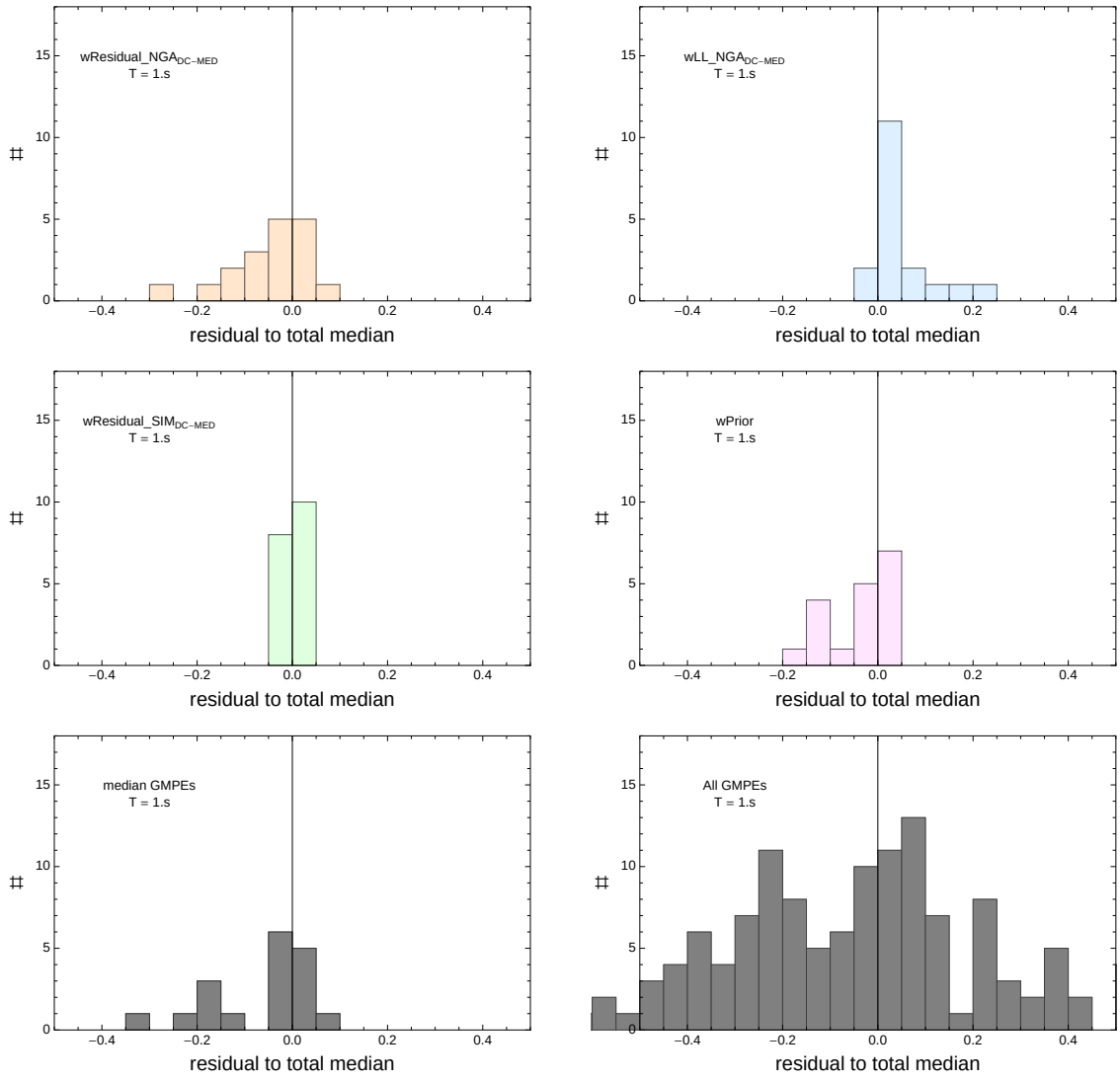



Figure 2.483: DCPPv4Histogram of differences for medians calculated with different weights to median calculated with total weights. Bottom row left shows differences between medians for the GMPE distribution to median calculated with total weights. Bottom row right shows differences between the original GMPEs (without uncertainty) to median calculated with total weights. For DCPP4, ModelA and $T = 1.$s.

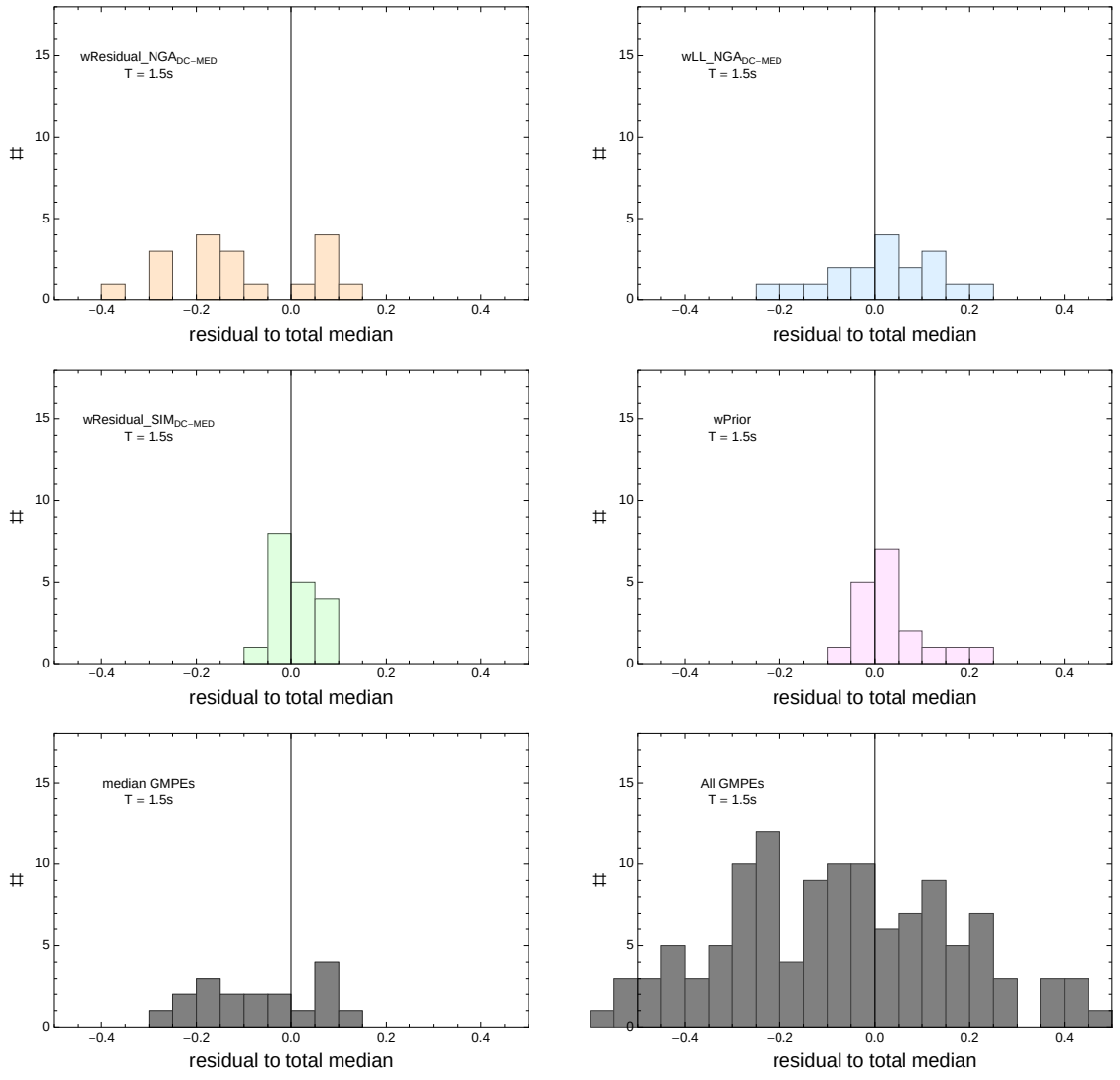



Figure 2.484: DCPPv4Histogram of differences for medians calculated with different weights to median calculated with total weights. Bottom row left shows differences between medians for the GMPE distribution to median calculated with total weights. Bottom row right shows differences between the original GMPEs (without uncertainty) to median calculated with total weights. For DCPP4, ModelA and $T = 1.5$s.

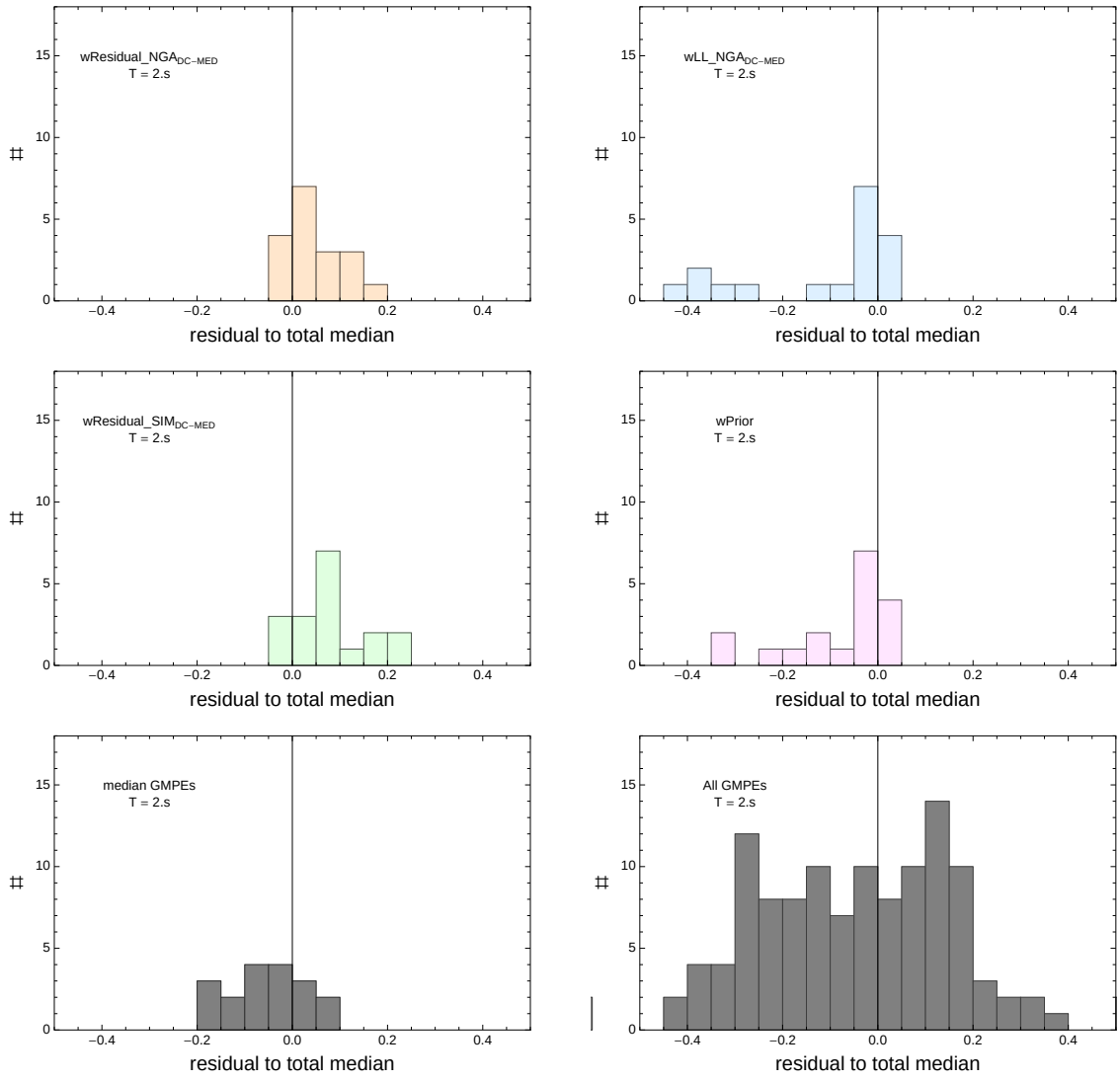



Figure 2.485: DCPPv4Histogram of differences for medians calculated with different weights to median calculated with total weights. Bottom row left shows differences between medians for the GMPE distribution to median calculated with total weights. Bottom row right shows differences between the original GMPEs (without uncertainty) to median calculated with total weights. For DCPP4, ModelA and $T = 2.$s.

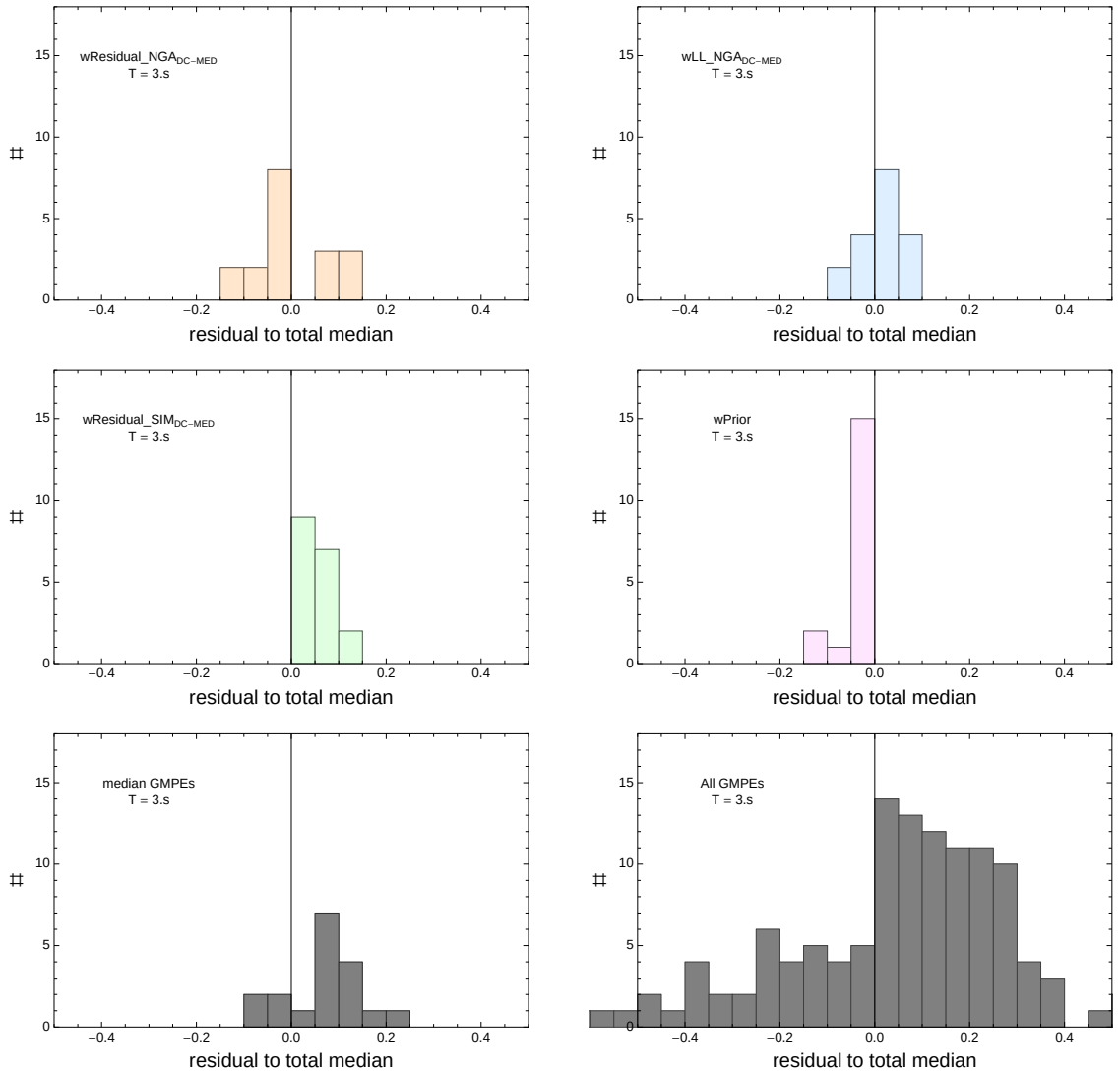



Figure 2.486: DCPPv4Histogram of differences for medians calculated with different weights to median calculated with total weights. Bottom row left shows differences between medians for the GMPE distribution to median calculated with total weights. Bottom row right shows differences between the original GMPEs (without uncertainty) to median calculated with total weights. For DCPP4, ModelA and $T = 3$.s.

# Chapter 3

# PVNGS – Model A

### 3.1.1 Deaggregation

**GM-Level 2**

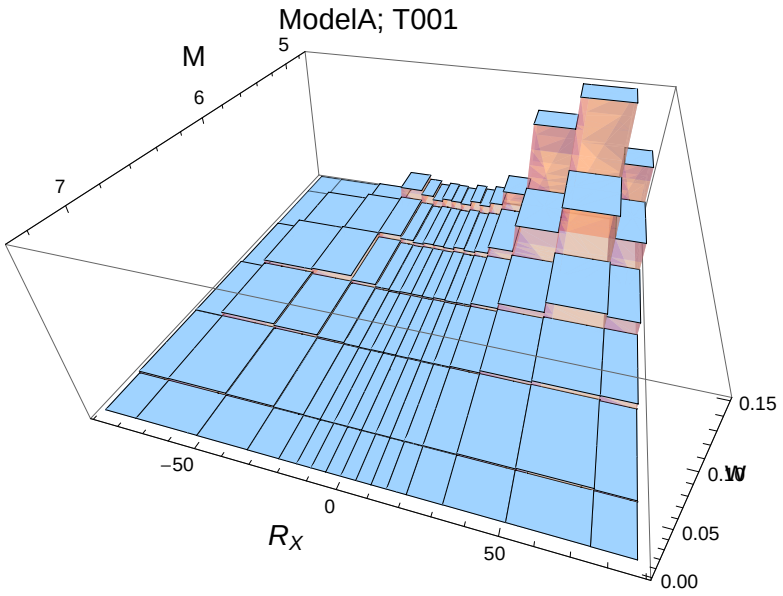



Figure 3.1: PVNGSv2: Deaggregation for a ground-motion level of 0.001g, calculated using a simple source model for PVNGS2 and the center model of the ModelA distribution. For $T = 0.01$s.

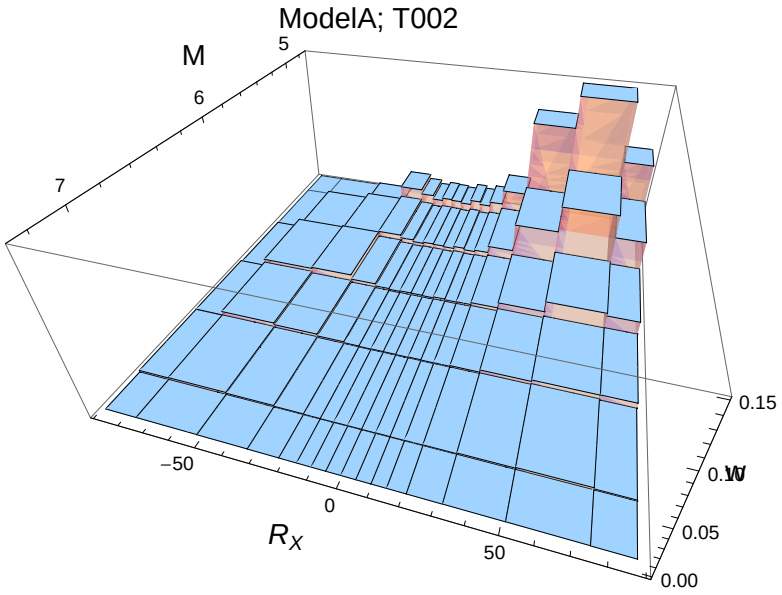



Figure 3.2: PVNGSv2: Deaggregation for a ground-motion level of 0.001g, calculated using a simple source model for PVNGS2 and the center model of the ModelA distribution. For $T = 0.02$s.

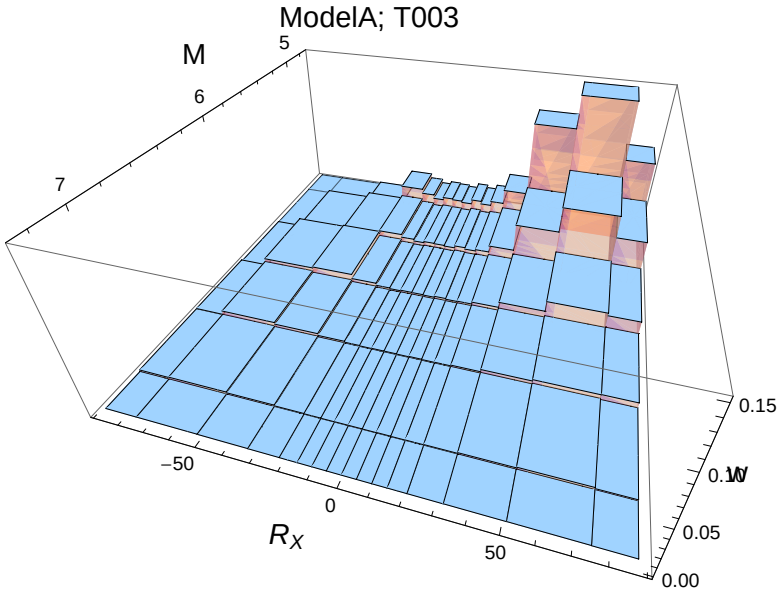



Figure 3.3: PVNGSv2: Deaggregation for a ground-motion level of 0.001g, calculated using a simple source model for PVNGS2 and the center model of the ModelA distribution. For $T = 0.03$s.

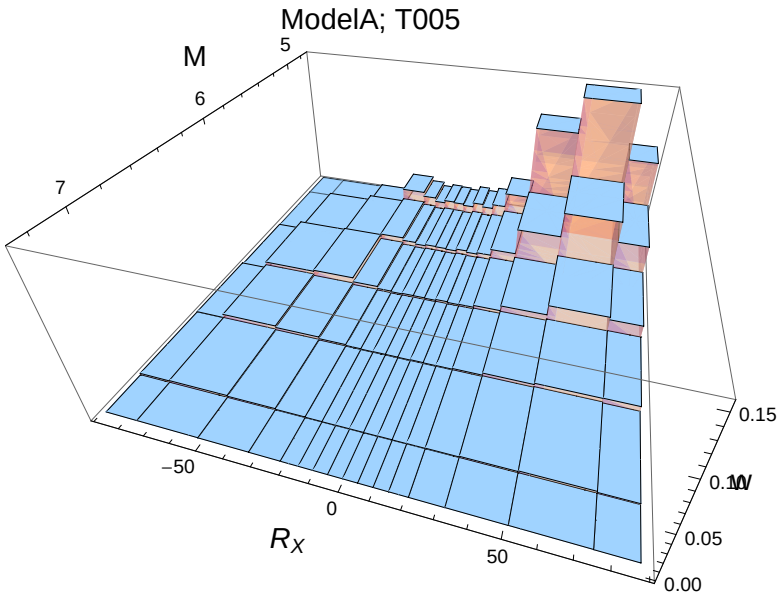



Figure 3.4: PVNGSv2: Deaggregation for a ground-motion level of 0.001g, calculated using a simple source model for PVNGS2 and the center model of the ModelA distribution. For $T = 0.05$s.

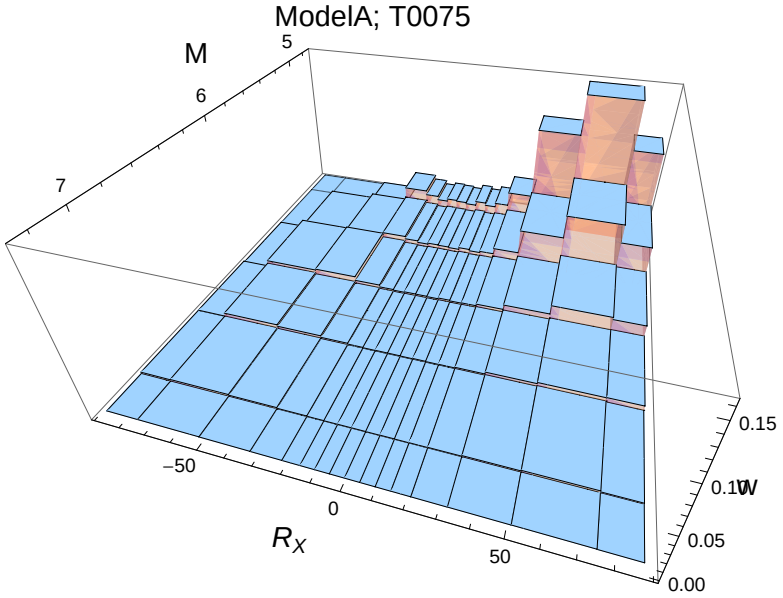



Figure 3.5: PVNGSv2: Deaggregation for a ground-motion level of 0.001g, calculated using a simple source model for PVNGS2 and the center model of the ModelA distribution. For $T = 0.075$s.

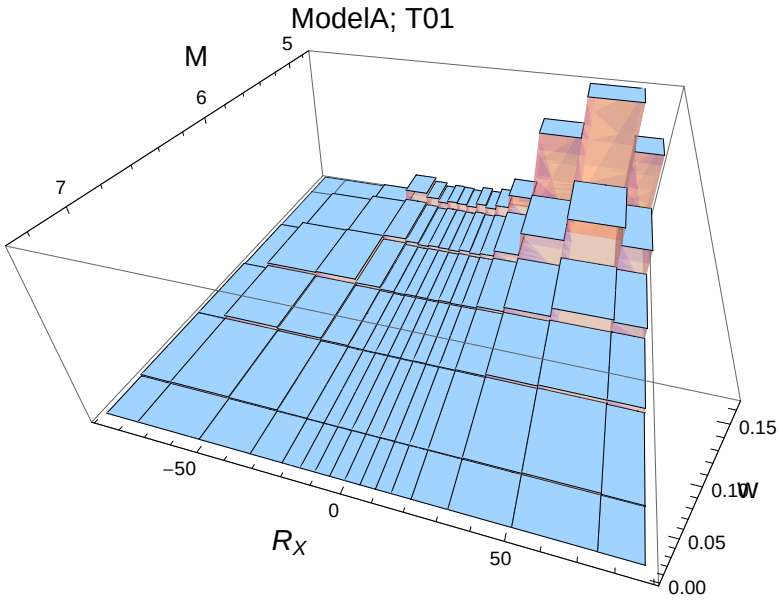



Figure 3.6: PVNGSv2: Deaggregation for a ground-motion level of 0.001g, calculated using a simple source model for PVNGS2 and the center model of the ModelA distribution. For $T = 0.1$s.

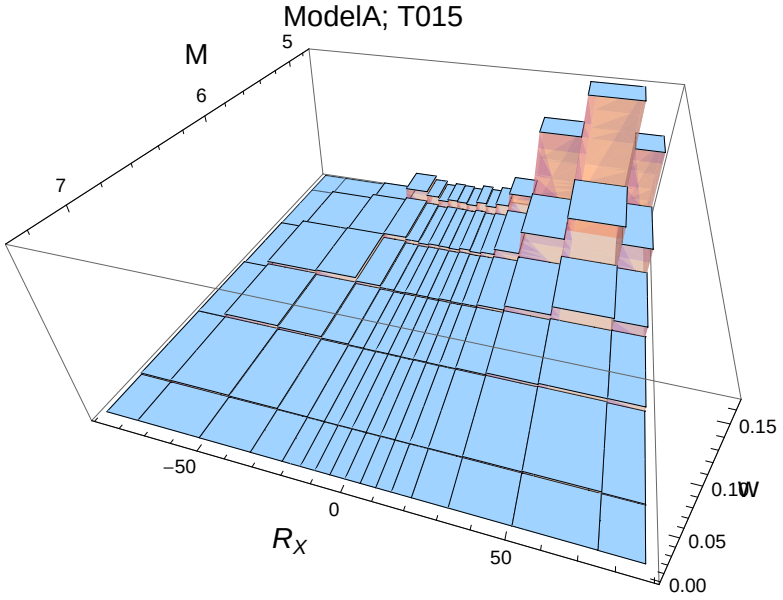



Figure 3.7: PVNGSv2: Deaggregation for a ground-motion level of 0.001g, calculated using a simple source model for PVNGS2 and the center model of the ModelA distribution. For $T = 0.15$s.

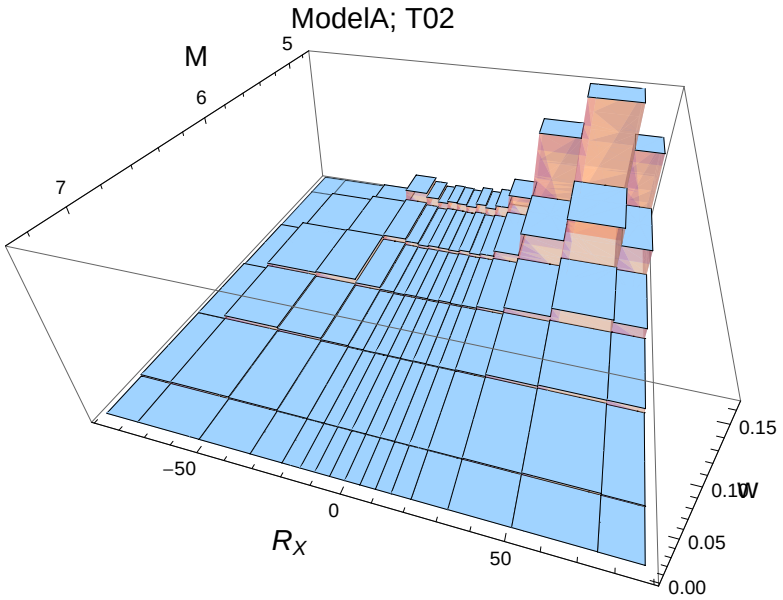



Figure 3.8: PVNGSv2: Deaggregation for a ground-motion level of 0.001g, calculated using a simple source model for PVNGS2 and the center model of the ModelA distribution. For $T = 0.2$s.

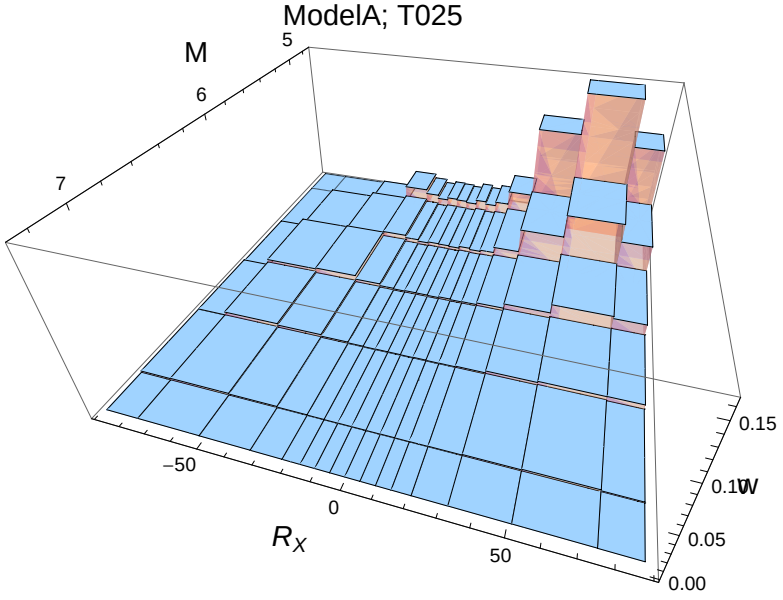



Figure 3.9: PVNGSv2: Deaggregation for a ground-motion level of 0.001g, calculated using a simple source model for PVNGS2 and the center model of the ModelA distribution. For $T = 0.25$s.

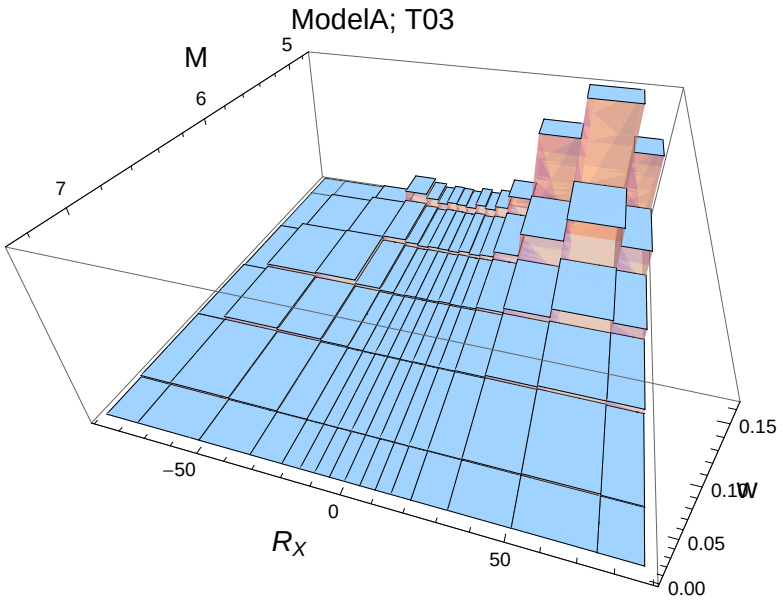



Figure 3.10: PVNGSv2: Deaggregation for a ground-motion level of 0.001g, calculated using a simple source model for PVNGS2 and the center model of the ModelA distribution. For $T = 0.3$s.

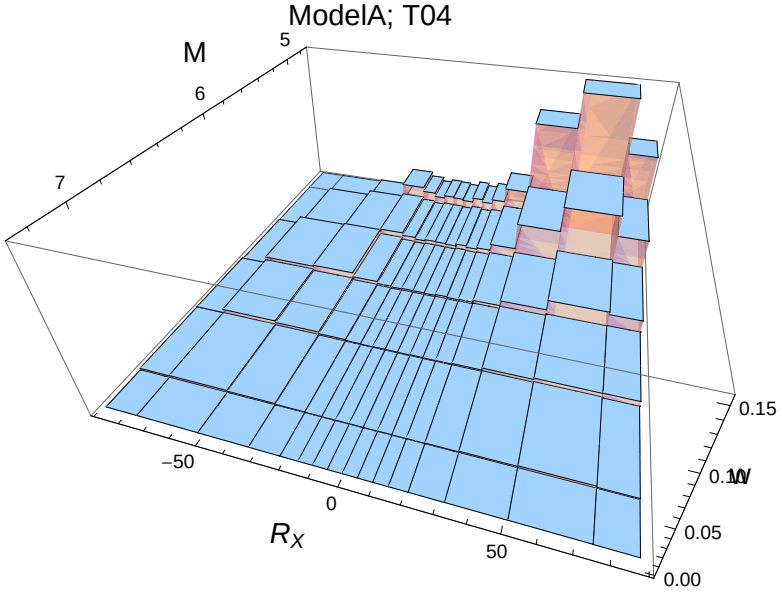



Figure 3.11: PVNGSv2: Deaggregation for a ground-motion level of 0.001g, calculated using a simple source model for PVNGS2 and the center model of the ModelA distribution. For $T = 0.4$s.

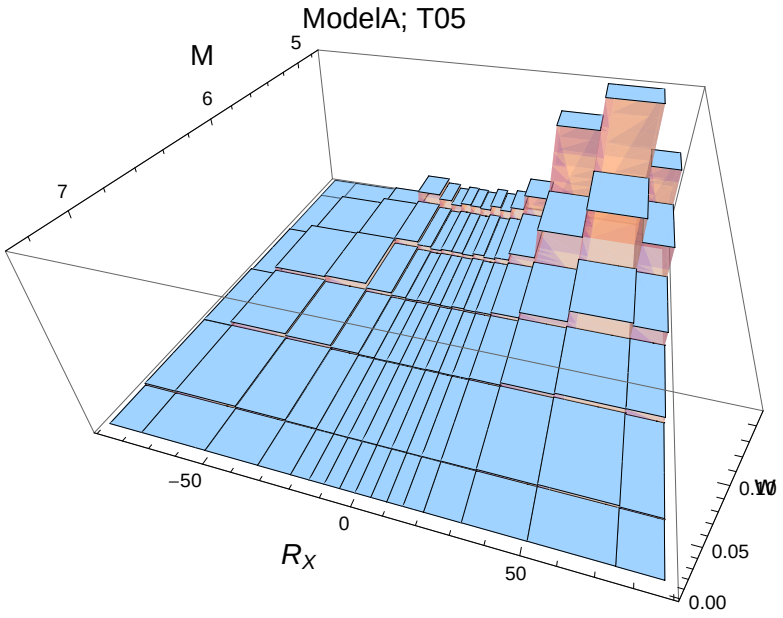



Figure 3.12: PVNGSv2: Deaggregation for a ground-motion level of 0.001g, calculated using a simple source model for PVNGS2 and the center model of the ModelA distribution. For $T = 0.5$s.

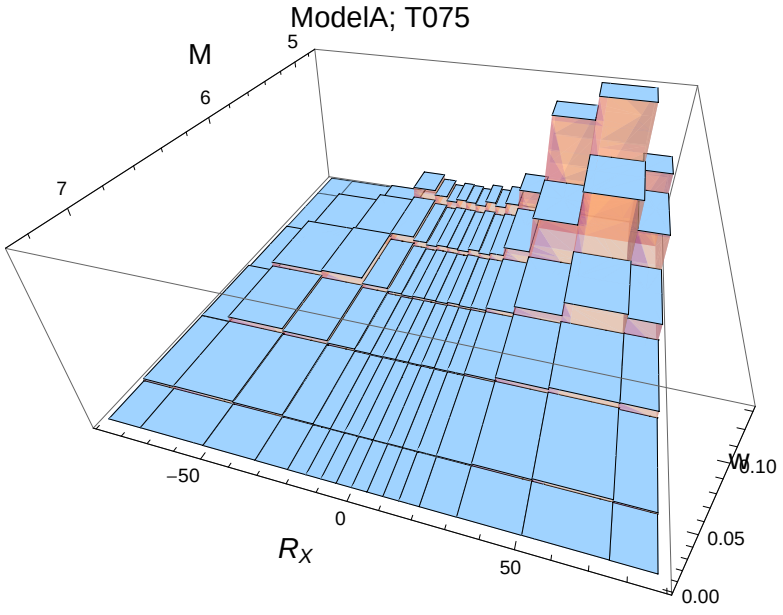



Figure 3.13: PVNGSv2: Deaggregation for a ground-motion level of 0.001g, calculated using a simple source model for PVNGS2 and the center model of the ModelA distribution. For $T = 0.75$s.

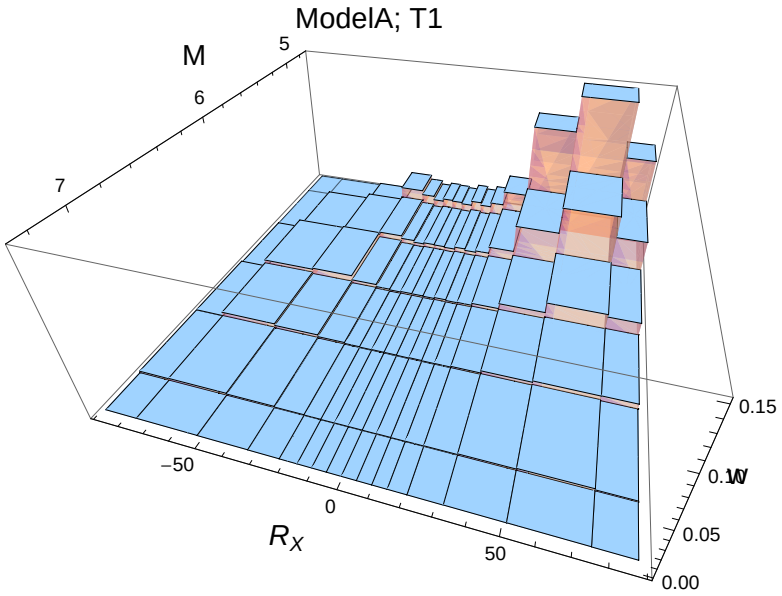



Figure 3.14: PVNGSv2: Deaggregation for a ground-motion level of 0.g, calculated using a simple source model for PVNGS2 and the center model of the ModelA distribution. For $T = 1$.s.

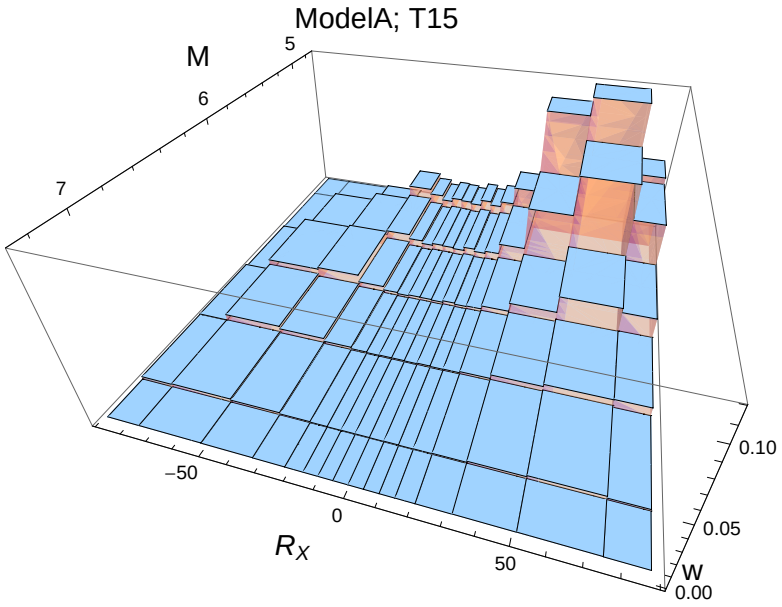



Figure 3.15: PVNGSv2: Deaggregation for a ground-motion level of 0.g, calculated using a simple source model for PVNGS2 and the center model of the ModelA distribution. For $T = 1.5$s.

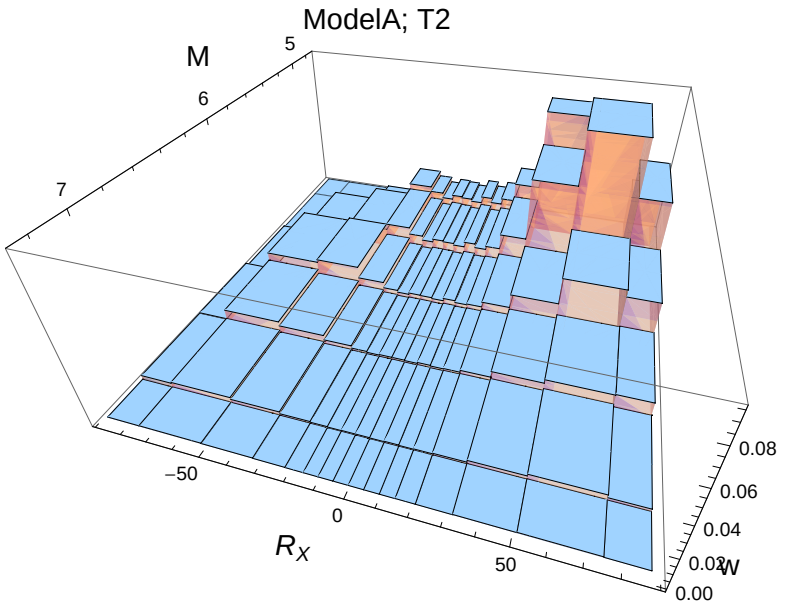



Figure 3.16: PVNGSv2: Deaggregation for a ground-motion level of 0.g, calculated using a simple source model for PVNGS2 and the center model of the ModelA distribution. For $T = 2$.s.

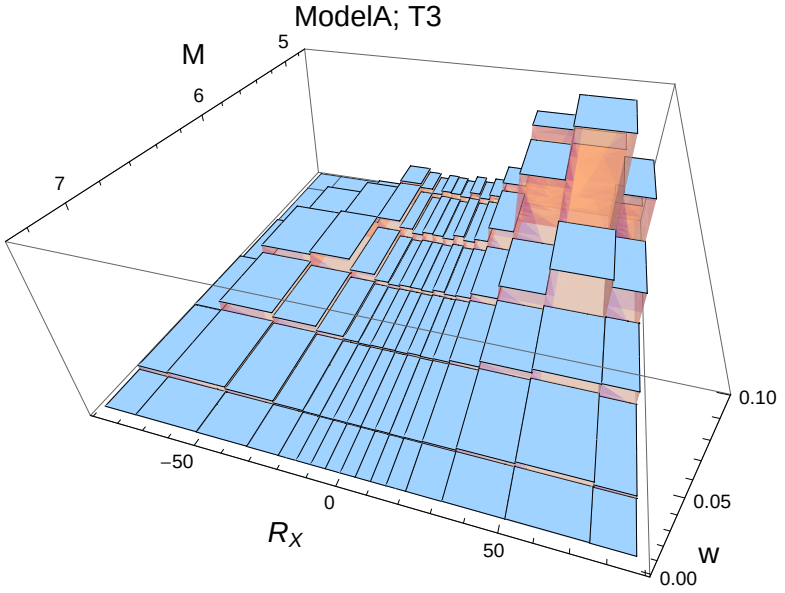



Figure 3.17: PVNGSv2: Deaggregation for a ground-motion level of 0.g, calculated using a simple source model for PVNGS2 and the center model of the ModelA distribution. For $T = 3$.s.

**GM-Level 8**

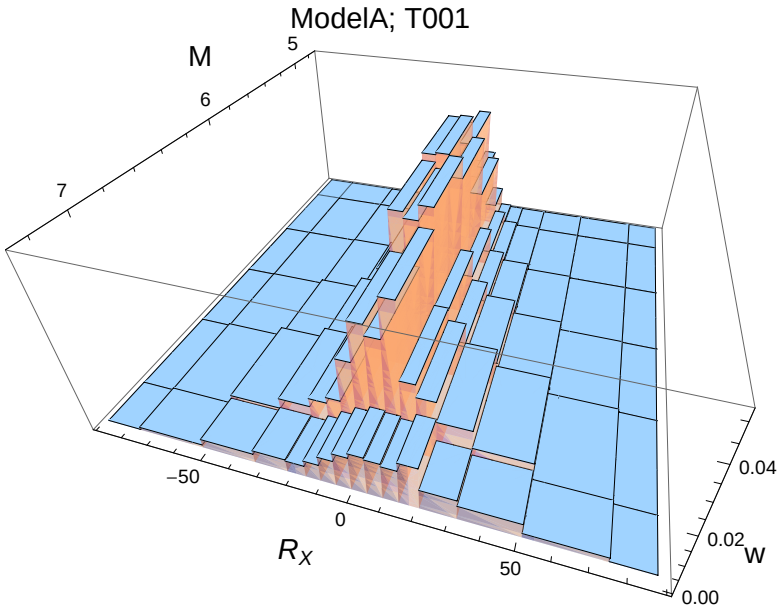



Figure 3.18: PVNGSv2: Deaggregation for a ground-motion level of 0.278g, calculated using a simple source model for PVNGS2 and the center model of the ModelA distribution. For $T = 0.01$s.

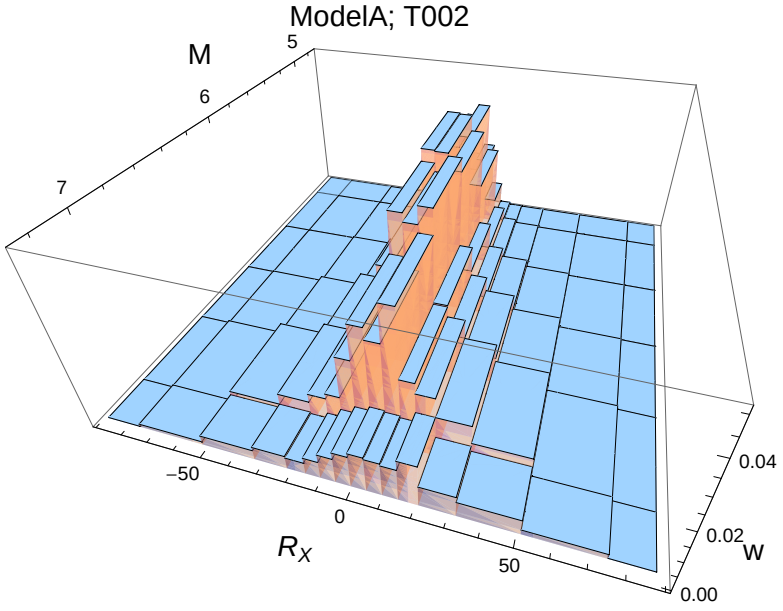



Figure 3.19: PVNGSv2: Deaggregation for a ground-motion level of 0.266g, calculated using a simple source model for PVNGS2 and the center model of the ModelA distribution. For $T = 0.02$s.

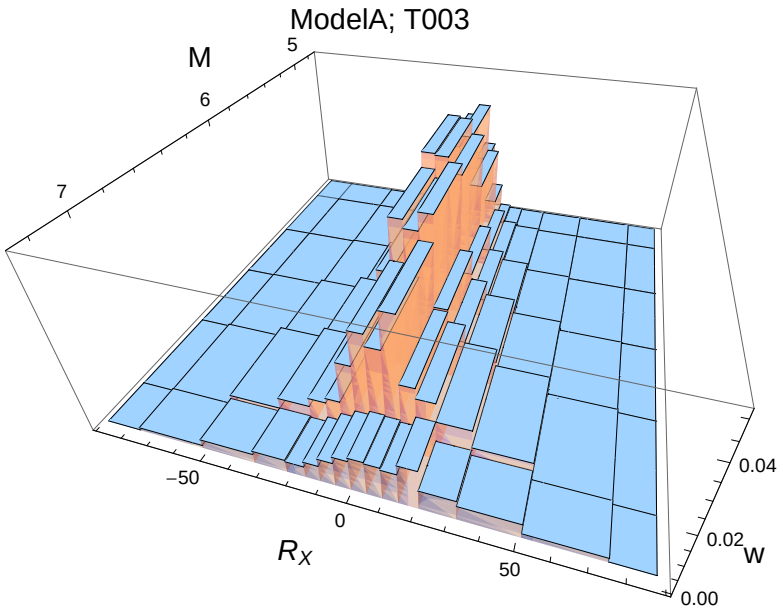



Figure 3.20: PVNGSv2: Deaggregation for a ground-motion level of 0.29g, calculated using a simple source model for PVNGS2 and the center model of the ModelA distribution. For $T = 0.03$s.

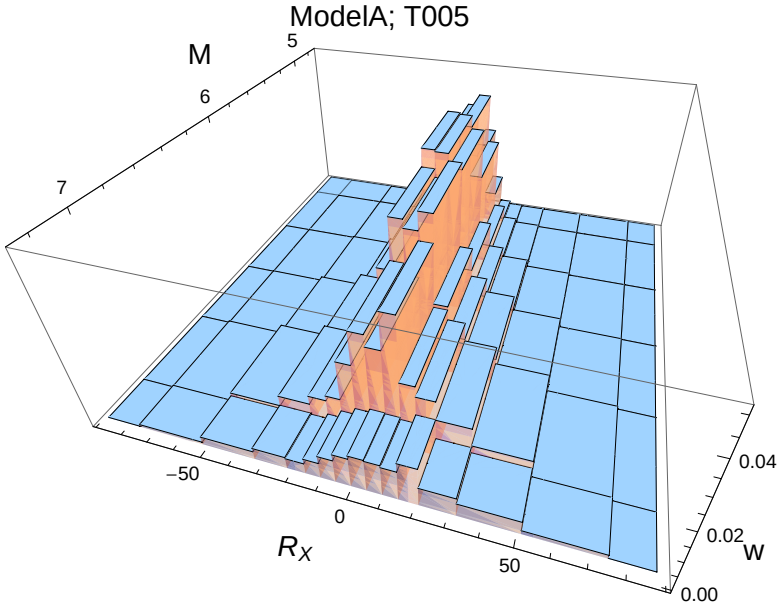



Figure 3.21: PVNGSv2: Deaggregation for a ground-motion level of 0.358g, calculated using a simple source model for PVNGS2 and the center model of the ModelA distribution. For $T = 0.05$s.

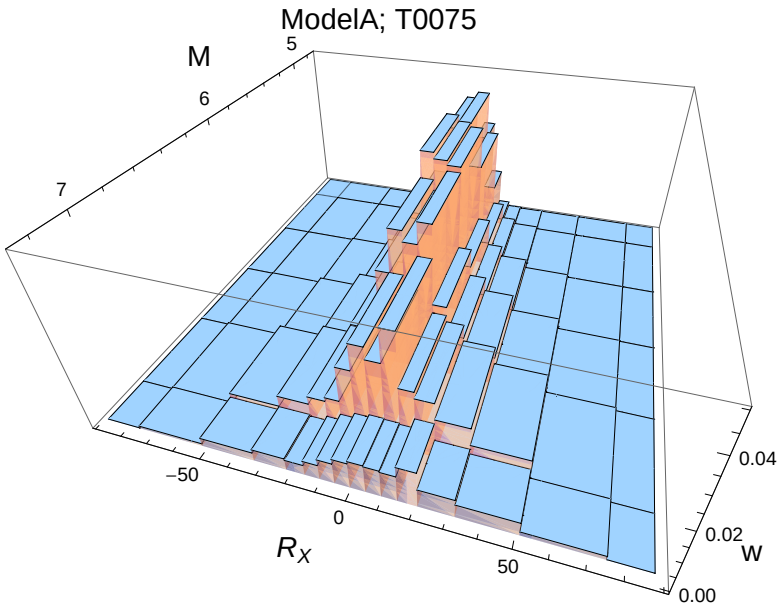



Figure 3.22: PVNGSv2: Deaggregation for a ground-motion level of 0.407g, calculated using a simple source model for PVNGS2 and the center model of the ModelA distribution. For $T = 0.075$s.

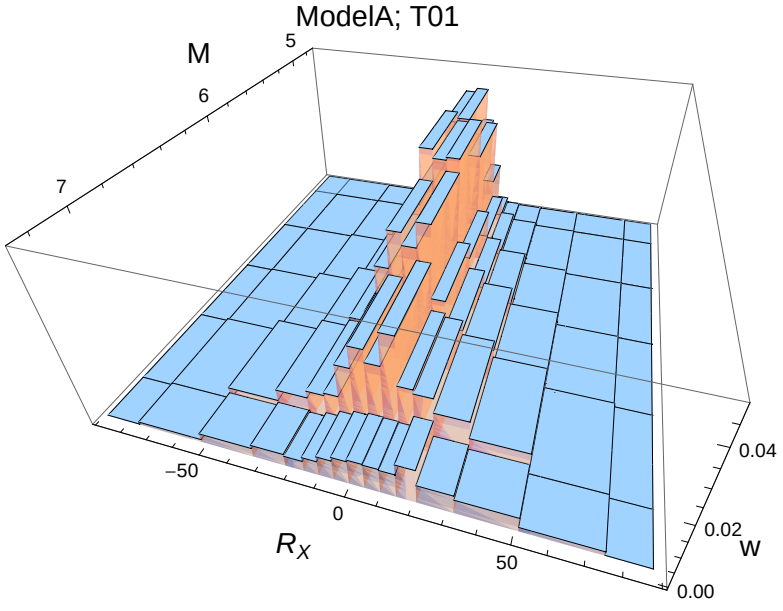



Figure 3.23: PVNGSv2: Deaggregation for a ground-motion level of 0.427g, calculated using a simple source model for PVNGS2 and the center model of the ModelA distribution. For $T = 0.1$s.

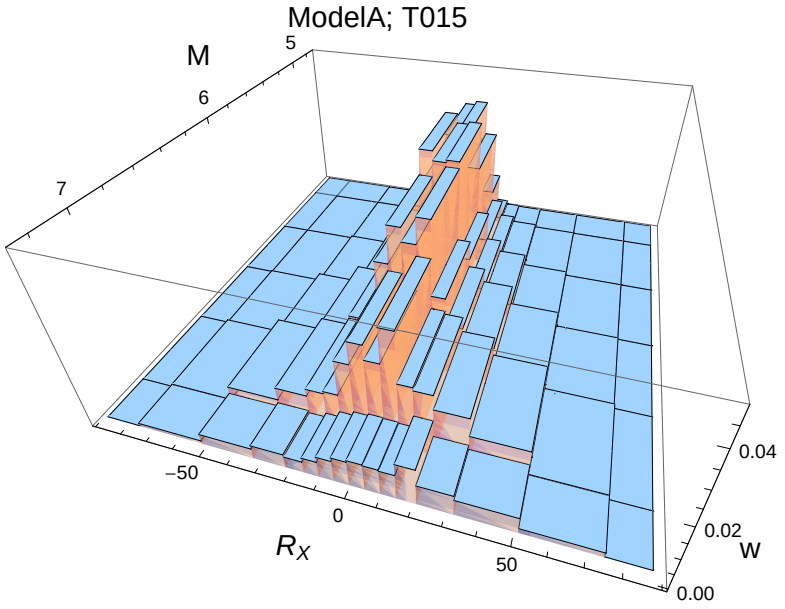



Figure 3.24: PVNGSv2: Deaggregation for a ground-motion level of 0.475g, calculated using a simple source model for PVNGS2 and the center model of the ModelA distribution. For $T = 0.15$s.

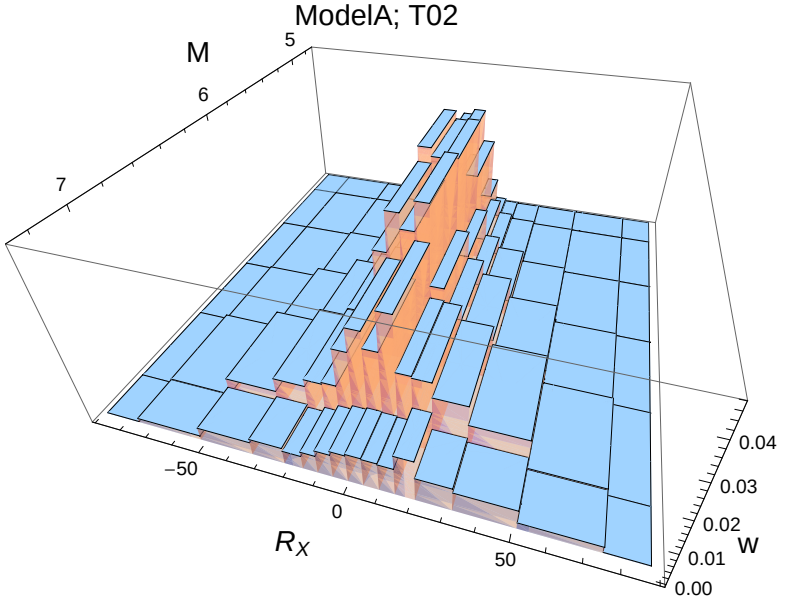



Figure 3.25: PVNGSv2: Deaggregation for a ground-motion level of 0.456g, calculated using a simple source model for PVNGS2 and the center model of the ModelA distribution. For $T = 0.2$s.

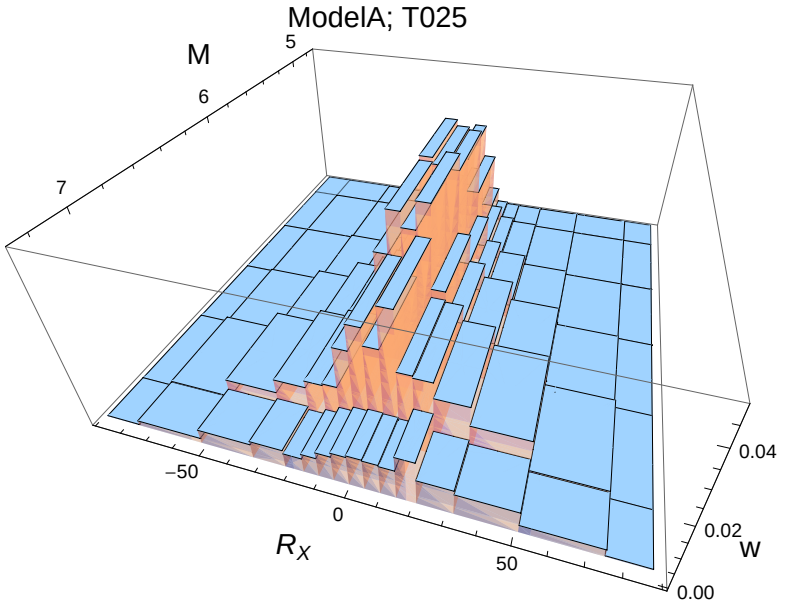



Figure 3.26: PVNGSv2: Deaggregation for a ground-motion level of 0.427g, calculated using a simple source model for PVNGS2 and the center model of the ModelA distribution. For $T = 0.25$s.

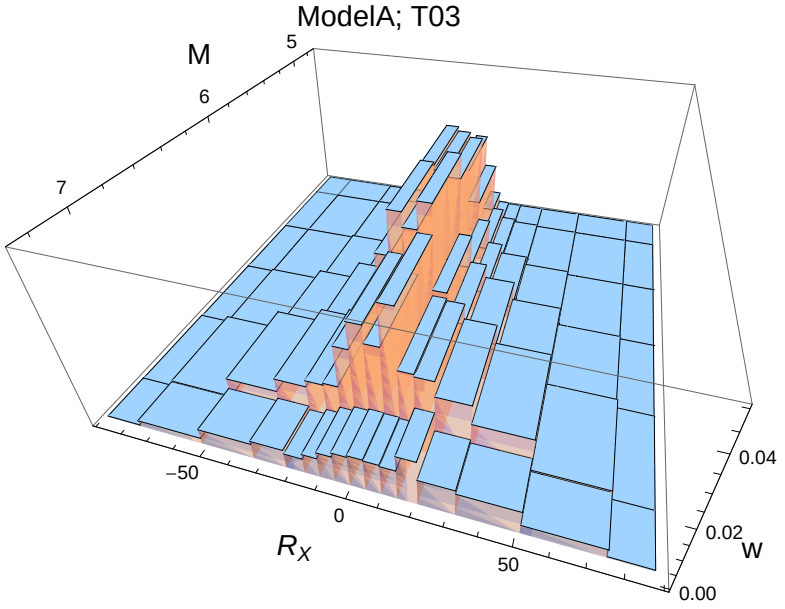



Figure 3.27: PVNGSv2: Deaggregation for a ground-motion level of 0.387g, calculated using a simple source model for PVNGS2 and the center model of the ModelA distribution. For $T = 0.3$s.

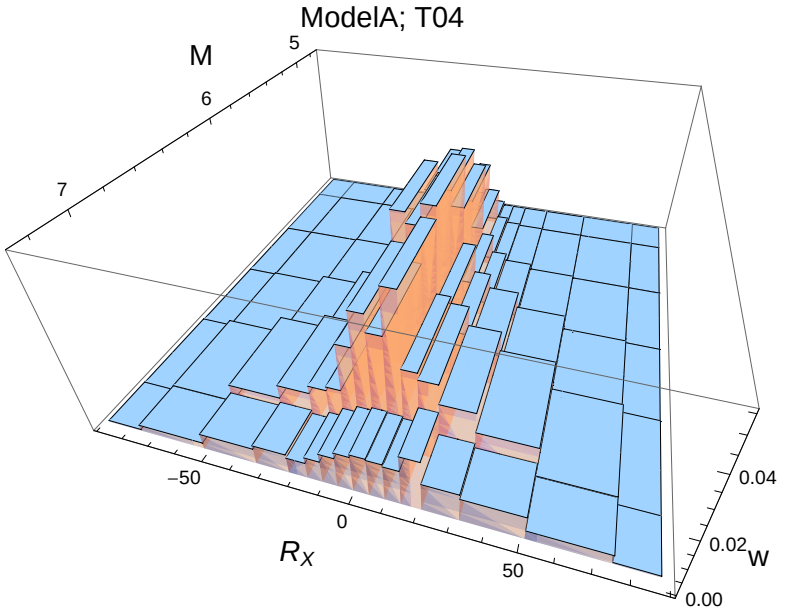



Figure 3.28: PVNGSv2: Deaggregation for a ground-motion level of 0.358g, calculated using a simple source model for PVNGS2 and the center model of the ModelA distribution. For $T = 0.4$s.

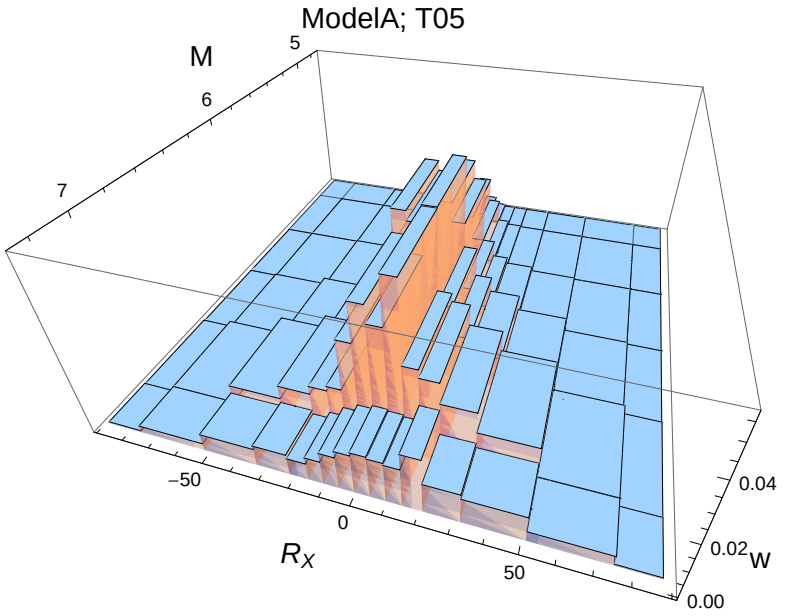



Figure 3.29: PVNGSv2: Deaggregation for a ground-motion level of 0.313g, calculated using a simple source model for PVNGS2 and the center model of the ModelA distribution. For $T = 0.5$s.

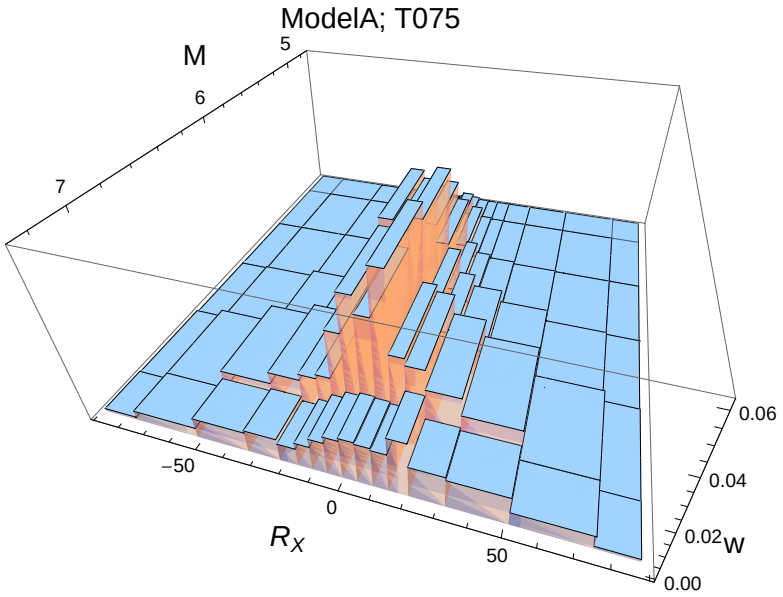



Figure 3.30: PVNGSv2: Deaggregation for a ground-motion level of 0.214g, calculated using a simple source model for PVNGS2 and the center model of the ModelA distribution. For $T = 0.75$s.

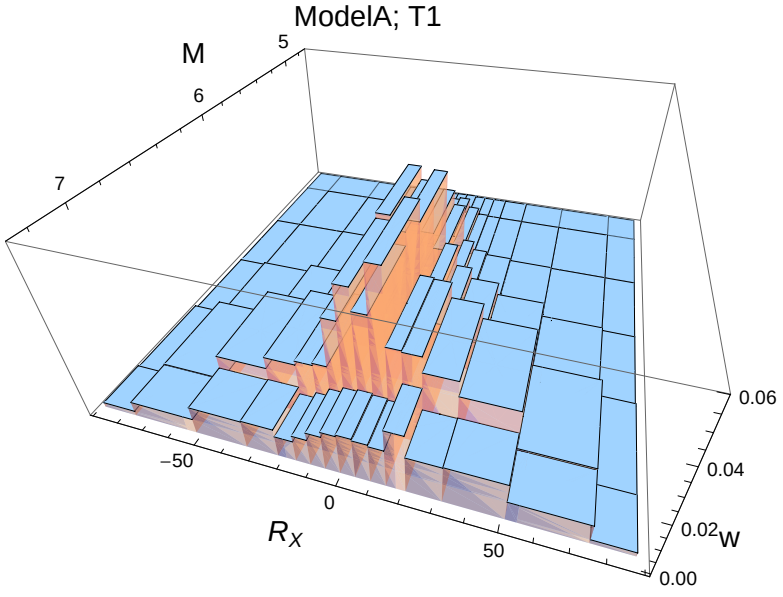



Figure 3.31: PVNGSv2: Deaggregation for a ground-motion level of 0.139g, calculated using a simple source model for PVNGS2 and the center model of the ModelA distribution. For $T = 1$.s.

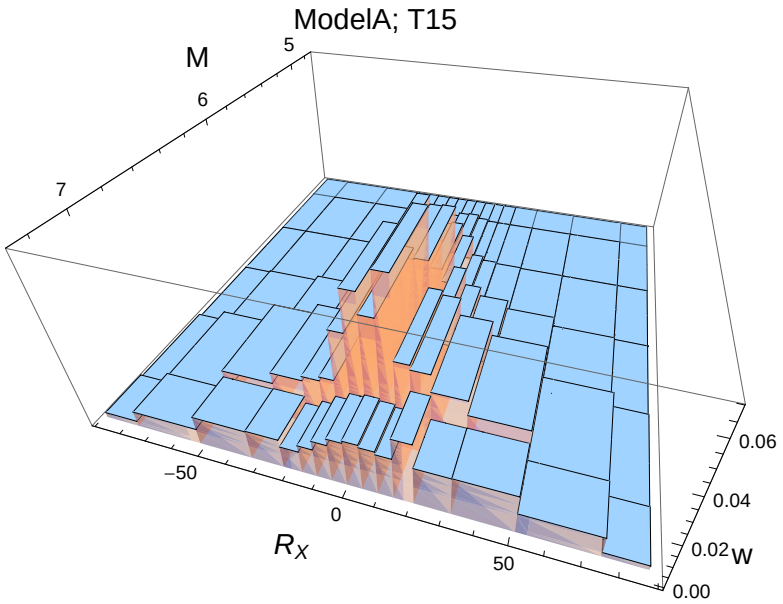



Figure 3.32: PVNGSv2: Deaggregation for a ground-motion level of 0.098g, calculated using a simple source model for PVNGS2 and the center model of the ModelA distribution. For $T = 1.5$s.

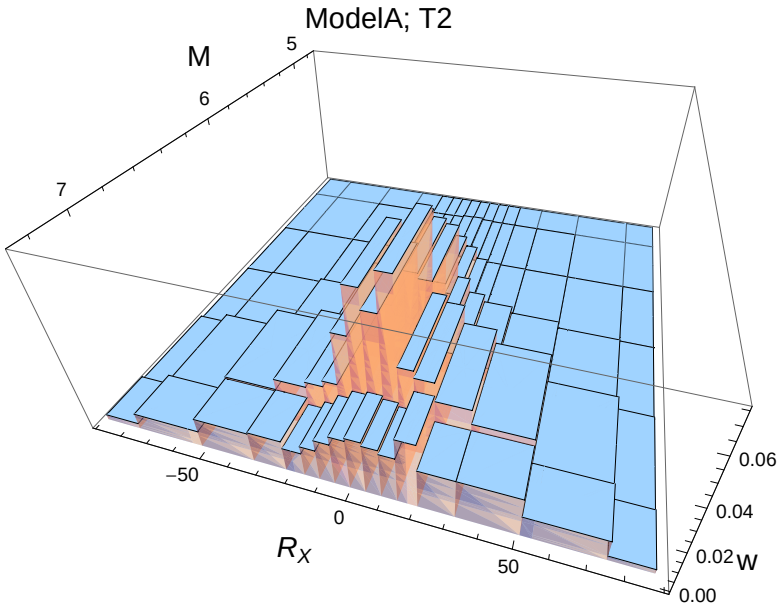



Figure 3.33: PVNGSv2: Deaggregation for a ground-motion level of 0.075g, calculated using a simple source model for PVNGS2 and the center model of the ModelA distribution. For $T = 2$.s.

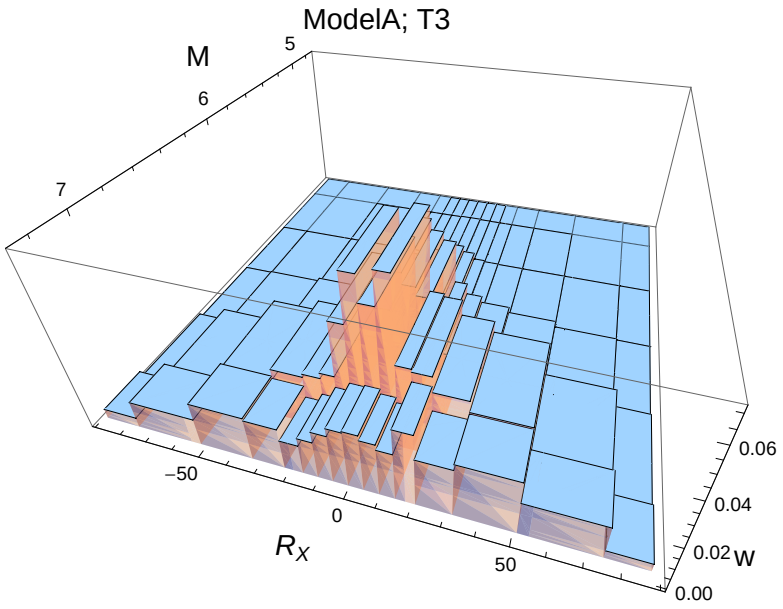



Figure 3.34: PVNGSv2: Deaggregation for a ground-motion level of 0.043g, calculated using a simple source model for PVNGS2 and the center model of the ModelA distribution. For $T = 3$.s.

### 3.1.2 Maps – Selection

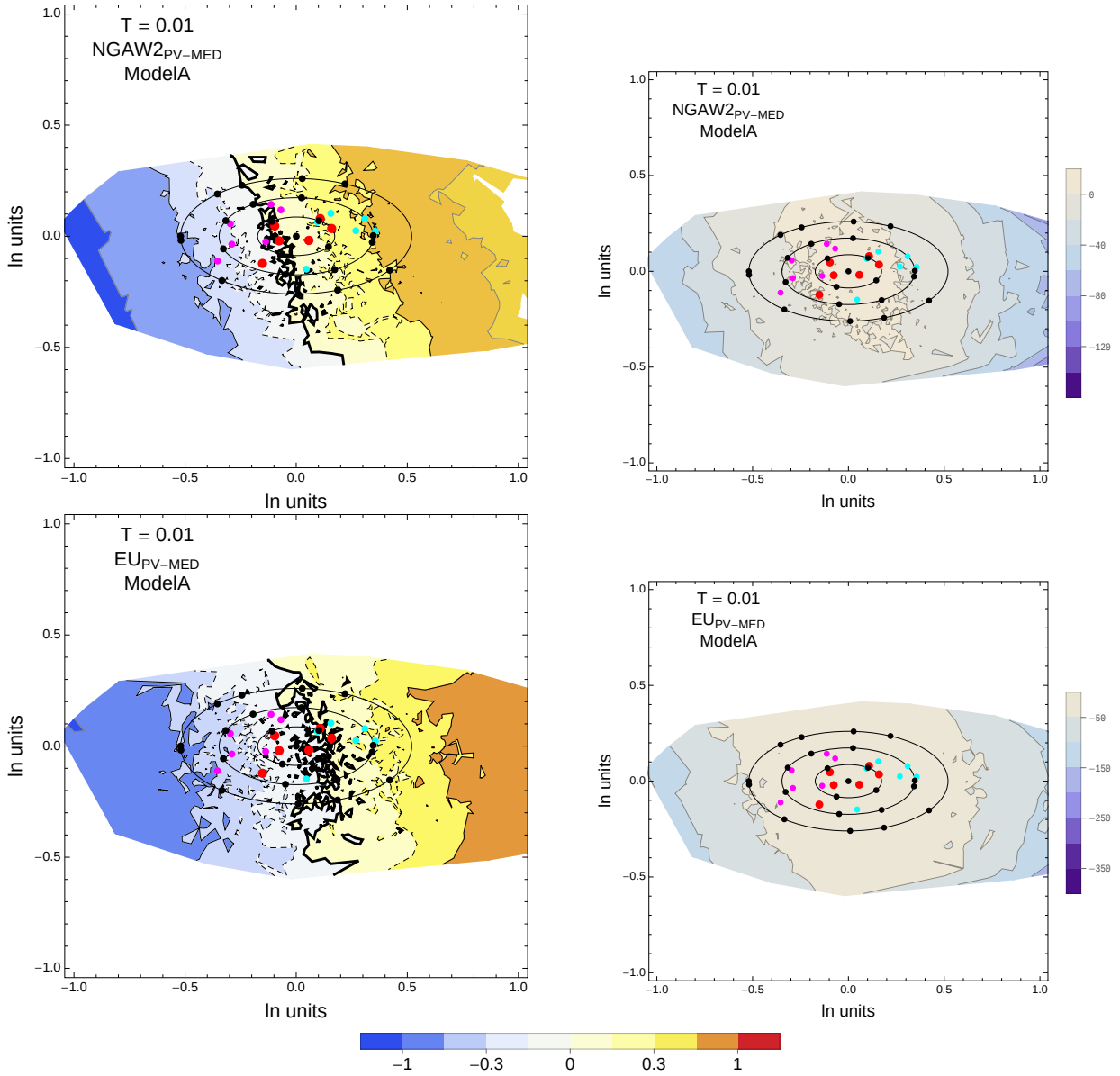



Figure 3.35: PVNGSv2: Contour Plots of mean residuals (top left) and likelihood (top right) for the NGA$_{PV-MED}$ dataset, and mean residuals (bottom left) and likelihood (top right) for the EU$_{PV-MED}$ dataset. Reference points are black dots. The original GMPEs are red dots,plus/minus uncertainty are magenta/cyan dots. The contour for the zero residual is a thick black line, the -0.15/0.15 contours are dashed black lines and the -0.3/0.3 contours are thin black lines. For $T = 0.01$s.

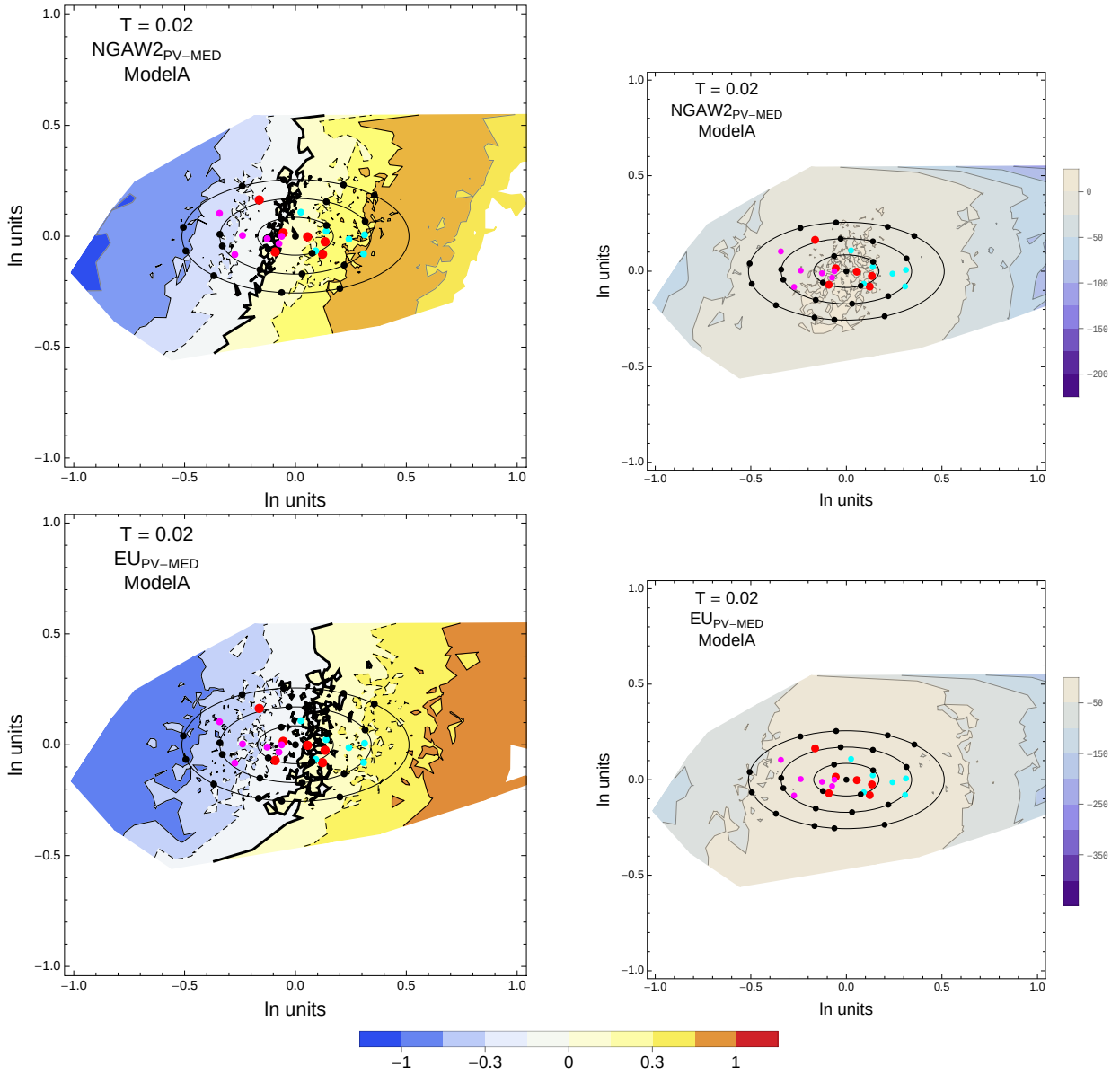



Figure 3.36: PVNGSv2: Contour Plots of mean residuals (top left) and likelihood (top right) for the NGA$_{PV-MED}$ dataset, and mean residuals (bottom left) and likelihood (top right) for the EU$_{PV-MED}$ dataset. Reference points are black dots. The original GMPEs are red dots,plus/minus uncertainty are magenta/cyan dots. The contour for the zero residual is a thick black line, the -0.15/0.15 contours are dashed black lines and the -0.3/0.3 contours are thin black lines. For $T = 0.02$s.

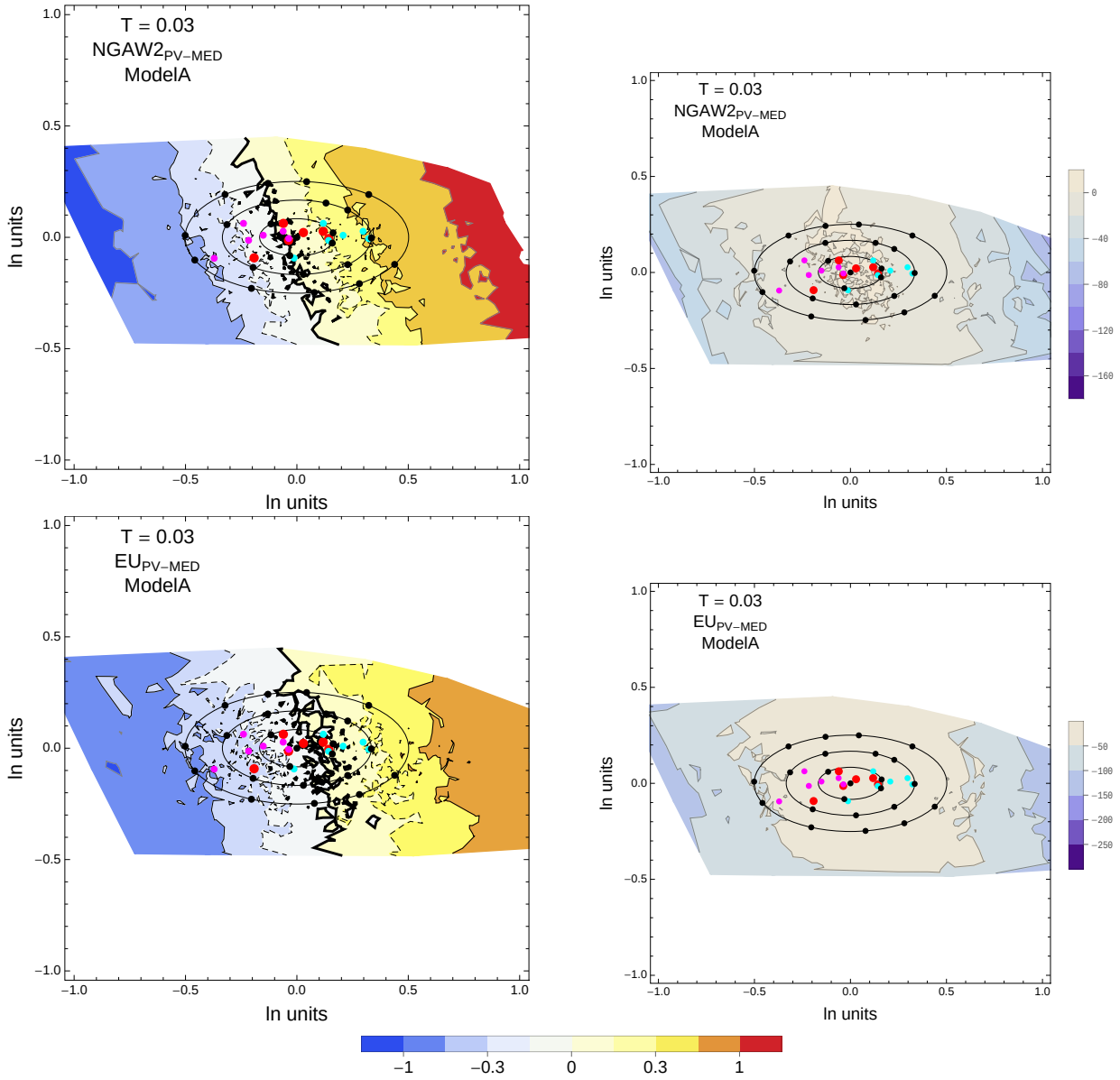



Figure 3.37: PVNGSv2: Contour Plots of mean residuals (top left) and likelihood (top right) for the NGA$_{PV-MED}$ dataset, and mean residuals (bottom left) and likelihood (top right) for the EU$_{PV-MED}$ dataset. Reference points are black dots. The original GMPEs are red dots,plus/minus uncertainty are magenta/cyan dots. The contour for the zero residual is a thick black line, the -0.15/0.15 contours are dashed black lines and the -0.3/0.3 contours are thin black lines. For $T = 0.03$s.

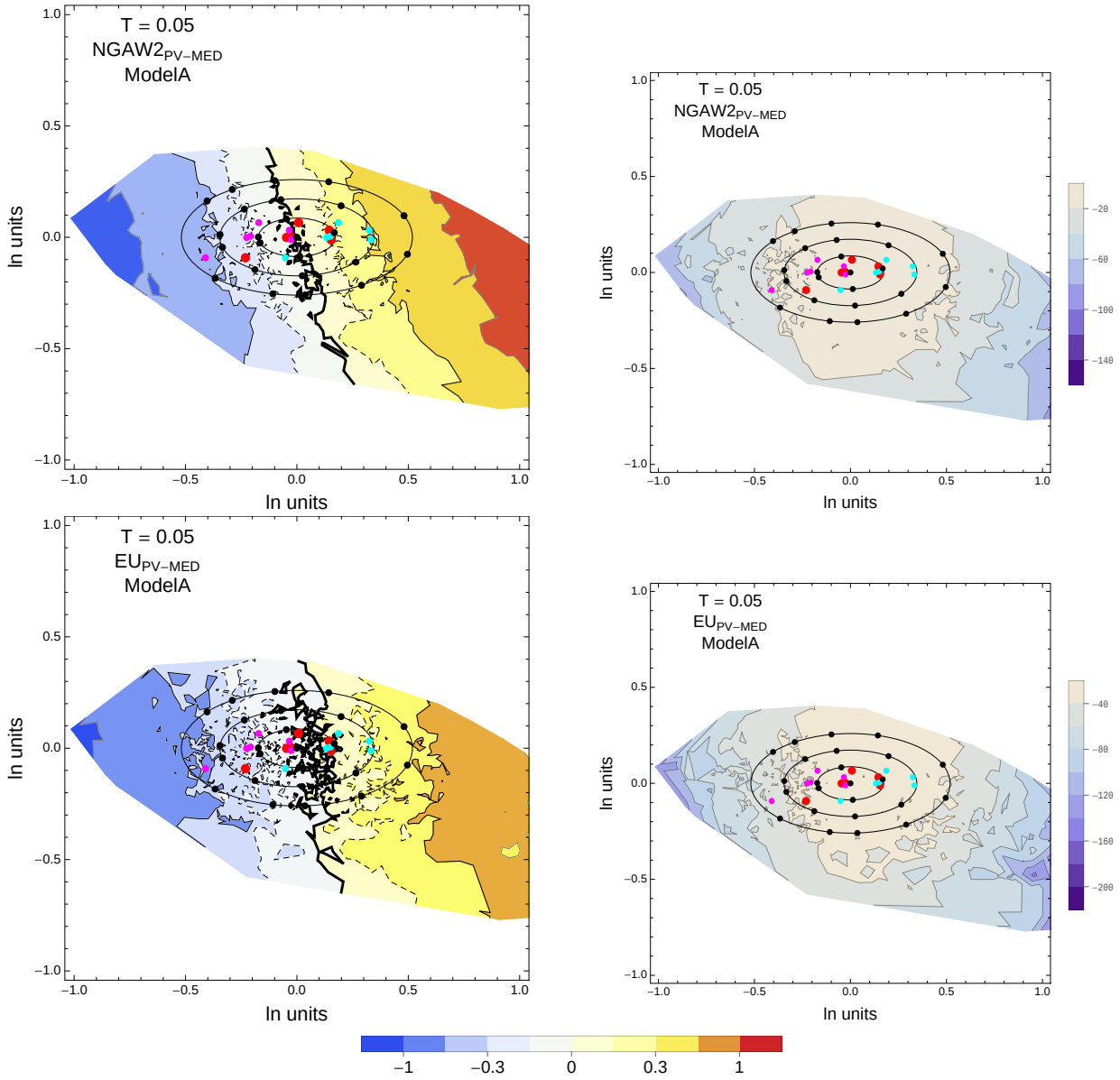



Figure 3.38: PVNGSv2: Contour Plots of mean residuals (top left) and likelihood (top right) for the NGA$_{PV-MED}$ dataset, and mean residuals (bottom left) and likelihood (top right) for the EU$_{PV-MED}$ dataset. Reference points are black dots. The original GMPEs are red dots,plus/minus uncertainty are magenta/cyan dots. The contour for the zero residual is a thick black line, the -0.15/0.15 contours are dashed black lines and the -0.3/0.3 contours are thin black lines. For $T = 0.05$s.

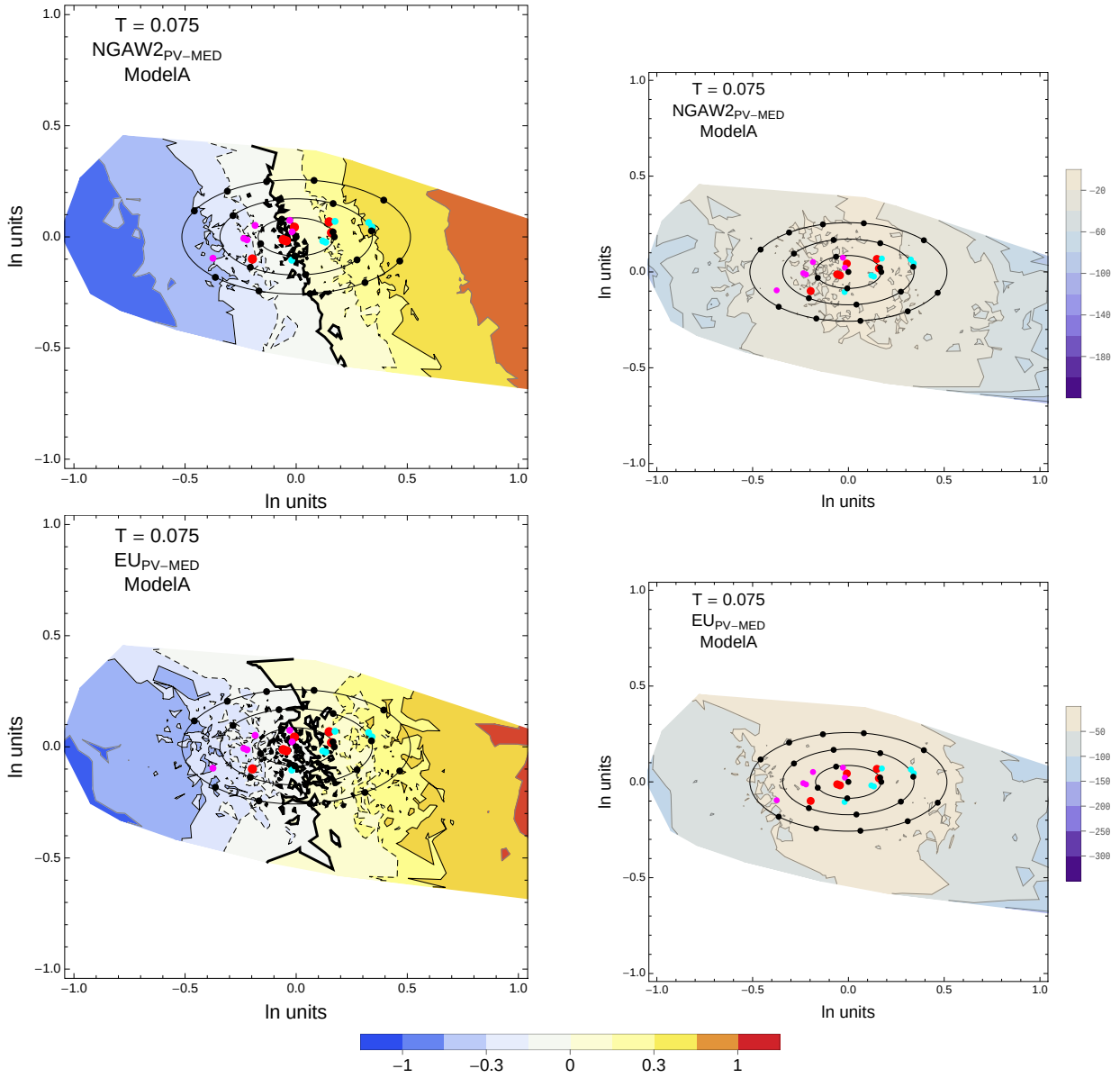



Figure 3.39: PVNGSv2: Contour Plots of mean residuals (top left) and likelihood (top right) for the NGA$_{PV-MED}$ dataset, and mean residuals (bottom left) and likelihood (top right) for the EU$_{PV-MED}$ dataset. Reference points are black dots. The original GMPEs are red dots,plus/minus uncertainty are magenta/cyan dots. The contour for the zero residual is a thick black line, the -0.15/0.15 contours are dashed black lines and the -0.3/0.3 contours are thin black lines. For $T = 0.075$s.

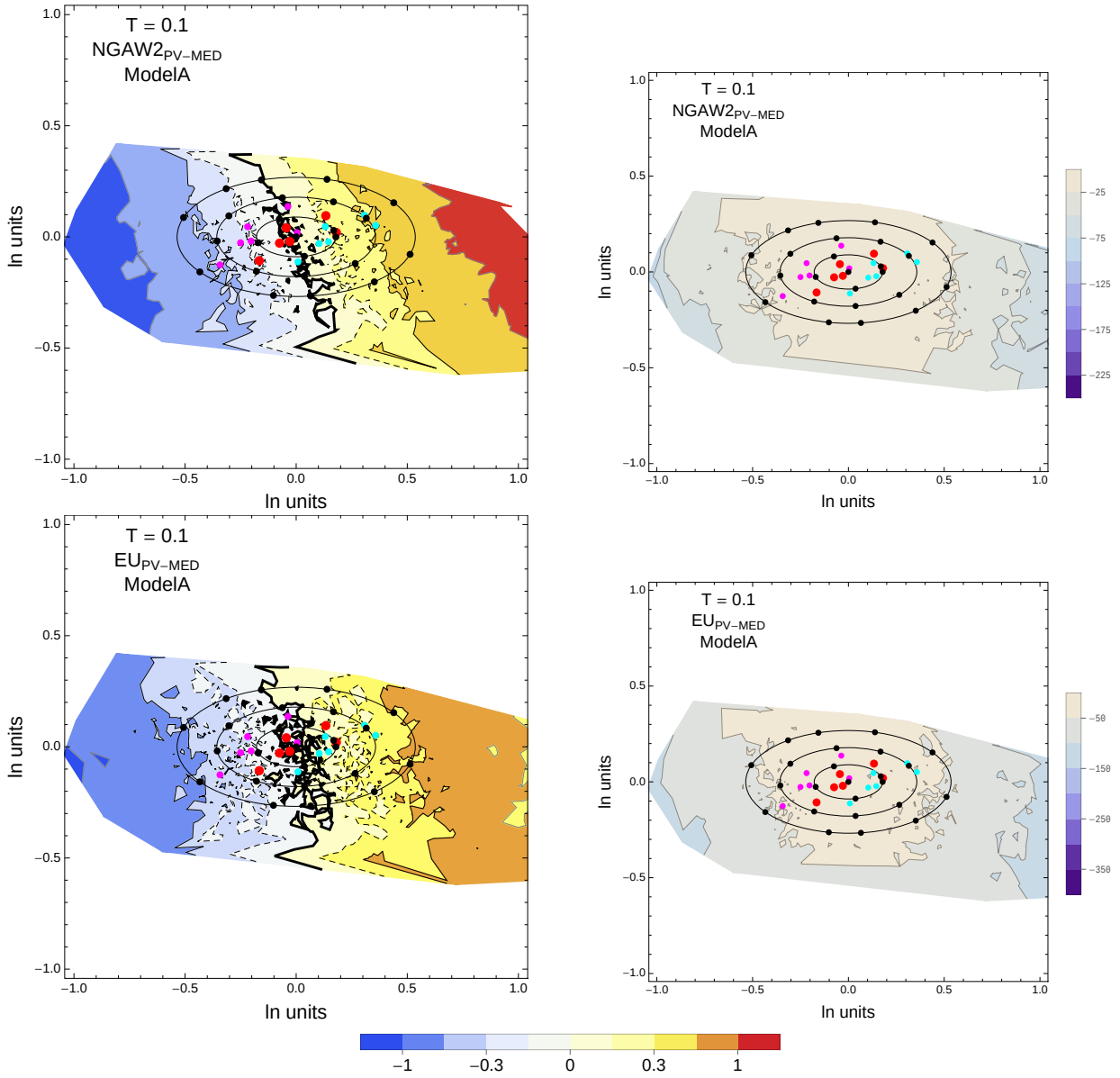



Figure 3.40: PVNGSv2: Contour Plots of mean residuals (top left) and likelihood (top right) for the NGA$_{PV-MED}$ dataset, and mean residuals (bottom left) and likelihood (top right) for the EU$_{PV-MED}$ dataset. Reference points are black dots. The original GMPEs are red dots,plus/minus uncertainty are magenta/cyan dots. The contour for the zero residual is a thick black line, the -0.15/0.15 contours are dashed black lines and the -0.3/0.3 contours are thin black lines. For $T = 0.1$s.

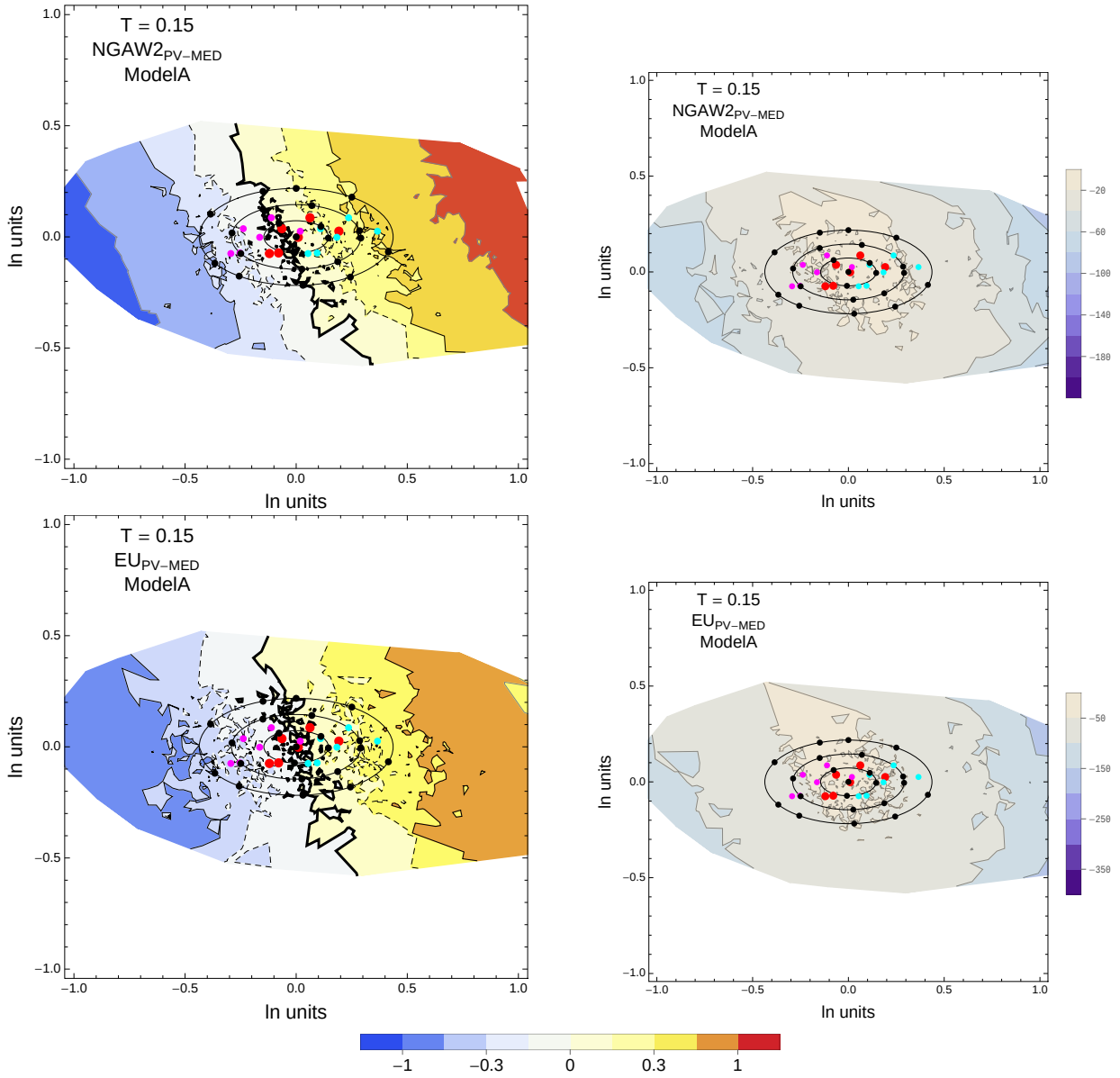



Figure 3.41: PVNGSv2: Contour Plots of mean residuals (top left) and likelihood (top right) for the NGA$_{PV-MED}$ dataset, and mean residuals (bottom left) and likelihood (top right) for the EU$_{PV-MED}$ dataset. Reference points are black dots. The original GMPEs are red dots,plus/minus uncertainty are magenta/cyan dots. The contour for the zero residual is a thick black line, the -0.15/0.15 contours are dashed black lines and the -0.3/0.3 contours are thin black lines. For $T = 0.15$s.

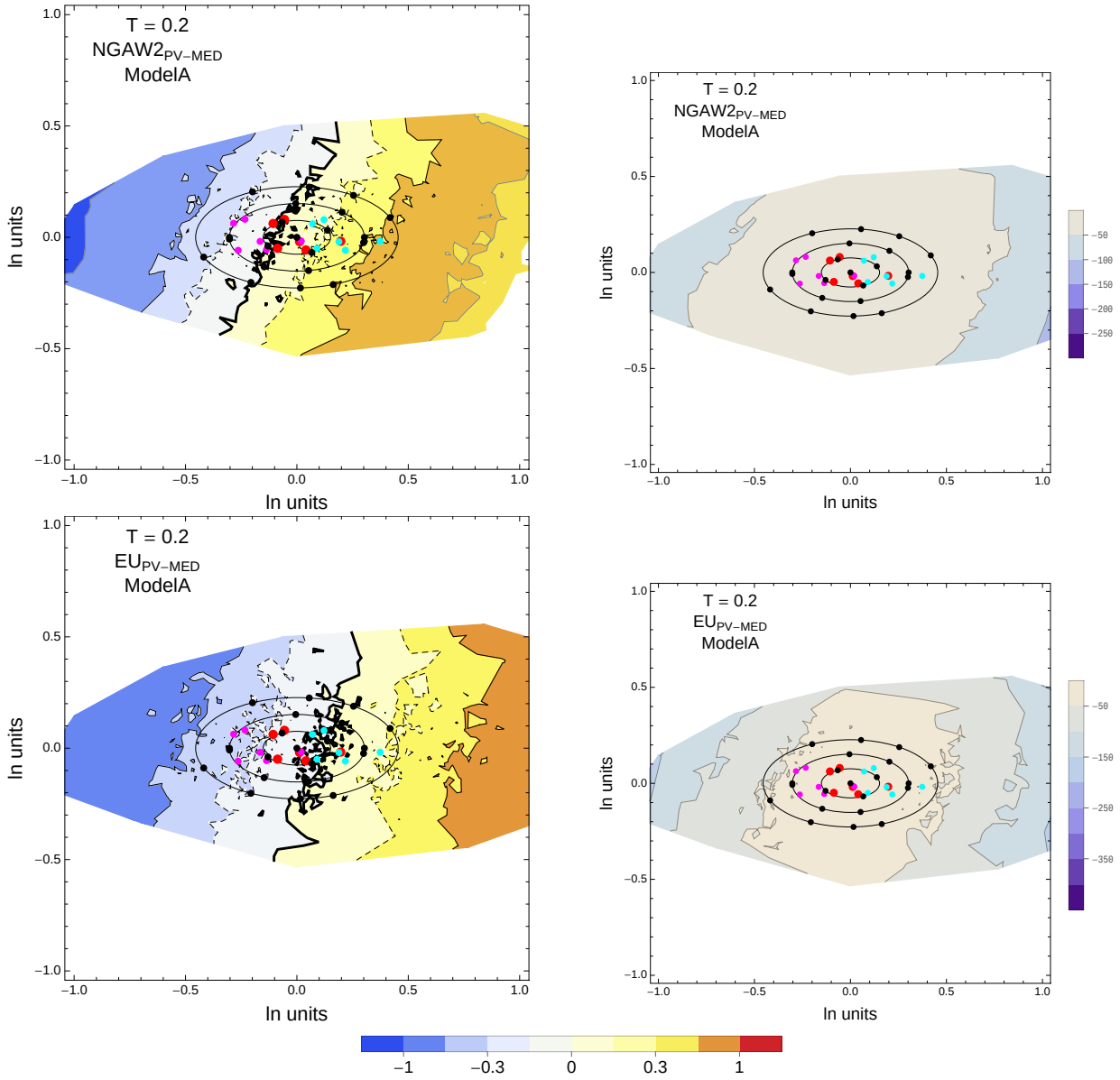



Figure 3.42: PVNGSv2: Contour Plots of mean residuals (top left) and likelihood (top right) for the NGA$_{PV-MED}$ dataset, and mean residuals (bottom left) and likelihood (top right) for the EU$_{PV-MED}$ dataset. Reference points are black dots. The original GMPEs are red dots,plus/minus uncertainty are magenta/cyan dots. The contour for the zero residual is a thick black line, the -0.15/0.15 contours are dashed black lines and the -0.3/0.3 contours are thin black lines. For $T = 0.2$s.

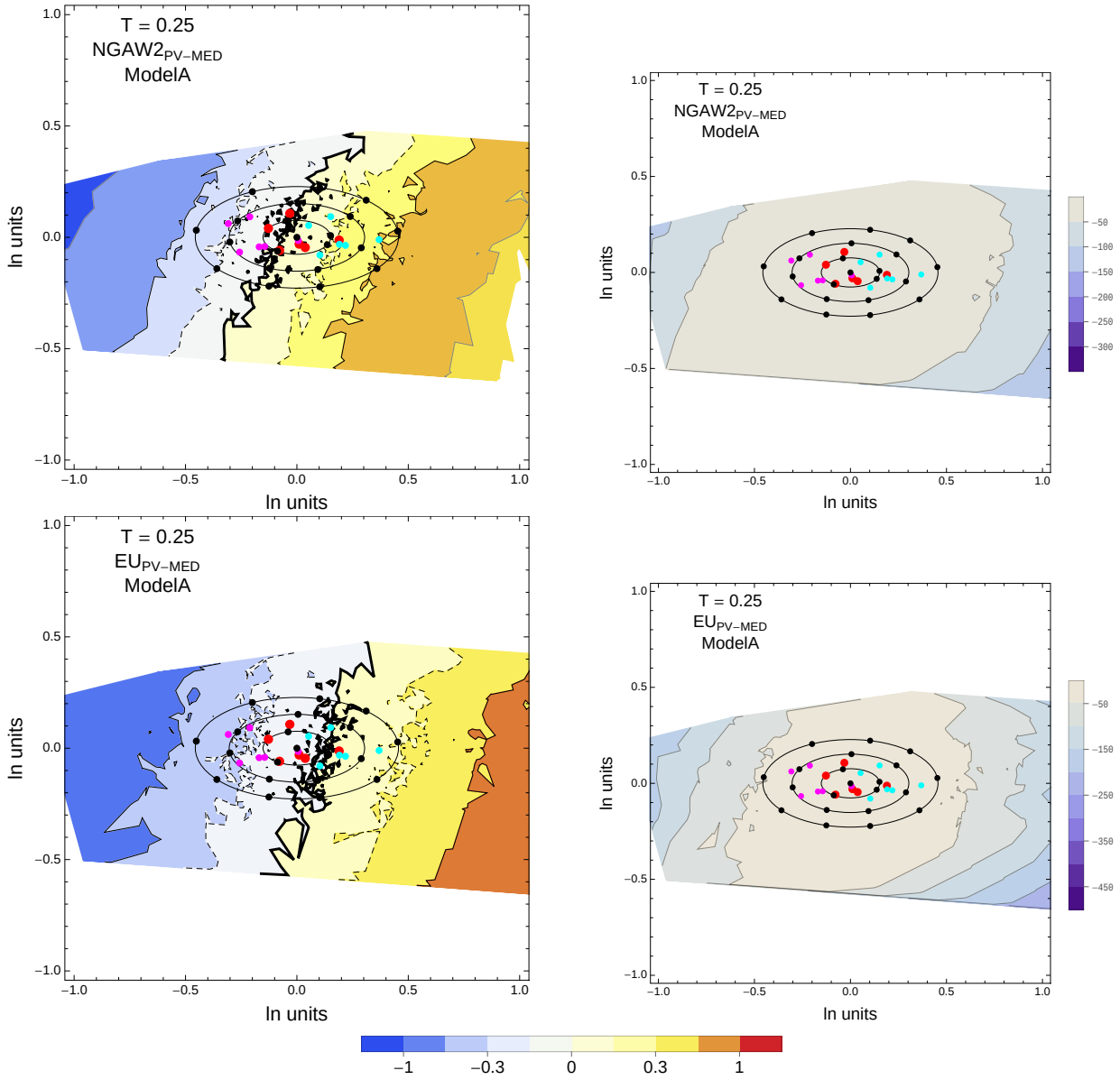



Figure 3.43: PVNGSv2: Contour Plots of mean residuals (top left) and likelihood (top right) for the NGA$_{PV-MED}$ dataset, and mean residuals (bottom left) and likelihood (top right) for the EU$_{PV-MED}$ dataset. Reference points are black dots. The original GMPEs are red dots,plus/minus uncertainty are magenta/cyan dots. The contour for the zero residual is a thick black line, the -0.15/0.15 contours are dashed black lines and the -0.3/0.3 contours are thin black lines. For $T = 0.25$s.

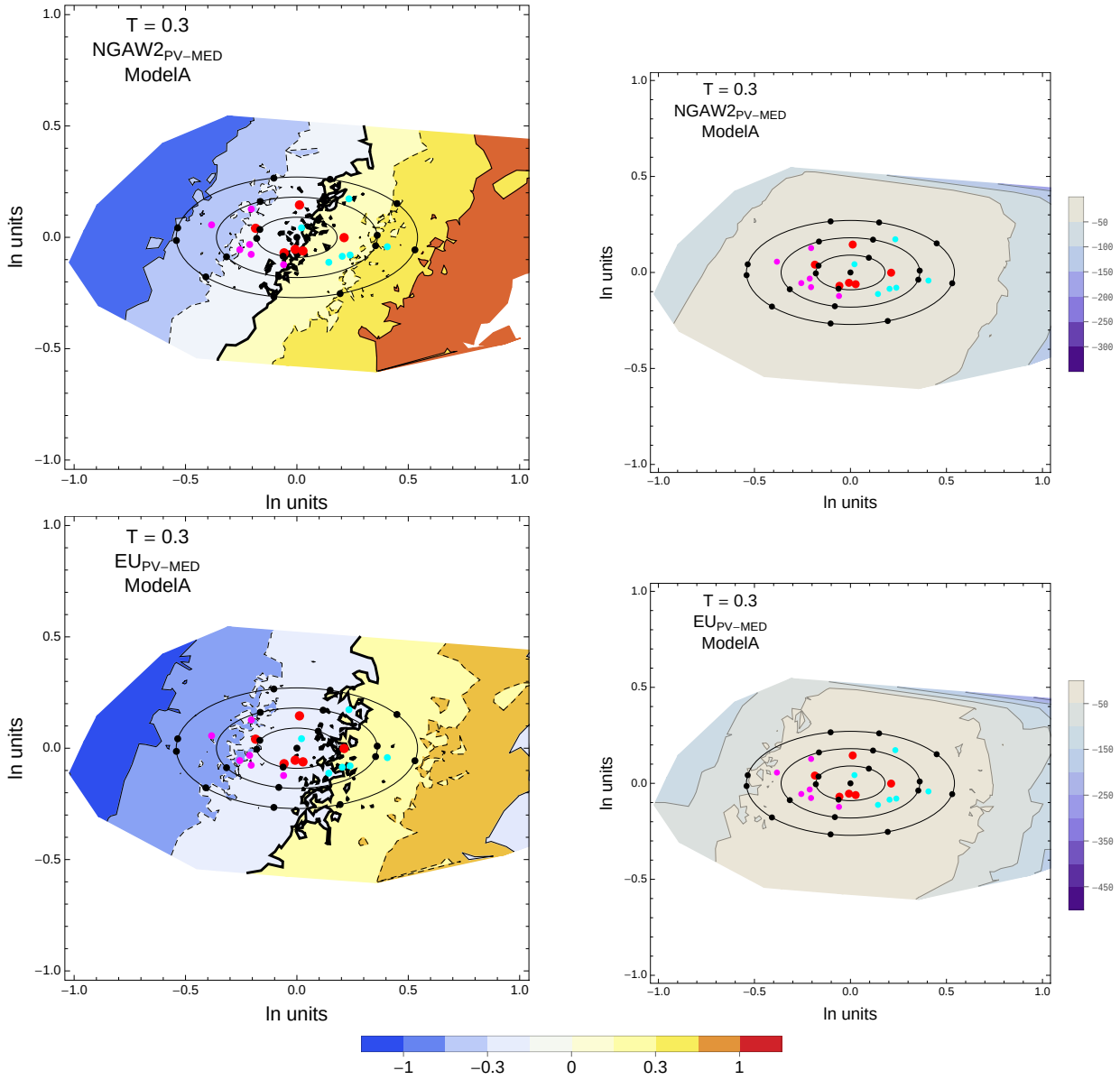



Figure 3.44: PVNGSv2: Contour Plots of mean residuals (top left) and likelihood (top right) for the NGA$_{PV-MED}$ dataset, and mean residuals (bottom left) and likelihood (top right) for the EU$_{PV-MED}$ dataset. Reference points are black dots. The original GMPEs are red dots,plus/minus uncertainty are magenta/cyan dots. The contour for the zero residual is a thick black line, the -0.15/0.15 contours are dashed black lines and the -0.3/0.3 contours are thin black lines. For $T = 0.3$s.

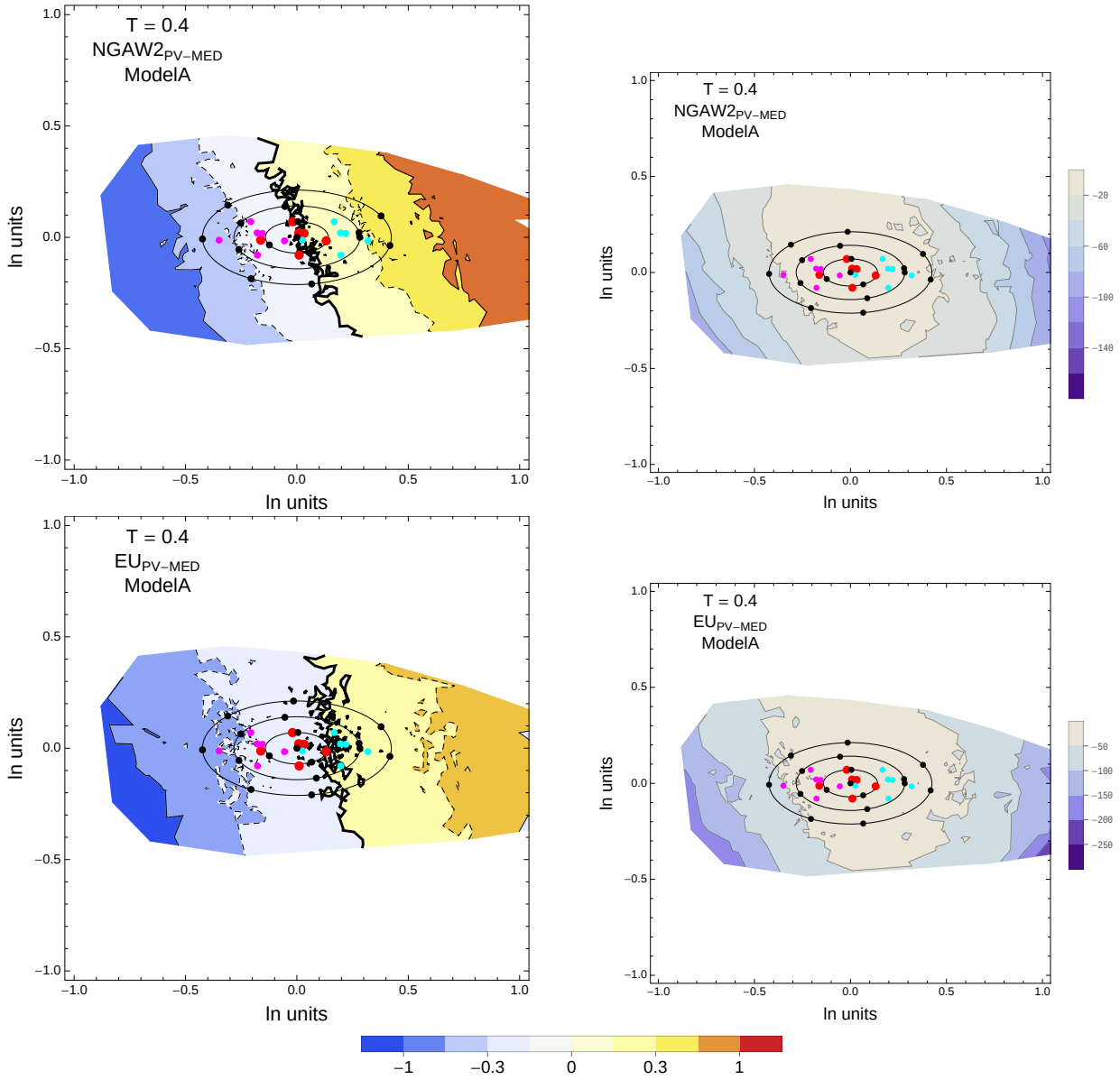



Figure 3.45: PVNGSv2: Contour Plots of mean residuals (top left) and likelihood (top right) for the NGA$_{PV-MED}$ dataset, and mean residuals (bottom left) and likelihood (top right) for the EU$_{PV-MED}$ dataset. Reference points are black dots. The original GMPEs are red dots,plus/minus uncertainty are magenta/cyan dots. The contour for the zero residual is a thick black line, the -0.15/0.15 contours are dashed black lines and the -0.3/0.3 contours are thin black lines. For $T = 0.4$s.

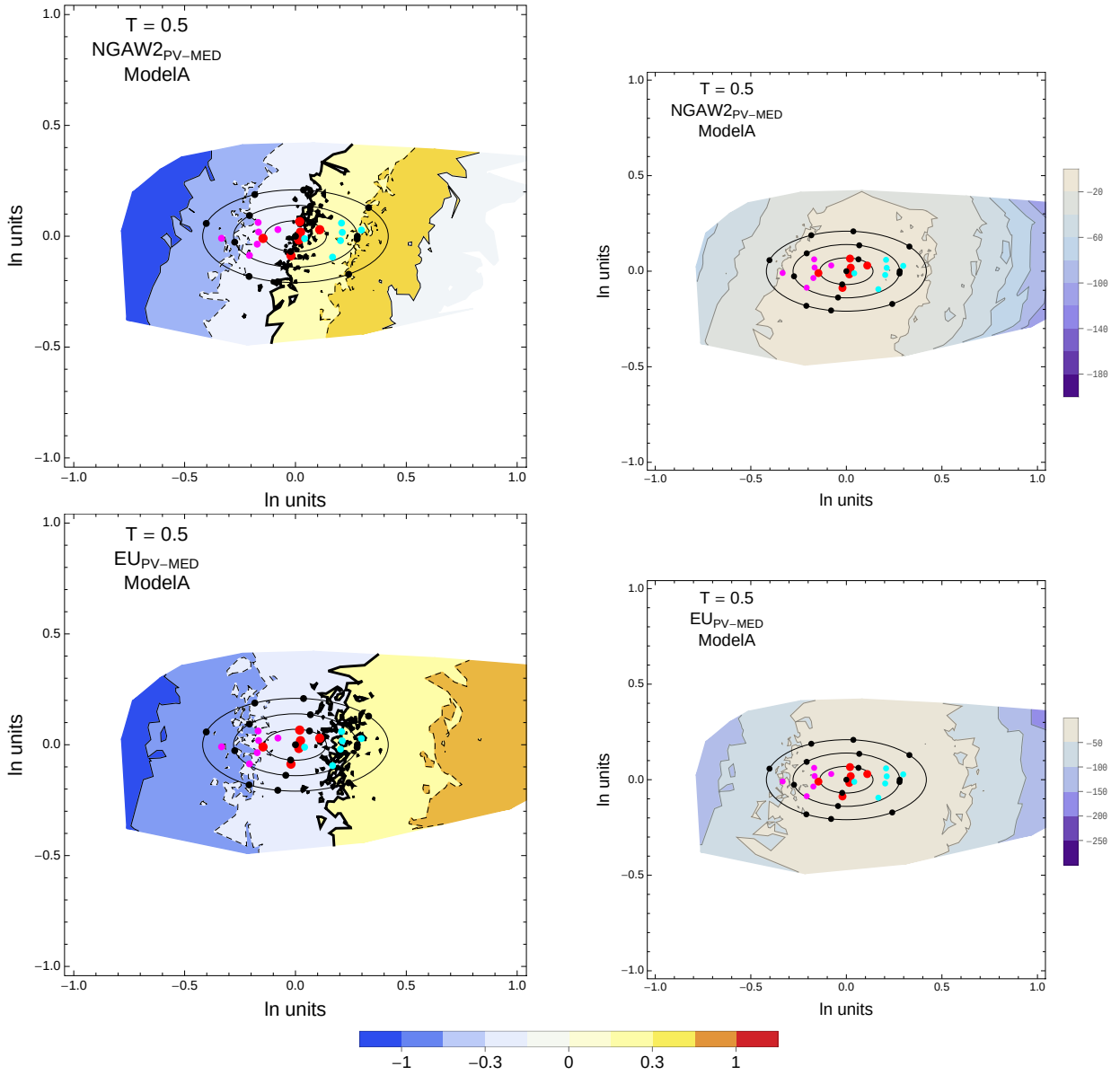



Figure 3.46: PVNGSv2: Contour Plots of mean residuals (top left) and likelihood (top right) for the NGA$_{PV-MED}$ dataset, and mean residuals (bottom left) and likelihood (top right) for the EU$_{PV-MED}$ dataset. Reference points are black dots. The original GMPEs are red dots,plus/minus uncertainty are magenta/cyan dots. The contour for the zero residual is a thick black line, the -0.15/0.15 contours are dashed black lines and the -0.3/0.3 contours are thin black lines. For $T = 0.5$s.

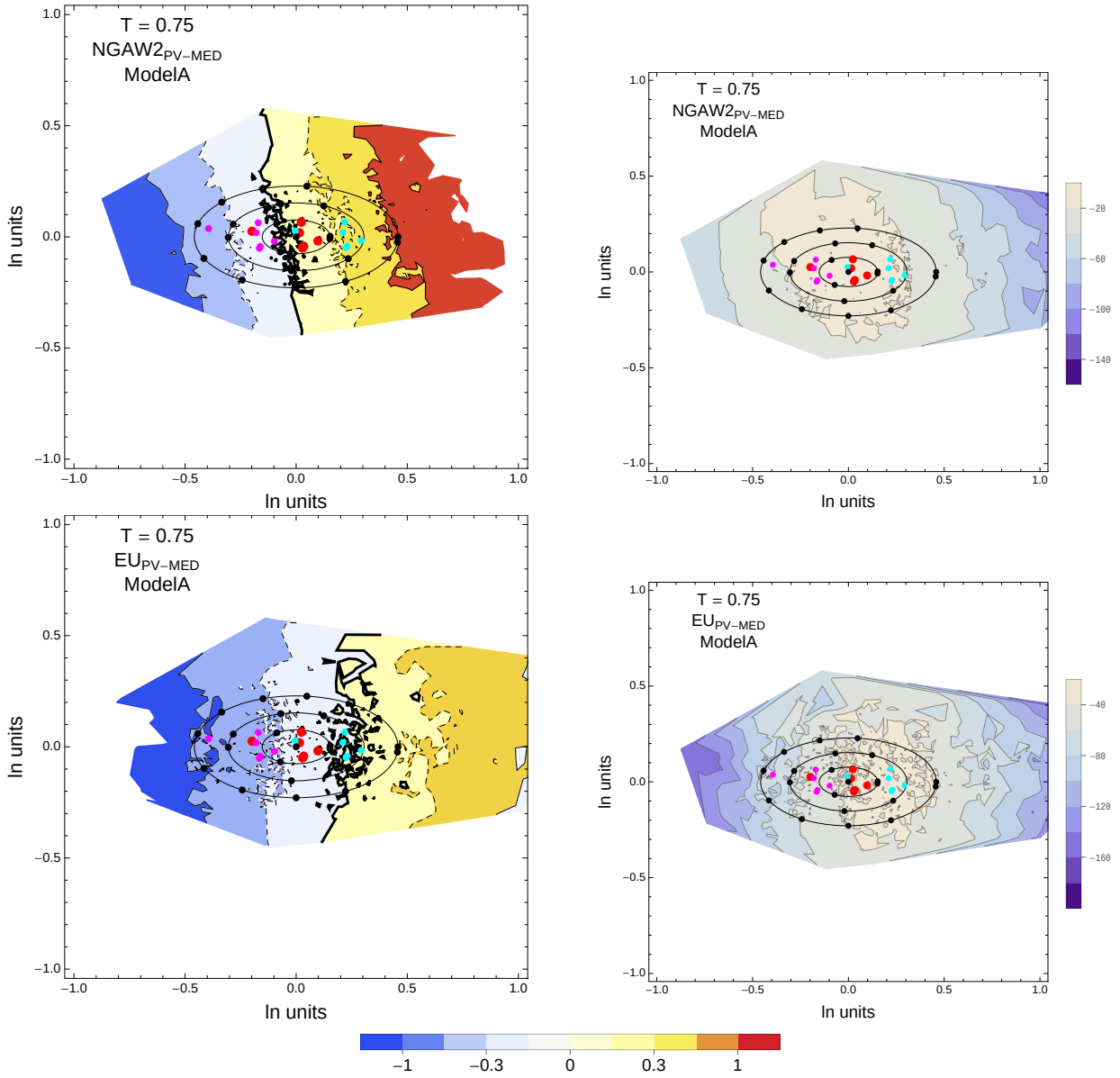



Figure 3.47: PVNGSv2: Contour Plots of mean residuals (top left) and likelihood (top right) for the NGA$_{PV-MED}$ dataset, and mean residuals (bottom left) and likelihood (top right) for the EU$_{PV-MED}$ dataset. Reference points are black dots. The original GMPEs are red dots,plus/minus uncertainty are magenta/cyan dots. The contour for the zero residual is a thick black line, the -0.15/0.15 contours are dashed black lines and the -0.3/0.3 contours are thin black lines. For $T = 0.75$s.

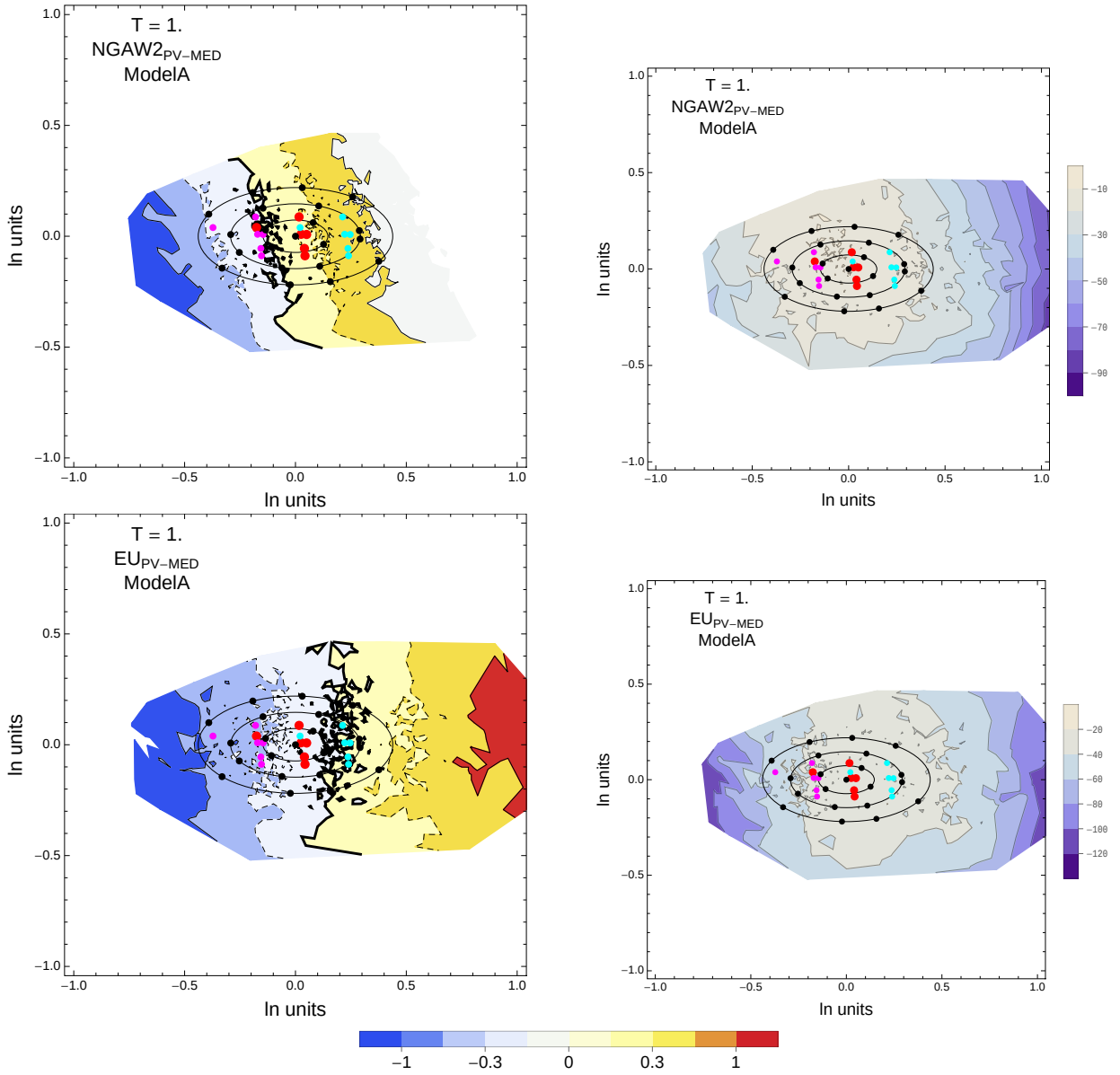



Figure 3.48: PVNGSv2: Contour Plots of mean residuals (top left) and likelihood (top right) for the NGA$_{PV-MED}$ dataset, and mean residuals (bottom left) and likelihood (top right) for the EU$_{PV-MED}$ dataset. Reference points are black dots. The original GMPEs are red dots,plus/minus uncertainty are magenta/cyan dots. The contour for the zero residual is a thick black line, the -0.15/0.15 contours are dashed black lines and the -0.3/0.3 contours are thin black lines. For $T = 1$.s.

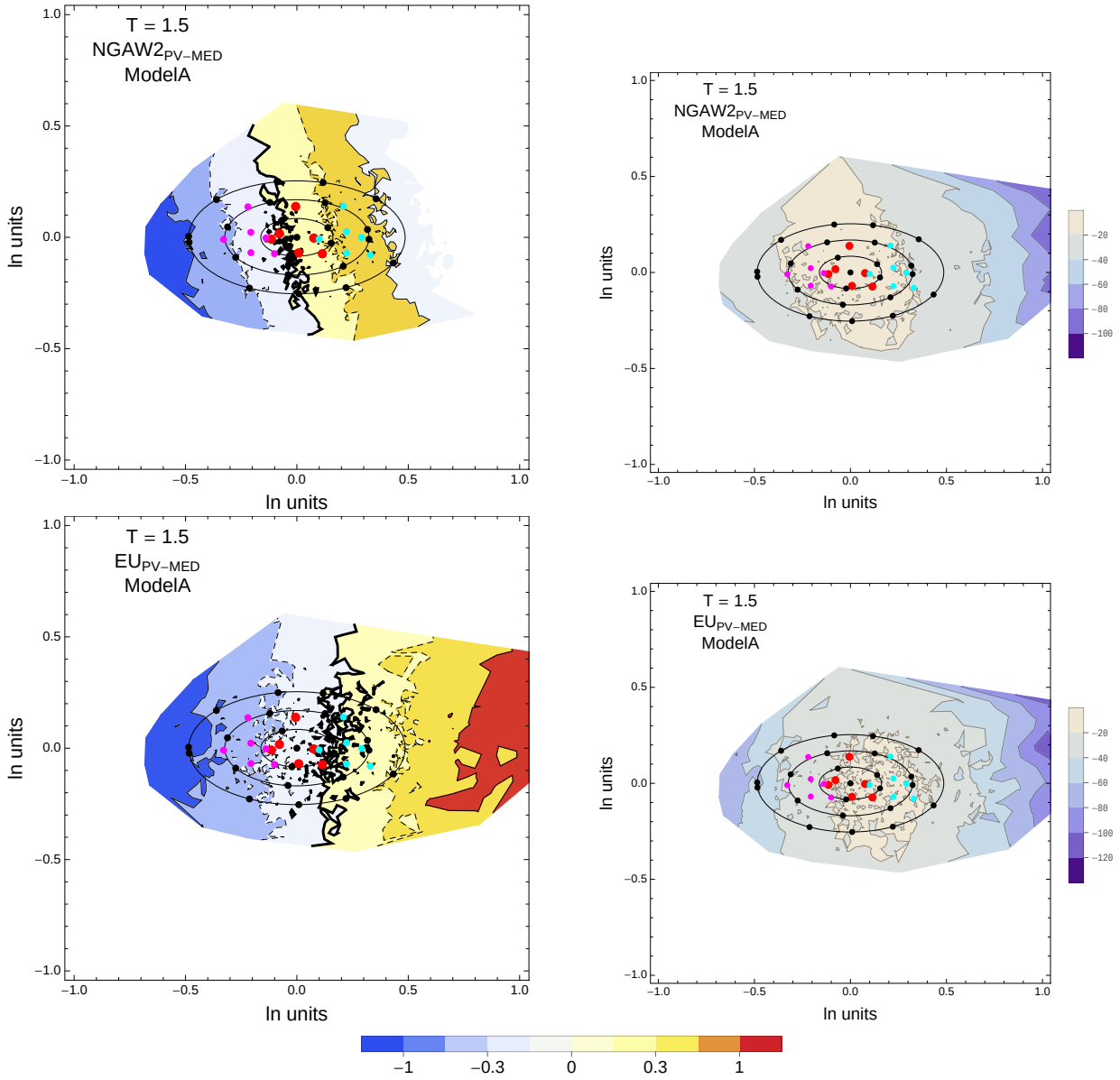



Figure 3.49: PVNGSv2: Contour Plots of mean residuals (top left) and likelihood (top right) for the NGA$_{PV-MED}$ dataset, and mean residuals (bottom left) and likelihood (top right) for the EU$_{PV-MED}$ dataset. Reference points are black dots. The original GMPEs are red dots,plus/minus uncertainty are magenta/cyan dots. The contour for the zero residual is a thick black line, the -0.15/0.15 contours are dashed black lines and the -0.3/0.3 contours are thin black lines. For $T = 1.5$s.

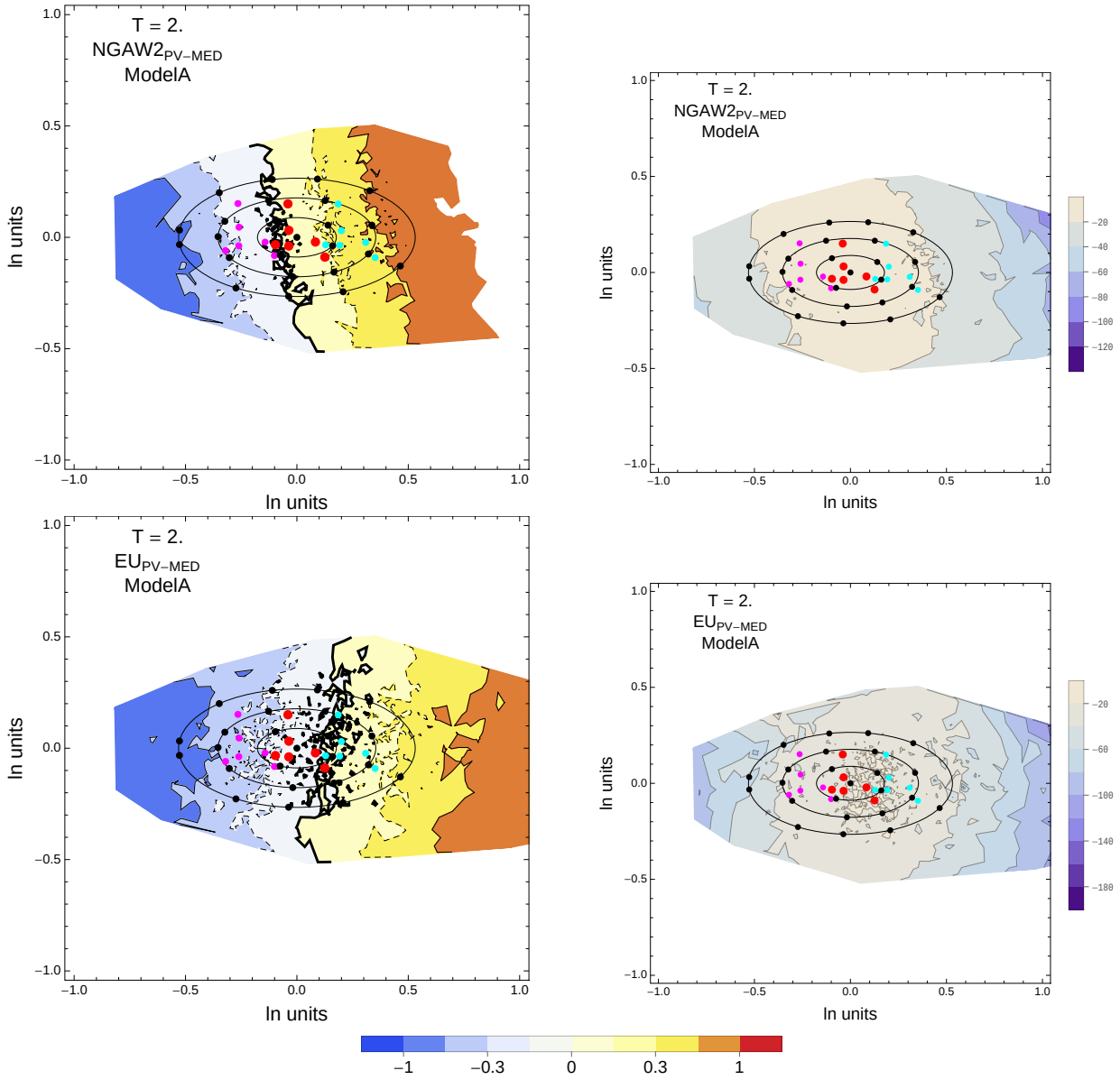



Figure 3.50: PVNGSv2: Contour Plots of mean residuals (top left) and likelihood (top right) for the NGA$_{PV-MED}$ dataset, and mean residuals (bottom left) and likelihood (top right) for the EU$_{PV-MED}$ dataset. Reference points are black dots. The original GMPEs are red dots,plus/minus uncertainty are magenta/cyan dots. The contour for the zero residual is a thick black line, the -0.15/0.15 contours are dashed black lines and the -0.3/0.3 contours are thin black lines. For $T = 2$.s.

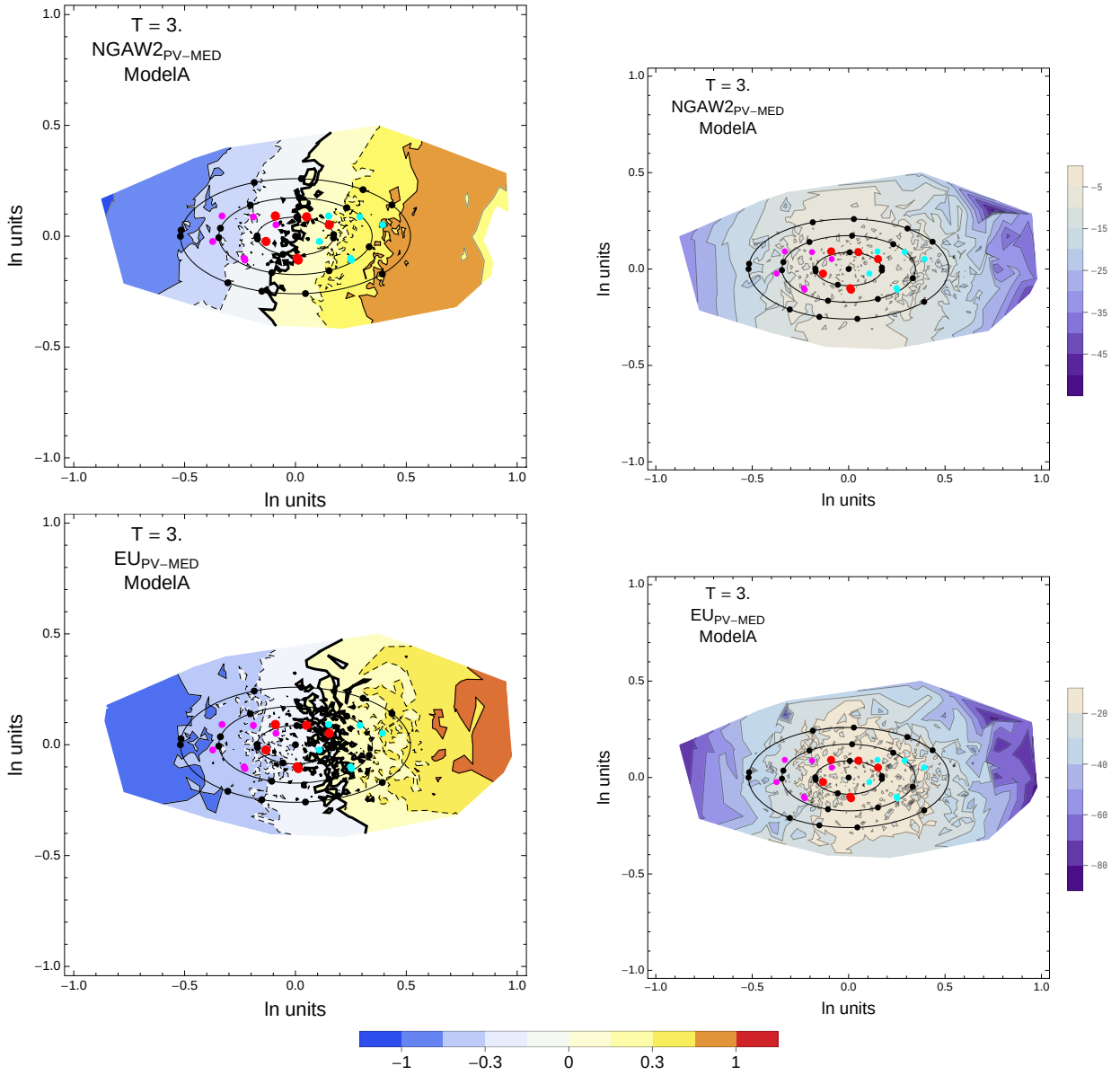



Figure 3.51: PVNGSv2: Contour Plots of mean residuals (top left) and likelihood (top right) for the NGA$_{PV-MED}$ dataset, and mean residuals (bottom left) and likelihood (top right) for the EU$_{PV-MED}$ dataset. Reference points are black dots. The original GMPEs are red dots,plus/minus uncertainty are magenta/cyan dots. The contour for the zero residual is a thick black line, the -0.15/0.15 contours are dashed black lines and the -0.3/0.3 contours are thin black lines. For $T = 3$.s.

### 3.1.3 Maps – Voronoi Cells

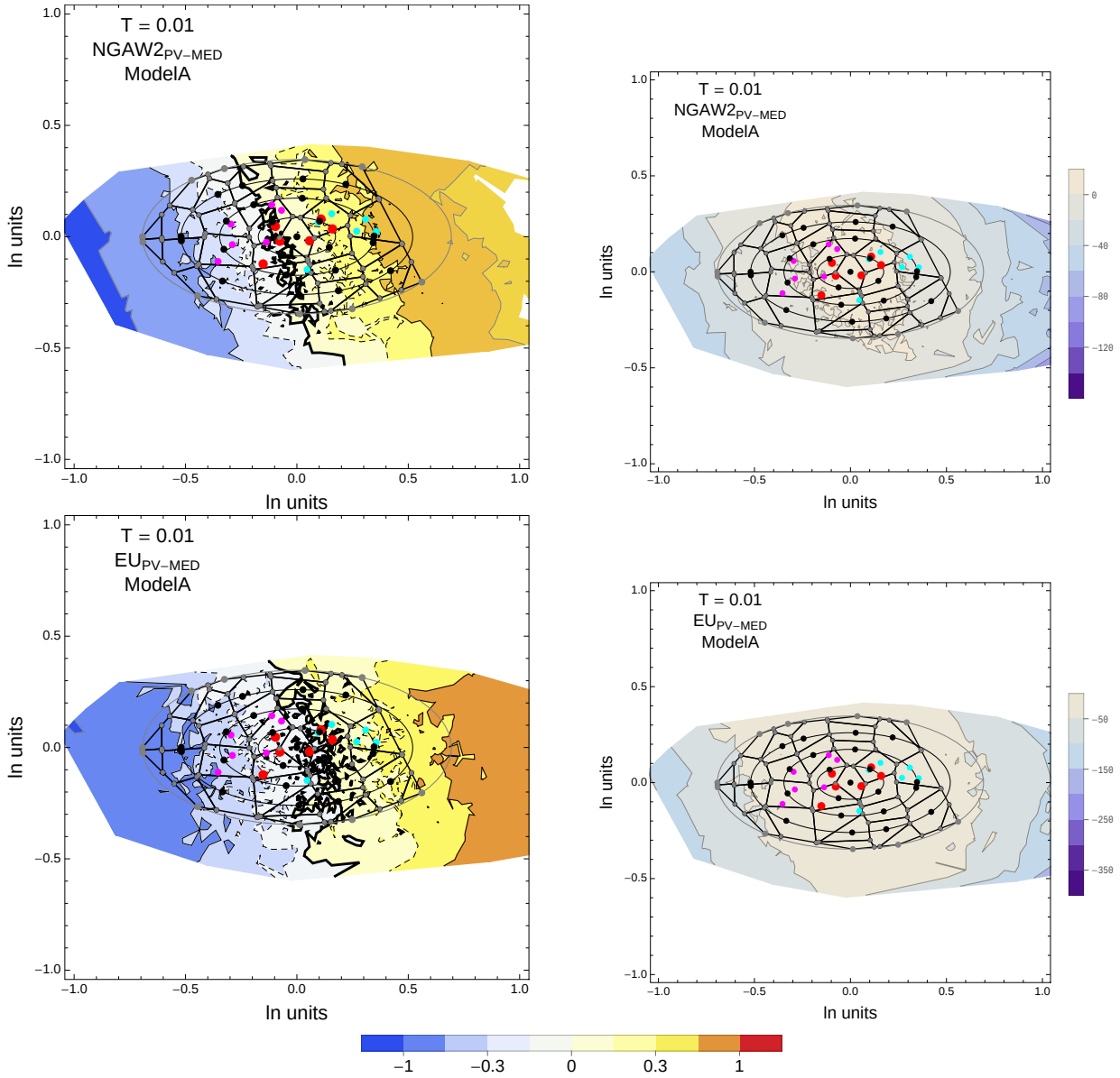



Figure 3.52: PVNGSv2: Contour Plots of selected mean residuals (top left) and likelihood (top right) for the NGA$_{PV-MED}$ dataset, and mean residuals (bottom left) and likelihood (top right) for the EU$_{PV-MED}$ dataset. The Voronoi cells used for selecting and weighting models are shown as black lines. The original GMPEs are red dots, plus/minus uncertainty are magenta/cyan dots. The contour for the zero residual is a thick black line, the -0.15/0.15 contours are dashed black lines and the -0.3/0.3 contours are thin black lines. For $T = 0.01$s.

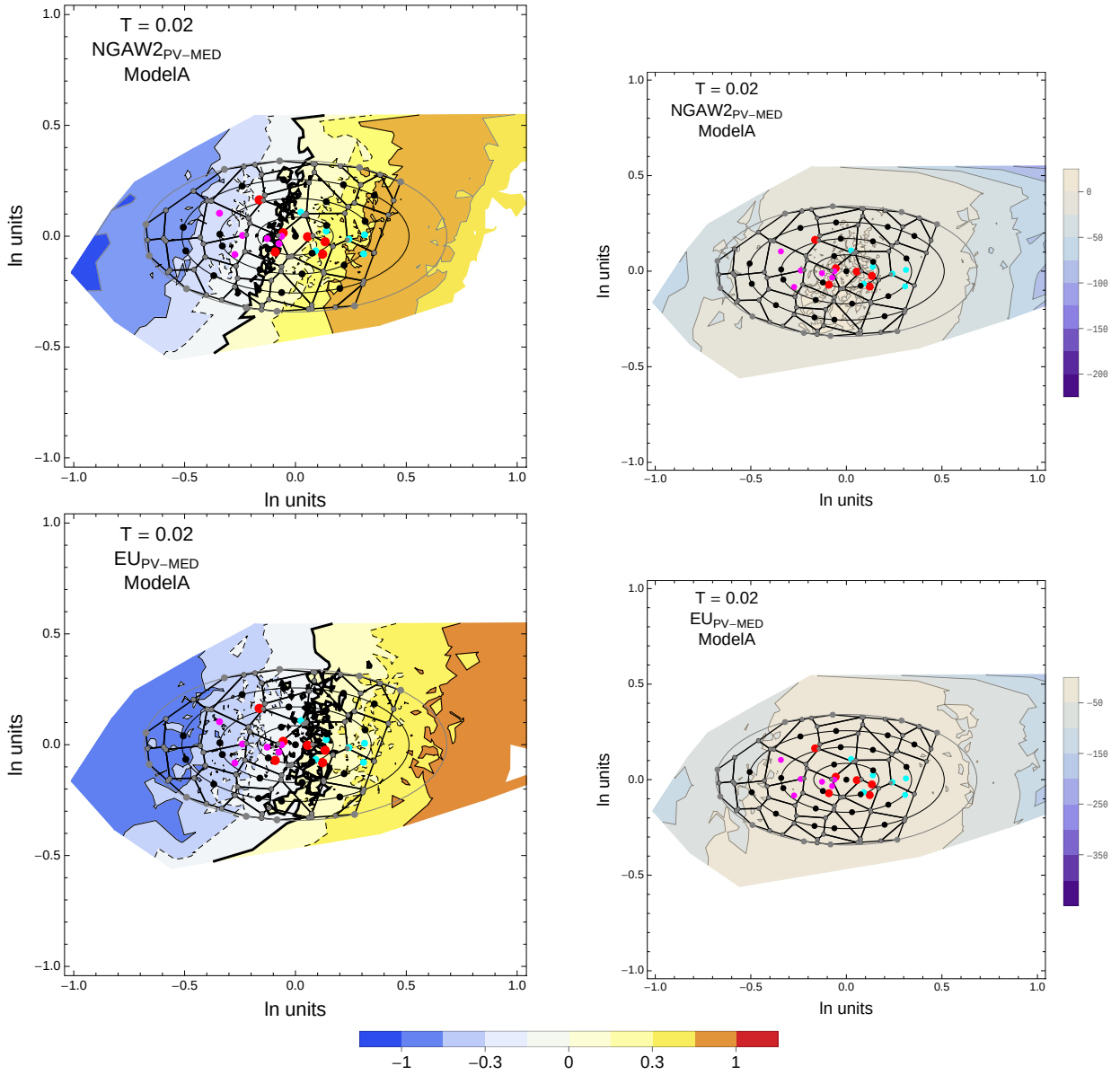



Figure 3.53: PVNGSv2: Contour Plots of selected mean residuals (top left) and likelihood (top right) for the NGA$_{PV-MED}$ dataset, and mean residuals (bottom left) and likelihood (top right) for the EU$_{PV-MED}$ dataset. The Voronoi cells used for selecting and weighting models are shown as black lines. The original GMPEs are red dots, plus/minus uncertainty are magenta/cyan dots. The contour for the zero residual is a thick black line, the -0.15/0.15 contours are dashed black lines and the -0.3/0.3 contours are thin black lines. For $T = 0.02$s.

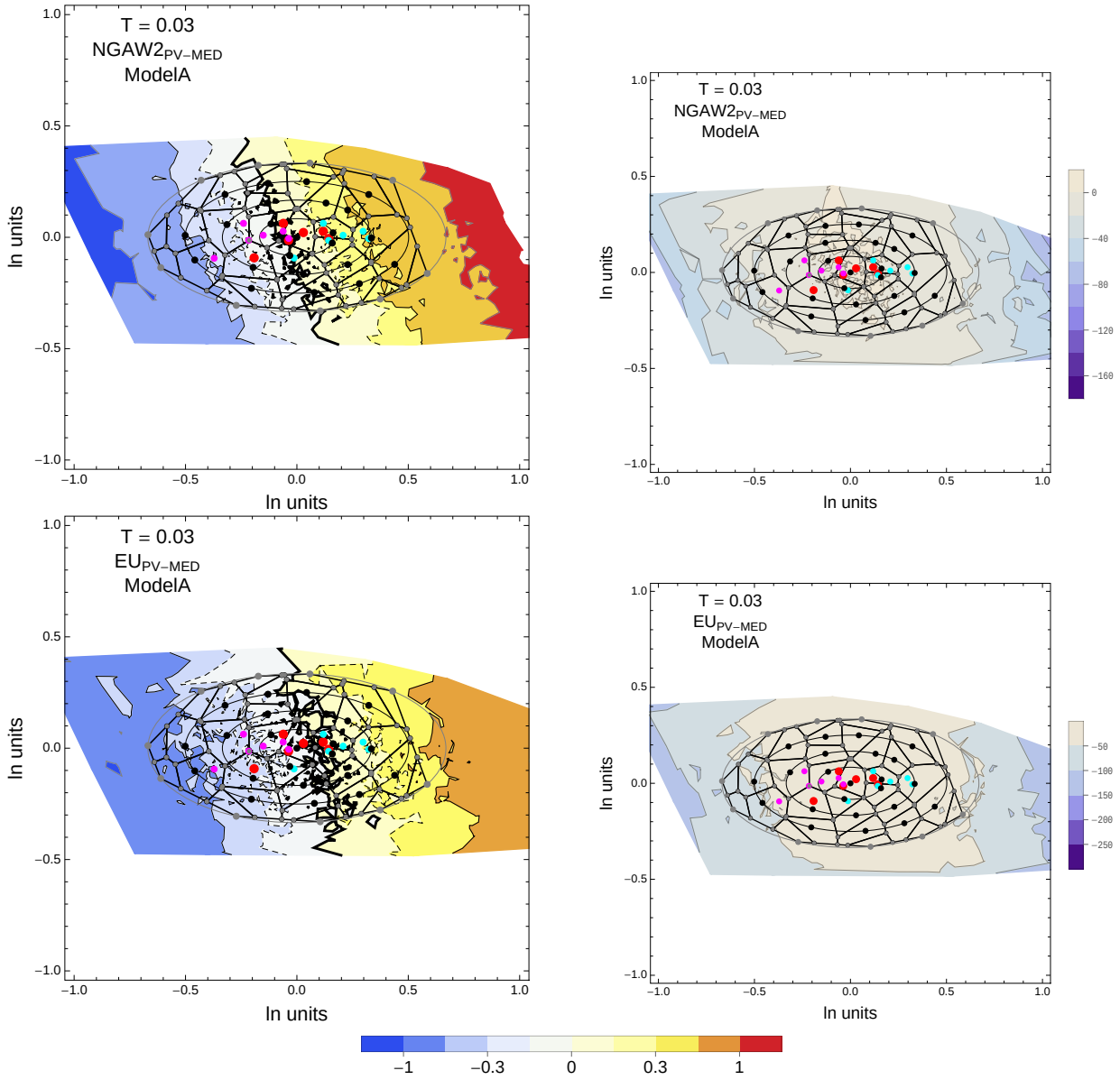



Figure 3.54: PVNGSv2: Contour Plots of selected mean residuals (top left) and likelihood (top right) for the NGA$_{PV-MED}$ dataset, and mean residuals (bottom left) and likelihood (top right) for the EU$_{PV-MED}$ dataset. The Voronoi cells used for selecting and weighting models are shown as black lines. The original GMPEs are red dots, plus/minus uncertainty are magenta/cyan dots. The contour for the zero residual is a thick black line, the -0.15/0.15 contours are dashed black lines and the -0.3/0.3 contours are thin black lines. For $T = 0.03$s.

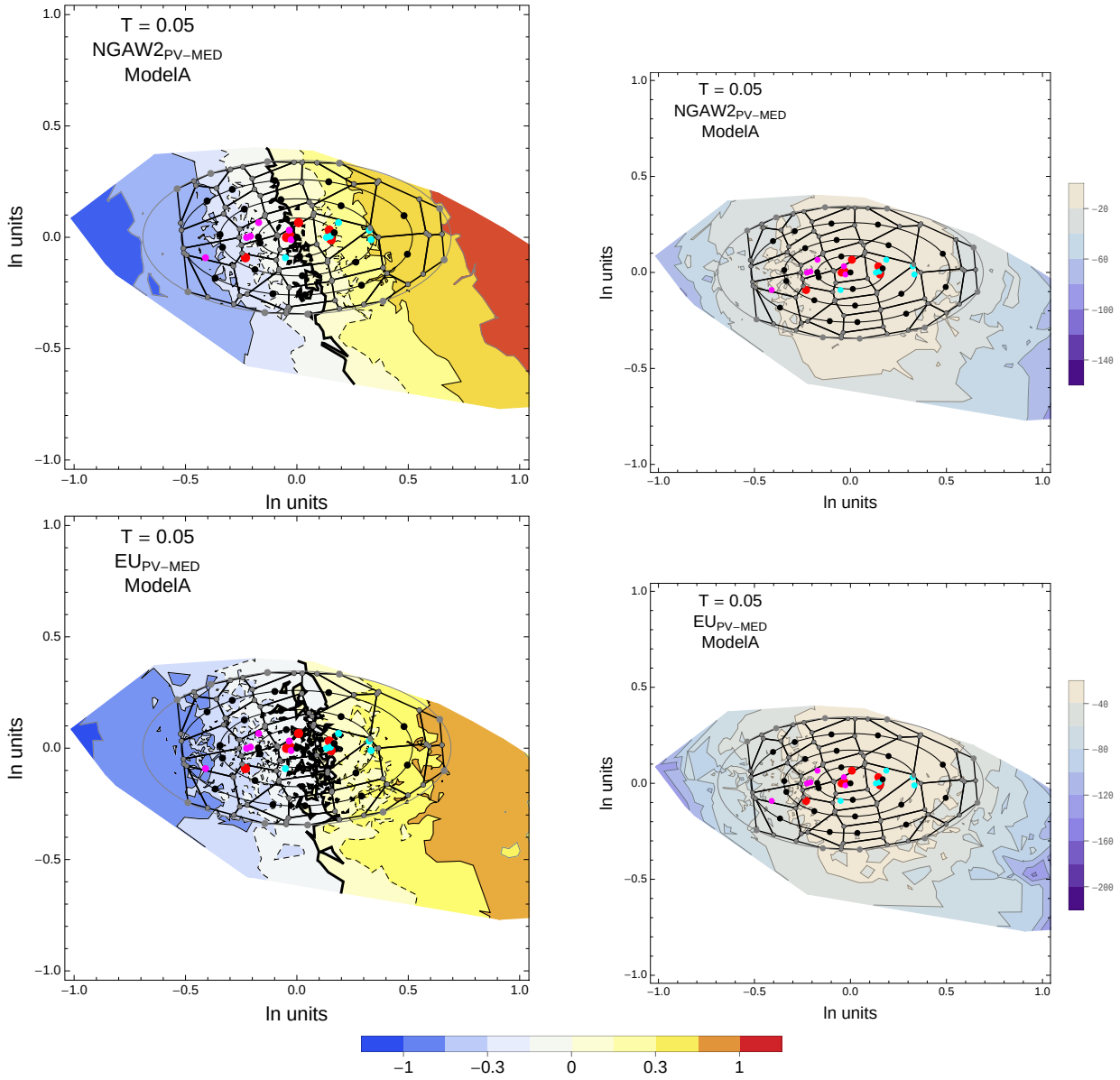



Figure 3.55: PVNGSv2: Contour Plots of selected mean residuals (top left) and likelihood (top right) for the NGA$_{PV-MED}$ dataset, and mean residuals (bottom left) and likelihood (top right) for the EU$_{PV-MED}$ dataset. The Voronoi cells used for selecting and weighting models are shown as black lines. The original GMPEs are red dots, plus/minus uncertainty are magenta/cyan dots. The contour for the zero residual is a thick black line, the -0.15/0.15 contours are dashed black lines and the -0.3/0.3 contours are thin black lines. For $T = 0.05$s.

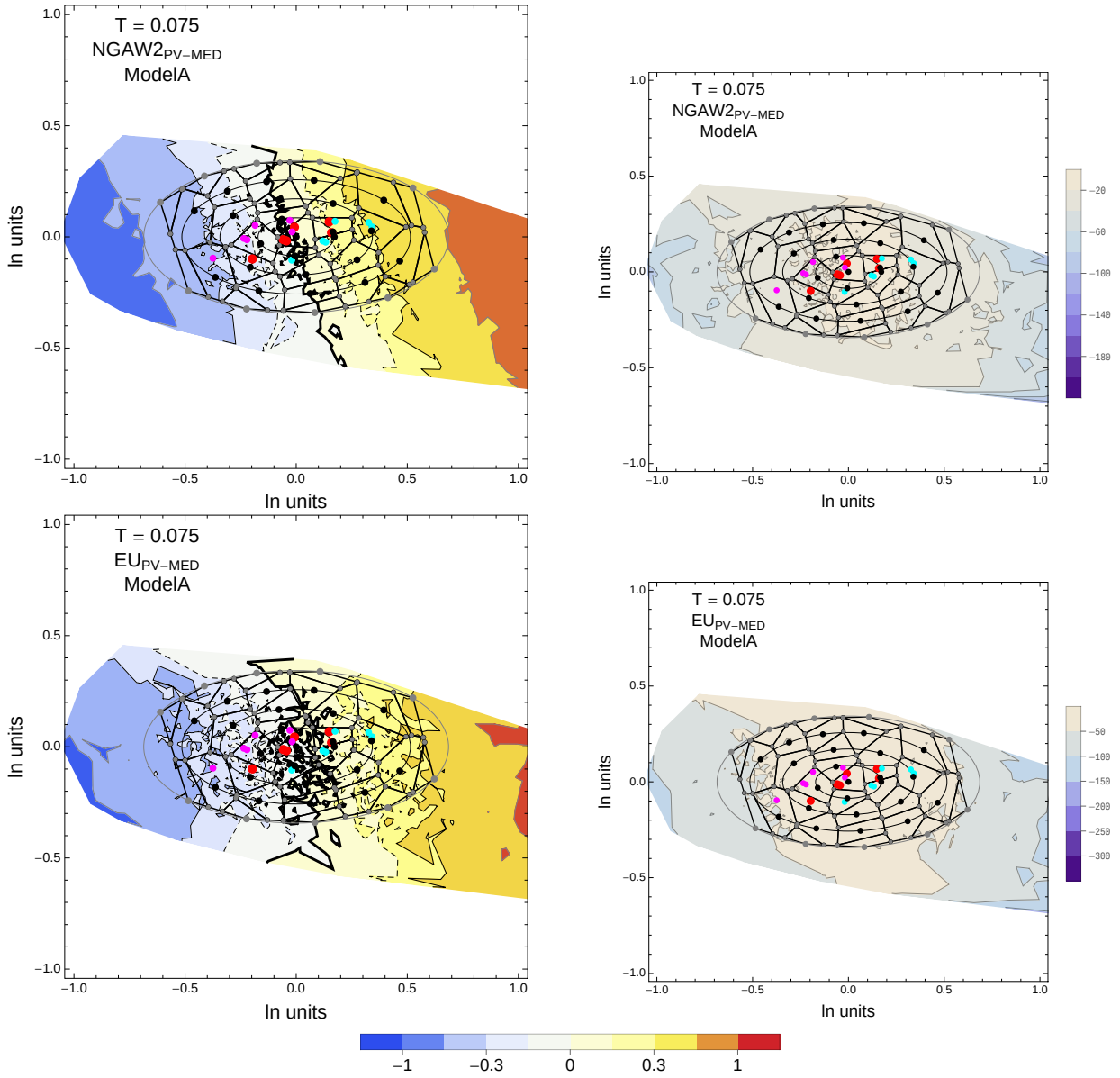



Figure 3.56: PVNGSv2: Contour Plots of selected mean residuals (top left) and likelihood (top right) for the NGA$_{PV-MED}$ dataset, and mean residuals (bottom left) and likelihood (top right) for the EU$_{PV-MED}$ dataset. The Voronoi cells used for selecting and weighting models are shown as black lines. The original GMPEs are red dots, plus/minus uncertainty are magenta/cyan dots. The contour for the zero residual is a thick black line, the -0.15/0.15 contours are dashed black lines and the -0.3/0.3 contours are thin black lines. For $T = 0.075$s.

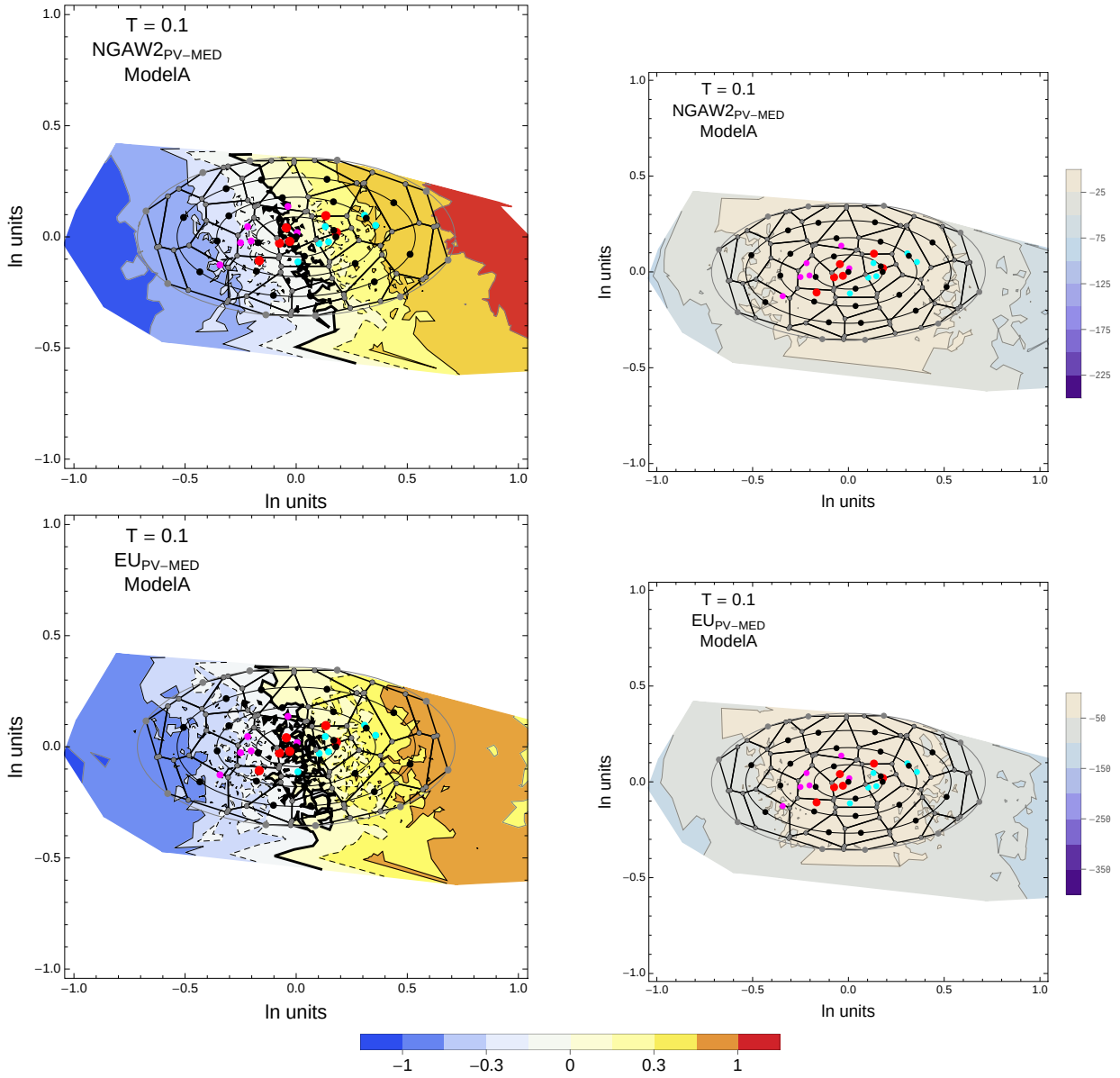



Figure 3.57: PVNGSv2: Contour Plots of selected mean residuals (top left) and likelihood (top right) for the NGA$_{PV-MED}$ dataset, and mean residuals (bottom left) and likelihood (top right) for the EU$_{PV-MED}$ dataset. The Voronoi cells used for selecting and weighting models are shown as black lines. The original GMPEs are red dots, plus/minus uncertainty are magenta/cyan dots. The contour for the zero residual is a thick black line, the -0.15/0.15 contours are dashed black lines and the -0.3/0.3 contours are thin black lines. For $T = 0.1$s.

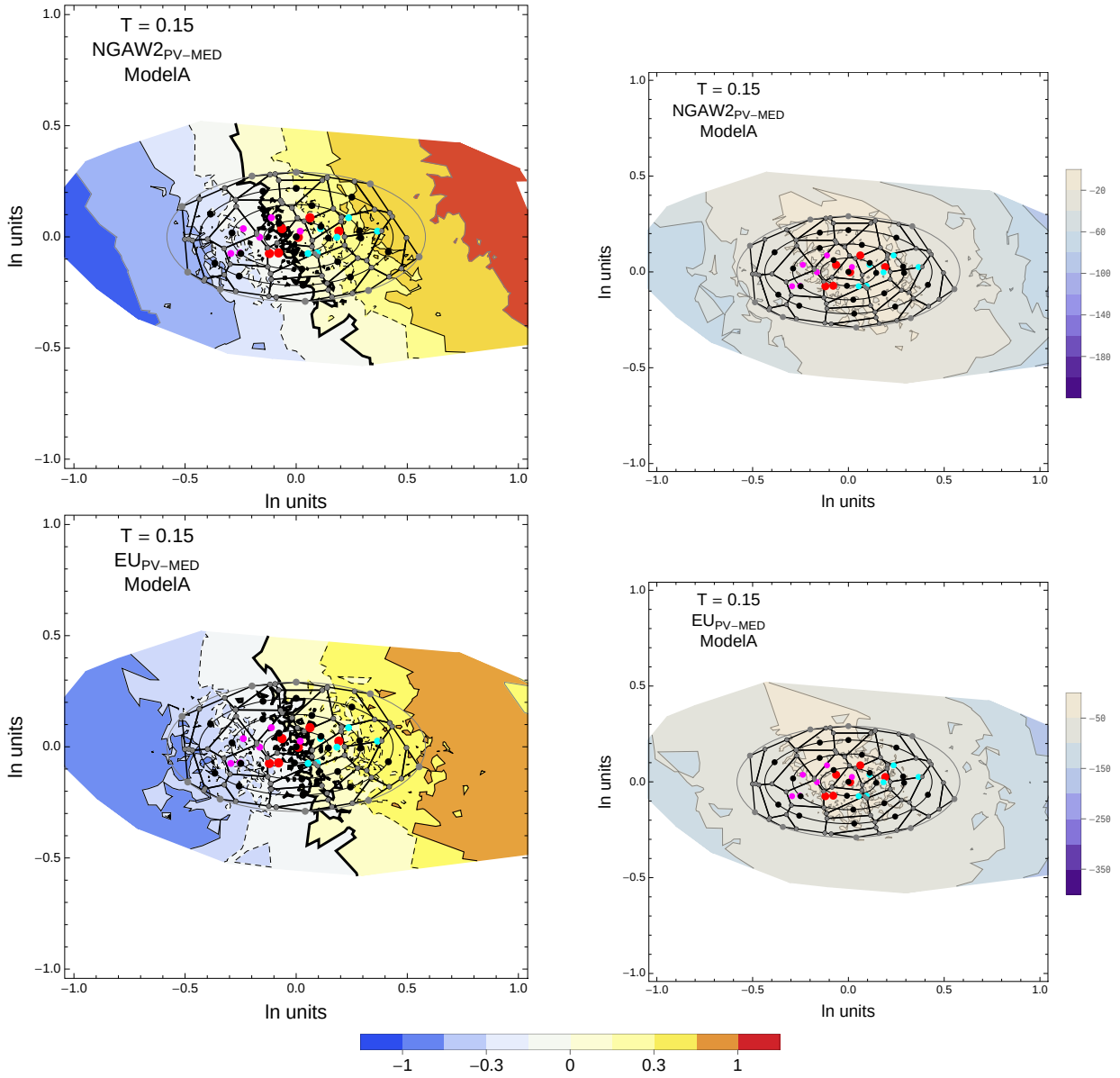



Figure 3.58: PVNGSv2: Contour Plots of selected mean residuals (top left) and likelihood (top right) for the NGA$_{PV-MED}$ dataset, and mean residuals (bottom left) and likelihood (top right) for the EU$_{PV-MED}$ dataset. The Voronoi cells used for selecting and weighting models are shown as black lines. The original GMPEs are red dots, plus/minus uncertainty are magenta/cyan dots. The contour for the zero residual is a thick black line, the -0.15/0.15 contours are dashed black lines and the -0.3/0.3 contours are thin black lines. For $T = 0.15$s.

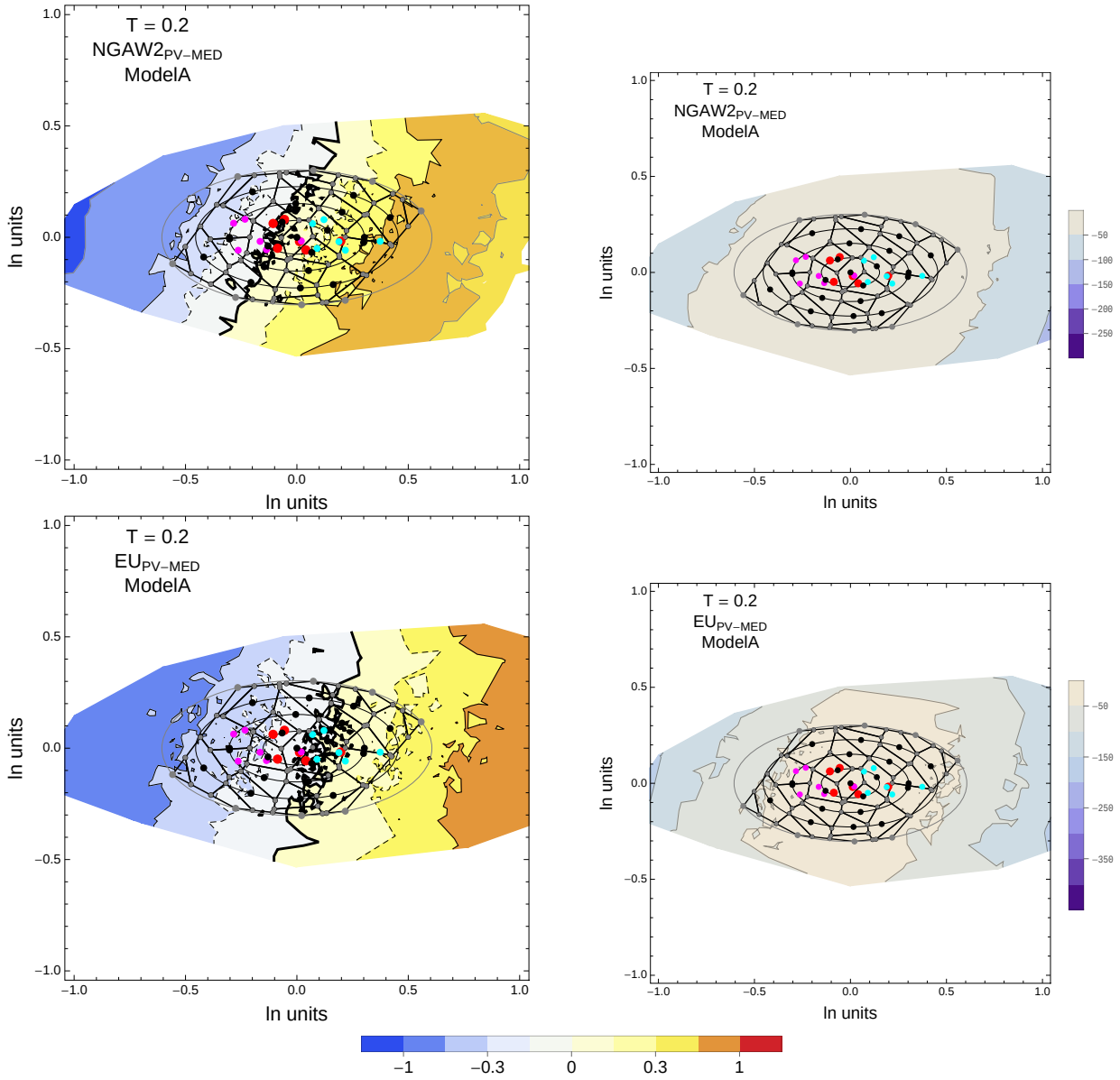



Figure 3.59: PVNGSv2: Contour Plots of selected mean residuals (top left) and likelihood (top right) for the NGA$_{PV-MED}$ dataset, and mean residuals (bottom left) and likelihood (top right) for the EU$_{PV-MED}$ dataset. The Voronoi cells used for selecting and weighting models are shown as black lines. The original GMPEs are red dots, plus/minus uncertainty are magenta/cyan dots. The contour for the zero residual is a thick black line, the -0.15/0.15 contours are dashed black lines and the -0.3/0.3 contours are thin black lines. For $T = 0.2$s.

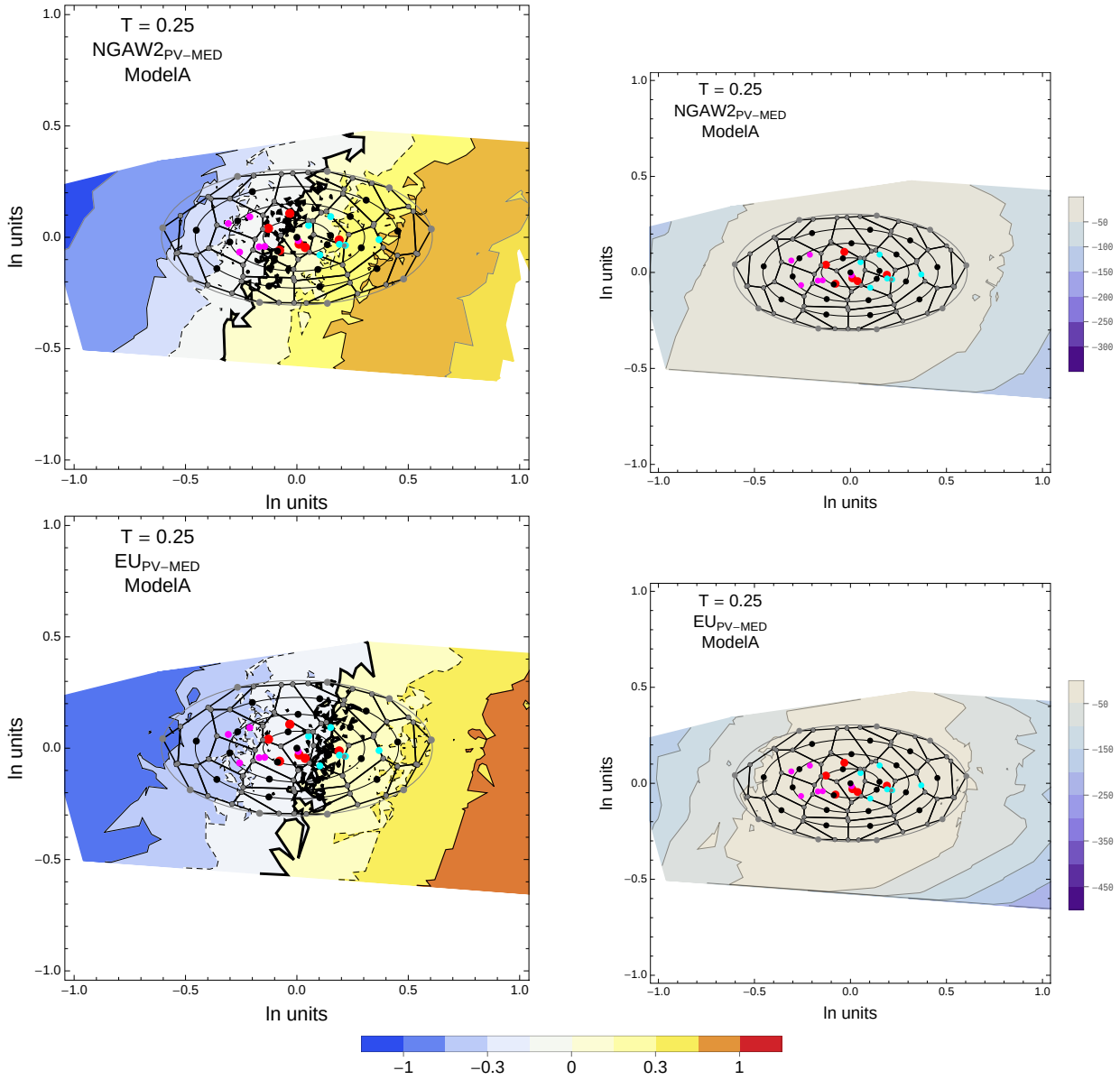



Figure 3.60: PVNGSv2: Contour Plots of selected mean residuals (top left) and likelihood (top right) for the NGA$_{PV-MED}$ dataset, and mean residuals (bottom left) and likelihood (top right) for the EU$_{PV-MED}$ dataset. The Voronoi cells used for selecting and weighting models are shown as black lines. The original GMPEs are red dots, plus/minus uncertainty are magenta/cyan dots. The contour for the zero residual is a thick black line, the -0.15/0.15 contours are dashed black lines and the -0.3/0.3 contours are thin black lines. For $T = 0.25$s.

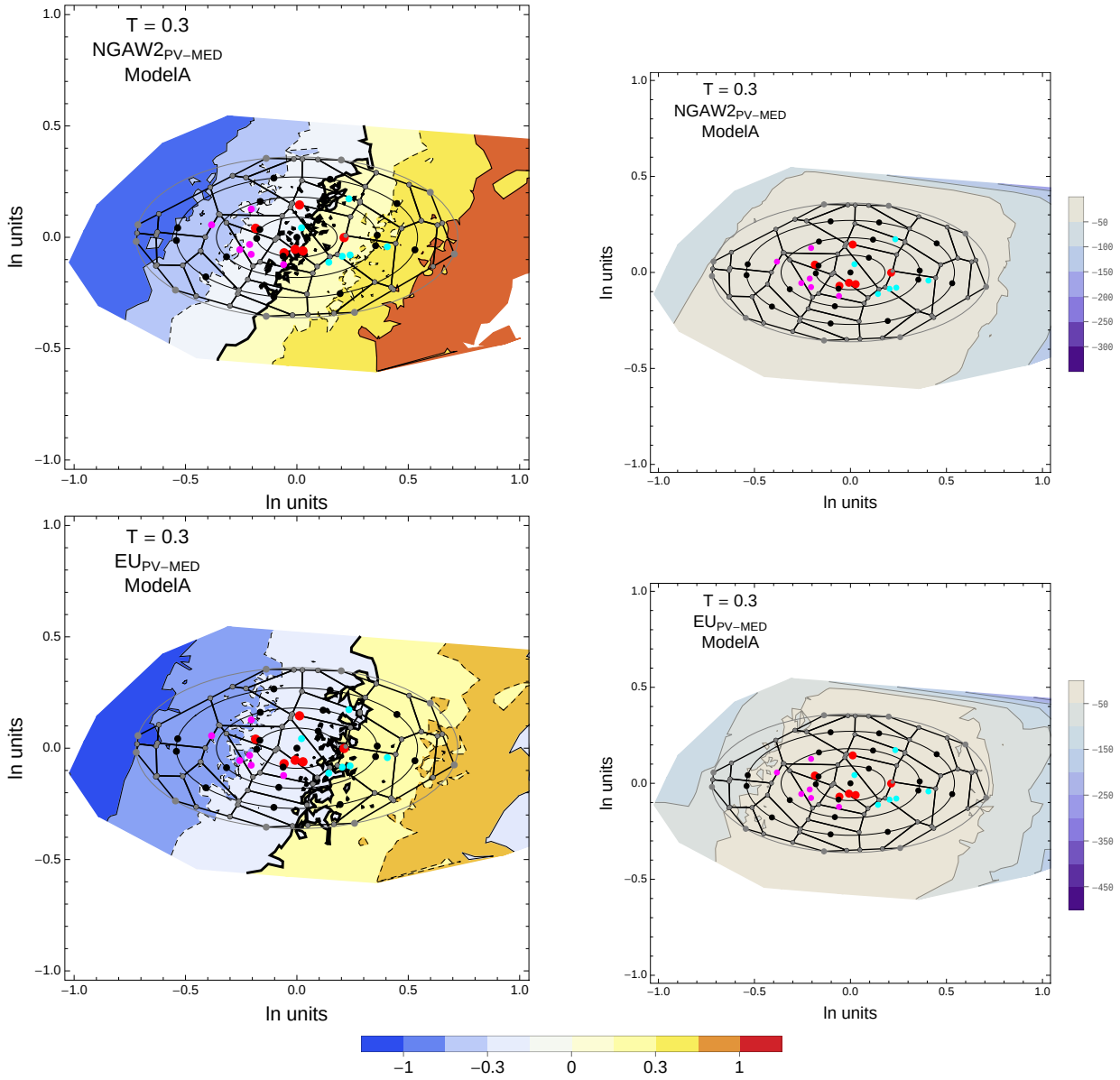



Figure 3.61: PVNGSv2: Contour Plots of selected mean residuals (top left) and likelihood (top right) for the NGA$_{PV-MED}$ dataset, and mean residuals (bottom left) and likelihood (top right) for the EU$_{PV-MED}$ dataset. The Voronoi cells used for selecting and weighting models are shown as black lines. The original GMPEs are red dots, plus/minus uncertainty are magenta/cyan dots. The contour for the zero residual is a thick black line, the -0.15/0.15 contours are dashed black lines and the -0.3/0.3 contours are thin black lines. For $T = 0.3$s.

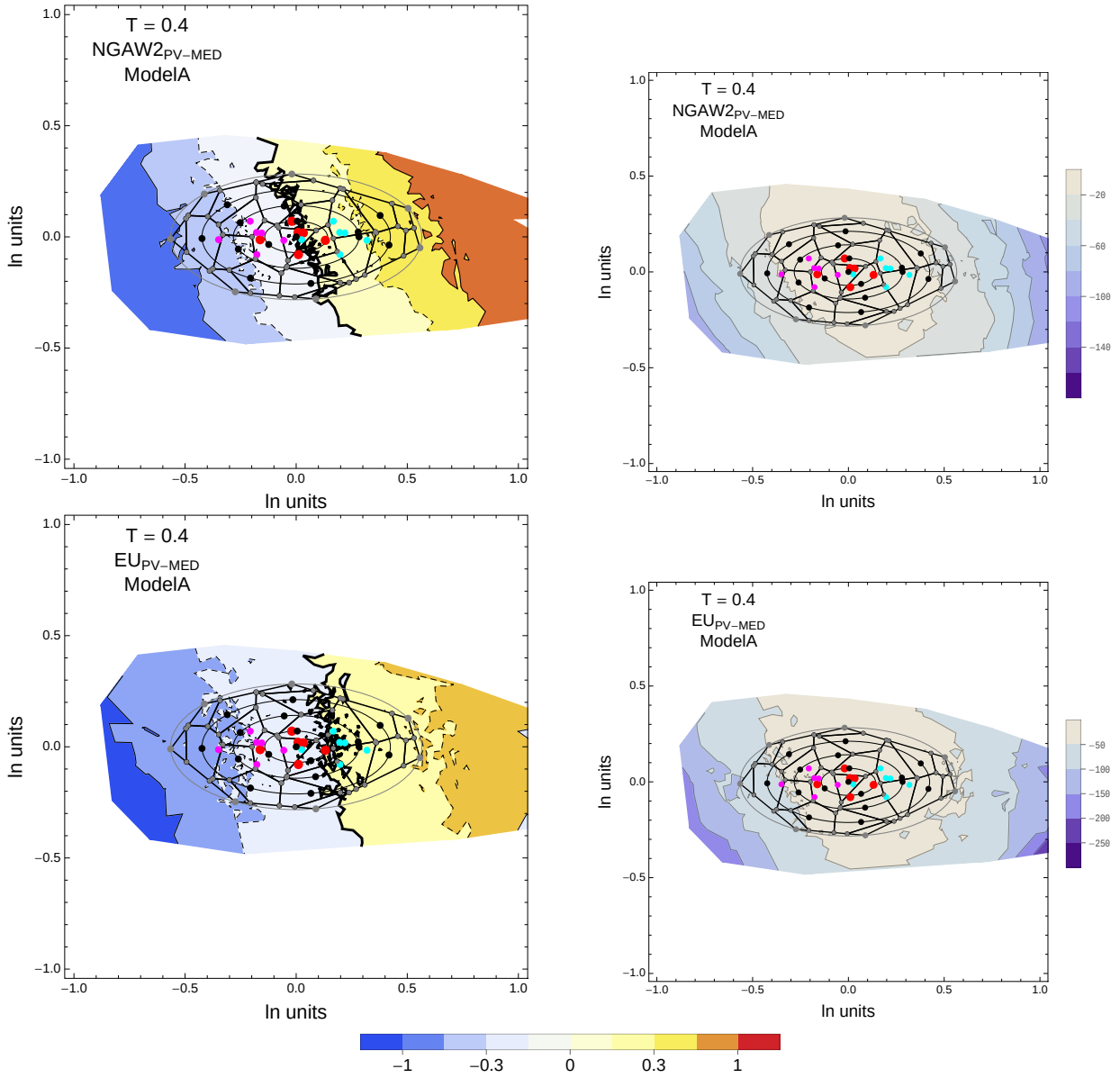



Figure 3.62: PVNGSv2: Contour Plots of selected mean residuals (top left) and likelihood (top right) for the NGA$_{PV-MED}$ dataset, and mean residuals (bottom left) and likelihood (top right) for the EU$_{PV-MED}$ dataset. The Voronoi cells used for selecting and weighting models are shown as black lines. The original GMPEs are red dots, plus/minus uncertainty are magenta/cyan dots. The contour for the zero residual is a thick black line, the -0.15/0.15 contours are dashed black lines and the -0.3/0.3 contours are thin black lines. For $T = 0.4$s.

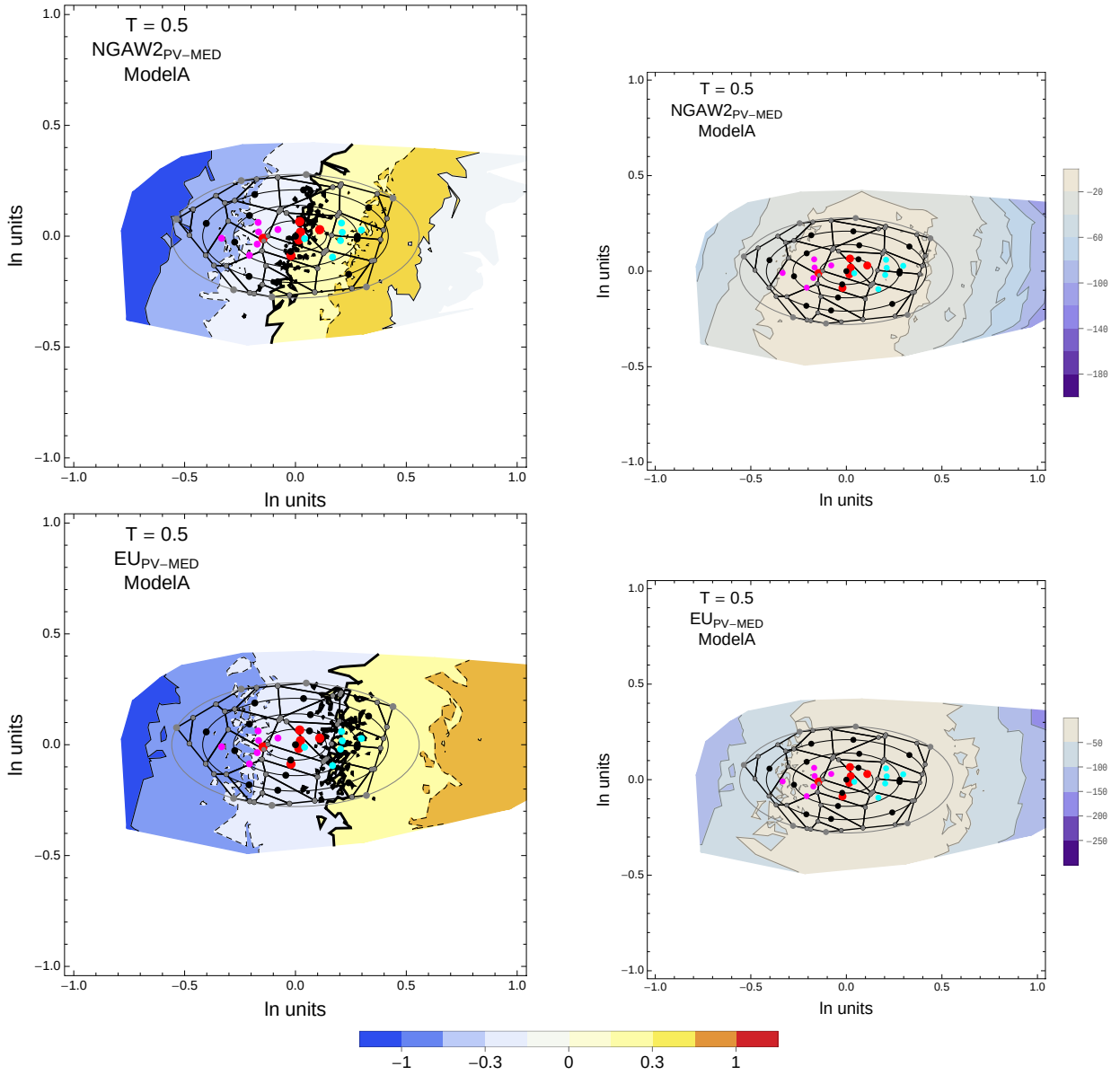



Figure 3.63: PVNGSv2: Contour Plots of selected mean residuals (top left) and likelihood (top right) for the $\text{NGA}_{PV-MED}$ dataset, and mean residuals (bottom left) and likelihood (top right) for the $\text{EU}_{PV-MED}$ dataset. The Voronoi cells used for selecting and weighting models are shown as black lines. The original GMPEs are red dots, plus/minus uncertainty are magenta/cyan dots. The contour for the zero residual is a thick black line, the -0.15/0.15 contours are dashed black lines and the -0.3/0.3 contours are thin black lines. For $T = 0.5$s.

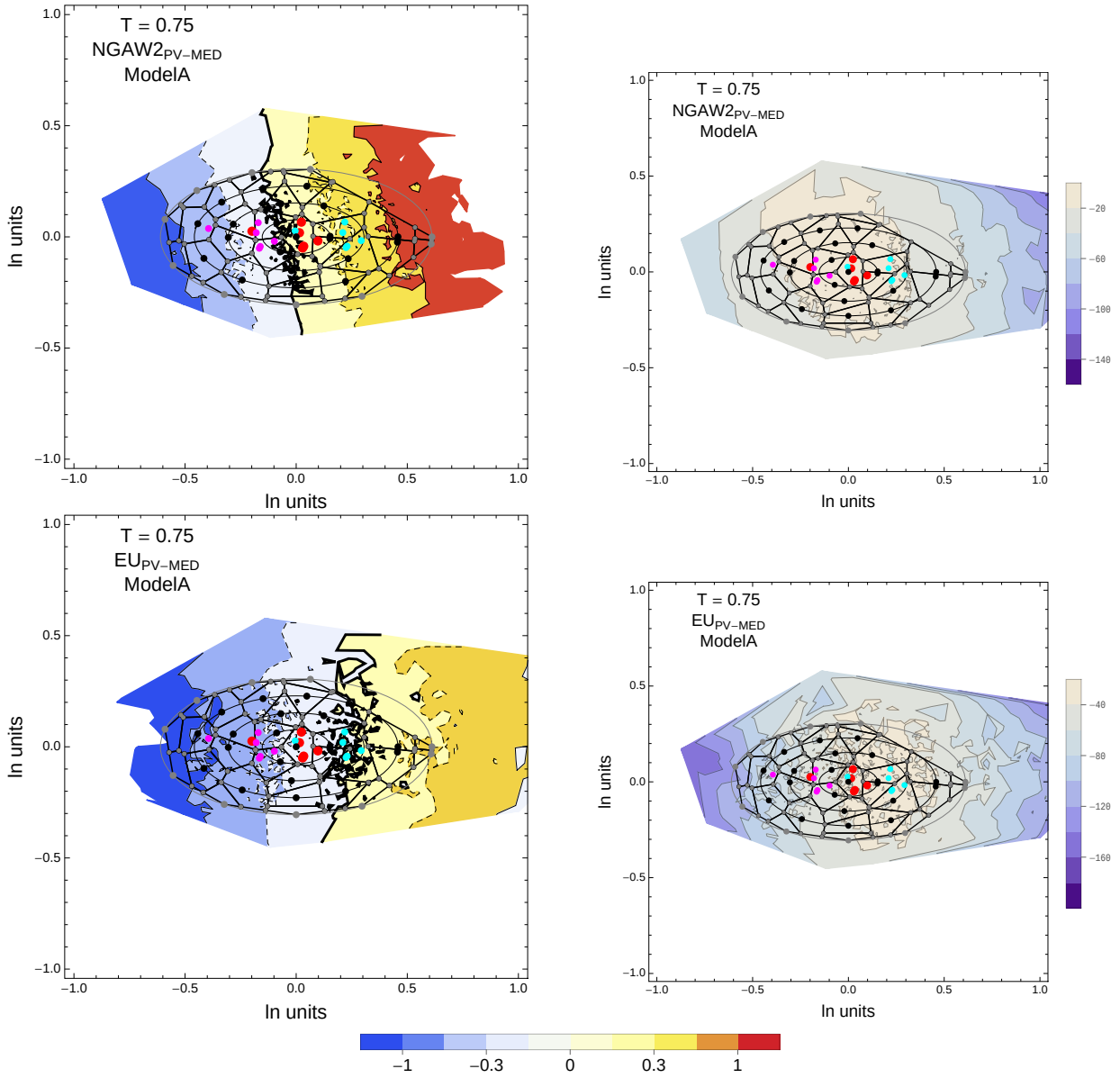



Figure 3.64: PVNGSv2: Contour Plots of selected mean residuals (top left) and likelihood (top right) for the NGA$_{PV-MED}$ dataset, and mean residuals (bottom left) and likelihood (top right) for the EU$_{PV-MED}$ dataset. The Voronoi cells used for selecting and weighting models are shown as black lines. The original GMPEs are red dots, plus/minus uncertainty are magenta/cyan dots. The contour for the zero residual is a thick black line, the -0.15/0.15 contours are dashed black lines and the -0.3/0.3 contours are thin black lines. For $T = 0.75$s.

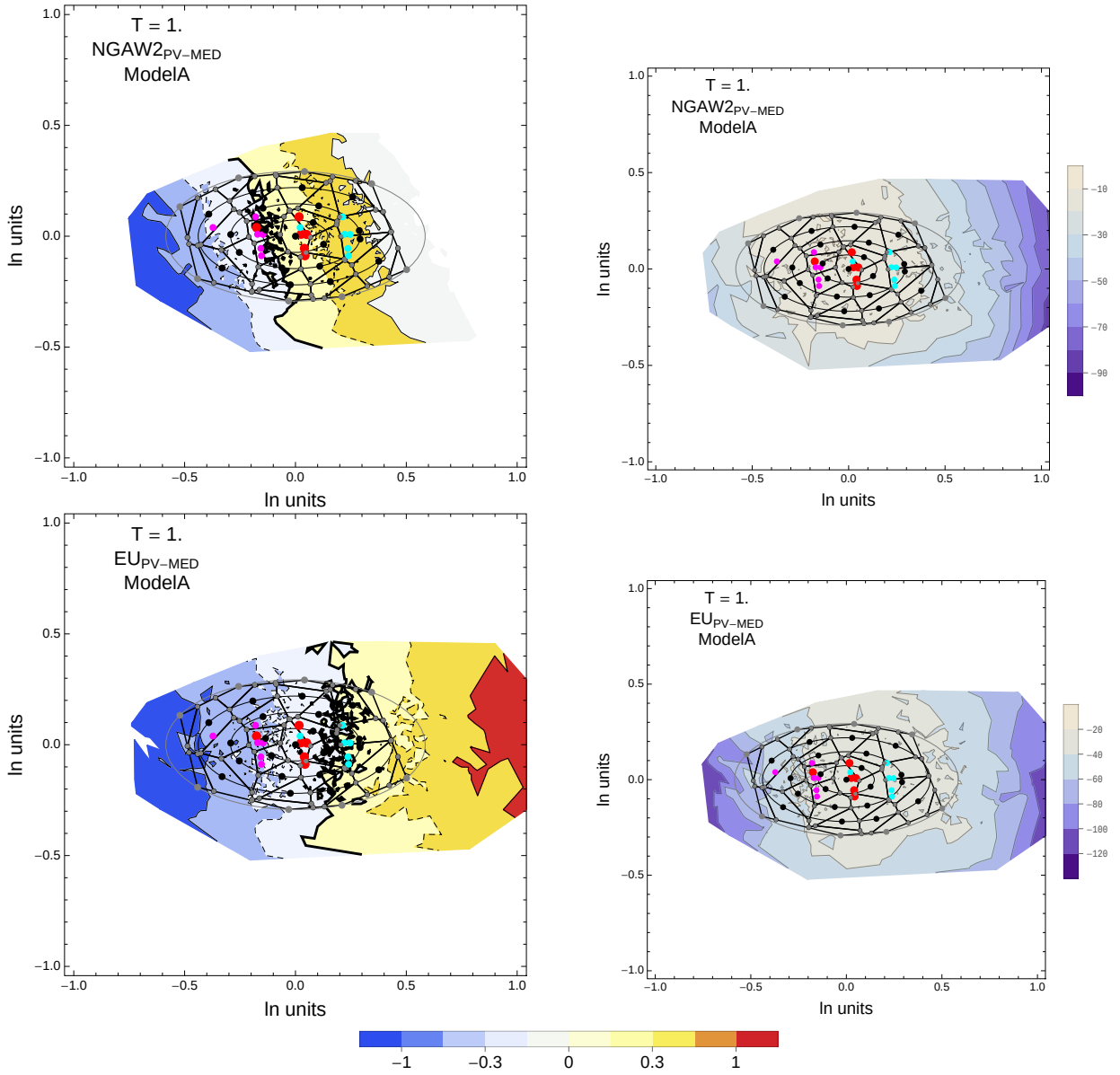



Figure 3.65: PVNGSv2: Contour Plots of selected mean residuals (top left) and likelihood (top right) for the $\text{NGA}_{PV-MED}$ dataset, and mean residuals (bottom left) and likelihood (top right) for the $\text{EU}_{PV-MED}$ dataset. The Voronoi cells used for selecting and weighting models are shown as black lines. The original GMPEs are red dots, plus/minus uncertainty are magenta/cyan dots. The contour for the zero residual is a thick black line, the -0.15/0.15 contours are dashed black lines and the -0.3/0.3 contours are thin black lines. For $T = 1$.s.

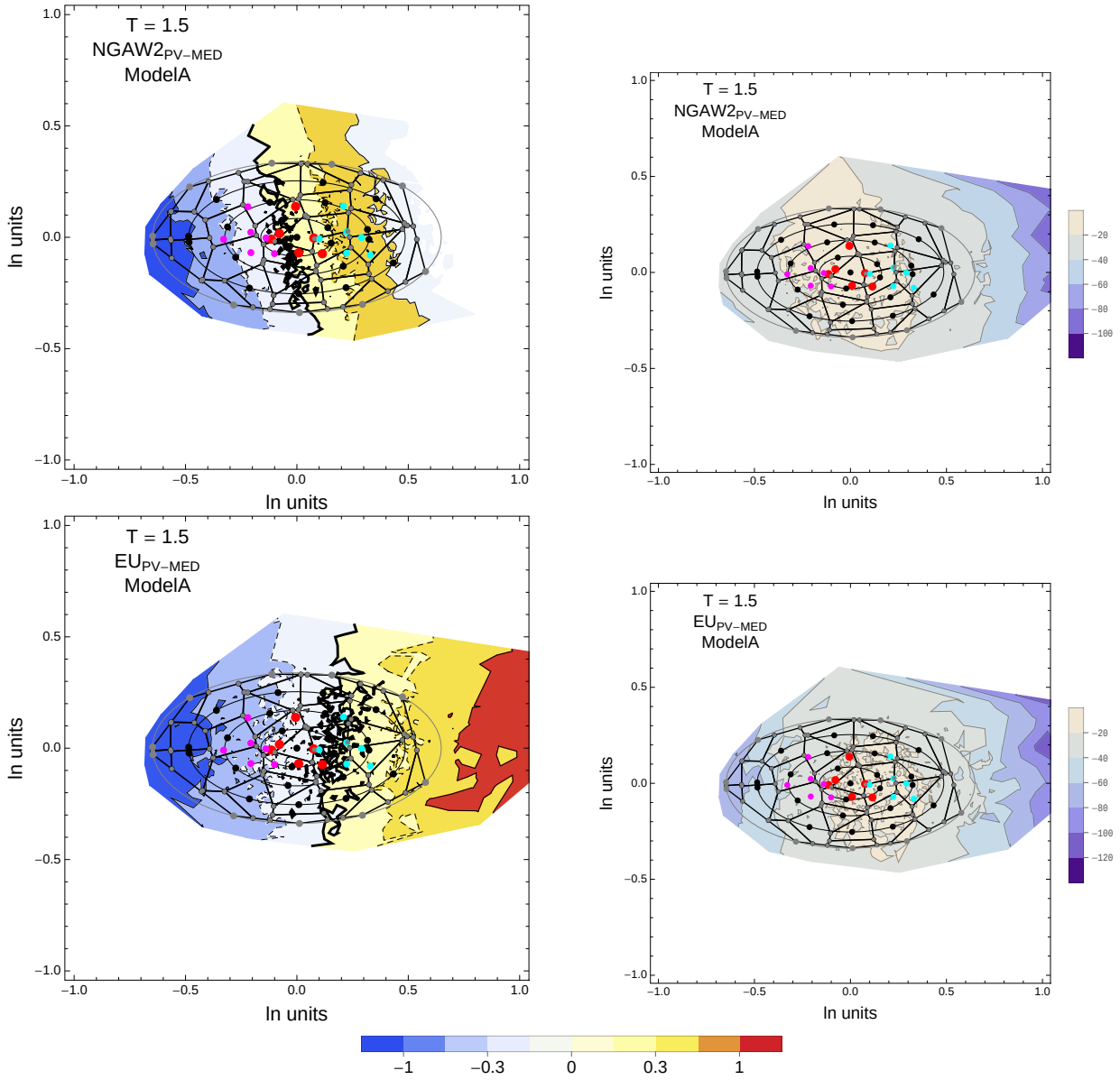



Figure 3.66: PVNGSv2: Contour Plots of selected mean residuals (top left) and likelihood (top right) for the NGA$_{PV-MED}$ dataset, and mean residuals (bottom left) and likelihood (top right) for the EU$_{PV-MED}$ dataset. The Voronoi cells used for selecting and weighting models are shown as black lines. The original GMPEs are red dots, plus/minus uncertainty are magenta/cyan dots. The contour for the zero residual is a thick black line, the -0.15/0.15 contours are dashed black lines and the -0.3/0.3 contours are thin black lines. For $T = 1.5$s.

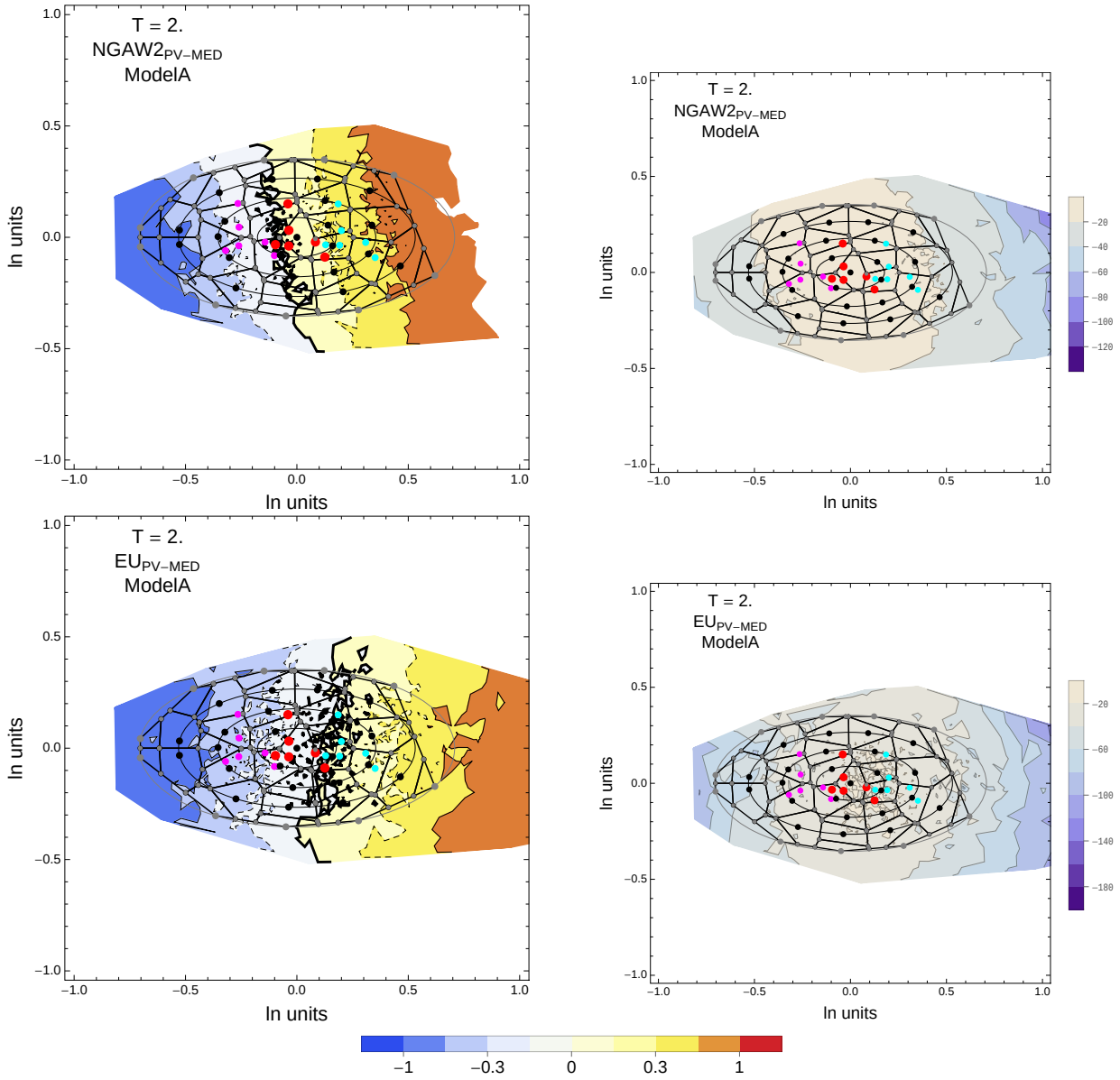



Figure 3.67: PVNGSv2: Contour Plots of selected mean residuals (top left) and likelihood (top right) for the $\text{NGA}_{PV-MED}$ dataset, and mean residuals (bottom left) and likelihood (top right) for the $\text{EU}_{PV-MED}$ dataset. The Voronoi cells used for selecting and weighting models are shown as black lines. The original GMPEs are red dots, plus/minus uncertainty are magenta/cyan dots. The contour for the zero residual is a thick black line, the -0.15/0.15 contours are dashed black lines and the -0.3/0.3 contours are thin black lines. For $T = 2$.s.

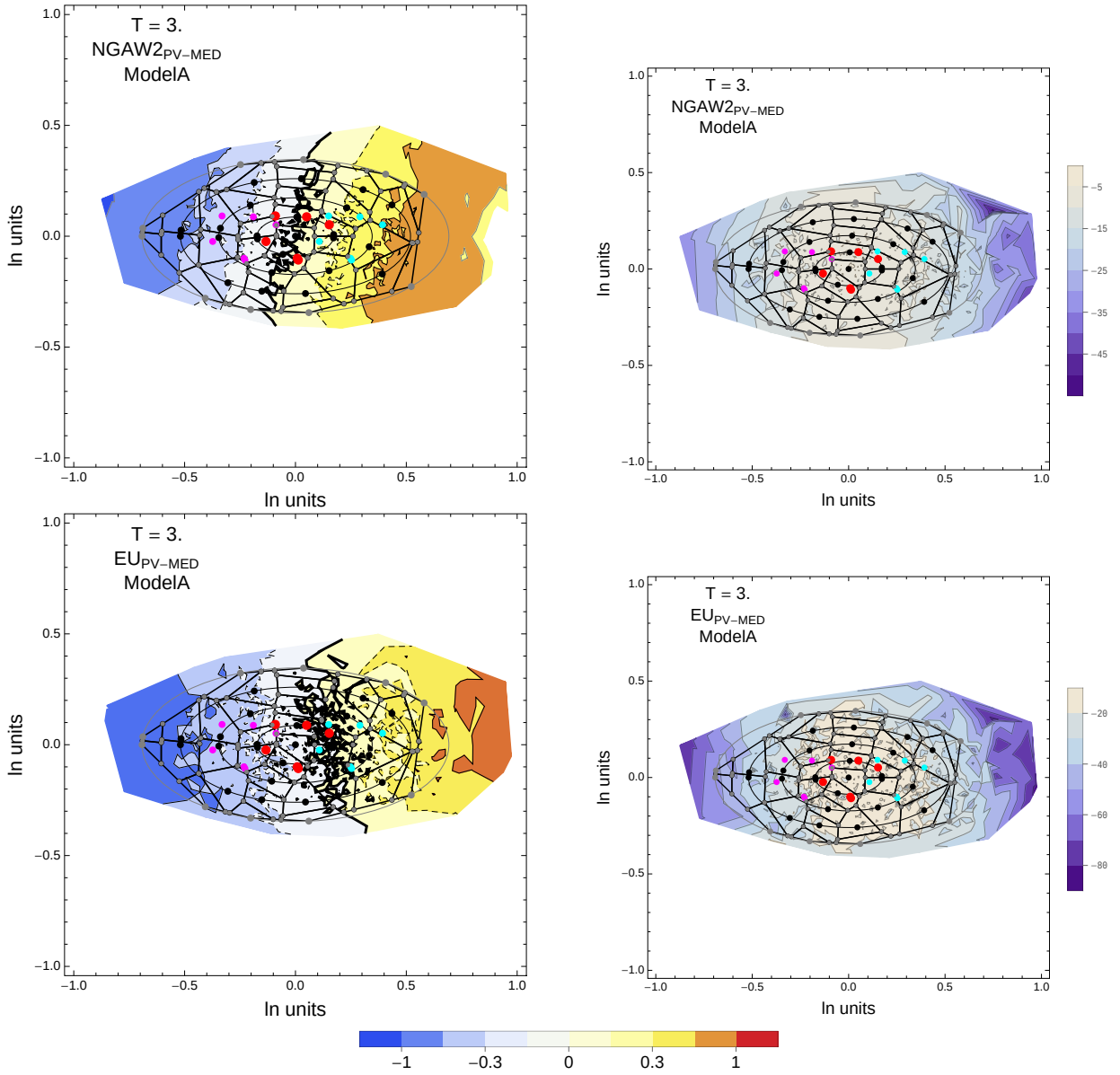



Figure 3.68: PVNGSv2: Contour Plots of selected mean residuals (top left) and likelihood (top right) for the $\text{NGA}_{PV-MED}$ dataset, and mean residuals (bottom left) and likelihood (top right) for the $\text{EU}_{PV-MED}$ dataset. The Voronoi cells used for selecting and weighting models are shown as black lines. The original GMPEs are red dots, plus/minus uncertainty are magenta/cyan dots. The contour for the zero residual is a thick black line, the -0.15/0.15 contours are dashed black lines and the -0.3/0.3 contours are thin black lines. For $T = 3$.s.

### 3.1.4 Hazard Curves

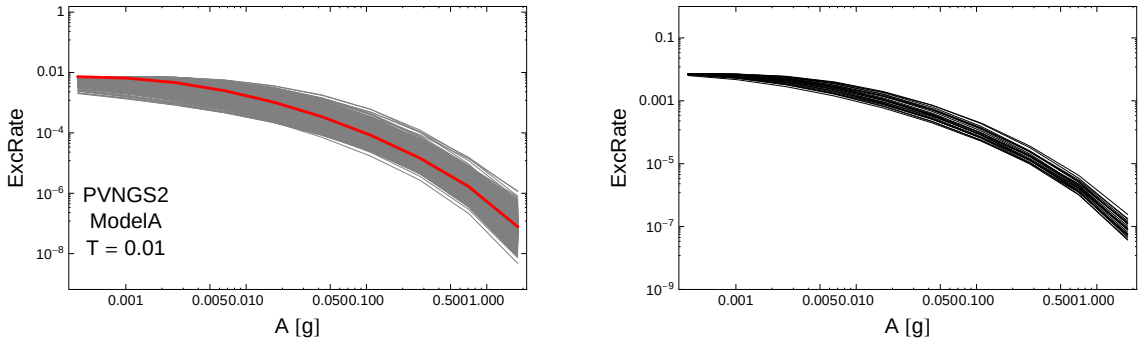



Figure 3.69: Hazard curves, calculated for a simple source model for PVNGS2. Left: 2000 hazard curves for all sampled A-models (gray) and the center model of the ModelA distribution (red); Right: hazard curves of selected models. For $T = 0.01$s.

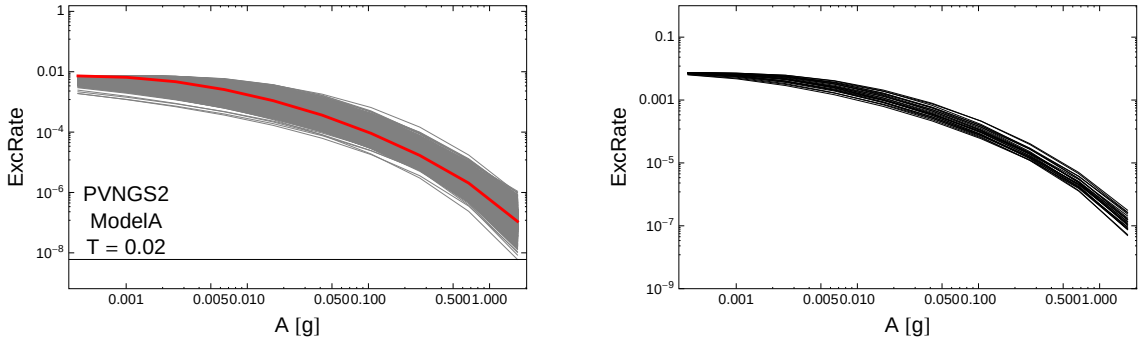



Figure 3.70: Hazard curves, calculated for a simple source model for PVNGS2. Left: 2000 hazard curves for all sampled A-models (gray) and the center model of the ModelA distribution (red); Right: hazard curves of selected models. For $T = 0.02$s.

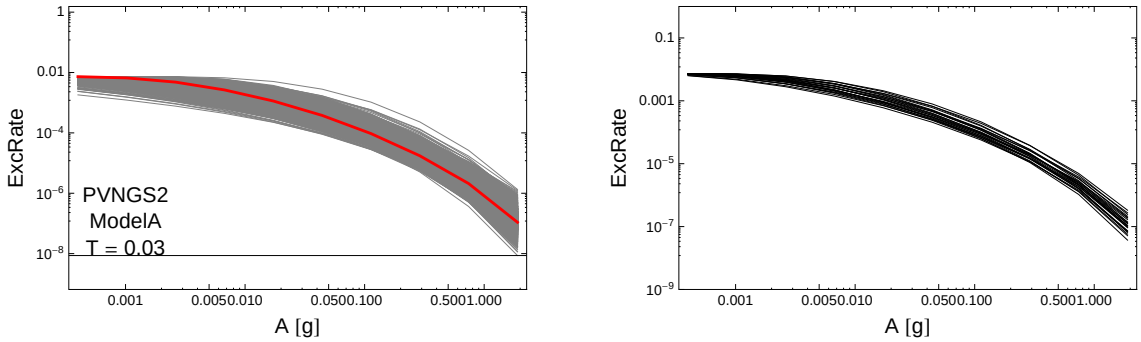



Figure 3.71: Hazard curves, calculated for a simple source model for PVNGS2. Left: 2000 hazard curves for all sampled A-models (gray) and the center model of the ModelA distribution (red); Right: hazard curves of selected models. For $T = 0.03$s.

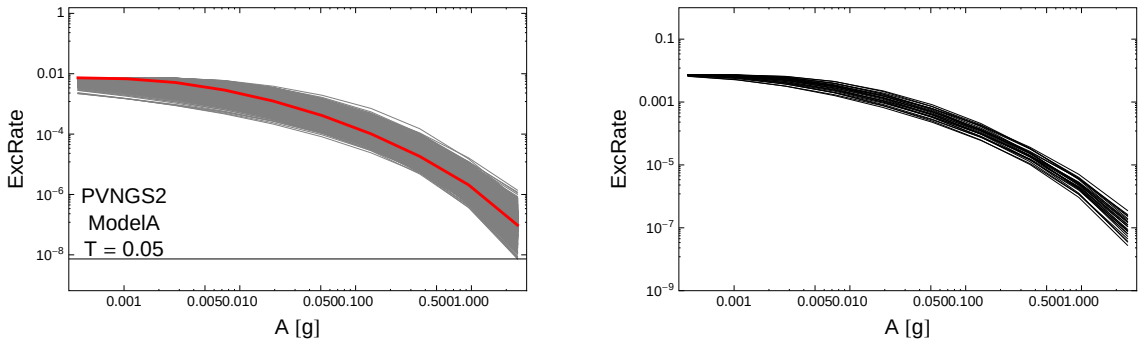



Figure 3.72: Hazard curves, calculated for a simple source model for PVNGS2. Left: 2000 hazard curves for all sampled A-models (gray) and the center model of the ModelA distribution (red); Right: hazard curves of selected models. For $T = 0.05$s.

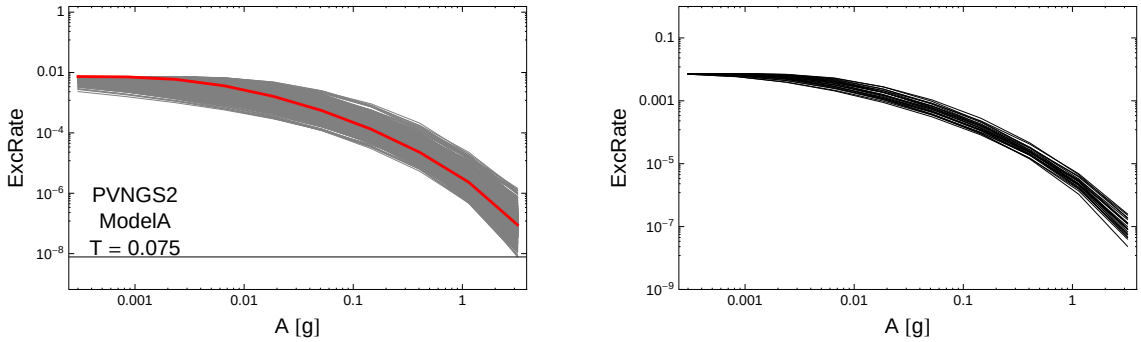



Figure 3.73: Hazard curves, calculated for a simple source model for PVNGS2. Left: 2000 hazard curves for all sampled A-models (gray) and the center model of the ModelA distribution (red); Right: hazard curves of selected models. For $T = 0.075$s.

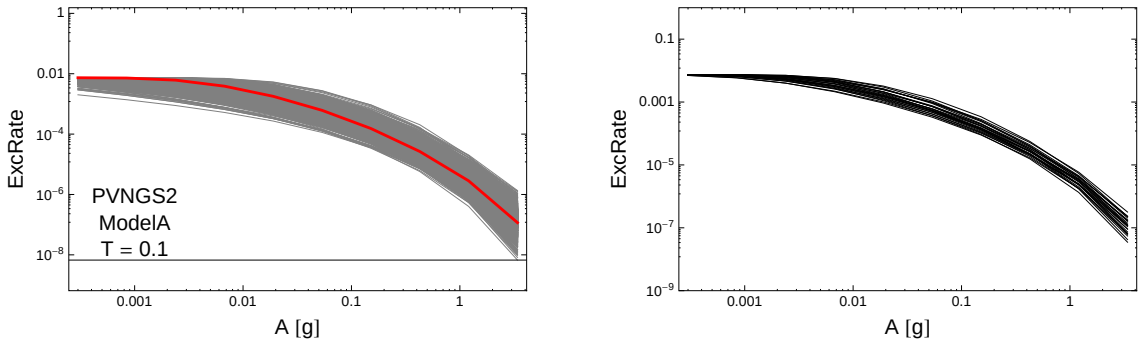



Figure 3.74: Hazard curves, calculated for a simple source model for PVNGS2. Left: 2000 hazard curves for all sampled A-models (gray) and the center model of the ModelA distribution (red); Right: hazard curves of selected models. For $T = 0.1$s.

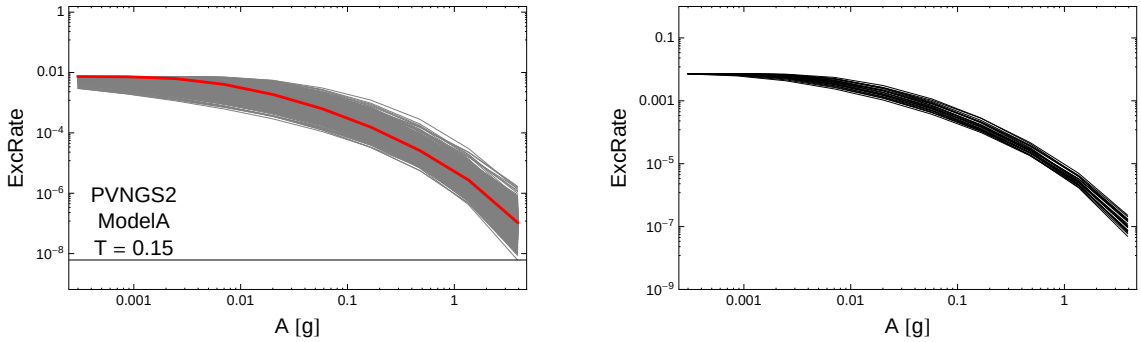



Figure 3.75: Hazard curves, calculated for a simple source model for PVNGS2. Left: 2000 hazard curves for all sampled A-models (gray) and the center model of the ModelA distribution (red); Right: hazard curves of selected models. For $T = 0.15$s.

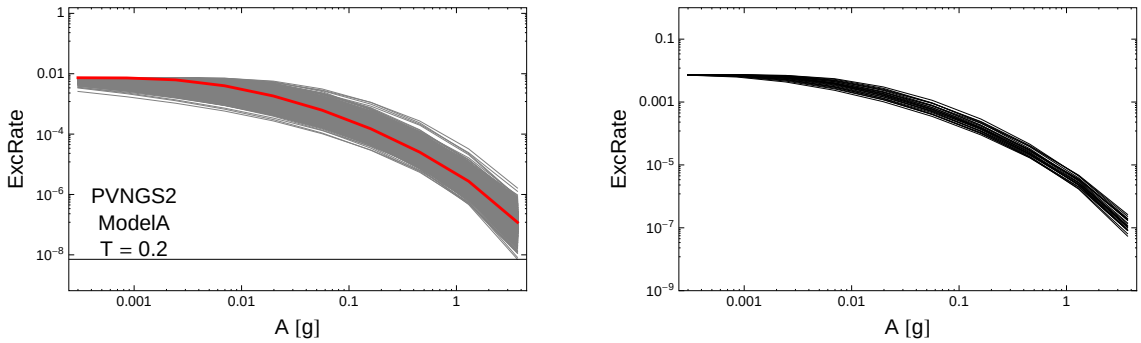



Figure 3.76: Hazard curves, calculated for a simple source model for PVNGS2. Left: 2000 hazard curves for all sampled A-models (gray) and the center model of the ModelA distribution (red); Right: hazard curves of selected models. For $T = 0.2$s.

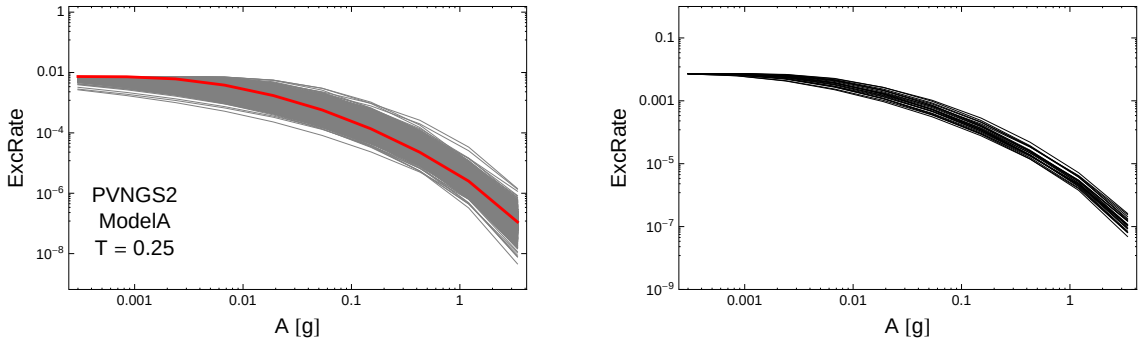



Figure 3.77: Hazard curves, calculated for a simple source model for PVNGS2. Left: 2000 hazard curves for all sampled A-models (gray) and the center model of the ModelA distribution (red); Right: hazard curves of selected models. For $T = 0.25$s.

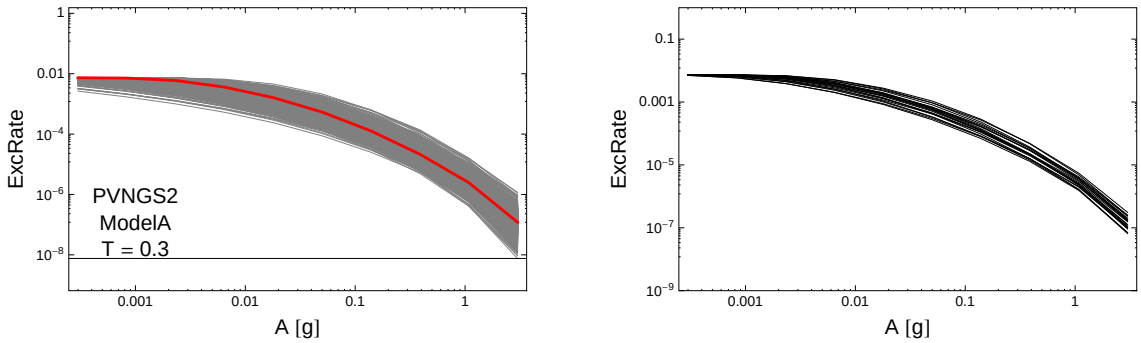



Figure 3.78: Hazard curves, calculated for a simple source model for PVNGS2. Left: 2000 hazard curves for all sampled A-models (gray) and the center model of the ModelA distribution (red); Right: hazard curves of selected models. For $T = 0.3$s.

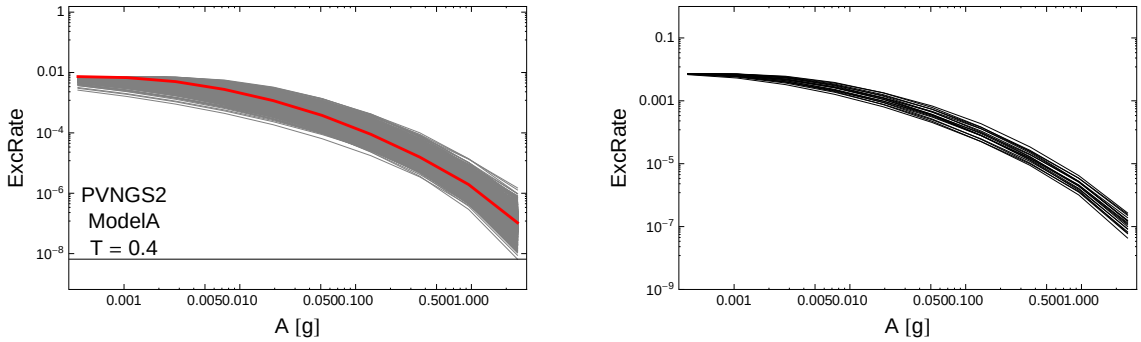



Figure 3.79: Hazard curves, calculated for a simple source model for PVNGS2. Left: 2000 hazard curves for all sampled A-models (gray) and the center model of the ModelA distribution (red); Right: hazard curves of selected models. For $T = 0.4$s.

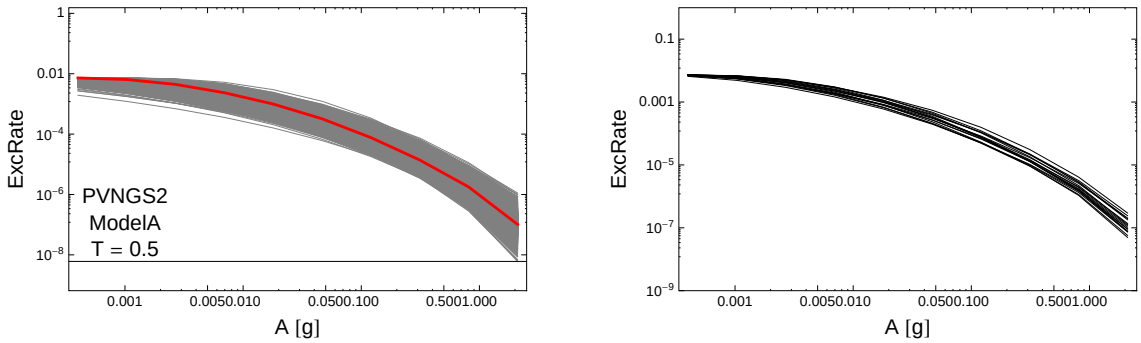



Figure 3.80: Hazard curves, calculated for a simple source model for PVNGS2. Left: 2000 hazard curves for all sampled A-models (gray) and the center model of the ModelA distribution (red); Right: hazard curves of selected models. For $T = 0.5$s.

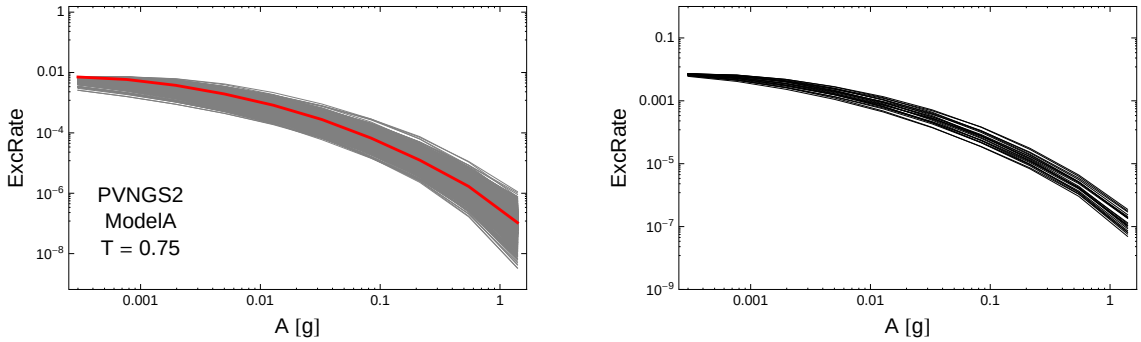



Figure 3.81: Hazard curves, calculated for a simple source model for PVNGS2. Left: 2000 hazard curves for all sampled A-models (gray) and the center model of the ModelA distribution (red); Right: hazard curves of selected models. For $T = 0.75$s.

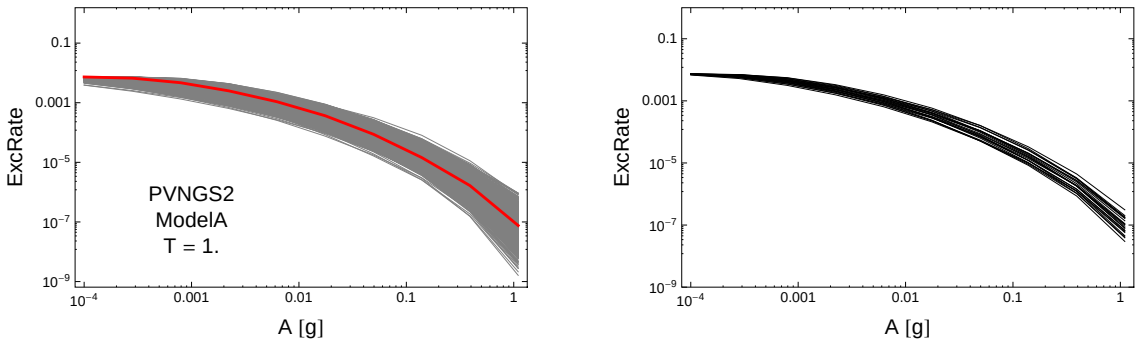



Figure 3.82: Hazard curves, calculated for a simple source model for PVNGS2. Left: 2000 hazard curves for all sampled A-models (gray) and the center model of the ModelA distribution (red); Right: hazard curves of selected models. For $T = 1$.s.

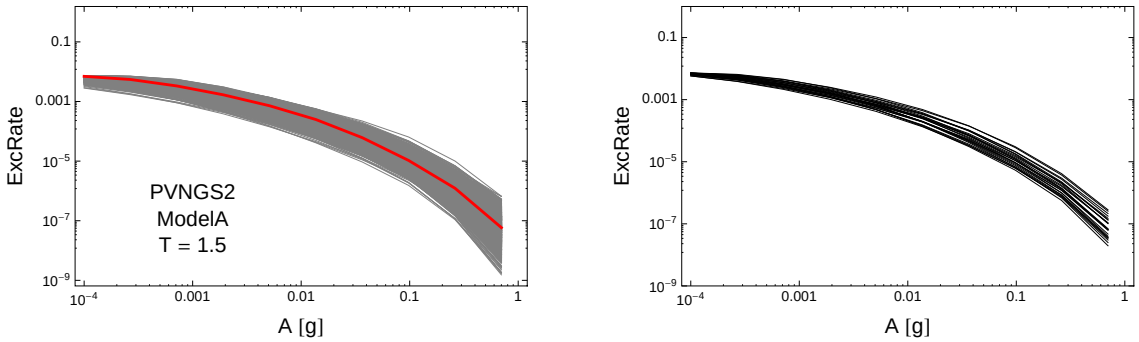



Figure 3.83: Hazard curves, calculated for a simple source model for PVNGS2. Left: 2000 hazard curves for all sampled A-models (gray) and the center model of the ModelA distribution (red); Right: hazard curves of selected models. For $T = 1.5$s.

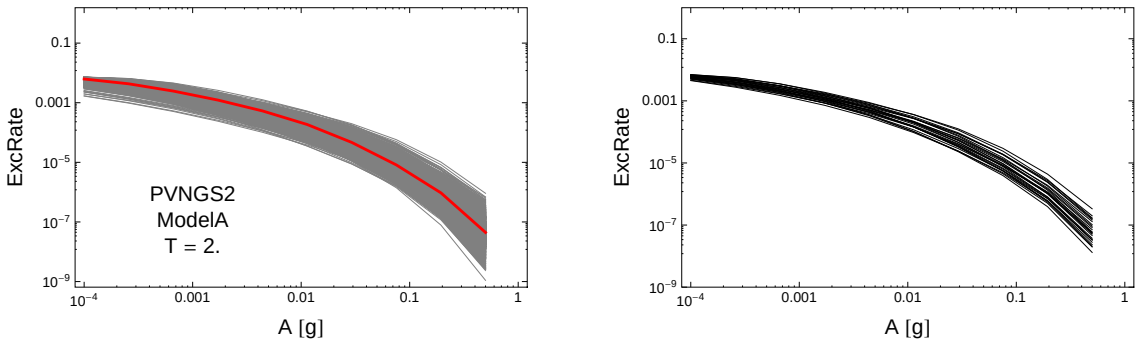



Figure 3.84: Hazard curves, calculated for a simple source model for PVNGS2. Left: 2000 hazard curves for all sampled A-models (gray) and the center model of the ModelA distribution (red); Right: hazard curves of selected models. For $T = 2.$s.

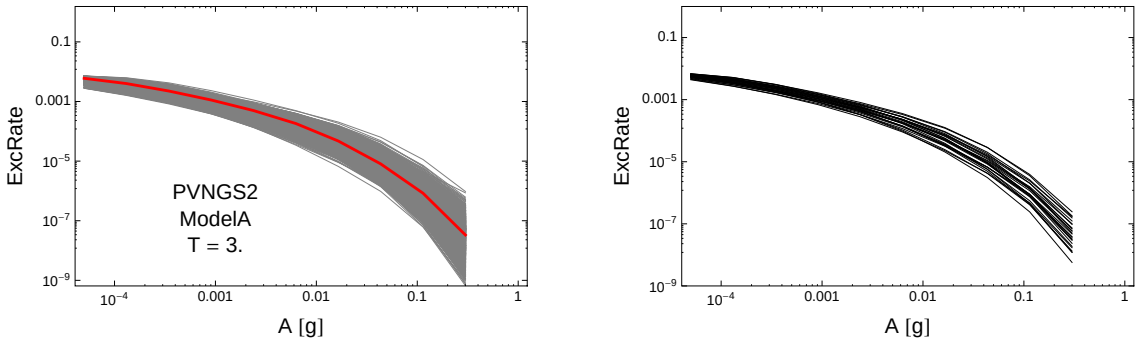



Figure 3.85: Hazard curves, calculated for a simple source model for PVNGS2. Left: 2000 hazard curves for all sampled A-models (gray) and the center model of the ModelA distribution (red); Right: hazard curves of selected models. For $T = 3$.s.

### 3.1.5 CDF Plots

**T = 0.01s**

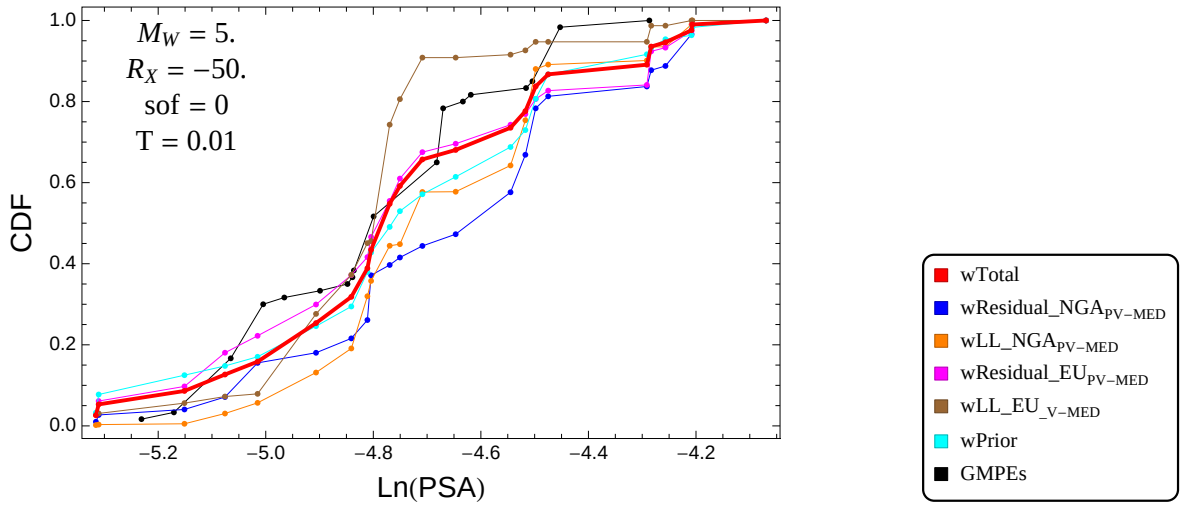



Figure 3.86: PVNGSv2: Cumulative distribution function of GMPEs (black) and selected models, for different sets of weights, for a scenario with $M = 5.$, $R_x = -50.$, $F = 0$, and $T = 0.01$s

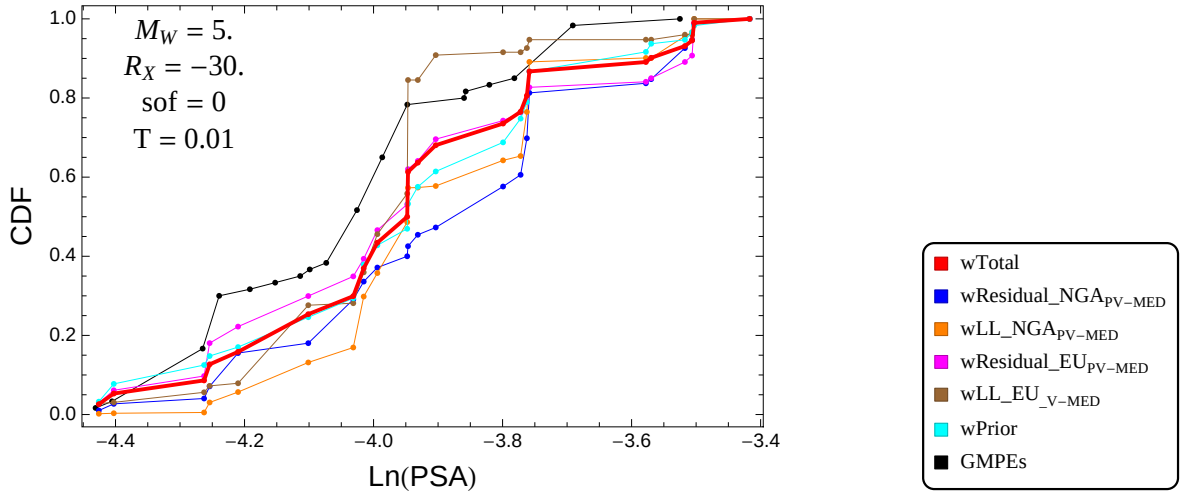



Figure 3.87: PVNGSv2: Cumulative distribution function of GMPEs (black) and selected models, for different sets of weights, for a scenario with $M = 5.$, $R_x = -30.$, $F = 0$, and $T = 0.01$s

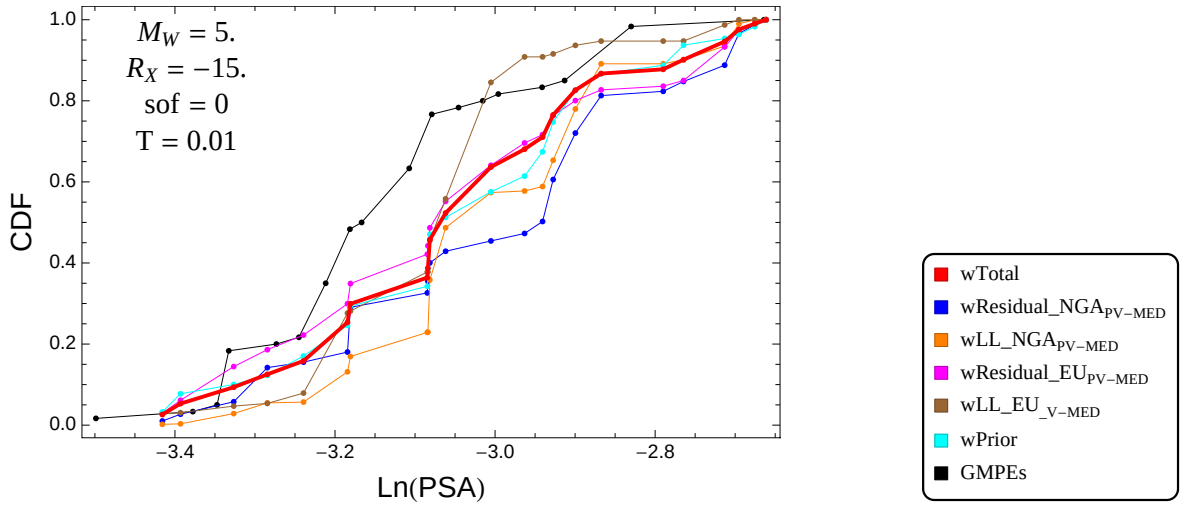



Figure 3.88: PVNGSv2: Cumulative distribution function of GMPEs (black) and selected models, for different sets of weights, for a scenario with $M = 5.$, $R_x = -15.$, $F = 0$, and $T = 0.01$s

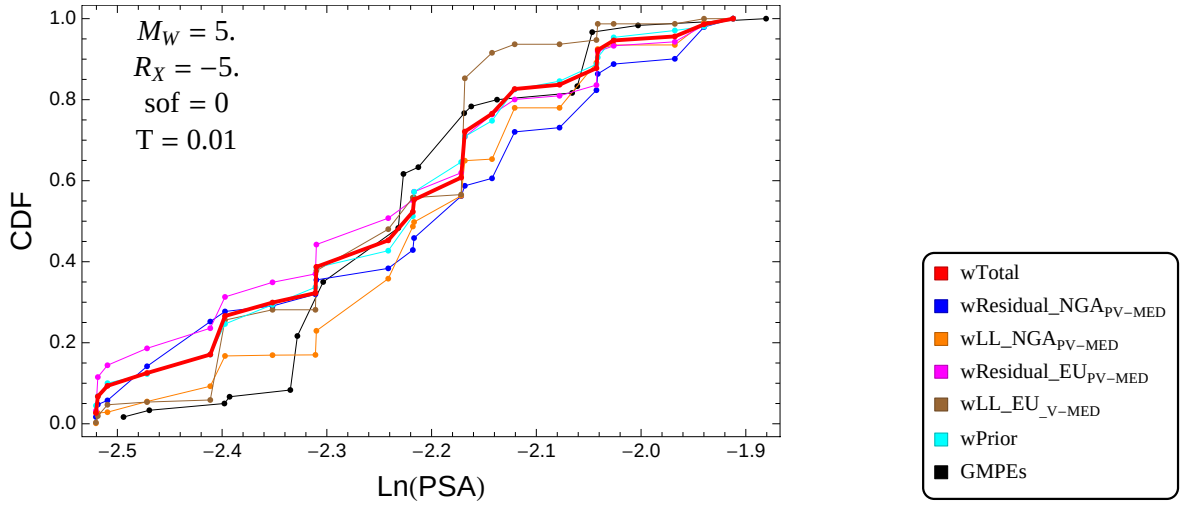



Figure 3.89: PVNGSv2: Cumulative distribution function of GMPEs (black) and selected models, for different sets of weights, for a scenario with $M = 5.$, $R_x = -5.$, $F = 0$, and $T = 0.01$s

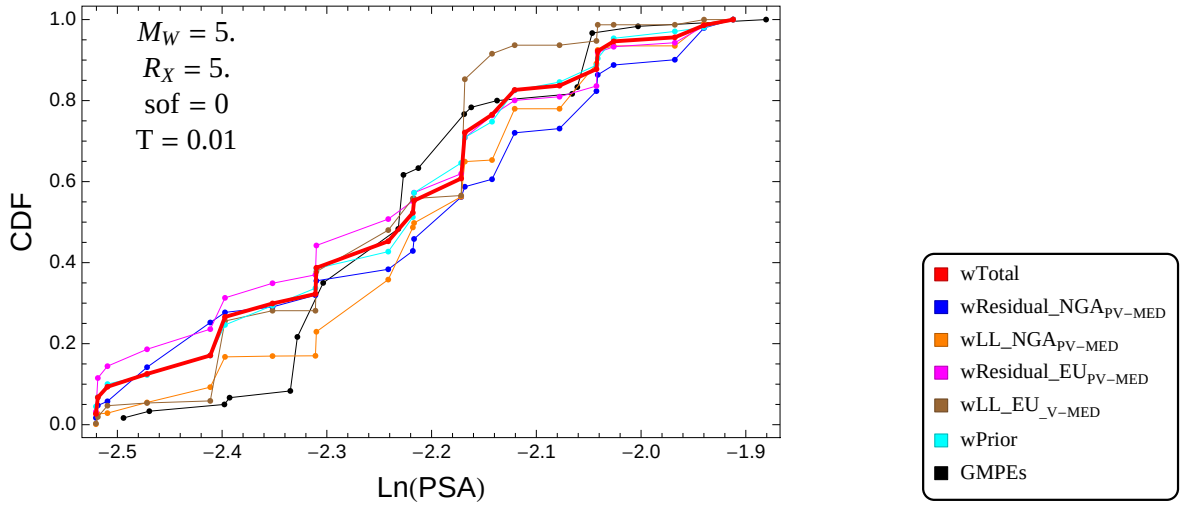



Figure 3.90: PVNGSv2: Cumulative distribution function of GMPEs (black) and selected models, for different sets of weights, for a scenario with $M = 5.$, $R_x = 5.$, $F = 0$, and $T = 0.01$s

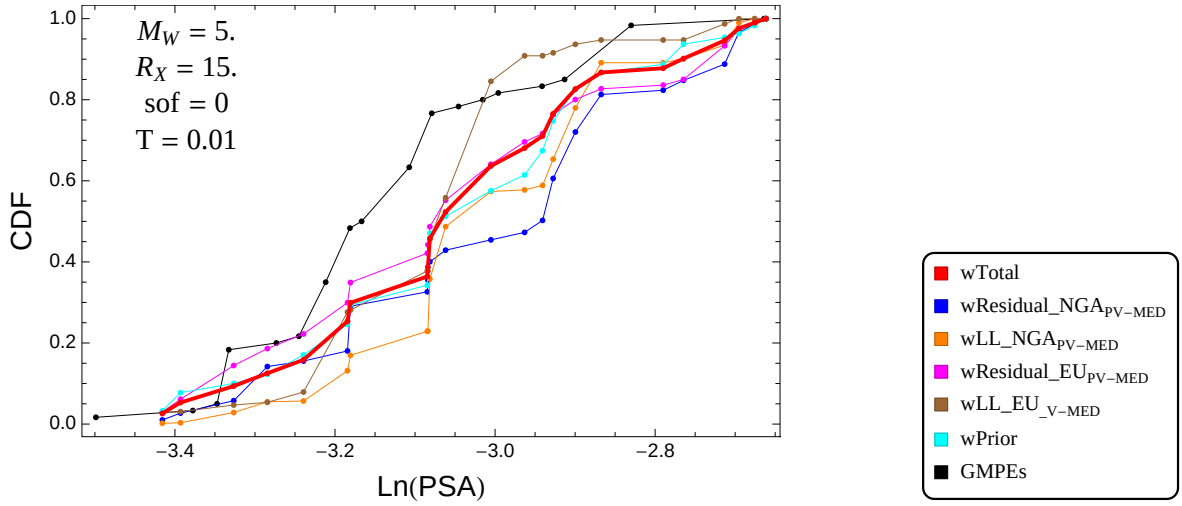



Figure 3.91: PVNGSv2: Cumulative distribution function of GMPEs (black) and selected models, for different sets of weights, for a scenario with $M = 5.$, $R_x = 15.$, $F = 0$, and $T = 0.01$s

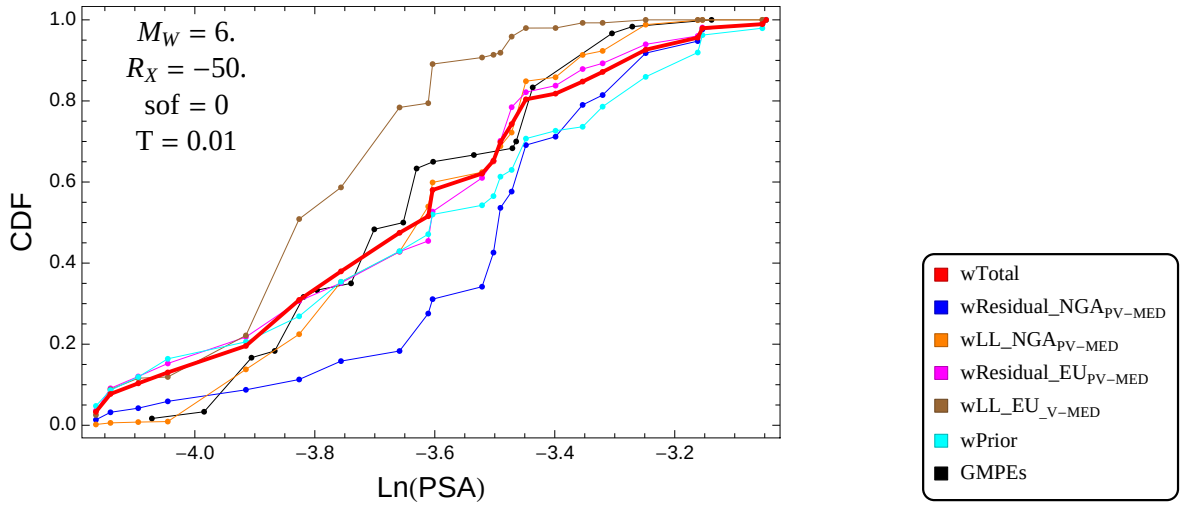



Figure 3.92: PVNGSv2: Cumulative distribution function of GMPEs (black) and selected models, for different sets of weights, for a scenario with $M = 6.$, $R_x = -50.$, $F = 0$, and $T = 0.01$s

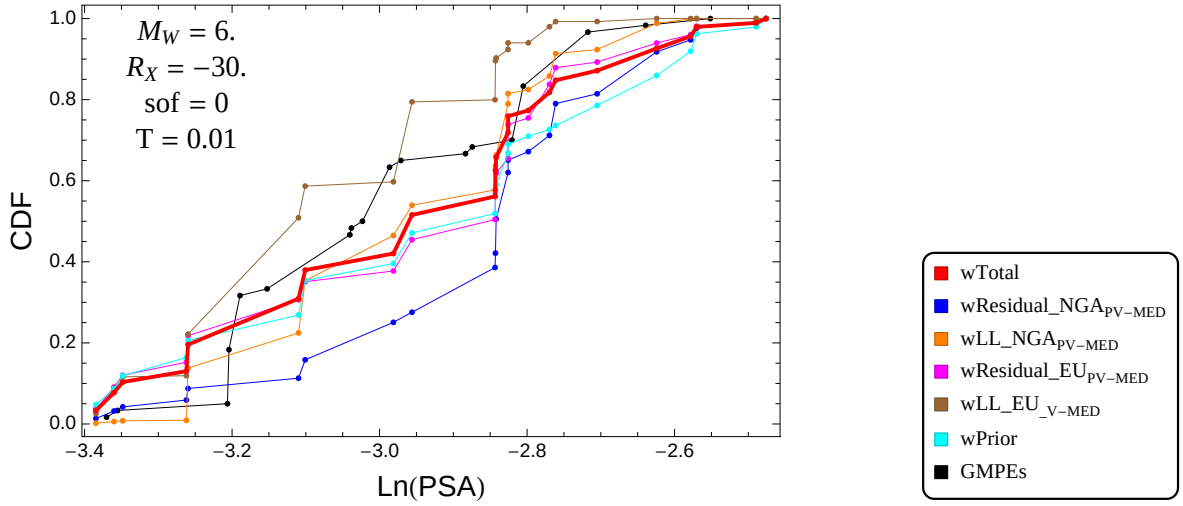



Figure 3.93: PVNGSv2: Cumulative distribution function of GMPEs (black) and selected models, for different sets of weights, for a scenario with $M = 6.$, $R_x = -30.$, $F = 0$, and $T = 0.01$s

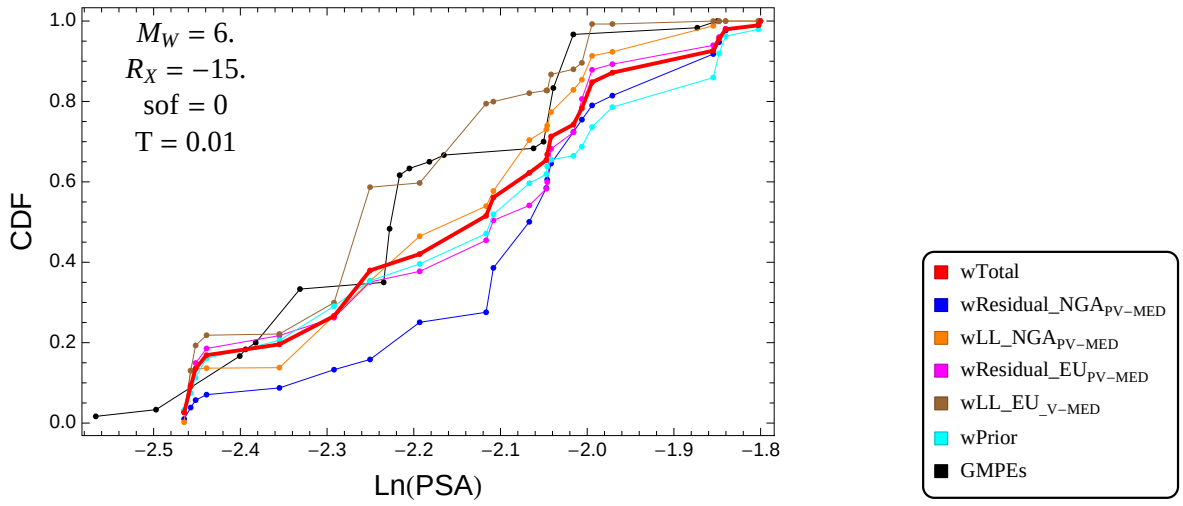



Figure 3.94: PVNGSv2: Cumulative distribution function of GMPEs (black) and selected models, for different sets of weights, for a scenario with $M = 6.$, $R_x = -15.$, $F = 0$, and $T = 0.01$s

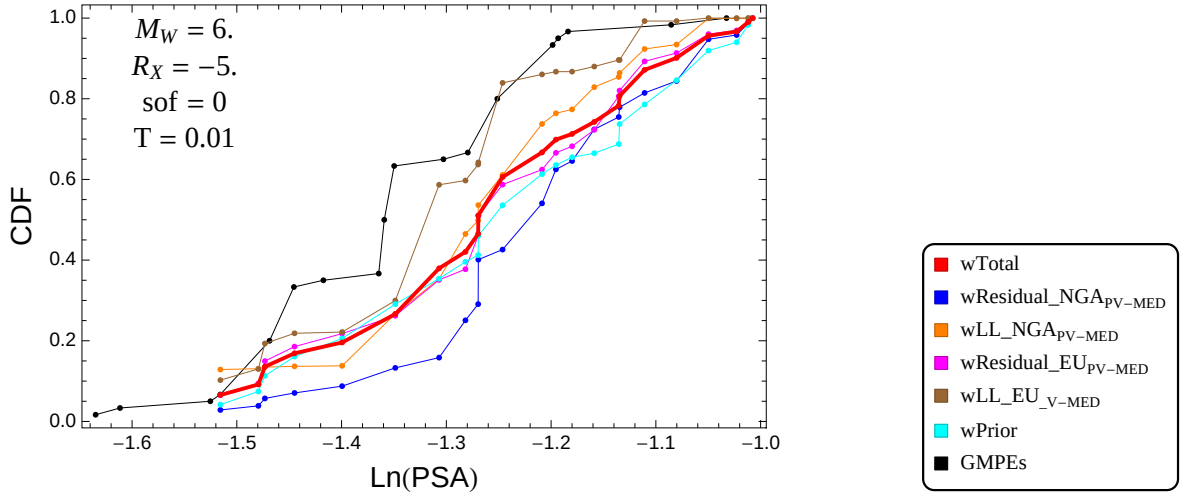



Figure 3.95: PVNGSv2: Cumulative distribution function of GMPEs (black) and selected models, for different sets of weights, for a scenario with $M = 6.$, $R_x = -5.$, $F = 0$, and $T = 0.01$s

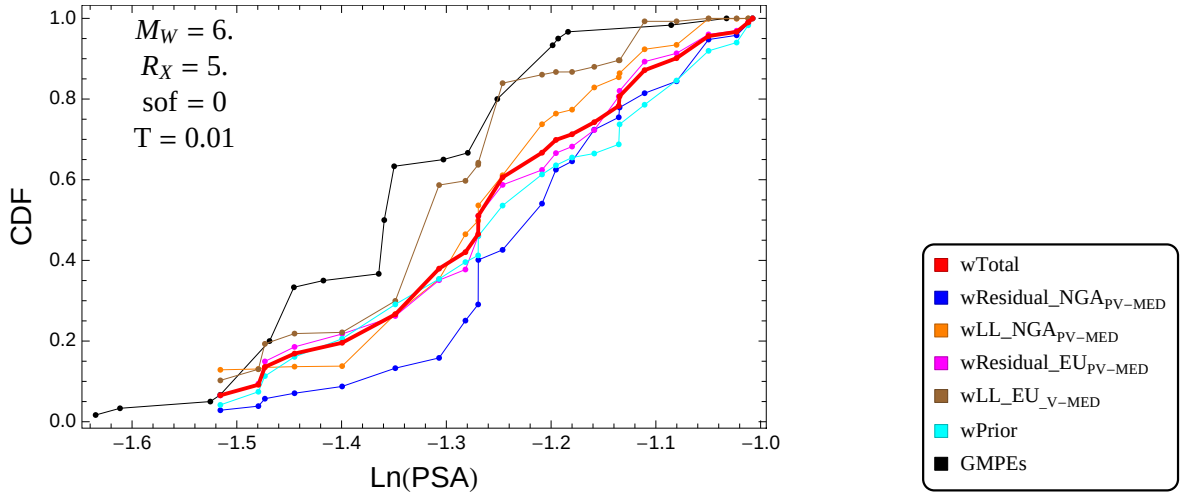



Figure 3.96: PVNGSv2: Cumulative distribution function of GMPEs (black) and selected models, for different sets of weights, for a scenario with $M = 6.$, $R_x = 5.$, $F = 0$, and $T = 0.01$s

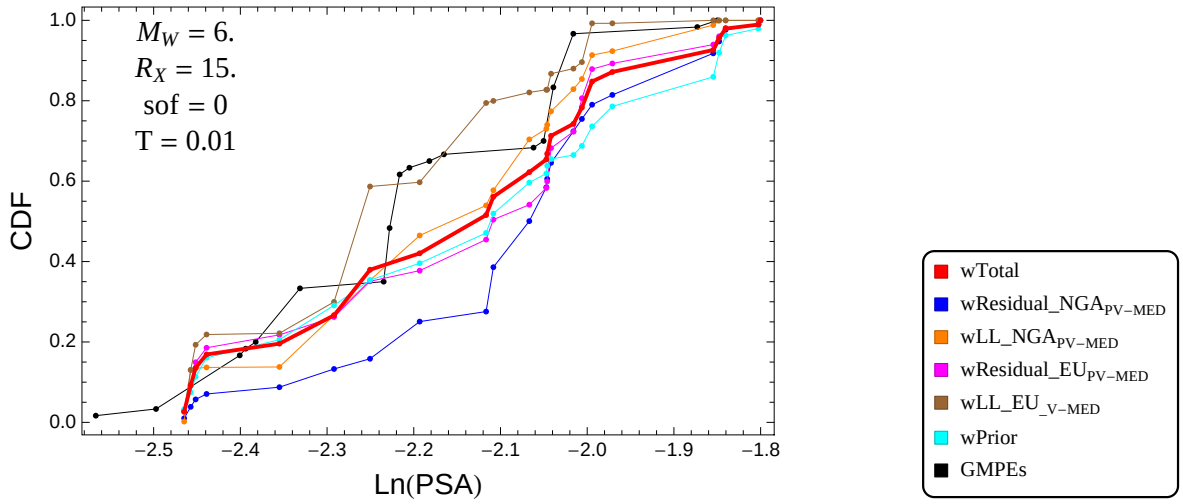



Figure 3.97: PVNGSv2: Cumulative distribution function of GMPEs (black) and selected models, for different sets of weights, for a scenario with $M = 6.$, $R_x = 15.$, $F = 0$, and $T = 0.01$s

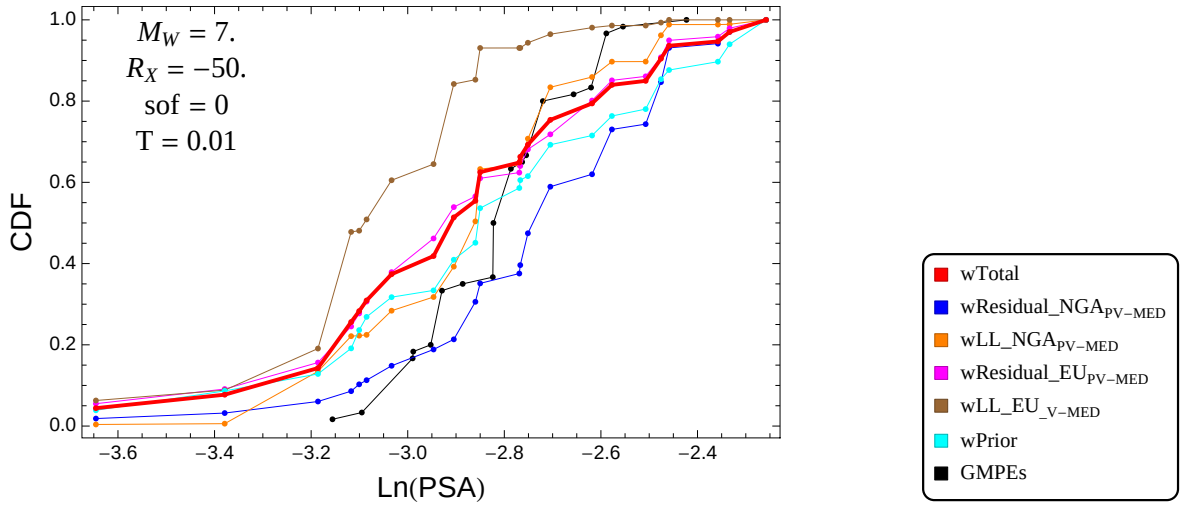



Figure 3.98: PVNGSv2: Cumulative distribution function of GMPEs (black) and selected models, for different sets of weights, for a scenario with $M = 7.$, $R_x = -50.$, $F = 0$, and $T = 0.01$s

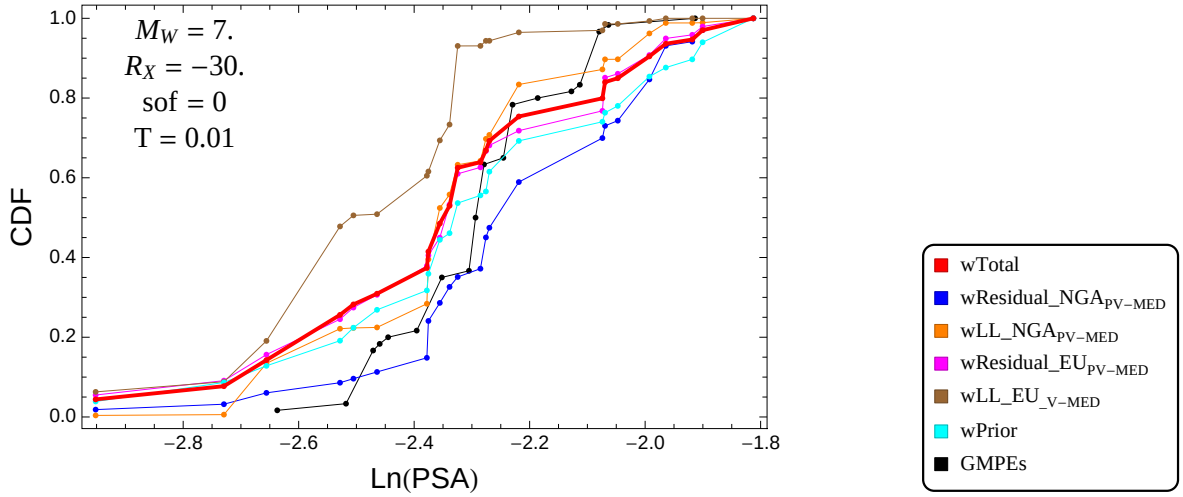



Figure 3.99: PVNGSv2: Cumulative distribution function of GMPEs (black) and selected models, for different sets of weights, for a scenario with $M = 7.$, $R_x = -30.$, $F = 0$, and $T = 0.01$s

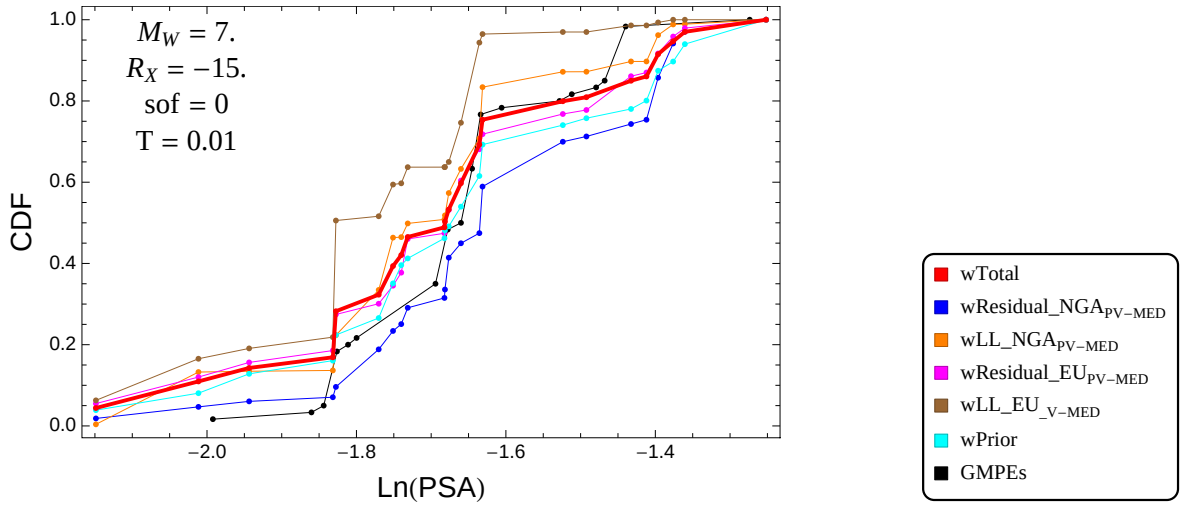



Figure 3.100: PVNGSv2: Cumulative distribution function of GMPEs (black) and selected models, for different sets of weights, for a scenario with $M = 7.$, $R_x = -15.$, $F = 0$, and $T = 0.01$s

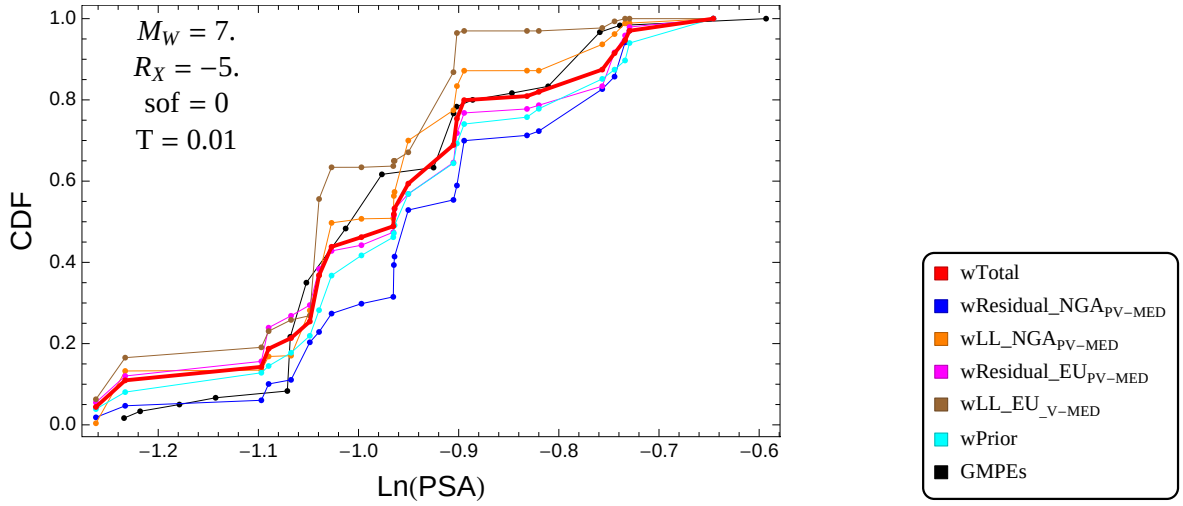



Figure 3.101: PVNGSv2: Cumulative distribution function of GMPEs (black) and selected models, for different sets of weights, for a scenario with $M = 7.$, $R_x = -5.$, $F = 0$, and $T = 0.01$s

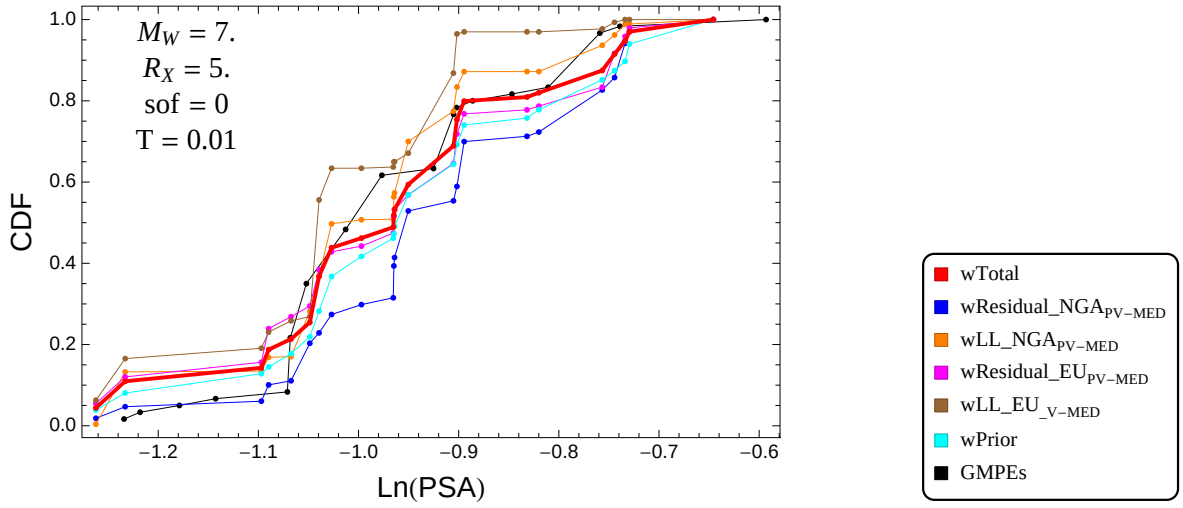



Figure 3.102: PVNGSv2: Cumulative distribution function of GMPEs (black) and selected models, for different sets of weights, for a scenario with $M = 7.$, $R_x = 5.$, $F = 0$, and $T = 0.01$s

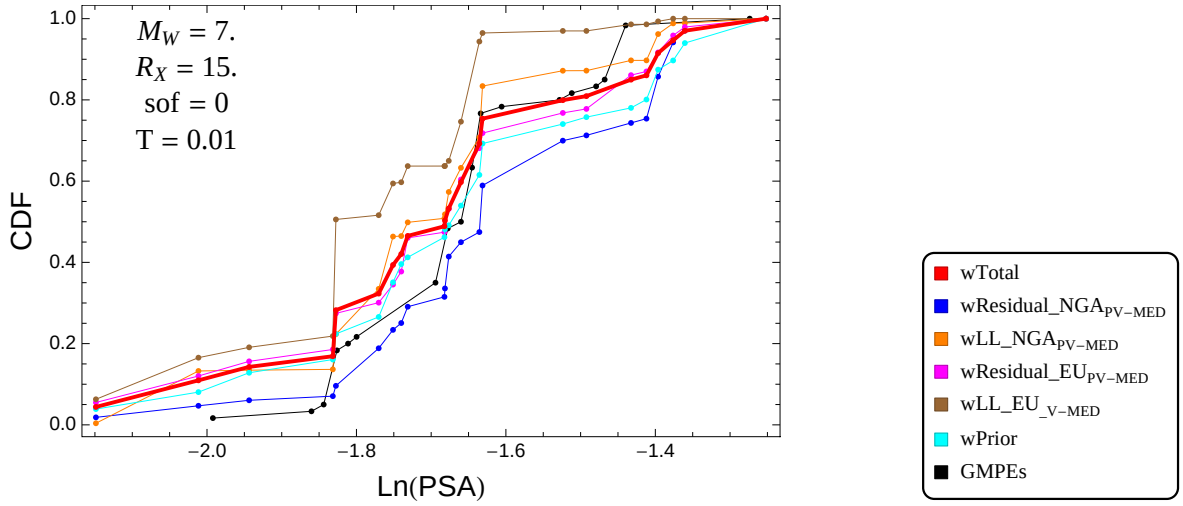



Figure 3.103: PVNGSv2: Cumulative distribution function of GMPEs (black) and selected models, for different sets of weights, for a scenario with $M = 7.$, $R_x = 15.$, $F = 0$, and $T = 0.01$s

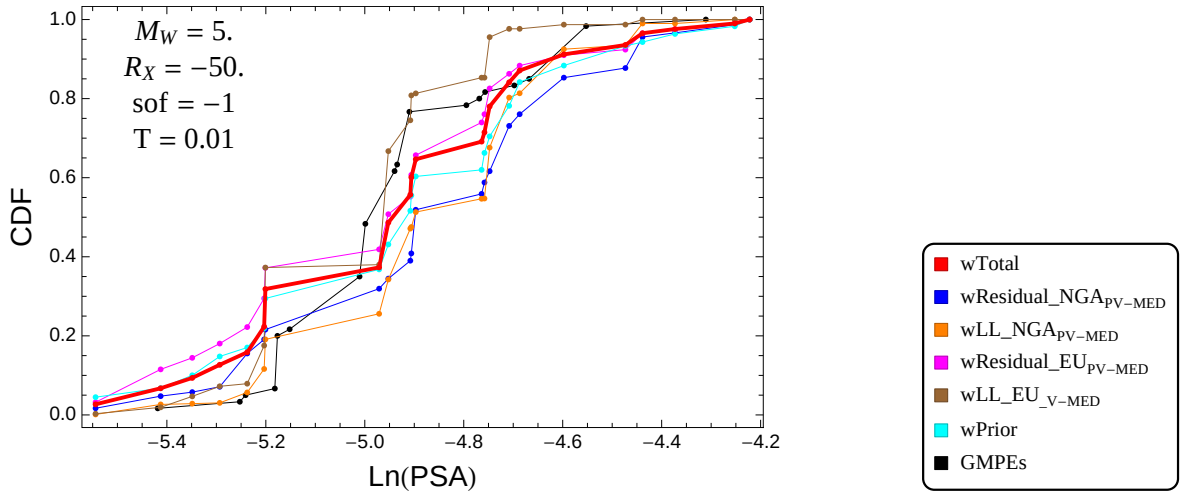



Figure 3.104: PVNGSv2: Cumulative distribution function of GMPEs (black) and selected models, for different sets of weights, for a scenario with $M = 5.$, $R_x = -50.$, $F = -1$, and $T = 0.01$s

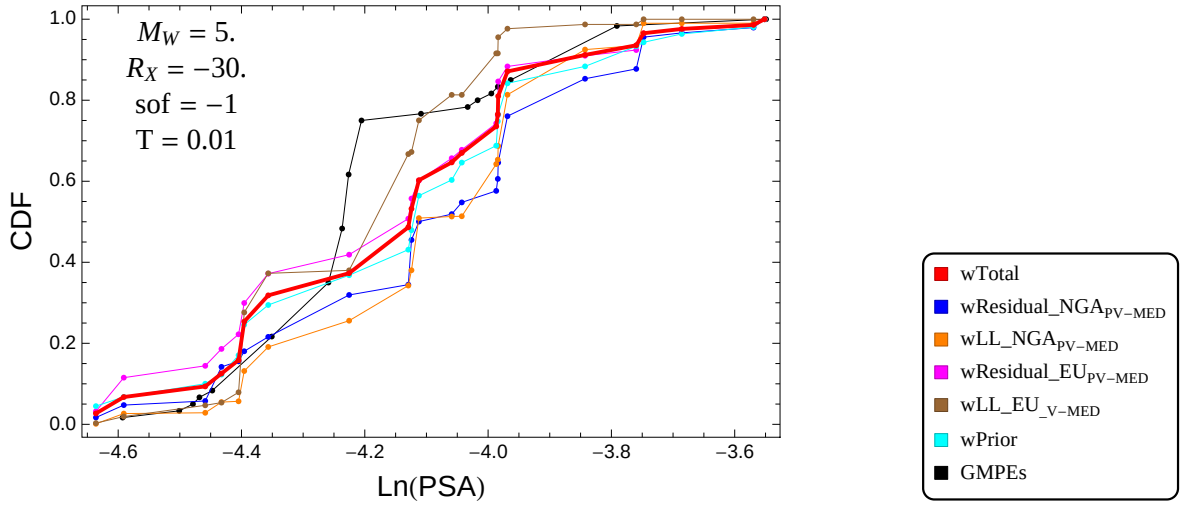



Figure 3.105: PVNGSv2: Cumulative distribution function of GMPEs (black) and selected models, for different sets of weights, for a scenario with $M = 5.$, $R_x = -30.$, $F = -1$, and $T = 0.01$s

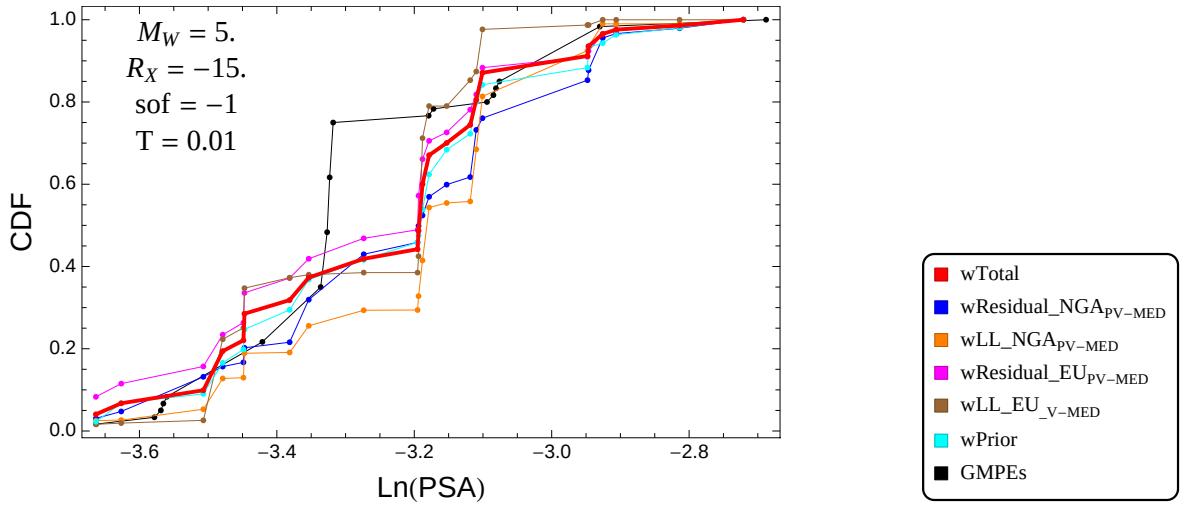



Figure 3.106: PVNGSv2: Cumulative distribution function of GMPEs (black) and selected models, for different sets of weights, for a scenario with $M = 5.$, $R_x = -15.$, $F = -1$, and $T = 0.01$s

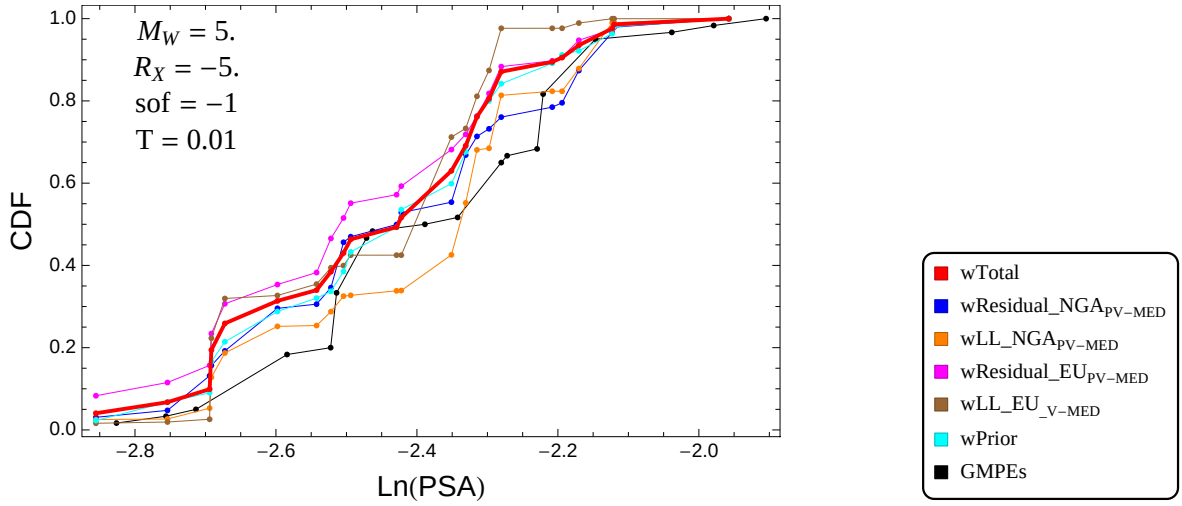



Figure 3.107: PVNGSv2: Cumulative distribution function of GMPEs (black) and selected models, for different sets of weights, for a scenario with $M = 5.$, $R_x = -5.$, $F = -1$, and $T = 0.01$s

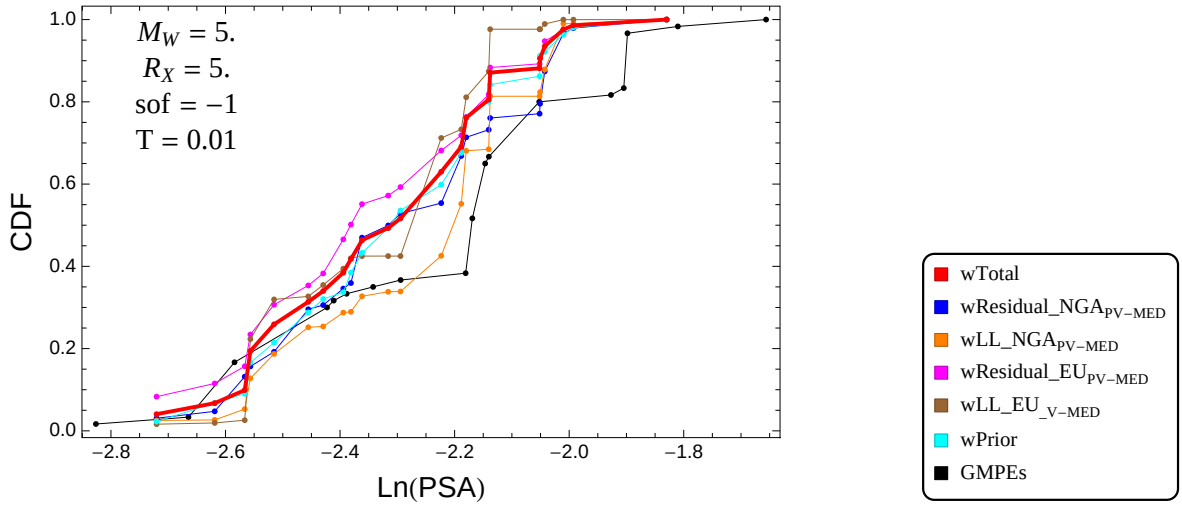



Figure 3.108: PVNGSv2: Cumulative distribution function of GMPEs (black) and selected models, for different sets of weights, for a scenario with $M = 5.$, $R_x = 5.$, $F = -1$, and $T = 0.01$s

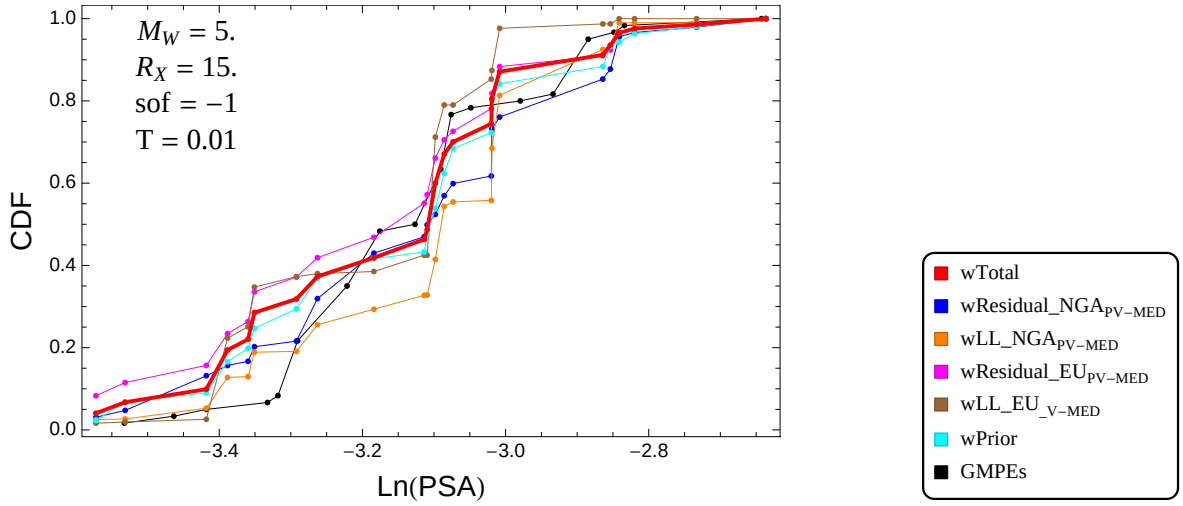



Figure 3.109: PVNGSv2: Cumulative distribution function of GMPEs (black) and selected models, for different sets of weights, for a scenario with $M = 5.$, $R_x = 15.$, $F = -1$, and $T = 0.01$s

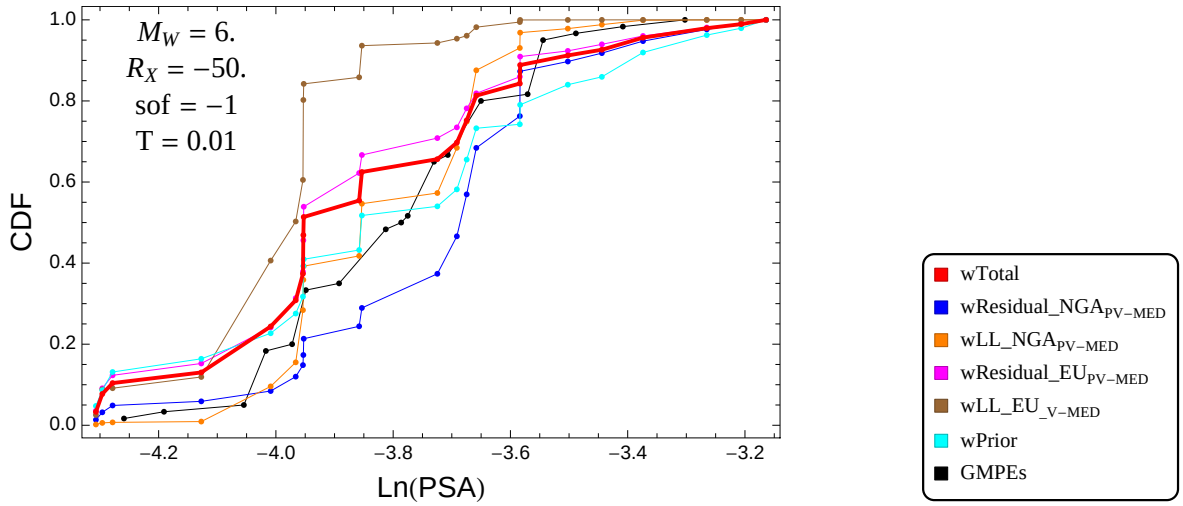



Figure 3.110: PVNGSv2: Cumulative distribution function of GMPEs (black) and selected models, for different sets of weights, for a scenario with $M = 6.$, $R_x = -50.$, $F = -1$, and $T = 0.01$s

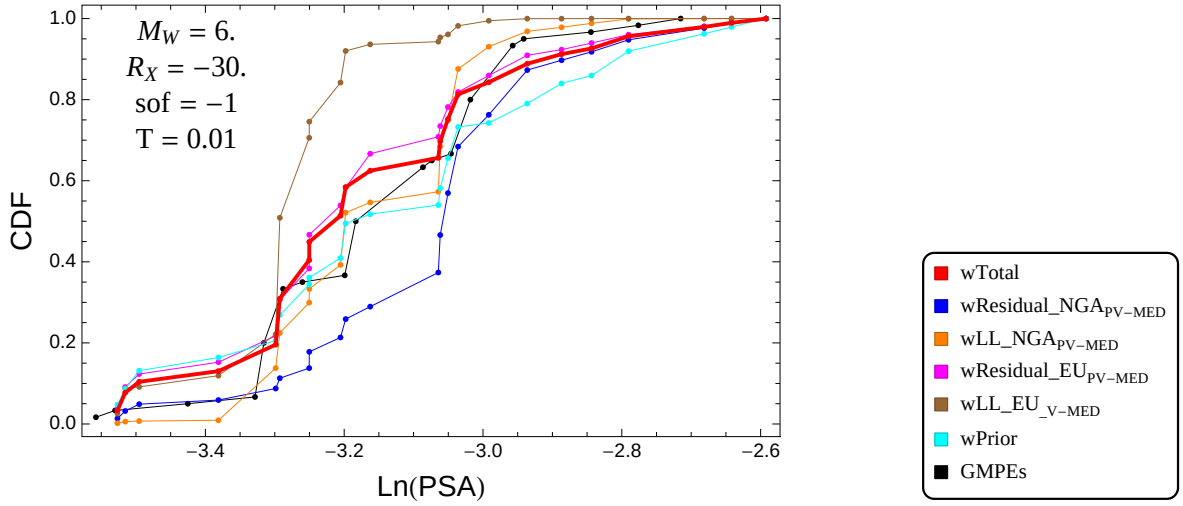



Figure 3.111: PVNGSv2: Cumulative distribution function of GMPEs (black) and selected models, for different sets of weights, for a scenario with $M = 6.$, $R_x = -30.$, $F = -1$, and $T = 0.01$s

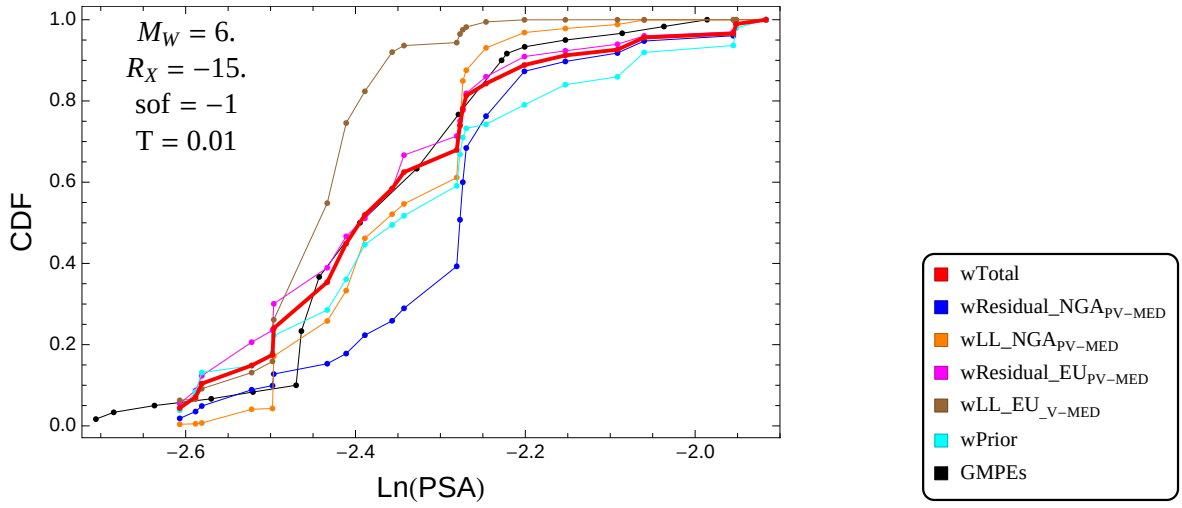



Figure 3.112: PVNGSv2: Cumulative distribution function of GMPEs (black) and selected models, for different sets of weights, for a scenario with $M = 6.$, $R_x = -15.$, $F = -1$, and $T = 0.01$s

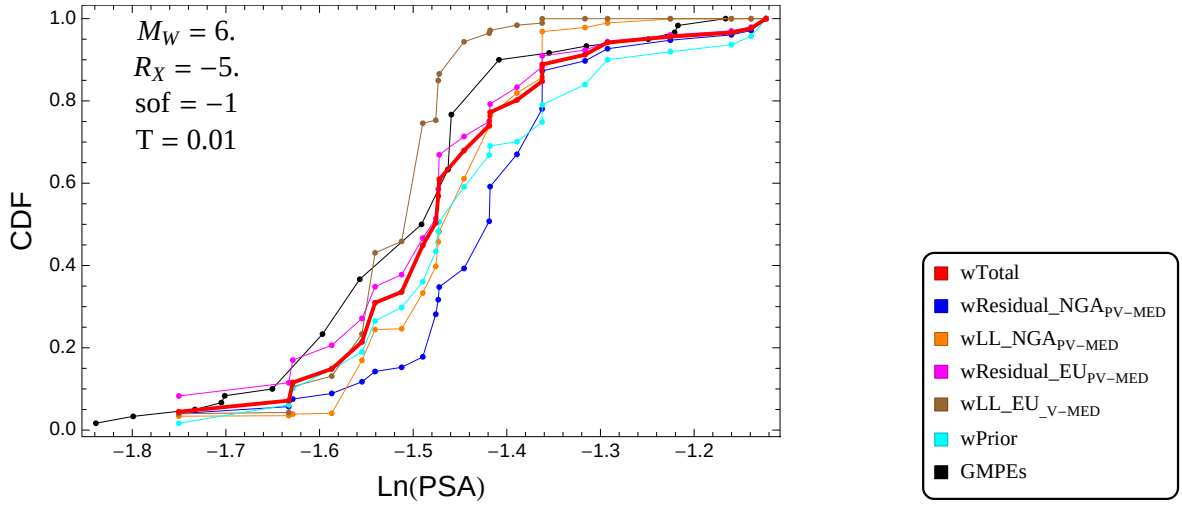



Figure 3.113: PVNGSv2: Cumulative distribution function of GMPEs (black) and selected models, for different sets of weights, for a scenario with $M = 6.$, $R_x = -5.$, $F = -1$, and $T = 0.01$s

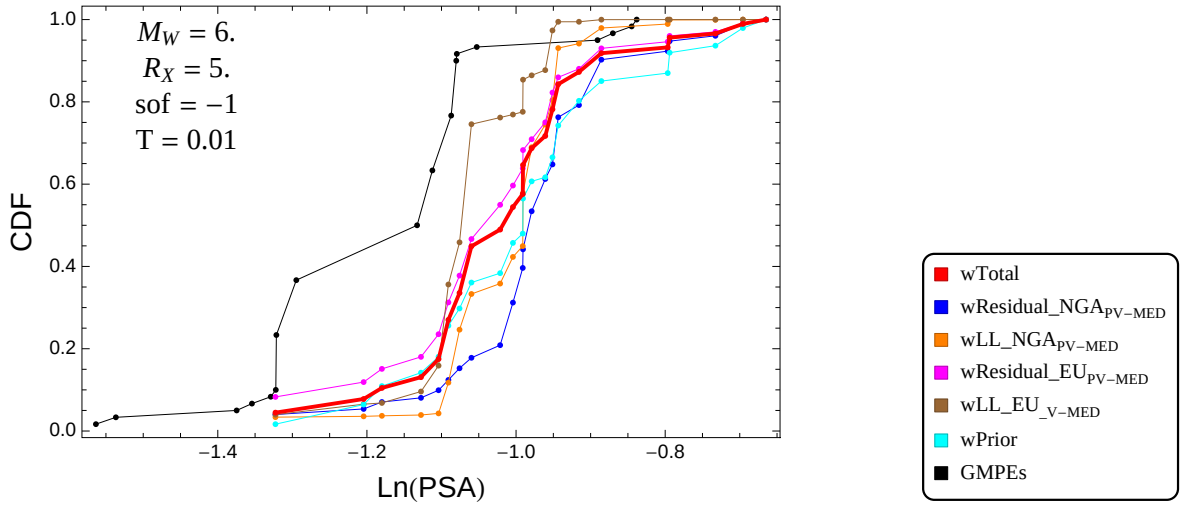



Figure 3.114: PVNGSv2: Cumulative distribution function of GMPEs (black) and selected models, for different sets of weights, for a scenario with $M = 6.$, $R_x = 5.$, $F = -1$, and $T = 0.01$s

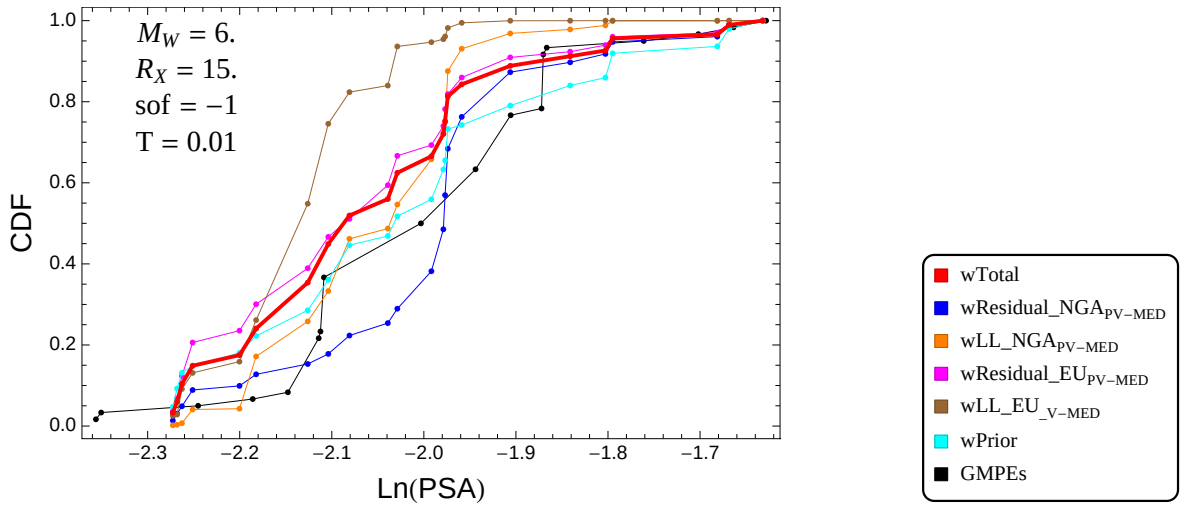



Figure 3.115: PVNGSv2: Cumulative distribution function of GMPEs (black) and selected models, for different sets of weights, for a scenario with $M = 6.$, $R_x = 15.$, $F = -1$, and $T = 0.01$s

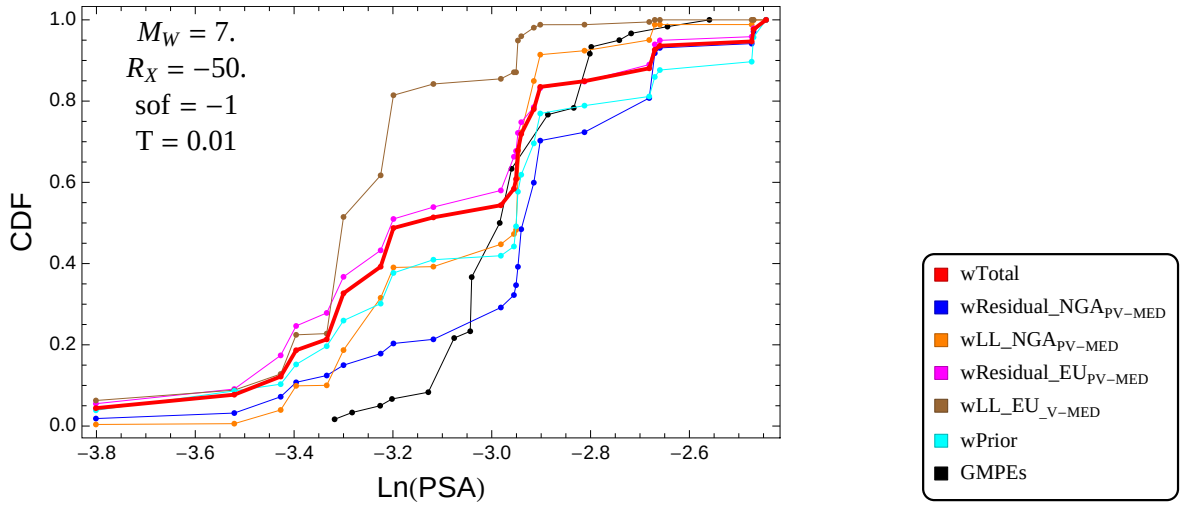



Figure 3.116: PVNGSv2: Cumulative distribution function of GMPEs (black) and selected models, for different sets of weights, for a scenario with $M = 7.$, $R_x = -50.$, $F = -1$, and $T = 0.01$s

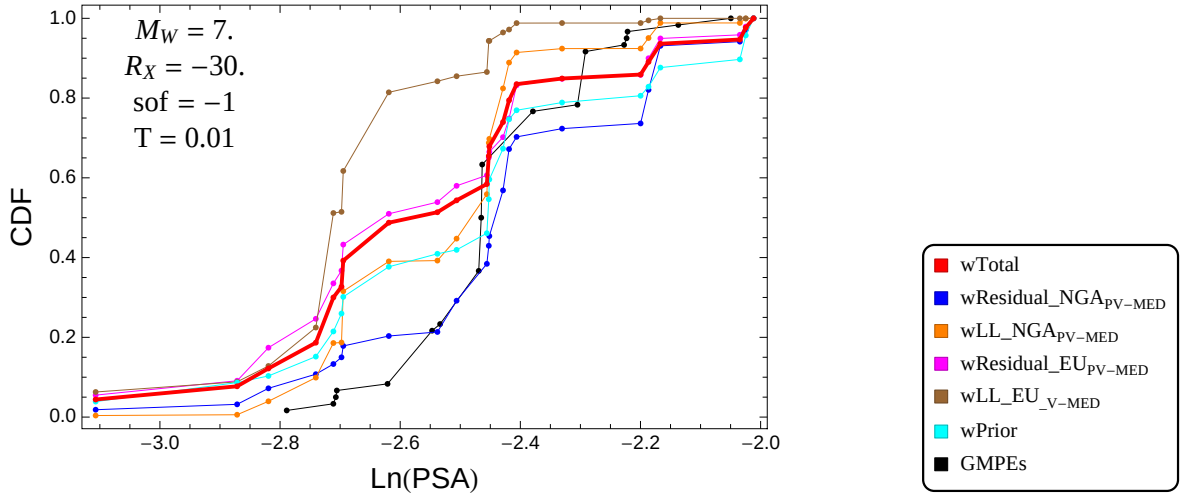



Figure 3.117: PVNGSv2: Cumulative distribution function of GMPEs (black) and selected models, for different sets of weights, for a scenario with $M = 7.$, $R_x = -30.$, $F = -1$, and $T = 0.01$s

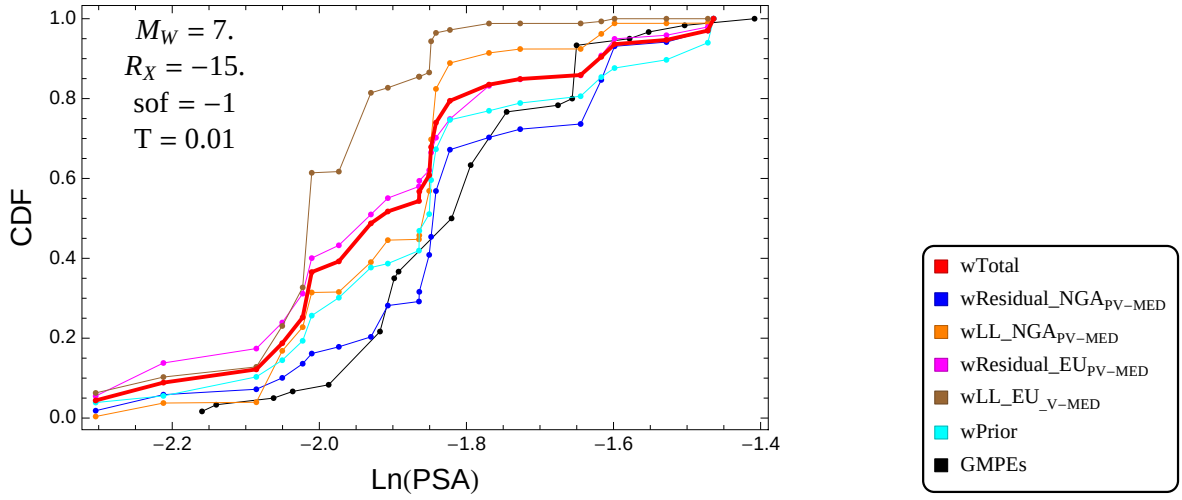



Figure 3.118: PVNGSv2: Cumulative distribution function of GMPEs (black) and selected models, for different sets of weights, for a scenario with $M = 7.$, $R_x = -15.$, $F = -1$, and $T = 0.01$s

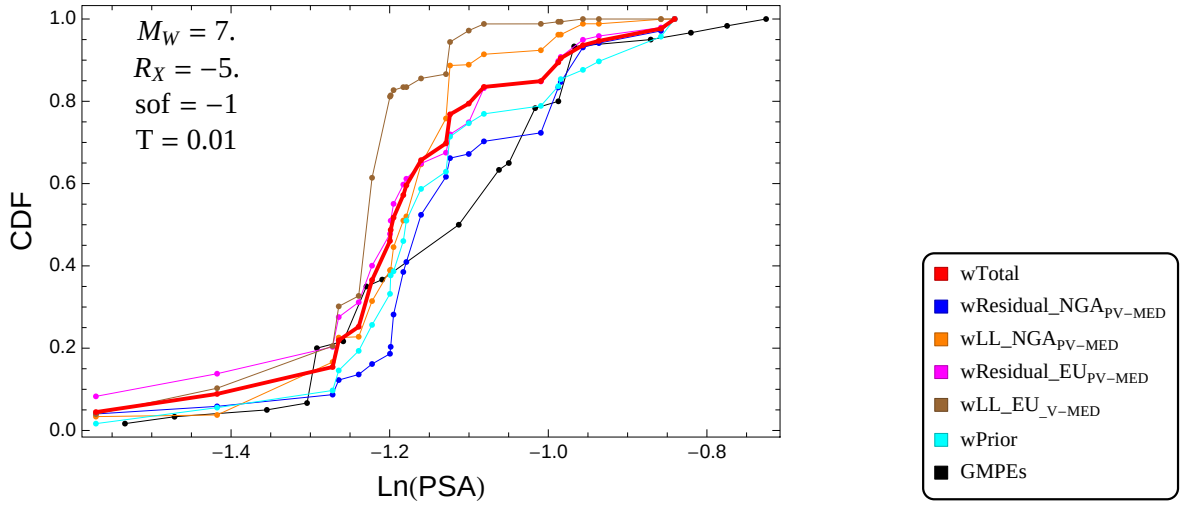



Figure 3.119: PVNGSv2: Cumulative distribution function of GMPEs (black) and selected models, for different sets of weights, for a scenario with $M = 7.$, $R_x = -5.$, $F = -1$, and $T = 0.01$s

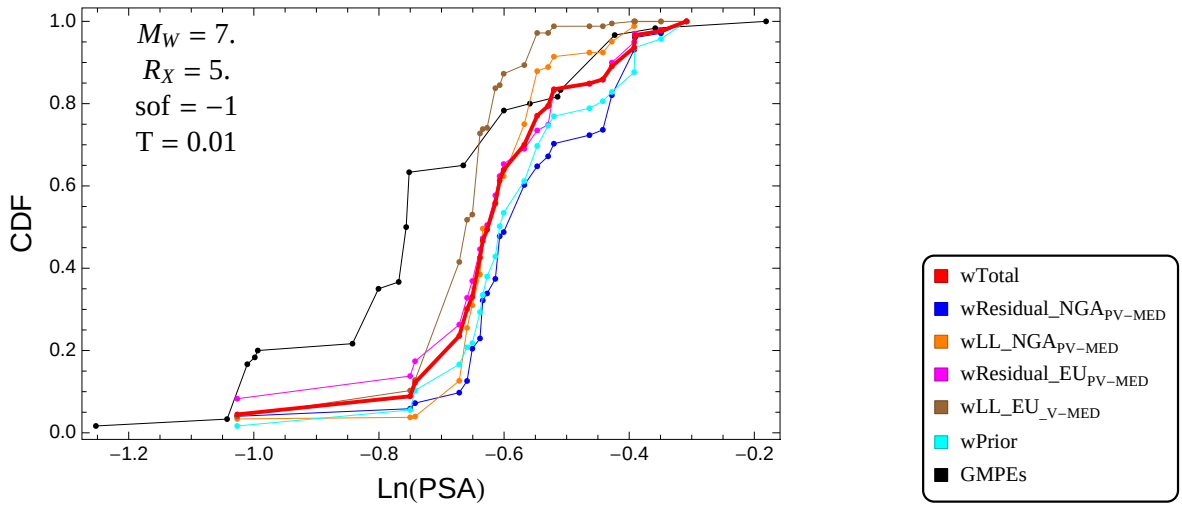



Figure 3.120: PVNGSv2: Cumulative distribution function of GMPEs (black) and selected models, for different sets of weights, for a scenario with $M = 7.$, $R_x = 5.$, $F = -1$, and $T = 0.01$s

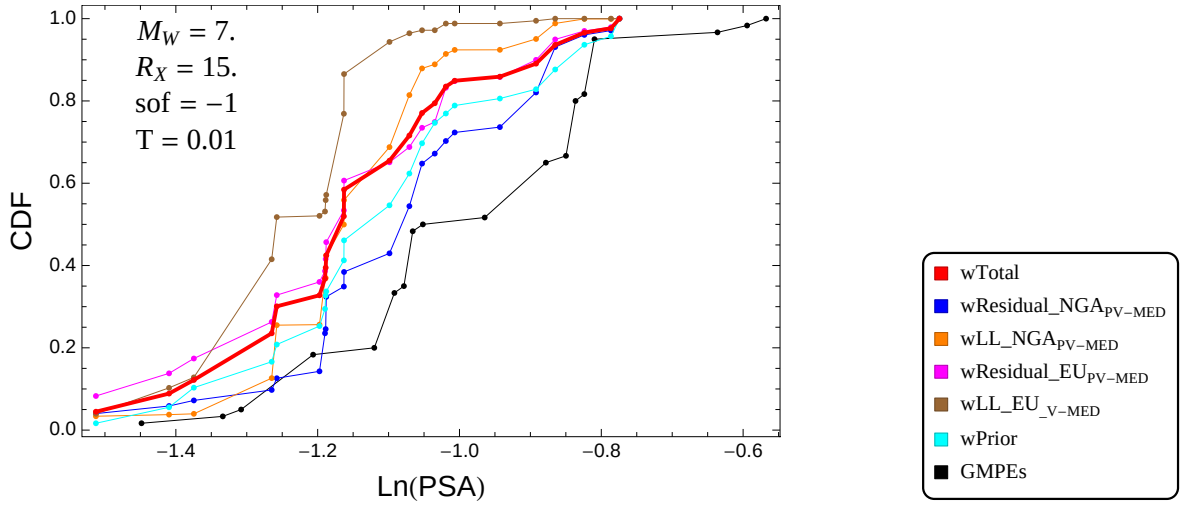



Figure 3.121: PVNGSv2: Cumulative distribution function of GMPEs (black) and selected models, for different sets of weights, for a scenario with $M = 7.$, $R_x = 15.$, $F = -1$, and $T = 0.01$s

**T = 0.2s**

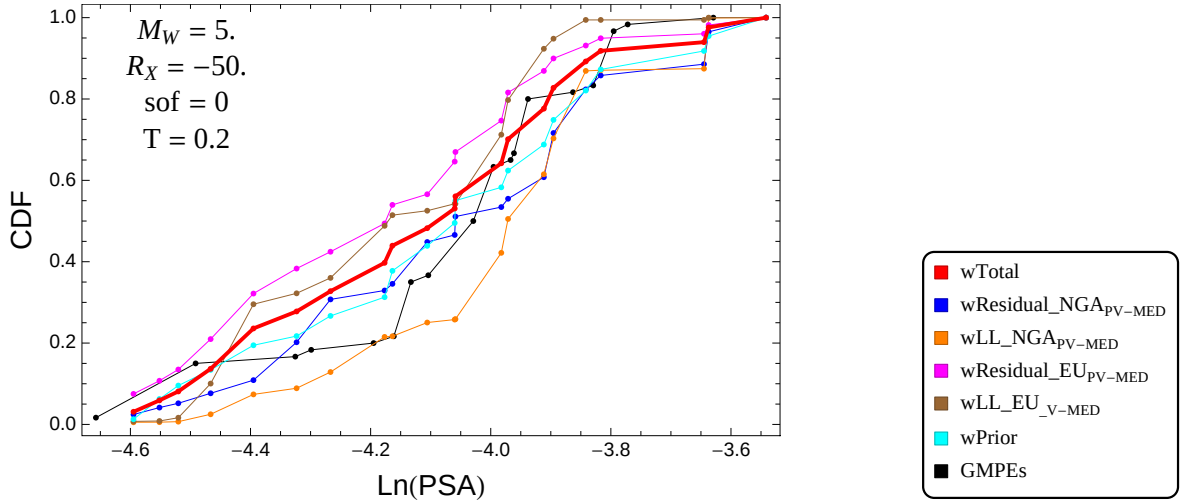



Figure 3.122: PVNGSv2: Cumulative distribution function of GMPEs (black) and selected models, for different sets of weights, for a scenario with $M = 5.$, $R_x = -50.$, $F = 0$, and $T = 0.2$s

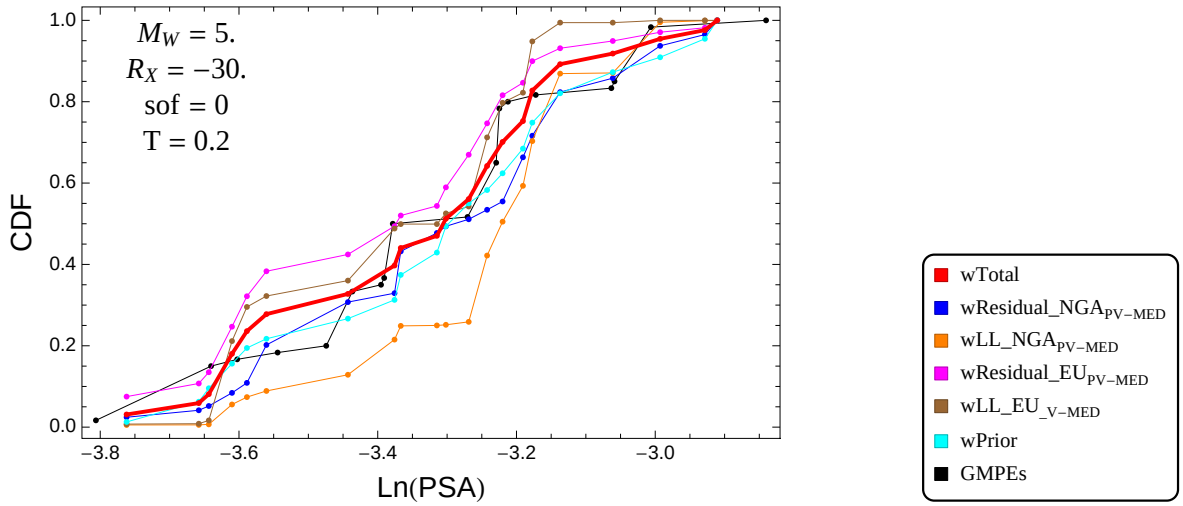



Figure 3.123: PVNGSv2: Cumulative distribution function of GMPEs (black) and selected models, for different sets of weights, for a scenario with $M = 5.$, $R_x = -30.$, $F = 0$, and $T = 0.2$s

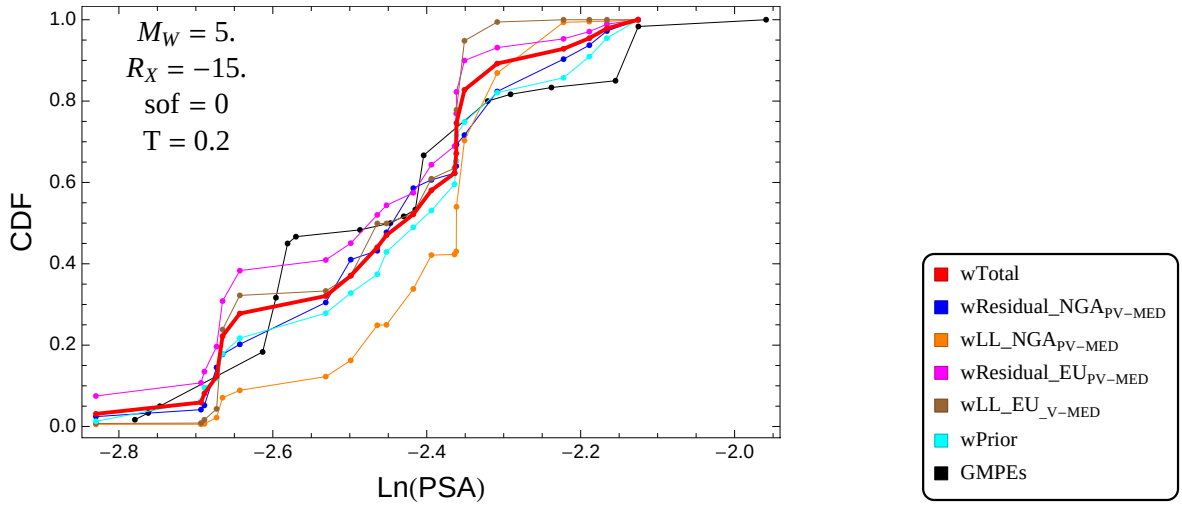



Figure 3.124: PVNGSv2: Cumulative distribution function of GMPEs (black) and selected models, for different sets of weights, for a scenario with $M = 5.$, $R_x = -15.$, $F = 0$, and $T = 0.2$s

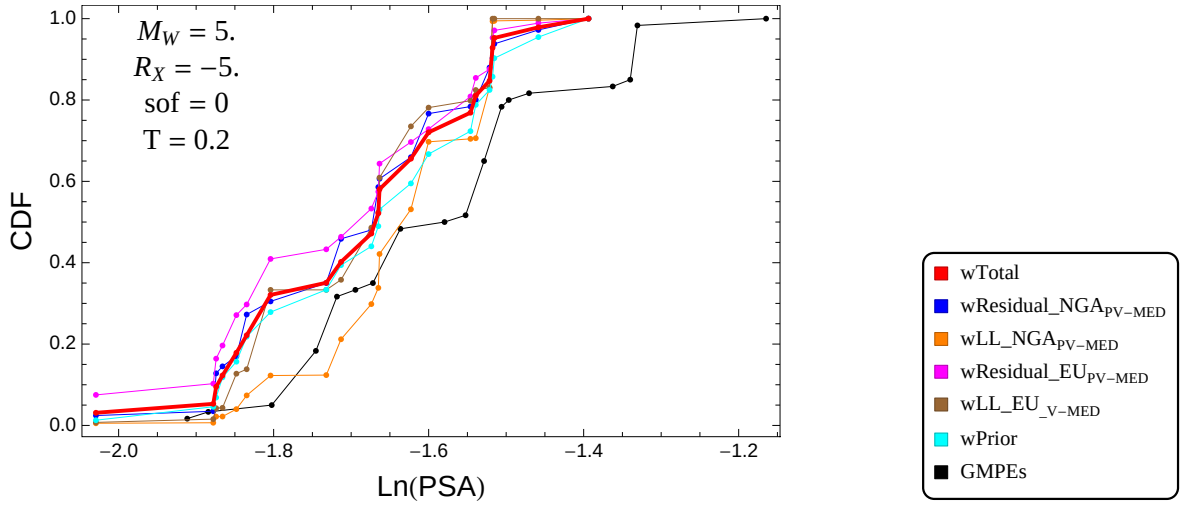



Figure 3.125: PVNGSv2: Cumulative distribution function of GMPEs (black) and selected models, for different sets of weights, for a scenario with $M = 5.$, $R_x = -5.$, $F = 0$, and $T = 0.2$s

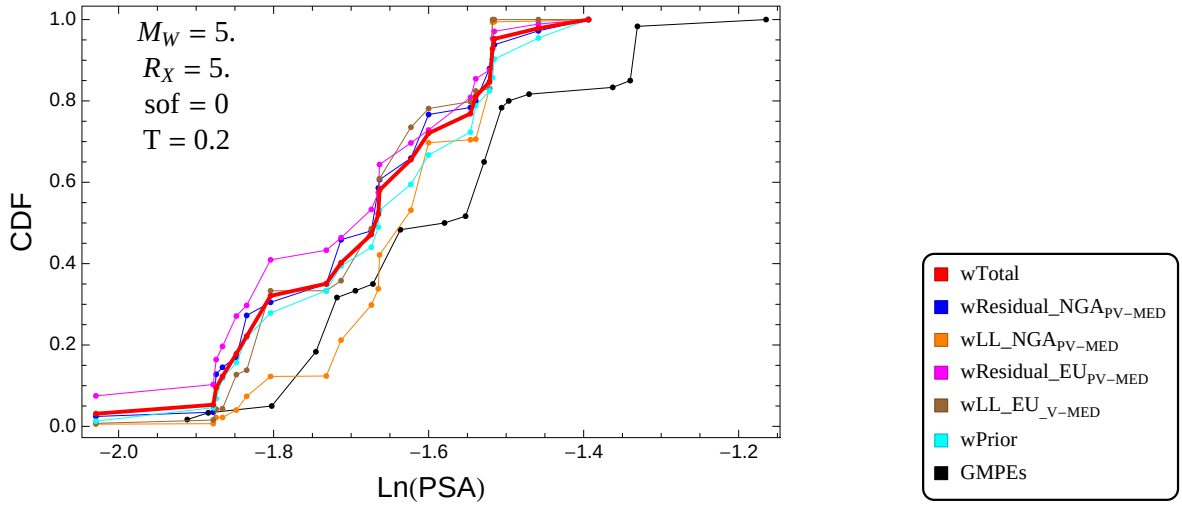



Figure 3.126: PVNGSv2: Cumulative distribution function of GMPEs (black) and selected models, for different sets of weights, for a scenario with $M = 5.$, $R_x = 5.$, $F = 0$, and $T = 0.2$s

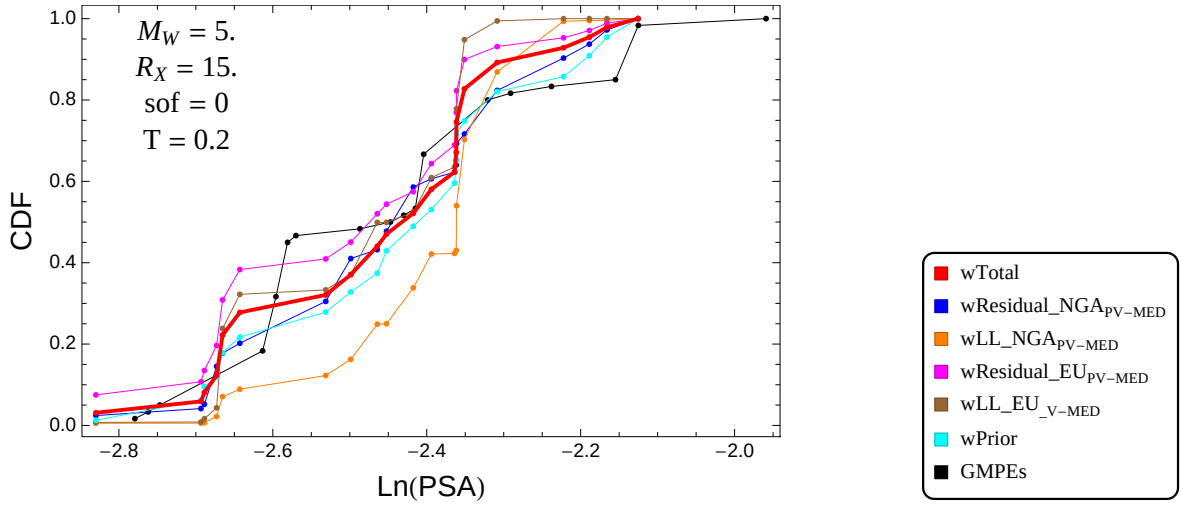



Figure 3.127: PVNGSv2: Cumulative distribution function of GMPEs (black) and selected models, for different sets of weights, for a scenario with $M = 5.$, $R_x = 15.$, $F = 0$, and $T = 0.2$s

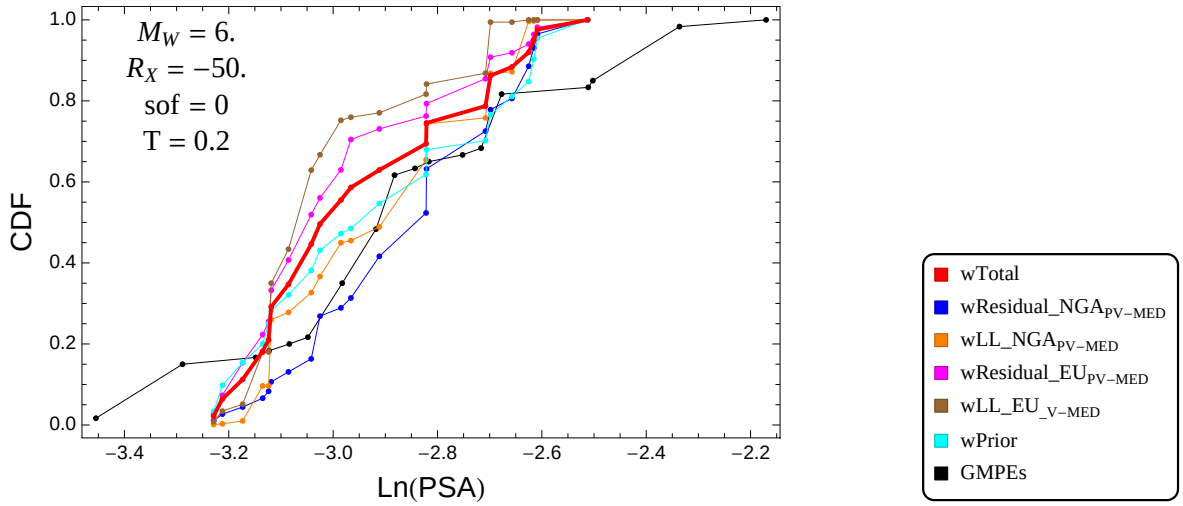



Figure 3.128: PVNGSv2: Cumulative distribution function of GMPEs (black) and selected models, for different sets of weights, for a scenario with $M = 6.$, $R_x = -50.$, $F = 0$, and $T = 0.2$s

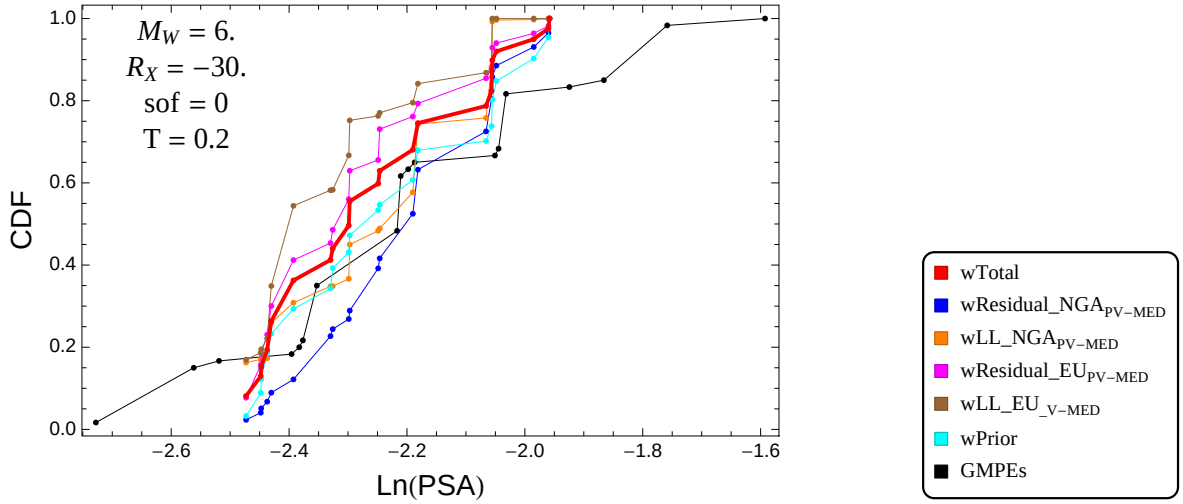



Figure 3.129: PVNGSv2: Cumulative distribution function of GMPEs (black) and selected models, for different sets of weights, for a scenario with $M = 6.$, $R_x = -30.$, $F = 0$, and $T = 0.2$s

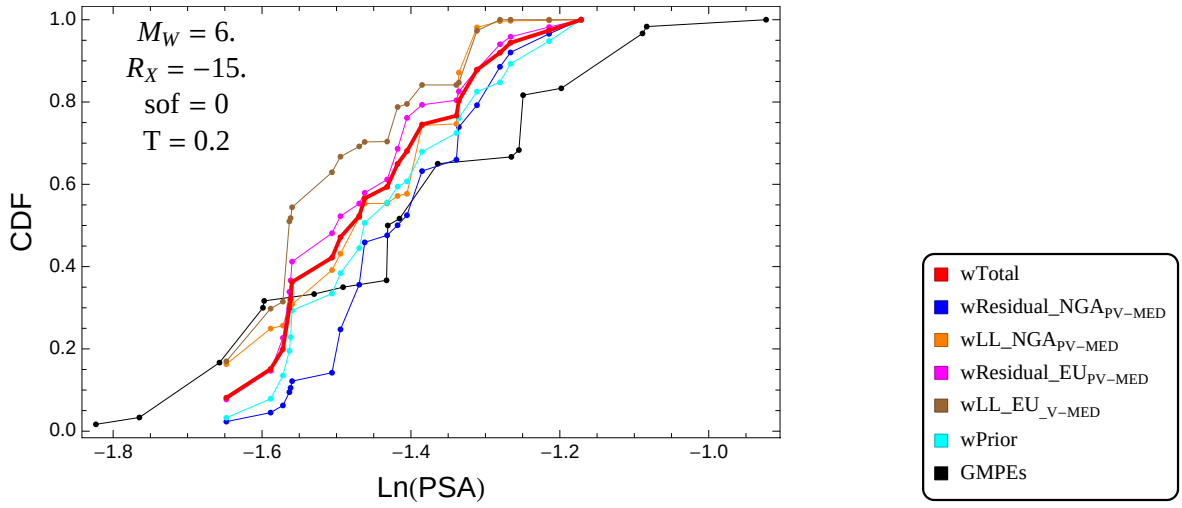



Figure 3.130: PVNGSv2: Cumulative distribution function of GMPEs (black) and selected models, for different sets of weights, for a scenario with $M = 6.$, $R_x = -15.$, $F = 0$, and $T = 0.2$s

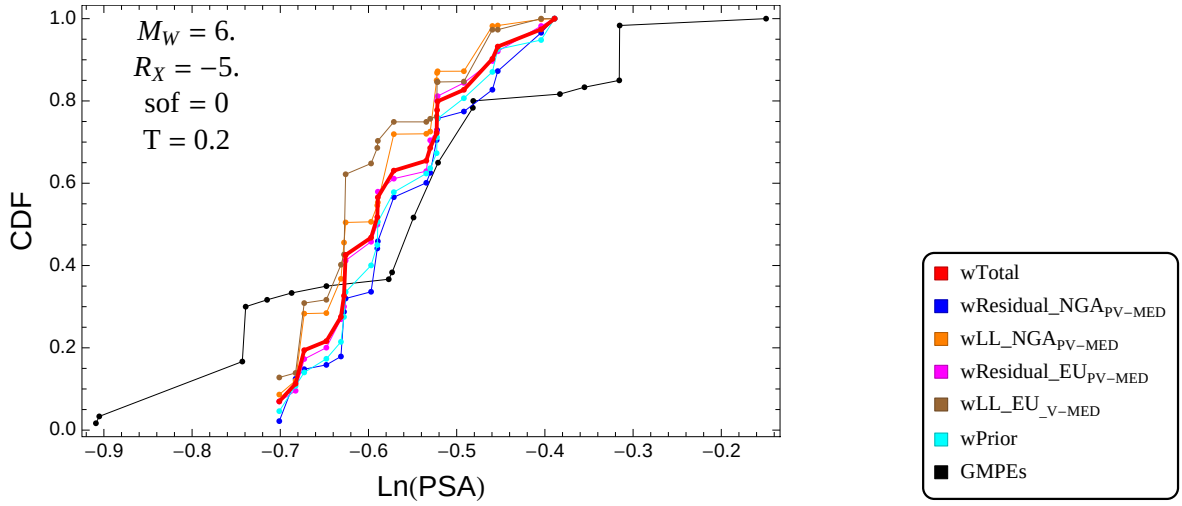



Figure 3.131: PVNGSv2: Cumulative distribution function of GMPEs (black) and selected models, for different sets of weights, for a scenario with $M = 6.$, $R_x = -5.$, $F = 0$, and $T = 0.2$s

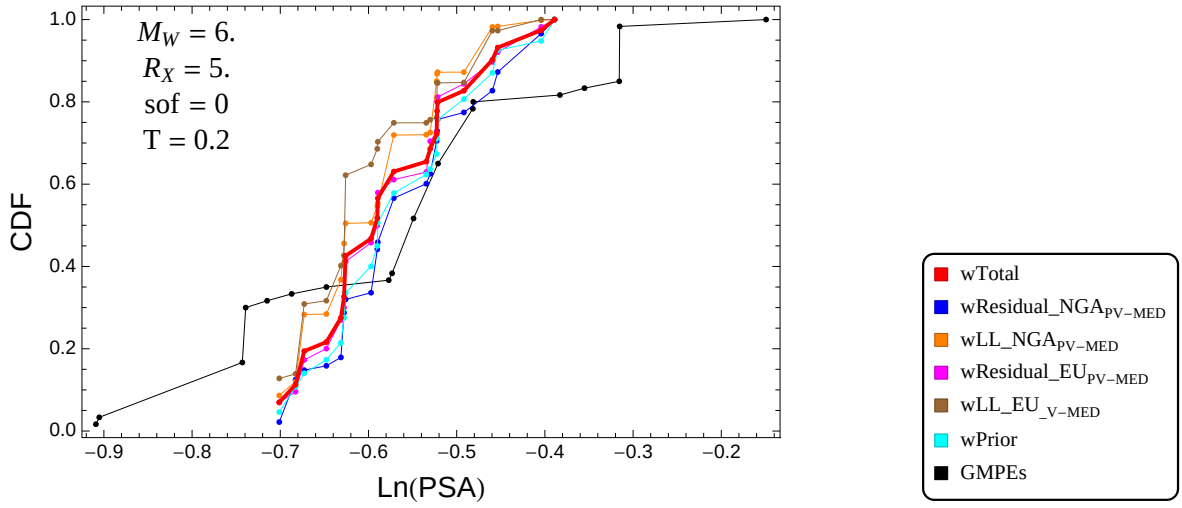



Figure 3.132: PVNGSv2: Cumulative distribution function of GMPEs (black) and selected models, for different sets of weights, for a scenario with $M = 6.$, $R_x = 5.$, $F = 0$, and $T = 0.2$s

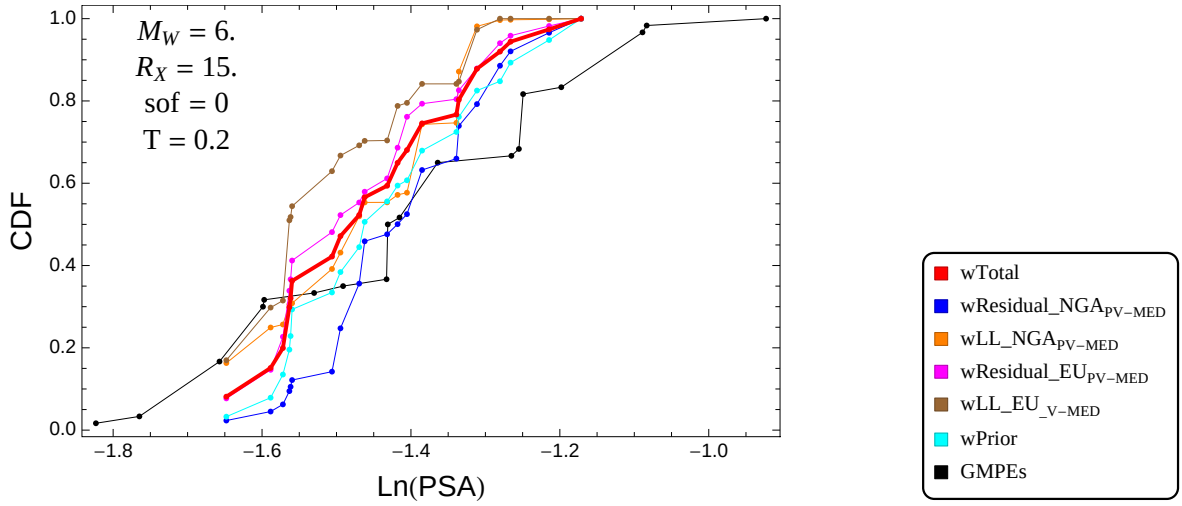



Figure 3.133: PVNGSv2: Cumulative distribution function of GMPEs (black) and selected models, for different sets of weights, for a scenario with $M = 6.$, $R_x = 15.$, $F = 0$, and $T = 0.2$s

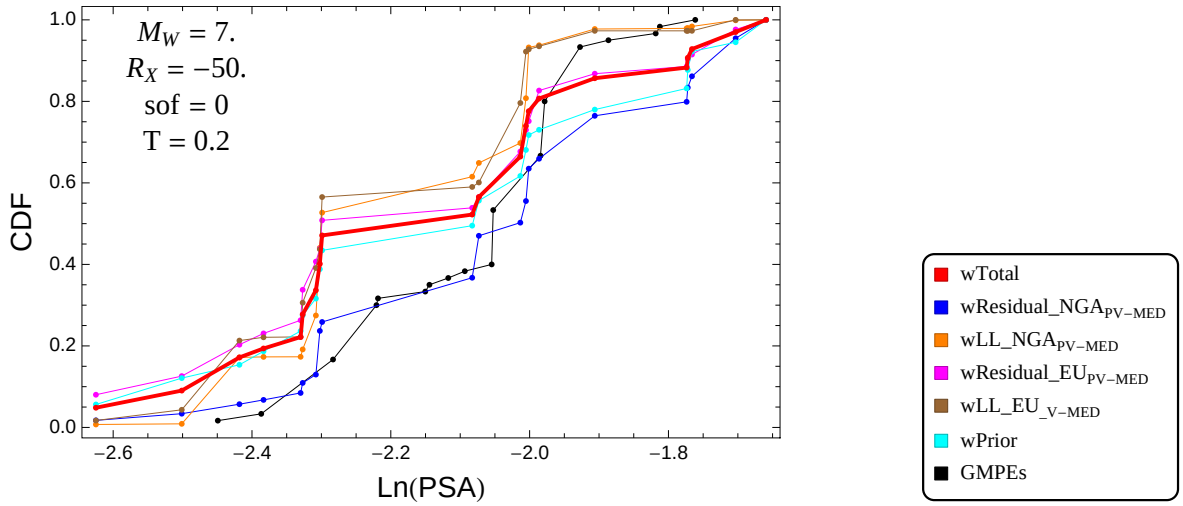



Figure 3.134: PVNGSv2: Cumulative distribution function of GMPEs (black) and selected models, for different sets of weights, for a scenario with $M = 7.$, $R_x = -50.$, $F = 0$, and $T = 0.2$s

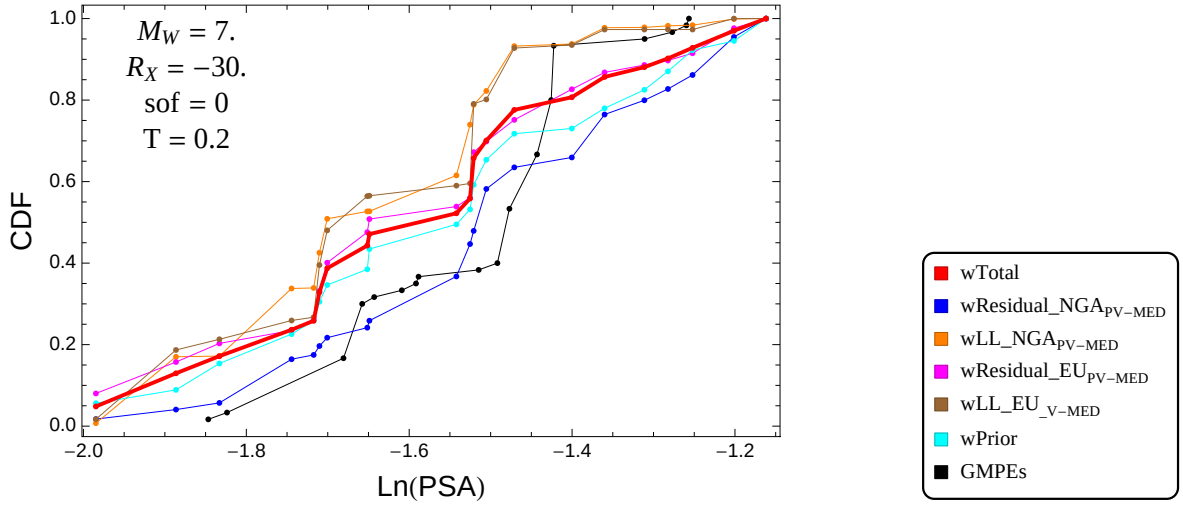



Figure 3.135: PVNGSv2: Cumulative distribution function of GMPEs (black) and selected models, for different sets of weights, for a scenario with $M = 7.$, $R_x = -30.$, $F = 0$, and $T = 0.2$s

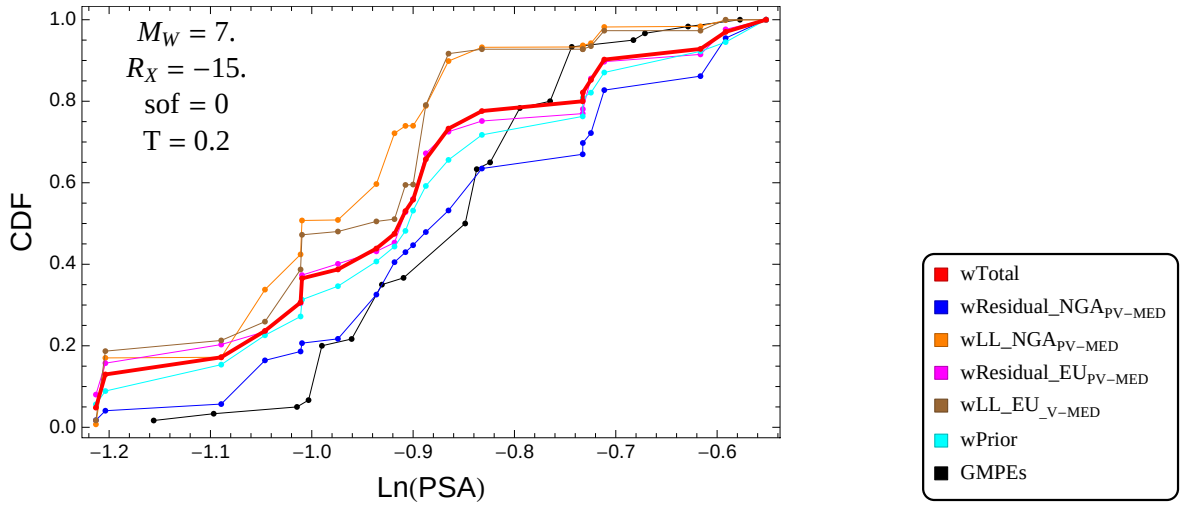



Figure 3.136: PVNGSv2: Cumulative distribution function of GMPEs (black) and selected models, for different sets of weights, for a scenario with $M = 7.$, $R_x = -15.$, $F = 0$, and $T = 0.2$s

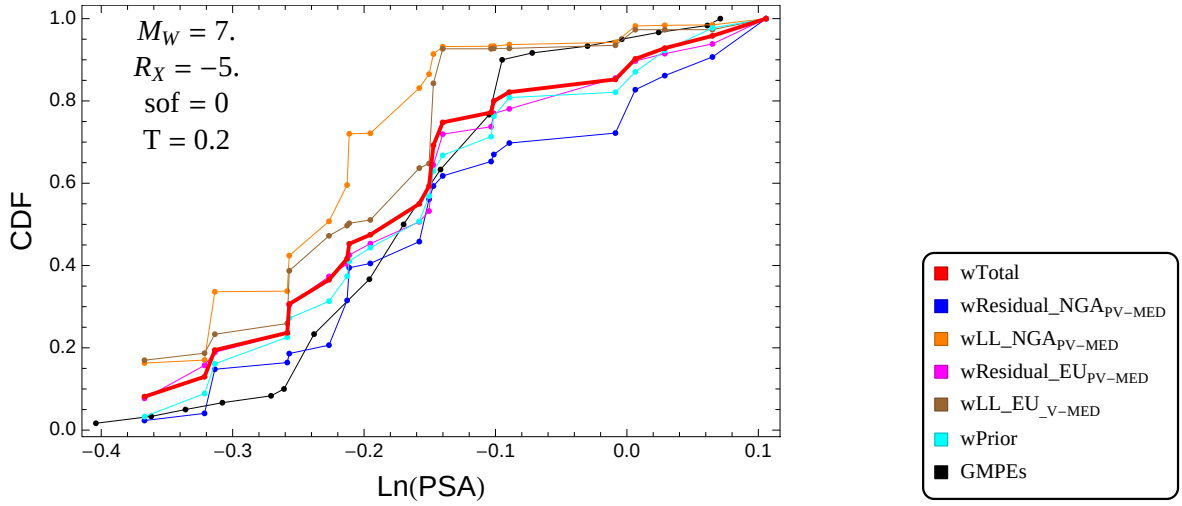



Figure 3.137: PVNGSv2: Cumulative distribution function of GMPEs (black) and selected models, for different sets of weights, for a scenario with $M = 7.$, $R_x = -5.$, $F = 0$, and $T = 0.2$s

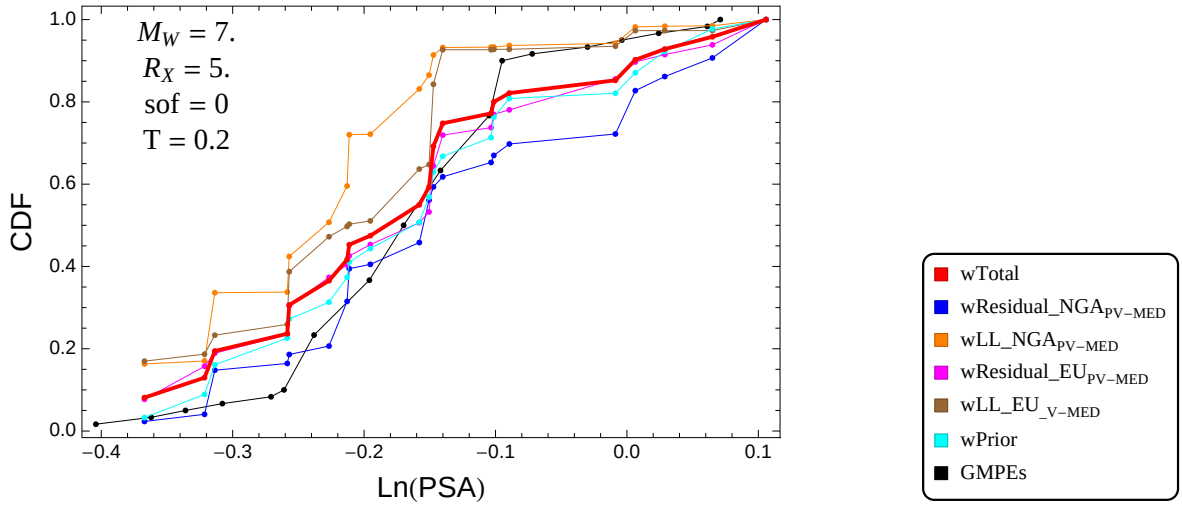



Figure 3.138: PVNGSv2: Cumulative distribution function of GMPEs (black) and selected models, for different sets of weights, for a scenario with $M = 7.$, $R_x = 5.$, $F = 0$, and $T = 0.2$s

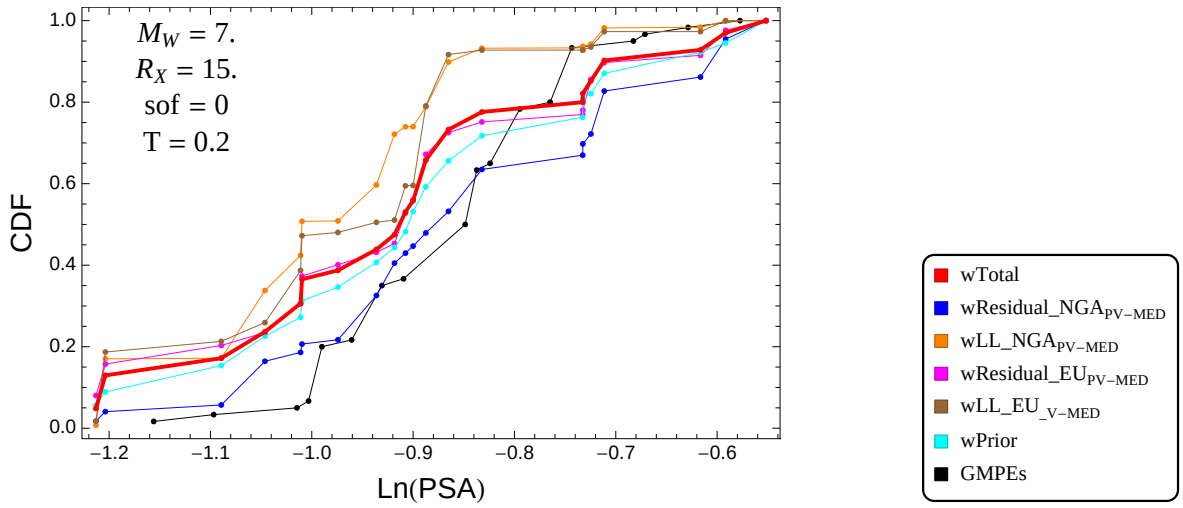



Figure 3.139: PVNGSv2: Cumulative distribution function of GMPEs (black) and selected models, for different sets of weights, for a scenario with $M = 7.$, $R_x = 15.$, $F = 0$, and $T = 0.2$s

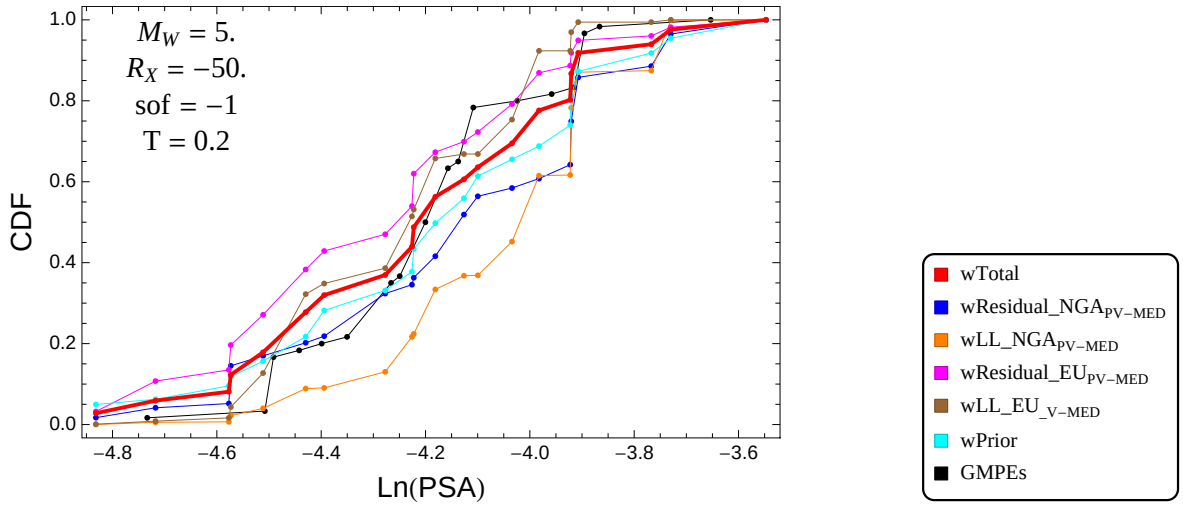



Figure 3.140: PVNGSv2: Cumulative distribution function of GMPEs (black) and selected models, for different sets of weights, for a scenario with $M = 5.$, $R_x = -50.$, $F = -1$, and $T = 0.2$s

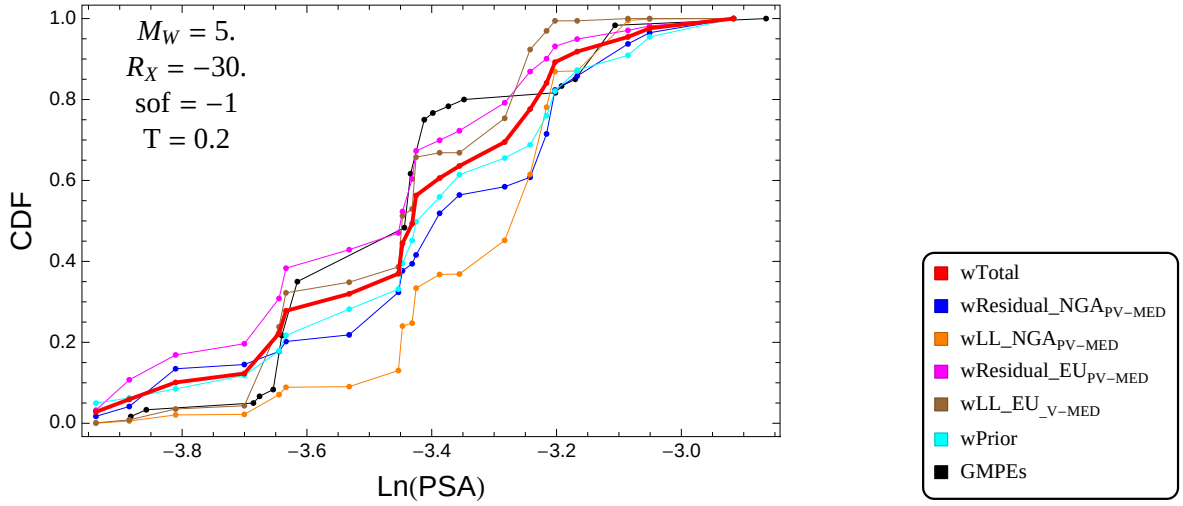



Figure 3.141: PVNGSv2: Cumulative distribution function of GMPEs (black) and selected models, for different sets of weights, for a scenario with $M = 5.$, $R_x = -30.$, $F = -1$, and $T = 0.2$s

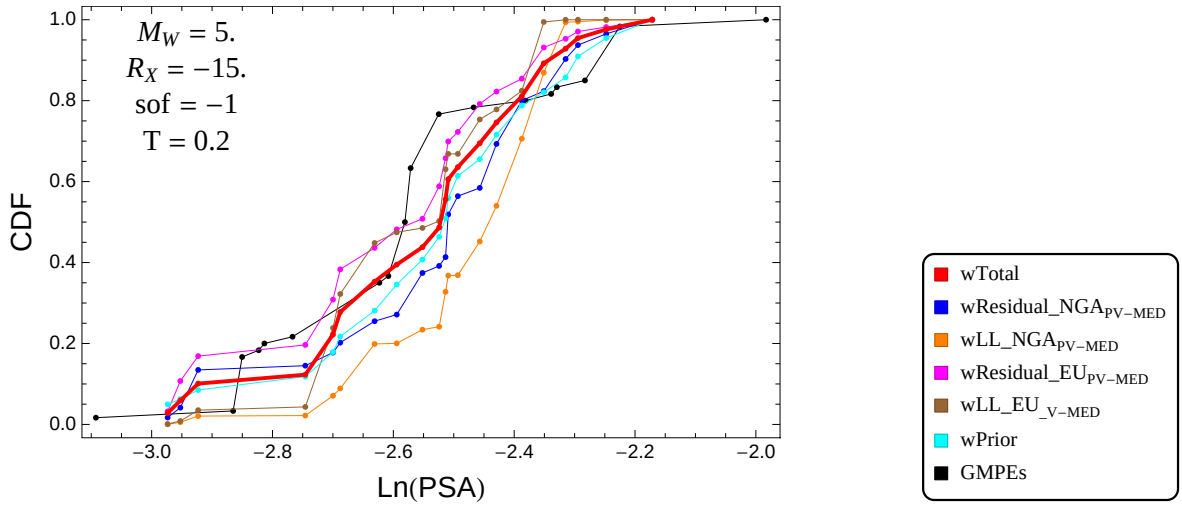



Figure 3.142: PVNGSv2: Cumulative distribution function of GMPEs (black) and selected models, for different sets of weights, for a scenario with $M = 5.$, $R_x = -15.$, $F = -1$, and $T = 0.2$s

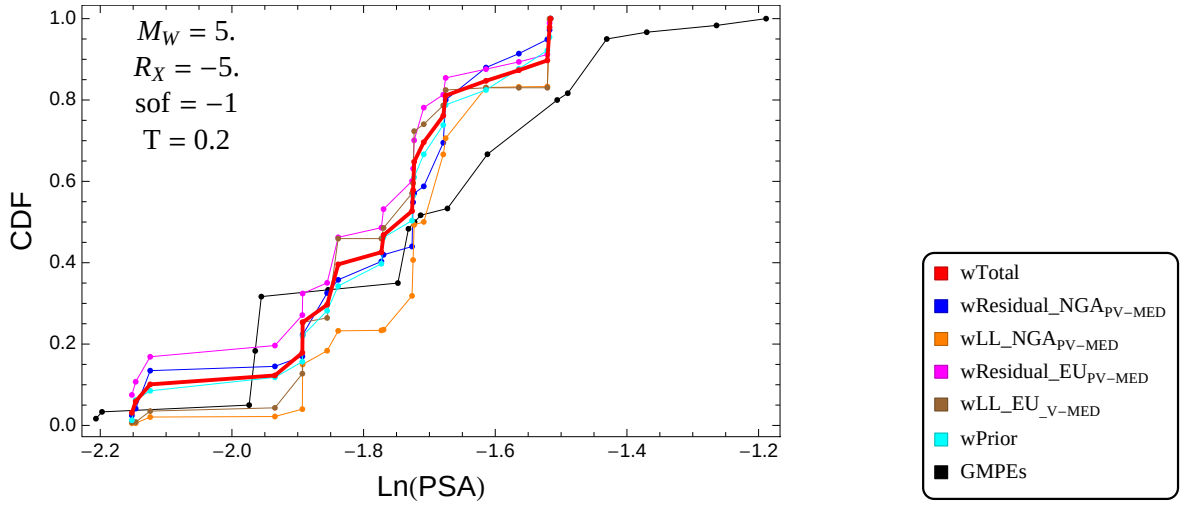



Figure 3.143: PVNGSv2: Cumulative distribution function of GMPEs (black) and selected models, for different sets of weights, for a scenario with $M = 5.$, $R_x = -5.$, $F = -1$, and $T = 0.2$s

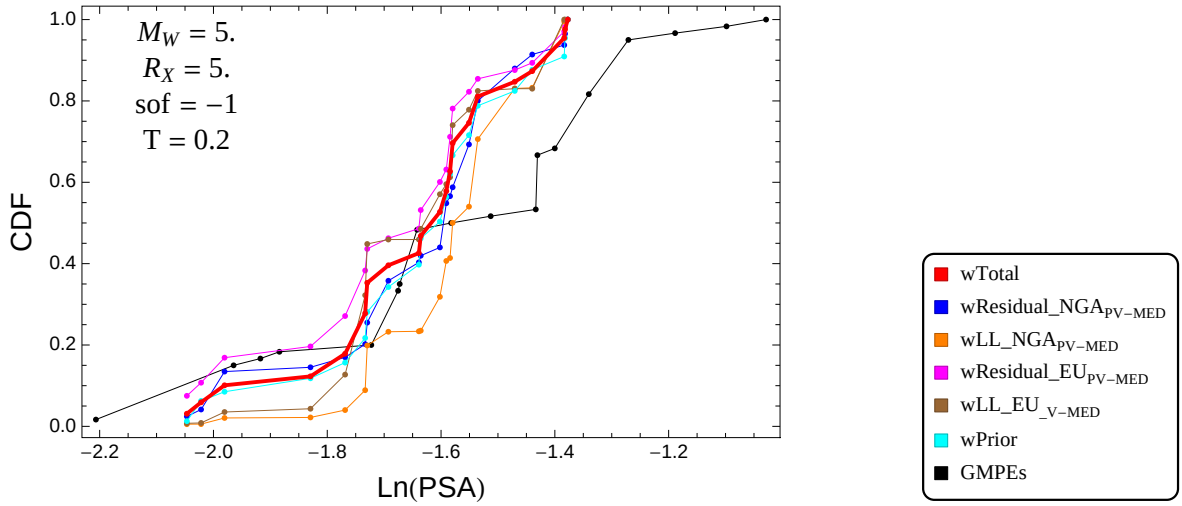



Figure 3.144: PVNGSv2: Cumulative distribution function of GMPEs (black) and selected models, for different sets of weights, for a scenario with $M = 5.$, $R_x = 5.$, $F = -1$, and $T = 0.2$s

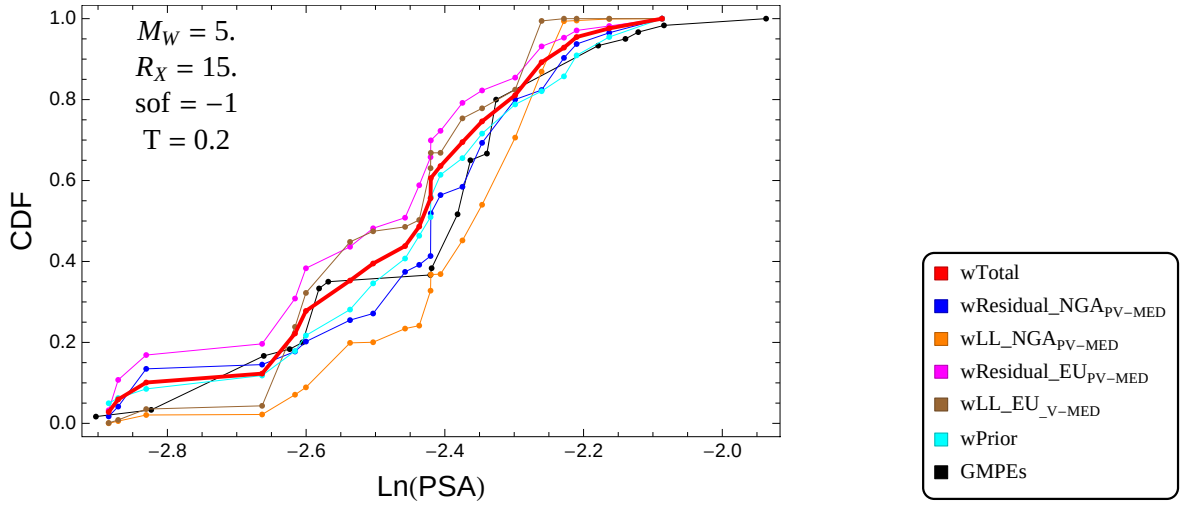



Figure 3.145: PVNGSv2: Cumulative distribution function of GMPEs (black) and selected models, for different sets of weights, for a scenario with $M = 5.$, $R_x = 15.$, $F = -1$, and $T = 0.2$s

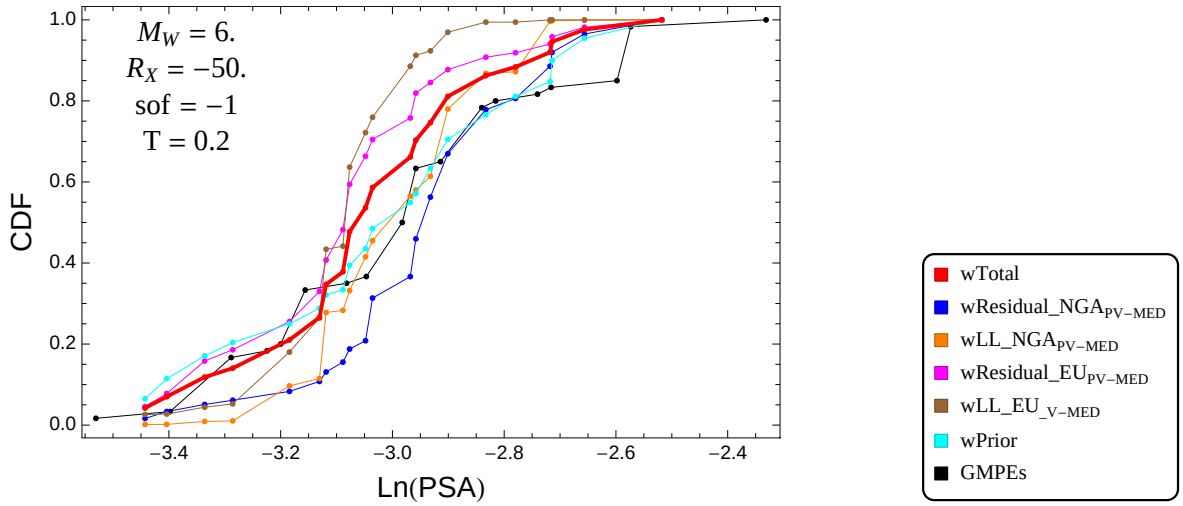



Figure 3.146: PVNGSv2: Cumulative distribution function of GMPEs (black) and selected models, for different sets of weights, for a scenario with $M = 6.$, $R_x = -50.$, $F = -1$, and $T = 0.2$s

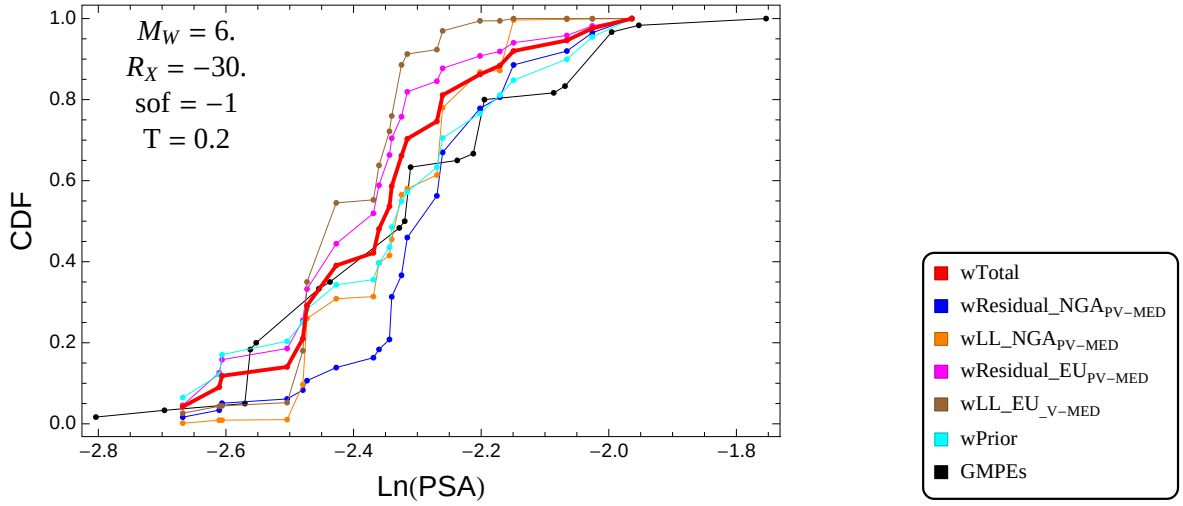



Figure 3.147: PVNGSv2: Cumulative distribution function of GMPEs (black) and selected models, for different sets of weights, for a scenario with $M = 6.$, $R_x = -30.$, $F = -1$, and $T = 0.2$s

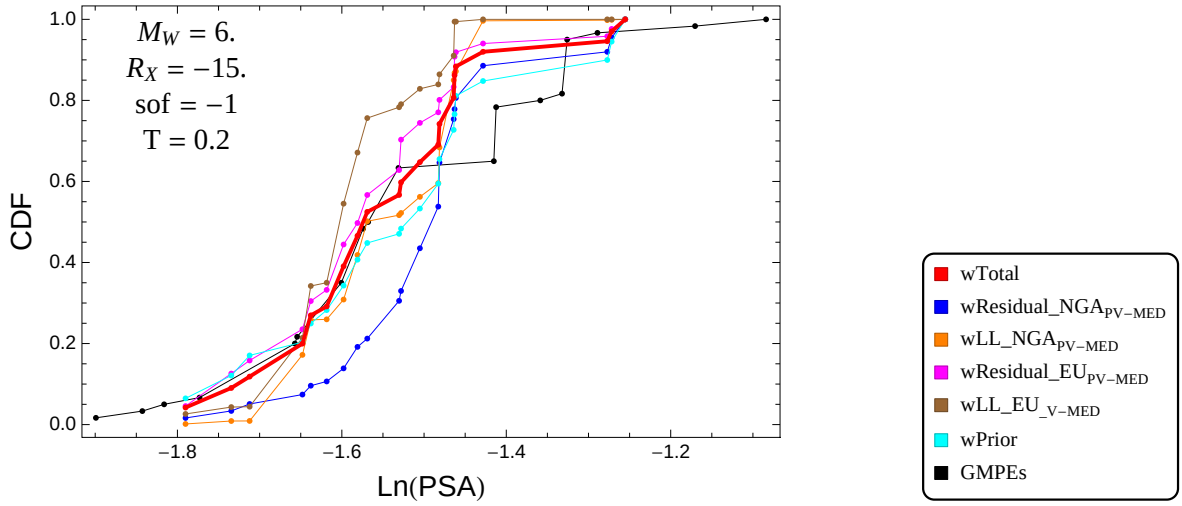



Figure 3.148: PVNGSv2: Cumulative distribution function of GMPEs (black) and selected models, for different sets of weights, for a scenario with $M = 6.$, $R_x = -15.$, $F = -1$, and $T = 0.2$s

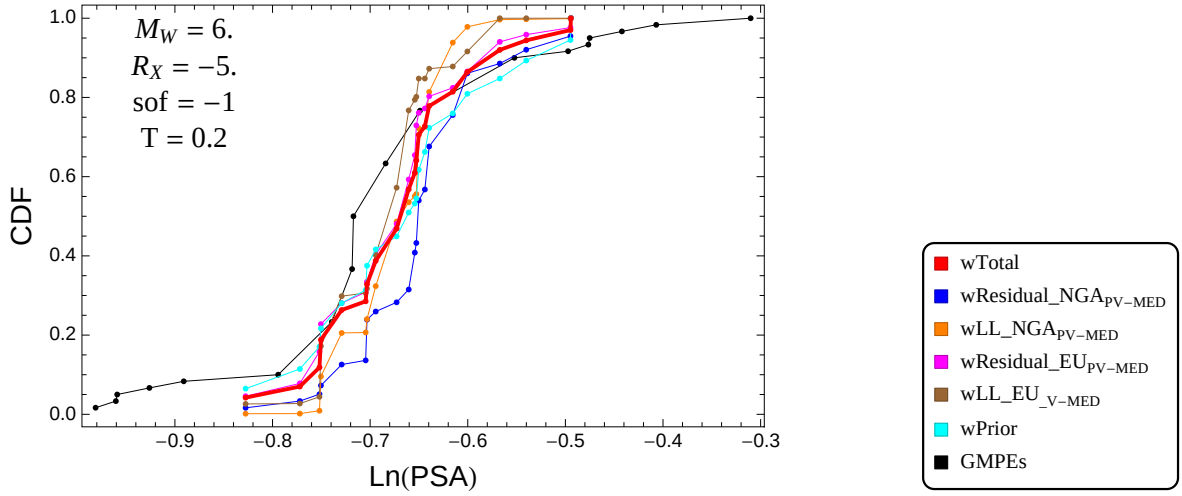



Figure 3.149: PVNGSv2: Cumulative distribution function of GMPEs (black) and selected models, for different sets of weights, for a scenario with $M = 6.$, $R_x = -5.$, $F = -1$, and $T = 0.2$s

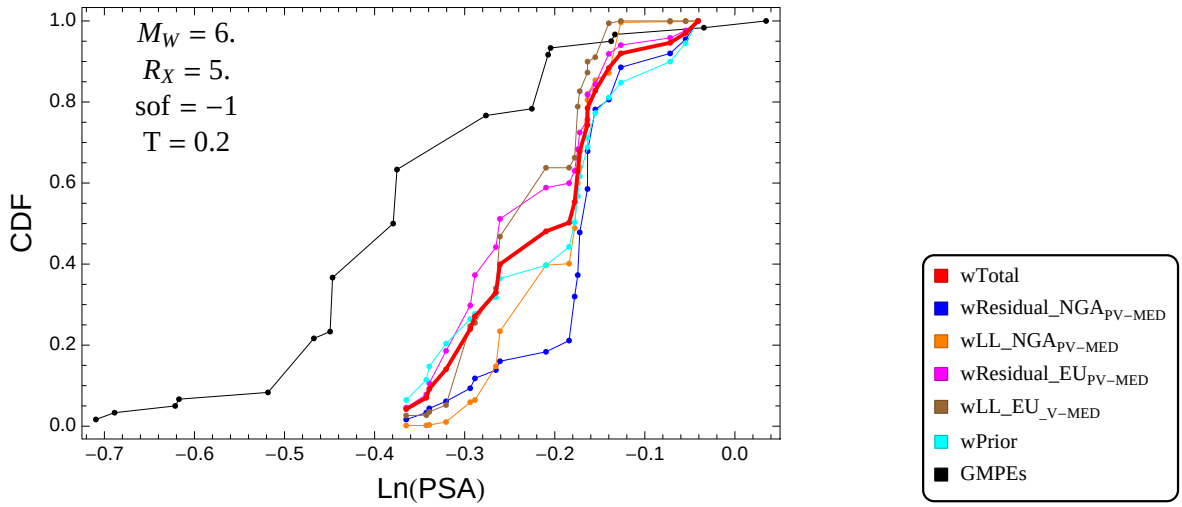



Figure 3.150: PVNGSv2: Cumulative distribution function of GMPEs (black) and selected models, for different sets of weights, for a scenario with $M = 6.$, $R_x = 5.$, $F = -1$, and $T = 0.2$s

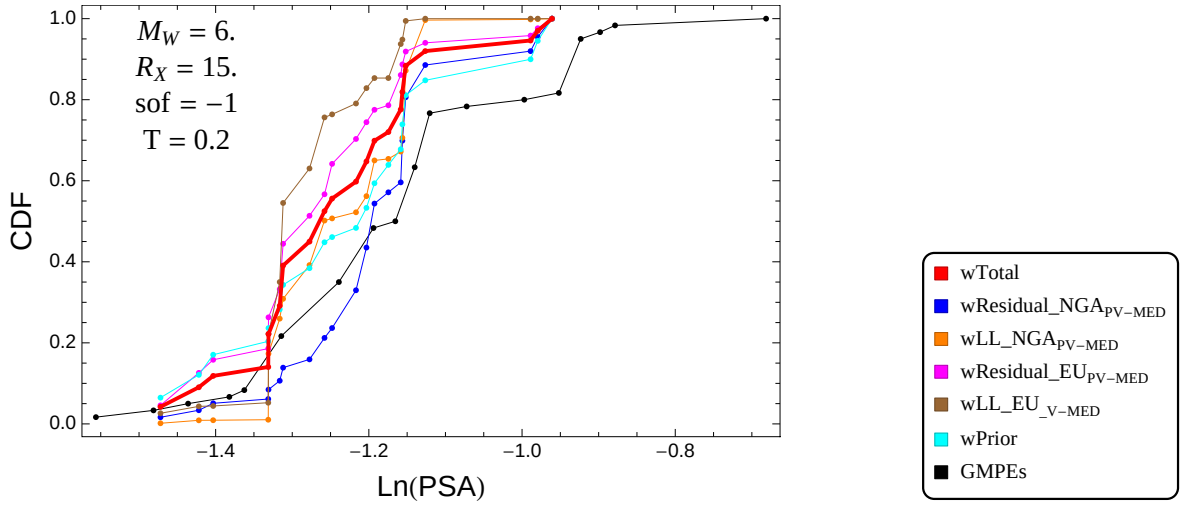



Figure 3.151: PVNGSv2: Cumulative distribution function of GMPEs (black) and selected models, for different sets of weights, for a scenario with $M = 6.$, $R_x = 15.$, $F = -1$, and $T = 0.2$s

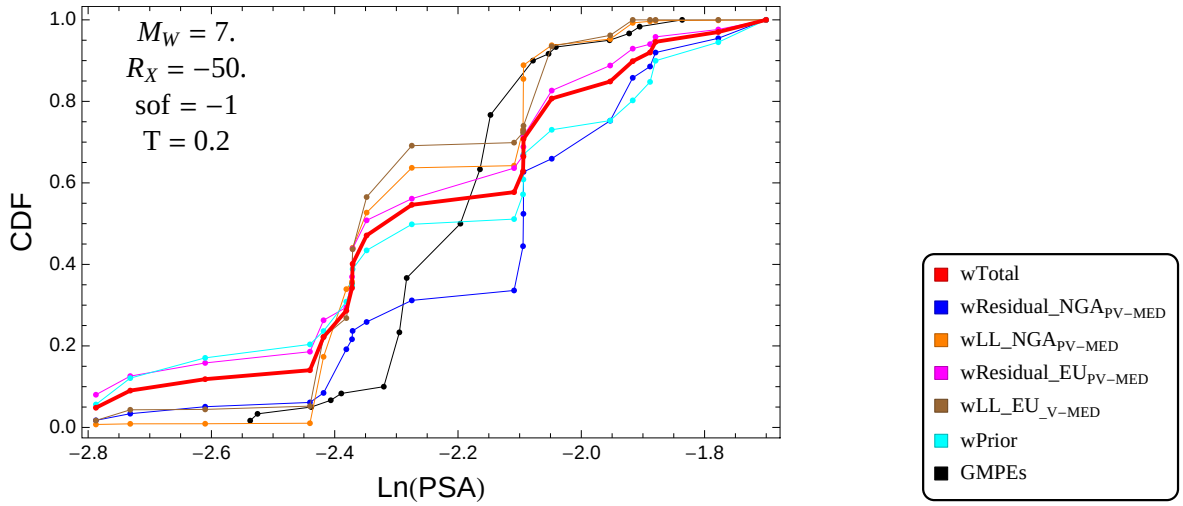



Figure 3.152: PVNGSv2: Cumulative distribution function of GMPEs (black) and selected models, for different sets of weights, for a scenario with $M = 7.$, $R_x = -50.$, $F = -1$, and $T = 0.2$s

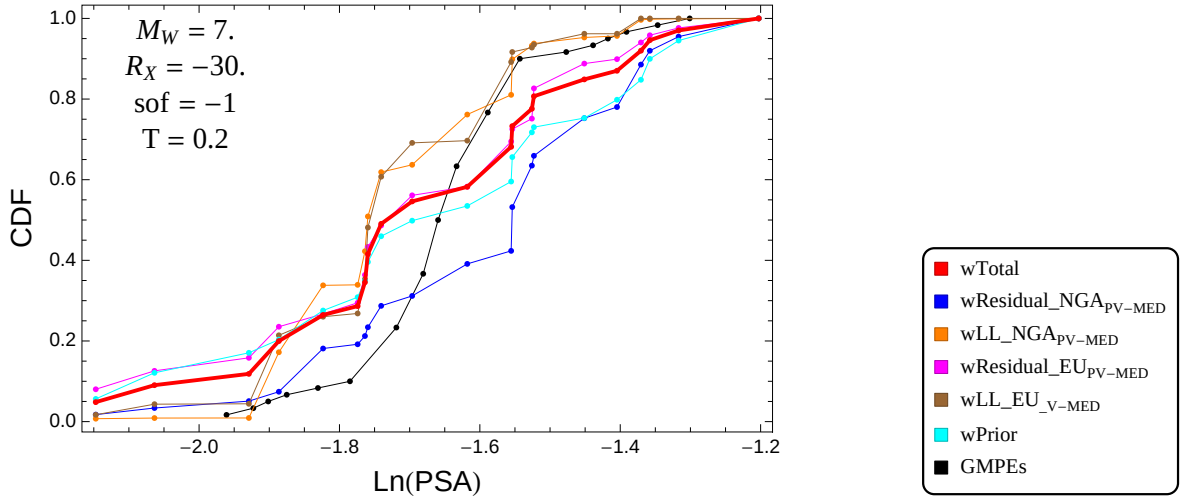



Figure 3.153: PVNGSv2: Cumulative distribution function of GMPEs (black) and selected models, for different sets of weights, for a scenario with $M = 7.$, $R_x = -30.$, $F = -1$, and $T = 0.2$s

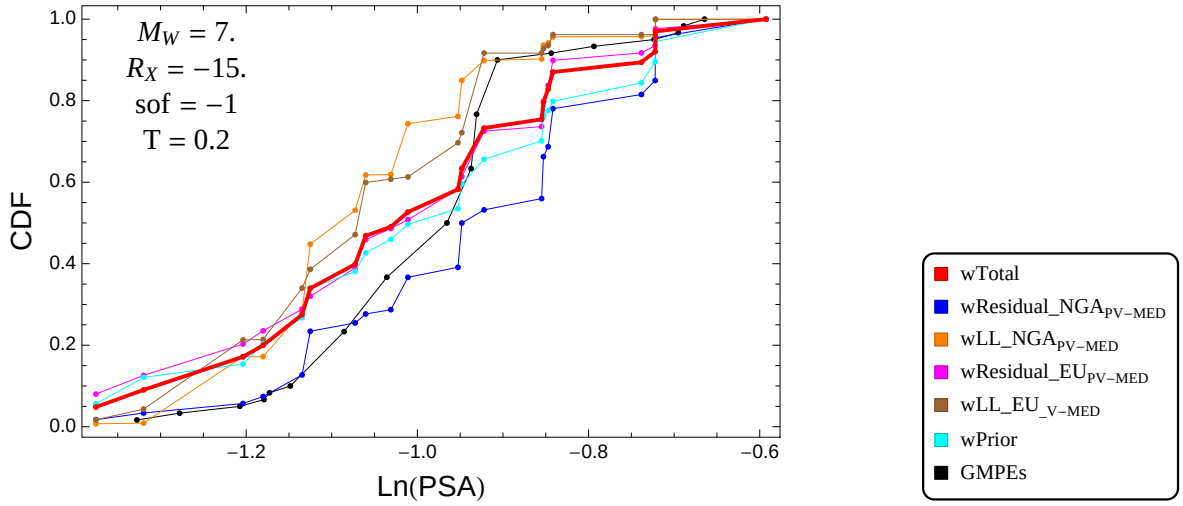



Figure 3.154: PVNGSv2: Cumulative distribution function of GMPEs (black) and selected models, for different sets of weights, for a scenario with $M = 7.$, $R_x = -15.$, $F = -1$, and $T = 0.2$s

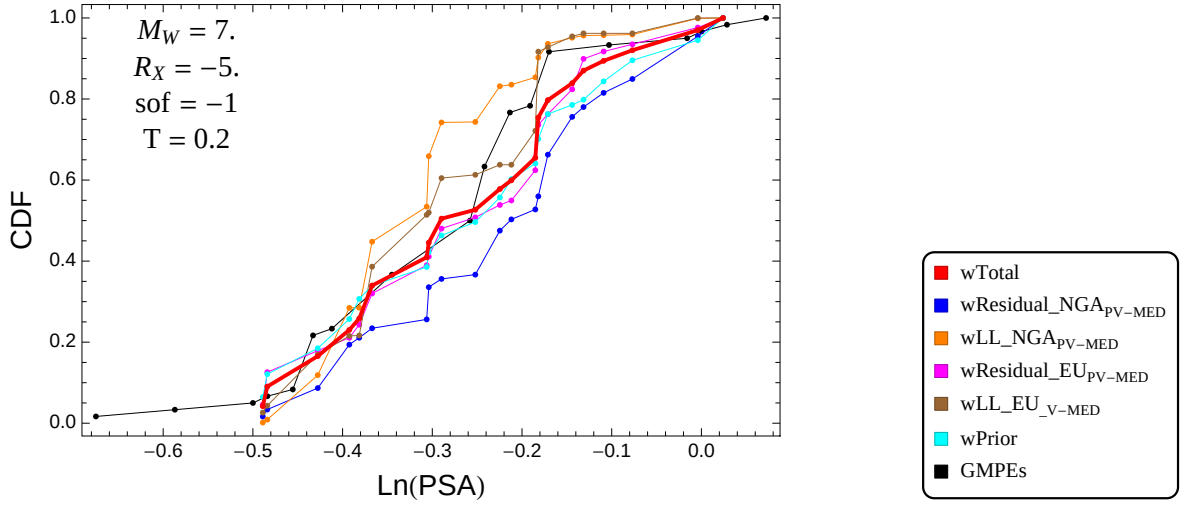



Figure 3.155: PVNGSv2: Cumulative distribution function of GMPEs (black) and selected models, for different sets of weights, for a scenario with $M = 7.$, $R_x = -5.$, $F = -1$, and $T = 0.2$s

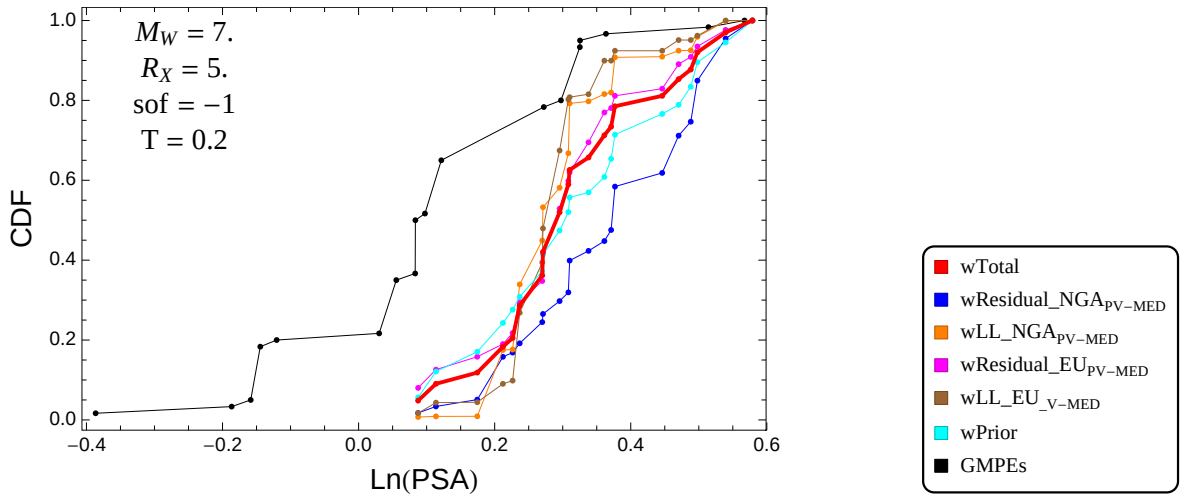



Figure 3.156: PVNGSv2: Cumulative distribution function of GMPEs (black) and selected models, for different sets of weights, for a scenario with $M = 7.$, $R_x = 5.$, $F = -1$, and $T = 0.2$s

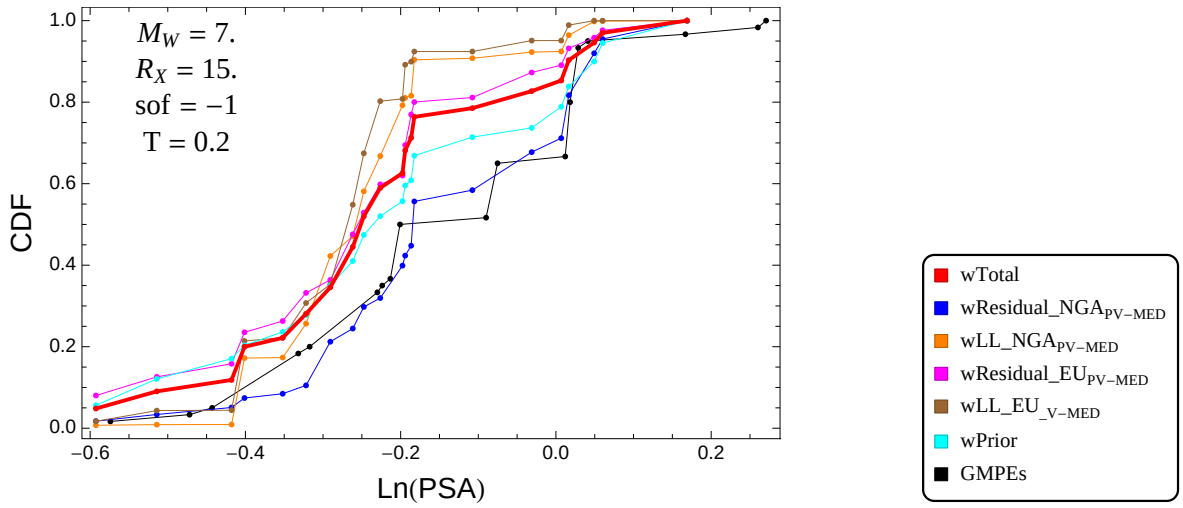



Figure 3.157: PVNGSv2: Cumulative distribution function of GMPEs (black) and selected models, for different sets of weights, for a scenario with $M = 7.$, $R_x = 15.$, $F = -1$, and $T = 0.2$s

**T = 0.5s**

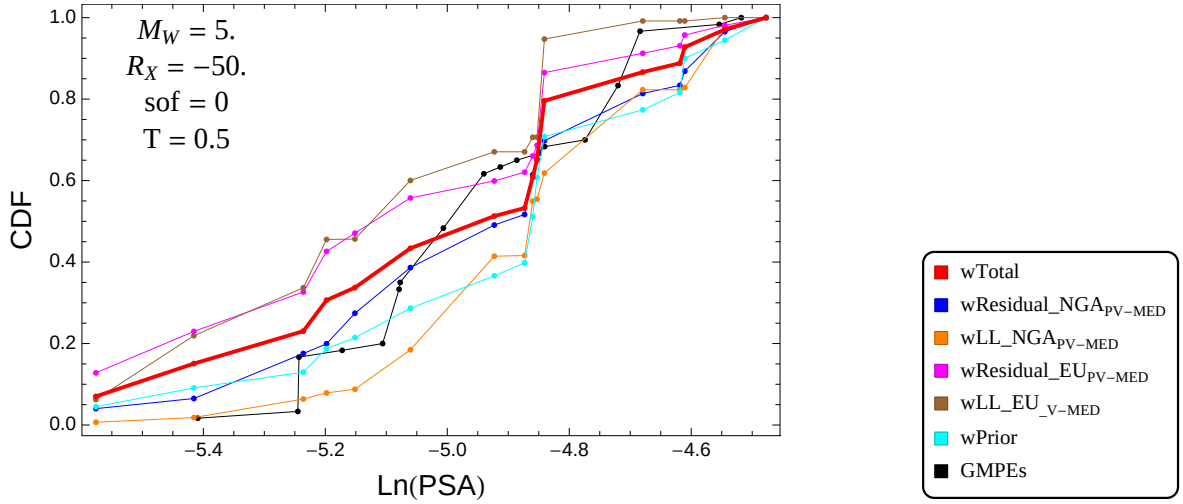



Figure 3.158: PVNGSv2: Cumulative distribution function of GMPEs (black) and selected models, for different sets of weights, for a scenario with $M = 5.$, $R_x = -50.$, $F = 0$, and $T = 0.5$s

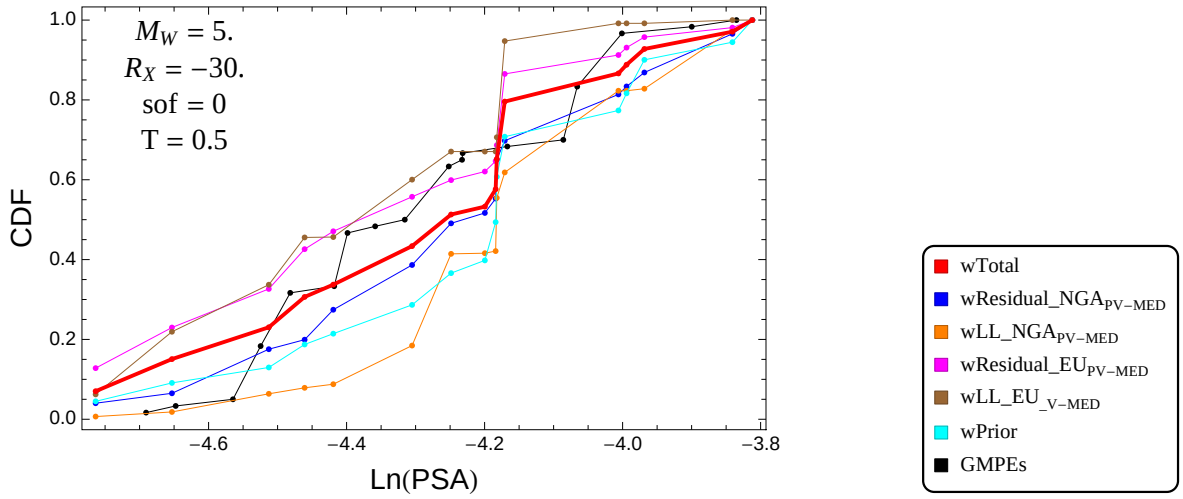



Figure 3.159: PVNGSv2: Cumulative distribution function of GMPEs (black) and selected models, for different sets of weights, for a scenario with $M = 5.$, $R_x = -30.$, $F = 0$, and $T = 0.5$s

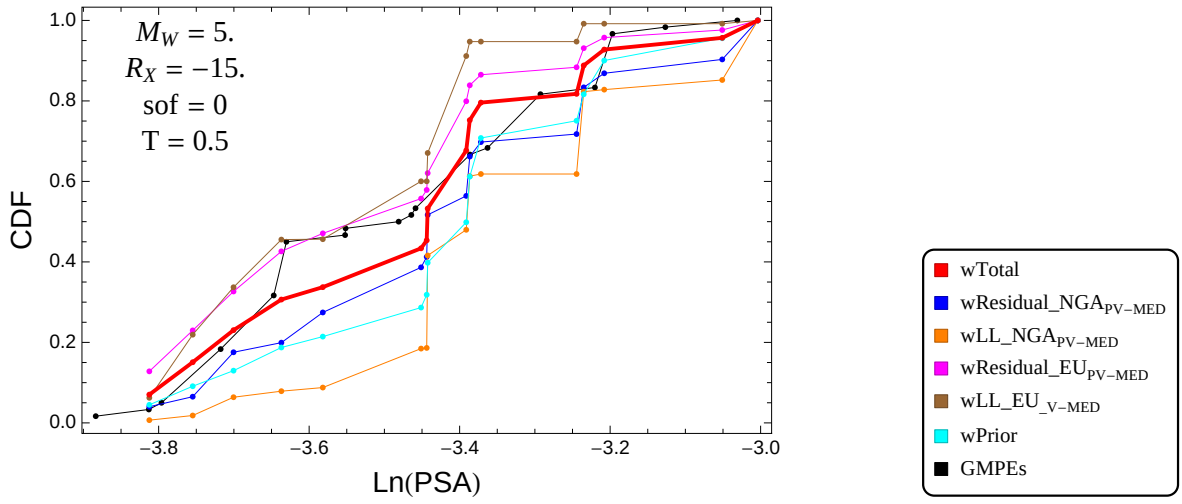



Figure 3.160: PVNGSv2: Cumulative distribution function of GMPEs (black) and selected models, for different sets of weights, for a scenario with $M = 5.$, $R_x = -15.$, $F = 0$, and $T = 0.5$s

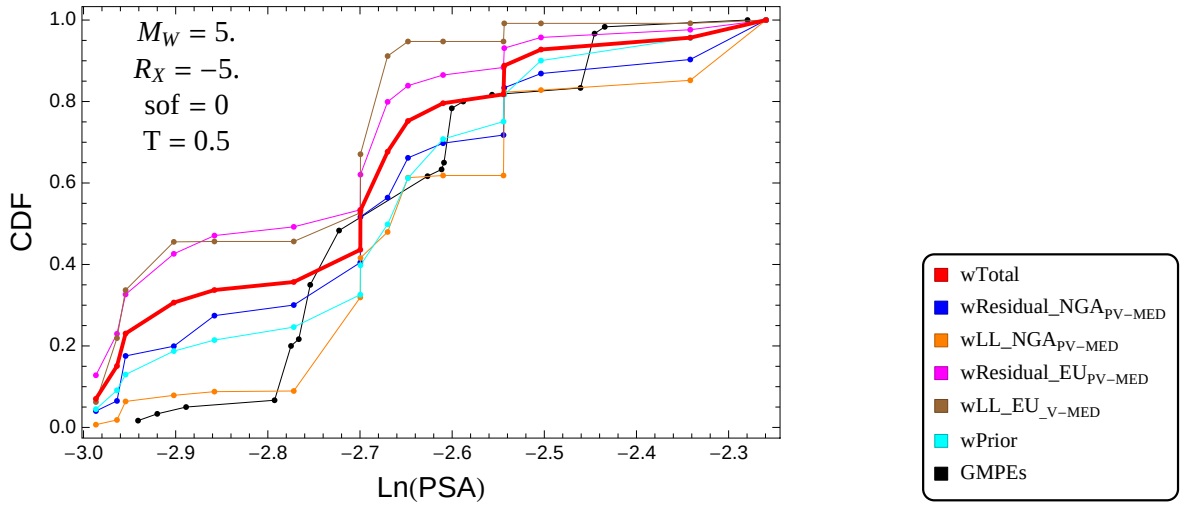



Figure 3.161: PVNGSv2: Cumulative distribution function of GMPEs (black) and selected models, for different sets of weights, for a scenario with $M = 5.$, $R_x = -5.$, $F = 0$, and $T = 0.5$s

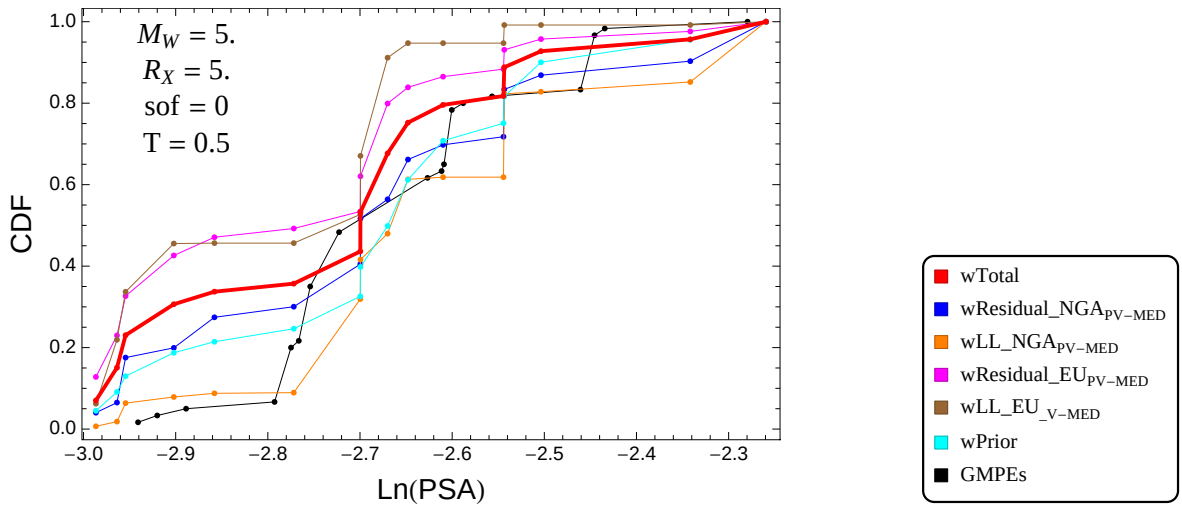



Figure 3.162: PVNGSv2: Cumulative distribution function of GMPEs (black) and selected models, for different sets of weights, for a scenario with $M = 5.$, $R_x = 5.$, $F = 0$, and $T = 0.5$s

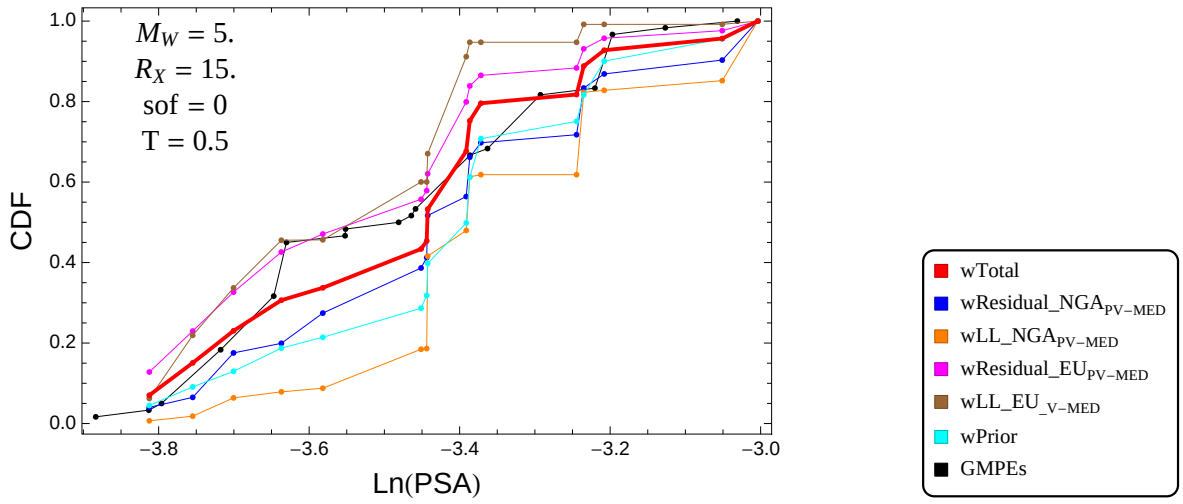



Figure 3.163: PVNGSv2: Cumulative distribution function of GMPEs (black) and selected models, for different sets of weights, for a scenario with $M = 5.$, $R_x = 15.$, $F = 0$, and $T = 0.5$s

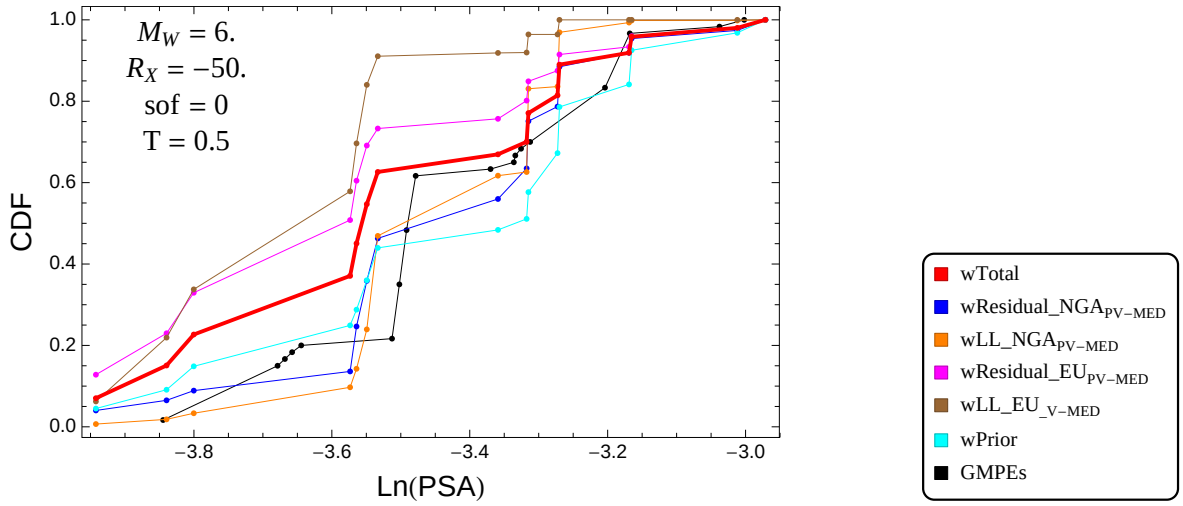



Figure 3.164: PVNGSv2: Cumulative distribution function of GMPEs (black) and selected models, for different sets of weights, for a scenario with $M = 6.$, $R_x = -50.$, $F = 0$, and $T = 0.5$s

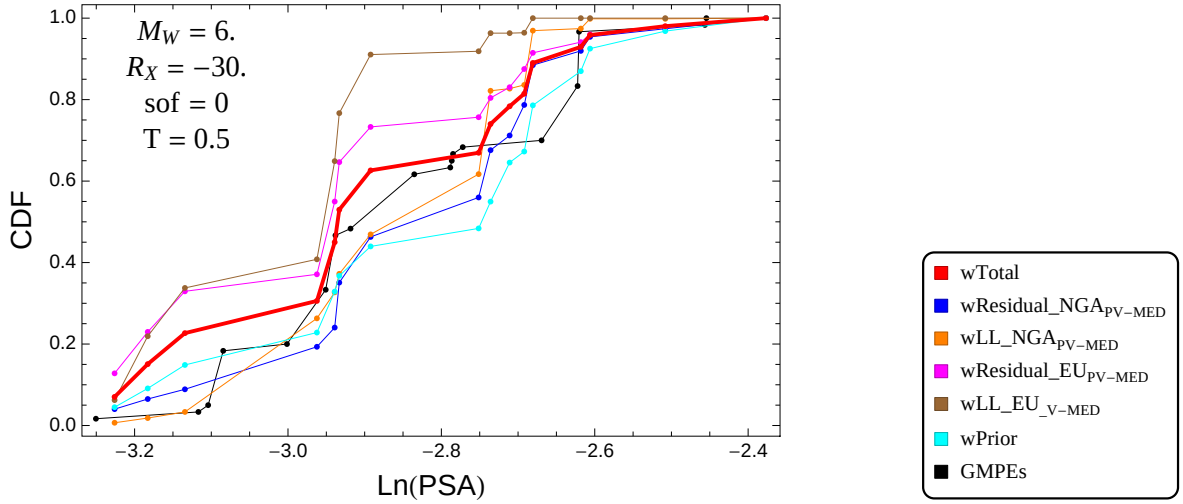



Figure 3.165: PVNGSv2: Cumulative distribution function of GMPEs (black) and selected models, for different sets of weights, for a scenario with $M = 6.$, $R_x = -30.$, $F = 0$, and $T = 0.5$s

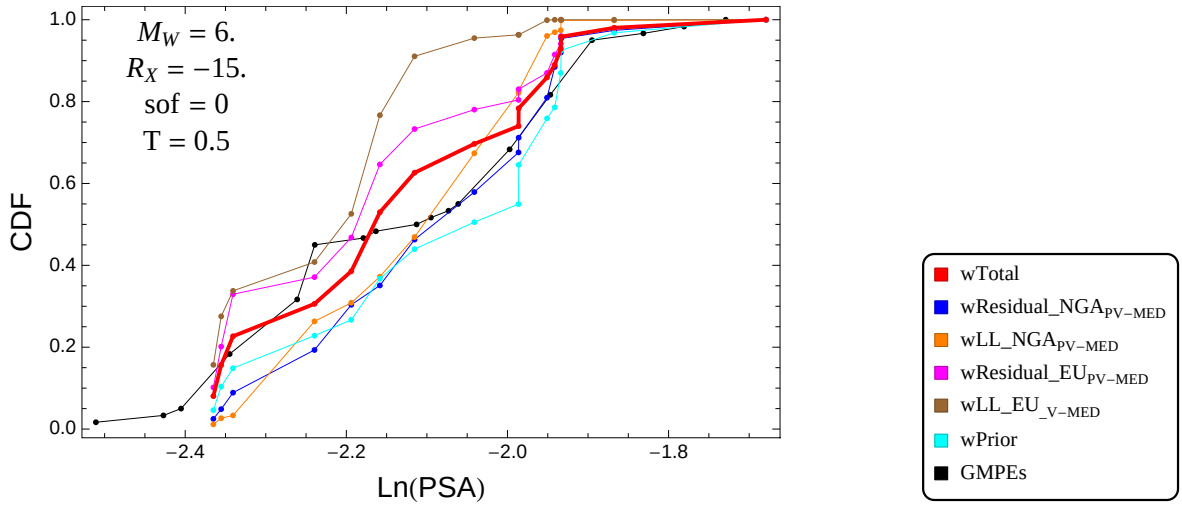



Figure 3.166: PVNGSv2: Cumulative distribution function of GMPEs (black) and selected models, for different sets of weights, for a scenario with $M = 6.$, $R_x = -15.$, $F = 0$, and $T = 0.5$s

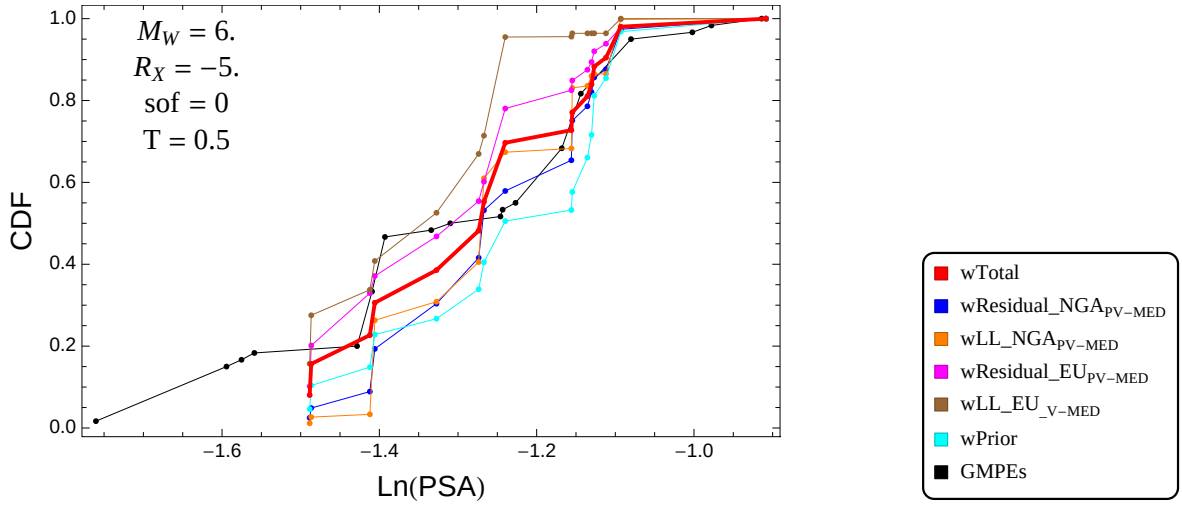



Figure 3.167: PVNGSv2: Cumulative distribution function of GMPEs (black) and selected models, for different sets of weights, for a scenario with $M = 6.$, $R_x = -5.$, $F = 0$, and $T = 0.5$s

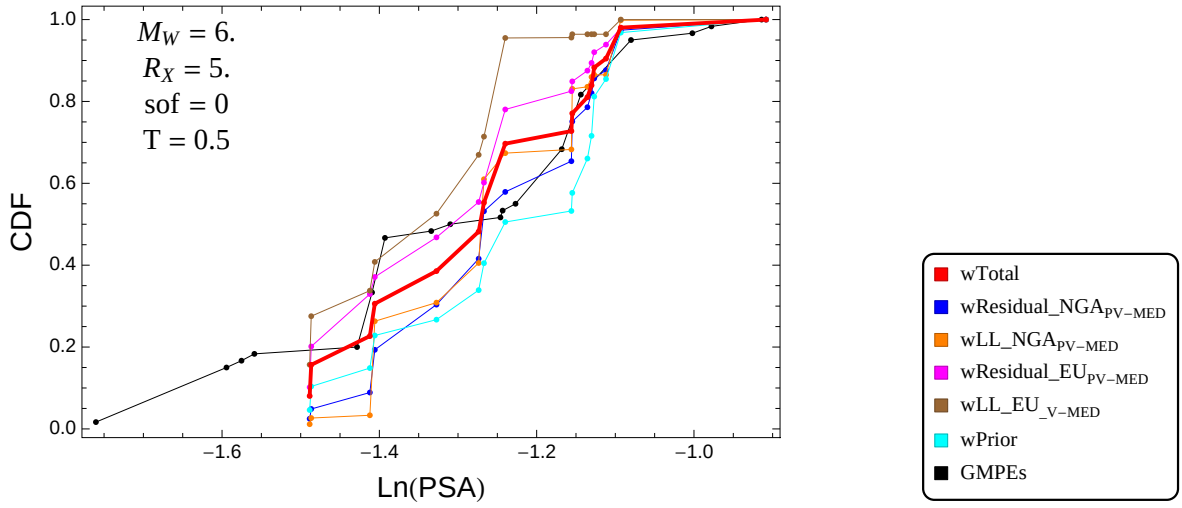



Figure 3.168: PVNGSv2: Cumulative distribution function of GMPEs (black) and selected models, for different sets of weights, for a scenario with $M = 6.$, $R_x = 5.$, $F = 0$, and $T = 0.5$s

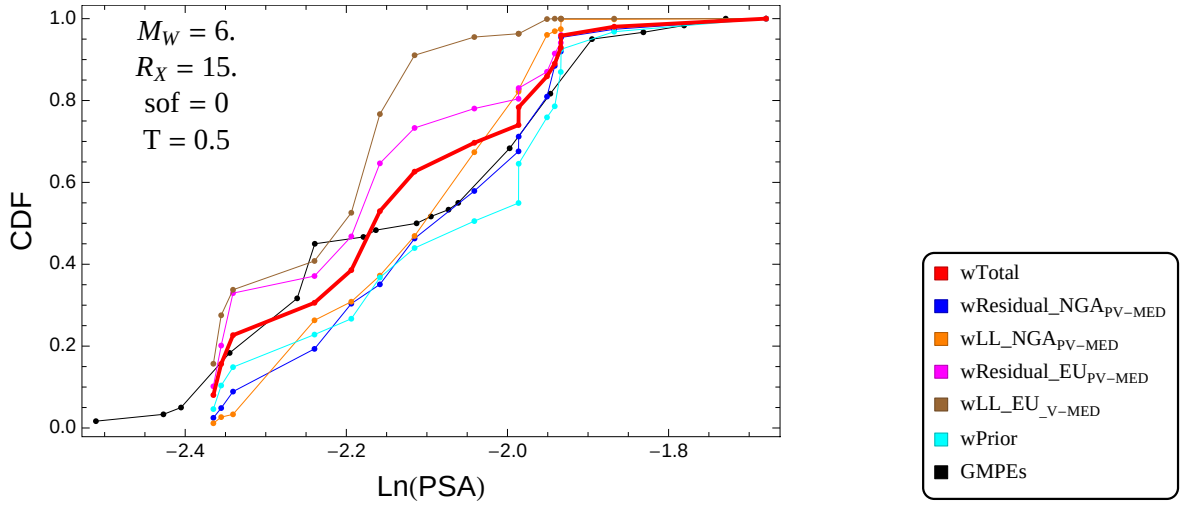



Figure 3.169: PVNGSv2: Cumulative distribution function of GMPEs (black) and selected models, for different sets of weights, for a scenario with $M = 6.$, $R_x = 15.$, $F = 0$, and $T = 0.5$s

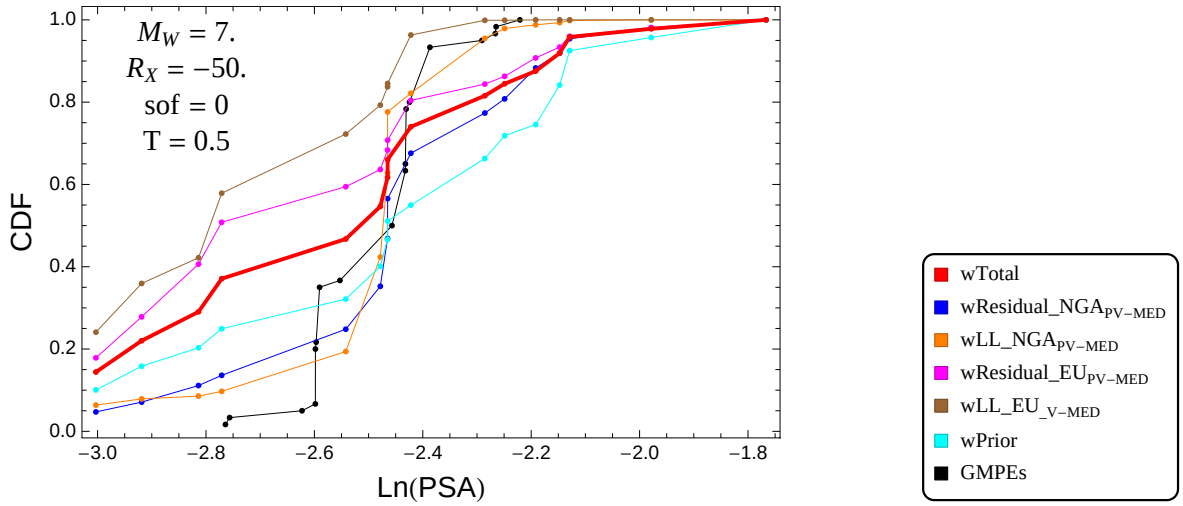



Figure 3.170: PVNGSv2: Cumulative distribution function of GMPEs (black) and selected models, for different sets of weights, for a scenario with $M = 7.$, $R_x = -50.$, $F = 0$, and $T = 0.5$s

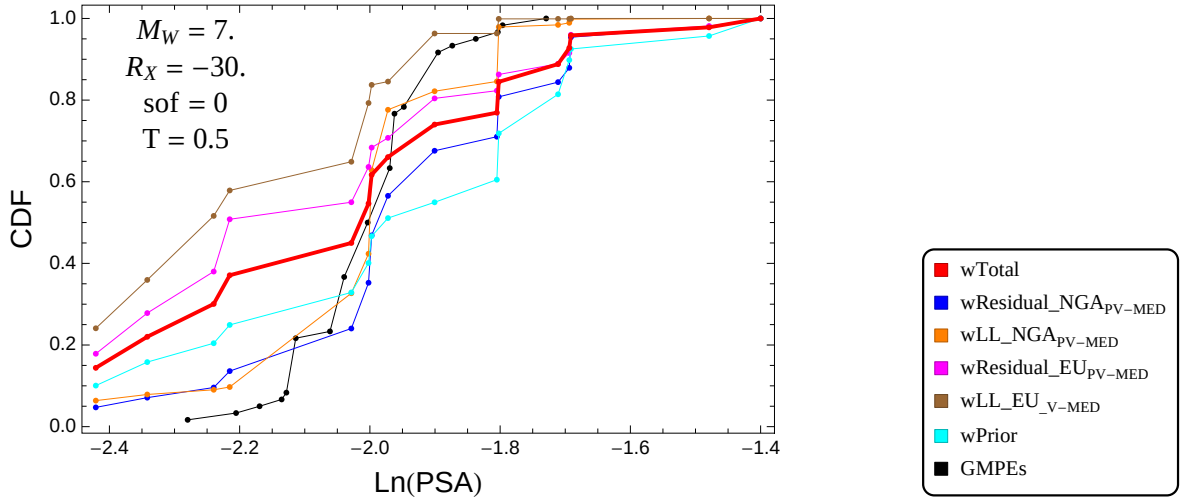



Figure 3.171: PVNGSv2: Cumulative distribution function of GMPEs (black) and selected models, for different sets of weights, for a scenario with $M = 7.$, $R_x = -30.$, $F = 0$, and $T = 0.5$s

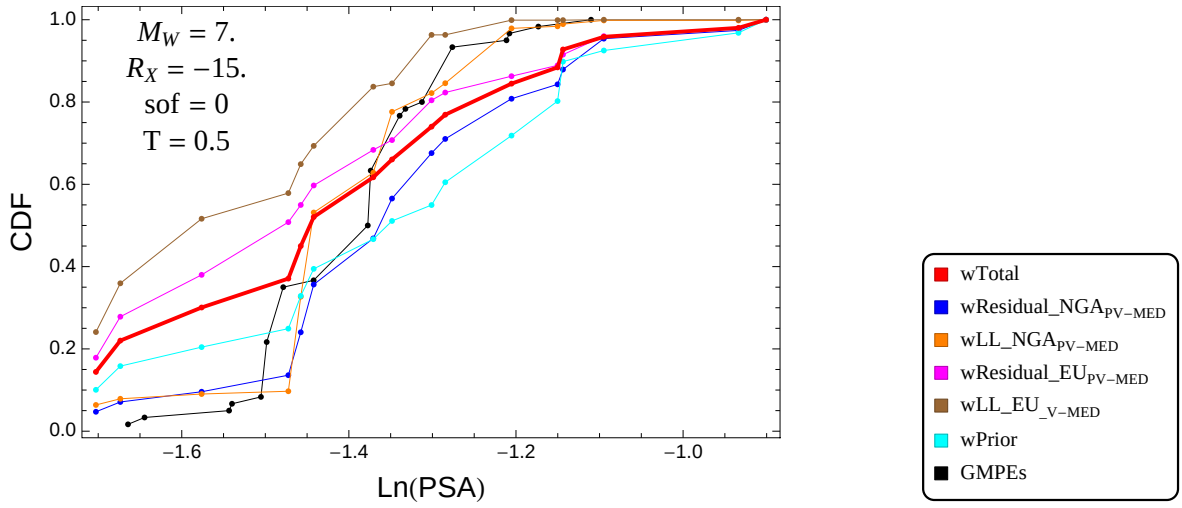



Figure 3.172: PVNGSv2: Cumulative distribution function of GMPEs (black) and selected models, for different sets of weights, for a scenario with $M = 7.$, $R_x = -15.$, $F = 0$, and $T = 0.5$s

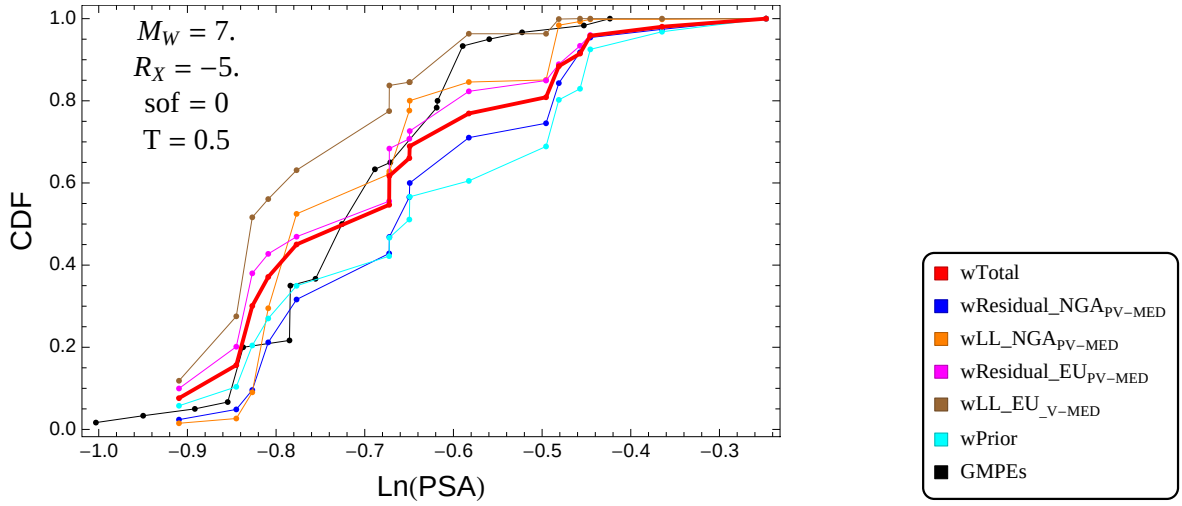



Figure 3.173: PVNGSv2: Cumulative distribution function of GMPEs (black) and selected models, for different sets of weights, for a scenario with $M = 7.$, $R_x = -5.$, $F = 0$, and $T = 0.5$s

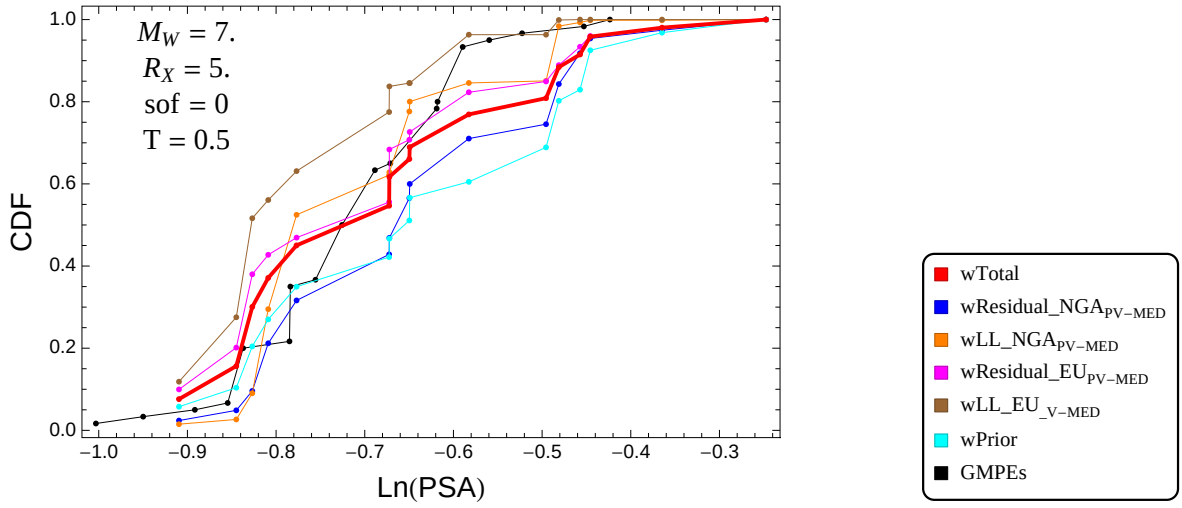



Figure 3.174: PVNGSv2: Cumulative distribution function of GMPEs (black) and selected models, for different sets of weights, for a scenario with $M = 7.$, $R_x = 5.$, $F = 0$, and $T = 0.5$s

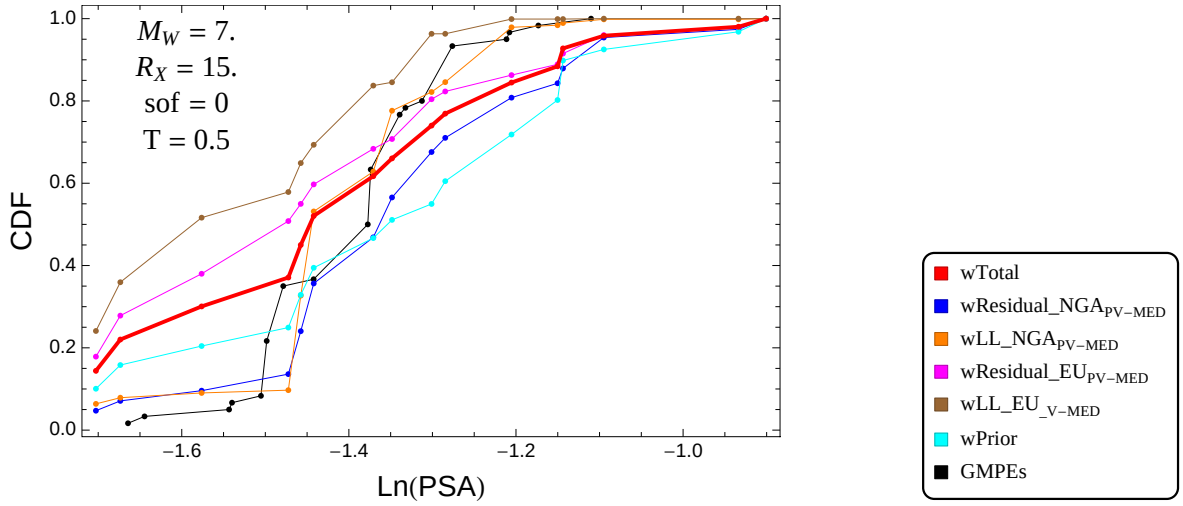



Figure 3.175: PVNGSv2: Cumulative distribution function of GMPEs (black) and selected models, for different sets of weights, for a scenario with $M = 7.$, $R_x = 15.$, $F = 0$, and $T = 0.5$s

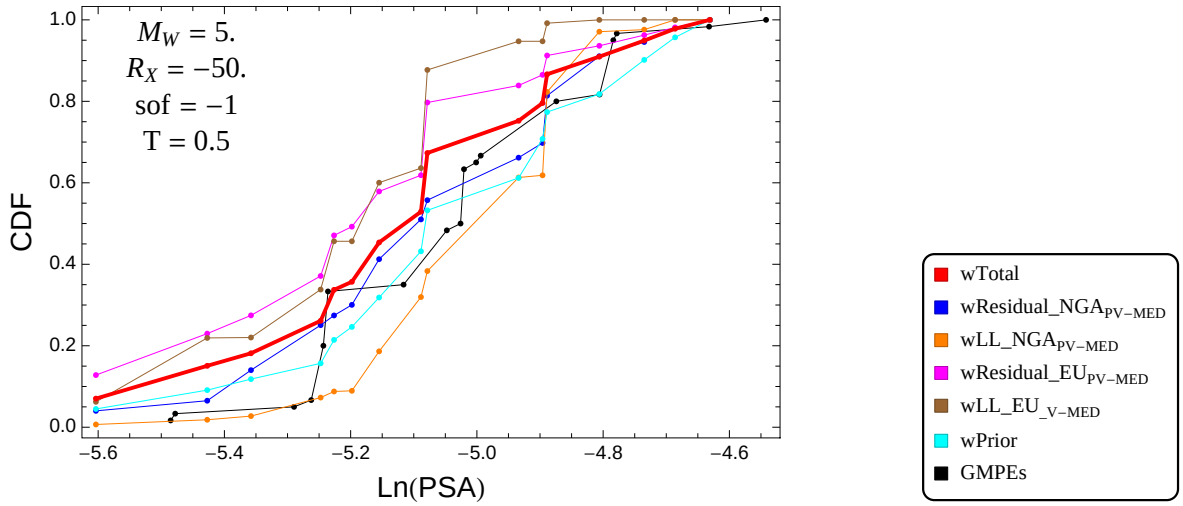



Figure 3.176: PVNGSv2: Cumulative distribution function of GMPEs (black) and selected models, for different sets of weights, for a scenario with $M = 5.$, $R_x = -50.$, $F = -1$, and $T = 0.5$s

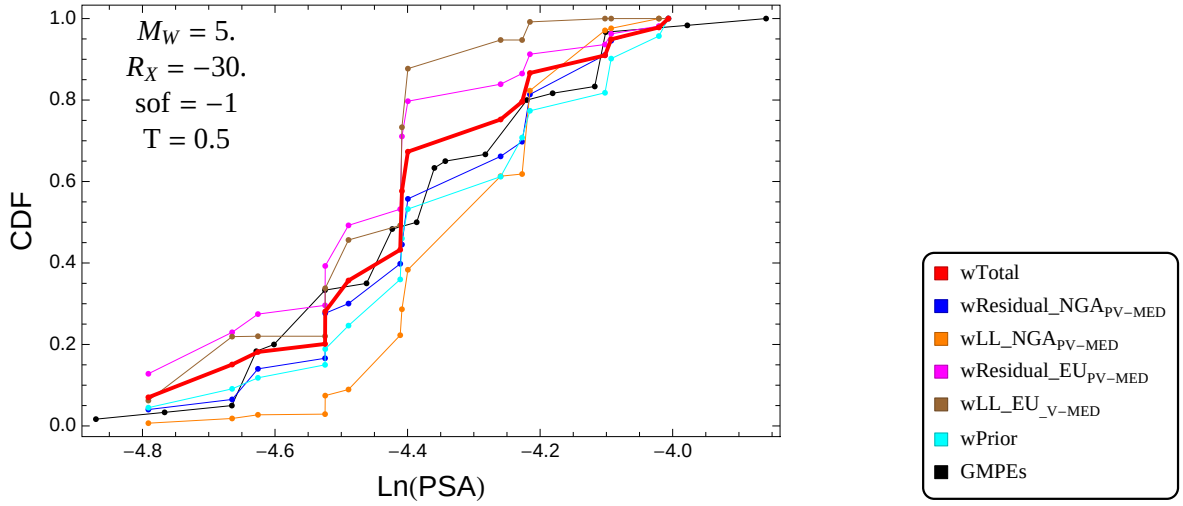



Figure 3.177: PVNGSv2: Cumulative distribution function of GMPEs (black) and selected models, for different sets of weights, for a scenario with $M = 5.$, $R_x = -30.$, $F = -1$, and $T = 0.5$s

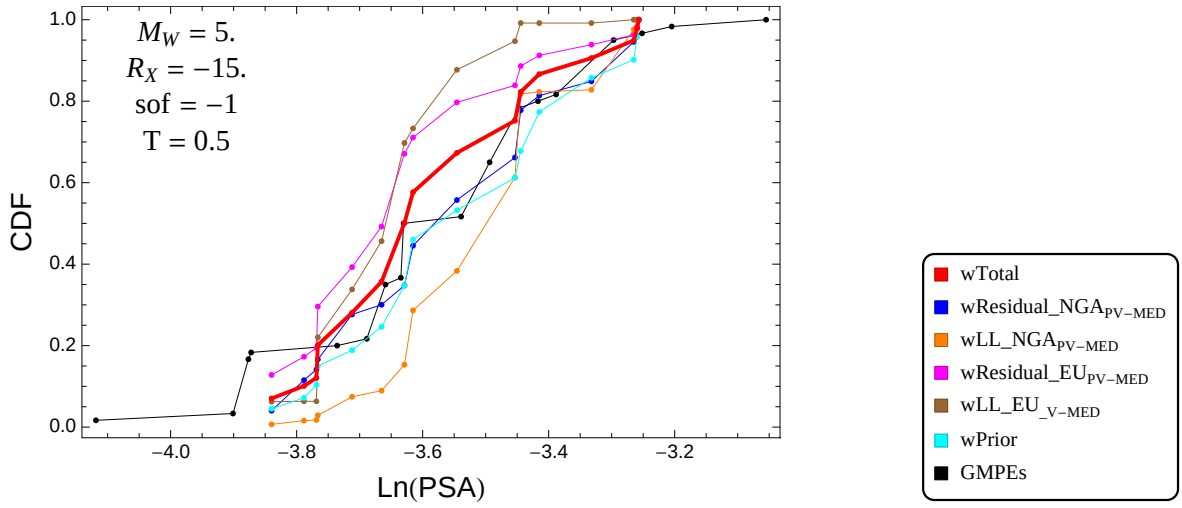



Figure 3.178: PVNGSv2: Cumulative distribution function of GMPEs (black) and selected models, for different sets of weights, for a scenario with $M = 5.$, $R_x = -15.$, $F = -1$, and $T = 0.5$s

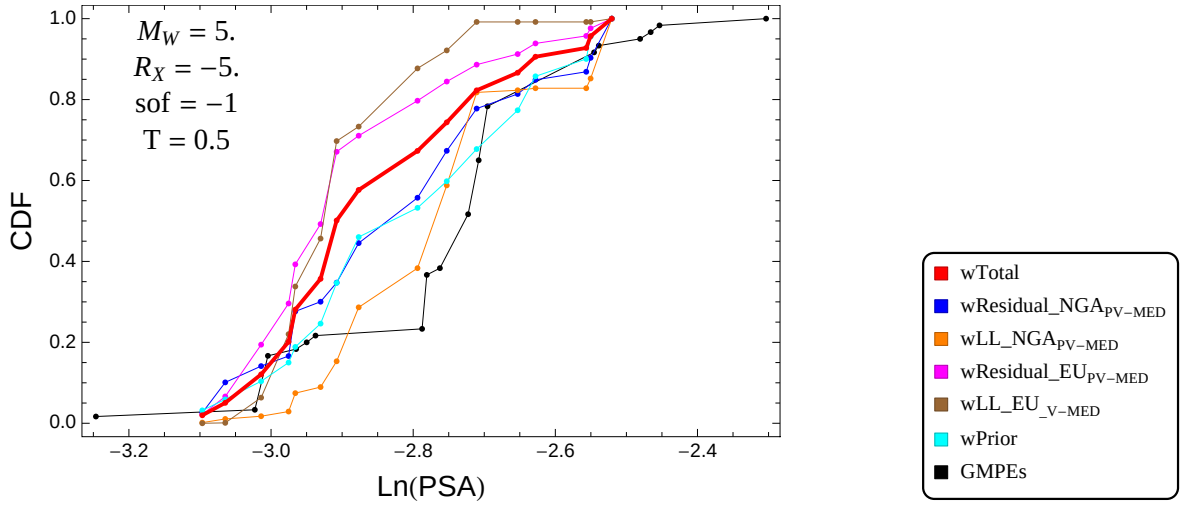



Figure 3.179: PVNGSv2: Cumulative distribution function of GMPEs (black) and selected models, for different sets of weights, for a scenario with $M = 5.$, $R_x = -5.$, $F = -1$, and $T = 0.5$s

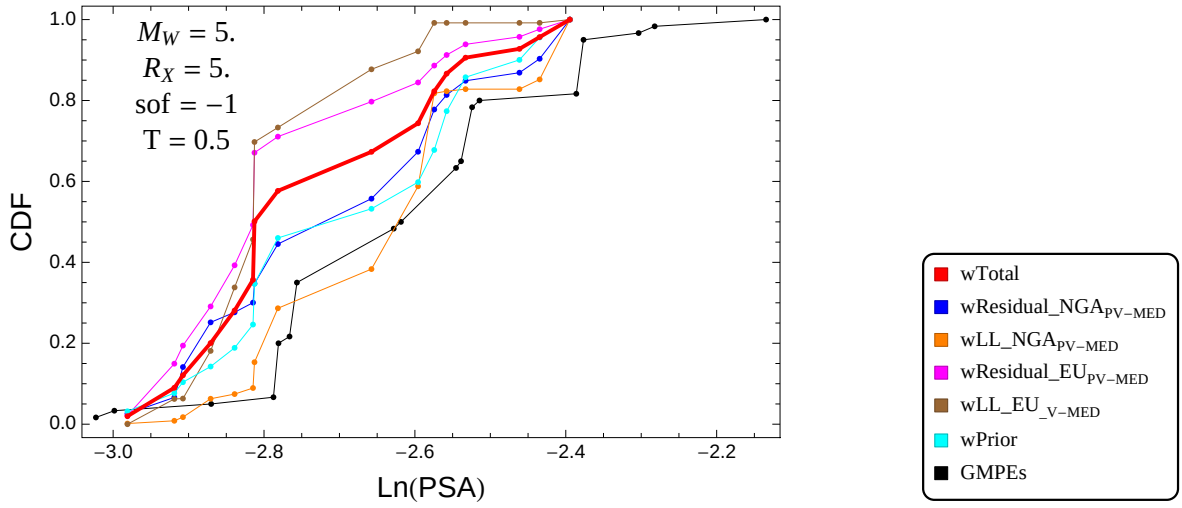



Figure 3.180: PVNGSv2: Cumulative distribution function of GMPEs (black) and selected models, for different sets of weights, for a scenario with $M = 5.$, $R_x = 5.$, $F = -1$, and $T = 0.5$s

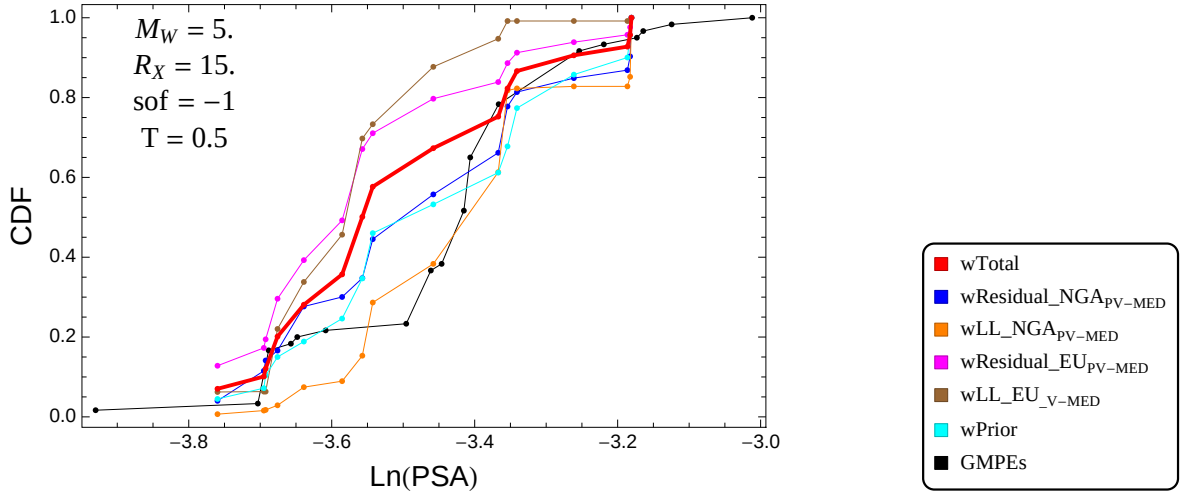



Figure 3.181: PVNGSv2: Cumulative distribution function of GMPEs (black) and selected models, for different sets of weights, for a scenario with $M = 5.$, $R_x = 15.$, $F = -1$, and $T = 0.5$s

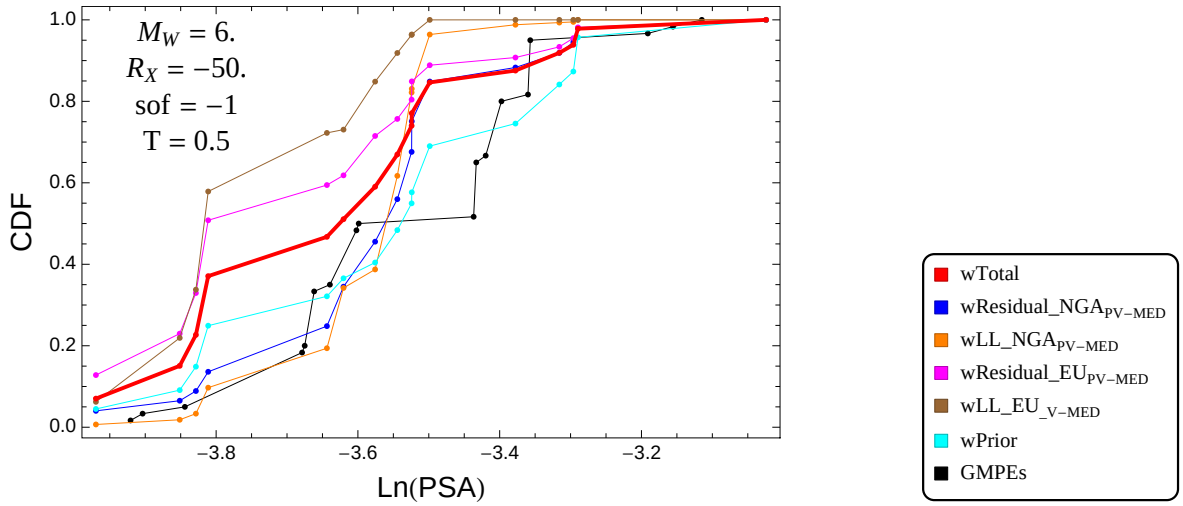



Figure 3.182: PVNGSv2: Cumulative distribution function of GMPEs (black) and selected models, for different sets of weights, for a scenario with $M = 6.$, $R_x = -50.$, $F = -1$, and $T = 0.5$s

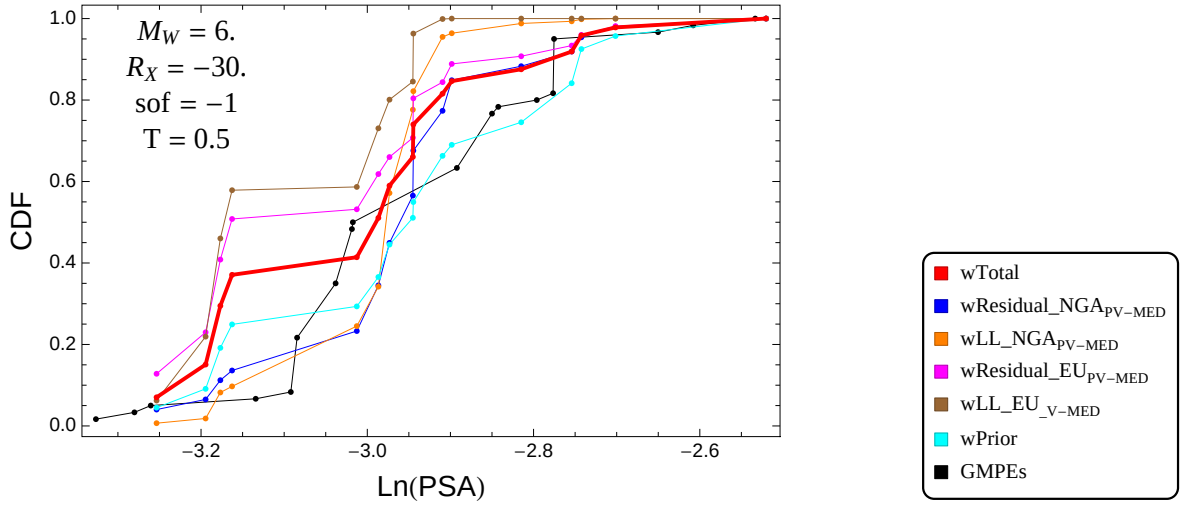



Figure 3.183: PVNGSv2: Cumulative distribution function of GMPEs (black) and selected models, for different sets of weights, for a scenario with $M = 6.$, $R_x = -30.$, $F = -1$, and $T = 0.5$s

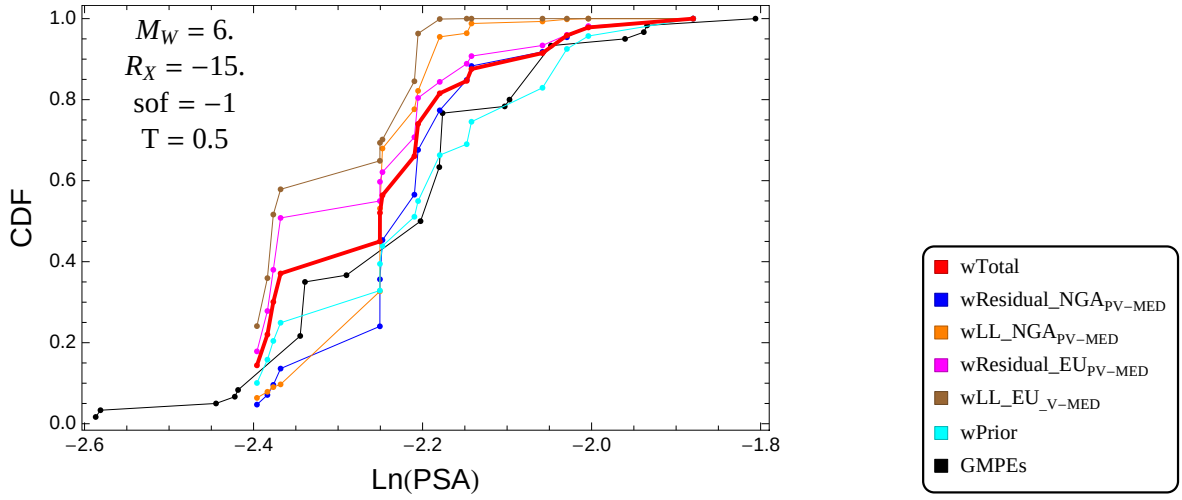



Figure 3.184: PVNGSv2: Cumulative distribution function of GMPEs (black) and selected models, for different sets of weights, for a scenario with $M = 6.$, $R_x = -15.$, $F = -1$, and $T = 0.5$s

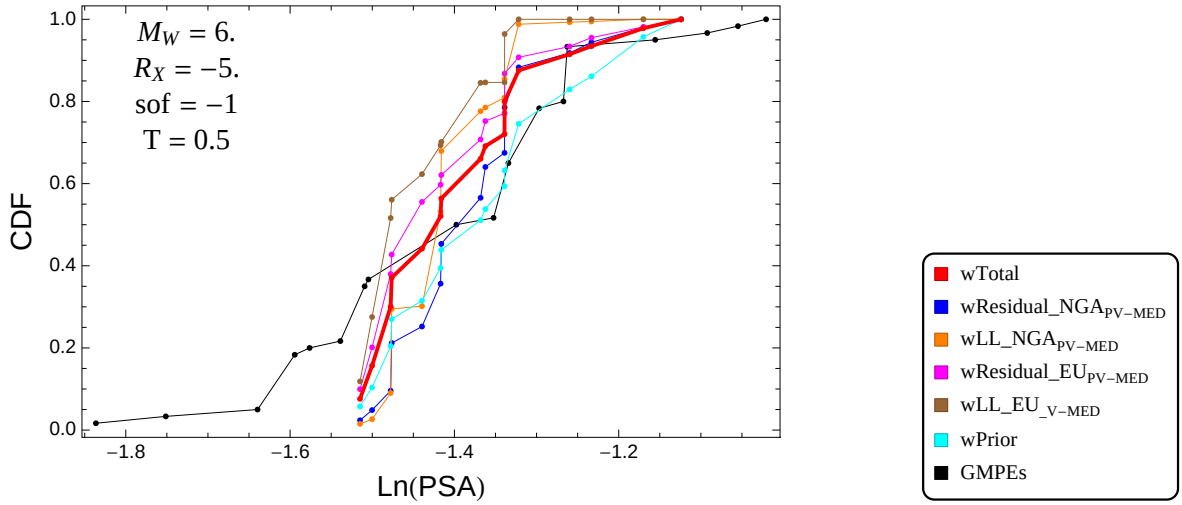



Figure 3.185: PVNGSv2: Cumulative distribution function of GMPEs (black) and selected models, for different sets of weights, for a scenario with $M = 6.$, $R_x = -5.$, $F = -1$, and $T = 0.5$s

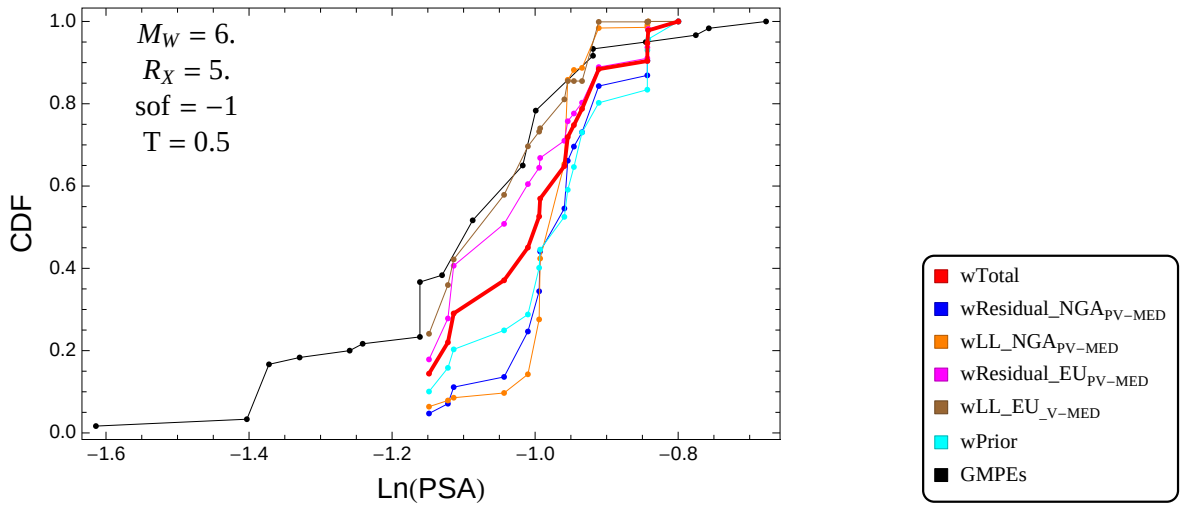



Figure 3.186: PVNGSv2: Cumulative distribution function of GMPEs (black) and selected models, for different sets of weights, for a scenario with $M = 6.$, $R_x = 5.$, $F = -1$, and $T = 0.5$s

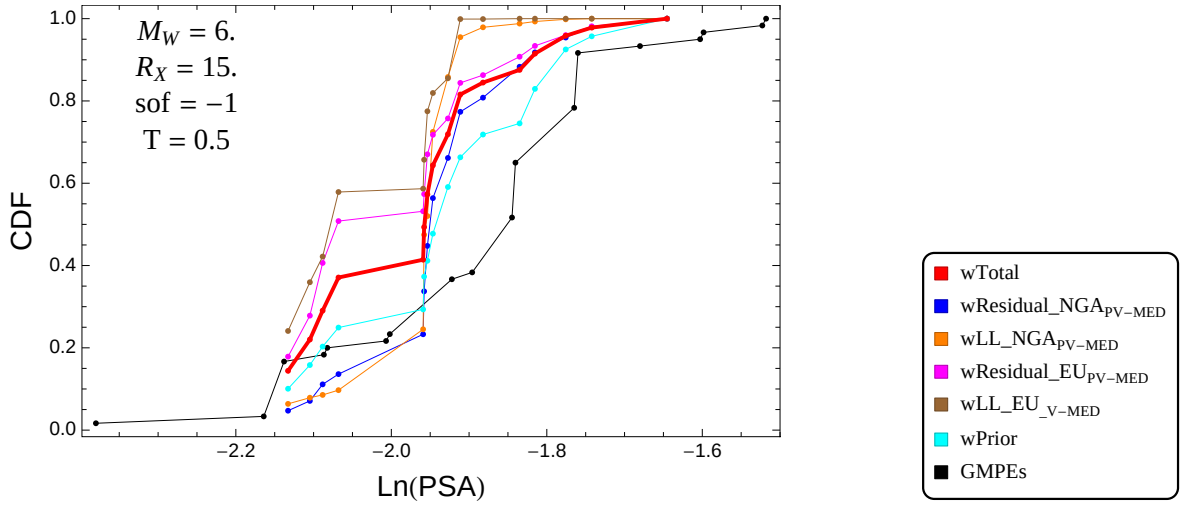



Figure 3.187: PVNGSv2: Cumulative distribution function of GMPEs (black) and selected models, for different sets of weights, for a scenario with $M = 6.$, $R_x = 15.$, $F = -1$, and $T = 0.5$s

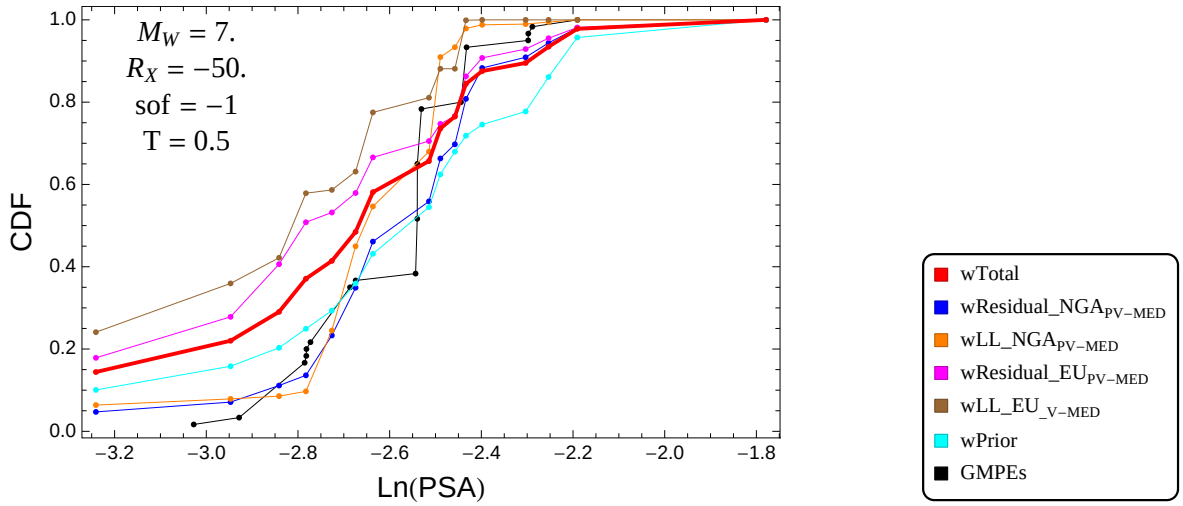



Figure 3.188: PVNGSv2: Cumulative distribution function of GMPEs (black) and selected models, for different sets of weights, for a scenario with $M = 7.$, $R_x = -50.$, $F = -1$, and $T = 0.5$s

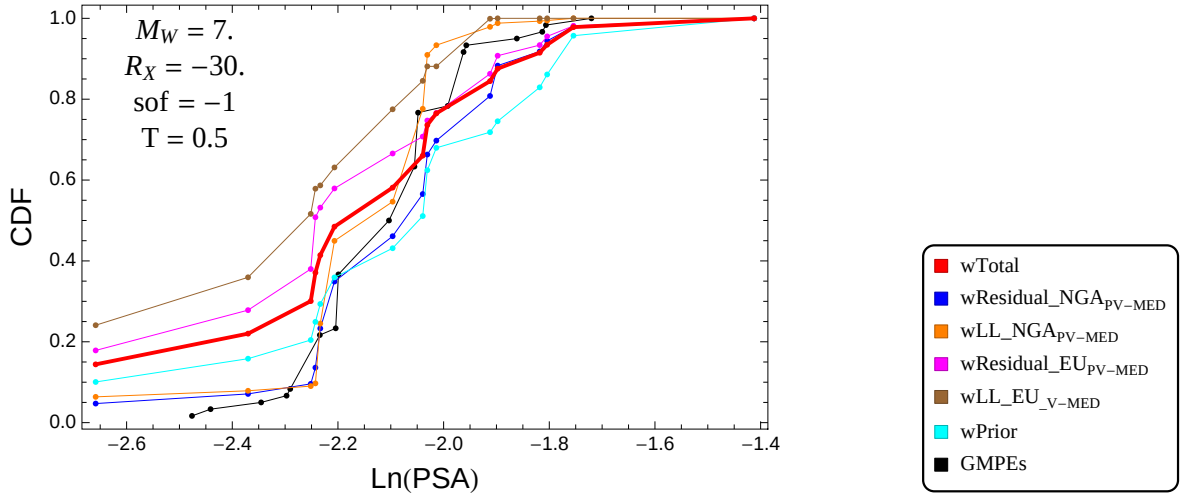



Figure 3.189: PVNGSv2: Cumulative distribution function of GMPEs (black) and selected models, for different sets of weights, for a scenario with $M = 7.$, $R_x = -30.$, $F = -1$, and $T = 0.5$s

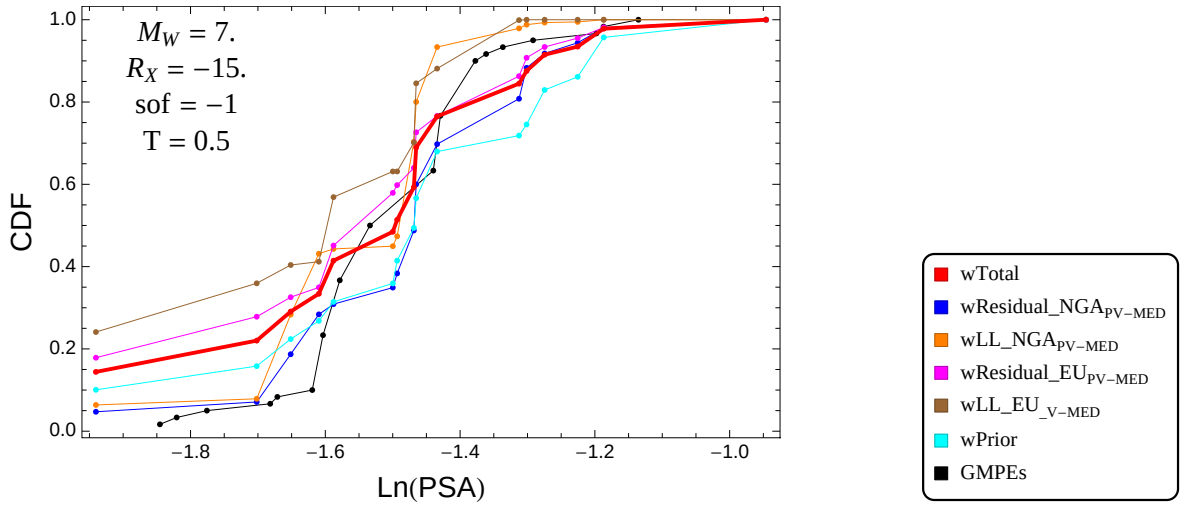



Figure 3.190: PVNGSv2: Cumulative distribution function of GMPEs (black) and selected models, for different sets of weights, for a scenario with $M = 7.$, $R_x = -15.$, $F = -1$, and $T = 0.5$s

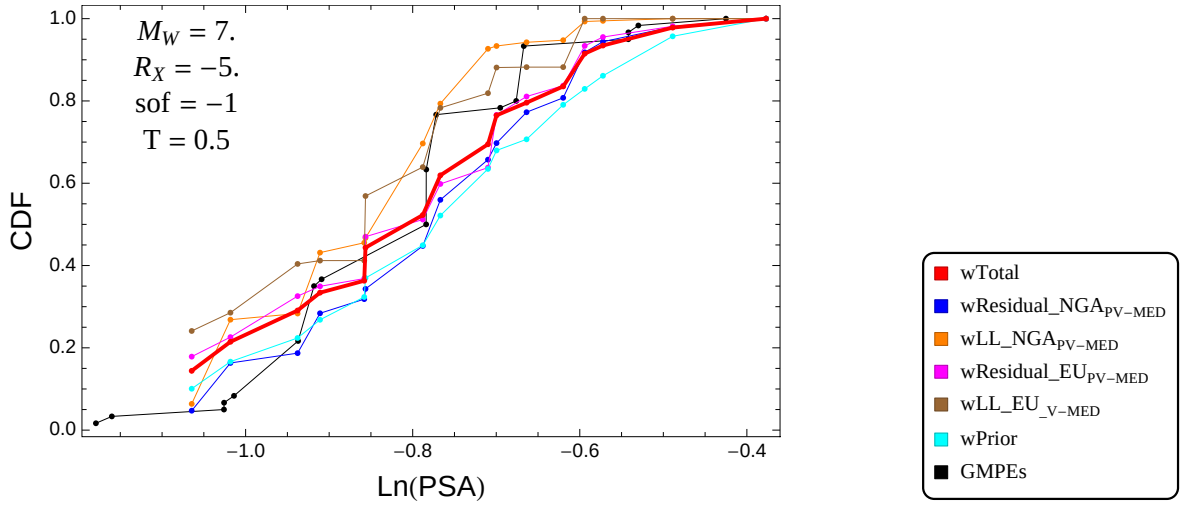



Figure 3.191: PVNGSv2: Cumulative distribution function of GMPEs (black) and selected models, for different sets of weights, for a scenario with $M = 7.$, $R_x = -5.$, $F = -1$, and $T = 0.5$s

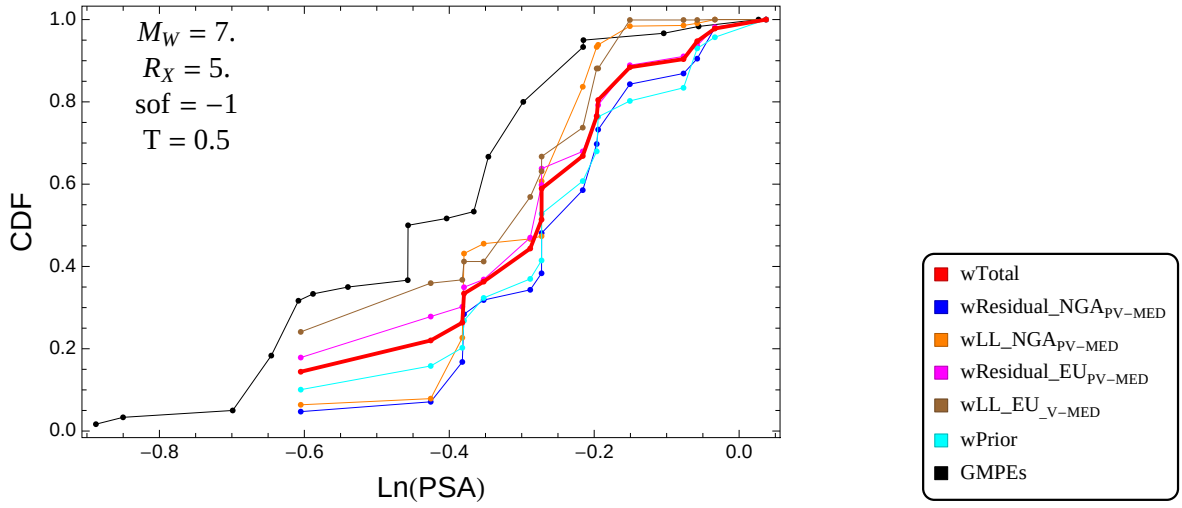



Figure 3.192: PVNGSv2: Cumulative distribution function of GMPEs (black) and selected models, for different sets of weights, for a scenario with $M = 7.$, $R_x = 5.$, $F = -1$, and $T = 0.5$s

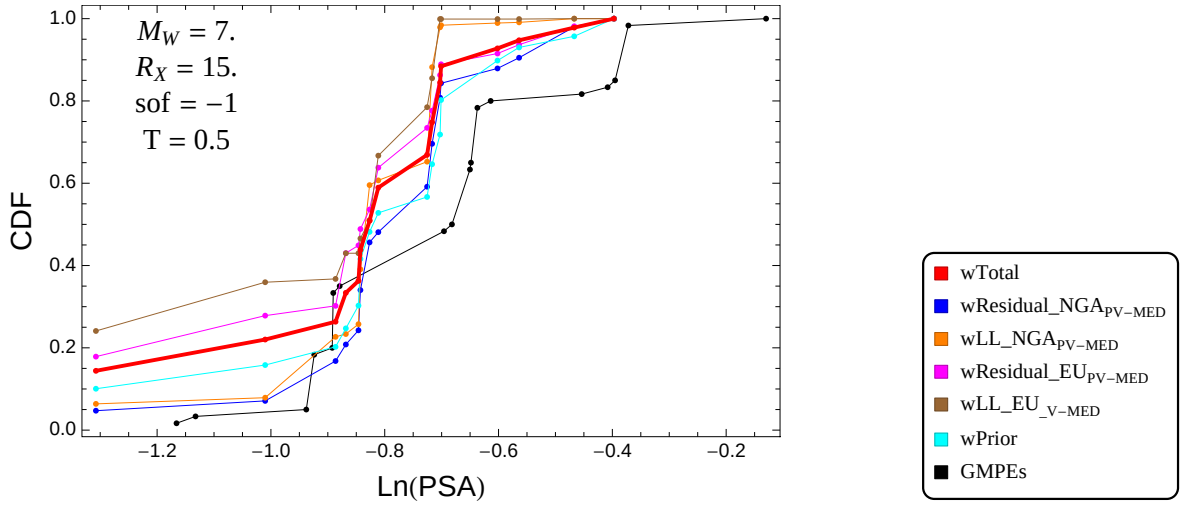



Figure 3.193: PVNGSv2: Cumulative distribution function of GMPEs (black) and selected models, for different sets of weights, for a scenario with $M = 7.$, $R_x = 15.$, $F = -1$, and $T = 0.5$s

**T = 1.s**

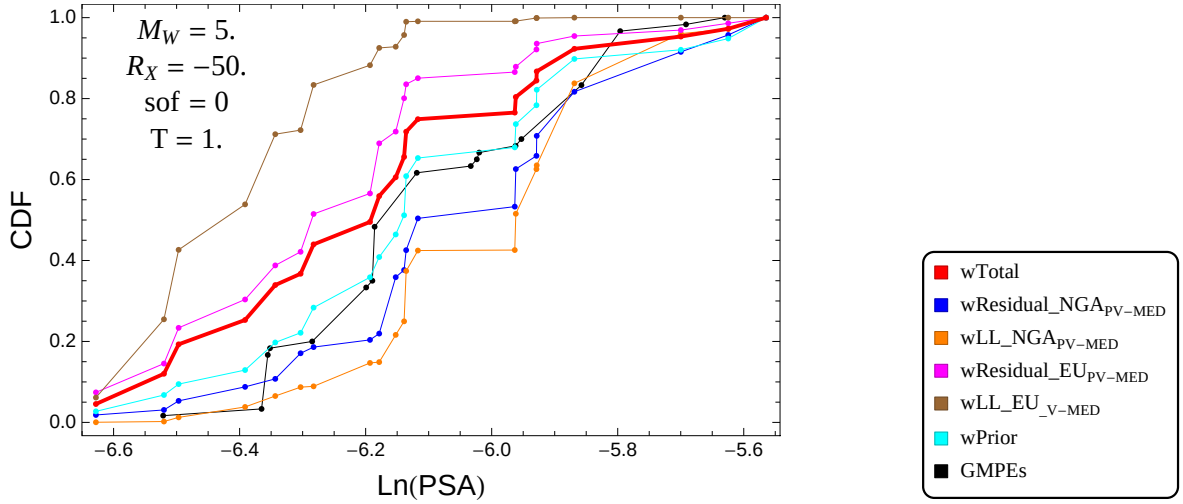



Figure 3.194: PVNGSv2: Cumulative distribution function of GMPEs (black) and selected models, for different sets of weights, for a scenario with $M = 5.$, $R_x = -50.$, $F = 0$, and $T = 1.$s

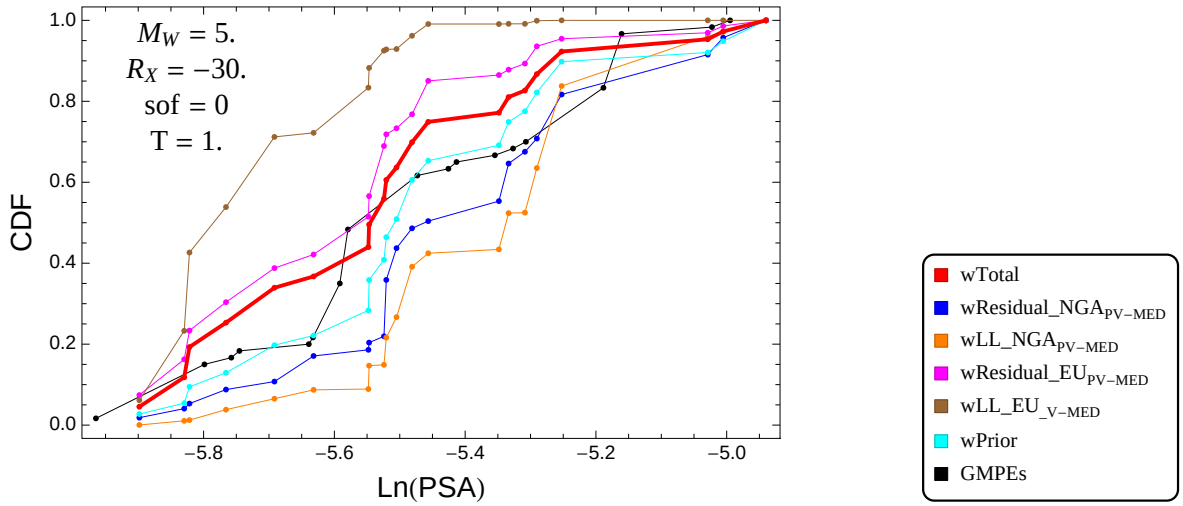



Figure 3.195: PVNGSv2: Cumulative distribution function of GMPEs (black) and selected models, for different sets of weights, for a scenario with $M = 5.$, $R_x = -30.$, $F = 0$, and $T = 1.$s

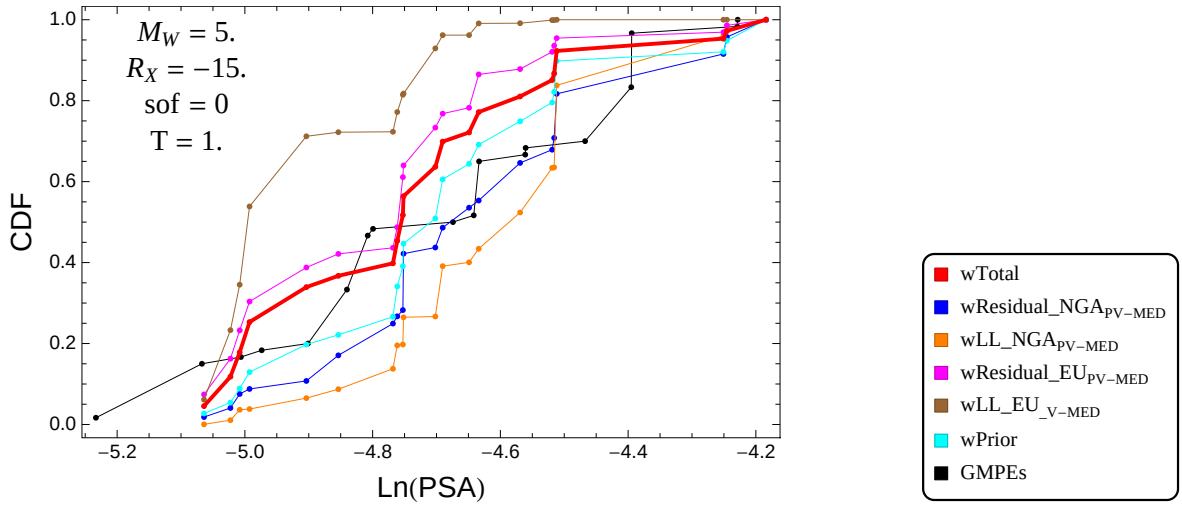



Figure 3.196: PVNGSv2: Cumulative distribution function of GMPEs (black) and selected models, for different sets of weights, for a scenario with $M = 5.$, $R_x = -15.$, $F = 0$, and $T = 1.$s

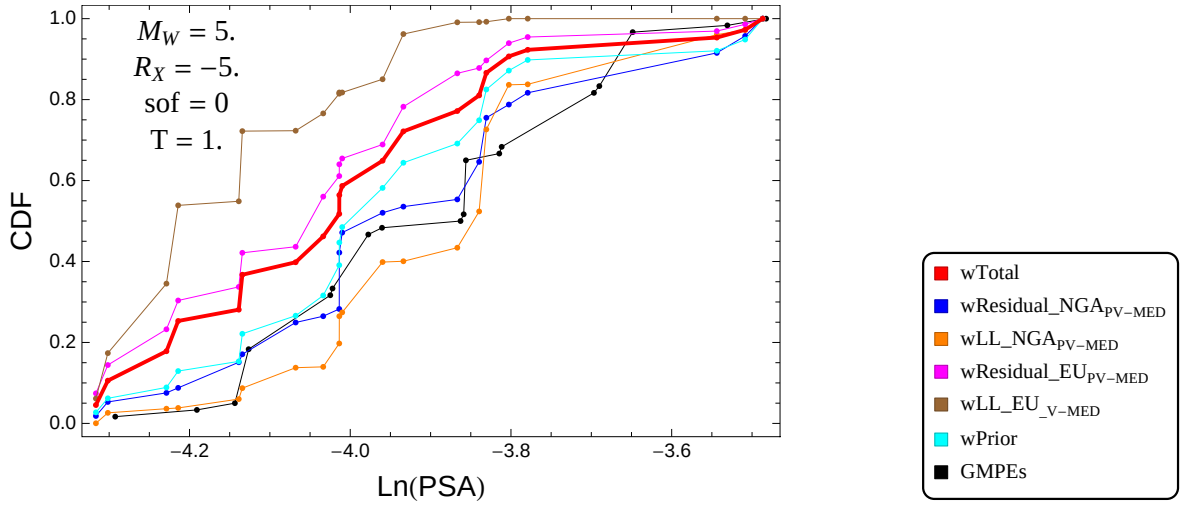



Figure 3.197: PVNGSv2: Cumulative distribution function of GMPEs (black) and selected models, for different sets of weights, for a scenario with $M = 5.$, $R_x = -5.$, $F = 0$, and $T = 1.$s

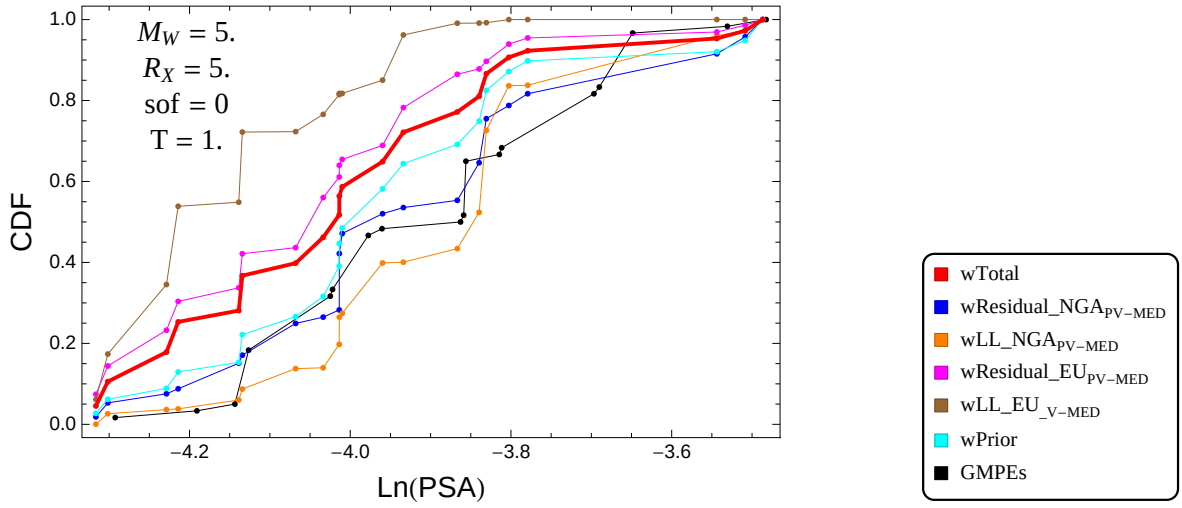



Figure 3.198: PVNGSv2: Cumulative distribution function of GMPEs (black) and selected models, for different sets of weights, for a scenario with $M = 5.$, $R_x = 5.$, $F = 0$, and $T = 1.$s

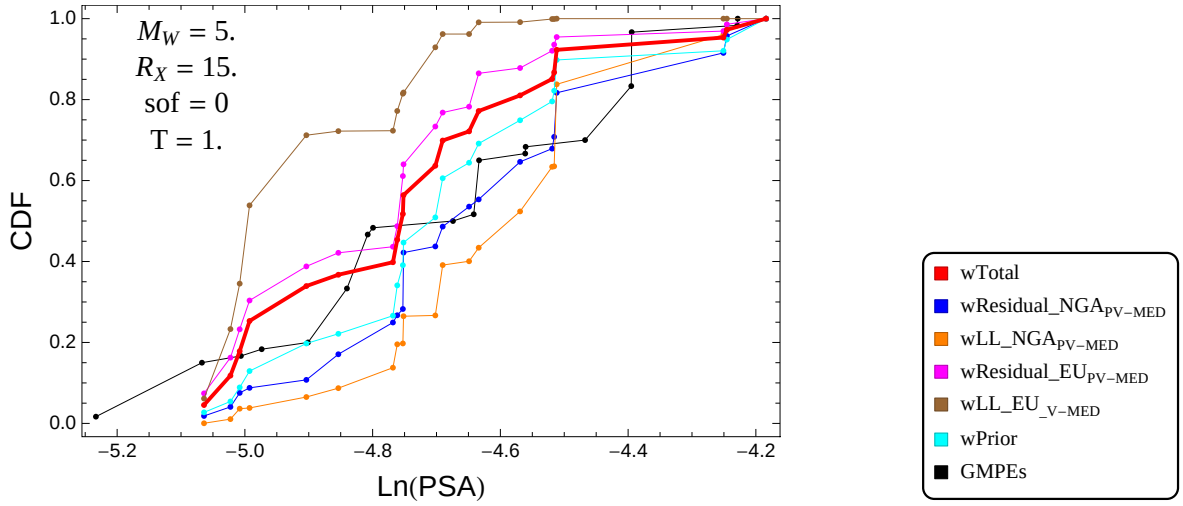



Figure 3.199: PVNGSv2: Cumulative distribution function of GMPEs (black) and selected models, for different sets of weights, for a scenario with $M = 5.$, $R_x = 15.$, $F = 0$, and $T = 1.$s

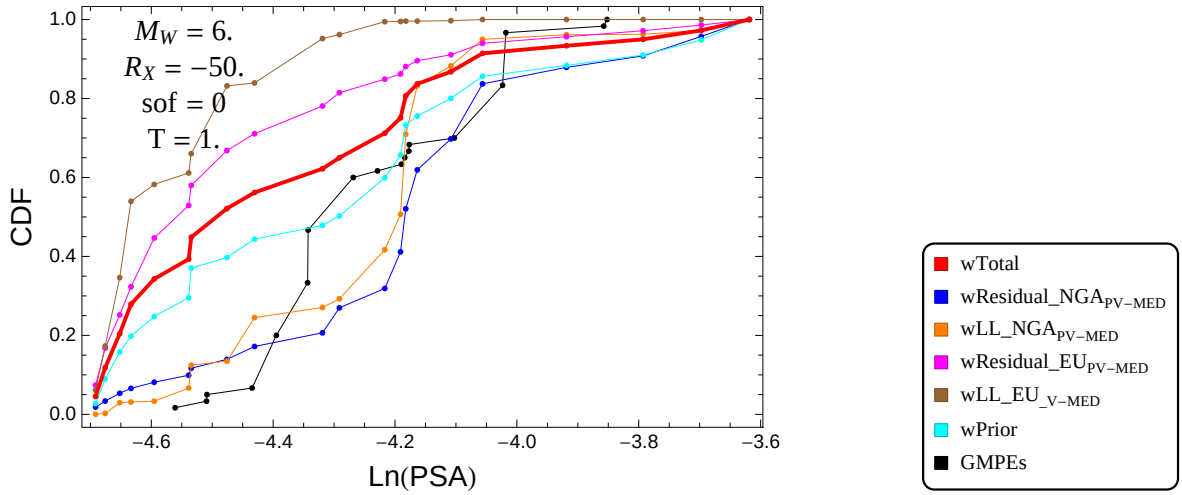



Figure 3.200: PVNGSv2: Cumulative distribution function of GMPEs (black) and selected models, for different sets of weights, for a scenario with $M = 6.$, $R_x = -50.$, $F = 0$, and $T = 1.$s

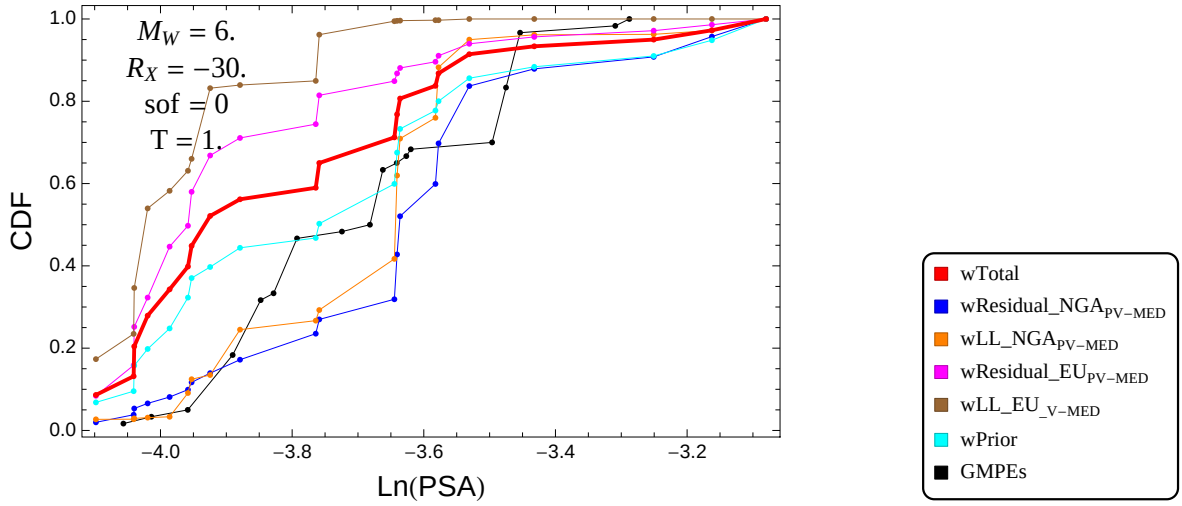



Figure 3.201: PVNGSv2: Cumulative distribution function of GMPEs (black) and selected models, for different sets of weights, for a scenario with $M = 6.$, $R_x = -30.$, $F = 0$, and $T = 1.$s

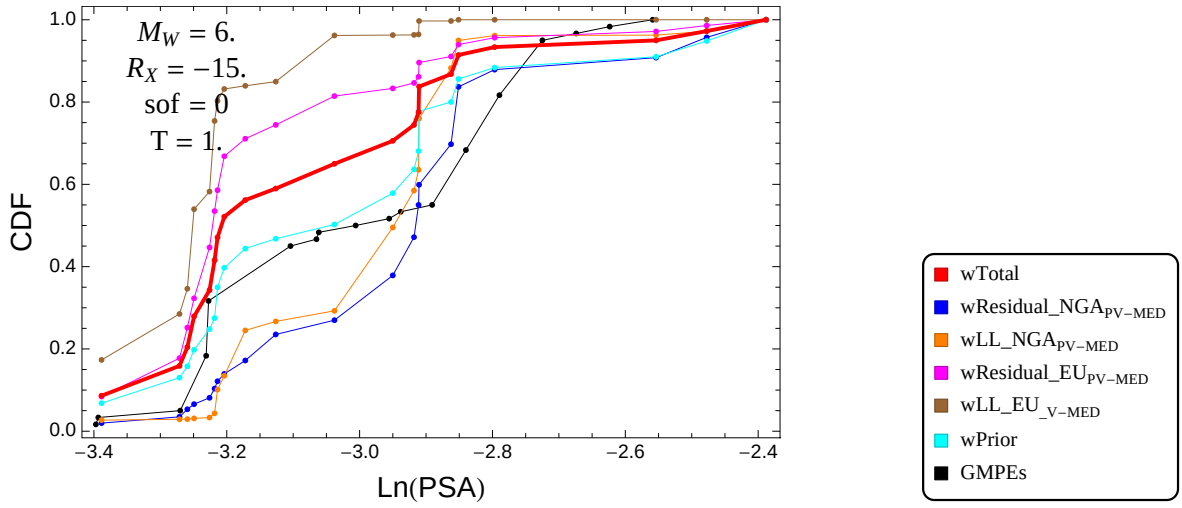



Figure 3.202: PVNGSv2: Cumulative distribution function of GMPEs (black) and selected models, for different sets of weights, for a scenario with $M = 6.$, $R_x = -15.$, $F = 0$, and $T = 1.$s

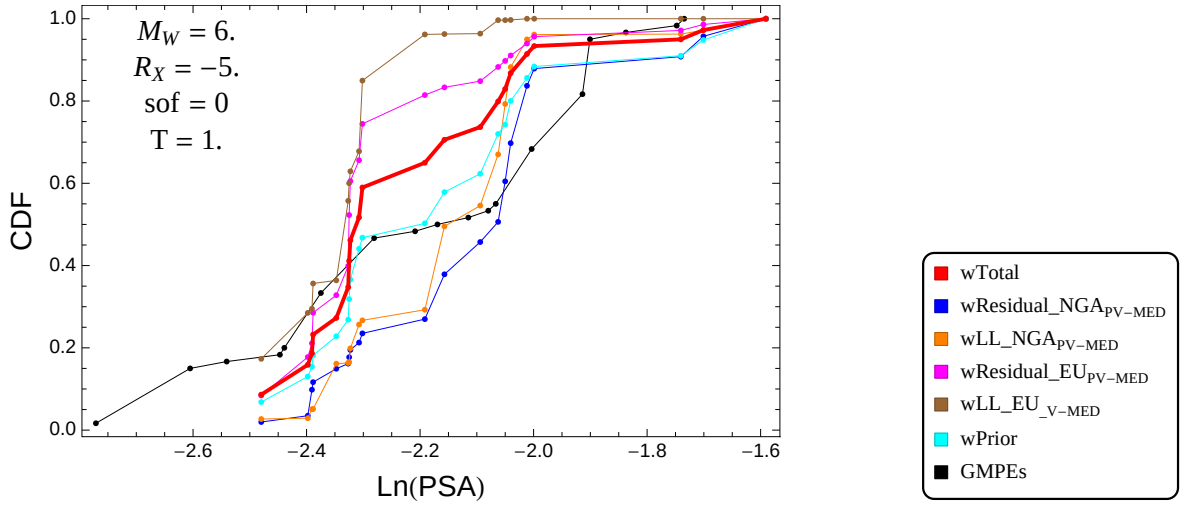



Figure 3.203: PVNGSv2: Cumulative distribution function of GMPEs (black) and selected models, for different sets of weights, for a scenario with $M = 6.$, $R_x = -5.$, $F = 0$, and $T = 1.$s

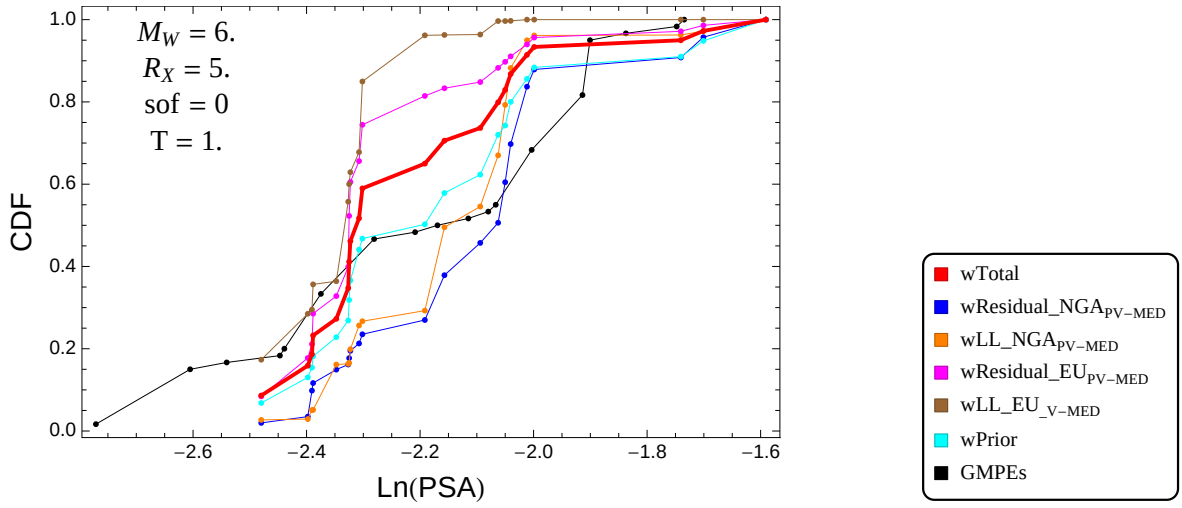



Figure 3.204: PVNGSv2: Cumulative distribution function of GMPEs (black) and selected models, for different sets of weights, for a scenario with $M = 6.$, $R_x = 5.$, $F = 0$, and $T = 1.$s

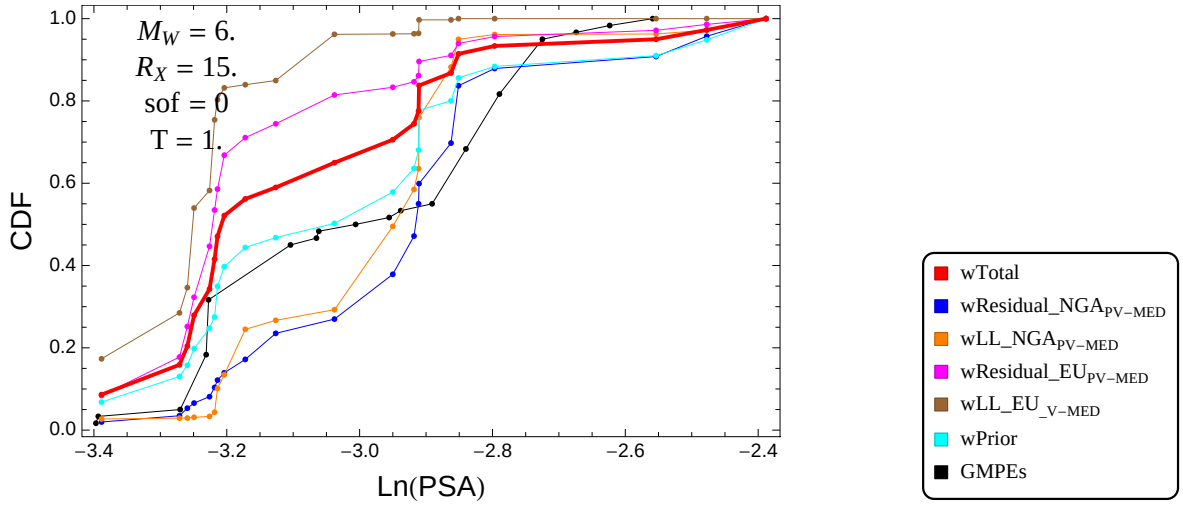



Figure 3.205: PVNGSv2: Cumulative distribution function of GMPEs (black) and selected models, for different sets of weights, for a scenario with $M = 6.$, $R_x = 15.$, $F = 0$, and $T = 1.$s

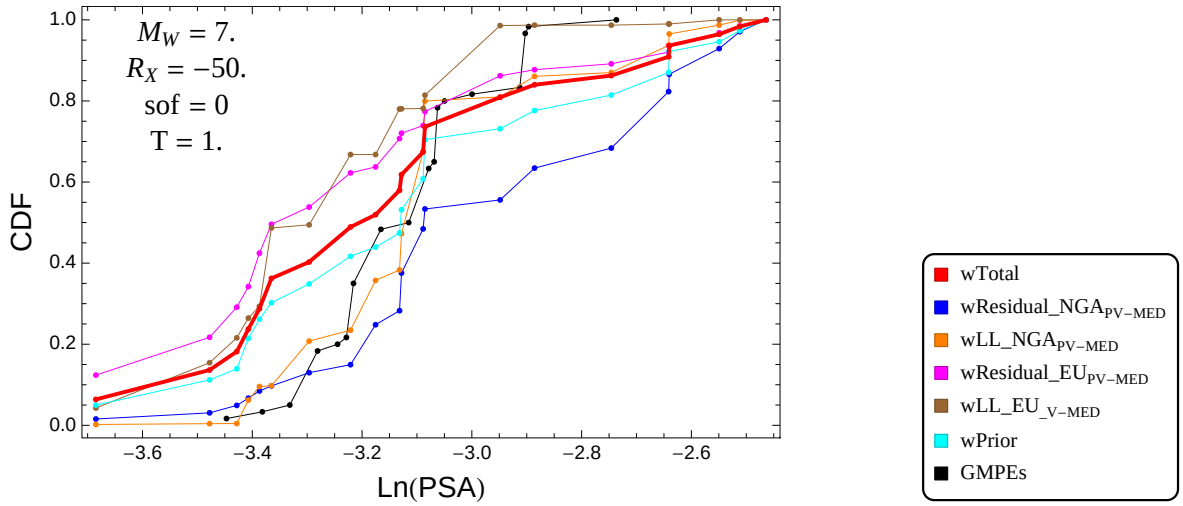



Figure 3.206: PVNGSv2: Cumulative distribution function of GMPEs (black) and selected models, for different sets of weights, for a scenario with $M = 7.$, $R_x = -50.$, $F = 0$, and $T = 1.$s

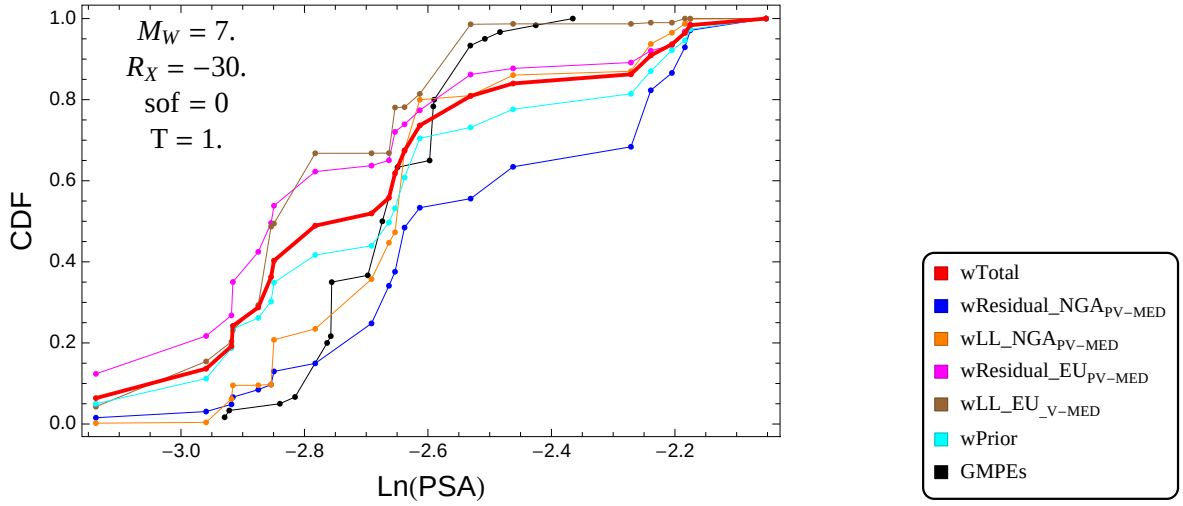



Figure 3.207: PVNGSv2: Cumulative distribution function of GMPEs (black) and selected models, for different sets of weights, for a scenario with $M = 7.$, $R_x = -30.$, $F = 0$, and $T = 1.$s

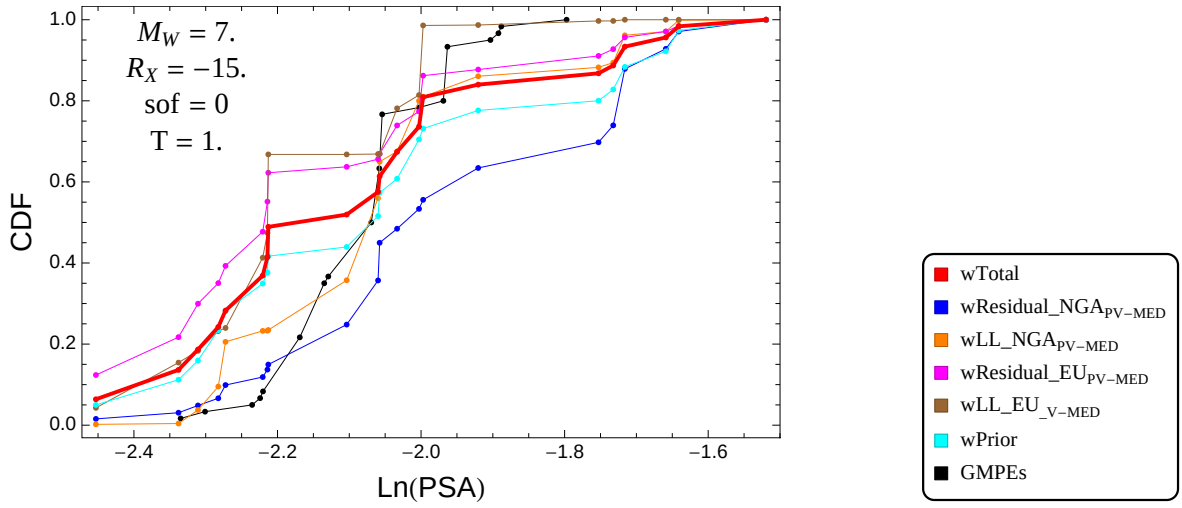



Figure 3.208: PVNGSv2: Cumulative distribution function of GMPEs (black) and selected models, for different sets of weights, for a scenario with $M = 7.$, $R_x = -15.$, $F = 0$, and $T = 1.$s

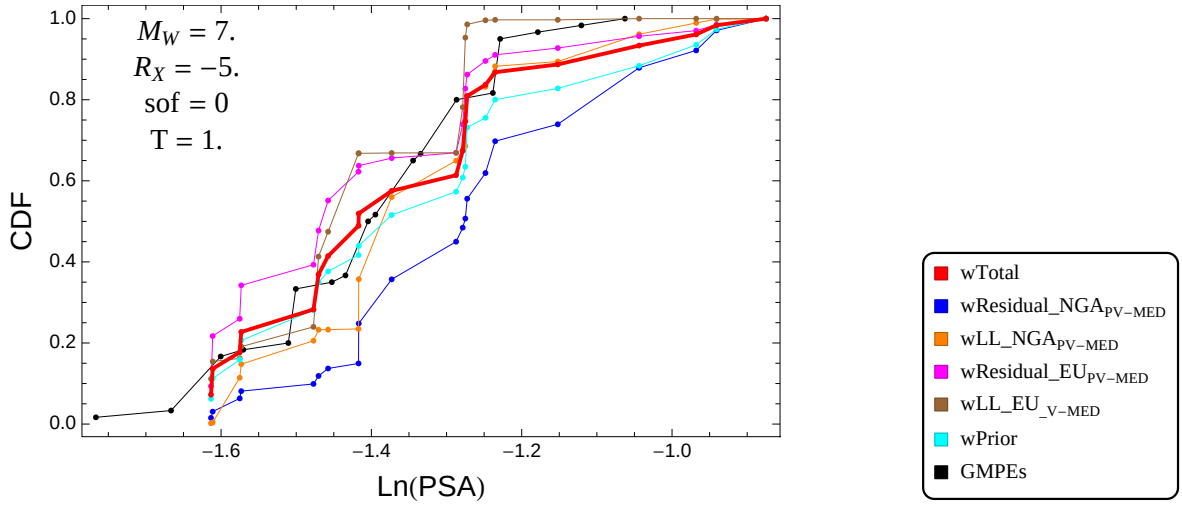



Figure 3.209: PVNGSv2: Cumulative distribution function of GMPEs (black) and selected models, for different sets of weights, for a scenario with $M = 7.$, $R_x = -5.$, $F = 0$, and $T = 1.$s

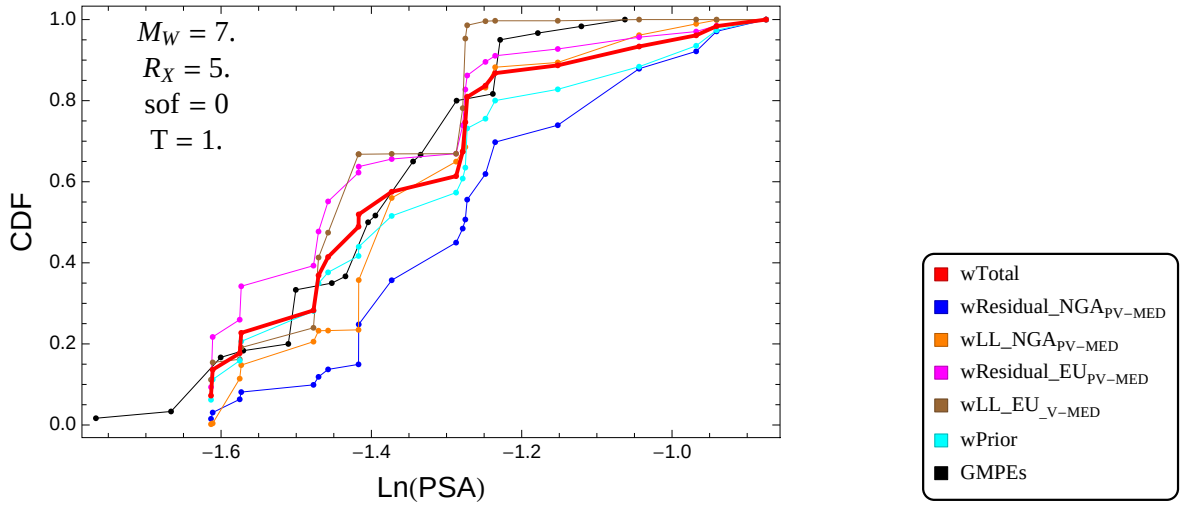



Figure 3.210: PVNGSv2: Cumulative distribution function of GMPEs (black) and selected models, for different sets of weights, for a scenario with $M = 7.$, $R_x = 5.$, $F = 0$, and $T = 1.$s

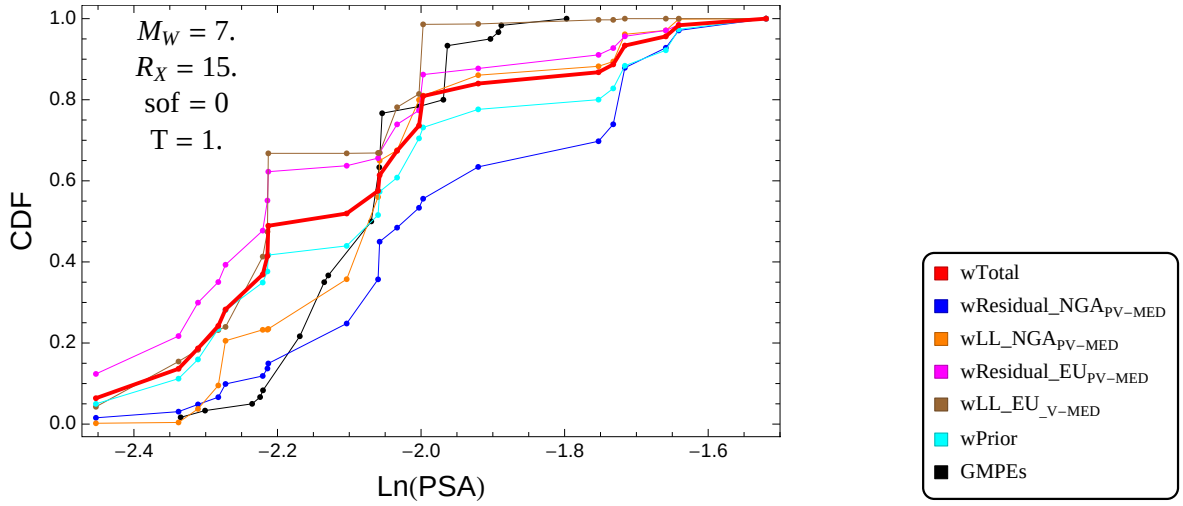



Figure 3.211: PVNGSv2: Cumulative distribution function of GMPEs (black) and selected models, for different sets of weights, for a scenario with $M = 7.$, $R_x = 15.$, $F = 0$, and $T = 1.$s

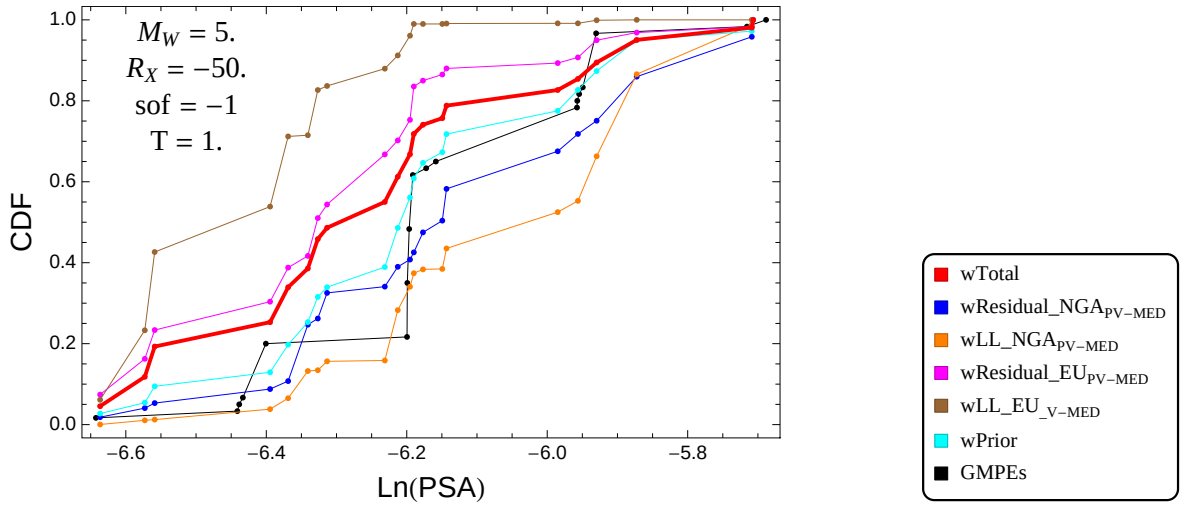



Figure 3.212: PVNGSv2: Cumulative distribution function of GMPEs (black) and selected models, for different sets of weights, for a scenario with $M = 5.$, $R_x = -50.$, $F = -1$, and $T = 1.$s

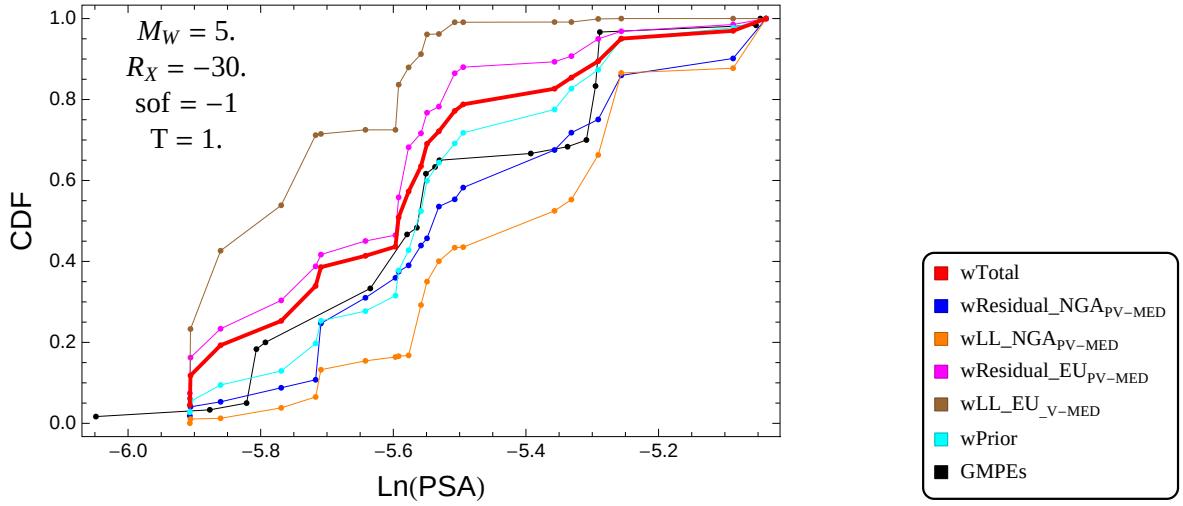



Figure 3.213: PVNGSv2: Cumulative distribution function of GMPEs (black) and selected models, for different sets of weights, for a scenario with $M = 5.$, $R_x = -30.$, $F = -1$, and $T = 1.$s

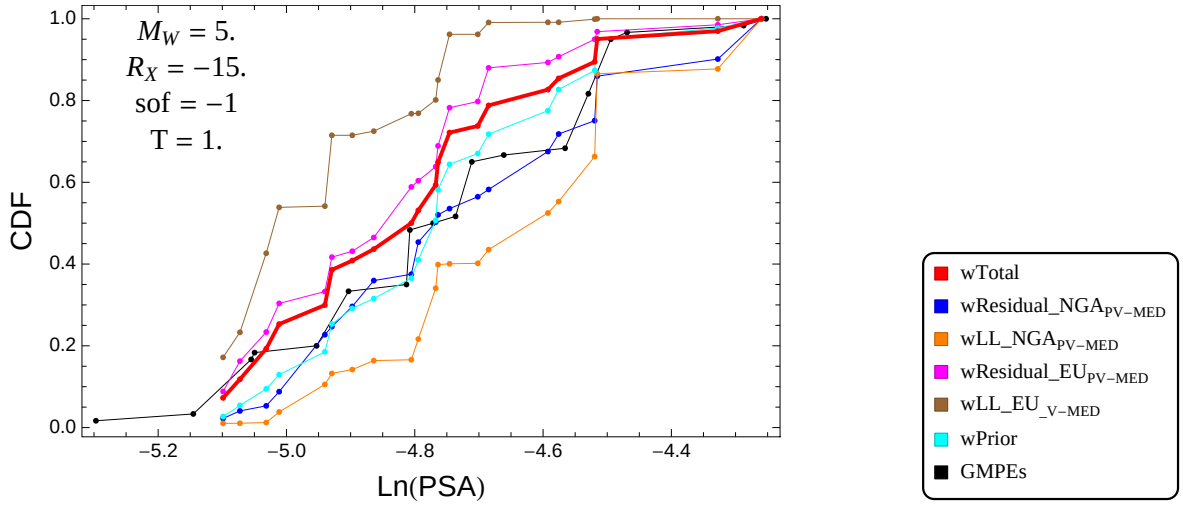



Figure 3.214: PVNGSv2: Cumulative distribution function of GMPEs (black) and selected models, for different sets of weights, for a scenario with $M = 5.$, $R_x = -15.$, $F = -1$, and $T = 1.$s

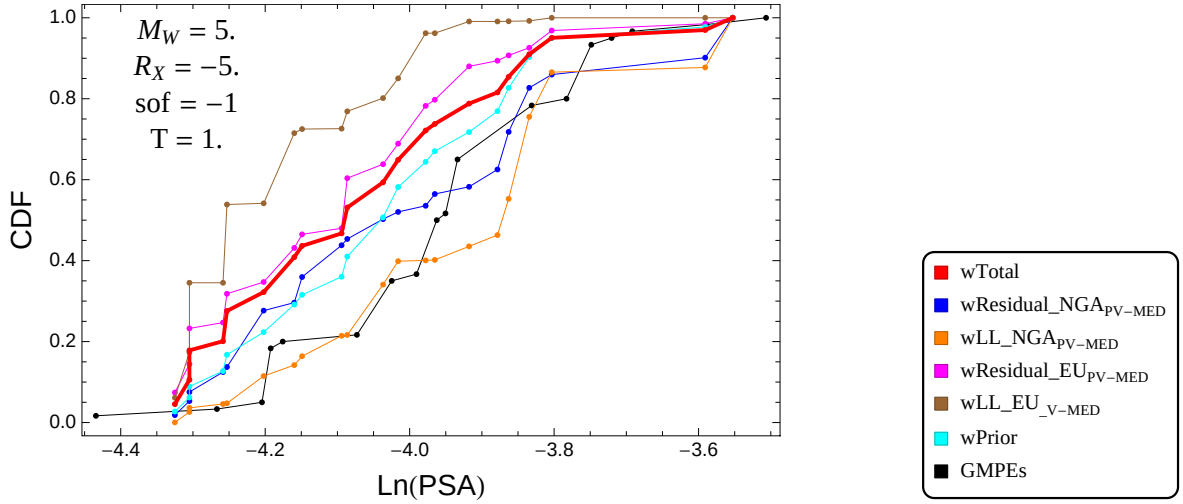



Figure 3.215: PVNGSv2: Cumulative distribution function of GMPEs (black) and selected models, for different sets of weights, for a scenario with $M = 5.$, $R_x = -5.$, $F = -1$, and $T = 1.$s

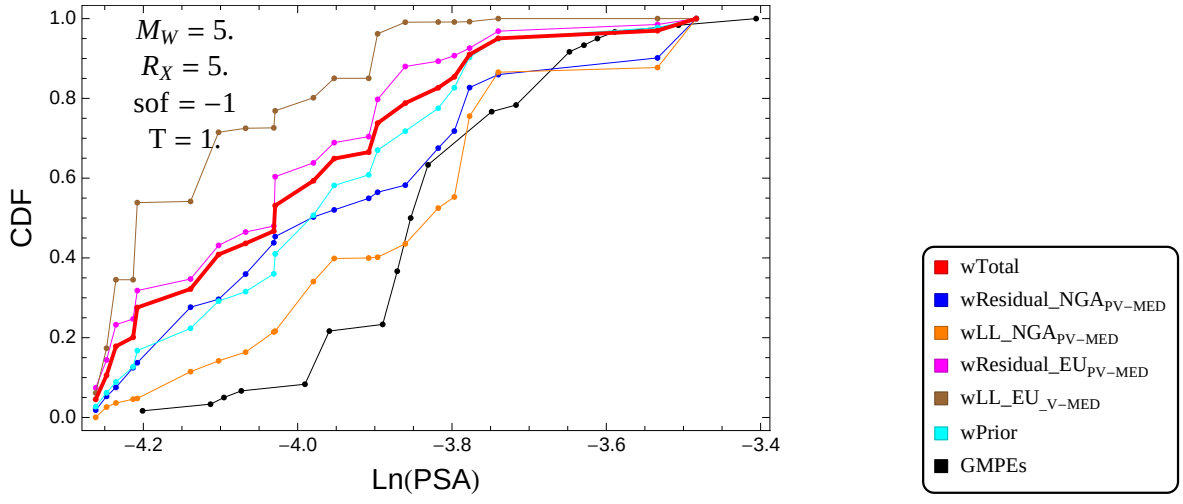



Figure 3.216: PVNGSv2: Cumulative distribution function of GMPEs (black) and selected models, for different sets of weights, for a scenario with $M = 5.$, $R_x = 5.$, $F = -1$, and $T = 1.$s

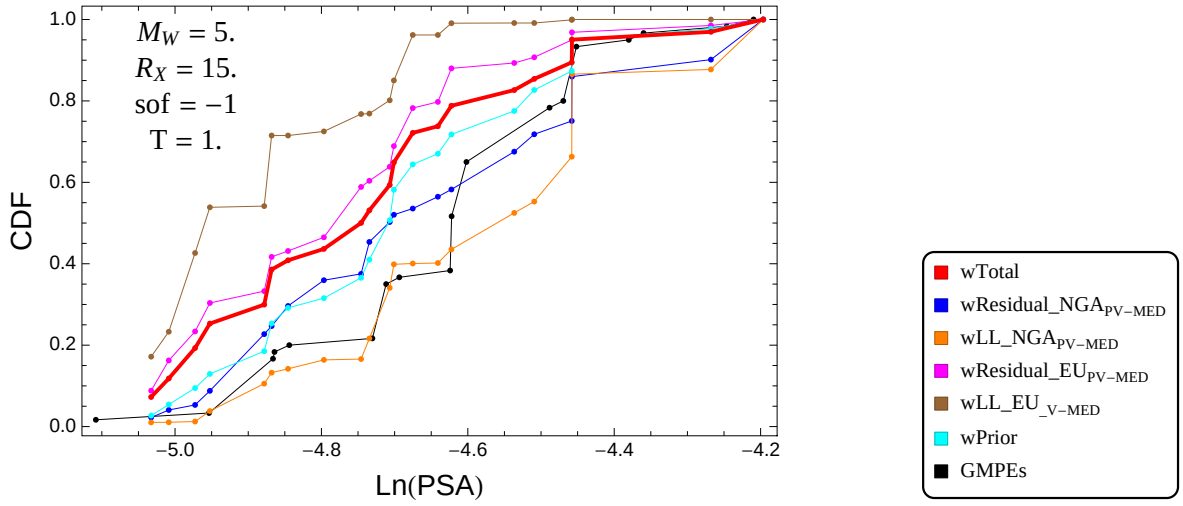



Figure 3.217: PVNGSv2: Cumulative distribution function of GMPEs (black) and selected models, for different sets of weights, for a scenario with $M = 5.$, $R_x = 15.$, $F = -1$, and $T = 1.$s

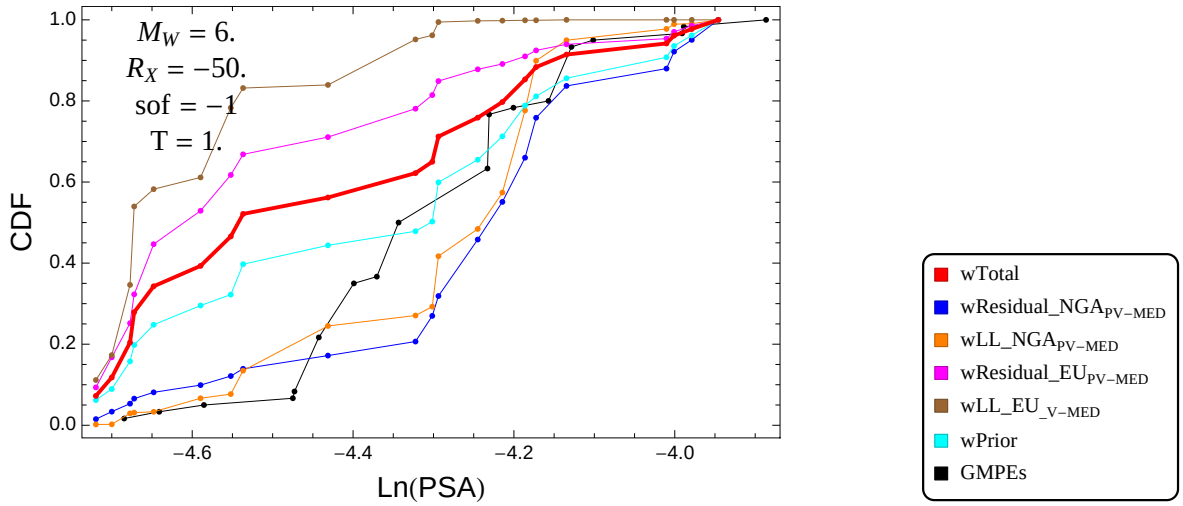



Figure 3.218: PVNGSv2: Cumulative distribution function of GMPEs (black) and selected models, for different sets of weights, for a scenario with $M = 6.$, $R_x = -50.$, $F = -1$, and $T = 1$.s

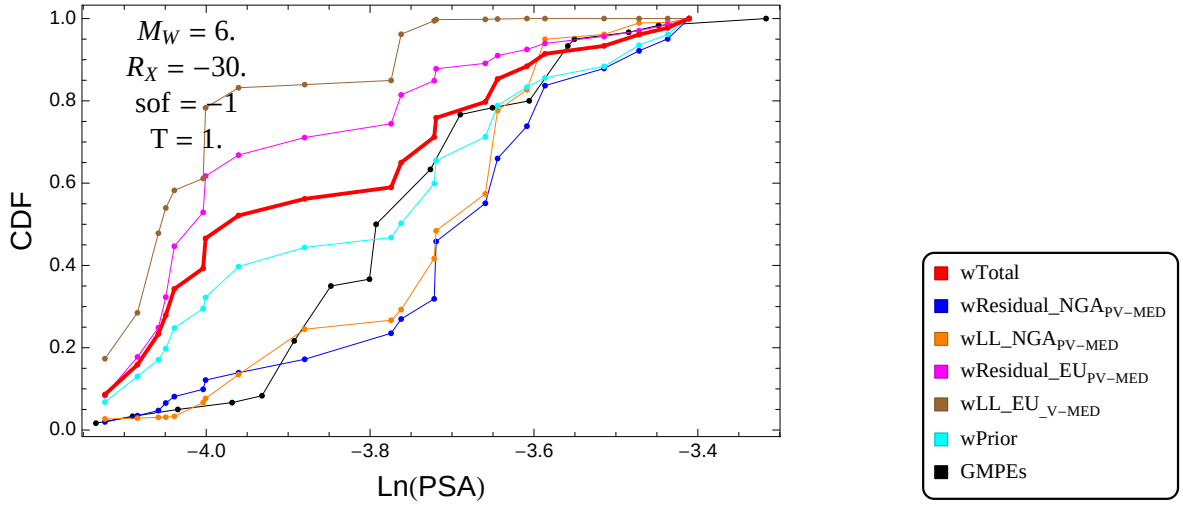



Figure 3.219: PVNGSv2: Cumulative distribution function of GMPEs (black) and selected models, for different sets of weights, for a scenario with $M = 6.$, $R_x = -30.$, $F = -1$, and $T = 1$.s

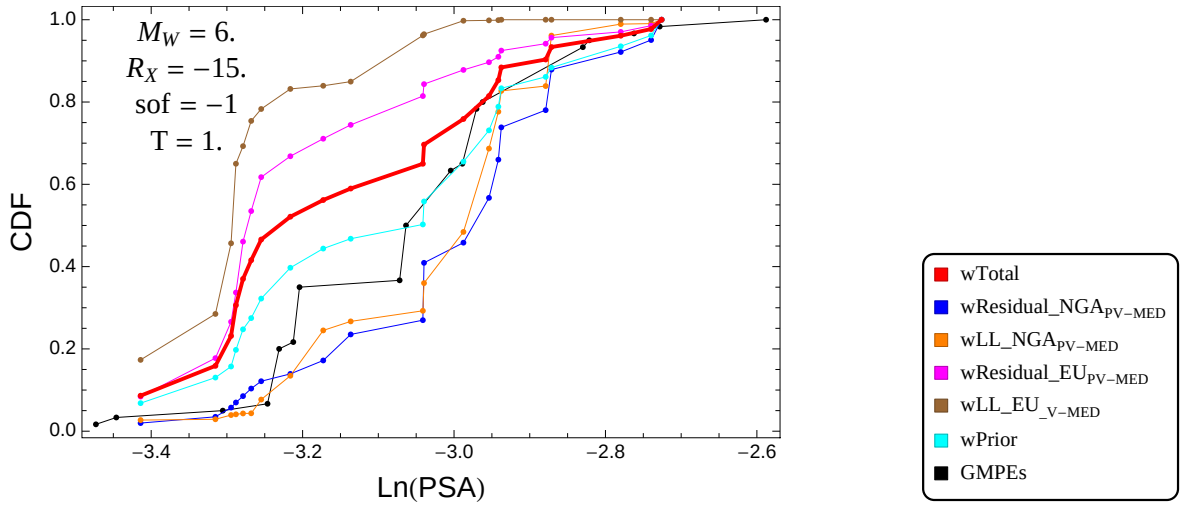



Figure 3.220: PVNGSv2: Cumulative distribution function of GMPEs (black) and selected models, for different sets of weights, for a scenario with $M = 6.$, $R_x = -15.$, $F = -1$, and $T = 1$.s

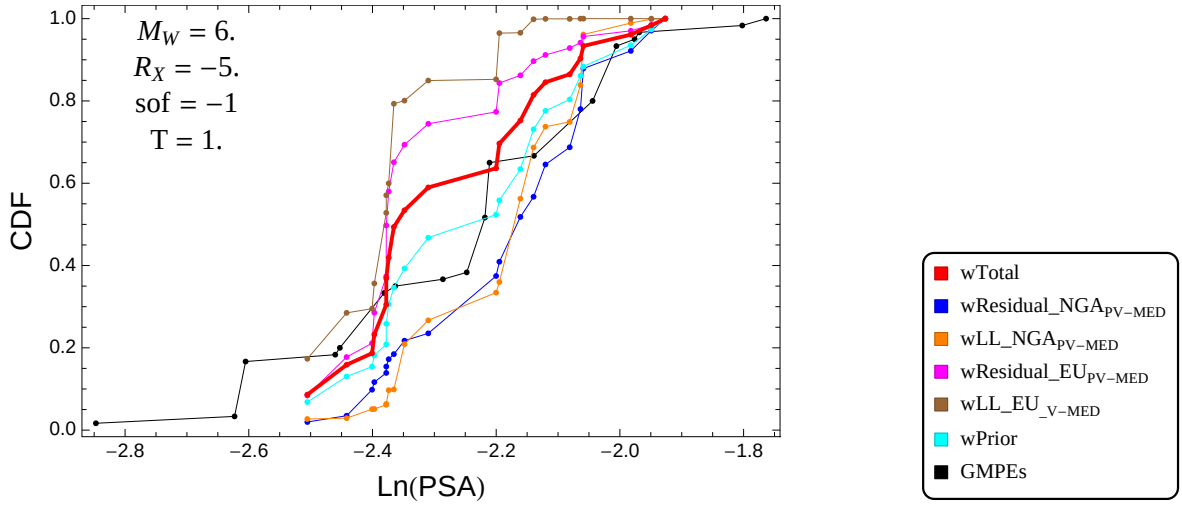



Figure 3.221: PVNGSv2: Cumulative distribution function of GMPEs (black) and selected models, for different sets of weights, for a scenario with $M = 6.$, $R_x = -5.$, $F = -1$, and $T = 1$.s

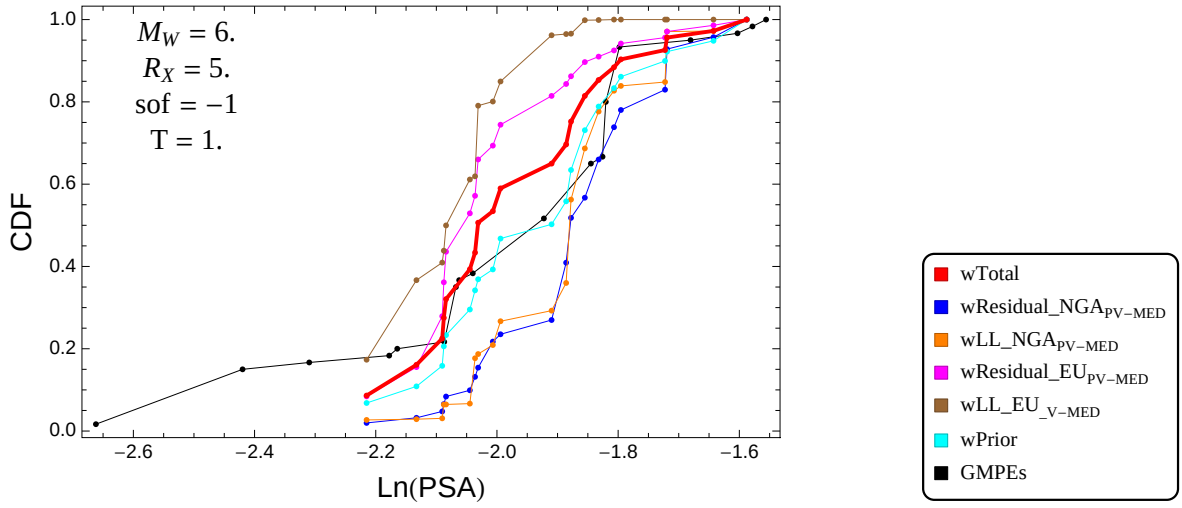



Figure 3.222: PVNGSv2: Cumulative distribution function of GMPEs (black) and selected models, for different sets of weights, for a scenario with $M = 6.$, $R_x = 5.$, $F = -1$, and $T = 1$.s

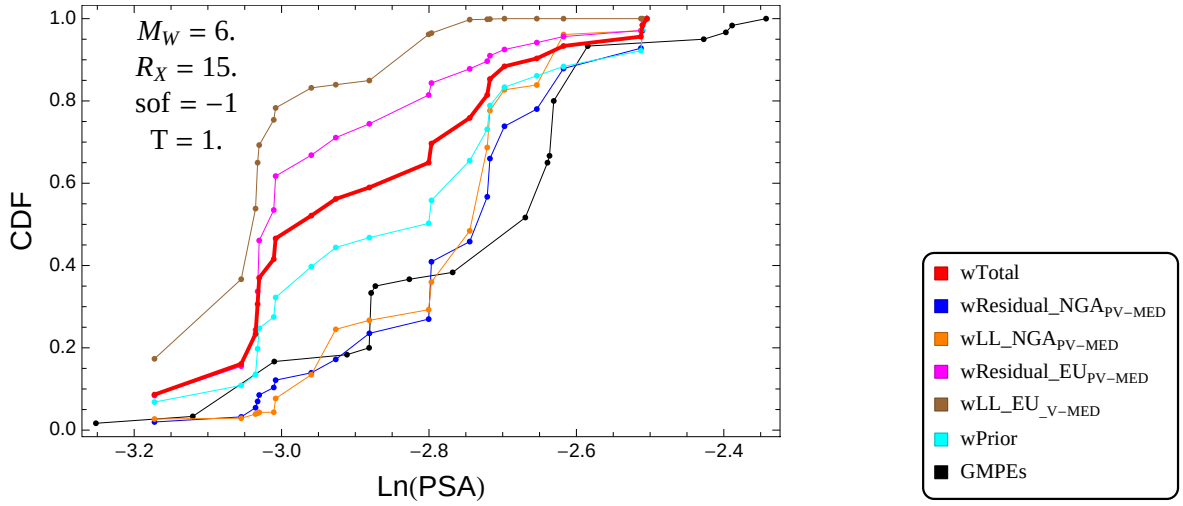



Figure 3.223: PVNGSv2: Cumulative distribution function of GMPEs (black) and selected models, for different sets of weights, for a scenario with $M = 6.$, $R_x = 15.$, $F = -1$, and $T = 1.$s

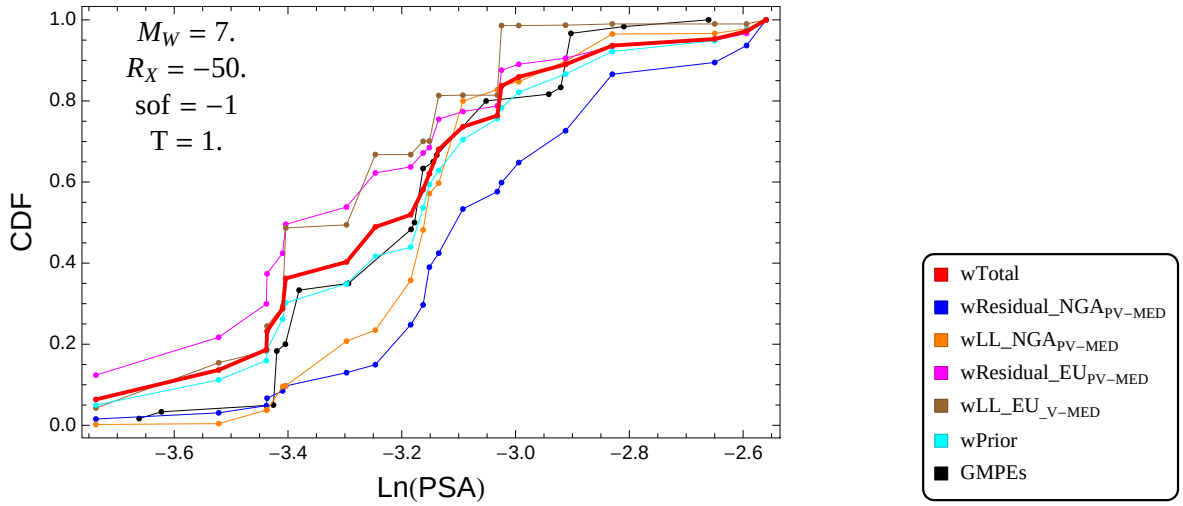



Figure 3.224: PVNGSv2: Cumulative distribution function of GMPEs (black) and selected models, for different sets of weights, for a scenario with $M = 7.$, $R_x = -50.$, $F = -1$, and $T = 1.$s

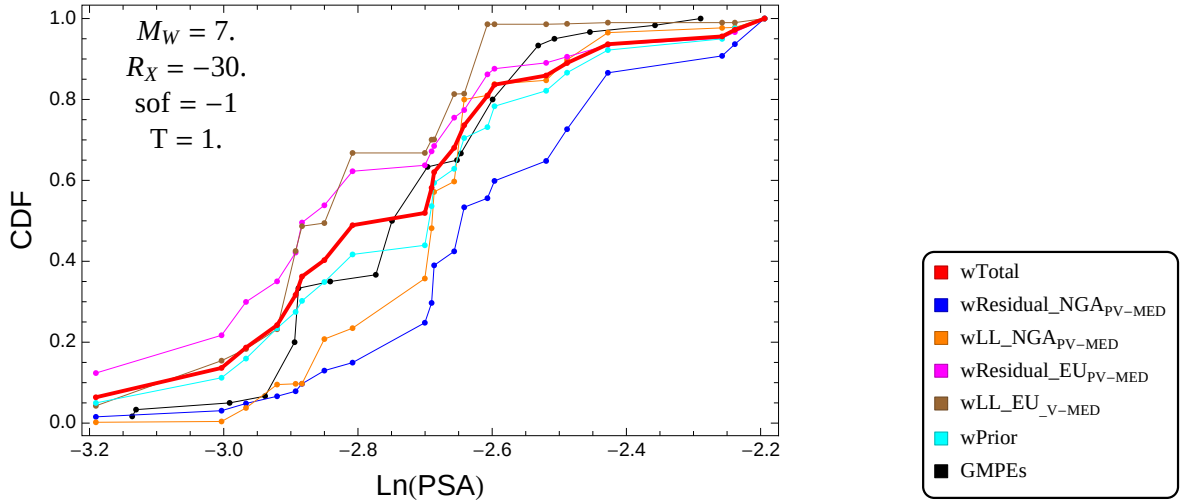



Figure 3.225: PVNGSv2: Cumulative distribution function of GMPEs (black) and selected models, for different sets of weights, for a scenario with $M = 7.$, $R_x = -30.$, $F = -1$, and $T = 1.$s

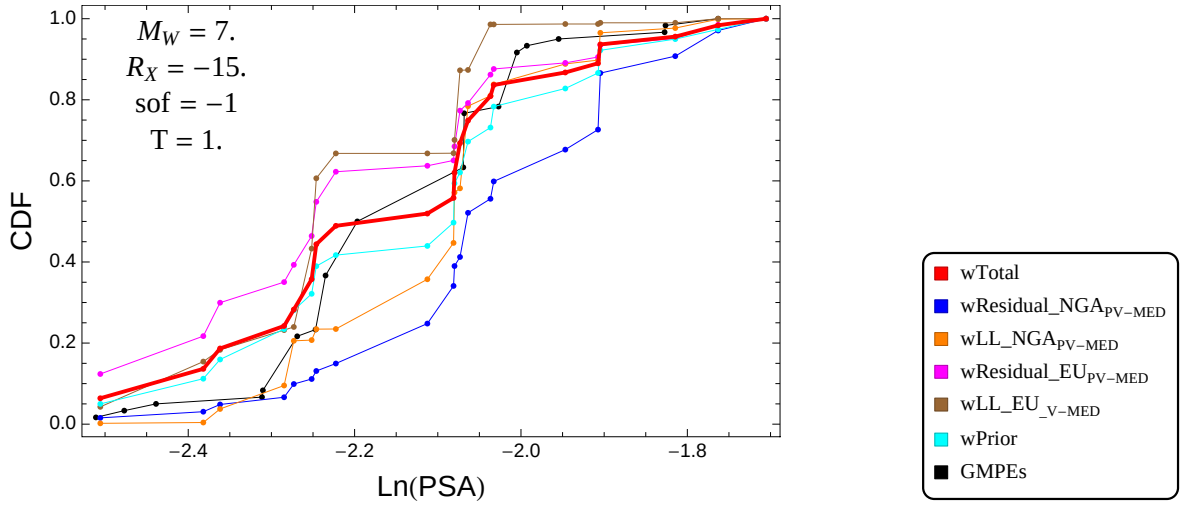



Figure 3.226: PVNGSv2: Cumulative distribution function of GMPEs (black) and selected models, for different sets of weights, for a scenario with $M = 7.$, $R_x = -15.$, $F = -1$, and $T = 1.$s

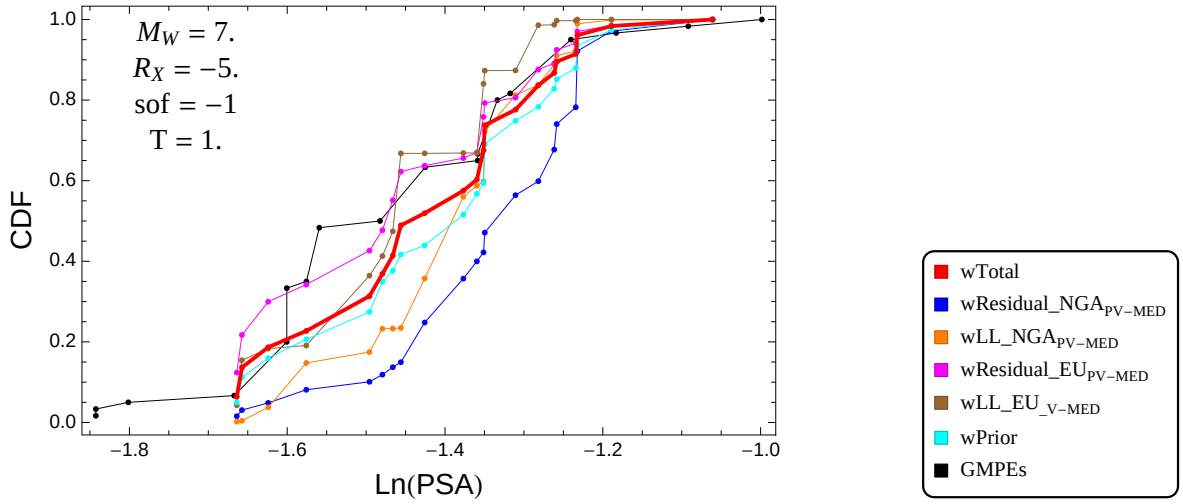



Figure 3.227: PVNGSv2: Cumulative distribution function of GMPEs (black) and selected models, for different sets of weights, for a scenario with $M = 7.$, $R_x = -5.$, $F = -1$, and $T = 1.$s

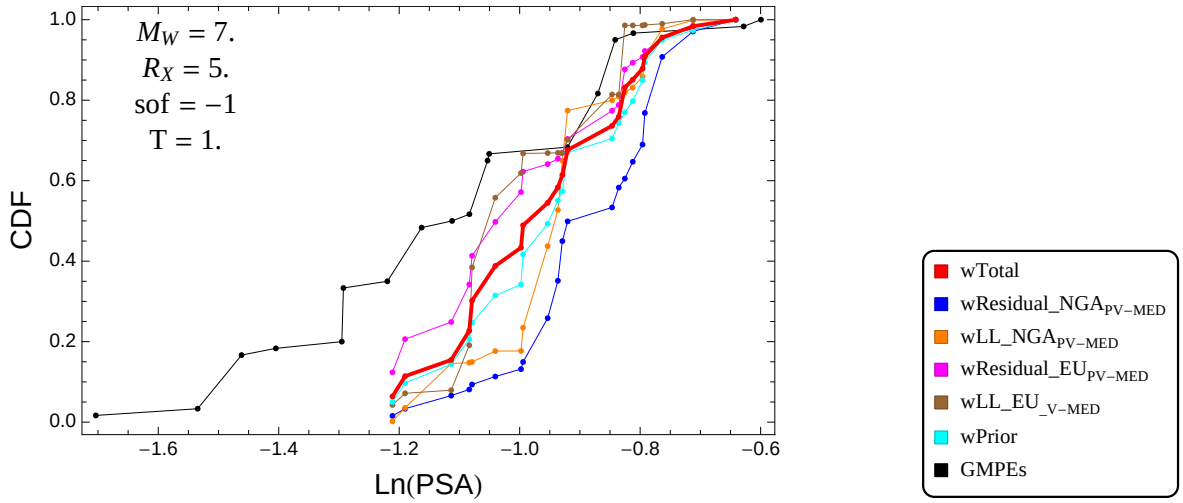



Figure 3.228: PVNGSv2: Cumulative distribution function of GMPEs (black) and selected models, for different sets of weights, for a scenario with $M = 7.$, $R_x = 5.$, $F = -1$, and $T = 1.$s

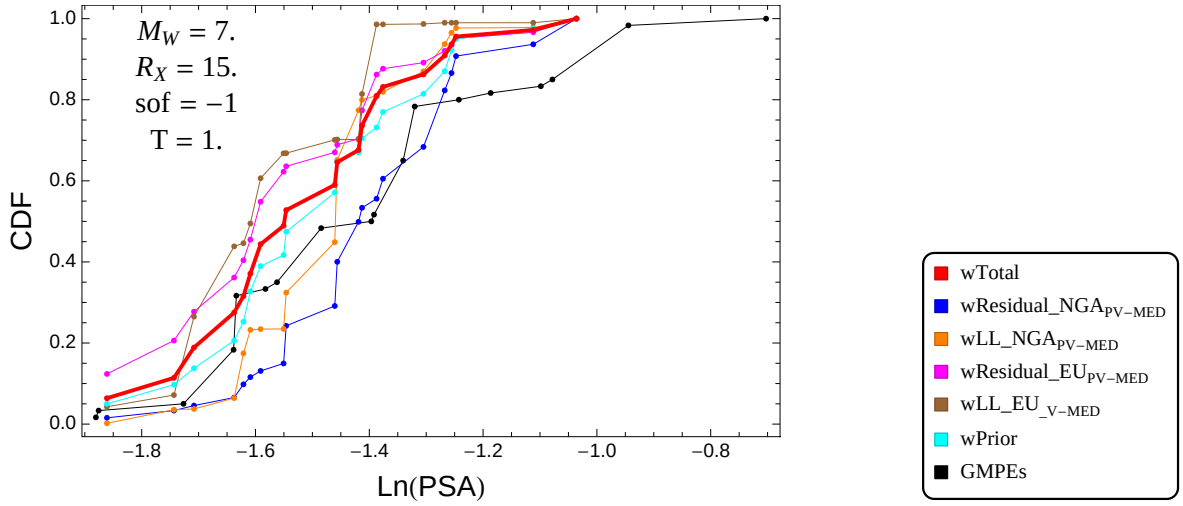



Figure 3.229: PVNGSv2: Cumulative distribution function of GMPEs (black) and selected models, for different sets of weights, for a scenario with $M = 7.$, $R_x = 15.$, $F = -1$, and $T = 1.$s

**T = 3.s**

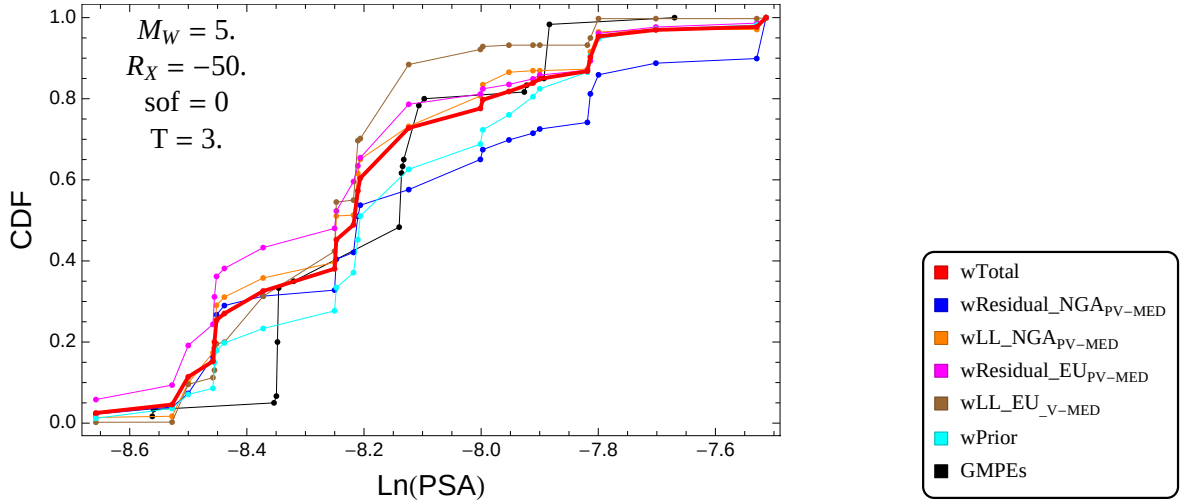



Figure 3.230: PVNGSv2: Cumulative distribution function of GMPEs (black) and selected models, for different sets of weights, for a scenario with $M = 5.$, $R_x = -50.$, $F = 0$, and $T = 3.$s

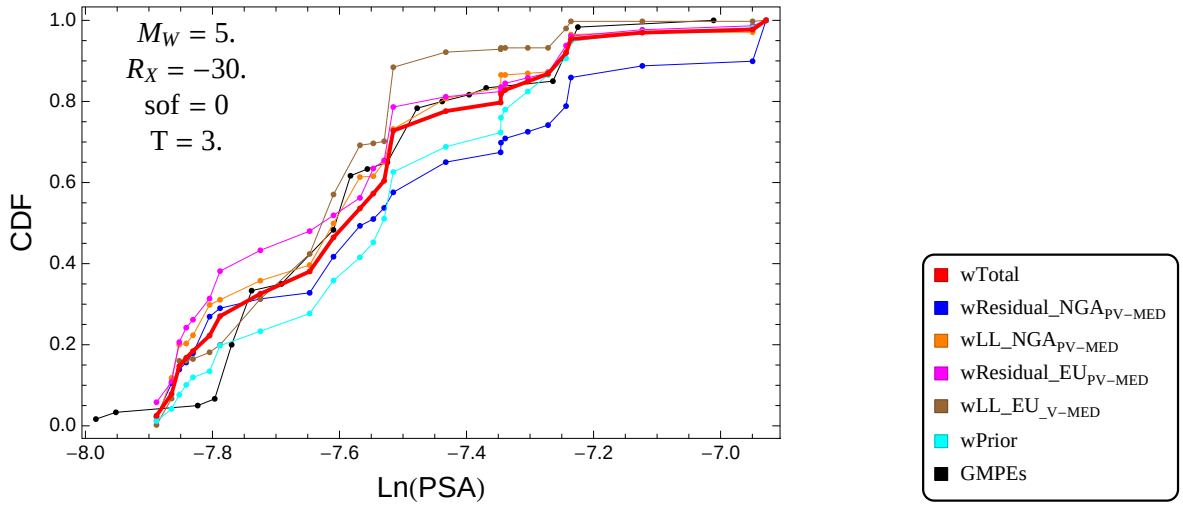



Figure 3.231: PVNGSv2: Cumulative distribution function of GMPEs (black) and selected models, for different sets of weights, for a scenario with $M = 5.$, $R_x = -30.$, $F = 0$, and $T = 3.$s

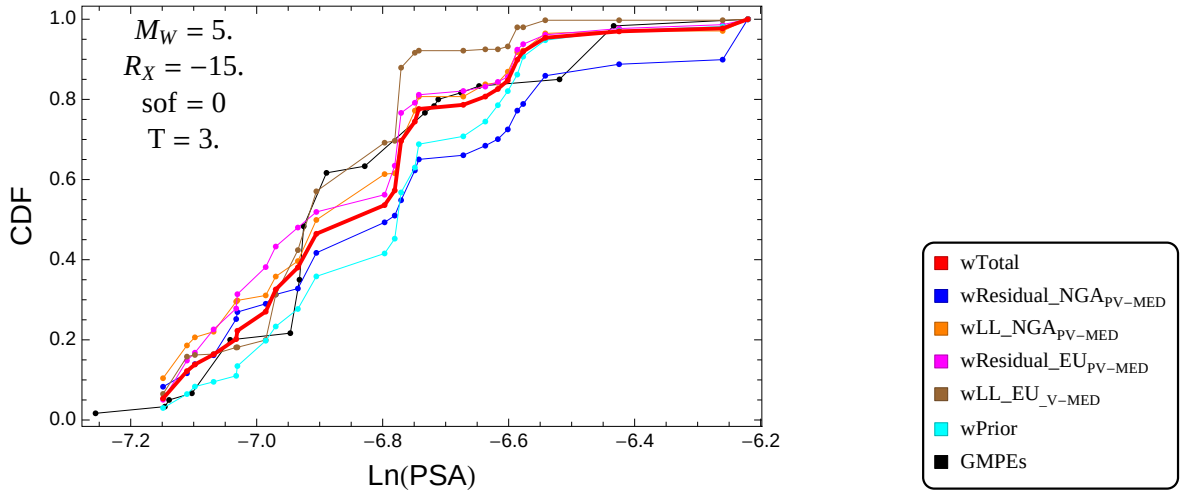



Figure 3.232: PVNGSv2: Cumulative distribution function of GMPEs (black) and selected models, for different sets of weights, for a scenario with $M = 5.$, $R_x = -15.$, $F = 0$, and $T = 3.$s

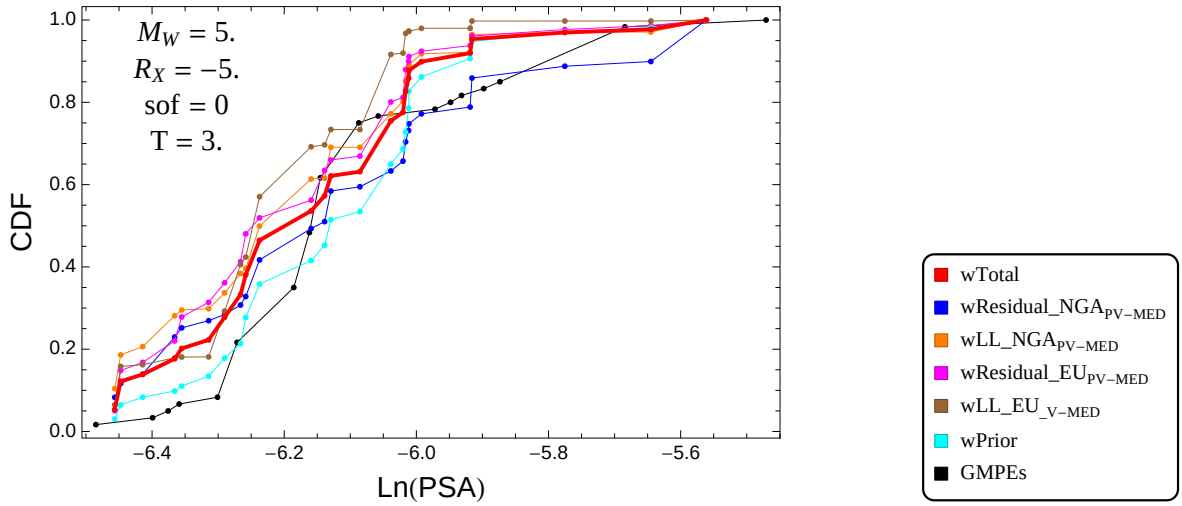



Figure 3.233: PVNGSv2: Cumulative distribution function of GMPEs (black) and selected models, for different sets of weights, for a scenario with $M = 5.$, $R_x = -5.$, $F = 0$, and $T = 3.$s

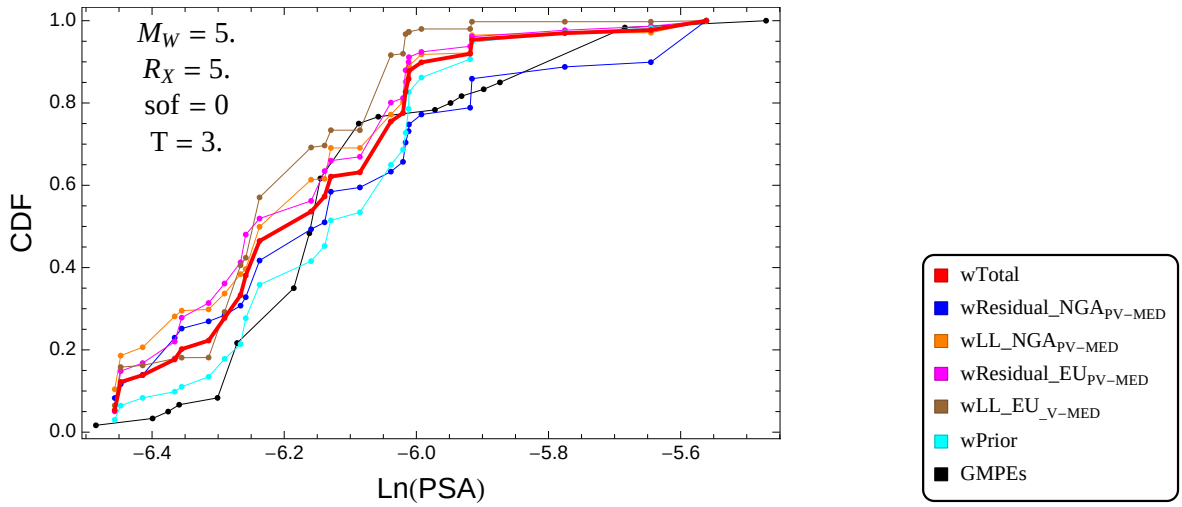



Figure 3.234: PVNGSv2: Cumulative distribution function of GMPEs (black) and selected models, for different sets of weights, for a scenario with $M = 5.$, $R_x = 5.$, $F = 0$, and $T = 3.$s

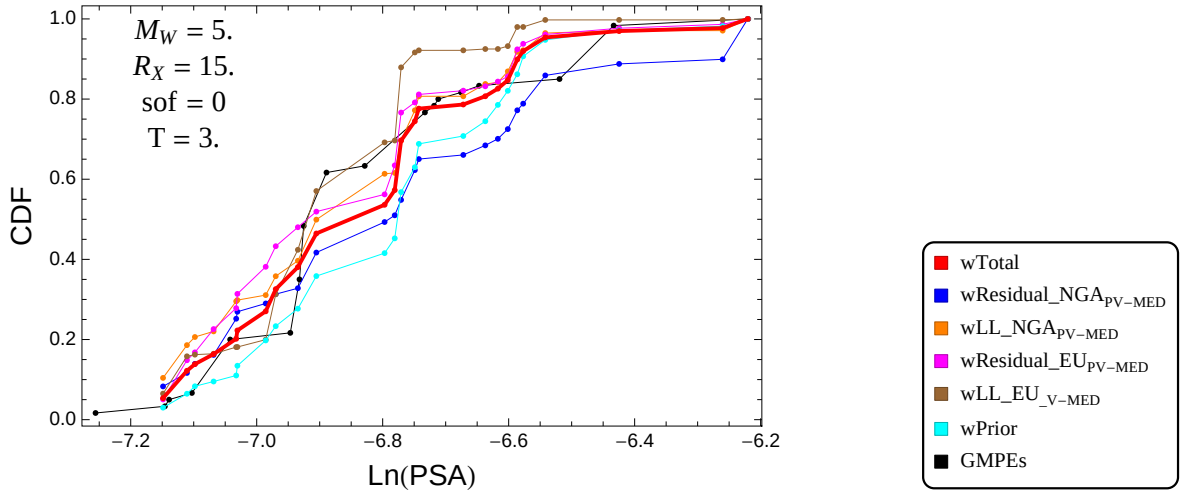



Figure 3.235: PVNGSv2: Cumulative distribution function of GMPEs (black) and selected models, for different sets of weights, for a scenario with $M = 5.$, $R_x = 15.$, $F = 0$, and $T = 3.$s

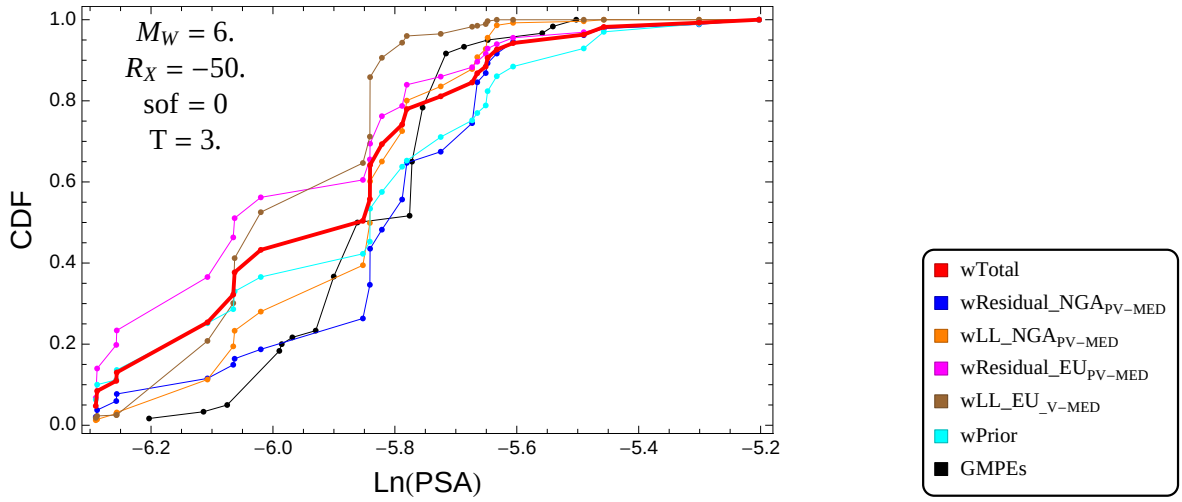



Figure 3.236: PVNGSv2: Cumulative distribution function of GMPEs (black) and selected models, for different sets of weights, for a scenario with $M = 6.$, $R_x = -50.$, $F = 0$, and $T = 3.$s

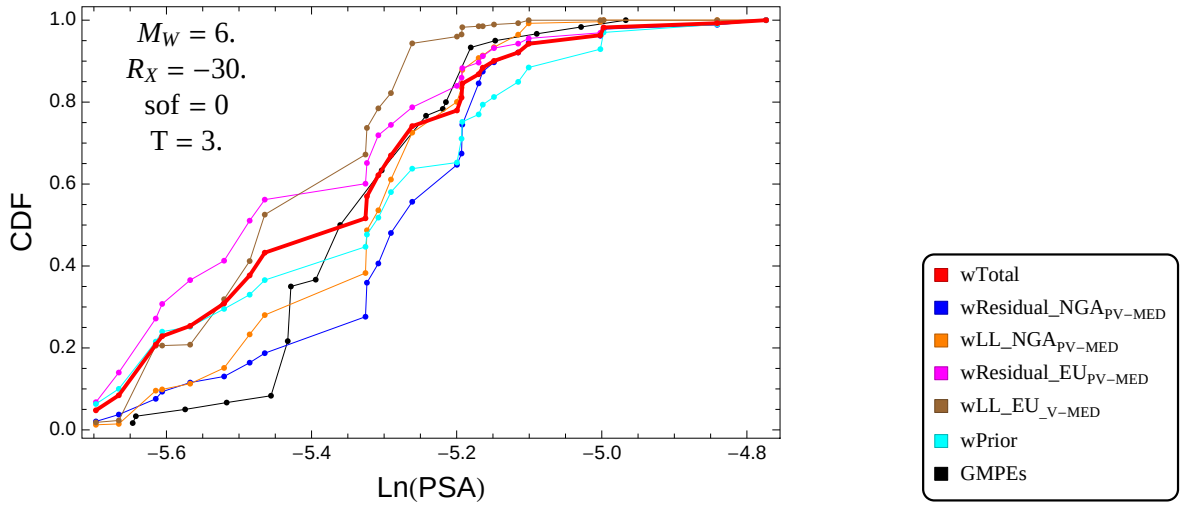



Figure 3.237: PVNGSv2: Cumulative distribution function of GMPEs (black) and selected models, for different sets of weights, for a scenario with $M = 6.$, $R_x = -30.$, $F = 0$, and $T = 3.$s

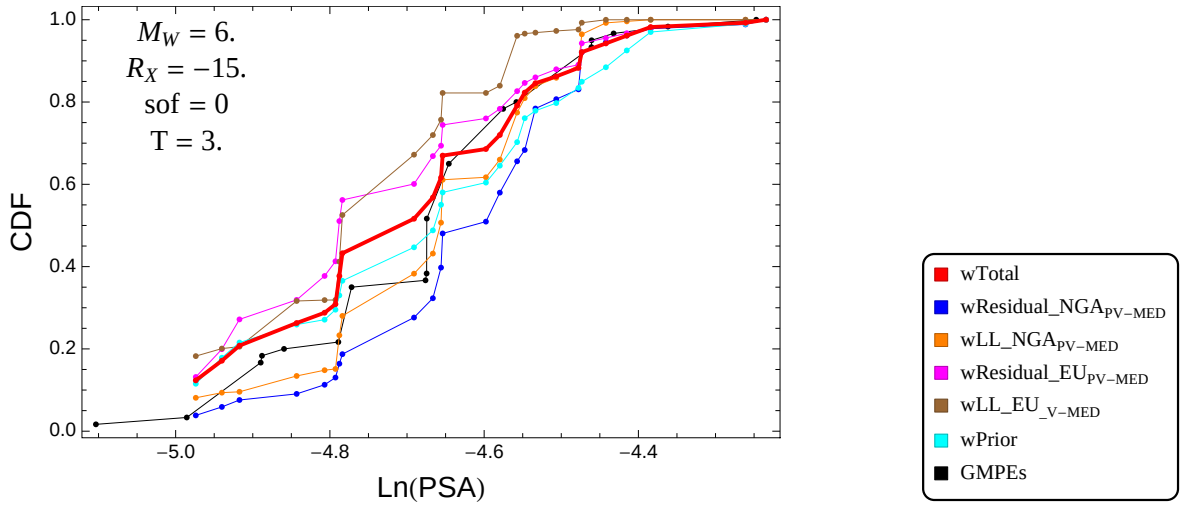



Figure 3.238: PVNGSv2: Cumulative distribution function of GMPEs (black) and selected models, for different sets of weights, for a scenario with $M = 6.$, $R_x = -15.$, $F = 0$, and $T = 3.$s

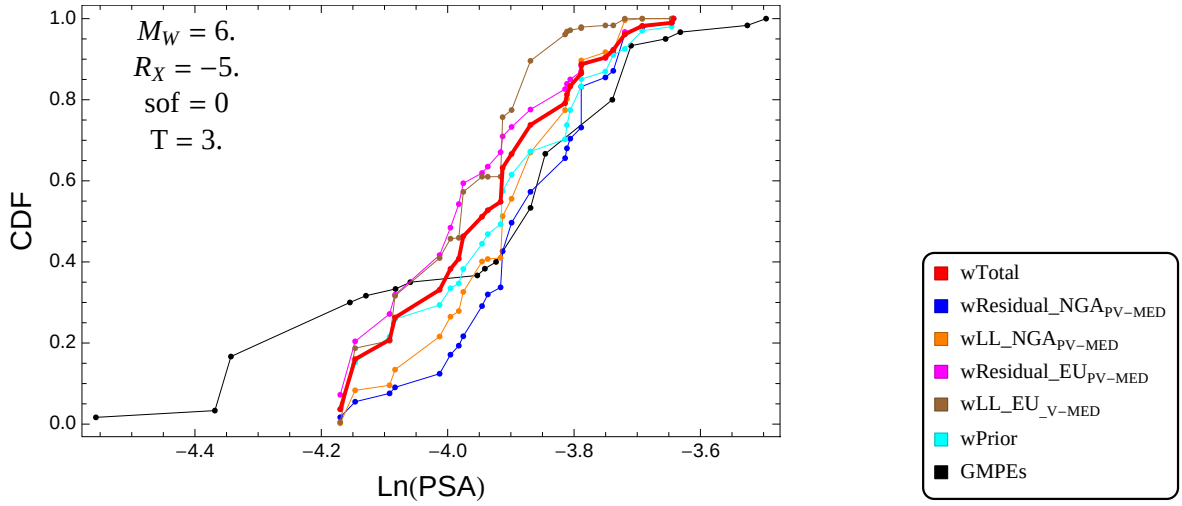



Figure 3.239: PVNGSv2: Cumulative distribution function of GMPEs (black) and selected models, for different sets of weights, for a scenario with $M = 6.$, $R_x = -5.$, $F = 0$, and $T = 3.$s

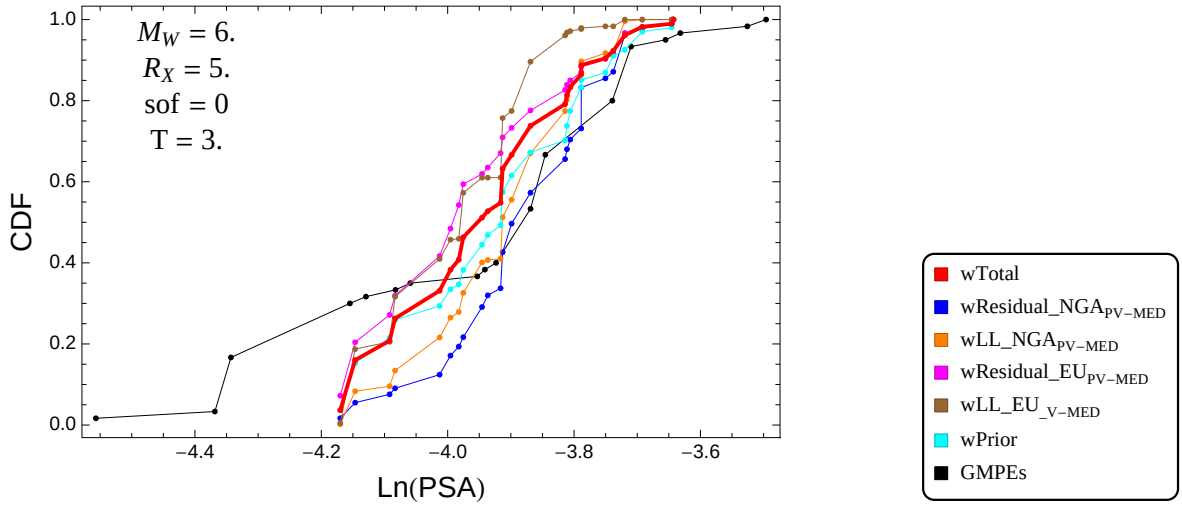



Figure 3.240: PVNGSv2: Cumulative distribution function of GMPEs (black) and selected models, for different sets of weights, for a scenario with $M = 6.$, $R_x = 5.$, $F = 0$, and $T = 3.$s

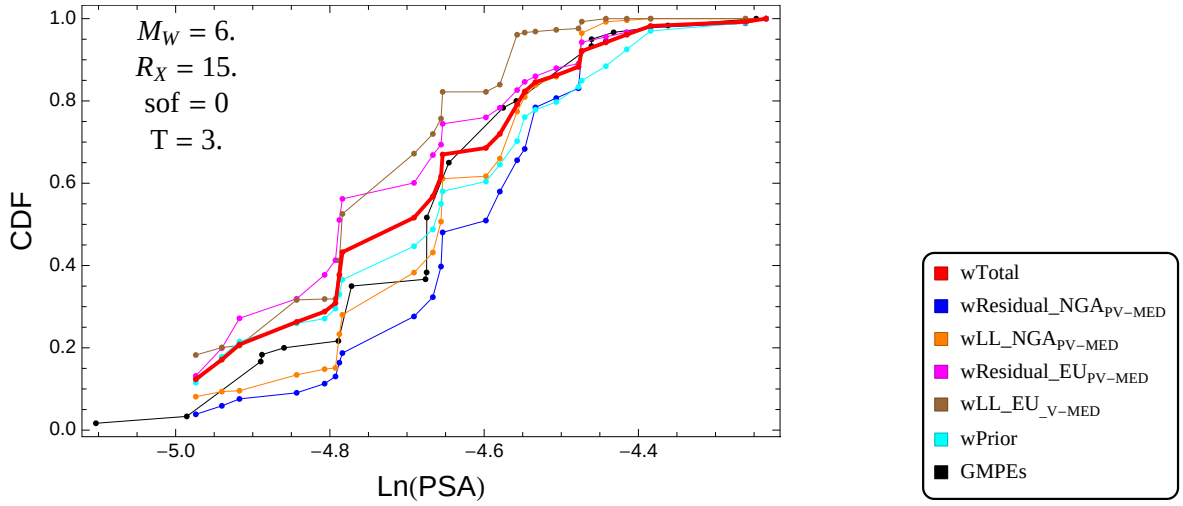



Figure 3.241: PVNGSv2: Cumulative distribution function of GMPEs (black) and selected models, for different sets of weights, for a scenario with $M = 6.$, $R_x = 15.$, $F = 0$, and $T = 3.$s

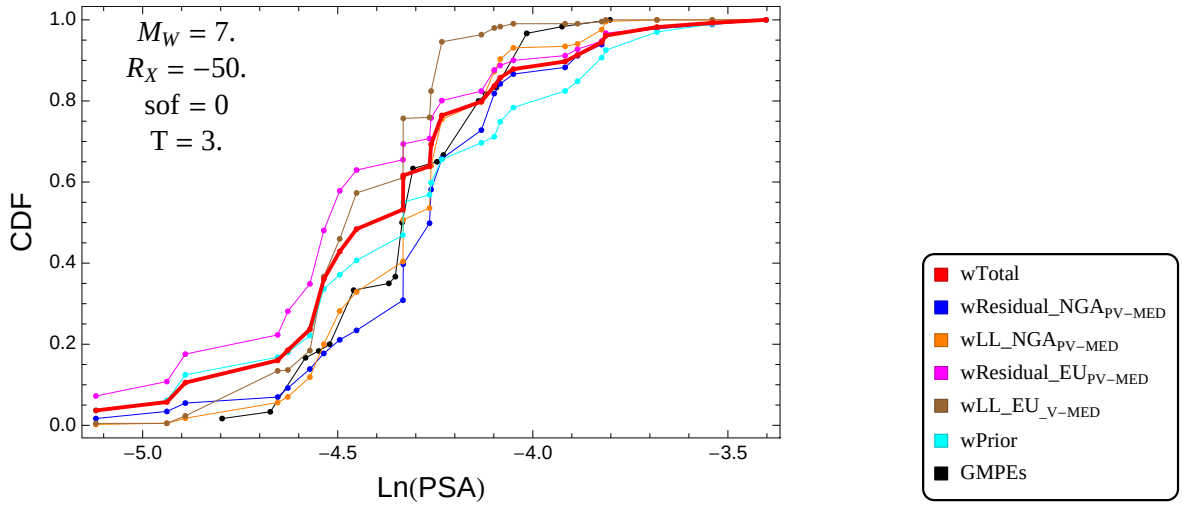



Figure 3.242: PVNGSv2: Cumulative distribution function of GMPEs (black) and selected models, for different sets of weights, for a scenario with $M = 7.$, $R_x = -50.$, $F = 0$, and $T = 3.$s

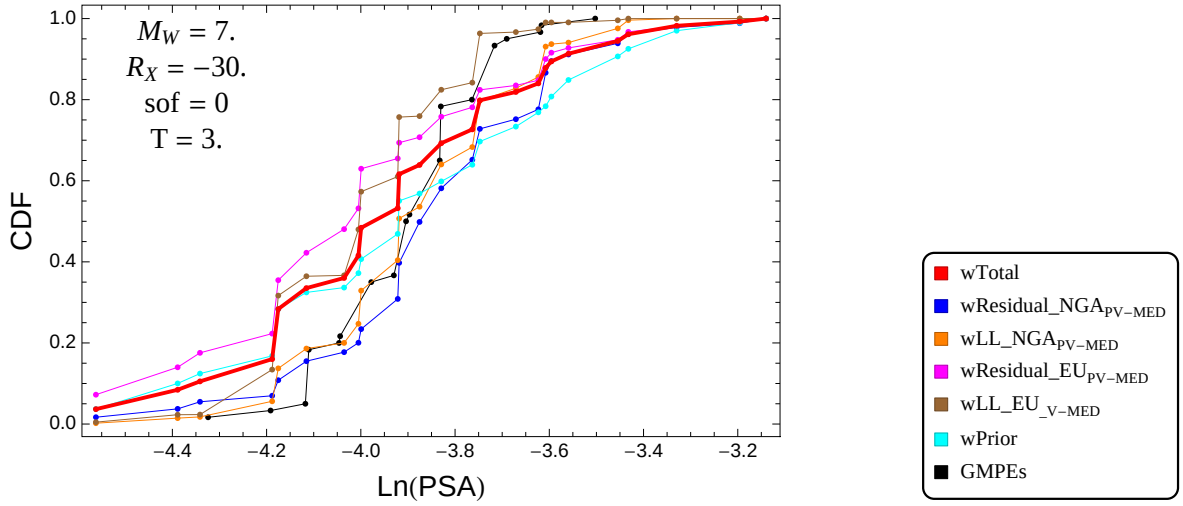



Figure 3.243: PVNGSv2: Cumulative distribution function of GMPEs (black) and selected models, for different sets of weights, for a scenario with $M = 7.$, $R_x = -30.$, $F = 0$, and $T = 3.$s

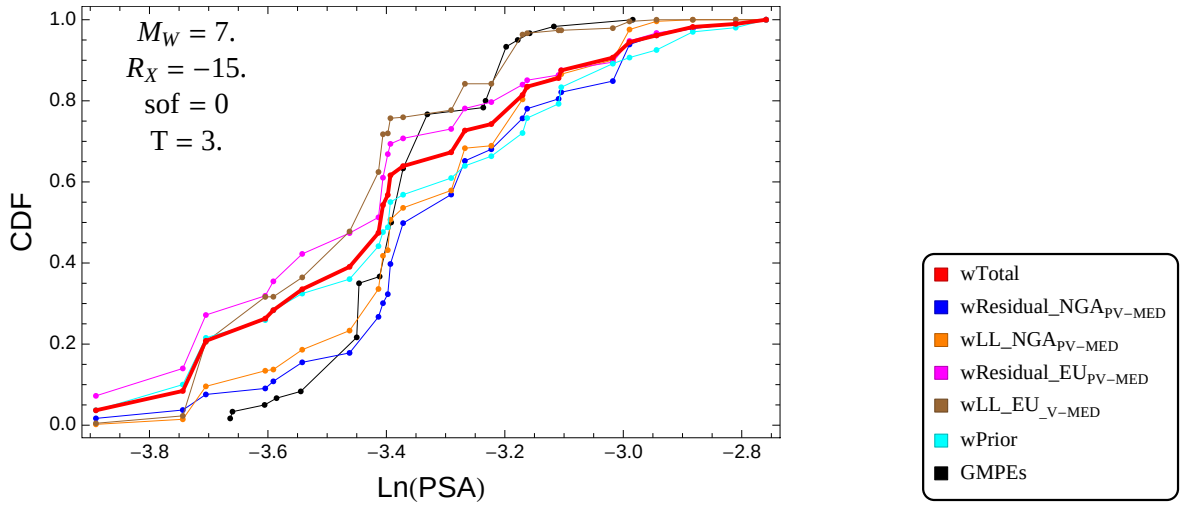



Figure 3.244: PVNGSv2: Cumulative distribution function of GMPEs (black) and selected models, for different sets of weights, for a scenario with $M = 7.$, $R_x = -15.$, $F = 0$, and $T = 3.$s

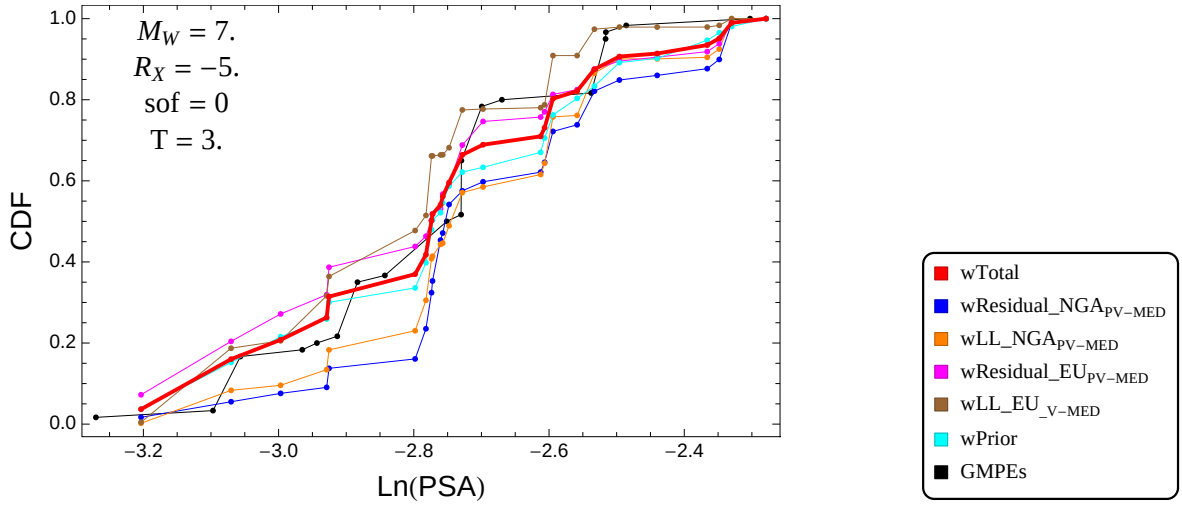



Figure 3.245: PVNGSv2: Cumulative distribution function of GMPEs (black) and selected models, for different sets of weights, for a scenario with $M = 7.$, $R_x = -5.$, $F = 0$, and $T = 3.$s

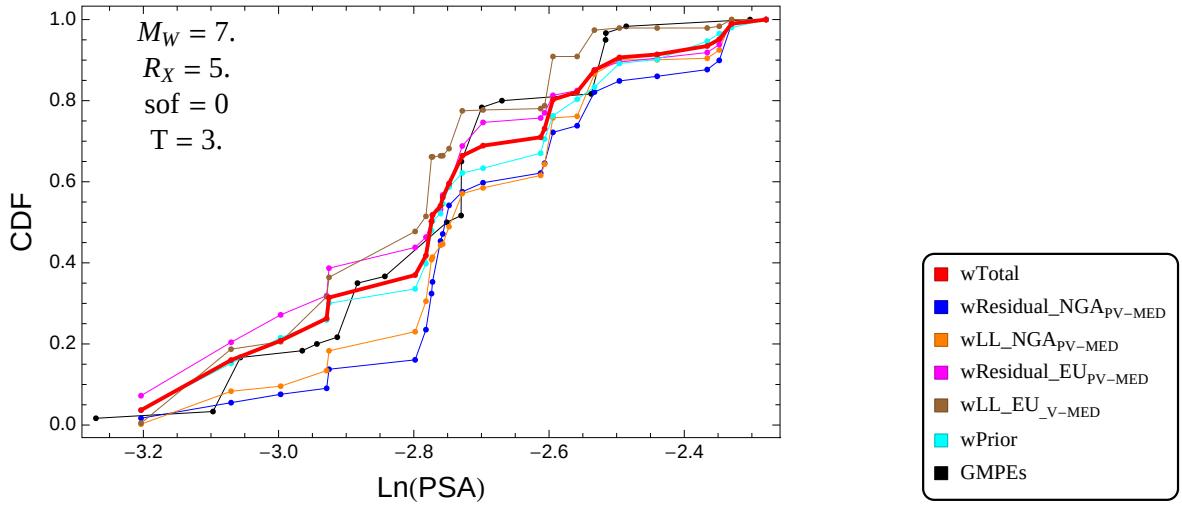



Figure 3.246: PVNGSv2: Cumulative distribution function of GMPEs (black) and selected models, for different sets of weights, for a scenario with $M = 7.$, $R_x = 5.$, $F = 0$, and $T = 3.$s

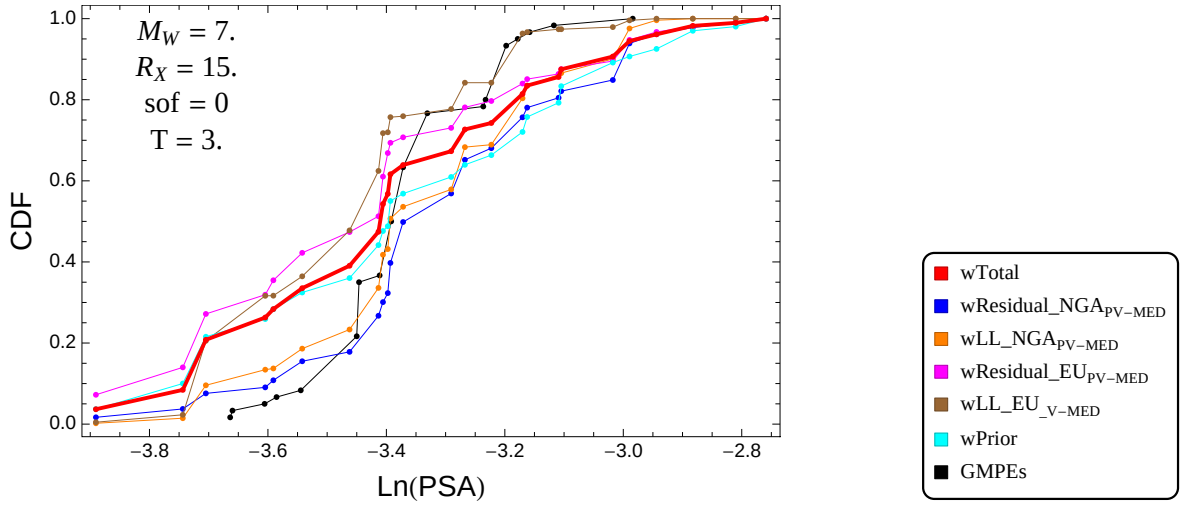



Figure 3.247: PVNGSv2: Cumulative distribution function of GMPEs (black) and selected models, for different sets of weights, for a scenario with $M = 7.$, $R_x = 15.$, $F = 0$, and $T = 3.$s

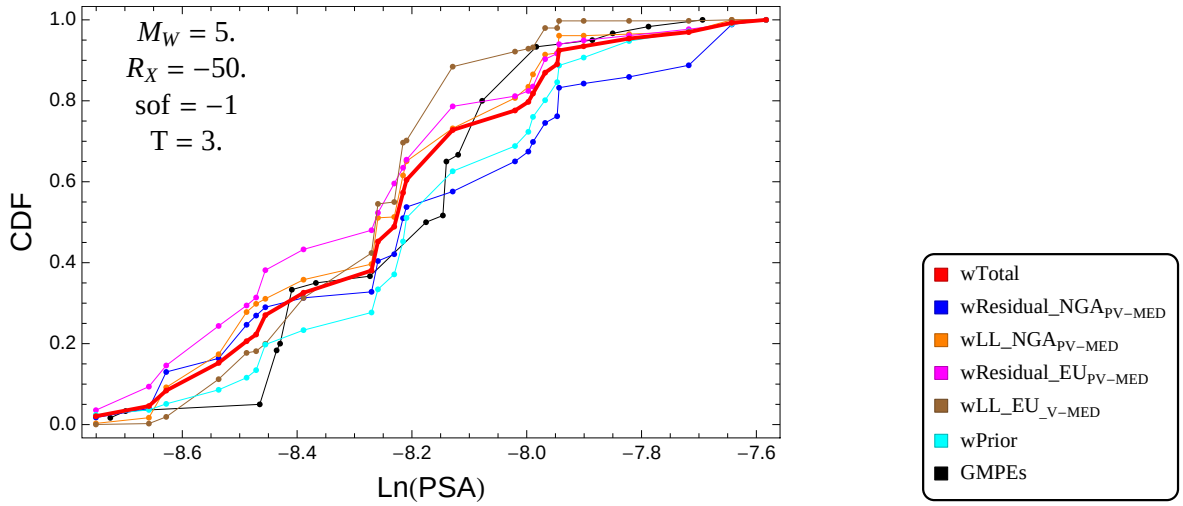



Figure 3.248: PVNGSv2: Cumulative distribution function of GMPEs (black) and selected models, for different sets of weights, for a scenario with $M = 5.$, $R_x = -50.$, $F = -1$, and $T = 3.$s

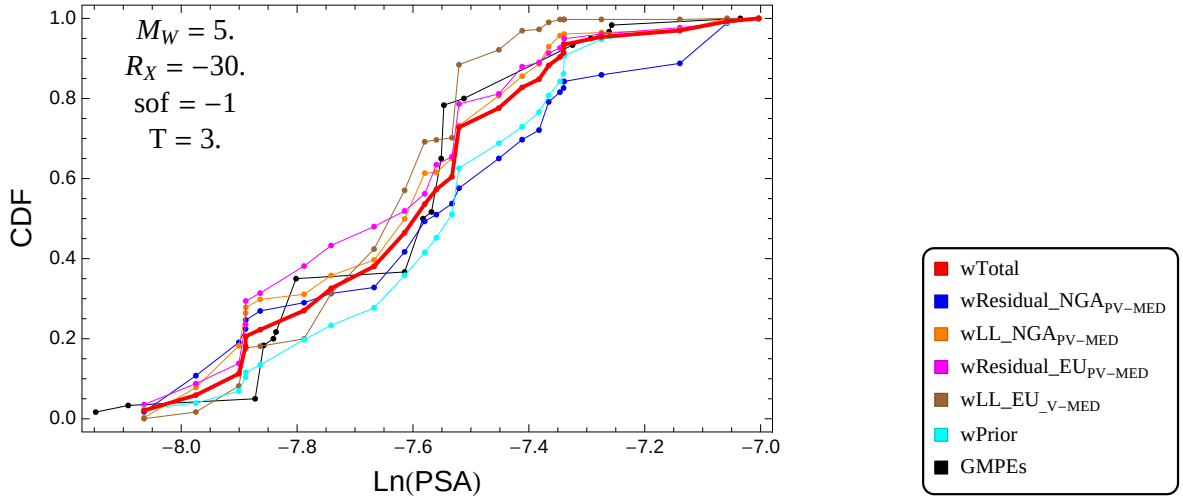



Figure 3.249: PVNGSv2: Cumulative distribution function of GMPEs (black) and selected models, for different sets of weights, for a scenario with $M = 5.$, $R_x = -30.$, $F = -1$, and $T = 3.$s

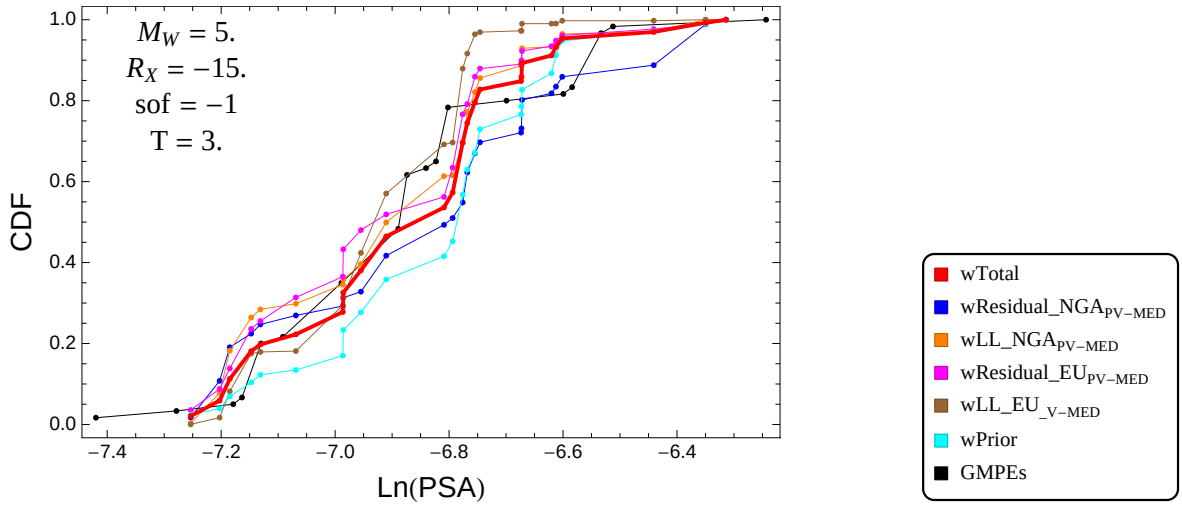



Figure 3.250: PVNGSv2: Cumulative distribution function of GMPEs (black) and selected models, for different sets of weights, for a scenario with $M = 5.$, $R_x = -15.$, $F = -1$, and $T = 3.$s

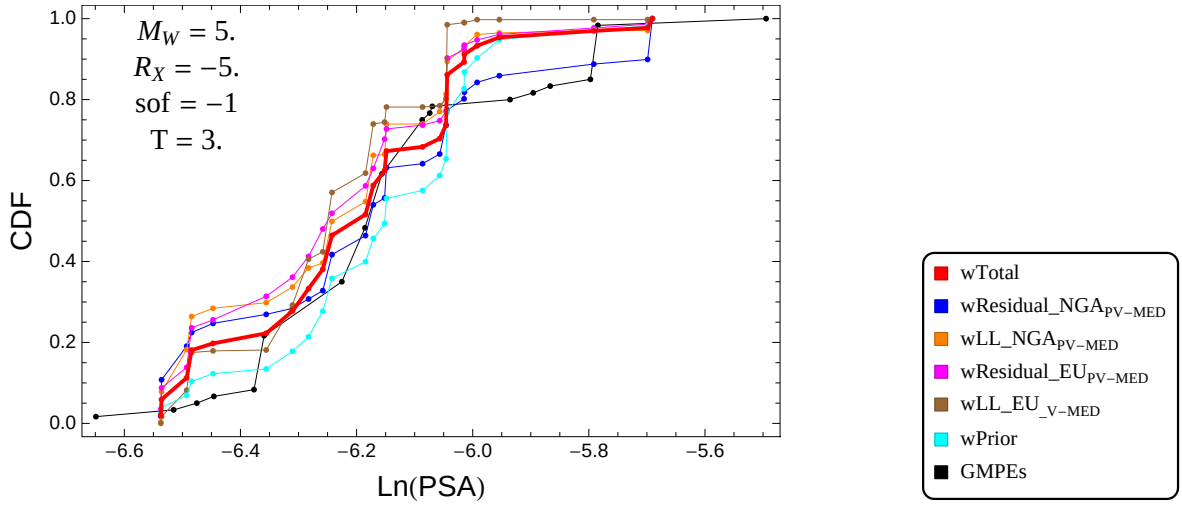



Figure 3.251: PVNGSv2: Cumulative distribution function of GMPEs (black) and selected models, for different sets of weights, for a scenario with $M = 5.$, $R_x = -5.$, $F = -1$, and $T = 3.$s

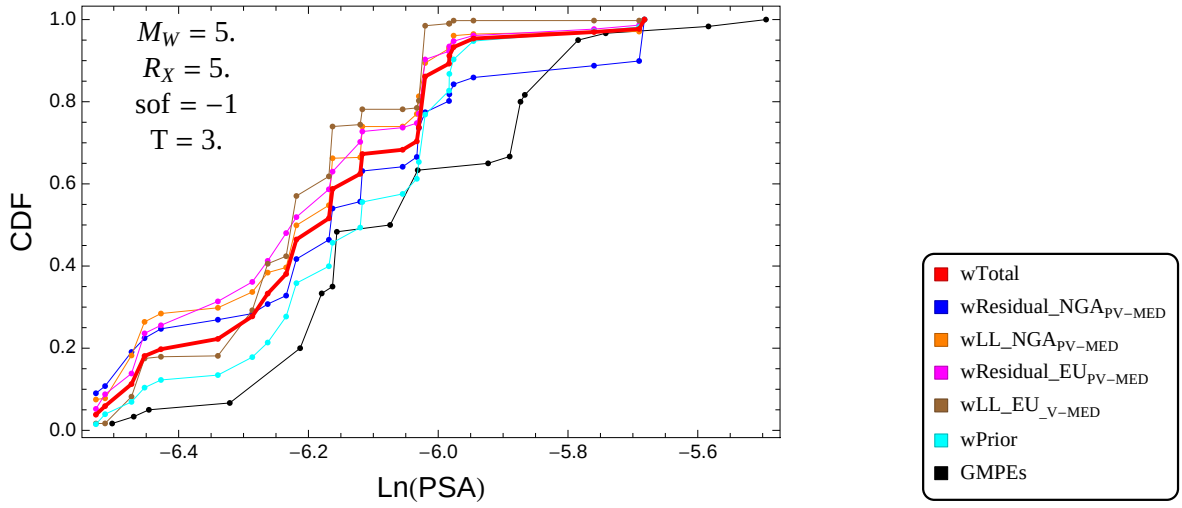



Figure 3.252: PVNGSv2: Cumulative distribution function of GMPEs (black) and selected models, for different sets of weights, for a scenario with $M = 5.$, $R_x = 5.$, $F = -1$, and $T = 3.$s

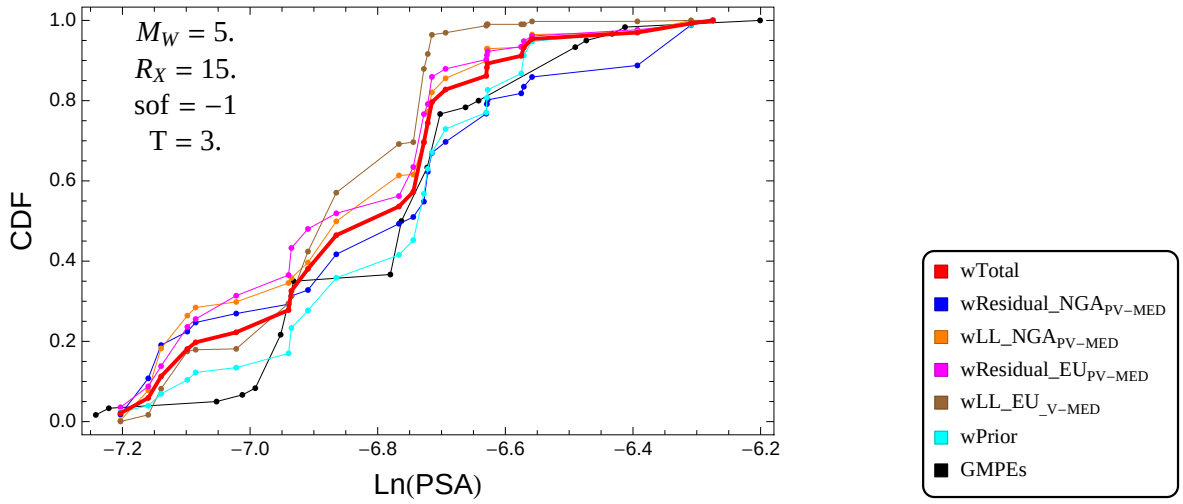



Figure 3.253: PVNGSv2: Cumulative distribution function of GMPEs (black) and selected models, for different sets of weights, for a scenario with $M = 5.$, $R_x = 15.$, $F = -1$, and $T = 3.$s

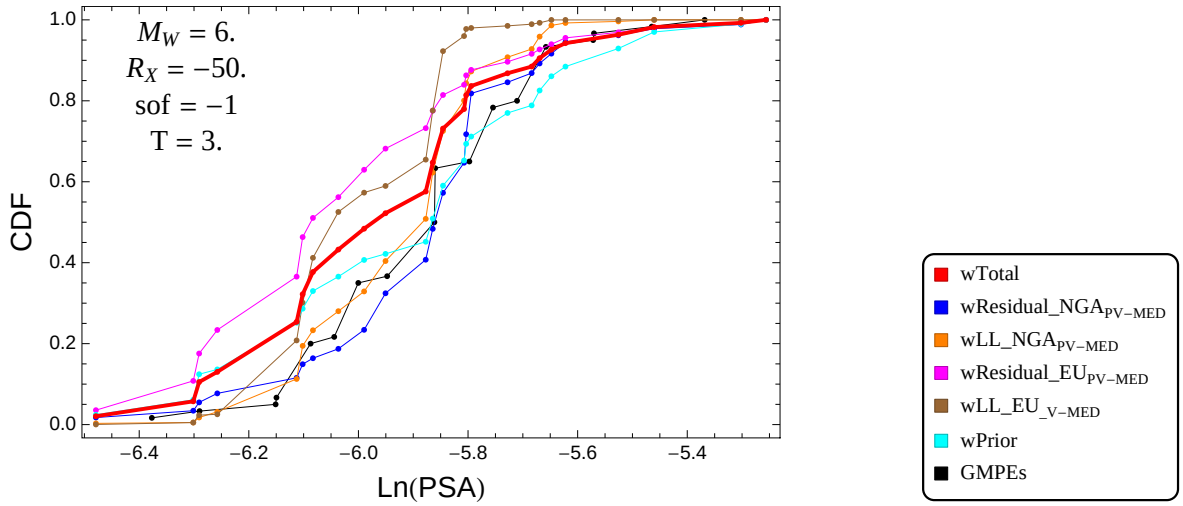



Figure 3.254: PVNGSv2: Cumulative distribution function of GMPEs (black) and selected models, for different sets of weights, for a scenario with $M = 6.$, $R_x = -50.$, $F = -1$, and $T = 3.$s

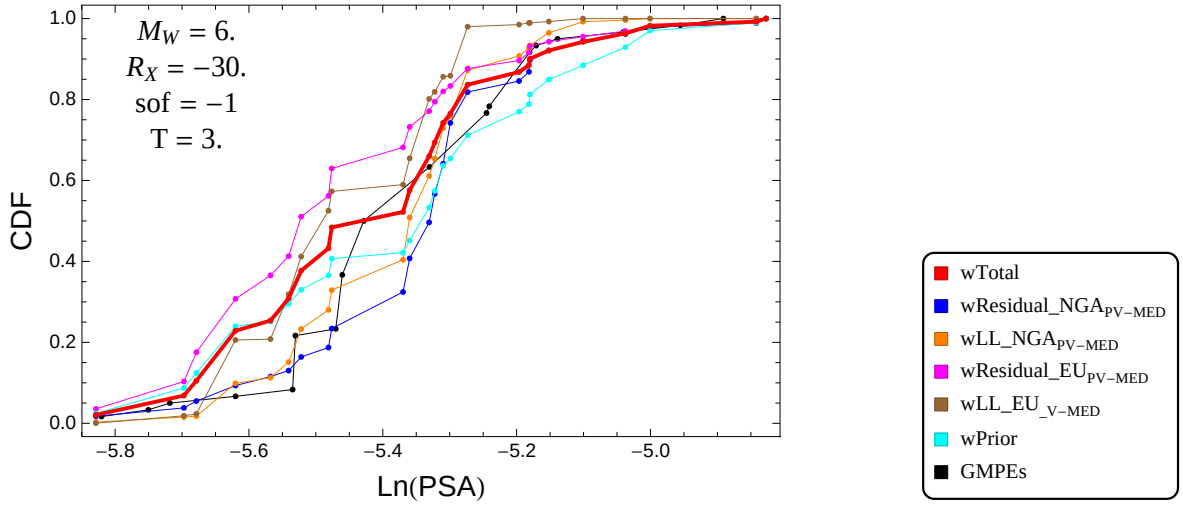



Figure 3.255: PVNGSv2: Cumulative distribution function of GMPEs (black) and selected models, for different sets of weights, for a scenario with $M = 6.$, $R_x = -30.$, $F = -1$, and $T = 3.$s

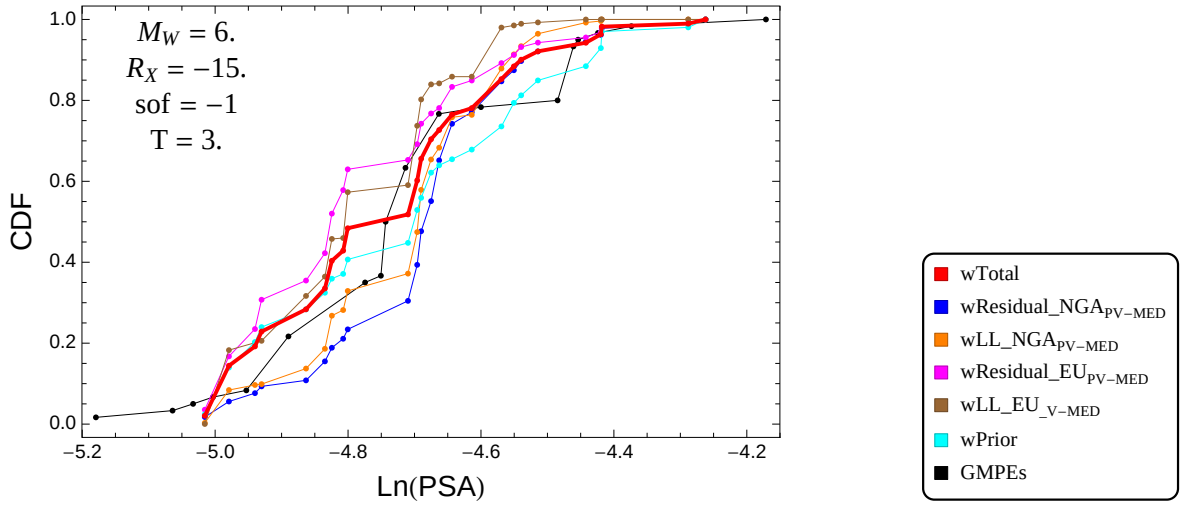



Figure 3.256: PVNGSv2: Cumulative distribution function of GMPEs (black) and selected models, for different sets of weights, for a scenario with $M = 6.$, $R_x = -15.$, $F = -1$, and $T = 3.$s

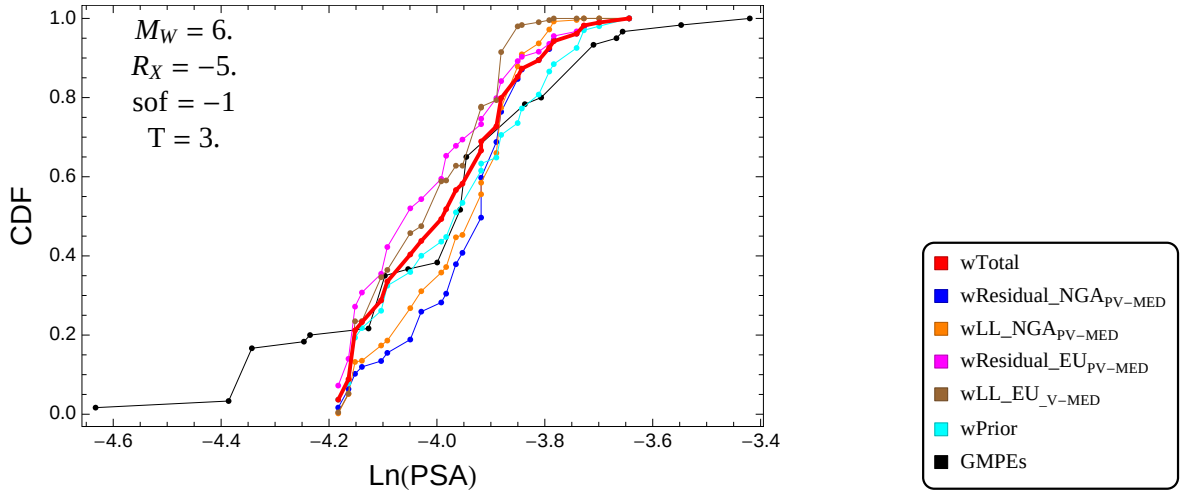



Figure 3.257: PVNGSv2: Cumulative distribution function of GMPEs (black) and selected models, for different sets of weights, for a scenario with $M = 6.$, $R_x = -5.$, $F = -1$, and $T = 3.$s

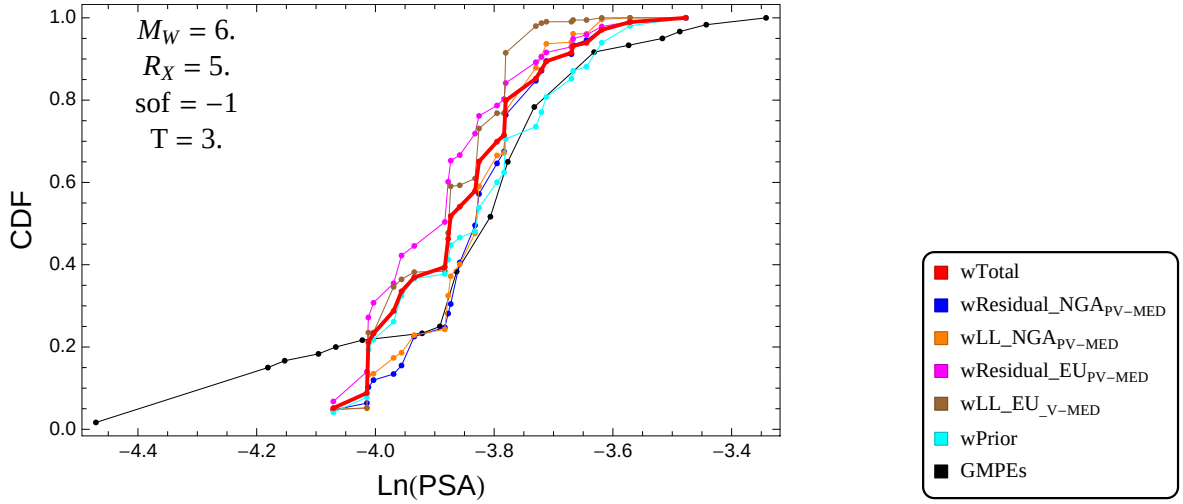



Figure 3.258: PVNGSv2: Cumulative distribution function of GMPEs (black) and selected models, for different sets of weights, for a scenario with $M = 6.$, $R_x = 5.$, $F = -1$, and $T = 3.$s

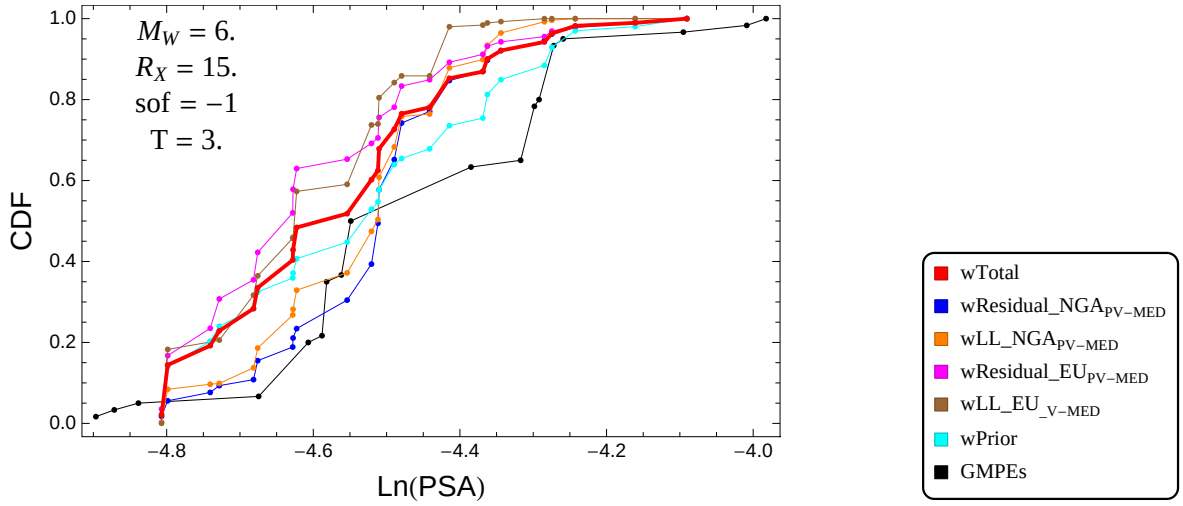



Figure 3.259: PVNGSv2: Cumulative distribution function of GMPEs (black) and selected models, for different sets of weights, for a scenario with $M = 6.$, $R_x = 15.$, $F = -1$, and $T = 3.$s

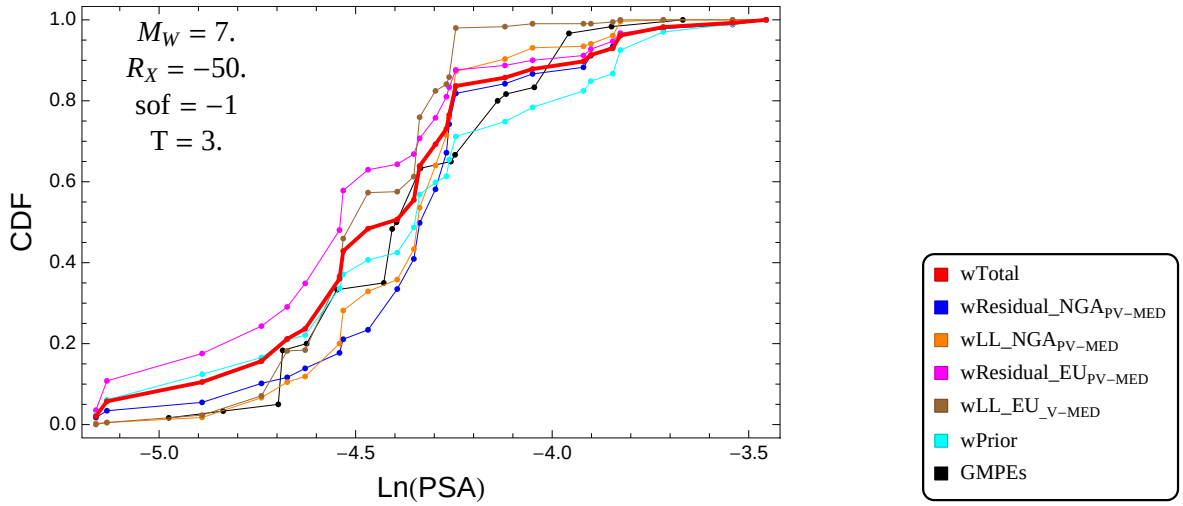



Figure 3.260: PVNGSv2: Cumulative distribution function of GMPEs (black) and selected models, for different sets of weights, for a scenario with $M = 7.$, $R_x = -50.$, $F = -1$, and $T = 3.$s

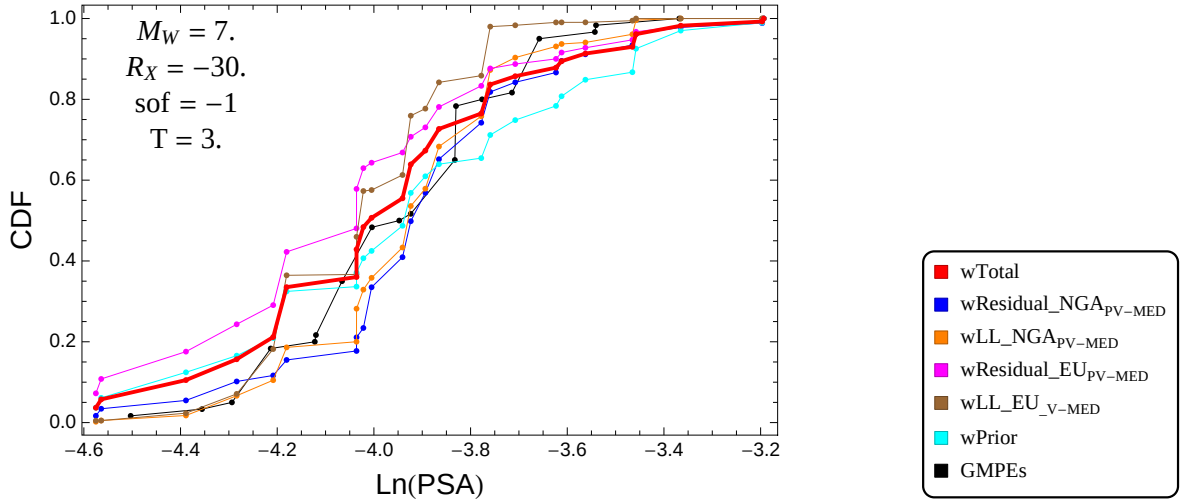



Figure 3.261: PVNGSv2: Cumulative distribution function of GMPEs (black) and selected models, for different sets of weights, for a scenario with $M = 7.$, $R_x = -30.$, $F = -1$, and $T = 3.$s

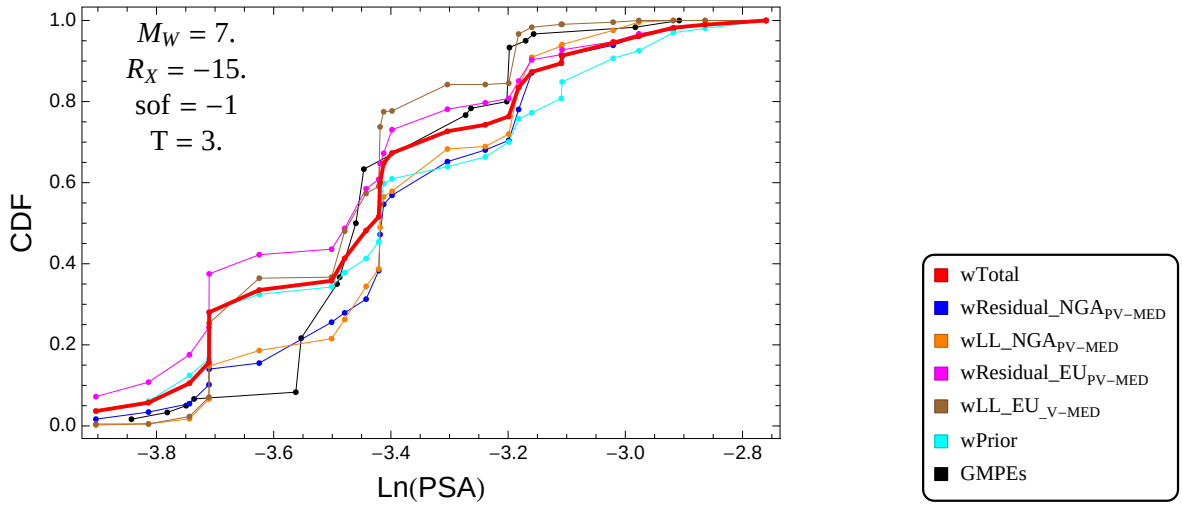



Figure 3.262: PVNGSv2: Cumulative distribution function of GMPEs (black) and selected models, for different sets of weights, for a scenario with $M = 7.$, $R_x = -15.$, $F = -1$, and $T = 3.$s

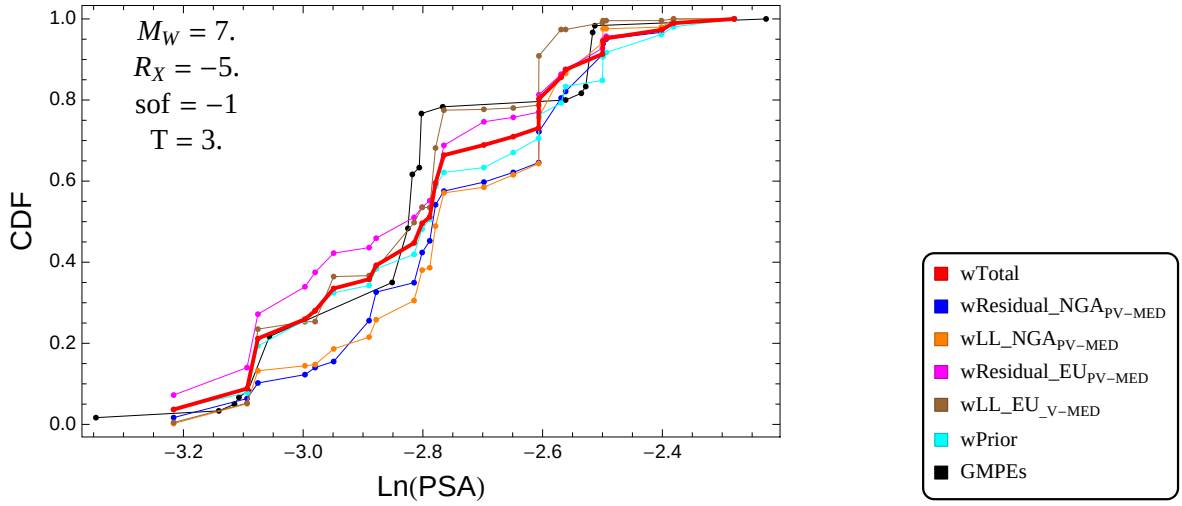



Figure 3.263: PVNGSv2: Cumulative distribution function of GMPEs (black) and selected models, for different sets of weights, for a scenario with $M = 7.$, $R_x = -5.$, $F = -1$, and $T = 3.$s

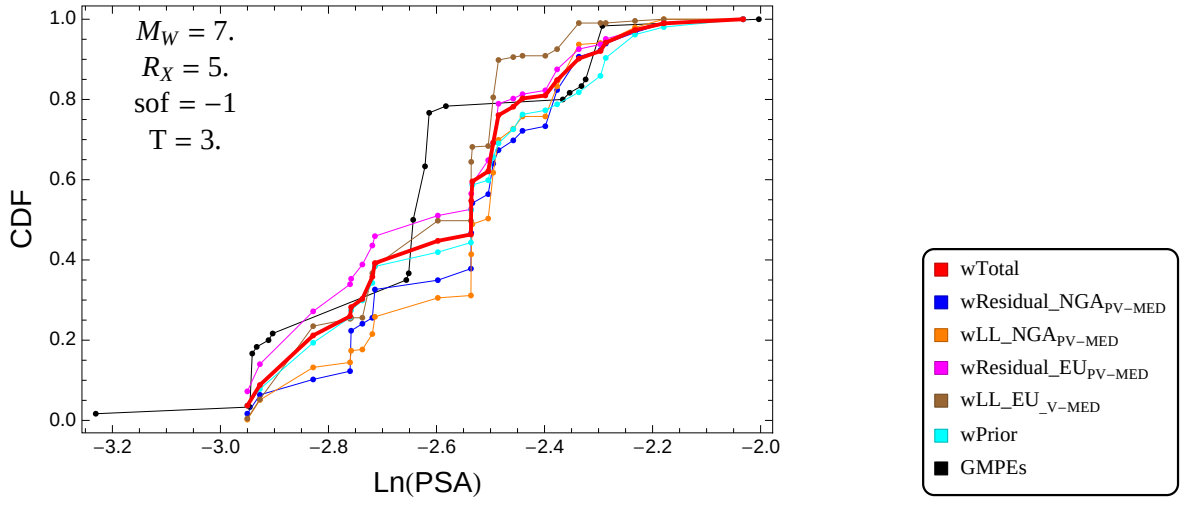



Figure 3.264: PVNGSv2: Cumulative distribution function of GMPEs (black) and selected models, for different sets of weights, for a scenario with $M = 7.$, $R_x = 5.$, $F = -1$, and $T = 3.$s

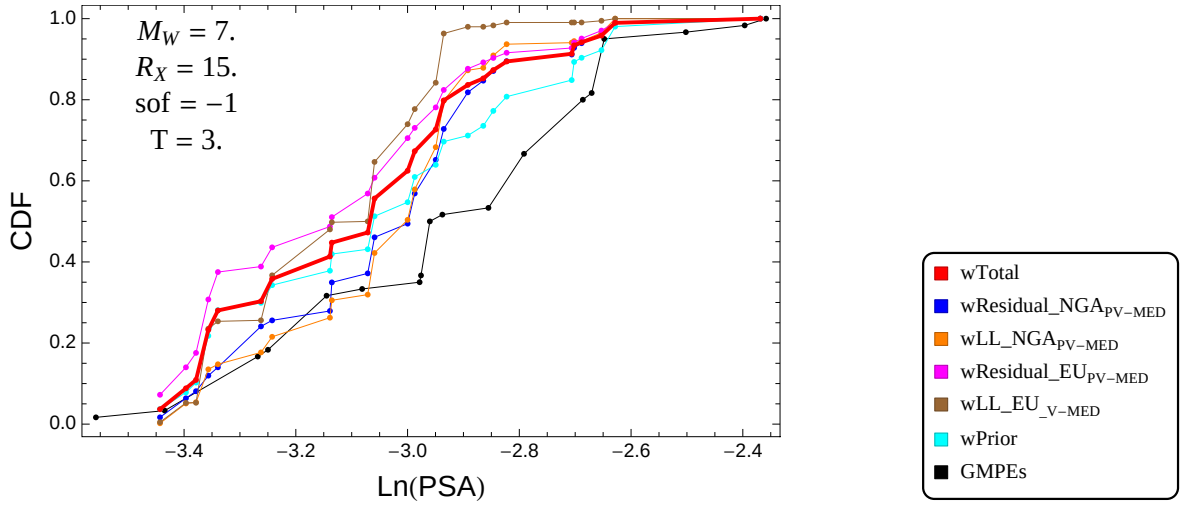



Figure 3.265: PVNGSv2: Cumulative distribution function of GMPEs (black) and selected models, for different sets of weights, for a scenario with $M = 7.$, $R_x = 15.$, $F = -1$, and $T = 3.$s

### 3.1.6 Quantile Plots vs. Distance

**T = 0.01s**

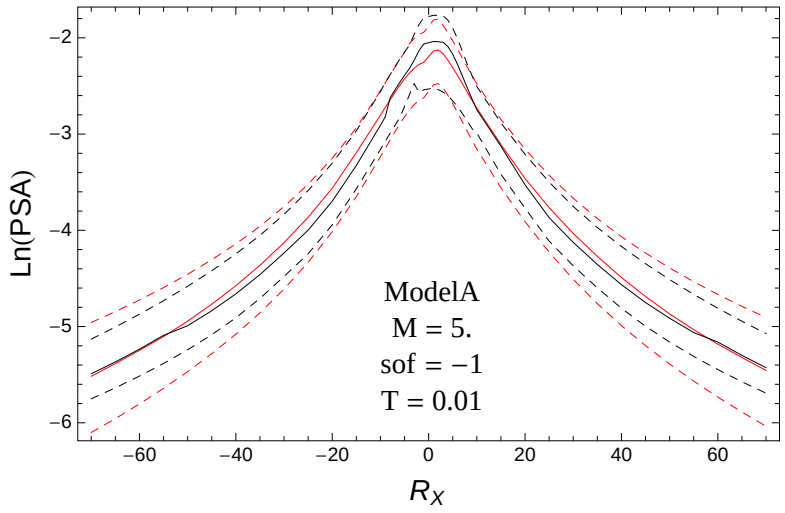



Figure 3.266: PVNGS2: Distance scaling of 0.05,0.5,0.95 quantile of the GMPE distribution (black) and the ModelA distribution (red) with total weights, for a scenario with $M = 5.$, $F = -1$, and $T = 0.01$.

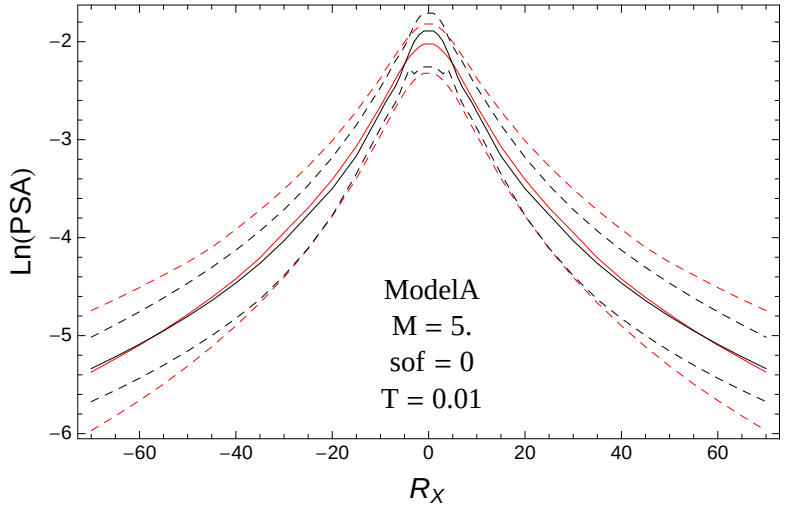



Figure 3.267: PVNGS2: Distance scaling of 0.05,0.5,0.95 quantile of the GMPE distribution (black) and the ModelA distribution (red) with total weights, for a scenario with $M = 5.$, $F = 0$, and $T = 0.01$.

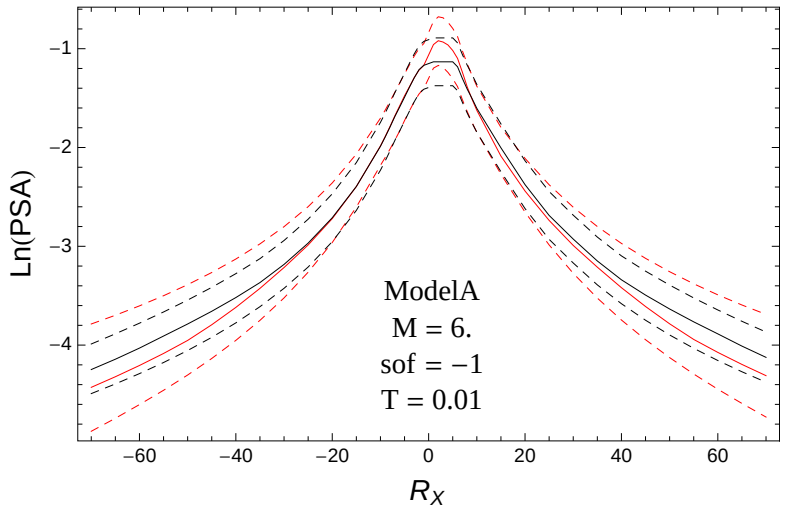



Figure 3.268: PVNGS2: Distance scaling of 0.05,0.5,0.95 quantile of the GMPE distribution (black) and the ModelA distribution (red) with total weights, for a scenario with $M = 6.$, $F = -1$, and $T = 0.01$.

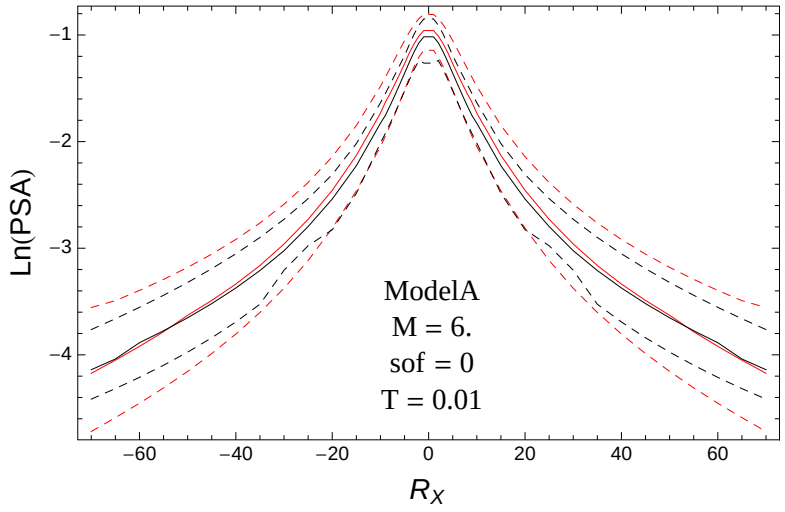



Figure 3.269: PVNGS2: Distance scaling of 0.05,0.5,0.95 quantile of the GMPE distribution (black) and the ModelA distribution (red) with total weights, for a scenario with $M = 6.$, $F = 0$, and $T = 0.01$.

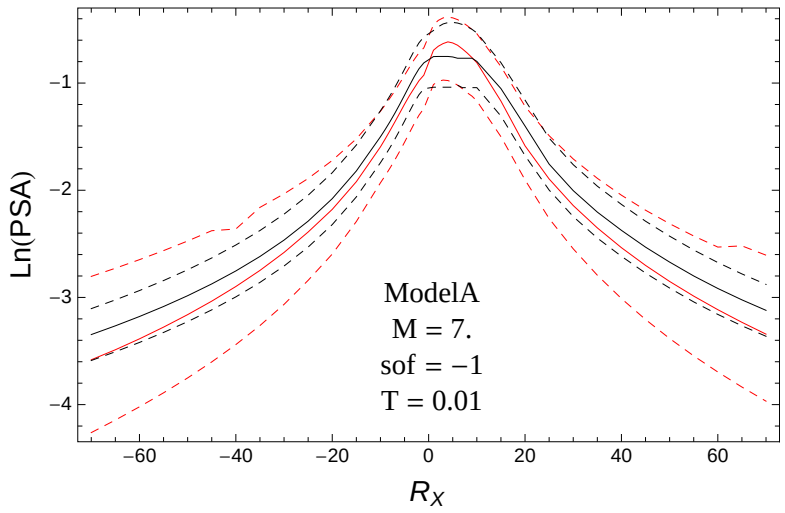



Figure 3.270: PVNGS2: Distance scaling of 0.05,0.5,0.95 quantile of the GMPE distribution (black) and the ModelA distribution (red) with total weights, for a scenario with $M = 7.$, $F = -1$, and $T = 0.01$.

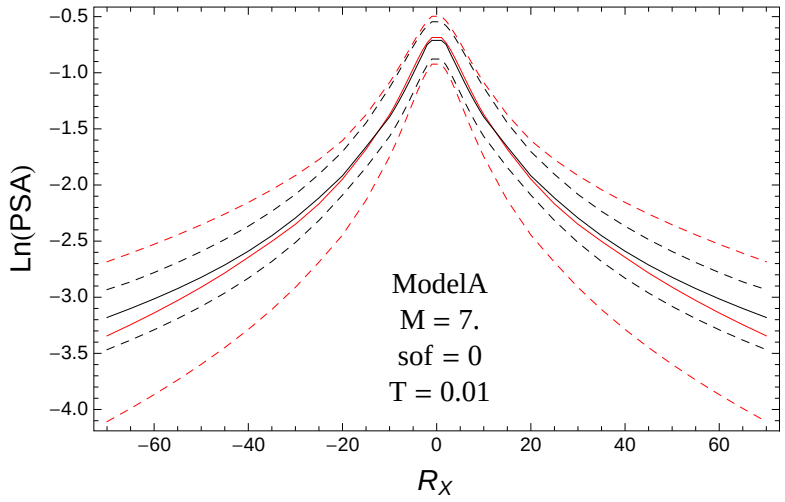



Figure 3.271: PVNGS2: Distance scaling of 0.05,0.5,0.95 quantile of the GMPE distribution (black) and the ModelA distribution (red) with total weights, for a scenario with $M = 7.$, $F = 0$, and $T = 0.01$.

**T = 0.2s**

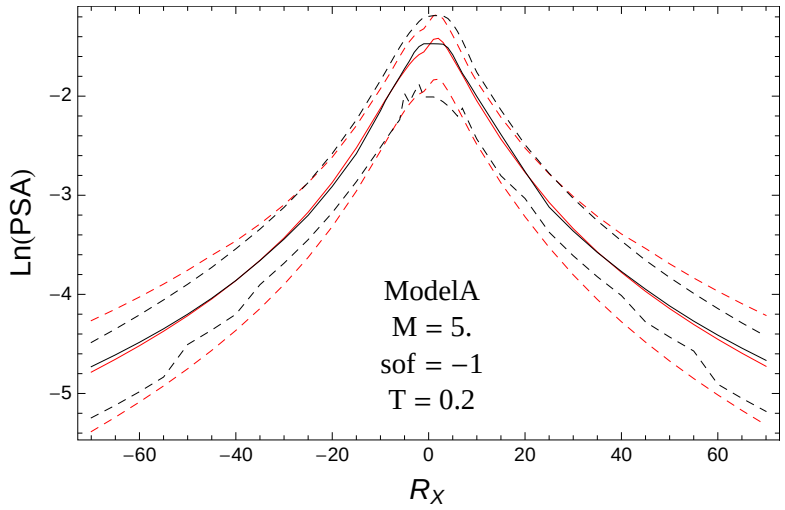



Figure 3.272: PVNGS2: Distance scaling of 0.05,0.5,0.95 quantile of the GMPE distribution (black) and the ModelA distribution (red) with total weights, for a scenario with $M = 5.$, $F = -1$, and $T = 0.2$.

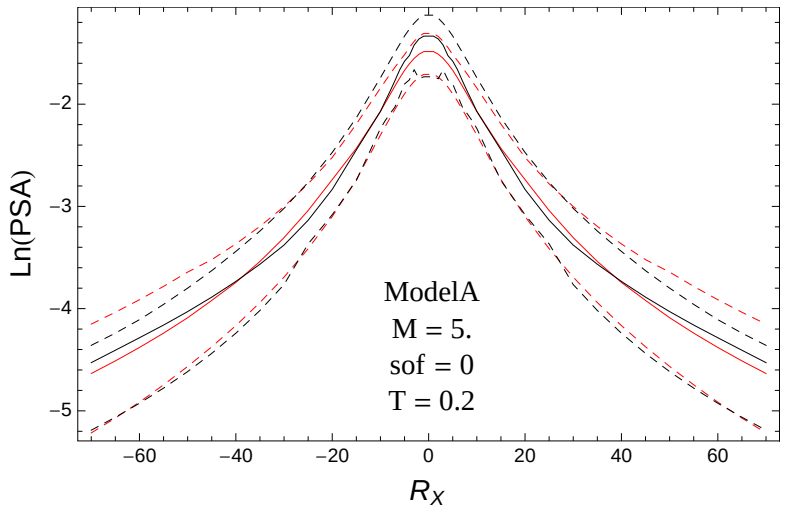



Figure 3.273: PVNGS2: Distance scaling of 0.05,0.5,0.95 quantile of the GMPE distribution (black) and the ModelA distribution (red) with total weights, for a scenario with $M = 5.$, $F = 0$, and $T = 0.2$.

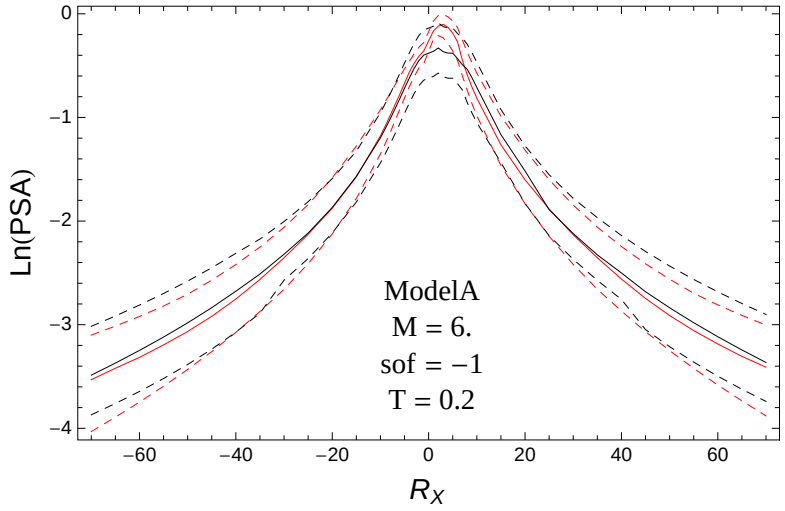



Figure 3.274: PVNGS2: Distance scaling of 0.05,0.5,0.95 quantile of the GMPE distribution (black) and the ModelA distribution (red) with total weights, for a scenario with $M = 6.$, $F = -1$, and $T = 0.2$.

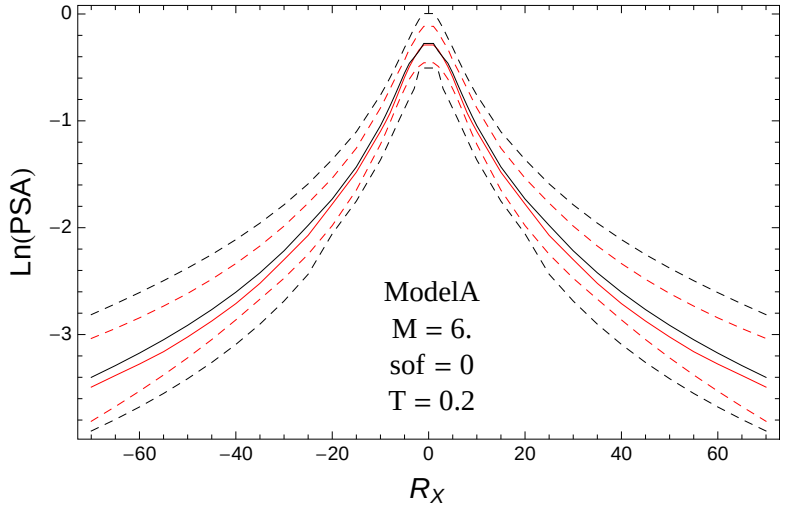



Figure 3.275: PVNGS2: Distance scaling of 0.05,0.5,0.95 quantile of the GMPE distribution (black) and the ModelA distribution (red) with total weights, for a scenario with $M = 6.$, $F = 0$, and $T = 0.2$.

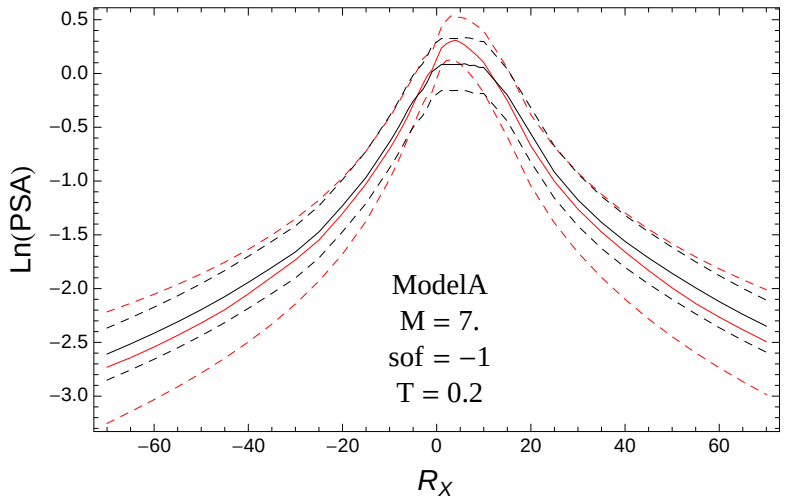



Figure 3.276: PVNGS2: Distance scaling of 0.05,0.5,0.95 quantile of the GMPE distribution (black) and the ModelA distribution (red) with total weights, for a scenario with $M = 7.$, $F = -1$, and $T = 0.2$.

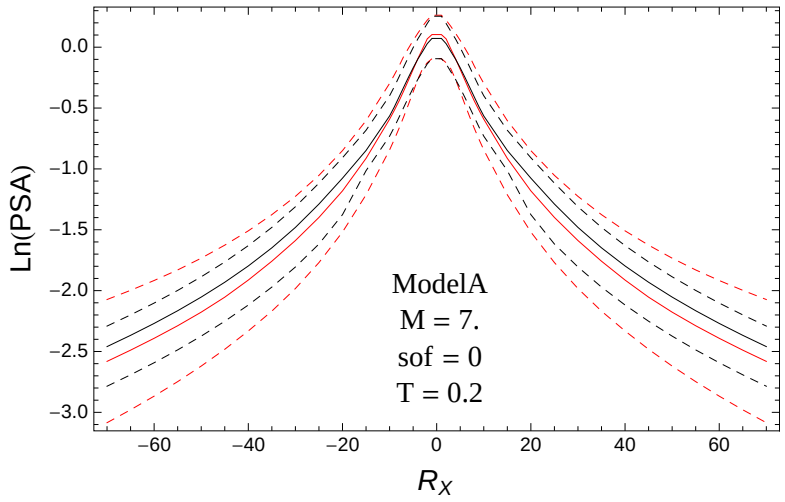



Figure 3.277: PVNGS2: Distance scaling of 0.05,0.5,0.95 quantile of the GMPE distribution (black) and the ModelA distribution (red) with total weights, for a scenario with $M = 7.$, $F = 0$, and $T = 0.2$.

**T = 0.5s**

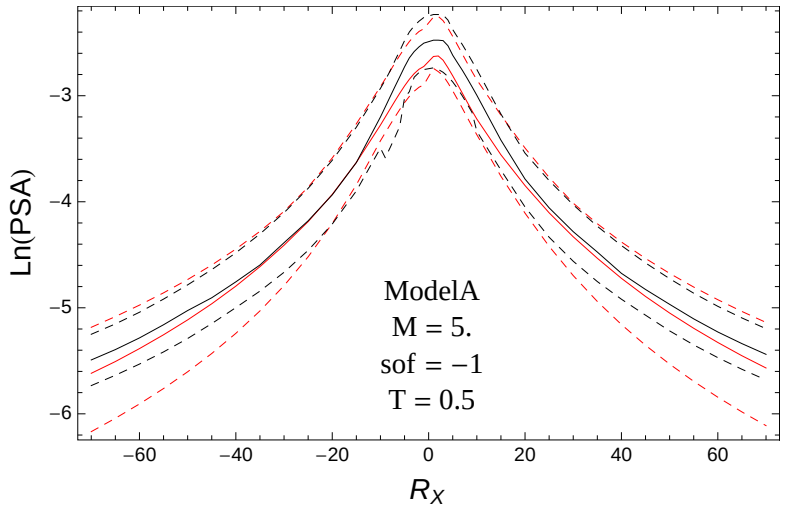



Figure 3.278: PVNGS2: Distance scaling of 0.05,0.5,0.95 quantile of the GMPE distribution (black) and the ModelA distribution (red) with total weights, for a scenario with $M = 5.$, $F = -1$, and $T = 0.5$.

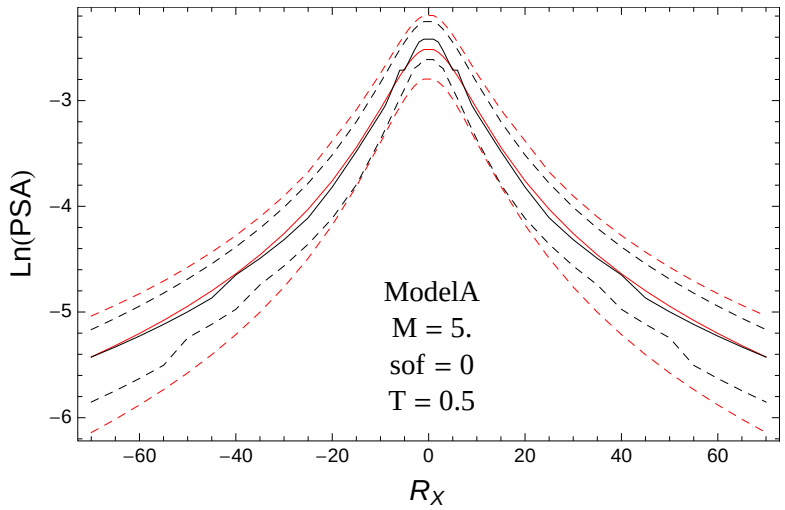



Figure 3.279: PVNGS2: Distance scaling of 0.05,0.5,0.95 quantile of the GMPE distribution (black) and the ModelA distribution (red) with total weights, for a scenario with $M = 5.$, $F = 0$, and $T = 0.5$.

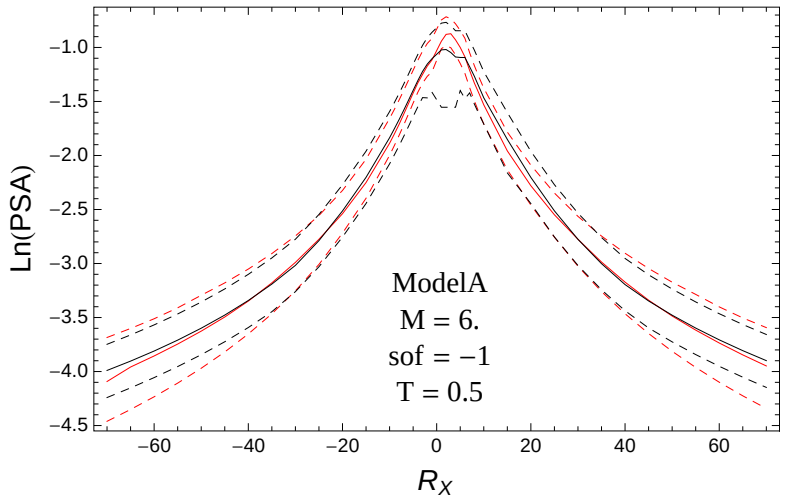



Figure 3.280: PVNGS2: Distance scaling of 0.05,0.5,0.95 quantile of the GMPE distribution (black) and the ModelA distribution (red) with total weights, for a scenario with $M = 6.$, $F = -1$, and $T = 0.5$.

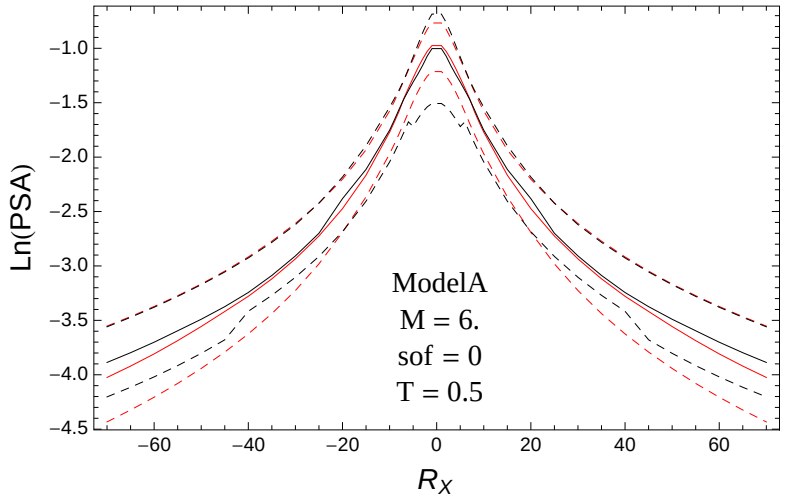



Figure 3.281: PVNGS2: Distance scaling of 0.05,0.5,0.95 quantile of the GMPE distribution (black) and the ModelA distribution (red) with total weights, for a scenario with $M = 6.$, $F = 0$, and $T = 0.5$.

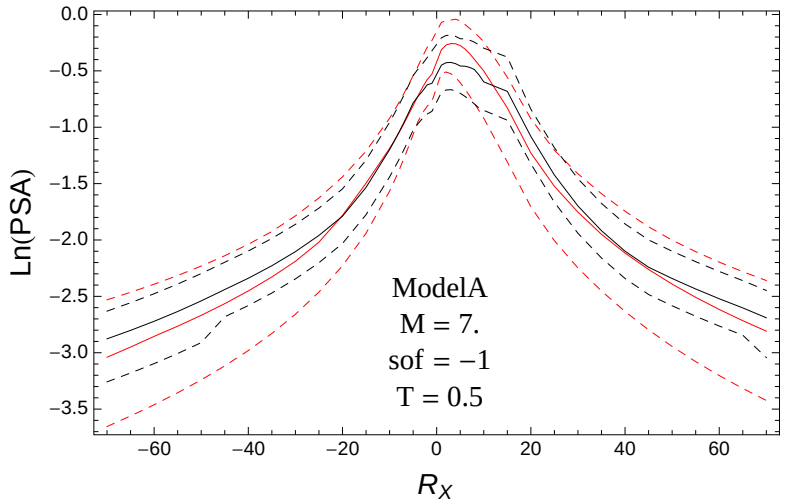



Figure 3.282: PVNGS2: Distance scaling of 0.05,0.5,0.95 quantile of the GMPE distribution (black) and the ModelA distribution (red) with total weights, for a scenario with $M = 7.$, $F = -1$, and $T = 0.5$.

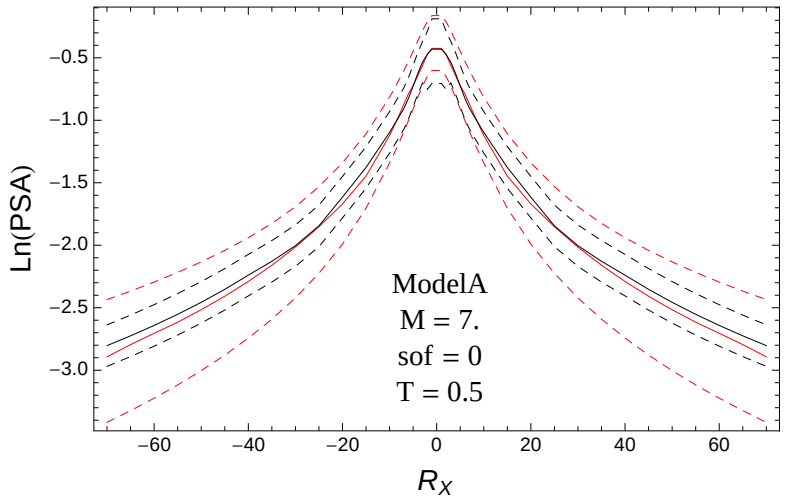



Figure 3.283: PVNGS2: Distance scaling of 0.05,0.5,0.95 quantile of the GMPE distribution (black) and the ModelA distribution (red) with total weights, for a scenario with $M = 7.$, $F = 0$, and $T = 0.5$.

**T = 1.s**

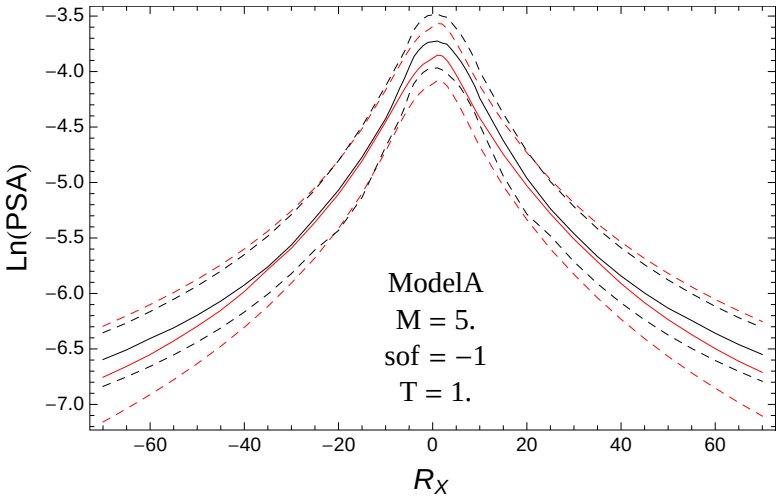



Figure 3.284: PVNGS2: Distance scaling of 0.05,0.5,0.95 quantile of the GMPE distribution (black) and the ModelA distribution (red) with total weights, for a scenario with $M = 5.$, $F = -1$, and $T = 1.$.

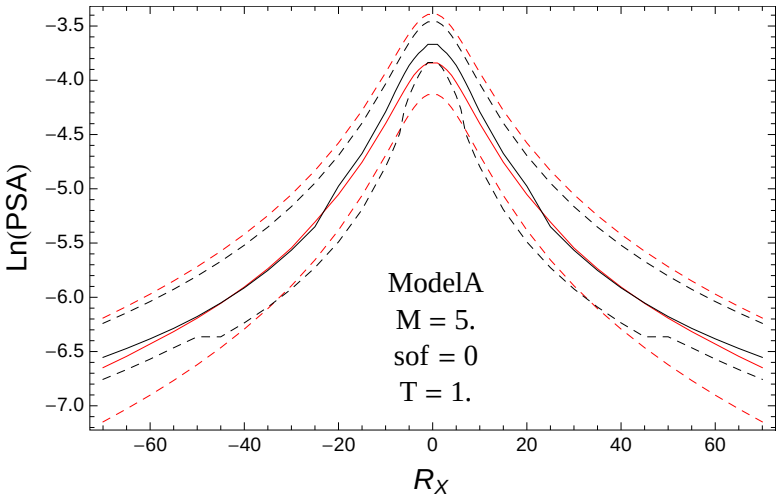



Figure 3.285: PVNGS2: Distance scaling of 0.05,0.5,0.95 quantile of the GMPE distribution (black) and the ModelA distribution (red) with total weights, for a scenario with $M = 5.$, $F = 0$, and $T = 1.$.

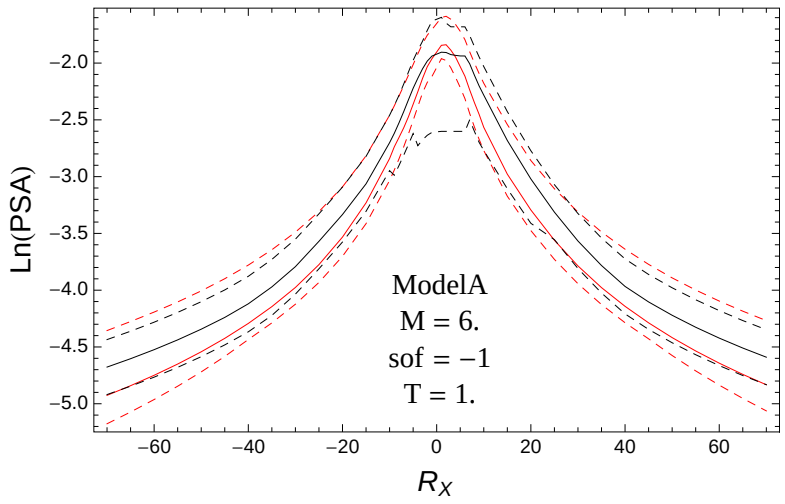



Figure 3.286: PVNGS2: Distance scaling of 0.05,0.5,0.95 quantile of the GMPE distribution (black) and the ModelA distribution (red) with total weights, for a scenario with $M = 6.$, $F = -1$, and $T = 1.$.

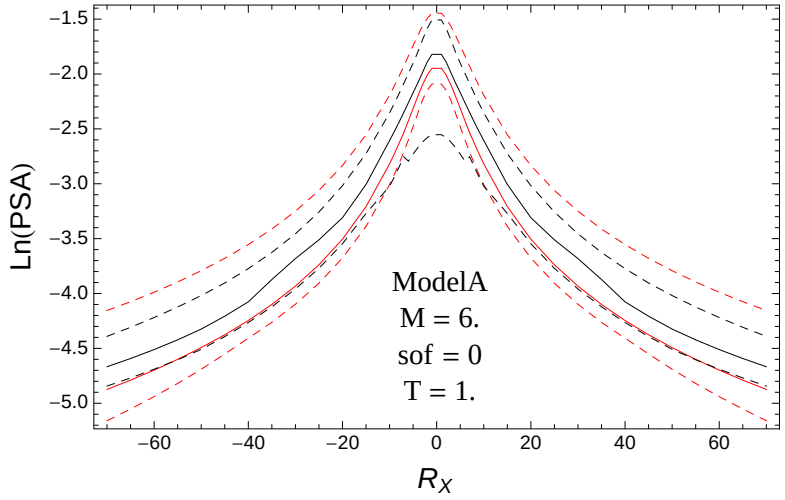



Figure 3.287: PVNGS2: Distance scaling of 0.05,0.5,0.95 quantile of the GMPE distribution (black) and the ModelA distribution (red) with total weights, for a scenario with $M = 6.$, $F = 0$, and $T = 1.$.

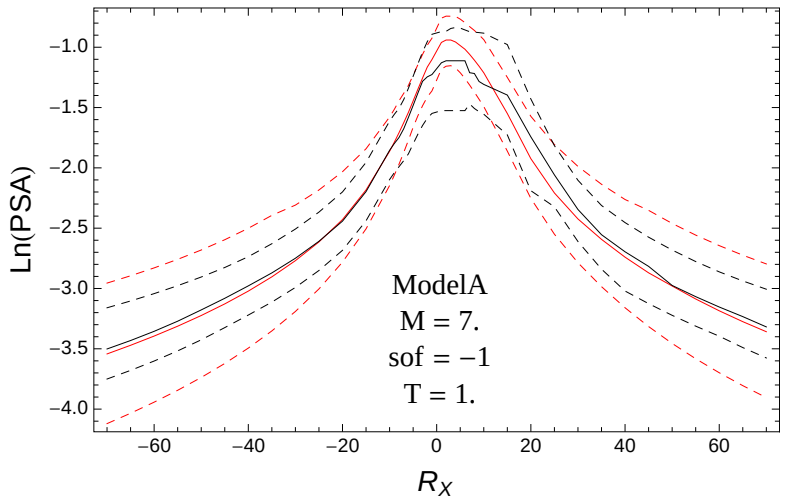



Figure 3.288: PVNGS2: Distance scaling of 0.05,0.5,0.95 quantile of the GMPE distribution (black) and the ModelA distribution (red) with total weights, for a scenario with $M = 7.$, $F = -1$, and $T = 1.$.

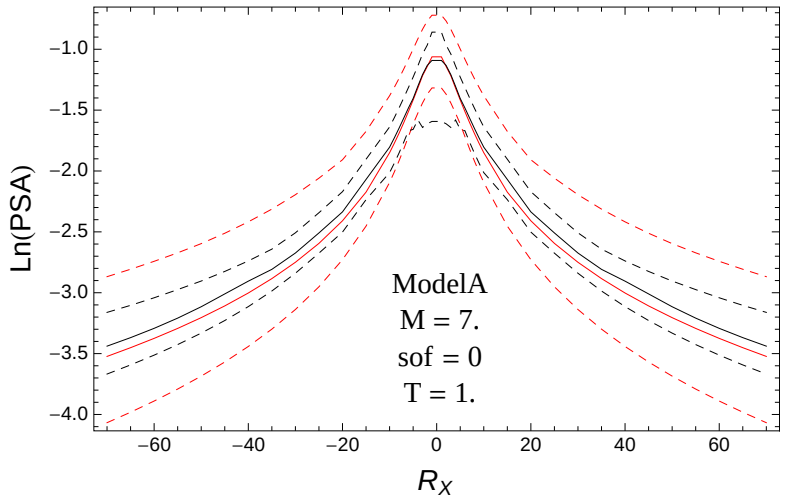



Figure 3.289: PVNGS2: Distance scaling of 0.05,0.5,0.95 quantile of the GMPE distribution (black) and the ModelA distribution (red) with total weights, for a scenario with $M = 7.$, $F = 0$, and $T = 1.$.

**T = 3.s**

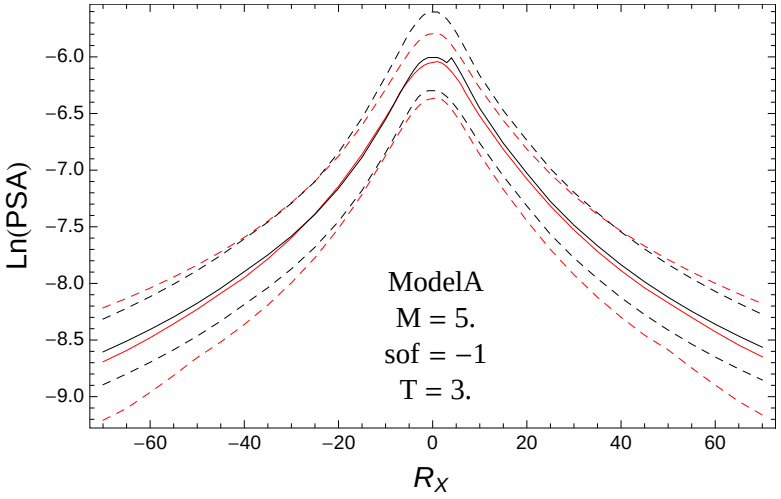



Figure 3.290: PVNGS2: Distance scaling of 0.05,0.5,0.95 quantile of the GMPE distribution (black) and the ModelA distribution (red) with total weights, for a scenario with $M = 5.$, $F = -1$, and $T = 3.$.

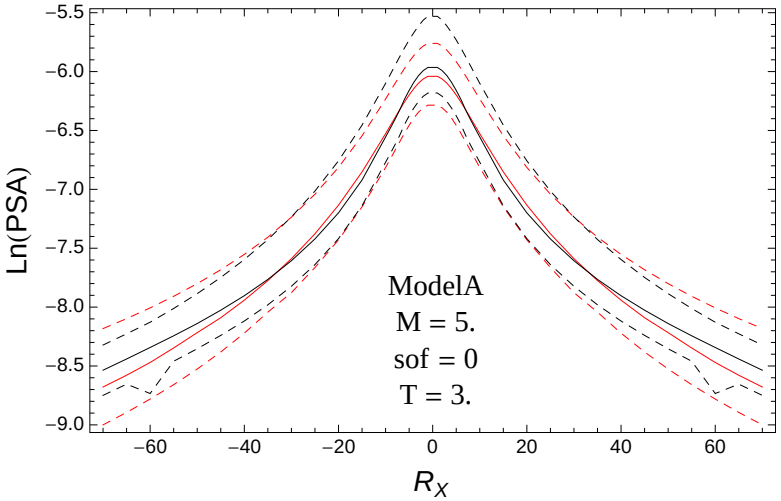



Figure 3.291: PVNGS2: Distance scaling of 0.05,0.5,0.95 quantile of the GMPE distribution (black) and the ModelA distribution (red) with total weights, for a scenario with $M = 5.$, $F = 0$, and $T = 3.$.

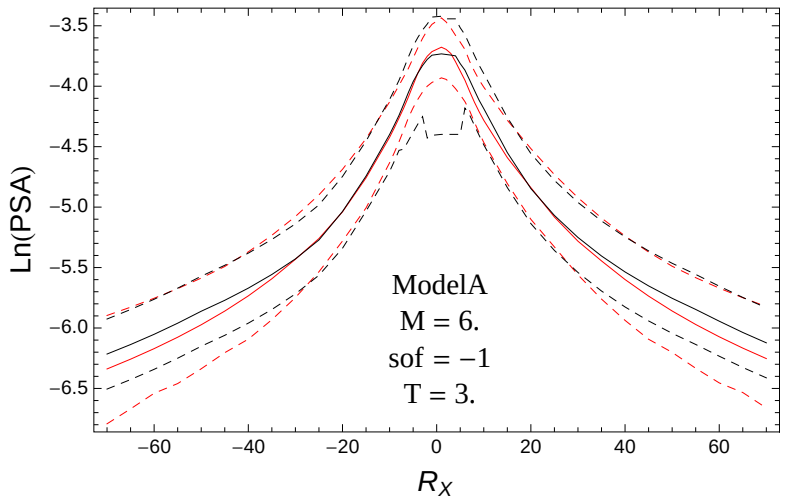



Figure 3.292: PVNGS2: Distance scaling of 0.05,0.5,0.95 quantile of the GMPE distribution (black) and the ModelA distribution (red) with total weights, for a scenario with $M = 6.$, $F = -1$, and $T = 3.$.

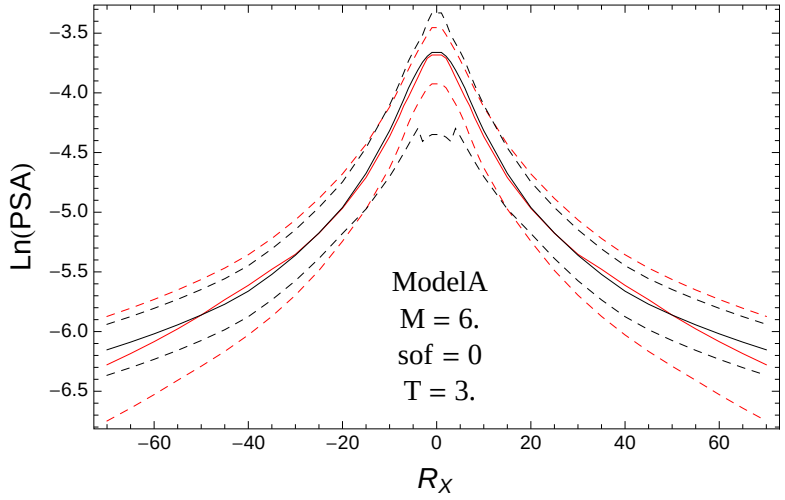



Figure 3.293: PVNGS2: Distance scaling of 0.05,0.5,0.95 quantile of the GMPE distribution (black) and the ModelA distribution (red) with total weights, for a scenario with $M = 6.$, $F = 0$, and $T = 3.$.

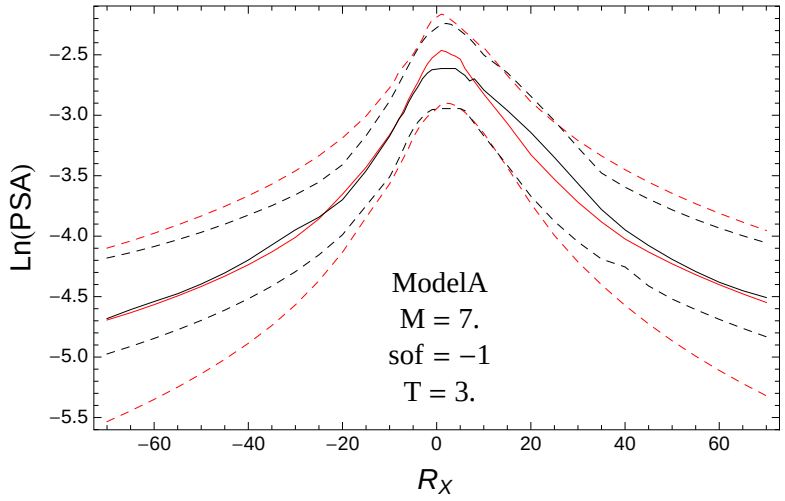



Figure 3.294: PVNGS2: Distance scaling of 0.05,0.5,0.95 quantile of the GMPE distribution (black) and the ModelA distribution (red) with total weights, for a scenario with $M = 7.$, $F = -1$, and $T = 3.$.

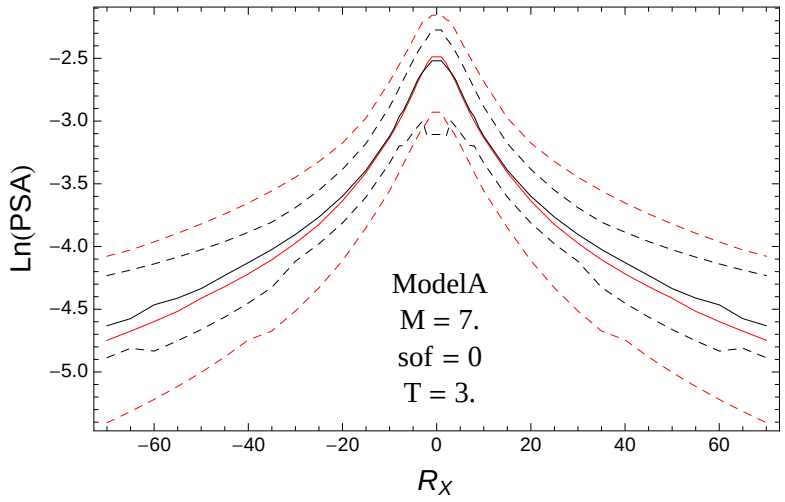



Figure 3.295: PVNGS2: Distance scaling of 0.05,0.5,0.95 quantile of the GMPE distribution (black) and the ModelA distribution (red) with total weights, for a scenario with $M = 7.$, $F = 0$, and $T = 3.$.

### 3.1.7 Quantile Plots vs. Distance with GMPEs

**T = 0.01s**

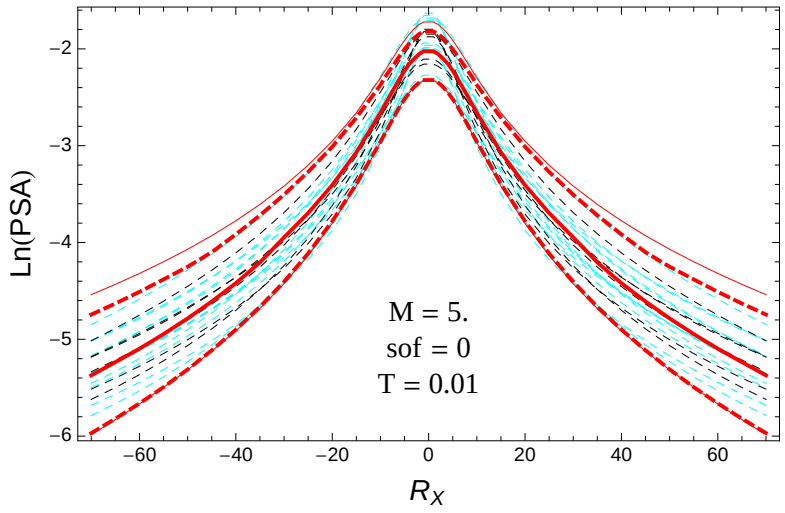



Figure 3.296: PVNGSv2: Distance scaling of the original GMPEs (dashed black), the original GMPEs with uncertainty model (dashed cyan) and 0.05,0.5,0.95 quantile of the ModelA distribution (red) with total weights, for a scenario with $M = 5.$, $F = 0$, and $T = 0.01$s.

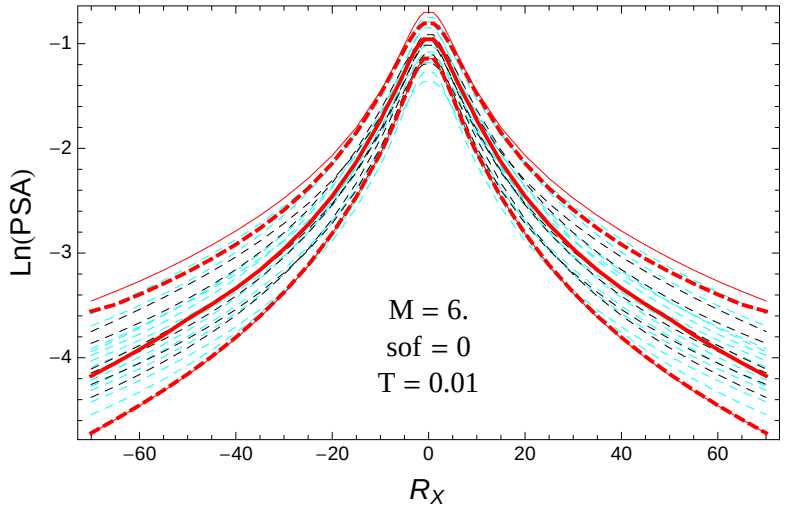



Figure 3.297: PVNGSv2: Distance scaling of the original GMPEs (dashed black), the original GMPEs with uncertainty model (dashed cyan) and 0.05,0.5,0.95 quantile of the ModelA distribution (red) with total weights, for a scenario with $M = 6.$, $F = 0$, and $T = 0.01$s.

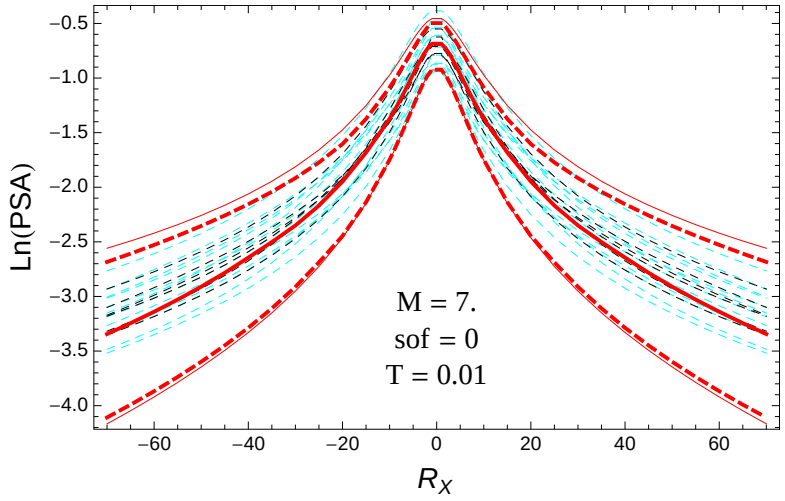



Figure 3.298: PVNGSv2: Distance scaling of the original GMPEs (dashed black), the original GMPEs with uncertainty model (dashed cyan) and 0.05,0.5,0.95 quantile of the ModelA distribution (red) with total weights, for a scenario with $M = 7.$, $F = 0$, and $T = 0.01$s.

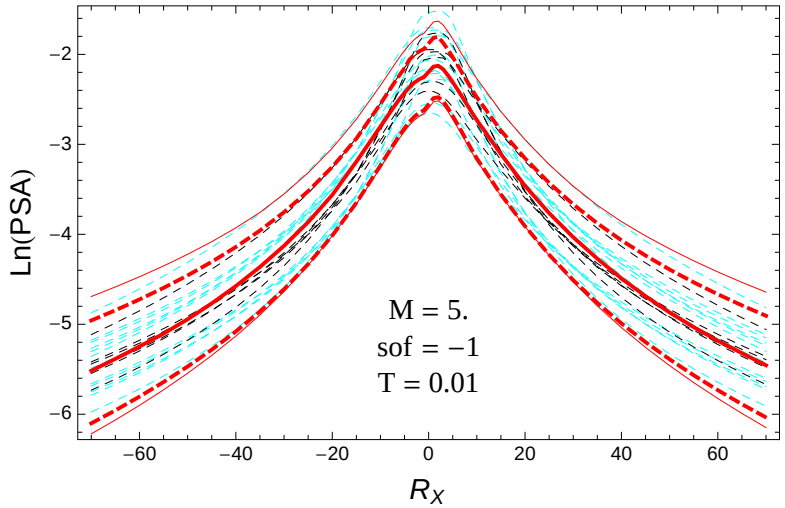



Figure 3.299: PVNGSv2: Distance scaling of the original GMPEs (dashed black), the original GMPEs with uncertainty model (dashed cyan) and 0.05,0.5,0.95 quantile of the ModelA distribution (red) with total weights, for a scenario with $M = 5.$, $F = -1$, and $T = 0.01$s.

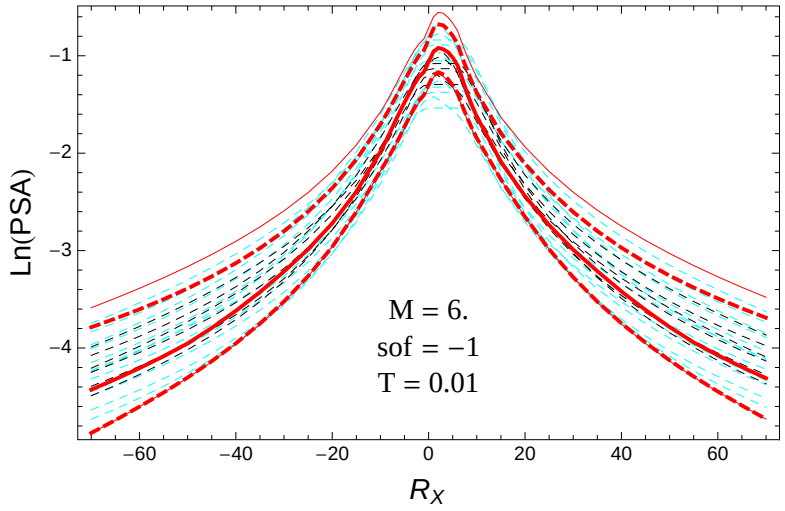



Figure 3.300: PVNGSv2: Distance scaling of the original GMPEs (dashed black), the original GMPEs with uncertainty model (dashed cyan) and 0.05,0.5,0.95 quantile of the ModelA distribution (red) with total weights, for a scenario with $M = 6.$, $F = -1$, and $T = 0.01$s.

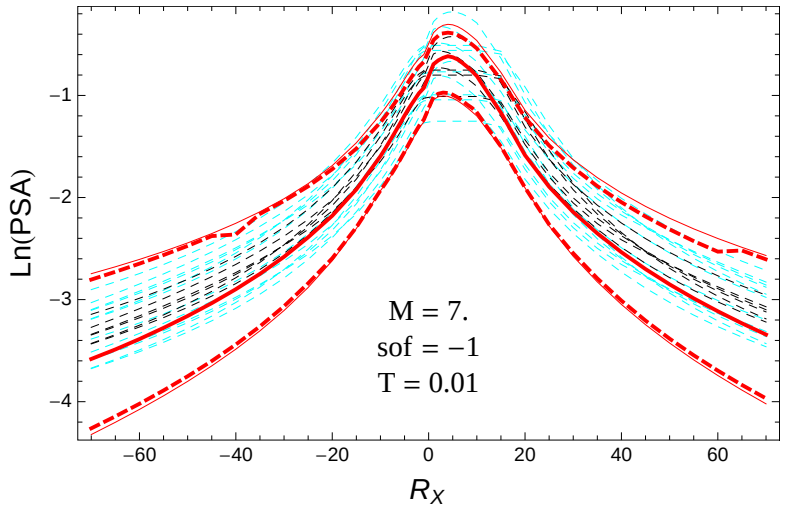



Figure 3.301: PVNGSv2: Distance scaling of the original GMPEs (dashed black), the original GMPEs with uncertainty model (dashed cyan) and 0.05,0.5,0.95 quantile of the ModelA distribution (red) with total weights, for a scenario with $M = 7.$, $F = -1$, and $T = 0.01$s.

**T = 0.2s**

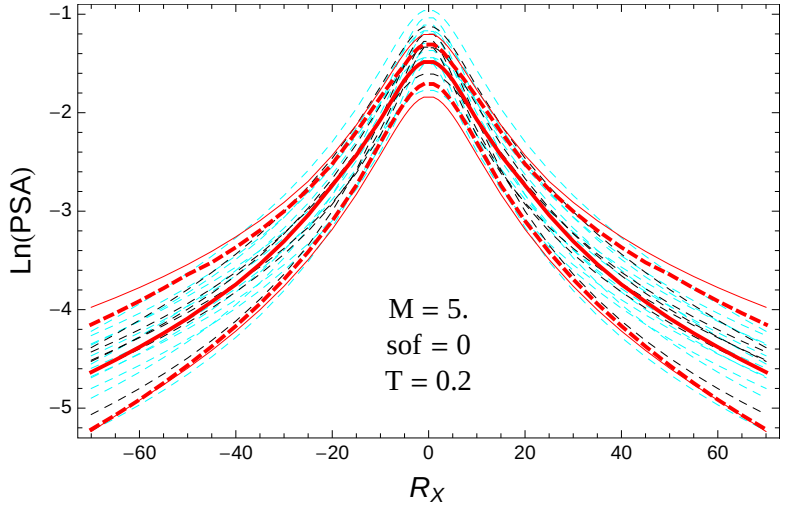



Figure 3.302: PVNGSv2: Distance scaling of the original GMPEs (dashed black), the original GMPEs with uncertainty model (dashed cyan) and 0.05,0.5,0.95 quantile of the ModelA distribution (red) with total weights, for a scenario with $M = 5.$, $F = 0$, and $T = 0.2$s.

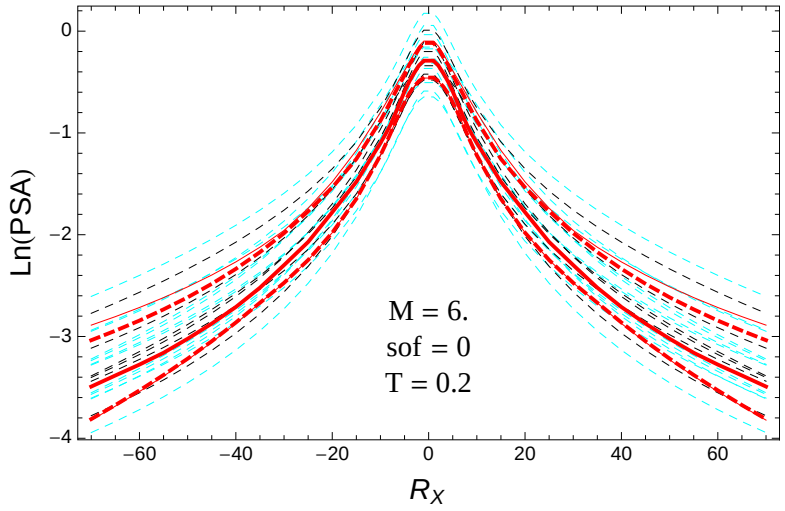



Figure 3.303: PVNGSv2: Distance scaling of the original GMPEs (dashed black), the original GMPEs with uncertainty model (dashed cyan) and 0.05,0.5,0.95 quantile of the ModelA distribution (red) with total weights, for a scenario with $M = 6.$, $F = 0$, and $T = 0.2$s.

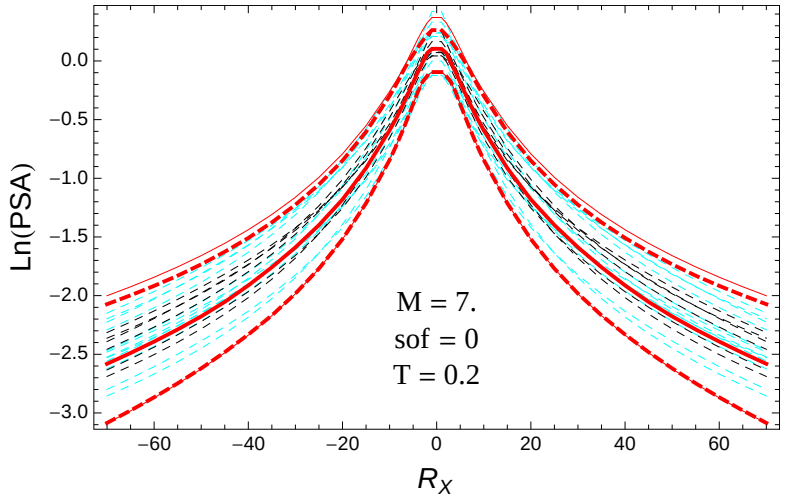



Figure 3.304: PVNGSv2: Distance scaling of the original GMPEs (dashed black), the original GMPEs with uncertainty model (dashed cyan) and 0.05,0.5,0.95 quantile of the ModelA distribution (red) with total weights, for a scenario with $M = 7.$, $F = 0$, and $T = 0.2$s.

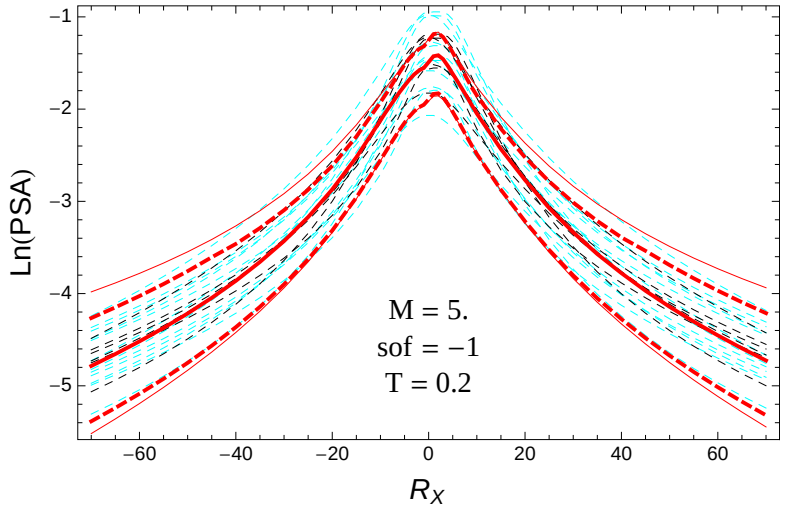



Figure 3.305: PVNGSv2: Distance scaling of the original GMPEs (dashed black), the original GMPEs with uncertainty model (dashed cyan) and 0.05,0.5,0.95 quantile of the ModelA distribution (red) with total weights, for a scenario with $M = 5.$, $F = -1$, and $T = 0.2$s.

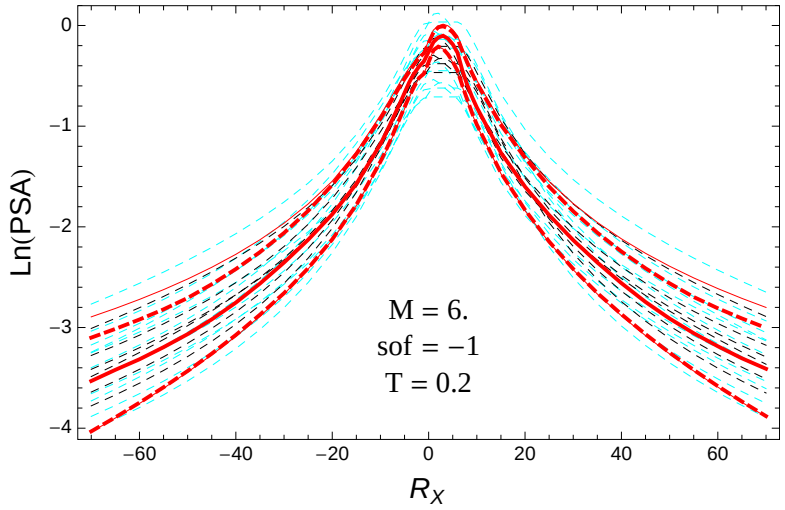



Figure 3.306: PVNGSv2: Distance scaling of the original GMPEs (dashed black), the original GMPEs with uncertainty model (dashed cyan) and 0.05,0.5,0.95 quantile of the ModelA distribution (red) with total weights, for a scenario with $M = 6.$, $F = -1$, and $T = 0.2$s.

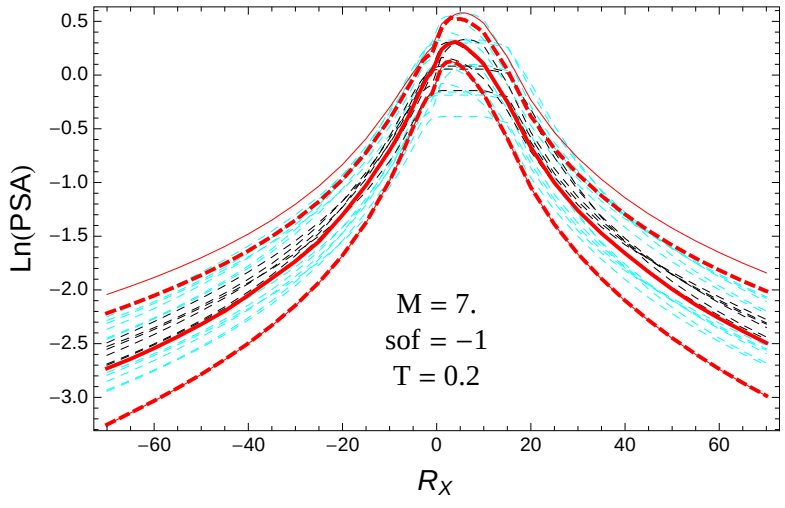



Figure 3.307: PVNGSv2: Distance scaling of the original GMPEs (dashed black), the original GMPEs with uncertainty model (dashed cyan) and 0.05,0.5,0.95 quantile of the ModelA distribution (red) with total weights, for a scenario with $M = 7.$, $F = -1$, and $T = 0.2$s.

**T = 0.5s**

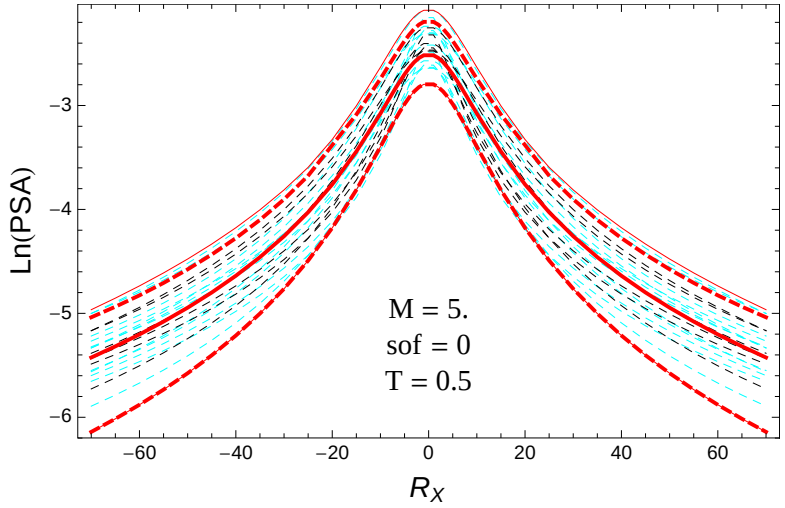



Figure 3.308: PVNGSv2: Distance scaling of the original GMPEs (dashed black), the original GMPEs with uncertainty model (dashed cyan) and 0.05,0.5,0.95 quantile of the ModelA distribution (red) with total weights, for a scenario with $M = 5.$, $F = 0$, and $T = 0.5$s.

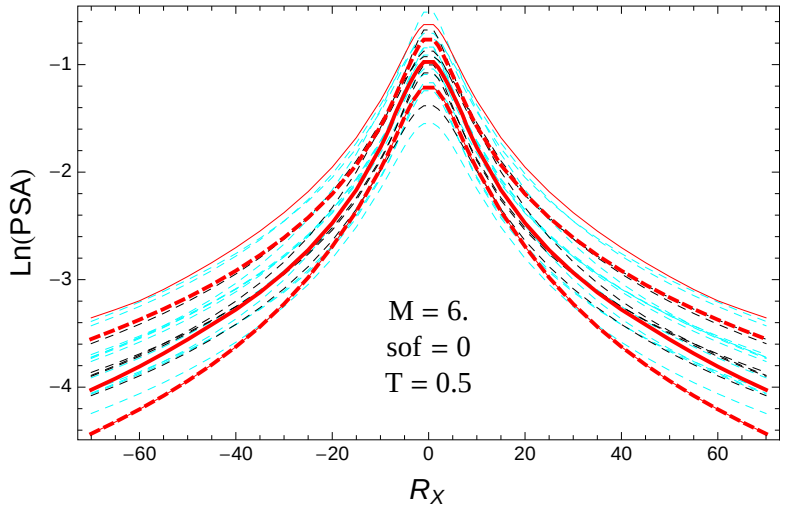



Figure 3.309: PVNGSv2: Distance scaling of the original GMPEs (dashed black), the original GMPEs with uncertainty model (dashed cyan) and 0.05,0.5,0.95 quantile of the ModelA distribution (red) with total weights, for a scenario with $M = 6.$, $F = 0$, and $T = 0.5$s.

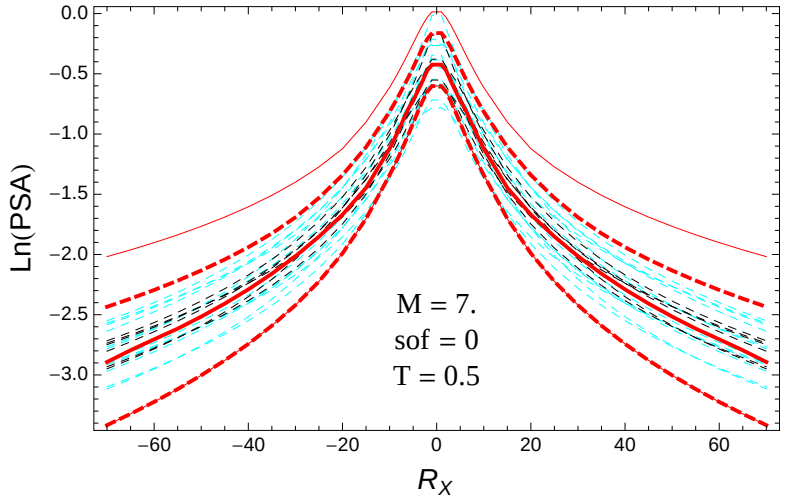



Figure 3.310: PVNGSv2: Distance scaling of the original GMPEs (dashed black), the original GMPEs with uncertainty model (dashed cyan) and 0.05,0.5,0.95 quantile of the ModelA distribution (red) with total weights, for a scenario with $M = 7.$, $F = 0$, and $T = 0.5$s.

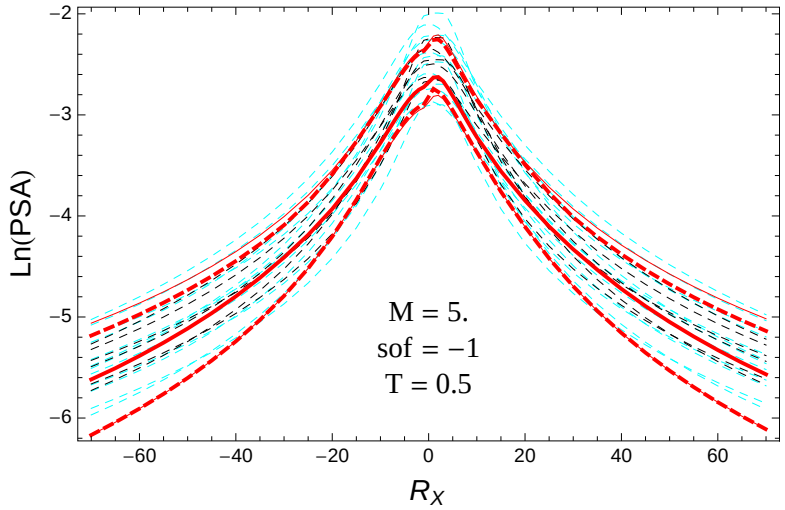



Figure 3.311: PVNGSv2: Distance scaling of the original GMPEs (dashed black), the original GMPEs with uncertainty model (dashed cyan) and 0.05,0.5,0.95 quantile of the ModelA distribution (red) with total weights, for a scenario with $M = 5.$, $F = -1$, and $T = 0.5$s.

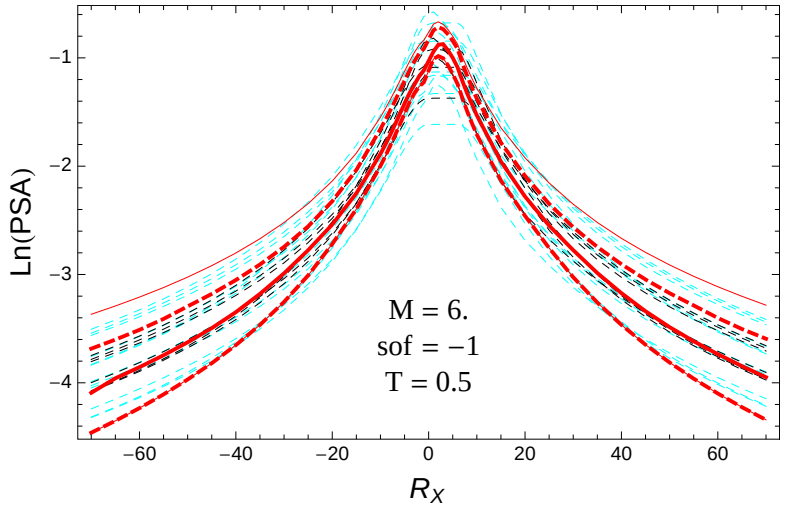



Figure 3.312: PVNGSv2: Distance scaling of the original GMPEs (dashed black), the original GMPEs with uncertainty model (dashed cyan) and 0.05,0.5,0.95 quantile of the ModelA distribution (red) with total weights, for a scenario with $M = 6.$, $F = -1$, and $T = 0.5$s.

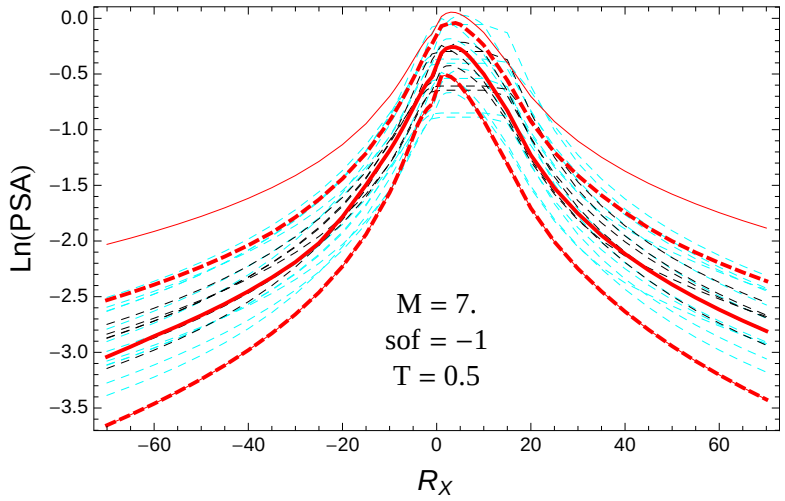



Figure 3.313: PVNGSv2: Distance scaling of the original GMPEs (dashed black), the original GMPEs with uncertainty model (dashed cyan) and 0.05,0.5,0.95 quantile of the ModelA distribution (red) with total weights, for a scenario with $M = 7.$, $F = -1$, and $T = 0.5$s.

**T = 1.s**

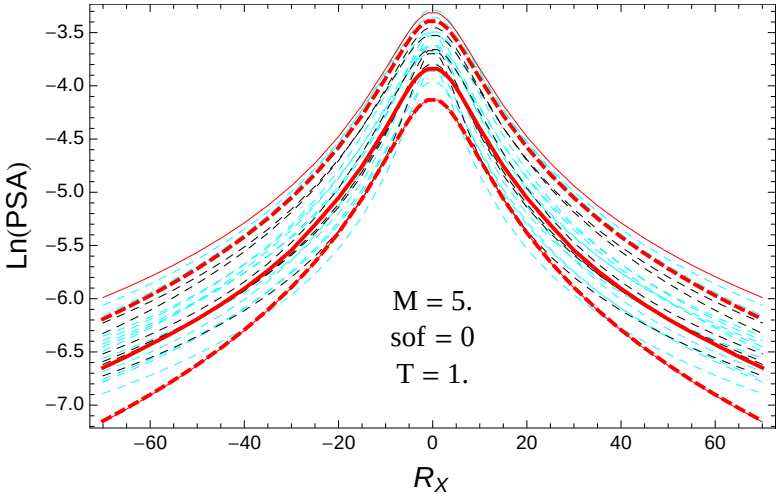



Figure 3.314: PVNGSv2: Distance scaling of the original GMPEs (dashed black), the original GMPEs with uncertainty model (dashed cyan) and 0.05,0.5,0.95 quantile of the ModelA distribution (red) with total weights, for a scenario with $M = 5.$, $F = 0$, and $T = 1.$s.

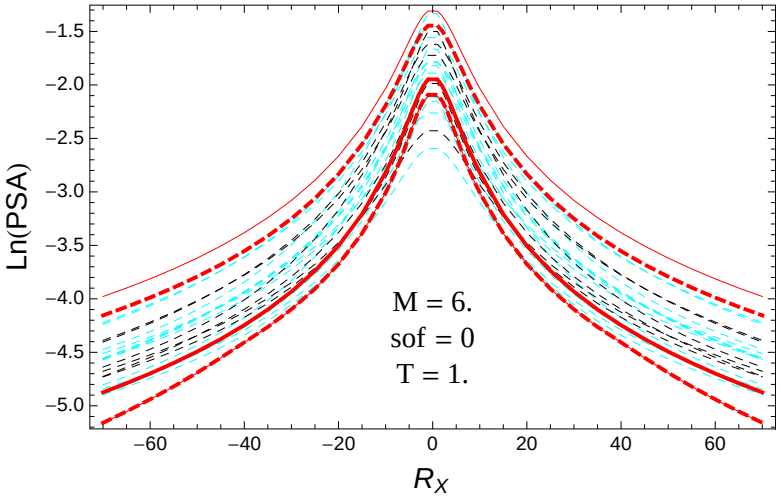



Figure 3.315: PVNGSv2: Distance scaling of the original GMPEs (dashed black), the original GMPEs with uncertainty model (dashed cyan) and 0.05,0.5,0.95 quantile of the ModelA distribution (red) with total weights, for a scenario with $M = 6.$, $F = 0$, and $T = 1.$s.

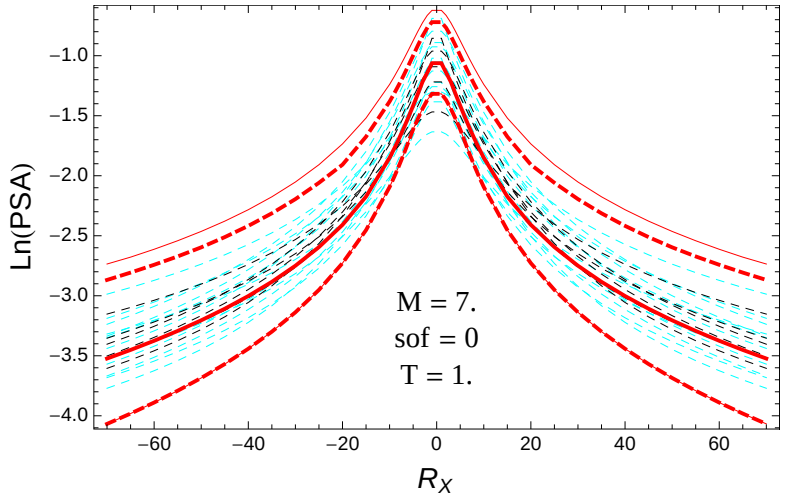



Figure 3.316: PVNGSv2: Distance scaling of the original GMPEs (dashed black), the original GMPEs with uncertainty model (dashed cyan) and 0.05,0.5,0.95 quantile of the ModelA distribution (red) with total weights, for a scenario with $M = 7.$, $F = 0$, and $T = 1.$s.

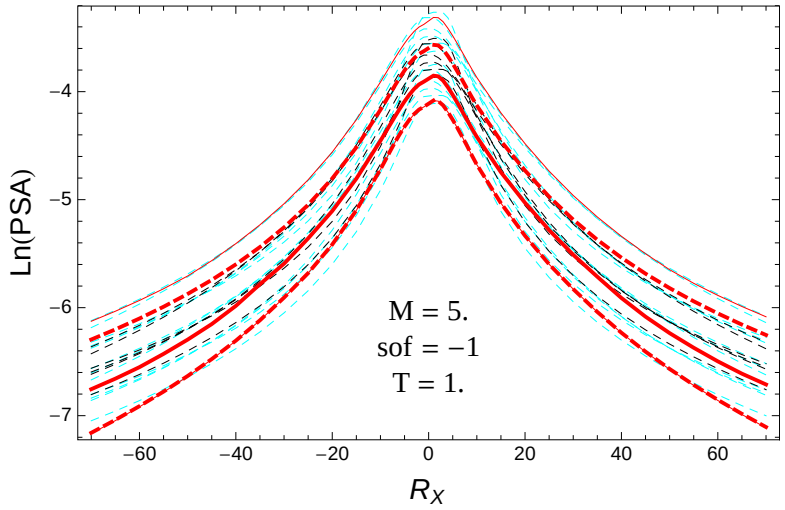



Figure 3.317: PVNGSv2: Distance scaling of the original GMPEs (dashed black), the original GMPEs with uncertainty model (dashed cyan) and 0.05,0.5,0.95 quantile of the ModelA distribution (red) with total weights, for a scenario with $M = 5.$, $F = -1$, and $T = 1.$s.

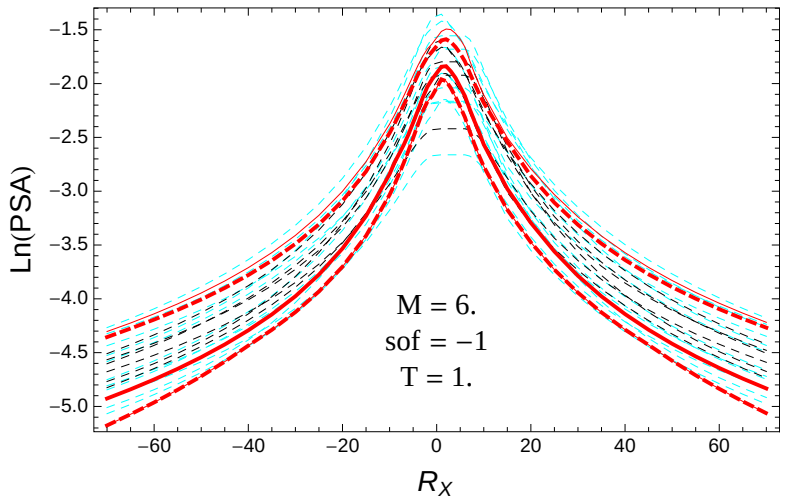



Figure 3.318: PVNGSv2: Distance scaling of the original GMPEs (dashed black), the original GMPEs with uncertainty model (dashed cyan) and 0.05,0.5,0.95 quantile of the ModelA distribution (red) with total weights, for a scenario with $M = 6.$, $F = -1$, and $T = 1.$s.

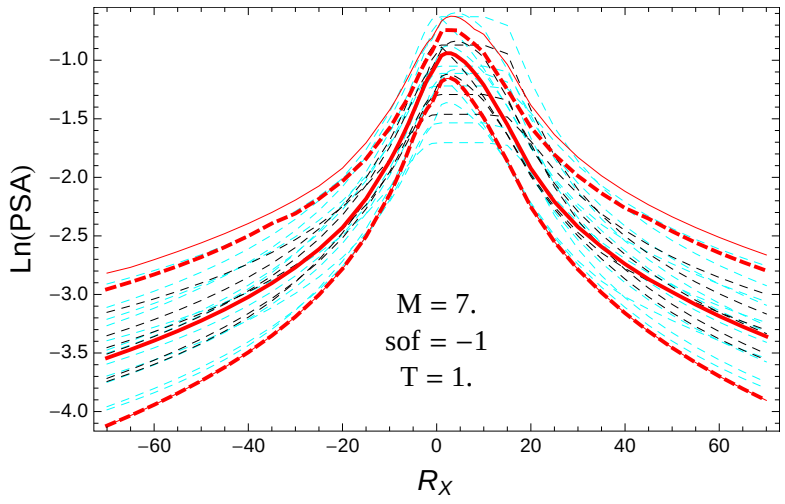



Figure 3.319: PVNGSv2: Distance scaling of the original GMPEs (dashed black), the original GMPEs with uncertainty model (dashed cyan) and 0.05,0.5,0.95 quantile of the ModelA distribution (red) with total weights, for a scenario with $M = 7.$, $F = -1$, and $T = 1.$s.

**T = 3.s**

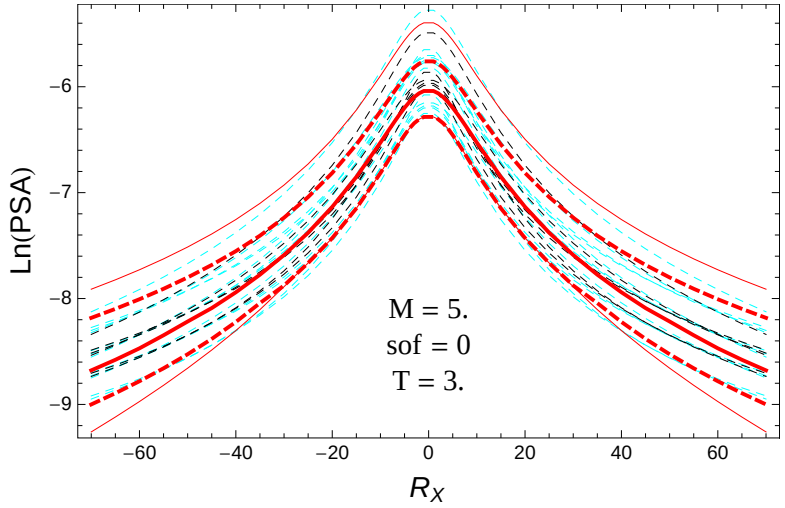



Figure 3.320: PVNGSv2: Distance scaling of the original GMPEs (dashed black), the original GMPEs with uncertainty model (dashed cyan) and 0.05,0.5,0.95 quantile of the ModelA distribution (red) with total weights, for a scenario with $M = 5.$, $F = 0$, and $T = 3.$s.

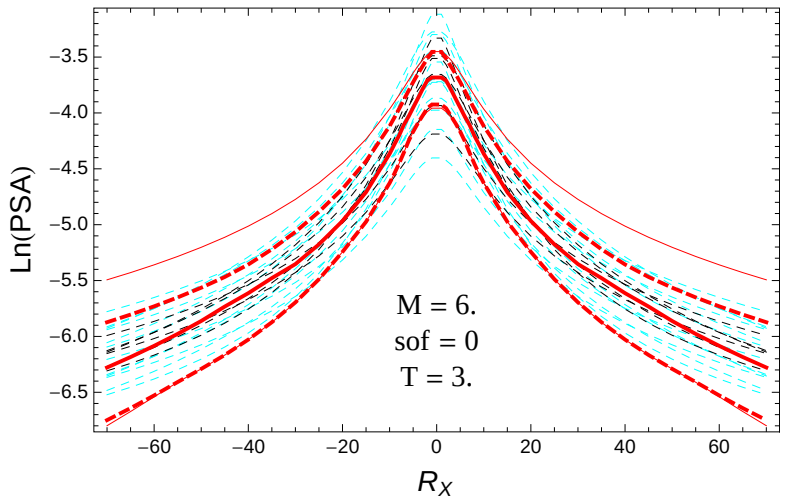



Figure 3.321: PVNGSv2: Distance scaling of the original GMPEs (dashed black), the original GMPEs with uncertainty model (dashed cyan) and 0.05,0.5,0.95 quantile of the ModelA distribution (red) with total weights, for a scenario with $M = 6.$, $F = 0$, and $T = 3.$s.

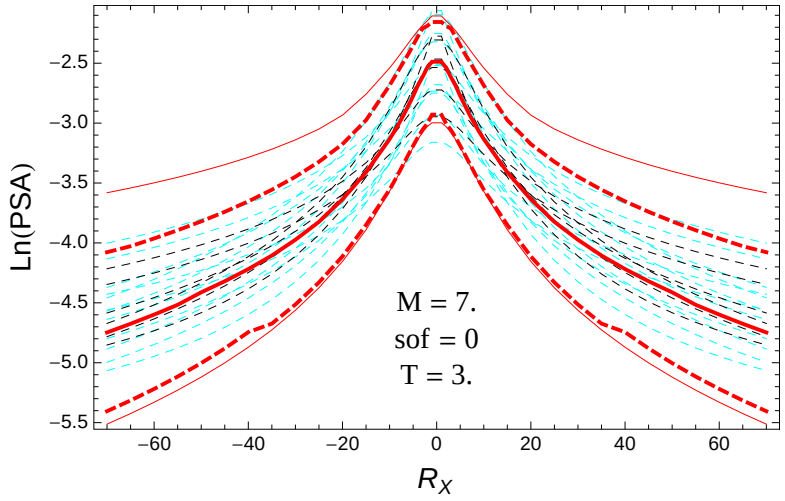



Figure 3.322: PVNGSv2: Distance scaling of the original GMPEs (dashed black), the original GMPEs with uncertainty model (dashed cyan) and 0.05,0.5,0.95 quantile of the ModelA distribution (red) with total weights, for a scenario with $M = 7.$, $F = 0$, and $T = 3.$s.

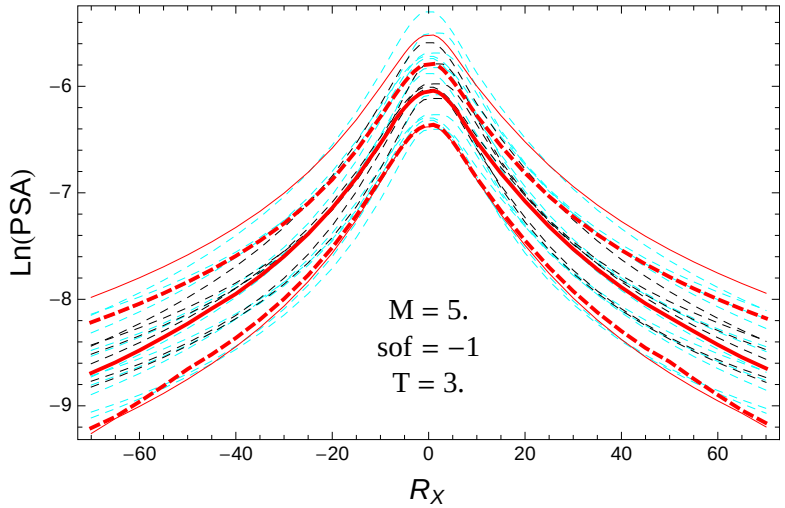



Figure 3.323: PVNGSv2: Distance scaling of the original GMPEs (dashed black), the original GMPEs with uncertainty model (dashed cyan) and 0.05,0.5,0.95 quantile of the ModelA distribution (red) with total weights, for a scenario with $M = 5.$, $F = -1$, and $T = 3.$s.

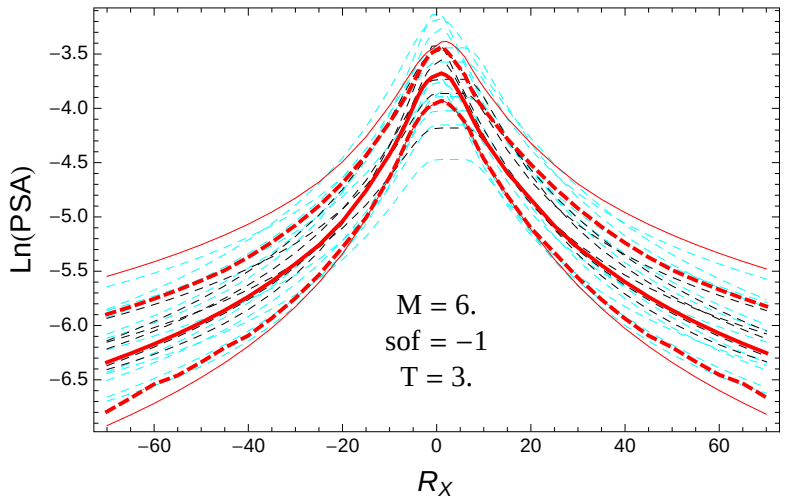



Figure 3.324: PVNGSv2: Distance scaling of the original GMPEs (dashed black), the original GMPEs with uncertainty model (dashed cyan) and 0.05,0.5,0.95 quantile of the ModelA distribution (red) with total weights, for a scenario with $M = 6.$, $F = -1$, and $T = 3.$s.

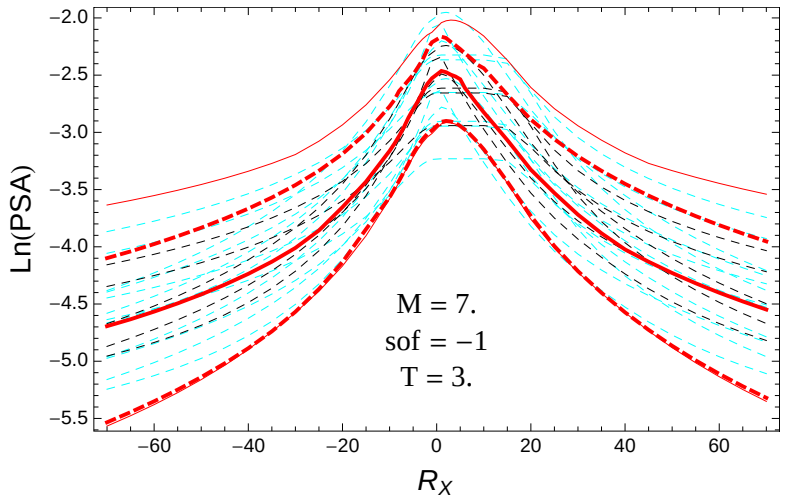



Figure 3.325: PVNGSv2: Distance scaling of the original GMPEs (dashed black), the original GMPEs with uncertainty model (dashed cyan) and 0.05,0.5,0.95 quantile of the ModelA distribution (red) with total weights, for a scenario with $M = 7.$, $F = -1$, and $T = 3.$s.

### 3.1.8 Quantile Plots vs. Magnitude

**T = 0.01s**

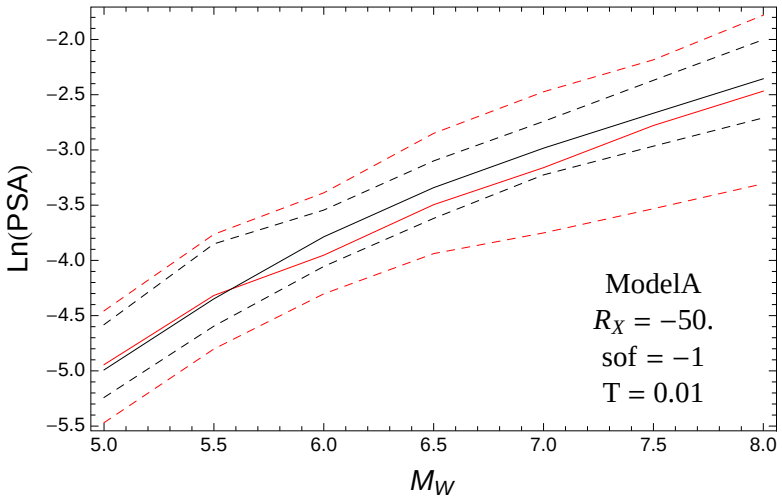



Figure 3.326: PVNGS2: Magnitude scaling of 0.05,0.5,0.95 quantile of the GMPE distribution (black) and the ModelA distribution (red) with total weights, for a scenario with $R_x = -50.$, $F = -1$, and $T = 0.01$.

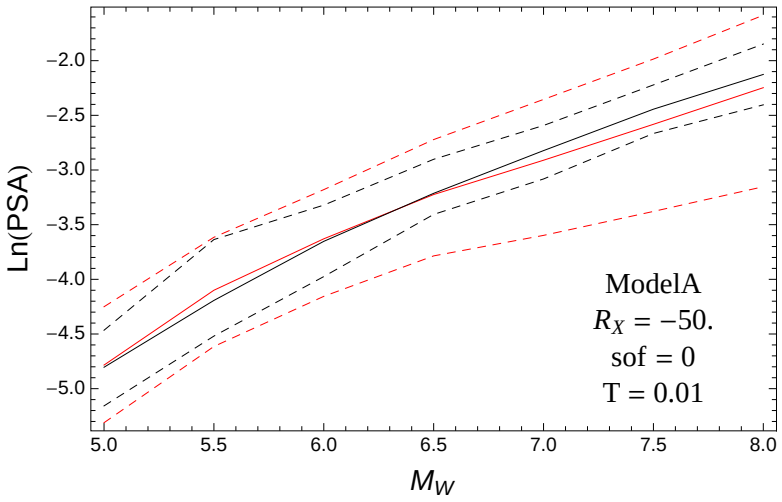



Figure 3.327: PVNGS2: Magnitude scaling of 0.05,0.5,0.95 quantile of the GMPE distribution (black) and the ModelA distribution (red) with total weights, for a scenario with $R_x = -50.$, $F = 0$, and $T = 0.01$.

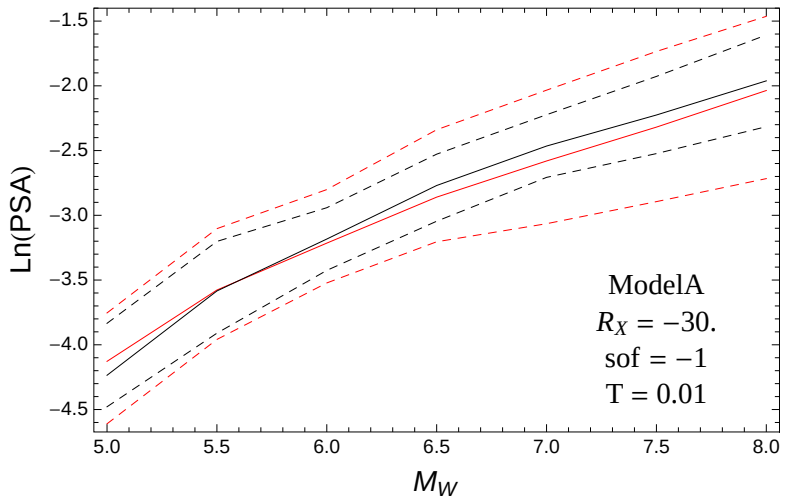



Figure 3.328: PVNGS2: Magnitude scaling of 0.05,0.5,0.95 quantile of the GMPE distribution (black) and the ModelA distribution (red) with total weights, for a scenario with $R_x = -30.$, $F = -1$, and $T = 0.01$.

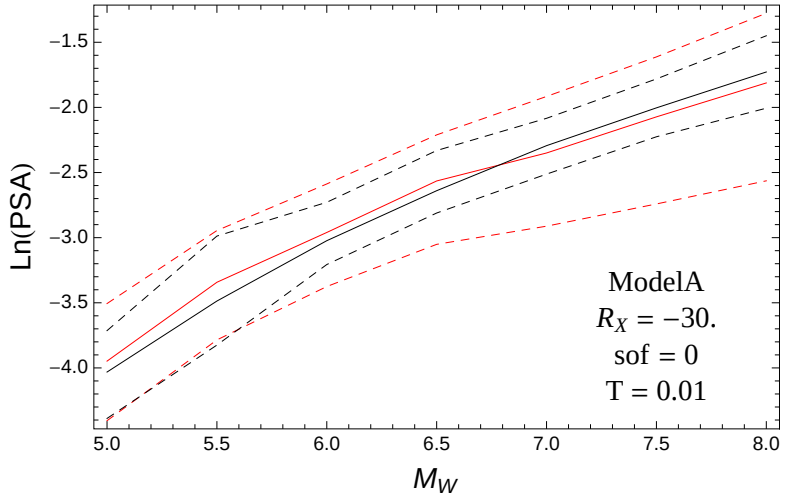



Figure 3.329: PVNGS2: Magnitude scaling of 0.05,0.5,0.95 quantile of the GMPE distribution (black) and the ModelA distribution (red) with total weights, for a scenario with $R_x = -30.$, $F = 0$, and $T = 0.01$.

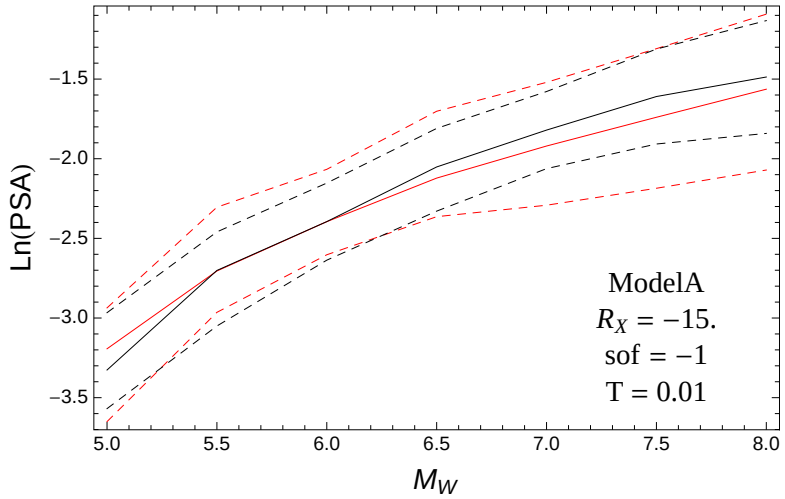



Figure 3.330: PVNGS2: Magnitude scaling of 0.05,0.5,0.95 quantile of the GMPE distribution (black) and the ModelA distribution (red) with total weights, for a scenario with $R_x = -15.$, $F = -1$, and $T = 0.01$.

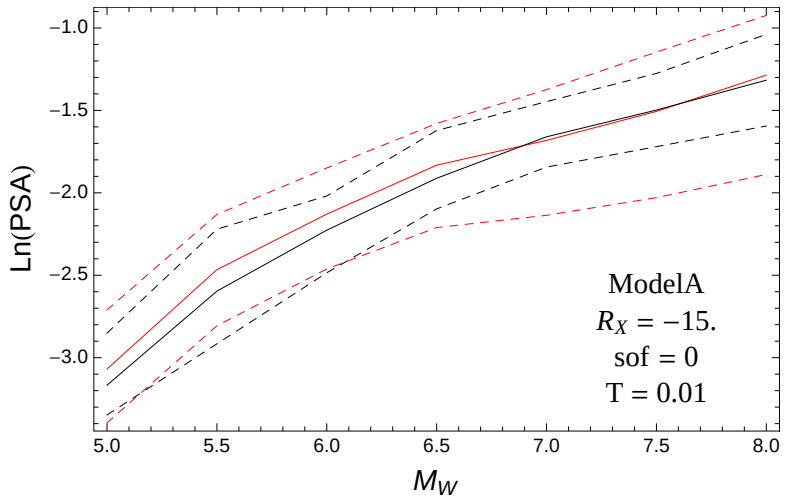



Figure 3.331: PVNGS2: Magnitude scaling of 0.05,0.5,0.95 quantile of the GMPE distribution (black) and the ModelA distribution (red) with total weights, for a scenario with $R_x = -15.$, $F = 0$, and $T = 0.01$.

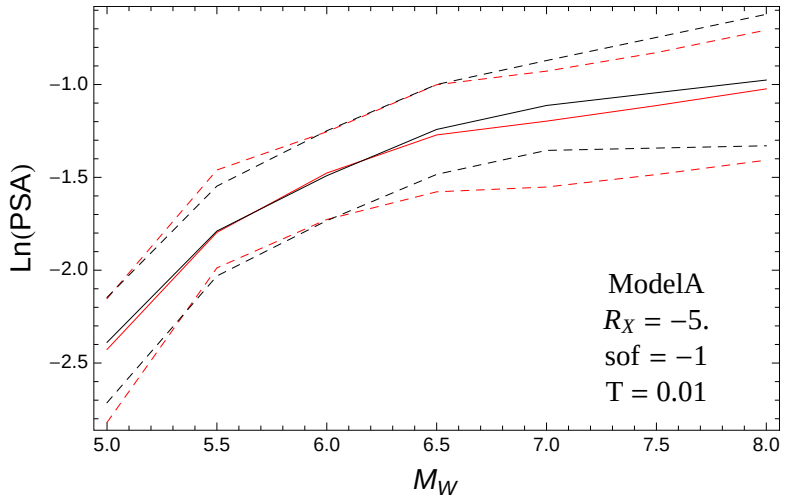



Figure 3.332: PVNGS2: Magnitude scaling of 0.05,0.5,0.95 quantile of the GMPE distribution (black) and the ModelA distribution (red) with total weights, for a scenario with $R_x = -5.$, $F = -1$, and $T = 0.01$.

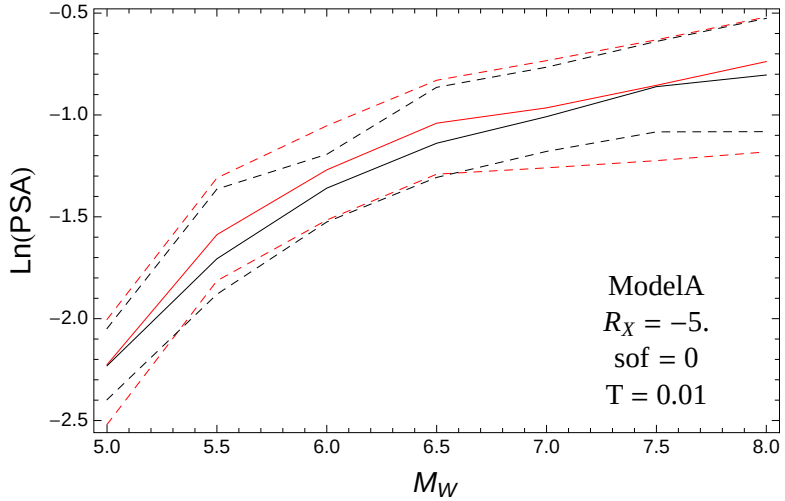



Figure 3.333: PVNGS2: Magnitude scaling of 0.05,0.5,0.95 quantile of the GMPE distribution (black) and the ModelA distribution (red) with total weights, for a scenario with $R_x = -5.$, $F = 0$, and $T = 0.01$.

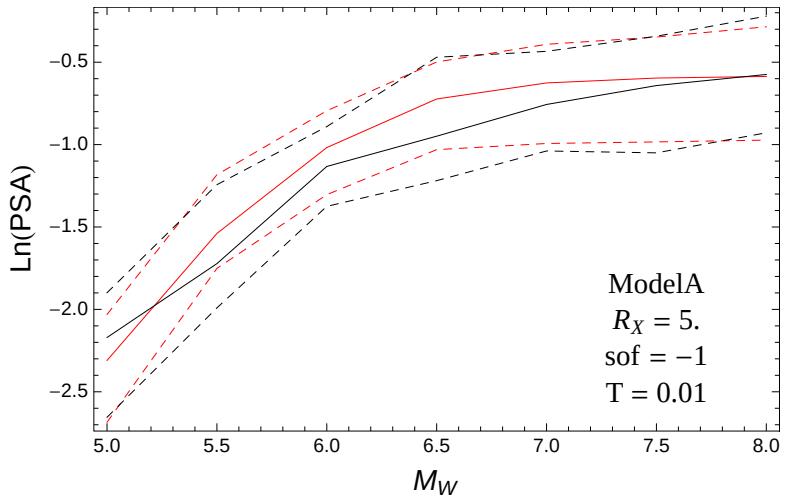



Figure 3.334: PVNGS2: Magnitude scaling of 0.05,0.5,0.95 quantile of the GMPE distribution (black) and the ModelA distribution (red) with total weights, for a scenario with $R_x = 5.$, $F = -1$, and $T = 0.01$.

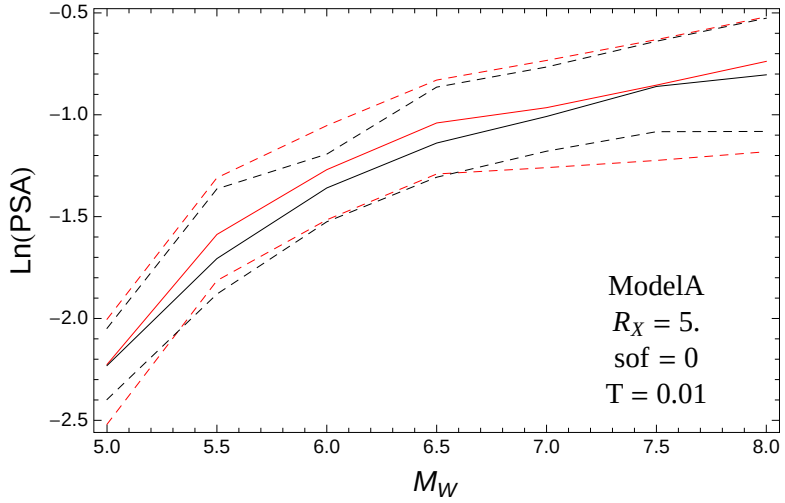



Figure 3.335: PVNGS2: Magnitude scaling of 0.05,0.5,0.95 quantile of the GMPE distribution (black) and the ModelA distribution (red) with total weights, for a scenario with $R_x = 5.$, $F = 0$, and $T = 0.01$.

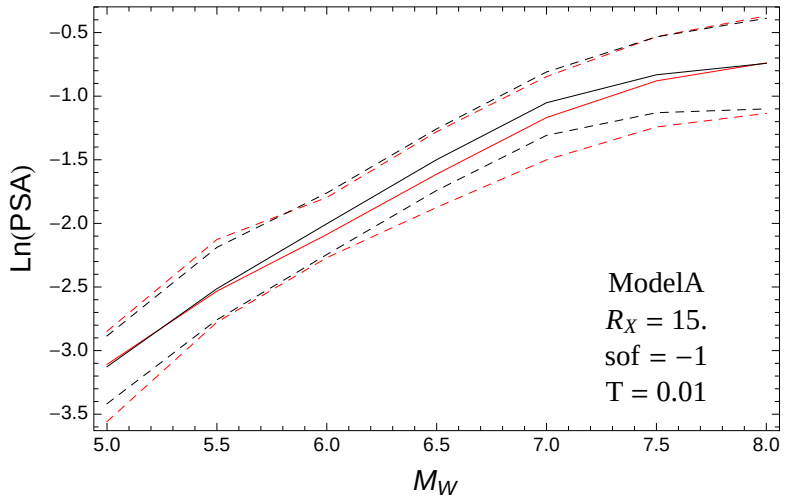



Figure 3.336: PVNGS2: Magnitude scaling of 0.05,0.5,0.95 quantile of the GMPE distribution (black) and the ModelA distribution (red) with total weights, for a scenario with $R_x = 15.$, $F = -1$, and $T = 0.01$.

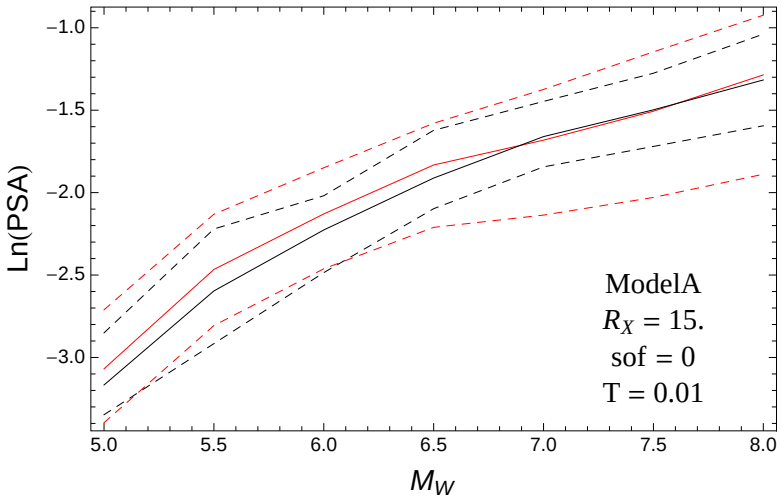



Figure 3.337: PVNGS2: Magnitude scaling of 0.05,0.5,0.95 quantile of the GMPE distribution (black) and the ModelA distribution (red) with total weights, for a scenario with $R_x = 15.$, $F = 0$, and $T = 0.01$.

**T = 0.2s**

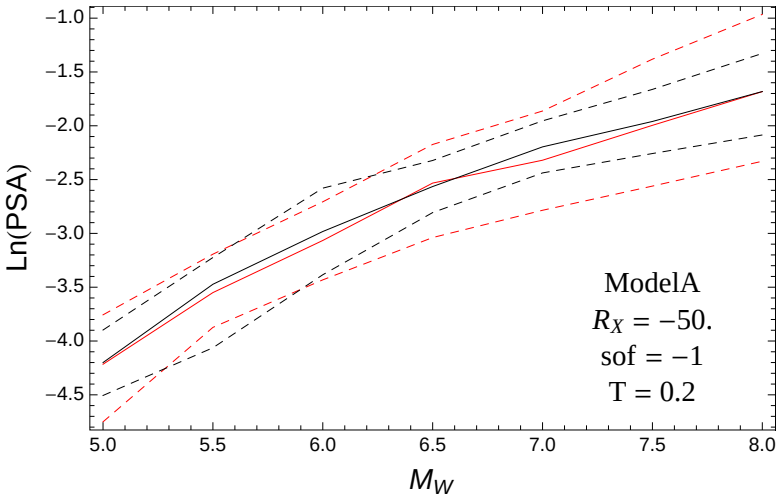



Figure 3.338: PVNGS2: Magnitude scaling of 0.05,0.5,0.95 quantile of the GMPE distribution (black) and the ModelA distribution (red) with total weights, for a scenario with $R_x = -50.$, $F = -1$, and $T = 0.2$.

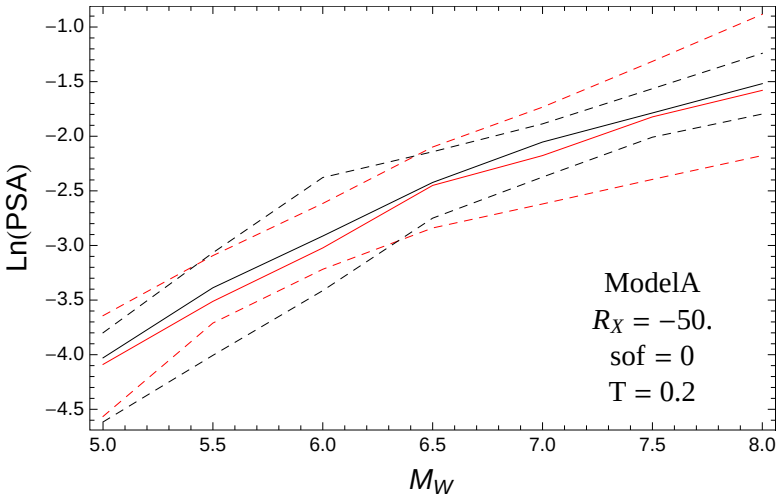



Figure 3.339: PVNGS2: Magnitude scaling of 0.05,0.5,0.95 quantile of the GMPE distribution (black) and the ModelA distribution (red) with total weights, for a scenario with $R_x = -50.$, $F = 0$, and $T = 0.2$.

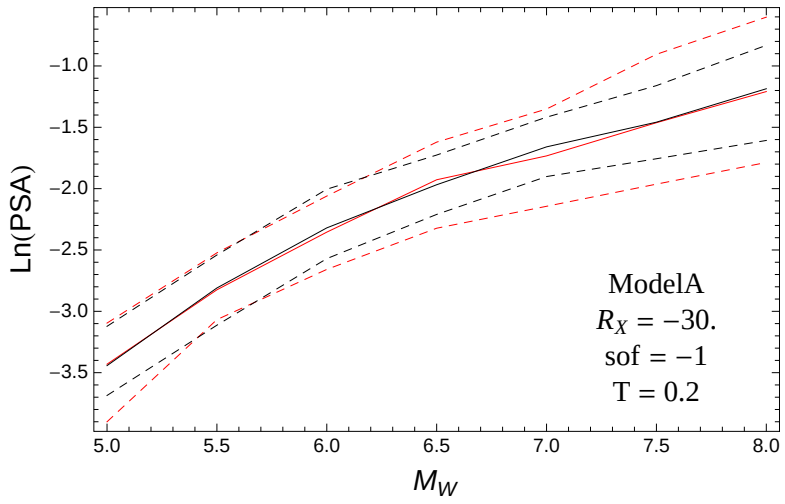



Figure 3.340: PVNGS2: Magnitude scaling of 0.05,0.5,0.95 quantile of the GMPE distribution (black) and the ModelA distribution (red) with total weights, for a scenario with $R_x = -30.$, $F = -1$, and $T = 0.2$.

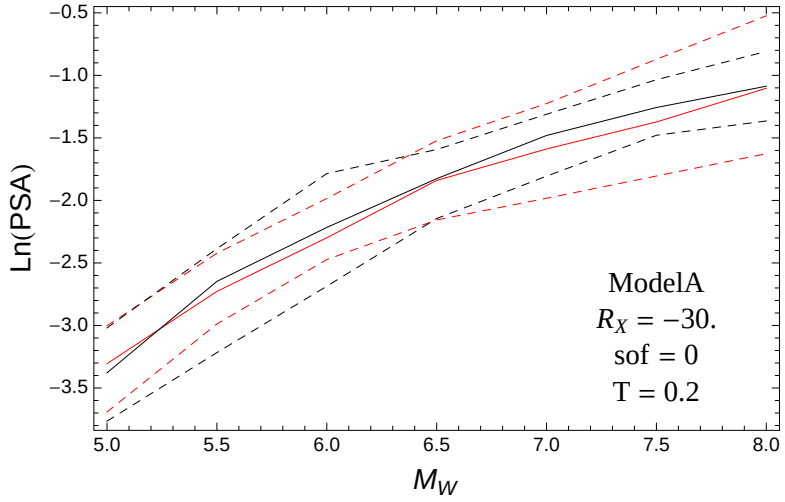



Figure 3.341: PVNGS2: Magnitude scaling of 0.05,0.5,0.95 quantile of the GMPE distribution (black) and the ModelA distribution (red) with total weights, for a scenario with $R_x = -30.$, $F = 0$, and $T = 0.2$.

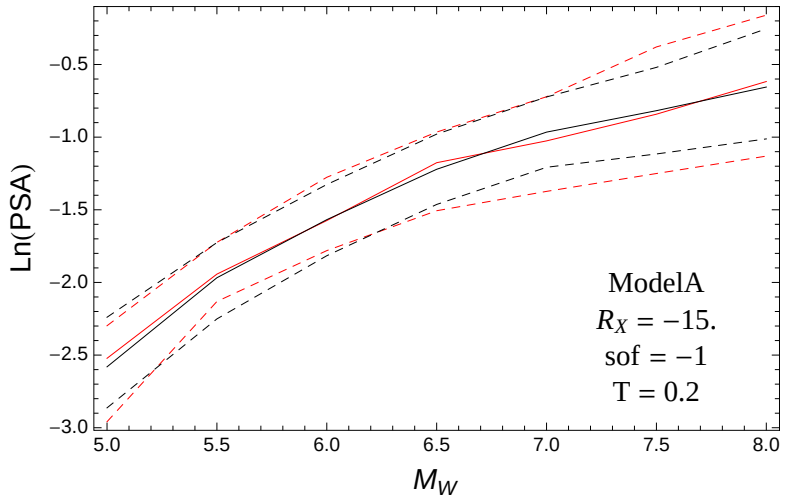



Figure 3.342: PVNGS2: Magnitude scaling of 0.05,0.5,0.95 quantile of the GMPE distribution (black) and the ModelA distribution (red) with total weights, for a scenario with $R_x = -15.$, $F = -1$, and $T = 0.2$.

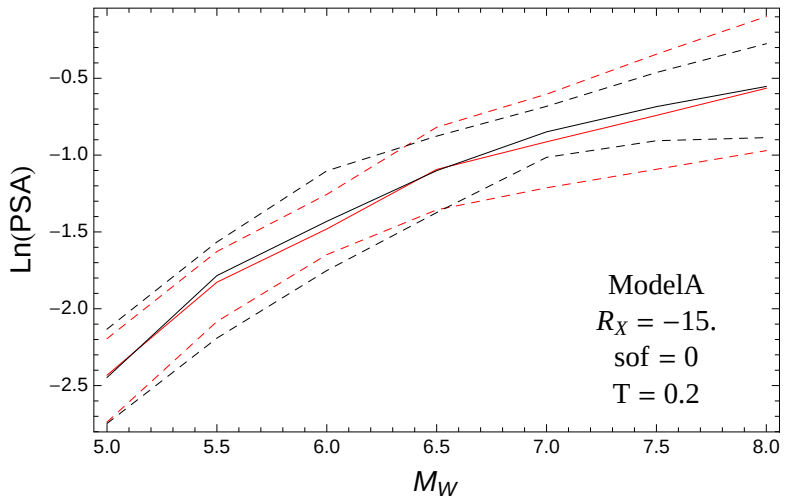



Figure 3.343: PVNGS2: Magnitude scaling of 0.05,0.5,0.95 quantile of the GMPE distribution (black) and the ModelA distribution (red) with total weights, for a scenario with $R_x = -15.$, $F = 0$, and $T = 0.2$.

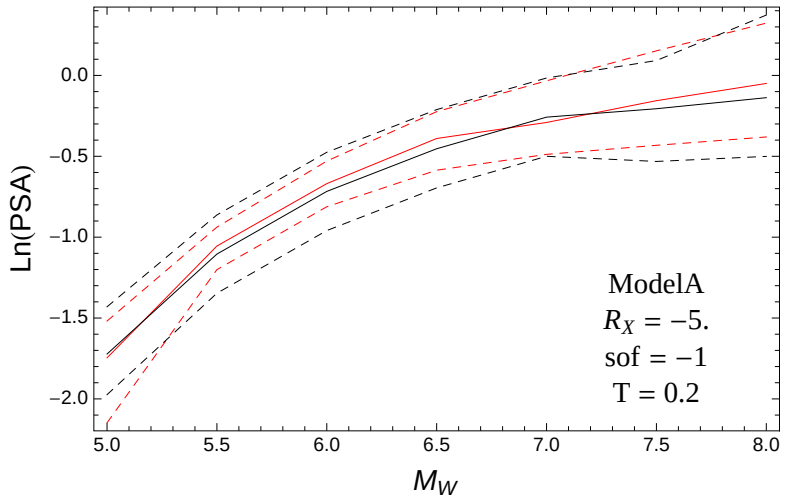



Figure 3.344: PVNGS2: Magnitude scaling of 0.05,0.5,0.95 quantile of the GMPE distribution (black) and the ModelA distribution (red) with total weights, for a scenario with $R_x = -5.$, $F = -1$, and $T = 0.2$.

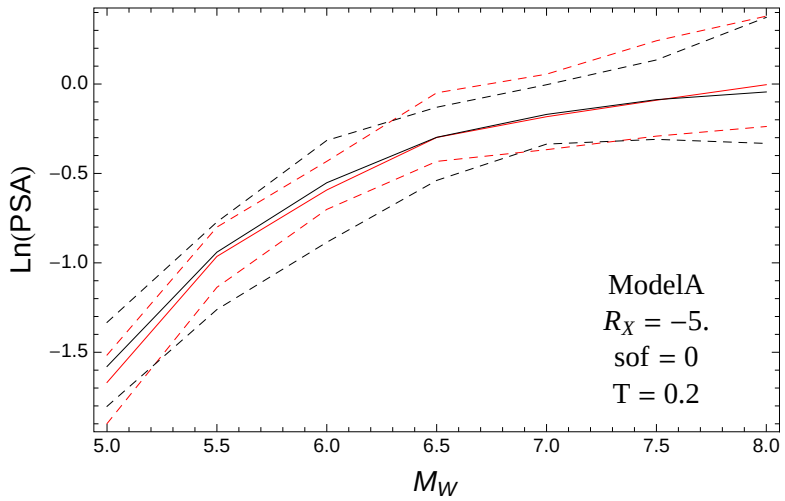



Figure 3.345: PVNGS2: Magnitude scaling of 0.05,0.5,0.95 quantile of the GMPE distribution (black) and the ModelA distribution (red) with total weights, for a scenario with $R_x = -5.$, $F = 0$, and $T = 0.2$.

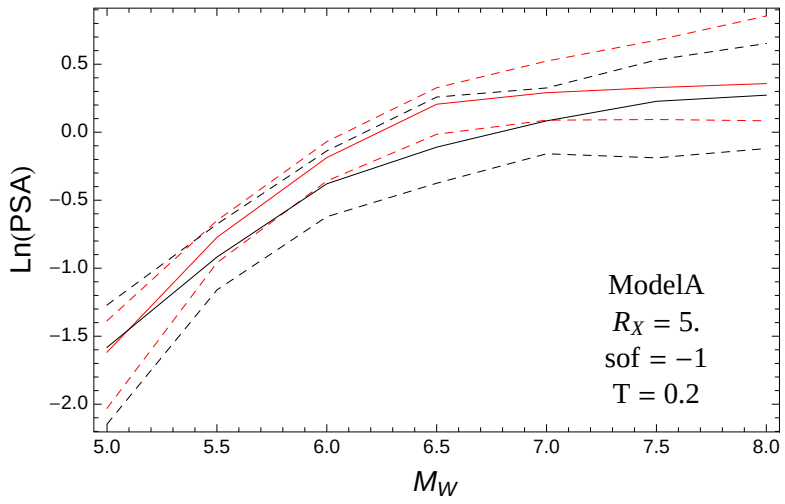



Figure 3.346: PVNGS2: Magnitude scaling of 0.05,0.5,0.95 quantile of the GMPE distribution (black) and the ModelA distribution (red) with total weights, for a scenario with $R_x = 5.$, $F = -1$, and $T = 0.2$.

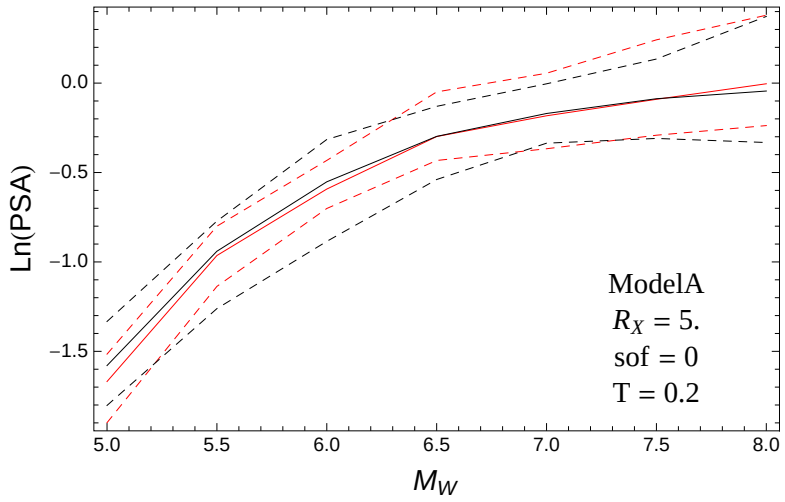



Figure 3.347: PVNGS2: Magnitude scaling of 0.05,0.5,0.95 quantile of the GMPE distribution (black) and the ModelA distribution (red) with total weights, for a scenario with $R_x = 5.$, $F = 0$, and $T = 0.2$.

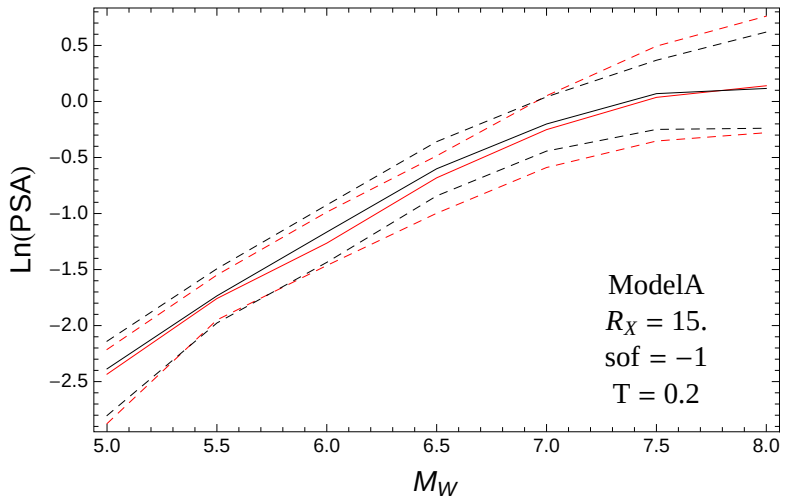



Figure 3.348: PVNGS2: Magnitude scaling of 0.05,0.5,0.95 quantile of the GMPE distribution (black) and the ModelA distribution (red) with total weights, for a scenario with $R_x = 15.$, $F = -1$, and $T = 0.2$.

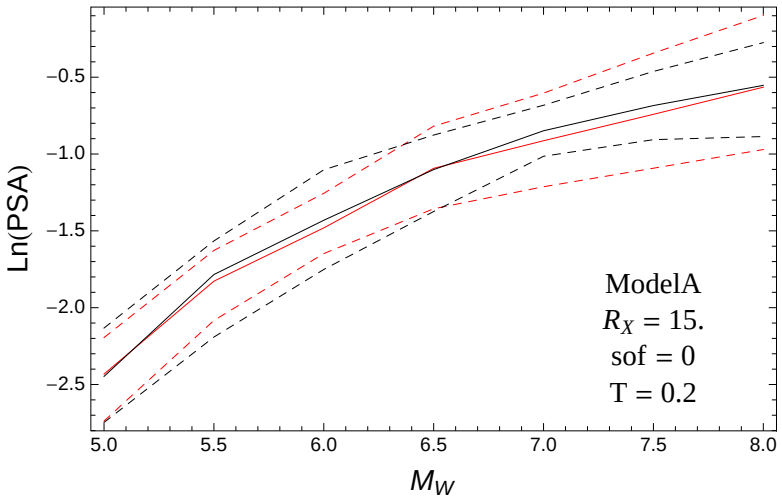



Figure 3.349: PVNGS2: Magnitude scaling of 0.05,0.5,0.95 quantile of the GMPE distribution (black) and the ModelA distribution (red) with total weights, for a scenario with $R_x = 15.$, $F = 0$, and $T = 0.2$.

**T = 0.5s**

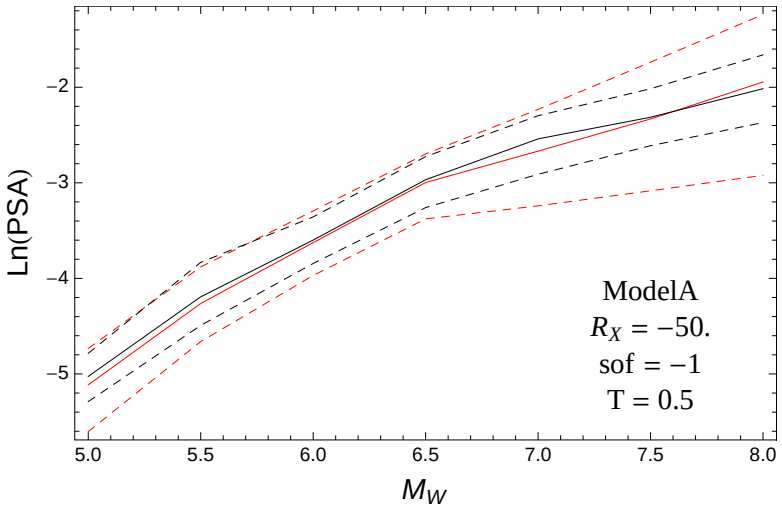



Figure 3.350: PVNGS2: Magnitude scaling of 0.05,0.5,0.95 quantile of the GMPE distribution (black) and the ModelA distribution (red) with total weights, for a scenario with $R_x = -50.$, $F = -1$, and $T = 0.5$.

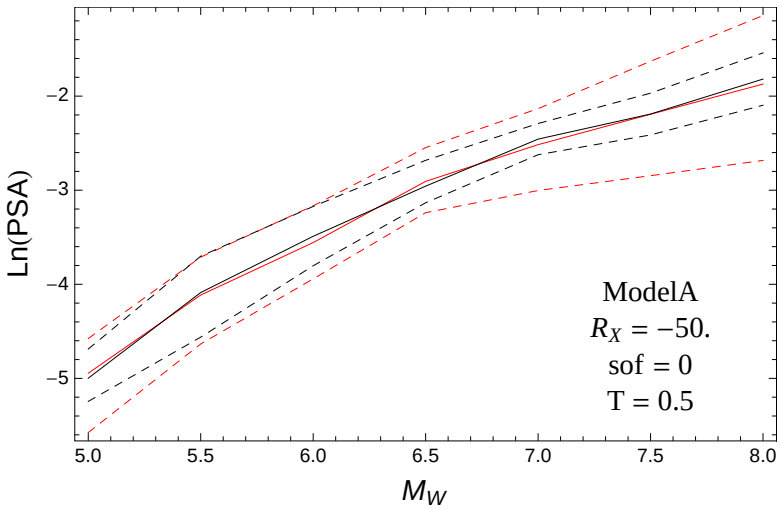



Figure 3.351: PVNGS2: Magnitude scaling of 0.05,0.5,0.95 quantile of the GMPE distribution (black) and the ModelA distribution (red) with total weights, for a scenario with $R_x = -50.$, $F = 0$, and $T = 0.5$.

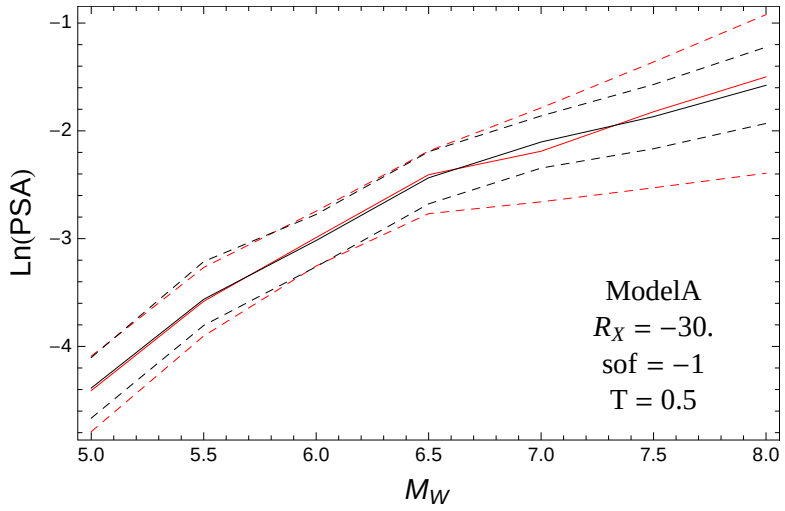



Figure 3.352: PVNGS2: Magnitude scaling of 0.05,0.5,0.95 quantile of the GMPE distribution (black) and the ModelA distribution (red) with total weights, for a scenario with $R_x = -30.$, $F = -1$, and $T = 0.5$.

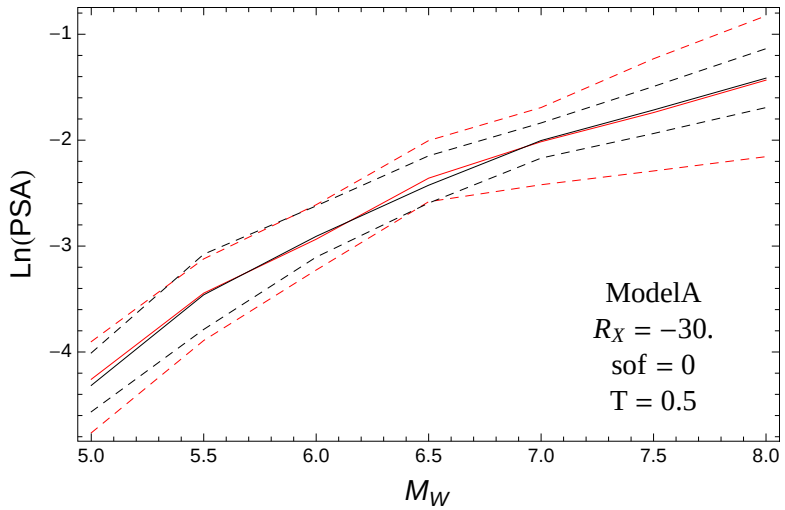



Figure 3.353: PVNGS2: Magnitude scaling of 0.05,0.5,0.95 quantile of the GMPE distribution (black) and the ModelA distribution (red) with total weights, for a scenario with $R_x = -30.$, $F = 0$, and $T = 0.5$.

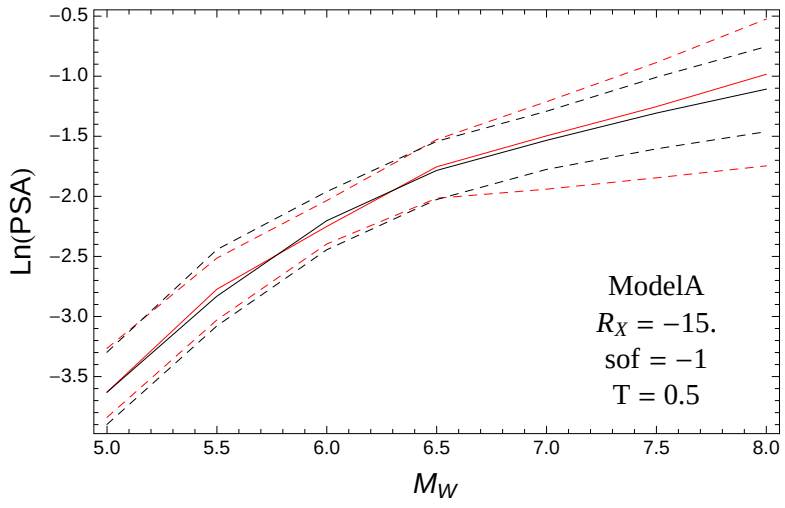



Figure 3.354: PVNGS2: Magnitude scaling of 0.05,0.5,0.95 quantile of the GMPE distribution (black) and the ModelA distribution (red) with total weights, for a scenario with $R_x = -15.$, $F = -1$, and $T = 0.5$.

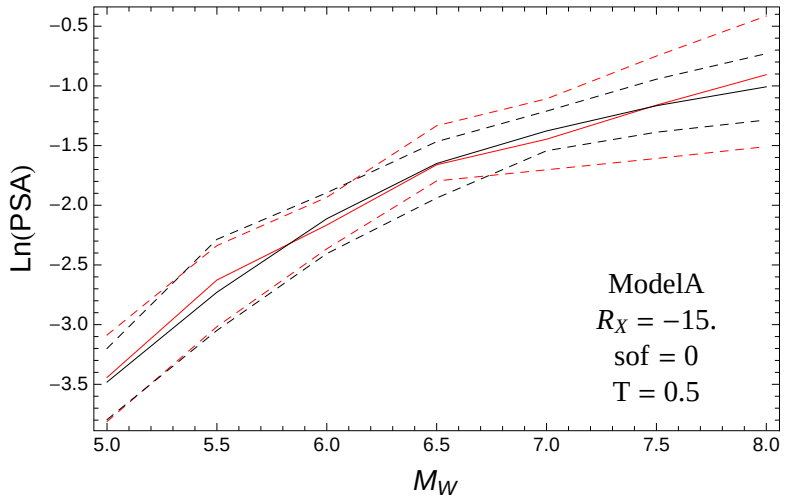



Figure 3.355: PVNGS2: Magnitude scaling of 0.05,0.5,0.95 quantile of the GMPE distribution (black) and the ModelA distribution (red) with total weights, for a scenario with $R_x = -15.$, $F = 0$, and $T = 0.5$.

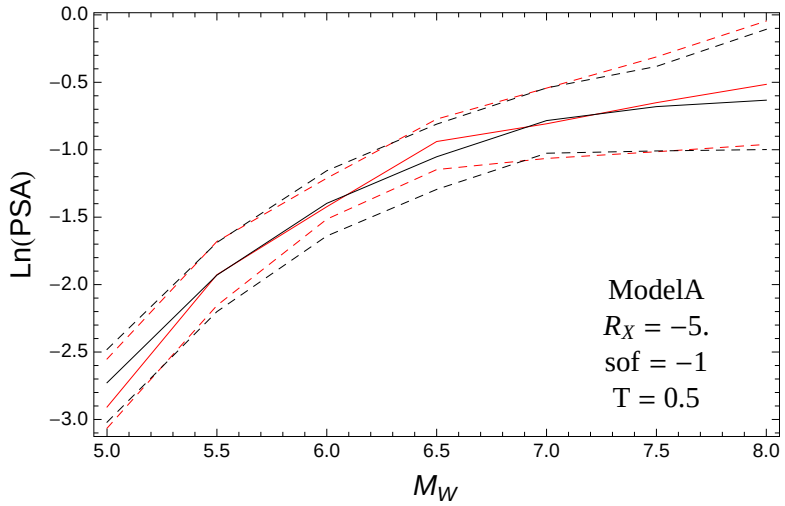



Figure 3.356: PVNGS2: Magnitude scaling of 0.05,0.5,0.95 quantile of the GMPE distribution (black) and the ModelA distribution (red) with total weights, for a scenario with $R_x = -5.$, $F = -1$, and $T = 0.5$.

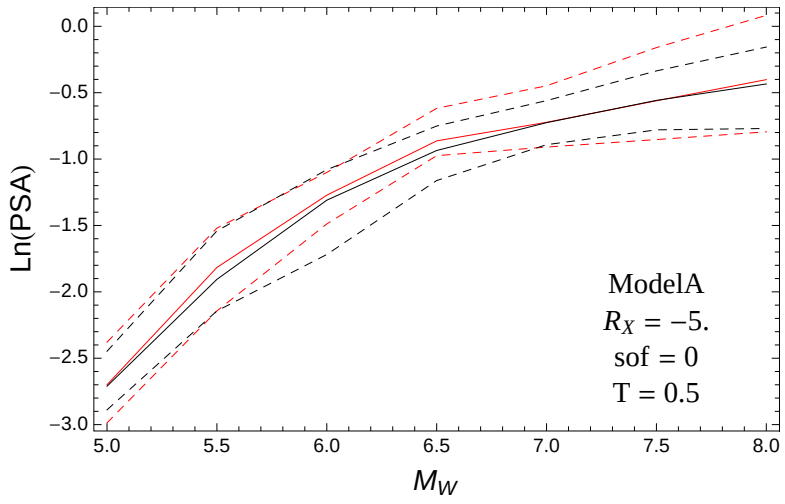



Figure 3.357: PVNGS2: Magnitude scaling of 0.05,0.5,0.95 quantile of the GMPE distribution (black) and the ModelA distribution (red) with total weights, for a scenario with $R_x = -5.$, $F = 0$, and $T = 0.5$.

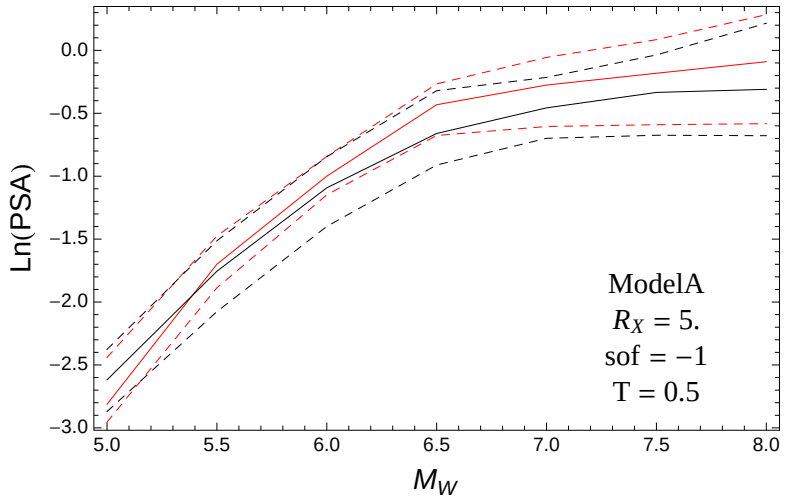



Figure 3.358: PVNGS2: Magnitude scaling of 0.05,0.5,0.95 quantile of the GMPE distribution (black) and the ModelA distribution (red) with total weights, for a scenario with $R_x = 5.$, $F = -1$, and $T = 0.5$.

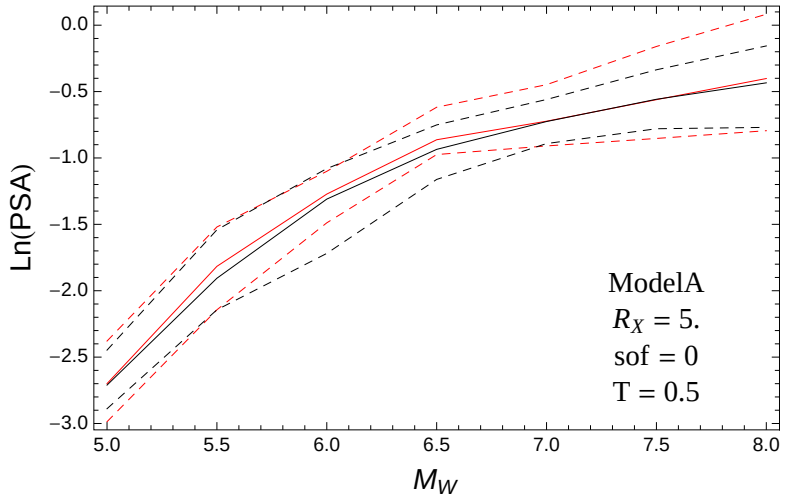



Figure 3.359: PVNGS2: Magnitude scaling of 0.05,0.5,0.95 quantile of the GMPE distribution (black) and the ModelA distribution (red) with total weights, for a scenario with $R_x = 5.$, $F = 0$, and $T = 0.5$.

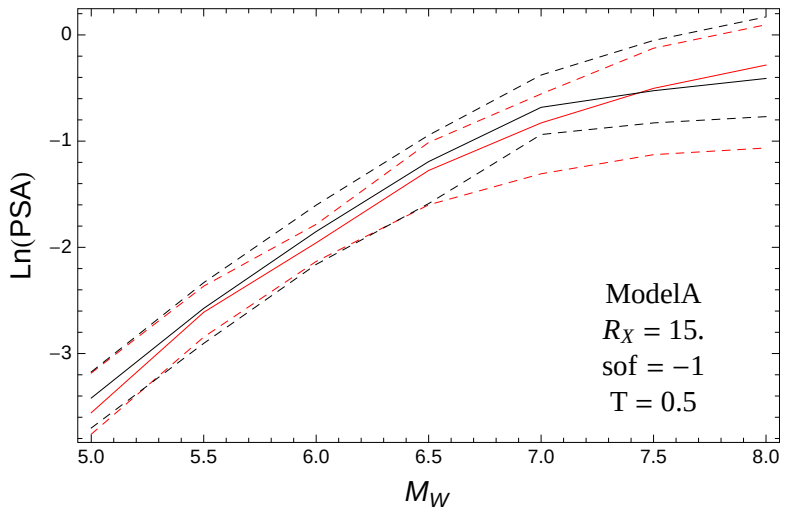



Figure 3.360: PVNGS2: Magnitude scaling of 0.05,0.5,0.95 quantile of the GMPE distribution (black) and the ModelA distribution (red) with total weights, for a scenario with $R_x = 15.$, $F = -1$, and $T = 0.5$.

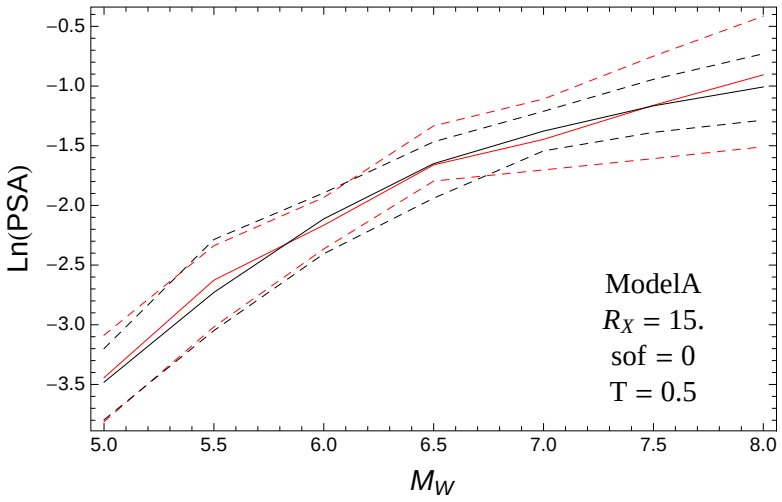



Figure 3.361: PVNGS2: Magnitude scaling of 0.05,0.5,0.95 quantile of the GMPE distribution (black) and the ModelA distribution (red) with total weights, for a scenario with $R_x = 15.$, $F = 0$, and $T = 0.5$.

**T = 1.s**

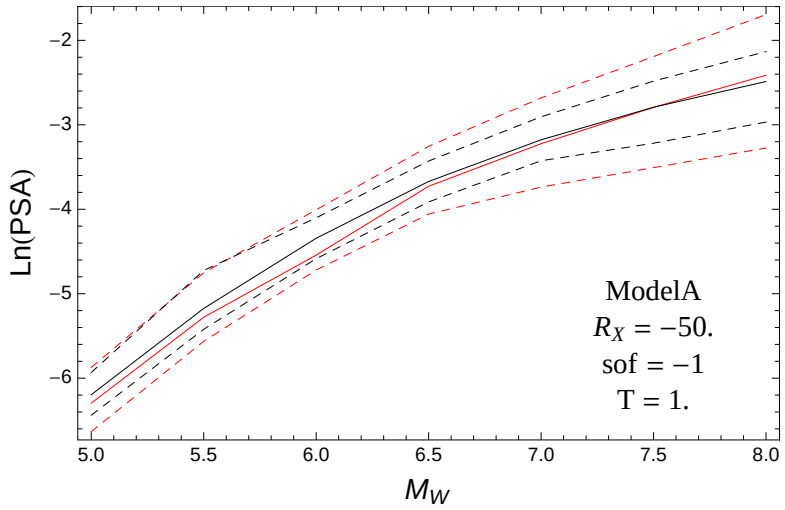



Figure 3.362: PVNGS2: Magnitude scaling of 0.05,0.5,0.95 quantile of the GMPE distribution (black) and the ModelA distribution (red) with total weights, for a scenario with $R_x = -50.$, $F = -1$, and $T = 1.$.

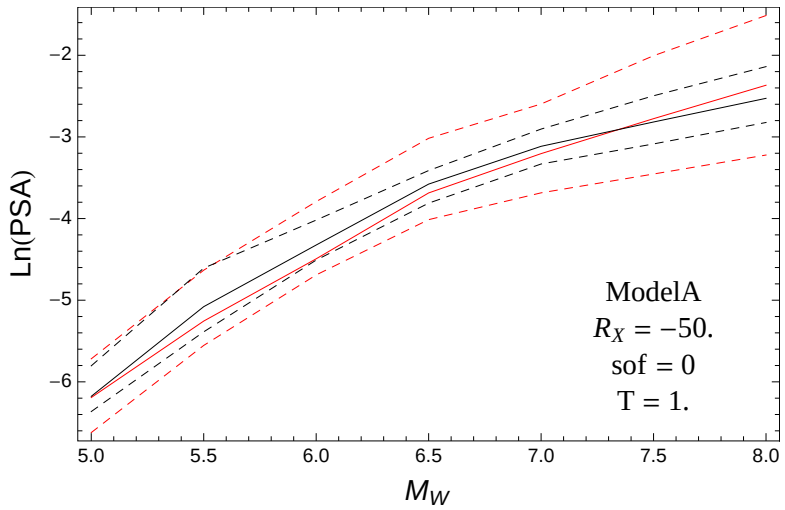



Figure 3.363: PVNGS2: Magnitude scaling of 0.05,0.5,0.95 quantile of the GMPE distribution (black) and the ModelA distribution (red) with total weights, for a scenario with $R_x = -50.$, $F = 0$, and $T = 1.$.

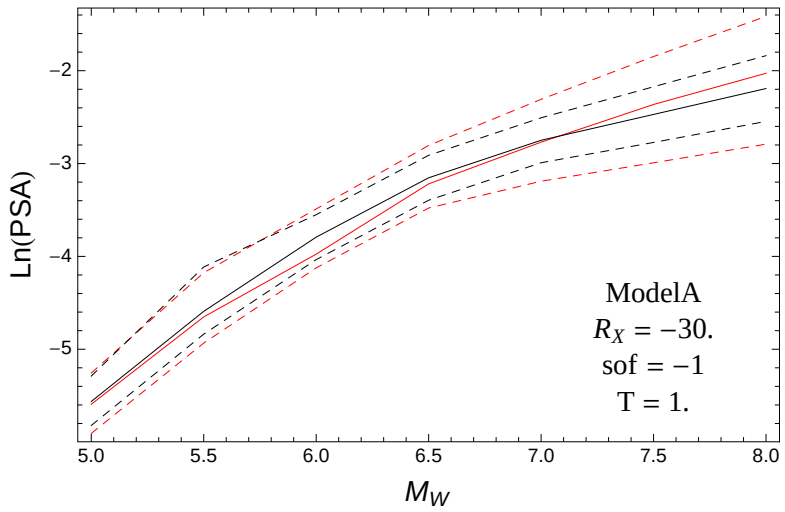



Figure 3.364: PVNGS2: Magnitude scaling of 0.05,0.5,0.95 quantile of the GMPE distribution (black) and the ModelA distribution (red) with total weights, for a scenario with $R_x = -30.$, $F = -1$, and $T = 1.$.

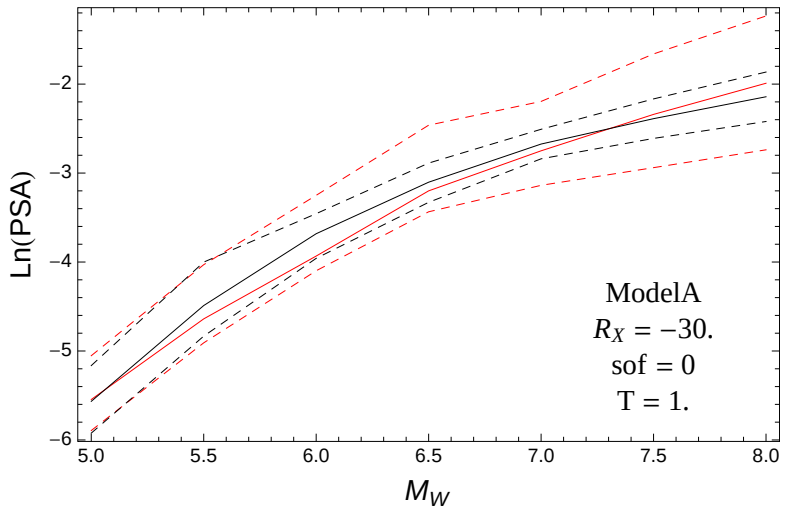



Figure 3.365: PVNGS2: Magnitude scaling of 0.05,0.5,0.95 quantile of the GMPE distribution (black) and the ModelA distribution (red) with total weights, for a scenario with $R_x = -30.$, $F = 0$, and $T = 1.$.

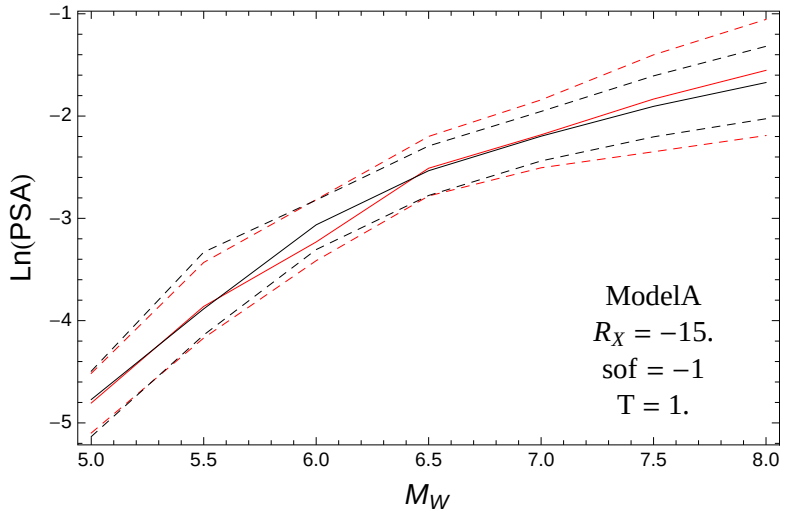



Figure 3.366: PVNGS2: Magnitude scaling of 0.05,0.5,0.95 quantile of the GMPE distribution (black) and the ModelA distribution (red) with total weights, for a scenario with $R_x = -15.$, $F = -1$, and $T = 1.$.

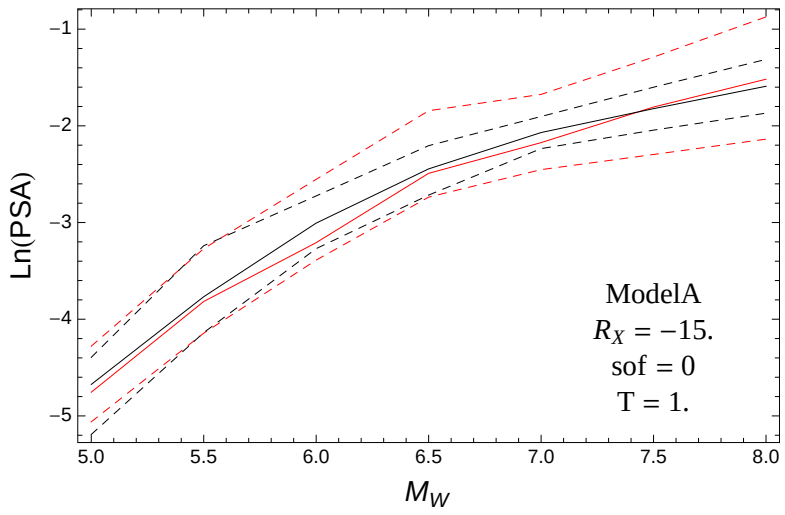



Figure 3.367: PVNGS2: Magnitude scaling of 0.05,0.5,0.95 quantile of the GMPE distribution (black) and the ModelA distribution (red) with total weights, for a scenario with $R_x = -15.$, $F = 0$, and $T = 1.$.

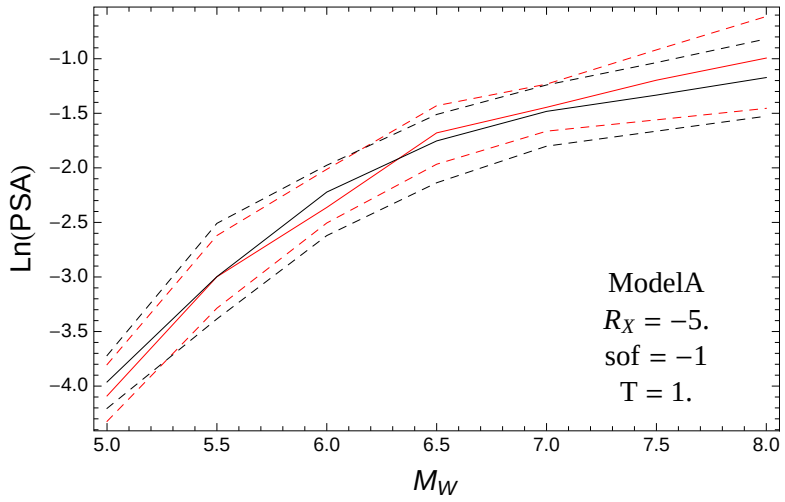



Figure 3.368: PVNGS2: Magnitude scaling of 0.05,0.5,0.95 quantile of the GMPE distribution (black) and the ModelA distribution (red) with total weights, for a scenario with $R_x = -5.$, $F = -1$, and $T = 1.$.

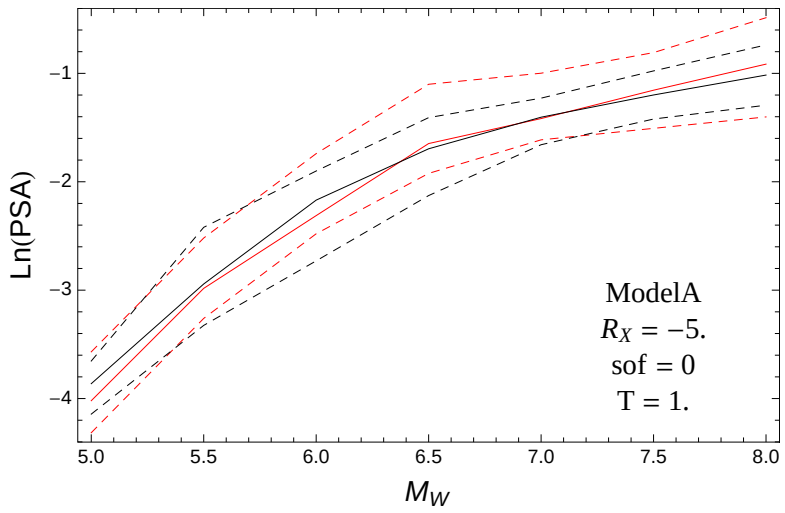



Figure 3.369: PVNGS2: Magnitude scaling of 0.05,0.5,0.95 quantile of the GMPE distribution (black) and the ModelA distribution (red) with total weights, for a scenario with $R_x = -5.$, $F = 0$, and $T = 1.$.

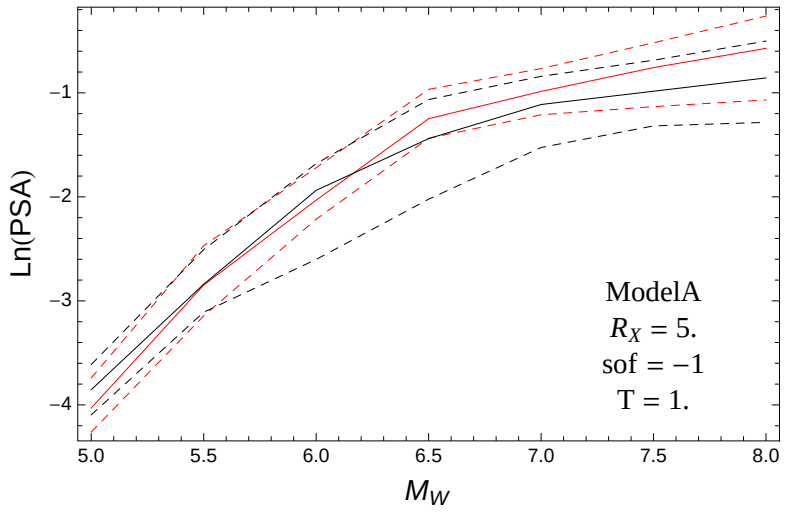



Figure 3.370: PVNGS2: Magnitude scaling of 0.05,0.5,0.95 quantile of the GMPE distribution (black) and the ModelA distribution (red) with total weights, for a scenario with $R_x = 5.$, $F = -1$, and $T = 1.$.

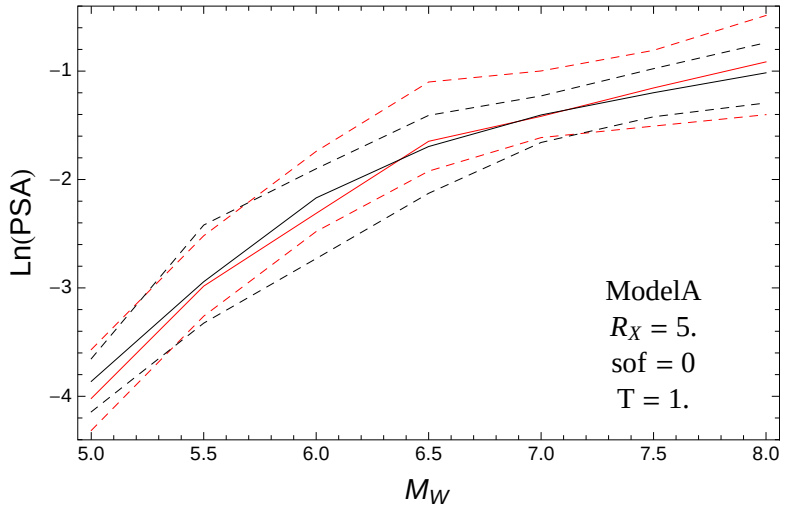



Figure 3.371: PVNGS2: Magnitude scaling of 0.05,0.5,0.95 quantile of the GMPE distribution (black) and the ModelA distribution (red) with total weights, for a scenario with $R_x = 5.$, $F = 0$, and $T = 1.$.

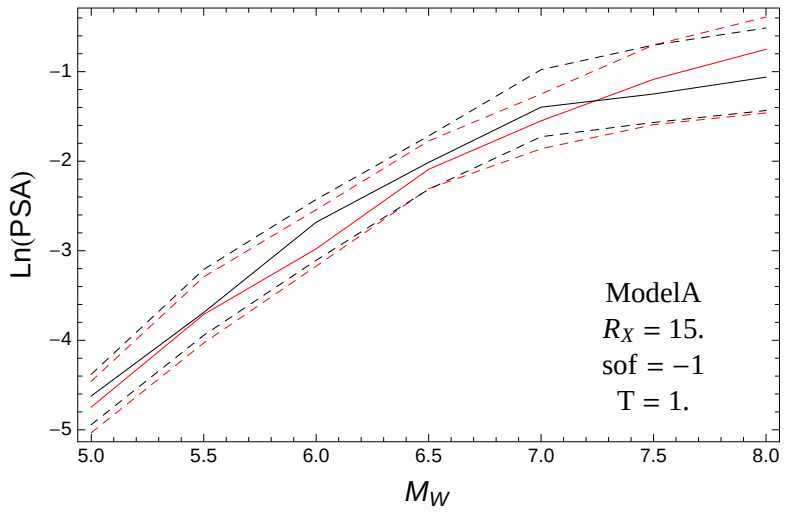



Figure 3.372: PVNGS2: Magnitude scaling of 0.05,0.5,0.95 quantile of the GMPE distribution (black) and the ModelA distribution (red) with total weights, for a scenario with $R_x = 15.$, $F = -1$, and $T = 1.$.

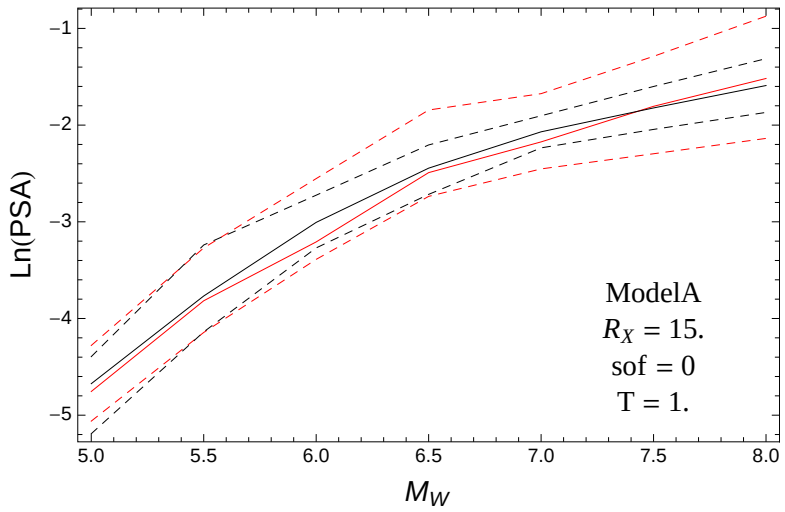



Figure 3.373: PVNGS2: Magnitude scaling of 0.05,0.5,0.95 quantile of the GMPE distribution (black) and the ModelA distribution (red) with total weights, for a scenario with $R_x = 15.$, $F = 0$, and $T = 1.$.

**T = 3.s**

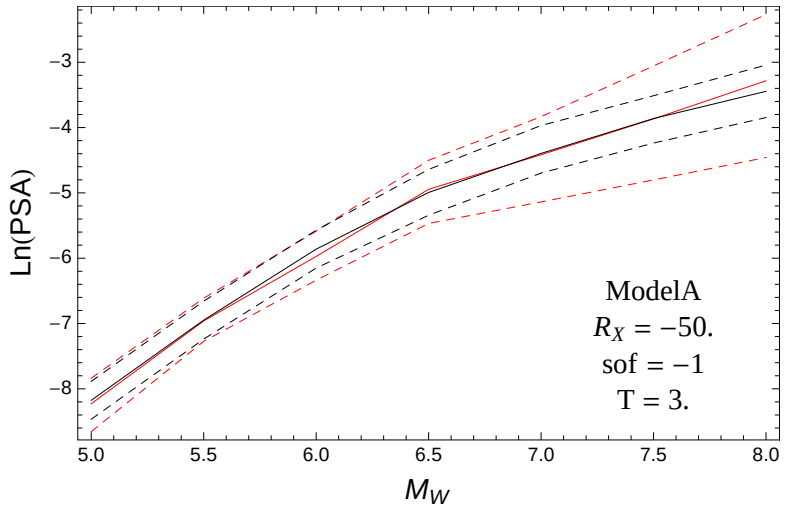



Figure 3.374: PVNGS2: Magnitude scaling of 0.05,0.5,0.95 quantile of the GMPE distribution (black) and the ModelA distribution (red) with total weights, for a scenario with $R_x = -50.$, $F = -1$, and $T = 3.$.

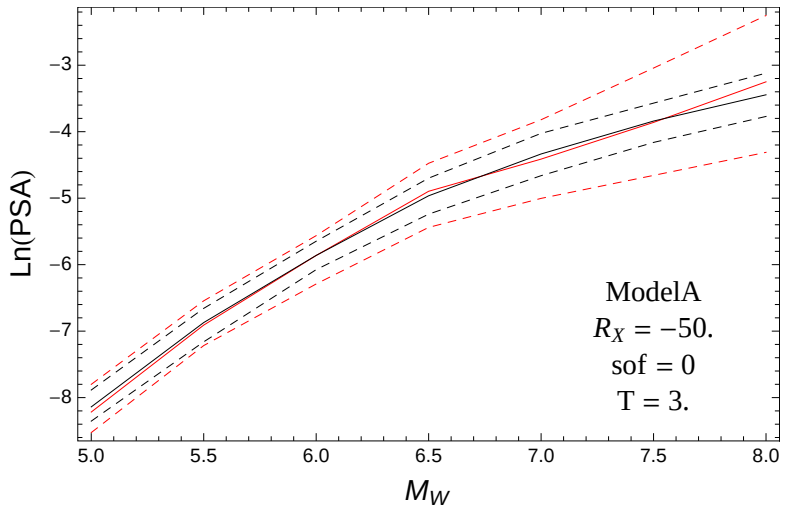



Figure 3.375: PVNGS2: Magnitude scaling of 0.05,0.5,0.95 quantile of the GMPE distribution (black) and the ModelA distribution (red) with total weights, for a scenario with $R_x = -50.$, $F = 0$, and $T = 3.$.

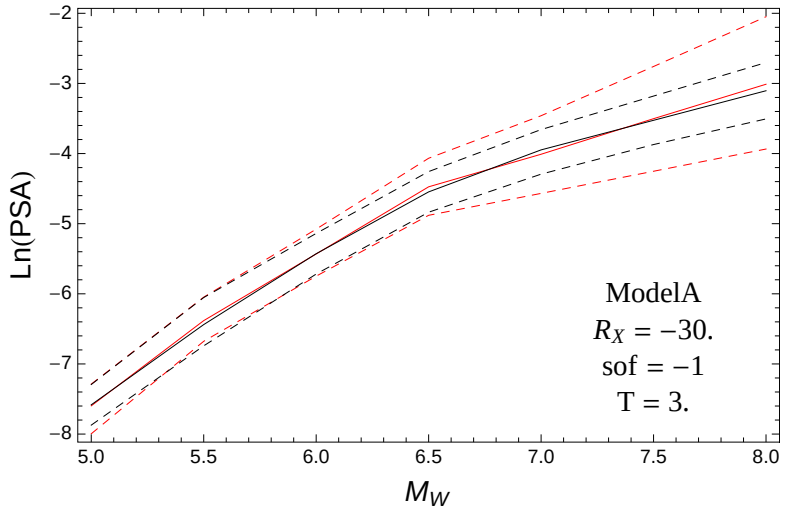



Figure 3.376: PVNGS2: Magnitude scaling of 0.05,0.5,0.95 quantile of the GMPE distribution (black) and the ModelA distribution (red) with total weights, for a scenario with $R_x = -30.$, $F = -1$, and $T = 3.$.

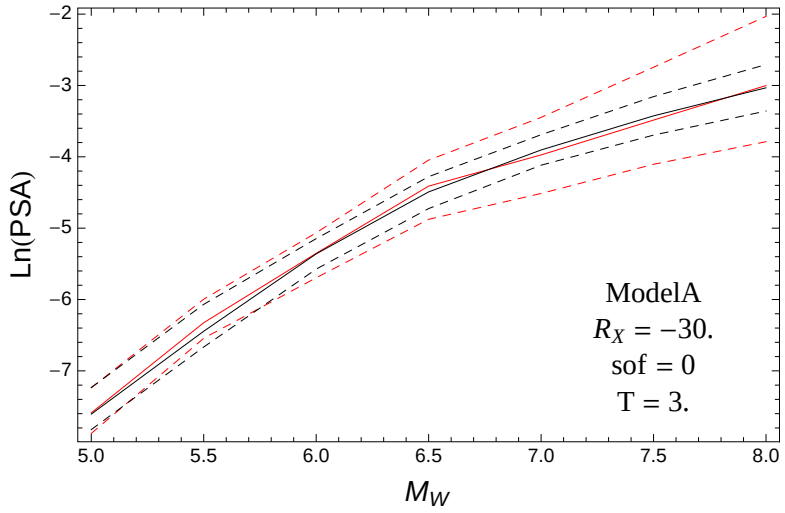



Figure 3.377: PVNGS2: Magnitude scaling of 0.05,0.5,0.95 quantile of the GMPE distribution (black) and the ModelA distribution (red) with total weights, for a scenario with $R_x = -30.$, $F = 0$, and $T = 3.$.

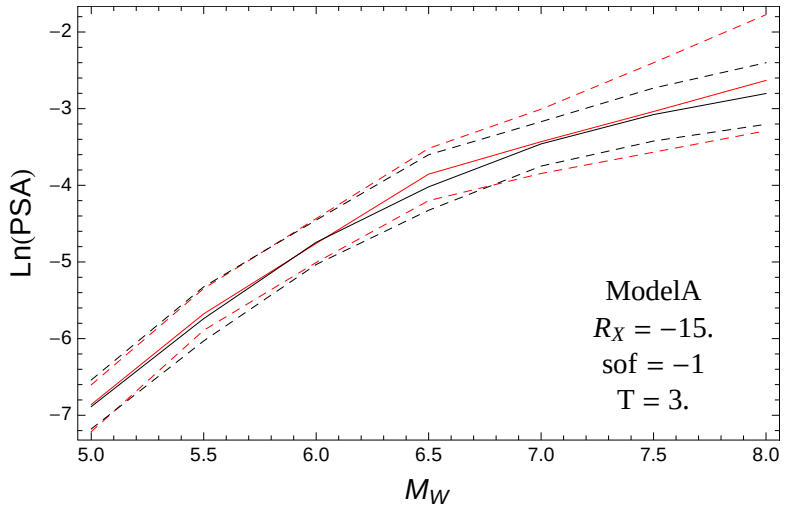



Figure 3.378: PVNGS2: Magnitude scaling of 0.05,0.5,0.95 quantile of the GMPE distribution (black) and the ModelA distribution (red) with total weights, for a scenario with $R_x = -15.$, $F = -1$, and $T = 3.$.

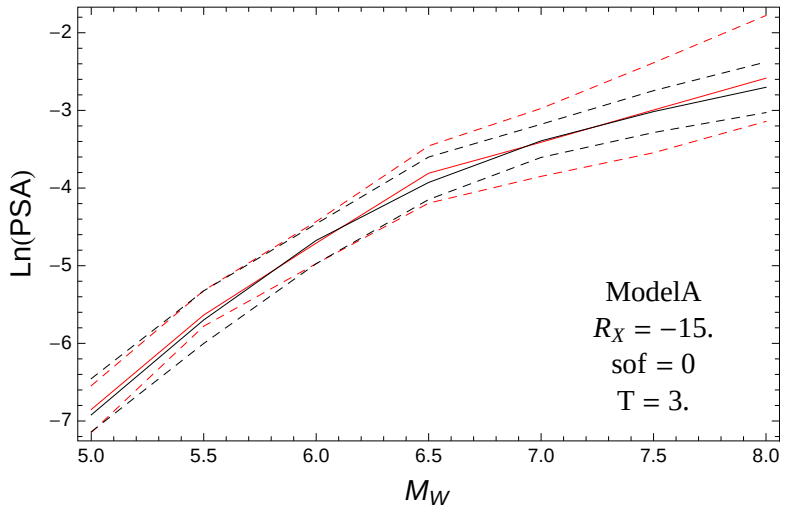



Figure 3.379: PVNGS2: Magnitude scaling of 0.05,0.5,0.95 quantile of the GMPE distribution (black) and the ModelA distribution (red) with total weights, for a scenario with $R_x = -15.$, $F = 0$, and $T = 3.$.

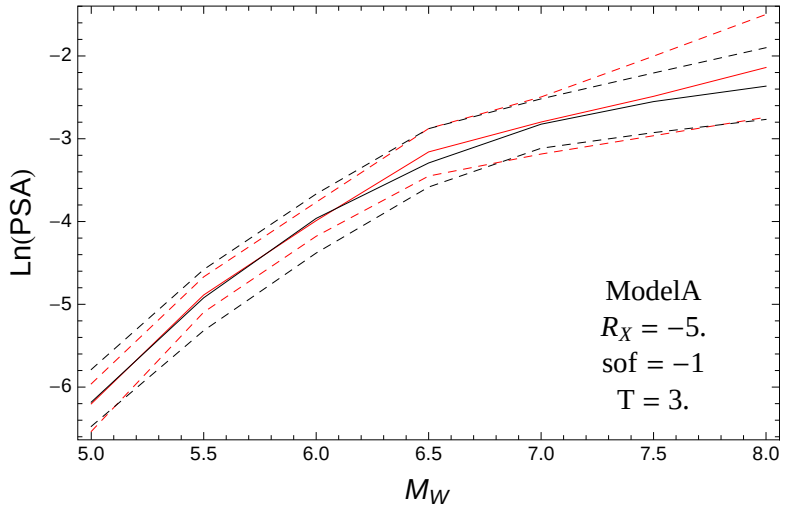



Figure 3.380: PVNGS2: Magnitude scaling of 0.05,0.5,0.95 quantile of the GMPE distribution (black) and the ModelA distribution (red) with total weights, for a scenario with $R_x = -5.$, $F = -1$, and $T = 3.$.

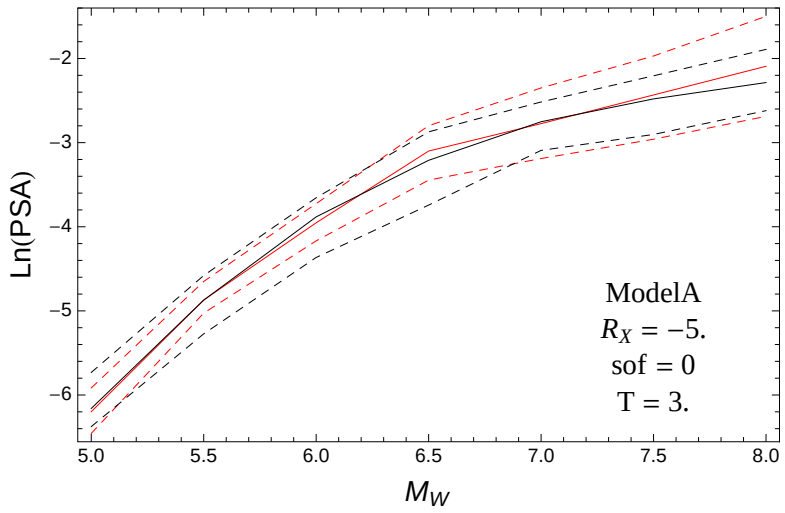



Figure 3.381: PVNGS2: Magnitude scaling of 0.05,0.5,0.95 quantile of the GMPE distribution (black) and the ModelA distribution (red) with total weights, for a scenario with $R_x = -5.$, $F = 0$, and $T = 3.$.

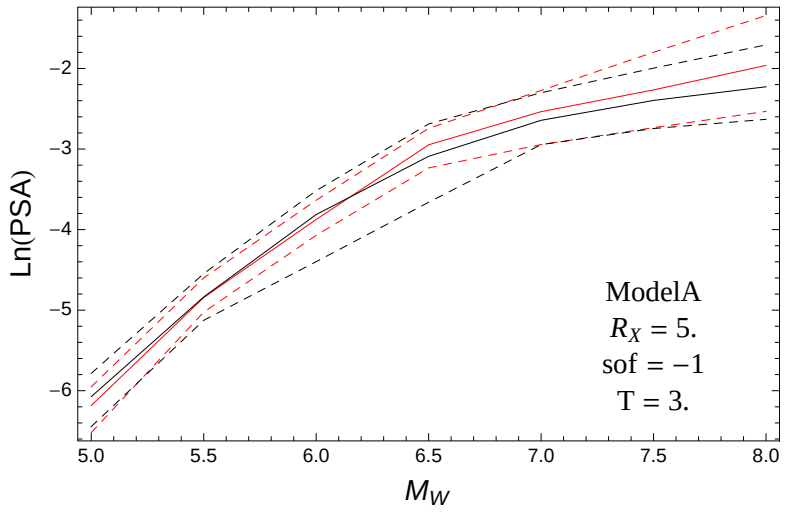



Figure 3.382: PVNGS2: Magnitude scaling of 0.05,0.5,0.95 quantile of the GMPE distribution (black) and the ModelA distribution (red) with total weights, for a scenario with $R_x = 5.$, $F = -1$, and $T = 3.$.

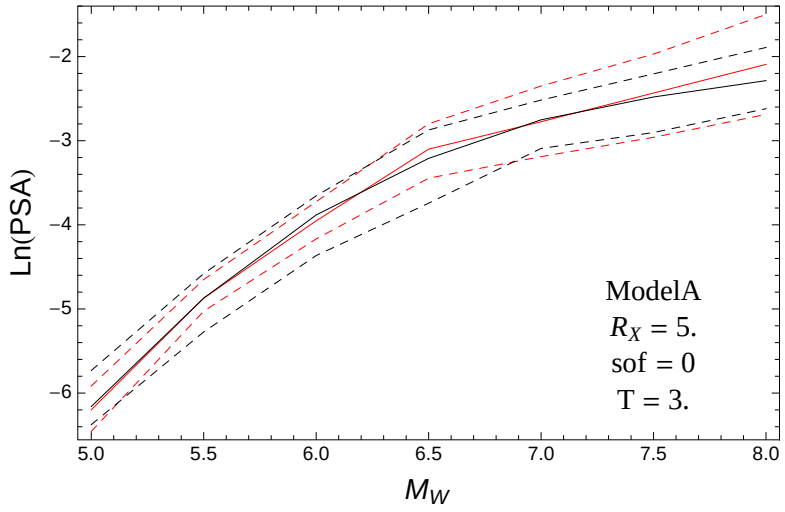



Figure 3.383: PVNGS2: Magnitude scaling of 0.05,0.5,0.95 quantile of the GMPE distribution (black) and the ModelA distribution (red) with total weights, for a scenario with $R_x = 5.$, $F = 0$, and $T = 3.$.

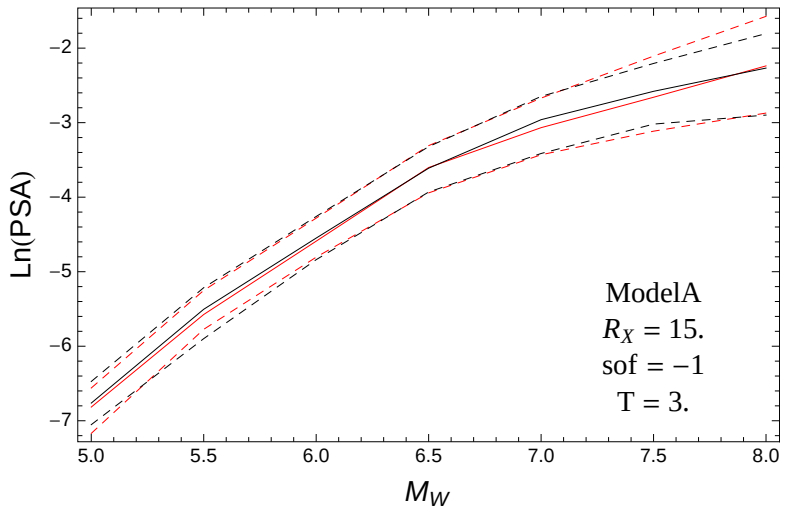



Figure 3.384: PVNGS2: Magnitude scaling of 0.05,0.5,0.95 quantile of the GMPE distribution (black) and the ModelA distribution (red) with total weights, for a scenario with $R_x = 15.$, $F = -1$, and $T = 3.$.

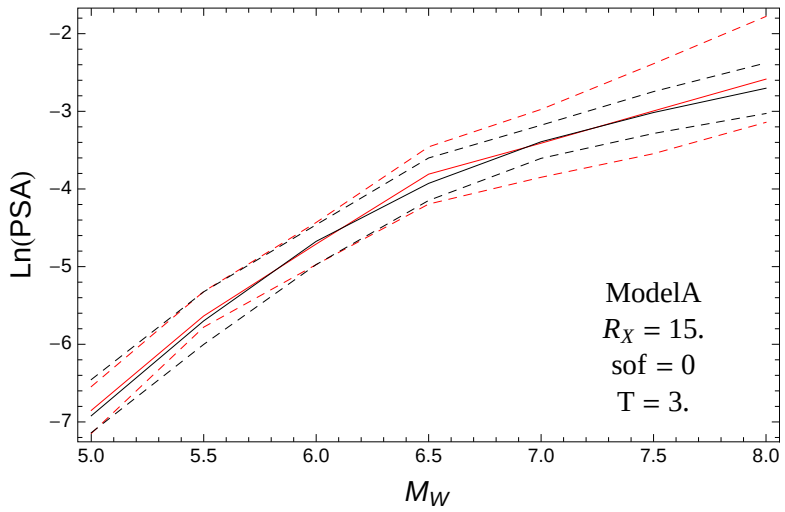



Figure 3.385: PVNGS2: Magnitude scaling of 0.05,0.5,0.95 quantile of the GMPE distribution (black) and the ModelA distribution (red) with total weights, for a scenario with $R_x = 15.$, $F = 0$, and $T = 3.$.

### 3.1.9 Quantile Plots vs. Period

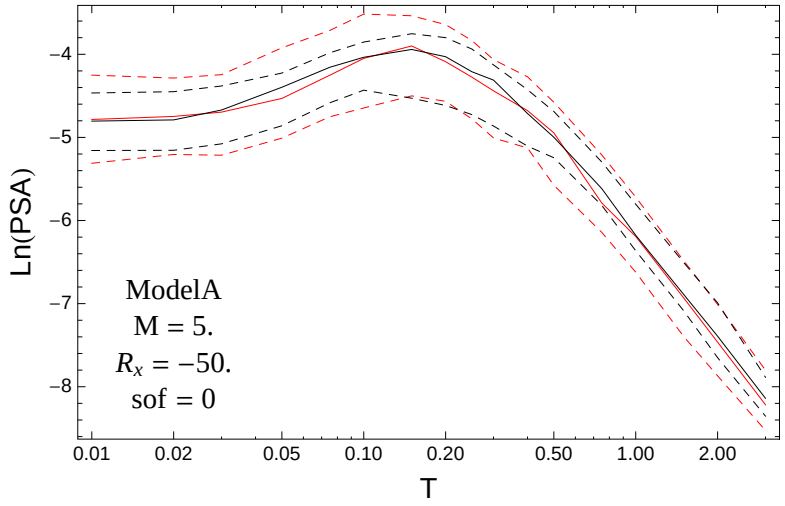



Figure 3.386: PVNGSv2: Spectra of 0.05,0.5,0.95 quantile of the GMPE distribution (black) and the model distribution (red) with total weights, for a scenario with $M_W = 5.$, $R_x = -50.$, $F = 0$.

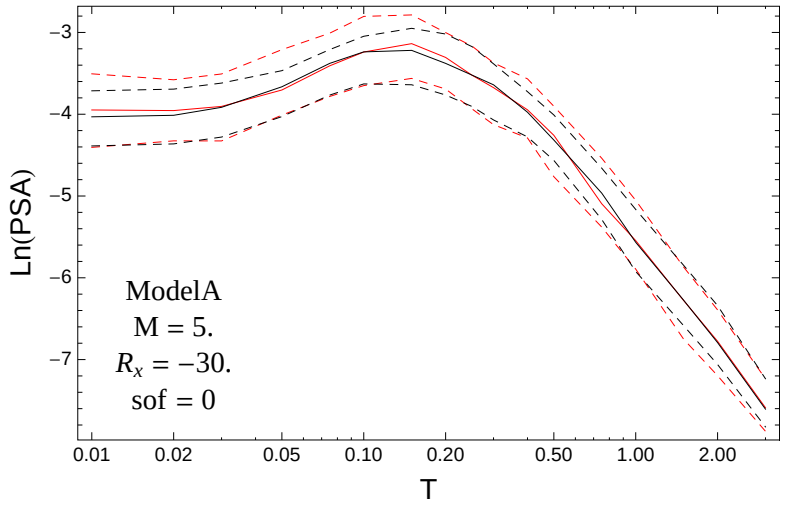



Figure 3.387: PVNGSv2: Spectra of 0.05,0.5,0.95 quantile of the GMPE distribution (black) and the model distribution (red) with total weights, for a scenario with $M_W = 5.$, $R_x = -30.$, $F = 0$.

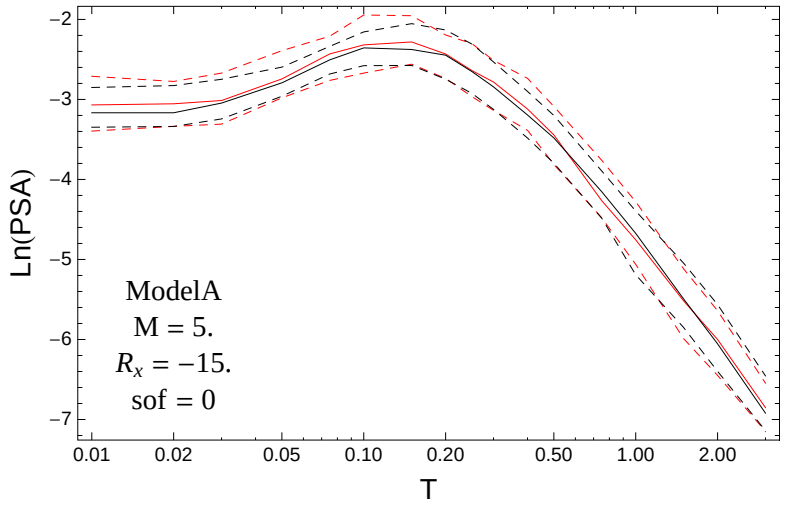



Figure 3.388: PVNGSv2: Spectra of 0.05,0.5,0.95 quantile of the GMPE distribution (black) and the model distribution (red) with total weights, for a scenario with $M_W = 5.$, $R_x = -15.$, $F = 0$.

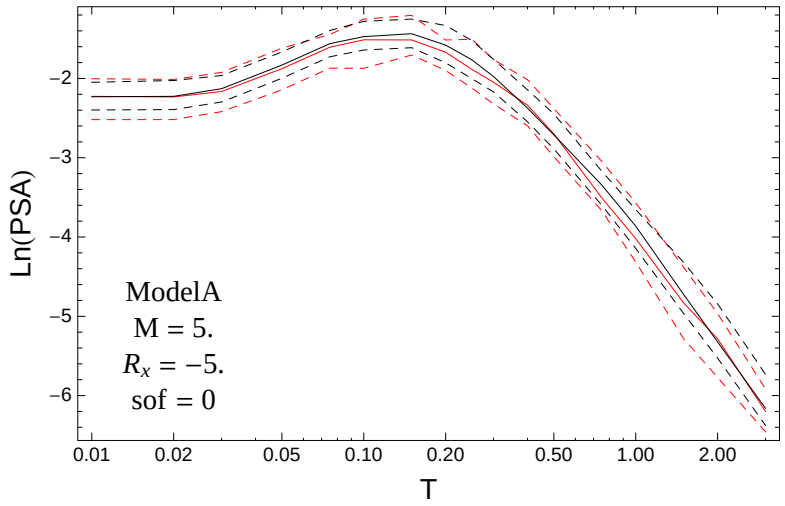



Figure 3.389: PVNGSv2: Spectra of 0.05,0.5,0.95 quantile of the GMPE distribution (black) and the model distribution (red) with total weights, for a scenario with $M_W = 5.$, $R_x = -5.$, $F = 0$.

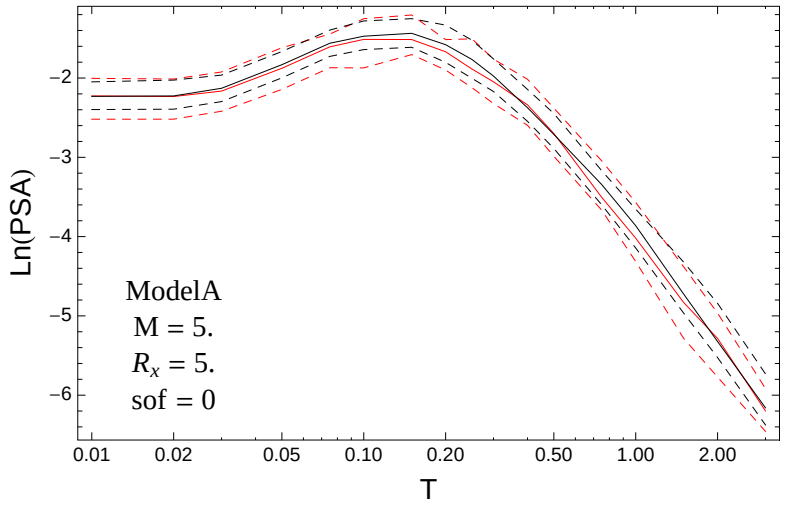



Figure 3.390: PVNGSv2: Spectra of 0.05,0.5,0.95 quantile of the GMPE distribution (black) and the model distribution (red) with total weights, for a scenario with $M_W = 5.$, $R_x = 5.$, $F = 0$.

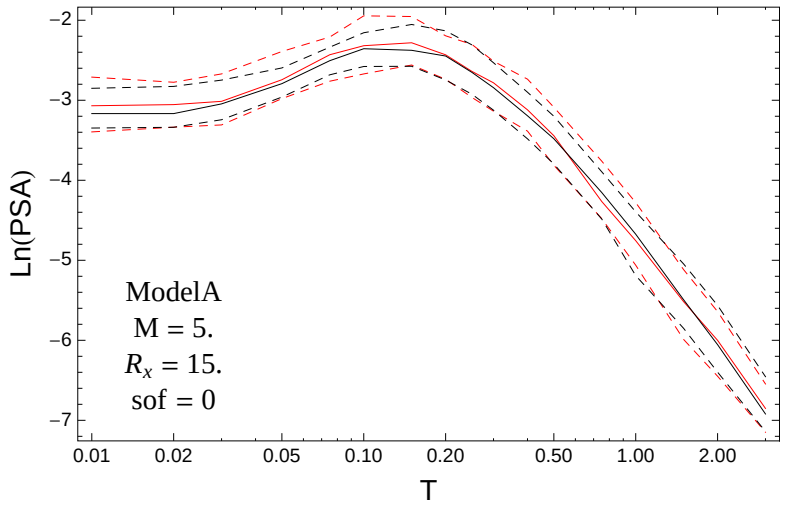



Figure 3.391: PVNGSv2: Spectra of 0.05,0.5,0.95 quantile of the GMPE distribution (black) and the model distribution (red) with total weights, for a scenario with $M_W = 5.$, $R_x = 15.$, $F = 0$.

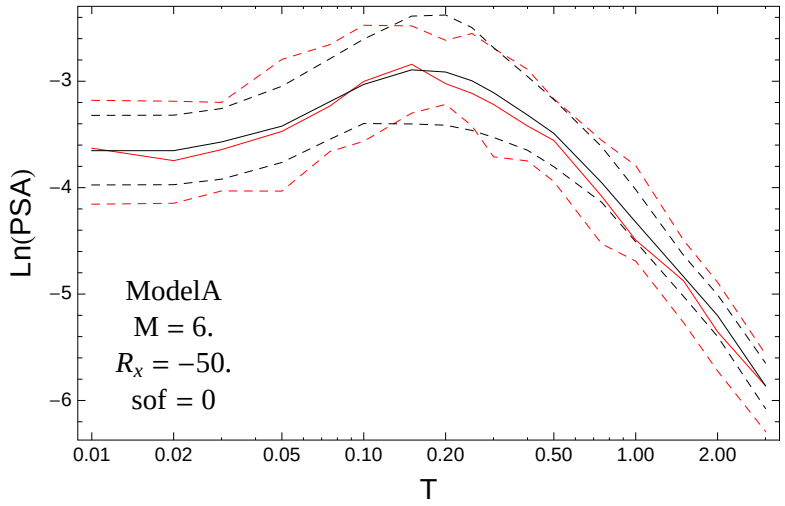



Figure 3.392: PVNGSv2: Spectra of 0.05,0.5,0.95 quantile of the GMPE distribution (black) and the model distribution (red) with total weights, for a scenario with $M_W = 6.$, $R_x = -50.$, $F = 0$.

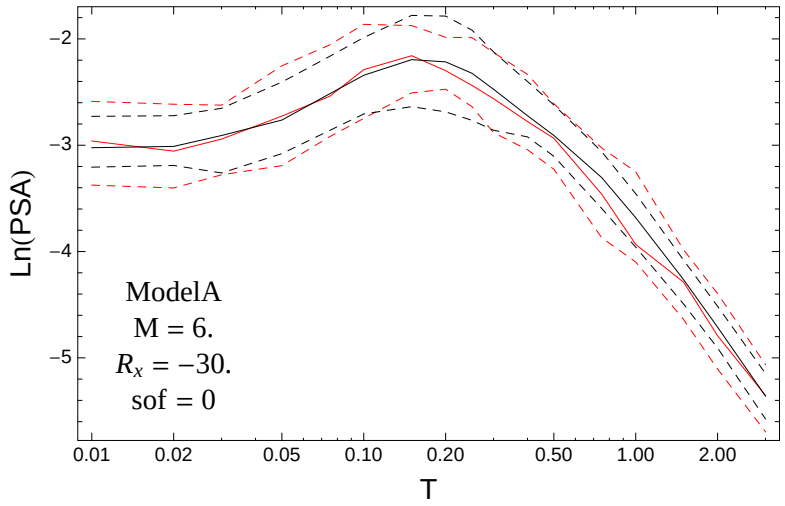



Figure 3.393: PVNGSv2: Spectra of 0.05,0.5,0.95 quantile of the GMPE distribution (black) and the model distribution (red) with total weights, for a scenario with $M_W = 6.$, $R_x = -30.$, $F = 0$.

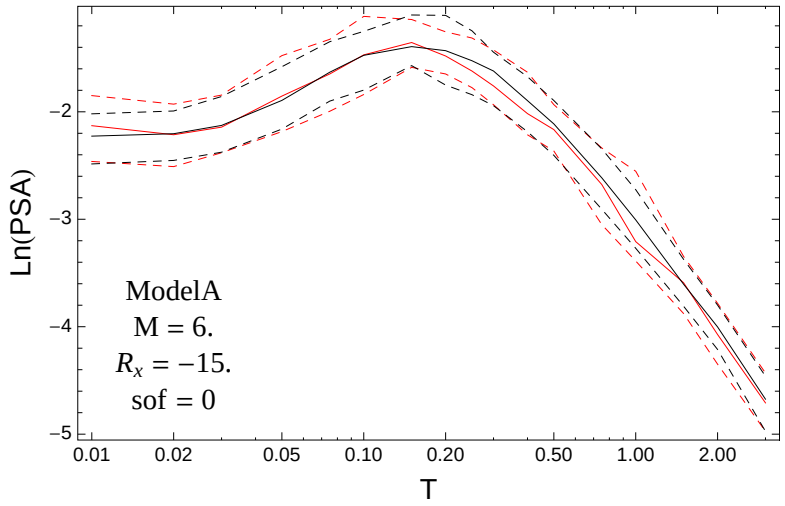



Figure 3.394: PVNGSv2: Spectra of 0.05,0.5,0.95 quantile of the GMPE distribution (black) and the model distribution (red) with total weights, for a scenario with $M_W = 6.$, $R_x = -15.$, $F = 0$.

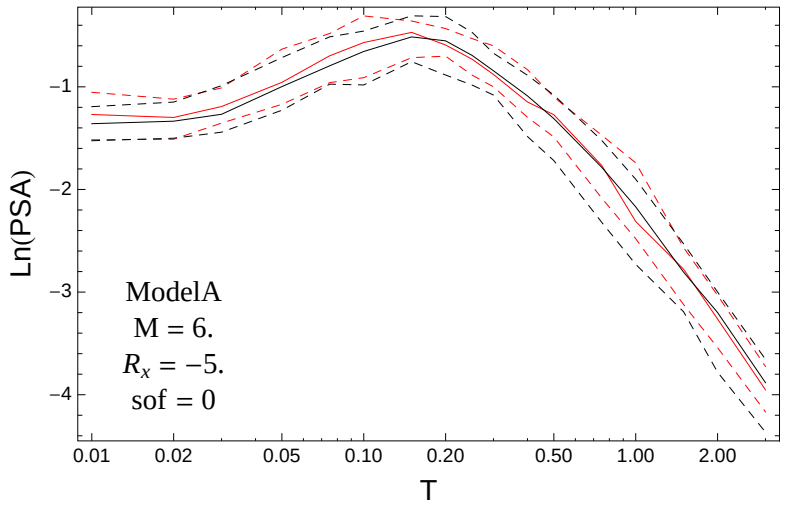



Figure 3.395: PVNGSv2: Spectra of 0.05,0.5,0.95 quantile of the GMPE distribution (black) and the model distribution (red) with total weights, for a scenario with $M_W = 6.$, $R_x = -5.$, $F = 0$.

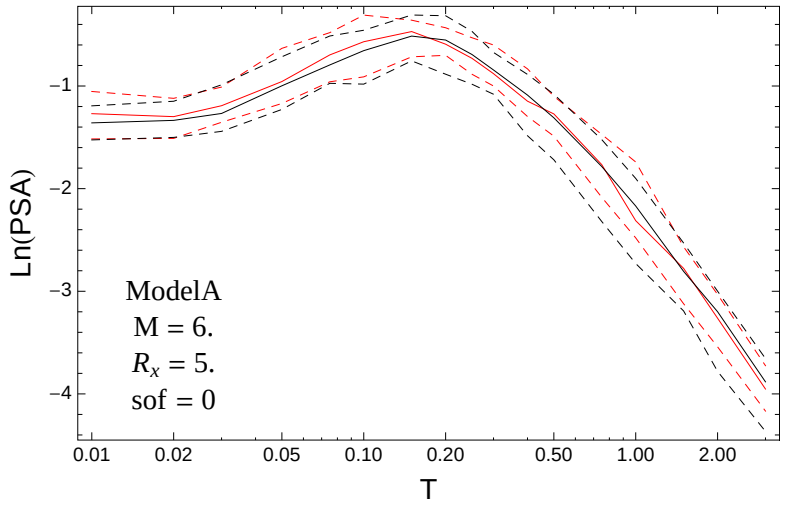



Figure 3.396: PVNGSv2: Spectra of 0.05,0.5,0.95 quantile of the GMPE distribution (black) and the model distribution (red) with total weights, for a scenario with $M_W = 6.$, $R_x = 5.$, $F = 0$.

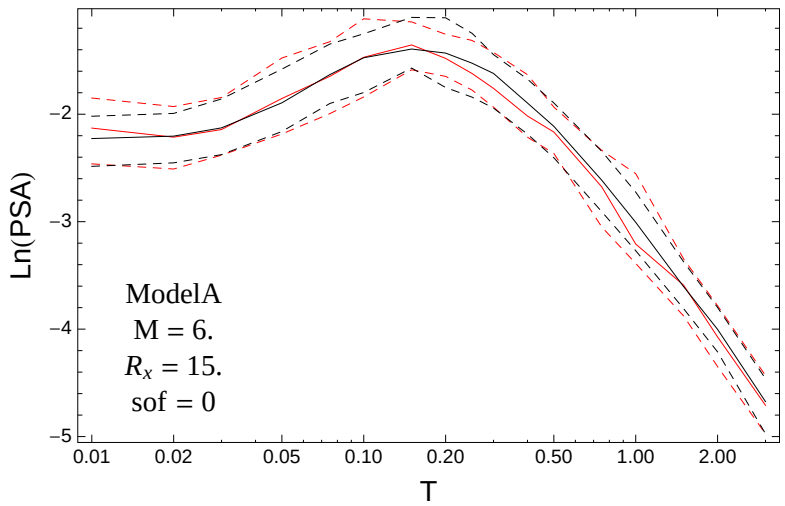



Figure 3.397: PVNGSv2: Spectra of 0.05,0.5,0.95 quantile of the GMPE distribution (black) and the model distribution (red) with total weights, for a scenario with $M_W = 6.$, $R_x = 15.$, $F = 0$.

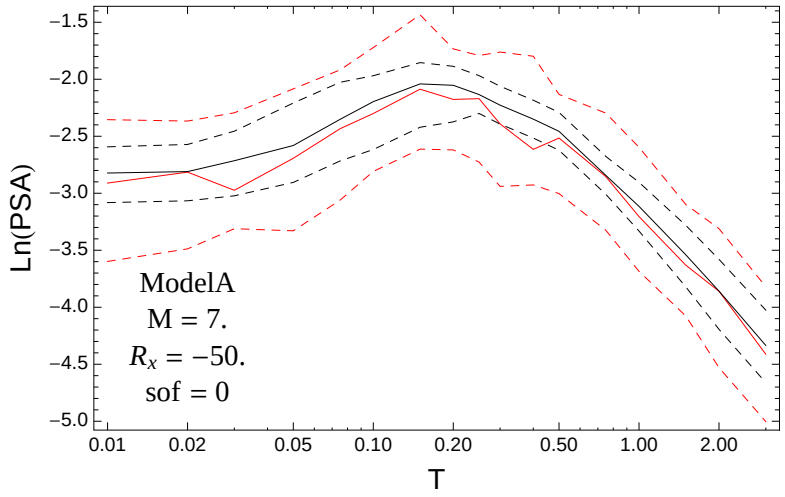



Figure 3.398: PVNGSv2: Spectra of 0.05,0.5,0.95 quantile of the GMPE distribution (black) and the model distribution (red) with total weights, for a scenario with $M_W = 7.$, $R_x = -50.$, $F = 0$.

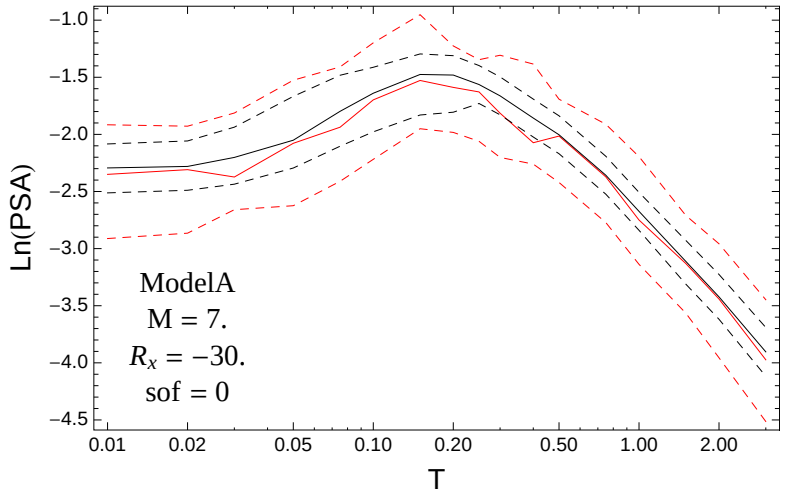



Figure 3.399: PVNGSv2: Spectra of 0.05,0.5,0.95 quantile of the GMPE distribution (black) and the model distribution (red) with total weights, for a scenario with $M_W = 7.$, $R_x = -30.$, $F = 0$.

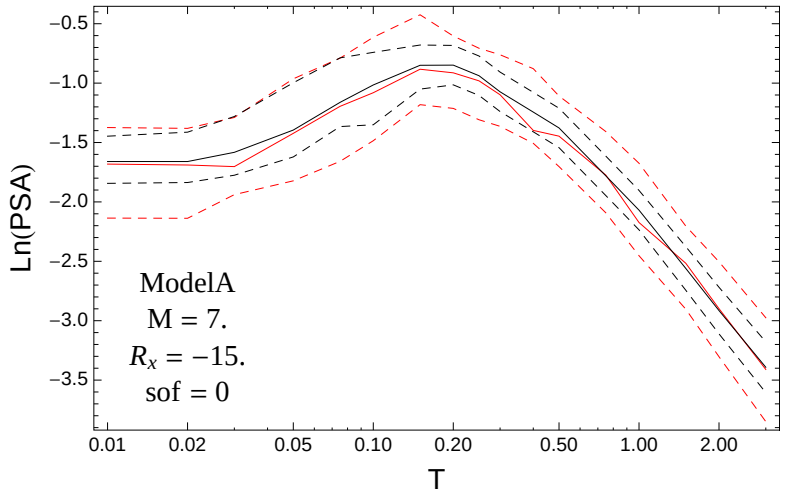



Figure 3.400: PVNGSv2: Spectra of 0.05,0.5,0.95 quantile of the GMPE distribution (black) and the model distribution (red) with total weights, for a scenario with $M_W = 7.$, $R_x = -15.$, $F = 0$.

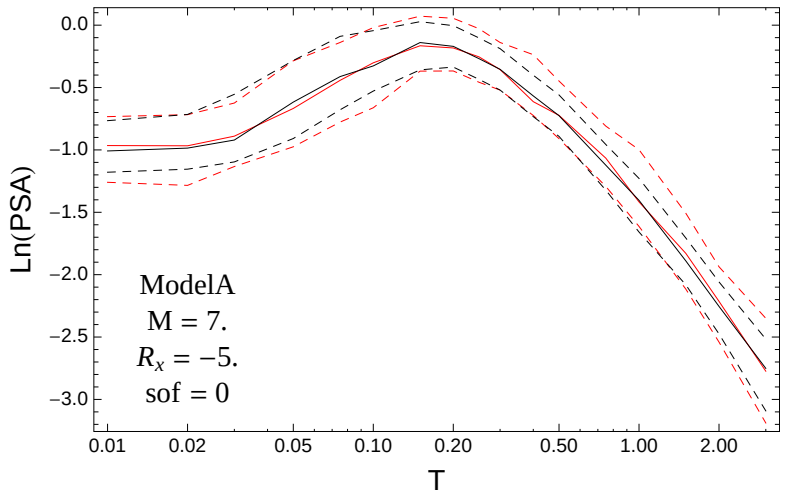



Figure 3.401: PVNGSv2: Spectra of 0.05,0.5,0.95 quantile of the GMPE distribution (black) and the model distribution (red) with total weights, for a scenario with $M_W = 7.$, $R_x = -5.$, $F = 0$.

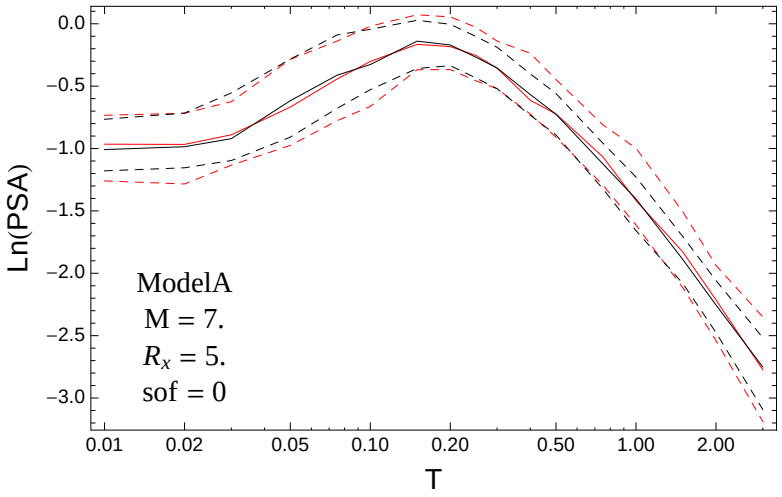



Figure 3.402: PVNGSv2: Spectra of 0.05,0.5,0.95 quantile of the GMPE distribution (black) and the model distribution (red) with total weights, for a scenario with $M_W = 7.$, $R_x = 5.$, $F = 0$.

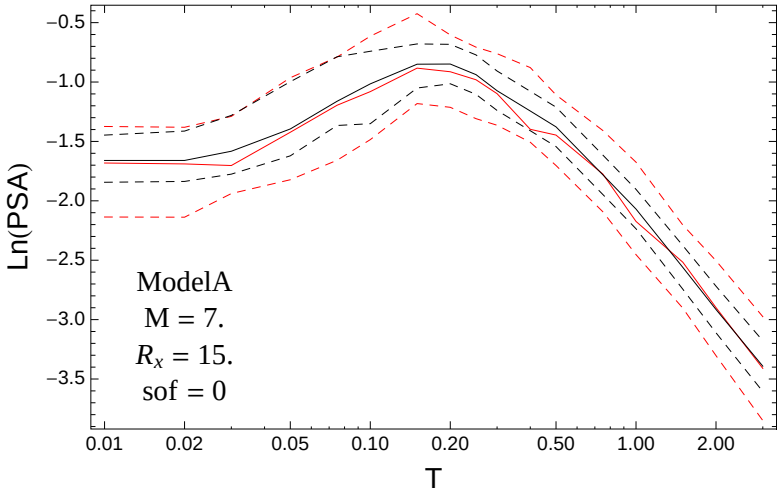



Figure 3.403: PVNGSv2: Spectra of 0.05,0.5,0.95 quantile of the GMPE distribution (black) and the model distribution (red) with total weights, for a scenario with $M_W = 7.$, $R_x = 15.$, $F = 0$.

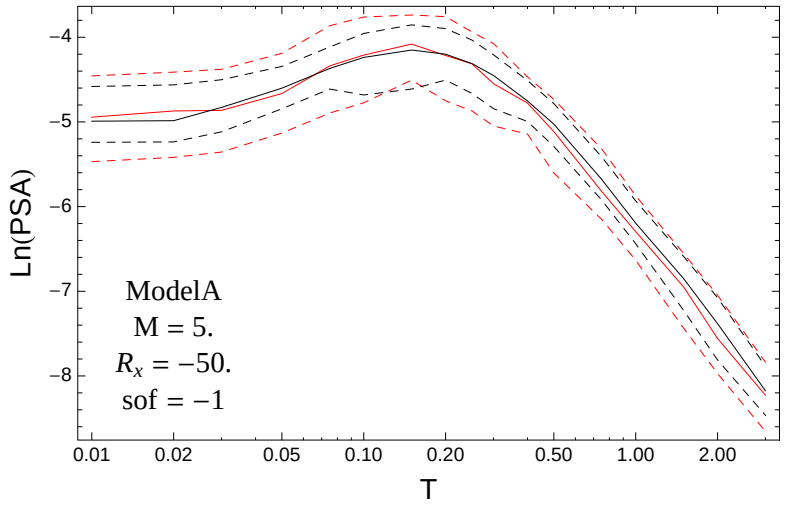



Figure 3.404: PVNGSv2: Spectra of 0.05,0.5,0.95 quantile of the GMPE distribution (black) and the model distribution (red) with total weights, for a scenario with $M_W = 5.$, $R_x = -50.$, $F = -1$.

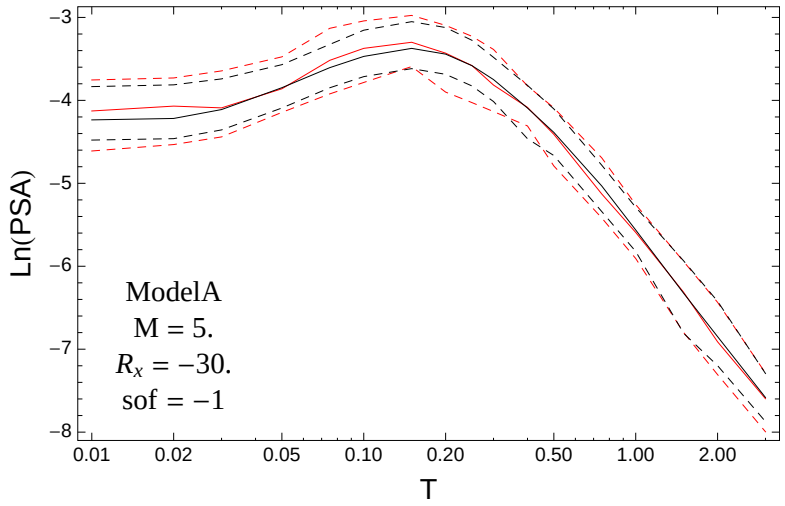



Figure 3.405: PVNGSv2: Spectra of 0.05,0.5,0.95 quantile of the GMPE distribution (black) and the model distribution (red) with total weights, for a scenario with $M_W = 5.$, $R_x = -30.$, $F = -1$.

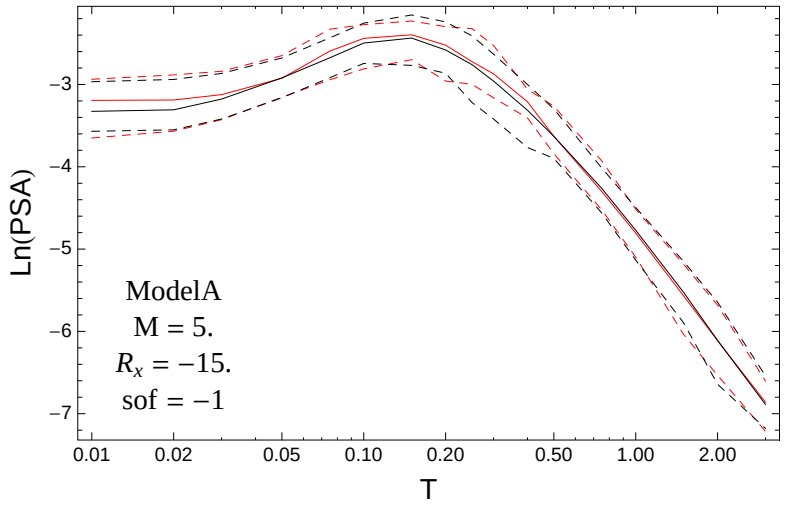



Figure 3.406: PVNGSv2: Spectra of 0.05,0.5,0.95 quantile of the GMPE distribution (black) and the model distribution (red) with total weights, for a scenario with $M_W = 5.$, $R_x = -15.$, $F = -1$.

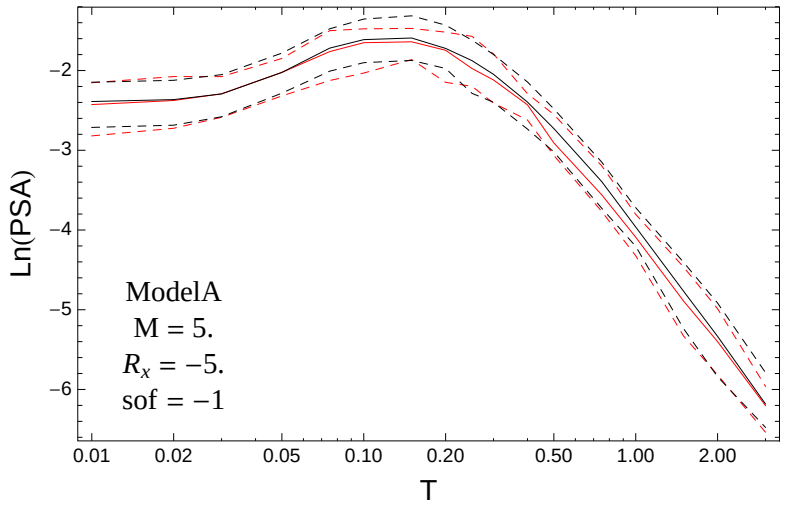



Figure 3.407: PVNGSv2: Spectra of 0.05,0.5,0.95 quantile of the GMPE distribution (black) and the model distribution (red) with total weights, for a scenario with $M_W = 5.$, $R_x = -5.$, $F = -1$.

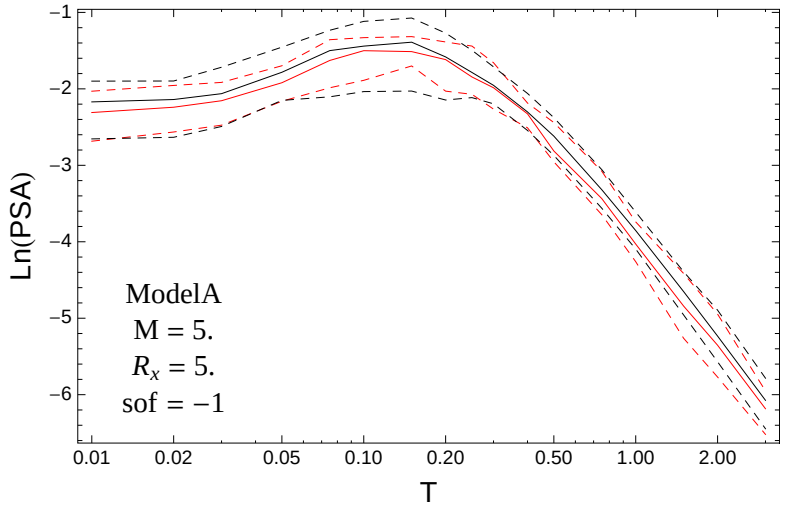



Figure 3.408: PVNGSv2: Spectra of 0.05,0.5,0.95 quantile of the GMPE distribution (black) and the model distribution (red) with total weights, for a scenario with $M_W = 5.$, $R_x = 5.$, $F = -1$.

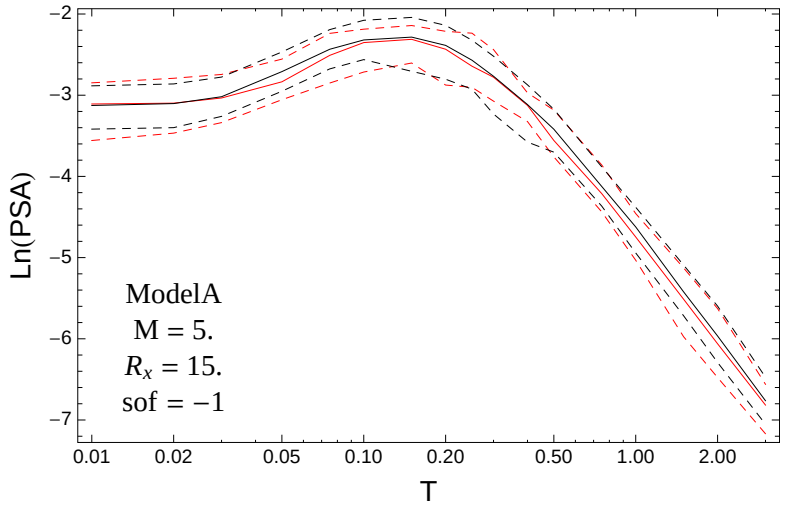



Figure 3.409: PVNGSv2: Spectra of 0.05,0.5,0.95 quantile of the GMPE distribution (black) and the model distribution (red) with total weights, for a scenario with $M_W = 5.$, $R_x = 15.$, $F = -1$.

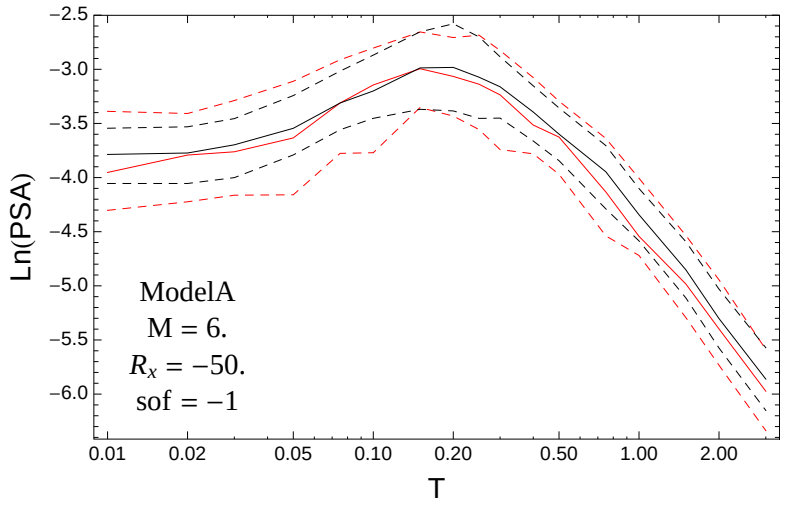



Figure 3.410: PVNGSv2: Spectra of 0.05,0.5,0.95 quantile of the GMPE distribution (black) and the model distribution (red) with total weights, for a scenario with $M_W = 6.$, $R_x = -50.$, $F = -1$.

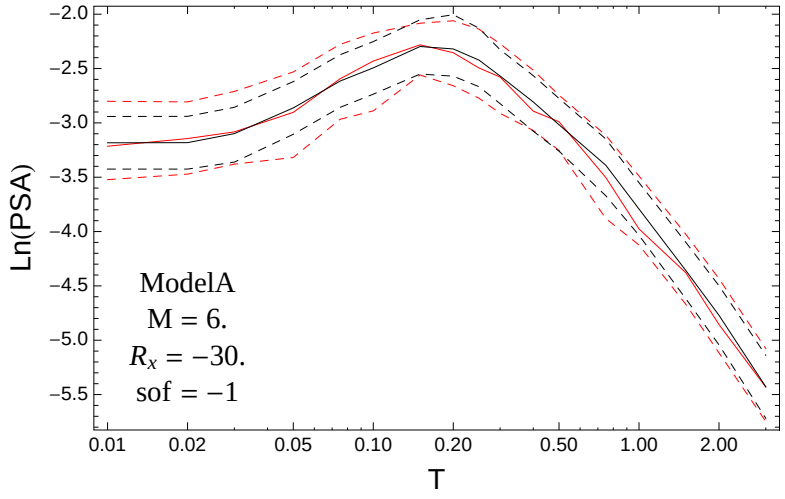



Figure 3.411: PVNGSv2: Spectra of 0.05,0.5,0.95 quantile of the GMPE distribution (black) and the model distribution (red) with total weights, for a scenario with $M_W = 6.$, $R_x = -30.$, $F = -1$.

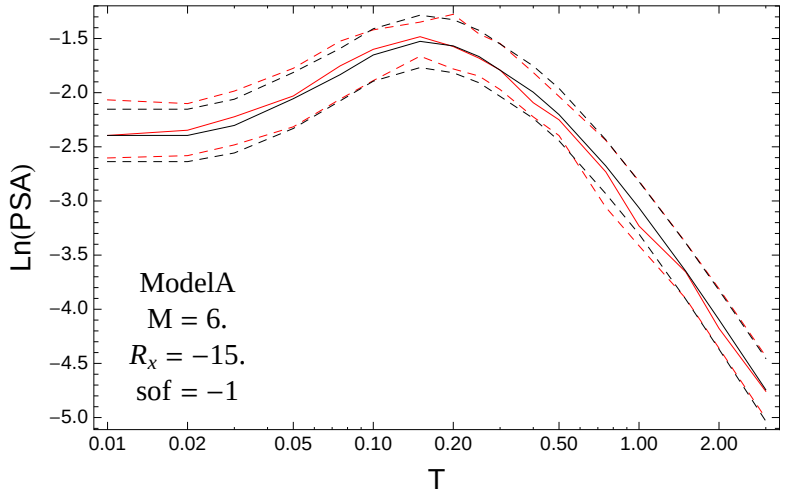



Figure 3.412: PVNGSv2: Spectra of 0.05,0.5,0.95 quantile of the GMPE distribution (black) and the model distribution (red) with total weights, for a scenario with $M_W = 6.$, $R_x = -15.$, $F = -1$.

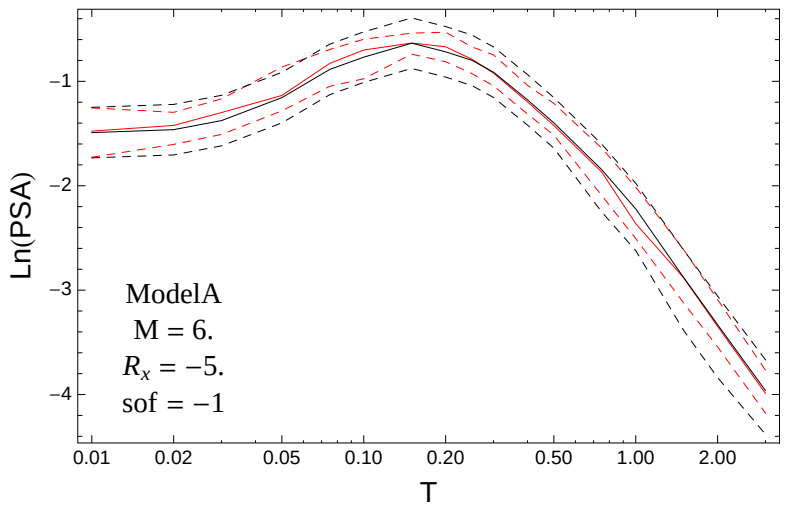



Figure 3.413: PVNGSv2: Spectra of 0.05,0.5,0.95 quantile of the GMPE distribution (black) and the model distribution (red) with total weights, for a scenario with $M_W = 6.$, $R_x = -5.$, $F = -1$.

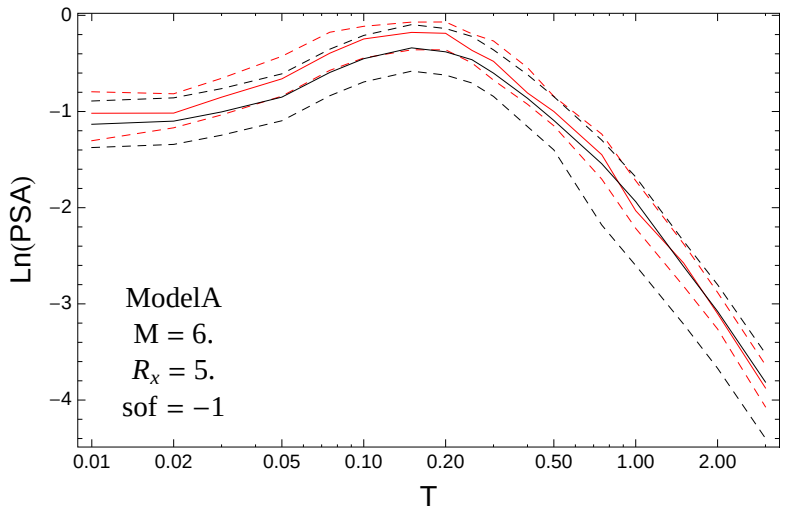



Figure 3.414: PVNGSv2: Spectra of 0.05,0.5,0.95 quantile of the GMPE distribution (black) and the model distribution (red) with total weights, for a scenario with $M_W = 6.$, $R_x = 5.$, $F = -1$.

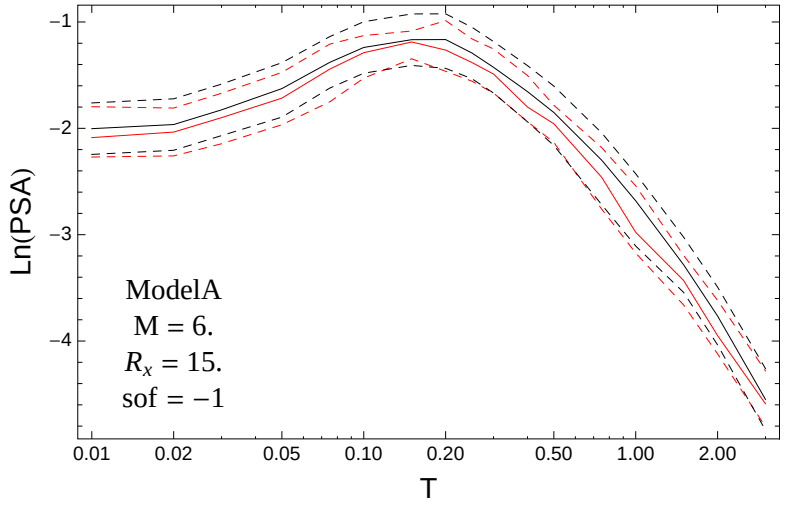



Figure 3.415: PVNGSv2: Spectra of 0.05,0.5,0.95 quantile of the GMPE distribution (black) and the model distribution (red) with total weights, for a scenario with $M_W = 6.$, $R_x = 15.$, $F = -1$.

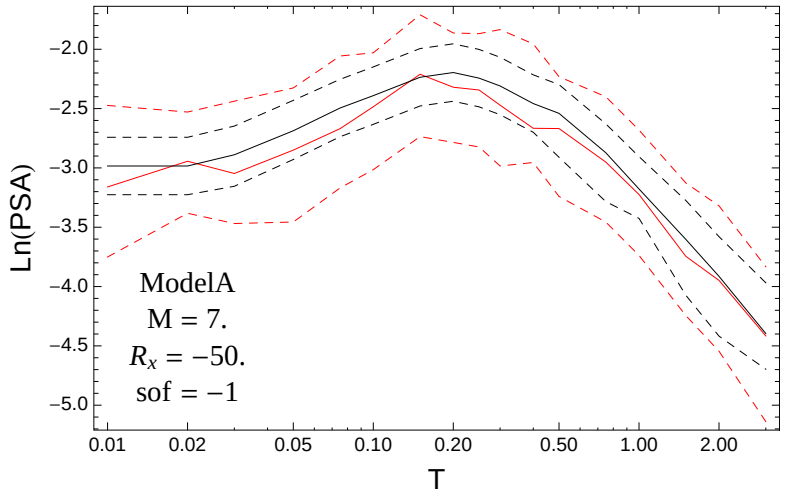



Figure 3.416: PVNGSv2: Spectra of 0.05,0.5,0.95 quantile of the GMPE distribution (black) and the model distribution (red) with total weights, for a scenario with $M_W = 7.$, $R_x = -50.$, $F = -1$.

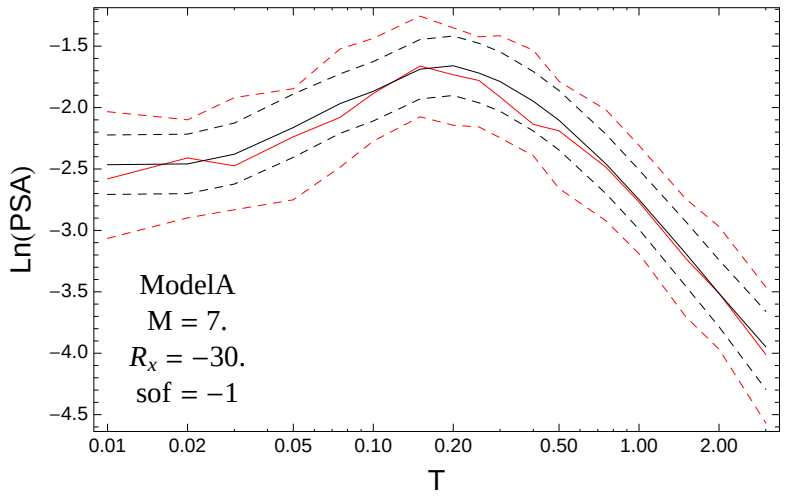



Figure 3.417: PVNGSv2: Spectra of 0.05,0.5,0.95 quantile of the GMPE distribution (black) and the model distribution (red) with total weights, for a scenario with $M_W = 7.$, $R_x = -30.$, $F = -1$.

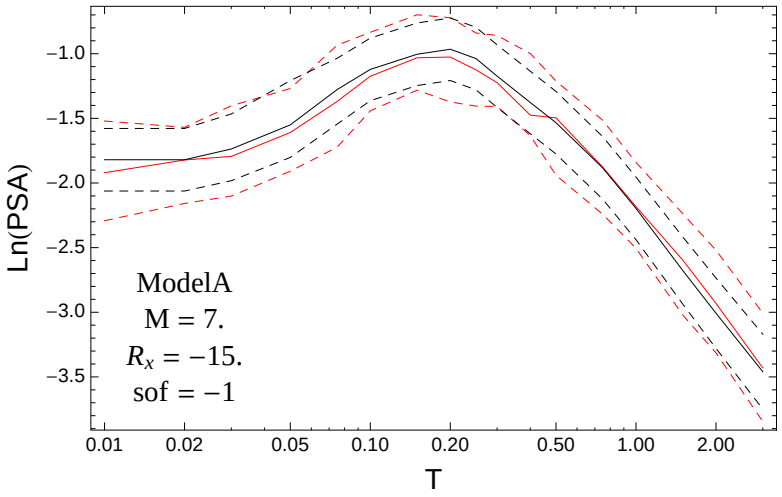



Figure 3.418: PVNGSv2: Spectra of 0.05,0.5,0.95 quantile of the GMPE distribution (black) and the model distribution (red) with total weights, for a scenario with $M_W = 7.$, $R_x = -15.$, $F = -1$.

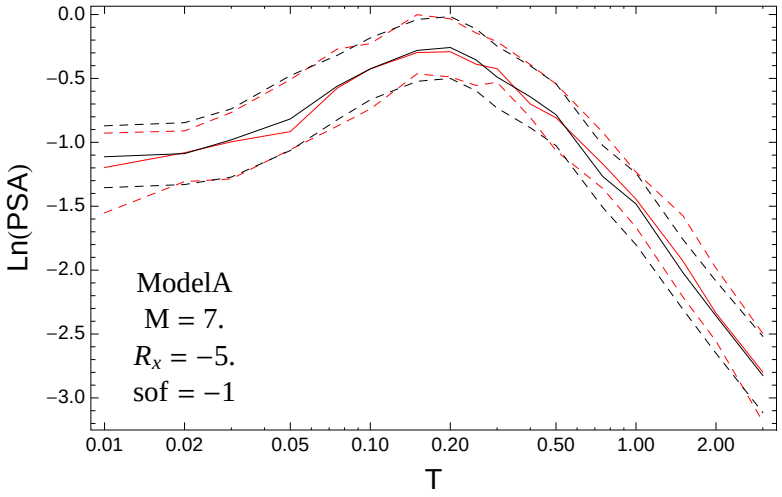



Figure 3.419: PVNGSv2: Spectra of 0.05,0.5,0.95 quantile of the GMPE distribution (black) and the model distribution (red) with total weights, for a scenario with $M_W = 7.$, $R_x = -5.$, $F = -1$.

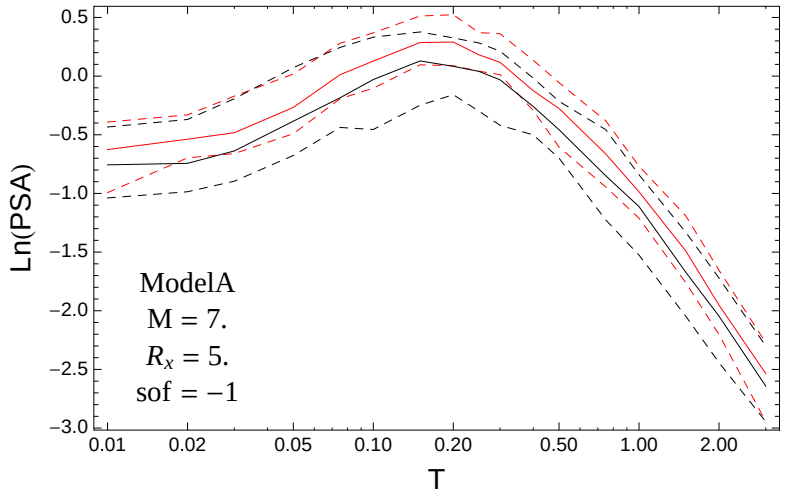



Figure 3.420: PVNGSv2: Spectra of 0.05,0.5,0.95 quantile of the GMPE distribution (black) and the model distribution (red) with total weights, for a scenario with $M_W = 7.$, $R_x = 5.$, $F = -1$.

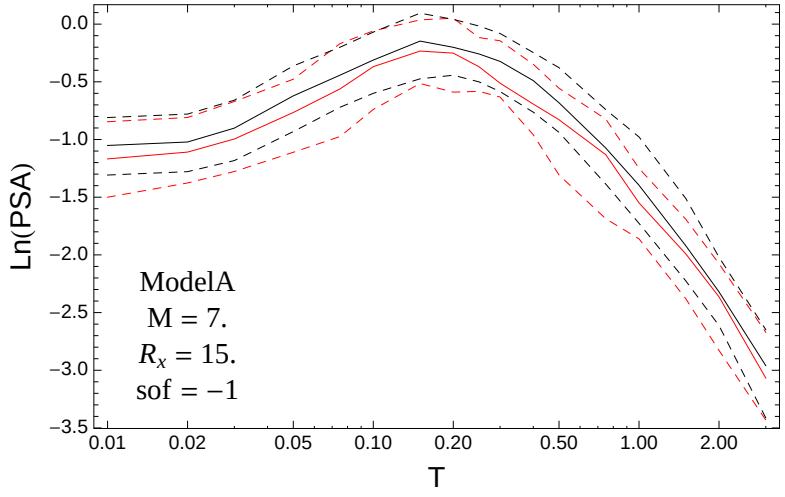



Figure 3.421: PVNGSv2: Spectra of 0.05,0.5,0.95 quantile of the GMPE distribution (black) and the model distribution (red) with total weights, for a scenario with $M_W = 7.$, $R_x = 15.$, $F = -1$.

### 3.1.10 Quantile Ratios vs. Distance

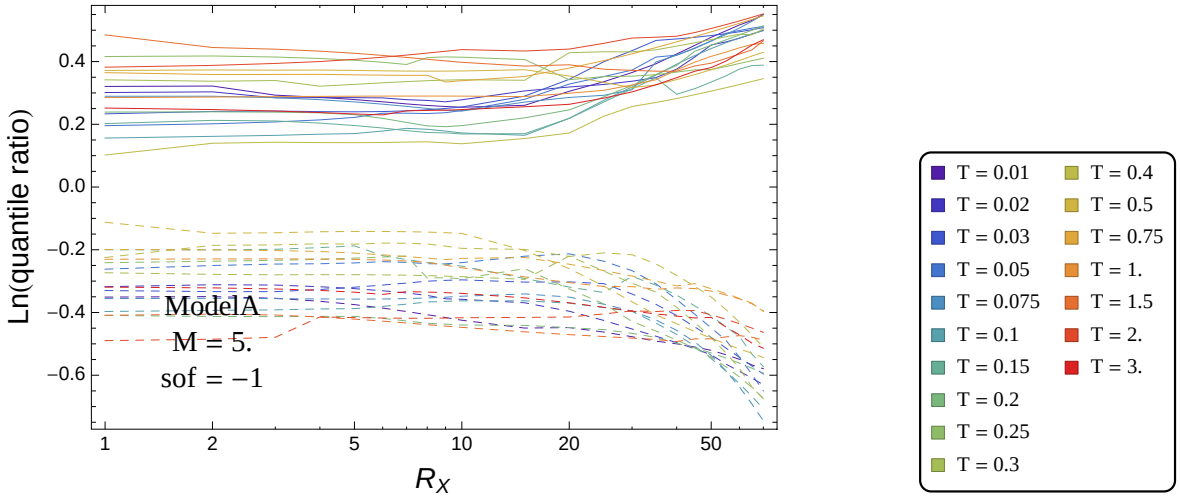



Figure 3.422: PVNGS2: Ratio of 0.05 to 0.5 (dashed) and ratio of 0.95 to 0.5 quantile (solid) of the ModelA-model distribution with total weights, for a scenario with $M = 5.$, $F = -1$, and all periods.

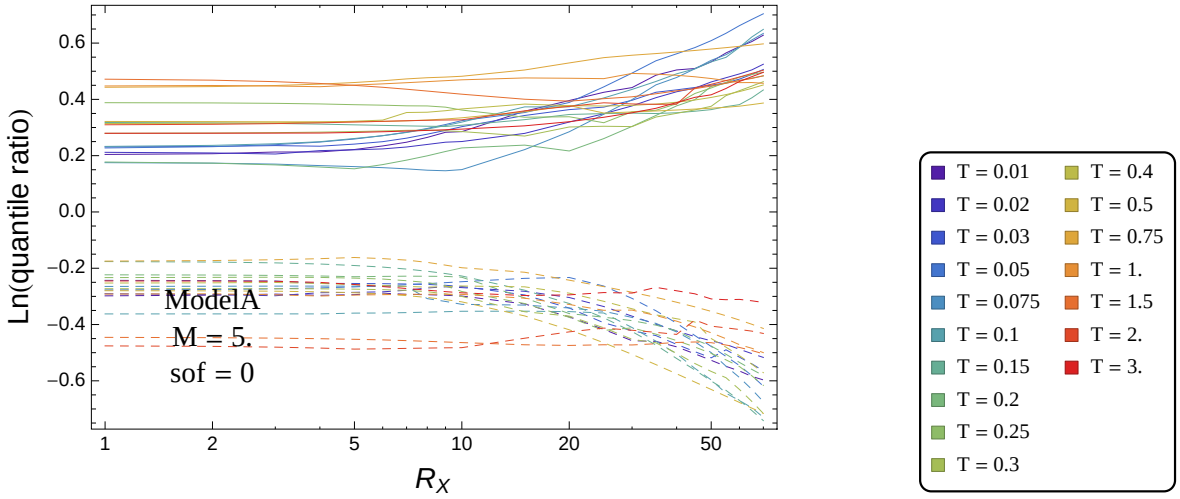



Figure 3.423: PVNGS2: Ratio of 0.05 to 0.5 (dashed) and ratio of 0.95 to 0.5 quantile (solid) of the ModelA-model distribution with total weights, for a scenario with $M = 5.$, $F = 0$, and all periods.

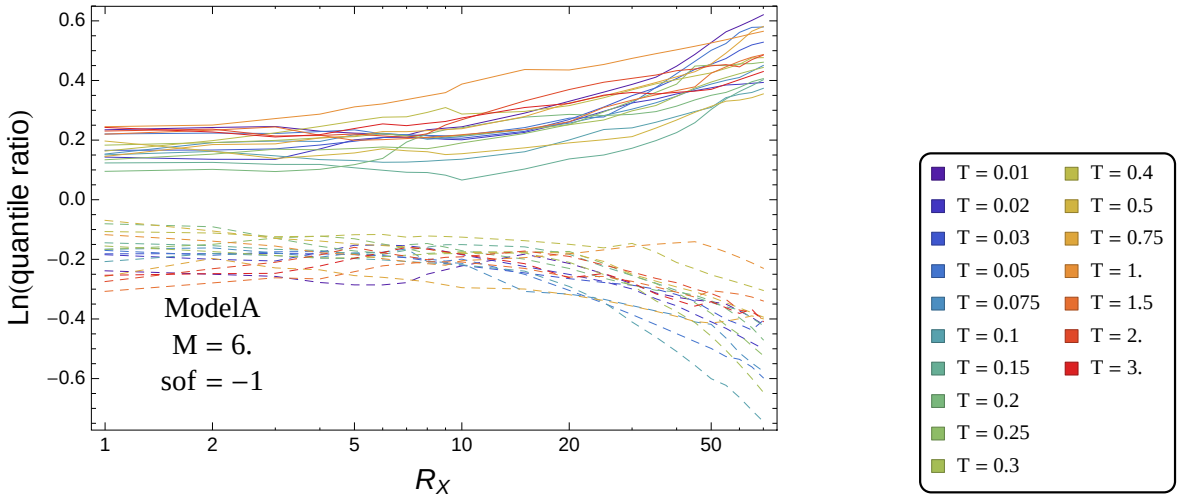



Figure 3.424: PVNGS2: Ratio of 0.05 to 0.5 (dashed) and ratio of 0.95 to 0.5 quantile (solid) of the ModelA-model distribution with total weights, for a scenario with $M = 6.$, $F = -1$, and all periods.

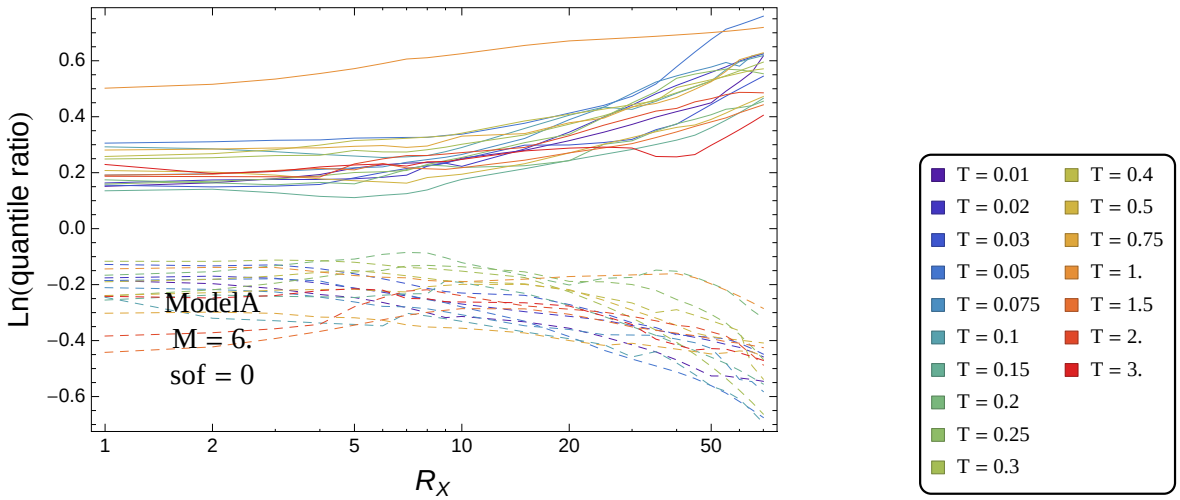



Figure 3.425: PVNGS2: Ratio of 0.05 to 0.5 (dashed) and ratio of 0.95 to 0.5 quantile (solid) of the ModelA-model distribution with total weights, for a scenario with $M = 6.$, $F = 0$, and all periods.

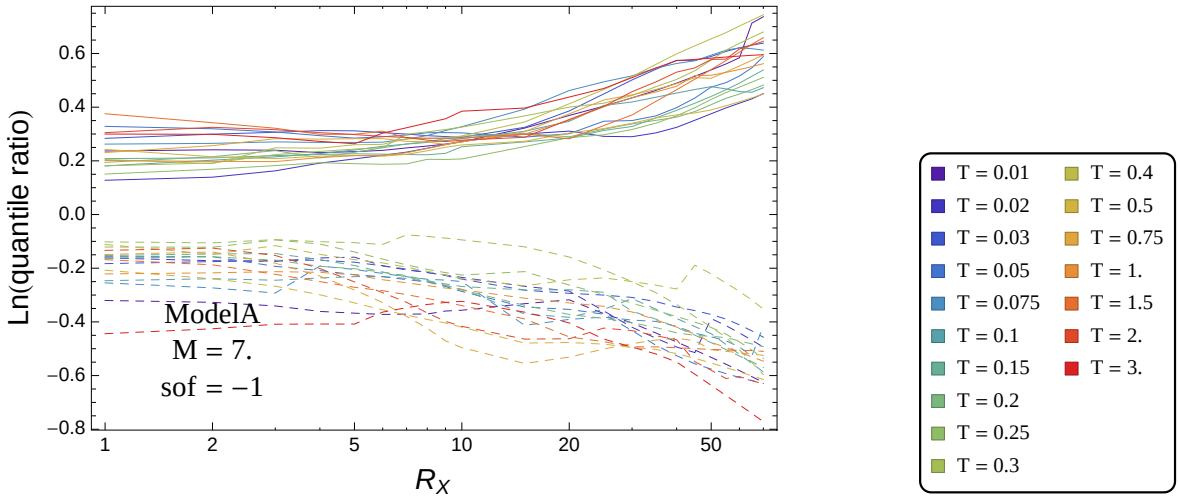



Figure 3.426: PVNGS2: Ratio of 0.05 to 0.5 (dashed) and ratio of 0.95 to 0.5 quantile (solid) of the ModelA-model distribution with total weights, for a scenario with $M = 7.$, $F = -1$, and all periods.

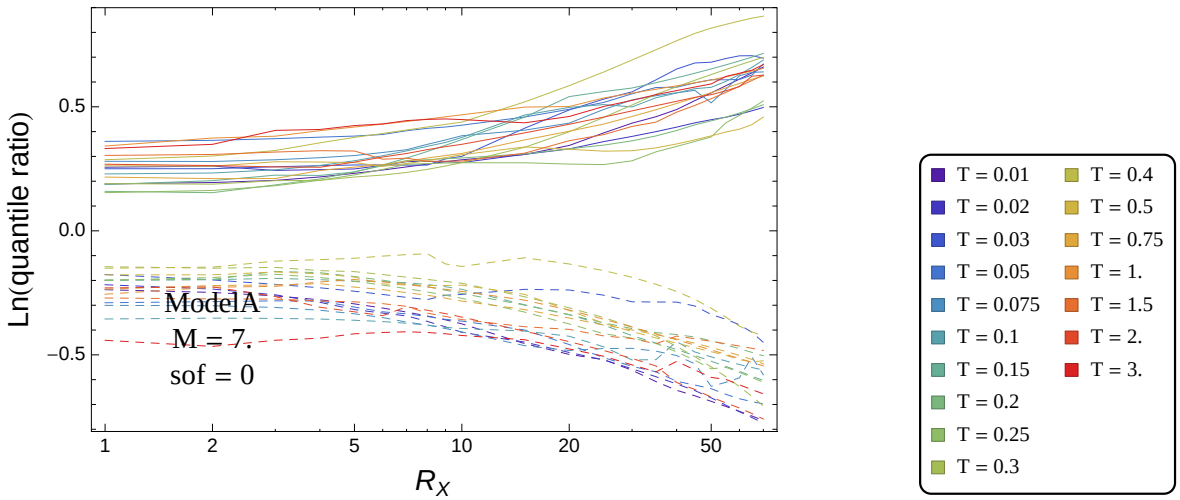



Figure 3.427: PVNGS2: Ratio of 0.05 to 0.5 (dashed) and ratio of 0.95 to 0.5 quantile (solid) of the ModelA-model distribution with total weights, for a scenario with $M = 7.$, $F = 0$, and all periods.

### 3.1.11 Magnitude Scaling with GMPEs

**T = 0.01s**

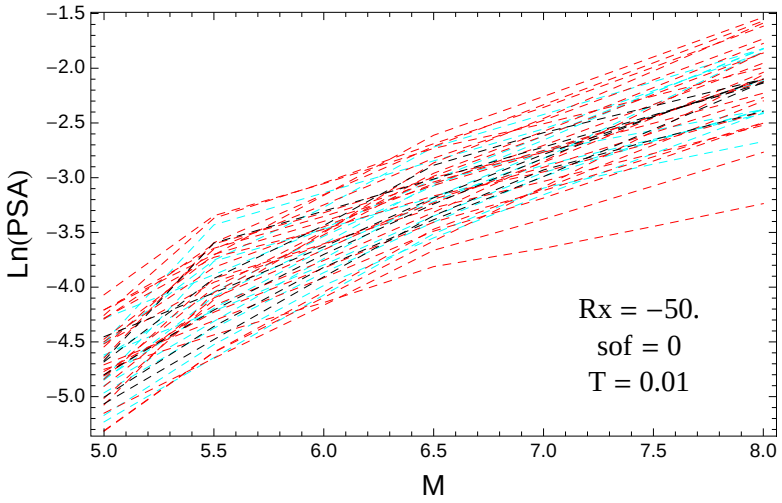



Figure 3.428: PVNGSv2: Magnitude scaling of the original GMPEs (dashed black), the original GMPEs with uncertainty model (dashed cyan) and selected A models (dashed red), for a scenario with $R_X = -50.$, $F = 0$, and $T = 0.01$s.

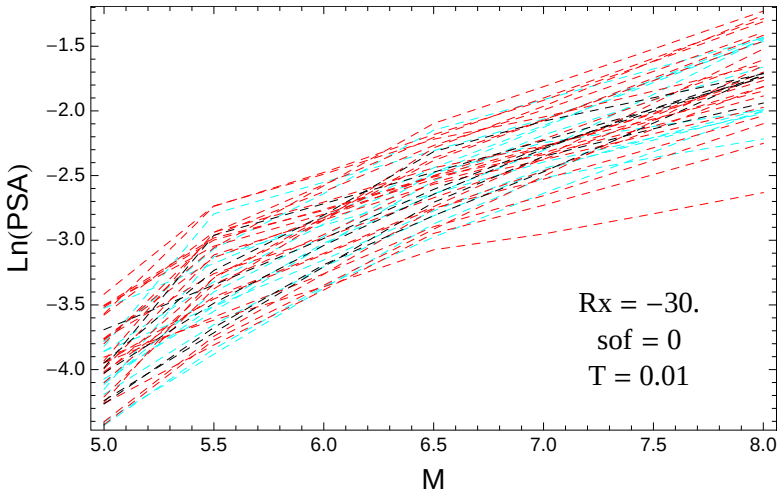



Figure 3.429: PVNGSv2: Magnitude scaling of the original GMPEs (dashed black), the original GMPEs with uncertainty model (dashed cyan) and selected A models (dashed red), for a scenario with $R_X = -30.$, $F = 0$, and $T = 0.01$s.

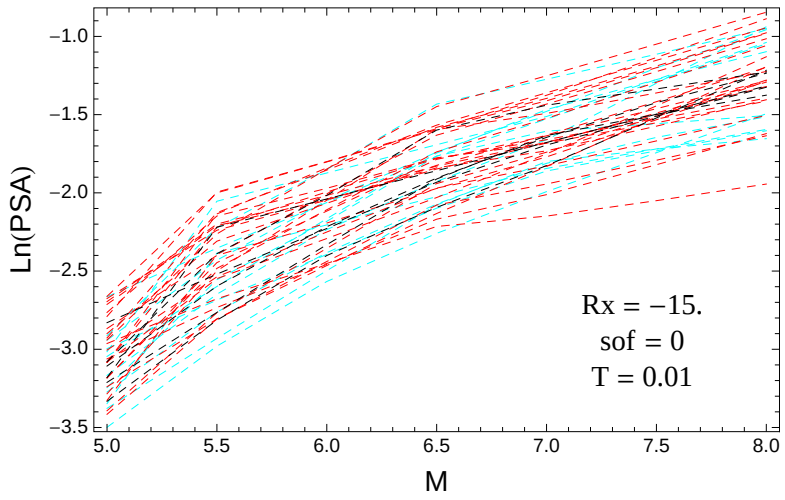



Figure 3.430: PVNGSv2: Magnitude scaling of the original GMPEs (dashed black), the original GMPEs with uncertainty model (dashed cyan) and selected A models (dashed red), for a scenario with $R_X = -15.$, $F = 0$, and $T = 0.01$s.

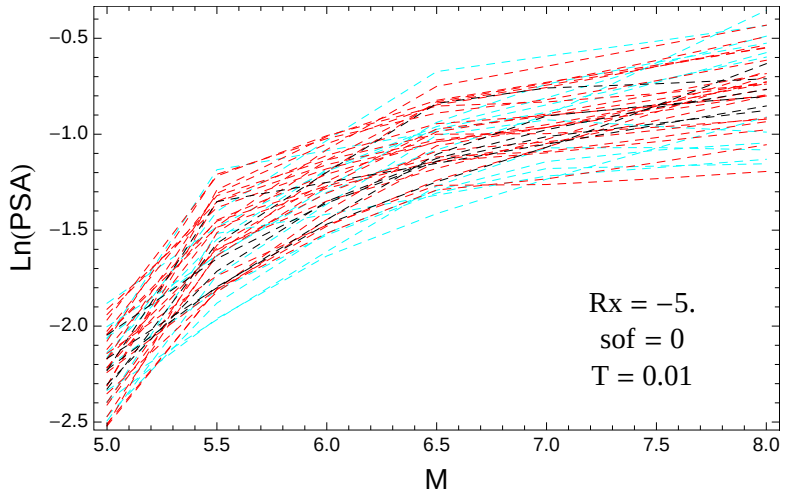



Figure 3.431: PVNGSv2: Magnitude scaling of the original GMPEs (dashed black), the original GMPEs with uncertainty model (dashed cyan) and selected A models (dashed red), for a scenario with $R_X = -5.$, $F = 0$, and $T = 0.01$s.

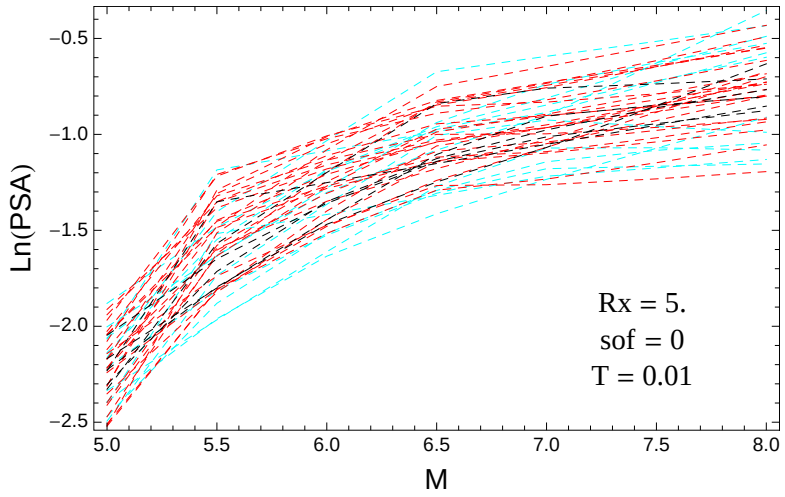



Figure 3.432: PVNGSv2: Magnitude scaling of the original GMPEs (dashed black), the original GMPEs with uncertainty model (dashed cyan) and selected A models (dashed red), for a scenario with $R_X = 5.$, $F = 0$, and $T = 0.01$s.

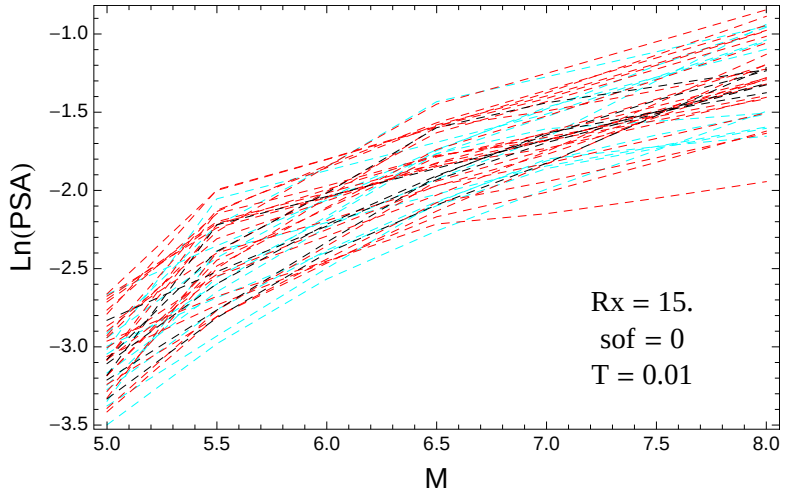



Figure 3.433: PVNGSv2: Magnitude scaling of the original GMPEs (dashed black), the original GMPEs with uncertainty model (dashed cyan) and selected A models (dashed red), for a scenario with $R_X = 15.$, $F = 0$, and $T = 0.01$s.

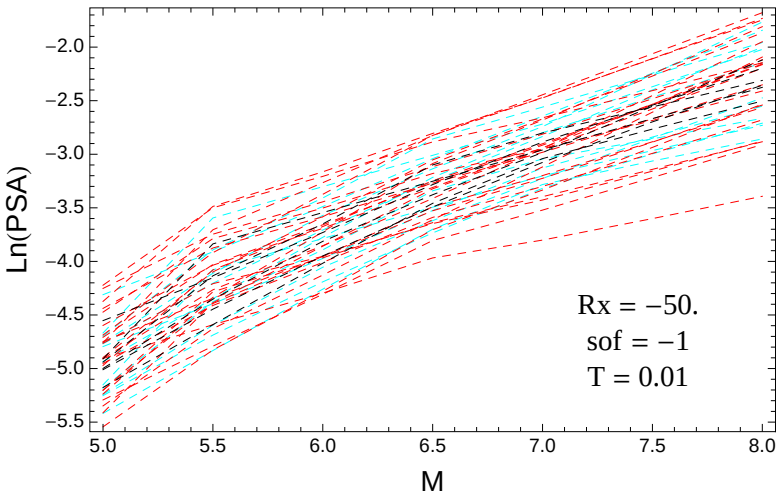



Figure 3.434: PVNGSv2: Magnitude scaling of the original GMPEs (dashed black), the original GMPEs with uncertainty model (dashed cyan) and selected A models (dashed red), for a scenario with $R_X = -50.$, $F = -1$, and $T = 0.01$s.

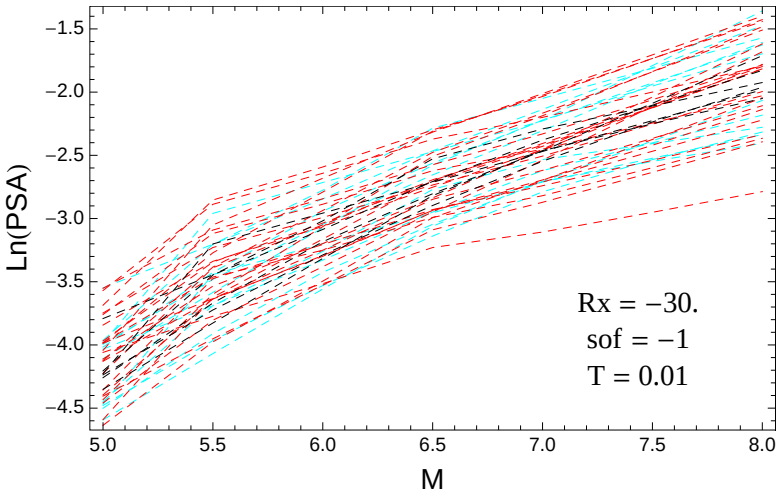



Figure 3.435: PVNGSv2: Magnitude scaling of the original GMPEs (dashed black), the original GMPEs with uncertainty model (dashed cyan) and selected A models (dashed red), for a scenario with $R_X = -30.$, $F = -1$, and $T = 0.01$s.

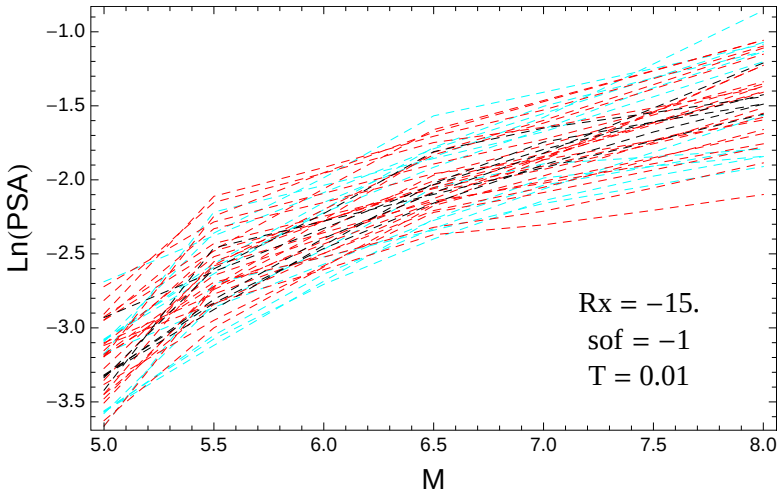



Figure 3.436: PVNGSv2: Magnitude scaling of the original GMPEs (dashed black), the original GMPEs with uncertainty model (dashed cyan) and selected A models (dashed red), for a scenario with $R_X = -15.$, $F = -1$, and $T = 0.01$s.

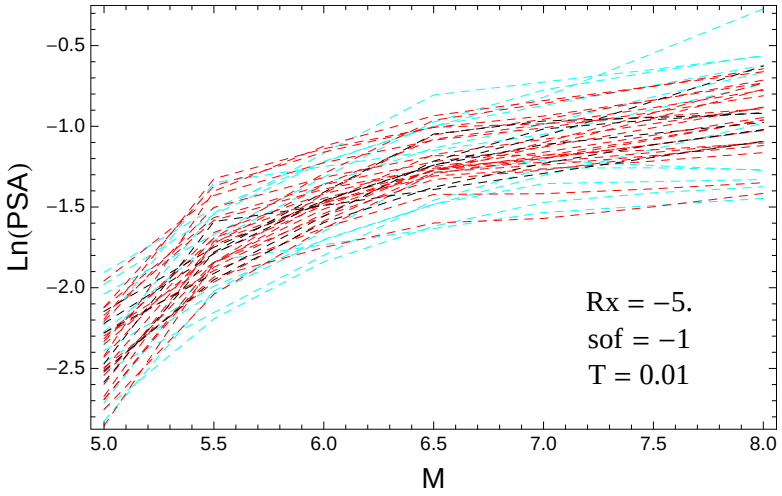



Figure 3.437: PVNGSv2: Magnitude scaling of the original GMPEs (dashed black), the original GMPEs with uncertainty model (dashed cyan) and selected A models (dashed red), for a scenario with $R_X = -5.$, $F = -1$, and $T = 0.01$s.

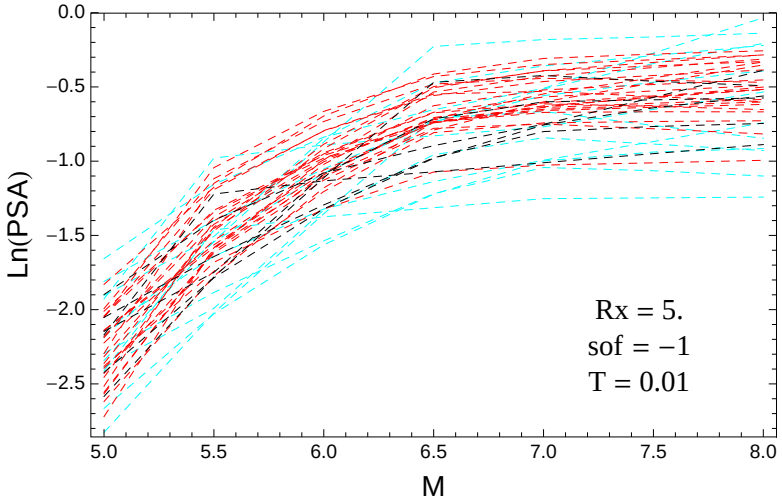



Figure 3.438: PVNGSv2: Magnitude scaling of the original GMPEs (dashed black), the original GMPEs with uncertainty model (dashed cyan) and selected A models (dashed red), for a scenario with $R_X = 5.$, $F = -1$, and $T = 0.01$s.

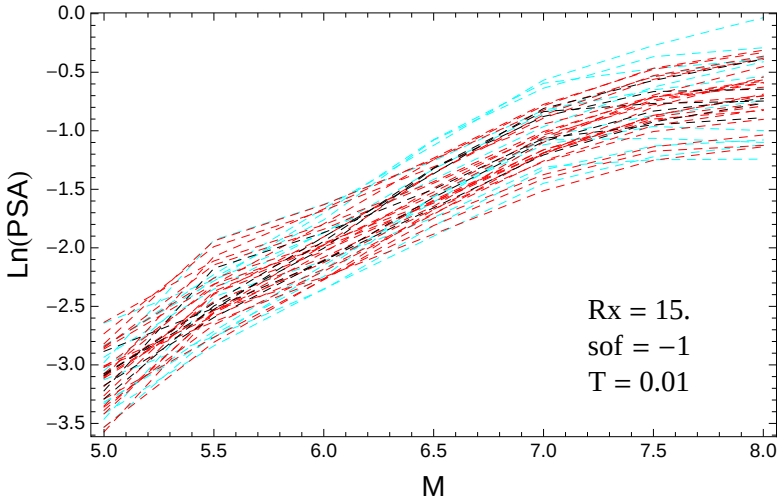



Figure 3.439: PVNGSv2: Magnitude scaling of the original GMPEs (dashed black), the original GMPEs with uncertainty model (dashed cyan) and selected A models (dashed red), for a scenario with $R_X = 15.$, $F = -1$, and $T = 0.01$s.

**T = 0.2s**

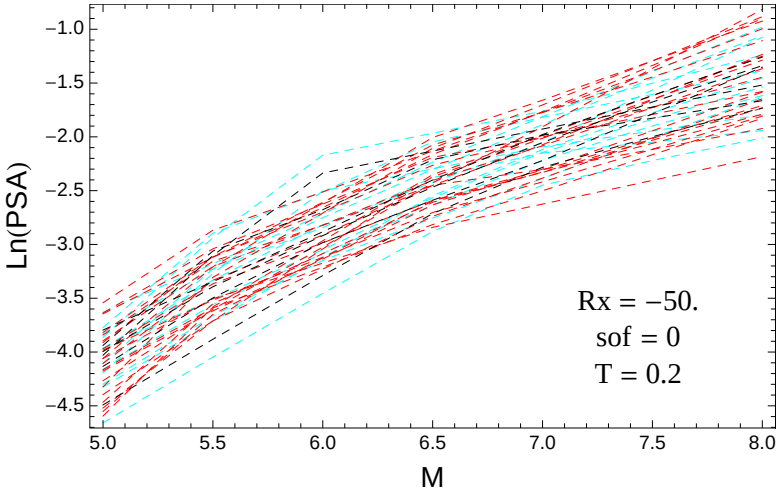



Figure 3.440: PVNGSv2: Magnitude scaling of the original GMPEs (dashed black), the original GMPEs with uncertainty model (dashed cyan) and selected A models (dashed red), for a scenario with $R_X = -50.$, $F = 0$, and $T = 0.2$s.

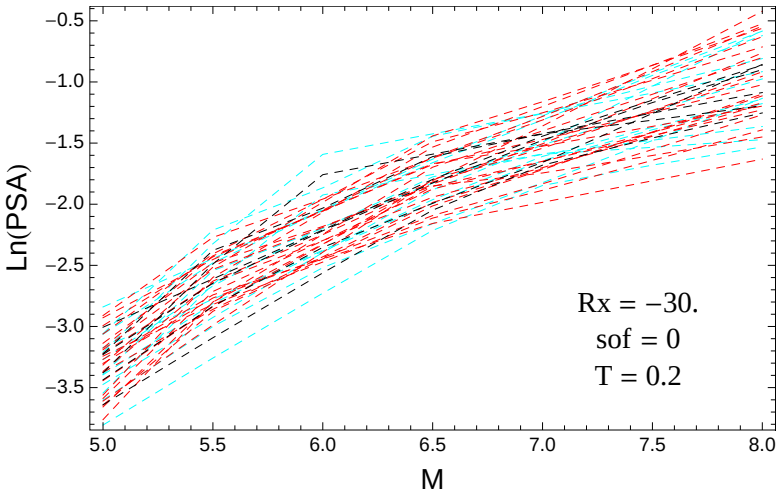



Figure 3.441: PVNGSv2: Magnitude scaling of the original GMPEs (dashed black), the original GMPEs with uncertainty model (dashed cyan) and selected A models (dashed red), for a scenario with $R_X = -30.$, $F = 0$, and $T = 0.2$s.

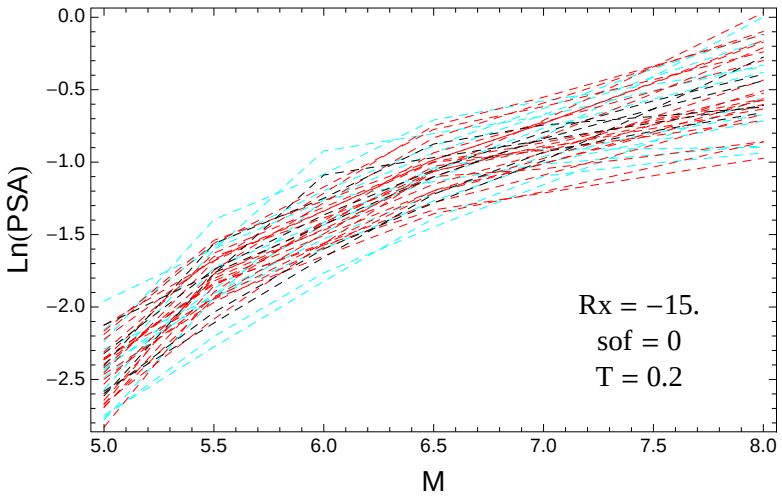



Figure 3.442: PVNGSv2: Magnitude scaling of the original GMPEs (dashed black), the original GMPEs with uncertainty model (dashed cyan) and selected A models (dashed red), for a scenario with $R_X = -15.$, $F = 0$, and $T = 0.2$s.

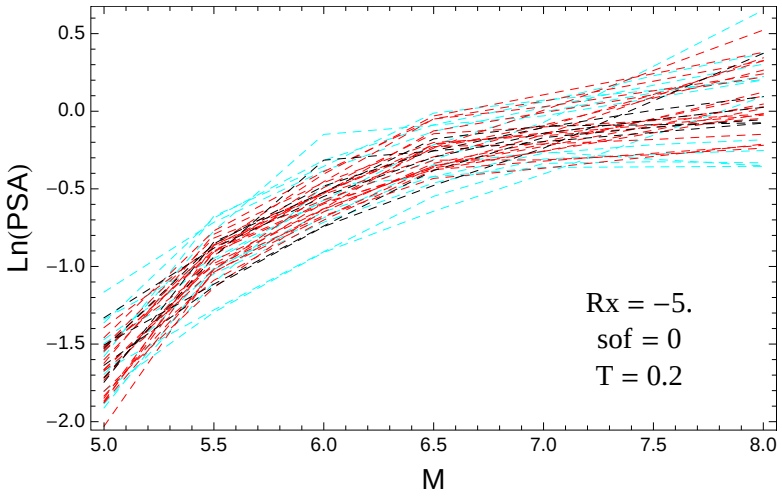



Figure 3.443: PVNGSv2: Magnitude scaling of the original GMPEs (dashed black), the original GMPEs with uncertainty model (dashed cyan) and selected A models (dashed red), for a scenario with $R_X = -5.$, $F = 0$, and $T = 0.2$s.

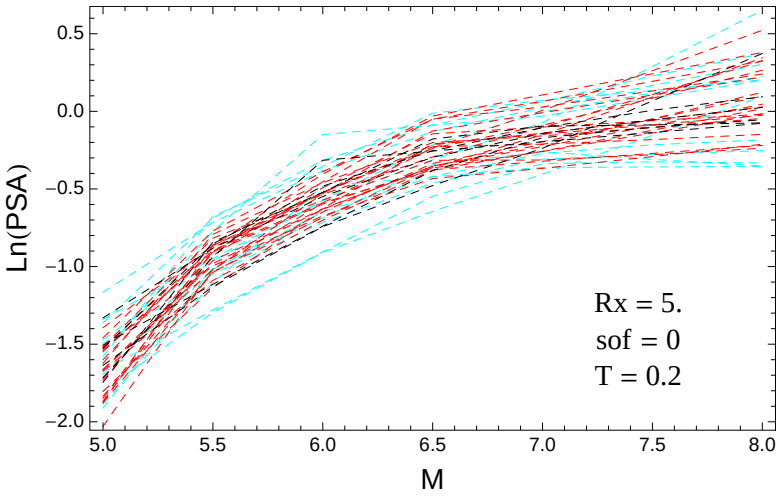



Figure 3.444: PVNGSv2: Magnitude scaling of the original GMPEs (dashed black), the original GMPEs with uncertainty model (dashed cyan) and selected A models (dashed red), for a scenario with $R_X = 5.$, $F = 0$, and $T = 0.2$s.

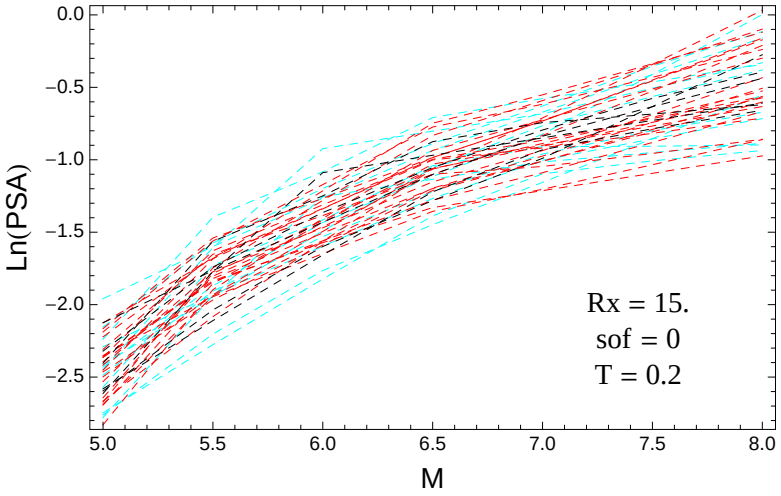



Figure 3.445: PVNGSv2: Magnitude scaling of the original GMPEs (dashed black), the original GMPEs with uncertainty model (dashed cyan) and selected A models (dashed red), for a scenario with $R_X = 15.$, $F = 0$, and $T = 0.2$s.

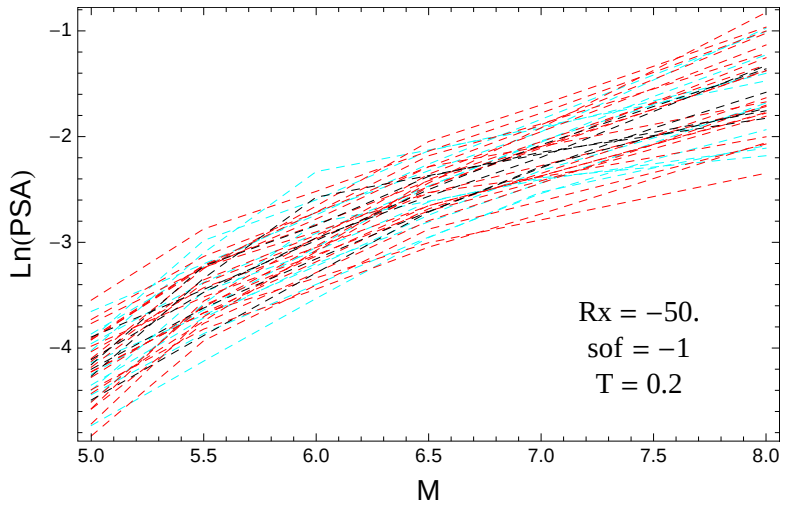



Figure 3.446: PVNGSv2: Magnitude scaling of the original GMPEs (dashed black), the original GMPEs with uncertainty model (dashed cyan) and selected A models (dashed red), for a scenario with $R_X = -50.$, $F = -1$, and $T = 0.2$s.

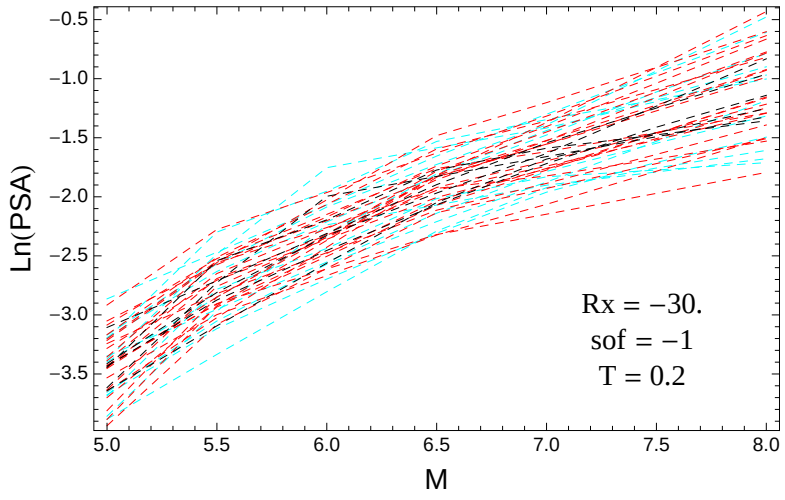



Figure 3.447: PVNGSv2: Magnitude scaling of the original GMPEs (dashed black), the original GMPEs with uncertainty model (dashed cyan) and selected A models (dashed red), for a scenario with $R_X = -30.$, $F = -1$, and $T = 0.2$s.

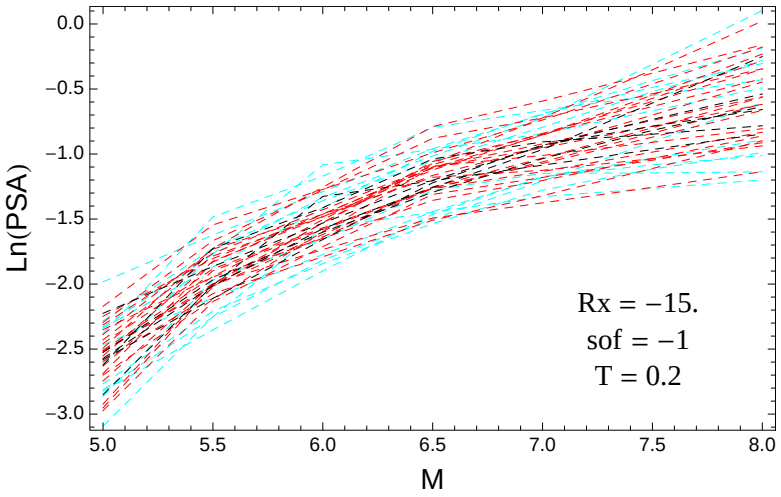



Figure 3.448: PVNGSv2: Magnitude scaling of the original GMPEs (dashed black), the original GMPEs with uncertainty model (dashed cyan) and selected A models (dashed red), for a scenario with $R_X = -15.$, $F = -1$, and $T = 0.2$s.

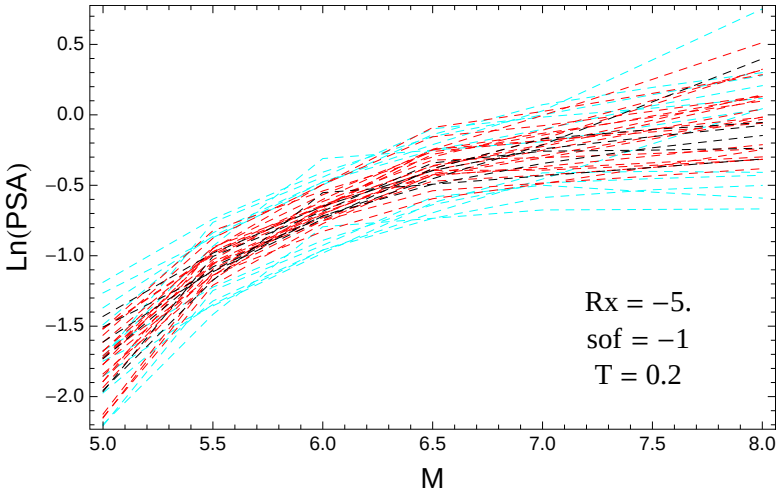



Figure 3.449: PVNGSv2: Magnitude scaling of the original GMPEs (dashed black), the original GMPEs with uncertainty model (dashed cyan) and selected A models (dashed red), for a scenario with $R_X = -5.$, $F = -1$, and $T = 0.2$s.

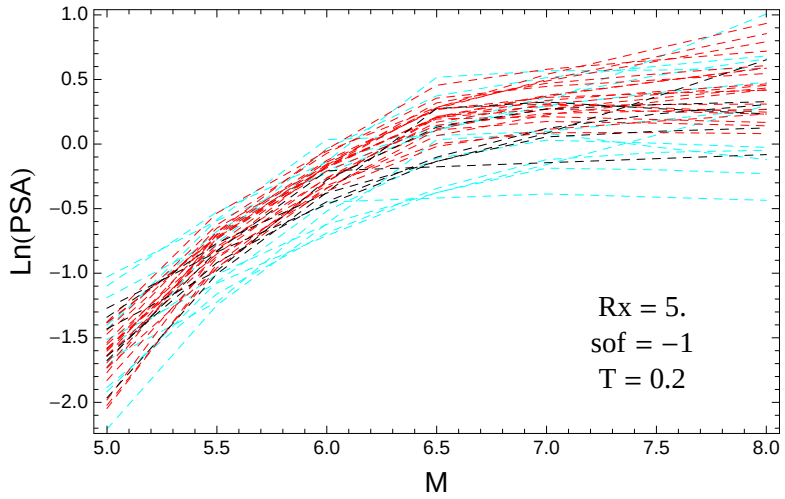



Figure 3.450: PVNGSv2: Magnitude scaling of the original GMPEs (dashed black), the original GMPEs with uncertainty model (dashed cyan) and selected A models (dashed red), for a scenario with $R_X = 5.$, $F = -1$, and $T = 0.2$s.

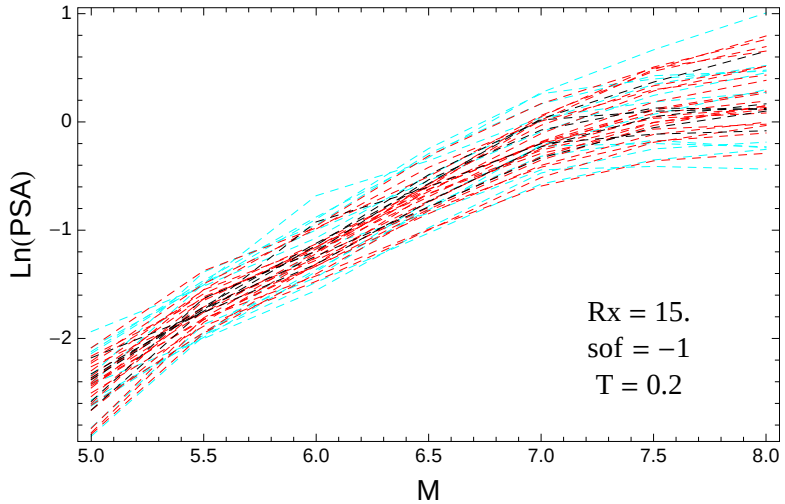



Figure 3.451: PVNGSv2: Magnitude scaling of the original GMPEs (dashed black), the original GMPEs with uncertainty model (dashed cyan) and selected A models (dashed red), for a scenario with $R_X = 15.$, $F = -1$, and $T = 0.2$s.

**T = 0.5s**

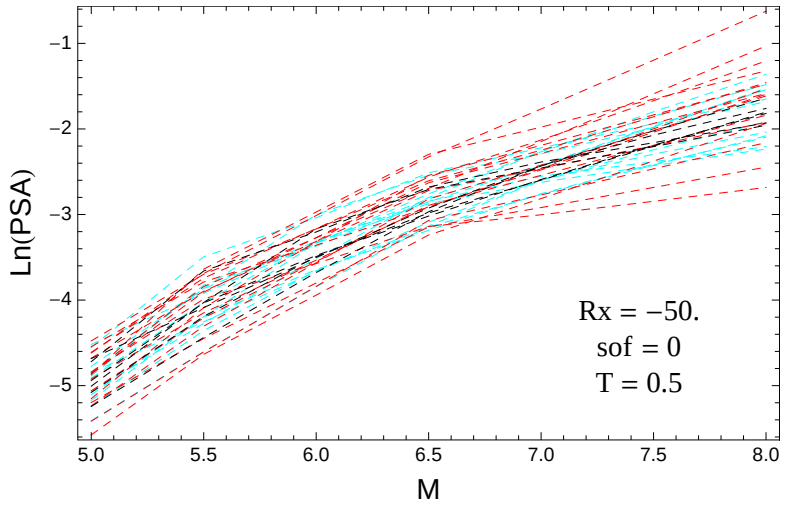



Figure 3.452: PVNGSv2: Magnitude scaling of the original GMPEs (dashed black), the original GMPEs with uncertainty model (dashed cyan) and selected A models (dashed red), for a scenario with $R_X = -50.$, $F = 0$, and $T = 0.5$s.

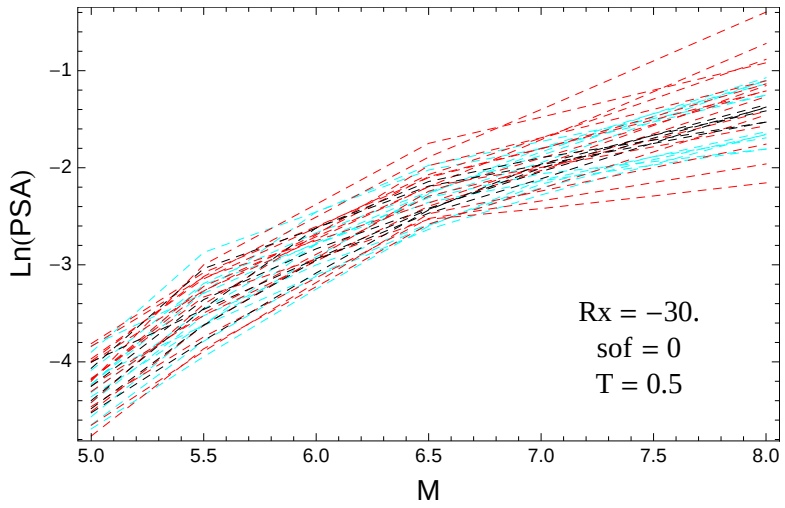



Figure 3.453: PVNGSv2: Magnitude scaling of the original GMPEs (dashed black), the original GMPEs with uncertainty model (dashed cyan) and selected A models (dashed red), for a scenario with $R_X = -30.$, $F = 0$, and $T = 0.5$s.

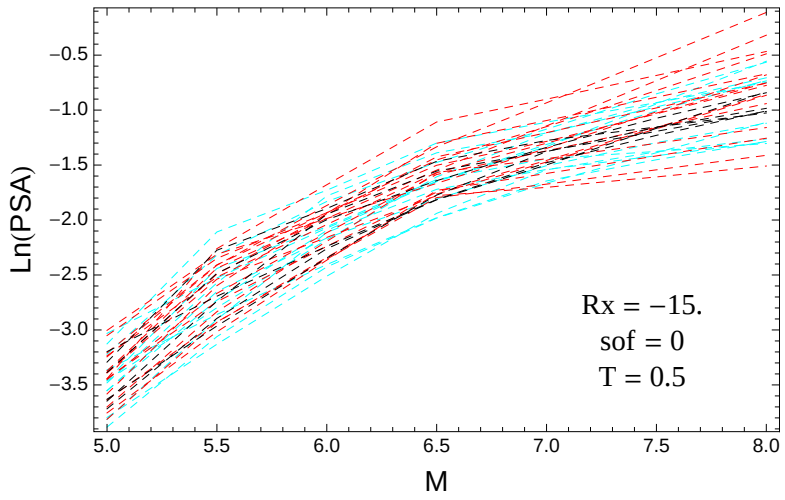



Figure 3.454: PVNGSv2: Magnitude scaling of the original GMPEs (dashed black), the original GMPEs with uncertainty model (dashed cyan) and selected A models (dashed red), for a scenario with $R_X = -15.$, $F = 0$, and $T = 0.5$s.

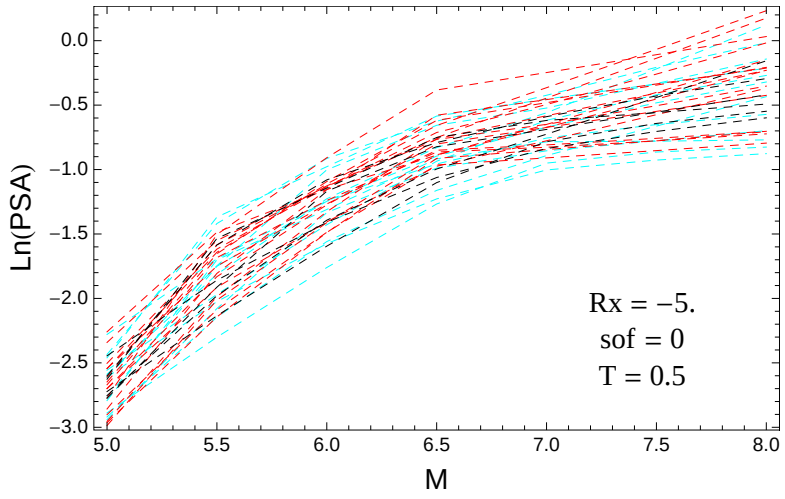



Figure 3.455: PVNGSv2: Magnitude scaling of the original GMPEs (dashed black), the original GMPEs with uncertainty model (dashed cyan) and selected A models (dashed red), for a scenario with $R_X = -5.$, $F = 0$, and $T = 0.5$s.

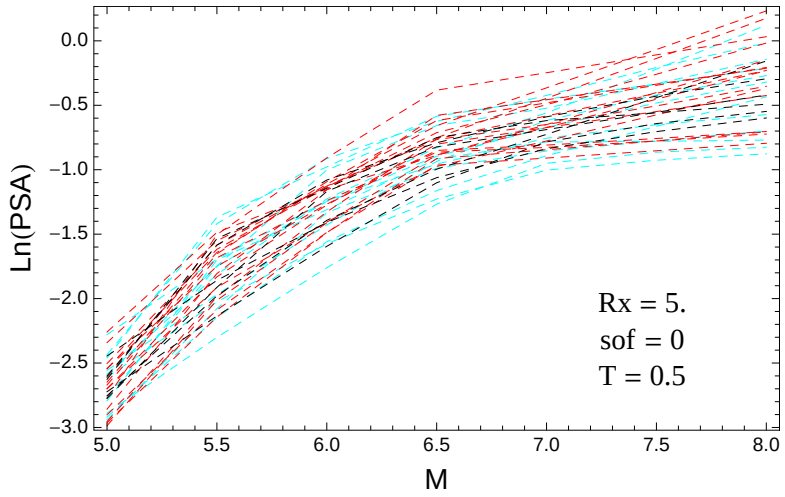



Figure 3.456: PVNGSv2: Magnitude scaling of the original GMPEs (dashed black), the original GMPEs with uncertainty model (dashed cyan) and selected A models (dashed red), for a scenario with $R_X = 5.$, $F = 0$, and $T = 0.5$s.

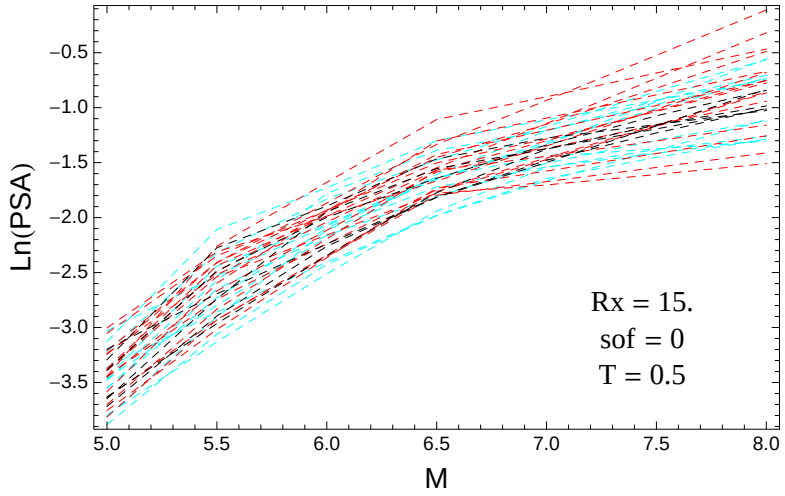



Figure 3.457: PVNGSv2: Magnitude scaling of the original GMPEs (dashed black), the original GMPEs with uncertainty model (dashed cyan) and selected A models (dashed red), for a scenario with $R_X = 15.$, $F = 0$, and $T = 0.5$s.

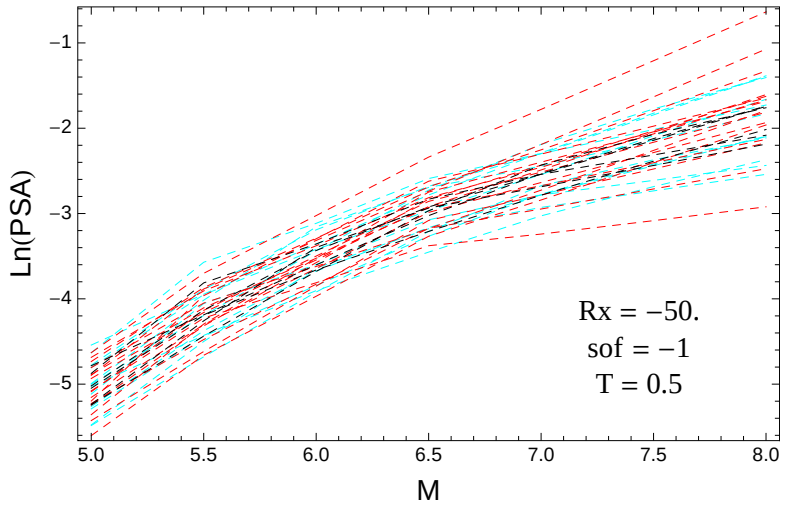



Figure 3.458: PVNGSv2: Magnitude scaling of the original GMPEs (dashed black), the original GMPEs with uncertainty model (dashed cyan) and selected A models (dashed red), for a scenario with $R_X = -50.$, $F = -1$, and $T = 0.5$s.

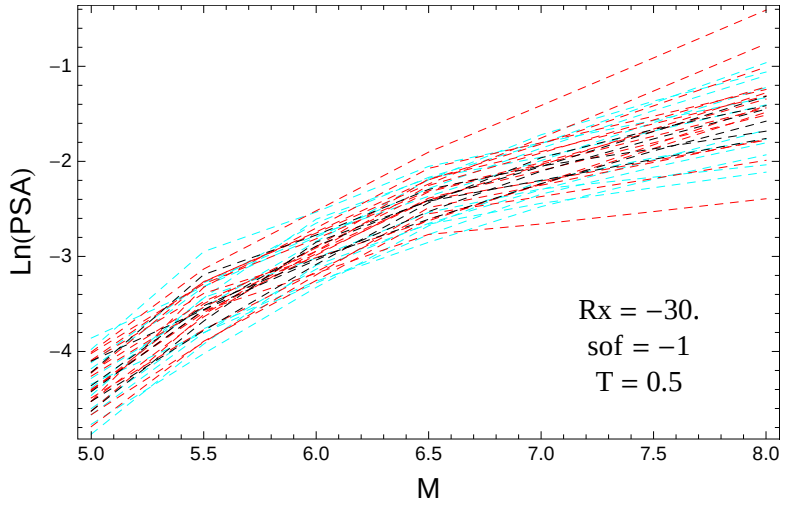



Figure 3.459: PVNGSv2: Magnitude scaling of the original GMPEs (dashed black), the original GMPEs with uncertainty model (dashed cyan) and selected A models (dashed red), for a scenario with $R_X = -30.$, $F = -1$, and $T = 0.5$s.

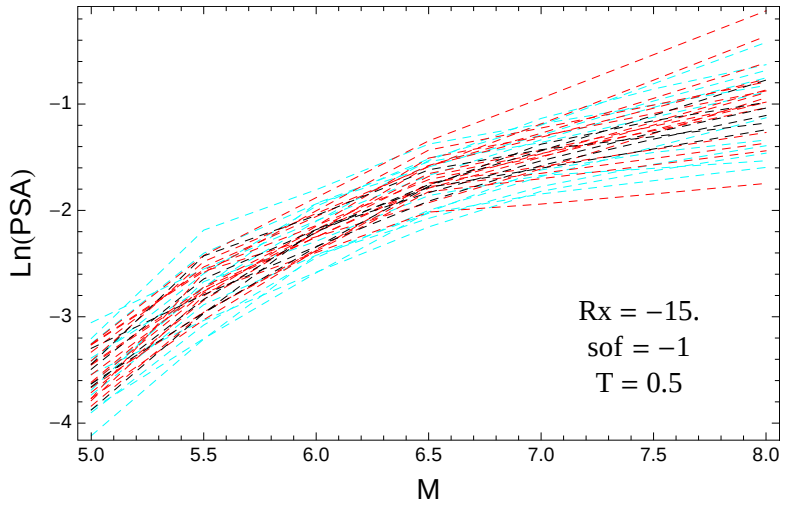



Figure 3.460: PVNGSv2: Magnitude scaling of the original GMPEs (dashed black), the original GMPEs with uncertainty model (dashed cyan) and selected A models (dashed red), for a scenario with $R_X = -15.$, $F = -1$, and $T = 0.5$s.

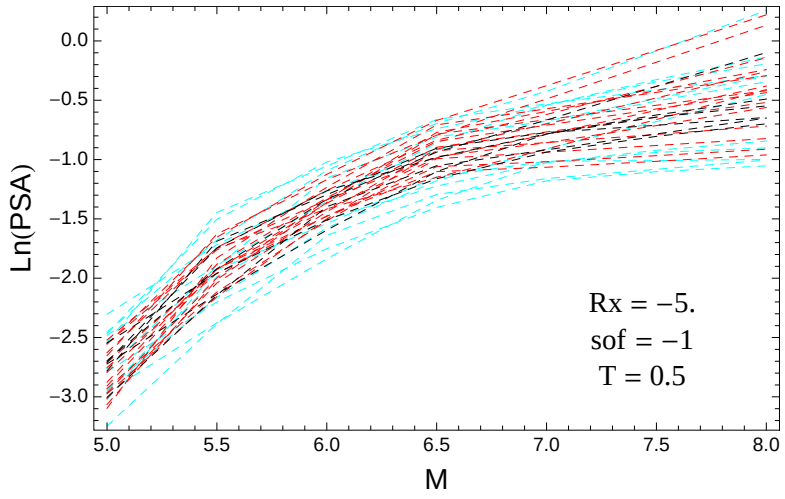



Figure 3.461: PVNGSv2: Magnitude scaling of the original GMPEs (dashed black), the original GMPEs with uncertainty model (dashed cyan) and selected A models (dashed red), for a scenario with $R_X = -5.$, $F = -1$, and $T = 0.5$s.

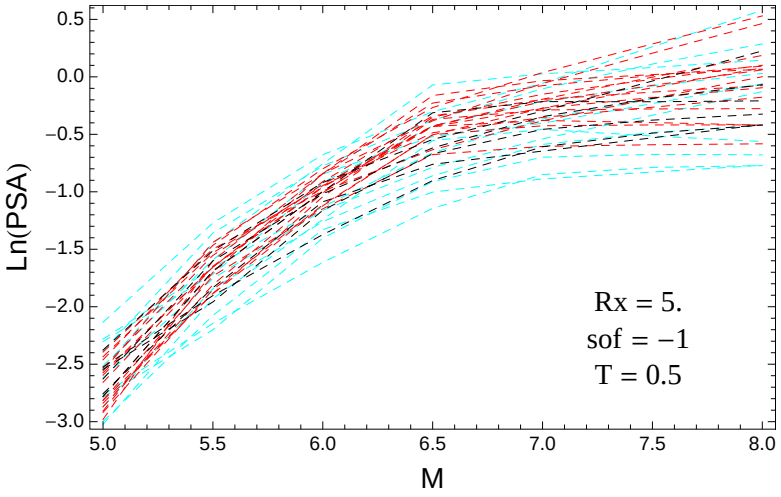



Figure 3.462: PVNGSv2: Magnitude scaling of the original GMPEs (dashed black), the original GMPEs with uncertainty model (dashed cyan) and selected A models (dashed red), for a scenario with $R_X = 5.$, $F = -1$, and $T = 0.5$s.

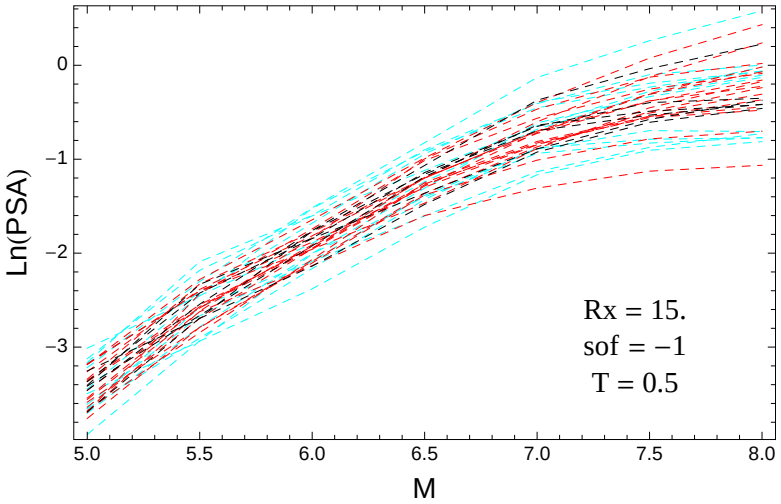



Figure 3.463: PVNGSv2: Magnitude scaling of the original GMPEs (dashed black), the original GMPEs with uncertainty model (dashed cyan) and selected A models (dashed red), for a scenario with $R_X = 15.$, $F = -1$, and $T = 0.5$s.

**T = 1.s**

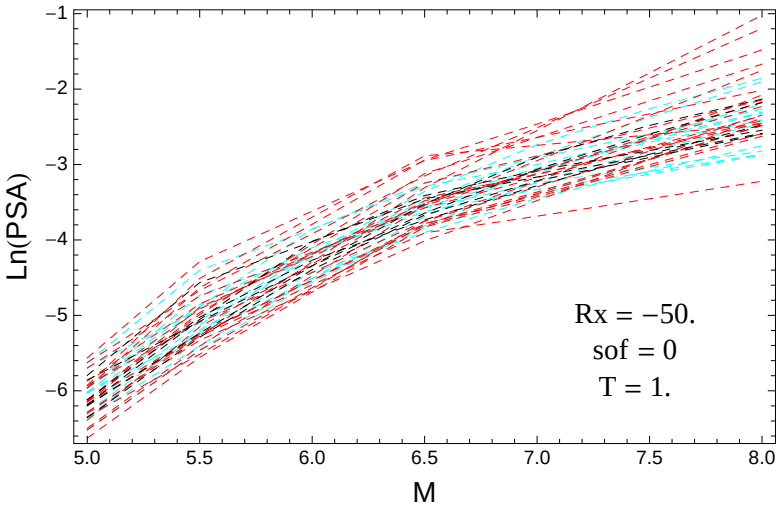



Figure 3.464: PVNGSv2: Magnitude scaling of the original GMPEs (dashed black), the original GMPEs with uncertainty model (dashed cyan) and selected A models (dashed red), for a scenario with $R_X = -50.$, $F = 0$, and $T = 1.$s.

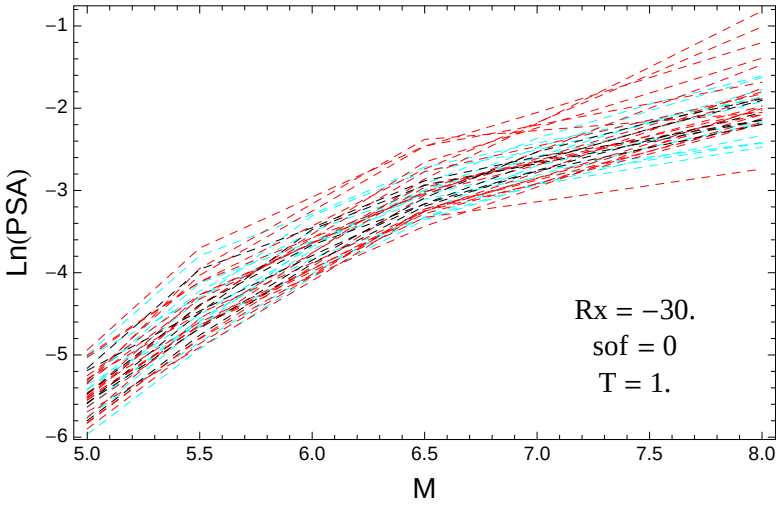



Figure 3.465: PVNGSv2: Magnitude scaling of the original GMPEs (dashed black), the original GMPEs with uncertainty model (dashed cyan) and selected A models (dashed red), for a scenario with $R_X = -30.$, $F = 0$, and $T = 1.$s.

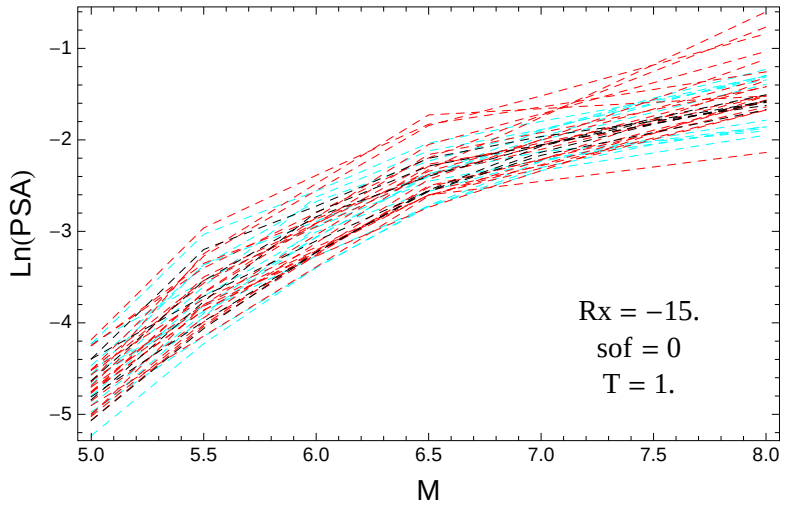



Figure 3.466: PVNGSv2: Magnitude scaling of the original GMPEs (dashed black), the original GMPEs with uncertainty model (dashed cyan) and selected A models (dashed red), for a scenario with $R_X = -15.$, $F = 0$, and $T = 1.$s.

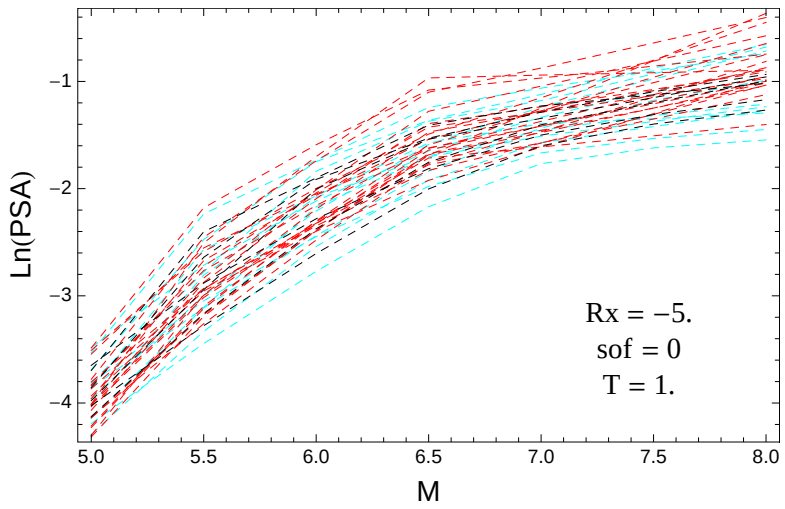



Figure 3.467: PVNGSv2: Magnitude scaling of the original GMPEs (dashed black), the original GMPEs with uncertainty model (dashed cyan) and selected A models (dashed red), for a scenario with $R_X = -5.$, $F = 0$, and $T = 1.$s.

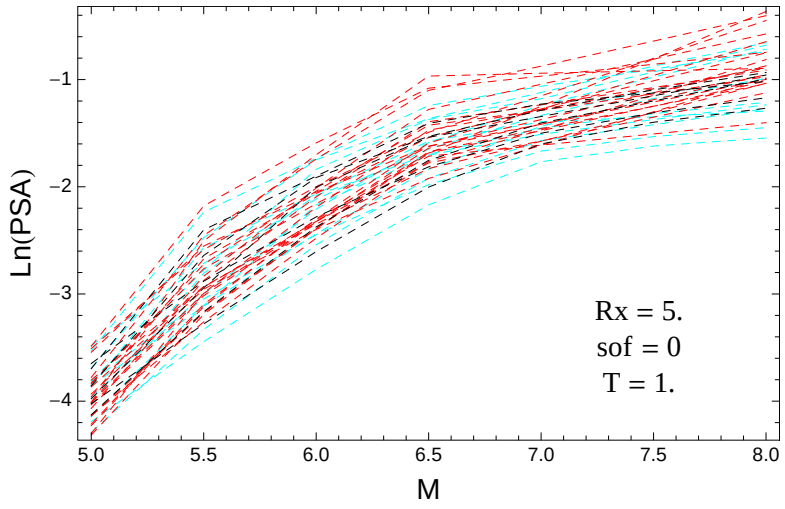



Figure 3.468: PVNGSv2: Magnitude scaling of the original GMPEs (dashed black), the original GMPEs with uncertainty model (dashed cyan) and selected A models (dashed red), for a scenario with $R_X = 5.$, $F = 0$, and $T = 1.$s.

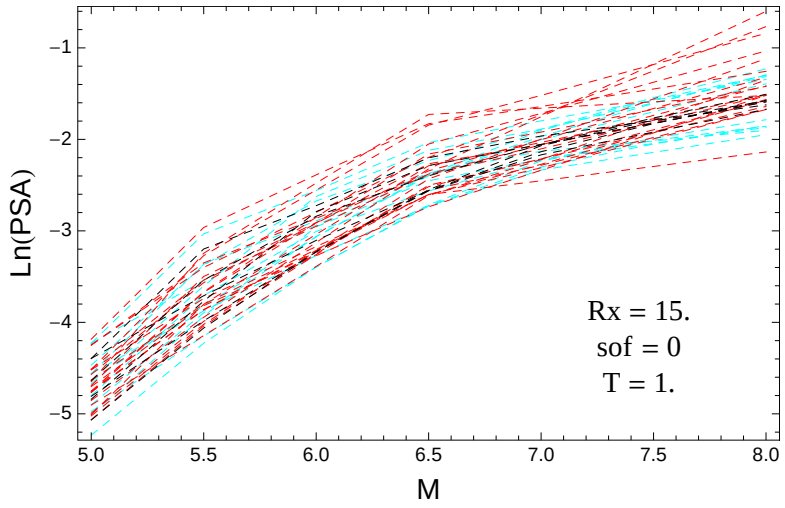



Figure 3.469: PVNGSv2: Magnitude scaling of the original GMPEs (dashed black), the original GMPEs with uncertainty model (dashed cyan) and selected A models (dashed red), for a scenario with $R_X = 15.$, $F = 0$, and $T = 1.$s.

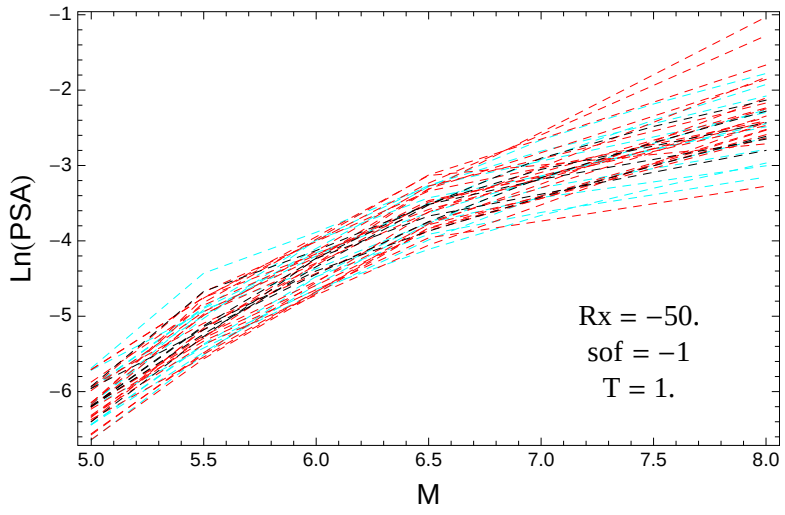



Figure 3.470: PVNGSv2: Magnitude scaling of the original GMPEs (dashed black), the original GMPEs with uncertainty model (dashed cyan) and selected A models (dashed red), for a scenario with $R_X = -50.$, $F = -1$, and $T = 1.$s.

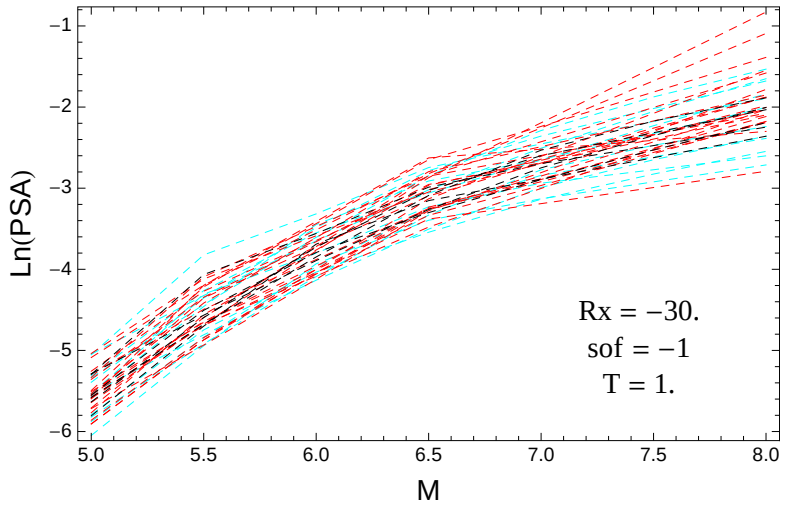



Figure 3.471: PVNGSv2: Magnitude scaling of the original GMPEs (dashed black), the original GMPEs with uncertainty model (dashed cyan) and selected A models (dashed red), for a scenario with $R_X = -30.$, $F = -1$, and $T = 1.$s.

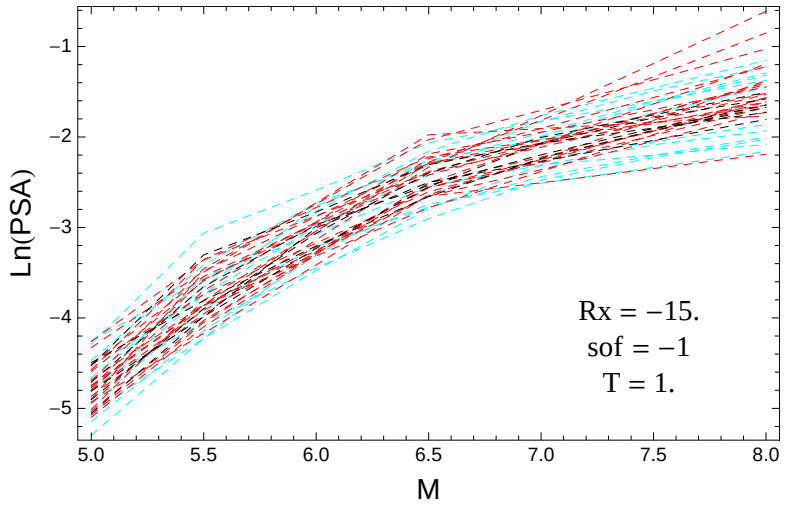



Figure 3.472: PVNGSv2: Magnitude scaling of the original GMPEs (dashed black), the original GMPEs with uncertainty model (dashed cyan) and selected A models (dashed red), for a scenario with $R_X = -15.$, $F = -1$, and $T = 1.$s.

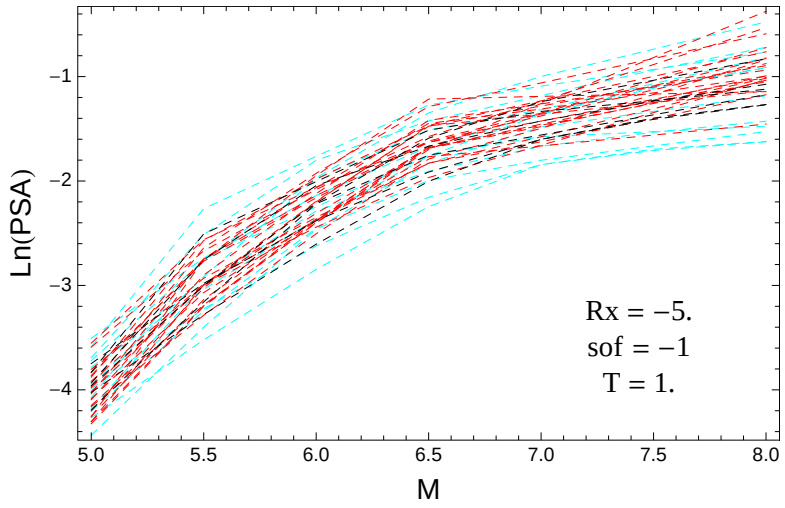



Figure 3.473: PVNGSv2: Magnitude scaling of the original GMPEs (dashed black), the original GMPEs with uncertainty model (dashed cyan) and selected A models (dashed red), for a scenario with $R_X = -5.$, $F = -1$, and $T = 1.$s.

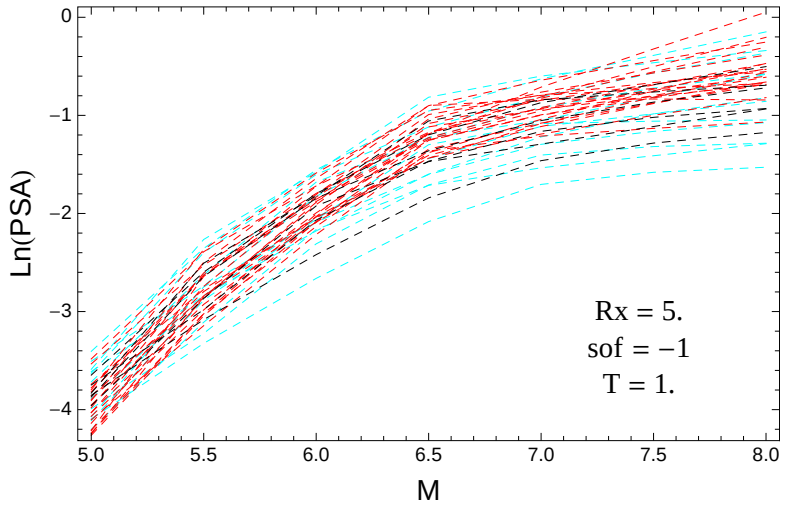



Figure 3.474: PVNGSv2: Magnitude scaling of the original GMPEs (dashed black), the original GMPEs with uncertainty model (dashed cyan) and selected A models (dashed red), for a scenario with $R_X = 5.$, $F = -1$, and $T = 1.$s.

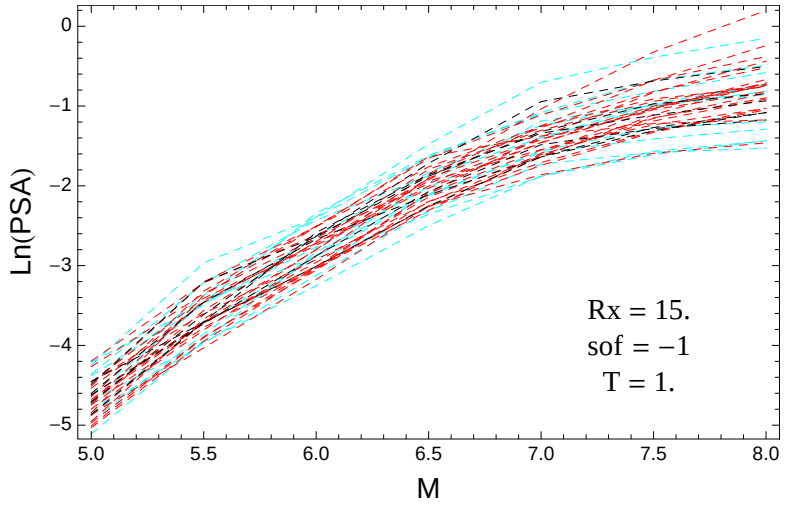



Figure 3.475: PVNGSv2: Magnitude scaling of the original GMPEs (dashed black), the original GMPEs with uncertainty model (dashed cyan) and selected A models (dashed red), for a scenario with $R_X = 15.$, $F = -1$, and $T = 1.$s.

**T = 3.s**

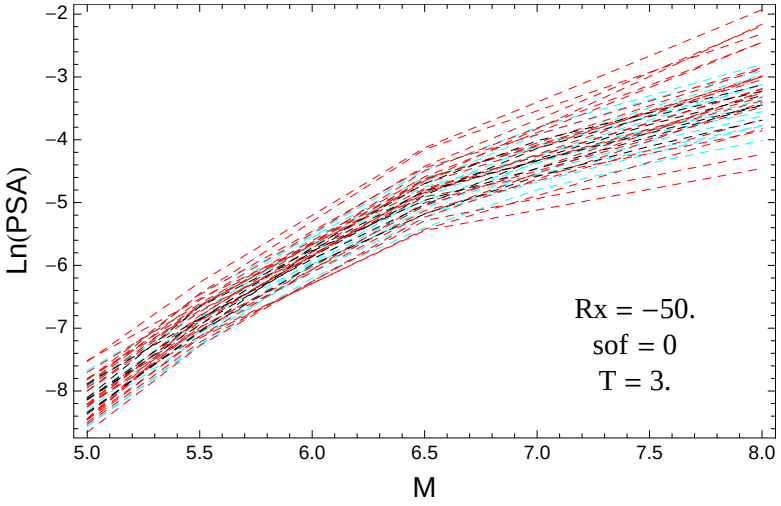



Figure 3.476: PVNGSv2: Magnitude scaling of the original GMPEs (dashed black), the original GMPEs with uncertainty model (dashed cyan) and selected A models (dashed red), for a scenario with $R_X = -50.$, $F = 0$, and $T = 3.$s.

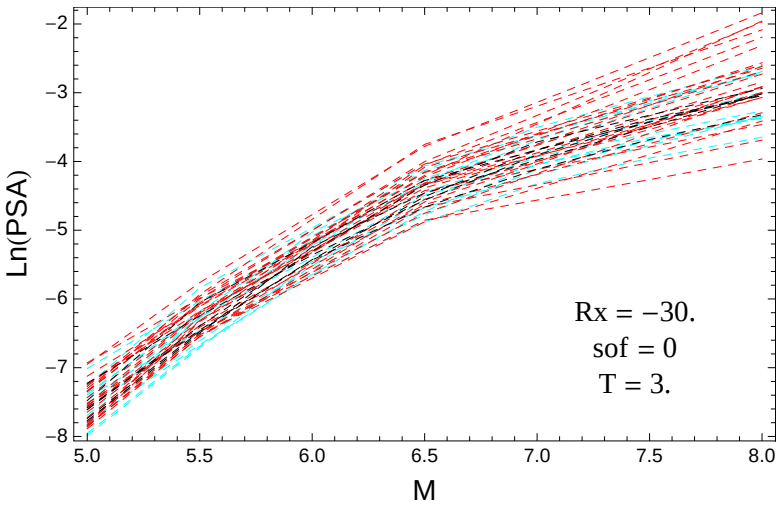



Figure 3.477: PVNGSv2: Magnitude scaling of the original GMPEs (dashed black), the original GMPEs with uncertainty model (dashed cyan) and selected A models (dashed red), for a scenario with $R_X = -30.$, $F = 0$, and $T = 3.$s.

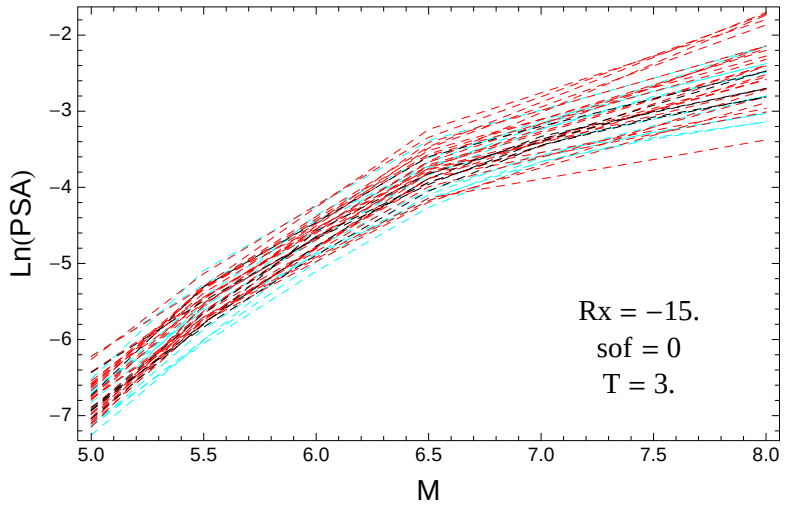



Figure 3.478: PVNGSv2: Magnitude scaling of the original GMPEs (dashed black), the original GMPEs with uncertainty model (dashed cyan) and selected A models (dashed red), for a scenario with $R_X = -15.$, $F = 0$, and $T = 3.$s.

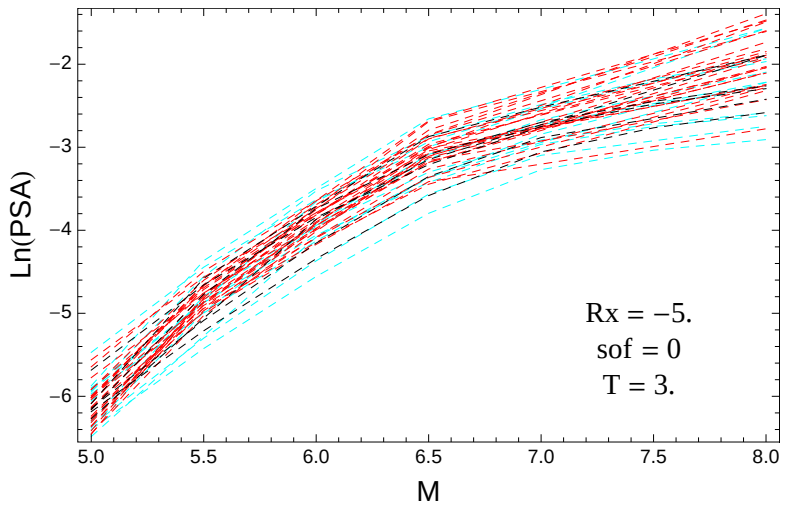



Figure 3.479: PVNGSv2: Magnitude scaling of the original GMPEs (dashed black), the original GMPEs with uncertainty model (dashed cyan) and selected A models (dashed red), for a scenario with $R_X = -5.$, $F = 0$, and $T = 3.$s.

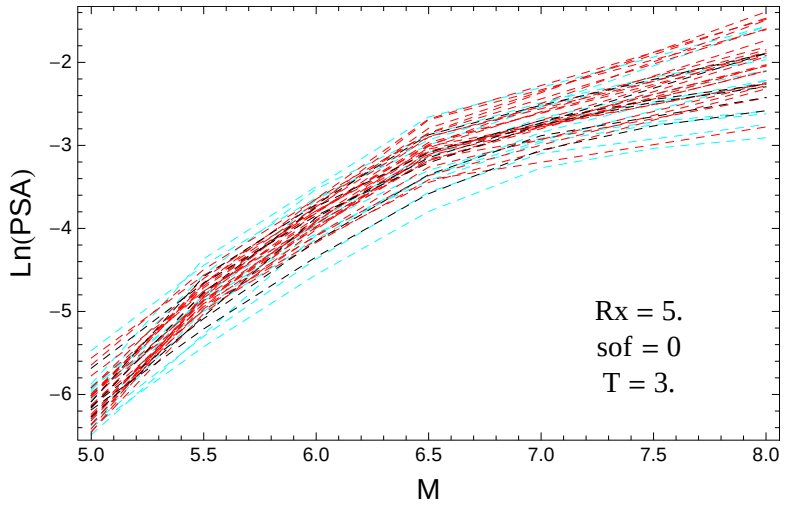



Figure 3.480: PVNGSv2: Magnitude scaling of the original GMPEs (dashed black), the original GMPEs with uncertainty model (dashed cyan) and selected A models (dashed red), for a scenario with $R_X = 5.$, $F = 0$, and $T = 3.$s.

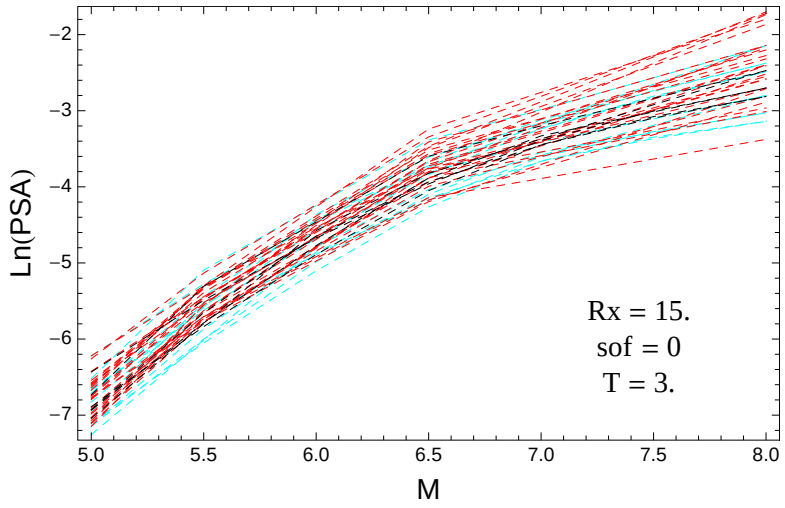



Figure 3.481: PVNGSv2: Magnitude scaling of the original GMPEs (dashed black), the original GMPEs with uncertainty model (dashed cyan) and selected A models (dashed red), for a scenario with $R_X = 15.$, $F = 0$, and $T = 3.$s.

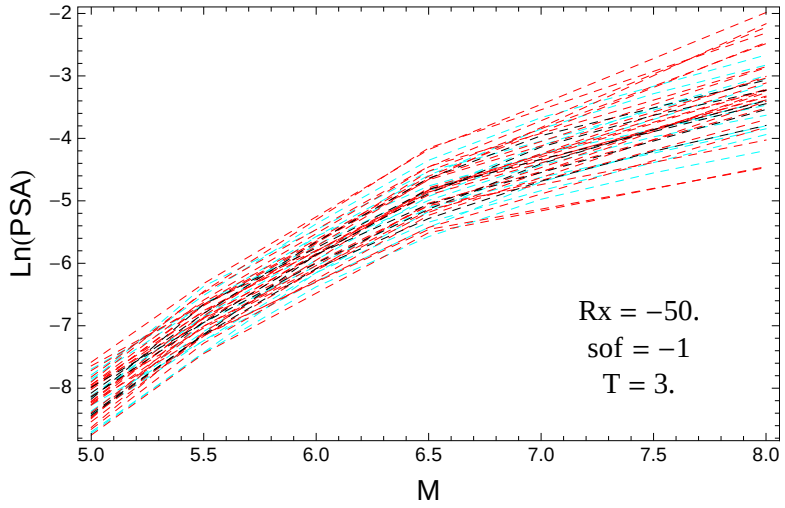



Figure 3.482: PVNGSv2: Magnitude scaling of the original GMPEs (dashed black), the original GMPEs with uncertainty model (dashed cyan) and selected A models (dashed red), for a scenario with $R_X = -50.$, $F = -1$, and $T = 3.$s.

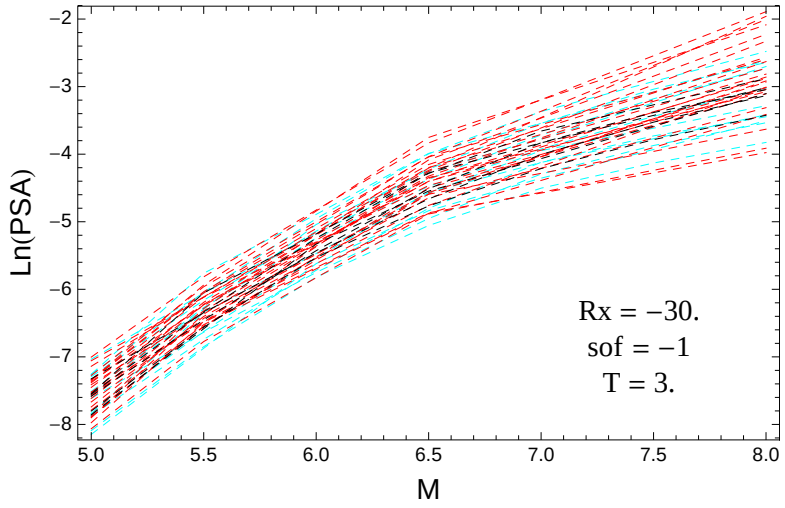



Figure 3.483: PVNGSv2: Magnitude scaling of the original GMPEs (dashed black), the original GMPEs with uncertainty model (dashed cyan) and selected A models (dashed red), for a scenario with $R_X = -30.$, $F = -1$, and $T = 3.$s.

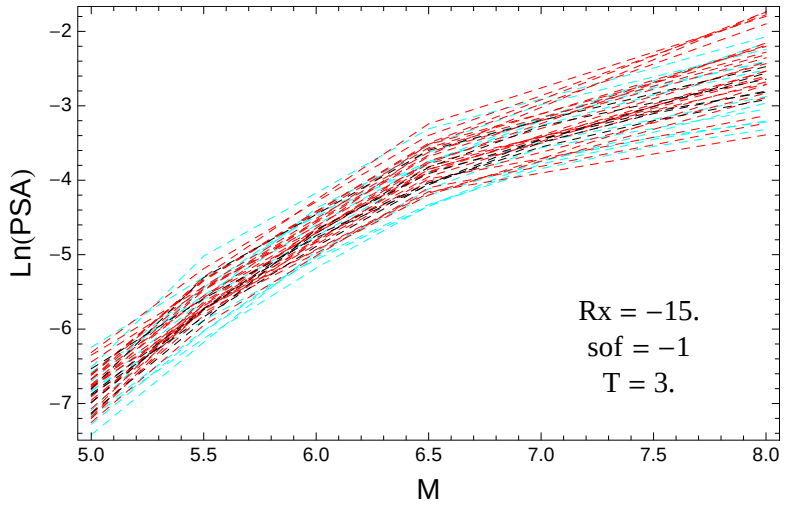



Figure 3.484: PVNGSv2: Magnitude scaling of the original GMPEs (dashed black), the original GMPEs with uncertainty model (dashed cyan) and selected A models (dashed red), for a scenario with $R_X = -15.$, $F = -1$, and $T = 3.$s.

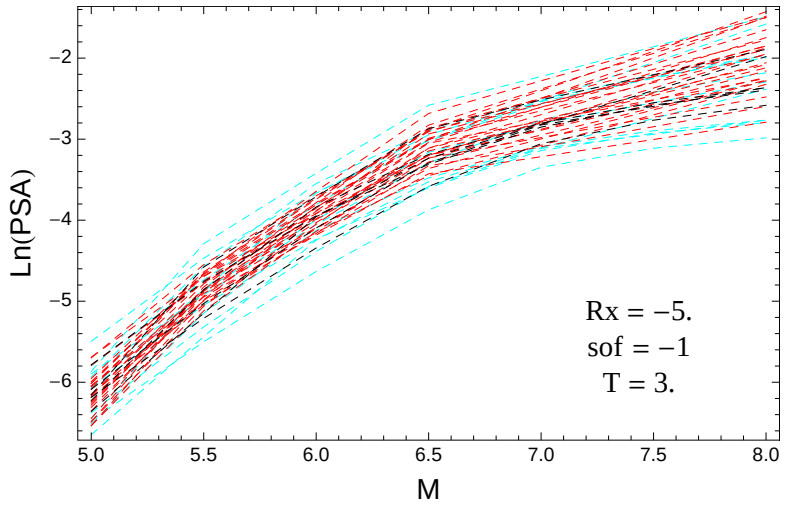



Figure 3.485: PVNGSv2: Magnitude scaling of the original GMPEs (dashed black), the original GMPEs with uncertainty model (dashed cyan) and selected A models (dashed red), for a scenario with $R_X = -5.$, $F = -1$, and $T = 3.$s.

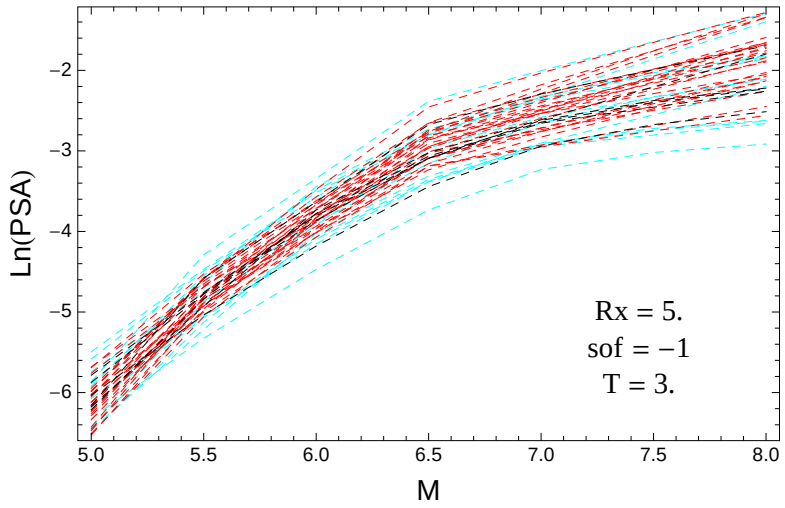



Figure 3.486: PVNGSv2: Magnitude scaling of the original GMPEs (dashed black), the original GMPEs with uncertainty model (dashed cyan) and selected A models (dashed red), for a scenario with $R_X = 5.$, $F = -1$, and $T = 3.$s.

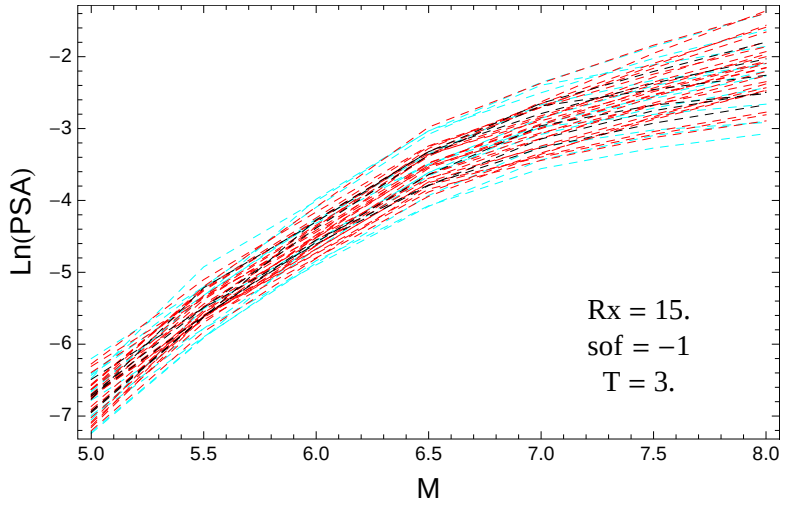



Figure 3.487: PVNGSv2: Magnitude scaling of the original GMPEs (dashed black), the original GMPEs with uncertainty model (dashed cyan) and selected A models (dashed red), for a scenario with $R_X = 15.$, $F = -1$, and $T = 3.$s.

### 3.1.12 Distance Scaling with GMPEs

**T = 0.01s**

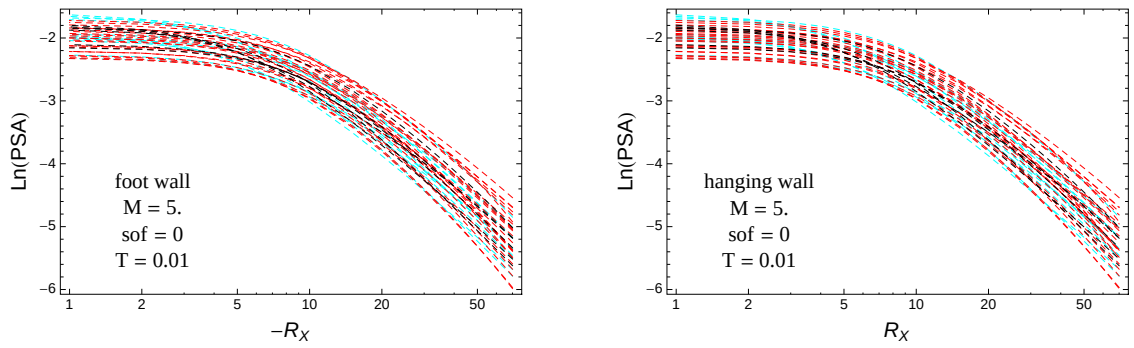



Figure 3.488: PVNGSv2: Distance scaling of the original GMPEs (dashed black), the original GMPEs with uncertainty model (dashed cyan) and selected A models (dashed red), for a scenario with $M = 5.$, $F = 0$, and $T = 0.01$s. Left: foot wall scaling; Right: hanging wall scaling.

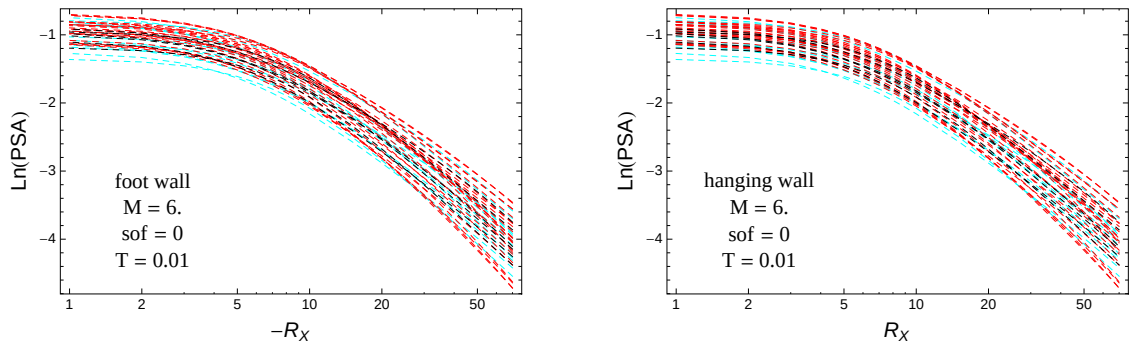



Figure 3.489: PVNGSv2: Distance scaling of the original GMPEs (dashed black), the original GMPEs with uncertainty model (dashed cyan) and selected A models (dashed red), for a scenario with $M = 6.$, $F = 0$, and $T = 0.01$s. Left: foot wall scaling; Right: hanging wall scaling.

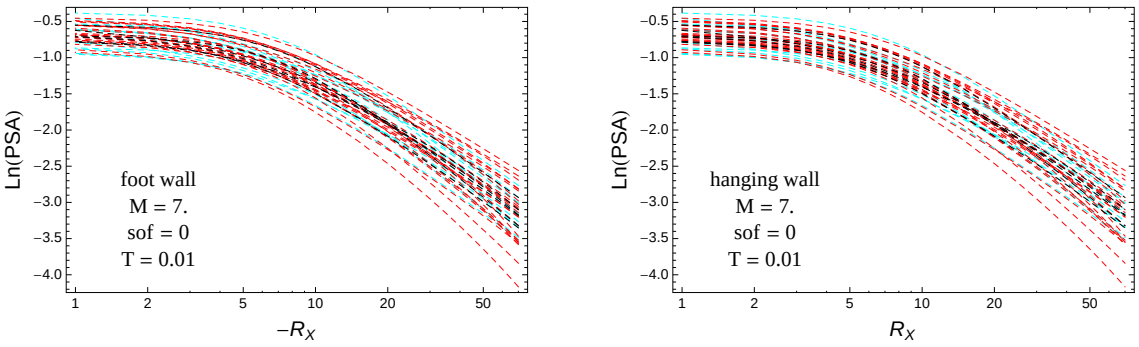



Figure 3.490: PVNGSv2: Distance scaling of the original GMPEs (dashed black), the original GMPEs with uncertainty model (dashed cyan) and selected A models (dashed red), for a scenario with $M = 7.$, $F = 0$, and $T = 0.01$s. Left: foot wall scaling; Right: hanging wall scaling.

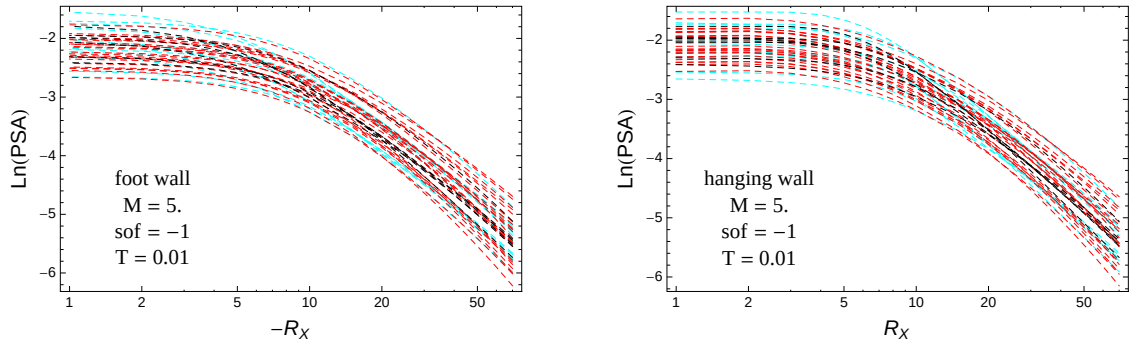



Figure 3.491: PVNGSv2: Distance scaling of the original GMPEs (dashed black), the original GMPEs with uncertainty model (dashed cyan) and selected A models (dashed red), for a scenario with $M = 5.$, $F = -1$, and $T = 0.01$s. Left: foot wall scaling; Right: hanging wall scaling.

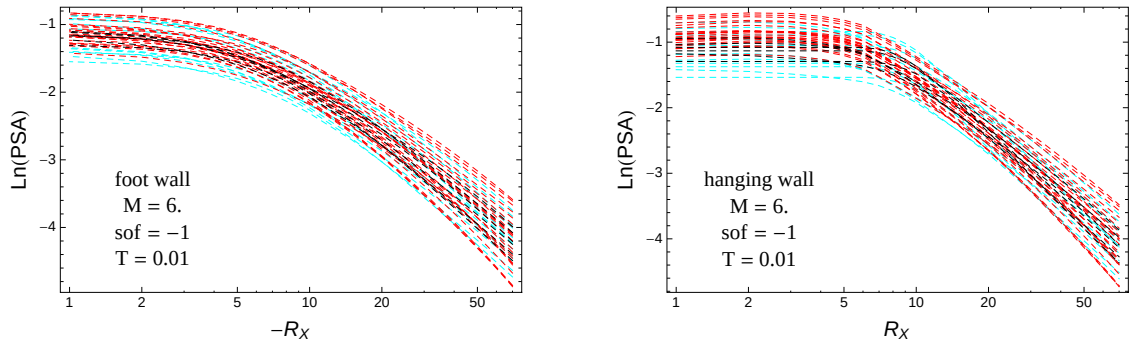



Figure 3.492: PVNGSv2: Distance scaling of the original GMPEs (dashed black), the original GMPEs with uncertainty model (dashed cyan) and selected A models (dashed red), for a scenario with $M = 6.$, $F = -1$, and $T = 0.01$s. Left: foot wall scaling; Right: hanging wall scaling.

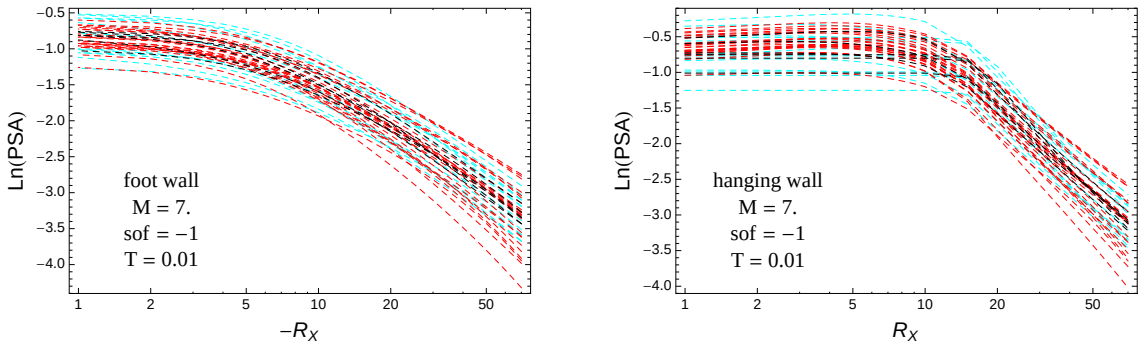



Figure 3.493: PVNGSv2: Distance scaling of the original GMPEs (dashed black), the original GMPEs with uncertainty model (dashed cyan) and selected A models (dashed red), for a scenario with $M = 7.$, $F = -1$, and $T = 0.01$s. Left: foot wall scaling; Right: hanging wall scaling.

**T = 0.2s**

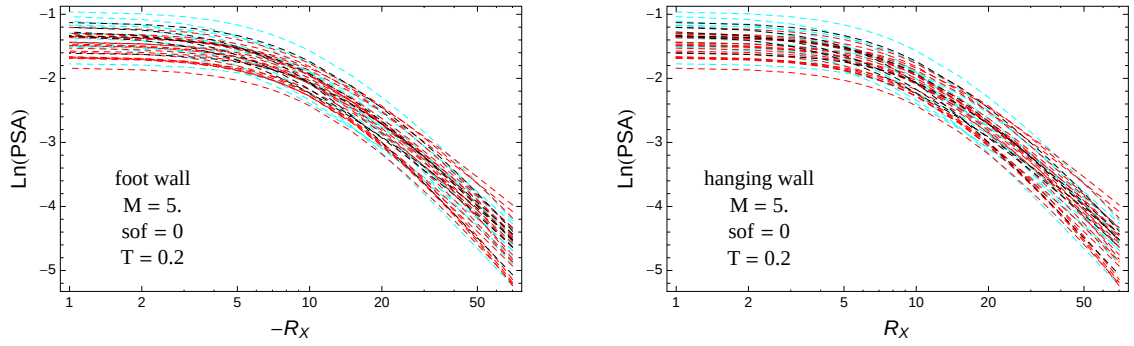



Figure 3.494: PVNGSv2: Distance scaling of the original GMPEs (dashed black), the original GMPEs with uncertainty model (dashed cyan) and selected A models (dashed red), for a scenario with $M = 5.$, $F = 0$, and $T = 0.2$s. Left: foot wall scaling; Right: hanging wall scaling.

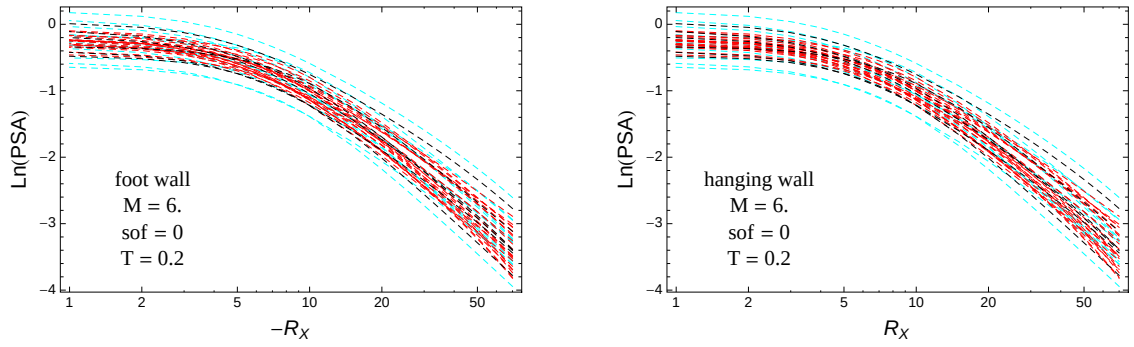



Figure 3.495: PVNGSv2: Distance scaling of the original GMPEs (dashed black), the original GMPEs with uncertainty model (dashed cyan) and selected A models (dashed red), for a scenario with $M = 6.$, $F = 0$, and $T = 0.2$s. Left: foot wall scaling; Right: hanging wall scaling.

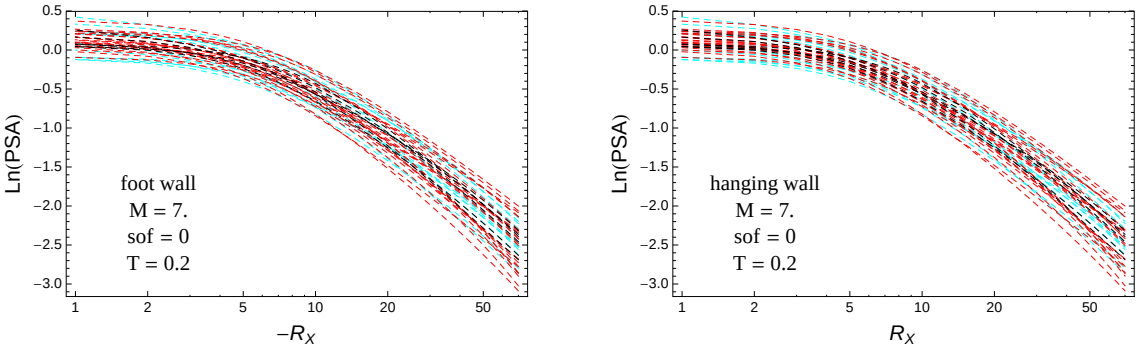



Figure 3.496: PVNGSv2: Distance scaling of the original GMPEs (dashed black), the original GMPEs with uncertainty model (dashed cyan) and selected A models (dashed red), for a scenario with $M = 7.$, $F = 0$, and $T = 0.2$s. Left: foot wall scaling; Right: hanging wall scaling.

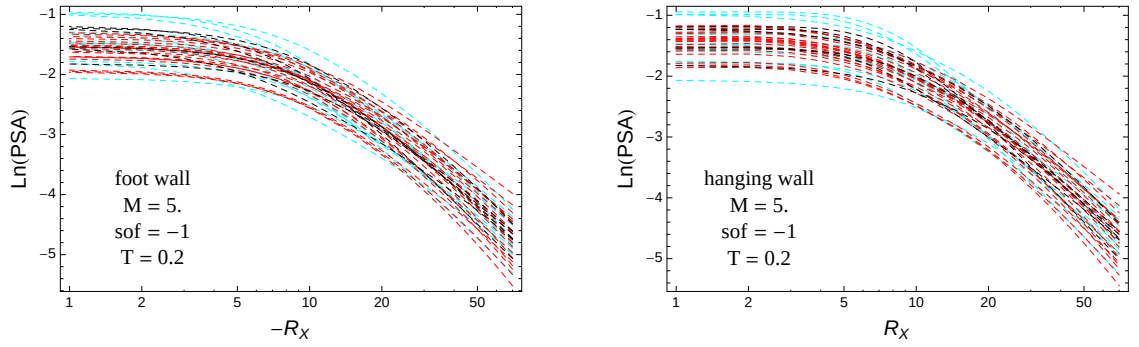



Figure 3.497: PVNGSv2: Distance scaling of the original GMPEs (dashed black), the original GMPEs with uncertainty model (dashed cyan) and selected A models (dashed red), for a scenario with $M = 5.$, $F = -1$, and $T = 0.2$s. Left: foot wall scaling; Right: hanging wall scaling.

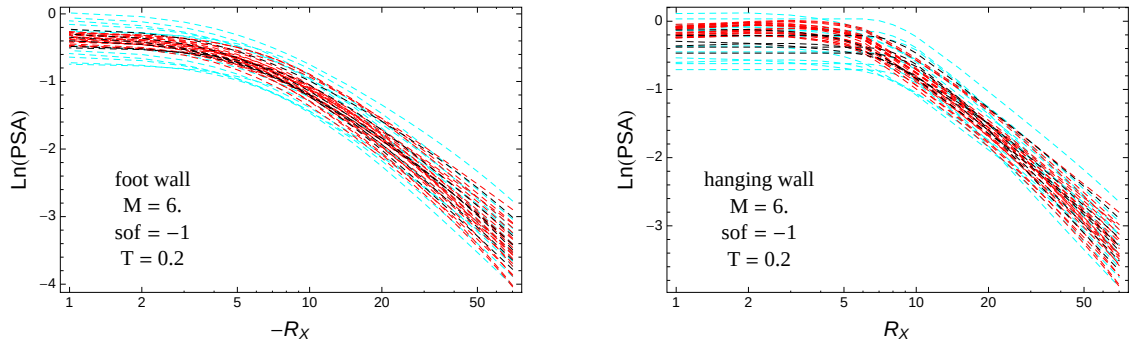



Figure 3.498: PVNGSv2: Distance scaling of the original GMPEs (dashed black), the original GMPEs with uncertainty model (dashed cyan) and selected A models (dashed red), for a scenario with $M = 6.$, $F = -1$, and $T = 0.2$s. Left: foot wall scaling; Right: hanging wall scaling.

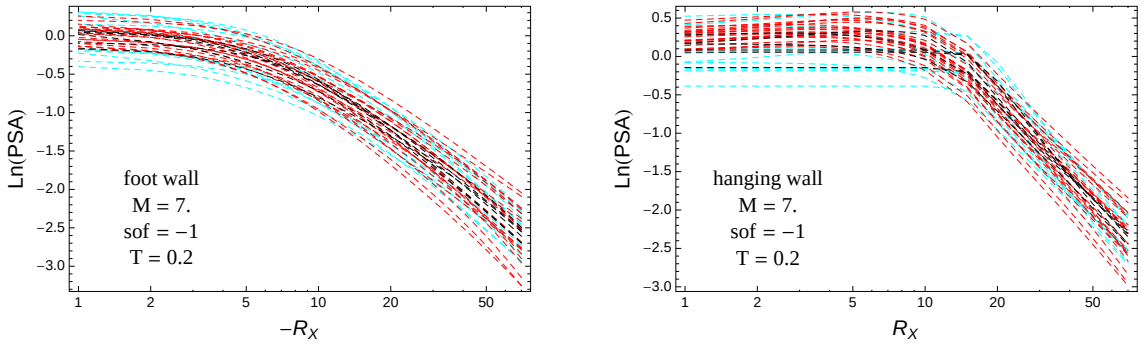



Figure 3.499: PVNGSv2: Distance scaling of the original GMPEs (dashed black), the original GMPEs with uncertainty model (dashed cyan) and selected A models (dashed red), for a scenario with $M = 7.$, $F = -1$, and $T = 0.2$s. Left: foot wall scaling; Right: hanging wall scaling.

**T = 0.5s**

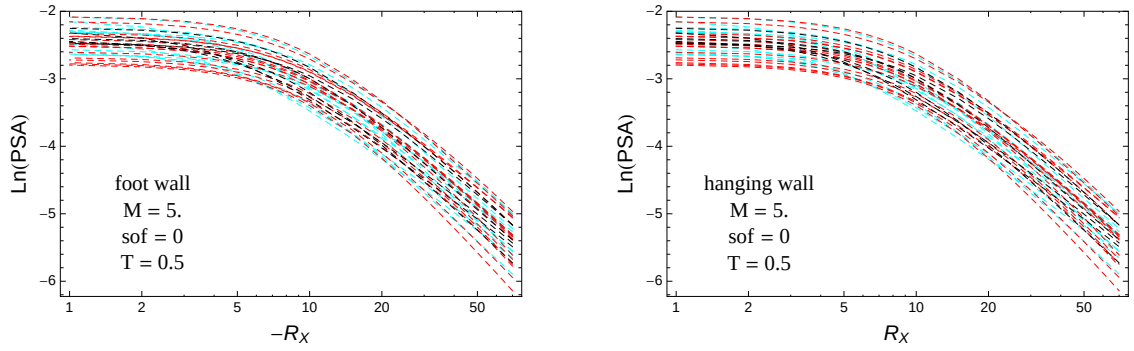



Figure 3.500: PVNGSv2: Distance scaling of the original GMPEs (dashed black), the original GMPEs with uncertainty model (dashed cyan) and selected A models (dashed red), for a scenario with $M = 5.$, $F = 0$, and $T = 0.5$s. Left: foot wall scaling; Right: hanging wall scaling.

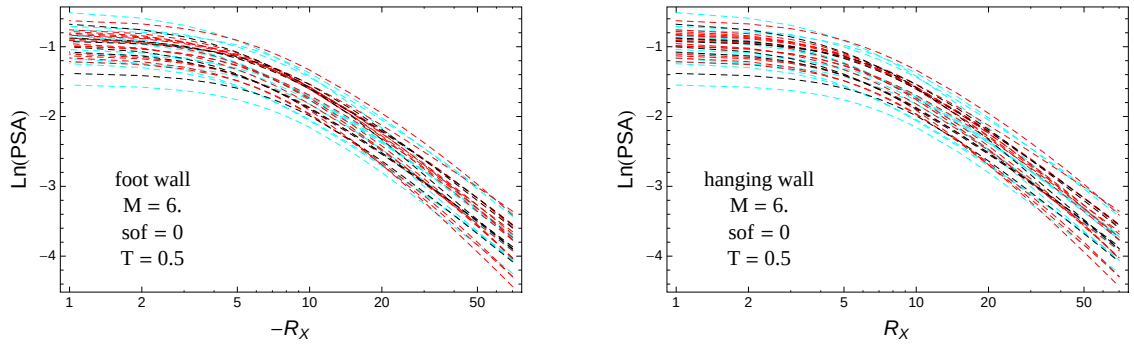



Figure 3.501: PVNGSv2: Distance scaling of the original GMPEs (dashed black), the original GMPEs with uncertainty model (dashed cyan) and selected A models (dashed red), for a scenario with $M = 6.$, $F = 0$, and $T = 0.5$s. Left: foot wall scaling; Right: hanging wall scaling.

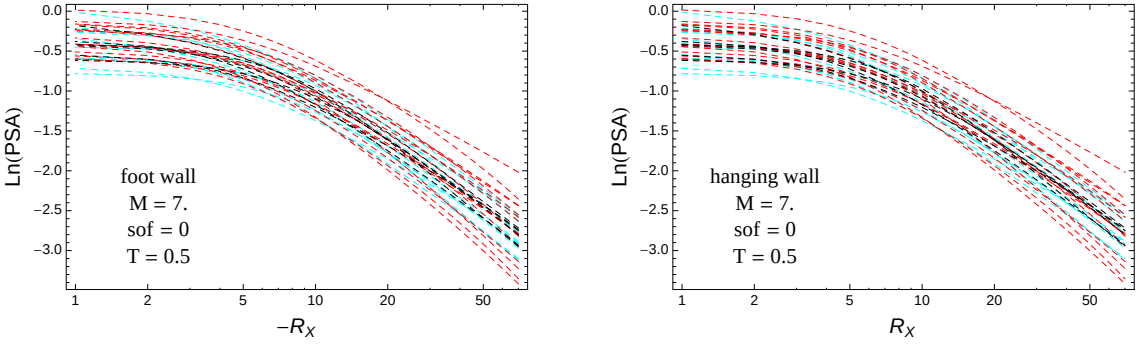



Figure 3.502: PVNGSv2: Distance scaling of the original GMPEs (dashed black), the original GMPEs with uncertainty model (dashed cyan) and selected A models (dashed red), for a scenario with $M = 7.$, $F = 0$, and $T = 0.5$s. Left: foot wall scaling; Right: hanging wall scaling.

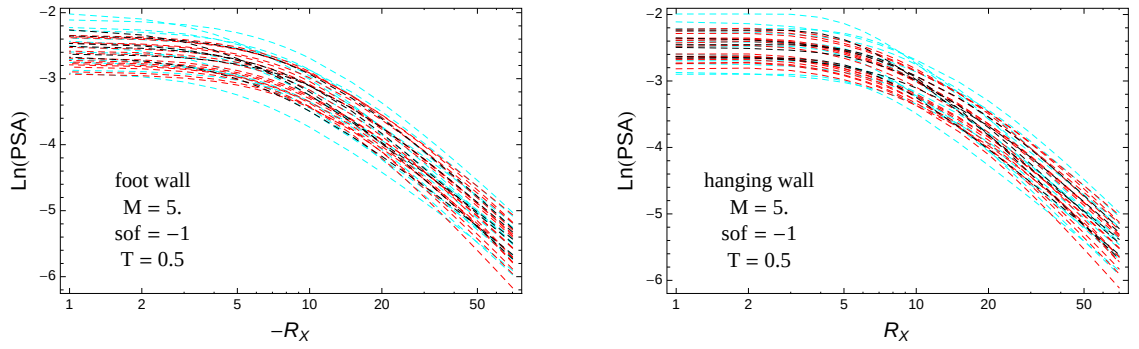



Figure 3.503: PVNGSv2: Distance scaling of the original GMPEs (dashed black), the original GMPEs with uncertainty model (dashed cyan) and selected A models (dashed red), for a scenario with $M = 5.$, $F = -1$, and $T = 0.5$s. Left: foot wall scaling; Right: hanging wall scaling.

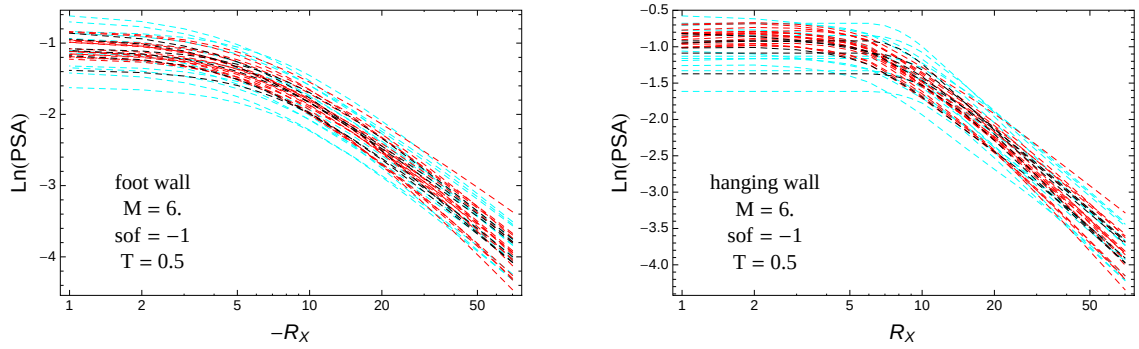



Figure 3.504: PVNGSv2: Distance scaling of the original GMPEs (dashed black), the original GMPEs with uncertainty model (dashed cyan) and selected A models (dashed red), for a scenario with $M = 6.$, $F = -1$, and $T = 0.5$s. Left: foot wall scaling; Right: hanging wall scaling.

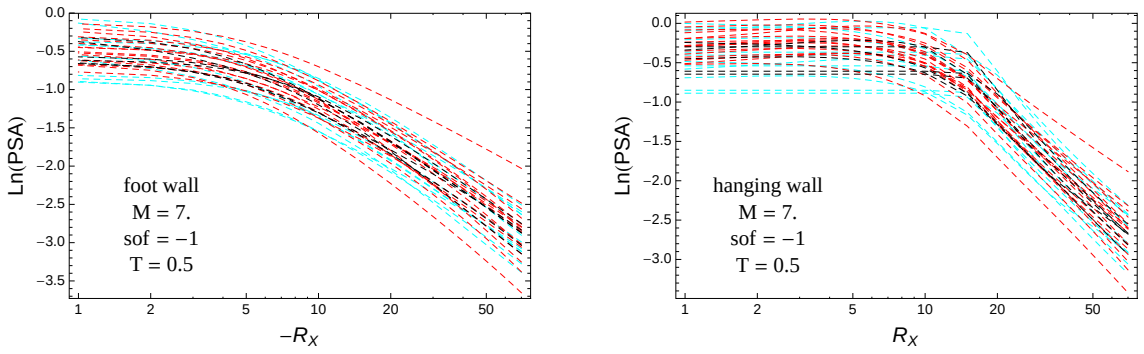



Figure 3.505: PVNGSv2: Distance scaling of the original GMPEs (dashed black), the original GMPEs with uncertainty model (dashed cyan) and selected A models (dashed red), for a scenario with $M = 7.$, $F = -1$, and $T = 0.5$s. Left: foot wall scaling; Right: hanging wall scaling.

**T = 1.s**

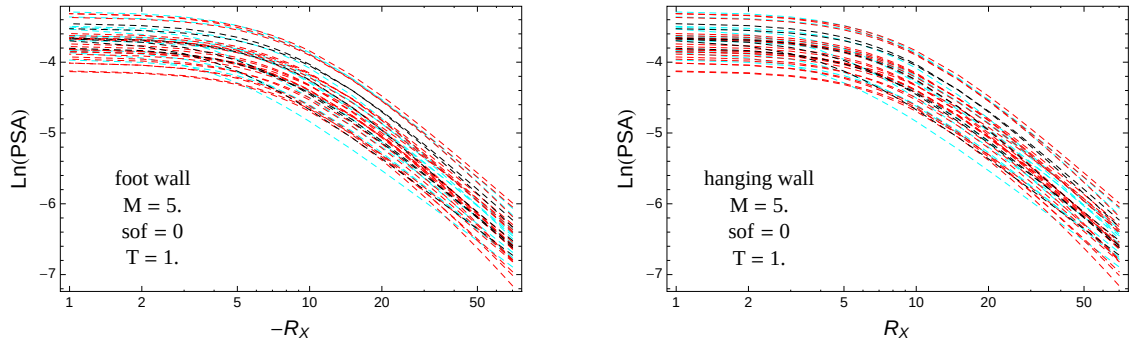



Figure 3.506: PVNGSv2: Distance scaling of the original GMPEs (dashed black), the original GMPEs with uncertainty model (dashed cyan) and selected A models (dashed red), for a scenario with $M = 5.$, $F = 0$, and $T = 1.$s. Left: foot wall scaling; Right: hanging wall scaling.

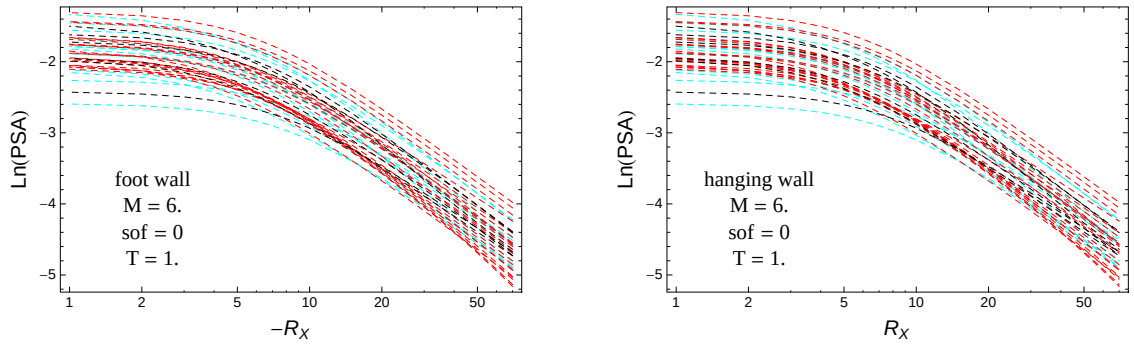



Figure 3.507: PVNGSv2: Distance scaling of the original GMPEs (dashed black), the original GMPEs with uncertainty model (dashed cyan) and selected A models (dashed red), for a scenario with $M = 6.$, $F = 0$, and $T = 1.$s. Left: foot wall scaling; Right: hanging wall scaling.

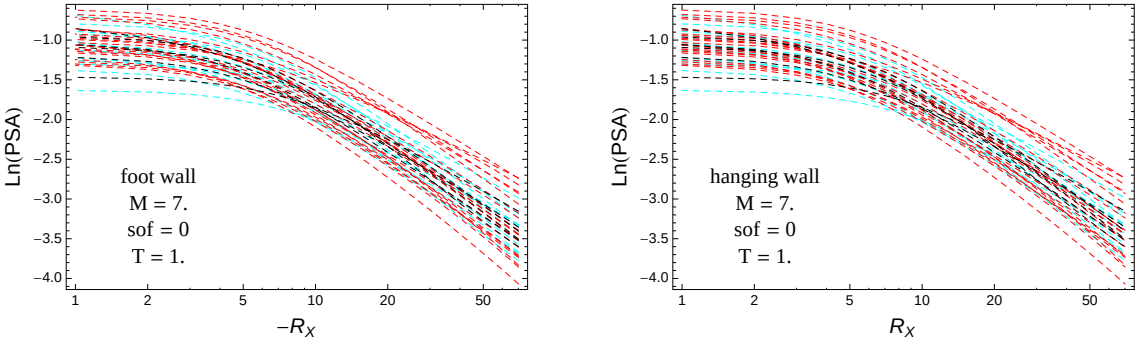



Figure 3.508: PVNGSv2: Distance scaling of the original GMPEs (dashed black), the original GMPEs with uncertainty model (dashed cyan) and selected A models (dashed red), for a scenario with $M = 7.$, $F = 0$, and $T = 1.$s. Left: foot wall scaling; Right: hanging wall scaling.

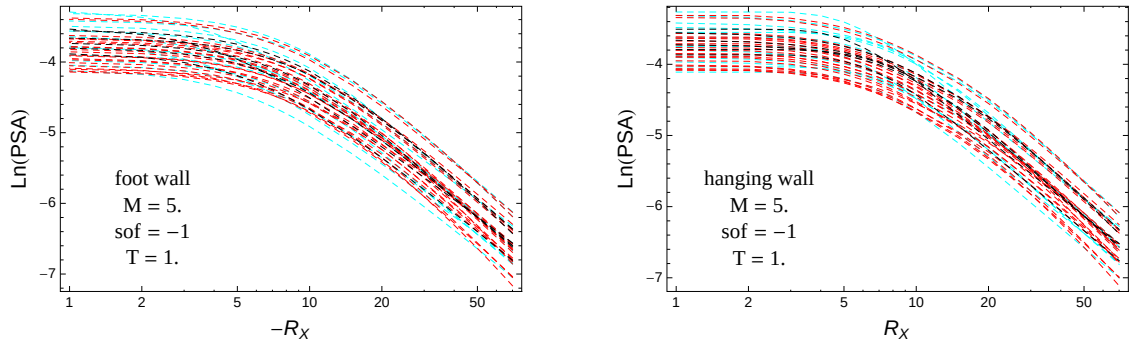



Figure 3.509: PVNGSv2: Distance scaling of the original GMPEs (dashed black), the original GMPEs with uncertainty model (dashed cyan) and selected A models (dashed red), for a scenario with $M = 5.$, $F = -1$, and $T = 1.$s. Left: foot wall scaling; Right: hanging wall scaling.

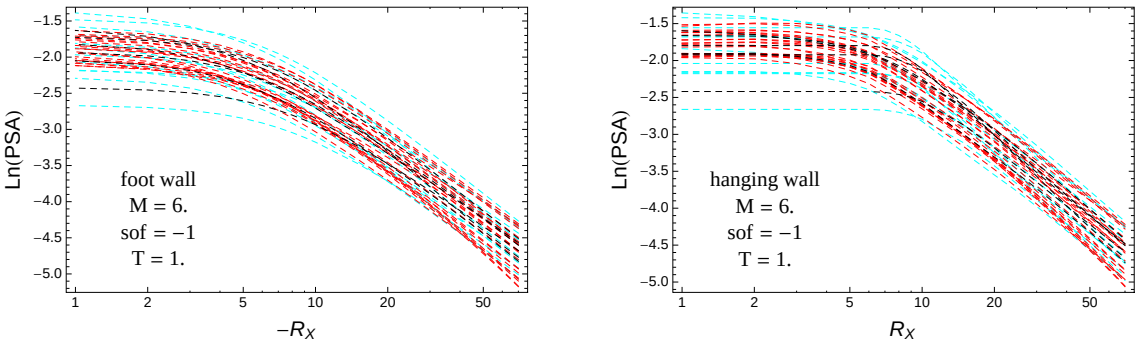



Figure 3.510: PVNGSv2: Distance scaling of the original GMPEs (dashed black), the original GMPEs with uncertainty model (dashed cyan) and selected A models (dashed red), for a scenario with $M = 6.$, $F = -1$, and $T = 1.$s. Left: foot wall scaling; Right: hanging wall scaling.

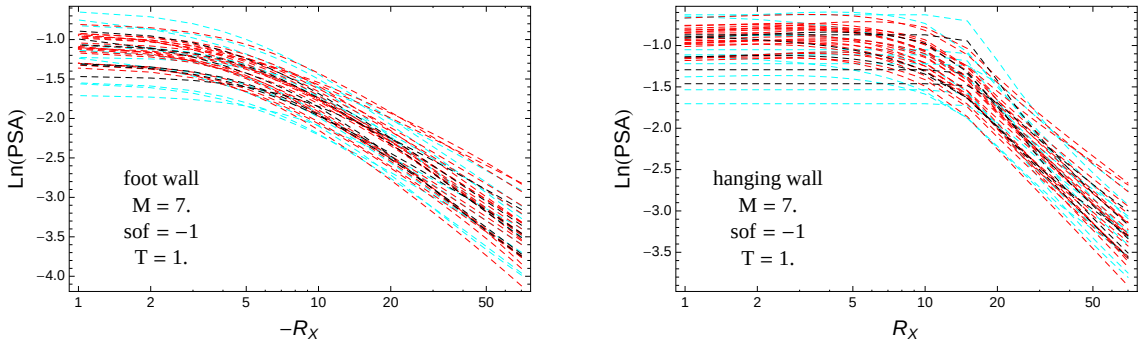



Figure 3.511: PVNGSv2: Distance scaling of the original GMPEs (dashed black), the original GMPEs with uncertainty model (dashed cyan) and selected A models (dashed red), for a scenario with $M = 7.$, $F = -1$, and $T = 1.$s. Left: foot wall scaling; Right: hanging wall scaling.

**T = 3.s**

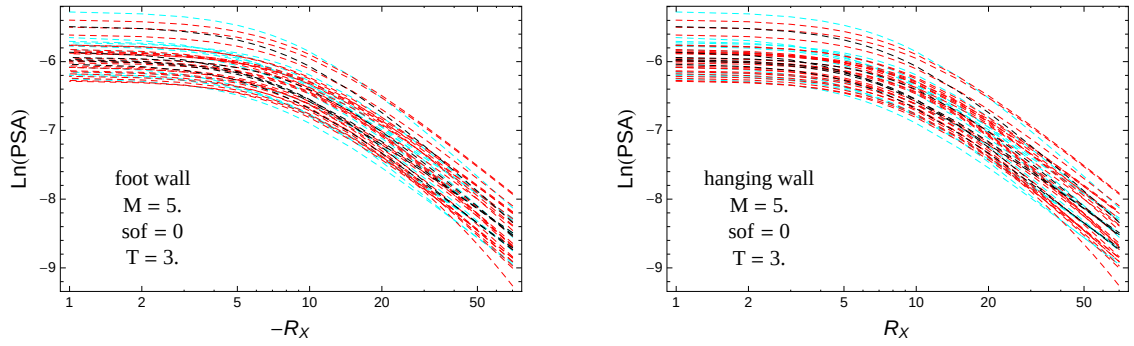



Figure 3.512: PVNGSv2: Distance scaling of the original GMPEs (dashed black), the original GMPEs with uncertainty model (dashed cyan) and selected A models (dashed red), for a scenario with $M = 5.$, $F = 0$, and $T = 3.$s. Left: foot wall scaling; Right: hanging wall scaling.

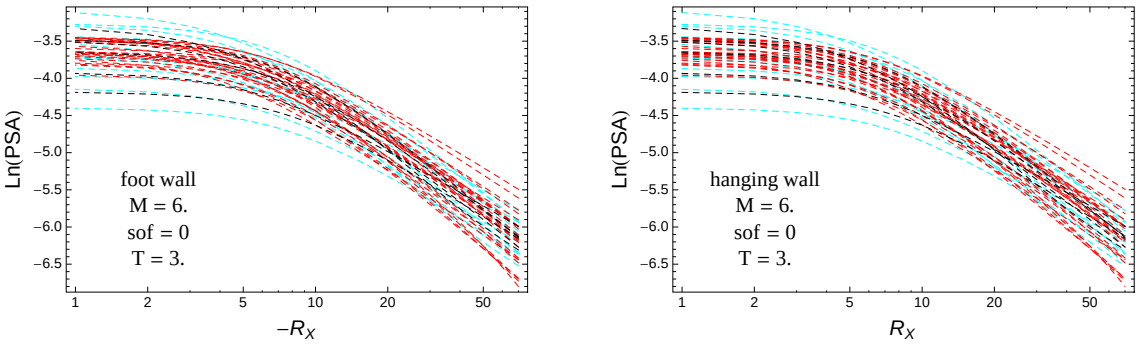



Figure 3.513: PVNGSv2: Distance scaling of the original GMPEs (dashed black), the original GMPEs with uncertainty model (dashed cyan) and selected A models (dashed red), for a scenario with $M = 6.$, $F = 0$, and $T = 3.$s. Left: foot wall scaling; Right: hanging wall scaling.

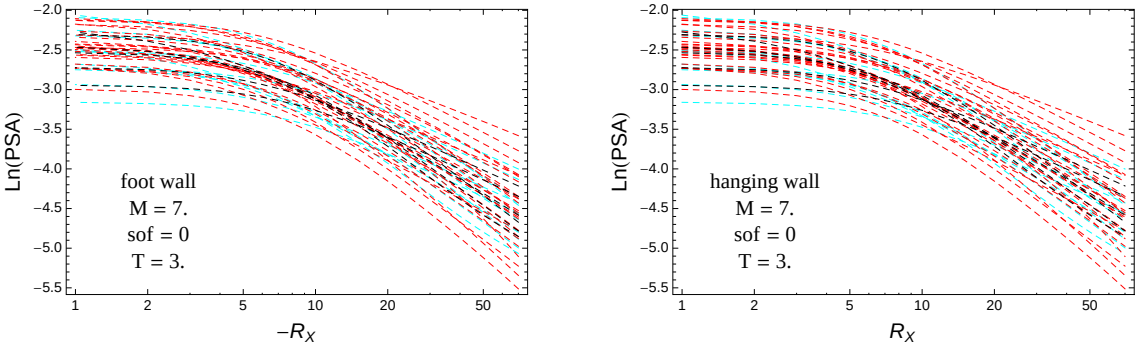



Figure 3.514: PVNGSv2: Distance scaling of the original GMPEs (dashed black), the original GMPEs with uncertainty model (dashed cyan) and selected A models (dashed red), for a scenario with $M = 7.$, $F = 0$, and $T = 3.$s. Left: foot wall scaling; Right: hanging wall scaling.

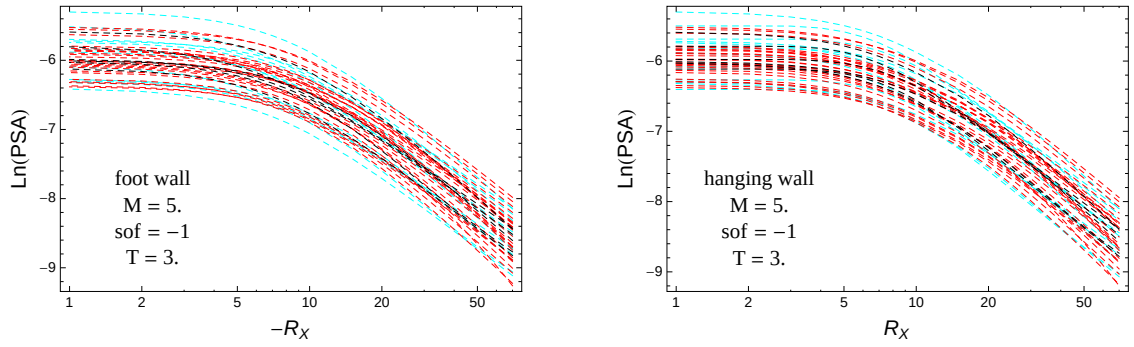



Figure 3.515: PVNGSv2: Distance scaling of the original GMPEs (dashed black), the original GMPEs with uncertainty model (dashed cyan) and selected A models (dashed red), for a scenario with $M = 5.$, $F = -1$, and $T = 3.$s. Left: foot wall scaling; Right: hanging wall scaling.

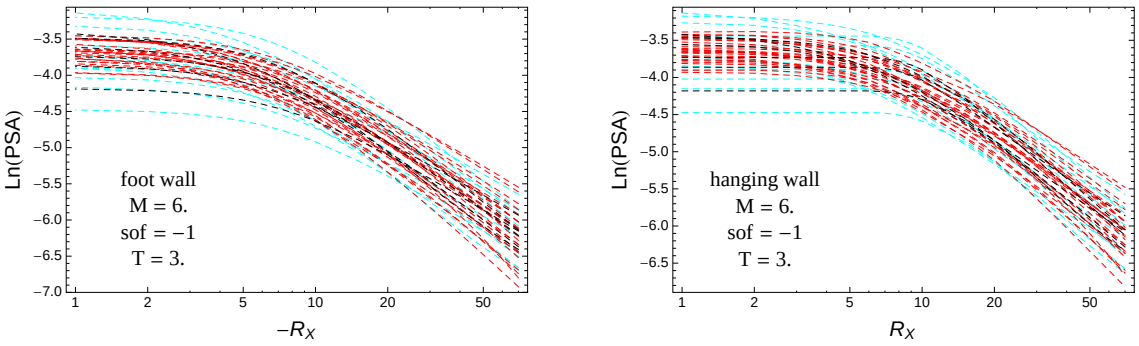



Figure 3.516: PVNGSv2: Distance scaling of the original GMPEs (dashed black), the original GMPEs with uncertainty model (dashed cyan) and selected A models (dashed red), for a scenario with $M = 6.$, $F = -1$, and $T = 3.$s. Left: foot wall scaling; Right: hanging wall scaling.

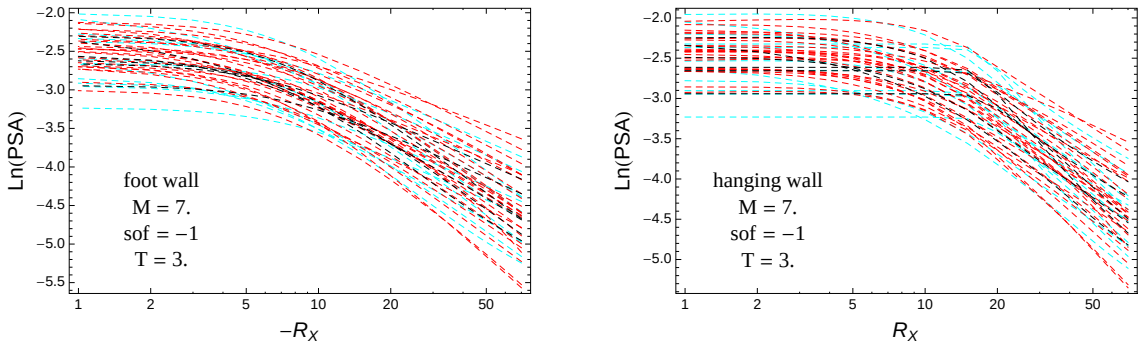



Figure 3.517: PVNGSv2: Distance scaling of the original GMPEs (dashed black), the original GMPEs with uncertainty model (dashed cyan) and selected A models (dashed red), for a scenario with $M = 7.$, $F = -1$, and $T = 3.$s. Left: foot wall scaling; Right: hanging wall scaling.

### 3.1.13 Quantile Plots vs. Magnitude with GMPEs

**T = 0.01s**

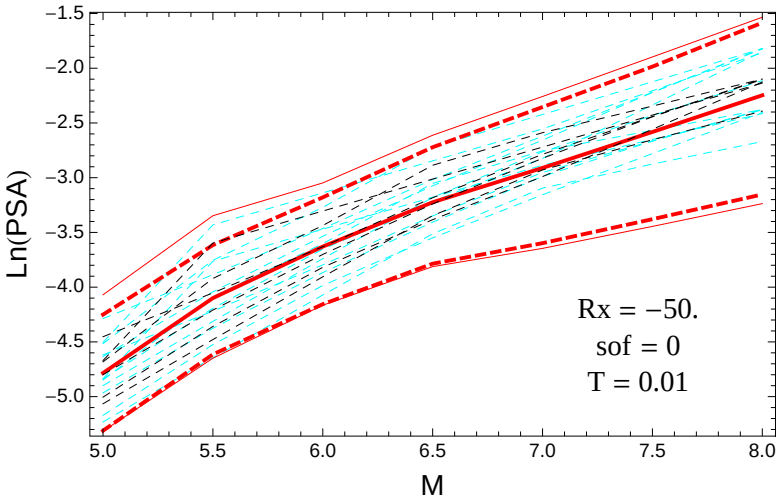



Figure 3.518: PVNGSv2: Magnitude scaling of the original GMPEs (dashed black), the original GMPEs with uncertainty model (dashed cyan) and 0.05,0.5,0.95 quantile of the ModelA distribution (red) with total weights, for a scenario with $R_X = -50.$, $F = 0$, and $T = 0.01$s.

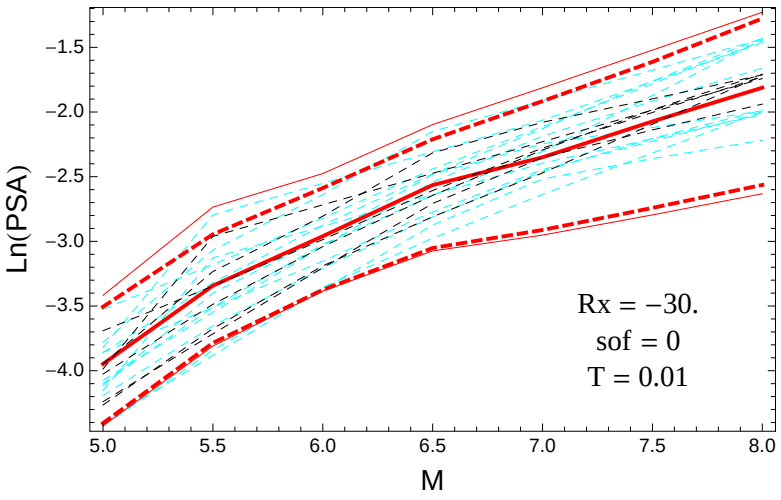



Figure 3.519: PVNGSv2: Magnitude scaling of the original GMPEs (dashed black), the original GMPEs with uncertainty model (dashed cyan) and 0.05,0.5,0.95 quantile of the ModelA distribution (red) with total weights, for a scenario with $R_X = -30.$, $F = 0$, and $T = 0.01$s.

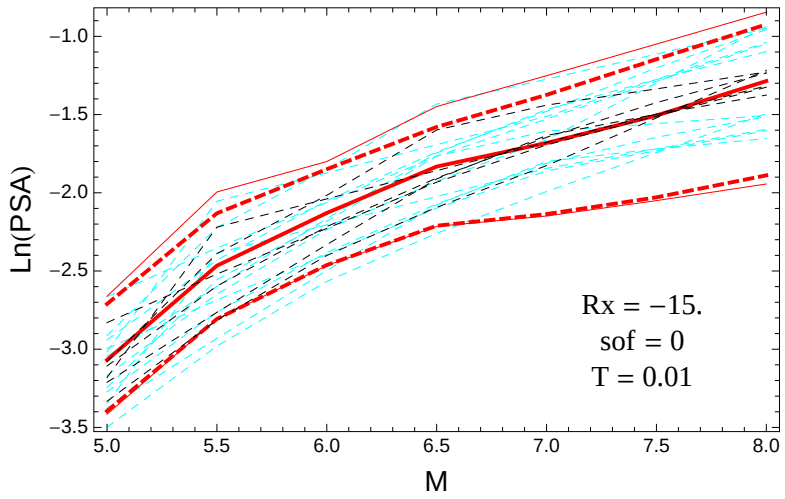



Figure 3.520: PVNGSv2: Magnitude scaling of the original GMPEs (dashed black), the original GMPEs with uncertainty model (dashed cyan) and 0.05,0.5,0.95 quantile of the ModelA distribution (red) with total weights, for a scenario with $R_X = -15.$, $F = 0$, and $T = 0.01$s.

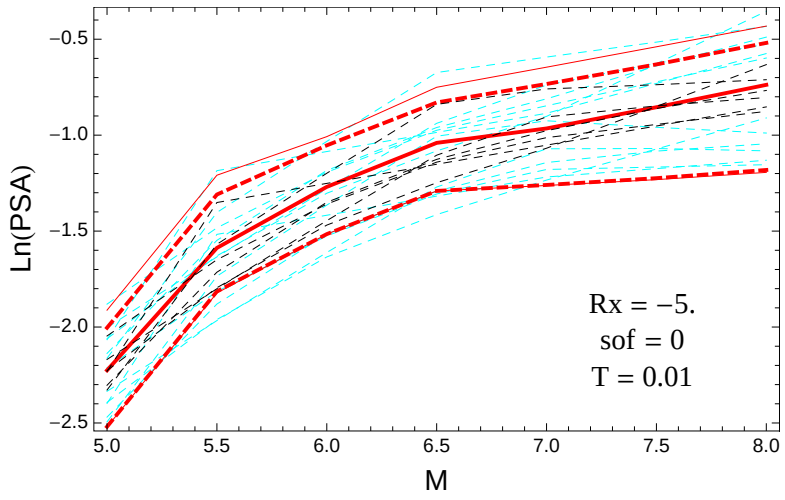



Figure 3.521: PVNGSv2: Magnitude scaling of the original GMPEs (dashed black), the original GMPEs with uncertainty model (dashed cyan) and 0.05,0.5,0.95 quantile of the ModelA distribution (red) with total weights, for a scenario with $R_X = -5.$, $F = 0$, and $T = 0.01$s.

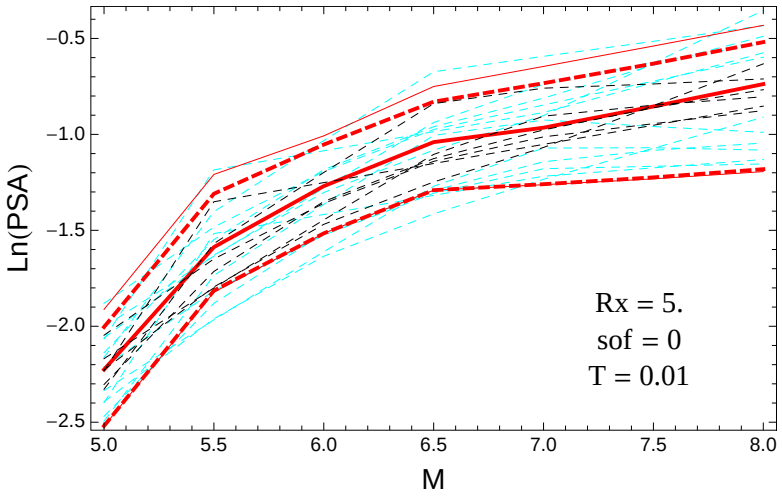



Figure 3.522: PVNGSv2: Magnitude scaling of the original GMPEs (dashed black), the original GMPEs with uncertainty model (dashed cyan) and 0.05,0.5,0.95 quantile of the ModelA distribution (red) with total weights, for a scenario with $R_X = 5.$, $F = 0$, and $T = 0.01$s.

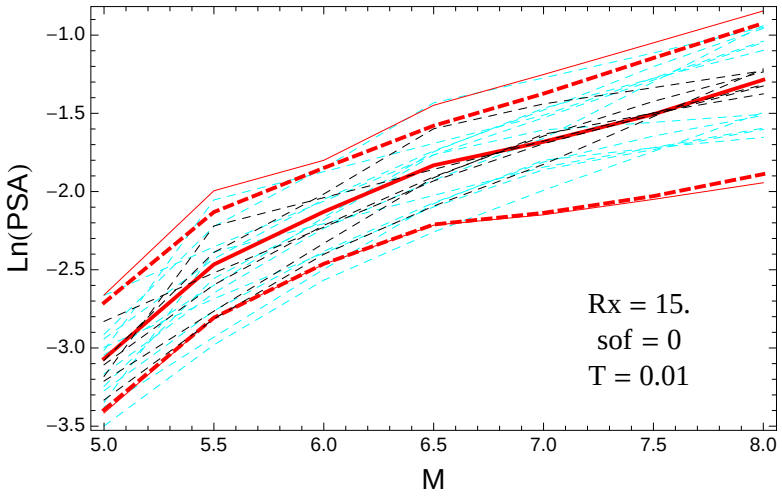



Figure 3.523: PVNGSv2: Magnitude scaling of the original GMPEs (dashed black), the original GMPEs with uncertainty model (dashed cyan) and 0.05,0.5,0.95 quantile of the ModelA distribution (red) with total weights, for a scenario with $R_X = 15.$, $F = 0$, and $T = 0.01$s.

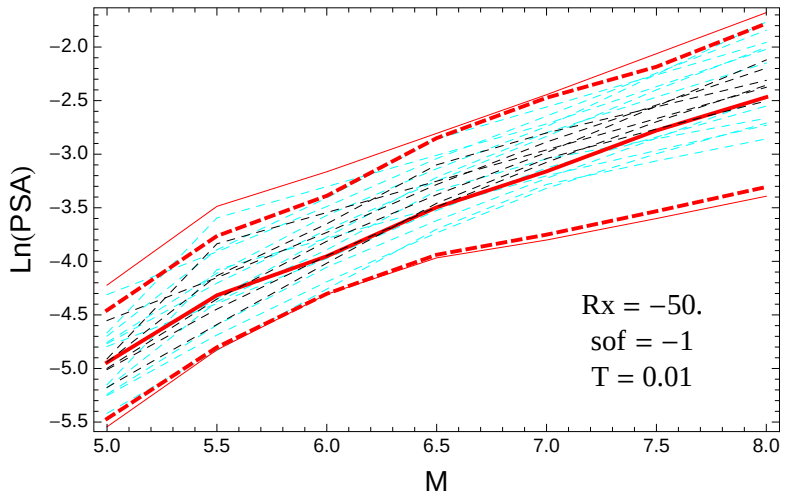



Figure 3.524: PVNGSv2: Magnitude scaling of the original GMPEs (dashed black), the original GMPEs with uncertainty model (dashed cyan) and 0.05,0.5,0.95 quantile of the ModelA distribution (red) with total weights, for a scenario with $R_X = -50.$, $F = -1$, and $T = 0.01$s.

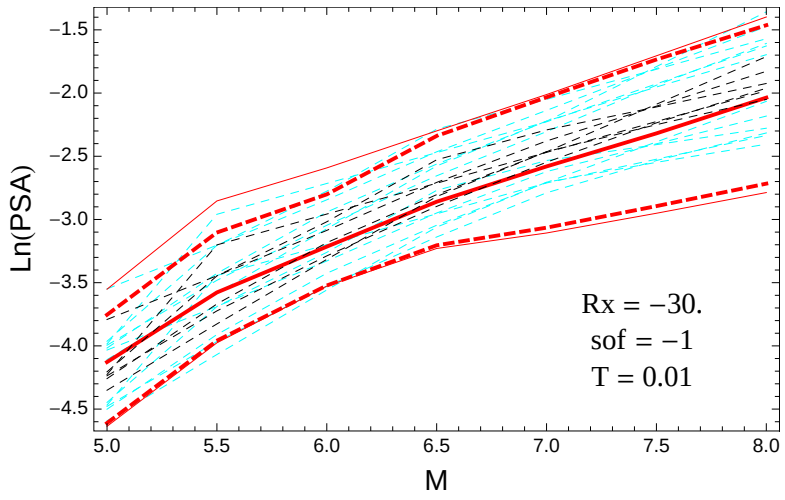



Figure 3.525: PVNGSv2: Magnitude scaling of the original GMPEs (dashed black), the original GMPEs with uncertainty model (dashed cyan) and 0.05,0.5,0.95 quantile of the ModelA distribution (red) with total weights, for a scenario with $R_X = -30.$, $F = -1$, and $T = 0.01$s.

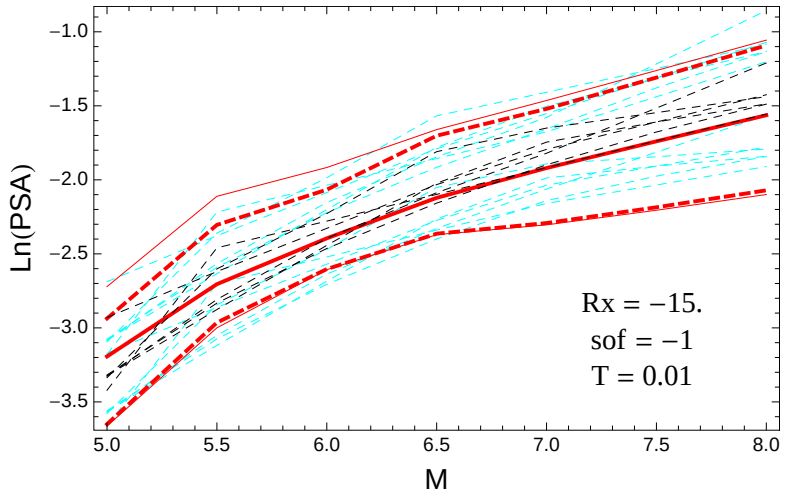



Figure 3.526: PVNGSv2: Magnitude scaling of the original GMPEs (dashed black), the original GMPEs with uncertainty model (dashed cyan) and 0.05,0.5,0.95 quantile of the ModelA distribution (red) with total weights, for a scenario with $R_X = -15.$, $F = -1$, and $T = 0.01$s.

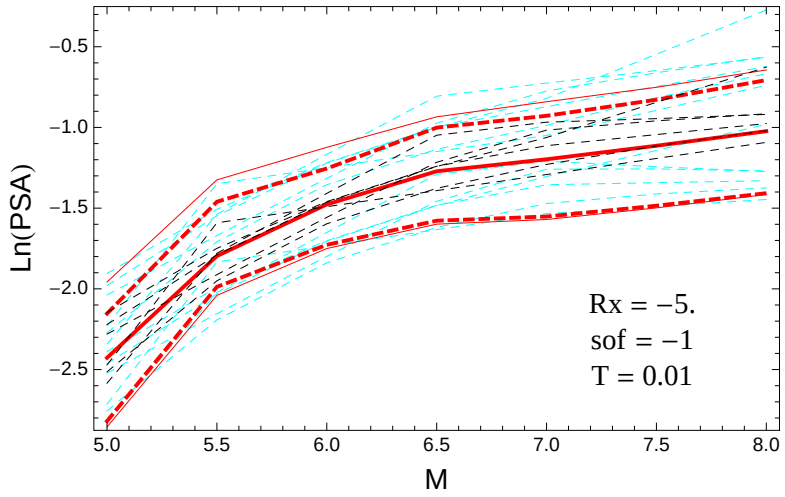



Figure 3.527: PVNGSv2: Magnitude scaling of the original GMPEs (dashed black), the original GMPEs with uncertainty model (dashed cyan) and 0.05,0.5,0.95 quantile of the ModelA distribution (red) with total weights, for a scenario with $R_X = -5.$, $F = -1$, and $T = 0.01$s.

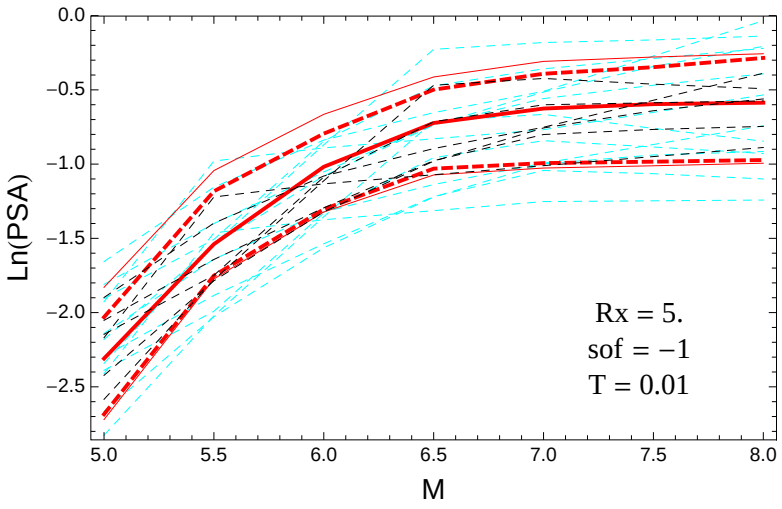



Figure 3.528: PVNGSv2: Magnitude scaling of the original GMPEs (dashed black), the original GMPEs with uncertainty model (dashed cyan) and 0.05,0.5,0.95 quantile of the ModelA distribution (red) with total weights, for a scenario with $R_X = 5.$, $F = -1$, and $T = 0.01$s.

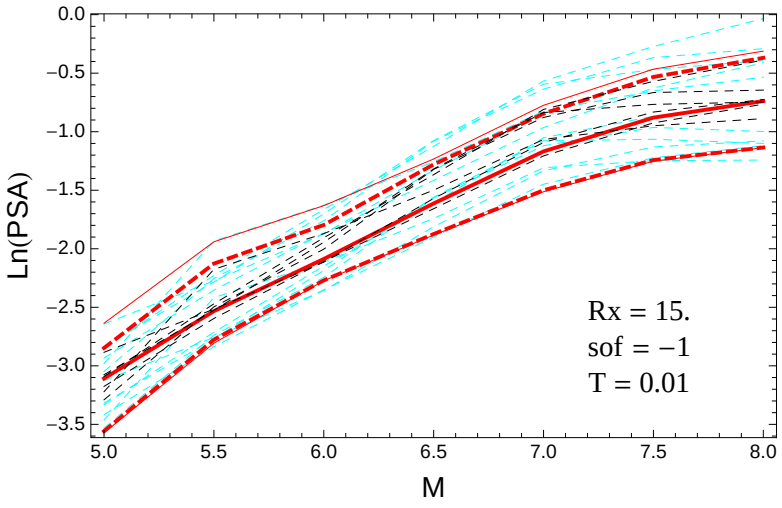



Figure 3.529: PVNGSv2: Magnitude scaling of the original GMPEs (dashed black), the original GMPEs with uncertainty model (dashed cyan) and 0.05,0.5,0.95 quantile of the ModelA distribution (red) with total weights, for a scenario with $R_X = 15.$, $F = -1$, and $T = 0.01$s.

**T = 0.2s**

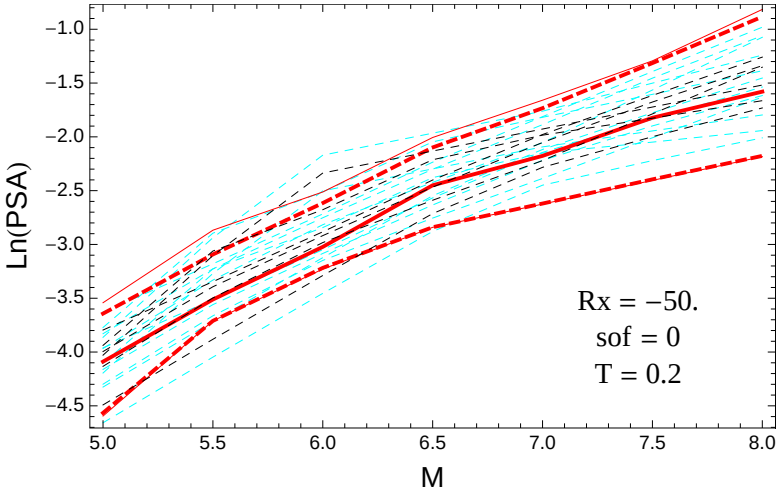



Figure 3.530: PVNGSv2: Magnitude scaling of the original GMPEs (dashed black), the original GMPEs with uncertainty model (dashed cyan) and 0.05,0.5,0.95 quantile of the ModelA distribution (red) with total weights, for a scenario with $R_X = -50.$, $F = 0$, and $T = 0.2$s.

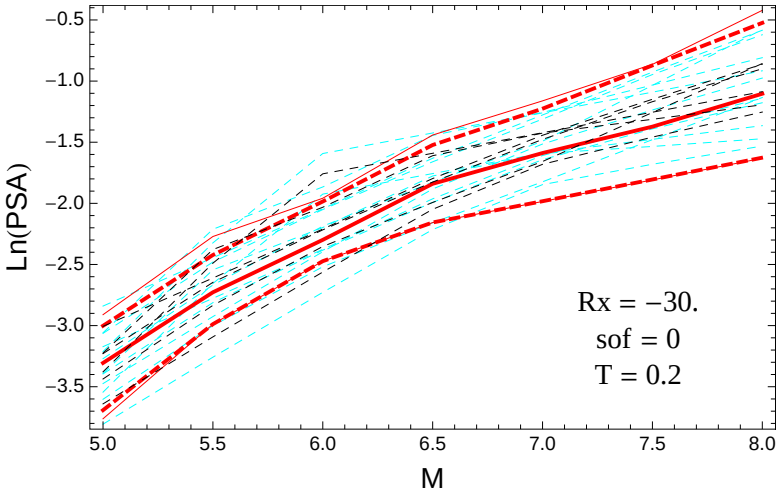



Figure 3.531: PVNGSv2: Magnitude scaling of the original GMPEs (dashed black), the original GMPEs with uncertainty model (dashed cyan) and 0.05,0.5,0.95 quantile of the ModelA distribution (red) with total weights, for a scenario with $R_X = -30.$, $F = 0$, and $T = 0.2$s.

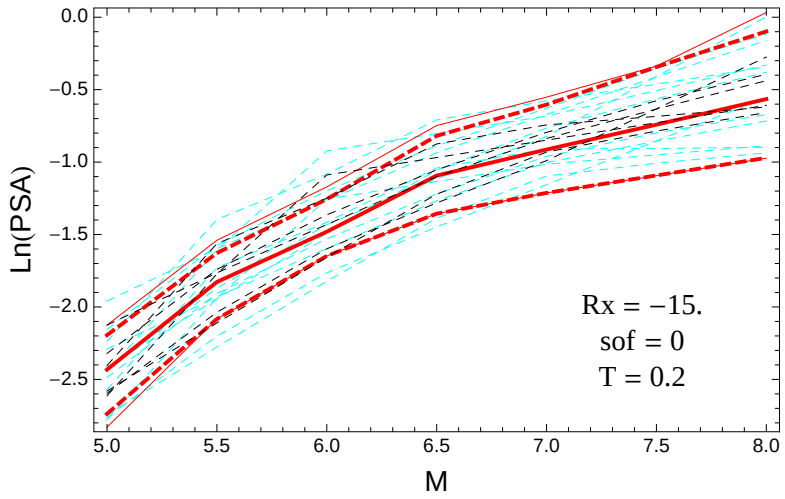



Figure 3.532: PVNGSv2: Magnitude scaling of the original GMPEs (dashed black), the original GMPEs with uncertainty model (dashed cyan) and 0.05,0.5,0.95 quantile of the ModelA distribution (red) with total weights, for a scenario with $R_X = -15.$, $F = 0$, and $T = 0.2$s.

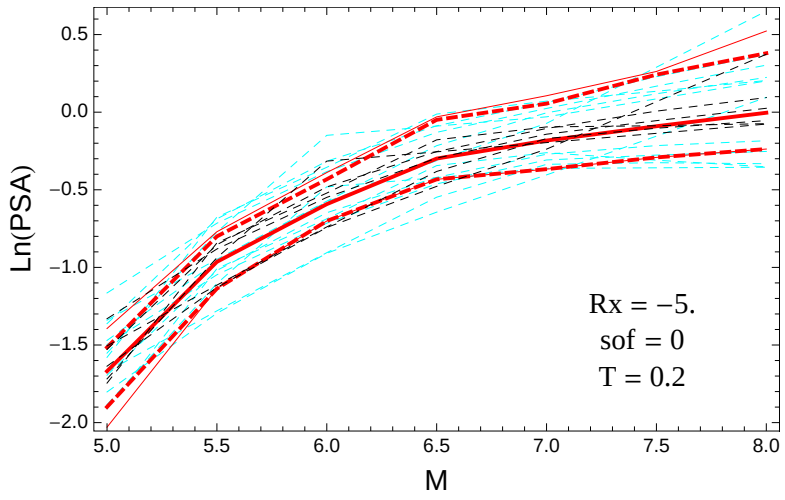



Figure 3.533: PVNGSv2: Magnitude scaling of the original GMPEs (dashed black), the original GMPEs with uncertainty model (dashed cyan) and 0.05,0.5,0.95 quantile of the ModelA distribution (red) with total weights, for a scenario with $R_X = -5.$, $F = 0$, and $T = 0.2$s.

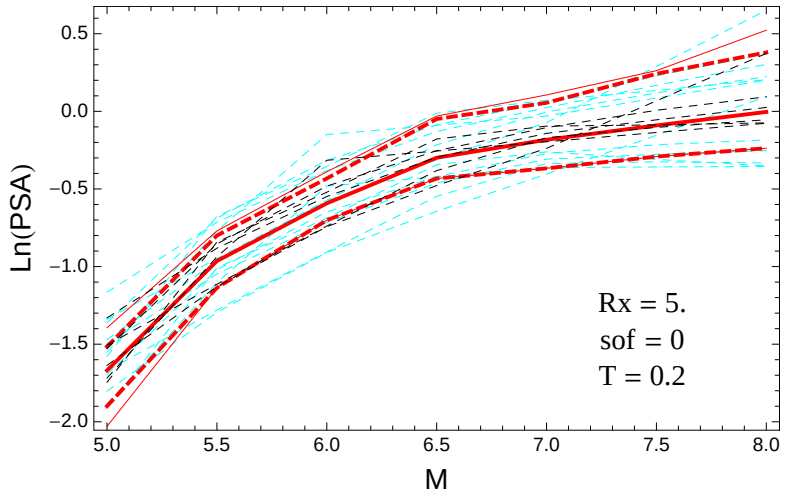



Figure 3.534: PVNGSv2: Magnitude scaling of the original GMPEs (dashed black), the original GMPEs with uncertainty model (dashed cyan) and 0.05,0.5,0.95 quantile of the ModelA distribution (red) with total weights, for a scenario with $R_X = 5.$, $F = 0$, and $T = 0.2$s.

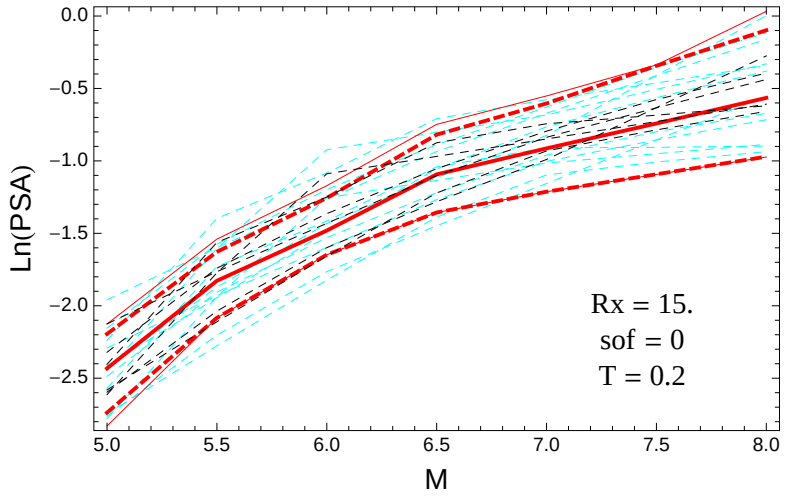



Figure 3.535: PVNGSv2: Magnitude scaling of the original GMPEs (dashed black), the original GMPEs with uncertainty model (dashed cyan) and 0.05,0.5,0.95 quantile of the ModelA distribution (red) with total weights, for a scenario with $R_X = 15.$, $F = 0$, and $T = 0.2$s.

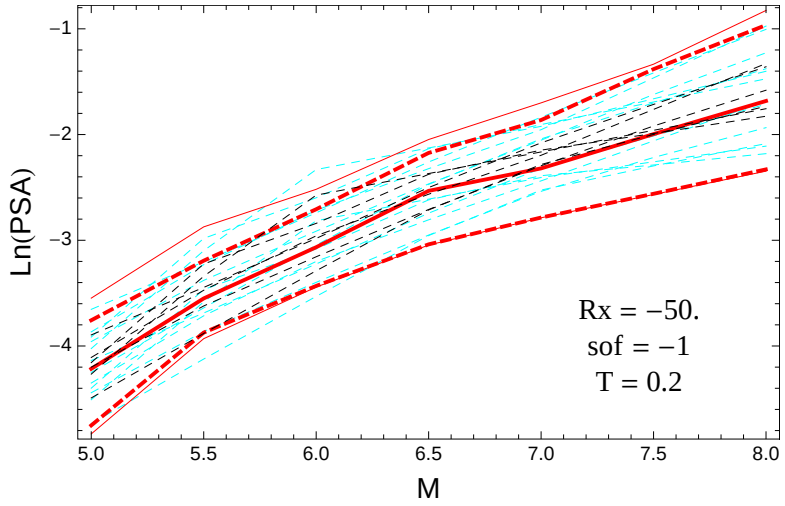



Figure 3.536: PVNGSv2: Magnitude scaling of the original GMPEs (dashed black), the original GMPEs with uncertainty model (dashed cyan) and 0.05,0.5,0.95 quantile of the ModelA distribution (red) with total weights, for a scenario with $R_X = -50.$, $F = -1$, and $T = 0.2$s.

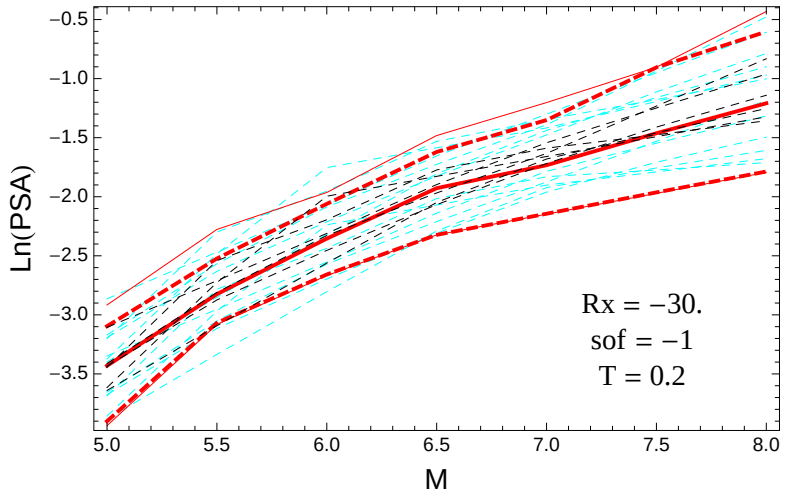



Figure 3.537: PVNGSv2: Magnitude scaling of the original GMPEs (dashed black), the original GMPEs with uncertainty model (dashed cyan) and 0.05,0.5,0.95 quantile of the ModelA distribution (red) with total weights, for a scenario with $R_X = -30.$, $F = -1$, and $T = 0.2$s.

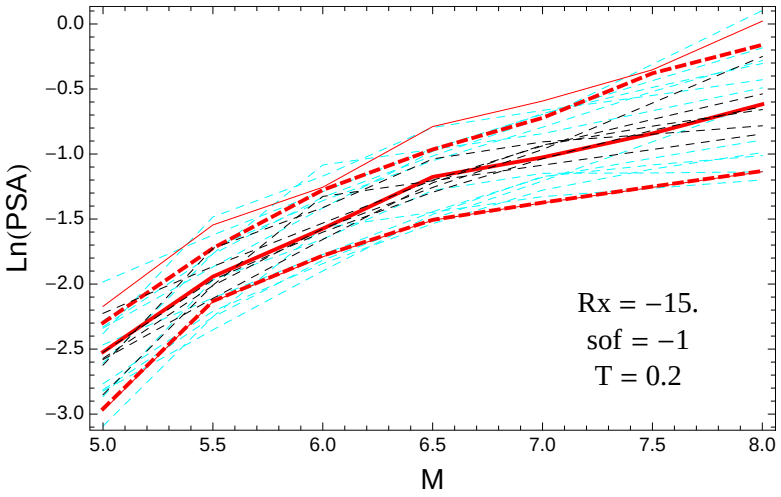



Figure 3.538: PVNGSv2: Magnitude scaling of the original GMPEs (dashed black), the original GMPEs with uncertainty model (dashed cyan) and 0.05,0.5,0.95 quantile of the ModelA distribution (red) with total weights, for a scenario with $R_X = -15.$, $F = -1$, and $T = 0.2$s.

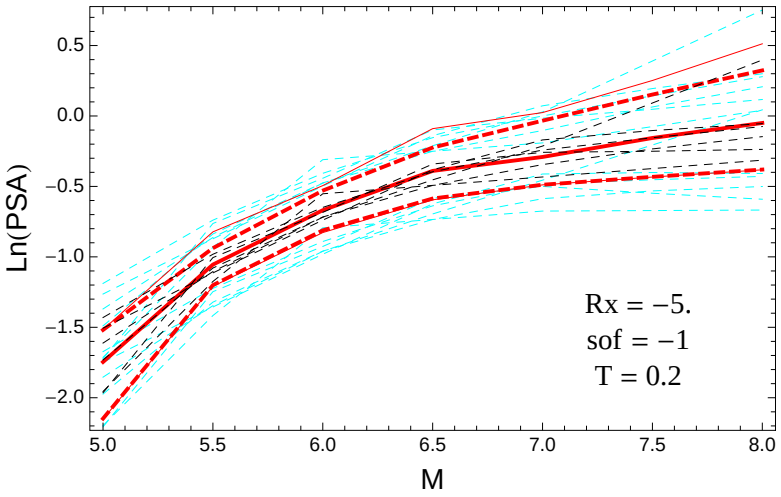



Figure 3.539: PVNGSv2: Magnitude scaling of the original GMPEs (dashed black), the original GMPEs with uncertainty model (dashed cyan) and 0.05,0.5,0.95 quantile of the ModelA distribution (red) with total weights, for a scenario with $R_X = -5.$, $F = -1$, and $T = 0.2$s.

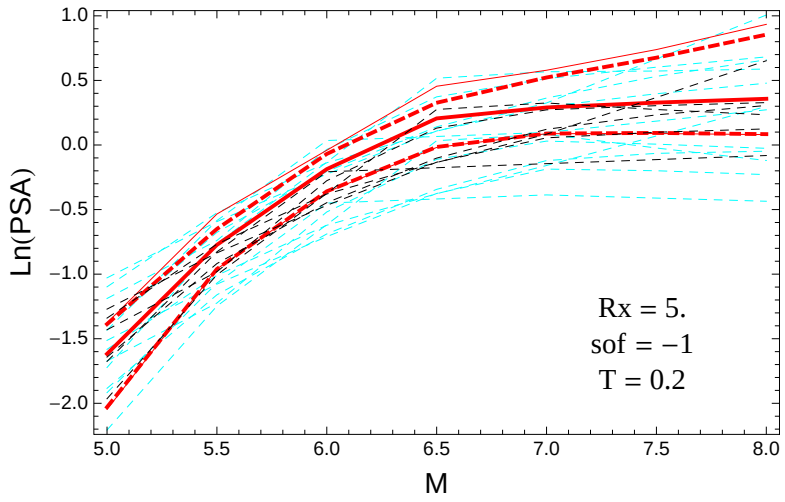



Figure 3.540: PVNGSv2: Magnitude scaling of the original GMPEs (dashed black), the original GMPEs with uncertainty model (dashed cyan) and 0.05,0.5,0.95 quantile of the ModelA distribution (red) with total weights, for a scenario with $R_X = 5.$, $F = -1$, and $T = 0.2$s.

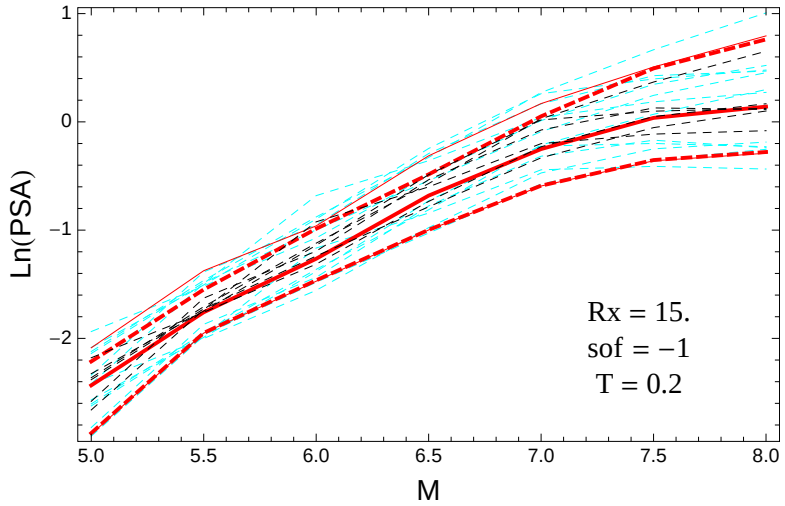



Figure 3.541: PVNGSv2: Magnitude scaling of the original GMPEs (dashed black), the original GMPEs with uncertainty model (dashed cyan) and 0.05,0.5,0.95 quantile of the ModelA distribution (red) with total weights, for a scenario with $R_X = 15.$, $F = -1$, and $T = 0.2$s.

**T = 0.5s**

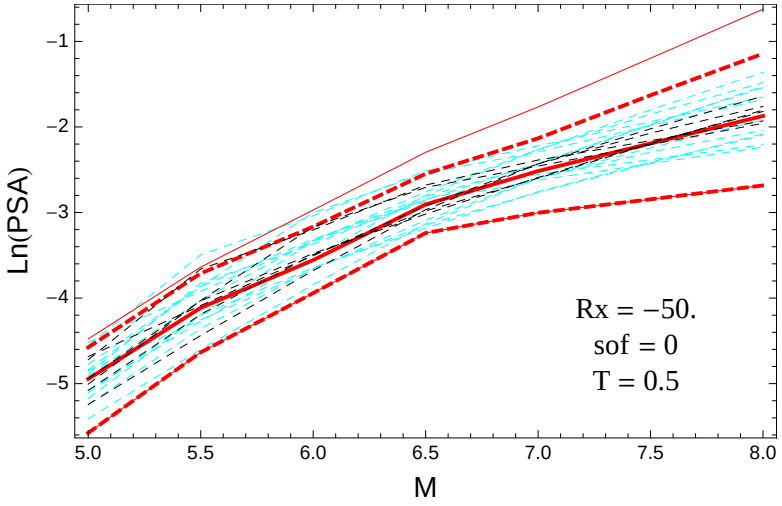



Figure 3.542: PVNGSv2: Magnitude scaling of the original GMPEs (dashed black), the original GMPEs with uncertainty model (dashed cyan) and 0.05,0.5,0.95 quantile of the ModelA distribution (red) with total weights, for a scenario with $R_X = -50.$, $F = 0$, and $T = 0.5$s.

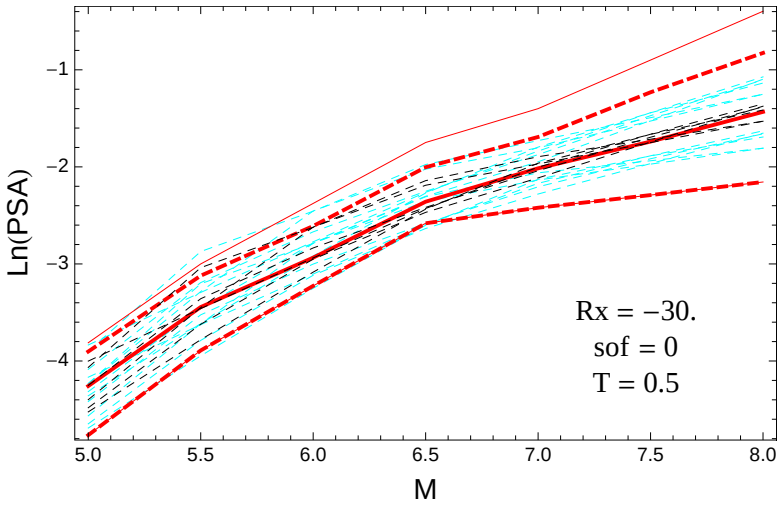



Figure 3.543: PVNGSv2: Magnitude scaling of the original GMPEs (dashed black), the original GMPEs with uncertainty model (dashed cyan) and 0.05,0.5,0.95 quantile of the ModelA distribution (red) with total weights, for a scenario with $R_X = -30.$, $F = 0$, and $T = 0.5$s.

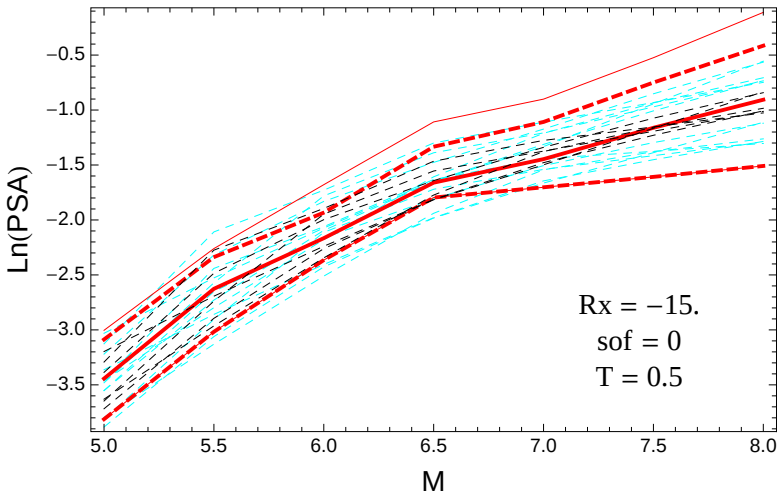



Figure 3.544: PVNGSv2: Magnitude scaling of the original GMPEs (dashed black), the original GMPEs with uncertainty model (dashed cyan) and 0.05,0.5,0.95 quantile of the ModelA distribution (red) with total weights, for a scenario with $R_X = -15.$, $F = 0$, and $T = 0.5$s.

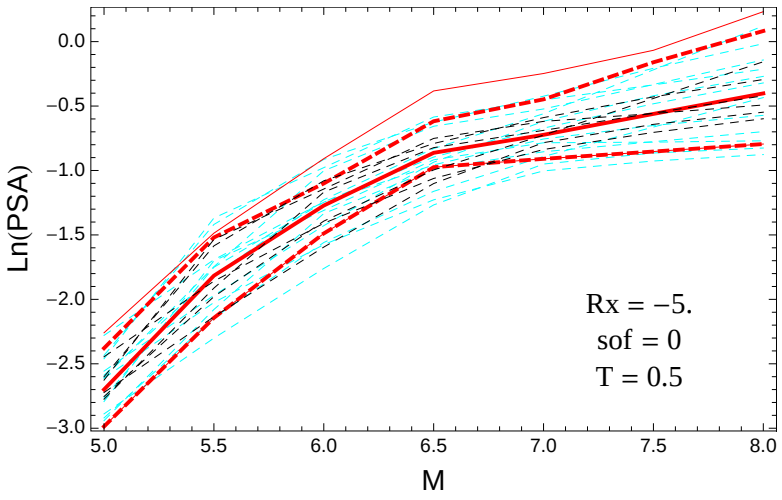



Figure 3.545: PVNGSv2: Magnitude scaling of the original GMPEs (dashed black), the original GMPEs with uncertainty model (dashed cyan) and 0.05,0.5,0.95 quantile of the ModelA distribution (red) with total weights, for a scenario with $R_X = -5.$, $F = 0$, and $T = 0.5$s.

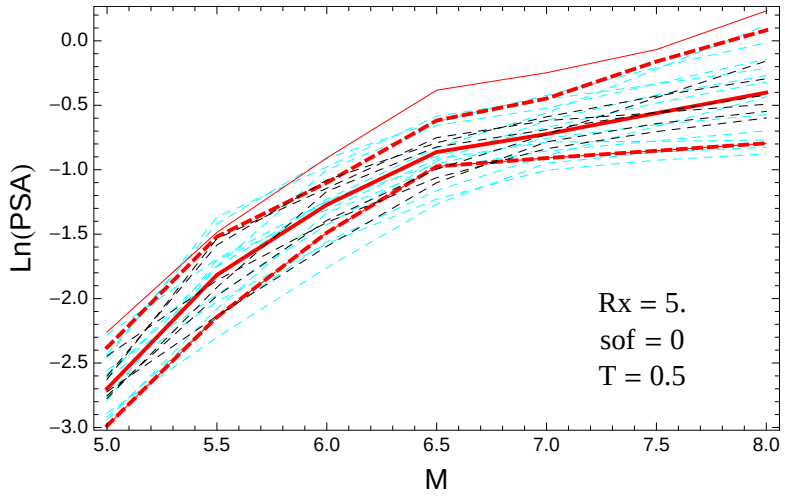



Figure 3.546: PVNGSv2: Magnitude scaling of the original GMPEs (dashed black), the original GMPEs with uncertainty model (dashed cyan) and 0.05,0.5,0.95 quantile of the ModelA distribution (red) with total weights, for a scenario with $R_X = 5.$, $F = 0$, and $T = 0.5$s.

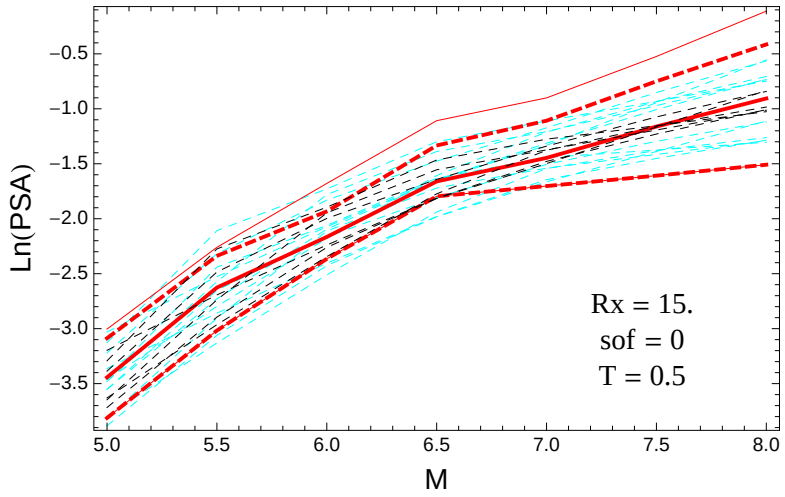



Figure 3.547: PVNGSv2: Magnitude scaling of the original GMPEs (dashed black), the original GMPEs with uncertainty model (dashed cyan) and 0.05,0.5,0.95 quantile of the ModelA distribution (red) with total weights, for a scenario with $R_X = 15.$, $F = 0$, and $T = 0.5$s.

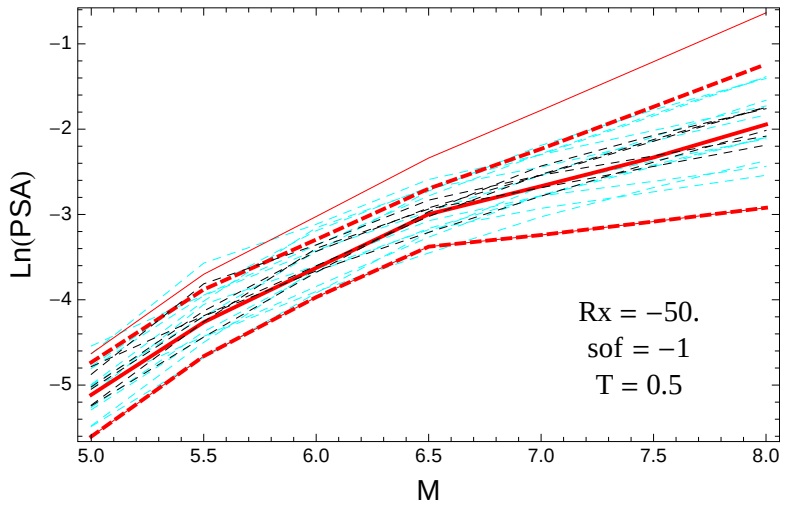



Figure 3.548: PVNGSv2: Magnitude scaling of the original GMPEs (dashed black), the original GMPEs with uncertainty model (dashed cyan) and 0.05,0.5,0.95 quantile of the ModelA distribution (red) with total weights, for a scenario with $R_X = -50.$, $F = -1$, and $T = 0.5$s.

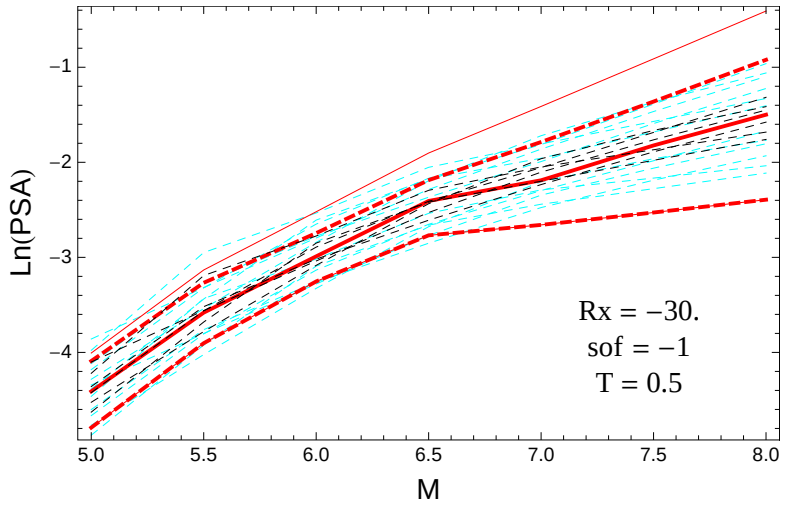



Figure 3.549: PVNGSv2: Magnitude scaling of the original GMPEs (dashed black), the original GMPEs with uncertainty model (dashed cyan) and 0.05,0.5,0.95 quantile of the ModelA distribution (red) with total weights, for a scenario with $R_X = -30.$, $F = -1$, and $T = 0.5$s.

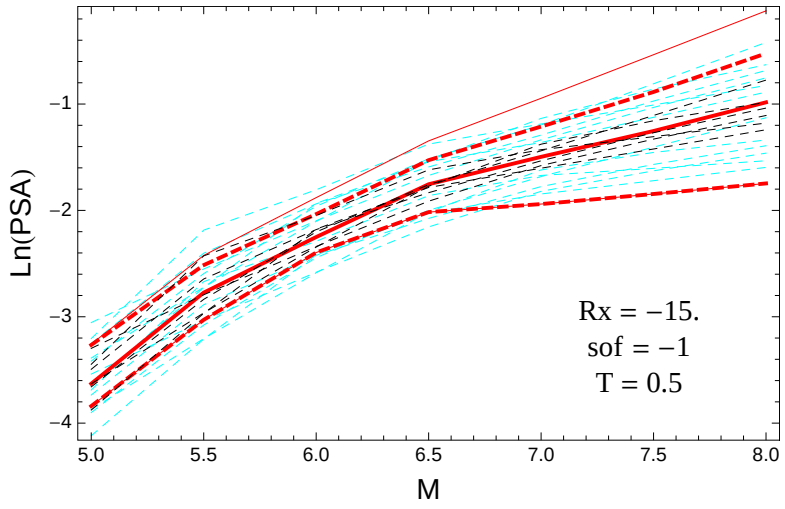



Figure 3.550: PVNGSv2: Magnitude scaling of the original GMPEs (dashed black), the original GMPEs with uncertainty model (dashed cyan) and 0.05,0.5,0.95 quantile of the ModelA distribution (red) with total weights, for a scenario with $R_X = -15.$, $F = -1$, and $T = 0.5$s.

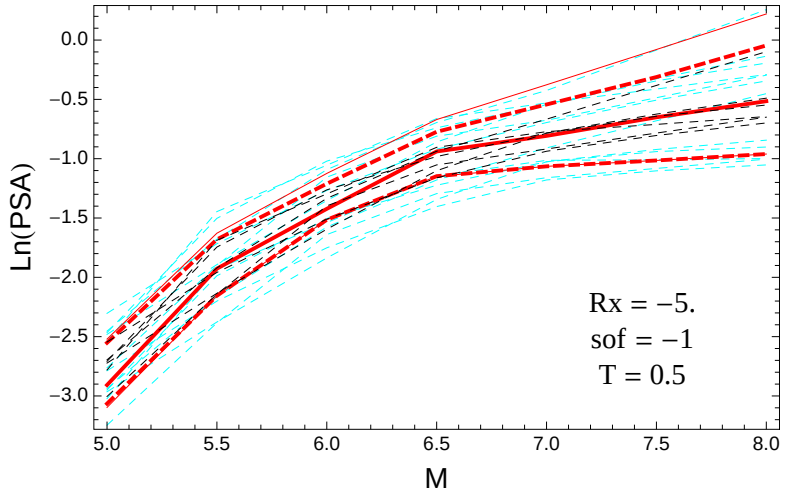



Figure 3.551: PVNGSv2: Magnitude scaling of the original GMPEs (dashed black), the original GMPEs with uncertainty model (dashed cyan) and 0.05,0.5,0.95 quantile of the ModelA distribution (red) with total weights, for a scenario with $R_X = -5.$, $F = -1$, and $T = 0.5$s.

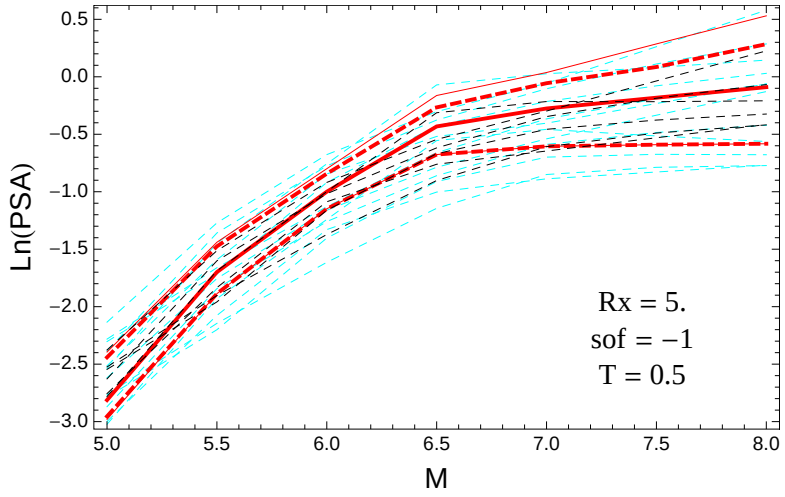



Figure 3.552: PVNGSv2: Magnitude scaling of the original GMPEs (dashed black), the original GMPEs with uncertainty model (dashed cyan) and 0.05,0.5,0.95 quantile of the ModelA distribution (red) with total weights, for a scenario with $R_X = 5.$, $F = -1$, and $T = 0.5$s.

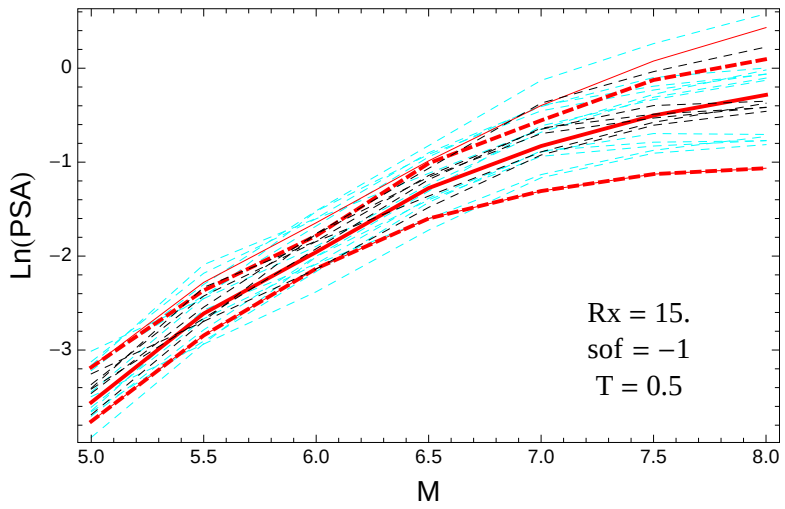



Figure 3.553: PVNGSv2: Magnitude scaling of the original GMPEs (dashed black), the original GMPEs with uncertainty model (dashed cyan) and 0.05,0.5,0.95 quantile of the ModelA distribution (red) with total weights, for a scenario with $R_X = 15.$, $F = -1$, and $T = 0.5$s.

**T = 1.s**

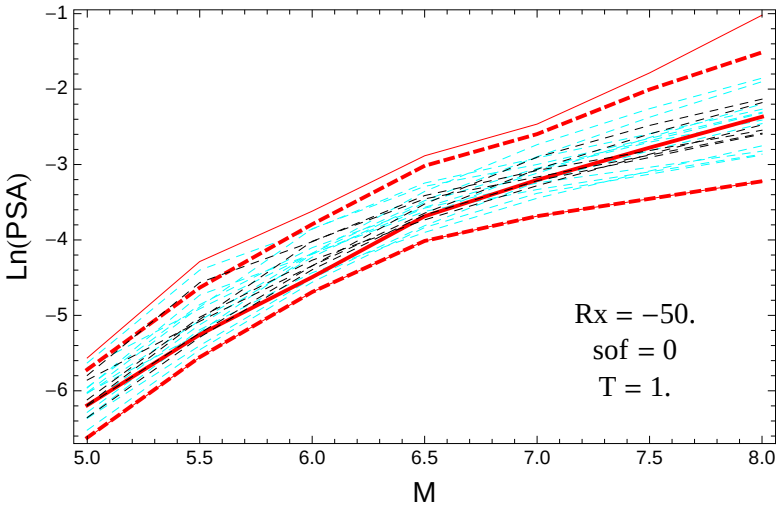



Figure 3.554: PVNGSv2: Magnitude scaling of the original GMPEs (dashed black), the original GMPEs with uncertainty model (dashed cyan) and 0.05,0.5,0.95 quantile of the ModelA distribution (red) with total weights, for a scenario with $R_X = -50.$, $F = 0$, and $T = 1.$s.

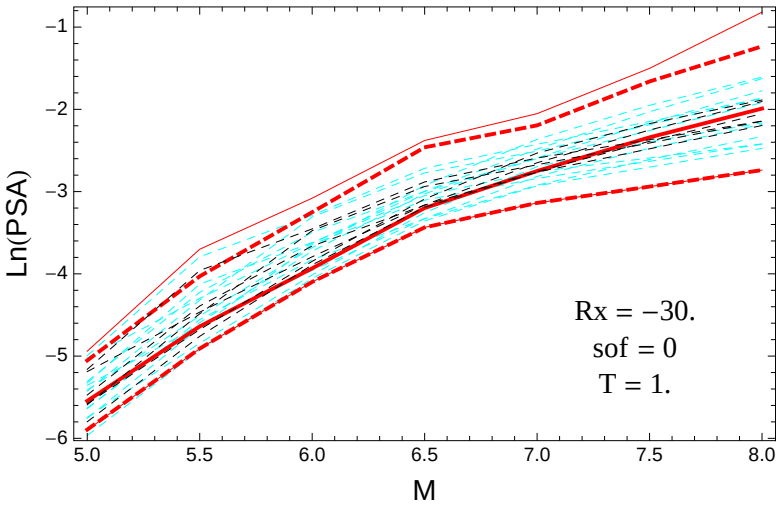



Figure 3.555: PVNGSv2: Magnitude scaling of the original GMPEs (dashed black), the original GMPEs with uncertainty model (dashed cyan) and 0.05,0.5,0.95 quantile of the ModelA distribution (red) with total weights, for a scenario with $R_X = -30.$, $F = 0$, and $T = 1.$s.

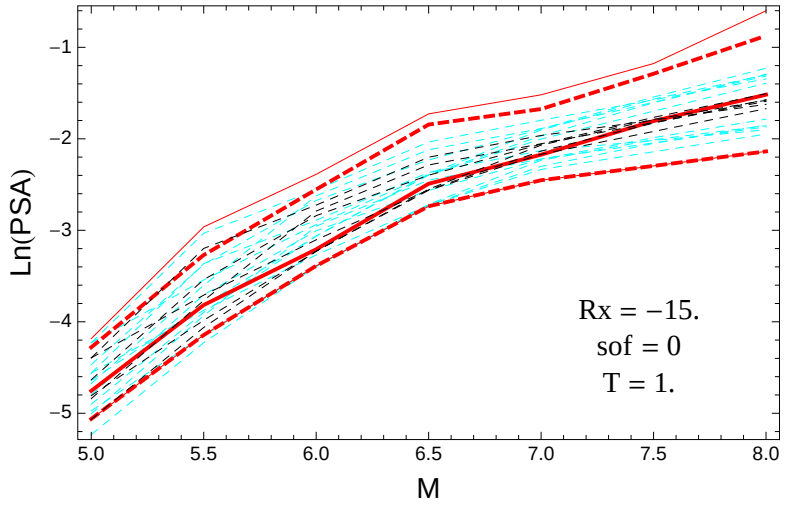



Figure 3.556: PVNGSv2: Magnitude scaling of the original GMPEs (dashed black), the original GMPEs with uncertainty model (dashed cyan) and 0.05,0.5,0.95 quantile of the ModelA distribution (red) with total weights, for a scenario with $R_X = -15.$, $F = 0$, and $T = 1.$s.

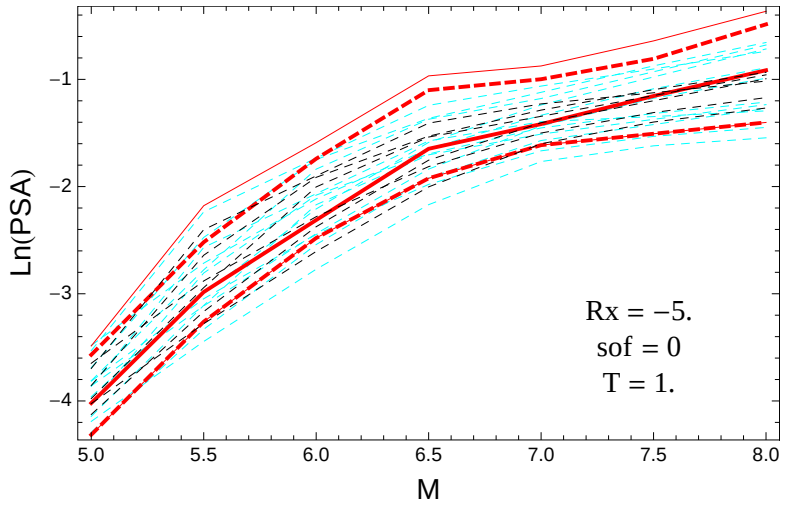



Figure 3.557: PVNGSv2: Magnitude scaling of the original GMPEs (dashed black), the original GMPEs with uncertainty model (dashed cyan) and 0.05,0.5,0.95 quantile of the ModelA distribution (red) with total weights, for a scenario with $R_X = -5.$, $F = 0$, and $T = 1.$s.

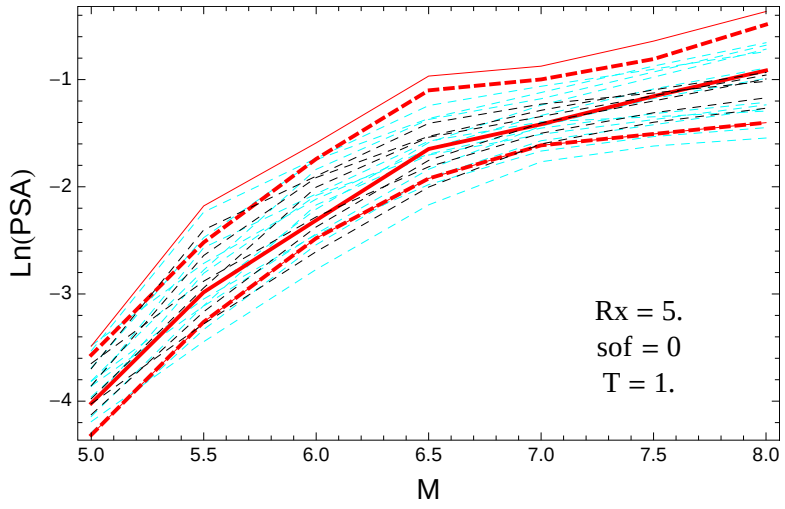



Figure 3.558: PVNGSv2: Magnitude scaling of the original GMPEs (dashed black), the original GMPEs with uncertainty model (dashed cyan) and 0.05,0.5,0.95 quantile of the ModelA distribution (red) with total weights, for a scenario with $R_X = 5.$, $F = 0$, and $T = 1.$s.

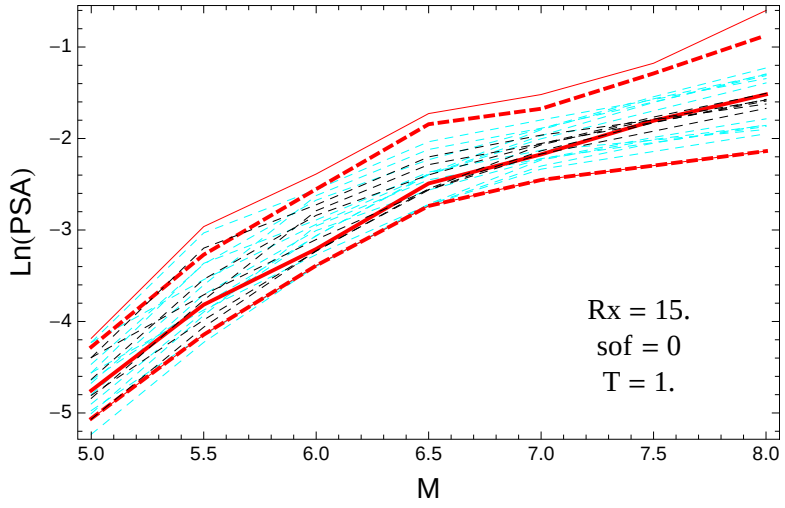



Figure 3.559: PVNGSv2: Magnitude scaling of the original GMPEs (dashed black), the original GMPEs with uncertainty model (dashed cyan) and 0.05,0.5,0.95 quantile of the ModelA distribution (red) with total weights, for a scenario with $R_X = 15.$, $F = 0$, and $T = 1.$s.

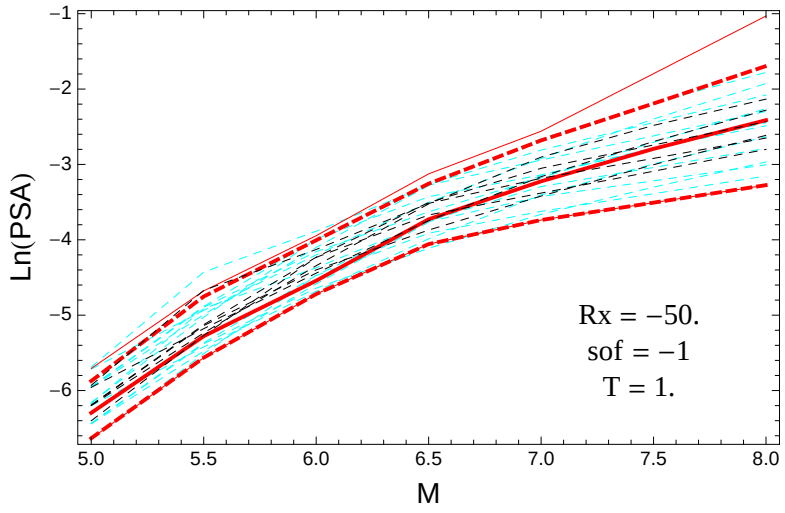



Figure 3.560: PVNGSv2: Magnitude scaling of the original GMPEs (dashed black), the original GMPEs with uncertainty model (dashed cyan) and 0.05,0.5,0.95 quantile of the ModelA distribution (red) with total weights, for a scenario with $R_X = -50.$, $F = -1$, and $T = 1.$s.

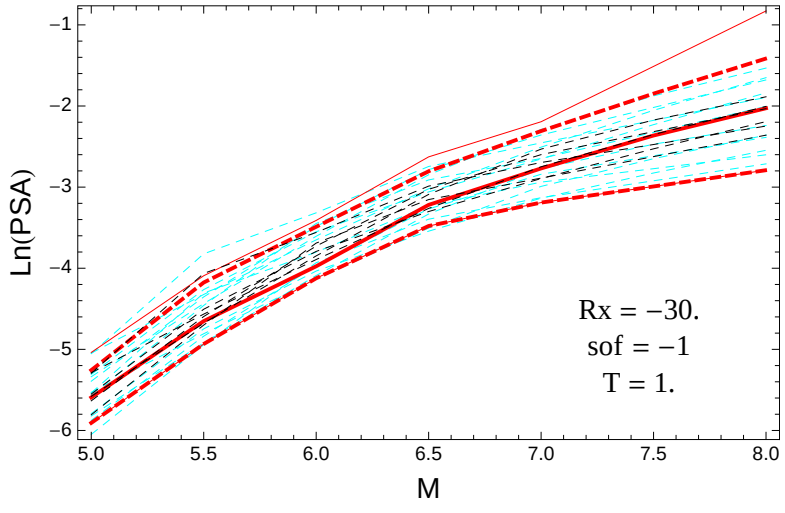



Figure 3.561: PVNGSv2: Magnitude scaling of the original GMPEs (dashed black), the original GMPEs with uncertainty model (dashed cyan) and 0.05,0.5,0.95 quantile of the ModelA distribution (red) with total weights, for a scenario with $R_X = -30.$, $F = -1$, and $T = 1.$s.

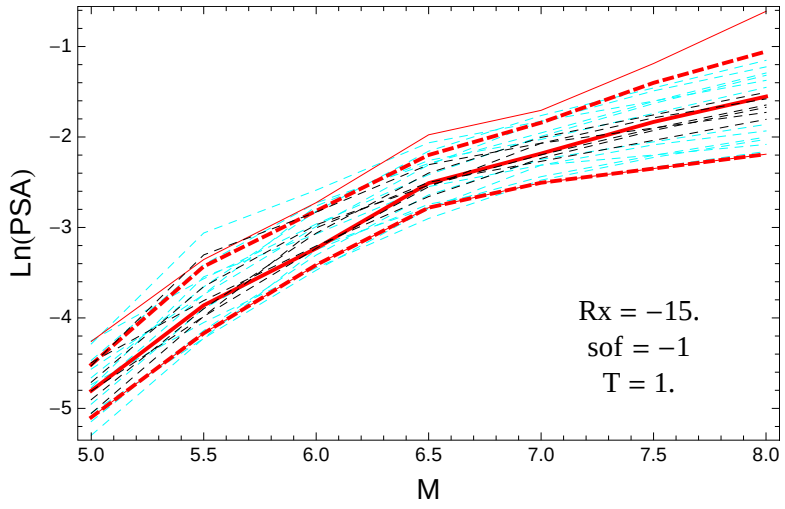



Figure 3.562: PVNGSv2: Magnitude scaling of the original GMPEs (dashed black), the original GMPEs with uncertainty model (dashed cyan) and 0.05,0.5,0.95 quantile of the ModelA distribution (red) with total weights, for a scenario with $R_X = -15.$, $F = -1$, and $T = 1.$s.

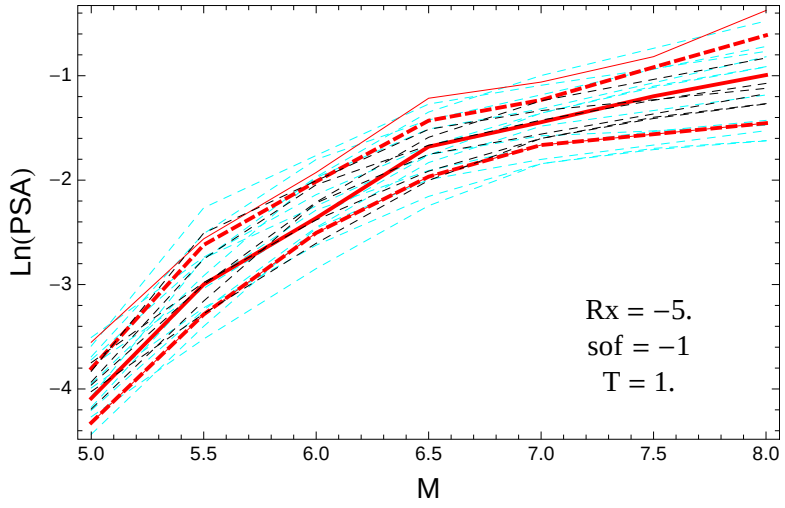



Figure 3.563: PVNGSv2: Magnitude scaling of the original GMPEs (dashed black), the original GMPEs with uncertainty model (dashed cyan) and 0.05,0.5,0.95 quantile of the ModelA distribution (red) with total weights, for a scenario with $R_X = -5.$, $F = -1$, and $T = 1.$s.

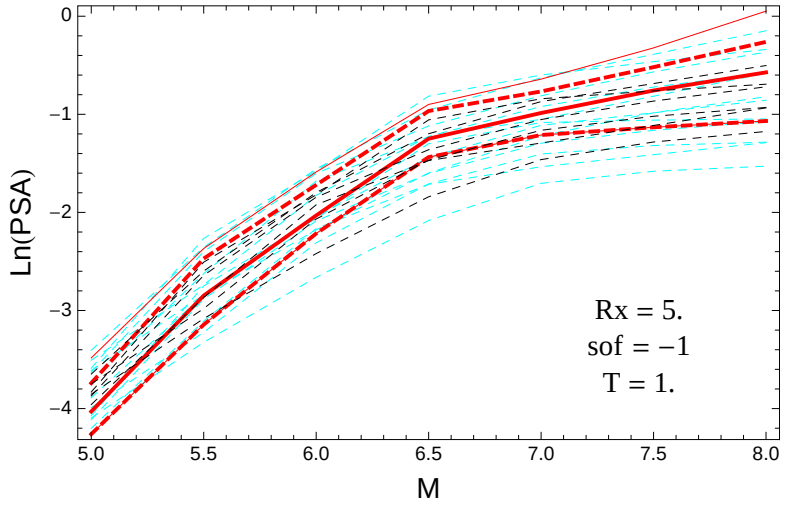



Figure 3.564: PVNGSv2: Magnitude scaling of the original GMPEs (dashed black), the original GMPEs with uncertainty model (dashed cyan) and 0.05,0.5,0.95 quantile of the ModelA distribution (red) with total weights, for a scenario with $R_X = 5.$, $F = -1$, and $T = 1.$s.

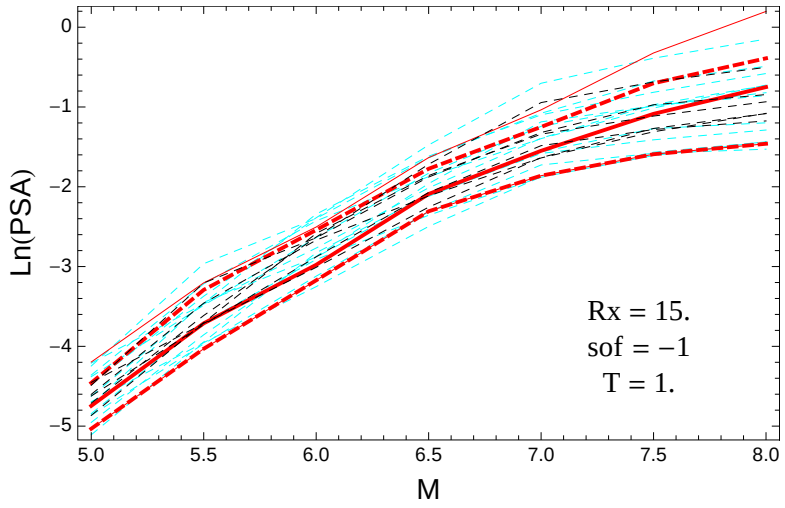



Figure 3.565: PVNGSv2: Magnitude scaling of the original GMPEs (dashed black), the original GMPEs with uncertainty model (dashed cyan) and 0.05,0.5,0.95 quantile of the ModelA distribution (red) with total weights, for a scenario with $R_X = 15.$, $F = -1$, and $T = 1.$s.

**T = 3.s**

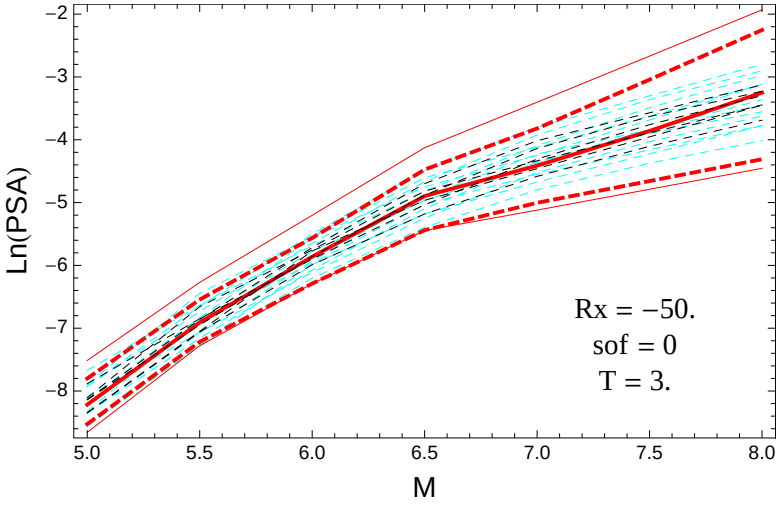



Figure 3.566: PVNGSv2: Magnitude scaling of the original GMPEs (dashed black), the original GMPEs with uncertainty model (dashed cyan) and 0.05,0.5,0.95 quantile of the ModelA distribution (red) with total weights, for a scenario with $R_X = -50.$, $F = 0$, and $T = 3.$s.

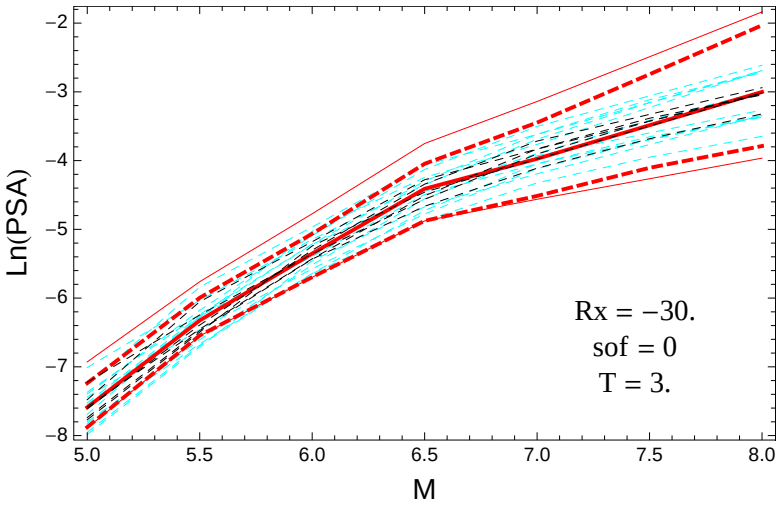



Figure 3.567: PVNGSv2: Magnitude scaling of the original GMPEs (dashed black), the original GMPEs with uncertainty model (dashed cyan) and 0.05,0.5,0.95 quantile of the ModelA distribution (red) with total weights, for a scenario with $R_X = -30.$, $F = 0$, and $T = 3.$s.

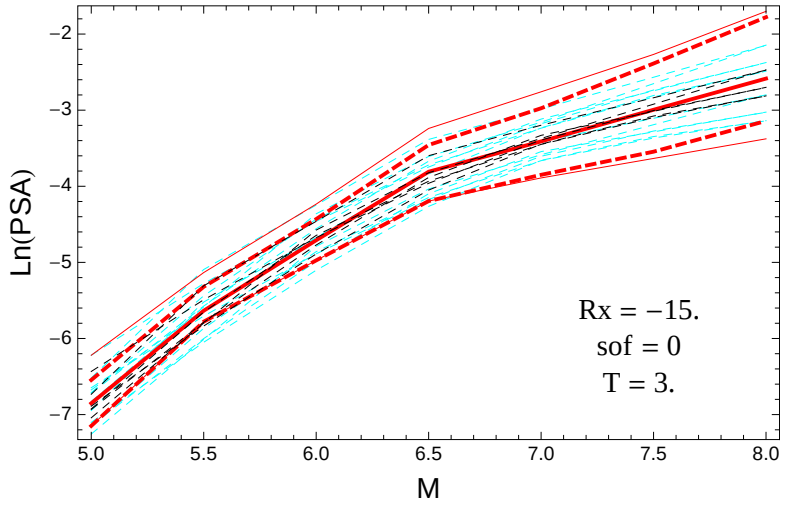



Figure 3.568: PVNGSv2: Magnitude scaling of the original GMPEs (dashed black), the original GMPEs with uncertainty model (dashed cyan) and 0.05,0.5,0.95 quantile of the ModelA distribution (red) with total weights, for a scenario with $R_X = -15.$, $F = 0$, and $T = 3.$s.

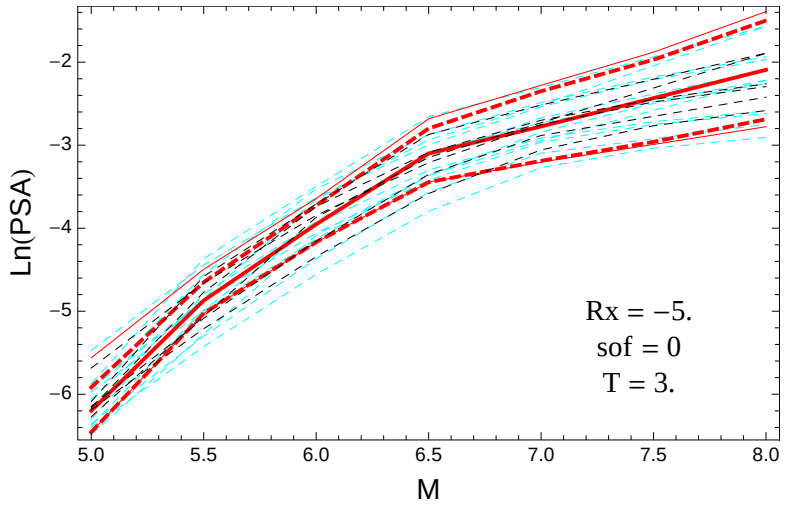



Figure 3.569: PVNGSv2: Magnitude scaling of the original GMPEs (dashed black), the original GMPEs with uncertainty model (dashed cyan) and 0.05,0.5,0.95 quantile of the ModelA distribution (red) with total weights, for a scenario with $R_X = -5.$, $F = 0$, and $T = 3.$s.

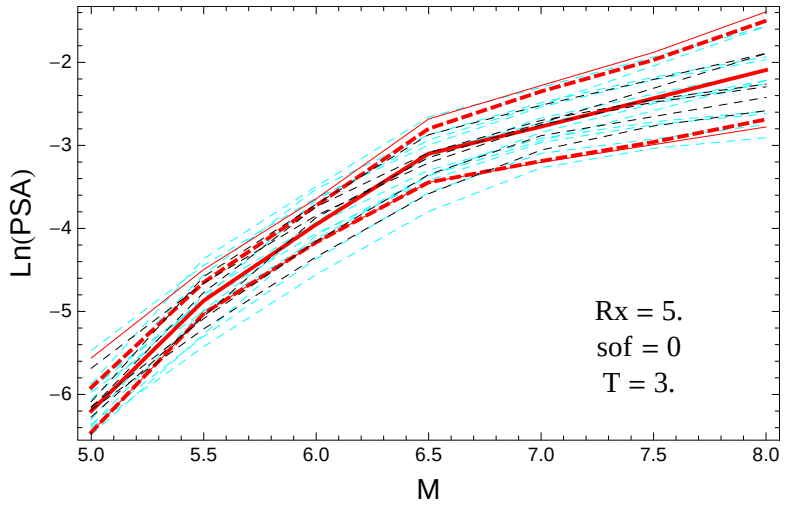



Figure 3.570: PVNGSv2: Magnitude scaling of the original GMPEs (dashed black), the original GMPEs with uncertainty model (dashed cyan) and 0.05,0.5,0.95 quantile of the ModelA distribution (red) with total weights, for a scenario with $R_X = 5.$, $F = 0$, and $T = 3.$s.

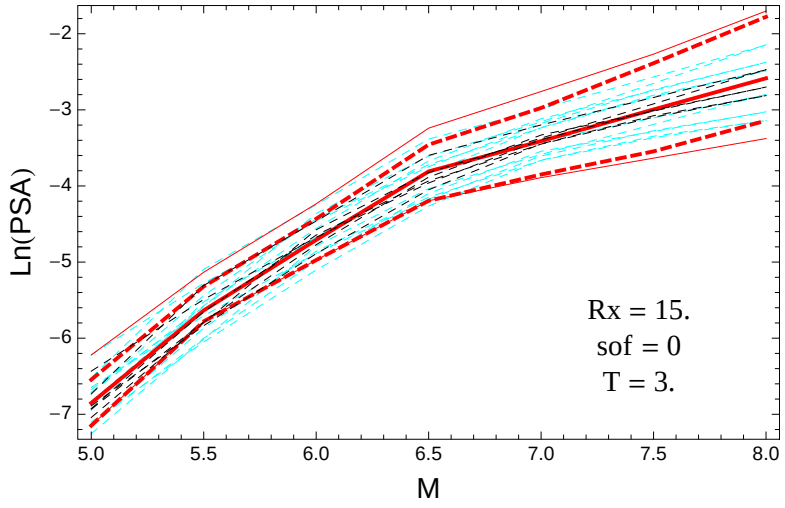



Figure 3.571: PVNGSv2: Magnitude scaling of the original GMPEs (dashed black), the original GMPEs with uncertainty model (dashed cyan) and 0.05,0.5,0.95 quantile of the ModelA distribution (red) with total weights, for a scenario with $R_X = 15.$, $F = 0$, and $T = 3.$s.

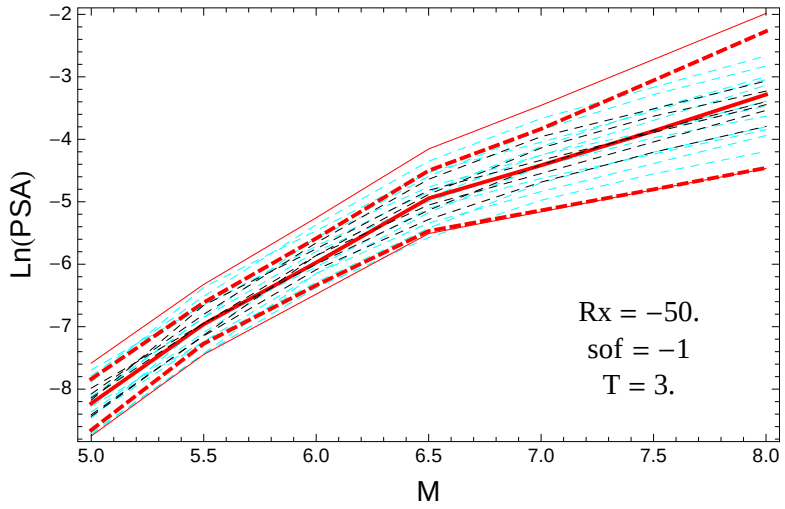



Figure 3.572: PVNGSv2: Magnitude scaling of the original GMPEs (dashed black), the original GMPEs with uncertainty model (dashed cyan) and 0.05,0.5,0.95 quantile of the ModelA distribution (red) with total weights, for a scenario with $R_X = -50.$, $F = -1$, and $T = 3.$s.

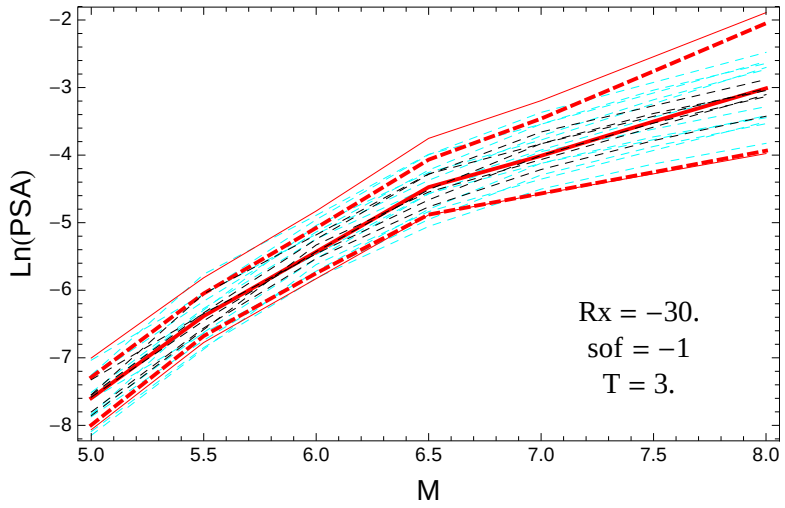



Figure 3.573: PVNGSv2: Magnitude scaling of the original GMPEs (dashed black), the original GMPEs with uncertainty model (dashed cyan) and 0.05,0.5,0.95 quantile of the ModelA distribution (red) with total weights, for a scenario with $R_X = -30.$, $F = -1$, and $T = 3.$s.

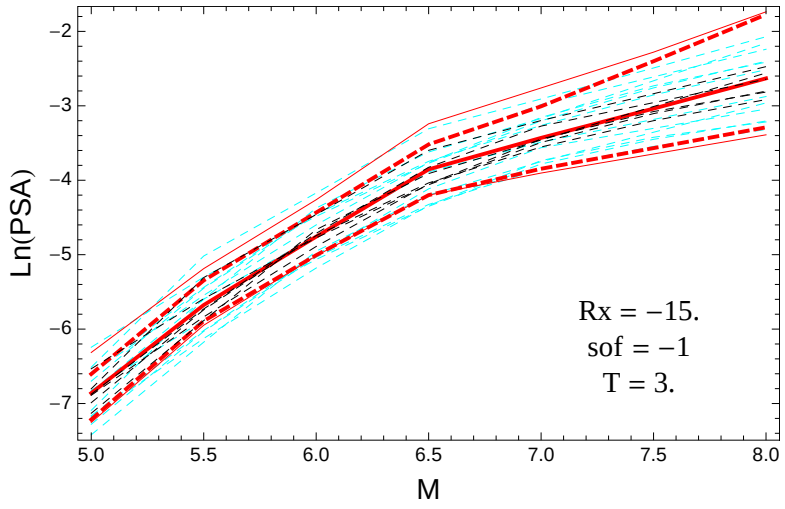



Figure 3.574: PVNGSv2: Magnitude scaling of the original GMPEs (dashed black), the original GMPEs with uncertainty model (dashed cyan) and 0.05,0.5,0.95 quantile of the ModelA distribution (red) with total weights, for a scenario with $R_X = -15.$, $F = -1$, and $T = 3.$s.

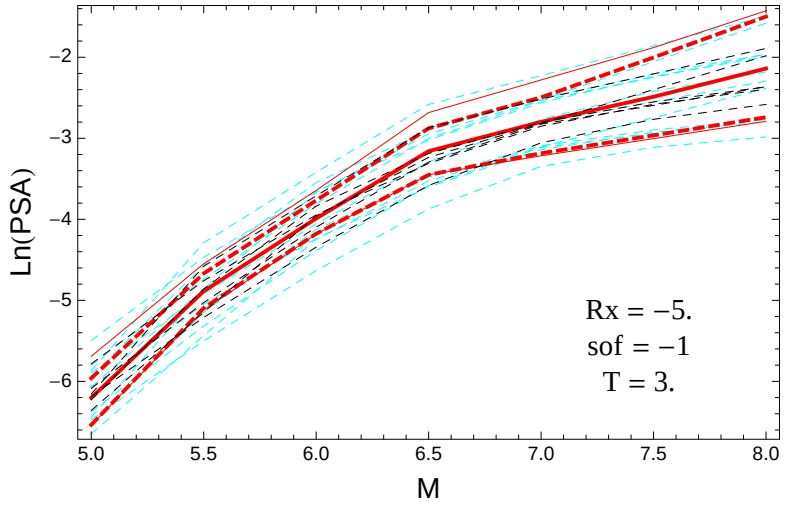



Figure 3.575: PVNGSv2: Magnitude scaling of the original GMPEs (dashed black), the original GMPEs with uncertainty model (dashed cyan) and 0.05,0.5,0.95 quantile of the ModelA distribution (red) with total weights, for a scenario with $R_X = -5.$, $F = -1$, and $T = 3.$s.

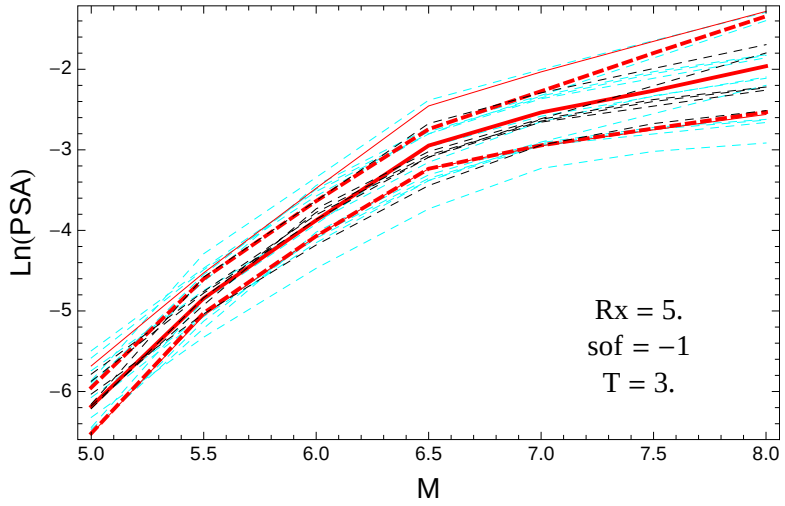



Figure 3.576: PVNGSv2: Magnitude scaling of the original GMPEs (dashed black), the original GMPEs with uncertainty model (dashed cyan) and 0.05,0.5,0.95 quantile of the ModelA distribution (red) with total weights, for a scenario with $R_X = 5.$, $F = -1$, and $T = 3.$s.

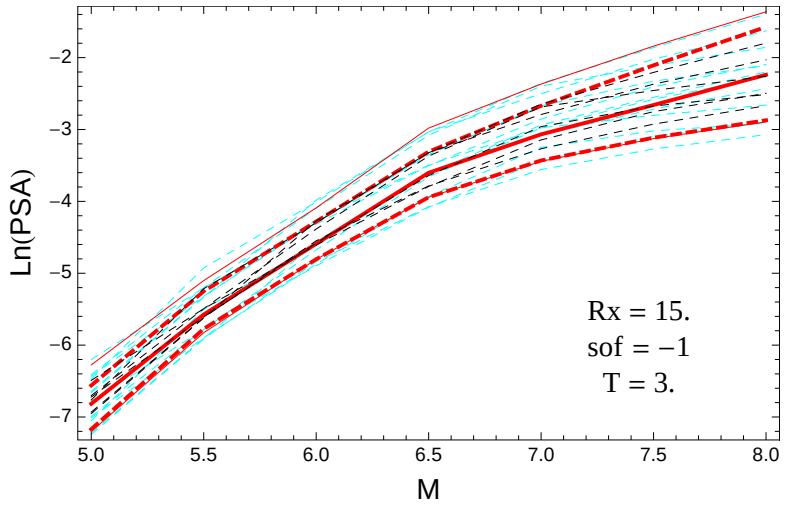



Figure 3.577: PVNGSv2: Magnitude scaling of the original GMPEs (dashed black), the original GMPEs with uncertainty model (dashed cyan) and 0.05,0.5,0.95 quantile of the ModelA distribution (red) with total weights, for a scenario with $R_X = 15.$, $F = -1$, and $T = 3.$s.

### 3.1.14 Quantile Plots vs. Period with GMPEs

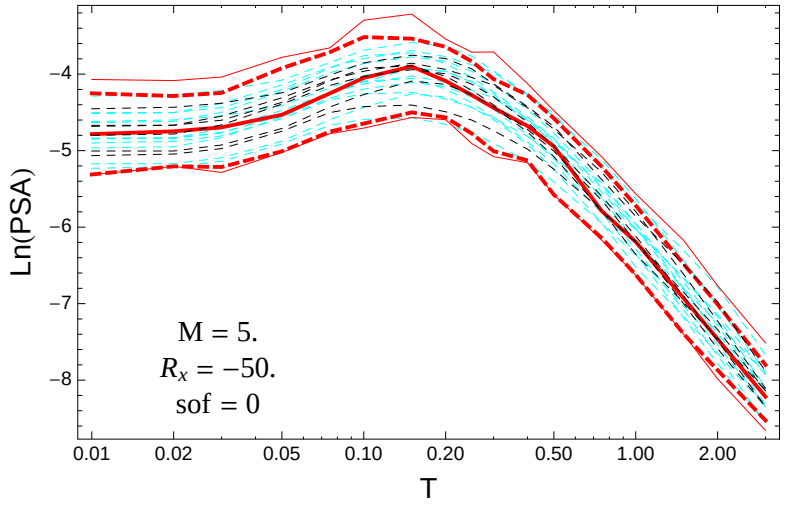



Figure 3.578: PVNGSv2: Spectra of 0.05,0.5,0.95 and the ModelA distribution (red) with total weights and original GMPEs (dashed black) and the original GMPEs with uncertainty model (dashed cyan), for a scenario with $M_W = 5.$, $R_x = -50.$, $F = 0$.

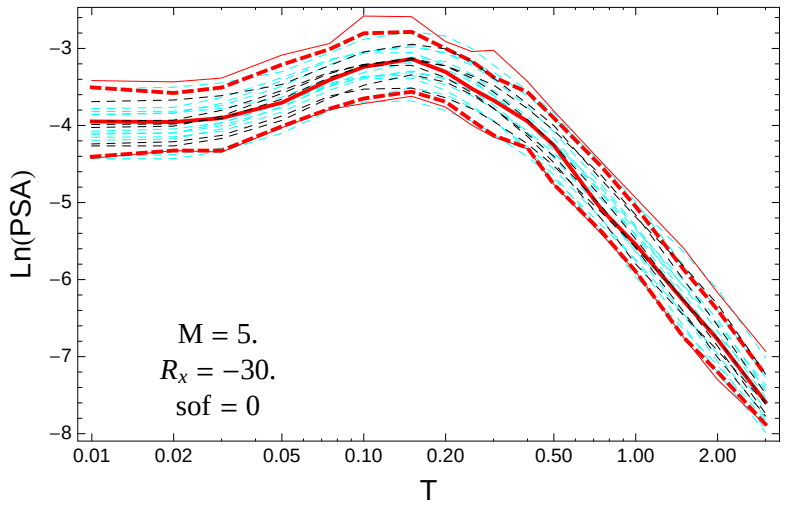



Figure 3.579: PVNGSv2: Spectra of 0.05,0.5,0.95 and the ModelA distribution (red) with total weights and original GMPEs (dashed black) and the original GMPEs with uncertainty model (dashed cyan), for a scenario with $M_W = 5.$, $R_x = -30.$, $F = 0$.

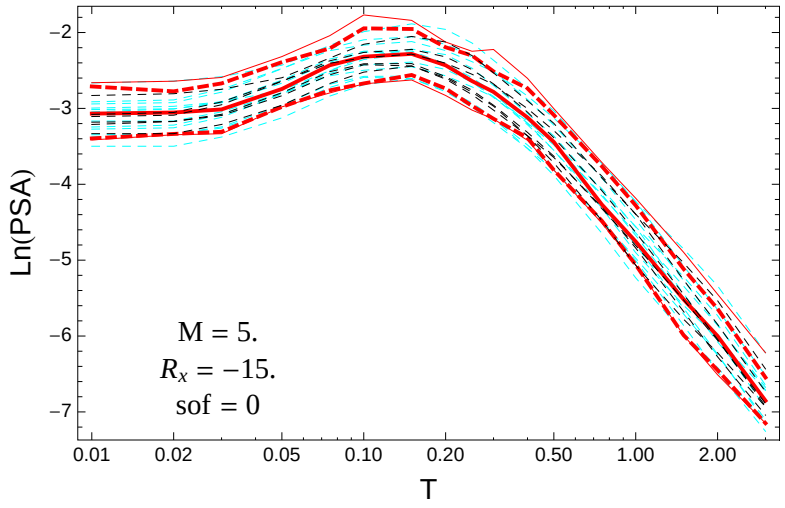



Figure 3.580: PVNGSv2: Spectra of 0.05,0.5,0.95 and the ModelA distribution (red) with total weights and original GMPEs (dashed black) and the original GMPEs with uncertainty model (dashed cyan), for a scenario with $M_W = 5.$, $R_x = -15.$, $F = 0$.

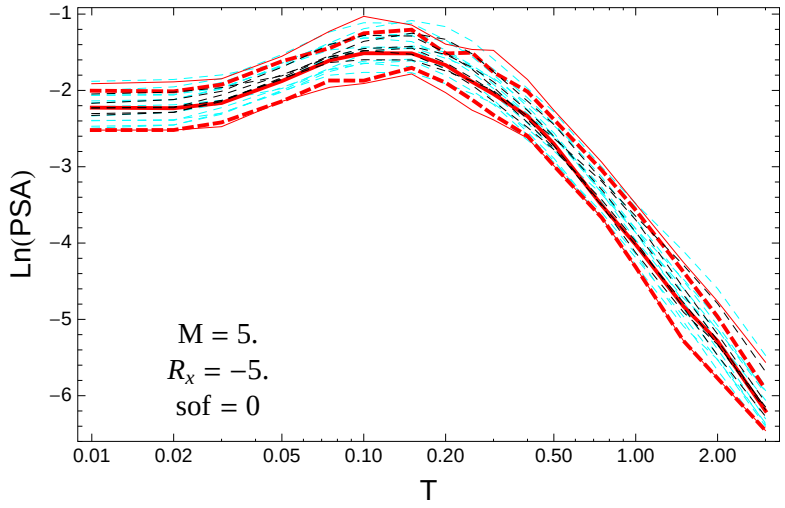



Figure 3.581: PVNGSv2: Spectra of 0.05,0.5,0.95 and the ModelA distribution (red) with total weights and original GMPEs (dashed black) and the original GMPEs with uncertainty model (dashed cyan), for a scenario with $M_W = 5.$, $R_x = -5.$, $F = 0$.

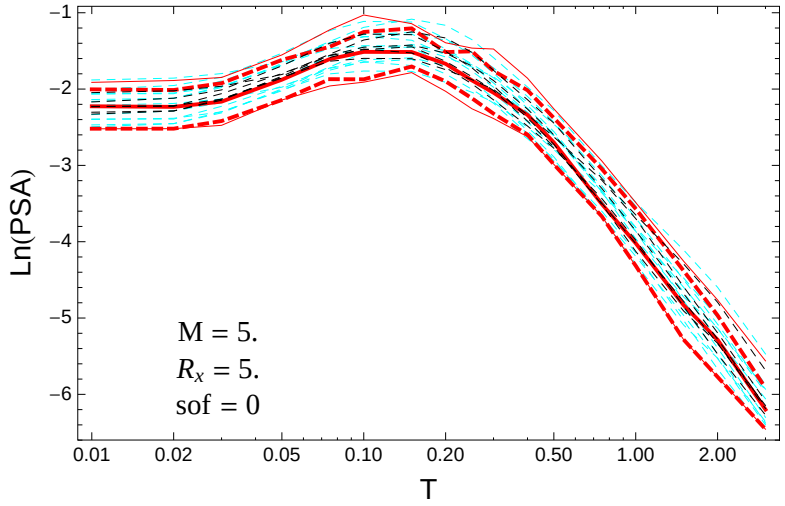



Figure 3.582: PVNGSv2: Spectra of 0.05,0.5,0.95 and the ModelA distribution (red) with total weights and original GMPEs (dashed black) and the original GMPEs with uncertainty model (dashed cyan), for a scenario with $M_W = 5.$, $R_x = 5.$, $F = 0$.

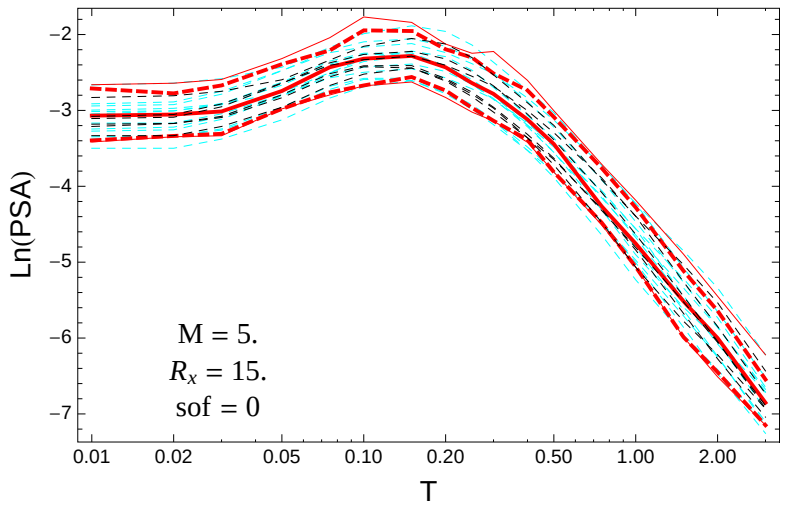



Figure 3.583: PVNGSv2: Spectra of 0.05,0.5,0.95 and the ModelA distribution (red) with total weights and original GMPEs (dashed black) and the original GMPEs with uncertainty model (dashed cyan), for a scenario with $M_W = 5.$, $R_x = 15.$, $F = 0$.

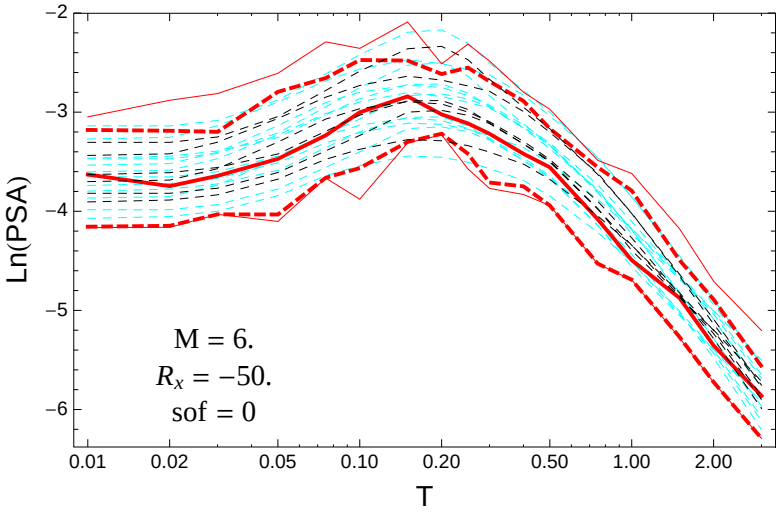



Figure 3.584: PVNGSv2: Spectra of 0.05,0.5,0.95 and the ModelA distribution (red) with total weights and original GMPEs (dashed black) and the original GMPEs with uncertainty model (dashed cyan), for a scenario with $M_W = 6.$, $R_x = -50.$, $F = 0.$

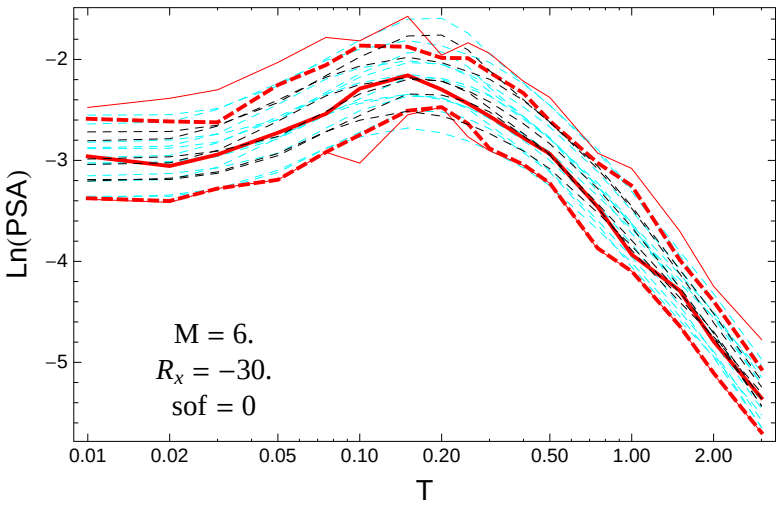



Figure 3.585: PVNGSv2: Spectra of 0.05,0.5,0.95 and the ModelA distribution (red) with total weights and original GMPEs (dashed black) and the original GMPEs with uncertainty model (dashed cyan), for a scenario with $M_W = 6.$, $R_x = -30.$, $F = 0.$

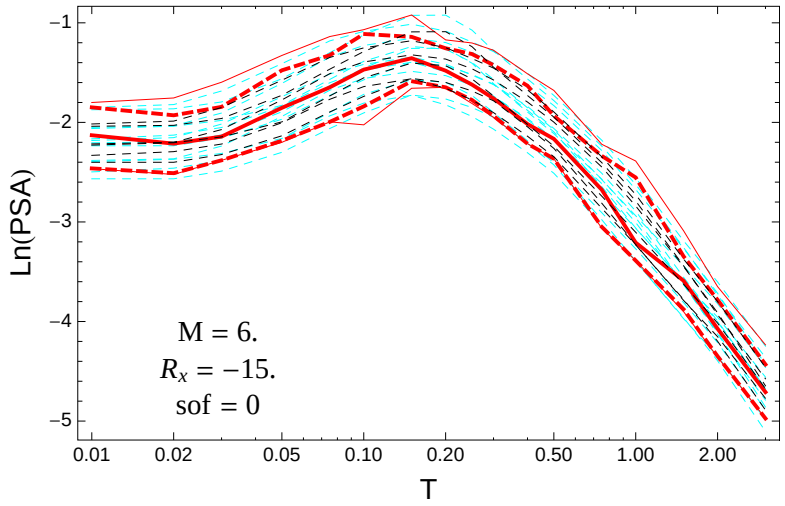



Figure 3.586: PVNGSv2: Spectra of 0.05,0.5,0.95 and the ModelA distribution (red) with total weights and original GMPEs (dashed black) and the original GMPEs with uncertainty model (dashed cyan), for a scenario with $M_W = 6.$, $R_x = -15.$, $F = 0$.

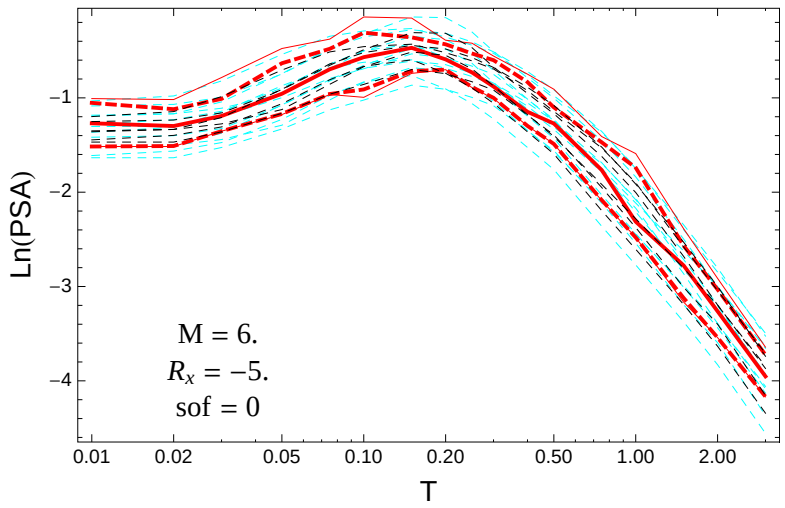



Figure 3.587: PVNGSv2: Spectra of 0.05,0.5,0.95 and the ModelA distribution (red) with total weights and original GMPEs (dashed black) and the original GMPEs with uncertainty model (dashed cyan), for a scenario with $M_W = 6.$, $R_x = -5.$, $F = 0$.

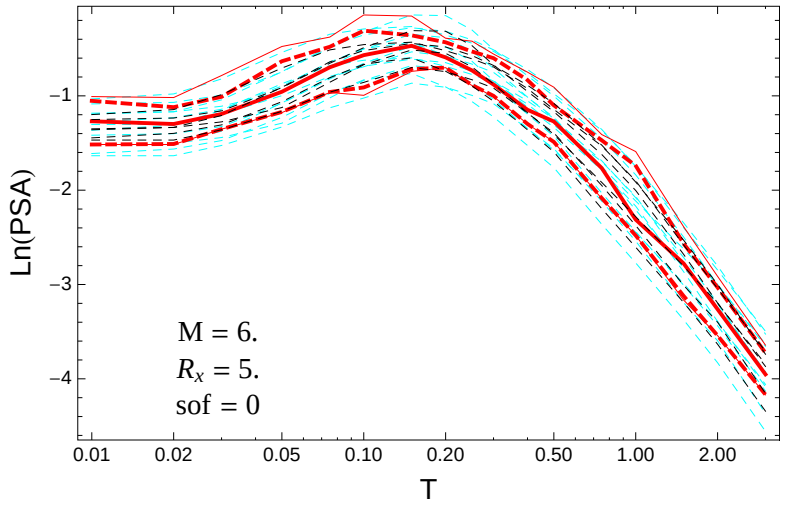



Figure 3.588: PVNGSv2: Spectra of 0.05,0.5,0.95 and the ModelA distribution (red) with total weights and original GMPEs (dashed black) and the original GMPEs with uncertainty model (dashed cyan), for a scenario with $M_W = 6.$, $R_x = 5.$, $F = 0$.

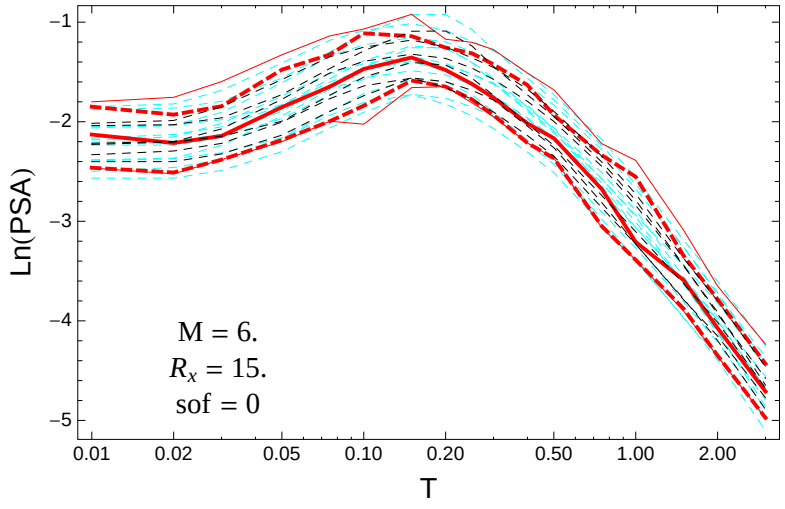



Figure 3.589: PVNGSv2: Spectra of 0.05,0.5,0.95 and the ModelA distribution (red) with total weights and original GMPEs (dashed black) and the original GMPEs with uncertainty model (dashed cyan), for a scenario with $M_W = 6.$, $R_x = 15.$, $F = 0$.

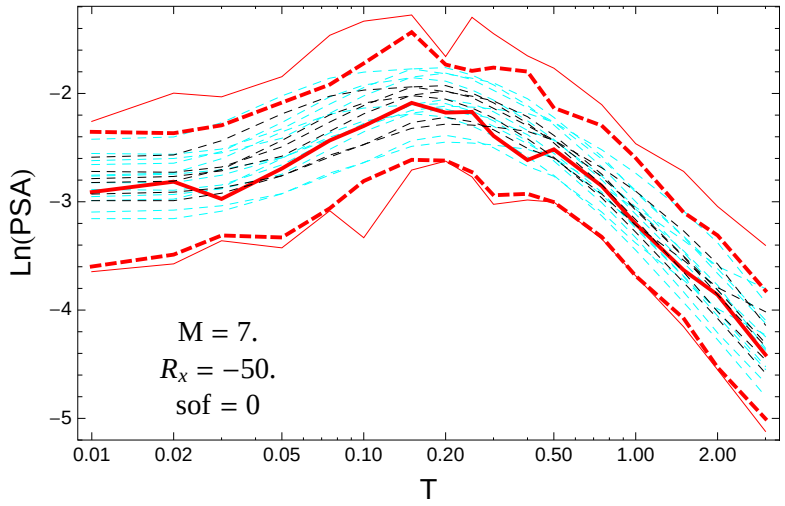



Figure 3.590: PVNGSv2: Spectra of 0.05,0.5,0.95 and the ModelA distribution (red) with total weights and original GMPEs (dashed black) and the original GMPEs with uncertainty model (dashed cyan), for a scenario with $M_W = 7.$, $R_x = -50.$, $F = 0$.

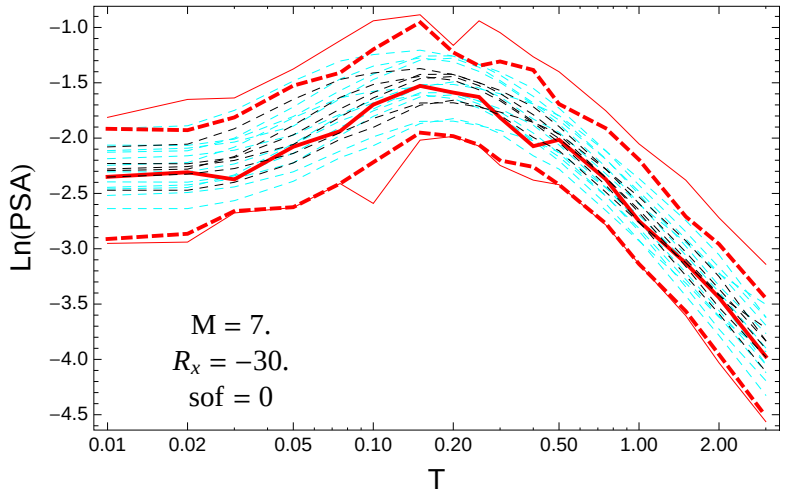



Figure 3.591: PVNGSv2: Spectra of 0.05,0.5,0.95 and the ModelA distribution (red) with total weights and original GMPEs (dashed black) and the original GMPEs with uncertainty model (dashed cyan), for a scenario with $M_W = 7.$, $R_x = -30.$, $F = 0$.

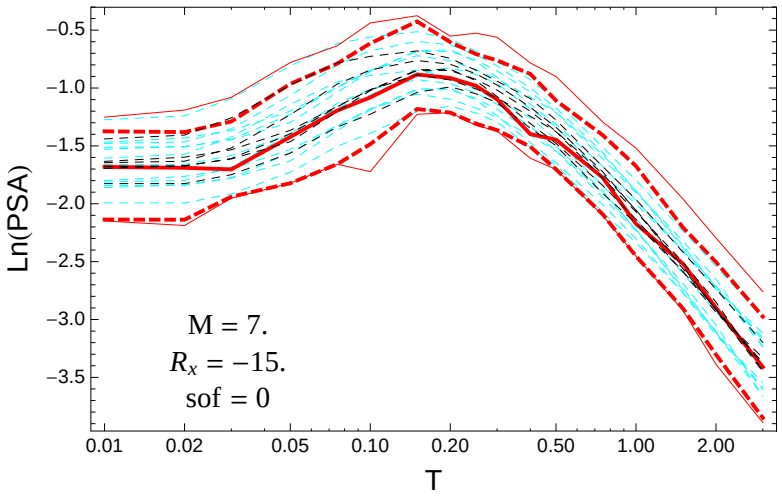



Figure 3.592: PVNGSv2: Spectra of 0.05,0.5,0.95 and the ModelA distribution (red) with total weights and original GMPEs (dashed black) and the original GMPEs with uncertainty model (dashed cyan), for a scenario with $M_W = 7.$, $R_x = -15.$, $F = 0$.

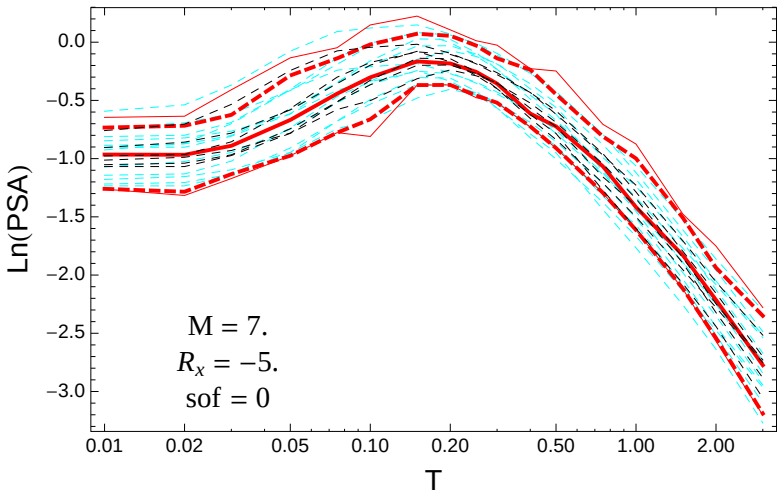



Figure 3.593: PVNGSv2: Spectra of 0.05,0.5,0.95 and the ModelA distribution (red) with total weights and original GMPEs (dashed black) and the original GMPEs with uncertainty model (dashed cyan), for a scenario with $M_W = 7.$, $R_x = -5.$, $F = 0$.

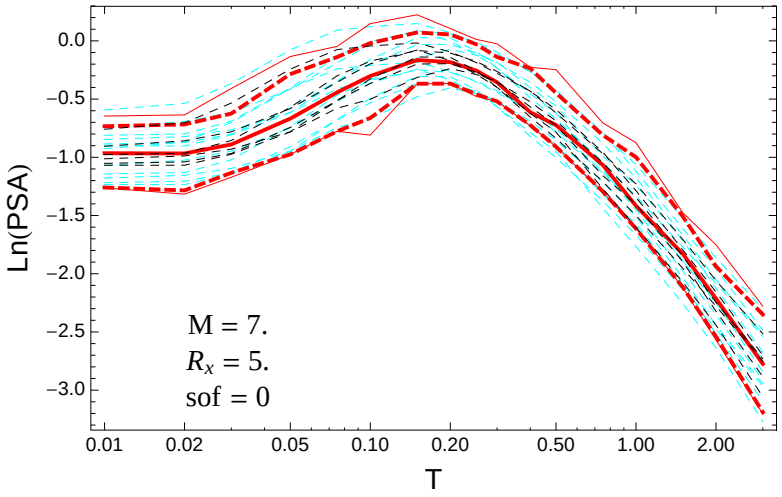



Figure 3.594: PVNGSv2: Spectra of 0.05,0.5,0.95 and the ModelA distribution (red) with total weights and original GMPEs (dashed black) and the original GMPEs with uncertainty model (dashed cyan), for a scenario with $M_W = 7.$, $R_x = 5.$, $F = 0$.

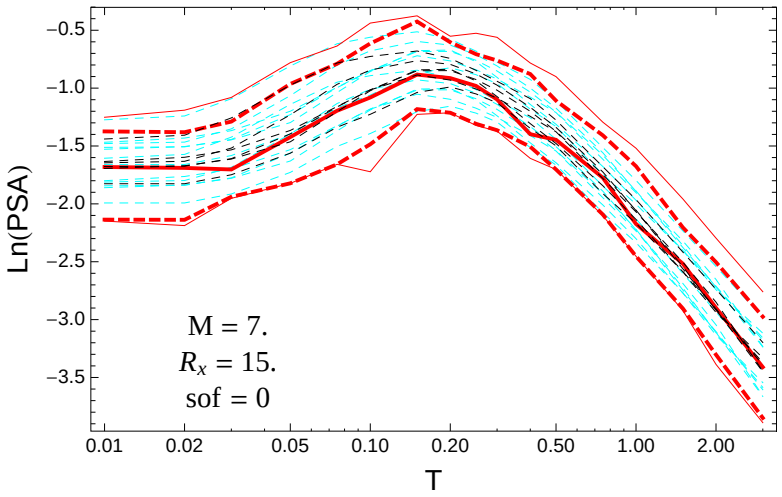



Figure 3.595: PVNGSv2: Spectra of 0.05,0.5,0.95 and the ModelA distribution (red) with total weights and original GMPEs (dashed black) and the original GMPEs with uncertainty model (dashed cyan), for a scenario with $M_W = 7.$, $R_x = 15.$, $F = 0$.

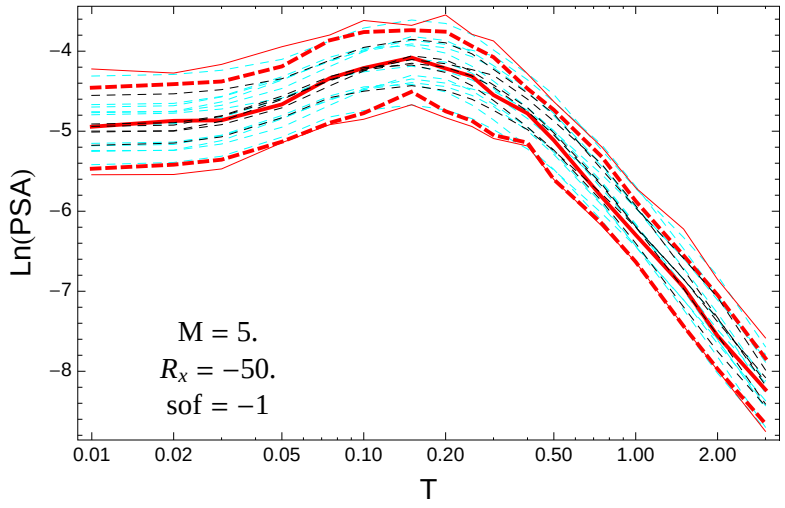



Figure 3.596: PVNGSv2: Spectra of 0.05,0.5,0.95 and the ModelA distribution (red) with total weights and original GMPEs (dashed black) and the original GMPEs with uncertainty model (dashed cyan), for a scenario with $M_W = 5.$, $R_x = -50.$, $F = -1$.

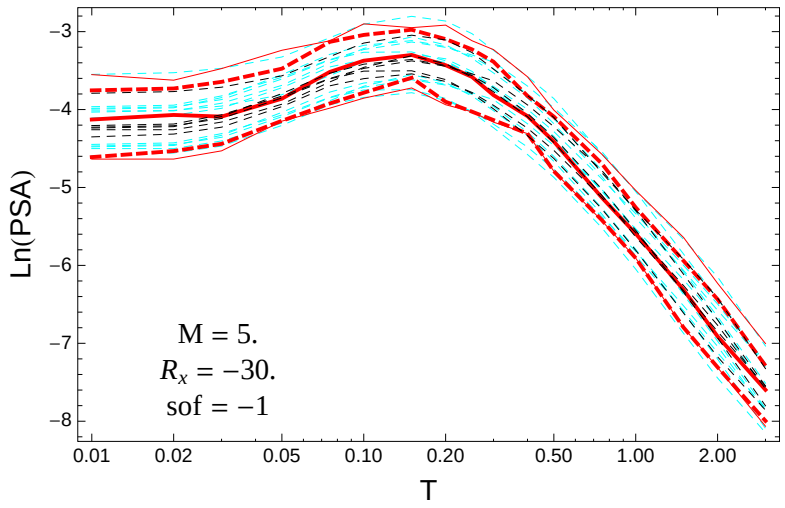



Figure 3.597: PVNGSv2: Spectra of 0.05,0.5,0.95 and the ModelA distribution (red) with total weights and original GMPEs (dashed black) and the original GMPEs with uncertainty model (dashed cyan), for a scenario with $M_W = 5.$, $R_x = -30.$, $F = -1$.

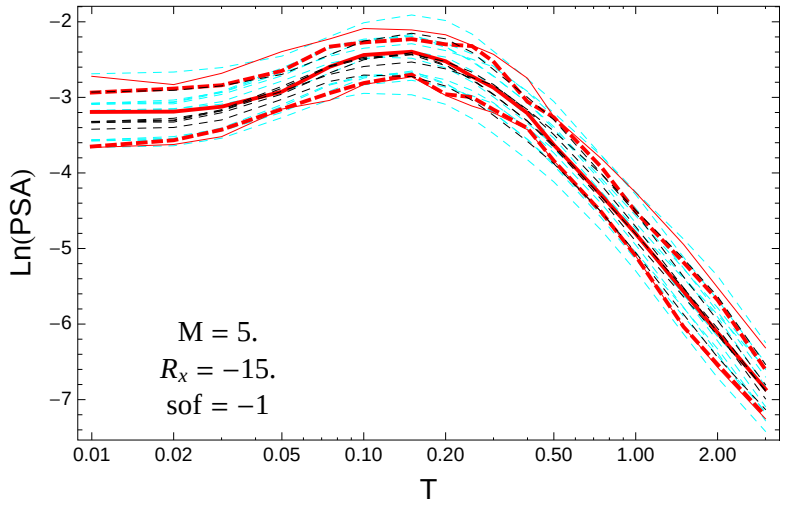



Figure 3.598: PVNGSv2: Spectra of 0.05,0.5,0.95 and the ModelA distribution (red) with total weights and original GMPEs (dashed black) and the original GMPEs with uncertainty model (dashed cyan), for a scenario with $M_W = 5.$, $R_x = -15.$, $F = -1$.

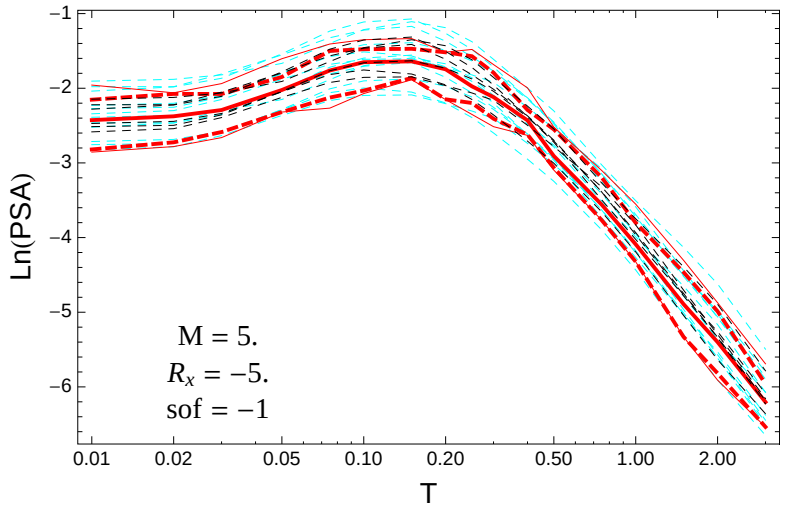



Figure 3.599: PVNGSv2: Spectra of 0.05,0.5,0.95 and the ModelA distribution (red) with total weights and original GMPEs (dashed black) and the original GMPEs with uncertainty model (dashed cyan), for a scenario with $M_W = 5.$, $R_x = -5.$, $F = -1$.

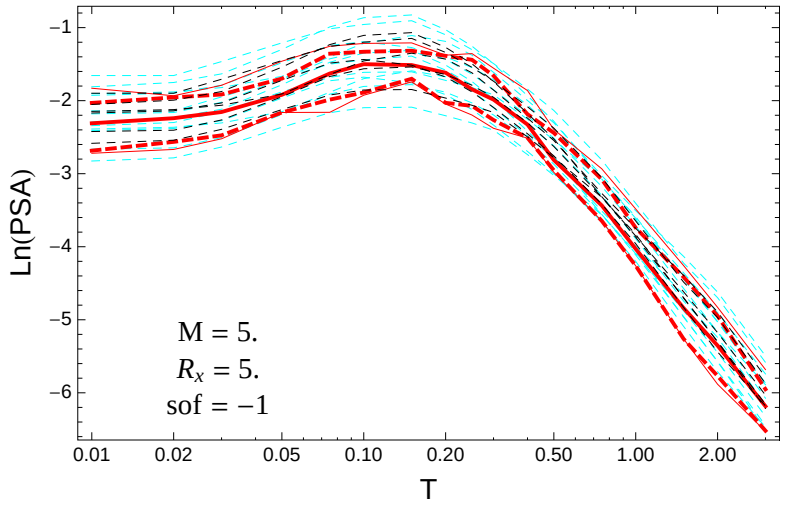



Figure 3.600: PVNGSv2: Spectra of 0.05,0.5,0.95 and the ModelA distribution (red) with total weights and original GMPEs (dashed black) and the original GMPEs with uncertainty model (dashed cyan), for a scenario with $M_W = 5.$, $R_x = 5.$, $F = -1$.

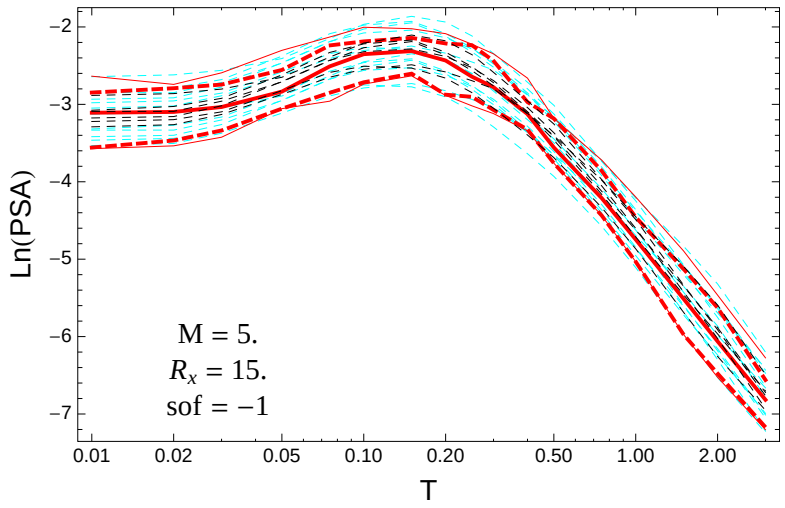



Figure 3.601: PVNGSv2: Spectra of 0.05,0.5,0.95 and the ModelA distribution (red) with total weights and original GMPEs (dashed black) and the original GMPEs with uncertainty model (dashed cyan), for a scenario with $M_W = 5.$, $R_x = 15.$, $F = -1$.

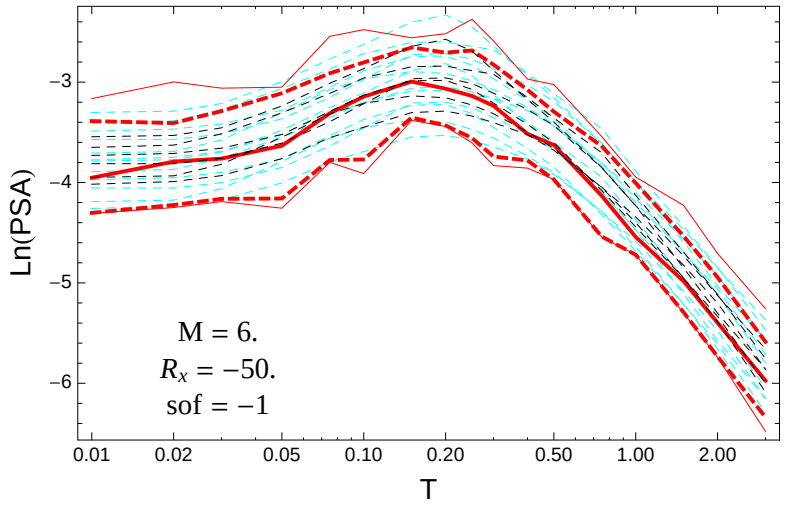



Figure 3.602: PVNGSv2: Spectra of 0.05,0.5,0.95 and the ModelA distribution (red) with total weights and original GMPEs (dashed black) and the original GMPEs with uncertainty model (dashed cyan), for a scenario with $M_W = 6.$, $R_x = -50.$, $F = -1$.

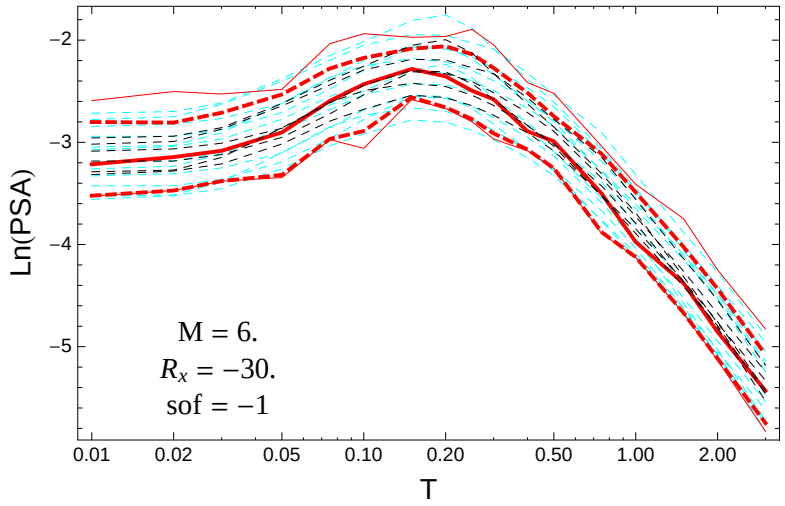



Figure 3.603: PVNGSv2: Spectra of 0.05,0.5,0.95 and the ModelA distribution (red) with total weights and original GMPEs (dashed black) and the original GMPEs with uncertainty model (dashed cyan), for a scenario with $M_W = 6.$, $R_x = -30.$, $F = -1$.

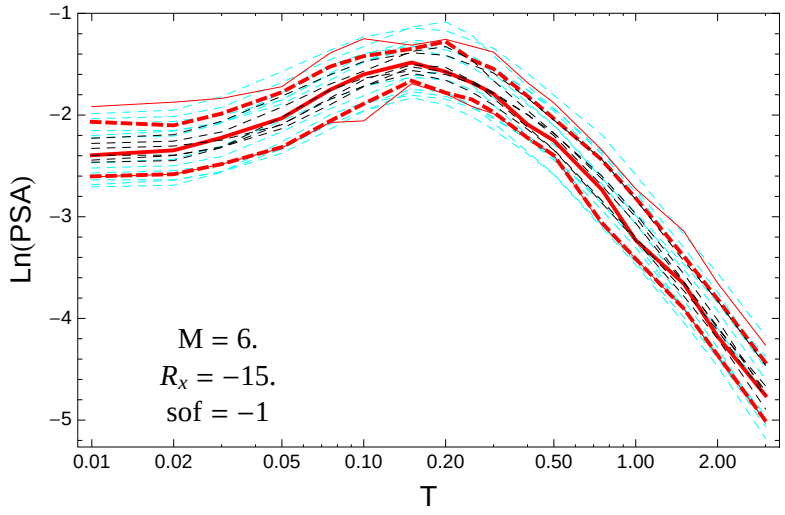



Figure 3.604: PVNGSv2: Spectra of 0.05,0.5,0.95 and the ModelA distribution (red) with total weights and original GMPEs (dashed black) and the original GMPEs with uncertainty model (dashed cyan), for a scenario with $M_W = 6.$, $R_x = -15.$, $F = -1$.

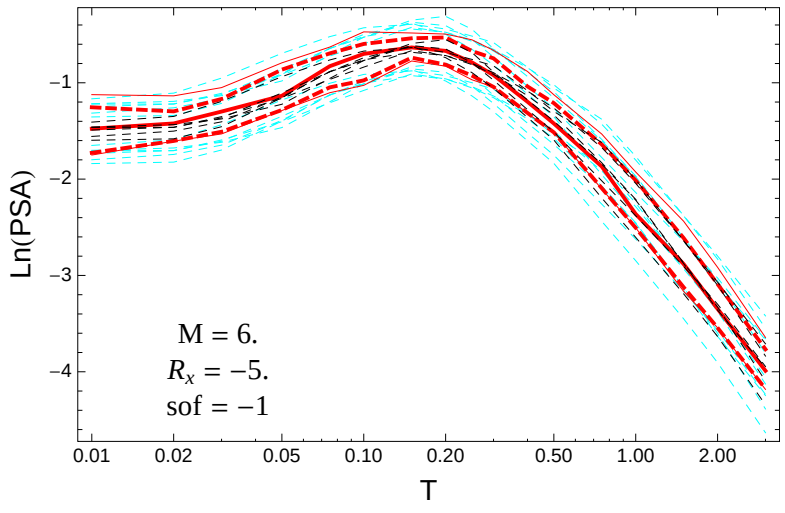



Figure 3.605: PVNGSv2: Spectra of 0.05,0.5,0.95 and the ModelA distribution (red) with total weights and original GMPEs (dashed black) and the original GMPEs with uncertainty model (dashed cyan), for a scenario with $M_W = 6.$, $R_x = -5.$, $F = -1$.

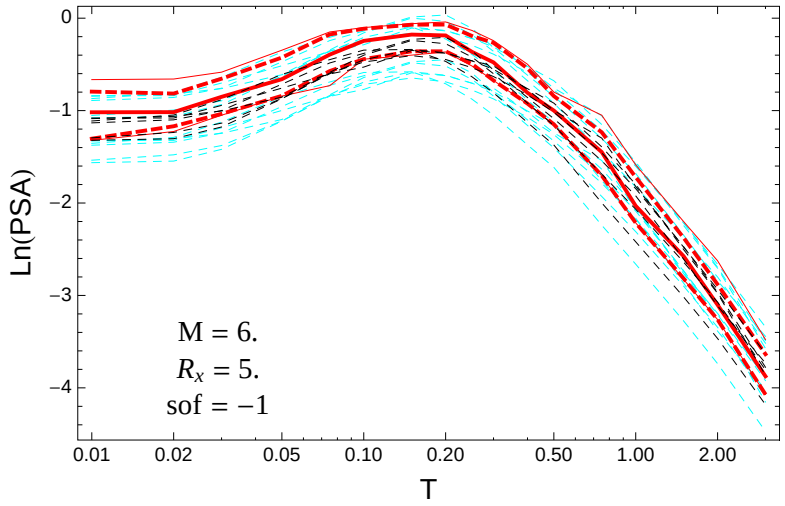



Figure 3.606: PVNGSv2: Spectra of 0.05,0.5,0.95 and the ModelA distribution (red) with total weights and original GMPEs (dashed black) and the original GMPEs with uncertainty model (dashed cyan), for a scenario with $M_W = 6.$, $R_x = 5.$, $F = -1$.

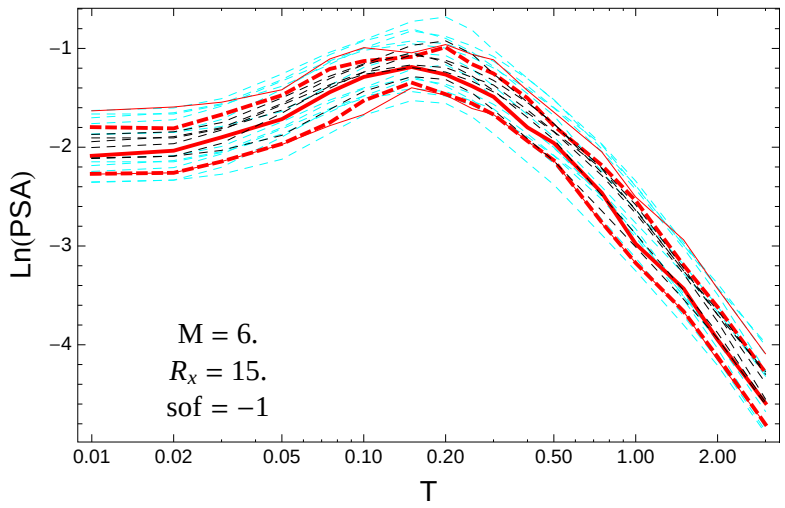



Figure 3.607: PVNGSv2: Spectra of 0.05,0.5,0.95 and the ModelA distribution (red) with total weights and original GMPEs (dashed black) and the original GMPEs with uncertainty model (dashed cyan), for a scenario with $M_W = 6.$, $R_x = 15.$, $F = -1$.

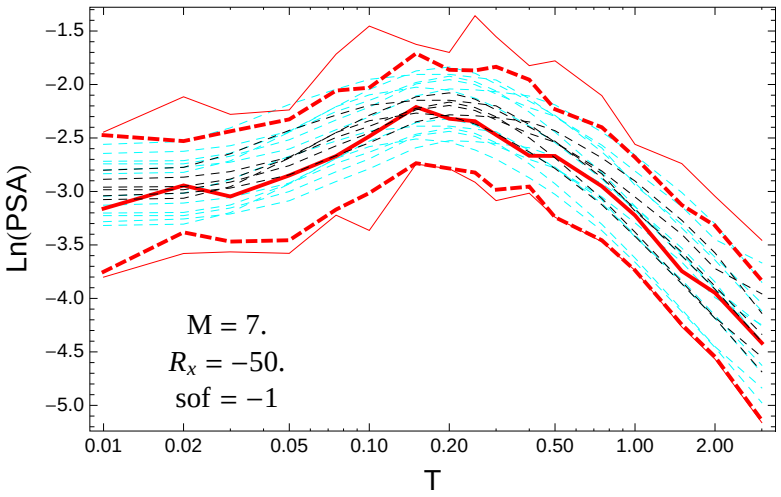



Figure 3.608: PVNGSv2: Spectra of 0.05,0.5,0.95 and the ModelA distribution (red) with total weights and original GMPEs (dashed black) and the original GMPEs with uncertainty model (dashed cyan), for a scenario with $M_W = 7.$, $R_x = -50.$, $F = -1$.

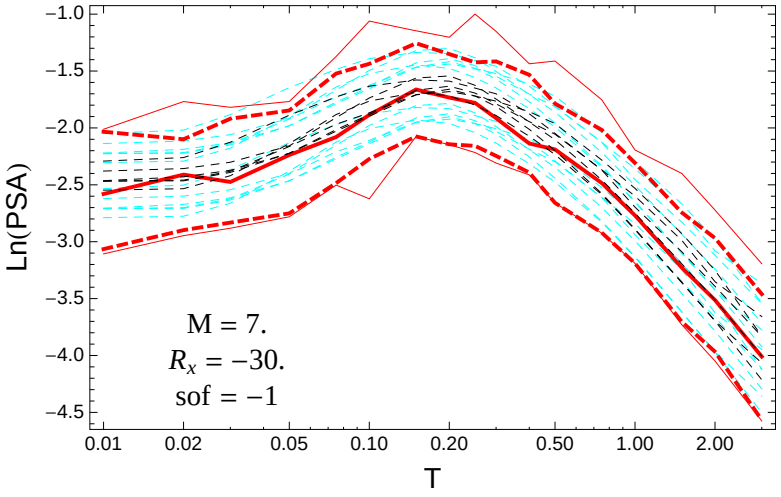



Figure 3.609: PVNGSv2: Spectra of 0.05,0.5,0.95 and the ModelA distribution (red) with total weights and original GMPEs (dashed black) and the original GMPEs with uncertainty model (dashed cyan), for a scenario with $M_W = 7.$, $R_x = -30.$, $F = -1$.

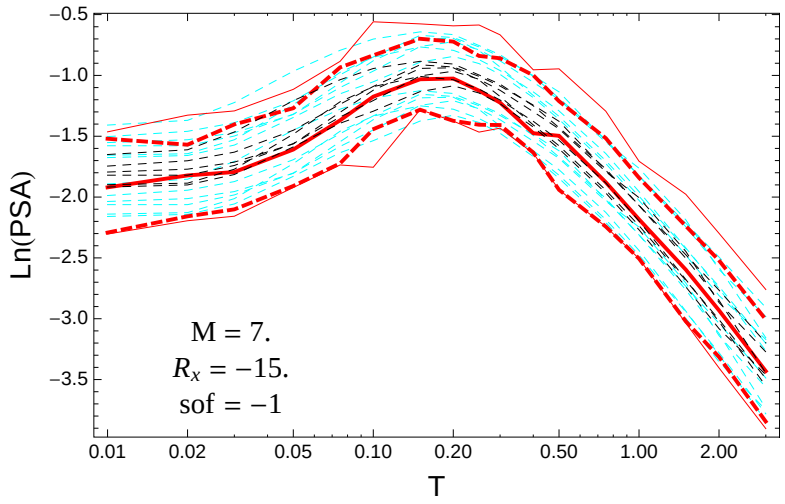



Figure 3.610: PVNGSv2: Spectra of 0.05,0.5,0.95 and the ModelA distribution (red) with total weights and original GMPEs (dashed black) and the original GMPEs with uncertainty model (dashed cyan), for a scenario with $M_W = 7.$, $R_x = -15.$, $F = -1$.

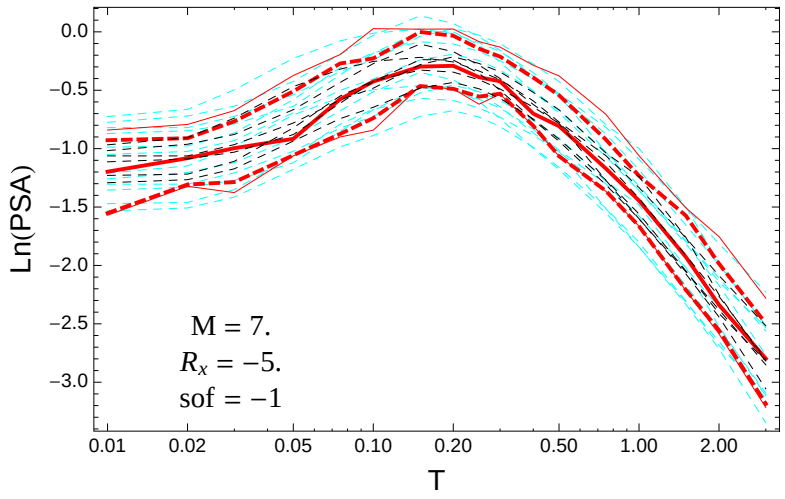



Figure 3.611: PVNGSv2: Spectra of 0.05,0.5,0.95 and the ModelA distribution (red) with total weights and original GMPEs (dashed black) and the original GMPEs with uncertainty model (dashed cyan), for a scenario with $M_W = 7.$, $R_x = -5.$, $F = -1$.

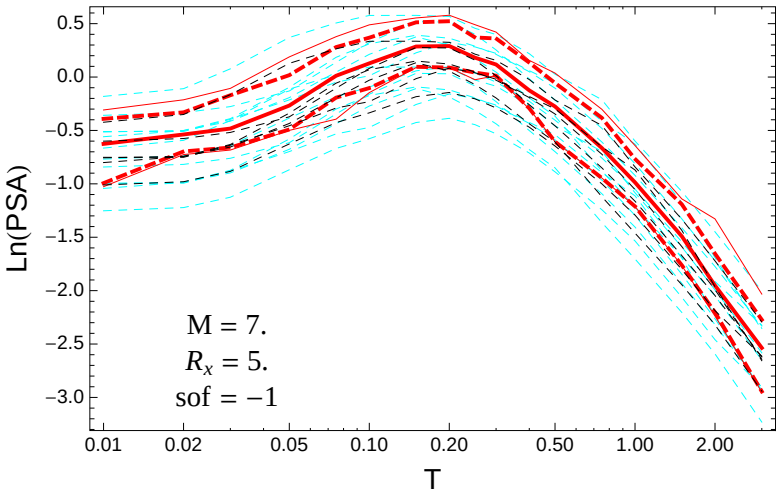



Figure 3.612: PVNGSv2: Spectra of 0.05,0.5,0.95 and the ModelA distribution (red) with total weights and original GMPEs (dashed black) and the original GMPEs with uncertainty model (dashed cyan), for a scenario with $M_W = 7.$, $R_x = 5.$, $F = -1$.

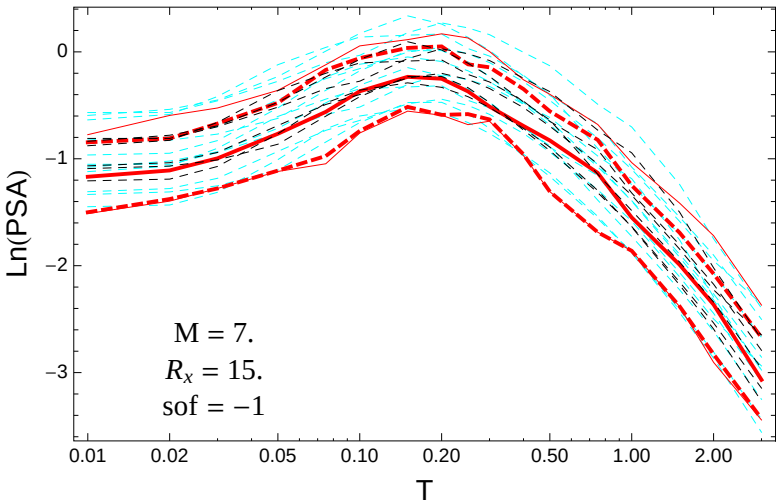



Figure 3.613: PVNGSv2: Spectra of 0.05,0.5,0.95 and the ModelA distribution (red) with total weights and original GMPEs (dashed black) and the original GMPEs with uncertainty model (dashed cyan), for a scenario with $M_W = 7.$, $R_x = 15.$, $F = -1$.

### 3.1.15 Median Residuals

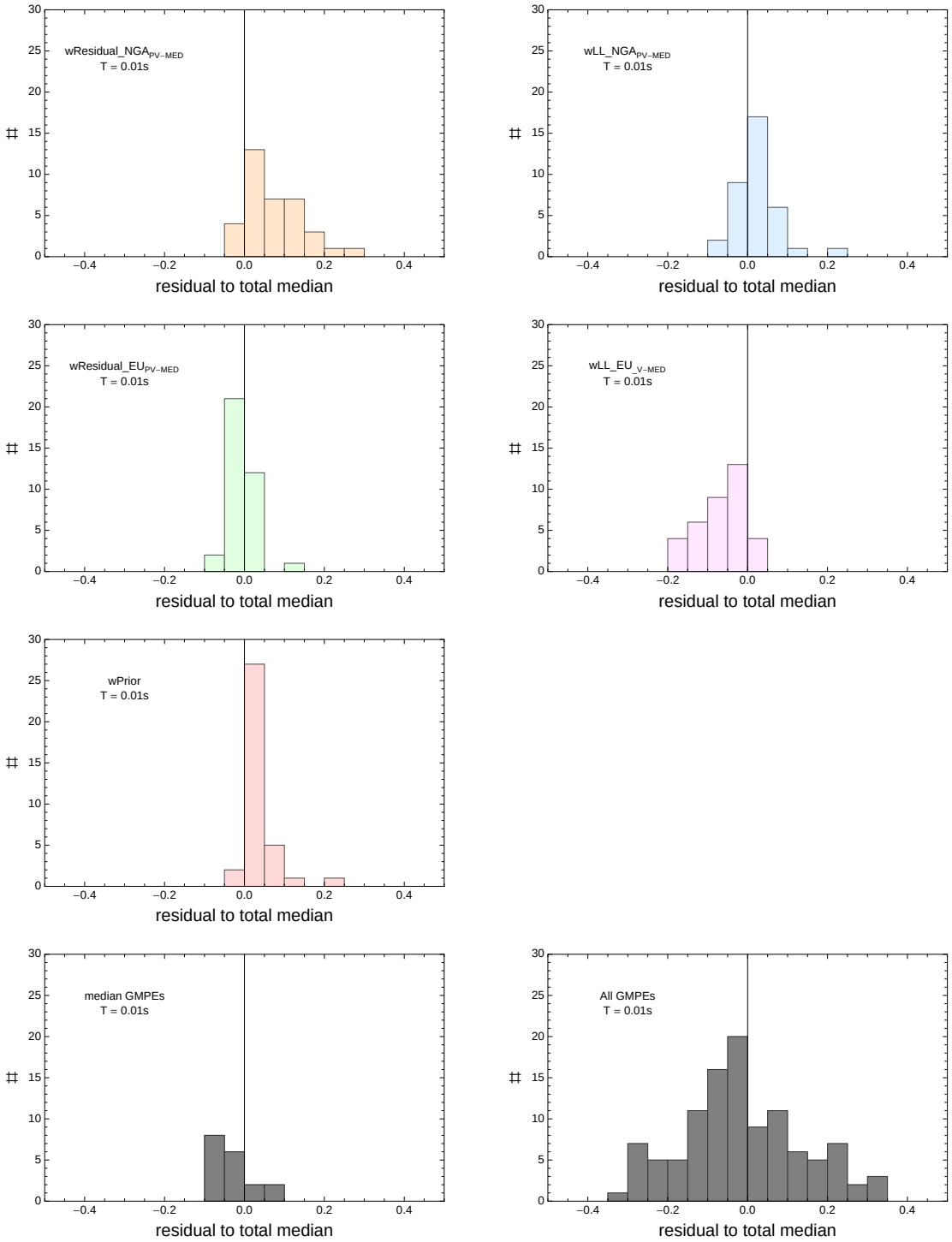



Figure 3.614: PVNGSv2: Histogram of differences for medians calculated with different weights to median calculated with total weights. Bottom row left shows differences between medians for the GMPE distribution to median calculated with total weights. Bottom row right shows differences between the original GMPEs (without uncertainty) to median calculated with total weights. For PVNGS2, ModelA and $T = 0.01$s.

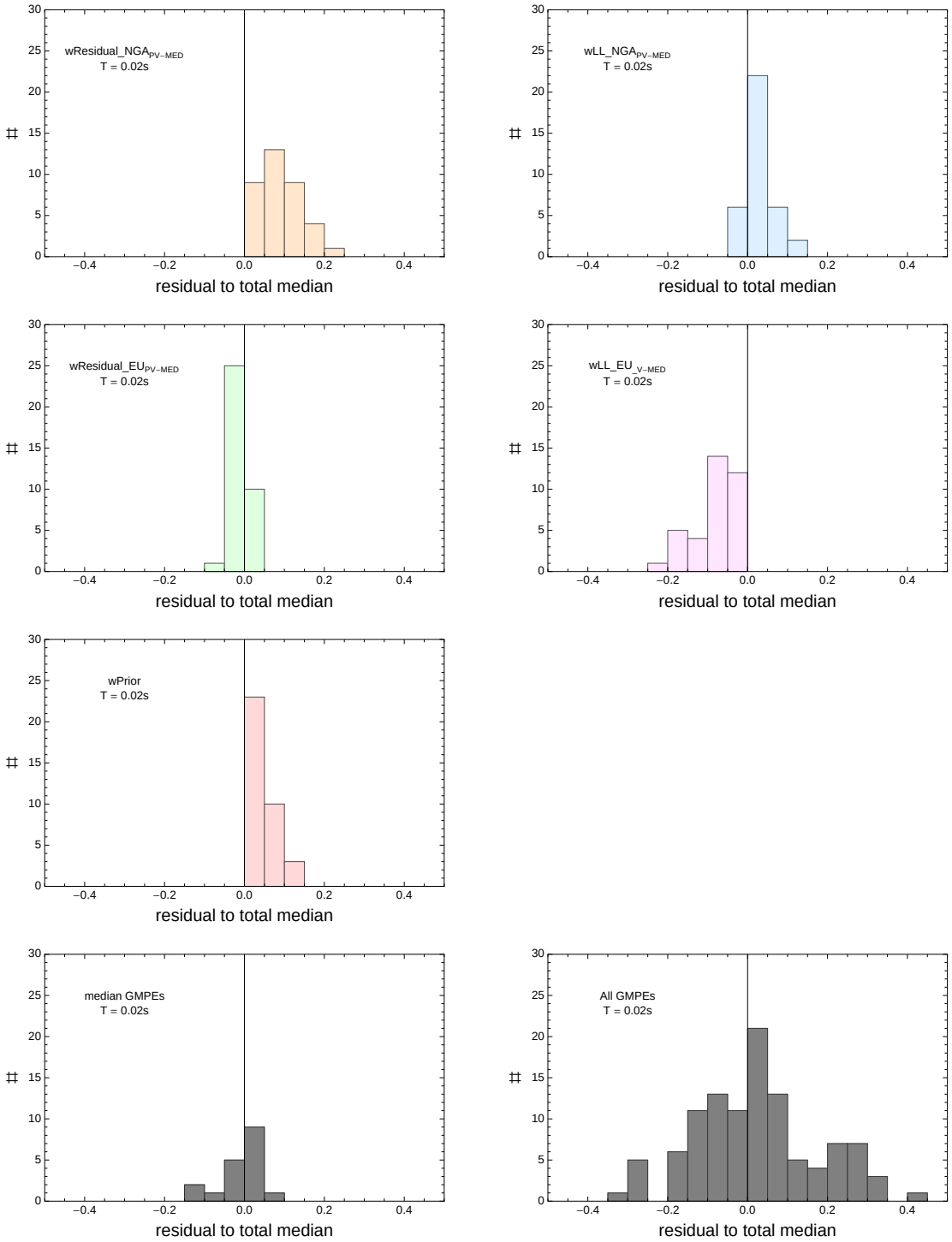



Figure 3.615: PVNGSv2: Histogram of differences for medians calculated with different weights to median calculated with total weights. Bottom row left shows differences between medians for the GMPE distribution to median calculated with total weights. Bottom row right shows differences between the original GMPEs (without uncertainty) to median calculated with total weights. For PVNGS2, ModelA and $T = 0.02$s.

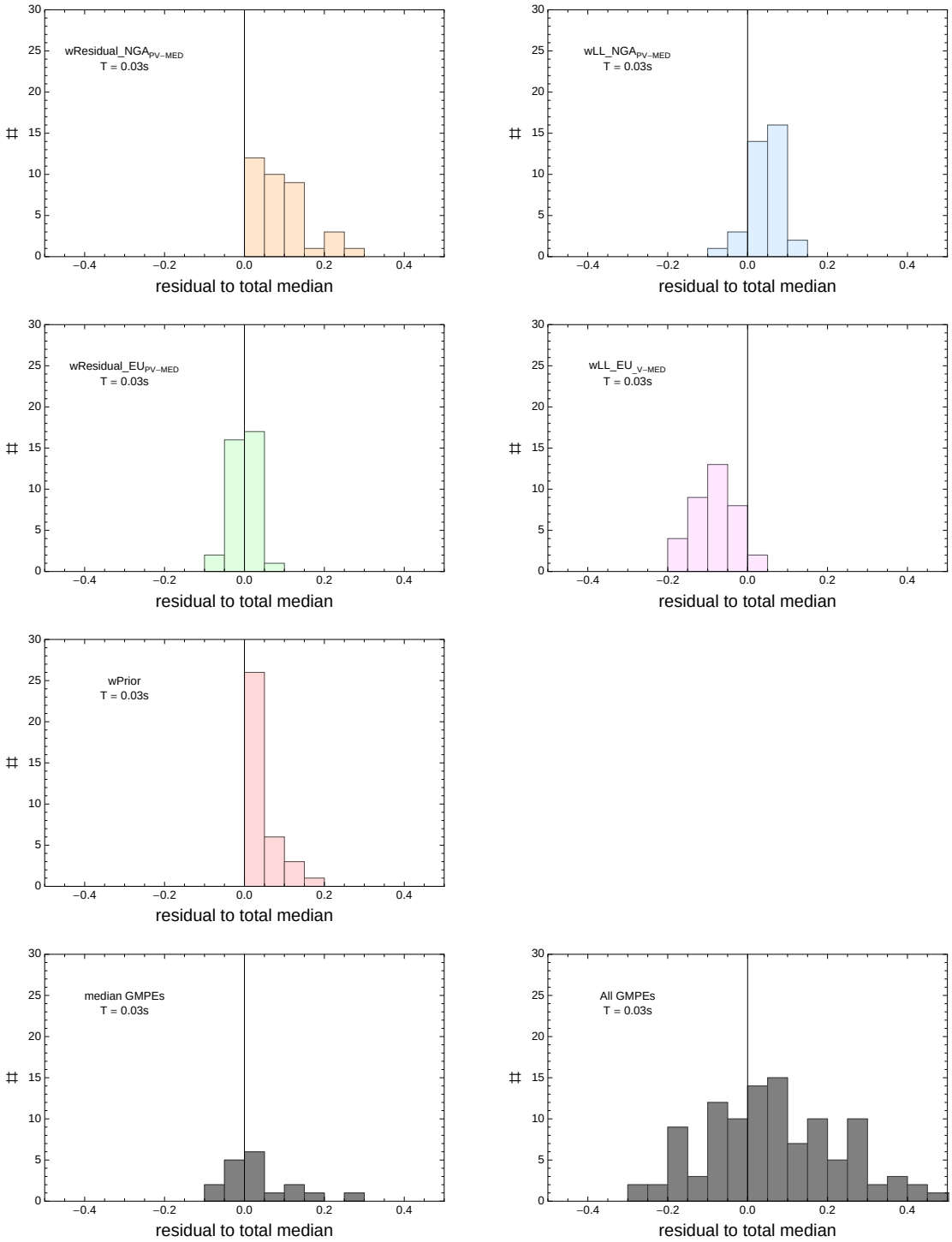



Figure 3.616: PVNGSv2: Histogram of differences for medians calculated with different weights to median calculated with total weights. Bottom row left shows differences between medians for the GMPE distribution to median calculated with total weights. Bottom row right shows differences between the original GMPEs (without uncertainty) to median calculated with total weights. For PVNGS2, ModelA and $T = 0.03$s.

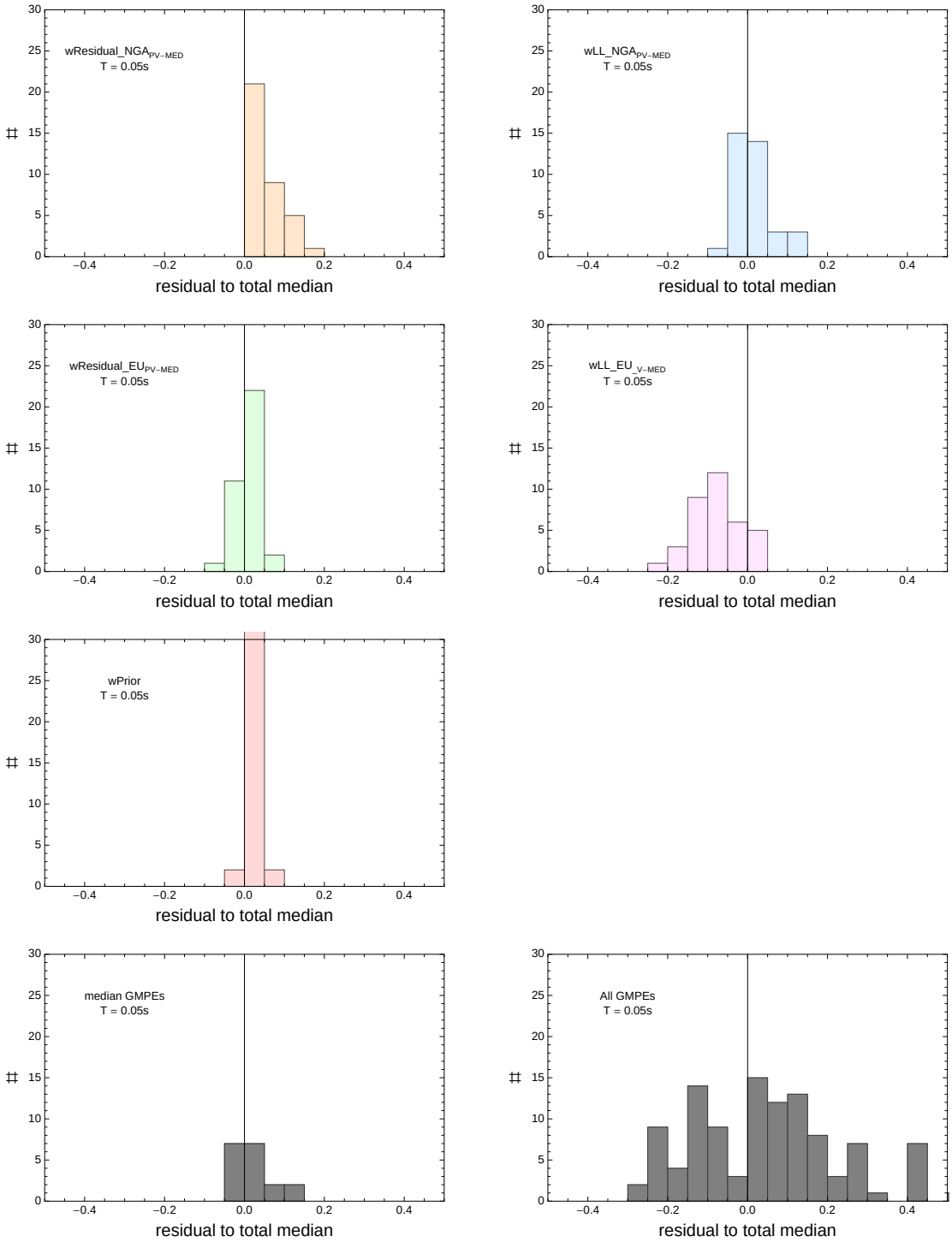



Figure 3.617: PVNGSv2: Histogram of differences for medians calculated with different weights to median calculated with total weights. Bottom row left shows differences between medians for the GMPE distribution to median calculated with total weights. Bottom row right shows differences between the original GMPEs (without uncertainty) to median calculated with total weights. For PVNGS2, ModelA and $T = 0.05$s.

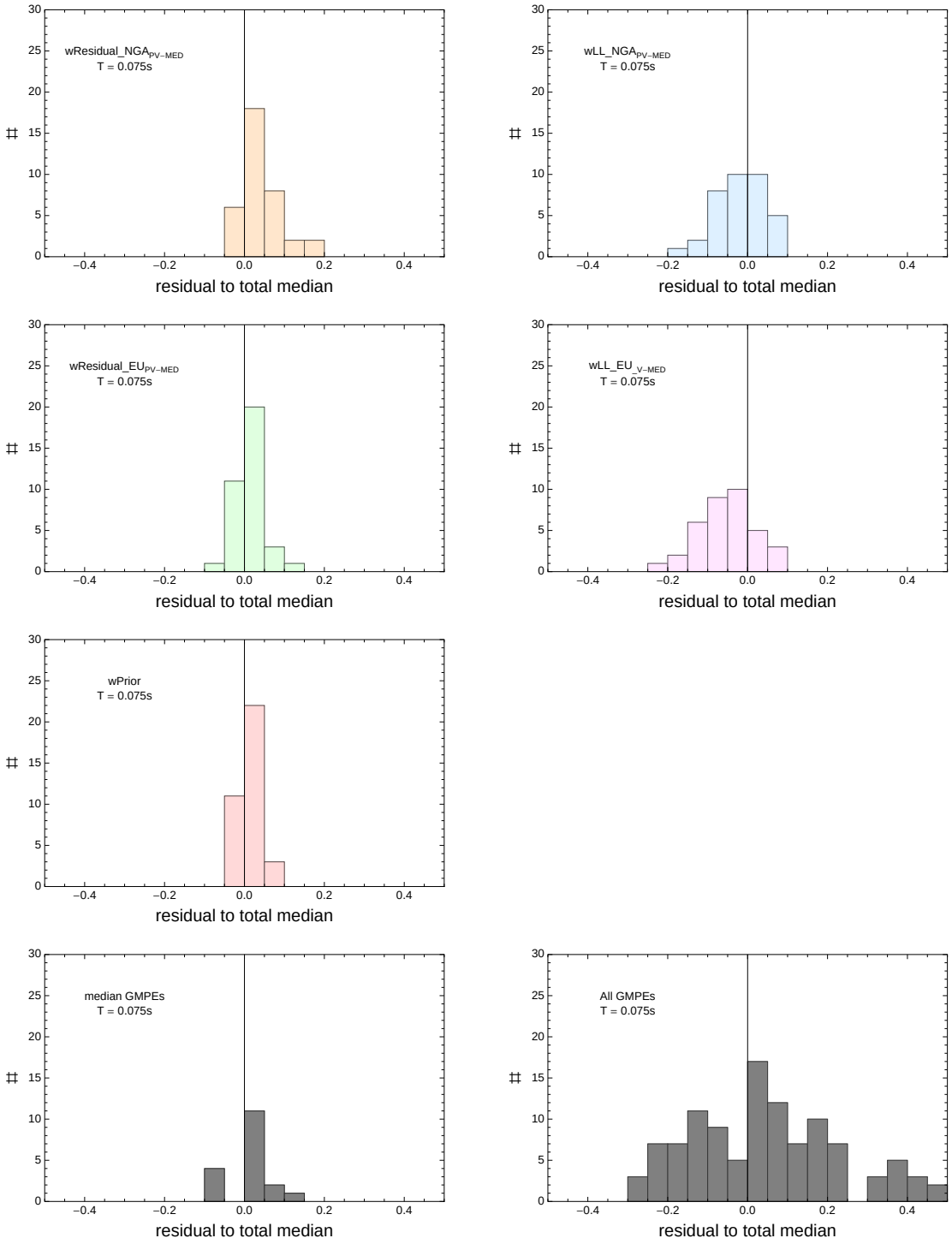



Figure 3.618: PVNGSv2: Histogram of differences for medians calculated with different weights to median calculated with total weights. Bottom row left shows differences between medians for the GMPE distribution to median calculated with total weights. Bottom row right shows differences between the original GMPEs (without uncertainty) to median calculated with total weights. For PVNGS2, ModelA and $T = 0.075$s.

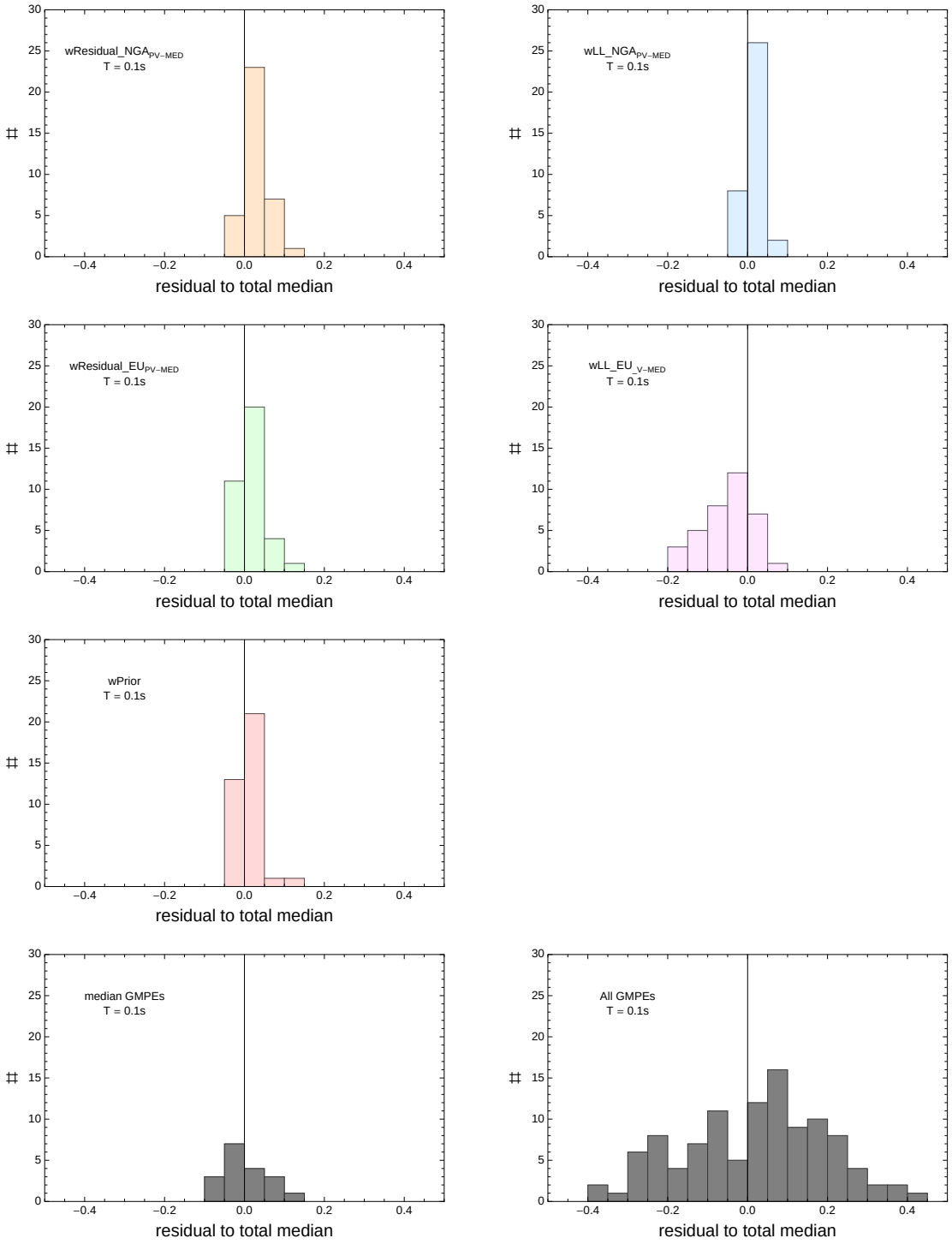



Figure 3.619: PVNGSv2: Histogram of differences for medians calculated with different weights to median calculated with total weights. Bottom row left shows differences between medians for the GMPE distribution to median calculated with total weights. Bottom row right shows differences between the original GMPEs (without uncertainty) to median calculated with total weights. For PVNGS2, ModelA and $T = 0.1$s.

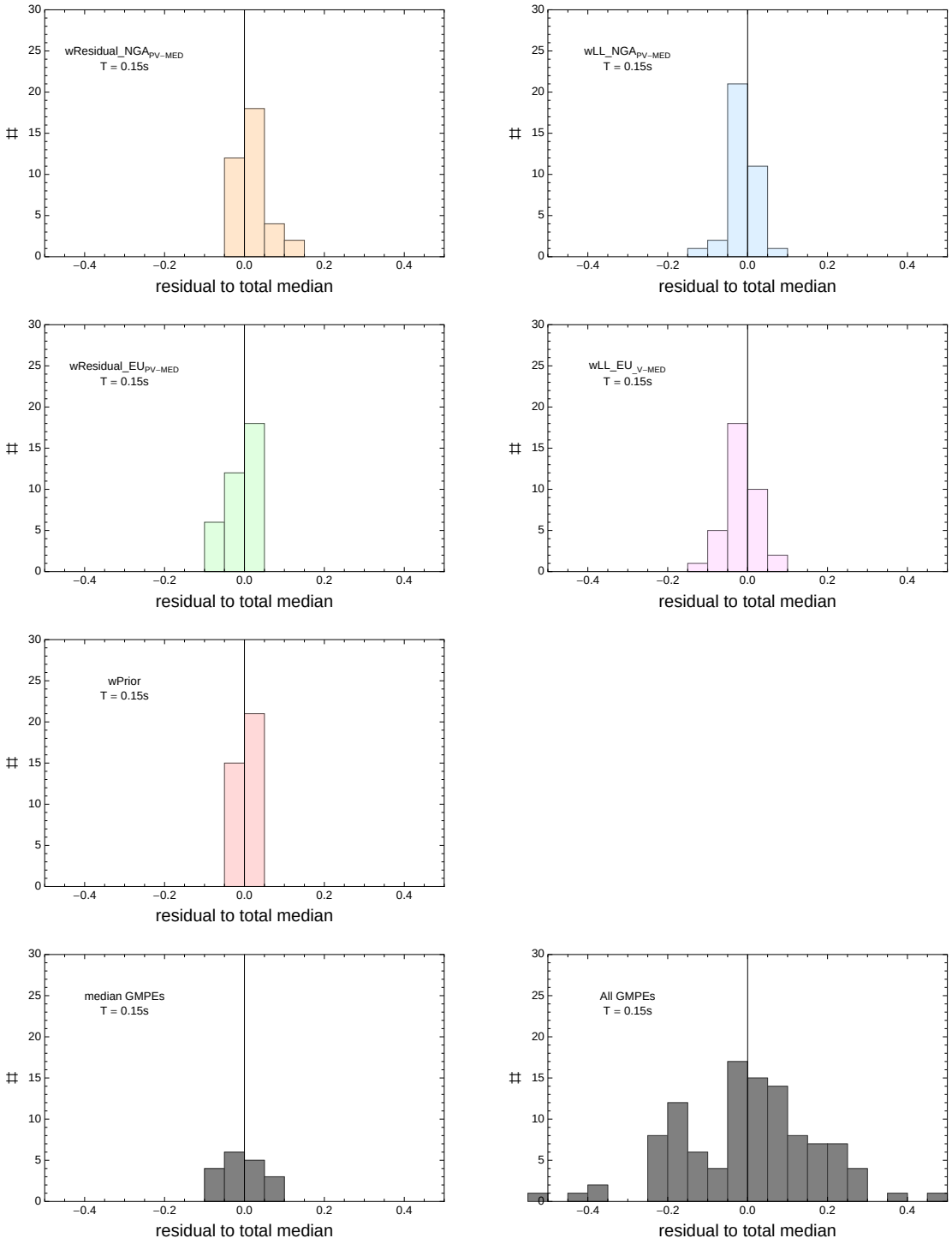



Figure 3.620: PVNGSv2: Histogram of differences for medians calculated with different weights to median calculated with total weights. Bottom row left shows differences between medians for the GMPE distribution to median calculated with total weights. Bottom row right shows differences between the original GMPEs (without uncertainty) to median calculated with total weights. For PVNGS2, ModelA and $T = 0.15$s.

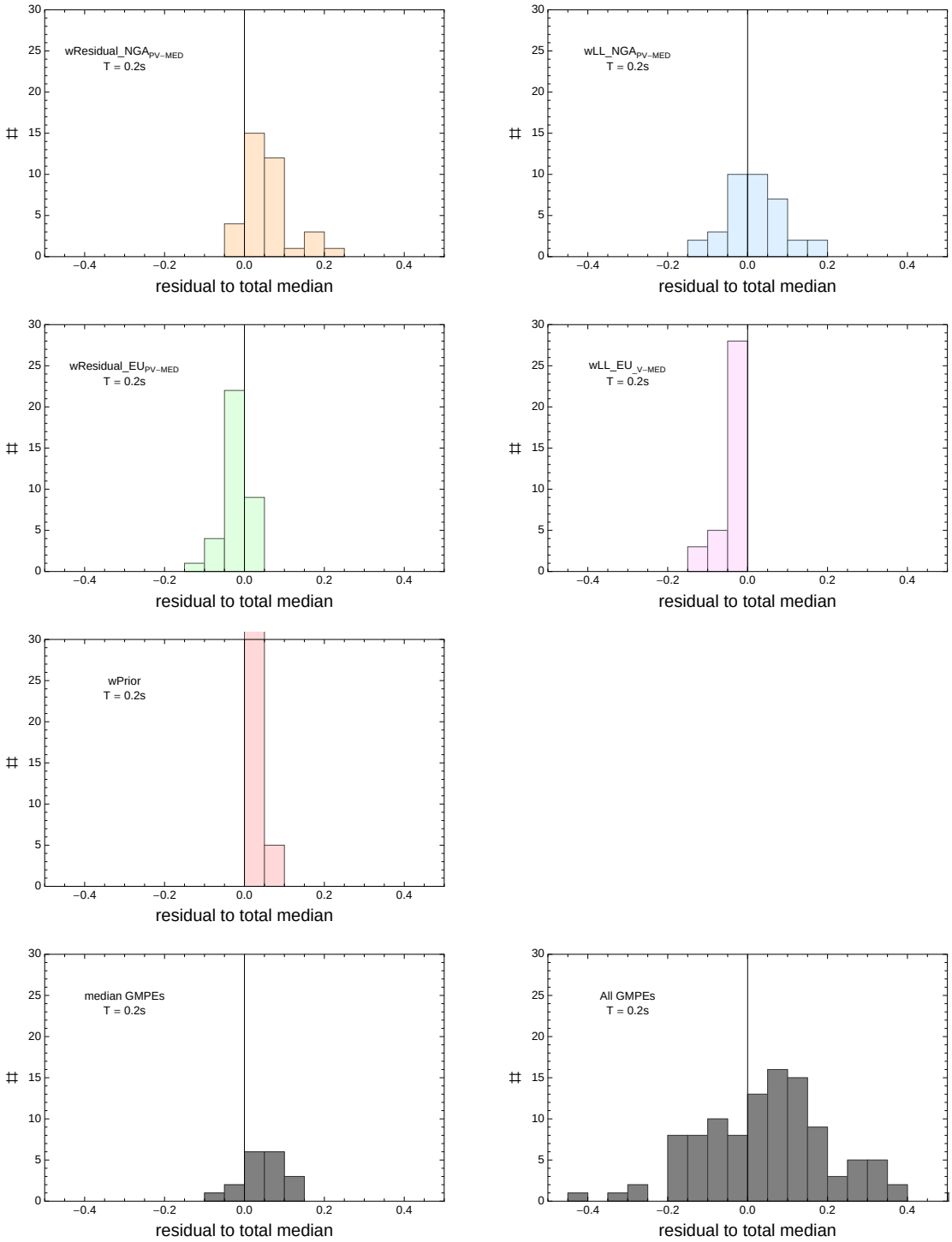



Figure 3.621: PVNGSv2: Histogram of differences for medians calculated with different weights to median calculated with total weights. Bottom row left shows differences between medians for the GMPE distribution to median calculated with total weights. Bottom row right shows differences between the original GMPEs (without uncertainty) to median calculated with total weights. For PVNGS2, ModelA and $T = 0.2$s.

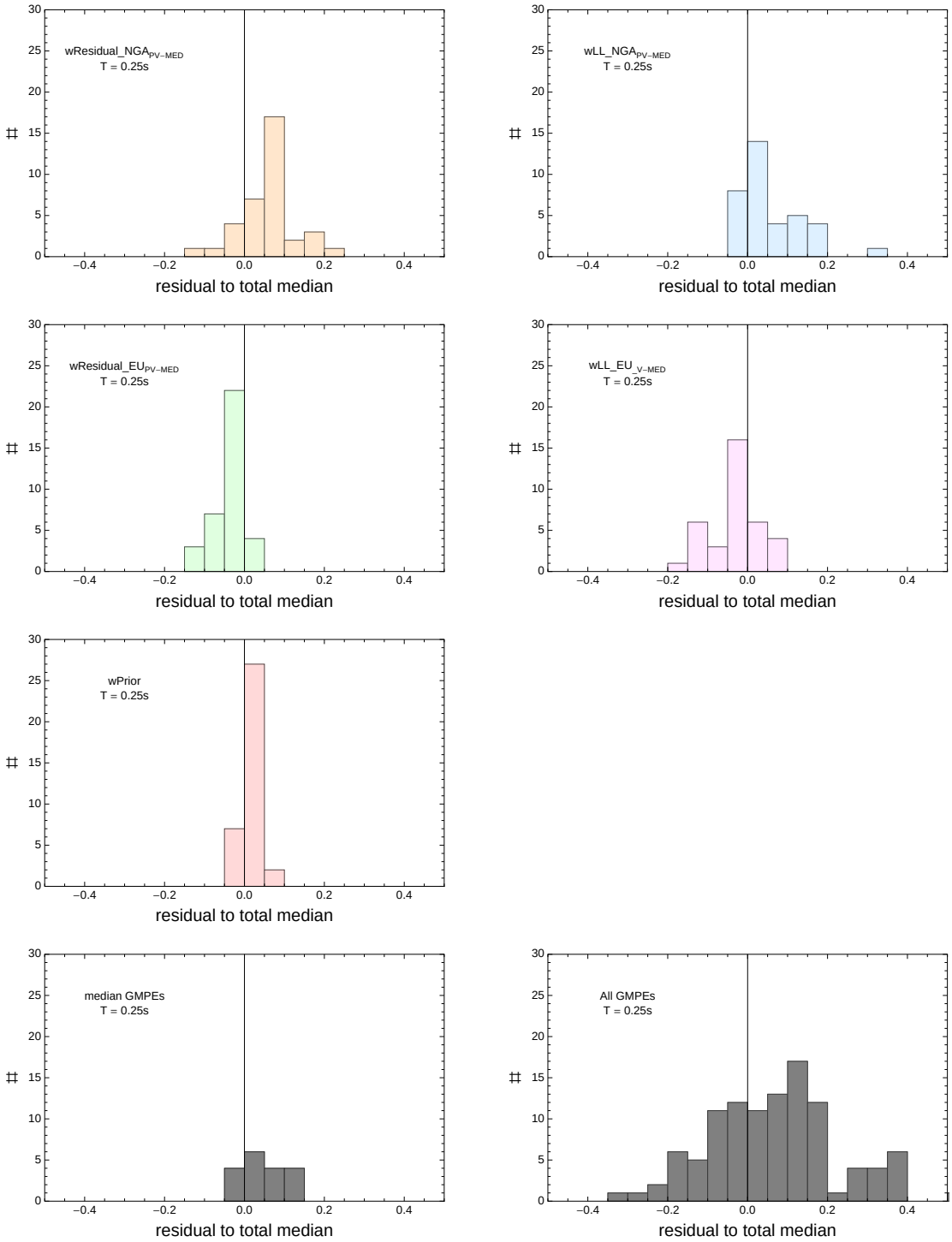



Figure 3.622: PVNGSv2: Histogram of differences for medians calculated with different weights to median calculated with total weights. Bottom row left shows differences between medians for the GMPE distribution to median calculated with total weights. Bottom row right shows differences between the original GMPEs (without uncertainty) to median calculated with total weights. For PVNGS2, ModelA and $T = 0.25$s.

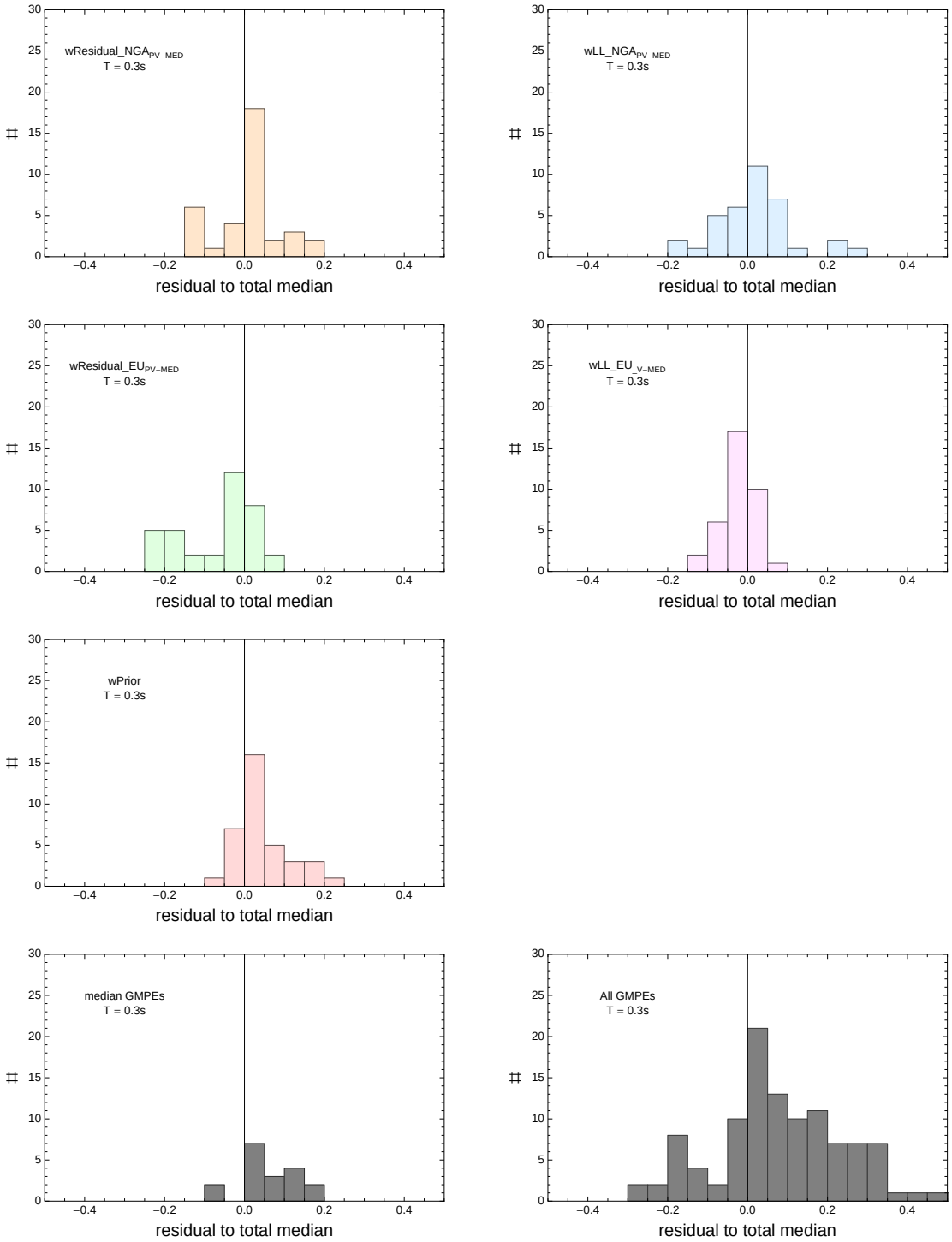



Figure 3.623: PVNGSv2: Histogram of differences for medians calculated with different weights to median calculated with total weights. Bottom row left shows differences between medians for the GMPE distribution to median calculated with total weights. Bottom row right shows differences between the original GMPEs (without uncertainty) to median calculated with total weights. For PVNGS2, ModelA and $T = 0.3$s.

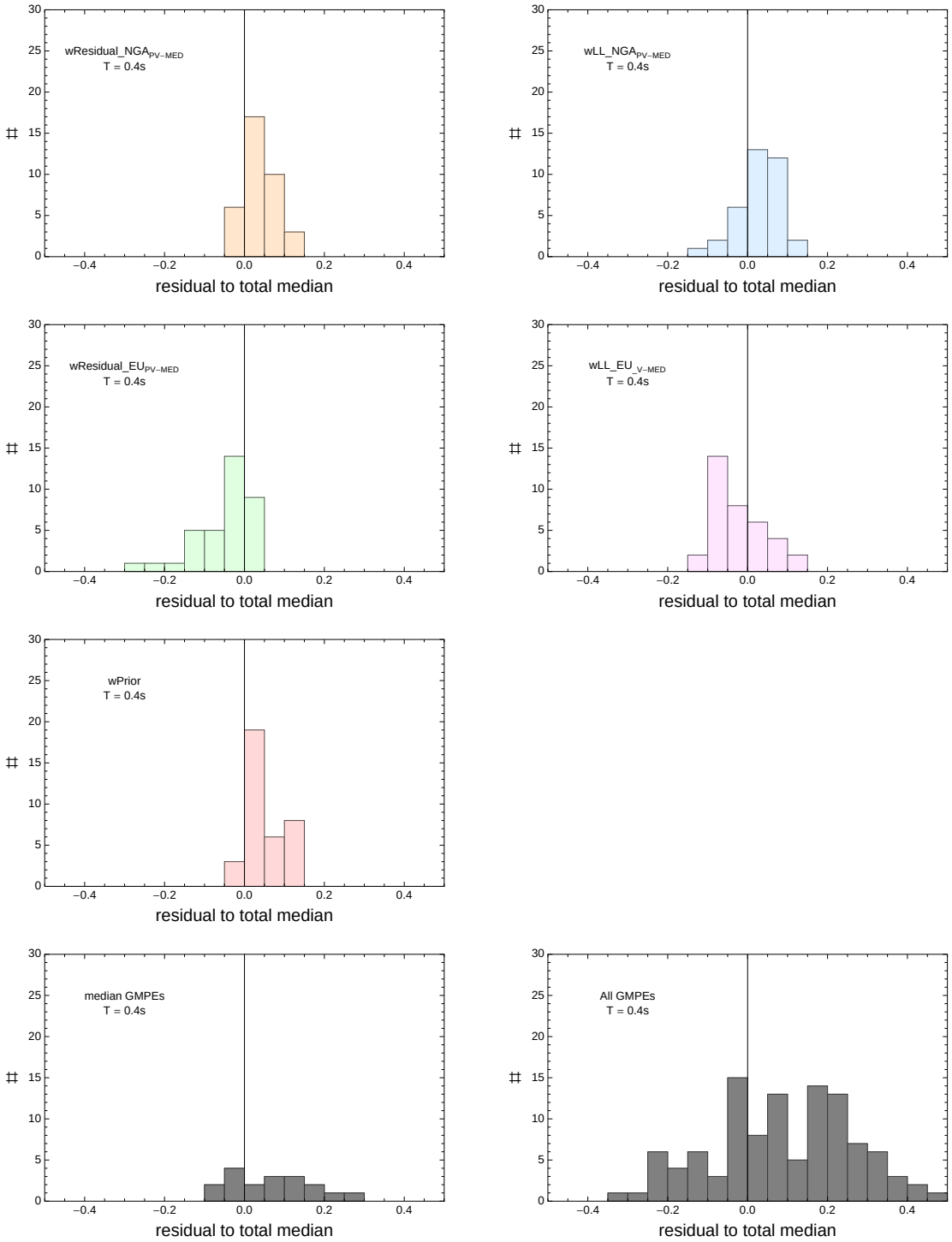



Figure 3.624: PVNGSv2: Histogram of differences for medians calculated with different weights to median calculated with total weights. Bottom row left shows differences between medians for the GMPE distribution to median calculated with total weights. Bottom row right shows differences between the original GMPEs (without uncertainty) to median calculated with total weights. For PVNGS2, ModelA and $T = 0.4$s.

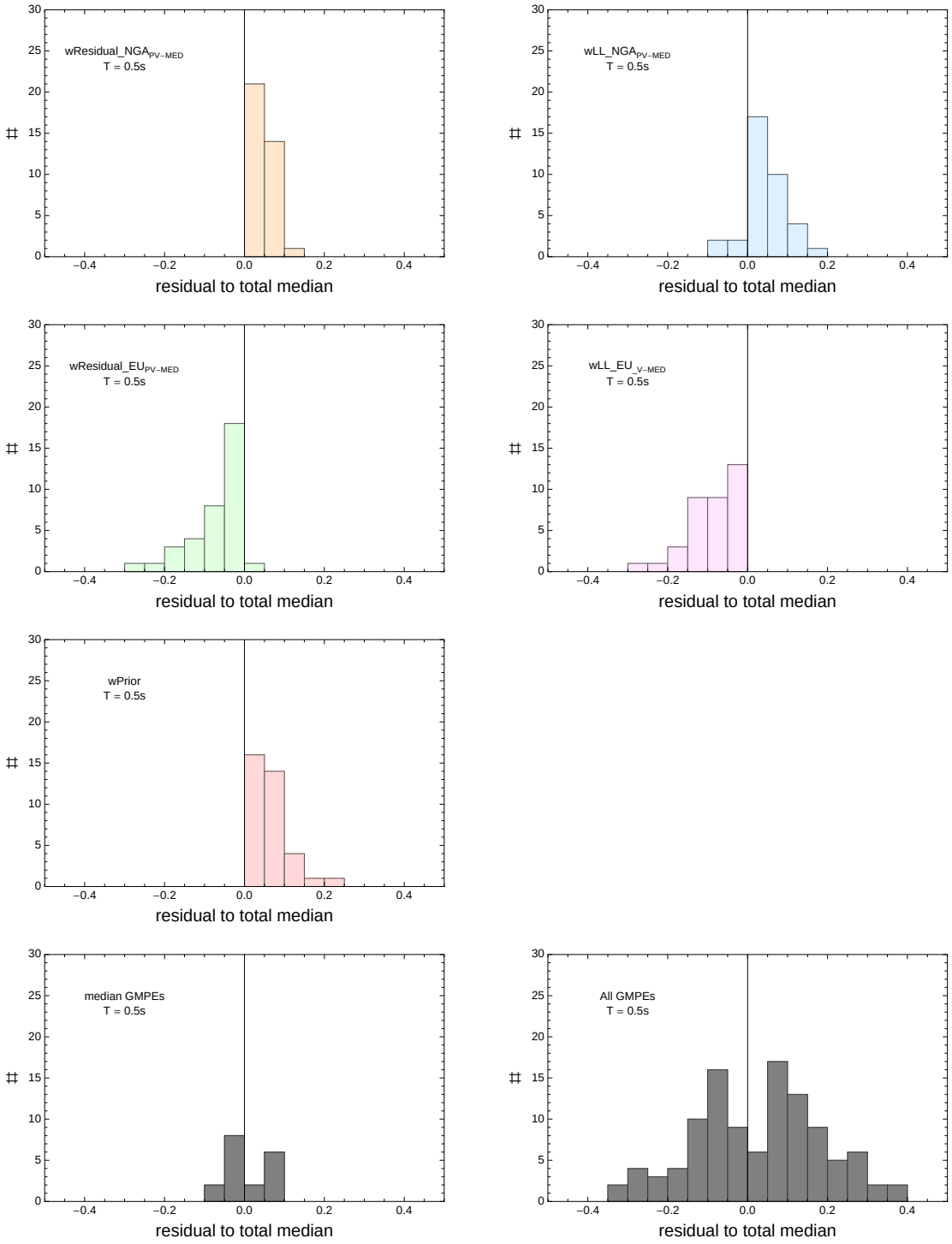



Figure 3.625: PVNGSv2: Histogram of differences for medians calculated with different weights to median calculated with total weights. Bottom row left shows differences between medians for the GMPE distribution to median calculated with total weights. Bottom row right shows differences between the original GMPEs (without uncertainty) to median calculated with total weights. For PVNGS2, ModelA and $T = 0.5$s.

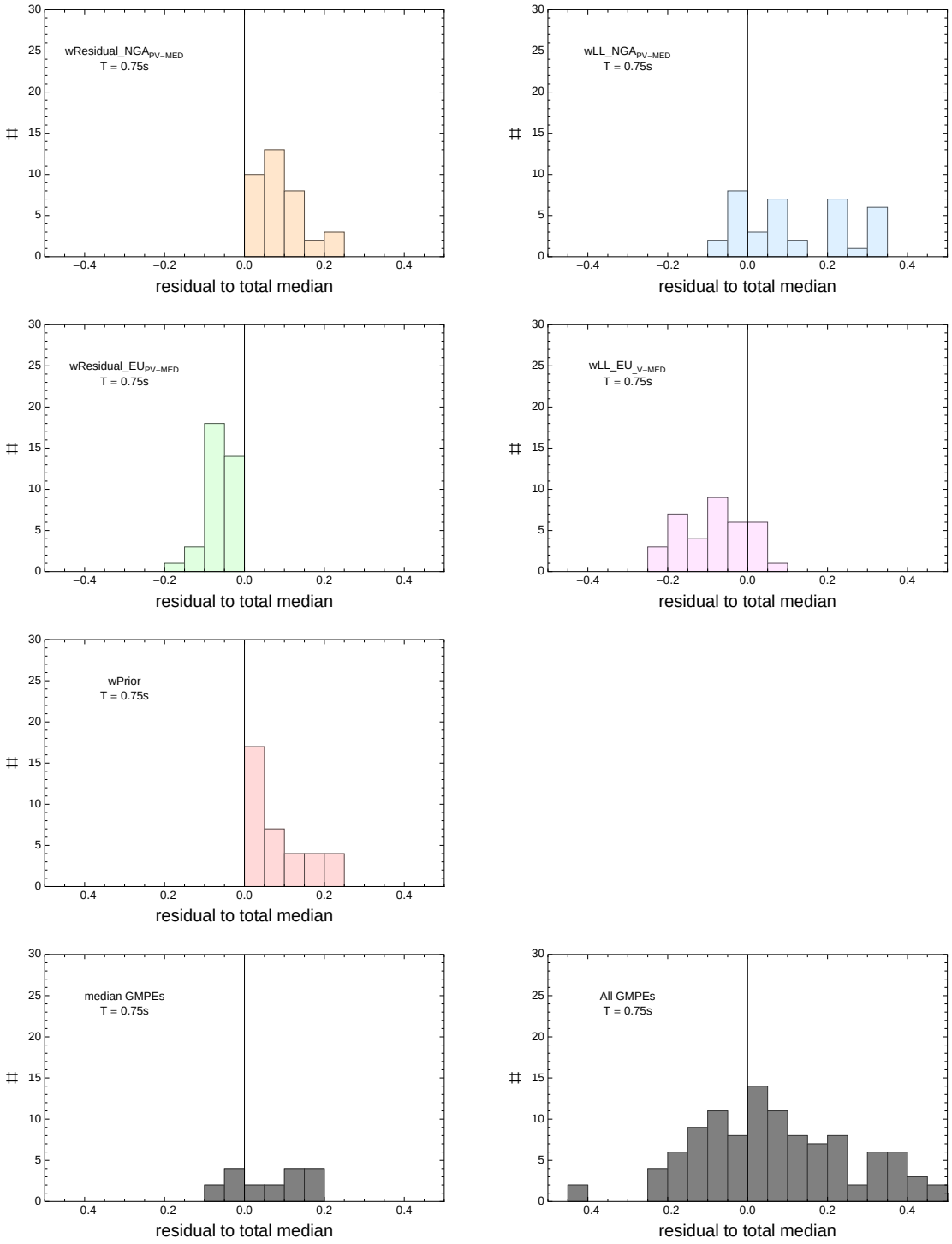



Figure 3.626: PVNGSv2: Histogram of differences for medians calculated with different weights to median calculated with total weights. Bottom row left shows differences between medians for the GMPE distribution to median calculated with total weights. Bottom row right shows differences between the original GMPEs (without uncertainty) to median calculated with total weights. For PVNGS2, ModelA and $T = 0.75$s.

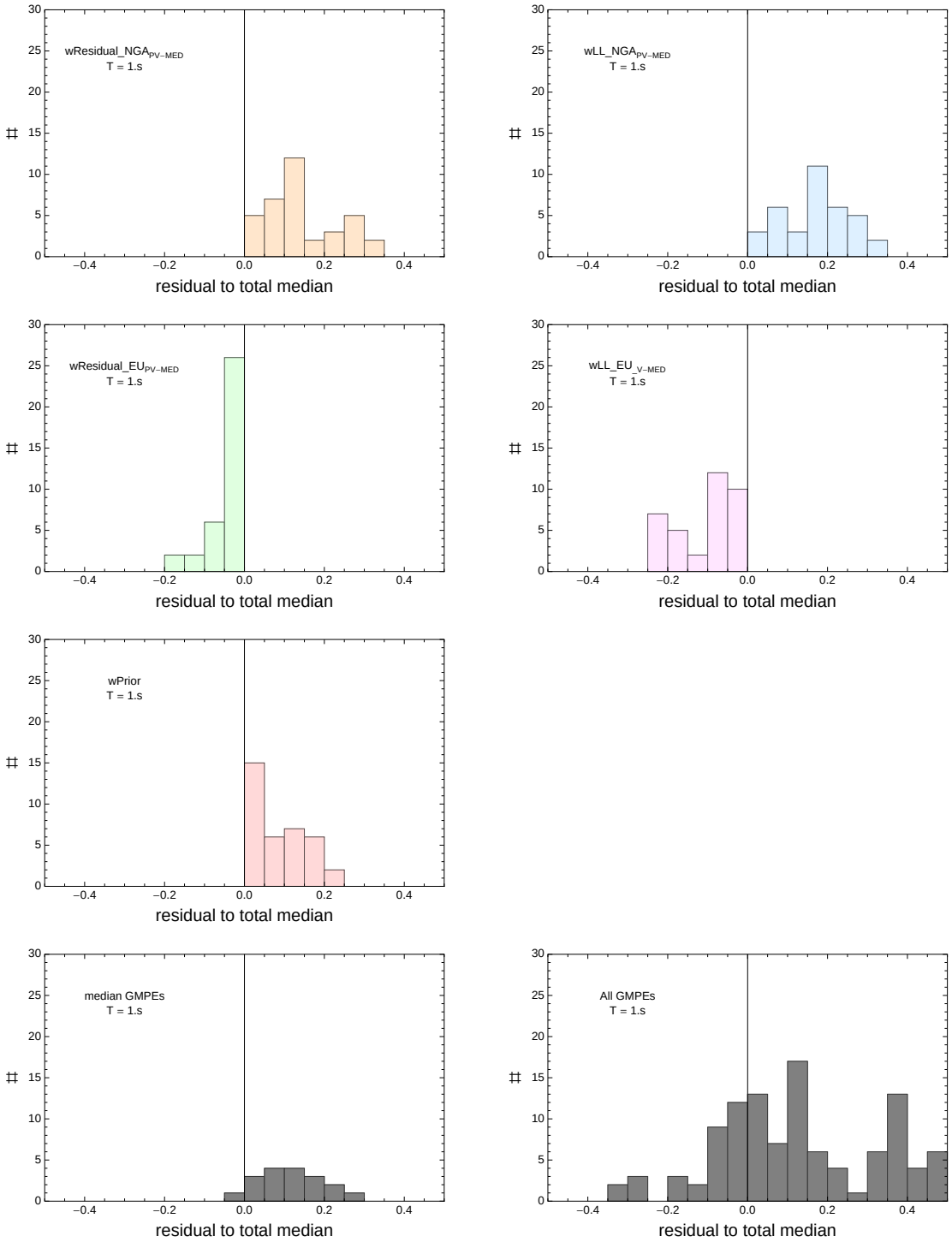



Figure 3.627: PVNGSv2: Histogram of differences for medians calculated with different weights to median calculated with total weights. Bottom row left shows differences between medians for the GMPE distribution to median calculated with total weights. Bottom row right shows differences between the original GMPEs (without uncertainty) to median calculated with total weights. For PVNGS2, ModelA and $T = 1.$s.

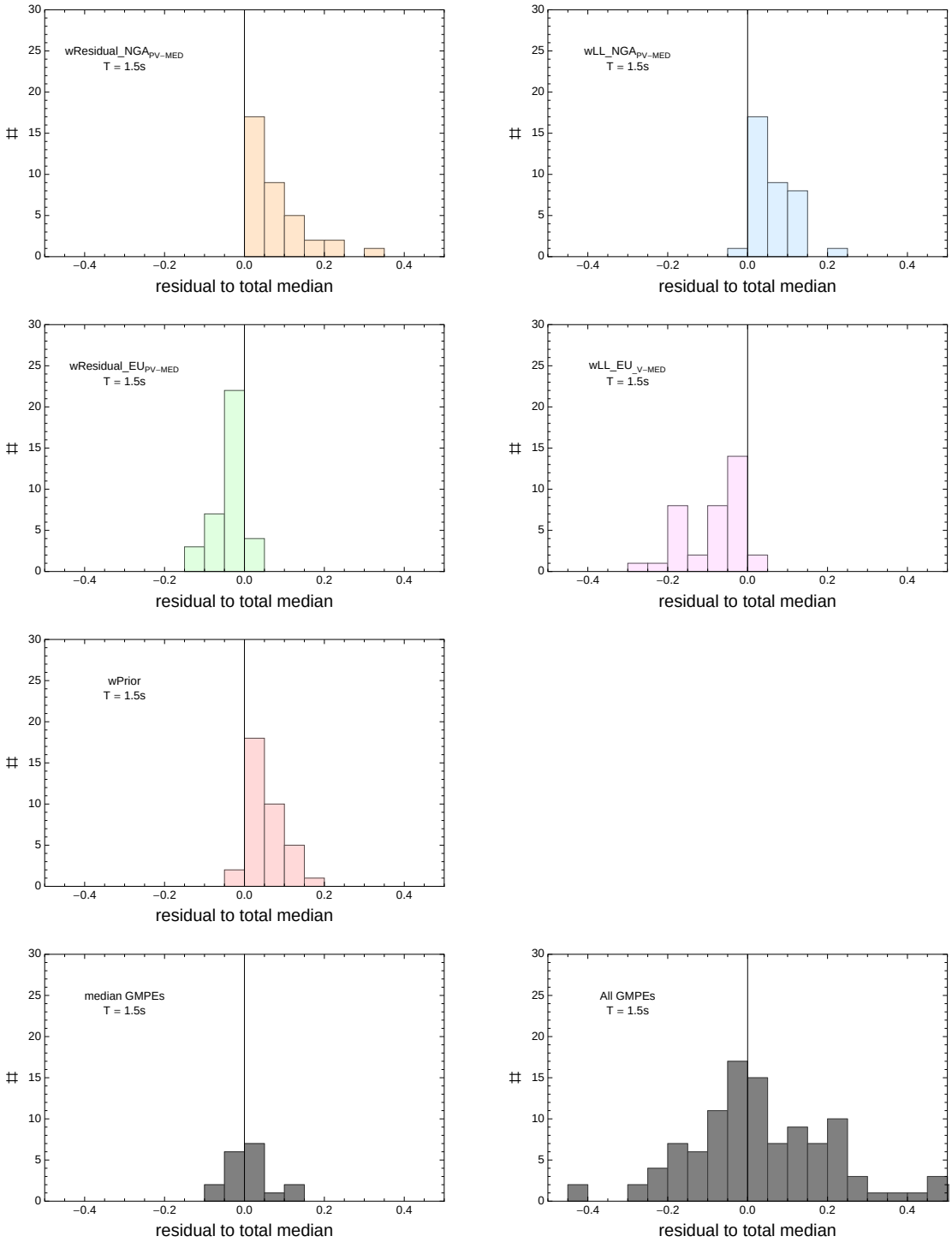



Figure 3.628: PVNGSv2: Histogram of differences for medians calculated with different weights to median calculated with total weights. Bottom row left shows differences between medians for the GMPE distribution to median calculated with total weights. Bottom row right shows differences between the original GMPEs (without uncertainty) to median calculated with total weights. For PVNGS2, ModelA and $T = 1.5$s.

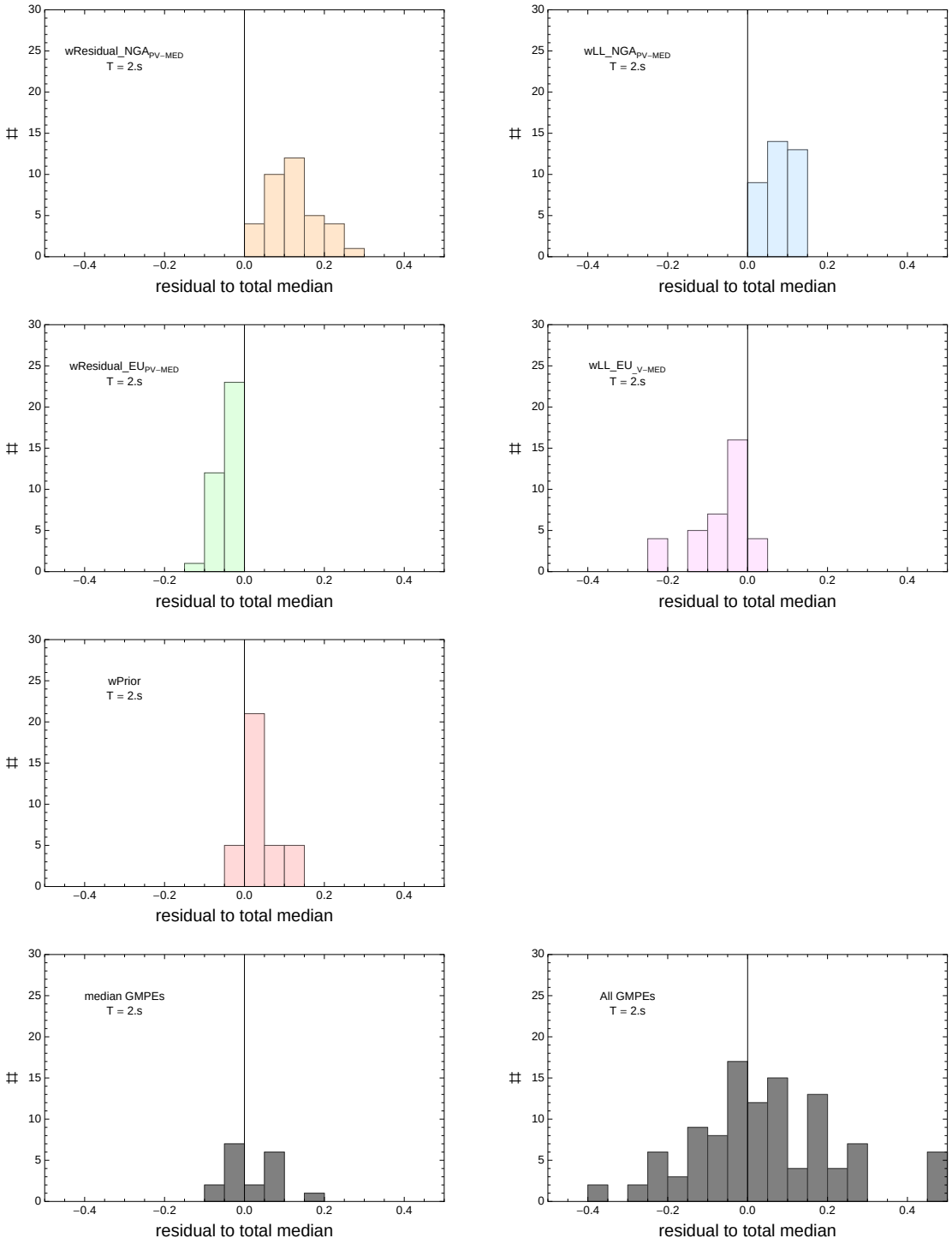



Figure 3.629: PVNGSv2: Histogram of differences for medians calculated with different weights to median calculated with total weights. Bottom row left shows differences between medians for the GMPE distribution to median calculated with total weights. Bottom row right shows differences between the original GMPEs (without uncertainty) to median calculated with total weights. For PVNGS2, ModelA and $T = 2.$s.

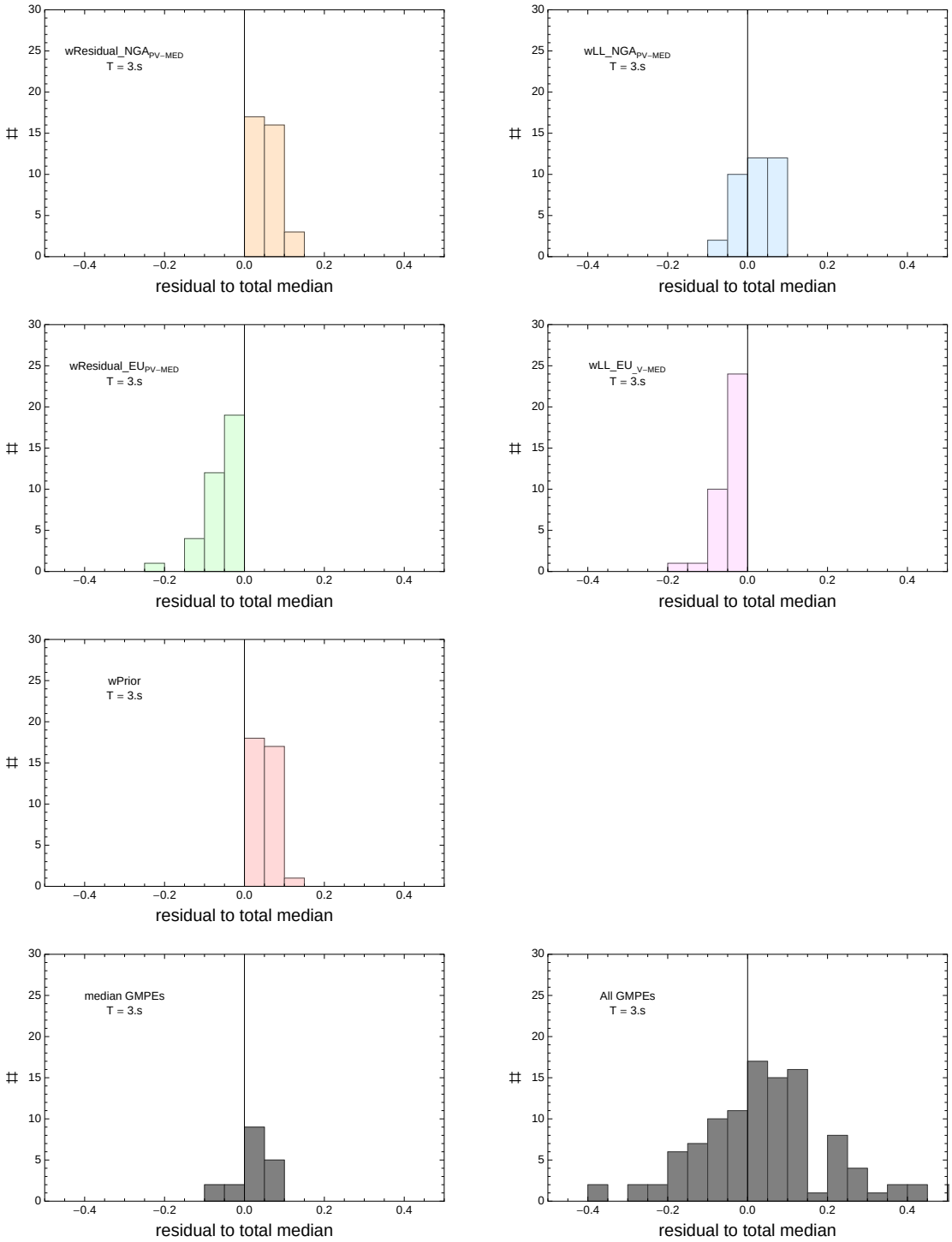



Figure 3.630: PVNGSv2: Histogram of differences for medians calculated with different weights to median calculated with total weights. Bottom row left shows differences between medians for the GMPE distribution to median calculated with total weights. Bottom row right shows differences between the original GMPEs (without uncertainty) to median calculated with total weights. For PVNGS2, ModelA and $T = 3$.s.

# Chapter 4

# PVNGS – Model B

### 4.1.1 Deaggregation

**GM-Level 2**

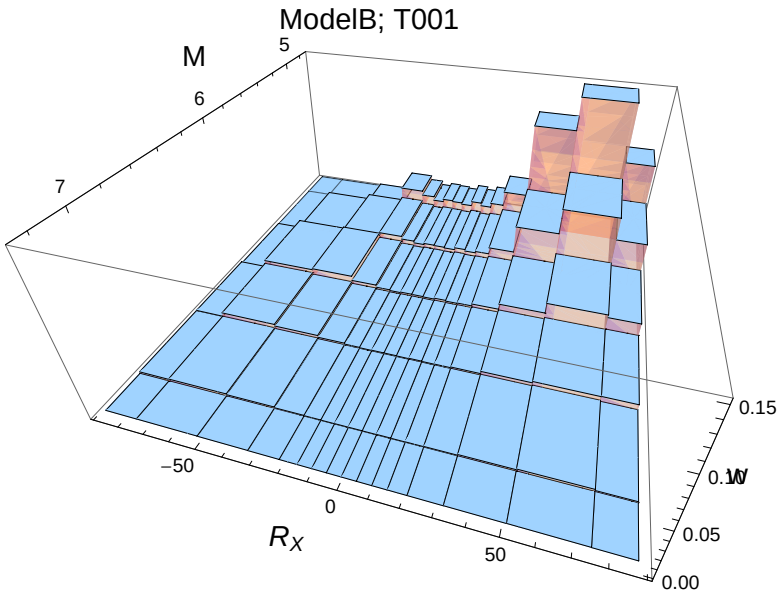



Figure 4.1: PVNGSv2: Deaggregation for a ground-motion level of 0.001g, calculated using a simple source model for PVNGS2 and the center model of the ModelB distribution. For $T = 0.01$s.

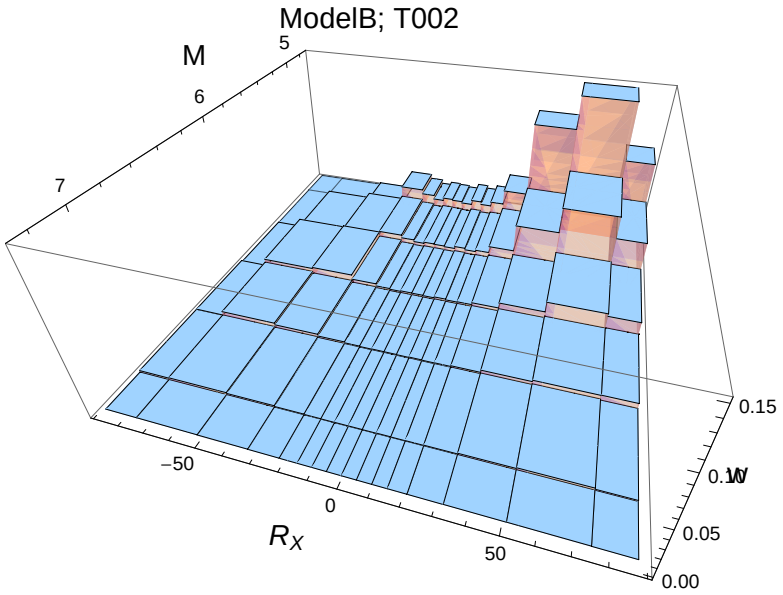



Figure 4.2: PVNGSv2: Deaggregation for a ground-motion level of 0.001g, calculated using a simple source model for PVNGS2 and the center model of the ModelB distribution. For $T = 0.02$s.

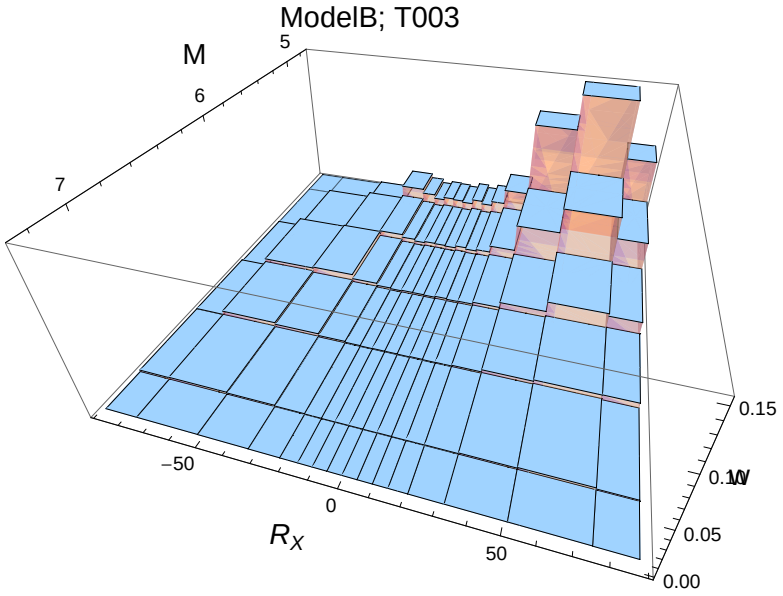



Figure 4.3: PVNGSv2: Deaggregation for a ground-motion level of 0.001g, calculated using a simple source model for PVNGS2 and the center model of the ModelB distribution. For $T = 0.03$s.

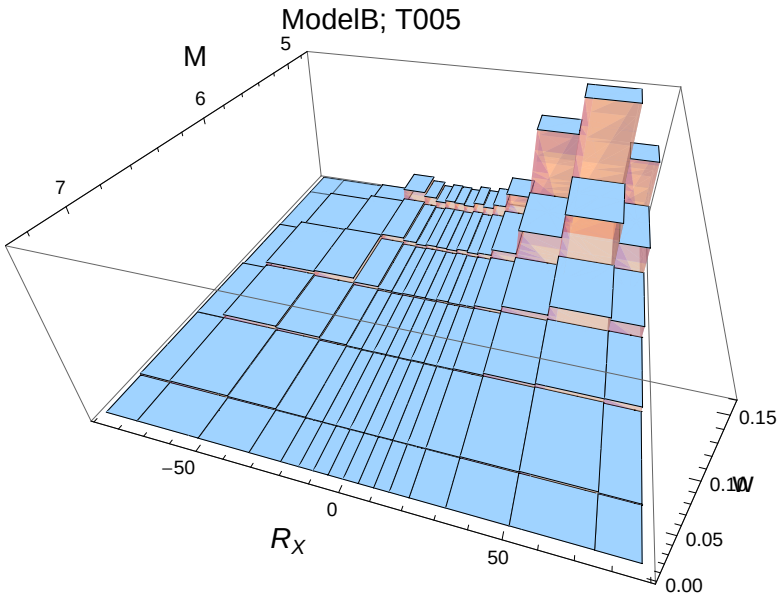



Figure 4.4: PVNGSv2: Deaggregation for a ground-motion level of 0.001g, calculated using a simple source model for PVNGS2 and the center model of the ModelB distribution. For $T = 0.05$s.

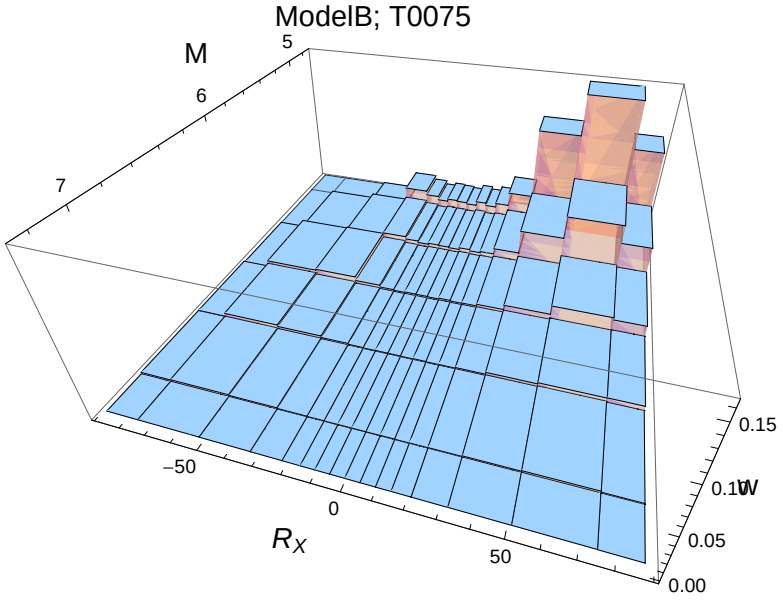



Figure 4.5: PVNGSv2: Deaggregation for a ground-motion level of 0.001g, calculated using a simple source model for PVNGS2 and the center model of the ModelB distribution. For $T = 0.075$s.

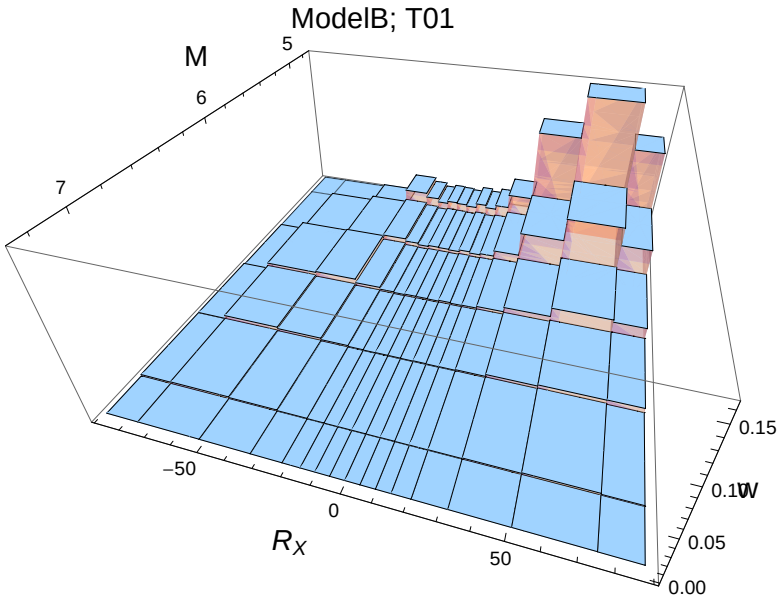



Figure 4.6: PVNGSv2: Deaggregation for a ground-motion level of 0.001g, calculated using a simple source model for PVNGS2 and the center model of the ModelB distribution. For $T = 0.1$s.

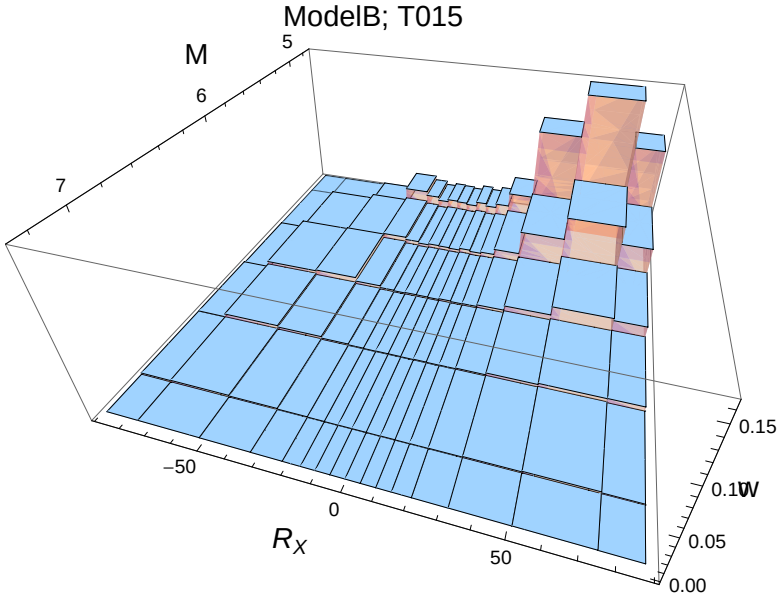



Figure 4.7: PVNGSv2: Deaggregation for a ground-motion level of 0.001g, calculated using a simple source model for PVNGS2 and the center model of the ModelB distribution. For $T = 0.15$s.

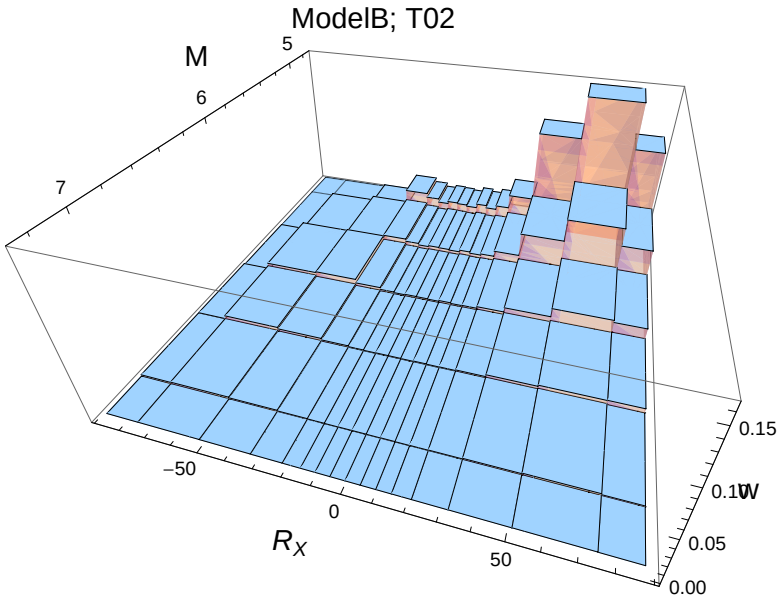



Figure 4.8: PVNGSv2: Deaggregation for a ground-motion level of 0.001g, calculated using a simple source model for PVNGS2 and the center model of the ModelB distribution. For $T = 0.2$s.

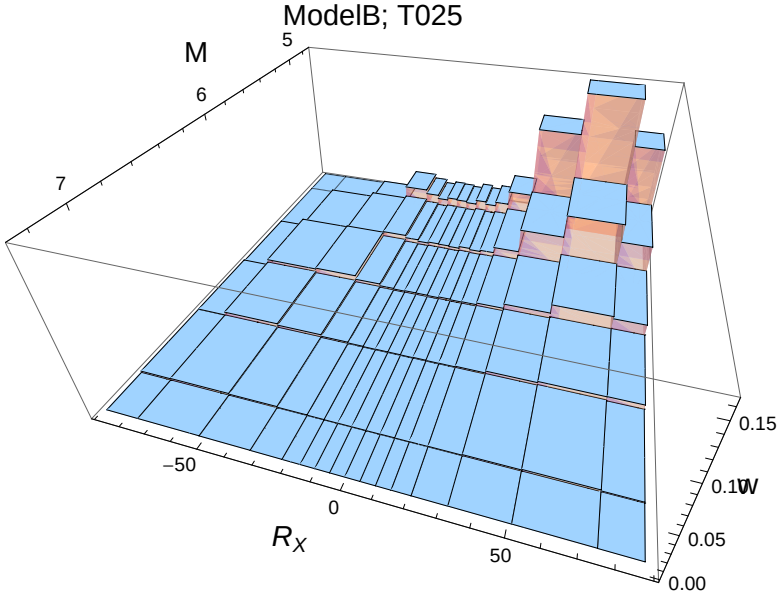



Figure 4.9: PVNGSv2: Deaggregation for a ground-motion level of 0.001g, calculated using a simple source model for PVNGS2 and the center model of the ModelB distribution. For $T = 0.25$s.

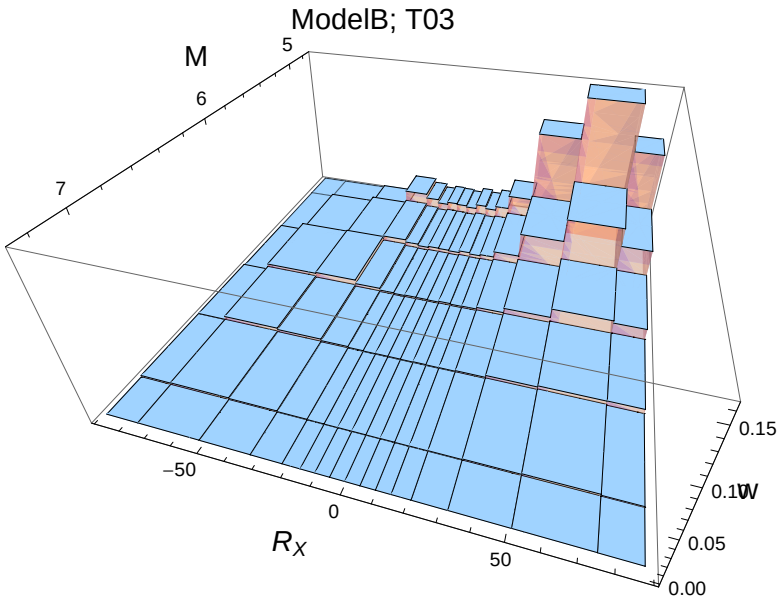



Figure 4.10: PVNGSv2: Deaggregation for a ground-motion level of 0.001g, calculated using a simple source model for PVNGS2 and the center model of the ModelB distribution. For $T = 0.3$s.

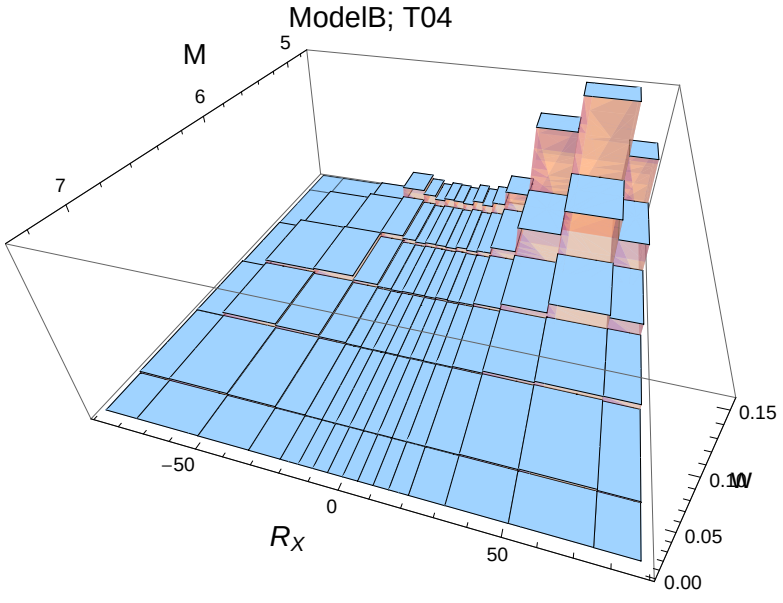



Figure 4.11: PVNGSv2: Deaggregation for a ground-motion level of 0.001g, calculated using a simple source model for PVNGS2 and the center model of the ModelB distribution. For $T = 0.4$s.

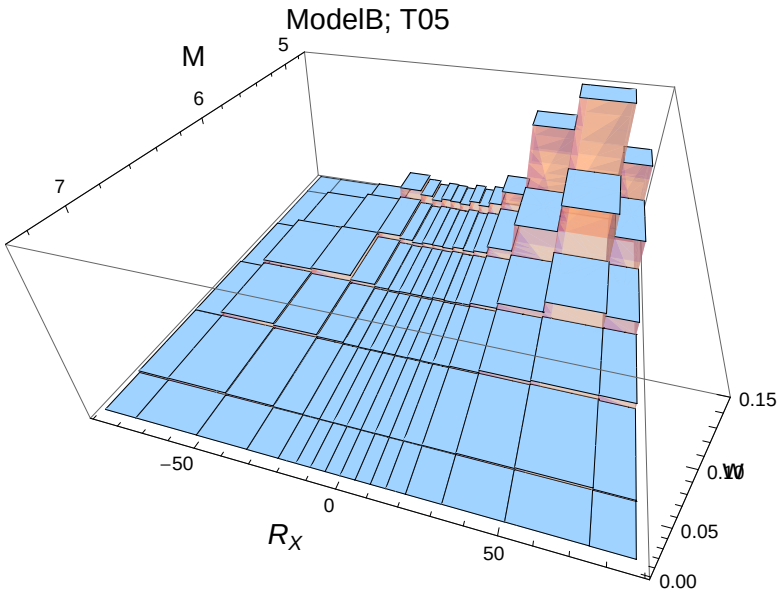



Figure 4.12: PVNGSv2: Deaggregation for a ground-motion level of 0.001g, calculated using a simple source model for PVNGS2 and the center model of the ModelB distribution. For $T = 0.5$s.

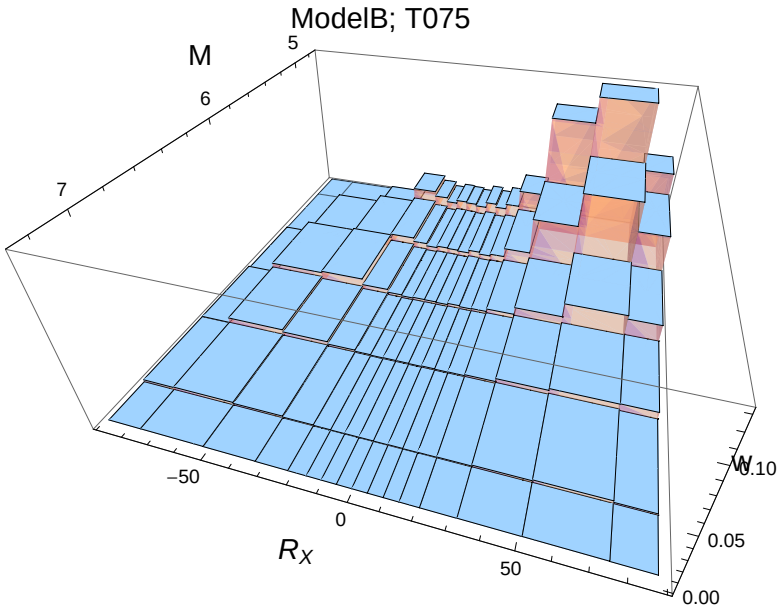



Figure 4.13: PVNGSv2: Deaggregation for a ground-motion level of 0.001g, calculated using a simple source model for PVNGS2 and the center model of the ModelB distribution. For $T = 0.75$s.

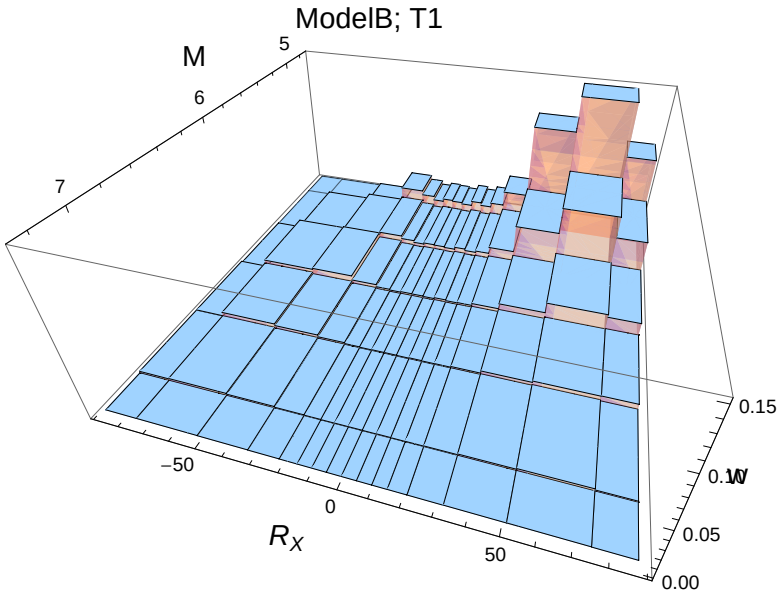



Figure 4.14: PVNGSv2: Deaggregation for a ground-motion level of 0.g, calculated using a simple source model for PVNGS2 and the center model of the ModelB distribution. For $T = 1$.s.

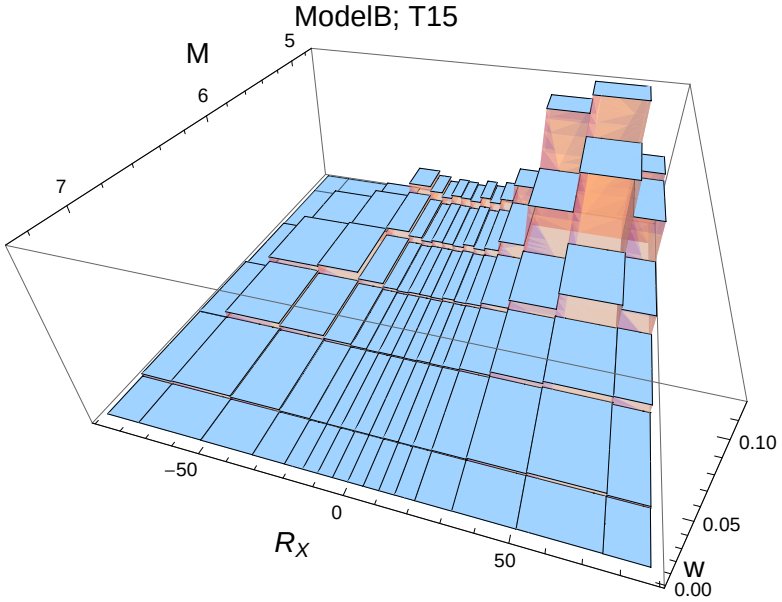



Figure 4.15: PVNGSv2: Deaggregation for a ground-motion level of 0.g, calculated using a simple source model for PVNGS2 and the center model of the ModelB distribution. For $T = 1.5$s.

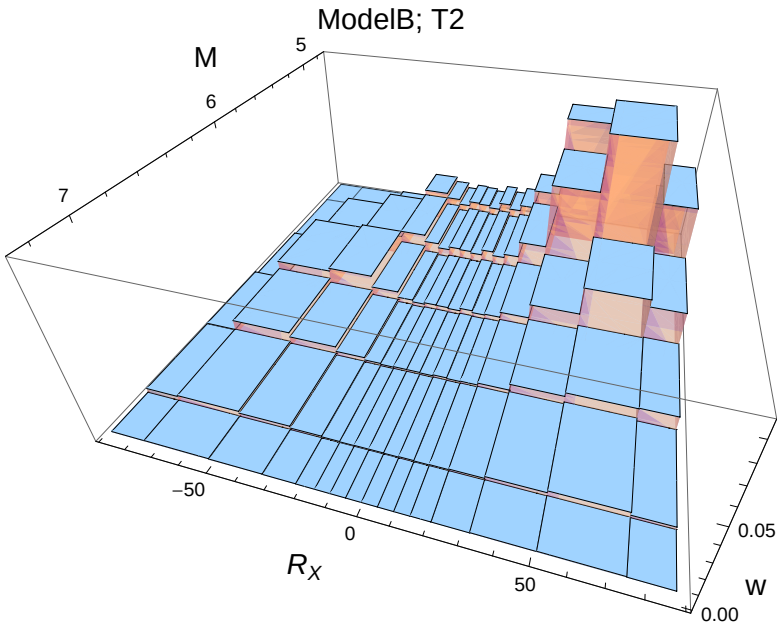



Figure 4.16: PVNGSv2: Deaggregation for a ground-motion level of 0.g, calculated using a simple source model for PVNGS2 and the center model of the ModelB distribution. For $T = 2$.s.

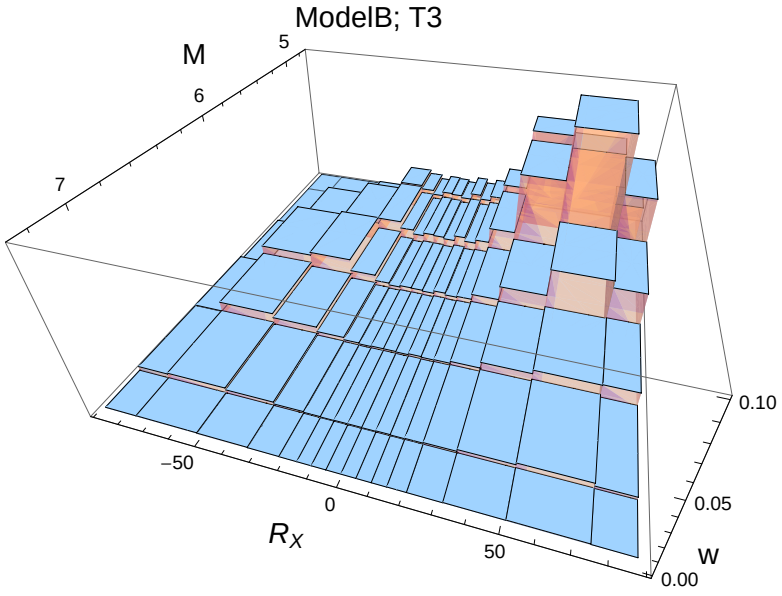



Figure 4.17: PVNGSv2: Deaggregation for a ground-motion level of 0.g, calculated using a simple source model for PVNGS2 and the center model of the ModelB distribution. For $T = 3$.s.

**GM-Level 8**

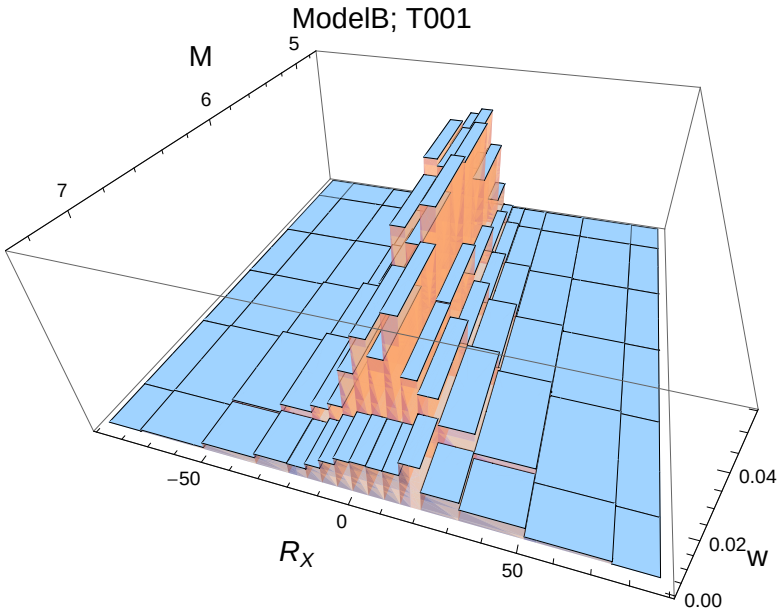



Figure 4.18: PVNGSv2: Deaggregation for a ground-motion level of 0.278g, calculated using a simple source model for PVNGS2 and the center model of the ModelB distribution. For $T = 0.01$s.

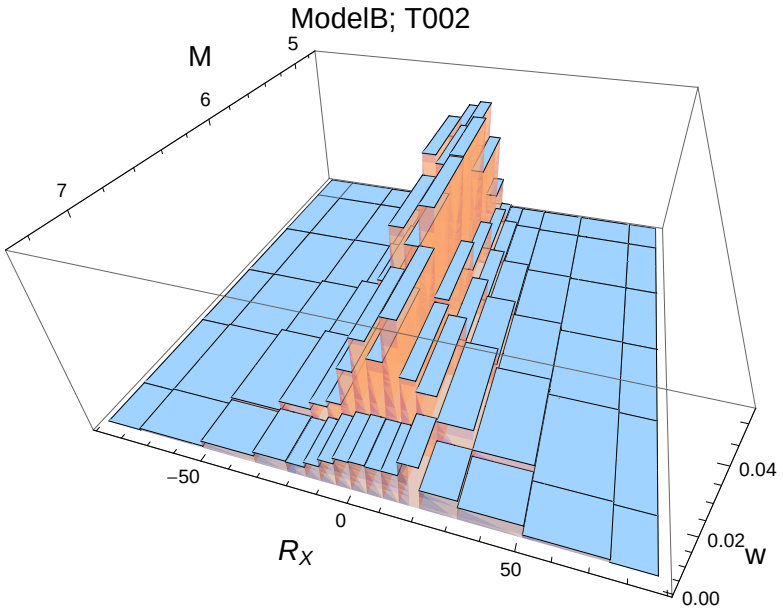



Figure 4.19: PVNGSv2: Deaggregation for a ground-motion level of 0.266g, calculated using a simple source model for PVNGS2 and the center model of the ModelB distribution. For $T = 0.02$s.

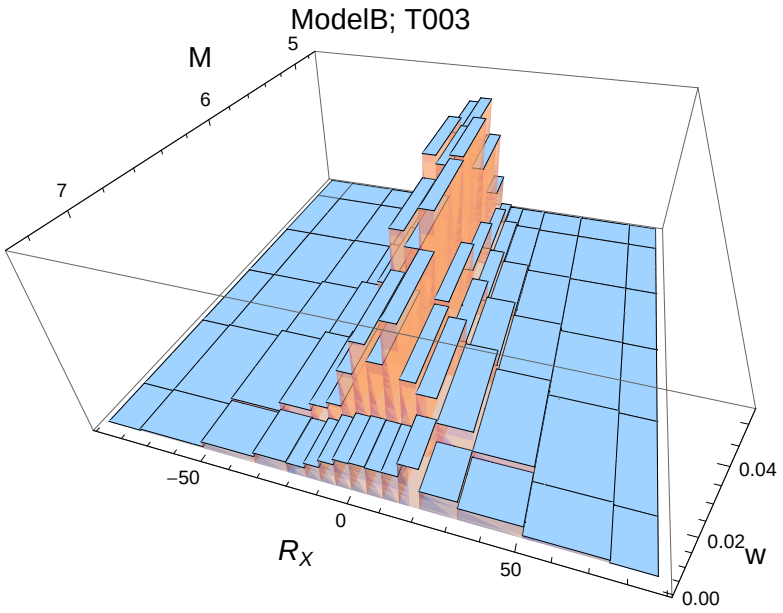



Figure 4.20: PVNGSv2: Deaggregation for a ground-motion level of 0.29g, calculated using a simple source model for PVNGS2 and the center model of the ModelB distribution. For $T = 0.03$s.

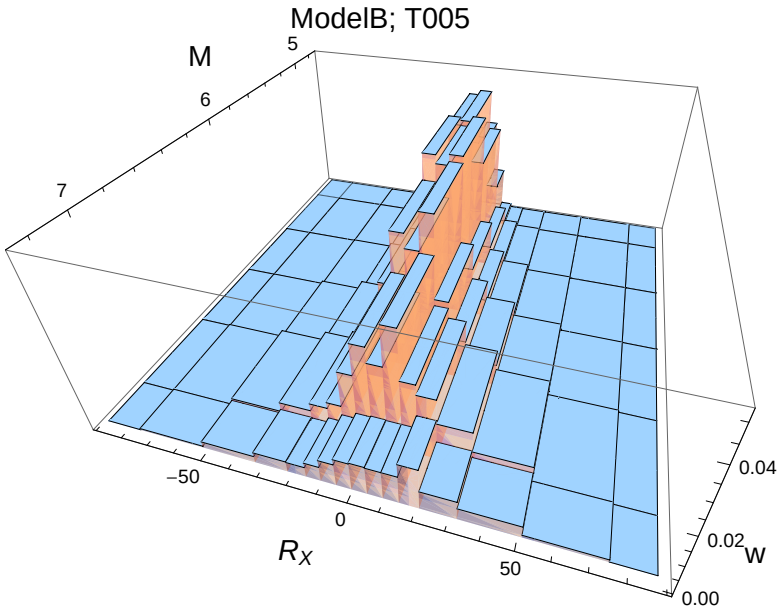



Figure 4.21: PVNGSv2: Deaggregation for a ground-motion level of 0.358g, calculated using a simple source model for PVNGS2 and the center model of the ModelB distribution. For $T = 0.05$s.

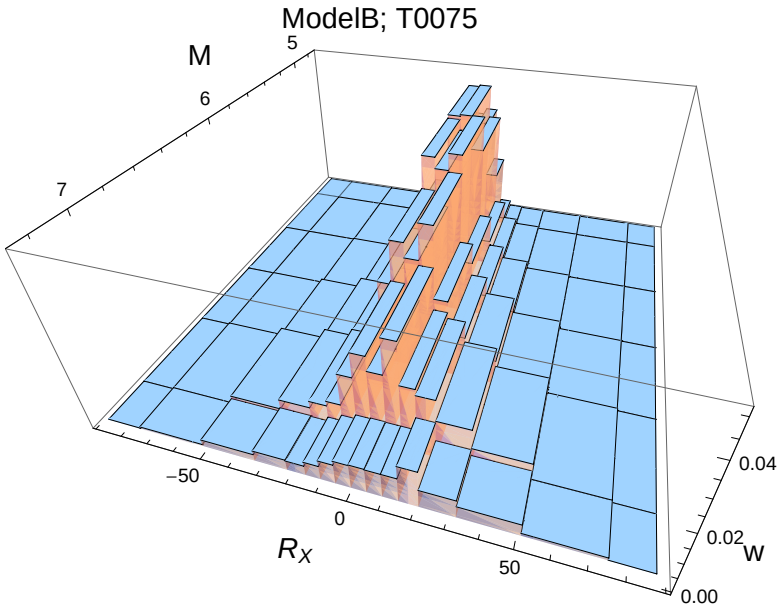



Figure 4.22: PVNGSv2: Deaggregation for a ground-motion level of 0.407g, calculated using a simple source model for PVNGS2 and the center model of the ModelB distribution. For $T = 0.075$s.

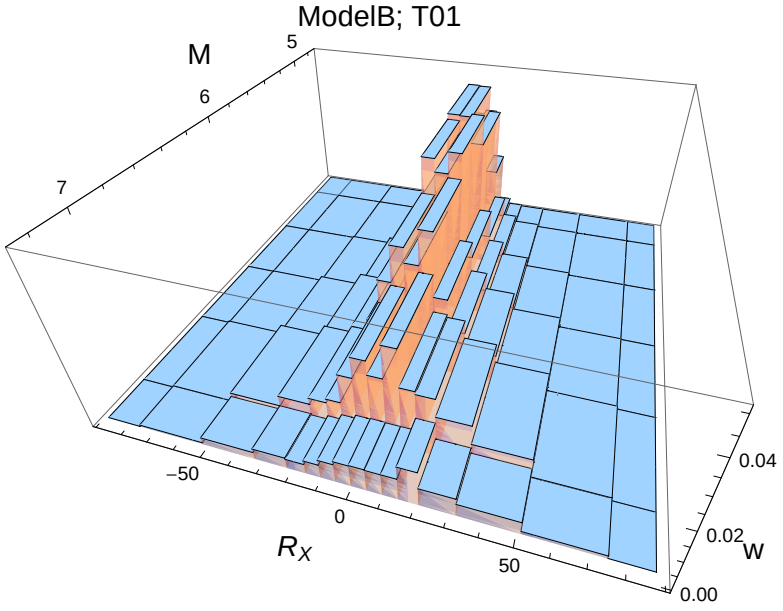



Figure 4.23: PVNGSv2: Deaggregation for a ground-motion level of 0.427g, calculated using a simple source model for PVNGS2 and the center model of the ModelB distribution. For $T = 0.1$s.

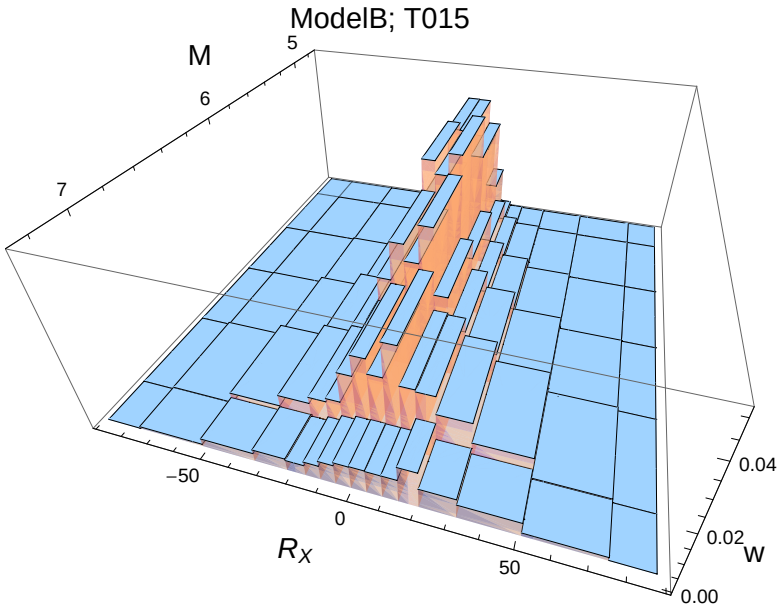



Figure 4.24: PVNGSv2: Deaggregation for a ground-motion level of 0.475g, calculated using a simple source model for PVNGS2 and the center model of the ModelB distribution. For $T = 0.15$s.

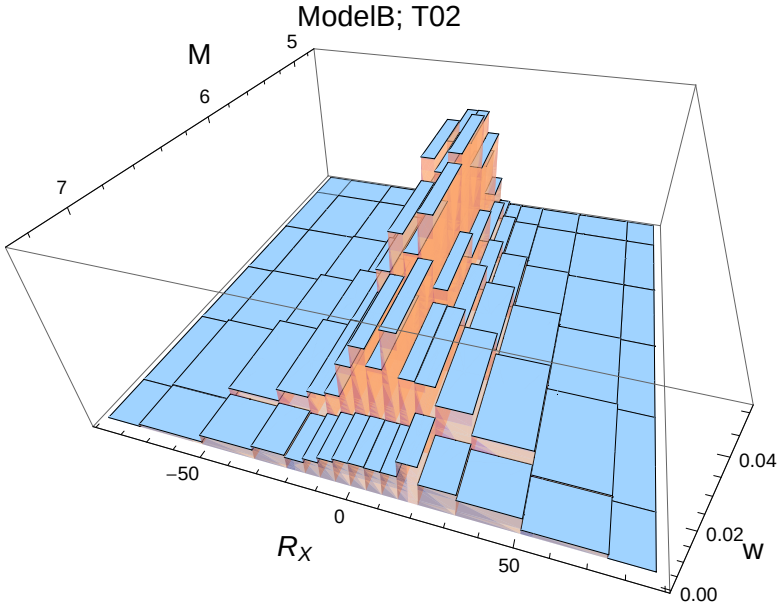



Figure 4.25: PVNGSv2: Deaggregation for a ground-motion level of 0.456g, calculated using a simple source model for PVNGS2 and the center model of the ModelB distribution. For $T = 0.2$s.

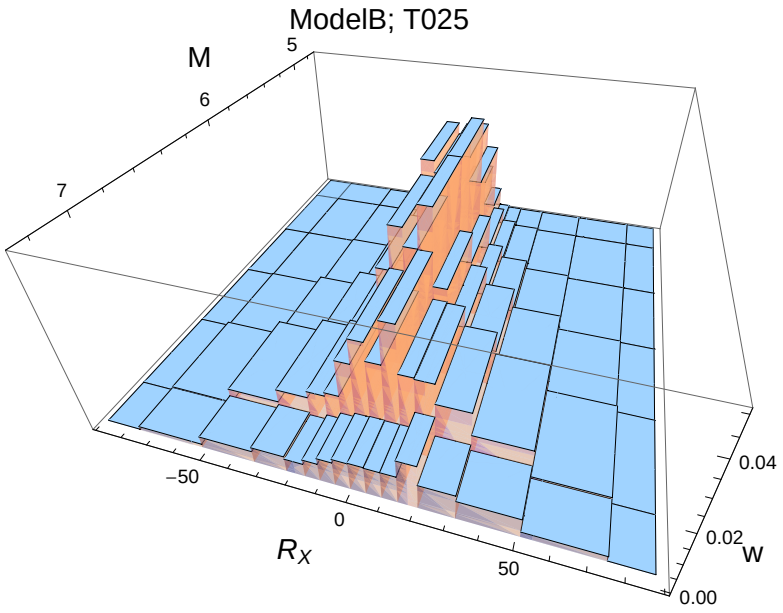



Figure 4.26: PVNGSv2: Deaggregation for a ground-motion level of 0.427g, calculated using a simple source model for PVNGS2 and the center model of the ModelB distribution. For $T = 0.25$s.

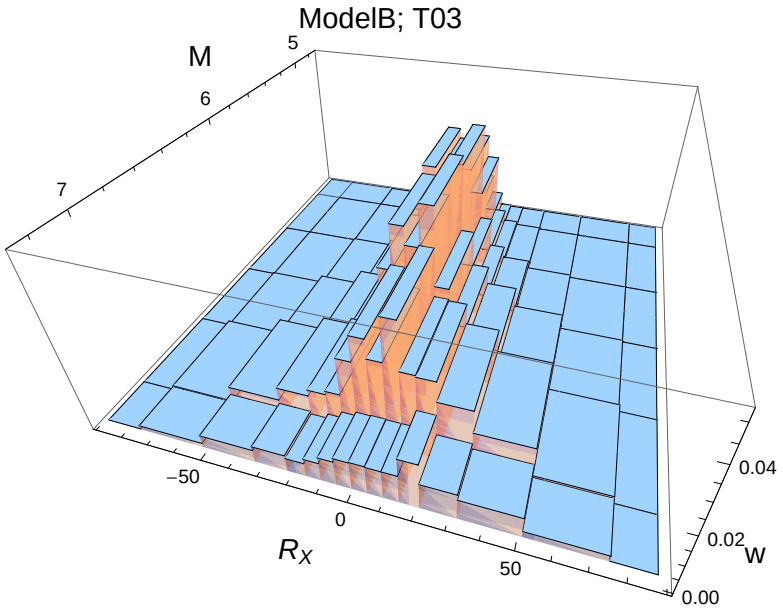



Figure 4.27: PVNGSv2: Deaggregation for a ground-motion level of 0.387g, calculated using a simple source model for PVNGS2 and the center model of the ModelB distribution. For $T = 0.3$s.

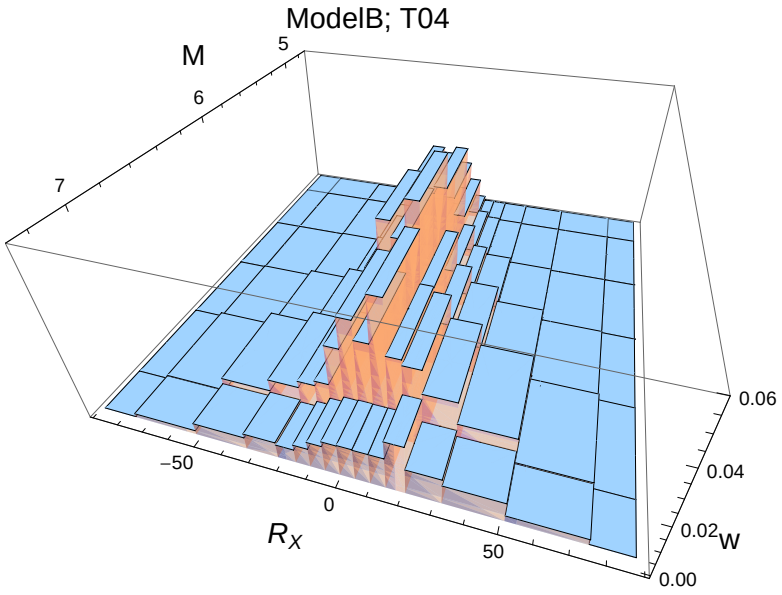



Figure 4.28: PVNGSv2: Deaggregation for a ground-motion level of 0.358g, calculated using a simple source model for PVNGS2 and the center model of the ModelB distribution. For $T = 0.4$s.

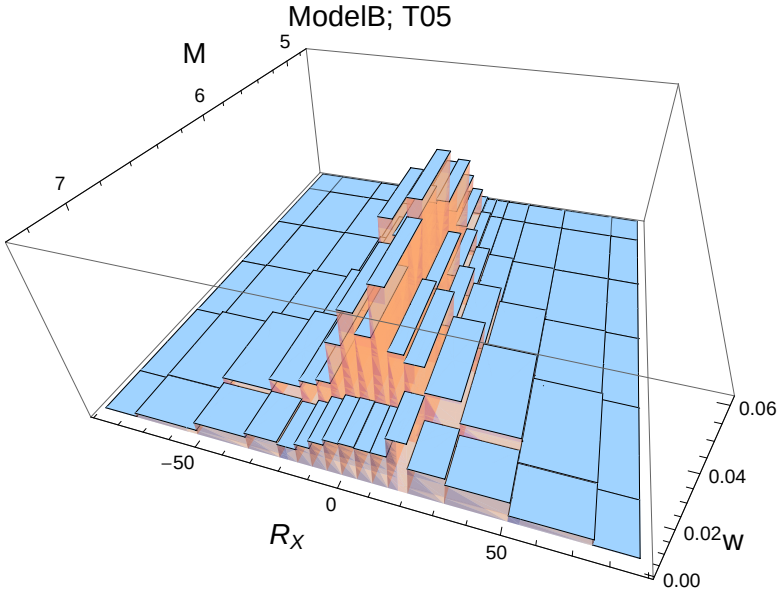



Figure 4.29: PVNGSv2: Deaggregation for a ground-motion level of 0.313g, calculated using a simple source model for PVNGS2 and the center model of the ModelB distribution. For $T = 0.5$s.

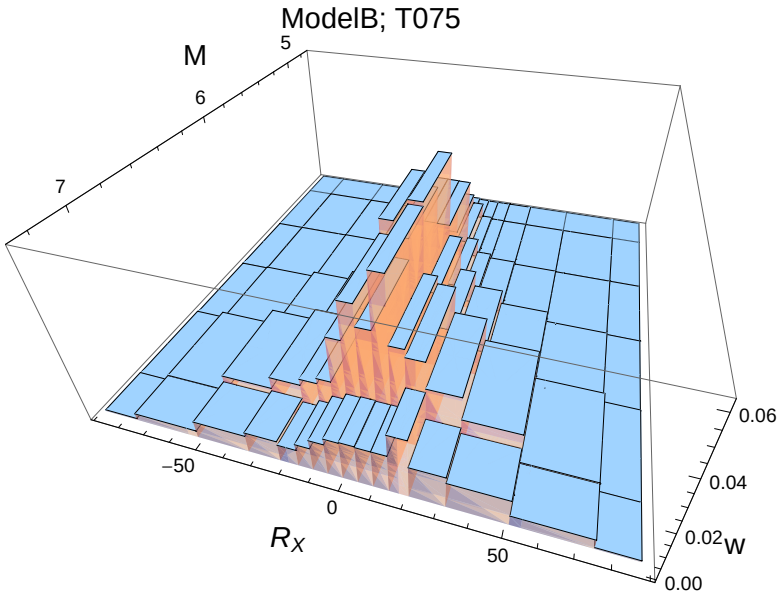



Figure 4.30: PVNGSv2: Deaggregation for a ground-motion level of 0.214g, calculated using a simple source model for PVNGS2 and the center model of the ModelB distribution. For $T = 0.75$s.

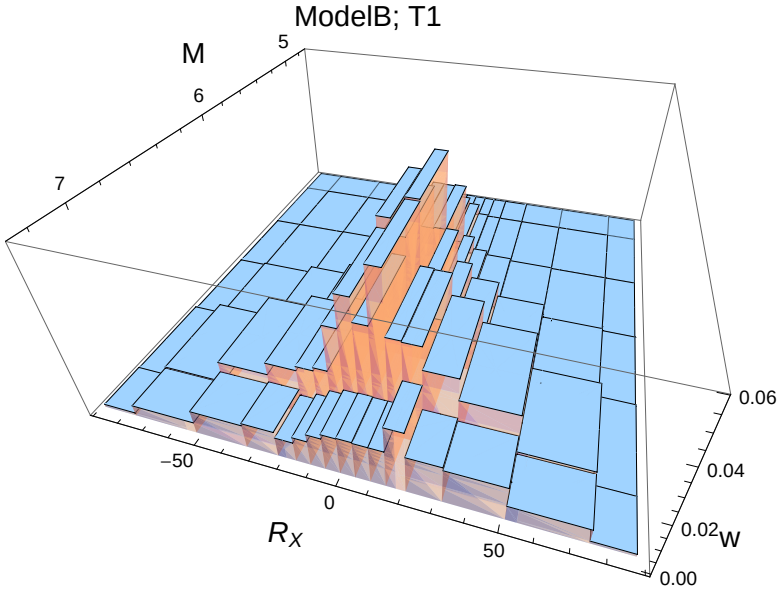



Figure 4.31: PVNGSv2: Deaggregation for a ground-motion level of 0.139g, calculated using a simple source model for PVNGS2 and the center model of the ModelB distribution. For $T = 1$.s.

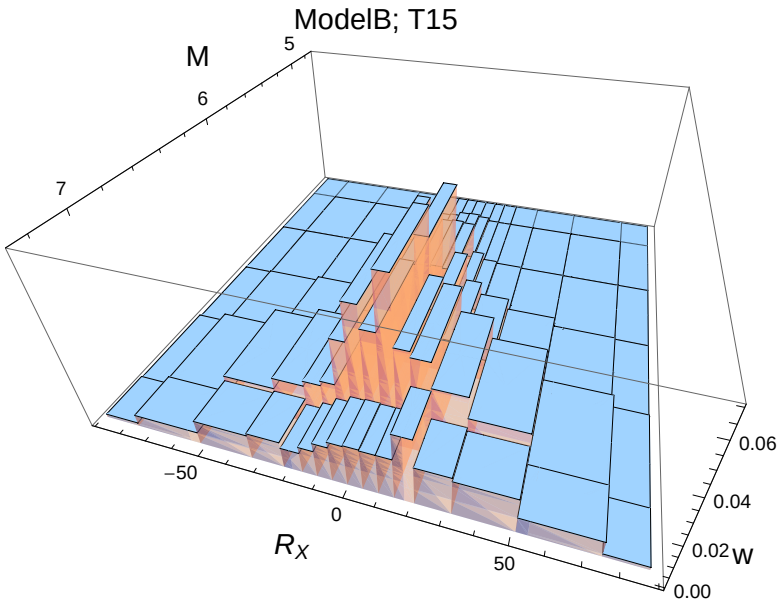



Figure 4.32: PVNGSv2: Deaggregation for a ground-motion level of 0.098g, calculated using a simple source model for PVNGS2 and the center model of the ModelB distribution. For $T = 1.5$s.

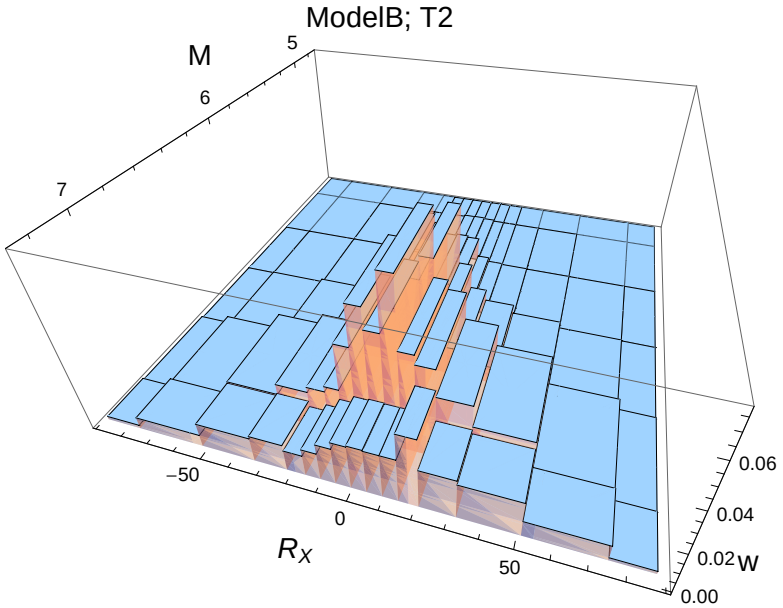



Figure 4.33: PVNGSv2: Deaggregation for a ground-motion level of 0.075g, calculated using a simple source model for PVNGS2 and the center model of the ModelB distribution. For $T = 2$.s.

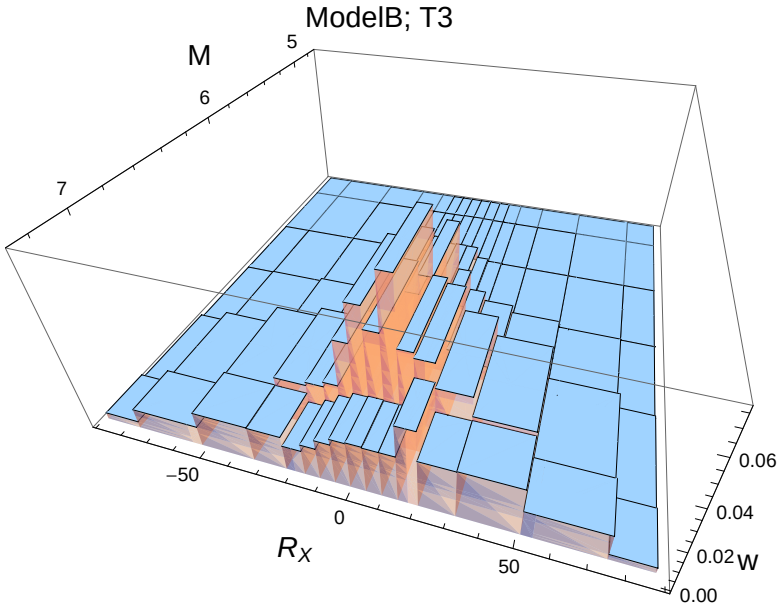



Figure 4.34: PVNGSv2: Deaggregation for a ground-motion level of 0.043g, calculated using a simple source model for PVNGS2 and the center model of the ModelB distribution. For $T = 3$.s.

### 4.1.2 Maps – Selection

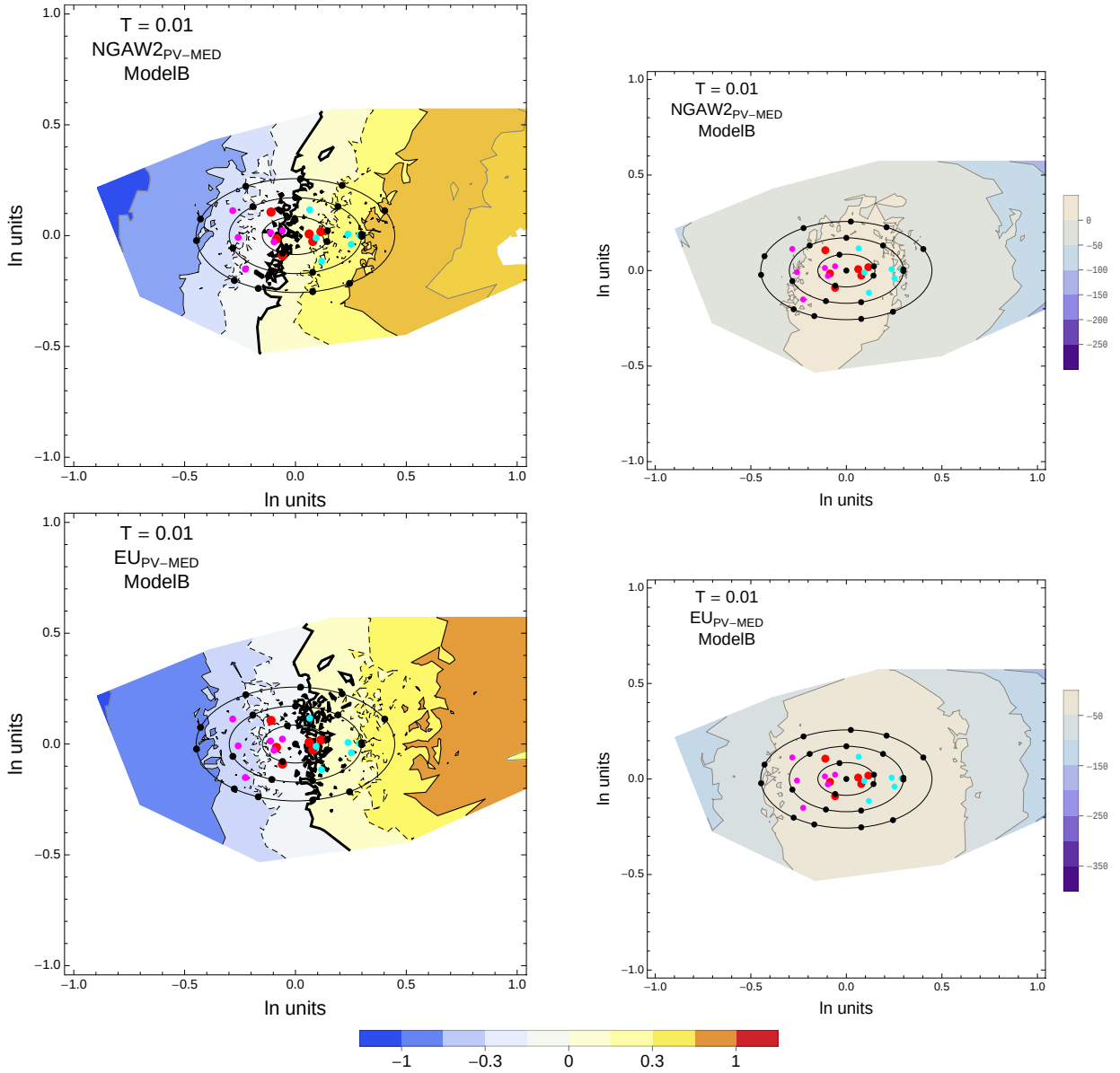



Figure 4.35: PVNGSv2: Contour Plots of mean residuals (top left) and likelihood (top right) for the NGA$_{PV-MED}$ dataset, and mean residuals (bottom left) and likelihood (top right) for the EU$_{PV-MED}$ dataset. Reference points are black dots. The original GMPEs are red dots,plus/minus uncertainty are magenta/cyan dots. The contour for the zero residual is a thick black line, the -0.15/0.15 contours are dashed black lines and the -0.3/0.3 contours are thin black lines. For $T = 0.01$s.

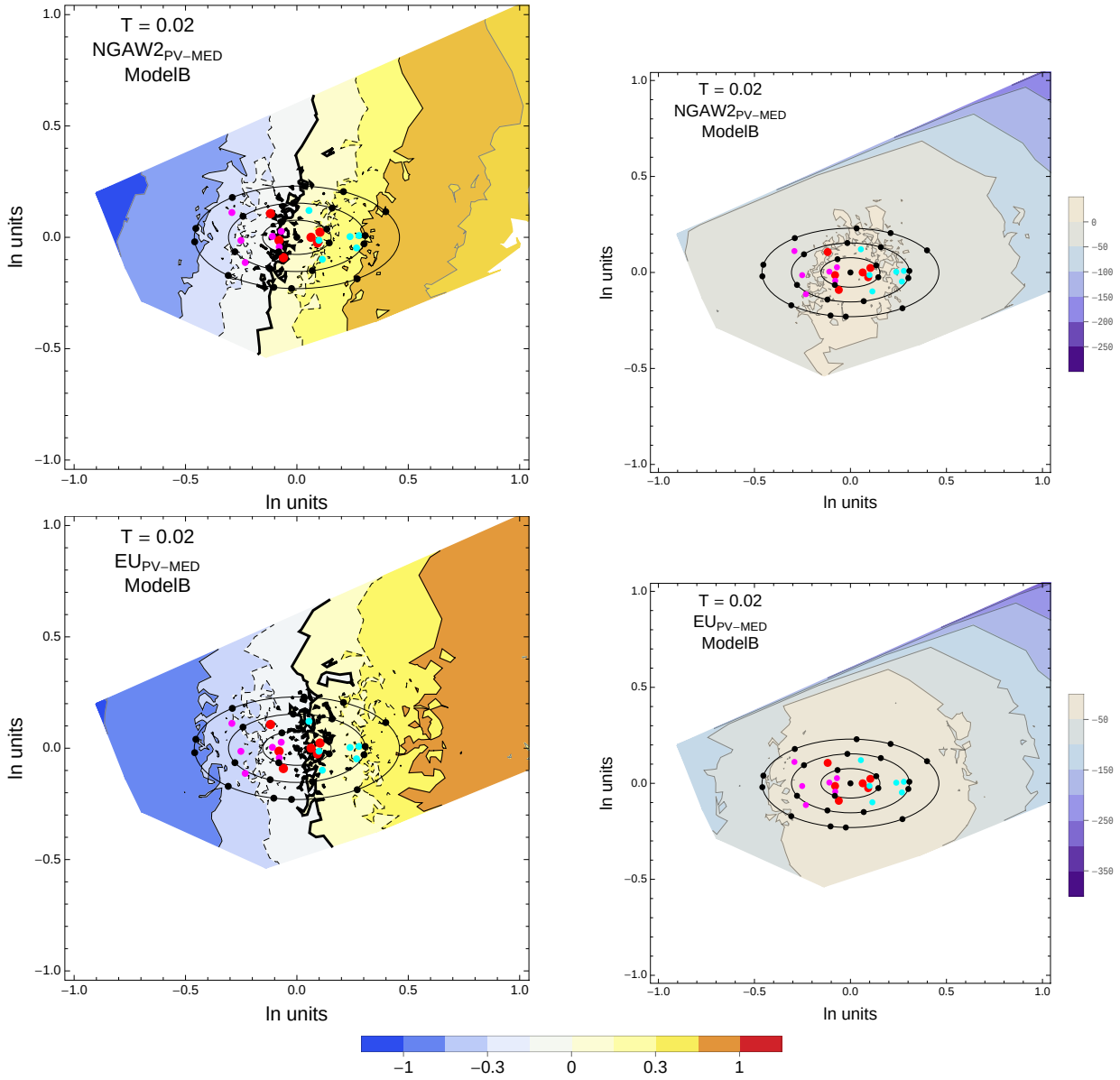



Figure 4.36: PVNGSv2: Contour Plots of mean residuals (top left) and likelihood (top right) for the NGA$_{PV-MED}$ dataset, and mean residuals (bottom left) and likelihood (top right) for the EU$_{PV-MED}$ dataset. Reference points are black dots. The original GMPEs are red dots,plus/minus uncertainty are magenta/cyan dots. The contour for the zero residual is a thick black line, the -0.15/0.15 contours are dashed black lines and the -0.3/0.3 contours are thin black lines. For $T = 0.02$s.

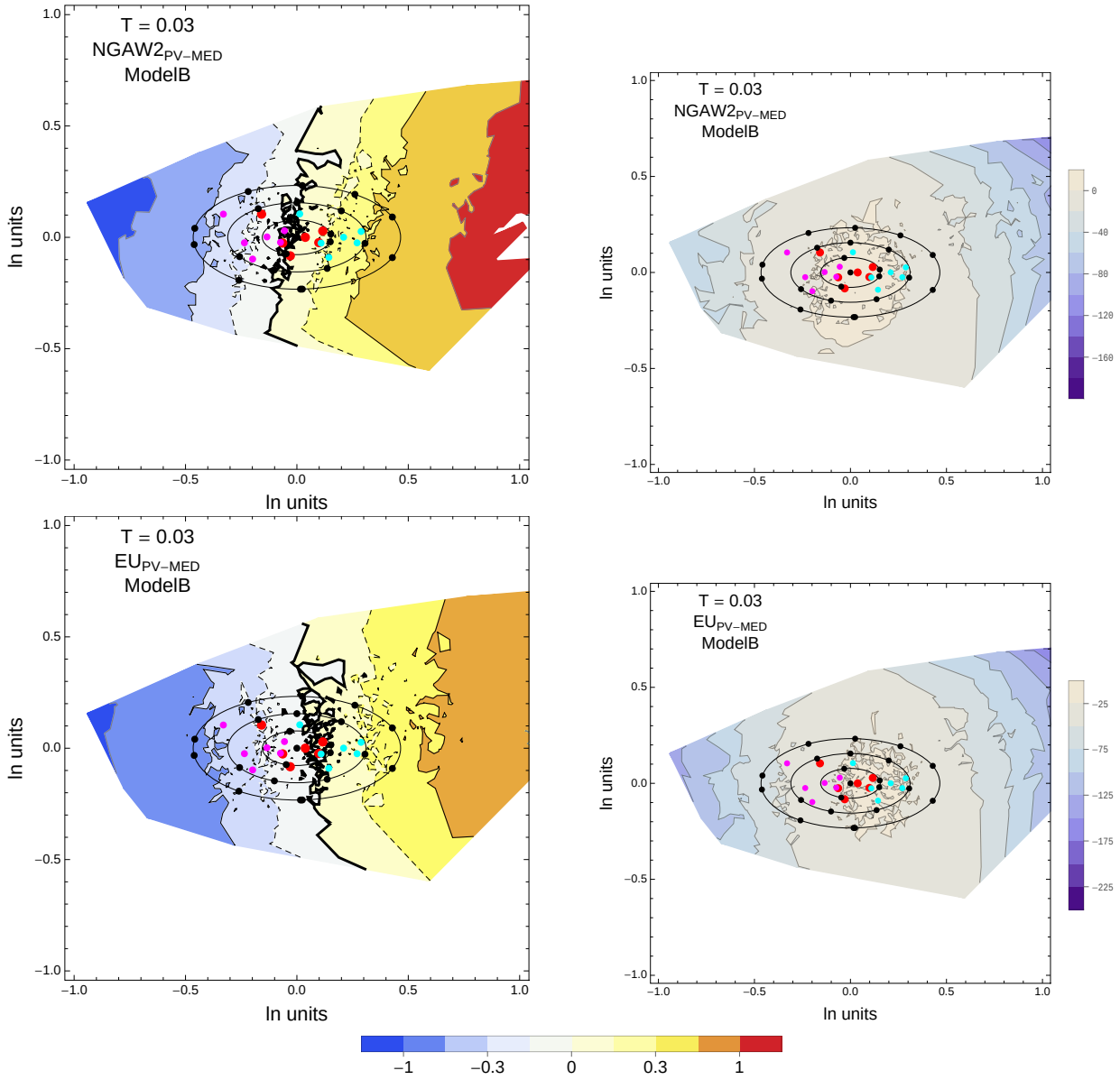



Figure 4.37: PVNGSv2: Contour Plots of mean residuals (top left) and likelihood (top right) for the NGA$_{PV-MED}$ dataset, and mean residuals (bottom left) and likelihood (top right) for the EU$_{PV-MED}$ dataset. Reference points are black dots. The original GMPEs are red dots,plus/minus uncertainty are magenta/cyan dots. The contour for the zero residual is a thick black line, the -0.15/0.15 contours are dashed black lines and the -0.3/0.3 contours are thin black lines. For $T = 0.03$s.

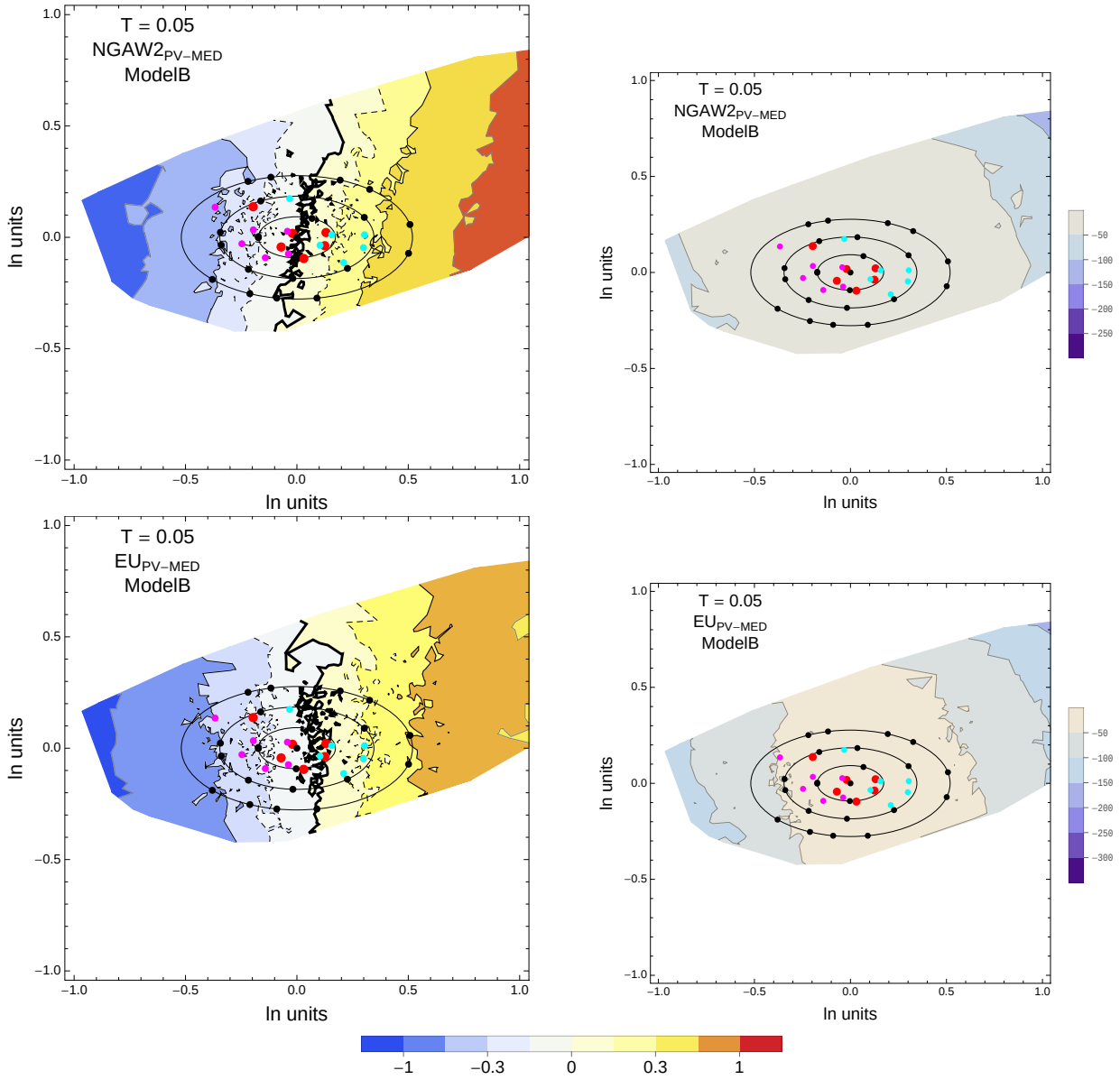



Figure 4.38: PVNGSv2: Contour Plots of mean residuals (top left) and likelihood (top right) for the NGA$_{PV-MED}$ dataset, and mean residuals (bottom left) and likelihood (top right) for the EU$_{PV-MED}$ dataset. Reference points are black dots. The original GMPEs are red dots,plus/minus uncertainty are magenta/cyan dots. The contour for the zero residual is a thick black line, the -0.15/0.15 contours are dashed black lines and the -0.3/0.3 contours are thin black lines. For $T = 0.05$s.

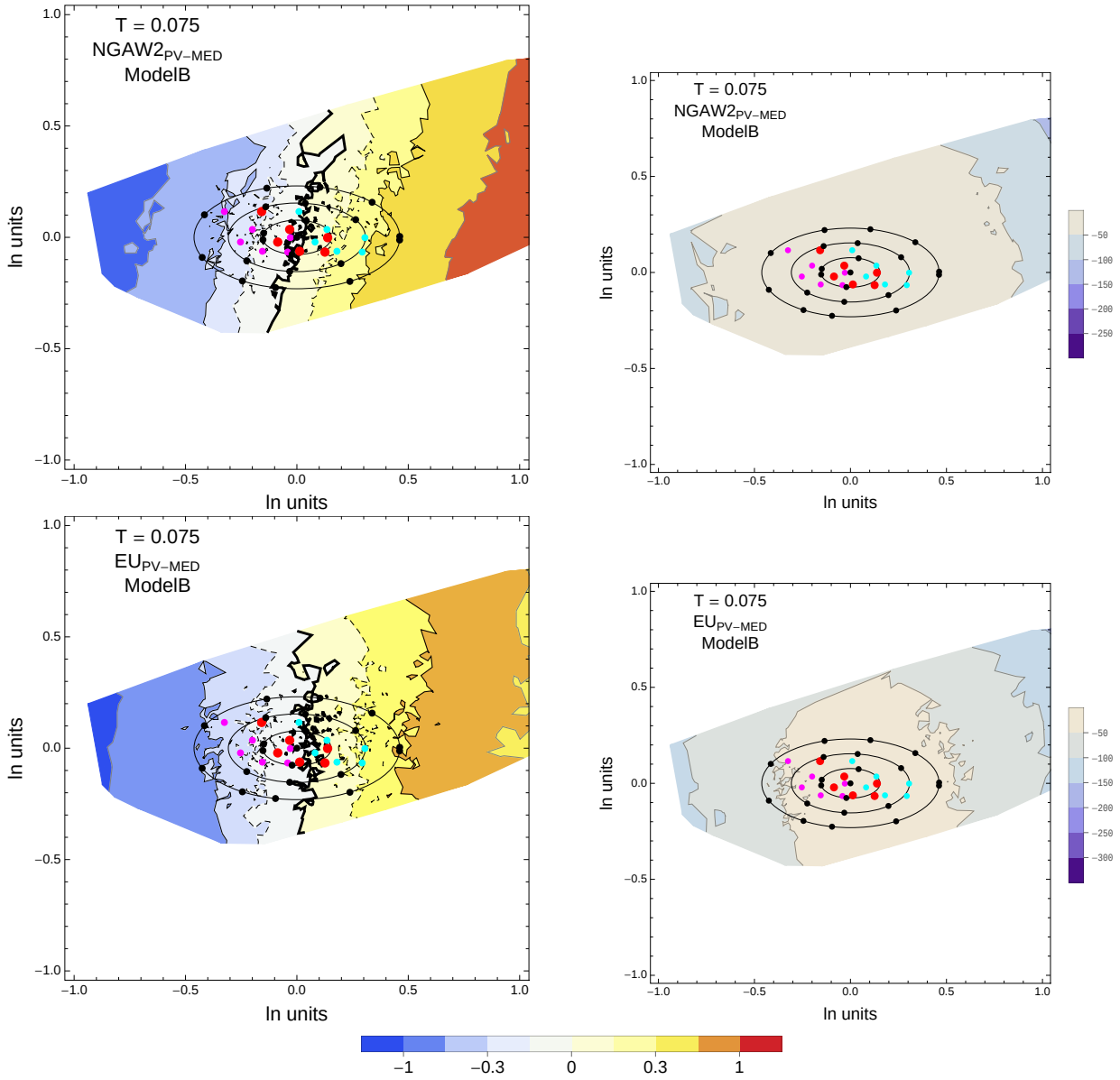



Figure 4.39: PVNGSv2: Contour Plots of mean residuals (top left) and likelihood (top right) for the NGA$_{PV-MED}$ dataset, and mean residuals (bottom left) and likelihood (top right) for the EU$_{PV-MED}$ dataset. Reference points are black dots. The original GMPEs are red dots,plus/minus uncertainty are magenta/cyan dots. The contour for the zero residual is a thick black line, the -0.15/0.15 contours are dashed black lines and the -0.3/0.3 contours are thin black lines. For $T = 0.075$s.

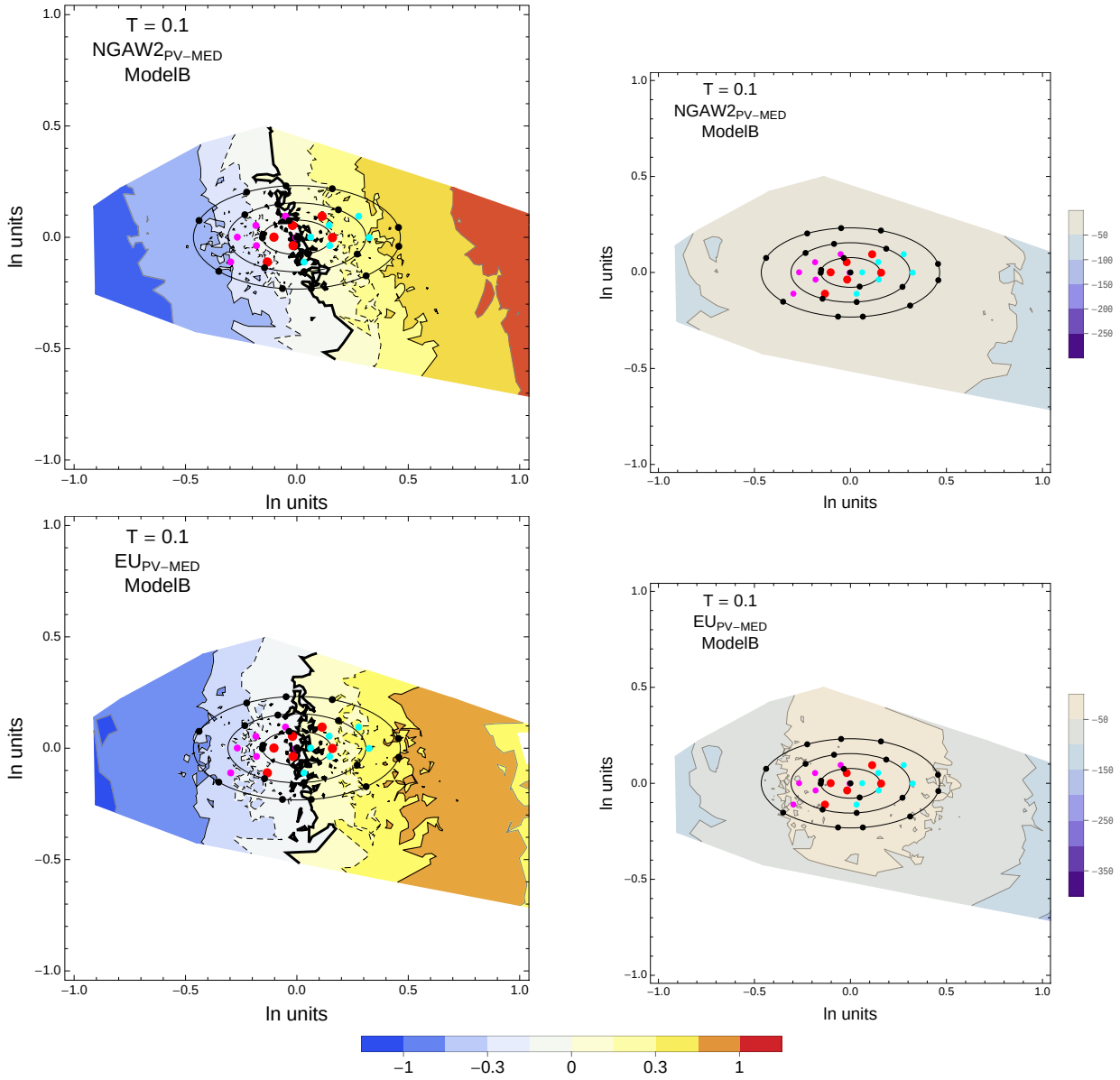



Figure 4.40: PVNGSv2: Contour Plots of mean residuals (top left) and likelihood (top right) for the NGA$_{PV-MED}$ dataset, and mean residuals (bottom left) and likelihood (top right) for the EU$_{PV-MED}$ dataset. Reference points are black dots. The original GMPEs are red dots,plus/minus uncertainty are magenta/cyan dots. The contour for the zero residual is a thick black line, the -0.15/0.15 contours are dashed black lines and the -0.3/0.3 contours are thin black lines. For $T = 0.1$s.

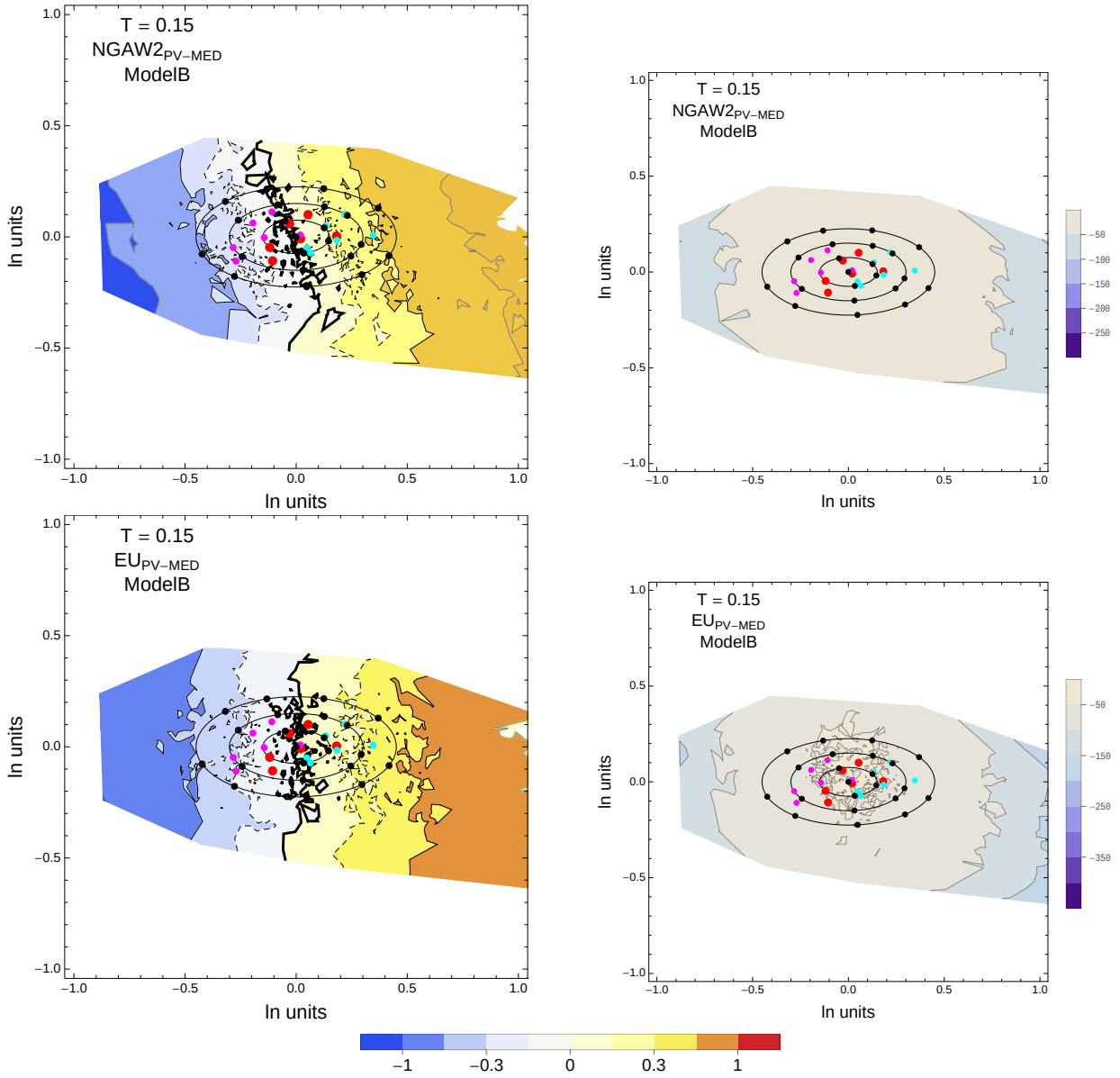



Figure 4.41: PVNGSv2: Contour Plots of mean residuals (top left) and likelihood (top right) for the NGA$_{PV-MED}$ dataset, and mean residuals (bottom left) and likelihood (top right) for the EU$_{PV-MED}$ dataset. Reference points are black dots. The original GMPEs are red dots,plus/minus uncertainty are magenta/cyan dots. The contour for the zero residual is a thick black line, the -0.15/0.15 contours are dashed black lines and the -0.3/0.3 contours are thin black lines. For $T = 0.15$s.

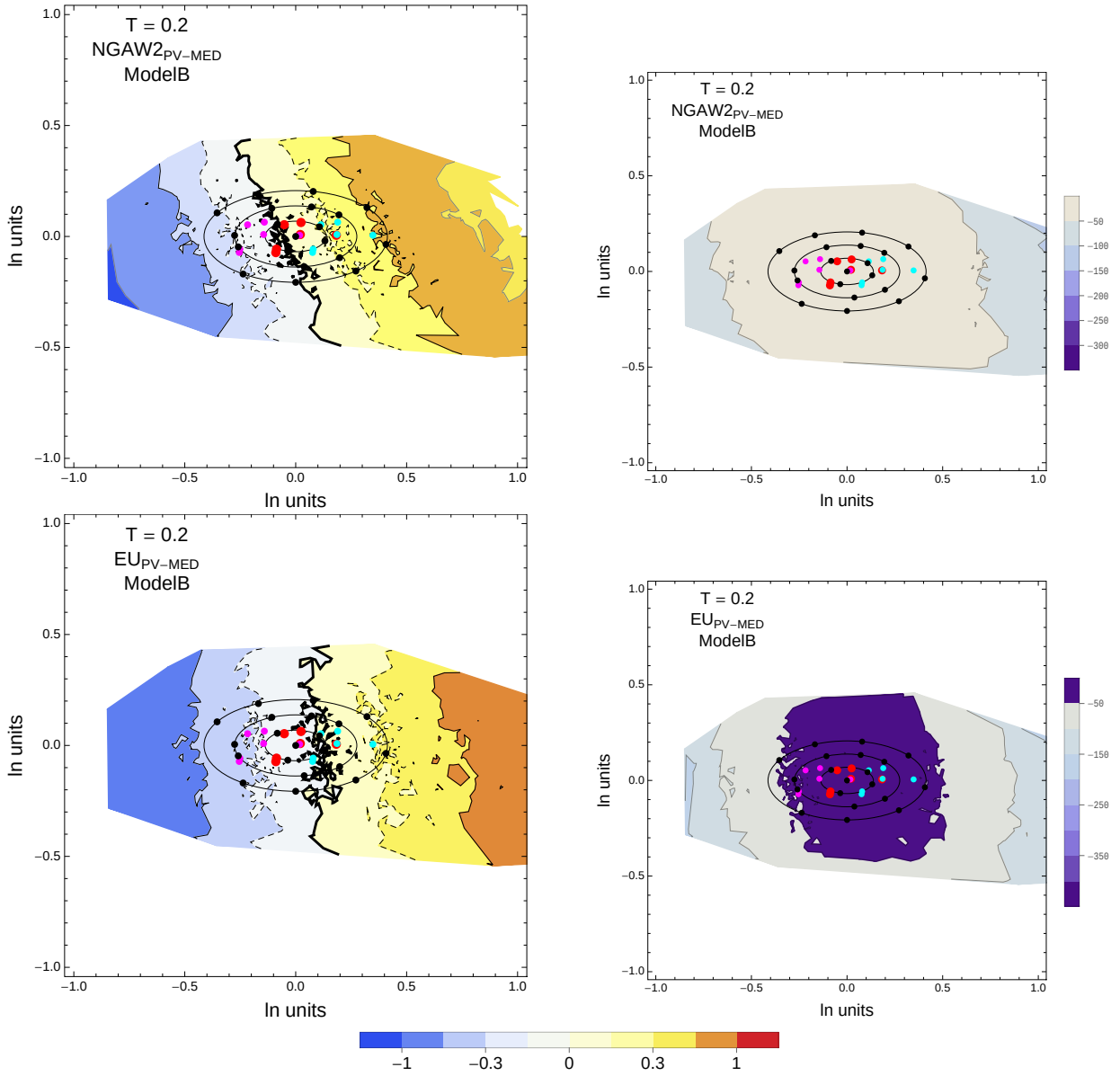



Figure 4.42: PVNGSv2: Contour Plots of mean residuals (top left) and likelihood (top right) for the NGA$_{PV-MED}$ dataset, and mean residuals (bottom left) and likelihood (top right) for the EU$_{PV-MED}$ dataset. Reference points are black dots. The original GMPEs are red dots,plus/minus uncertainty are magenta/cyan dots. The contour for the zero residual is a thick black line, the -0.15/0.15 contours are dashed black lines and the -0.3/0.3 contours are thin black lines. For $T = 0.2$s.

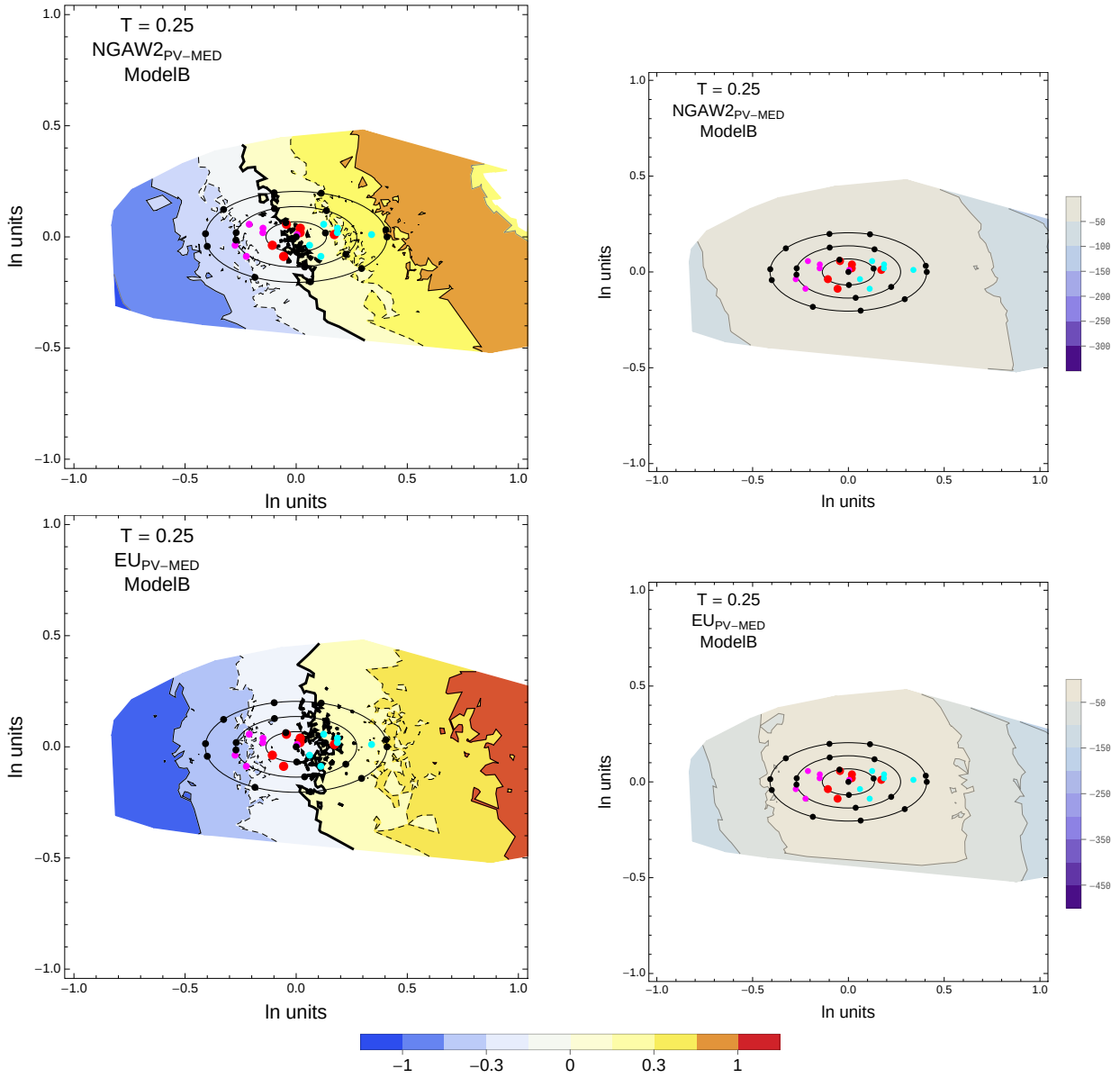



Figure 4.43: PVNGSv2: Contour Plots of mean residuals (top left) and likelihood (top right) for the NGA$_{PV-MED}$ dataset, and mean residuals (bottom left) and likelihood (top right) for the EU$_{PV-MED}$ dataset. Reference points are black dots. The original GMPEs are red dots,plus/minus uncertainty are magenta/cyan dots. The contour for the zero residual is a thick black line, the -0.15/0.15 contours are dashed black lines and the -0.3/0.3 contours are thin black lines. For $T = 0.25$s.

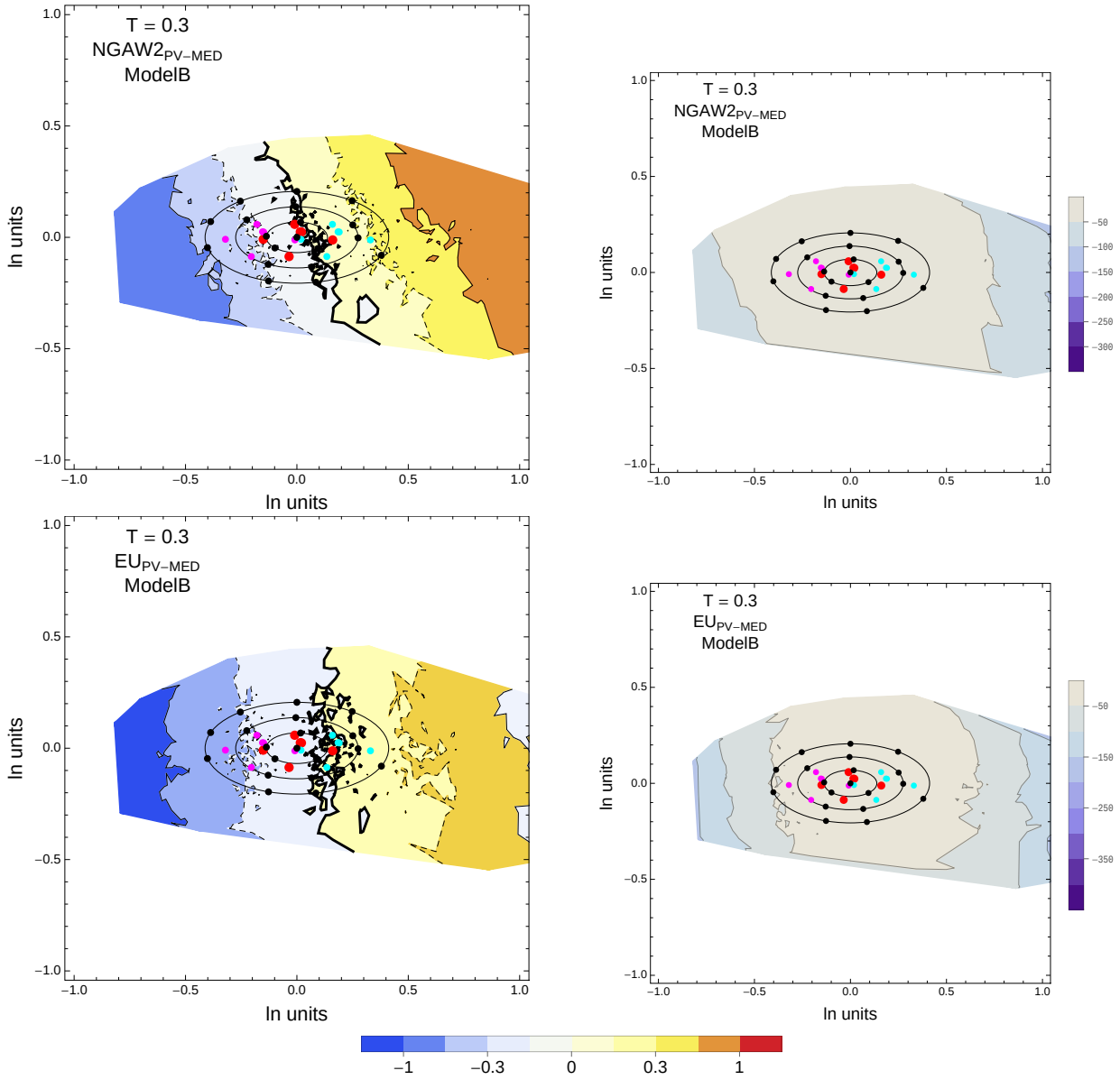



Figure 4.44: PVNGSv2: Contour Plots of mean residuals (top left) and likelihood (top right) for the NGA$_{PV-MED}$ dataset, and mean residuals (bottom left) and likelihood (top right) for the EU$_{PV-MED}$ dataset. Reference points are black dots. The original GMPEs are red dots,plus/minus uncertainty are magenta/cyan dots. The contour for the zero residual is a thick black line, the -0.15/0.15 contours are dashed black lines and the -0.3/0.3 contours are thin black lines. For $T = 0.3$s.

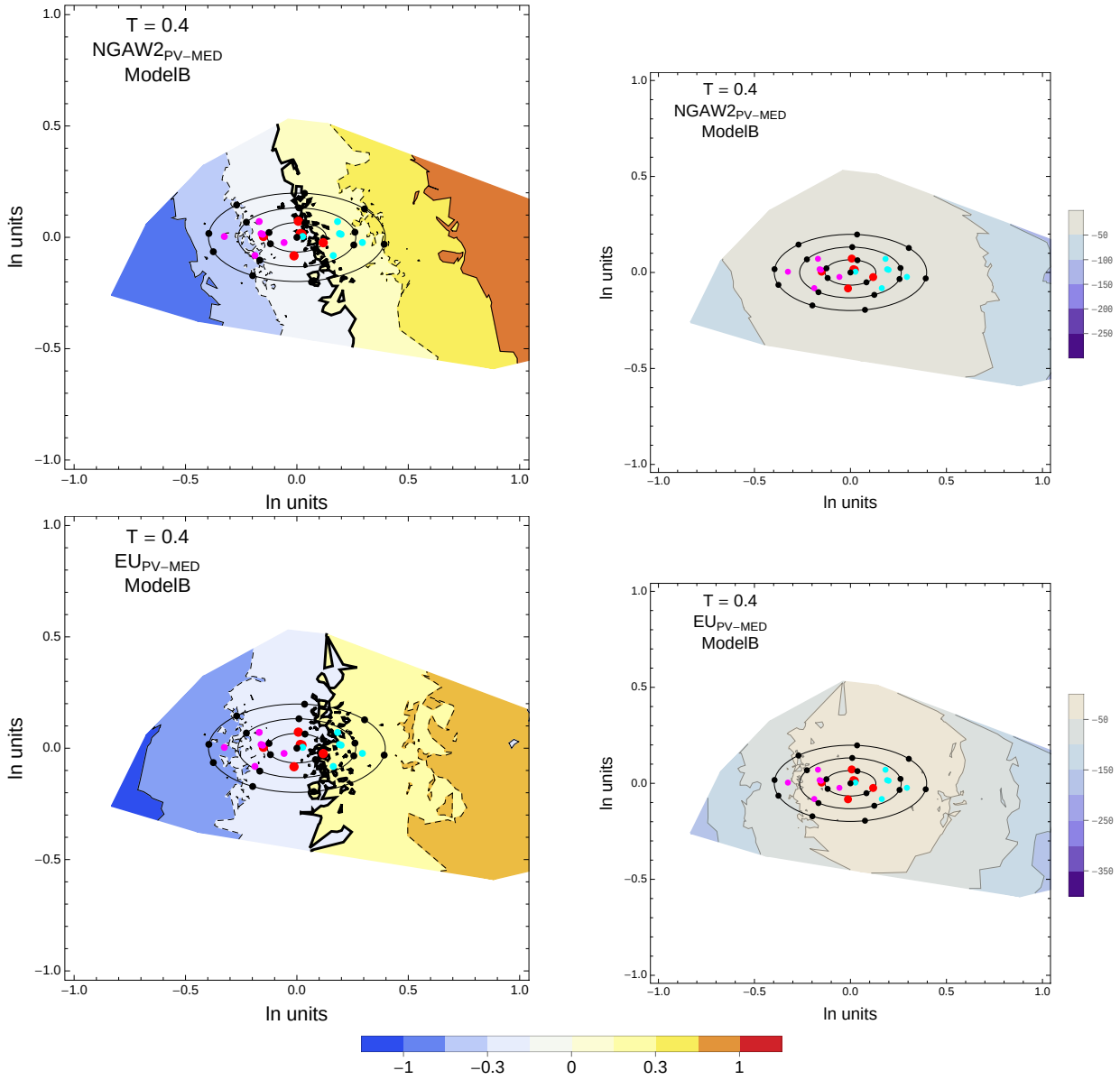



Figure 4.45: PVNGSv2: Contour Plots of mean residuals (top left) and likelihood (top right) for the NGA$_{PV-MED}$ dataset, and mean residuals (bottom left) and likelihood (top right) for the EU$_{PV-MED}$ dataset. Reference points are black dots. The original GMPEs are red dots,plus/minus uncertainty are magenta/cyan dots. The contour for the zero residual is a thick black line, the -0.15/0.15 contours are dashed black lines and the -0.3/0.3 contours are thin black lines. For $T = 0.4$s.

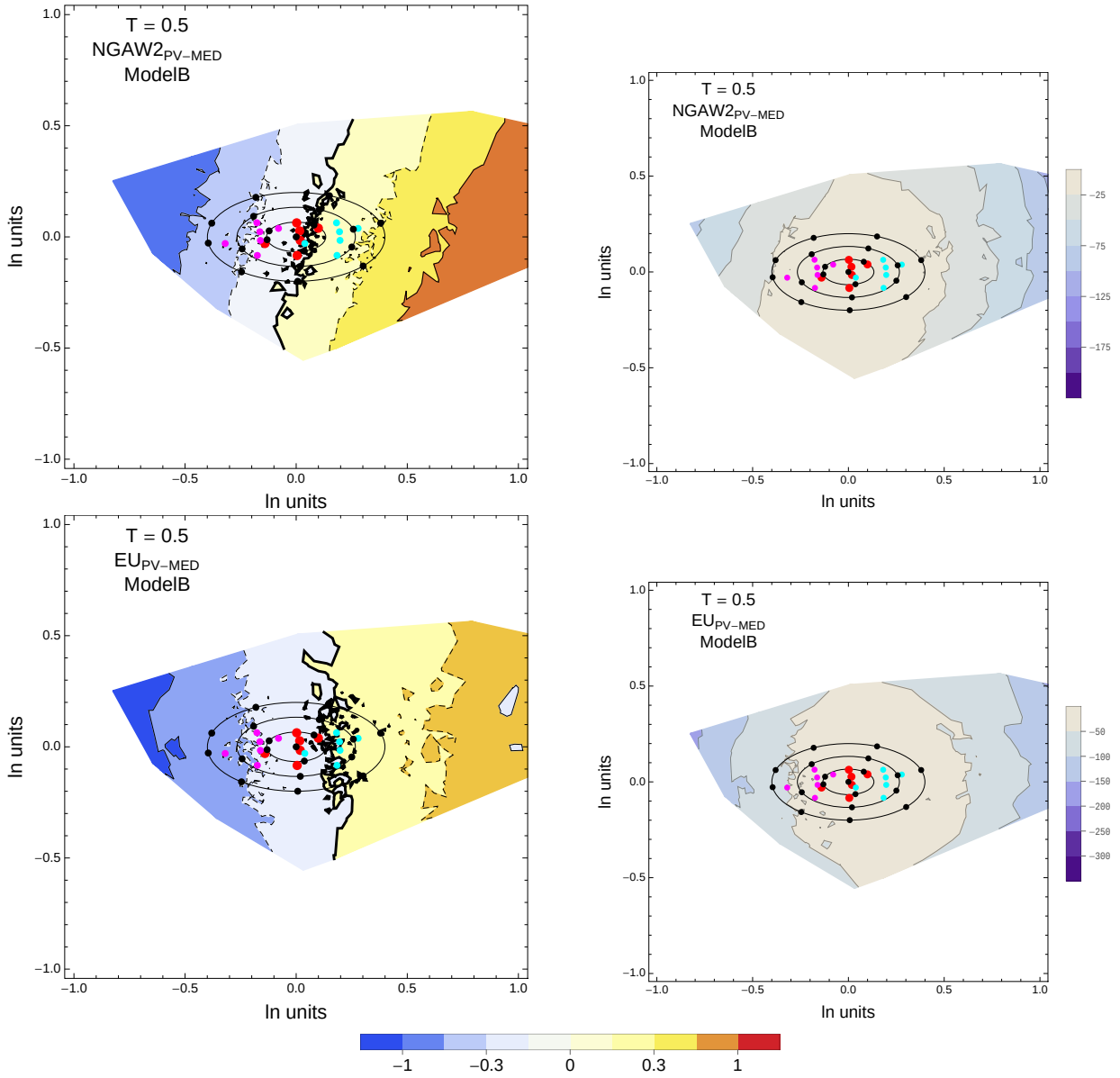



Figure 4.46: PVNGSv2: Contour Plots of mean residuals (top left) and likelihood (top right) for the NGA$_{PV-MED}$ dataset, and mean residuals (bottom left) and likelihood (top right) for the EU$_{PV-MED}$ dataset. Reference points are black dots. The original GMPEs are red dots,plus/minus uncertainty are magenta/cyan dots. The contour for the zero residual is a thick black line, the -0.15/0.15 contours are dashed black lines and the -0.3/0.3 contours are thin black lines. For $T = 0.5$s.

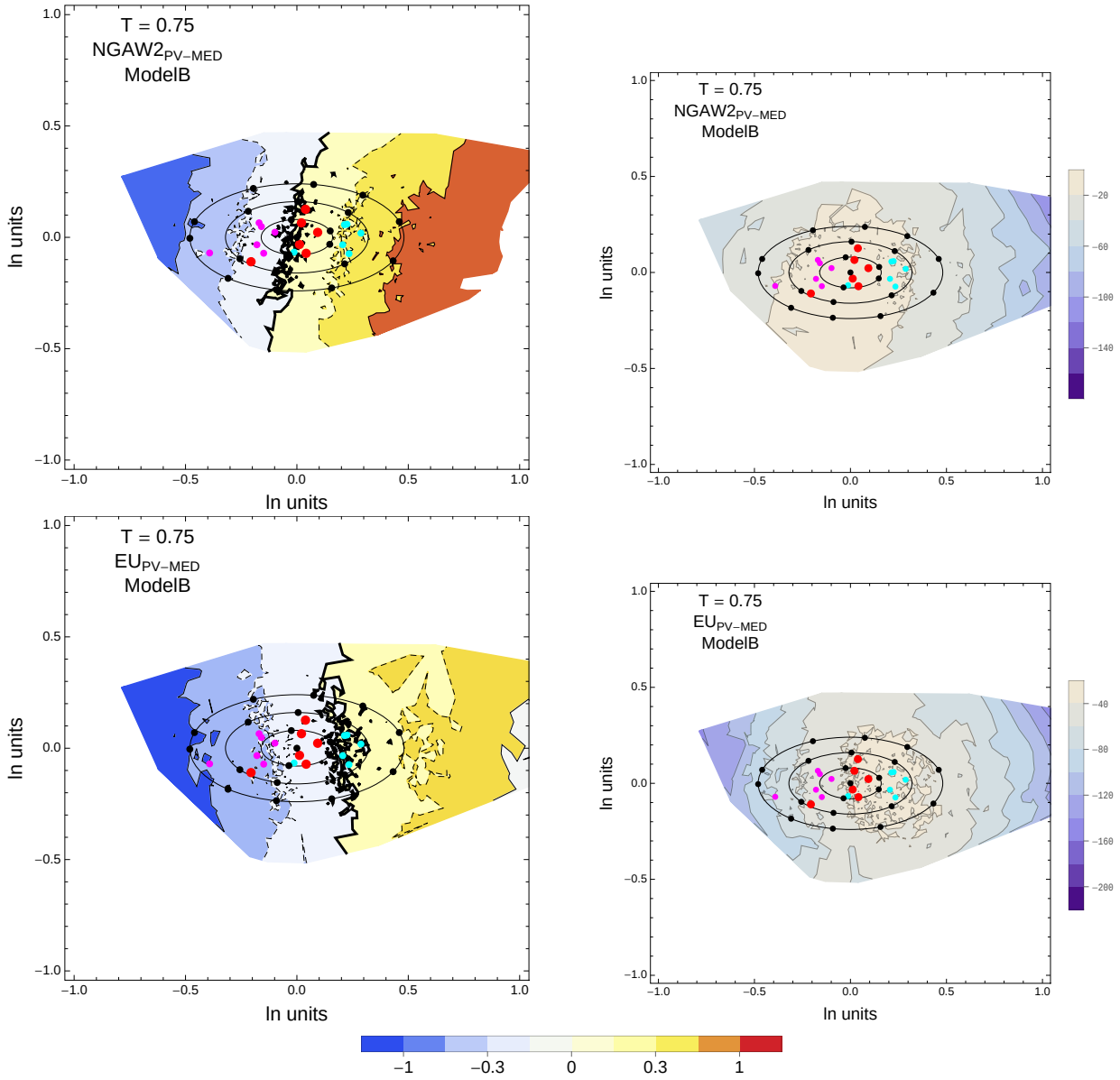



Figure 4.47: PVNGSv2: Contour Plots of mean residuals (top left) and likelihood (top right) for the NGA$_{PV-MED}$ dataset, and mean residuals (bottom left) and likelihood (top right) for the EU$_{PV-MED}$ dataset. Reference points are black dots. The original GMPEs are red dots,plus/minus uncertainty are magenta/cyan dots. The contour for the zero residual is a thick black line, the -0.15/0.15 contours are dashed black lines and the -0.3/0.3 contours are thin black lines. For $T = 0.75$s.

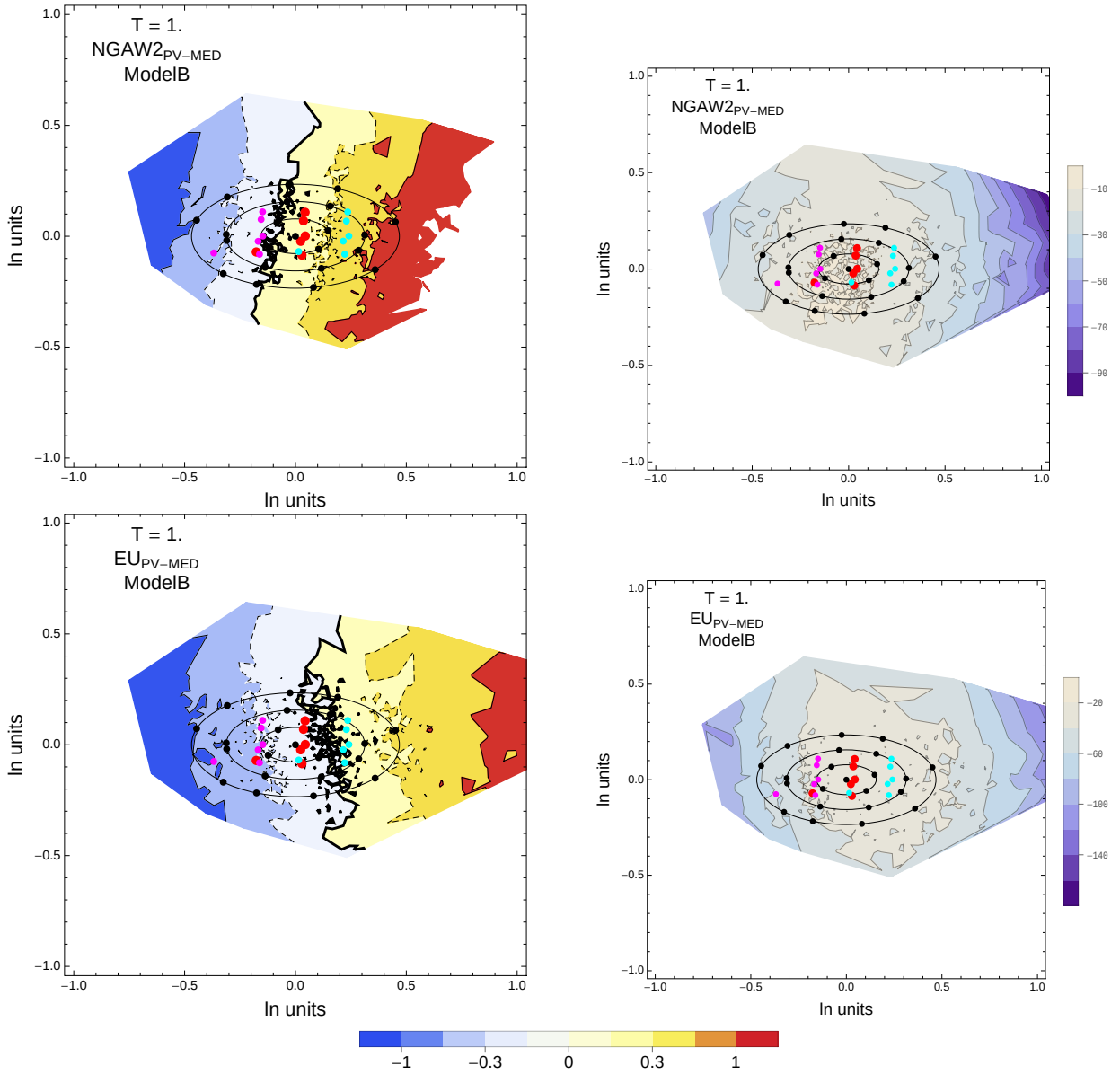



Figure 4.48: PVNGSv2: Contour Plots of mean residuals (top left) and likelihood (top right) for the NGA$_{PV-MED}$ dataset, and mean residuals (bottom left) and likelihood (top right) for the EU$_{PV-MED}$ dataset. Reference points are black dots. The original GMPEs are red dots,plus/minus uncertainty are magenta/cyan dots. The contour for the zero residual is a thick black line, the -0.15/0.15 contours are dashed black lines and the -0.3/0.3 contours are thin black lines. For $T = 1$.s.

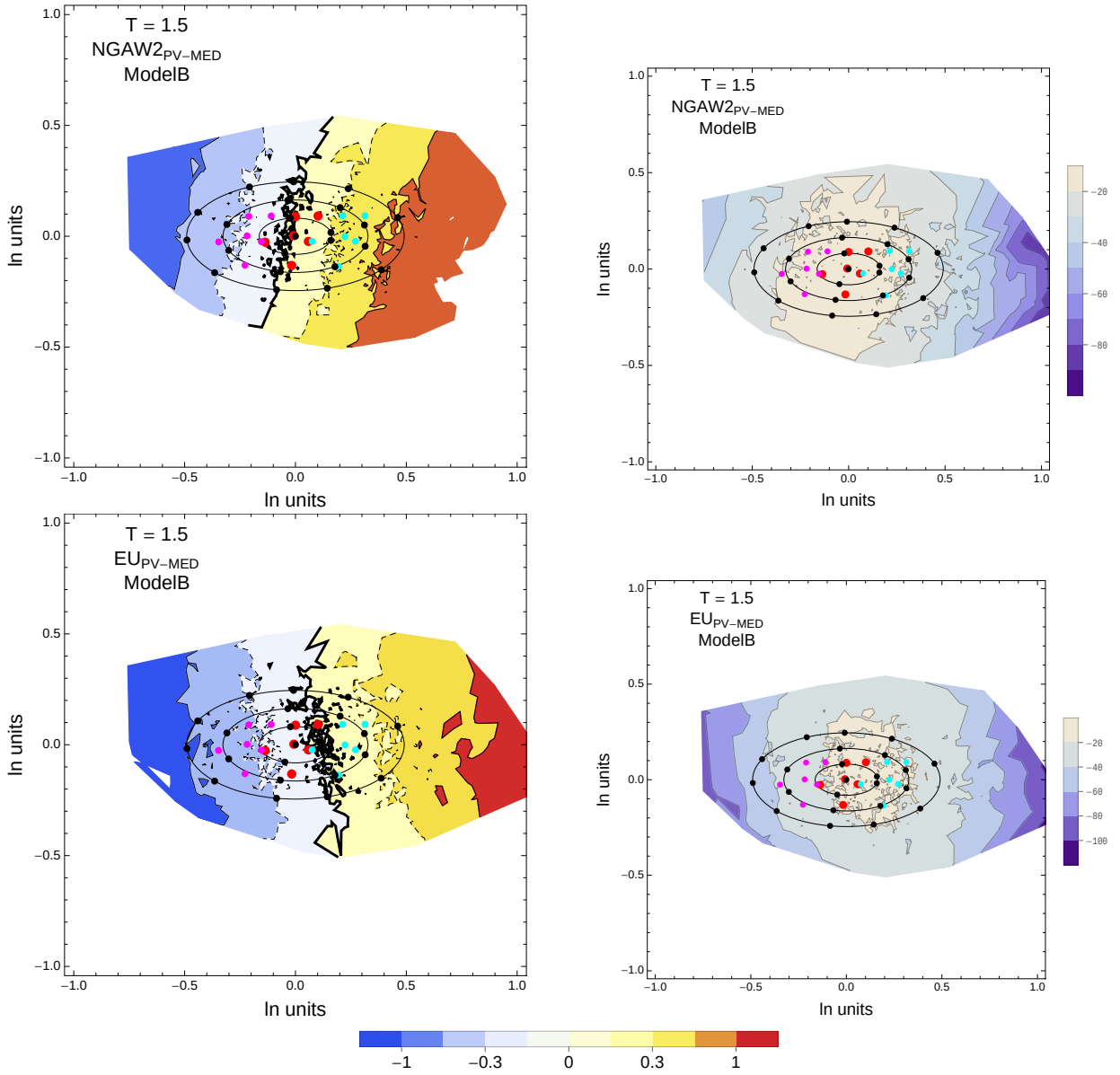



Figure 4.49: PVNGSv2: Contour Plots of mean residuals (top left) and likelihood (top right) for the NGA$_{PV-MED}$ dataset, and mean residuals (bottom left) and likelihood (top right) for the EU$_{PV-MED}$ dataset. Reference points are black dots. The original GMPEs are red dots,plus/minus uncertainty are magenta/cyan dots. The contour for the zero residual is a thick black line, the -0.15/0.15 contours are dashed black lines and the -0.3/0.3 contours are thin black lines. For $T = 1.5$s.

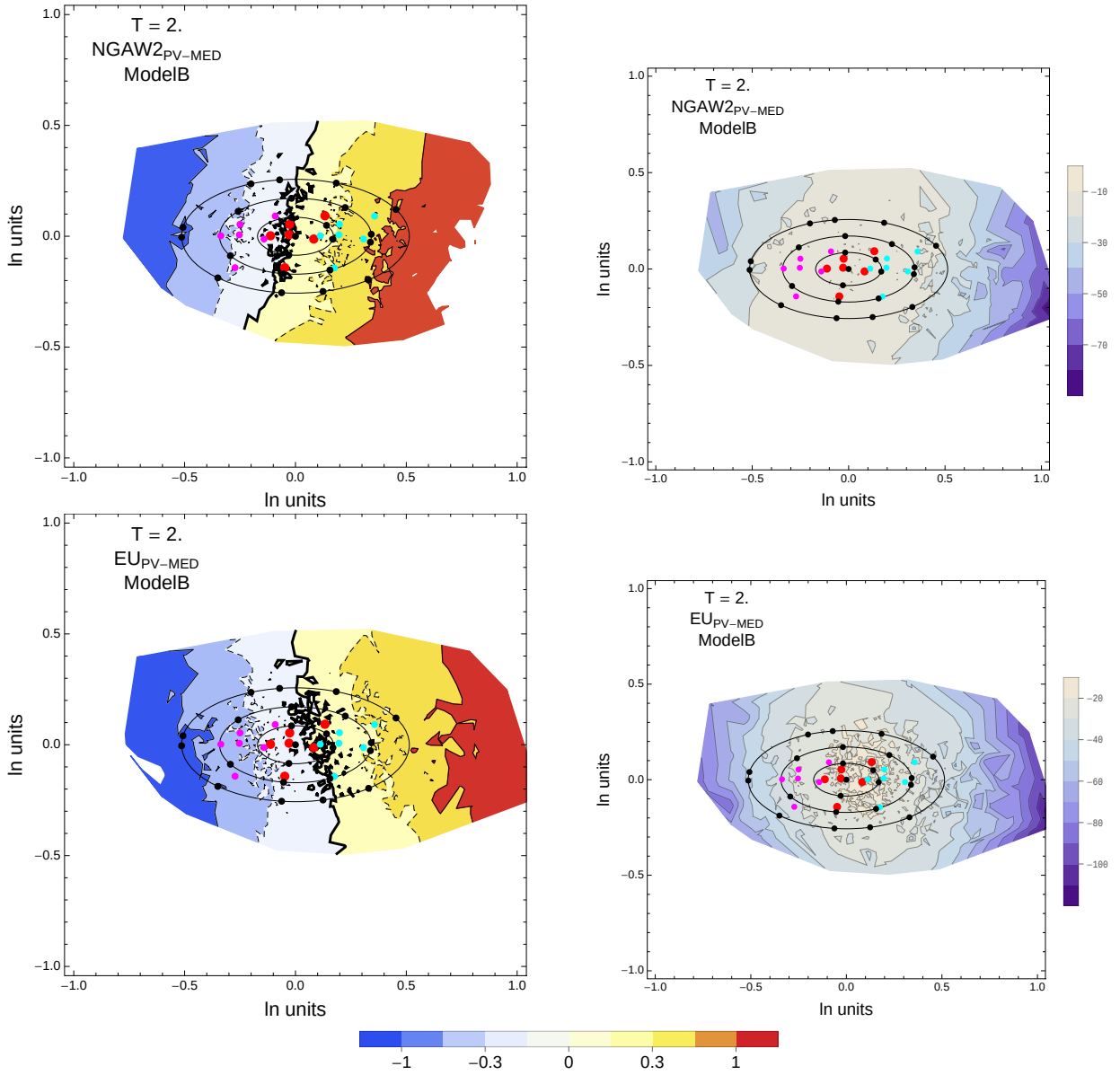



Figure 4.50: PVNGSv2: Contour Plots of mean residuals (top left) and likelihood (top right) for the NGA$_{PV-MED}$ dataset, and mean residuals (bottom left) and likelihood (top right) for the EU$_{PV-MED}$ dataset. Reference points are black dots. The original GMPEs are red dots,plus/minus uncertainty are magenta/cyan dots. The contour for the zero residual is a thick black line, the -0.15/0.15 contours are dashed black lines and the -0.3/0.3 contours are thin black lines. For $T = 2$.s.

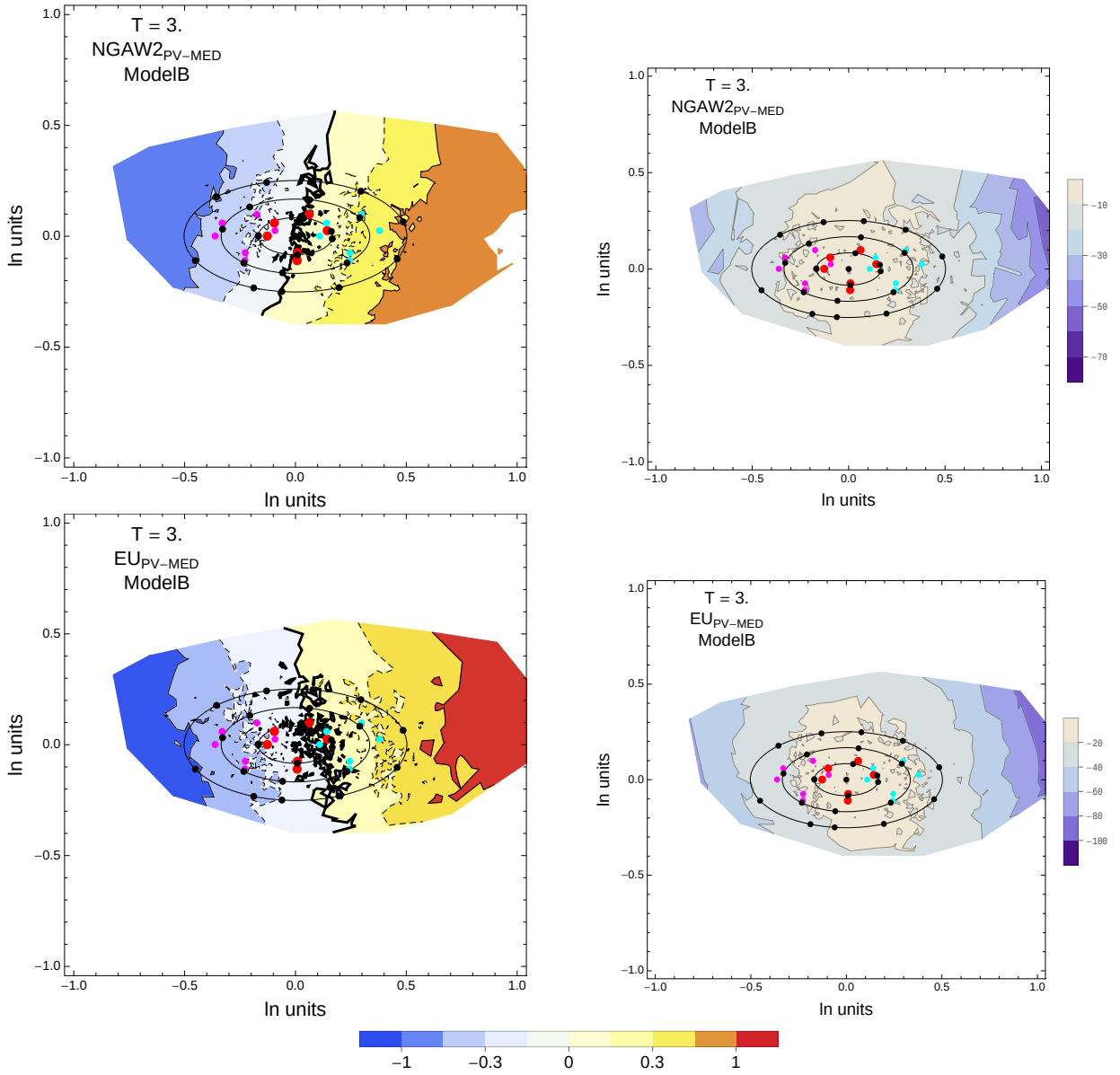



Figure 4.51: PVNGSv2: Contour Plots of mean residuals (top left) and likelihood (top right) for the NGA$_{PV-MED}$ dataset, and mean residuals (bottom left) and likelihood (top right) for the EU$_{PV-MED}$ dataset. Reference points are black dots. The original GMPEs are red dots,plus/minus uncertainty are magenta/cyan dots. The contour for the zero residual is a thick black line, the -0.15/0.15 contours are dashed black lines and the -0.3/0.3 contours are thin black lines. For $T = 3$.s.

### 4.1.3 Maps – Voronoi Cells

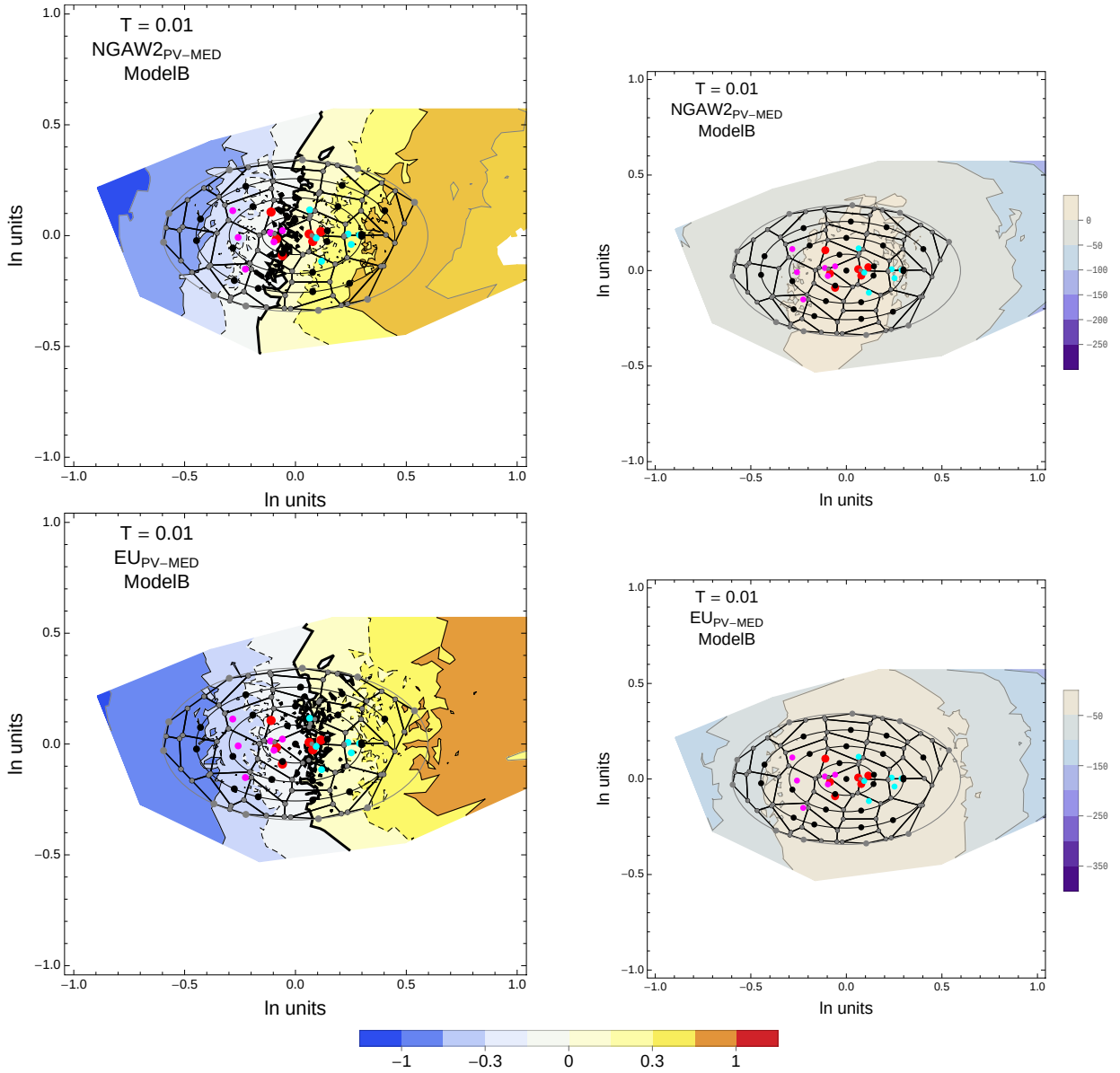



Figure 4.52: PVNGSv2: Contour Plots of selected mean residuals (top left) and likelihood (top right) for the NGA$_{PV-MED}$ dataset, and mean residuals (bottom left) and likelihood (top right) for the EU$_{PV-MED}$ dataset. The Voronoi cells used for selecting and weighting models are shown as black lines. The original GMPEs are red dots, plus/minus uncertainty are magenta/cyan dots. The contour for the zero residual is a thick black line, the -0.15/0.15 contours are dashed black lines and the -0.3/0.3 contours are thin black lines. For $T = 0.01$s.

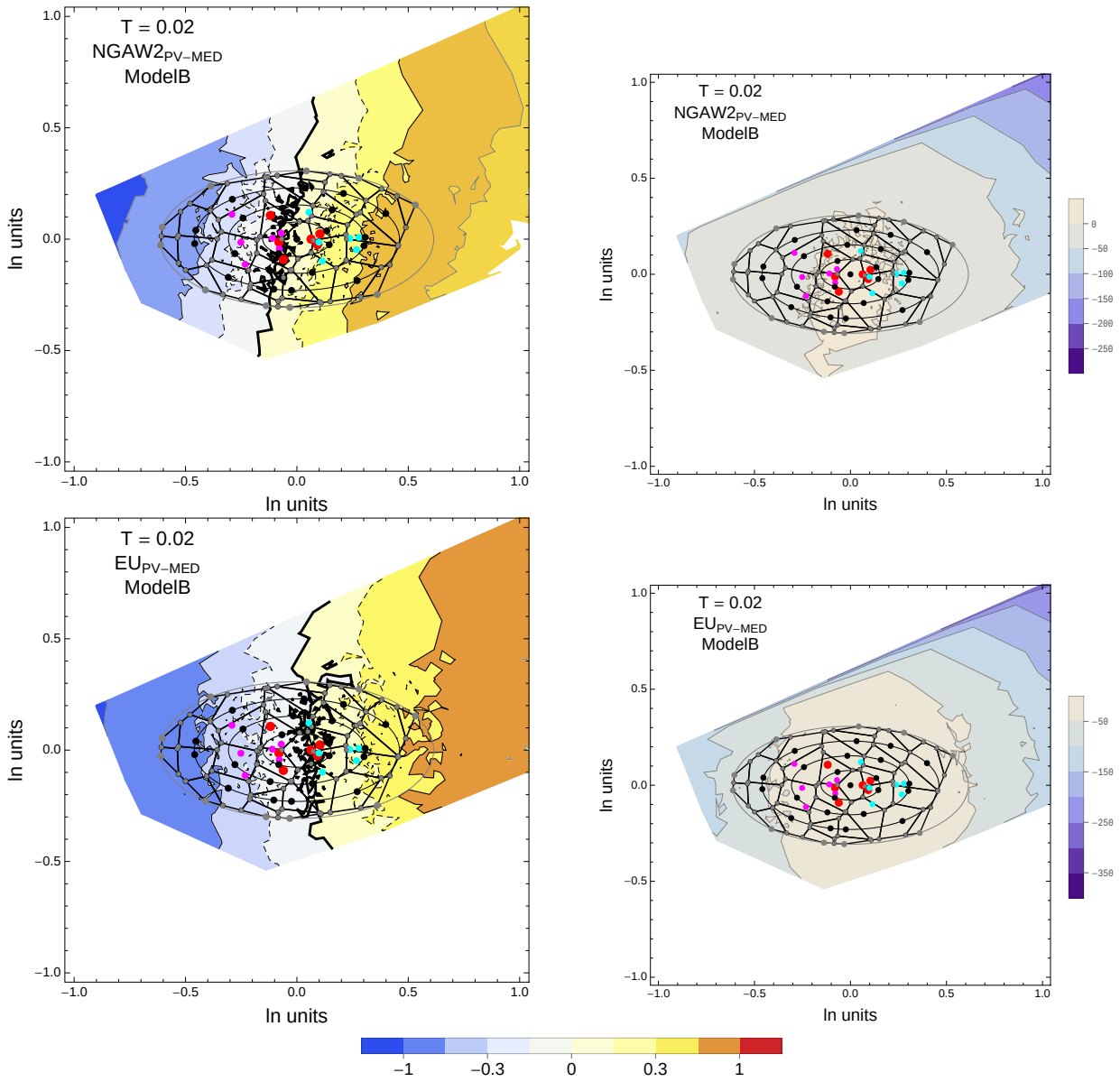



Figure 4.53: PVNGSv2: Contour Plots of selected mean residuals (top left) and likelihood (top right) for the NGA$_{PV-MED}$ dataset, and mean residuals (bottom left) and likelihood (top right) for the EU$_{PV-MED}$ dataset. The Voronoi cells used for selecting and weighting models are shown as black lines. The original GMPEs are red dots, plus/minus uncertainty are magenta/cyan dots. The contour for the zero residual is a thick black line, the -0.15/0.15 contours are dashed black lines and the -0.3/0.3 contours are thin black lines. For $T = 0.02$s.

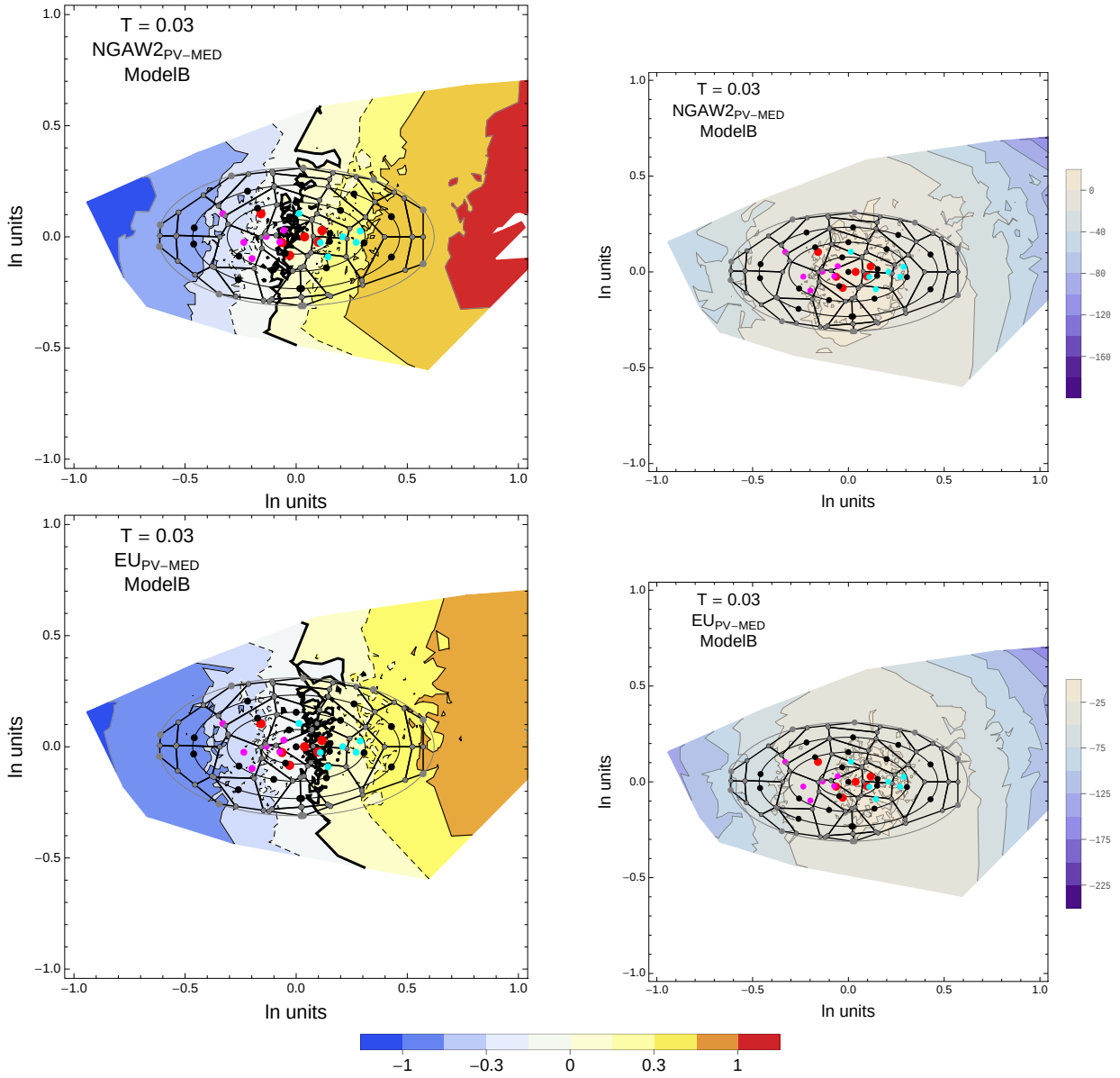



Figure 4.54: PVNGSv2: Contour Plots of selected mean residuals (top left) and likelihood (top right) for the NGA$_{PV-MED}$ dataset, and mean residuals (bottom left) and likelihood (top right) for the EU$_{PV-MED}$ dataset. The Voronoi cells used for selecting and weighting models are shown as black lines. The original GMPEs are red dots, plus/minus uncertainty are magenta/cyan dots. The contour for the zero residual is a thick black line, the -0.15/0.15 contours are dashed black lines and the -0.3/0.3 contours are thin black lines. For $T = 0.03$s.

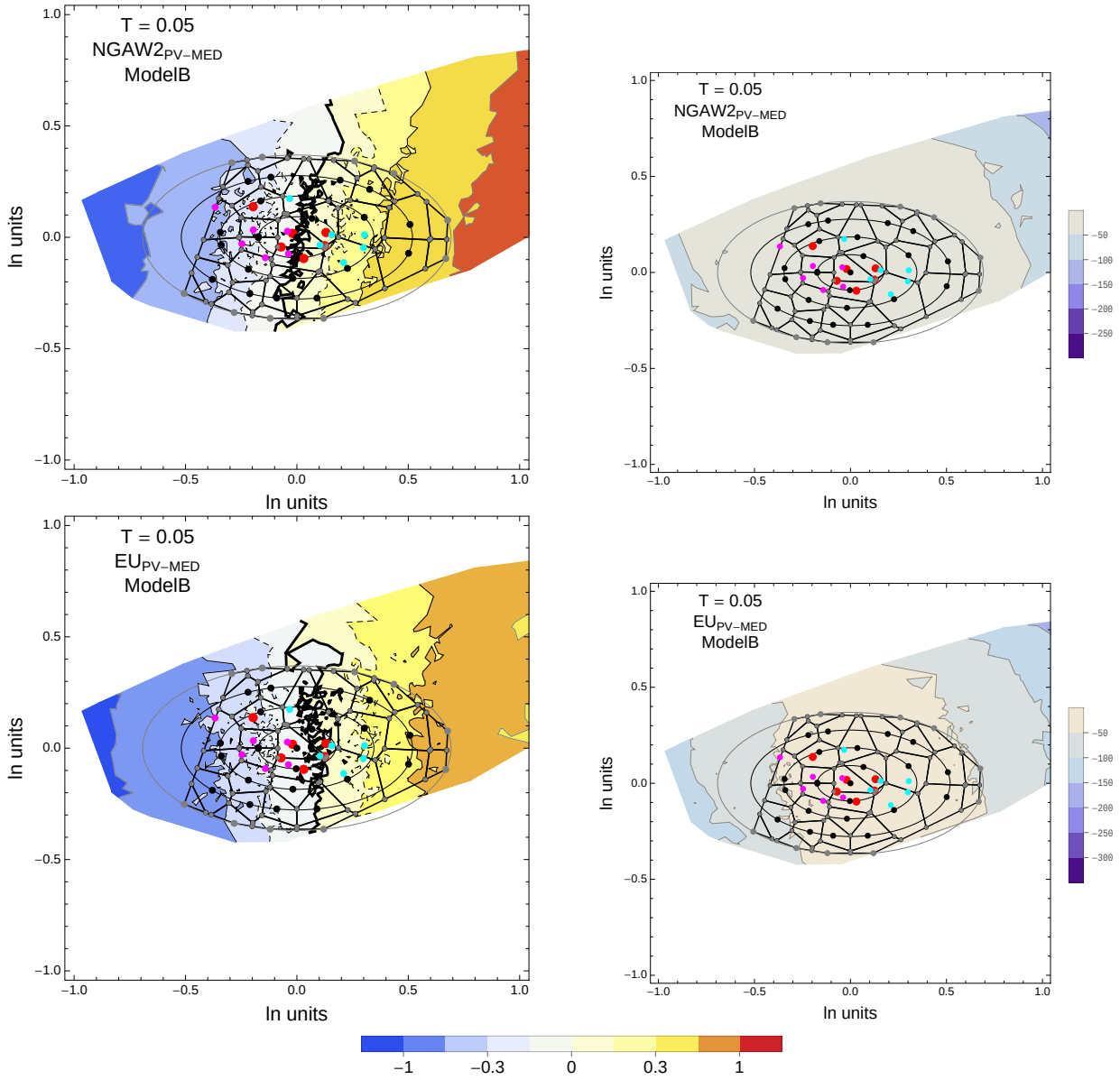



Figure 4.55: PVNGSv2: Contour Plots of selected mean residuals (top left) and likelihood (top right) for the NGA$_{PV-MED}$ dataset, and mean residuals (bottom left) and likelihood (top right) for the EU$_{PV-MED}$ dataset. The Voronoi cells used for selecting and weighting models are shown as black lines. The original GMPEs are red dots, plus/minus uncertainty are magenta/cyan dots. The contour for the zero residual is a thick black line, the -0.15/0.15 contours are dashed black lines and the -0.3/0.3 contours are thin black lines. For $T = 0.05$s.

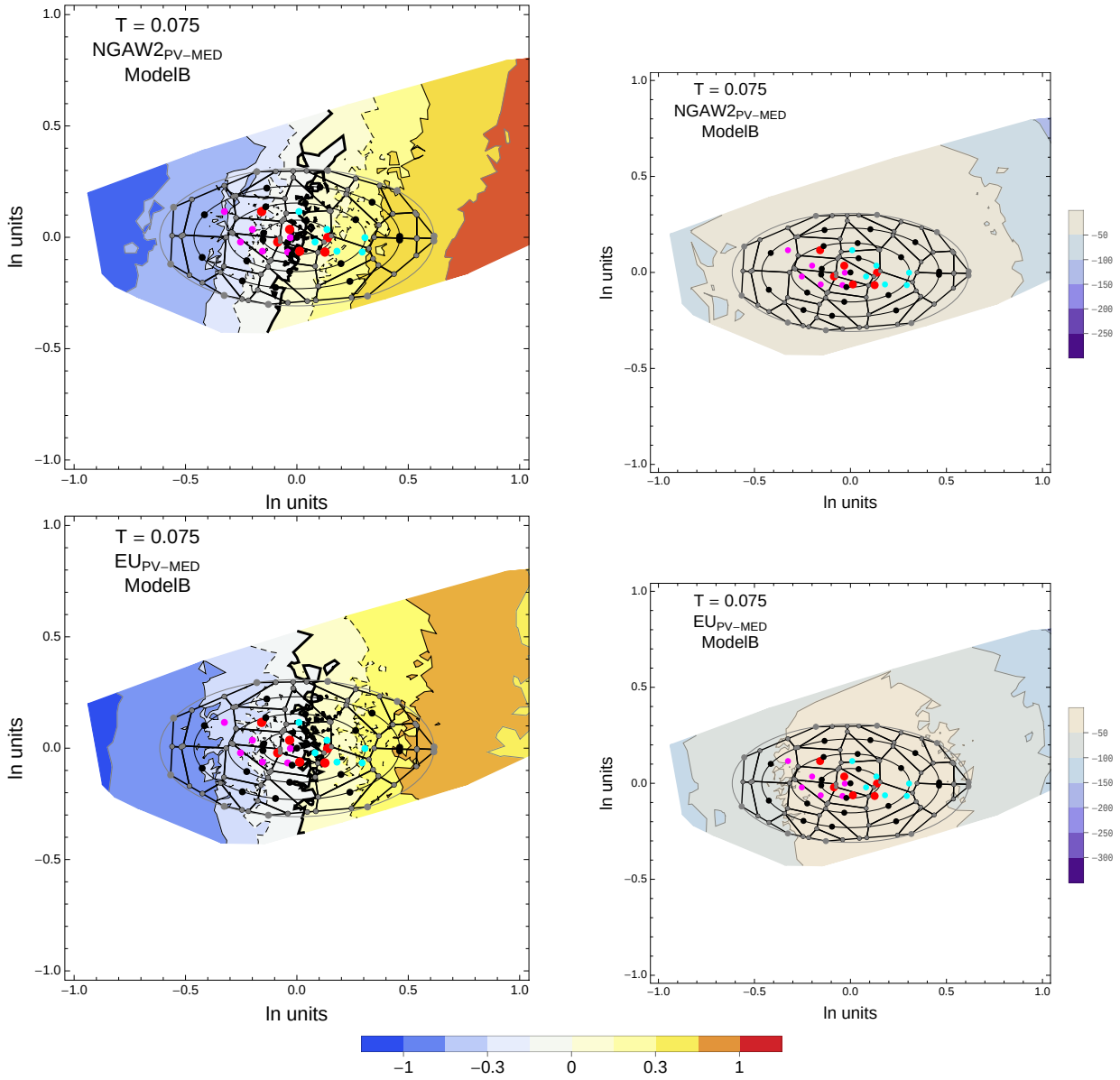



Figure 4.56: PVNGSv2: Contour Plots of selected mean residuals (top left) and likelihood (top right) for the NGA$_{PV-MED}$ dataset, and mean residuals (bottom left) and likelihood (top right) for the EU$_{PV-MED}$ dataset. The Voronoi cells used for selecting and weighting models are shown as black lines. The original GMPEs are red dots, plus/minus uncertainty are magenta/cyan dots. The contour for the zero residual is a thick black line, the -0.15/0.15 contours are dashed black lines and the -0.3/0.3 contours are thin black lines. For $T = 0.075$s.

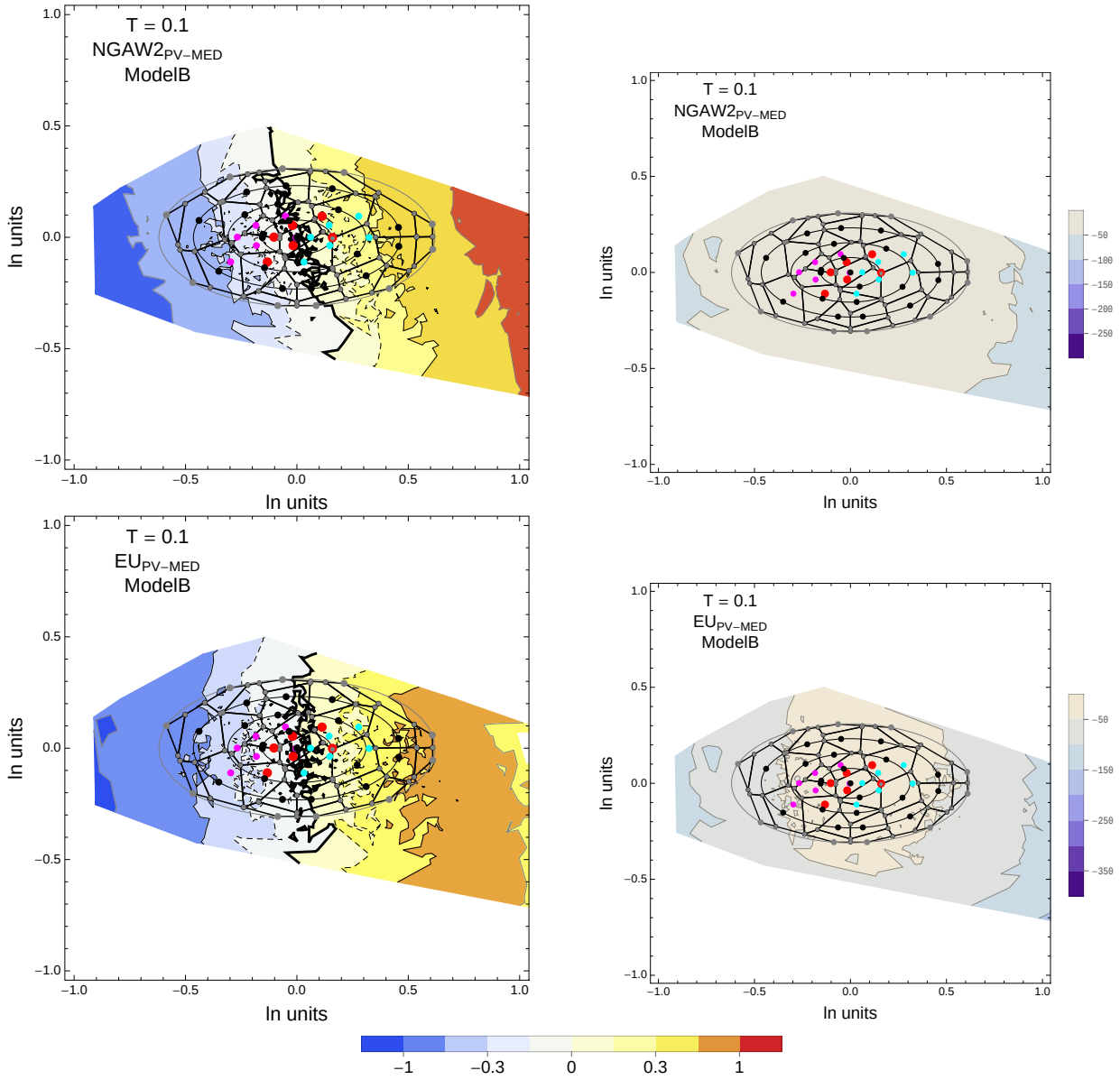



Figure 4.57: PVNGSv2: Contour Plots of selected mean residuals (top left) and likelihood (top right) for the NGA$_{PV-MED}$ dataset, and mean residuals (bottom left) and likelihood (top right) for the EU$_{PV-MED}$ dataset. The Voronoi cells used for selecting and weighting models are shown as black lines. The original GMPEs are red dots, plus/minus uncertainty are magenta/cyan dots. The contour for the zero residual is a thick black line, the -0.15/0.15 contours are dashed black lines and the -0.3/0.3 contours are thin black lines. For $T = 0.1$s.

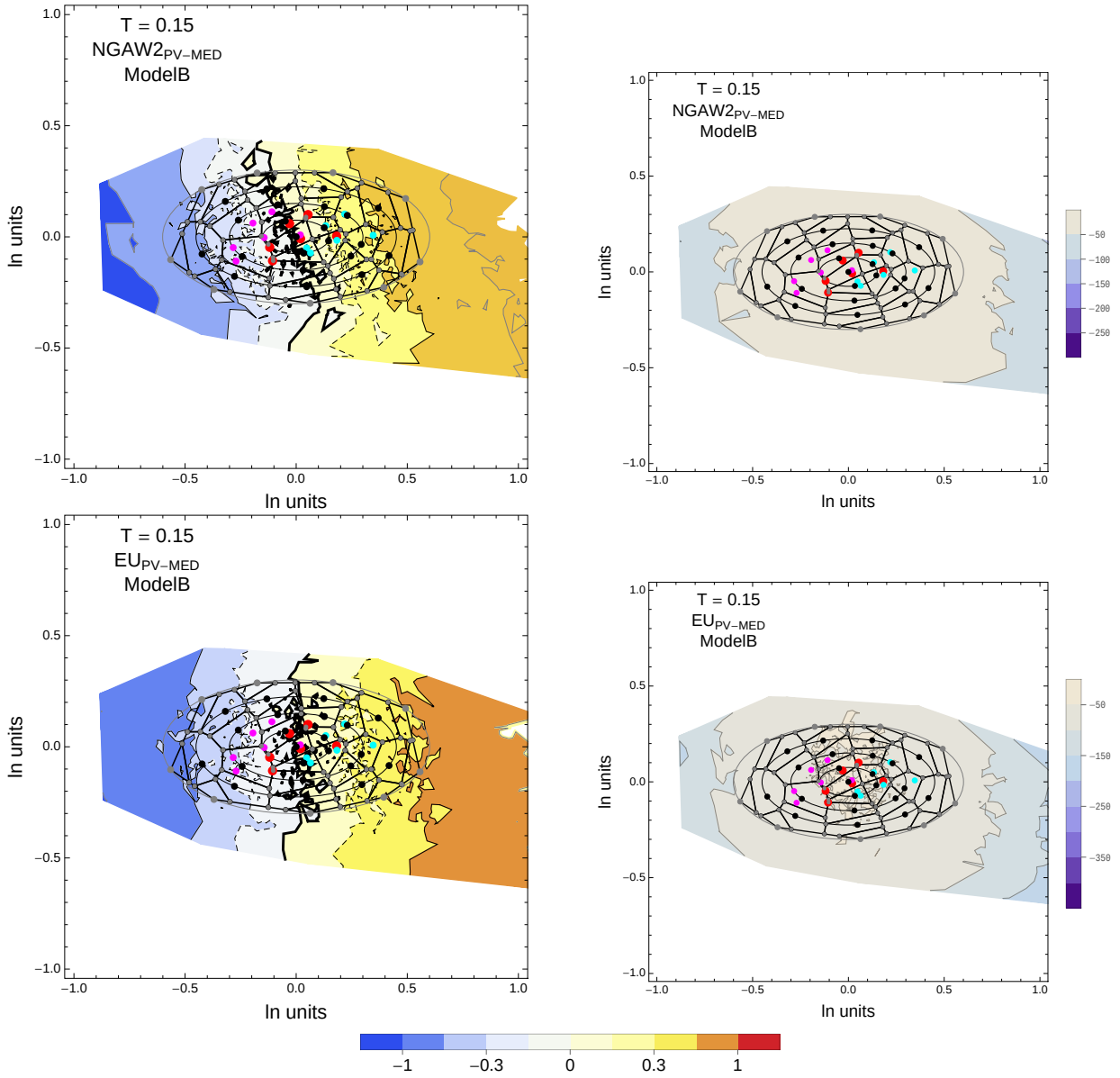



Figure 4.58: PVNGSv2: Contour Plots of selected mean residuals (top left) and likelihood (top right) for the NGA$_{PV-MED}$ dataset, and mean residuals (bottom left) and likelihood (top right) for the EU$_{PV-MED}$ dataset. The Voronoi cells used for selecting and weighting models are shown as black lines. The original GMPEs are red dots, plus/minus uncertainty are magenta/cyan dots. The contour for the zero residual is a thick black line, the -0.15/0.15 contours are dashed black lines and the -0.3/0.3 contours are thin black lines. For $T = 0.15$s.

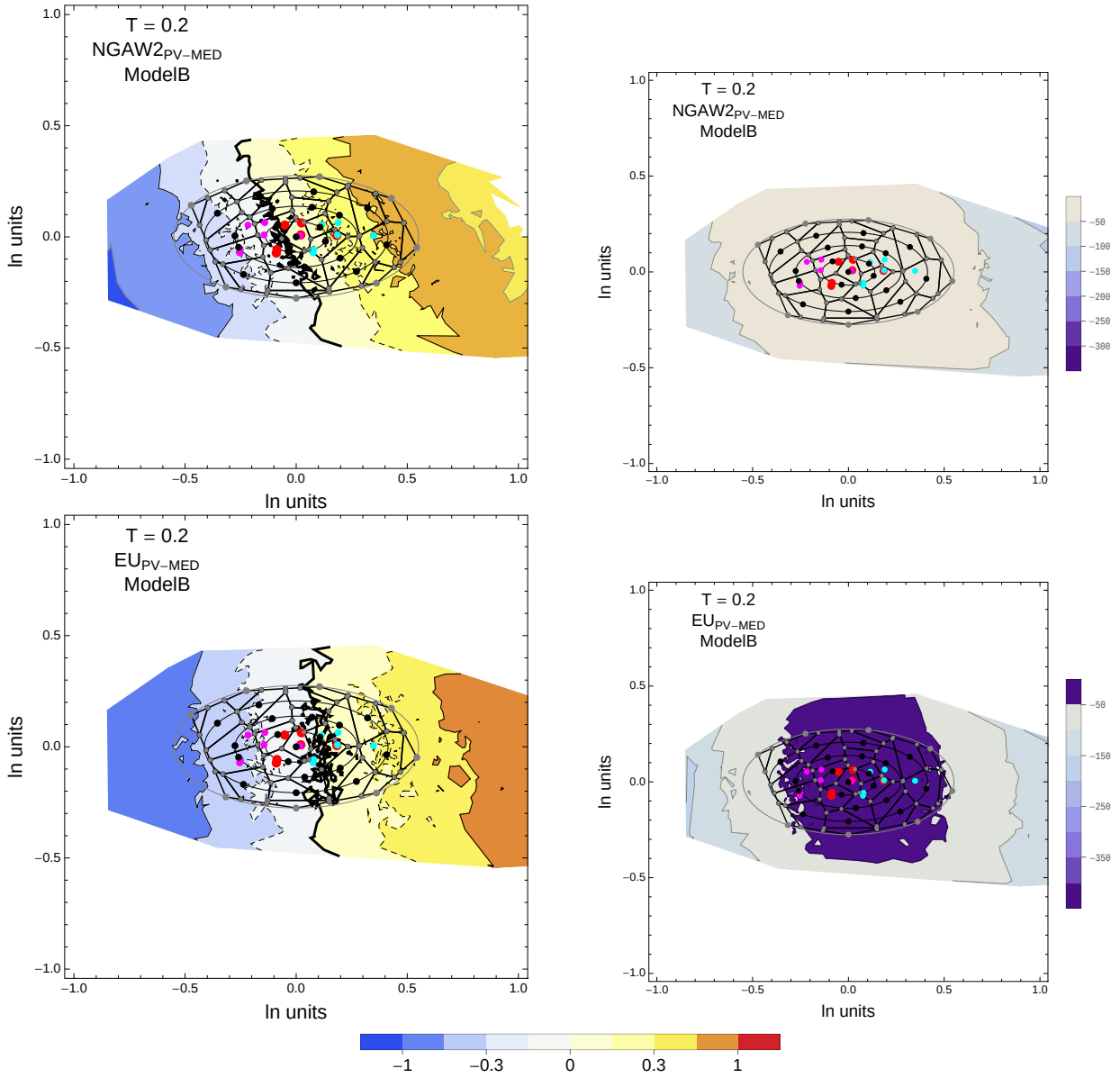



Figure 4.59: PVNGSv2: Contour Plots of selected mean residuals (top left) and likelihood (top right) for the NGA$_{PV-MED}$ dataset, and mean residuals (bottom left) and likelihood (top right) for the EU$_{PV-MED}$ dataset. The Voronoi cells used for selecting and weighting models are shown as black lines. The original GMPEs are red dots, plus/minus uncertainty are magenta/cyan dots. The contour for the zero residual is a thick black line, the -0.15/0.15 contours are dashed black lines and the -0.3/0.3 contours are thin black lines. For $T = 0.2$s.

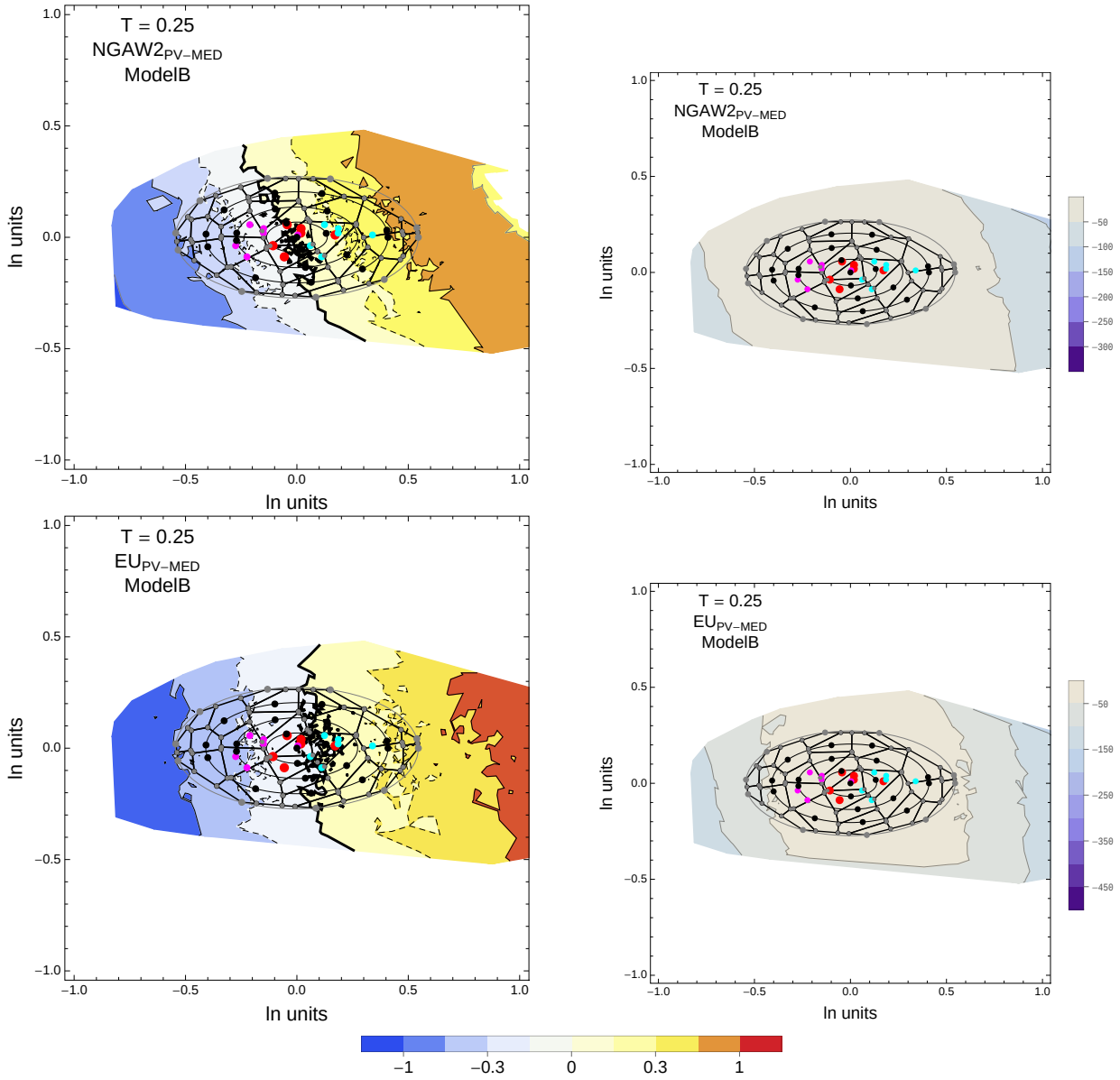



Figure 4.60: PVNGSv2: Contour Plots of selected mean residuals (top left) and likelihood (top right) for the NGA$_{PV-MED}$ dataset, and mean residuals (bottom left) and likelihood (top right) for the EU$_{PV-MED}$ dataset. The Voronoi cells used for selecting and weighting models are shown as black lines. The original GMPEs are red dots, plus/minus uncertainty are magenta/cyan dots. The contour for the zero residual is a thick black line, the -0.15/0.15 contours are dashed black lines and the -0.3/0.3 contours are thin black lines. For $T = 0.25$s.

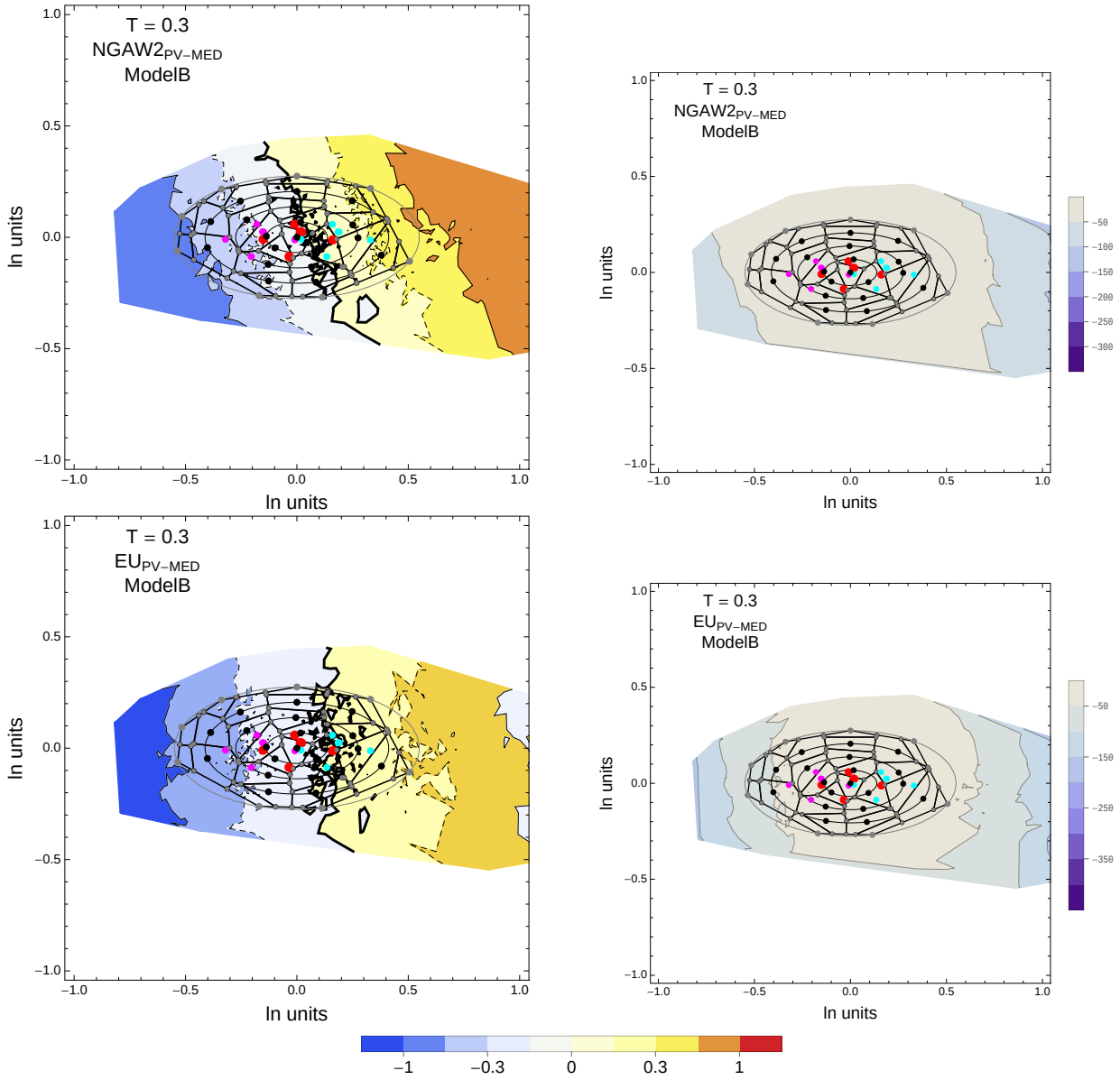



Figure 4.61: PVNGSv2: Contour Plots of selected mean residuals (top left) and likelihood (top right) for the NGA$_{PV-MED}$ dataset, and mean residuals (bottom left) and likelihood (top right) for the EU$_{PV-MED}$ dataset. The Voronoi cells used for selecting and weighting models are shown as black lines. The original GMPEs are red dots, plus/minus uncertainty are magenta/cyan dots. The contour for the zero residual is a thick black line, the -0.15/0.15 contours are dashed black lines and the -0.3/0.3 contours are thin black lines. For $T = 0.3$s.

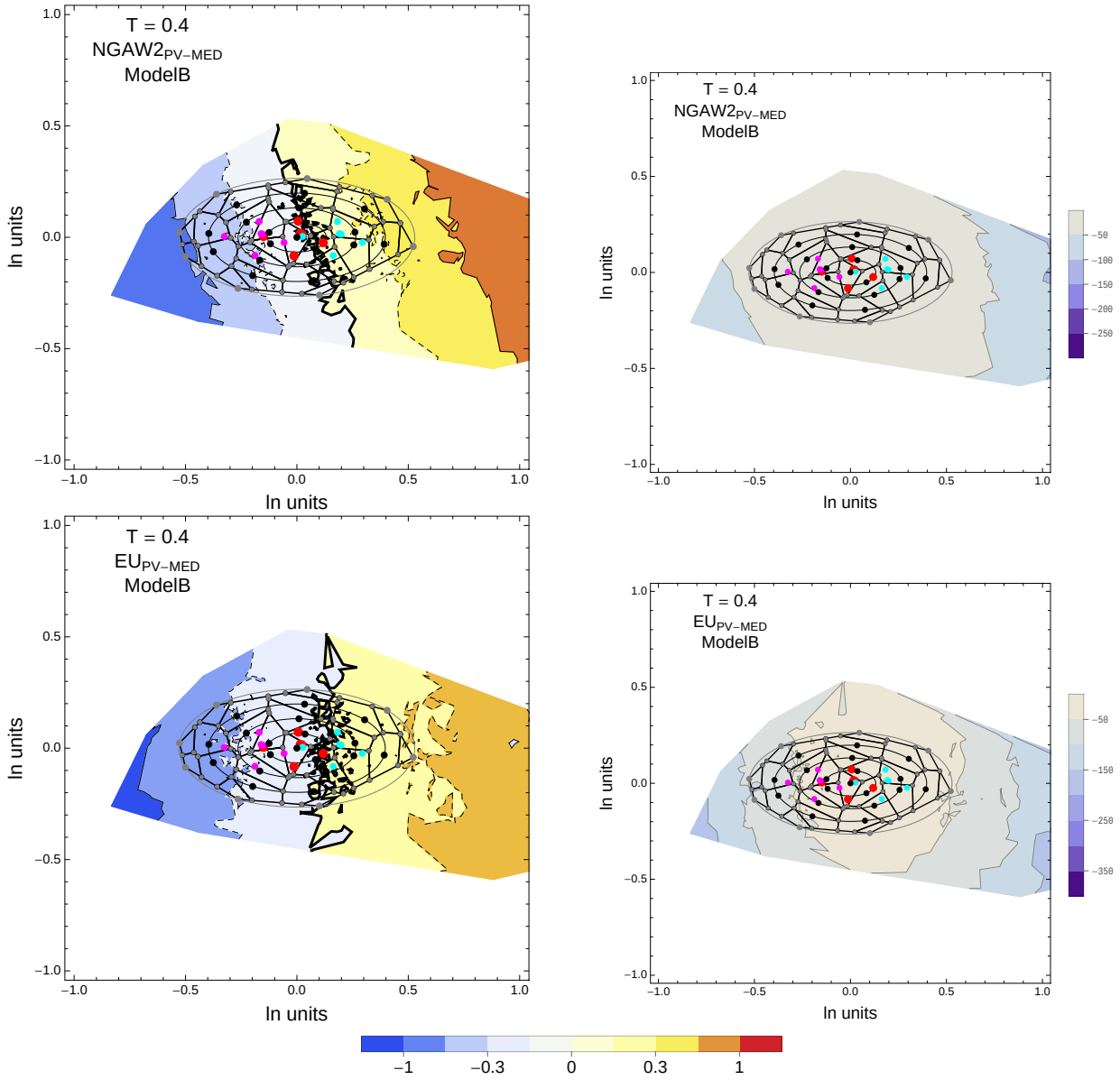



Figure 4.62: PVNGSv2: Contour Plots of selected mean residuals (top left) and likelihood (top right) for the NGA$_{PV-MED}$ dataset, and mean residuals (bottom left) and likelihood (top right) for the EU$_{PV-MED}$ dataset. The Voronoi cells used for selecting and weighting models are shown as black lines. The original GMPEs are red dots, plus/minus uncertainty are magenta/cyan dots. The contour for the zero residual is a thick black line, the -0.15/0.15 contours are dashed black lines and the -0.3/0.3 contours are thin black lines. For $T = 0.4$s.

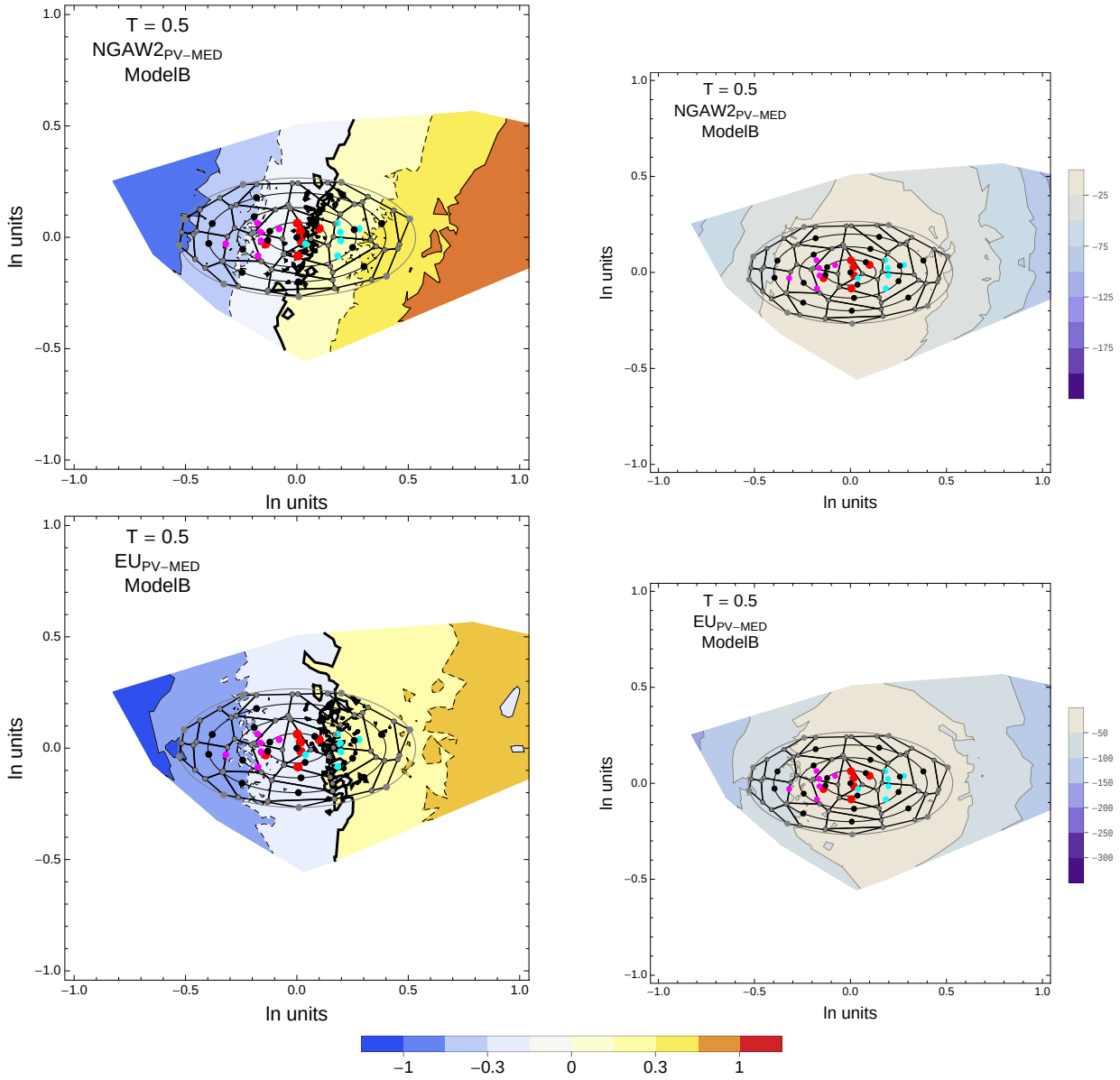



Figure 4.63: PVNGSv2: Contour Plots of selected mean residuals (top left) and likelihood (top right) for the NGA$_{PV-MED}$ dataset, and mean residuals (bottom left) and likelihood (top right) for the EU$_{PV-MED}$ dataset. The Voronoi cells used for selecting and weighting models are shown as black lines. The original GMPEs are red dots, plus/minus uncertainty are magenta/cyan dots. The contour for the zero residual is a thick black line, the -0.15/0.15 contours are dashed black lines and the -0.3/0.3 contours are thin black lines. For $T = 0.5$s.

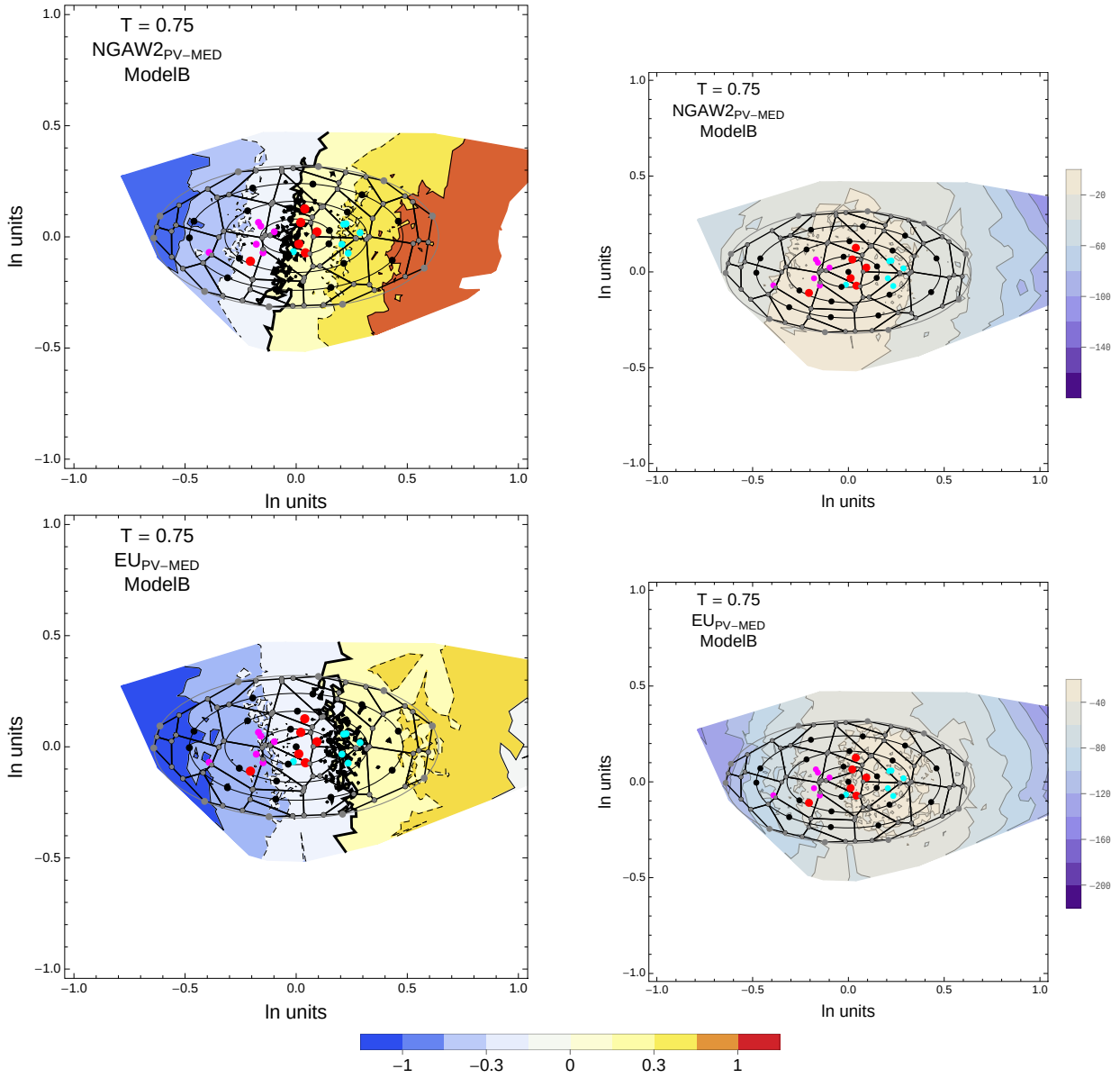



Figure 4.64: PVNGSv2: Contour Plots of selected mean residuals (top left) and likelihood (top right) for the NGA$_{PV-MED}$ dataset, and mean residuals (bottom left) and likelihood (top right) for the EU$_{PV-MED}$ dataset. The Voronoi cells used for selecting and weighting models are shown as black lines. The original GMPEs are red dots, plus/minus uncertainty are magenta/cyan dots. The contour for the zero residual is a thick black line, the -0.15/0.15 contours are dashed black lines and the -0.3/0.3 contours are thin black lines. For $T = 0.75$s.

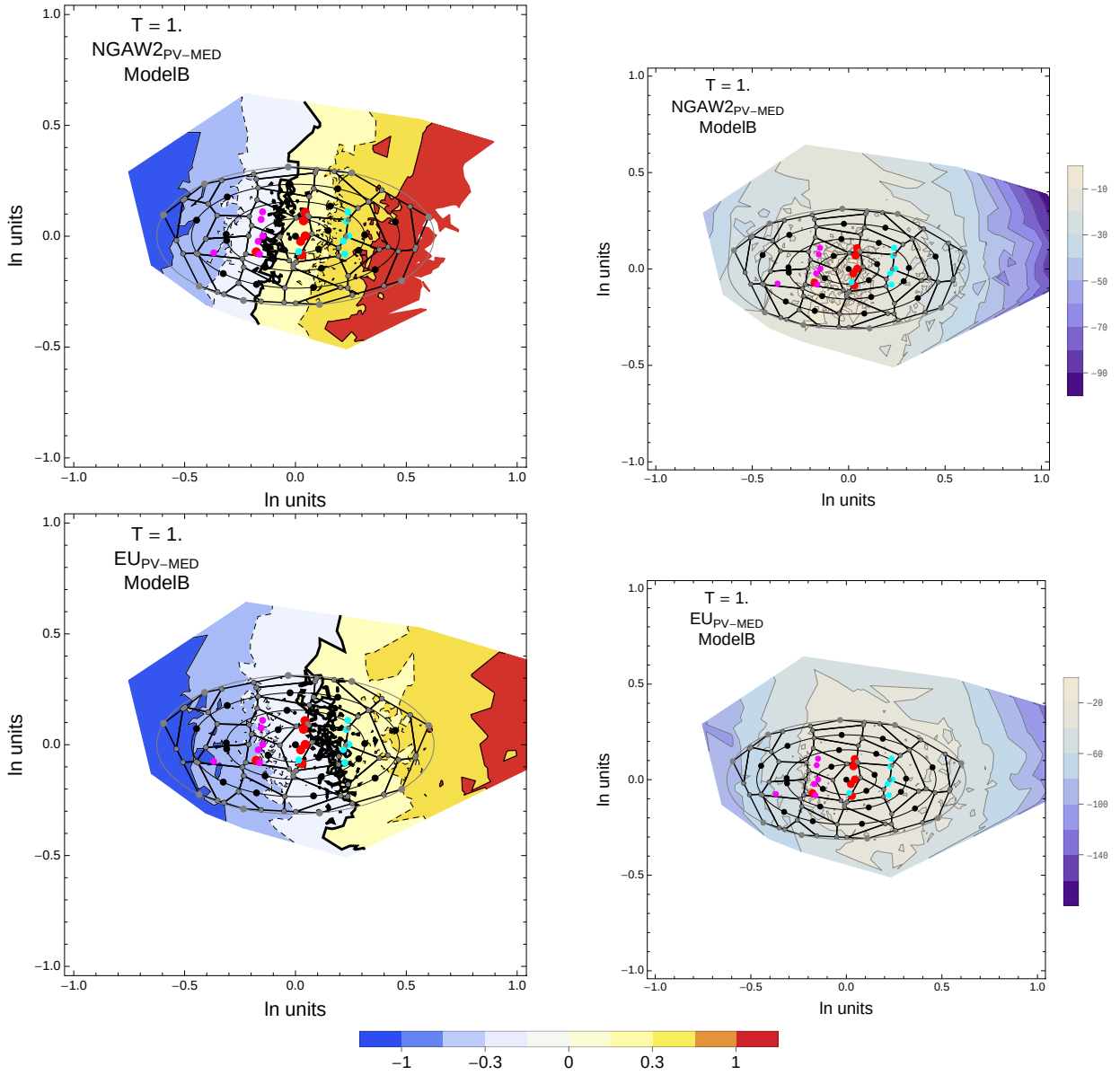



Figure 4.65: PVNGSv2: Contour Plots of selected mean residuals (top left) and likelihood (top right) for the NGA$_{PV-MED}$ dataset, and mean residuals (bottom left) and likelihood (top right) for the EU$_{PV-MED}$ dataset. The Voronoi cells used for selecting and weighting models are shown as black lines. The original GMPEs are red dots, plus/minus uncertainty are magenta/cyan dots. The contour for the zero residual is a thick black line, the -0.15/0.15 contours are dashed black lines and the -0.3/0.3 contours are thin black lines. For $T = 1$.s.

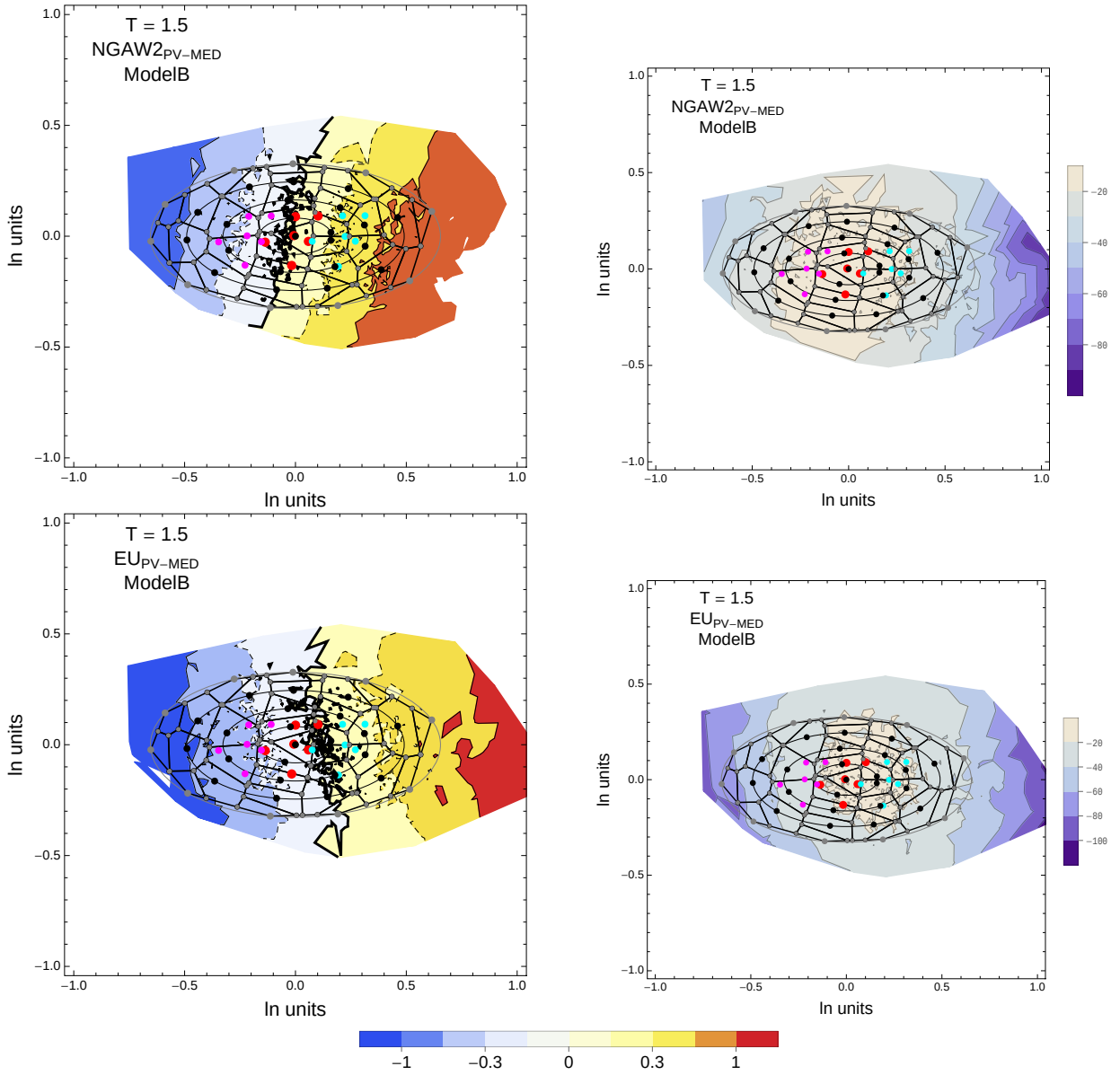



Figure 4.66: PVNGSv2: Contour Plots of selected mean residuals (top left) and likelihood (top right) for the NGA$_{PV-MED}$ dataset, and mean residuals (bottom left) and likelihood (top right) for the EU$_{PV-MED}$ dataset. The Voronoi cells used for selecting and weighting models are shown as black lines. The original GMPEs are red dots, plus/minus uncertainty are magenta/cyan dots. The contour for the zero residual is a thick black line, the -0.15/0.15 contours are dashed black lines and the -0.3/0.3 contours are thin black lines. For $T = 1.5$s.

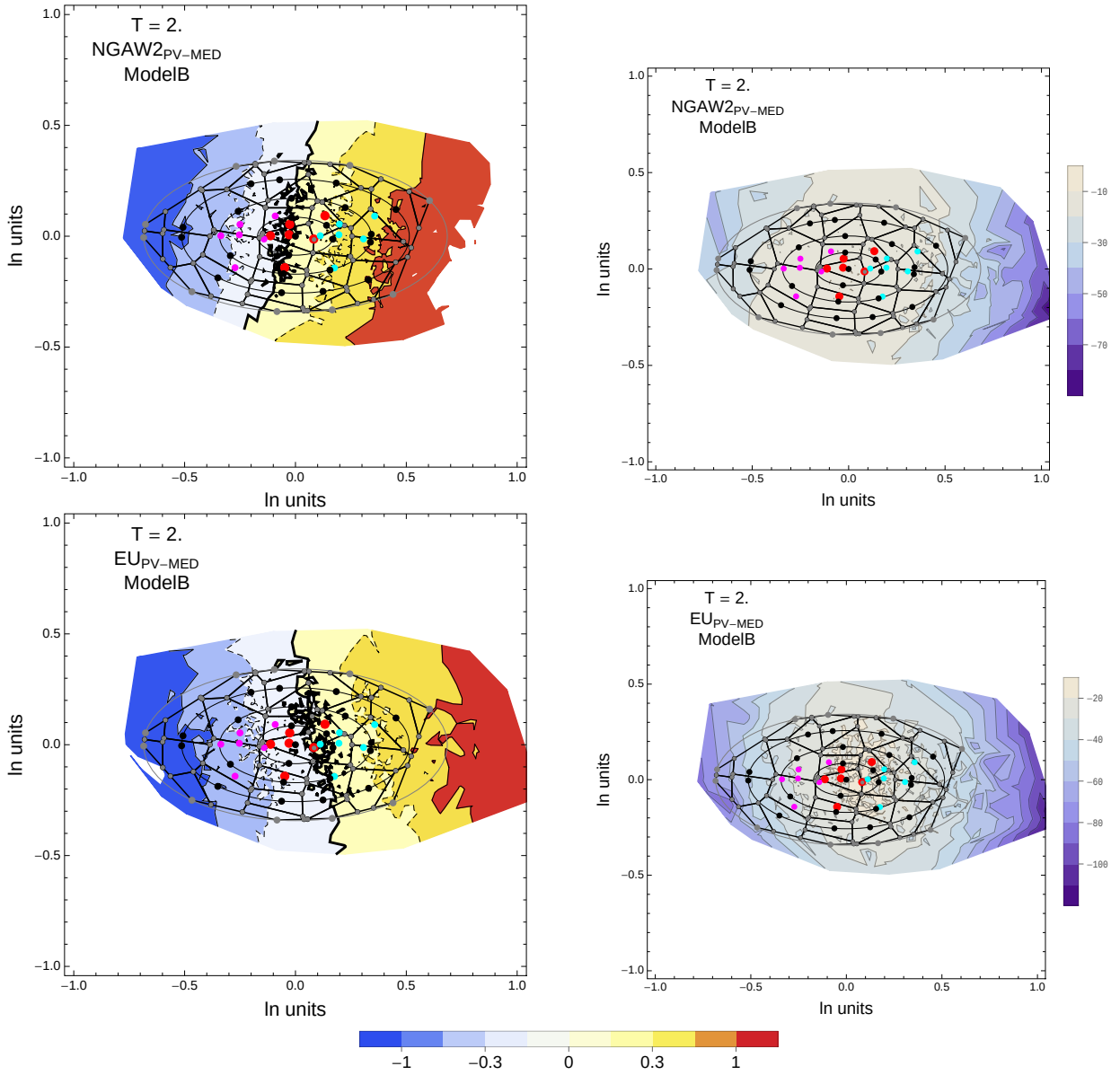



Figure 4.67: PVNGSv2: Contour Plots of selected mean residuals (top left) and likelihood (top right) for the $\text{NGA}_{PV-MED}$ dataset, and mean residuals (bottom left) and likelihood (top right) for the $\text{EU}_{PV-MED}$ dataset. The Voronoi cells used for selecting and weighting models are shown as black lines. The original GMPEs are red dots, plus/minus uncertainty are magenta/cyan dots. The contour for the zero residual is a thick black line, the -0.15/0.15 contours are dashed black lines and the -0.3/0.3 contours are thin black lines. For $T = 2$.s.

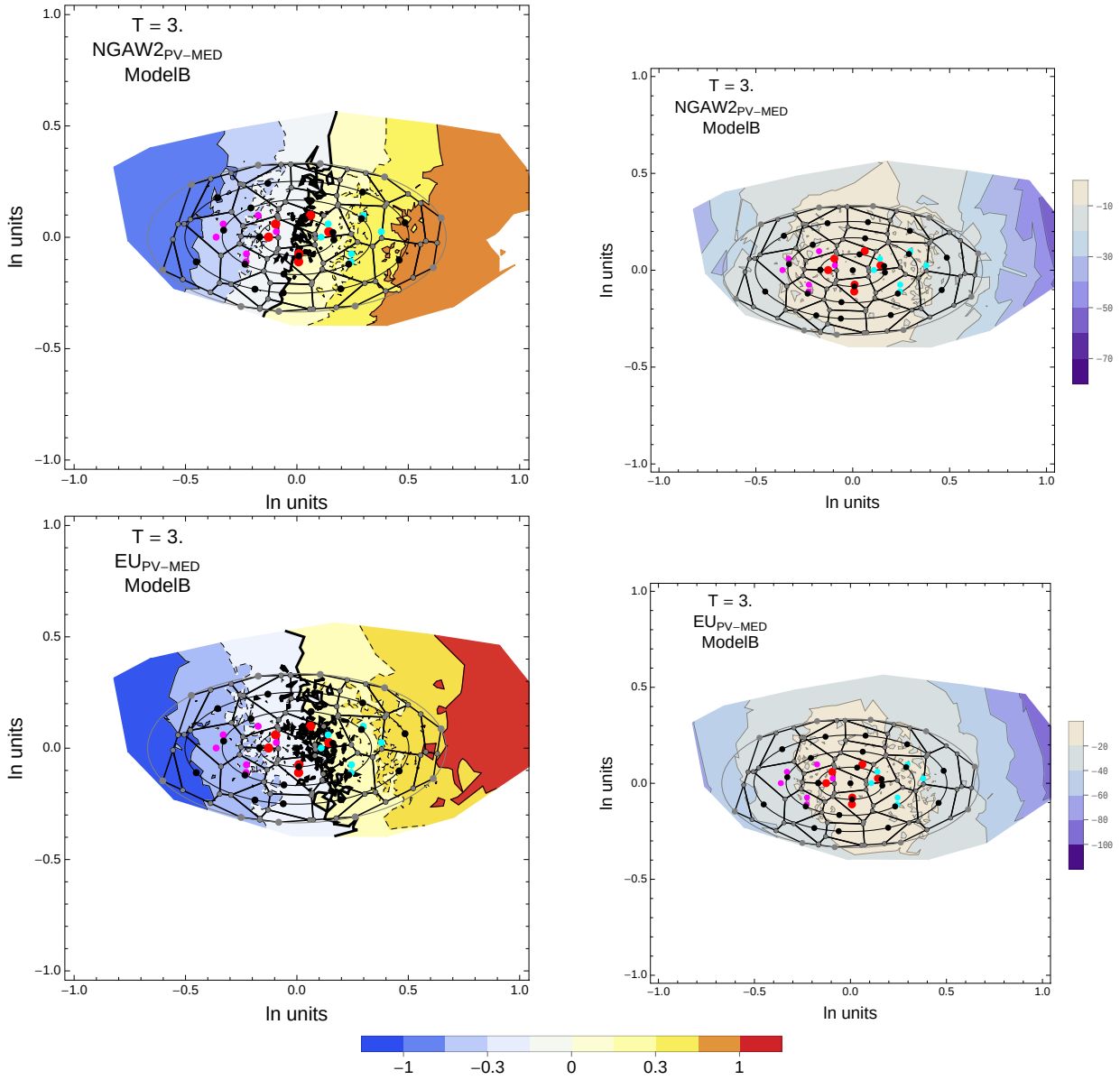



Figure 4.68: PVNGSv2: Contour Plots of selected mean residuals (top left) and likelihood (top right) for the NGA$_{PV-MED}$ dataset, and mean residuals (bottom left) and likelihood (top right) for the EU$_{PV-MED}$ dataset. The Voronoi cells used for selecting and weighting models are shown as black lines. The original GMPEs are red dots, plus/minus uncertainty are magenta/cyan dots. The contour for the zero residual is a thick black line, the -0.15/0.15 contours are dashed black lines and the -0.3/0.3 contours are thin black lines. For $T = 3$.s.

### 4.1.4 Hazard Curves

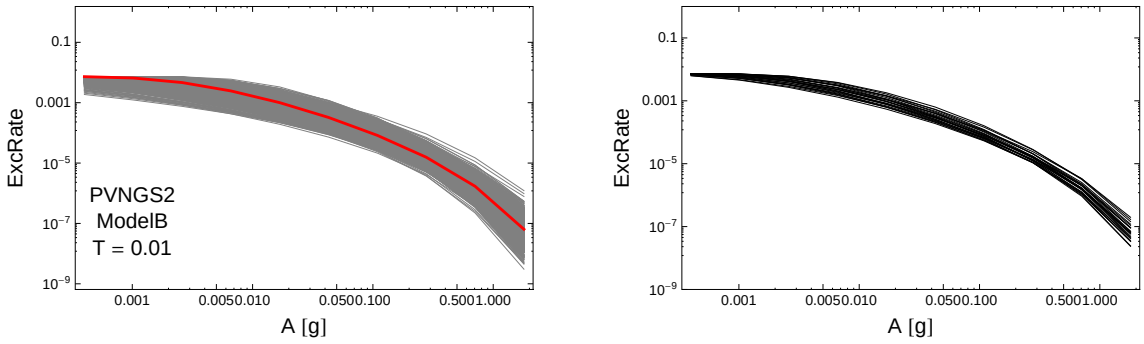



Figure 4.69: Hazard curves, calculated for a simple source model for PVNGS2. Left: 2000 hazard curves for all sampled B-models (gray) and the center model of the ModelB distribution (red); Right: hazard curves of selected models. For $T = 0.01$s.

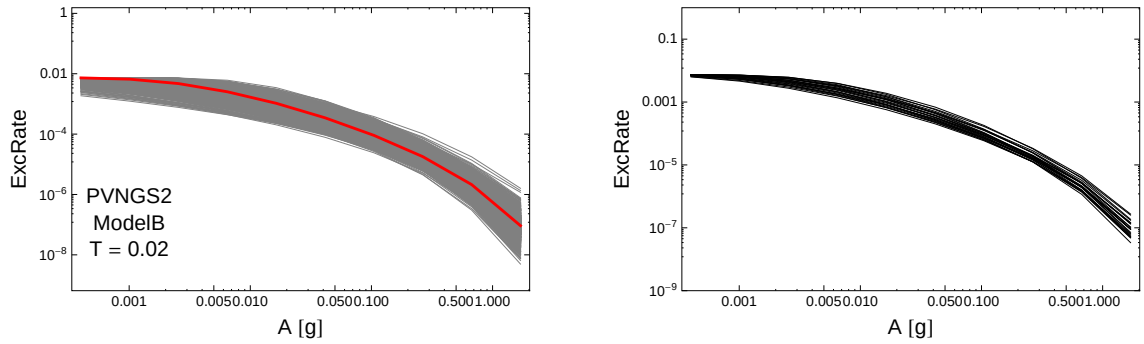



Figure 4.70: Hazard curves, calculated for a simple source model for PVNGS2. Left: 2000 hazard curves for all sampled B-models (gray) and the center model of the ModelB distribution (red); Right: hazard curves of selected models. For $T = 0.02$s.

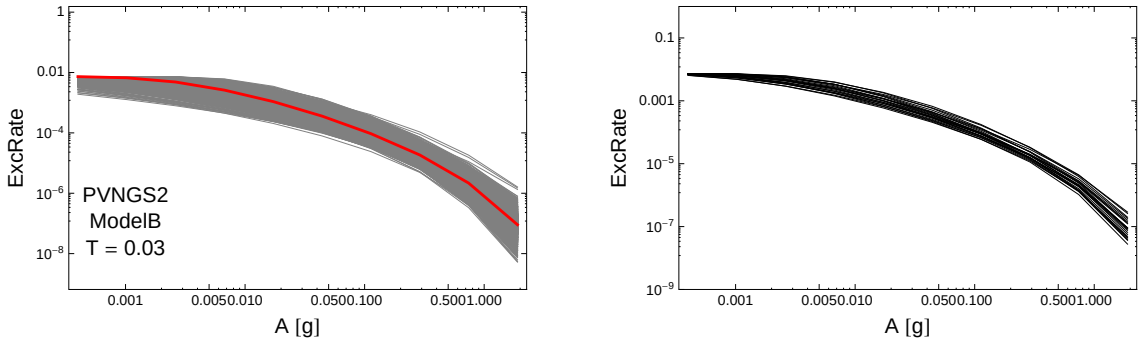



Figure 4.71: Hazard curves, calculated for a simple source model for PVNGS2. Left: 2000 hazard curves for all sampled B-models (gray) and the center model of the ModelB distribution (red); Right: hazard curves of selected models. For $T = 0.03$s.

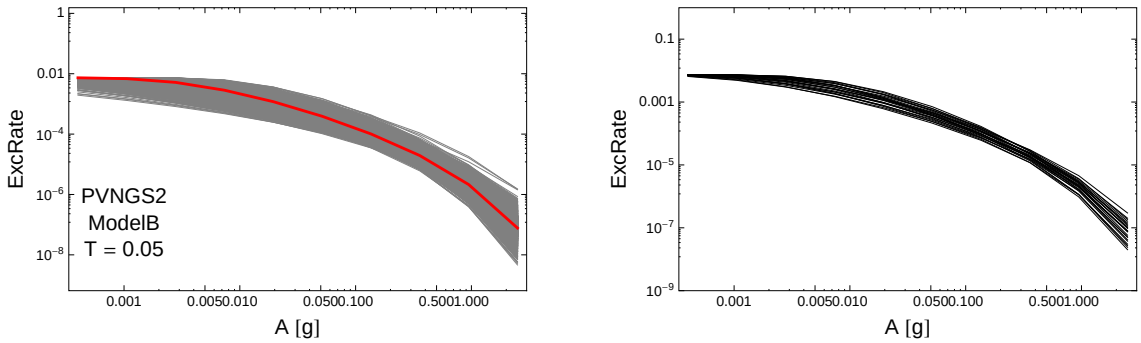



Figure 4.72: Hazard curves, calculated for a simple source model for PVNGS2. Left: 2000 hazard curves for all sampled B-models (gray) and the center model of the ModelB distribution (red); Right: hazard curves of selected models. For $T = 0.05$s.

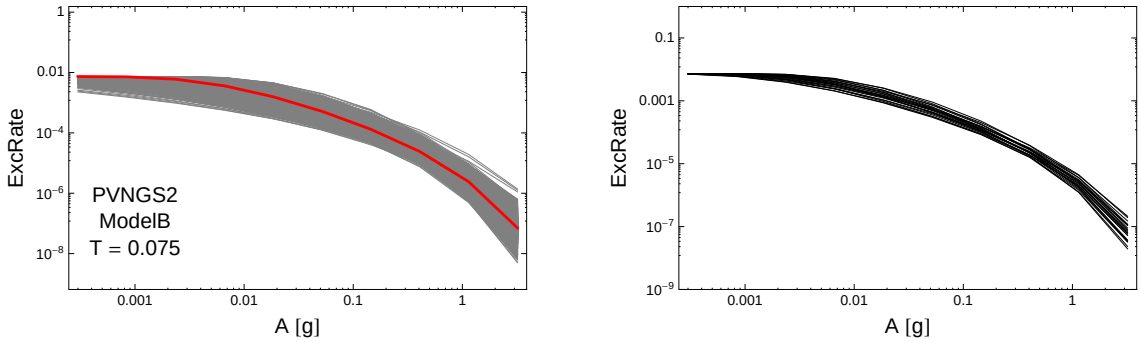



Figure 4.73: Hazard curves, calculated for a simple source model for PVNGS2. Left: 2000 hazard curves for all sampled B-models (gray) and the center model of the ModelB distribution (red); Right: hazard curves of selected models. For $T = 0.075$s.

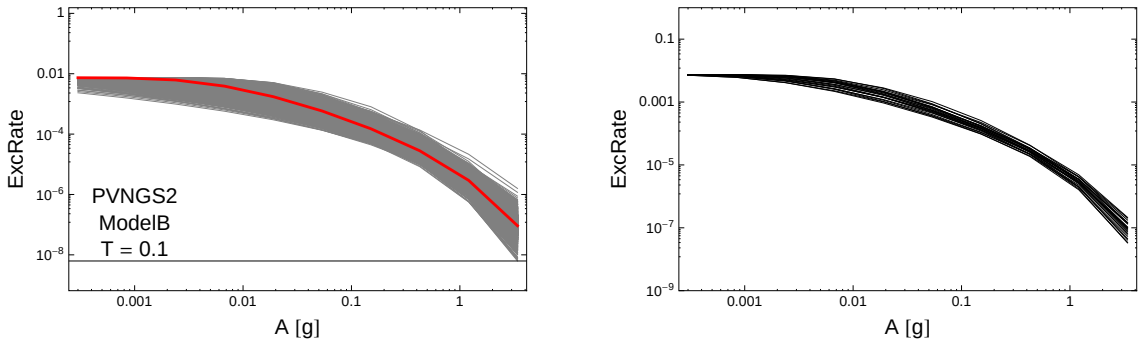



Figure 4.74: Hazard curves, calculated for a simple source model for PVNGS2. Left: 2000 hazard curves for all sampled B-models (gray) and the center model of the ModelB distribution (red); Right: hazard curves of selected models. For $T = 0.1$s.

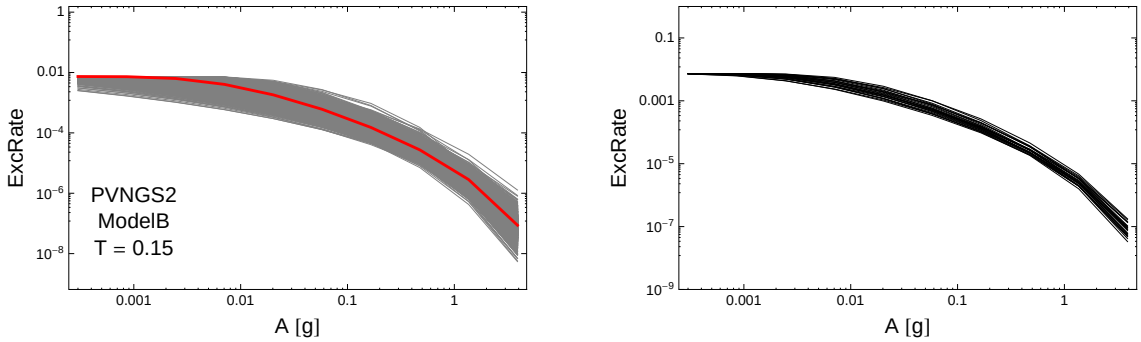



Figure 4.75: Hazard curves, calculated for a simple source model for PVNGS2. Left: 2000 hazard curves for all sampled B-models (gray) and the center model of the ModelB distribution (red); Right: hazard curves of selected models. For $T = 0.15$s.

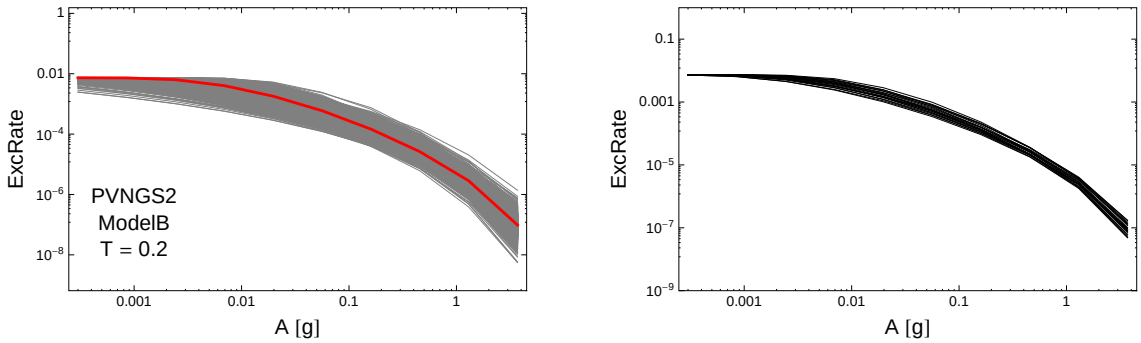



Figure 4.76: Hazard curves, calculated for a simple source model for PVNGS2. Left: 2000 hazard curves for all sampled B-models (gray) and the center model of the ModelB distribution (red); Right: hazard curves of selected models. For $T = 0.2$s.

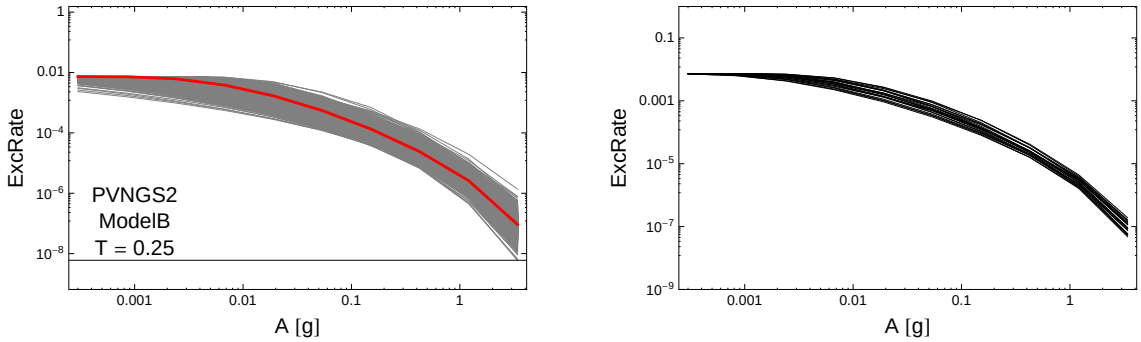



Figure 4.77: Hazard curves, calculated for a simple source model for PVNGS2. Left: 2000 hazard curves for all sampled B-models (gray) and the center model of the ModelB distribution (red); Right: hazard curves of selected models. For $T = 0.25$s.

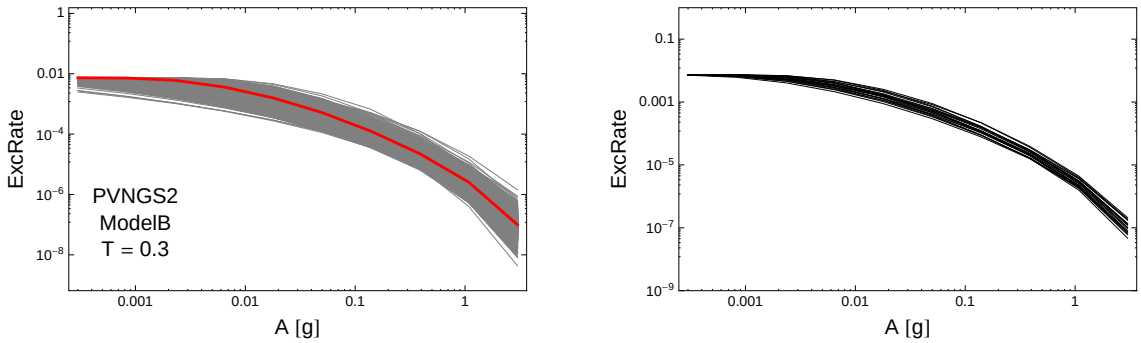



Figure 4.78: Hazard curves, calculated for a simple source model for PVNGS2. Left: 2000 hazard curves for all sampled B-models (gray) and the center model of the ModelB distribution (red); Right: hazard curves of selected models. For $T = 0.3$s.

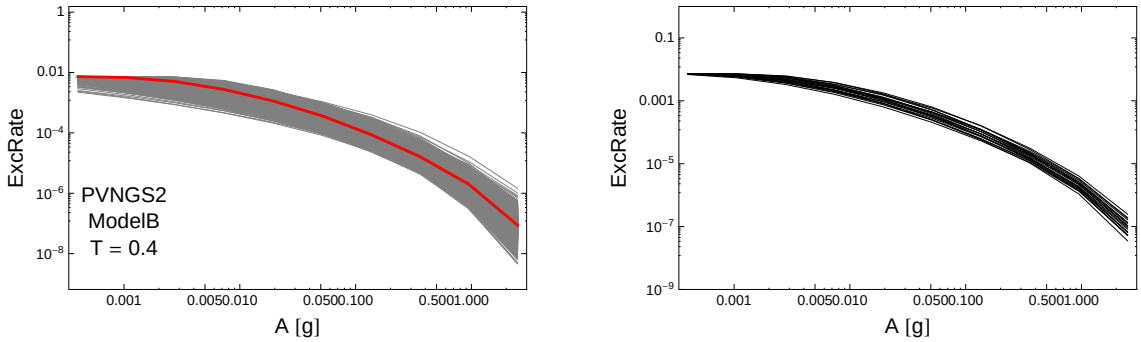



Figure 4.79: Hazard curves, calculated for a simple source model for PVNGS2. Left: 2000 hazard curves for all sampled B-models (gray) and the center model of the ModelB distribution (red); Right: hazard curves of selected models. For $T = 0.4$s.

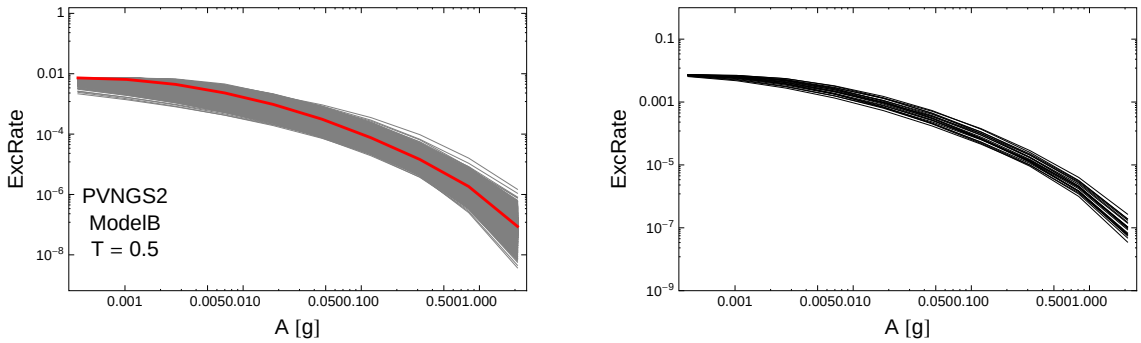



Figure 4.80: Hazard curves, calculated for a simple source model for PVNGS2. Left: 2000 hazard curves for all sampled B-models (gray) and the center model of the ModelB distribution (red); Right: hazard curves of selected models. For $T = 0.5$s.

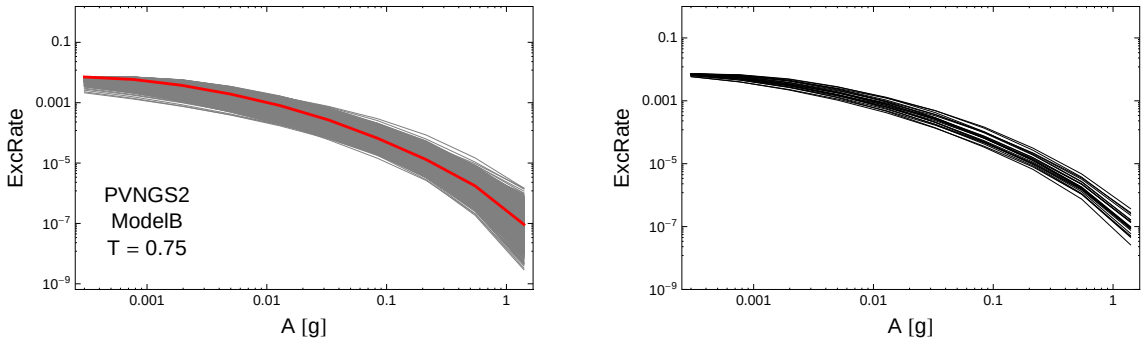



Figure 4.81: Hazard curves, calculated for a simple source model for PVNGS2. Left: 2000 hazard curves for all sampled B-models (gray) and the center model of the ModelB distribution (red); Right: hazard curves of selected models. For $T = 0.75$s.

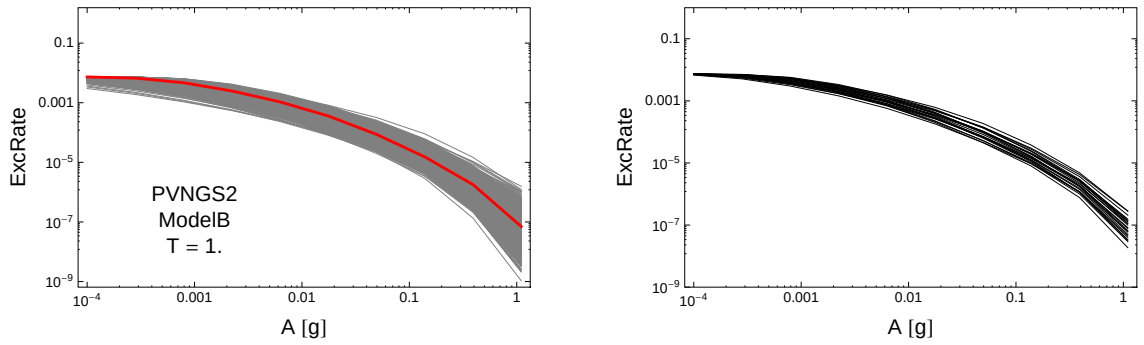



Figure 4.82: Hazard curves, calculated for a simple source model for PVNGS2. Left: 2000 hazard curves for all sampled B-models (gray) and the center model of the ModelB distribution (red); Right: hazard curves of selected models. For $T = 1$.s.

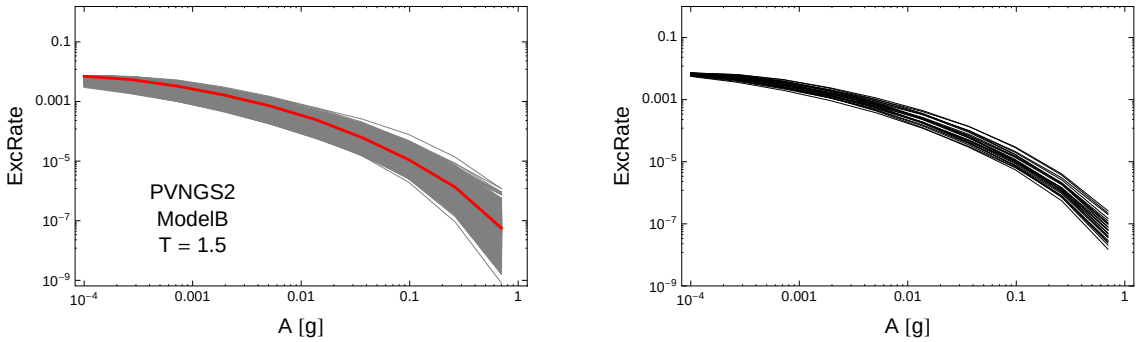



Figure 4.83: Hazard curves, calculated for a simple source model for PVNGS2. Left: 2000 hazard curves for all sampled B-models (gray) and the center model of the ModelB distribution (red); Right: hazard curves of selected models. For $T = 1.5$s.

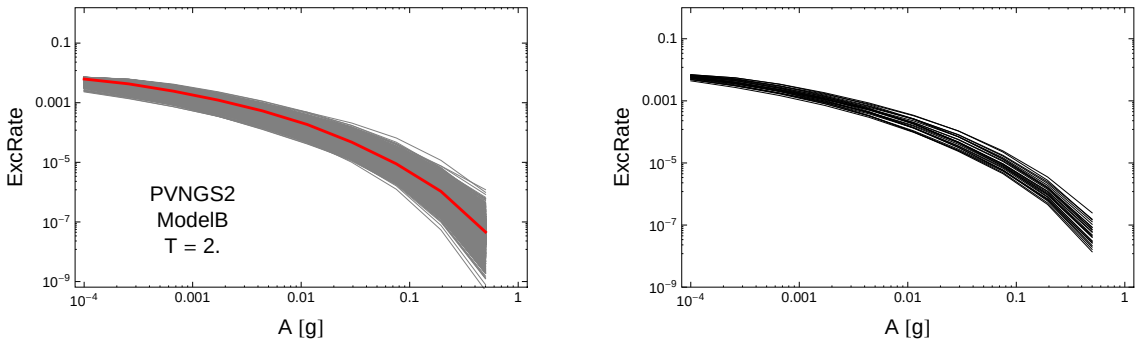



Figure 4.84: Hazard curves, calculated for a simple source model for PVNGS2. Left: 2000 hazard curves for all sampled B-models (gray) and the center model of the ModelB distribution (red); Right: hazard curves of selected models. For $T = 2.$s.

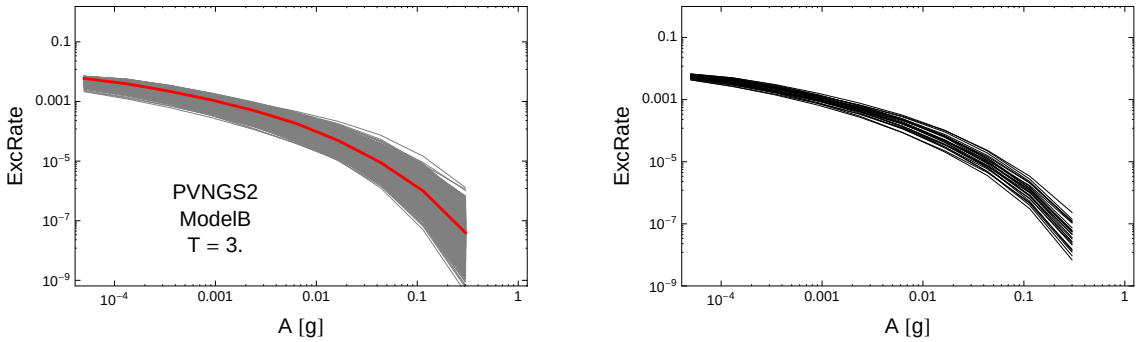



Figure 4.85: Hazard curves, calculated for a simple source model for PVNGS2. Left: 2000 hazard curves for all sampled B-models (gray) and the center model of the ModelB distribution (red); Right: hazard curves of selected models. For $T = 3$.s.

### 4.1.5 CDF Plots

**T = 0.01s**

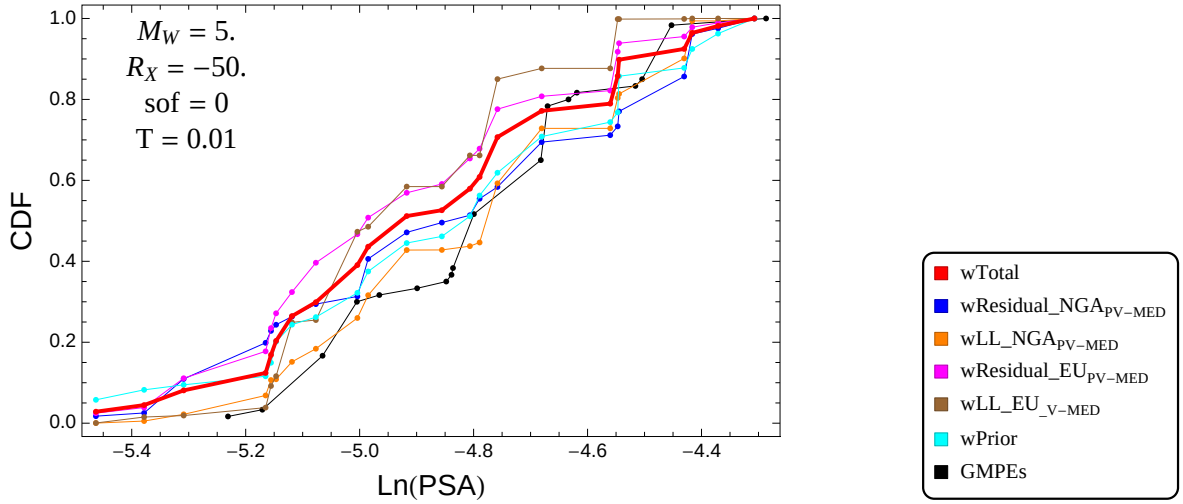



Figure 4.86: PVNGSv2: Cumulative distribution function of GMPEs (black) and selected models, for different sets of weights, for a scenario with $M = 5.$, $R_x = -50.$, $F = 0$, and $T = 0.01$s

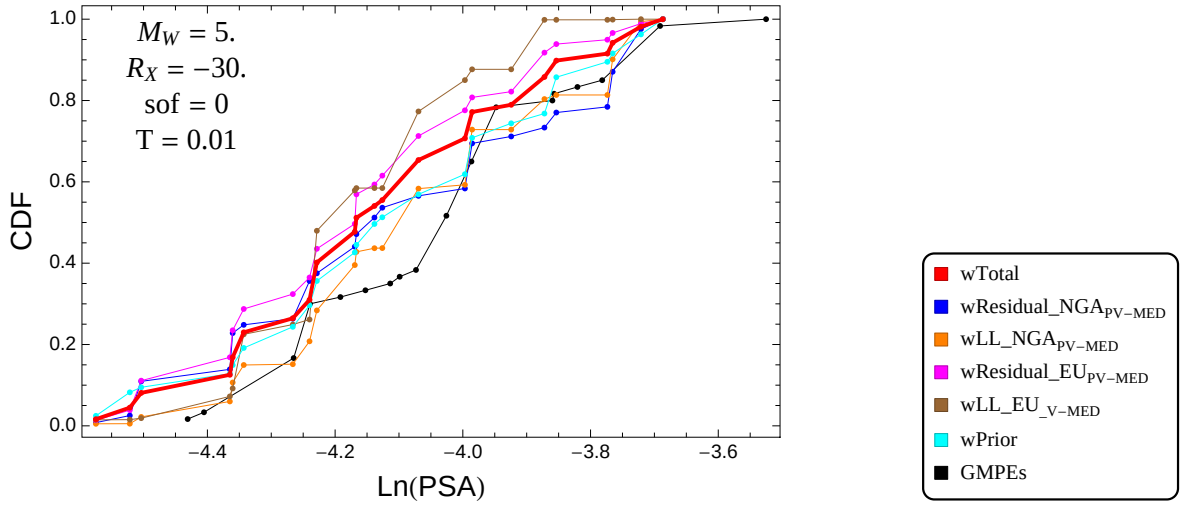



Figure 4.87: PVNGSv2: Cumulative distribution function of GMPEs (black) and selected models, for different sets of weights, for a scenario with $M = 5.$, $R_x = -30.$, $F = 0$, and $T = 0.01$s

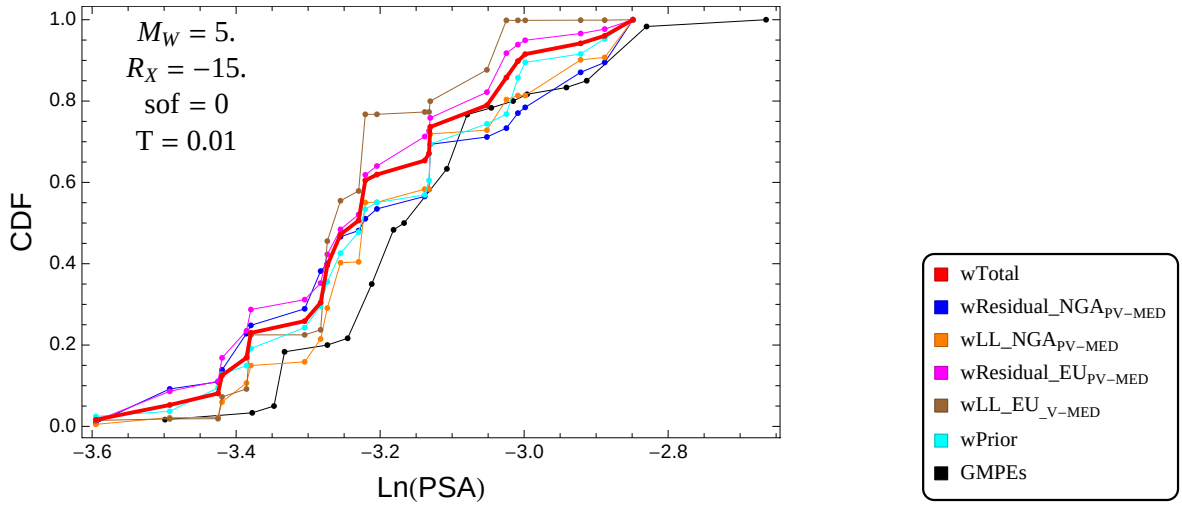



Figure 4.88: PVNGSv2: Cumulative distribution function of GMPEs (black) and selected models, for different sets of weights, for a scenario with $M = 5.$, $R_x = -15.$, $F = 0$, and $T = 0.01$s

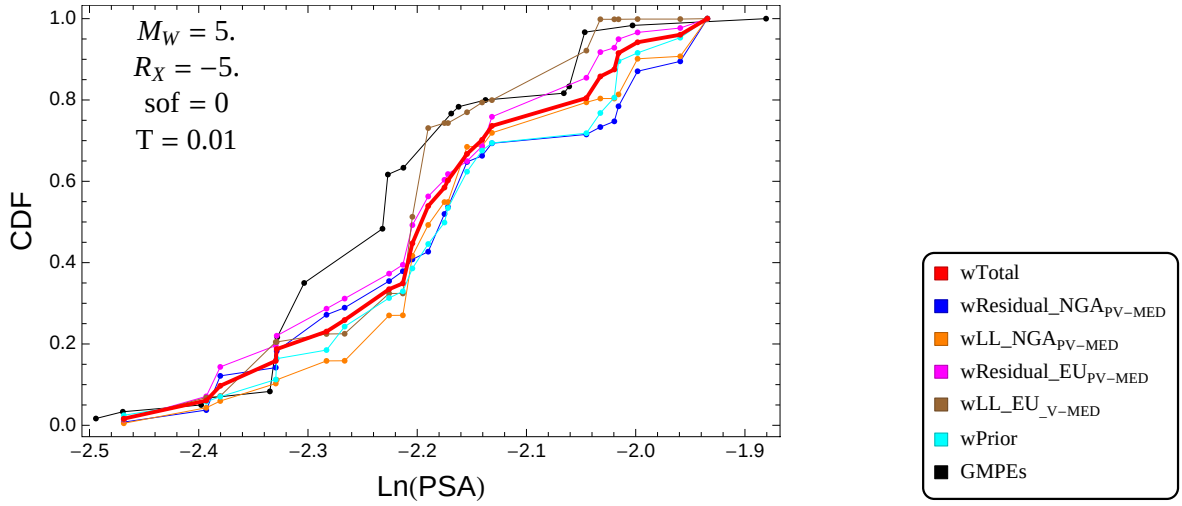



Figure 4.89: PVNGSv2: Cumulative distribution function of GMPEs (black) and selected models, for different sets of weights, for a scenario with $M = 5.$, $R_x = -5.$, $F = 0$, and $T = 0.01$s

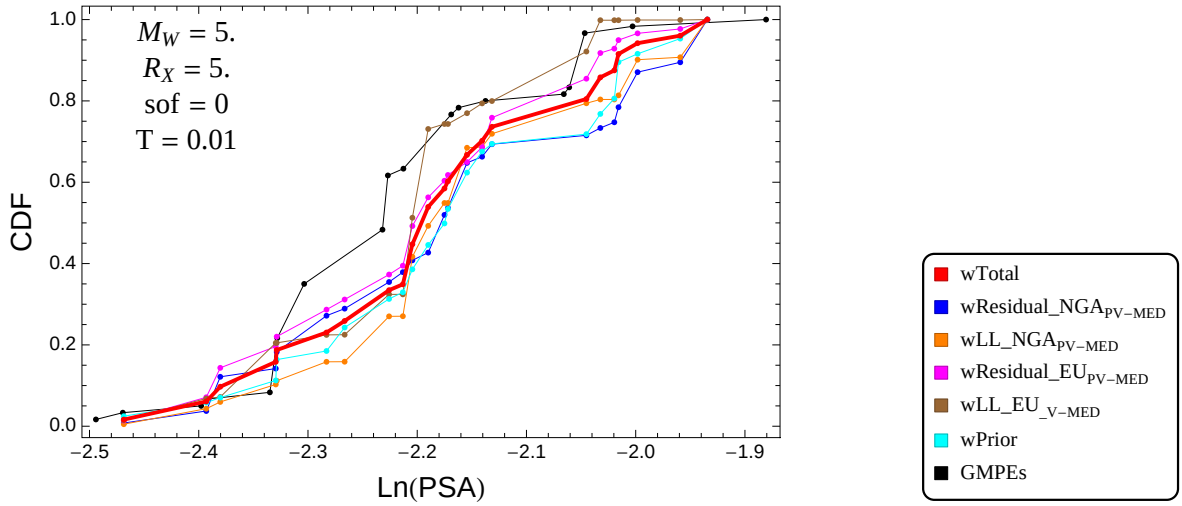



Figure 4.90: PVNGSv2: Cumulative distribution function of GMPEs (black) and selected models, for different sets of weights, for a scenario with $M = 5.$, $R_x = 5.$, $F = 0$, and $T = 0.01$s

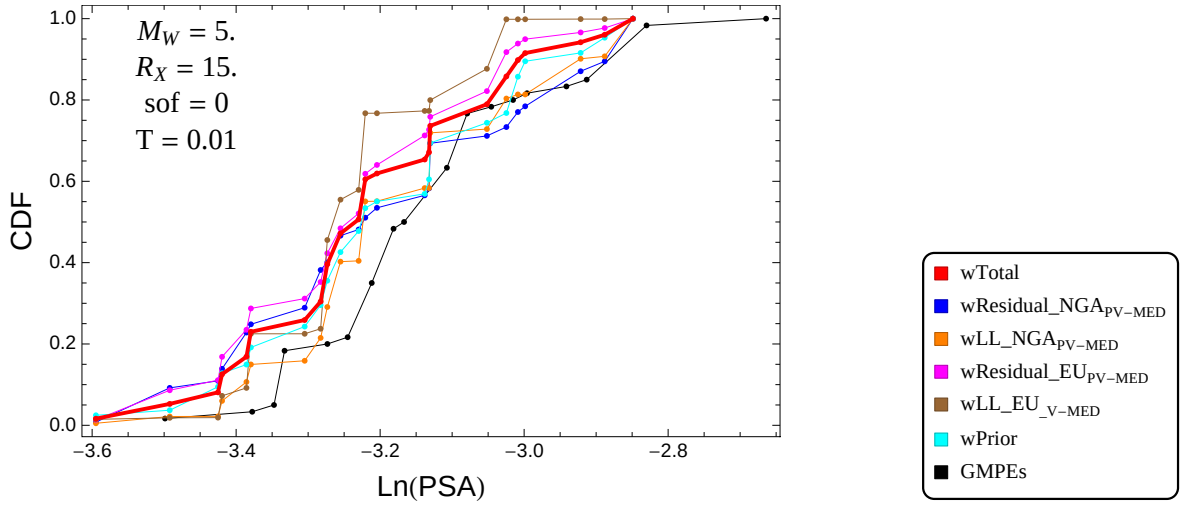



Figure 4.91: PVNGSv2: Cumulative distribution function of GMPEs (black) and selected models, for different sets of weights, for a scenario with $M = 5.$, $R_x = 15.$, $F = 0$, and $T = 0.01$s

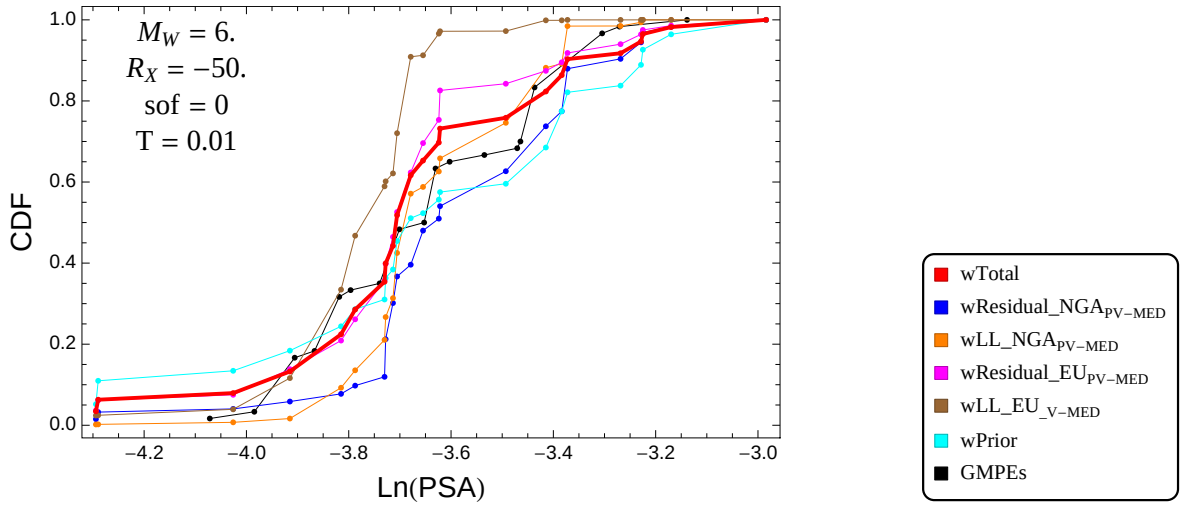



Figure 4.92: PVNGSv2: Cumulative distribution function of GMPEs (black) and selected models, for different sets of weights, for a scenario with $M = 6.$, $R_x = -50.$, $F = 0$, and $T = 0.01$s

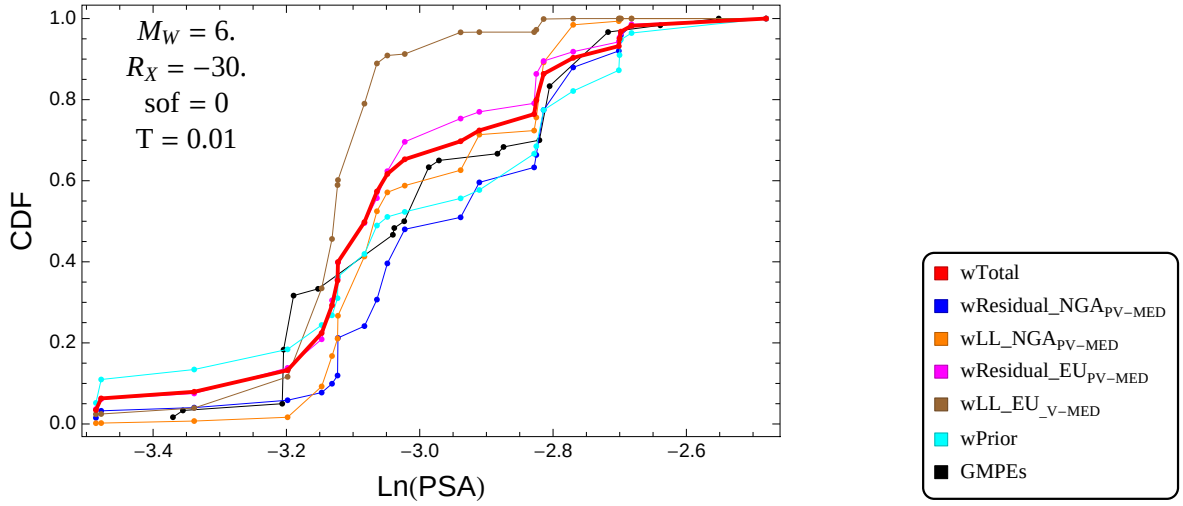



Figure 4.93: PVNGSv2: Cumulative distribution function of GMPEs (black) and selected models, for different sets of weights, for a scenario with $M = 6.$, $R_x = -30.$, $F = 0$, and $T = 0.01$s

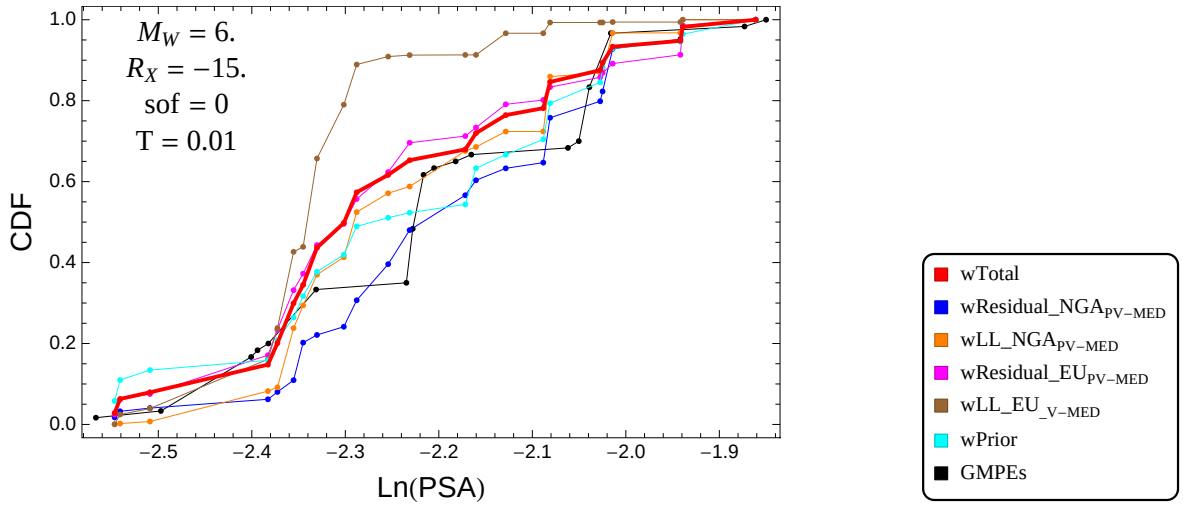



Figure 4.94: PVNGSv2: Cumulative distribution function of GMPEs (black) and selected models, for different sets of weights, for a scenario with $M = 6.$, $R_x = -15.$, $F = 0$, and $T = 0.01$s

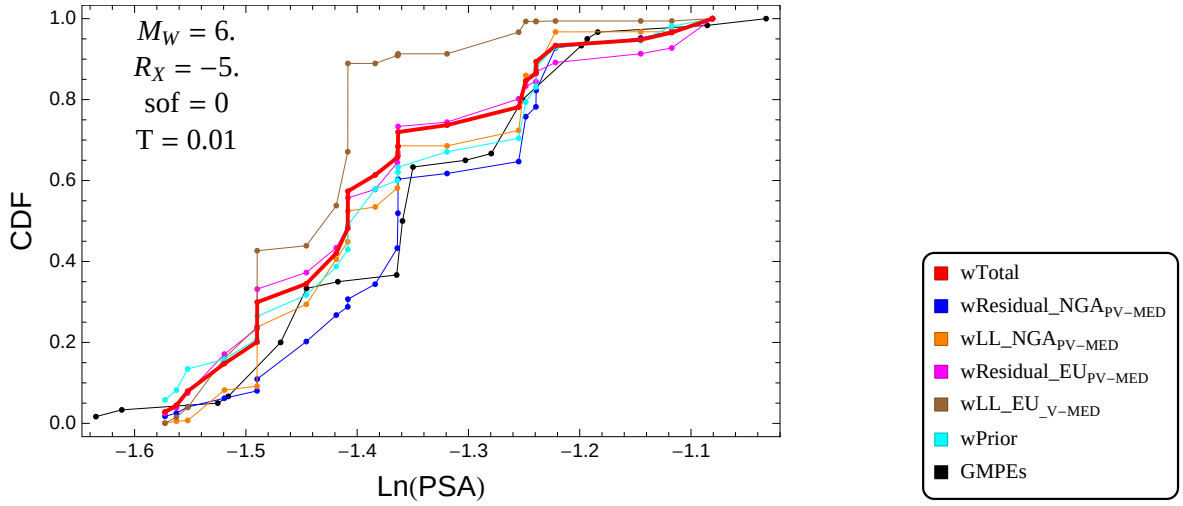



Figure 4.95: PVNGSv2: Cumulative distribution function of GMPEs (black) and selected models, for different sets of weights, for a scenario with $M = 6.$, $R_x = -5.$, $F = 0$, and $T = 0.01$s

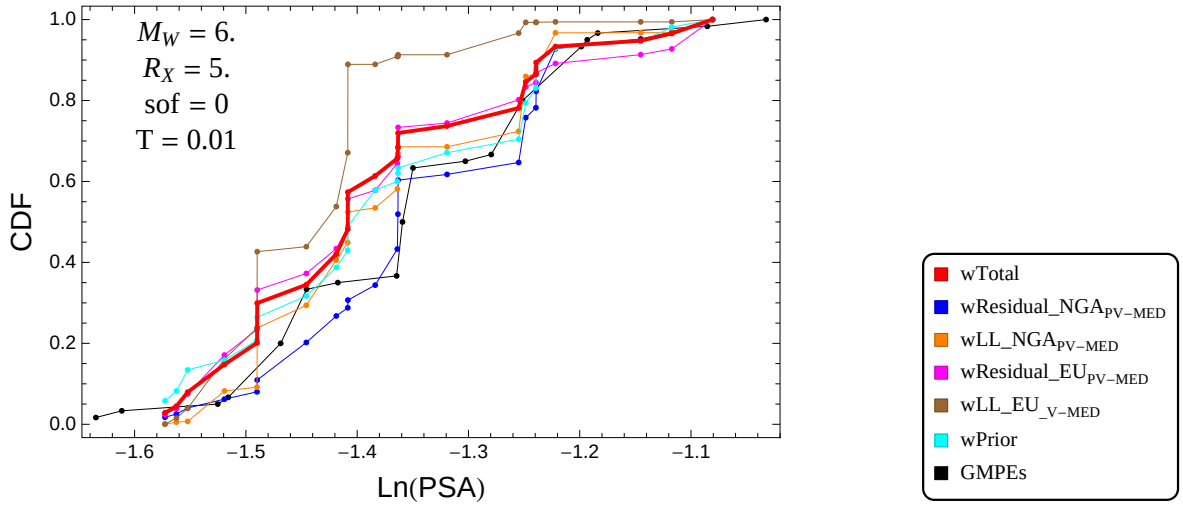



Figure 4.96: PVNGSv2: Cumulative distribution function of GMPEs (black) and selected models, for different sets of weights, for a scenario with $M = 6.$, $R_x = 5.$, $F = 0$, and $T = 0.01$s

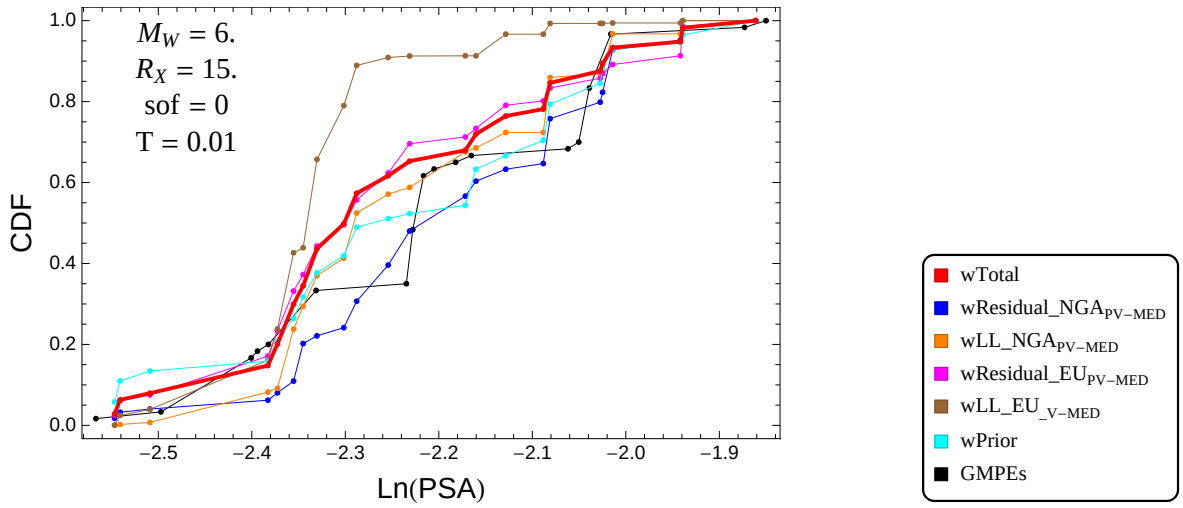



Figure 4.97: PVNGSv2: Cumulative distribution function of GMPEs (black) and selected models, for different sets of weights, for a scenario with $M = 6.$, $R_x = 15.$, $F = 0$, and $T = 0.01$s

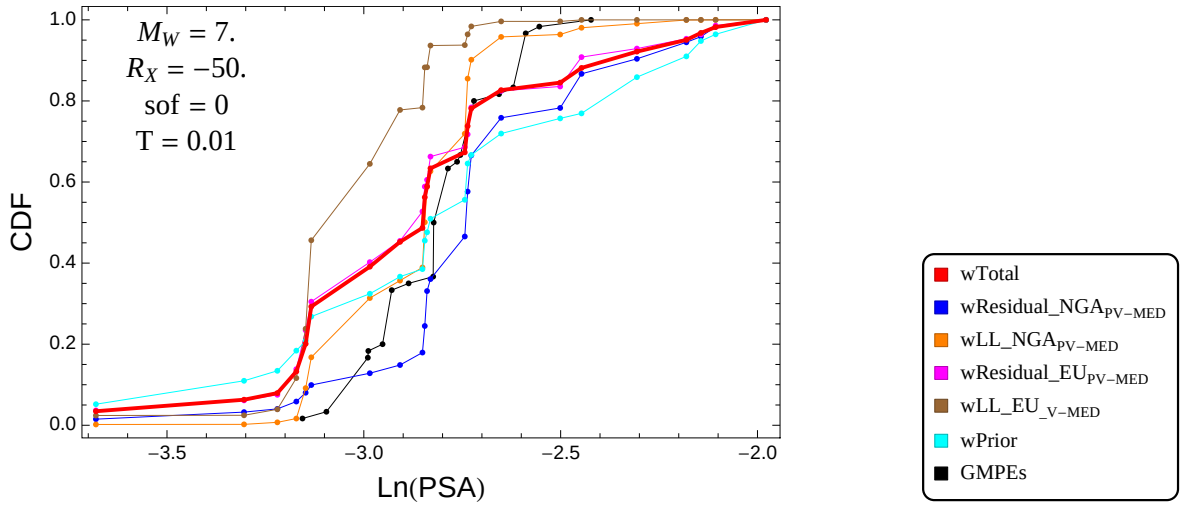



Figure 4.98: PVNGSv2: Cumulative distribution function of GMPEs (black) and selected models, for different sets of weights, for a scenario with $M = 7.$, $R_x = -50.$, $F = 0$, and $T = 0.01$s

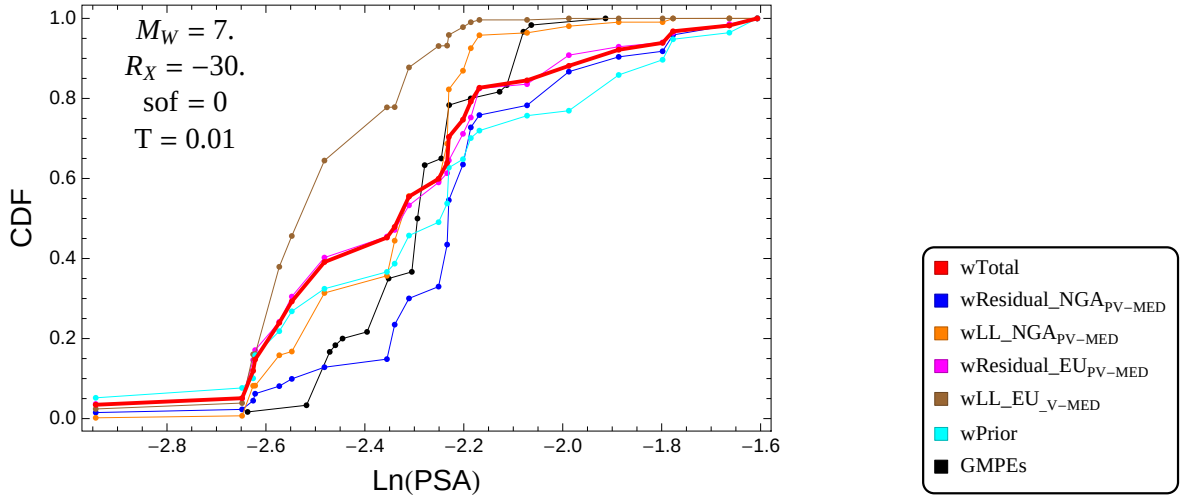



Figure 4.99: PVNGSv2: Cumulative distribution function of GMPEs (black) and selected models, for different sets of weights, for a scenario with $M = 7.$, $R_x = -30.$, $F = 0$, and $T = 0.01$s

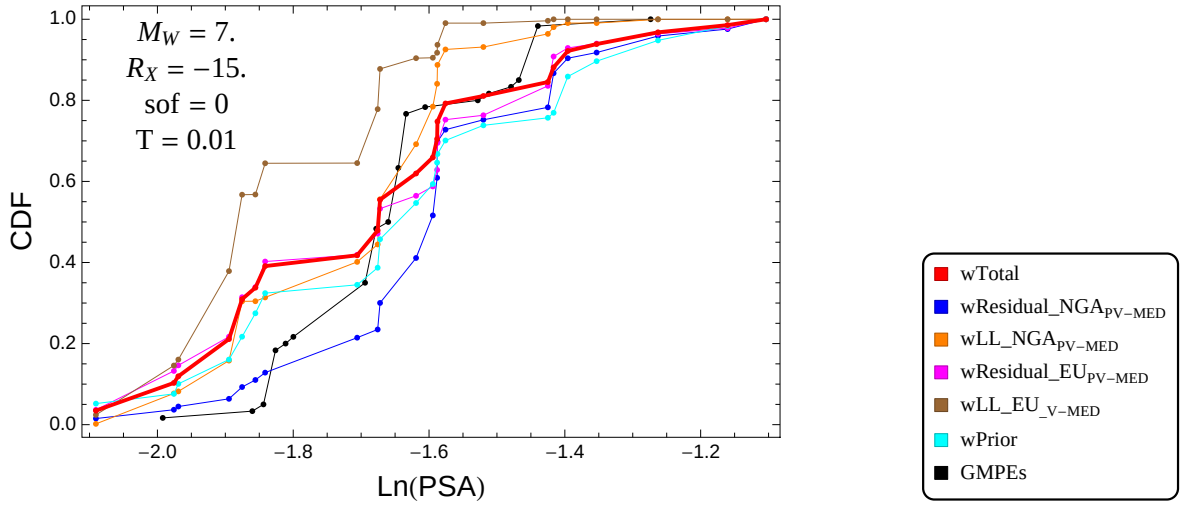



Figure 4.100: PVNGSv2: Cumulative distribution function of GMPEs (black) and selected models, for different sets of weights, for a scenario with $M = 7.$, $R_x = -15.$, $F = 0$, and $T = 0.01$s

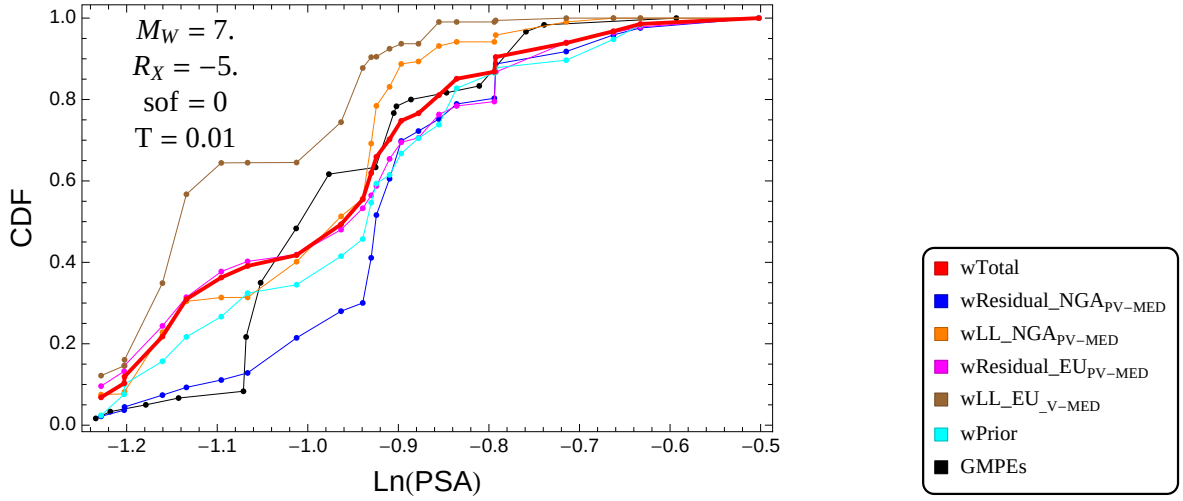



Figure 4.101: PVNGSv2: Cumulative distribution function of GMPEs (black) and selected models, for different sets of weights, for a scenario with $M = 7.$, $R_x = -5.$, $F = 0$, and $T = 0.01$s

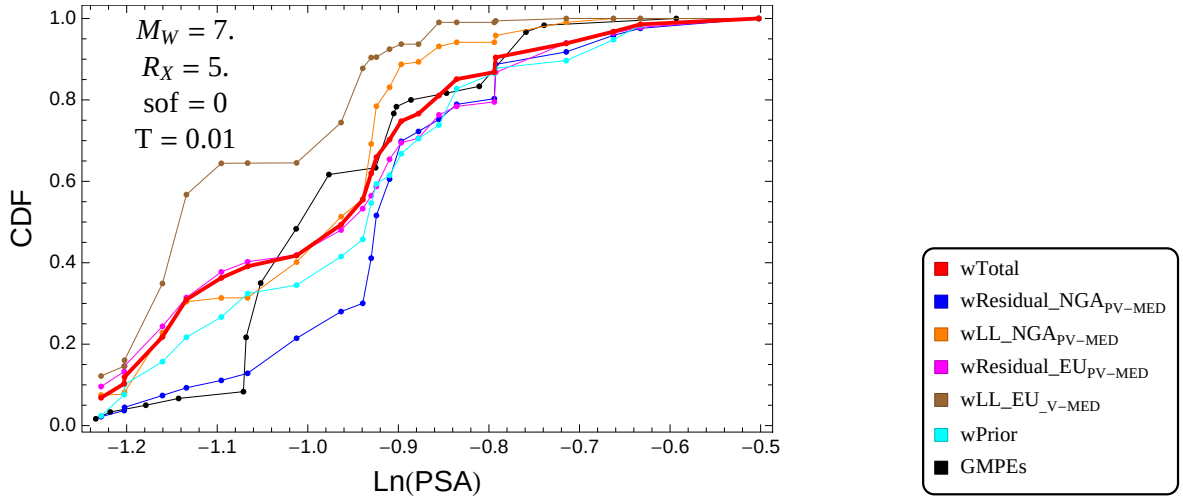



Figure 4.102: PVNGSv2: Cumulative distribution function of GMPEs (black) and selected models, for different sets of weights, for a scenario with $M = 7.$, $R_x = 5.$, $F = 0$, and $T = 0.01$s

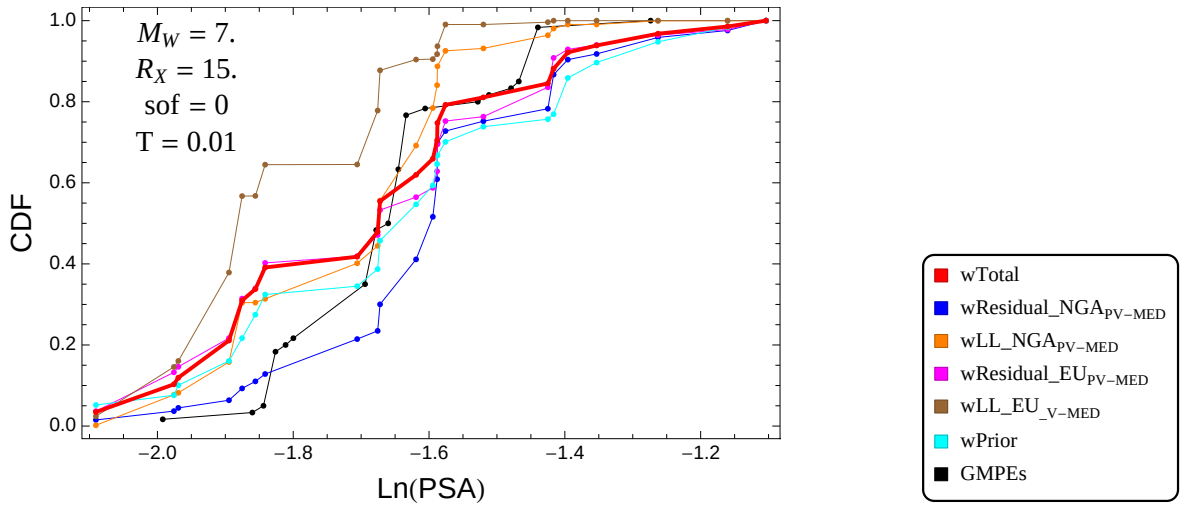



Figure 4.103: PVNGSv2: Cumulative distribution function of GMPEs (black) and selected models, for different sets of weights, for a scenario with $M = 7.$, $R_x = 15.$, $F = 0$, and $T = 0.01$s

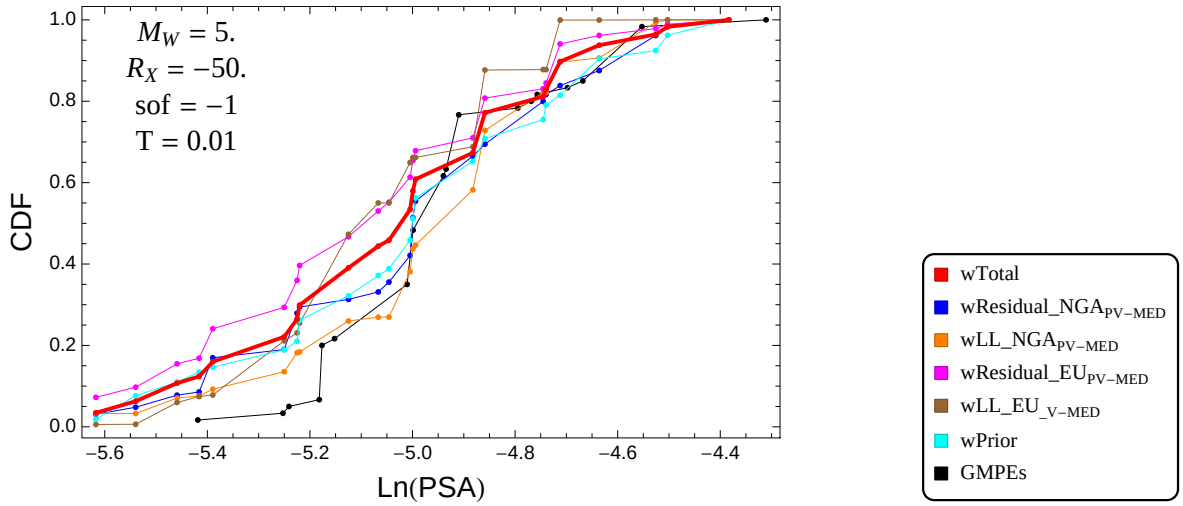



Figure 4.104: PVNGSv2: Cumulative distribution function of GMPEs (black) and selected models, for different sets of weights, for a scenario with $M = 5.$, $R_x = -50.$, $F = -1$, and $T = 0.01$s

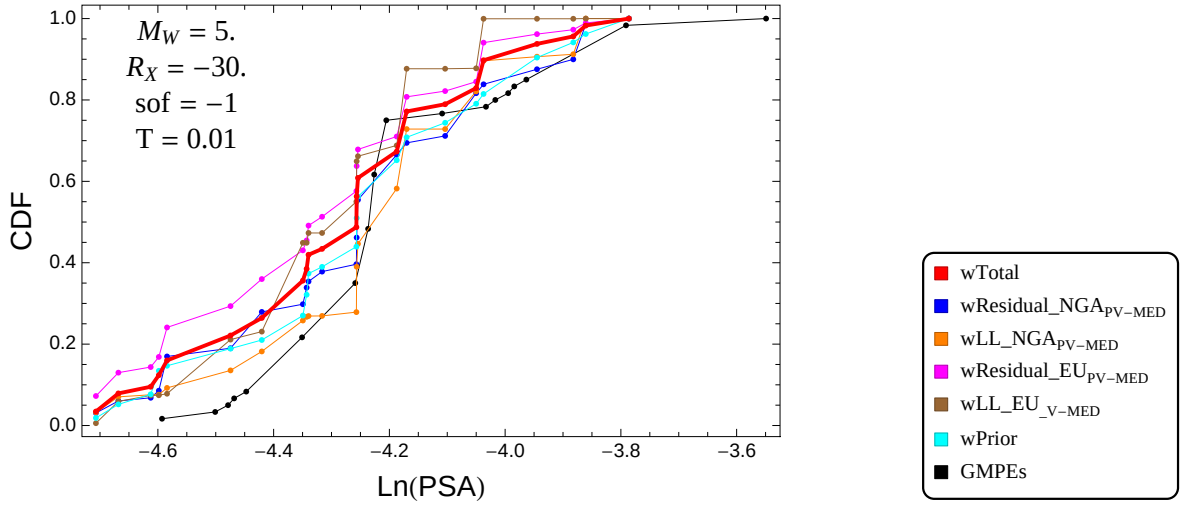



Figure 4.105: PVNGSv2: Cumulative distribution function of GMPEs (black) and selected models, for different sets of weights, for a scenario with $M = 5.$, $R_x = -30.$, $F = -1$, and $T = 0.01$s

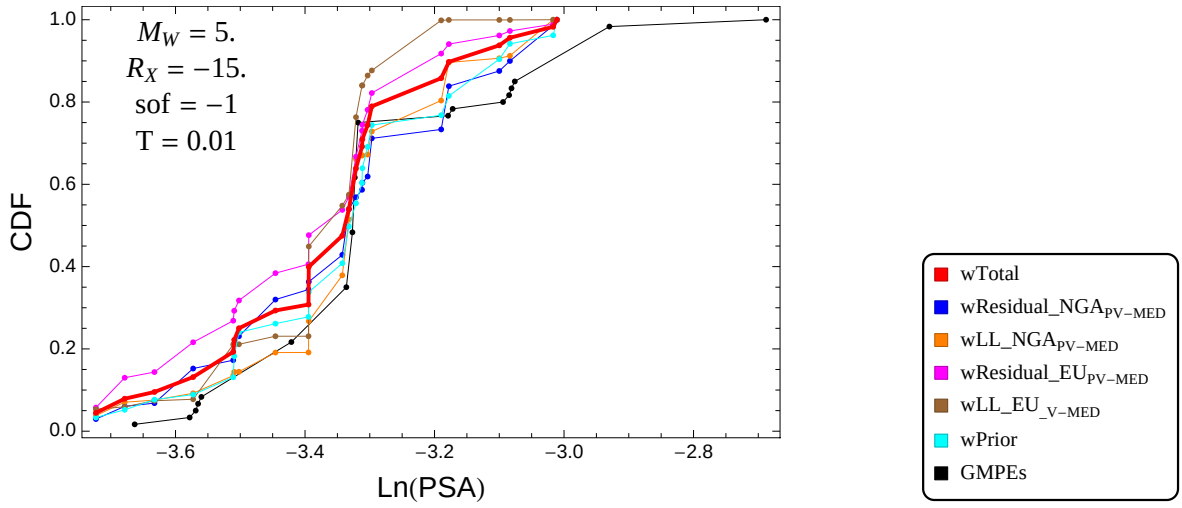



Figure 4.106: PVNGSv2: Cumulative distribution function of GMPEs (black) and selected models, for different sets of weights, for a scenario with $M = 5.$, $R_x = -15.$, $F = -1$, and $T = 0.01$s

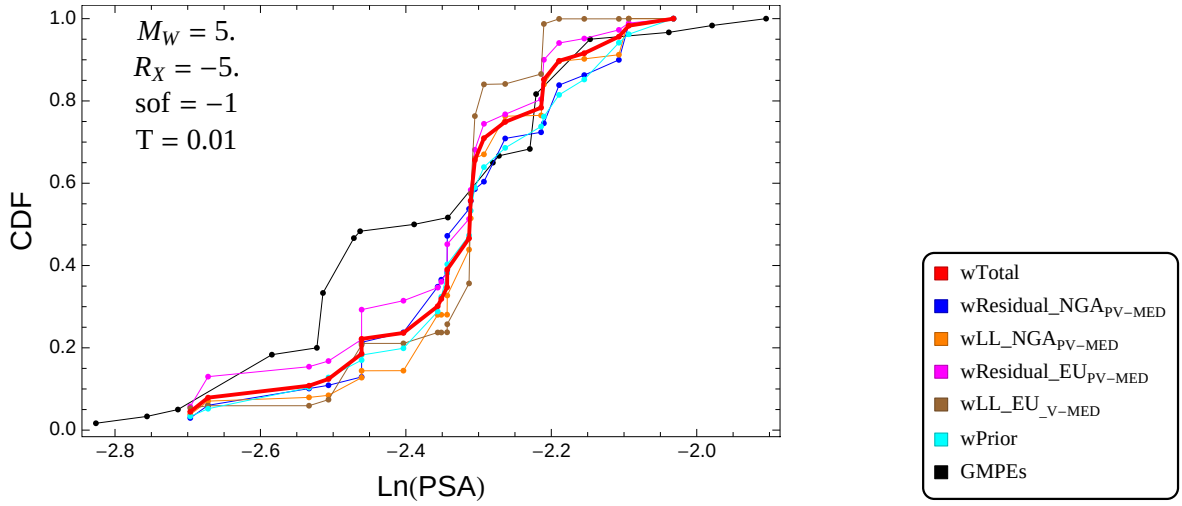



Figure 4.107: PVNGSv2: Cumulative distribution function of GMPEs (black) and selected models, for different sets of weights, for a scenario with $M = 5.$, $R_x = -5.$, $F = -1$, and $T = 0.01$s

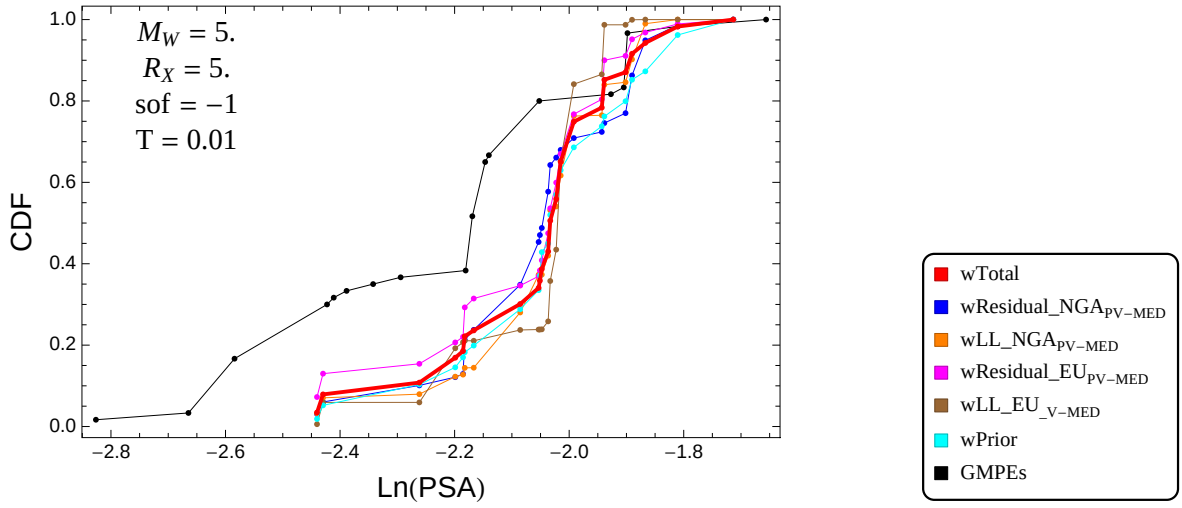



Figure 4.108: PVNGSv2: Cumulative distribution function of GMPEs (black) and selected models, for different sets of weights, for a scenario with $M = 5.$, $R_x = 5.$, $F = -1$, and $T = 0.01$s

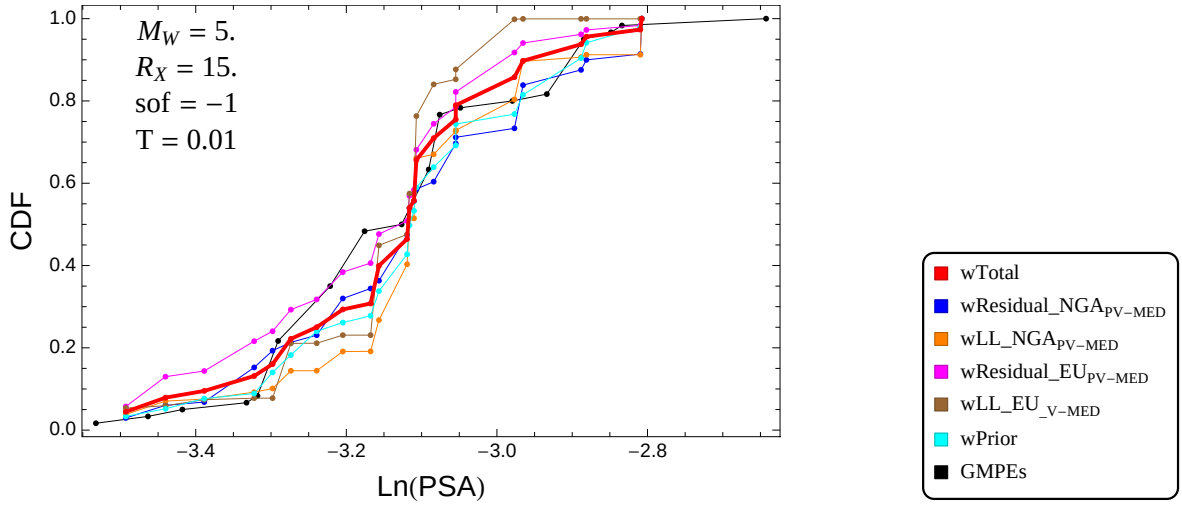



Figure 4.109: PVNGSv2: Cumulative distribution function of GMPEs (black) and selected models, for different sets of weights, for a scenario with $M = 5.$, $R_x = 15.$, $F = -1$, and $T = 0.01$s

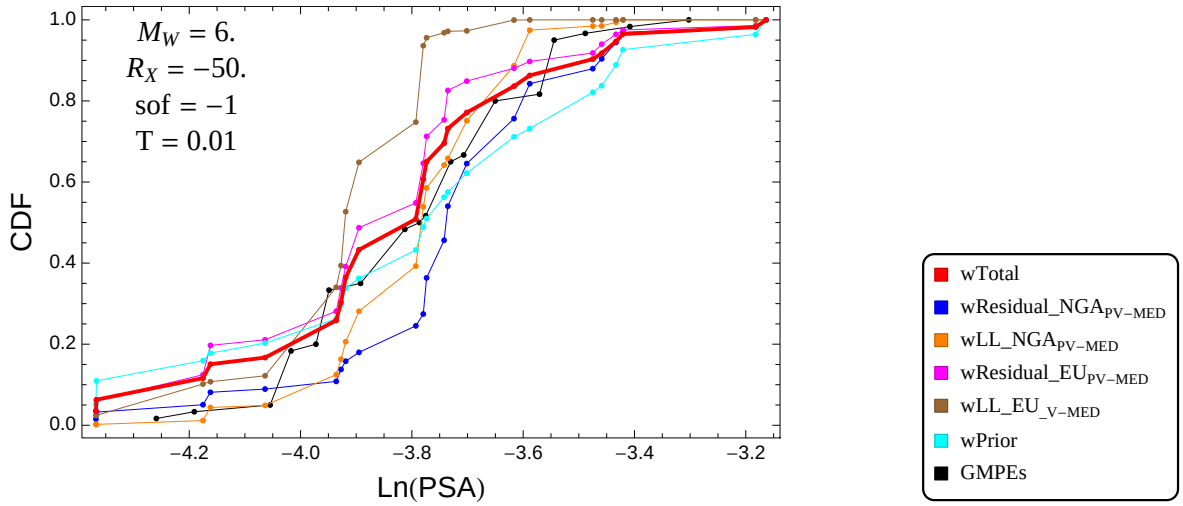



Figure 4.110: PVNGSv2: Cumulative distribution function of GMPEs (black) and selected models, for different sets of weights, for a scenario with $M = 6.$, $R_x = -50.$, $F = -1$, and $T = 0.01$s

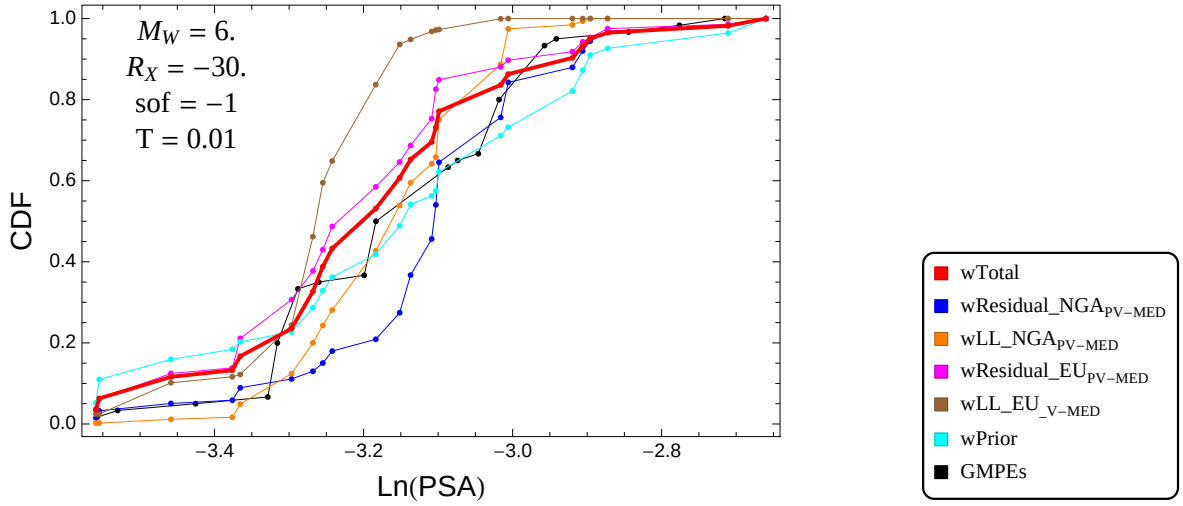



Figure 4.111: PVNGSv2: Cumulative distribution function of GMPEs (black) and selected models, for different sets of weights, for a scenario with $M = 6.$, $R_x = -30.$, $F = -1$, and $T = 0.01$s

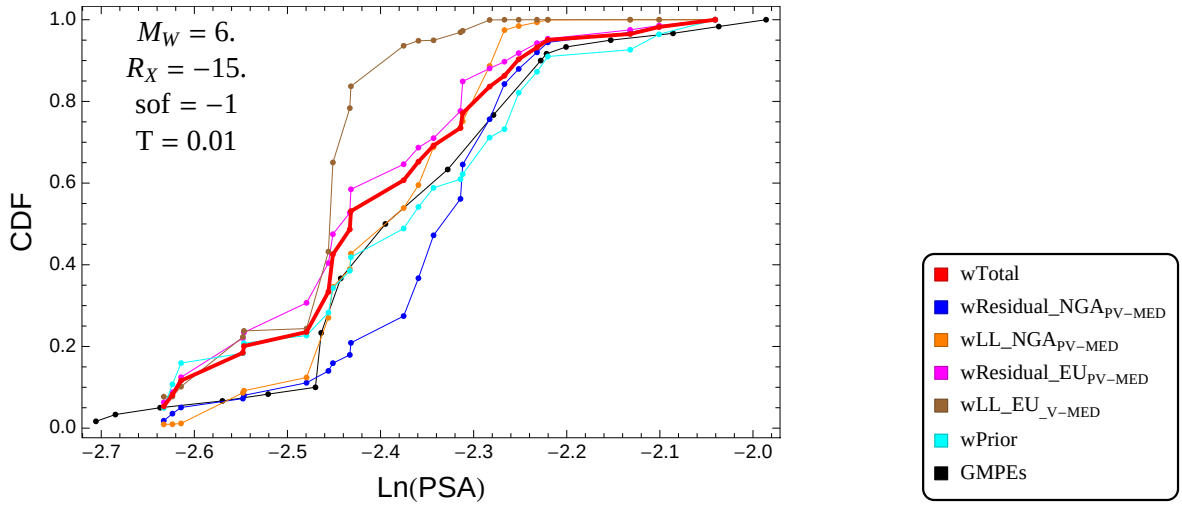



Figure 4.112: PVNGSv2: Cumulative distribution function of GMPEs (black) and selected models, for different sets of weights, for a scenario with $M = 6.$, $R_x = -15.$, $F = -1$, and $T = 0.01$s

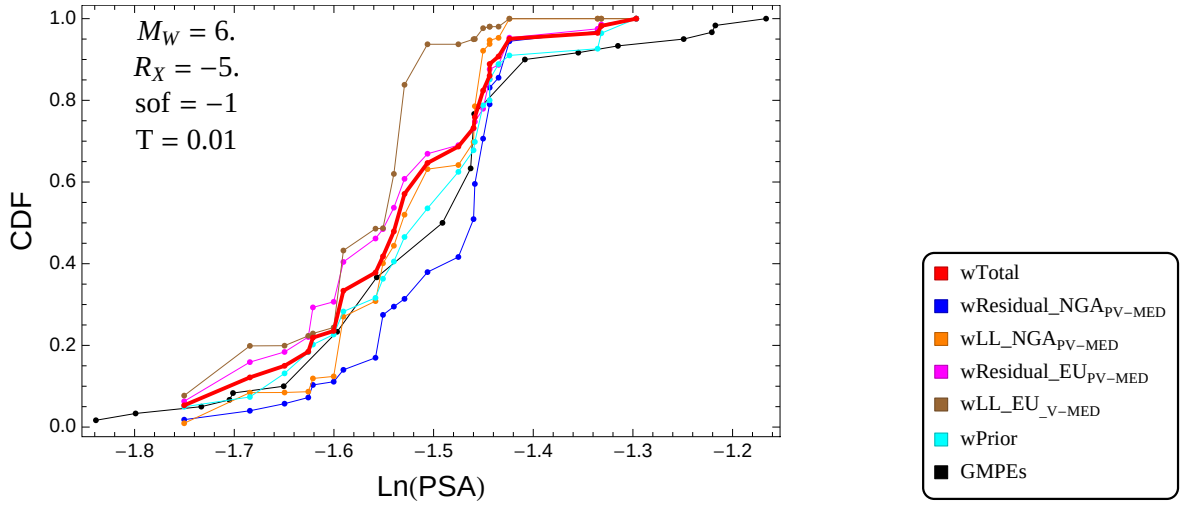



Figure 4.113: PVNGSv2: Cumulative distribution function of GMPEs (black) and selected models, for different sets of weights, for a scenario with $M = 6.$, $R_x = -5.$, $F = -1$, and $T = 0.01$s

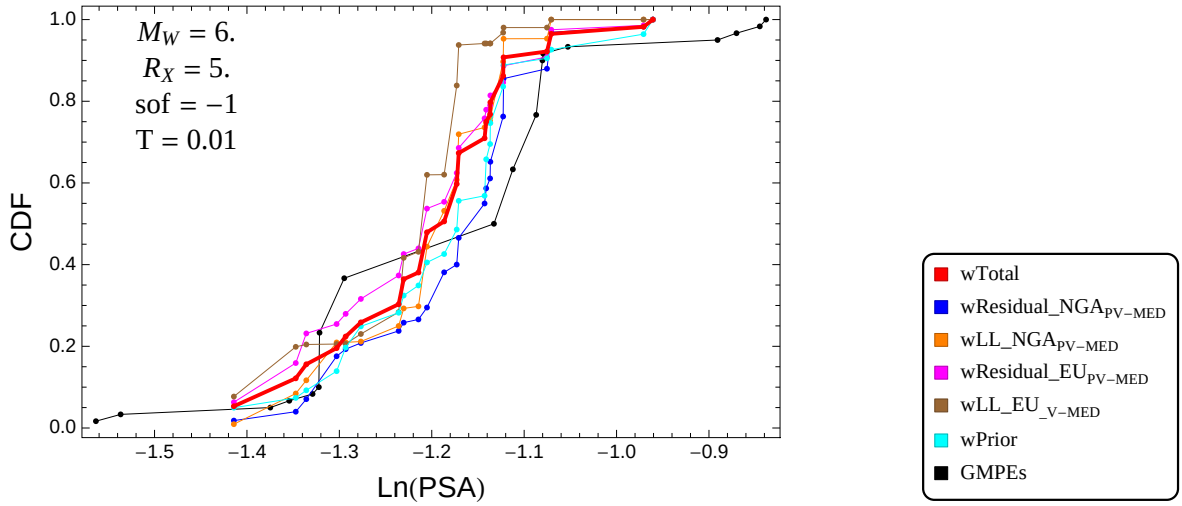



Figure 4.114: PVNGSv2: Cumulative distribution function of GMPEs (black) and selected models, for different sets of weights, for a scenario with $M = 6.$, $R_x = 5.$, $F = -1$, and $T = 0.01$s

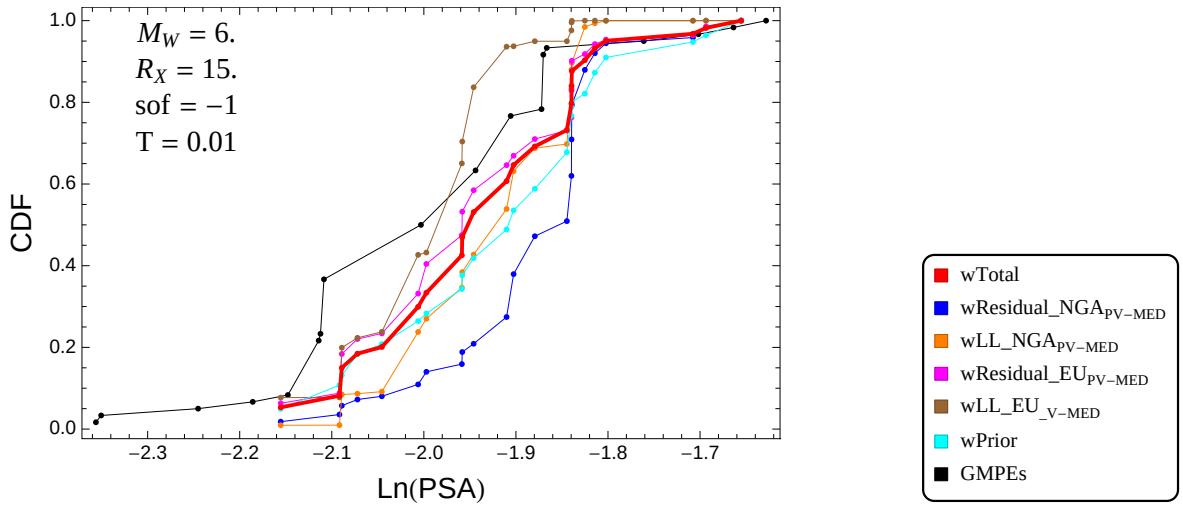



Figure 4.115: PVNGSv2: Cumulative distribution function of GMPEs (black) and selected models, for different sets of weights, for a scenario with $M = 6.$, $R_x = 15.$, $F = -1$, and $T = 0.01$s

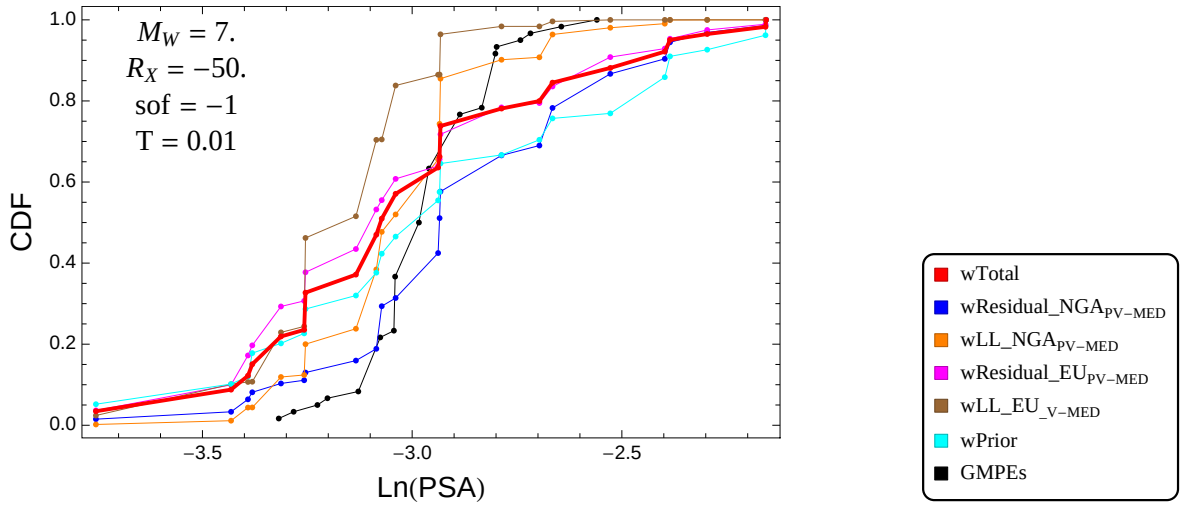



Figure 4.116: PVNGSv2: Cumulative distribution function of GMPEs (black) and selected models, for different sets of weights, for a scenario with $M = 7.$, $R_x = -50.$, $F = -1$, and $T = 0.01$s

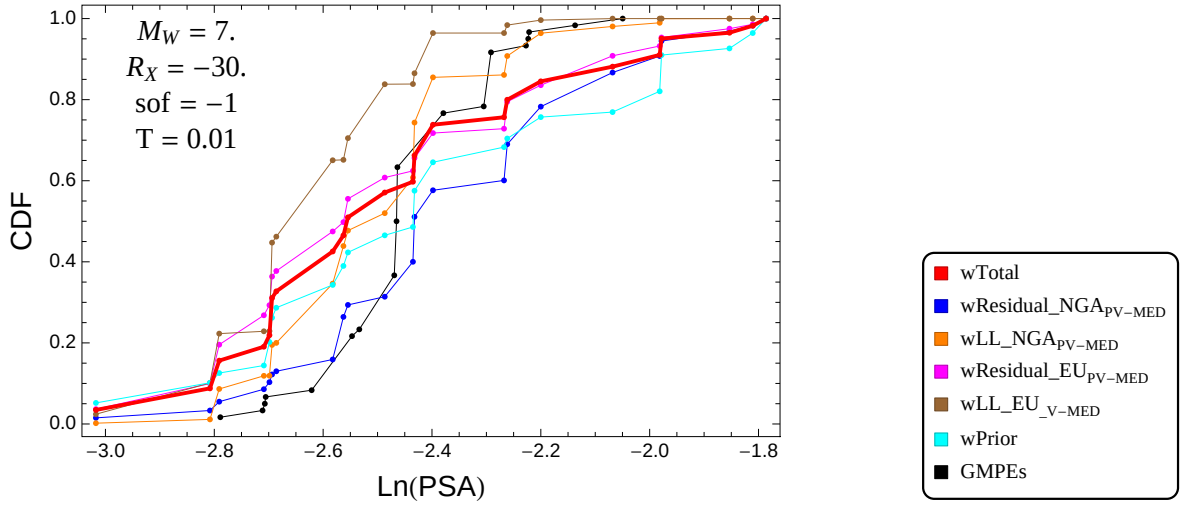



Figure 4.117: PVNGSv2: Cumulative distribution function of GMPEs (black) and selected models, for different sets of weights, for a scenario with $M = 7.$, $R_x = -30.$, $F = -1$, and $T = 0.01$s

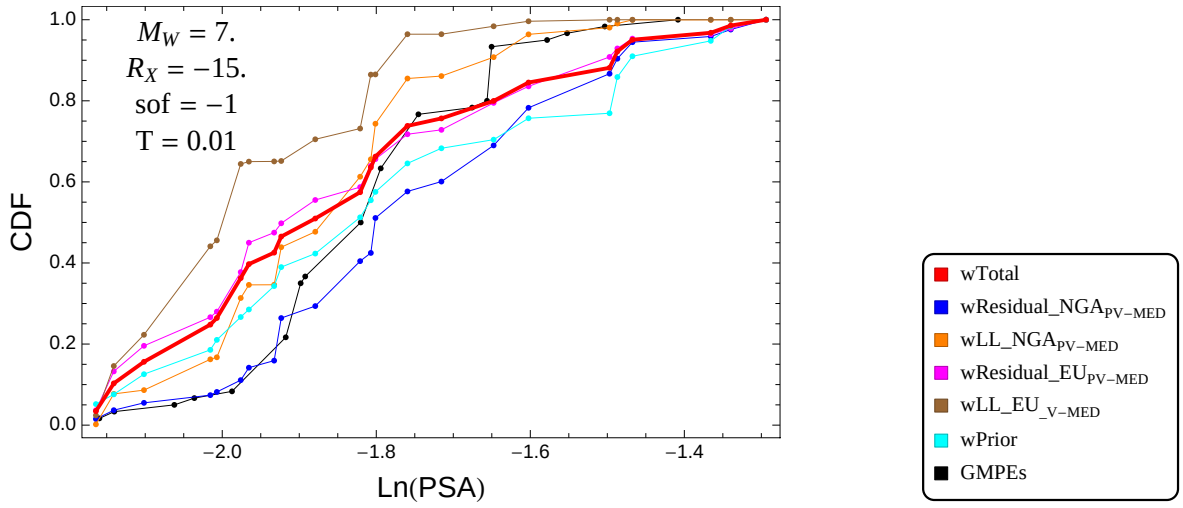



Figure 4.118: PVNGSv2: Cumulative distribution function of GMPEs (black) and selected models, for different sets of weights, for a scenario with $M = 7.$, $R_x = -15.$, $F = -1$, and $T = 0.01$s

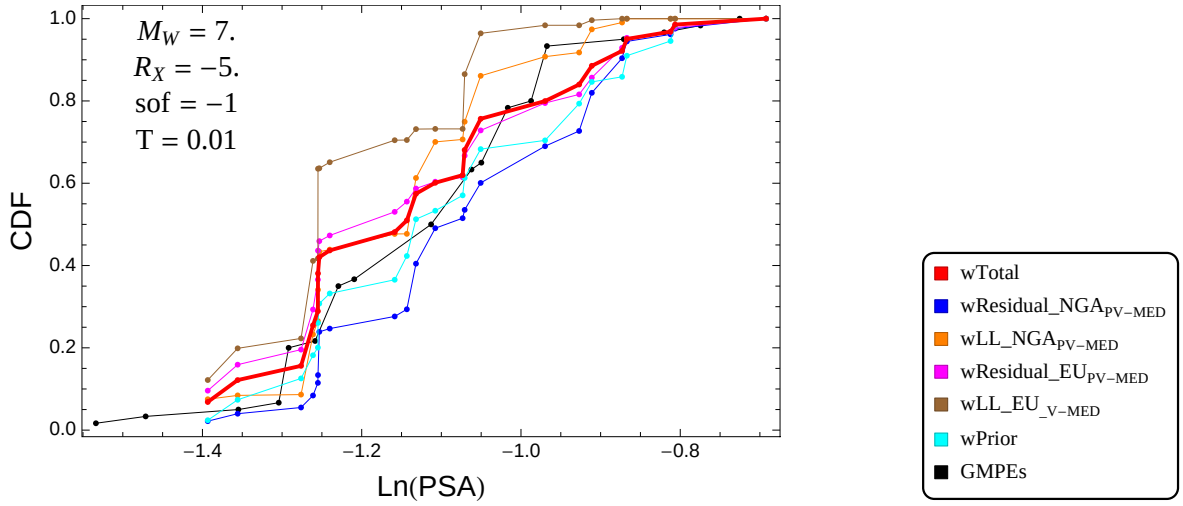



Figure 4.119: PVNGSv2: Cumulative distribution function of GMPEs (black) and selected models, for different sets of weights, for a scenario with $M = 7.$, $R_x = -5.$, $F = -1$, and $T = 0.01$s

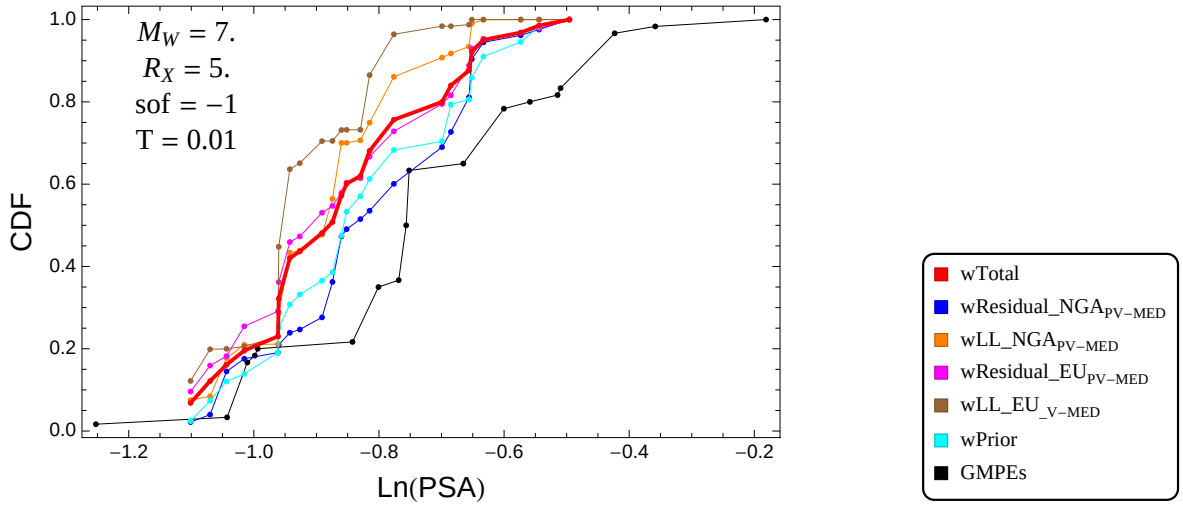



Figure 4.120: PVNGSv2: Cumulative distribution function of GMPEs (black) and selected models, for different sets of weights, for a scenario with $M = 7.$, $R_x = 5.$, $F = -1$, and $T = 0.01$s

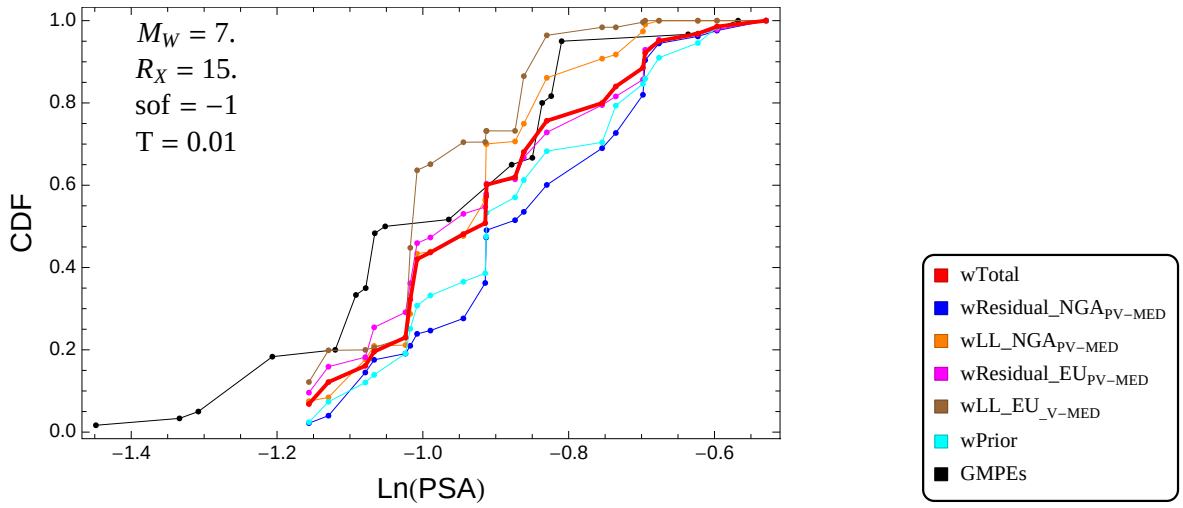



Figure 4.121: PVNGSv2: Cumulative distribution function of GMPEs (black) and selected models, for different sets of weights, for a scenario with $M = 7.$, $R_x = 15.$, $F = -1$, and $T = 0.01$s

**T = 0.2s**

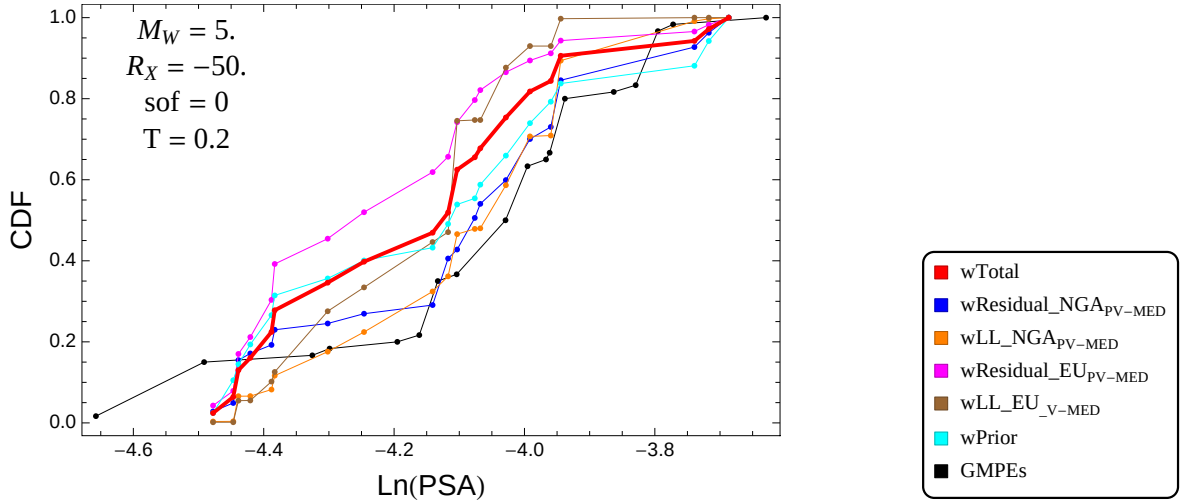



Figure 4.122: PVNGSv2: Cumulative distribution function of GMPEs (black) and selected models, for different sets of weights, for a scenario with $M = 5.$, $R_x = -50.$, $F = 0$, and $T = 0.2$s

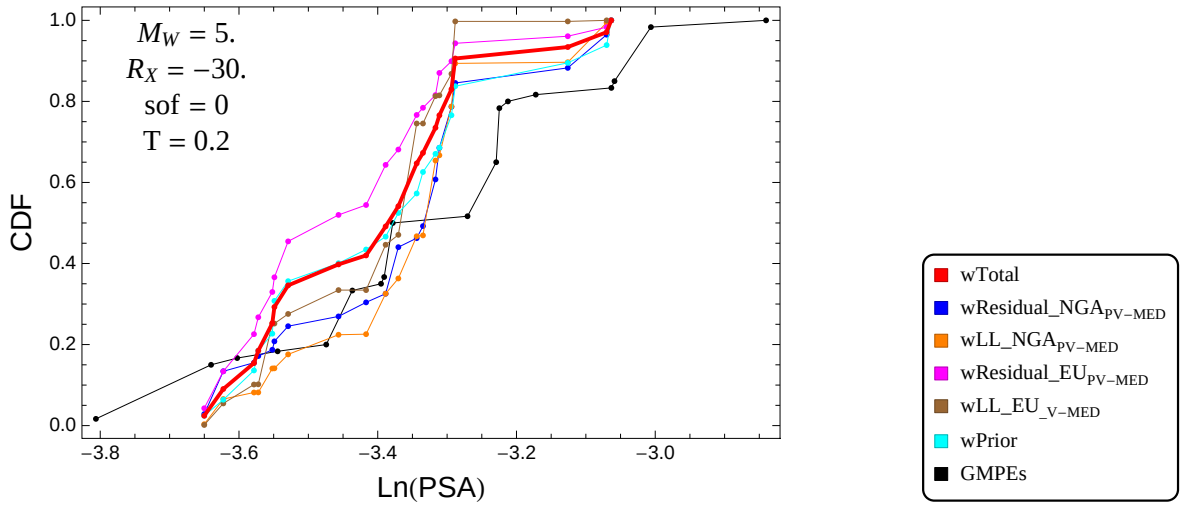



Figure 4.123: PVNGSv2: Cumulative distribution function of GMPEs (black) and selected models, for different sets of weights, for a scenario with $M = 5.$, $R_x = -30.$, $F = 0$, and $T = 0.2$s

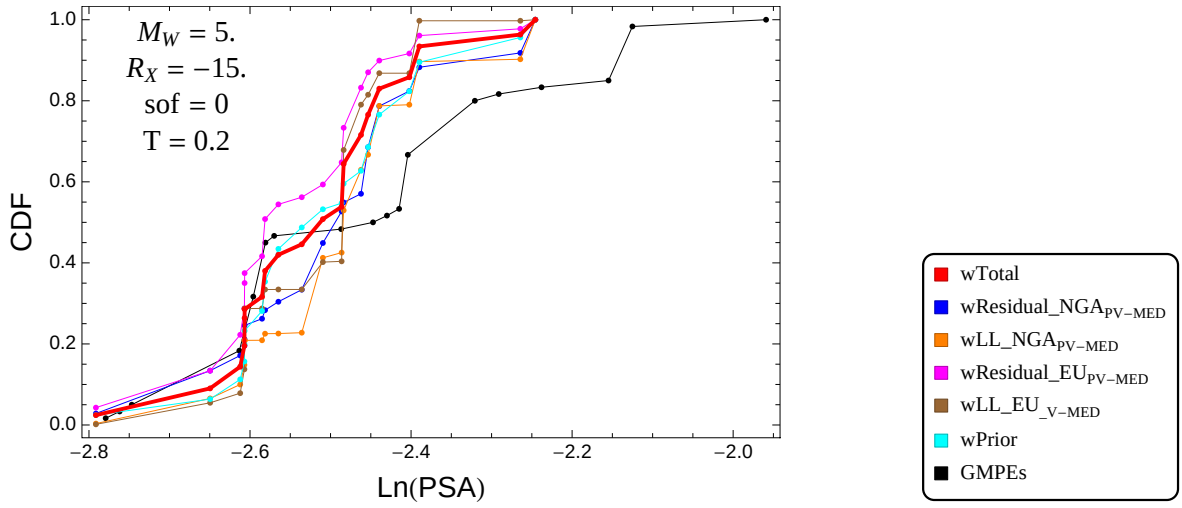



Figure 4.124: PVNGSv2: Cumulative distribution function of GMPEs (black) and selected models, for different sets of weights, for a scenario with $M = 5.$, $R_x = -15.$, $F = 0$, and $T = 0.2$s

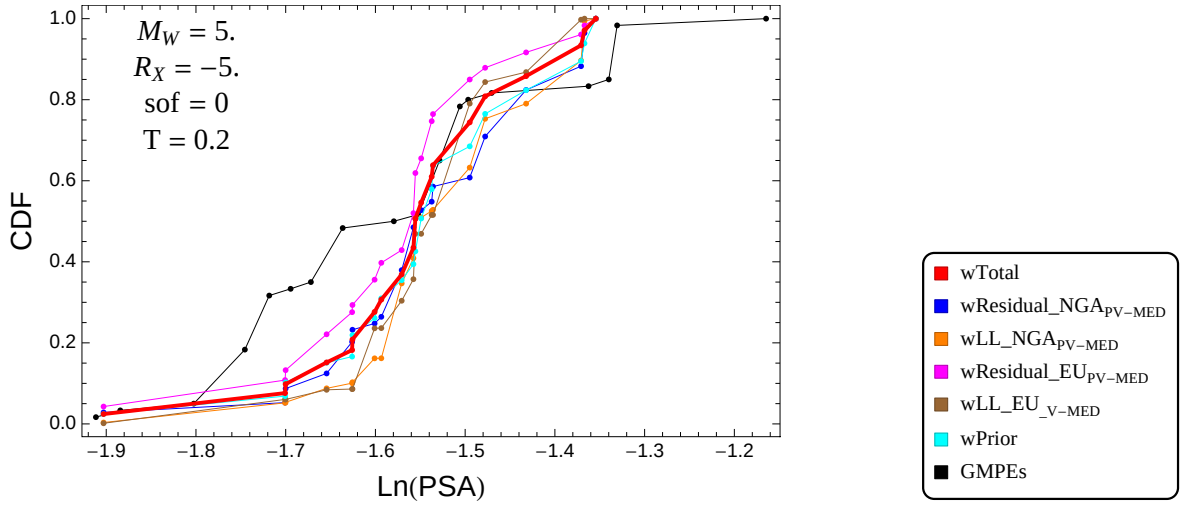



Figure 4.125: PVNGSv2: Cumulative distribution function of GMPEs (black) and selected models, for different sets of weights, for a scenario with $M = 5.$, $R_x = -5.$, $F = 0$, and $T = 0.2$s

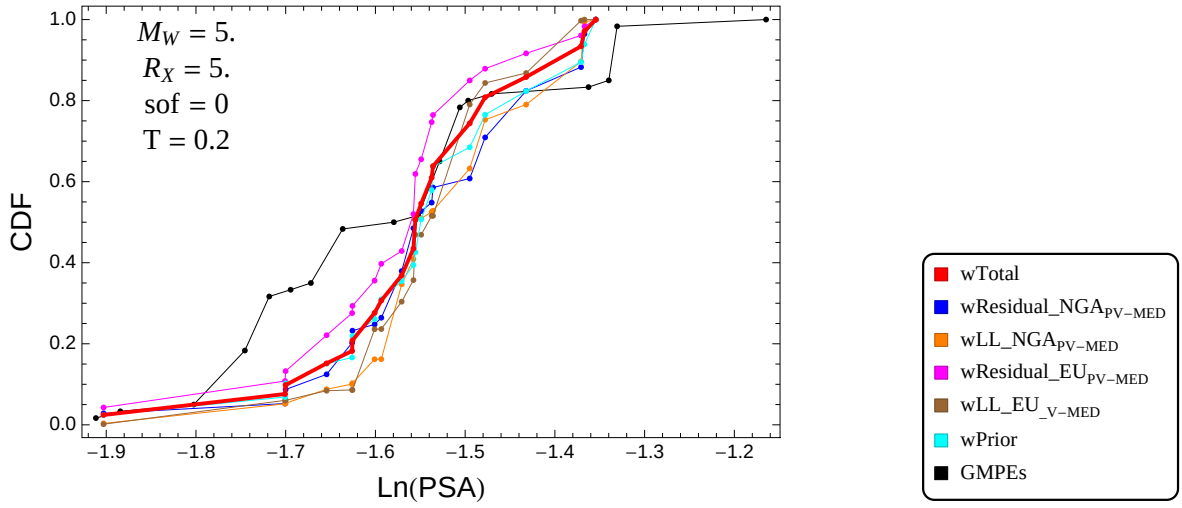



Figure 4.126: PVNGSv2: Cumulative distribution function of GMPEs (black) and selected models, for different sets of weights, for a scenario with $M = 5.$, $R_x = 5.$, $F = 0$, and $T = 0.2$s

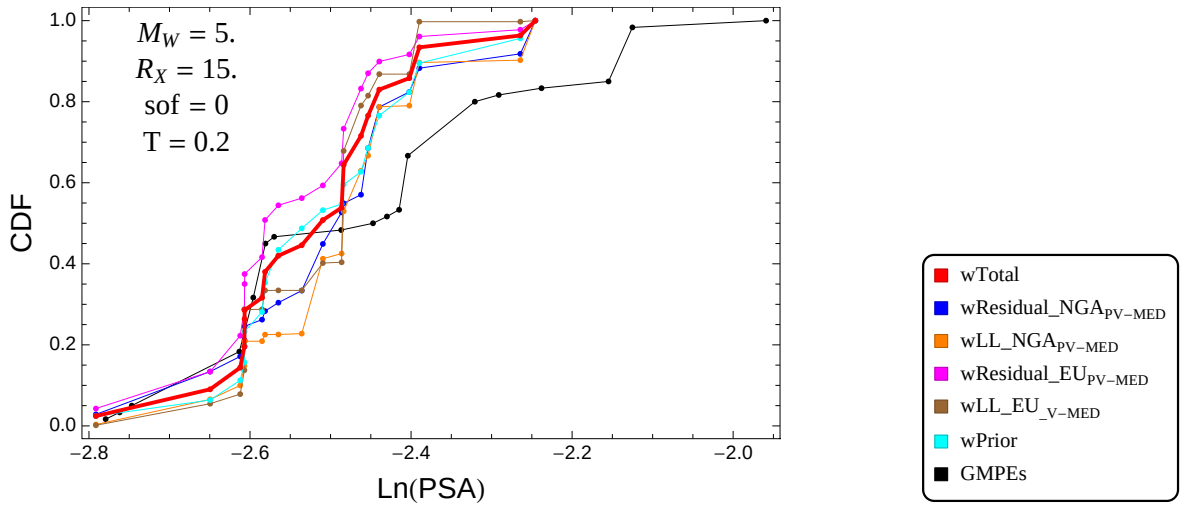



Figure 4.127: PVNGSv2: Cumulative distribution function of GMPEs (black) and selected models, for different sets of weights, for a scenario with $M = 5.$, $R_x = 15.$, $F = 0$, and $T = 0.2$s

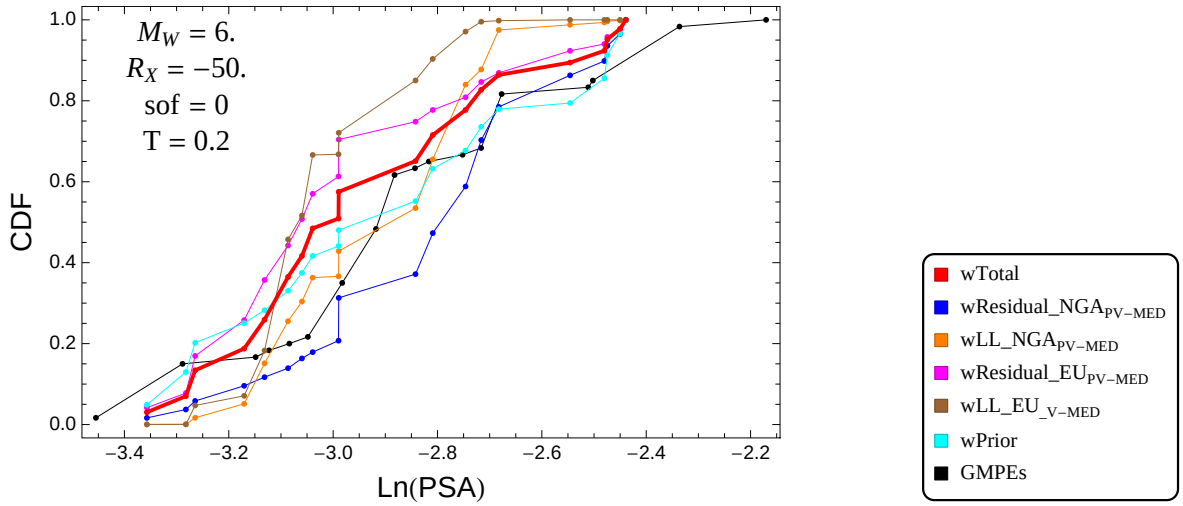



Figure 4.128: PVNGSv2: Cumulative distribution function of GMPEs (black) and selected models, for different sets of weights, for a scenario with $M = 6.$, $R_x = -50.$, $F = 0$, and $T = 0.2$s

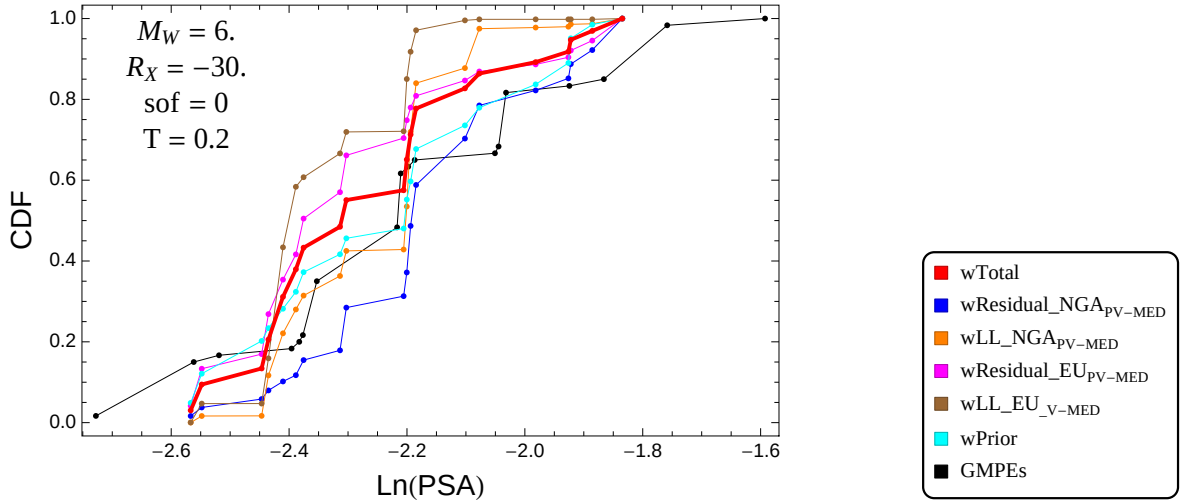



Figure 4.129: PVNGSv2: Cumulative distribution function of GMPEs (black) and selected models, for different sets of weights, for a scenario with $M = 6.$, $R_x = -30.$, $F = 0$, and $T = 0.2$s

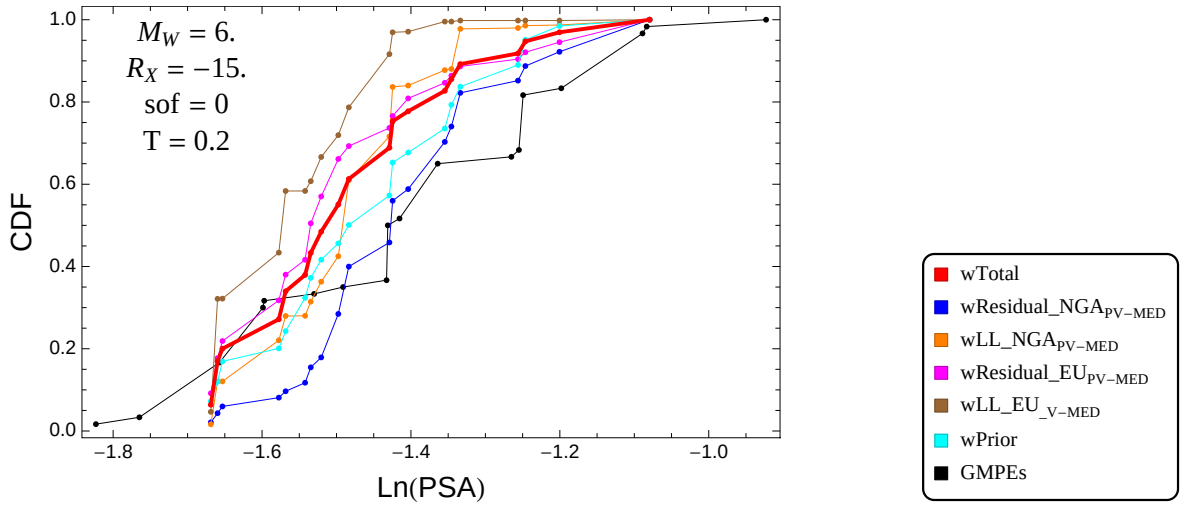



Figure 4.130: PVNGSv2: Cumulative distribution function of GMPEs (black) and selected models, for different sets of weights, for a scenario with $M = 6.$, $R_x = -15.$, $F = 0$, and $T = 0.2$s

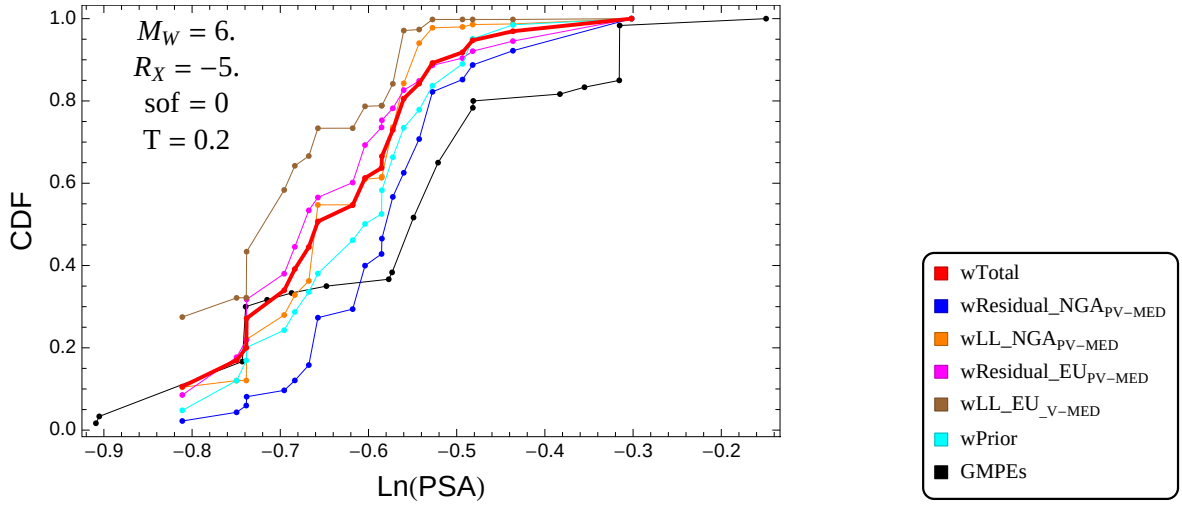



Figure 4.131: PVNGSv2: Cumulative distribution function of GMPEs (black) and selected models, for different sets of weights, for a scenario with $M = 6.$, $R_x = -5.$, $F = 0$, and $T = 0.2$s

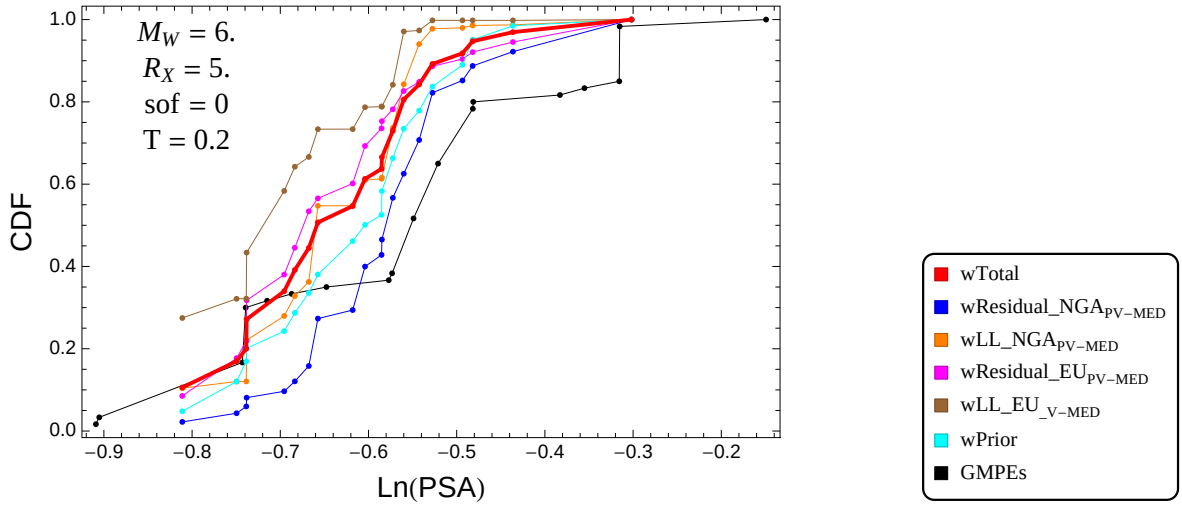



Figure 4.132: PVNGSv2: Cumulative distribution function of GMPEs (black) and selected models, for different sets of weights, for a scenario with $M = 6.$, $R_x = 5.$, $F = 0$, and $T = 0.2$s

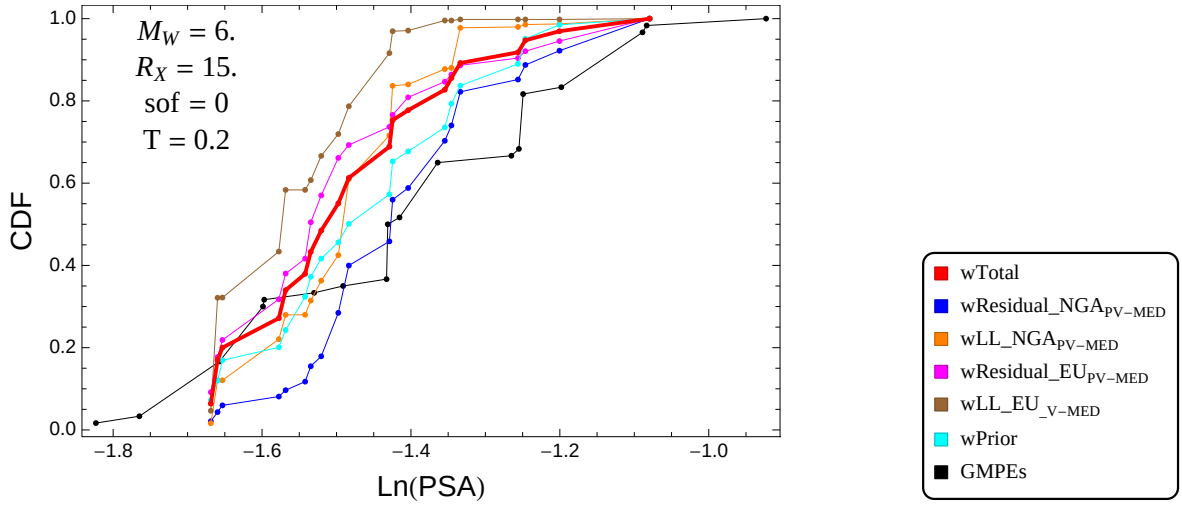



Figure 4.133: PVNGSv2: Cumulative distribution function of GMPEs (black) and selected models, for different sets of weights, for a scenario with $M = 6.$, $R_x = 15.$, $F = 0$, and $T = 0.2$s

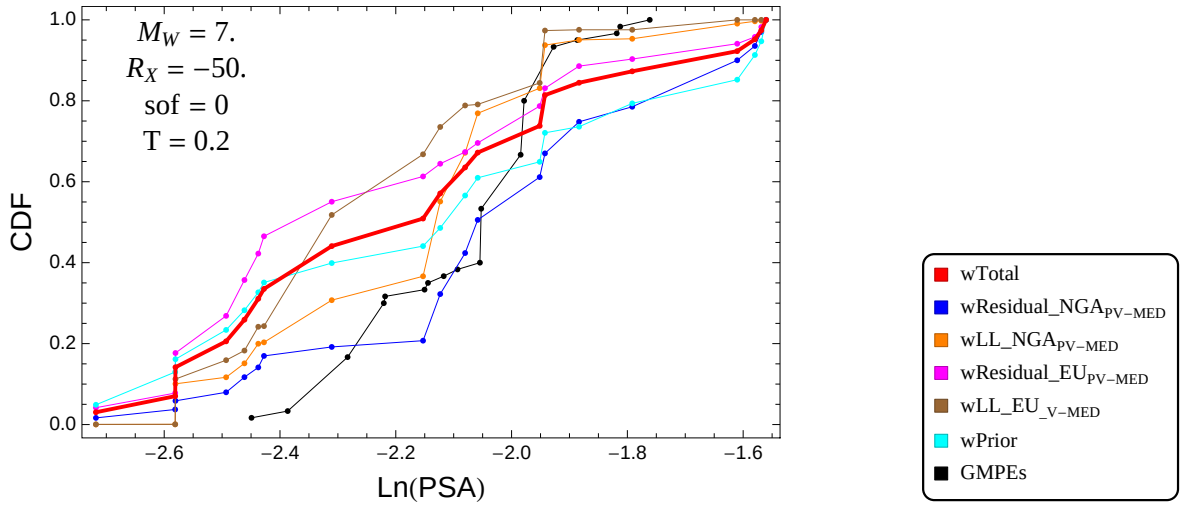



Figure 4.134: PVNGSv2: Cumulative distribution function of GMPEs (black) and selected models, for different sets of weights, for a scenario with $M = 7.$, $R_x = -50.$, $F = 0$, and $T = 0.2$s

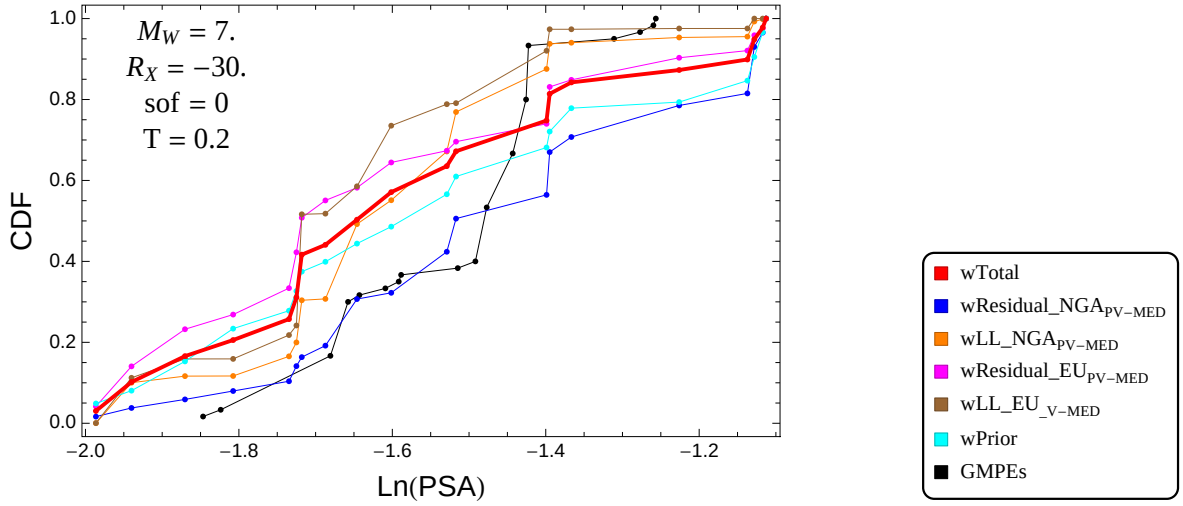



Figure 4.135: PVNGSv2: Cumulative distribution function of GMPEs (black) and selected models, for different sets of weights, for a scenario with $M = 7.$, $R_x = -30.$, $F = 0$, and $T = 0.2$s

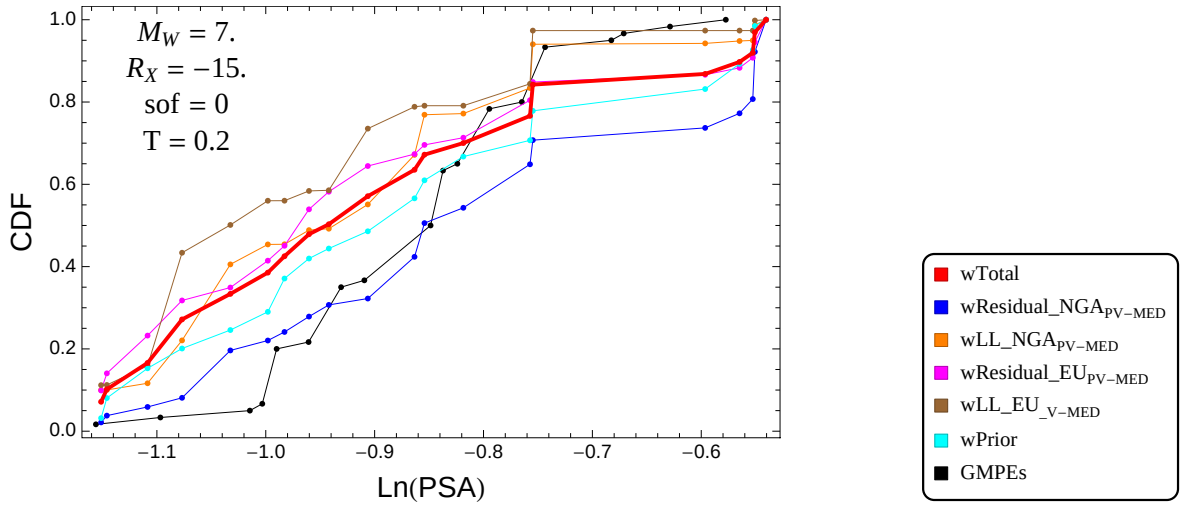



Figure 4.136: PVNGSv2: Cumulative distribution function of GMPEs (black) and selected models, for different sets of weights, for a scenario with $M = 7.$, $R_x = -15.$, $F = 0$, and $T = 0.2$s

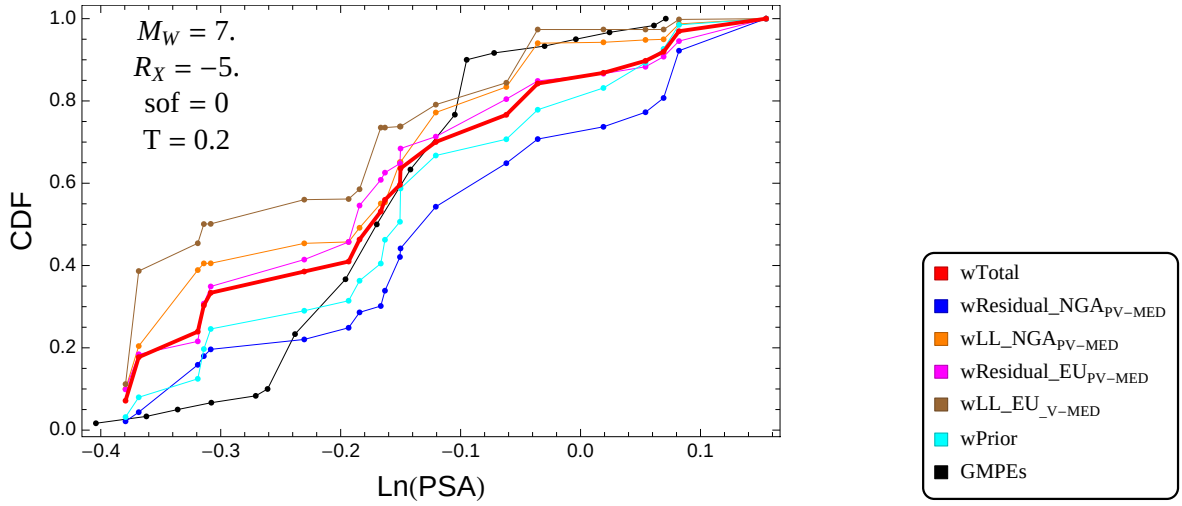



Figure 4.137: PVNGSv2: Cumulative distribution function of GMPEs (black) and selected models, for different sets of weights, for a scenario with $M = 7.$, $R_x = -5.$, $F = 0$, and $T = 0.2$s

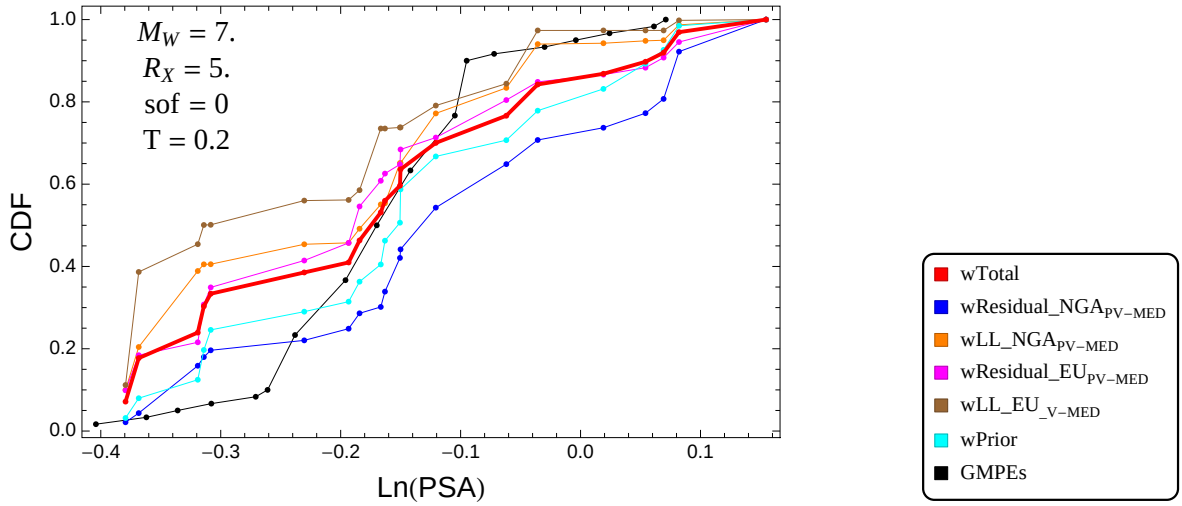



Figure 4.138: PVNGSv2: Cumulative distribution function of GMPEs (black) and selected models, for different sets of weights, for a scenario with $M = 7.$, $R_x = 5.$, $F = 0$, and $T = 0.2$s

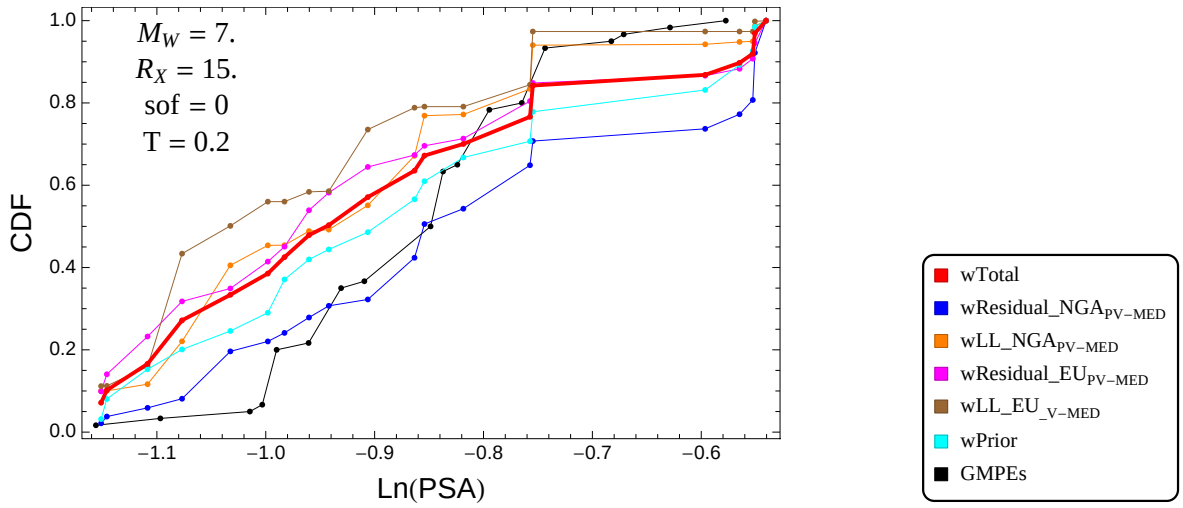



Figure 4.139: PVNGSv2: Cumulative distribution function of GMPEs (black) and selected models, for different sets of weights, for a scenario with $M = 7.$, $R_x = 15.$, $F = 0$, and $T = 0.2$s

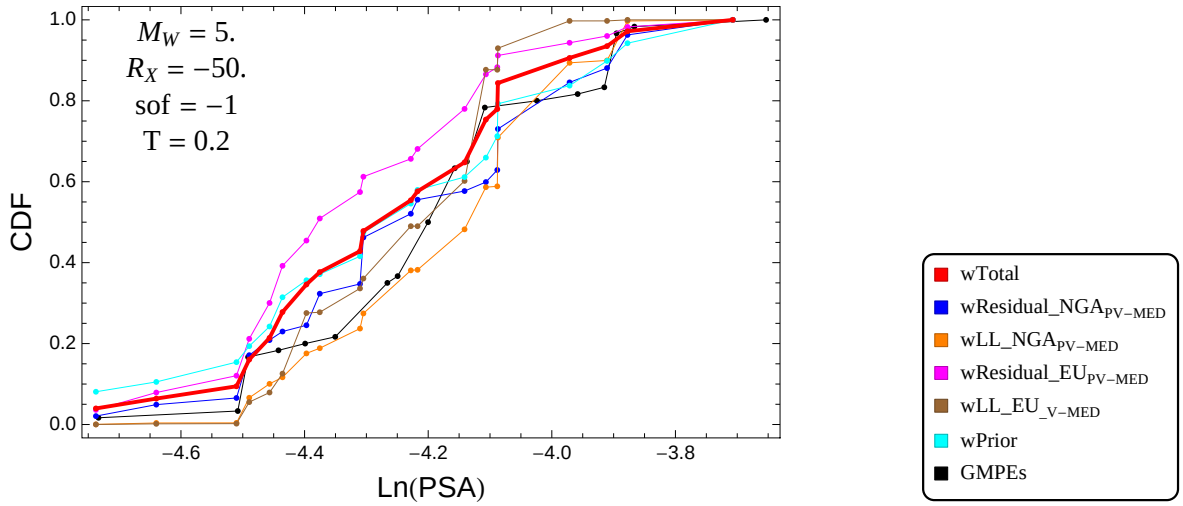



Figure 4.140: PVNGSv2: Cumulative distribution function of GMPEs (black) and selected models, for different sets of weights, for a scenario with $M = 5.$, $R_x = -50.$, $F = -1$, and $T = 0.2$s

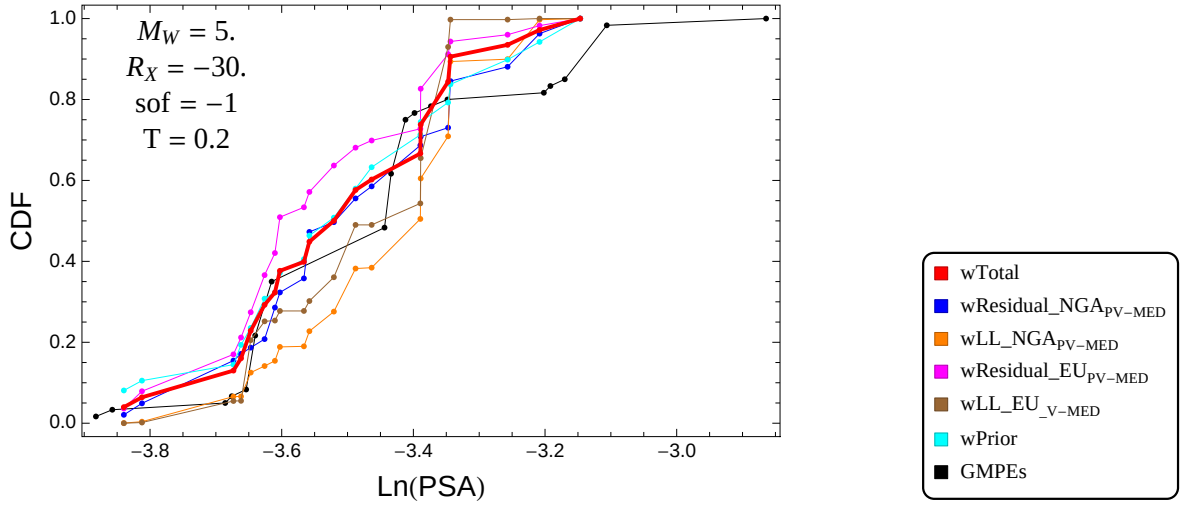



Figure 4.141: PVNGSv2: Cumulative distribution function of GMPEs (black) and selected models, for different sets of weights, for a scenario with $M = 5.$, $R_x = -30.$, $F = -1$, and $T = 0.2$s

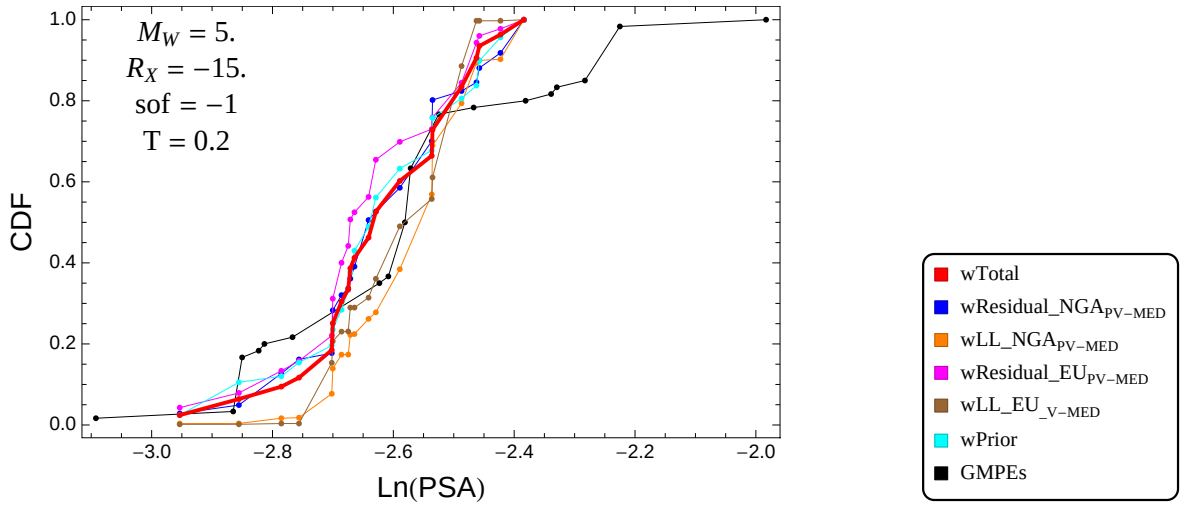



Figure 4.142: PVNGSv2: Cumulative distribution function of GMPEs (black) and selected models, for different sets of weights, for a scenario with $M = 5.$, $R_x = -15.$, $F = -1$, and $T = 0.2$s

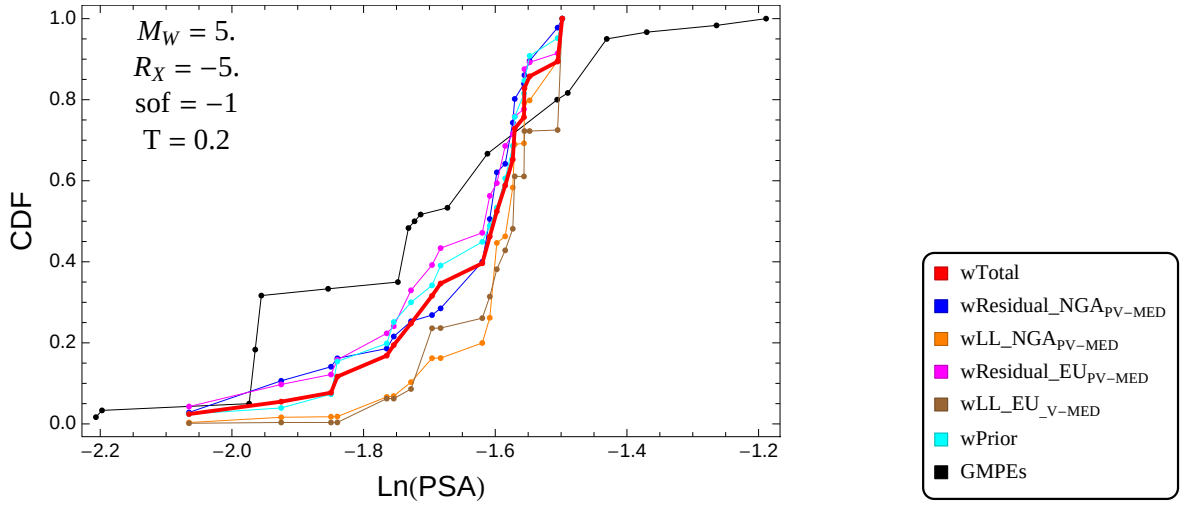



Figure 4.143: PVNGSv2: Cumulative distribution function of GMPEs (black) and selected models, for different sets of weights, for a scenario with $M = 5.$, $R_x = -5.$, $F = -1$, and $T = 0.2$s

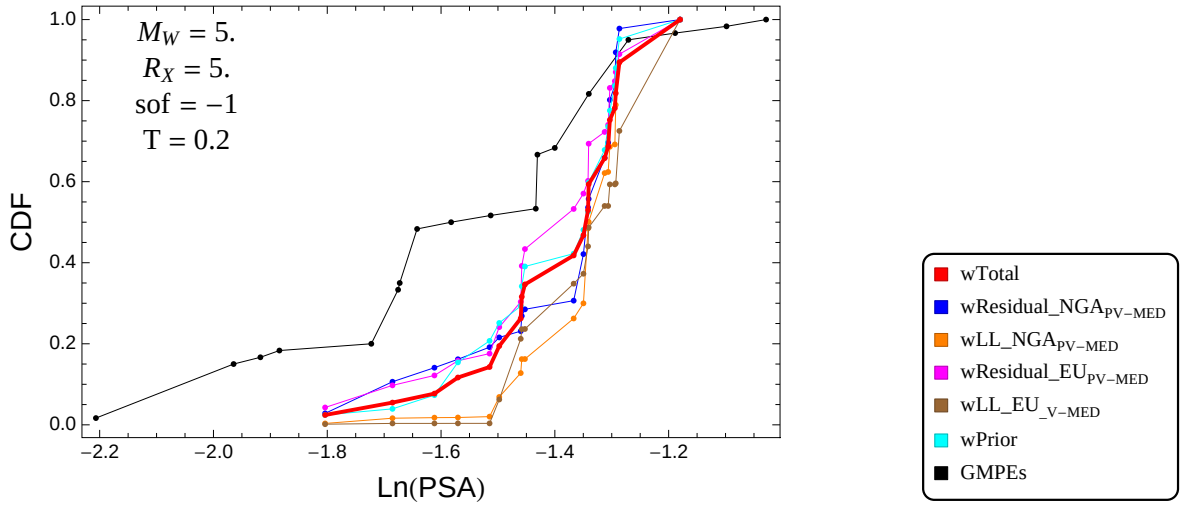



Figure 4.144: PVNGSv2: Cumulative distribution function of GMPEs (black) and selected models, for different sets of weights, for a scenario with $M = 5.$, $R_x = 5.$, $F = -1$, and $T = 0.2$s

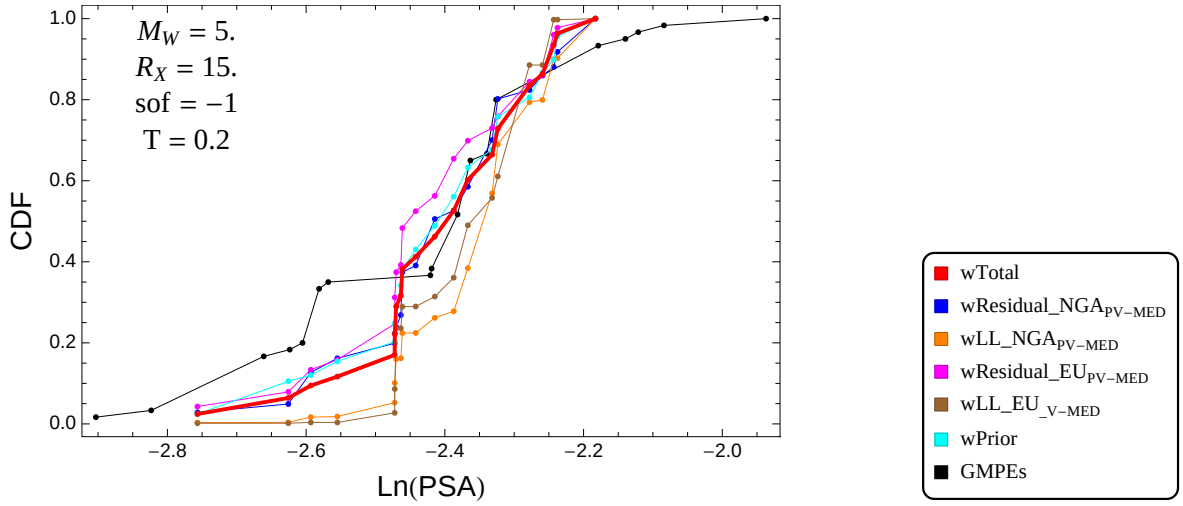



Figure 4.145: PVNGSv2: Cumulative distribution function of GMPEs (black) and selected models, for different sets of weights, for a scenario with $M = 5.$, $R_x = 15.$, $F = -1$, and $T = 0.2$s

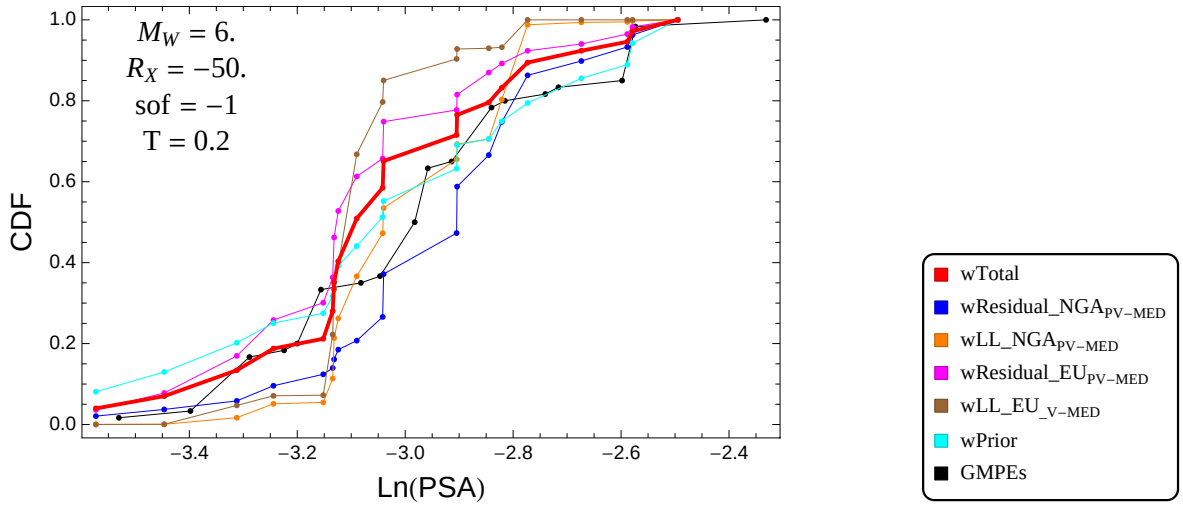



Figure 4.146: PVNGSv2: Cumulative distribution function of GMPEs (black) and selected models, for different sets of weights, for a scenario with $M = 6.$, $R_x = -50.$, $F = -1$, and $T = 0.2$s

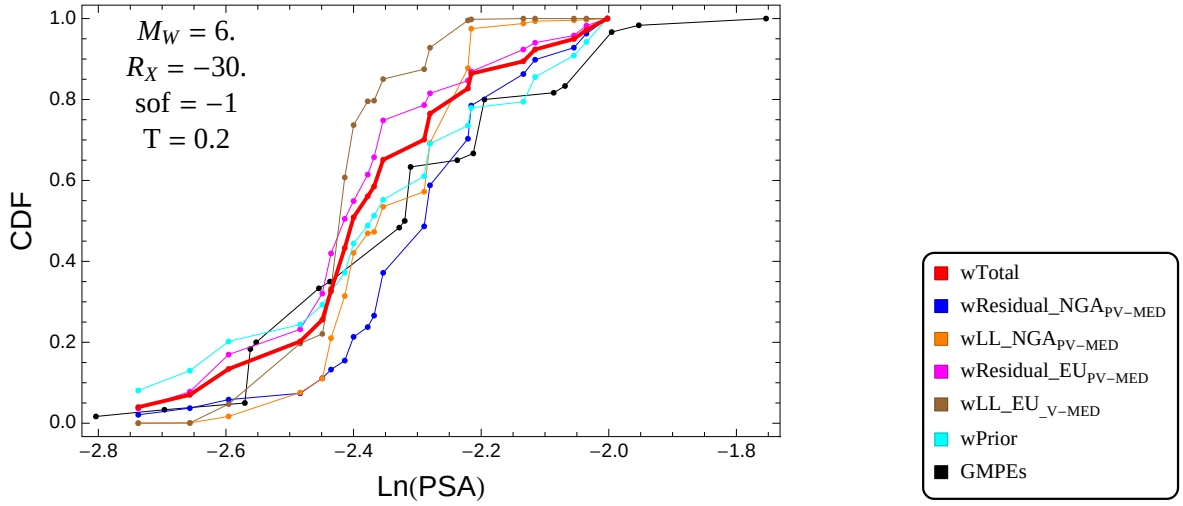



Figure 4.147: PVNGSv2: Cumulative distribution function of GMPEs (black) and selected models, for different sets of weights, for a scenario with $M = 6.$, $R_x = -30.$, $F = -1$, and $T = 0.2$s

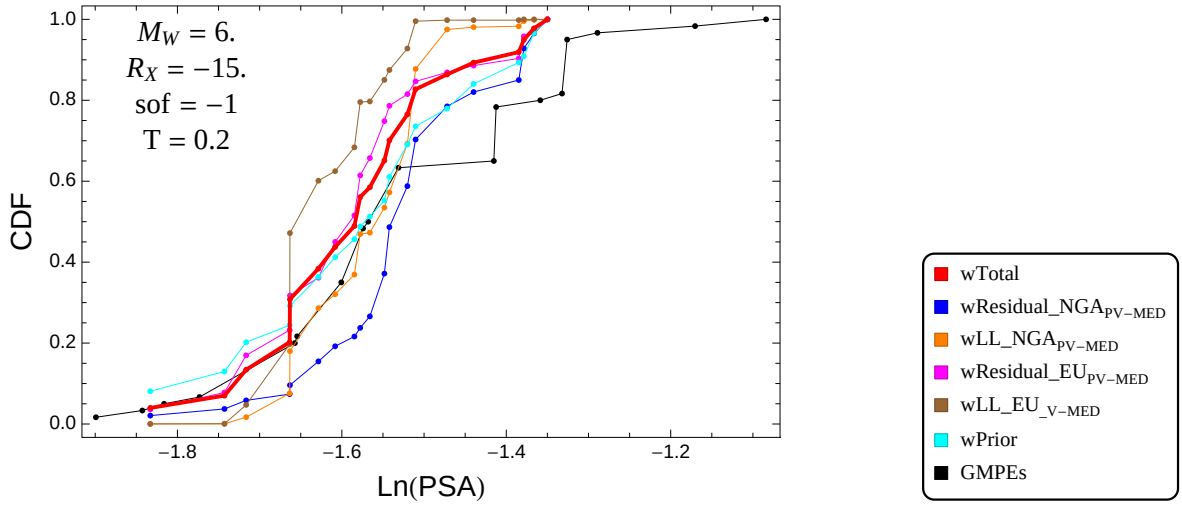



Figure 4.148: PVNGSv2: Cumulative distribution function of GMPEs (black) and selected models, for different sets of weights, for a scenario with $M = 6.$, $R_x = -15.$, $F = -1$, and $T = 0.2$s

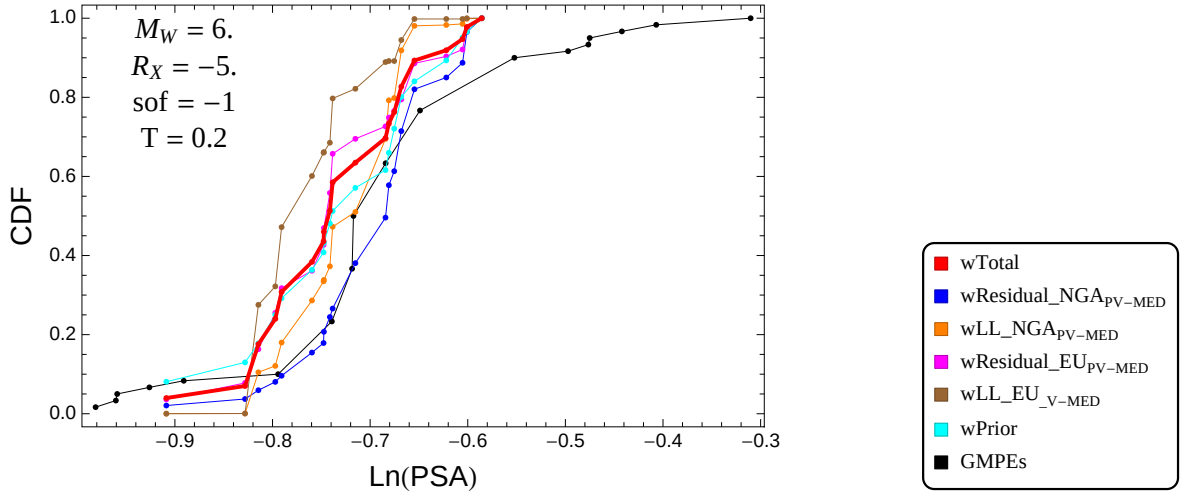



Figure 4.149: PVNGSv2: Cumulative distribution function of GMPEs (black) and selected models, for different sets of weights, for a scenario with $M = 6.$, $R_x = -5.$, $F = -1$, and $T = 0.2$s

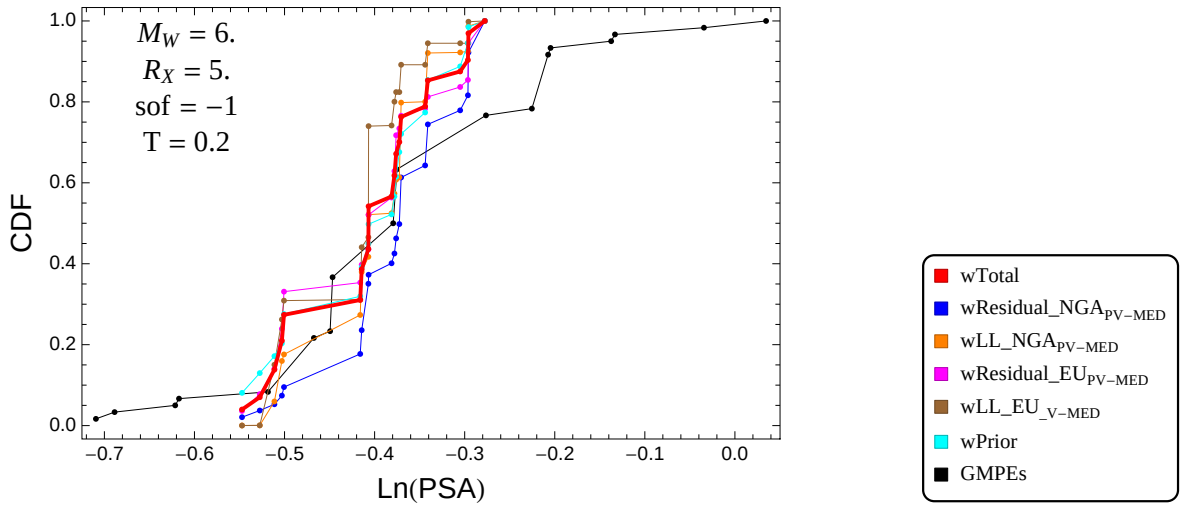



Figure 4.150: PVNGSv2: Cumulative distribution function of GMPEs (black) and selected models, for different sets of weights, for a scenario with $M = 6.$, $R_x = 5.$, $F = -1$, and $T = 0.2$s

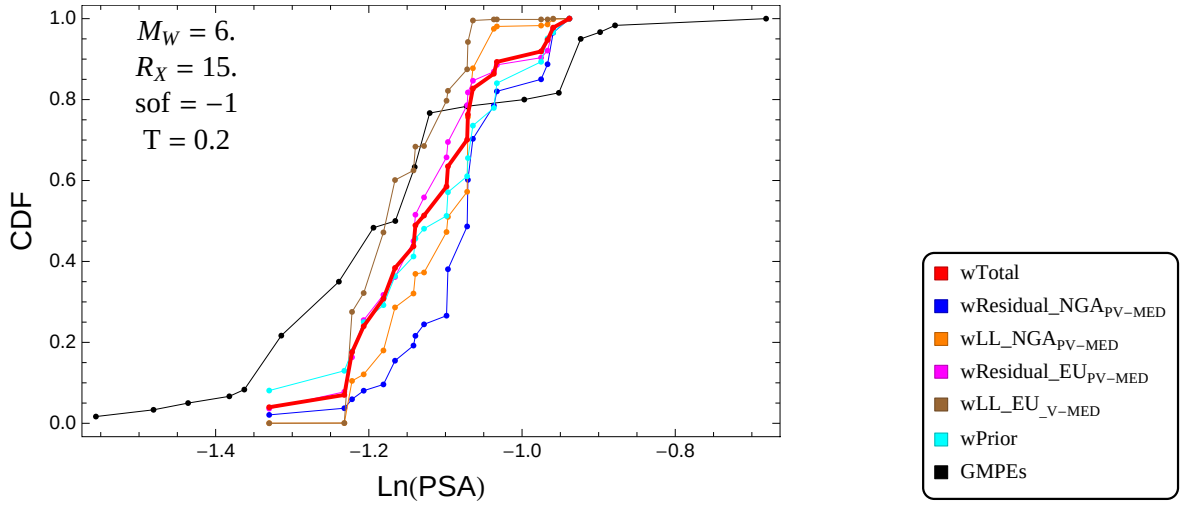



Figure 4.151: PVNGSv2: Cumulative distribution function of GMPEs (black) and selected models, for different sets of weights, for a scenario with $M = 6.$, $R_x = 15.$, $F = -1$, and $T = 0.2$s

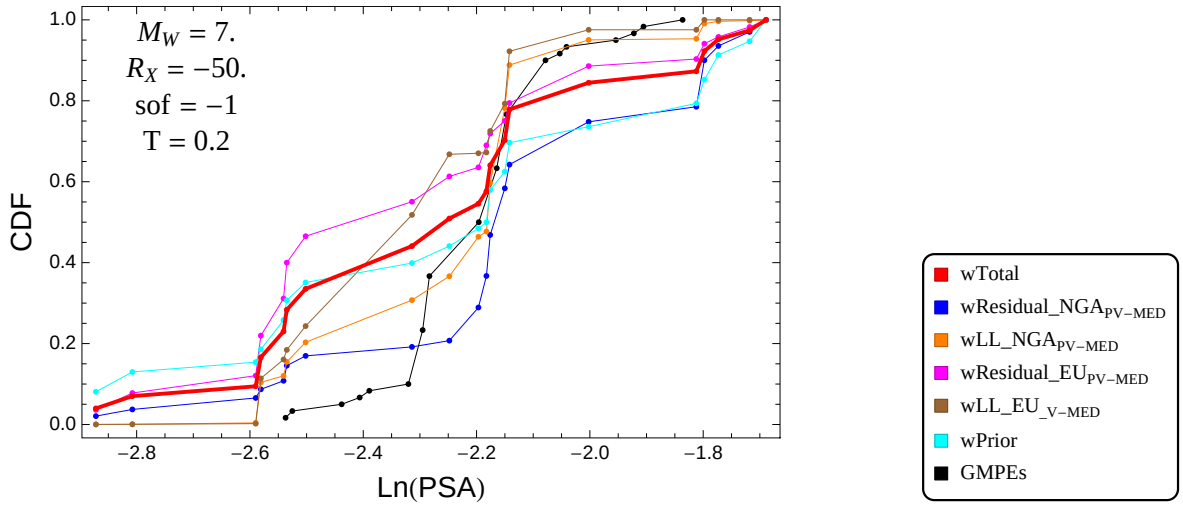



Figure 4.152: PVNGSv2: Cumulative distribution function of GMPEs (black) and selected models, for different sets of weights, for a scenario with $M = 7.$, $R_x = -50.$, $F = -1$, and $T = 0.2$s

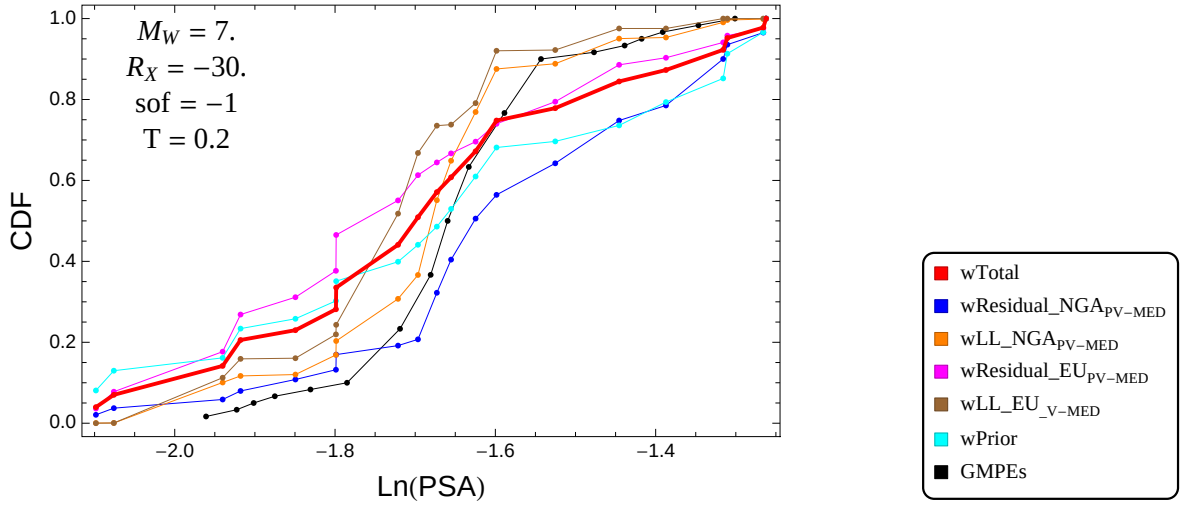



Figure 4.153: PVNGSv2: Cumulative distribution function of GMPEs (black) and selected models, for different sets of weights, for a scenario with $M = 7.$, $R_x = -30.$, $F = -1$, and $T = 0.2$s

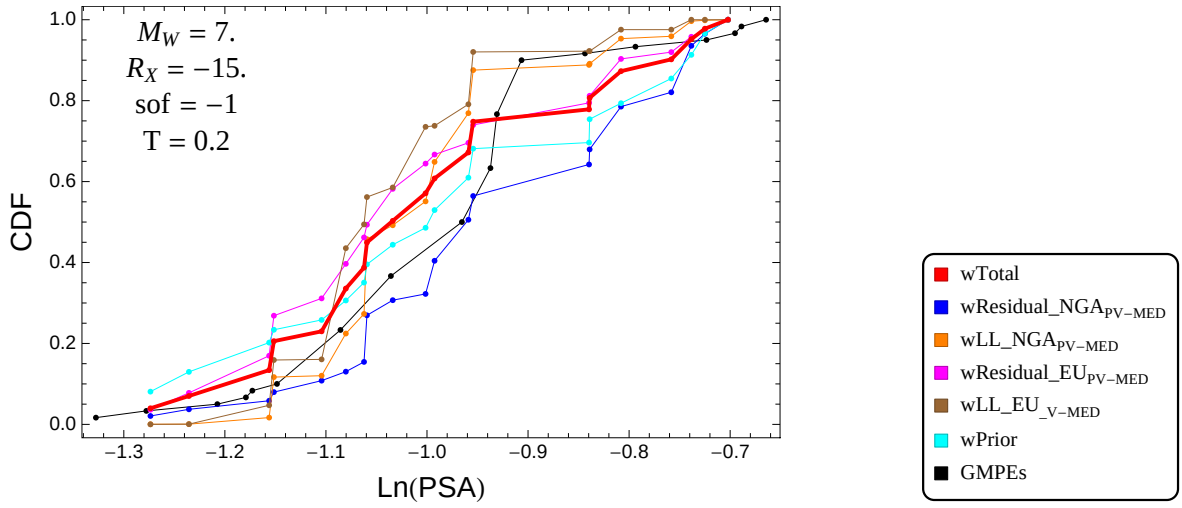



Figure 4.154: PVNGSv2: Cumulative distribution function of GMPEs (black) and selected models, for different sets of weights, for a scenario with $M = 7.$, $R_x = -15.$, $F = -1$, and $T = 0.2$s

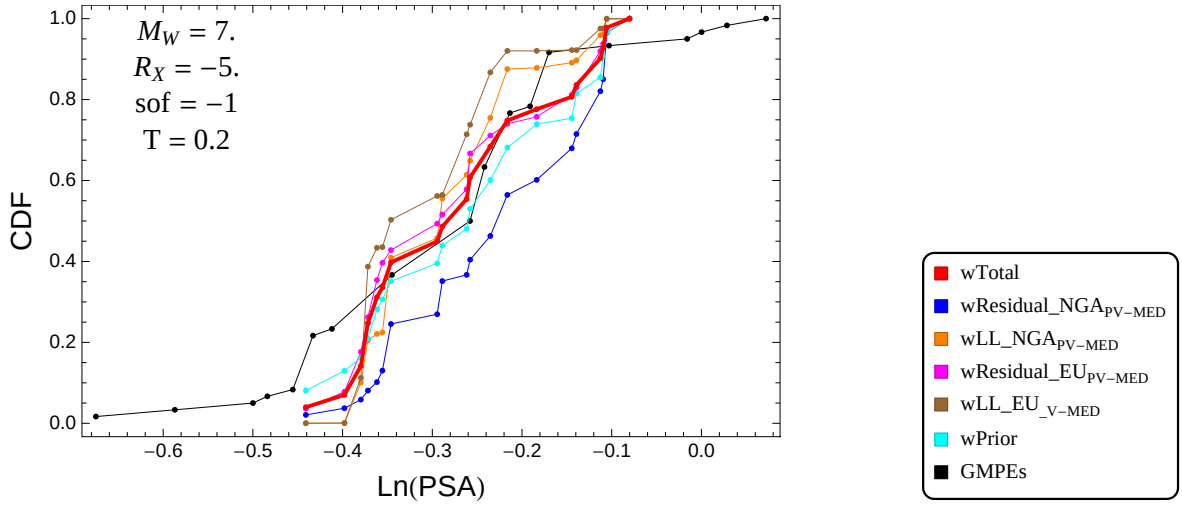



Figure 4.155: PVNGSv2: Cumulative distribution function of GMPEs (black) and selected models, for different sets of weights, for a scenario with $M = 7.$, $R_x = -5.$, $F = -1$, and $T = 0.2$s

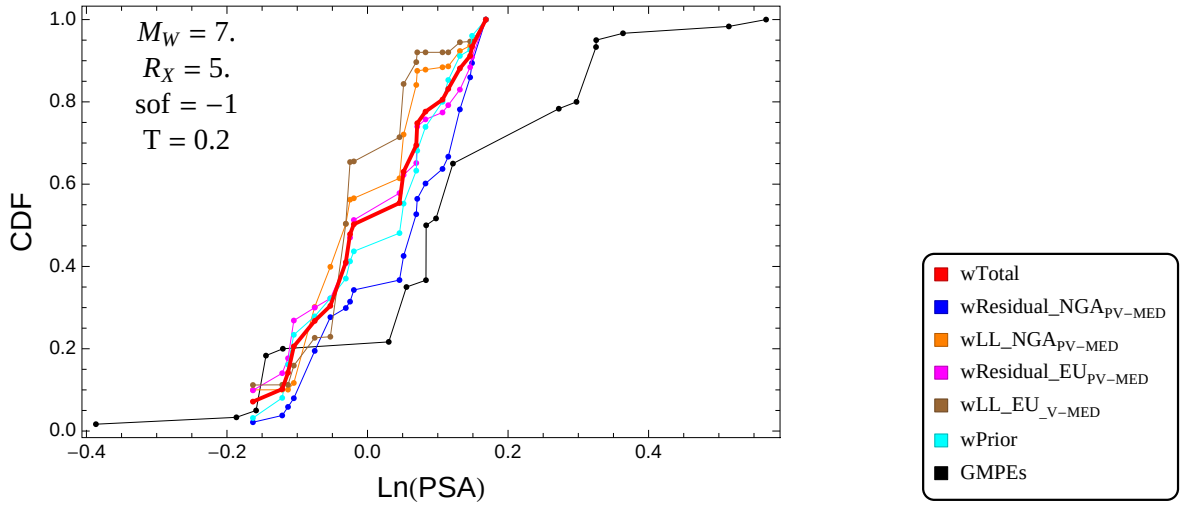



Figure 4.156: PVNGSv2: Cumulative distribution function of GMPEs (black) and selected models, for different sets of weights, for a scenario with $M = 7.$, $R_x = 5.$, $F = -1$, and $T = 0.2$s

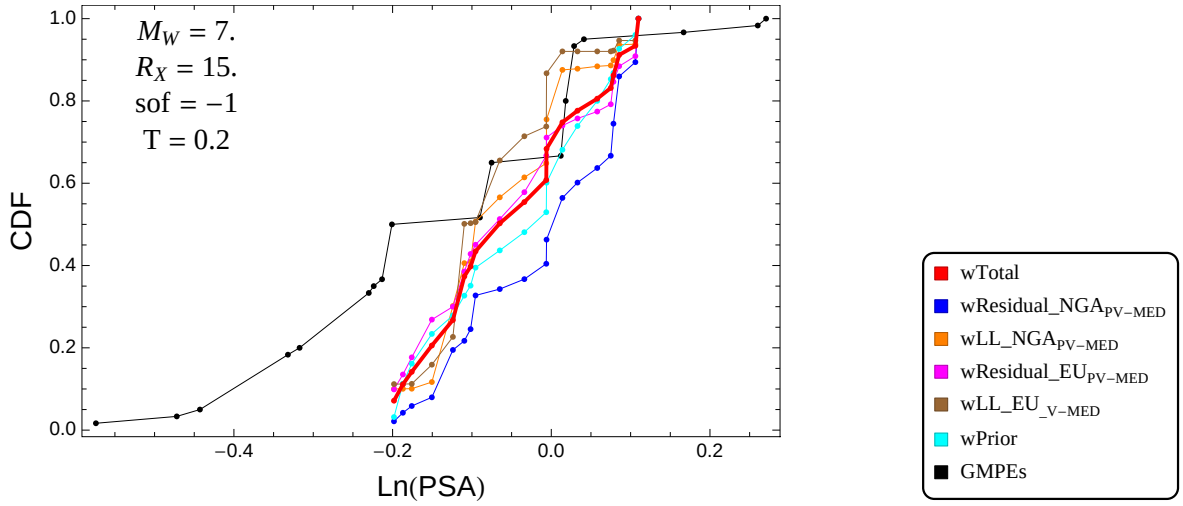



Figure 4.157: PVNGSv2: Cumulative distribution function of GMPEs (black) and selected models, for different sets of weights, for a scenario with $M = 7.$, $R_x = 15.$, $F = -1$, and $T = 0.2$s

**T = 0.5s**

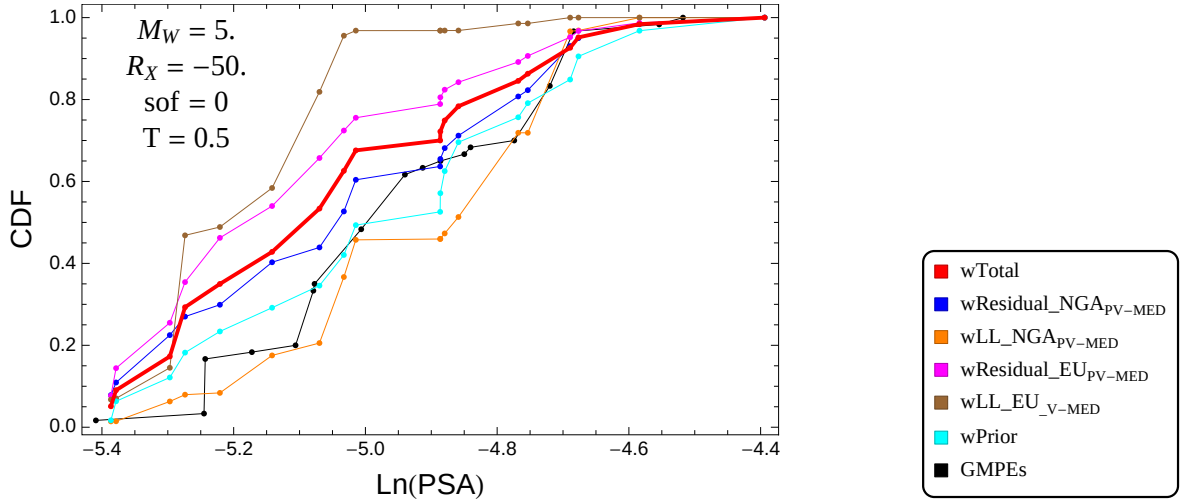



Figure 4.158: PVNGSv2: Cumulative distribution function of GMPEs (black) and selected models, for different sets of weights, for a scenario with $M = 5.$, $R_x = -50.$, $F = 0$, and $T = 0.5$s

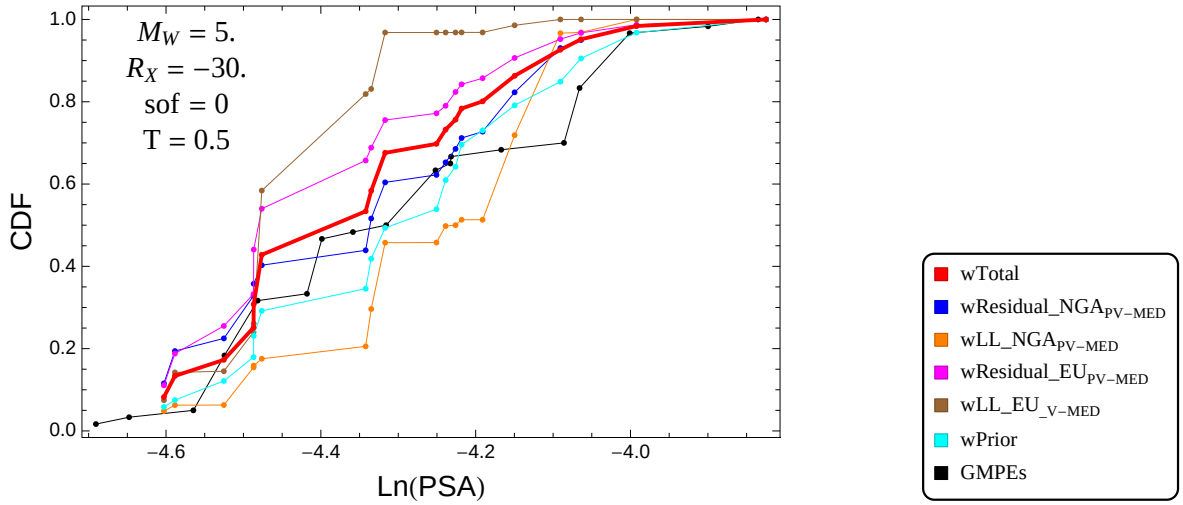



Figure 4.159: PVNGSv2: Cumulative distribution function of GMPEs (black) and selected models, for different sets of weights, for a scenario with $M = 5.$, $R_x = -30.$, $F = 0$, and $T = 0.5$s

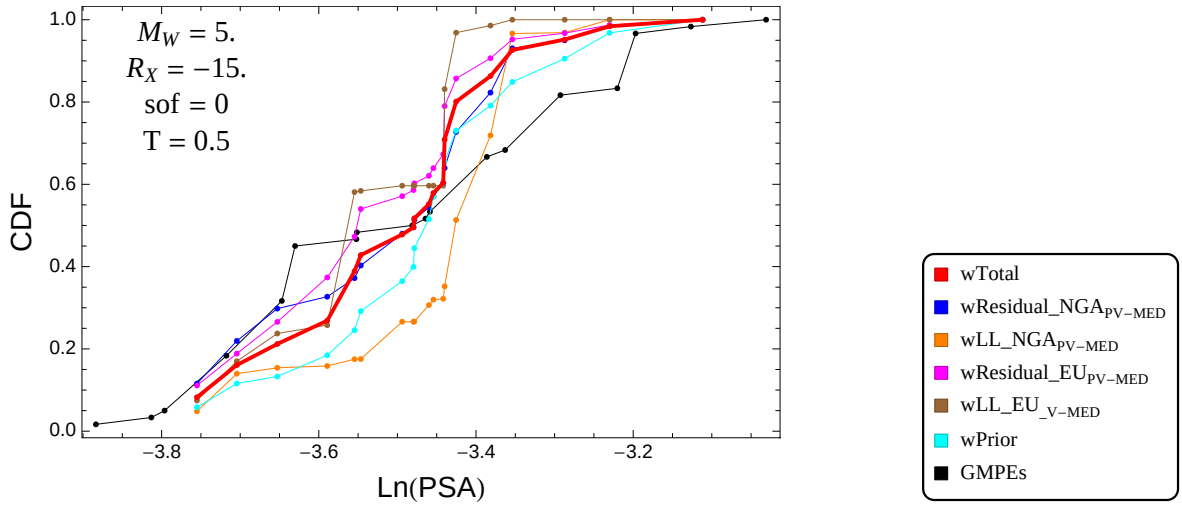



Figure 4.160: PVNGSv2: Cumulative distribution function of GMPEs (black) and selected models, for different sets of weights, for a scenario with $M = 5.$, $R_x = -15.$, $F = 0$, and $T = 0.5$s

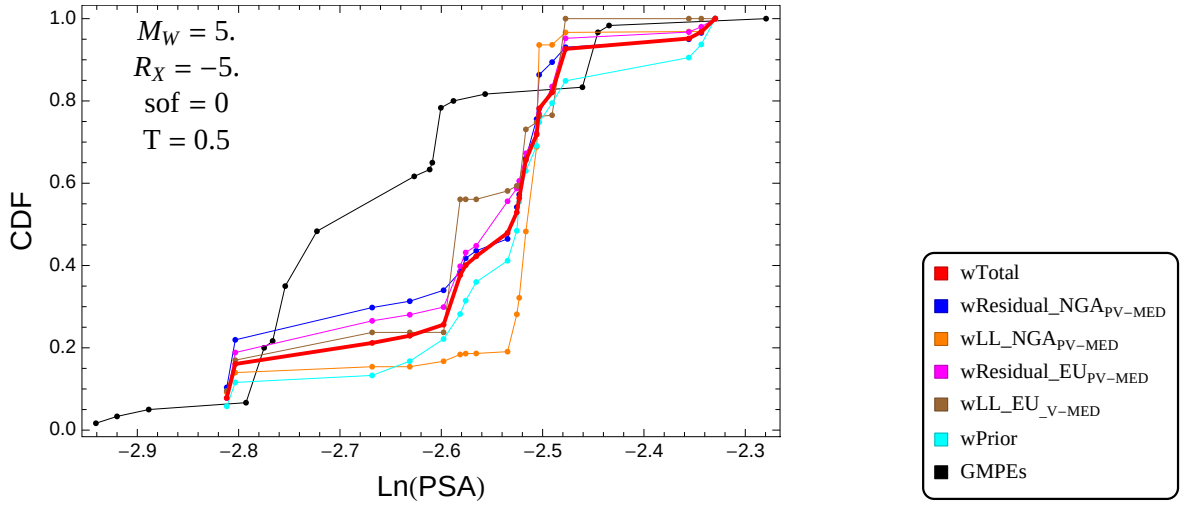



Figure 4.161: PVNGSv2: Cumulative distribution function of GMPEs (black) and selected models, for different sets of weights, for a scenario with $M = 5.$, $R_x = -5.$, $F = 0$, and $T = 0.5$s

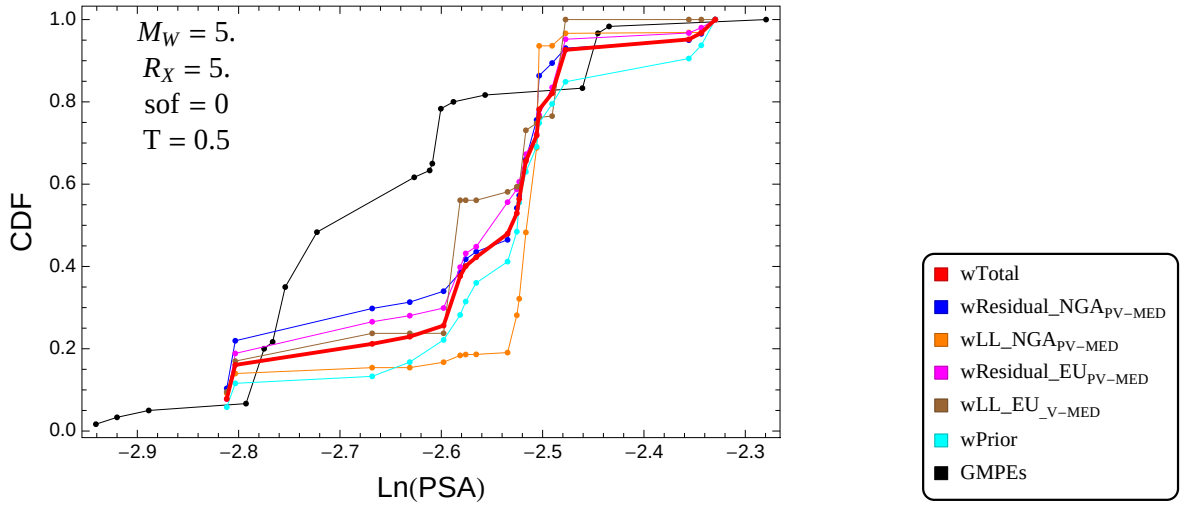



Figure 4.162: PVNGSv2: Cumulative distribution function of GMPEs (black) and selected models, for different sets of weights, for a scenario with $M = 5.$, $R_x = 5.$, $F = 0$, and $T = 0.5$s

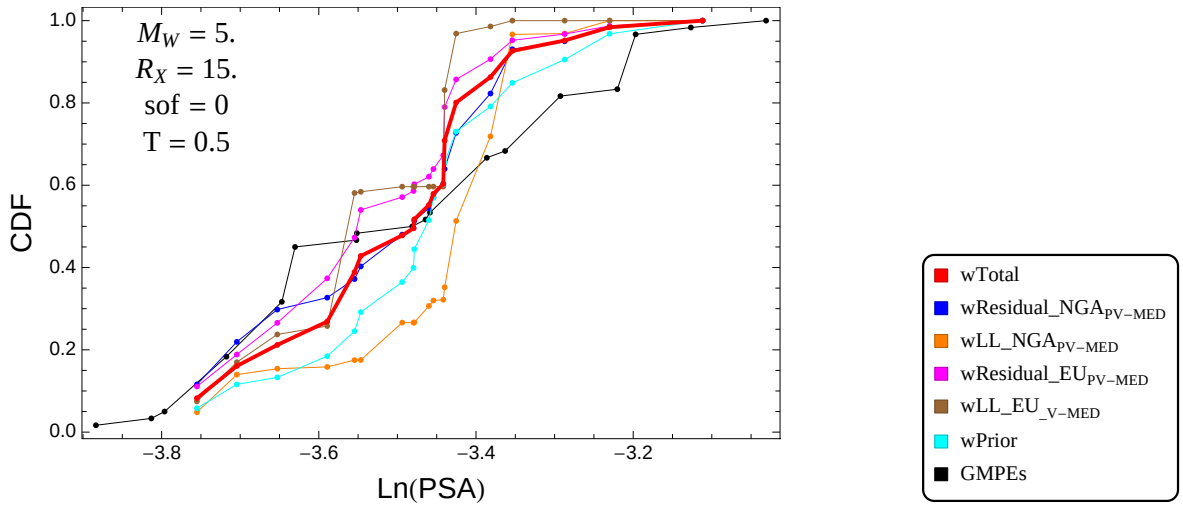



Figure 4.163: PVNGSv2: Cumulative distribution function of GMPEs (black) and selected models, for different sets of weights, for a scenario with $M = 5.$, $R_x = 15.$, $F = 0$, and $T = 0.5$s

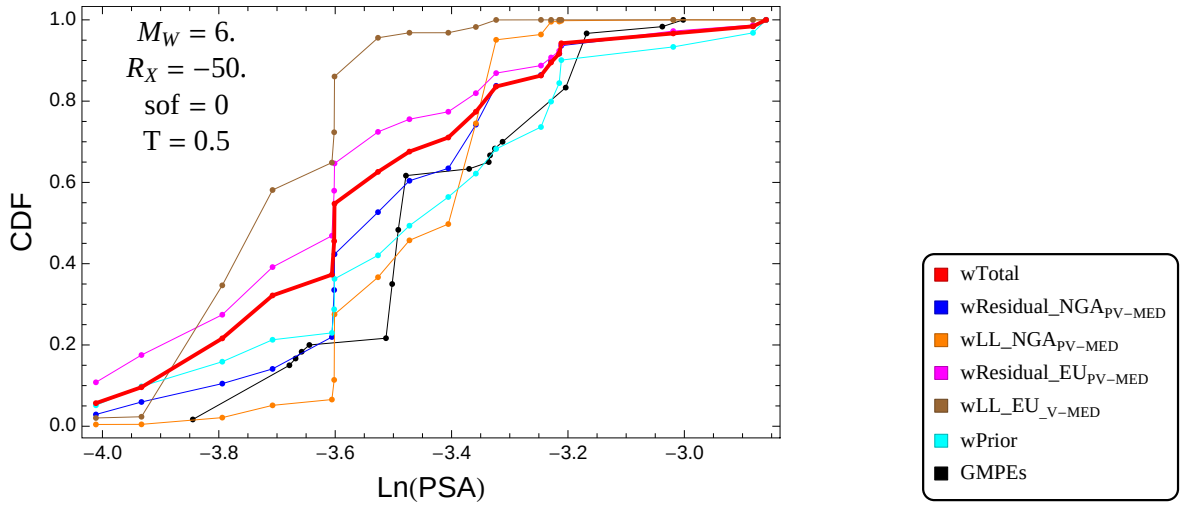



Figure 4.164: PVNGSv2: Cumulative distribution function of GMPEs (black) and selected models, for different sets of weights, for a scenario with $M = 6.$, $R_x = -50.$, $F = 0$, and $T = 0.5$s

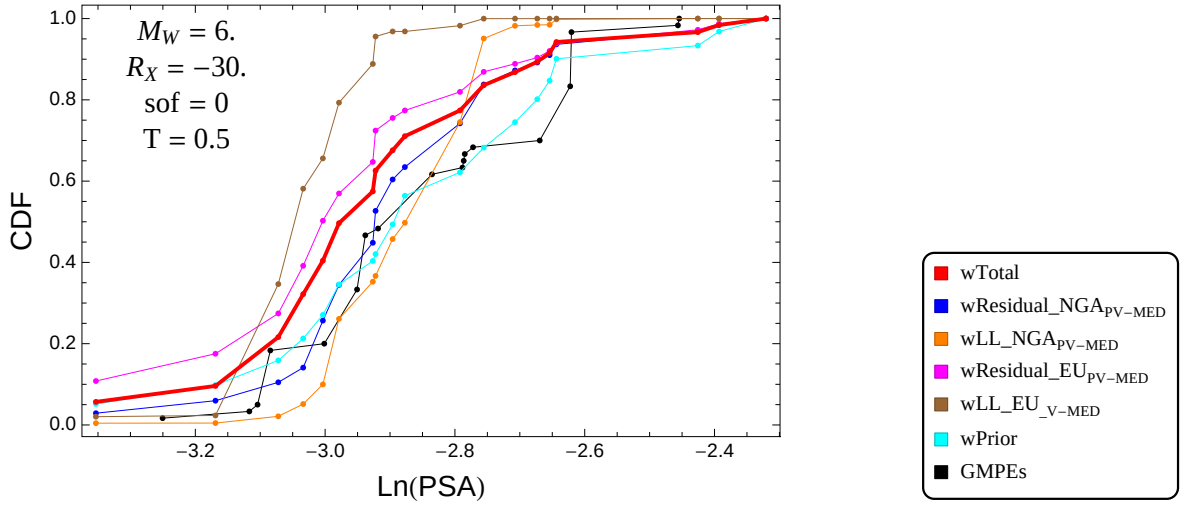



Figure 4.165: PVNGSv2: Cumulative distribution function of GMPEs (black) and selected models, for different sets of weights, for a scenario with $M = 6.$, $R_x = -30.$, $F = 0$, and $T = 0.5$s

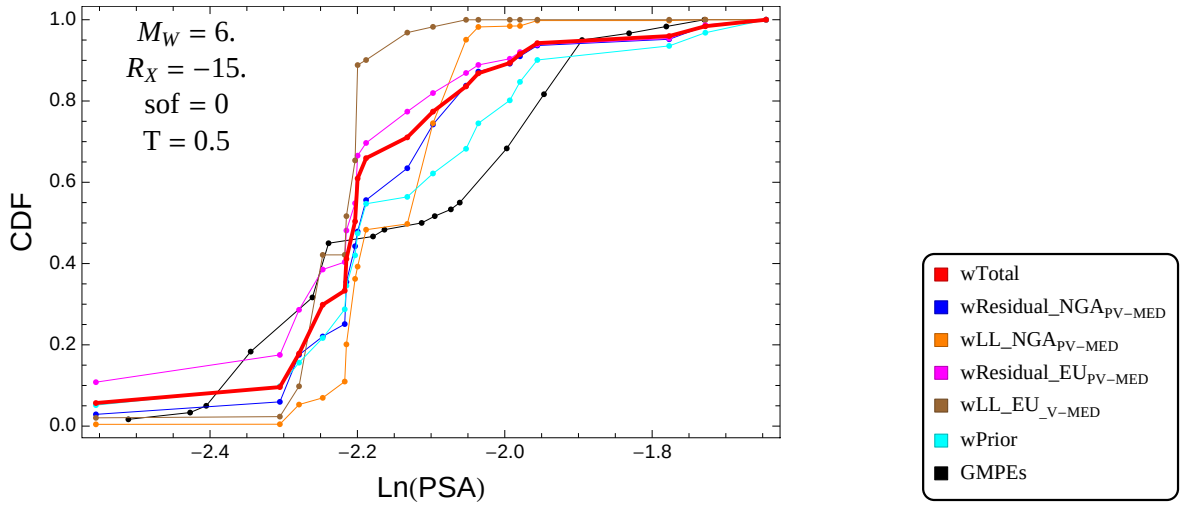



Figure 4.166: PVNGSv2: Cumulative distribution function of GMPEs (black) and selected models, for different sets of weights, for a scenario with $M = 6.$, $R_x = -15.$, $F = 0$, and $T = 0.5$s

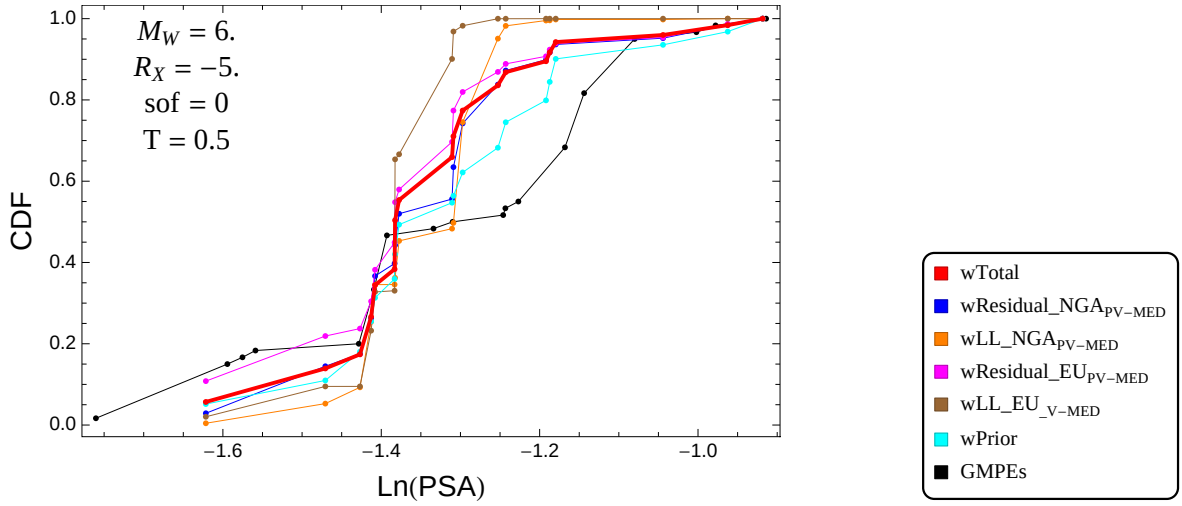



Figure 4.167: PVNGSv2: Cumulative distribution function of GMPEs (black) and selected models, for different sets of weights, for a scenario with $M = 6.$, $R_x = -5.$, $F = 0$, and $T = 0.5$s

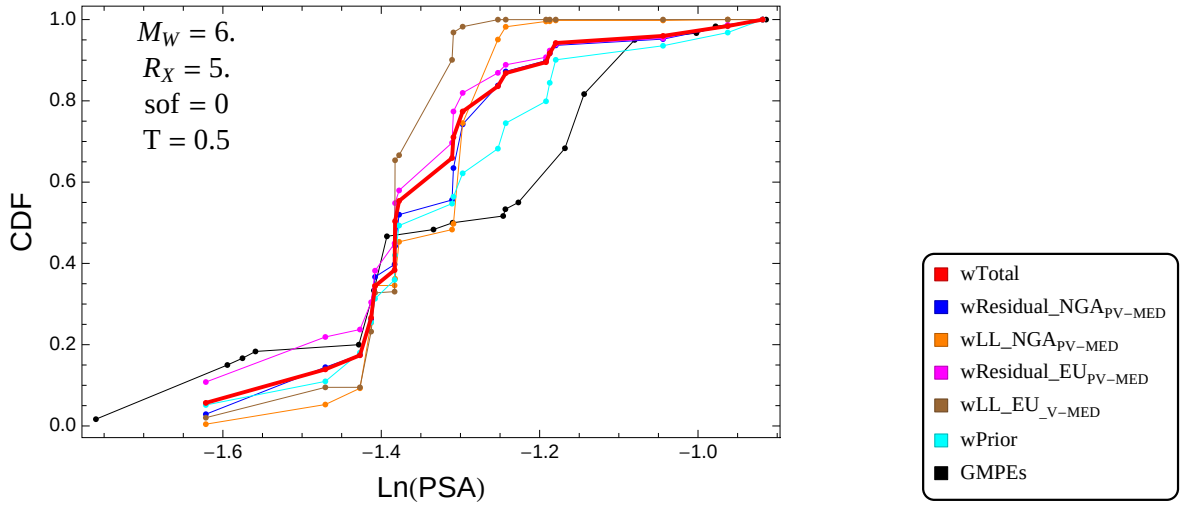



Figure 4.168: PVNGSv2: Cumulative distribution function of GMPEs (black) and selected models, for different sets of weights, for a scenario with $M = 6.$, $R_x = 5.$, $F = 0$, and $T = 0.5$s

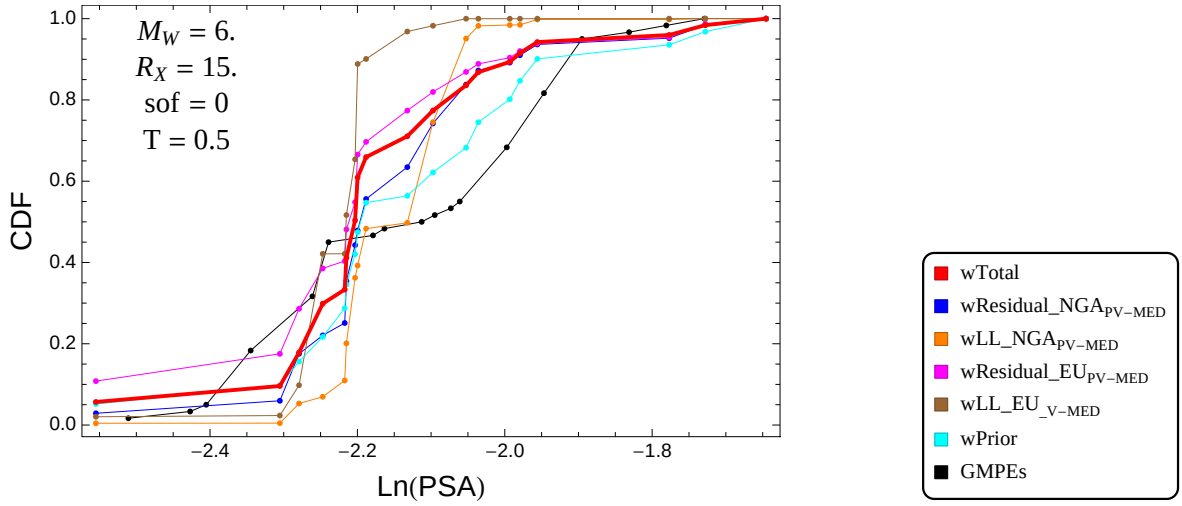



Figure 4.169: PVNGSv2: Cumulative distribution function of GMPEs (black) and selected models, for different sets of weights, for a scenario with $M = 6.$, $R_x = 15.$, $F = 0$, and $T = 0.5$s

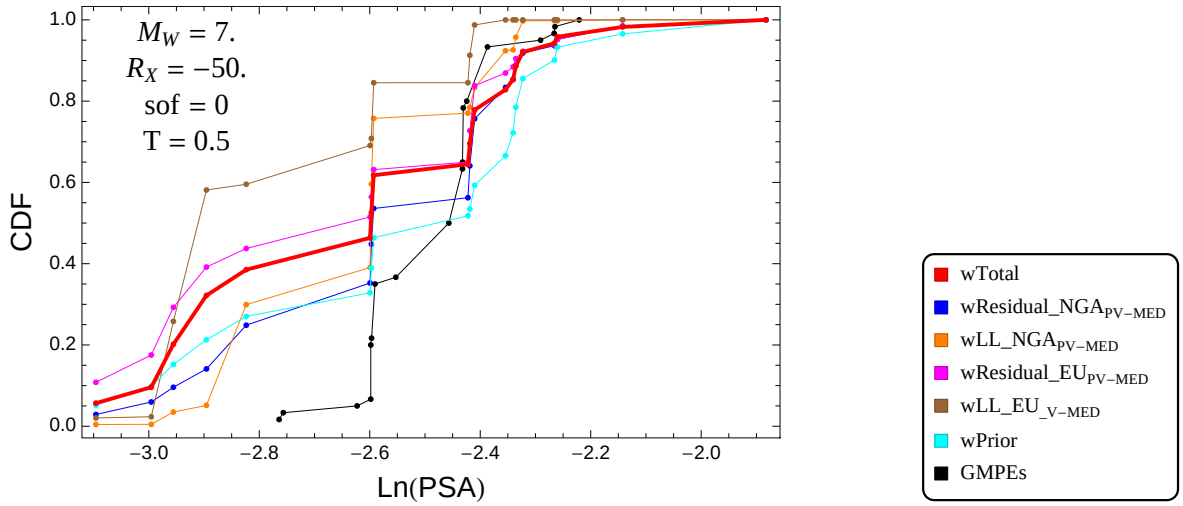



Figure 4.170: PVNGSv2: Cumulative distribution function of GMPEs (black) and selected models, for different sets of weights, for a scenario with $M = 7.$, $R_x = -50.$, $F = 0$, and $T = 0.5$s

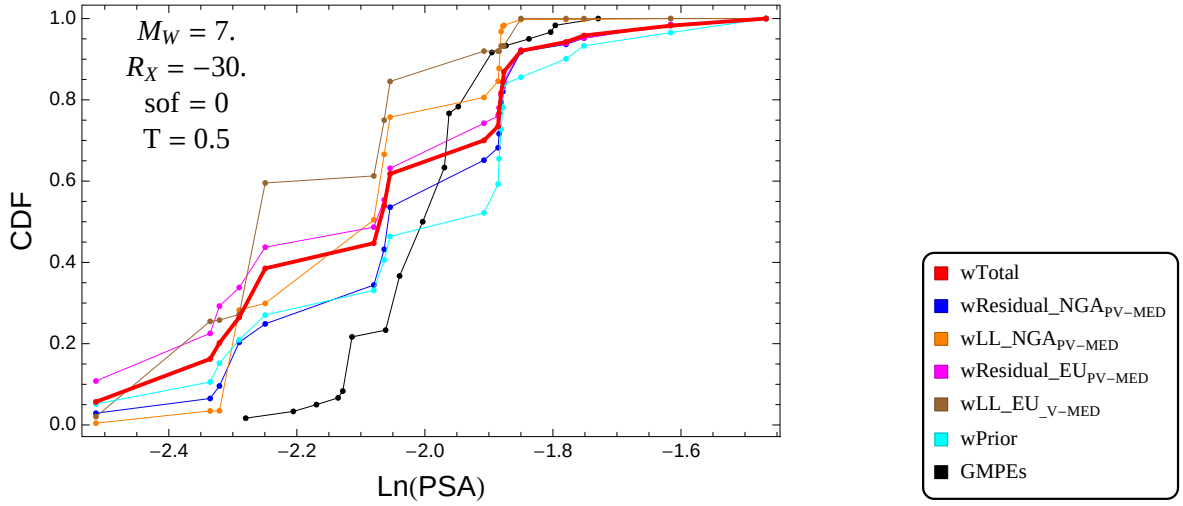



Figure 4.171: PVNGSv2: Cumulative distribution function of GMPEs (black) and selected models, for different sets of weights, for a scenario with $M = 7.$, $R_x = -30.$, $F = 0$, and $T = 0.5$s

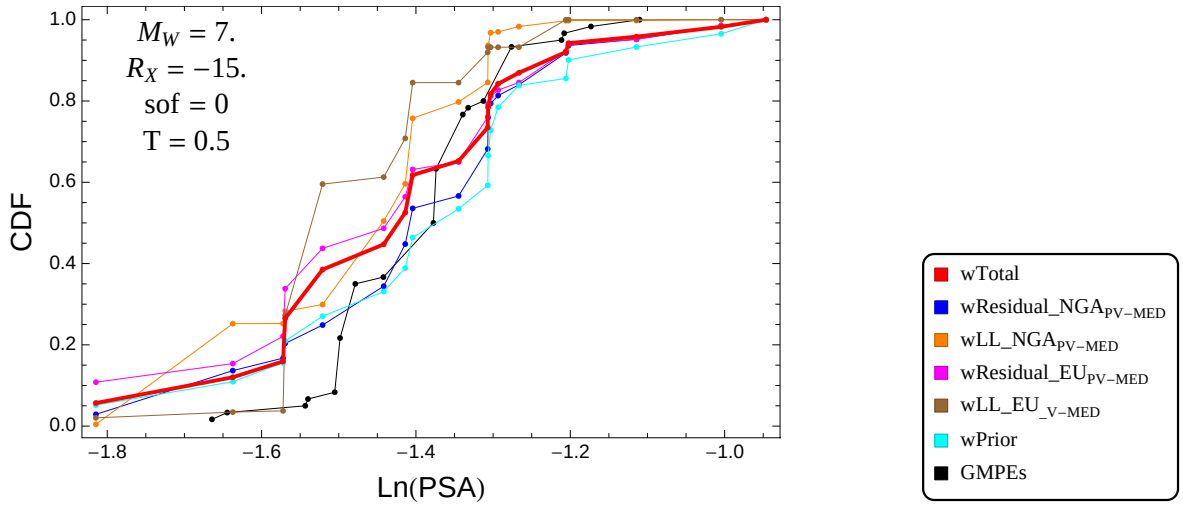



Figure 4.172: PVNGSv2: Cumulative distribution function of GMPEs (black) and selected models, for different sets of weights, for a scenario with $M = 7.$, $R_x = -15.$, $F = 0$, and $T = 0.5$s

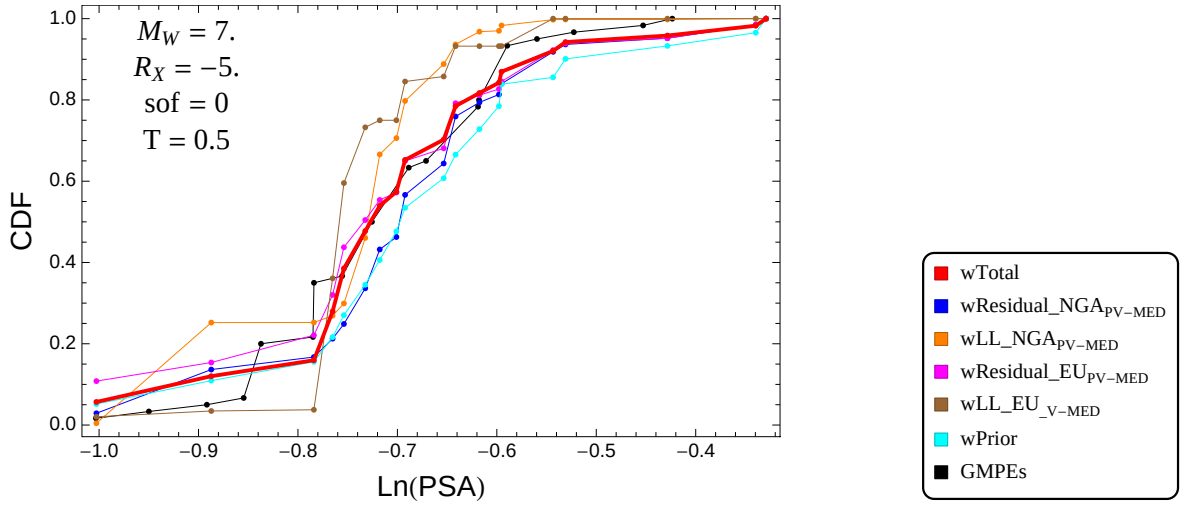



Figure 4.173: PVNGSv2: Cumulative distribution function of GMPEs (black) and selected models, for different sets of weights, for a scenario with $M = 7.$, $R_x = -5.$, $F = 0$, and $T = 0.5$s

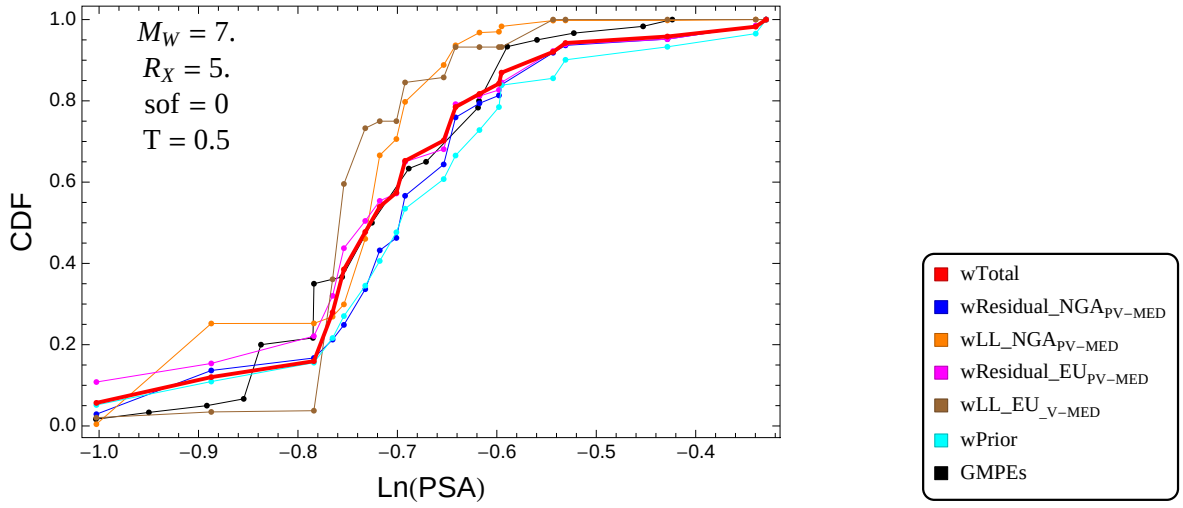



Figure 4.174: PVNGSv2: Cumulative distribution function of GMPEs (black) and selected models, for different sets of weights, for a scenario with $M = 7.$, $R_x = 5.$, $F = 0$, and $T = 0.5$s

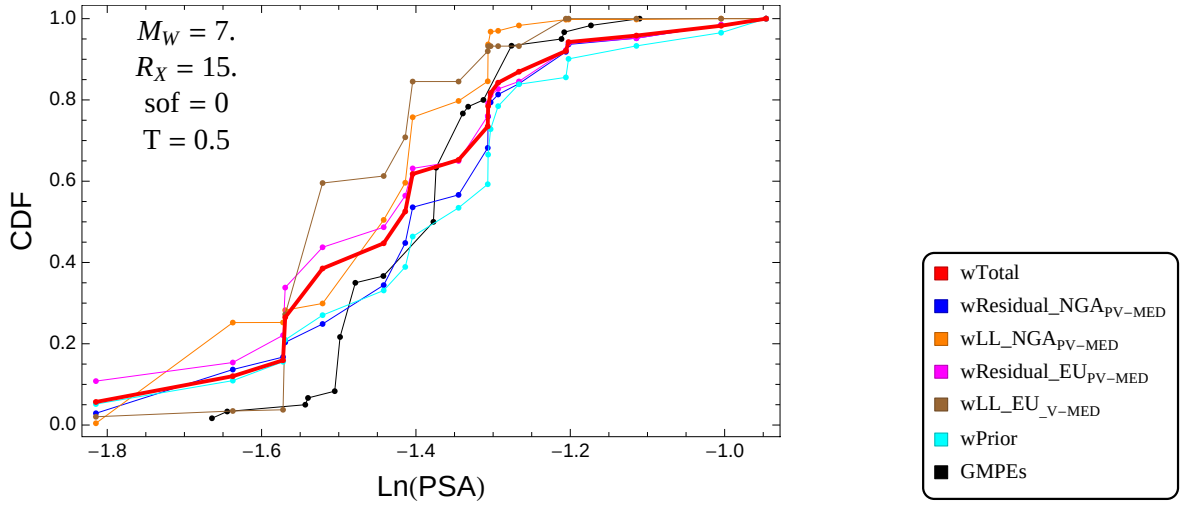



Figure 4.175: PVNGSv2: Cumulative distribution function of GMPEs (black) and selected models, for different sets of weights, for a scenario with $M = 7.$, $R_x = 15.$, $F = 0$, and $T = 0.5$s

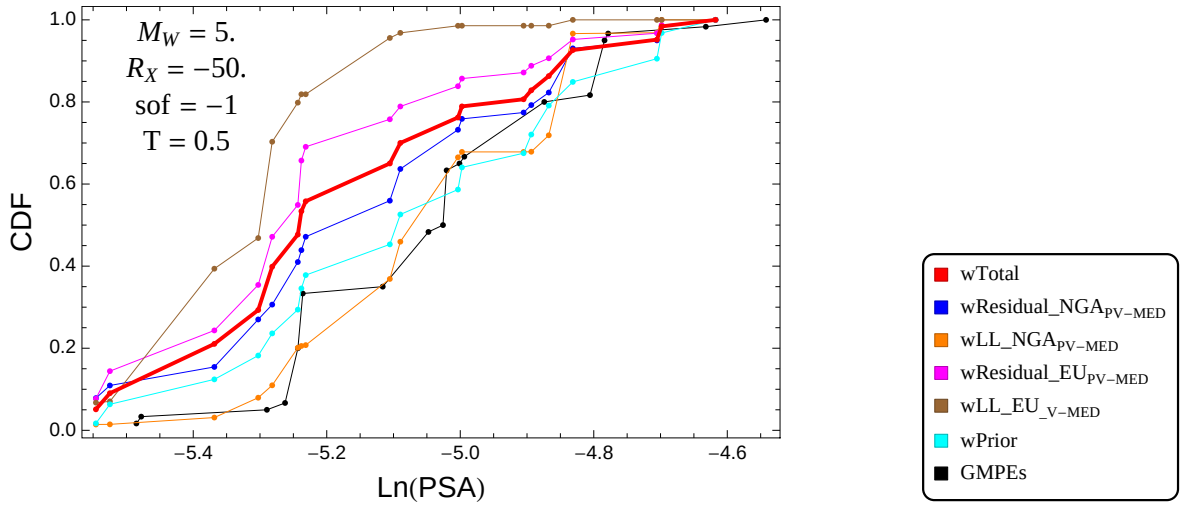



Figure 4.176: PVNGSv2: Cumulative distribution function of GMPEs (black) and selected models, for different sets of weights, for a scenario with $M = 5.$, $R_x = -50.$, $F = -1$, and $T = 0.5$s

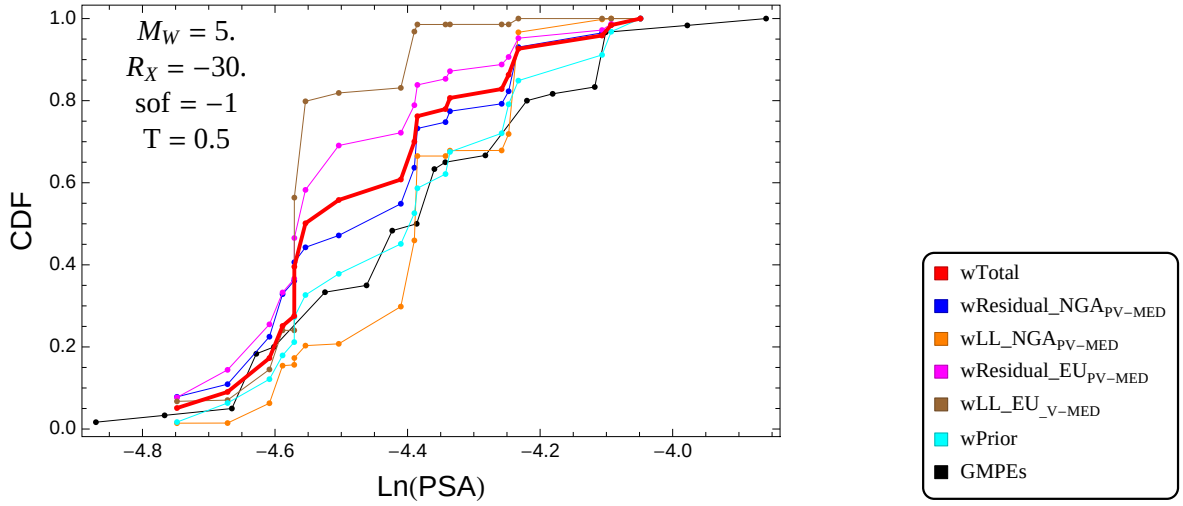



Figure 4.177: PVNGSv2: Cumulative distribution function of GMPEs (black) and selected models, for different sets of weights, for a scenario with $M = 5.$, $R_x = -30.$, $F = -1$, and $T = 0.5$s

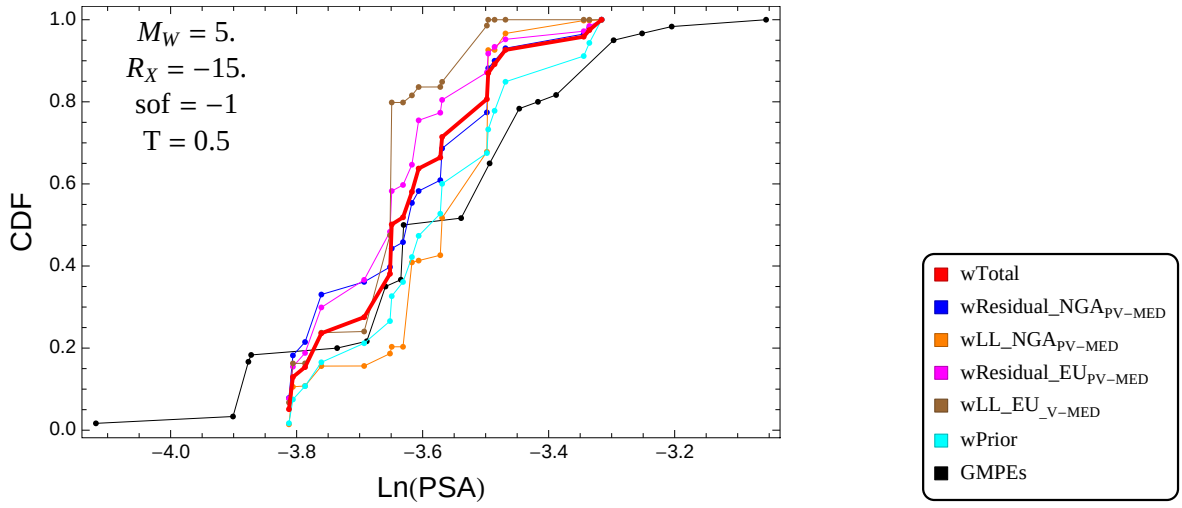



Figure 4.178: PVNGSv2: Cumulative distribution function of GMPEs (black) and selected models, for different sets of weights, for a scenario with $M = 5.$, $R_x = -15.$, $F = -1$, and $T = 0.5$s

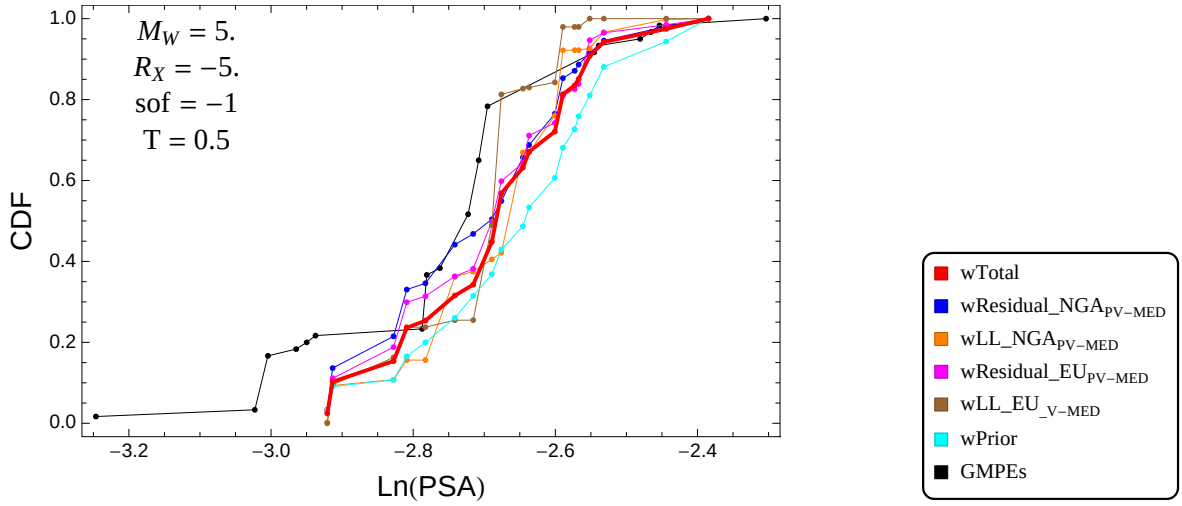



Figure 4.179: PVNGSv2: Cumulative distribution function of GMPEs (black) and selected models, for different sets of weights, for a scenario with $M = 5.$, $R_x = -5.$, $F = -1$, and $T = 0.5$s

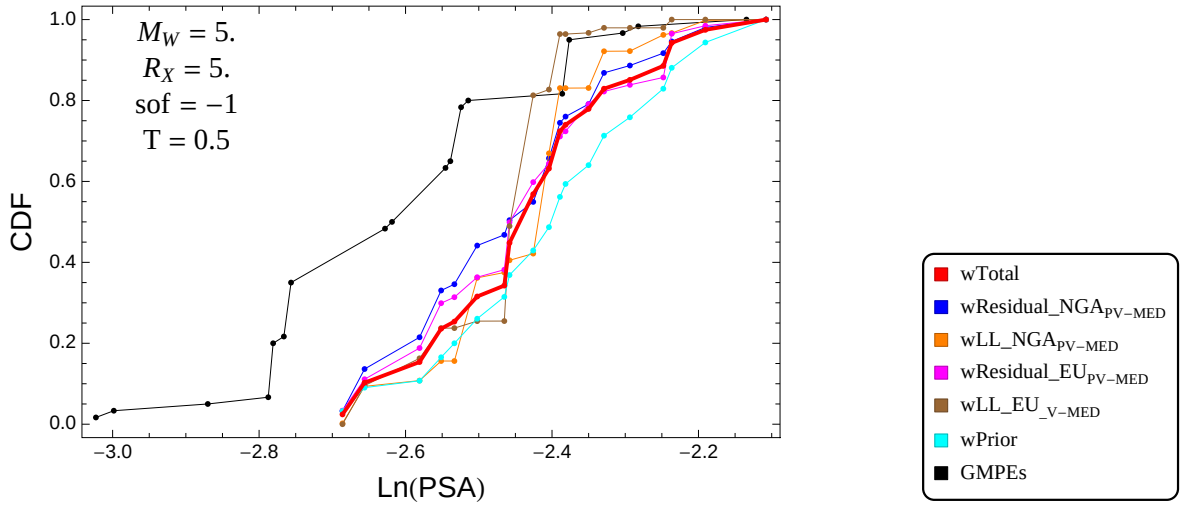



Figure 4.180: PVNGSv2: Cumulative distribution function of GMPEs (black) and selected models, for different sets of weights, for a scenario with $M = 5.$, $R_x = 5.$, $F = -1$, and $T = 0.5$s

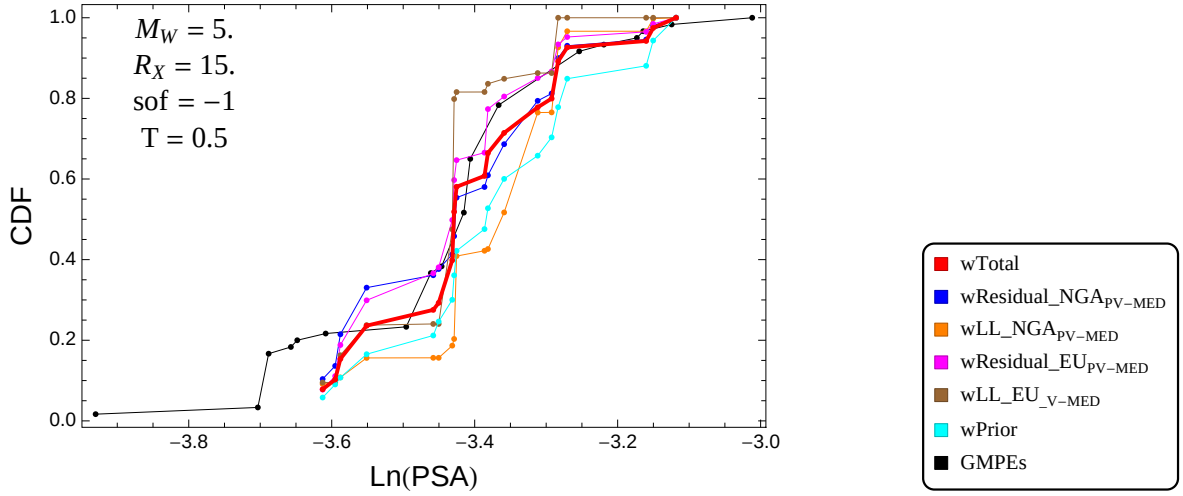



Figure 4.181: PVNGSv2: Cumulative distribution function of GMPEs (black) and selected models, for different sets of weights, for a scenario with $M = 5.$, $R_x = 15.$, $F = -1$, and $T = 0.5$s

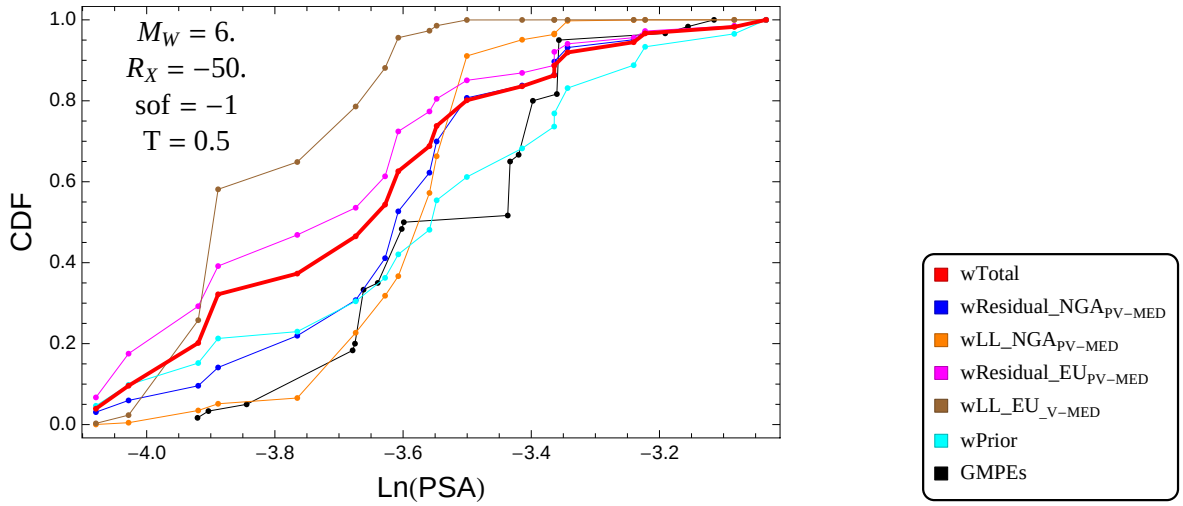



Figure 4.182: PVNGSv2: Cumulative distribution function of GMPEs (black) and selected models, for different sets of weights, for a scenario with $M = 6.$, $R_x = -50.$, $F = -1$, and $T = 0.5$s

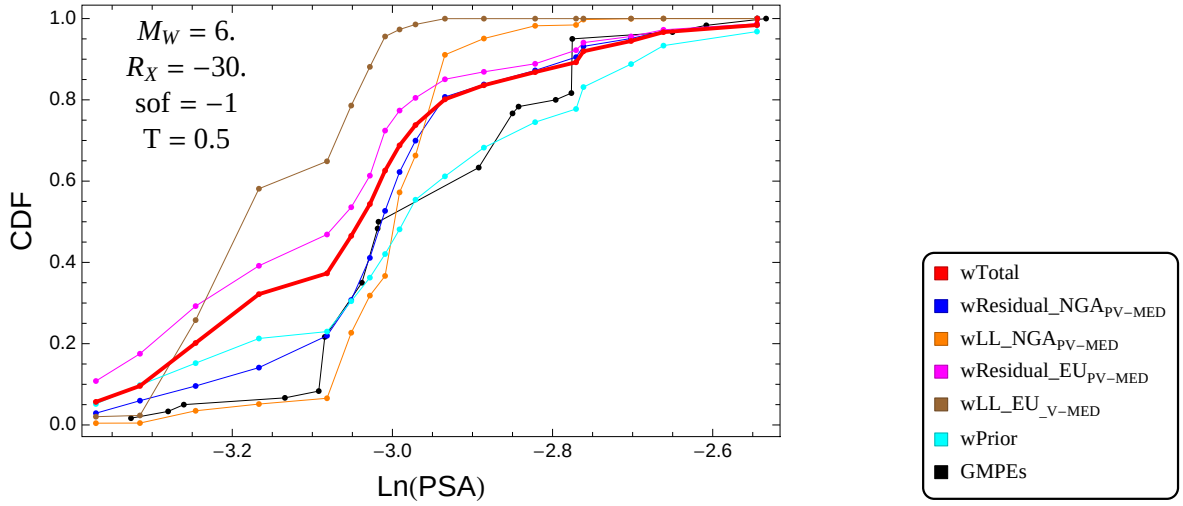



Figure 4.183: PVNGSv2: Cumulative distribution function of GMPEs (black) and selected models, for different sets of weights, for a scenario with $M = 6.$, $R_x = -30.$, $F = -1$, and $T = 0.5$s

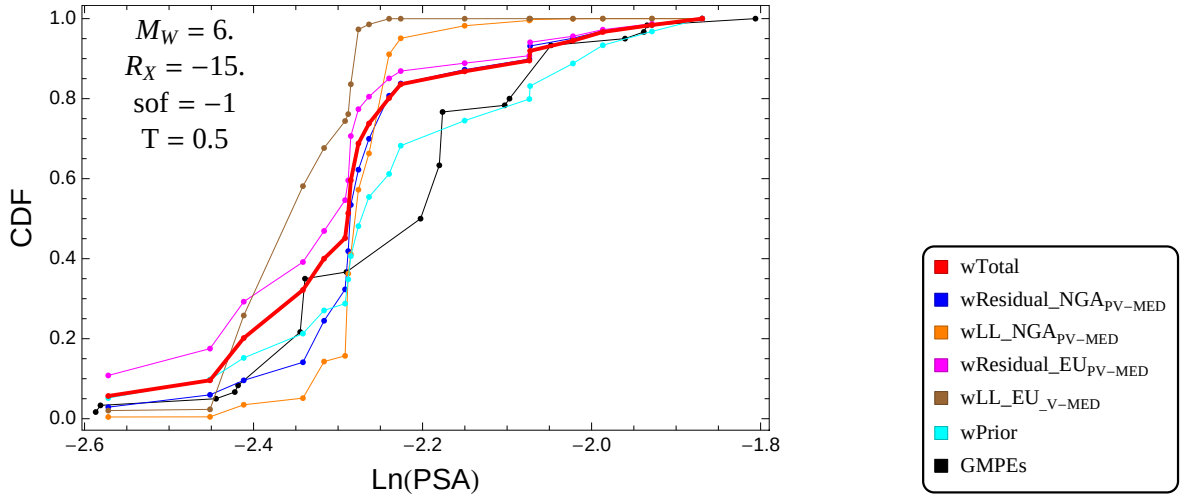



Figure 4.184: PVNGSv2: Cumulative distribution function of GMPEs (black) and selected models, for different sets of weights, for a scenario with $M = 6.$, $R_x = -15.$, $F = -1$, and $T = 0.5$s

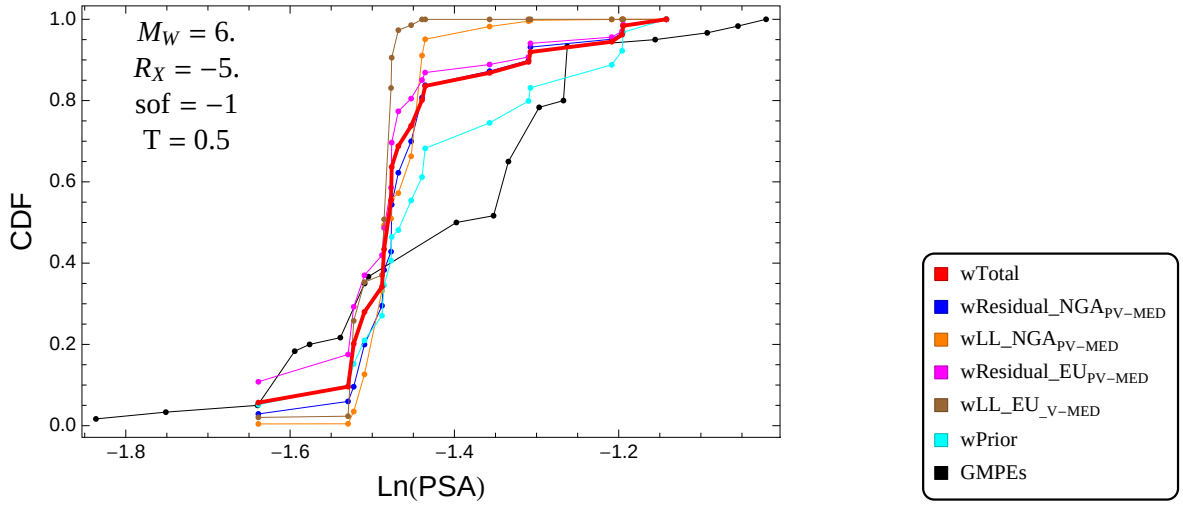



Figure 4.185: PVNGSv2: Cumulative distribution function of GMPEs (black) and selected models, for different sets of weights, for a scenario with $M = 6.$, $R_x = -5.$, $F = -1$, and $T = 0.5$s

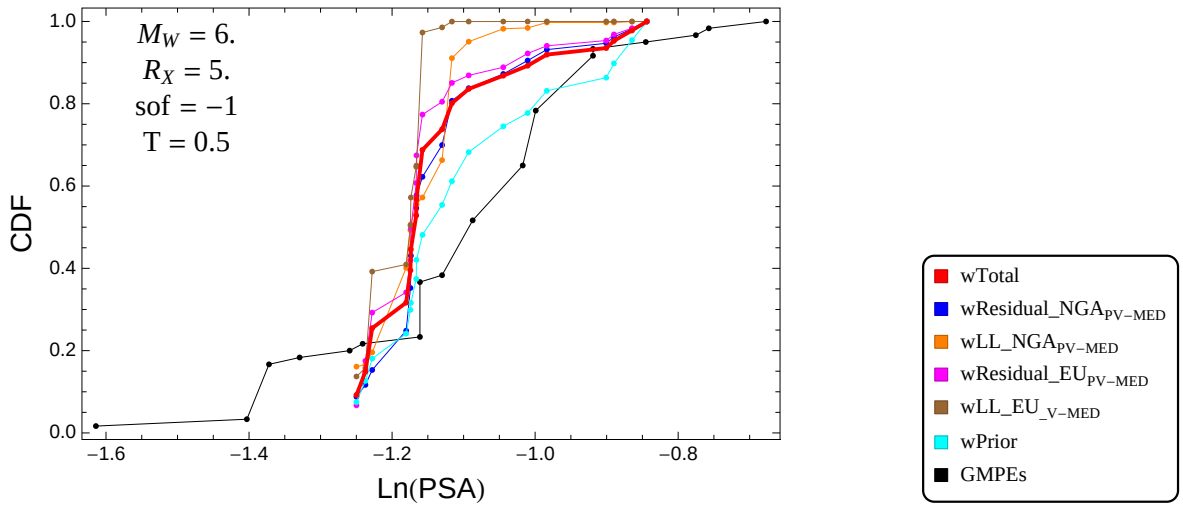



Figure 4.186: PVNGSv2: Cumulative distribution function of GMPEs (black) and selected models, for different sets of weights, for a scenario with $M = 6.$, $R_x = 5.$, $F = -1$, and $T = 0.5$s

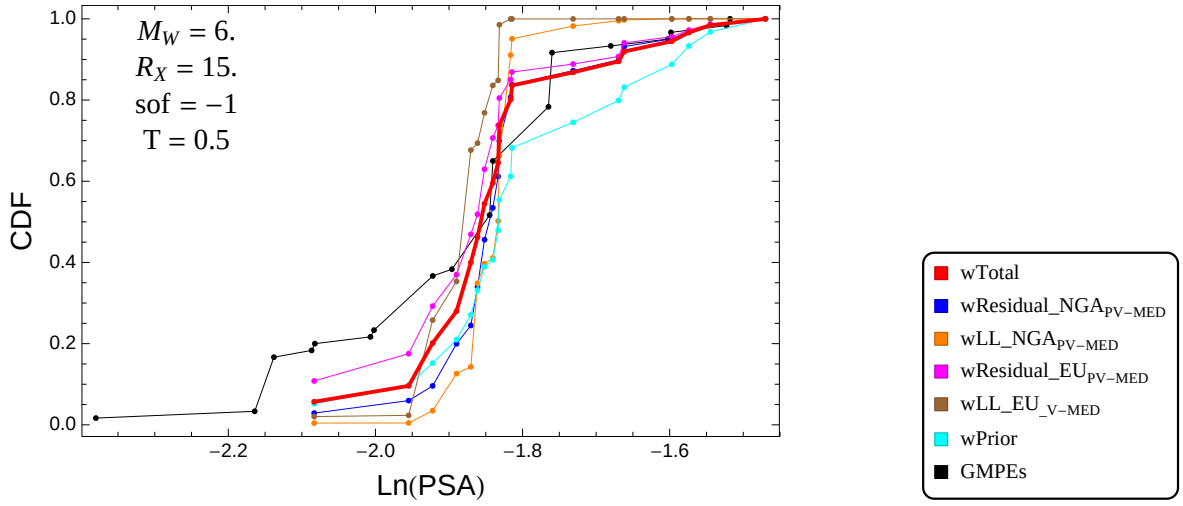



Figure 4.187: PVNGSv2: Cumulative distribution function of GMPEs (black) and selected models, for different sets of weights, for a scenario with $M = 6.$, $R_x = 15.$, $F = -1$, and $T = 0.5$s

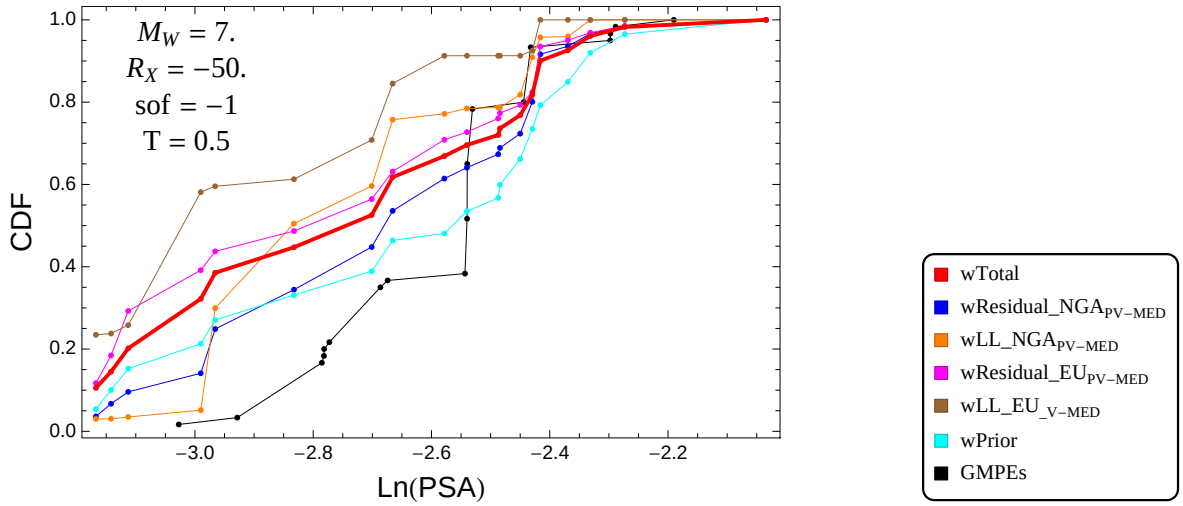



Figure 4.188: PVNGSv2: Cumulative distribution function of GMPEs (black) and selected models, for different sets of weights, for a scenario with $M = 7.$, $R_x = -50.$, $F = -1$, and $T = 0.5$s

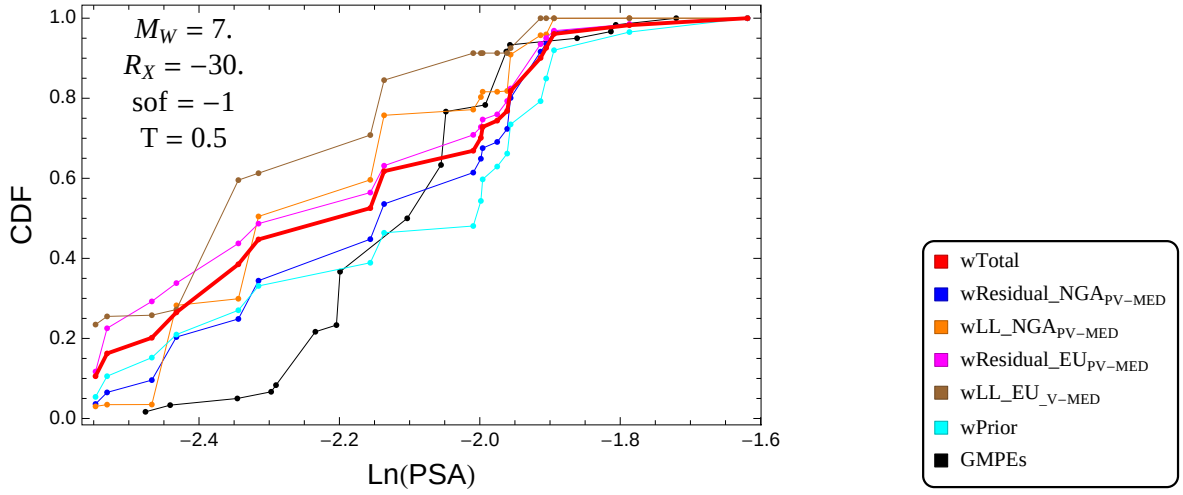



Figure 4.189: PVNGSv2: Cumulative distribution function of GMPEs (black) and selected models, for different sets of weights, for a scenario with $M = 7.$, $R_x = -30.$, $F = -1$, and $T = 0.5$s

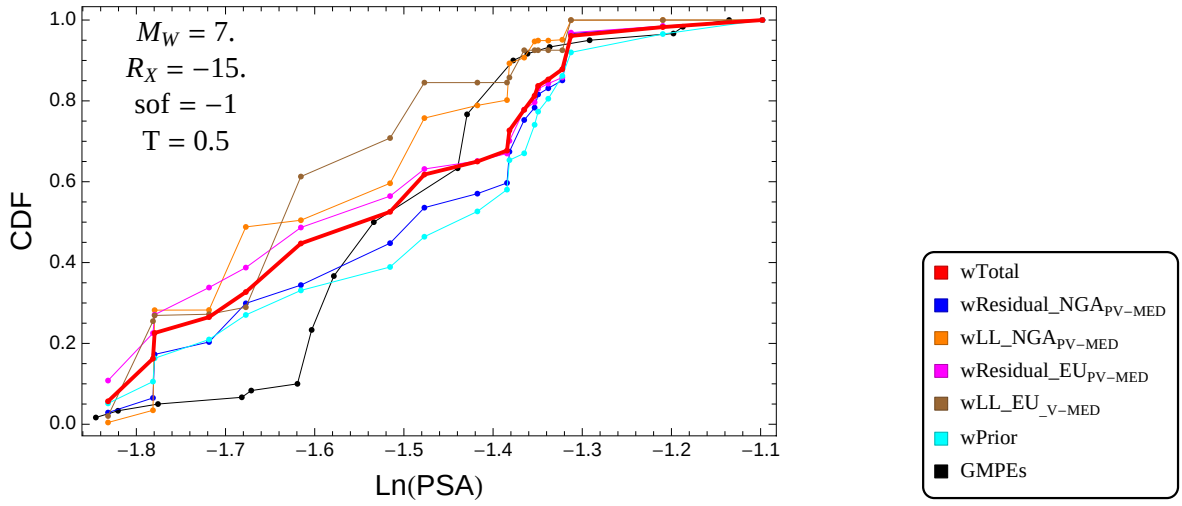



Figure 4.190: PVNGSv2: Cumulative distribution function of GMPEs (black) and selected models, for different sets of weights, for a scenario with $M = 7.$, $R_x = -15.$, $F = -1$, and $T = 0.5$s

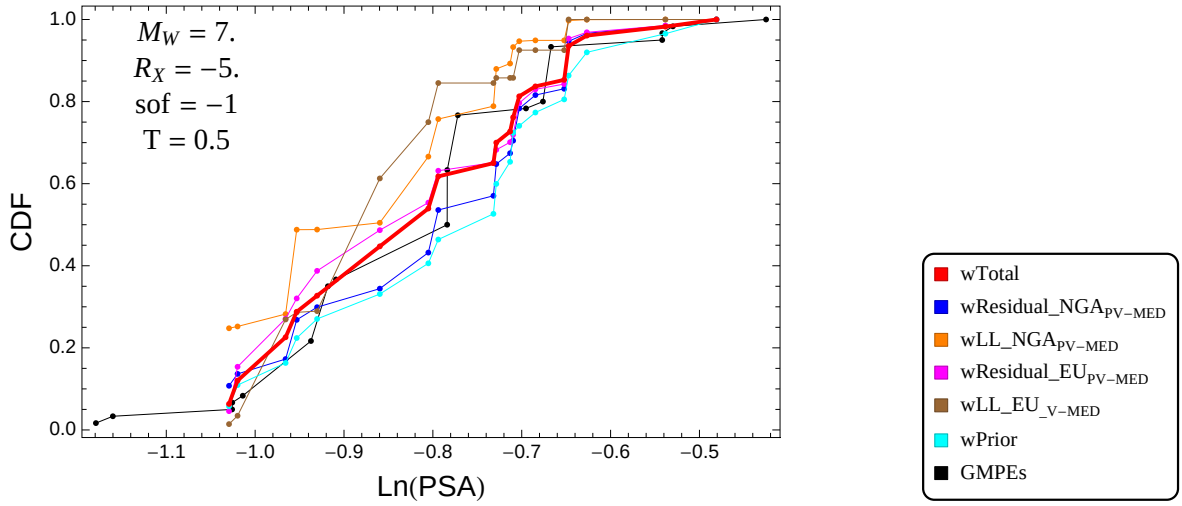



Figure 4.191: PVNGSv2: Cumulative distribution function of GMPEs (black) and selected models, for different sets of weights, for a scenario with $M = 7.$, $R_x = -5.$, $F = -1$, and $T = 0.5$s

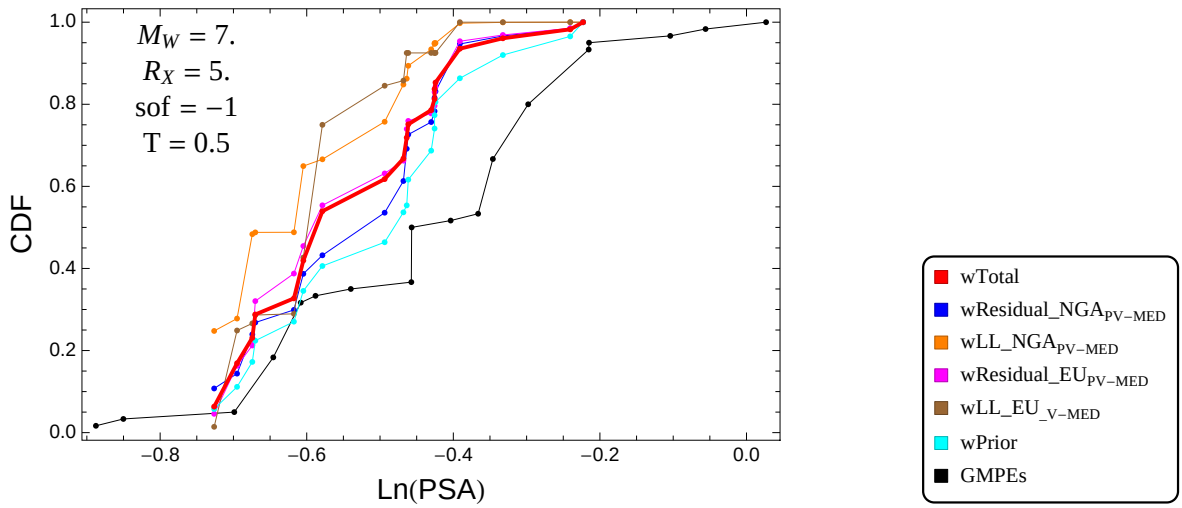



Figure 4.192: PVNGSv2: Cumulative distribution function of GMPEs (black) and selected models, for different sets of weights, for a scenario with $M = 7.$, $R_x = 5.$, $F = -1$, and $T = 0.5$s

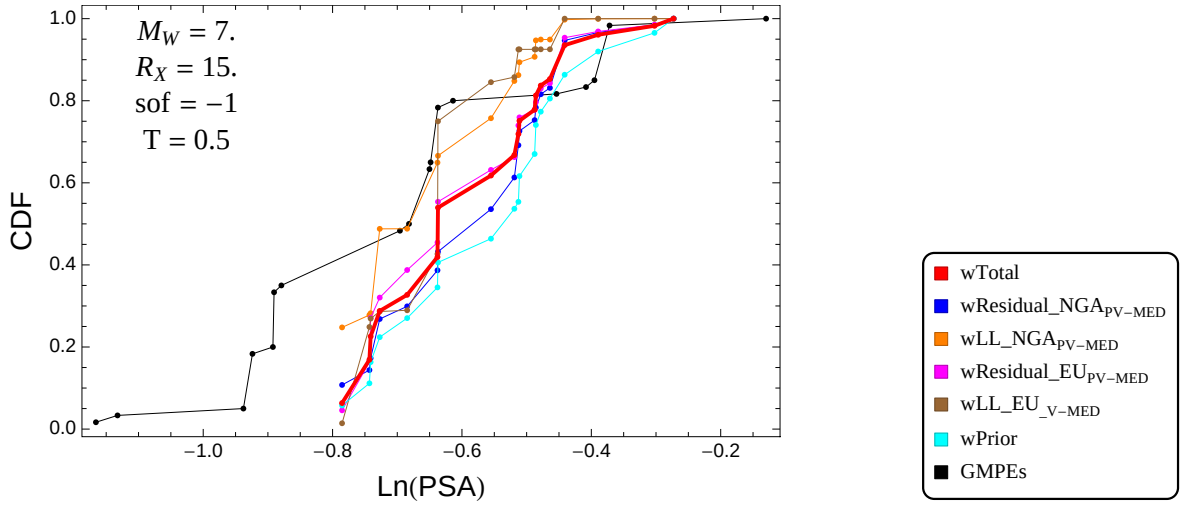



Figure 4.193: PVNGSv2: Cumulative distribution function of GMPEs (black) and selected models, for different sets of weights, for a scenario with $M = 7.$, $R_x = 15.$, $F = -1$, and $T = 0.5$s

**T = 1.s**

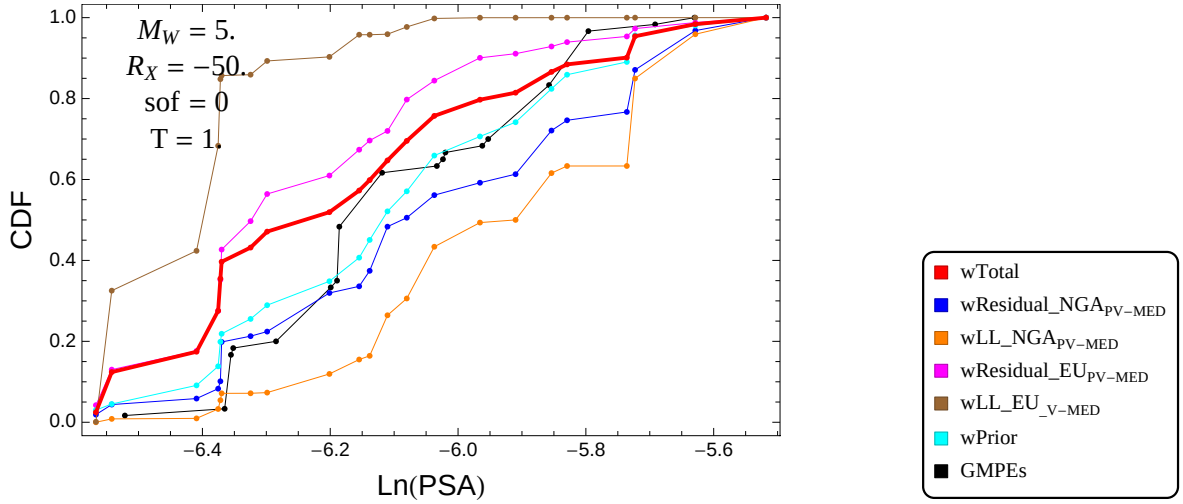



Figure 4.194: PVNGSv2: Cumulative distribution function of GMPEs (black) and selected models, for different sets of weights, for a scenario with $M = 5.$, $R_x = -50.$, $F = 0$, and $T = 1.$s

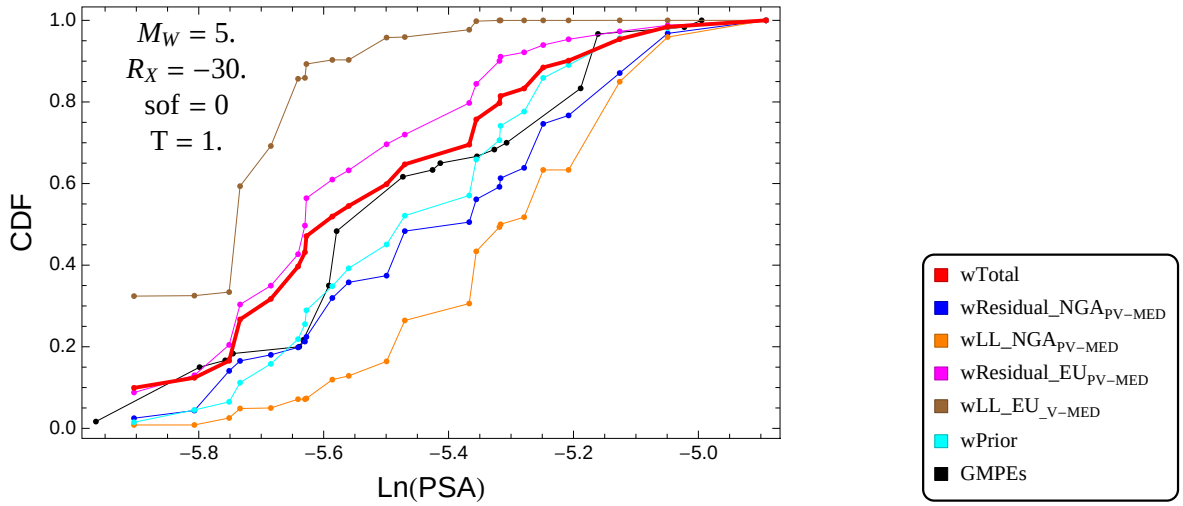



Figure 4.195: PVNGSv2: Cumulative distribution function of GMPEs (black) and selected models, for different sets of weights, for a scenario with $M = 5.$, $R_x = -30.$, $F = 0$, and $T = 1.$s

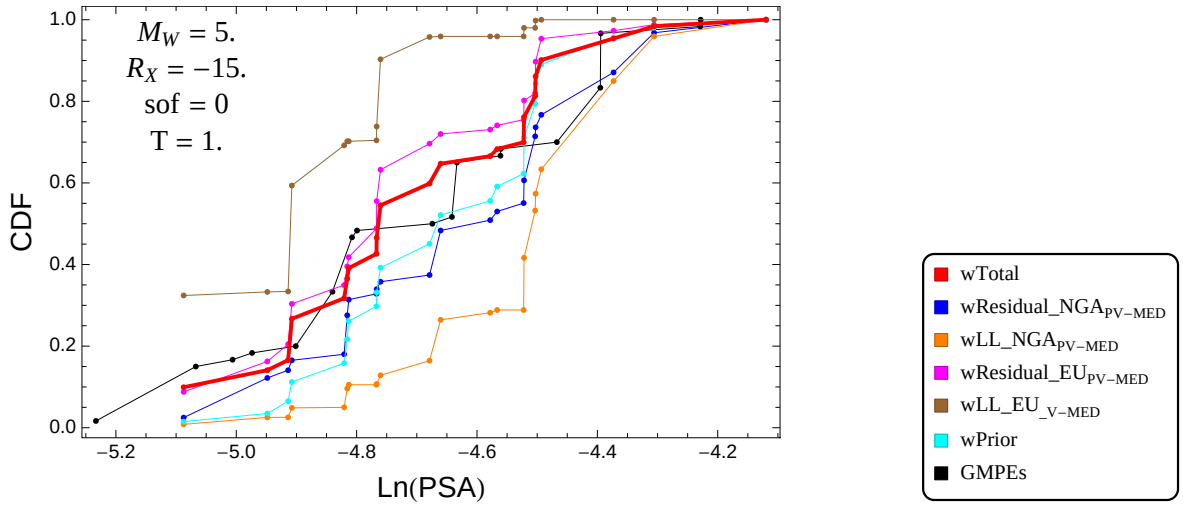



Figure 4.196: PVNGSv2: Cumulative distribution function of GMPEs (black) and selected models, for different sets of weights, for a scenario with $M = 5.$, $R_x = -15.$, $F = 0$, and $T = 1.$s

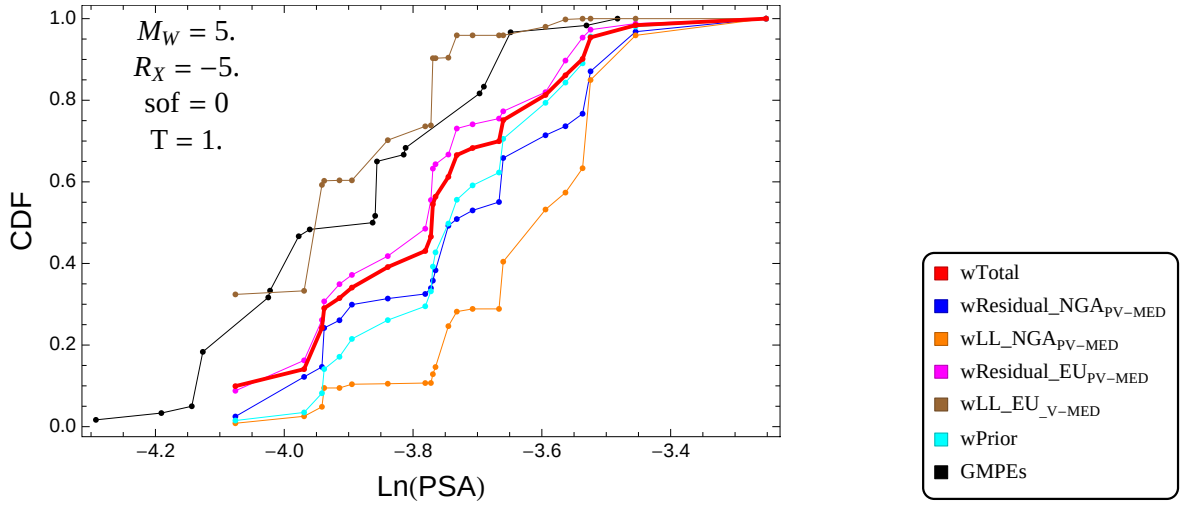



Figure 4.197: PVNGSv2: Cumulative distribution function of GMPEs (black) and selected models, for different sets of weights, for a scenario with $M = 5.$, $R_x = -5.$, $F = 0$, and $T = 1.$s

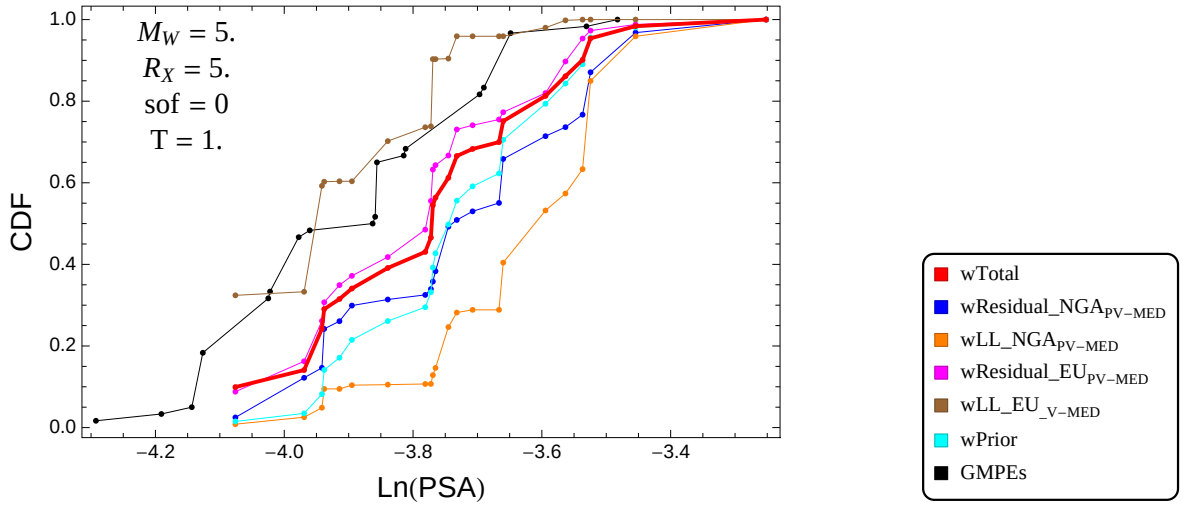



Figure 4.198: PVNGSv2: Cumulative distribution function of GMPEs (black) and selected models, for different sets of weights, for a scenario with $M = 5.$, $R_x = 5.$, $F = 0$, and $T = 1.$s

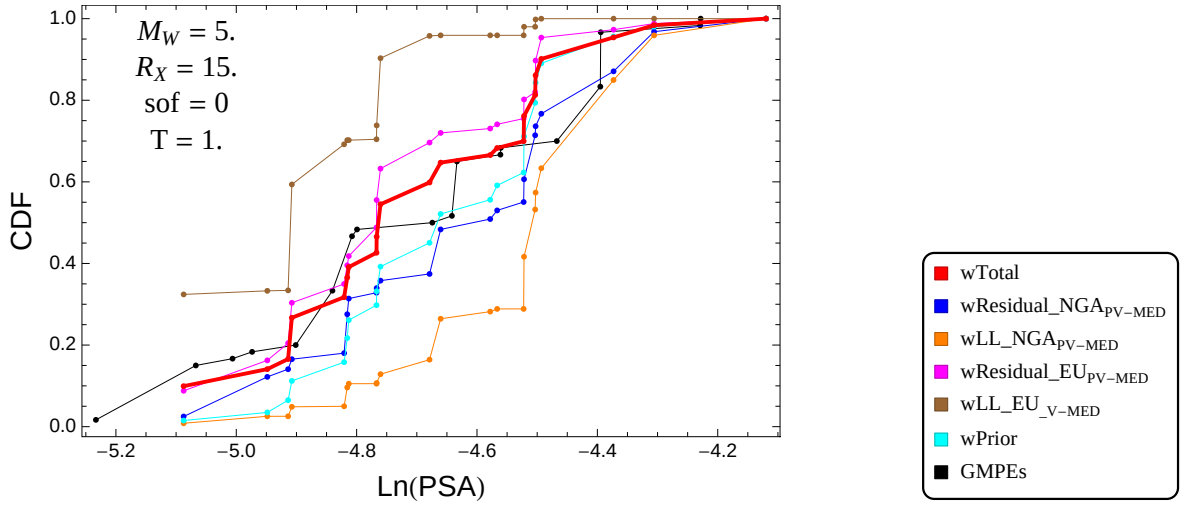



Figure 4.199: PVNGSv2: Cumulative distribution function of GMPEs (black) and selected models, for different sets of weights, for a scenario with $M = 5.$, $R_x = 15.$, $F = 0$, and $T = 1.$s

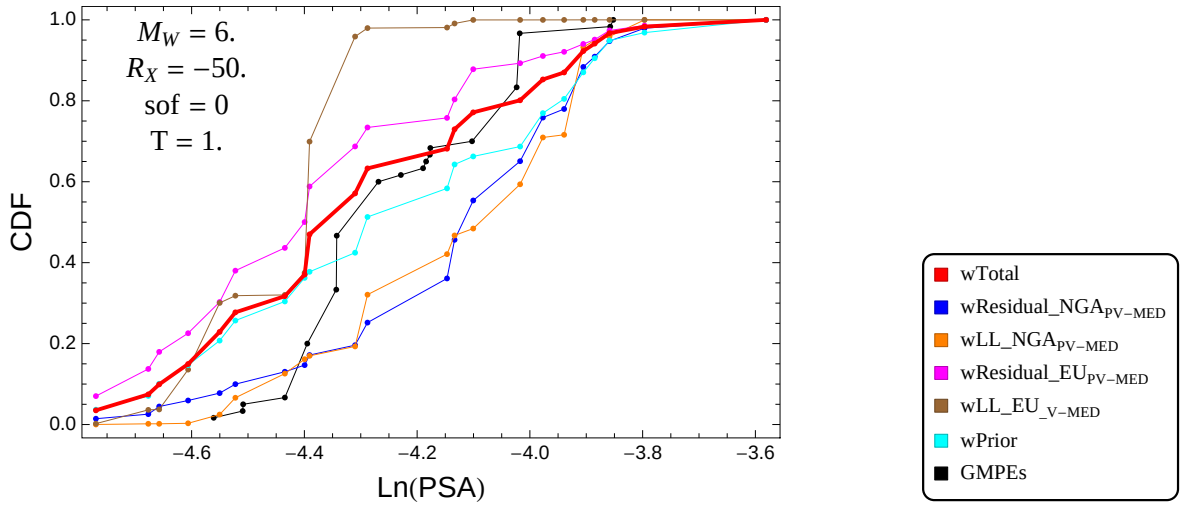



Figure 4.200: PVNGSv2: Cumulative distribution function of GMPEs (black) and selected models, for different sets of weights, for a scenario with $M = 6.$, $R_x = -50.$, $F = 0$, and $T = 1.$s

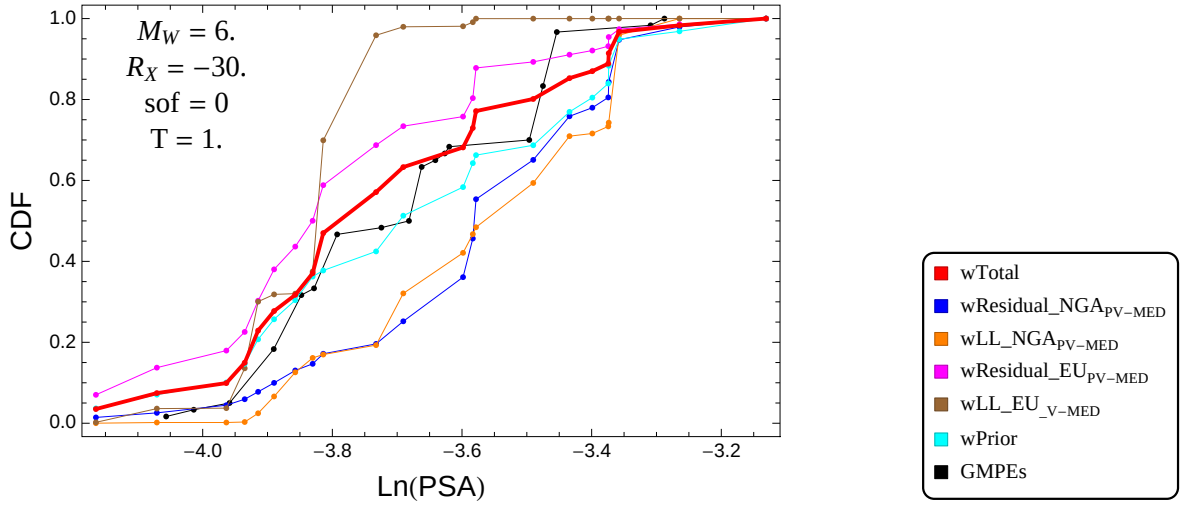



Figure 4.201: PVNGSv2: Cumulative distribution function of GMPEs (black) and selected models, for different sets of weights, for a scenario with $M = 6.$, $R_x = -30.$, $F = 0$, and $T = 1.$s

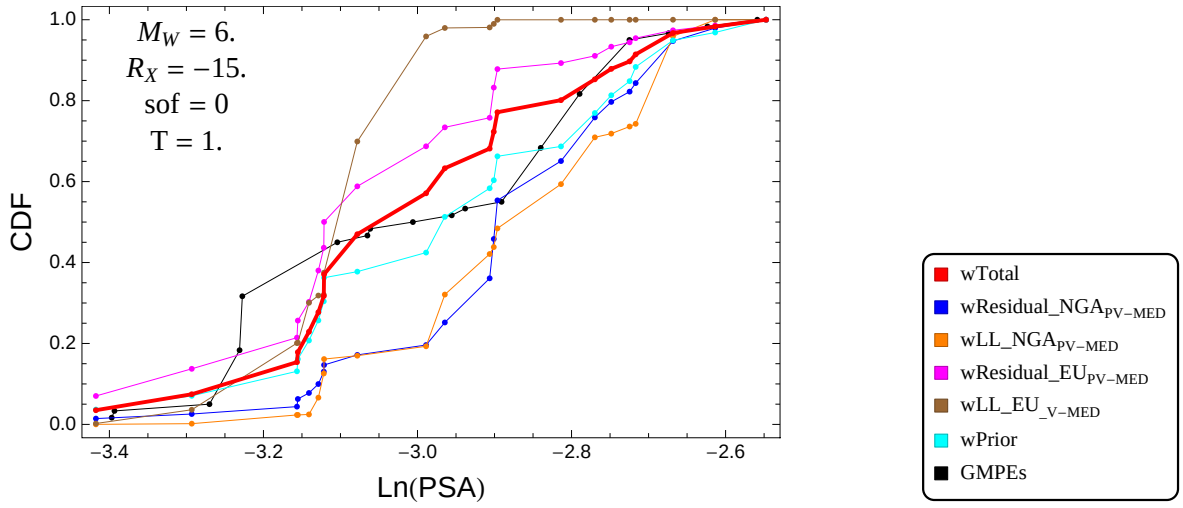



Figure 4.202: PVNGSv2: Cumulative distribution function of GMPEs (black) and selected models, for different sets of weights, for a scenario with $M = 6.$, $R_x = -15.$, $F = 0$, and $T = 1.$s

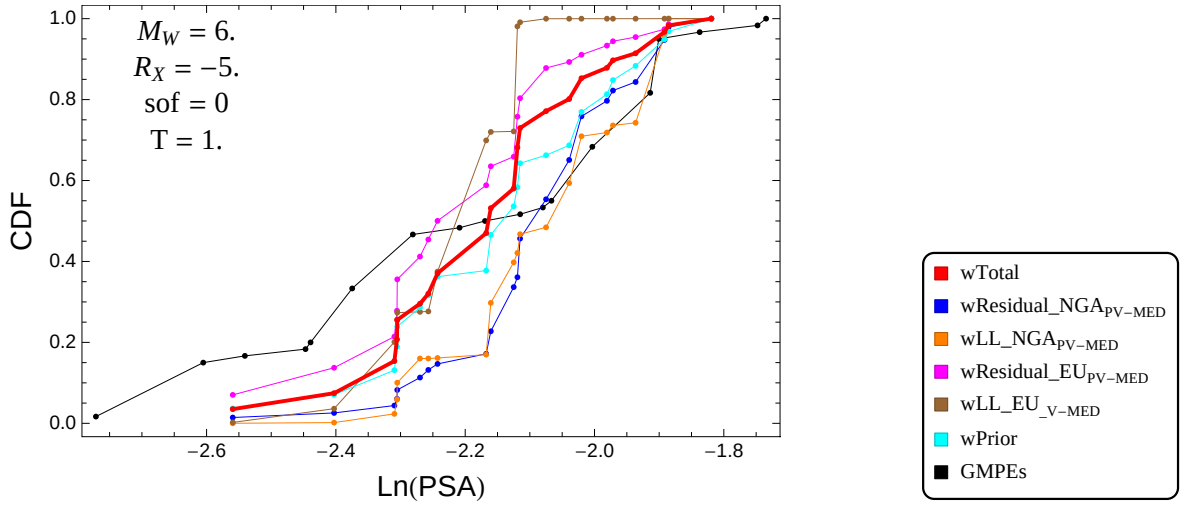



Figure 4.203: PVNGSv2: Cumulative distribution function of GMPEs (black) and selected models, for different sets of weights, for a scenario with $M = 6.$, $R_x = -5.$, $F = 0$, and $T = 1.$s

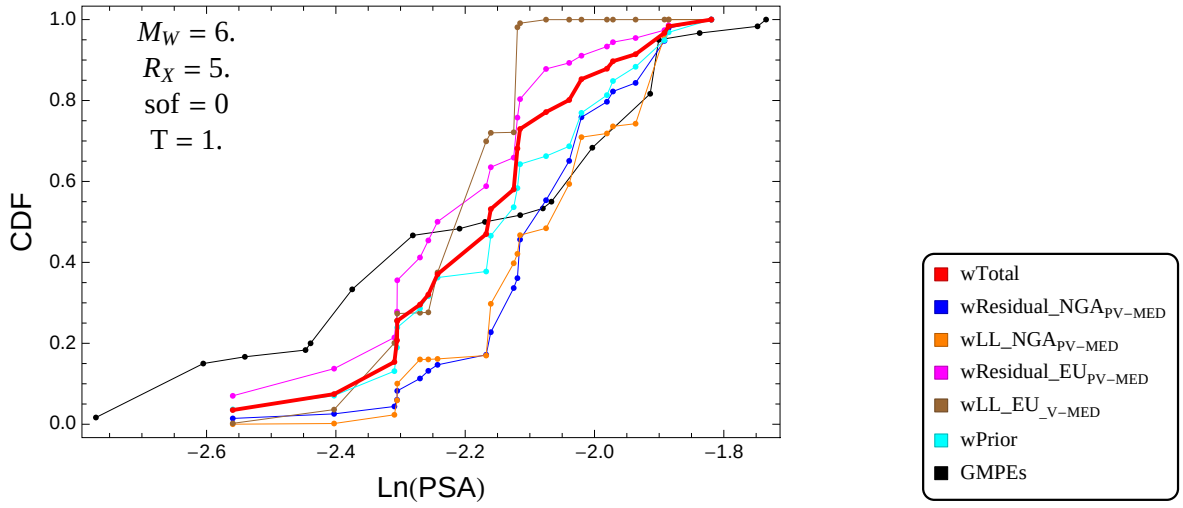



Figure 4.204: PVNGSv2: Cumulative distribution function of GMPEs (black) and selected models, for different sets of weights, for a scenario with $M = 6.$, $R_x = 5.$, $F = 0$, and $T = 1.$s

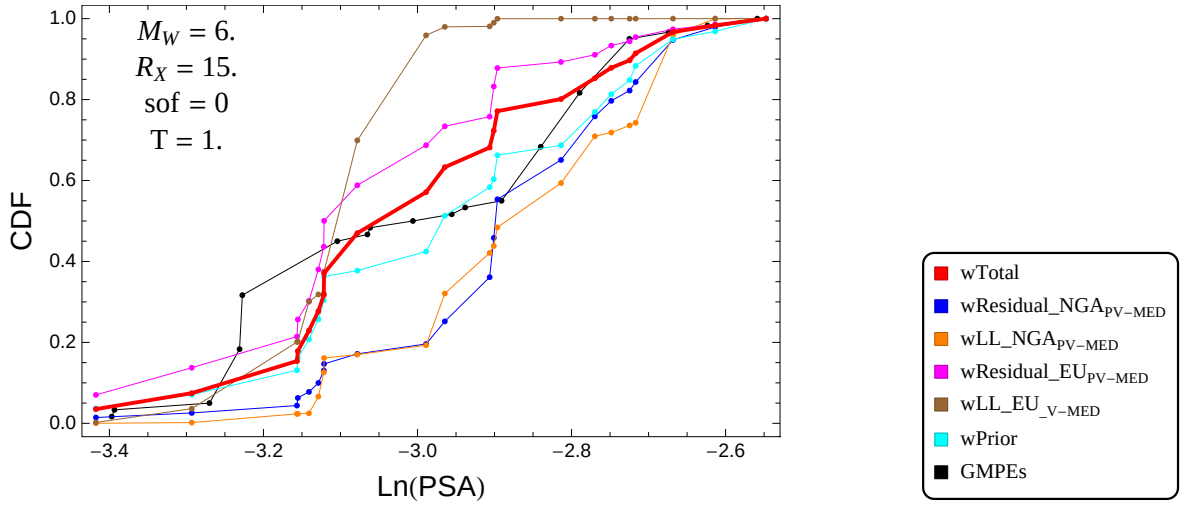



Figure 4.205: PVNGSv2: Cumulative distribution function of GMPEs (black) and selected models, for different sets of weights, for a scenario with $M = 6.$, $R_x = 15.$, $F = 0$, and $T = 1.$s

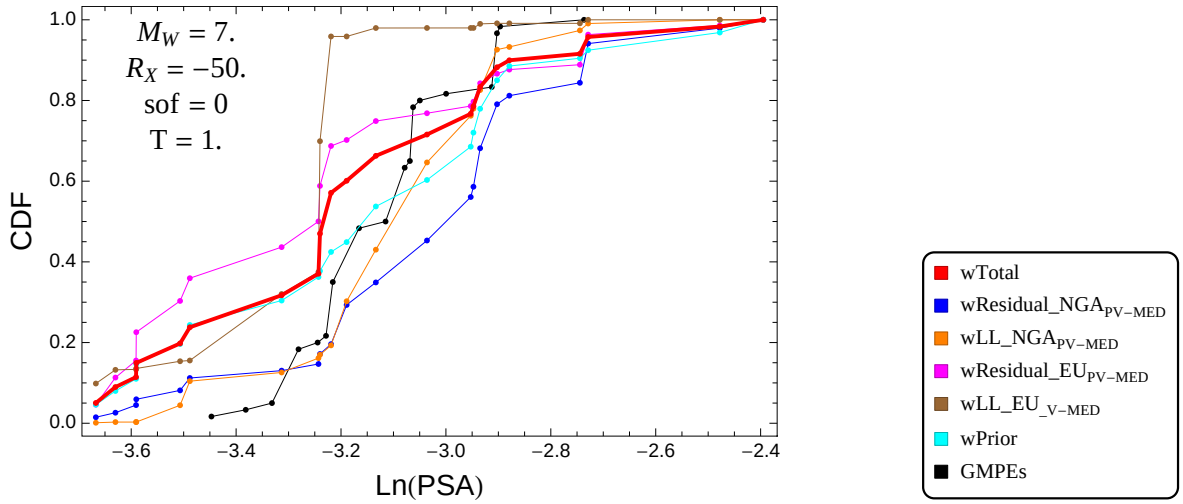



Figure 4.206: PVNGSv2: Cumulative distribution function of GMPEs (black) and selected models, for different sets of weights, for a scenario with $M = 7.$, $R_x = -50.$, $F = 0$, and $T = 1.$s

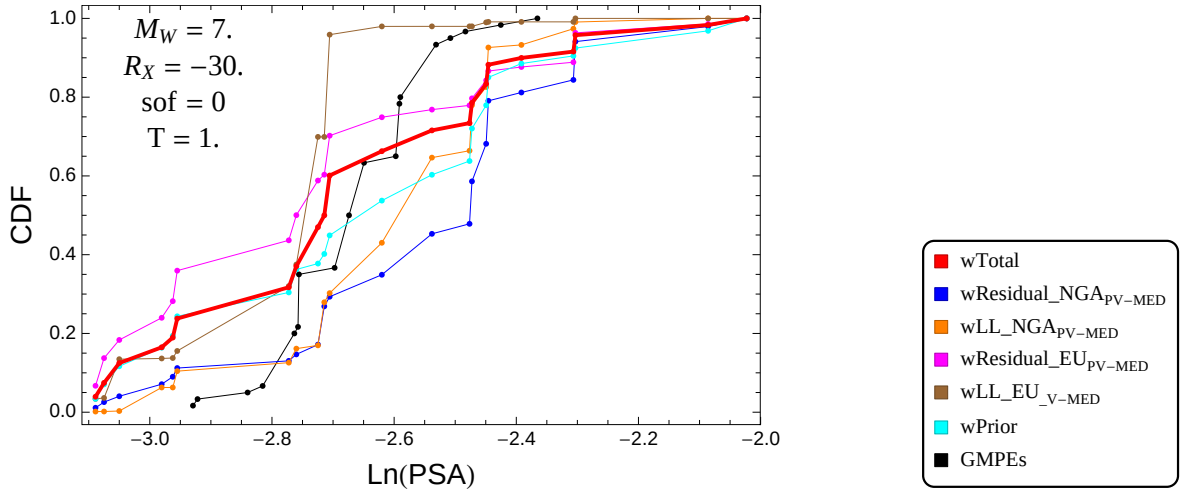



Figure 4.207: PVNGSv2: Cumulative distribution function of GMPEs (black) and selected models, for different sets of weights, for a scenario with $M = 7.$, $R_x = -30.$, $F = 0$, and $T = 1.$s

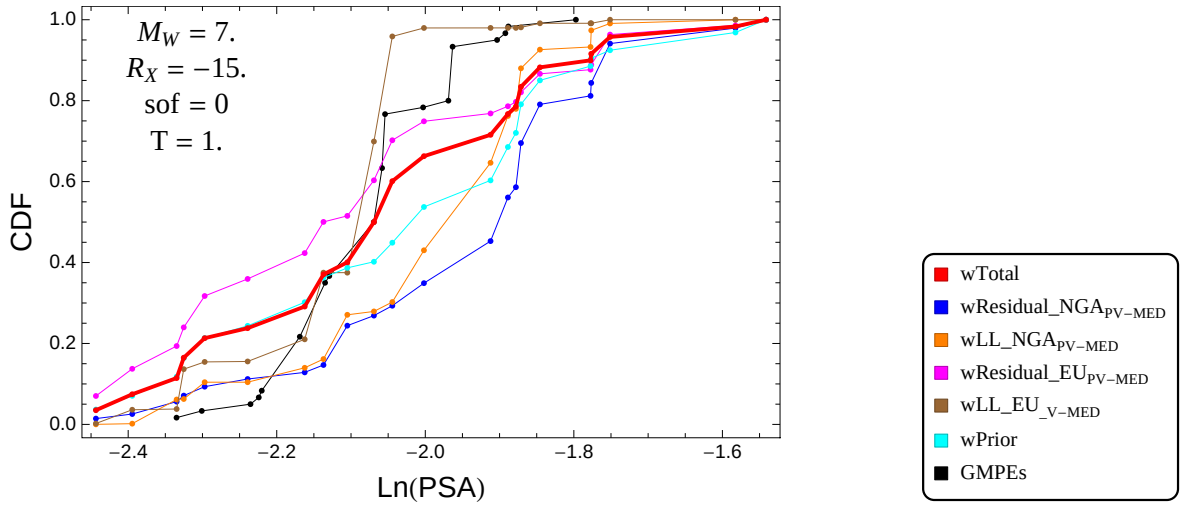



Figure 4.208: PVNGSv2: Cumulative distribution function of GMPEs (black) and selected models, for different sets of weights, for a scenario with $M = 7.$, $R_x = -15.$, $F = 0$, and $T = 1.$s

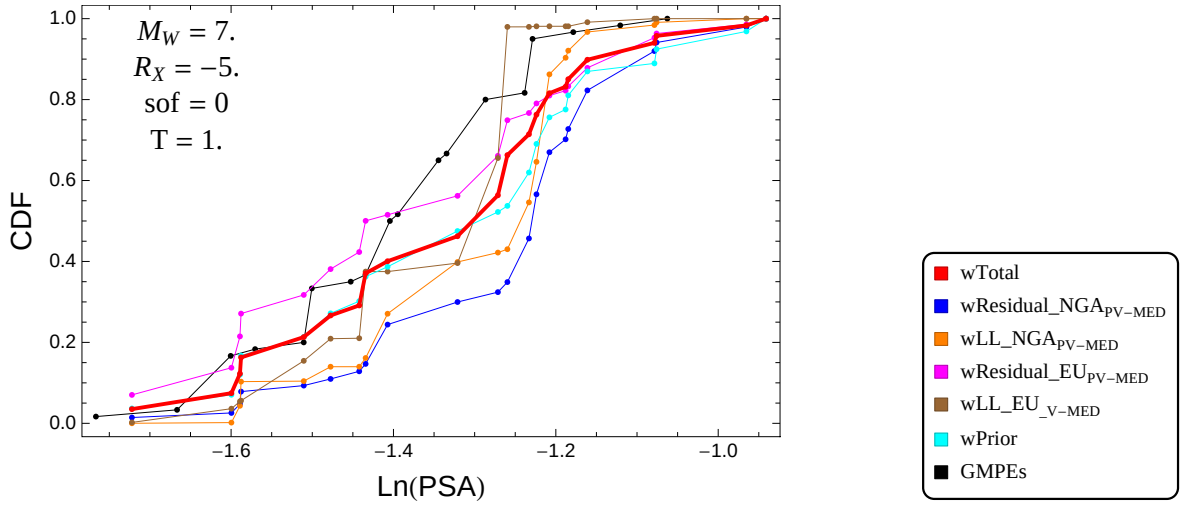



Figure 4.209: PVNGSv2: Cumulative distribution function of GMPEs (black) and selected models, for different sets of weights, for a scenario with $M = 7.$, $R_x = -5.$, $F = 0$, and $T = 1.$s

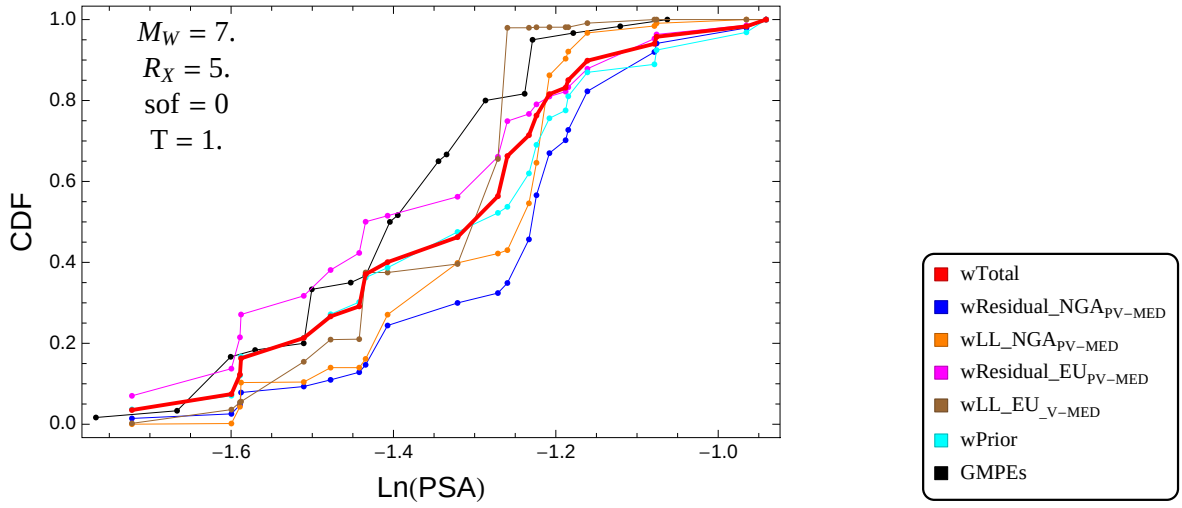



Figure 4.210: PVNGSv2: Cumulative distribution function of GMPEs (black) and selected models, for different sets of weights, for a scenario with $M = 7.$, $R_x = 5.$, $F = 0$, and $T = 1.$s

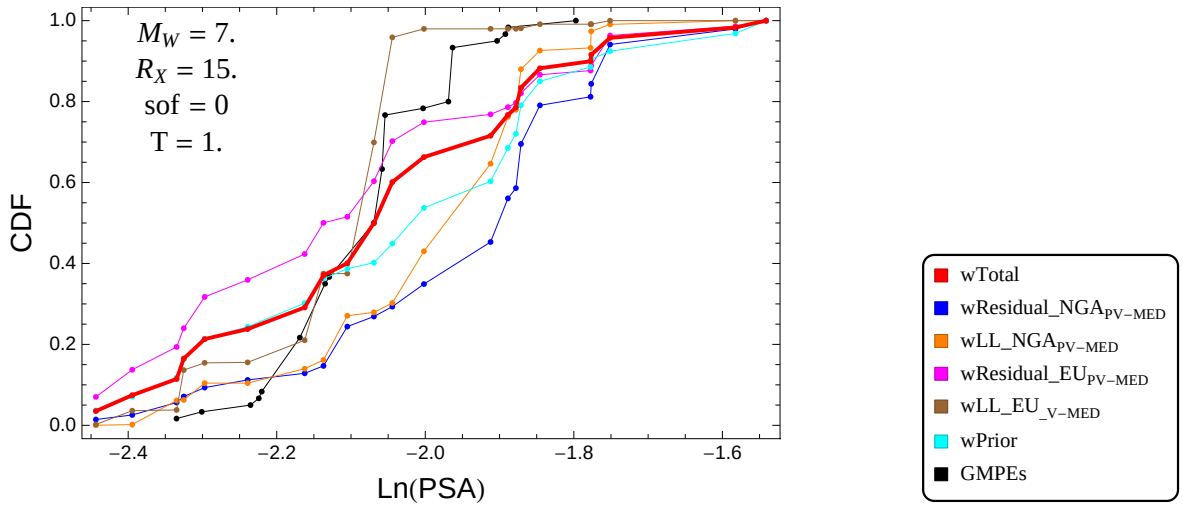



Figure 4.211: PVNGSv2: Cumulative distribution function of GMPEs (black) and selected models, for different sets of weights, for a scenario with $M = 7.$, $R_x = 15.$, $F = 0$, and $T = 1.$s

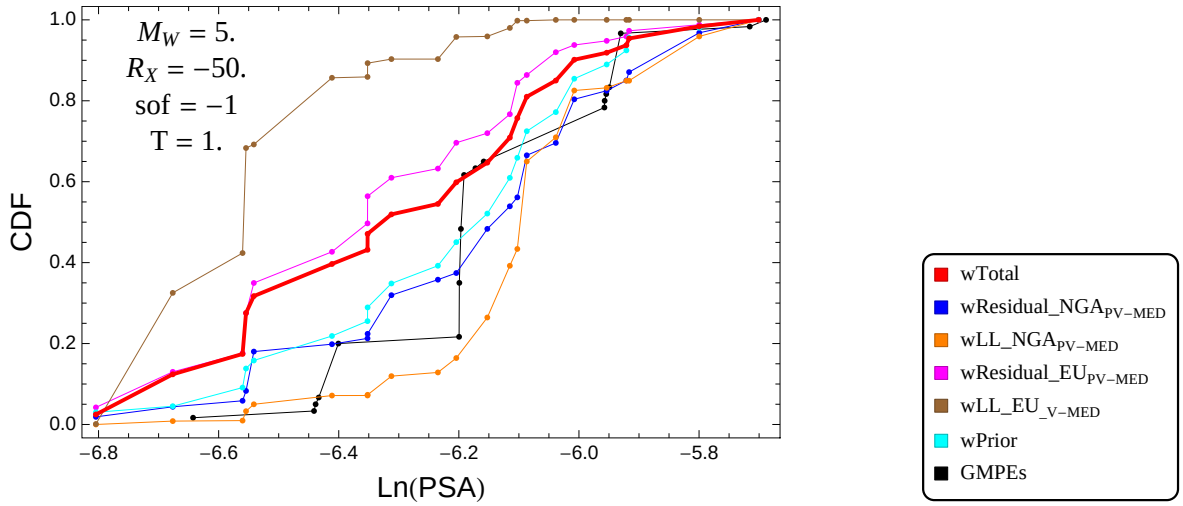



Figure 4.212: PVNGSv2: Cumulative distribution function of GMPEs (black) and selected models, for different sets of weights, for a scenario with $M = 5.$, $R_x = -50.$, $F = -1$, and $T = 1$.s

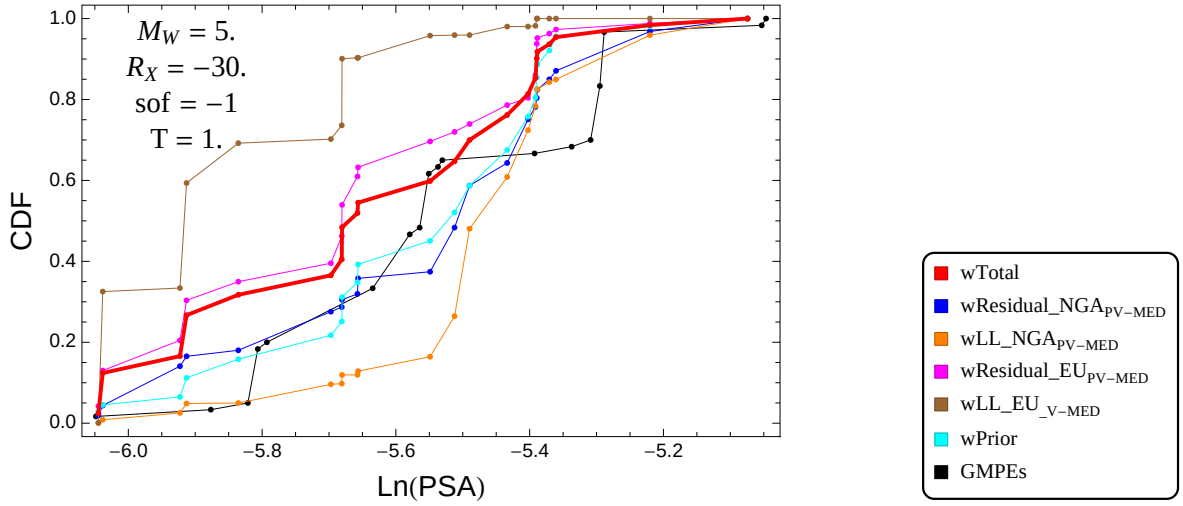



Figure 4.213: PVNGSv2: Cumulative distribution function of GMPEs (black) and selected models, for different sets of weights, for a scenario with $M = 5.$, $R_x = -30.$, $F = -1$, and $T = 1$.s

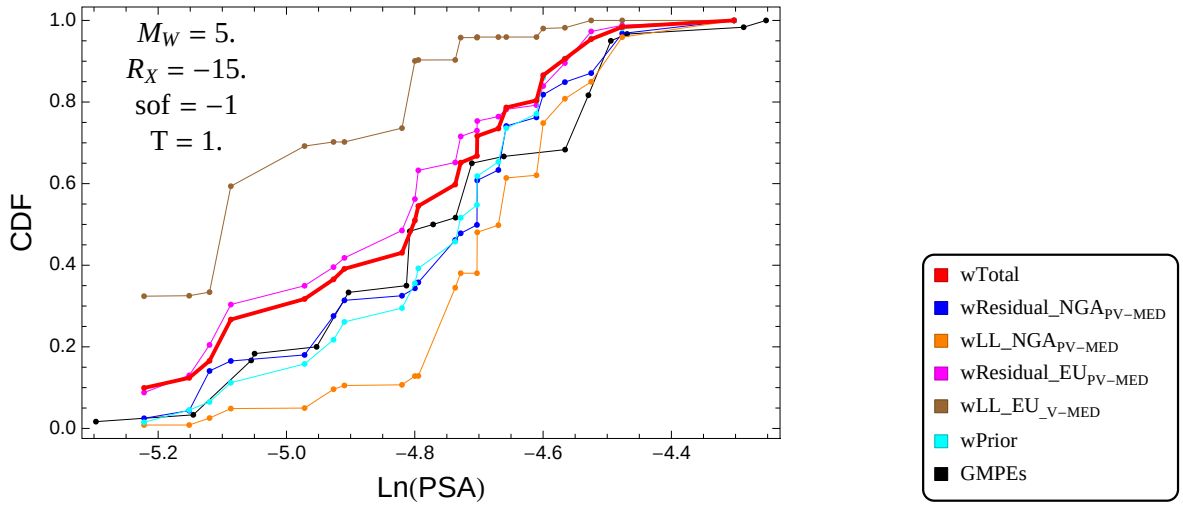



Figure 4.214: PVNGSv2: Cumulative distribution function of GMPEs (black) and selected models, for different sets of weights, for a scenario with $M = 5.$, $R_x = -15.$, $F = -1$, and $T = 1.$s

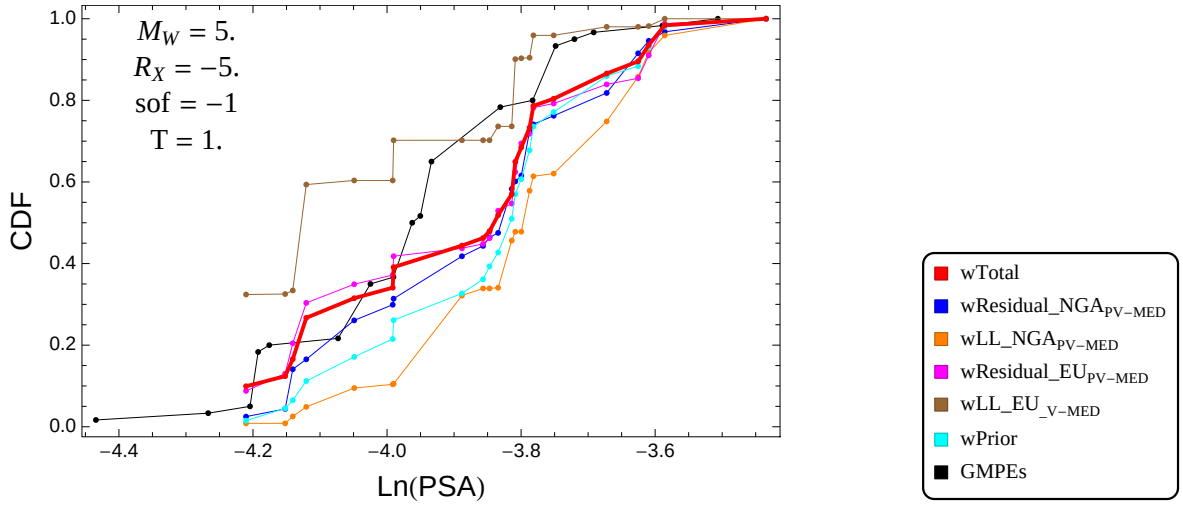



Figure 4.215: PVNGSv2: Cumulative distribution function of GMPEs (black) and selected models, for different sets of weights, for a scenario with $M = 5.$, $R_x = -5.$, $F = -1$, and $T = 1.$s

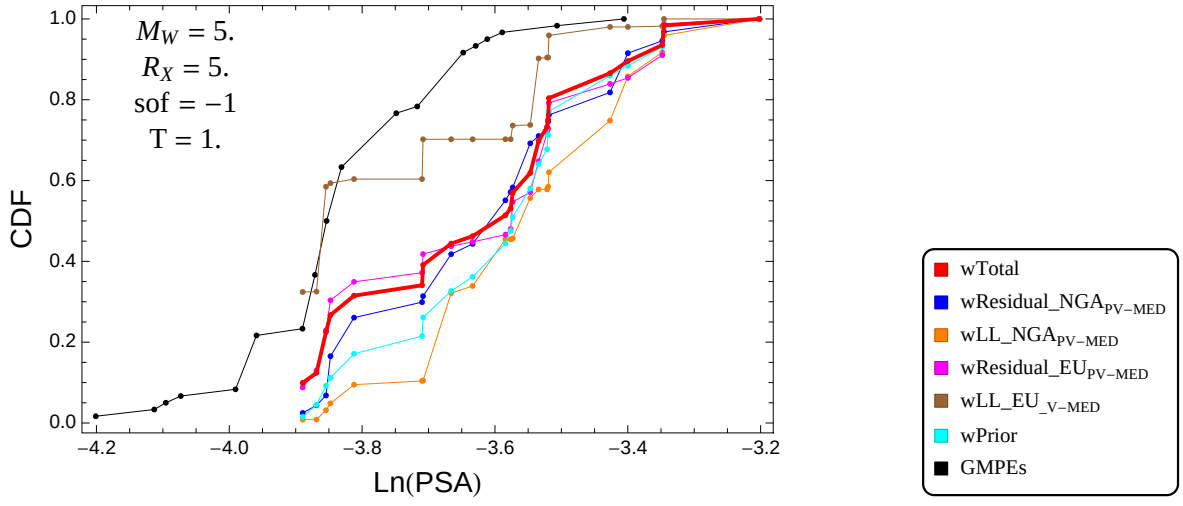



Figure 4.216: PVNGSv2: Cumulative distribution function of GMPEs (black) and selected models, for different sets of weights, for a scenario with $M = 5.$, $R_x = 5.$, $F = -1$, and $T = 1.$s

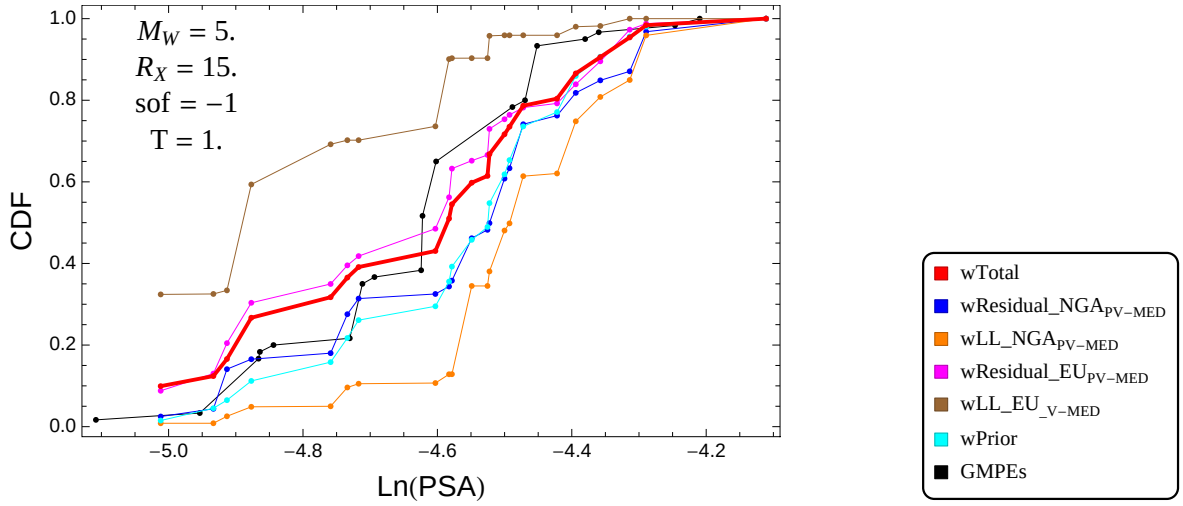



Figure 4.217: PVNGSv2: Cumulative distribution function of GMPEs (black) and selected models, for different sets of weights, for a scenario with $M = 5.$, $R_x = 15.$, $F = -1$, and $T = 1.$s

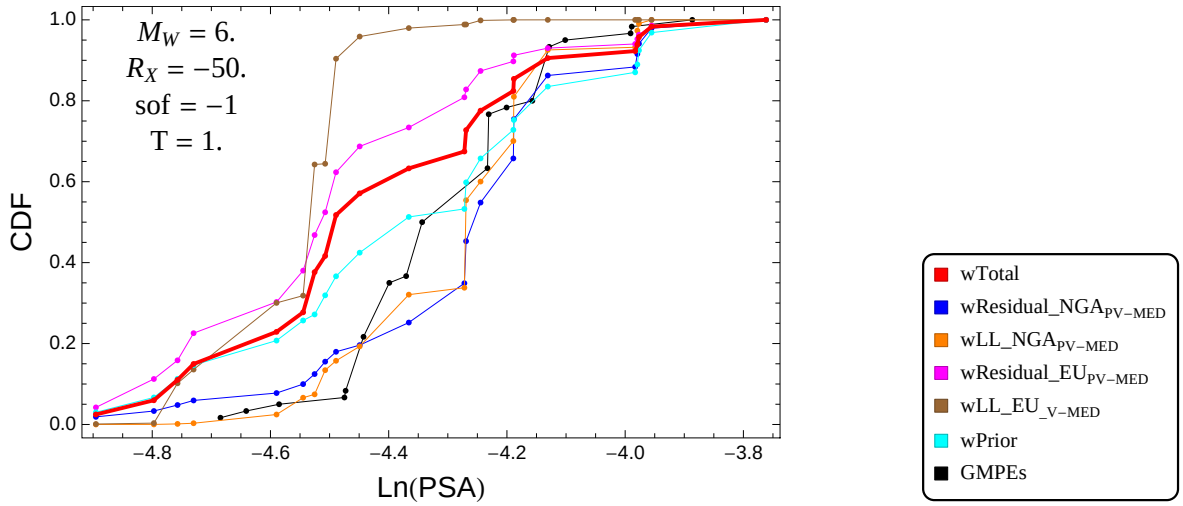



Figure 4.218: PVNGSv2: Cumulative distribution function of GMPEs (black) and selected models, for different sets of weights, for a scenario with $M = 6.$, $R_x = -50.$, $F = -1$, and $T = 1$.s

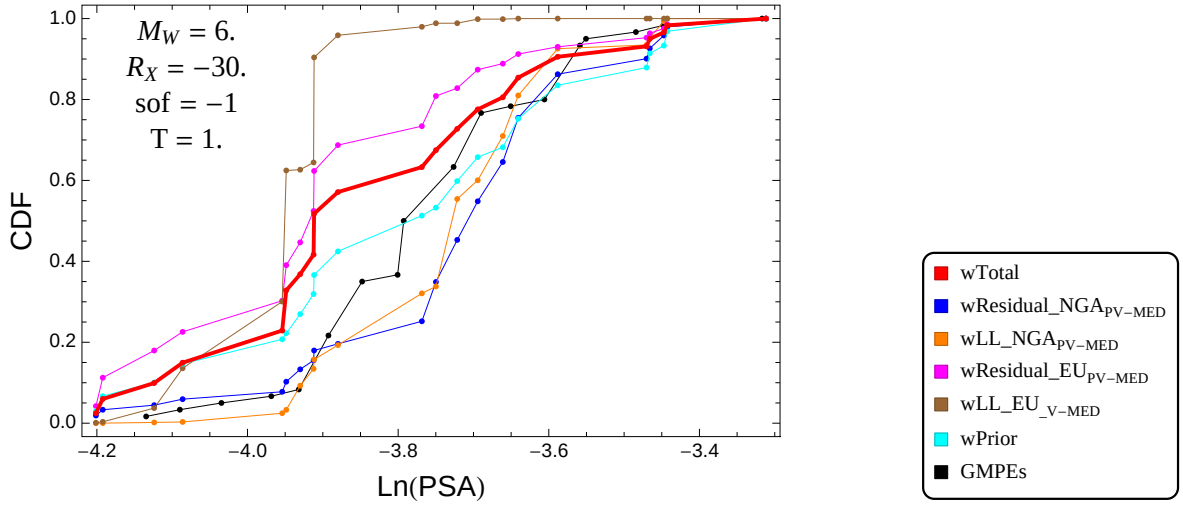



Figure 4.219: PVNGSv2: Cumulative distribution function of GMPEs (black) and selected models, for different sets of weights, for a scenario with $M = 6.$, $R_x = -30.$, $F = -1$, and $T = 1$.s

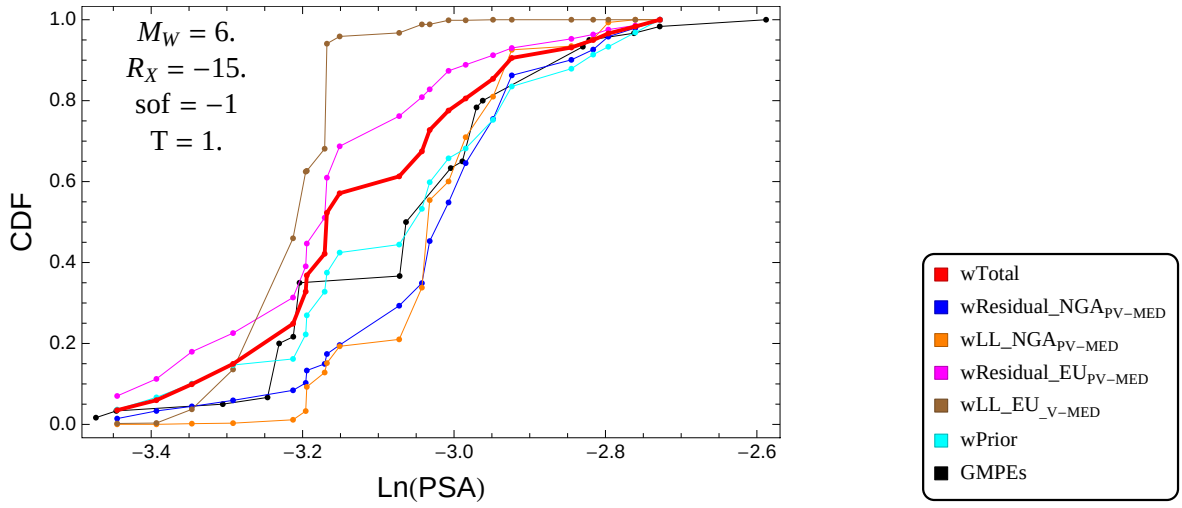



Figure 4.220: PVNGSv2: Cumulative distribution function of GMPEs (black) and selected models, for different sets of weights, for a scenario with $M = 6.$, $R_x = -15.$, $F = -1$, and $T = 1$.s

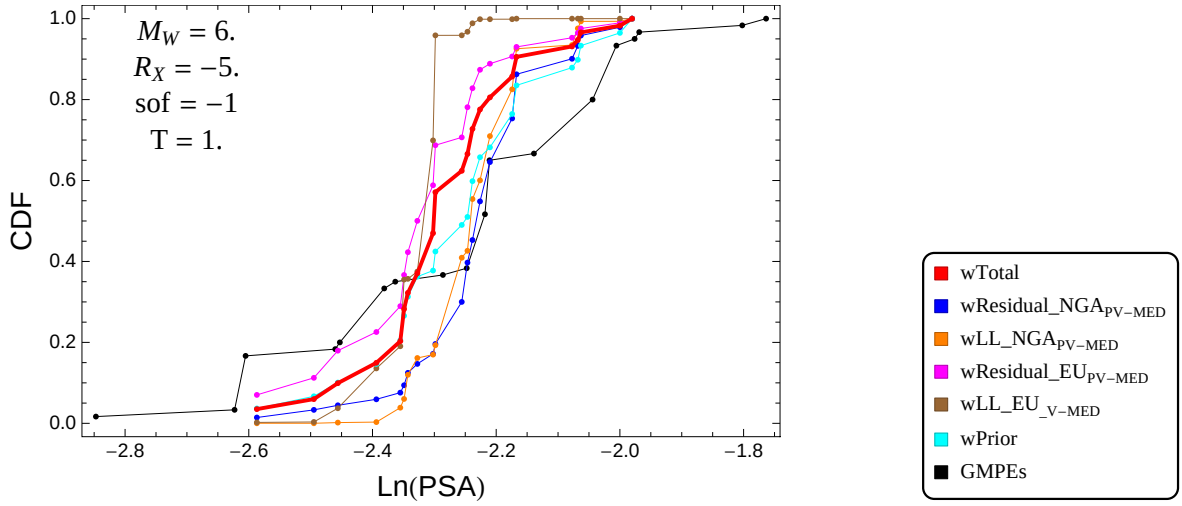



Figure 4.221: PVNGSv2: Cumulative distribution function of GMPEs (black) and selected models, for different sets of weights, for a scenario with $M = 6.$, $R_x = -5.$, $F = -1$, and $T = 1$.s

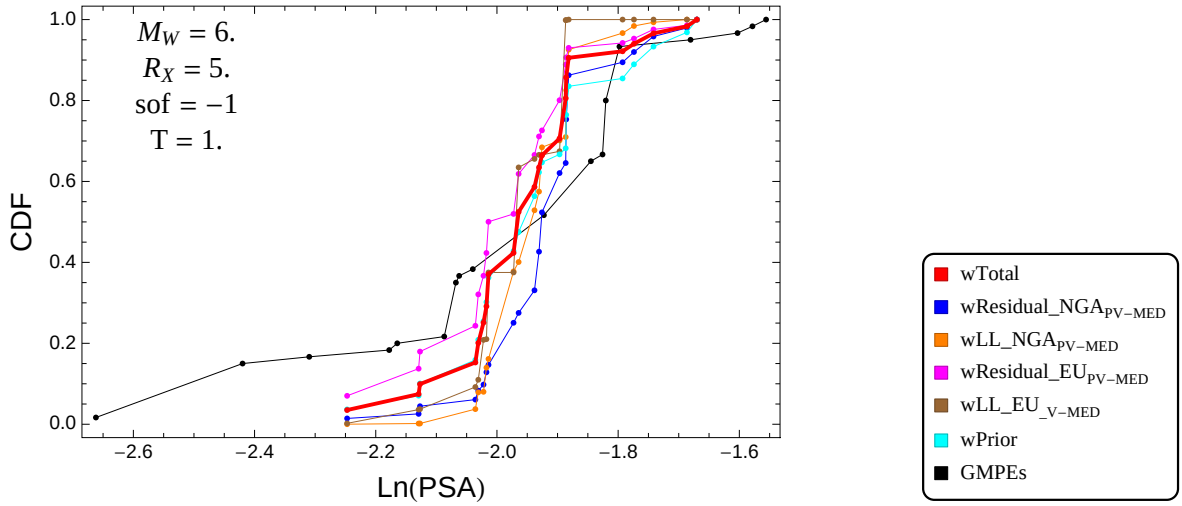



Figure 4.222: PVNGSv2: Cumulative distribution function of GMPEs (black) and selected models, for different sets of weights, for a scenario with $M = 6.$, $R_x = 5.$, $F = -1$, and $T = 1$.s

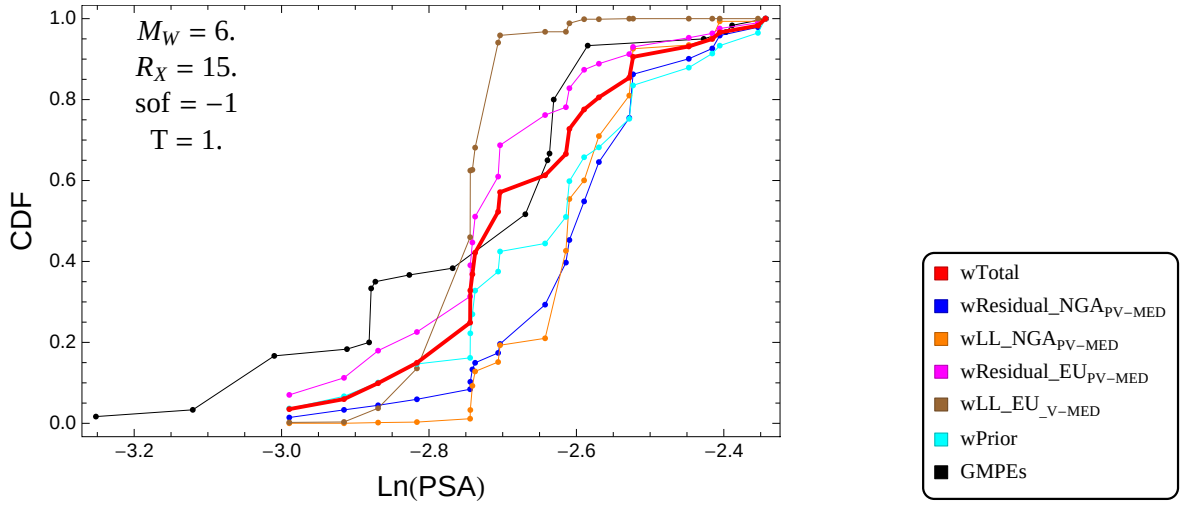



Figure 4.223: PVNGSv2: Cumulative distribution function of GMPEs (black) and selected models, for different sets of weights, for a scenario with $M = 6.$, $R_x = 15.$, $F = -1$, and $T = 1.$s

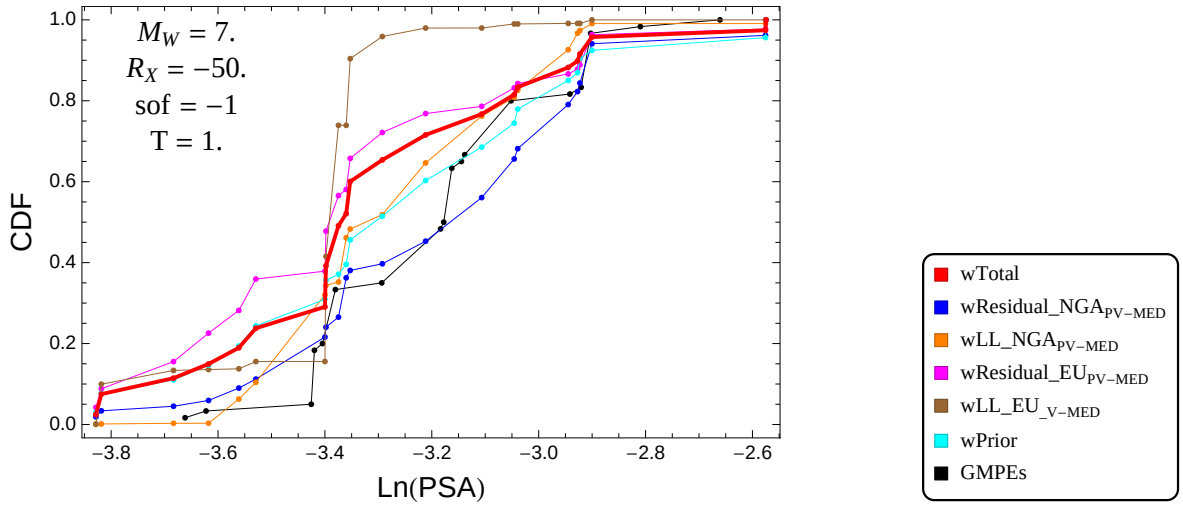



Figure 4.224: PVNGSv2: Cumulative distribution function of GMPEs (black) and selected models, for different sets of weights, for a scenario with $M = 7.$, $R_x = -50.$, $F = -1$, and $T = 1.$s

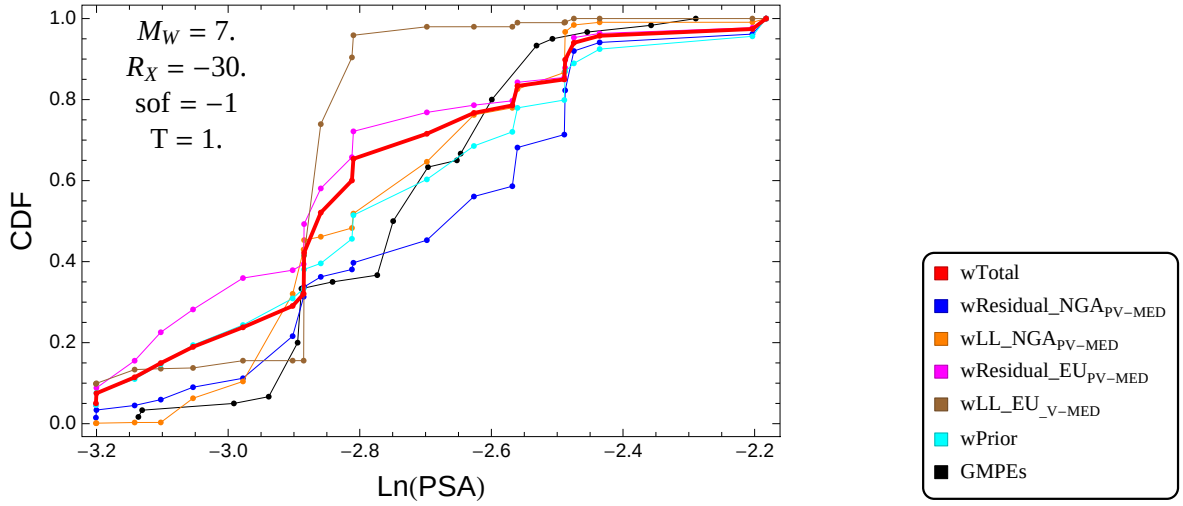



Figure 4.225: PVNGSv2: Cumulative distribution function of GMPEs (black) and selected models, for different sets of weights, for a scenario with $M = 7.$, $R_x = -30.$, $F = -1$, and $T = 1.$s

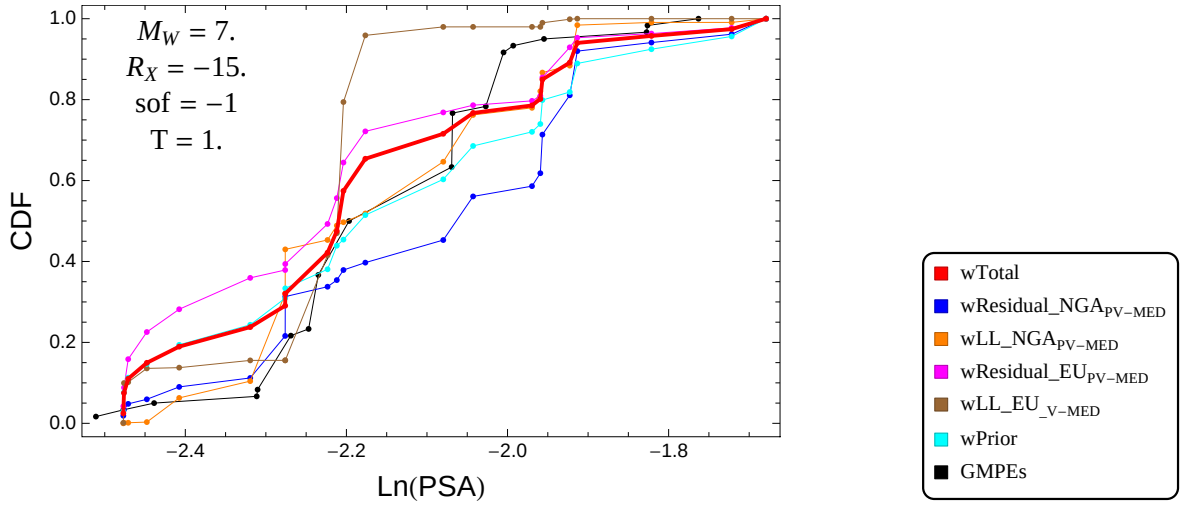



Figure 4.226: PVNGSv2: Cumulative distribution function of GMPEs (black) and selected models, for different sets of weights, for a scenario with $M = 7.$, $R_x = -15.$, $F = -1$, and $T = 1.$s

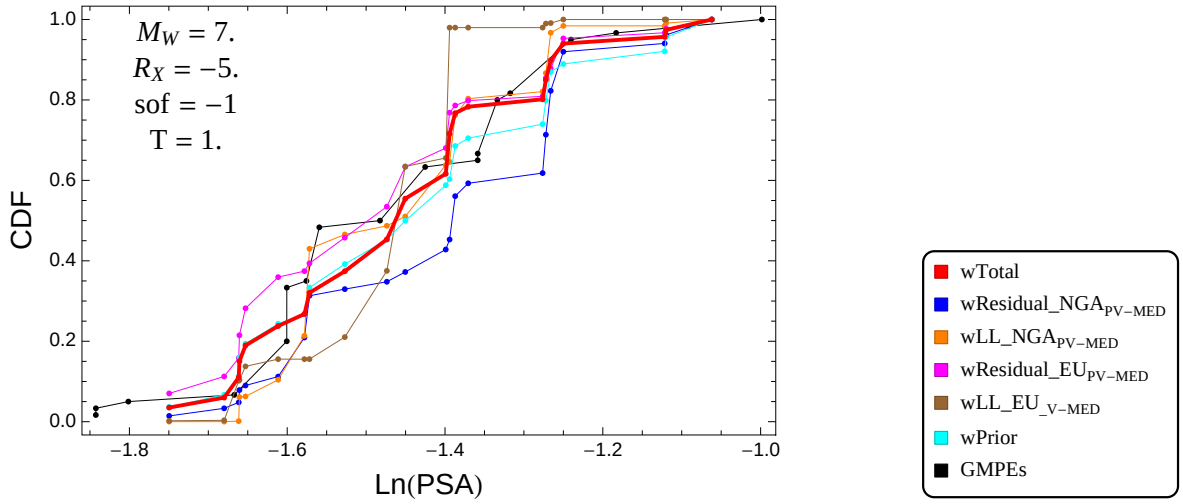



Figure 4.227: PVNGSv2: Cumulative distribution function of GMPEs (black) and selected models, for different sets of weights, for a scenario with $M = 7.$, $R_x = -5.$, $F = -1$, and $T = 1.$s

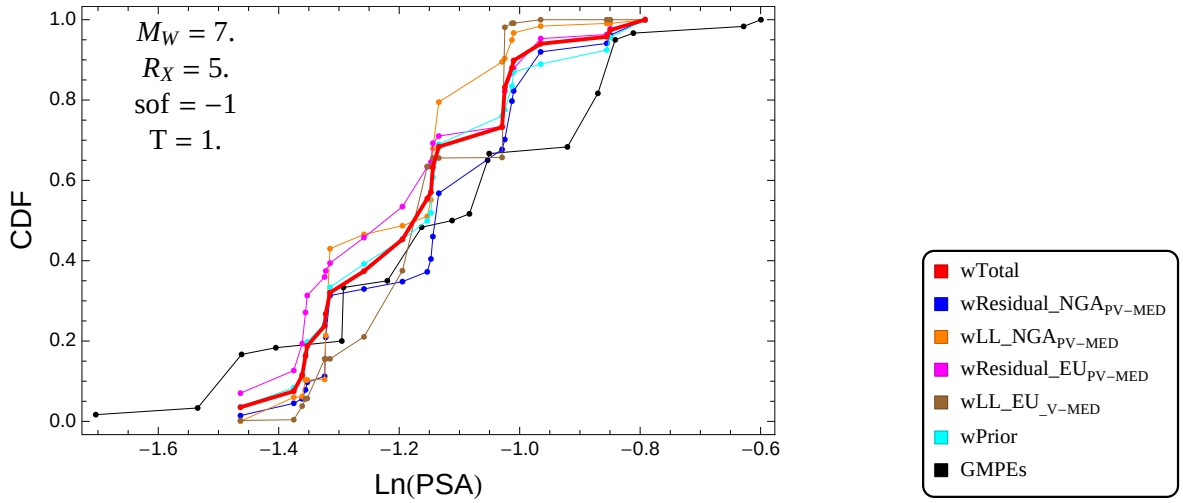



Figure 4.228: PVNGSv2: Cumulative distribution function of GMPEs (black) and selected models, for different sets of weights, for a scenario with $M = 7.$, $R_x = 5.$, $F = -1$, and $T = 1.$s

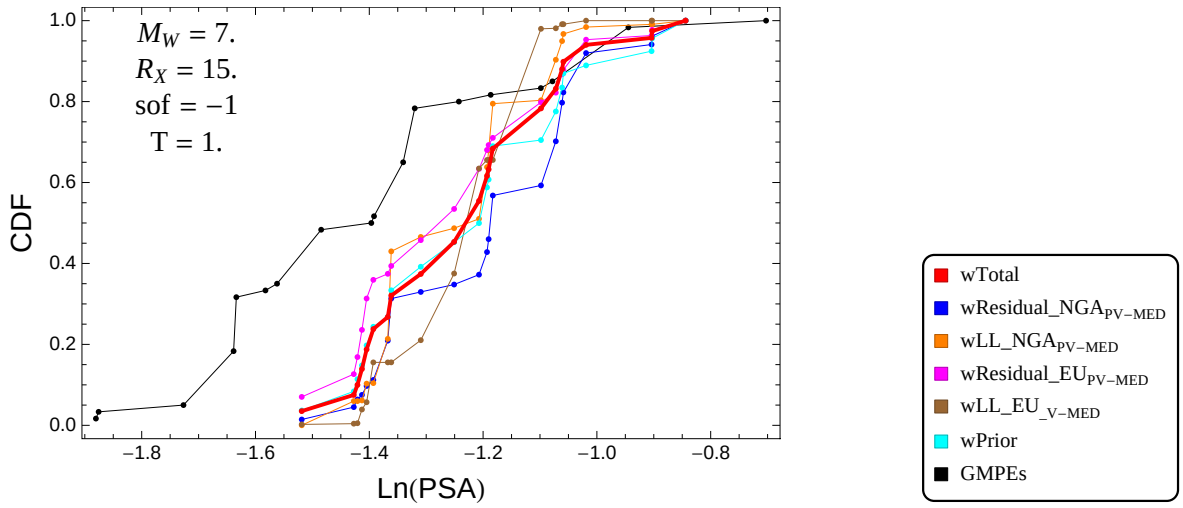



Figure 4.229: PVNGSv2: Cumulative distribution function of GMPEs (black) and selected models, for different sets of weights, for a scenario with $M = 7.$, $R_x = 15.$, $F = -1$, and $T = 1.$s

**T = 3.s**

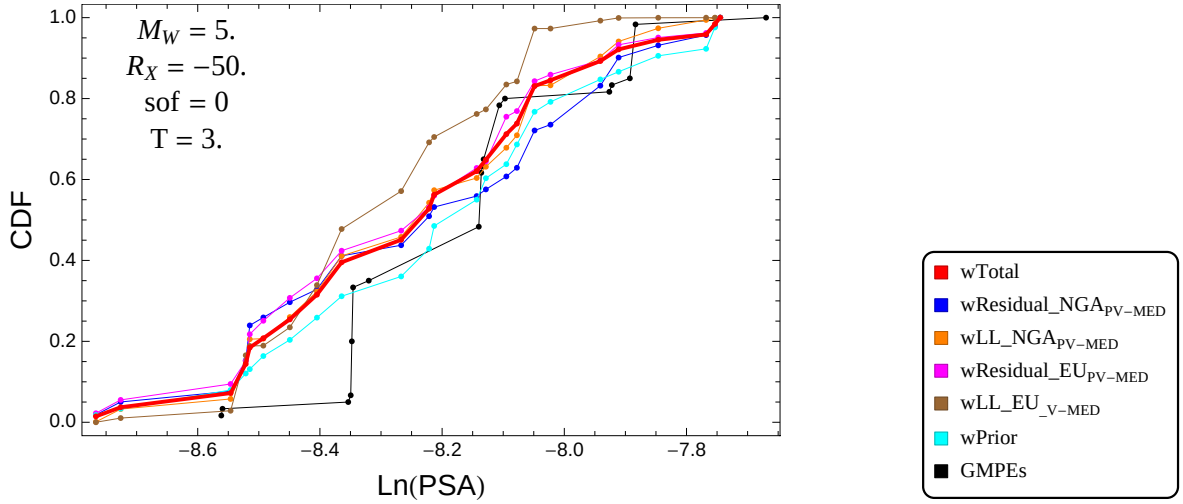



Figure 4.230: PVNGSv2: Cumulative distribution function of GMPEs (black) and selected models, for different sets of weights, for a scenario with $M = 5.$, $R_x = -50.$, $F = 0$, and $T = 3.$s

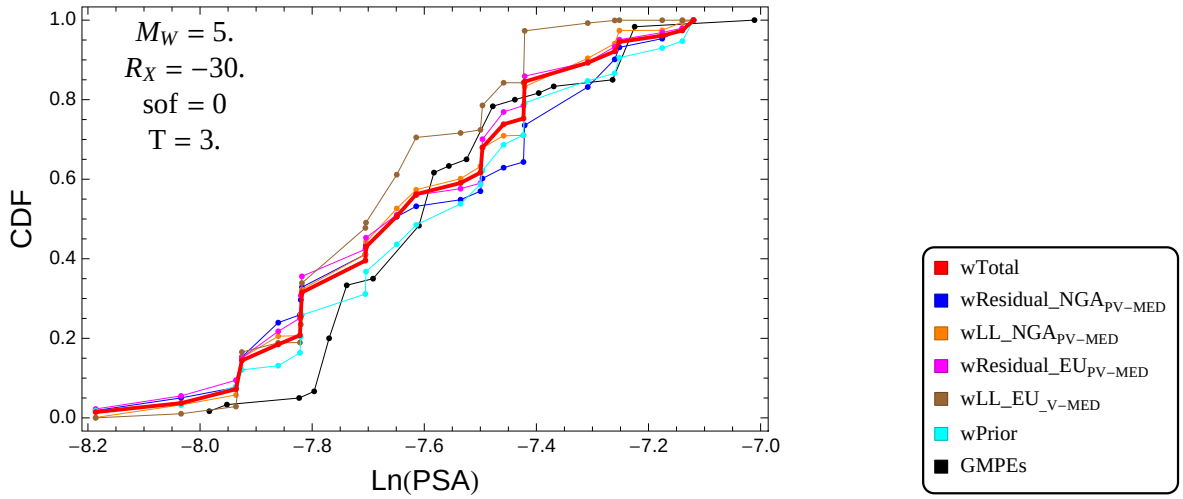



Figure 4.231: PVNGSv2: Cumulative distribution function of GMPEs (black) and selected models, for different sets of weights, for a scenario with $M = 5.$, $R_x = -30.$, $F = 0$, and $T = 3.$s

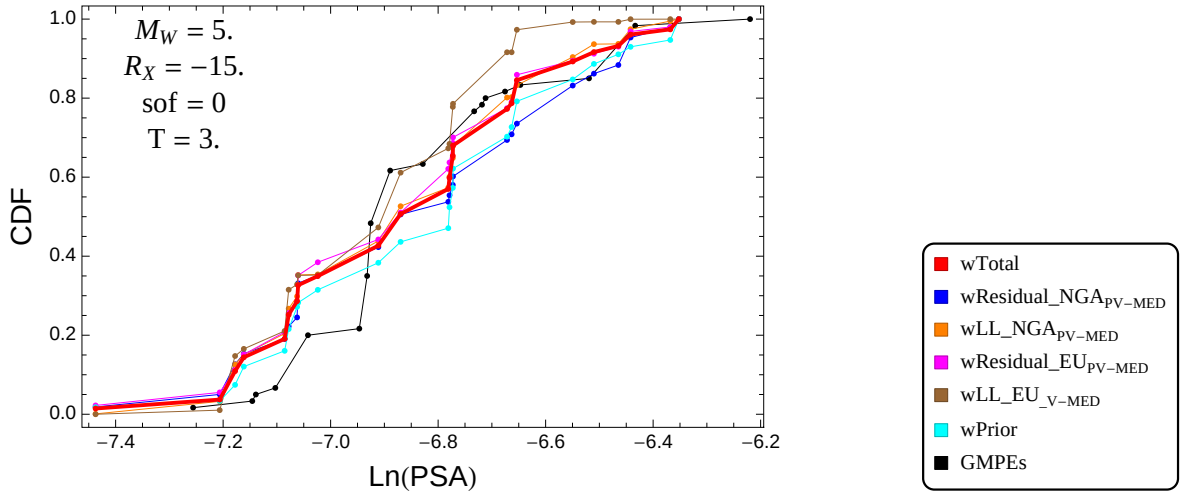



Figure 4.232: PVNGSv2: Cumulative distribution function of GMPEs (black) and selected models, for different sets of weights, for a scenario with $M = 5.$, $R_x = -15.$, $F = 0$, and $T = 3.$s

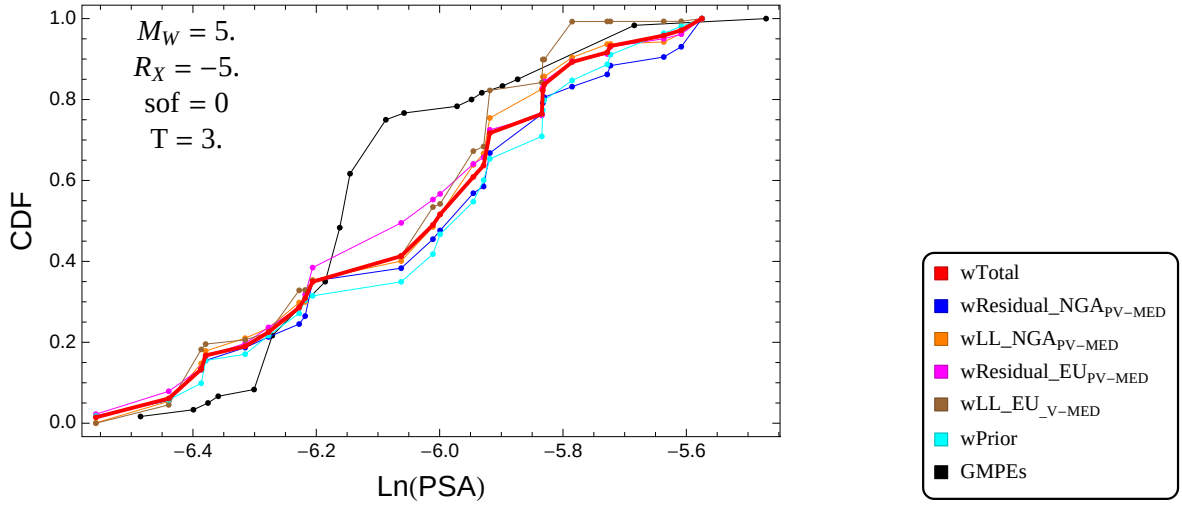



Figure 4.233: PVNGSv2: Cumulative distribution function of GMPEs (black) and selected models, for different sets of weights, for a scenario with $M = 5.$, $R_x = -5.$, $F = 0$, and $T = 3.$s

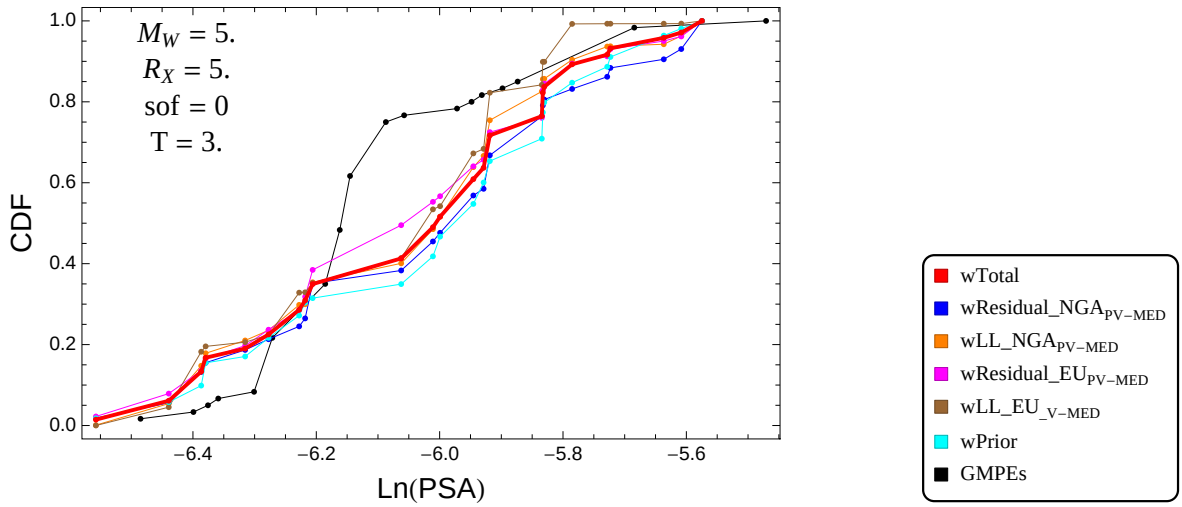



Figure 4.234: PVNGSv2: Cumulative distribution function of GMPEs (black) and selected models, for different sets of weights, for a scenario with $M = 5.$, $R_x = 5.$, $F = 0$, and $T = 3.$s

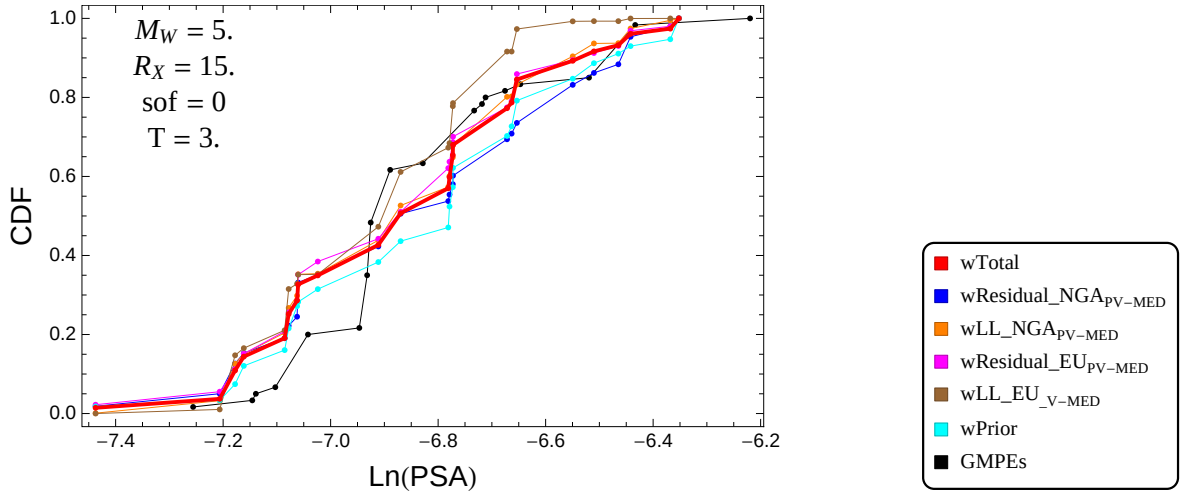



Figure 4.235: PVNGSv2: Cumulative distribution function of GMPEs (black) and selected models, for different sets of weights, for a scenario with $M = 5.$, $R_x = 15.$, $F = 0$, and $T = 3.$s

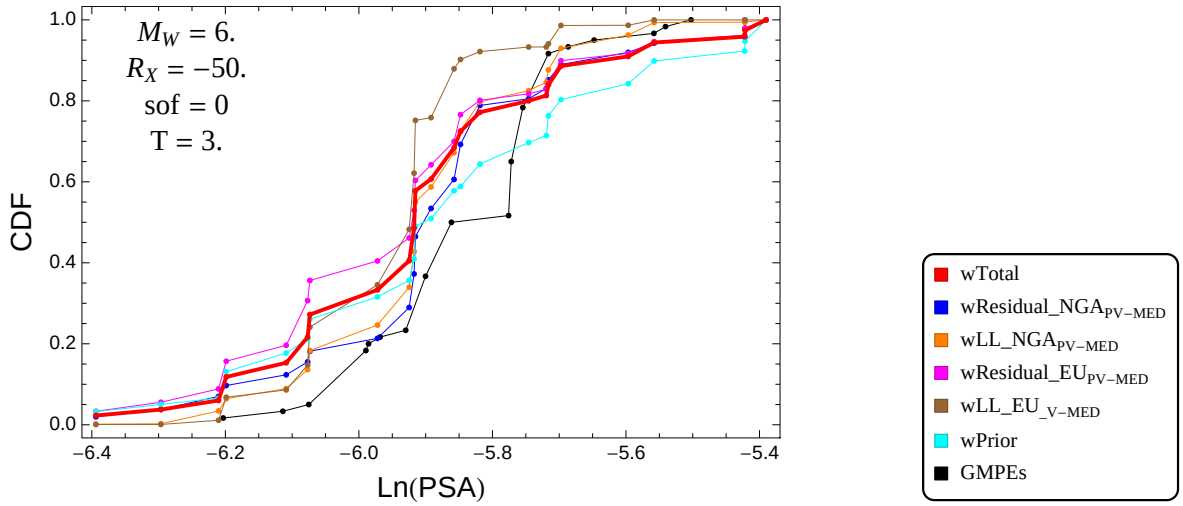



Figure 4.236: PVNGSv2: Cumulative distribution function of GMPEs (black) and selected models, for different sets of weights, for a scenario with $M = 6.$, $R_x = -50.$, $F = 0$, and $T = 3.$s

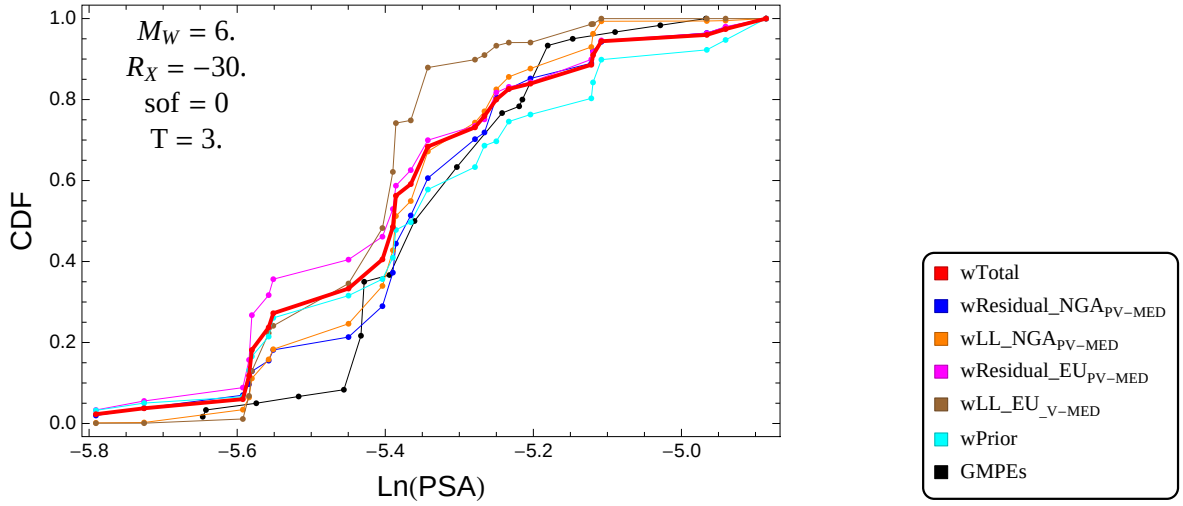



Figure 4.237: PVNGSv2: Cumulative distribution function of GMPEs (black) and selected models, for different sets of weights, for a scenario with $M = 6.$, $R_x = -30.$, $F = 0$, and $T = 3.$s

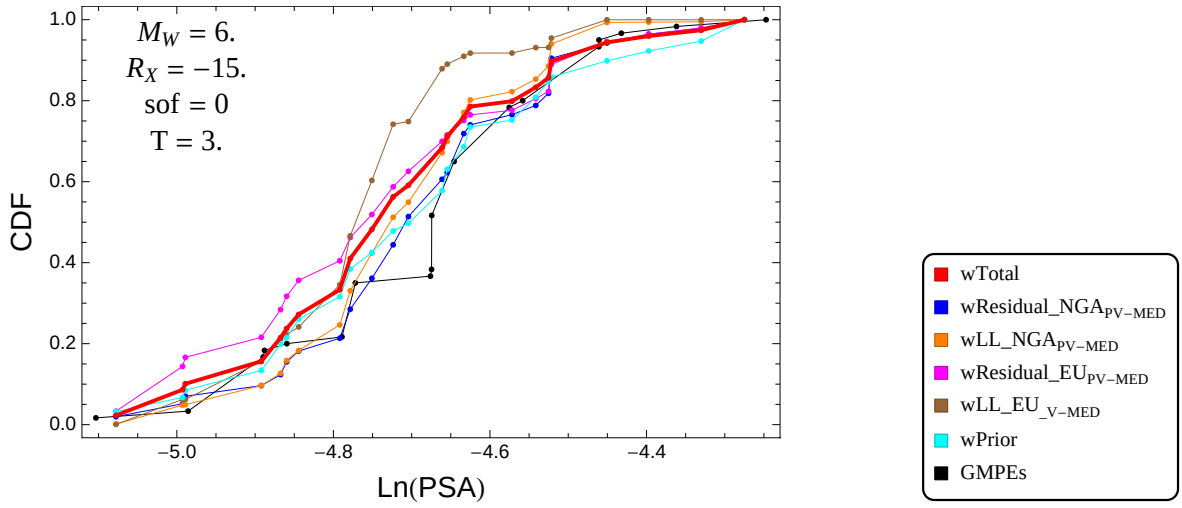



Figure 4.238: PVNGSv2: Cumulative distribution function of GMPEs (black) and selected models, for different sets of weights, for a scenario with $M = 6.$, $R_x = -15.$, $F = 0$, and $T = 3.$s

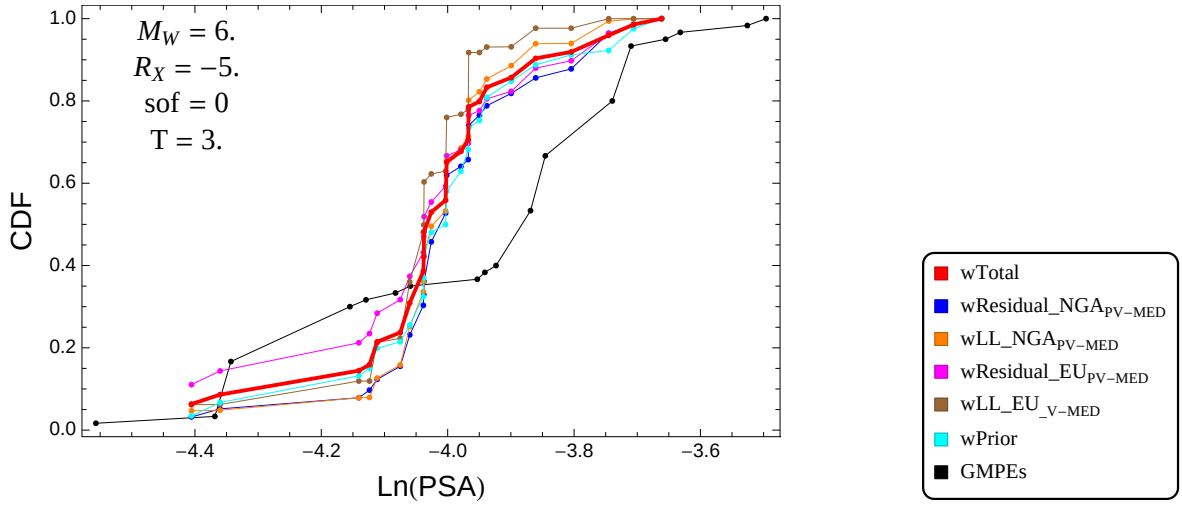



Figure 4.239: PVNGSv2: Cumulative distribution function of GMPEs (black) and selected models, for different sets of weights, for a scenario with $M = 6.$, $R_x = -5.$, $F = 0$, and $T = 3.$s

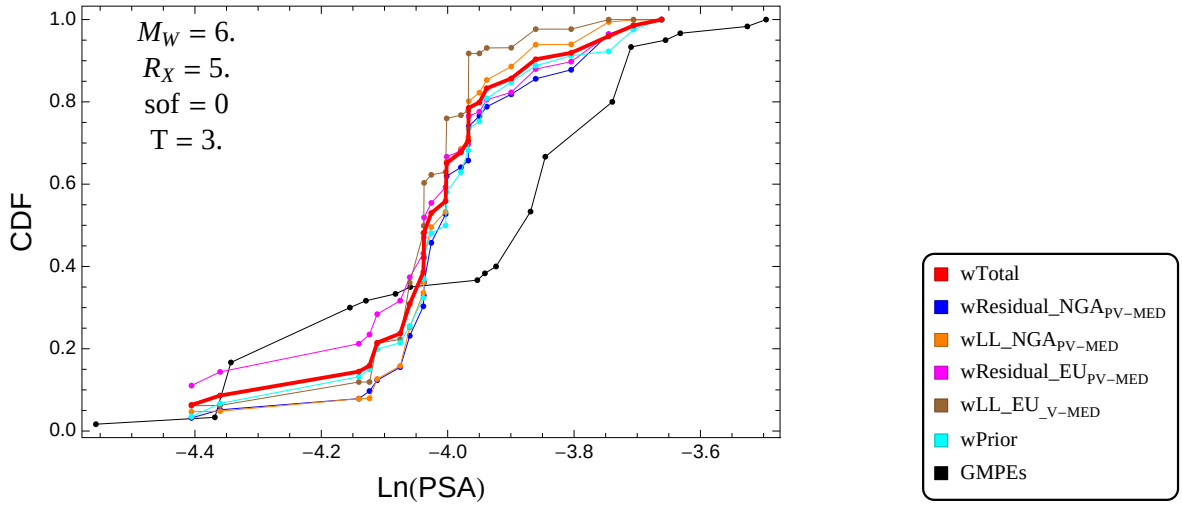



Figure 4.240: PVNGSv2: Cumulative distribution function of GMPEs (black) and selected models, for different sets of weights, for a scenario with $M = 6.$, $R_x = 5.$, $F = 0$, and $T = 3.$s

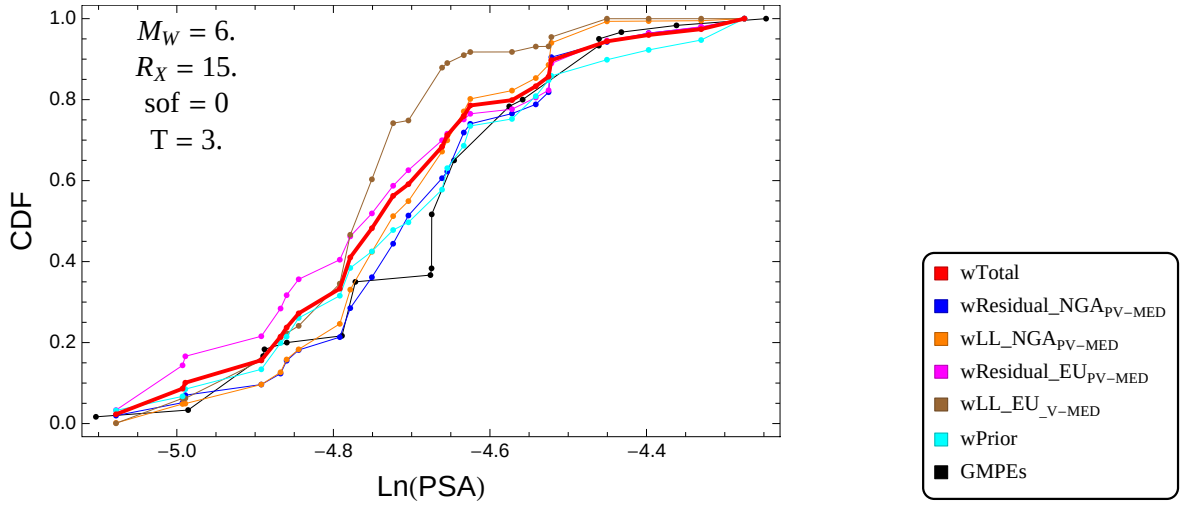



Figure 4.241: PVNGSv2: Cumulative distribution function of GMPEs (black) and selected models, for different sets of weights, for a scenario with $M = 6.$, $R_x = 15.$, $F = 0$, and $T = 3.$s

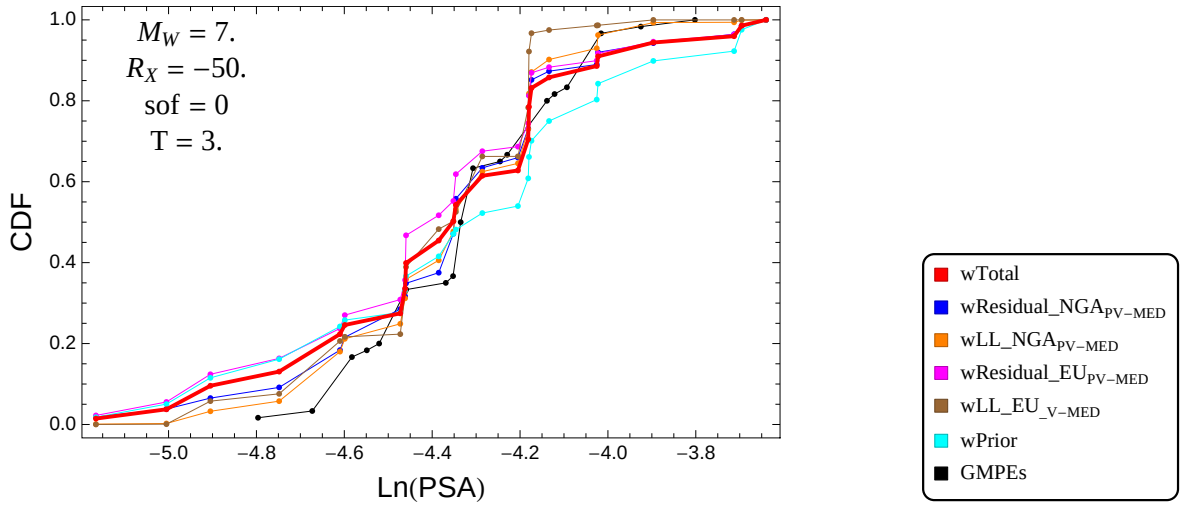



Figure 4.242: PVNGSv2: Cumulative distribution function of GMPEs (black) and selected models, for different sets of weights, for a scenario with $M = 7.$, $R_x = -50.$, $F = 0$, and $T = 3.$s

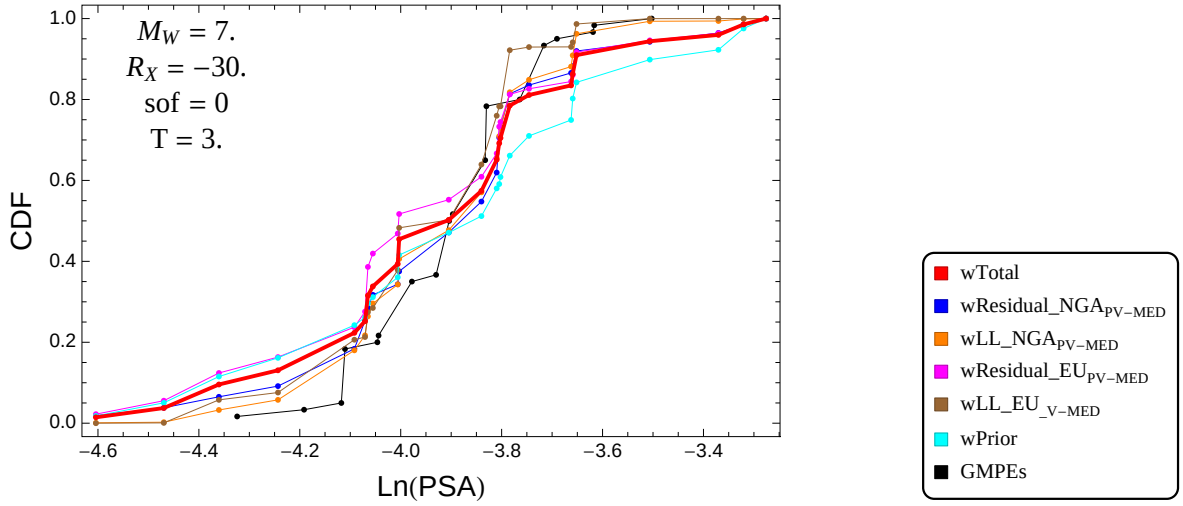



Figure 4.243: PVNGSv2: Cumulative distribution function of GMPEs (black) and selected models, for different sets of weights, for a scenario with $M = 7.$, $R_x = -30.$, $F = 0$, and $T = 3.$s

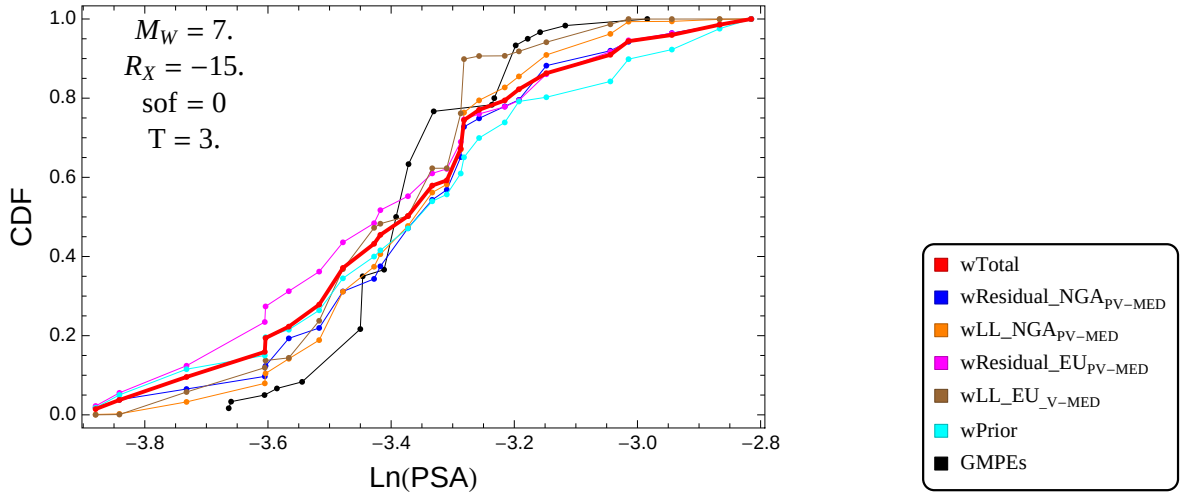



Figure 4.244: PVNGSv2: Cumulative distribution function of GMPEs (black) and selected models, for different sets of weights, for a scenario with $M = 7.$, $R_x = -15.$, $F = 0$, and $T = 3.$s

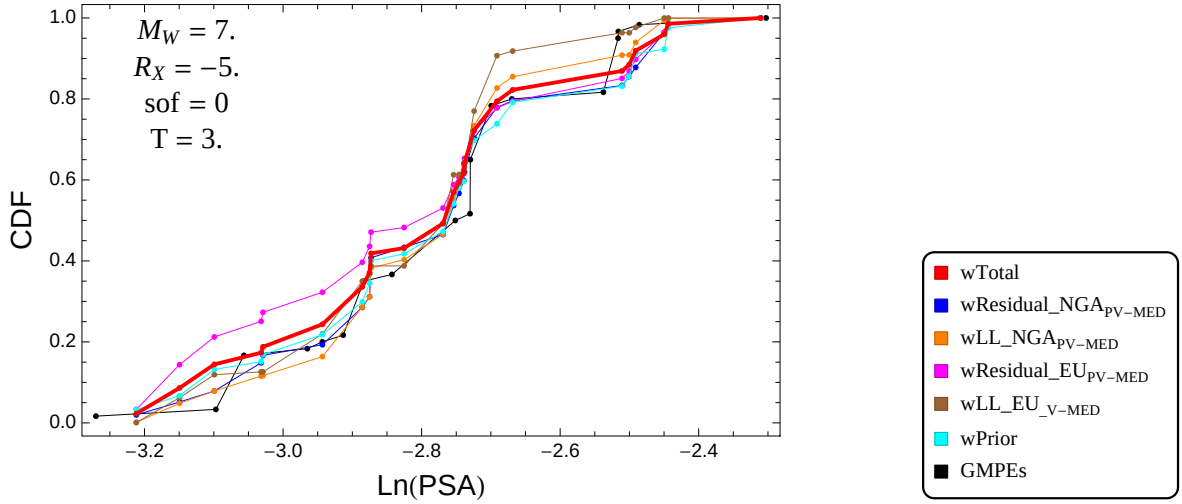



Figure 4.245: PVNGSv2: Cumulative distribution function of GMPEs (black) and selected models, for different sets of weights, for a scenario with $M = 7.$, $R_x = -5.$, $F = 0$, and $T = 3.$s

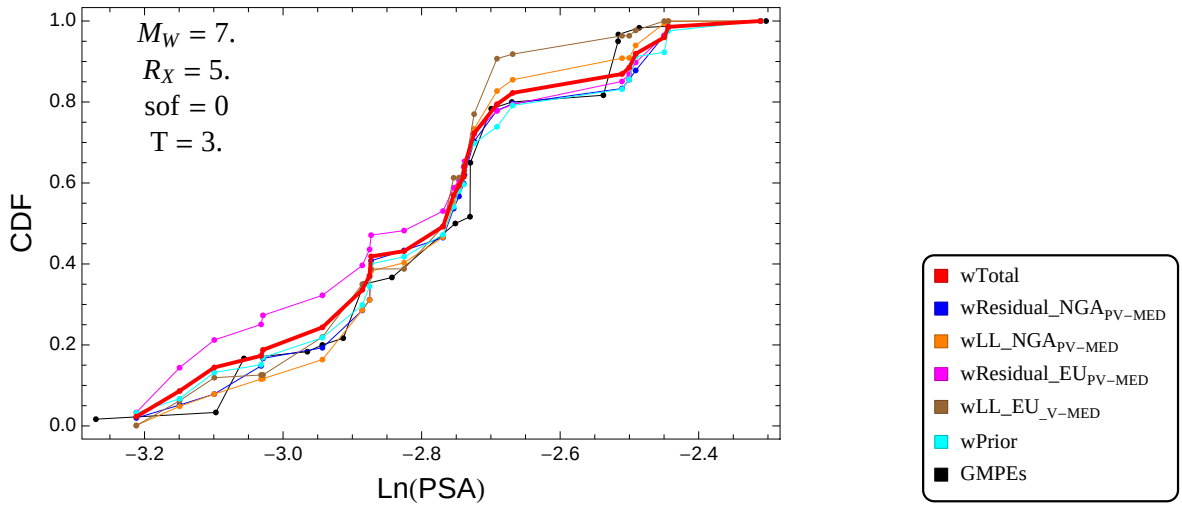



Figure 4.246: PVNGSv2: Cumulative distribution function of GMPEs (black) and selected models, for different sets of weights, for a scenario with $M = 7.$, $R_x = 5.$, $F = 0$, and $T = 3.$s

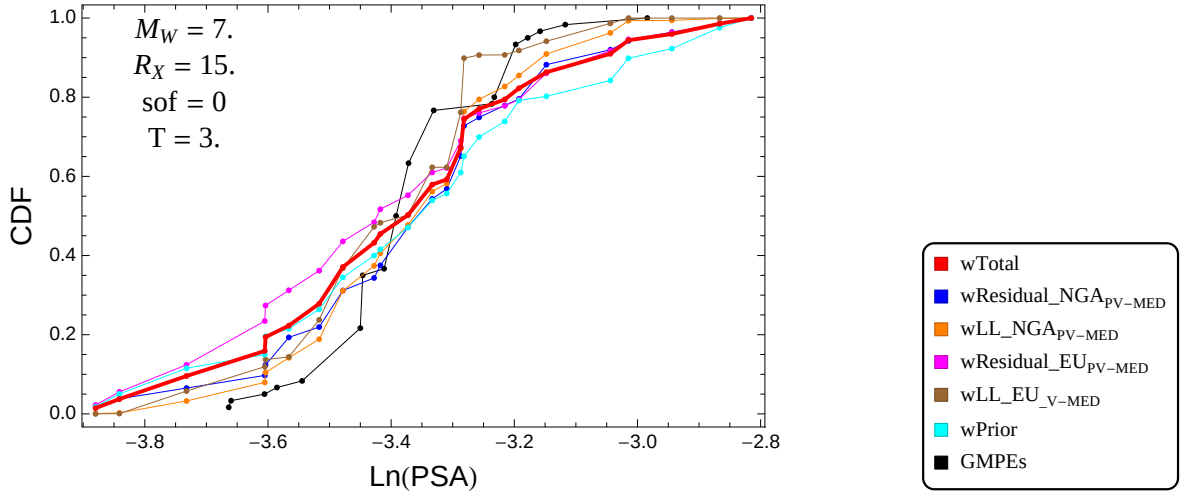



Figure 4.247: PVNGSv2: Cumulative distribution function of GMPEs (black) and selected models, for different sets of weights, for a scenario with $M = 7.$, $R_x = 15.$, $F = 0$, and $T = 3.$s

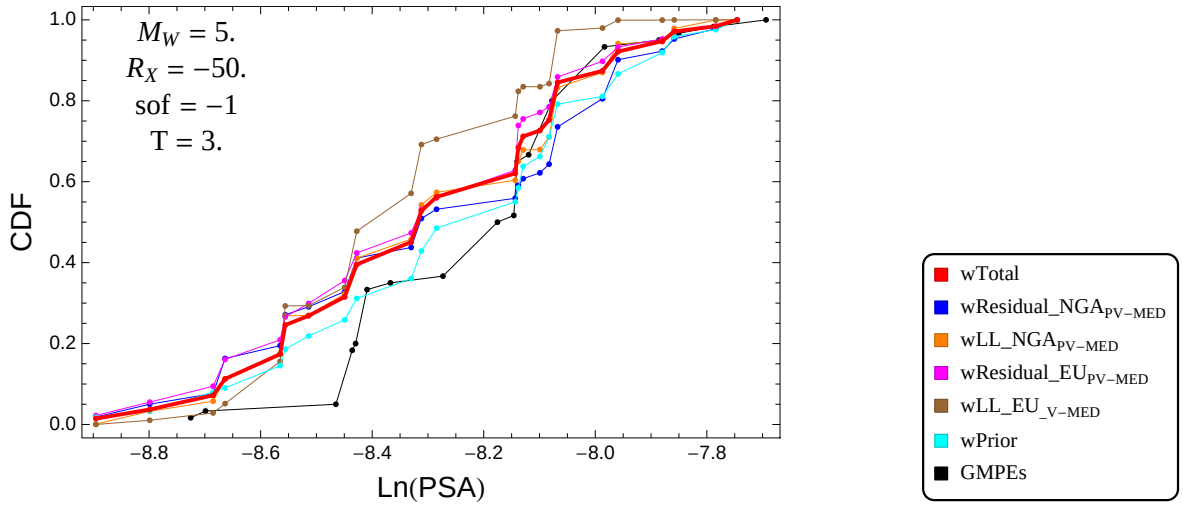



Figure 4.248: PVNGSv2: Cumulative distribution function of GMPEs (black) and selected models, for different sets of weights, for a scenario with $M = 5.$, $R_x = -50.$, $F = -1$, and $T = 3.$s

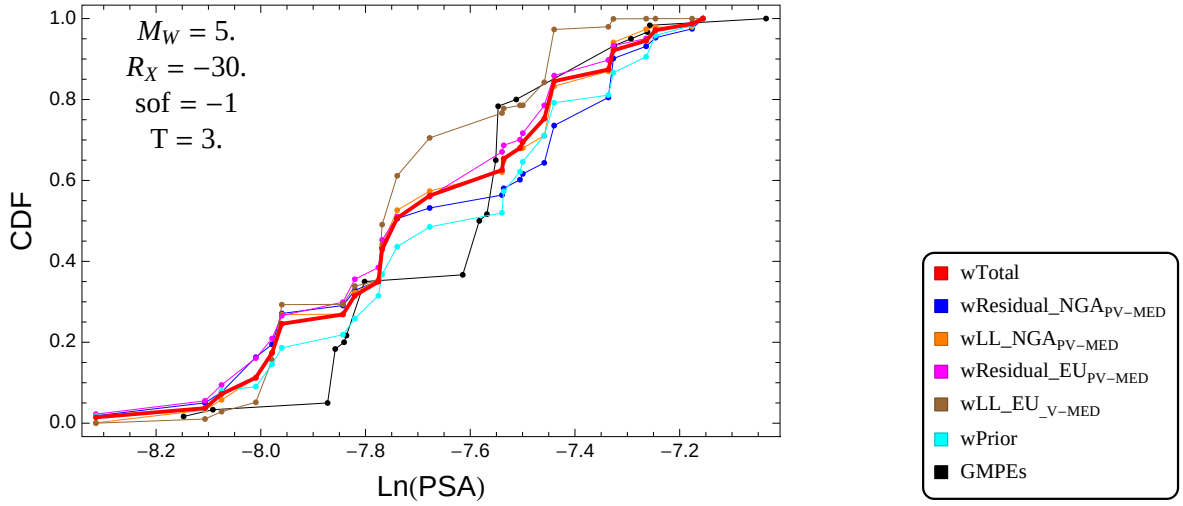



Figure 4.249: PVNGSv2: Cumulative distribution function of GMPEs (black) and selected models, for different sets of weights, for a scenario with $M = 5.$, $R_x = -30.$, $F = -1$, and $T = 3.$s

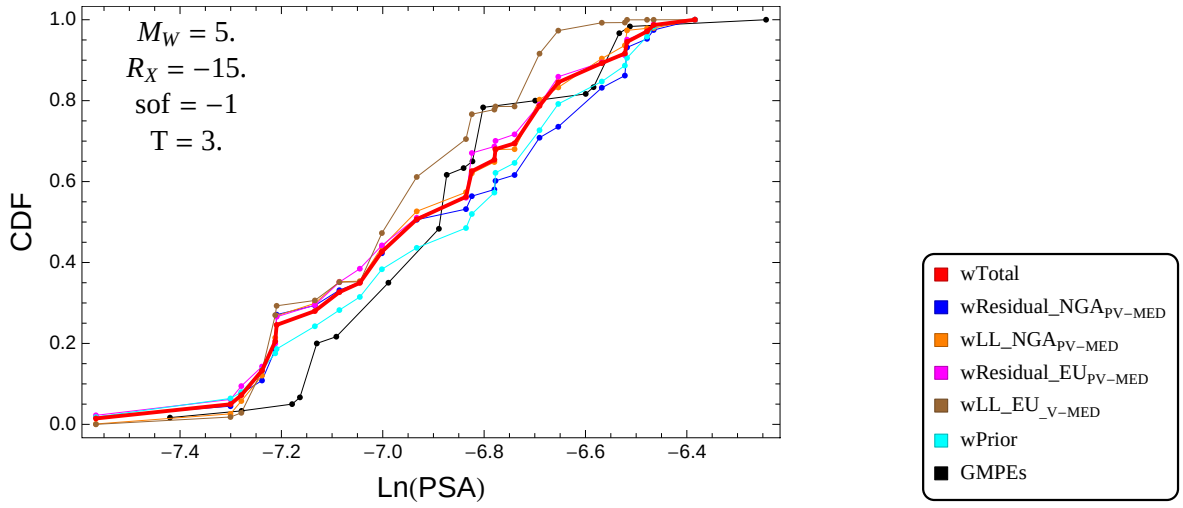



Figure 4.250: PVNGSv2: Cumulative distribution function of GMPEs (black) and selected models, for different sets of weights, for a scenario with $M = 5.$, $R_x = -15.$, $F = -1$, and $T = 3.$s

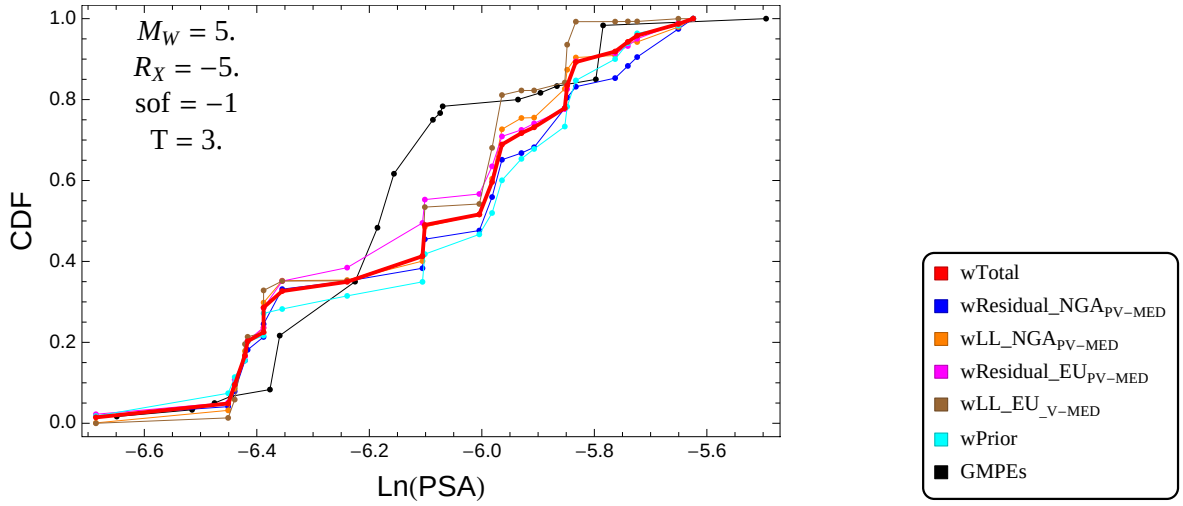



Figure 4.251: PVNGSv2: Cumulative distribution function of GMPEs (black) and selected models, for different sets of weights, for a scenario with $M = 5.$, $R_x = -5.$, $F = -1$, and $T = 3.$s

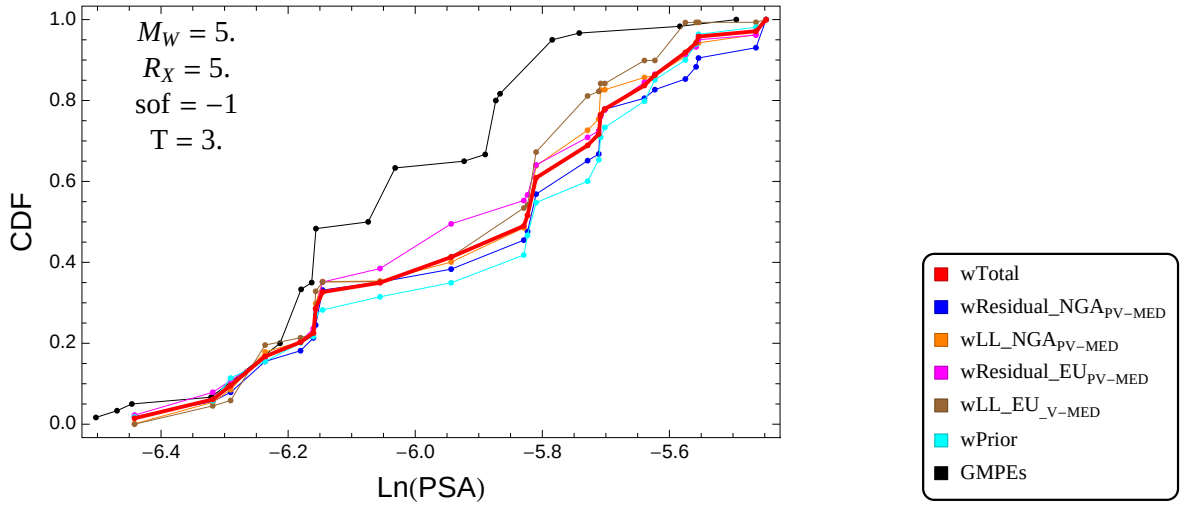



Figure 4.252: PVNGSv2: Cumulative distribution function of GMPEs (black) and selected models, for different sets of weights, for a scenario with $M = 5.$, $R_x = 5.$, $F = -1$, and $T = 3.$s

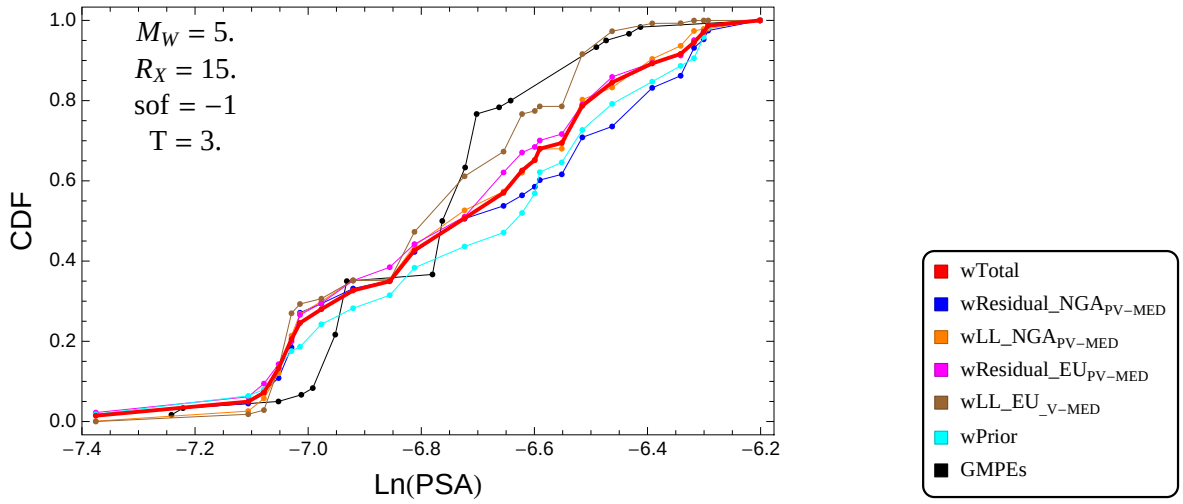



Figure 4.253: PVNGSv2: Cumulative distribution function of GMPEs (black) and selected models, for different sets of weights, for a scenario with $M = 5.$, $R_x = 15.$, $F = -1$, and $T = 3.$s

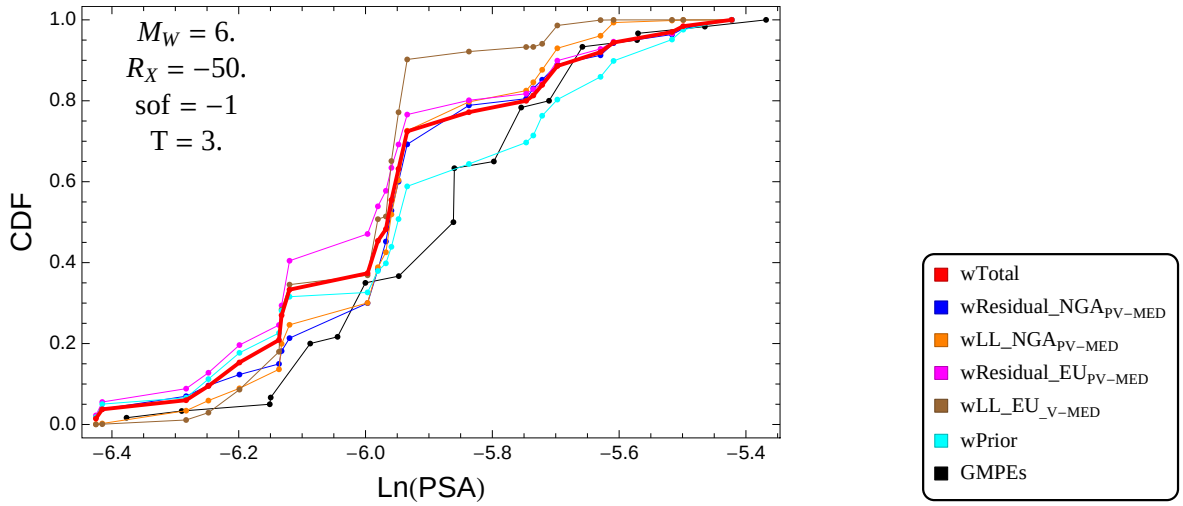



Figure 4.254: PVNGSv2: Cumulative distribution function of GMPEs (black) and selected models, for different sets of weights, for a scenario with $M = 6.$, $R_x = -50.$, $F = -1$, and $T = 3.$s

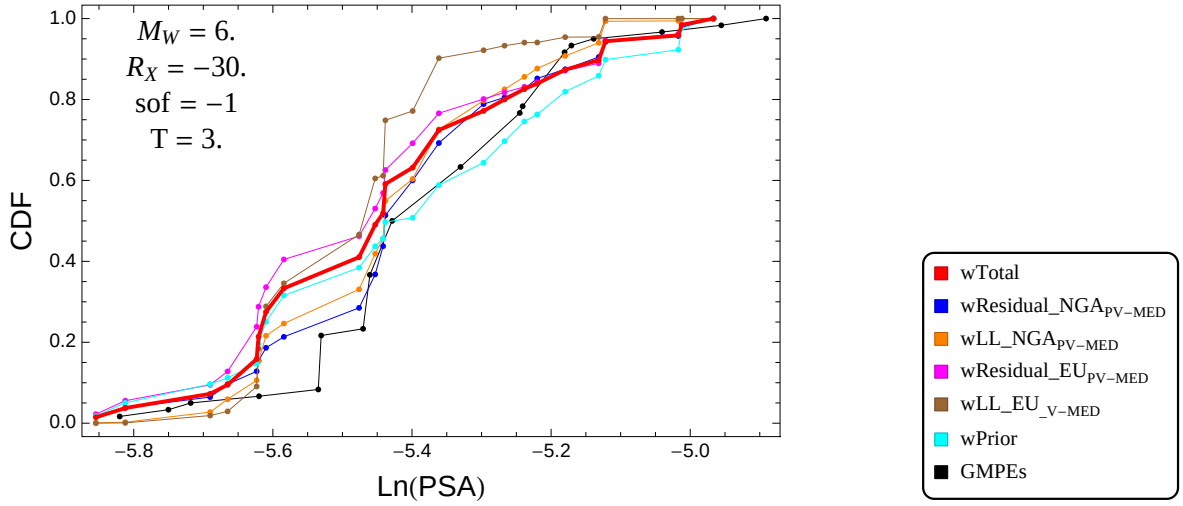



Figure 4.255: PVNGSv2: Cumulative distribution function of GMPEs (black) and selected models, for different sets of weights, for a scenario with $M = 6.$, $R_x = -30.$, $F = -1$, and $T = 3.$s

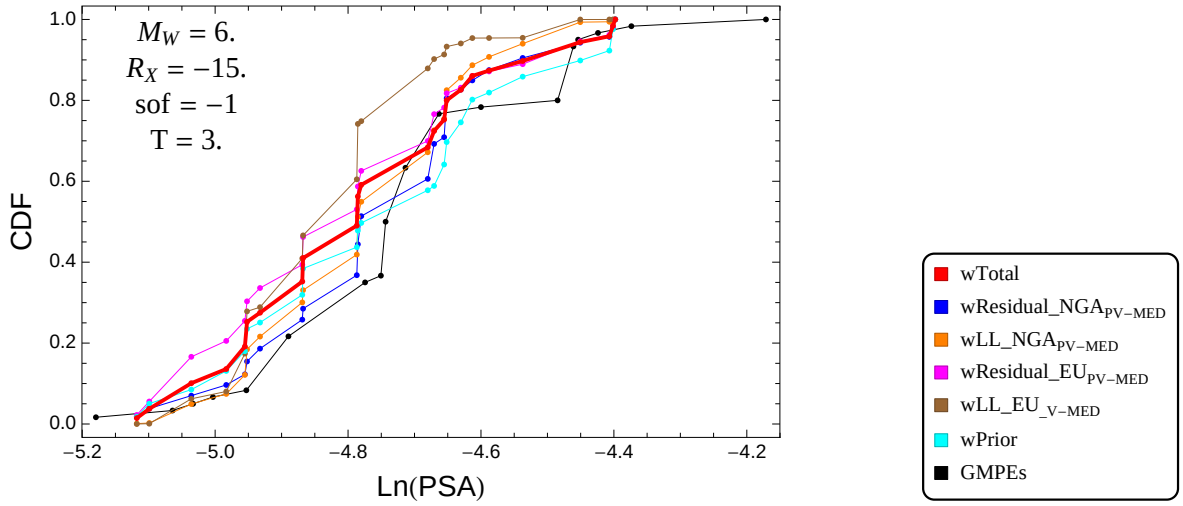



Figure 4.256: PVNGSv2: Cumulative distribution function of GMPEs (black) and selected models, for different sets of weights, for a scenario with $M = 6.$, $R_x = -15.$, $F = -1$, and $T = 3.$s

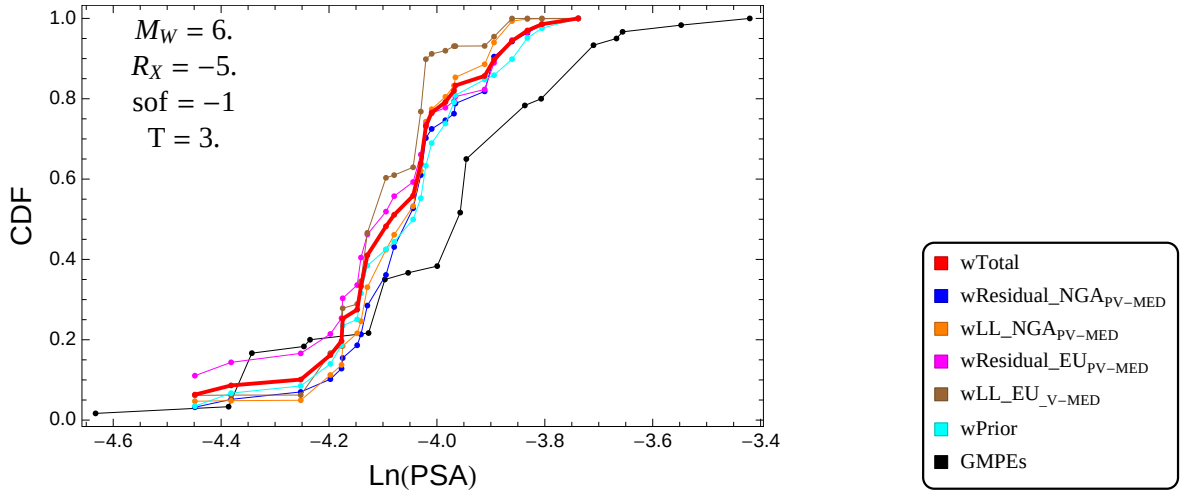



Figure 4.257: PVNGSv2: Cumulative distribution function of GMPEs (black) and selected models, for different sets of weights, for a scenario with $M = 6.$, $R_x = -5.$, $F = -1$, and $T = 3.$s

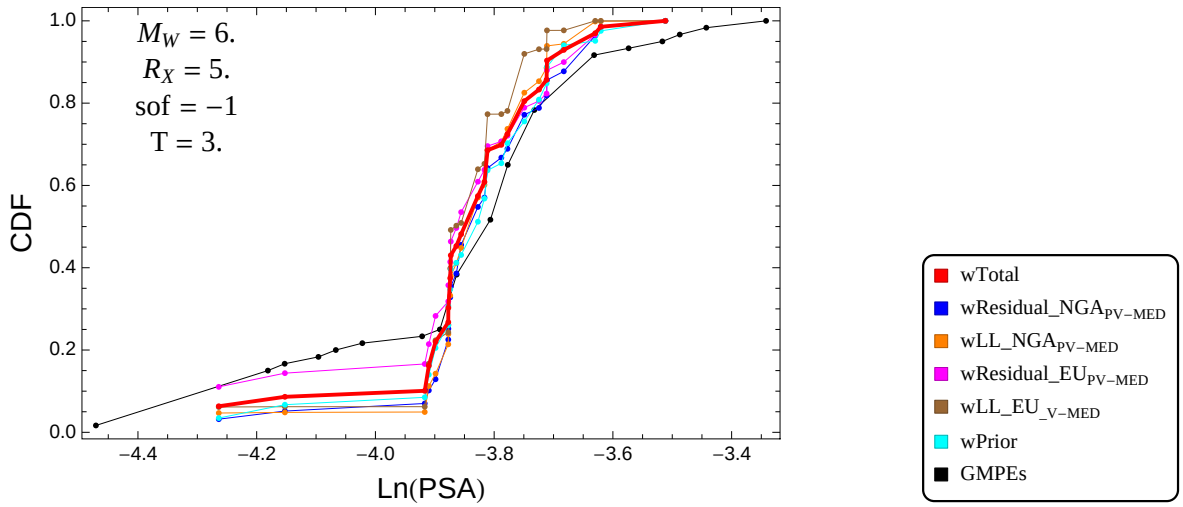



Figure 4.258: PVNGSv2: Cumulative distribution function of GMPEs (black) and selected models, for different sets of weights, for a scenario with $M = 6.$, $R_x = 5.$, $F = -1$, and $T = 3.$s

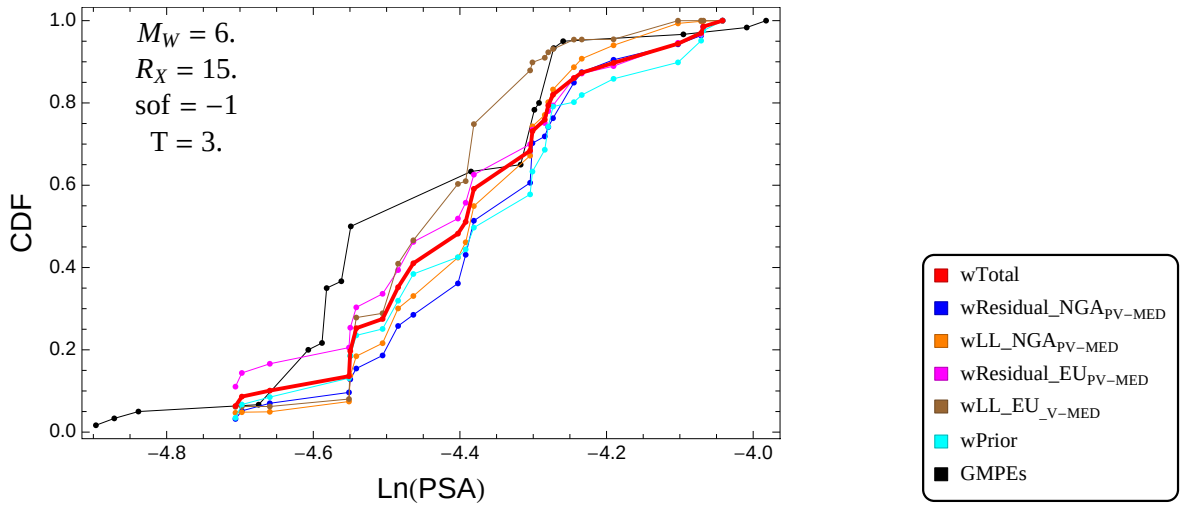



Figure 4.259: PVNGSv2: Cumulative distribution function of GMPEs (black) and selected models, for different sets of weights, for a scenario with $M = 6.$, $R_x = 15.$, $F = -1$, and $T = 3.$s

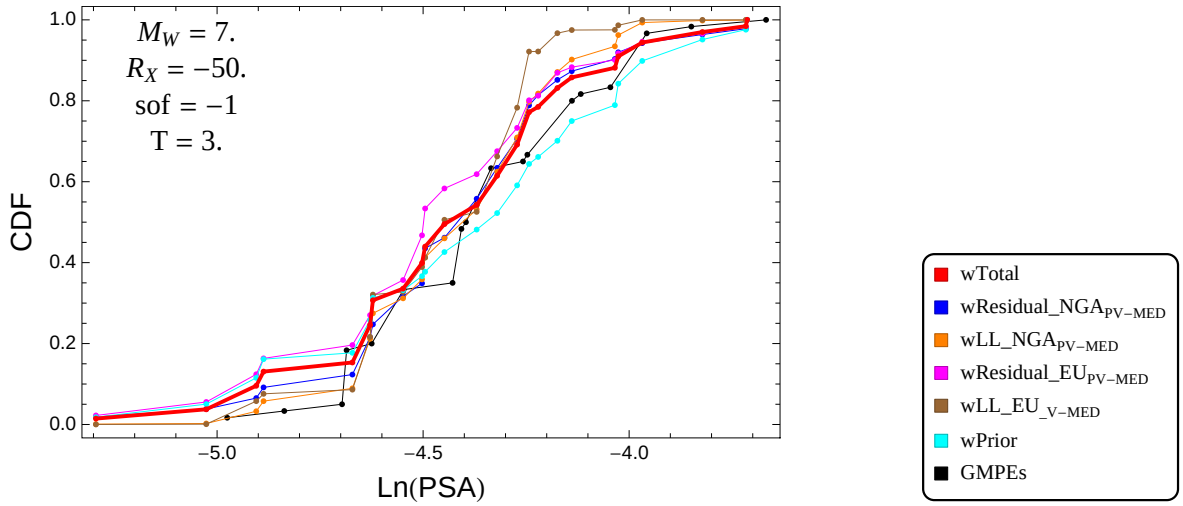



Figure 4.260: PVNGSv2: Cumulative distribution function of GMPEs (black) and selected models, for different sets of weights, for a scenario with $M = 7.$, $R_x = -50.$, $F = -1$, and $T = 3.$s

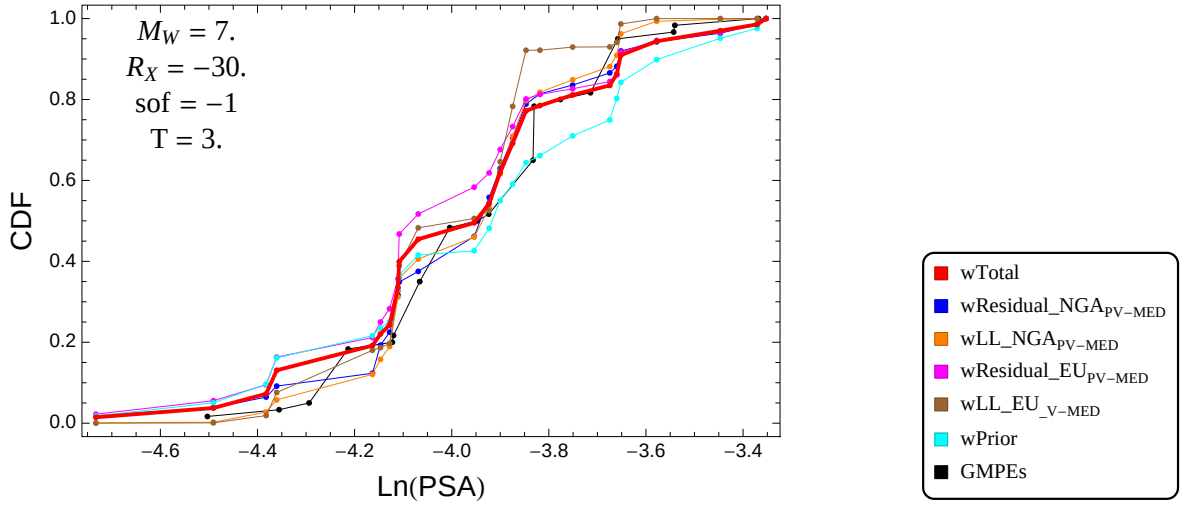



Figure 4.261: PVNGSv2: Cumulative distribution function of GMPEs (black) and selected models, for different sets of weights, for a scenario with $M = 7.$, $R_x = -30.$, $F = -1$, and $T = 3.$s

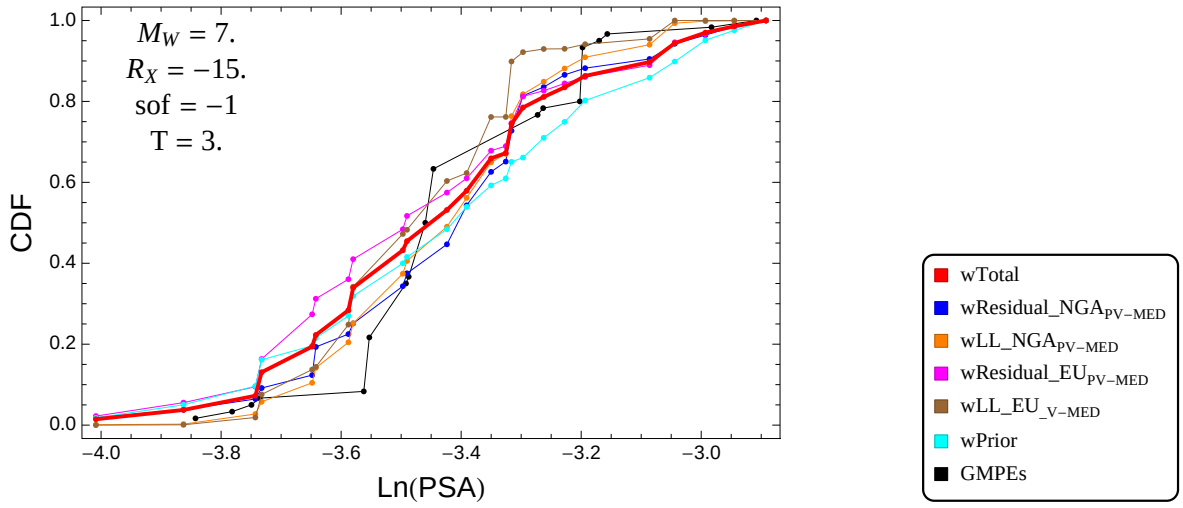



Figure 4.262: PVNGSv2: Cumulative distribution function of GMPEs (black) and selected models, for different sets of weights, for a scenario with $M = 7.$, $R_x = -15.$, $F = -1$, and $T = 3.$s

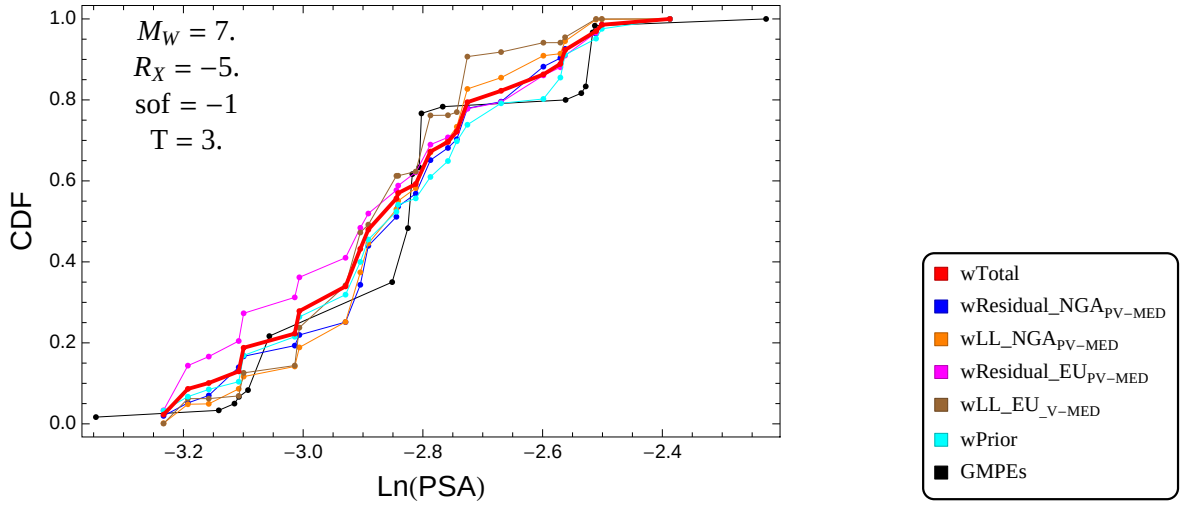



Figure 4.263: PVNGSv2: Cumulative distribution function of GMPEs (black) and selected models, for different sets of weights, for a scenario with $M = 7.$, $R_x = -5.$, $F = -1$, and $T = 3.$s

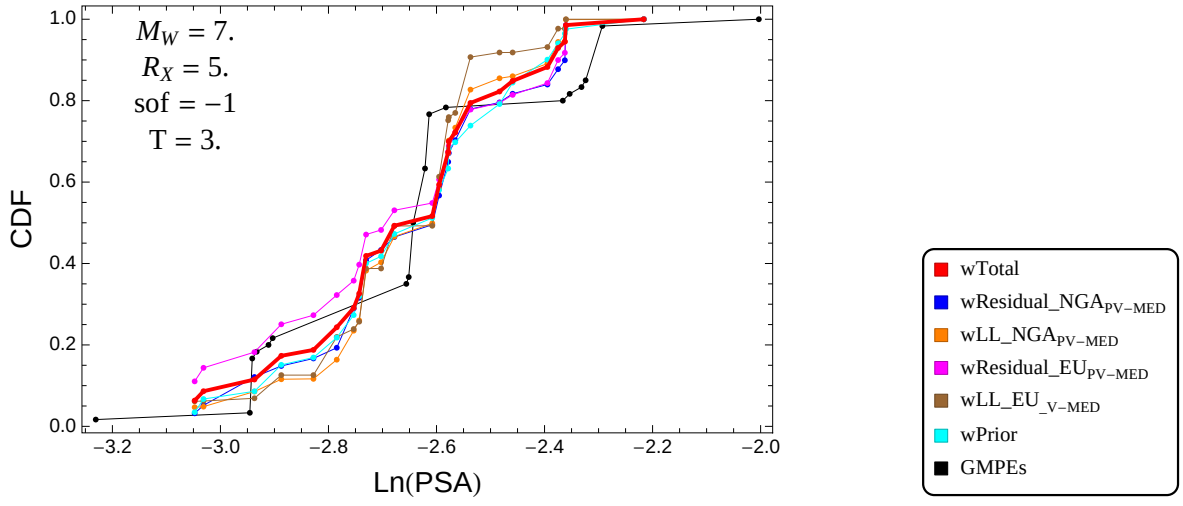



Figure 4.264: PVNGSv2: Cumulative distribution function of GMPEs (black) and selected models, for different sets of weights, for a scenario with $M = 7.$, $R_x = 5.$, $F = -1$, and $T = 3.$s

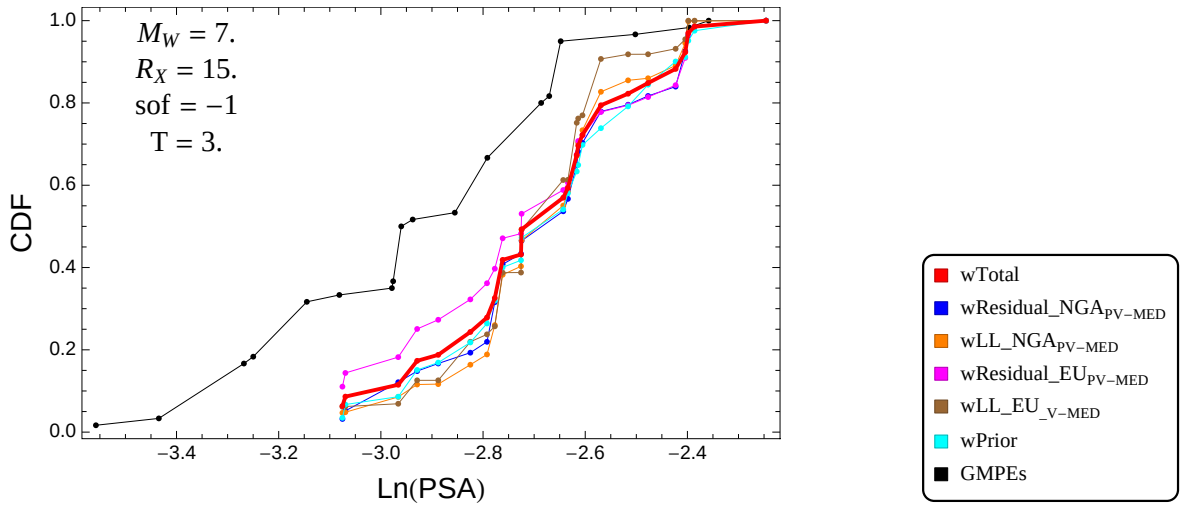



Figure 4.265: PVNGSv2: Cumulative distribution function of GMPEs (black) and selected models, for different sets of weights, for a scenario with $M = 7.$, $R_x = 15.$, $F = -1$, and $T = 3.$s

### 4.1.6 Quantile Plots vs. Distance

**T = 0.01s**

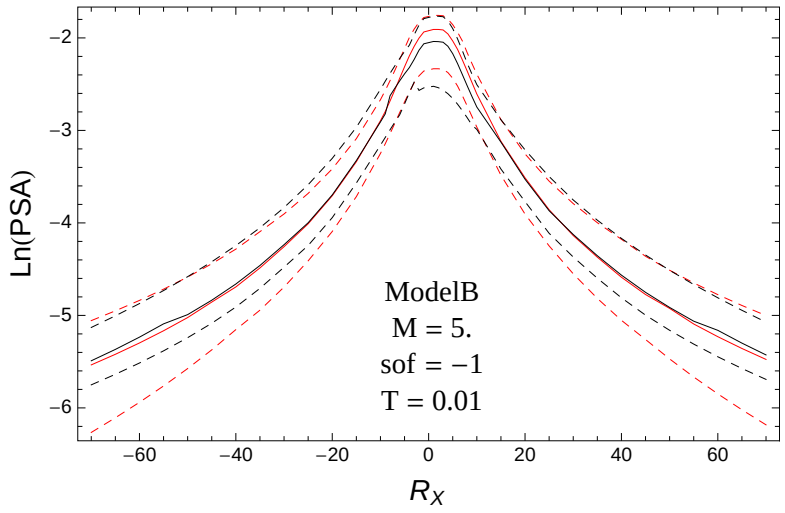



Figure 4.266: PVNGS2: Distance scaling of 0.05,0.5,0.95 quantile of the GMPE distribution (black) and the ModelB distribution (red) with total weights, for a scenario with $M = 5.$, $F = -1$, and $T = 0.01$.

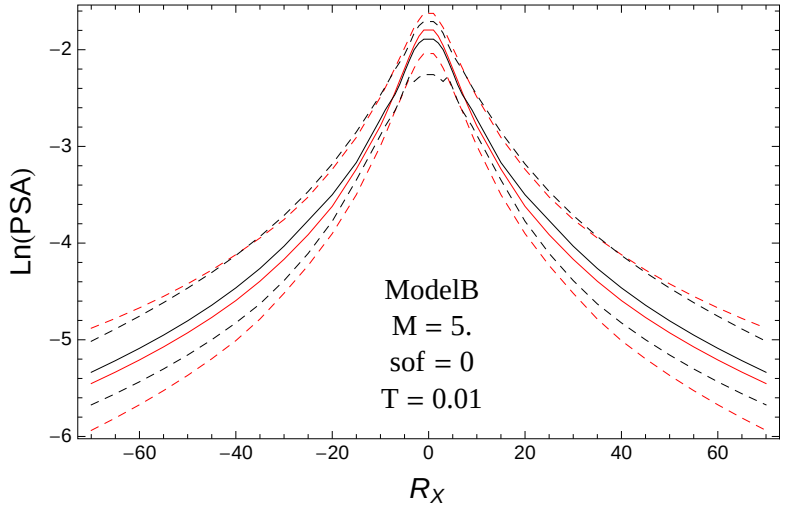



Figure 4.267: PVNGS2: Distance scaling of 0.05,0.5,0.95 quantile of the GMPE distribution (black) and the ModelB distribution (red) with total weights, for a scenario with $M = 5.$, $F = 0$, and $T = 0.01$.

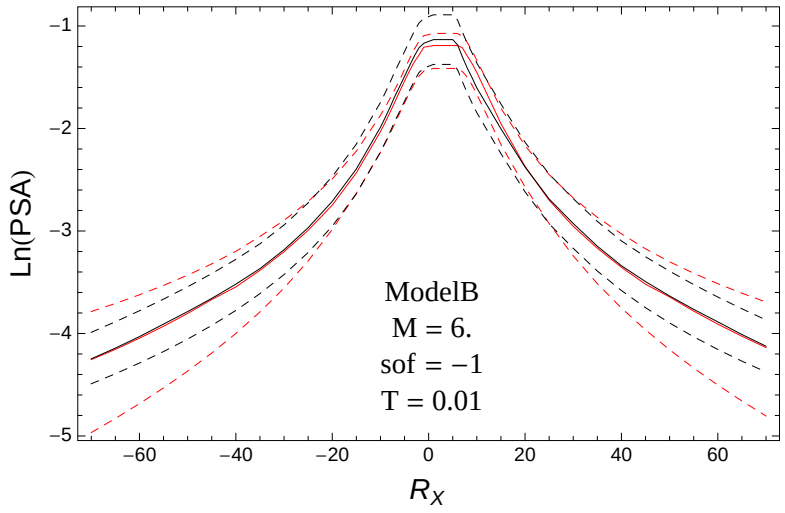



Figure 4.268: PVNGS2: Distance scaling of 0.05,0.5,0.95 quantile of the GMPE distribution (black) and the ModelB distribution (red) with total weights, for a scenario with $M = 6.$, $F = -1$, and $T = 0.01$.

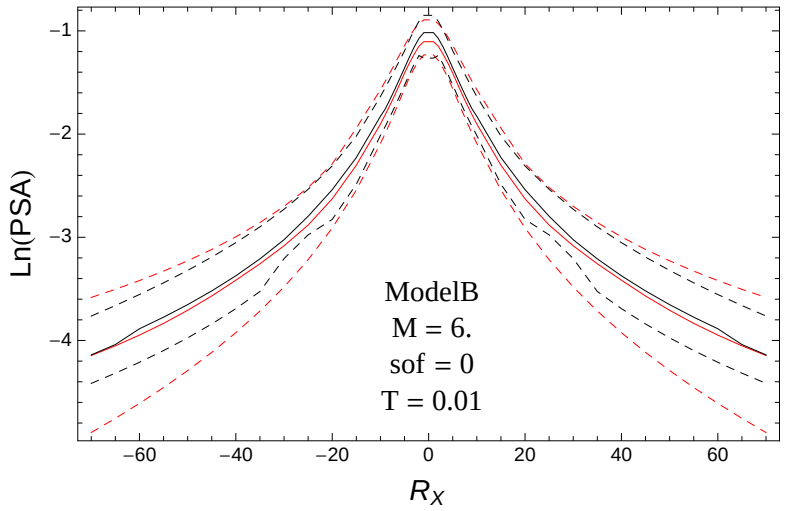



Figure 4.269: PVNGS2: Distance scaling of 0.05,0.5,0.95 quantile of the GMPE distribution (black) and the ModelB distribution (red) with total weights, for a scenario with $M = 6.$, $F = 0$, and $T = 0.01$.

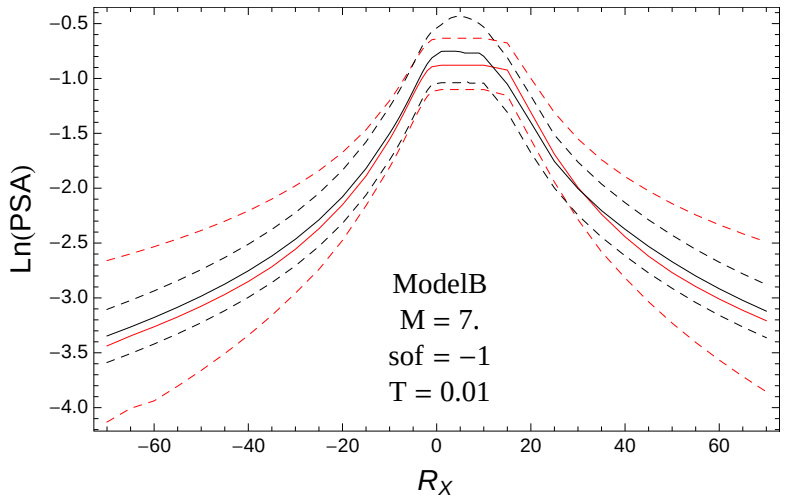



Figure 4.270: PVNGS2: Distance scaling of 0.05,0.5,0.95 quantile of the GMPE distribution (black) and the ModelB distribution (red) with total weights, for a scenario with $M = 7.$, $F = -1$, and $T = 0.01$.

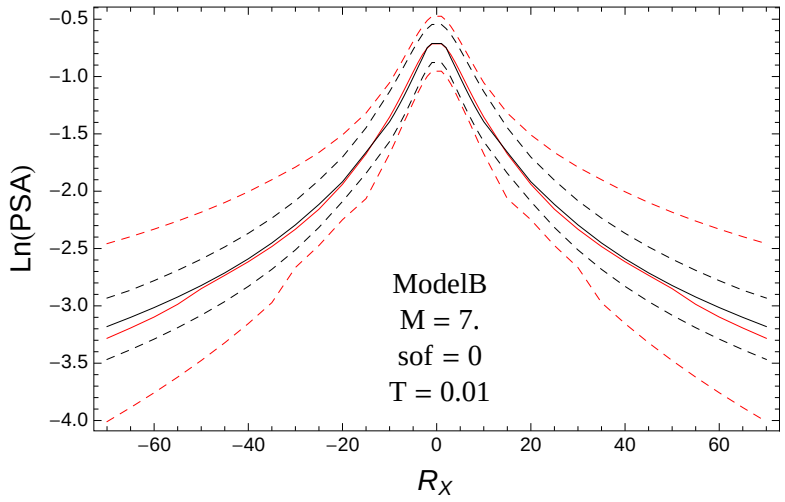



Figure 4.271: PVNGS2: Distance scaling of 0.05,0.5,0.95 quantile of the GMPE distribution (black) and the ModelB distribution (red) with total weights, for a scenario with $M = 7.$, $F = 0$, and $T = 0.01$.

**T = 0.2s**

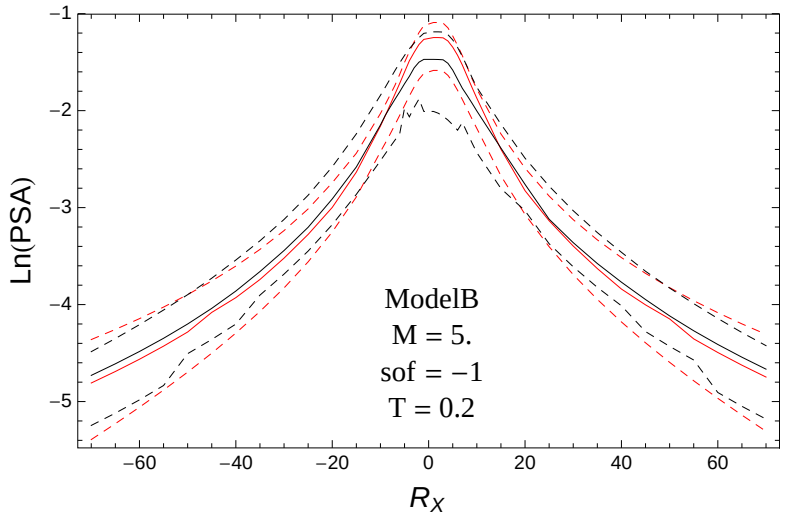



Figure 4.272: PVNGS2: Distance scaling of 0.05,0.5,0.95 quantile of the GMPE distribution (black) and the ModelB distribution (red) with total weights, for a scenario with $M = 5.$, $F = -1$, and $T = 0.2$.

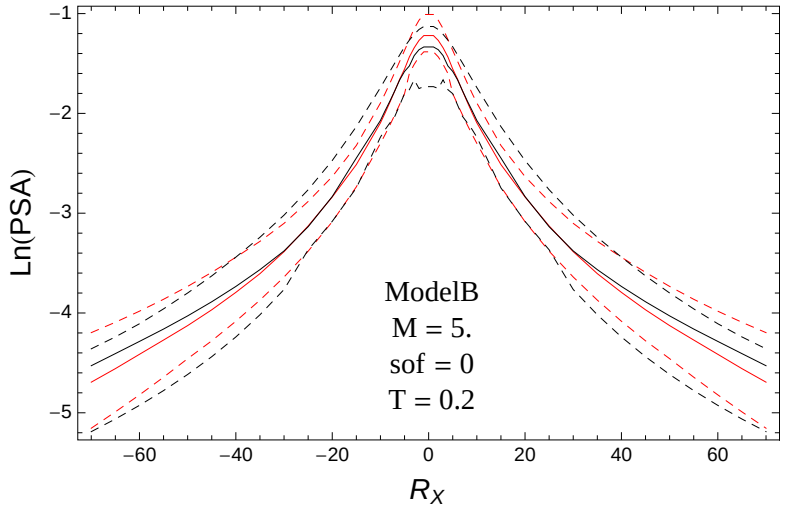



Figure 4.273: PVNGS2: Distance scaling of 0.05,0.5,0.95 quantile of the GMPE distribution (black) and the ModelB distribution (red) with total weights, for a scenario with $M = 5.$, $F = 0$, and $T = 0.2$.

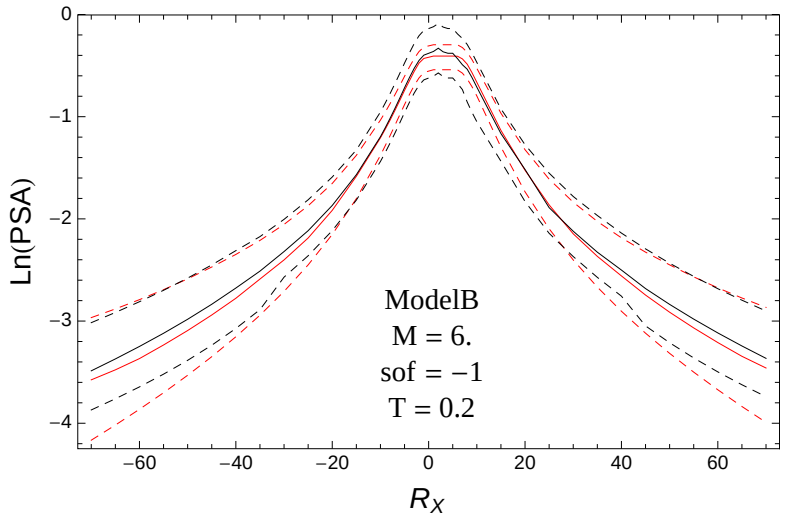



Figure 4.274: PVNGS2: Distance scaling of 0.05,0.5,0.95 quantile of the GMPE distribution (black) and the ModelB distribution (red) with total weights, for a scenario with $M = 6.$, $F = -1$, and $T = 0.2$.

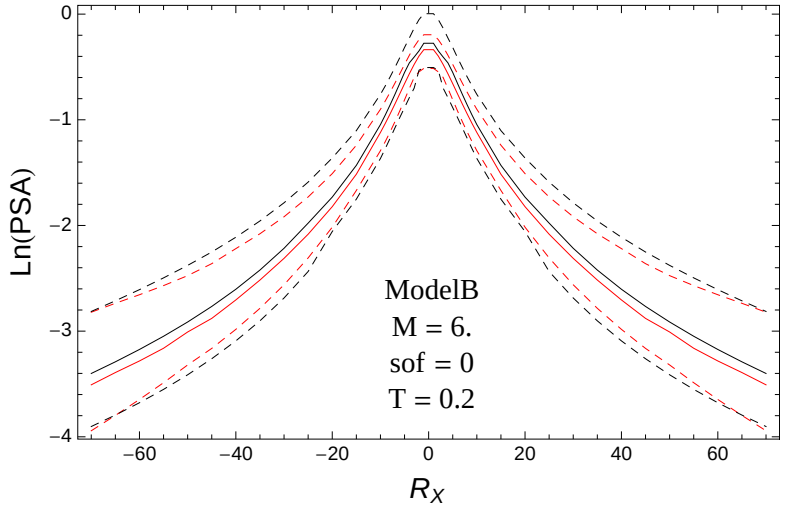



Figure 4.275: PVNGS2: Distance scaling of 0.05,0.5,0.95 quantile of the GMPE distribution (black) and the ModelB distribution (red) with total weights, for a scenario with $M = 6.$, $F = 0$, and $T = 0.2$.

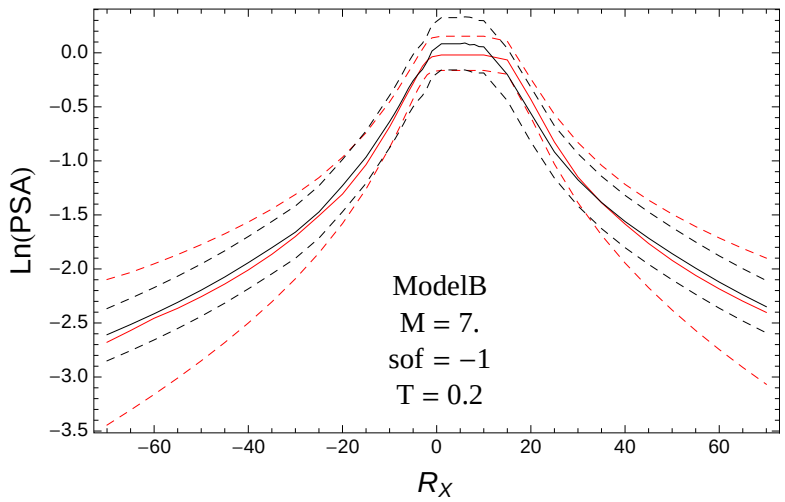



Figure 4.276: PVNGS2: Distance scaling of 0.05,0.5,0.95 quantile of the GMPE distribution (black) and the ModelB distribution (red) with total weights, for a scenario with $M = 7.$, $F = -1$, and $T = 0.2$.

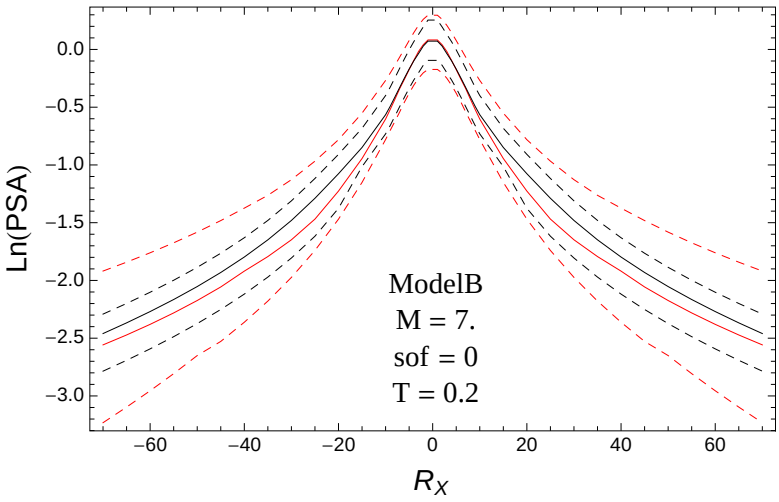



Figure 4.277: PVNGS2: Distance scaling of 0.05,0.5,0.95 quantile of the GMPE distribution (black) and the ModelB distribution (red) with total weights, for a scenario with $M = 7.$, $F = 0$, and $T = 0.2$.

**T = 0.5s**

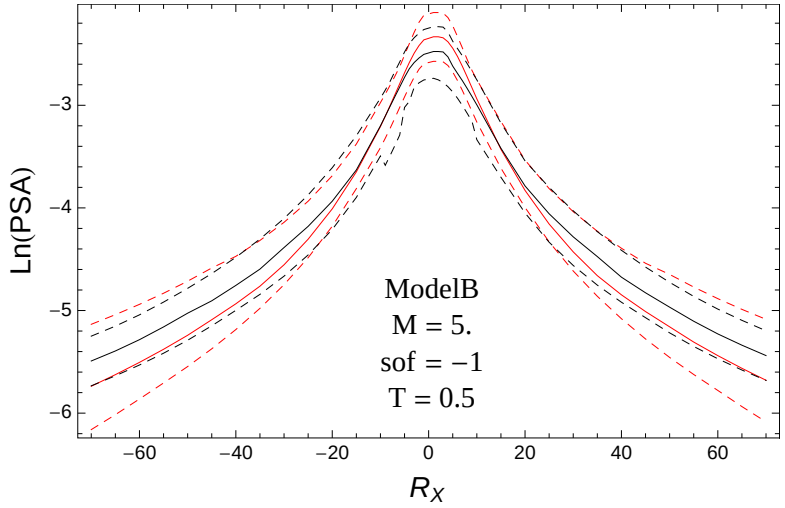



Figure 4.278: PVNGS2: Distance scaling of 0.05,0.5,0.95 quantile of the GMPE distribution (black) and the ModelB distribution (red) with total weights, for a scenario with $M = 5.$, $F = -1$, and $T = 0.5$.

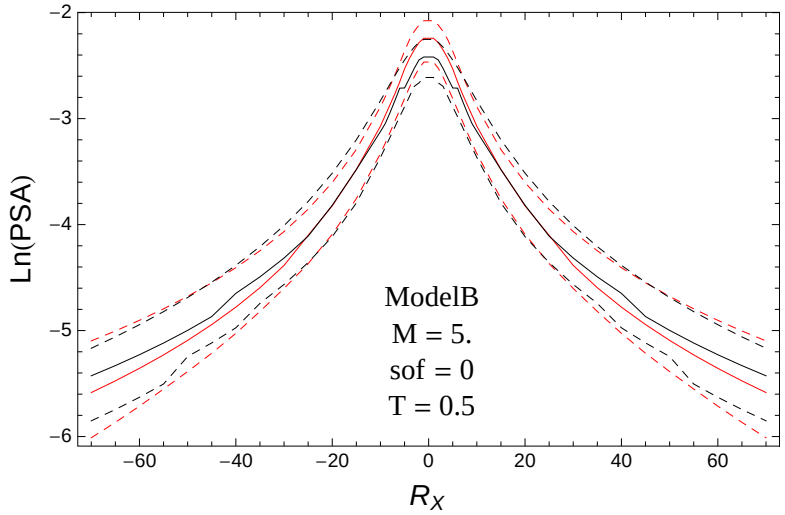



Figure 4.279: PVNGS2: Distance scaling of 0.05,0.5,0.95 quantile of the GMPE distribution (black) and the ModelB distribution (red) with total weights, for a scenario with $M = 5.$, $F = 0$, and $T = 0.5$.

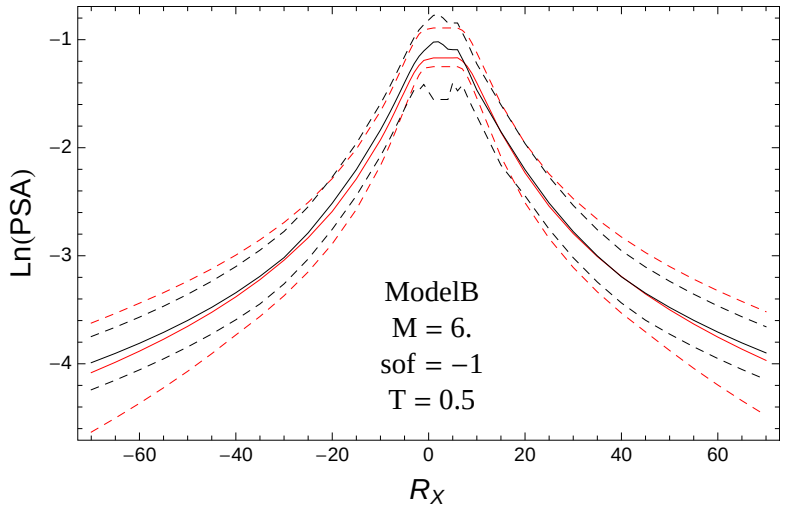



Figure 4.280: PVNGS2: Distance scaling of 0.05,0.5,0.95 quantile of the GMPE distribution (black) and the ModelB distribution (red) with total weights, for a scenario with $M = 6.$, $F = -1$, and $T = 0.5$.

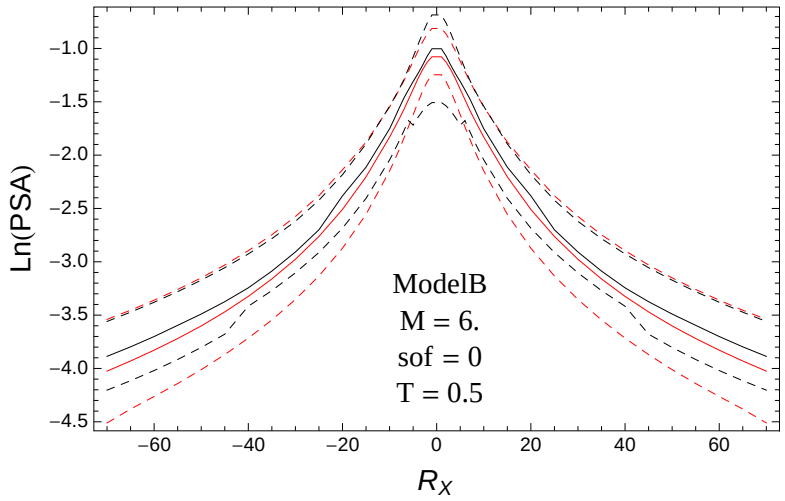



Figure 4.281: PVNGS2: Distance scaling of 0.05,0.5,0.95 quantile of the GMPE distribution (black) and the ModelB distribution (red) with total weights, for a scenario with $M = 6.$, $F = 0$, and $T = 0.5$.

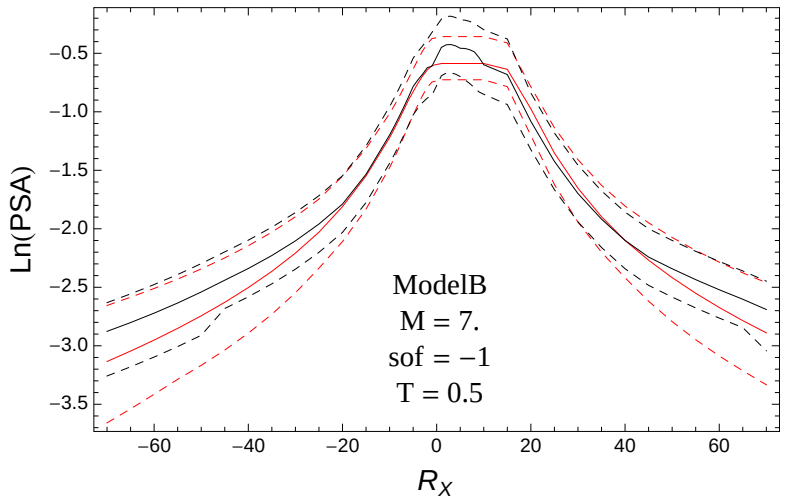



Figure 4.282: PVNGS2: Distance scaling of 0.05,0.5,0.95 quantile of the GMPE distribution (black) and the ModelB distribution (red) with total weights, for a scenario with $M = 7.$, $F = -1$, and $T = 0.5$.

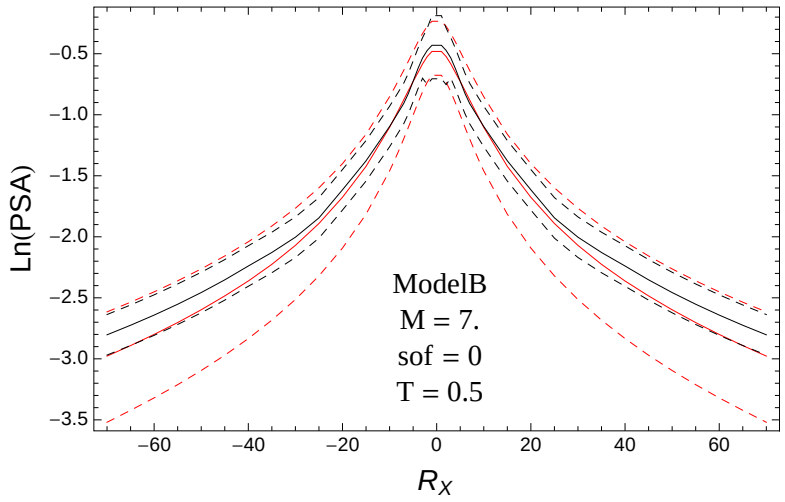



Figure 4.283: PVNGS2: Distance scaling of 0.05,0.5,0.95 quantile of the GMPE distribution (black) and the ModelB distribution (red) with total weights, for a scenario with $M = 7.$, $F = 0$, and $T = 0.5$.

**T = 1.s**

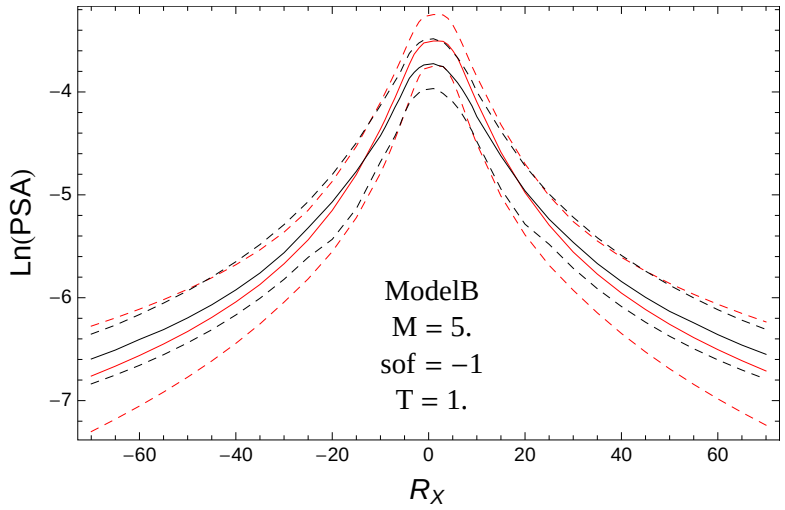



Figure 4.284: PVNGS2: Distance scaling of 0.05,0.5,0.95 quantile of the GMPE distribution (black) and the ModelB distribution (red) with total weights, for a scenario with $M = 5.$, $F = -1$, and $T = 1.$.

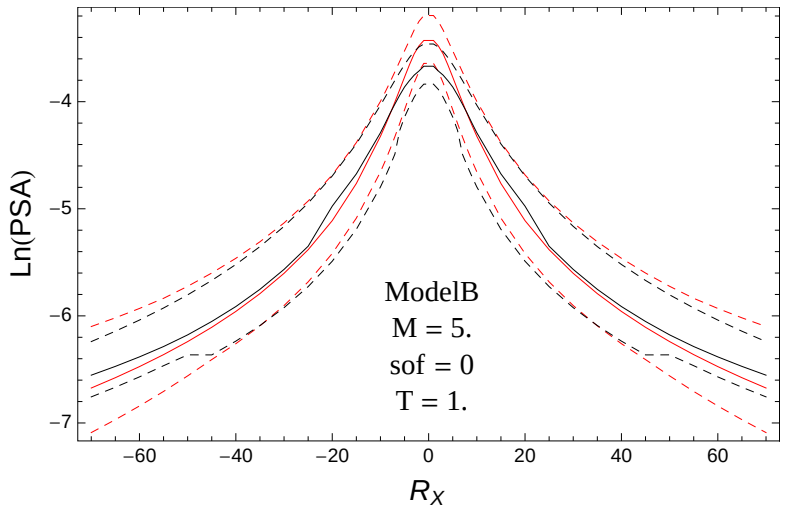



Figure 4.285: PVNGS2: Distance scaling of 0.05,0.5,0.95 quantile of the GMPE distribution (black) and the ModelB distribution (red) with total weights, for a scenario with $M = 5.$, $F = 0$, and $T = 1.$.

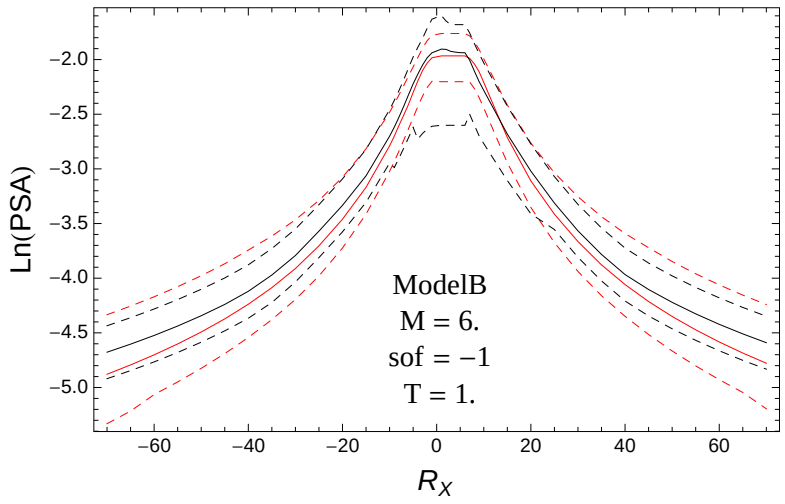



Figure 4.286: PVNGS2: Distance scaling of 0.05,0.5,0.95 quantile of the GMPE distribution (black) and the ModelB distribution (red) with total weights, for a scenario with $M = 6.$, $F = -1$, and $T = 1.$.

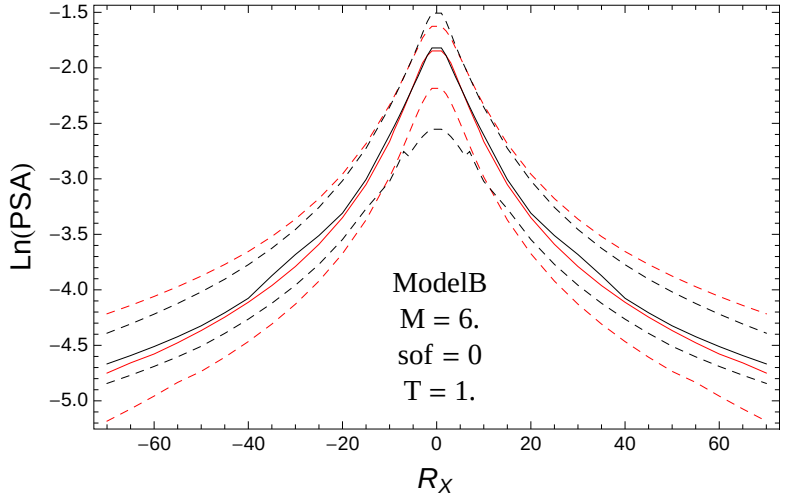



Figure 4.287: PVNGS2: Distance scaling of 0.05,0.5,0.95 quantile of the GMPE distribution (black) and the ModelB distribution (red) with total weights, for a scenario with $M = 6.$, $F = 0$, and $T = 1.$.

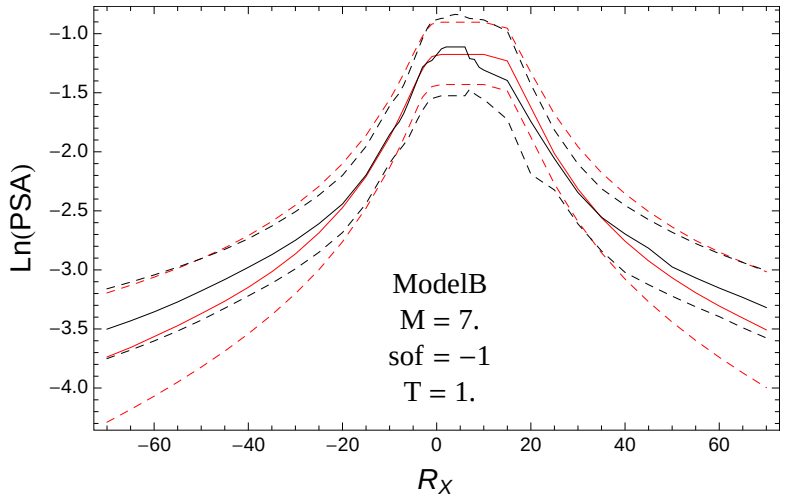



Figure 4.288: PVNGS2: Distance scaling of 0.05,0.5,0.95 quantile of the GMPE distribution (black) and the ModelB distribution (red) with total weights, for a scenario with $M = 7.$, $F = -1$, and $T = 1.$.

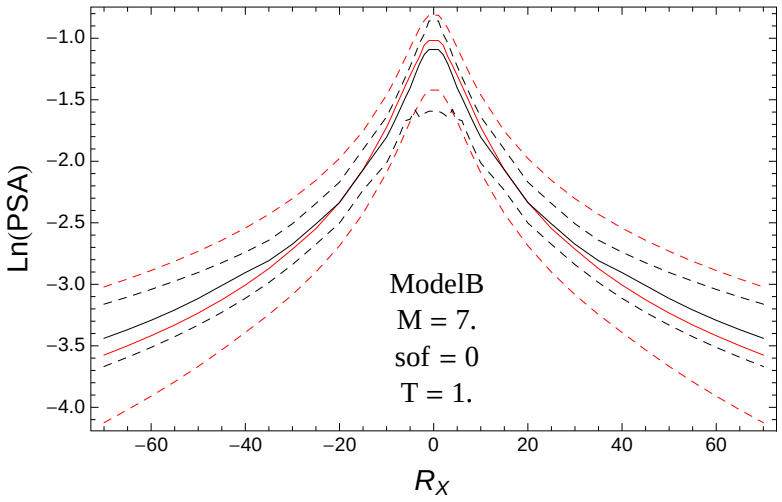



Figure 4.289: PVNGS2: Distance scaling of 0.05,0.5,0.95 quantile of the GMPE distribution (black) and the ModelB distribution (red) with total weights, for a scenario with $M = 7.$, $F = 0$, and $T = 1.$.

**T = 3.s**

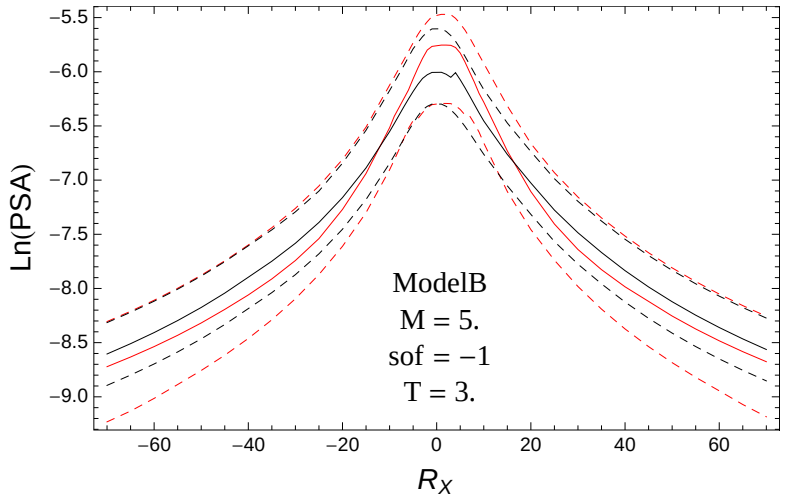



Figure 4.290: PVNGS2: Distance scaling of 0.05,0.5,0.95 quantile of the GMPE distribution (black) and the ModelB distribution (red) with total weights, for a scenario with $M = 5.$, $F = -1$, and $T = 3.$.

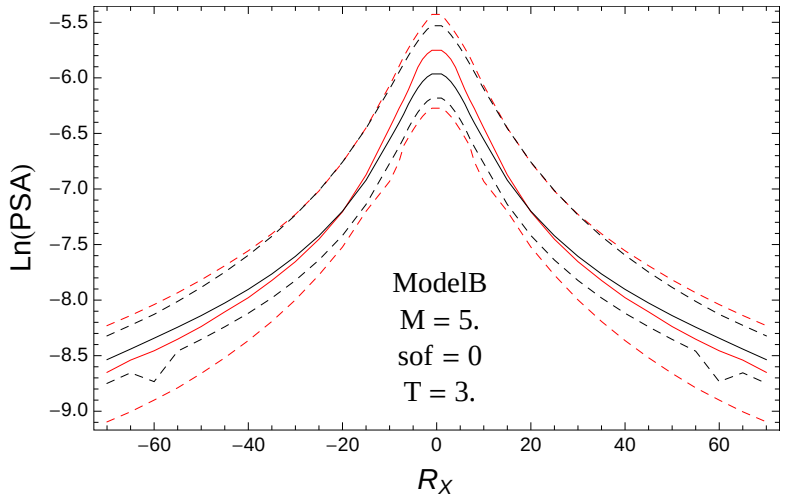



Figure 4.291: PVNGS2: Distance scaling of 0.05,0.5,0.95 quantile of the GMPE distribution (black) and the ModelB distribution (red) with total weights, for a scenario with $M = 5.$, $F = 0$, and $T = 3.$.

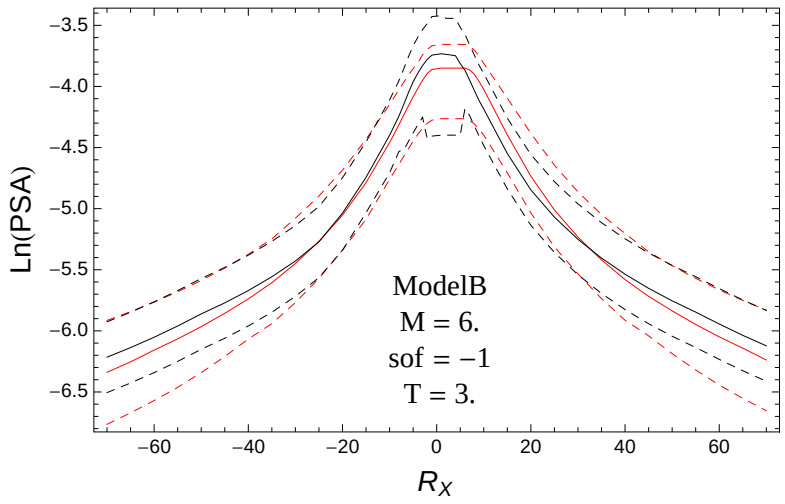



Figure 4.292: PVNGS2: Distance scaling of 0.05,0.5,0.95 quantile of the GMPE distribution (black) and the ModelB distribution (red) with total weights, for a scenario with $M = 6.$, $F = -1$, and $T = 3.$.

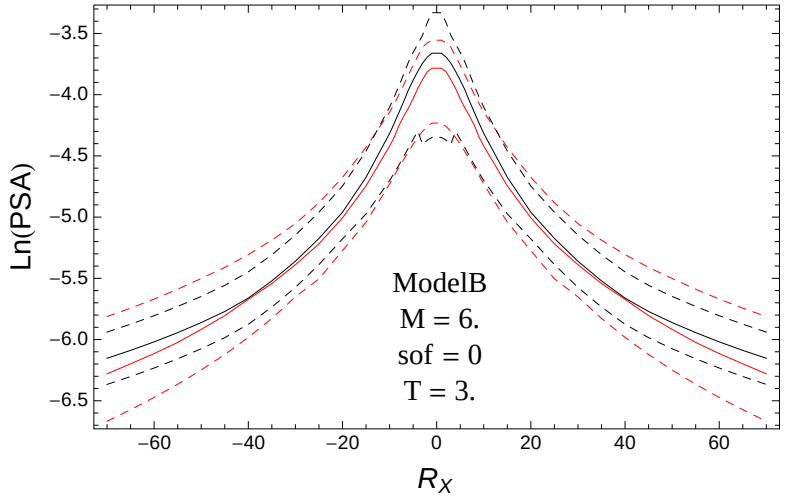



Figure 4.293: PVNGS2: Distance scaling of 0.05,0.5,0.95 quantile of the GMPE distribution (black) and the ModelB distribution (red) with total weights, for a scenario with $M = 6.$, $F = 0$, and $T = 3.$.

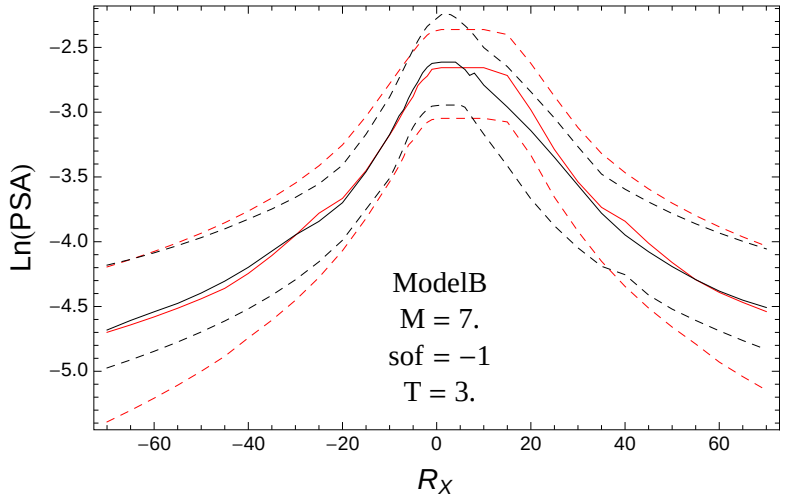



Figure 4.294: PVNGS2: Distance scaling of 0.05,0.5,0.95 quantile of the GMPE distribution (black) and the ModelB distribution (red) with total weights, for a scenario with $M = 7.$, $F = -1$, and $T = 3.$.

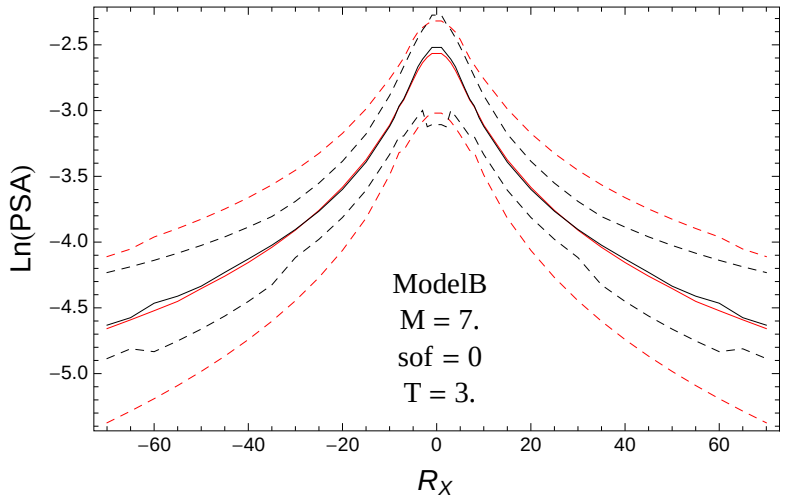



Figure 4.295: PVNGS2: Distance scaling of 0.05,0.5,0.95 quantile of the GMPE distribution (black) and the ModelB distribution (red) with total weights, for a scenario with $M = 7.$, $F = 0$, and $T = 3.$.

### 4.1.7 Quantile Plots vs. Distance with GMPEs

**T = 0.01s**

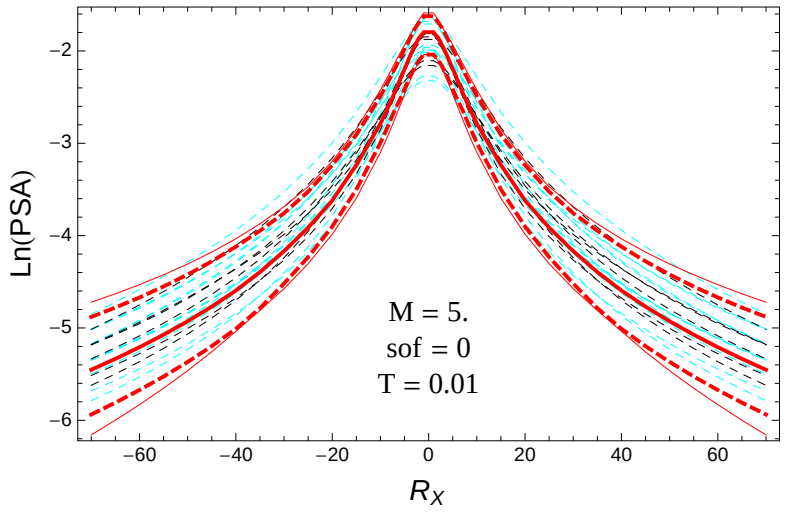



Figure 4.296: PVNGSv2: Distance scaling of the original GMPEs (dashed black), the original GMPEs with uncertainty model (dashed cyan) and 0.05,0.5,0.95 quantile of the ModelB distribution (red) with total weights, for a scenario with $M = 5.$, $F = 0$, and $T = 0.01$s.

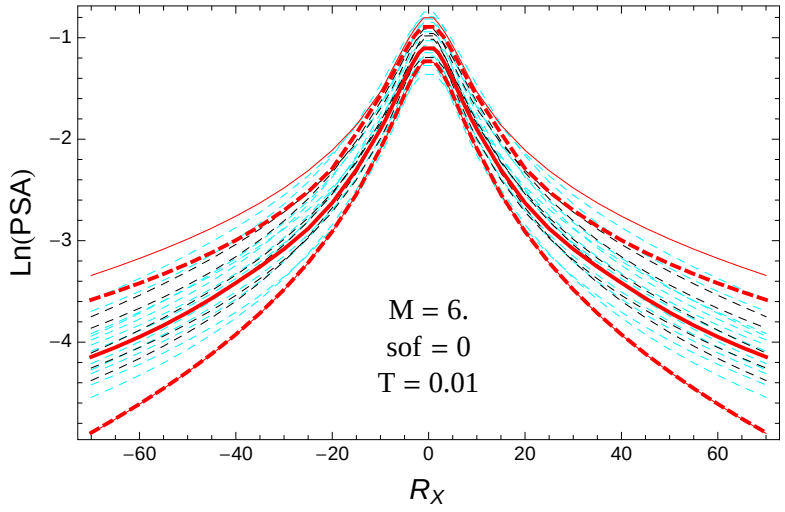



Figure 4.297: PVNGSv2: Distance scaling of the original GMPEs (dashed black), the original GMPEs with uncertainty model (dashed cyan) and 0.05,0.5,0.95 quantile of the ModelB distribution (red) with total weights, for a scenario with $M = 6.$, $F = 0$, and $T = 0.01$s.

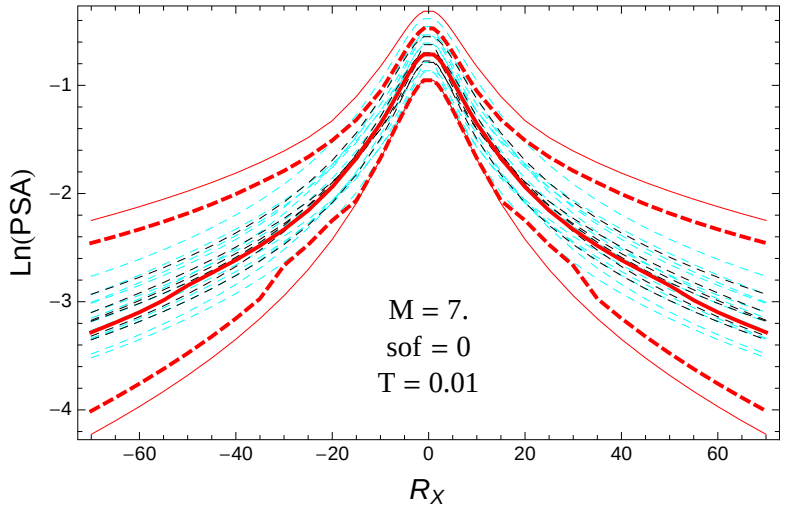



Figure 4.298: PVNGSv2: Distance scaling of the original GMPEs (dashed black), the original GMPEs with uncertainty model (dashed cyan) and 0.05,0.5,0.95 quantile of the ModelB distribution (red) with total weights, for a scenario with $M = 7.$, $F = 0$, and $T = 0.01$s.

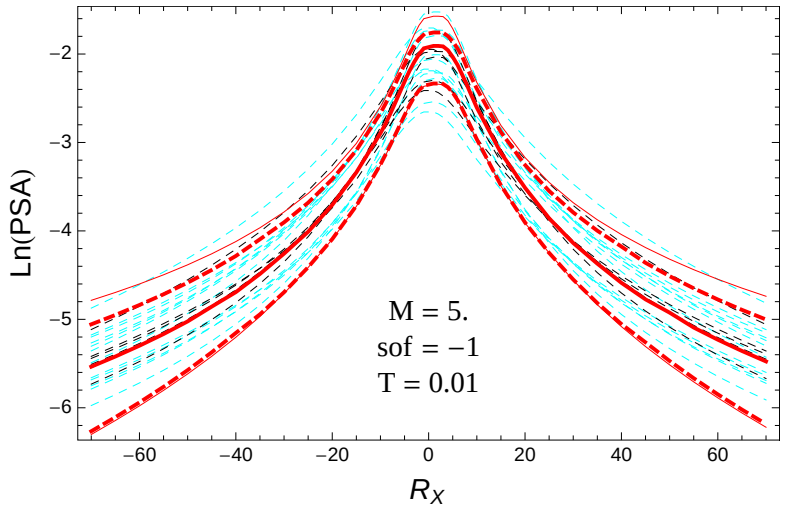



Figure 4.299: PVNGSv2: Distance scaling of the original GMPEs (dashed black), the original GMPEs with uncertainty model (dashed cyan) and 0.05,0.5,0.95 quantile of the ModelB distribution (red) with total weights, for a scenario with $M = 5.$, $F = -1$, and $T = 0.01$s.

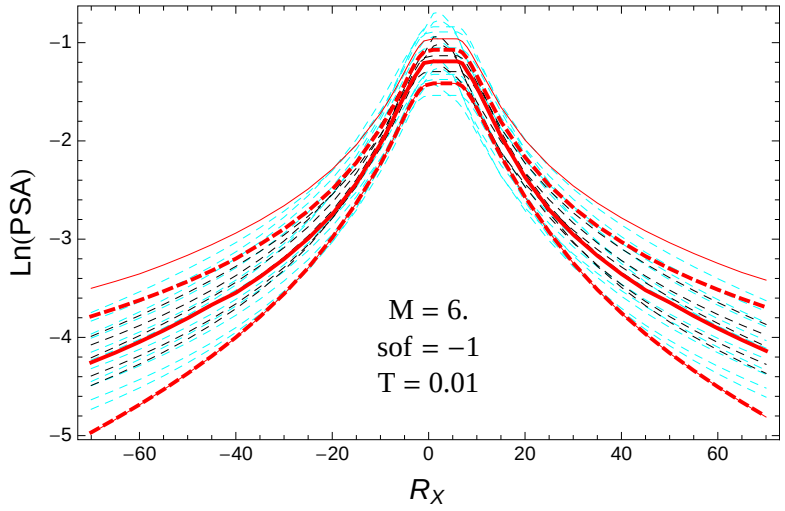



Figure 4.300: PVNGSv2: Distance scaling of the original GMPEs (dashed black), the original GMPEs with uncertainty model (dashed cyan) and 0.05,0.5,0.95 quantile of the ModelB distribution (red) with total weights, for a scenario with $M = 6.$, $F = -1$, and $T = 0.01$s.

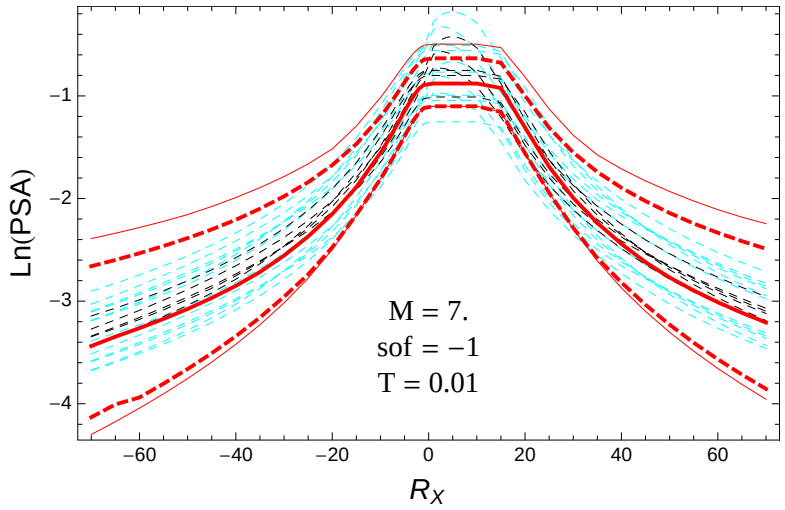



Figure 4.301: PVNGSv2: Distance scaling of the original GMPEs (dashed black), the original GMPEs with uncertainty model (dashed cyan) and 0.05,0.5,0.95 quantile of the ModelB distribution (red) with total weights, for a scenario with $M = 7.$, $F = -1$, and $T = 0.01$s.

**T = 0.2s**

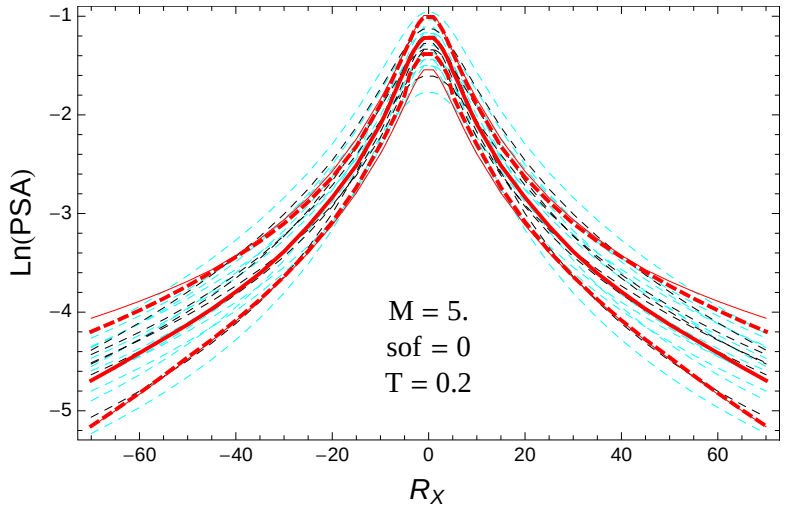



Figure 4.302: PVNGSv2: Distance scaling of the original GMPEs (dashed black), the original GMPEs with uncertainty model (dashed cyan) and 0.05,0.5,0.95 quantile of the ModelB distribution (red) with total weights, for a scenario with $M = 5.$, $F = 0$, and $T = 0.2$s.

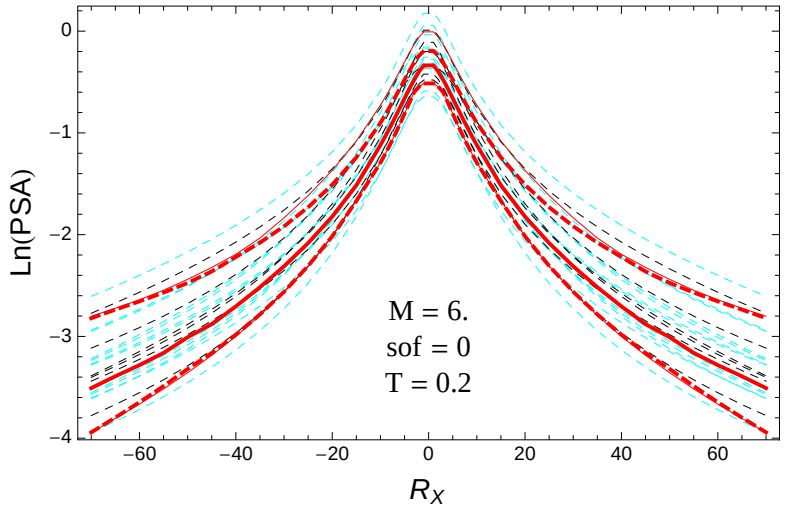



Figure 4.303: PVNGSv2: Distance scaling of the original GMPEs (dashed black), the original GMPEs with uncertainty model (dashed cyan) and 0.05,0.5,0.95 quantile of the ModelB distribution (red) with total weights, for a scenario with $M = 6.$, $F = 0$, and $T = 0.2$s.

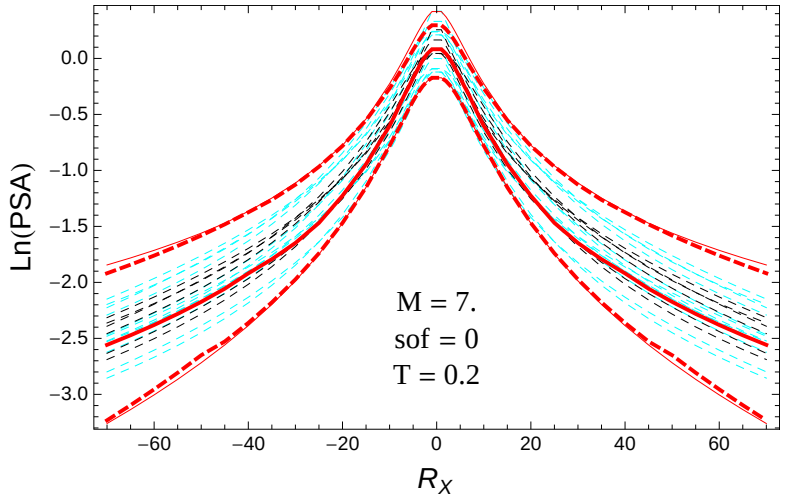



Figure 4.304: PVNGSv2: Distance scaling of the original GMPEs (dashed black), the original GMPEs with uncertainty model (dashed cyan) and 0.05,0.5,0.95 quantile of the ModelB distribution (red) with total weights, for a scenario with $M = 7.$, $F = 0$, and $T = 0.2$s.

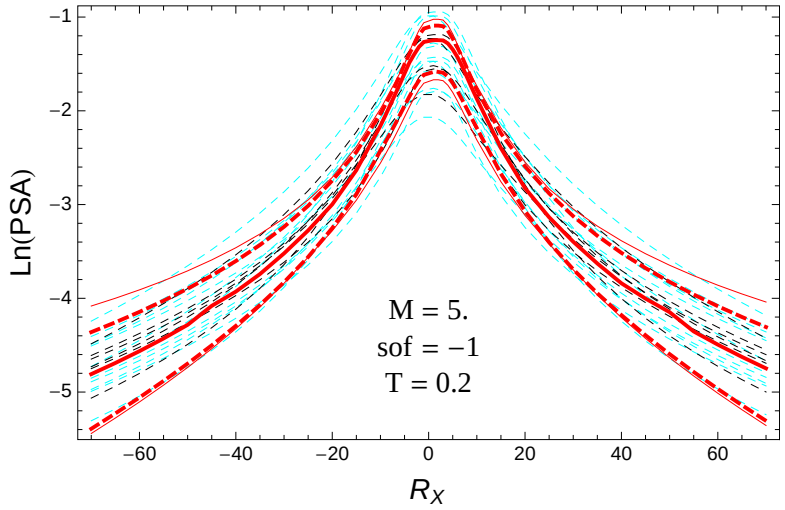



Figure 4.305: PVNGSv2: Distance scaling of the original GMPEs (dashed black), the original GMPEs with uncertainty model (dashed cyan) and 0.05,0.5,0.95 quantile of the ModelB distribution (red) with total weights, for a scenario with $M = 5.$, $F = -1$, and $T = 0.2$s.

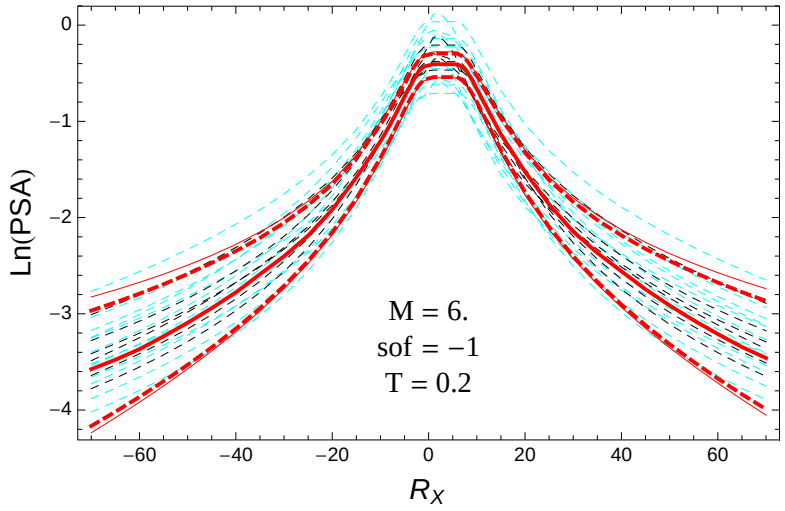



Figure 4.306: PVNGSv2: Distance scaling of the original GMPEs (dashed black), the original GMPEs with uncertainty model (dashed cyan) and 0.05,0.5,0.95 quantile of the ModelB distribution (red) with total weights, for a scenario with $M = 6.$, $F = -1$, and $T = 0.2$s.

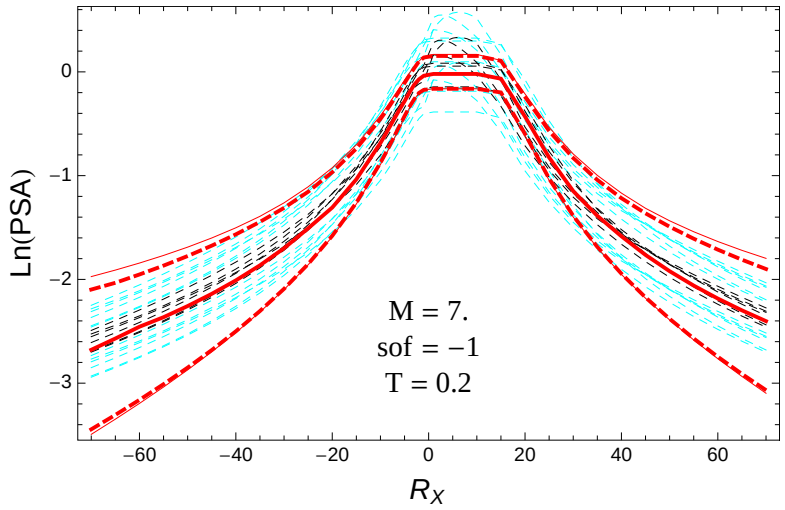



Figure 4.307: PVNGSv2: Distance scaling of the original GMPEs (dashed black), the original GMPEs with uncertainty model (dashed cyan) and 0.05,0.5,0.95 quantile of the ModelB distribution (red) with total weights, for a scenario with $M = 7.$, $F = -1$, and $T = 0.2$s.

**T = 0.5s**

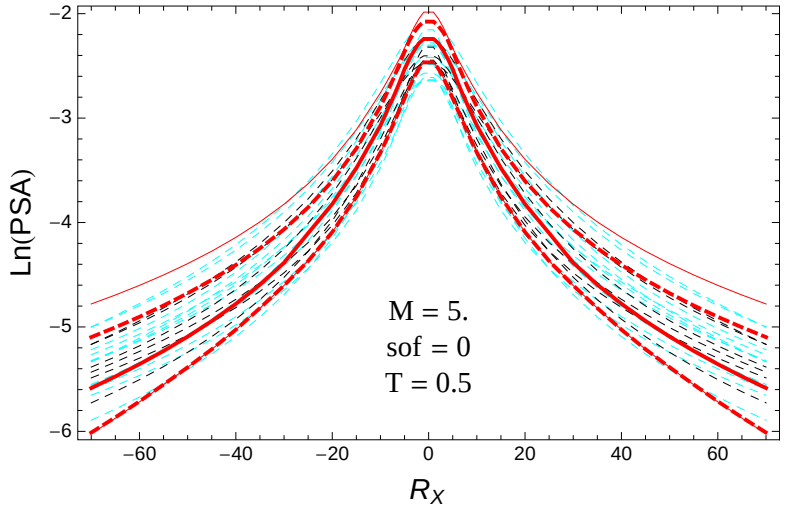



Figure 4.308: PVNGSv2: Distance scaling of the original GMPEs (dashed black), the original GMPEs with uncertainty model (dashed cyan) and 0.05,0.5,0.95 quantile of the ModelB distribution (red) with total weights, for a scenario with $M = 5.$, $F = 0$, and $T = 0.5$s.

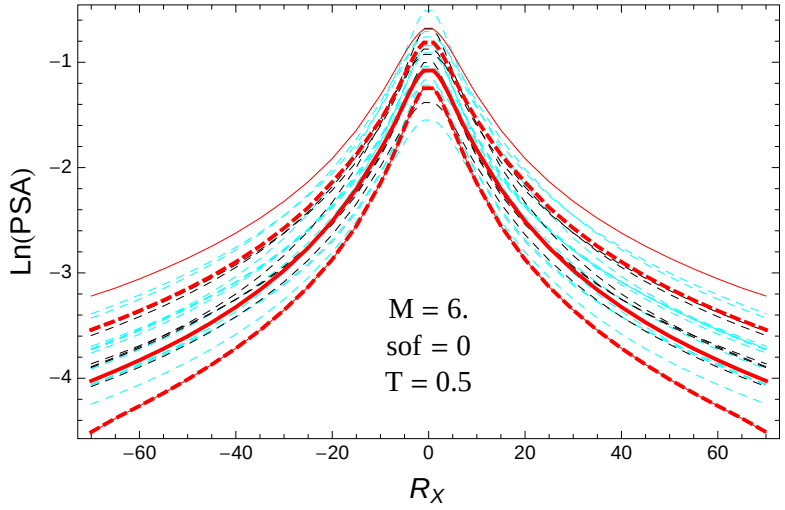



Figure 4.309: PVNGSv2: Distance scaling of the original GMPEs (dashed black), the original GMPEs with uncertainty model (dashed cyan) and 0.05,0.5,0.95 quantile of the ModelB distribution (red) with total weights, for a scenario with $M = 6.$, $F = 0$, and $T = 0.5$s.

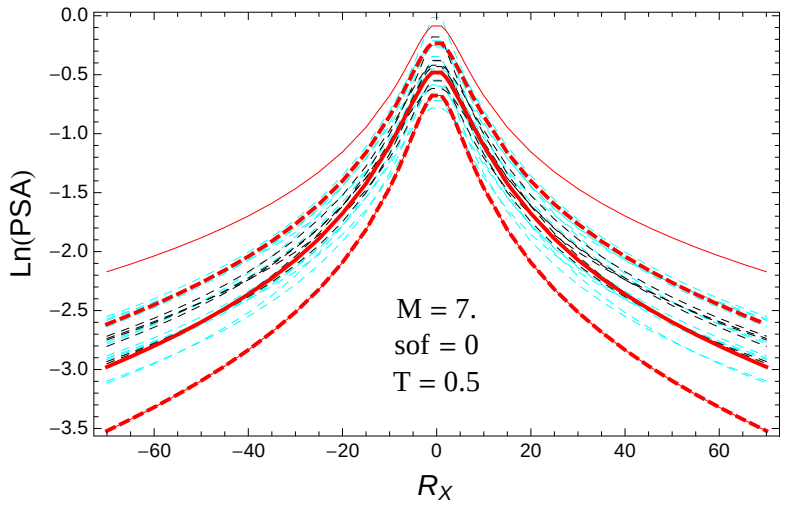



Figure 4.310: PVNGSv2: Distance scaling of the original GMPEs (dashed black), the original GMPEs with uncertainty model (dashed cyan) and 0.05,0.5,0.95 quantile of the ModelB distribution (red) with total weights, for a scenario with $M = 7.$, $F = 0$, and $T = 0.5$s.

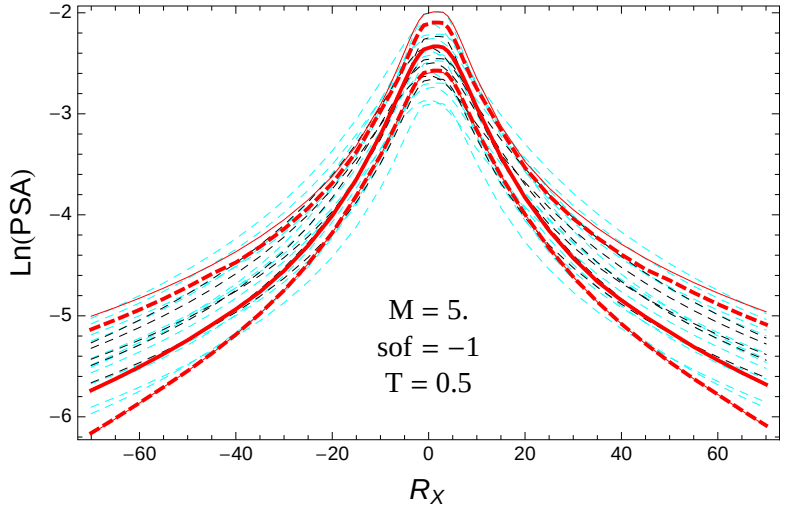



Figure 4.311: PVNGSv2: Distance scaling of the original GMPEs (dashed black), the original GMPEs with uncertainty model (dashed cyan) and 0.05,0.5,0.95 quantile of the ModelB distribution (red) with total weights, for a scenario with $M = 5.$, $F = -1$, and $T = 0.5$s.

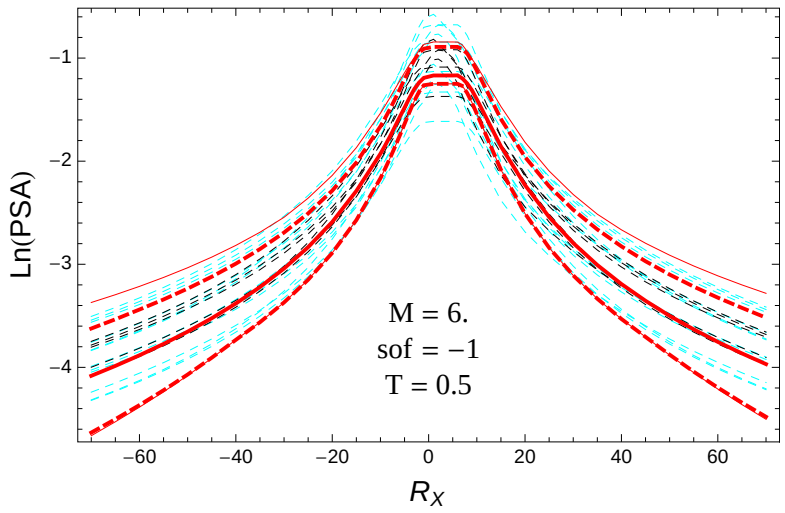



Figure 4.312: PVNGSv2: Distance scaling of the original GMPEs (dashed black), the original GMPEs with uncertainty model (dashed cyan) and 0.05,0.5,0.95 quantile of the ModelB distribution (red) with total weights, for a scenario with $M = 6.$, $F = -1$, and $T = 0.5$s.

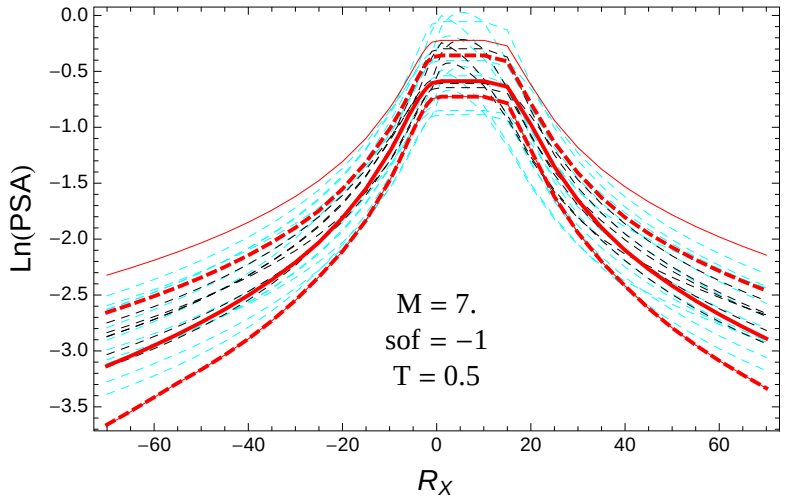



Figure 4.313: PVNGSv2: Distance scaling of the original GMPEs (dashed black), the original GMPEs with uncertainty model (dashed cyan) and 0.05,0.5,0.95 quantile of the ModelB distribution (red) with total weights, for a scenario with $M = 7.$, $F = -1$, and $T = 0.5$s.

**T = 1.s**

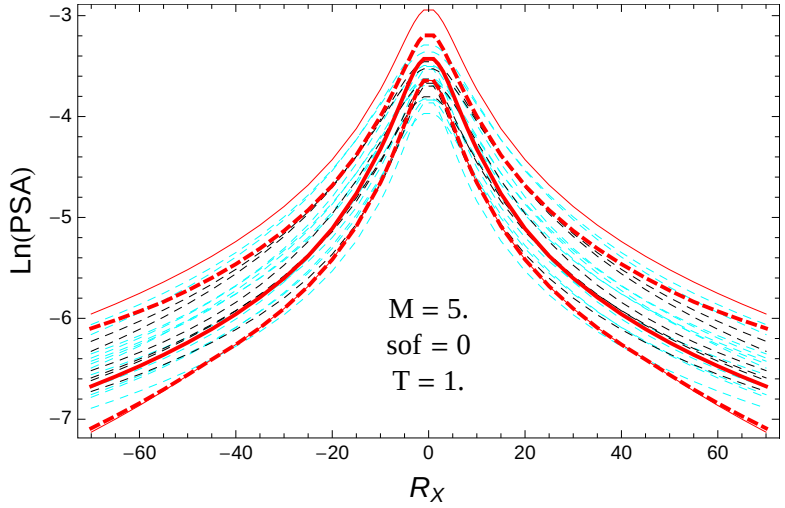



Figure 4.314: PVNGSv2: Distance scaling of the original GMPEs (dashed black), the original GMPEs with uncertainty model (dashed cyan) and 0.05,0.5,0.95 quantile of the ModelB distribution (red) with total weights, for a scenario with $M = 5.$, $F = 0$, and $T = 1.$s.

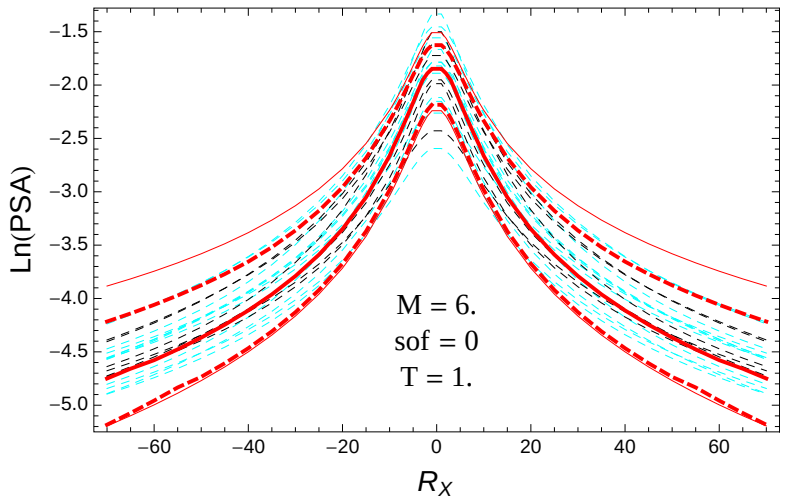



Figure 4.315: PVNGSv2: Distance scaling of the original GMPEs (dashed black), the original GMPEs with uncertainty model (dashed cyan) and 0.05,0.5,0.95 quantile of the ModelB distribution (red) with total weights, for a scenario with $M = 6.$, $F = 0$, and $T = 1.$s.

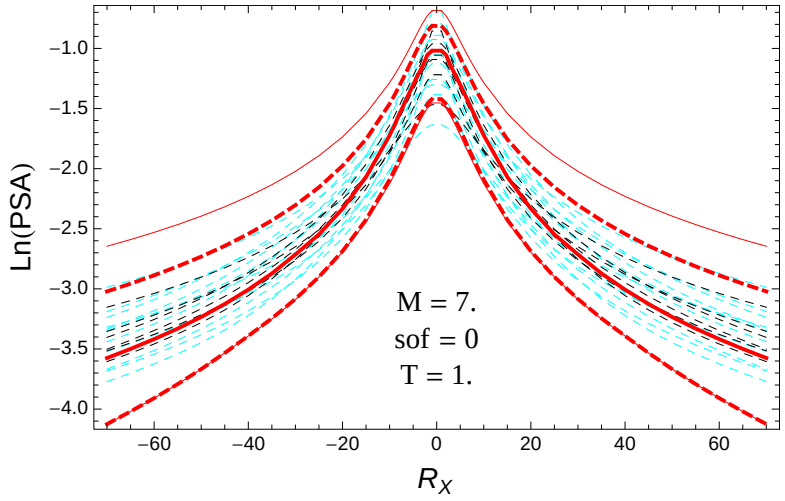



Figure 4.316: PVNGSv2: Distance scaling of the original GMPEs (dashed black), the original GMPEs with uncertainty model (dashed cyan) and 0.05,0.5,0.95 quantile of the ModelB distribution (red) with total weights, for a scenario with $M = 7.$, $F = 0$, and $T = 1.$s.

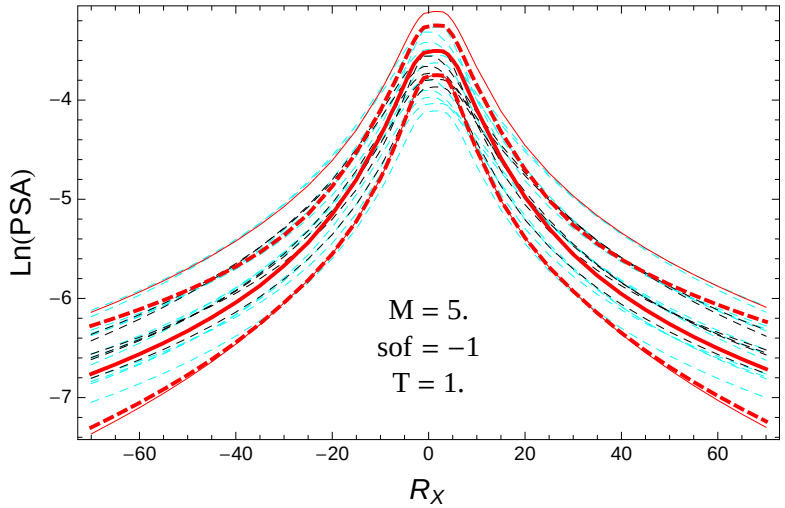



Figure 4.317: PVNGSv2: Distance scaling of the original GMPEs (dashed black), the original GMPEs with uncertainty model (dashed cyan) and 0.05,0.5,0.95 quantile of the ModelB distribution (red) with total weights, for a scenario with $M = 5.$, $F = -1$, and $T = 1.$s.

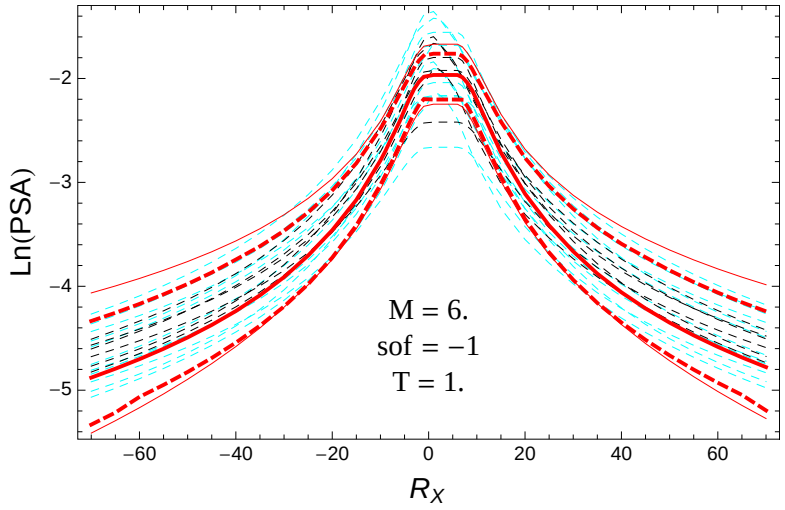



Figure 4.318: PVNGSv2: Distance scaling of the original GMPEs (dashed black), the original GMPEs with uncertainty model (dashed cyan) and 0.05,0.5,0.95 quantile of the ModelB distribution (red) with total weights, for a scenario with $M = 6.$, $F = -1$, and $T = 1.$s.

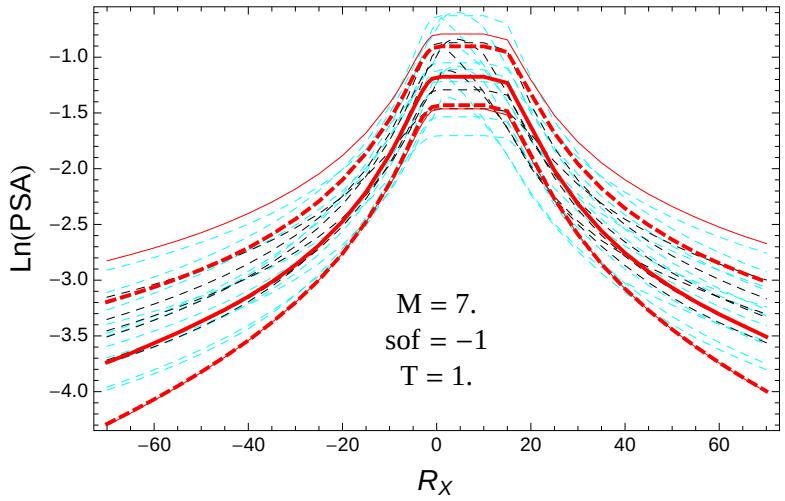



Figure 4.319: PVNGSv2: Distance scaling of the original GMPEs (dashed black), the original GMPEs with uncertainty model (dashed cyan) and 0.05,0.5,0.95 quantile of the ModelB distribution (red) with total weights, for a scenario with $M = 7.$, $F = -1$, and $T = 1.$s.

**T = 3.s**

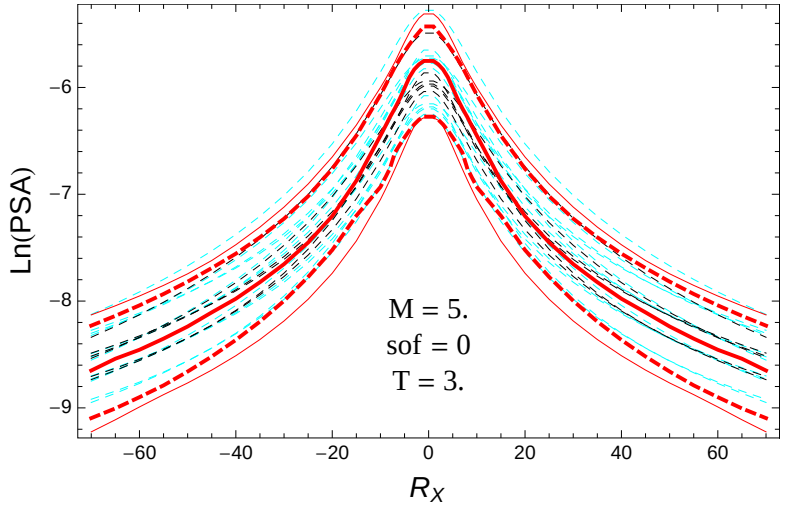



Figure 4.320: PVNGSv2: Distance scaling of the original GMPEs (dashed black), the original GMPEs with uncertainty model (dashed cyan) and 0.05,0.5,0.95 quantile of the ModelB distribution (red) with total weights, for a scenario with $M = 5.$, $F = 0$, and $T = 3.$s.

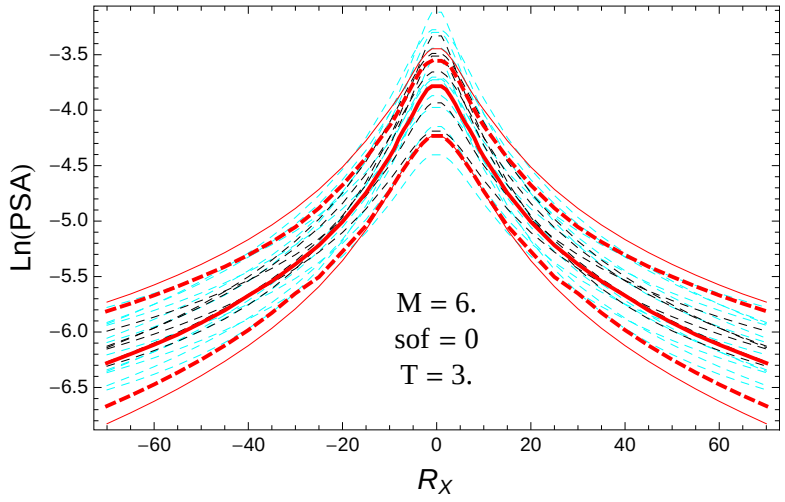



Figure 4.321: PVNGSv2: Distance scaling of the original GMPEs (dashed black), the original GMPEs with uncertainty model (dashed cyan) and 0.05,0.5,0.95 quantile of the ModelB distribution (red) with total weights, for a scenario with $M = 6.$, $F = 0$, and $T = 3.$s.

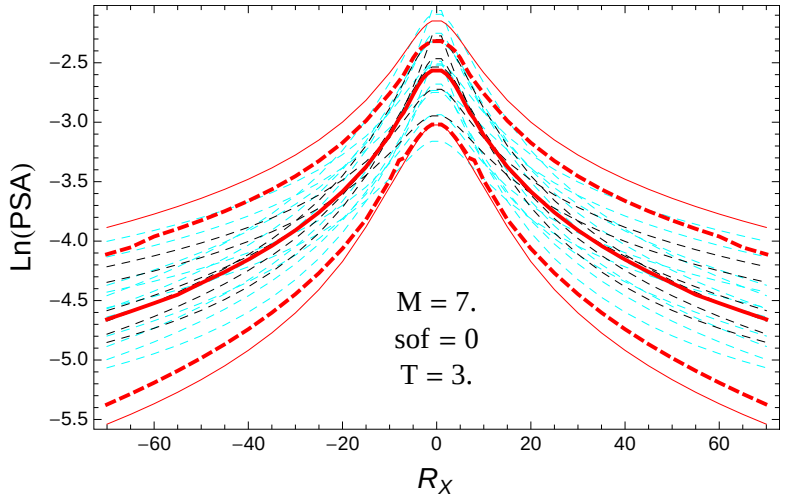



Figure 4.322: PVNGSv2: Distance scaling of the original GMPEs (dashed black), the original GMPEs with uncertainty model (dashed cyan) and 0.05,0.5,0.95 quantile of the ModelB distribution (red) with total weights, for a scenario with $M = 7.$, $F = 0$, and $T = 3.$s.

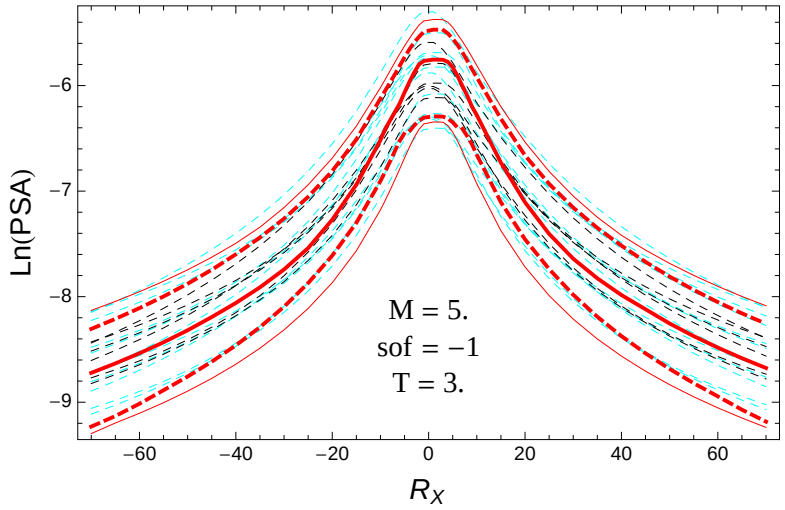



Figure 4.323: PVNGSv2: Distance scaling of the original GMPEs (dashed black), the original GMPEs with uncertainty model (dashed cyan) and 0.05,0.5,0.95 quantile of the ModelB distribution (red) with total weights, for a scenario with $M = 5.$, $F = -1$, and $T = 3.$s.

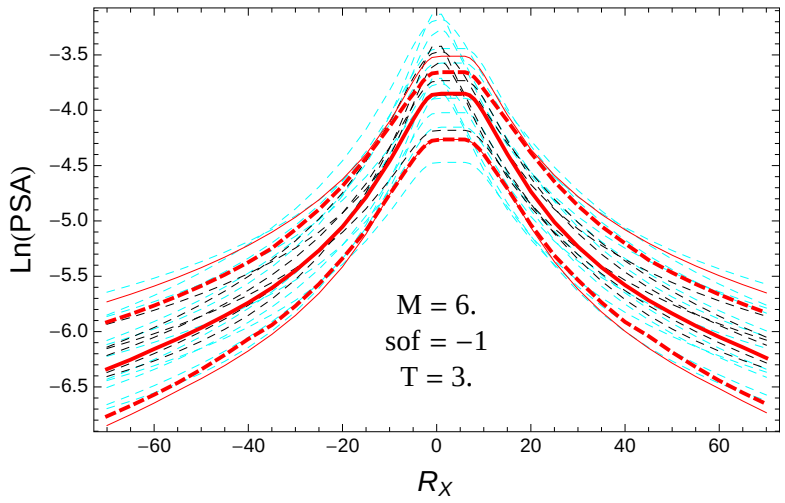



Figure 4.324: PVNGSv2: Distance scaling of the original GMPEs (dashed black), the original GMPEs with uncertainty model (dashed cyan) and 0.05,0.5,0.95 quantile of the ModelB distribution (red) with total weights, for a scenario with $M = 6.$, $F = -1$, and $T = 3.$s.

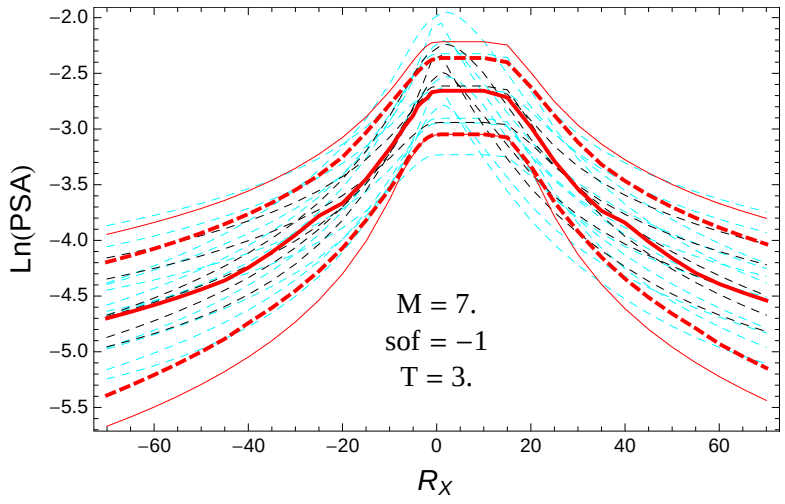



Figure 4.325: PVNGSv2: Distance scaling of the original GMPEs (dashed black), the original GMPEs with uncertainty model (dashed cyan) and 0.05,0.5,0.95 quantile of the ModelB distribution (red) with total weights, for a scenario with $M = 7.$, $F = -1$, and $T = 3.$s.

### 4.1.8 Quantile Plots vs. Magnitude

**T = 0.01s**

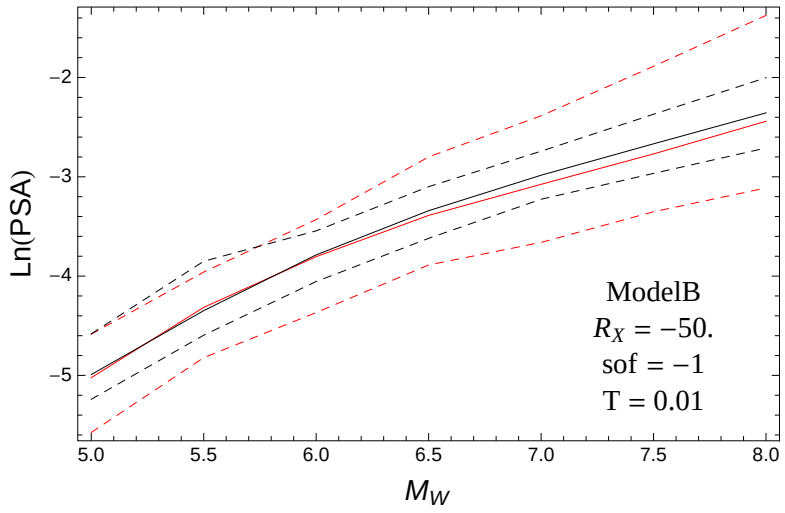



Figure 4.326: PVNGS2: Magnitude scaling of 0.05,0.5,0.95 quantile of the GMPE distribution (black) and the ModelB distribution (red) with total weights, for a scenario with $R_x = -50.$, $F = -1$, and $T = 0.01$.

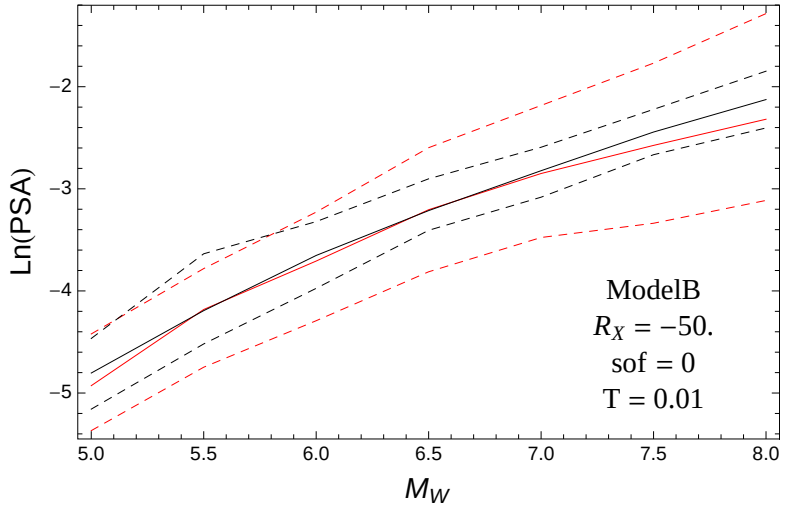



Figure 4.327: PVNGS2: Magnitude scaling of 0.05,0.5,0.95 quantile of the GMPE distribution (black) and the ModelB distribution (red) with total weights, for a scenario with $R_x = -50.$, $F = 0$, and $T = 0.01$.

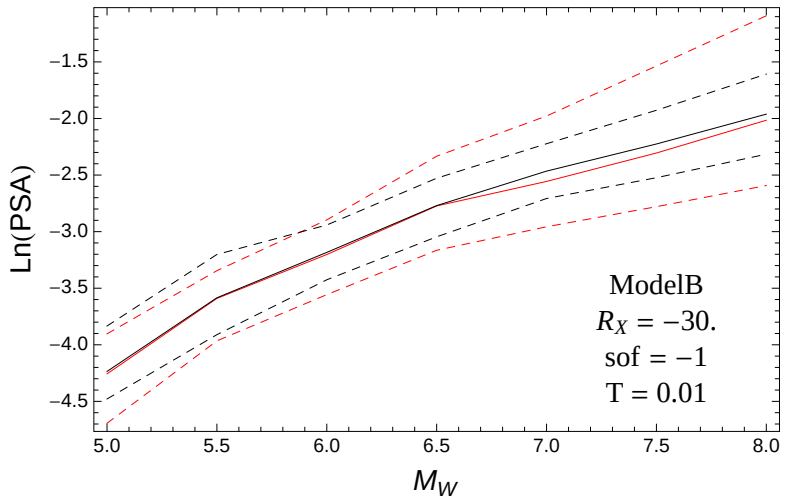



Figure 4.328: PVNGS2: Magnitude scaling of 0.05,0.5,0.95 quantile of the GMPE distribution (black) and the ModelB distribution (red) with total weights, for a scenario with $R_x = -30.$, $F = -1$, and $T = 0.01$.

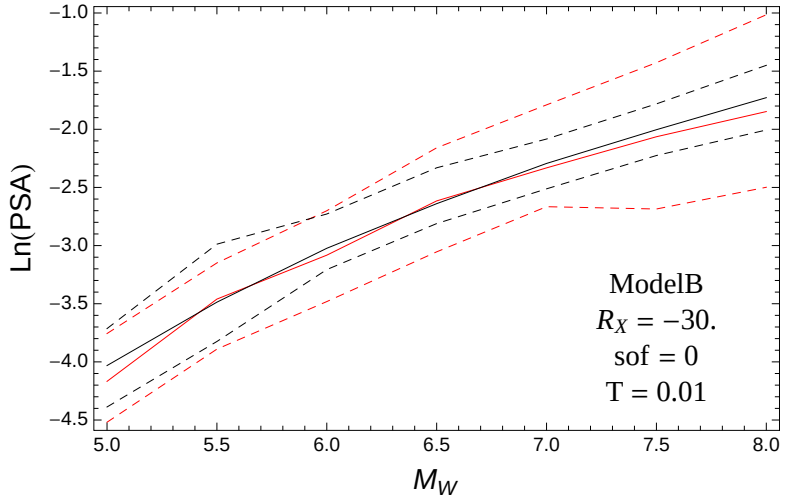



Figure 4.329: PVNGS2: Magnitude scaling of 0.05,0.5,0.95 quantile of the GMPE distribution (black) and the ModelB distribution (red) with total weights, for a scenario with $R_x = -30.$, $F = 0$, and $T = 0.01$.

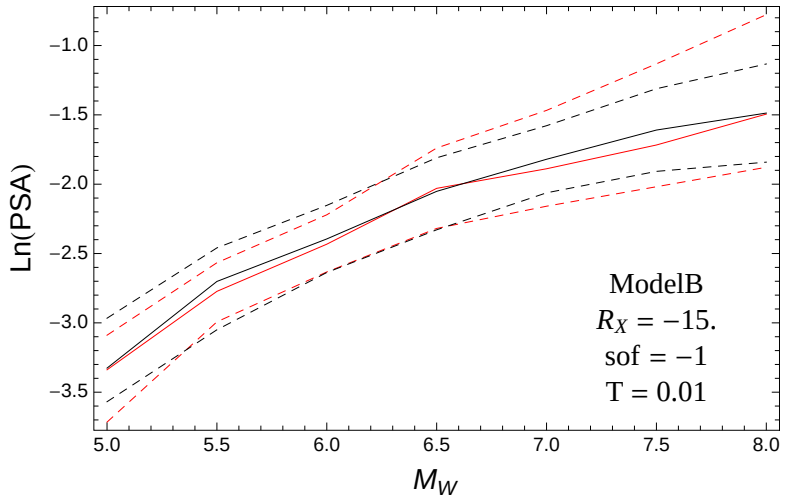



Figure 4.330: PVNGS2: Magnitude scaling of 0.05,0.5,0.95 quantile of the GMPE distribution (black) and the ModelB distribution (red) with total weights, for a scenario with $R_x = -15.$, $F = -1$, and $T = 0.01$.

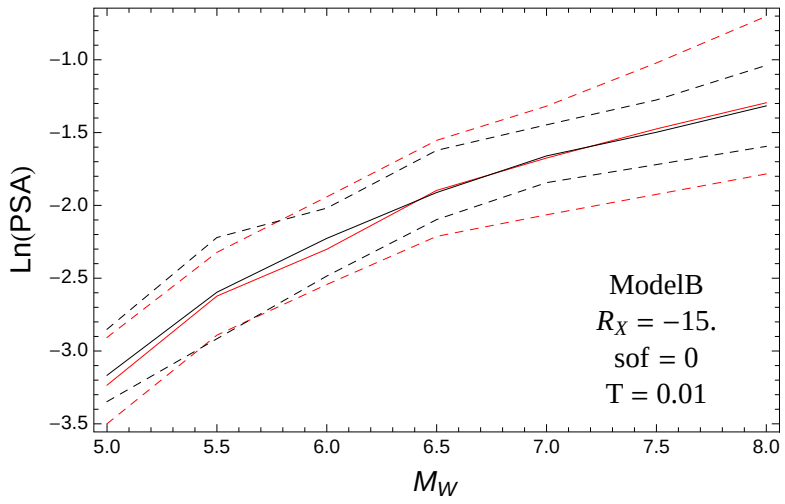



Figure 4.331: PVNGS2: Magnitude scaling of 0.05,0.5,0.95 quantile of the GMPE distribution (black) and the ModelB distribution (red) with total weights, for a scenario with $R_x = -15.$, $F = 0$, and $T = 0.01$.

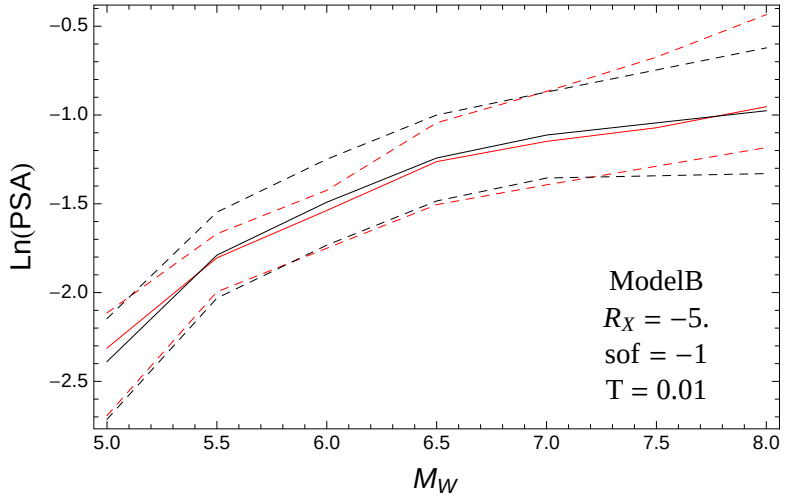



Figure 4.332: PVNGS2: Magnitude scaling of 0.05,0.5,0.95 quantile of the GMPE distribution (black) and the ModelB distribution (red) with total weights, for a scenario with $R_x = -5.$, $F = -1$, and $T = 0.01$.

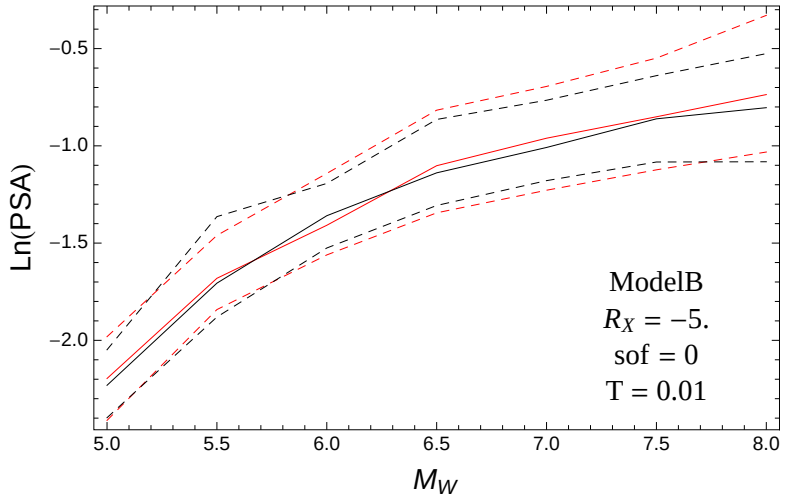



Figure 4.333: PVNGS2: Magnitude scaling of 0.05,0.5,0.95 quantile of the GMPE distribution (black) and the ModelB distribution (red) with total weights, for a scenario with $R_x = -5.$, $F = 0$, and $T = 0.01$.

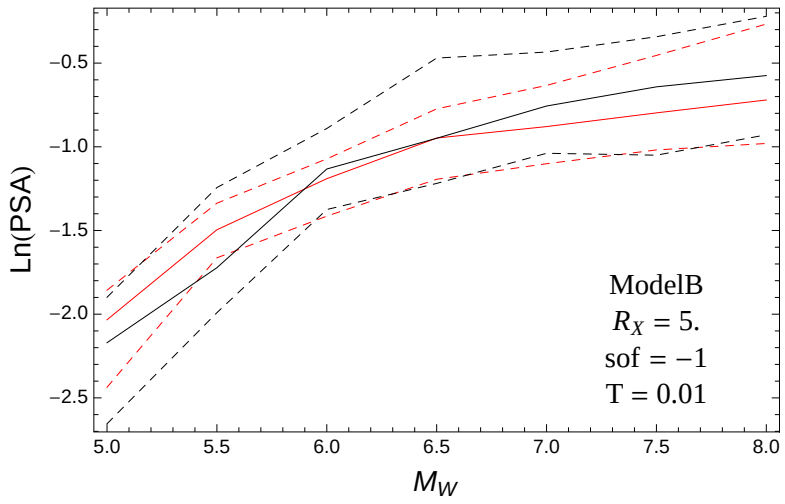



Figure 4.334: PVNGS2: Magnitude scaling of 0.05,0.5,0.95 quantile of the GMPE distribution (black) and the ModelB distribution (red) with total weights, for a scenario with $R_x = 5.$, $F = -1$, and $T = 0.01$.

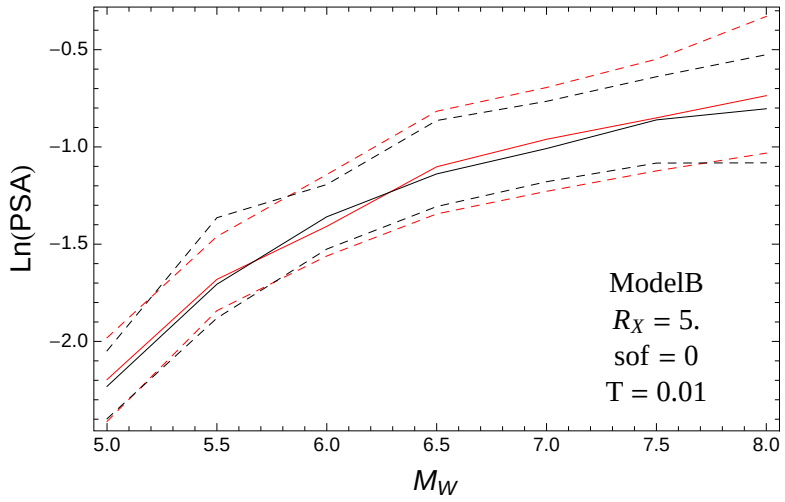



Figure 4.335: PVNGS2: Magnitude scaling of 0.05,0.5,0.95 quantile of the GMPE distribution (black) and the ModelB distribution (red) with total weights, for a scenario with $R_x = 5.$, $F = 0$, and $T = 0.01$.

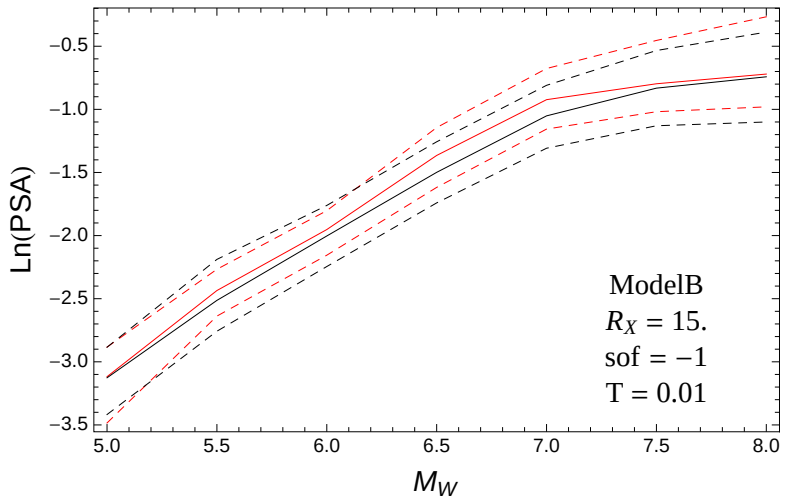



Figure 4.336: PVNGS2: Magnitude scaling of 0.05,0.5,0.95 quantile of the GMPE distribution (black) and the ModelB distribution (red) with total weights, for a scenario with $R_x = 15.$, $F = -1$, and $T = 0.01$.

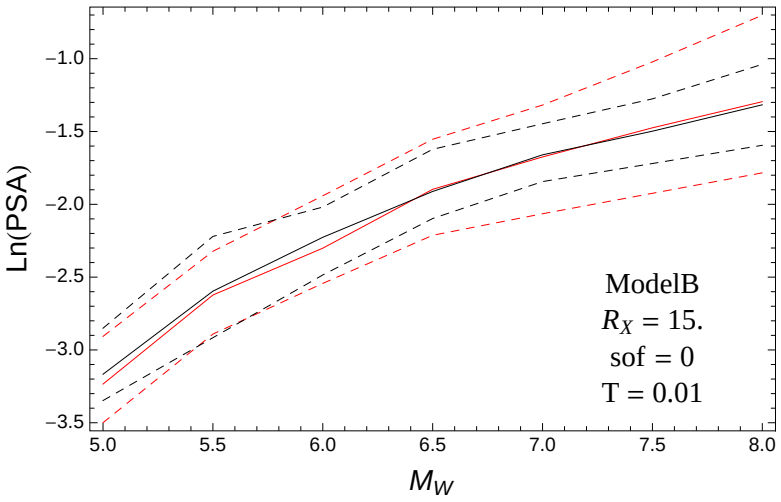



Figure 4.337: PVNGS2: Magnitude scaling of 0.05,0.5,0.95 quantile of the GMPE distribution (black) and the ModelB distribution (red) with total weights, for a scenario with $R_x = 15.$, $F = 0$, and $T = 0.01$.

**T = 0.2s**

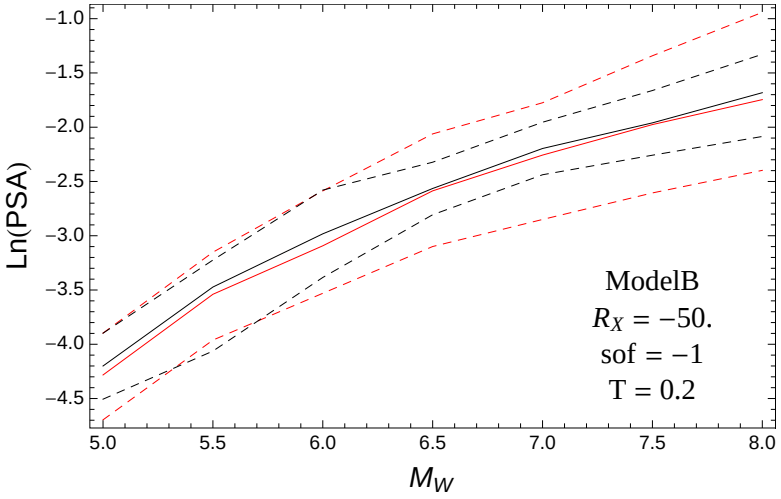



Figure 4.338: PVNGS2: Magnitude scaling of 0.05,0.5,0.95 quantile of the GMPE distribution (black) and the ModelB distribution (red) with total weights, for a scenario with $R_x = -50.$, $F = -1$, and $T = 0.2$.

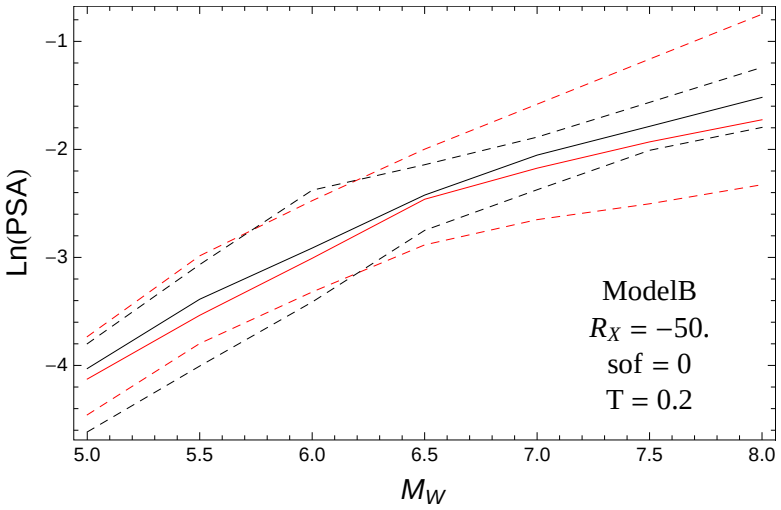



Figure 4.339: PVNGS2: Magnitude scaling of 0.05,0.5,0.95 quantile of the GMPE distribution (black) and the ModelB distribution (red) with total weights, for a scenario with $R_x = -50.$, $F = 0$, and $T = 0.2$.

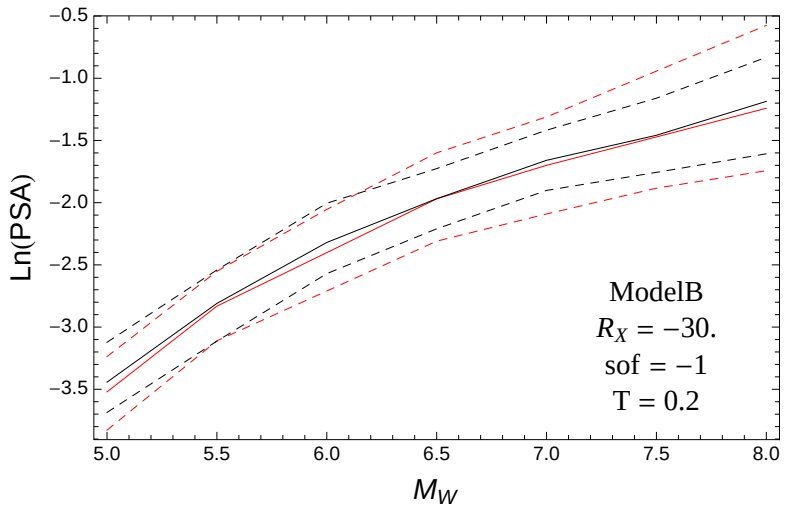



Figure 4.340: PVNGS2: Magnitude scaling of 0.05,0.5,0.95 quantile of the GMPE distribution (black) and the ModelB distribution (red) with total weights, for a scenario with $R_x = -30.$, $F = -1$, and $T = 0.2$.

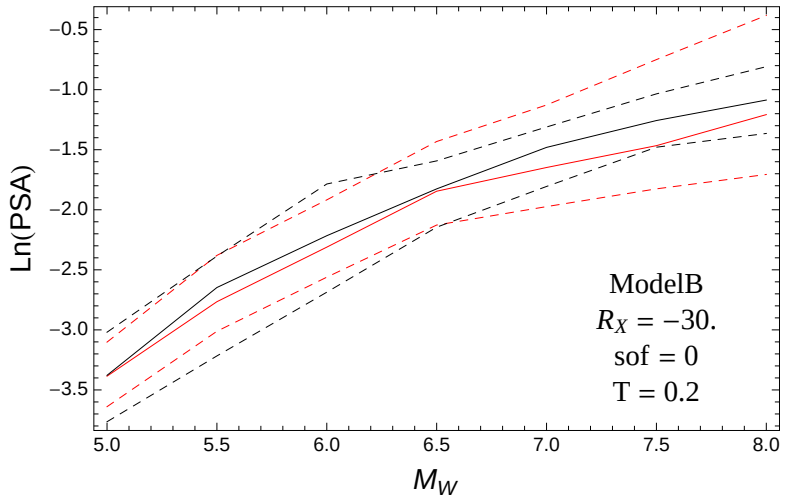



Figure 4.341: PVNGS2: Magnitude scaling of 0.05,0.5,0.95 quantile of the GMPE distribution (black) and the ModelB distribution (red) with total weights, for a scenario with $R_x = -30.$, $F = 0$, and $T = 0.2$.

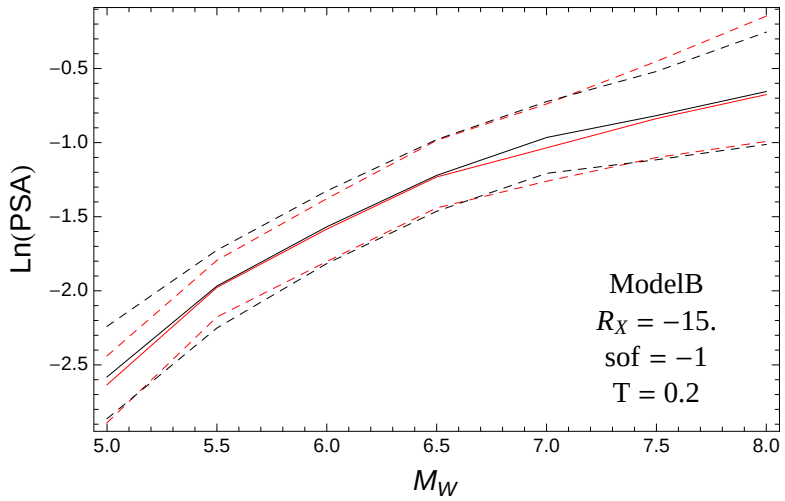



Figure 4.342: PVNGS2: Magnitude scaling of 0.05,0.5,0.95 quantile of the GMPE distribution (black) and the ModelB distribution (red) with total weights, for a scenario with $R_x = -15.$, $F = -1$, and $T = 0.2$.

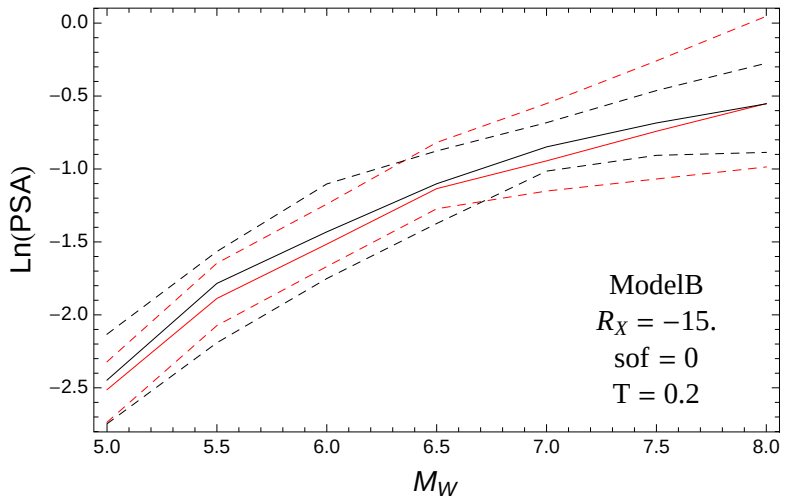



Figure 4.343: PVNGS2: Magnitude scaling of 0.05,0.5,0.95 quantile of the GMPE distribution (black) and the ModelB distribution (red) with total weights, for a scenario with $R_x = -15.$, $F = 0$, and $T = 0.2$.

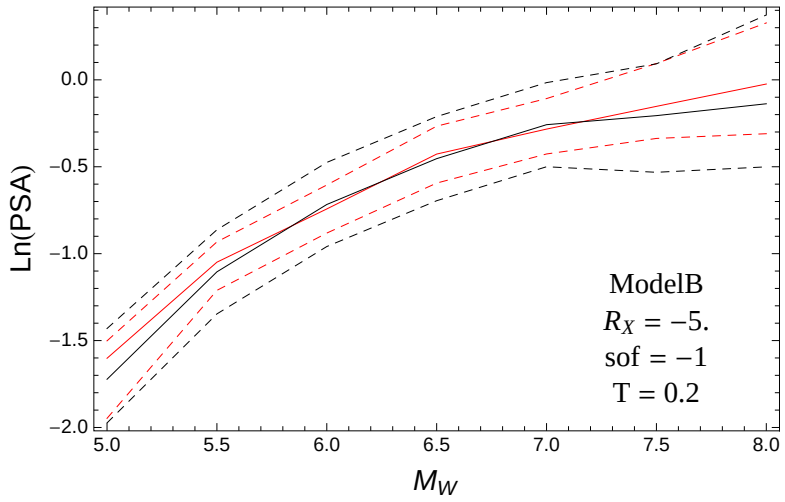



Figure 4.344: PVNGS2: Magnitude scaling of 0.05,0.5,0.95 quantile of the GMPE distribution (black) and the ModelB distribution (red) with total weights, for a scenario with $R_x = -5.$, $F = -1$, and $T = 0.2$.

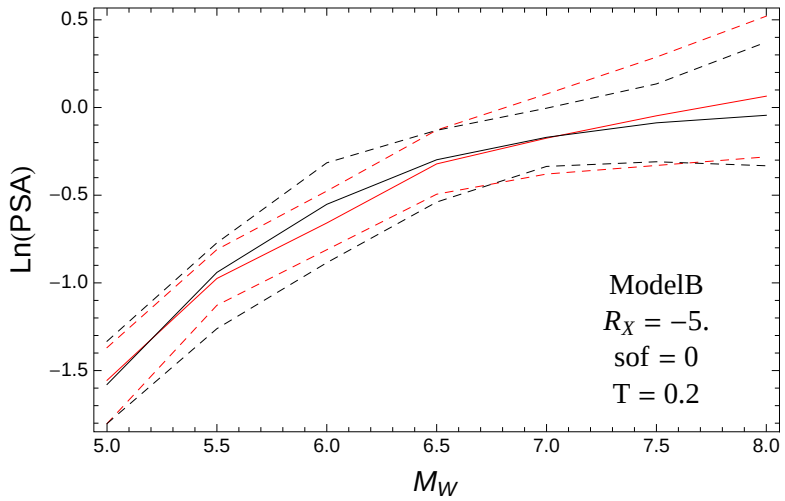



Figure 4.345: PVNGS2: Magnitude scaling of 0.05,0.5,0.95 quantile of the GMPE distribution (black) and the ModelB distribution (red) with total weights, for a scenario with $R_x = -5.$, $F = 0$, and $T = 0.2$.

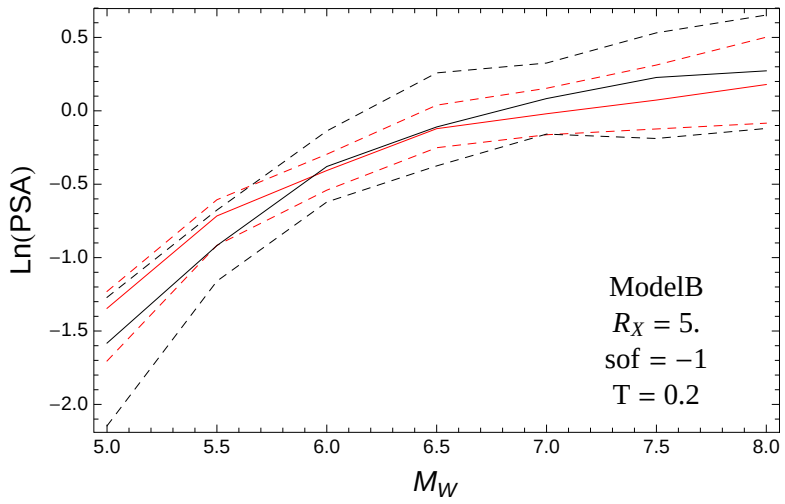



Figure 4.346: PVNGS2: Magnitude scaling of 0.05,0.5,0.95 quantile of the GMPE distribution (black) and the ModelB distribution (red) with total weights, for a scenario with $R_x = 5.$, $F = -1$, and $T = 0.2$.

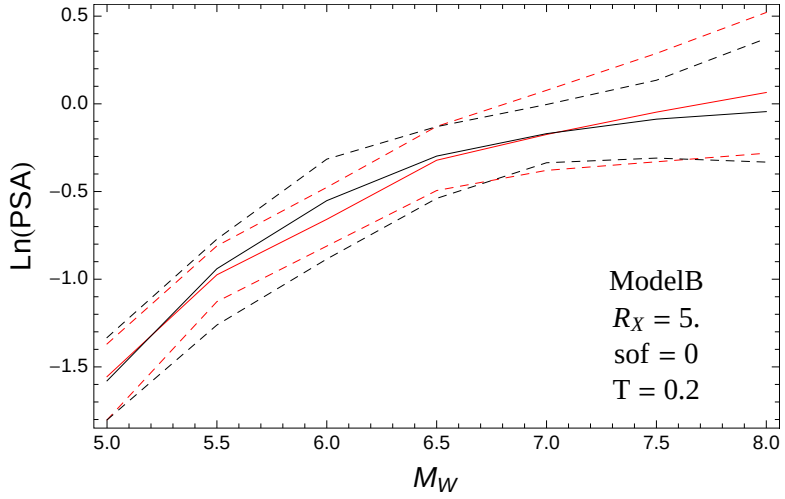



Figure 4.347: PVNGS2: Magnitude scaling of 0.05,0.5,0.95 quantile of the GMPE distribution (black) and the ModelB distribution (red) with total weights, for a scenario with $R_x = 5.$, $F = 0$, and $T = 0.2$.

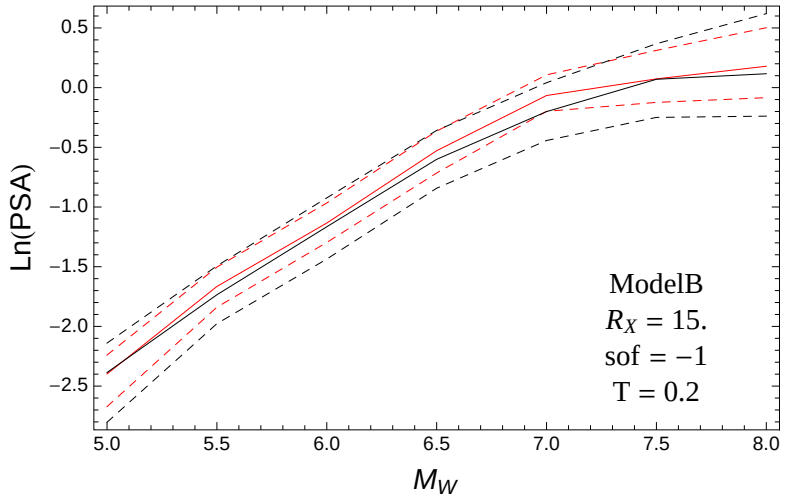



Figure 4.348: PVNGS2: Magnitude scaling of 0.05,0.5,0.95 quantile of the GMPE distribution (black) and the ModelB distribution (red) with total weights, for a scenario with $R_x = 15.$, $F = -1$, and $T = 0.2$.

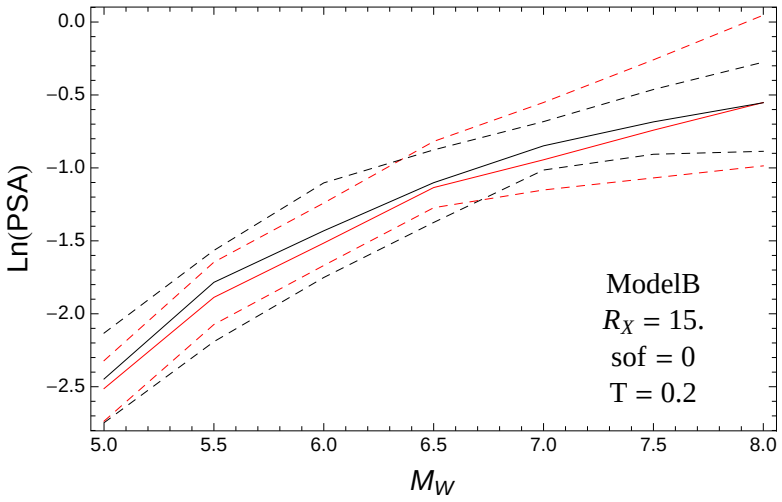



Figure 4.349: PVNGS2: Magnitude scaling of 0.05,0.5,0.95 quantile of the GMPE distribution (black) and the ModelB distribution (red) with total weights, for a scenario with $R_x = 15.$, $F = 0$, and $T = 0.2$.

**T = 0.5s**

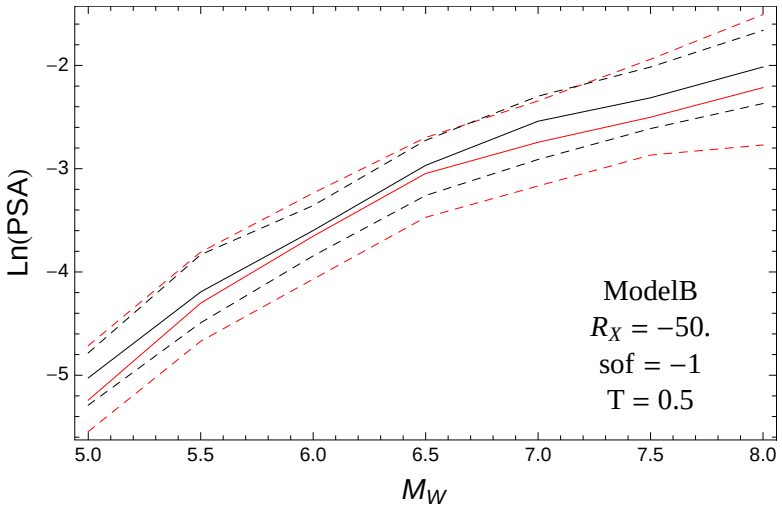



Figure 4.350: PVNGS2: Magnitude scaling of 0.05,0.5,0.95 quantile of the GMPE distribution (black) and the ModelB distribution (red) with total weights, for a scenario with $R_x = -50.$, $F = -1$, and $T = 0.5$.

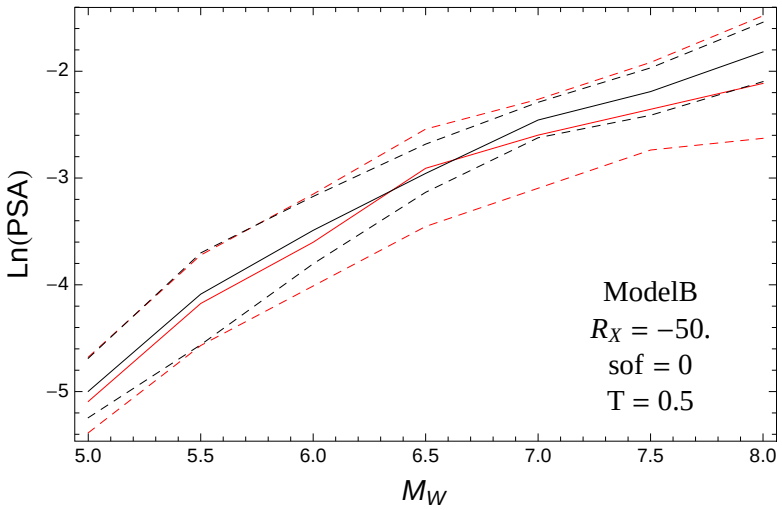



Figure 4.351: PVNGS2: Magnitude scaling of 0.05,0.5,0.95 quantile of the GMPE distribution (black) and the ModelB distribution (red) with total weights, for a scenario with $R_x = -50.$, $F = 0$, and $T = 0.5$.

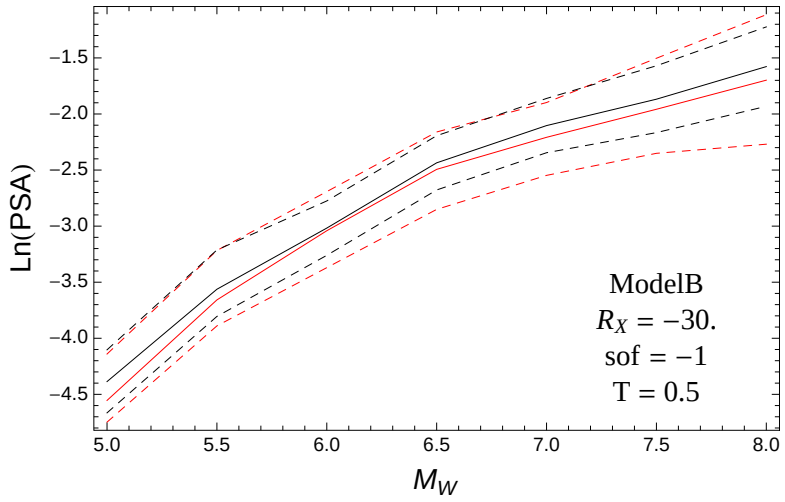



Figure 4.352: PVNGS2: Magnitude scaling of 0.05,0.5,0.95 quantile of the GMPE distribution (black) and the ModelB distribution (red) with total weights, for a scenario with $R_x = -30.$, $F = -1$, and $T = 0.5$.

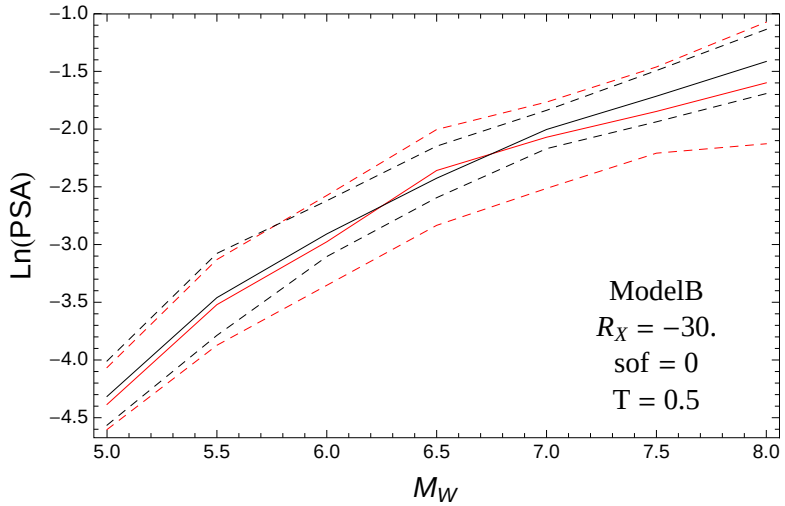



Figure 4.353: PVNGS2: Magnitude scaling of 0.05,0.5,0.95 quantile of the GMPE distribution (black) and the ModelB distribution (red) with total weights, for a scenario with $R_x = -30.$, $F = 0$, and $T = 0.5$.

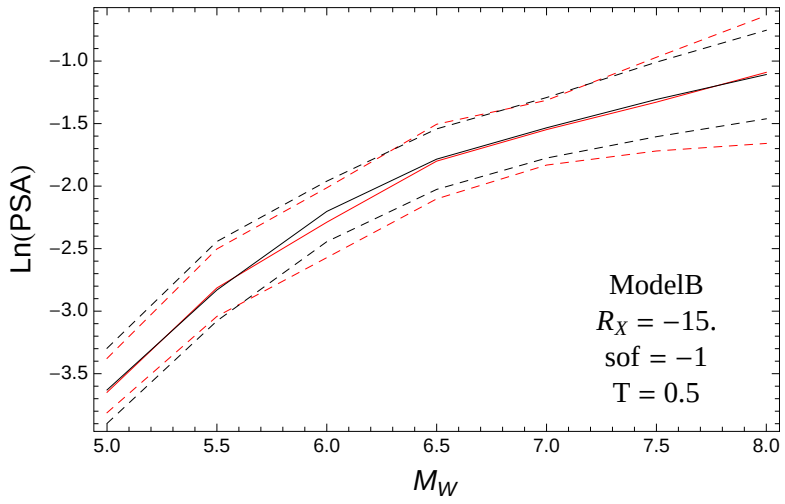



Figure 4.354: PVNGS2: Magnitude scaling of 0.05,0.5,0.95 quantile of the GMPE distribution (black) and the ModelB distribution (red) with total weights, for a scenario with $R_x = -15.$, $F = -1$, and $T = 0.5$.

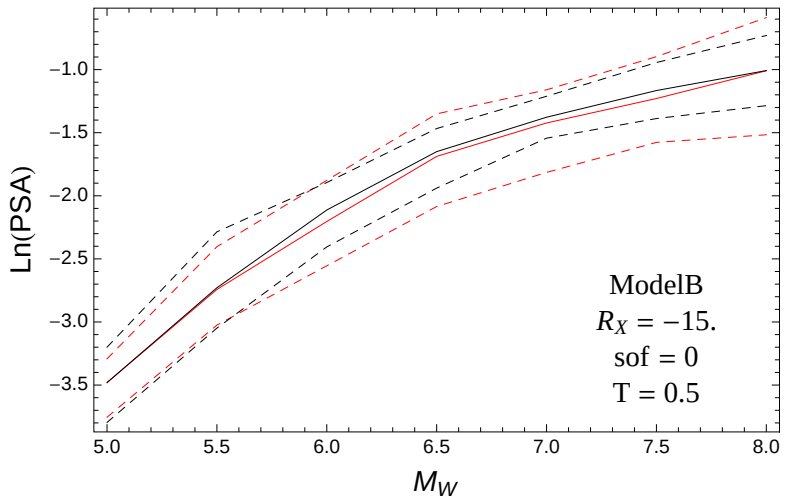



Figure 4.355: PVNGS2: Magnitude scaling of 0.05,0.5,0.95 quantile of the GMPE distribution (black) and the ModelB distribution (red) with total weights, for a scenario with $R_x = -15.$, $F = 0$, and $T = 0.5$.

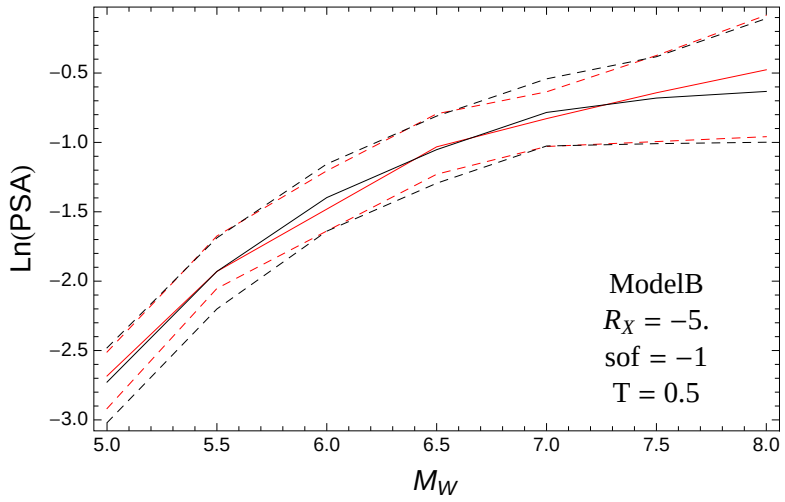



Figure 4.356: PVNGS2: Magnitude scaling of 0.05,0.5,0.95 quantile of the GMPE distribution (black) and the ModelB distribution (red) with total weights, for a scenario with $R_x = -5.$, $F = -1$, and $T = 0.5$.

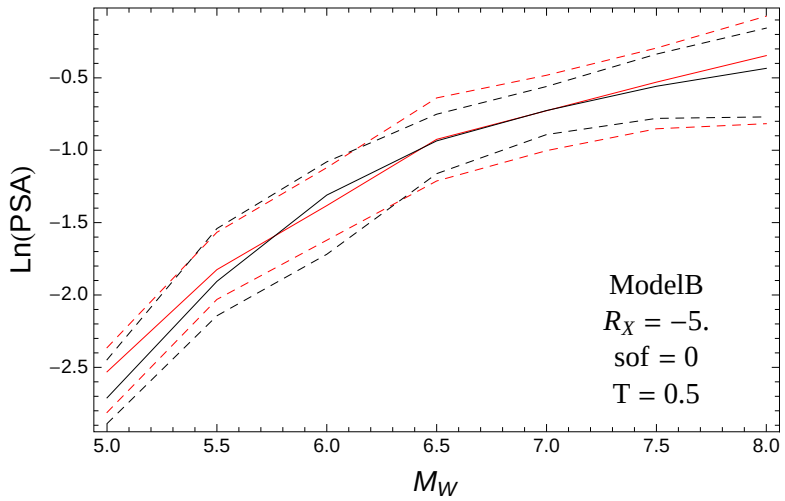



Figure 4.357: PVNGS2: Magnitude scaling of 0.05,0.5,0.95 quantile of the GMPE distribution (black) and the ModelB distribution (red) with total weights, for a scenario with $R_x = -5.$, $F = 0$, and $T = 0.5$.

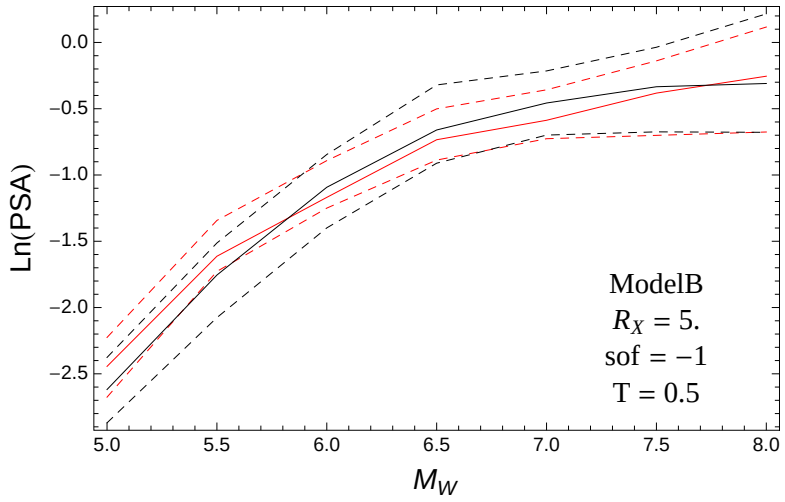



Figure 4.358: PVNGS2: Magnitude scaling of 0.05,0.5,0.95 quantile of the GMPE distribution (black) and the ModelB distribution (red) with total weights, for a scenario with $R_x = 5.$, $F = -1$, and $T = 0.5$.

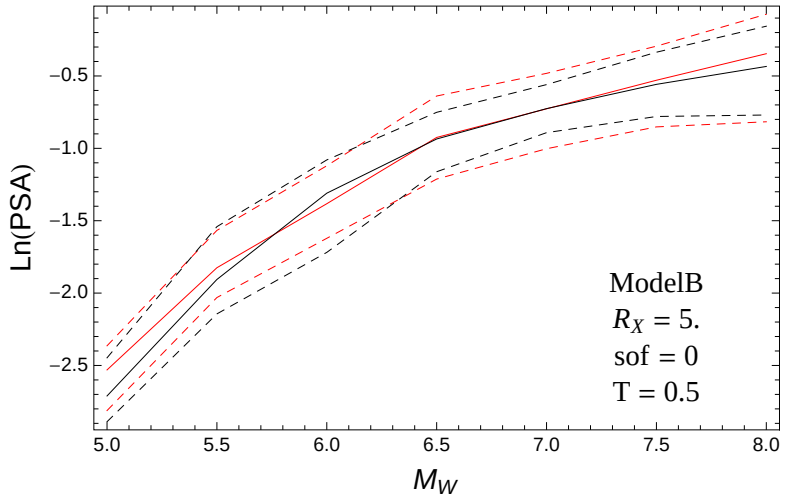



Figure 4.359: PVNGS2: Magnitude scaling of 0.05,0.5,0.95 quantile of the GMPE distribution (black) and the ModelB distribution (red) with total weights, for a scenario with $R_x = 5.$, $F = 0$, and $T = 0.5$.

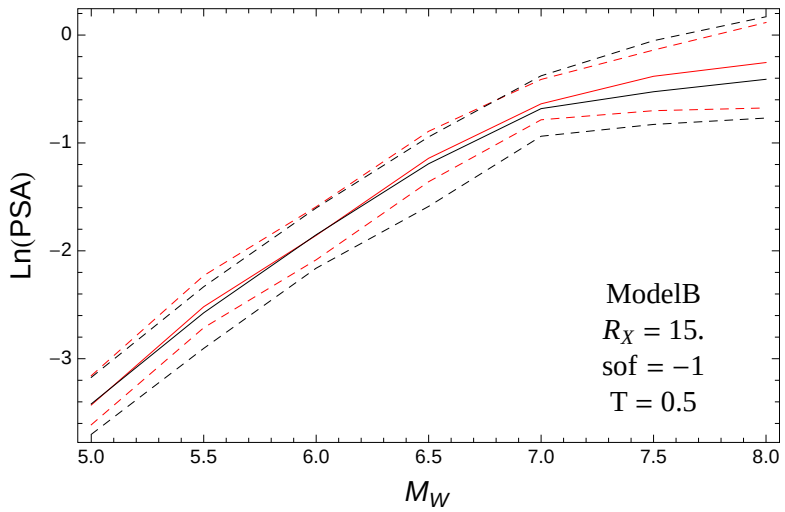



Figure 4.360: PVNGS2: Magnitude scaling of 0.05,0.5,0.95 quantile of the GMPE distribution (black) and the ModelB distribution (red) with total weights, for a scenario with $R_x = 15.$, $F = -1$, and $T = 0.5$.

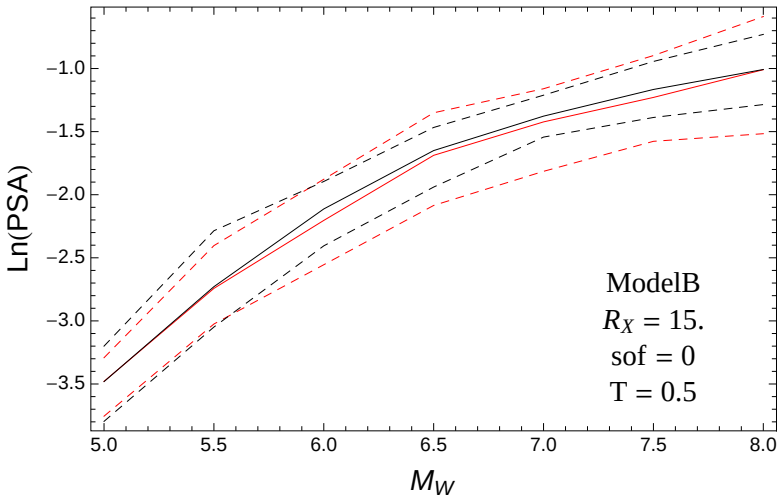



Figure 4.361: PVNGS2: Magnitude scaling of 0.05,0.5,0.95 quantile of the GMPE distribution (black) and the ModelB distribution (red) with total weights, for a scenario with $R_x = 15.$, $F = 0$, and $T = 0.5$.

**T = 1.s**

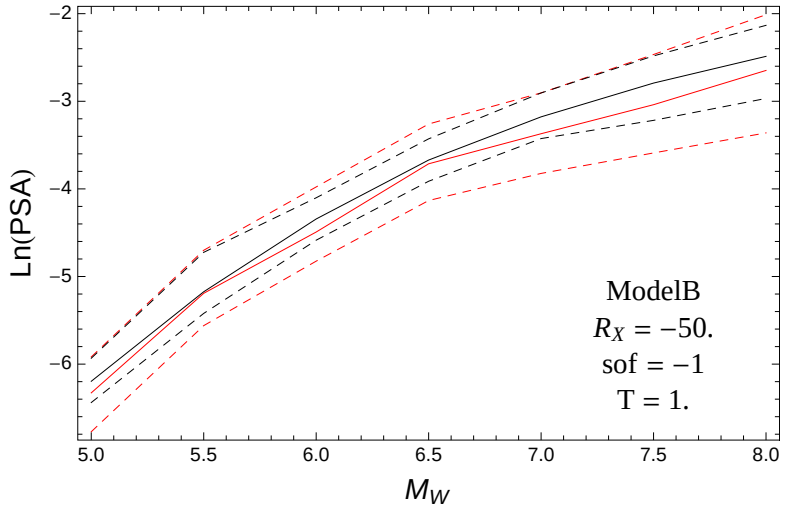



Figure 4.362: PVNGS2: Magnitude scaling of 0.05,0.5,0.95 quantile of the GMPE distribution (black) and the ModelB distribution (red) with total weights, for a scenario with $R_x = -50.$, $F = -1$, and $T = 1.$.

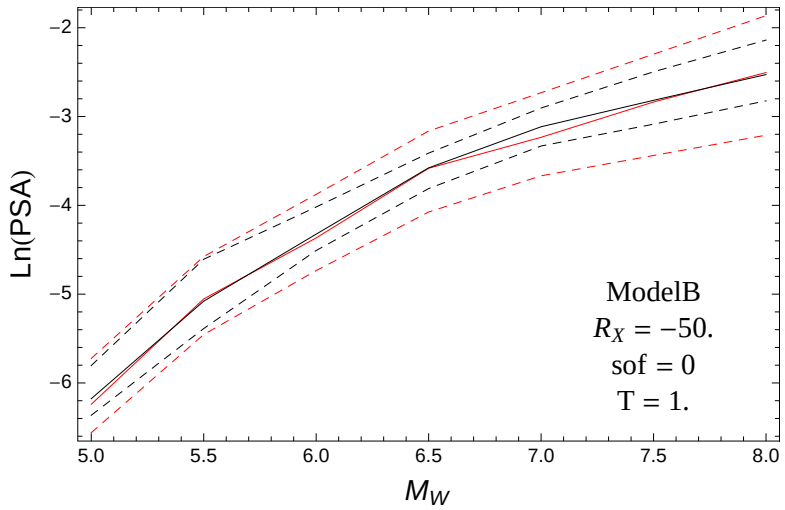



Figure 4.363: PVNGS2: Magnitude scaling of 0.05,0.5,0.95 quantile of the GMPE distribution (black) and the ModelB distribution (red) with total weights, for a scenario with $R_x = -50.$, $F = 0$, and $T = 1.$.

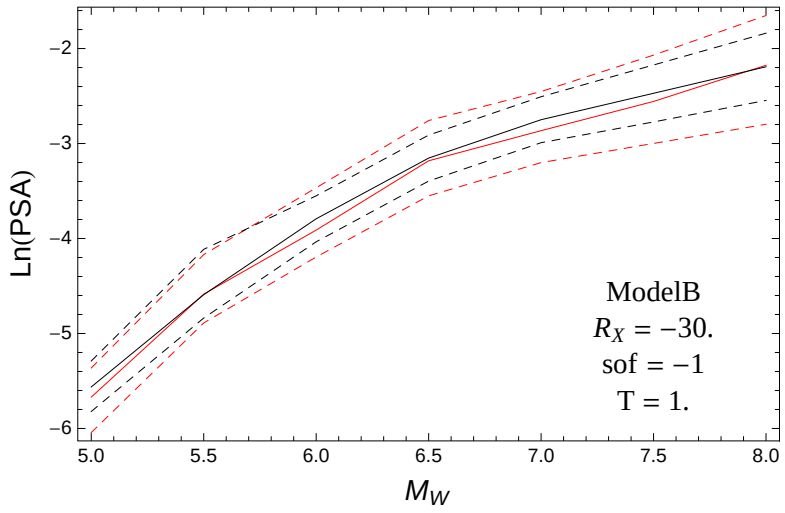



Figure 4.364: PVNGS2: Magnitude scaling of 0.05,0.5,0.95 quantile of the GMPE distribution (black) and the ModelB distribution (red) with total weights, for a scenario with $R_x = -30.$, $F = -1$, and $T = 1.$.

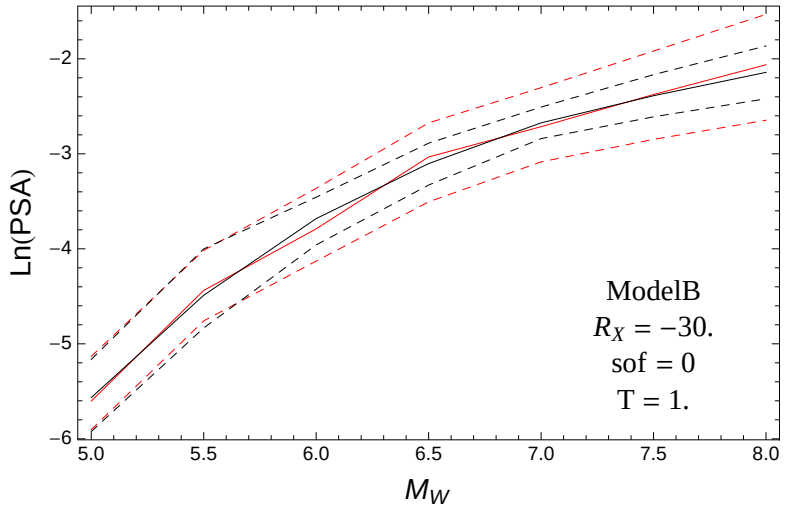



Figure 4.365: PVNGS2: Magnitude scaling of 0.05,0.5,0.95 quantile of the GMPE distribution (black) and the ModelB distribution (red) with total weights, for a scenario with $R_x = -30.$, $F = 0$, and $T = 1.$.

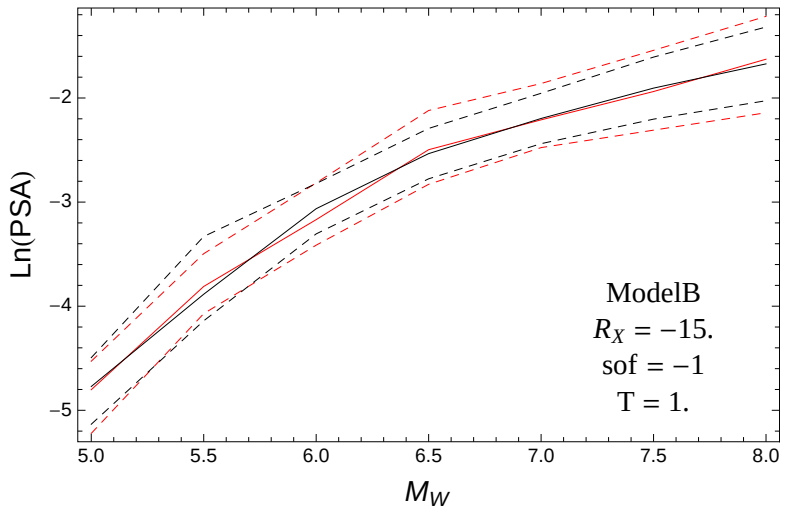



Figure 4.366: PVNGS2: Magnitude scaling of 0.05,0.5,0.95 quantile of the GMPE distribution (black) and the ModelB distribution (red) with total weights, for a scenario with $R_x = -15.$, $F = -1$, and $T = 1.$.

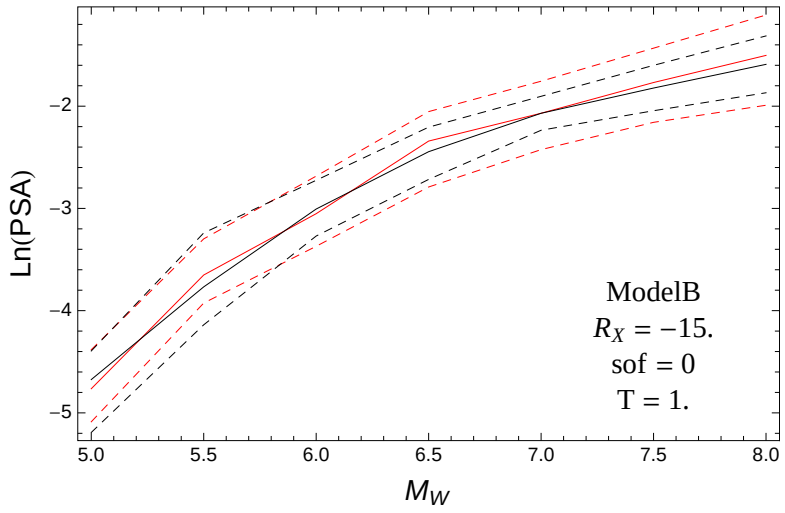



Figure 4.367: PVNGS2: Magnitude scaling of 0.05,0.5,0.95 quantile of the GMPE distribution (black) and the ModelB distribution (red) with total weights, for a scenario with $R_x = -15.$, $F = 0$, and $T = 1.$.

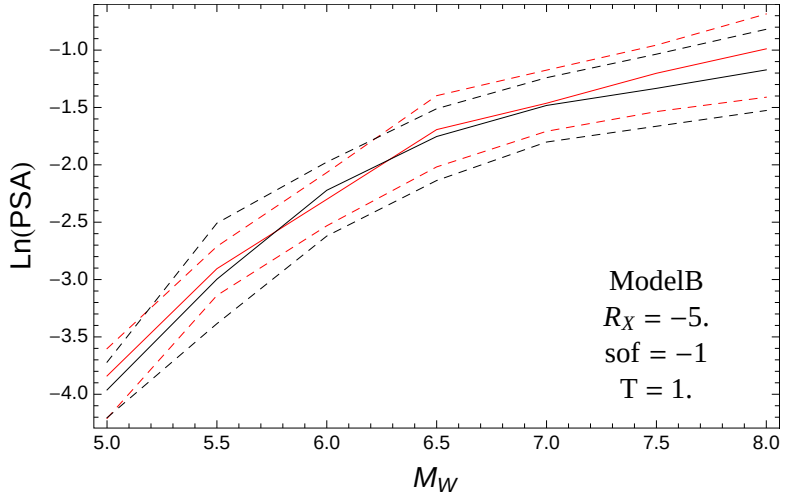



Figure 4.368: PVNGS2: Magnitude scaling of 0.05,0.5,0.95 quantile of the GMPE distribution (black) and the ModelB distribution (red) with total weights, for a scenario with $R_x = -5.$, $F = -1$, and $T = 1.$.

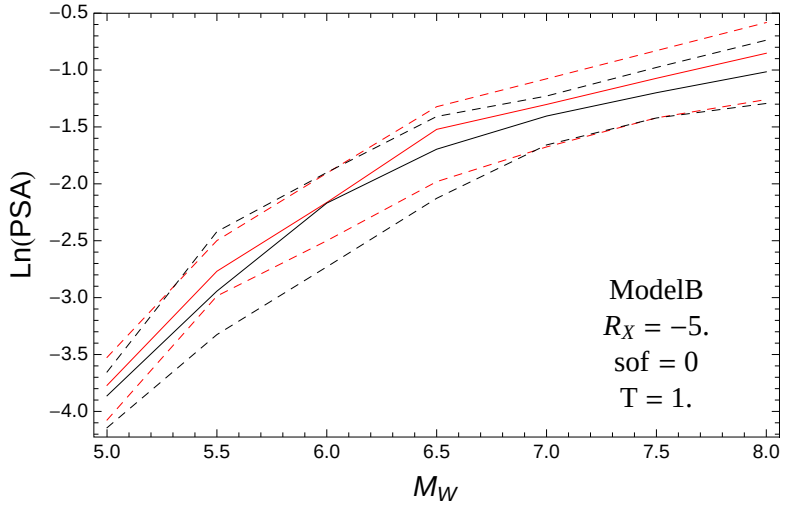



Figure 4.369: PVNGS2: Magnitude scaling of 0.05,0.5,0.95 quantile of the GMPE distribution (black) and the ModelB distribution (red) with total weights, for a scenario with $R_x = -5.$, $F = 0$, and $T = 1.$.

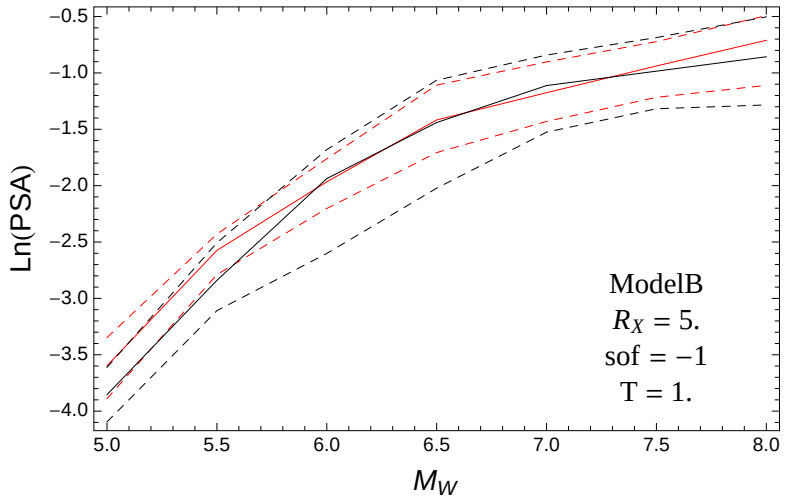



Figure 4.370: PVNGS2: Magnitude scaling of 0.05,0.5,0.95 quantile of the GMPE distribution (black) and the ModelB distribution (red) with total weights, for a scenario with $R_x = 5.$, $F = -1$, and $T = 1.$.

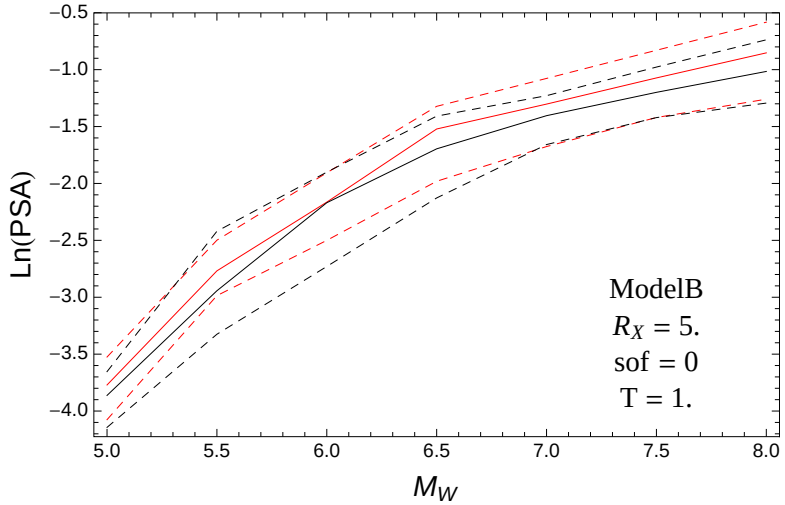



Figure 4.371: PVNGS2: Magnitude scaling of 0.05,0.5,0.95 quantile of the GMPE distribution (black) and the ModelB distribution (red) with total weights, for a scenario with $R_x = 5.$, $F = 0$, and $T = 1.$.

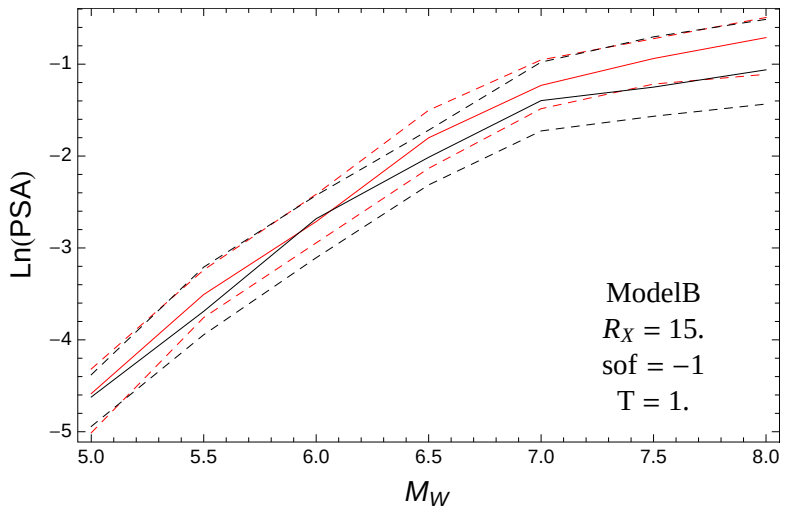



Figure 4.372: PVNGS2: Magnitude scaling of 0.05,0.5,0.95 quantile of the GMPE distribution (black) and the ModelB distribution (red) with total weights, for a scenario with $R_x = 15.$, $F = -1$, and $T = 1.$.

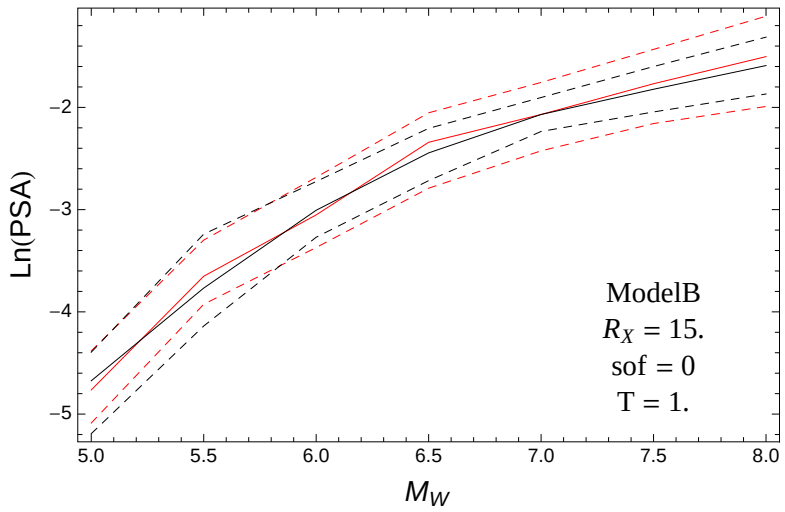



Figure 4.373: PVNGS2: Magnitude scaling of 0.05,0.5,0.95 quantile of the GMPE distribution (black) and the ModelB distribution (red) with total weights, for a scenario with $R_x = 15.$, $F = 0$, and $T = 1.$.

**T = 3.s**

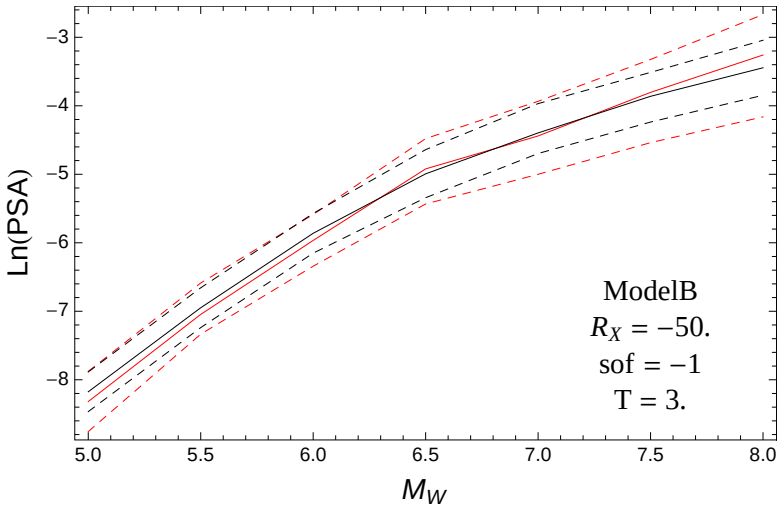



Figure 4.374: PVNGS2: Magnitude scaling of 0.05,0.5,0.95 quantile of the GMPE distribution (black) and the ModelB distribution (red) with total weights, for a scenario with $R_x = -50.$, $F = -1$, and $T = 3.$.

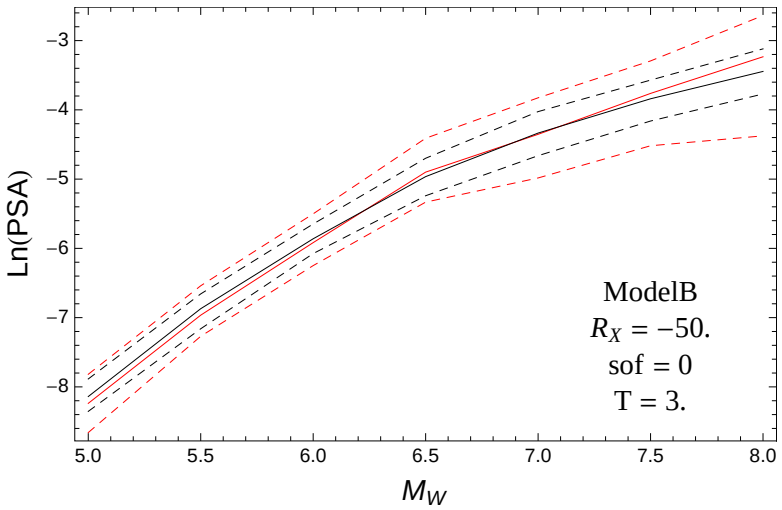



Figure 4.375: PVNGS2: Magnitude scaling of 0.05,0.5,0.95 quantile of the GMPE distribution (black) and the ModelB distribution (red) with total weights, for a scenario with $R_x = -50.$, $F = 0$, and $T = 3.$.

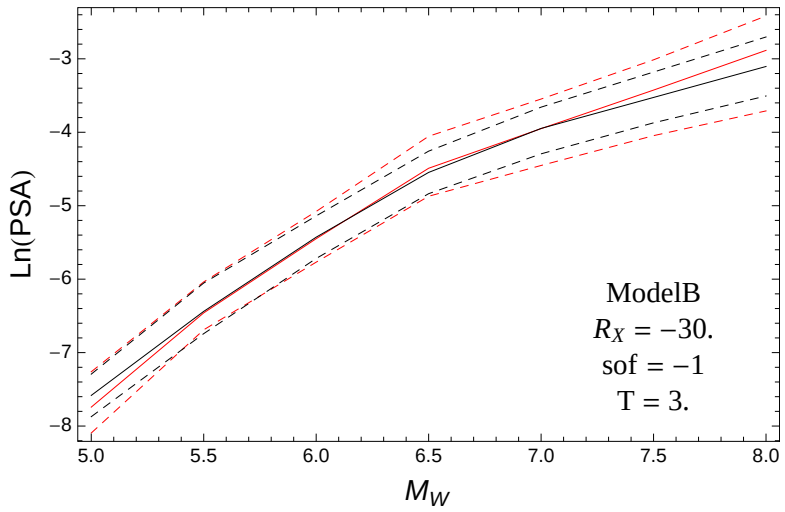



Figure 4.376: PVNGS2: Magnitude scaling of 0.05,0.5,0.95 quantile of the GMPE distribution (black) and the ModelB distribution (red) with total weights, for a scenario with $R_x = -30.$, $F = -1$, and $T = 3.$.

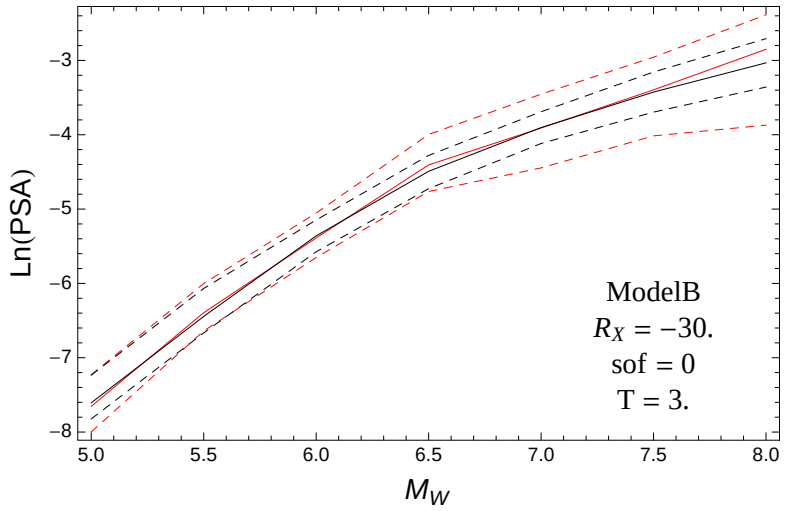



Figure 4.377: PVNGS2: Magnitude scaling of 0.05,0.5,0.95 quantile of the GMPE distribution (black) and the ModelB distribution (red) with total weights, for a scenario with $R_x = -30.$, $F = 0$, and $T = 3.$.

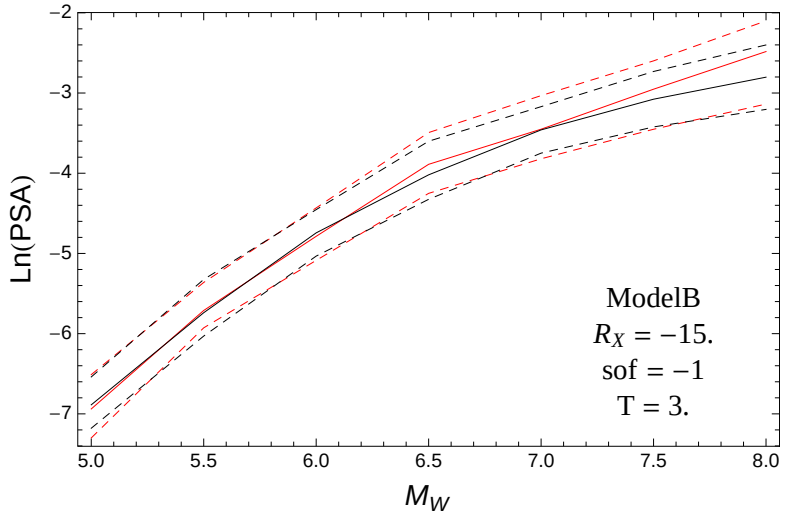



Figure 4.378: PVNGS2: Magnitude scaling of 0.05,0.5,0.95 quantile of the GMPE distribution (black) and the ModelB distribution (red) with total weights, for a scenario with $R_x = -15.$, $F = -1$, and $T = 3.$.

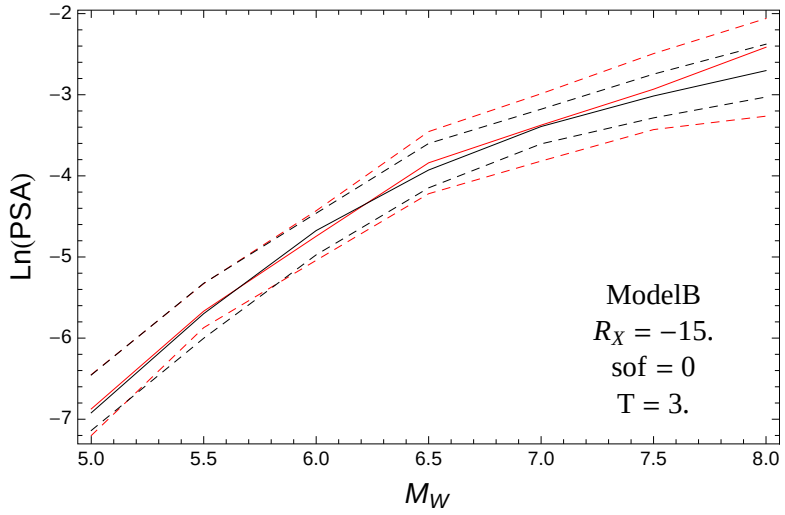



Figure 4.379: PVNGS2: Magnitude scaling of 0.05,0.5,0.95 quantile of the GMPE distribution (black) and the ModelB distribution (red) with total weights, for a scenario with $R_x = -15.$, $F = 0$, and $T = 3.$.

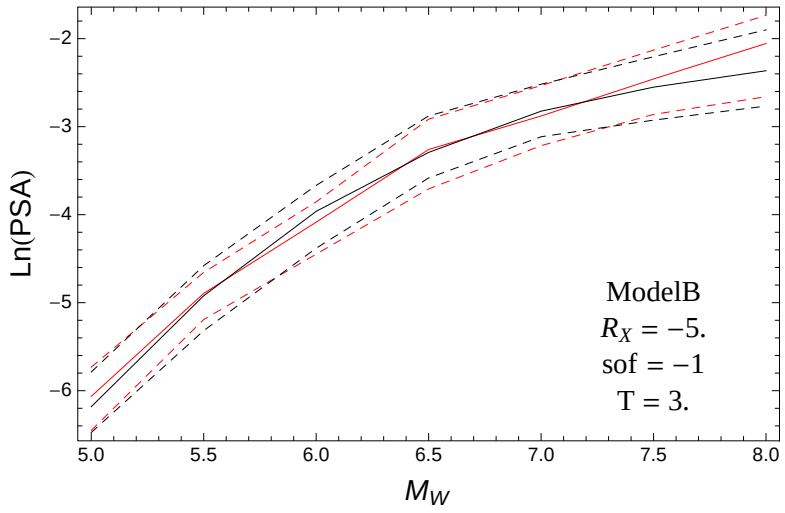



Figure 4.380: PVNGS2: Magnitude scaling of 0.05,0.5,0.95 quantile of the GMPE distribution (black) and the ModelB distribution (red) with total weights, for a scenario with $R_x = -5.$, $F = -1$, and $T = 3.$.

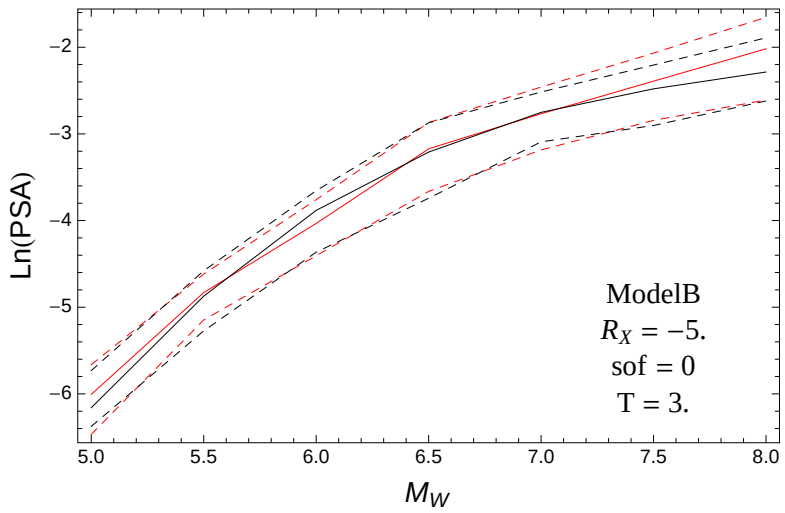



Figure 4.381: PVNGS2: Magnitude scaling of 0.05,0.5,0.95 quantile of the GMPE distribution (black) and the ModelB distribution (red) with total weights, for a scenario with $R_x = -5.$, $F = 0$, and $T = 3.$.

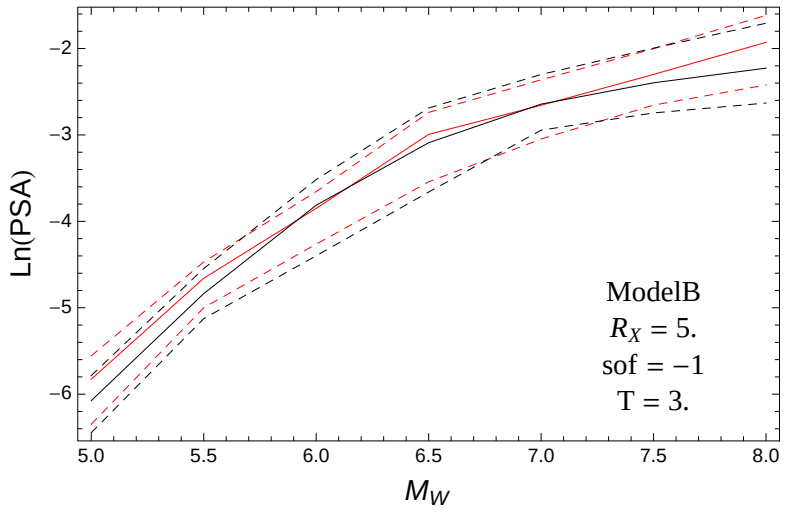



Figure 4.382: PVNGS2: Magnitude scaling of 0.05,0.5,0.95 quantile of the GMPE distribution (black) and the ModelB distribution (red) with total weights, for a scenario with $R_x = 5.$, $F = -1$, and $T = 3.$.

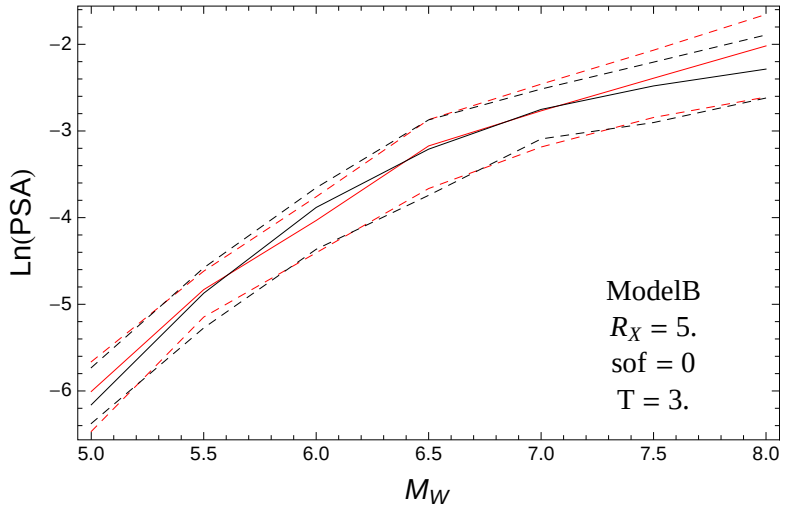



Figure 4.383: PVNGS2: Magnitude scaling of 0.05,0.5,0.95 quantile of the GMPE distribution (black) and the ModelB distribution (red) with total weights, for a scenario with $R_x = 5.$, $F = 0$, and $T = 3.$.

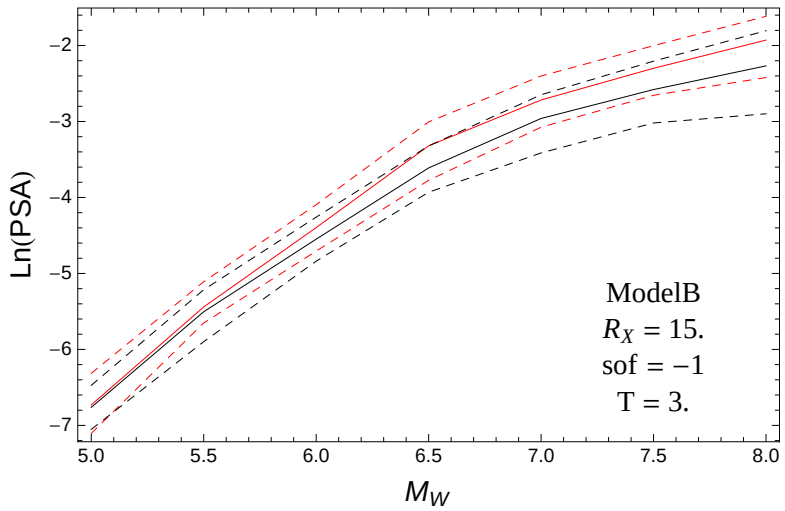



Figure 4.384: PVNGS2: Magnitude scaling of 0.05,0.5,0.95 quantile of the GMPE distribution (black) and the ModelB distribution (red) with total weights, for a scenario with $R_x = 15.$, $F = -1$, and $T = 3.$.

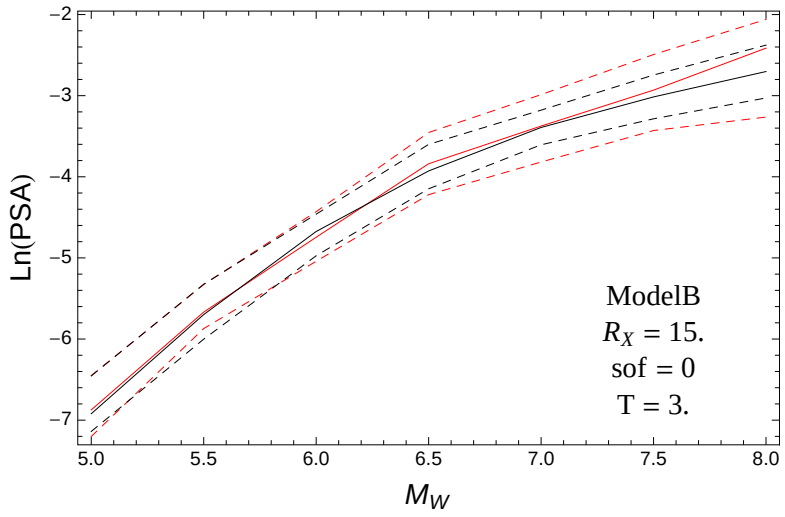



Figure 4.385: PVNGS2: Magnitude scaling of 0.05,0.5,0.95 quantile of the GMPE distribution (black) and the ModelB distribution (red) with total weights, for a scenario with $R_x = 15.$, $F = 0$, and $T = 3.$.

### 4.1.9 Quantile Plots vs. Period

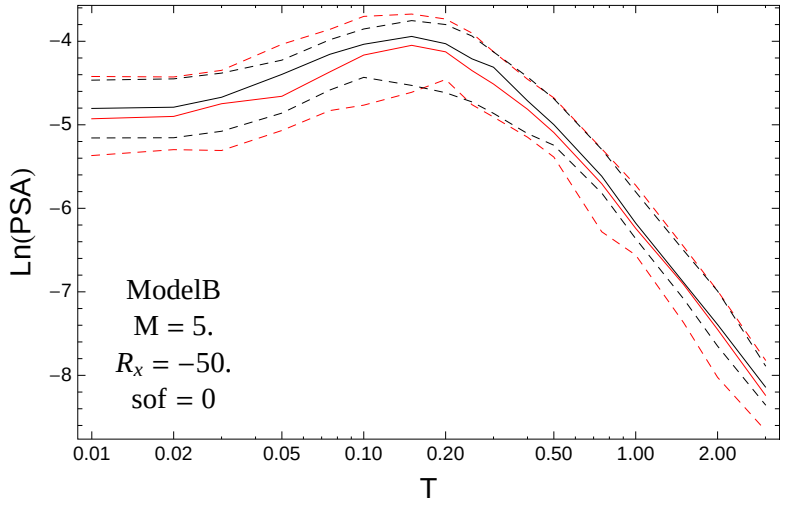



Figure 4.386: PVNGSv2: Spectra of 0.05,0.5,0.95 quantile of the GMPE distribution (black) and the model distribution (red) with total weights, for a scenario with $M_W = 5.$, $R_x = -50.$, $F = 0$.

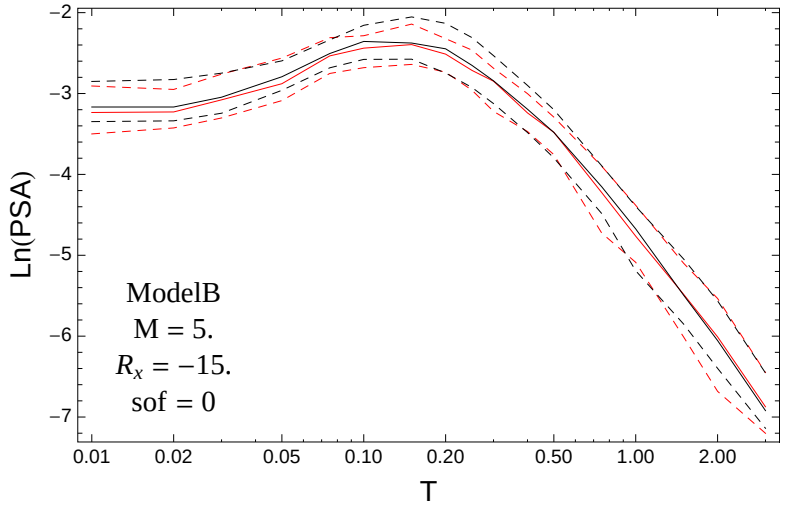



Figure 4.387: PVNGSv2: Spectra of 0.05,0.5,0.95 quantile of the GMPE distribution (black) and the model distribution (red) with total weights, for a scenario with $M_W = 5.$, $R_x = -15.$, $F = 0$.

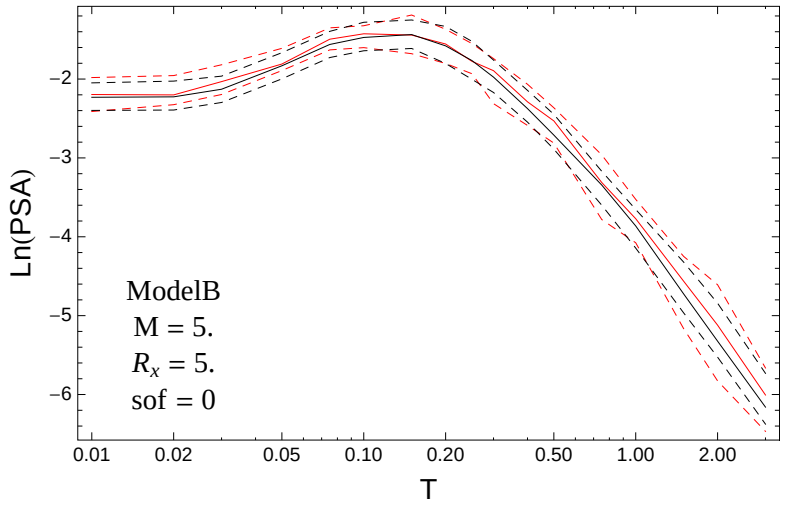



Figure 4.388: PVNGSv2: Spectra of 0.05,0.5,0.95 quantile of the GMPE distribution (black) and the model distribution (red) with total weights, for a scenario with $M_W = 5.$, $R_x = 5.$, $F = 0$.

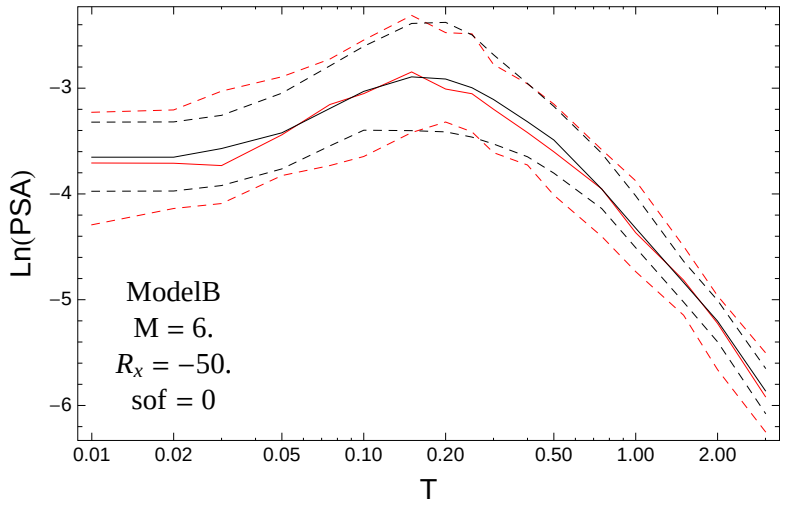



Figure 4.389: PVNGSv2: Spectra of 0.05,0.5,0.95 quantile of the GMPE distribution (black) and the model distribution (red) with total weights, for a scenario with $M_W = 6.$, $R_x = -50.$, $F = 0$.

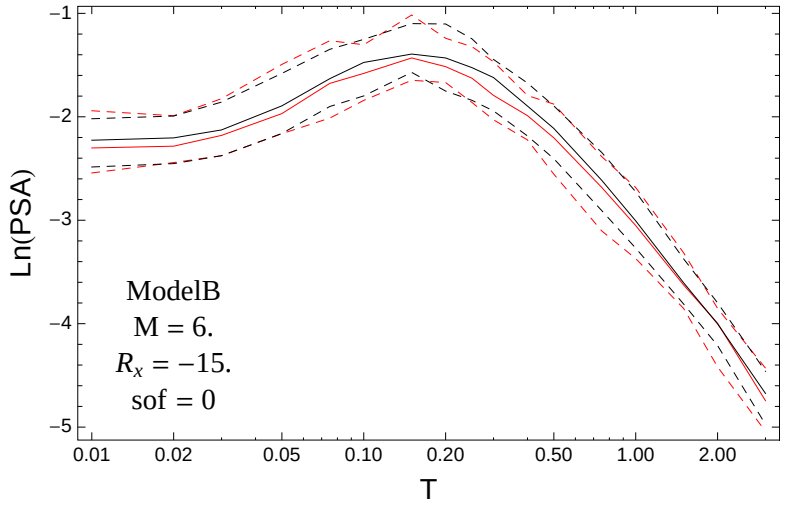



Figure 4.390: PVNGSv2: Spectra of 0.05,0.5,0.95 quantile of the GMPE distribution (black) and the model distribution (red) with total weights, for a scenario with $M_W = 6.$, $R_x = -15.$, $F = 0$.

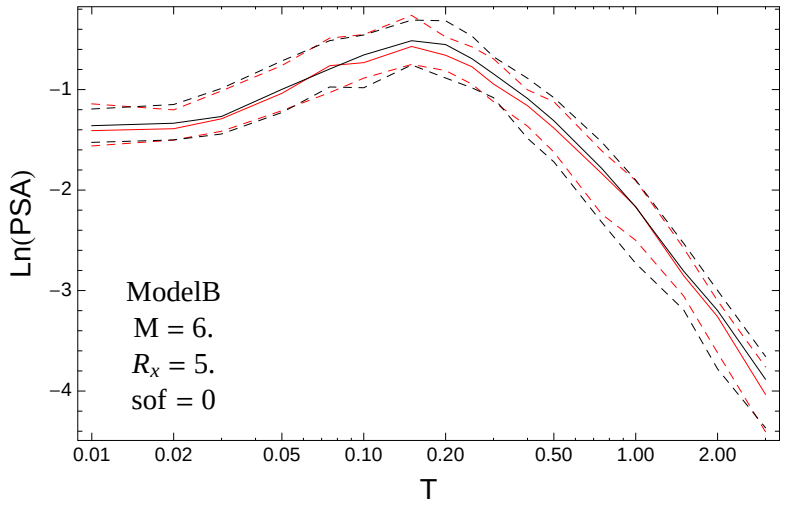



Figure 4.391: PVNGSv2: Spectra of 0.05,0.5,0.95 quantile of the GMPE distribution (black) and the model distribution (red) with total weights, for a scenario with $M_W = 6.$, $R_x = 5.$, $F = 0$.

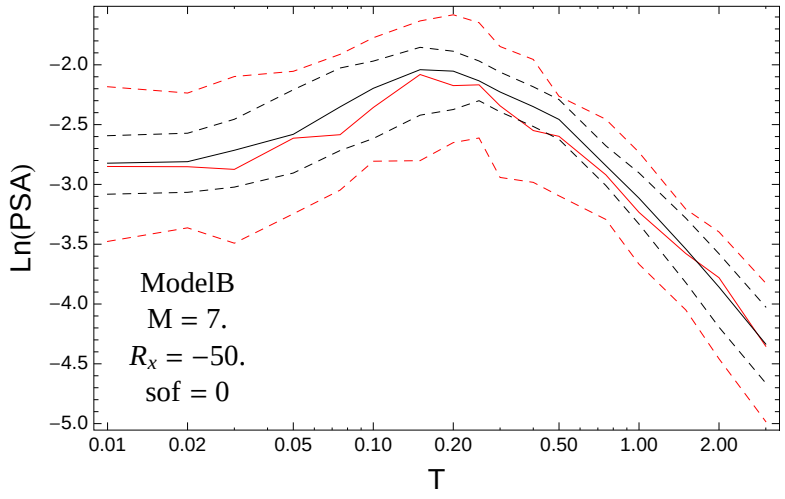



Figure 4.392: PVNGSv2: Spectra of 0.05,0.5,0.95 quantile of the GMPE distribution (black) and the model distribution (red) with total weights, for a scenario with $M_W = 7.$, $R_x = -50.$, $F = 0$.

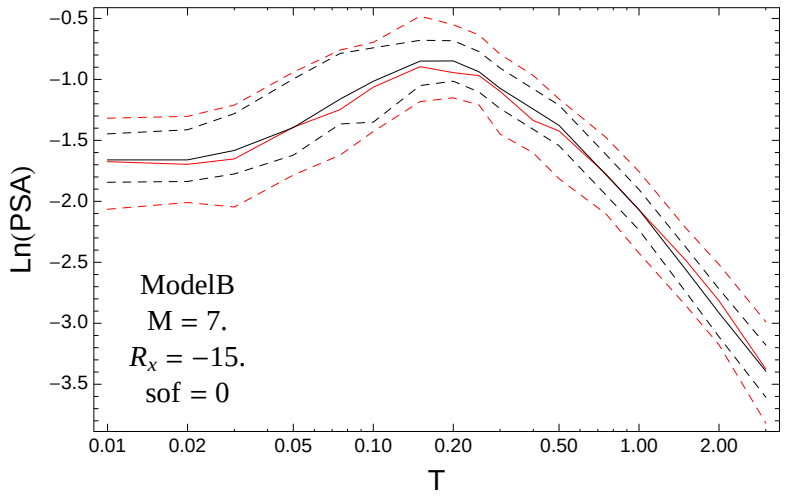



Figure 4.393: PVNGSv2: Spectra of 0.05,0.5,0.95 quantile of the GMPE distribution (black) and the model distribution (red) with total weights, for a scenario with $M_W = 7.$, $R_x = -15.$, $F = 0$.

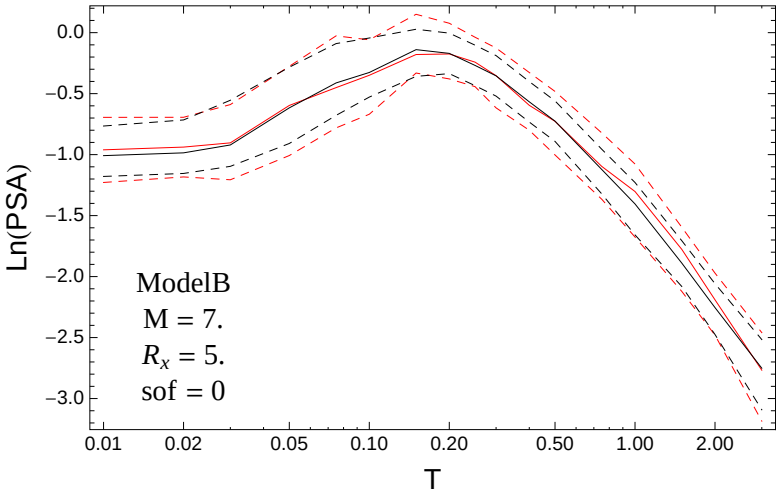



Figure 4.394: PVNGSv2: Spectra of 0.05,0.5,0.95 quantile of the GMPE distribution (black) and the model distribution (red) with total weights, for a scenario with $M_W = 7.$, $R_x = 5.$, $F = 0$.

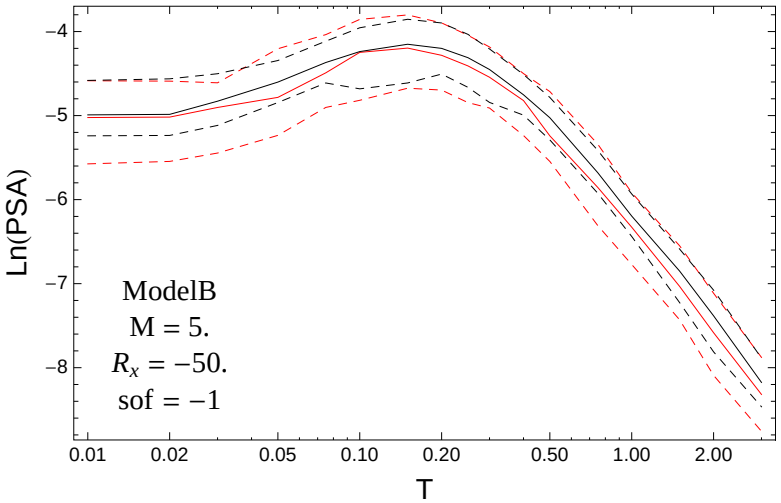



Figure 4.395: PVNGSv2: Spectra of 0.05,0.5,0.95 quantile of the GMPE distribution (black) and the model distribution (red) with total weights, for a scenario with $M_W = 5.$, $R_x = -50.$, $F = -1$.

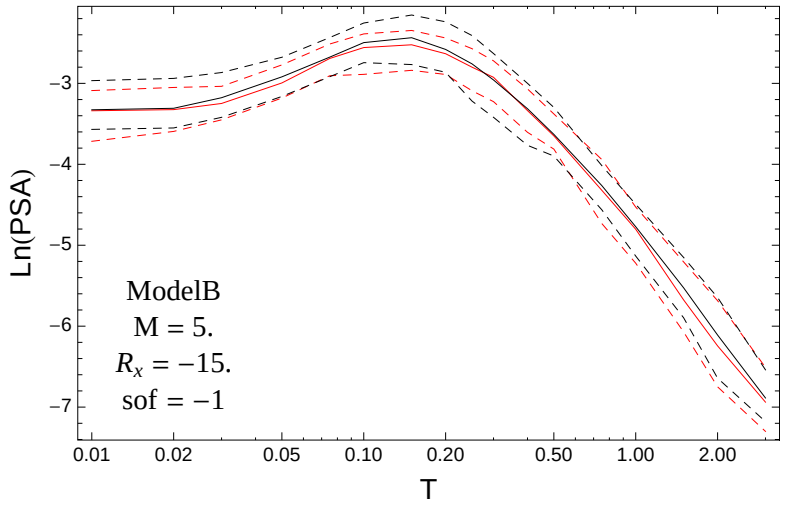



Figure 4.396: PVNGSv2: Spectra of 0.05,0.5,0.95 quantile of the GMPE distribution (black) and the model distribution (red) with total weights, for a scenario with $M_W = 5.$, $R_x = -15.$, $F = -1$.

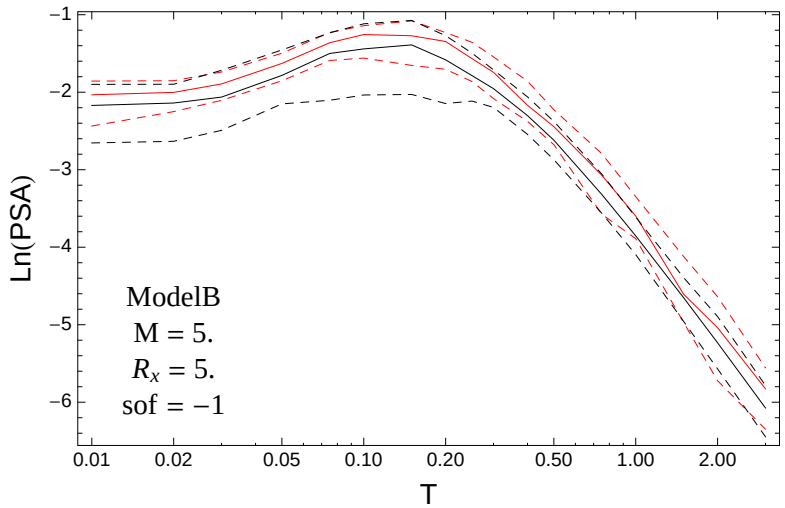



Figure 4.397: PVNGSv2: Spectra of 0.05,0.5,0.95 quantile of the GMPE distribution (black) and the model distribution (red) with total weights, for a scenario with $M_W = 5.$, $R_x = 5.$, $F = -1$.

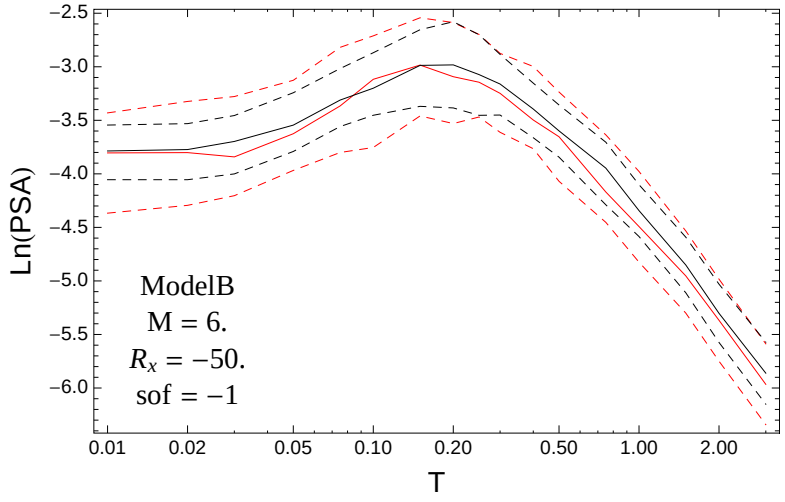



Figure 4.398: PVNGSv2: Spectra of 0.05,0.5,0.95 quantile of the GMPE distribution (black) and the model distribution (red) with total weights, for a scenario with $M_W = 6.$, $R_x = -50.$, $F = -1$.

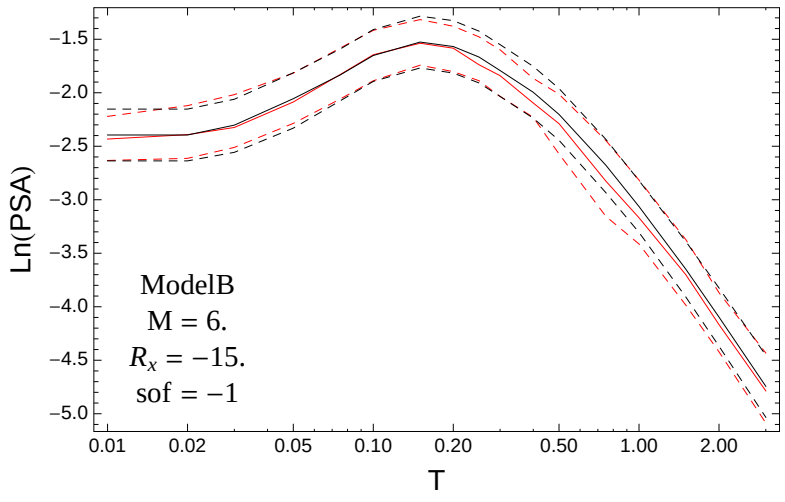



Figure 4.399: PVNGSv2: Spectra of 0.05,0.5,0.95 quantile of the GMPE distribution (black) and the model distribution (red) with total weights, for a scenario with $M_W = 6.$, $R_x = -15.$, $F = -1$.

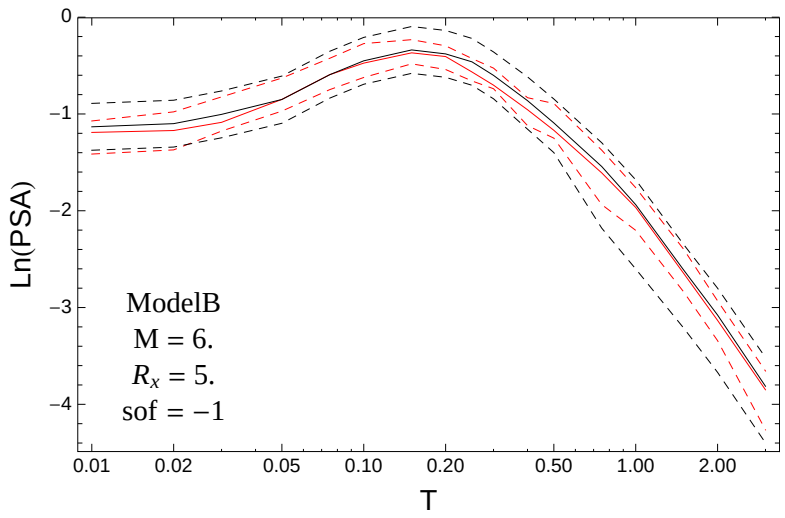



Figure 4.400: PVNGSv2: Spectra of 0.05,0.5,0.95 quantile of the GMPE distribution (black) and the model distribution (red) with total weights, for a scenario with $M_W = 6.$, $R_x = 5.$, $F = -1$.

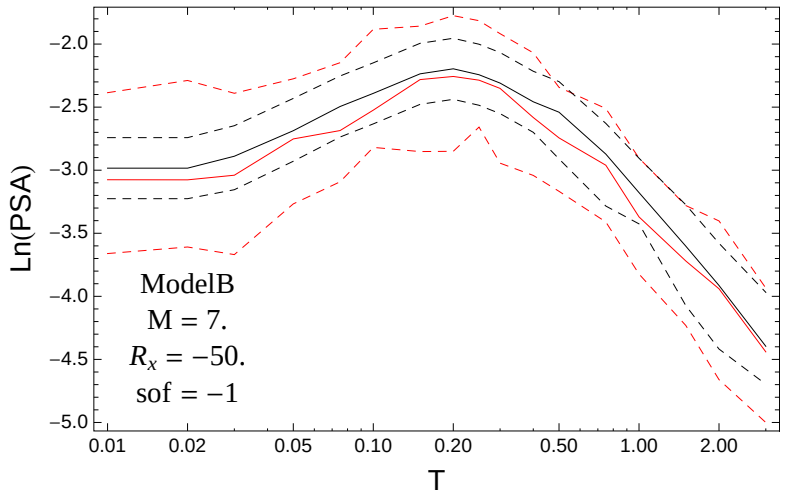



Figure 4.401: PVNGSv2: Spectra of 0.05,0.5,0.95 quantile of the GMPE distribution (black) and the model distribution (red) with total weights, for a scenario with $M_W = 7.$, $R_x = -50.$, $F = -1$.

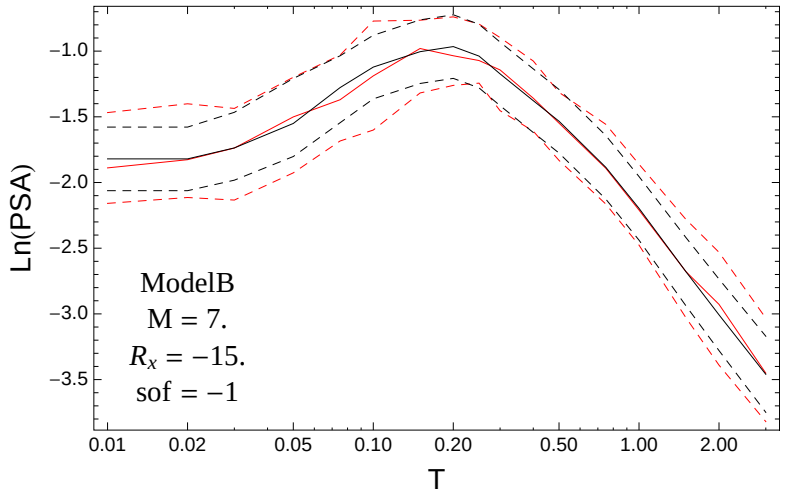



Figure 4.402: PVNGSv2: Spectra of 0.05,0.5,0.95 quantile of the GMPE distribution (black) and the model distribution (red) with total weights, for a scenario with $M_W = 7.$, $R_x = -15.$, $F = -1$.

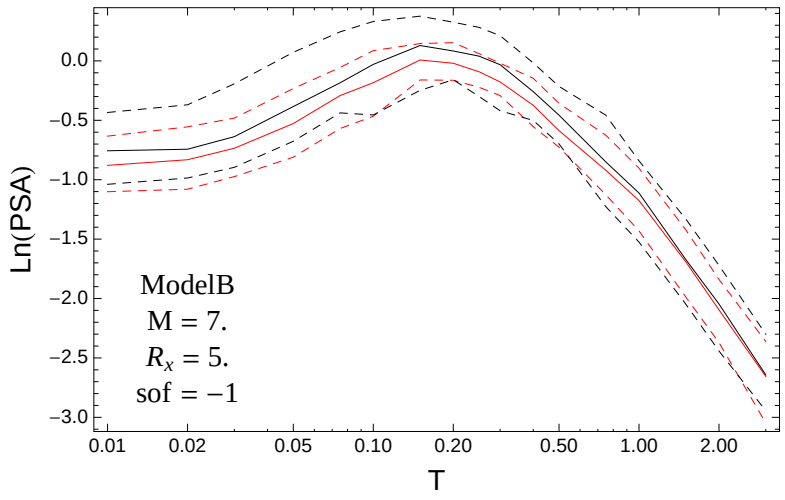



Figure 4.403: PVNGSv2: Spectra of 0.05,0.5,0.95 quantile of the GMPE distribution (black) and the model distribution (red) with total weights, for a scenario with $M_W = 7.$, $R_x = 5.$, $F = -1$.

### 4.1.10 Quantile Ratios vs. Distance

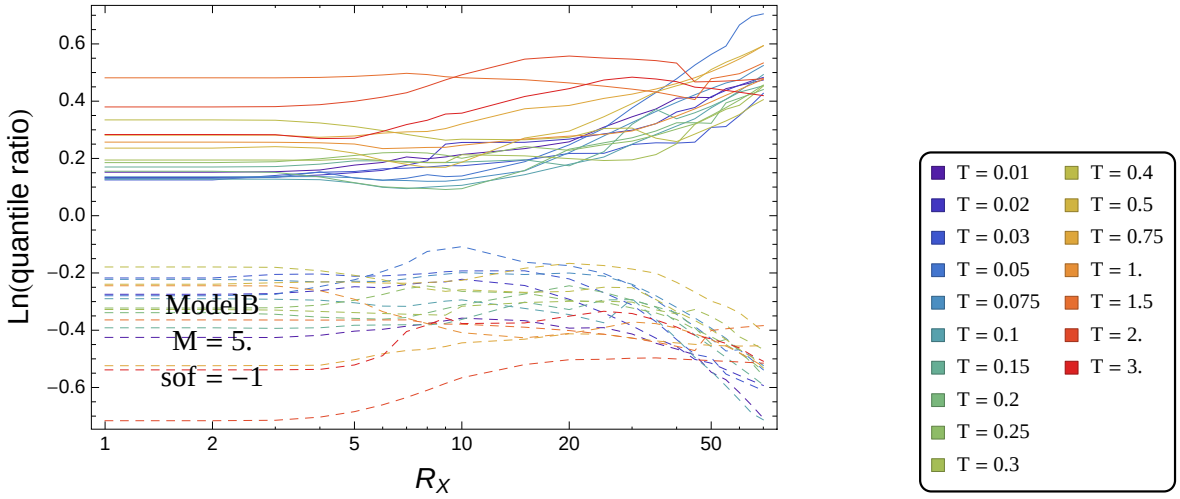



Figure 4.404: PVNGS2: Ratio of 0.05 to 0.5 (dashed) and ratio of 0.95 to 0.5 quantile (solid) of the ModelB-model distribution with total weights, for a scenario with $M = 5.$, $F = -1$, and all periods.

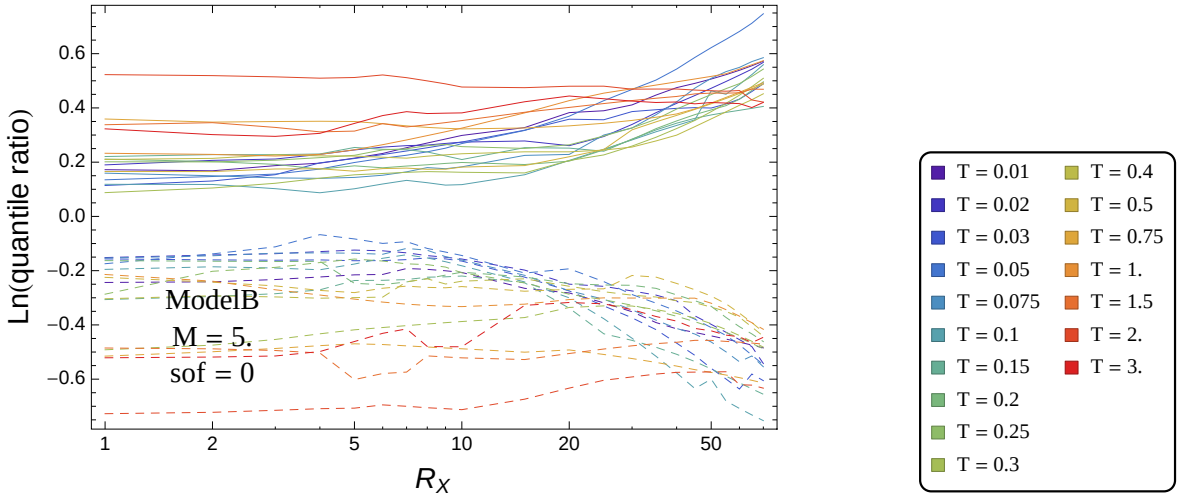



Figure 4.405: PVNGS2: Ratio of 0.05 to 0.5 (dashed) and ratio of 0.95 to 0.5 quantile (solid) of the ModelB-model distribution with total weights, for a scenario with $M = 5.$, $F = 0$, and all periods.

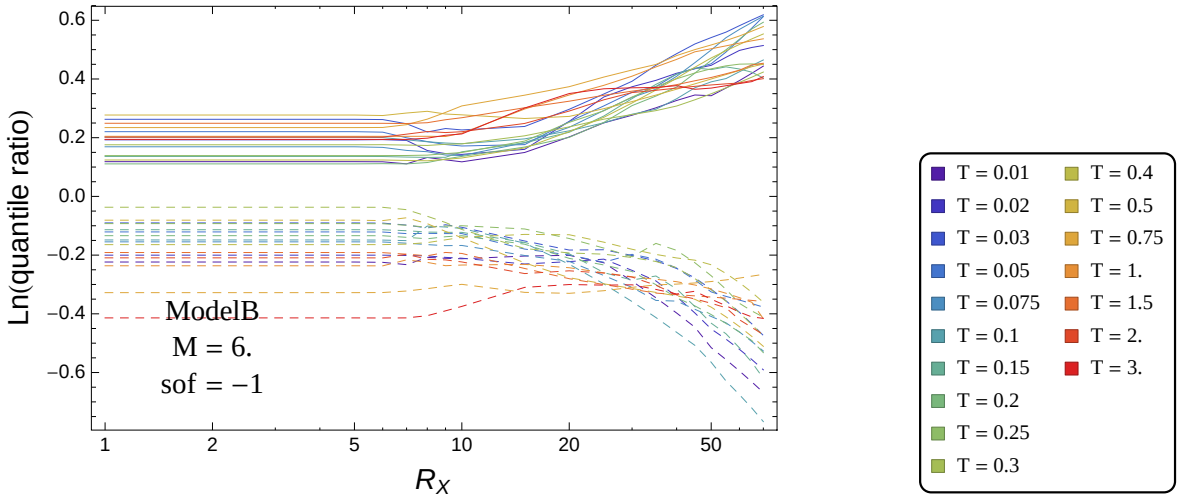



Figure 4.406: PVNGS2: Ratio of 0.05 to 0.5 (dashed) and ratio of 0.95 to 0.5 quantile (solid) of the ModelB-model distribution with total weights, for a scenario with $M = 6.$, $F = -1$, and all periods.

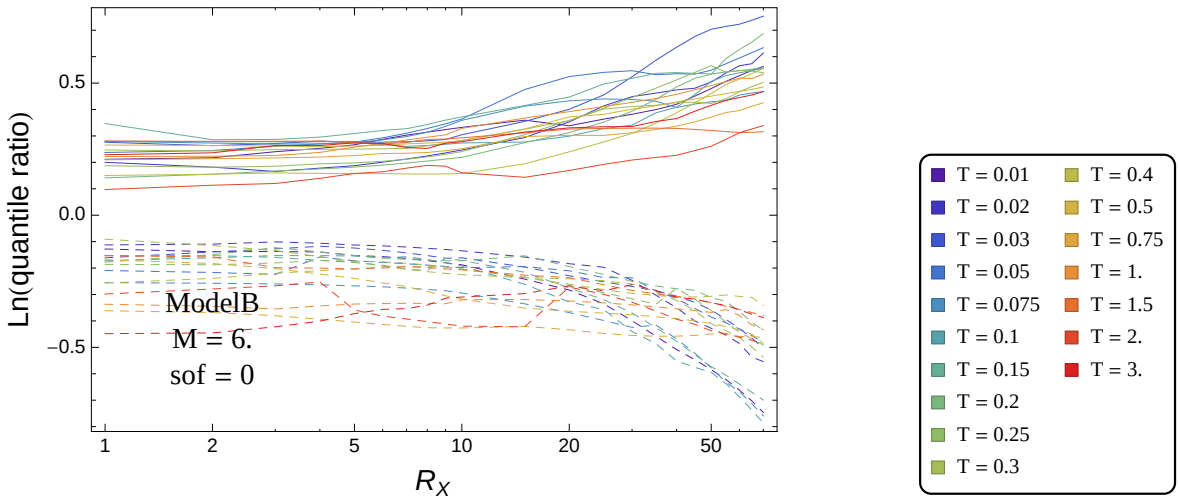



Figure 4.407: PVNGS2: Ratio of 0.05 to 0.5 (dashed) and ratio of 0.95 to 0.5 quantile (solid) of the ModelB-model distribution with total weights, for a scenario with $M = 6.$, $F = 0$, and all periods.

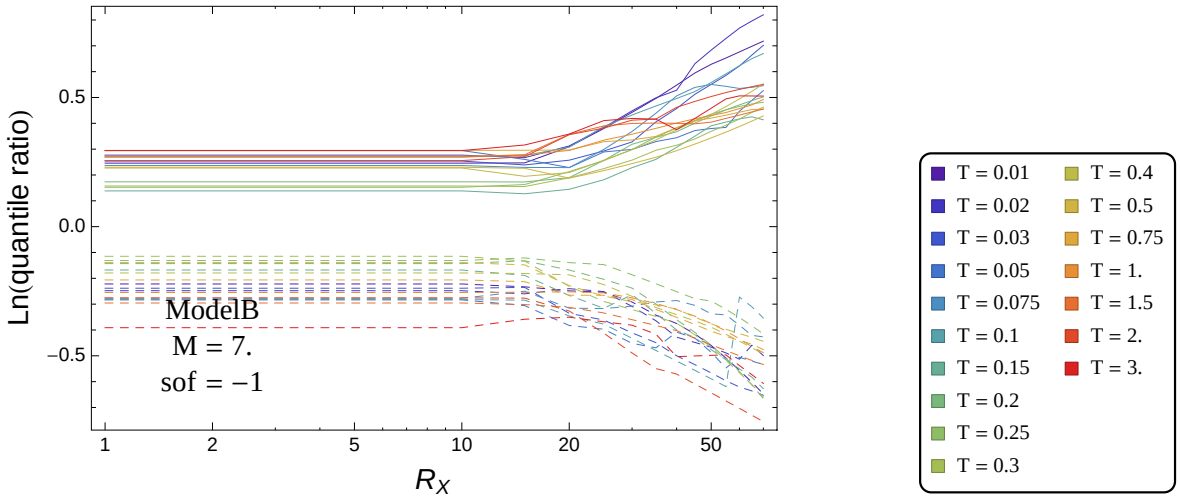



Figure 4.408: PVNGS2: Ratio of 0.05 to 0.5 (dashed) and ratio of 0.95 to 0.5 quantile (solid) of the ModelB-model distribution with total weights, for a scenario with $M = 7.$, $F = -1$, and all periods.

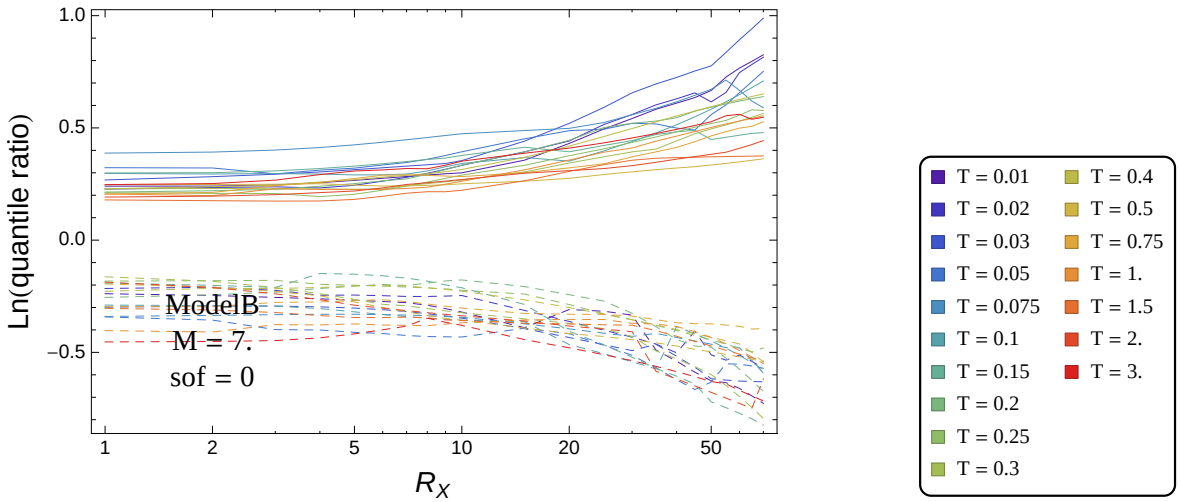



Figure 4.409: PVNGS2: Ratio of 0.05 to 0.5 (dashed) and ratio of 0.95 to 0.5 quantile (solid) of the ModelB-model distribution with total weights, for a scenario with $M = 7.$, $F = 0$, and all periods.

### 4.1.11 Magnitude Scaling with GMPEs

**T = 0.01s**

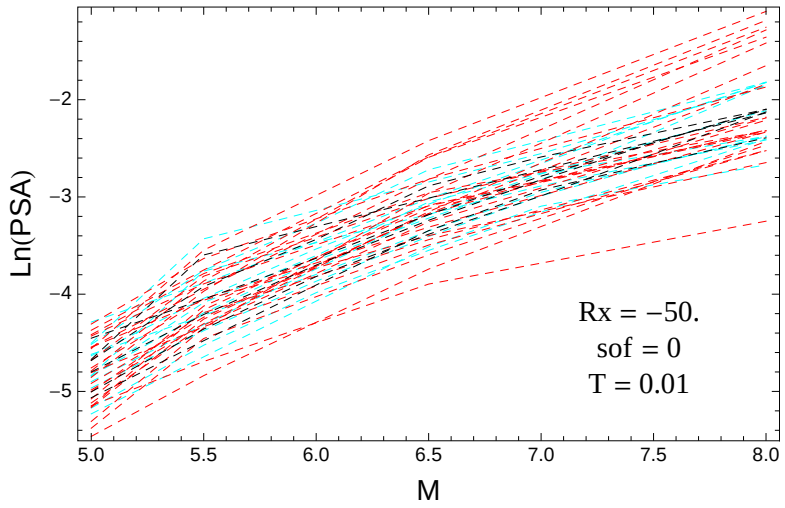



Figure 4.410: PVNGSv2: Magnitude scaling of the original GMPEs (dashed black), the original GMPEs with uncertainty model (dashed cyan) and selected B models (dashed red), for a scenario with $R_X = -50.$, $F = 0$, and $T = 0.01$s.

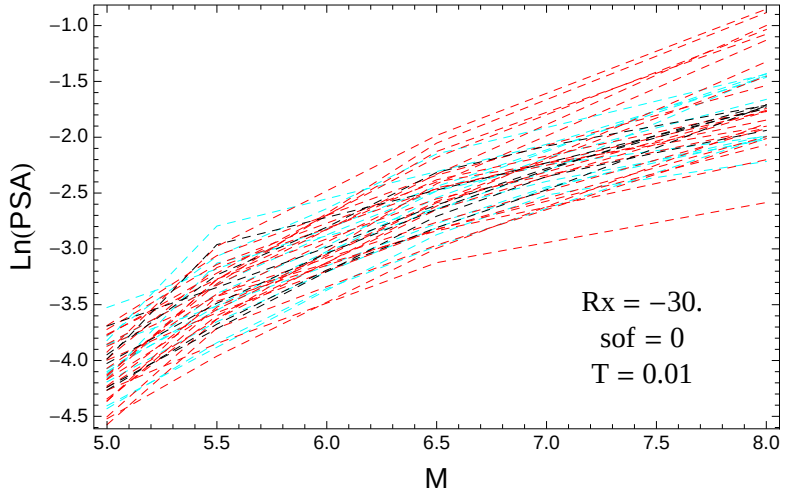



Figure 4.411: PVNGSv2: Magnitude scaling of the original GMPEs (dashed black), the original GMPEs with uncertainty model (dashed cyan) and selected B models (dashed red), for a scenario with $R_X = -30.$, $F = 0$, and $T = 0.01$s.

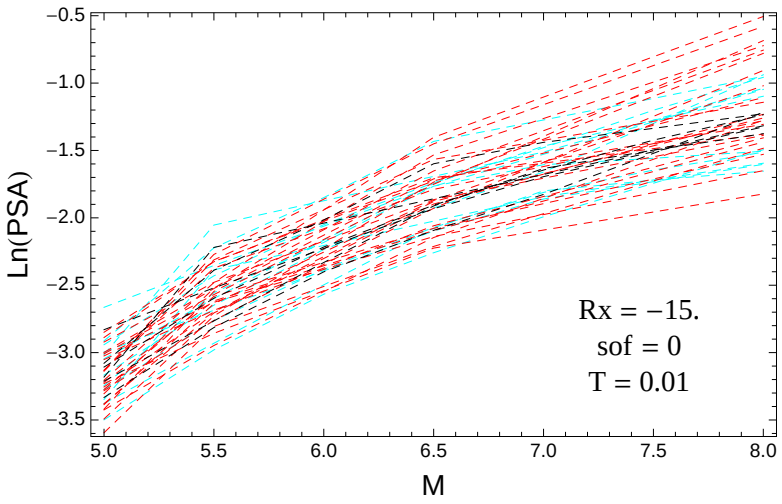



Figure 4.412: PVNGSv2: Magnitude scaling of the original GMPEs (dashed black), the original GMPEs with uncertainty model (dashed cyan) and selected B models (dashed red), for a scenario with $R_X = -15.$, $F = 0$, and $T = 0.01$s.

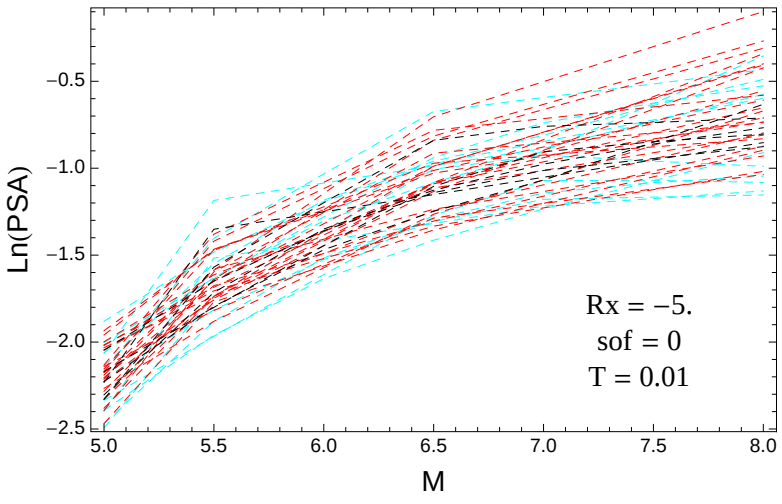



Figure 4.413: PVNGSv2: Magnitude scaling of the original GMPEs (dashed black), the original GMPEs with uncertainty model (dashed cyan) and selected B models (dashed red), for a scenario with $R_X = -5.$, $F = 0$, and $T = 0.01$s.

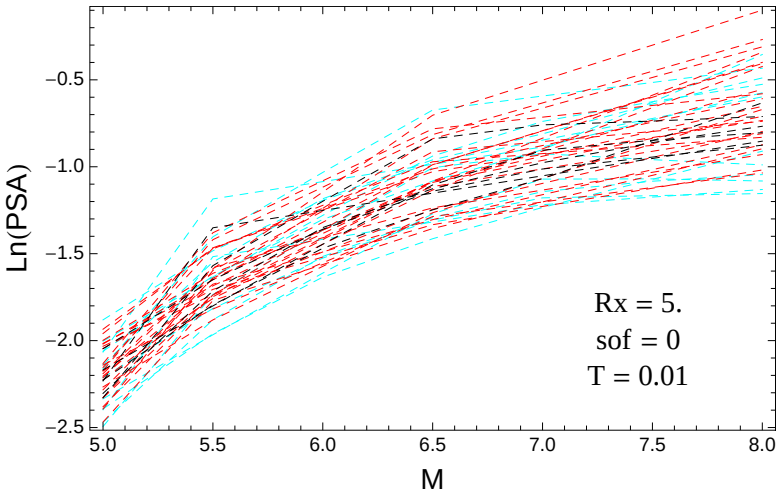



Figure 4.414: PVNGSv2: Magnitude scaling of the original GMPEs (dashed black), the original GMPEs with uncertainty model (dashed cyan) and selected B models (dashed red), for a scenario with $R_X = 5.$, $F = 0$, and $T = 0.01$s.

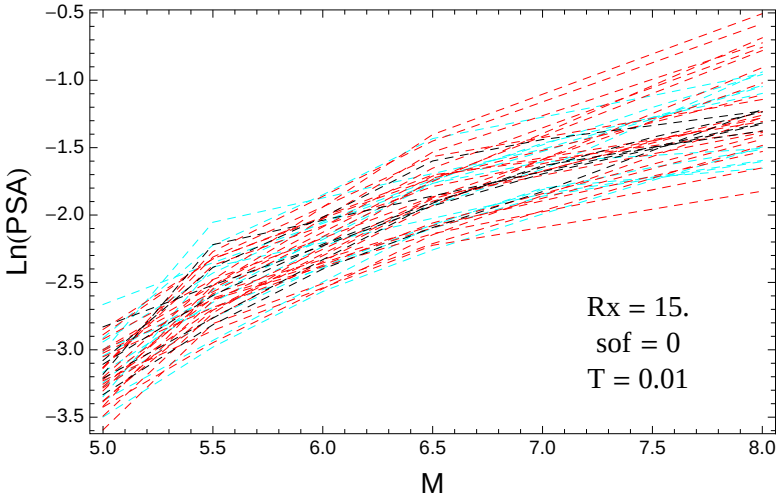



Figure 4.415: PVNGSv2: Magnitude scaling of the original GMPEs (dashed black), the original GMPEs with uncertainty model (dashed cyan) and selected B models (dashed red), for a scenario with $R_X = 15.$, $F = 0$, and $T = 0.01$s.

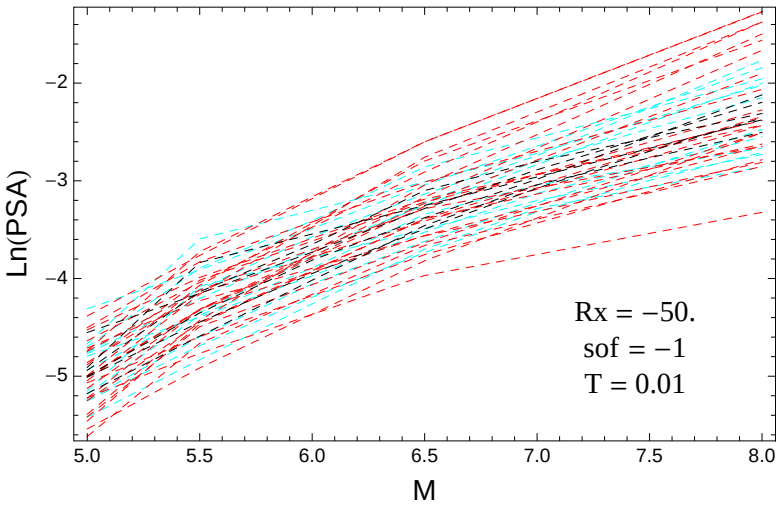



Figure 4.416: PVNGSv2: Magnitude scaling of the original GMPEs (dashed black), the original GMPEs with uncertainty model (dashed cyan) and selected B models (dashed red), for a scenario with $R_X = -50.$, $F = -1$, and $T = 0.01$s.

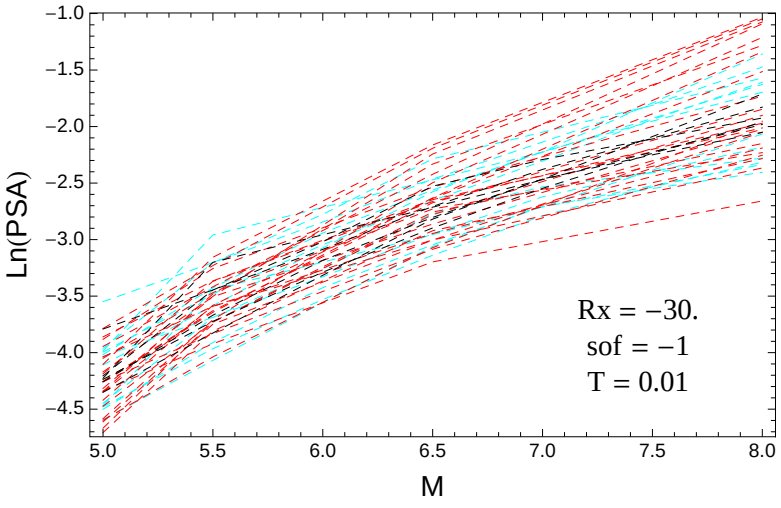



Figure 4.417: PVNGSv2: Magnitude scaling of the original GMPEs (dashed black), the original GMPEs with uncertainty model (dashed cyan) and selected B models (dashed red), for a scenario with $R_X = -30.$, $F = -1$, and $T = 0.01$s.

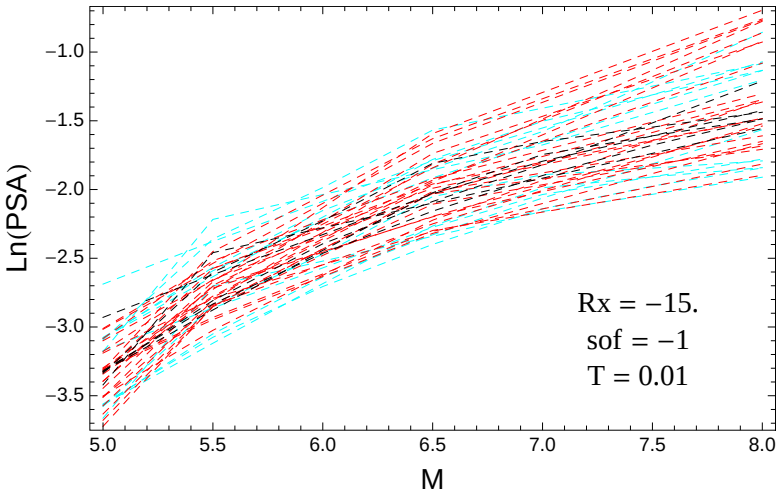



Figure 4.418: PVNGSv2: Magnitude scaling of the original GMPEs (dashed black), the original GMPEs with uncertainty model (dashed cyan) and selected B models (dashed red), for a scenario with $R_X = -15.$, $F = -1$, and $T = 0.01$s.

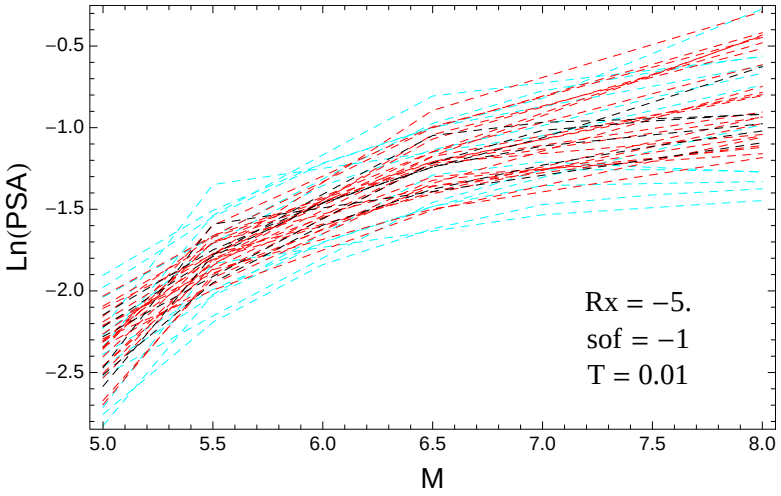



Figure 4.419: PVNGSv2: Magnitude scaling of the original GMPEs (dashed black), the original GMPEs with uncertainty model (dashed cyan) and selected B models (dashed red), for a scenario with $R_X = -5.$, $F = -1$, and $T = 0.01$s.

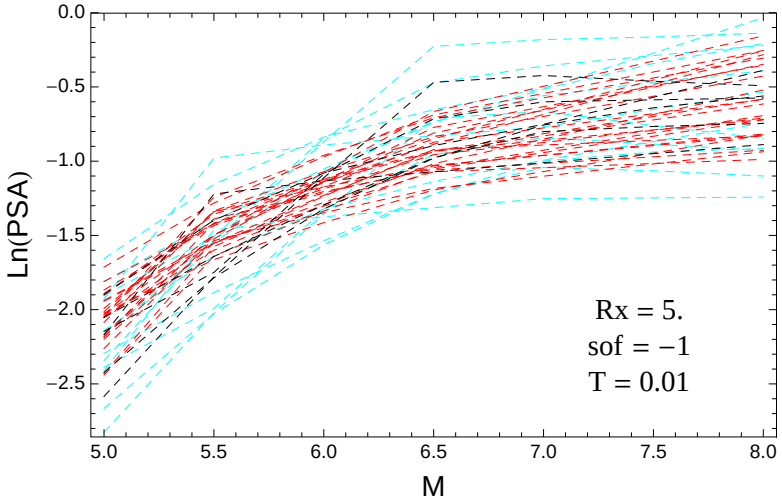



Figure 4.420: PVNGSv2: Magnitude scaling of the original GMPEs (dashed black), the original GMPEs with uncertainty model (dashed cyan) and selected B models (dashed red), for a scenario with $R_X = 5.$, $F = -1$, and $T = 0.01$s.

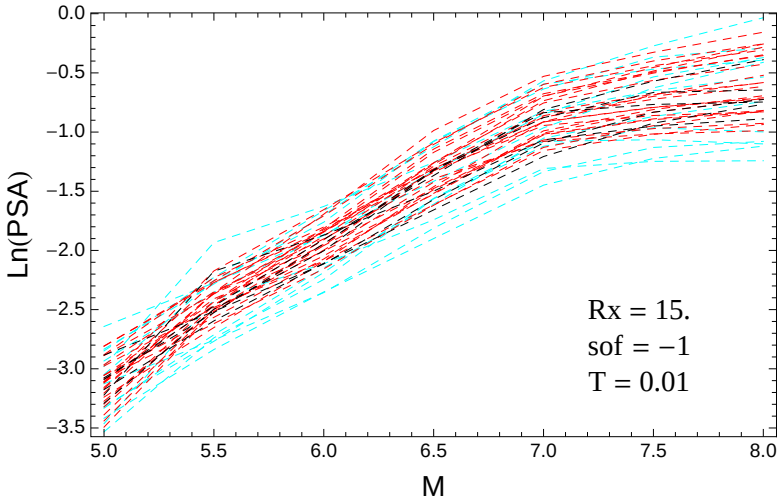



Figure 4.421: PVNGSv2: Magnitude scaling of the original GMPEs (dashed black), the original GMPEs with uncertainty model (dashed cyan) and selected B models (dashed red), for a scenario with $R_X = 15.$, $F = -1$, and $T = 0.01$s.

**T = 0.2s**

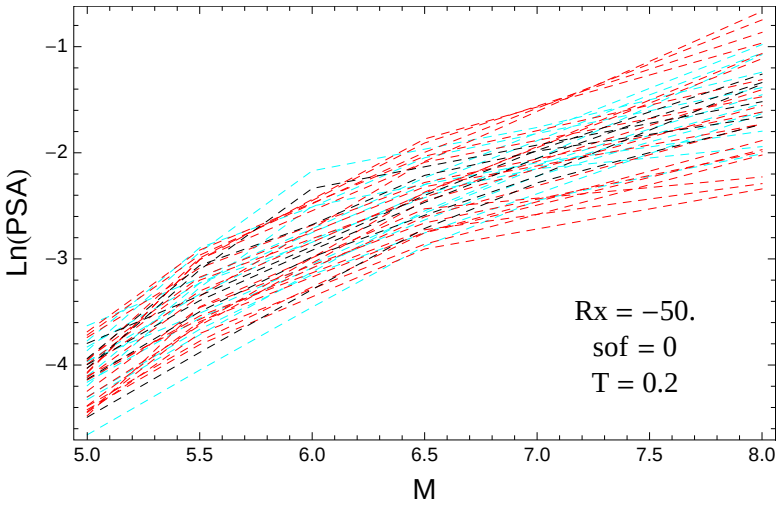



Figure 4.422: PVNGSv2: Magnitude scaling of the original GMPEs (dashed black), the original GMPEs with uncertainty model (dashed cyan) and selected B models (dashed red), for a scenario with $R_X = -50.$, $F = 0$, and $T = 0.2$s.

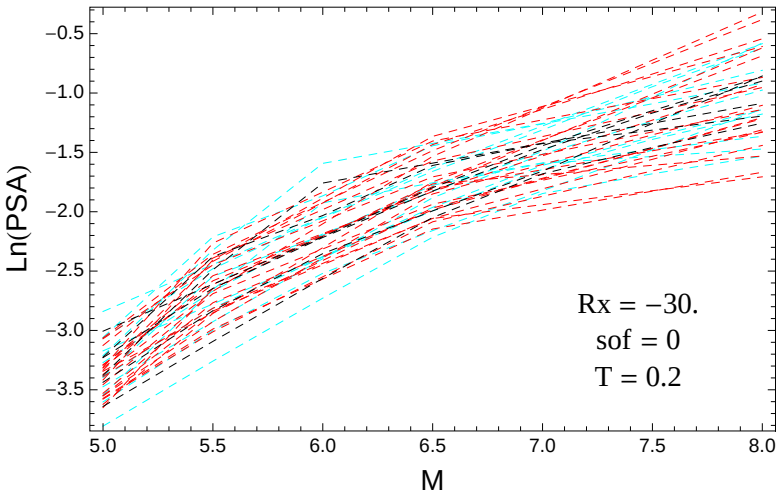



Figure 4.423: PVNGSv2: Magnitude scaling of the original GMPEs (dashed black), the original GMPEs with uncertainty model (dashed cyan) and selected B models (dashed red), for a scenario with $R_X = -30.$, $F = 0$, and $T = 0.2$s.

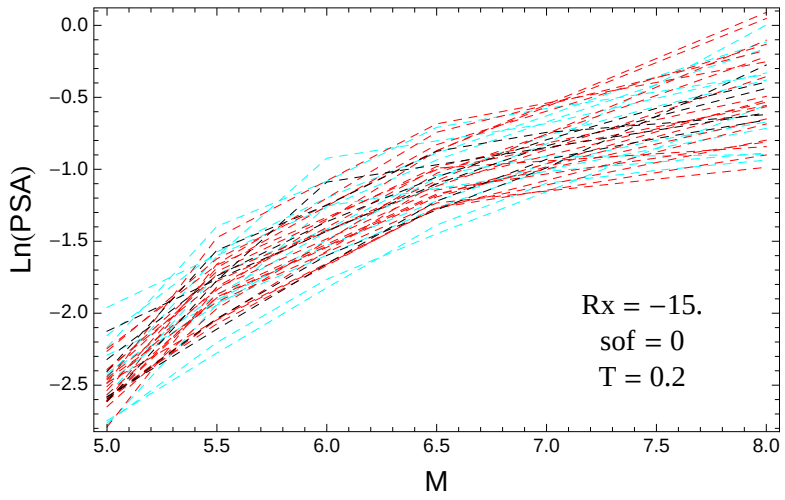



Figure 4.424: PVNGSv2: Magnitude scaling of the original GMPEs (dashed black), the original GMPEs with uncertainty model (dashed cyan) and selected B models (dashed red), for a scenario with $R_X = -15.$, $F = 0$, and $T = 0.2$s.

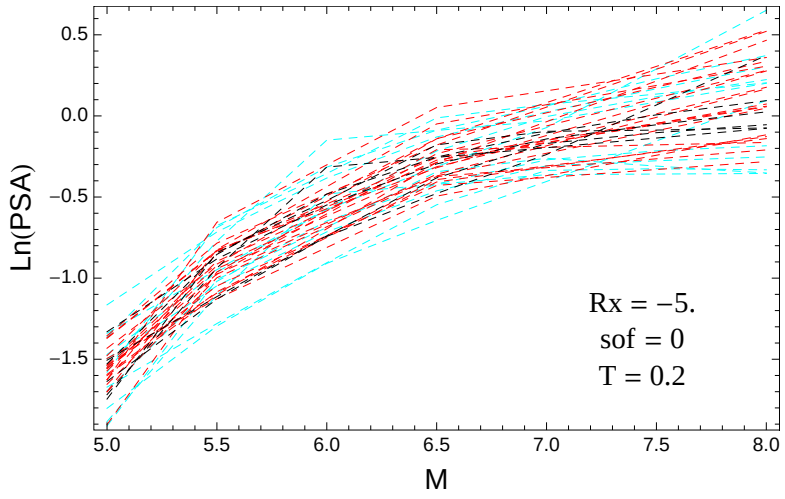



Figure 4.425: PVNGSv2: Magnitude scaling of the original GMPEs (dashed black), the original GMPEs with uncertainty model (dashed cyan) and selected B models (dashed red), for a scenario with $R_X = -5.$, $F = 0$, and $T = 0.2$s.

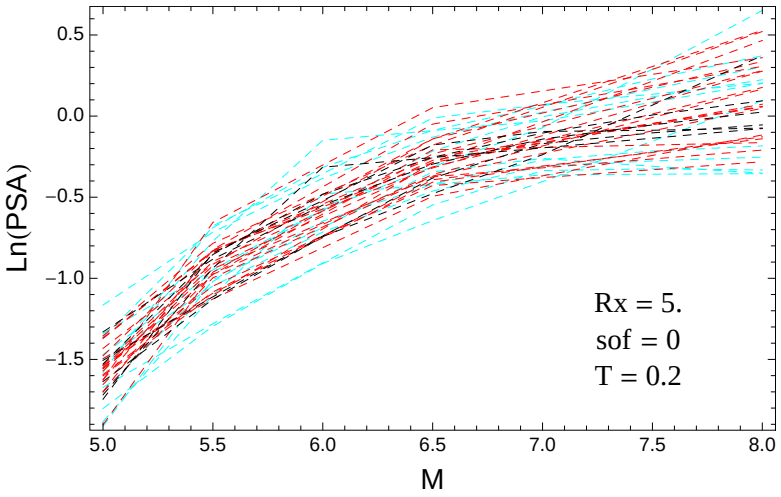



Figure 4.426: PVNGSv2: Magnitude scaling of the original GMPEs (dashed black), the original GMPEs with uncertainty model (dashed cyan) and selected B models (dashed red), for a scenario with $R_X = 5.$, $F = 0$, and $T = 0.2$s.

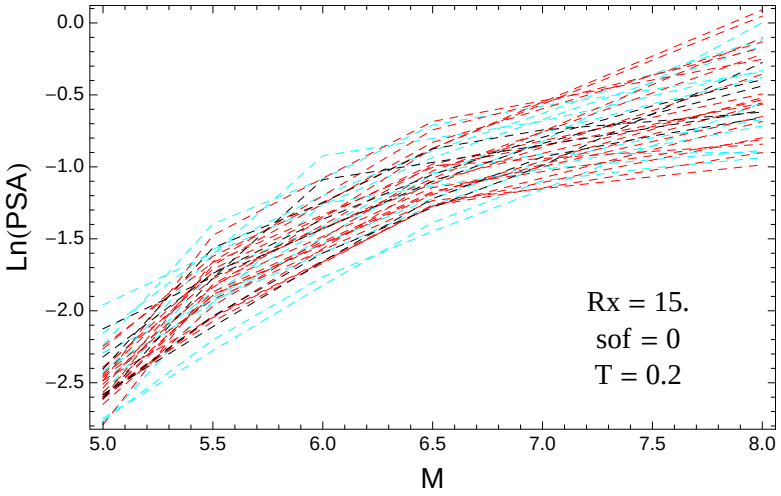



Figure 4.427: PVNGSv2: Magnitude scaling of the original GMPEs (dashed black), the original GMPEs with uncertainty model (dashed cyan) and selected B models (dashed red), for a scenario with $R_X = 15.$, $F = 0$, and $T = 0.2$s.

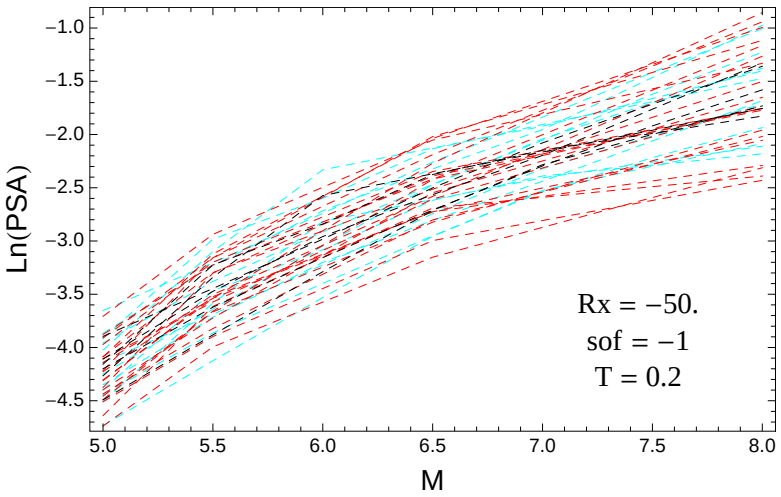



Figure 4.428: PVNGSv2: Magnitude scaling of the original GMPEs (dashed black), the original GMPEs with uncertainty model (dashed cyan) and selected B models (dashed red), for a scenario with $R_X = -50.$, $F = -1$, and $T = 0.2$s.

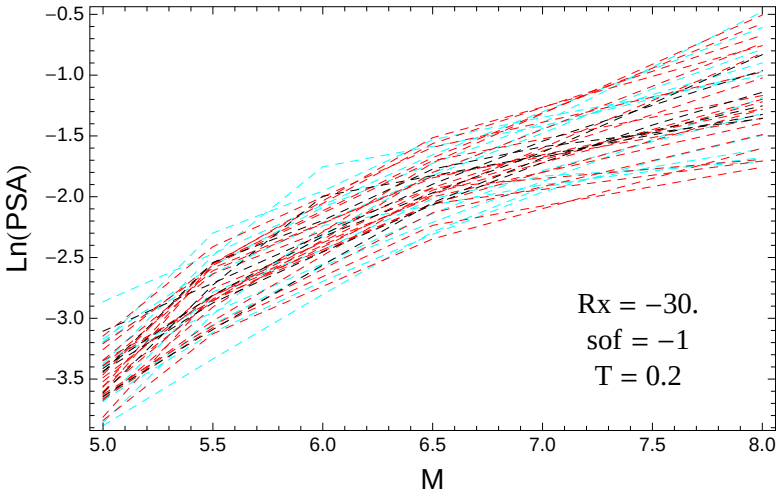



Figure 4.429: PVNGSv2: Magnitude scaling of the original GMPEs (dashed black), the original GMPEs with uncertainty model (dashed cyan) and selected B models (dashed red), for a scenario with $R_X = -30.$, $F = -1$, and $T = 0.2$s.

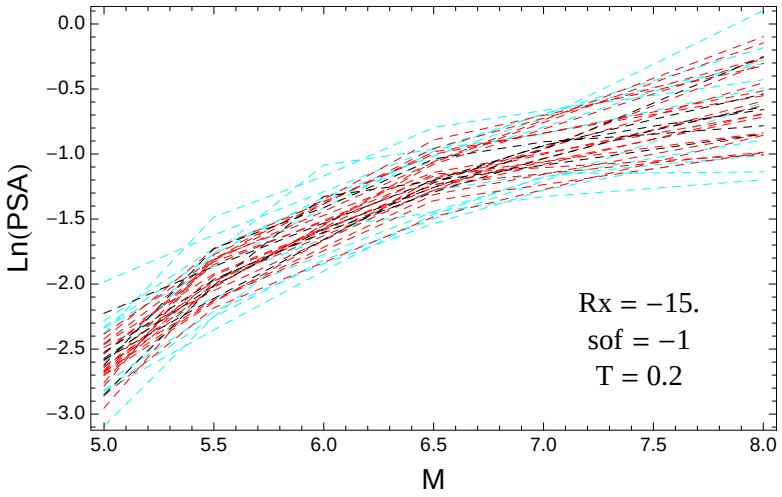



Figure 4.430: PVNGSv2: Magnitude scaling of the original GMPEs (dashed black), the original GMPEs with uncertainty model (dashed cyan) and selected B models (dashed red), for a scenario with $R_X = -15.$, $F = -1$, and $T = 0.2$s.

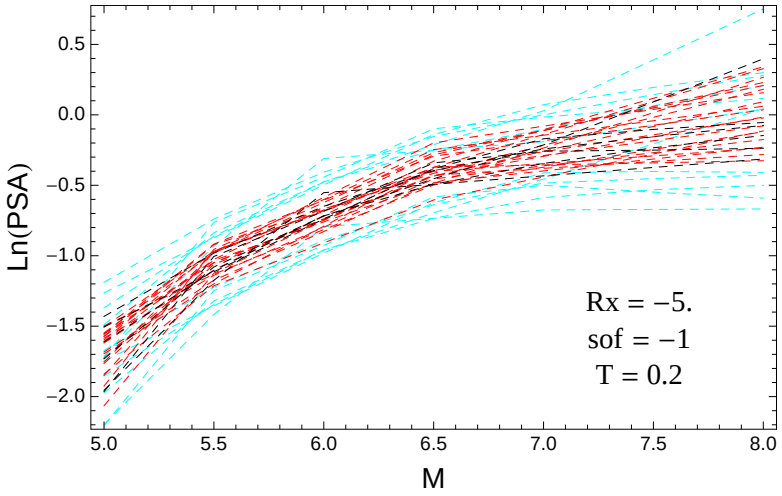



Figure 4.431: PVNGSv2: Magnitude scaling of the original GMPEs (dashed black), the original GMPEs with uncertainty model (dashed cyan) and selected B models (dashed red), for a scenario with $R_X = -5.$, $F = -1$, and $T = 0.2$s.

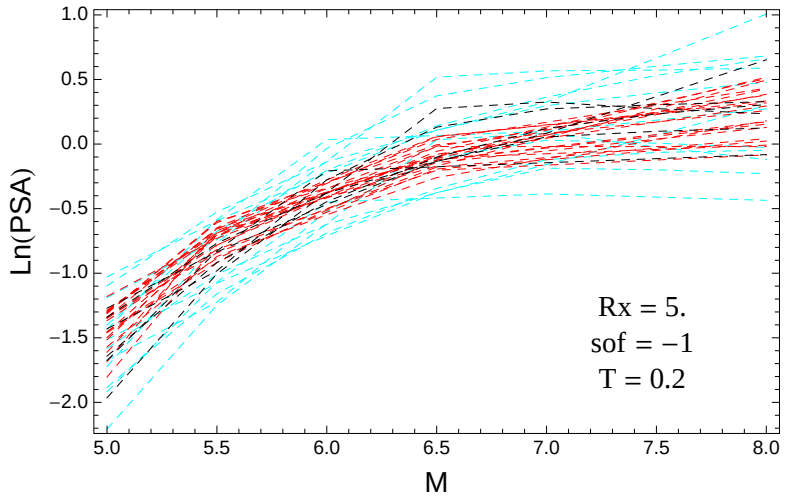



Figure 4.432: PVNGSv2: Magnitude scaling of the original GMPEs (dashed black), the original GMPEs with uncertainty model (dashed cyan) and selected B models (dashed red), for a scenario with $R_X = 5.$, $F = -1$, and $T = 0.2$s.

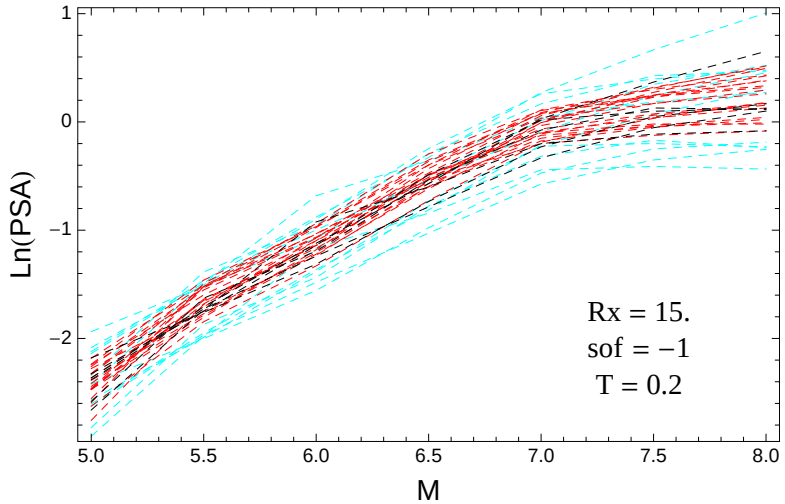



Figure 4.433: PVNGSv2: Magnitude scaling of the original GMPEs (dashed black), the original GMPEs with uncertainty model (dashed cyan) and selected B models (dashed red), for a scenario with $R_X = 15.$, $F = -1$, and $T = 0.2$s.

**T = 0.5s**

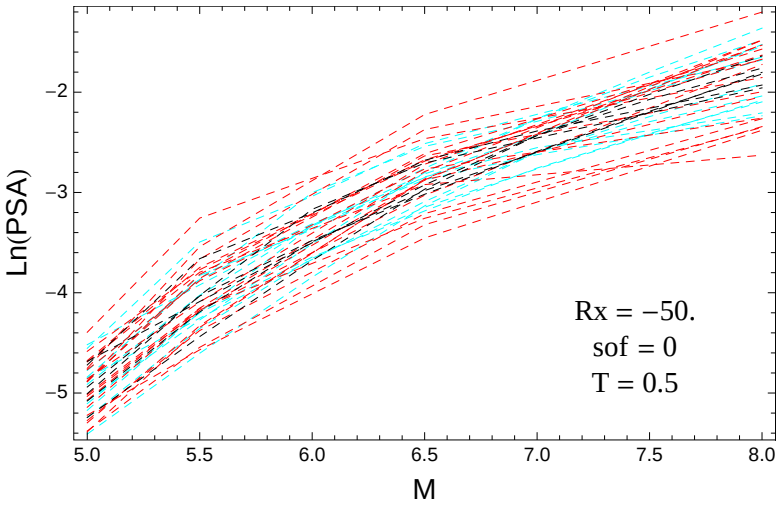



Figure 4.434: PVNGSv2: Magnitude scaling of the original GMPEs (dashed black), the original GMPEs with uncertainty model (dashed cyan) and selected B models (dashed red), for a scenario with $R_X = -50.$, $F = 0$, and $T = 0.5$s.

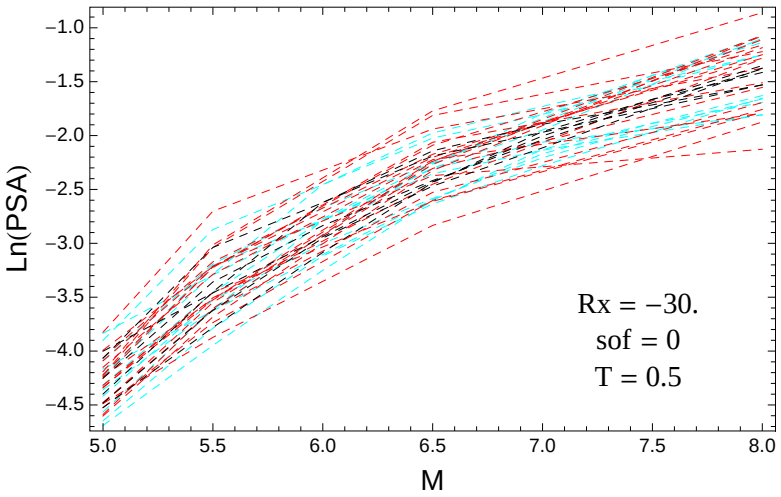



Figure 4.435: PVNGSv2: Magnitude scaling of the original GMPEs (dashed black), the original GMPEs with uncertainty model (dashed cyan) and selected B models (dashed red), for a scenario with $R_X = -30.$, $F = 0$, and $T = 0.5$s.

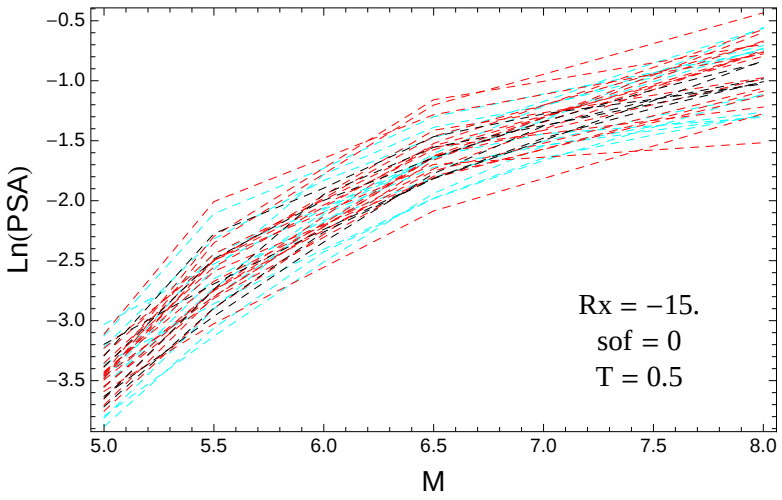



Figure 4.436: PVNGSv2: Magnitude scaling of the original GMPEs (dashed black), the original GMPEs with uncertainty model (dashed cyan) and selected B models (dashed red), for a scenario with $R_X = -15.$, $F = 0$, and $T = 0.5$s.

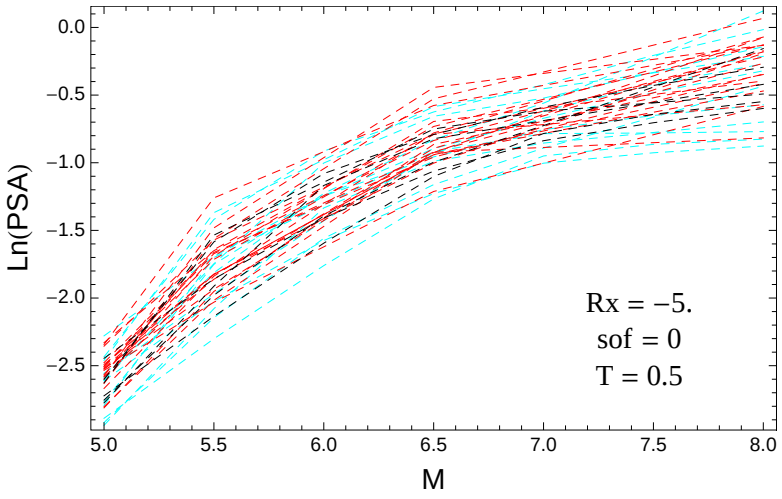



Figure 4.437: PVNGSv2: Magnitude scaling of the original GMPEs (dashed black), the original GMPEs with uncertainty model (dashed cyan) and selected B models (dashed red), for a scenario with $R_X = -5.$, $F = 0$, and $T = 0.5$s.

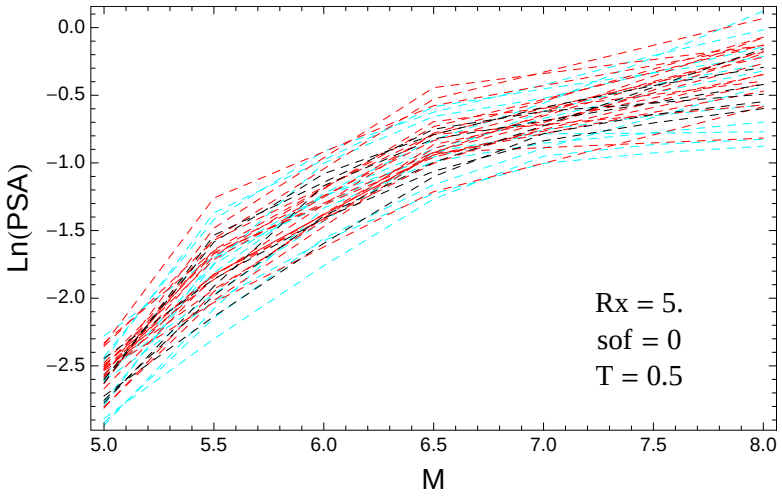



Figure 4.438: PVNGSv2: Magnitude scaling of the original GMPEs (dashed black), the original GMPEs with uncertainty model (dashed cyan) and selected B models (dashed red), for a scenario with $R_X = 5.$, $F = 0$, and $T = 0.5$s.

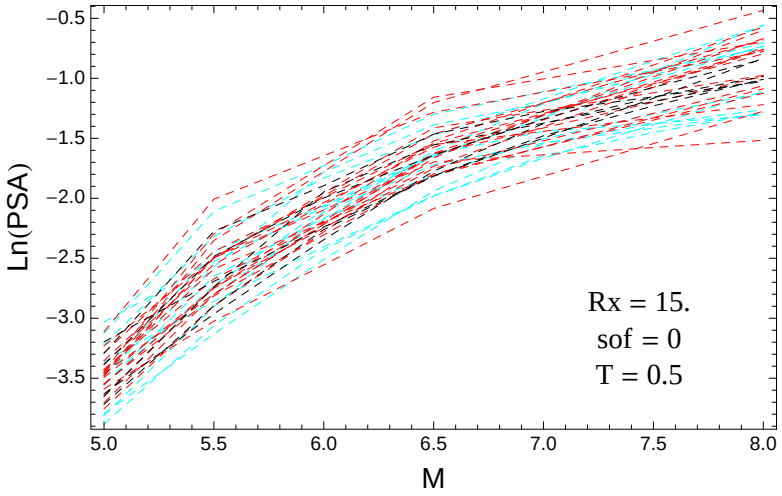



Figure 4.439: PVNGSv2: Magnitude scaling of the original GMPEs (dashed black), the original GMPEs with uncertainty model (dashed cyan) and selected B models (dashed red), for a scenario with $R_X = 15.$, $F = 0$, and $T = 0.5$s.

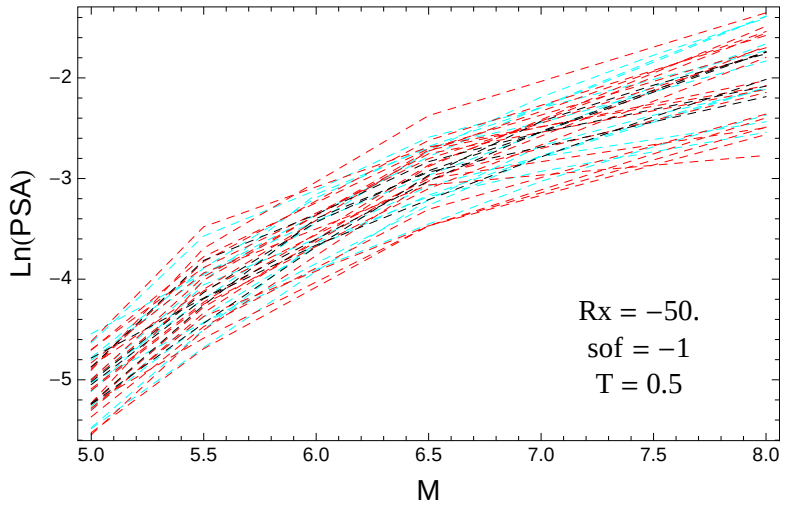



Figure 4.440: PVNGSv2: Magnitude scaling of the original GMPEs (dashed black), the original GMPEs with uncertainty model (dashed cyan) and selected B models (dashed red), for a scenario with $R_X = -50.$, $F = -1$, and $T = 0.5$s.

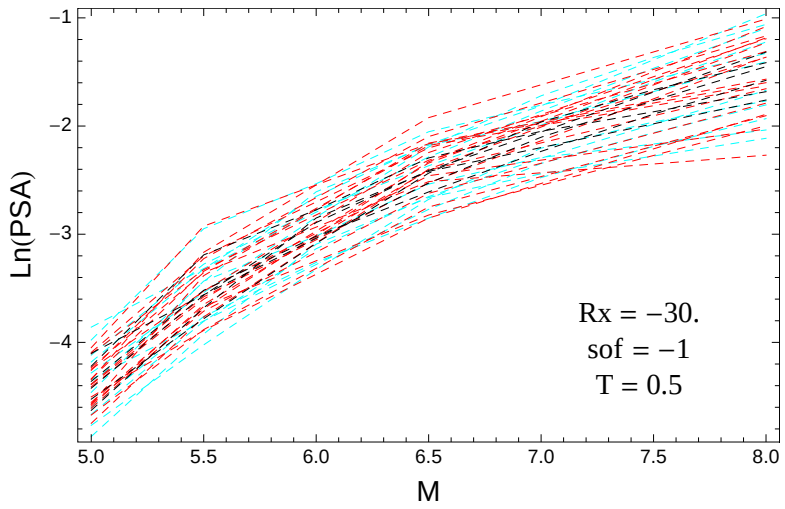



Figure 4.441: PVNGSv2: Magnitude scaling of the original GMPEs (dashed black), the original GMPEs with uncertainty model (dashed cyan) and selected B models (dashed red), for a scenario with $R_X = -30.$, $F = -1$, and $T = 0.5$s.

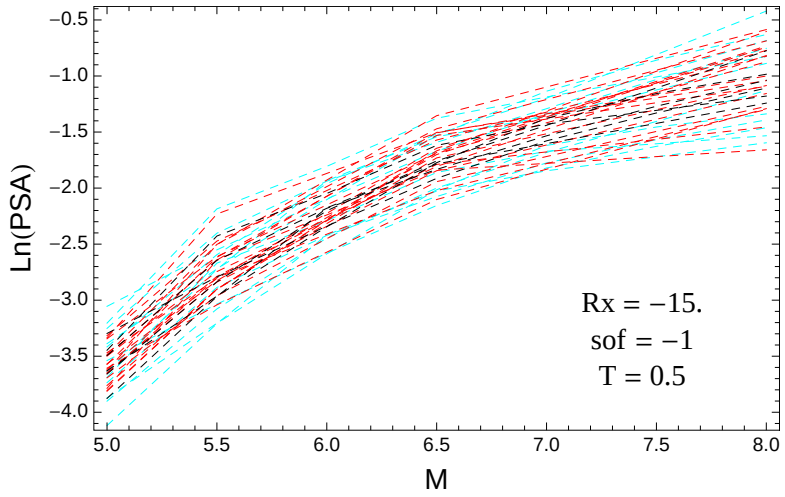



Figure 4.442: PVNGSv2: Magnitude scaling of the original GMPEs (dashed black), the original GMPEs with uncertainty model (dashed cyan) and selected B models (dashed red), for a scenario with $R_X = -15.$, $F = -1$, and $T = 0.5$s.

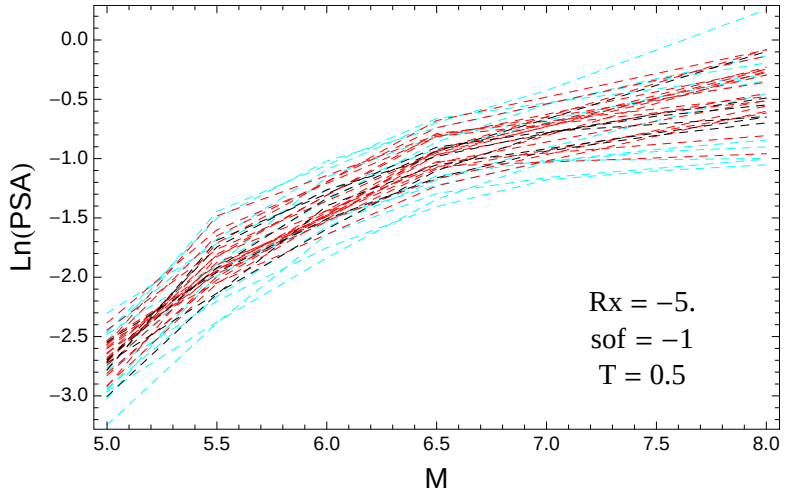



Figure 4.443: PVNGSv2: Magnitude scaling of the original GMPEs (dashed black), the original GMPEs with uncertainty model (dashed cyan) and selected B models (dashed red), for a scenario with $R_X = -5.$, $F = -1$, and $T = 0.5$s.

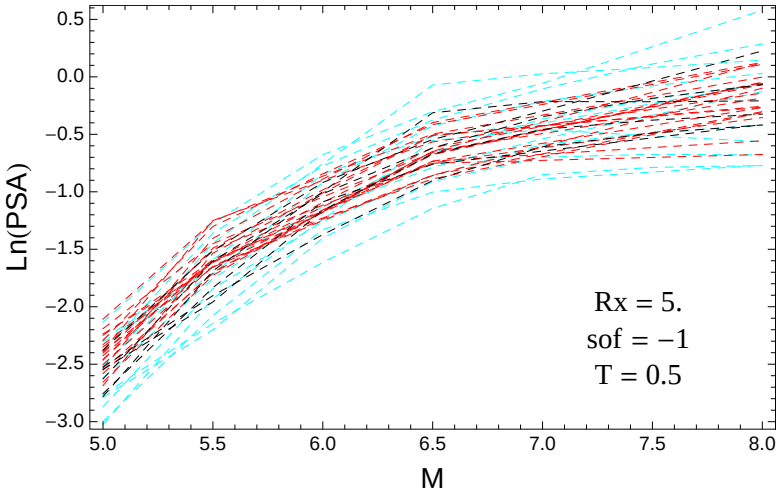



Figure 4.444: PVNGSv2: Magnitude scaling of the original GMPEs (dashed black), the original GMPEs with uncertainty model (dashed cyan) and selected B models (dashed red), for a scenario with $R_X = 5.$, $F = -1$, and $T = 0.5$s.

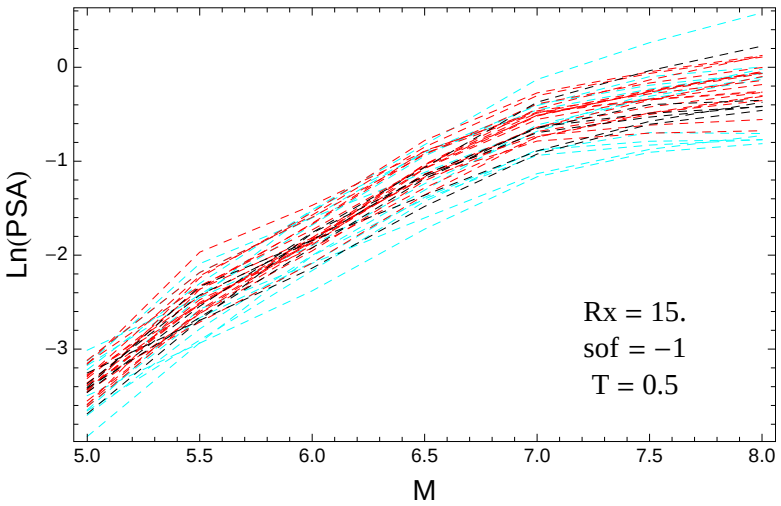



Figure 4.445: PVNGSv2: Magnitude scaling of the original GMPEs (dashed black), the original GMPEs with uncertainty model (dashed cyan) and selected B models (dashed red), for a scenario with $R_X = 15.$, $F = -1$, and $T = 0.5$s.

**T = 1.s**

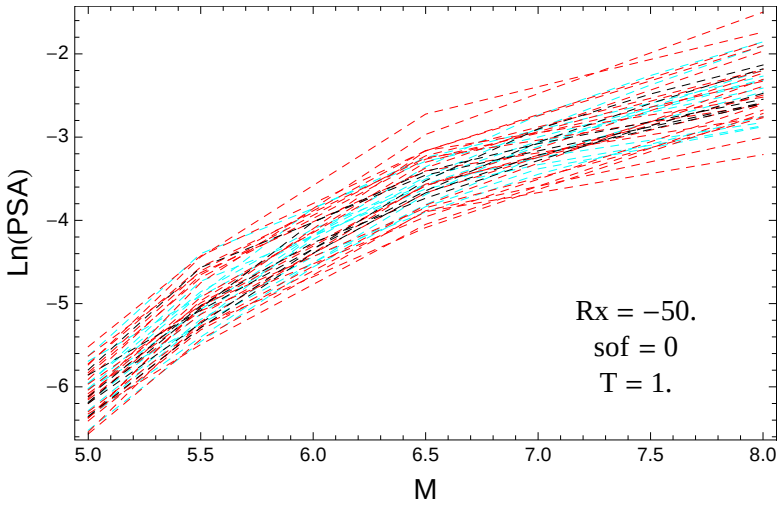



Figure 4.446: PVNGSv2: Magnitude scaling of the original GMPEs (dashed black), the original GMPEs with uncertainty model (dashed cyan) and selected B models (dashed red), for a scenario with $R_X = -50.$, $F = 0$, and $T = 1.$s.

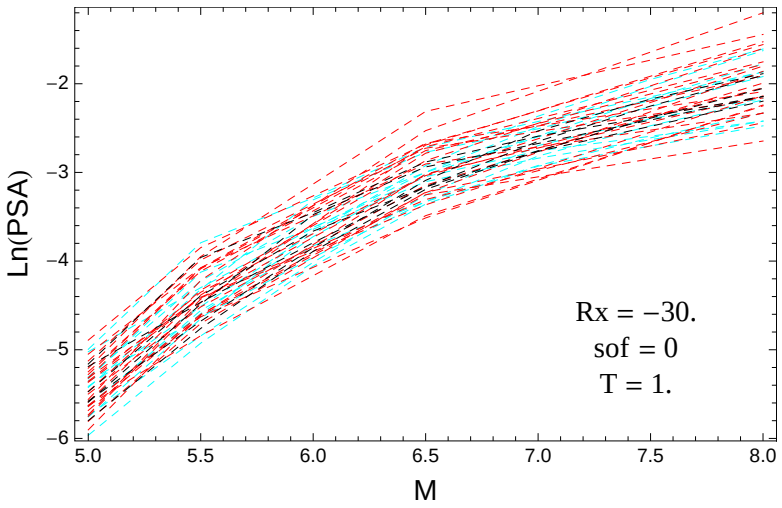



Figure 4.447: PVNGSv2: Magnitude scaling of the original GMPEs (dashed black), the original GMPEs with uncertainty model (dashed cyan) and selected B models (dashed red), for a scenario with $R_X = -30.$, $F = 0$, and $T = 1.$s.

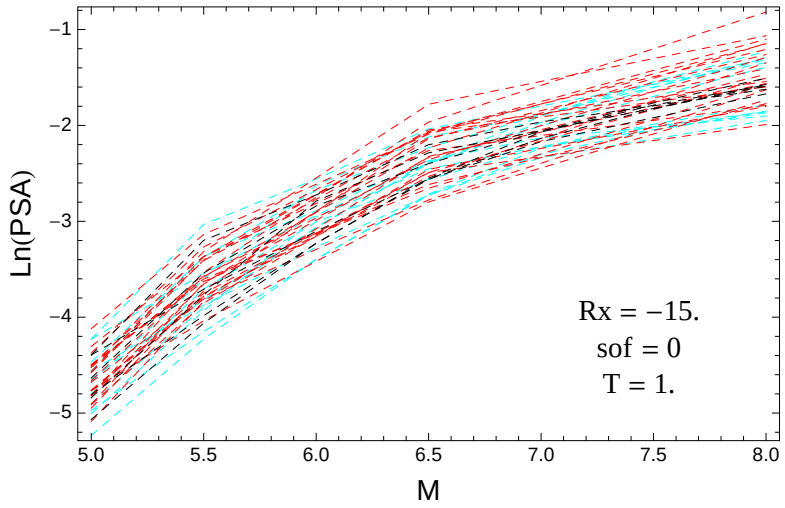



Figure 4.448: PVNGSv2: Magnitude scaling of the original GMPEs (dashed black), the original GMPEs with uncertainty model (dashed cyan) and selected B models (dashed red), for a scenario with $R_X = -15.$, $F = 0$, and $T = 1.$s.

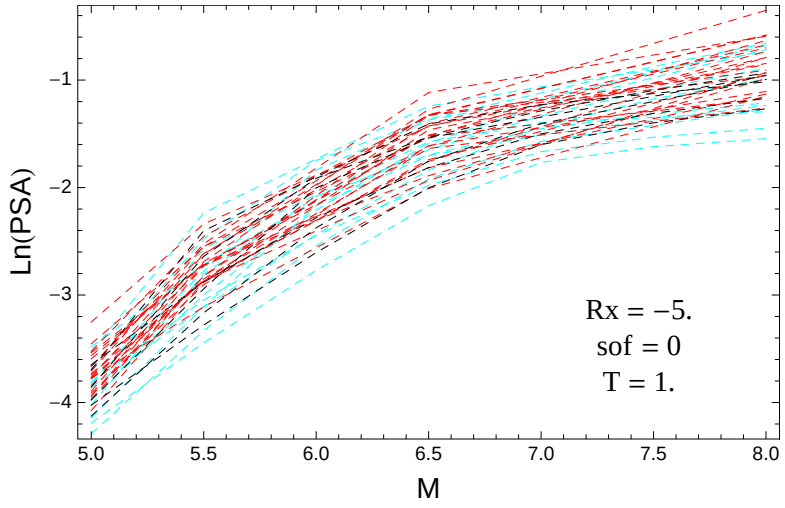



Figure 4.449: PVNGSv2: Magnitude scaling of the original GMPEs (dashed black), the original GMPEs with uncertainty model (dashed cyan) and selected B models (dashed red), for a scenario with $R_X = -5.$, $F = 0$, and $T = 1.$s.

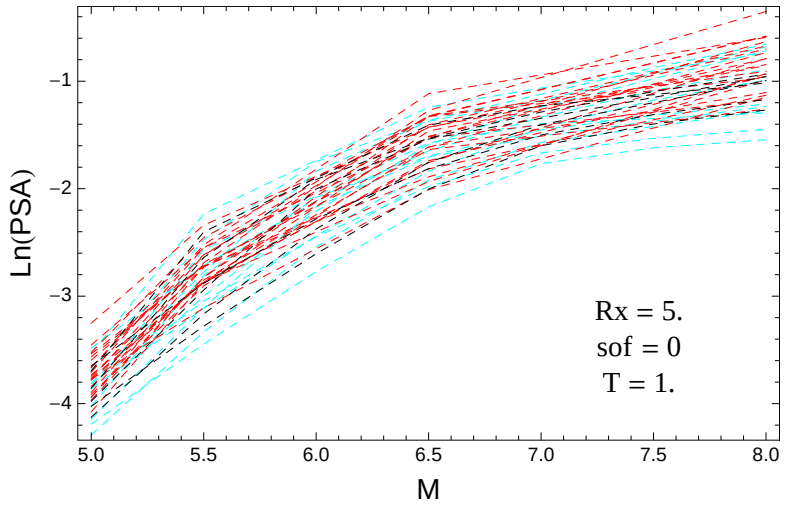



Figure 4.450: PVNGSv2: Magnitude scaling of the original GMPEs (dashed black), the original GMPEs with uncertainty model (dashed cyan) and selected B models (dashed red), for a scenario with $R_X = 5.$, $F = 0$, and $T = 1.$s.

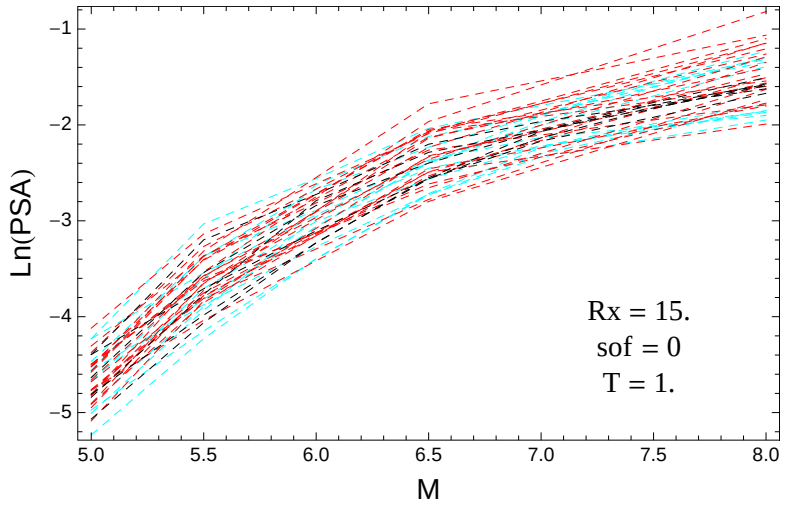



Figure 4.451: PVNGSv2: Magnitude scaling of the original GMPEs (dashed black), the original GMPEs with uncertainty model (dashed cyan) and selected B models (dashed red), for a scenario with $R_X = 15.$, $F = 0$, and $T = 1.$s.

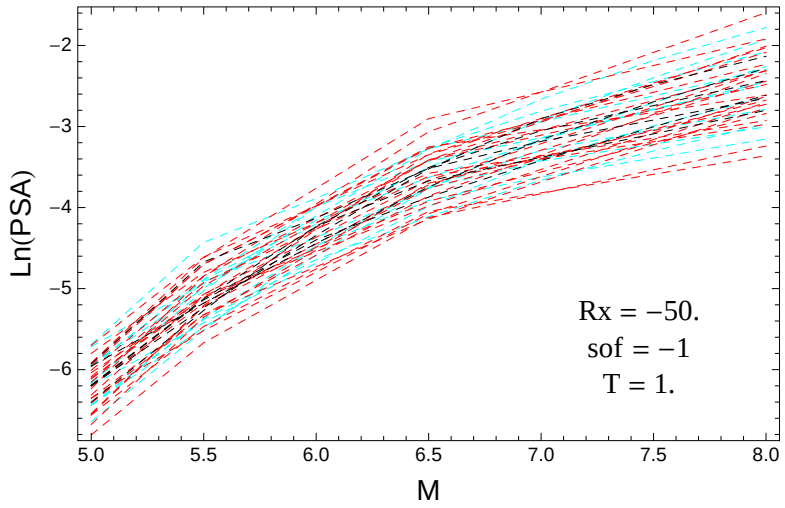



Figure 4.452: PVNGSv2: Magnitude scaling of the original GMPEs (dashed black), the original GMPEs with uncertainty model (dashed cyan) and selected B models (dashed red), for a scenario with $R_X = -50.$, $F = -1$, and $T = 1.$s.

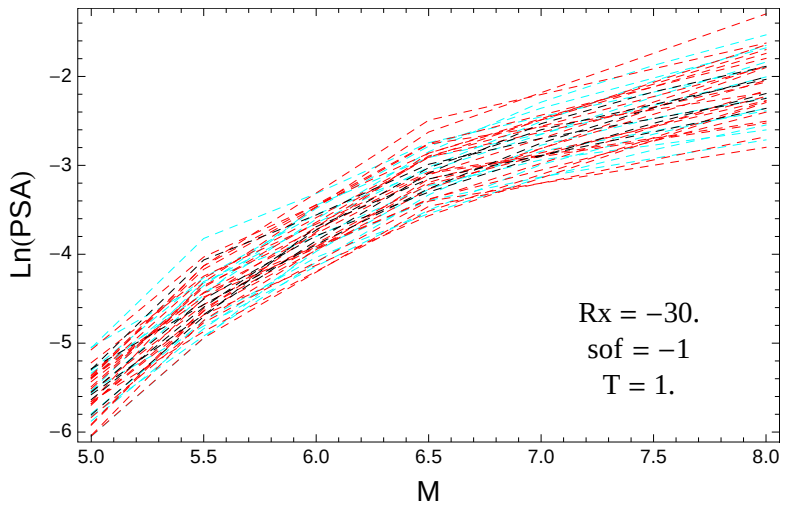



Figure 4.453: PVNGSv2: Magnitude scaling of the original GMPEs (dashed black), the original GMPEs with uncertainty model (dashed cyan) and selected B models (dashed red), for a scenario with $R_X = -30.$, $F = -1$, and $T = 1.$s.

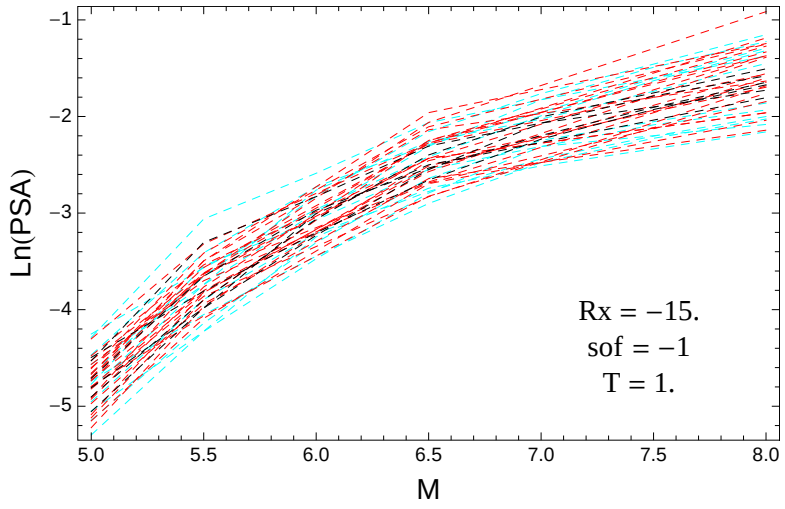



Figure 4.454: PVNGSv2: Magnitude scaling of the original GMPEs (dashed black), the original GMPEs with uncertainty model (dashed cyan) and selected B models (dashed red), for a scenario with $R_X = -15.$, $F = -1$, and $T = 1.$s.

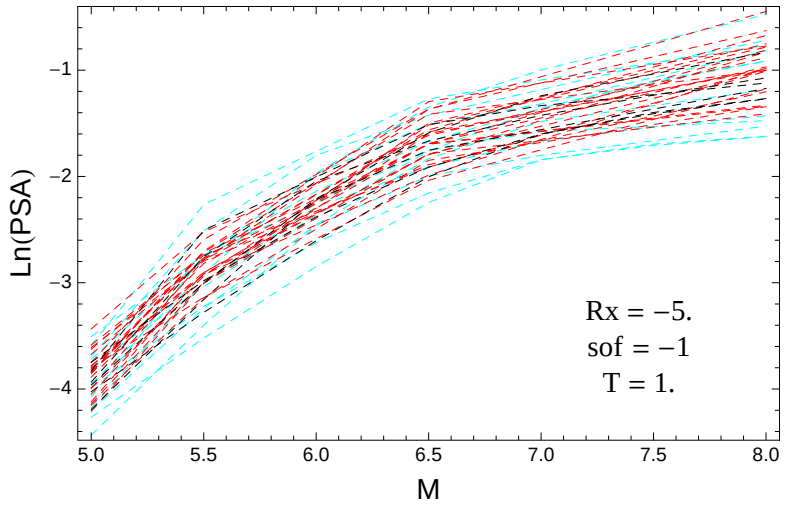



Figure 4.455: PVNGSv2: Magnitude scaling of the original GMPEs (dashed black), the original GMPEs with uncertainty model (dashed cyan) and selected B models (dashed red), for a scenario with $R_X = -5.$, $F = -1$, and $T = 1.$s.

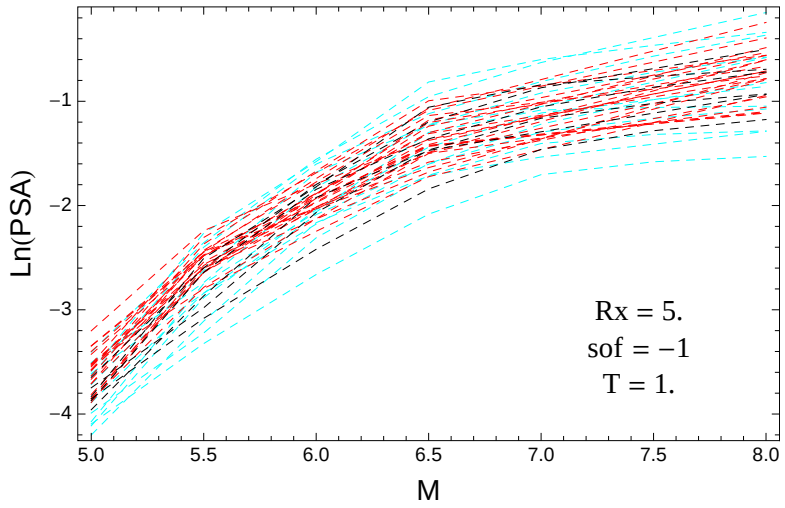



Figure 4.456: PVNGSv2: Magnitude scaling of the original GMPEs (dashed black), the original GMPEs with uncertainty model (dashed cyan) and selected B models (dashed red), for a scenario with $R_X = 5.$, $F = -1$, and $T = 1.$s.

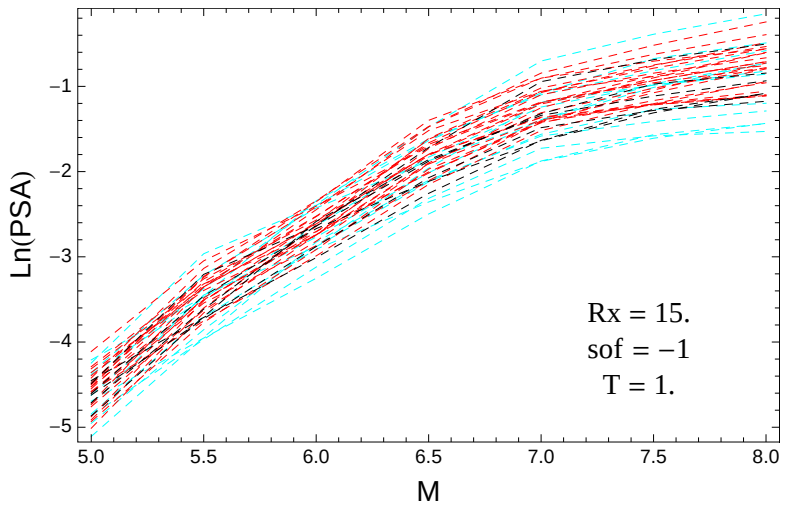



Figure 4.457: PVNGSv2: Magnitude scaling of the original GMPEs (dashed black), the original GMPEs with uncertainty model (dashed cyan) and selected B models (dashed red), for a scenario with $R_X = 15.$, $F = -1$, and $T = 1.$s.

**T = 3.s**

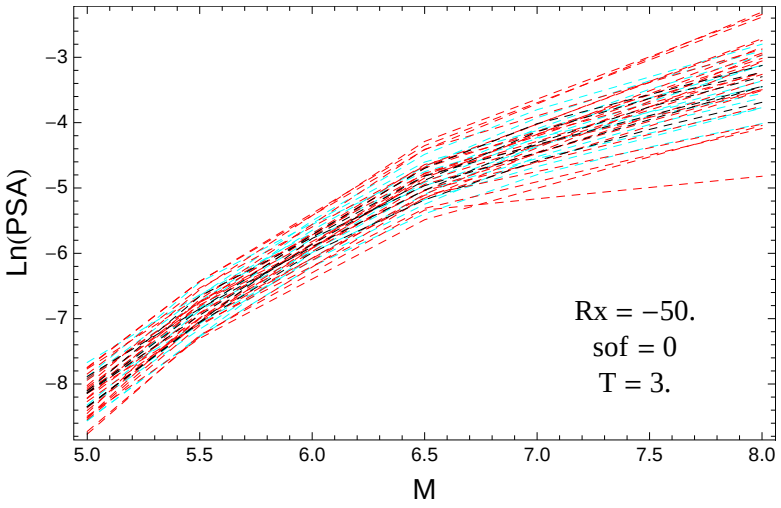



Figure 4.458: PVNGSv2: Magnitude scaling of the original GMPEs (dashed black), the original GMPEs with uncertainty model (dashed cyan) and selected B models (dashed red), for a scenario with $R_X = -50.$, $F = 0$, and $T = 3.$s.

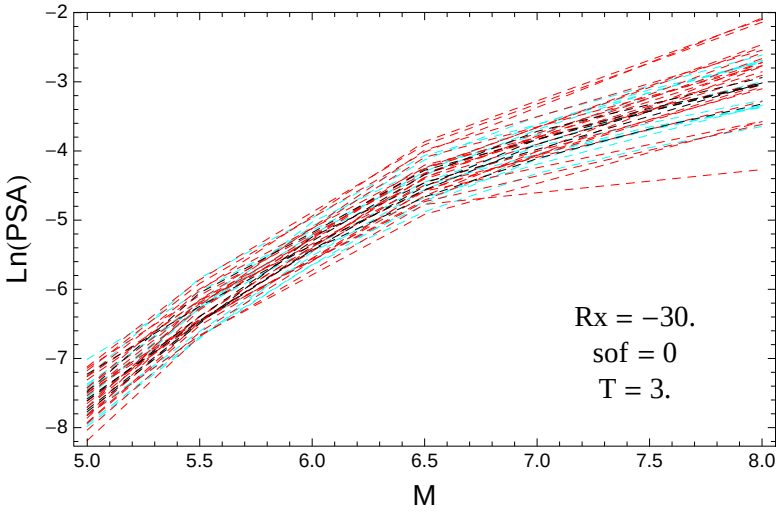



Figure 4.459: PVNGSv2: Magnitude scaling of the original GMPEs (dashed black), the original GMPEs with uncertainty model (dashed cyan) and selected B models (dashed red), for a scenario with $R_X = -30.$, $F = 0$, and $T = 3.$s.

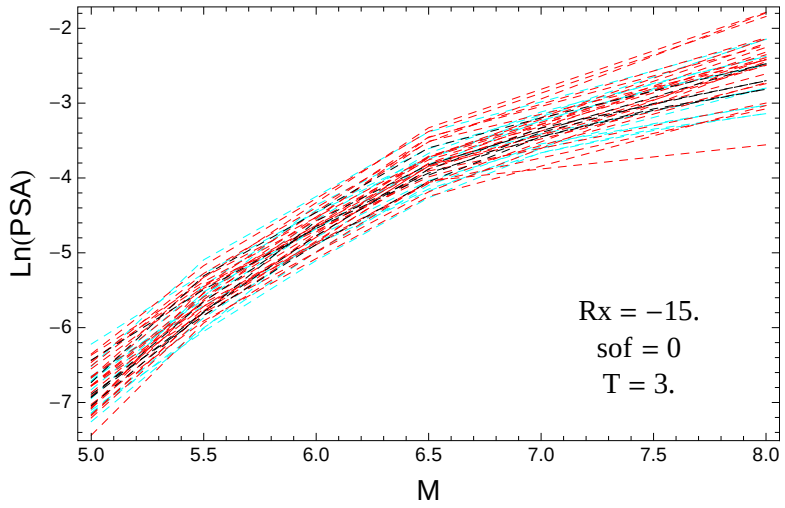



Figure 4.460: PVNGSv2: Magnitude scaling of the original GMPEs (dashed black), the original GMPEs with uncertainty model (dashed cyan) and selected B models (dashed red), for a scenario with $R_X = -15.$, $F = 0$, and $T = 3.$s.

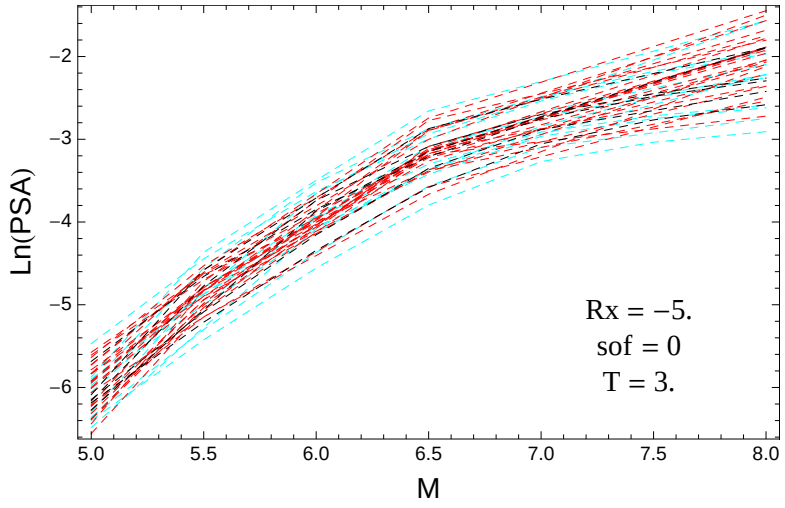



Figure 4.461: PVNGSv2: Magnitude scaling of the original GMPEs (dashed black), the original GMPEs with uncertainty model (dashed cyan) and selected B models (dashed red), for a scenario with $R_X = -5.$, $F = 0$, and $T = 3.$s.

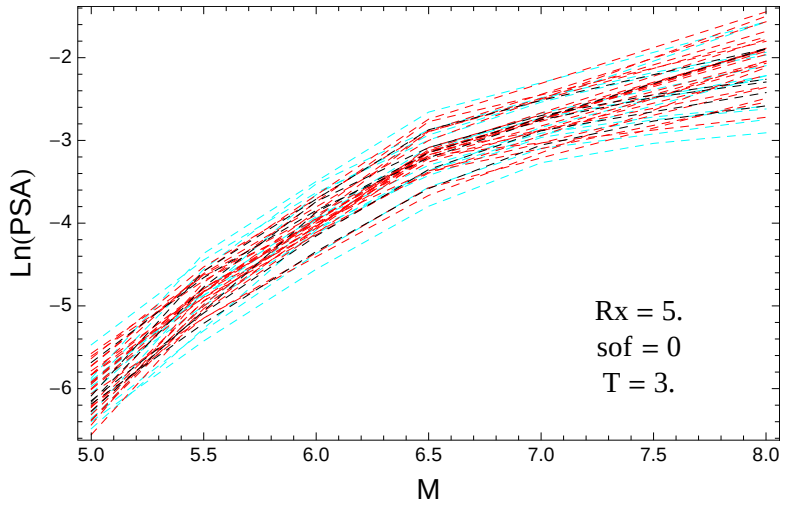



Figure 4.462: PVNGSv2: Magnitude scaling of the original GMPEs (dashed black), the original GMPEs with uncertainty model (dashed cyan) and selected B models (dashed red), for a scenario with $R_X = 5.$, $F = 0$, and $T = 3.$s.

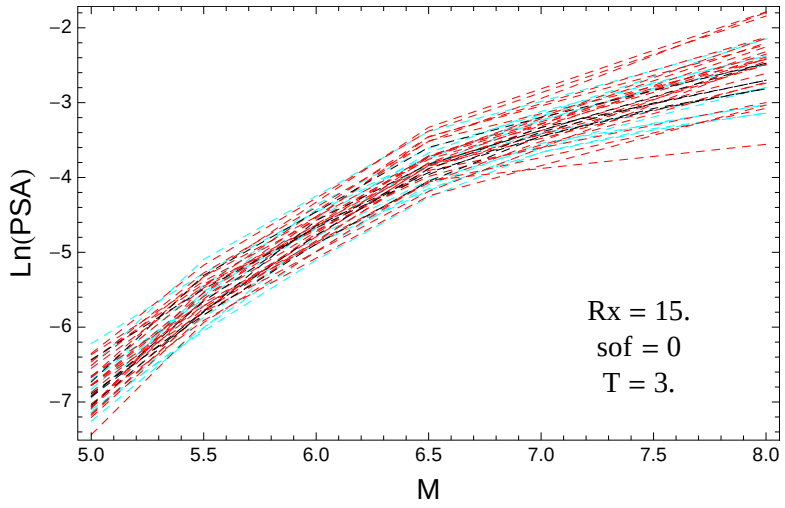



Figure 4.463: PVNGSv2: Magnitude scaling of the original GMPEs (dashed black), the original GMPEs with uncertainty model (dashed cyan) and selected B models (dashed red), for a scenario with $R_X = 15.$, $F = 0$, and $T = 3.$s.

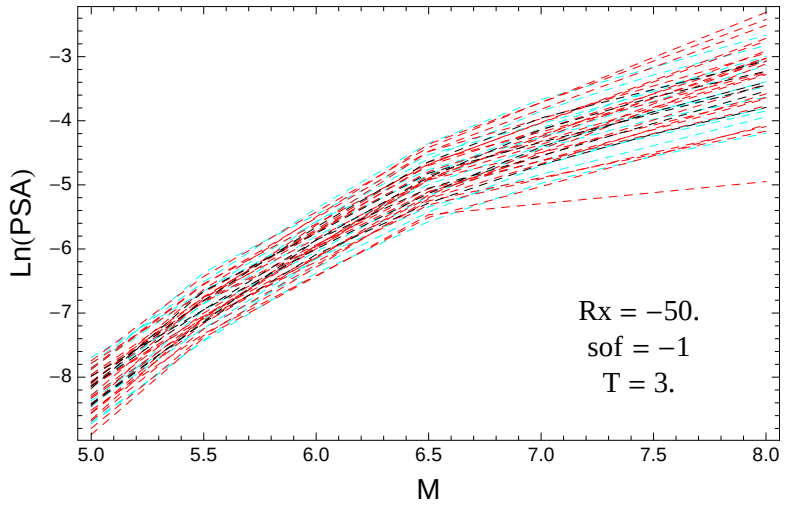



Figure 4.464: PVNGSv2: Magnitude scaling of the original GMPEs (dashed black), the original GMPEs with uncertainty model (dashed cyan) and selected B models (dashed red), for a scenario with $R_X = -50.$, $F = -1$, and $T = 3.$s.

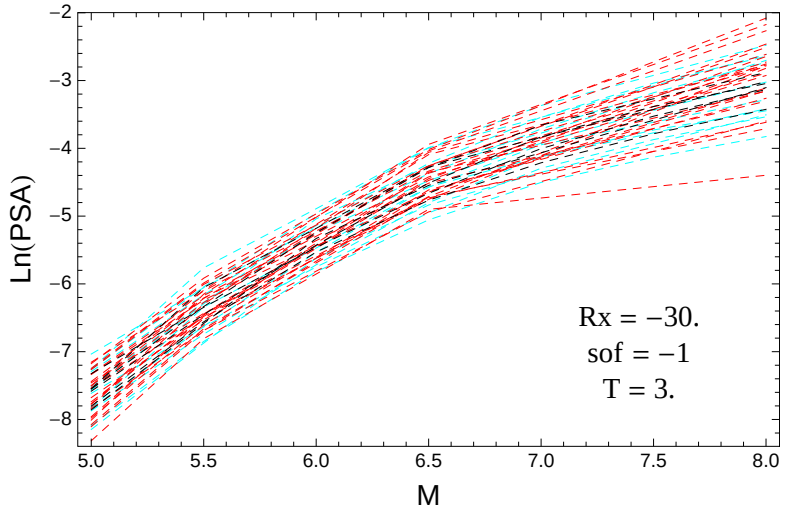



Figure 4.465: PVNGSv2: Magnitude scaling of the original GMPEs (dashed black), the original GMPEs with uncertainty model (dashed cyan) and selected B models (dashed red), for a scenario with $R_X = -30.$, $F = -1$, and $T = 3.$s.

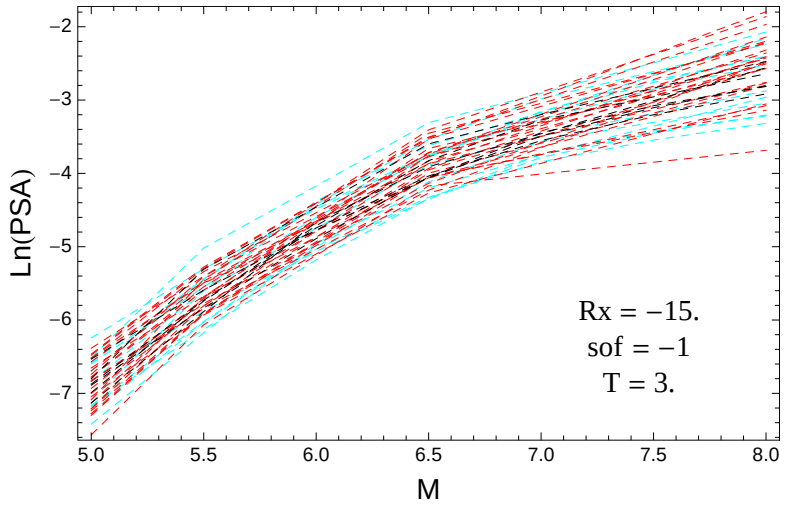



Figure 4.466: PVNGSv2: Magnitude scaling of the original GMPEs (dashed black), the original GMPEs with uncertainty model (dashed cyan) and selected B models (dashed red), for a scenario with $R_X = -15.$, $F = -1$, and $T = 3.$s.

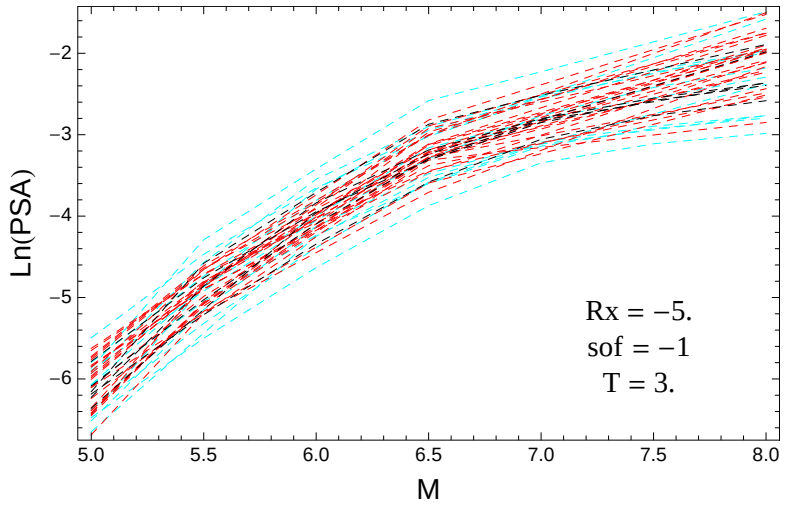



Figure 4.467: PVNGSv2: Magnitude scaling of the original GMPEs (dashed black), the original GMPEs with uncertainty model (dashed cyan) and selected B models (dashed red), for a scenario with $R_X = -5.$, $F = -1$, and $T = 3.$s.

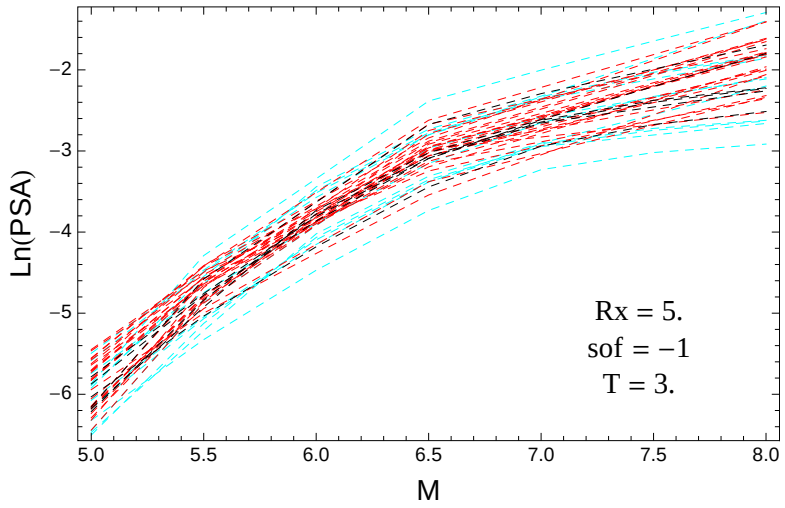



Figure 4.468: PVNGSv2: Magnitude scaling of the original GMPEs (dashed black), the original GMPEs with uncertainty model (dashed cyan) and selected B models (dashed red), for a scenario with $R_X = 5.$, $F = -1$, and $T = 3.$s.

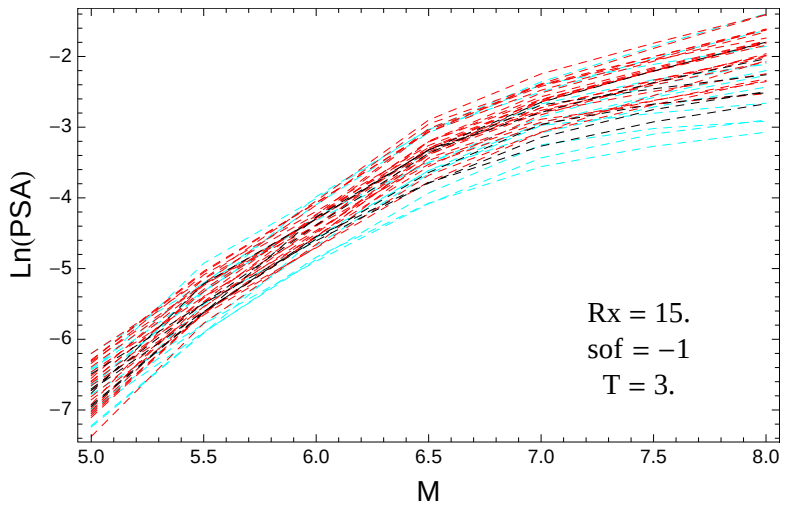



Figure 4.469: PVNGSv2: Magnitude scaling of the original GMPEs (dashed black), the original GMPEs with uncertainty model (dashed cyan) and selected B models (dashed red), for a scenario with $R_X = 15.$, $F = -1$, and $T = 3.$s.

### 4.1.12 Distance Scaling with GMPEs

**T = 0.01s**

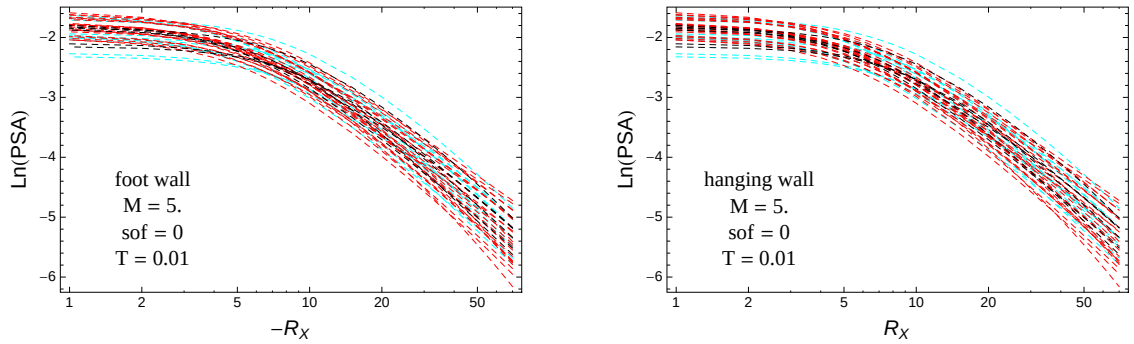



Figure 4.470: PVNGSv2: Distance scaling of the original GMPEs (dashed black), the original GMPEs with uncertainty model (dashed cyan) and selected B models (dashed red), for a scenario with $M = 5.$, $F = 0$, and $T = 0.01$s. Left: foot wall scaling; Right: hanging wall scaling.

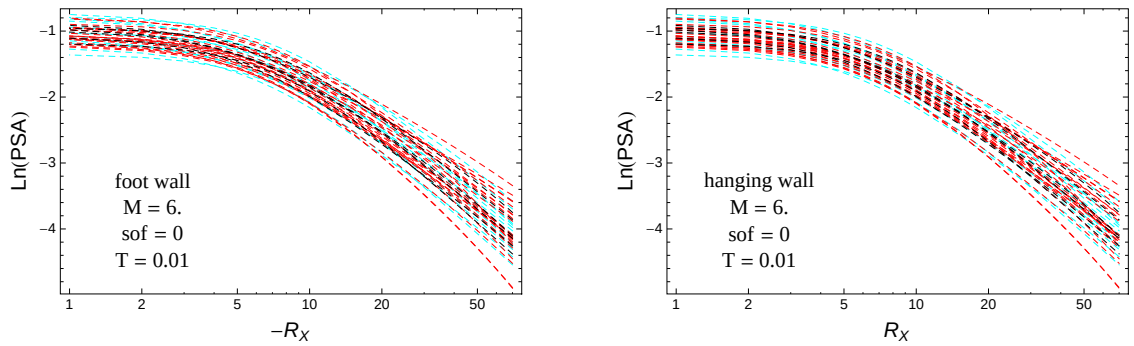



Figure 4.471: PVNGSv2: Distance scaling of the original GMPEs (dashed black), the original GMPEs with uncertainty model (dashed cyan) and selected B models (dashed red), for a scenario with $M = 6.$, $F = 0$, and $T = 0.01$s. Left: foot wall scaling; Right: hanging wall scaling.

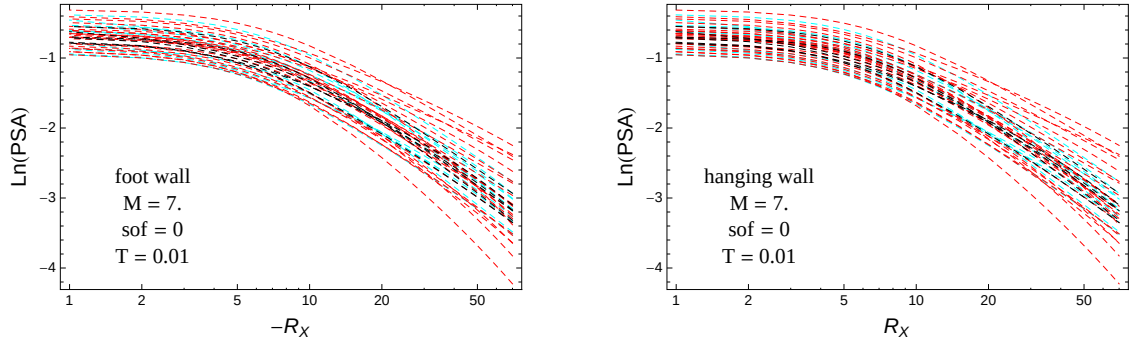



Figure 4.472: PVNGSv2: Distance scaling of the original GMPEs (dashed black), the original GMPEs with uncertainty model (dashed cyan) and selected B models (dashed red), for a scenario with $M = 7.$, $F = 0$, and $T = 0.01$s. Left: foot wall scaling; Right: hanging wall scaling.

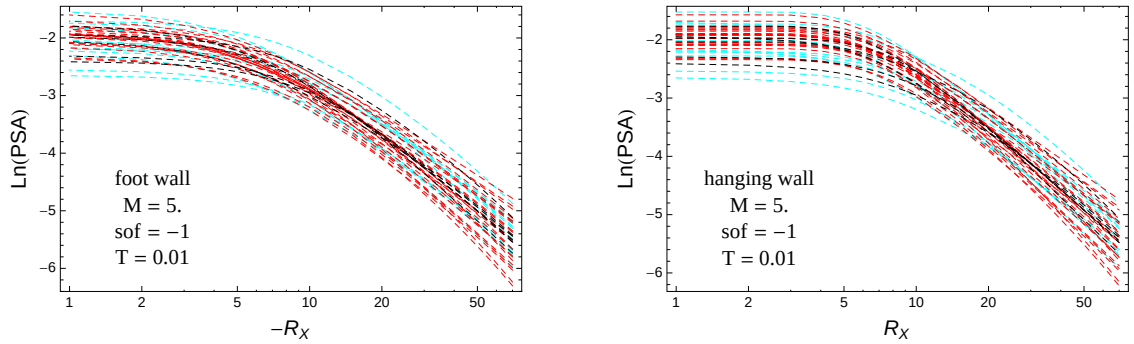



Figure 4.473: PVNGSv2: Distance scaling of the original GMPEs (dashed black), the original GMPEs with uncertainty model (dashed cyan) and selected B models (dashed red), for a scenario with $M = 5.$, $F = -1$, and $T = 0.01$s. Left: foot wall scaling; Right: hanging wall scaling.

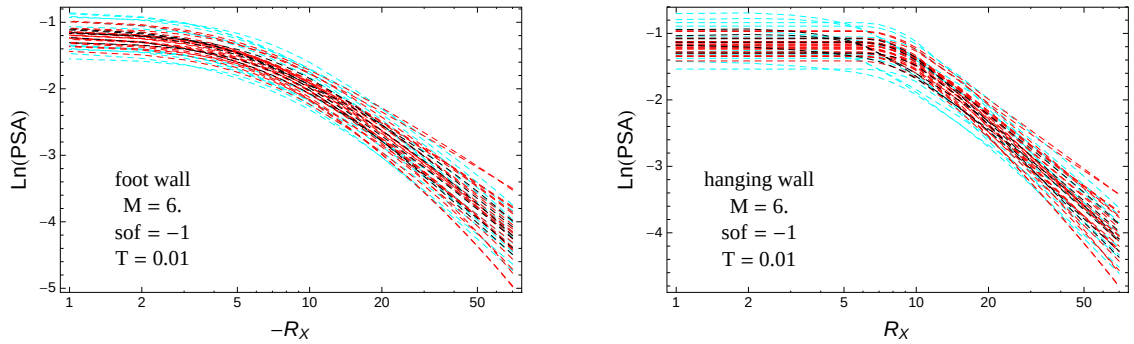



Figure 4.474: PVNGSv2: Distance scaling of the original GMPEs (dashed black), the original GMPEs with uncertainty model (dashed cyan) and selected B models (dashed red), for a scenario with $M = 6.$, $F = -1$, and $T = 0.01$s. Left: foot wall scaling; Right: hanging wall scaling.

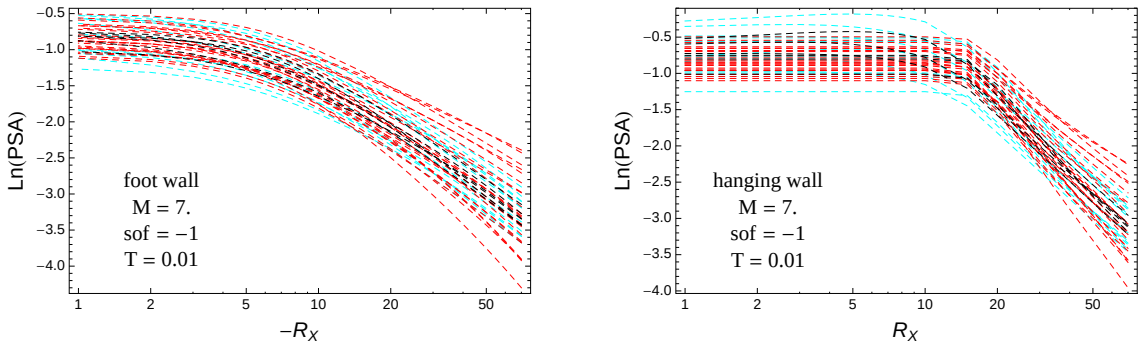



Figure 4.475: PVNGSv2: Distance scaling of the original GMPEs (dashed black), the original GMPEs with uncertainty model (dashed cyan) and selected B models (dashed red), for a scenario with $M = 7.$, $F = -1$, and $T = 0.01$s. Left: foot wall scaling; Right: hanging wall scaling.

**T = 0.2s**

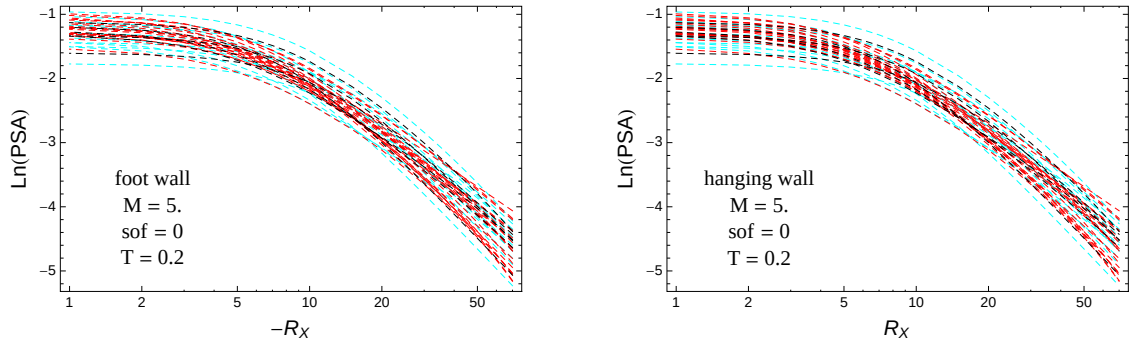



Figure 4.476: PVNGSv2: Distance scaling of the original GMPEs (dashed black), the original GMPEs with uncertainty model (dashed cyan) and selected B models (dashed red), for a scenario with $M = 5.$, $F = 0$, and $T = 0.2$s. Left: foot wall scaling; Right: hanging wall scaling.

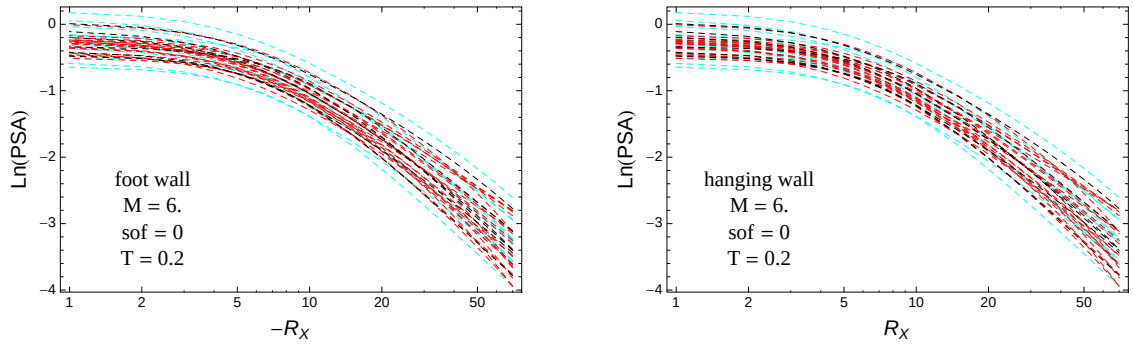



Figure 4.477: PVNGSv2: Distance scaling of the original GMPEs (dashed black), the original GMPEs with uncertainty model (dashed cyan) and selected B models (dashed red), for a scenario with $M = 6.$, $F = 0$, and $T = 0.2$s. Left: foot wall scaling; Right: hanging wall scaling.

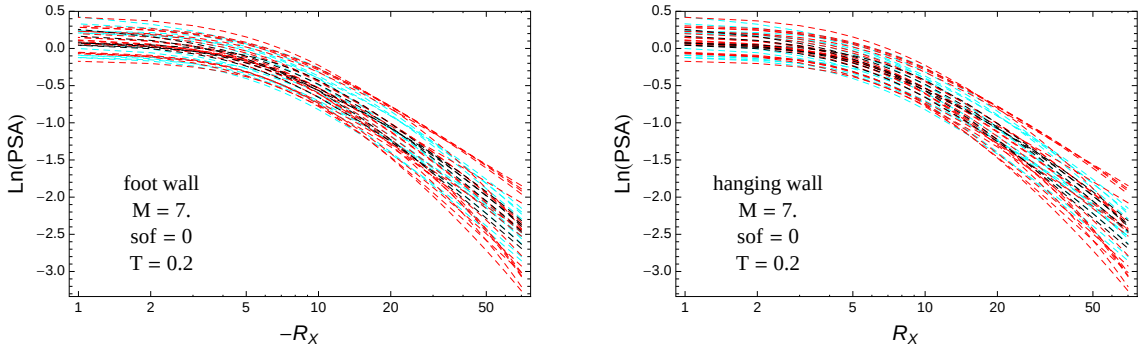



Figure 4.478: PVNGSv2: Distance scaling of the original GMPEs (dashed black), the original GMPEs with uncertainty model (dashed cyan) and selected B models (dashed red), for a scenario with $M = 7.$, $F = 0$, and $T = 0.2$s. Left: foot wall scaling; Right: hanging wall scaling.

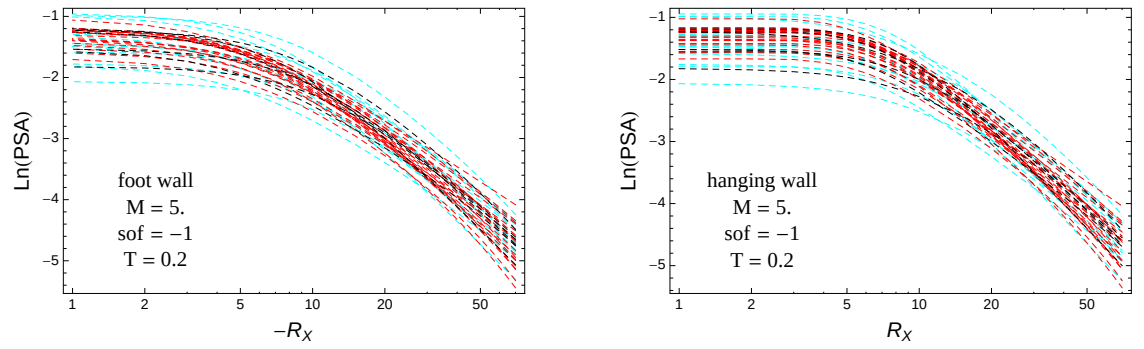



Figure 4.479: PVNGSv2: Distance scaling of the original GMPEs (dashed black), the original GMPEs with uncertainty model (dashed cyan) and selected B models (dashed red), for a scenario with $M = 5.$, $F = -1$, and $T = 0.2$s. Left: foot wall scaling; Right: hanging wall scaling.

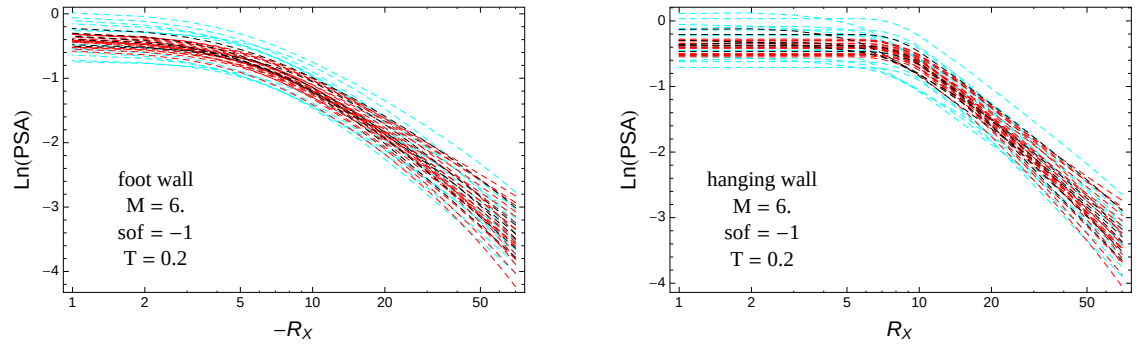



Figure 4.480: PVNGSv2: Distance scaling of the original GMPEs (dashed black), the original GMPEs with uncertainty model (dashed cyan) and selected B models (dashed red), for a scenario with $M = 6.$, $F = -1$, and $T = 0.2$s. Left: foot wall scaling; Right: hanging wall scaling.

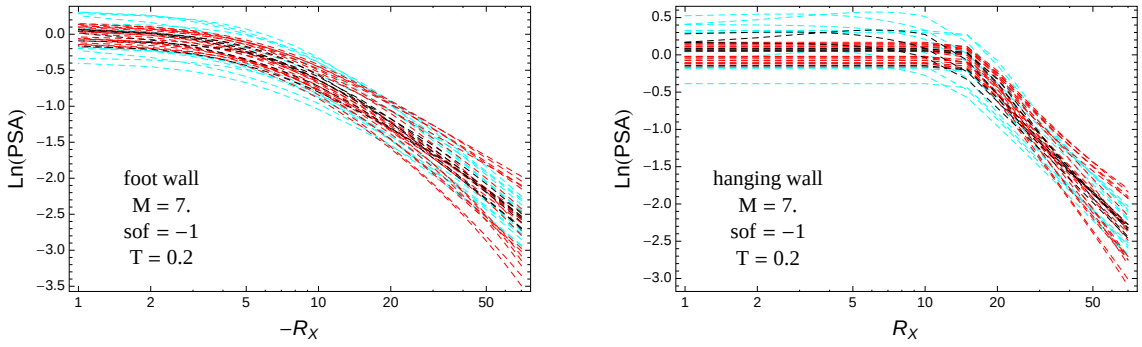



Figure 4.481: PVNGSv2: Distance scaling of the original GMPEs (dashed black), the original GMPEs with uncertainty model (dashed cyan) and selected B models (dashed red), for a scenario with $M = 7.$, $F = -1$, and $T = 0.2$s. Left: foot wall scaling; Right: hanging wall scaling.

**T = 0.5s**

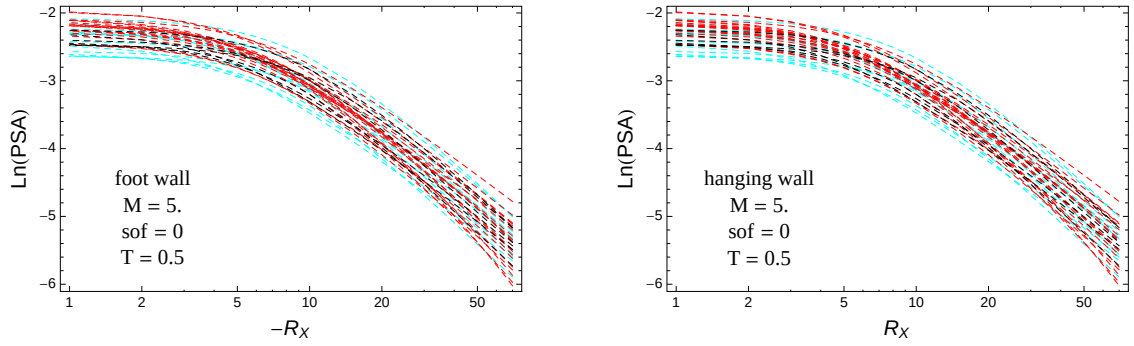



Figure 4.482: PVNGSv2: Distance scaling of the original GMPEs (dashed black), the original GMPEs with uncertainty model (dashed cyan) and selected B models (dashed red), for a scenario with $M = 5.$, $F = 0$, and $T = 0.5$s. Left: foot wall scaling; Right: hanging wall scaling.

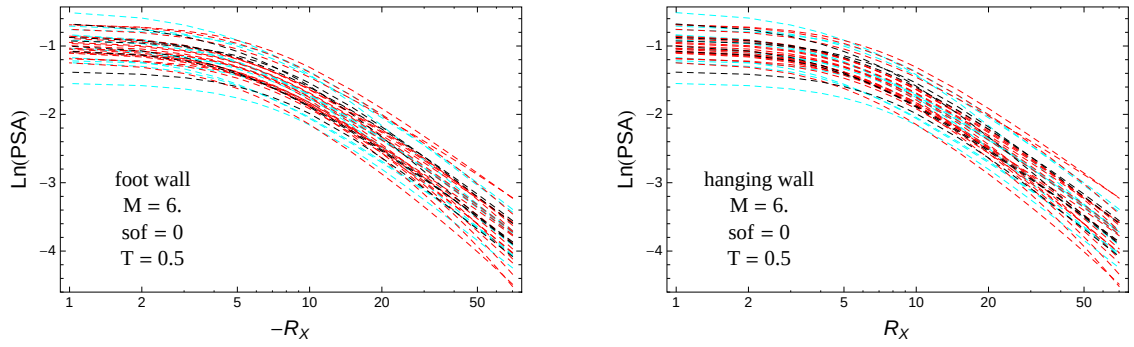



Figure 4.483: PVNGSv2: Distance scaling of the original GMPEs (dashed black), the original GMPEs with uncertainty model (dashed cyan) and selected B models (dashed red), for a scenario with $M = 6.$, $F = 0$, and $T = 0.5$s. Left: foot wall scaling; Right: hanging wall scaling.

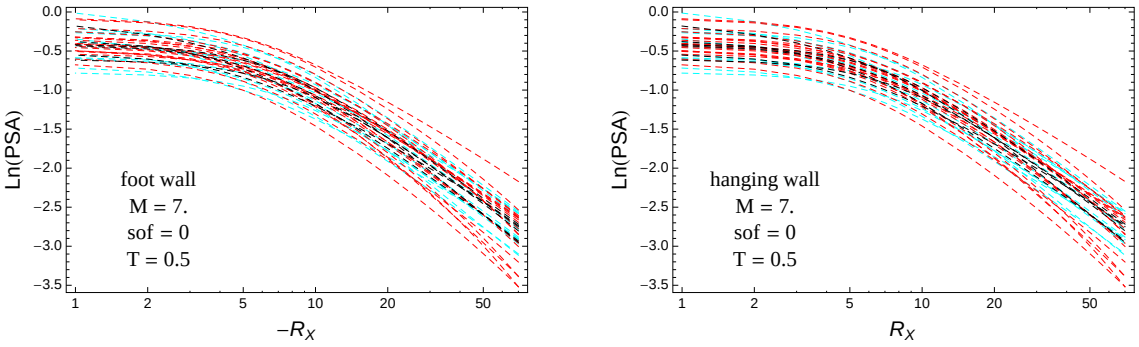



Figure 4.484: PVNGSv2: Distance scaling of the original GMPEs (dashed black), the original GMPEs with uncertainty model (dashed cyan) and selected B models (dashed red), for a scenario with $M = 7.$, $F = 0$, and $T = 0.5$s. Left: foot wall scaling; Right: hanging wall scaling.

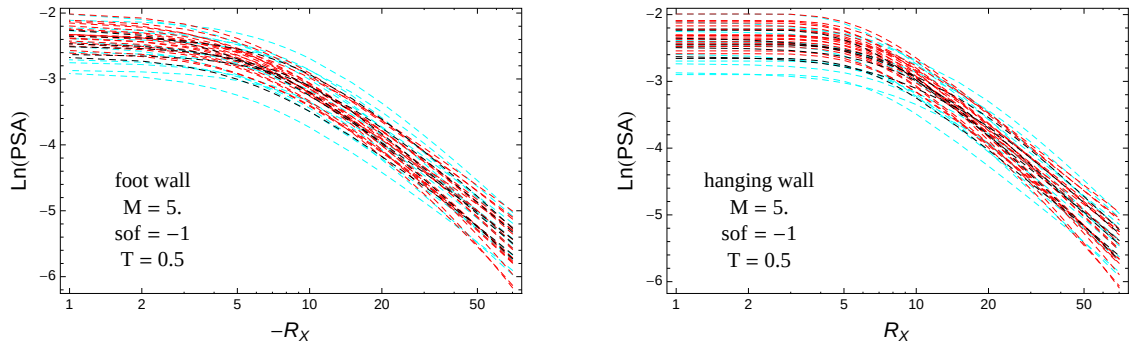



Figure 4.485: PVNGSv2: Distance scaling of the original GMPEs (dashed black), the original GMPEs with uncertainty model (dashed cyan) and selected B models (dashed red), for a scenario with $M = 5.$, $F = -1$, and $T = 0.5$s. Left: foot wall scaling; Right: hanging wall scaling.

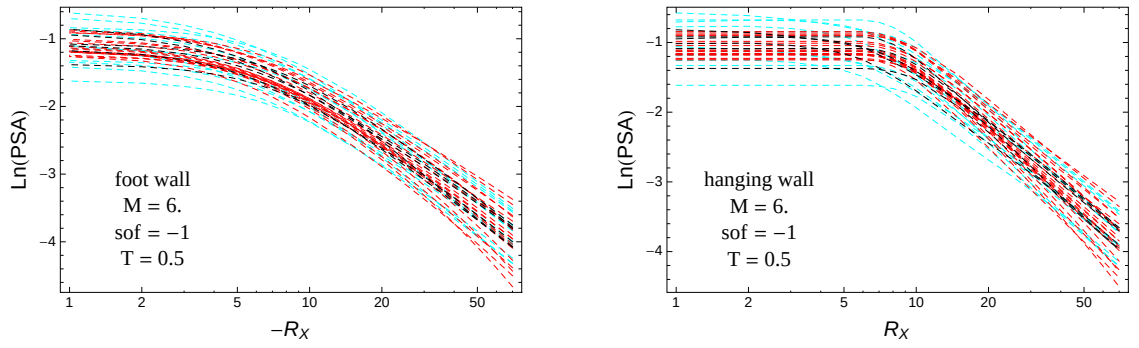



Figure 4.486: PVNGSv2: Distance scaling of the original GMPEs (dashed black), the original GMPEs with uncertainty model (dashed cyan) and selected B models (dashed red), for a scenario with $M = 6.$, $F = -1$, and $T = 0.5$s. Left: foot wall scaling; Right: hanging wall scaling.

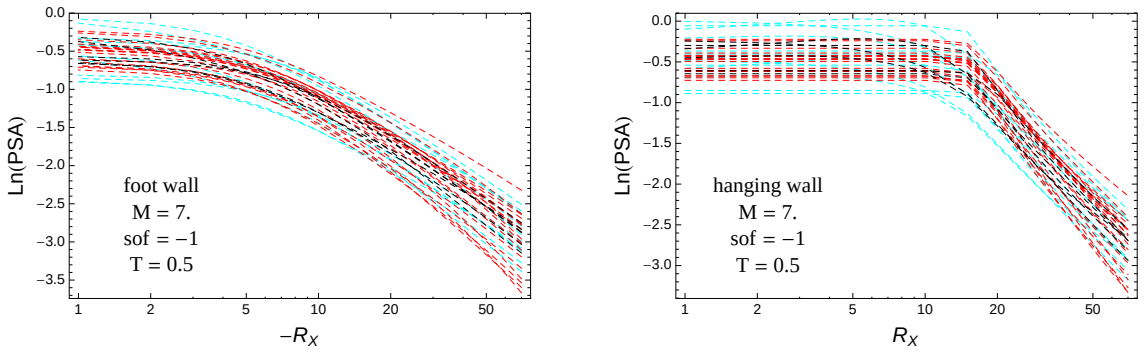



Figure 4.487: PVNGSv2: Distance scaling of the original GMPEs (dashed black), the original GMPEs with uncertainty model (dashed cyan) and selected B models (dashed red), for a scenario with $M = 7.$, $F = -1$, and $T = 0.5$s. Left: foot wall scaling; Right: hanging wall scaling.

**T = 1.s**

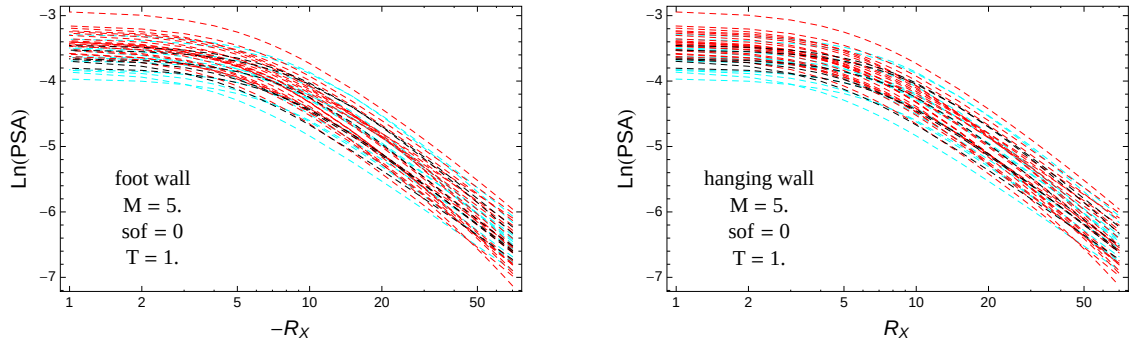



Figure 4.488: PVNGSv2: Distance scaling of the original GMPEs (dashed black), the original GMPEs with uncertainty model (dashed cyan) and selected B models (dashed red), for a scenario with $M = 5.$, $F = 0$, and $T = 1.$s. Left: foot wall scaling; Right: hanging wall scaling.

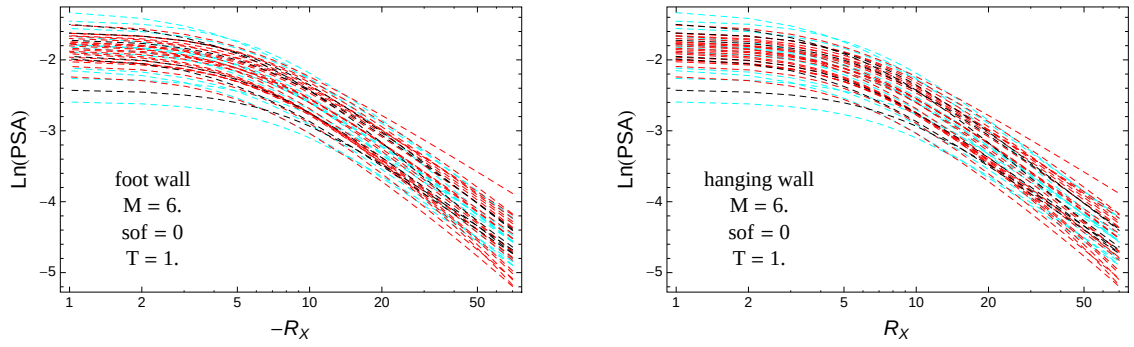



Figure 4.489: PVNGSv2: Distance scaling of the original GMPEs (dashed black), the original GMPEs with uncertainty model (dashed cyan) and selected B models (dashed red), for a scenario with $M = 6.$, $F = 0$, and $T = 1.$s. Left: foot wall scaling; Right: hanging wall scaling.

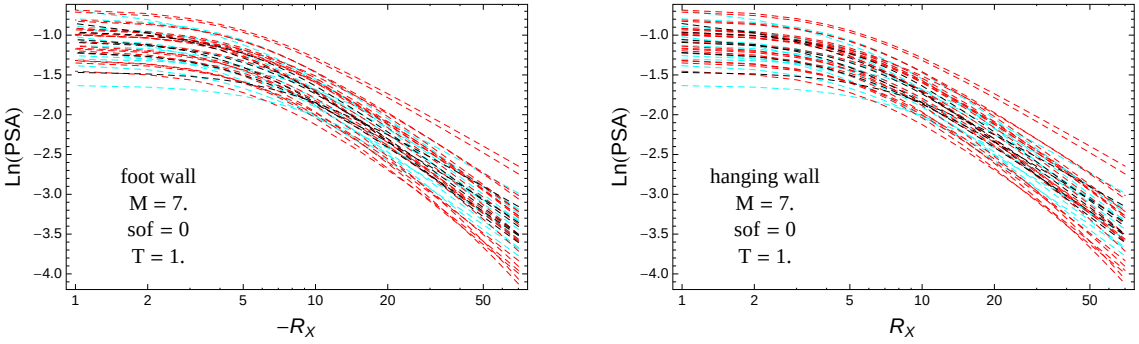



Figure 4.490: PVNGSv2: Distance scaling of the original GMPEs (dashed black), the original GMPEs with uncertainty model (dashed cyan) and selected B models (dashed red), for a scenario with $M = 7.$, $F = 0$, and $T = 1.$s. Left: foot wall scaling; Right: hanging wall scaling.

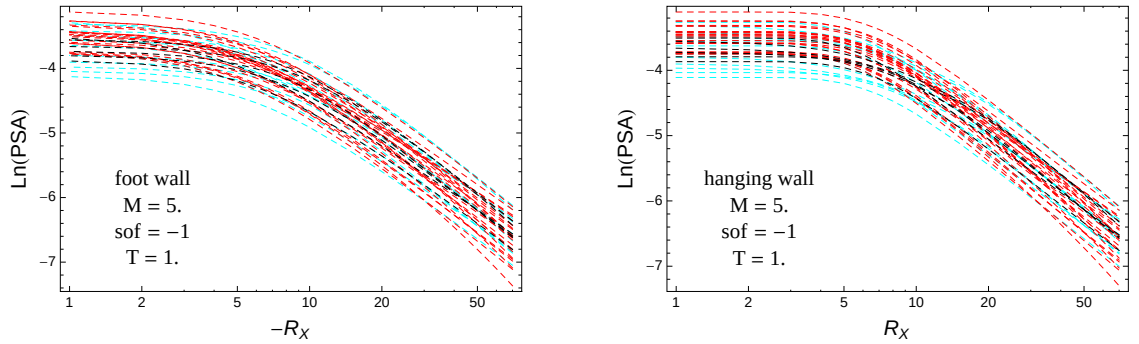



Figure 4.491: PVNGSv2: Distance scaling of the original GMPEs (dashed black), the original GMPEs with uncertainty model (dashed cyan) and selected B models (dashed red), for a scenario with $M = 5.$, $F = -1$, and $T = 1.$s. Left: foot wall scaling; Right: hanging wall scaling.

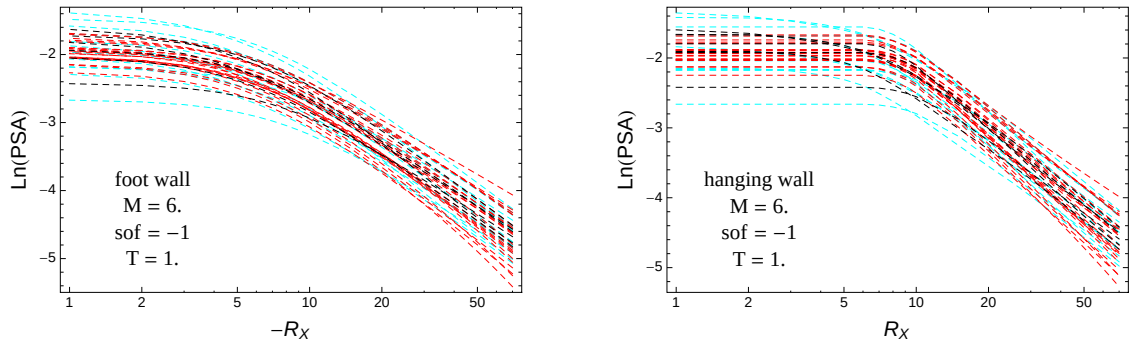



Figure 4.492: PVNGSv2: Distance scaling of the original GMPEs (dashed black), the original GMPEs with uncertainty model (dashed cyan) and selected B models (dashed red), for a scenario with $M = 6.$, $F = -1$, and $T = 1.$s. Left: foot wall scaling; Right: hanging wall scaling.

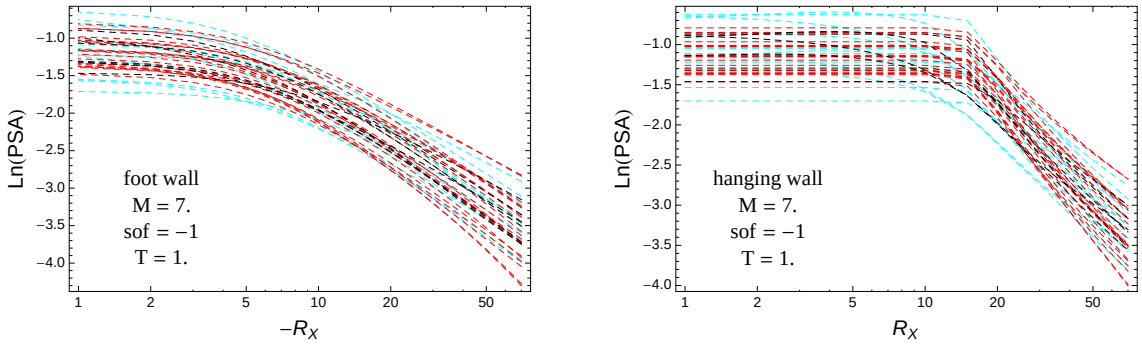



Figure 4.493: PVNGSv2: Distance scaling of the original GMPEs (dashed black), the original GMPEs with uncertainty model (dashed cyan) and selected B models (dashed red), for a scenario with $M = 7.$, $F = -1$, and $T = 1.$s. Left: foot wall scaling; Right: hanging wall scaling.

**T = 3.s**

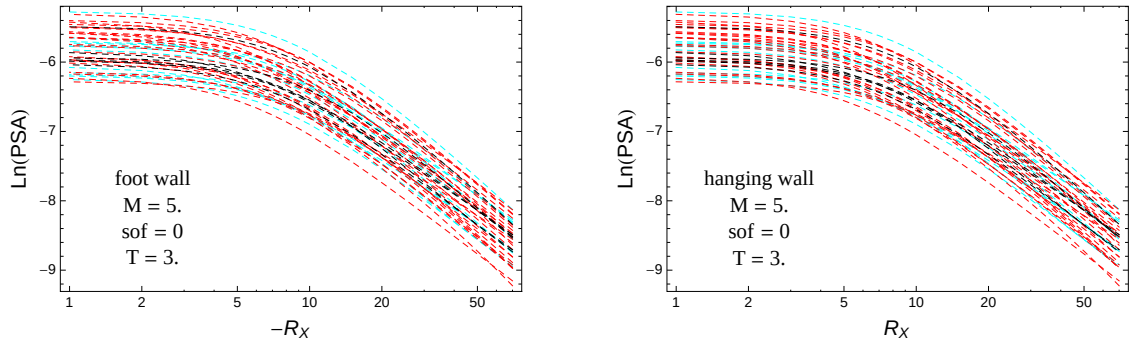



Figure 4.494: PVNGSv2: Distance scaling of the original GMPEs (dashed black), the original GMPEs with uncertainty model (dashed cyan) and selected B models (dashed red), for a scenario with $M = 5.$, $F = 0$, and $T = 3.$s. Left: foot wall scaling; Right: hanging wall scaling.

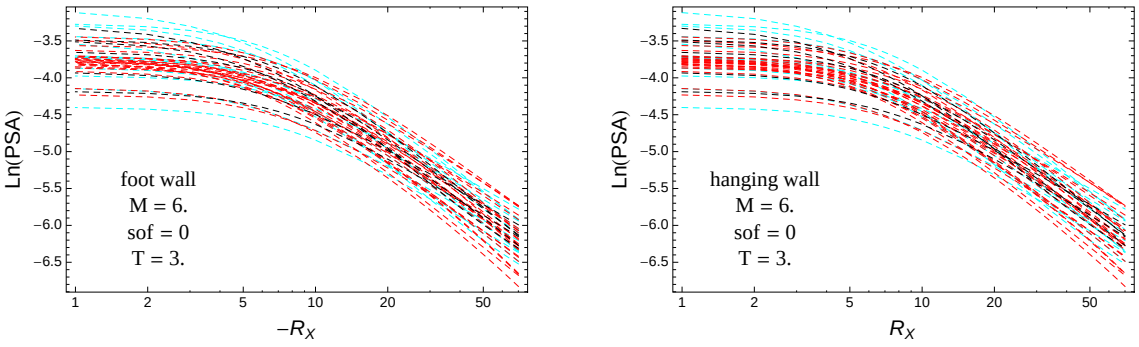



Figure 4.495: PVNGSv2: Distance scaling of the original GMPEs (dashed black), the original GMPEs with uncertainty model (dashed cyan) and selected B models (dashed red), for a scenario with $M = 6.$, $F = 0$, and $T = 3.$s. Left: foot wall scaling; Right: hanging wall scaling.

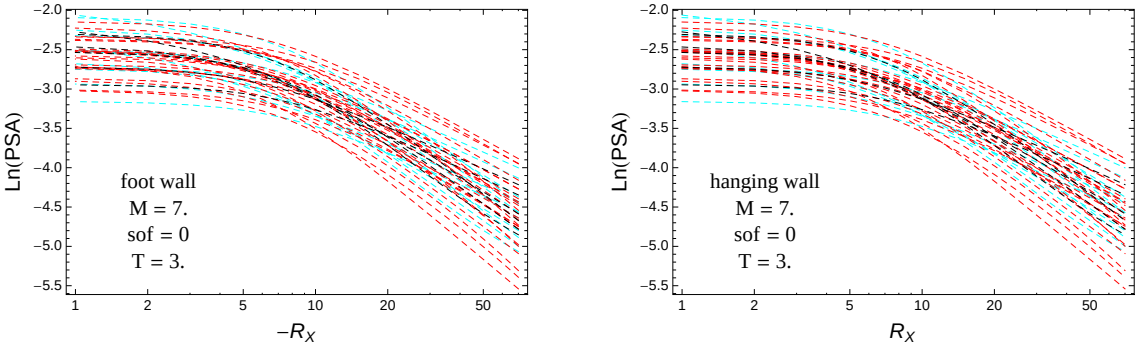



Figure 4.496: PVNGSv2: Distance scaling of the original GMPEs (dashed black), the original GMPEs with uncertainty model (dashed cyan) and selected B models (dashed red), for a scenario with $M = 7.$, $F = 0$, and $T = 3.$s. Left: foot wall scaling; Right: hanging wall scaling.

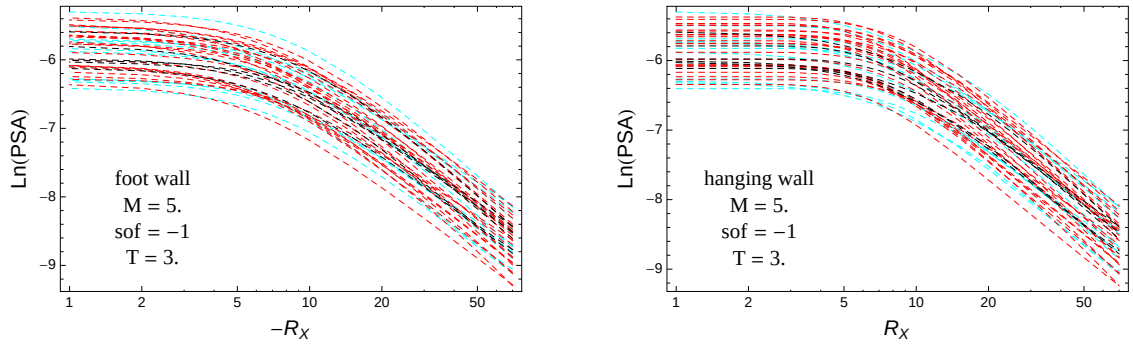



Figure 4.497: PVNGSv2: Distance scaling of the original GMPEs (dashed black), the original GMPEs with uncertainty model (dashed cyan) and selected B models (dashed red), for a scenario with $M = 5.$, $F = -1$, and $T = 3.$s. Left: foot wall scaling; Right: hanging wall scaling.

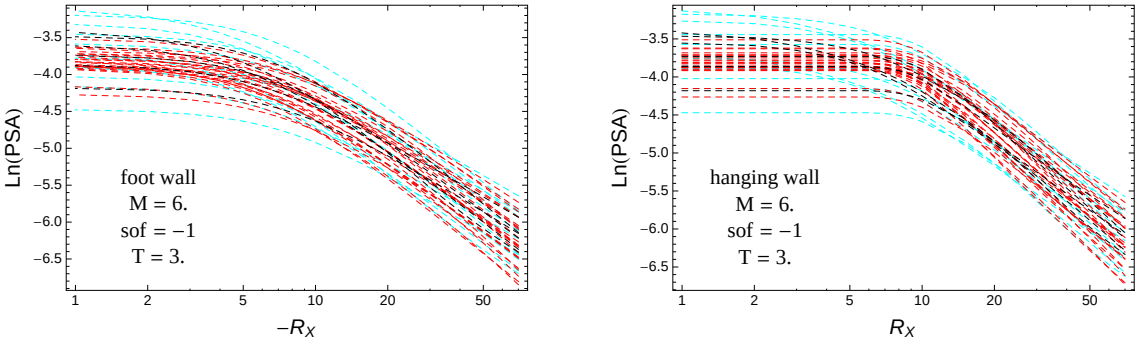



Figure 4.498: PVNGSv2: Distance scaling of the original GMPEs (dashed black), the original GMPEs with uncertainty model (dashed cyan) and selected B models (dashed red), for a scenario with $M = 6.$, $F = -1$, and $T = 3.$s. Left: foot wall scaling; Right: hanging wall scaling.

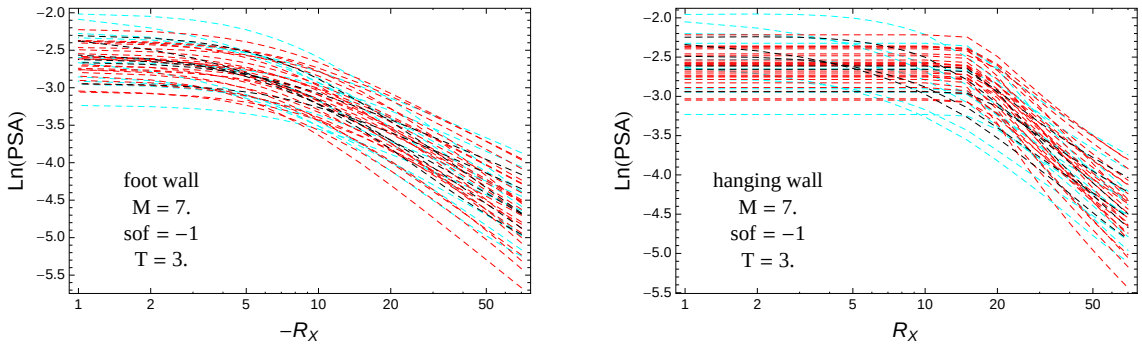



Figure 4.499: PVNGSv2: Distance scaling of the original GMPEs (dashed black), the original GMPEs with uncertainty model (dashed cyan) and selected B models (dashed red), for a scenario with $M = 7.$, $F = -1$, and $T = 3.$s. Left: foot wall scaling; Right: hanging wall scaling.

### 4.1.13 Quantile Plots vs. Magnitude with GMPEs

**T = 0.01s**

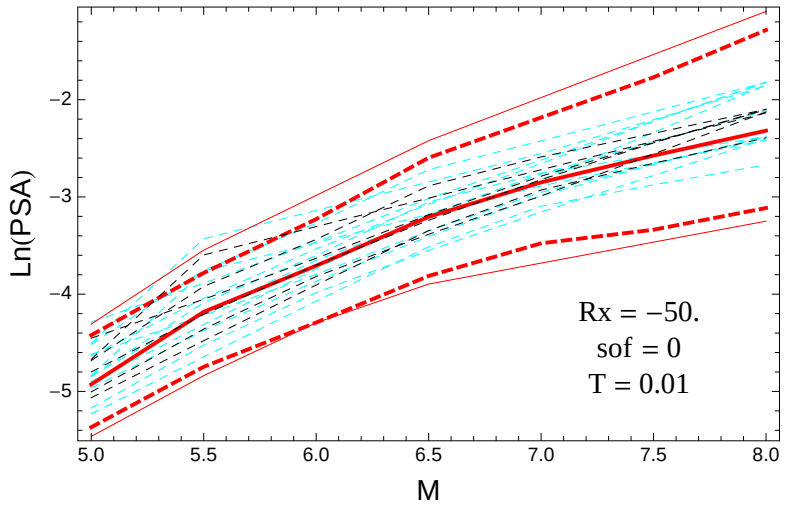



Figure 4.500: PVNGSv2: Magnitude scaling of the original GMPEs (dashed black), the original GMPEs with uncertainty model (dashed cyan) and 0.05,0.5,0.95 quantile of the ModelB distribution (red) with total weights, for a scenario with $R_X = -50.$, $F = 0$, and $T = 0.01$s.

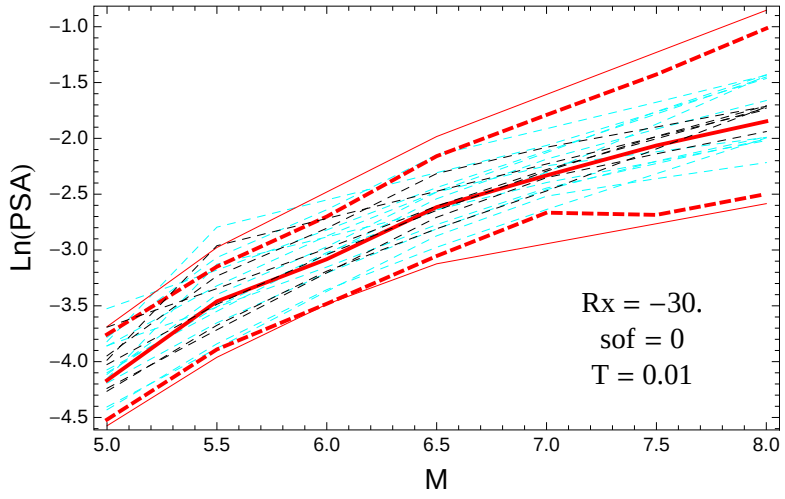



Figure 4.501: PVNGSv2: Magnitude scaling of the original GMPEs (dashed black), the original GMPEs with uncertainty model (dashed cyan) and 0.05,0.5,0.95 quantile of the ModelB distribution (red) with total weights, for a scenario with $R_X = -30.$, $F = 0$, and $T = 0.01$s.

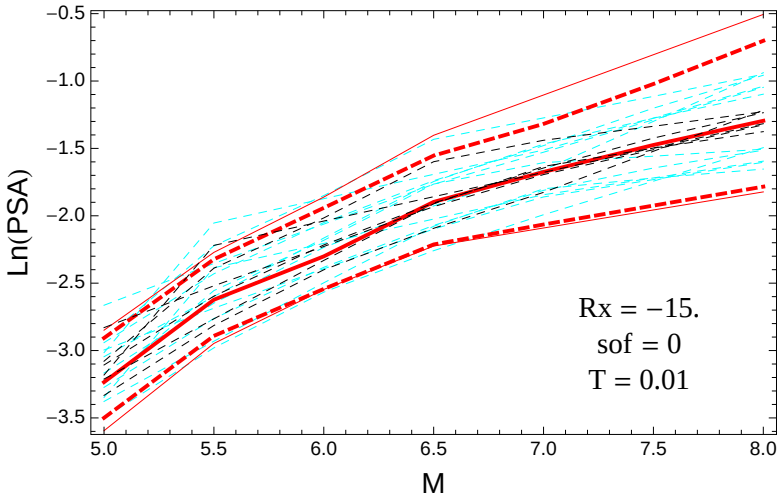



Figure 4.502: PVNGSv2: Magnitude scaling of the original GMPEs (dashed black), the original GMPEs with uncertainty model (dashed cyan) and 0.05,0.5,0.95 quantile of the ModelB distribution (red) with total weights, for a scenario with $R_X = -15.$, $F = 0$, and $T = 0.01$s.

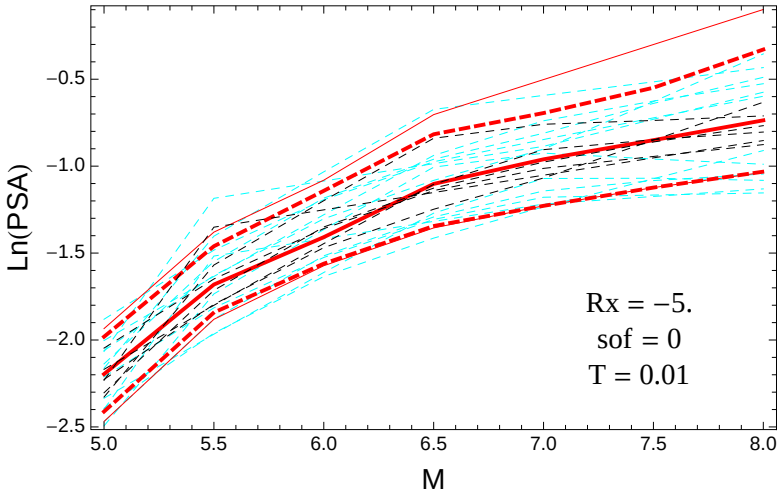



Figure 4.503: PVNGSv2: Magnitude scaling of the original GMPEs (dashed black), the original GMPEs with uncertainty model (dashed cyan) and 0.05,0.5,0.95 quantile of the ModelB distribution (red) with total weights, for a scenario with $R_X = -5.$, $F = 0$, and $T = 0.01$s.

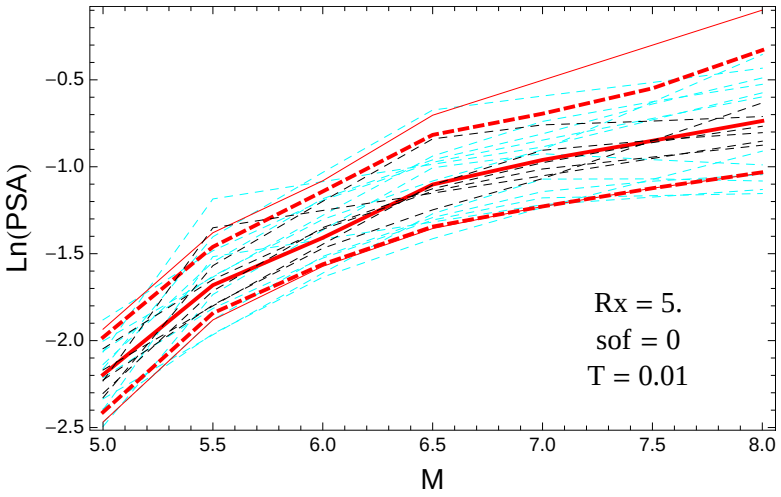



Figure 4.504: PVNGSv2: Magnitude scaling of the original GMPEs (dashed black), the original GMPEs with uncertainty model (dashed cyan) and 0.05,0.5,0.95 quantile of the ModelB distribution (red) with total weights, for a scenario with $R_X = 5.$, $F = 0$, and $T = 0.01$s.

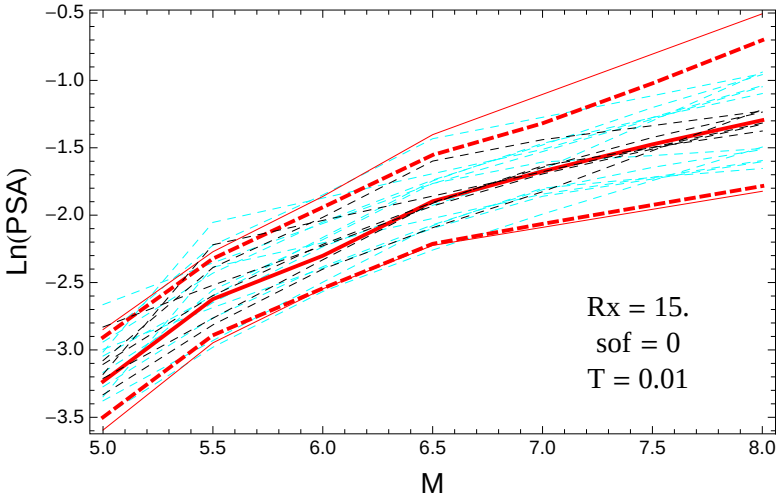



Figure 4.505: PVNGSv2: Magnitude scaling of the original GMPEs (dashed black), the original GMPEs with uncertainty model (dashed cyan) and 0.05,0.5,0.95 quantile of the ModelB distribution (red) with total weights, for a scenario with $R_X = 15.$, $F = 0$, and $T = 0.01$s.

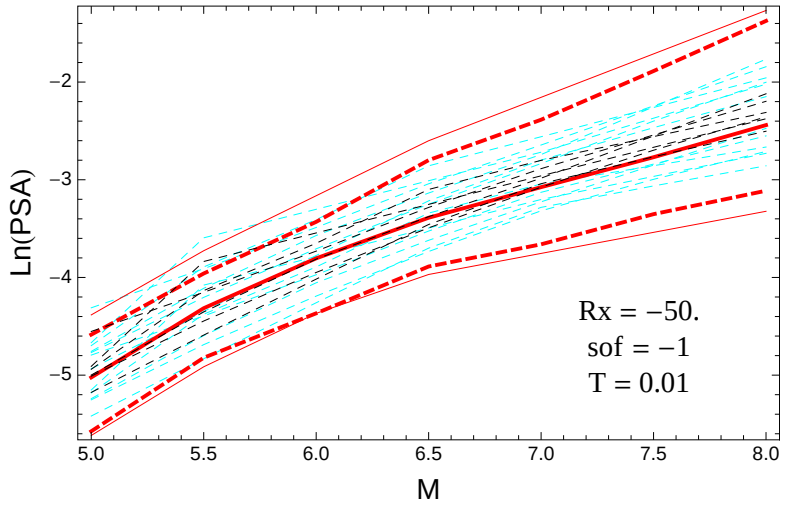



Figure 4.506: PVNGSv2: Magnitude scaling of the original GMPEs (dashed black), the original GMPEs with uncertainty model (dashed cyan) and 0.05,0.5,0.95 quantile of the ModelB distribution (red) with total weights, for a scenario with $R_X = -50.$, $F = -1$, and $T = 0.01$s.

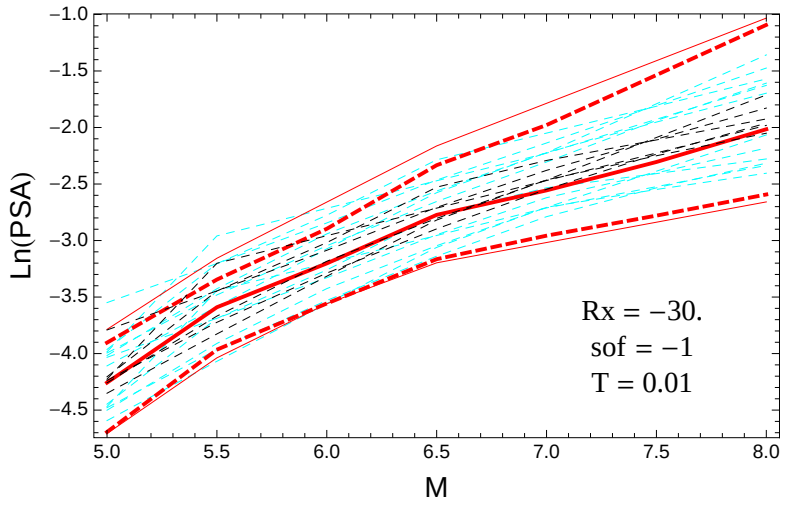



Figure 4.507: PVNGSv2: Magnitude scaling of the original GMPEs (dashed black), the original GMPEs with uncertainty model (dashed cyan) and 0.05,0.5,0.95 quantile of the ModelB distribution (red) with total weights, for a scenario with $R_X = -30.$, $F = -1$, and $T = 0.01$s.

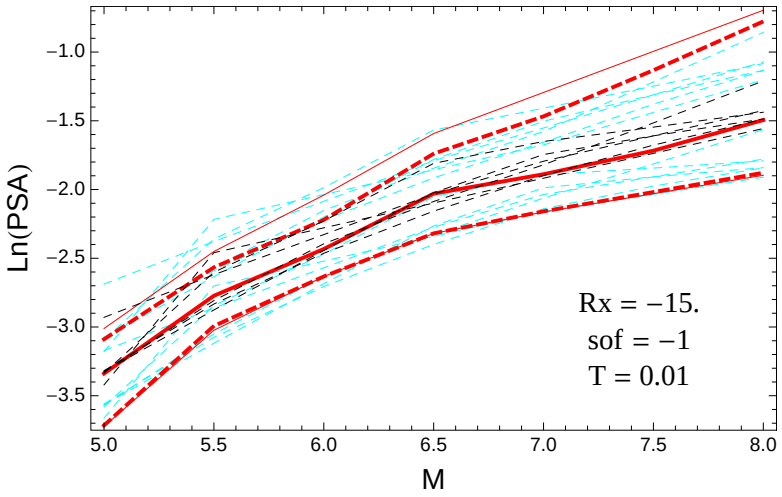



Figure 4.508: PVNGSv2: Magnitude scaling of the original GMPEs (dashed black), the original GMPEs with uncertainty model (dashed cyan) and 0.05,0.5,0.95 quantile of the ModelB distribution (red) with total weights, for a scenario with $R_X = -15.$, $F = -1$, and $T = 0.01$s.

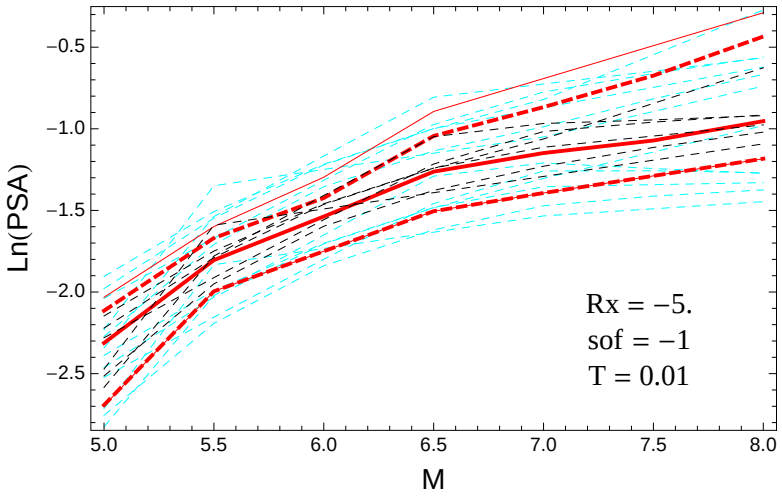



Figure 4.509: PVNGSv2: Magnitude scaling of the original GMPEs (dashed black), the original GMPEs with uncertainty model (dashed cyan) and 0.05,0.5,0.95 quantile of the ModelB distribution (red) with total weights, for a scenario with $R_X = -5.$, $F = -1$, and $T = 0.01$s.

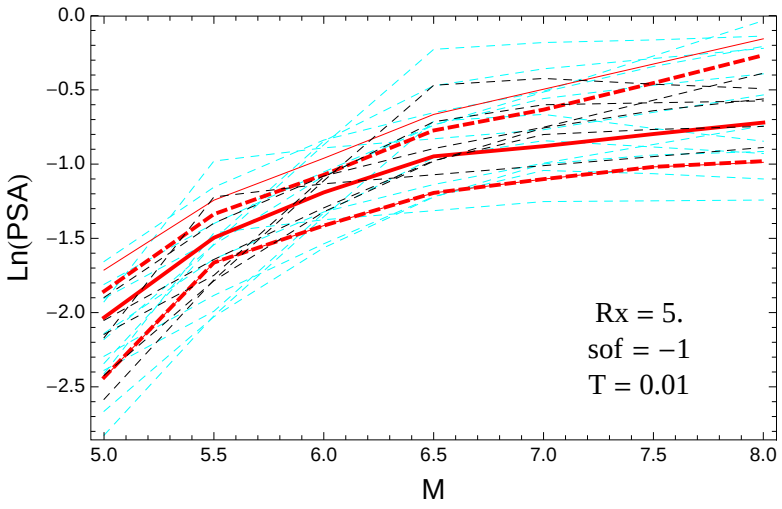



Figure 4.510: PVNGSv2: Magnitude scaling of the original GMPEs (dashed black), the original GMPEs with uncertainty model (dashed cyan) and 0.05,0.5,0.95 quantile of the ModelB distribution (red) with total weights, for a scenario with $R_X = 5.$, $F = -1$, and $T = 0.01$s.

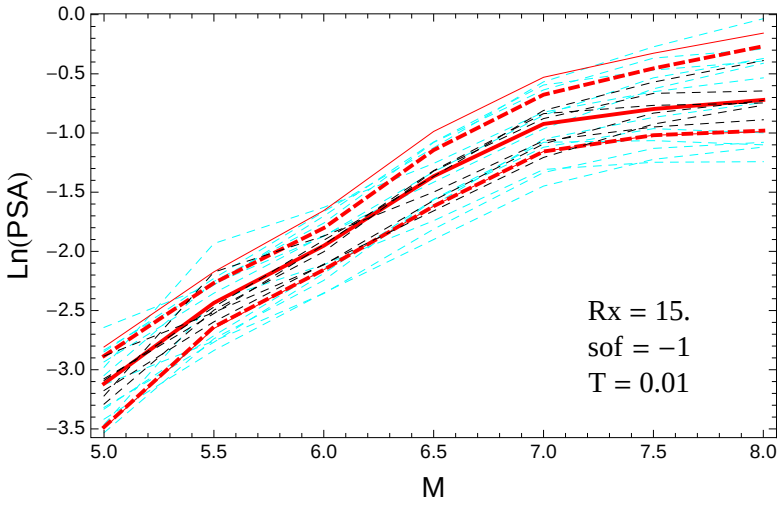



Figure 4.511: PVNGSv2: Magnitude scaling of the original GMPEs (dashed black), the original GMPEs with uncertainty model (dashed cyan) and 0.05,0.5,0.95 quantile of the ModelB distribution (red) with total weights, for a scenario with $R_X = 15.$, $F = -1$, and $T = 0.01$s.

**T = 0.2s**

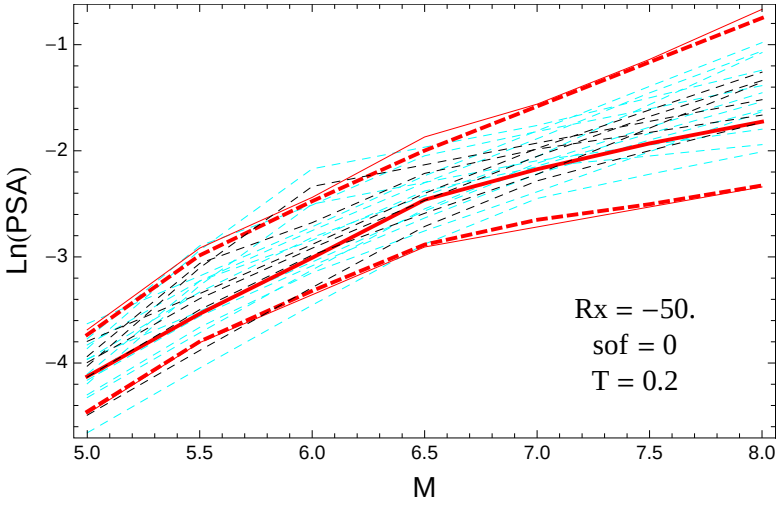



Figure 4.512: PVNGSv2: Magnitude scaling of the original GMPEs (dashed black), the original GMPEs with uncertainty model (dashed cyan) and 0.05,0.5,0.95 quantile of the ModelB distribution (red) with total weights, for a scenario with $R_X = -50.$, $F = 0$, and $T = 0.2$s.

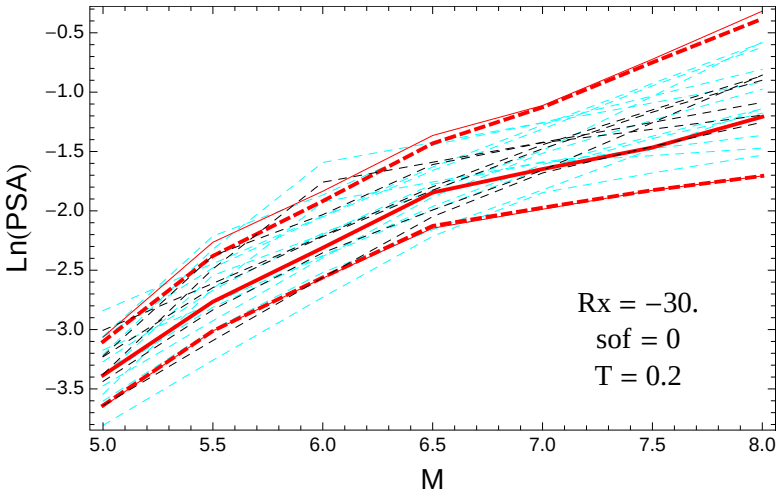



Figure 4.513: PVNGSv2: Magnitude scaling of the original GMPEs (dashed black), the original GMPEs with uncertainty model (dashed cyan) and 0.05,0.5,0.95 quantile of the ModelB distribution (red) with total weights, for a scenario with $R_X = -30.$, $F = 0$, and $T = 0.2$s.

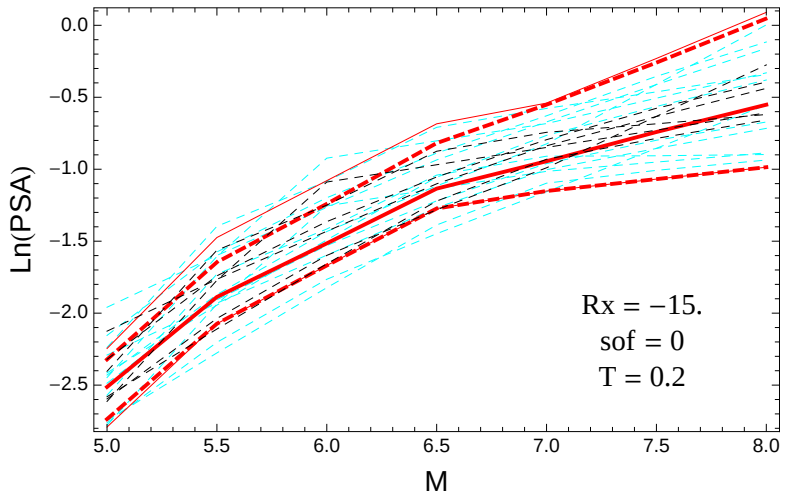



Figure 4.514: PVNGSv2: Magnitude scaling of the original GMPEs (dashed black), the original GMPEs with uncertainty model (dashed cyan) and 0.05,0.5,0.95 quantile of the ModelB distribution (red) with total weights, for a scenario with $R_X = -15.$, $F = 0$, and $T = 0.2$s.

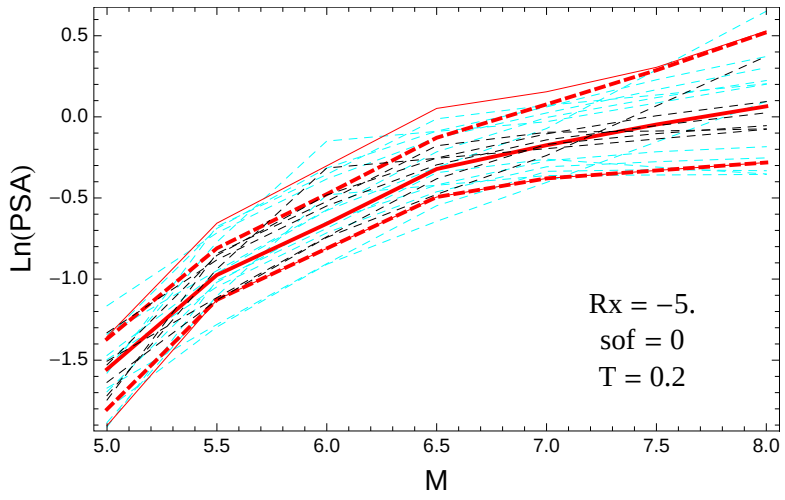



Figure 4.515: PVNGSv2: Magnitude scaling of the original GMPEs (dashed black), the original GMPEs with uncertainty model (dashed cyan) and 0.05,0.5,0.95 quantile of the ModelB distribution (red) with total weights, for a scenario with $R_X = -5.$, $F = 0$, and $T = 0.2$s.

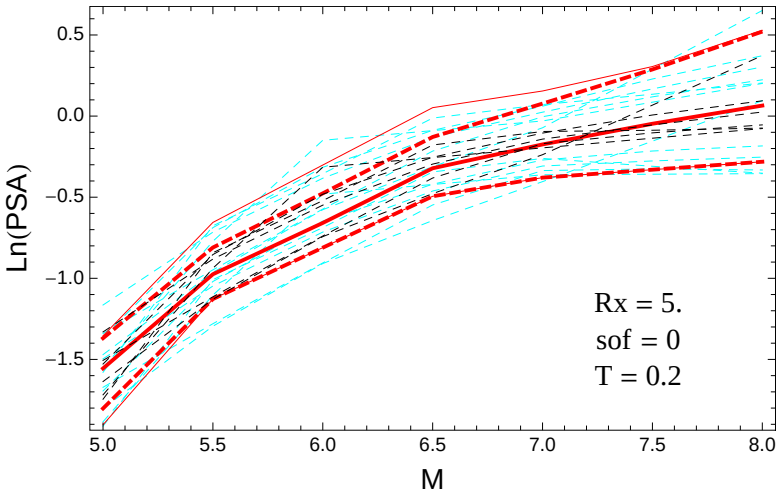



Figure 4.516: PVNGSv2: Magnitude scaling of the original GMPEs (dashed black), the original GMPEs with uncertainty model (dashed cyan) and 0.05,0.5,0.95 quantile of the ModelB distribution (red) with total weights, for a scenario with $R_X = 5.$, $F = 0$, and $T = 0.2$s.

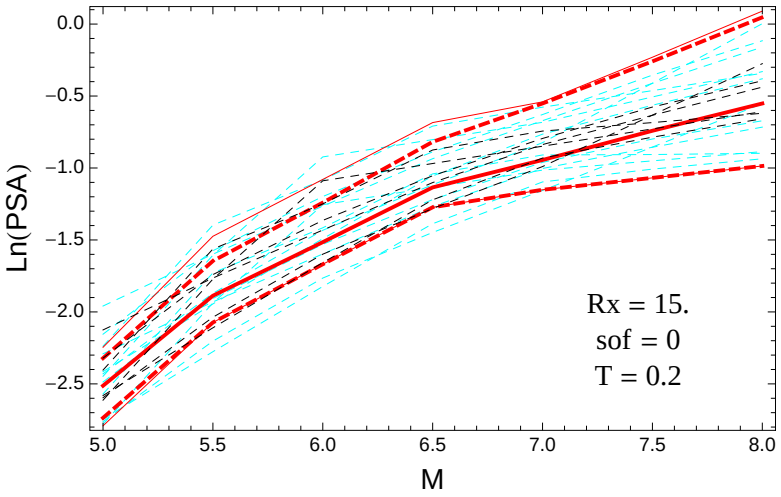



Figure 4.517: PVNGSv2: Magnitude scaling of the original GMPEs (dashed black), the original GMPEs with uncertainty model (dashed cyan) and 0.05,0.5,0.95 quantile of the ModelB distribution (red) with total weights, for a scenario with $R_X = 15.$, $F = 0$, and $T = 0.2$s.

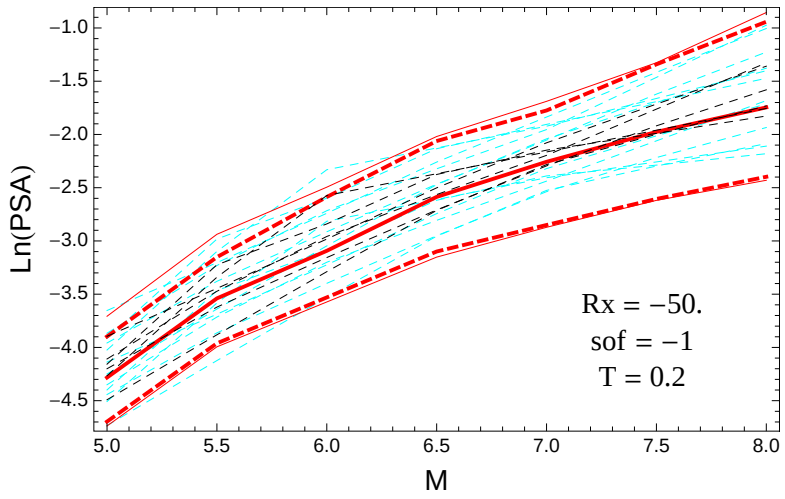



Figure 4.518: PVNGSv2: Magnitude scaling of the original GMPEs (dashed black), the original GMPEs with uncertainty model (dashed cyan) and 0.05,0.5,0.95 quantile of the ModelB distribution (red) with total weights, for a scenario with $R_X = -50.$, $F = -1$, and $T = 0.2$s.

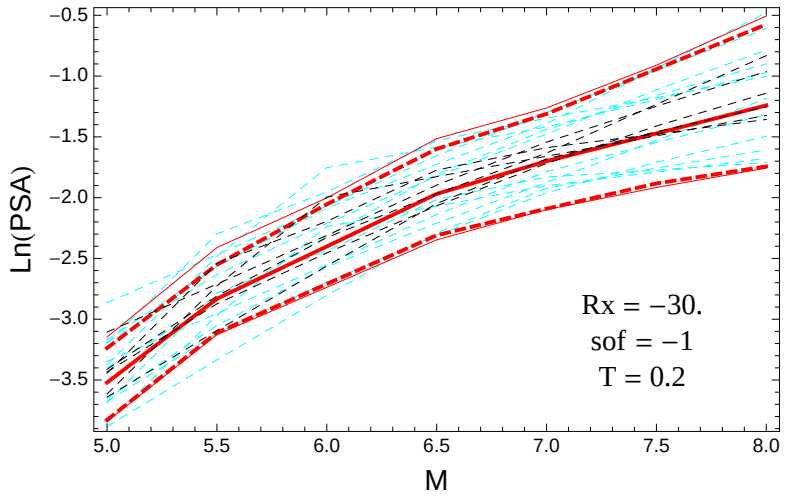



Figure 4.519: PVNGSv2: Magnitude scaling of the original GMPEs (dashed black), the original GMPEs with uncertainty model (dashed cyan) and 0.05,0.5,0.95 quantile of the ModelB distribution (red) with total weights, for a scenario with $R_X = -30.$, $F = -1$, and $T = 0.2$s.

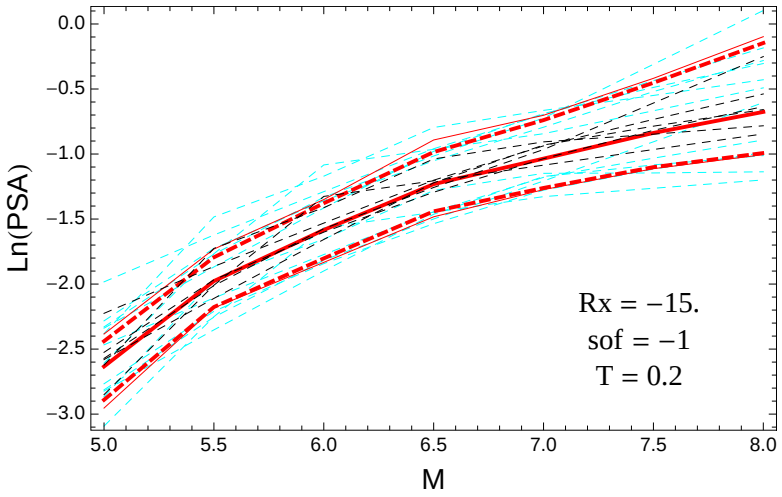



Figure 4.520: PVNGSv2: Magnitude scaling of the original GMPEs (dashed black), the original GMPEs with uncertainty model (dashed cyan) and 0.05,0.5,0.95 quantile of the ModelB distribution (red) with total weights, for a scenario with $R_X = -15.$, $F = -1$, and $T = 0.2$s.

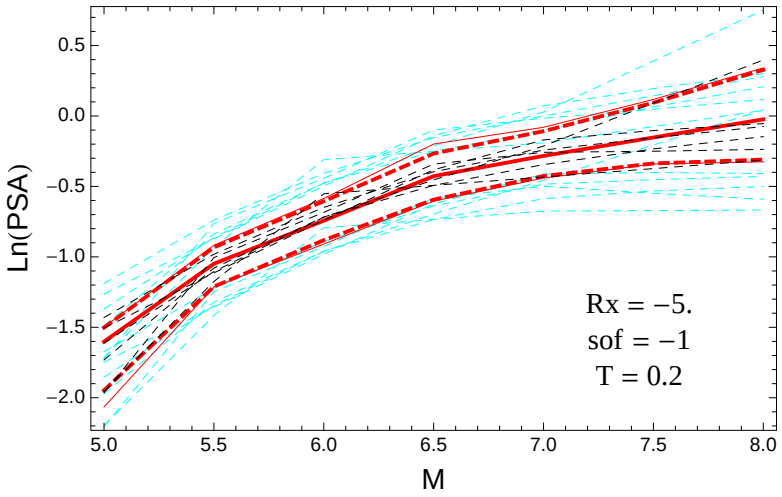



Figure 4.521: PVNGSv2: Magnitude scaling of the original GMPEs (dashed black), the original GMPEs with uncertainty model (dashed cyan) and 0.05,0.5,0.95 quantile of the ModelB distribution (red) with total weights, for a scenario with $R_X = -5.$, $F = -1$, and $T = 0.2$s.

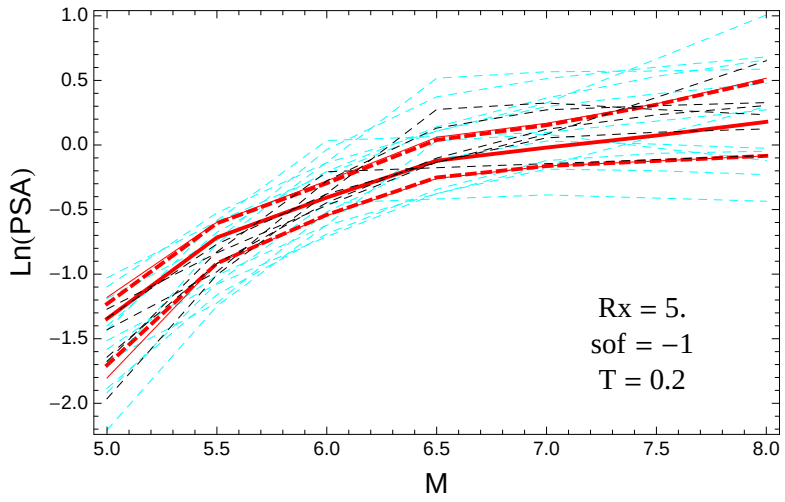



Figure 4.522: PVNGSv2: Magnitude scaling of the original GMPEs (dashed black), the original GMPEs with uncertainty model (dashed cyan) and 0.05,0.5,0.95 quantile of the ModelB distribution (red) with total weights, for a scenario with $R_X = 5.$, $F = -1$, and $T = 0.2$s.

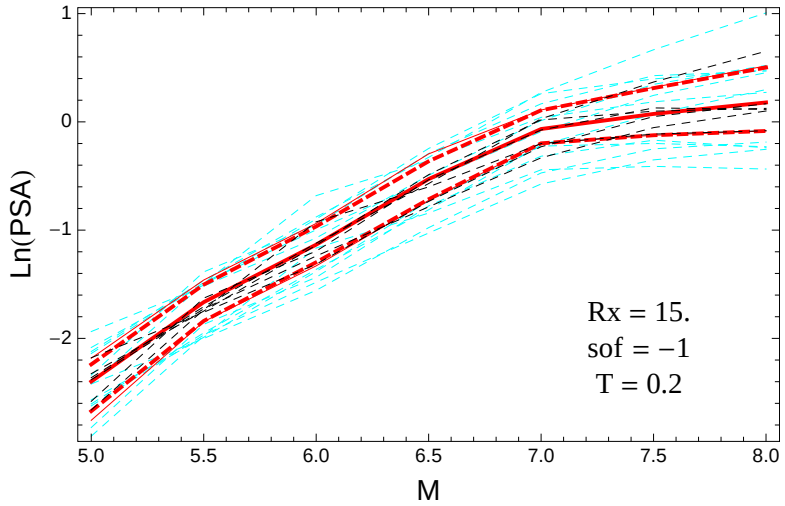



Figure 4.523: PVNGSv2: Magnitude scaling of the original GMPEs (dashed black), the original GMPEs with uncertainty model (dashed cyan) and 0.05,0.5,0.95 quantile of the ModelB distribution (red) with total weights, for a scenario with $R_X = 15.$, $F = -1$, and $T = 0.2$s.

**T = 0.5s**

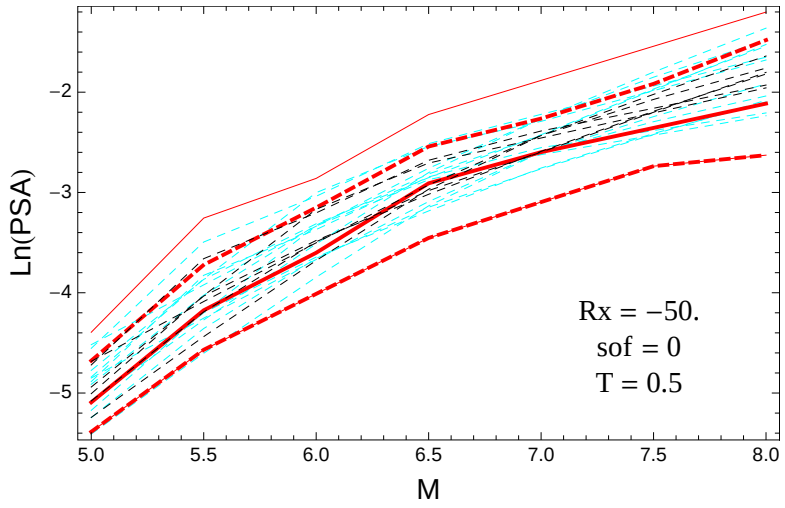



Figure 4.524: PVNGSv2: Magnitude scaling of the original GMPEs (dashed black), the original GMPEs with uncertainty model (dashed cyan) and 0.05,0.5,0.95 quantile of the ModelB distribution (red) with total weights, for a scenario with $R_X = -50.$, $F = 0$, and $T = 0.5$s.

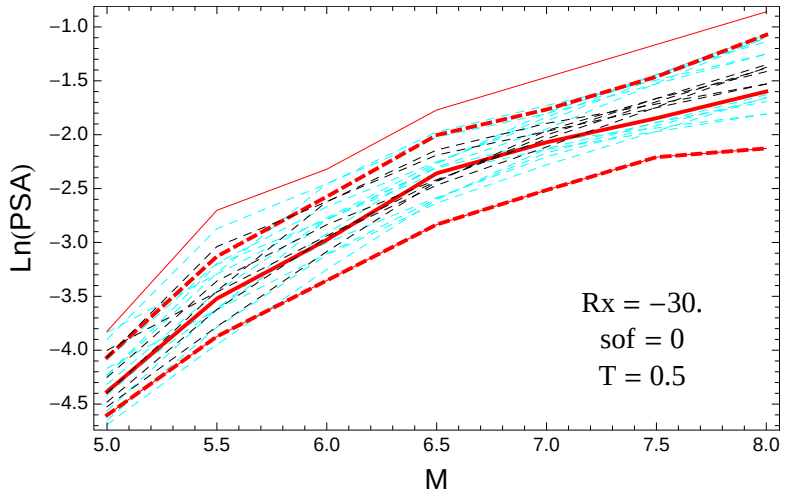



Figure 4.525: PVNGSv2: Magnitude scaling of the original GMPEs (dashed black), the original GMPEs with uncertainty model (dashed cyan) and 0.05,0.5,0.95 quantile of the ModelB distribution (red) with total weights, for a scenario with $R_X = -30.$, $F = 0$, and $T = 0.5$s.

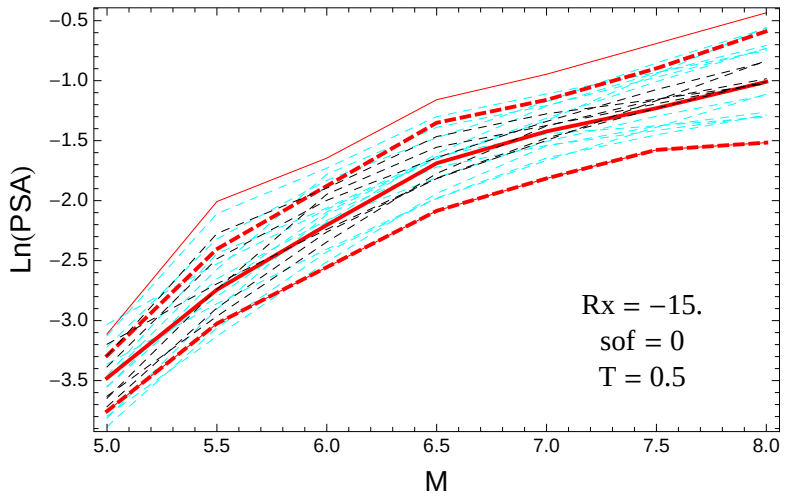



Figure 4.526: PVNGSv2: Magnitude scaling of the original GMPEs (dashed black), the original GMPEs with uncertainty model (dashed cyan) and 0.05,0.5,0.95 quantile of the ModelB distribution (red) with total weights, for a scenario with $R_X = -15.$, $F = 0$, and $T = 0.5$s.

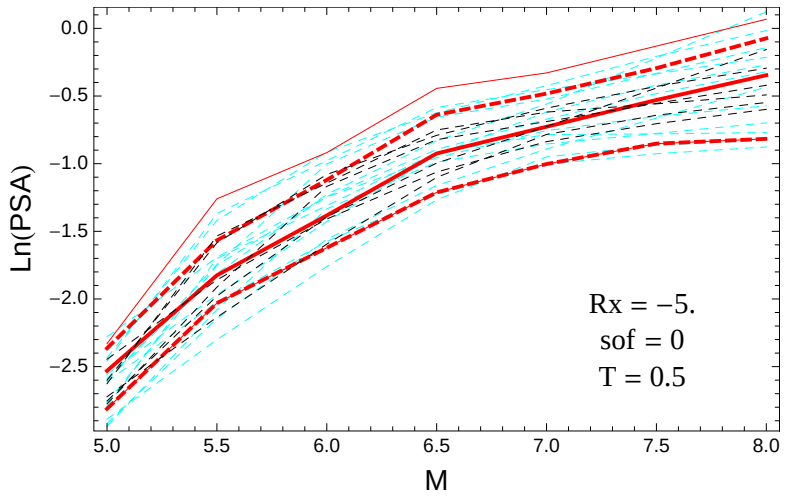



Figure 4.527: PVNGSv2: Magnitude scaling of the original GMPEs (dashed black), the original GMPEs with uncertainty model (dashed cyan) and 0.05,0.5,0.95 quantile of the ModelB distribution (red) with total weights, for a scenario with $R_X = -5.$, $F = 0$, and $T = 0.5$s.

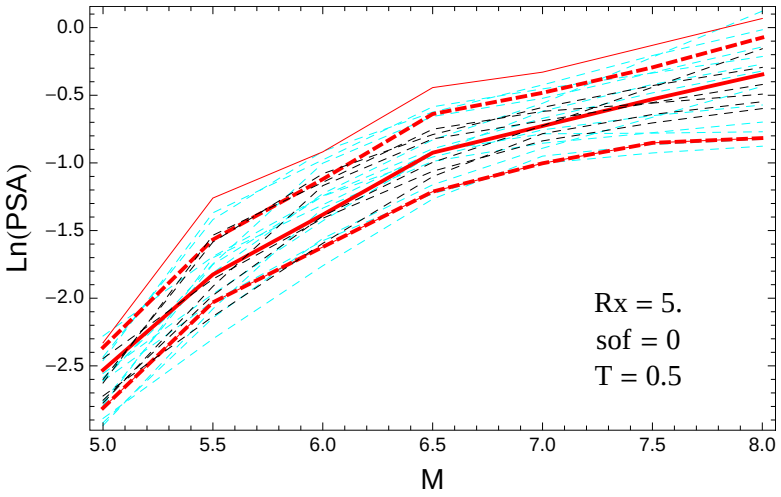



Figure 4.528: PVNGSv2: Magnitude scaling of the original GMPEs (dashed black), the original GMPEs with uncertainty model (dashed cyan) and 0.05,0.5,0.95 quantile of the ModelB distribution (red) with total weights, for a scenario with $R_X = 5.$, $F = 0$, and $T = 0.5$s.

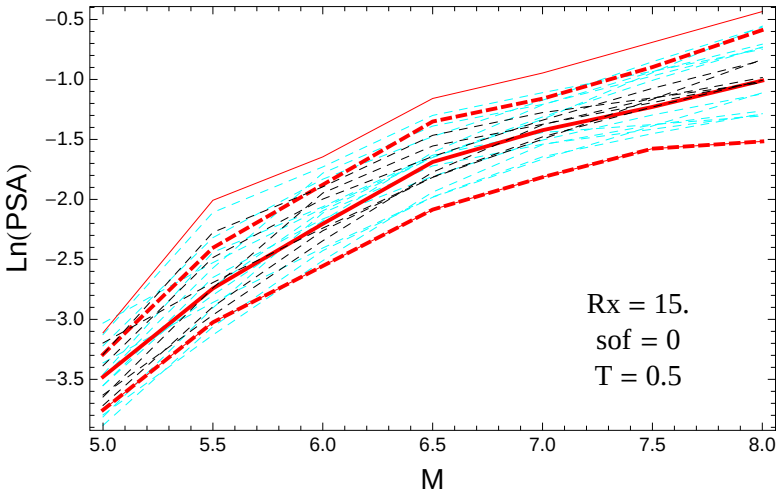



Figure 4.529: PVNGSv2: Magnitude scaling of the original GMPEs (dashed black), the original GMPEs with uncertainty model (dashed cyan) and 0.05,0.5,0.95 quantile of the ModelB distribution (red) with total weights, for a scenario with $R_X = 15.$, $F = 0$, and $T = 0.5$s.

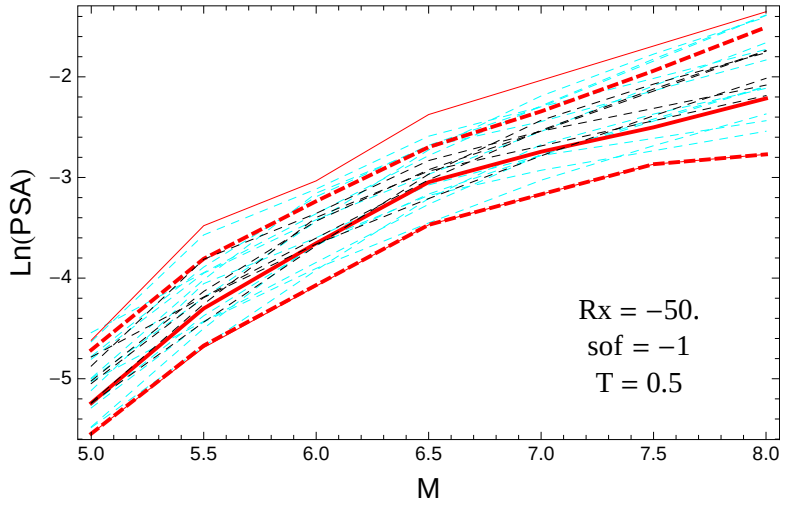



Figure 4.530: PVNGSv2: Magnitude scaling of the original GMPEs (dashed black), the original GMPEs with uncertainty model (dashed cyan) and 0.05,0.5,0.95 quantile of the ModelB distribution (red) with total weights, for a scenario with $R_X = -50.$, $F = -1$, and $T = 0.5$s.

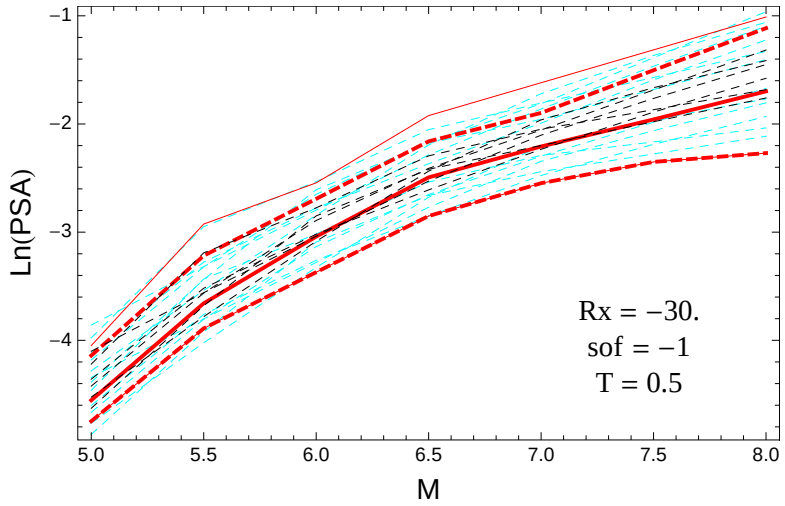



Figure 4.531: PVNGSv2: Magnitude scaling of the original GMPEs (dashed black), the original GMPEs with uncertainty model (dashed cyan) and 0.05,0.5,0.95 quantile of the ModelB distribution (red) with total weights, for a scenario with $R_X = -30.$, $F = -1$, and $T = 0.5$s.

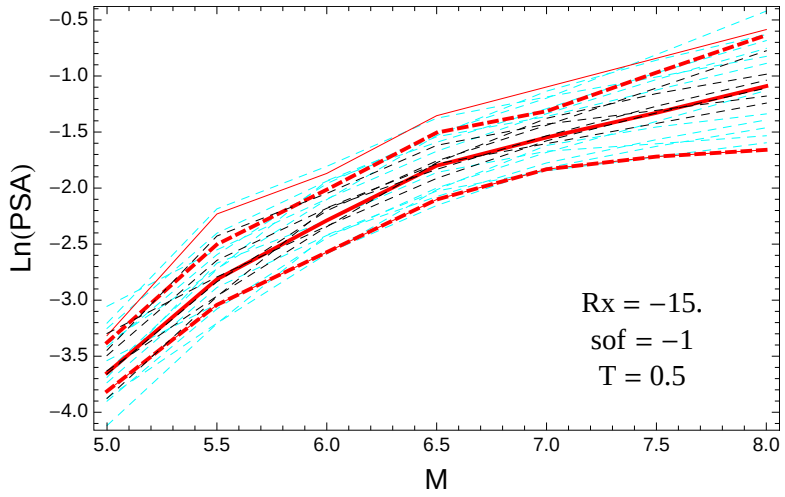



Figure 4.532: PVNGSv2: Magnitude scaling of the original GMPEs (dashed black), the original GMPEs with uncertainty model (dashed cyan) and 0.05,0.5,0.95 quantile of the ModelB distribution (red) with total weights, for a scenario with $R_X = -15.$, $F = -1$, and $T = 0.5$s.

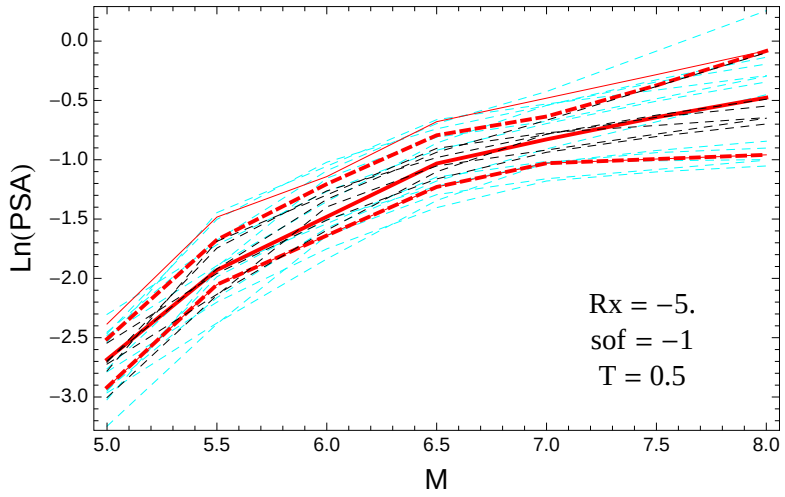



Figure 4.533: PVNGSv2: Magnitude scaling of the original GMPEs (dashed black), the original GMPEs with uncertainty model (dashed cyan) and 0.05,0.5,0.95 quantile of the ModelB distribution (red) with total weights, for a scenario with $R_X = -5.$, $F = -1$, and $T = 0.5$s.

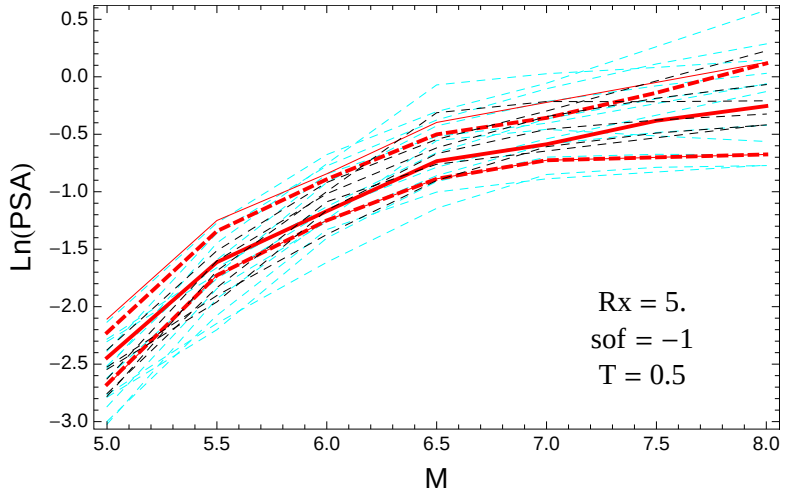



Figure 4.534: PVNGSv2: Magnitude scaling of the original GMPEs (dashed black), the original GMPEs with uncertainty model (dashed cyan) and 0.05,0.5,0.95 quantile of the ModelB distribution (red) with total weights, for a scenario with $R_X = 5.$, $F = -1$, and $T = 0.5$s.

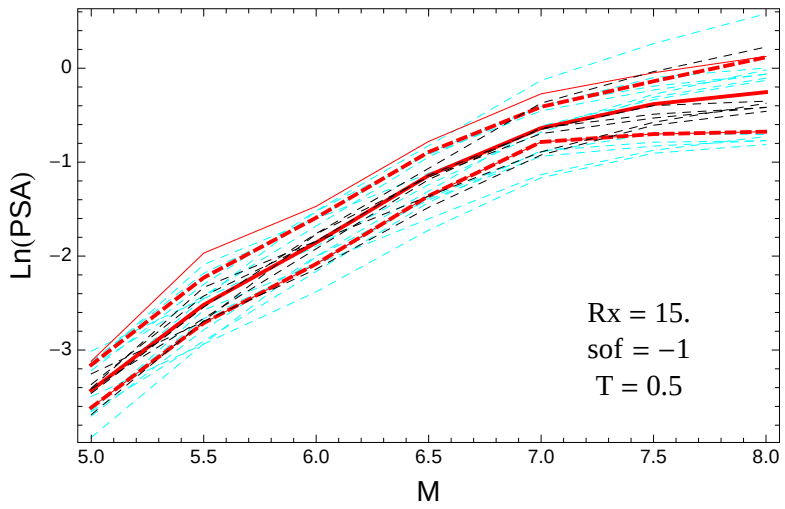



Figure 4.535: PVNGSv2: Magnitude scaling of the original GMPEs (dashed black), the original GMPEs with uncertainty model (dashed cyan) and 0.05,0.5,0.95 quantile of the ModelB distribution (red) with total weights, for a scenario with $R_X = 15.$, $F = -1$, and $T = 0.5$s.

**T = 1.s**

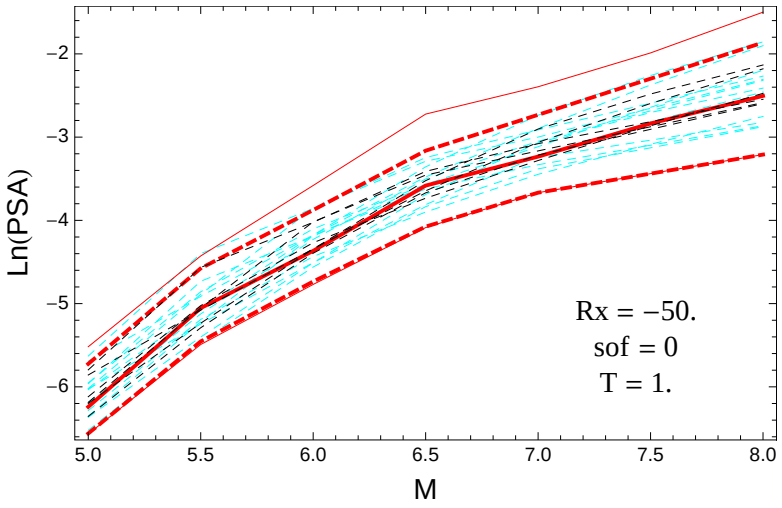



Figure 4.536: PVNGSv2: Magnitude scaling of the original GMPEs (dashed black), the original GMPEs with uncertainty model (dashed cyan) and 0.05,0.5,0.95 quantile of the ModelB distribution (red) with total weights, for a scenario with $R_X = -50.$, $F = 0$, and $T = 1.$s.

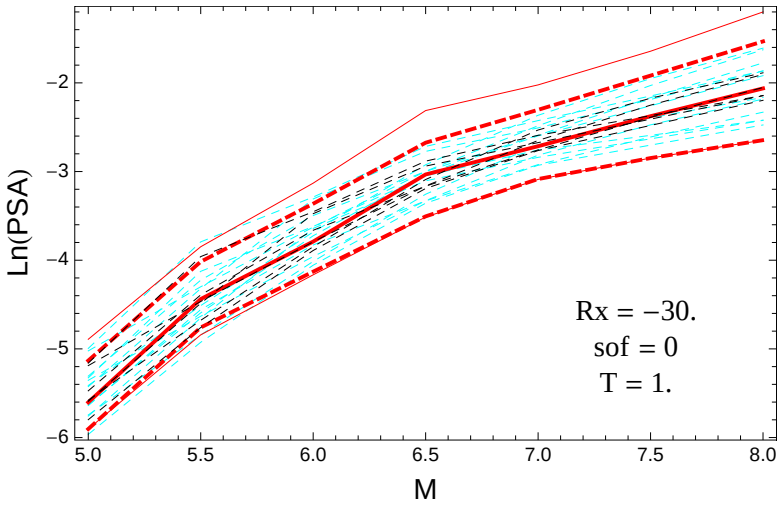



Figure 4.537: PVNGSv2: Magnitude scaling of the original GMPEs (dashed black), the original GMPEs with uncertainty model (dashed cyan) and 0.05,0.5,0.95 quantile of the ModelB distribution (red) with total weights, for a scenario with $R_X = -30.$, $F = 0$, and $T = 1.$s.

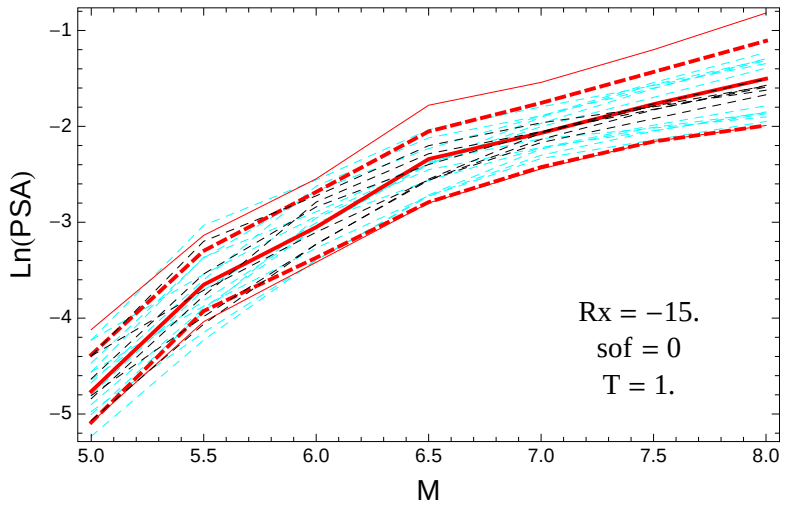



Figure 4.538: PVNGSv2: Magnitude scaling of the original GMPEs (dashed black), the original GMPEs with uncertainty model (dashed cyan) and 0.05,0.5,0.95 quantile of the ModelB distribution (red) with total weights, for a scenario with $R_X = -15.$, $F = 0$, and $T = 1.$s.

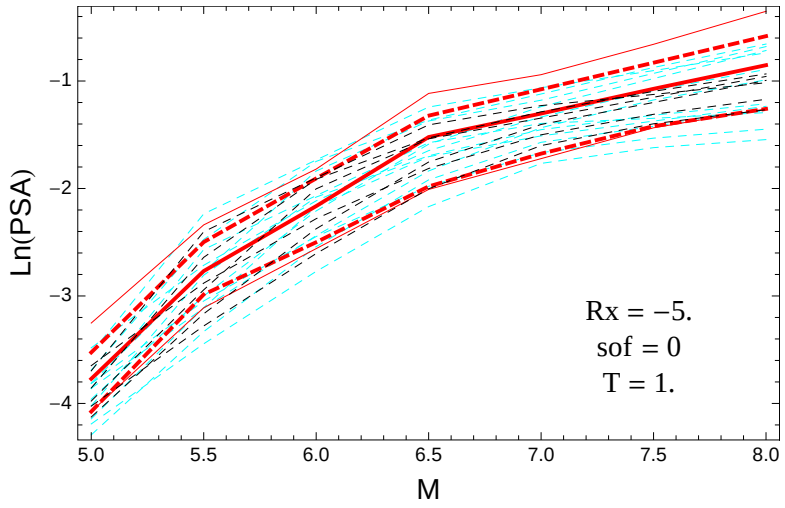



Figure 4.539: PVNGSv2: Magnitude scaling of the original GMPEs (dashed black), the original GMPEs with uncertainty model (dashed cyan) and 0.05,0.5,0.95 quantile of the ModelB distribution (red) with total weights, for a scenario with $R_X = -5.$, $F = 0$, and $T = 1.$s.

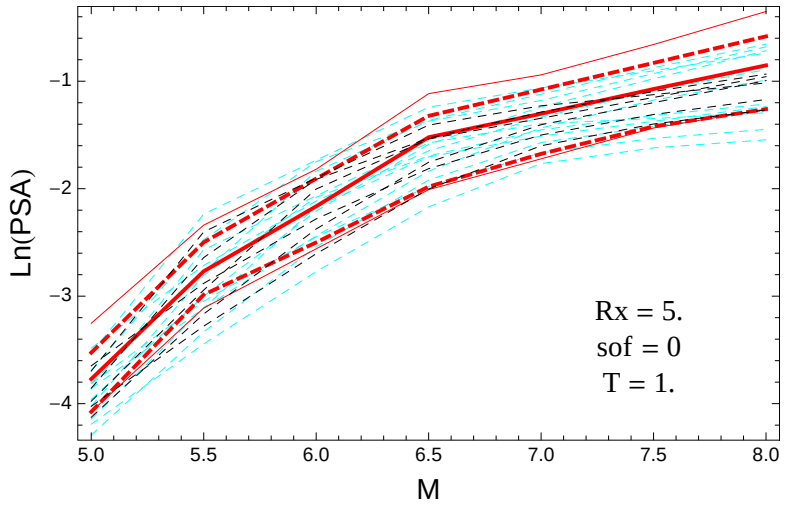



Figure 4.540: PVNGSv2: Magnitude scaling of the original GMPEs (dashed black), the original GMPEs with uncertainty model (dashed cyan) and 0.05,0.5,0.95 quantile of the ModelB distribution (red) with total weights, for a scenario with $R_X = 5.$, $F = 0$, and $T = 1.$s.

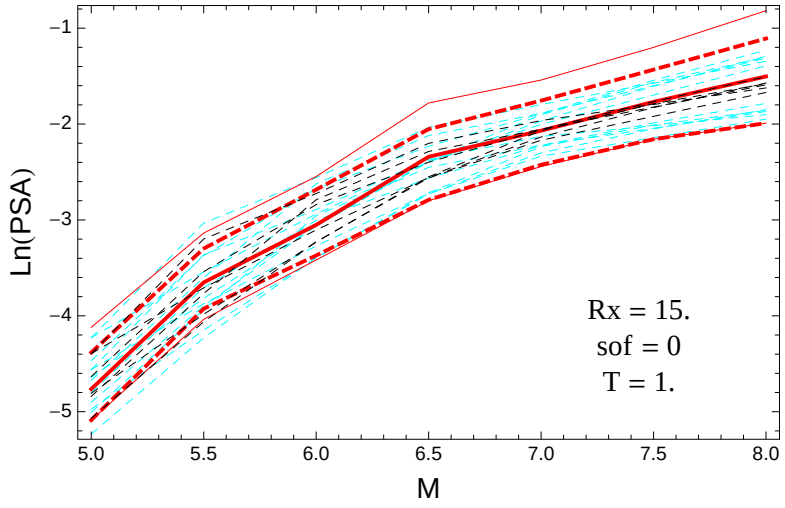



Figure 4.541: PVNGSv2: Magnitude scaling of the original GMPEs (dashed black), the original GMPEs with uncertainty model (dashed cyan) and 0.05,0.5,0.95 quantile of the ModelB distribution (red) with total weights, for a scenario with $R_X = 15.$, $F = 0$, and $T = 1.$s.

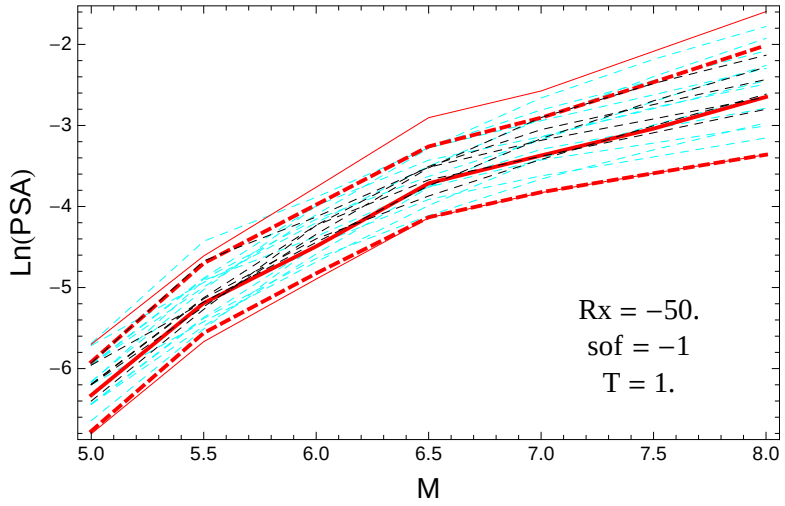



Figure 4.542: PVNGSv2: Magnitude scaling of the original GMPEs (dashed black), the original GMPEs with uncertainty model (dashed cyan) and 0.05,0.5,0.95 quantile of the ModelB distribution (red) with total weights, for a scenario with $R_X = -50.$, $F = -1$, and $T = 1.$s.

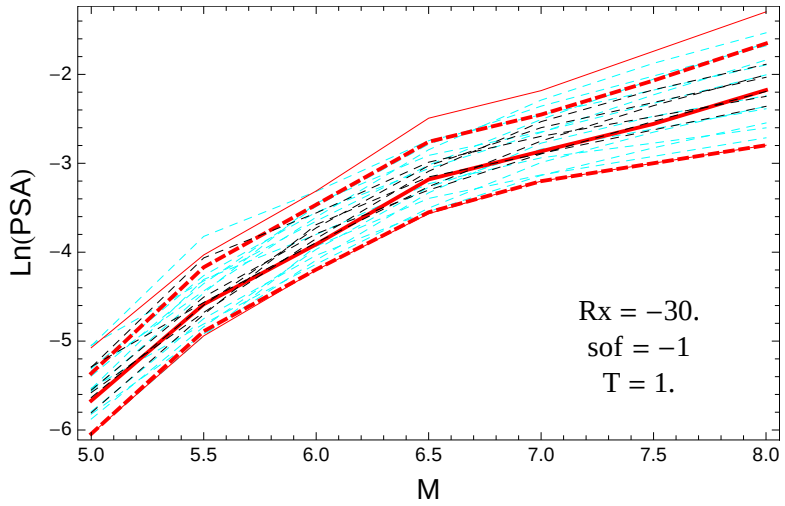



Figure 4.543: PVNGSv2: Magnitude scaling of the original GMPEs (dashed black), the original GMPEs with uncertainty model (dashed cyan) and 0.05,0.5,0.95 quantile of the ModelB distribution (red) with total weights, for a scenario with $R_X = -30.$, $F = -1$, and $T = 1.$s.

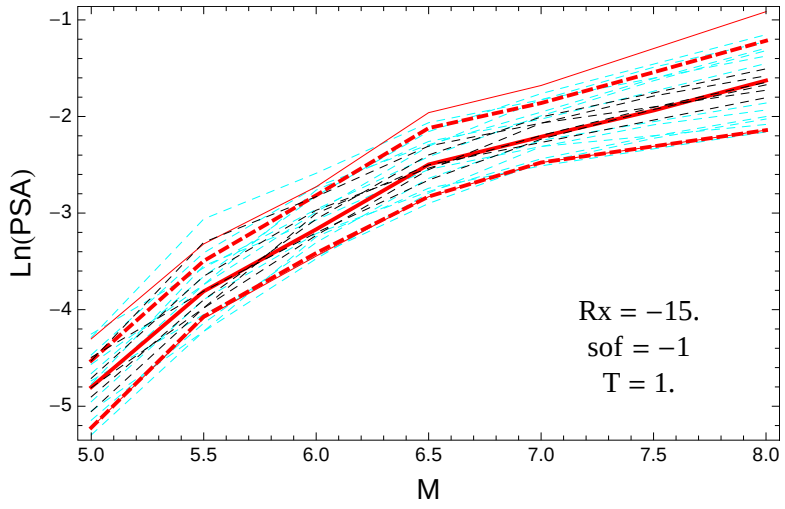



Figure 4.544: PVNGSv2: Magnitude scaling of the original GMPEs (dashed black), the original GMPEs with uncertainty model (dashed cyan) and 0.05,0.5,0.95 quantile of the ModelB distribution (red) with total weights, for a scenario with $R_X = -15.$, $F = -1$, and $T = 1.$s.

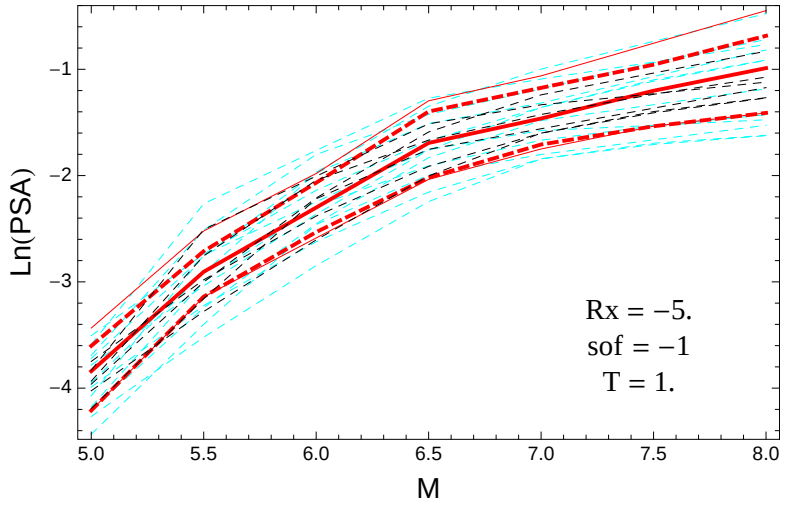



Figure 4.545: PVNGSv2: Magnitude scaling of the original GMPEs (dashed black), the original GMPEs with uncertainty model (dashed cyan) and 0.05,0.5,0.95 quantile of the ModelB distribution (red) with total weights, for a scenario with $R_X = -5.$, $F = -1$, and $T = 1.$s.

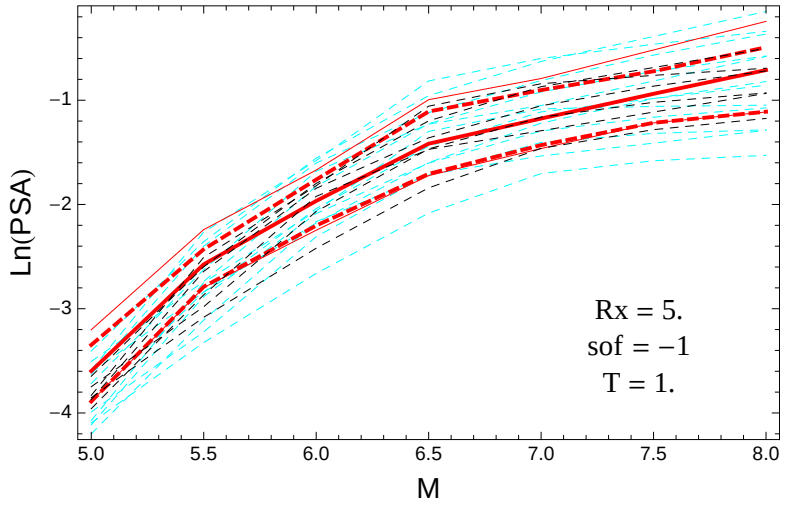



Figure 4.546: PVNGSv2: Magnitude scaling of the original GMPEs (dashed black), the original GMPEs with uncertainty model (dashed cyan) and 0.05,0.5,0.95 quantile of the ModelB distribution (red) with total weights, for a scenario with $R_X = 5.$, $F = -1$, and $T = 1.$s.

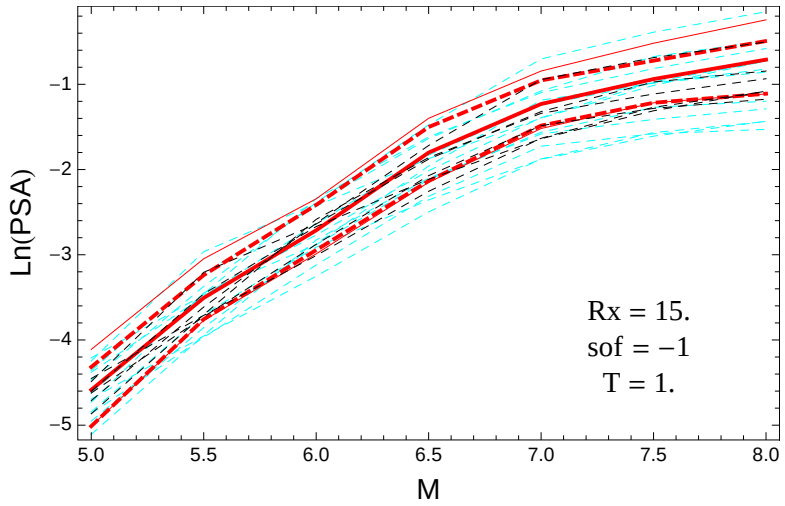



Figure 4.547: PVNGSv2: Magnitude scaling of the original GMPEs (dashed black), the original GMPEs with uncertainty model (dashed cyan) and 0.05,0.5,0.95 quantile of the ModelB distribution (red) with total weights, for a scenario with $R_X = 15.$, $F = -1$, and $T = 1.$s.

**T = 3.s**

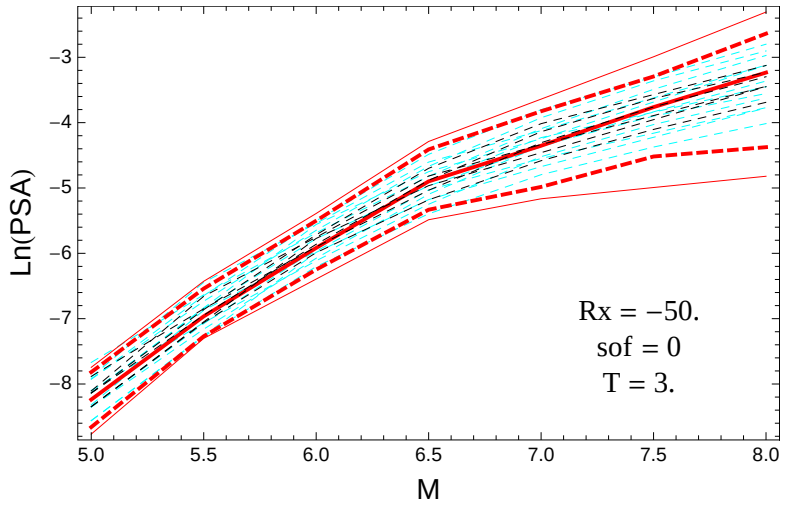



Figure 4.548: PVNGSv2: Magnitude scaling of the original GMPEs (dashed black), the original GMPEs with uncertainty model (dashed cyan) and 0.05,0.5,0.95 quantile of the ModelB distribution (red) with total weights, for a scenario with $R_X = -50.$, $F = 0$, and $T = 3.$s.

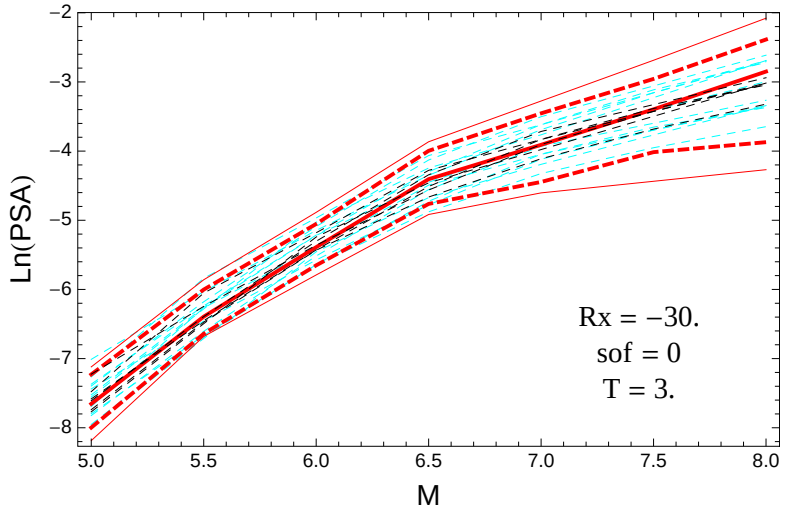



Figure 4.549: PVNGSv2: Magnitude scaling of the original GMPEs (dashed black), the original GMPEs with uncertainty model (dashed cyan) and 0.05,0.5,0.95 quantile of the ModelB distribution (red) with total weights, for a scenario with $R_X = -30.$, $F = 0$, and $T = 3.$s.

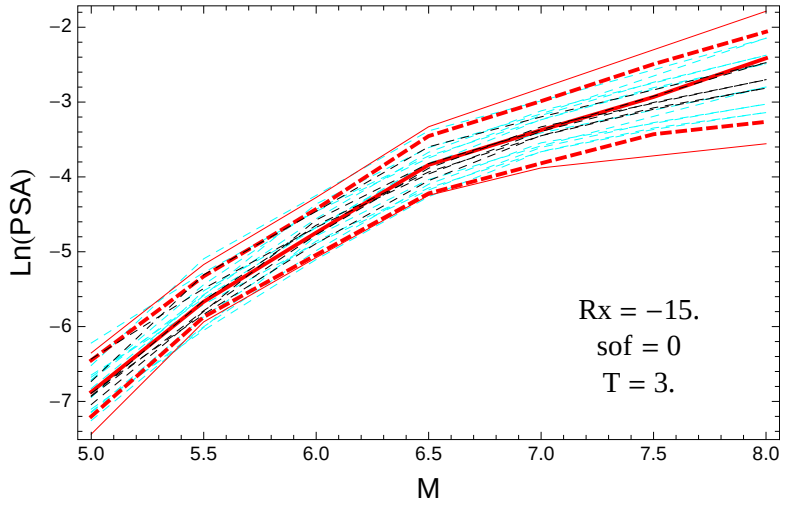



Figure 4.550: PVNGSv2: Magnitude scaling of the original GMPEs (dashed black), the original GMPEs with uncertainty model (dashed cyan) and 0.05,0.5,0.95 quantile of the ModelB distribution (red) with total weights, for a scenario with $R_X = -15.$, $F = 0$, and $T = 3.$s.

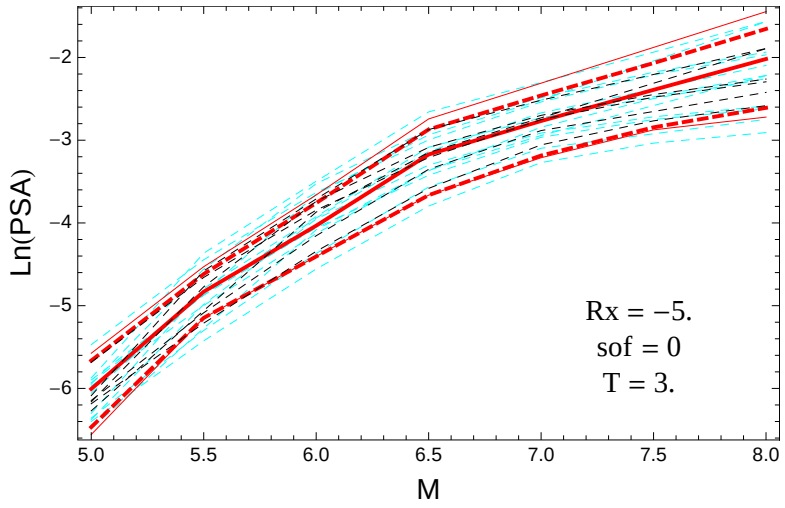



Figure 4.551: PVNGSv2: Magnitude scaling of the original GMPEs (dashed black), the original GMPEs with uncertainty model (dashed cyan) and 0.05,0.5,0.95 quantile of the ModelB distribution (red) with total weights, for a scenario with $R_X = -5.$, $F = 0$, and $T = 3.$s.

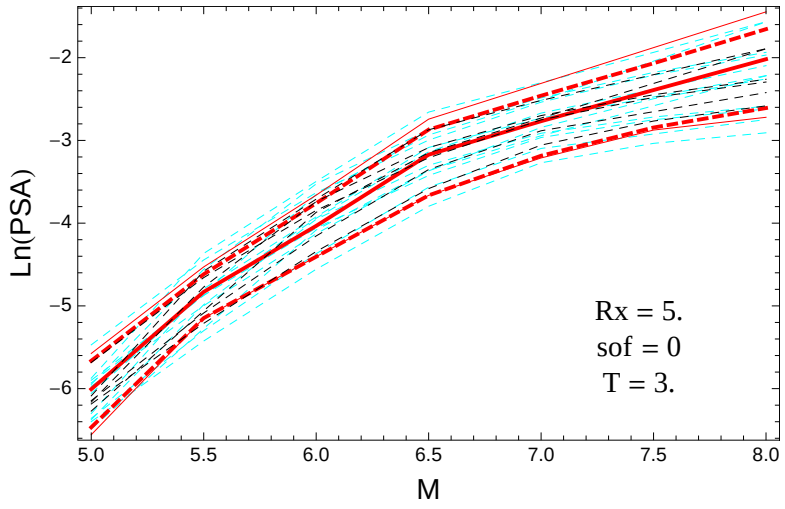



Figure 4.552: PVNGSv2: Magnitude scaling of the original GMPEs (dashed black), the original GMPEs with uncertainty model (dashed cyan) and 0.05,0.5,0.95 quantile of the ModelB distribution (red) with total weights, for a scenario with $R_X = 5.$, $F = 0$, and $T = 3.$s.

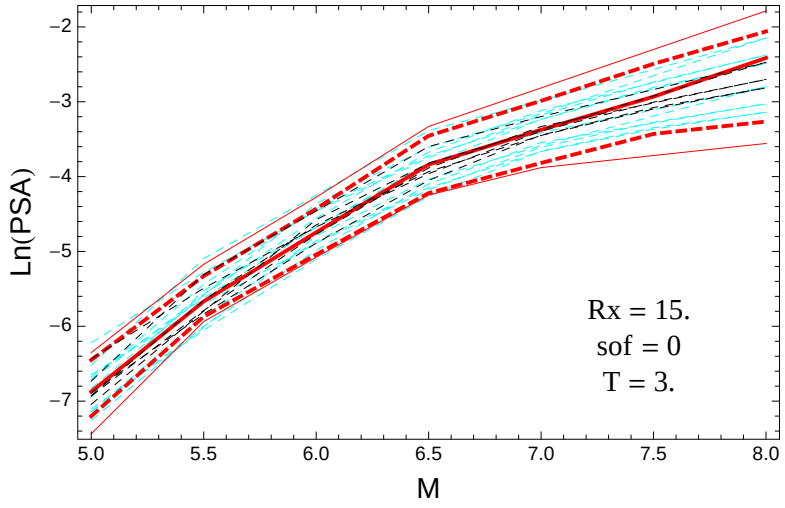



Figure 4.553: PVNGSv2: Magnitude scaling of the original GMPEs (dashed black), the original GMPEs with uncertainty model (dashed cyan) and 0.05,0.5,0.95 quantile of the ModelB distribution (red) with total weights, for a scenario with $R_X = 15.$, $F = 0$, and $T = 3.$s.

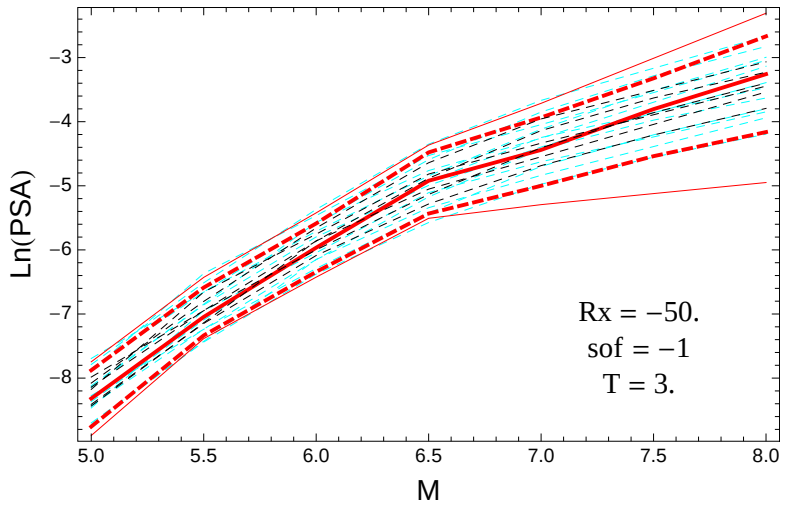



Figure 4.554: PVNGSv2: Magnitude scaling of the original GMPEs (dashed black), the original GMPEs with uncertainty model (dashed cyan) and 0.05,0.5,0.95 quantile of the ModelB distribution (red) with total weights, for a scenario with $R_X = -50.$, $F = -1$, and $T = 3.$s.

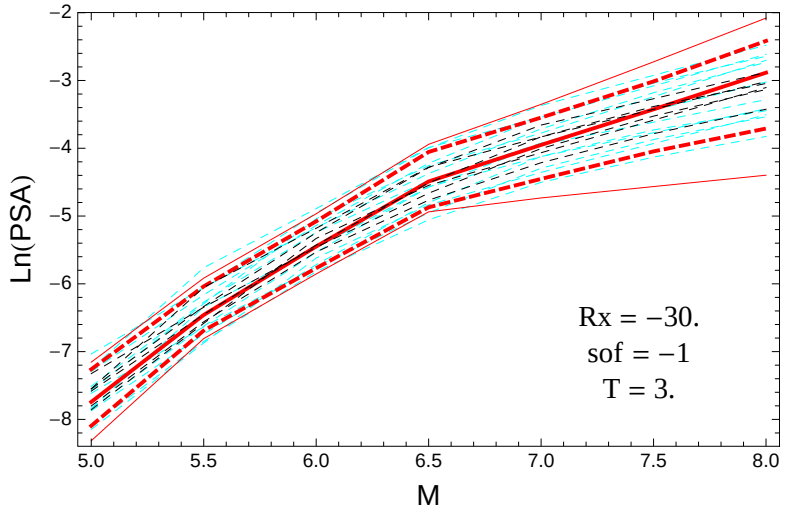



Figure 4.555: PVNGSv2: Magnitude scaling of the original GMPEs (dashed black), the original GMPEs with uncertainty model (dashed cyan) and 0.05,0.5,0.95 quantile of the ModelB distribution (red) with total weights, for a scenario with $R_X = -30.$, $F = -1$, and $T = 3.$s.

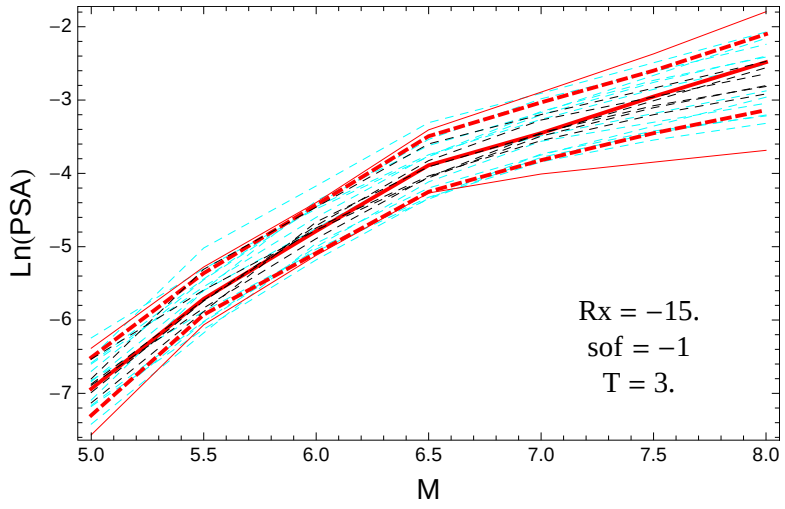



Figure 4.556: PVNGSv2: Magnitude scaling of the original GMPEs (dashed black), the original GMPEs with uncertainty model (dashed cyan) and 0.05,0.5,0.95 quantile of the ModelB distribution (red) with total weights, for a scenario with $R_X = -15.$, $F = -1$, and $T = 3.$s.

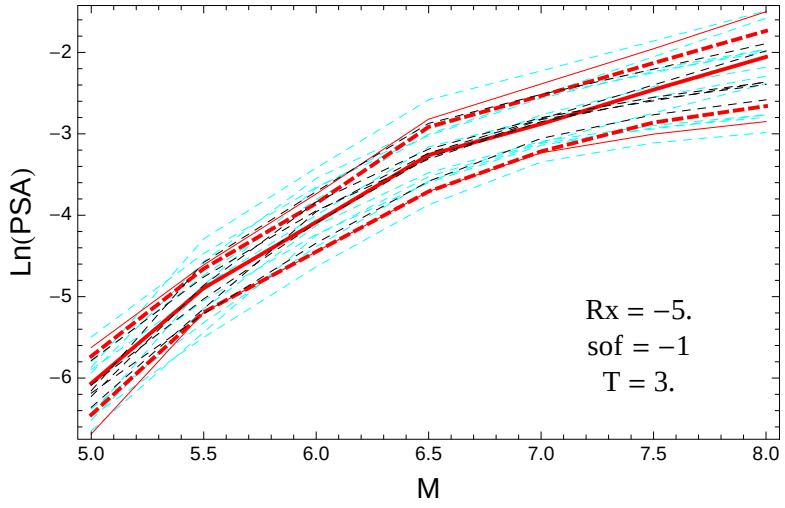



Figure 4.557: PVNGSv2: Magnitude scaling of the original GMPEs (dashed black), the original GMPEs with uncertainty model (dashed cyan) and 0.05,0.5,0.95 quantile of the ModelB distribution (red) with total weights, for a scenario with $R_X = -5.$, $F = -1$, and $T = 3.$s.

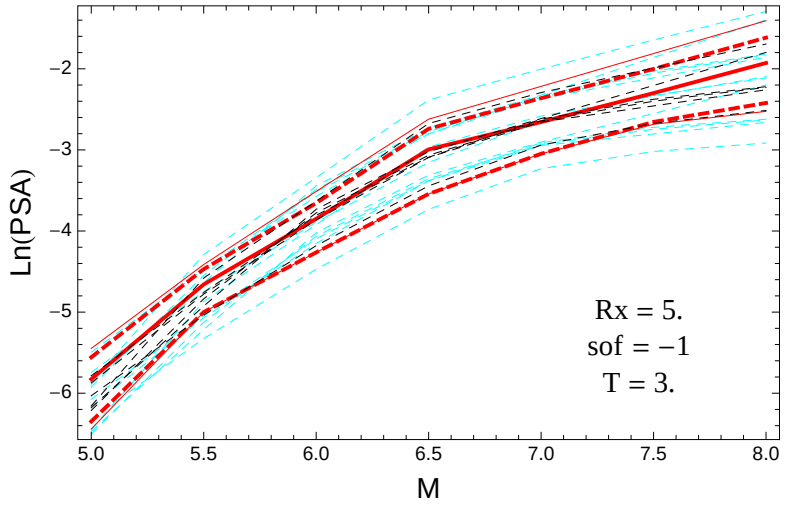



Figure 4.558: PVNGSv2: Magnitude scaling of the original GMPEs (dashed black), the original GMPEs with uncertainty model (dashed cyan) and 0.05,0.5,0.95 quantile of the ModelB distribution (red) with total weights, for a scenario with $R_X = 5.$, $F = -1$, and $T = 3.$s.

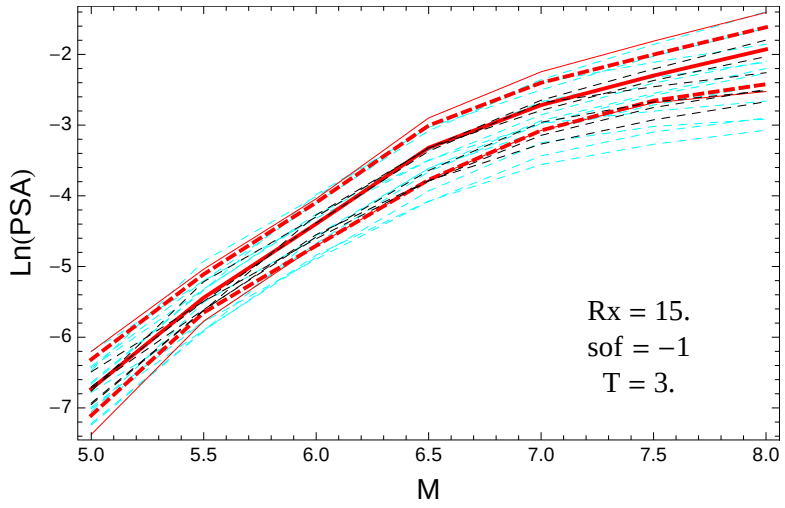



Figure 4.559: PVNGSv2: Magnitude scaling of the original GMPEs (dashed black), the original GMPEs with uncertainty model (dashed cyan) and 0.05,0.5,0.95 quantile of the ModelB distribution (red) with total weights, for a scenario with $R_X = 15.$, $F = -1$, and $T = 3.$s.

### 4.1.14 Quantile Plots vs. Period with GMPEs

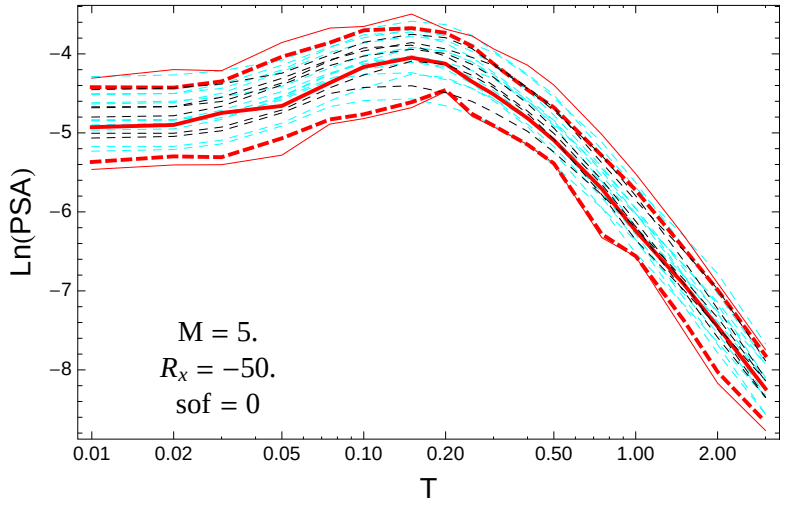



Figure 4.560: PVNGSv2: Spectra of 0.05,0.5,0.95 and the ModelB distribution (red) with total weights, original GMPEs (dashed black) and the original GMPEs with uncertainty model (dashed cyan) for a scenario with $M_W = 5.$, $R_x = -50.$, $F = 0$.

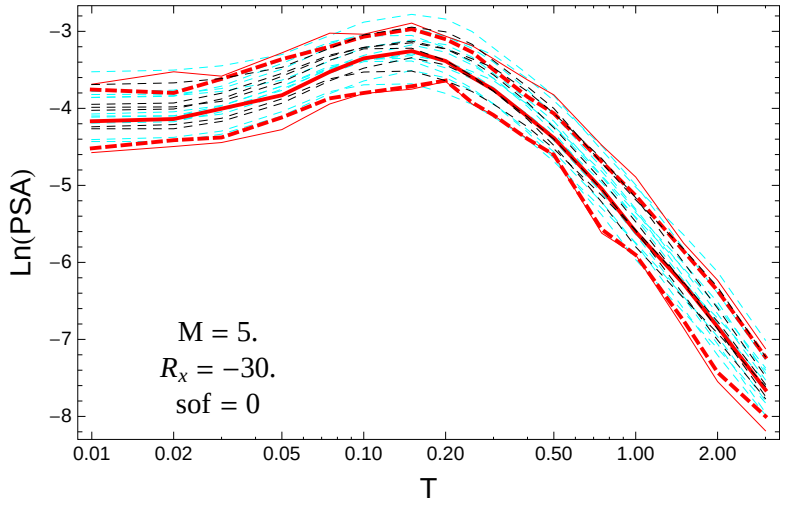



Figure 4.561: PVNGSv2: Spectra of 0.05,0.5,0.95 and the ModelB distribution (red) with total weights, original GMPEs (dashed black) and the original GMPEs with uncertainty model (dashed cyan) for a scenario with $M_W = 5.$, $R_x = -30.$, $F = 0$.

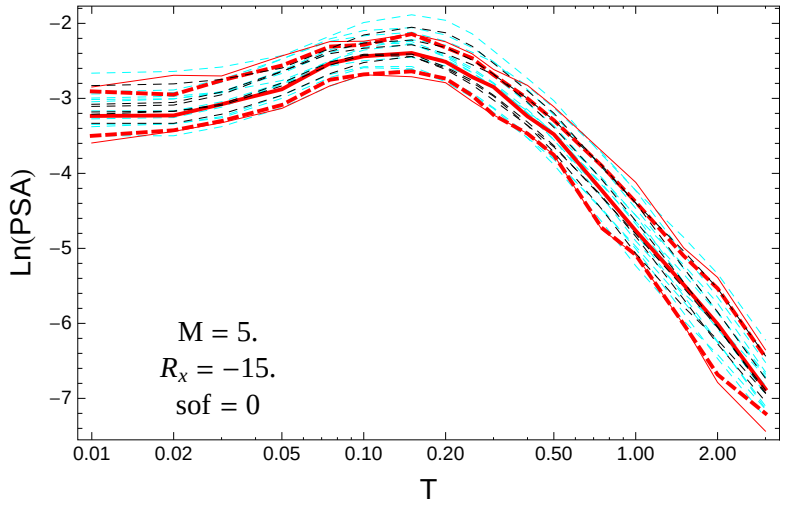



Figure 4.562: PVNGSv2: Spectra of 0.05,0.5,0.95 and the ModelB distribution (red) with total weights, original GMPEs (dashed black) and the original GMPEs with uncertainty model (dashed cyan) for a scenario with $M_W = 5.$, $R_x = -15.$, $F = 0$.

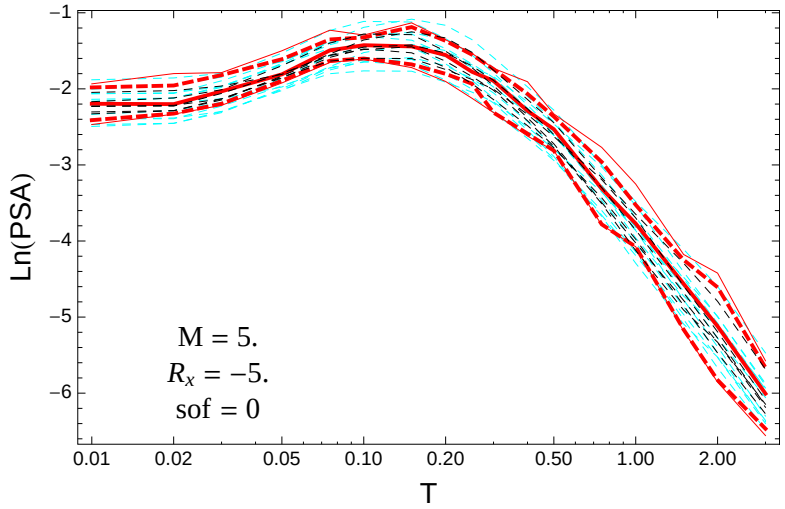



Figure 4.563: PVNGSv2: Spectra of 0.05,0.5,0.95 and the ModelB distribution (red) with total weights, original GMPEs (dashed black) and the original GMPEs with uncertainty model (dashed cyan) for a scenario with $M_W = 5.$, $R_x = -5.$, $F = 0$.

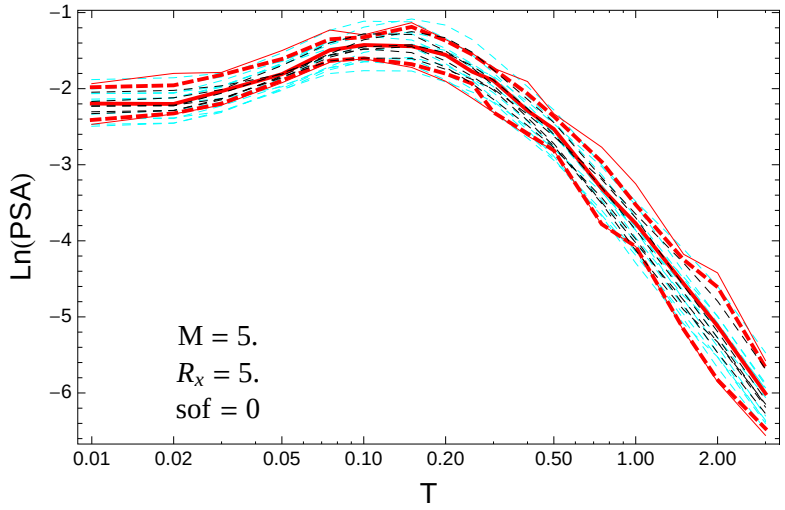



Figure 4.564: PVNGSv2: Spectra of 0.05,0.5,0.95 and the ModelB distribution (red) with total weights, original GMPEs (dashed black) and the original GMPEs with uncertainty model (dashed cyan) for a scenario with $M_W = 5.$, $R_x = 5.$, $F = 0$.

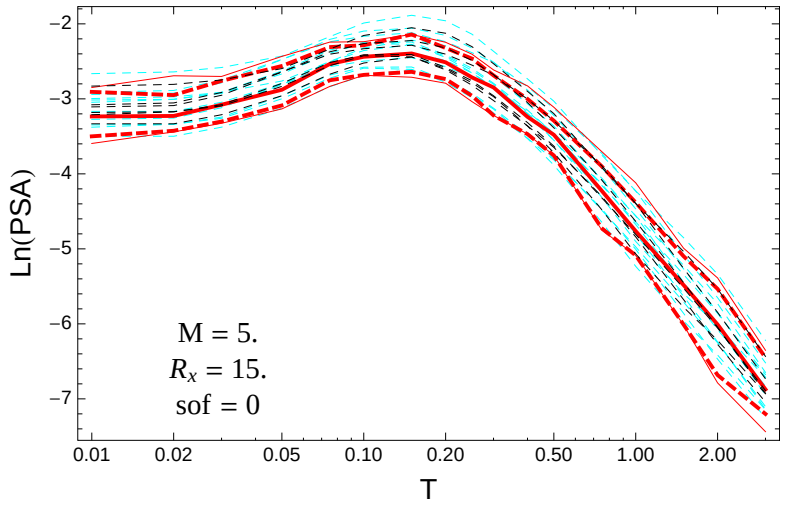



Figure 4.565: PVNGSv2: Spectra of 0.05,0.5,0.95 and the ModelB distribution (red) with total weights, original GMPEs (dashed black) and the original GMPEs with uncertainty model (dashed cyan) for a scenario with $M_W = 5.$, $R_x = 15.$, $F = 0$.

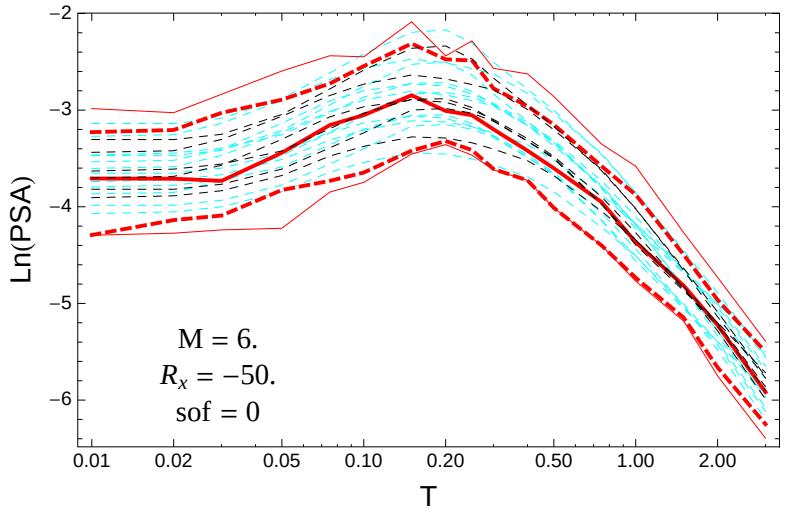



Figure 4.566: PVNGSv2: Spectra of 0.05,0.5,0.95 and the ModelB distribution (red) with total weights, original GMPEs (dashed black) and the original GMPEs with uncertainty model (dashed cyan) for a scenario with $M_W = 6.$, $R_x = -50.$, $F = 0$.

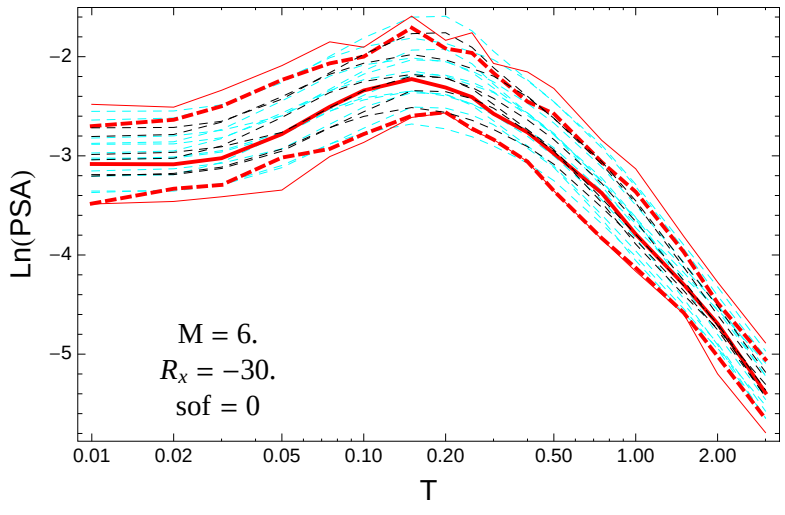



Figure 4.567: PVNGSv2: Spectra of 0.05,0.5,0.95 and the ModelB distribution (red) with total weights, original GMPEs (dashed black) and the original GMPEs with uncertainty model (dashed cyan) for a scenario with $M_W = 6.$, $R_x = -30.$, $F = 0$.

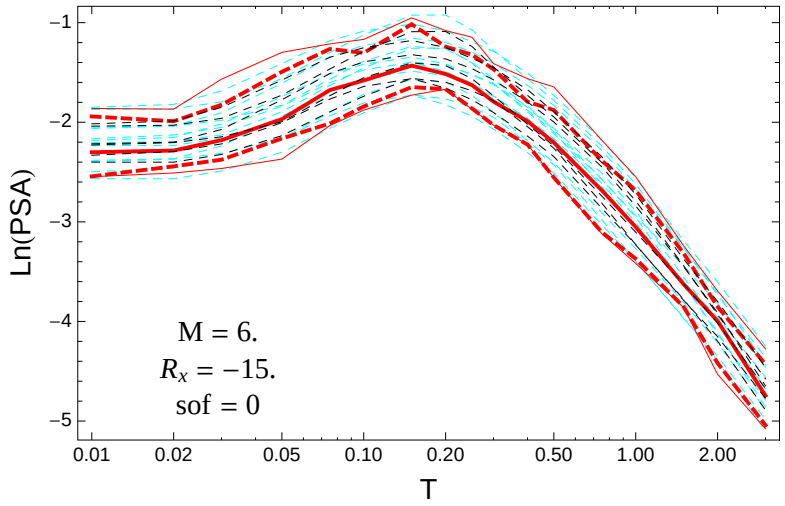



Figure 4.568: PVNGSv2: Spectra of 0.05,0.5,0.95 and the ModelB distribution (red) with total weights, original GMPEs (dashed black) and the original GMPEs with uncertainty model (dashed cyan) for a scenario with $M_W = 6.$, $R_x = -15.$, $F = 0$.

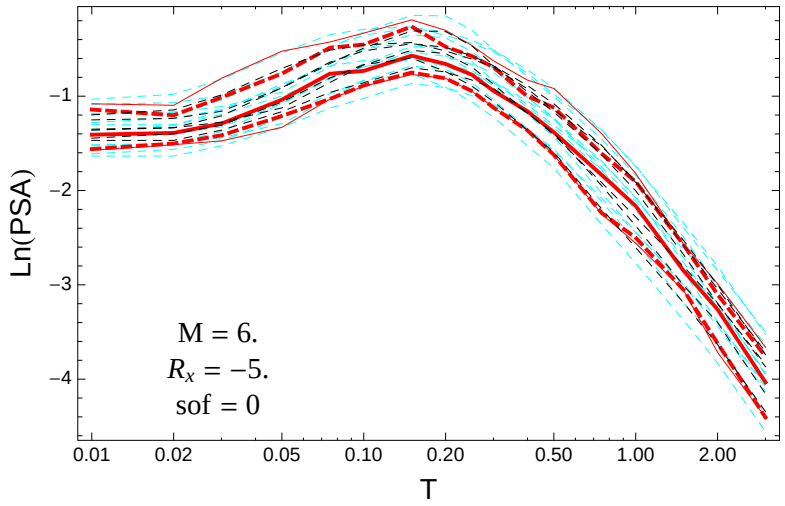



Figure 4.569: PVNGSv2: Spectra of 0.05,0.5,0.95 and the ModelB distribution (red) with total weights, original GMPEs (dashed black) and the original GMPEs with uncertainty model (dashed cyan) for a scenario with $M_W = 6.$, $R_x = -5.$, $F = 0$.

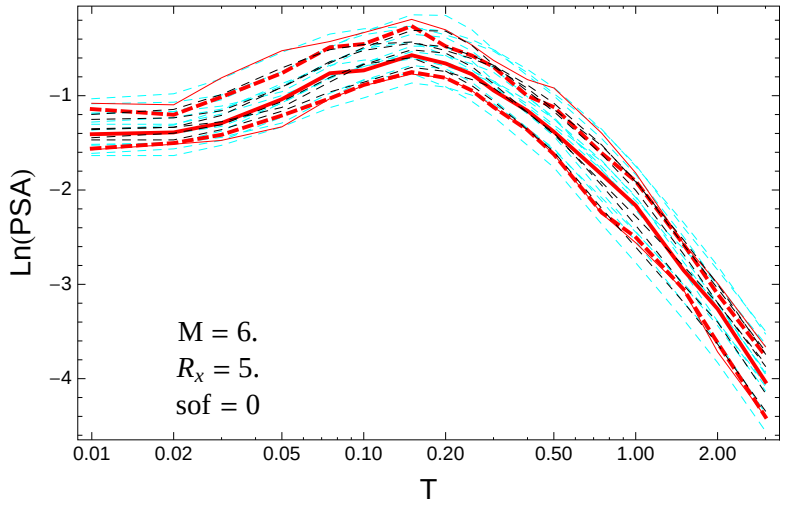



Figure 4.570: PVNGSv2: Spectra of 0.05,0.5,0.95 and the ModelB distribution (red) with total weights, original GMPEs (dashed black) and the original GMPEs with uncertainty model (dashed cyan) for a scenario with $M_W = 6.$, $R_x = 5.$, $F = 0$.

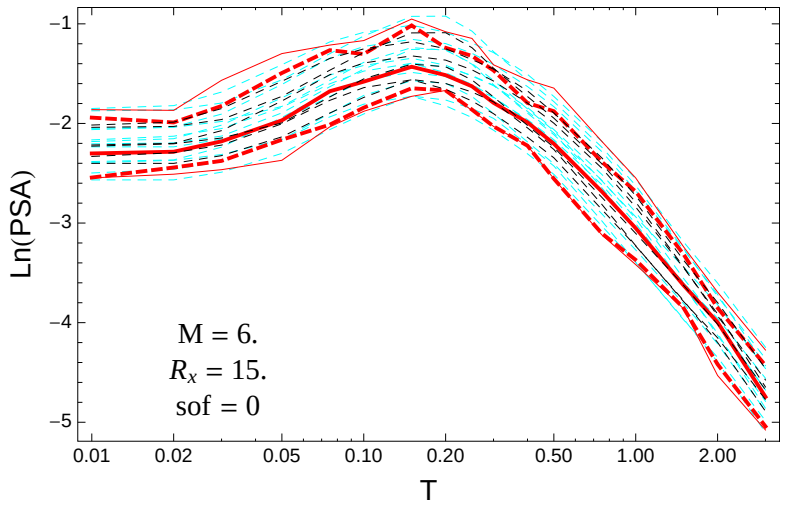



Figure 4.571: PVNGSv2: Spectra of 0.05,0.5,0.95 and the ModelB distribution (red) with total weights, original GMPEs (dashed black) and the original GMPEs with uncertainty model (dashed cyan) for a scenario with $M_W = 6.$, $R_x = 15.$, $F = 0$.

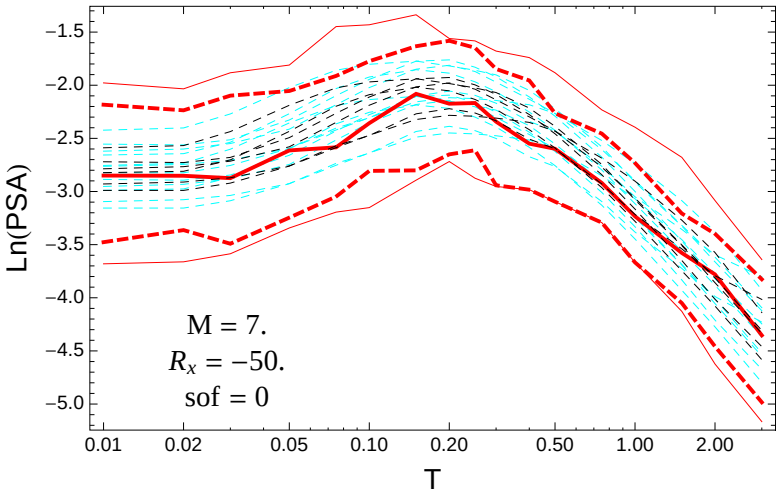



Figure 4.572: PVNGSv2: Spectra of 0.05,0.5,0.95 and the ModelB distribution (red) with total weights, original GMPEs (dashed black) and the original GMPEs with uncertainty model (dashed cyan) for a scenario with $M_W = 7.$, $R_x = -50.$, $F = 0$.

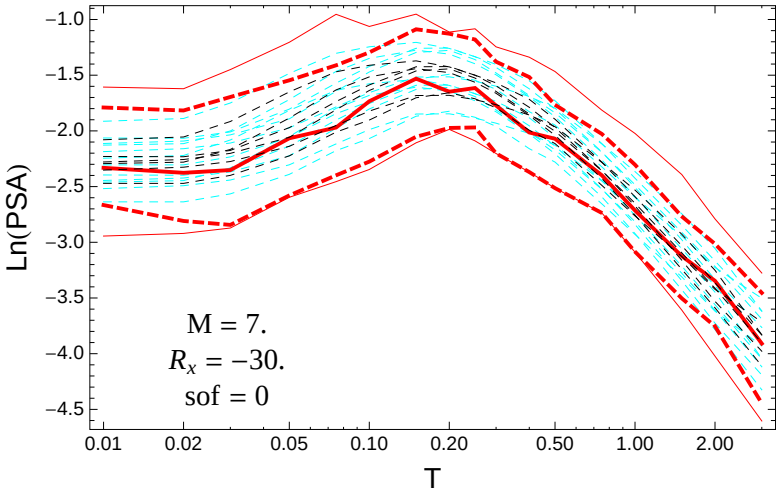



Figure 4.573: PVNGSv2: Spectra of 0.05,0.5,0.95 and the ModelB distribution (red) with total weights, original GMPEs (dashed black) and the original GMPEs with uncertainty model (dashed cyan) for a scenario with $M_W = 7.$, $R_x = -30.$, $F = 0$.

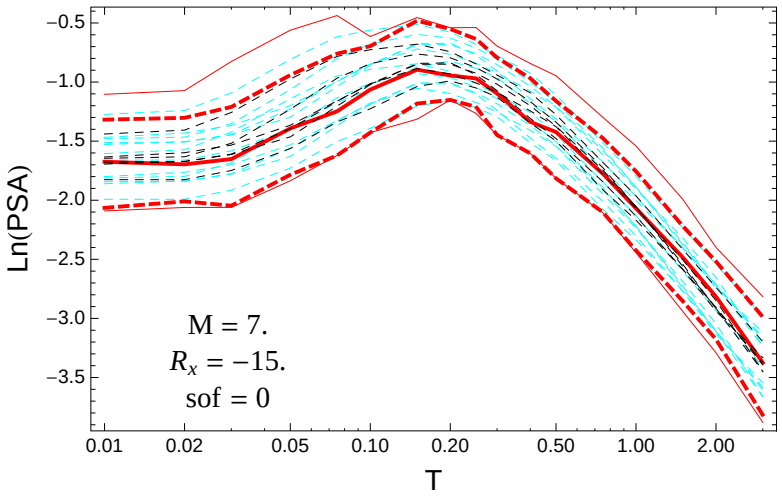



Figure 4.574: PVNGSv2: Spectra of 0.05,0.5,0.95 and the ModelB distribution (red) with total weights, original GMPEs (dashed black) and the original GMPEs with uncertainty model (dashed cyan) for a scenario with $M_W = 7.$, $R_x = -15.$, $F = 0$.

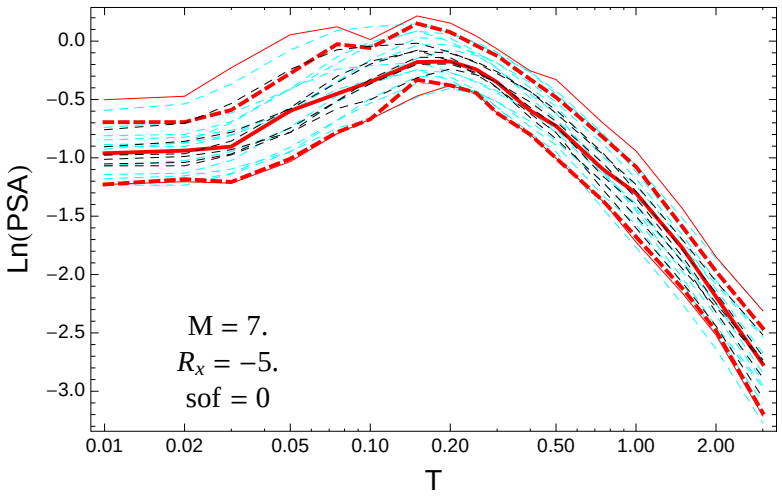



Figure 4.575: PVNGSv2: Spectra of 0.05,0.5,0.95 and the ModelB distribution (red) with total weights, original GMPEs (dashed black) and the original GMPEs with uncertainty model (dashed cyan) for a scenario with $M_W = 7.$, $R_x = -5.$, $F = 0$.

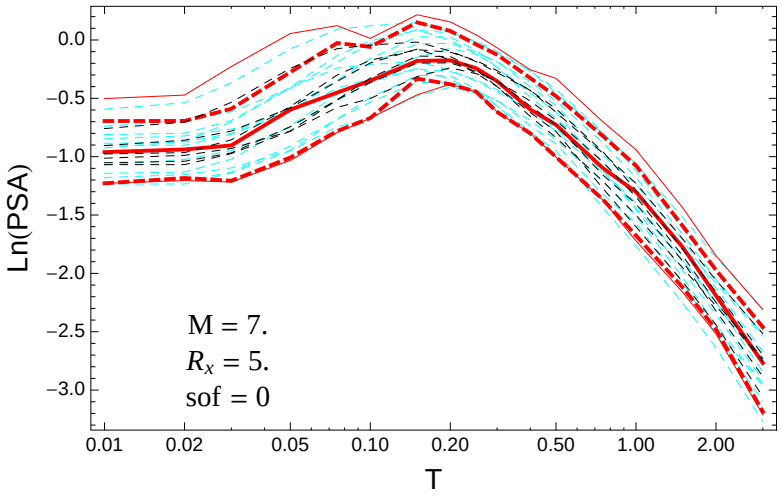



Figure 4.576: PVNGSv2: Spectra of 0.05,0.5,0.95 and the ModelB distribution (red) with total weights, original GMPEs (dashed black) and the original GMPEs with uncertainty model (dashed cyan) for a scenario with $M_W = 7.$, $R_x = 5.$, $F = 0$.

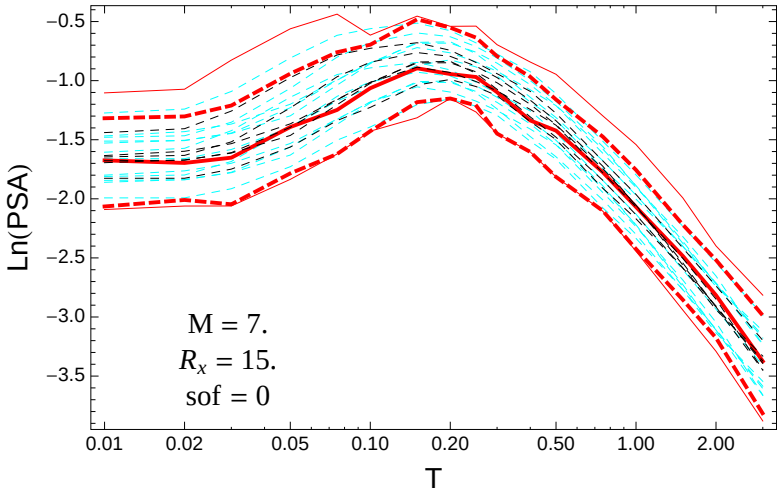



Figure 4.577: PVNGSv2: Spectra of 0.05,0.5,0.95 and the ModelB distribution (red) with total weights, original GMPEs (dashed black) and the original GMPEs with uncertainty model (dashed cyan) for a scenario with $M_W = 7.$, $R_x = 15.$, $F = 0$.

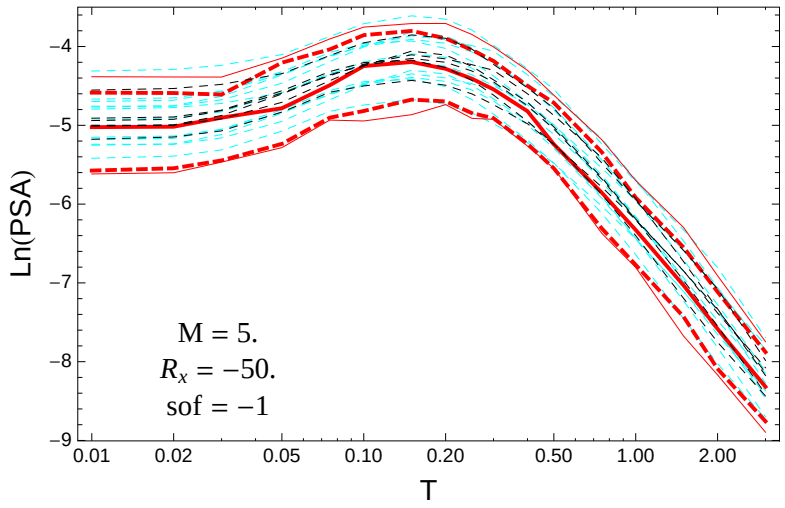



Figure 4.578: PVNGSv2: Spectra of 0.05,0.5,0.95 and the ModelB distribution (red) with total weights, original GMPEs (dashed black) and the original GMPEs with uncertainty model (dashed cyan) for a scenario with $M_W = 5.$, $R_x = -50.$, $F = -1$.

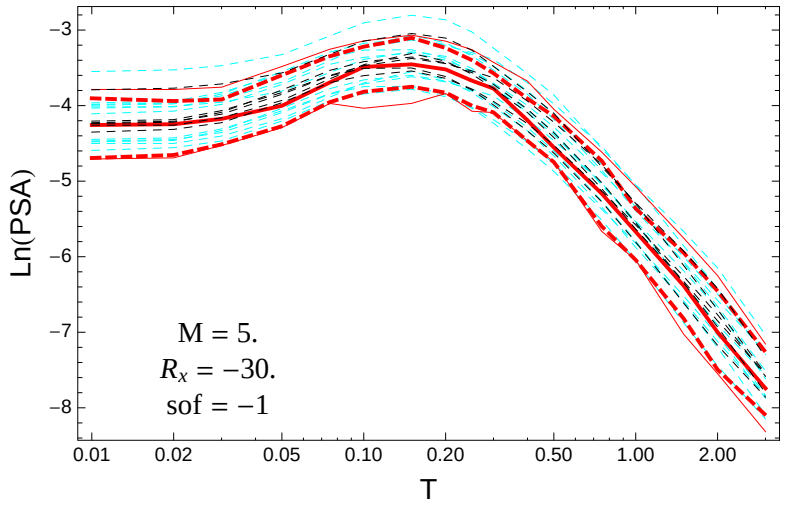



Figure 4.579: PVNGSv2: Spectra of 0.05,0.5,0.95 and the ModelB distribution (red) with total weights, original GMPEs (dashed black) and the original GMPEs with uncertainty model (dashed cyan) for a scenario with $M_W = 5.$, $R_x = -30.$, $F = -1$.

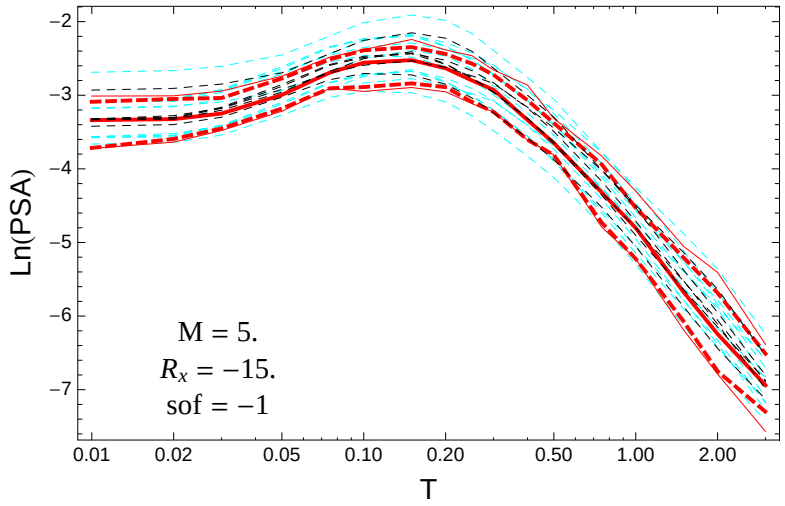



Figure 4.580: PVNGSv2: Spectra of 0.05,0.5,0.95 and the ModelB distribution (red) with total weights, original GMPEs (dashed black) and the original GMPEs with uncertainty model (dashed cyan) for a scenario with $M_W = 5.$, $R_x = -15.$, $F = -1$.

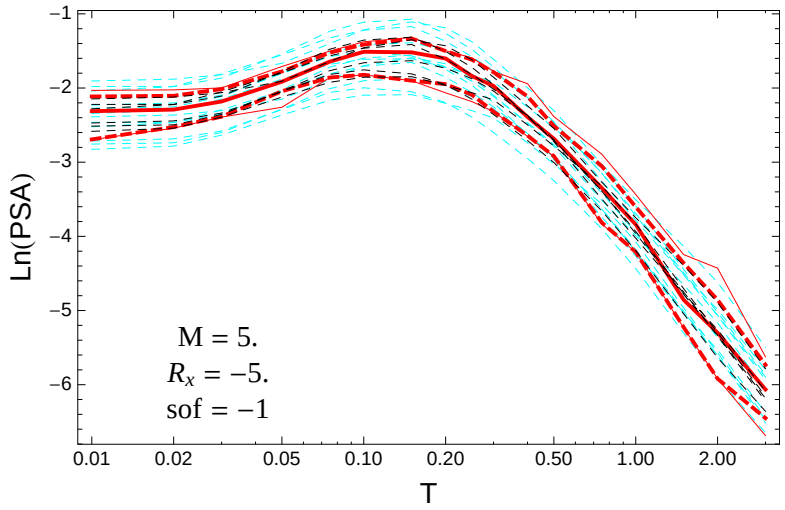



Figure 4.581: PVNGSv2: Spectra of 0.05,0.5,0.95 and the ModelB distribution (red) with total weights, original GMPEs (dashed black) and the original GMPEs with uncertainty model (dashed cyan) for a scenario with $M_W = 5.$, $R_x = -5.$, $F = -1$.

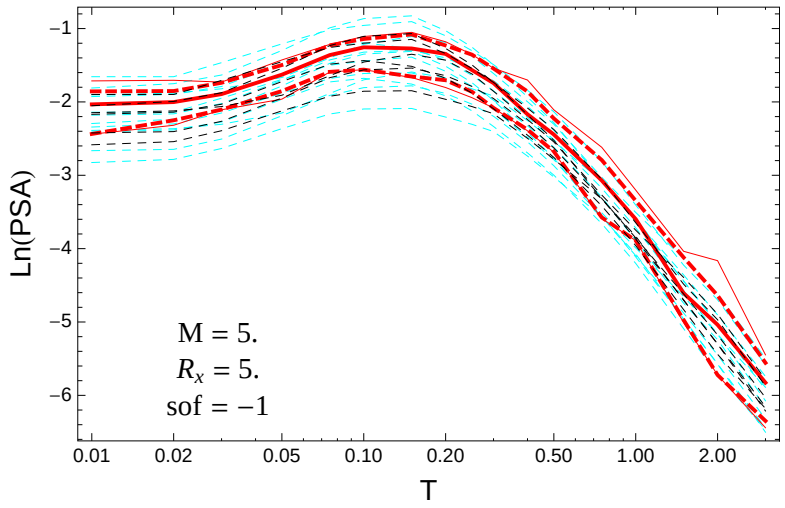



Figure 4.582: PVNGSv2: Spectra of 0.05,0.5,0.95 and the ModelB distribution (red) with total weights, original GMPEs (dashed black) and the original GMPEs with uncertainty model (dashed cyan) for a scenario with $M_W = 5.$, $R_x = 5.$, $F = -1$.

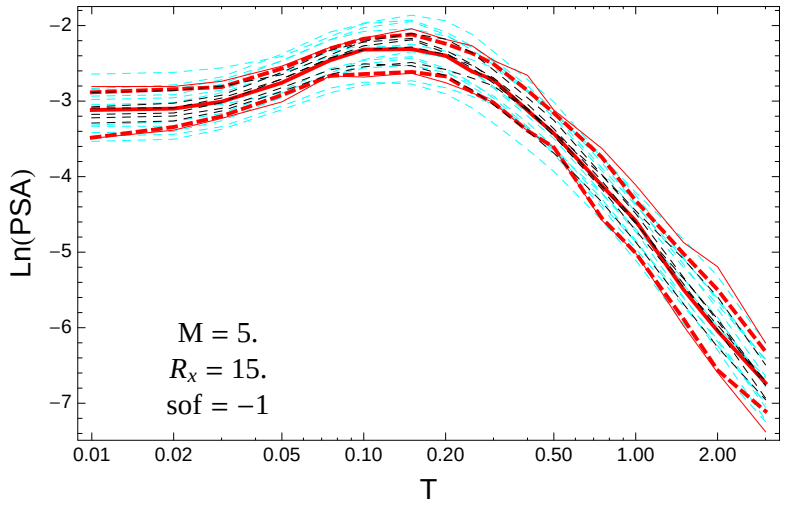



Figure 4.583: PVNGSv2: Spectra of 0.05,0.5,0.95 and the ModelB distribution (red) with total weights, original GMPEs (dashed black) and the original GMPEs with uncertainty model (dashed cyan) for a scenario with $M_W = 5.$, $R_x = 15.$, $F = -1$.

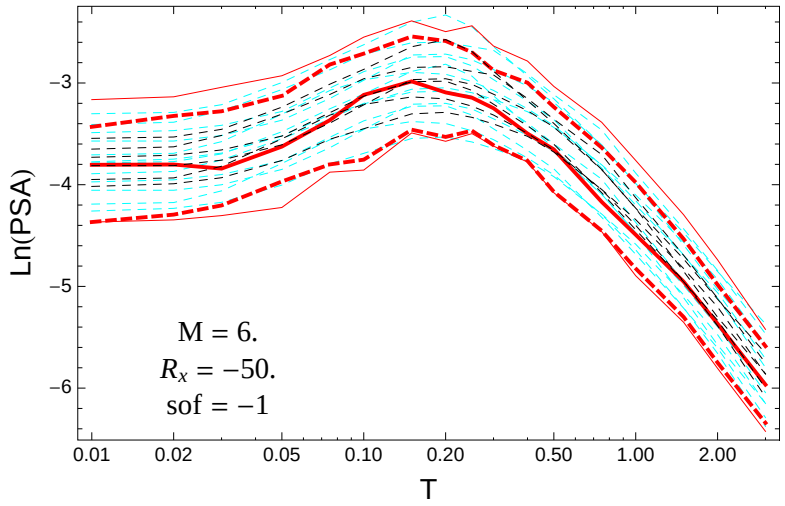



Figure 4.584: PVNGSv2: Spectra of 0.05,0.5,0.95 and the ModelB distribution (red) with total weights, original GMPEs (dashed black) and the original GMPEs with uncertainty model (dashed cyan) for a scenario with $M_W = 6.$, $R_x = -50.$, $F = -1$.

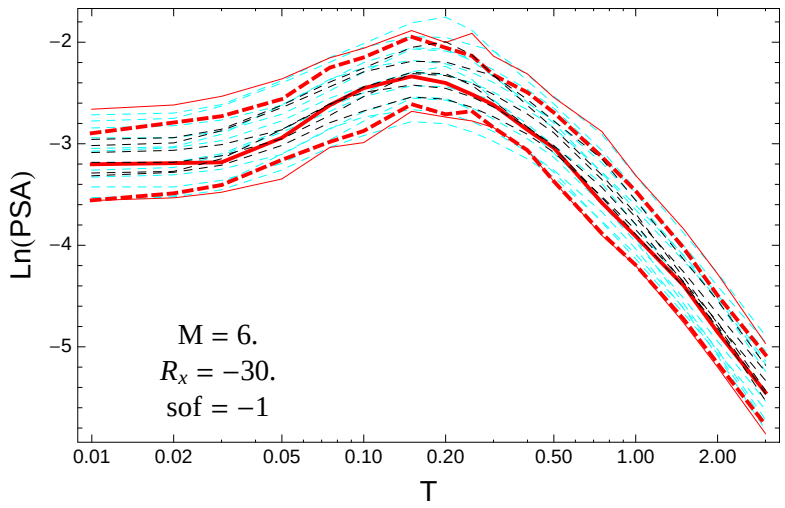



Figure 4.585: PVNGSv2: Spectra of 0.05,0.5,0.95 and the ModelB distribution (red) with total weights, original GMPEs (dashed black) and the original GMPEs with uncertainty model (dashed cyan) for a scenario with $M_W = 6.$, $R_x = -30.$, $F = -1$.

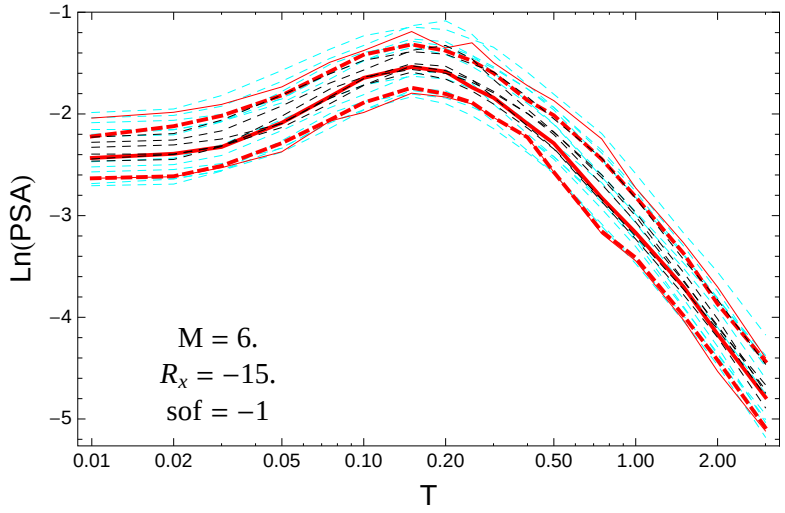



Figure 4.586: PVNGSv2: Spectra of 0.05,0.5,0.95 and the ModelB distribution (red) with total weights, original GMPEs (dashed black) and the original GMPEs with uncertainty model (dashed cyan) for a scenario with $M_W = 6.$, $R_x = -15.$, $F = -1$.

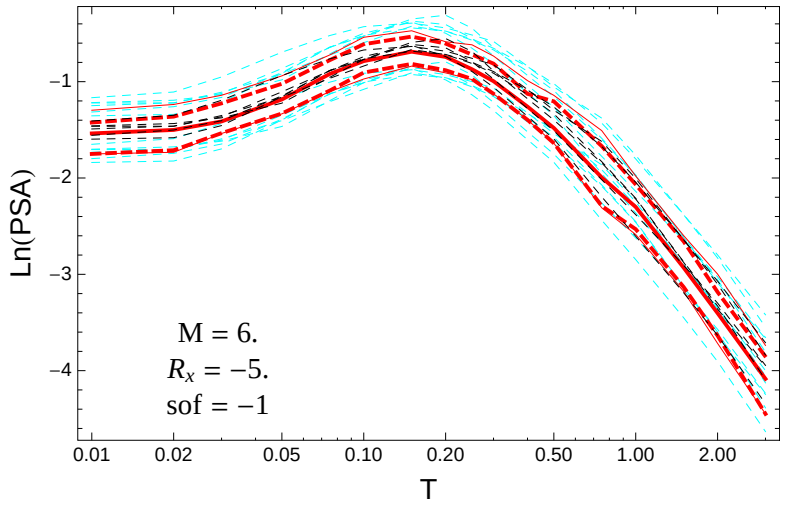



Figure 4.587: PVNGSv2: Spectra of 0.05,0.5,0.95 and the ModelB distribution (red) with total weights, original GMPEs (dashed black) and the original GMPEs with uncertainty model (dashed cyan) for a scenario with $M_W = 6.$, $R_x = -5.$, $F = -1$.

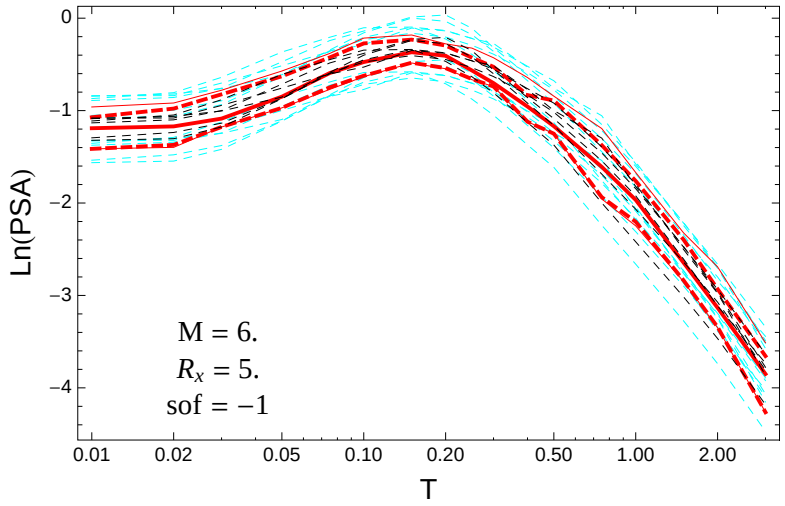



Figure 4.588: PVNGSv2: Spectra of 0.05,0.5,0.95 and the ModelB distribution (red) with total weights, original GMPEs (dashed black) and the original GMPEs with uncertainty model (dashed cyan) for a scenario with $M_W = 6.$, $R_x = 5.$, $F = -1.$

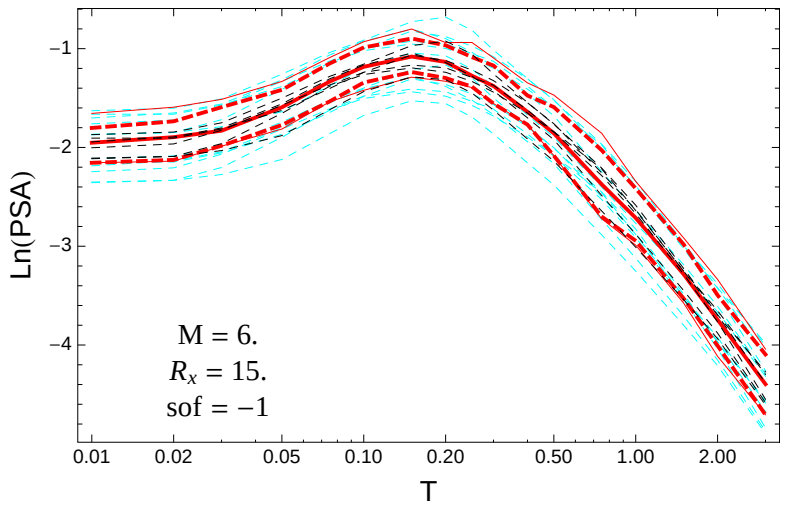



Figure 4.589: PVNGSv2: Spectra of 0.05,0.5,0.95 and the ModelB distribution (red) with total weights, original GMPEs (dashed black) and the original GMPEs with uncertainty model (dashed cyan) for a scenario with $M_W = 6.$, $R_x = 15.$, $F = -1.$

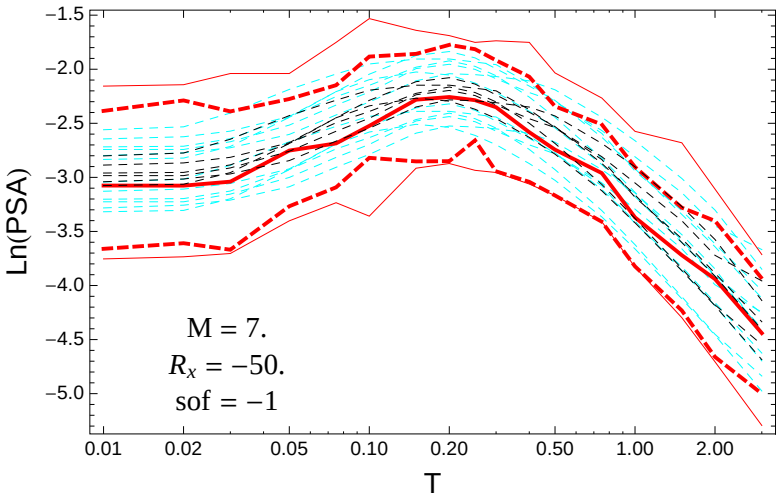



Figure 4.590: PVNGSv2: Spectra of 0.05,0.5,0.95 and the ModelB distribution (red) with total weights, original GMPEs (dashed black) and the original GMPEs with uncertainty model (dashed cyan) for a scenario with $M_W = 7.$, $R_x = -50.$, $F = -1$.

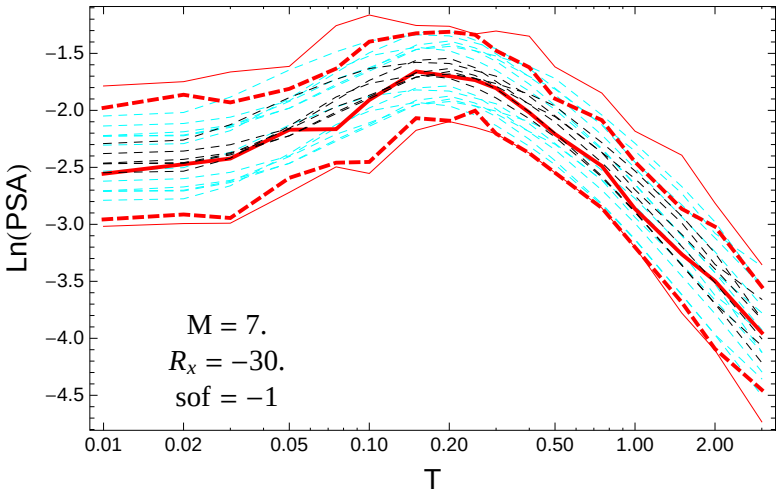



Figure 4.591: PVNGSv2: Spectra of 0.05,0.5,0.95 and the ModelB distribution (red) with total weights, original GMPEs (dashed black) and the original GMPEs with uncertainty model (dashed cyan) for a scenario with $M_W = 7.$, $R_x = -30.$, $F = -1$.

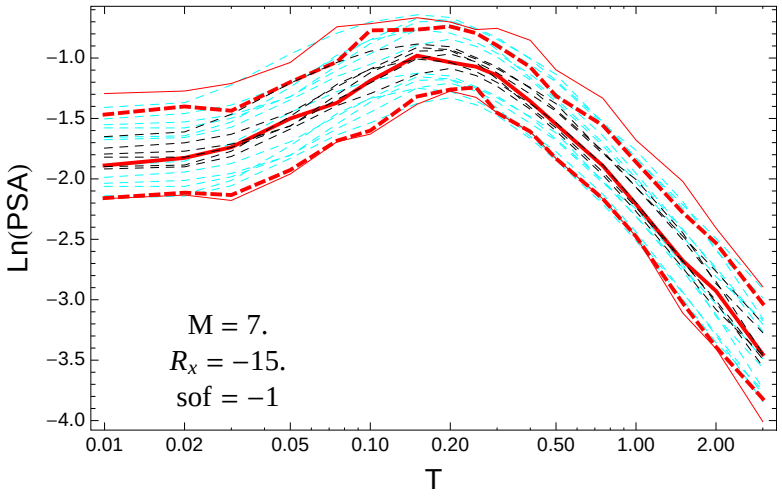



Figure 4.592: PVNGSv2: Spectra of 0.05,0.5,0.95 and the ModelB distribution (red) with total weights, original GMPEs (dashed black) and the original GMPEs with uncertainty model (dashed cyan) for a scenario with $M_W = 7.$, $R_x = -15.$, $F = -1$.

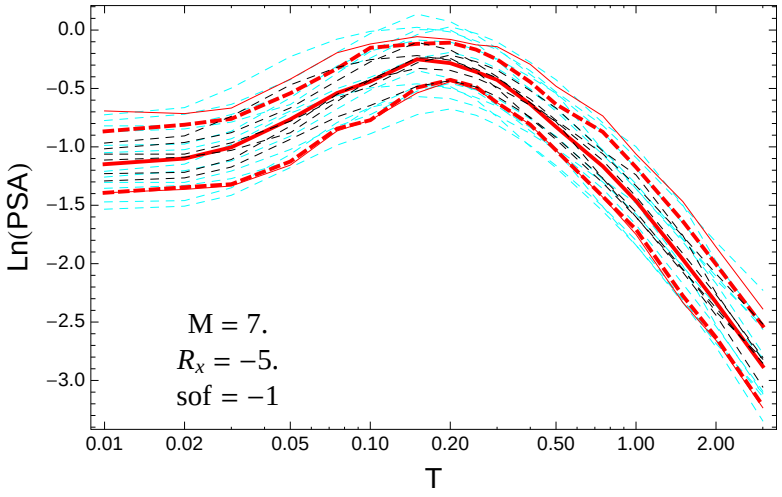



Figure 4.593: PVNGSv2: Spectra of 0.05,0.5,0.95 and the ModelB distribution (red) with total weights, original GMPEs (dashed black) and the original GMPEs with uncertainty model (dashed cyan) for a scenario with $M_W = 7.$, $R_x = -5.$, $F = -1$.

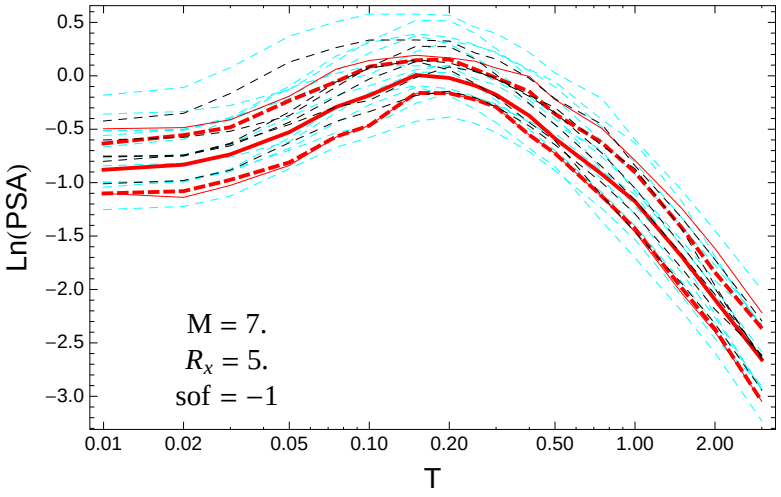



Figure 4.594: PVNGSv2: Spectra of 0.05,0.5,0.95 and the ModelB distribution (red) with total weights, original GMPEs (dashed black) and the original GMPEs with uncertainty model (dashed cyan) for a scenario with $M_W = 7.$, $R_x = 5.$, $F = -1$.

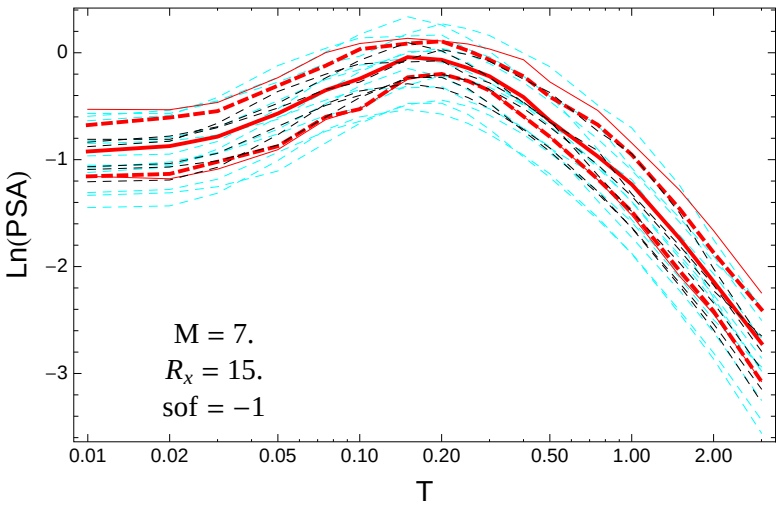



Figure 4.595: PVNGSv2: Spectra of 0.05,0.5,0.95 and the ModelB distribution (red) with total weights, original GMPEs (dashed black) and the original GMPEs with uncertainty model (dashed cyan) for a scenario with $M_W = 7.$, $R_x = 15.$, $F = -1$.

### 4.1.15 Median Residuals

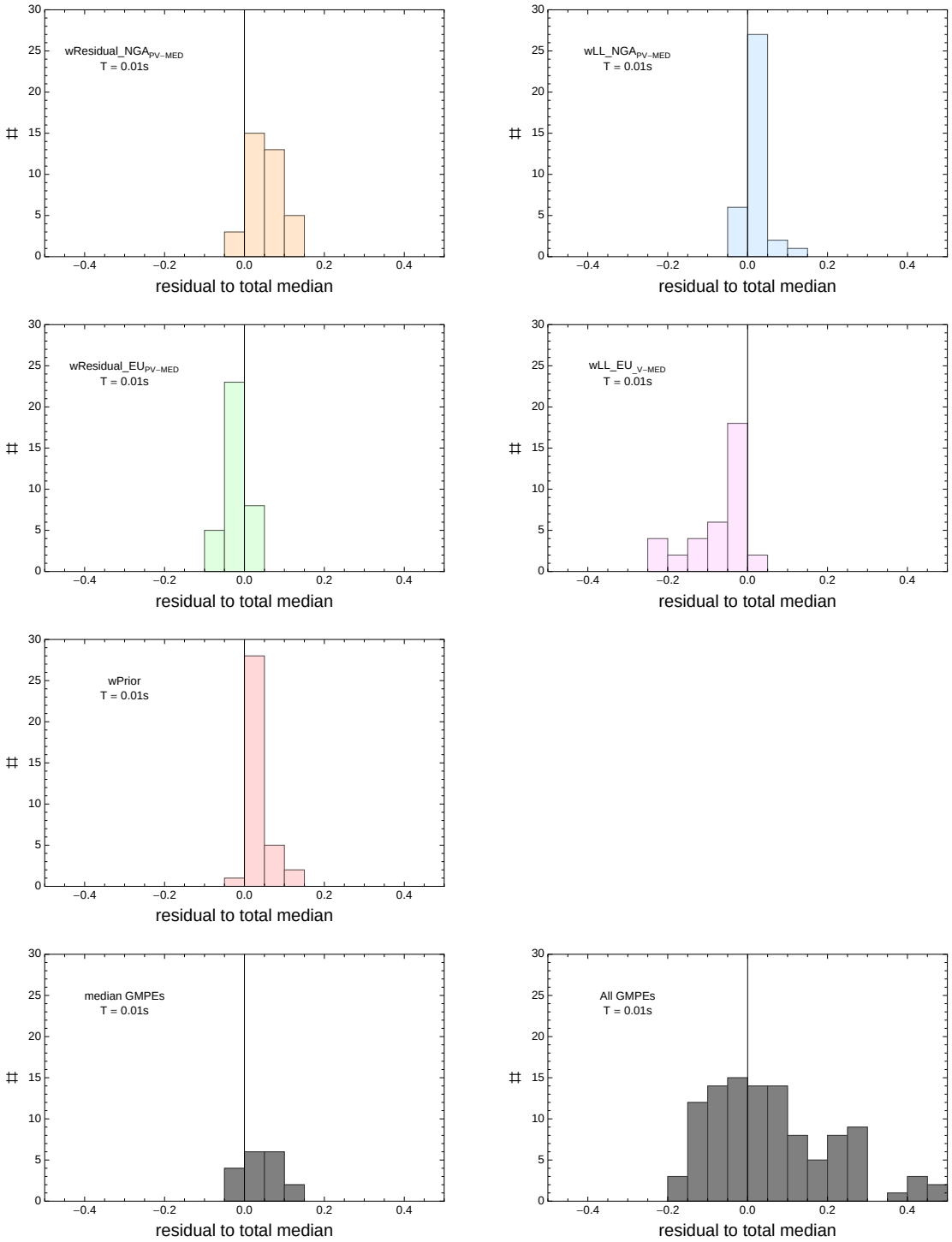



Figure 4.596: PVNGSv2: Histogram of differences for medians calculated with different weights to median calculated with total weights. Bottom row left shows differences between medians for the GMPE distribution to median calculated with total weights. Bottom row right shows differences between the original GMPEs (without uncertainty) to median calculated with total weights. For PVNGS2, ModelB and $T = 0.01$s.

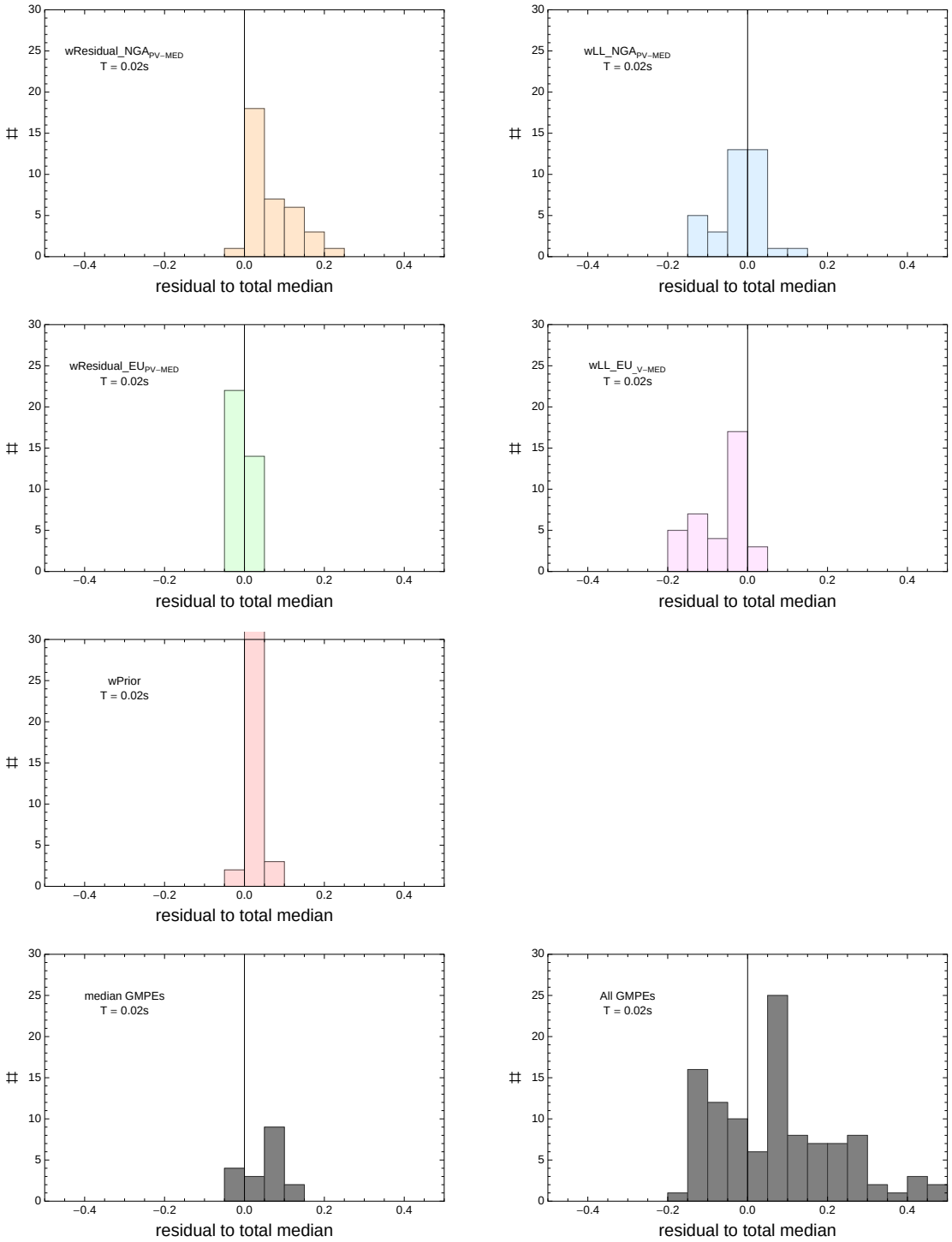



Figure 4.597: PVNGSv2: Histogram of differences for medians calculated with different weights to median calculated with total weights. Bottom row left shows differences between medians for the GMPE distribution to median calculated with total weights. Bottom row right shows differences between the original GMPEs (without uncertainty) to median calculated with total weights. For PVNGS2, ModelB and $T = 0.02$s.

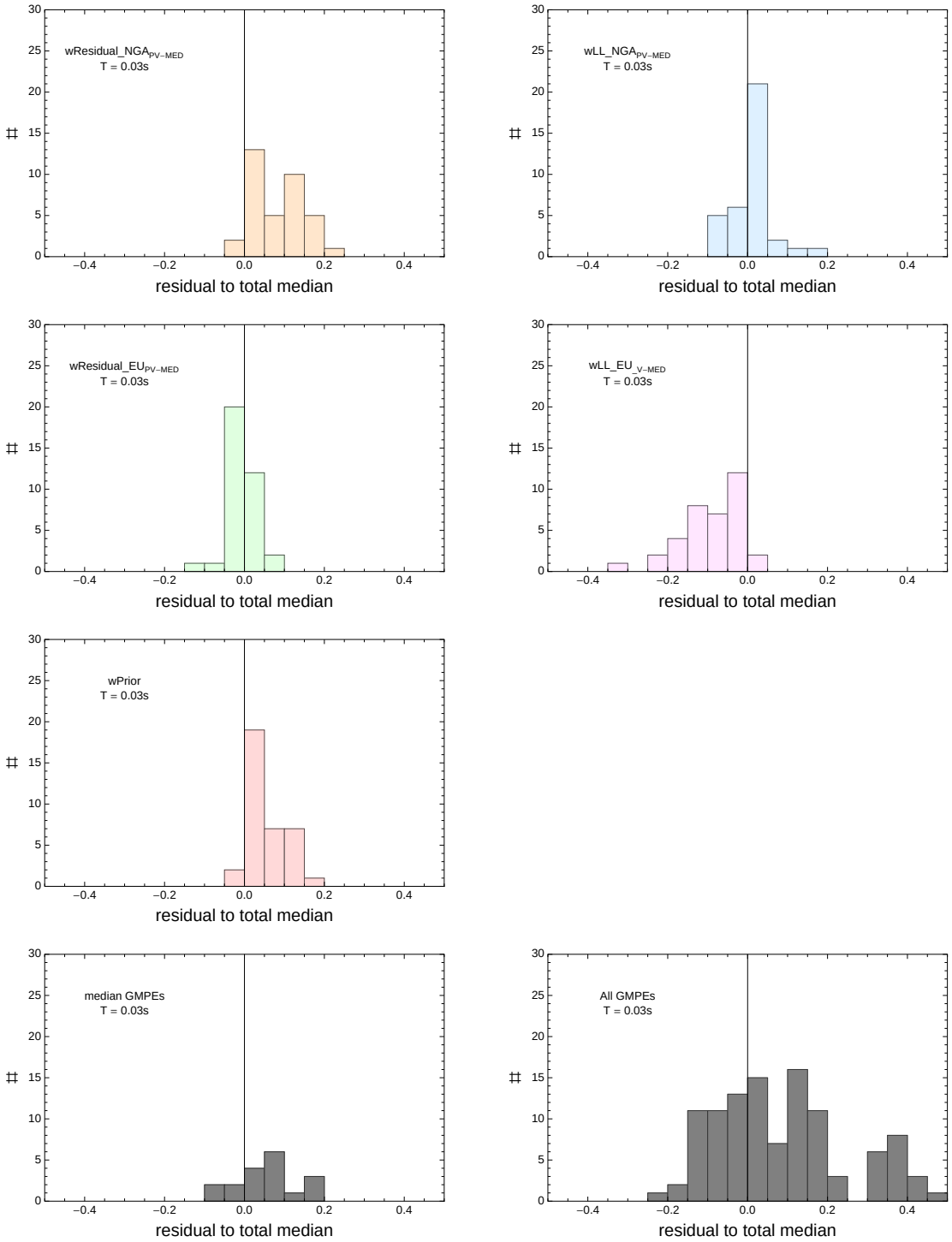



Figure 4.598: PVNGSv2: Histogram of differences for medians calculated with different weights to median calculated with total weights. Bottom row left shows differences between medians for the GMPE distribution to median calculated with total weights. Bottom row right shows differences between the original GMPEs (without uncertainty) to median calculated with total weights. For PVNGS2, ModelB and $T = 0.03$s.

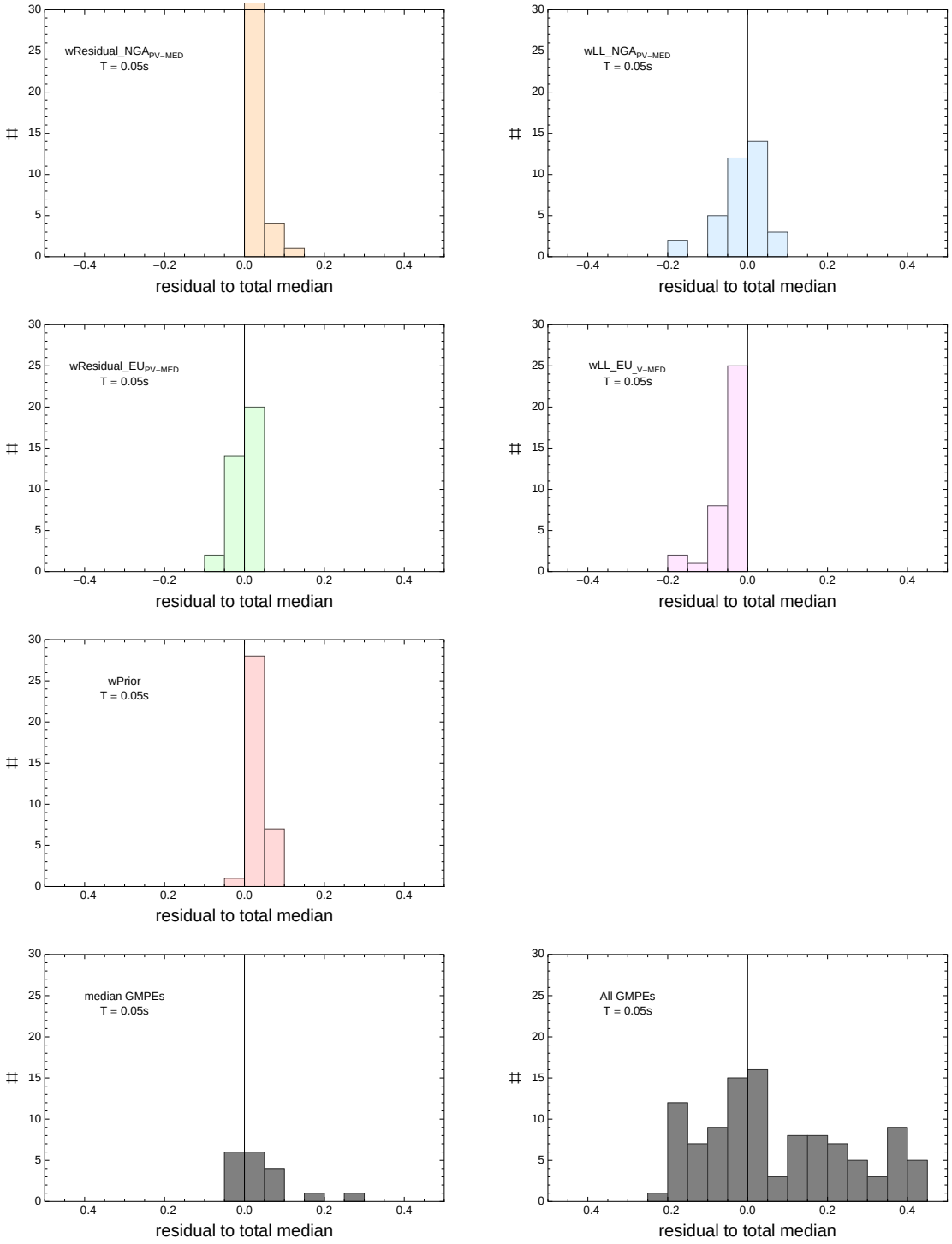



Figure 4.599: PVNGSv2: Histogram of differences for medians calculated with different weights to median calculated with total weights. Bottom row left shows differences between medians for the GMPE distribution to median calculated with total weights. Bottom row right shows differences between the original GMPEs (without uncertainty) to median calculated with total weights. For PVNGS2, ModelB and $T = 0.05$s.

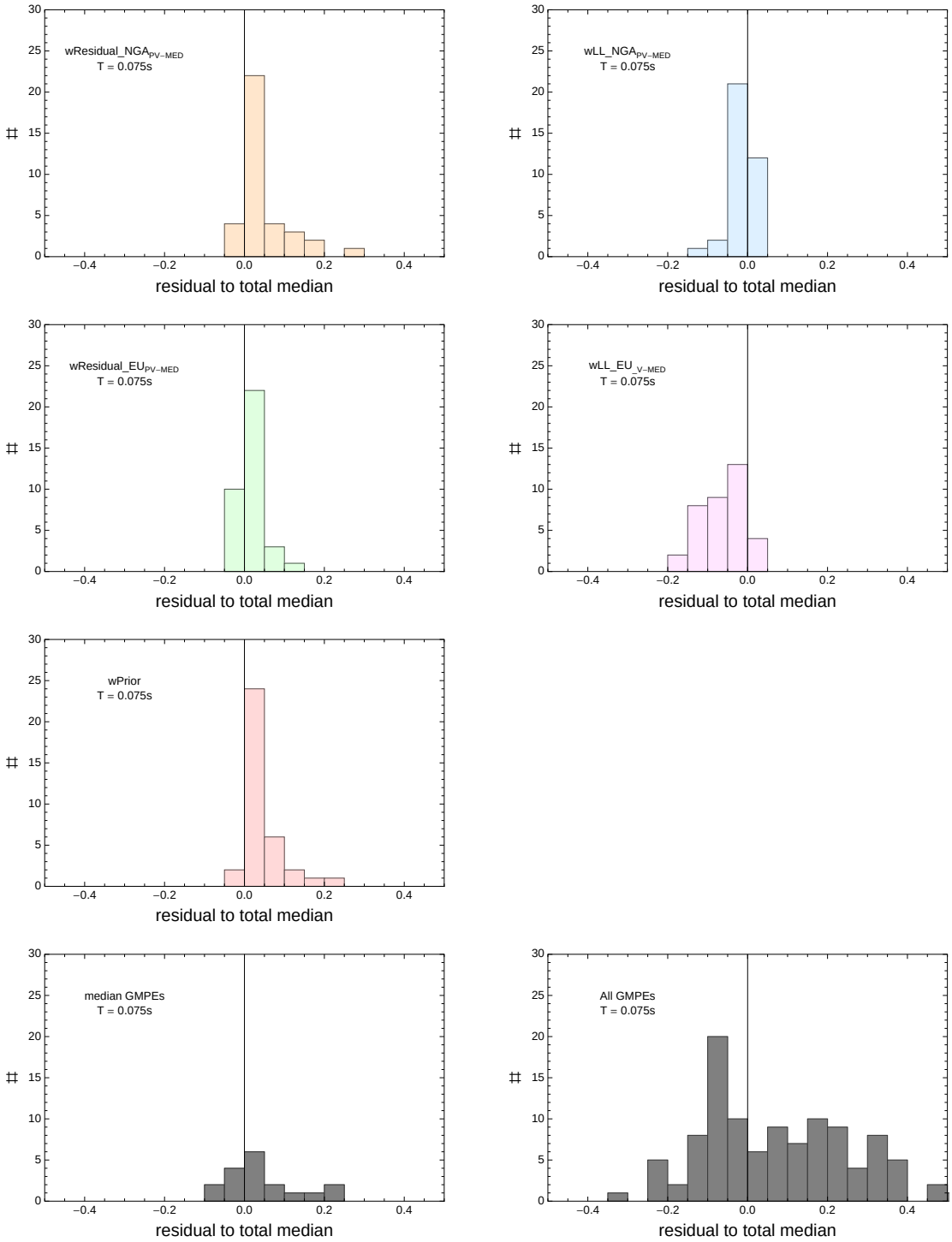



Figure 4.600: PVNGSv2: Histogram of differences for medians calculated with different weights to median calculated with total weights. Bottom row left shows differences between medians for the GMPE distribution to median calculated with total weights. Bottom row right shows differences between the original GMPEs (without uncertainty) to median calculated with total weights. For PVNGS2, ModelB and $T = 0.075$s.

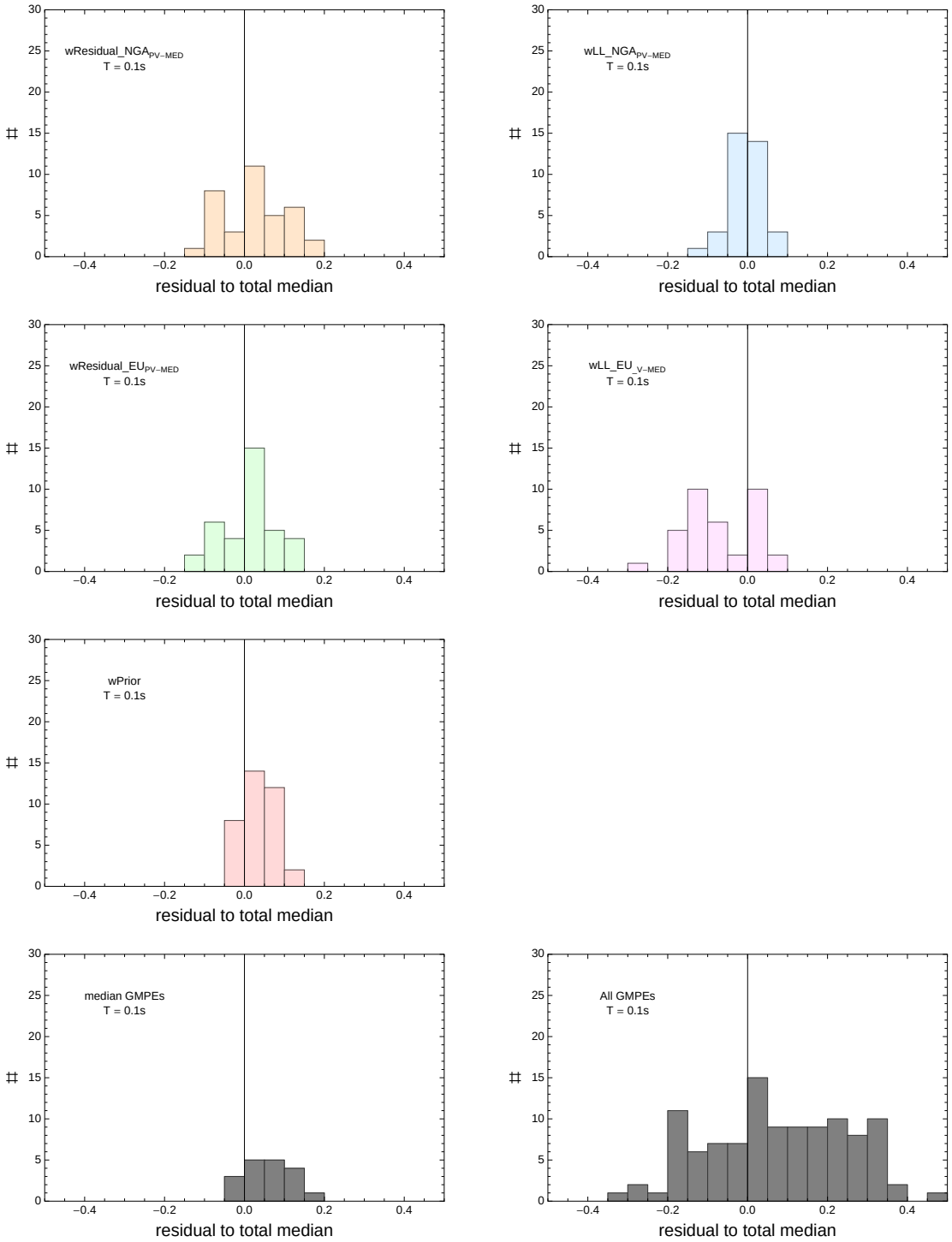



Figure 4.601: PVNGSv2: Histogram of differences for medians calculated with different weights to median calculated with total weights. Bottom row left shows differences between medians for the GMPE distribution to median calculated with total weights. Bottom row right shows differences between the original GMPEs (without uncertainty) to median calculated with total weights. For PVNGS2, ModelB and $T = 0.1$s.

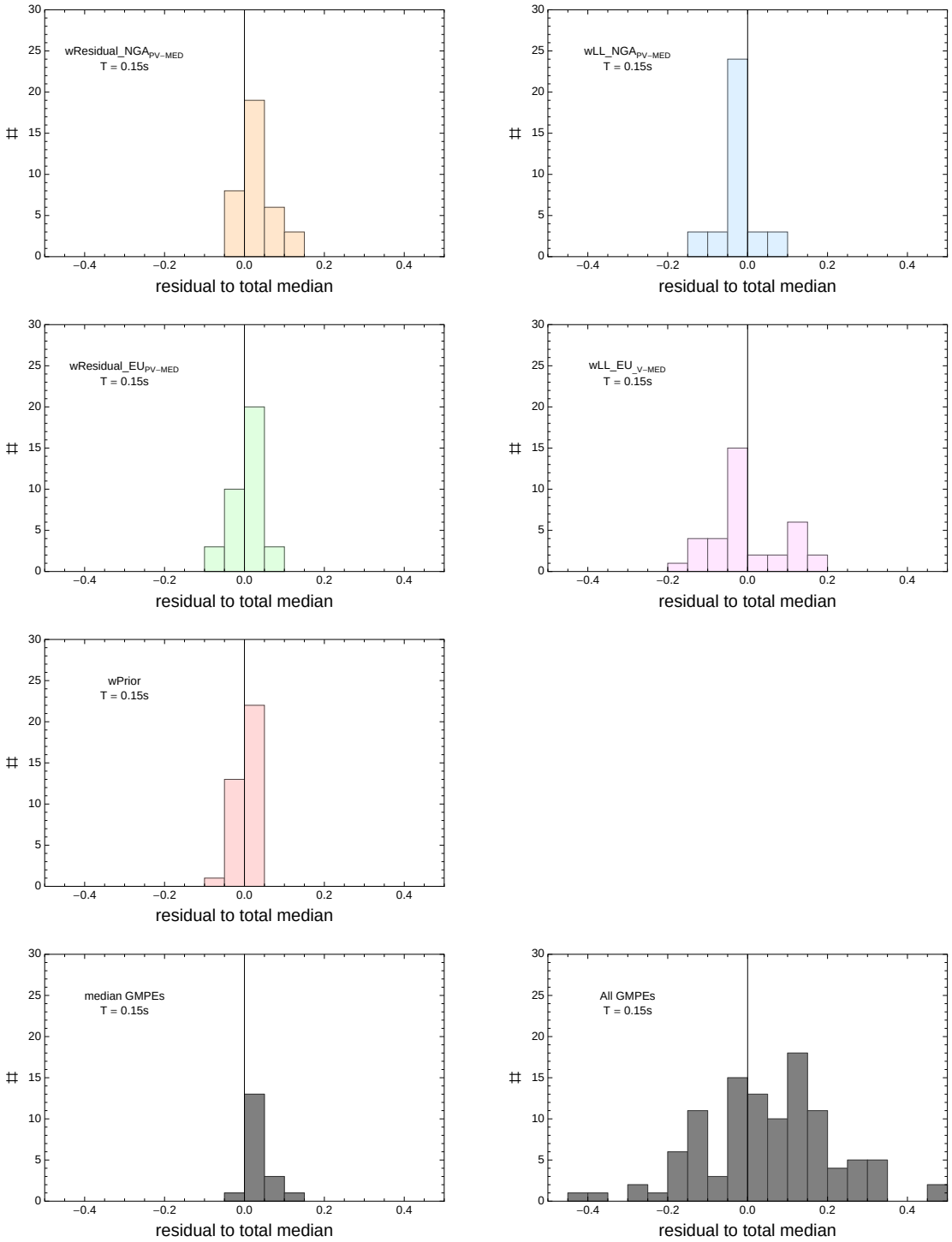



Figure 4.602: PVNGSv2: Histogram of differences for medians calculated with different weights to median calculated with total weights. Bottom row left shows differences between medians for the GMPE distribution to median calculated with total weights. Bottom row right shows differences between the original GMPEs (without uncertainty) to median calculated with total weights. For PVNGS2, ModelB and $T = 0.15$s.

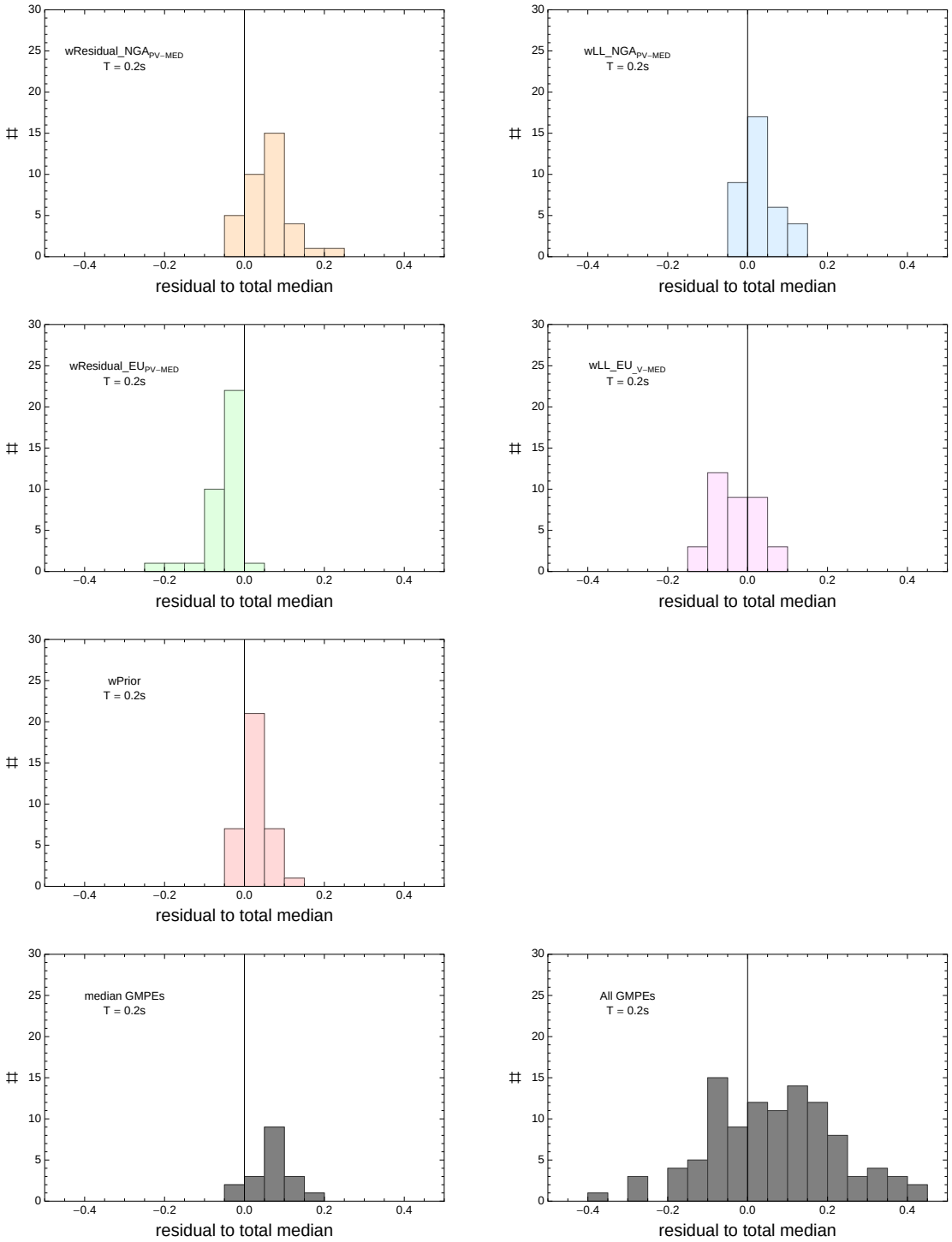



Figure 4.603: PVNGSv2: Histogram of differences for medians calculated with different weights to median calculated with total weights. Bottom row left shows differences between medians for the GMPE distribution to median calculated with total weights. Bottom row right shows differences between the original GMPEs (without uncertainty) to median calculated with total weights. For PVNGS2, ModelB and $T = 0.2$s.

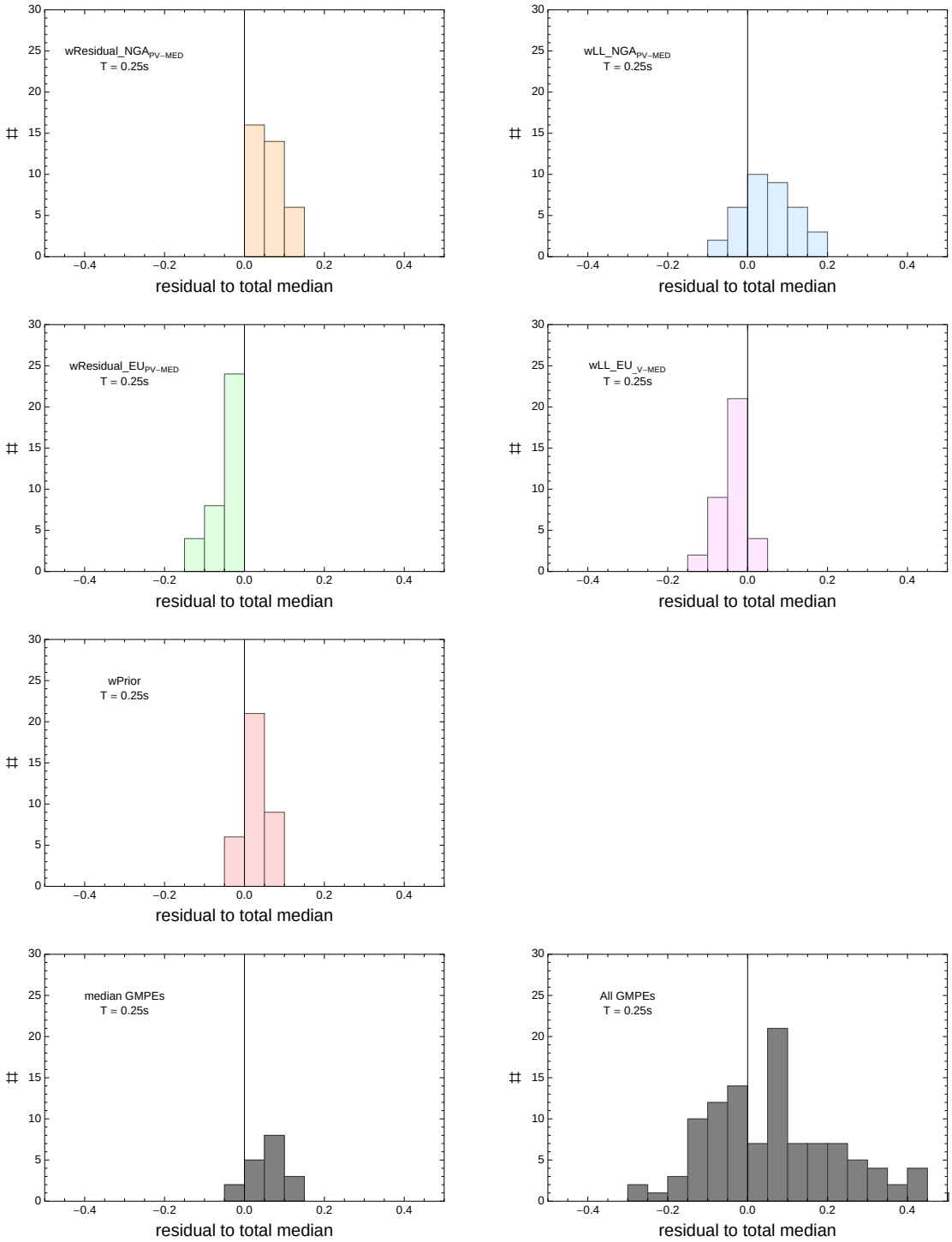



Figure 4.604: PVNGSv2: Histogram of differences for medians calculated with different weights to median calculated with total weights. Bottom row left shows differences between medians for the GMPE distribution to median calculated with total weights. Bottom row right shows differences between the original GMPEs (without uncertainty) to median calculated with total weights. For PVNGS2, ModelB and $T = 0.25$s.

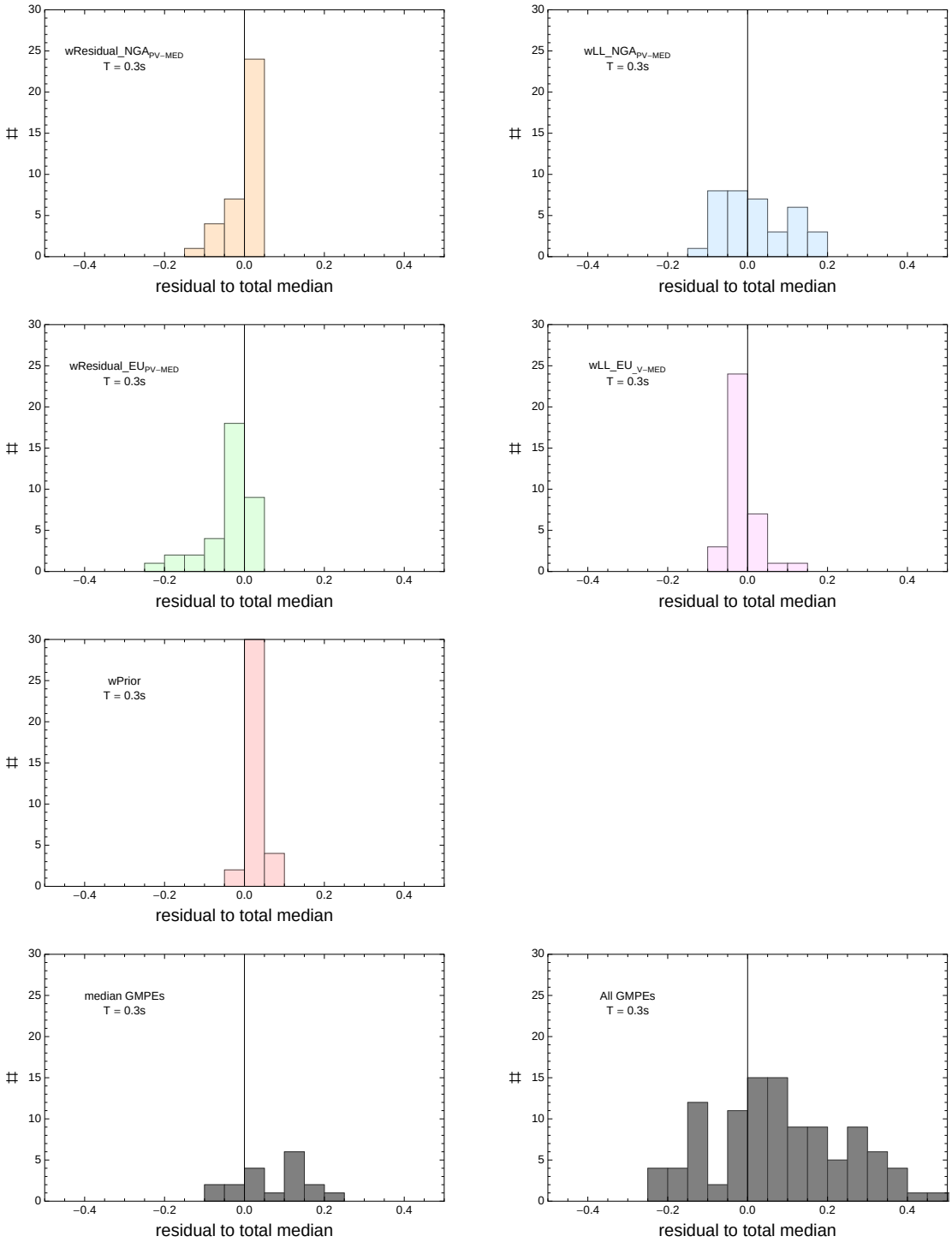



Figure 4.605: PVNGSv2: Histogram of differences for medians calculated with different weights to median calculated with total weights. Bottom row left shows differences between medians for the GMPE distribution to median calculated with total weights. Bottom row right shows differences between the original GMPEs (without uncertainty) to median calculated with total weights. For PVNGS2, ModelB and $T = 0.3$s.

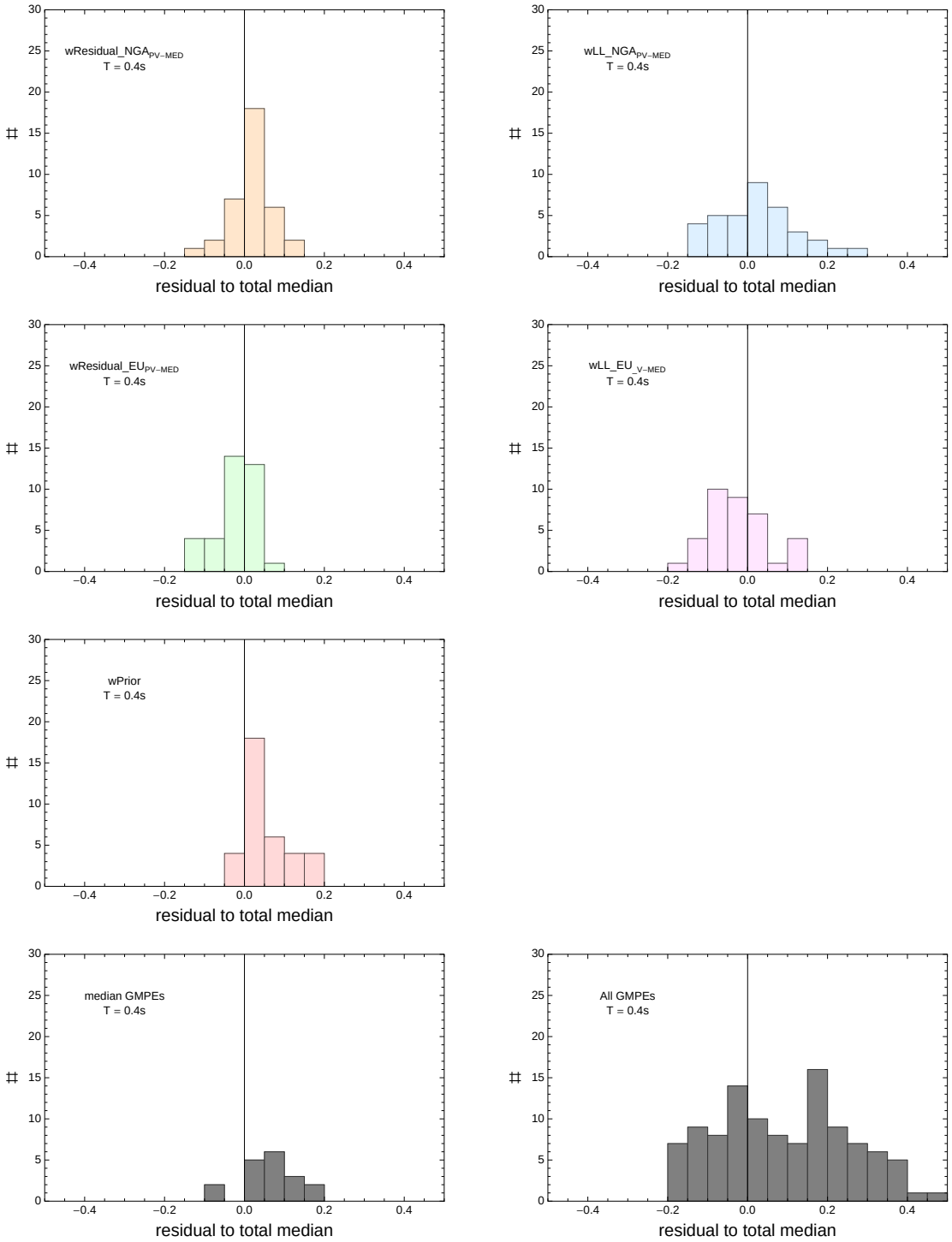



Figure 4.606: PVNGSv2: Histogram of differences for medians calculated with different weights to median calculated with total weights. Bottom row left shows differences between medians for the GMPE distribution to median calculated with total weights. Bottom row right shows differences between the original GMPEs (without uncertainty) to median calculated with total weights. For PVNGS2, ModelB and $T = 0.4$s.

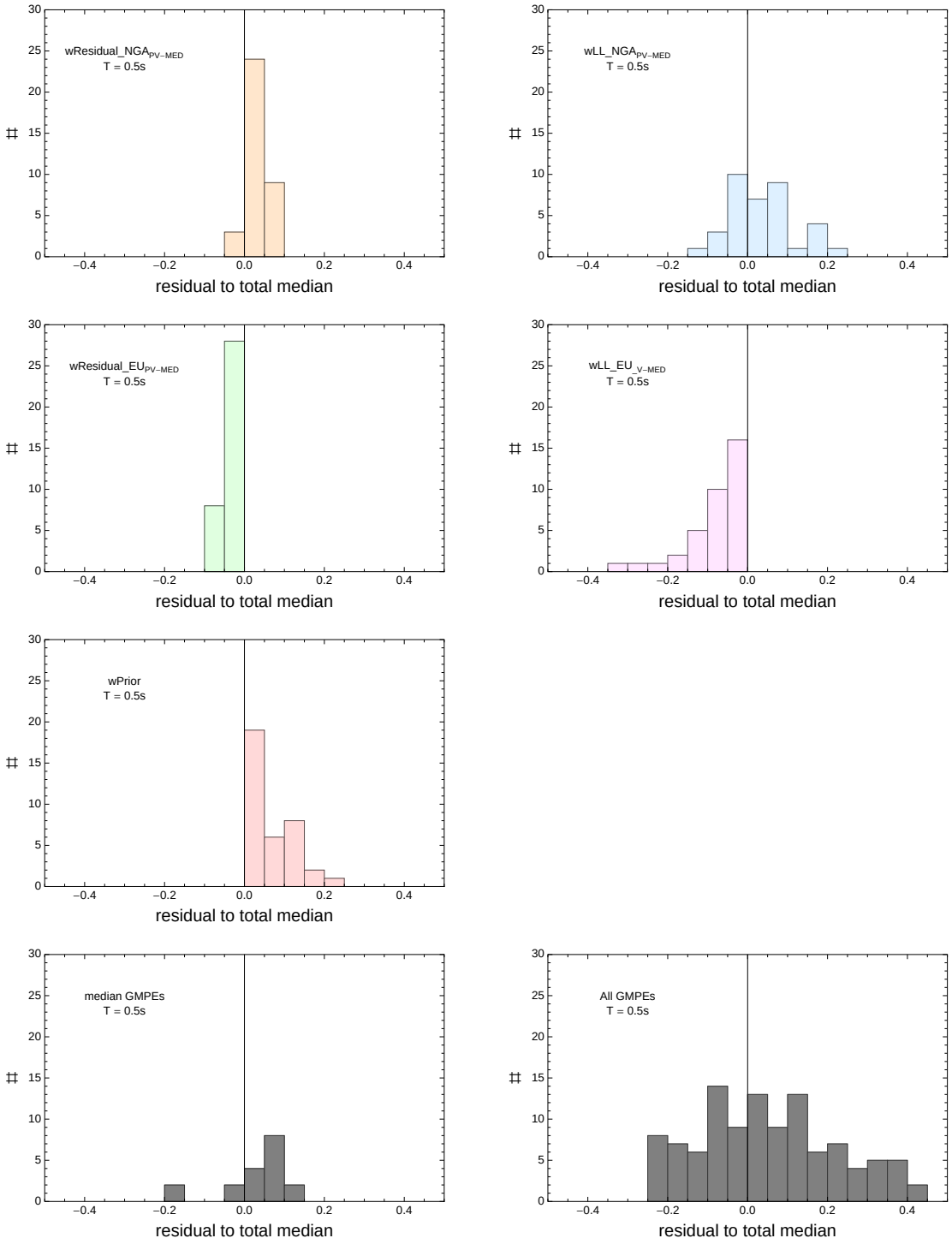



Figure 4.607: PVNGSv2: Histogram of differences for medians calculated with different weights to median calculated with total weights. Bottom row left shows differences between medians for the GMPE distribution to median calculated with total weights. Bottom row right shows differences between the original GMPEs (without uncertainty) to median calculated with total weights. For PVNGS2, ModelB and $T = 0.5$s.

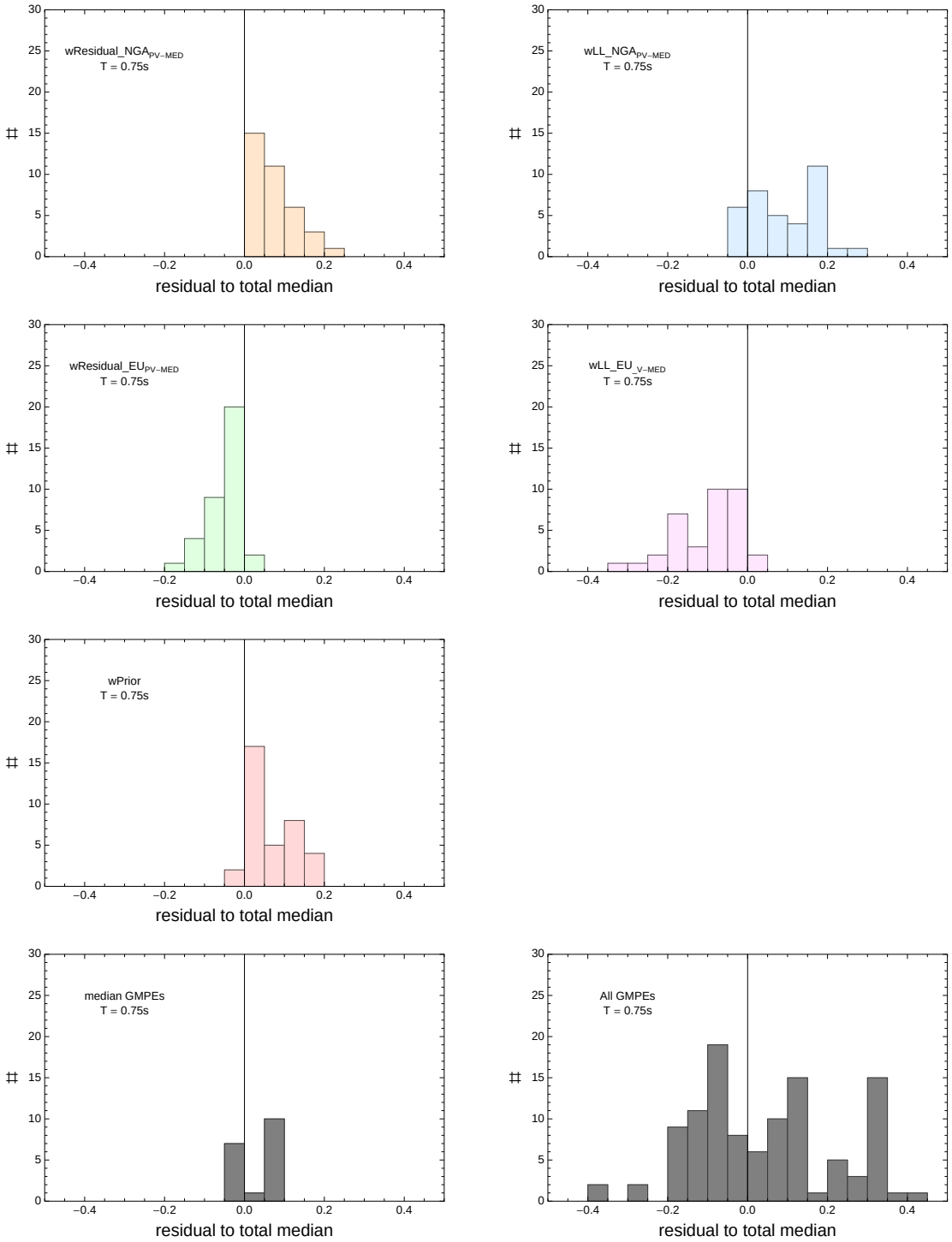



Figure 4.608: PVNGSv2: Histogram of differences for medians calculated with different weights to median calculated with total weights. Bottom row left shows differences between medians for the GMPE distribution to median calculated with total weights. Bottom row right shows differences between the original GMPEs (without uncertainty) to median calculated with total weights. For PVNGS2, ModelB and $T = 0.75$s.

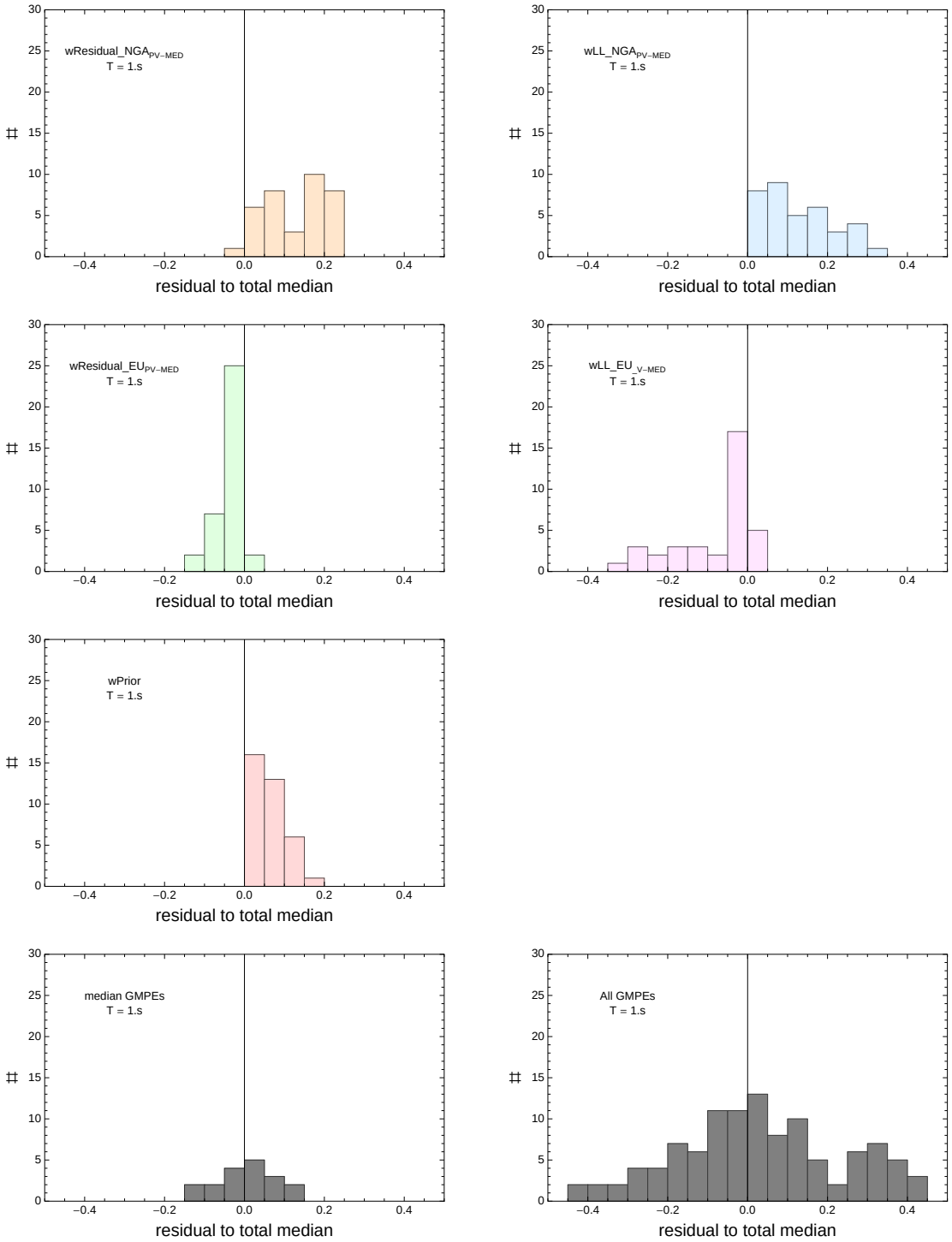



Figure 4.609: PVNGSv2: Histogram of differences for medians calculated with different weights to median calculated with total weights. Bottom row left shows differences between medians for the GMPE distribution to median calculated with total weights. Bottom row right shows differences between the original GMPEs (without uncertainty) to median calculated with total weights. For PVNGS2, ModelB and $T = 1.$s.

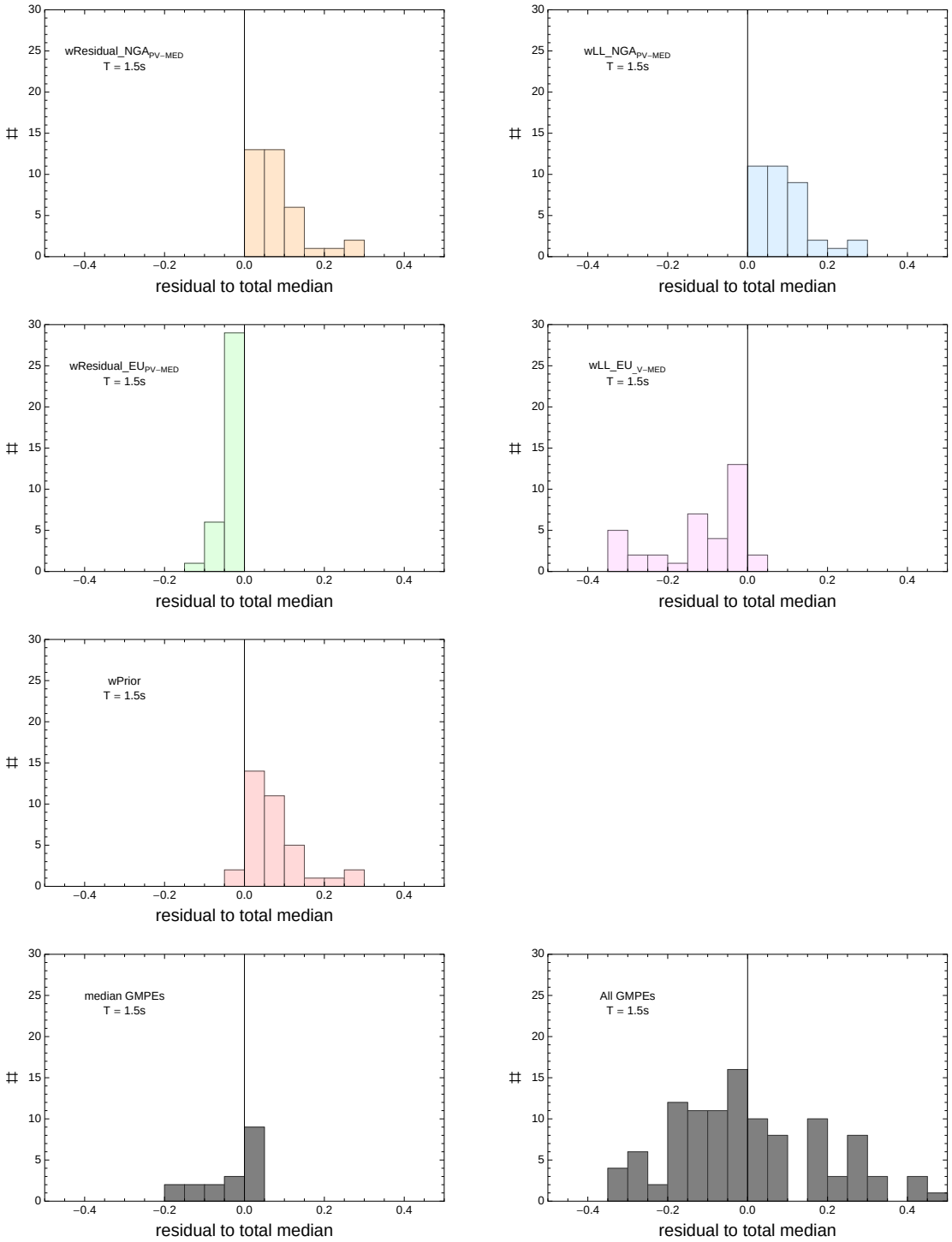



Figure 4.610: PVNGSv2: Histogram of differences for medians calculated with different weights to median calculated with total weights. Bottom row left shows differences between medians for the GMPE distribution to median calculated with total weights. Bottom row right shows differences between the original GMPEs (without uncertainty) to median calculated with total weights. For PVNGS2, ModelB and $T = 1.5$s.

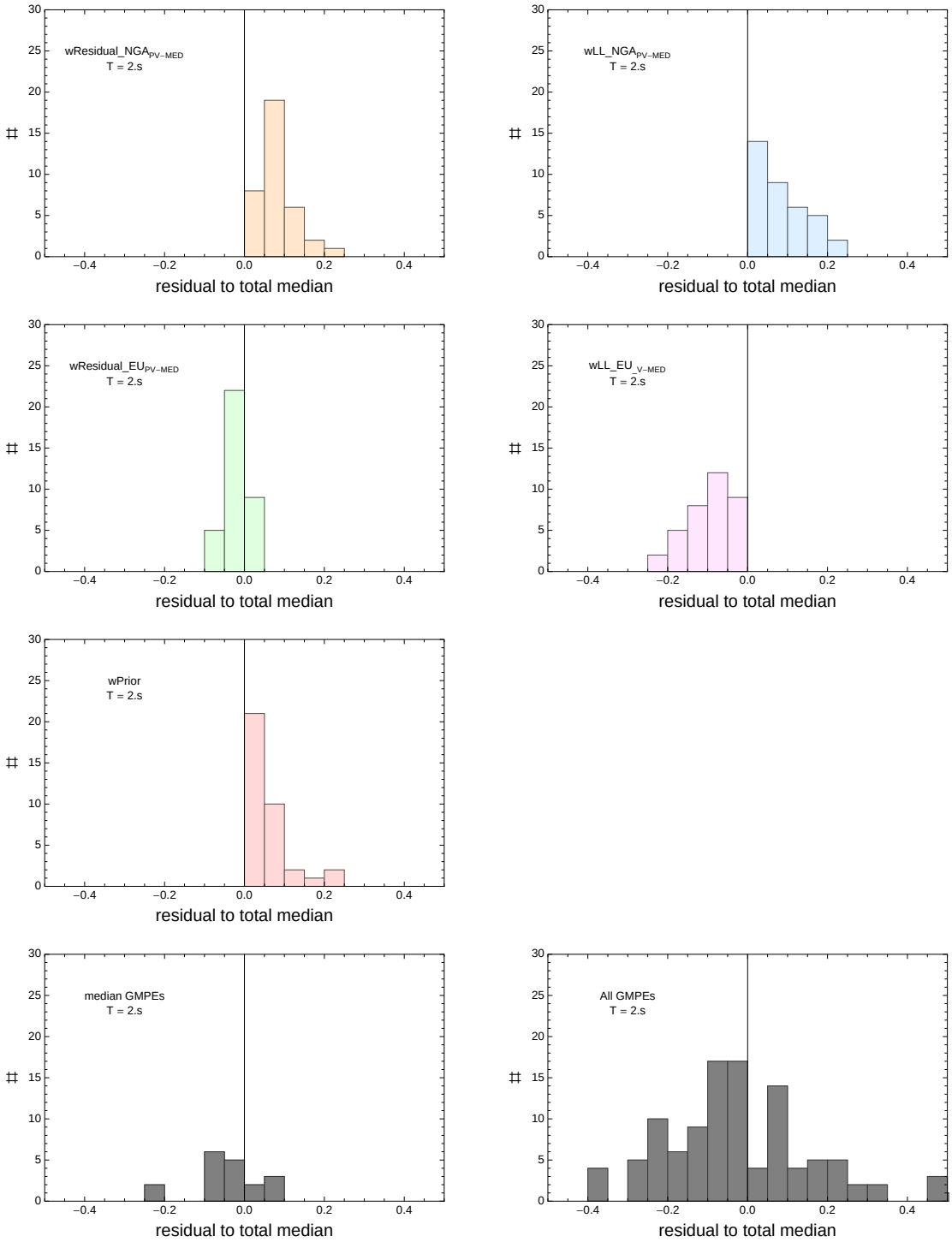



Figure 4.611: PVNGSv2: Histogram of differences for medians calculated with different weights to median calculated with total weights. Bottom row left shows differences between medians for the GMPE distribution to median calculated with total weights. Bottom row right shows differences between the original GMPEs (without uncertainty) to median calculated with total weights. For PVNGS2, ModelB and $T = 2.$s.

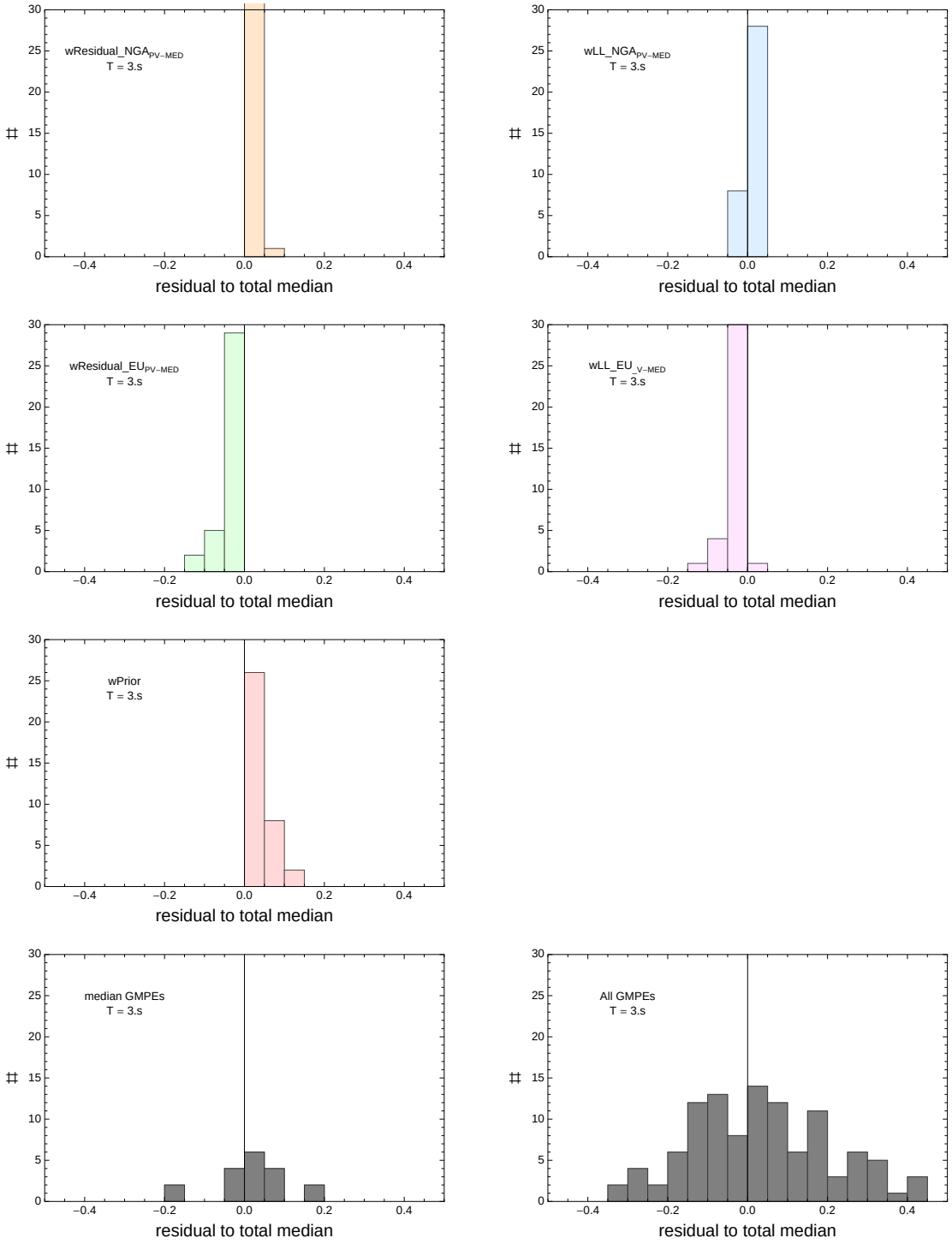



Figure 4.612: PVNGSv2: Histogram of differences for medians calculated with different weights to median calculated with total weights. Bottom row left shows differences between medians for the GMPE distribution to median calculated with total weights. Bottom row right shows differences between the original GMPEs (without uncertainty) to median calculated with total weights. For PVNGS2, ModelB and $T = 3.$s.

# Chapter 5

# PVNGS – Model AB

### 5.1.1 Combined Maps

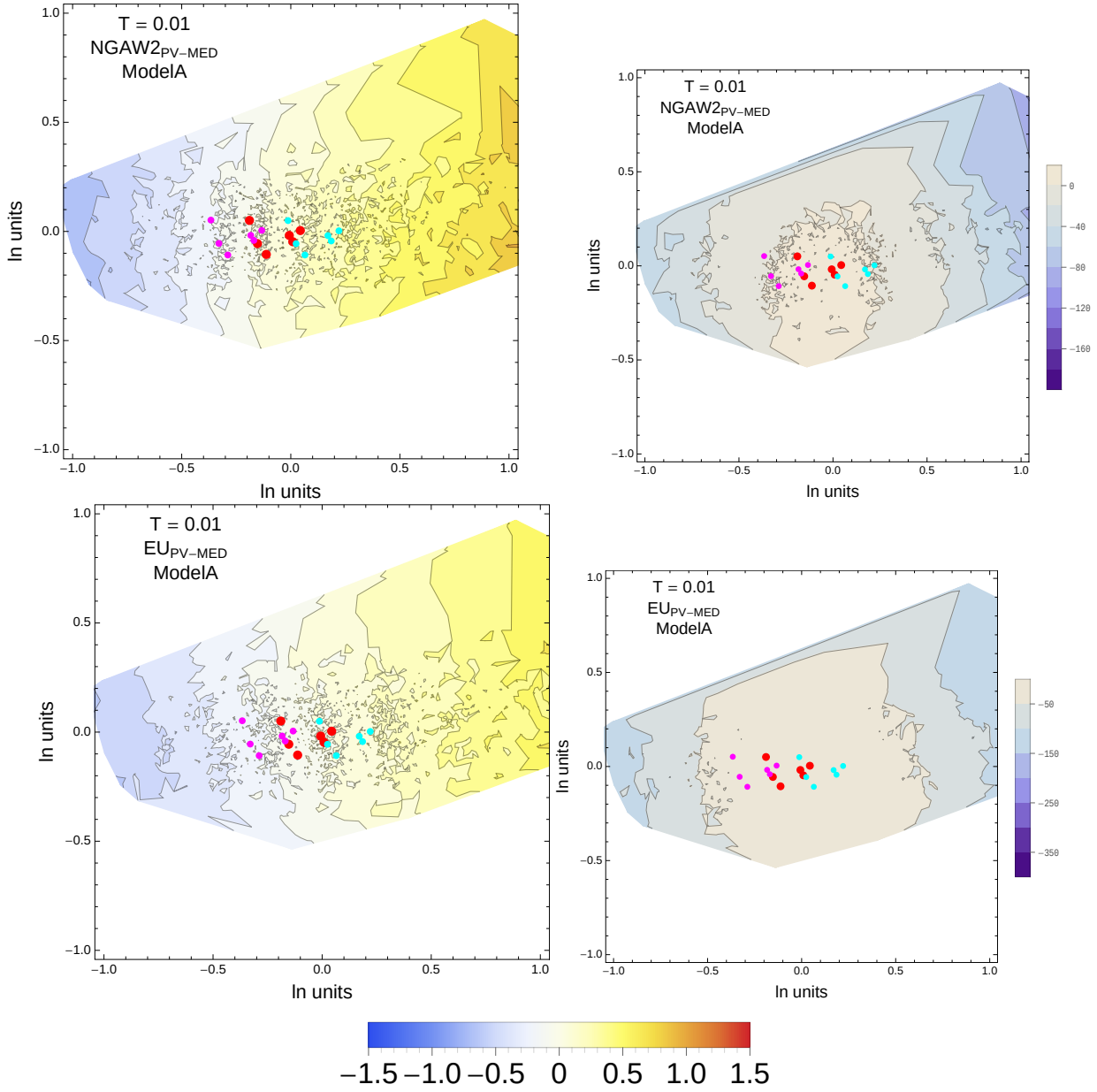



Figure 5.1: PVNGSv2: Contour Plots of mean residuals (top left) and likelihood (top right) for the NGA$_{PV-MED}$ dataset, and mean residuals (bottom left) and likelihood (top right) for the EU$_{PV-MED}$ dataset. The map is based on both Model A and B. The original GMPEs are red dots, plus/minus uncertainty are magenta/cyan dots. For $T = 0.01$s.

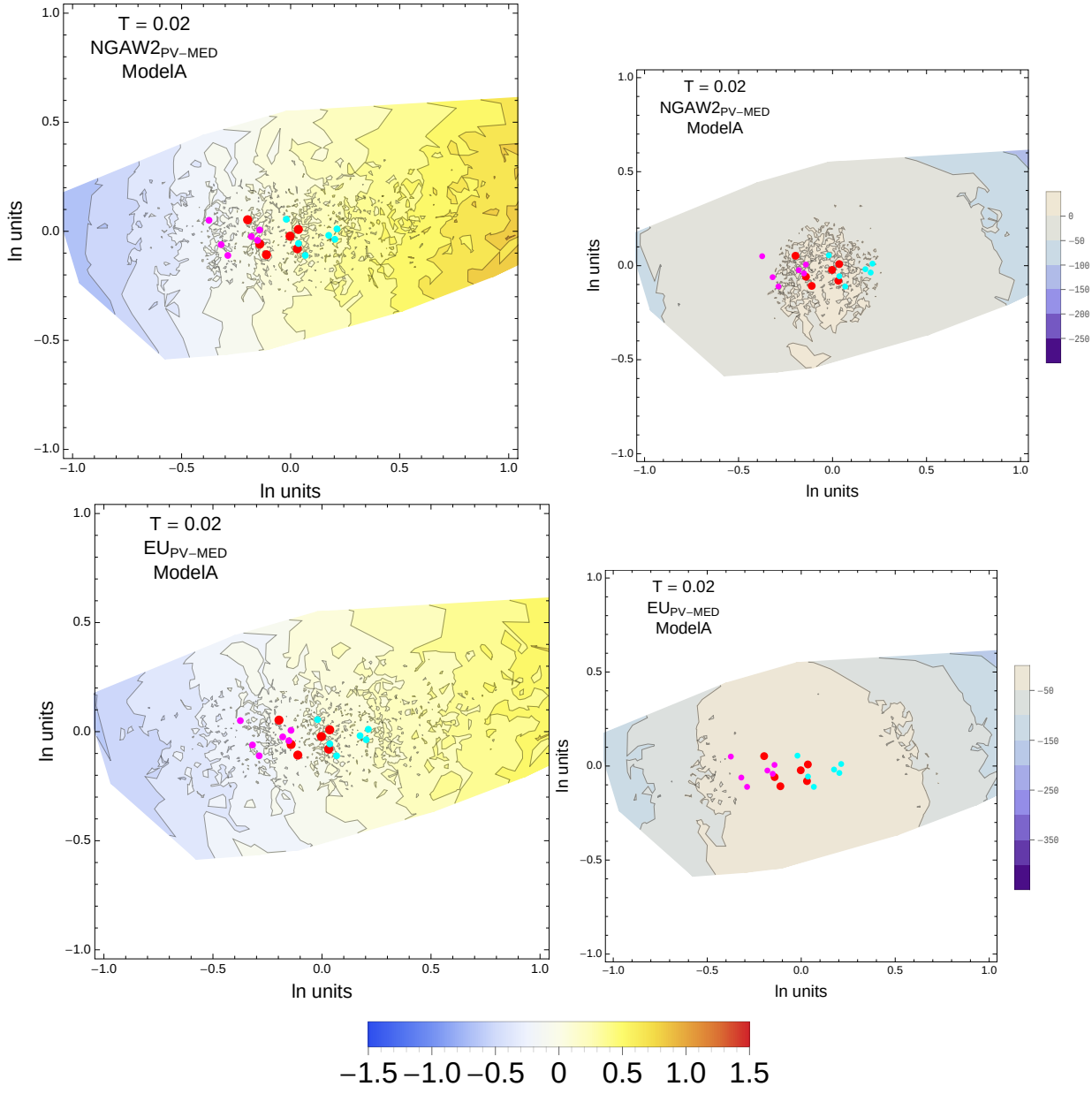



Figure 5.2: PVNGSv2: Contour Plots of mean residuals (top left) and likelihood (top right) for the NGA$_{PV-MED}$ dataset, and mean residuals (bottom left) and likelihood (top right) for the EU$_{PV-MED}$ dataset. The map is based on both Model A and B. The original GMPEs are red dots, plus/minus uncertainty are magenta/cyan dots. For $T = 0.02$s.

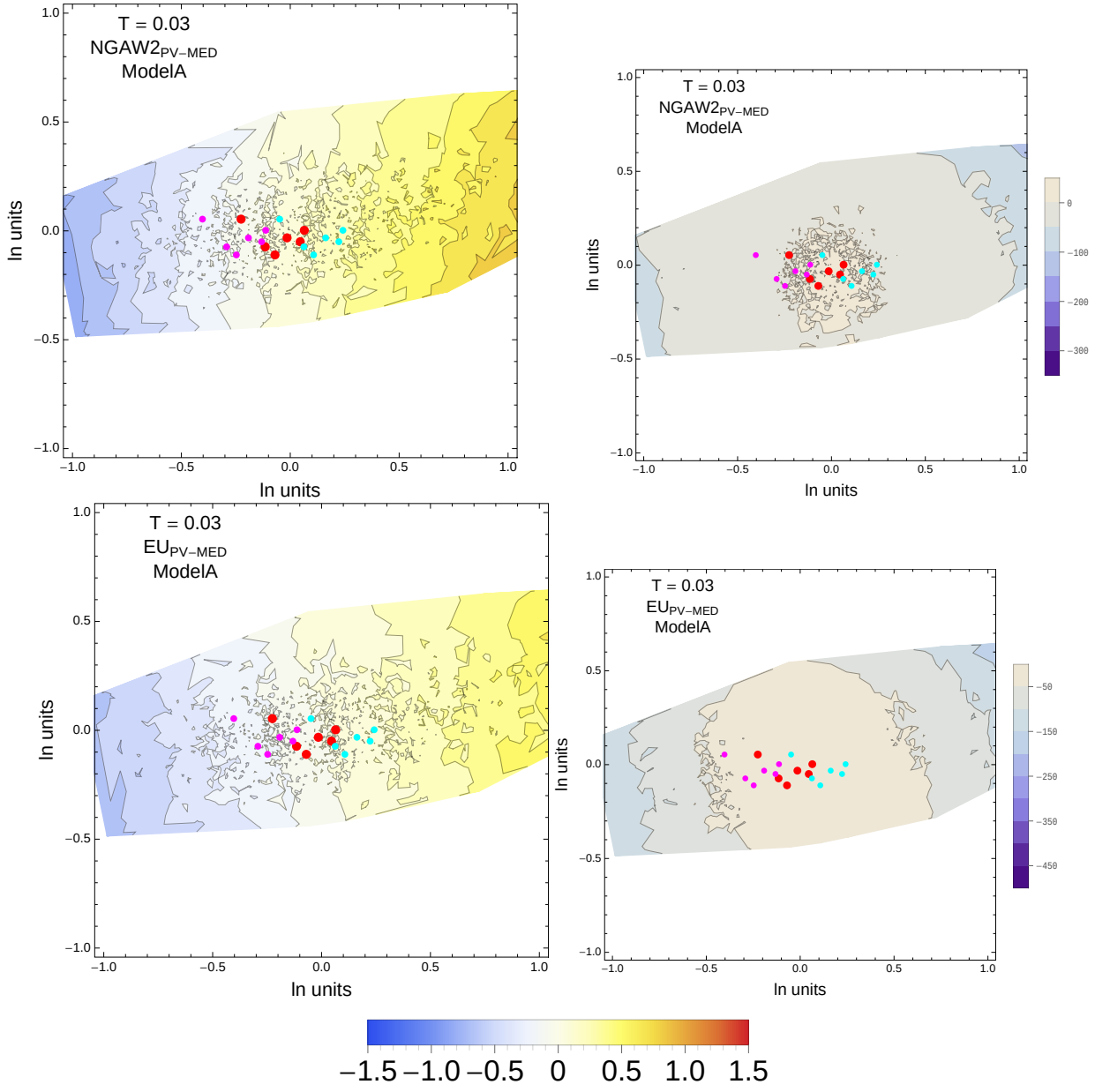



Figure 5.3: PVNGSv2: Contour Plots of mean residuals (top left) and likelihood (top right) for the NGA$_{PV-MED}$ dataset, and mean residuals (bottom left) and likelihood (top right) for the EU$_{PV-MED}$ dataset. The map is based on both Model A and B. The original GMPEs are red dots, plus/minus uncertainty are magenta/cyan dots. For $T = 0.03$s.

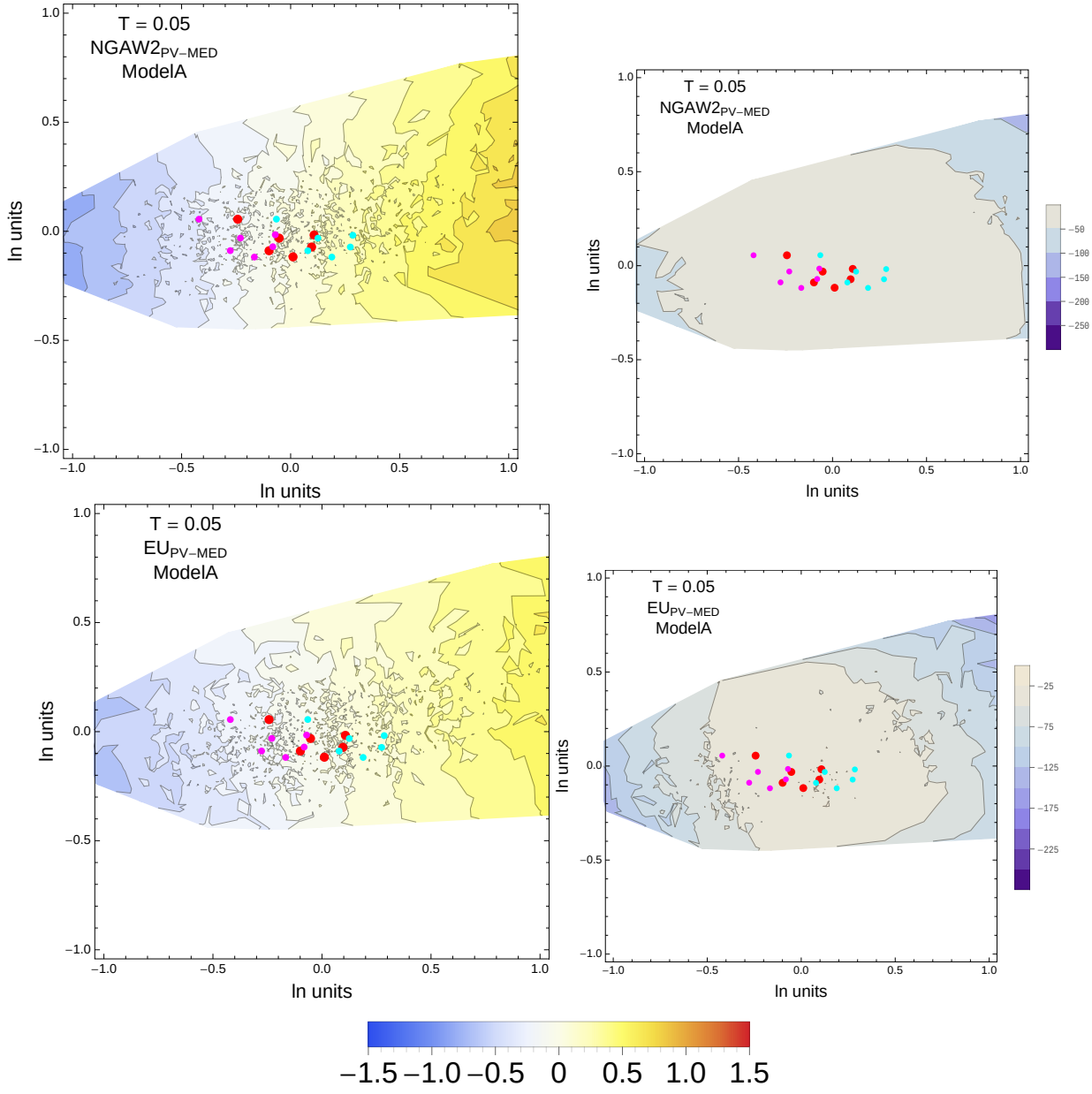



Figure 5.4: PVNGSv2: Contour Plots of mean residuals (top left) and likelihood (top right) for the NGA$_{PV-MED}$ dataset, and mean residuals (bottom left) and likelihood (top right) for the EU$_{PV-MED}$ dataset. The map is based on both Model A and B. The original GMPEs are red dots, plus/minus uncertainty are magenta/cyan dots. For $T = 0.05$s.

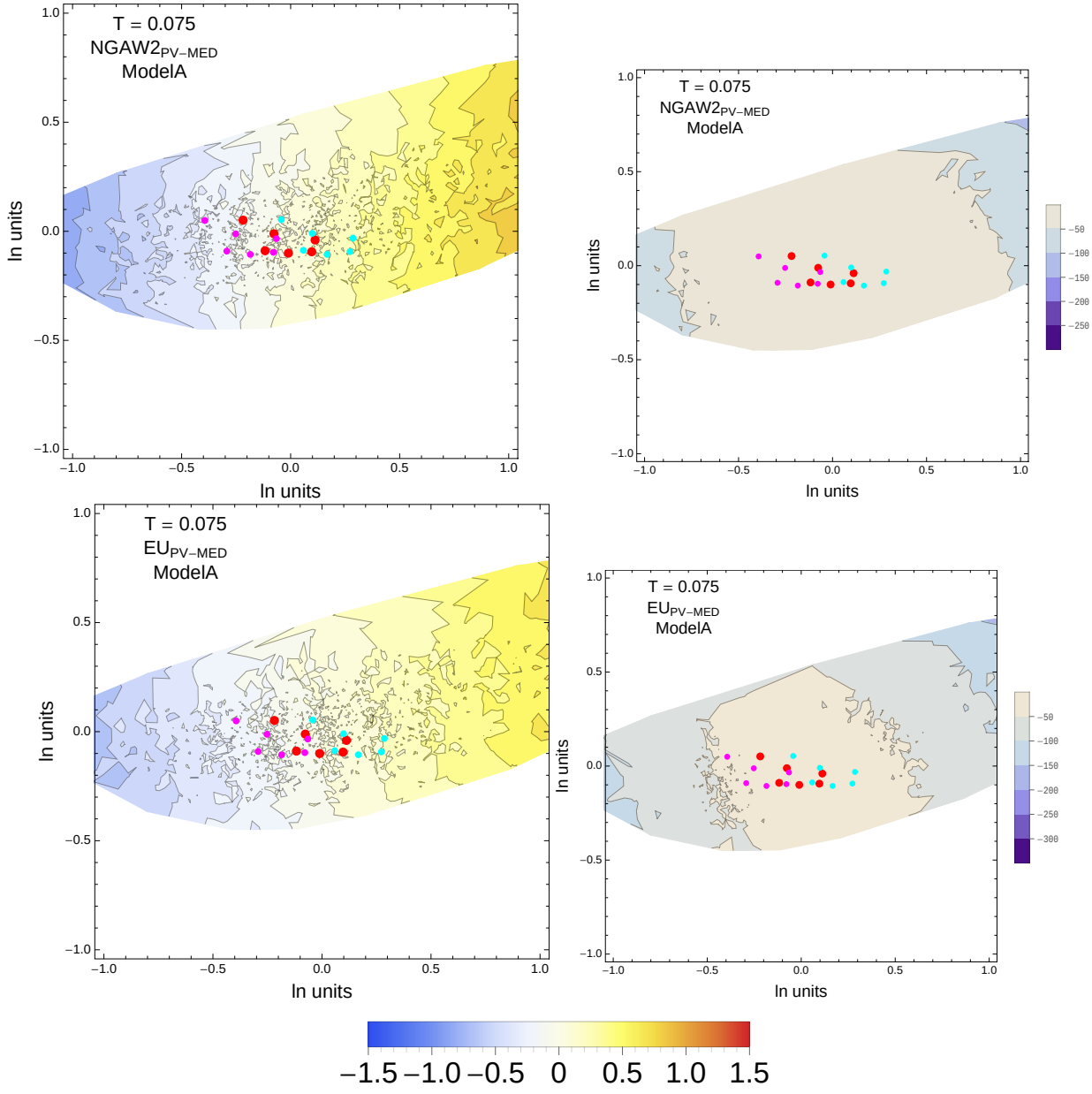



Figure 5.5: PVNGSv2: Contour Plots of mean residuals (top left) and likelihood (top right) for the NGA$_{PV-MED}$ dataset, and mean residuals (bottom left) and likelihood (top right) for the EU$_{PV-MED}$ dataset. The map is based on both Model A and B. The original GMPEs are red dots, plus/minus uncertainty are magenta/cyan dots. For $T = 0.075$s.

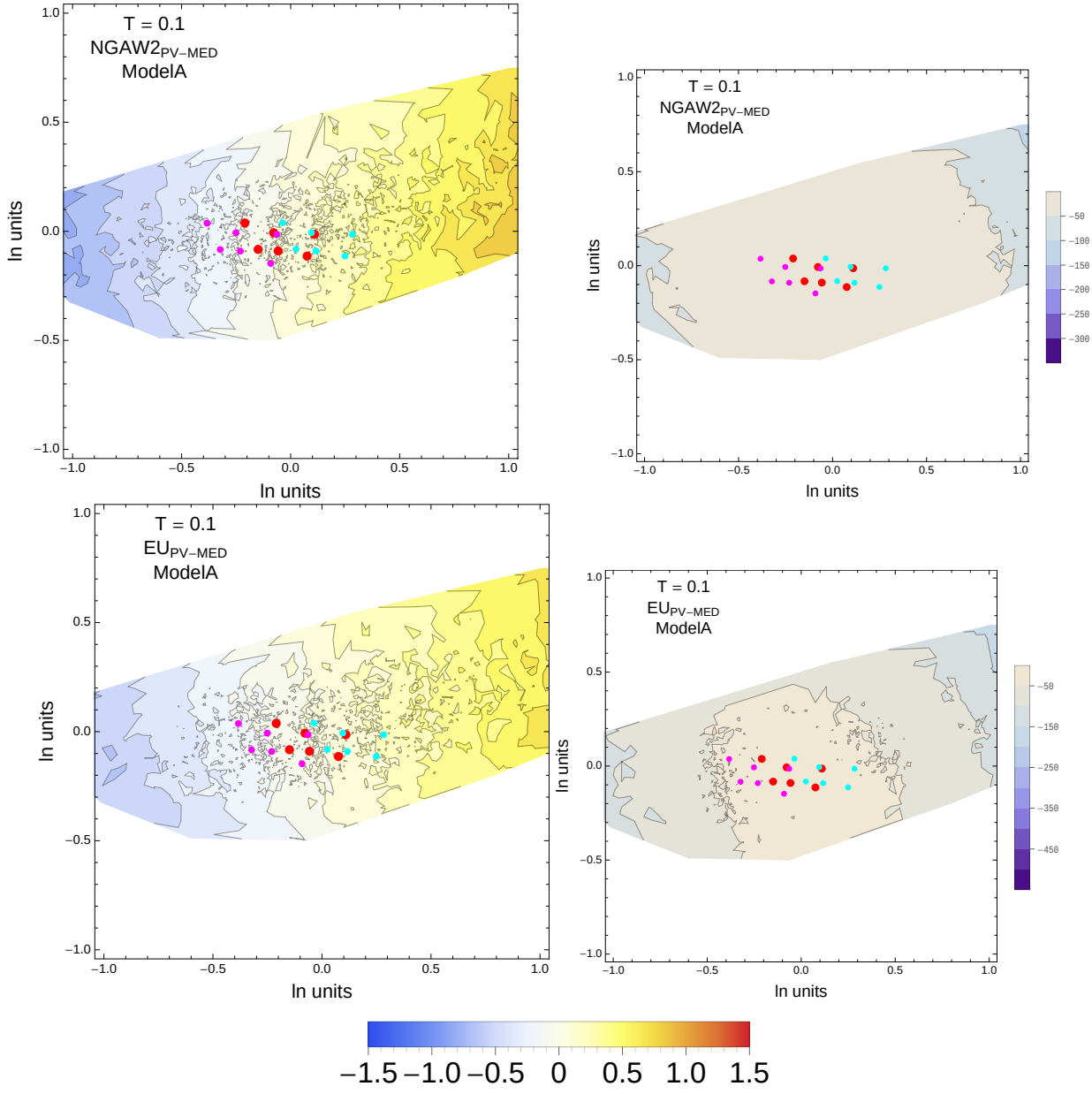



Figure 5.6: PVNGSv2: Contour Plots of mean residuals (top left) and likelihood (top right) for the NGA$_{PV-MED}$ dataset, and mean residuals (bottom left) and likelihood (top right) for the EU$_{PV-MED}$ dataset. The map is based on both Model A and B. The original GMPEs are red dots, plus/minus uncertainty are magenta/cyan dots. For $T = 0.1$s.

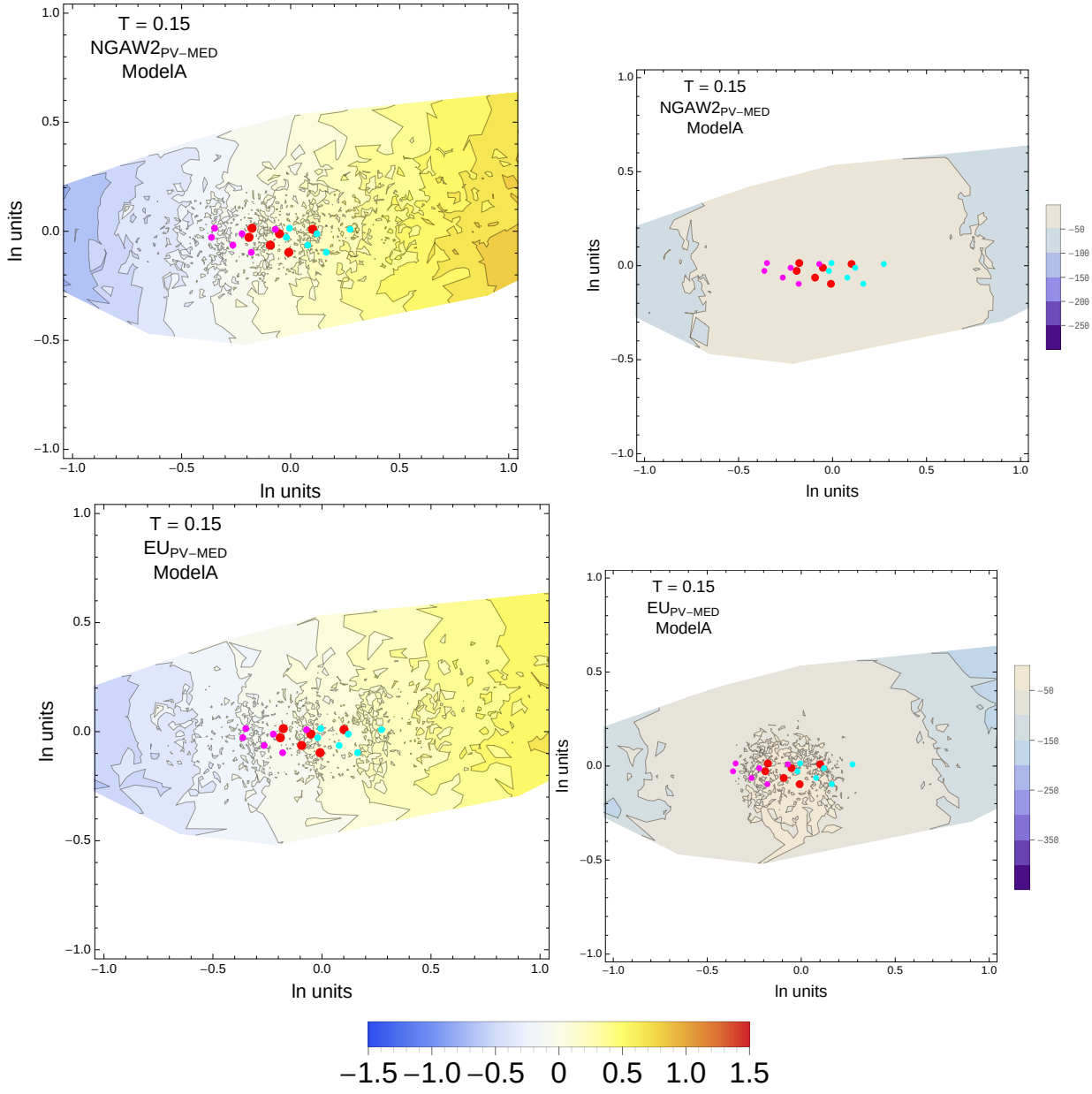



Figure 5.7: PVNGSv2: Contour Plots of mean residuals (top left) and likelihood (top right) for the NGA$_{PV-MED}$ dataset, and mean residuals (bottom left) and likelihood (top right) for the EU$_{PV-MED}$ dataset. The map is based on both Model A and B. The original GMPEs are red dots, plus/minus uncertainty are magenta/cyan dots. For $T = 0.15$s.

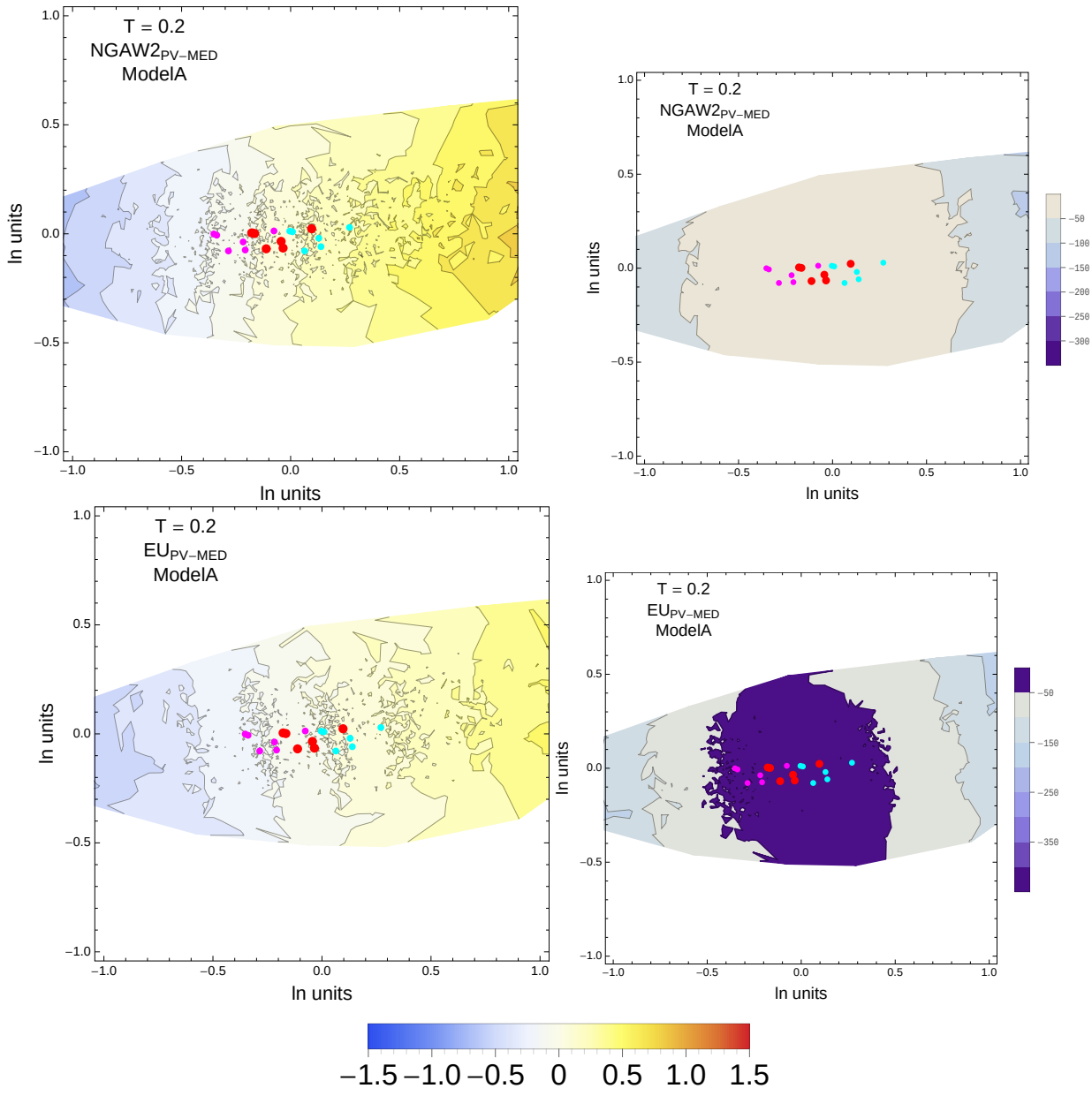



Figure 5.8: PVNGSv2: Contour Plots of mean residuals (top left) and likelihood (top right) for the NGA$_{PV-MED}$ dataset, and mean residuals (bottom left) and likelihood (top right) for the EU$_{PV-MED}$ dataset. The map is based on both Model A and B. The original GMPEs are red dots, plus/minus uncertainty are magenta/cyan dots. For $T = 0.2$s.

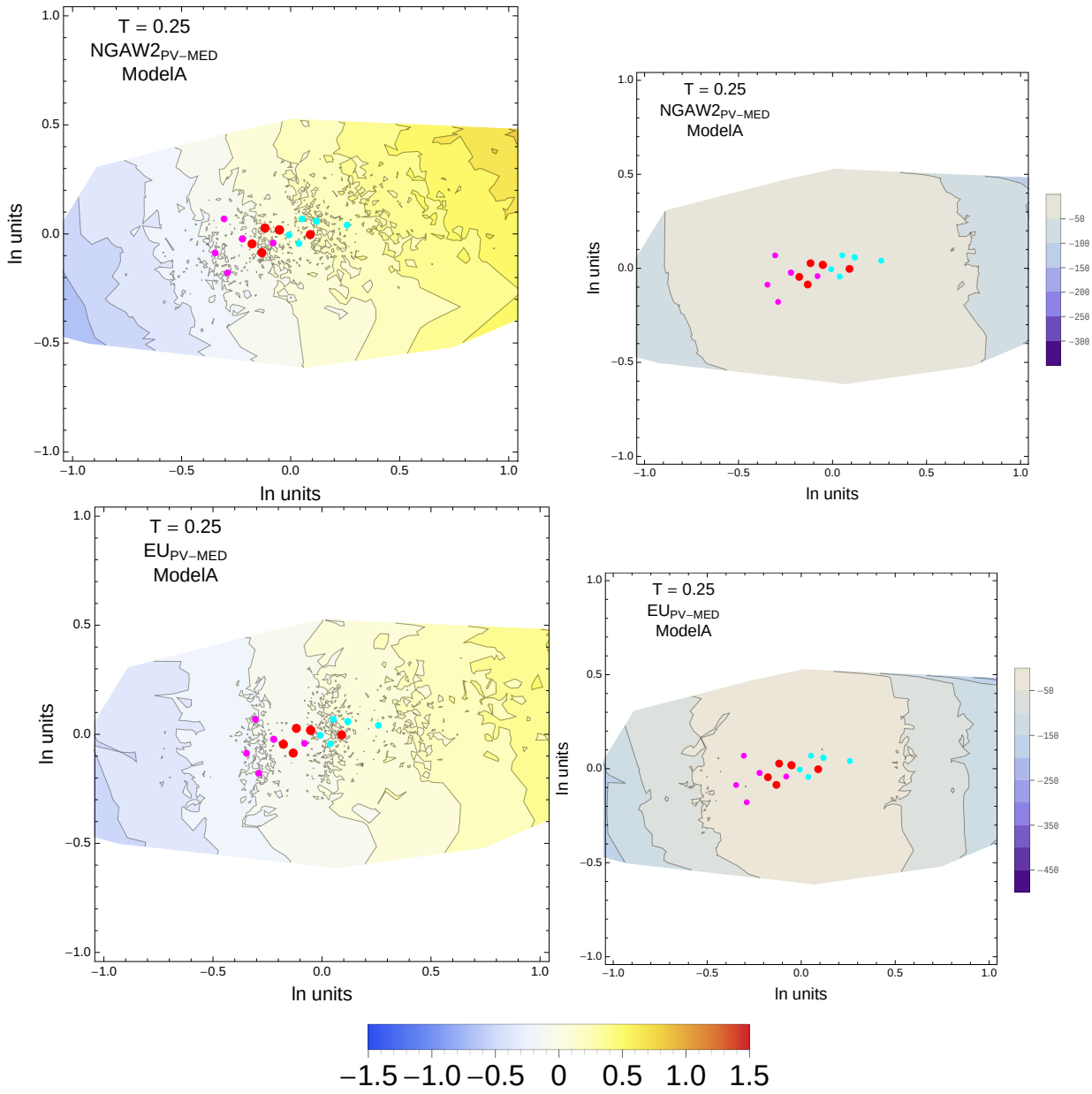



Figure 5.9: PVNGSv2: Contour Plots of mean residuals (top left) and likelihood (top right) for the NGA$_{PV-MED}$ dataset, and mean residuals (bottom left) and likelihood (top right) for the EU$_{PV-MED}$ dataset. The map is based on both Model A and B. The original GMPEs are red dots, plus/minus uncertainty are magenta/cyan dots. For $T = 0.25$s.

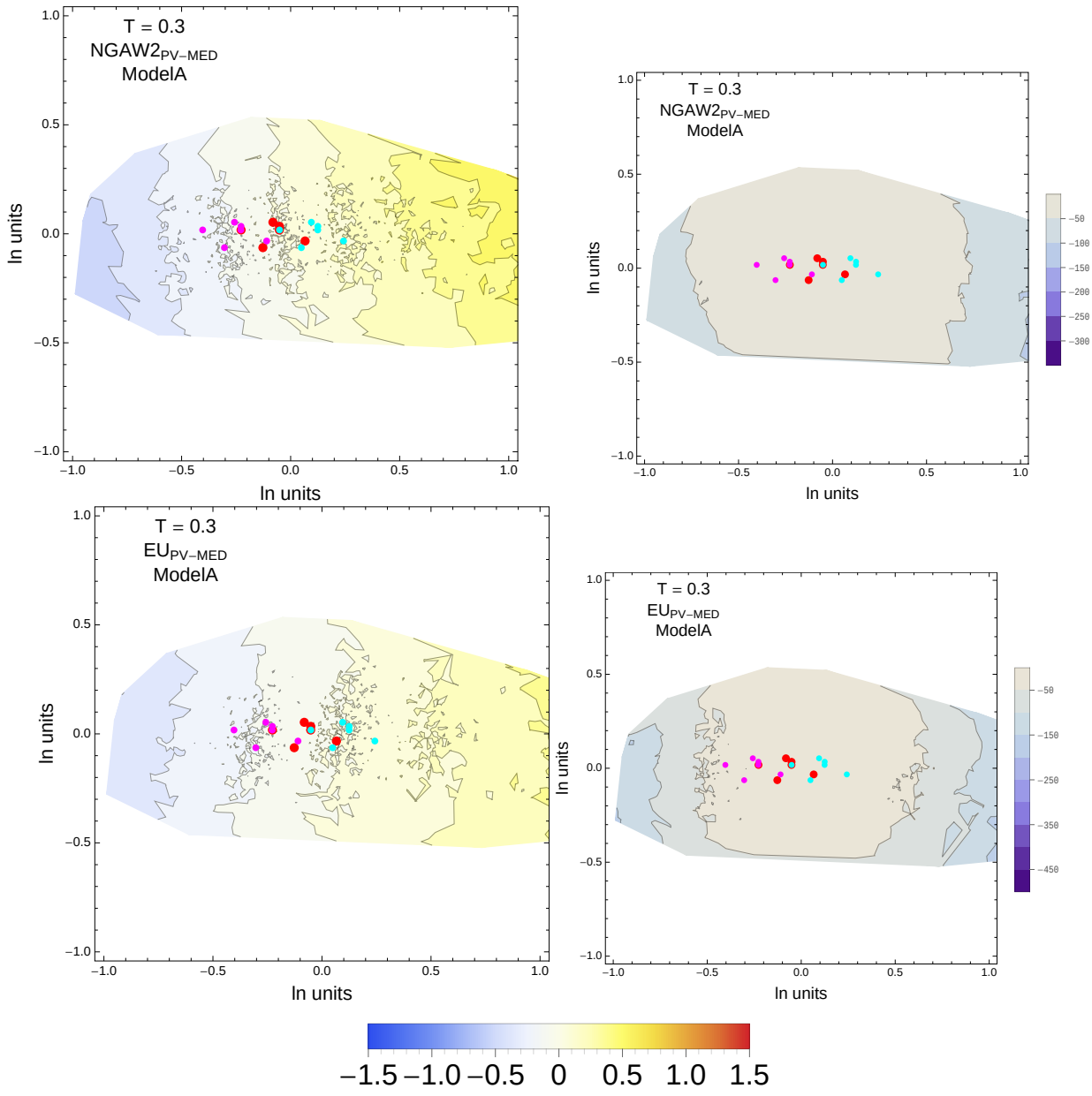



Figure 5.10: PVNGSv2: Contour Plots of mean residuals (top left) and likelihood (top right) for the NGA$_{PV-MED}$ dataset, and mean residuals (bottom left) and likelihood (top right) for the EU$_{PV-MED}$ dataset. The map is based on both Model A and B. The original GMPEs are red dots, plus/minus uncertainty are magenta/cyan dots. For $T = 0.3$s.

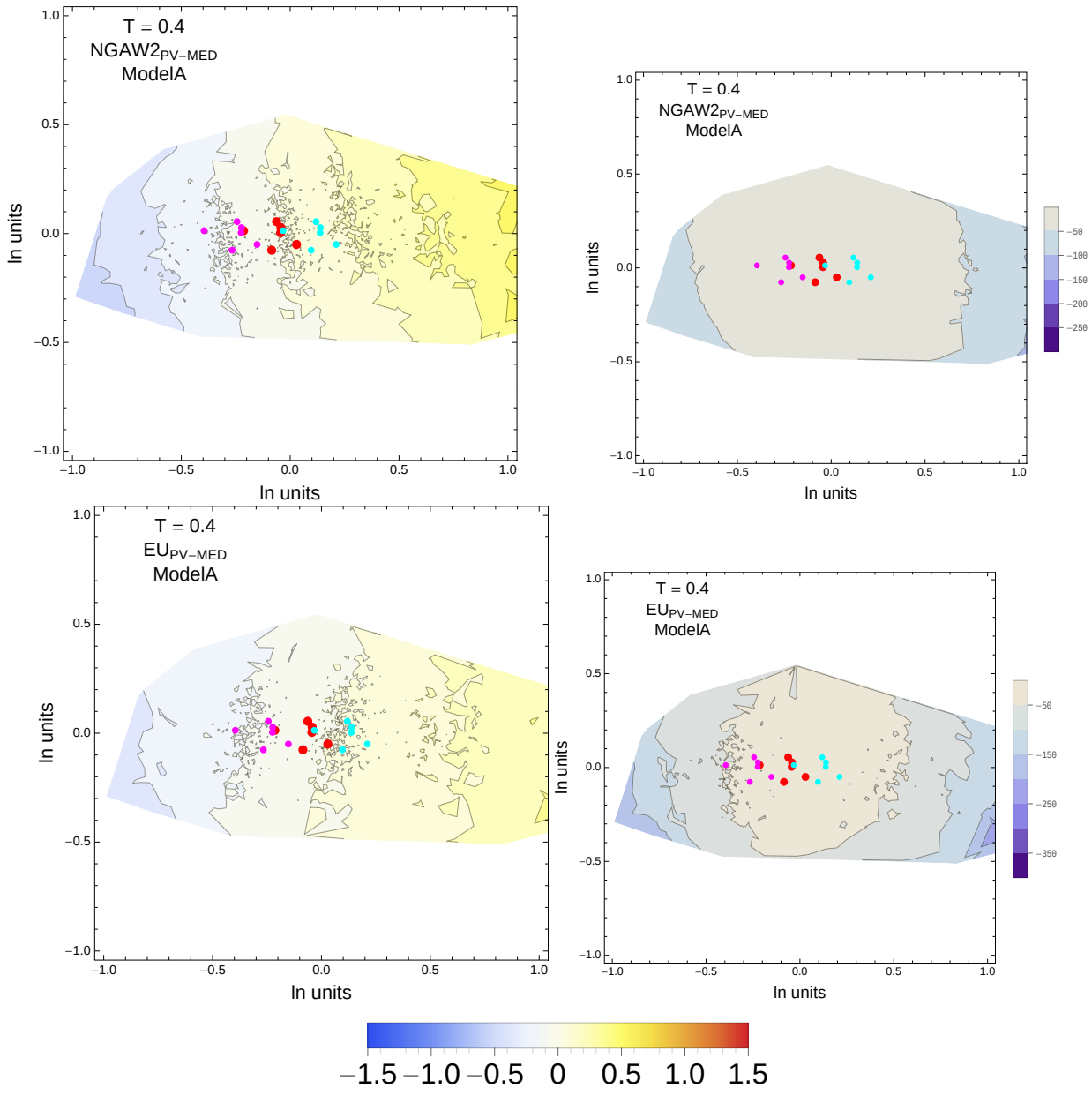



Figure 5.11: PVNGSv2: Contour Plots of mean residuals (top left) and likelihood (top right) for the NGA$_{PV-MED}$ dataset, and mean residuals (bottom left) and likelihood (top right) for the EU$_{PV-MED}$ dataset. The map is based on both Model A and B. The original GMPEs are red dots, plus/minus uncertainty are magenta/cyan dots. For $T = 0.4$s.

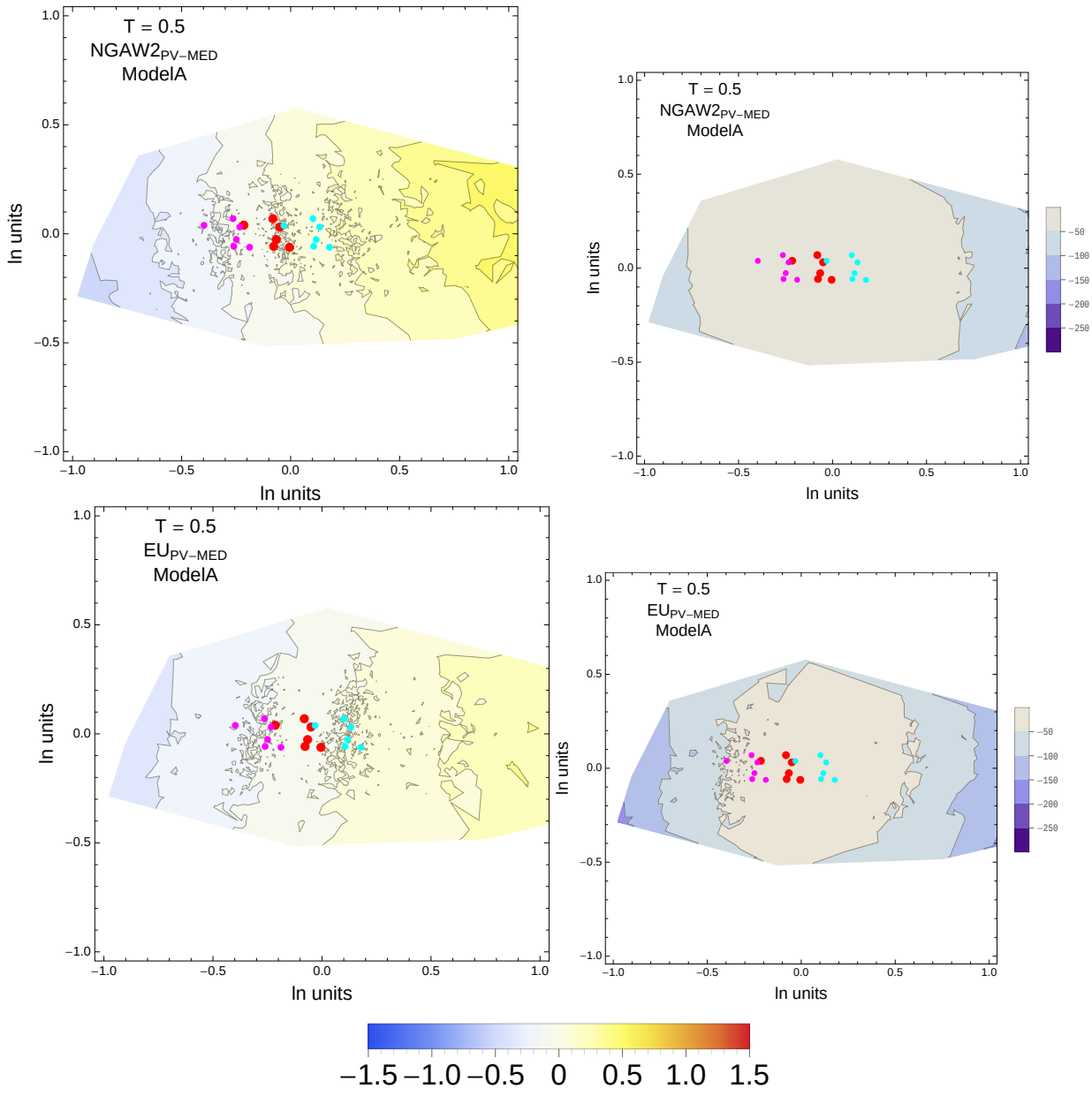



Figure 5.12: PVNGSv2: Contour Plots of mean residuals (top left) and likelihood (top right) for the NGA$_{PV-MED}$ dataset, and mean residuals (bottom left) and likelihood (top right) for the EU$_{PV-MED}$ dataset. The map is based on both Model A and B. The original GMPEs are red dots, plus/minus uncertainty are magenta/cyan dots. For $T = 0.5$s.

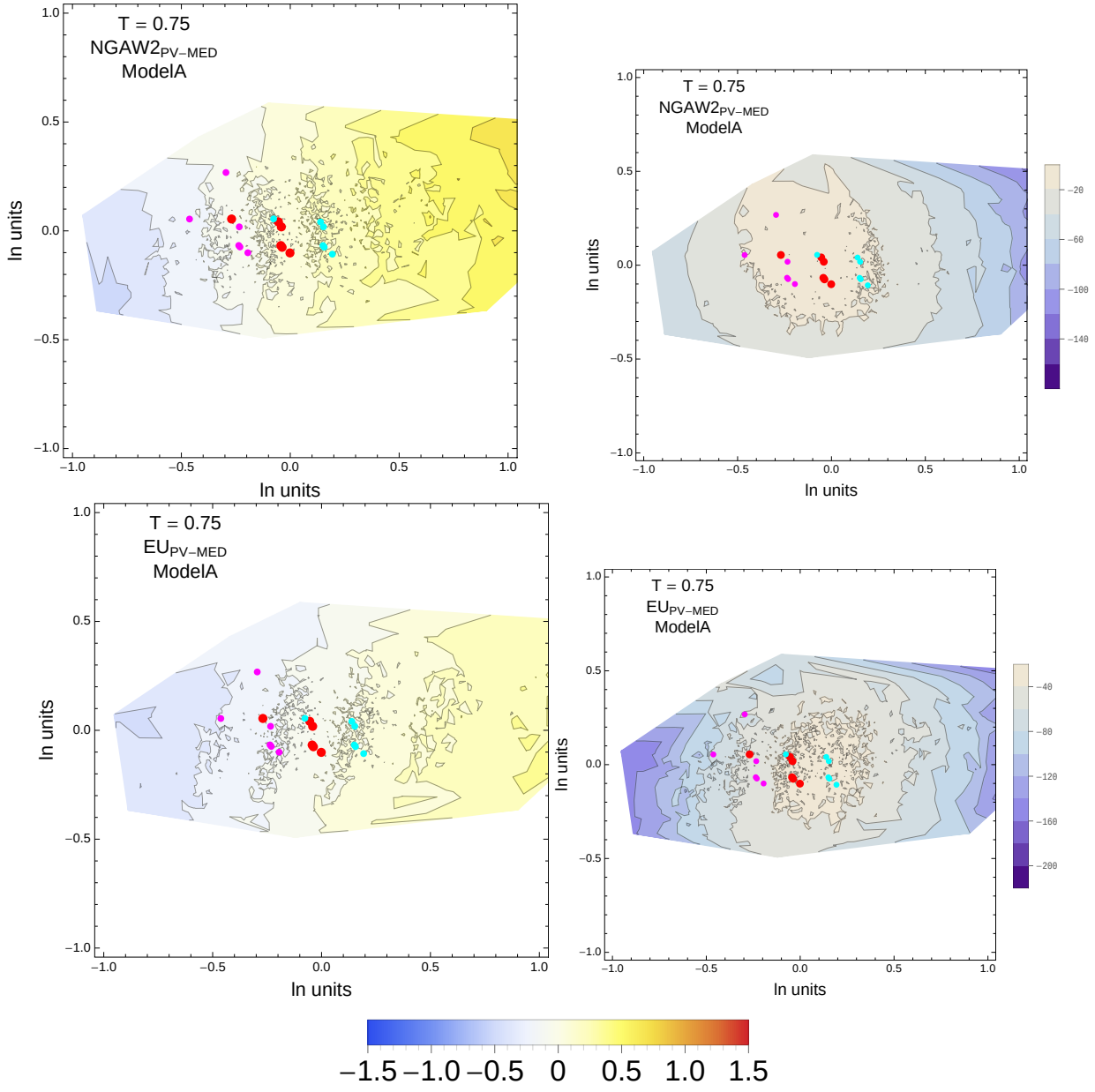



Figure 5.13: PVNGSv2: Contour Plots of mean residuals (top left) and likelihood (top right) for the NGA$_{PV-MED}$ dataset, and mean residuals (bottom left) and likelihood (top right) for the EU$_{PV-MED}$ dataset. The map is based on both Model A and B. The original GMPEs are red dots, plus/minus uncertainty are magenta/cyan dots. For $T = 0.75$s.

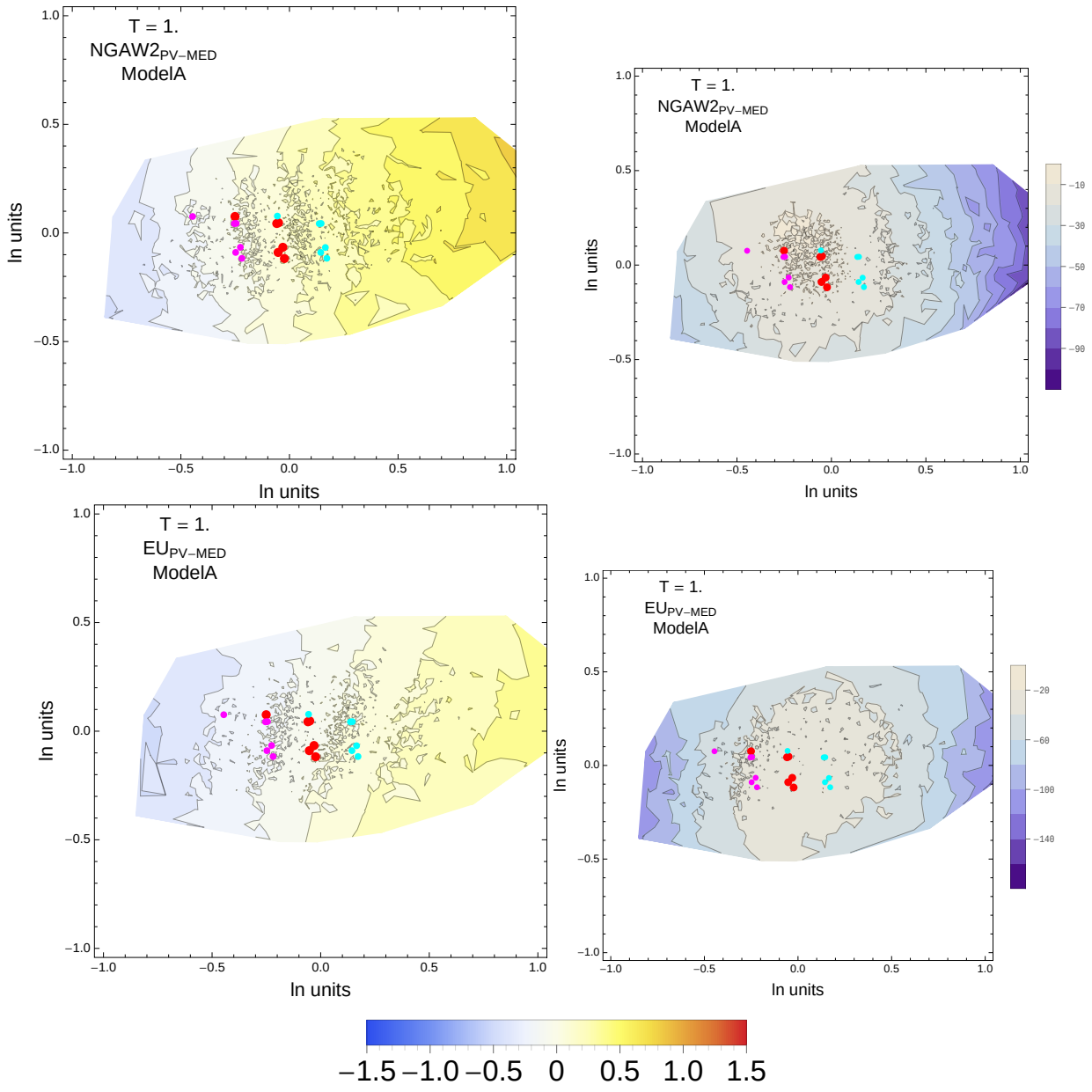



Figure 5.14: PVNGSv2: Contour Plots of mean residuals (top left) and likelihood (top right) for the NGA$_{PV-MED}$ dataset, and mean residuals (bottom left) and likelihood (top right) for the EU$_{PV-MED}$ dataset. The map is based on both Model A and B. The original GMPEs are red dots, plus/minus uncertainty are magenta/cyan dots. For $T = 1$.s.

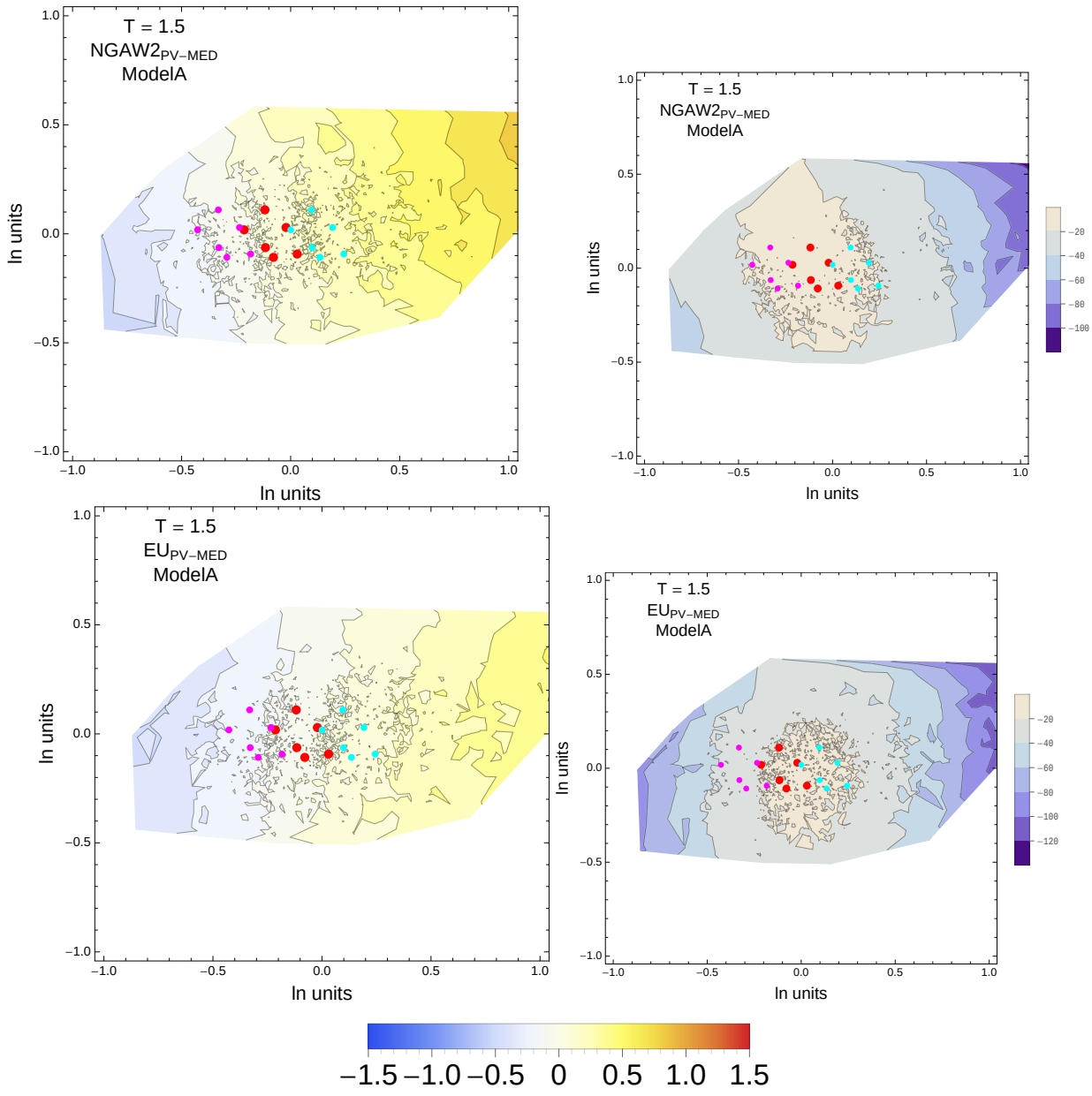



Figure 5.15: PVNGSv2: Contour Plots of mean residuals (top left) and likelihood (top right) for the NGA$_{PV-MED}$ dataset, and mean residuals (bottom left) and likelihood (top right) for the EU$_{PV-MED}$ dataset. The map is based on both Model A and B. The original GMPEs are red dots, plus/minus uncertainty are magenta/cyan dots. For $T = 1.5$s.

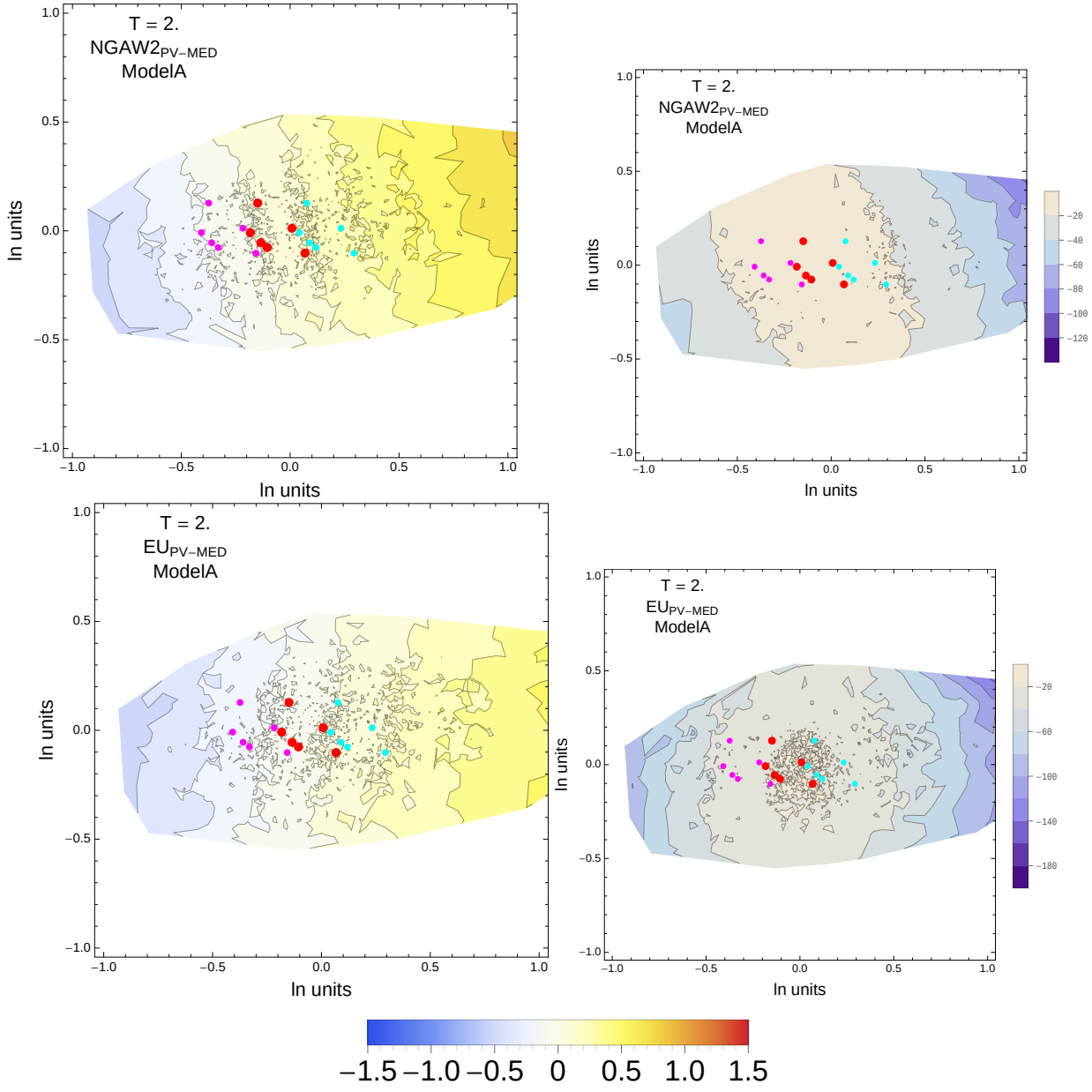



Figure 5.16: PVNGSv2: Contour Plots of mean residuals (top left) and likelihood (top right) for the NGA$_{PV-MED}$ dataset, and mean residuals (bottom left) and likelihood (top right) for the EU$_{PV-MED}$ dataset. The map is based on both Model A and B. The original GMPEs are red dots, plus/minus uncertainty are magenta/cyan dots. For $T = 2$.s.

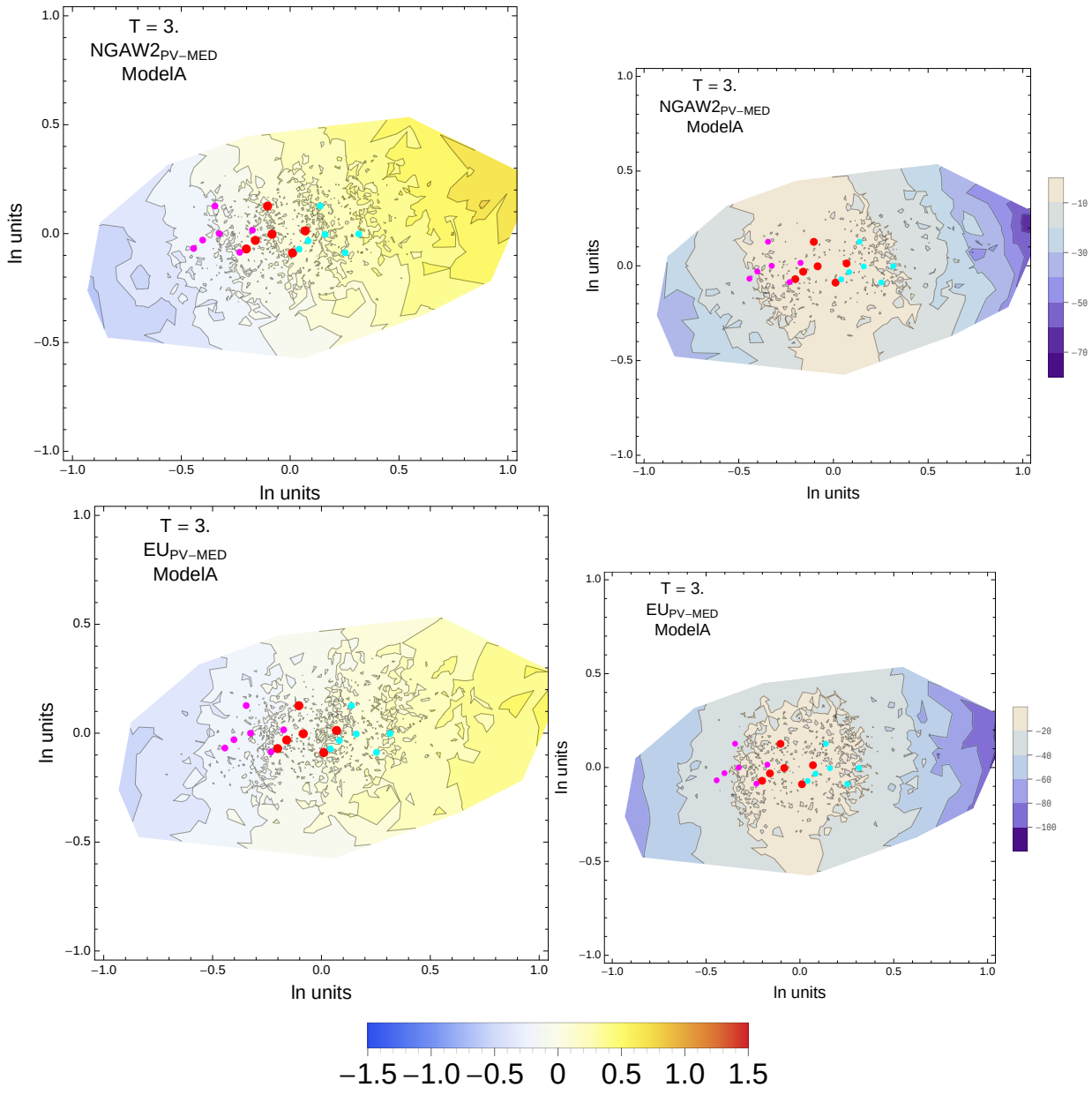



Figure 5.17: PVNGSv2: Contour Plots of mean residuals (top left) and likelihood (top right) for the NGA$_{PV-MED}$ dataset, and mean residuals (bottom left) and likelihood (top right) for the EU$_{PV-MED}$ dataset. The map is based on both Model A and B. The original GMPEs are red dots, plus/minus uncertainty are magenta/cyan dots. For $T = 3$.s.

### 5.1.2 Combined Quantile Plots vs. Distance with GMPEs

**T = 0.01s**

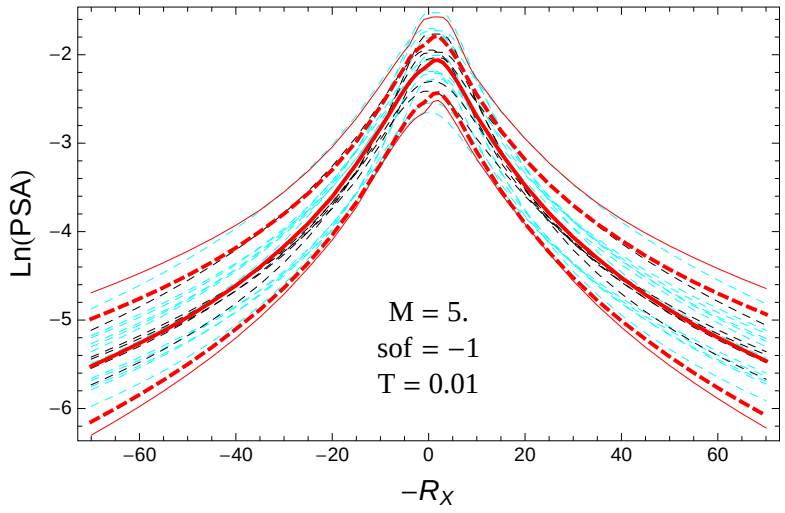



Figure 5.18: PVNGSv2: Distance scaling of the original GMPEs (dashed black), the original GMPEs with uncertainty model (dashed cyan) and 0.05,0.5,0.95 quantile of the combined ModelA and ModelB distribution (red) with total weights, for a scenario with $M = 5.$, $F = -1$, and $T = 0.01$s.

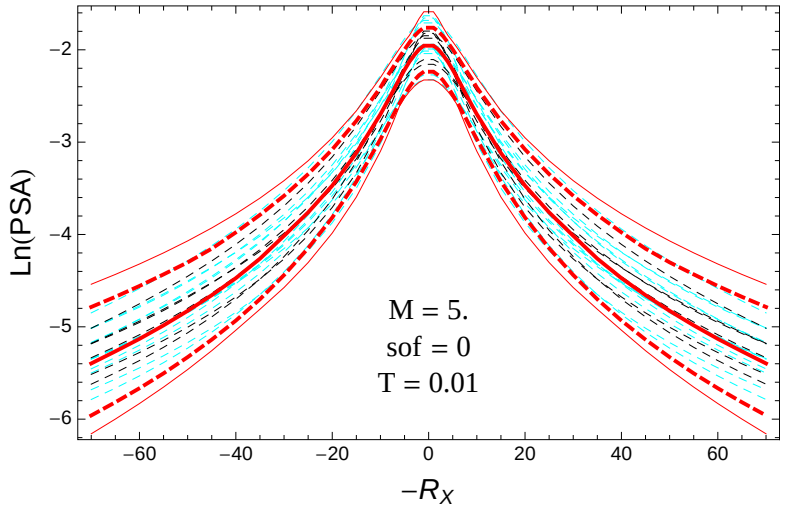



Figure 5.19: PVNGSv2: Distance scaling of the original GMPEs (dashed black), the original GMPEs with uncertainty model (dashed cyan) and 0.05,0.5,0.95 quantile of the combined ModelA and ModelB distribution (red) with total weights, for a scenario with $M = 5.$, $F = 0$, and $T = 0.01$s.

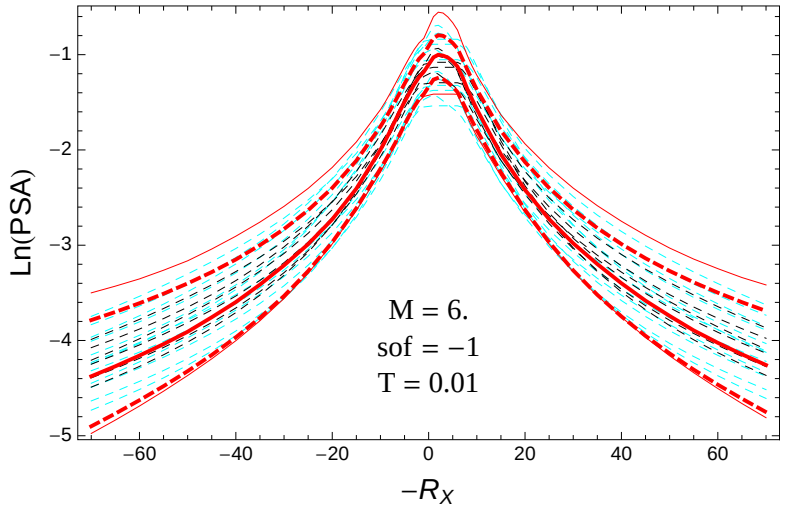



Figure 5.20: PVNGSv2: Distance scaling of the original GMPEs (dashed black), the original GMPEs with uncertainty model (dashed cyan) and 0.05,0.5,0.95 quantile of the combined ModelA and ModelB distribution (red) with total weights, for a scenario with $M = 6.$, $F = -1$, and $T = 0.01$s.

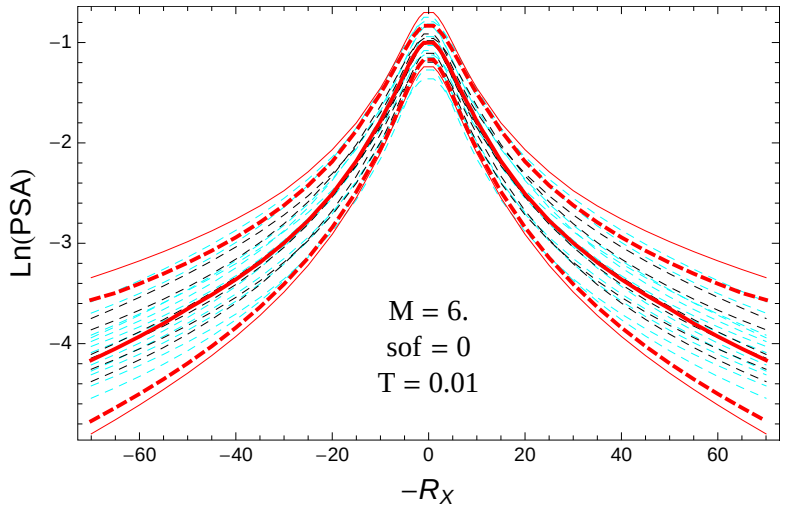



Figure 5.21: PVNGSv2: Distance scaling of the original GMPEs (dashed black), the original GMPEs with uncertainty model (dashed cyan) and 0.05,0.5,0.95 quantile of the combined ModelA and ModelB distribution (red) with total weights, for a scenario with $M = 6.$, $F = 0$, and $T = 0.01$s.

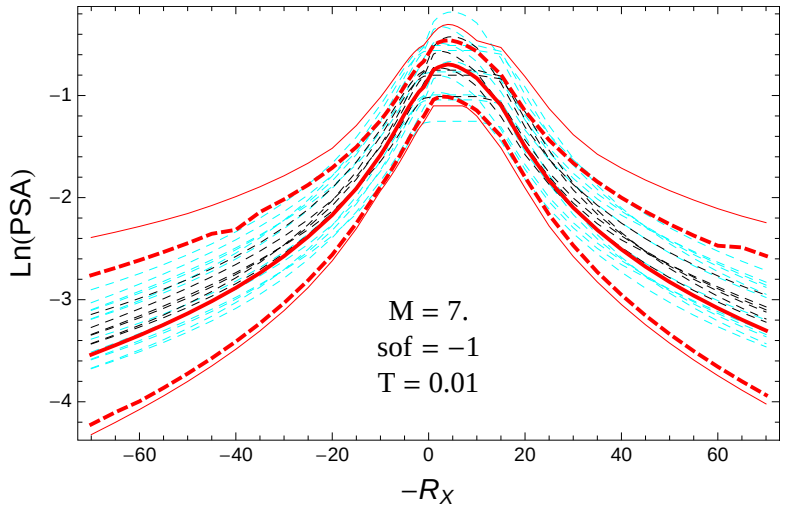



Figure 5.22: PVNGSv2: Distance scaling of the original GMPEs (dashed black), the original GMPEs with uncertainty model (dashed cyan) and 0.05,0.5,0.95 quantile of the combined ModelA and ModelB distribution (red) with total weights, for a scenario with $M = 7.$, $F = -1$, and $T = 0.01$s.

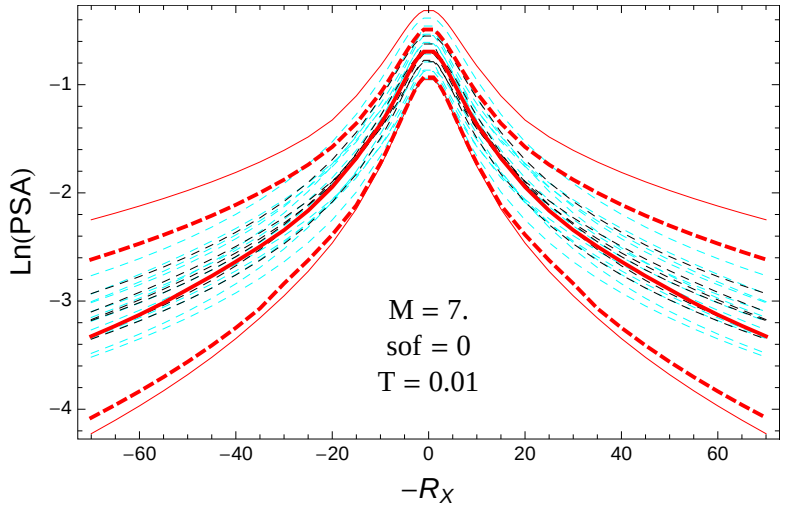



Figure 5.23: PVNGSv2: Distance scaling of the original GMPEs (dashed black), the original GMPEs with uncertainty model (dashed cyan) and 0.05,0.5,0.95 quantile of the combined ModelA and ModelB distribution (red) with total weights, for a scenario with $M = 7.$, $F = 0$, and $T = 0.01$s.

**T = 0.2s**

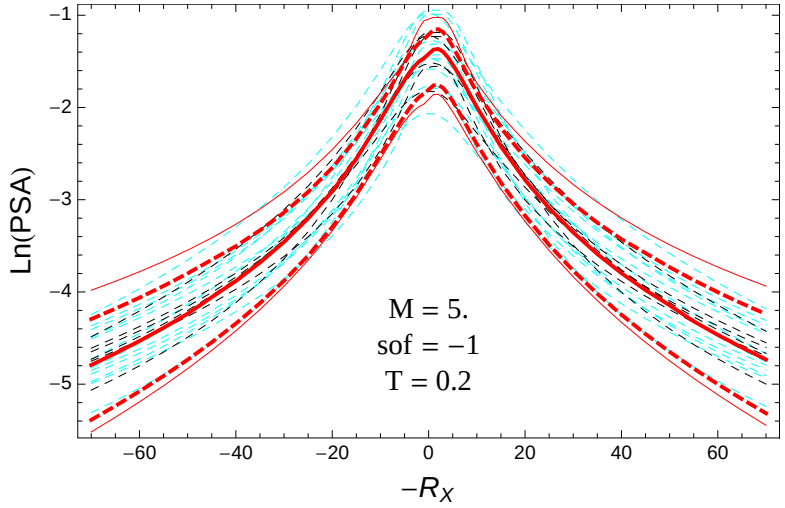



Figure 5.24: PVNGSv2: Distance scaling of the original GMPEs (dashed black), the original GMPEs with uncertainty model (dashed cyan) and 0.05,0.5,0.95 quantile of the combined ModelA and ModelB distribution (red) with total weights, for a scenario with $M = 5.$, $F = -1$, and $T = 0.2$s.

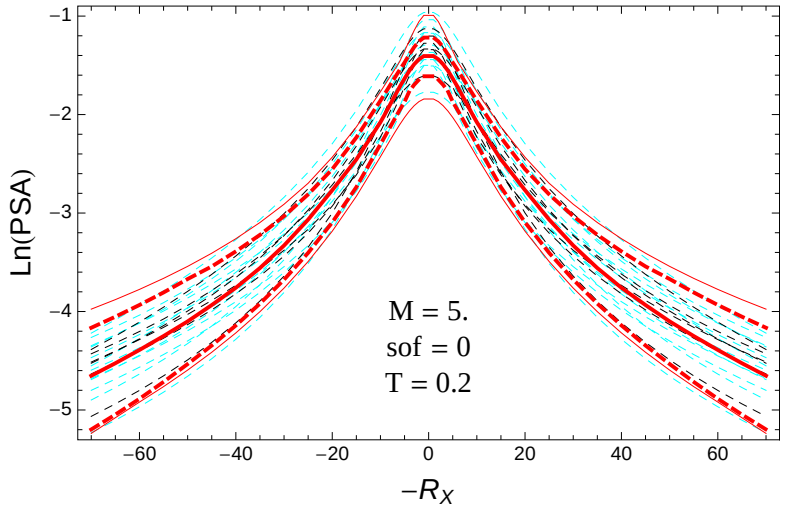



Figure 5.25: PVNGSv2: Distance scaling of the original GMPEs (dashed black), the original GMPEs with uncertainty model (dashed cyan) and 0.05,0.5,0.95 quantile of the combined ModelA and ModelB distribution (red) with total weights, for a scenario with $M = 5.$, $F = 0$, and $T = 0.2$s.

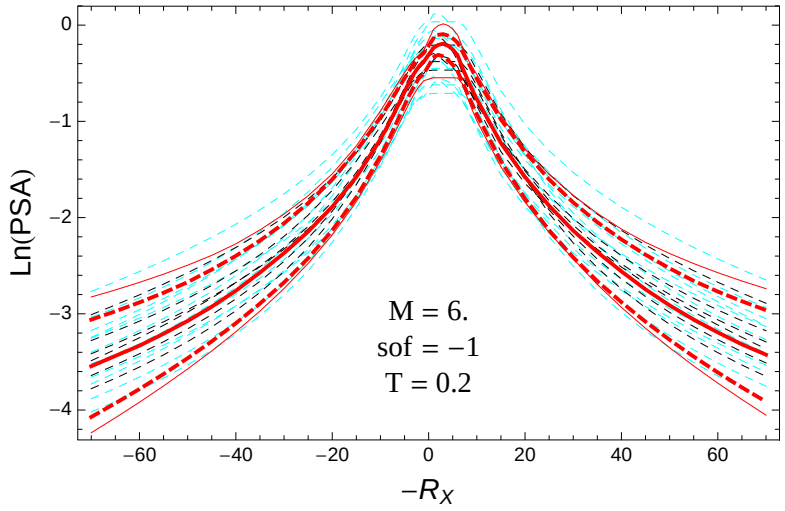



Figure 5.26: PVNGSv2: Distance scaling of the original GMPEs (dashed black), the original GMPEs with uncertainty model (dashed cyan) and 0.05,0.5,0.95 quantile of the combined ModelA and ModelB distribution (red) with total weights, for a scenario with $M = 6.$, $F = -1$, and $T = 0.2$s.

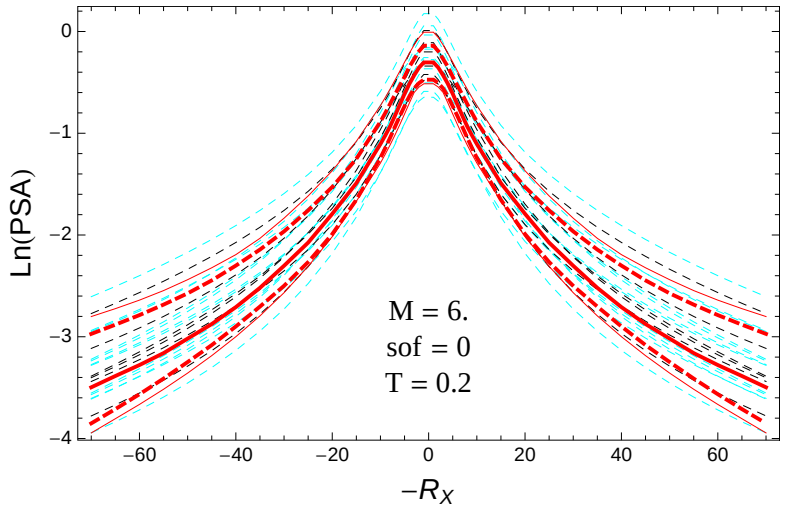



Figure 5.27: PVNGSv2: Distance scaling of the original GMPEs (dashed black), the original GMPEs with uncertainty model (dashed cyan) and 0.05,0.5,0.95 quantile of the combined ModelA and ModelB distribution (red) with total weights, for a scenario with $M = 6.$, $F = 0$, and $T = 0.2$s.

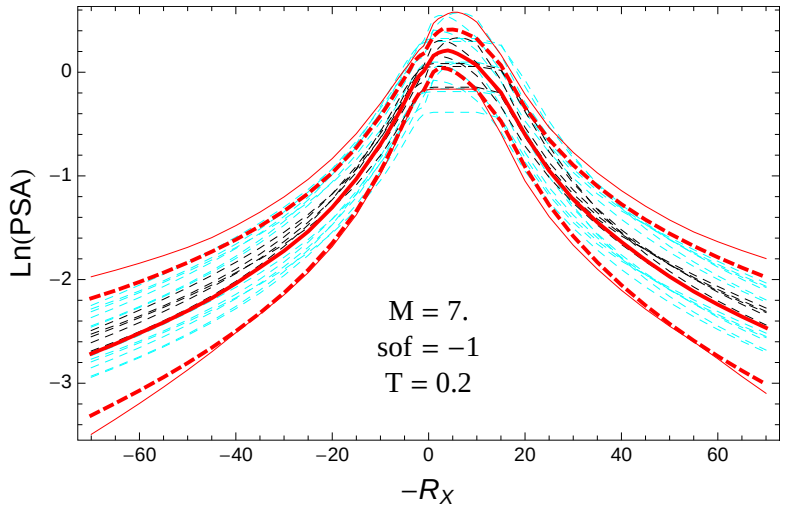



Figure 5.28: PVNGSv2: Distance scaling of the original GMPEs (dashed black), the original GMPEs with uncertainty model (dashed cyan) and 0.05,0.5,0.95 quantile of the combined ModelA and ModelB distribution (red) with total weights, for a scenario with $M = 7.$, $F = -1$, and $T = 0.2$s.

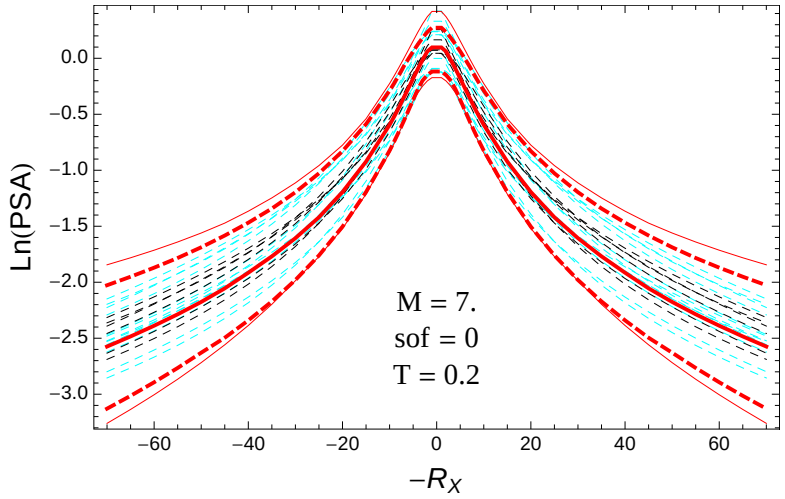



Figure 5.29: PVNGSv2: Distance scaling of the original GMPEs (dashed black), the original GMPEs with uncertainty model (dashed cyan) and 0.05,0.5,0.95 quantile of the combined ModelA and ModelB distribution (red) with total weights, for a scenario with $M = 7.$, $F = 0$, and $T = 0.2$s.

**T = 0.5s**

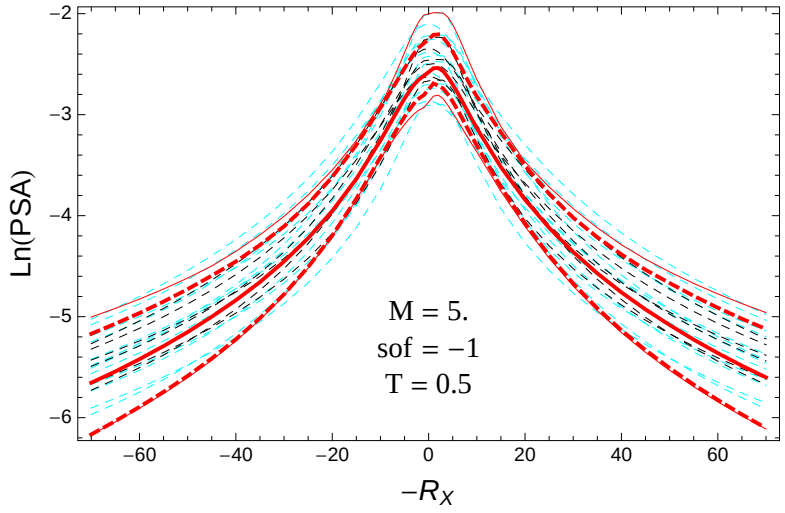



Figure 5.30: PVNGSv2: Distance scaling of the original GMPEs (dashed black), the original GMPEs with uncertainty model (dashed cyan) and 0.05,0.5,0.95 quantile of the combined ModelA and ModelB distribution (red) with total weights, for a scenario with $M = 5.$, $F = -1$, and $T = 0.5$s.

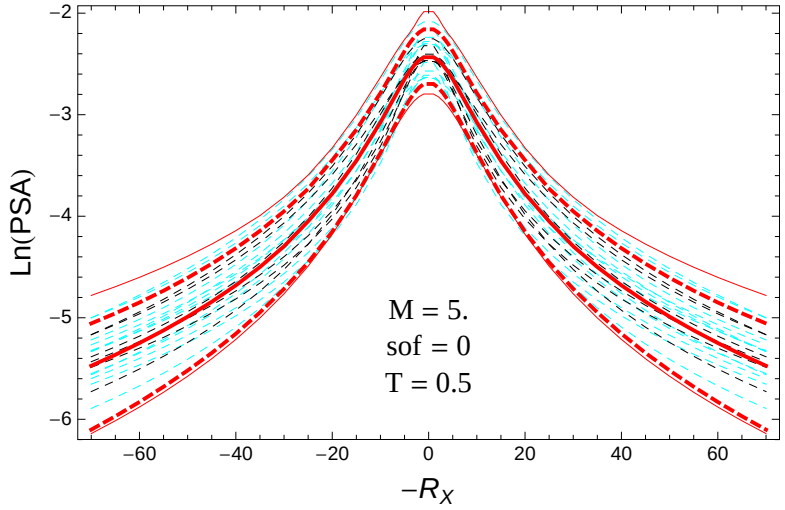



Figure 5.31: PVNGSv2: Distance scaling of the original GMPEs (dashed black), the original GMPEs with uncertainty model (dashed cyan) and 0.05,0.5,0.95 quantile of the combined ModelA and ModelB distribution (red) with total weights, for a scenario with $M = 5.$, $F = 0$, and $T = 0.5$s.

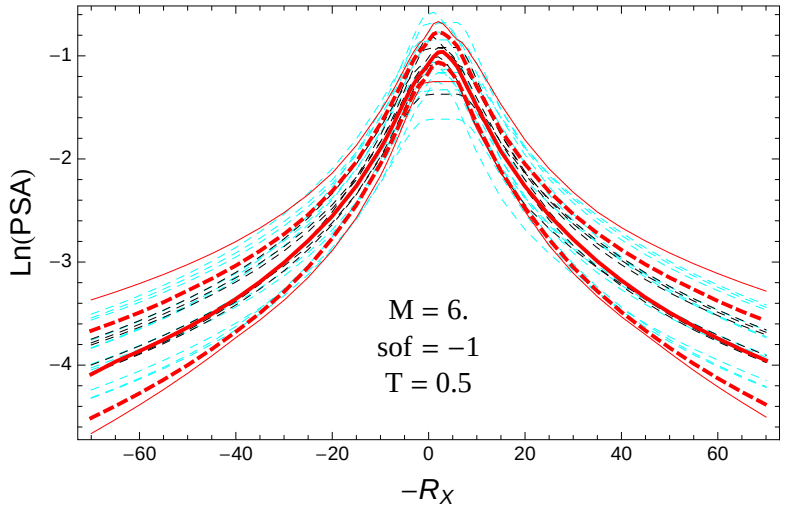



Figure 5.32: PVNGSv2: Distance scaling of the original GMPEs (dashed black), the original GMPEs with uncertainty model (dashed cyan) and 0.05,0.5,0.95 quantile of the combined ModelA and ModelB distribution (red) with total weights, for a scenario with $M = 6.$, $F = -1$, and $T = 0.5$s.

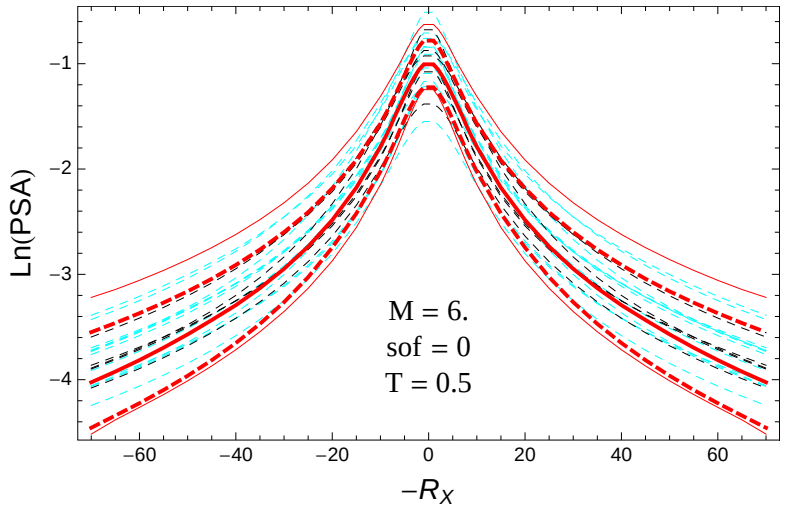



Figure 5.33: PVNGSv2: Distance scaling of the original GMPEs (dashed black), the original GMPEs with uncertainty model (dashed cyan) and 0.05,0.5,0.95 quantile of the combined ModelA and ModelB distribution (red) with total weights, for a scenario with $M = 6.$, $F = 0$, and $T = 0.5$s.

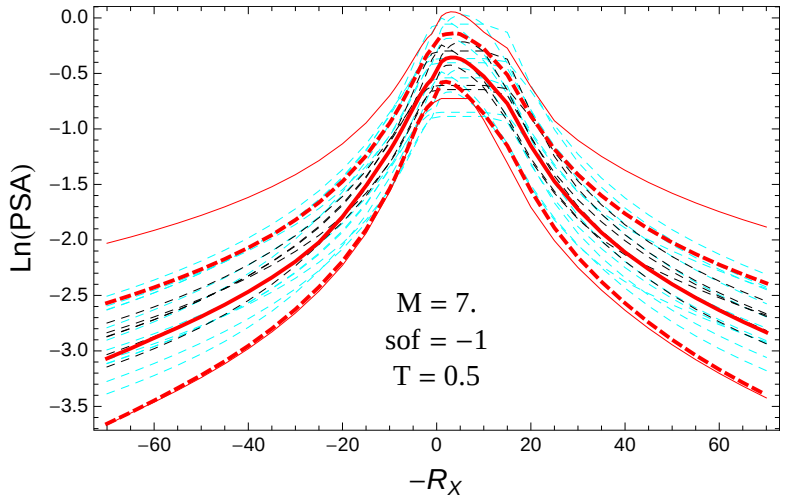



Figure 5.34: PVNGSv2: Distance scaling of the original GMPEs (dashed black), the original GMPEs with uncertainty model (dashed cyan) and 0.05,0.5,0.95 quantile of the combined ModelA and ModelB distribution (red) with total weights, for a scenario with $M = 7.$, $F = -1$, and $T = 0.5$s.

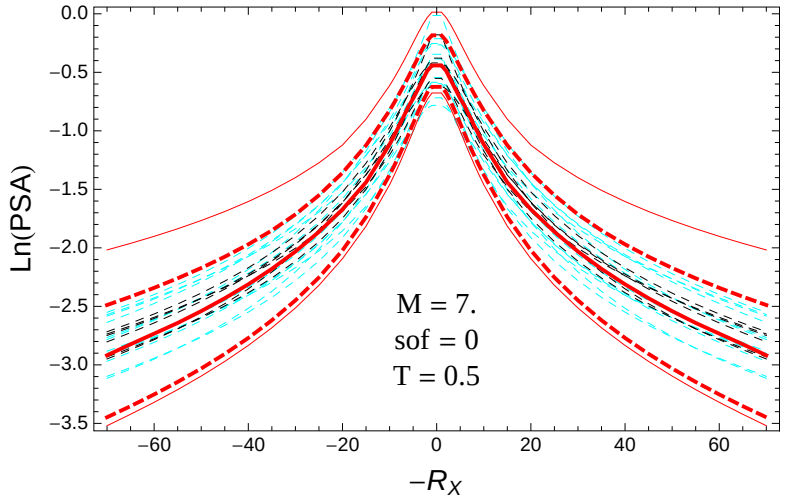



Figure 5.35: PVNGSv2: Distance scaling of the original GMPEs (dashed black), the original GMPEs with uncertainty model (dashed cyan) and 0.05,0.5,0.95 quantile of the combined ModelA and ModelB distribution (red) with total weights, for a scenario with $M = 7.$, $F = 0$, and $T = 0.5$s.

**T = 1.s**

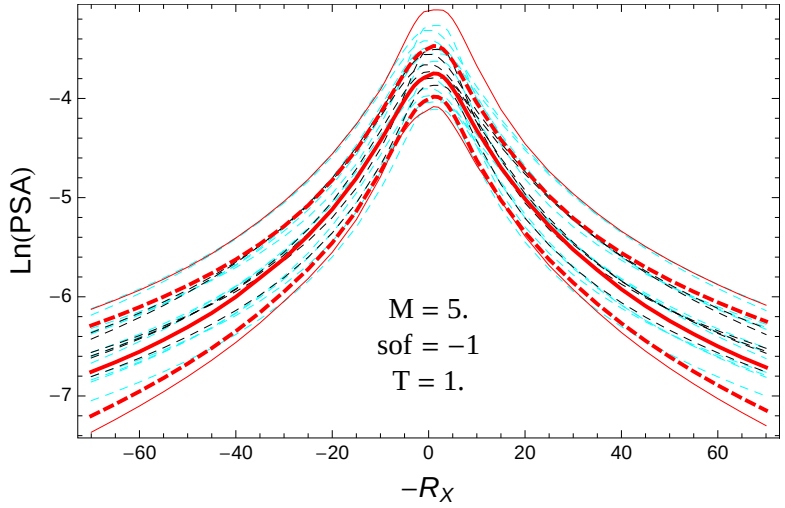



Figure 5.36: PVNGSv2: Distance scaling of the original GMPEs (dashed black), the original GMPEs with uncertainty model (dashed cyan) and 0.05,0.5,0.95 quantile of the combined ModelA and ModelB distribution (red) with total weights, for a scenario with $M = 5.$, $F = -1$, and $T = 1.$s.

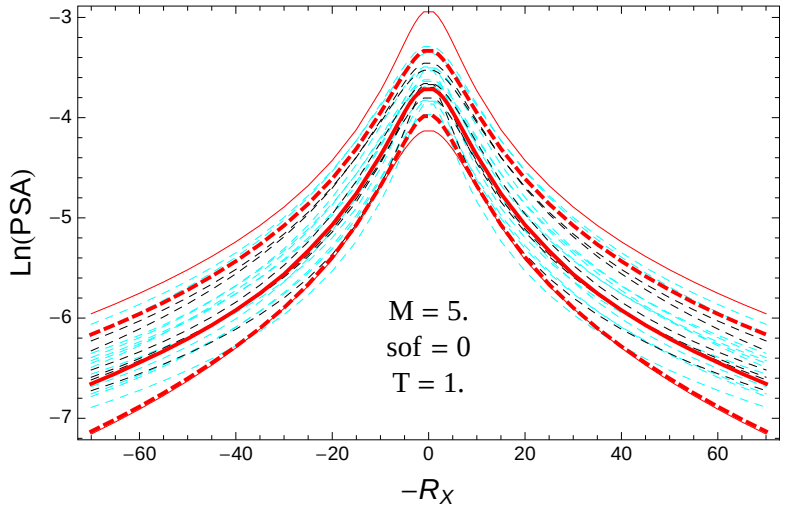



Figure 5.37: PVNGSv2: Distance scaling of the original GMPEs (dashed black), the original GMPEs with uncertainty model (dashed cyan) and 0.05,0.5,0.95 quantile of the combined ModelA and ModelB distribution (red) with total weights, for a scenario with $M = 5.$, $F = 0$, and $T = 1.$s.

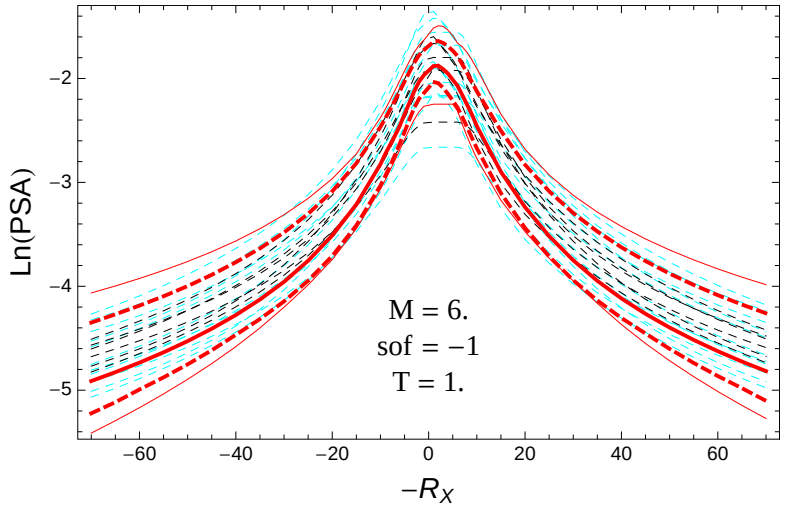



Figure 5.38: PVNGSv2: Distance scaling of the original GMPEs (dashed black), the original GMPEs with uncertainty model (dashed cyan) and 0.05,0.5,0.95 quantile of the combined ModelA and ModelB distribution (red) with total weights, for a scenario with $M = 6.$, $F = -1$, and $T = 1.$s.

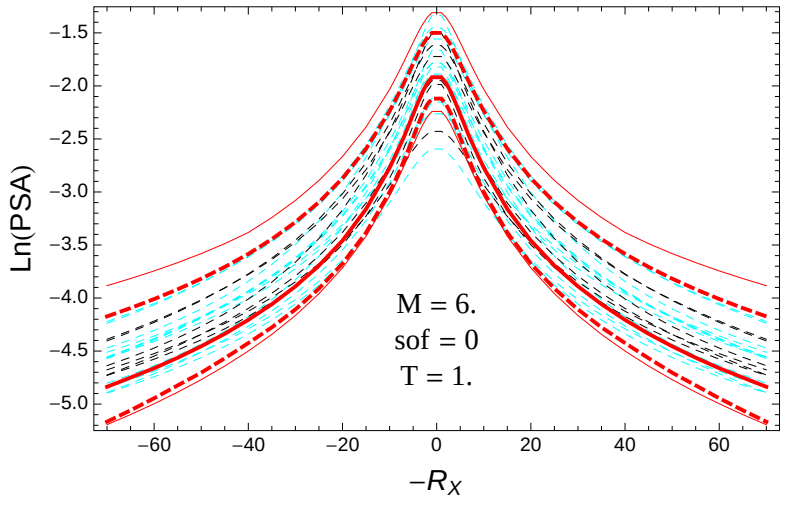



Figure 5.39: PVNGSv2: Distance scaling of the original GMPEs (dashed black), the original GMPEs with uncertainty model (dashed cyan) and 0.05,0.5,0.95 quantile of the combined ModelA and ModelB distribution (red) with total weights, for a scenario with $M = 6.$, $F = 0$, and $T = 1.$s.

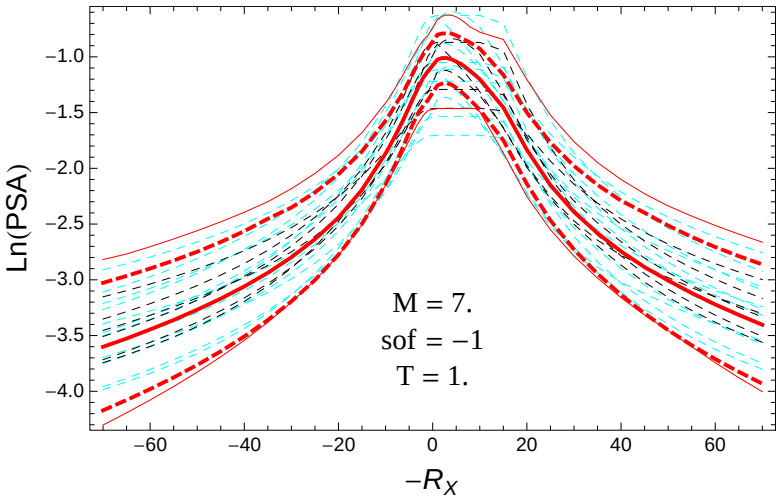



Figure 5.40: PVNGSv2: Distance scaling of the original GMPEs (dashed black), the original GMPEs with uncertainty model (dashed cyan) and 0.05,0.5,0.95 quantile of the combined ModelA and ModelB distribution (red) with total weights, for a scenario with $M = 7.$, $F = -1$, and $T = 1.$s.

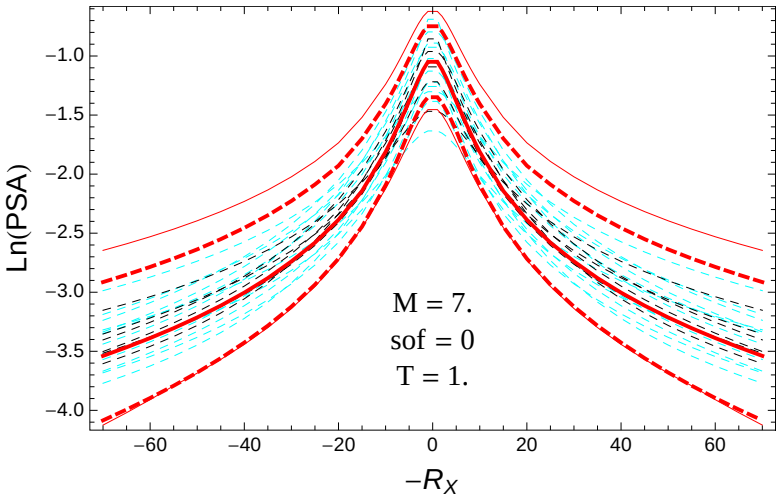



Figure 5.41: PVNGSv2: Distance scaling of the original GMPEs (dashed black), the original GMPEs with uncertainty model (dashed cyan) and 0.05,0.5,0.95 quantile of the combined ModelA and ModelB distribution (red) with total weights, for a scenario with $M = 7.$, $F = 0$, and $T = 1.$s.

**T = 2.s**

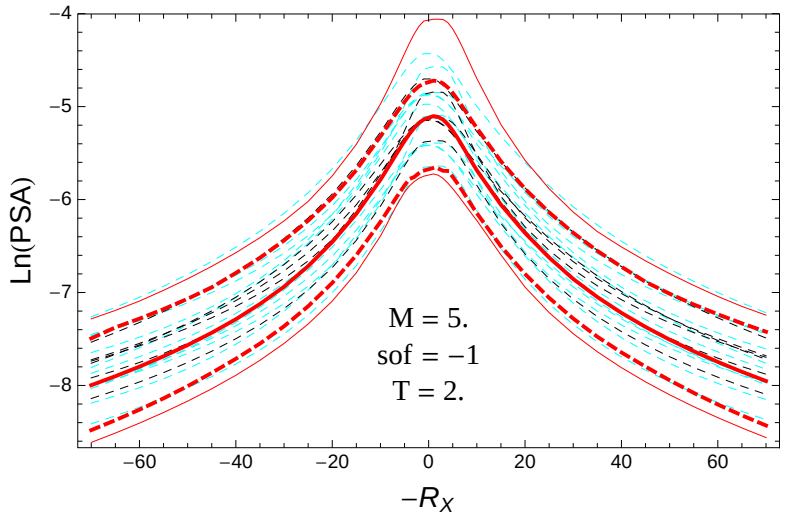



Figure 5.42: PVNGSv2: Distance scaling of the original GMPEs (dashed black), the original GMPEs with uncertainty model (dashed cyan) and 0.05,0.5,0.95 quantile of the combined ModelA and ModelB distribution (red) with total weights, for a scenario with $M = 5.$, $F = -1$, and $T = 2.$s.

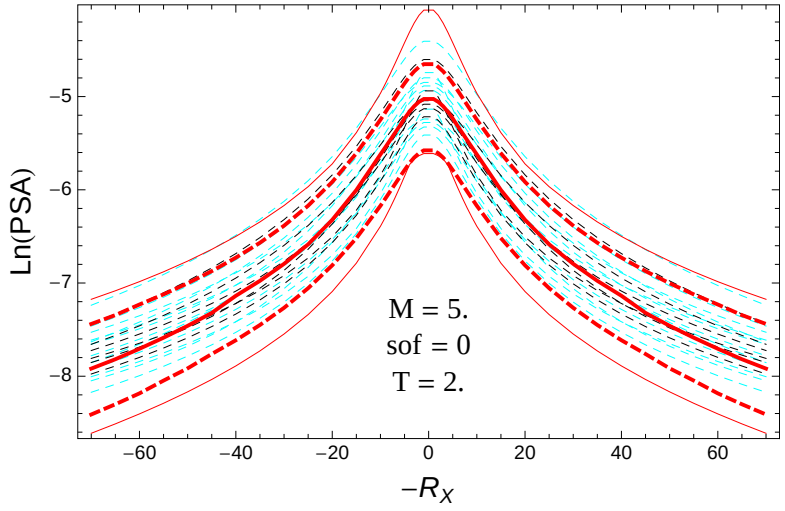



Figure 5.43: PVNGSv2: Distance scaling of the original GMPEs (dashed black), the original GMPEs with uncertainty model (dashed cyan) and 0.05,0.5,0.95 quantile of the combined ModelA and ModelB distribution (red) with total weights, for a scenario with $M = 5.$, $F = 0$, and $T = 2.$s.

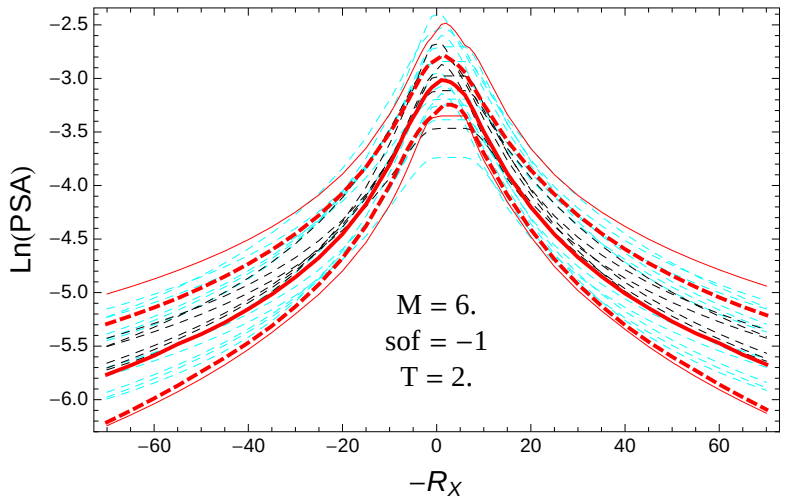



Figure 5.44: PVNGSv2: Distance scaling of the original GMPEs (dashed black), the original GMPEs with uncertainty model (dashed cyan) and 0.05,0.5,0.95 quantile of the combined ModelA and ModelB distribution (red) with total weights, for a scenario with $M = 6.$, $F = -1$, and $T = 2.$s.

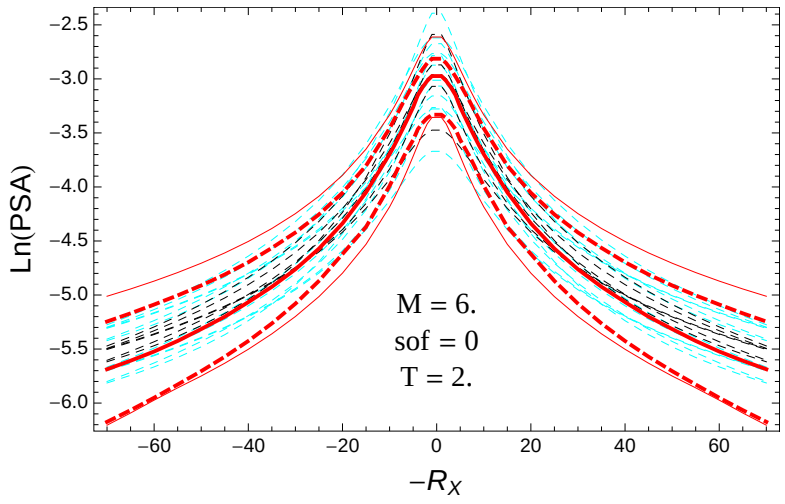



Figure 5.45: PVNGSv2: Distance scaling of the original GMPEs (dashed black), the original GMPEs with uncertainty model (dashed cyan) and 0.05,0.5,0.95 quantile of the combined ModelA and ModelB distribution (red) with total weights, for a scenario with $M = 6.$, $F = 0$, and $T = 2.$s.

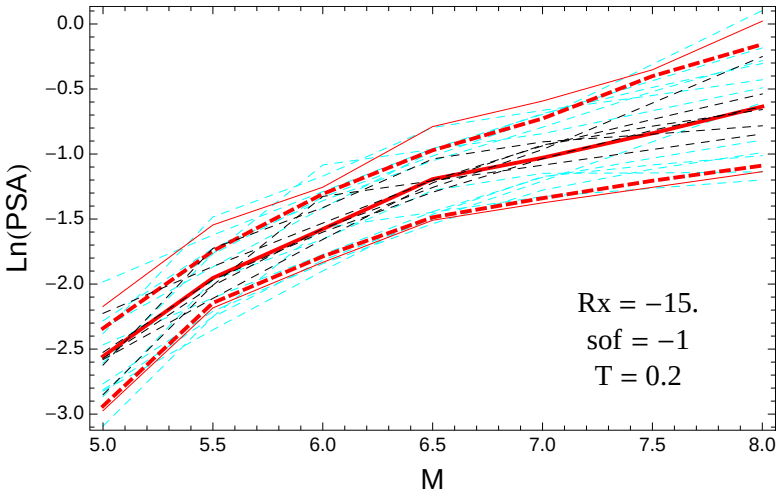



Figure 5.106: PVNGSv2: Magnitude scaling of the original GMPEs (dashed black), the original GMPEs with uncertainty model (dashed cyan) and 0.05,0.5,0.95 quantile of the combined ModelA and ModelB distribution (red) with total weights, for a scenario with $R_X = -15.$, $F = -1$, and $T = 0.2$s.

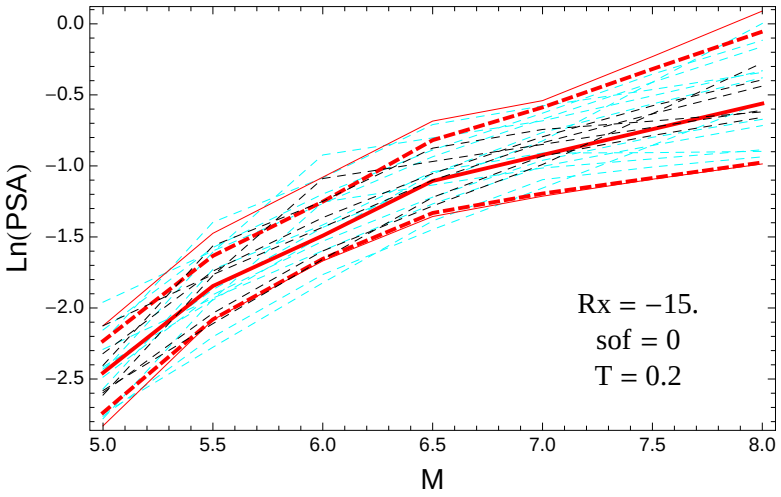



Figure 5.107: PVNGSv2: Magnitude scaling of the original GMPEs (dashed black), the original GMPEs with uncertainty model (dashed cyan) and 0.05,0.5,0.95 quantile of the combined ModelA and ModelB distribution (red) with total weights, for a scenario with $R_X = -15.$, $F = 0$, and $T = 0.2$s.

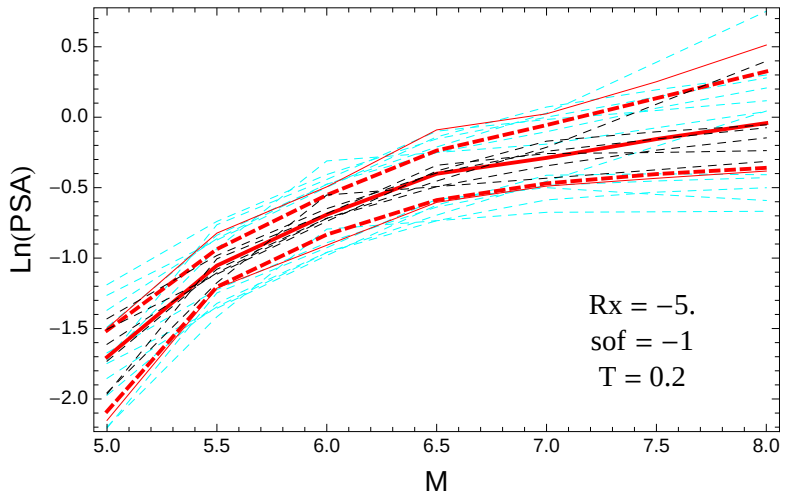



Figure 5.108: PVNGSv2: Magnitude scaling of the original GMPEs (dashed black), the original GMPEs with uncertainty model (dashed cyan) and 0.05,0.5,0.95 quantile of the combined ModelA and ModelB distribution (red) with total weights, for a scenario with $R_X = -5.$, $F = -1$, and $T = 0.2$s.

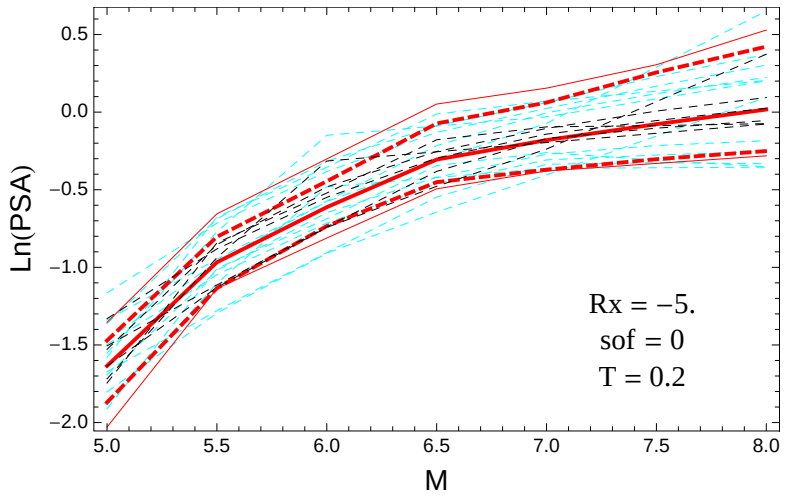



Figure 5.109: PVNGSv2: Magnitude scaling of the original GMPEs (dashed black), the original GMPEs with uncertainty model (dashed cyan) and 0.05,0.5,0.95 quantile of the combined ModelA and ModelB distribution (red) with total weights, for a scenario with $R_X = -5.$, $F = 0$, and $T = 0.2$s.

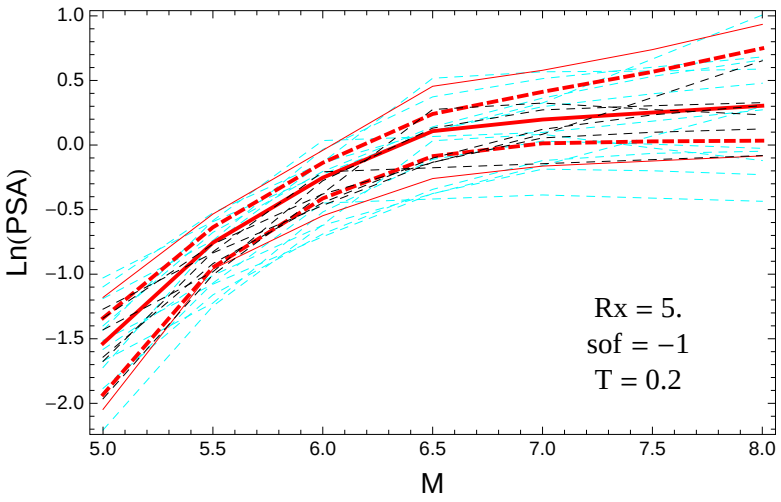



Figure 5.110: PVNGSv2: Magnitude scaling of the original GMPEs (dashed black), the original GMPEs with uncertainty model (dashed cyan) and 0.05,0.5,0.95 quantile of the combined ModelA and ModelB distribution (red) with total weights, for a scenario with $R_X = 5.$, $F = -1$, and $T = 0.2$s.

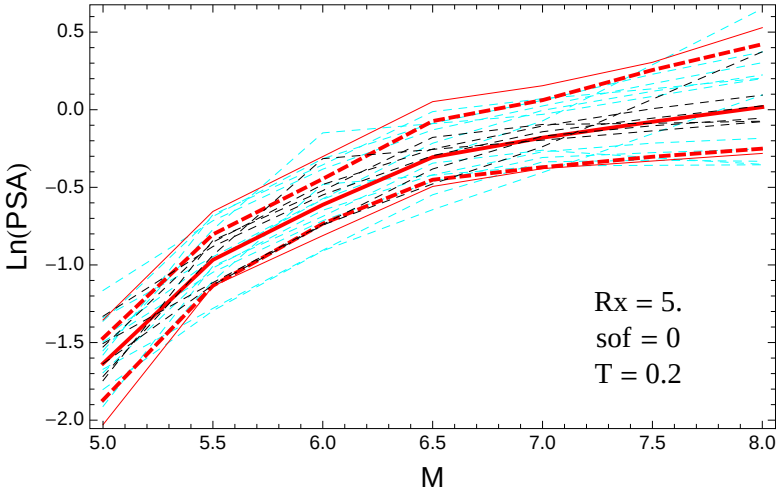



Figure 5.111: PVNGSv2: Magnitude scaling of the original GMPEs (dashed black), the original GMPEs with uncertainty model (dashed cyan) and 0.05,0.5,0.95 quantile of the combined ModelA and ModelB distribution (red) with total weights, for a scenario with $R_X = 5.$, $F = 0$, and $T = 0.2$s.

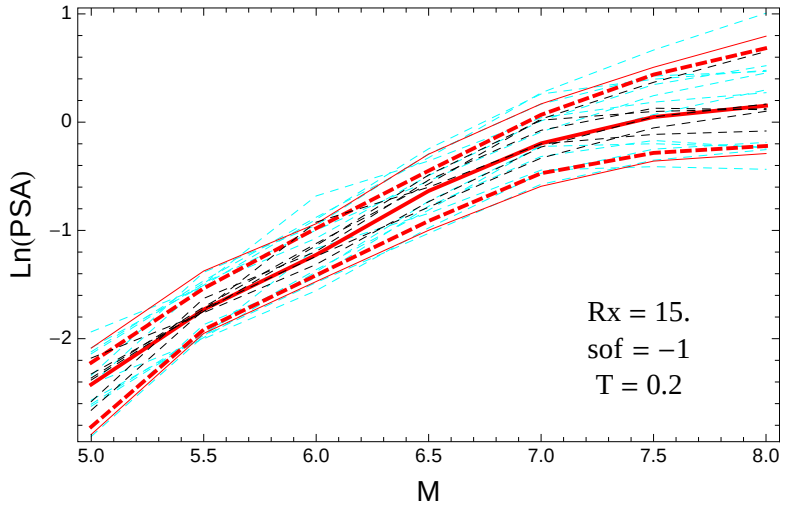



Figure 5.112: PVNGSv2: Magnitude scaling of the original GMPEs (dashed black), the original GMPEs with uncertainty model (dashed cyan) and 0.05,0.5,0.95 quantile of the combined ModelA and ModelB distribution (red) with total weights, for a scenario with $R_X = 15.$, $F = -1$, and $T = 0.2$s.

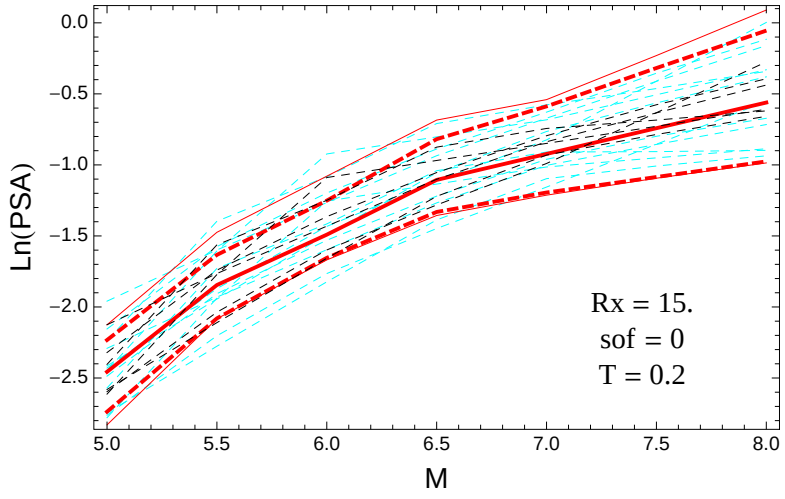



Figure 5.113: PVNGSv2: Magnitude scaling of the original GMPEs (dashed black), the original GMPEs with uncertainty model (dashed cyan) and 0.05,0.5,0.95 quantile of the combined ModelA and ModelB distribution (red) with total weights, for a scenario with $R_X = 15.$, $F = 0$, and $T = 0.2$s.

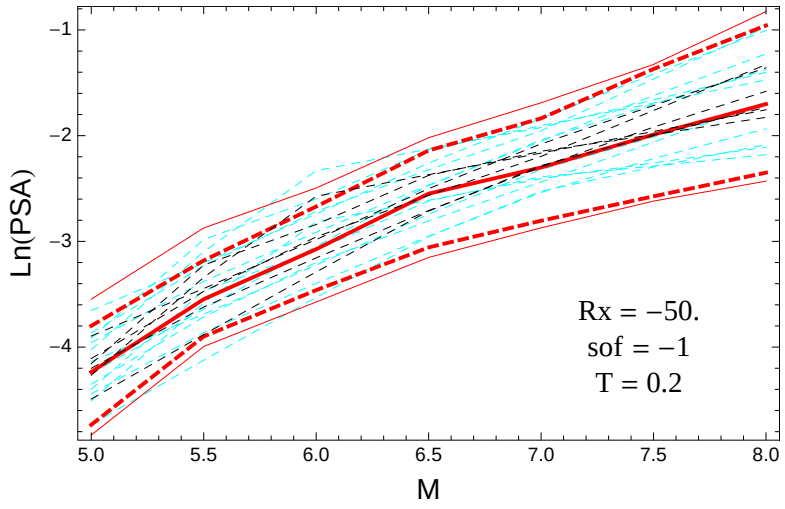



Figure 5.114: PVNGSv2: Magnitude scaling of the original GMPEs (dashed black), the original GMPEs with uncertainty model (dashed cyan) and 0.05,0.5,0.95 quantile of the combined ModelA and ModelB distribution (red) with total weights, for a scenario with $R_X = -50.$, $F = -1$, and $T = 0.2$s.

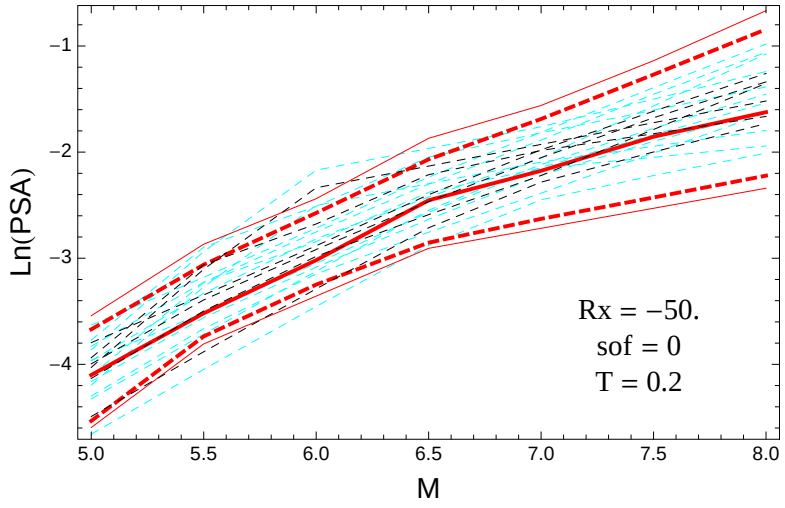



Figure 5.115: PVNGSv2: Magnitude scaling of the original GMPEs (dashed black), the original GMPEs with uncertainty model (dashed cyan) and 0.05,0.5,0.95 quantile of the combined ModelA and ModelB distribution (red) with total weights, for a scenario with $R_X = -50.$, $F = 0$, and $T = 0.2$s.

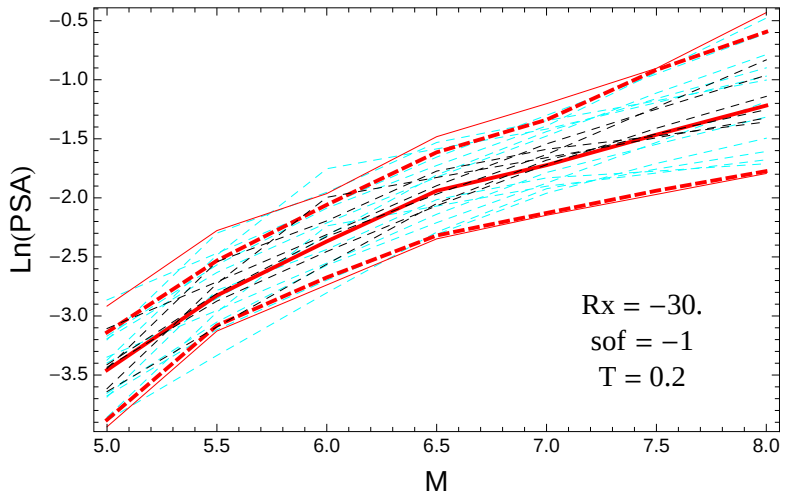



Figure 5.116: PVNGSv2: Magnitude scaling of the original GMPEs (dashed black), the original GMPEs with uncertainty model (dashed cyan) and 0.05,0.5,0.95 quantile of the combined ModelA and ModelB distribution (red) with total weights, for a scenario with $R_X = -30.$, $F = -1$, and $T = 0.2$s.

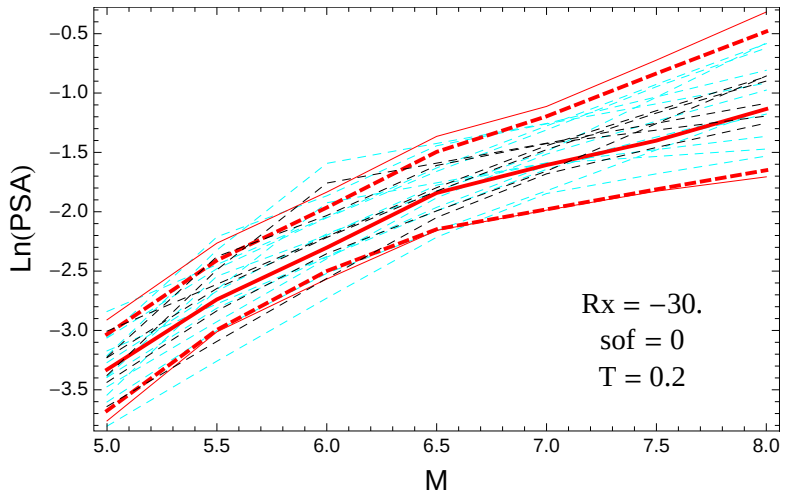



Figure 5.117: PVNGSv2: Magnitude scaling of the original GMPEs (dashed black), the original GMPEs with uncertainty model (dashed cyan) and 0.05,0.5,0.95 quantile of the combined ModelA and ModelB distribution (red) with total weights, for a scenario with $R_X = -30.$, $F = 0$, and $T = 0.2$s.

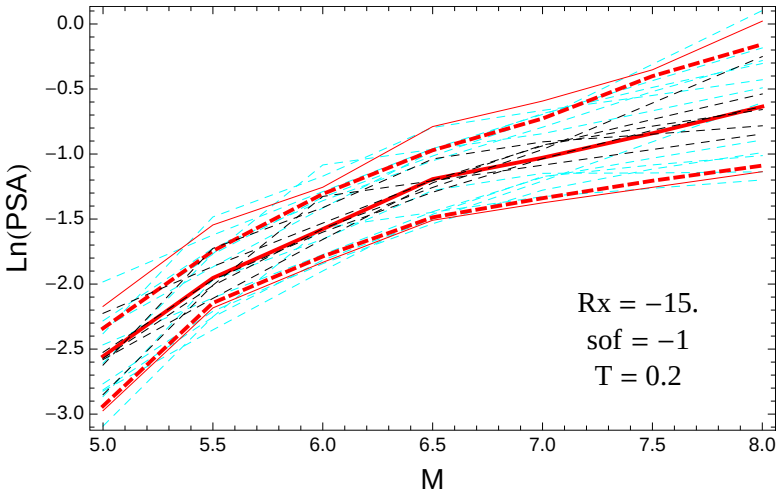



Figure 5.118: PVNGSv2: Magnitude scaling of the original GMPEs (dashed black), the original GMPEs with uncertainty model (dashed cyan) and 0.05,0.5,0.95 quantile of the combined ModelA and ModelB distribution (red) with total weights, for a scenario with $R_X = -15.$, $F = -1$, and $T = 0.2$s.

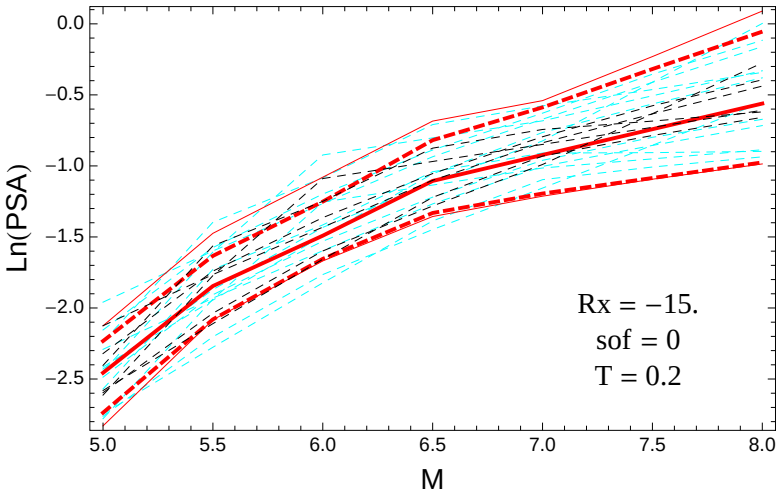



Figure 5.119: PVNGSv2: Magnitude scaling of the original GMPEs (dashed black), the original GMPEs with uncertainty model (dashed cyan) and 0.05,0.5,0.95 quantile of the combined ModelA and ModelB distribution (red) with total weights, for a scenario with $R_X = -15.$, $F = 0$, and $T = 0.2$s.

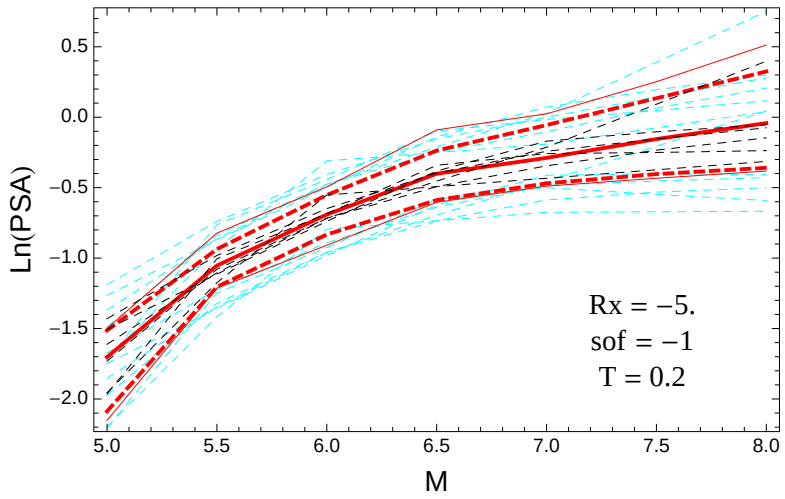



Figure 5.120: PVNGSv2: Magnitude scaling of the original GMPEs (dashed black), the original GMPEs with uncertainty model (dashed cyan) and 0.05,0.5,0.95 quantile of the combined ModelA and ModelB distribution (red) with total weights, for a scenario with $R_X = -5.$, $F = -1$, and $T = 0.2$s.

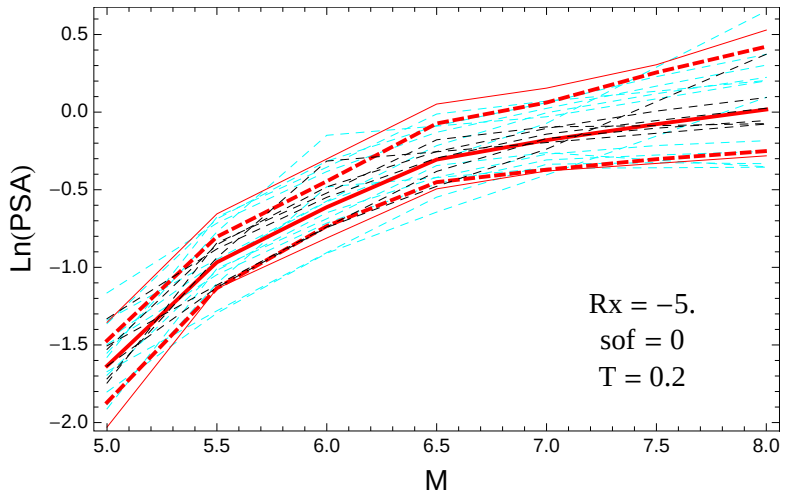



Figure 5.121: PVNGSv2: Magnitude scaling of the original GMPEs (dashed black), the original GMPEs with uncertainty model (dashed cyan) and 0.05,0.5,0.95 quantile of the combined ModelA and ModelB distribution (red) with total weights, for a scenario with $R_X = -5.$, $F = 0$, and $T = 0.2$s.

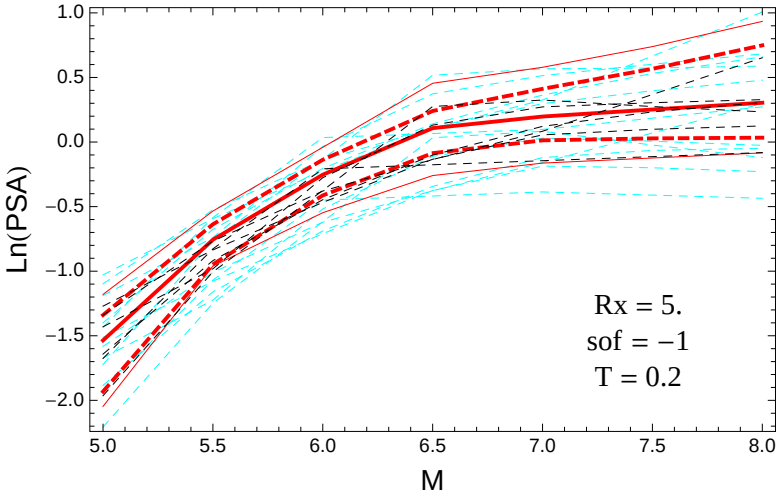



Figure 5.122: PVNGSv2: Magnitude scaling of the original GMPEs (dashed black), the original GMPEs with uncertainty model (dashed cyan) and 0.05,0.5,0.95 quantile of the combined ModelA and ModelB distribution (red) with total weights, for a scenario with $R_X = 5.$, $F = -1$, and $T = 0.2$s.

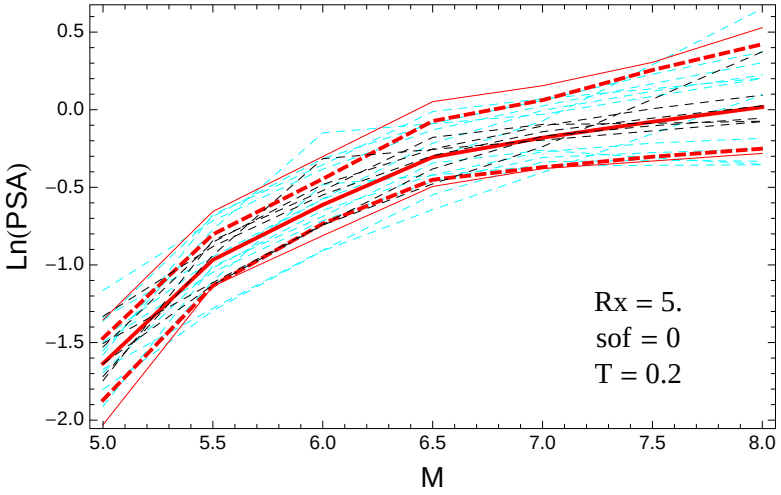



Figure 5.123: PVNGSv2: Magnitude scaling of the original GMPEs (dashed black), the original GMPEs with uncertainty model (dashed cyan) and 0.05,0.5,0.95 quantile of the combined ModelA and ModelB distribution (red) with total weights, for a scenario with $R_X = 5.$, $F = 0$, and $T = 0.2$s.

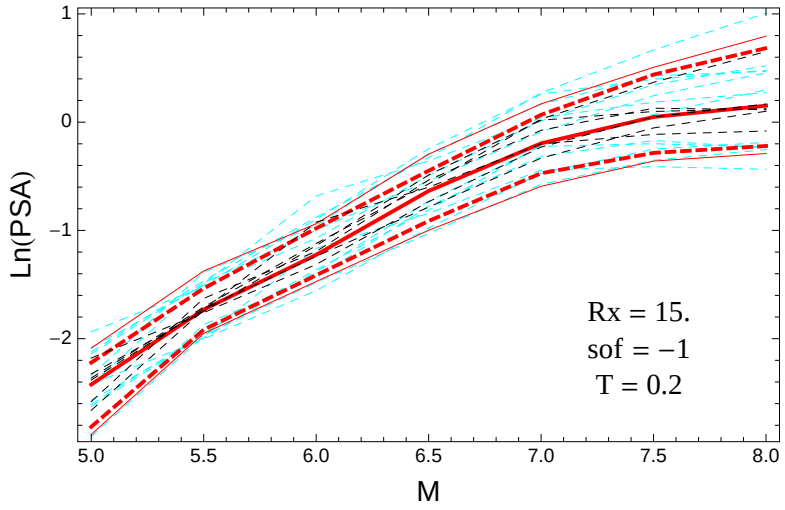



Figure 5.124: PVNGSv2: Magnitude scaling of the original GMPEs (dashed black), the original GMPEs with uncertainty model (dashed cyan) and 0.05,0.5,0.95 quantile of the combined ModelA and ModelB distribution (red) with total weights, for a scenario with $R_X = 15.$, $F = -1$, and $T = 0.2$s.

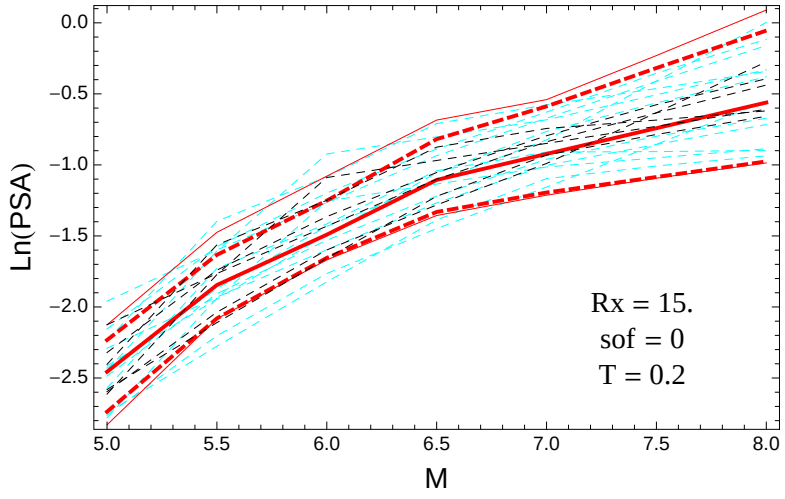



Figure 5.125: PVNGSv2: Magnitude scaling of the original GMPEs (dashed black), the original GMPEs with uncertainty model (dashed cyan) and 0.05,0.5,0.95 quantile of the combined ModelA and ModelB distribution (red) with total weights, for a scenario with $R_X = 15.$, $F = 0$, and $T = 0.2$s.

**T = 0.5s**

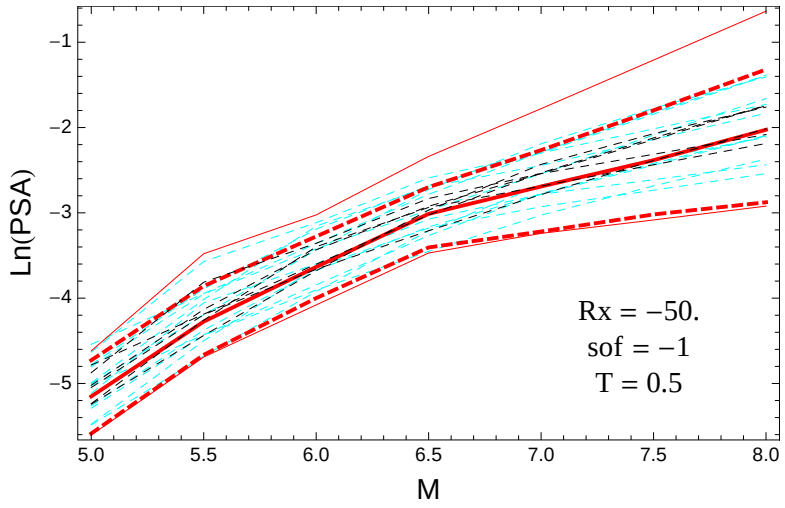



Figure 5.126: PVNGSv2: Magnitude scaling of the original GMPEs (dashed black), the original GMPEs with uncertainty model (dashed cyan) and 0.05,0.5,0.95 quantile of the combined ModelA and ModelB distribution (red) with total weights, for a scenario with $R_X = -50.$, $F = -1$, and $T = 0.5$s.

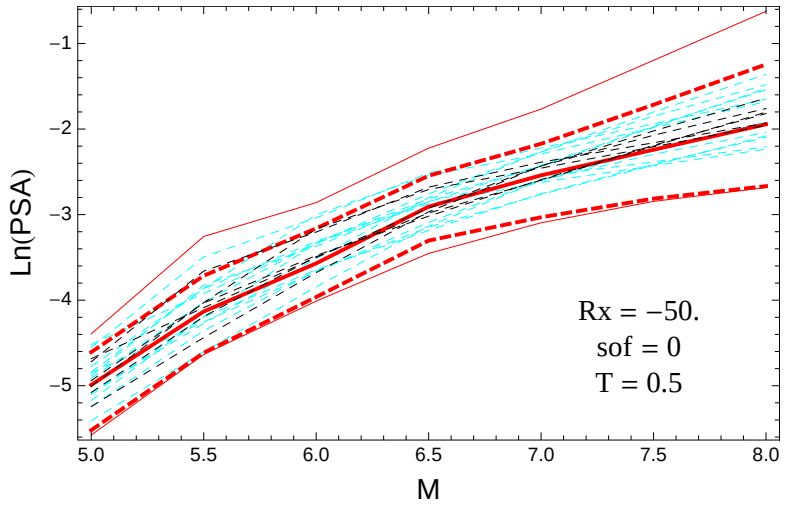



Figure 5.127: PVNGSv2: Magnitude scaling of the original GMPEs (dashed black), the original GMPEs with uncertainty model (dashed cyan) and 0.05,0.5,0.95 quantile of the combined ModelA and ModelB distribution (red) with total weights, for a scenario with $R_X = -50.$, $F = 0$, and $T = 0.5$s.

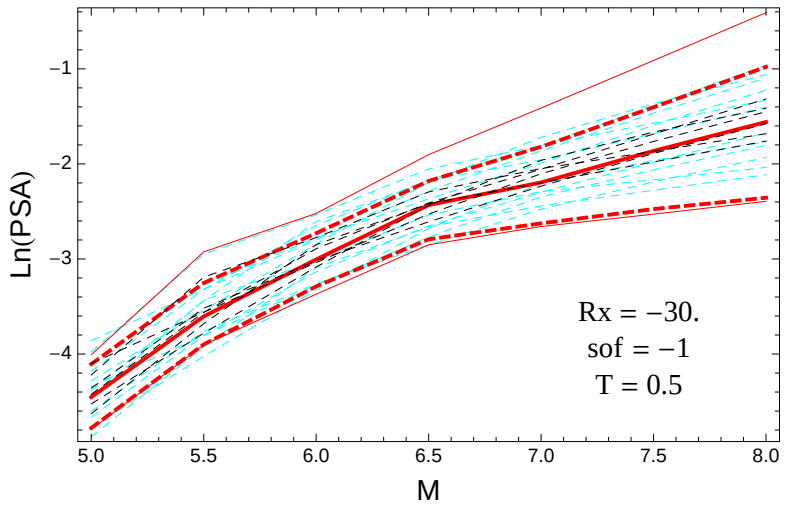



Figure 5.128: PVNGSv2: Magnitude scaling of the original GMPEs (dashed black), the original GMPEs with uncertainty model (dashed cyan) and 0.05,0.5,0.95 quantile of the combined ModelA and ModelB distribution (red) with total weights, for a scenario with $R_X = -30.$, $F = -1$, and $T = 0.5$s.

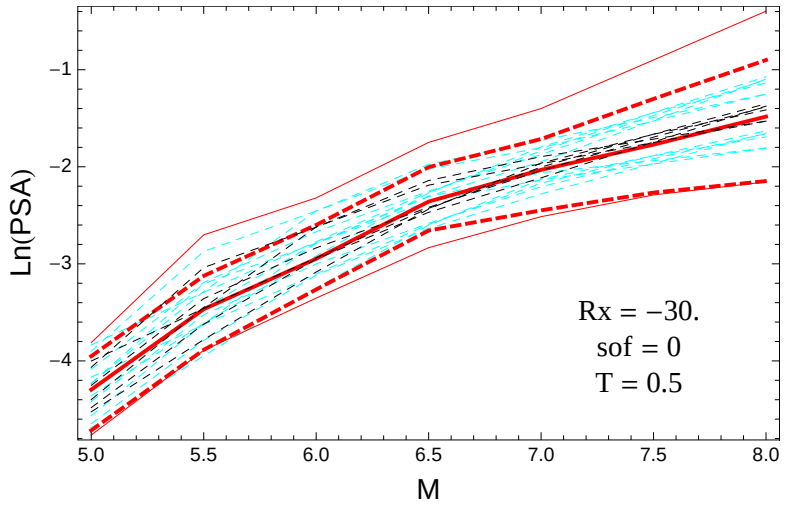



Figure 5.129: PVNGSv2: Magnitude scaling of the original GMPEs (dashed black), the original GMPEs with uncertainty model (dashed cyan) and 0.05,0.5,0.95 quantile of the combined ModelA and ModelB distribution (red) with total weights, for a scenario with $R_X = -30.$, $F = 0$, and $T = 0.5$s.

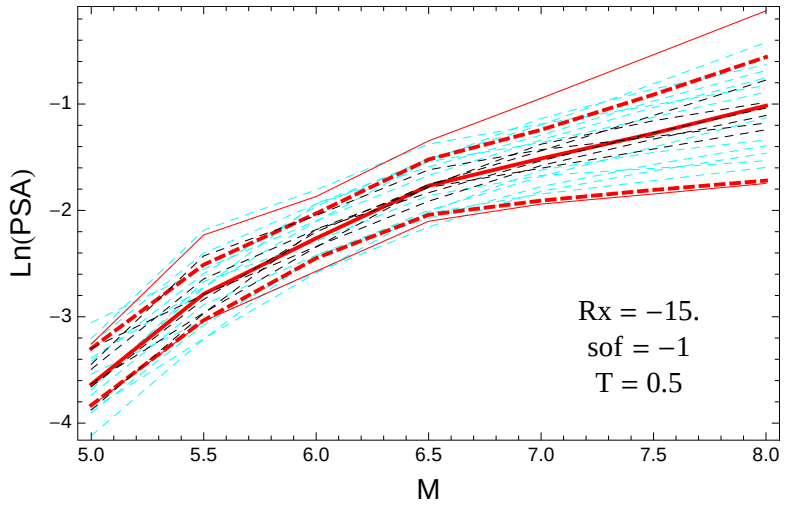



Figure 5.130: PVNGSv2: Magnitude scaling of the original GMPEs (dashed black), the original GMPEs with uncertainty model (dashed cyan) and 0.05,0.5,0.95 quantile of the combined ModelA and ModelB distribution (red) with total weights, for a scenario with $R_X = -15.$, $F = -1$, and $T = 0.5$s.

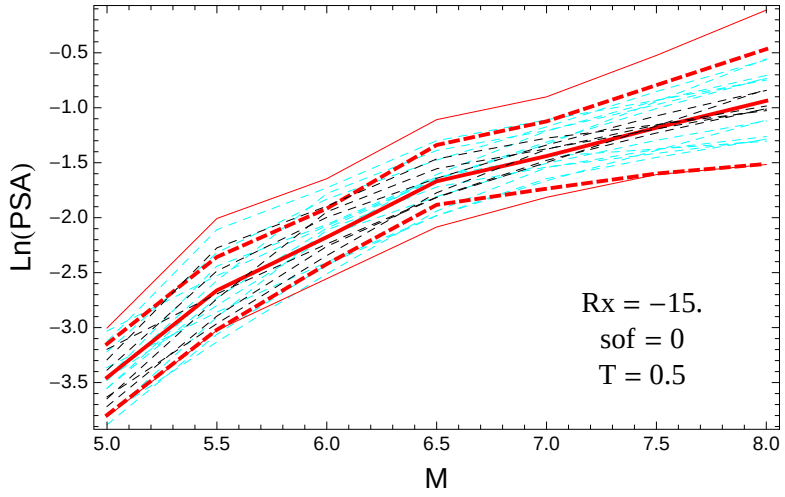



Figure 5.131: PVNGSv2: Magnitude scaling of the original GMPEs (dashed black), the original GMPEs with uncertainty model (dashed cyan) and 0.05,0.5,0.95 quantile of the combined ModelA and ModelB distribution (red) with total weights, for a scenario with $R_X = -15.$, $F = 0$, and $T = 0.5$s.

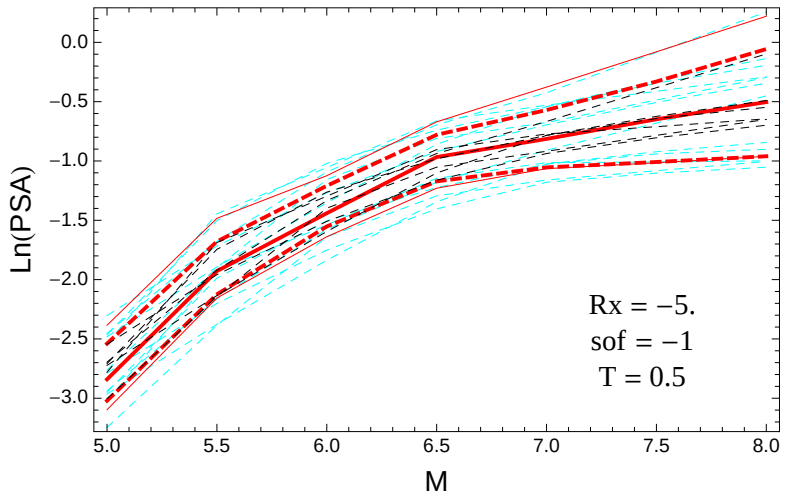



Figure 5.132: PVNGSv2: Magnitude scaling of the original GMPEs (dashed black), the original GMPEs with uncertainty model (dashed cyan) and 0.05,0.5,0.95 quantile of the combined ModelA and ModelB distribution (red) with total weights, for a scenario with $R_X = -5.$, $F = -1$, and $T = 0.5$s.

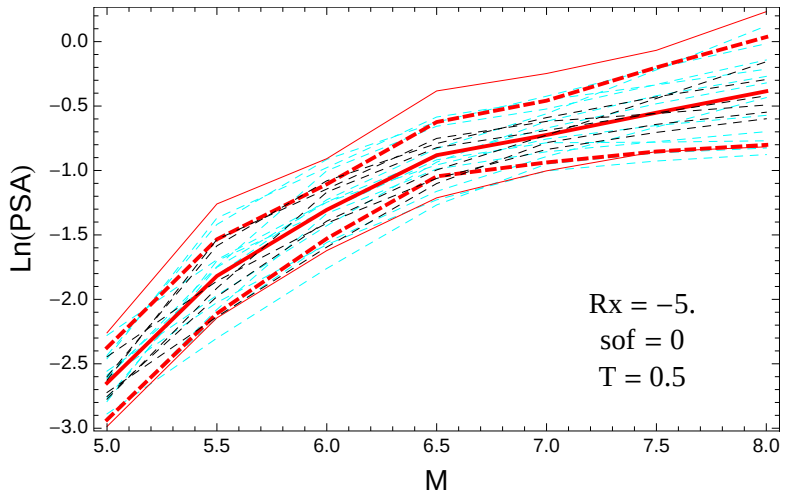



Figure 5.133: PVNGSv2: Magnitude scaling of the original GMPEs (dashed black), the original GMPEs with uncertainty model (dashed cyan) and 0.05,0.5,0.95 quantile of the combined ModelA and ModelB distribution (red) with total weights, for a scenario with $R_X = -5.$, $F = 0$, and $T = 0.5$s.

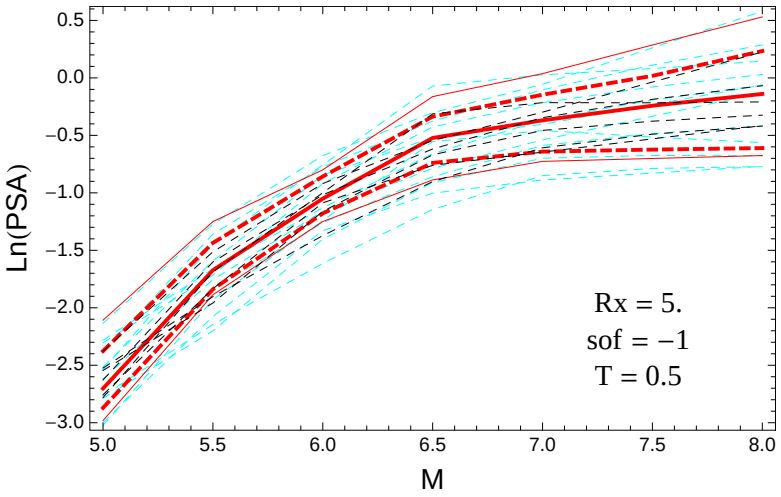



Figure 5.134: PVNGSv2: Magnitude scaling of the original GMPEs (dashed black), the original GMPEs with uncertainty model (dashed cyan) and 0.05,0.5,0.95 quantile of the combined ModelA and ModelB distribution (red) with total weights, for a scenario with $R_X = 5.$, $F = -1$, and $T = 0.5$s.

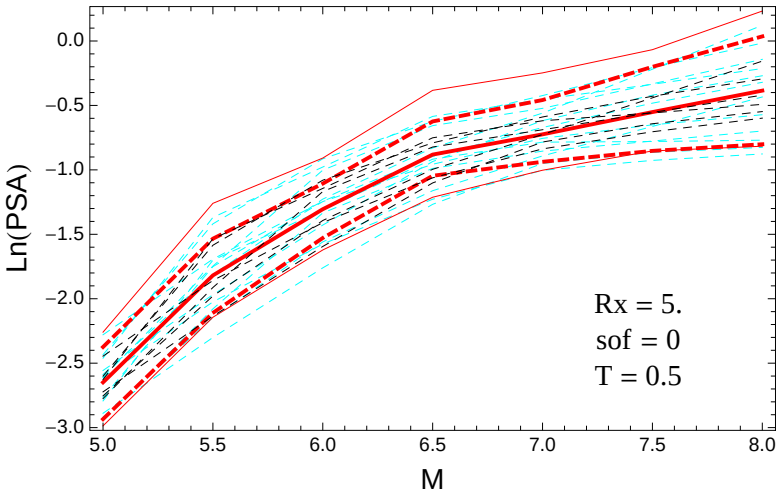



Figure 5.135: PVNGSv2: Magnitude scaling of the original GMPEs (dashed black), the original GMPEs with uncertainty model (dashed cyan) and 0.05,0.5,0.95 quantile of the combined ModelA and ModelB distribution (red) with total weights, for a scenario with $R_X = 5.$, $F = 0$, and $T = 0.5$s.

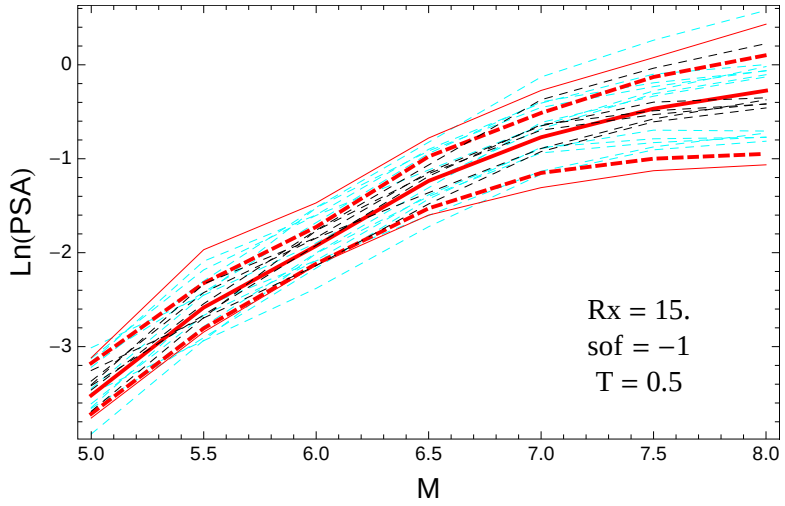



Figure 5.136: PVNGSv2: Magnitude scaling of the original GMPEs (dashed black), the original GMPEs with uncertainty model (dashed cyan) and 0.05,0.5,0.95 quantile of the combined ModelA and ModelB distribution (red) with total weights, for a scenario with $R_X = 15.$, $F = -1$, and $T = 0.5$s.

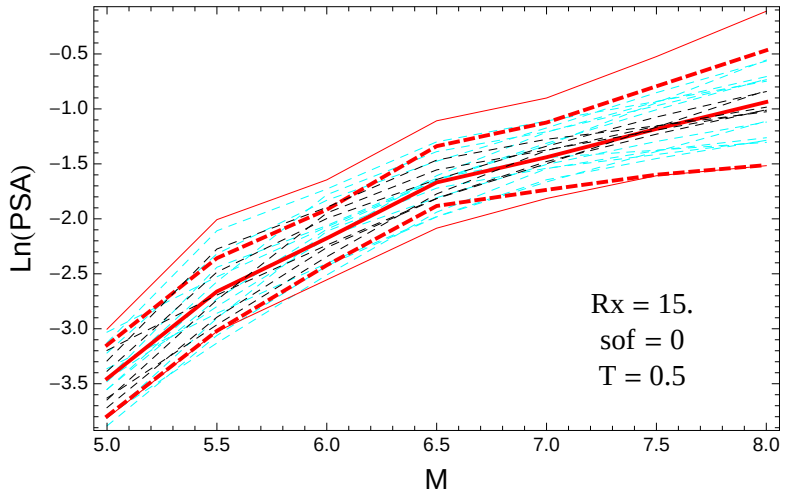



Figure 5.137: PVNGSv2: Magnitude scaling of the original GMPEs (dashed black), the original GMPEs with uncertainty model (dashed cyan) and 0.05,0.5,0.95 quantile of the combined ModelA and ModelB distribution (red) with total weights, for a scenario with $R_X = 15.$, $F = 0$, and $T = 0.5$s.

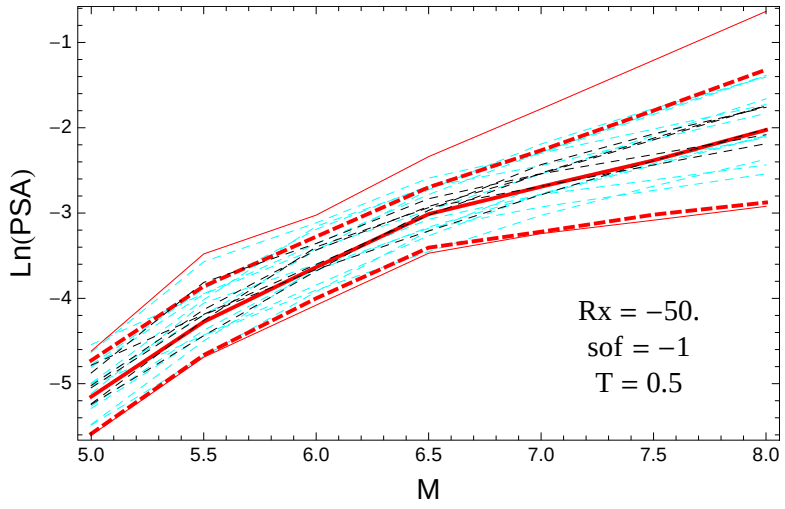



Figure 5.138: PVNGSv2: Magnitude scaling of the original GMPEs (dashed black), the original GMPEs with uncertainty model (dashed cyan) and 0.05,0.5,0.95 quantile of the combined ModelA and ModelB distribution (red) with total weights, for a scenario with $R_X = -50.$, $F = -1$, and $T = 0.5$s.

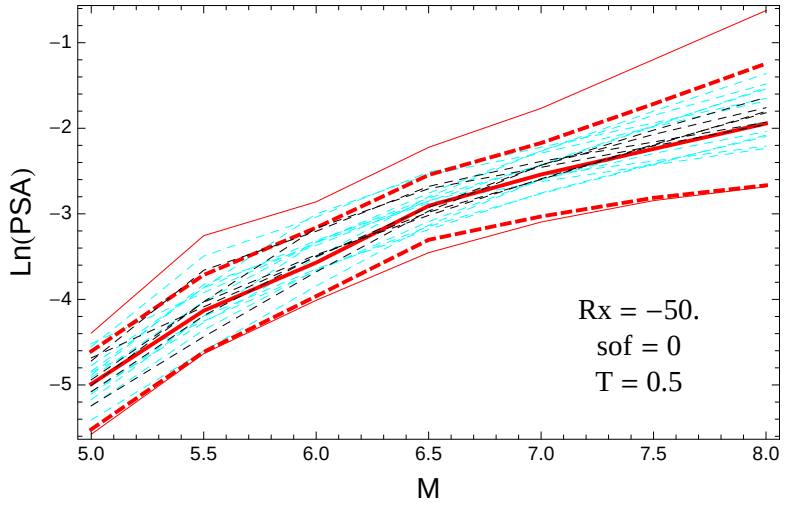



Figure 5.139: PVNGSv2: Magnitude scaling of the original GMPEs (dashed black), the original GMPEs with uncertainty model (dashed cyan) and 0.05,0.5,0.95 quantile of the combined ModelA and ModelB distribution (red) with total weights, for a scenario with $R_X = -50.$, $F = 0$, and $T = 0.5$s.

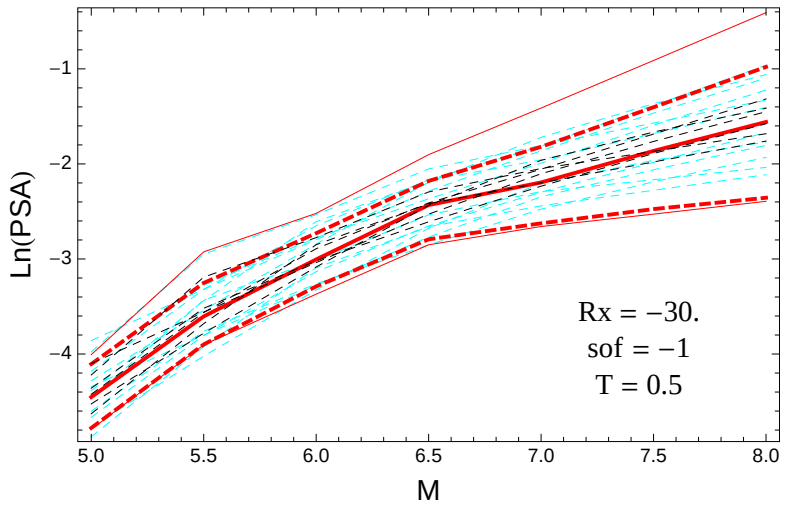



Figure 5.140: PVNGSv2: Magnitude scaling of the original GMPEs (dashed black), the original GMPEs with uncertainty model (dashed cyan) and 0.05,0.5,0.95 quantile of the combined ModelA and ModelB distribution (red) with total weights, for a scenario with $R_X = -30.$, $F = -1$, and $T = 0.5$s.

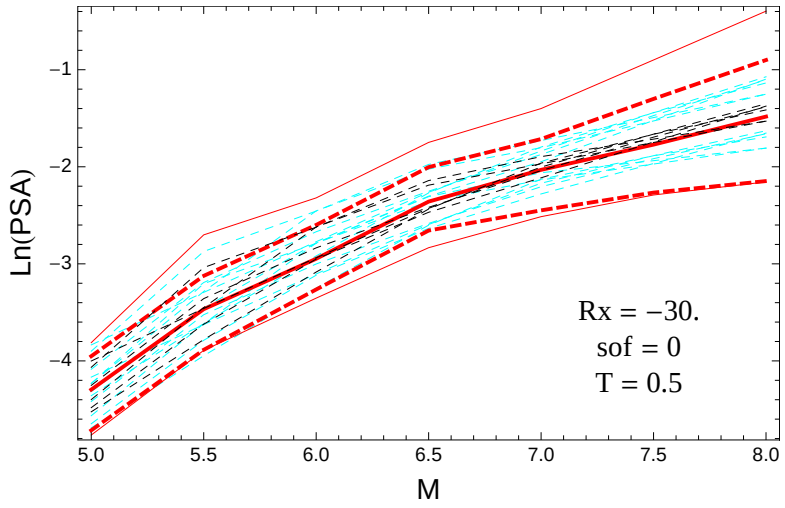



Figure 5.141: PVNGSv2: Magnitude scaling of the original GMPEs (dashed black), the original GMPEs with uncertainty model (dashed cyan) and 0.05,0.5,0.95 quantile of the combined ModelA and ModelB distribution (red) with total weights, for a scenario with $R_X = -30.$, $F = 0$, and $T = 0.5$s.

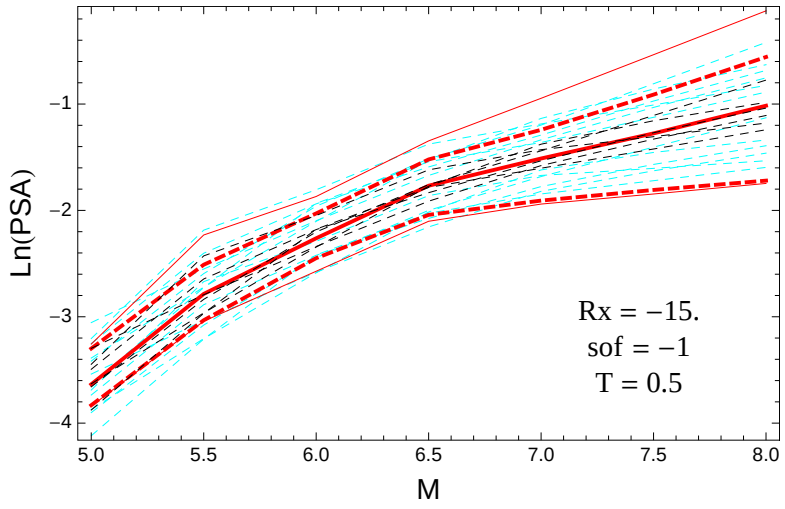



Figure 5.142: PVNGSv2: Magnitude scaling of the original GMPEs (dashed black), the original GMPEs with uncertainty model (dashed cyan) and 0.05,0.5,0.95 quantile of the combined ModelA and ModelB distribution (red) with total weights, for a scenario with $R_X = -15.$, $F = -1$, and $T = 0.5$s.

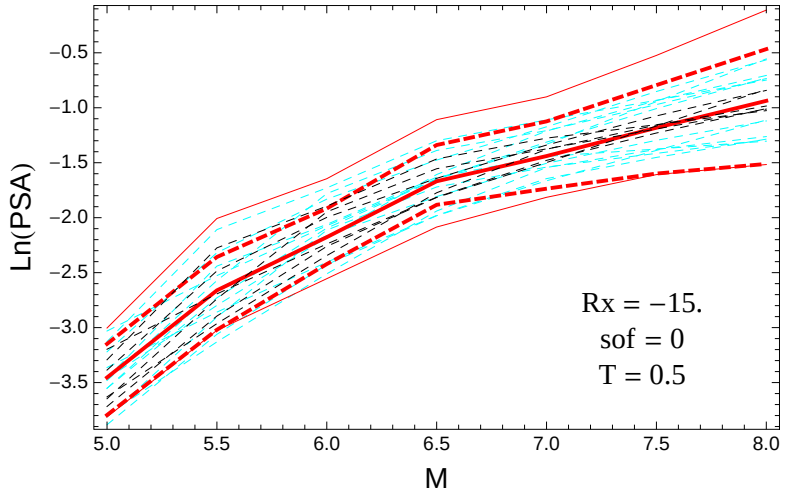



Figure 5.143: PVNGSv2: Magnitude scaling of the original GMPEs (dashed black), the original GMPEs with uncertainty model (dashed cyan) and 0.05,0.5,0.95 quantile of the combined ModelA and ModelB distribution (red) with total weights, for a scenario with $R_X = -15.$, $F = 0$, and $T = 0.5$s.

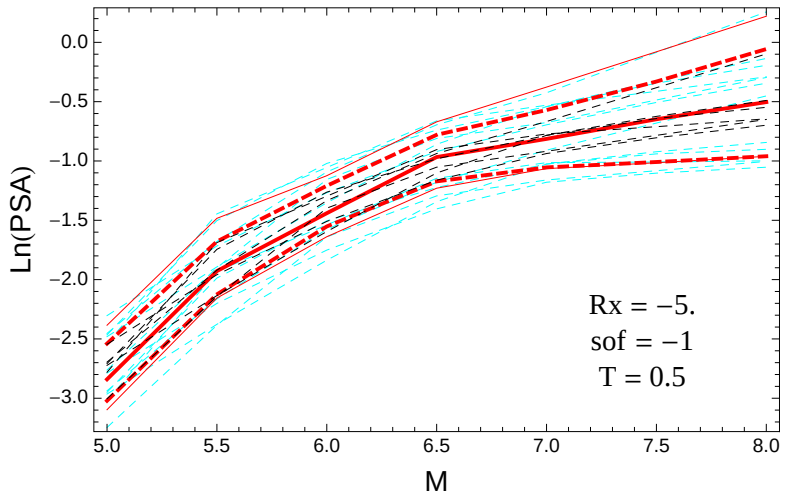



Figure 5.144: PVNGSv2: Magnitude scaling of the original GMPEs (dashed black), the original GMPEs with uncertainty model (dashed cyan) and 0.05,0.5,0.95 quantile of the combined ModelA and ModelB distribution (red) with total weights, for a scenario with $R_X = -5.$, $F = -1$, and $T = 0.5$s.

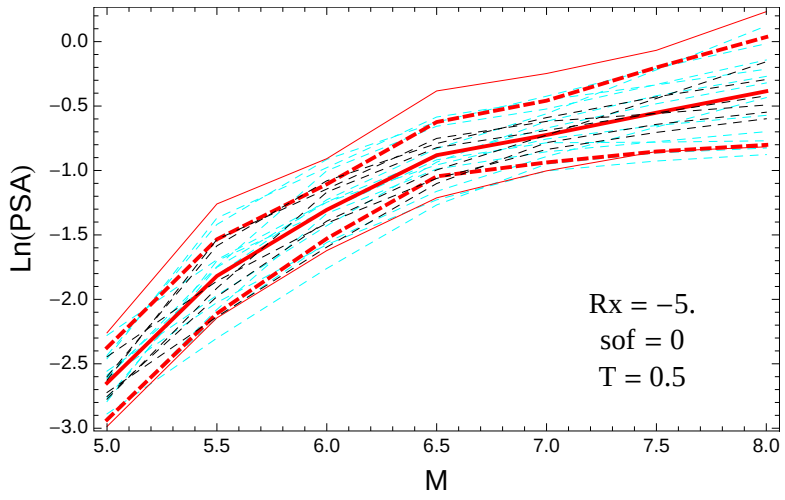



Figure 5.145: PVNGSv2: Magnitude scaling of the original GMPEs (dashed black), the original GMPEs with uncertainty model (dashed cyan) and 0.05,0.5,0.95 quantile of the combined ModelA and ModelB distribution (red) with total weights, for a scenario with $R_X = -5.$, $F = 0$, and $T = 0.5$s.

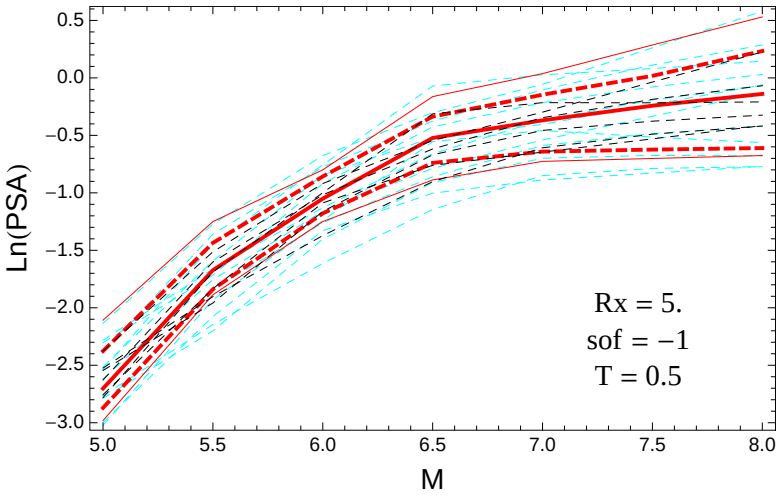



Figure 5.146: PVNGSv2: Magnitude scaling of the original GMPEs (dashed black), the original GMPEs with uncertainty model (dashed cyan) and 0.05,0.5,0.95 quantile of the combined ModelA and ModelB distribution (red) with total weights, for a scenario with $R_X = 5.$, $F = -1$, and $T = 0.5$s.

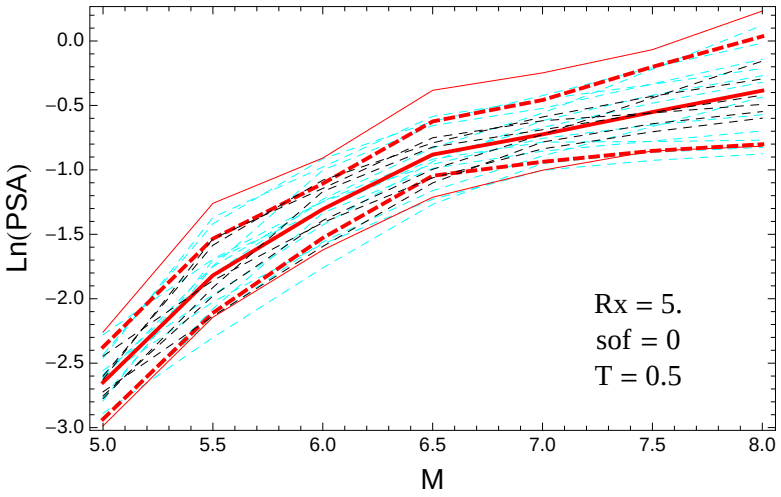



Figure 5.147: PVNGSv2: Magnitude scaling of the original GMPEs (dashed black), the original GMPEs with uncertainty model (dashed cyan) and 0.05,0.5,0.95 quantile of the combined ModelA and ModelB distribution (red) with total weights, for a scenario with $R_X = 5.$, $F = 0$, and $T = 0.5$s.

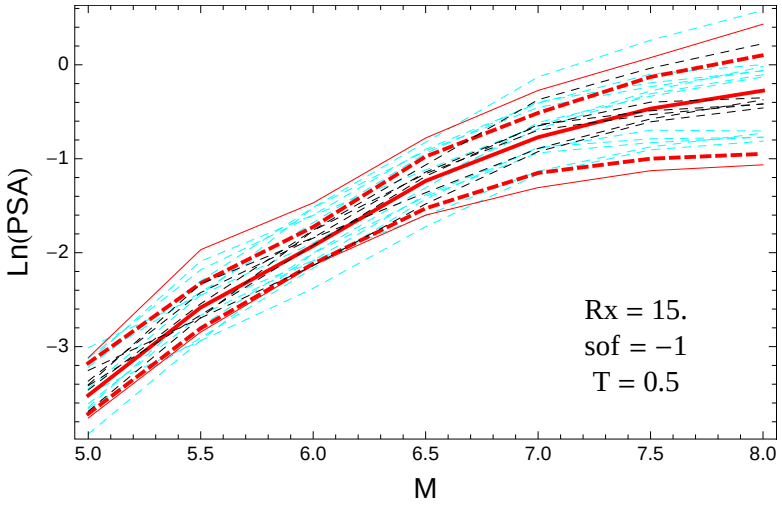



Figure 5.148: PVNGSv2: Magnitude scaling of the original GMPEs (dashed black), the original GMPEs with uncertainty model (dashed cyan) and 0.05,0.5,0.95 quantile of the combined ModelA and ModelB distribution (red) with total weights, for a scenario with $R_X = 15.$, $F = -1$, and $T = 0.5$s.

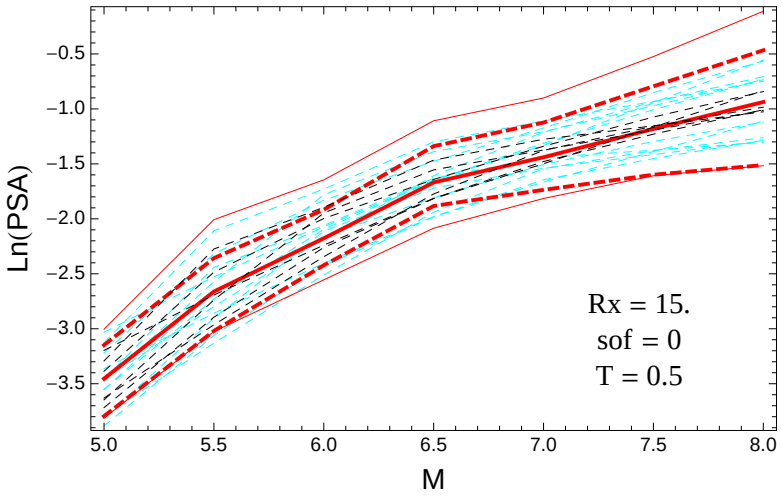



Figure 5.149: PVNGSv2: Magnitude scaling of the original GMPEs (dashed black), the original GMPEs with uncertainty model (dashed cyan) and 0.05,0.5,0.95 quantile of the combined ModelA and ModelB distribution (red) with total weights, for a scenario with $R_X = 15.$, $F = 0$, and $T = 0.5$s.

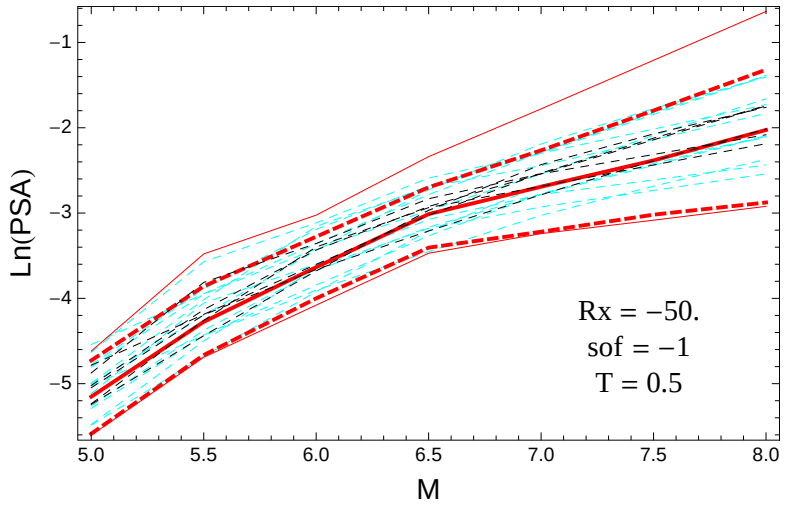



Figure 5.150: PVNGSv2: Magnitude scaling of the original GMPEs (dashed black), the original GMPEs with uncertainty model (dashed cyan) and 0.05,0.5,0.95 quantile of the combined ModelA and ModelB distribution (red) with total weights, for a scenario with $R_X = -50.$, $F = -1$, and $T = 0.5$s.

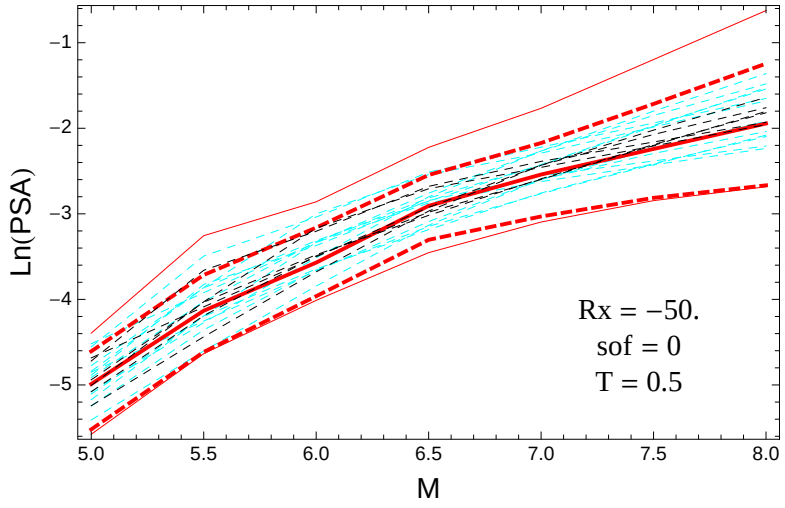



Figure 5.151: PVNGSv2: Magnitude scaling of the original GMPEs (dashed black), the original GMPEs with uncertainty model (dashed cyan) and 0.05,0.5,0.95 quantile of the combined ModelA and ModelB distribution (red) with total weights, for a scenario with $R_X = -50.$, $F = 0$, and $T = 0.5$s.

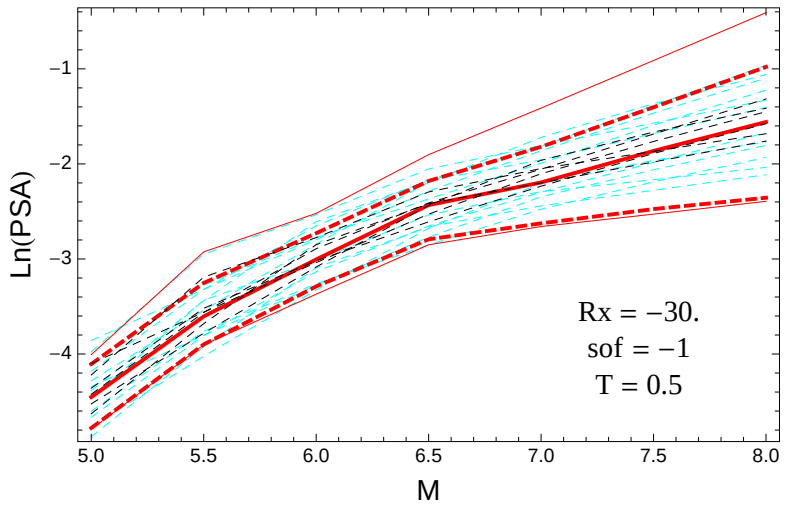



Figure 5.152: PVNGSv2: Magnitude scaling of the original GMPEs (dashed black), the original GMPEs with uncertainty model (dashed cyan) and 0.05,0.5,0.95 quantile of the combined ModelA and ModelB distribution (red) with total weights, for a scenario with $R_X = -30.$, $F = -1$, and $T = 0.5$s.

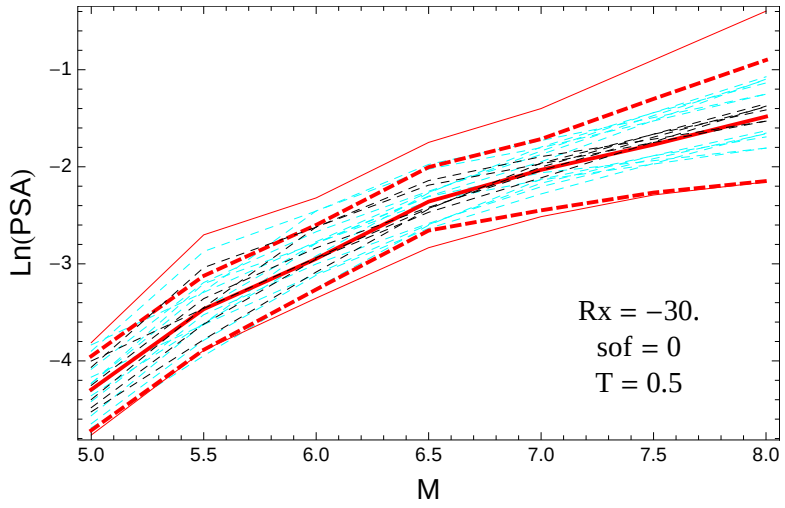



Figure 5.153: PVNGSv2: Magnitude scaling of the original GMPEs (dashed black), the original GMPEs with uncertainty model (dashed cyan) and 0.05,0.5,0.95 quantile of the combined ModelA and ModelB distribution (red) with total weights, for a scenario with $R_X = -30.$, $F = 0$, and $T = 0.5$s.

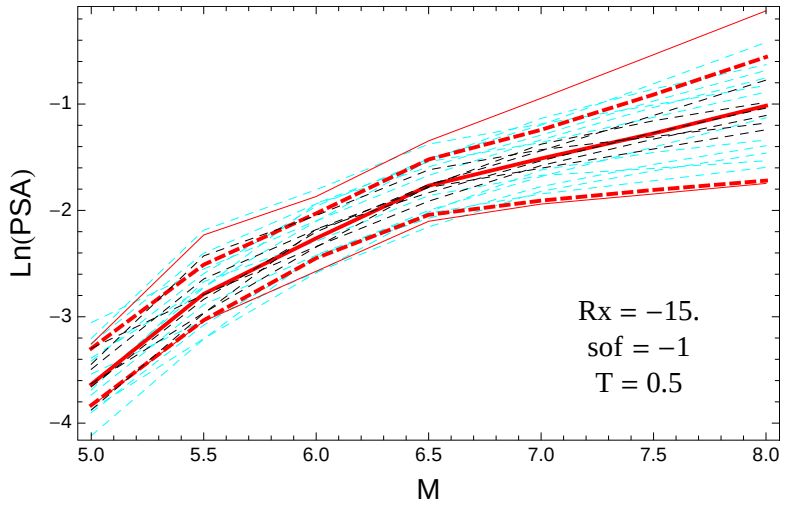



Figure 5.154: PVNGSv2: Magnitude scaling of the original GMPEs (dashed black), the original GMPEs with uncertainty model (dashed cyan) and 0.05,0.5,0.95 quantile of the combined ModelA and ModelB distribution (red) with total weights, for a scenario with $R_X = -15.$, $F = -1$, and $T = 0.5$s.

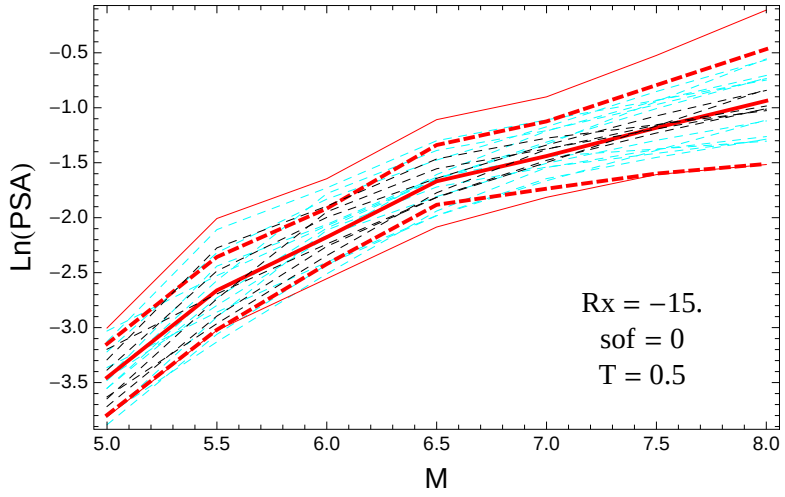



Figure 5.155: PVNGSv2: Magnitude scaling of the original GMPEs (dashed black), the original GMPEs with uncertainty model (dashed cyan) and 0.05,0.5,0.95 quantile of the combined ModelA and ModelB distribution (red) with total weights, for a scenario with $R_X = -15.$, $F = 0$, and $T = 0.5$s.

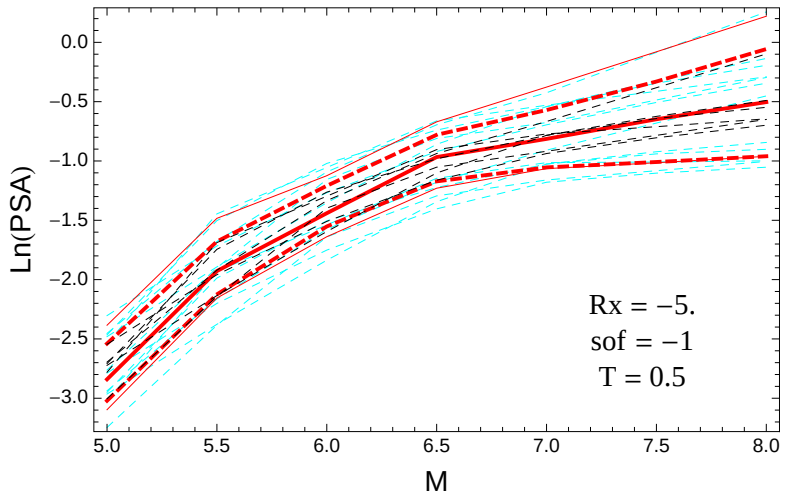



Figure 5.156: PVNGSv2: Magnitude scaling of the original GMPEs (dashed black), the original GMPEs with uncertainty model (dashed cyan) and 0.05,0.5,0.95 quantile of the combined ModelA and ModelB distribution (red) with total weights, for a scenario with $R_X = -5.$, $F = -1$, and $T = 0.5$s.

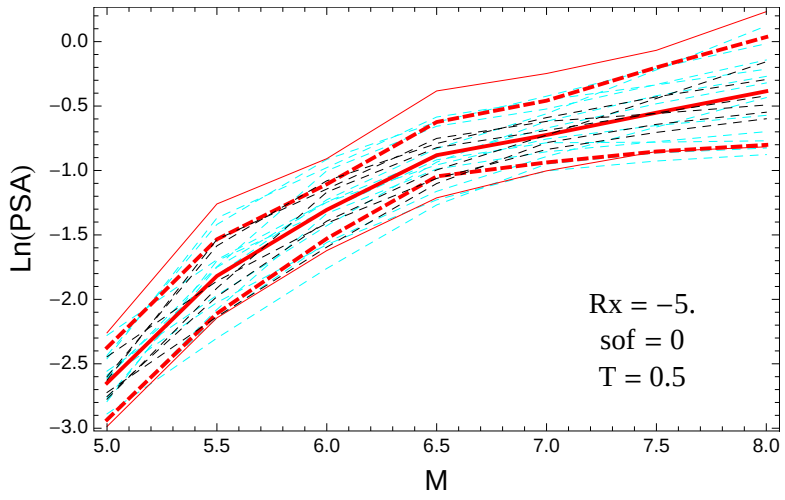



Figure 5.157: PVNGSv2: Magnitude scaling of the original GMPEs (dashed black), the original GMPEs with uncertainty model (dashed cyan) and 0.05,0.5,0.95 quantile of the combined ModelA and ModelB distribution (red) with total weights, for a scenario with $R_X = -5.$, $F = 0$, and $T = 0.5$s.

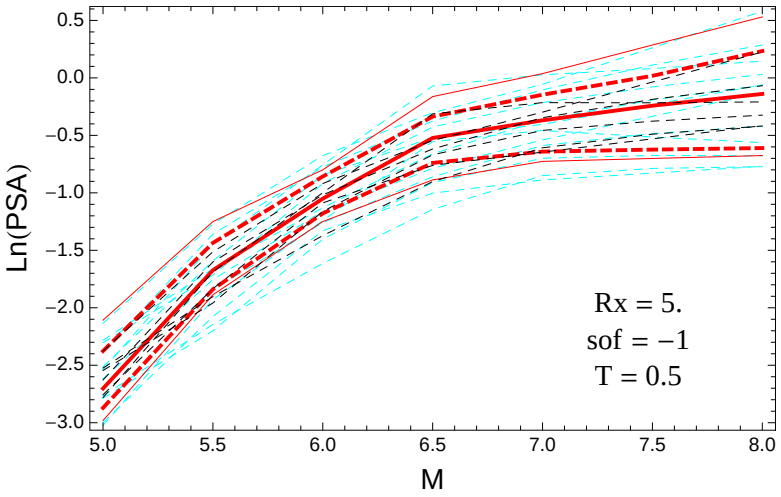



Figure 5.158: PVNGSv2: Magnitude scaling of the original GMPEs (dashed black), the original GMPEs with uncertainty model (dashed cyan) and 0.05,0.5,0.95 quantile of the combined ModelA and ModelB distribution (red) with total weights, for a scenario with $R_X = 5.$, $F = -1$, and $T = 0.5$s.

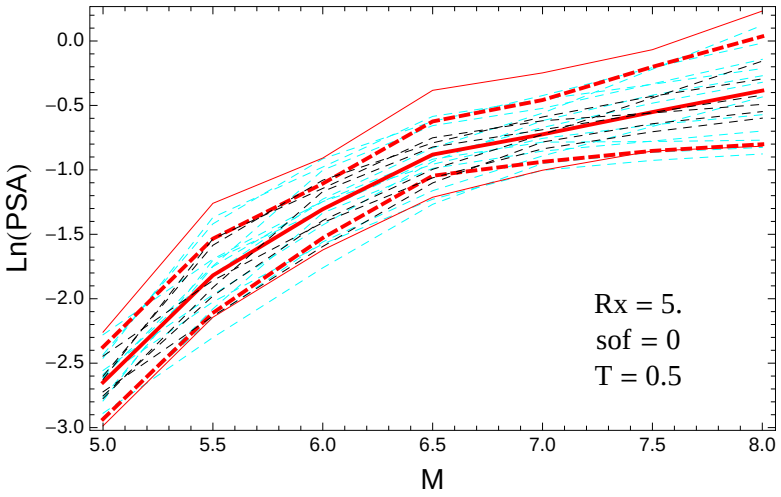



Figure 5.159: PVNGSv2: Magnitude scaling of the original GMPEs (dashed black), the original GMPEs with uncertainty model (dashed cyan) and 0.05,0.5,0.95 quantile of the combined ModelA and ModelB distribution (red) with total weights, for a scenario with $R_X = 5.$, $F = 0$, and $T = 0.5$s.

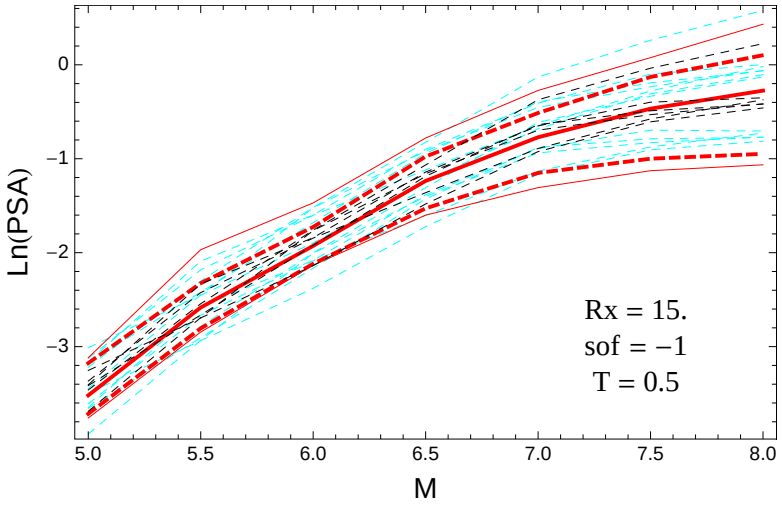



Figure 5.160: PVNGSv2: Magnitude scaling of the original GMPEs (dashed black), the original GMPEs with uncertainty model (dashed cyan) and 0.05,0.5,0.95 quantile of the combined ModelA and ModelB distribution (red) with total weights, for a scenario with $R_X = 15.$, $F = -1$, and $T = 0.5$s.

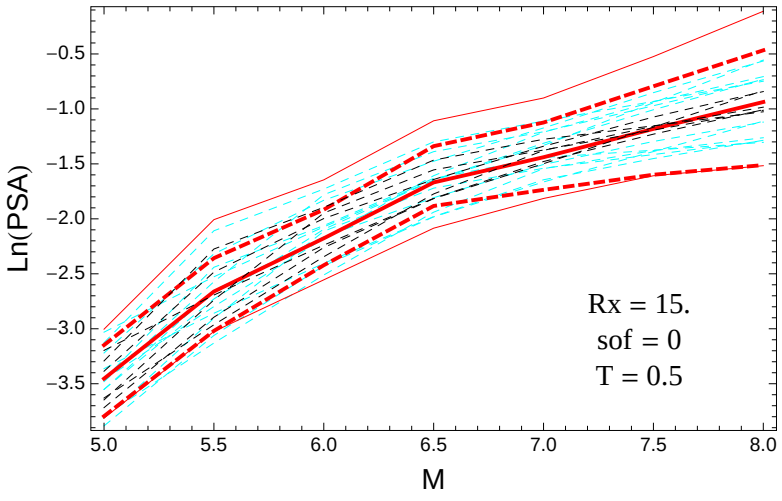



Figure 5.161: PVNGSv2: Magnitude scaling of the original GMPEs (dashed black), the original GMPEs with uncertainty model (dashed cyan) and 0.05,0.5,0.95 quantile of the combined ModelA and ModelB distribution (red) with total weights, for a scenario with $R_X = 15.$, $F = 0$, and $T = 0.5$s.

**T = 1.s**

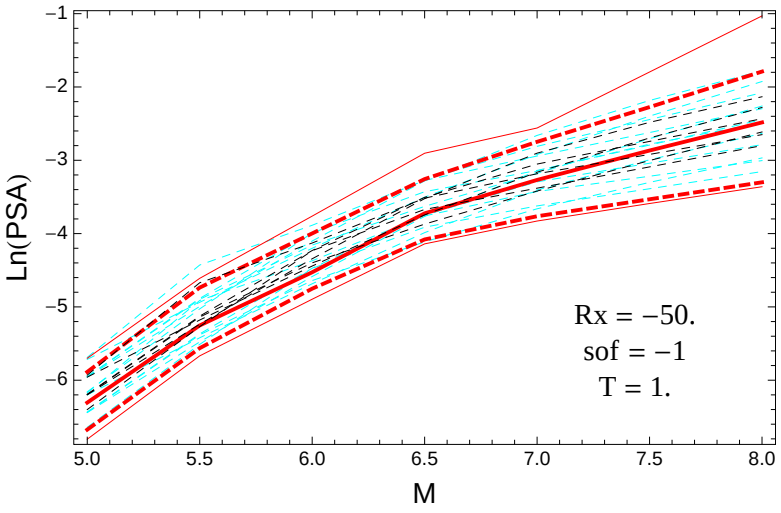



Figure 5.162: PVNGSv2: Magnitude scaling of the original GMPEs (dashed black), the original GMPEs with uncertainty model (dashed cyan) and 0.05,0.5,0.95 quantile of the combined ModelA and ModelB distribution (red) with total weights, for a scenario with $R_X = -50.$, $F = -1$, and $T = 1.$s.

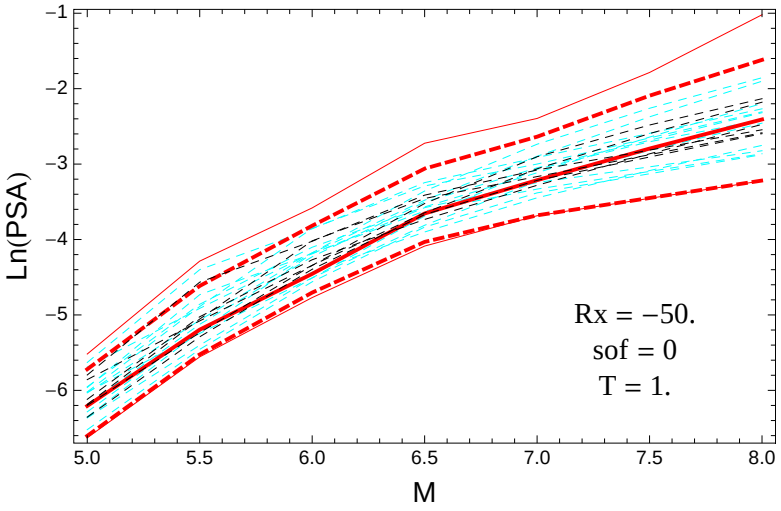



Figure 5.163: PVNGSv2: Magnitude scaling of the original GMPEs (dashed black), the original GMPEs with uncertainty model (dashed cyan) and 0.05,0.5,0.95 quantile of the combined ModelA and ModelB distribution (red) with total weights, for a scenario with $R_X = -50.$, $F = 0$, and $T = 1.$s.

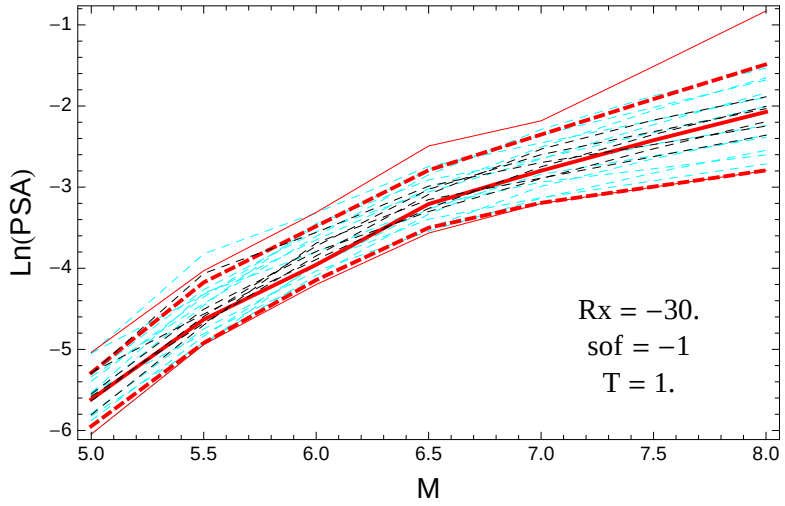



Figure 5.164: PVNGSv2: Magnitude scaling of the original GMPEs (dashed black), the original GMPEs with uncertainty model (dashed cyan) and 0.05,0.5,0.95 quantile of the combined ModelA and ModelB distribution (red) with total weights, for a scenario with $R_X = -30.$, $F = -1$, and $T = 1.$s.

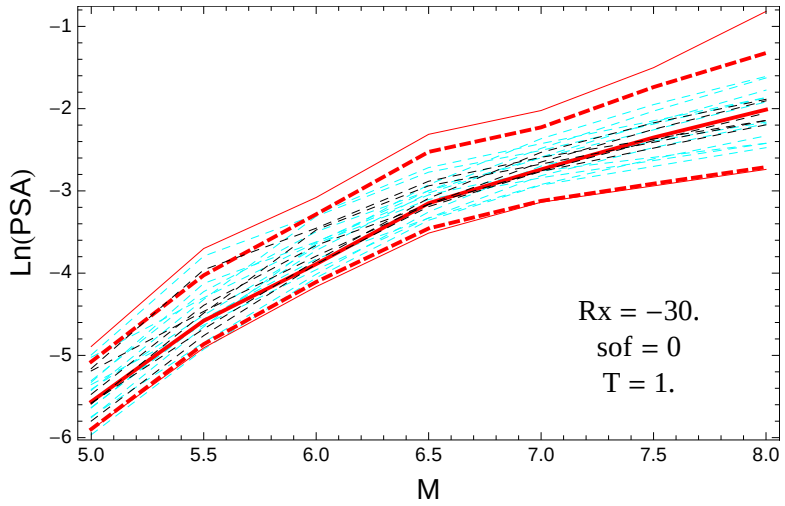



Figure 5.165: PVNGSv2: Magnitude scaling of the original GMPEs (dashed black), the original GMPEs with uncertainty model (dashed cyan) and 0.05,0.5,0.95 quantile of the combined ModelA and ModelB distribution (red) with total weights, for a scenario with $R_X = -30.$, $F = 0$, and $T = 1.$s.

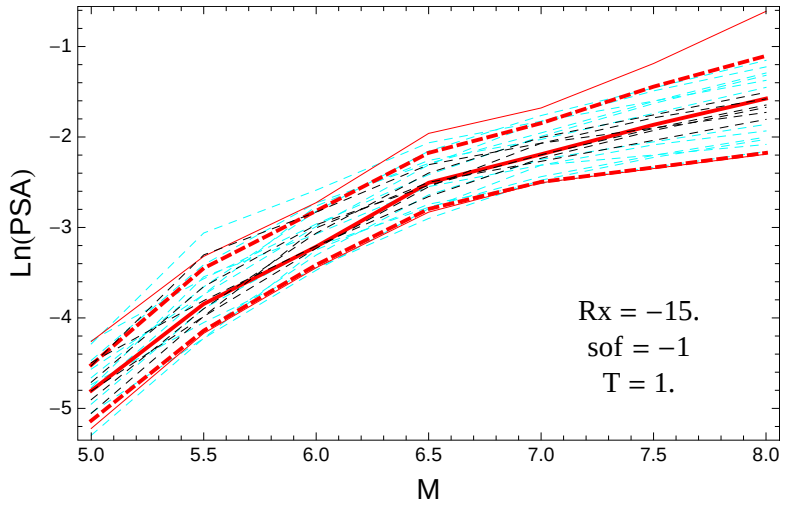



Figure 5.166: PVNGSv2: Magnitude scaling of the original GMPEs (dashed black), the original GMPEs with uncertainty model (dashed cyan) and 0.05,0.5,0.95 quantile of the combined ModelA and ModelB distribution (red) with total weights, for a scenario with $R_X = -15.$, $F = -1$, and $T = 1.$s.

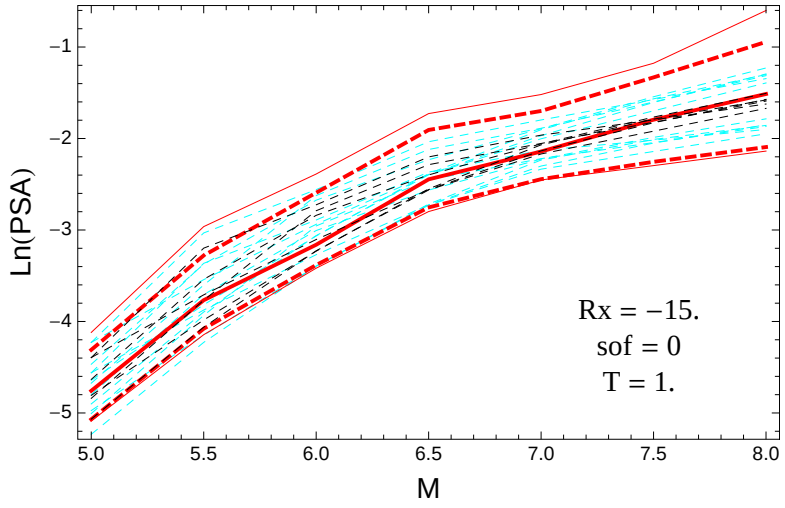



Figure 5.167: PVNGSv2: Magnitude scaling of the original GMPEs (dashed black), the original GMPEs with uncertainty model (dashed cyan) and 0.05,0.5,0.95 quantile of the combined ModelA and ModelB distribution (red) with total weights, for a scenario with $R_X = -15.$, $F = 0$, and $T = 1.$s.

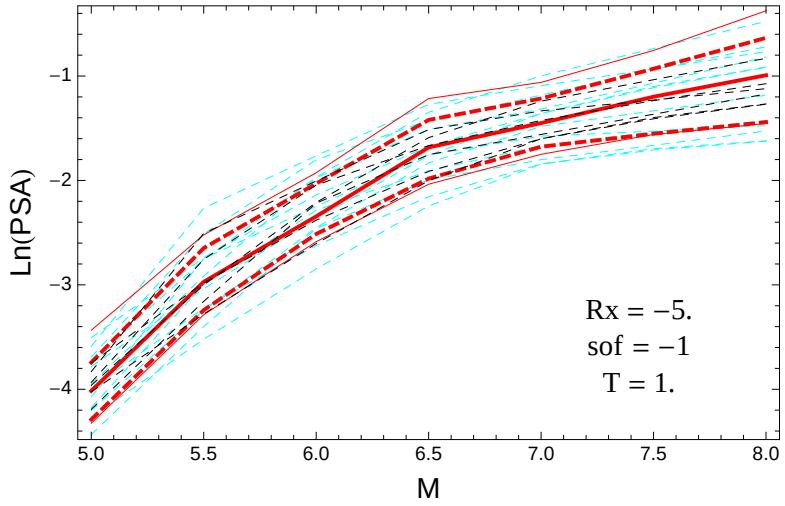



Figure 5.168: PVNGSv2: Magnitude scaling of the original GMPEs (dashed black), the original GMPEs with uncertainty model (dashed cyan) and 0.05,0.5,0.95 quantile of the combined ModelA and ModelB distribution (red) with total weights, for a scenario with $R_X = -5.$, $F = -1$, and $T = 1.$s.

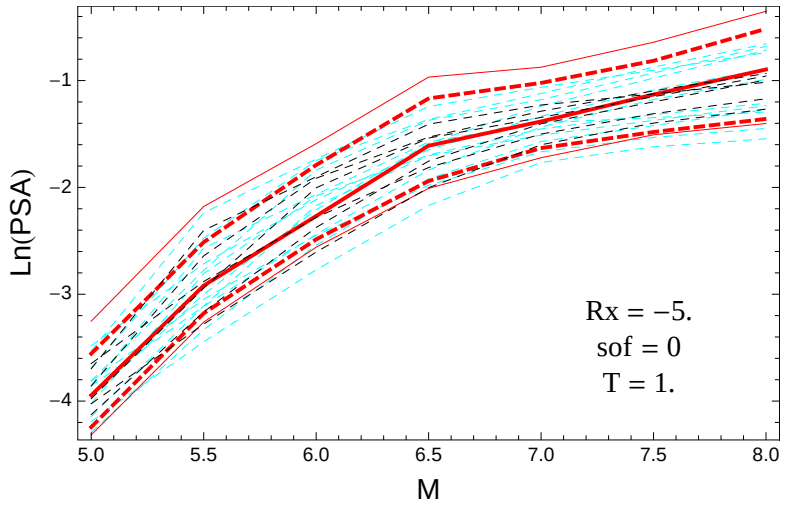



Figure 5.169: PVNGSv2: Magnitude scaling of the original GMPEs (dashed black), the original GMPEs with uncertainty model (dashed cyan) and 0.05,0.5,0.95 quantile of the combined ModelA and ModelB distribution (red) with total weights, for a scenario with $R_X = -5.$, $F = 0$, and $T = 1.$s.

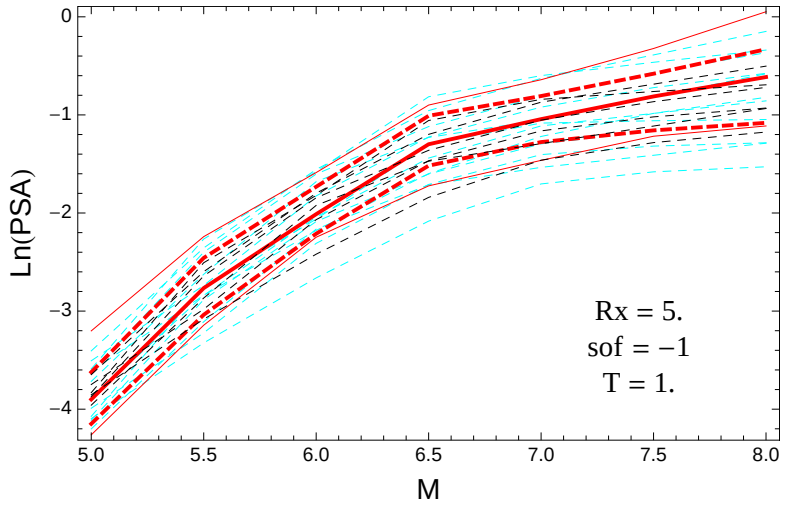



Figure 5.170: PVNGSv2: Magnitude scaling of the original GMPEs (dashed black), the original GMPEs with uncertainty model (dashed cyan) and 0.05,0.5,0.95 quantile of the combined ModelA and ModelB distribution (red) with total weights, for a scenario with $R_X = 5.$, $F = -1$, and $T = 1.$s.

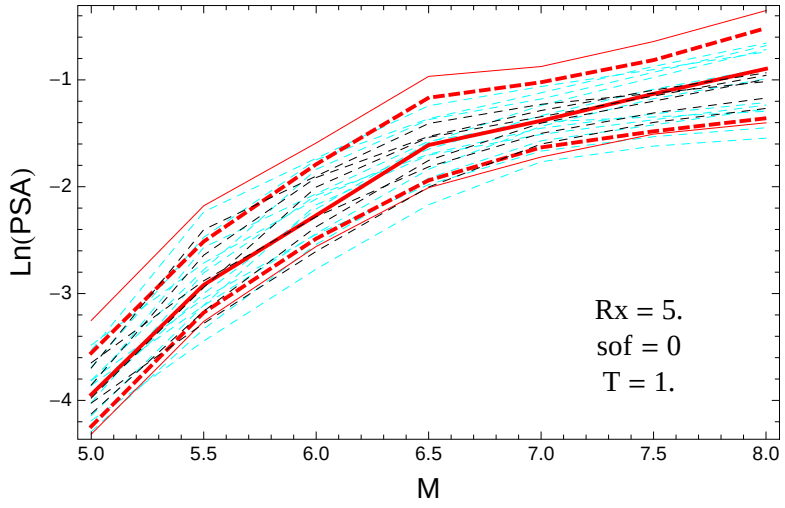



Figure 5.171: PVNGSv2: Magnitude scaling of the original GMPEs (dashed black), the original GMPEs with uncertainty model (dashed cyan) and 0.05,0.5,0.95 quantile of the combined ModelA and ModelB distribution (red) with total weights, for a scenario with $R_X = 5.$, $F = 0$, and $T = 1.$s.

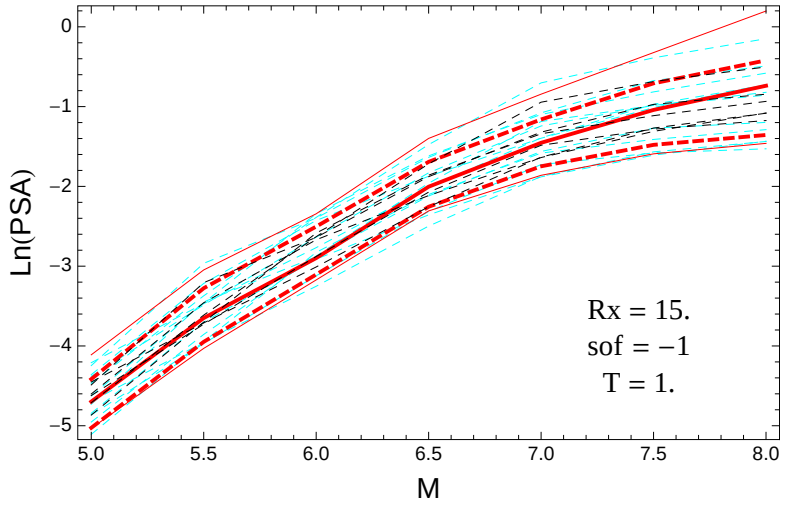



Figure 5.172: PVNGSv2: Magnitude scaling of the original GMPEs (dashed black), the original GMPEs with uncertainty model (dashed cyan) and 0.05,0.5,0.95 quantile of the combined ModelA and ModelB distribution (red) with total weights, for a scenario with $R_X = 15.$, $F = -1$, and $T = 1.$s.

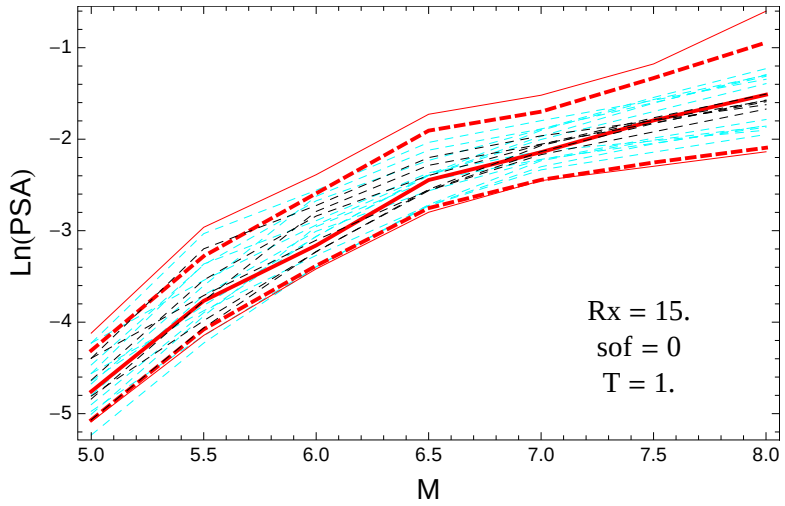



Figure 5.173: PVNGSv2: Magnitude scaling of the original GMPEs (dashed black), the original GMPEs with uncertainty model (dashed cyan) and 0.05,0.5,0.95 quantile of the combined ModelA and ModelB distribution (red) with total weights, for a scenario with $R_X = 15.$, $F = 0$, and $T = 1.$s.

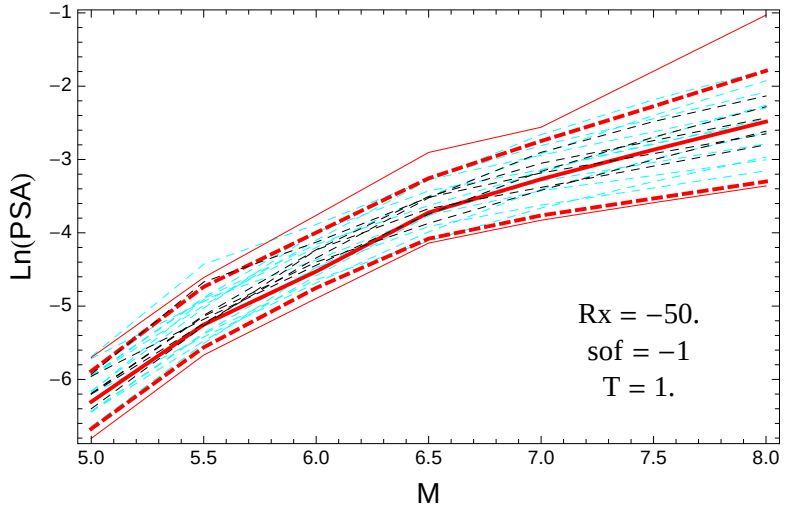



Figure 5.174: PVNGSv2: Magnitude scaling of the original GMPEs (dashed black), the original GMPEs with uncertainty model (dashed cyan) and 0.05,0.5,0.95 quantile of the combined ModelA and ModelB distribution (red) with total weights, for a scenario with $R_X = -50.$, $F = -1$, and $T = 1.$s.

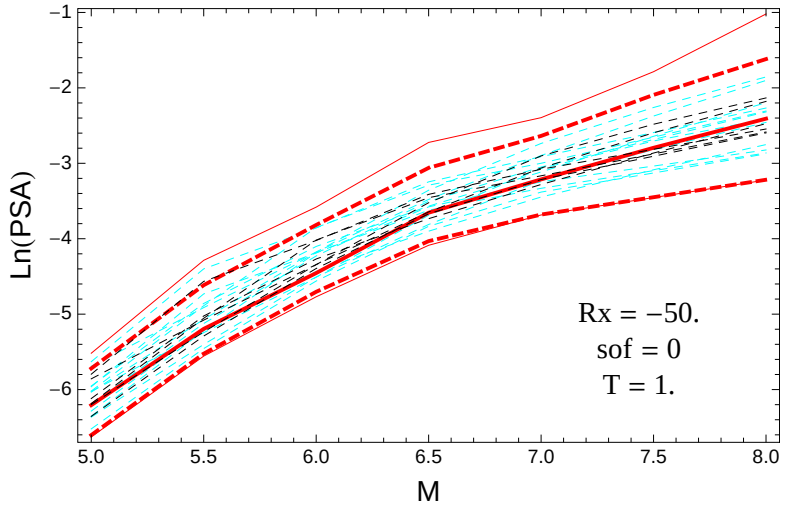



Figure 5.175: PVNGSv2: Magnitude scaling of the original GMPEs (dashed black), the original GMPEs with uncertainty model (dashed cyan) and 0.05,0.5,0.95 quantile of the combined ModelA and ModelB distribution (red) with total weights, for a scenario with $R_X = -50.$, $F = 0$, and $T = 1.$s.

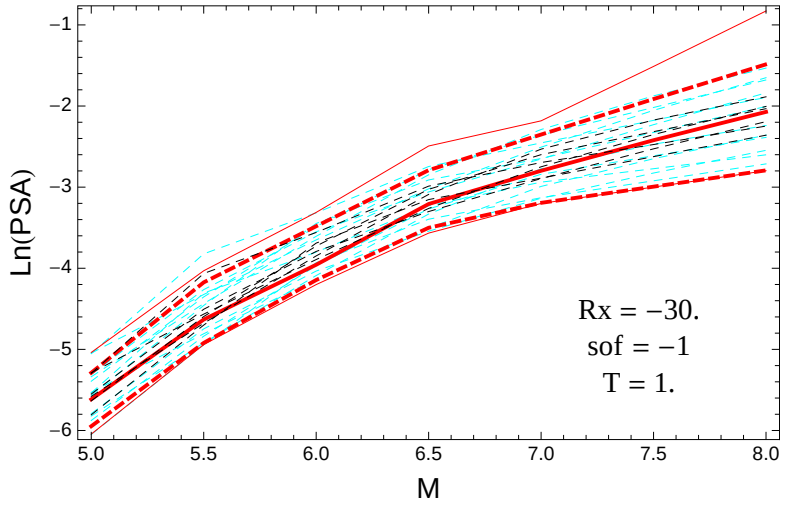



Figure 5.176: PVNGSv2: Magnitude scaling of the original GMPEs (dashed black), the original GMPEs with uncertainty model (dashed cyan) and 0.05,0.5,0.95 quantile of the combined ModelA and ModelB distribution (red) with total weights, for a scenario with $R_X = -30.$, $F = -1$, and $T = 1.$s.

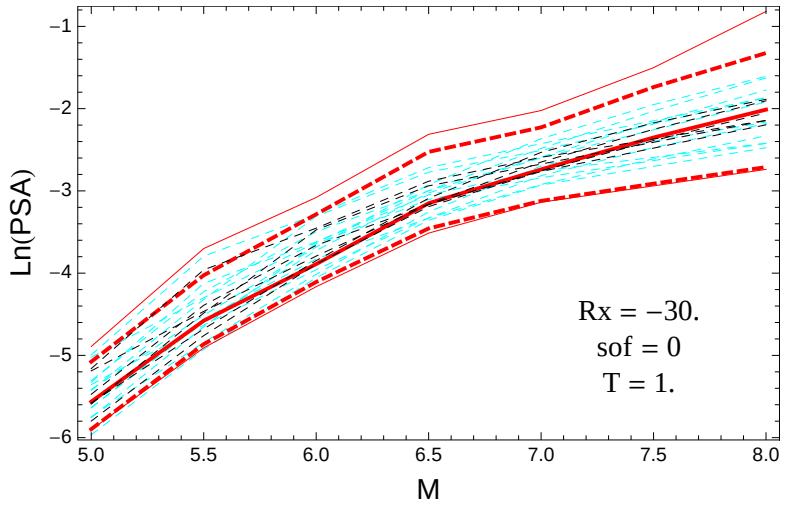



Figure 5.177: PVNGSv2: Magnitude scaling of the original GMPEs (dashed black), the original GMPEs with uncertainty model (dashed cyan) and 0.05,0.5,0.95 quantile of the combined ModelA and ModelB distribution (red) with total weights, for a scenario with $R_X = -30.$, $F = 0$, and $T = 1.$s.

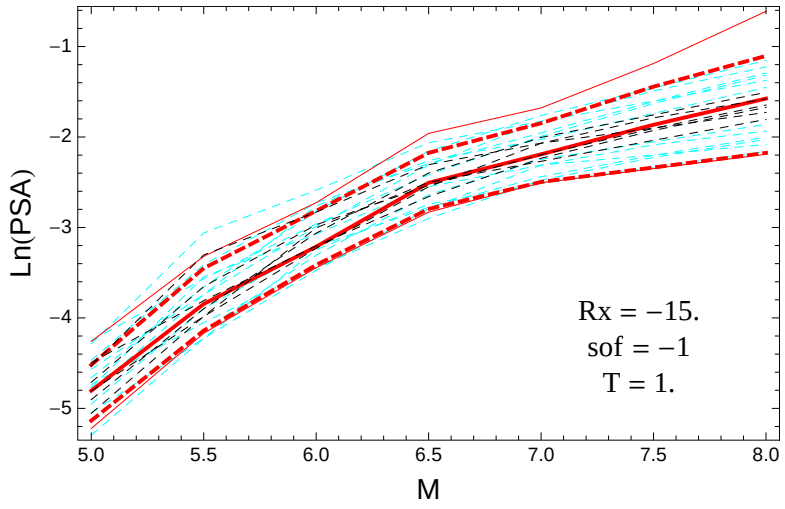



Figure 5.178: PVNGSv2: Magnitude scaling of the original GMPEs (dashed black), the original GMPEs with uncertainty model (dashed cyan) and 0.05,0.5,0.95 quantile of the combined ModelA and ModelB distribution (red) with total weights, for a scenario with $R_X = -15.$, $F = -1$, and $T = 1.$s.

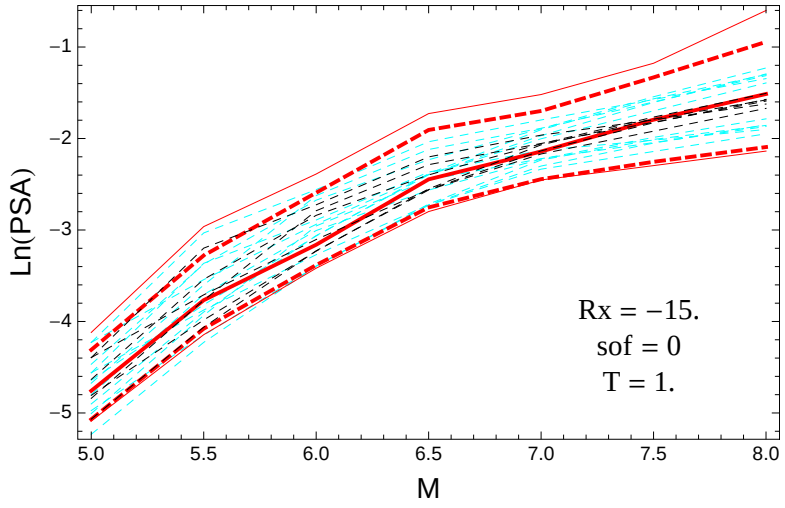



Figure 5.179: PVNGSv2: Magnitude scaling of the original GMPEs (dashed black), the original GMPEs with uncertainty model (dashed cyan) and 0.05,0.5,0.95 quantile of the combined ModelA and ModelB distribution (red) with total weights, for a scenario with $R_X = -15.$, $F = 0$, and $T = 1.$s.

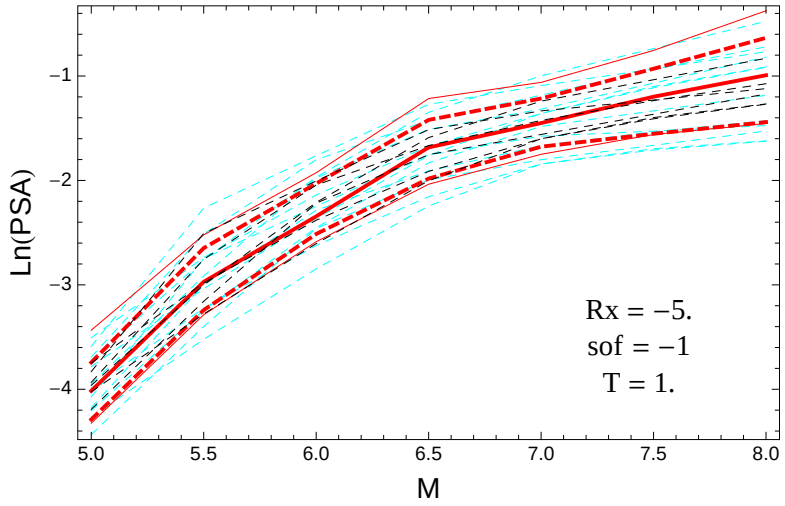



Figure 5.180: PVNGSv2: Magnitude scaling of the original GMPEs (dashed black), the original GMPEs with uncertainty model (dashed cyan) and 0.05,0.5,0.95 quantile of the combined ModelA and ModelB distribution (red) with total weights, for a scenario with $R_X = -5.$, $F = -1$, and $T = 1.$s.

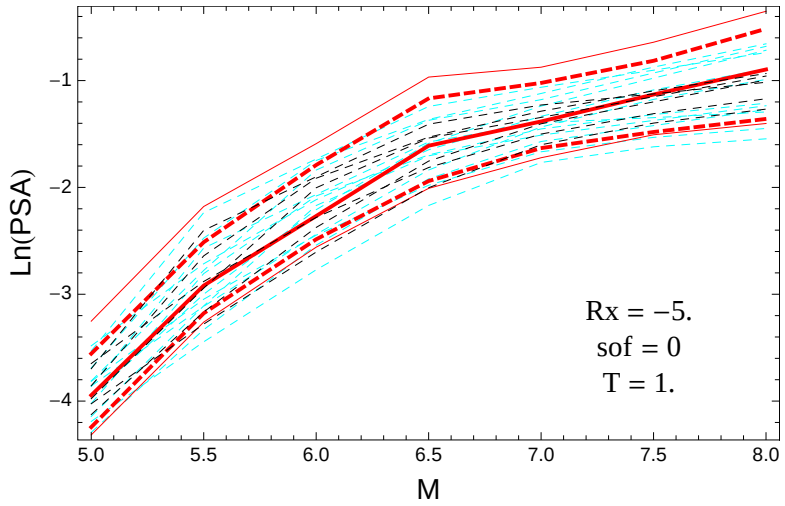



Figure 5.181: PVNGSv2: Magnitude scaling of the original GMPEs (dashed black), the original GMPEs with uncertainty model (dashed cyan) and 0.05,0.5,0.95 quantile of the combined ModelA and ModelB distribution (red) with total weights, for a scenario with $R_X = -5.$, $F = 0$, and $T = 1.$s.

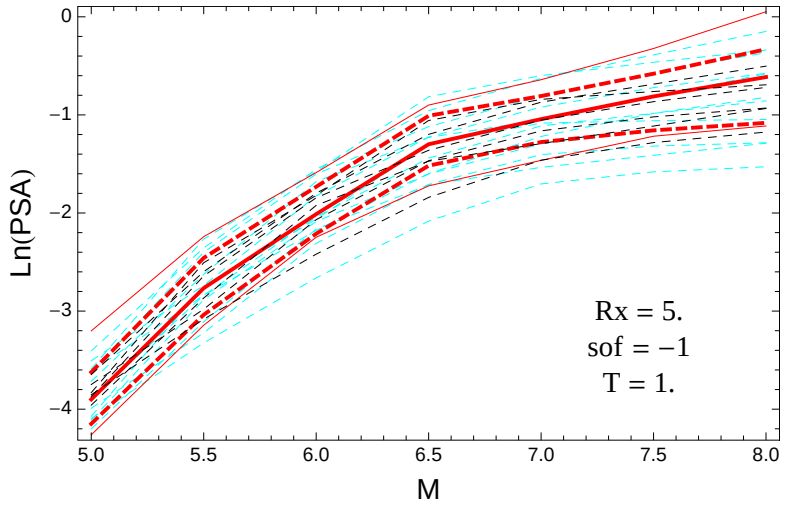



Figure 5.182: PVNGSv2: Magnitude scaling of the original GMPEs (dashed black), the original GMPEs with uncertainty model (dashed cyan) and 0.05,0.5,0.95 quantile of the combined ModelA and ModelB distribution (red) with total weights, for a scenario with $R_X = 5.$, $F = -1$, and $T = 1.$s.

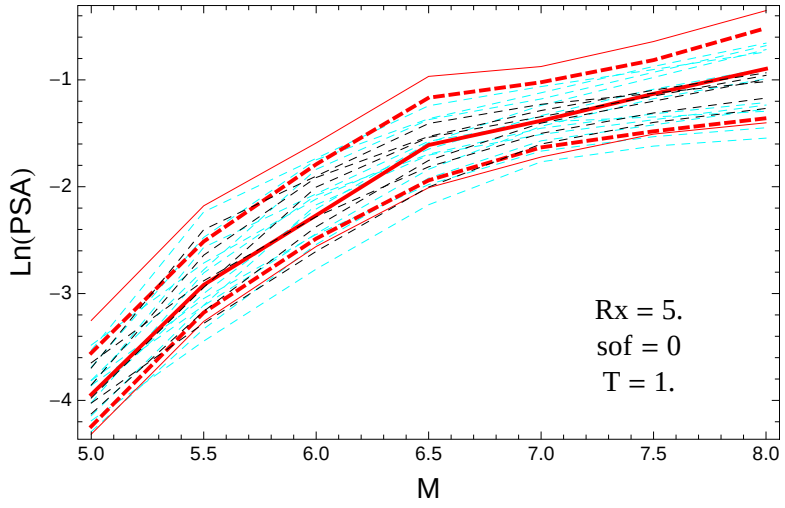



Figure 5.183: PVNGSv2: Magnitude scaling of the original GMPEs (dashed black), the original GMPEs with uncertainty model (dashed cyan) and 0.05,0.5,0.95 quantile of the combined ModelA and ModelB distribution (red) with total weights, for a scenario with $R_X = 5.$, $F = 0$, and $T = 1.$s.

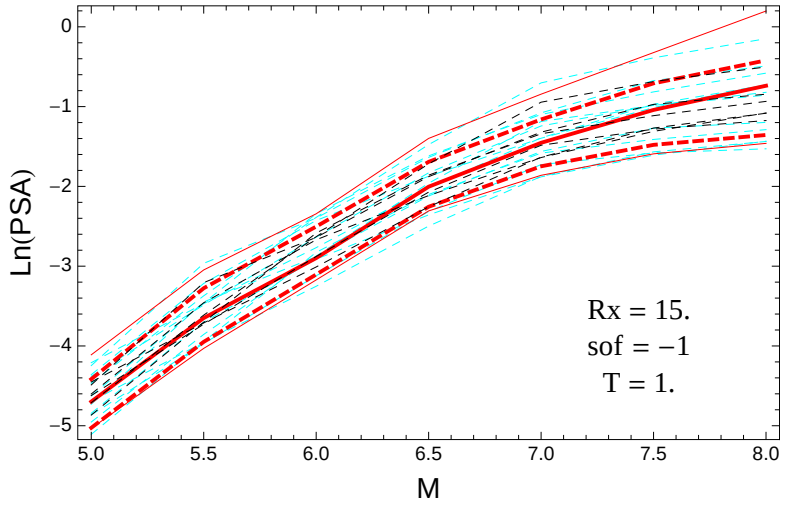



Figure 5.184: PVNGSv2: Magnitude scaling of the original GMPEs (dashed black), the original GMPEs with uncertainty model (dashed cyan) and 0.05,0.5,0.95 quantile of the combined ModelA and ModelB distribution (red) with total weights, for a scenario with $R_X = 15.$, $F = -1$, and $T = 1.$s.

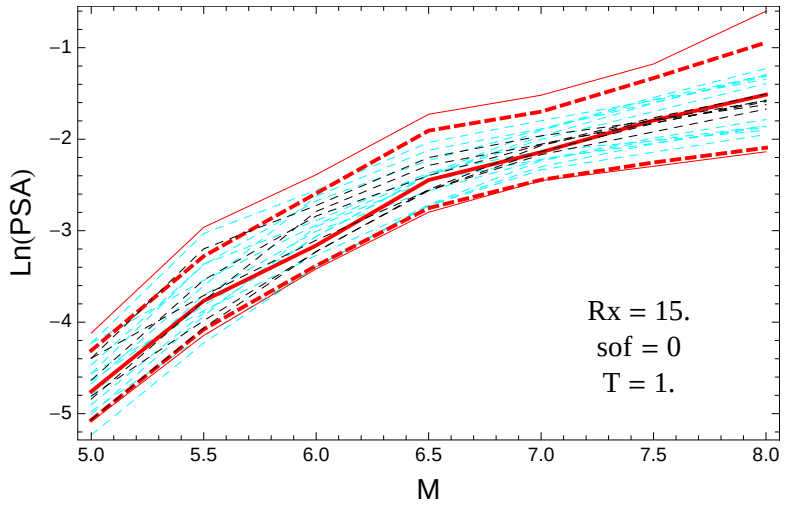



Figure 5.185: PVNGSv2: Magnitude scaling of the original GMPEs (dashed black), the original GMPEs with uncertainty model (dashed cyan) and 0.05,0.5,0.95 quantile of the combined ModelA and ModelB distribution (red) with total weights, for a scenario with $R_X = 15.$, $F = 0$, and $T = 1.$s.

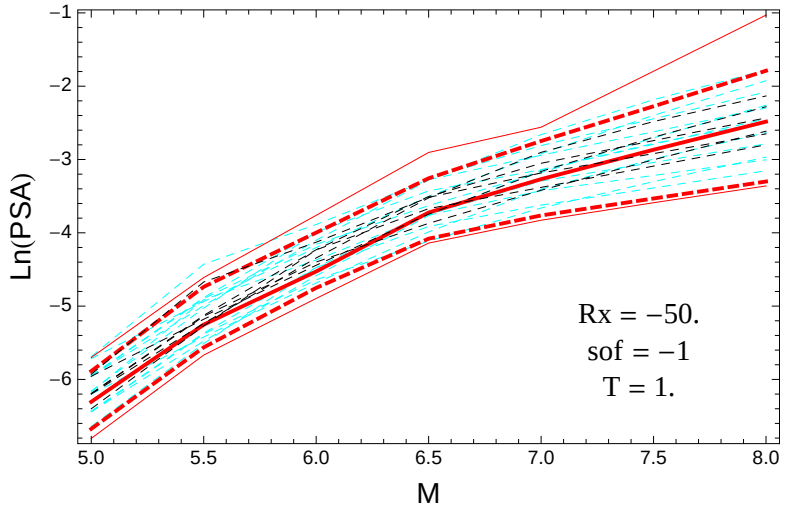



Figure 5.186: PVNGSv2: Magnitude scaling of the original GMPEs (dashed black), the original GMPEs with uncertainty model (dashed cyan) and 0.05,0.5,0.95 quantile of the combined ModelA and ModelB distribution (red) with total weights, for a scenario with $R_X = -50.$, $F = -1$, and $T = 1.$s.

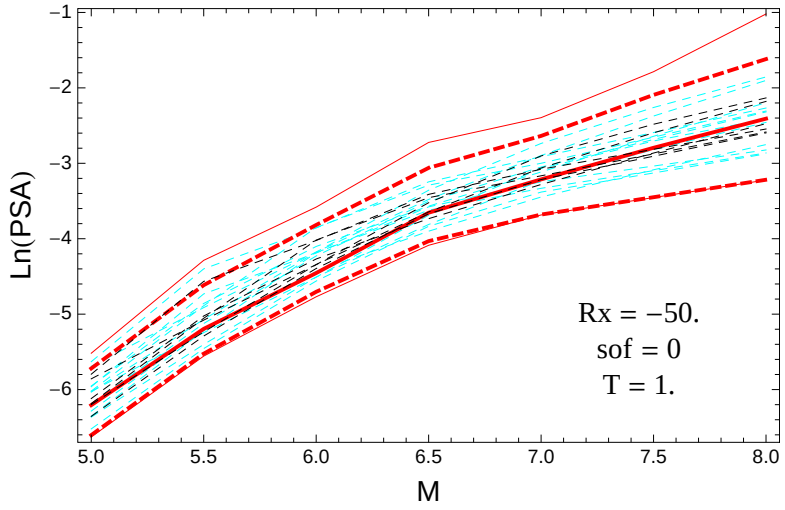



Figure 5.187: PVNGSv2: Magnitude scaling of the original GMPEs (dashed black), the original GMPEs with uncertainty model (dashed cyan) and 0.05,0.5,0.95 quantile of the combined ModelA and ModelB distribution (red) with total weights, for a scenario with $R_X = -50.$, $F = 0$, and $T = 1.$s.

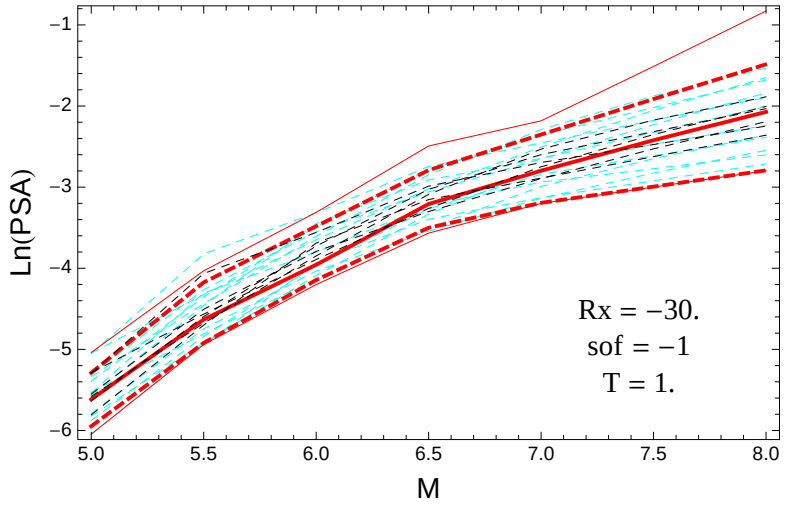



Figure 5.188: PVNGSv2: Magnitude scaling of the original GMPEs (dashed black), the original GMPEs with uncertainty model (dashed cyan) and 0.05,0.5,0.95 quantile of the combined ModelA and ModelB distribution (red) with total weights, for a scenario with $R_X = -30.$, $F = -1$, and $T = 1.$s.

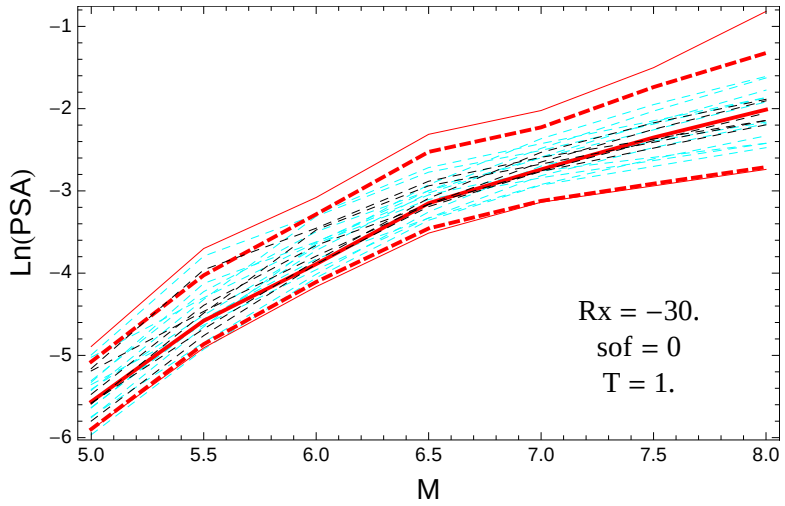



Figure 5.189: PVNGSv2: Magnitude scaling of the original GMPEs (dashed black), the original GMPEs with uncertainty model (dashed cyan) and 0.05,0.5,0.95 quantile of the combined ModelA and ModelB distribution (red) with total weights, for a scenario with $R_X = -30.$, $F = 0$, and $T = 1.$s.

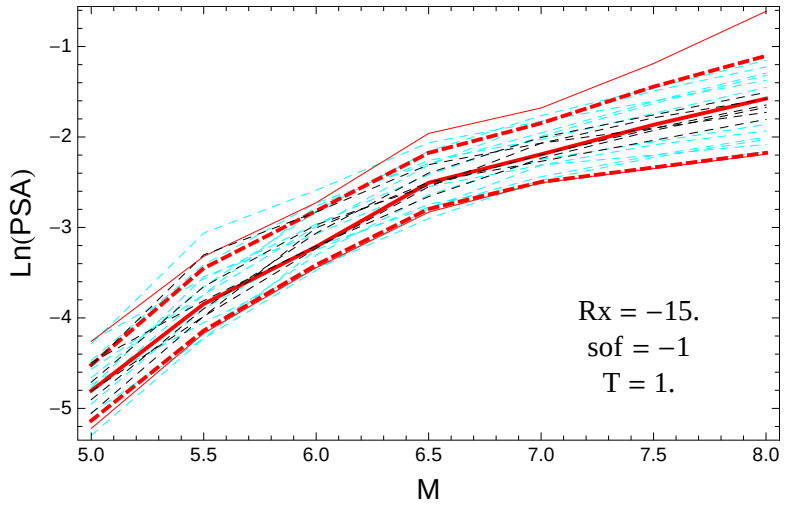



Figure 5.190: PVNGSv2: Magnitude scaling of the original GMPEs (dashed black), the original GMPEs with uncertainty model (dashed cyan) and 0.05,0.5,0.95 quantile of the combined ModelA and ModelB distribution (red) with total weights, for a scenario with $R_X = -15.$, $F = -1$, and $T = 1.$s.

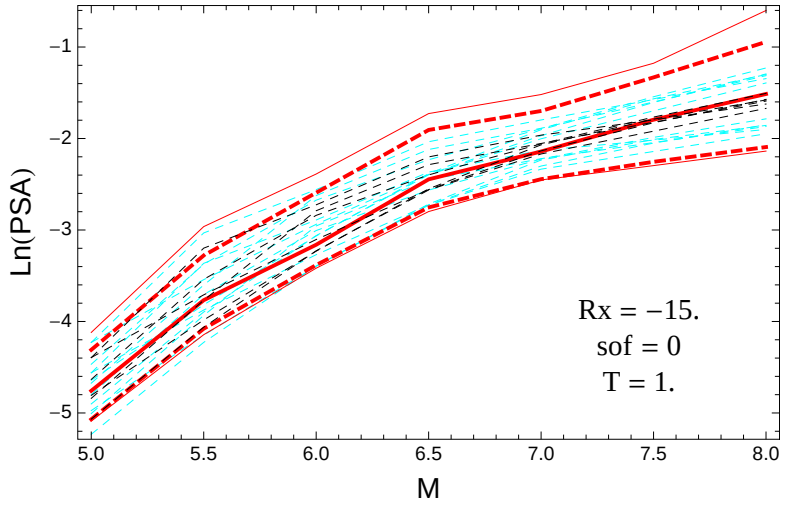



Figure 5.191: PVNGSv2: Magnitude scaling of the original GMPEs (dashed black), the original GMPEs with uncertainty model (dashed cyan) and 0.05,0.5,0.95 quantile of the combined ModelA and ModelB distribution (red) with total weights, for a scenario with $R_X = -15.$, $F = 0$, and $T = 1.$s.

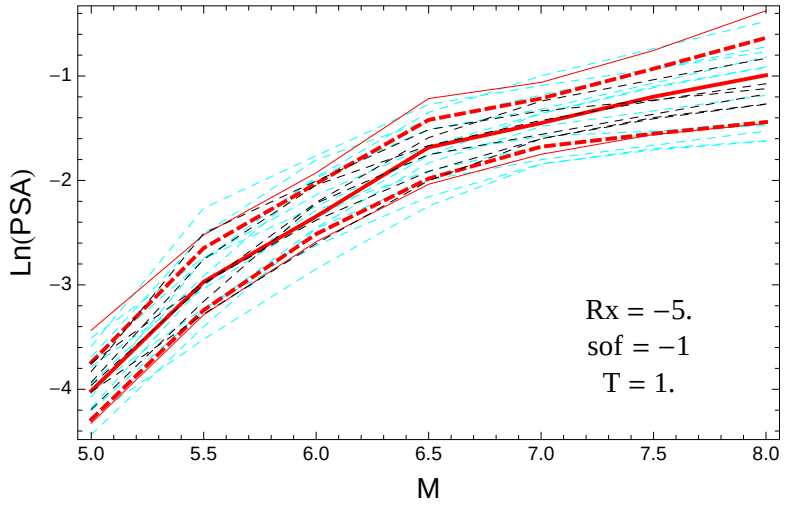



Figure 5.192: PVNGSv2: Magnitude scaling of the original GMPEs (dashed black), the original GMPEs with uncertainty model (dashed cyan) and 0.05,0.5,0.95 quantile of the combined ModelA and ModelB distribution (red) with total weights, for a scenario with $R_X = -5.$, $F = -1$, and $T = 1.$s.

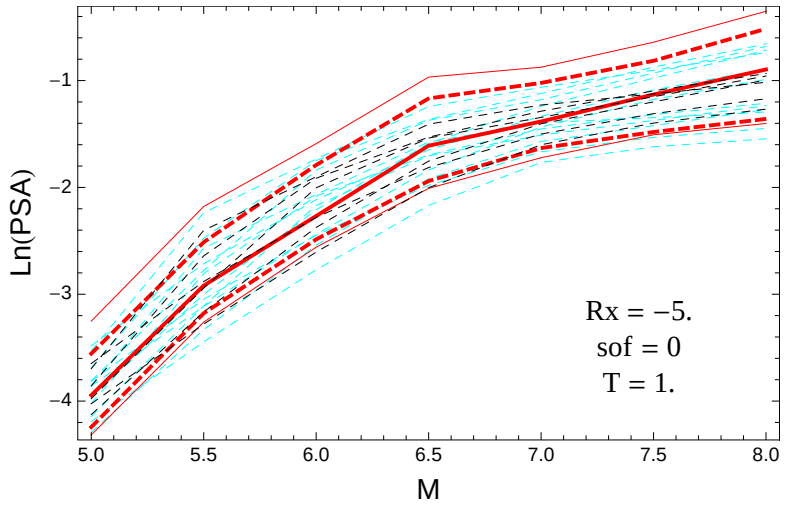



Figure 5.193: PVNGSv2: Magnitude scaling of the original GMPEs (dashed black), the original GMPEs with uncertainty model (dashed cyan) and 0.05,0.5,0.95 quantile of the combined ModelA and ModelB distribution (red) with total weights, for a scenario with $R_X = -5.$, $F = 0$, and $T = 1.$s.

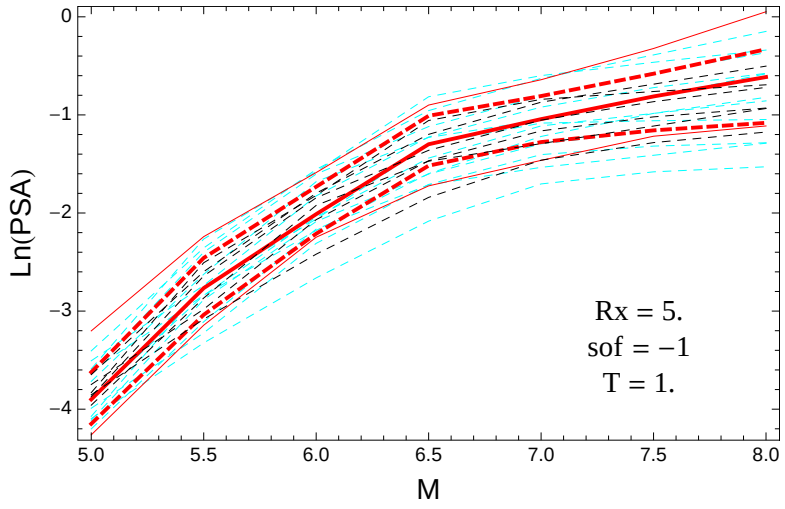



Figure 5.194: PVNGSv2: Magnitude scaling of the original GMPEs (dashed black), the original GMPEs with uncertainty model (dashed cyan) and 0.05,0.5,0.95 quantile of the combined ModelA and ModelB distribution (red) with total weights, for a scenario with $R_X = 5.$, $F = -1$, and $T = 1.$s.

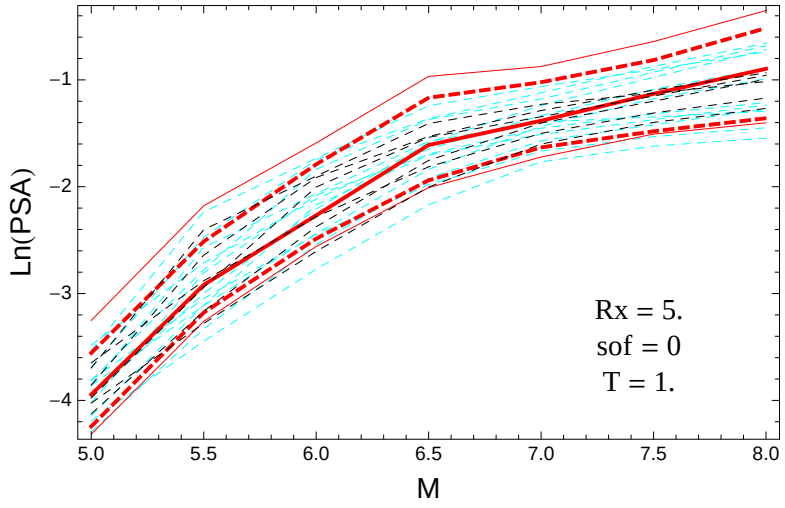



Figure 5.195: PVNGSv2: Magnitude scaling of the original GMPEs (dashed black), the original GMPEs with uncertainty model (dashed cyan) and 0.05,0.5,0.95 quantile of the combined ModelA and ModelB distribution (red) with total weights, for a scenario with $R_X = 5.$, $F = 0$, and $T = 1.$s.

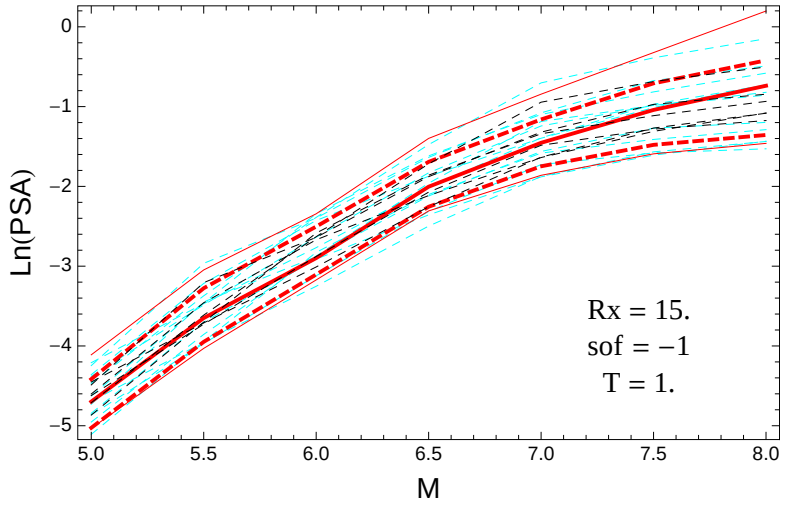



Figure 5.196: PVNGSv2: Magnitude scaling of the original GMPEs (dashed black), the original GMPEs with uncertainty model (dashed cyan) and 0.05,0.5,0.95 quantile of the combined ModelA and ModelB distribution (red) with total weights, for a scenario with $R_X = 15.$, $F = -1$, and $T = 1.$s.

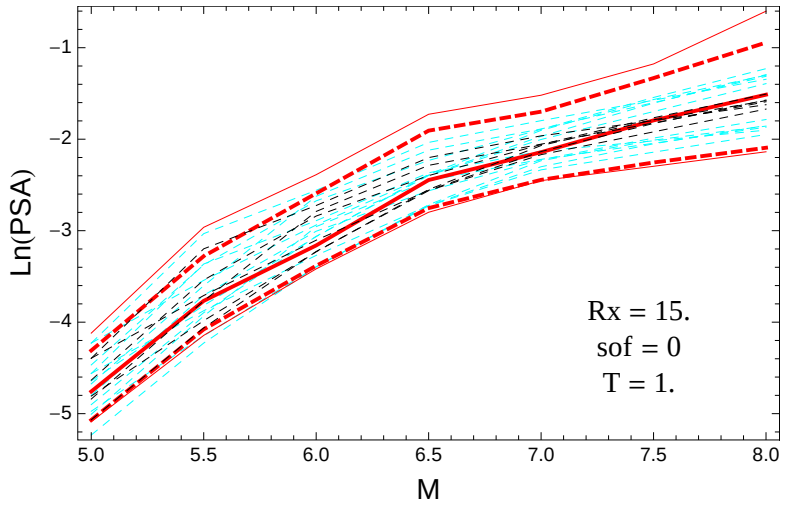



Figure 5.197: PVNGSv2: Magnitude scaling of the original GMPEs (dashed black), the original GMPEs with uncertainty model (dashed cyan) and 0.05,0.5,0.95 quantile of the combined ModelA and ModelB distribution (red) with total weights, for a scenario with $R_X = 15.$, $F = 0$, and $T = 1.$s.

**T = 2.s**

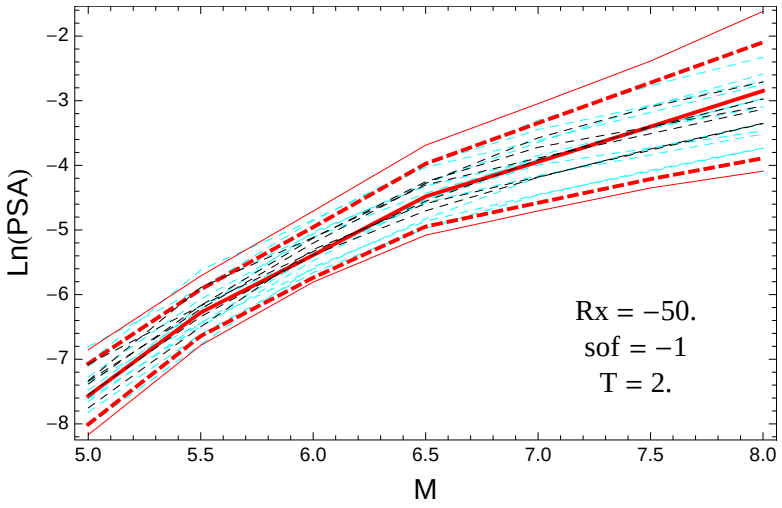



Figure 5.198: PVNGSv2: Magnitude scaling of the original GMPEs (dashed black), the original GMPEs with uncertainty model (dashed cyan) and 0.05,0.5,0.95 quantile of the combined ModelA and ModelB distribution (red) with total weights, for a scenario with $R_X = -50.$, $F = -1$, and $T = 2.$s.

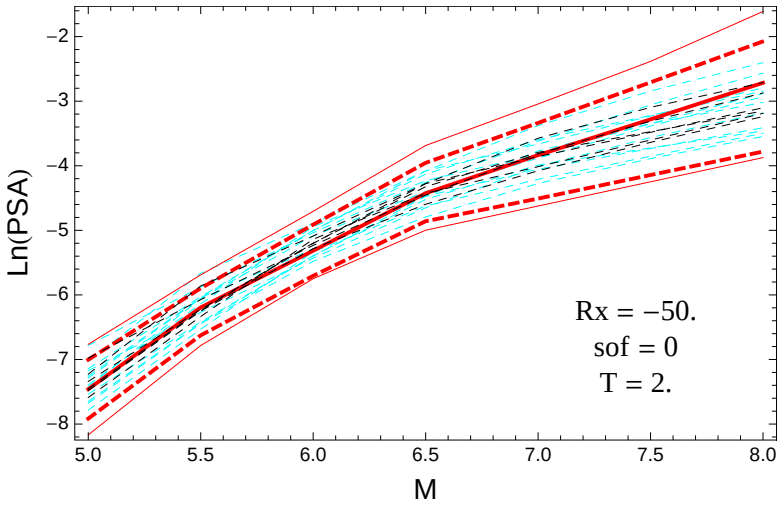



Figure 5.199: PVNGSv2: Magnitude scaling of the original GMPEs (dashed black), the original GMPEs with uncertainty model (dashed cyan) and 0.05,0.5,0.95 quantile of the combined ModelA and ModelB distribution (red) with total weights, for a scenario with $R_X = -50.$, $F = 0$, and $T = 2.$s.

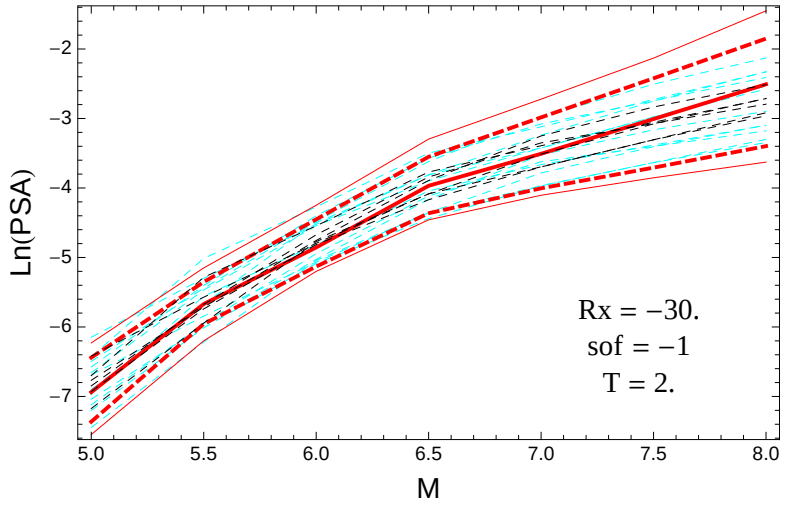



Figure 5.200: PVNGSv2: Magnitude scaling of the original GMPEs (dashed black), the original GMPEs with uncertainty model (dashed cyan) and 0.05,0.5,0.95 quantile of the combined ModelA and ModelB distribution (red) with total weights, for a scenario with $R_X = -30.$, $F = -1$, and $T = 2.$s.

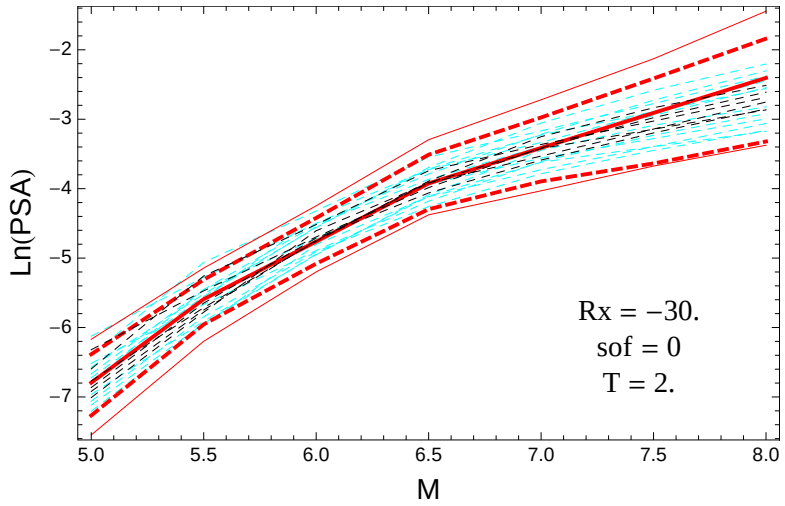



Figure 5.201: PVNGSv2: Magnitude scaling of the original GMPEs (dashed black), the original GMPEs with uncertainty model (dashed cyan) and 0.05,0.5,0.95 quantile of the combined ModelA and ModelB distribution (red) with total weights, for a scenario with $R_X = -30.$, $F = 0$, and $T = 2.$s.

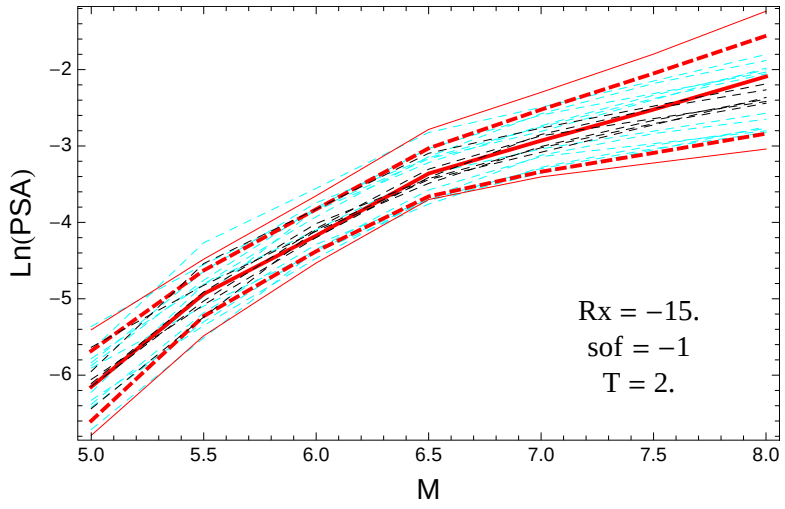



Figure 5.202: PVNGSv2: Magnitude scaling of the original GMPEs (dashed black), the original GMPEs with uncertainty model (dashed cyan) and 0.05,0.5,0.95 quantile of the combined ModelA and ModelB distribution (red) with total weights, for a scenario with $R_X = -15.$, $F = -1$, and $T = 2.$s.

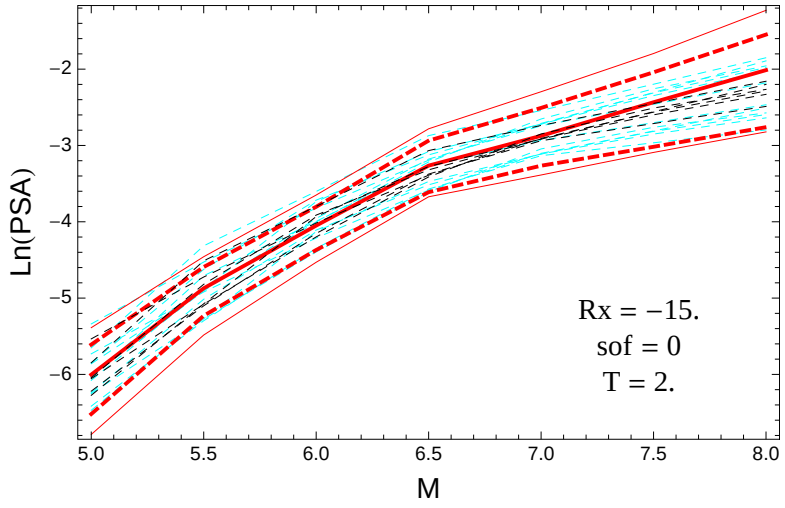



Figure 5.203: PVNGSv2: Magnitude scaling of the original GMPEs (dashed black), the original GMPEs with uncertainty model (dashed cyan) and 0.05,0.5,0.95 quantile of the combined ModelA and ModelB distribution (red) with total weights, for a scenario with $R_X = -15.$, $F = 0$, and $T = 2.$s.

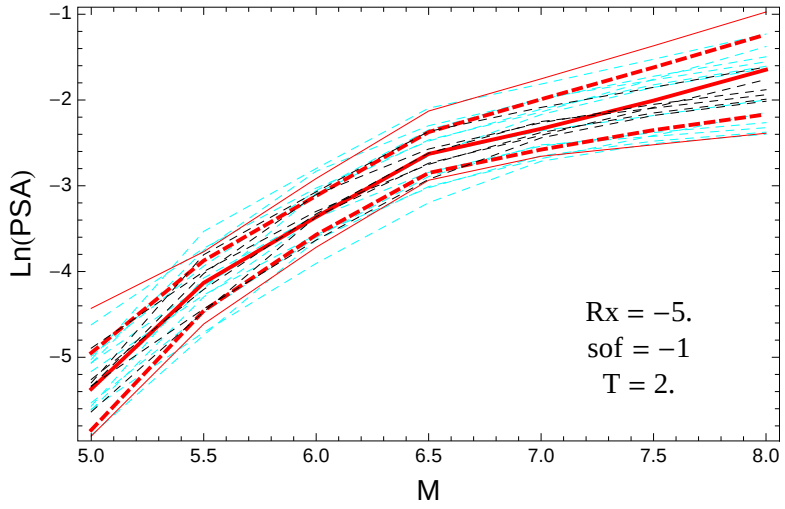



Figure 5.204: PVNGSv2: Magnitude scaling of the original GMPEs (dashed black), the original GMPEs with uncertainty model (dashed cyan) and 0.05,0.5,0.95 quantile of the combined ModelA and ModelB distribution (red) with total weights, for a scenario with $R_X = -5.$, $F = -1$, and $T = 2.$s.

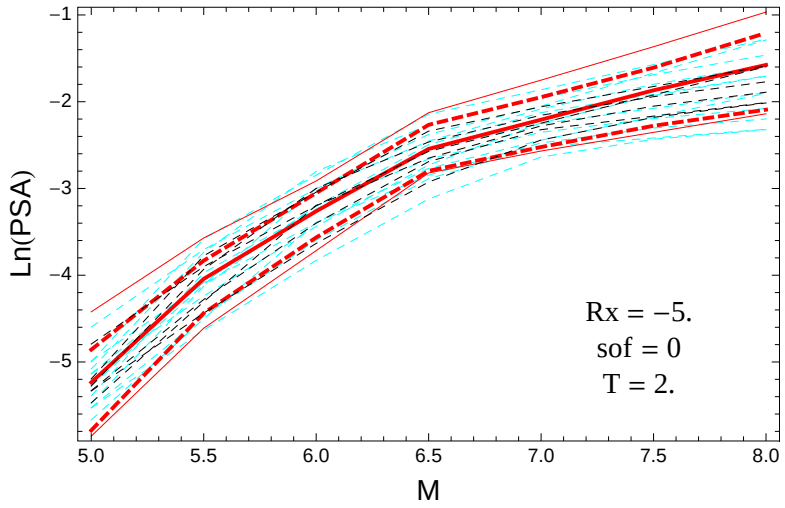



Figure 5.205: PVNGSv2: Magnitude scaling of the original GMPEs (dashed black), the original GMPEs with uncertainty model (dashed cyan) and 0.05,0.5,0.95 quantile of the combined ModelA and ModelB distribution (red) with total weights, for a scenario with $R_X = -5.$, $F = 0$, and $T = 2.$s.

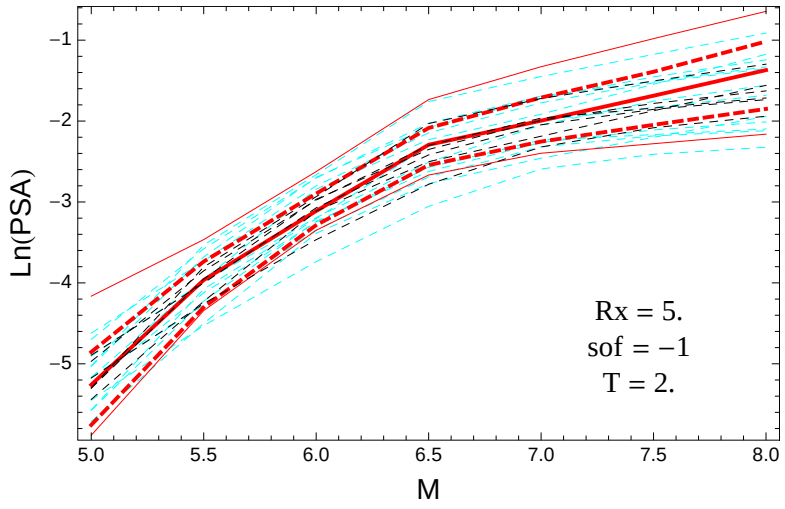



Figure 5.206: PVNGSv2: Magnitude scaling of the original GMPEs (dashed black), the original GMPEs with uncertainty model (dashed cyan) and 0.05,0.5,0.95 quantile of the combined ModelA and ModelB distribution (red) with total weights, for a scenario with $R_X = 5.$, $F = -1$, and $T = 2.$s.

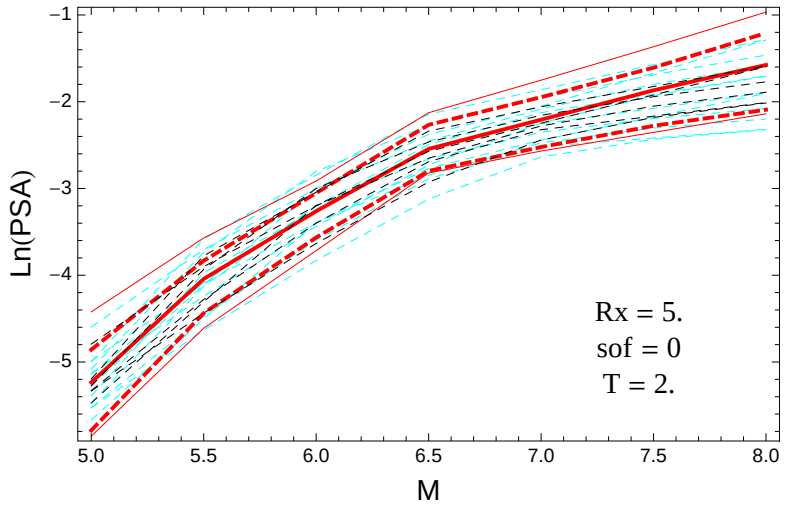



Figure 5.207: PVNGSv2: Magnitude scaling of the original GMPEs (dashed black), the original GMPEs with uncertainty model (dashed cyan) and 0.05,0.5,0.95 quantile of the combined ModelA and ModelB distribution (red) with total weights, for a scenario with $R_X = 5.$, $F = 0$, and $T = 2.$s.

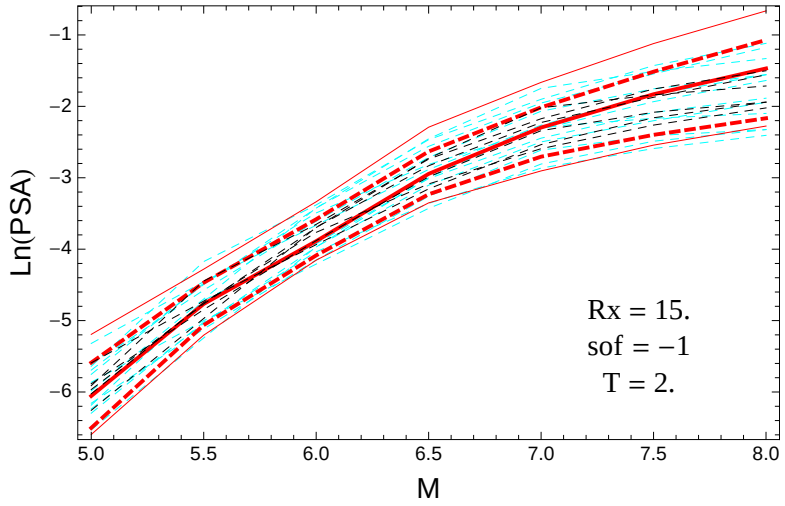



Figure 5.208: PVNGSv2: Magnitude scaling of the original GMPEs (dashed black), the original GMPEs with uncertainty model (dashed cyan) and 0.05,0.5,0.95 quantile of the combined ModelA and ModelB distribution (red) with total weights, for a scenario with $R_X = 15.$, $F = -1$, and $T = 2.$s.

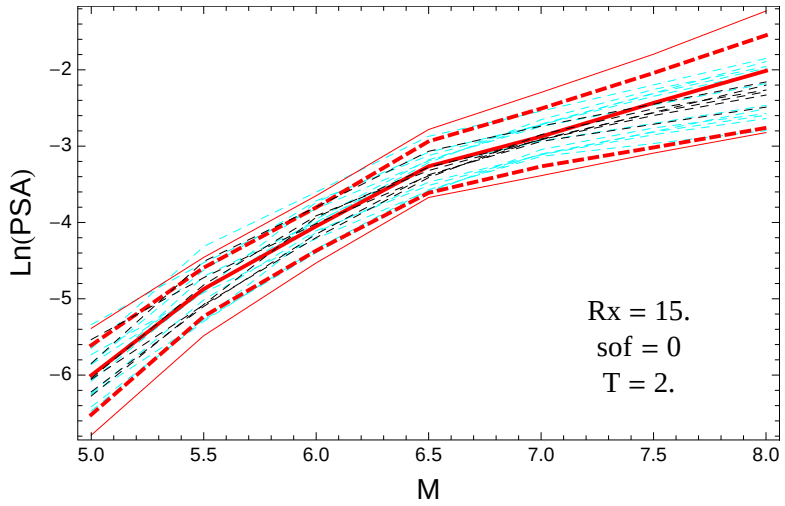



Figure 5.209: PVNGSv2: Magnitude scaling of the original GMPEs (dashed black), the original GMPEs with uncertainty model (dashed cyan) and 0.05,0.5,0.95 quantile of the combined ModelA and ModelB distribution (red) with total weights, for a scenario with $R_X = 15.$, $F = 0$, and $T = 2.$s.

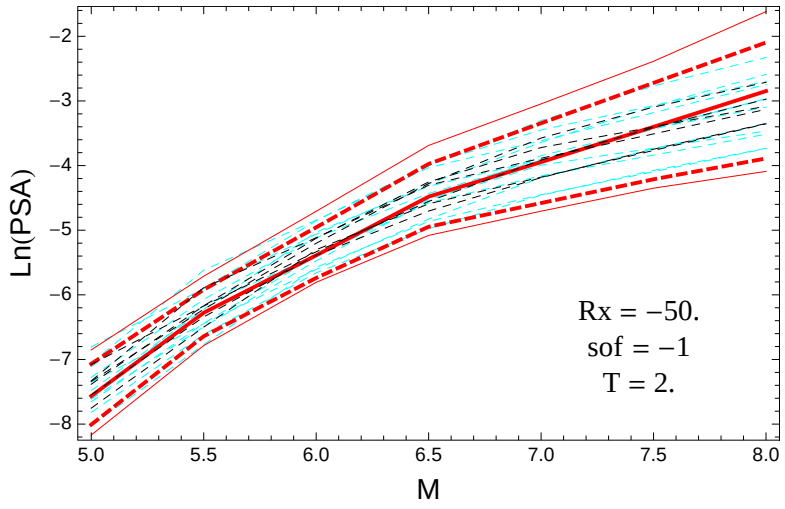



Figure 5.210: PVNGSv2: Magnitude scaling of the original GMPEs (dashed black), the original GMPEs with uncertainty model (dashed cyan) and 0.05,0.5,0.95 quantile of the combined ModelA and ModelB distribution (red) with total weights, for a scenario with $R_X = -50.$, $F = -1$, and $T = 2.$s.

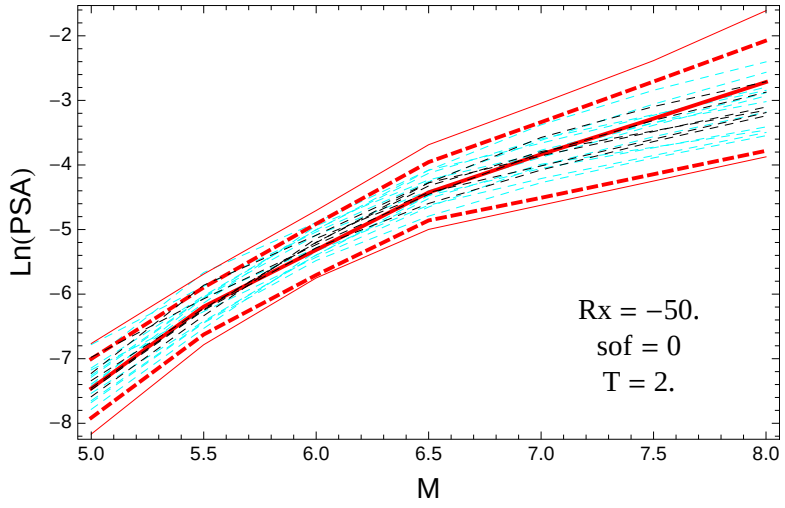



Figure 5.211: PVNGSv2: Magnitude scaling of the original GMPEs (dashed black), the original GMPEs with uncertainty model (dashed cyan) and 0.05,0.5,0.95 quantile of the combined ModelA and ModelB distribution (red) with total weights, for a scenario with $R_X = -50.$, $F = 0$, and $T = 2.$s.

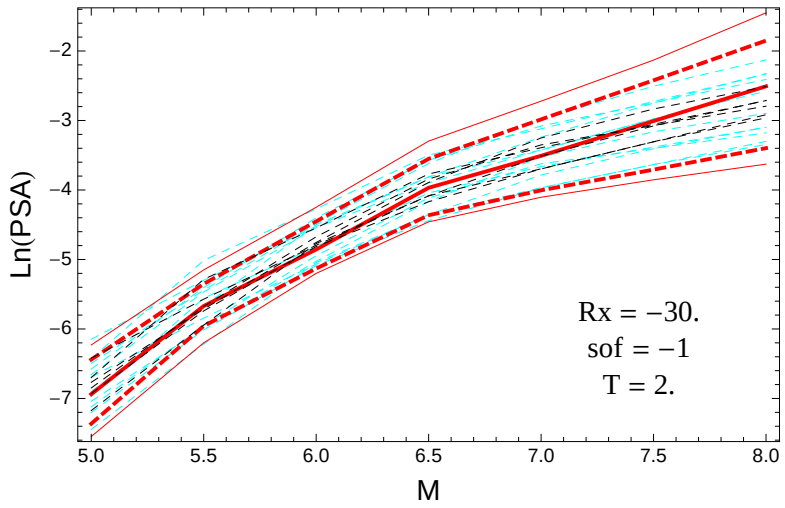



Figure 5.212: PVNGSv2: Magnitude scaling of the original GMPEs (dashed black), the original GMPEs with uncertainty model (dashed cyan) and 0.05,0.5,0.95 quantile of the combined ModelA and ModelB distribution (red) with total weights, for a scenario with $R_X = -30.$, $F = -1$, and $T = 2.$s.

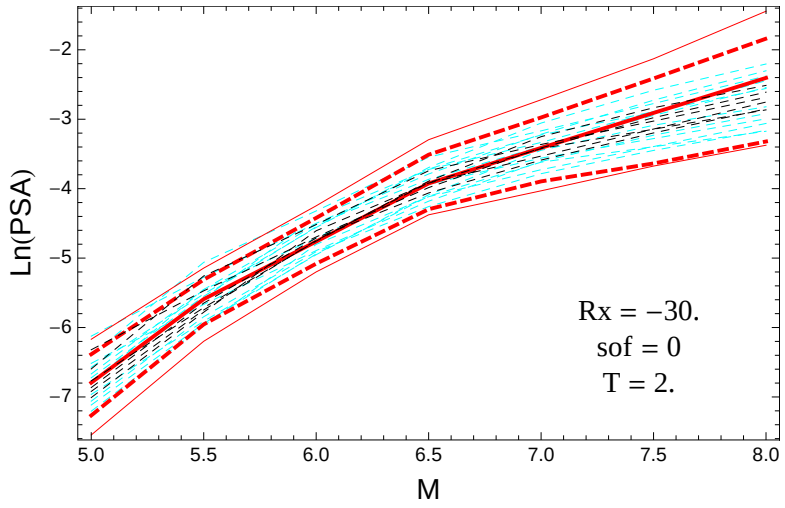



Figure 5.213: PVNGSv2: Magnitude scaling of the original GMPEs (dashed black), the original GMPEs with uncertainty model (dashed cyan) and 0.05,0.5,0.95 quantile of the combined ModelA and ModelB distribution (red) with total weights, for a scenario with $R_X = -30.$, $F = 0$, and $T = 2.$s.

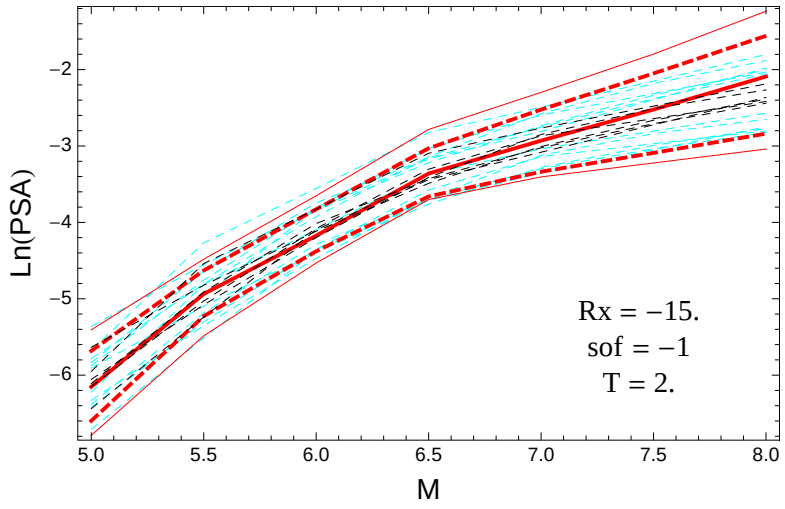



Figure 5.214: PVNGSv2: Magnitude scaling of the original GMPEs (dashed black), the original GMPEs with uncertainty model (dashed cyan) and 0.05,0.5,0.95 quantile of the combined ModelA and ModelB distribution (red) with total weights, for a scenario with $R_X = -15.$, $F = -1$, and $T = 2.$s.

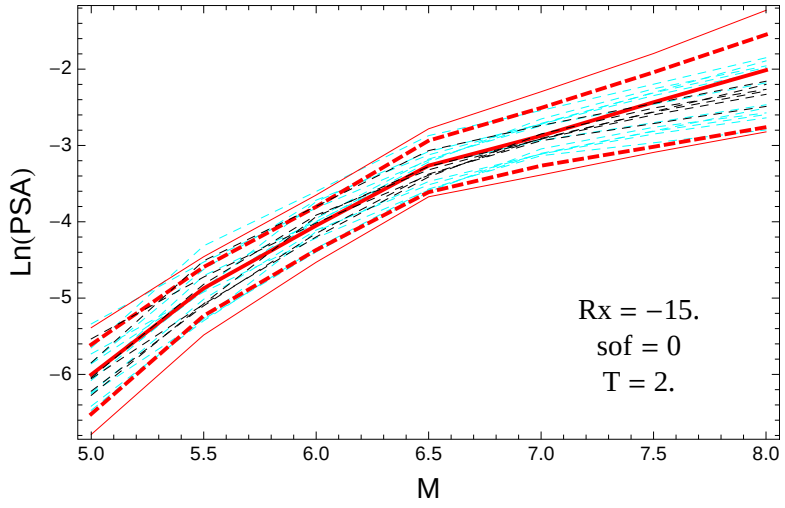



Figure 5.215: PVNGSv2: Magnitude scaling of the original GMPEs (dashed black), the original GMPEs with uncertainty model (dashed cyan) and 0.05,0.5,0.95 quantile of the combined ModelA and ModelB distribution (red) with total weights, for a scenario with $R_X = -15.$, $F = 0$, and $T = 2.$s.

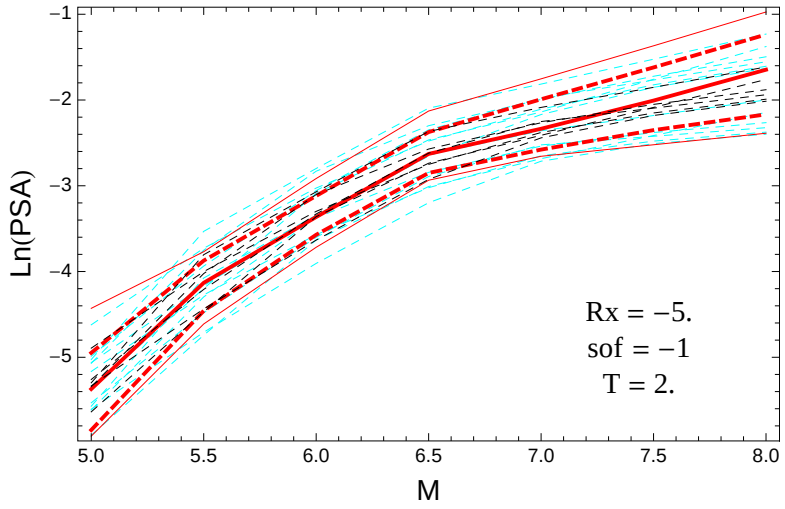



Figure 5.216: PVNGSv2: Magnitude scaling of the original GMPEs (dashed black), the original GMPEs with uncertainty model (dashed cyan) and 0.05,0.5,0.95 quantile of the combined ModelA and ModelB distribution (red) with total weights, for a scenario with $R_X = -5.$, $F = -1$, and $T = 2.$s.

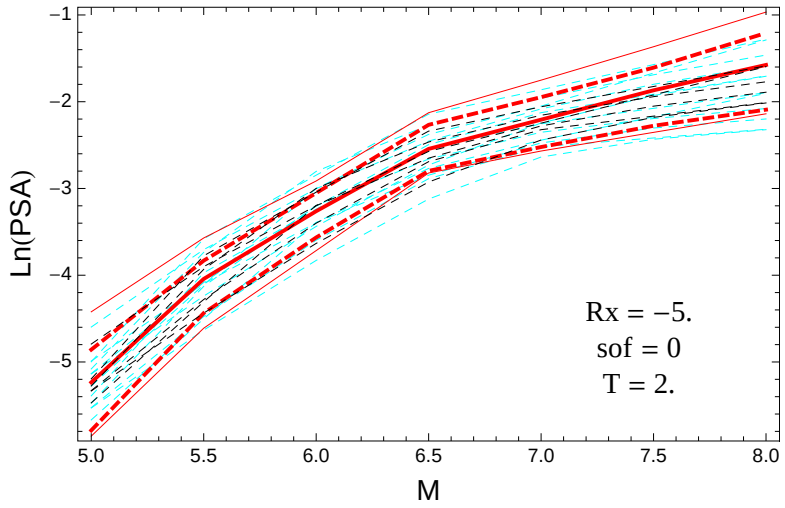



Figure 5.217: PVNGSv2: Magnitude scaling of the original GMPEs (dashed black), the original GMPEs with uncertainty model (dashed cyan) and 0.05,0.5,0.95 quantile of the combined ModelA and ModelB distribution (red) with total weights, for a scenario with $R_X = -5.$, $F = 0$, and $T = 2.$s.

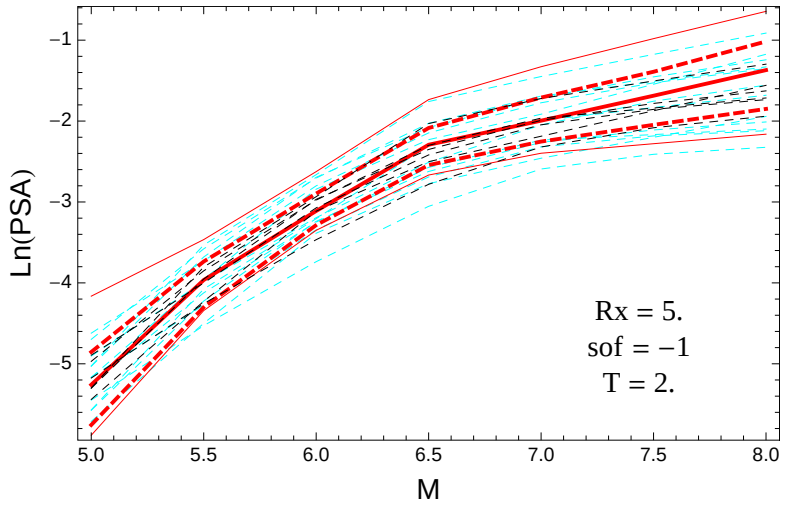



Figure 5.218: PVNGSv2: Magnitude scaling of the original GMPEs (dashed black), the original GMPEs with uncertainty model (dashed cyan) and 0.05,0.5,0.95 quantile of the combined ModelA and ModelB distribution (red) with total weights, for a scenario with $R_X = 5.$, $F = -1$, and $T = 2.$s.

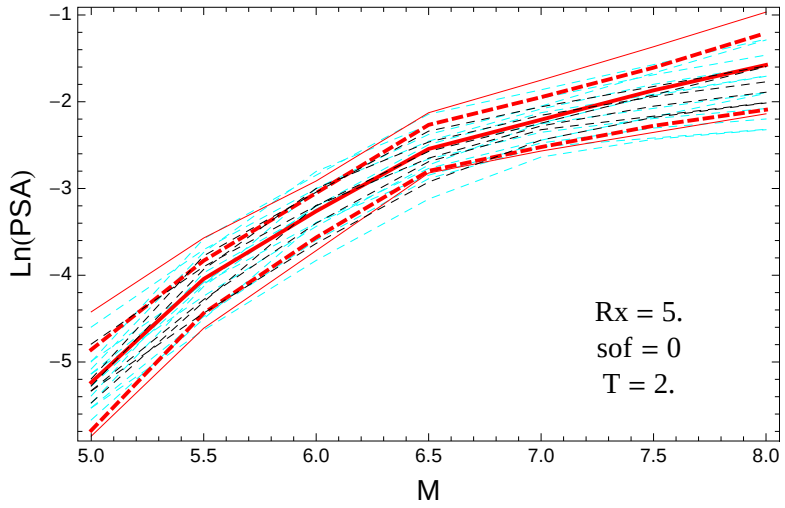



Figure 5.219: PVNGSv2: Magnitude scaling of the original GMPEs (dashed black), the original GMPEs with uncertainty model (dashed cyan) and 0.05,0.5,0.95 quantile of the combined ModelA and ModelB distribution (red) with total weights, for a scenario with $R_X = 5.$, $F = 0$, and $T = 2.$s.

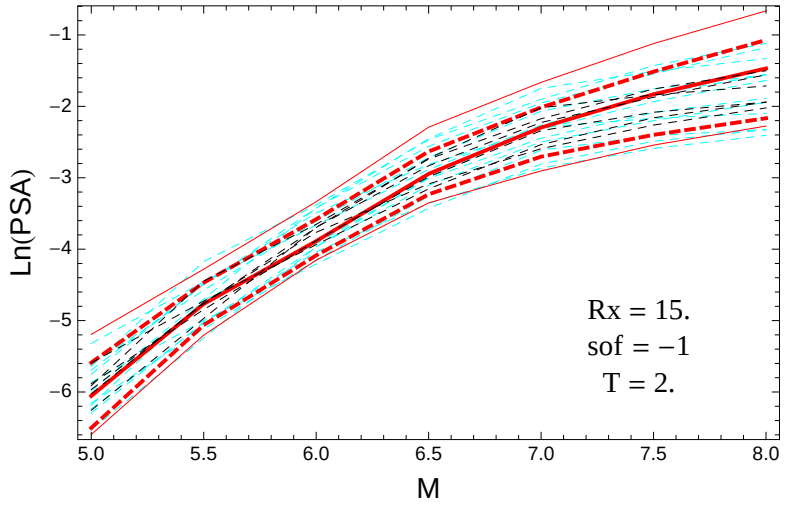



Figure 5.220: PVNGSv2: Magnitude scaling of the original GMPEs (dashed black), the original GMPEs with uncertainty model (dashed cyan) and 0.05,0.5,0.95 quantile of the combined ModelA and ModelB distribution (red) with total weights, for a scenario with $R_X = 15.$, $F = -1$, and $T = 2.$s.

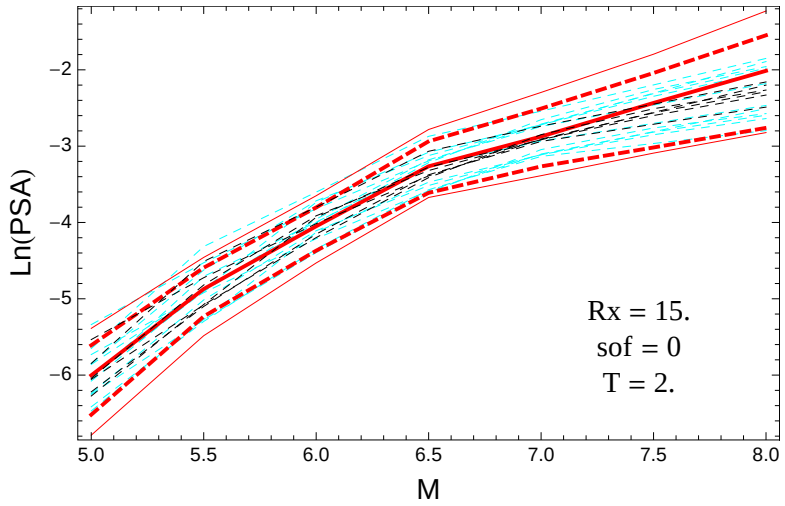



Figure 5.221: PVNGSv2: Magnitude scaling of the original GMPEs (dashed black), the original GMPEs with uncertainty model (dashed cyan) and 0.05,0.5,0.95 quantile of the combined ModelA and ModelB distribution (red) with total weights, for a scenario with $R_X = 15.$, $F = 0$, and $T = 2.$s.

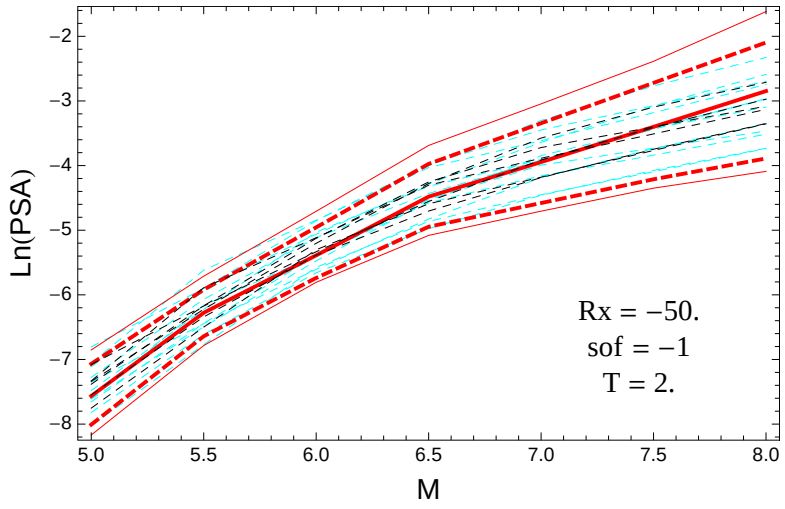



Figure 5.222: PVNGSv2: Magnitude scaling of the original GMPEs (dashed black), the original GMPEs with uncertainty model (dashed cyan) and 0.05,0.5,0.95 quantile of the combined ModelA and ModelB distribution (red) with total weights, for a scenario with $R_X = -50.$, $F = -1$, and $T = 2.$s.

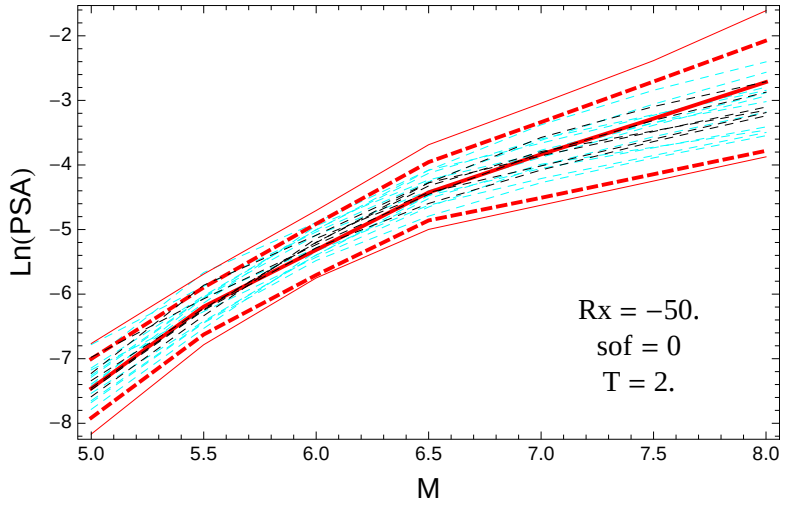



Figure 5.223: PVNGSv2: Magnitude scaling of the original GMPEs (dashed black), the original GMPEs with uncertainty model (dashed cyan) and 0.05,0.5,0.95 quantile of the combined ModelA and ModelB distribution (red) with total weights, for a scenario with $R_X = -50.$, $F = 0$, and $T = 2.$s.

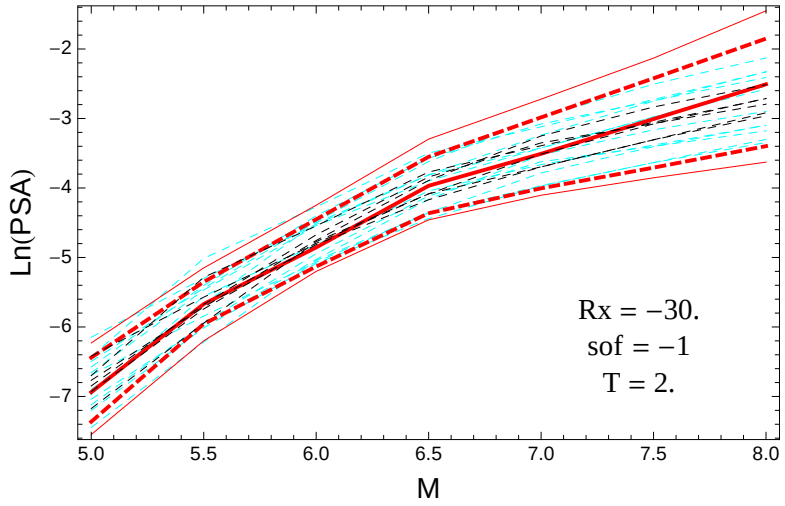



Figure 5.224: PVNGSv2: Magnitude scaling of the original GMPEs (dashed black), the original GMPEs with uncertainty model (dashed cyan) and 0.05,0.5,0.95 quantile of the combined ModelA and ModelB distribution (red) with total weights, for a scenario with $R_X = -30.$, $F = -1$, and $T = 2.$s.

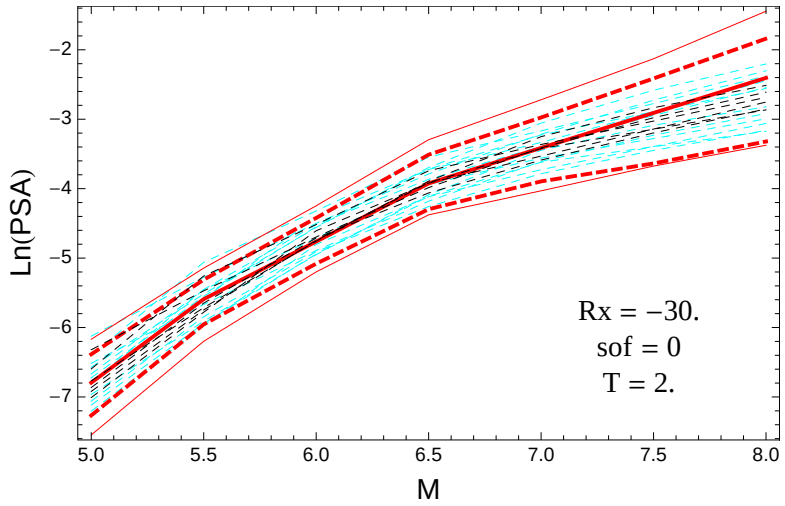



Figure 5.225: PVNGSv2: Magnitude scaling of the original GMPEs (dashed black), the original GMPEs with uncertainty model (dashed cyan) and 0.05,0.5,0.95 quantile of the combined ModelA and ModelB distribution (red) with total weights, for a scenario with $R_X = -30.$, $F = 0$, and $T = 2.$s.

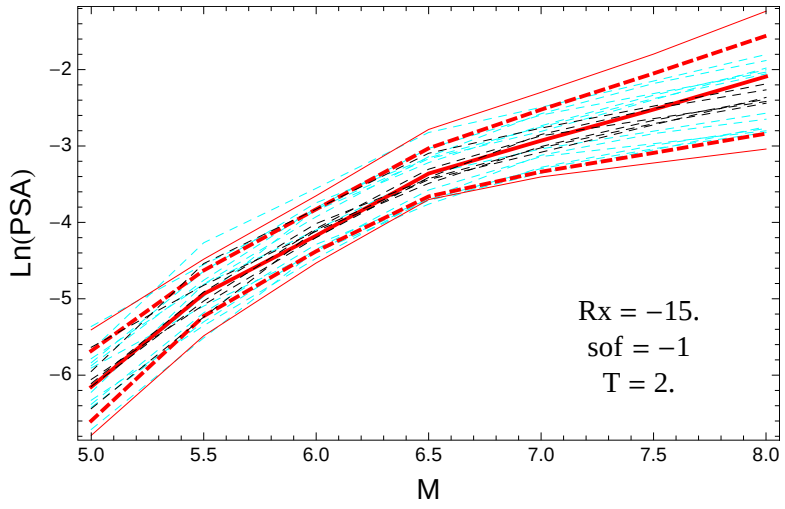



Figure 5.226: PVNGSv2: Magnitude scaling of the original GMPEs (dashed black), the original GMPEs with uncertainty model (dashed cyan) and 0.05,0.5,0.95 quantile of the combined ModelA and ModelB distribution (red) with total weights, for a scenario with $R_X = -15.$, $F = -1$, and $T = 2.$s.

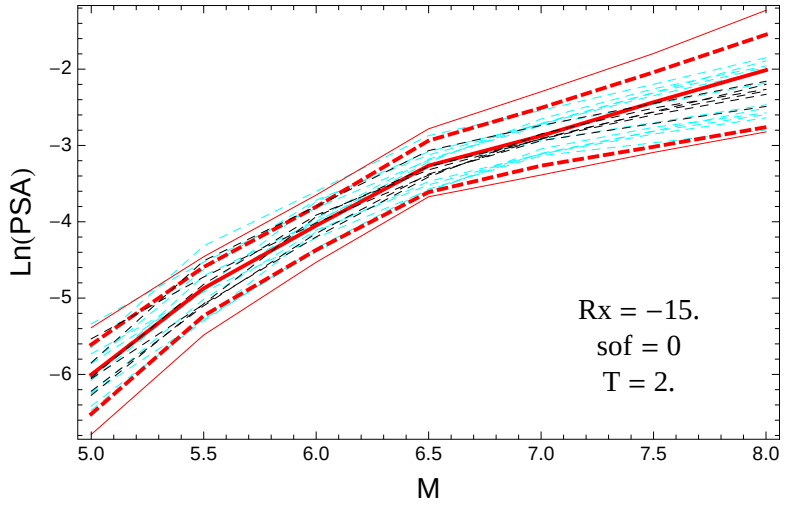



Figure 5.227: PVNGSv2: Magnitude scaling of the original GMPEs (dashed black), the original GMPEs with uncertainty model (dashed cyan) and 0.05,0.5,0.95 quantile of the combined ModelA and ModelB distribution (red) with total weights, for a scenario with $R_X = -15.$, $F = 0$, and $T = 2.$s.

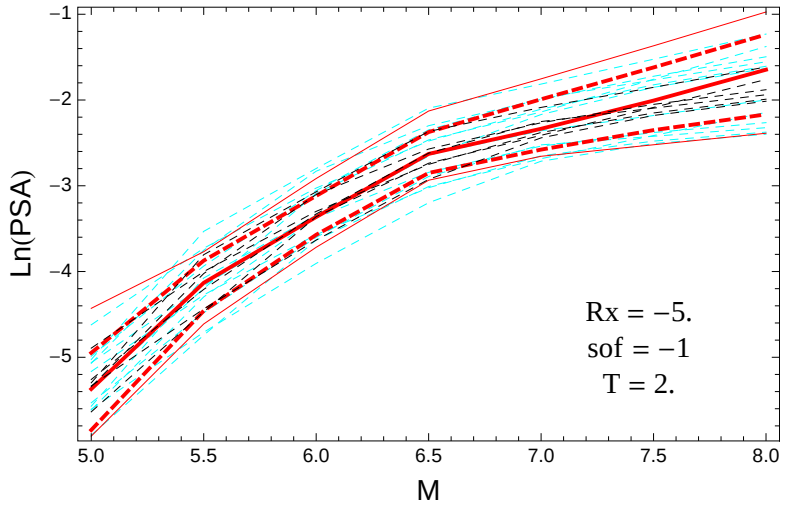



Figure 5.228: PVNGSv2: Magnitude scaling of the original GMPEs (dashed black), the original GMPEs with uncertainty model (dashed cyan) and 0.05,0.5,0.95 quantile of the combined ModelA and ModelB distribution (red) with total weights, for a scenario with $R_X = -5.$, $F = -1$, and $T = 2.$s.

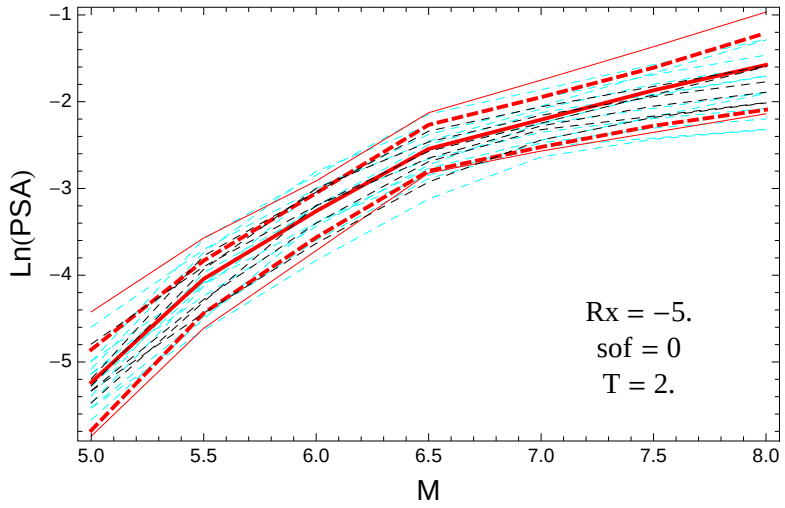



Figure 5.229: PVNGSv2: Magnitude scaling of the original GMPEs (dashed black), the original GMPEs with uncertainty model (dashed cyan) and 0.05,0.5,0.95 quantile of the combined ModelA and ModelB distribution (red) with total weights, for a scenario with $R_X = -5.$, $F = 0$, and $T = 2.$s.

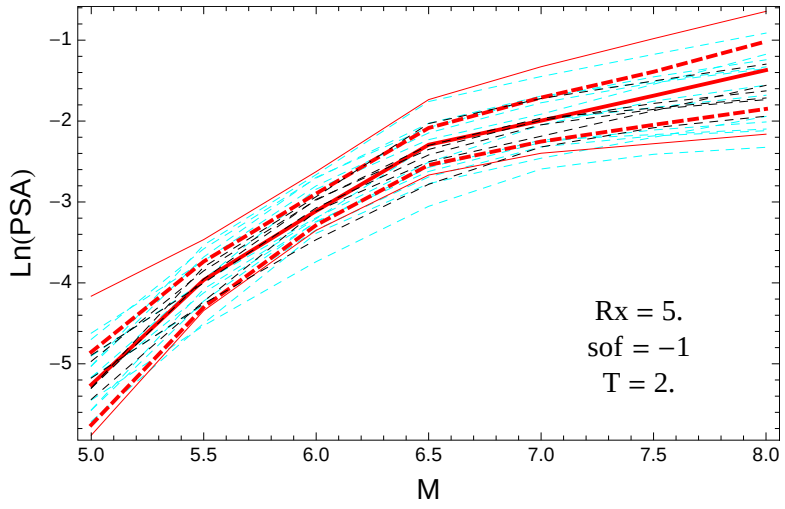



Figure 5.230: PVNGSv2: Magnitude scaling of the original GMPEs (dashed black), the original GMPEs with uncertainty model (dashed cyan) and 0.05,0.5,0.95 quantile of the combined ModelA and ModelB distribution (red) with total weights, for a scenario with $R_X = 5.$, $F = -1$, and $T = 2.$s.

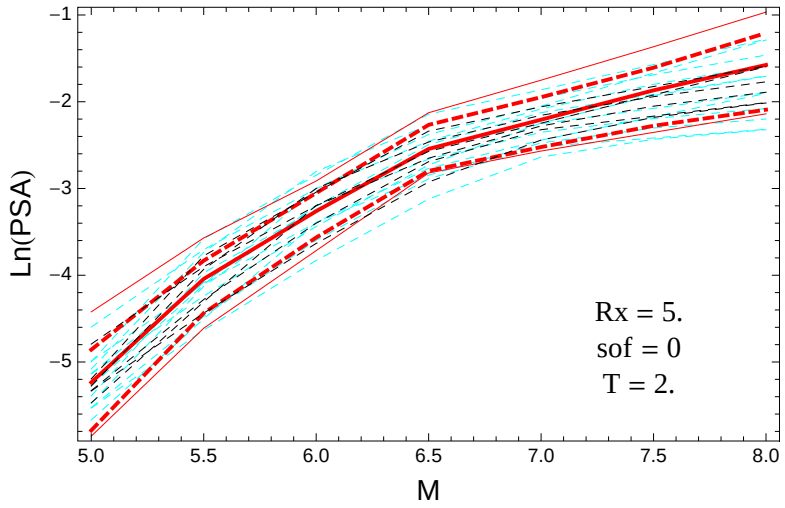



Figure 5.231: PVNGSv2: Magnitude scaling of the original GMPEs (dashed black), the original GMPEs with uncertainty model (dashed cyan) and 0.05,0.5,0.95 quantile of the combined ModelA and ModelB distribution (red) with total weights, for a scenario with $R_X = 5.$, $F = 0$, and $T = 2.$s.

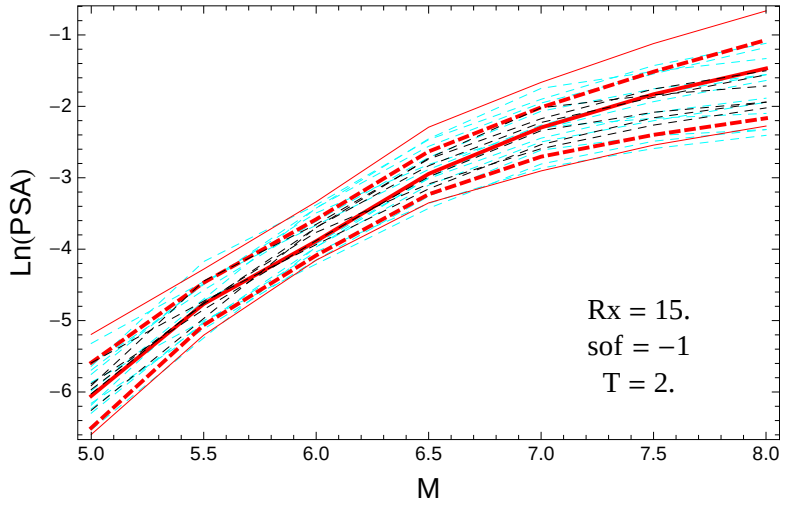



Figure 5.232: PVNGSv2: Magnitude scaling of the original GMPEs (dashed black), the original GMPEs with uncertainty model (dashed cyan) and 0.05,0.5,0.95 quantile of the combined ModelA and ModelB distribution (red) with total weights, for a scenario with $R_X = 15.$, $F = -1$, and $T = 2.$s.

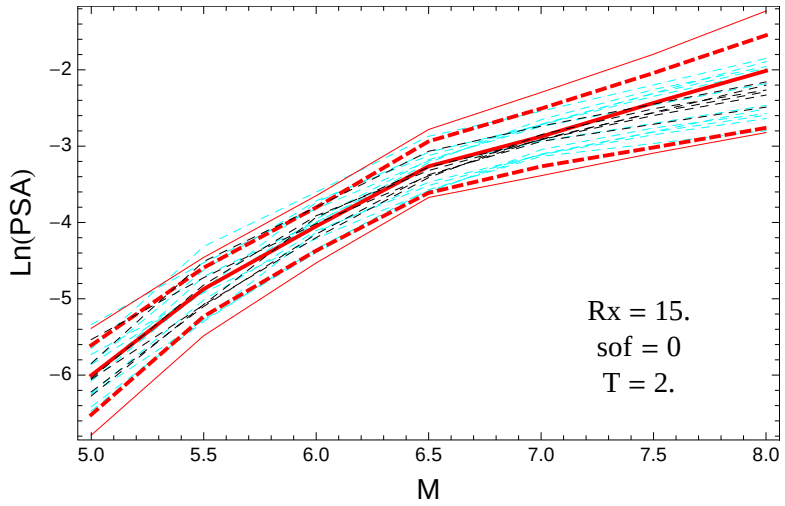



Figure 5.233: PVNGSv2: Magnitude scaling of the original GMPEs (dashed black), the original GMPEs with uncertainty model (dashed cyan) and 0.05,0.5,0.95 quantile of the combined ModelA and ModelB distribution (red) with total weights, for a scenario with $R_X = 15.$, $F = 0$, and $T = 2.$s.

**T = 3.s**

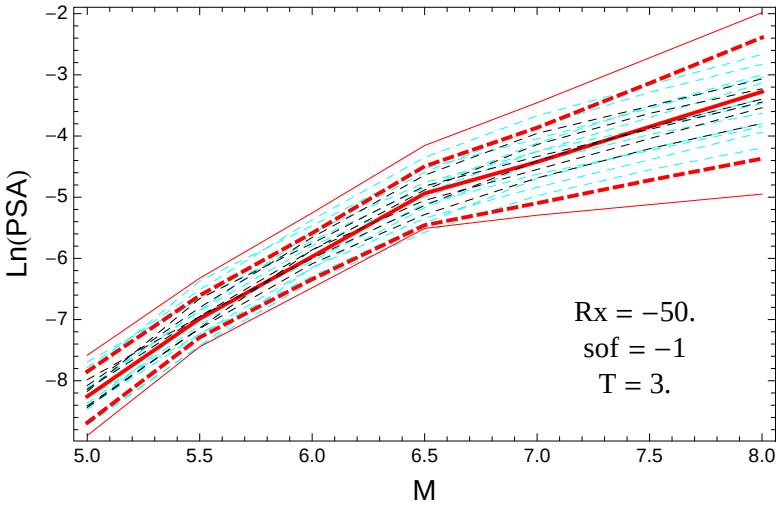



Figure 5.234: PVNGSv2: Magnitude scaling of the original GMPEs (dashed black), the original GMPEs with uncertainty model (dashed cyan) and 0.05,0.5,0.95 quantile of the combined ModelA and ModelB distribution (red) with total weights, for a scenario with $R_X = -50.$, $F = -1$, and $T = 3.$s.

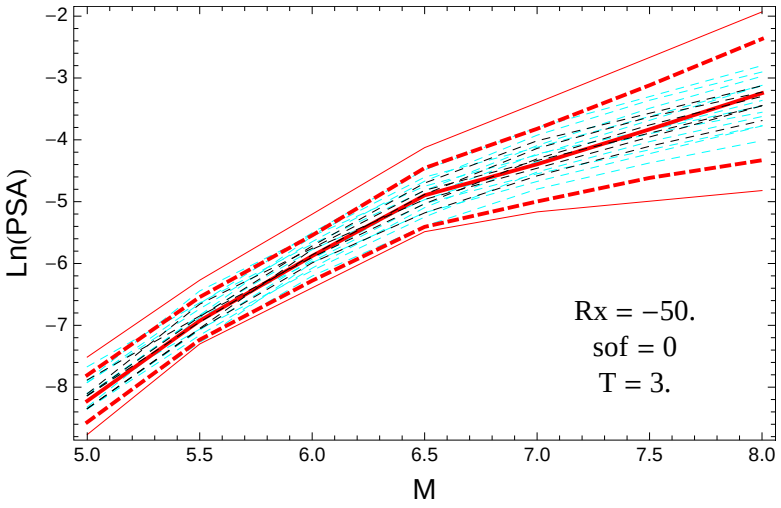



Figure 5.235: PVNGSv2: Magnitude scaling of the original GMPEs (dashed black), the original GMPEs with uncertainty model (dashed cyan) and 0.05,0.5,0.95 quantile of the combined ModelA and ModelB distribution (red) with total weights, for a scenario with $R_X = -50.$, $F = 0$, and $T = 3.$s.

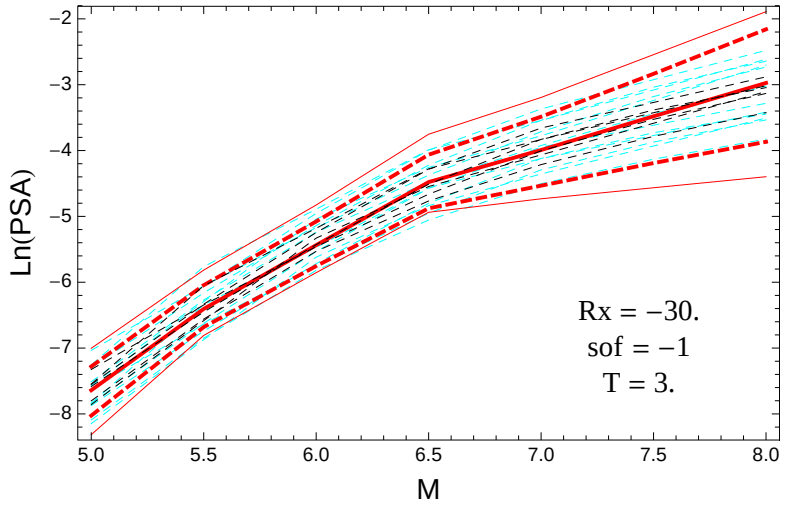



Figure 5.236: PVNGSv2: Magnitude scaling of the original GMPEs (dashed black), the original GMPEs with uncertainty model (dashed cyan) and 0.05,0.5,0.95 quantile of the combined ModelA and ModelB distribution (red) with total weights, for a scenario with $R_X = -30.$, $F = -1$, and $T = 3.$s.

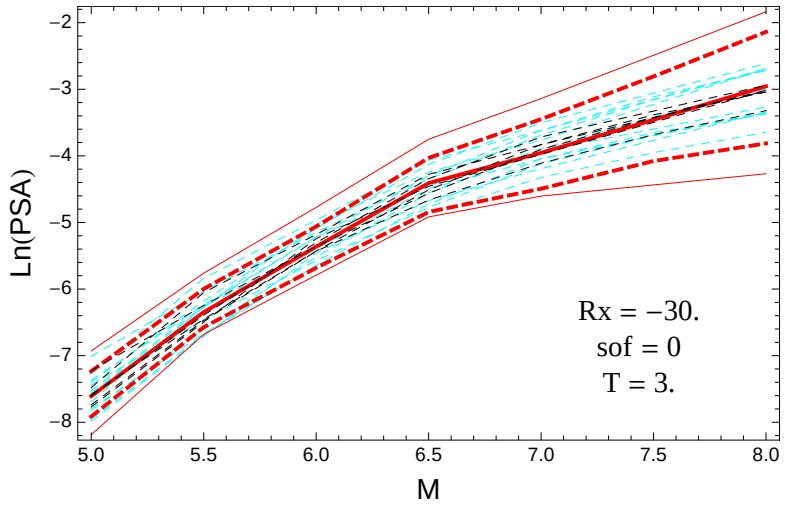



Figure 5.237: PVNGSv2: Magnitude scaling of the original GMPEs (dashed black), the original GMPEs with uncertainty model (dashed cyan) and 0.05,0.5,0.95 quantile of the combined ModelA and ModelB distribution (red) with total weights, for a scenario with $R_X = -30.$, $F = 0$, and $T = 3.$s.

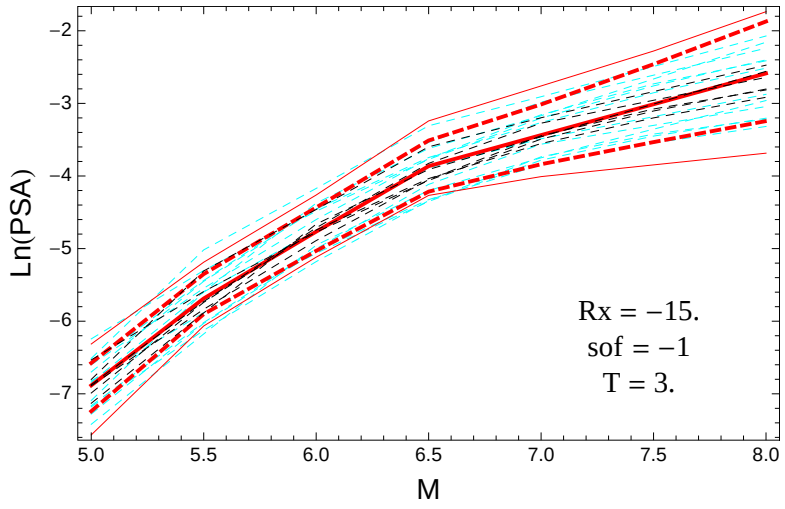



Figure 5.238: PVNGSv2: Magnitude scaling of the original GMPEs (dashed black), the original GMPEs with uncertainty model (dashed cyan) and 0.05,0.5,0.95 quantile of the combined ModelA and ModelB distribution (red) with total weights, for a scenario with $R_X = -15.$, $F = -1$, and $T = 3.$s.

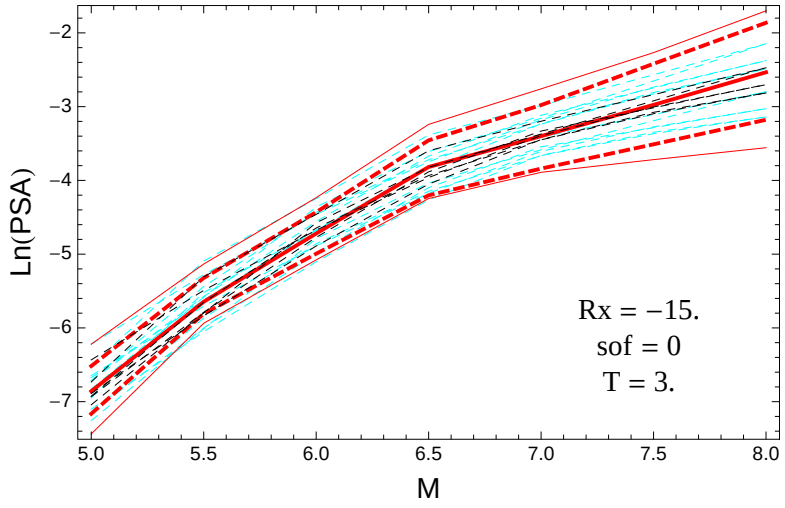



Figure 5.239: PVNGSv2: Magnitude scaling of the original GMPEs (dashed black), the original GMPEs with uncertainty model (dashed cyan) and 0.05,0.5,0.95 quantile of the combined ModelA and ModelB distribution (red) with total weights, for a scenario with $R_X = -15.$, $F = 0$, and $T = 3.$s.

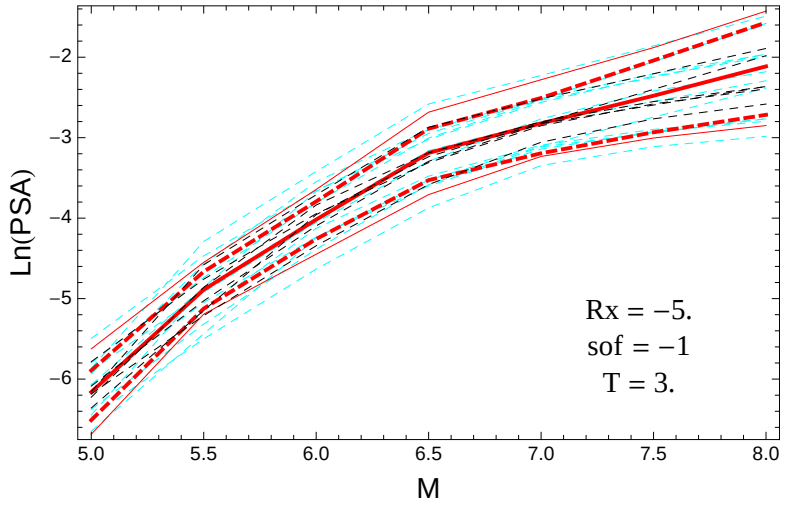



Figure 5.240: PVNGSv2: Magnitude scaling of the original GMPEs (dashed black), the original GMPEs with uncertainty model (dashed cyan) and 0.05,0.5,0.95 quantile of the combined ModelA and ModelB distribution (red) with total weights, for a scenario with $R_X = -5.$, $F = -1$, and $T = 3.$s.

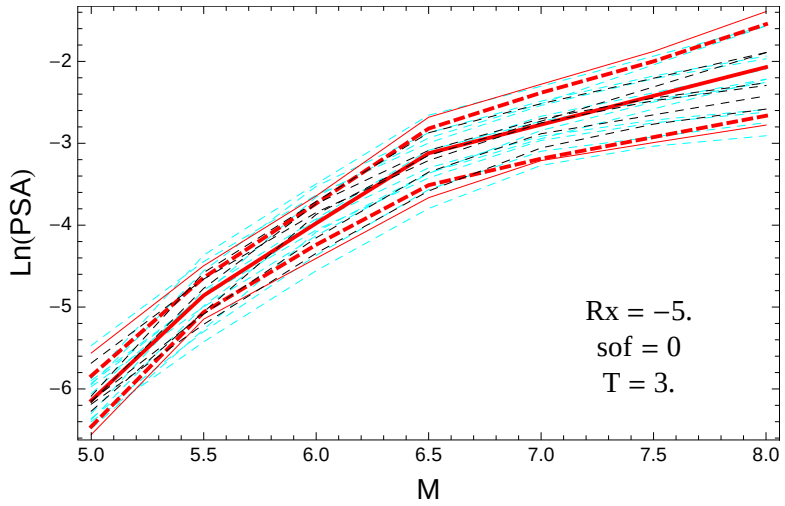



Figure 5.241: PVNGSv2: Magnitude scaling of the original GMPEs (dashed black), the original GMPEs with uncertainty model (dashed cyan) and 0.05,0.5,0.95 quantile of the combined ModelA and ModelB distribution (red) with total weights, for a scenario with $R_X = -5.$, $F = 0$, and $T = 3.$s.

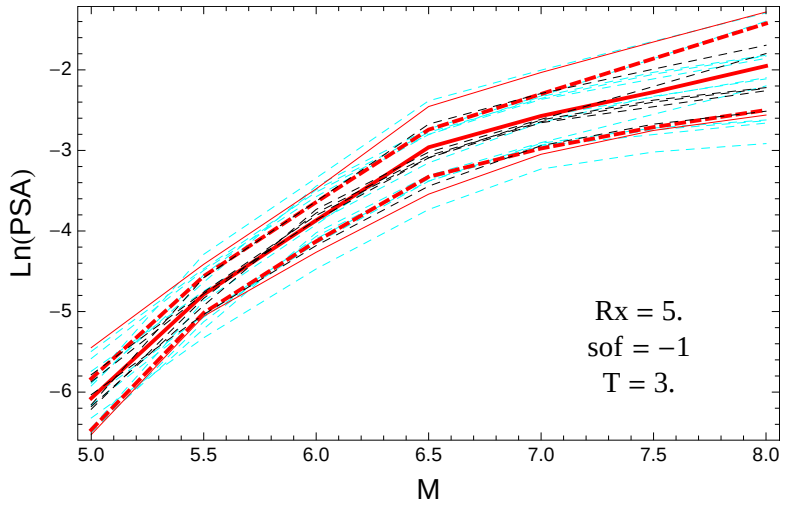



Figure 5.242: PVNGSv2: Magnitude scaling of the original GMPEs (dashed black), the original GMPEs with uncertainty model (dashed cyan) and 0.05,0.5,0.95 quantile of the combined ModelA and ModelB distribution (red) with total weights, for a scenario with $R_X = 5.$, $F = -1$, and $T = 3.$s.

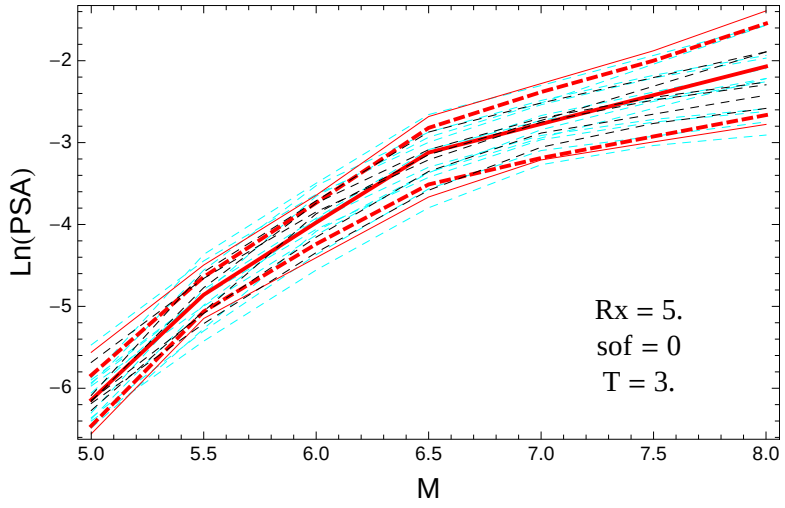



Figure 5.243: PVNGSv2: Magnitude scaling of the original GMPEs (dashed black), the original GMPEs with uncertainty model (dashed cyan) and 0.05,0.5,0.95 quantile of the combined ModelA and ModelB distribution (red) with total weights, for a scenario with $R_X = 5.$, $F = 0$, and $T = 3.$s.

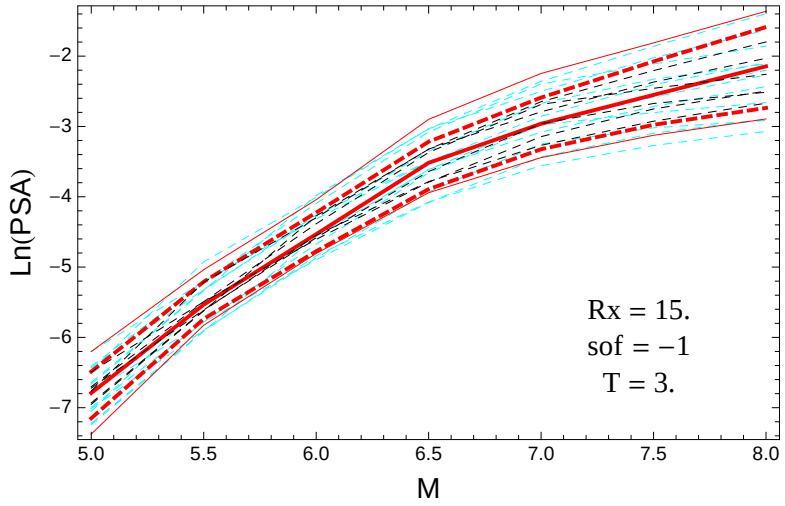



Figure 5.244: PVNGSv2: Magnitude scaling of the original GMPEs (dashed black), the original GMPEs with uncertainty model (dashed cyan) and 0.05,0.5,0.95 quantile of the combined ModelA and ModelB distribution (red) with total weights, for a scenario with $R_X = 15.$, $F = -1$, and $T = 3.$s.

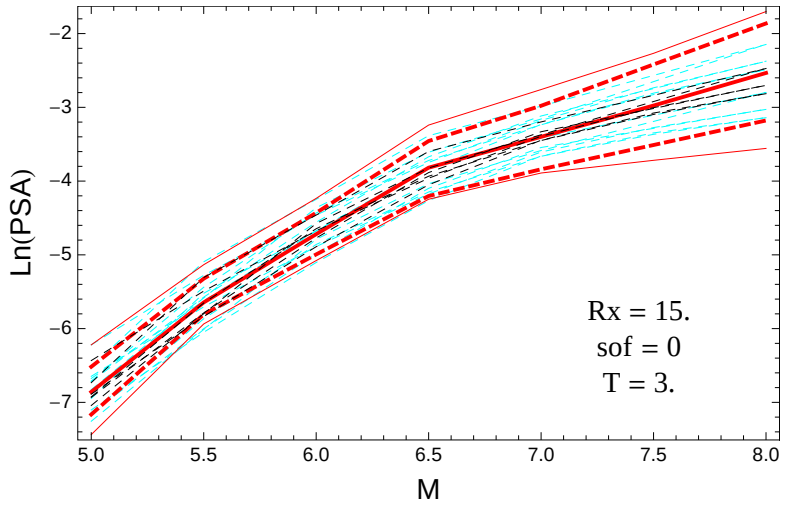



Figure 5.245: PVNGSv2: Magnitude scaling of the original GMPEs (dashed black), the original GMPEs with uncertainty model (dashed cyan) and 0.05,0.5,0.95 quantile of the combined ModelA and ModelB distribution (red) with total weights, for a scenario with $R_X = 15.$, $F = 0$, and $T = 3.$s.

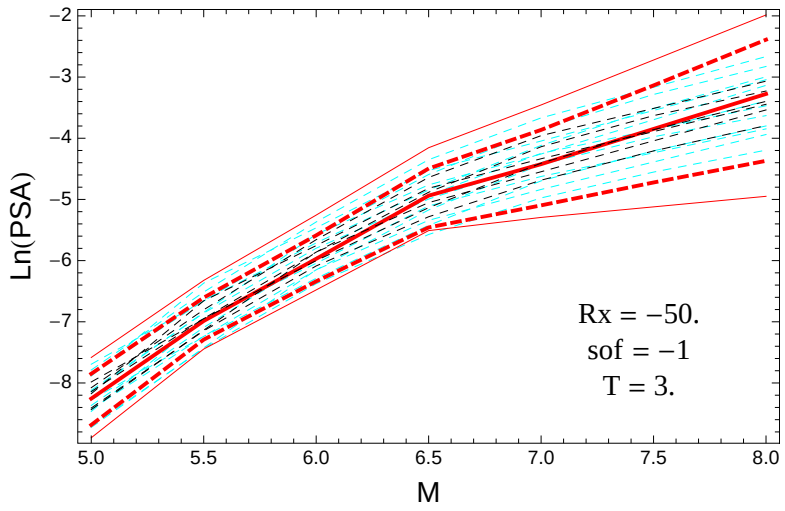



Figure 5.246: PVNGSv2: Magnitude scaling of the original GMPEs (dashed black), the original GMPEs with uncertainty model (dashed cyan) and 0.05,0.5,0.95 quantile of the combined ModelA and ModelB distribution (red) with total weights, for a scenario with $R_X = -50.$, $F = -1$, and $T = 3$.s.

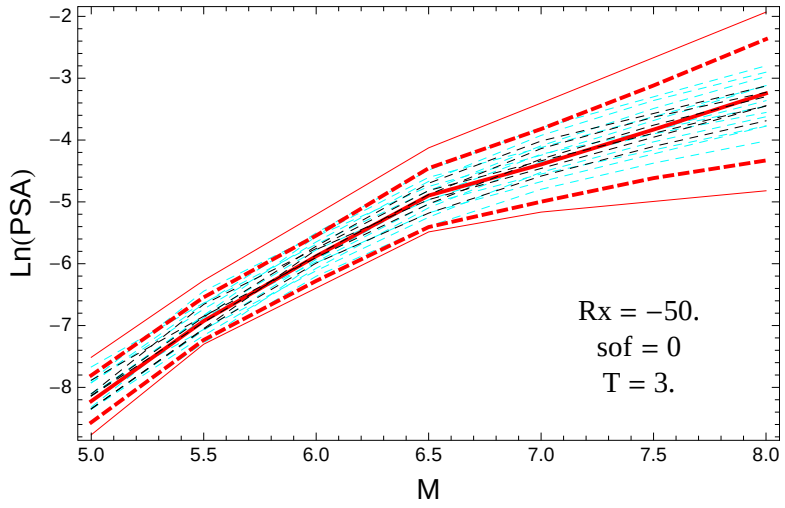



Figure 5.247: PVNGSv2: Magnitude scaling of the original GMPEs (dashed black), the original GMPEs with uncertainty model (dashed cyan) and 0.05,0.5,0.95 quantile of the combined ModelA and ModelB distribution (red) with total weights, for a scenario with $R_X = -50.$, $F = 0$, and $T = 3$.s.

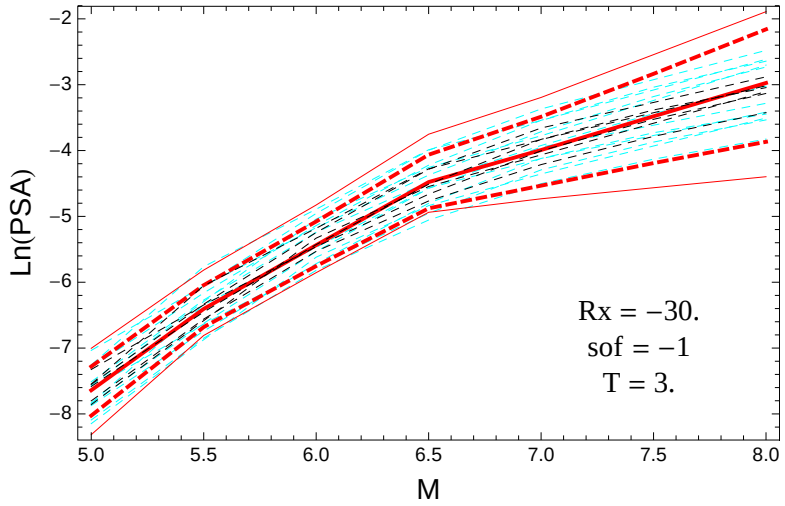



Figure 5.248: PVNGSv2: Magnitude scaling of the original GMPEs (dashed black), the original GMPEs with uncertainty model (dashed cyan) and 0.05,0.5,0.95 quantile of the combined ModelA and ModelB distribution (red) with total weights, for a scenario with $R_X = -30.$, $F = -1$, and $T = 3.$s.

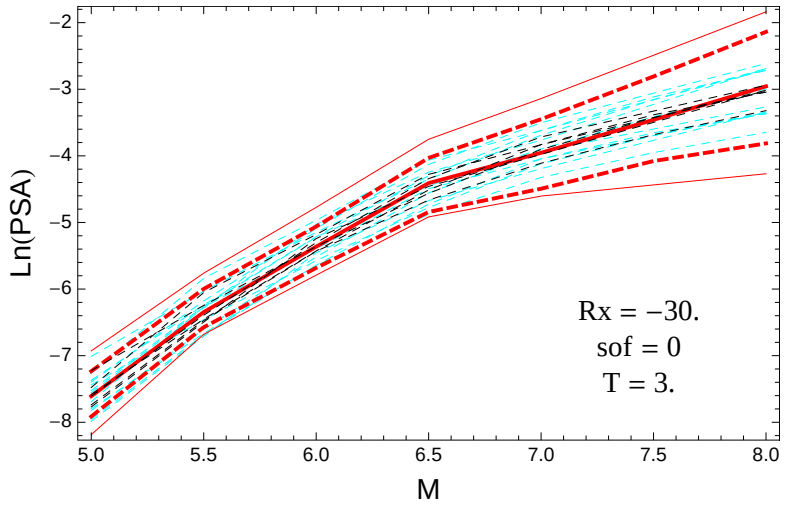



Figure 5.249: PVNGSv2: Magnitude scaling of the original GMPEs (dashed black), the original GMPEs with uncertainty model (dashed cyan) and 0.05,0.5,0.95 quantile of the combined ModelA and ModelB distribution (red) with total weights, for a scenario with $R_X = -30.$, $F = 0$, and $T = 3.$s.

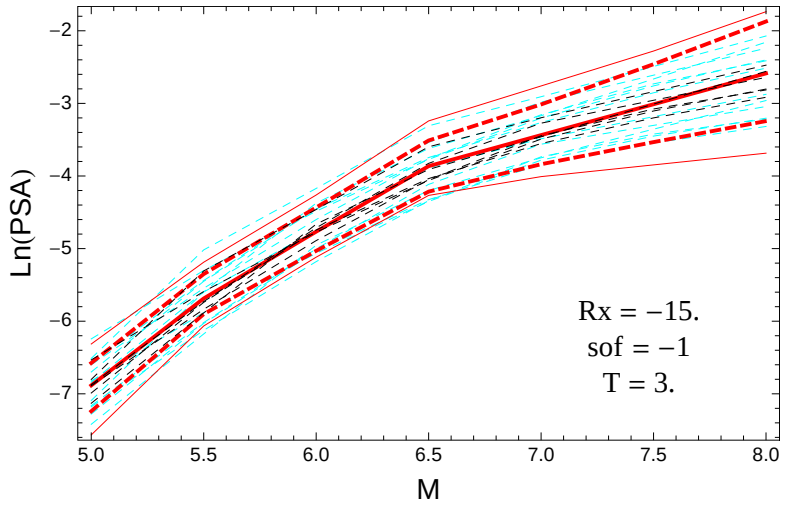



Figure 5.250: PVNGSv2: Magnitude scaling of the original GMPEs (dashed black), the original GMPEs with uncertainty model (dashed cyan) and 0.05,0.5,0.95 quantile of the combined ModelA and ModelB distribution (red) with total weights, for a scenario with $R_X = -15.$, $F = -1$, and $T = 3.$s.

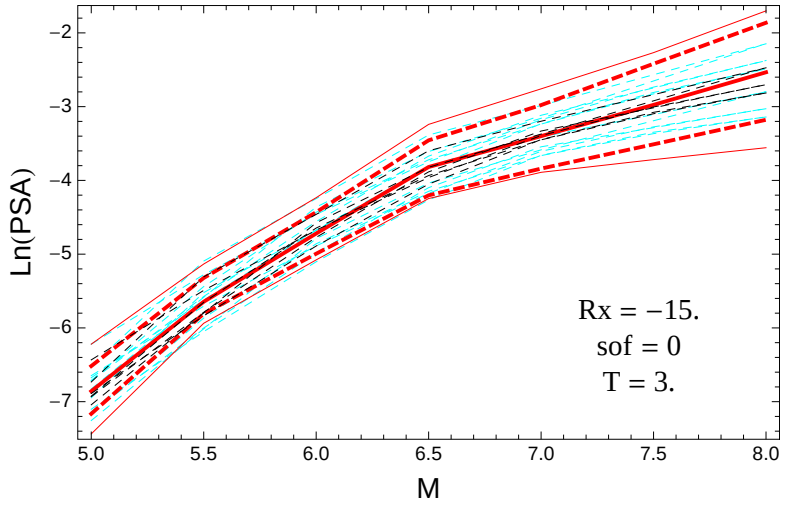



Figure 5.251: PVNGSv2: Magnitude scaling of the original GMPEs (dashed black), the original GMPEs with uncertainty model (dashed cyan) and 0.05,0.5,0.95 quantile of the combined ModelA and ModelB distribution (red) with total weights, for a scenario with $R_X = -15.$, $F = 0$, and $T = 3.$s.

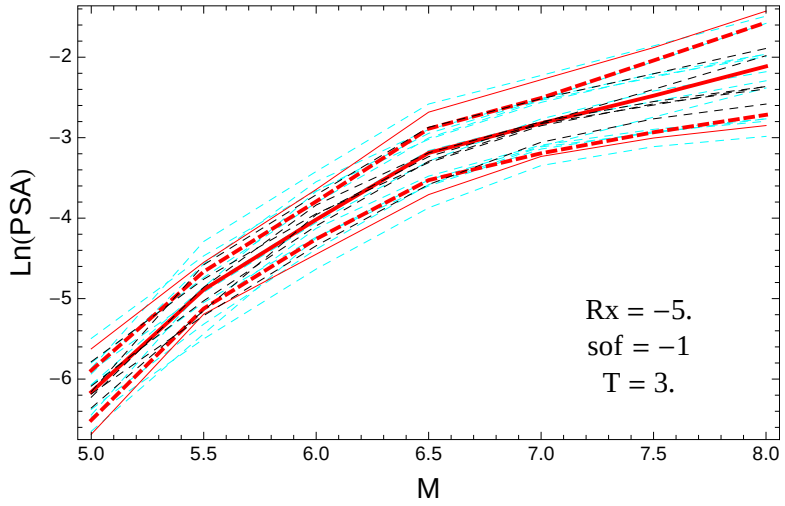



Figure 5.252: PVNGSv2: Magnitude scaling of the original GMPEs (dashed black), the original GMPEs with uncertainty model (dashed cyan) and 0.05,0.5,0.95 quantile of the combined ModelA and ModelB distribution (red) with total weights, for a scenario with $R_X = -5.$, $F = -1$, and $T = 3.$s.

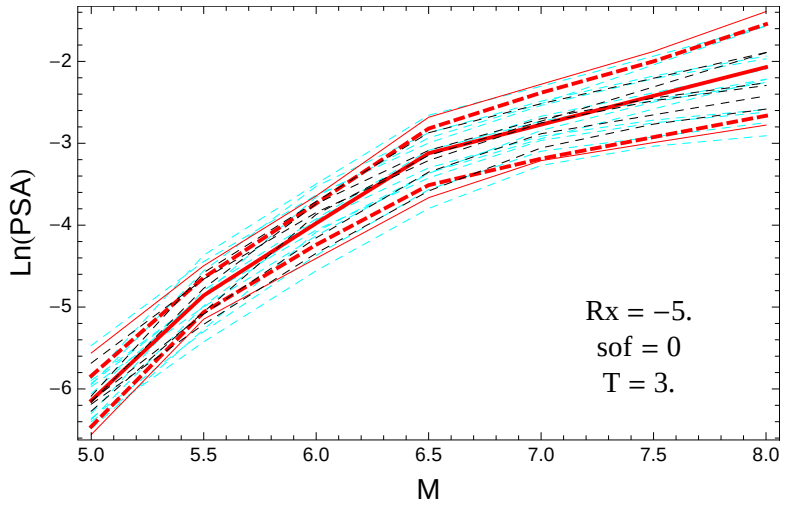



Figure 5.253: PVNGSv2: Magnitude scaling of the original GMPEs (dashed black), the original GMPEs with uncertainty model (dashed cyan) and 0.05,0.5,0.95 quantile of the combined ModelA and ModelB distribution (red) with total weights, for a scenario with $R_X = -5.$, $F = 0$, and $T = 3.$s.

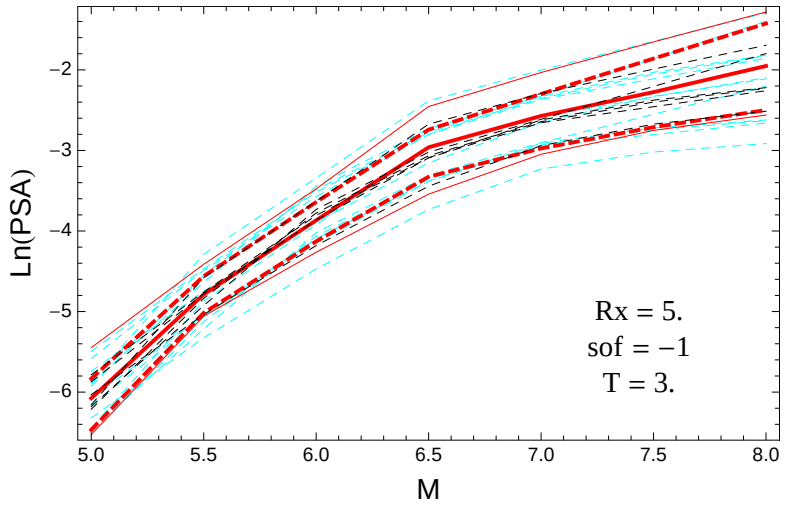



Figure 5.254: PVNGSv2: Magnitude scaling of the original GMPEs (dashed black), the original GMPEs with uncertainty model (dashed cyan) and 0.05,0.5,0.95 quantile of the combined ModelA and ModelB distribution (red) with total weights, for a scenario with $R_X = 5.$, $F = -1$, and $T = 3.$s.

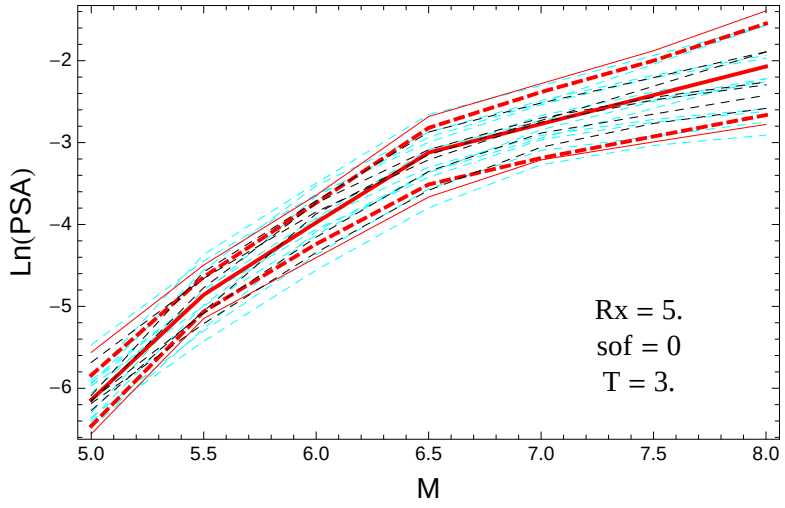



Figure 5.255: PVNGSv2: Magnitude scaling of the original GMPEs (dashed black), the original GMPEs with uncertainty model (dashed cyan) and 0.05,0.5,0.95 quantile of the combined ModelA and ModelB distribution (red) with total weights, for a scenario with $R_X = 5.$, $F = 0$, and $T = 3.$s.

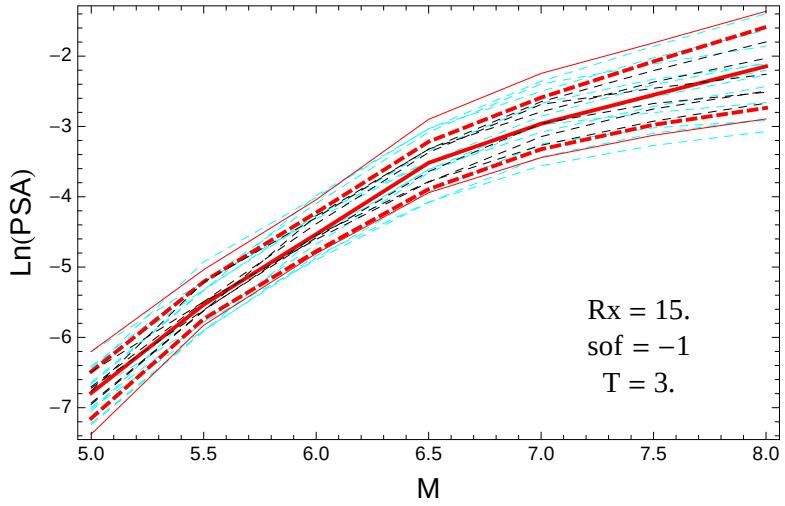



Figure 5.256: PVNGSv2: Magnitude scaling of the original GMPEs (dashed black), the original GMPEs with uncertainty model (dashed cyan) and 0.05,0.5,0.95 quantile of the combined ModelA and ModelB distribution (red) with total weights, for a scenario with $R_X = 15.$, $F = -1$, and $T = 3.$s.

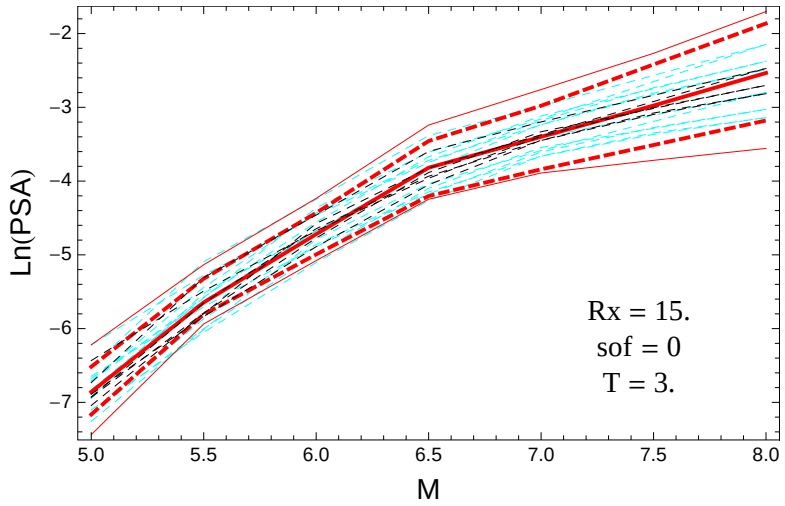



Figure 5.257: PVNGSv2: Magnitude scaling of the original GMPEs (dashed black), the original GMPEs with uncertainty model (dashed cyan) and 0.05,0.5,0.95 quantile of the combined ModelA and ModelB distribution (red) with total weights, for a scenario with $R_X = 15.$, $F = 0$, and $T = 3.$s.

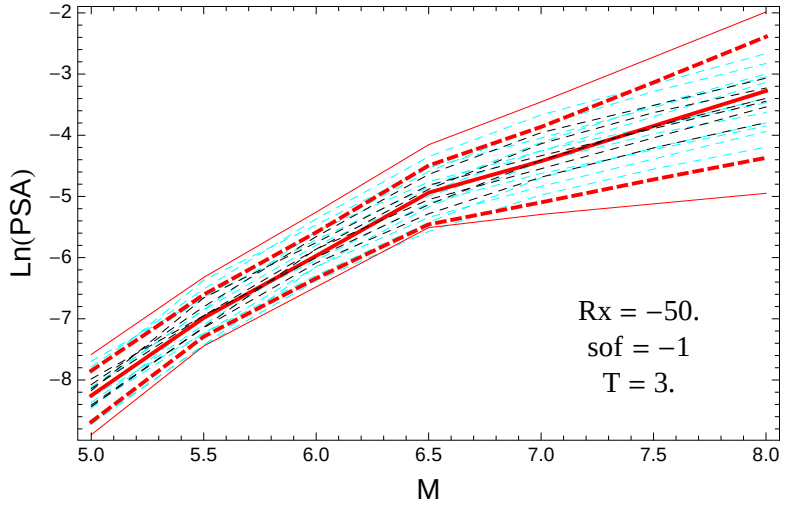



Figure 5.258: PVNGSv2: Magnitude scaling of the original GMPEs (dashed black), the original GMPEs with uncertainty model (dashed cyan) and 0.05,0.5,0.95 quantile of the combined ModelA and ModelB distribution (red) with total weights, for a scenario with $R_X = -50.$, $F = -1$, and $T = 3.$s.

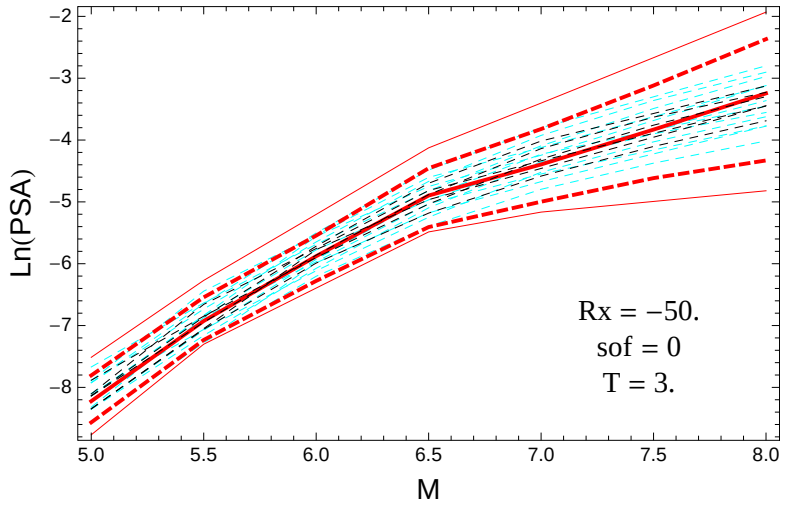



Figure 5.259: PVNGSv2: Magnitude scaling of the original GMPEs (dashed black), the original GMPEs with uncertainty model (dashed cyan) and 0.05,0.5,0.95 quantile of the combined ModelA and ModelB distribution (red) with total weights, for a scenario with $R_X = -50.$, $F = 0$, and $T = 3.$s.

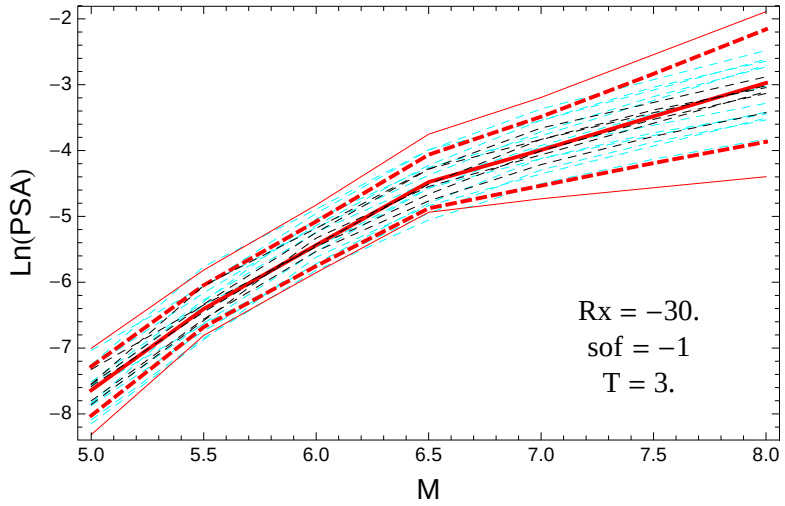



Figure 5.260: PVNGSv2: Magnitude scaling of the original GMPEs (dashed black), the original GMPEs with uncertainty model (dashed cyan) and 0.05,0.5,0.95 quantile of the combined ModelA and ModelB distribution (red) with total weights, for a scenario with $R_X = -30.$, $F = -1$, and $T = 3.$s.

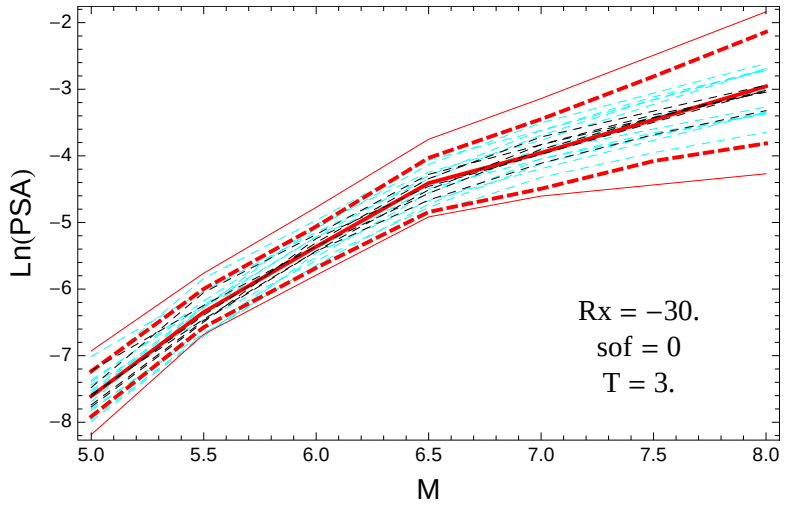



Figure 5.261: PVNGSv2: Magnitude scaling of the original GMPEs (dashed black), the original GMPEs with uncertainty model (dashed cyan) and 0.05,0.5,0.95 quantile of the combined ModelA and ModelB distribution (red) with total weights, for a scenario with $R_X = -30.$, $F = 0$, and $T = 3.$s.

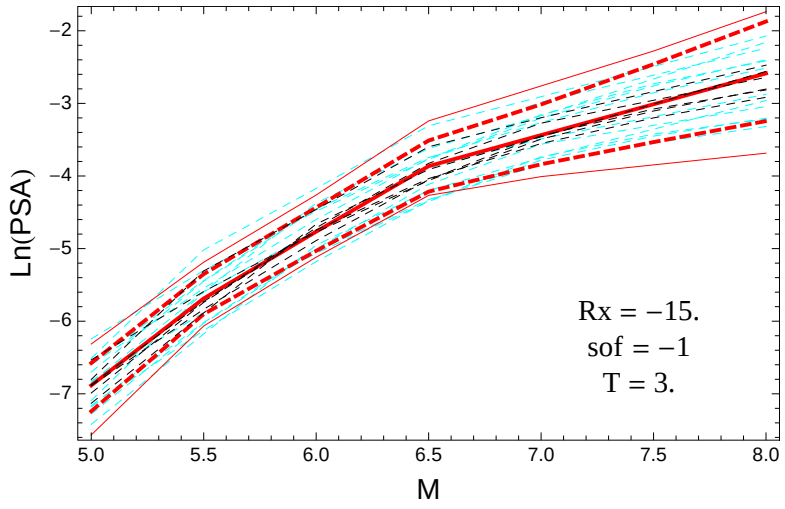



Figure 5.262: PVNGSv2: Magnitude scaling of the original GMPEs (dashed black), the original GMPEs with uncertainty model (dashed cyan) and 0.05,0.5,0.95 quantile of the combined ModelA and ModelB distribution (red) with total weights, for a scenario with $R_X = -15.$, $F = -1$, and $T = 3.$s.

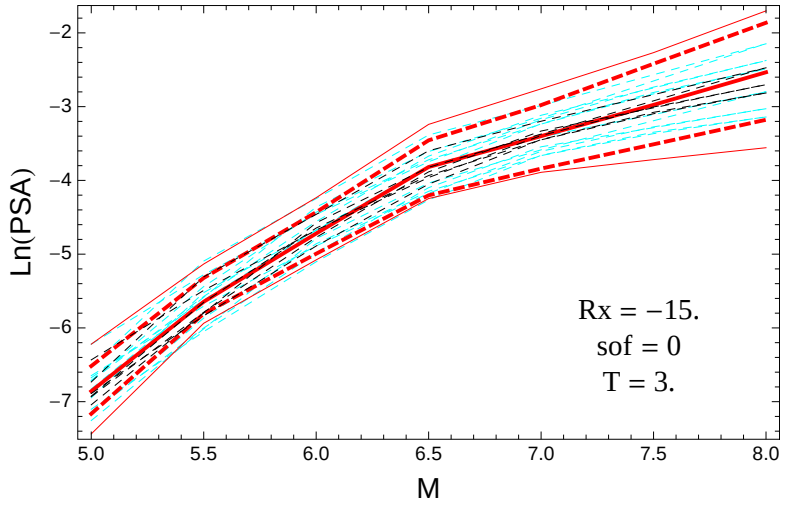



Figure 5.263: PVNGSv2: Magnitude scaling of the original GMPEs (dashed black), the original GMPEs with uncertainty model (dashed cyan) and 0.05,0.5,0.95 quantile of the combined ModelA and ModelB distribution (red) with total weights, for a scenario with $R_X = -15.$, $F = 0$, and $T = 3.$s.

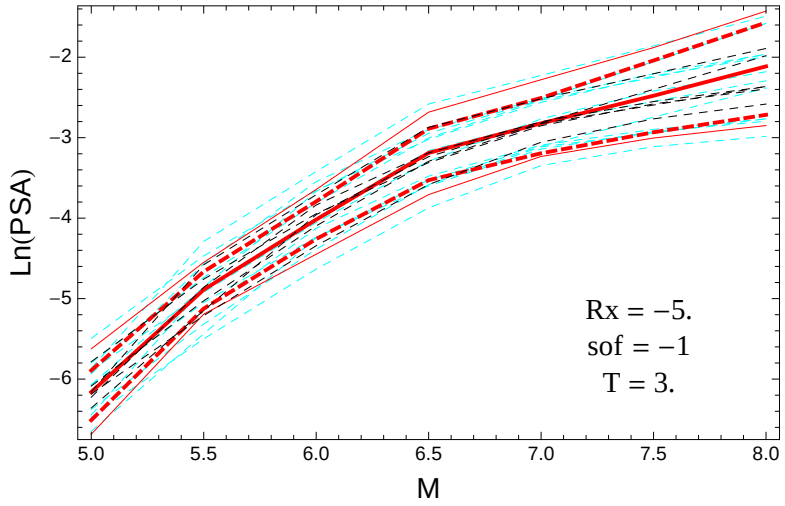



Figure 5.264: PVNGSv2: Magnitude scaling of the original GMPEs (dashed black), the original GMPEs with uncertainty model (dashed cyan) and 0.05,0.5,0.95 quantile of the combined ModelA and ModelB distribution (red) with total weights, for a scenario with $R_X = -5.$, $F = -1$, and $T = 3.$s.

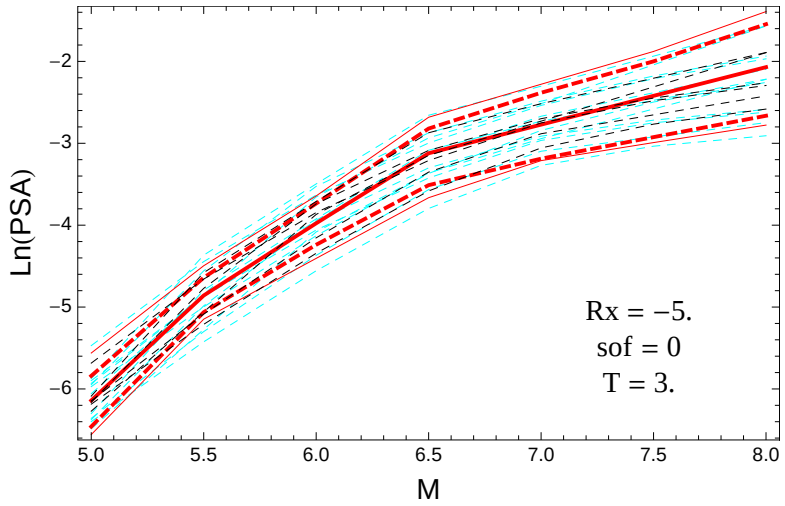



Figure 5.265: PVNGSv2: Magnitude scaling of the original GMPEs (dashed black), the original GMPEs with uncertainty model (dashed cyan) and 0.05,0.5,0.95 quantile of the combined ModelA and ModelB distribution (red) with total weights, for a scenario with $R_X = -5.$, $F = 0$, and $T = 3.$s.

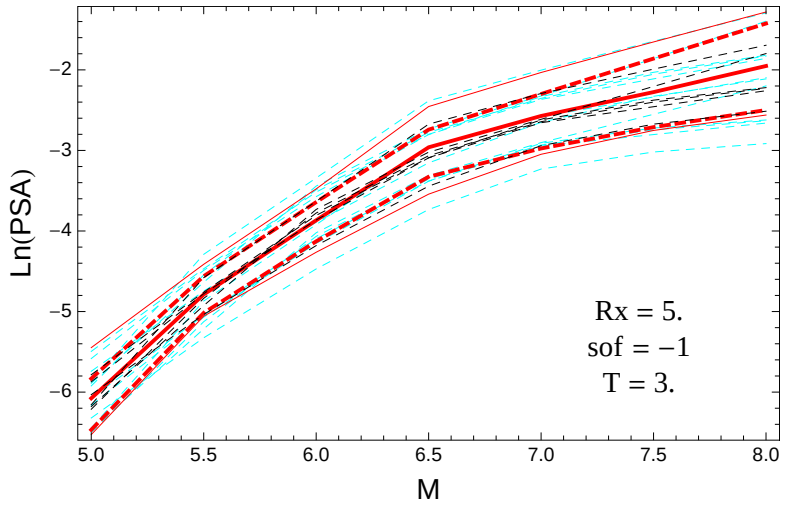



Figure 5.266: PVNGSv2: Magnitude scaling of the original GMPEs (dashed black), the original GMPEs with uncertainty model (dashed cyan) and 0.05,0.5,0.95 quantile of the combined ModelA and ModelB distribution (red) with total weights, for a scenario with $R_X = 5.$, $F = -1$, and $T = 3.$s.

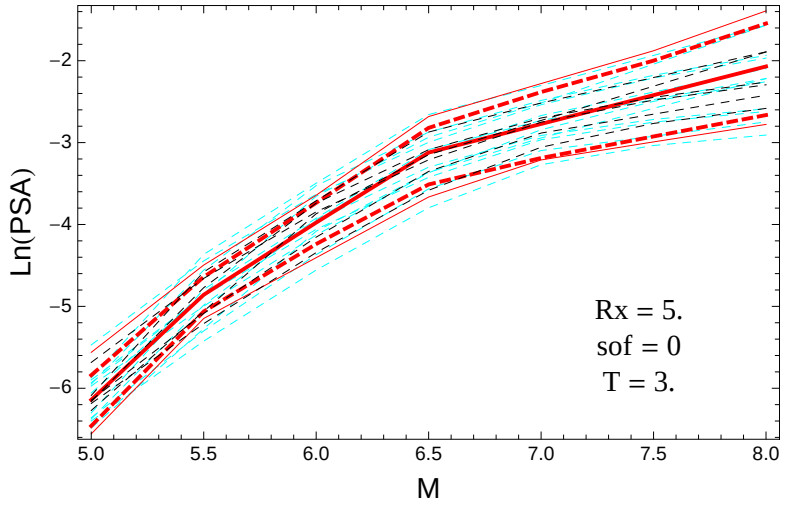



Figure 5.267: PVNGSv2: Magnitude scaling of the original GMPEs (dashed black), the original GMPEs with uncertainty model (dashed cyan) and 0.05,0.5,0.95 quantile of the combined ModelA and ModelB distribution (red) with total weights, for a scenario with $R_X = 5.$, $F = 0$, and $T = 3.$s.

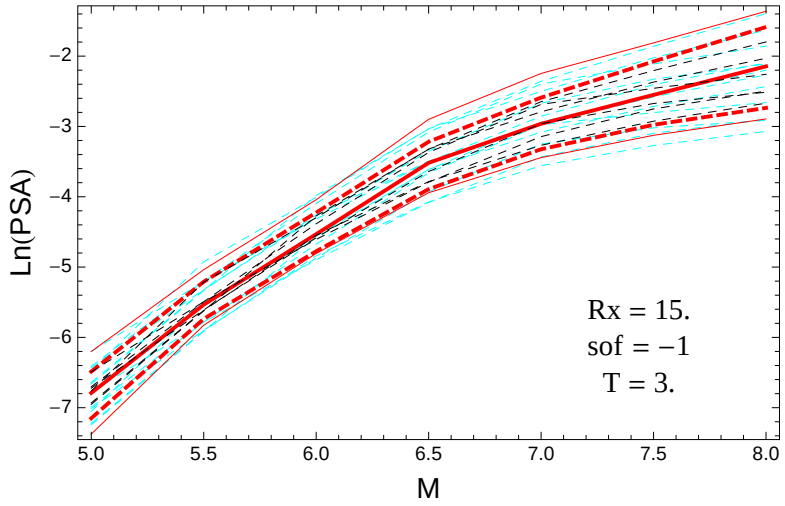



Figure 5.268: PVNGSv2: Magnitude scaling of the original GMPEs (dashed black), the original GMPEs with uncertainty model (dashed cyan) and 0.05,0.5,0.95 quantile of the combined ModelA and ModelB distribution (red) with total weights, for a scenario with $R_X = 15.$, $F = -1$, and $T = 3.$s.

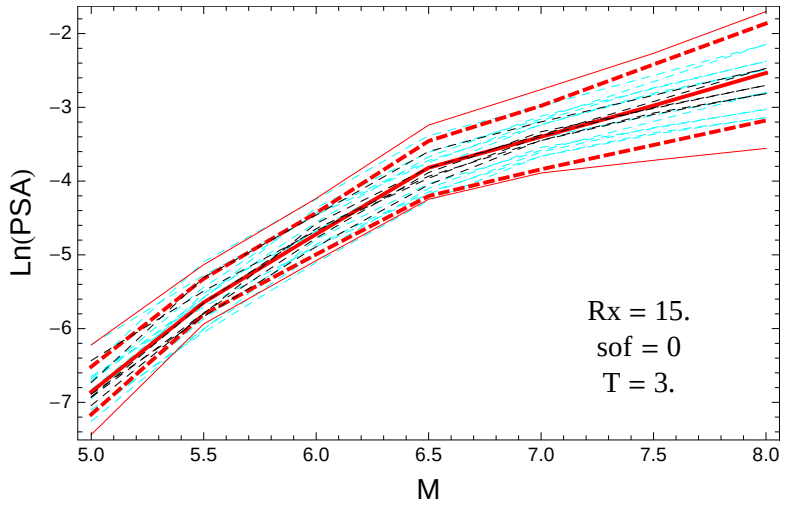



Figure 5.269: PVNGSv2: Magnitude scaling of the original GMPEs (dashed black), the original GMPEs with uncertainty model (dashed cyan) and 0.05,0.5,0.95 quantile of the combined ModelA and ModelB distribution (red) with total weights, for a scenario with $R_X = 15.$, $F = 0$, and $T = 3.$s.

### 5.1.4 Combined Quantile Plots vs. Period with GMPEs

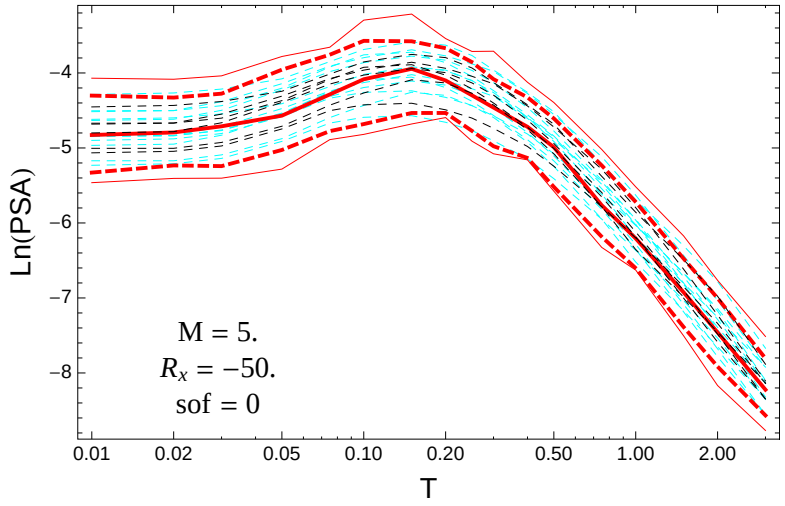



Figure 5.270: PVNGSv2: Spectra of 0.05,0.5,0.95 and the combined ModelA and ModelB distribution (red) with total weights, original GMPEs (dashed black) and the original GMPEs with uncertainty model (dashed cyan), for a scenario with $M_W = 5.$, $R_x = -50.$, $F = 0$.

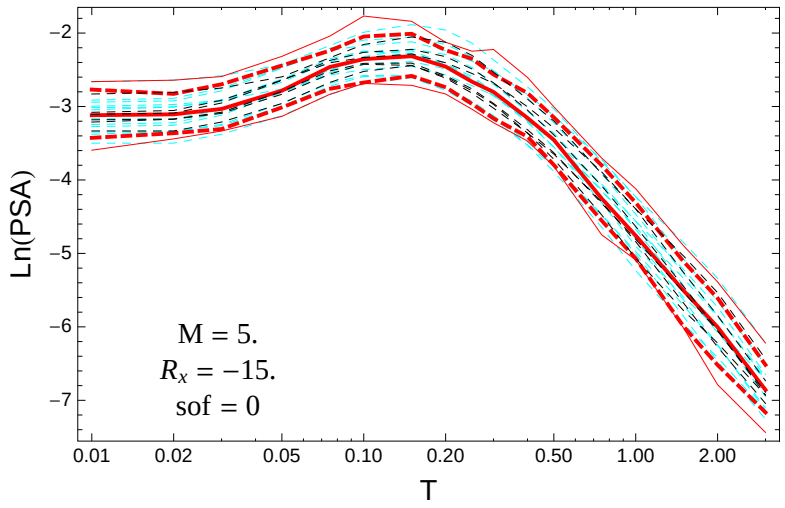



Figure 5.271: PVNGSv2: Spectra of 0.05,0.5,0.95 and the combined ModelA and ModelB distribution (red) with total weights, original GMPEs (dashed black) and the original GMPEs with uncertainty model (dashed cyan), for a scenario with $M_W = 5.$, $R_x = -15.$, $F = 0$.

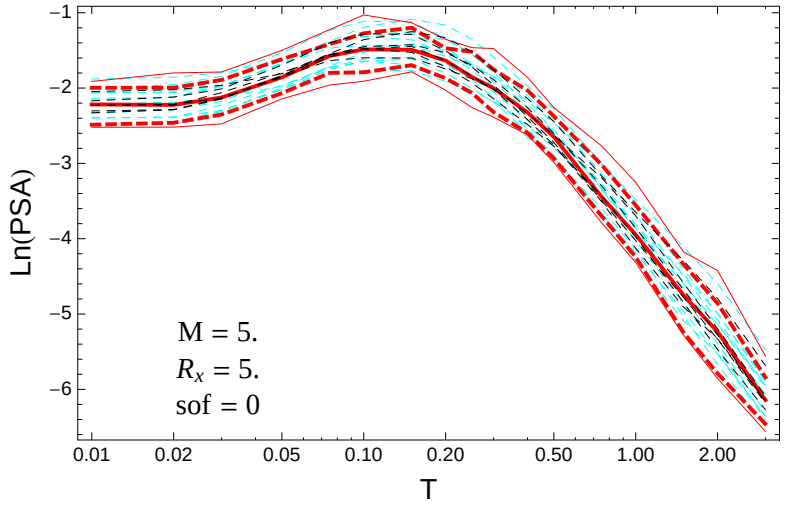



Figure 5.272: PVNGSv2: Spectra of 0.05,0.5,0.95 and the combined ModelA and ModelB distribution (red) with total weights, original GMPEs (dashed black) and the original GMPEs with uncertainty model (dashed cyan), for a scenario with $M_W = 5.$, $R_x = 5.$, $F = 0$.

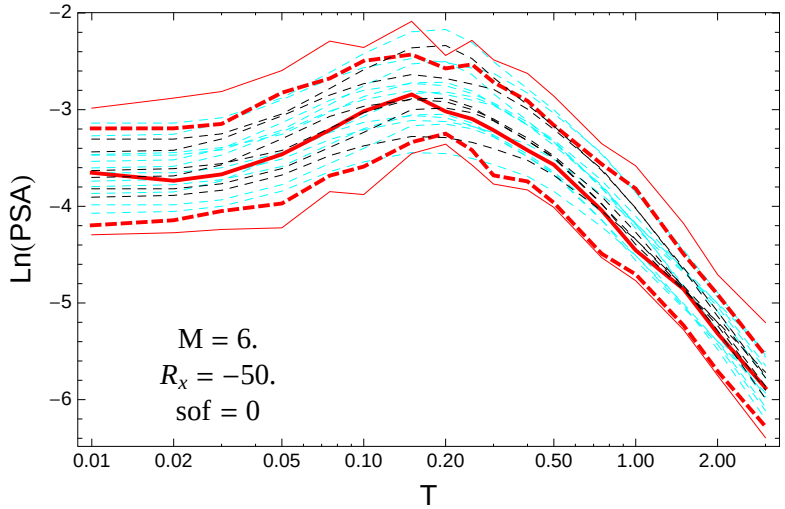



Figure 5.273: PVNGSv2: Spectra of 0.05,0.5,0.95 and the combined ModelA and ModelB distribution (red) with total weights, original GMPEs (dashed black) and the original GMPEs with uncertainty model (dashed cyan), for a scenario with $M_W = 6.$, $R_x = -50.$, $F = 0$.

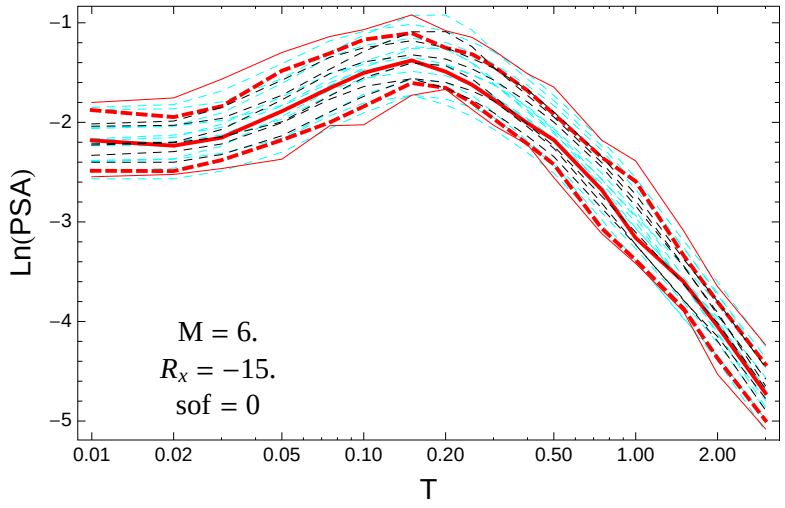



Figure 5.274: PVNGSv2: Spectra of 0.05,0.5,0.95 and the combined ModelA and ModelB distribution (red) with total weights, original GMPEs (dashed black) and the original GMPEs with uncertainty model (dashed cyan), for a scenario with $M_W = 6.$, $R_x = -15.$, $F = 0$.

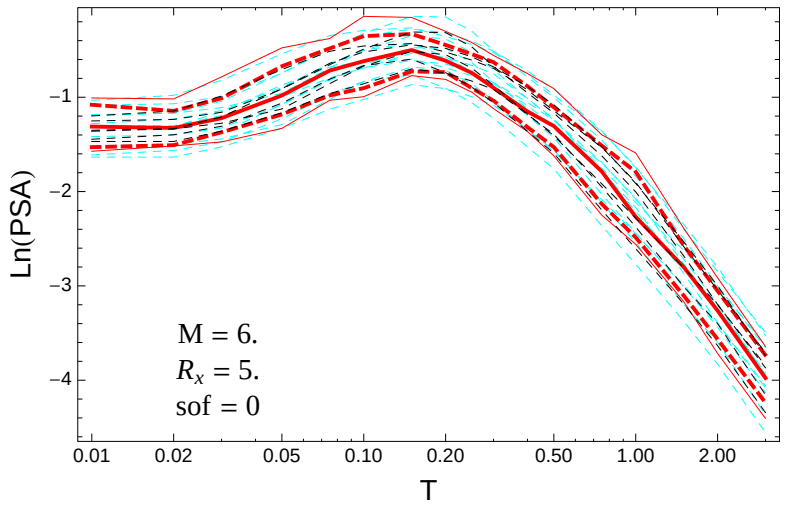



Figure 5.275: PVNGSv2: Spectra of 0.05,0.5,0.95 and the combined ModelA and ModelB distribution (red) with total weights, original GMPEs (dashed black) and the original GMPEs with uncertainty model (dashed cyan), for a scenario with $M_W = 6.$, $R_x = 5.$, $F = 0$.

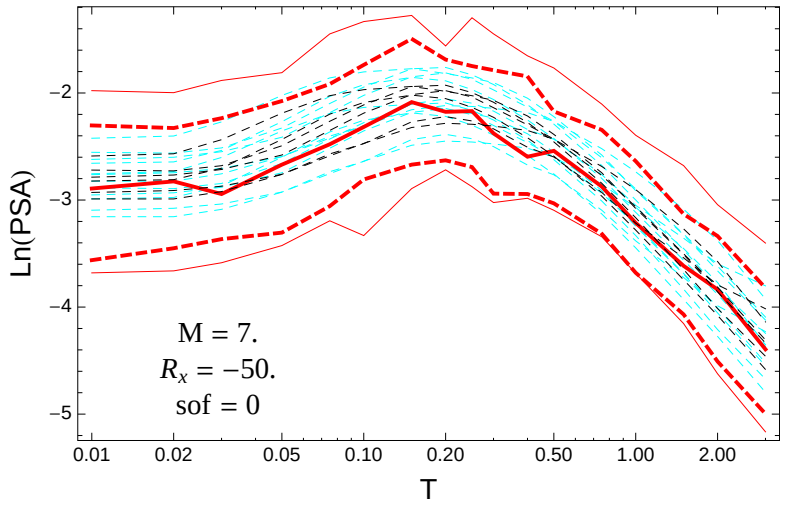



Figure 5.276: PVNGSv2: Spectra of 0.05,0.5,0.95 and the combined ModelA and ModelB distribution (red) with total weights, original GMPEs (dashed black) and the original GMPEs with uncertainty model (dashed cyan), for a scenario with $M_W = 7.$, $R_x = -50.$, $F = 0$.

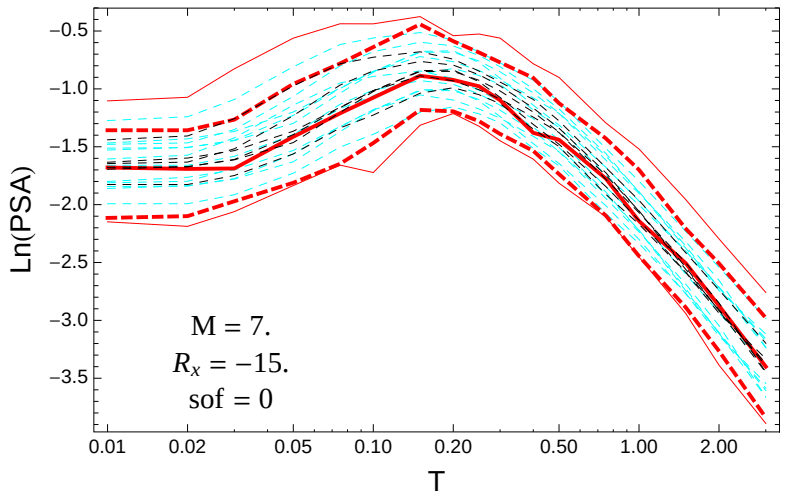



Figure 5.277: PVNGSv2: Spectra of 0.05,0.5,0.95 and the combined ModelA and ModelB distribution (red) with total weights, original GMPEs (dashed black) and the original GMPEs with uncertainty model (dashed cyan), for a scenario with $M_W = 7.$, $R_x = -15.$, $F = 0$.

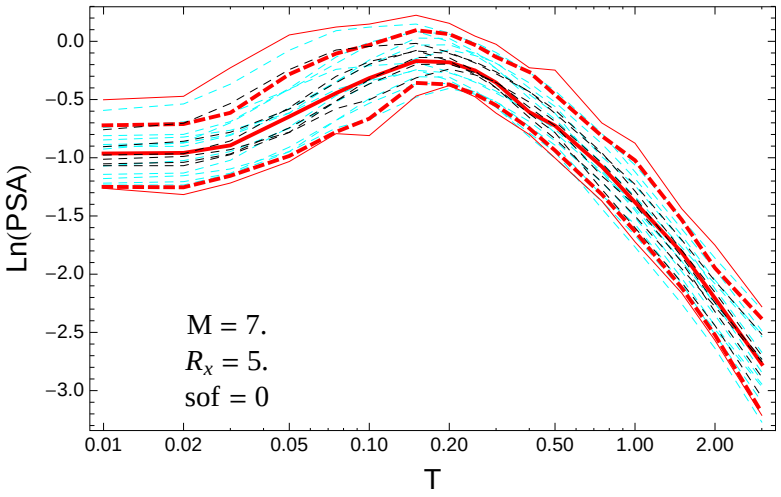



Figure 5.278: PVNGSv2: Spectra of 0.05,0.5,0.95 and the combined ModelA and ModelB distribution (red) with total weights, original GMPEs (dashed black) and the original GMPEs with uncertainty model (dashed cyan), for a scenario with $M_W = 7.$, $R_x = 5.$, $F = 0$.

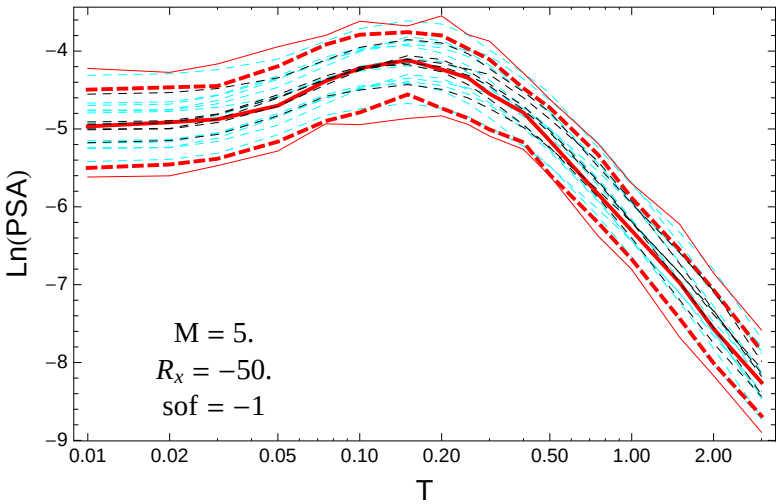



Figure 5.279: PVNGSv2: Spectra of 0.05,0.5,0.95 and the combined ModelA and ModelB distribution (red) with total weights, original GMPEs (dashed black) and the original GMPEs with uncertainty model (dashed cyan), for a scenario with $M_W = 5.$, $R_x = -50.$, $F = -1$.

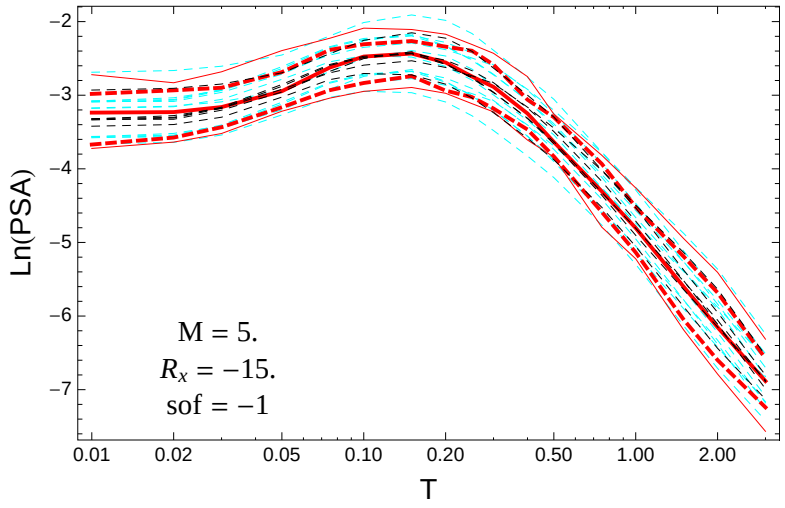



Figure 5.280: PVNGSv2: Spectra of 0.05,0.5,0.95 and the combined ModelA and ModelB distribution (red) with total weights, original GMPEs (dashed black) and the original GMPEs with uncertainty model (dashed cyan), for a scenario with $M_W = 5.$, $R_x = -15.$, $F = -1$.

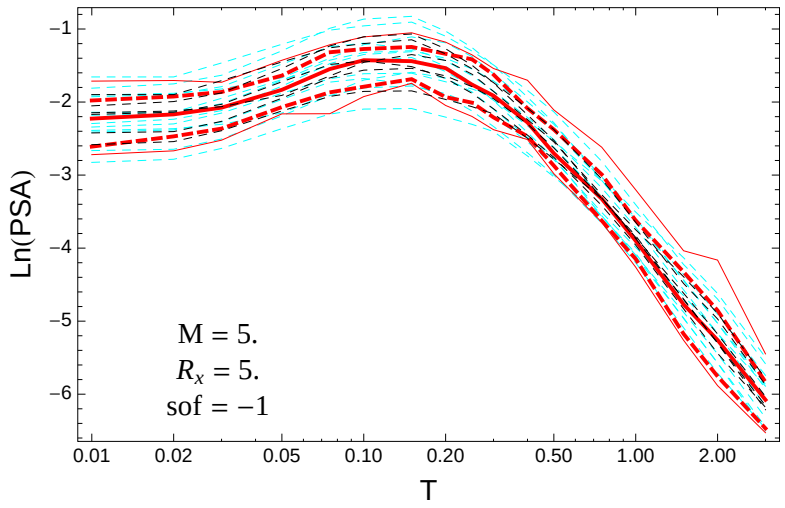



Figure 5.281: PVNGSv2: Spectra of 0.05,0.5,0.95 and the combined ModelA and ModelB distribution (red) with total weights, original GMPEs (dashed black) and the original GMPEs with uncertainty model (dashed cyan), for a scenario with $M_W = 5.$, $R_x = 5.$, $F = -1$.

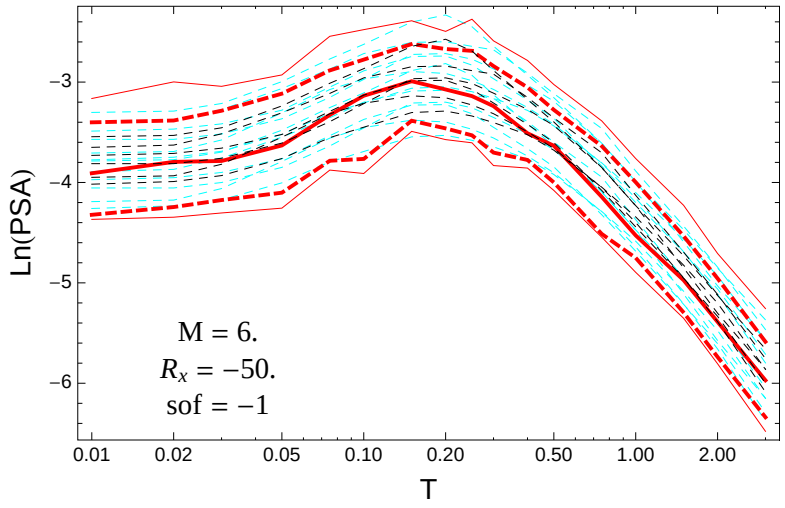



Figure 5.282: PVNGSv2: Spectra of 0.05,0.5,0.95 and the combined ModelA and ModelB distribution (red) with total weights, original GMPEs (dashed black) and the original GMPEs with uncertainty model (dashed cyan), for a scenario with $M_W = 6.$, $R_x = -50.$, $F = -1$.

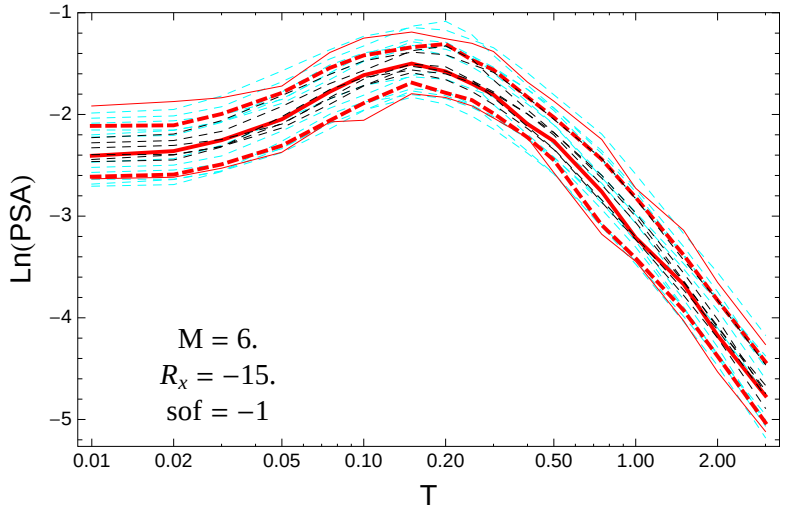



Figure 5.283: PVNGSv2: Spectra of 0.05,0.5,0.95 and the combined ModelA and ModelB distribution (red) with total weights, original GMPEs (dashed black) and the original GMPEs with uncertainty model (dashed cyan), for a scenario with $M_W = 6.$, $R_x = -15.$, $F = -1$.

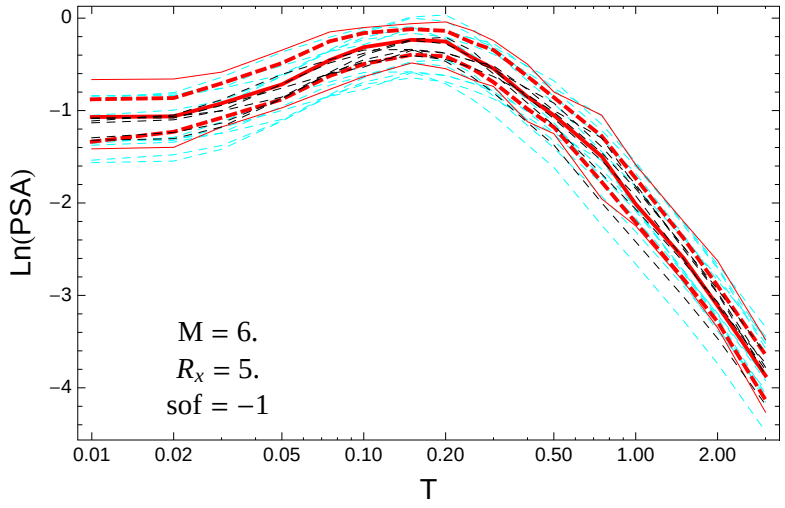



Figure 5.284: PVNGSv2: Spectra of 0.05,0.5,0.95 and the combined ModelA and ModelB distribution (red) with total weights, original GMPEs (dashed black) and the original GMPEs with uncertainty model (dashed cyan), for a scenario with $M_W = 6.$, $R_x = 5.$, $F = -1$.

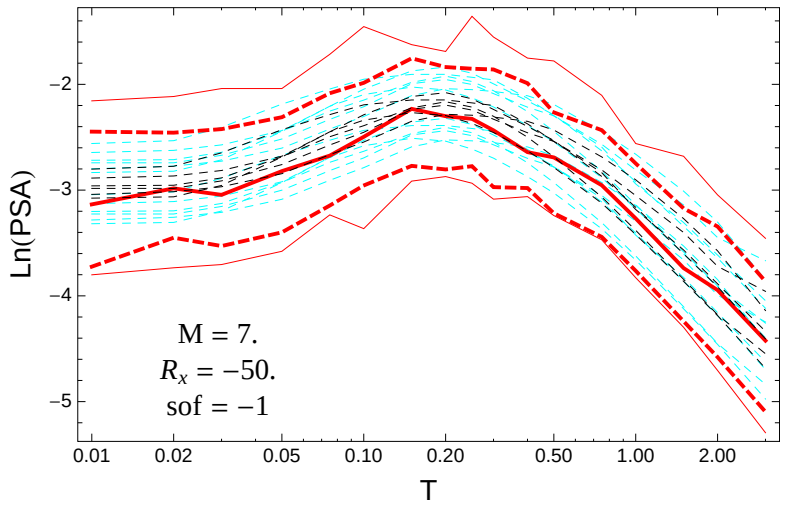



Figure 5.285: PVNGSv2: Spectra of 0.05,0.5,0.95 and the combined ModelA and ModelB distribution (red) with total weights, original GMPEs (dashed black) and the original GMPEs with uncertainty model (dashed cyan), for a scenario with $M_W = 7.$, $R_x = -50.$, $F = -1$.

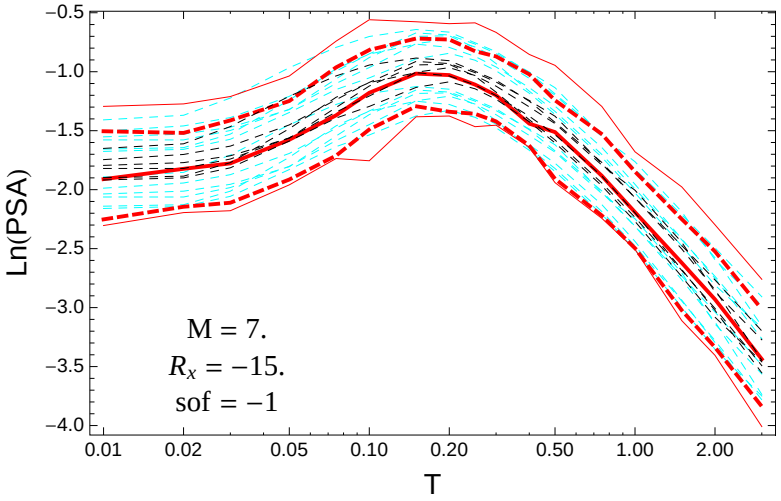



Figure 5.286: PVNGSv2: Spectra of 0.05,0.5,0.95 and the combined ModelA and ModelB distribution (red) with total weights, original GMPEs (dashed black) and the original GMPEs with uncertainty model (dashed cyan), for a scenario with $M_W = 7.$, $R_x = -15.$, $F = -1$.

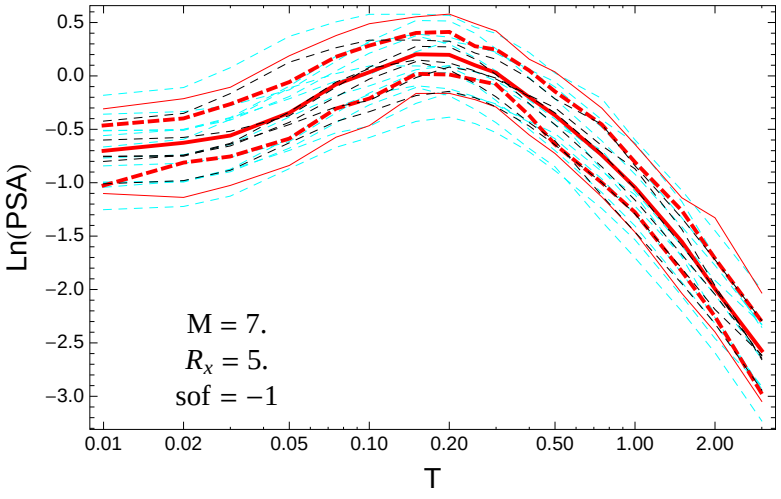



Figure 5.287: PVNGSv2: Spectra of 0.05,0.5,0.95 and the combined ModelA and ModelB distribution (red) with total weights, original GMPEs (dashed black) and the original GMPEs with uncertainty model (dashed cyan), for a scenario with $M_W = 7.$, $R_x = 5.$, $F = -1$.

### 5.1.5 Median Residuals

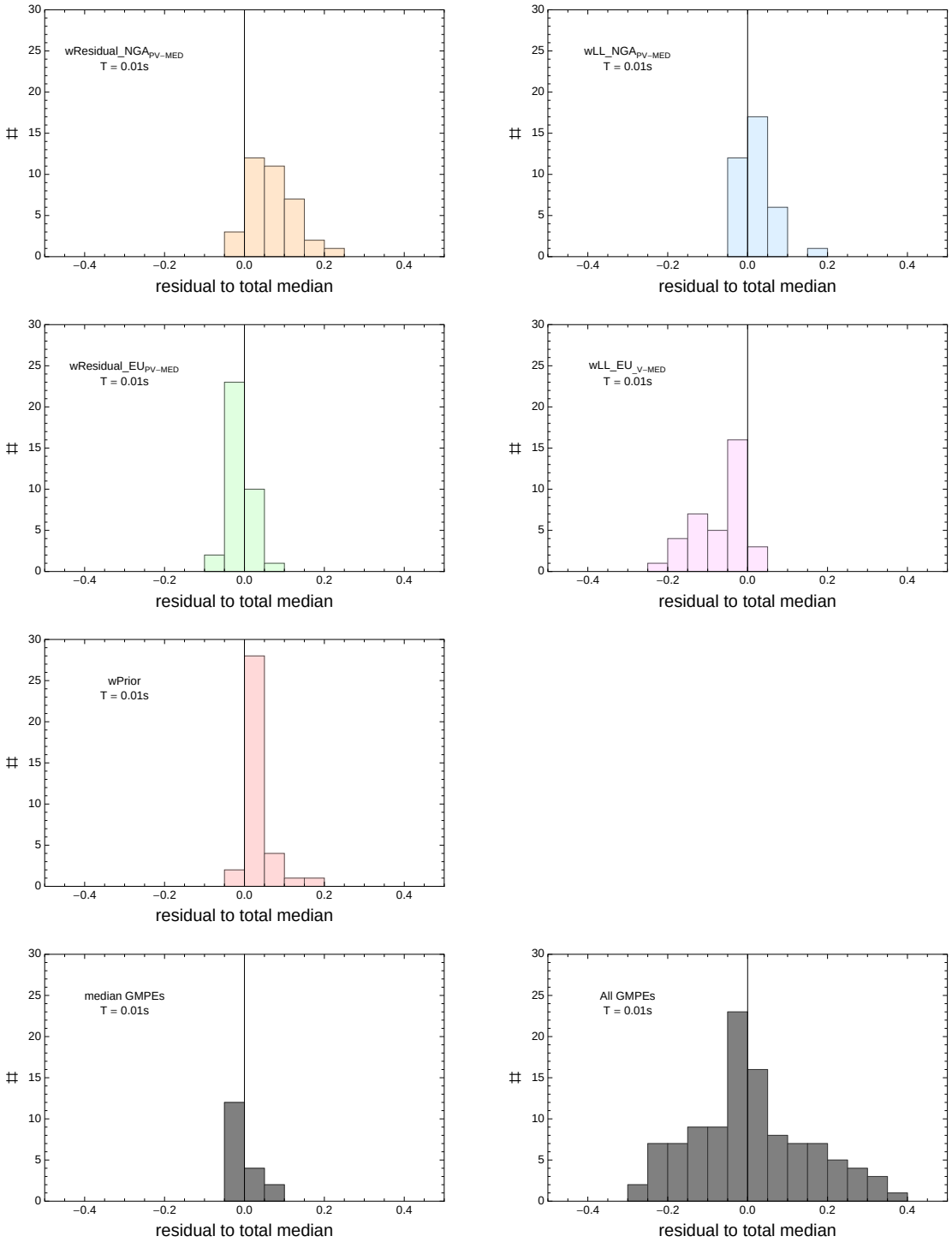



Figure 5.288: PVNGSv2: Histogram of differences for medians calculated with different weights to median calculated with total weights. Bottom row left shows differences between medians for the GMPE distribution to median calculated with total weights. Bottom row right shows differences between the original GMPEs (without uncertainty) to median calculated with total weights. For PVNGS2, combined Model A and B and $T = 0.01$s.

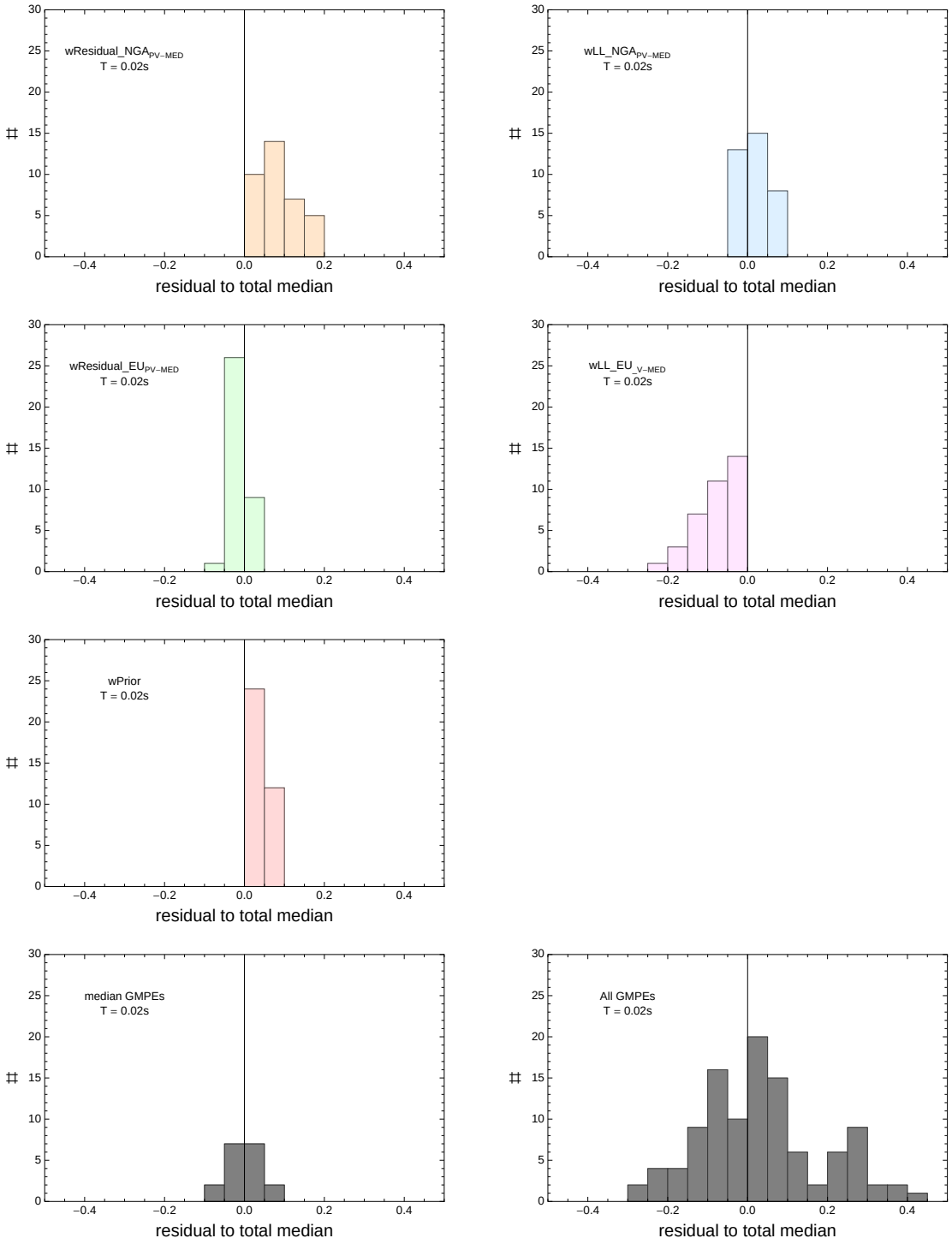



Figure 5.289: PVNGSv2: Histogram of differences for medians calculated with different weights to median calculated with total weights. Bottom row left shows differences between medians for the GMPE distribution to median calculated with total weights. Bottom row right shows differences between the original GMPEs (without uncertainty) to median calculated with total weights. For PVNGS2, combined Model A and B and $T = 0.02$s.

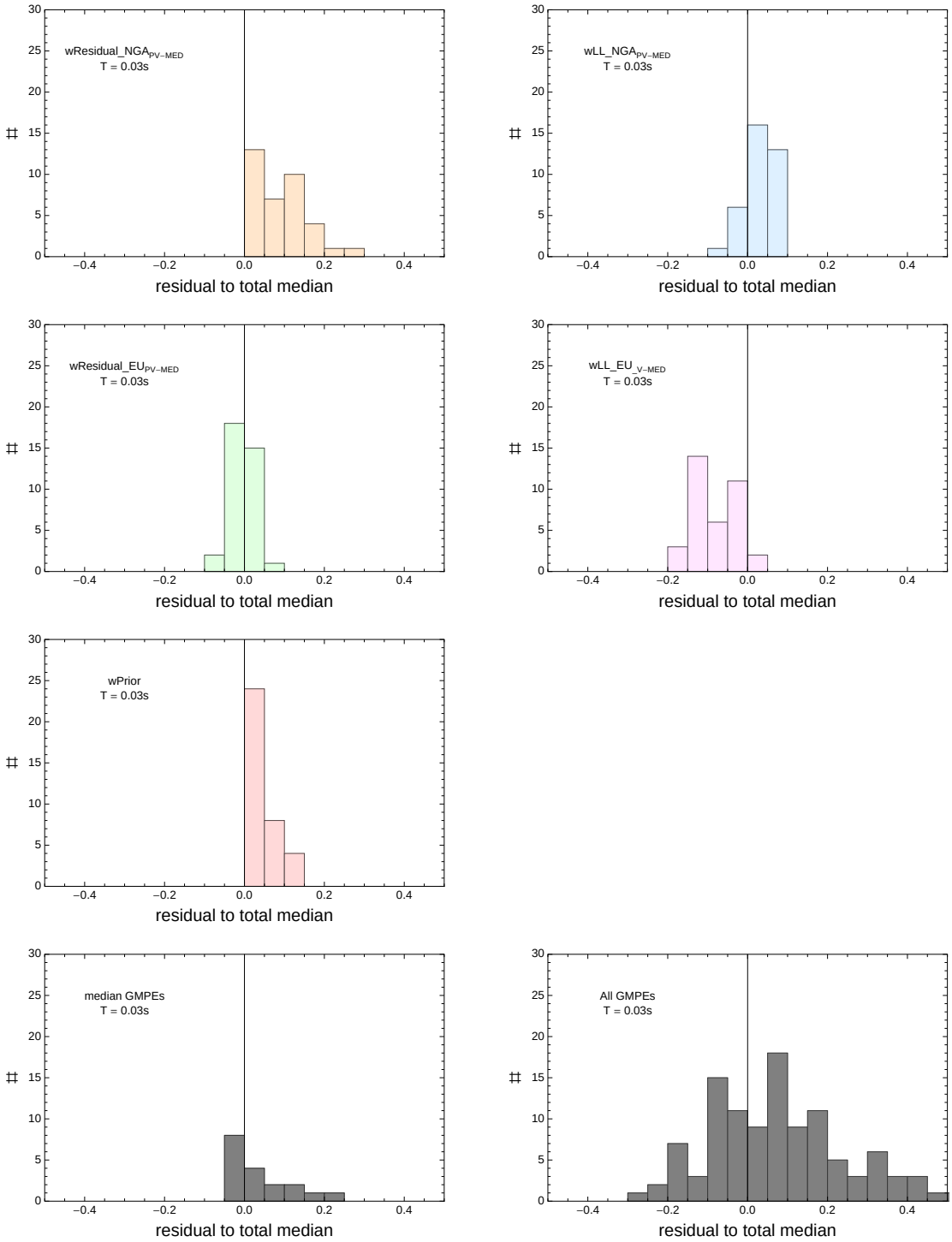



Figure 5.290: PVNGSv2: Histogram of differences for medians calculated with different weights to median calculated with total weights. Bottom row left shows differences between medians for the GMPE distribution to median calculated with total weights. Bottom row right shows differences between the original GMPEs (without uncertainty) to median calculated with total weights. For PVNGS2, combined Model A and B and $T = 0.03$s.

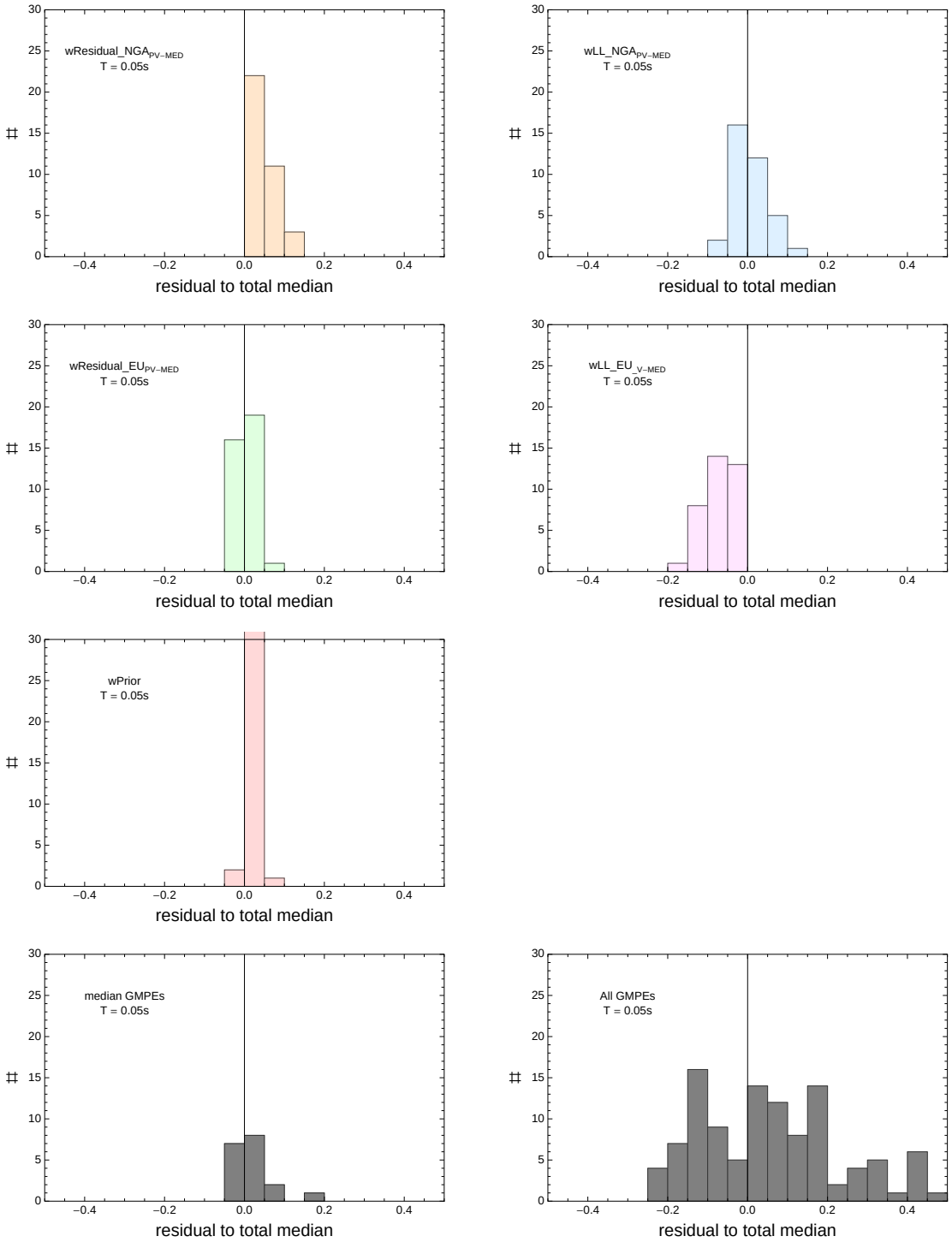



Figure 5.291: PVNGSv2: Histogram of differences for medians calculated with different weights to median calculated with total weights. Bottom row left shows differences between medians for the GMPE distribution to median calculated with total weights. Bottom row right shows differences between the original GMPEs (without uncertainty) to median calculated with total weights. For PVNGS2, combined Model A and B and $T = 0.05$s.

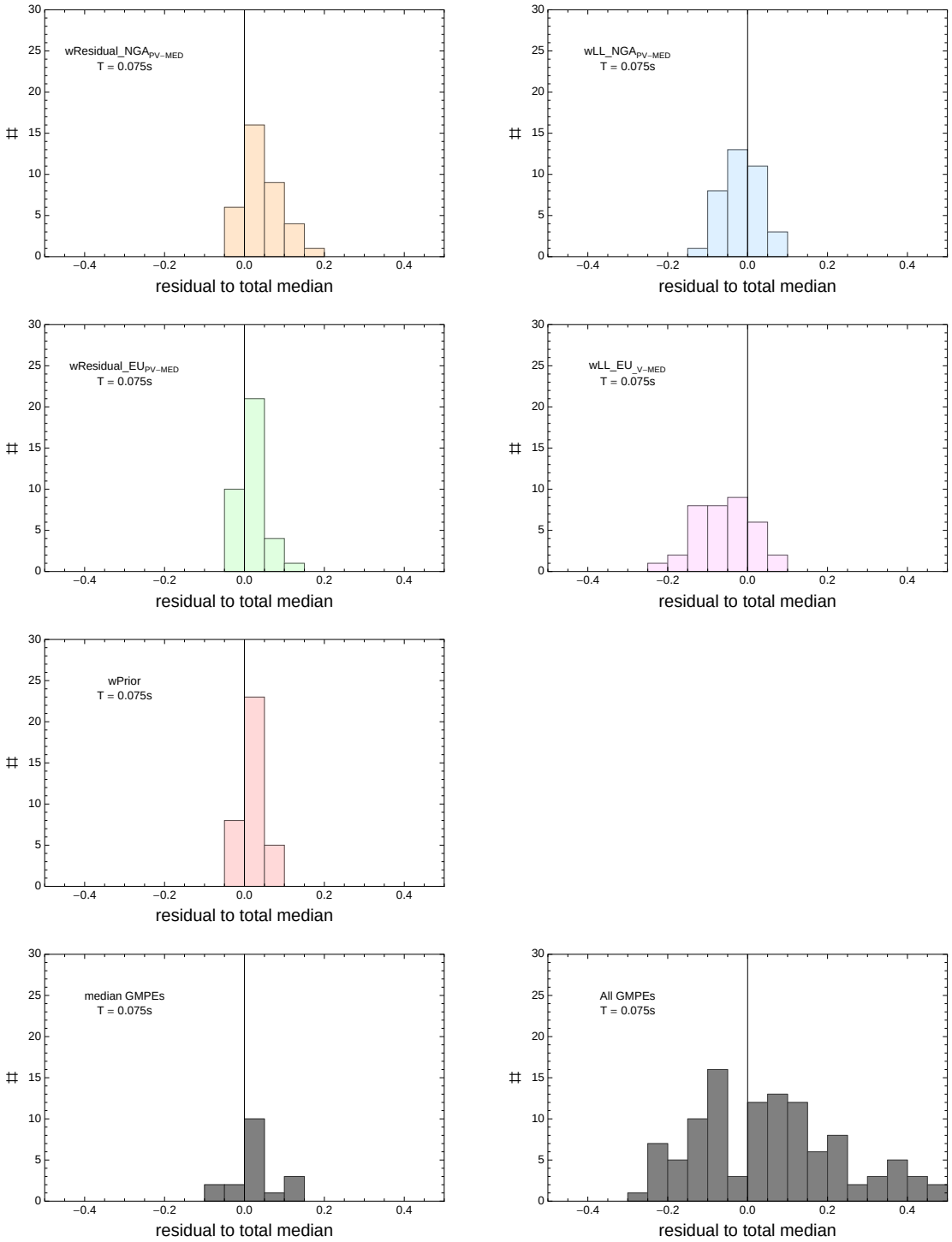



Figure 5.292: PVNGSv2: Histogram of differences for medians calculated with different weights to median calculated with total weights. Bottom row left shows differences between medians for the GMPE distribution to median calculated with total weights. Bottom row right shows differences between the original GMPEs (without uncertainty) to median calculated with total weights. For PVNGS2, combined Model A and B and $T = 0.075$s.

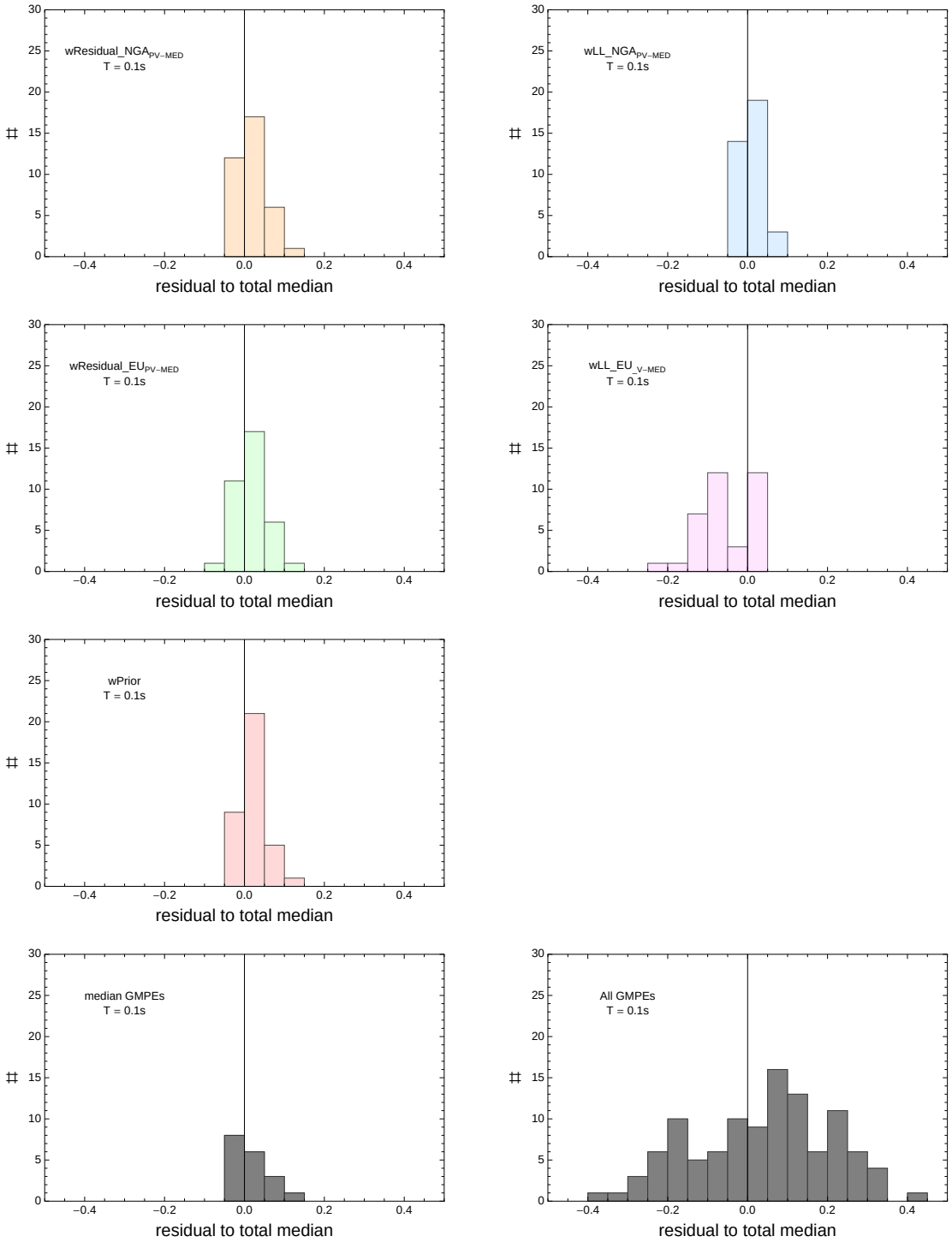



Figure 5.293: PVNGSv2: Histogram of differences for medians calculated with different weights to median calculated with total weights. Bottom row left shows differences between medians for the GMPE distribution to median calculated with total weights. Bottom row right shows differences between the original GMPEs (without uncertainty) to median calculated with total weights. For PVNGS2, combined Model A and B and $T = 0.1$s.

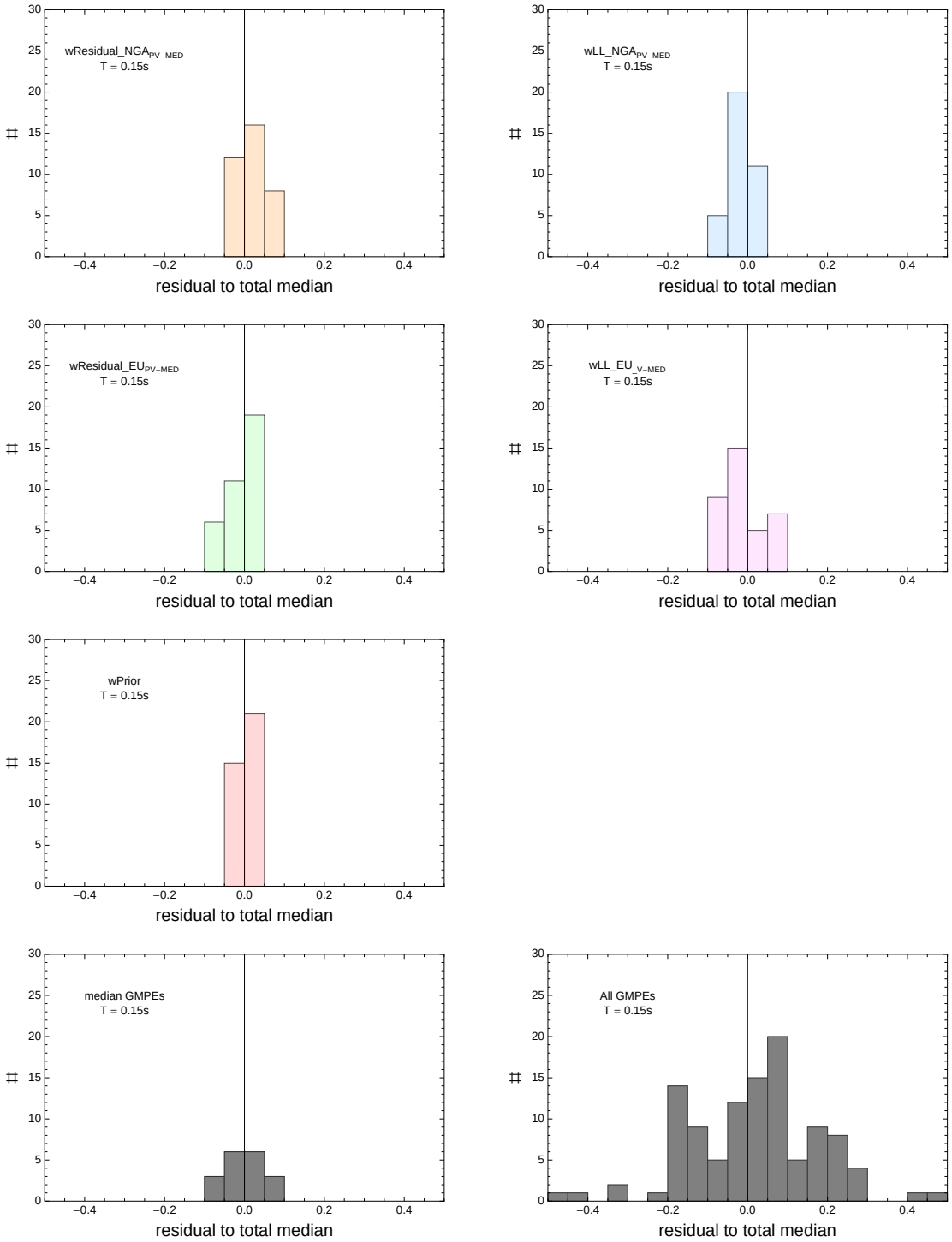



Figure 5.294: PVNGSv2: Histogram of differences for medians calculated with different weights to median calculated with total weights. Bottom row left shows differences between medians for the GMPE distribution to median calculated with total weights. Bottom row right shows differences between the original GMPEs (without uncertainty) to median calculated with total weights. For PVNGS2, combined Model A and B and $T = 0.15$s.

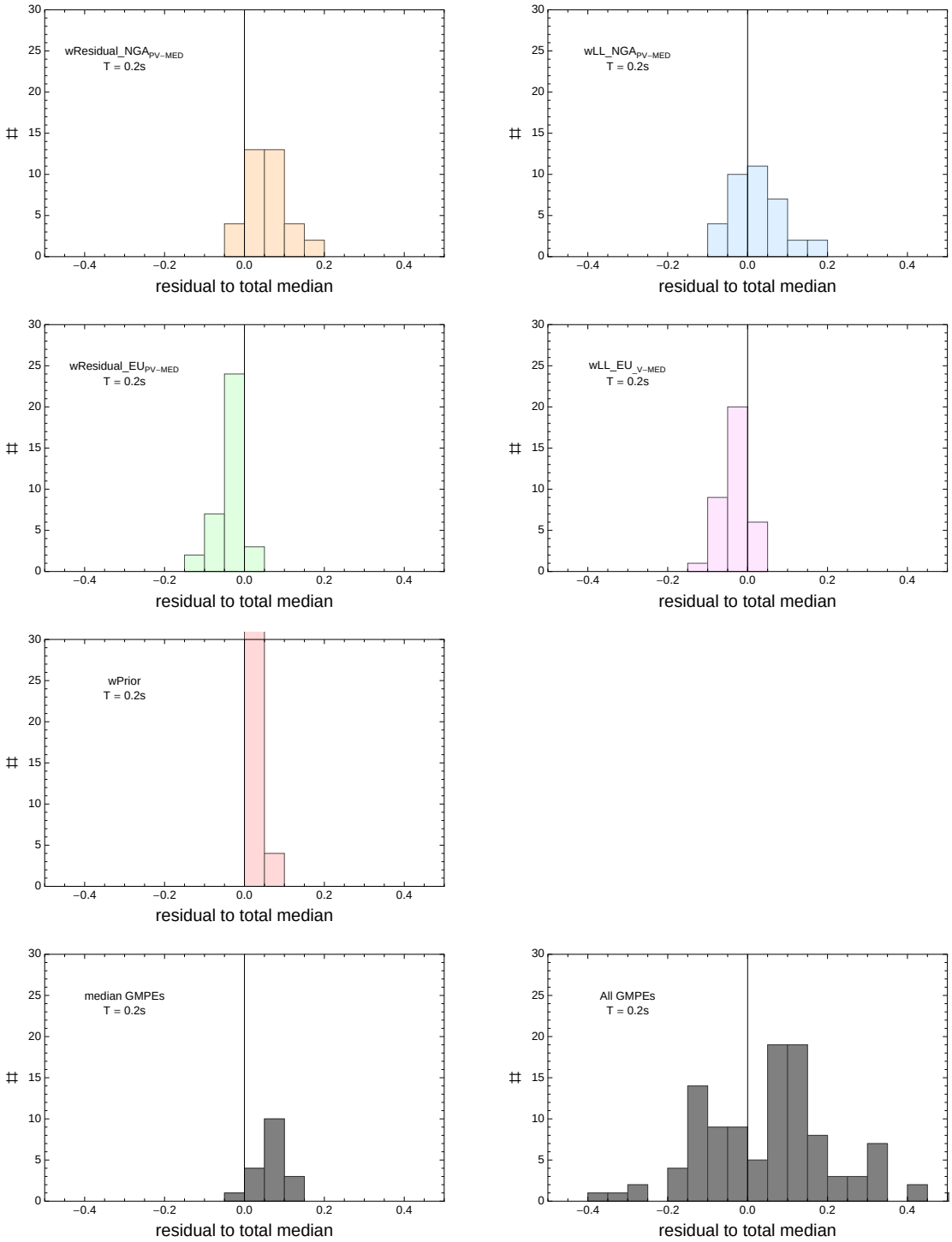



Figure 5.295: PVNGSv2: Histogram of differences for medians calculated with different weights to median calculated with total weights. Bottom row left shows differences between medians for the GMPE distribution to median calculated with total weights. Bottom row right shows differences between the original GMPEs (without uncertainty) to median calculated with total weights. For PVNGS2, combined Model A and B and $T = 0.2$s.

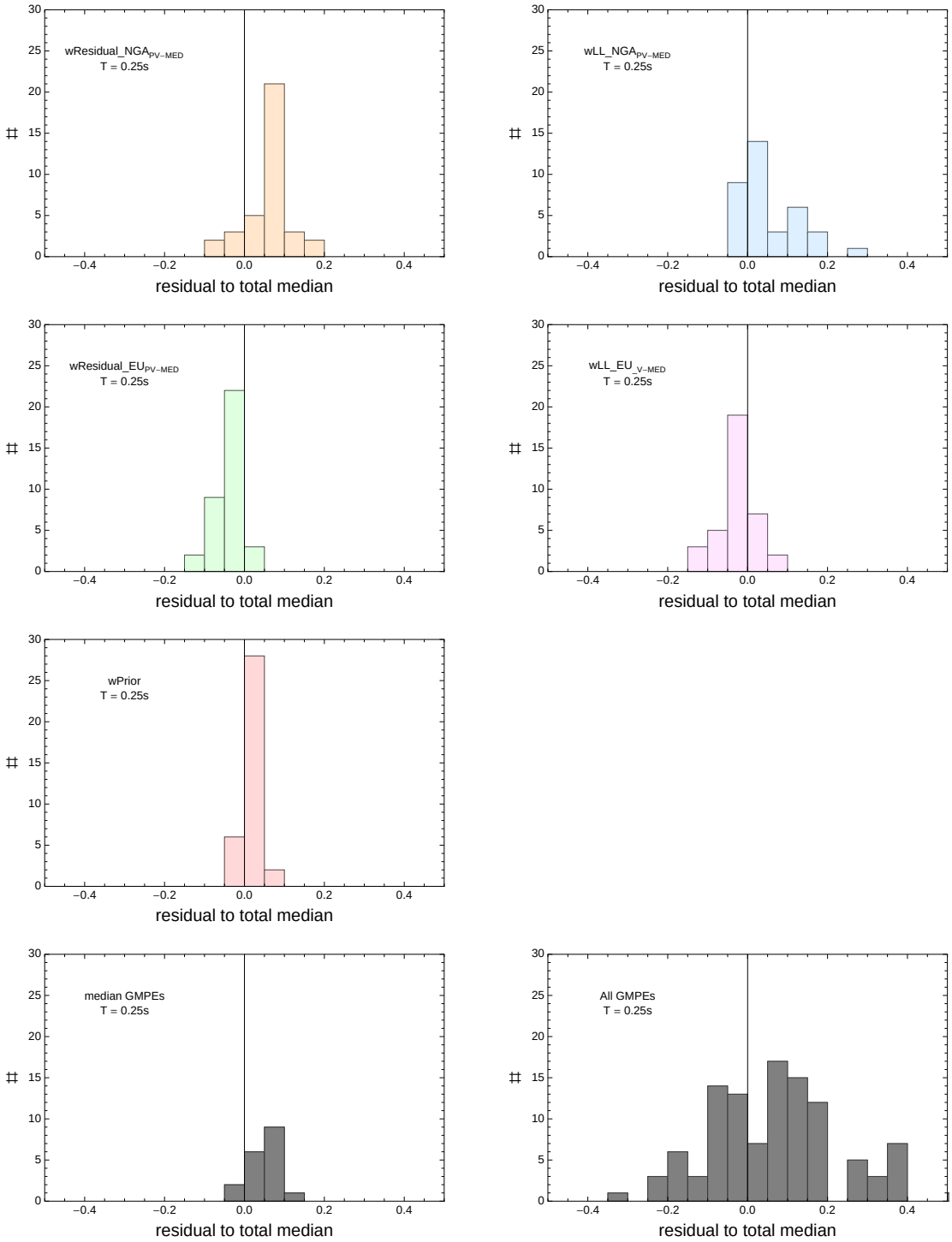



Figure 5.296: PVNGSv2: Histogram of differences for medians calculated with different weights to median calculated with total weights. Bottom row left shows differences between medians for the GMPE distribution to median calculated with total weights. Bottom row right shows differences between the original GMPEs (without uncertainty) to median calculated with total weights. For PVNGS2, combined Model A and B and $T = 0.25$s.

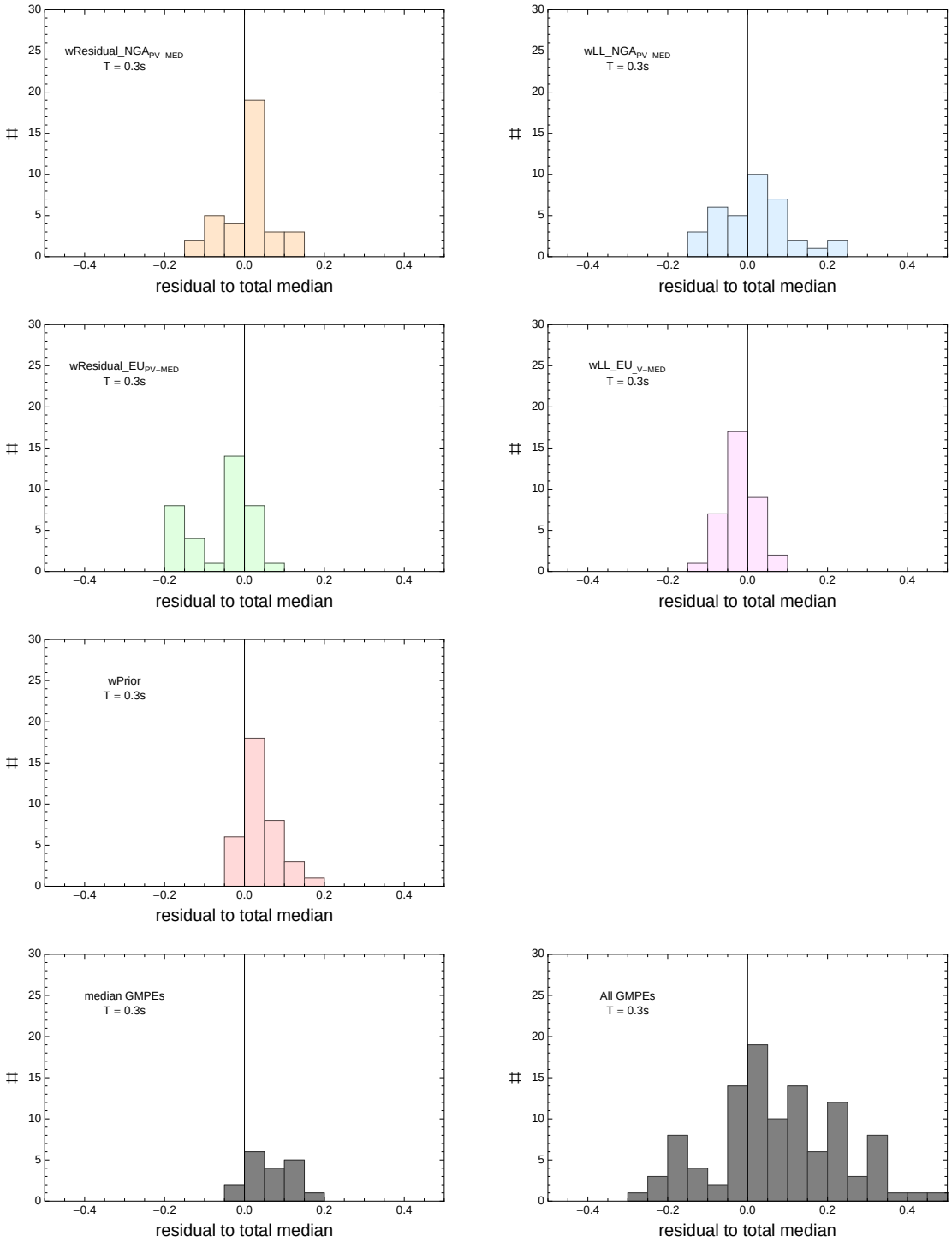



Figure 5.297: PVNGSv2: Histogram of differences for medians calculated with different weights to median calculated with total weights. Bottom row left shows differences between medians for the GMPE distribution to median calculated with total weights. Bottom row right shows differences between the original GMPEs (without uncertainty) to median calculated with total weights. For PVNGS2, combined Model A and B and $T = 0.3$s.

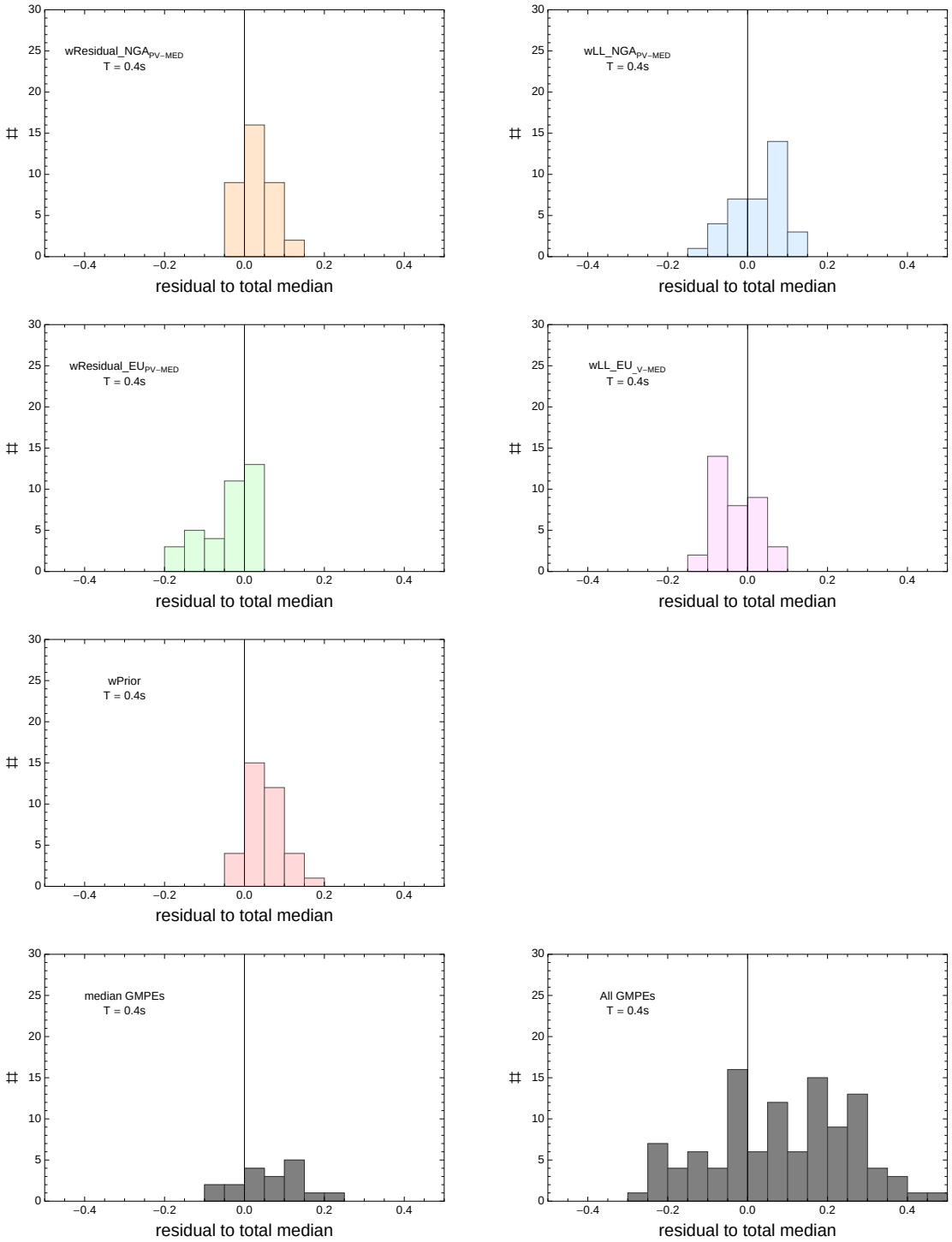



Figure 5.298: PVNGSv2: Histogram of differences for medians calculated with different weights to median calculated with total weights. Bottom row left shows differences between medians for the GMPE distribution to median calculated with total weights. Bottom row right shows differences between the original GMPEs (without uncertainty) to median calculated with total weights. For PVNGS2, combined Model A and B and $T = 0.4$s.

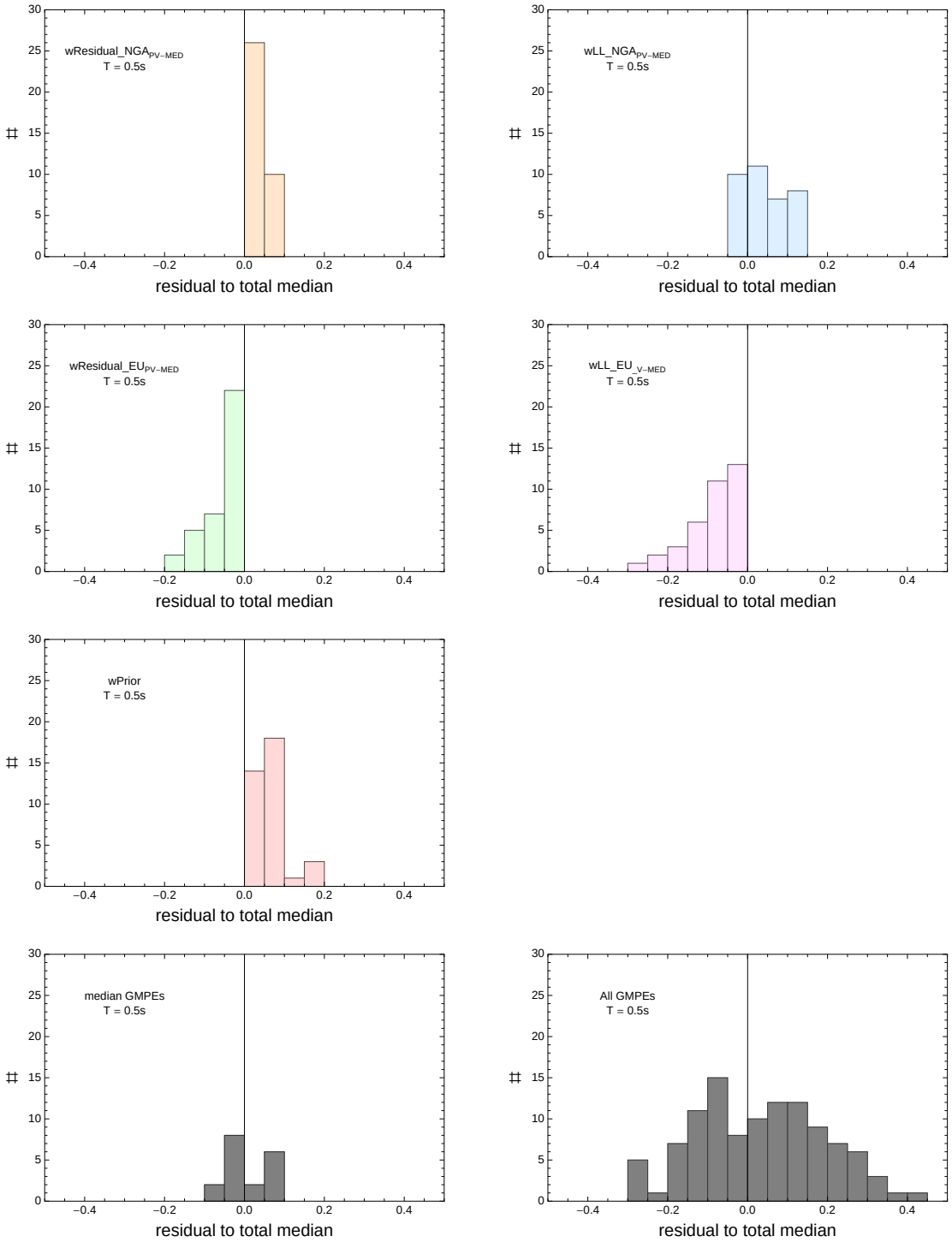



Figure 5.299: PVNGSv2: Histogram of differences for medians calculated with different weights to median calculated with total weights. Bottom row left shows differences between medians for the GMPE distribution to median calculated with total weights. Bottom row right shows differences between the original GMPEs (without uncertainty) to median calculated with total weights. For PVNGS2, combined Model A and B and $T = 0.5$s.

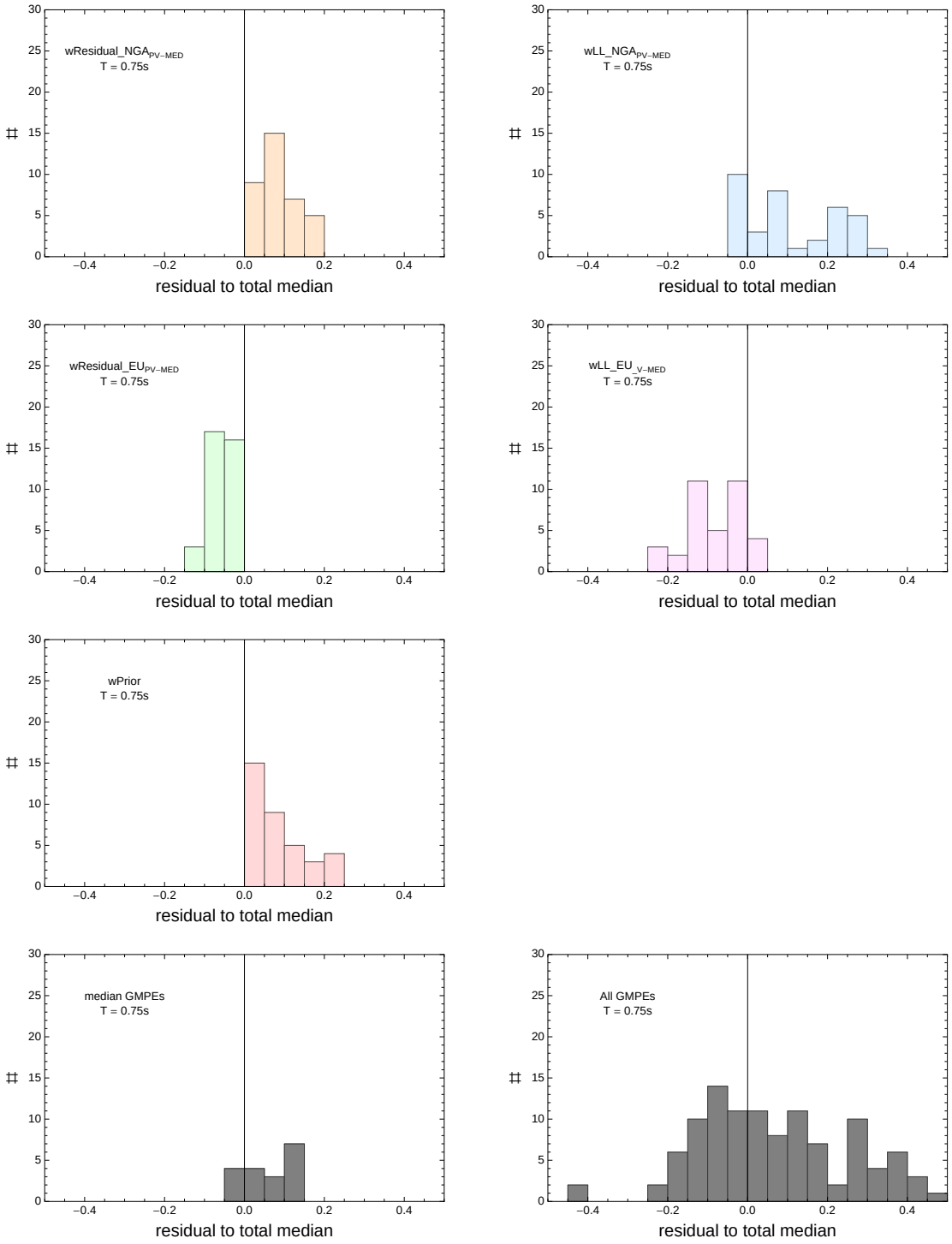



Figure 5.300: PVNGSv2: Histogram of differences for medians calculated with different weights to median calculated with total weights. Bottom row left shows differences between medians for the GMPE distribution to median calculated with total weights. Bottom row right shows differences between the original GMPEs (without uncertainty) to median calculated with total weights. For PVNGS2, combined Model A and B and $T = 0.75$s.

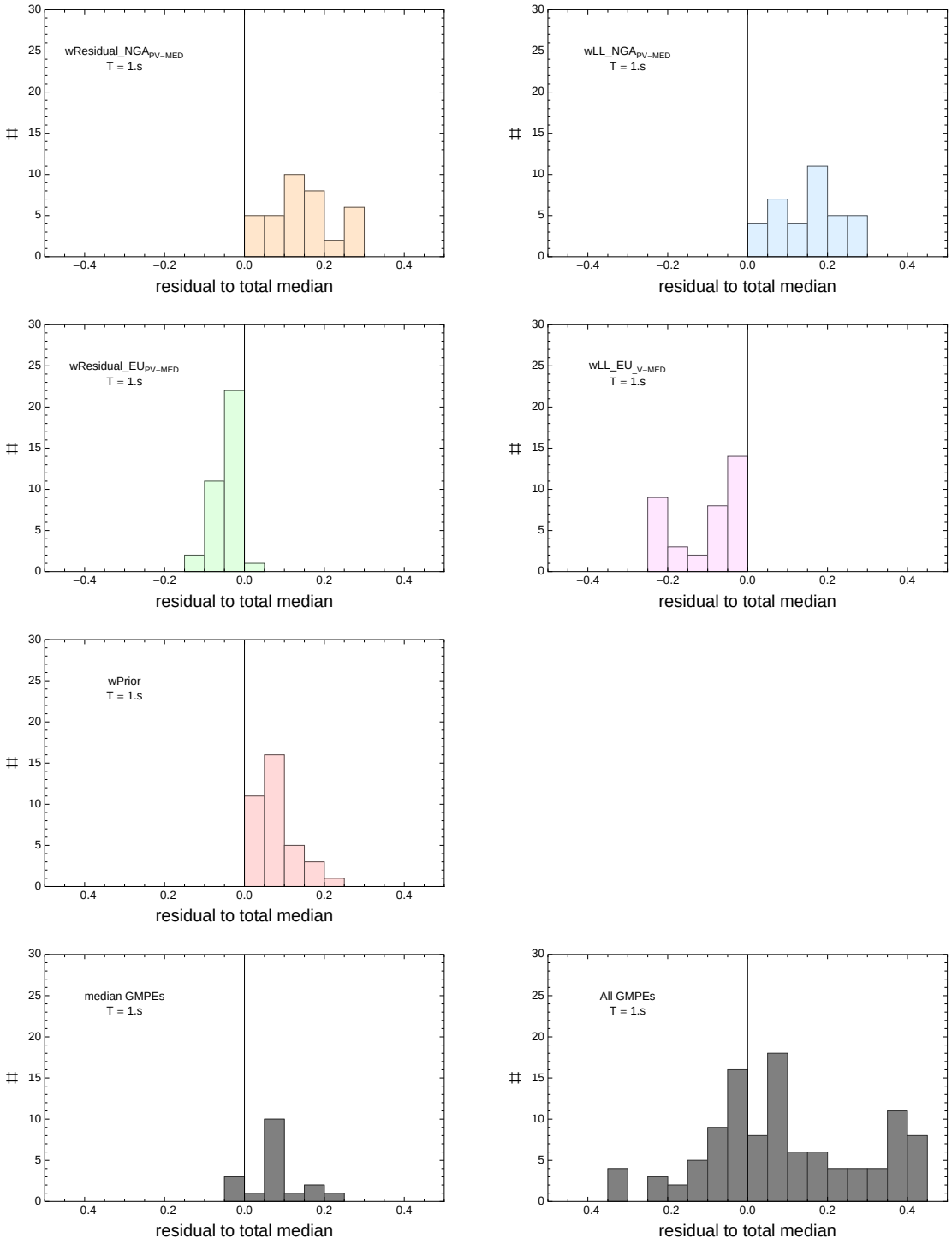



Figure 5.301: PVNGSv2: Histogram of differences for medians calculated with different weights to median calculated with total weights. Bottom row left shows differences between medians for the GMPE distribution to median calculated with total weights. Bottom row right shows differences between the original GMPEs (without uncertainty) to median calculated with total weights. For PVNGS2, combined Model A and B and $T = 1.$s.

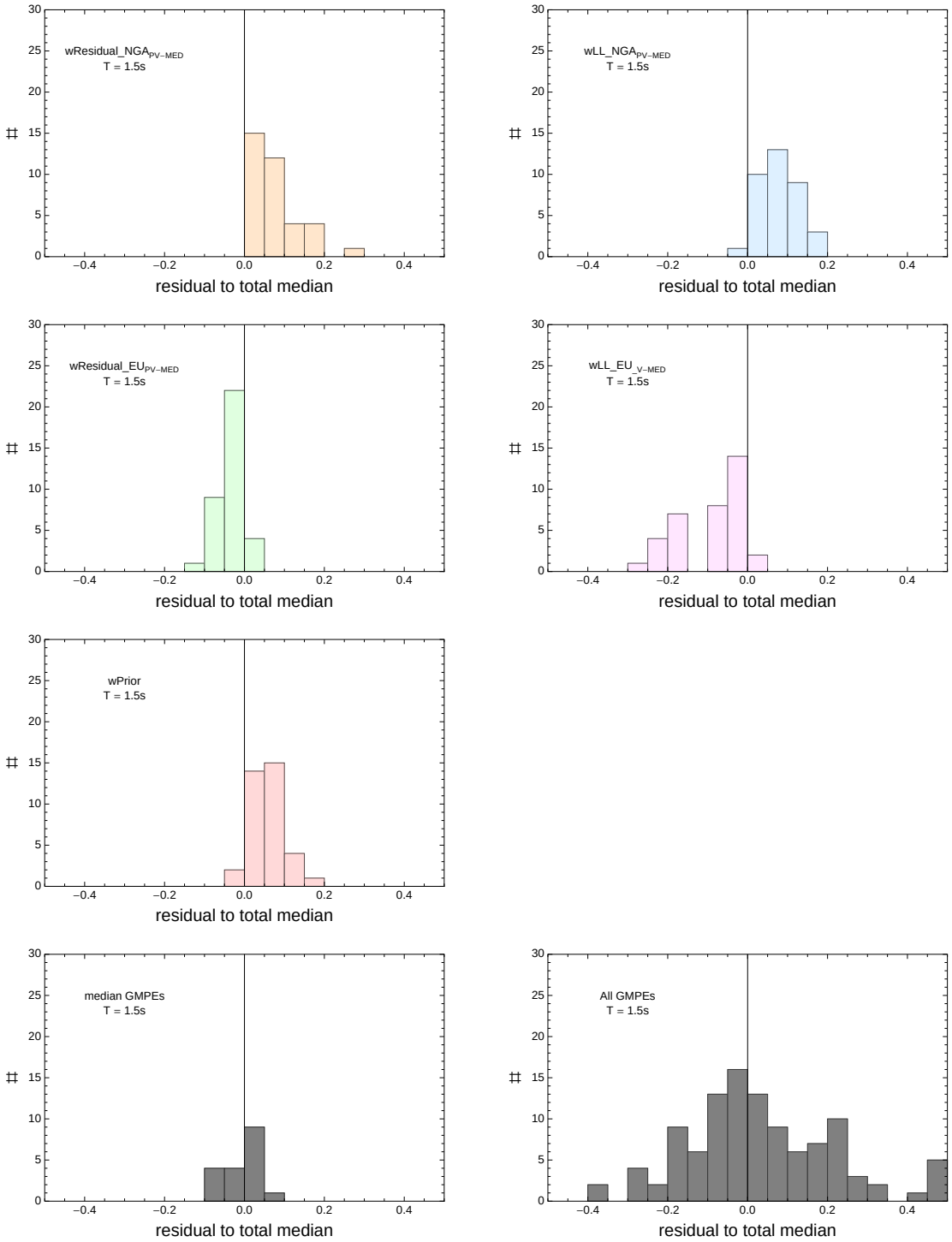



Figure 5.302: PVNGSv2: Histogram of differences for medians calculated with different weights to median calculated with total weights. Bottom row left shows differences between medians for the GMPE distribution to median calculated with total weights. Bottom row right shows differences between the original GMPEs (without uncertainty) to median calculated with total weights. For PVNGS2, combined Model A and B and $T = 1.5$s.

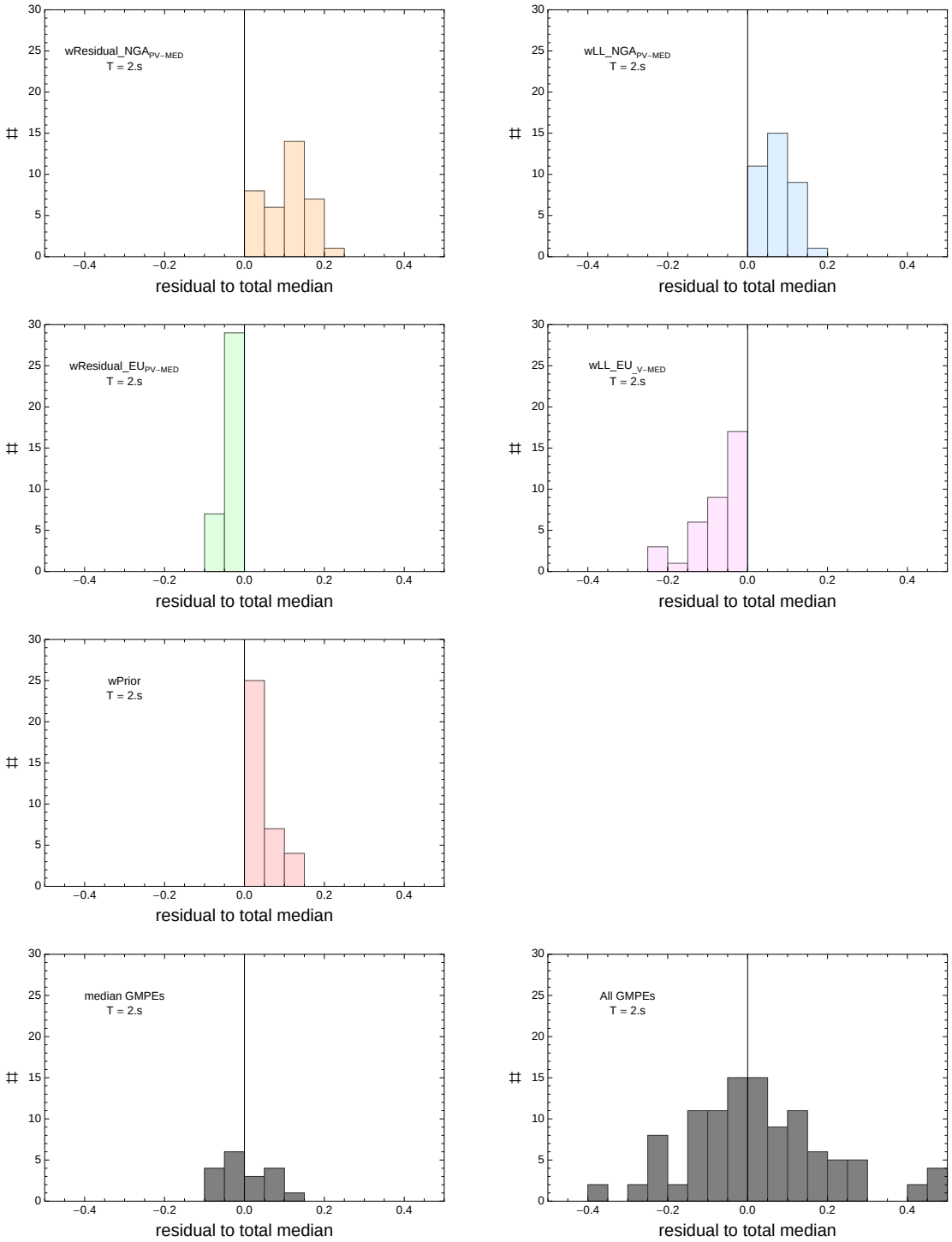



Figure 5.303: PVNGSv2: Histogram of differences for medians calculated with different weights to median calculated with total weights. Bottom row left shows differences between medians for the GMPE distribution to median calculated with total weights. Bottom row right shows differences between the original GMPEs (without uncertainty) to median calculated with total weights. For PVNGS2, combined Model A and B and $T = 2$.s.

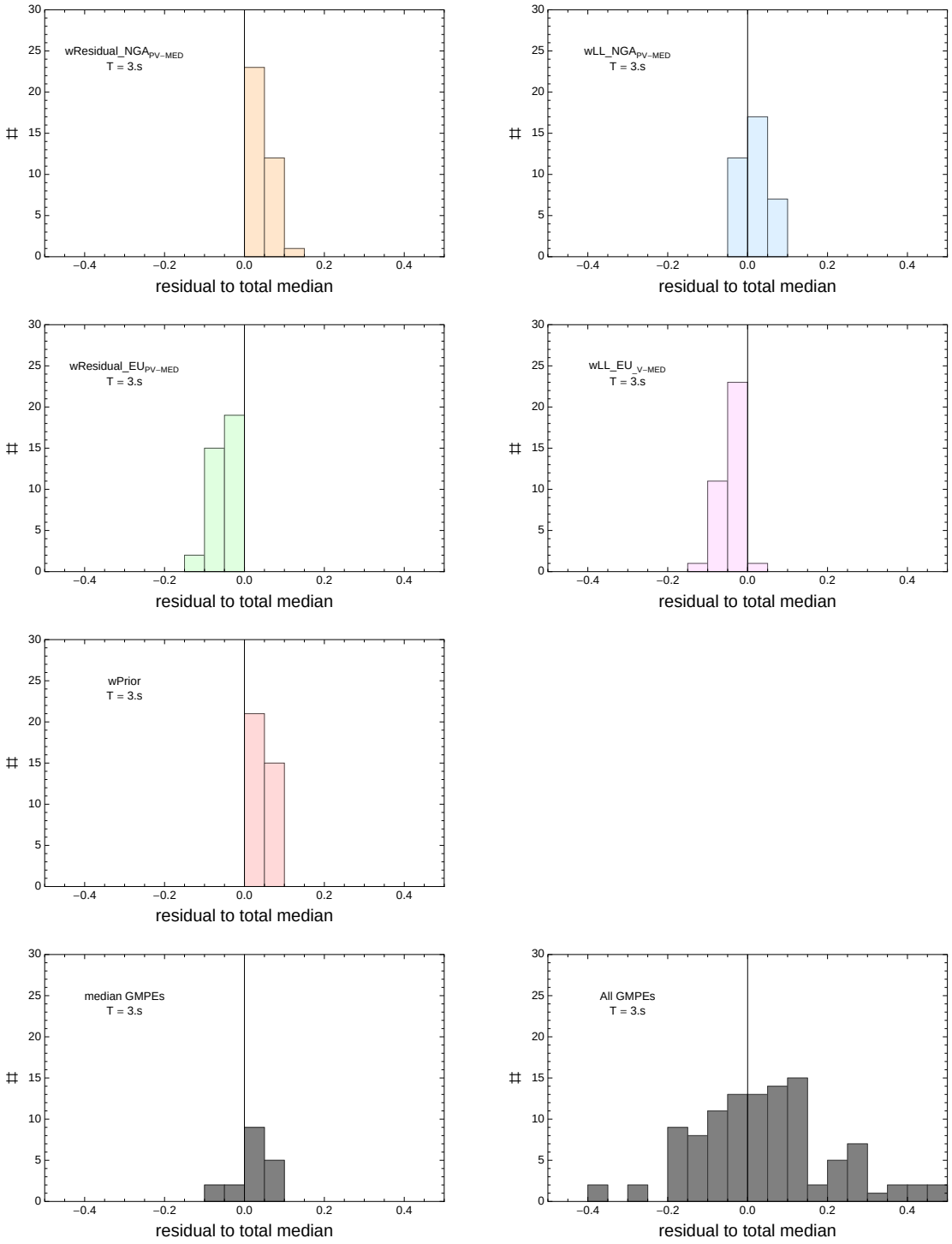



Figure 5.304: PVNGSv2: Histogram of differences for medians calculated with different weights to median calculated with total weights. Bottom row left shows differences between medians for the GMPE distribution to median calculated with total weights. Bottom row right shows differences between the original GMPEs (without uncertainty) to median calculated with total weights. For PVNGS2, combined Model A and B and $T = 3$.s.

# Bibliography


[1] N. A. Abrahamson, W. J. Silva, and R. Kamai. Summary of the ASK14 Ground Motion Relation for Active Crustal Regions. *Earthquake Spectra*, 30(3):1025–1055, 2014.

[2] S. Akkar and Z. Cagnan. A Local Ground-Motion Predictive Model for Turkey, and Its Comparison with Other Regional and Global Ground-Motion Models. *Bulletin of the Seismological Society of America*, 100(6):2978–2995, 2010.

[3] S. Akkar, M. A. Sandkkaya, and J. J. Bommer. Empirical ground-motion models for point- and extended-source crustal earthquake scenarios in Europe and the Middle East. *Bulletin of Earthquake Engineering*, 12(1):359–387, 2014a.

[4] S. Akkar, M. A. Sandkkaya, and J. J. Bommer. Erratum to: Empirical ground-motion models for point- and extended-source crustal earthquake scenarios in Europe and the Middle East. *Bulletin of Earthquake Engineering*, 12(1):389–390, 2014b.

[5] L. Al-Atik and R. R. Youngs. Epistemic Uncertainty for NGA-West2 Models. *Earthquake Spectra*, 30(3):1301–1318, 2014.

[6] G. M. Atkinson, J. J. Bommer, and N. A. Abrahamson. Alternative Approaches to Modeling Epistemic Uncertainty in Ground Motions in Probabilistic Seismic-Hazard Analysis. *Seismological Research Letters*, 85(6):1141–1144, 2014.

[7] D. Bindi, M. Massa, L. Luzi, G. Ameri, F. Pacor, R. Puglia, and P. Augliera. Pan-European ground-motion prediction equations for the average horizontal component of PGA, PGV, and 5 %-damped PSA at spectral periods up to 3.0 s using the RESORCE dataset. *Bulletin of Earthquake Engineering*, 12(1):391–430, 2014a.

[8] D. Bindi, M. Massa, L. Luzi, G. Ameri, F. Pacor, R. Puglia, and P. Augliera. Erratum to: Pan-European ground-motion prediction equations for the average horizontal component of PGA, PGV, and 5%-damped PSA at spectral periods up to 3.0 s using the RESORCE dataset. *Bulletin of Earthquake Engineering*, 12(1):431–448, 2014b.

[9] D. M. Boore, J. P. Stewart, E. Seyhan, and G. M. Atkinson. NGA-West2 Equations for Predicting PGA, PGV, and 5% Damped PSA for Shallow Crustal Earthquakes. *Earthquake Spectra*, 30(3):1057–1085, 2014.

[10] S. S. Bora, F. Scherbaum, N. Kuehn, and P. Stafford. Fourier spectral- and duration models for the generation of response spectra adjustable to different source-, propagation-, and site conditions. *Bulletin of Earthquake Engineering*, 12(1):467–493, 2014.

[11] K. W. Campbell and Y. Bozorgnia. NGA-West2 Ground Motion Model for the Average Horizontal Components of PGA, PGV, and 5% Damped Linear Acceleration Response Spectra. *Earthquake Spectra*, 30(3):1087–1115, 2014.

[12] B. S.-J. Chiou and R. R. Youngs. Update of the Chiou and Youngs NGA Model for the Average Horizontal Component of Peak Ground Motion and Response Spectra. *Earthquake Spectra*, 30(3):1117–1153, 2014.

[13] J.-M. Geusebroek, G. J. Burghouts, and A. W.M. Smeulders. The Amsterdam Library of Object Images. *International Journal of Computer Vision*, 61(1):103–112, 2005.

[14] V. Graizer. Updated Graizer-Kalkan Ground-Motion Prediction Equations for Western United States. In *Proceedings of 10th U.S. National Conference on Earthquake Engineering Frontiers of Earthquake Engineering*, July 21-25, 2014. Anchorage, Alaska, Paper ID 1097, 11 pp.

[15] H. Hotelling. Analysis of a complex of statistical variables into principal components. *Journal of Educational Psychology*, 24(6):417–441, 1933.

[16] I. M. Idriss. An NGA-West2 Empirical Model for Estimating the Horizontal Spectral Values Generated by Shallow Crustal Earthquakes. *Earthquake Spectra*, 30(3):1155–1177, 2014.

[17] J. W. Sammon. A nonlinear mapping for data structure analysis. *IEEE Transactions on computers*, C-18:401–409, 1969.

[18] F. Scherbaum, N. M. Kuehn, M. Ohrnberger, and A. Koehler. Exploring the Proximity of Ground-Motion Models Using High-Dimensional Visualization Techniques. *Earthquake Spectra*, 26(4):1117–1138, 2010.

[19] J. X. Zhao, J. Zhang, A. Asano, Y. Ohno, T. Oouchi, T. Takahashi, H. Ogawa, K. Irikura, H. K. Thio, P. G. Somerville, and Y. Fukushima. Attenuation Relations of Strong Ground Motion in Japan Using Site Classification Based on Predominant Period. *Bulletin of the Seismological Society of America*, 96(3):898–913, 2006.

# APPENDIX I

# GROUND MOTIONS FOR THE WELLS (NV) EARTHQUAKE

## I.1 Background and Motivation

The Wells, Nevada earthquake occurred on February 21, 2008 approximately 10 km northeast of the town of Wells, Nevada. This event had a moment magnitude of 6.0, a normal focal mechanism, and occurred on a previously unmapped fault (USGS, 2014). A finite-fault model for this rupture was developed by Dreger et al. (2011), as shown on Figure I-1. A rupture plane with an area of approximately 100 $km^2$ exhibited slip during the event. The slip was concentrated on a plane with a dip of approximately $50^o$, at a strike of $N40^oE$. The hypocenter was located at a depth of 7.0 km and slip occurred over a depth range of 5 to 11 km.

The tectonic setting, magnitude, and focal mechanism of this earthquake are all consistent with the seismic sources in the Greater Arizona region that contribute significantly to the hazard at high frequencies at the Palo Verde Nuclear Generating Station (PVNGS), as discussed in Section 4.2.3. Additionally, large magnitude normal earthquakes are not well sampled in the PEER Ground Motion database (Ancheta et al., 2014) used to develop the NGA-West2 ground-motion prediction equations (GMPEs). For these reasons, the ground motions from the Wells, Nevada event were compiled and compared to the GMPEs to provide additional data for testing the applicability of the GMPEs to local earthquakes in Arizona.

## I.2 Data Availability and Processing

### *I.2.1 Available Ground-Motion Recordings*

The current study of the Wells, Nevada event included identifying available strong ground-motion recordings in the vicinity of the earthquake epicenter. Very few permanent strong motion recording stations existed in the Wells, Nevada area prior to the Wells event. A review of the permanent networks from the IRIS DMC database identified one permanent station within 100 km of the epicenter of the Wells event. The ELK station from the United States National Seismic Network (network code US) is located in Elko, Nevada and is located 56 km southwest of the Wells event epicenter. In addition to this permanent station, the USArray Transportable Array (network code TA) was deployed in the area at the

time of the earthquake. A total of seven TA temporary stations were deployed within 100 km of the epicenter: M11A, M12A, M13A, N11A, N12A, N13A and O12A. These stations were equipped with broadband seismometers sampling 40 samples per second, with a basically flat sensor response in the 0.01 - 15 Hz frequency range, as shown in Figure I-2 for one the TA stations (114A) which has the same sensor response as the TA stations that recorded the Wells ground motions. The limitations of the TA recordings for use in the comparison with GMPEs are addressed in Section I.3.2. In total ground motions were recorded at eight locations within 100 km. The locations of these stations relative to the earthquake epicenter are shown on Figure I-1.

### *I.2.2 Site Conditions*

The surface geology for the region surrounding the Wells, Nevada event is shown on Figure I-3; the shapefiles in this figure are based on the USGS (2007) database. In this figure various geologic sub-units were grouped into the general categories:

- **Soft Soil to Soil** - Playa, Mudflat, Eolian Deposits, Loess and Lake or Marine Sediment
- **Soil to Stiff Soil** - Alluvium, Colluvium, Glacial Till, Glacial Sediment, Terraces
- **Stiff Soil to Soft Rock** - Sedimentary rock including Sandstone, Siltstone, Claystone, Mudstone and Shale
- **Soft Rock to Hard Rock** - Igneous rock including Granite, Diorite, Rhyolite, Gabbro and Basalt
- **Hard Rock** - Metamorphic rock including Gneiss, Schist, Marble and Quartzite

The best estimate $V_{S30}$ from the Wills and Clahan (2006) database for each geologic category was selected: 280 m/s for soft soil to soil; 350 m/s for soil to stiff soil; 450 m/s for stiff soil to soft rock; 600 m/s for soft rock to hard rock; and 750 m/s for hard rock. Using these categories, a $V_{S30}$ was assigned to each recording station from this geologic proxy; the site geology and inferred $V_{S30}$ value for each station with usable ground motions (as inferred from the results of the data processing described in Section I.2.3) are summarized on Figure I-3. Station M12A was not characterized because, as shown later, the data are not usable. The Wills and Clahan (2006) relationships between surface geologic units and $V_{S30}$ are based on California data and geology; as such, the relationships might not be appropriate for Nevada. The issues of the performance of the proxy in estimating $V_{S30}$ values (median and standard deviation), and regional variability of the proxies (surface geology - Wills and Clahan, 2006; GMX 3rd letter - Chiou et al., 2008; topographic slope - Wald and Allen, 2007); terrain - Yong et al., 2012; geomorphology - Matsuoka et al., 2006), were addressed in Seyhan et al. (2014). Table 4 in Seyhan et al. (2014) shows that the regional differences in the median $V_{S30}$, with respect to the published proxy models, range from -0.14 to 0.13 (ln units). For ease of analysis, the impact of the uncertainty in the $V_{S30}$ of $\pm$ 0.15 (ln units) for the recording sites in Nevada is addressed in Section I.3.2.

### *I.2.3 Data Processing*

The data for these stations was retrieved using the IRIS DMC time series java application; the application was used to convert the units of the velocity traces from counts to cm/s. The raw data that was downloaded included two orthogonal horizontal velocity traces from each station. The horizontal components were oriented north-south and east-west at each location (see Figures I-4 and I-5). The as-recorded velocity traces are plotted on Figure I-6 in orbital plots with the north-south velocity on the y-axis and the east-west velocity on the x-axis. As shown on Figure I-4, the peak intensities from each component of the recording at TA station M12A were clipped at the equipment maximum velocity of 1.6 cm/s; due to the clipping, this recording was discarded. For reference, the focal mechanism for the Wells event is shown on Figures I-4 through I-6; this focal mechanism is based on the solution developed by the UCB Seismological Laboratory (UCB, 2014), but the finite-fault inversion by Dreger et al. (2011) was used to determine the distances.

Preliminary processing was performed on the ground-motion records in accordance with the methodology carried out for the PEER Ground Motion database records (Chiou et al., 2008). Each horizontal component was converted to an acceleration, zero-order corrected (mean removed), and filtered with a high pass filter (Butterworth filter with 8 poles and a corner frequency of 0.1 Hz). Finally, the records were baseline corrected and the acceleration, velocity and displacement time histories are plotted for visual inspection on Figures I-7 through I-13. Response spectra were calculated for these records and are plotted on Figures I-14 and I-15 for visual inspection.

## I.3 Data Analysis

### *I.3.1 Peak Ground Velocities*

Figures I-4 and I-6 show the Peak Ground Velocities (PGVs) at the seven locations with usable data. An azimuthally-dependent trend is not noticed.

### *I.3.2 Comparison with Candidate GMPEs*

The residuals from the Wells event are computed using the pre-selected GMPEs for the Greater Arizona sources. The candidate GMPEs for the Greater Arizona sources are (see Section 6.2.2): Abrahamson et al. (2014 – ASK14), Boore et al. (2014 – BSSA14), Campbell and Bozorgnia (2014 – CB14), Chiou and Youngs (2014 – CY14), Idriss (2014 – Id14), Akkar et al. (2014a, 2014b – ASB14), and Bindi et al. (2014a, 2014b – Bi14). The Id14 model is not used for computing the residuals because it only applies to sites with $V_{S30}$ > 450 m/s and some of the sites have inferred $V_{S30}$ values less than 450 m/s.

Due to the reliable bandwidth of the TA stations, the residuals with respect of the GMPEs are judged to be reliable below 12 Hz. Accordingly, the residuals are not shown nor evaluated for periods below 0.075 sec.

The distance dependence of the residuals for five spectral periods (0.1, 0.2, 0.4, 1.0, and 2.0 sec) was evaluated for the six GMPEs, as shown in Figures I-16 for ASK14, BSSA14, CB14, CY14, ASB14 and Bi14. For the shorter periods, the residuals show a significant trend with distance: the stations at distances less than 40 km tend to have negative residuals and the stations at distances greater than 80 km tend to have positive residuals. This type of a distance trend can affect the interpretation of the mean residuals because the mean value will depend on the relative number of stations at short and large distances.

The mean residuals for all six GMPEs are shown in Figure I-17. At short periods(less than 0.2 sec), data are in general agreement with the GMPEs with an average residual between -0.3 and 0.3 natural log units, which is about one standard deviation of the between-event variability seen in the candidate GMPEs. In particular, the residuals from the NGA-West2 models are systematically lower than the residuals from the European models, reflecting the reduced ground motions for normal-faulting earthquakes in the European GMPEs. At this short-period range, the NGA-West2 residuals are negative or near zero whereas the European model residuals are positive, indicating that, on average, the NGA-West2 models are a better fit the short periods.

At intermediate periods (T = 0.2 to 0.5 sec), both the NGA-West2 and European models show a trend of the mean residuals becoming more negative as the period increases. In this period range, the NGA-West2 models over-predict the ground motions and the European models are closer to the zero residual line than the NGA-West2 models. At long periods (T > 0.5 sec), both the NGA-West2 models and the European models strongly over-predict the ground motions, and the residuals become more negative (-0.5 to -1.2 natural log units)

As noted in Section I.2.2, the regional differences in the median $V_{S30}$ are within about $\pm$ 0.15 (ln units) of the published proxy models. The TI Team judged that the differences between the $V_{S30}$ proxy for Nevada and California would be within the global range. Using a $\pm$ 0.15 leads to a change in the total PSA residuals of between 7% at periods between 0.075 and 0.3 sec, and 11% at periods between 0.3 and 3 sec when averaged over the six candidate GMPEs. This uncertainty is small compared to the range of the mean residuals (about +0.5 to -1 in ln units), thus the uncertainty in the $V_{S30}$ estimate is not critical for the evaluation of the Wells earthquake data.

## I.4 References

Abrahamson, N.A., Silva, W.J., and Kamai, R. (2014). Summary of the AKS14 Ground-Motion Relation for Active Crustal Regions, *Earthquake Spectra*, Vol. 30(3), 1025-1055, DOI: 10.1193/070913EQS198M.

Akkar, S., Sandikkaya, M.A., and Bommer, J.J. (2014a). Empirical ground-motion models for point- and extended-source crustal earthquake scenarios in Europe and the Middle East, *Bull. Earthquake Eng*., Vol. 12(1), 359-387, DOI: 10.1007/s10518-013-9461-4.

Akkar, S., Sandikkaya, M.A., and Bommer, J.J. (2014b). Erratum to: Empirical ground-motion models for point- and extended-source crustal earthquake scenarios in Europe and the Middle East, *Bull. Earthquake Eng.*, Vol. 12(1), 389-390, DOI: 10.1007/s10518-013-9508-6.

Ancheta, T.D., Darragh, R.B., Stewart, J.P., Seyhan, E., Silva, W.J., Chiou, B.S.-J., Wooddell, K.E., Graves, R.W., Kottke, A.R., Boore, D.M., Kishida, T., and Donahue, J.L. (2014). NGA-West2 Database, *Earthquake Spectra*, Vol. 30(3), 989-1005.

Bindi D., Massa M., Luzi L., Ameri G., Pacor F., Puglia R., and Augliera, P. (2014a). Pan-European Ground-Motion Prediction Equations for the Average Horizontal Component of PGA, PGV, and 5%-Damped PSA at Spectral Periods up to 3.0 s using the RESORCE dataset, *Bull. Earthquake Eng*., Vol. 12, 391-430, DOI: 10.1007/s10518-013-9525-5.

Bindi D., Massa M., Luzi L., Ameri G., Pacor F., Puglia R., and Augliera, P. (2014b). Erratum to: Pan-European Ground-Motion Prediction Equations for the Average Horizontal Component of PGA, PGV, and 5%-Damped PSA at Spectral Periods up to 3.0 s using the RESORCE dataset, *Bull. Earthquake Eng*., Vol. 12, 431-448, DOI: 10.1007/s10518-014-9589-x.

Boore, D.M., Stewart, J.P., Seyhan, E., and Atkinson, G.M. (2014). NGA-West 2 Equations for Predicting PGA, PGV, and 5%-Damped PSA for Shallow Crustal Earthquakes, *Earthquake Spectra*, Vol. 30(3), 1057-1085, DOI: 10.1193/070113EQS184M.

Campbell, K.W., and Bozorgnia, Y. (2014). NGA-West2 Ground Motion Model for the Average Horizontal Components of PGA, PGV, and 5%-Damped Linear Acceleration Response Spectra, *Earthquake Spectra*, Vol. 30(3), 1087-1115, DOI: 10.1193/062913EQS175M.

Chiou, B., Darragh, R., Gregor, N., and Silva, W. (2008). NGA project strong-motion database, *Earthquake Spectra*, Vol. 24(1), 23-44.

Chiou, B.S.-J., and Youngs, R.R. (2014). Update of the Chiou and Youngs NGA Model for the Average Horizontal Component of Peak Ground Motion and Response Spectra, *Earthquake Spectra*, Vol. 30(3), 1117-1153, DOI: 10.1193/072813EQS219M.

Dreger, D.S. Dreger, Ford, S.R, and Ryder, I. (2011). Preliminary Finite-Source Study of the February 21, 2008 Wells, Nevada Earthquake, *Nevada Bureau of Mines and Geology Special Publication*, Vol. 36, 147-156.

Idriss, I.M. (2014). An NGA-West2 Empirical Model for Estimating the Horizontal Spectral Values Generated by Shallow Crustal Earthquakes, *Earthquake* Spectra, Vol. 30(3), 1155-1177, DOI: 10.1193/070613EQS195M.

Leonard, M. (2010). Earthquake Fault Scaling: Self-Consistent Relating of Rupture Length, Width, Average Displacement, and Moment Release, *Bull. Seism. Soc. Am.*, Vol. 100(5A), 1971-1988.

Matsuoka, M., Wakamatsu, K., Fujimoto, F., Midorikawa, S. (2006). Average shear-wave velocity mapping using Japan engineering geomorphologic classification map, *J. Struct. Mecha. Earthq. Eng.*, Vol. 23(1), 57s–68s.

Seyhan, E., Stewart, J.P., Ancheta, T.D., Darragh, R.B., and Graves, R.W. (2014). NGA-West2 Site Database, *Earthquake Spectra*, Vol. 30(3), 1007-1024.

United States Geologic Survey – USGS (2007). Preliminary integrated geologic map databases for the United States: Western States, California, Nevada, Arizona, Washington, Oregon, Idaho, and Utah, Version 1.3, *Open File Report 2005-1305*, available at [http://pubs.usgs.gov/of/2005/1305/], updated December 2007.

United States Geologic Survey – USGS (2014). Magnitude 6.0 – NEVADA: Earthquake Summary, available at [http://earthquake.usgs.gov/earthquakes/eqinthenews/2008/us2008nsa9/#summary]; page last modified July 2014.

UCB (2014). Moment tensor solutions, available at http://seismo.berkeley.edu/mt/

Wald, D.J., and Allen, T.I. (2007). Topographic slope as a proxy for seismic site conditions and amplification, *Bull. Seismol. Soc. Am.*, Vol. 97, 1379–1395.

Wills C.J., Clahan K.B. (2006). Developing a map of geologically defined site- condition categories for California, *Bull. Seism. Soc. Am.*, Vol. 96, 1483-1501.

Yong, A., Hough, S.E., Iwahashi, J., and Braverman, A. (2012). Terrain-based site conditions map of California with implications for the contiguous United States, *Bull. Seismol. Soc. Am.*, Vol. 102, 114–128.

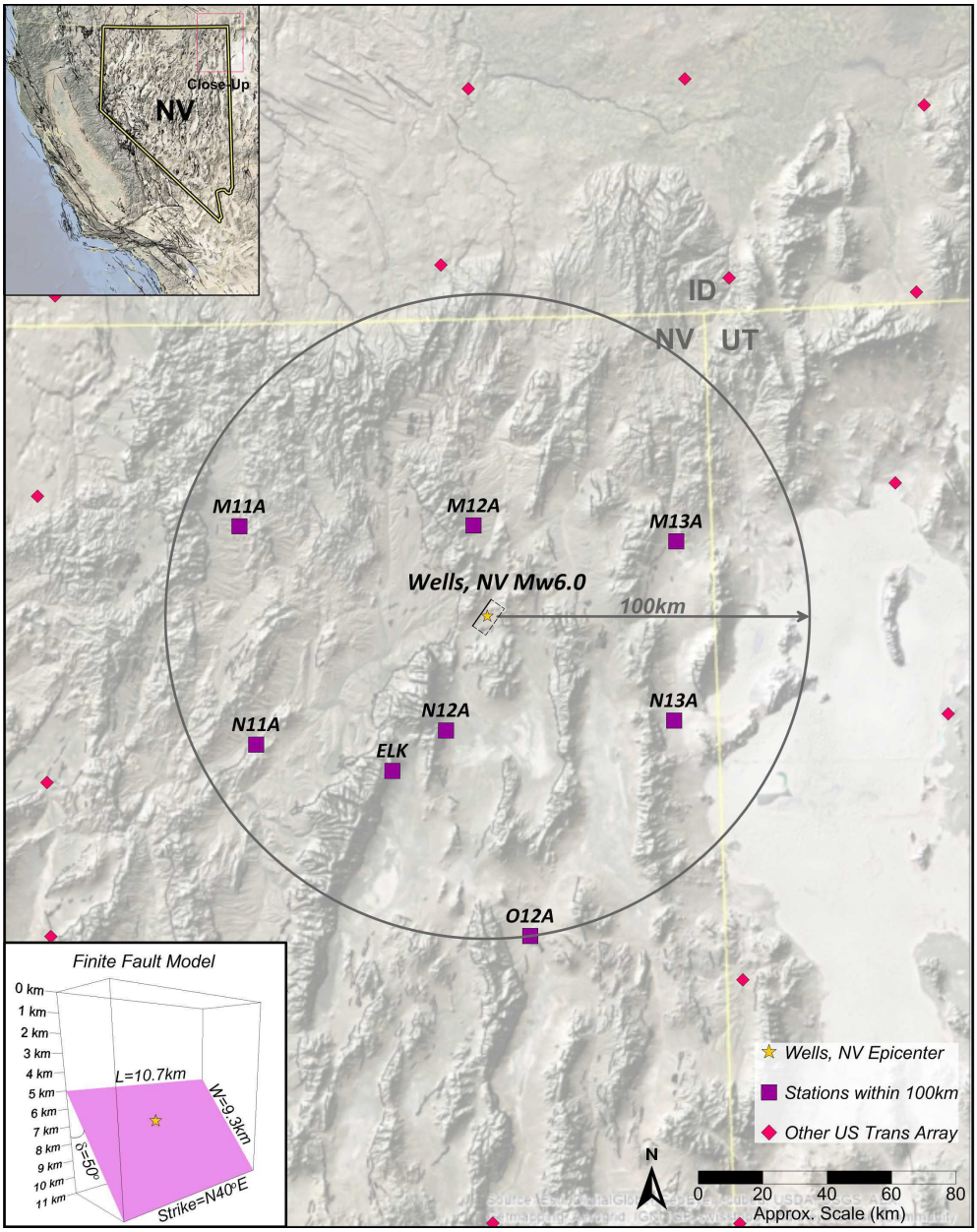



**Figure I-1:** Wells, NV earthquake location and distribution of recording stations in the proximity of the epicenter. The Dreger et al. (2011) finite-fault rupture model is shown in the box located in the left bottom corner.

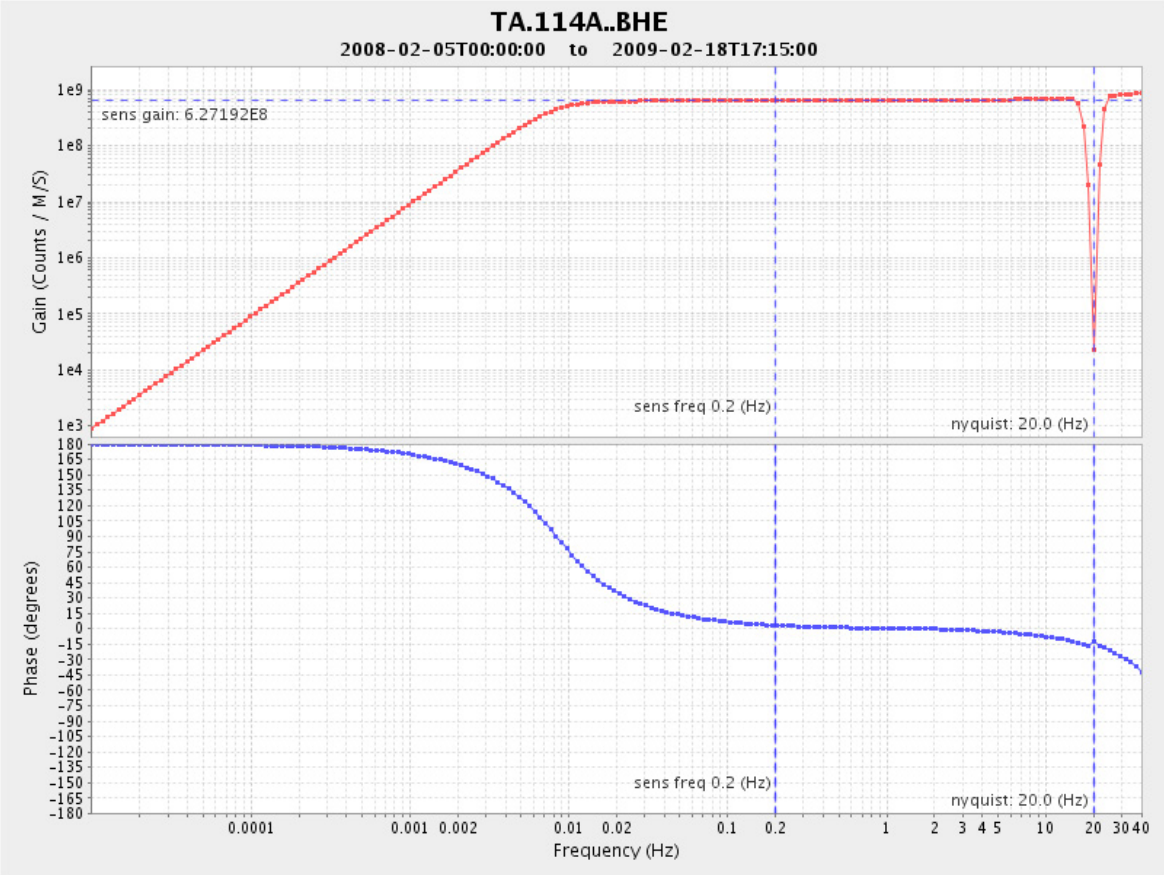
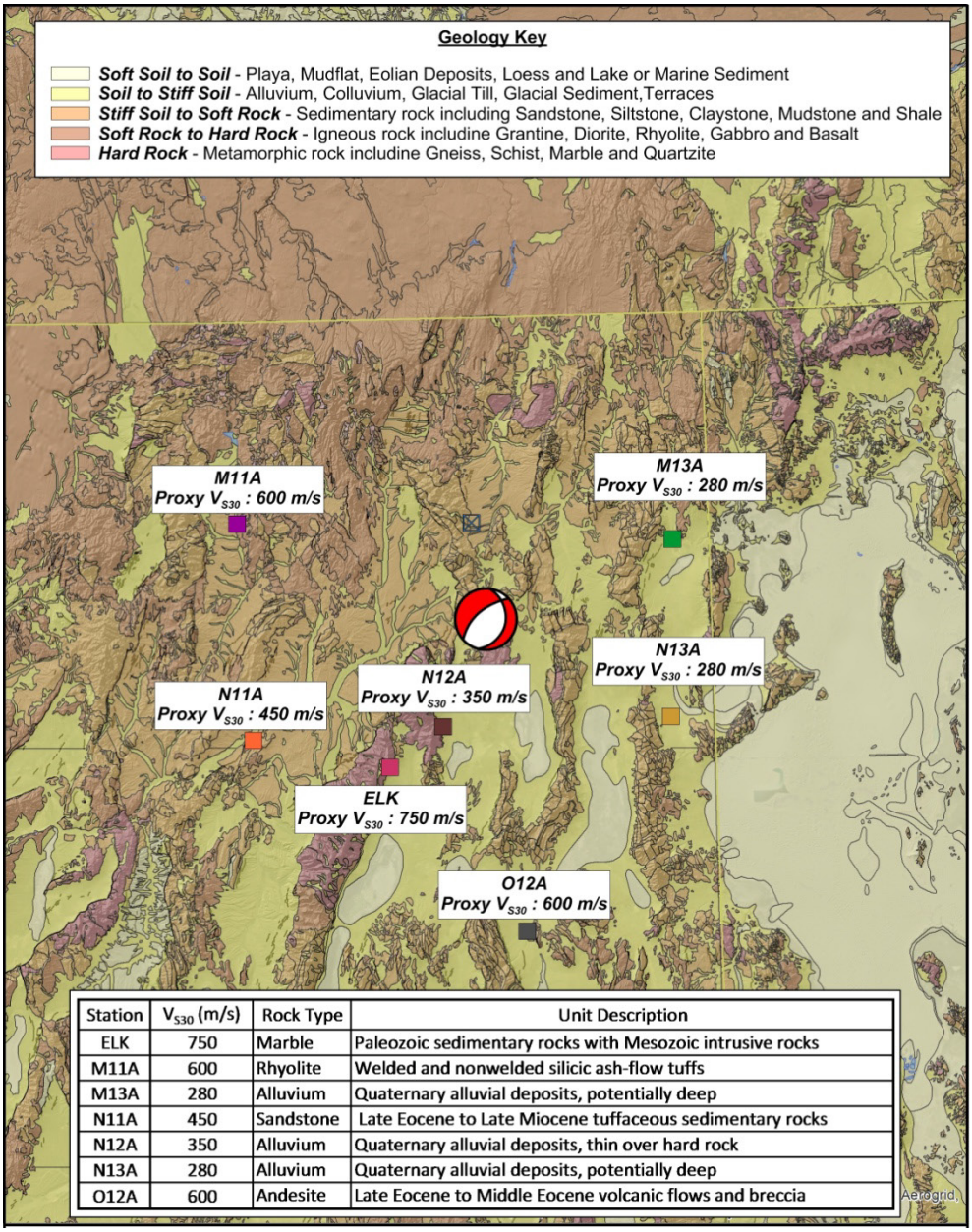



**Figure I-2:** Example of instrument response for the USArray (TA) stations. The Nyquist frequency is 20 Hz because the TA has a low sampling rate of 40 Hz. An anti-alias filter is applied to the TA data at about 80% of the Nyquist frequency with a corner frequency near 16 Hz, thus the instrument response is flat from 0.01 to about 15 Hz.




| Station | $V_{S30}$ (m/s) | Rock Type | Unit Description |
|---|---|---|---|
| ELK | 750 | Marble | Paleozoic sedimentary rocks with Mesozoic intrusive rocks |
| M11A | 600 | Rhyolite | Welded and nonwelded silicic ash-flow tuffs |
| M13A | 280 | Alluvium | Quaternary alluvial deposits, potentially deep |
| N11A | 450 | Sandstone | Late Eocene to Late Miocene tuffaceous sedimentary rocks |
| N12A | 350 | Alluvium | Quaternary alluvial deposits, thin over hard rock |
| N13A | 280 | Alluvium | Quaternary alluvial deposits, potentially deep |
| O12A | 600 | Andesite | Late Eocene to Middle Eocene volcanic flows and breccia |

**Figure I-3:** Surface geology for the region surrounding the Wells, Nevada event, based on the USGS (2007) database. $V_{S30}$ values assigned to each of the stations with usable data based on the Wills and Clahan (2006) geology proxy approach are shown in the table located at the bottom of the Figure.

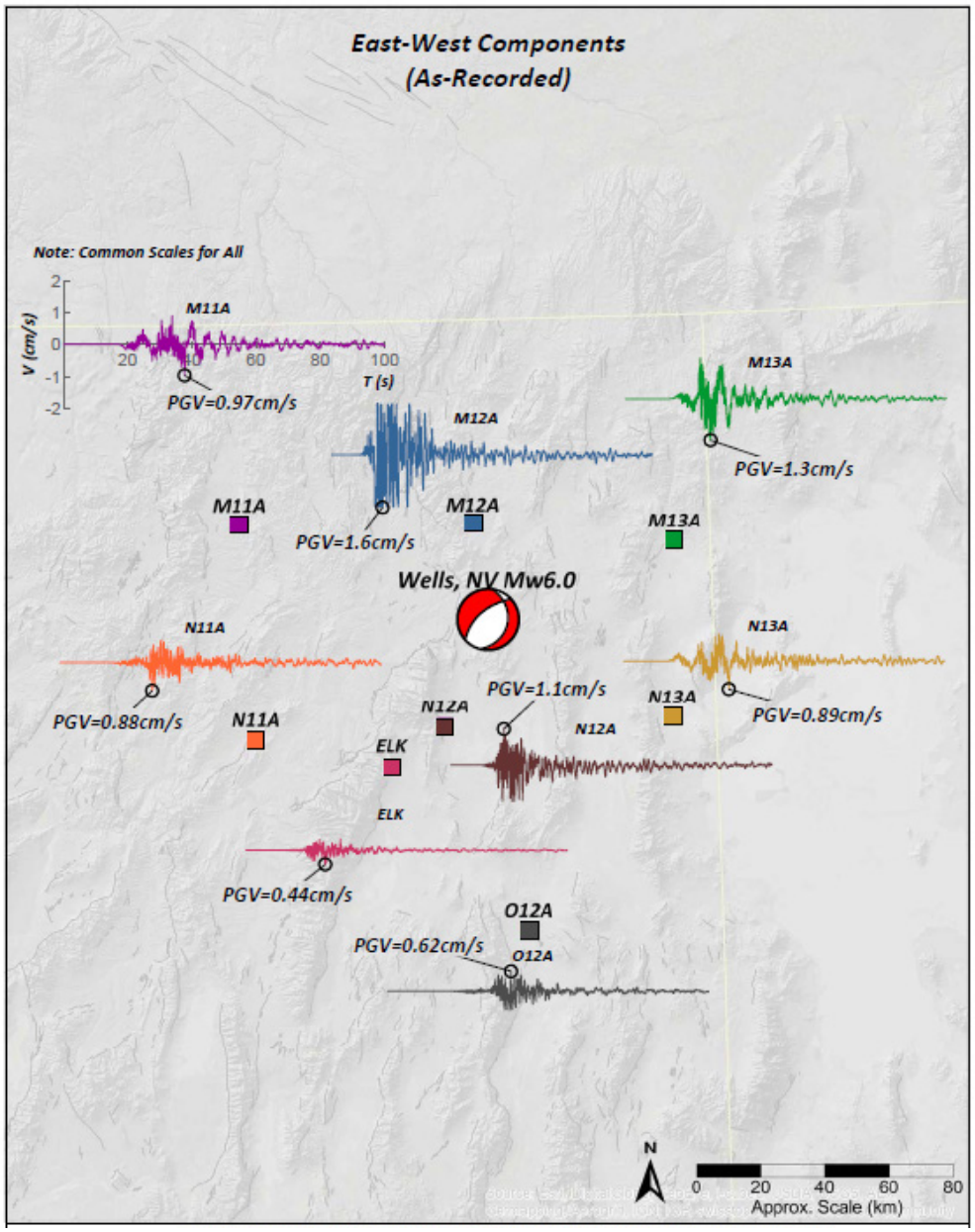



**Figure I-4:** East-West components of the velocity traces for the Wells recordings. The velocity traces are shown as recorded, i.e. prior to the signal processing. PGV values for each recording are shown as well.

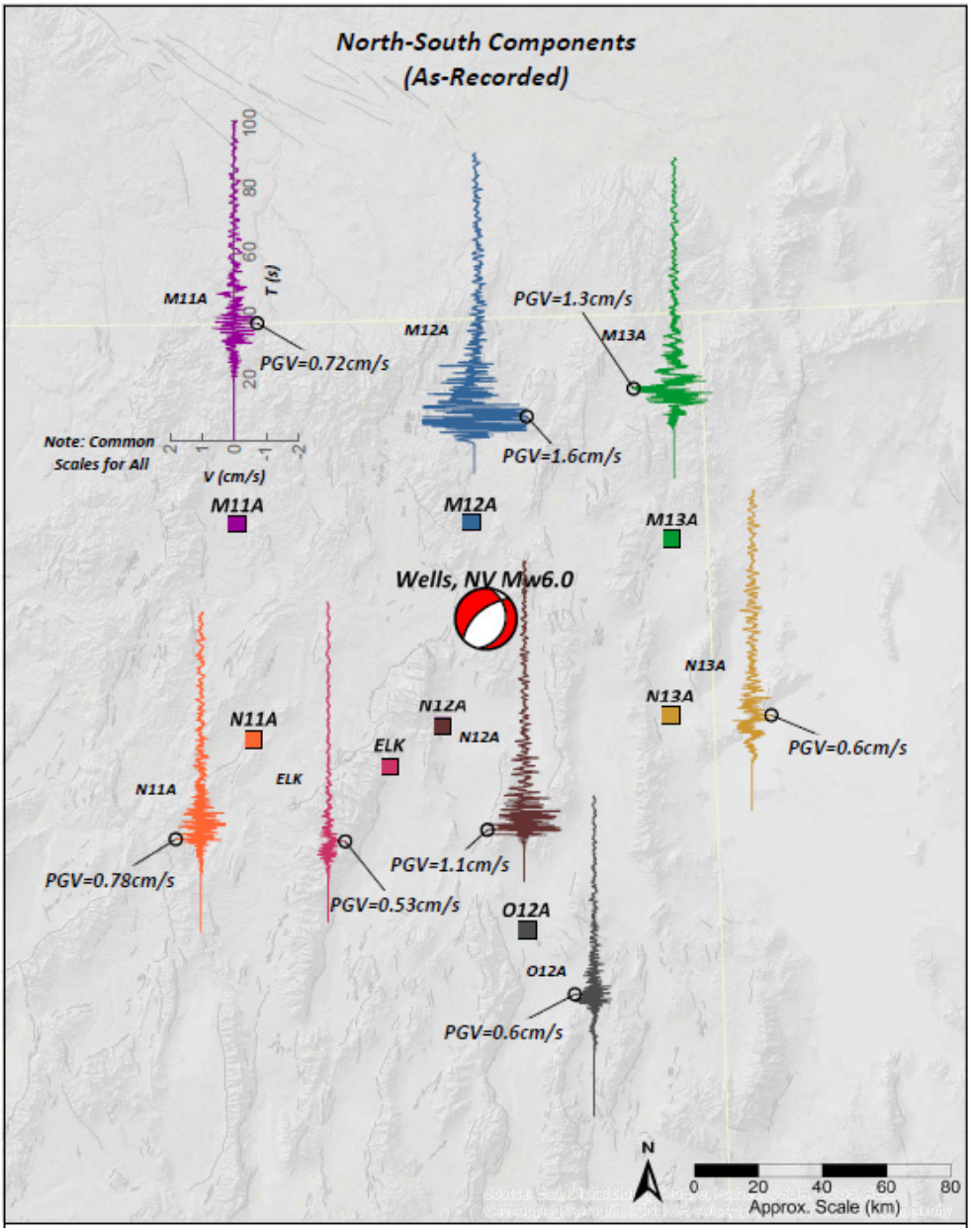



**Figure I-5:** North-South components of the velocity traces for the Wells recordings. The velocity traces are shown as recorded, i.e. prior to the signal processing. PGV values for each recording are shown as well.

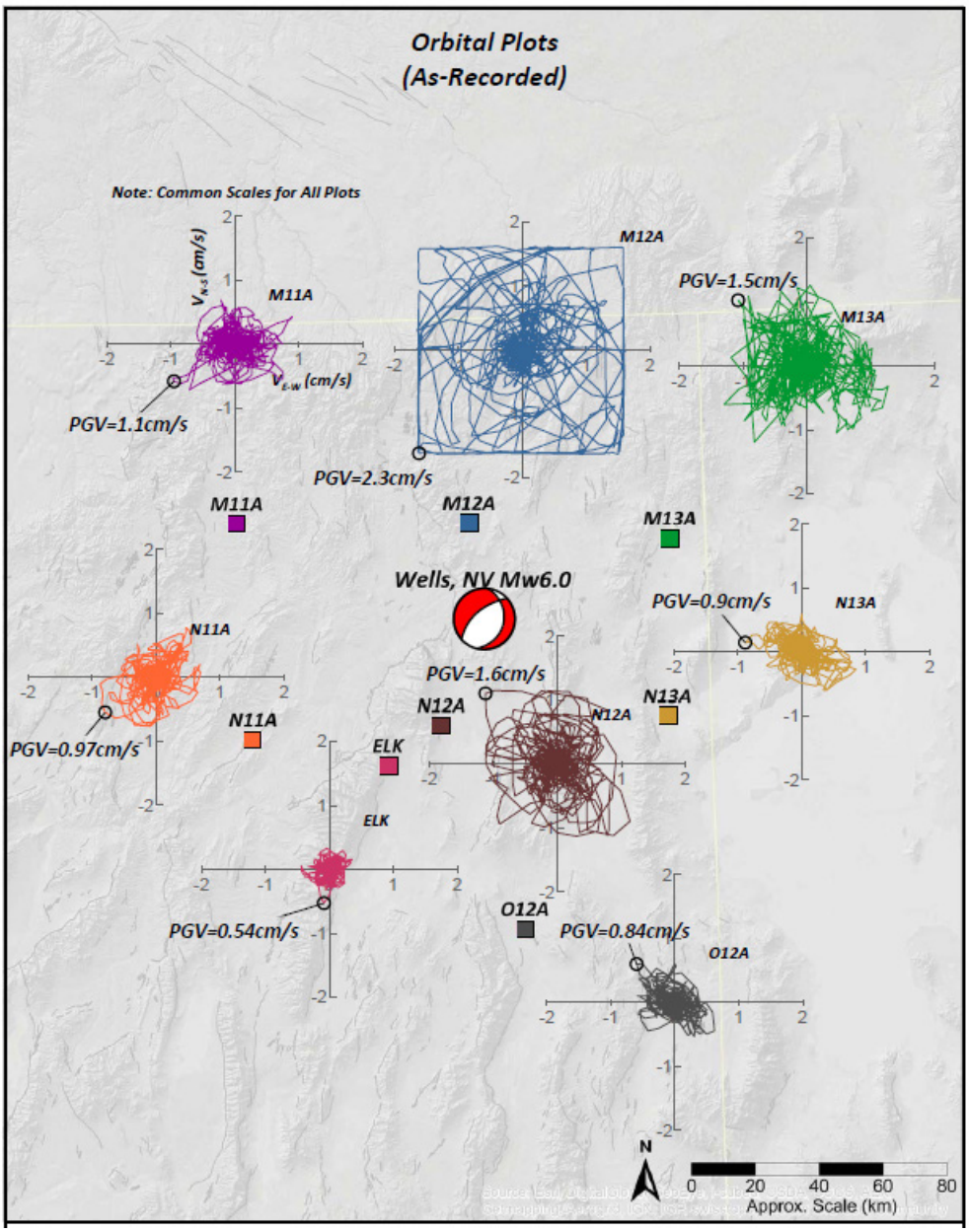



**Figure I-6**: Orbital plots of the as-recorded velocity. The positive y-axis is North and positive x-axis is East.

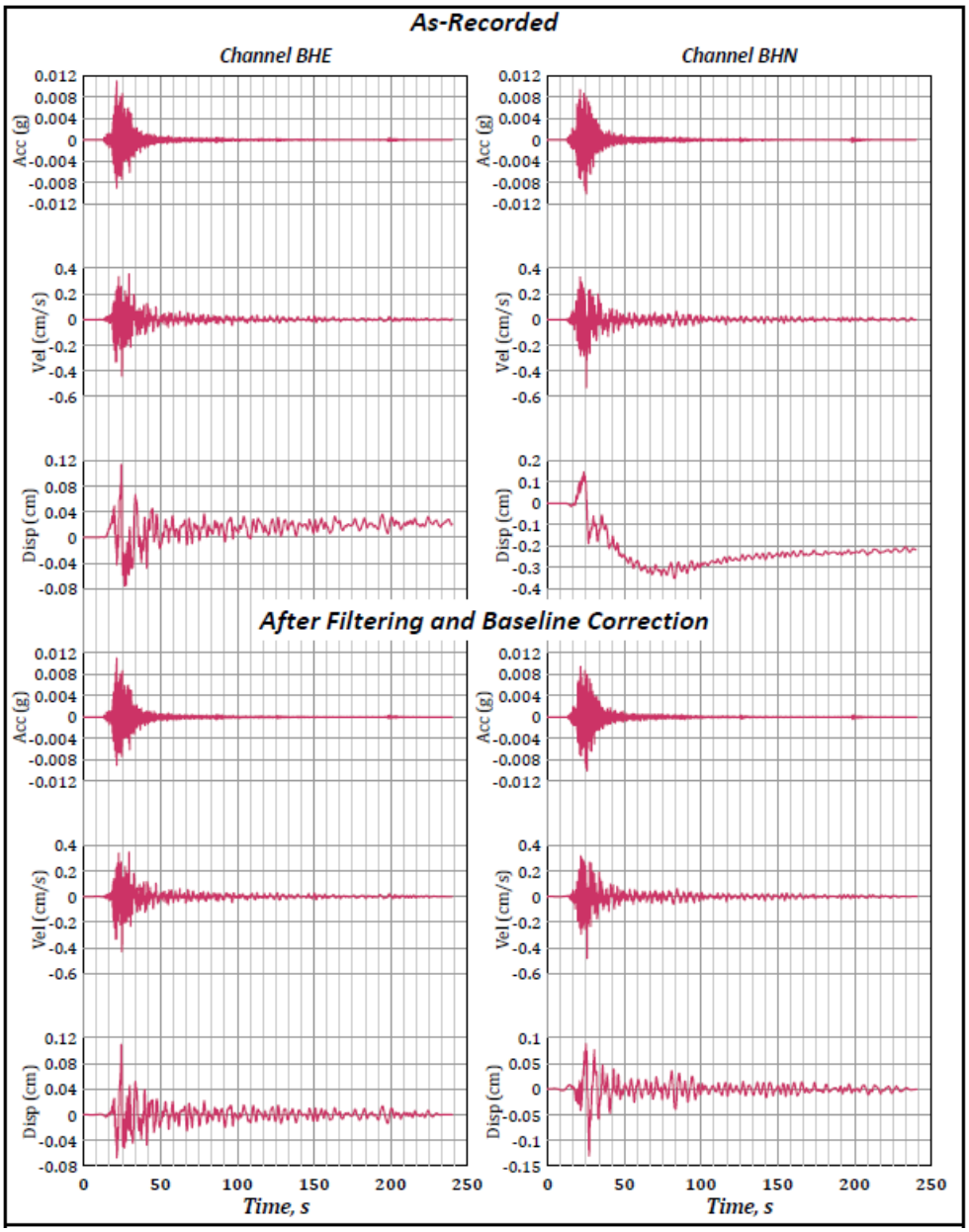



**Figure I-7:** Comparison of the as-recorded versus processed time series (acceleration, velocity and displacement) from the ELK station.

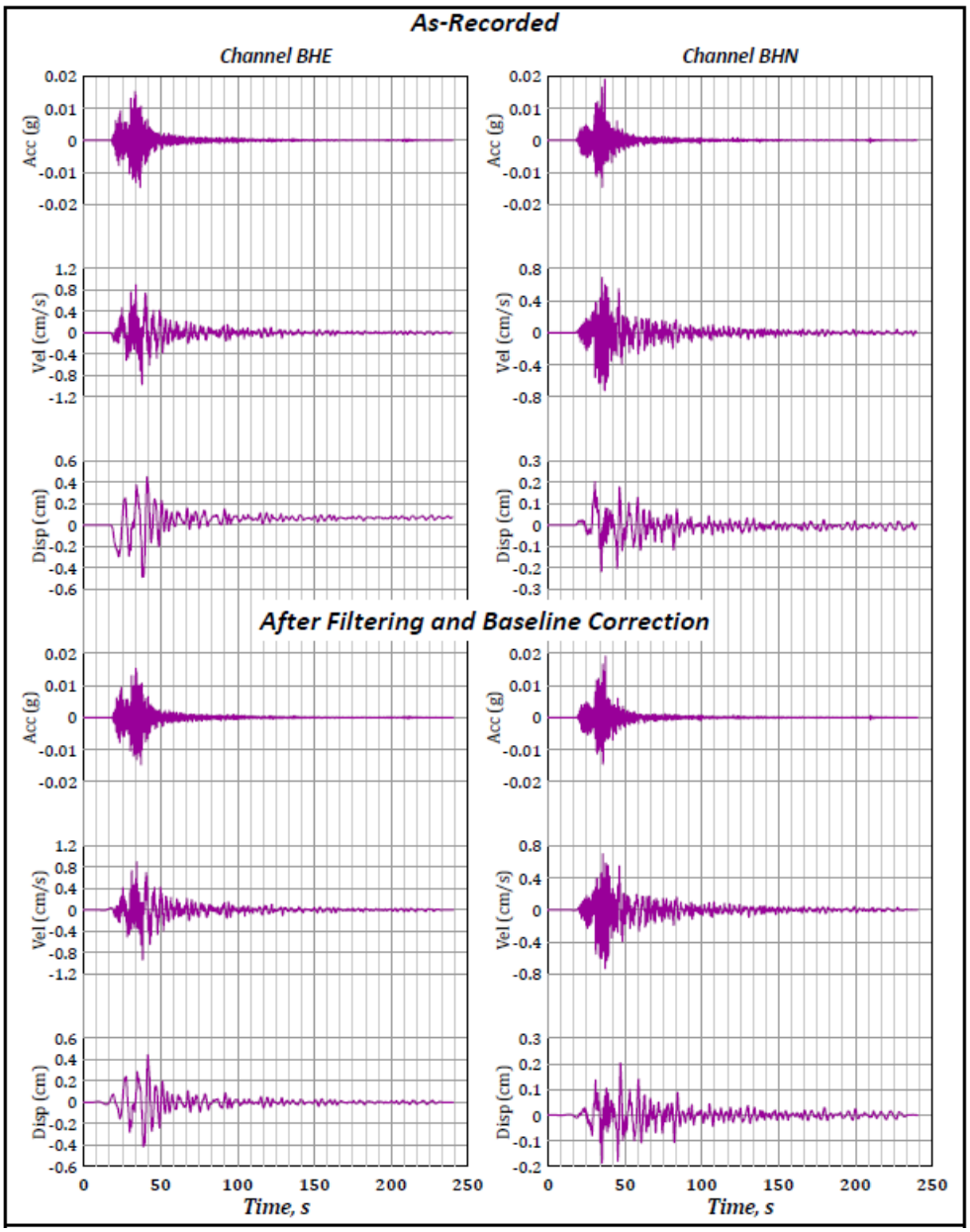



**Figure I-8:** Comparison of the as-recorded versus processed time series (acceleration, velocity and displacement) from the M11A station.

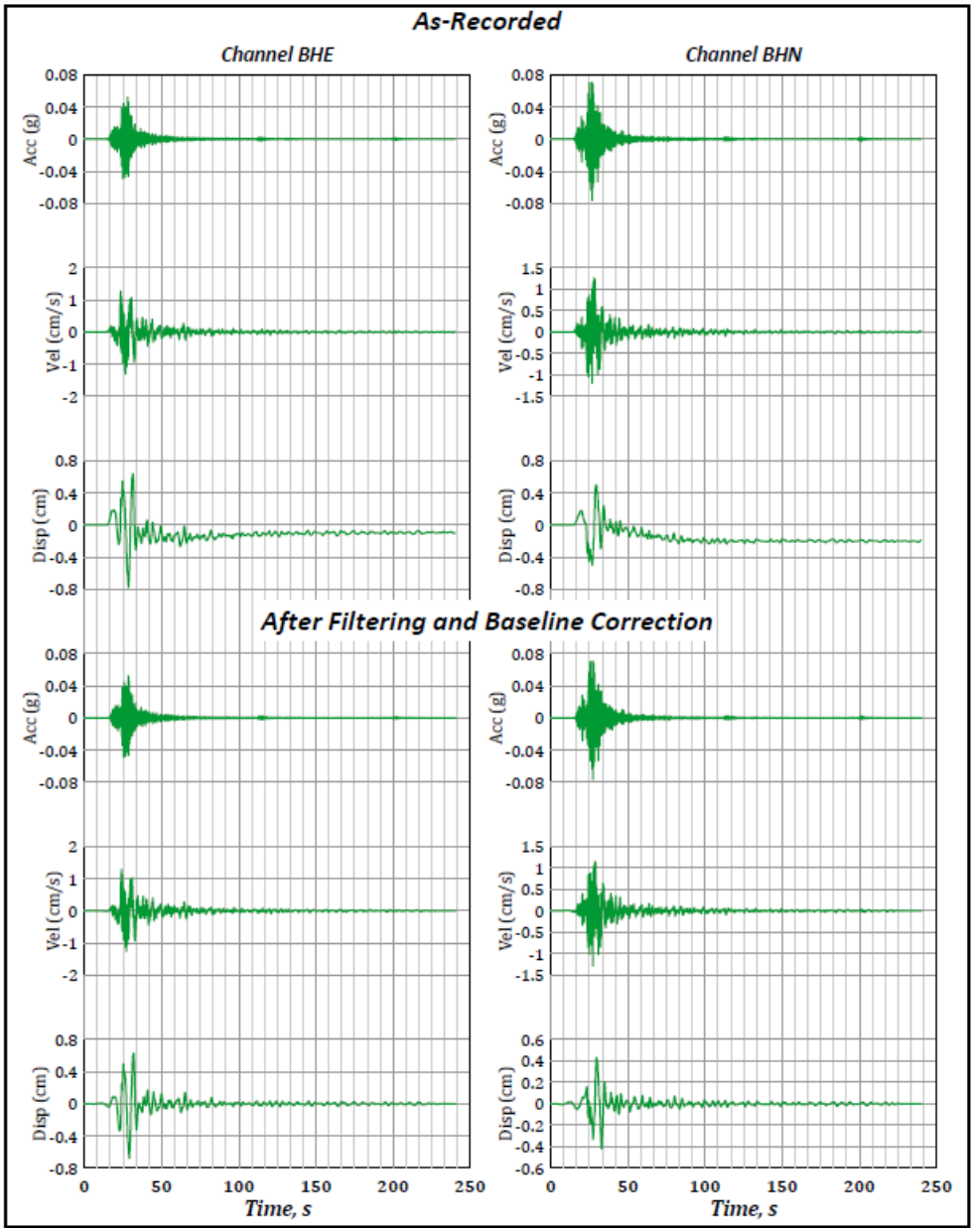



**Figure I-9:** Comparison of the as-recorded versus processed time series (acceleration, velocity and displacement) from the M13A station.

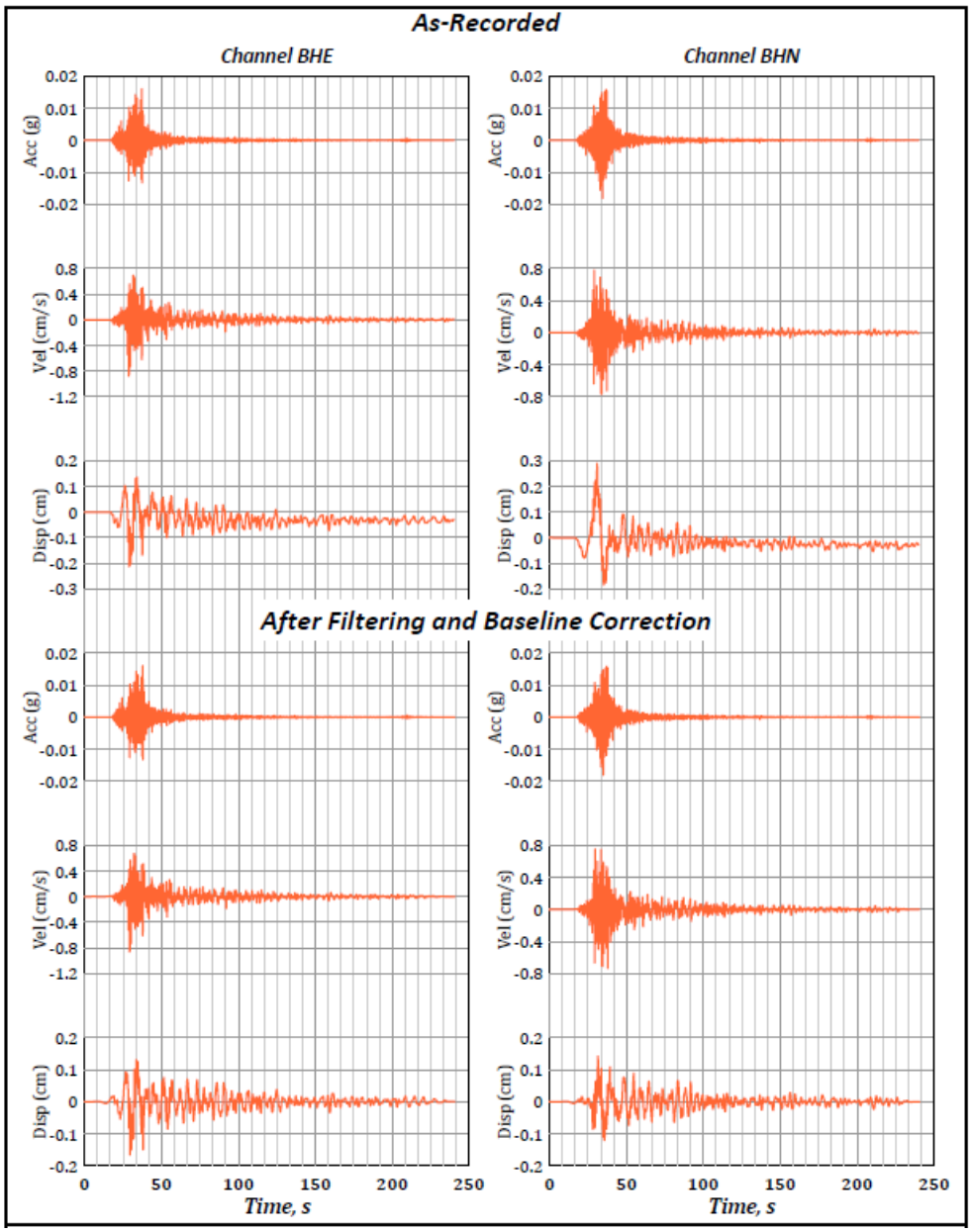



**Figure I-10:** Comparison of the as-recorded versus processed time series (acceleration, velocity and displacement) from the N11A station.

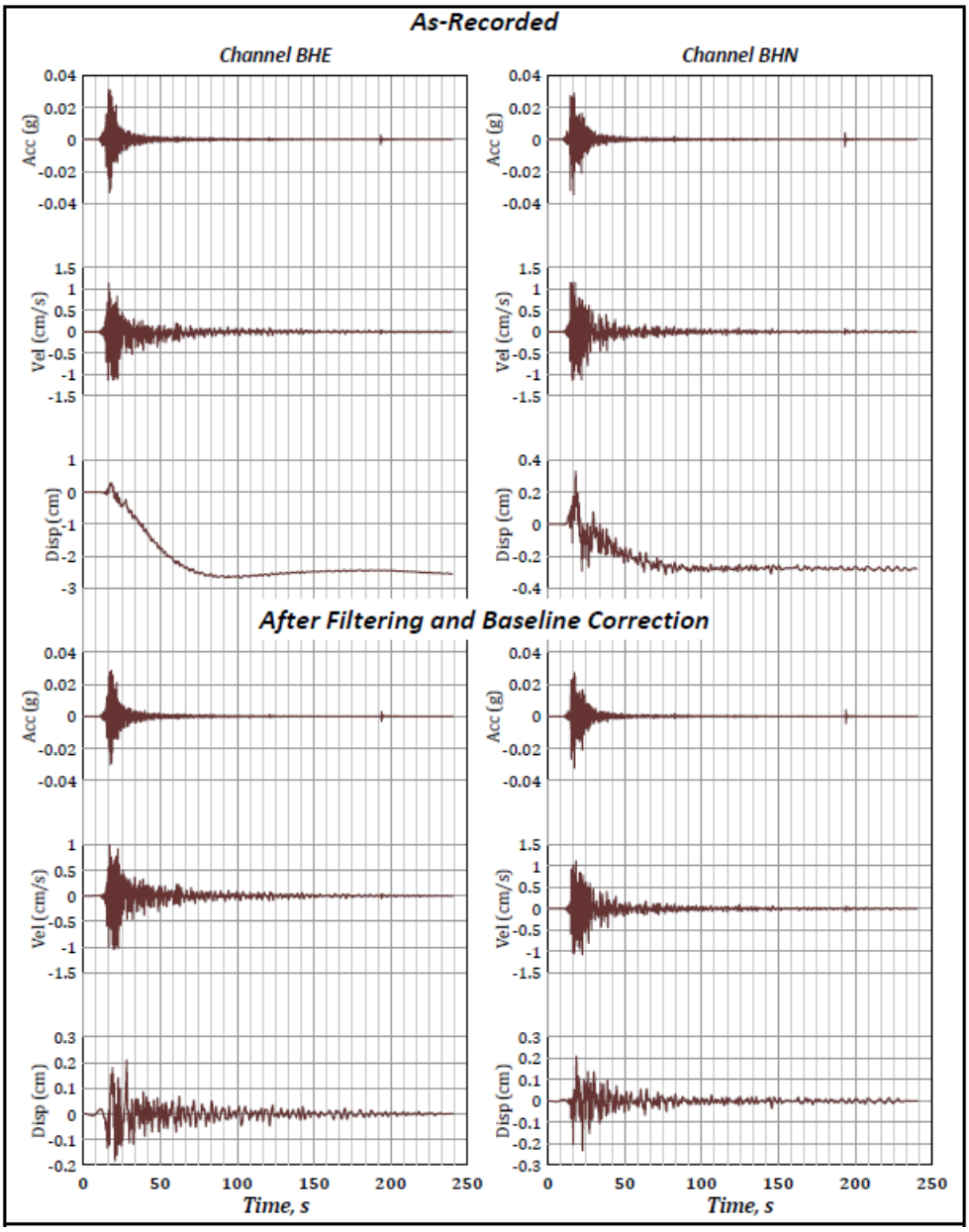



**Figure I-11:** Comparison of the as-recorded versus processed time series (acceleration, velocity and displacement) from the N12A station.

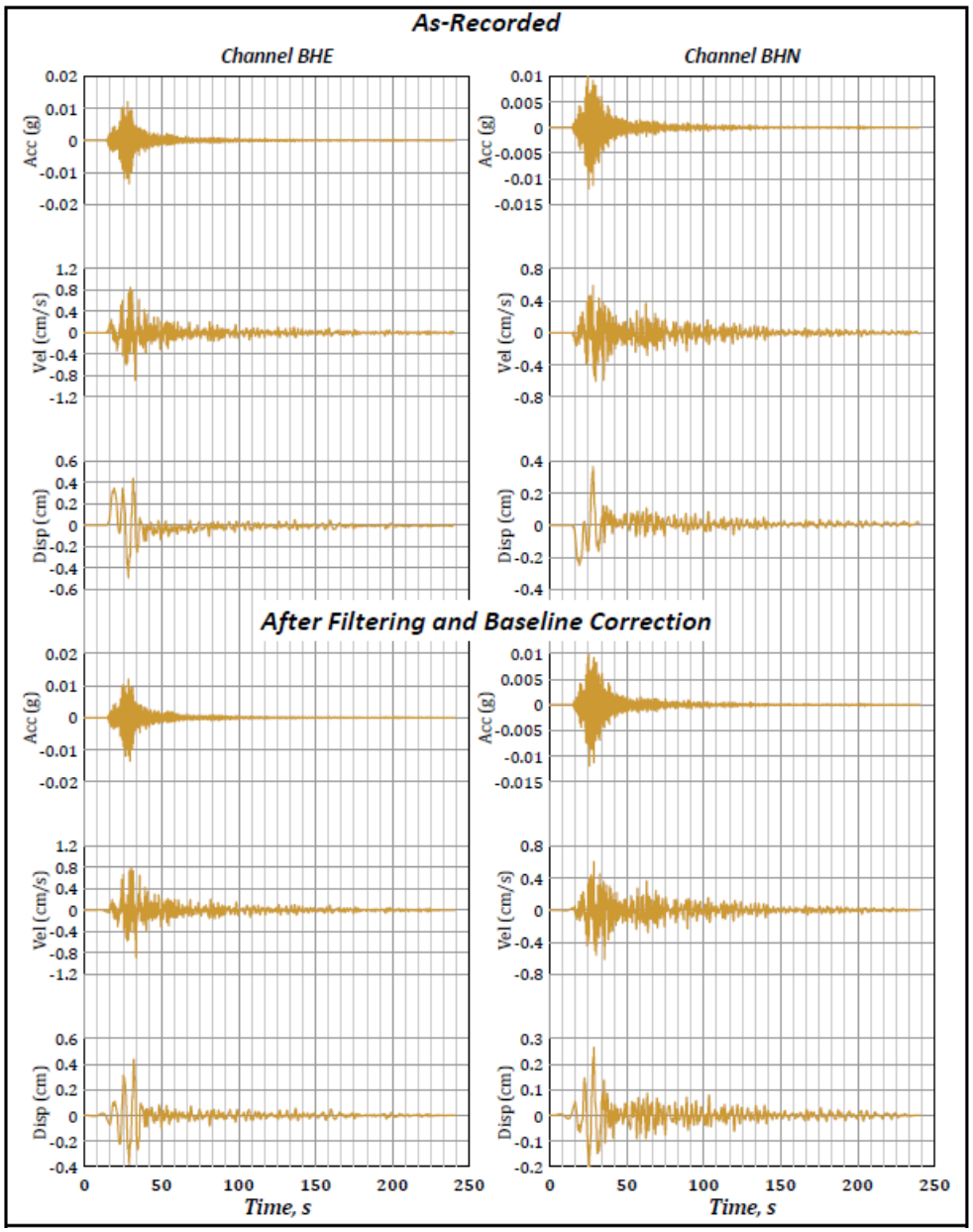



**Figure I-12:** Comparison of the as-recorded versus processed time series (acceleration, velocity and displacement) from the N13A station.

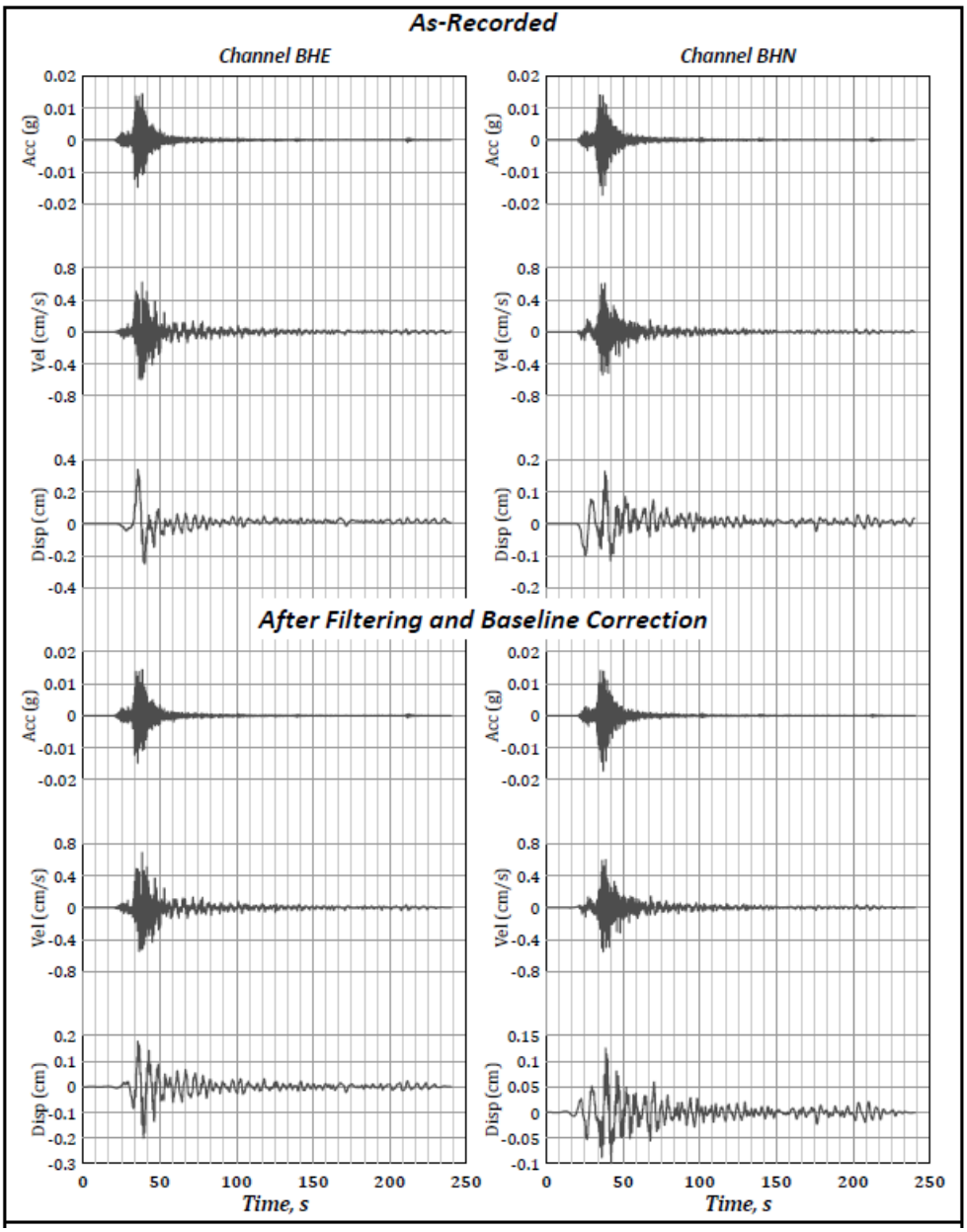



**Figure I-13:** Comparison of the as-recorded versus processed time series (acceleration, velocity and displacement) from the O12A station.

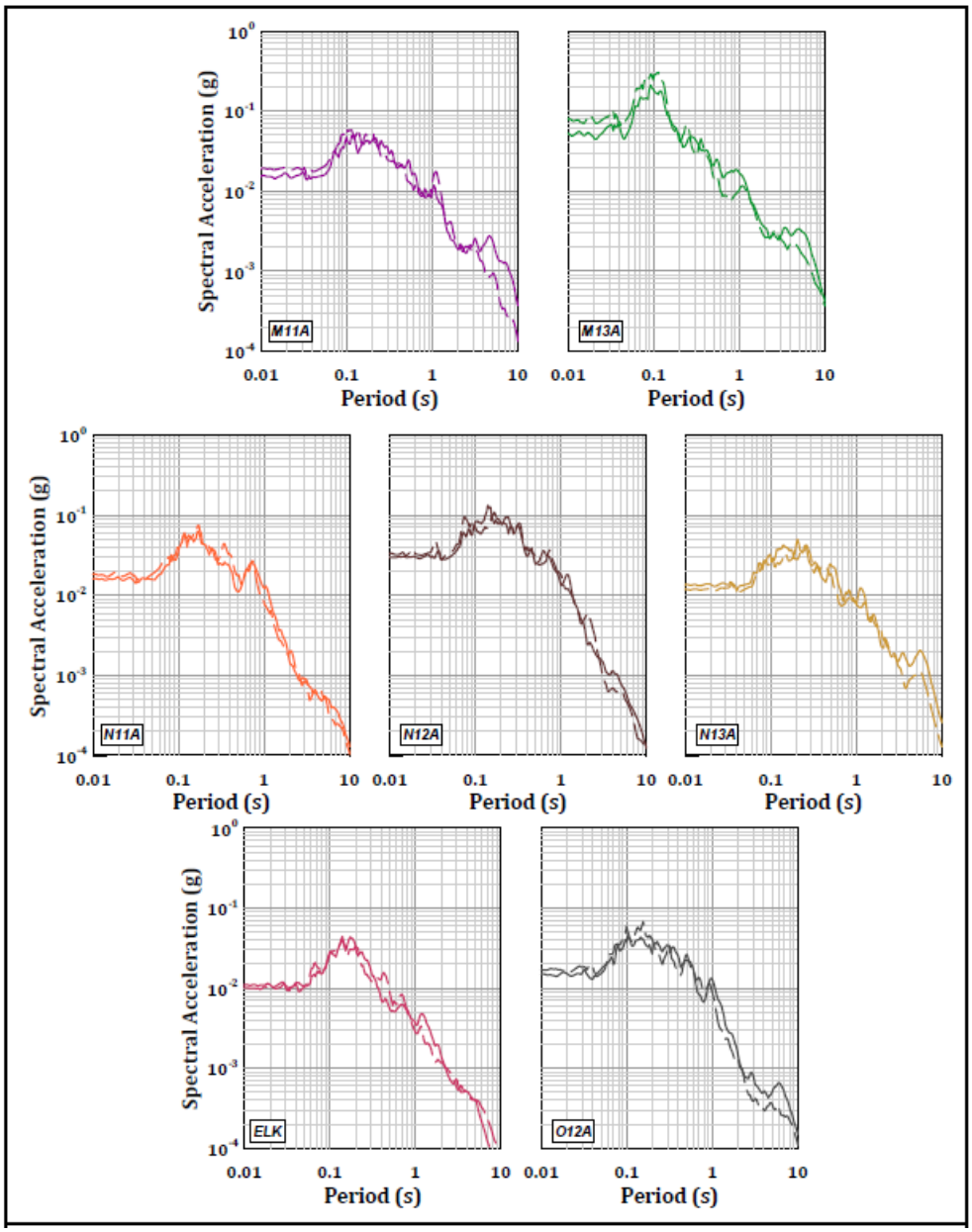



**Figure I-14:** 5%-damped response spectra of the processed N-S and E-W components for the Wells event recorded at the seven stations with usable data.

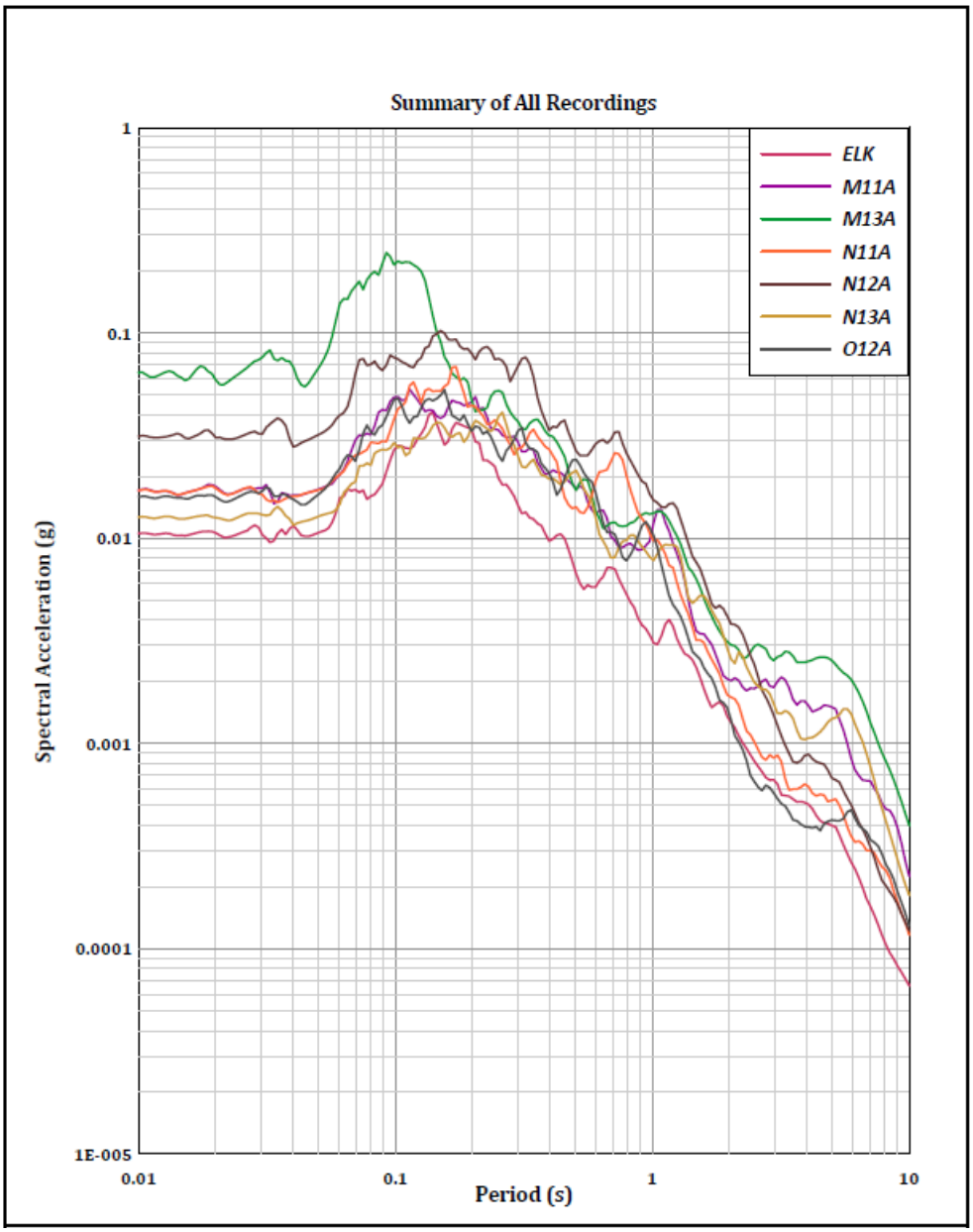



**Figure I-15:** Geometric mean of the response spectra from the two horizontal components for the seven stations with usable recordings.

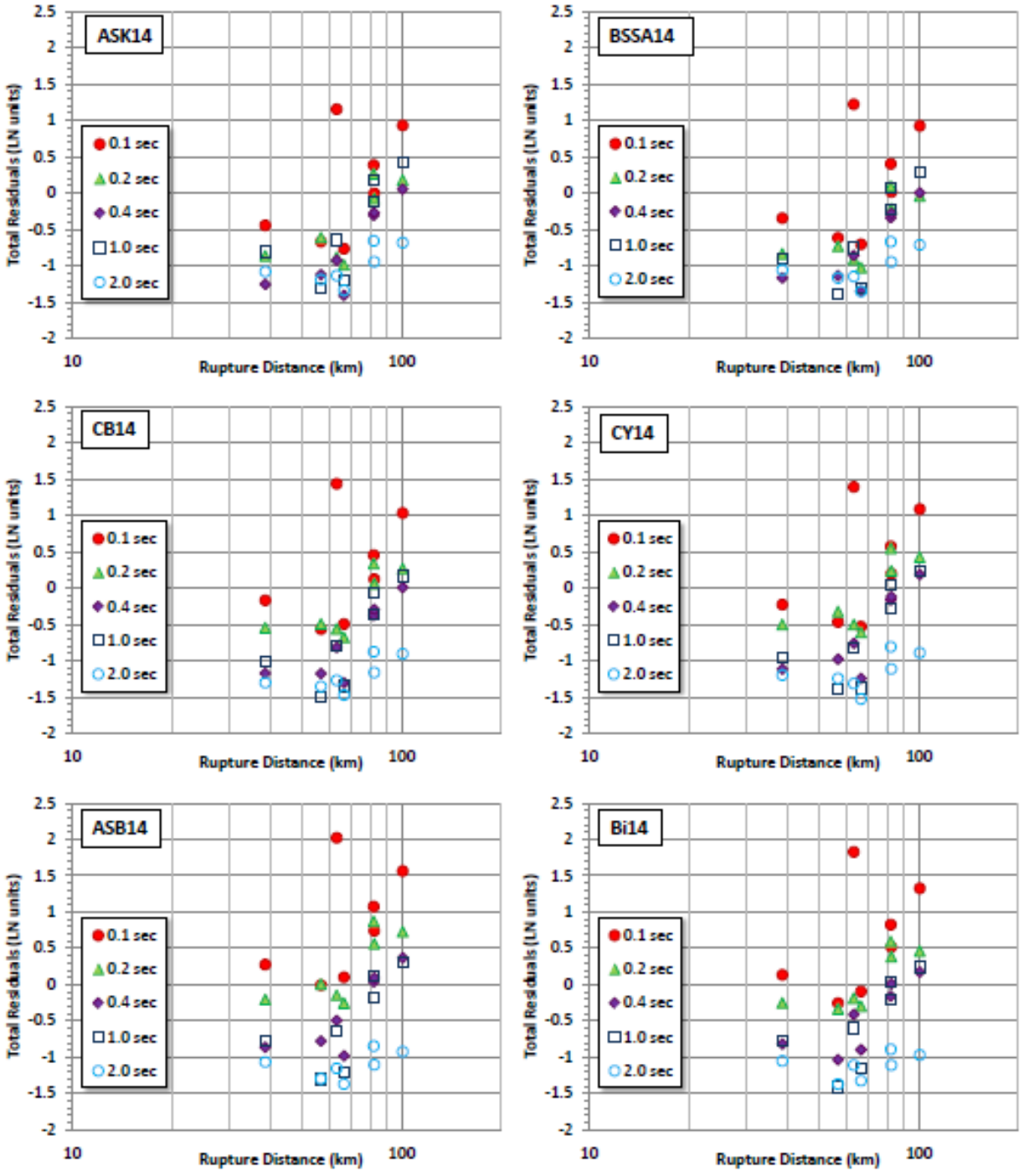



**Figure I-16:** Residuals from the seven recordings for the Wells, Nevada earthquake, computed for the six candidate GMPEs.

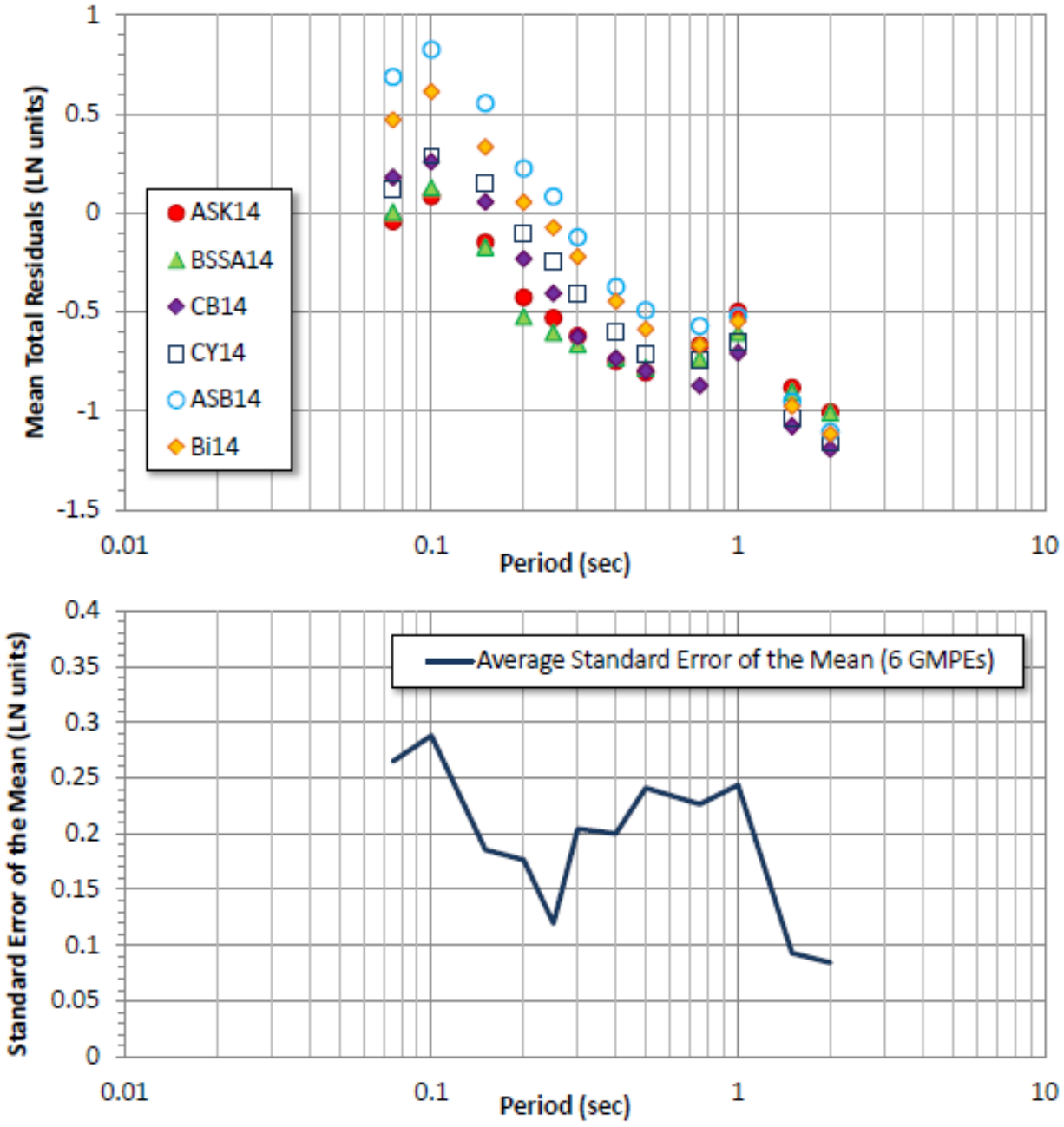



**Figure I-17:** Mean residuals from the seven recordings for the Wells, Nevada earthquake, evaluated for the six applicable GMPEs (Top). Average of the standard error of the mean (ln units) for the six sets of residuals (Bottom).

# APPENDIX J

# FORWARD FINITE-FAULT SIMULATIONS FOR SWUS

## J.1 Finite Fault Simulations Models

A data base of ground motions from numerical, broadband, finite-fault simulations was compiled from methods implemented on the Southern California Earthquake Center (SCEC) Broadband Platform (BBP) (e.g. Maechling et al., 2015), and which passed a peer-review process in terms of median pseudo spectral acceleration motions (Dreger et al., 2015). These motions were used to determine the appropriate mixing of ground-motion prediction equations (GMPE) for splay and complex rupture scenarios (Section J.4), and to extend GMPE hanging-wall terms to lower magnitude (Section J.5). In addition, simulations for single rupture plane cases were used to develop ground motions for use in the characterization of the Sammon's GMPE space (Table 8.4-1) to develop logic tree weights for the median ground-motion base models (e.g. Figure 8.2-2). The simulation validation process and the construction of simulation scenarios for the project's objectives are described in the following.

### *J.1.1 Evaluation of the Models*

The SCEC BBP has implemented 5 broadband, finite-source simulation methods, all of which have their approaches described in the peer-reviewed literature. There is one purely stochastic approach utilizing a band-limited white-noise model (EXSIM, Assatourians and Atkinson, 2015), two approaches that utilize deterministic Green's functions to describe the wave propagation and different models for the characterization of the spatio-temporal heterogeneity of the kinematic seismic source process (CSM, Anderson, 2015; and UCSB, Crempien and Archuleta, 2015), and two hybrid approaches that use stochastic motions for frequencies greater than 1 Hz, and deterministic motions for frequencies less than 1 Hz (GP, Graves and Pitarka, 2015; and SDSU, Olsen and Takedatsu, 2015).

The five methods were evaluated for suitability for simulation of strong ground motion for engineering applications in terms of the RotD50 spectra. RotD50 spectra is defined as the median value of the 5%-damped pseudo-spectral acceleration (PSA) computed as the resultant of two horizontal components of ground motion over each degree of rotation from 1 to 180 degrees independent of period (Boore, 2010). The RotD50 spectra were computed for 63 discrete periods in the range from 0.01 to 10 seconds for the validation. Goulet et al. (2015) describes the formal validation framework, and the details of the two components of the validation namely, Part A, which is a comparison against event specific observed

RotD50 spectra, and Part B, which is a comparison against published GMPEs. The evaluation process benefitted from the structure of the BBP in which the simulation software adhered to a strict version control, and method lock-in in which methods could not be modified as they were being evaluated against the PSA data and the GMPEs. Additionally, the BBP is structured such that independent third party operators may utilize the software to generate the simulated motions thereby maintaining the strict developer-separated framework making objective evaluation of the method performance possible.

A seven person panel was constructed consisting of Douglas Dreger (UC Berkeley, Chair), Gregory Beroza (Stanford University), Steven Day (San Diego State University), Christine Goulet (UC Berkeley), Thomas Jordan (USC), Jonathan Stewart (UCLA) and Paul Spudich (USGS) to evaluate the performance of the BBP and the implemented methods for version 13.6.1. The process included a two-day workshop (June 11-12, 2013) in which the developers presented their methods and had a broad discussion regarding method differences and similarities, as well as a preliminary review of simulation results. This workshop was followed by a formal one-day working meeting (July 1, 2013) in which the panel reviewed the validation results and subjected the developers to questioning. Materials provided at this meeting were used as part of a detailed review of the methods, which was submitted to SCEC on August 1, 2013, and is included in the Attachment B, and is available online by pasting the following link into a web browser: "http://scec.usc.edu/scecpedia/SCEC_BBP_Phase_1_Evaluation". The panel findings have also been published in the peer-reviewed literature (Dreger et al., 2015). The following is an excerpt of the panel findings.

In the Part A validation, the methods were studied using the bias of simulation results with respect to observations for seven specific events. Bias is defined as the value of the residual of the natural logarithm of the observed PSA to that for each simulation method. A suite of 63 periods was used to define the PSA from 0.01 to 10 sec. For each event 40 stations providing good azimuthal coverage of the source and providing coverage within 200 km (1 to 193 km) of closest rupture distance were used in the validation. Part A examined the mean bias for the events, individually and collectively. Assessment criteria included; (1) the ability to match observed RotD50 spectra relative to thresholds of 0.35 natural log units representing 0.1 magnitude unit at long-periods, (2) a lack of trends in bias within discrete period bins, (3) a measure of distance-period dependence of the bias, and (4) consistency of simulated RotD50 spectra with published GMPEs. The results of the Part A validation show that three version 13.6.1 methods, EXSIM (Atkinson and Assatourians, 2015), GP (Graves and Pitarka, 2015) and SDSU (Olsen and Takedatsu, 2015), were deemed suitable for broadband simulation of PSA from 0.01 to 3 seconds period over the entire distance range for **M**5.89 to **M**7.22. At periods longer than 3 seconds the simulation methods, with the exception of EXSIM, displayed increased levels of bias

Figure J.1.1-1 shows an example of the metric combining the absolute value of the mean bias and the mean of the absolute value of the bias. This metric was used because it could identify trends in bias from positive to negative with zero mean. To facilitate comparison, this metric is shown in four period

bins, and four distance bins for the three passing simulation methods, and published NGA-West1 GMPEs. Green indicates that the mean bias is less than 0.35 in natural logarithm units, and red indicates that the mean bias is larger than 0.69 in LN units (a factor of two difference in simulated and observed ground motions). The detailed discussion of the different goodness of fit measures and evaluation criteria can be found in the SCEC review report (Attachment B), and in Dreger et al., (2015). It was the judgment of the SCEC validation panel that the performance of the simulation methods should be better than a factor of 2 in ground motion or 0.69 in LN units as a minimum passing condition. Finally, the validation panel noted that in the 0.01 to 1 second period range that cases with large bias (red, and some of the white cells) the GMPE fit also shows comparable misfit indicating the presence of an event term, which when accounted for results in good agreement for all three methods in median PSA across this broad period range. At longer periods the bias is observed to increase in which the simulation methods, with the exception of EXSIM (Atkinson and Assatourians, 2015), tend to over-estimate the PSA motions.

The second validation test, Part B, considered a comparison of simulated PSA with published GMPEs at two distances, 20 and 50 km for **M**6.2 and **M**6.6 strike-slip, and reverse-slip scenarios. The Part B acceptance criterion permits simulation mean motions to deviate only up to a preset amount from the mean of the NGA-West 1 GMPEs (AS08 [Abrahamson and Silva, 2008], CB08 [Campbell and Bozorgnia, 2008], CY08 [Chiou and Youngs, 2008], BA08 [Boore and Atkinson, 2008]), as described in Goulet et al. (2015). The permissible deviation was defined as the largest and smallest prediction at any period from all of the NGA-West2 GMPEs (ASK14 [Abrahamson et al., 2014], CB14 [Campbell and Bozorgnia, 2014], CY14 [Chiou and Youngs, 2014], and BSSA14 [Boore et al., 2014]). The largest value was then increased by 15% and the smallest value was decreased by 15%, and these maximum acceptable deviations were then applied uniformly to all periods. The dashed lines in Figure J.1.1-2 show the maximum acceptable deviations, and span a range in ground motion that is slightly larger than a factor of 3. While all methods satisfied the evaluation criteria for at least one of the cases, only EXSIM (Atkinson and Assatourians, 2015), GP (Graves and Pitarka, 2015) and SDSU (Olsen and Takedatsu, 2015) satisfy the acceptance criteria for all of the Part B cases. Figure J.1.1-2 shows an example of Part B comparison for these three methods. A full inventory of such comparisons is provided in the SCEC review report provided in Attachment B.

Based on the Part A and Part B validation tests the review panel deemed that the EXSIM (Atkinson and Assatourians, 2015), GP (Graves and Pitarka, 2015) and SDSU (Olsen and Takedatsu, 2015) methods are considered suitable for broadband simulation of median PSA from 0.01 to 3 seconds period within the validation magnitude range (**M**5.9 – 7.2; Dreger et al., 2013; **M**5.5 – 7.2, Dreger et al., 2015); and that they are suitable from **M**5.5 to **M**8 for the purposes of assessing relative effects of changes in source geometry, rupture direction, presence of secondary slip on splays, hanging-wall effects, etc. Although the panel did not utilize a specific metric to assess hanging-wall effects, Donahue and Abrahamson (2014) used simulations from the GP method to develop a hanging-wall factor to be used with GMPEs

and comparisons with the very sparse hanging-wall data set was positive. The panel noted that for periods above 1 second there is increased bias relative to recordings, and above 3 seconds period there are significant deviations from GMPEs, and that further analysis will be required to understand the source of this additional bias.

The TI Team judged that meeting the acceptance criteria laid out by the validation panel makes the methods suitable for determining the appropriate mixing of the GMPEs for splay and complex rupture scenarios (Section J.4), extending the GMPE hanging-wall terms to lower magnitude (Section J.5), and developing ground motions from single rupture planes that are ultimately used to develop logic tree weights for the median ground-motion base models (Figure 8.2-2).

It is also noted that subsequent to this review the three passing methods were successful in a broadened Part A data set that added 5 additional small magnitude **M**4.6-5.8 events as well as a broadened Part B comparison (Goulet et al., 2015 Dreger et al., 2015).

| | | PSA Period Range | | | | | | | | | | | | | | | |
|---|---|---|---|---|---|---|---|---|---|---|---|---|---|---|---|---|---|
| | | 0.01<= T <= 0.1 s | | | | 0.1 < T < 1 s | | | | 1 <= T <= 3 s | | | | T > 3 s | | | |
| | Event (Mw, Mech.) | EXSIM | G&P | SDSU | GMPE | EXSIM | G&P | SDSU | GMPE | EXSIM | G&P | SDSU | GMPE | EXSIM | G&P | SDSU | GMPE |
| 0 <= Rrup <= 5 km | Whittier Narrows (5.89, REV) | | | | | | | | | | | | | | | | |
| | North Palm Springs (6.12, ROBL) | 0.38 | 0.07 | 0.44 | 0.16 | 0.23 | 0.12 | 0.31 | 0.16 | 0.20 | 0.60 | 0.65 | 0.15 | 0.08 | 1.08 | 1.09 | 0.50 |
| | Tottori (6.59, SS) | 1.18 | 0.10 | 0.35 | 0.23 | 0.41 | 0.45 | 0.54 | 0.62 | 0.19 | 0.21 | 0.22 | 0.11 | 0.23 | 0.41 | 0.41 | 0.41 |
| | Niigata (6.65, REV) | | | | | | | | | | | | | | | | |
| | Northridge (6.73, REV) | | | | | | | | | | | | | | | | |
| | Loma Prieta (6.94, ROBL) | 0.23 | 0.22 | 0.22 | 0.25 | 0.25 | 0.18 | 0.25 | 0.21 | 0.66 | 0.50 | 0.54 | 0.59 | 0.33 | 0.66 | 0.67 | 0.31 |
| | Landers (7.22, SS) | 0.70 | 0.76 | 0.90 | 1.05 | 0.24 | 0.41 | 0.34 | 0.69 | 0.63 | 0.35 | 0.29 | 0.93 | 1.07 | 0.29 | 0.29 | 1.17 |
| | **Average CA** | 0.36 | 0.26 | 0.40 | 0.32 | 0.24 | 0.22 | 0.28 | 0.29 | 0.56 | 0.42 | 0.46 | 0.55 | 0.61 | 0.42 | 0.42 | 0.54 |
| | **Average ALL** | 0.29 | 0.21 | 0.33 | 0.31 | 0.24 | 0.25 | 0.33 | 0.35 | 0.47 | 0.39 | 0.42 | 0.48 | 0.48 | 0.42 | 0.42 | 0.42 |
| 5 < Rrup <=20 km | Whittier Narrows (5.89, REV) | 0.28 | 0.26 | 0.28 | 0.30 | 0.32 | 0.20 | 0.18 | 0.21 | 0.21 | 0.50 | 0.56 | 0.44 | 0.37 | 1.12 | 1.05 | 0.81 |
| | North Palm Springs (6.12, ROBL) | 0.23 | 0.33 | 0.24 | 0.25 | 0.27 | 0.33 | 0.32 | 0.28 | 0.26 | 0.47 | 0.54 | 0.39 | 0.29 | 0.16 | 0.16 | 0.45 |
| | Tottori (6.59, SS) | 0.47 | 0.28 | 0.50 | 0.60 | 0.21 | 0.32 | 0.23 | 0.60 | 0.21 | 0.25 | 0.29 | 0.22 | 0.37 | 0.25 | 0.25 | 0.22 |
| | Niigata (6.65, REV) | 0.34 | 0.40 | 0.40 | 0.48 | 0.39 | 0.36 | 0.27 | 0.42 | 0.34 | 0.62 | 0.67 | 0.47 | 0.34 | 0.62 | 0.64 | 0.61 |
| | Northridge (6.73, REV) | 0.30 | 0.25 | 0.27 | 0.20 | 0.37 | 0.36 | 0.23 | 0.32 | 0.38 | 0.25 | 0.30 | 0.36 | 0.36 | 0.27 | 0.28 | 0.29 |
| | Loma Prieta (6.94, ROBL) | 0.33 | 0.20 | 0.25 | 0.26 | 0.27 | 0.21 | 0.25 | 0.29 | 0.27 | 0.62 | 0.67 | 0.18 | 0.27 | 0.46 | 0.46 | 0.23 |
| | Landers (7.22, SS) | 0.46 | 0.60 | 0.56 | 0.33 | 0.34 | 0.38 | 0.38 | 0.32 | 0.44 | 0.54 | 0.56 | 0.23 | 0.48 | 0.97 | 0.97 | 0.43 |
| | **Average CA** | 0.28 | 0.22 | 0.27 | 0.22 | 0.29 | 0.22 | 0.23 | 0.25 | 0.23 | 0.44 | 0.49 | 0.26 | 0.29 | 0.45 | 0.45 | 0.25 |
| | **Average ALL** | 0.25 | 0.20 | 0.30 | 0.25 | 0.28 | 0.25 | 0.23 | 0.31 | 0.24 | 0.44 | 0.48 | 0.26 | 0.28 | 0.43 | 0.43 | 0.28 |
| 20 < Rrup <= 70 km | Whittier Narrows (5.89, REV) | 0.40 | 0.21 | 0.31 | 0.31 | 0.35 | 0.23 | 0.29 | 0.27 | 0.30 | 0.49 | 0.54 | 0.52 | 0.14 | 0.52 | 0.52 | 0.31 |
| | North Palm Springs (6.12, ROBL) | 0.62 | 0.41 | 0.46 | 0.42 | 0.31 | 0.25 | 0.28 | 0.29 | 0.44 | 0.27 | 0.33 | 0.41 | 0.34 | 0.50 | 0.50 | 0.09 |
| | Tottori (6.59, SS) | 0.31 | 0.75 | 0.26 | 1.08 | 0.34 | 0.35 | 0.37 | 0.53 | 0.50 | 0.70 | 0.74 | 0.49 | 0.20 | 0.55 | 0.55 | 0.36 |
| | Niigata (6.65, REV) | 0.31 | 0.49 | 0.29 | 0.48 | 0.29 | 0.35 | 0.38 | 0.33 | 0.52 | 0.97 | 1.00 | 0.67 | 0.40 | 1.12 | 1.12 | 0.72 |
| | Northridge (6.73, REV) | 0.21 | 0.18 | 0.59 | 0.32 | 0.29 | 0.24 | 0.52 | 0.24 | 0.57 | 0.38 | 0.44 | 0.38 | 0.35 | 0.63 | 0.63 | 0.27 |
| | Loma Prieta (6.94, ROBL) | 0.27 | 0.38 | 0.38 | 0.34 | 0.28 | 0.34 | 0.31 | 0.24 | 0.38 | 0.65 | 0.68 | 0.24 | 0.39 | 0.42 | 0.42 | 0.48 |
| | Landers (7.22, SS) | 0.25 | 0.52 | 0.33 | 0.30 | 0.39 | 0.48 | 0.39 | 0.29 | 0.70 | 0.71 | 0.74 | 0.48 | 0.44 | 0.91 | 0.91 | 0.41 |
| | **Average CA** | 0.28 | 0.28 | 0.33 | 0.27 | 0.26 | 0.30 | 0.35 | 0.25 | 0.49 | 0.53 | 0.58 | 0.40 | 0.30 | 0.70 | 0.70 | 0.27 |
| | **Average ALL** | 0.29 | 0.27 | 0.31 | 0.30 | 0.28 | 0.31 | 0.35 | 0.26 | 0.50 | 0.63 | 0.67 | 0.45 | 0.31 | 0.78 | 0.78 | 0.42 |
| 70 < Rrup <= 200 km | Whittier Narrows (5.89, REV) | | | | | | | | | | | | | | | | |
| | North Palm Springs (6.12, ROBL) | 0.15 | 0.14 | 0.20 | 0.25 | 0.46 | 0.37 | 0.43 | 0.43 | 0.46 | 0.39 | 0.30 | 0.35 | | | | |
| | Tottori (6.59, SS) | 0.54 | 0.77 | 0.35 | 0.63 | 0.53 | 0.43 | 0.61 | 0.38 | 0.52 | 0.55 | 0.55 | 0.51 | 0.81 | 0.48 | 0.45 | 0.32 |
| | Niigata (6.65, REV) | 0.31 | 0.33 | 0.40 | 0.49 | 0.44 | 0.65 | 0.32 | 0.81 | 0.52 | 1.32 | 1.12 | 1.05 | 0.33 | 1.53 | 1.22 | 0.92 |
| | Northridge (6.73, REV) | 0.27 | 0.48 | 0.33 | 0.18 | 0.32 | 0.55 | 0.44 | 0.40 | 0.87 | 0.48 | 0.51 | 0.56 | 0.58 | 0.29 | 0.29 | 0.18 |
| | Loma Prieta (6.94, ROBL) | 0.60 | 0.55 | 0.65 | 0.45 | 0.64 | 0.69 | 0.85 | 0.73 | 0.88 | 0.57 | 0.54 | 1.19 | 0.48 | 0.37 | 0.37 | 0.79 |
| | Landers (7.22, SS) | 0.08 | 0.14 | 0.30 | 0.18 | 0.32 | 0.22 | 0.41 | 0.22 | 0.37 | 0.20 | 0.21 | 0.45 | 0.35 | 0.24 | 0.43 | 0.78 |
| | **Average CA** | 0.22 | 0.21 | 0.23 | 0.23 | 0.25 | 0.28 | 0.31 | 0.34 | 0.36 | 0.29 | 0.28 | 0.56 | 0.36 | 0.25 | 0.40 | 0.77 |
| | **Average ALL** | 0.33 | 0.39 | 0.31 | 0.33 | 0.29 | 0.31 | 0.39 | 0.34 | 0.36 | 0.63 | 0.57 | 0.52 | 0.46 | 0.85 | 0.71 | 0.50 |

**Figure J.1.1-1:** Goodness of fit defined as the equally weighted absolute value of the mean bias and the mean of the absolute value of the bias. Green shows bias less than 0.35 LN units and red shows bias greater than 0.69 LN units. The values are provided in four period bins and four distance bins.

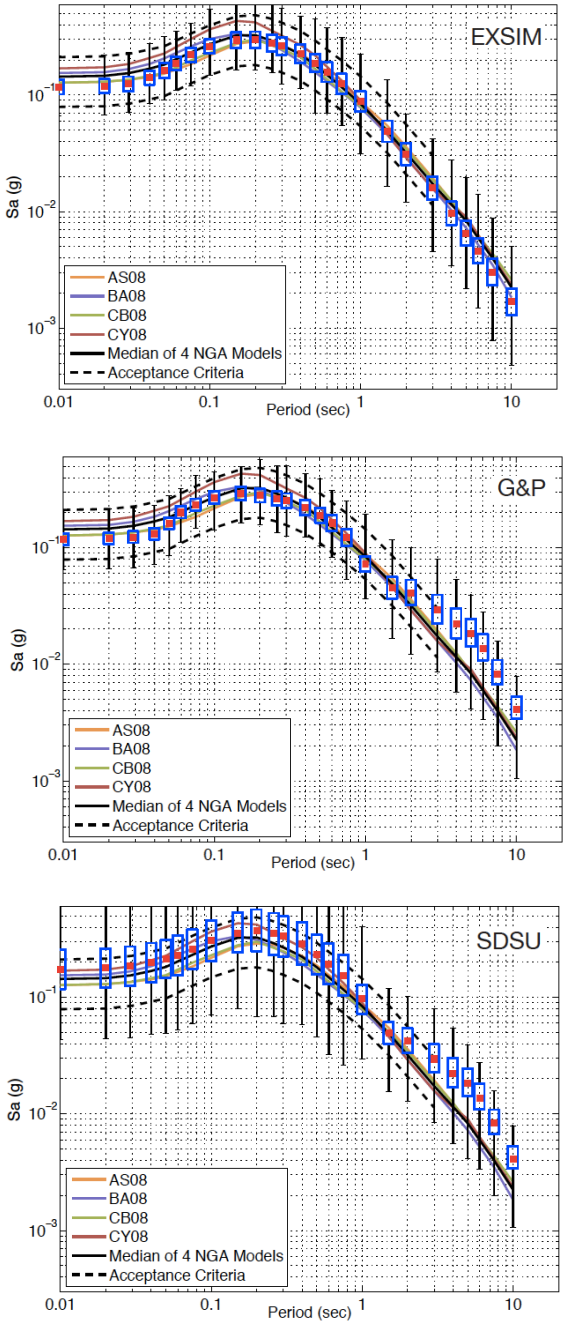



**Figure J.1.1-2:** Part B comparison for a **M**6.6 Reverse fault case at a distance of 20 km and $Z_{TOR}$ = 3 km. The solid black line is the median of four NGA-West1 GMPEs. The dashed curves are the maximum and minimum from the four NGA-West2 GMPE models applied to all periods equally in which the maximum was multiplied by 1.15 and the minimum by 0.85. Red squares and blue boxes are the median and standard deviation of 50 source realizations. The bars show the extremes of all 50 simulations. The red squares falling within the dashed lines were used as a passing criterion for the methods.

## J.2 Cases for Forward Simulations

As discussed in the previous section, based on the findings of the SCEC BBP peer-review panel, three methods were deemed satisfactory for use in determining numerical, finite-fault median pseudo spectral acceleration ground motions for the project. These methods are the stochastic EXSIM (Atkinson and Assatourians, 2015), and the hybrid GP (Graves and Pitarka, 2015), and SDSU (Olsen and Takedatsu, 2015) methods. The following describes the setup and parameterization of the various rupture scenarios that were used.

### *J.2.1 Simple Planar Ruptures*

Simple planar ruptures were run to constrain the hanging-wall effect for low magnitude scenarios in the **M**5.5 to **M**6 range and to compare scaling between models in the mid-magnitude (**M**6.5 to **M**7) range. All simulations used the Leonard (2010) relationship, M=log10(A) + 4, for scaling, where A is the rupture area in $km^2$ and **M** is the moment magnitude ($M_W$).

In total 36 simple planar scenarios (different magnitude, dip and $Z_{TOR}$ cases) were computed on the SCEC Broadband Platform using each of the three methods that passed the SCEC validation exercise: GP (2015), SDSU (Olsen and Takedatsu, 2015), and EXSIM (Atkinson and Assatourians, 2015). For each of the methods, simulations for 32 random hypocenters and slip models (realizations) were computed for each of the 36 scenarios at 182 stations. The station layout is shown (Figure J.2.1-1) with respect to the **M**5.5, **M**6.0, and **M**6.5 scenarios with a dip of 45 degrees.

Table J.2.1-1 summarizes the scenarios that were run for each of the three simulation methods. The scenarios are reverse earthquakes that range in magnitude from **M**5.5 to **M**7.0, dip from 10 to 60 degrees, and have a depth to the top of rupture from 0 to 12 kilometers. Because the **M**7.0 simulations take substantially more computational resources it was necessary to limit those calculations to only the 45 degree dip case. The M6.5 simulations were found behave in a very systematic manner with respect to fault dip, and based on the TI teams understanding of the simulation methods there is no reason that the behavior of the corresponding **M**7.0 cases would differ.

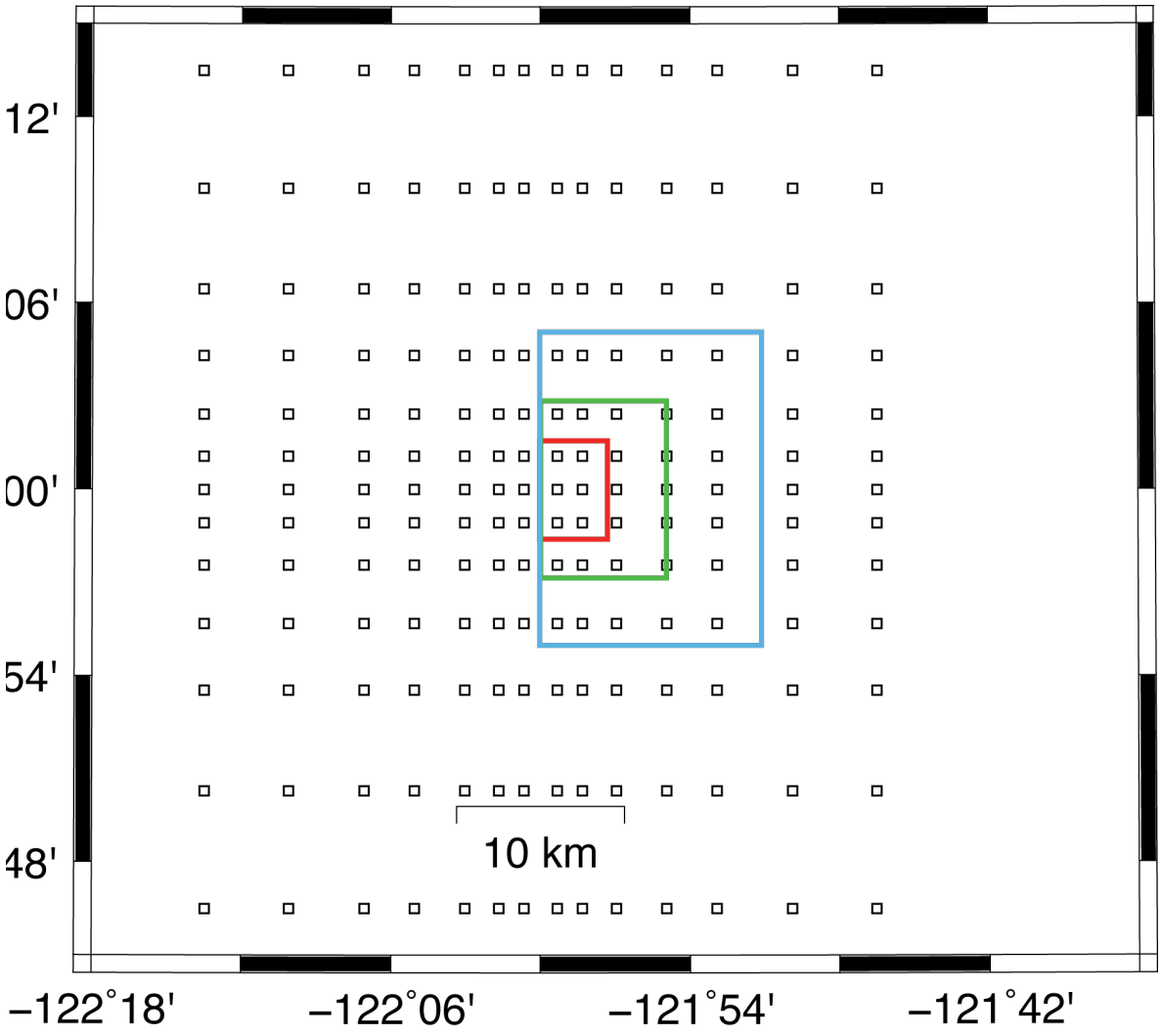



**Figure J.2.1-1:** Station Layout for the Simple Planar Ruptures with respect to the **M**5.5 (red), **M**6.0 (green), and **M**6.5 (blue) faults. The fault projections are for a dip of 45 degrees.

**Table J.2.1-1:** Single Planar fault scenarios.

| SCENARIO | METHODS | REALIZATIONS | M | RAKE | DIP | $Z_{TOR}$ (km) | STATIONS |
|---|---|---|---|---|---|---|---|
| 00 | GP, SDSU, EXSIM | 32 | 5.5 | 90 | 10 | 2.5 | 182 |
| 01 | GP, SDSU, EXSIM | 32 | 5.5 | 90 | 10 | 7.0 | 182 |
| 02 | GP, SDSU, EXSIM | 32 | 5.5 | 90 | 10 | 12.0 | 182 |
| 03 | GP, SDSU, EXSIM | 32 | 5.5 | 90 | 20 | 2.5 | 182 |
| 04 | GP, SDSU, EXSIM | 32 | 5.5 | 90 | 20 | 7.0 | 182 |
| 05 | GP, SDSU, EXSIM | 32 | 5.5 | 90 | 20 | 12.0 | 182 |
| 06 | GP, SDSU, EXSIM | 32 | 5.5 | 90 | 30 | 2.5 | 182 |
| 07 | GP, SDSU, EXSIM | 32 | 5.5 | 90 | 30 | 7.0 | 182 |
| 08 | GP, SDSU, EXSIM | 32 | 5.5 | 90 | 30 | 12.0 | 182 |
| 09 | GP, SDSU, EXSIM | 32 | 5.5 | 90 | 45 | 2.5 | 182 |
| 10 | GP, SDSU, EXSIM | 32 | 5.5 | 90 | 45 | 7.0 | 182 |
| 11 | GP, SDSU, EXSIM | 32 | 5.5 | 90 | 45 | 12.0 | 182 |
| 12 | GP, SDSU, EXSIM | 32 | 5.5 | 90 | 60 | 2.5 | 182 |
| 13 | GP, SDSU, EXSIM | 32 | 5.5 | 90 | 60 | 7.0 | 182 |
| 14 | GP, SDSU, EXSIM | 32 | 5.5 | 90 | 60 | 12.0 | 182 |
| 15 | GP, SDSU, EXSIM | 32 | 6.0 | 90 | 10 | 2.5 | 182 |
| 16 | GP, SDSU, EXSIM | 32 | 6.0 | 90 | 10 | 7.0 | 182 |
| 17 | GP, SDSU, EXSIM | 32 | 6.0 | 90 | 10 | 12.0 | 182 |
| 18 | GP, SDSU, EXSIM | 32 | 6.0 | 90 | 20 | 2.5 | 182 |
| 19 | GP, SDSU, EXSIM | 32 | 6.0 | 90 | 20 | 7.0 | 182 |
| 20 | GP, SDSU, EXSIM | 32 | 6.0 | 90 | 20 | 12.0 | 182 |
| 21 | GP, SDSU, EXSIM | 32 | 6.0 | 90 | 30 | 2.5 | 182 |
| 22 | GP, SDSU, EXSIM | 32 | 6.0 | 90 | 30 | 7.0 | 182 |
| 23 | GP, SDSU, EXSIM | 32 | 6.0 | 90 | 30 | 12.0 | 182 |
| 24 | GP, SDSU, EXSIM | 32 | 6.0 | 90 | 45 | 2.5 | 182 |
| 25 | GP, SDSU, EXSIM | 32 | 6.0 | 90 | 45 | 7.0 | 182 |
| 26 | GP, SDSU, EXSIM | 32 | 6.0 | 90 | 45 | 12.0 | 182 |
| 27 | GP, SDSU, EXSIM | 32 | 6.0 | 90 | 60 | 2.5 | 182 |
| 28 | GP, SDSU, EXSIM | 32 | 6.0 | 90 | 60 | 7.0 | 182 |
| 29 | GP, SDSU, EXSIM | 32 | 6.0 | 90 | 60 | 12.0 | 182 |
| 30 | GP, SDSU, EXSIM | 32 | 6.5 | 90 | 10 | 0.0 | 182 |
| 31 | GP, SDSU, EXSIM | 32 | 6.5 | 90 | 20 | 0.0 | 182 |
| 32 | GP, SDSU, EXSIM | 32 | 6.5 | 90 | 30 | 0.0 | 182 |
| 33 | GP, SDSU, EXSIM | 32 | 6.5 | 90 | 45 | 0.0 | 182 |
| 34 | GP, SDSU, EXSIM | 32 | 6.5 | 90 | 60 | 0.0 | 182 |
| 35 | GP, SDSU, EXSIM | 32 | 7.0 | 90 | 45 | 0.0 | 109 |

### *J.2.2 Complex Ruptures*

The SWUS GMC project was given two complex rupture scenarios from the DCPP SSC TI Team, as described in Chapter 4 Section 1 and Chapter 6 Section 7. The scenarios are simplified cases specifically designed by the SSC project for conducting the BBP simulations. Each scenario consists of a combined rupture of two separate planar faults, for which simulations have been performed: Hosgri-Los Osos, and Shoreline-San Luis Bay. The GMC TI and SSC Teams discussed how to best define the scenario events at great length throughout the course of the project. The major predicament was having both **M** and the rupture dimension, length (L) and width (W), specified by the SSC. As a result, the magnitude scaling laws used in developing, testing, and validating the simulation methods would not be followed. To resolve this issue, it was decided to start with **M** in place of L, which is a departure from using mapped length values, and in general moves away from the source characterization recommended by the SSC. Based on suggestions by Robert Graves (personal communication), the GMC TI Team developed a methodology for assigning rupture scenario dimension based on a starting magnitude (**M**). Given an **M** assigned by the SSC, the fault dimensions for all scenarios were back calculated consistent with the Leonard (2010) scaling relationships.

The basic sets of relations from Leonard (2010) are:

$$\mathbf{M} = \log_{10}(A) + 4 \qquad \text{(Eq. J.2.2-1)}$$

$$W = C * L^{(2/3)} \qquad \text{(Eq. J.2.2-2)}$$

where **M** = moment magnitude

A = rupture area in km^2 = L*W

L = fault length in km

W = down-dip fault width in km

C = empirically derived constant;

C = 1.75 for dip-slip faults

C = 1.5 for strike slip faults up to **M** = 7.1,

for **M** > 7.1 fix W = 22km and use L = A/W to get length

Equation (J.2.2-1) is satisfied in all of our simulation cases. For all scenario faults, the W comes from equation (J.2.2-2) except that for strike slip faults, this width saturates at 22km (cases where **M** > 7.1). For scenarios which combine reverse and strike-slip segments, the scaling relations for strike slip faults has been used to define the overall geometry. Each scenario has 3 magnitude cases from which the

dimensions were derived: **M** = 7.0, 7.2, and 7.4. Whenever the magnitude-area relation required shortening of the fault length with respect to the length assigned by the SSC, the southern endpoint was held fixed and the northern endpoint was moved south to achieve the shorter fault length. The TI Team made this decision because the major complexities are located in the southern portion of the fault scenarios. The detailed parameters used to define the scenarios are listed in Tables J.2.2-1 and J.2.2-2.

For single plane simulations within the validated magnitude range, the simulations may be used to generate a simulation GMPE as used in Chapter 8. The complex scenarios were based on the SSC guidelines, but not exactly due to the recommendations of the simulation methods developers in which the Leonard (2010) scaling relations were used to define fault length and fault width. Thus complex scenarios were not used for site-specific ground-motion estimation. Rather, they were only used to develop ratios describing how to mix GMPEs to compute ground motion for non-planar faults.

### *J.2.2.1 Complex Scenario 1: Hosgri – Los Osos*

Complex Scenario 1 is based on the Hosgri – Los Osos fault geometry. It involves two segments: one is strike-slip and the other is reverse in which the site is closer to the reverse segment on the hanging wall (Figure J.2.2-1). Table J.2.2-1 lists the fault parameters for this case for the three considered magnitudes.

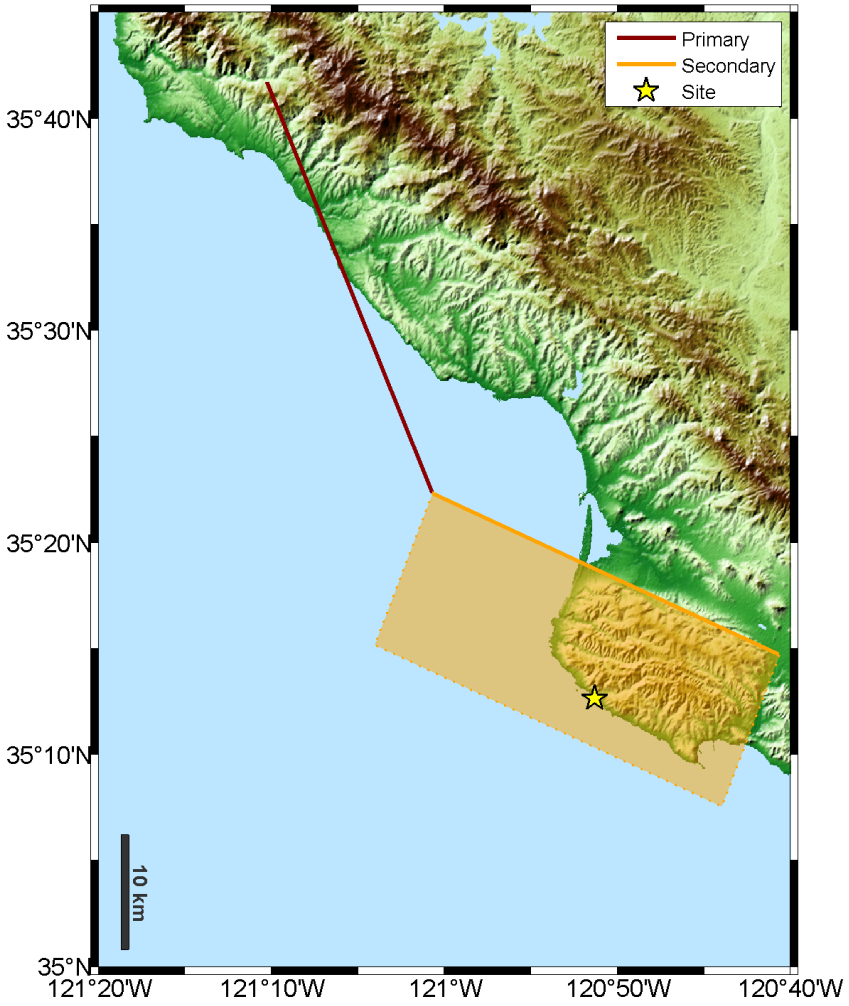



**Figure J.2.2-1:** Simplified complex Scenario 1 based on the Hosgri to Los Osos scenario. The red line shows the Hosgri Fault and the orange line and rectangle the surface projection of the dipping Los Osos fault. The star shows the site of ground-motion characterization.

**Table J.2.2-1:** Parameters defining the Complex Scenario 1 based on the Hosgri (blue parameters) and Los Osos (green parameters) faults.

| Name | M total | Strike 1 | Dip 1 | Rake 1 | Length 1 | M 1 | Strike 2 | Dip 2 | Rake 2 | Length 2 | M 2 |
|---|---|---|---|---|---|---|---|---|---|---|---|
| Complex Scenario 1A | 7.0 | 338.14 | 90 | 180 | 16.27 | 6.66 | 115.25 | 50 | 90 | 33.20 | 6.88 |
| Complex Scenario 1B | 7.2 | 338.14 | 90 | 180 | 38.84 | 7.02 | 115.25 | 50 | 90 | 33.20 | 6.98 |
| Complex Scenario 1C | 7.4 | 338.14 | 90 | 180 | 80.98 | 7.30 | 115.25 | 50 | 90 | 33.20 | 7.02 |

### *J.2.2.2 Complex Scenario 2: Shoreline – San Luis Bay*

Complex scenario 2 is based on the Shoreline – San Louis Bay fault geometry. It involves two segments: one is strike-slip and the other is reverse in which the site is closer to the strike-slip segment (Figure J.2.2-2). Table J.2.2-2 lists the fault parameters for this case for the three considered magnitudes.




**Figure J.2.2-2:** Simplified complex Scenario 2 based on the Shoreline to San Luis Bay complex scenario. The red line shows the trace of the modeled Shoreline Fault and the orange line and rectangle show the surface projection of the dipping San Luis Bay Fault. The star shows the position of the site for characterizing ground motions.

**Table J.2.2-2:** Parameters defining the Complex Scenario 2, based on the Shoreline (blue parameters) and San Luis Bay (green parameters) faults.

| Name | M total | Strike 1 | Dip 1 | Rake 1 | Length 1 | M 1 | Strike 2 | Dip 2 | Rake 2 | Length 2 | M 2 |
|---|---|---|---|---|---|---|---|---|---|---|---|
| Complex Scenario 2A | 7.0 | 299.86 | 90 | 180 | 41.67 | 6.96 | 273.19 | 70 | 90 | 7.80 | 6.42 |
| Complex Scenario 2B | 7.2 | 299.86 | 90 | 180 | 64.24 | 7.18 | 273.19 | 70 | 90 | 7.80 | 6.47 |
| Complex Scenario 2C | 7.4 | 299.86 | 90 | 180 | 106.38 | 7.39 | 273.19 | 70 | 90 | 7.80 | 6.51 |

### *J.2.3 Splay Ruptures*

Similar to the methodology used in the complex case, the splay scenarios were defined by considering a combination of factors. The TI Team first considered the SSC recommendations for **M**, location, dimensions, and style of faulting, and were adjusted to be consistent with Leonard (2010) scaling since all of the BBP methods have been calibrated to the Leonard magnitude-area scaling relation. Finally, the TI Team wanted to have scenarios that would contribute in a meaningful way to the research goals (section J.1). In doing so, the magnitude for some of the secondary ruptures were increased relative to what the SSC would consider possible (or perhaps even realistic) in order to ensure that the secondary ruptures would impact the ground motions for the analysis.

The terminology used to describe the splay ruptures is shown in Figure J.2.3-1. Each scenario has been based on two SSC cases, i.e. the Hosgri-Shoreline, and Los Osos-San Luis Bay scenarios. Each scenario consists of a combined rupture of two separate planar faults (termed the primary and secondary segments).

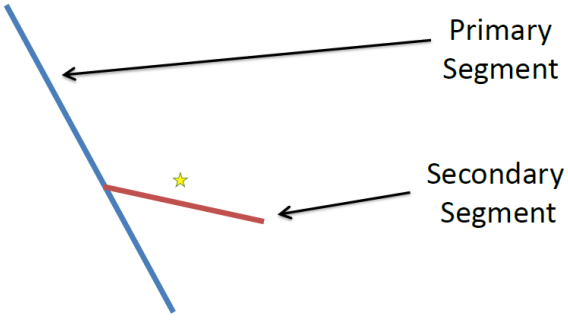



**Figure J.2.3-1:** Terminology for splay faults.

For both splay scenarios, the TI Team begins the process of determining the scenario properties with the primary segment. Starting from **M**, the primary fault dimensions are back calculated consistent with the Leonard (2010) scaling relationships, as described in the previous section. The southern endpoint of the primary segment is then fixed at the location specified by the SSC, and the northern endpoint is based on the scenario magnitude and corresponding length.

The secondary segment scenario properties were handled differently for each case. For the Hosgri-Shoreline splay scenario, both the primary and secondary segments are strike slip, as shown in Figure J.2.3-2. First, to define the secondary segment properties the average slip from the primary segment simulations was calculated by summing slip on each subfault and dividing by the total number of subfaults. Then, to define the secondary segment properties, this average slip was then scaled by 25% and the slip for the secondary segment was adjusted to the average. The TI Team originally used a scaling of 10%, as recommended by the SSC, however this lead to insignificant ground-motion contributions from the secondary fault. For this reason, the TI Team decided to increase the slip on the secondary fault to 25%. This slip is used in the Leonard (2010) relationship to define L, W, and **M** for the secondary fault. The northwest end of the segment is fixed at the intersection point of the two faults, as specified by the SSC.

For the Los Osos-San Luis Bay splay scenario, both the primary and secondary segments are reverse and meet at depth as shown in Figure J.2.3-3. Keeping the fault surface traces in the proper locations and using the correct dip angles, with the geometry shown in Figure J.2.3-3, it was necessary to keep the fault width of the secondary segment fixed for all scenarios. Otherwise, the secondary segment would not meet at depth with the primary segment. The required fault width for the secondary segment using the SSC fault surface trace locations and dip angles is 12.7 km. The Leonard (2010) relationships for reverse faults were then used to estimate L (19.55 km) and **M** (6.39) from this width. The southern end of this segment was then fixed at the location specified by the SSC.

As with the complex cases, equation (J.2.2-1) from Section J.2.2 is satisfied in all of the simulation cases.

Each scenario has 3 magnitude cases (on the primary segments) from which the dimensions were derived: **M** = 7.0, 7.2, and 7.4. The magnitudes for the secondary segments were determined using the process outlined above. The detailed parameters used to define the scenarios are listed in Tables J.2.3-1 and J.2.3-2.

For single plane simulations within the validated magnitude range, the simulations may be used to generate a simulation GMPE as used in Chapter 8. The splay scenarios were based on the SSC, but not exactly due to the recommendations of the simulation methods developers in which the Leonard (2010) scaling relations were used to define fault length and fault width. Thus, splay scenarios were not used for site-specific ground-motion estimation. Rather, they were only used to develop ratios describing how to mix GMPEs to compute ground motion for non-planar faults.

### *J.2.3.1 Splay Scenario 1: Hosgri – Shoreline*

Splay scenario 1 is based on the Hosgri-Shoreline splay scenario, where both the primary and secondary segments are strike slip. The site is closest to the secondary segment.

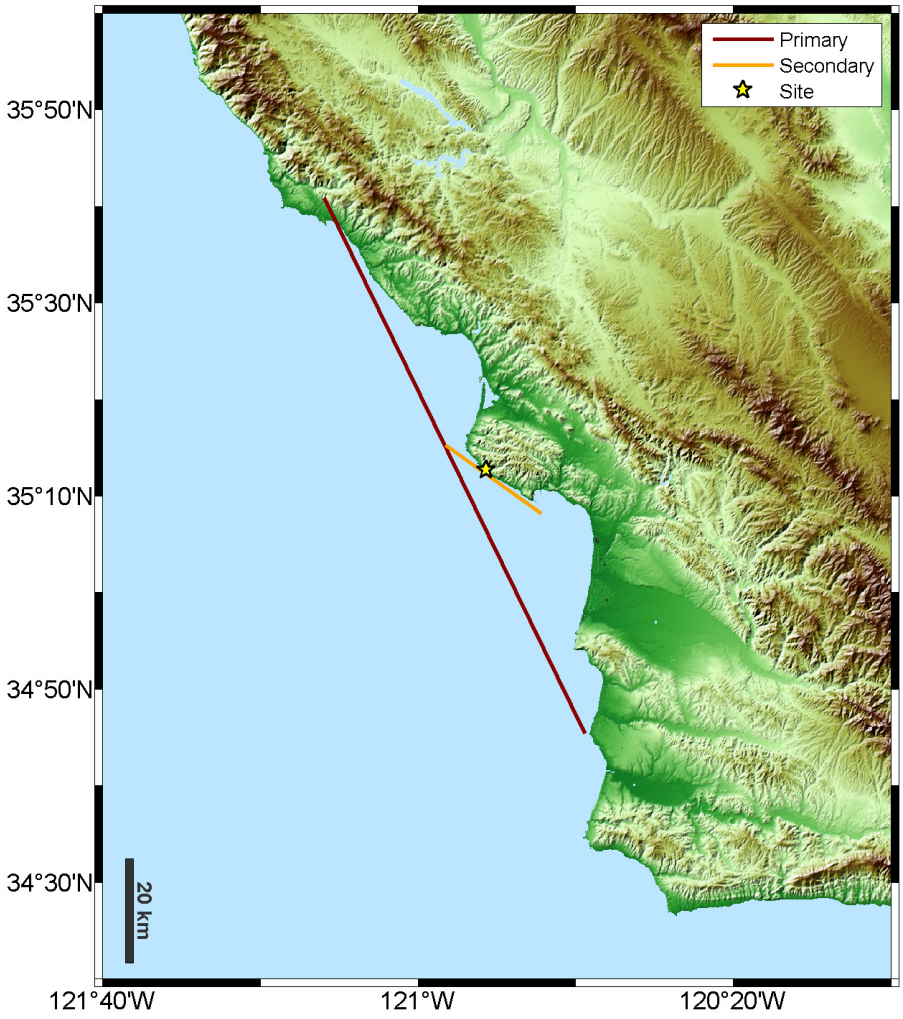



**Figure J.2.3-2:** Splay Scenario 1 (based on the Hosgri-Shoreline splay scenario). Red line shows the Hosgri fault and the orange line the Shoreline fault. The star shows the site for ground-motion characterization.

**Table J.2.3-1:** Parameters defining the Splay Scenarios 1 (based on the Hosgri-Shoreline splay scenario).

| | Segment | M | Strike | Rake | Dip | $Z_{TOR}$ | L | W |
|---|---|---|---|---|---|---|---|---|
| **M** Case 1 | Primary | 7.0 | 334.2 | 180 | 90 | 0 | 49.47 | 20.21 |
| | Secondary | 6.05 | 305.7 | 180 | 90 | 0 | 13.26 | 8.4 |
| **M** Case 2 | Primary | 7.2 | 334.2 | 180 | 90 | 0 | 72.04 | 22.0 |
| | Secondary | 6.22 | 305.7 | 180 | 90 | 0 | 16.86 | 9.86 |
| **M** Case 3 | Primary | 7.4 | 334.2 | 180 | 90 | 0 | 114.18 | 22.0 |
| | Secondary | 6.43 | 305.7 | 180 | 90 | 0 | 22.44 | 11.93 |

### *J.2.3.2 Splay Scenario 2: Los Osos – San Luis Bay*

Splay scenario 2 is based on the Los Osos-San Luis Bay splay scenario. Both the primary and secondary segments are reverse and intersect at depth with the primary rupture truncating the secondary rupture. The site is on the hanging wall of both segments, very close to the secondary segment surface trace.

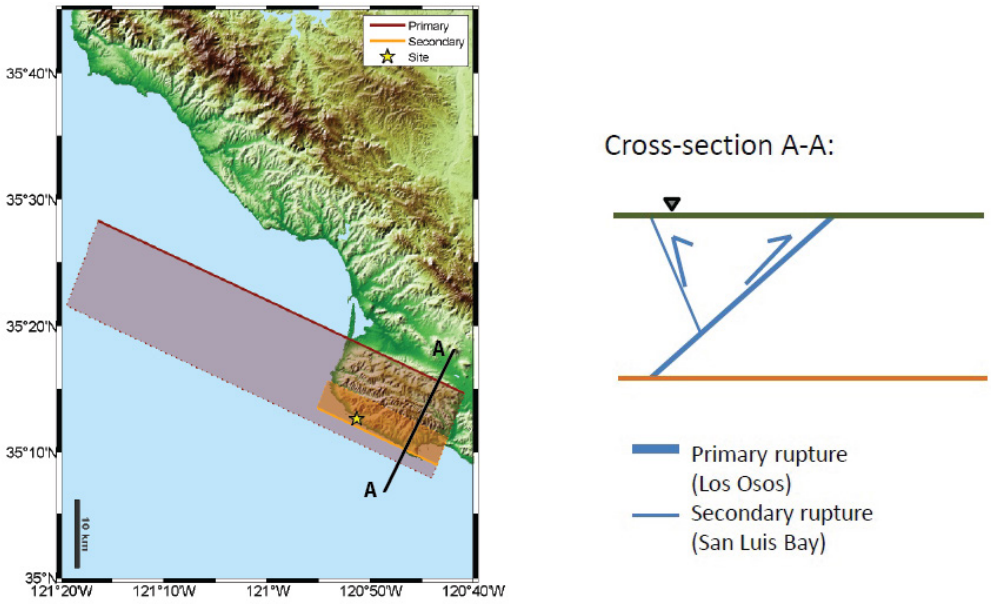



**Figure J.2.3-3:** Splay Scenario 2 (based on the Los Osos – San Luis Bay splay scenario). Solid lines are the surface traces of the faults, and the translucent yellow and red rectangles are the surface projections of the dipping San Luis Bay and Los Osos fault planes. The star shows the site for ground-motion characterization.

**Table J.2.3-2:** Parameters defining the Splay Scenarios 2 (based on the Los Osos-San Luis Bay splay scenarios.

| | Segment | M | Strike | Rake | Dip | $Z_{TOR}$ | L | W |
|---|---|---|---|---|---|---|---|---|
| **M** Case 1 | Primary | 7.00 | 115.4 | 90 | 60 | 0 | 44.82 | 22.08 |
| | Secondary | 6.39 | 295.4 | 90 | 70 | 0 | 19.55 | 12.7 |
| **M** Case 2 | Primary | 7.20 | 115.4 | 90 | 60 | 0 | 59.26 | 26.6 |
| | Secondary | 6.39 | 295.4 | 90 | 70 | 0 | 19.55 | 12.7 |
| **M** Case 3 | Primary | 7.40 | 115.4 | 90 | 60 | 0 | 78.19 | 32.0 |
| | Secondary | 6.39 | 295.4 | 90 | 70 | 0 | 19.55 | 12.7 |

## J.3 Forward Simulations Processing

The processing steps outlined below pertain to each of the three categories of simulations: simple planar ruptures, complex ruptures, and splay ruptures.

- Simulations were run on the validated version of the Broadband Platform: v13.6.1
- All scenarios were run using each of the three simulation techniques: GP (Graves and Pitarka, 2015), SDSU (Olsen and Takedatsu, 2015), and EXSIM (Atkinson and Assatourians, 2015).
- 32 realizations of random hypocenter locations and slip models were run for each scenario, and hypocenters were allowed to distribute themselves anywhere along the length of the primary fault (or anywhere along the entire fault in the complex scenarios, see clarification below).
- For each of the scenario realizations, standard output of the BBP includes: a figure showing the slip contours and rupture front, time histories (displacement, velocity, and acceleration), and RotD50 ground-motion spectra.

Source and station inputs required for standard processing on the BBP include: magnitude-area scaling parameters (**M** and fault dimension), fault parameters (depth to top of rupture, strike, rake, and dip), hypocenter location, rupture discretization parameters, and station coordinates. Because the Broadband Platform is only equipped to simulate simple planar ruptures, the complicated nature of the complex and splay ruptures required special processing beyond what is currently implemented on the SCEC BBP. The special processing for these scenarios is described below.

### *J.3.1 Simple Planar Ruptures*

The process used for computing the simple planar ruptures includes:

1. Creating the source and station input files for each planar rupture scenario,
2. Running simulations for each scenario on the BBP, and
3. Utilizing the BBP computed RotD50 spectra for Ground-motion Analysis.

### *J.3.2 Complex Ruptures*

Simulations with version 13.6.1 are available only for single-segment, planar faults. A BBP simulation is described by: **M**, strike, dip, rake, fault dimensions, hypocenter location, and fault location.

The process used for the complex ruptures includes:

1. Specifying one source description for the total **M** event,
2. Creating the SRF file (see below),
3. Separating the SRF file into two pieces with lengths corresponding to the fault segments in the complex scenario,
4. Rotating the desired segment,
5. Running simulations for both segments individually, and
6. Combining the results.

The source rupture file (SRF) is a file format defined by Robert Graves and adopted by the SCEC BBP that describes fault surfaces as a distribution of point sources. Each point source description contains all of the necessary information to compute the contribution of that point to the total response of the fault rupture. Using BBP v13.6.1 rupture described in the SRF must be planar.

This procedure resulted in a rupture scenario with a single **M**, no slip velocity discontinuity, and a single hypocenter. Radiation pattern and rake continuity are maintained. This process of "bending" of the SRF was repeated for each realization.

Once the SRF files were separated and "bent", simulations were run for both of the segments. Simulated acceleration time series from the two segments are combined in the time domain, and the RotD50 is computed from the two combined horizontal components.

Following this approach, the correct rupture time information is embedded in the SRF files, so the time series are simply summed in the time domain to produce the waveforms for the complex rupture cases. Unlike the GP and SDSU methods, the EXSIM method does not use an SRF file because this method assumes a stochastic rupture process. For the EXSIM method, separate source descriptions for both segments are developed such the total moment of the complex rupture scenario is preserved. The time series of the second rupture must then be shifted (or delayed) in time before the waveforms are summed in the time domain. The time delay is computed using an assumed rupture velocity ($V_r$) of 3 km/s, the distance between the hypocenter in the initial segment, and the junction (or "bend" point) of the two segments.

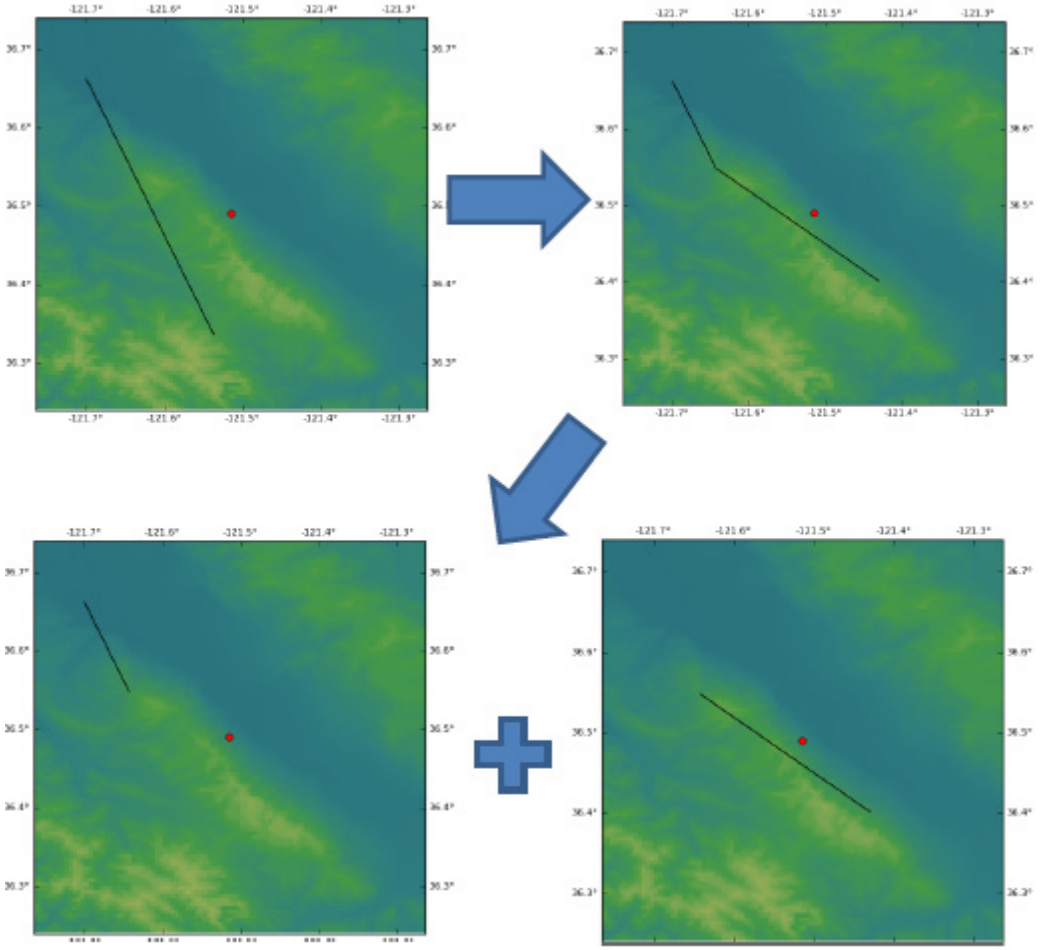


**Figure J.3.2-1:** An example of the "bending" process of the rupture description on the BBP. Black lines are the rupture surface traces and the red dots are the simulations sites. The colored shading represents elevation (yellow is an elevation high and blue is an elevation low), though elevation has no effect on "bending" process.

### *J.3.2.1 RotD50 Factors*

The TI Team computed RotD50 spectra for each of the 32 randomized hypocenter source realizations for both the two individual scenario segments and also for the combined rupture source. These RotD50 spectra are averaged to get one result for each simulation method. Because the GMPEs are suitable for single planar ruptures, it is not obvious how the ground motions from individual segments should be combined to represent a complex rupture scenario. To select the best method for computing GMPE ground motions for scenarios involving non-planar ruptures, the TI Team computed ground-motion

factors from simulations at the plant site for each simulation method. For the complex simulations, the ground-motion factors are the natural log ratio of the average RotD50 spectra for the total complex rupture (numerator) to the average RotD50 spectra from the single segment that is closest to the site (denominator.) The average is taken over the results from all of the simulation source realizations for a given rupture scenario. The ground-motion factors from simulations are representative of the relative increase of the RotD50 due to adding the fault complexity of the non-planar rupture scenario. The purpose of computing the ground-motion factors from simulations is that they can then be compared with ground-motion factors obtained from GMPEs that have been computed using various rules for defining GMPE input parameters. The rules for computing the ground-motion factors are discussed in Section J.4.

#### *J.3.2.2 Additional Comments*

For complex scenarios with both a strike-slip and reverse component, it was required to begin with two planar SRFs representing the entire **M** scenario - one strike slip, and one reverse - with identical source descriptions except for the average rake and dip parameters. Both the strike slip and reverse scenario SRF files were separated into two files with dimensions corresponding to the fault segments in the complex scenario. Then the desired segment was manually rotated (or "bent" as described above) to obtain a pair of geometrically appropriate segments; one each from the strike slip and the reverse scenarios. This process maintains radiation pattern and rake continuity between the segment edges, even though there is a physical discontinuity at the junction of the vertical strike slip segment and the dipping reverse segment. The results were verified by plotting the entire **M** scenario SRFs (a single plane) along with the individual segment files (comprising the complex scenario). These plots were inspected before performing BBP simulations. Simulations were then combined using the appropriate strike-slip and reverse segments.

### *J.3.3 Splay Ruptures*

Hypocenters were allowed anywhere along the length of the primary segment fault, but secondary segment hypocenters were treated differently for the two scenarios. For the Hosgri-Shoreline splay scenario (both strike-slip segments) the secondary segment hypocenter was placed at the connection point of the primary and secondary segments at the same depth as the randomized hypocenter from the primary segment. If the primary segment hypocenter was deeper than the secondary segment fault plane total depth for a particular realization, the hypocenter was placed at the bottom of the secondary segment. For the Los Osos – San Luis Bay scenarios (both reverse, meeting at depth) the primary segment hypocenter was allowed to be anywhere along strike, but at the bottom of the fault. For corresponding realizations of the secondary segment the hypocenter was placed at the same location (in space) along strike as the primary segment. If this was not possible, because the primary segments are longer and also deeper, the secondary hypocenter was placed on the end of the secondary segment

fault plane at the edge closest to the primary segment hypocenter. In all cases the secondary segment hypocenters were along the bottom edge of the secondary segment fault plane. Hypocenter locations for the Los Osos – San Luis Bay simulations are shown in map view in Figure J.3.3-1.

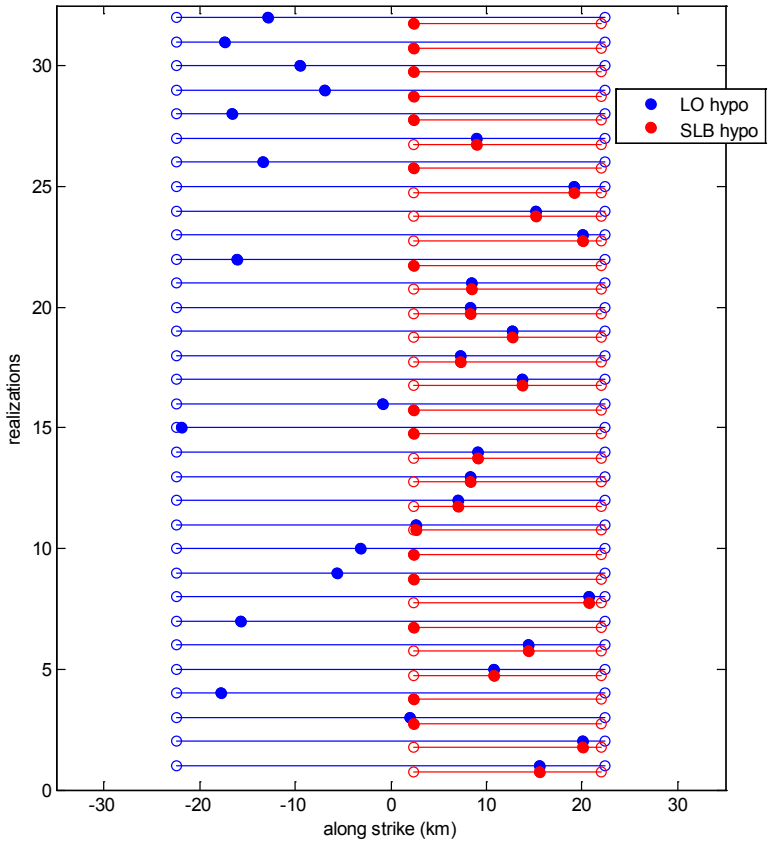



**Figure J.3.3-1:** Example of hypocenter locations along strike for 32 realizations of the Los Osos (LO) – San Luis Bay (SLB) simulations.

The process used for the splay ruptures includes:

1. Specifying one source description for the primary segment,
2. Specifying a second source description for the secondary segment,
3. Creating two planar SRF files using BBP v13.6.1,
4. Running simulations for both segments individually, and
5. Combining the results (see Figure J.3.3-2).

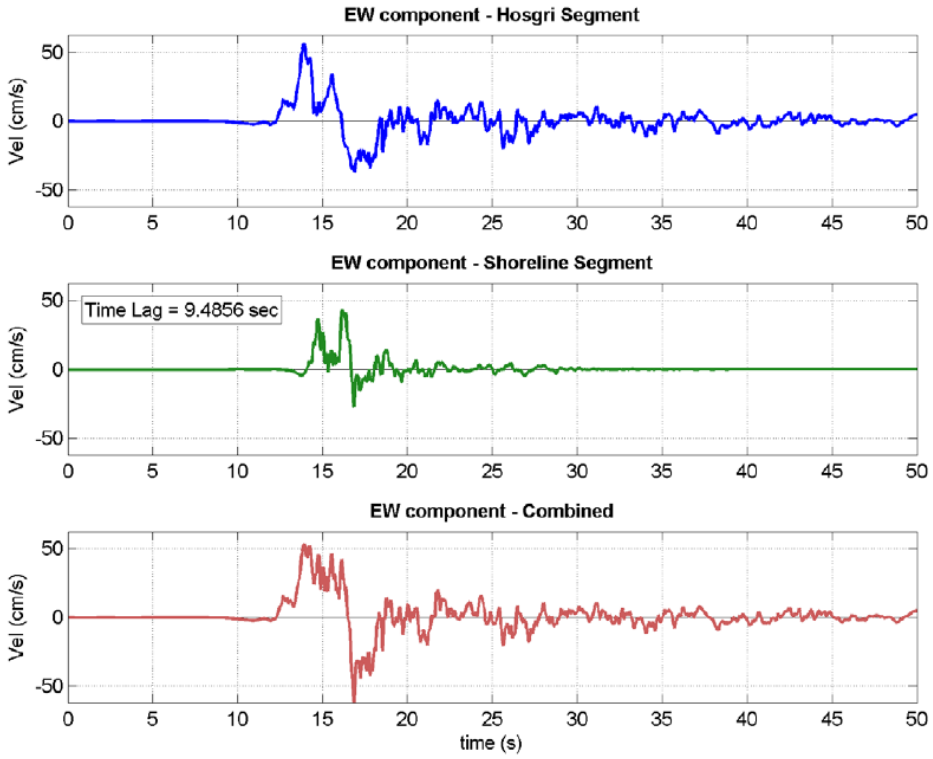



**Figure J.3.3-2:** Example simulated velocity waveforms from the Hosgri-Shoreline splay simulation. The top panel is the primary segment (Hosgri) synthetic, the middle panel is the secondary segment (Shoreline) synthetic, and the bottom panel is the combined synthetic. RotD50 is computed using the two orthogonal synthetics.

Unlike the complex simulations, for which the correct rupture time information was embedded in the SRF files, the splay simulations for the primary and secondary segments are independent of one another. Therefore, for all three simulation methods a time lag has been applied to the secondary segment synthetics before combining in the time domain (Figure J.3.3-2, middle panel). The time lag is added in the secondary segment for all source realizations because the hypocenters were placed on the primary segment in every realization. The time delay is computed using an assumed rupture velocity ($V_r$) of 3 km/s, the distance between the hypocenter in the primary segment, and the junction between the two segments. As discussed above, the hypocenter for the secondary segment is placed at the junction between the primary and secondary segments at the same depth as the randomized hypocenter from the primary segment.

### *J.3.3.1 RotD50 Factors*

The TI Team computed RotD50 spectra for each of the 32 randomized hypocenter source realizations for both the two individual scenario segments and also for the combined rupture source (Figure J.3.3-3). These RotD50 spectra are averaged to get one result for each simulation method. Because the GMPEs are for single planar ruptures, it is not obvious how the ground motions from individual segments should be combined to represent a splay rupture scenario. To select the best method for computing GMPE ground motions for scenarios involving non-planar ruptures, the TI Team computed ground-motion factors from simulations at the plant site for each simulation method. For the splay simulations, the ground-motion factors are the natural log ratio of the average RotD50 spectra for the total splay rupture (numerator) to the average RotD50 spectra from the single segment that is closest to the site (denominator.) The average is taken over the results from all of the simulation source realizations for a given rupture scenario. The ground-motion factors from simulations are representative of the relative increase of the RotD50 due to adding the fault complexity of the non-planar rupture scenario. The purpose of computing the ground-motion factors from simulations is that they can then be compared with ground-motion factors obtained from GMPEs that have been computed using various rules for defining GMPE input parameters. The rules for computing the ground-motion factors are discussed in Section J.4.

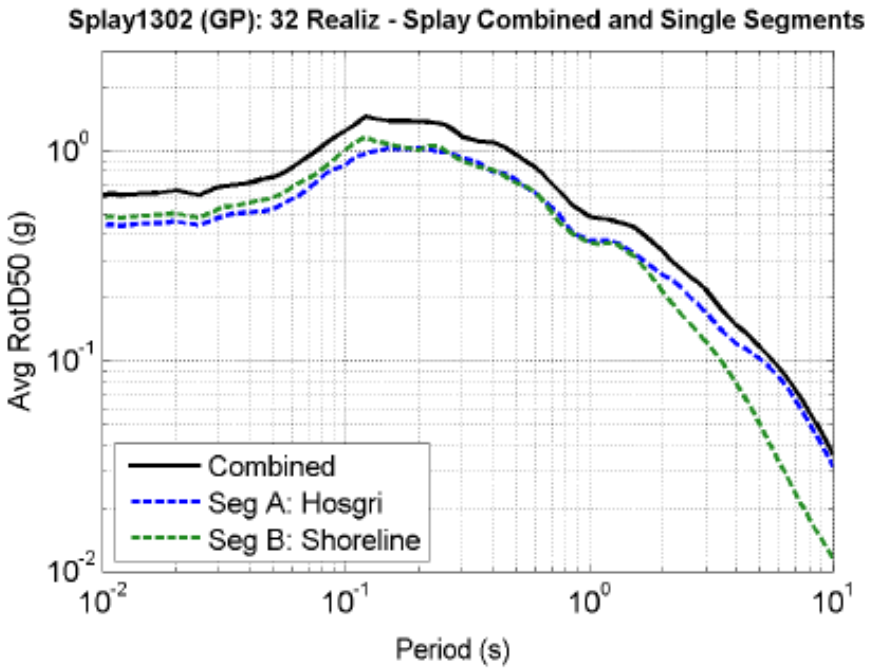



**Figure J.3.3-3:** Example results from the Hosgri-Shoreline splay simulations, GP simulation method. Spectra are the average RotD50 of the 32 randomized hypocenter source realizations for the primary and secondary segments individually, and also for the combined rupture.

## J.4 Models for Ground-Motion Computation for Splay and Complex ruptures

Broadband Platform (BBP) simulations were used to inform the decision of the TI Team regarding how to utilize Ground Motion Prediction Equations (GMPEs) to compute ground motions for splay and complex rupture types at the DCPP site. Because the GMPEs are only applicable for single, planar rupture surfaces with a single style of faulting, it is not clear what parameters are appropriate to use in the models to compute ground motions for ruptures with complicated geometries and/or mixed styles of faulting. The BBP simulations were used to study the characteristics of the ground motions that result from these complicated rupture types, and comparisons between ground-motion factors from simulations and GMPEs were made to support the development of a model for the computation of ground motions for splay and complex ruptures using GMPEs.

The expectation for a splay rupture is that the ground motion at a site will be different for the joint rupture of the primary and secondary fault segments than for the rupture of the primary segment alone. For a complex rupture, it is expected that the ground motion should be at least as high for the joint rupture of the two contributing segments than that from the segment closest to the site alone. Thus, the idea behind computing ground-motion factors is to develop a sense of how much the secondary fault can potentially increase the ground motion over what would be predicted at the site from the primary segment alone for both the splay and complex rupture cases. The ground-motion factors from simulations (as discussed in Section J.3) are mostly positive, meaning that the simulation results agree with the expected result that motions are larger in the more complex ruptures. Following an approach similar to that for computing the ground-motion factors from simulations, the ground-motion factors from GMPEs (in LN units) were computed using a combined RotD50 spectrum in the numerator and either the RotD50 spectrum for the closest segment (for complex ruptures) or the RotD50 spectrum for the primary segment (for splay ruptures) in the denominator, as illustrated by Figure J.4-1. The procedure for computing the combined RotD50 spectra from the complex and splay rupture simulations is outlined in Sections J.3.2 and J.3.3 respectively. The procedures for computing the combined RotD50 spectra from the GMPEs are outlined below. In the results that follow, it is shown that the ground-motion factors from GMPEs can be either positive or negative depending on which of the four methods is used for computing the combined RotD50 spectra.

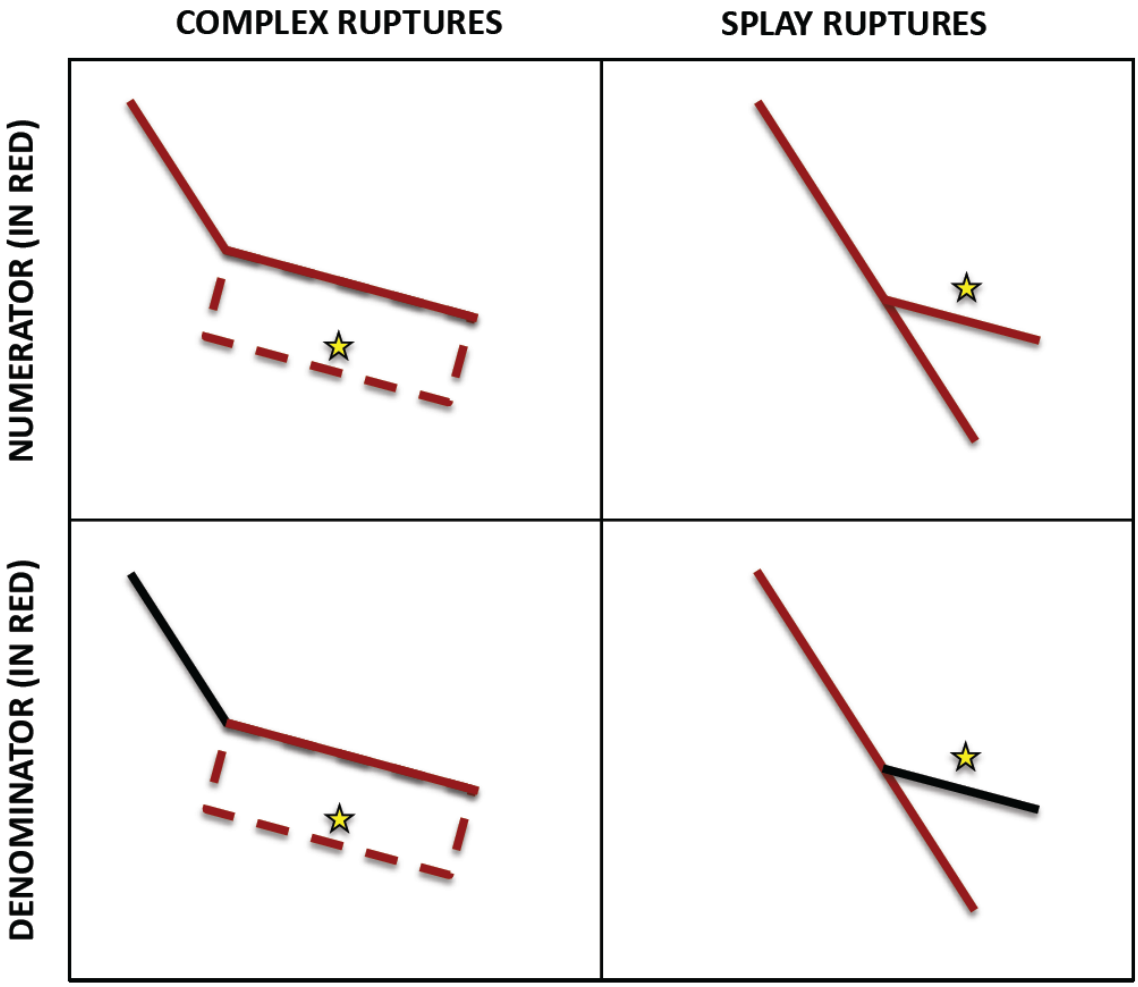



**Figure J.4-1:** Segments used in the factor numerator and denominator for both the complex and splay faulting cases.

### *J.4.1 Alternative Methods*

Four methods were evaluated for computing combined RotD50 spectra from the GMPEs, with the preference given to the method that yields ground-motion factors from GMPEs that resemble those from simulations. The four methods for computing GMPE ground motions include:

METHOD 1: Square Root of the Sum of the Squares (SRSS) of Multiple Fault Segments

METHOD 2: Approximate as Single Fault using Fault Parameters Averaged by Area

METHOD 3: Approximate as Single Fault using Fault Parameters Averaged by $1/R^2$

METHOD 4: Approximate as Single Fault using Closest Segment Parameters

#### *J.4.1.1 METHOD 1: SRSS Multiple Fault Segments*

Method 1 takes the approach of computing the SRSS of the resulting RotD50 spectra from each of the individual participating rupture segments. For the complex rupture case, this means that a RotD50 spectrum is computed for each of the single, planar segments that comprise the complex rupture. Similarly, for the splay case, RotD50 spectra were computed separately for the Primary and Secondary faults. In both cases the individual spectra are combined using the SRSS technique:

$$PSA_{SRSS} = \sqrt{\left(PSA_{Fault1}^2 + PSA_{Fault2}^2\right)} \qquad \text{(Eq. J.4.1-1)}$$

where PSA is the pseudo-spectral acceleration. Method 1 is distinct from Methods 2, 3, and 4 in that it is the only method in which the individual rupture segments are treated separately in the GMPEs and then the RotD50 spectra are combined in an additional step. Methods 2, 3, and 4 represent different ways of creating a single representative rupture to use directly in the GMPEs.

#### *J.4.1.2 METHOD 2: Approximate as Single Fault using Fault Parameters Averaged by Area*

The approach of Method 2 is to calculate average fault parameters (rake, dip, and down-dip width) weighted by fault area. The first step in this approach is to compute the full scenario magnitude based on the combined area for each of the participating complex or splay rupture segments. Weighted averages for rake, dip, and down-dip width are then computed based on the area of each of the individual participating rupture segments. The GMPEs use the distance metrics ($R_{RUP}$, $R_{JB}$, and $R_X$) that correspond to the closest point on the rupture plane from the site of interest and the estimated average fault parameters to compute a single response spectrum that represents either the full complex or splay rupture.

#### *J.4.1.3 METHOD 3: Approximate as Single Fault using Fault Parameters Averaged by $1/R^2$*

Method 3 calculates the average fault parameters (rake, dip, and down-dip width) weighted by $1/R^2$. The fault ruptures are discretized and weighted averages for rake, dip, and down-dip width are computed based on inverse-squared distance to the rupture plane ($1/R^2$) in the following way:

$$Dip_{ave} = \frac{\sum\left(Dip_i \times \frac{1}{R_i^2}\right)}{\sum \frac{1}{R_i^2}} \qquad \text{(Eq. J.4.1-2)}$$

where i represents a discrete fault element. Similar weighted averages are used for the rake and the rupture width. The distance metrics ($R_{RUP}$, $R_{JB}$, and $R_X$) are based on the distances for the closest point on the rupture plane from the site of interest. The magnitude is the magnitude for the combined ruptures.

The average fault parameters are then applied to the GMPEs to compute a single response spectrum that represents either the full complex or splay rupture.

#### *J.4.1.4 METHOD 4: Approximate as Single Fault using Closest Segment Parameters*

Method 4 is perhaps the most simple of the four approaches. This method simply uses the full scenario magnitude computed from the combined area of each of the participating complex or splay rupture segments. The fault parameters and the distance metrics are taken from the closest point along the rupture to the site of interest.

### *J.4.2 Model for Complex Ruptures*

The model for complex fault ruptures is based on the analysis of two complex fault scenarios based on the Hosgri-Los Osos system (Figure J.2.2-1; Table J.2.2-1), and on the Shoreline – San Luis Bay system (Figure J.2.2-3; Table J.2.2-3). Further details regarding the scenario design may be found in Section J.2.2.

#### *J.4.2.1 Complex Scenario 1: Hosgri – Los Osos Complex Fault System*

The geometric relationship between the vertical, strike-slip Hosgri and the 50-degree dipping, reverse Los Osos faults is shown in Figure J.2.2-1. Fault parameters for each of the participating fault segments are listed in Table J.2.2-1 for the three Hosgri – Los Osos cases considered: Case 1 (Hosgri **M**7.0), Case 2 (Hosgri **M**7.2), and Case 3 (Hosgri **M**7.4).

Using Case 2 as an example, the computed fault parameters and distance metrics for each of the four methods of computing ground motions using GMPEs is shown in Table J.4.2-1. For each method, the numbers in this table represent the fault parameters that are used to compute each GMPE RotD50 spectrum. The additional step of computing the SRSS of the two individual fault segment RotD50 spectra is required to obtain a single RotD50 spectrum for Method 1.

**Table J.4.2-1:** Computed fault parameters and distance metrics for the Case 2 Complex Scenario 1 (Hosgri-Los Osos, with **M**7.2 on Hosgri segment).

| | $R_{RUP}$ (km) | $R_{JB}$ (km) | $R_X$ (km) | Mag | dip | rake | Down Dip Width (km) |
|---|---|---|---|---|---|---|---|
| **Hosgri Method 1** | 22.8 | 22.8 | 22.8 | 6.93 | 90 | 180 | 22 |
| **Los Osos Method 1** | 7.8 | 0 | 10.2 | 6.87 | 50 | 90 | 22 |
| **Complex Method 2** | 7.8 | 0 | 10.2 | 7.2 | 71.5 | 138.3 | 22 |
| **Complex Method 3** | 7.8 | 0 | 10.2 | 7.2 | 55 | 101.2 | 22 |
| **Complex Method 4** | 7.8 | 0 | 10.2 | 7.2 | 50 | 90 | 22 |

Figure J.4.2-1 provides a comparison between the BBP RotD50 spectra for the three ground-motion simulation methods (GP, SDSU, and EXSIM) and the RotD50 spectra obtained from the GMPEs using each of the four different methods for assigning predictor variables. This comparison shows that the GP and SDSU simulation methods produce ground motions that are slightly higher than the GMPEs at low frequency (≤ 1Hz). The EXSIM approach, on the other hand, produces ground motions that are generally consistent with the GMPEs at low frequency. At frequencies above 1Hz, the SDSU simulation method produces the highest ground motions of the three simulation techniques. Based on the period and GMPE method it is compared against, the SDSU method either produces the highest ground motions or is consistent with the upper bound of the GMPEs. At high frequencies, the GP and EXSIM simulations generally produce ground motions that are consistent with the upper bound from the GMPEs for each GMPE method.

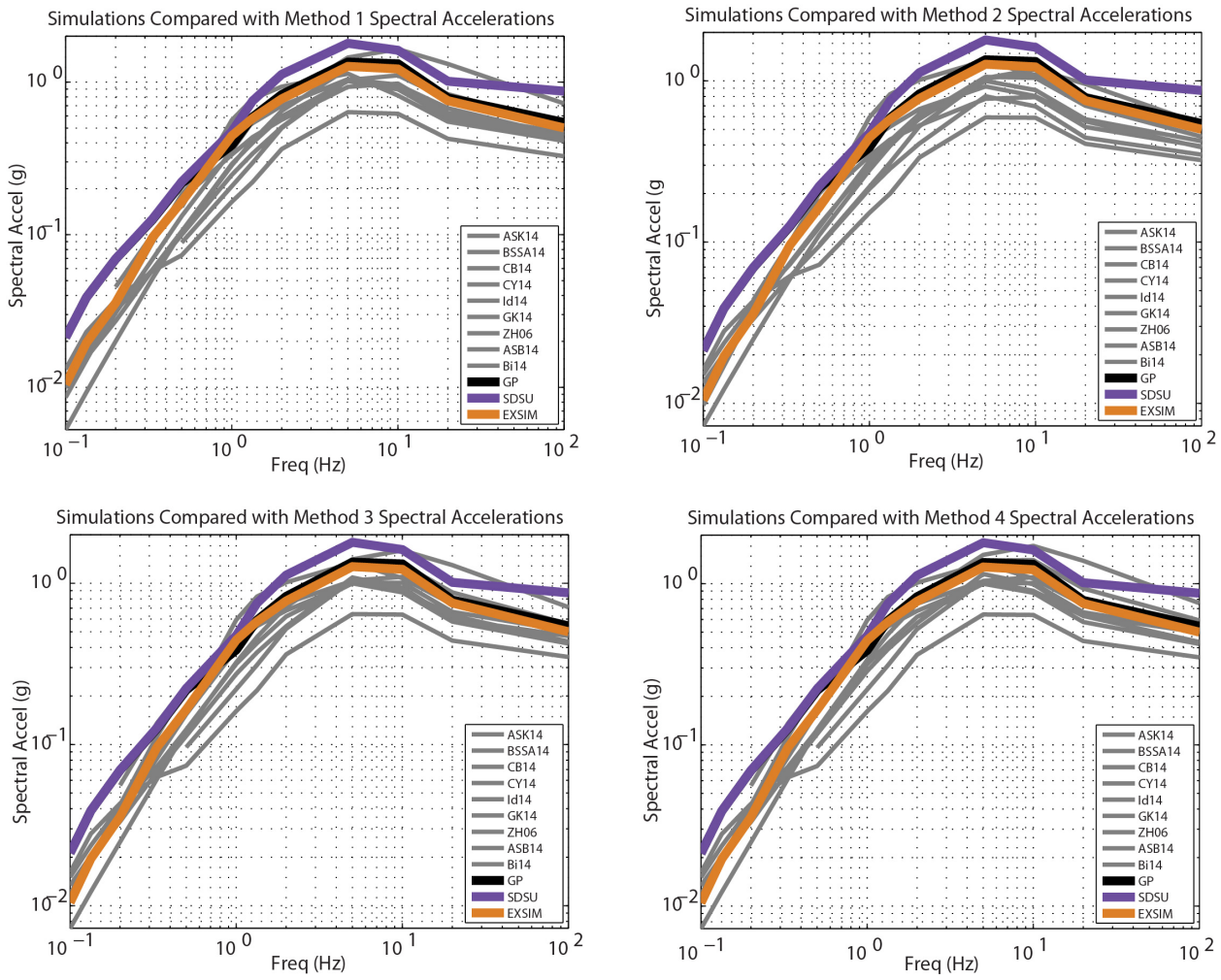



**Figure J.4.2-1** Comparison of the RotD50 spectra for the three simulation methods: GP (black), SDSU (violet), and EXSIM (orange) with the various methods of computing RotD50 spectra from the GMPEs (grey).

Ground-motion factors computed from the three simulation methods are shown in Figure J.4.2-2. In Figure J.4.2-3 the ground-motion factors from simulations (grey lines) are compared to those from the GMPEs.

Comparing the ground-motion factors from simulations (grey lines) with those from GMPEs (colored dots) in Figure J.4.2-3 clearly shows that the ground-motion factors obtained using the SRSS approach (Method 1) best follow the amplitude and overall trend of the factors computed from the three simulation methods over all spectral periods.

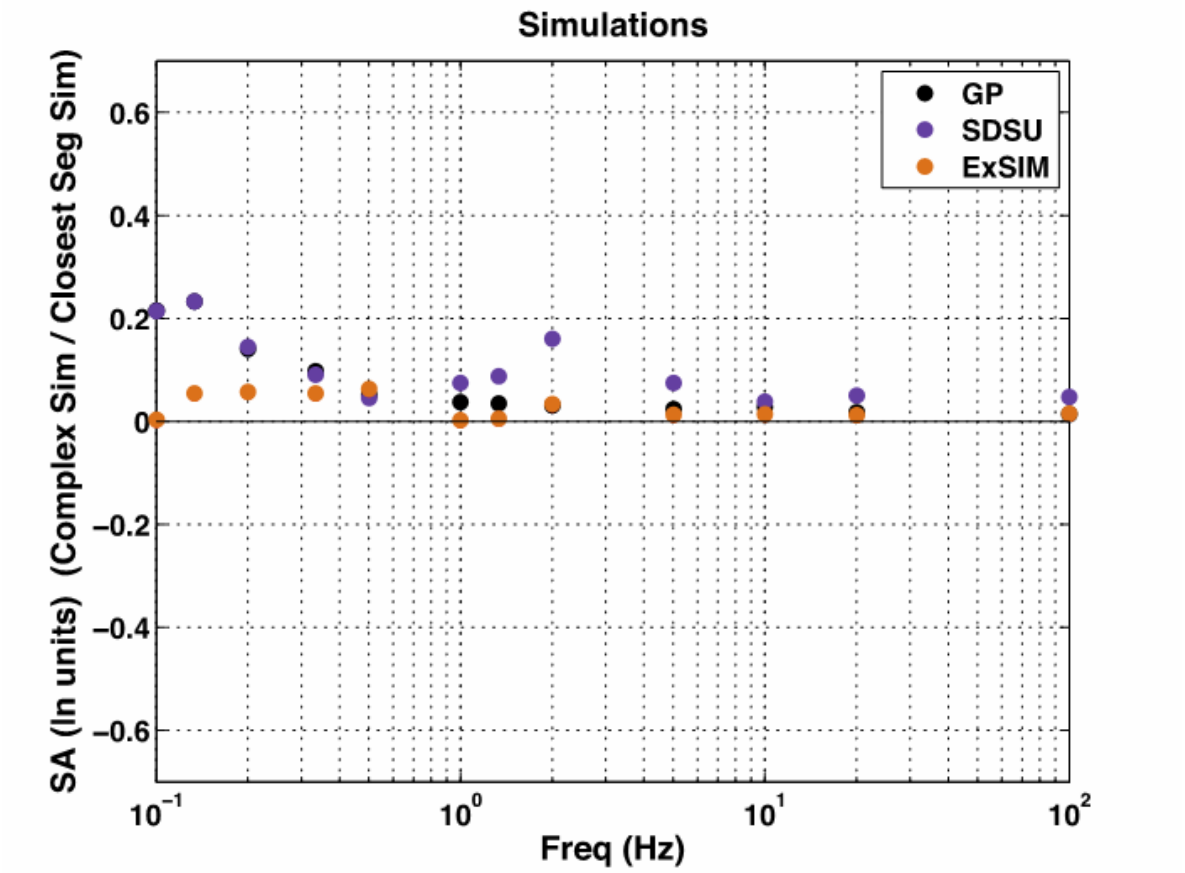



**Figure J.4.2-2:** Ground-Motion Factors for the three simulation methods: GP (black), SDSU (violet), and EXSIM (orange).

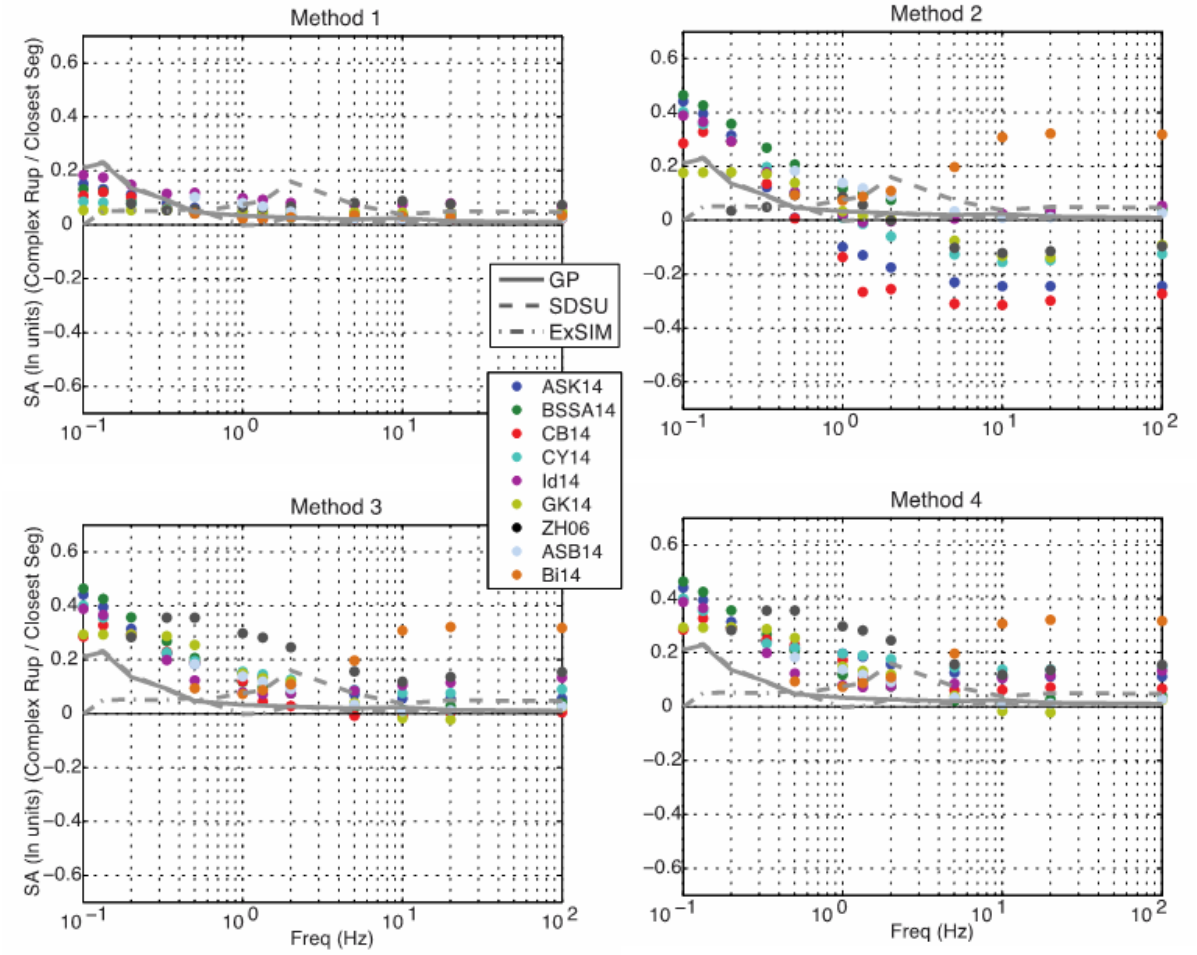



**Figure J.4.2-3:** Ground-Motion Factors for the three simulation methods (grey lines) compared with factors from the various GMPE approaches (colored dots).

The SRSS approach (Method 1) yields small factors because DCPP is located on the hanging wall of the Los Osos fault and far from the Hosgri. As a result, most of the ground-motion contribution at DCPP comes from the Los Osos fault, and the ground motions in the denominator (the Los Osos alone) are very similar to the ground motions in the numerator (SRSS of the Los Osos and the Hosgri).

Method 2 produces the lowest factors at frequencies above about 1 Hz because averaging fault parameters by area results in a steeper dip than that for the Los Osos and a reverse-oblique mechanism because the relative area of the **M**7.2 Hosgri fault is large. Both of these factors tend to decrease the ground motions in the numerator relative to the denominator. The large spread in the ground-motion factors from GMPEs for Method 2 shows the differences in the treatment of the hanging wall term between the GMPEs.

Methods 3 and 4 are very similar. Averaging the fault parameters by closest distance (Method 3) and taking the fault parameters of the nearest segment (Method 4) both result in average fault parameters that are more similar to the parameters of the Los Osos fault. The main reason for factors that are higher for Methods 3 and 4 than for Method 1 is that the magnitude computed from the average fault parameters is based on the total area of the complex rupture system in Methods 3 and 4. In Method 1, the magnitudes used in the GMPEs are computed separately based on the areas of the individual fault segments, in this case the Hosgri and Los Osos fault. As a result, if Method 1 is followed, two response spectra are computed using lower magnitude parameters than are obtained by Methods 2, 3, and 4. These response spectra are then combined to produce a RotD50 spectra that is lower than

### *J.4.2.2 Complex Scenario 2: Shoreline – San Luis Bay Complex Fault System*

The geometric relationship between the vertical, strike-slip Shoreline and the 70-degree dipping, reverse San Luis Bay faults is shown in Figure J.2.2-2. Fault parameters for each of the participating fault segments are listed in Table J.2.2-2 for the three Shoreline – San Luis Bay cases considered: Case 1 (Shoreline **M**7.0), Case 2 (Shoreline **M**7.2), and Case 3 (Shoreline **M**7.4).

Using Case 2 as an example, the computed fault parameters and distance metrics for each of the four methods to compute ground-motion factors from GMPEs is shown in Table J.4.2-2. For each method, the numbers in this table represent the fault parameters that are used to compute each GMPE RotD50 spectrum. The additional step of computing the SRSS of the two individual fault segment RotD50 spectra is required to obtain a single RotD50 spectrum for Method 1.

**Table J.4.2-2:** Computed fault parameters and distance metrics for the Case 2 Complex Scenario 2 (based on the Shoreline-San Luis Bay complex scenarios, with **M**7.2 on the Shoreline segment).

| | $R_{RUP}$ (km) | $R_{JB}$ (km) | $R_X$ (km) | Mag | dip | rake | Down Dip Width (km) |
|---|---|---|---|---|---|---|---|
| **Shoreline Method 1** | 0.7 | 0.7 | 0.7 | 7.15 | 90 | 180 | 22 |
| **San Luis Bay Method1** | 6.4 | 5.5 | 6.5 | 6.23 | 70 | 90 | 22 |
| **Complex Method 2** | 0.7 | 0.7 | 0.7 | 7.2 | 87.8 | 170.3 | 22 |
| **Complex Method 3** | 0.7 | 0.7 | 0.7 | 7.2 | 89.6 | 178.2 | 22 |
| **Complex Method 4** | 0.7 | 0.7 | 0.7 | 7.2 | 90 | 180 | 22 |

Figure J.4.2-4 provides a comparison between the BBP RotD50 spectra from the three simulation methods (GP, SDSU, and EXSIM) and the RotD50 spectra obtained from using the different methodologies to compute predictor variables to use in the GMPEs. This comparison shows that the GP and SDSU simulation methods produce ground motions that are slightly higher than the GMPEs at low frequency (≤ 1Hz). The EXSIM approach, on the other hand, produces ground motions that are generally consistent with the GMPEs at low frequency. At frequencies above 1Hz, the EXSIM produces the highest ground motions of the three simulation techniques. With the exception of Method 1 at T = 0.05 sec, the EXSIM ground motions are higher than the range of the GMPEs. The GP and SDSU methods produce ground motions that are generally consistent with the upper bound of the GMPE range at high frequency and they show fairly good agreement with each other.

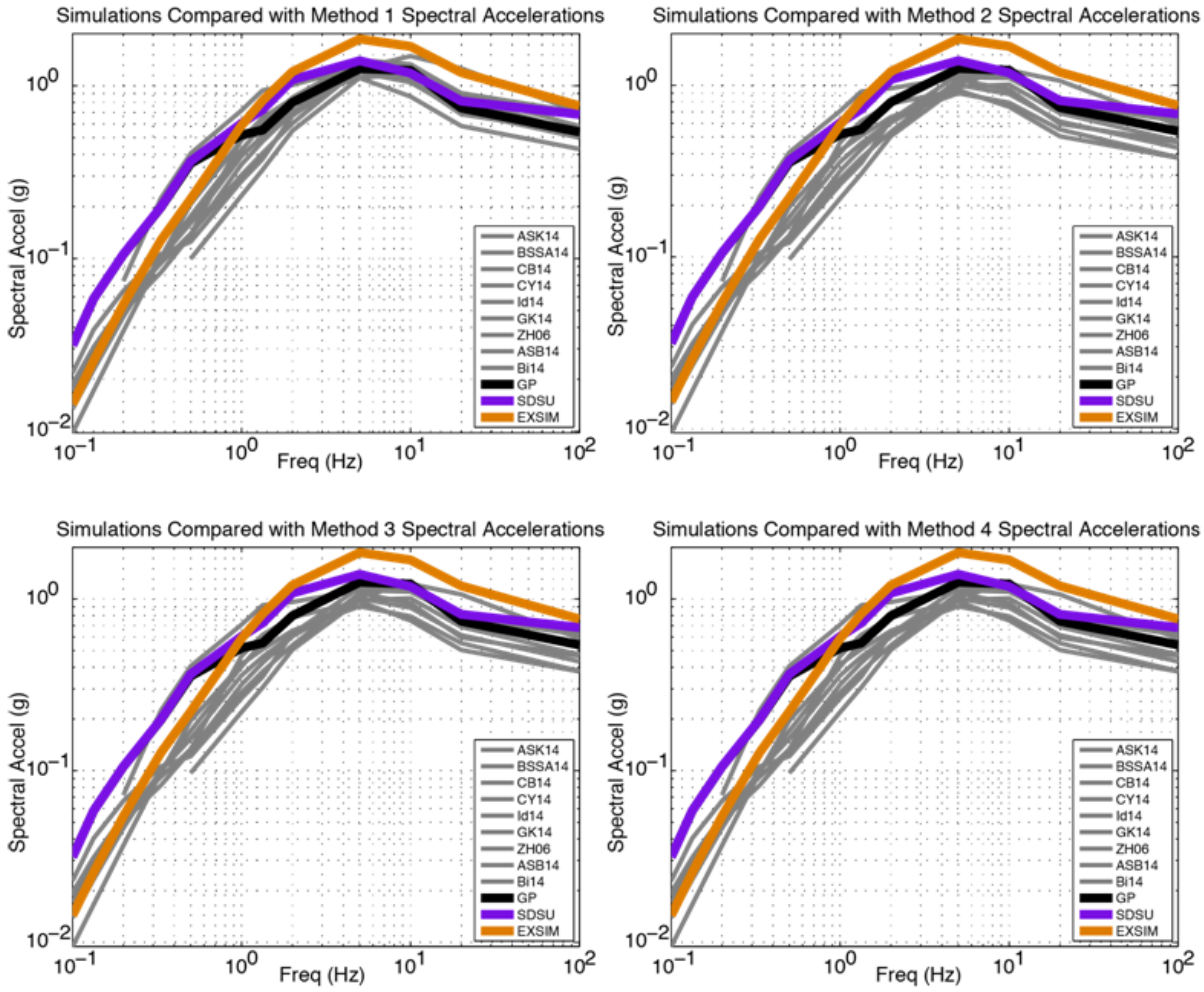



**Figure J.4.2-4:** Comparison of the RotD50 spectra for the three simulation methods: GP (black), SDSU (violet), and EXSIM (orange) with the various methods of computing RotD50 spectra from the GMPEs (grey).

Ground-motion factors computed from the three simulation methods are shown in Figure J.4.2-5. Figure J.4.2-6 compares the ground-motion factors from simulations (grey lines) with those from the GMPEs.

Comparing the ground-motion factors from simulations (grey lines) with those from the GMPEs (colored dots) in Figure J.4.2-6 clearly shows that the ground-motion factors obtained using the SRSS approach (Method 1) best follow the amplitude and overall trend over all spectral periods.

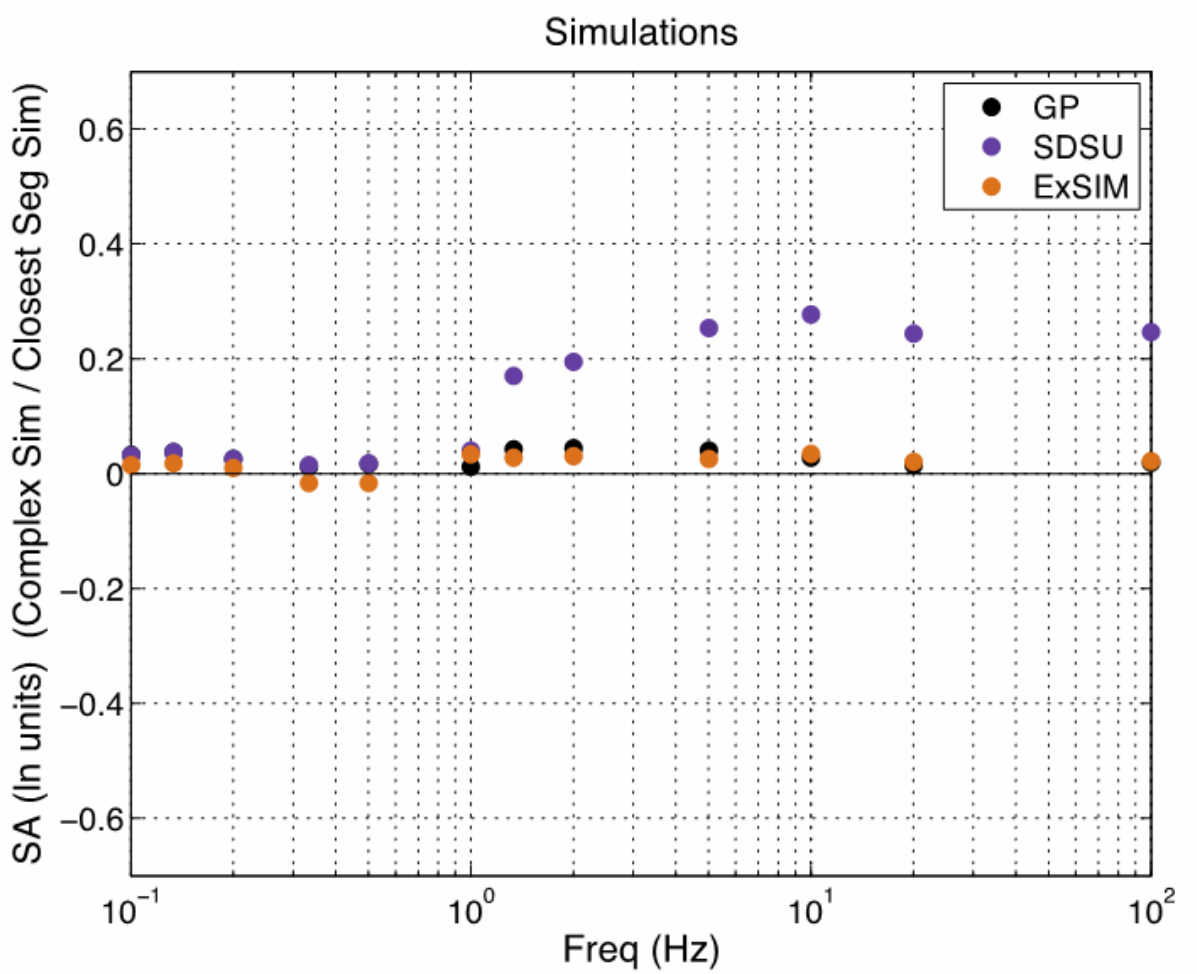



**Figure J.4.2-5:** Ground-Motion Factors for the Three Simulation Methods: GP (black), SDSU (violet), and EXSIM (orange).

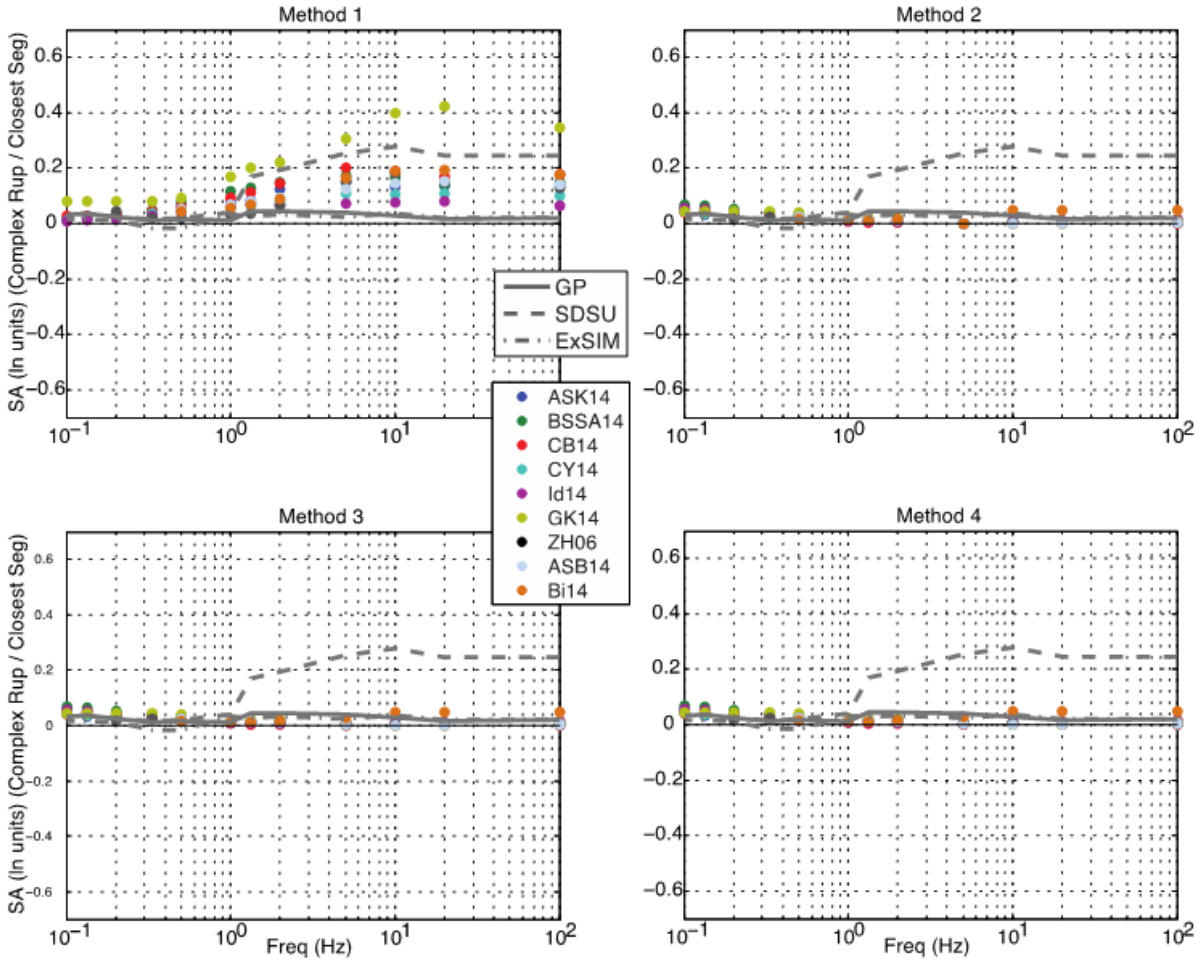



**Figure J.4.2-6:** Ground-Motion Factors for the Three Simulation Methods (grey lines) compared with factors from the various GMPE approaches (colored dots).

The SRSS approach (Method 1) yields the largest factors because DCPP is located along the vertical, strike-slip Shoreline fault but near to the rupture plane of the reverse, dipping San Luis Bay Fault. As a result, the ground-motion contribution at DCPP comes both from the Shoreline fault and the Los Osos fault, and the ground motions in the denominator (the Shoreline Fault) are smaller than the ground motions in the numerator (SRSS of the Shoreline and San Luis Bay faults).

Methods 2, 3, and 4 all produce similar results; very small ground-motion factors over all frequencies. The reason is that both the parameter averaging techniques (Methods 2 and 3) and the approach of taking parameters from the nearest segment (Method 4) result in a vertical to near vertical, strike-slip fault. Thus, each of Methods 2, 3, and 4 misses the important contribution of the small, but close San Luis Bay fault.

The TI Team used the SRSS approach (Method 1) to compute the ground motions for complex faults at the DCPP site. This decision is based on the observation that the GMPE predictor variables computed using Method 1 result in ground-motion factors from GMPEs that follow the same trend observed in the ground-motion factors from simulations for both the Hosgri – Los Osos and the Shoreline – San Luis Bay cases. For the Hosgri – Los Osos scenario, the ground-motion factors from both the simulations and GMPEs are relatively high and steadily decreasing between 0.1 and 1 Hz. Between 1 and 100 Hz, the factors are lower and essentially stable. For this scenario, Methods 2, 3, and 4 lead to more variability in the ground-motion factors from GMPEs than in those estimated from simulations. Also, due to the way the predictor variables are computed in Method 2, the resulting ground-motions factors for this scenario are negative at high frequency for some of the GMPEs. For the Shoreline – San Luis Bay scenario, the ground-motion factors for both the GMPEs and simulations have relatively small values that remain essentially constant from 0.1 to 1 Hz. Above 1 Hz, both sets of ground-motion factors show a definite increase that appears to be somewhat constant at higher frequency. For this case, observations for Methods 2, 3 and 4 show the opposite trend.

### *J.4.3 Model for Splay Ruptures*

The model for splay fault ruptures is based on the analysis of two splay fault scenarios: The Hosgri-Shoreline system (Figure J.2.3-2; Table J.2.3-1), and the Los Osos – San Luis Bay system (Figure J.2.3-3; Table J.2.3-2). Further details regarding the scenario design may be found in Sections J.2.3.

#### *J.4.3.1 Splay Scenario 1: Hosgri – Shoreline Splay Fault System*

The geometric relationship between the vertical, strike-slip Hosgri and Shoreline faults is shown in Figure J.2.3-2. Fault parameters for each of the participating fault segments are listed in Table J.2.3-1 for the three Hosgri – Shoreline cases considered: Case 1 (Hosgri **M**7.0), Case 2 (Hosgri **M**7.2), and Case 3 (Hosgri **M**7.4).

Using Case 3 as an example, the computed fault parameters and distance metrics for each of the four methodologies of computing ground-motion factors from GMPEs is shown in Table J.4.3-1. For each method, the numbers in this table represent the fault parameters that are used to compute each GMPE RotD50 spectrum. The additional step of computing the SRSS of the two individual fault segment RotD50 spectra is required to obtain a single RotD50 spectrum for Method 1.

**Table J.4.3-1:** Computed fault parameters and distance metrics for the Case 3 Splay Scenario 1 (based on the Hosgri-Shoreline splay scenarios, with **M**7.4 on the Hosgri segment).

| | $R_{RUP}$ (km) | $R_{JB}$ (km) | $R_X$ (km) | Mag | dip | rake | Down Dip Width (km) |
|---|---|---|---|---|---|---|---|
| **Hosgri: Method 1** | 5.10 | 5.10 | 5.10 | 7.40 | 90 | 180 | 22.00 |
| **Shoreline: Method 1** | 0.66 | 0.66 | 0.66 | 6.43 | 90 | 180 | 11.93 |
| **Splay Method 2** | 0.66 | 0.66 | 0.66 | 7.44 | 90 | 180 | 20.35 |
| **Splay Method 3** | 0.66 | 0.66 | 0.66 | 7.44 | 90 | 180 | 13.06 |
| **Splay Method 4** | 0.66 | 0.66 | 0.66 | 7.44 | 90 | 180 | 11.93 |

Figure J.4.3-1 provides a comparison between the BBP RotD50 spectra for the three methods (GP, SDSU, and EXSIM) and the RotD50 spectra obtained from the GMPEs. This comparison shows that the GP and SDSU simulations are generally higher than the GMPEs at low frequency, but roughly in agreement with the GMPEs at high frequency (Figure J.4.3-1). EXSIM, on the other hand is in agreement with the GMPEs at low frequency and higher than both the GMPEs and the other simulations at high frequency (Figure J.4.3-1). In fact, peak amplitudes for EXSIM are (in some cases) as much as a factor of two higher than peak amplitudes for GP and SDSU. This result is expected by Dr. Gail Atkinson because the GMPEs have stronger saturation than the EXSIM model at very close distance. Overall, Method 1 RotD50 spectra provide the best agreement with the simulation results because the range obtained from the GMPE spectra utilizing Method 1 to generate the predictor variables (**M**, R, dip, rake, and down-dip width) comes the closest to enveloping the simulation RotD50 spectra. As will also be shown later in this Section, trends in ground-motion factors from GMPEs computed using Method 1 follow the same trends as those computed from the simulations.

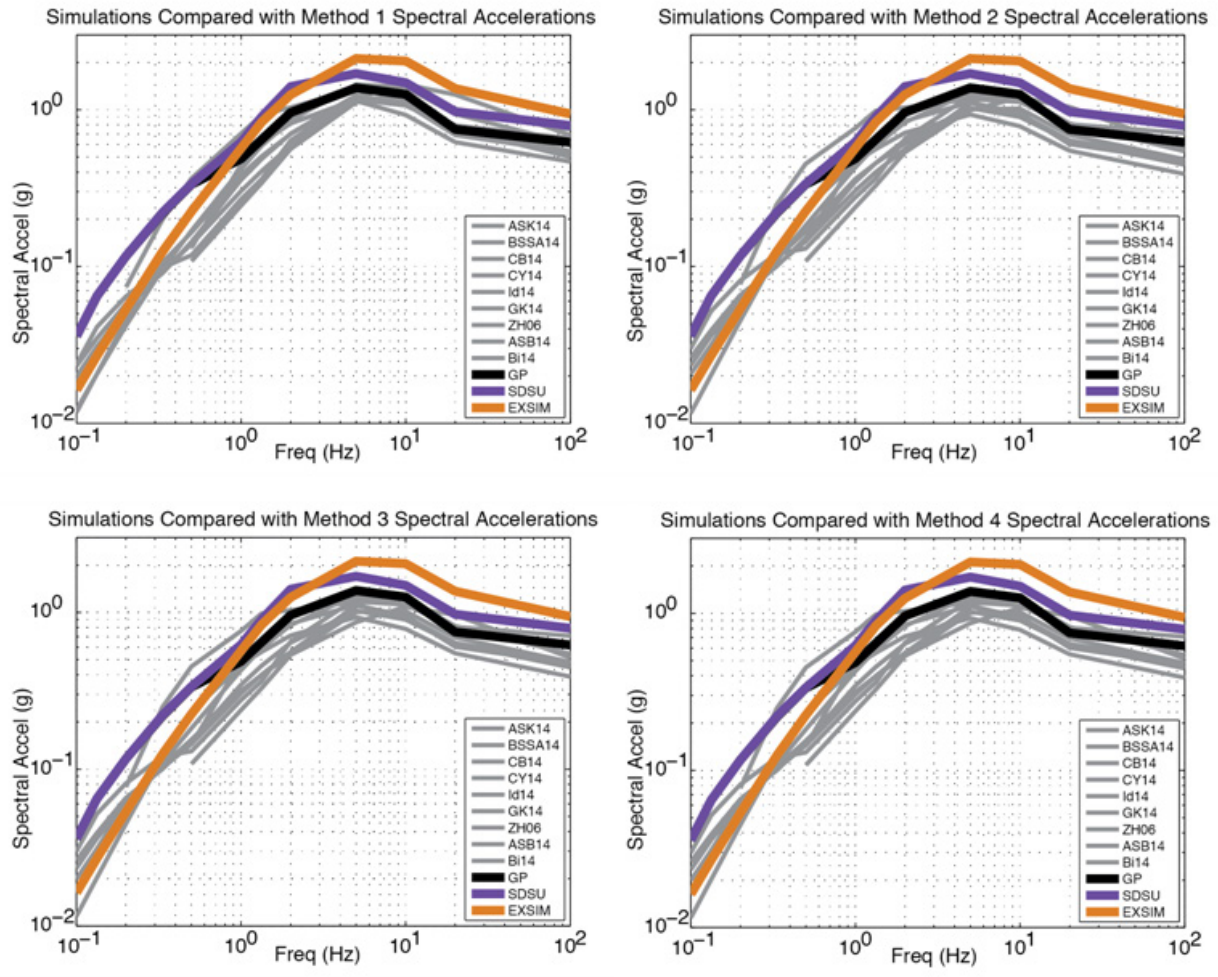



**Figure J.4.3-1**: Comparison of the RotD50 spectra for the three simulation methods: GP (black), SDSU (violet), and EXSIM (orange) with the various methods of computing RotD50 spectra from the GMPEs (grey).

Simulation factors are shown in Figure J.4.3-2. The large factors for the EXSIM approach at high frequency result, in part, from the fact that EXSIM does not saturate at close distances. EXSIM also predicts lower ground motions for the Primary ruptures and higher ground motions for the secondary ruptures at high frequencies. Both of these trends contribute to the large splay rupture factors for the EXSIM method at high frequency.

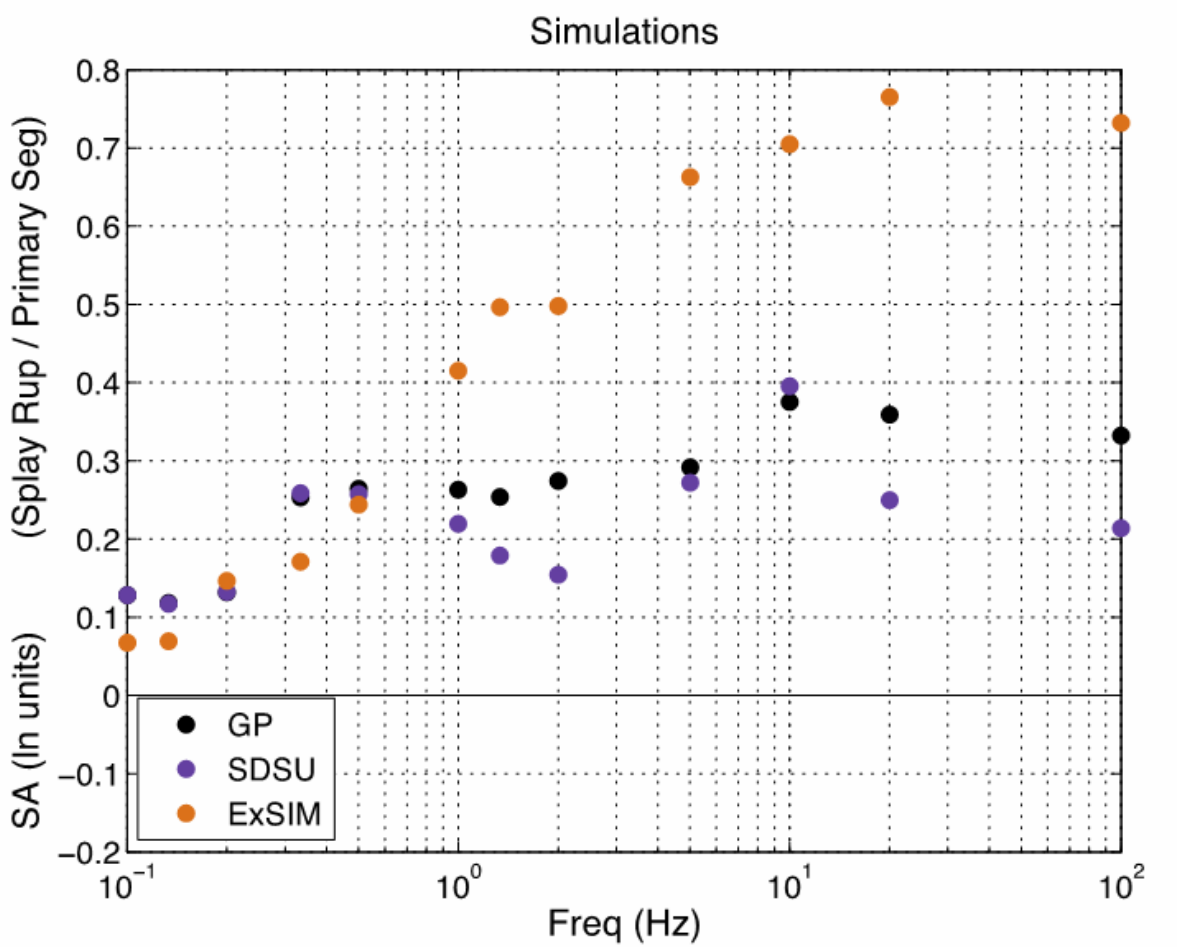



**Figure J.4.3-2:** Ground-Motion Factors for the Three Simulation Methods: GP (black), SDSU (violet), and EXSIM (orange).

Comparing the ground-motion factors from simulations (grey lines) with those from GMPEs (colored dots) in Figure J.4.3-3 reveals that at low frequency (≤ 1Hz), splay rupture ground-motion factors obtained using the SRSS approach (Method 1) are most consistent. At higher frequencies (≥ 1Hz), splay rupture ground-motion factors from GMPEs obtained using the SRSS approach (Method 1) generally follow the amplitude and overall trend of the ground-motion factors computed from GP and SDSU simulations (Figure J.4.3-3).

Ground-motion factors from GMPEs computed with Methods 2, 3, and 4 are very similar because the dip for both the primary and secondary faults is 90 degrees, and the rake is 180 degrees. The only difference in fault parameters between these two segments is the rupture width. Thus, only the rupture width varies between the methods when determining average fault parameters to use in the GMPEs for this case.

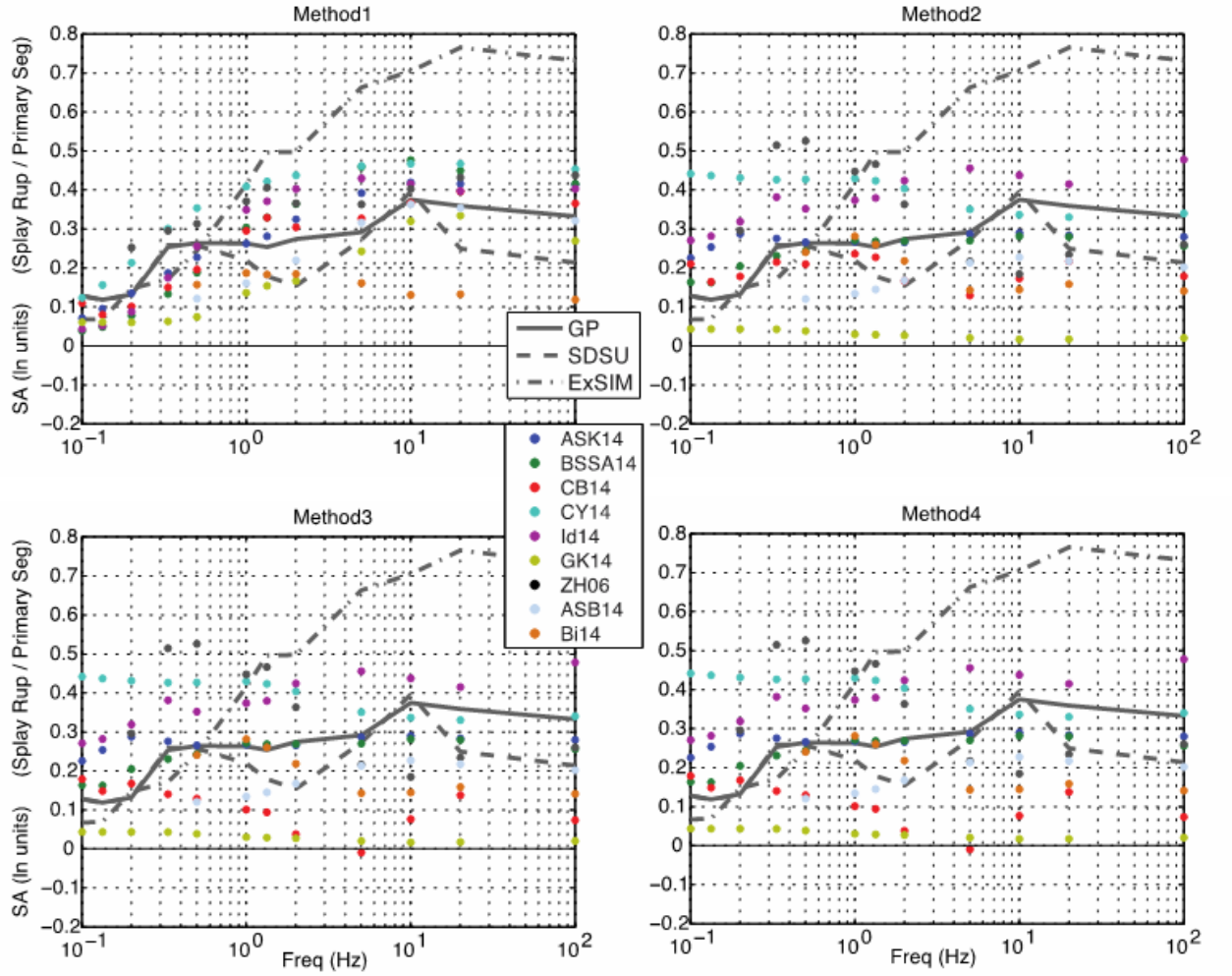



**Figure J.4.3-3:** Ground-Motion Factors for the Three Simulation Methods (grey lines) compared with factors from the various GMPE approaches (colored dots).

### *J.4.3.2 Splay Scenario 2: Los Osos – San Luis Bay Splay Fault System*

The geometric relationship between the 60 degree dipping, reverse Los Osos and the 70-degree dipping, reverse San Luis Bay faults is shown in Figure J.2.3-3. Fault parameters for each of the participating fault segments are listed in Table J.4.3-2 for the three Los Osos – San Luis Bay cases considered: Case 1 (Los Osos **M**7.0), Case 2 (Los Osos **M**7.2), and Case 3 (Los Osos **M**7.4).

Using Case 3 as an example, the computed fault parameters and distance metrics for each of the four GMPE methodologies is shown in Table J.4.2-2. For each method, the numbers in this table represent the fault parameters that are used to compute each GMPE RotD50 spectrum. The additional step of

computing the SRSS of the two individual fault segment RotD50 spectra is required to obtain a single RotD50 spectrum for Method 1.

**Table J.4.3-2**: Computed fault parameters and distance metrics for the Case 3 Splay Scenario 2 (based on the Los Osos-San Luis Bay splay scenarios, with **M**7.4 on the Los Osos segment).

| | $R_{RUP}$ (km) | $R_{JB}$ (km) | $R_X$ (km) | Mag | dip | rake | Down Dip Width (km) |
|---|---|---|---|---|---|---|---|
| **Los Osos: Method 1** | 8.57 | 0.0 | 9.90 | 7.40 | 60.0 | 90 | 32.0 |
| **San Luis Bay: Method 1** | 1.00 | 0.0 | 1.07 | 6.40 | 70.0 | 90 | 12.7 |
| **Splay Method 2** | 1.00 | 0.0 | 1.07 | 7.44 | 62.00 | 90 | 28.14 |
| **Splay Method 3** | 1.00 | 0.0 | 1.07 | 7.44 | 69.20 | 90 | 14.24 |
| **Splay Method 4** | 1.00 | 0.0 | 1.07 | 7.44 | 70.0 | 90 | 12.7 |

Figure J.4.3-4 provides a comparison between the BBP RotD50 spectra for the three methods (GP, SDSU, and EXSIM) and the RotD50 spectra obtained from the GMPEs. This comparison shows that the GP and SDSU simulations are generally higher than the EXSIM simulation and the GMPEs at low frequency (≤ 1Hz). At higher frequency (≥ 10Hz) all simulation methods appear to be in agreement with the GMPEs and the SDSU and EXSIM simulation methods show good agreement with each other. Between 1Hz and 10Hz the simulation ground motions (especially EXSIM and SDSU) appear to be higher than the GMPEs for many of the methods. Overall, Method 1 RotD50 spectra provide the best agreement with the simulation results.

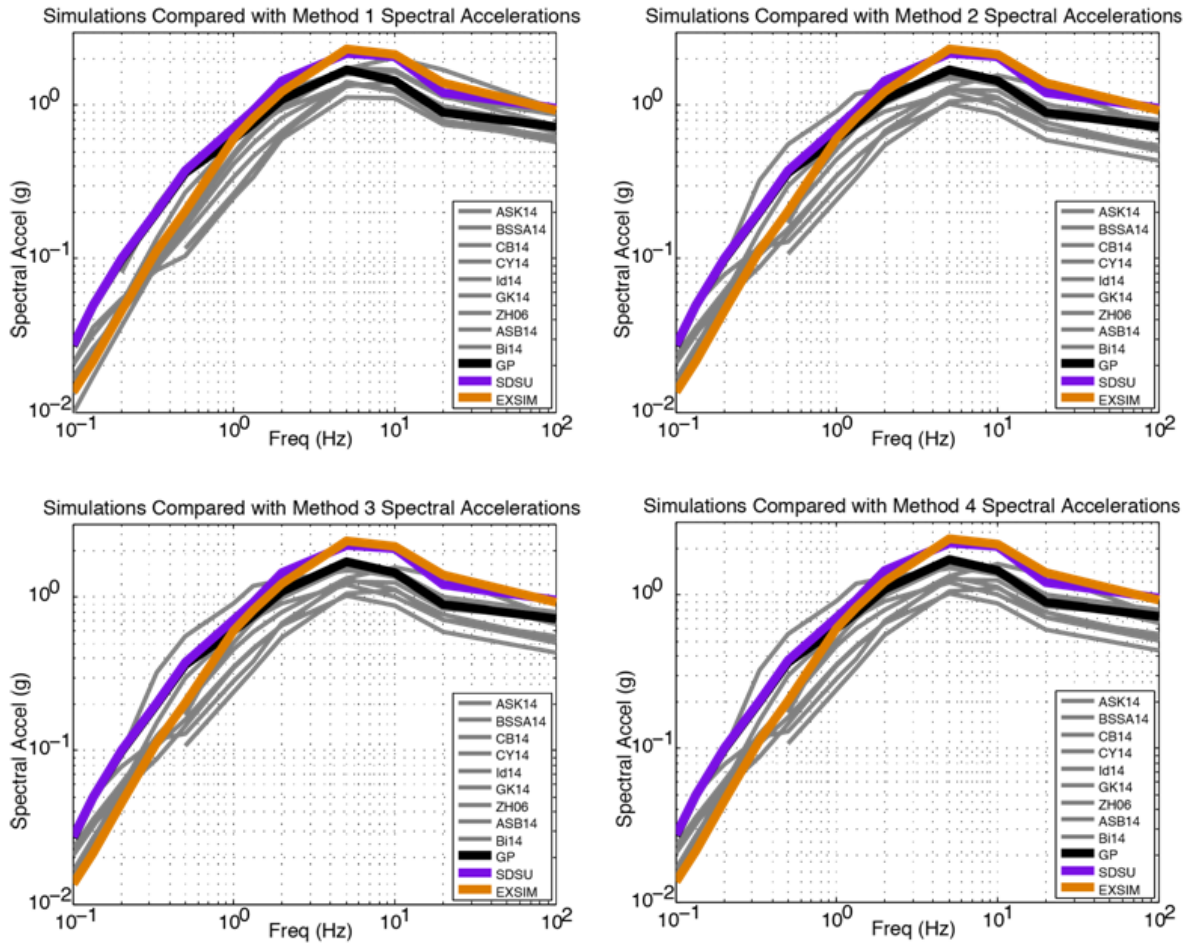



**Figure J.4.3-4:** Comparison of the RotD50 spectra for the three simulation methods: GP (black), SDSU (violet), and EXSIM (orange) with the various methods of computing RotD50 spectra from the GMPEs (grey).

Ground-motion factors computed from the three simulation methods are shown in Figure J.4.3-5. The large factors for EXSIM at high frequency result, in part, from the fact that EXSIM does not saturate at close distances. EXSIM also predicts lower ground motions for the Primary ruptures and higher ground motions for the secondary ruptures at high frequencies. Both of these trends contribute to the large splay rupture factors for the EXSIM method at high frequency.

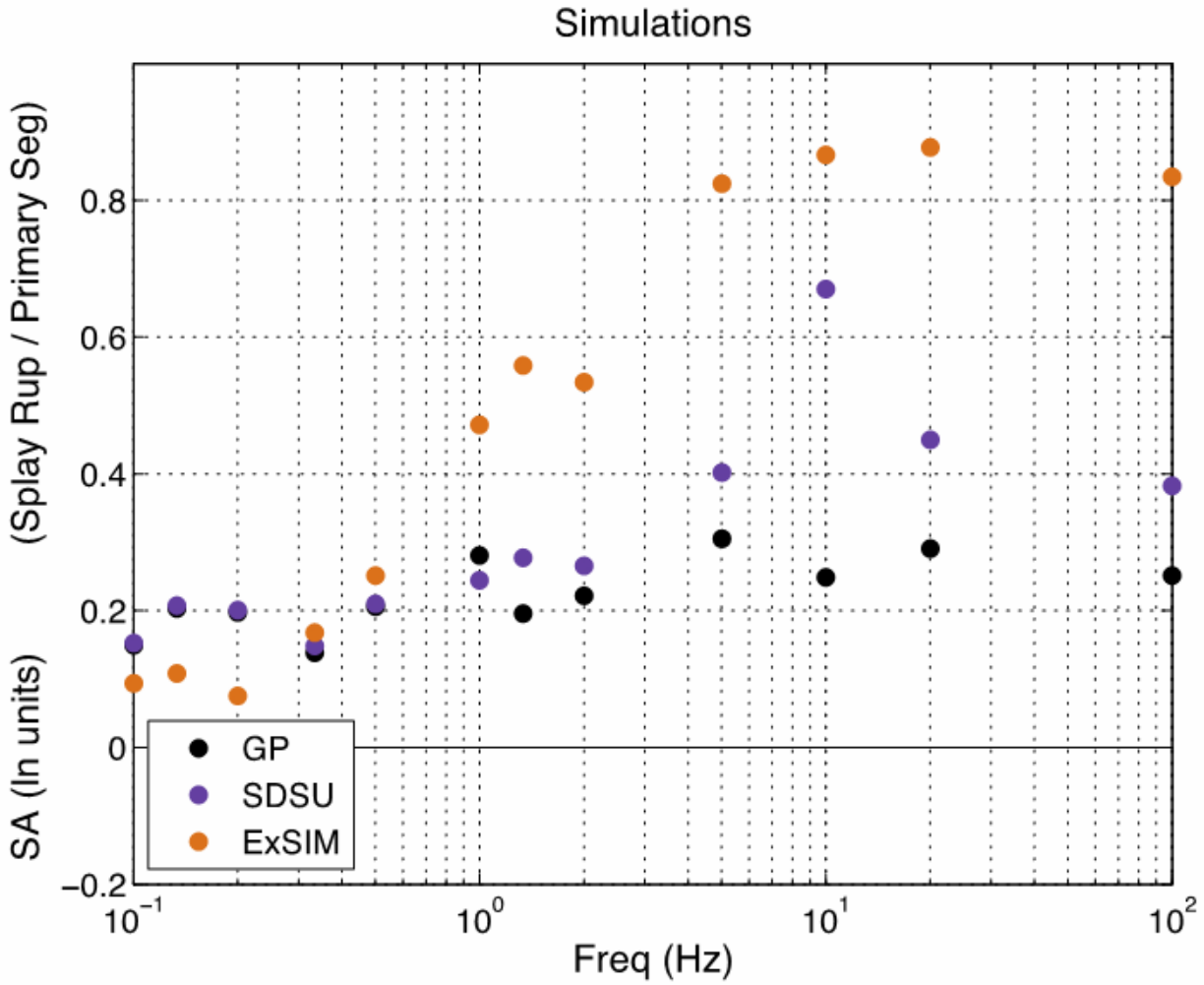



**Figure J.4.3-5:** Ground-Motion Factors for the Three Simulation Methods: GP (black), SDSU (violet), and $_{EXSIM}$ (orange).

Comparing the ground-motion factors from simulations (grey lines) with those from GMPEs (colored dots) in Figure J.4.3-6 reveals that at low frequency (≤ 1Hz), splay rupture ground-motion factors obtained using the SRSS approach (Method 1) generally follows the amplitude and overall trend of the ground-motion factors computed from the three simulation methods (Figure J.4.3-6). At higher frequencies (≥ 1Hz), splay rupture ground-motion factors obtained using the SRSS approach (Method 1) generally follow the amplitude and overall trend of the ground-motion factors computed from GP and SDSU simulations (with the exception of the peak at 10 Hz) (Figure J.4.3-6).

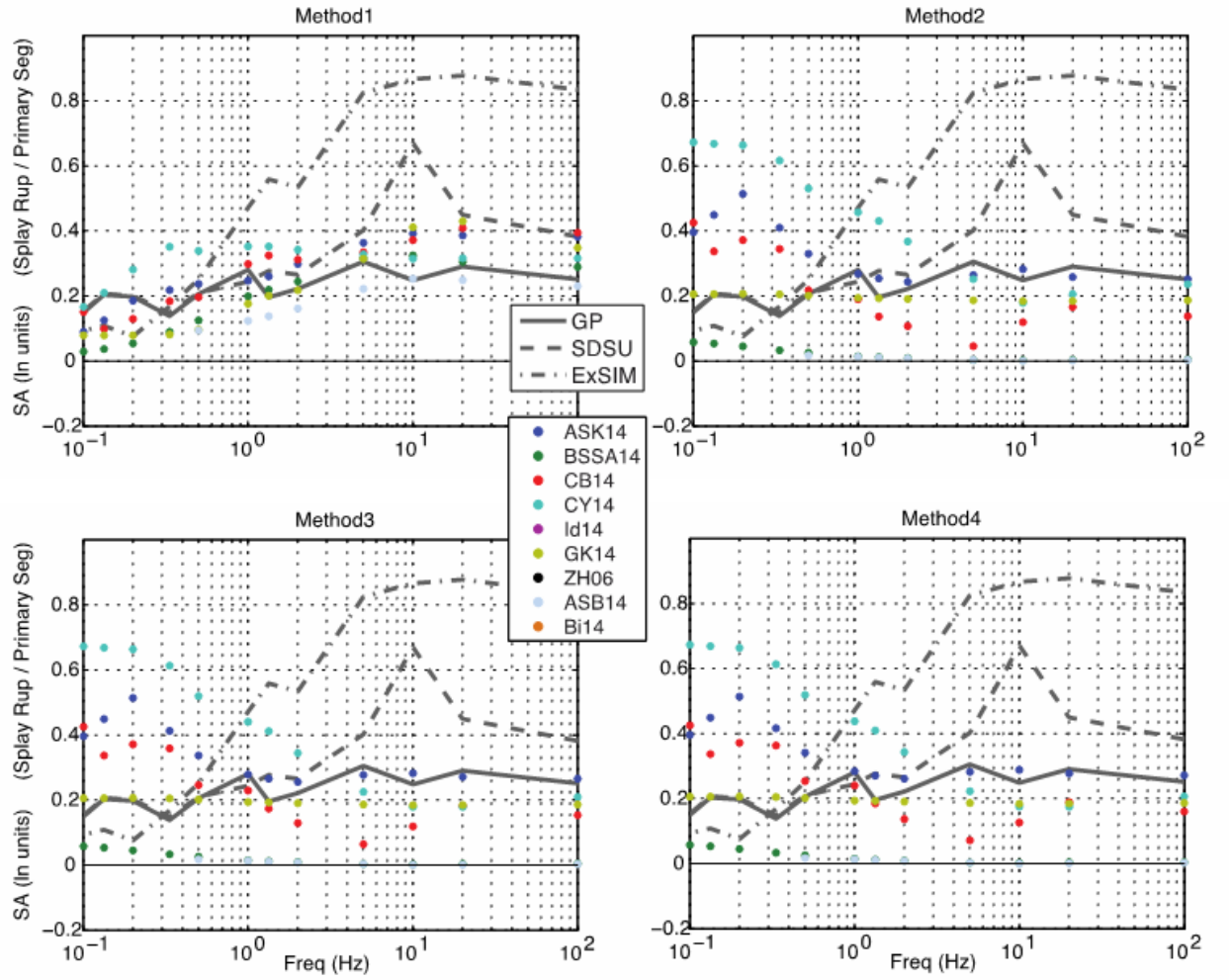



**Figure J.4.3-6:** Ground-Motion Factors for the Three Simulation Methods (grey lines) compared with factors from the various GMPE approaches (colored dots).

The TI Team used the SRSS approach (Method 1) to compute the ground motions for splay faults at the DCPP site. This decision is based on the observation that the GMPE predictor variables computed using Method 1 result in ground-motion factors from GMPEs that follow the same trend observed in the ground-motion factors from simulations for both the Hosgri – Shoreline and the Los Osos – San Luis Bay cases. For the Hosgri – Shoreline scenario, the ground-motion factors from both the GMPEs and simulations begin low and steadily increase between 0.1 and 1 Hz. Between 1 and 100 Hz, the ground-motion factors are higher and essentially stable. For this scenario, Methods 2, 3, and 4 result in significant variability in the ground-motion factors between each of the GMPEs. Also, when considered separately, the GMPEs do not all display the same trends in their respective ground-motion factors. For the Los Osos – San Luis Bay scenario, the ground-motion factors for both the GMPEs and the simulations

have relatively small values that increase steadily from 0.1 to 10 Hz. Above 10 Hz, the ground-motion factors for both GMPEs and simulations appear rather constant. For this case, comparisons for Methods 2, 3 and 4 show the opposite trend.

## J.5 Simulations for Hanging-Wall Scaling

### *J.5.1 Previous simulations used to constraint HW scaling*

Donahue and Abrahamson (2014) used broadband finite-source simulations to develop a hanging-wall functional form. This form was then applied to implement hanging-wall terms in the ASK14 (Abrahamson et al., 2014) GMPE. Two other NGA-West2 GMPE relationships (CY14: Chiou and Youngs, 2014; CB14: Campbell and Bozorgnia, 2014) utilized hanging-wall terms informed from broadband simulations. These studies utilized simulations for **M** ≥ 6.0 and the limited data to constrain the hanging-wall terms. ASK14 and CB14 both applied magnitude tapers in which the hanging-wall terms tapers to zero from **M** 6.5 to 5.5, and for **M** ≤ 5.5 the hanging-wall term is zero. The CY14 formulation does not have an explicit magnitude taper.

### *J.5.2 Comparison between Finite Fault Simulations and Hanging-Wall scaling from GMPEs*

For this project it is necessary to apply hanging-wall terms to lower magnitudes, and therefore a series of simulations were performed to generate ground-motion data for reverse events for a suite of magnitudes (5.5, 6.0 and 6.5), a suite of depth to the top of the fault ($Z_{TOR}$) (12.0 7.0 and 2.5 km), and for a suite of fault dip (10, 20, 30, 45, and 60 degrees). These simulations, described in Section J.2.1, were used for 1) comparison with published GMPE with hanging-wall terms to assess the need for extending hanging-wall terms to lower magnitude, and 2) to test a SWUS hanging-wall term developed by this project to be applied to the Common Functional Form median motion GMPE (Section 6.3) that was used in the hazard calculation.

For each of these scenarios there were 32 source realizations computed at a fixed array of 182 stations. Figure J.5.2-1 shows the distribution of the stations and the surface projection for the **M**5.5, **M**6.0 and **M**6.5 scenarios for a fault dip of 45 degrees. The RotD50 PSA output from the BBP was used in the analysis.

The simulations were compared to the NGA-West2 GMPE hanging-wall terms by first constructing a fault perpendicular profile defined by distance to the top edge of the fault ($R_X$). For each $R_X$ the simulated PSA was averaged for all sites located within the north and south extent of the surface projection rupture plane for each scenario (e.g. Figure J.5.2-1). Then the simulation footwall motions ($R_X < 0$) were fit with an $R_{RUP}$ model, defined as $LN(y)=a+b*LN(R_{RUP})$, where $R_{RUP}$ is the distance to the closest point of the rupture. For sites on the footwall the closest point is always the top edge of the fault. The

fitted $R_{RUP}$ model was then projected to the hanging-wall side to illustrate the hanging-wall effect of the simulations, and to then test the published hanging-wall terms. This approach was first tested by generating ground motions for a suite of $R_X$ for each of the published GMPE. Figure J.5.2-2 shows a comparison for the ASK14 GMPE for **M**6.5, $Z_{TOR}$=7 km and dips of 45 and 60 degrees. The near exact comparison with the published motions demonstrates the viability of the analysis procedure.

The simulations were then compared to the three GMPE hanging-wall terms. Figure J.5.2-3 compares the **M**5.5, **M**6.0 and **M**6.5 cases for $Z_{TOR}$=7 km and dip=45 degrees for the ASK14 model. This model invokes a **M** taper that zeros the hanging-wall term for **M** ≤ 5.5, and for this case the simulations show larger motions on the hanging-wall. The hanging-wall term for **M**6 and **M**6.5 agree well with the simulations. Figure J.5.2-4 compares the **M**5.5, **M**6.0 and **M**6.5 cases for $Z_{TOR}$=7 km and dip=45 degrees for the CB14 model, which shows similar behavior.

It is noted that the SDSU method in Figure J.5.2-3 for the **M**5.5 and **M**6.0 cases shows lower values on the hanging wall than the other two simulation methods, and there also appears to more overall scatter in values for different $R_X$. For the **M**6.5 case all three simulation methods show elevated motions on the hanging wall. Because both the GP and EXSIM methods for the shown 45 degree dip case and other fault dip cases, as well as the SDSU method having values more consistent with the other two methods for the other dip and $Z_{TOR}$ cases, it was the judgment of the TI Team that the simulations do show hanging-wall amplifications for **M** < 6.5.

For the CY14 GMPE there is not an explicit **M** scaling of the hanging-wall term, but rather the scaling is accomplished through a hyperbolic tangent function of $R_X$ that grows larger for increasing values of $R_X$ that is then truncated by a distance taper that is a function of both $R_{JB}$ and $R_{RUP}$ and has a minimum value for $R_{JB}$=0, when the site is over the dipping fault. Thus for a larger rupture the distance taper remains near unity due to $R_{JB}$ remaining zero for larger $R_X$ over the surface projection of the fault, which leads to an increase in amplitude of the hanging-wall term. Figure J.5.2-5 compares the **M**5.5, **M**6.0 and **M**6.5 cases for $Z_{TOR}$=7 km and dip=45 degrees for the CY14 model.

The sensitivity of the published hanging-wall terms was examined for different dips, and $Z_{TOR}$. Based on this analysis the simulations show that hanging-wall effects may be important for magnitude as low as **M**5.5. Modifications to the **M** tapers for each of the NGA-West2 GMPE were examined, however it was determined that a better approach was to develop an independent SWUS hanging-wall term that can be applied directly to the Common Functional-Form GMPE (see Section 6.4). The SWUS hanging-wall term is compared to the ground-motion simulations in Section 6.3.

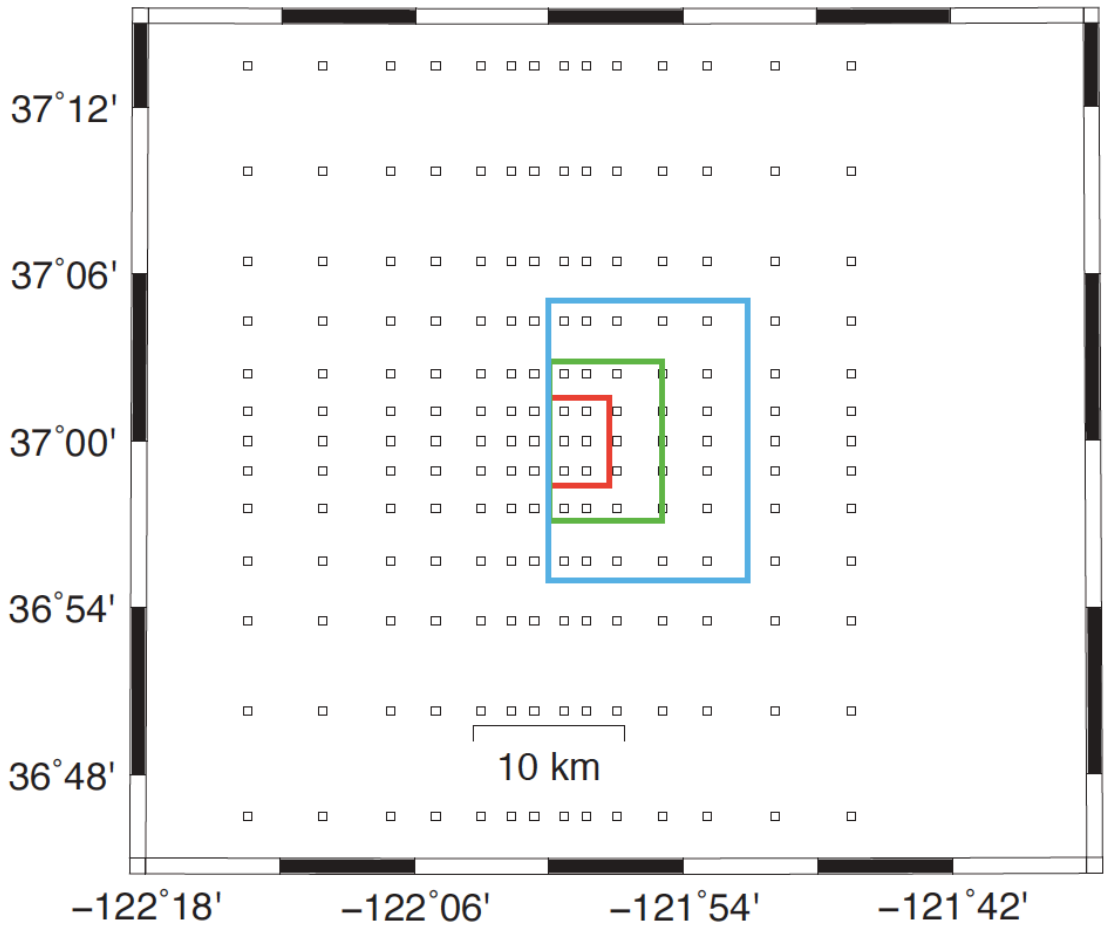



**Figure J.5.2-1:** Map showing the locations of the 182 stations (squares), and the surface projection of the 45-degree dipping cases for **M**5.5 (red), **M**6.0 (green) and **M**6.5 (blue). To construct the ground-motion profiles in $R_X$ the rows of stations contained within the upper and lower extent of each scenario were averaged.

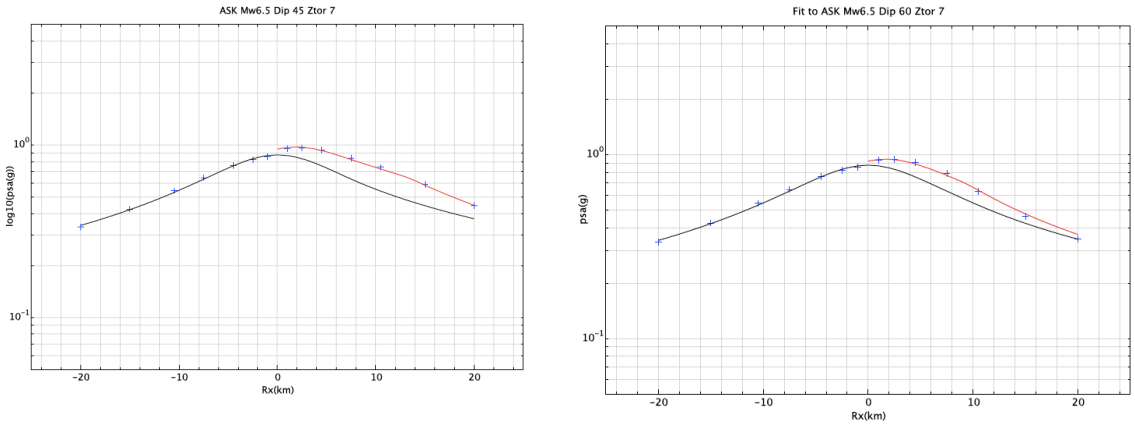



**Figure J.5.2-2:** Actual ASK14 GMPE motions computed from the published equations (plusses) are compared to the method for analyzing hanging-wall terms (lines). The black line shows a $R_{RUP}$ relation obtained by fitting a line to the natural logarithm of the footwall motions ($R_X < 0$). This relationship is then projected to the hanging wall (black line, $R_X \geq 0$). The red line shows the $R_{RUP}$ relationship with the ASK14 hanging-wall term applied.

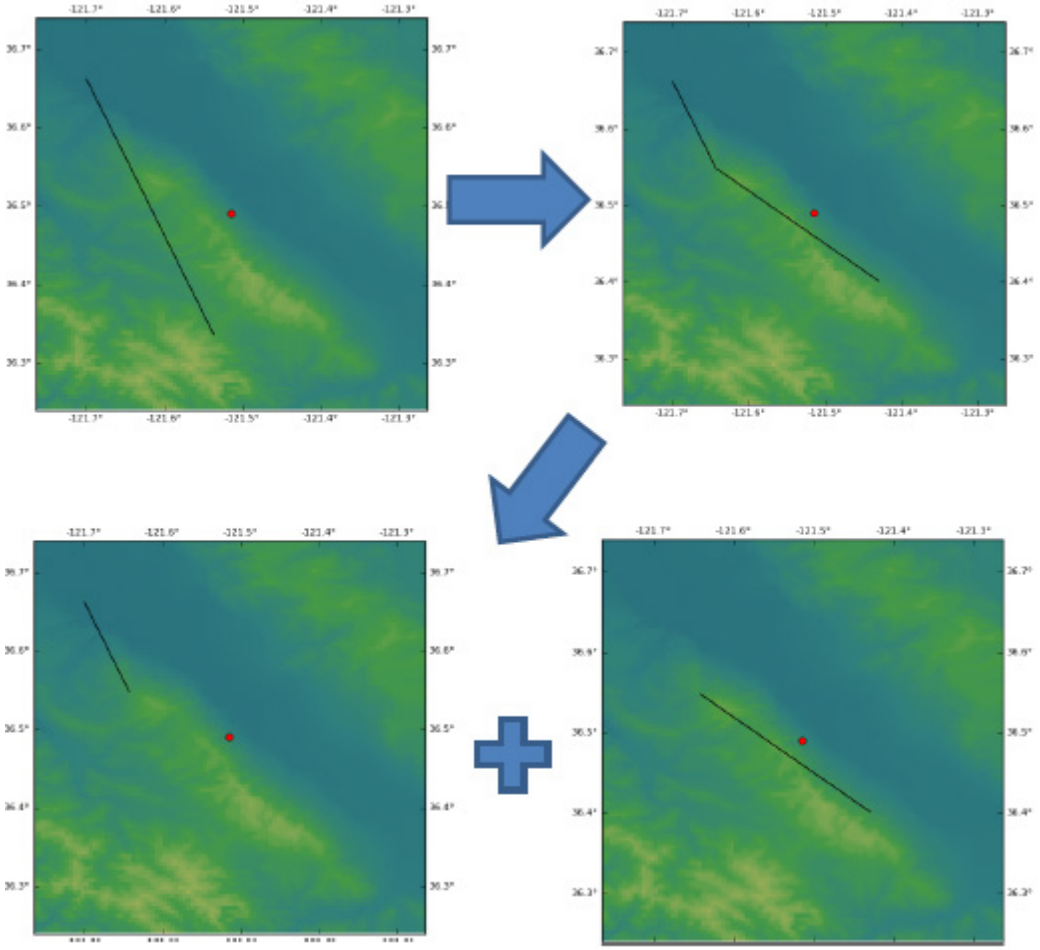


**Figure J.3.2-1:** An example of the "bending" process of the rupture description on the BBP. Black lines are the rupture surface traces and the red dots are the simulations sites. The colored shading represents elevation (yellow is an elevation high and blue is an elevation low), though elevation has no effect on "bending" process.

### *J.3.2.1 RotD50 Factors*

The TI Team computed RotD50 spectra for each of the 32 randomized hypocenter source realizations for both the two individual scenario segments and also for the combined rupture source. These RotD50 spectra are averaged to get one result for each simulation method. Because the GMPEs are suitable for single planar ruptures, it is not obvious how the ground motions from individual segments should be combined to represent a complex rupture scenario. To select the best method for computing GMPE ground motions for scenarios involving non-planar ruptures, the TI Team computed ground-motion

factors from simulations at the plant site for each simulation method. For the complex simulations, the ground-motion factors are the natural log ratio of the average RotD50 spectra for the total complex rupture (numerator) to the average RotD50 spectra from the single segment that is closest to the site (denominator.) The average is taken over the results from all of the simulation source realizations for a given rupture scenario. The ground-motion factors from simulations are representative of the relative increase of the RotD50 due to adding the fault complexity of the non-planar rupture scenario. The purpose of computing the ground-motion factors from simulations is that they can then be compared with ground-motion factors obtained from GMPEs that have been computed using various rules for defining GMPE input parameters. The rules for computing the ground-motion factors are discussed in Section J.4.

#### *J.3.2.2 Additional Comments*

For complex scenarios with both a strike-slip and reverse component, it was required to begin with two planar SRFs representing the entire **M** scenario - one strike slip, and one reverse - with identical source descriptions except for the average rake and dip parameters. Both the strike slip and reverse scenario SRF files were separated into two files with dimensions corresponding to the fault segments in the complex scenario. Then the desired segment was manually rotated (or "bent" as described above) to obtain a pair of geometrically appropriate segments; one each from the strike slip and the reverse scenarios. This process maintains radiation pattern and rake continuity between the segment edges, even though there is a physical discontinuity at the junction of the vertical strike slip segment and the dipping reverse segment. The results were verified by plotting the entire **M** scenario SRFs (a single plane) along with the individual segment files (comprising the complex scenario). These plots were inspected before performing BBP simulations. Simulations were then combined using the appropriate strike-slip and reverse segments.

### *J.3.3 Splay Ruptures*

Hypocenters were allowed anywhere along the length of the primary segment fault, but secondary segment hypocenters were treated differently for the two scenarios. For the Hosgri-Shoreline splay scenario (both strike-slip segments) the secondary segment hypocenter was placed at the connection point of the primary and secondary segments at the same depth as the randomized hypocenter from the primary segment. If the primary segment hypocenter was deeper than the secondary segment fault plane total depth for a particular realization, the hypocenter was placed at the bottom of the secondary segment. For the Los Osos – San Luis Bay scenarios (both reverse, meeting at depth) the primary segment hypocenter was allowed to be anywhere along strike, but at the bottom of the fault. For corresponding realizations of the secondary segment the hypocenter was placed at the same location (in space) along strike as the primary segment. If this was not possible, because the primary segments are longer and also deeper, the secondary hypocenter was placed on the end of the secondary segment

fault plane at the edge closest to the primary segment hypocenter. In all cases the secondary segment hypocenters were along the bottom edge of the secondary segment fault plane. Hypocenter locations for the Los Osos – San Luis Bay simulations are shown in map view in Figure J.3.3-1.

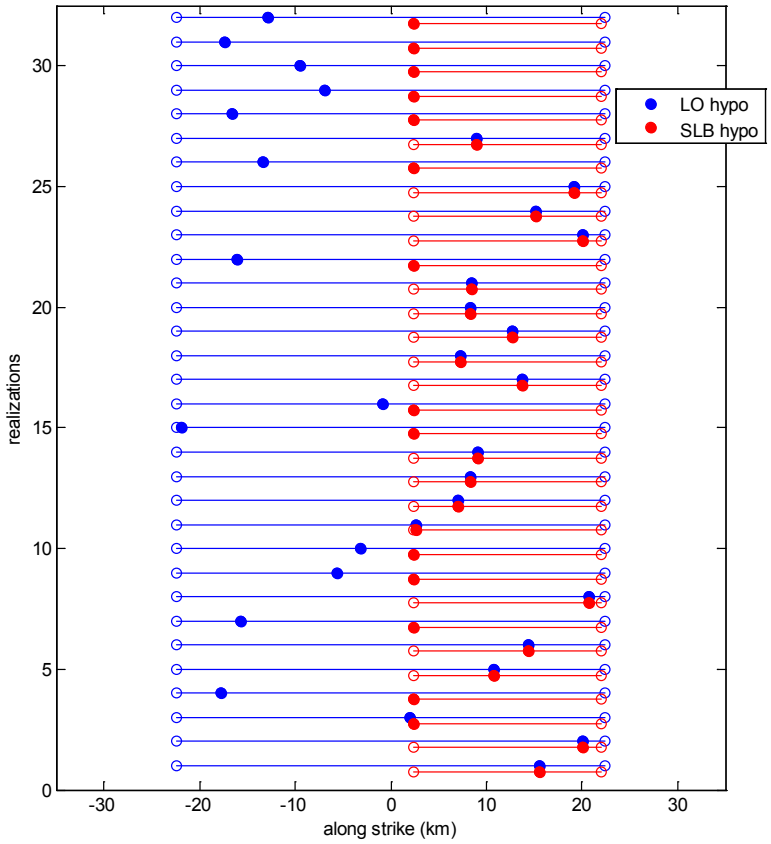



**Figure J.3.3-1:** Example of hypocenter locations along strike for 32 realizations of the Los Osos (LO) – San Luis Bay (SLB) simulations.

The process used for the splay ruptures includes:

1. Specifying one source description for the primary segment,
2. Specifying a second source description for the secondary segment,
3. Creating two planar SRF files using BBP v13.6.1,
4. Running simulations for both segments individually, and
5. Combining the results (see Figure J.3.3-2).

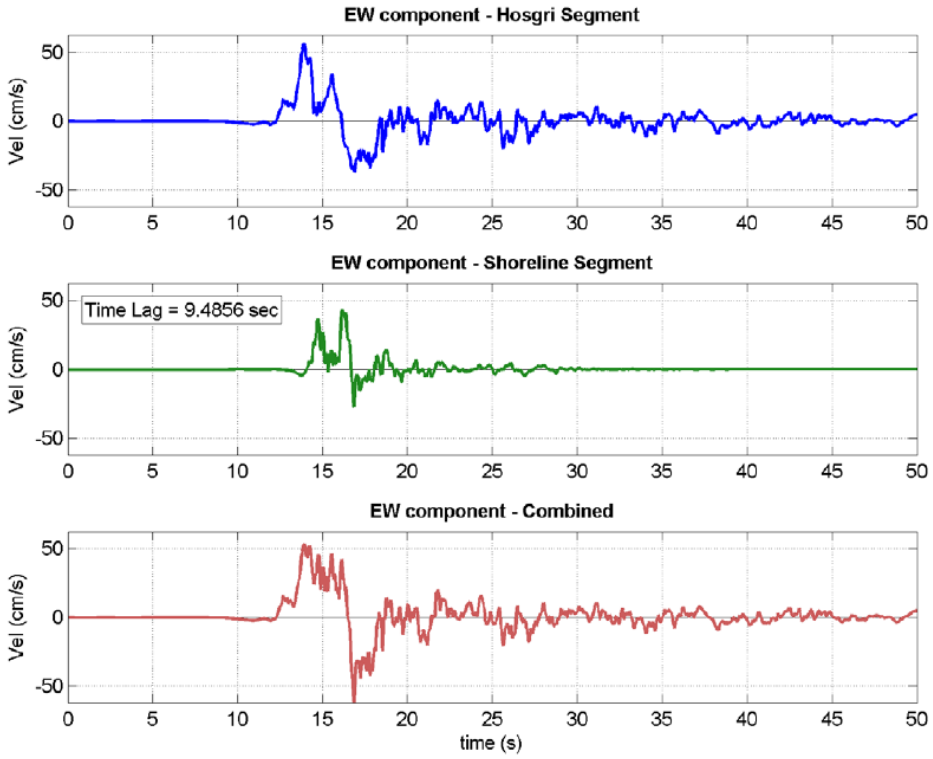



**Figure J.3.3-2:** Example simulated velocity waveforms from the Hosgri-Shoreline splay simulation. The top panel is the primary segment (Hosgri) synthetic, the middle panel is the secondary segment (Shoreline) synthetic, and the bottom panel is the combined synthetic. RotD50 is computed using the two orthogonal synthetics.

Unlike the complex simulations, for which the correct rupture time information was embedded in the SRF files, the splay simulations for the primary and secondary segments are independent of one another. Therefore, for all three simulation methods a time lag has been applied to the secondary segment synthetics before combining in the time domain (Figure J.3.3-2, middle panel). The time lag is added in the secondary segment for all source realizations because the hypocenters were placed on the primary segment in every realization. The time delay is computed using an assumed rupture velocity ($V_r$) of 3 km/s, the distance between the hypocenter in the primary segment, and the junction between the two segments. As discussed above, the hypocenter for the secondary segment is placed at the junction between the primary and secondary segments at the same depth as the randomized hypocenter from the primary segment.

### *J.3.3.1 RotD50 Factors*

The TI Team computed RotD50 spectra for each of the 32 randomized hypocenter source realizations for both the two individual scenario segments and also for the combined rupture source (Figure J.3.3-3). These RotD50 spectra are averaged to get one result for each simulation method. Because the GMPEs are for single planar ruptures, it is not obvious how the ground motions from individual segments should be combined to represent a splay rupture scenario. To select the best method for computing GMPE ground motions for scenarios involving non-planar ruptures, the TI Team computed ground-motion factors from simulations at the plant site for each simulation method. For the splay simulations, the ground-motion factors are the natural log ratio of the average RotD50 spectra for the total splay rupture (numerator) to the average RotD50 spectra from the single segment that is closest to the site (denominator.) The average is taken over the results from all of the simulation source realizations for a given rupture scenario. The ground-motion factors from simulations are representative of the relative increase of the RotD50 due to adding the fault complexity of the non-planar rupture scenario. The purpose of computing the ground-motion factors from simulations is that they can then be compared with ground-motion factors obtained from GMPEs that have been computed using various rules for defining GMPE input parameters. The rules for computing the ground-motion factors are discussed in Section J.4.

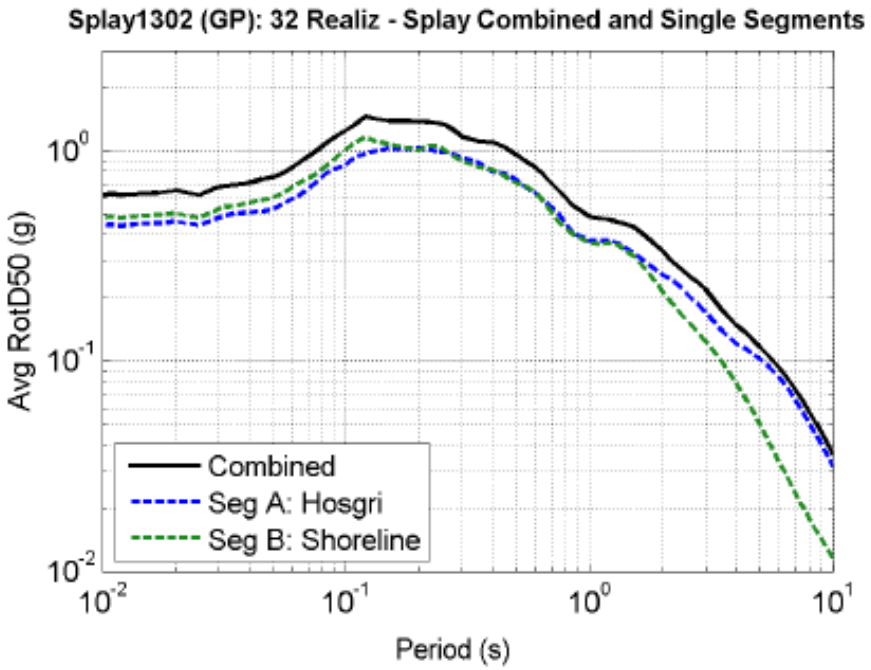



**Figure J.3.3-3:** Example results from the Hosgri-Shoreline splay simulations, GP simulation method. Spectra are the average RotD50 of the 32 randomized hypocenter source realizations for the primary and secondary segments individually, and also for the combined rupture.

## J.4 Models for Ground-Motion Computation for Splay and Complex ruptures

Broadband Platform (BBP) simulations were used to inform the decision of the TI Team regarding how to utilize Ground Motion Prediction Equations (GMPEs) to compute ground motions for splay and complex rupture types at the DCPP site. Because the GMPEs are only applicable for single, planar rupture surfaces with a single style of faulting, it is not clear what parameters are appropriate to use in the models to compute ground motions for ruptures with complicated geometries and/or mixed styles of faulting. The BBP simulations were used to study the characteristics of the ground motions that result from these complicated rupture types, and comparisons between ground-motion factors from simulations and GMPEs were made to support the development of a model for the computation of ground motions for splay and complex ruptures using GMPEs.

The expectation for a splay rupture is that the ground motion at a site will be different for the joint rupture of the primary and secondary fault segments than for the rupture of the primary segment alone. For a complex rupture, it is expected that the ground motion should be at least as high for the joint rupture of the two contributing segments than that from the segment closest to the site alone. Thus, the idea behind computing ground-motion factors is to develop a sense of how much the secondary fault can potentially increase the ground motion over what would be predicted at the site from the primary segment alone for both the splay and complex rupture cases. The ground-motion factors from simulations (as discussed in Section J.3) are mostly positive, meaning that the simulation results agree with the expected result that motions are larger in the more complex ruptures. Following an approach similar to that for computing the ground-motion factors from simulations, the ground-motion factors from GMPEs (in LN units) were computed using a combined RotD50 spectrum in the numerator and either the RotD50 spectrum for the closest segment (for complex ruptures) or the RotD50 spectrum for the primary segment (for splay ruptures) in the denominator, as illustrated by Figure J.4-1. The procedure for computing the combined RotD50 spectra from the complex and splay rupture simulations is outlined in Sections J.3.2 and J.3.3 respectively. The procedures for computing the combined RotD50 spectra from the GMPEs are outlined below. In the results that follow, it is shown that the ground-motion factors from GMPEs can be either positive or negative depending on which of the four methods is used for computing the combined RotD50 spectra.

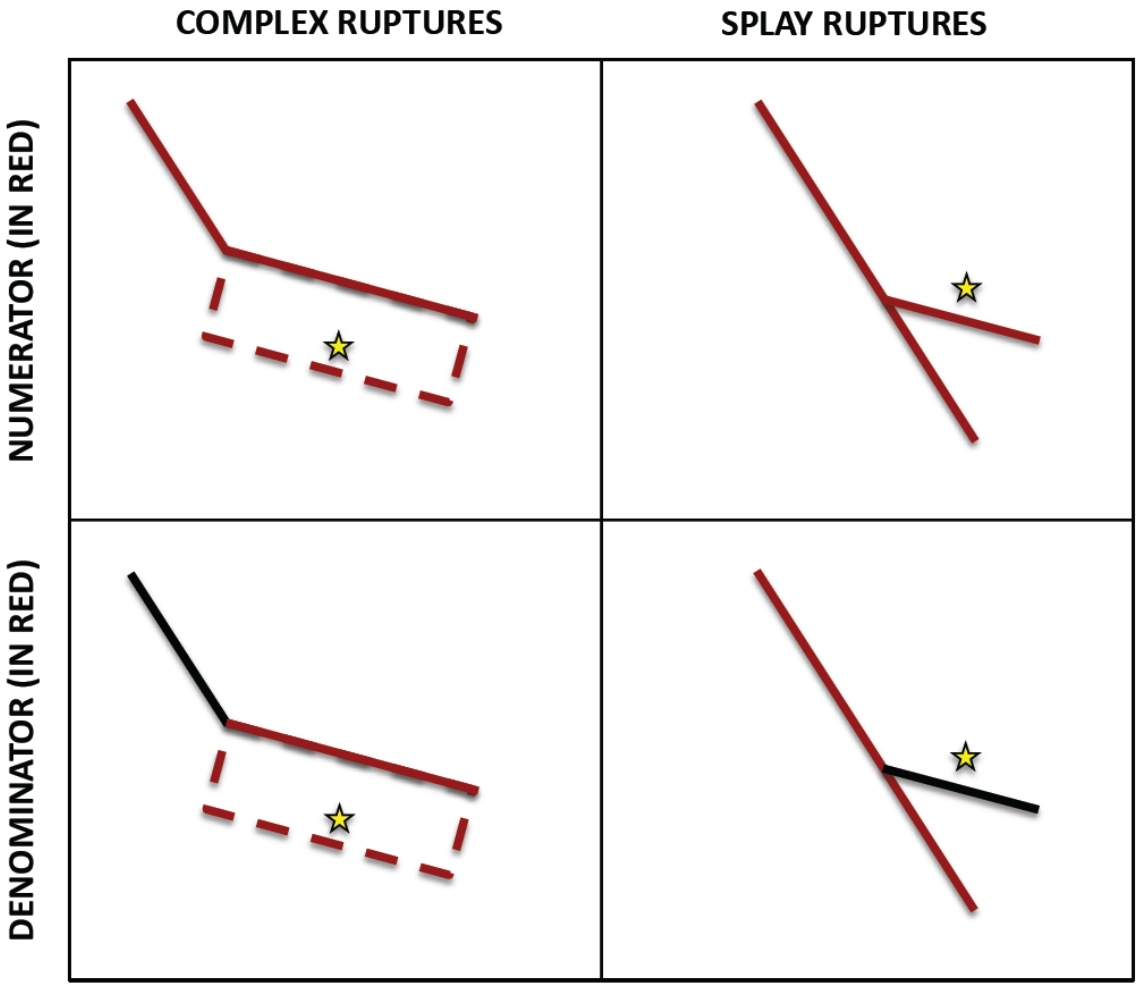



**Figure J.4-1:** Segments used in the factor numerator and denominator for both the complex and splay faulting cases.

### *J.4.1 Alternative Methods*

Four methods were evaluated for computing combined RotD50 spectra from the GMPEs, with the preference given to the method that yields ground-motion factors from GMPEs that resemble those from simulations. The four methods for computing GMPE ground motions include:

METHOD 1: Square Root of the Sum of the Squares (SRSS) of Multiple Fault Segments

METHOD 2: Approximate as Single Fault using Fault Parameters Averaged by Area

METHOD 3: Approximate as Single Fault using Fault Parameters Averaged by $1/R^2$

METHOD 4: Approximate as Single Fault using Closest Segment Parameters

#### *J.4.1.1 METHOD 1: SRSS Multiple Fault Segments*

Method 1 takes the approach of computing the SRSS of the resulting RotD50 spectra from each of the individual participating rupture segments. For the complex rupture case, this means that a RotD50 spectrum is computed for each of the single, planar segments that comprise the complex rupture. Similarly, for the splay case, RotD50 spectra were computed separately for the Primary and Secondary faults. In both cases the individual spectra are combined using the SRSS technique:

$$PSA_{SRSS} = \sqrt{\left(PSA_{Fault1}^2 + PSA_{Fault2}^2\right)} \qquad \text{(Eq. J.4.1-1)}$$

where PSA is the pseudo-spectral acceleration. Method 1 is distinct from Methods 2, 3, and 4 in that it is the only method in which the individual rupture segments are treated separately in the GMPEs and then the RotD50 spectra are combined in an additional step. Methods 2, 3, and 4 represent different ways of creating a single representative rupture to use directly in the GMPEs.

#### *J.4.1.2 METHOD 2: Approximate as Single Fault using Fault Parameters Averaged by Area*

The approach of Method 2 is to calculate average fault parameters (rake, dip, and down-dip width) weighted by fault area. The first step in this approach is to compute the full scenario magnitude based on the combined area for each of the participating complex or splay rupture segments. Weighted averages for rake, dip, and down-dip width are then computed based on the area of each of the individual participating rupture segments. The GMPEs use the distance metrics ($R_{RUP}$, $R_{JB}$, and $R_X$) that correspond to the closest point on the rupture plane from the site of interest and the estimated average fault parameters to compute a single response spectrum that represents either the full complex or splay rupture.

#### *J.4.1.3 METHOD 3: Approximate as Single Fault using Fault Parameters Averaged by $1/R^2$*

Method 3 calculates the average fault parameters (rake, dip, and down-dip width) weighted by $1/R^2$. The fault ruptures are discretized and weighted averages for rake, dip, and down-dip width are computed based on inverse-squared distance to the rupture plane ($1/R^2$) in the following way:

$$Dip_{ave} = \frac{\sum\left(Dip_i \times \frac{1}{R_i^2}\right)}{\sum \frac{1}{R_i^2}} \qquad \text{(Eq. J.4.1-2)}$$

where i represents a discrete fault element. Similar weighted averages are used for the rake and the rupture width. The distance metrics ($R_{RUP}$, $R_{JB}$, and $R_X$) are based on the distances for the closest point on the rupture plane from the site of interest. The magnitude is the magnitude for the combined ruptures.

The average fault parameters are then applied to the GMPEs to compute a single response spectrum that represents either the full complex or splay rupture.

#### *J.4.1.4 METHOD 4: Approximate as Single Fault using Closest Segment Parameters*

Method 4 is perhaps the most simple of the four approaches. This method simply uses the full scenario magnitude computed from the combined area of each of the participating complex or splay rupture segments. The fault parameters and the distance metrics are taken from the closest point along the rupture to the site of interest.

### *J.4.2 Model for Complex Ruptures*

The model for complex fault ruptures is based on the analysis of two complex fault scenarios based on the Hosgri-Los Osos system (Figure J.2.2-1; Table J.2.2-1), and on the Shoreline – San Luis Bay system (Figure J.2.2-3; Table J.2.2-3). Further details regarding the scenario design may be found in Section J.2.2.

#### *J.4.2.1 Complex Scenario 1: Hosgri – Los Osos Complex Fault System*

The geometric relationship between the vertical, strike-slip Hosgri and the 50-degree dipping, reverse Los Osos faults is shown in Figure J.2.2-1. Fault parameters for each of the participating fault segments are listed in Table J.2.2-1 for the three Hosgri – Los Osos cases considered: Case 1 (Hosgri **M**7.0), Case 2 (Hosgri **M**7.2), and Case 3 (Hosgri **M**7.4).

Using Case 2 as an example, the computed fault parameters and distance metrics for each of the four methods of computing ground motions using GMPEs is shown in Table J.4.2-1. For each method, the numbers in this table represent the fault parameters that are used to compute each GMPE RotD50 spectrum. The additional step of computing the SRSS of the two individual fault segment RotD50 spectra is required to obtain a single RotD50 spectrum for Method 1.

**Table J.4.2-1:** Computed fault parameters and distance metrics for the Case 2 Complex Scenario 1 (Hosgri-Los Osos, with **M**7.2 on Hosgri segment).

| | $R_{RUP}$ (km) | $R_{JB}$ (km) | $R_X$ (km) | Mag | dip | rake | Down Dip Width (km) |
|---|---|---|---|---|---|---|---|
| **Hosgri Method 1** | 22.8 | 22.8 | 22.8 | 6.93 | 90 | 180 | 22 |
| **Los Osos Method 1** | 7.8 | 0 | 10.2 | 6.87 | 50 | 90 | 22 |
| **Complex Method 2** | 7.8 | 0 | 10.2 | 7.2 | 71.5 | 138.3 | 22 |
| **Complex Method 3** | 7.8 | 0 | 10.2 | 7.2 | 55 | 101.2 | 22 |
| **Complex Method 4** | 7.8 | 0 | 10.2 | 7.2 | 50 | 90 | 22 |

Figure J.4.2-1 provides a comparison between the BBP RotD50 spectra for the three ground-motion simulation methods (GP, SDSU, and EXSIM) and the RotD50 spectra obtained from the GMPEs using each of the four different methods for assigning predictor variables. This comparison shows that the GP and SDSU simulation methods produce ground motions that are slightly higher than the GMPEs at low frequency (≤ 1Hz). The EXSIM approach, on the other hand, produces ground motions that are generally consistent with the GMPEs at low frequency. At frequencies above 1Hz, the SDSU simulation method produces the highest ground motions of the three simulation techniques. Based on the period and GMPE method it is compared against, the SDSU method either produces the highest ground motions or is consistent with the upper bound of the GMPEs. At high frequencies, the GP and EXSIM simulations generally produce ground motions that are consistent with the upper bound from the GMPEs for each GMPE method.

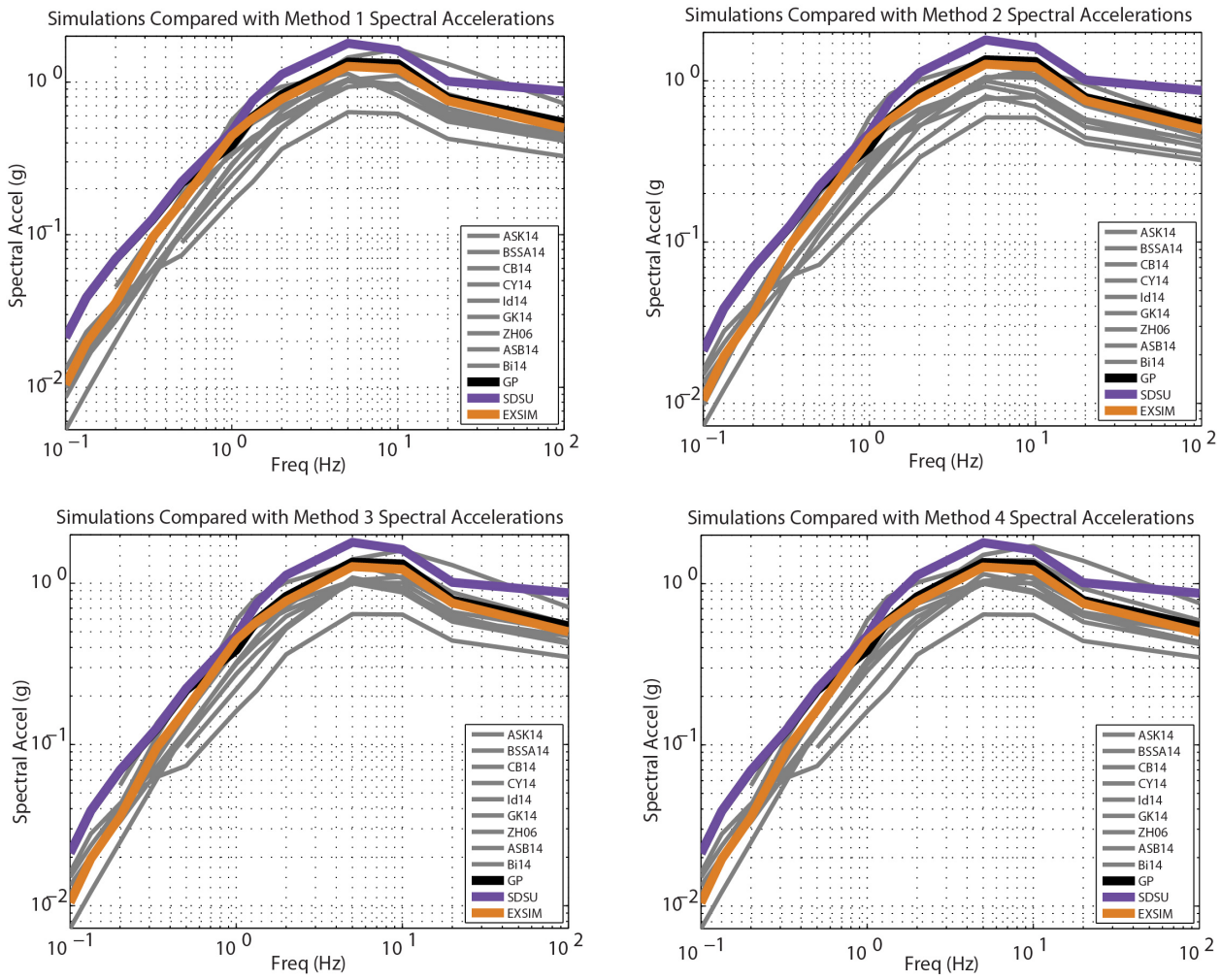



**Figure J.4.2-1** Comparison of the RotD50 spectra for the three simulation methods: GP (black), SDSU (violet), and EXSIM (orange) with the various methods of computing RotD50 spectra from the GMPEs (grey).

Ground-motion factors computed from the three simulation methods are shown in Figure J.4.2-2. In Figure J.4.2-3 the ground-motion factors from simulations (grey lines) are compared to those from the GMPEs.

Comparing the ground-motion factors from simulations (grey lines) with those from GMPEs (colored dots) in Figure J.4.2-3 clearly shows that the ground-motion factors obtained using the SRSS approach (Method 1) best follow the amplitude and overall trend of the factors computed from the three simulation methods over all spectral periods.

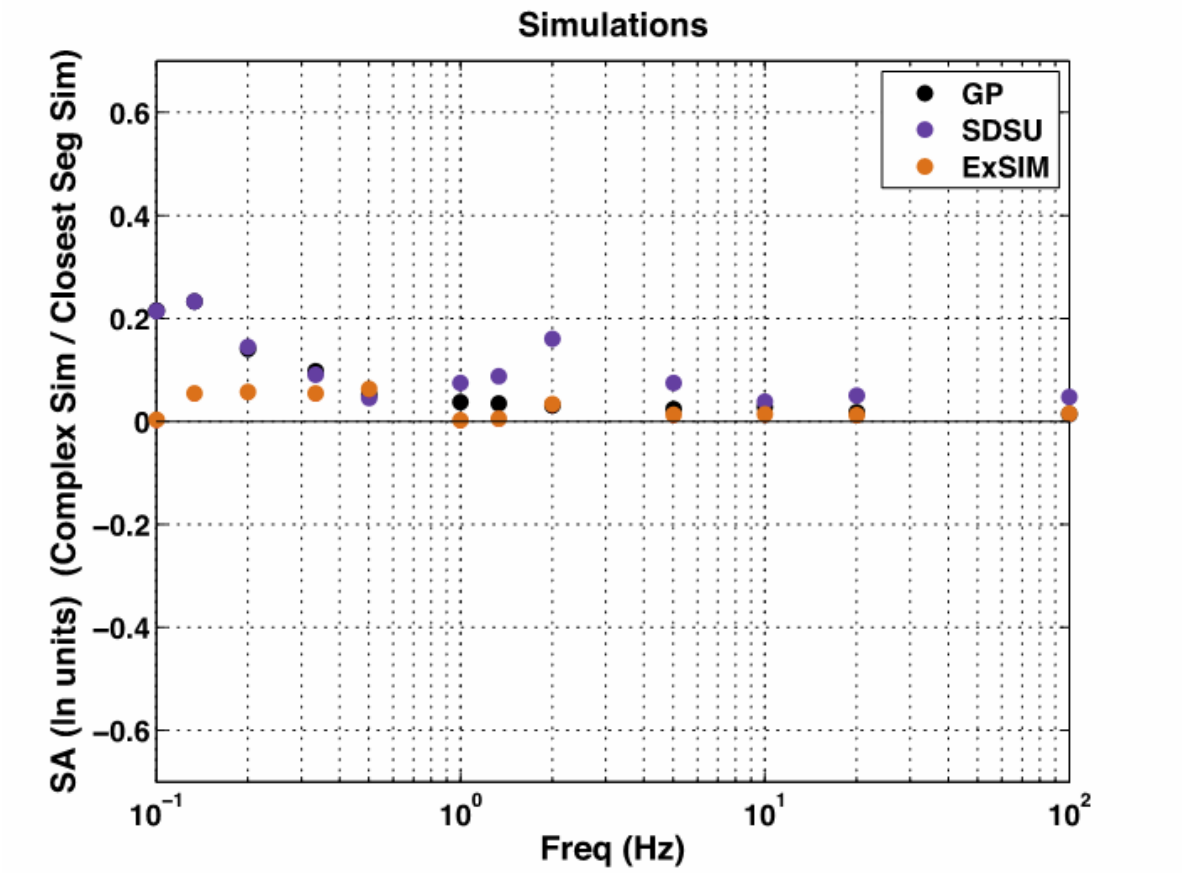



**Figure J.4.2-2:** Ground-Motion Factors for the three simulation methods: GP (black), SDSU (violet), and EXSIM (orange).

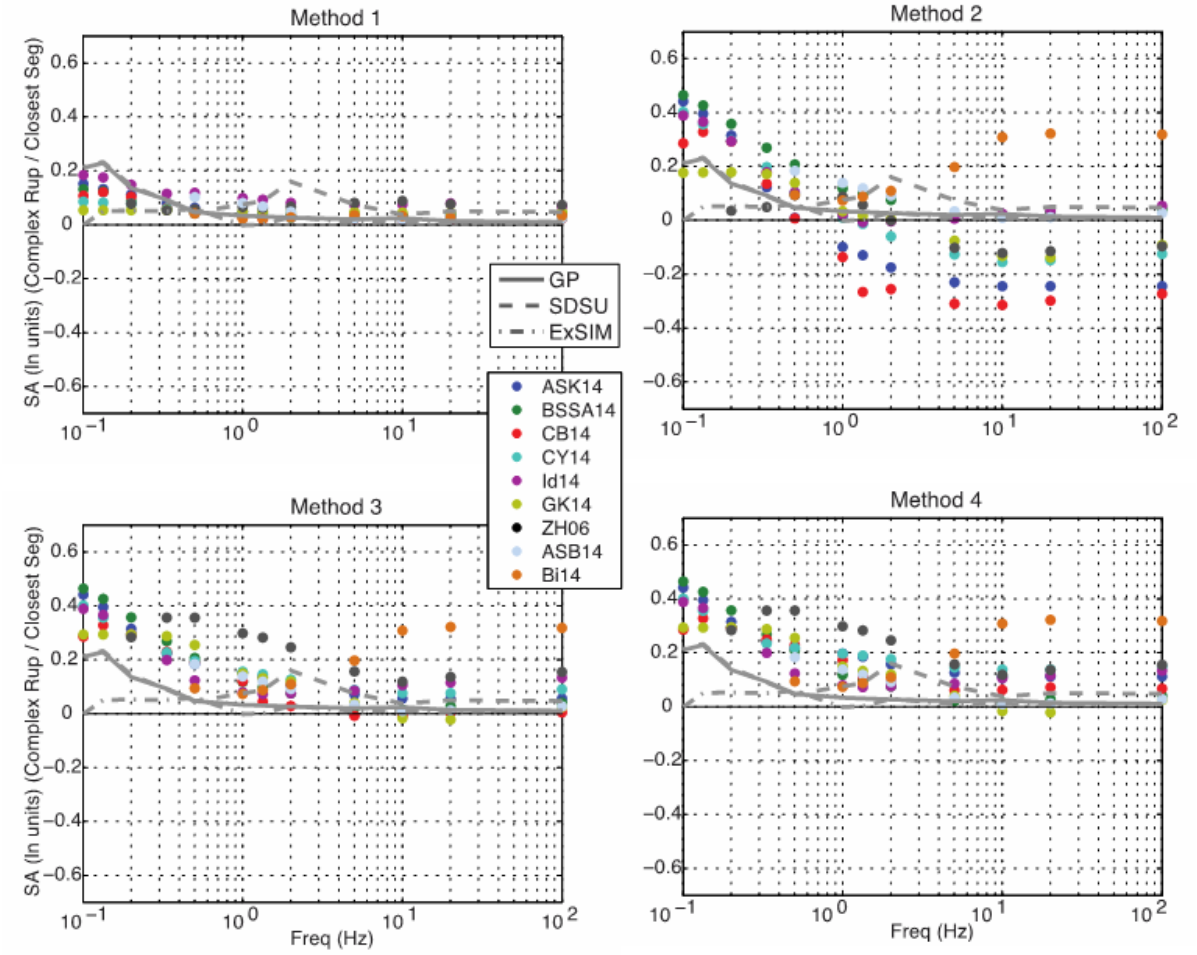



**Figure J.4.2-3:** Ground-Motion Factors for the three simulation methods (grey lines) compared with factors from the various GMPE approaches (colored dots).

The SRSS approach (Method 1) yields small factors because DCPP is located on the hanging wall of the Los Osos fault and far from the Hosgri. As a result, most of the ground-motion contribution at DCPP comes from the Los Osos fault, and the ground motions in the denominator (the Los Osos alone) are very similar to the ground motions in the numerator (SRSS of the Los Osos and the Hosgri).

Method 2 produces the lowest factors at frequencies above about 1 Hz because averaging fault parameters by area results in a steeper dip than that for the Los Osos and a reverse-oblique mechanism because the relative area of the **M**7.2 Hosgri fault is large. Both of these factors tend to decrease the ground motions in the numerator relative to the denominator. The large spread in the ground-motion factors from GMPEs for Method 2 shows the differences in the treatment of the hanging wall term between the GMPEs.

Methods 3 and 4 are very similar. Averaging the fault parameters by closest distance (Method 3) and taking the fault parameters of the nearest segment (Method 4) both result in average fault parameters that are more similar to the parameters of the Los Osos fault. The main reason for factors that are higher for Methods 3 and 4 than for Method 1 is that the magnitude computed from the average fault parameters is based on the total area of the complex rupture system in Methods 3 and 4. In Method 1, the magnitudes used in the GMPEs are computed separately based on the areas of the individual fault segments, in this case the Hosgri and Los Osos fault. As a result, if Method 1 is followed, two response spectra are computed using lower magnitude parameters than are obtained by Methods 2, 3, and 4. These response spectra are then combined to produce a RotD50 spectra that is lower than

### *J.4.2.2 Complex Scenario 2: Shoreline – San Luis Bay Complex Fault System*

The geometric relationship between the vertical, strike-slip Shoreline and the 70-degree dipping, reverse San Luis Bay faults is shown in Figure J.2.2-2. Fault parameters for each of the participating fault segments are listed in Table J.2.2-2 for the three Shoreline – San Luis Bay cases considered: Case 1 (Shoreline **M**7.0), Case 2 (Shoreline **M**7.2), and Case 3 (Shoreline **M**7.4).

Using Case 2 as an example, the computed fault parameters and distance metrics for each of the four methods to compute ground-motion factors from GMPEs is shown in Table J.4.2-2. For each method, the numbers in this table represent the fault parameters that are used to compute each GMPE RotD50 spectrum. The additional step of computing the SRSS of the two individual fault segment RotD50 spectra is required to obtain a single RotD50 spectrum for Method 1.

**Table J.4.2-2:** Computed fault parameters and distance metrics for the Case 2 Complex Scenario 2 (based on the Shoreline-San Luis Bay complex scenarios, with **M**7.2 on the Shoreline segment).

| | $R_{RUP}$ (km) | $R_{JB}$ (km) | $R_X$ (km) | Mag | dip | rake | Down Dip Width (km) |
|---|---|---|---|---|---|---|---|
| **Shoreline Method 1** | 0.7 | 0.7 | 0.7 | 7.15 | 90 | 180 | 22 |
| **San Luis Bay Method1** | 6.4 | 5.5 | 6.5 | 6.23 | 70 | 90 | 22 |
| **Complex Method 2** | 0.7 | 0.7 | 0.7 | 7.2 | 87.8 | 170.3 | 22 |
| **Complex Method 3** | 0.7 | 0.7 | 0.7 | 7.2 | 89.6 | 178.2 | 22 |
| **Complex Method 4** | 0.7 | 0.7 | 0.7 | 7.2 | 90 | 180 | 22 |

Figure J.4.2-4 provides a comparison between the BBP RotD50 spectra from the three simulation methods (GP, SDSU, and EXSIM) and the RotD50 spectra obtained from using the different methodologies to compute predictor variables to use in the GMPEs. This comparison shows that the GP and SDSU simulation methods produce ground motions that are slightly higher than the GMPEs at low frequency (≤ 1Hz). The EXSIM approach, on the other hand, produces ground motions that are generally consistent with the GMPEs at low frequency. At frequencies above 1Hz, the EXSIM produces the highest ground motions of the three simulation techniques. With the exception of Method 1 at T = 0.05 sec, the EXSIM ground motions are higher than the range of the GMPEs. The GP and SDSU methods produce ground motions that are generally consistent with the upper bound of the GMPE range at high frequency and they show fairly good agreement with each other.

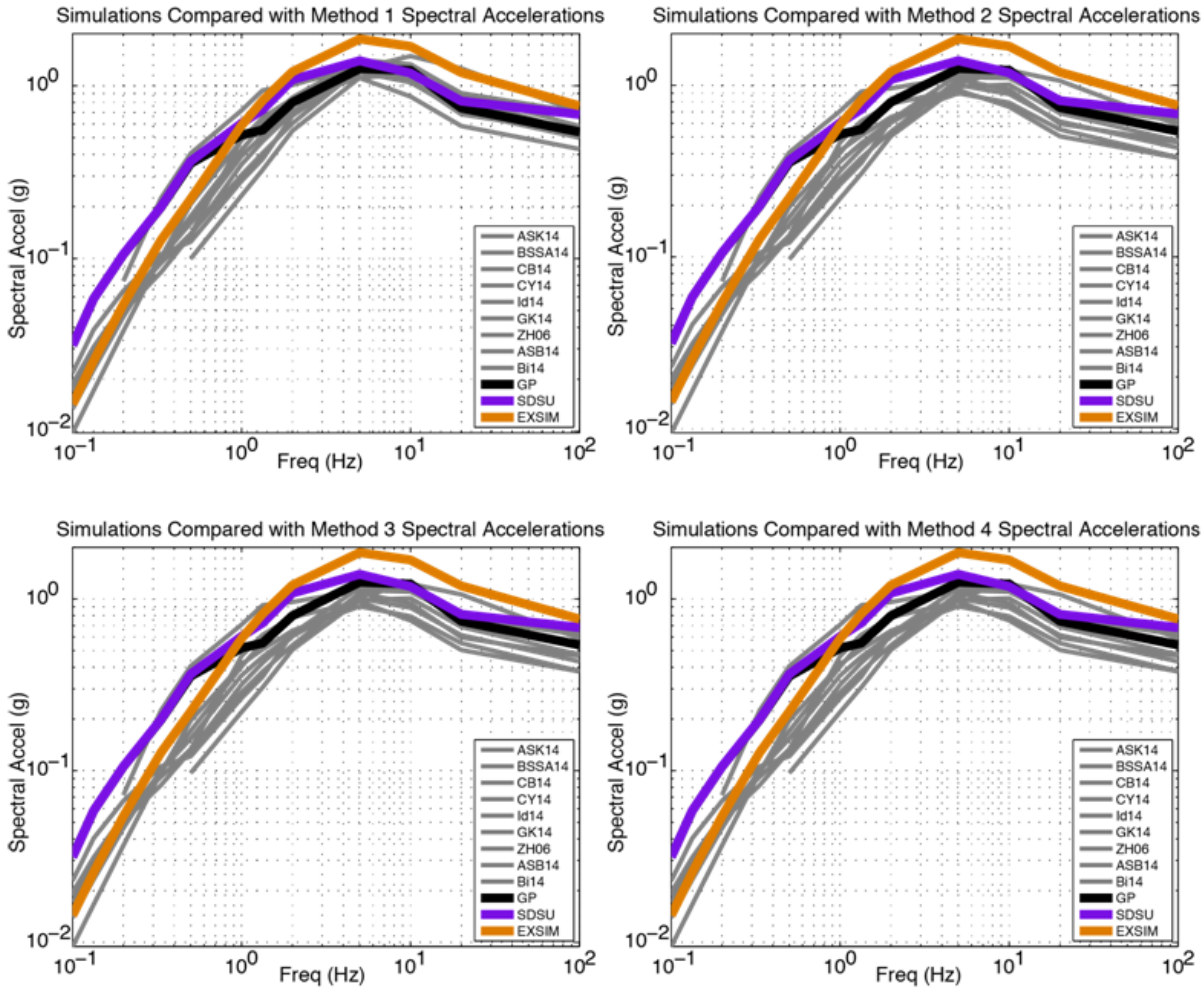



**Figure J.4.2-4:** Comparison of the RotD50 spectra for the three simulation methods: GP (black), SDSU (violet), and EXSIM (orange) with the various methods of computing RotD50 spectra from the GMPEs (grey).

Ground-motion factors computed from the three simulation methods are shown in Figure J.4.2-5. Figure J.4.2-6 compares the ground-motion factors from simulations (grey lines) with those from the GMPEs.

Comparing the ground-motion factors from simulations (grey lines) with those from the GMPEs (colored dots) in Figure J.4.2-6 clearly shows that the ground-motion factors obtained using the SRSS approach (Method 1) best follow the amplitude and overall trend over all spectral periods.

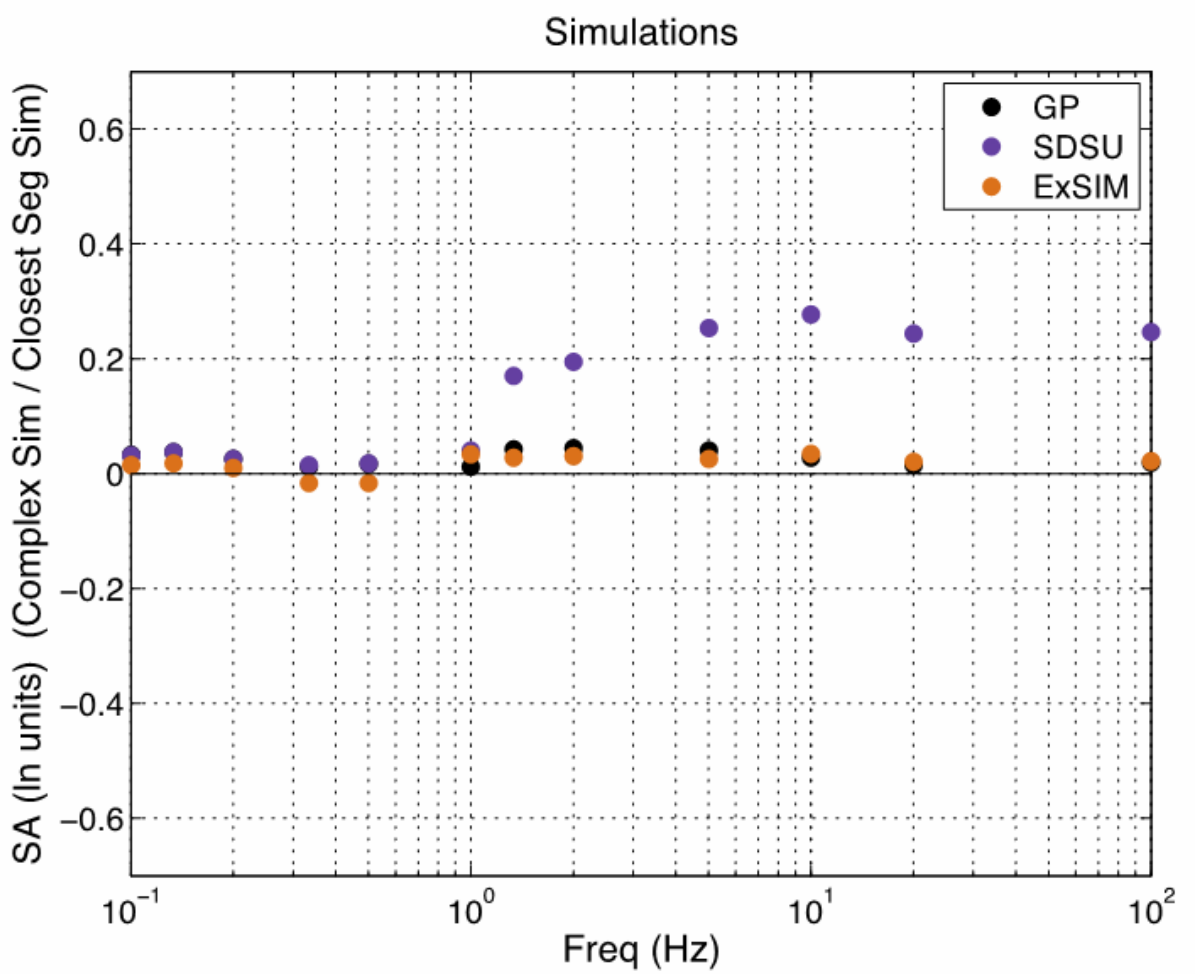



**Figure J.4.2-5:** Ground-Motion Factors for the Three Simulation Methods: GP (black), SDSU (violet), and EXSIM (orange).

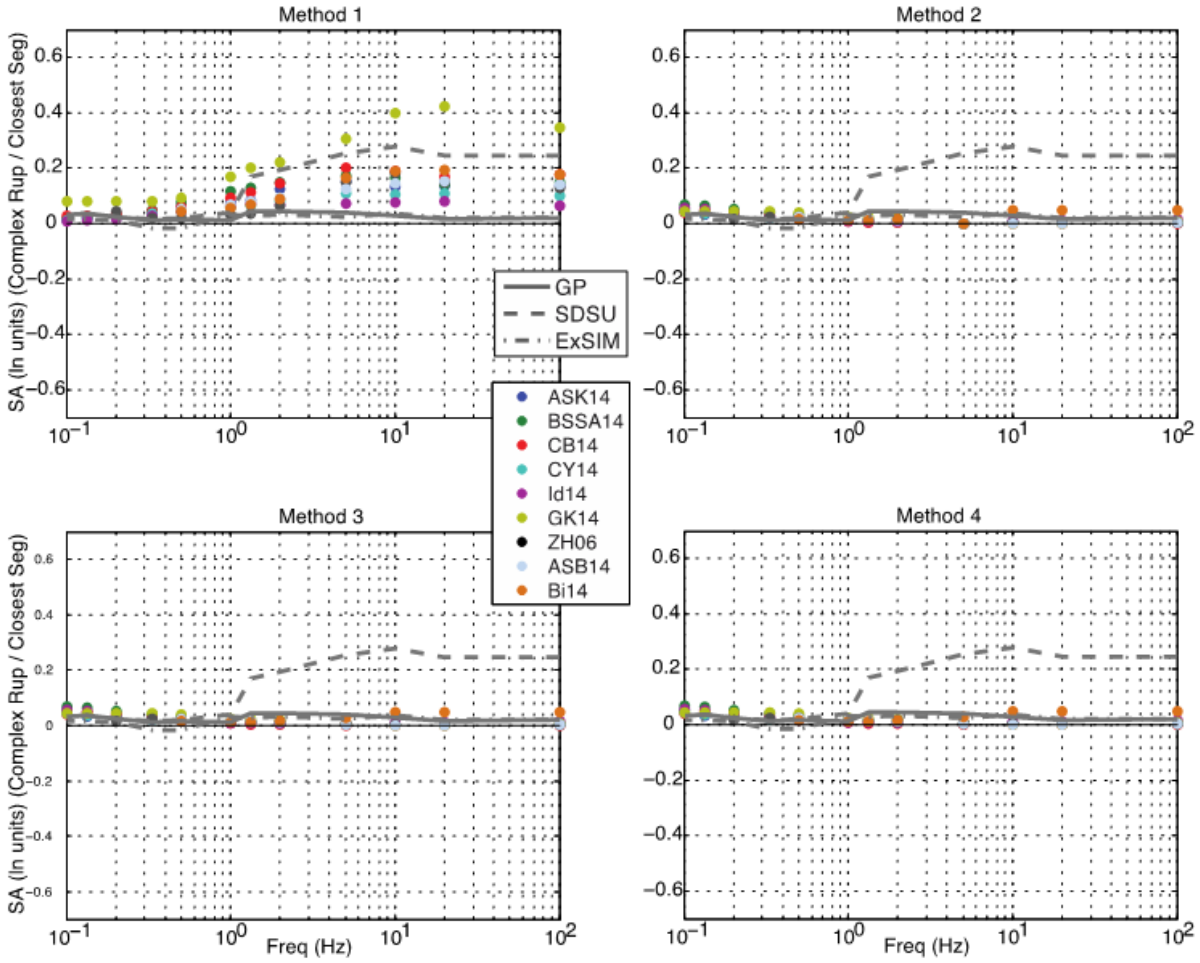



**Figure J.4.2-6:** Ground-Motion Factors for the Three Simulation Methods (grey lines) compared with factors from the various GMPE approaches (colored dots).

The SRSS approach (Method 1) yields the largest factors because DCPP is located along the vertical, strike-slip Shoreline fault but near to the rupture plane of the reverse, dipping San Luis Bay Fault. As a result, the ground-motion contribution at DCPP comes both from the Shoreline fault and the Los Osos fault, and the ground motions in the denominator (the Shoreline Fault) are smaller than the ground motions in the numerator (SRSS of the Shoreline and San Luis Bay faults).

Methods 2, 3, and 4 all produce similar results; very small ground-motion factors over all frequencies. The reason is that both the parameter averaging techniques (Methods 2 and 3) and the approach of taking parameters from the nearest segment (Method 4) result in a vertical to near vertical, strike-slip fault. Thus, each of Methods 2, 3, and 4 misses the important contribution of the small, but close San Luis Bay fault.

The TI Team used the SRSS approach (Method 1) to compute the ground motions for complex faults at the DCPP site. This decision is based on the observation that the GMPE predictor variables computed using Method 1 result in ground-motion factors from GMPEs that follow the same trend observed in the ground-motion factors from simulations for both the Hosgri – Los Osos and the Shoreline – San Luis Bay cases. For the Hosgri – Los Osos scenario, the ground-motion factors from both the simulations and GMPEs are relatively high and steadily decreasing between 0.1 and 1 Hz. Between 1 and 100 Hz, the factors are lower and essentially stable. For this scenario, Methods 2, 3, and 4 lead to more variability in the ground-motion factors from GMPEs than in those estimated from simulations. Also, due to the way the predictor variables are computed in Method 2, the resulting ground-motions factors for this scenario are negative at high frequency for some of the GMPEs. For the Shoreline – San Luis Bay scenario, the ground-motion factors for both the GMPEs and simulations have relatively small values that remain essentially constant from 0.1 to 1 Hz. Above 1 Hz, both sets of ground-motion factors show a definite increase that appears to be somewhat constant at higher frequency. For this case, observations for Methods 2, 3 and 4 show the opposite trend.

### *J.4.3 Model for Splay Ruptures*

The model for splay fault ruptures is based on the analysis of two splay fault scenarios: The Hosgri-Shoreline system (Figure J.2.3-2; Table J.2.3-1), and the Los Osos – San Luis Bay system (Figure J.2.3-3; Table J.2.3-2). Further details regarding the scenario design may be found in Sections J.2.3.

#### *J.4.3.1 Splay Scenario 1: Hosgri – Shoreline Splay Fault System*

The geometric relationship between the vertical, strike-slip Hosgri and Shoreline faults is shown in Figure J.2.3-2. Fault parameters for each of the participating fault segments are listed in Table J.2.3-1 for the three Hosgri – Shoreline cases considered: Case 1 (Hosgri **M**7.0), Case 2 (Hosgri **M**7.2), and Case 3 (Hosgri **M**7.4).

Using Case 3 as an example, the computed fault parameters and distance metrics for each of the four methodologies of computing ground-motion factors from GMPEs is shown in Table J.4.3-1. For each method, the numbers in this table represent the fault parameters that are used to compute each GMPE RotD50 spectrum. The additional step of computing the SRSS of the two individual fault segment RotD50 spectra is required to obtain a single RotD50 spectrum for Method 1.

**Table J.4.3-1:** Computed fault parameters and distance metrics for the Case 3 Splay Scenario 1 (based on the Hosgri-Shoreline splay scenarios, with **M**7.4 on the Hosgri segment).

| | $R_{RUP}$ (km) | $R_{JB}$ (km) | $R_X$ (km) | Mag | dip | rake | Down Dip Width (km) |
|---|---|---|---|---|---|---|---|
| **Hosgri: Method 1** | 5.10 | 5.10 | 5.10 | 7.40 | 90 | 180 | 22.00 |
| **Shoreline: Method 1** | 0.66 | 0.66 | 0.66 | 6.43 | 90 | 180 | 11.93 |
| **Splay Method 2** | 0.66 | 0.66 | 0.66 | 7.44 | 90 | 180 | 20.35 |
| **Splay Method 3** | 0.66 | 0.66 | 0.66 | 7.44 | 90 | 180 | 13.06 |
| **Splay Method 4** | 0.66 | 0.66 | 0.66 | 7.44 | 90 | 180 | 11.93 |

Figure J.4.3-1 provides a comparison between the BBP RotD50 spectra for the three methods (GP, SDSU, and EXSIM) and the RotD50 spectra obtained from the GMPEs. This comparison shows that the GP and SDSU simulations are generally higher than the GMPEs at low frequency, but roughly in agreement with the GMPEs at high frequency (Figure J.4.3-1). EXSIM, on the other hand is in agreement with the GMPEs at low frequency and higher than both the GMPEs and the other simulations at high frequency (Figure J.4.3-1). In fact, peak amplitudes for EXSIM are (in some cases) as much as a factor of two higher than peak amplitudes for GP and SDSU. This result is expected by Dr. Gail Atkinson because the GMPEs have stronger saturation than the EXSIM model at very close distance. Overall, Method 1 RotD50 spectra provide the best agreement with the simulation results because the range obtained from the GMPE spectra utilizing Method 1 to generate the predictor variables (**M**, R, dip, rake, and down-dip width) comes the closest to enveloping the simulation RotD50 spectra. As will also be shown later in this Section, trends in ground-motion factors from GMPEs computed using Method 1 follow the same trends as those computed from the simulations.

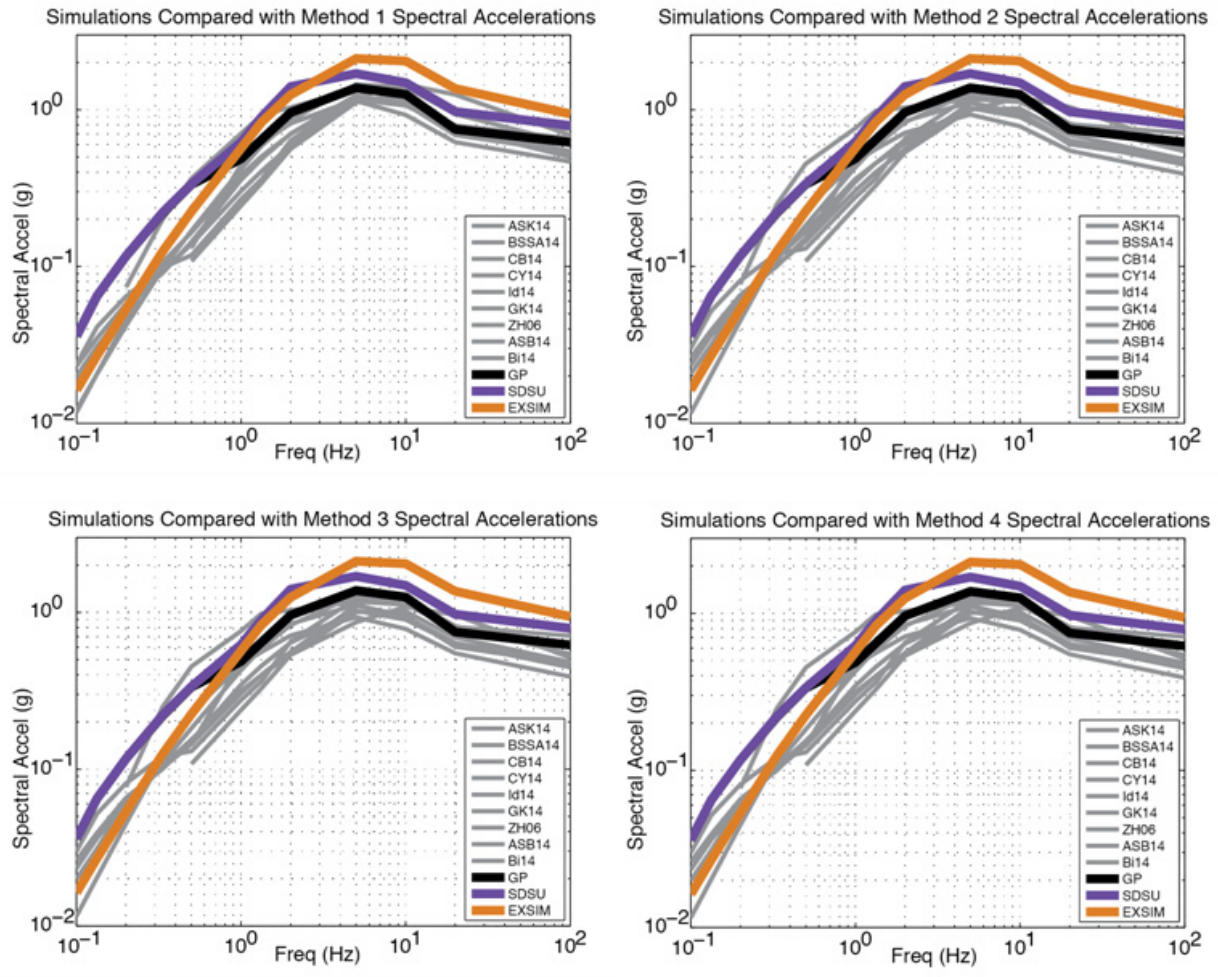



**Figure J.4.3-1**: Comparison of the RotD50 spectra for the three simulation methods: GP (black), SDSU (violet), and EXSIM (orange) with the various methods of computing RotD50 spectra from the GMPEs (grey).

Simulation factors are shown in Figure J.4.3-2. The large factors for the EXSIM approach at high frequency result, in part, from the fact that EXSIM does not saturate at close distances. EXSIM also predicts lower ground motions for the Primary ruptures and higher ground motions for the secondary ruptures at high frequencies. Both of these trends contribute to the large splay rupture factors for the EXSIM method at high frequency.

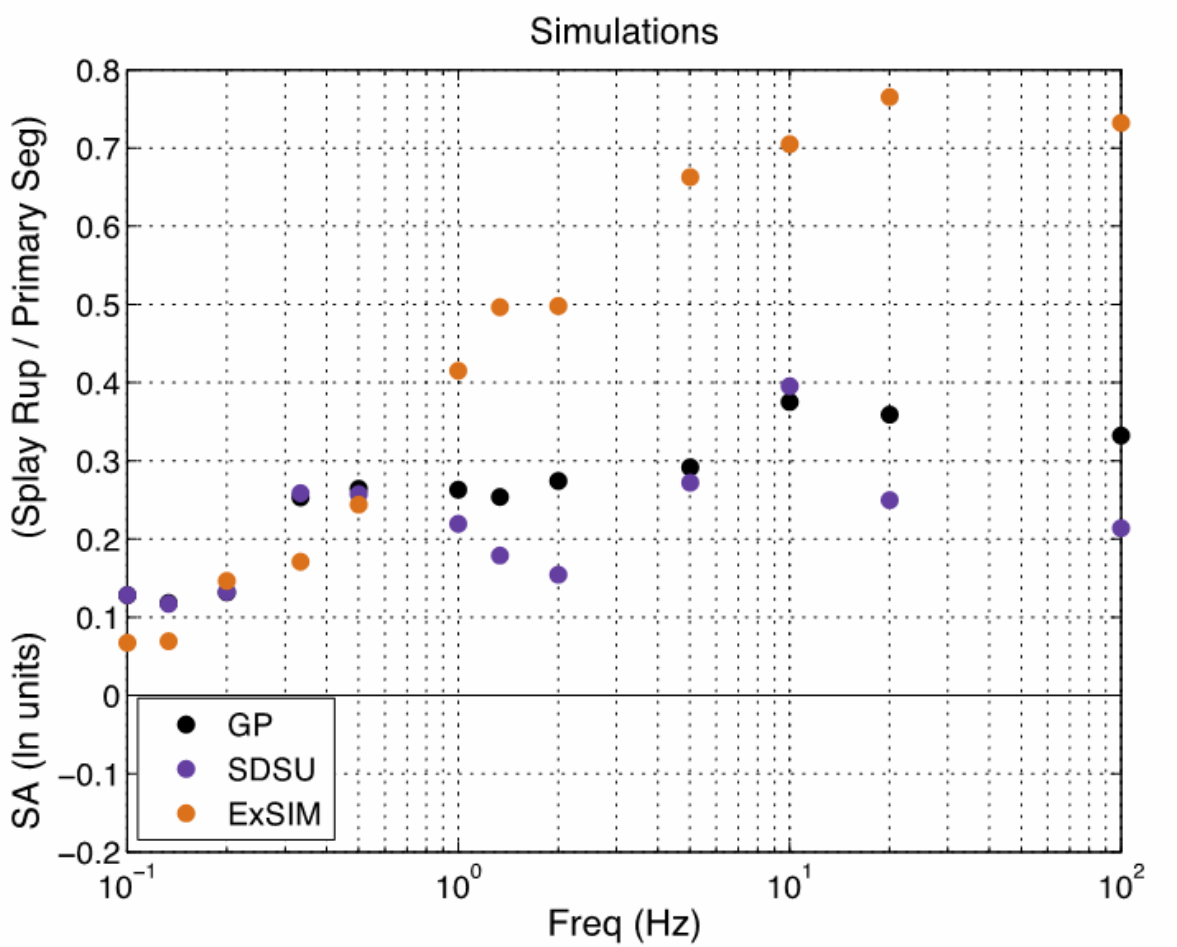



**Figure J.4.3-2:** Ground-Motion Factors for the Three Simulation Methods: GP (black), SDSU (violet), and EXSIM (orange).

Comparing the ground-motion factors from simulations (grey lines) with those from GMPEs (colored dots) in Figure J.4.3-3 reveals that at low frequency (≤ 1Hz), splay rupture ground-motion factors obtained using the SRSS approach (Method 1) are most consistent. At higher frequencies (≥ 1Hz), splay rupture ground-motion factors from GMPEs obtained using the SRSS approach (Method 1) generally follow the amplitude and overall trend of the ground-motion factors computed from GP and SDSU simulations (Figure J.4.3-3).

Ground-motion factors from GMPEs computed with Methods 2, 3, and 4 are very similar because the dip for both the primary and secondary faults is 90 degrees, and the rake is 180 degrees. The only difference in fault parameters between these two segments is the rupture width. Thus, only the rupture width varies between the methods when determining average fault parameters to use in the GMPEs for this case.

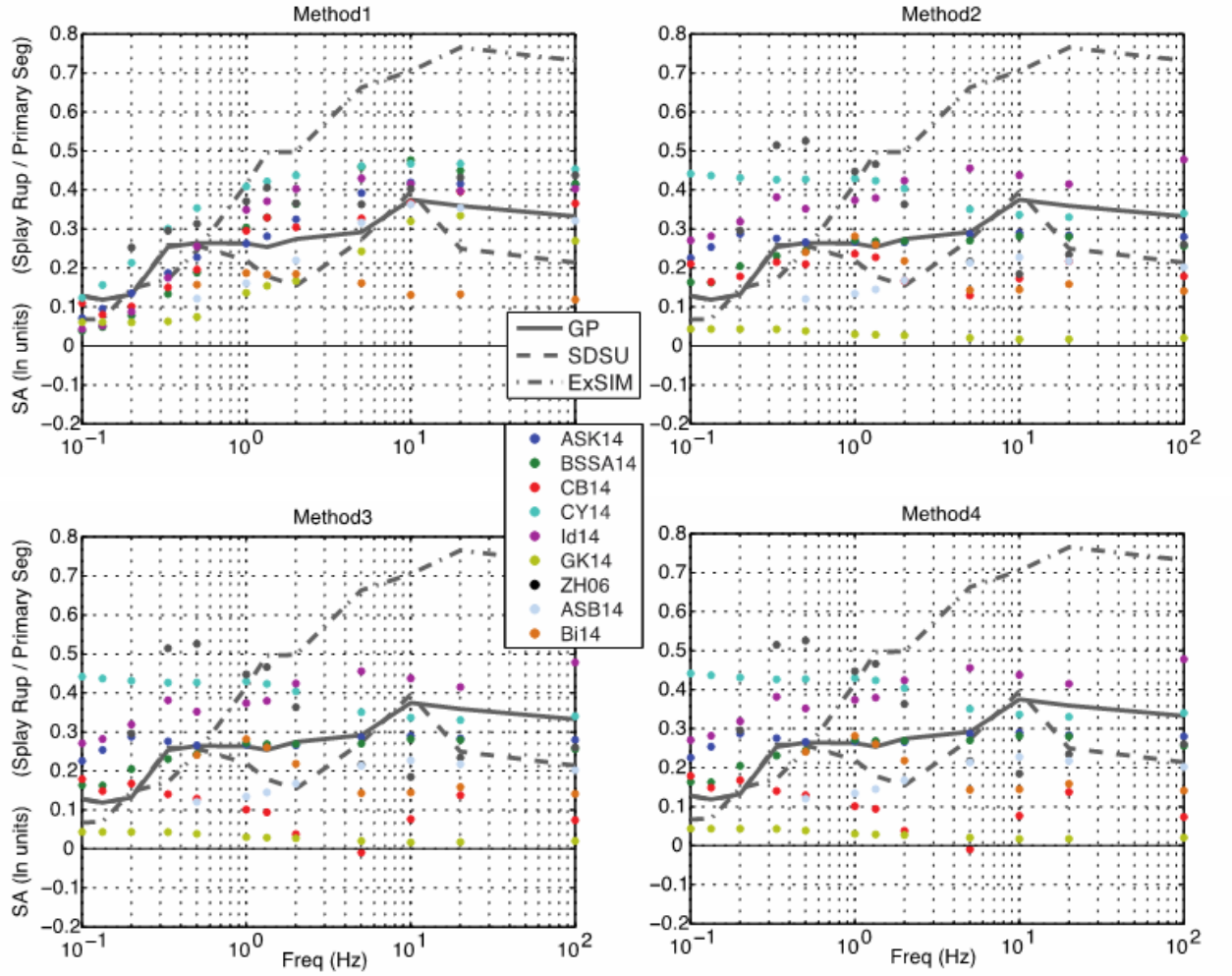



**Figure J.4.3-3:** Ground-Motion Factors for the Three Simulation Methods (grey lines) compared with factors from the various GMPE approaches (colored dots).

### *J.4.3.2 Splay Scenario 2: Los Osos – San Luis Bay Splay Fault System*

The geometric relationship between the 60 degree dipping, reverse Los Osos and the 70-degree dipping, reverse San Luis Bay faults is shown in Figure J.2.3-3. Fault parameters for each of the participating fault segments are listed in Table J.4.3-2 for the three Los Osos – San Luis Bay cases considered: Case 1 (Los Osos **M**7.0), Case 2 (Los Osos **M**7.2), and Case 3 (Los Osos **M**7.4).

Using Case 3 as an example, the computed fault parameters and distance metrics for each of the four GMPE methodologies is shown in Table J.4.2-2. For each method, the numbers in this table represent the fault parameters that are used to compute each GMPE RotD50 spectrum. The additional step of

computing the SRSS of the two individual fault segment RotD50 spectra is required to obtain a single RotD50 spectrum for Method 1.

**Table J.4.3-2**: Computed fault parameters and distance metrics for the Case 3 Splay Scenario 2 (based on the Los Osos-San Luis Bay splay scenarios, with **M**7.4 on the Los Osos segment).

| | $R_{RUP}$ (km) | $R_{JB}$ (km) | $R_X$ (km) | Mag | dip | rake | Down Dip Width (km) |
|---|---|---|---|---|---|---|---|
| **Los Osos: Method 1** | 8.57 | 0.0 | 9.90 | 7.40 | 60.0 | 90 | 32.0 |
| **San Luis Bay: Method 1** | 1.00 | 0.0 | 1.07 | 6.40 | 70.0 | 90 | 12.7 |
| **Splay Method 2** | 1.00 | 0.0 | 1.07 | 7.44 | 62.00 | 90 | 28.14 |
| **Splay Method 3** | 1.00 | 0.0 | 1.07 | 7.44 | 69.20 | 90 | 14.24 |
| **Splay Method 4** | 1.00 | 0.0 | 1.07 | 7.44 | 70.0 | 90 | 12.7 |

Figure J.4.3-4 provides a comparison between the BBP RotD50 spectra for the three methods (GP, SDSU, and EXSIM) and the RotD50 spectra obtained from the GMPEs. This comparison shows that the GP and SDSU simulations are generally higher than the EXSIM simulation and the GMPEs at low frequency (≤ 1Hz). At higher frequency (≥ 10Hz) all simulation methods appear to be in agreement with the GMPEs and the SDSU and EXSIM simulation methods show good agreement with each other. Between 1Hz and 10Hz the simulation ground motions (especially EXSIM and SDSU) appear to be higher than the GMPEs for many of the methods. Overall, Method 1 RotD50 spectra provide the best agreement with the simulation results.

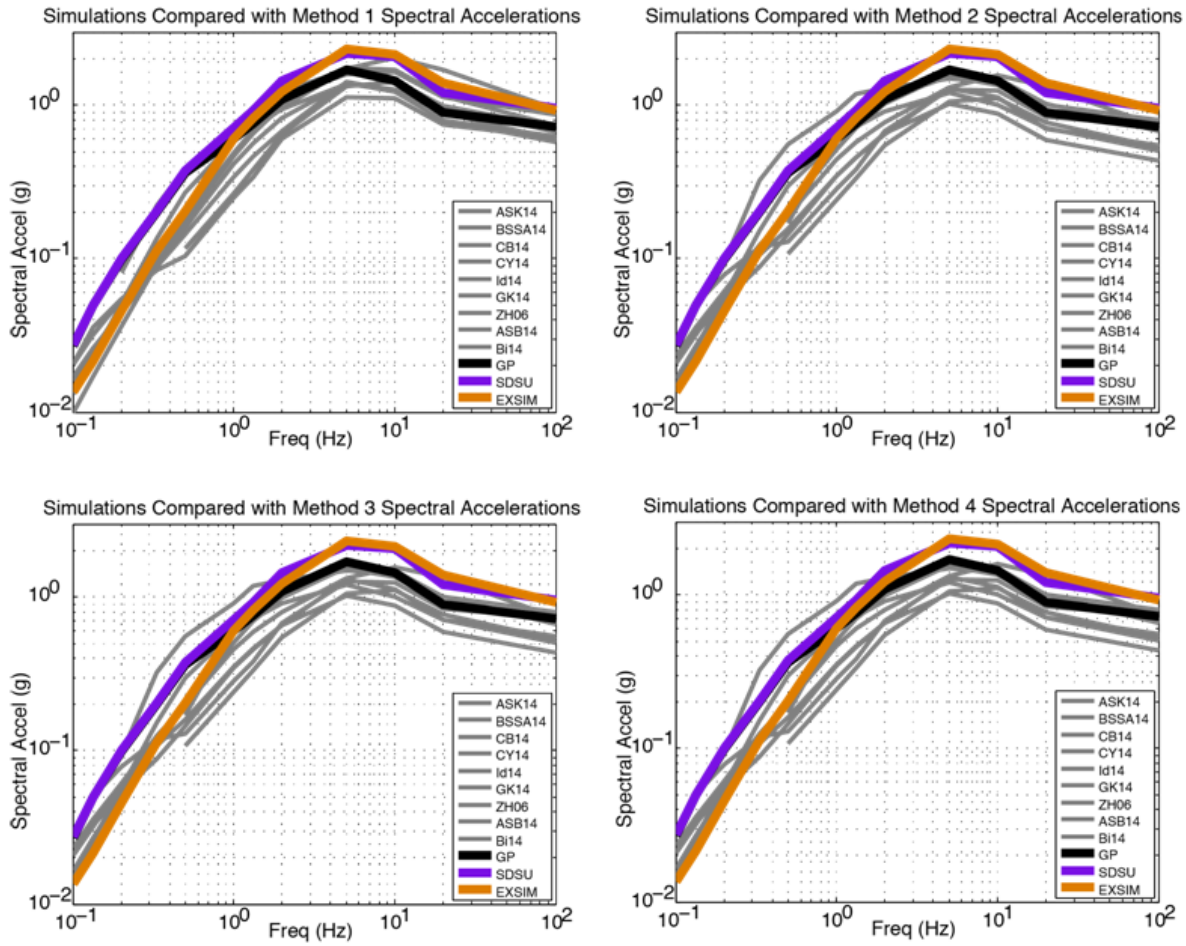



**Figure J.4.3-4:** Comparison of the RotD50 spectra for the three simulation methods: GP (black), SDSU (violet), and EXSIM (orange) with the various methods of computing RotD50 spectra from the GMPEs (grey).

Ground-motion factors computed from the three simulation methods are shown in Figure J.4.3-5. The large factors for EXSIM at high frequency result, in part, from the fact that EXSIM does not saturate at close distances. EXSIM also predicts lower ground motions for the Primary ruptures and higher ground motions for the secondary ruptures at high frequencies. Both of these trends contribute to the large splay rupture factors for the EXSIM method at high frequency.

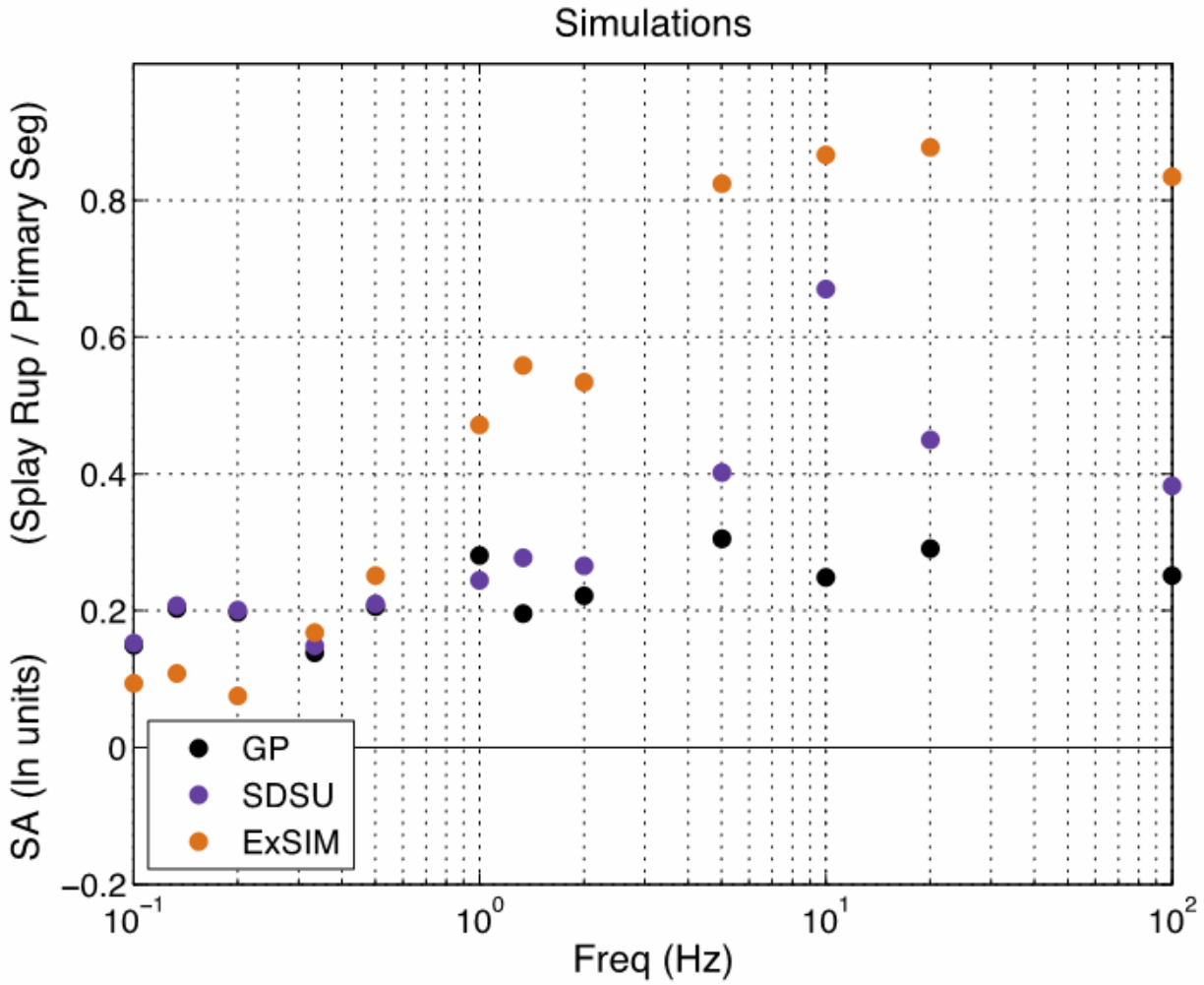



**Figure J.4.3-5:** Ground-Motion Factors for the Three Simulation Methods: GP (black), SDSU (violet), and $_{EXSIM}$ (orange).

Comparing the ground-motion factors from simulations (grey lines) with those from GMPEs (colored dots) in Figure J.4.3-6 reveals that at low frequency (≤ 1Hz), splay rupture ground-motion factors obtained using the SRSS approach (Method 1) generally follows the amplitude and overall trend of the ground-motion factors computed from the three simulation methods (Figure J.4.3-6). At higher frequencies (≥ 1Hz), splay rupture ground-motion factors obtained using the SRSS approach (Method 1) generally follow the amplitude and overall trend of the ground-motion factors computed from GP and SDSU simulations (with the exception of the peak at 10 Hz) (Figure J.4.3-6).

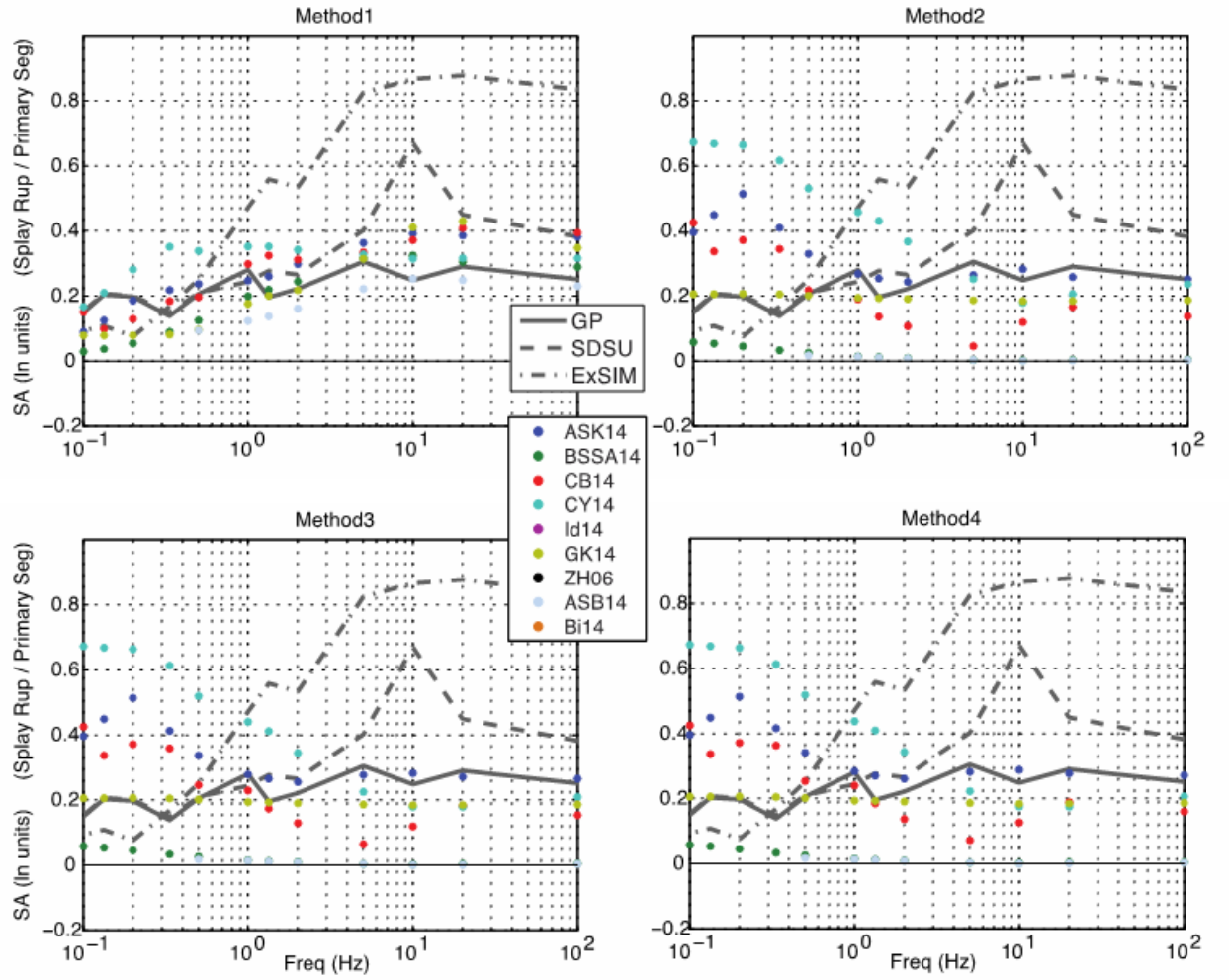



**Figure J.4.3-6:** Ground-Motion Factors for the Three Simulation Methods (grey lines) compared with factors from the various GMPE approaches (colored dots).

The TI Team used the SRSS approach (Method 1) to compute the ground motions for splay faults at the DCPP site. This decision is based on the observation that the GMPE predictor variables computed using Method 1 result in ground-motion factors from GMPEs that follow the same trend observed in the ground-motion factors from simulations for both the Hosgri – Shoreline and the Los Osos – San Luis Bay cases. For the Hosgri – Shoreline scenario, the ground-motion factors from both the GMPEs and simulations begin low and steadily increase between 0.1 and 1 Hz. Between 1 and 100 Hz, the ground-motion factors are higher and essentially stable. For this scenario, Methods 2, 3, and 4 result in significant variability in the ground-motion factors between each of the GMPEs. Also, when considered separately, the GMPEs do not all display the same trends in their respective ground-motion factors. For the Los Osos – San Luis Bay scenario, the ground-motion factors for both the GMPEs and the simulations

have relatively small values that increase steadily from 0.1 to 10 Hz. Above 10 Hz, the ground-motion factors for both GMPEs and simulations appear rather constant. For this case, comparisons for Methods 2, 3 and 4 show the opposite trend.

## J.5 Simulations for Hanging-Wall Scaling

### *J.5.1 Previous simulations used to constraint HW scaling*

Donahue and Abrahamson (2014) used broadband finite-source simulations to develop a hanging-wall functional form. This form was then applied to implement hanging-wall terms in the ASK14 (Abrahamson et al., 2014) GMPE. Two other NGA-West2 GMPE relationships (CY14: Chiou and Youngs, 2014; CB14: Campbell and Bozorgnia, 2014) utilized hanging-wall terms informed from broadband simulations. These studies utilized simulations for **M** ≥ 6.0 and the limited data to constrain the hanging-wall terms. ASK14 and CB14 both applied magnitude tapers in which the hanging-wall terms tapers to zero from **M** 6.5 to 5.5, and for **M** ≤ 5.5 the hanging-wall term is zero. The CY14 formulation does not have an explicit magnitude taper.

### *J.5.2 Comparison between Finite Fault Simulations and Hanging-Wall scaling from GMPEs*

For this project it is necessary to apply hanging-wall terms to lower magnitudes, and therefore a series of simulations were performed to generate ground-motion data for reverse events for a suite of magnitudes (5.5, 6.0 and 6.5), a suite of depth to the top of the fault ($Z_{TOR}$) (12.0 7.0 and 2.5 km), and for a suite of fault dip (10, 20, 30, 45, and 60 degrees). These simulations, described in Section J.2.1, were used for 1) comparison with published GMPE with hanging-wall terms to assess the need for extending hanging-wall terms to lower magnitude, and 2) to test a SWUS hanging-wall term developed by this project to be applied to the Common Functional Form median motion GMPE (Section 6.3) that was used in the hazard calculation.

For each of these scenarios there were 32 source realizations computed at a fixed array of 182 stations. Figure J.5.2-1 shows the distribution of the stations and the surface projection for the **M**5.5, **M**6.0 and **M**6.5 scenarios for a fault dip of 45 degrees. The RotD50 PSA output from the BBP was used in the analysis.

The simulations were compared to the NGA-West2 GMPE hanging-wall terms by first constructing a fault perpendicular profile defined by distance to the top edge of the fault ($R_X$). For each $R_X$ the simulated PSA was averaged for all sites located within the north and south extent of the surface projection rupture plane for each scenario (e.g. Figure J.5.2-1). Then the simulation footwall motions ($R_X < 0$) were fit with an $R_{RUP}$ model, defined as $LN(y)=a+b*LN(R_{RUP})$, where $R_{RUP}$ is the distance to the closest point of the rupture. For sites on the footwall the closest point is always the top edge of the fault. The

fitted $R_{RUP}$ model was then projected to the hanging-wall side to illustrate the hanging-wall effect of the simulations, and to then test the published hanging-wall terms. This approach was first tested by generating ground motions for a suite of $R_X$ for each of the published GMPE. Figure J.5.2-2 shows a comparison for the ASK14 GMPE for **M**6.5, $Z_{TOR}$=7 km and dips of 45 and 60 degrees. The near exact comparison with the published motions demonstrates the viability of the analysis procedure.

The simulations were then compared to the three GMPE hanging-wall terms. Figure J.5.2-3 compares the **M**5.5, **M**6.0 and **M**6.5 cases for $Z_{TOR}$=7 km and dip=45 degrees for the ASK14 model. This model invokes a **M** taper that zeros the hanging-wall term for **M** ≤ 5.5, and for this case the simulations show larger motions on the hanging-wall. The hanging-wall term for **M**6 and **M**6.5 agree well with the simulations. Figure J.5.2-4 compares the **M**5.5, **M**6.0 and **M**6.5 cases for $Z_{TOR}$=7 km and dip=45 degrees for the CB14 model, which shows similar behavior.

It is noted that the SDSU method in Figure J.5.2-3 for the **M**5.5 and **M**6.0 cases shows lower values on the hanging wall than the other two simulation methods, and there also appears to more overall scatter in values for different $R_X$. For the **M**6.5 case all three simulation methods show elevated motions on the hanging wall. Because both the GP and EXSIM methods for the shown 45 degree dip case and other fault dip cases, as well as the SDSU method having values more consistent with the other two methods for the other dip and $Z_{TOR}$ cases, it was the judgment of the TI Team that the simulations do show hanging-wall amplifications for **M** < 6.5.

For the CY14 GMPE there is not an explicit **M** scaling of the hanging-wall term, but rather the scaling is accomplished through a hyperbolic tangent function of $R_X$ that grows larger for increasing values of $R_X$ that is then truncated by a distance taper that is a function of both $R_{JB}$ and $R_{RUP}$ and has a minimum value for $R_{JB}$=0, when the site is over the dipping fault. Thus for a larger rupture the distance taper remains near unity due to $R_{JB}$ remaining zero for larger $R_X$ over the surface projection of the fault, which leads to an increase in amplitude of the hanging-wall term. Figure J.5.2-5 compares the **M**5.5, **M**6.0 and **M**6.5 cases for $Z_{TOR}$=7 km and dip=45 degrees for the CY14 model.

The sensitivity of the published hanging-wall terms was examined for different dips, and $Z_{TOR}$. Based on this analysis the simulations show that hanging-wall effects may be important for magnitude as low as **M**5.5. Modifications to the **M** tapers for each of the NGA-West2 GMPE were examined, however it was determined that a better approach was to develop an independent SWUS hanging-wall term that can be applied directly to the Common Functional-Form GMPE (see Section 6.4). The SWUS hanging-wall term is compared to the ground-motion simulations in Section 6.3.

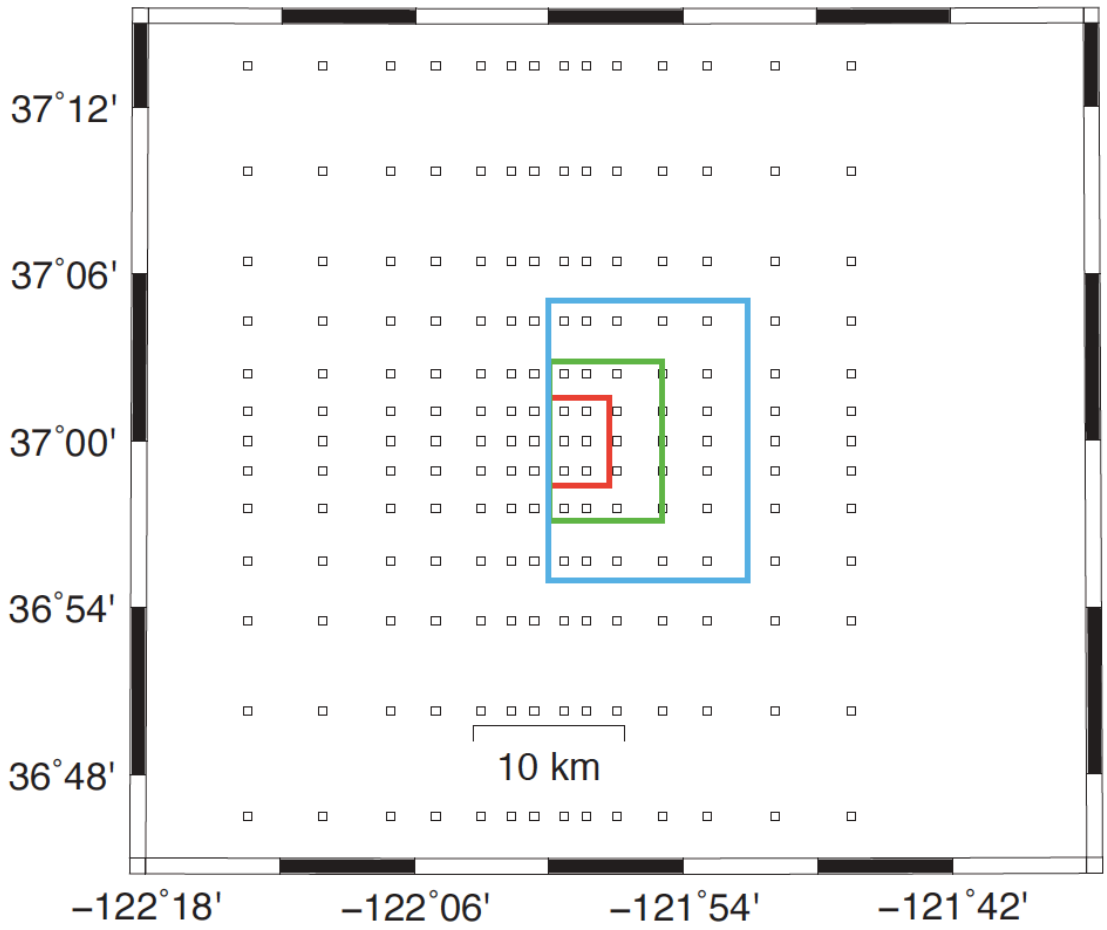



**Figure J.5.2-1:** Map showing the locations of the 182 stations (squares), and the surface projection of the 45-degree dipping cases for **M**5.5 (red), **M**6.0 (green) and **M**6.5 (blue). To construct the ground-motion profiles in $R_X$ the rows of stations contained within the upper and lower extent of each scenario were averaged.

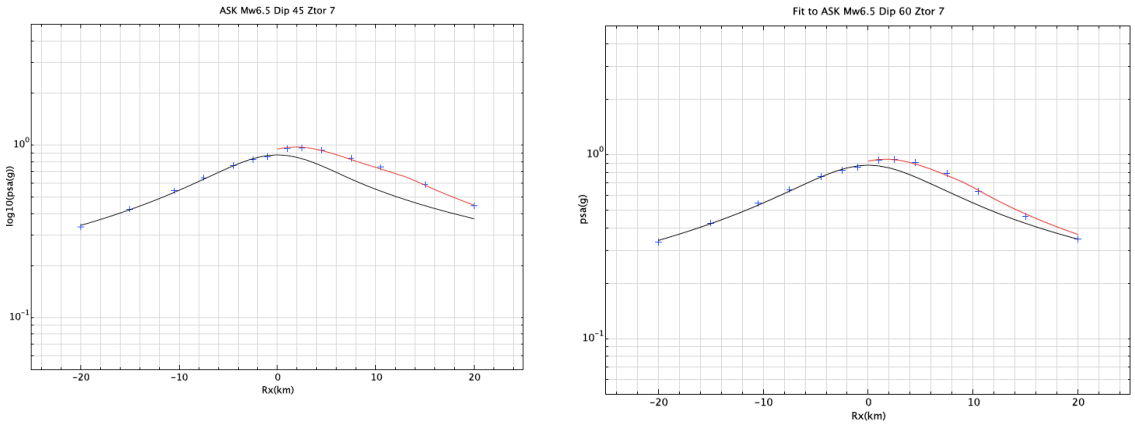



**Figure J.5.2-2:** Actual ASK14 GMPE motions computed from the published equations (plusses) are compared to the method for analyzing hanging-wall terms (lines). The black line shows a $R_{RUP}$ relation obtained by fitting a line to the natural logarithm of the footwall motions ($R_X < 0$). This relationship is then projected to the hanging wall (black line, $R_X \geq 0$). The red line shows the $R_{RUP}$ relationship with the ASK14 hanging-wall term applied.

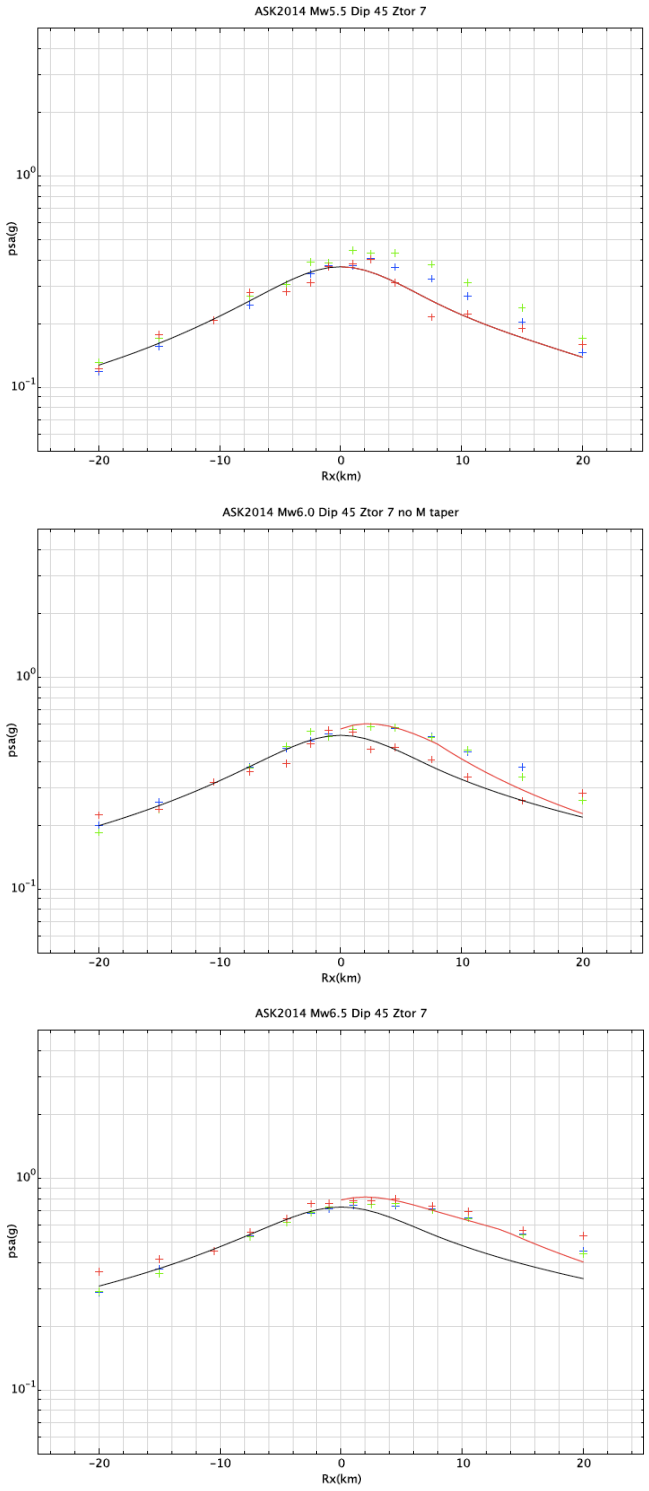



**Figure J.5.2-3:** Comparison of ASK14 hanging-wall term (red line) with simulations EXSIM (green plusses), GP (blue plusses) and SDSU (red plusses) for **M**5.5, 6.0 and 6.5 with dip=45 degrees and $Z_{TOR}$=7 km.

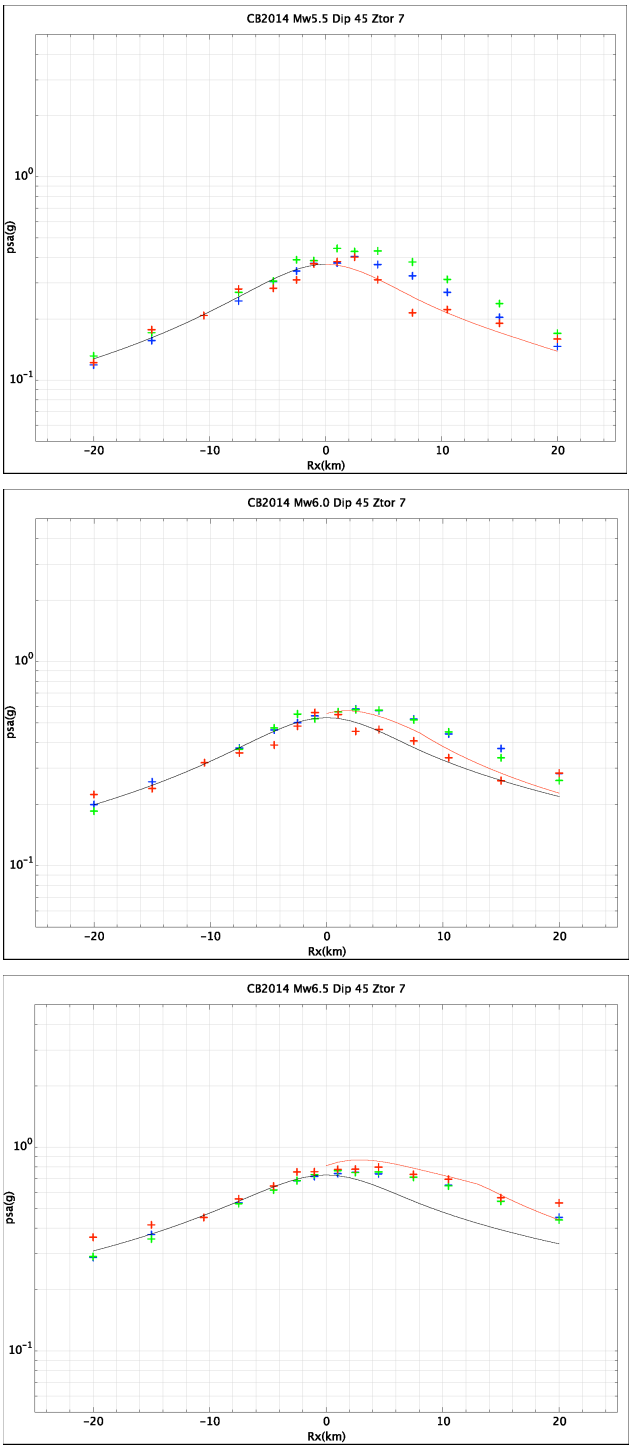



**Figure J.5.2-4:** Comparison of CB14 hanging-wall term (red line) with simulations EXSIM (green plusses), GP (blue plusses) and SDSU (red plusses) for **M**5.5, **M**6.0 and **M**6.5 with dip=45 degrees and $Z_{TOR}$=7 km.

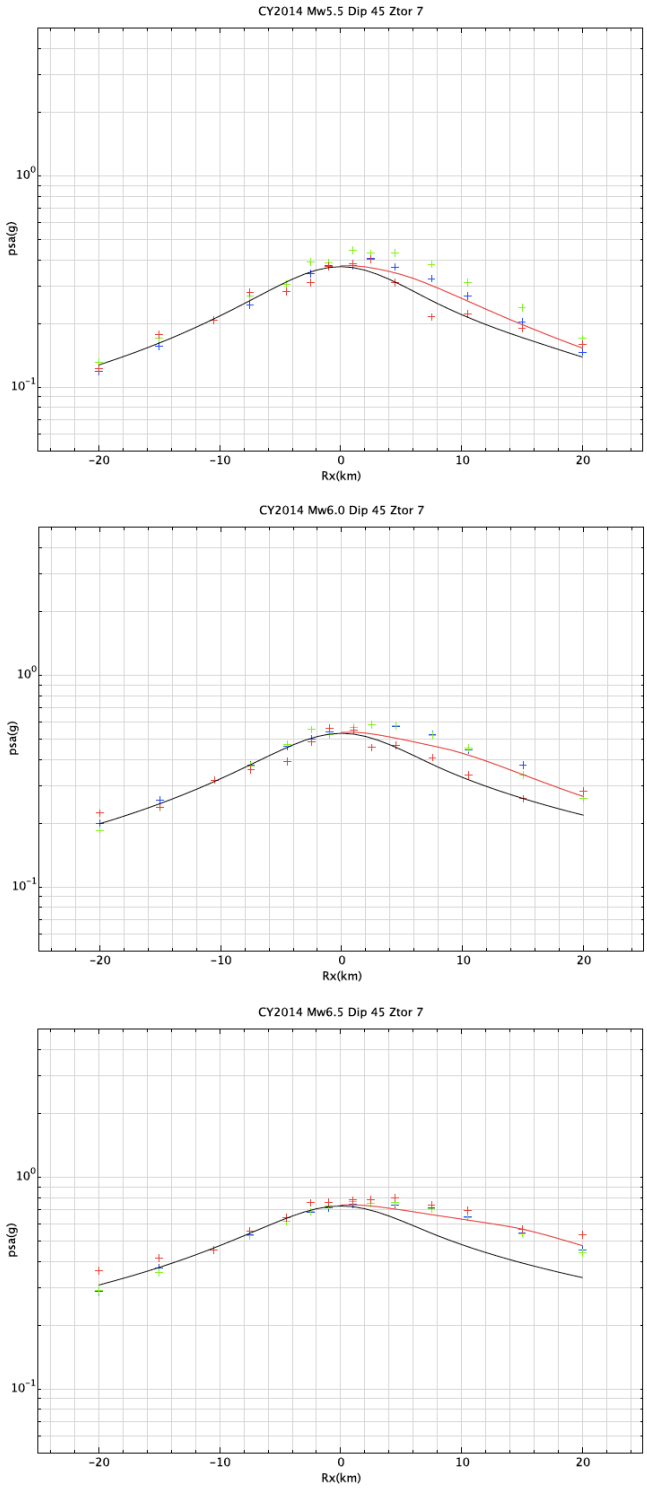



**Figure J.5.2-5:** Comparison of CY14 hanging-wall term (red line) with simulations EXSIM (green plusses), GP (blue plusses) and SDSU (red plusses) for **M**5.5, **M**6.0 and **M**6.5 with dip=45 degrees and $Z_{TOR}$=7 km.

## J.6 Additional Evaluations on Simulations

### *J.6.1 Potential for missing 3D effects using 1D simulations*

The BBP is currently utilizing Green's functions computed from 1D velocity models. There are two velocity models that are being used on the BBP, one based on average southern California structure and the other for northern California. For this project the simulations used the northern California model. Future BBP work will incorporate 3D velocity models, but for now the simulations only take into account 1D velocity structure. Although EXSIM does not explicitly use a velocity model to compute Green's functions it does take into account regional geometrical spreading and attenuation (Q). As implemented the methods are simulating motions to an effective rock site with a shear wave velocity ($V_S$) of 863 m/s. Both GP and SDSU utilize deterministic Green's functions for periods longer than 1 second. For periods shorter than 1 second both models use stochastic formulations that are not affected by the 1D model approximation.

To examine the suitability of the BBP northern California velocity model for use in DCPP ground-motion simulations broadband, three-component waveforms with frequency-wavenumber synthetics for an **M**4.7 San Simeon aftershock were compared. For periods longer than 1 second, the period range where deterministic Green's functions are employed by the simulation methods, this event is effectively a point-source, and the complexity in the observed waveforms is dominated by wave propagation. In Figure J.6.1-1 four S-wave velocity models are compared. The red curve is the velocity model used by the BBP, the two gray models have been proposed for the central coast ranges (Walter and Mooney, 1982; McLaren and Savage, 2001), and the black GIL7 curve was developed through broadband waveform modeling and is currently used by the Berkeley Seismological Laboratory (BSL) to routinely estimate seismic moment tensors in northern California (e.g. Pasyanos et al., 1996). As Figure J.6.1-1 shows the BBP northern California model is similar to the other three central coast models in terms of 1) the thickness of the crust (24-25 km), 2) the depth of a mid-crustal discontinuity (14-17 km), although there is variation in the size of the discontinuity, and 3) the presence of a pronounced velocity gradient in the shallow crust (less than 5 km depth).

In Figure J.6.1-2 broadband synthetics (frequencies from 0 to 25 Hz) are compared with the observations recorded at the BSL PKD site, located 56.5 km from the earthquake. There are no known 3D structures along this path that significantly affect the waveforms, although the presence of coda indicates 3D scattering at later times in the record. The strike, rake, dip, scalar seismic moment and source depth parameters (286°, 93°, 62°, 1.33e+23 dyne cm, 5.5 km) from the Berkeley Moment Tensor Catalog (http://ncedc.org) were assumed. The frequency wave-number Green's functions were convolved with a source time function with a rise time of 0.3 seconds, which is appropriate for the **M**4.7 earthquake. The top row shows the transverse, radial and vertical component data in black, and the synthetics calculated

with the GIL7 1D velocity model (e.g. Pasyanos et al., 1996), which is considered appropriate for the central coast ranges based on broadband waveform modeling (Dreger and Romanowicz, 1994; Rolandone et al., 2006) . The other four rows compare synthetic seismograms for the four 1D models. On balance, the simulated waveforms based on the BBP Norcal profile agree with the key features of the observed waveforms at least as well as those based on alternative available 1D models, and qualitatively fits the data in terms of the long-period P-wave on the radial and vertical components, the Love wave dispersion on the transverse component, and the Rayleigh wave dispersion on the radial and vertical components.

In Figure J.6.1-3 the same data and synthetics are compared for frequencies less than 1 Hz, which is the passband where the GP and SDSU methods are using deterministic Green's functions to simulate PSA. At these frequencies the waveforms are essentially a point-source response for a **M**4.7 event, and as the figure shows there is very good agreement between the GIL7 velocity model and the observations. The BBP northern California velocity model is also shown to be equally consistent with the data in this frequency band.

Based on the comparisons of the BBP 1D velocity model with others proposed for the region, and the test comparing point-source simulations with the broadband records for the **M**4.7 event, it is the judgment of the TI team that the use of the 1D velocity model simulation results for the ground-motion objectives of the project is justified.

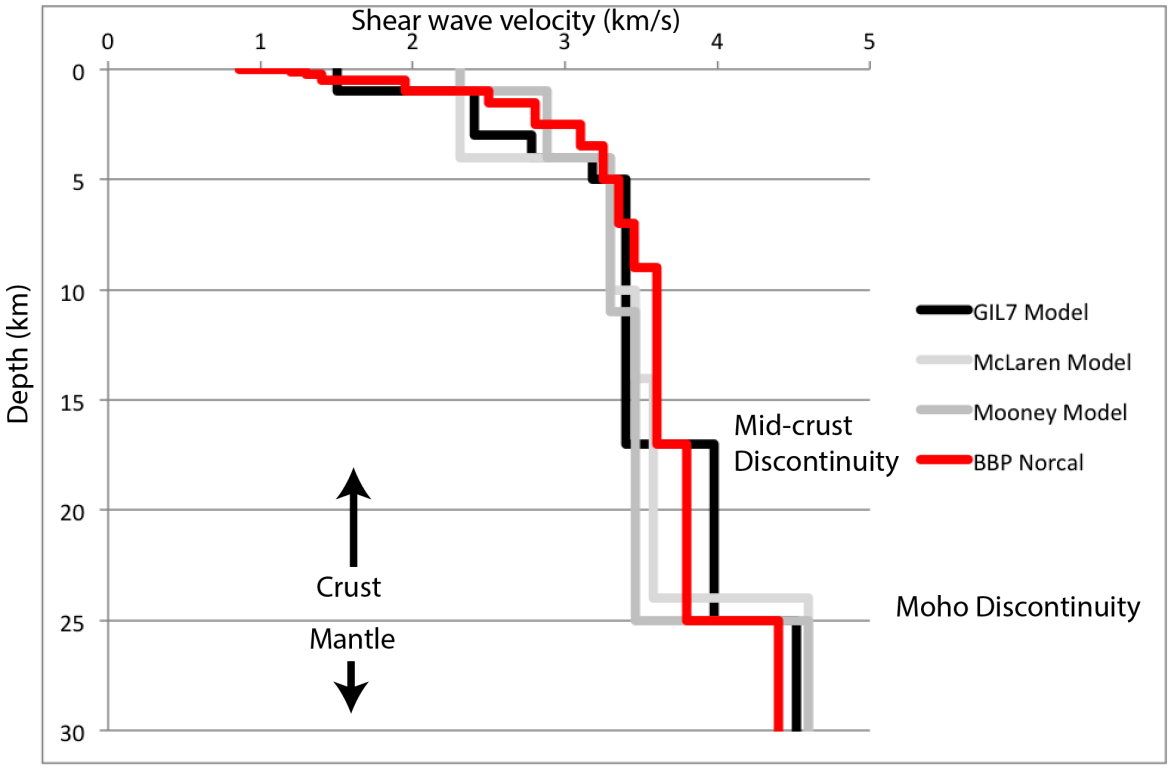



**Figure J.6.1-1:** Comparison of 1D velocity models for the Central Coast Region. S-wave velocity is shown in km/s. The red curve show the velocity model used in the SWUS simulations.

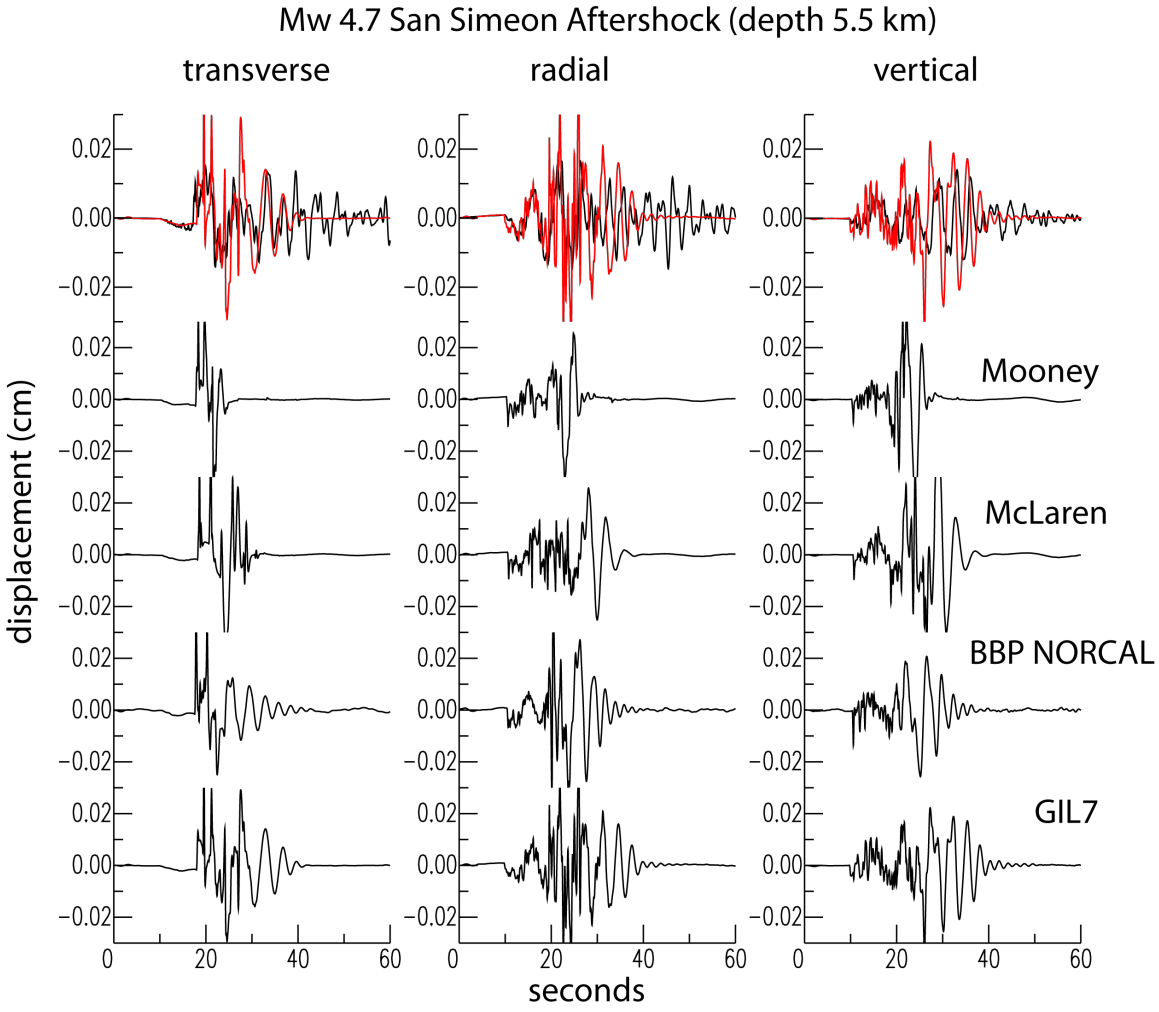



**Figure J.6.1-2:** (top row) Comparison of broadband (0 to 25 Hz) data (black) recorded at PKD and GIL7 synthetic seismogram (red). Rows 2-5 compare the broadband synthetics for three central coast velocity models with the BBP northern California model.

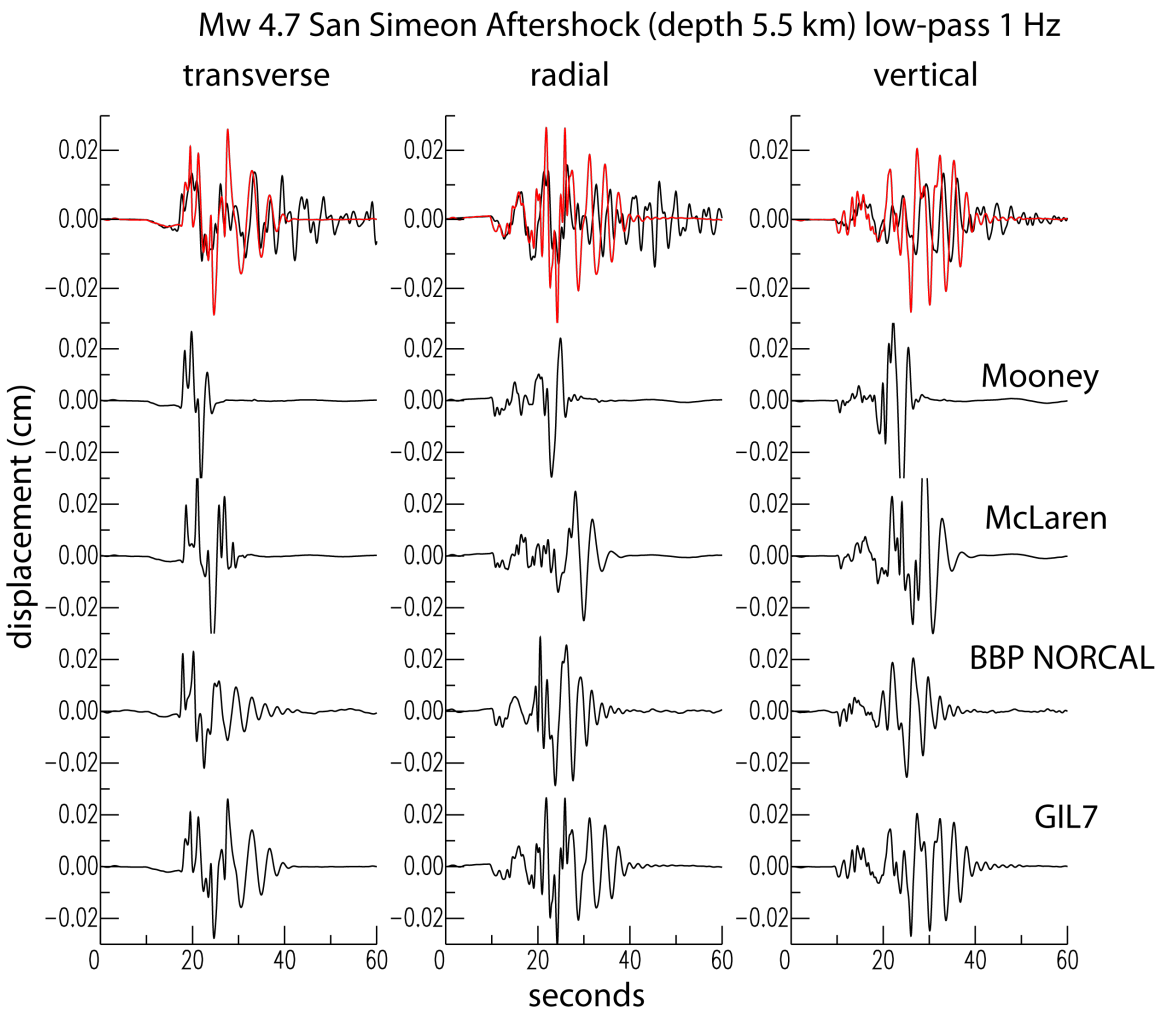



**Figure J.6.1-3:** Same as figure J.6.1-2 except that the records have been low-pass filtered at 1 Hz with an acausal, 4-pole Butterworth filter.

### *J.6.2 Comparison of slip and long periods motions*

At the SWUS Workshop #2 it was remarked (see Appendix F) that long-period (static to several seconds period) motions at sites close to the fault are most sensitive to nearby slip on the fault, and that if ground motions are simply scaled in terms of magnitude, as is done with GMPEs, that this may oversimplify the problem since fault slip is variable along strike, and variable from event to event. In this section several related aspects of this question are examined using the simulations for the 1992 Landers earthquake that was a part of the method validation exercise (Dreger et al., 2013). First, the distribution of slip for sites distributed along strike for a single source realization are compared to the distribution of slip for a single site for 50 source realizations. Second, relationships between long-period ground-motion parameters to different characterizations of fault slip are examined. Finally, the observed spectral

displacement (SD) are compared to SD for 50 source realizations at the two closest stations to the fault (less than 5 km), namely LCN and JOS (Figure J.6.2-1), and also with the NGA-West2 GMPE.

For the BBP validation 50 random source realizations were simulated. Figure J.6.2-2A shows the slip distribution for one of these realizations for the GP method. Since the SDSU method uses the same Green's functions, and source model as the GP method at long-periods, and EXSIM is not designed for long-period, near-fault ground motions, this analysis was performed using only the GP simulation results.

Relationships between simulated long-period peak displacement, static displacement and SD were compared to features of the slip models, such as the nearest surface slip as recommended at Workshop 2, as well as with the geometric mean of the maximum value of the radiation pattern weighted fault-parallel (FP) and fault-normal (FN) slip (defined in the next paragraph), and the geometric mean of the FP and FN radiation pattern weighted slip.

Figure J.6.2-3A compares the distribution of nearest surface fault slip at station LCN for 50 source realizations (blue bars) with the nearest surface slip at 13 stations distributed along the length of the fault for source realization 0000 (cyan bars, and shown in Figure J.6.2-2A). The comparison shows that while there is considerably variability of nearest surface slip, which has been suggested to be controlling of the near-fault ground motions, along the strike of the fault that 50 source realizations effectively captures this range. It will be shown in the following that nearest surface slip is in fact not a good indicator of the scaling of near-fault ground motions when stations are located several km from the source, and that a better indicator is a spatial average of slip in the vicinity of the station. Figure J.6.2-3B compares the distribution of radiation pattern weighted slip (described in the next paragraph) at station LCN for 50 source realizations (blue bars) with the radiation pattern averaged fault slip at the 13 stations distributed along the length of the fault for source realization 0000 (cyan bars). This figure demonstrates that the use of 10's of source realizations effectively captures the variability in fault slip for sites located along the length of a fault, and if a correlation with long-period ground motion to nearby fault slip can be found that it therefore effectively captures the variability in the long-period ground motion.

It is shown later that the nearest surface slip alone did not correlate with the long-period ground-motion parameters, which is not surprising since there can be large contributions to the ground motions from slip on shallow portions on the fault that are nearby, but not necessarily closest to the site. To address this the radiation pattern sensitivity function was calculated by first computing the SH and SV radiation pattern coefficients (equations 4.90 and 4.91; Aki and Richards, 2002) for each point on the fault for each of the two stations (LCN and JOS, Figure J.6.2-1), as well as for the 13 equally spaced stations located 5 km from the fault trace. These functions are also scaled by a geometrical spreading term. The SH and SV radiation sensitivity is then rotated into the fault parallel (FP) and fault normal (FN) radiation sensitivity, which is shown in Figure J.6.2-2BC for station LCN. This function essentially shows the spatial extent of the fault that is expected to contribute significantly to the FP and FN motions at a given site, in

this case LCN. The FP radiation sensitivity is strongest at the fault adjacent to the site, whereas the FN radiation sensitivity is more complicated and extends to larger distance on the fault from the site.

Figure J.6.2-4 compares the FP and FN displacement time histories at LCN and JOS for the 50 source realizations. The different sign of the static offset is due to the two stations being on opposite sides of the fault. Station JOS has static terms on both the FP and FN components because it is located near the end of the fault.

Plots of simulated static displacement and peak FP and FN displacement with nearest surface slip showed considerable scatter, which is not surprising since at a distance of 5 km an area of the fault contributes to strong near-fault signals as well as the single point location of nearest surface slip (Figure J.6.2-5). Furthermore the small slope of the fitted lines indicates a lack of correlation between the point value of nearest surface slip and the different ground-motion parameters. On the other hand, the right column of Figure J.6.2-5 shows the same ground-motion parameters plotted against the radiation pattern averaged estimate of fault slip. In each case there are clear correlations between the ground-motion parameters and the estimate of fault slip. The strongest correlations are for the FP component as theoretically expected, because the static displacement and the FP peak displacement correlate better with nearby fault slip than the FN peak displacement, which will be sensitive to contributions integrated over the length of the fault, and which will also be affected by directivity. Similar correlations are found for station JOS. Figure J.6.2-5 demonstrates that the level of long-period motions do not scale with the closest surface slip, but do scale with a spatial average of nearby fault slip.

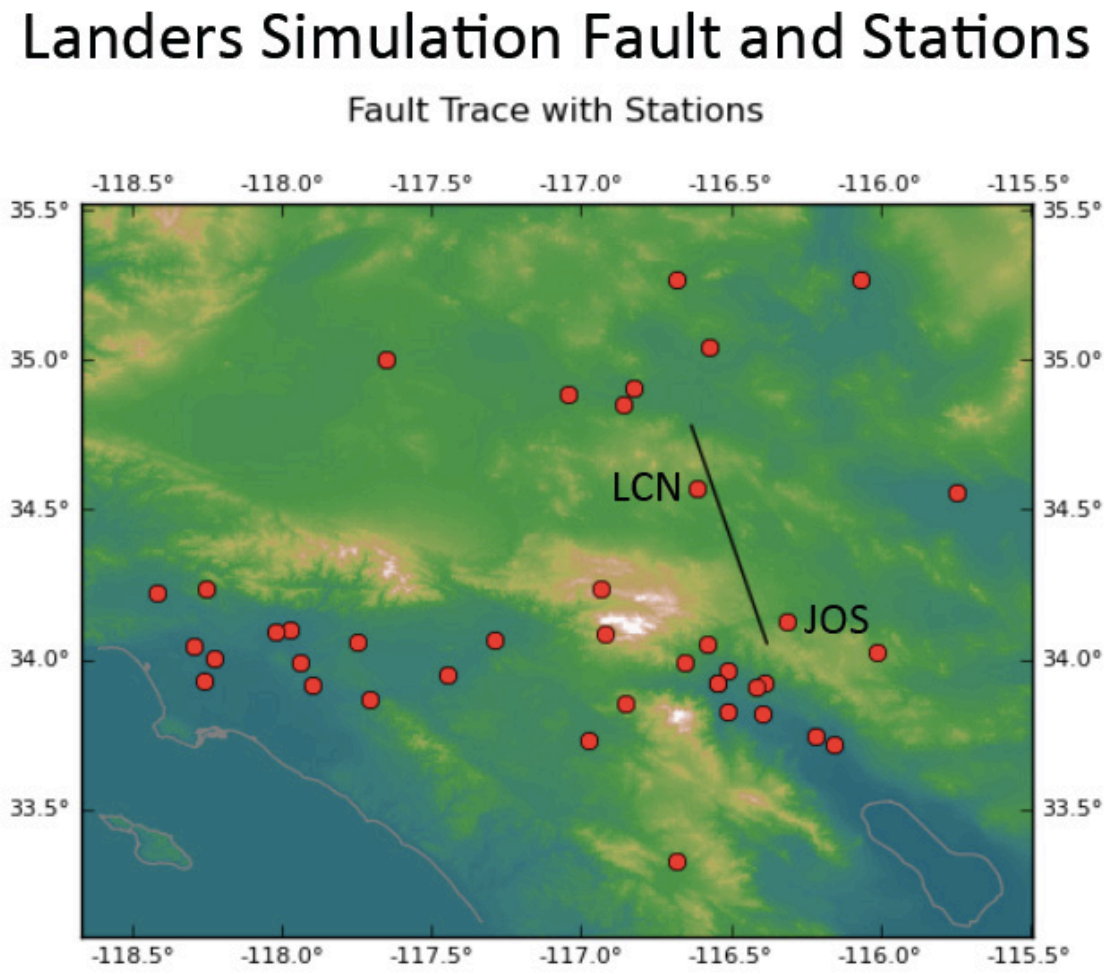



**Figure J.6.2-1:** Map showing the location of the vertically dipping, planar fault model (black line), and stations (red circles) used in the BBP Landers earthquake validation exercise. The two closest stations are LCN and JOS.

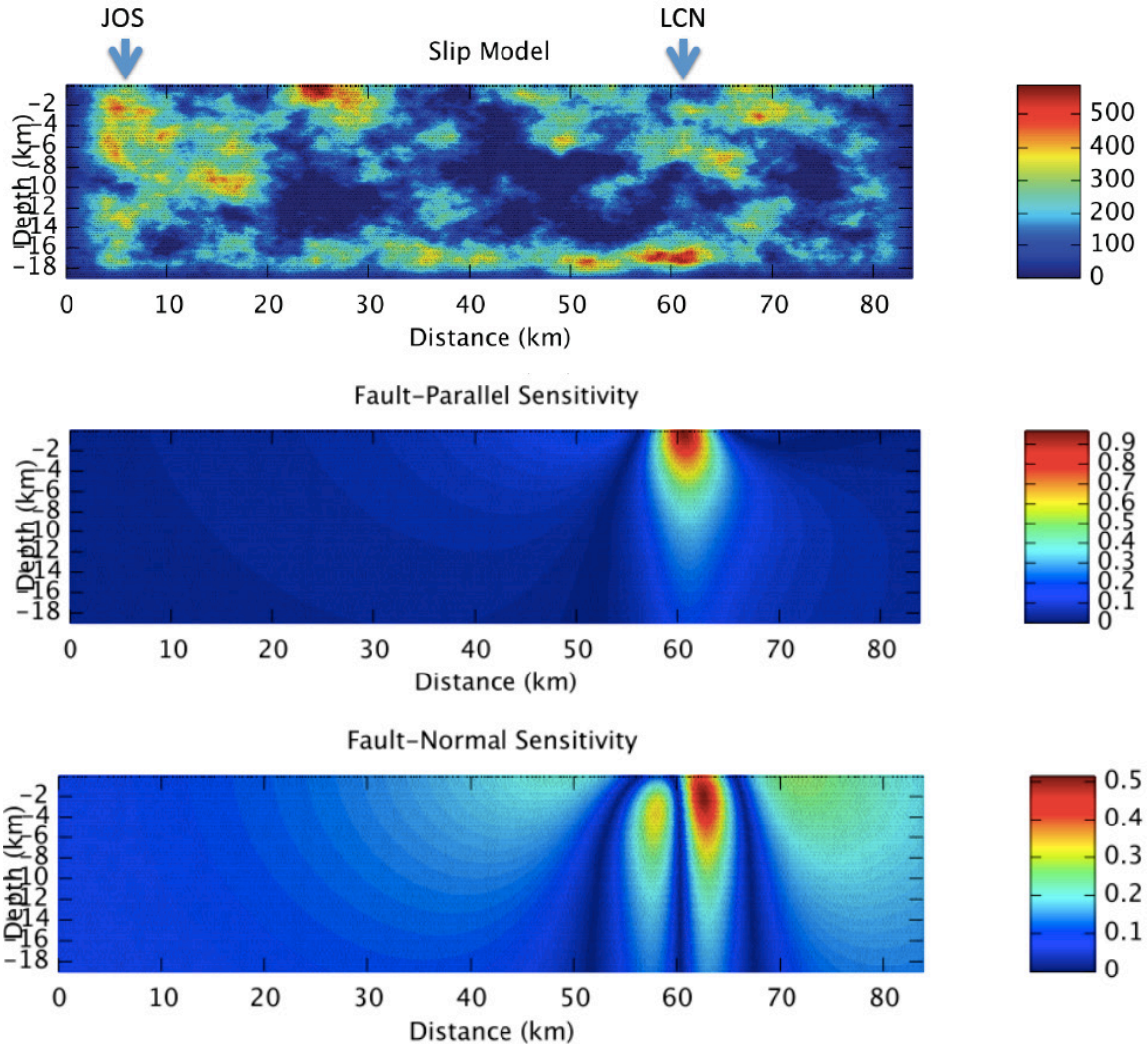



**Figure J.6.2-2:** A) Example of fault slip (cm) for one of the 50 Landers random slip realizations. B) The FP radiation sensitivity for station LCN. The highest sensitivity (reds). C) The FN radiation sensitivity.

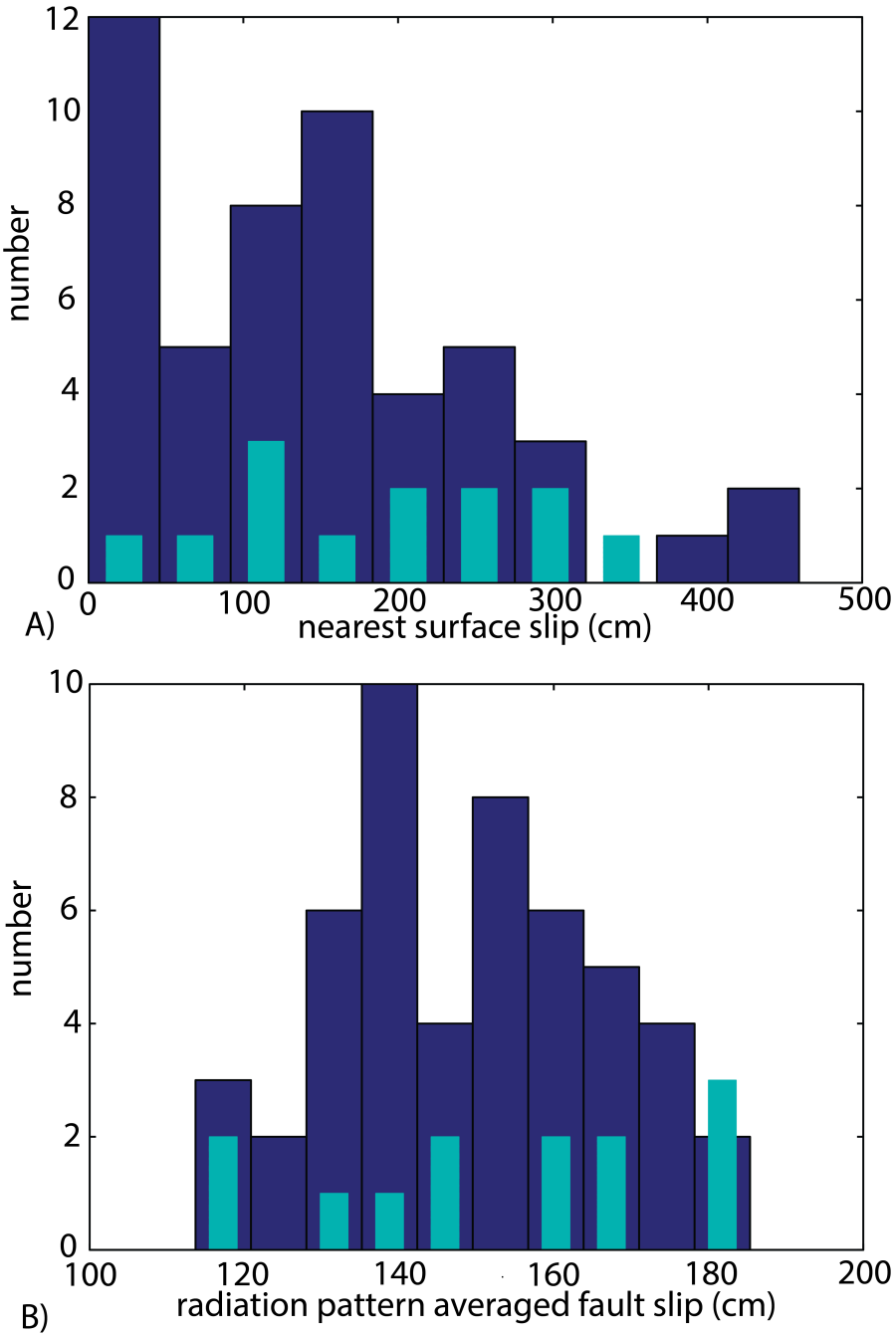



**Figure J.6.2-3:** A) Nearest surface slip for station LCN for 50 fault slip realizations (blue bars) is compared to nearest surface slip at 13 stations equally spaced along the fault (Figure J.6.2-1) for the single fault slip model shown in Figure J.6.2-2A (cyan bars). B) Radiation pattern averaged fault slip for station LCN for 50 fault slip realizations (blue bars) is compared to radiation pattern averaged slip at 13 stations equally spaced along the fault (Figure J.6.2-1) for the single fault slip model shown in Figure J.6.2-2A (cyan bars).

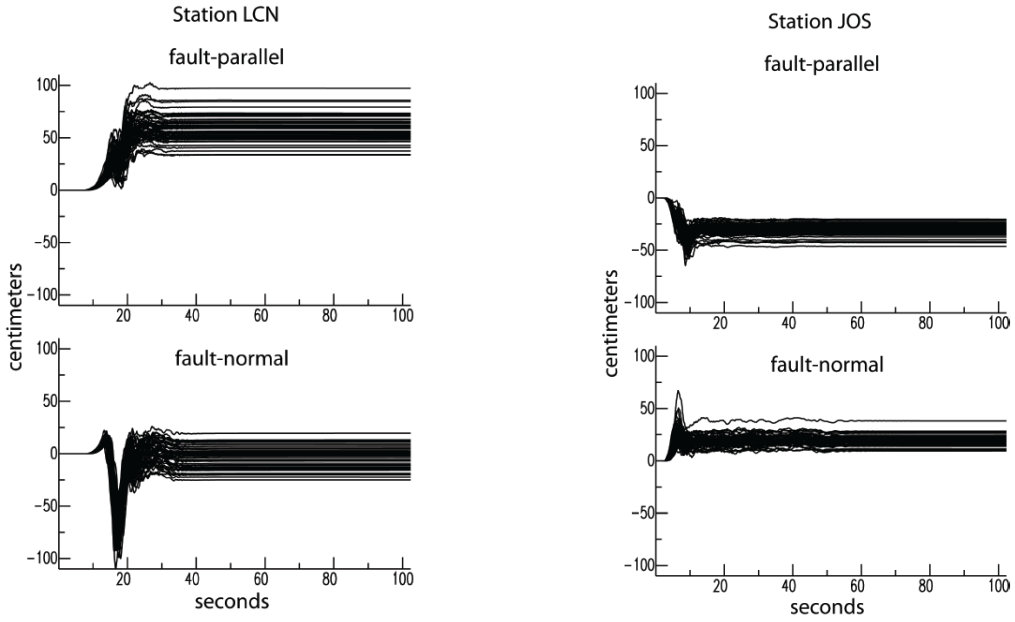



**Figure J.6.2-4:** Comparison of FP and FN displacement time histories for the 50 random source realizations at stations LCN and JOS. Note that the difference in sign of the static offset is due to the stations being on opposite sides of the fault.

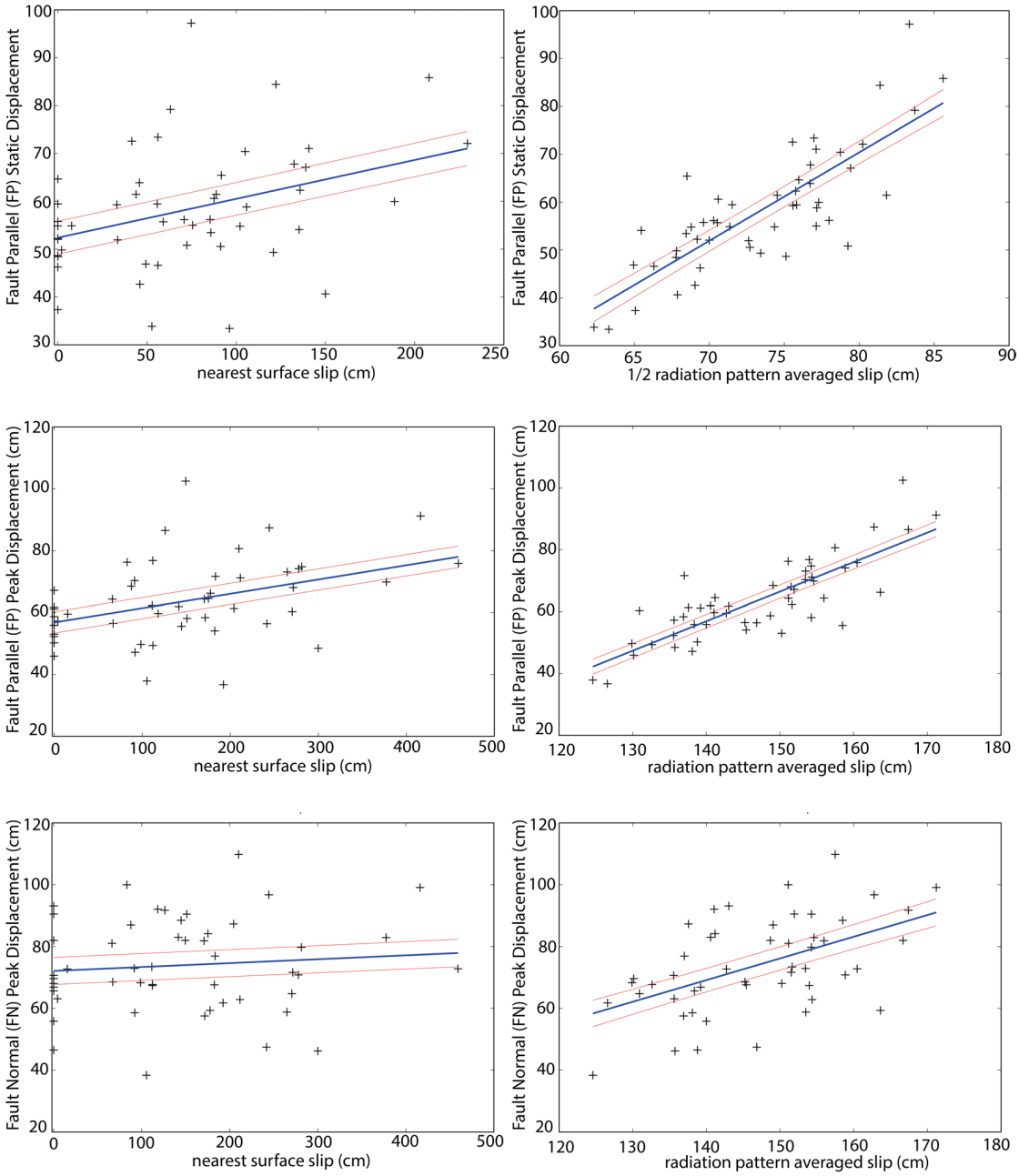



**Figure J.6.2-5:** The left column compares FP static, FP peak, and FN peak ground motions (plusses) at station LCN for 50 source realizations plotted against surface slip. In the first panel the static ground motion is compared to ½ of the surface slip since it theoretically is proportional to ½ of the fault slip. The right column compares FP static, FP peak and FN peak ground motions (plusses) at LCN for 50 source realizations plotted against the radiation pattern averaged slip. The blue lines show linear regressions of the simulated ground-motion data and the red lines show the 95% confidence regions.

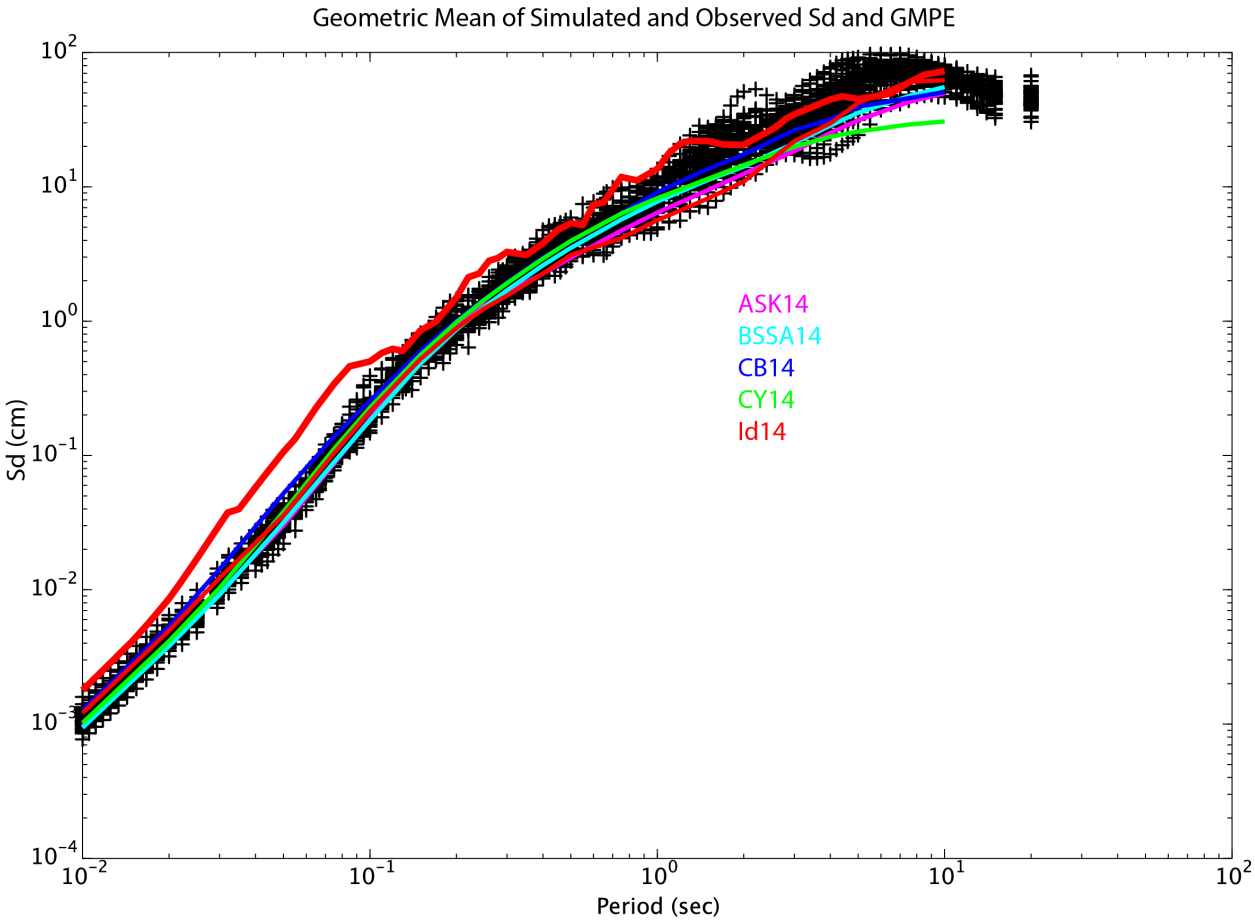



**Figure J.6.2-6:** Comparison of the geometric mean of the observed FP and FN SD (thick red line), the geometric mean of simulated FP and FN SD for the 50 source realizations (plusses), and the median SD from the NGA-West2 GMPE relationship for station LCN.

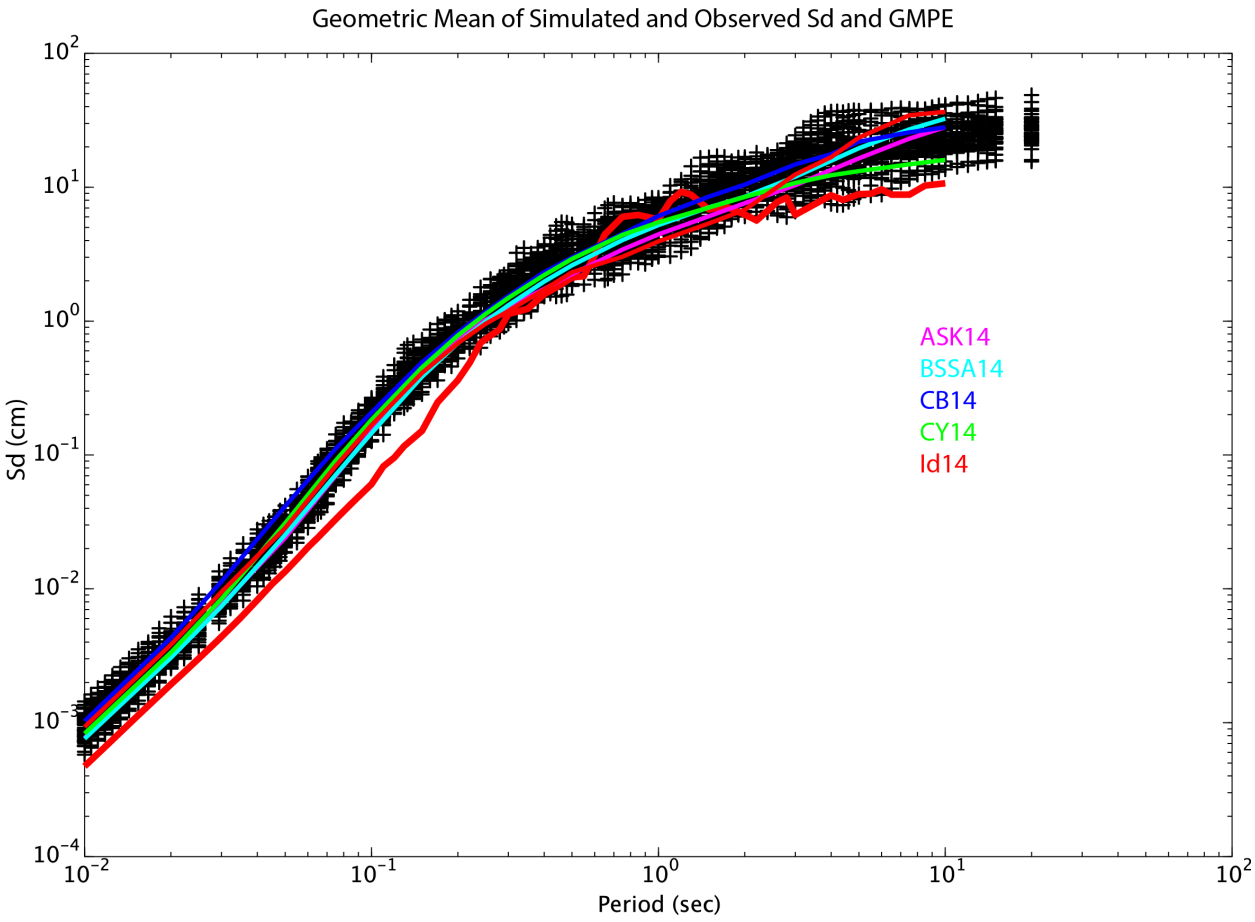



**Figure J.6.2-7:** Comparison of the geometric mean of the observed FP and FN SD (thick red line), the geometric mean of simulated FP and FN SD for the 50 source realizations (plusses), and the median SD from the NGA-West2 GMPE relationship for station JOS.

For stations LCN and JOS Figures J.6.2-6 and J.6.2-7 show the geometric mean of the FP and FN simulated motions from the 50 random source simulations as plusses, the NGA-West2 GMPE relationships for spectral displacement (SD) as the thin colored lines, and the observed SD is shown as the thick red lines. The simulations generally agree with the observed SD, however they under-predict SD at LCN at short periods, and for JOS the short periods are over-predicted. But overall the simulations are consistent with the observations. The median NGA-West2 SD motions are also seen to agree well with the simulation results, which is consistent with the observations made during the validation of the simulation codes (e.g. Dreger et al., 2013; and Figure J.1.1-2). The GMPE motions are scaled simply by magnitude, and this analysis shows that the long-period simulated motions from the 50 finite-source slip realizations are consistent with them on average, and that the range of the simulated motions spans that of the individual GMPEs.

There are several conclusions to draw from the analysis of this section. First, it was shown that along strike variability in slip for realistic complex slip models is effectively captured at a given site with the use of 10's of source realizations. Second, long-period motions such as static and peak displacement scale with a radiation pattern averaged estimate of nearby fault slip. Thus along strike variability in long-period motions should be effectively captured with the use of 10's of source realizations for given site. Third, simulations of SD at recording sites LCN and JOS are generally consistent with observed SD at those sites, particularly at longer periods. Finally, simulated SD from the 50 source realizations encompasses the SD estimated from the NGA-West2 GMPEs in which their estimates are scaled by the magnitude parameter.

## J.7 References

Abrahamson, N.A., and Silva, W. (2008). Summary of the Abrahamson & Silva NGA Ground-Motion Relations, *Earthquake Spectra*, Vol. 24(1), 67-97.

Abrahamson, N.A., Silva, W.J., and Kamai, R. (2014). Summary of the AKS14 Ground-Motion Relation for Active Crustal Regions, *Earthquake Spectra*, Vol. 30(3), 1025-1055, DOI: 10.1193/070913EQS198M

Aki, K. and P. G. Richards (2002). Quantitative Seismology, 2nd edition, University Science Books, Sausalito, California, 700p,

Atkinson, G.M, and Assatourians, K. (2015). Implementation and validation of EXSIM (a stochastic finite-fault ground-motion simulation algorithm) on the SCEC broadband platform, *Seismol. Res. Letts Letts*., Vol. 86(1), 48-60, DOI: 10.1785/0220140097.

Boore, D.M., and Atkinson, G.M. (2008). Ground-Motion Prediction Equations for the Average Horizontal Component of PGA, PGV, and 5%-Damped PSA at Spectral Periods between 0.01s and 10.0s, *Earthquake Spectra*, Vol. 24(1), 99-138.

Boore, D.M., Stewart, J.P., Seyhan, E., and Atkinson, G.M. (2014). NGA-West 2 Equations for Predicting PGA, PGV, and 5%-Damped PSA for Shallow Crustal Earthquakes, *Earthquake Spectra*, Vol. 30(3), 1057-1085, DOI: 10.1193/070113EQS184M.

Campbell, K.W., and Bozorgnia, Y. (2008). NGA Ground Motion Model for the Geometric Mean Horizontal Component of PGA, PGV, PGD and 5% Damped Linear Elastic Response Spectra for Periods Ranging from 0.01 to 10 s, *Earthquake Spectra*, Vol. 24(1), 139-171.

Campbell, K.W., and Bozorgnia, Y. (2014). NGA-West2 Ground Motion Model for the Average Horizontal Components of PGA, PGV, and 5%-Damped Linear Acceleration Response Spectra, Earthquake Spectra, Vol. 30(3), 1117-1153, DOI: 10.1193/062913EQS175M.

Chiou, B.S.-J., and Youngs R.R. (2008), An NGA model for the average horizontal component of peak ground motion and response spectra, *Earthquake Spectra*, Vol. 24(1), 173-215.

Chiou, B.S.-J., and Youngs, R.R. (2014). Update of the Chiou and Youngs NGA Model for the Average Horizontal Component of Peak Ground Motion and Response Spectra, *Earthquake Spectra*, Vol. 30(3), 1117-1153, DOI: 10.1193/072813EQS219M.

Donahue, J., and Abrahamson, N.A. (2014). Simulation-based Hanging-Wall Effects, *Earthquake Spectra*, Vol. 30(3), 1269-1284, DOI: 10.1193/071113EQS200M.

Dreger, D., and B. Romanowicz (1994). Source characteristics of events in the San Francisco Bay region, *U.S. Geol. Surv. Open-File Report*. 94-176, 301-309.

Dreger, D.S., Beroza, G.C., Day, S.M., Goulet, C.A., Jordan, T.H., Spudich, P.A, and Stewart, J.P. (2013). Evaluation of SCEC Broadband Platform Phase 1 Ground Motion Simulation Results, 33 pp. plus Appendices, Report submitted to SCEC, Aug. 1 2013 and available at http://scec.usc.edu/scecpedia/SCEC_BBP_Phase_1_Evaluation

Dreger, D. S., G. C. Beroza, S. M. Day, C. A. Goulet, T. H. Jordan, P. A. Spudich, and J. P. Stewart (2015). Validation of the SCEC broadband platform v14.3 simulation methods using pseudospectral acceleration data, *Seismol. Res. Lett.*, Vol. 86(1), 39-47, DOI: 10.1785/0220140118.

Graves, R.W. and Pitarka, A. (2015). Refinements of the Graves and Pitarka (2010) Broadband Ground-Motion Simulation Method, *Seismol. Res. Letts*., Vol. 86(1), 75-80, DOI: 10.1785/0220140101.

Goulet, C. A., N. A. Abrahamson, P. G. Somerville, and K. E. Wooddell (2015). The SCEC Broadband Platform validation exercise: Methodology for code validation in the context of seismic hazard analyses, Seismol. Res. Lett., Vol. 86(1), 17-26, DOI: 10.1785/0220140104.

Leonard, M. (2010). Earthquake Fault Scaling: Self-Consistent Relating of Rupture Length, Width, Average Displacement, and Moment Release, *Bull. Seismol. Soc. Am.*, Vol. 100, 1971-1988.

Maechling, P.J., Silva, F., Callaghan, S., and Jordan, T.H. (2015). Broadband Platform: System Architecture and Software Implementation, *Seismol. Res. Letts*., Vol. 86(1), 27-38, DOI: 10.1785/0220140125

McLaren, M.K., and Savage, W.U. (2001). Seismicity of South-Central Coastal California: October 1987 through January 1997, *Bull. Seism. Soc. Am*., Vol. 91, 1629-1658.

Olsen, K. and Takedatsu, R. (2015). The SDSU Broadband Ground Motion Generation Module BBtoolbox Version 1.5, *Seismol. Res. Letts*., Vol. 86(1), 81-88, DOI: 10.1785/0220140102.

Pasyanos, M., Dreger, D.S., and Romanowicz, B. (1996). Toward real-time estimation of regional moment tensors, *Bull. Seism. Soc. Am*., Vol. 86, 12255-1269.

Rolandone, F., D. Dreger, M. Murray, and R. Burgmann (2006). Coseismic slip distribution of the 2003 Mw6.6 San Simeon earthquake, California, determined from GPS measurements and seismic waveform data, *Geophys. Res. Lett.*, Vol. 33, L16315, DOI:10.1029/2006GL027079.

Walter, A.W., and Mooney, W.D. (1982). Crustal structure of the Diablo Gabilan Ranges, Central California; a reinterpretation of existing data, *Bull. Seism. Soc. Am*., Vol. 72, 1567-1590.

# APPENDIX K

# $\phi_{SS}$ EVALUATION

This Appendix presents the evaluation of the $\phi_{SS}$ values for several periods with respect their dependence on main predictors, such as magnitude, distance, style-of-faulting and $V_{S30}$.

## K.1 NGA-West2 and Lin et al. (2010) Subsets for $\phi_{SS}$

$\phi_{SS}$ was analyzed using the four NGA-West2 datasets (dataset of ASK14 [Abrahamson et al., 2014], BSSA14 [Boore et al., 2014], CB14 [Campbell and Bozorgnia, 2014], and CY14 [Chiou and Youngs, 2014]), each supplemented by the Lin et al. (2011) Taiwanese dataset (GLOBAL$_{PHISS\text{-}ASK14}$, GLOBAL$_{PHISS\text{-}BSSA14}$, GLOBAL$_{PHISS\text{-}CY14}$ and GLOBAL$_{PHISS\text{-}CB14}$). The datasets are described in Section 5.4.1.

Stations with a minimum of 3 recordings per site were used in the analysis. Figures K.1-1 and K.1-2 show a comparison of constant $\phi_{SS}$ versus period for the four NGA-West2 datasets and Lin et al. (2011) Taiwan dataset as well as for a subset with California data only. The California subsets are described in Section 5.4.3 and are referred to as NGA-W2$_{CA\text{-}PHISS\text{-}ASK14}$, NGA-W2$_{CA\text{-}PHISS\text{-}BSSA14}$, NGA-W2$_{CA\text{-}PHISS\text{-}CB14}$, and NGA-W2$_{CA\text{-}PHISS\text{-}CY14}$. These plots show that $\phi_{SS}$ results are consistent among the NGA-West2 datasets and that the Taiwanese data show lower $\phi_{SS}$ at short periods than the NGA-West2 data. Figure K.1-3 shows the magnitude-dependence of $\phi_{SS}$ at PGA and T = 1 sec for the NGA-West2 California subset and the Taiwanese Lin et al. (2011) dataset. This figure shows that the four NGA-West2 California datasets show similar magnitude-dependence. Figures K.1-4 and K.1-5 show the magnitude and distance dependence of the five datasets at PGA and T = 1 sec, respectively. Figure K.1-6 shows the $V_{S30}$-dependence of NGA-West2 California subset and the Taiwanese Lin et al. (2011) dataset PGA and T = 1 sec. Figure K.1-4 shows that $\phi_{SS}$ binned by magnitude and distance for Taiwan is generally similar to that of the NGA-West2 California subset except for the small magnitude and large distance where $\phi_{SS}$ for Taiwan is lower than the four NGA-West2 California subsets.

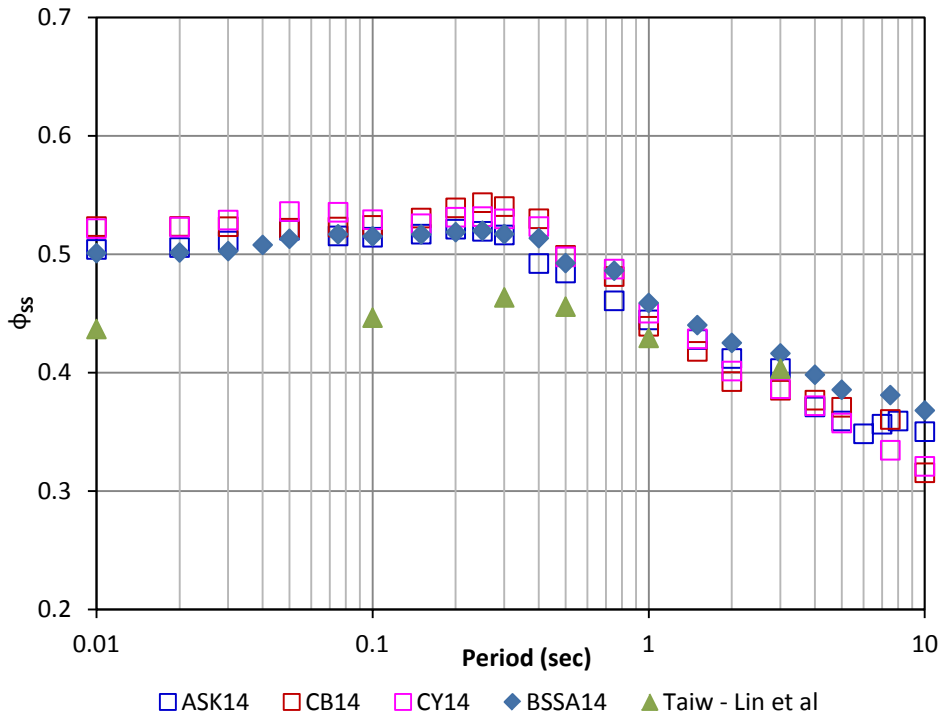



**Figure K.1-1**: Comparison of constant $\phi_{SS}$ versus period for the four NGA-West2 datasets and the Lin et al. (2011) Taiwanese dataset ($GLOBAL_{PHISS\text{-}ASK14}$, $GLOBAL_{PHISS\text{-}BSSA14}$, $GLOBAL_{PHISS\text{-}CY14}$ and $GLOBAL_{PHISS\text{-}CB14}$).

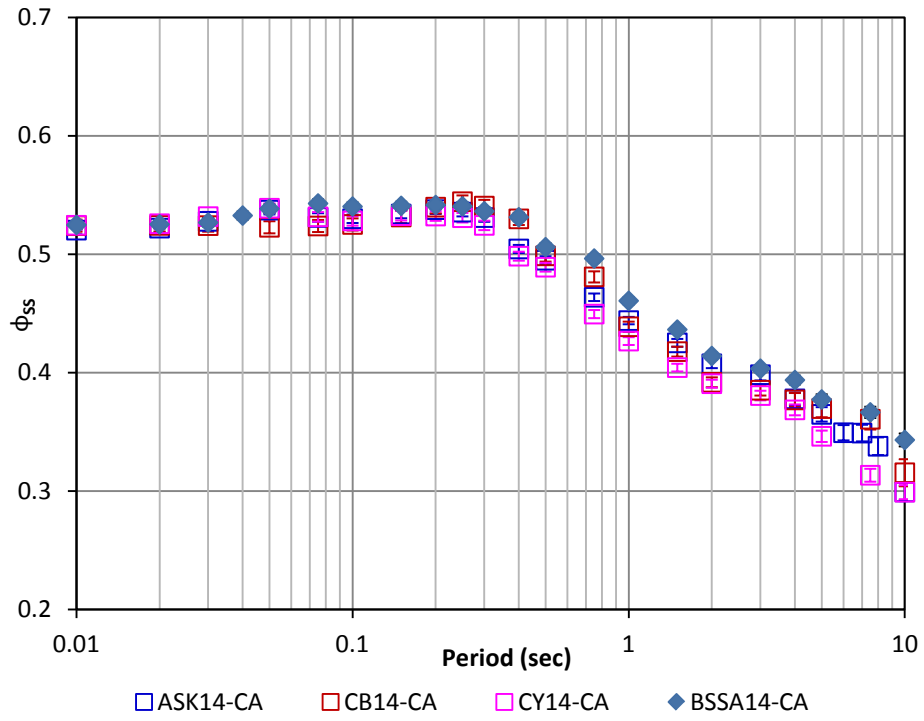



**Figure K.1-2:** Comparison of constant $\phi_{SS}$ versus period for the four NGA-West2 datasets for only California (NGA-W2$_{CA\text{-}PHISS\text{-}ASK14}$, NGA-W2$_{CA\text{-}PHISS\text{-}BSSA14}$, NGA-W2$_{CA\text{-}PHISS\text{-}CB14}$ and NGA-W2$_{CA\text{-}PHISS\text{-}CY14}$).

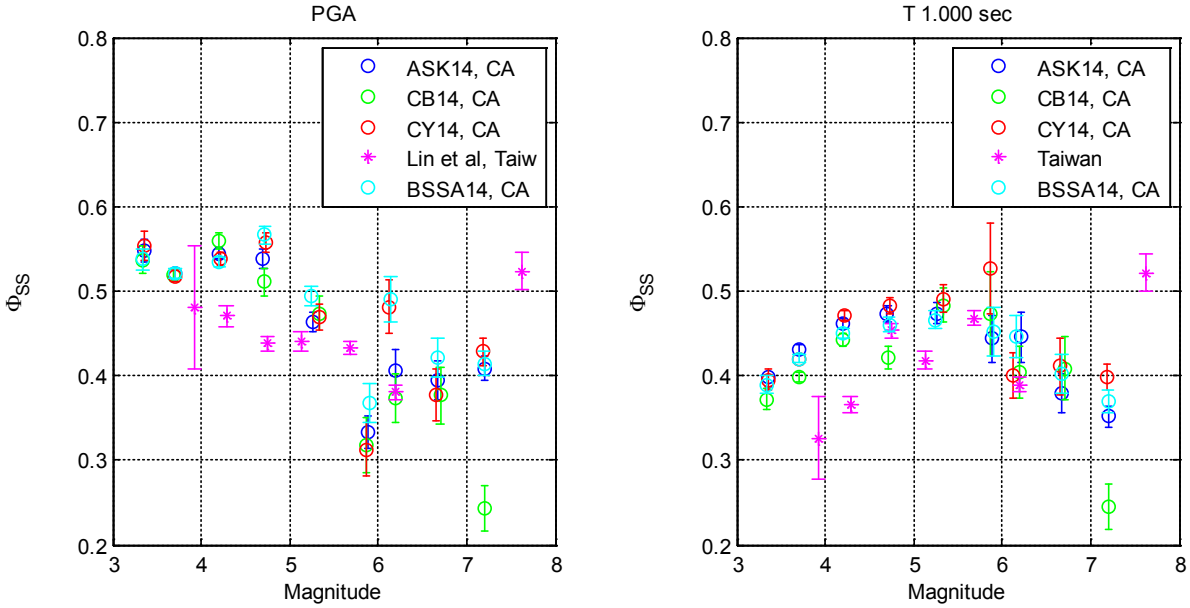



**Figure K.1-3:** Magnitude-dependence of NGA-West2 California $\phi_{SS}$ (NGA-W2$_{CA\text{-}PHISS\text{-}ASK14}$, NGA-W2$_{CA\text{-}PHISS\text{-}BSSA14}$, NGA-W2$_{CA\text{-}PHISS\text{-}CB14}$ and NGA-W2$_{CA\text{-}PHISS\text{-}CY14}$) and of Taiwan Lin et al. (2011) $\phi_{SS}$ at PGA and T =1 sec.

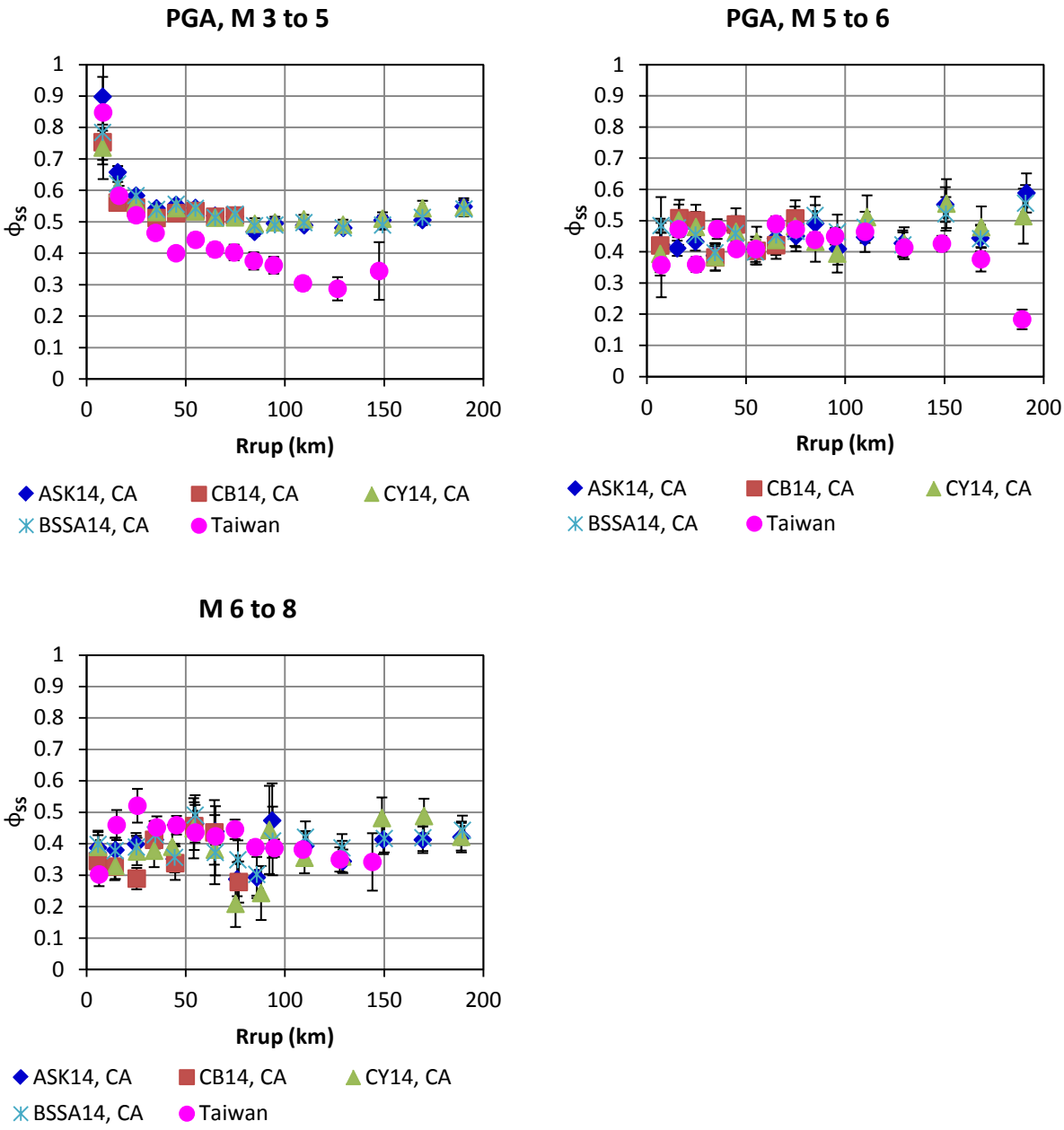



**Figure K.1-4:** Magnitude and distance-dependence of NGA-West2 California $\phi_{SS}$ (NGA-W2$_{\text{CA-PHISS-ASK14}}$, NGA-W2$_{\text{CA-PHISS-BSSA14}}$, NGA-W2$_{\text{CA-PHISS-CB14}}$ and NGA-W2$_{\text{CA-PHISS-CY14}}$) and of Taiwan Lin et al. (2011) $\phi_{SS}$ at PGA.

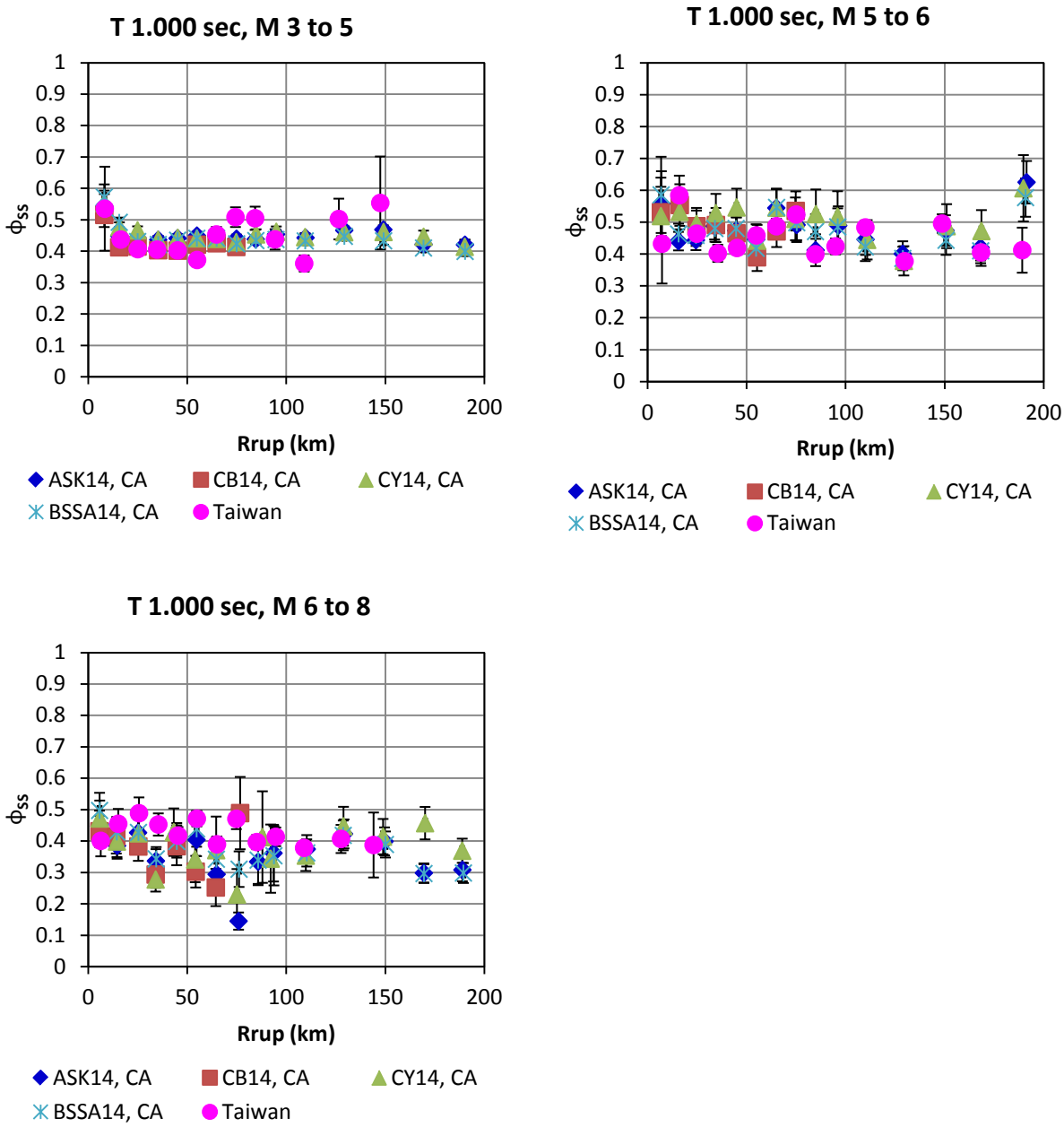



**Figure K.1-5:** Magnitude and distance-dependence of NGA-West2 California $\phi_{SS}$ (NGA-W2$_{CA\text{-}PHISS\text{-}ASK14}$, NGA-W2$_{CA\text{-}PHISS\text{-}BSSA14}$, NGA-W2$_{CA\text{-}PHISS\text{-}CB14}$ and NGA-W2$_{CA\text{-}PHISS\text{-}CY14}$) and of Taiwan Lin et al. (2011) $\phi_{SS}$ at T = 1 sec.

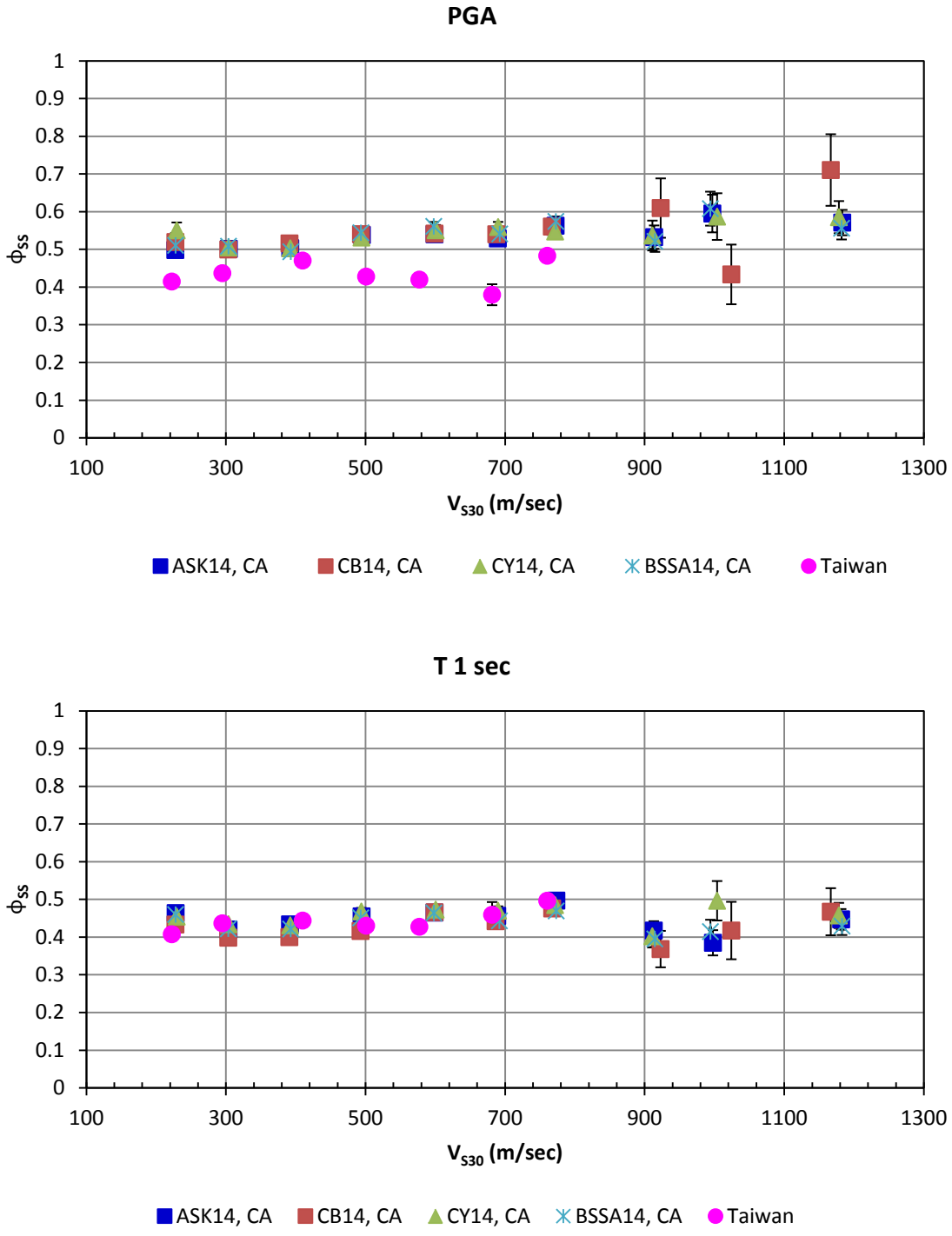



**Figure K.1-6:** $V_{S30}$-dependence of NGA-West2 California $\phi_{SS}$ (NGA-$W2_{CA\text{-}PHISS\text{-}ASK14}$, NGA-$W2_{CA\text{-}PHISS\text{-}BSSA14}$, NGA-$W2_{CA\text{-}PHISS\text{-}CB14}$ and NGA-$W2_{CA\text{-}PHISS\text{-}CY14}$) and of Taiwan Lin et al. (2011) $\phi_{SS}$ at PGA and T = 1 sec.

## K.2 European Dataset

The European dataset $EUR_{PHISS}$ (subset of the Akkar et al., 2014a and b) was used to evaluate $\phi_{SS}$ using only stations with a minimum of 3 recordings per site. Description of the $EUR_{PHISS}$ is provided in Section 5.4.2). The plots in Figures K.2-1 to K.2-5 show the evaluation of $\phi_{SS}$ for the European dataset (for the entire dataset and in different magnitude and distance ranges). Trends of $\phi_{SS}$ versus magnitude, distance, $V_{S30}$, and style-of-faulting are presented at PGA and at spectral period of 1 sec.

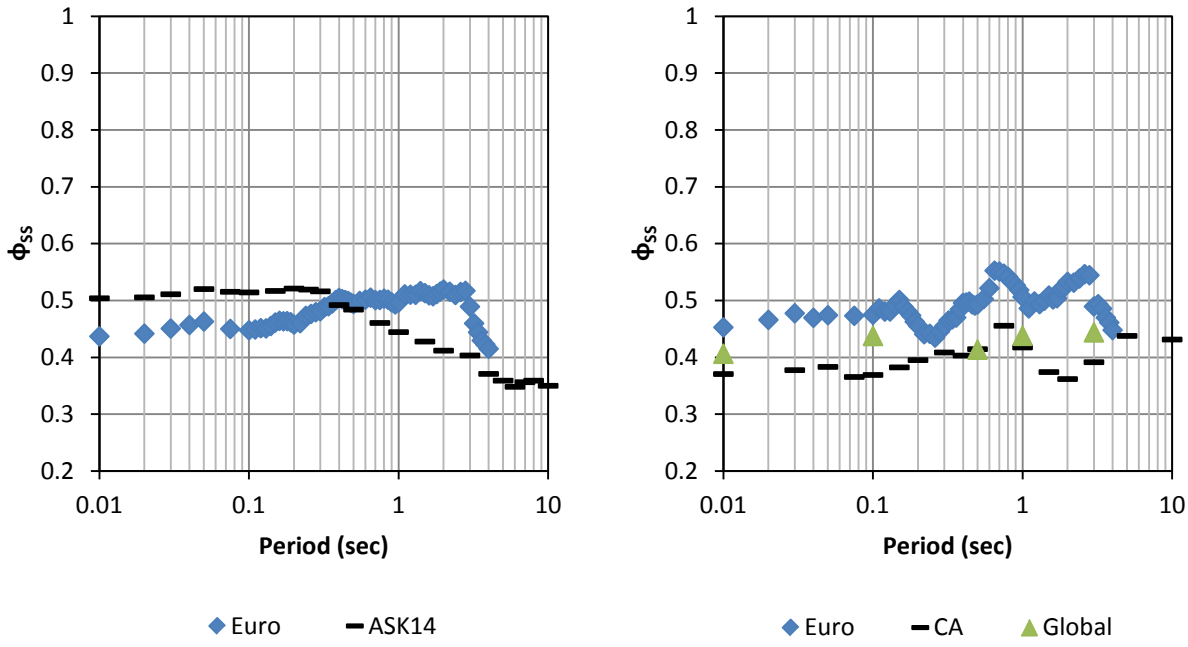



**Figure K.2-1:** Comparison of constant $\phi_{SS}$ over all magnitude and distances for the European dataset $EUR_{PHISS}$ and ASK14 dataset $GLOBAL_{PHISS\text{-}ASK14}$ (left), and for **M** ≥ 5.5 and distance less than 50 km for the European dataset $EUR_{PHISS}$, the ASK14 California subset $NGA\text{-}W2_{CA\text{-}PHISS\text{-}ASK14}$ and the global ASK14 plus Lin et al. (2011)) datasets $GLOBAL_{PHISS\text{-}ASK14}$ (right).

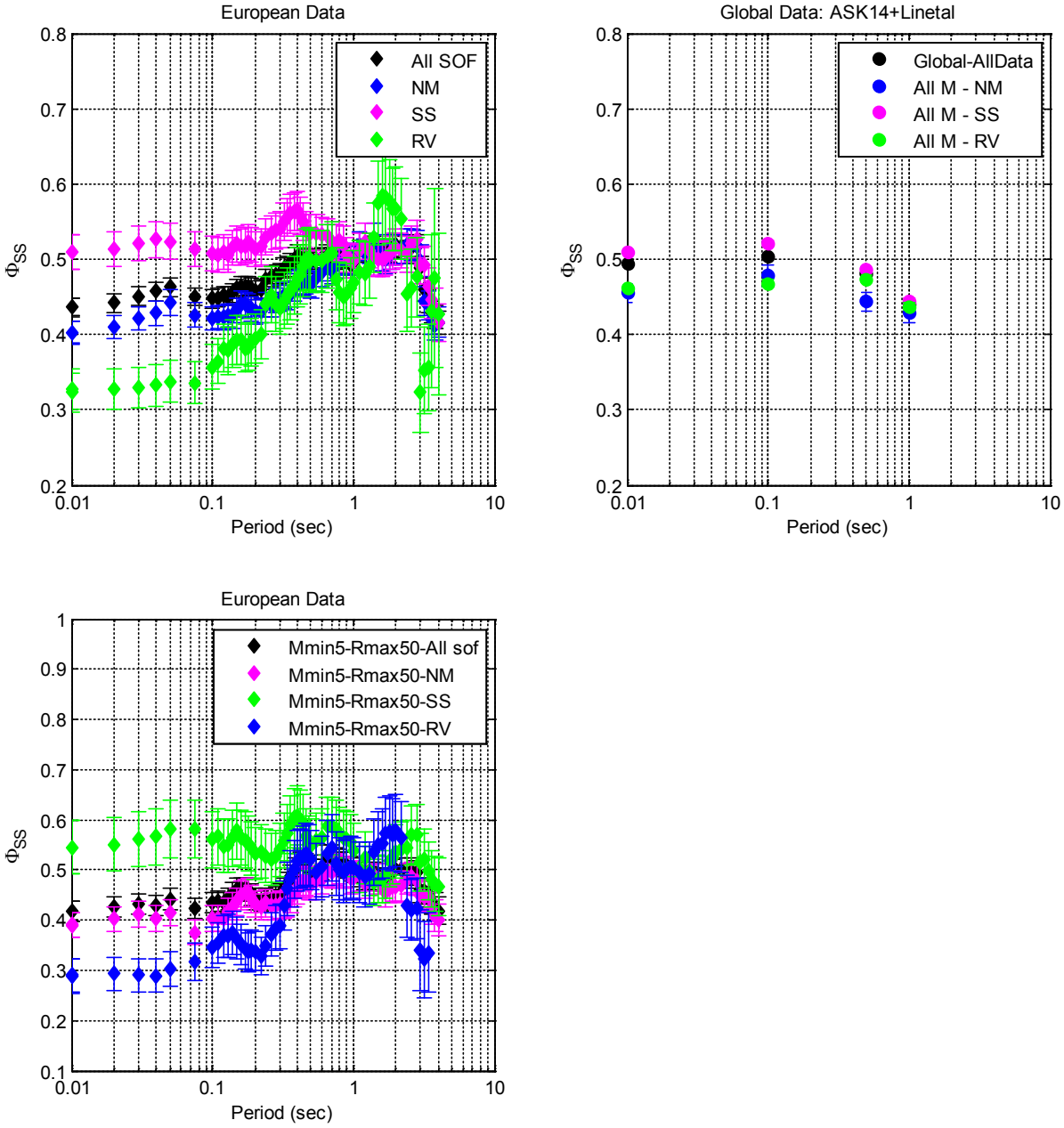



**Figure K.2-2:** Style-of-faulting dependence of $\phi_{SS}$ for the European dataset $EUR_{PHISS}$ and the global ASK14 dataset $GLOBAL_{PHISS\text{-}ASK14}$ (top plots), and for the European dataset $EUR_{PHISS}$ with **M** ≥ 5.0 and distance less than 50 km (bottom plot).

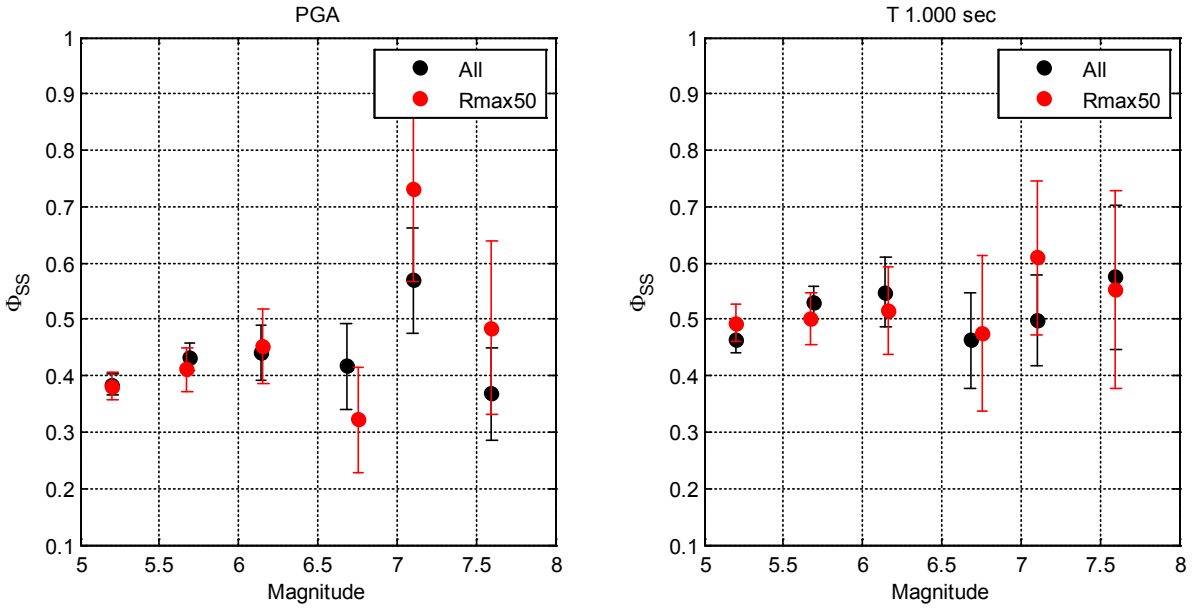



**Figure K.2-3:** Magnitude-dependence of $\phi_{SS}$ for the European dataset $EUR_{PHISS}$ (all distances and distance less than 50 km) at PGA (left) and T = 1 sec (right)

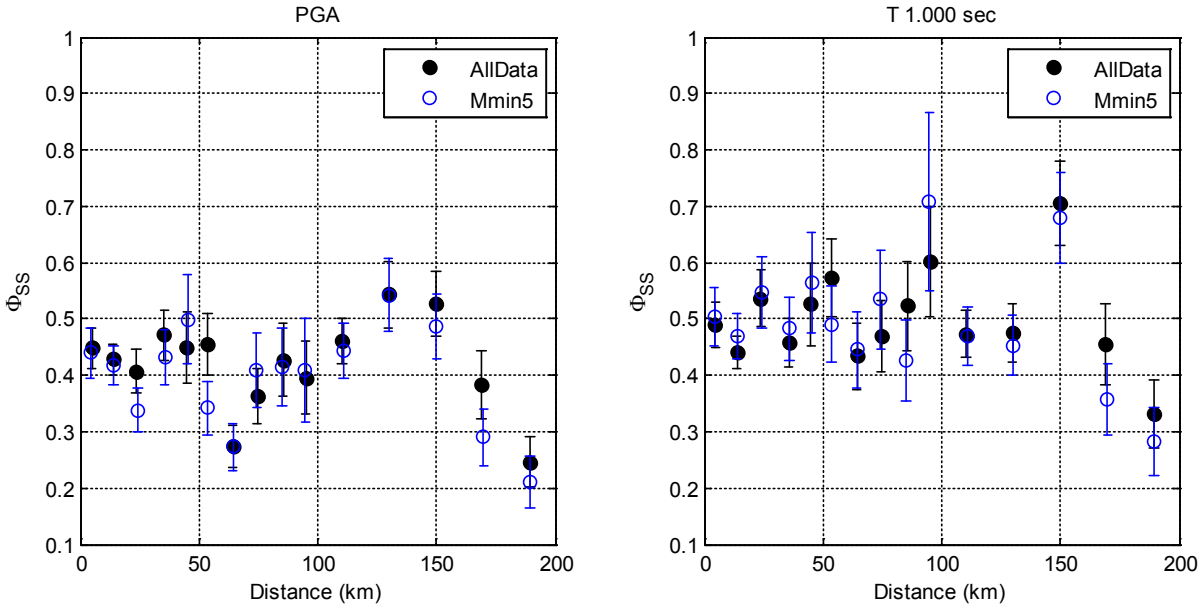



**Figure K.2-4:** Distance-dependence of $\phi_{SS}$ for the European dataset $EUR_{PHISS}$ (all distances and **M** ≥ 5.0) at PGA (left) and T = 1 sec (right).

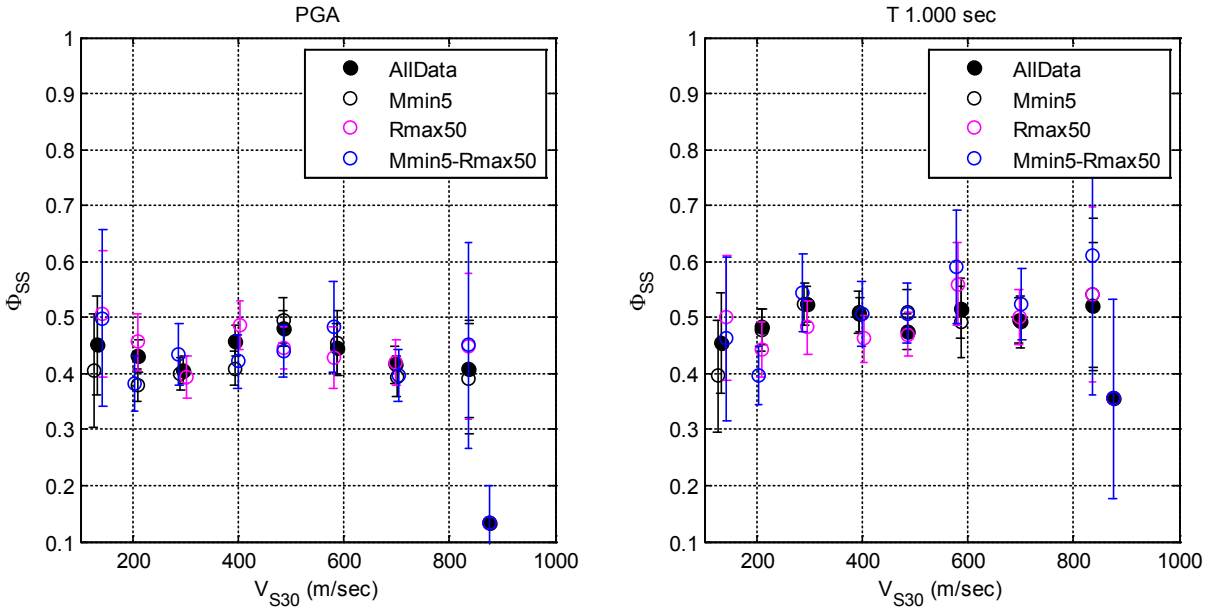



**Figure K.2-5:** $V_{S30}$-dependence of $\phi_{SS}$ for the European dataset $EUR_{PHISS}$ at PGA (left) and T = 1 sec (right).

## K.3 References

Abrahamson, N.A., Silva, W.J., and Kamai, R. (2014). Summary of the AKS14 Ground-Motion Relation for Active Crustal Regions, *Earthquake Spectra*, Vol. 30(3), 1025-1055, DOI: 10.1193/070913EQS198M.

Akkar, S., Sandikkaya, M.A., and Bommer, J.J. (2014a). Empirical ground-motion models for point- and extended-source crustal earthquake scenarios in Europe and the Middle East, *Bull. Earthquake Eng*., Vol. 12(1), 359-387, DOI 10.1007/s10518-013-9461-4.

Akkar, S., Sandikkaya, M.A., and Bommer, J.J. (2014b). Erratum to: Empirical ground-motion models for point- and extended-source crustal earthquake scenarios in Europe and the Middle East, *Bull. Earthquake Eng*, Vol. 12(1), 389-390, DOI 10.1007/s10518-013-9508-6.

Boore, D.M., Stewart, J.P., Seyhan, E., and Atkinson, G.M. (2014). NGA-West 2 Equations for Predicting PGA, PGV, and 5%-Damped PSA for Shallow Crustal Earthquakes, *Earthquake Spectra*, Vol. 30(3), 1057-1085, DOI: 10.1193/070113EQS184M.

Campbell, K.W., and Bozorgnia, Y. (2014). NGA-West2 Ground Motion Model for the Average Horizontal Components of PGA, PGV, and 5%-Damped Linear Acceleration Response Spectra, *Earthquake Spectra*, Vol. 30(3), 1087-1115, DOI: 10.1193/062913EQS175M.

Chiou, B.S.-J., and Youngs, R.R. (2014). Update of the Chiou and Youngs NGA Model for the Average Horizontal Component of Peak Ground Motion and Response Spectra, *Earthquake Spectra*, Vol. 30(3), 1117-1153, DOI: 10.1193/072813EQS219M.

Lin, P.-S., Chiou, B., Abrahamson, N., Walling, M., Lee, C.-T., and Cheng, C.-T. (2011). Repeatable source, site, and path effects on the standard deviation for empirical ground-motion prediction models, *Bull. Seismol. Soc. Am.,* Vol. 101(5), 2281-2295, DOI: 10.1785/012009031.

# *APPENDIX L*

## PVNGS KEY INTERFACE ISSUES

# GeoPentech

SWUS GMC SSHAC Level 3 Project Project No.12024B
October 27, 2014

Arizona Public Service Company
Palo Verde Nuclear Generating Station (PVNGS)
*Wandell, Christopher J.*
Senior Consulting "Chief" Civil Engineer
Phone: (623) 393-6741
E-mail: christopher.wandell@aps.com

**Subject: Revision 1.0 to Transmittal of material to facilitate the interface between SWUS GMC SSHAC Level 3 project and PVNGS Site Response effort**

Dear Mr. Wandell:

This transmittal contains the material intended to facilitate the interface between the Southwestern US Ground Motion Characterization (SWUS GMC) SSHAC Level 3 Project and the Site Response effort for PVNGS PSHA Project, and was originally transmitted on October 3, 2014. This revision is Rev. 1 and is prepared at the request of Dr. Gabriel Toro of LCI to accommodate some clarification on the host kappa value and on the target kappa value with its uncertainty. This revision includes information on the host density profile associated to the host $V_S$ profile, which was not previously included in Rev. 0.

Specifically, this Rev.1 addresses the following topics: a) Host kappa value – *Updated*; b) Host profile ($V_S$ and Density) – *Updated*; c) Target kappa value and its uncertainty – *Updated*; and d) Target $V_S$ profile – *Original*.

The technical details are provided below.

### a) Host kappa value - *Updated*

Analysis of kappa estimates associated to the seven proponent GMPEs applied to the PVNGS site, for the reference $V_{S30}$ condition of 760 m/s, was conducted by Linda Al-Atik in September 2014. A document describing the methodology applied to obtain the kappa estimates and the resulting values is attached digitally to this transmittal, and is labeled "Host

Kappa_LindaAlAtik-09222014.docx". The document will be integrated in the SWUS GMC Report as appropriate. Table 1 is extracted from the document, and shows the kappa estimates for the proponent GMPEs at reference site conditions as follows:

**Table 1. Best estimate host kappa values for the 7 candidate GMPEs for a reference $V_{S30}$ of 760 m/sec.**

| GMPE | ASK14 | BSSA14 | CB14 | CY14 | ASB13 | Bindi13 | Zhao06 |
|---|---|---|---|---|---|---|---|
| Host Kappa (sec) | 0.045 | 0.038 | 0.037 | 0.041 | 0.042 | 0.045 | 0.042 |

The geometric mean of the above estimates is 0.041 seconds, and represents the host kappa value for the SWUS GMC Project. Epistemic uncertainty to this kappa value is not provided.

No epistemic uncertainty in the host kappa value should be considered in the calculation of adjustment factors from Reference-rock to PVNGS rock because this uncertainty is captured by the variation in high-frequency spectral shape within the SWUS GMC common form based models.

### b) Host profile ($V_S$ and Density) - *Updated*

The excel file labeled "WUS_VsProfile-10272014.xls", attached digitally to this transmittal, contains the information on the $V_S$ profile and density utilized in the host kappa analysis.

The $V_S$ values in the profiles are consistent with Peninsula Range base profile in Kamai et al. (2013) 2013/12 PEER Report, available at the following URL:

http://peer.berkeley.edu/publications/peer_reports/reports_2013/webPEER-2013-12-Kamai_et_al.pdf

The density values were calculated from the above Vs values using the widely used approach recommended by Dr. David Boore of the USGS. This approach is documented in the following URL:

http://daveboore.com/daves_notes/daves_notes_on_relating_density_to_velocity_v1.2.pdf

Evaluation of alternative density profiles was not part of the SWUS GMC TI Team's scope of work.

### c) Target kappa value and its uncertainty - *Updated*

Analysis of the kappa estimates for sites around PVNGS is documented in the Kishida et al. (2014) 2014/09 PEER Report available at the following URL:
http://peer.berkeley.edu/publications/peer_reports/reports_2014/webPEER-2014-09-Arizona.pdf

The kappa estimates from the PEER report are 0.033 sec with a logarithmic standard deviation of 0.5 (natural logarithm base), and they are associated to reference conditions. This value represents a bedrock kappa estimate.

**d) Target $V_S$ profile - *Original***

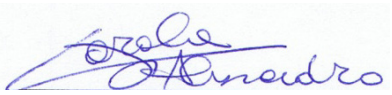
The digitized profiles used for the 2014/09 PEER Report study were provided by Walt Silva on September 18, 2014. The two profiles are called 113A.PAR and Z14A.PAR, and are digitally attached to this communication.

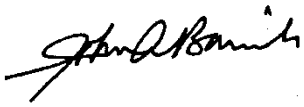
Per Walt Silva's communication, the two profiles we used for computing the amplification associated to the target kappa analysis. The two profiles were obtained via SASW inversion documented in the 2014/09 PEER Report, and they merged into the host $V_S$ profile at depth. Profile Z14A was used for stiff soil sites (i.e. $V_{S30} \leq$ 670 m/s), and profile 113A was used for firm rock.

Should you have any question, or require more information, please do not hesitate to contact us.

Sincerely,

**GeoPentech**





Carola Di Alessandro
Project Manager

John A. Barneich
Principal

CC:
PVNGS Project Technical Integrator: Robin McGuire
PVNGS Hazard Analysts: Melanie Walling and Gabriel Toro
SWUS GMC TI Team Lead: Norm Abrahamson

# REFERENCES

Kishida, T., Kayen, R.E., Ktenidou, O-J., Silva, W.J., Darragh, R.B., and Watson-Lamprey, J. (2014). PEER Arizona Strong-Motion Database and GMPEs Evaluation, *PEER Report 2014/09*, Pacific Earthquake Engineering Research Center, University of California, Berkeley, CA, June 2014, 136 pp.

Kamai, R., Abrahamson, N.A., and Silva, W.J. (2013). Nonlinear Horizontal Site Response for the NGA-West2 Project, *PEER Report 2013/12*, Pacific Earthquake Engineering Research Center, University of California, Berkeley, CA, May 2013, 70 pp

# APPENDIX M

## HOST KAPPA

The ground-motion prediction equations (GMPEs) used in this project (Section 5.5) capture the site effects using the shear-wave velocity in the top 30 m ($V_{S30}$) and the depth of the soil. The point-source stochastic model (SMSIM), widely applied in the Central and Eastern North America (CENA), has an additional site parameter, called kappa, that describes the high-frequency spectral content for hard-rock site and has a large effect on the high-frequency (> 10 Hz) ground motion. Because the empirical ground-motion data sets are dominated by soil and soft-rock sites (e.g. Section 5.1 and figures therein), the GMPEs are not well constrained for high $V_{S30}$ values. To use the empirical GMPEs in the range that they are better constrained, the SWUS GMC project used a reference rock condition for a soft-rock site with $V_{S30}$ = 760 m/s. The adjustment of the reference soft-rock ground motion to the site-specific rock site condition is part of the site response study that is conducted outside of the SWUS GMC project. For hard-rock sites, the adjustment should consider both the effects of kappa as well as the effect of the $V_S$ profile.

Unless kappa is included explicitly as a prediction parameter, GMPEs reflect the average kappa-$V_{S30}$ correlation of the regions that contributed the ground-motion data from which they were derived (host region or regions). Therefore, kappa implied by the spectral shape of the GMPEs is referred to as "host" kappa. This Appendix presents the methodology for estimating host kappa for the candidate GMPEs used for the Palo Verde Nuclear Generation Station (PVNGS) and Diablo Canyon Power Plant (DCPP) sites, and shows results for to the reference soft-rock condition ($V_{S30}$ = 760 m/s) adopted for the SWUS GMC project. The main use of the host kappa values is to allow for a comparison of the site-specific kappa with the kappa implied by the candidate GMPEs. If the site-specific kappa is different from the host kappa, then a kappa correction can be made to the response spectra from the probabilistic seismic hazard analysis (PSHA) as part of the site response study.

### M.1 Kappa Components and Terminology

Kappa is a measure of the observed high-frequency decay of Fourier amplitude spectra (FAS) of ground motion. The mechanism causing the observed high-frequency fall-off has been subject of debate for the last 30 years. Detailed description of the origins of kappa can be found in Campbell (2009), Campbell et al. (2014) and Hashash et al. (2014). Kappa estimated at a site from a given earthquake scenario is referred to as $\kappa_{obs}$ and reflects the combined effects of source ($\kappa_{source}$), path ($\kappa_{path}$), and site ($\kappa_{site}$) on spectral decay:

$$\kappa_{obs} = \kappa_{source} + \kappa_{path} + \kappa_{site}. \quad \text{(Eq. M-1)}$$

Studies of ground-motion recordings at a single station from earthquakes at multiple source-to-site distances show that $\kappa_{obs}$ increases with source-to-site distance in a manner consistent with the effects of anelastic attenuation (e.g., Anderson and Hough, 1984). The distance dependence of kappa reflects the incremental attenuation due to the horizontal propagation of shear waves through the crust. Zero-distance kappa, $\kappa_0$, can be obtained after removing the path attenuation effects from $\kappa_{obs}$. Assuming that average $\kappa_{source}$ is negligible (Purvance and Anderson, 2003; Van Houtte et al., 2011), $\kappa_0$ approximates $\kappa_{site}$ with $\kappa_{site}$ representing the attenuation due to the propagation of shear waves through subsurface materials below and near the site within distances of hundreds meters to a few kilometers.

Kappa estimated using the inverse random vibration theory (IRVT) approach (Al Atik et al., 2013) is the average of $\kappa_{obs}$ inferred from short distance scenarios (5, 10, and 20 km) and is referred to as $\kappa_1$. Assuming that the distance contribution to kappa is negligible for these short distance scenarios, $\kappa_1$ approximates $\kappa_0$.

## M.2 Methodology

Host kappa values were estimated using the IRVT approach for the following GMPEs for a reference $V_{S30}$ of 760 m/sec: Abrahamson et al. (2014) (ASK14), Boore et al. (2014) (BSSA14), Campbell and Bozorgnia (2014) (CB14), Chiou and Youngs (2014) (CY14), Bindi et al. (2014a, 2104b) (Bi14), Akkar et al. (2014a, 2014b) (ASB14), and Zhao et al. (2006) (ZH06). The Idriss (2014) model is not evaluated for host kappa because it is for a broad soft-rock category rather than the reference $V_{S30}$ = 760 m/s. For the Idriss (2014) candidate GMPE used for DCPP, the kappa is assumed to be the same as for the other NGA-West2 GMPEs because they use similar data sets for the $V_{S30}$ > 450 m/s as used by Idriss (2014).

The IRVT approach relies upon deriving Fourier amplitude spectra (FAS) from the GMPE response spectra using IRVT as implemented in the computer program STRATA (Kottke and Rathje, 2008). The input to STRATA consists of the GMPE response spectra and ground-motion duration estimates for the scenarios considered. The GMPE host kappa values for each GMPE are estimated using the high-frequency slope of the FAS according to the Anderson and Hough (1984) method. The scenarios are restricted to short distances to reduce the impact of anelastic attenuation (Q) on the high-frequency part of the response spectra and FAS. To decouple kappa from site amplification effects, the FAS are divided by the representative site amplification factors before estimating host kappa.

As discussed in Al Atik et al. (2013), response spectra with strong high-frequency attenuation, such as the Western United States (WUS) spectra, are subject to saturation effects resulting from the increased contribution of Fourier amplitudes at lower frequencies to the high-frequency response spectral accelerations. That is, for frequencies well above the frequency of the peak in the response spectrum, the response spectral values are affected by the FAS at the lower frequencies and not just by the FAS

near the oscillator frequency. This makes it difficult to resolve the FAS at high frequencies (greater than about 30 to 35 Hz for WUS GMPEs) from the shape of the response spectrum, resulting in potentially inaccurate FAS estimates at these high frequencies. In many cases, the inverted FAS will drift off at very high frequencies due to this issue, making it difficult to find the best slope of the high-frequency FAS. As a result, frequencies larger than 30 Hz are not used for estimating GMPEs host kappa values.

## M.3 Host Kappa Values

The main application of the kappa correction is for PVNGS, so the scenarios selected for estimating the host kappa were based on the PVNGS source characterization. In particular, the host kappa values were estimated for the seven candidate GMPEs using the IRVT approach for nine normal-faulting scenarios with a dip angle of 50 degrees, for magnitude 5.0, 6.0, and 7.0 and $R_X$ distances of 5, 10, and 20 km on the footwall. These magnitude, distance, and style-of-faulting scenarios were selected to be consistent with the sources contributing to the hazard at PVNGS at high frequency (Sections 4.2.2 and 4.2.3). Moreover, short-distance scenarios are selected to decouple the near-site attenuation effects from the distance attenuation effects as described in the previous section. To compute the distance metrics required for the GMPEs given the magnitude, dip, and Rx values, the rupture geometry needs to be defined. The rupture width was calculated according to Wells and Coppersmith (1994); the hypocenter was assumed to be located at the center of the fault rupture; the depth to top of rupture was calculated using the relation given by Chiou and Youngs (2014). The IRVT method requires the duration of the ground motion, which was estimated using the duration model in the WUS stochastic point-source model of Campbell (2003) with a stress drop of 100 bars. The duration used in the IRVT is the sum of the source and path durations.

The western U.S. (WUS) $V_S$ profile of Kamai et al. (2013) with a $V_{S30}$ of 760 m/sec was used as a representative $V_S$ profile for the host region as shown in Figure M-1. Linear site amplification factors for the host $V_S$ profile were developed using the square-root impedance (SRI) or quarter wavelength (QWL) method as implemented in the computer program SMSIM (Boore, 2005). The amplification factors were derived at the surface of the profile with respect to the half-space located at a depth of 9.6 km with $V_S$ of 3.5 km/sec. Default densities based on WUS $V_S$-density relationships built into the QWL program were used. The approach to relate $V_S$ and density is documented in the following URL: http://daveboore.com/daves_notes/daves_notes_on_relating_density_to_velocity_v1.2.pdf. Evaluation of alternative density profiles was not part of the SWUS GMC TI Team's scope of work.

An angle of incidence at the source of zero degrees (i.e. the wave-front is parallel to the surface and its raypath is perpendicular, or normal, to the interface) was adopted. Figure M-2 shows the QWL site amplification factors for the WUS rock site with $V_{S30}$=760 m/s. The sensitivity of the QWL site amplification factors to using an angle of incidence of 30 degrees was evaluated with the results shown in Figure M-2. While an angle of incidence of 30 degrees is considered to be more appropriate for deep

earthquake sources, the difference in the resulting site amplification factors is small (less than 10%). Moreover, Figure M-2 shows that the high-frequency slopes of the site amplification factors are similar between frequencies of about 5 to 20 Hz for the two angles of incidence. As a result, the impact of using an angle of incidence of 30 degrees versus 0 degrees on the resulting host kappa values is expected to be small. Finally, an angle of incidence of zero degrees is considered to be generally more consistent with 1-D site response analyses and was therefore adopted by the TI Team.

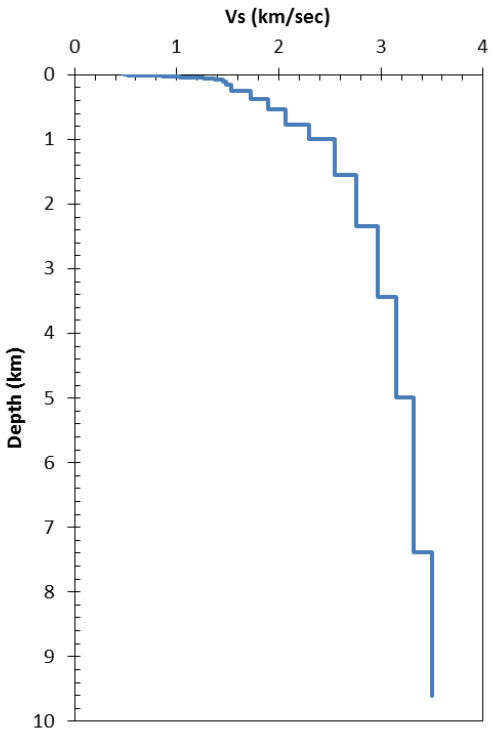



**Figure M-1:** Host $V_S$ profile with $V_{S30}$ of 760 m/sec based on Kamai et al. (2013).

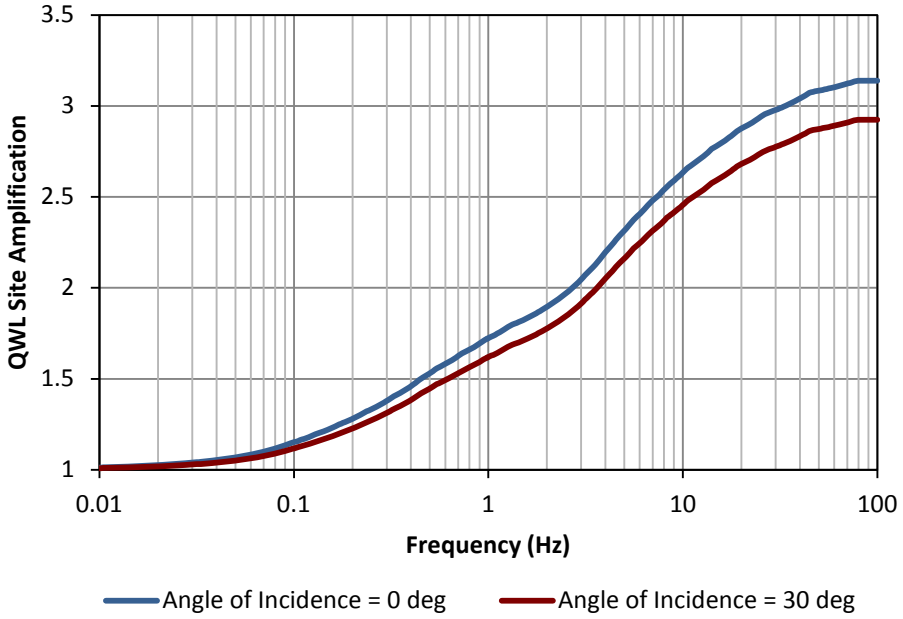



**Figure M-2:** QWL linear site amplification factors for the WUS $V_S$ profile with $V_{S30}$ of 760 m/sec, for and angle of incidence of zero degrees (blue line) and 30 degrees (red line).

The FAS were derived from the GMPEs response spectra using the IRVT approach for the nine scenarios described above (3 magnitudes and 3 distances) and then divided by the host site amplification factors shown in Figure M-2 for an angle of incidence of zero degrees to decouple the site amplification from kappa effects at high frequency. The resulting FAS were then inspected to select the start and end frequencies (f1 and f2) over which log(FAS) versus frequency is approximately linear. Kappa for each of the nine selected scenarios was estimated by fitting the Anderson and Hough (1984) exponential kappa scaling function to the FAS between f1 and f2. Estimated kappa values were averaged for the nine selected scenarios to define the host kappa ($\kappa_1$) for the seven candidate GMPEs.

The $\kappa_1$ estimates are sensitive to the choice of f1 and f2. Figure M-3 shows an example of the effect of different f1 and f2 choices on the resulting $\kappa_1$ estimates for CY14 for the magnitude 6.0 and $R_X$ = 10 km scenario. Figure M-3 shows that for three different f1 and f2 picks, log(FAS) versus frequency is linear but the resulting $\kappa_1$ estimates are 0.037, 0.040 and 0.042 sec. The $\kappa_1$ values for the seven candidate GMPEs were derived for the best visual picks of f1 and f2. Figures M-4 to M-10 show the high-frequency slope fit to the IRVT-derived FAS for the seven candidate GMPEs for the nine scenarios. The $\kappa_1$ values estimated for the nine selected scenarios were averaged for each GMPE. The averaged $\kappa_1$ estimates are listed in Table M-1 along with their standard deviations for each GMPE.

**Table M-1:** Best estimate $\kappa_1$ values for the 7 candidate GMPEs for a reference $V_{S30}$ of 760 m/sec.

| GMPE | ASK14 | BSSA14 | CB14 | CY14 | ASB14 | Bi14 | ZH06 |
|---|---|---|---|---|---|---|---|
| Average $\kappa_1$ (sec) | 0.045 | 0.038 | 0.037 | 0.041 | 0.042 | 0.045 | 0.042 |
| Standard Deviation | 0.0014 | 0.0033 | 0.0028 | 0.0014 | 0.0034 | 0.0052 | 0.0022 |

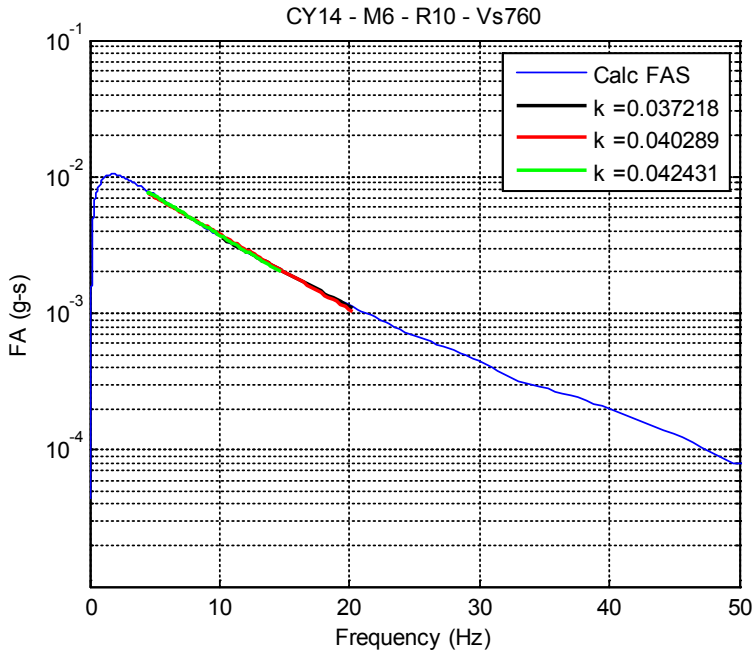



**Figure M-3:** Sensitivity of $\kappa_1$ estimates to the choice of f1 and f2 for CY14 for a scenario with magnitude 6.0 and distance of 10 km.

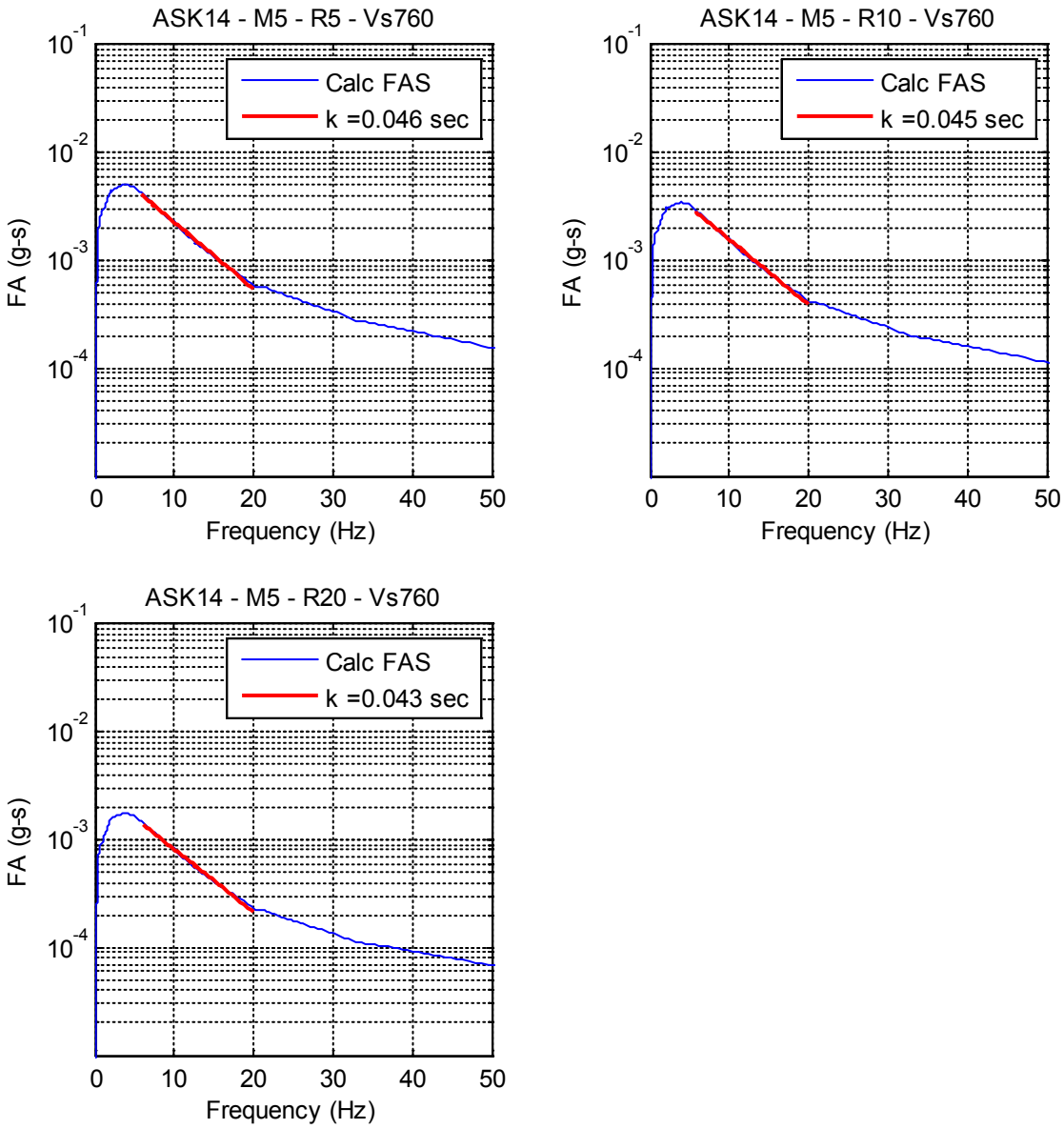



**Figure M-4a:** Fit of the high-frequency FAS for ASK14 for the **M**5.0 and $R_x$ = 5, 10, and 20 km scenarios.

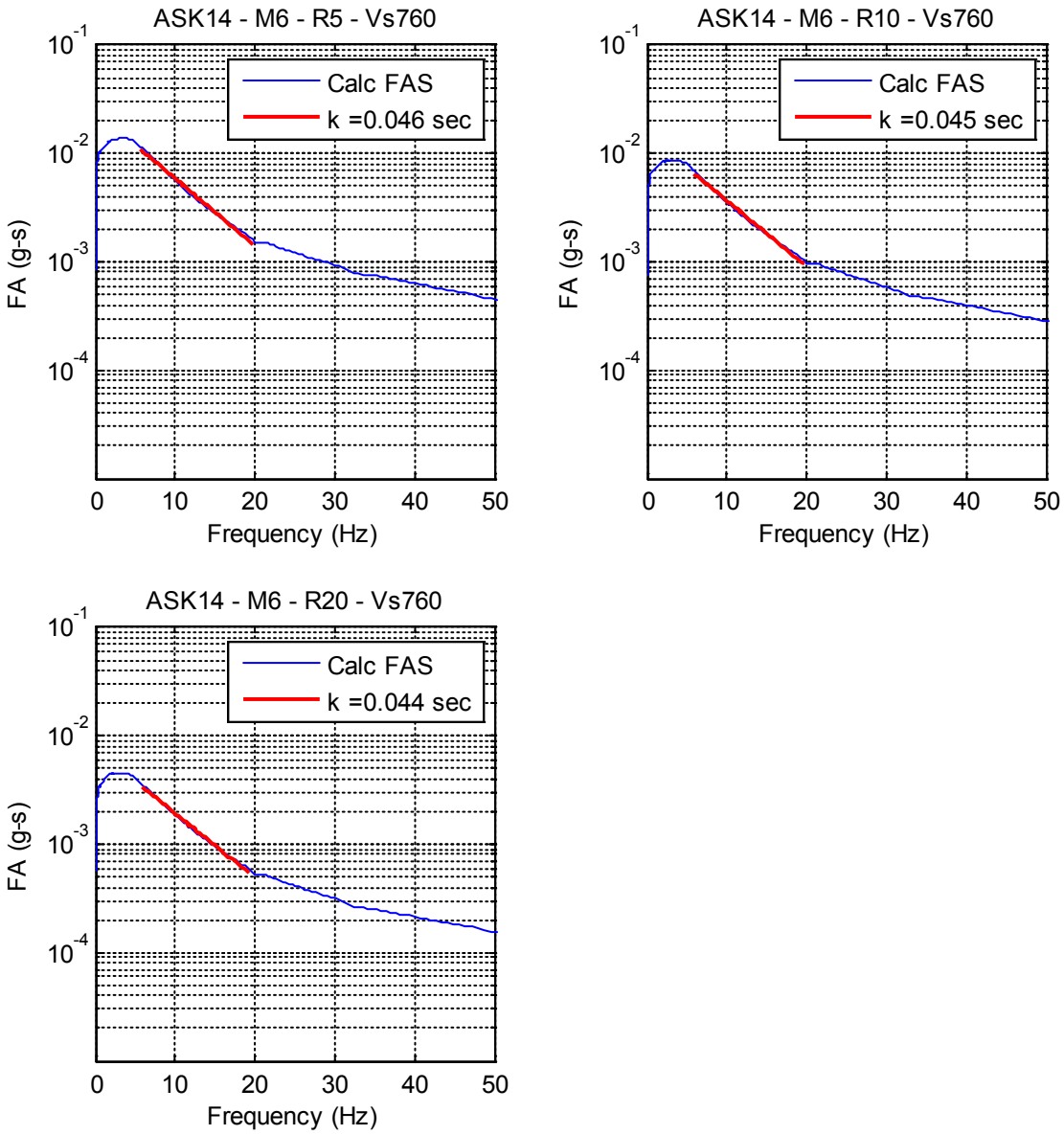



**Figure M-4b:** Fit of the high-frequency FAS for ASK14 for the **M**6.0 and $R_x$ = 5, 10 and 20 km scenarios.

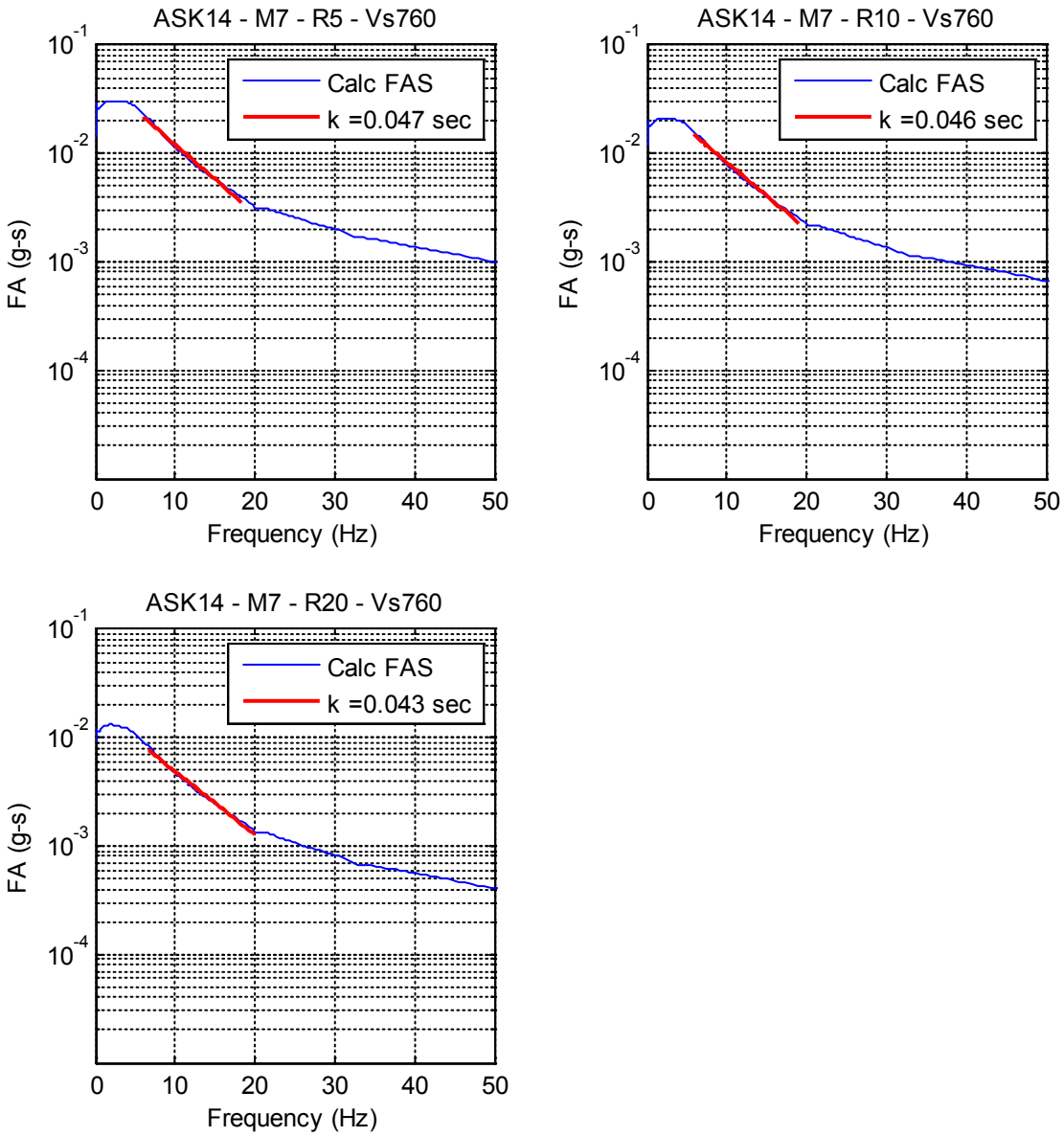



**Figure M-4c:** Fit of the high-frequency FAS for ASK14 for the **M**7.0 and $R_x$ = 5, 10, and 20 km scenarios.

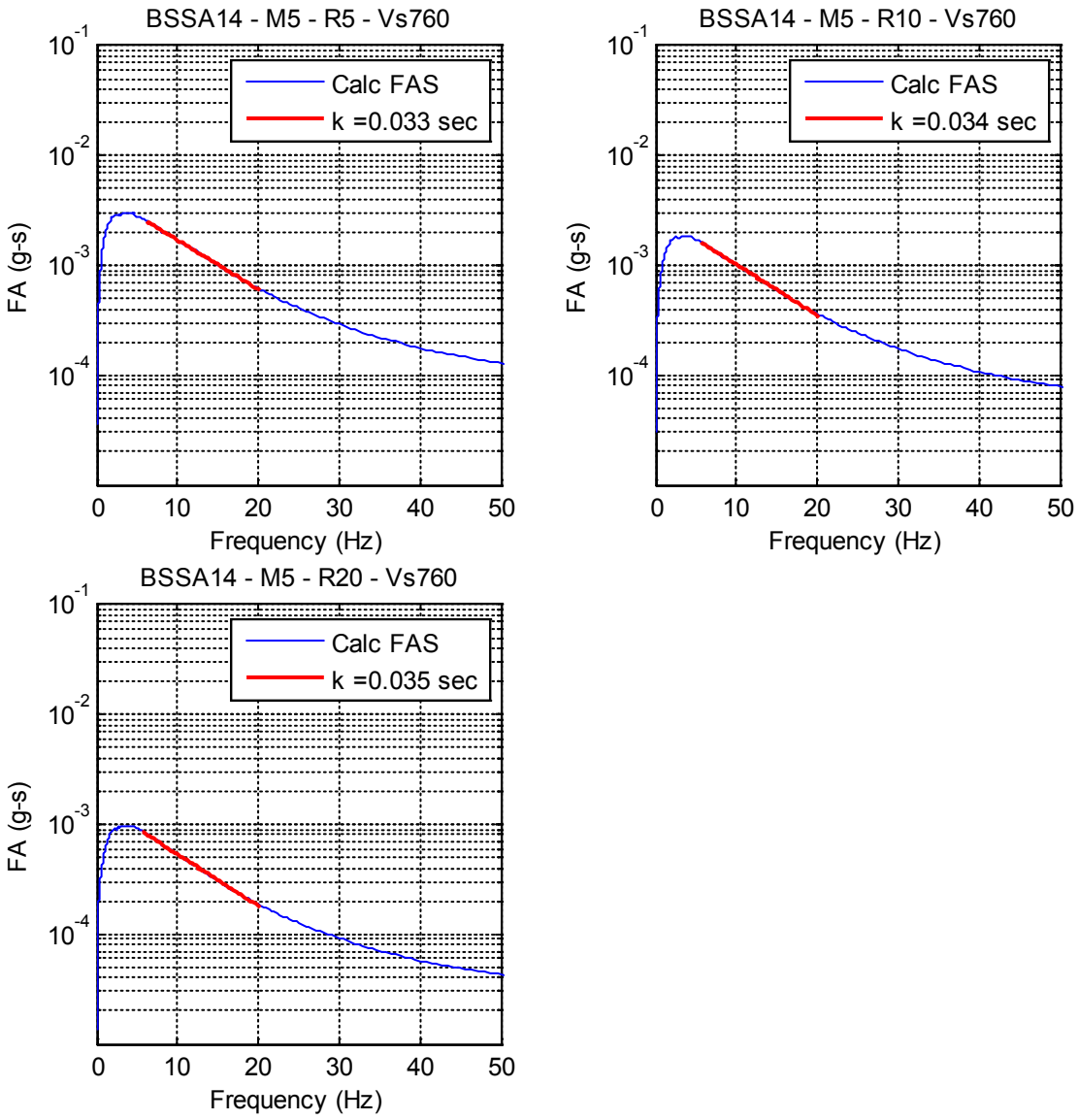



**Figure M-5a:** Fit of the high-frequency FAS for BSSA14 for the **M**5.0 and $R_x$ = 5, 10, and 20 km scenarios.

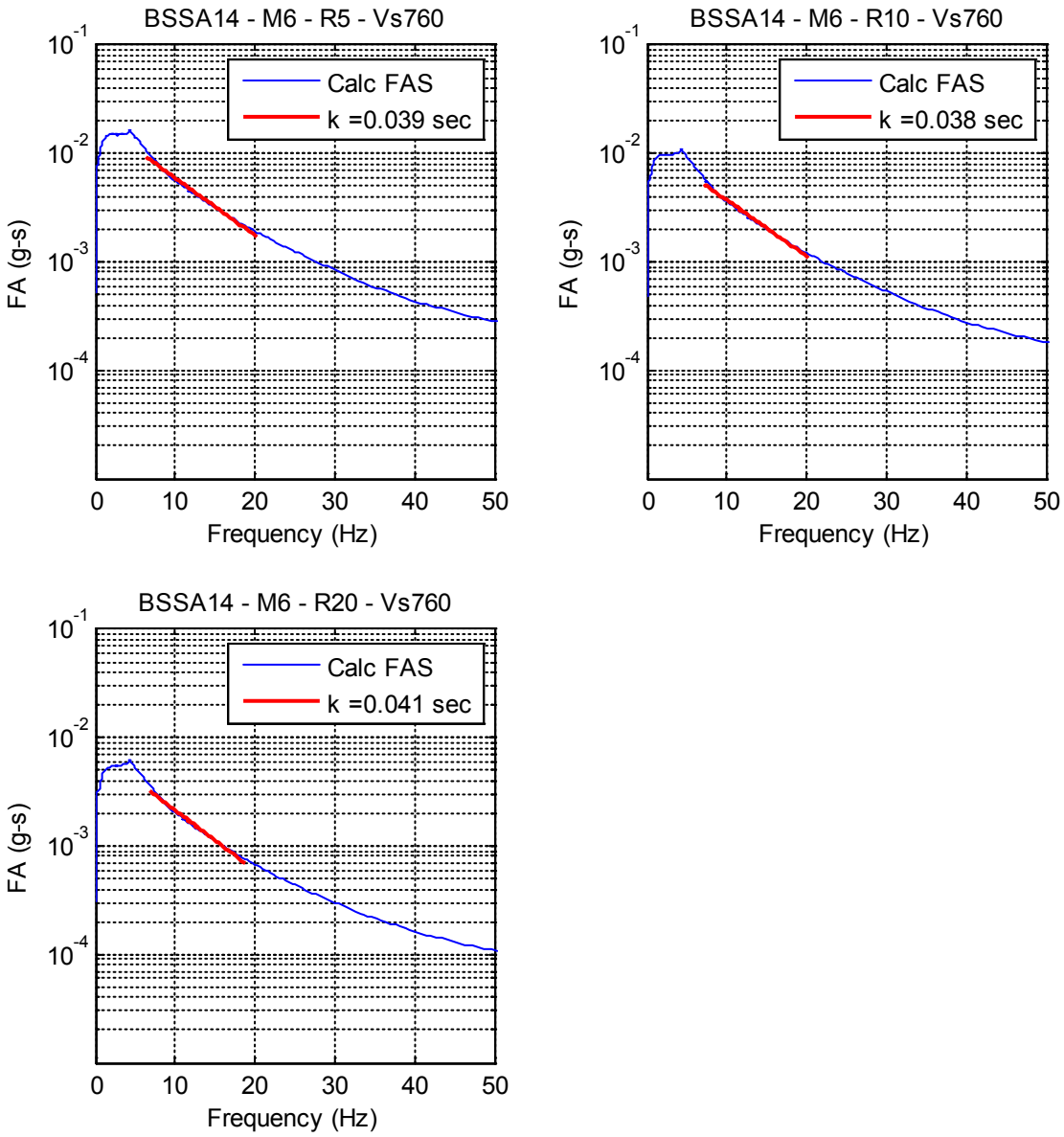



**Figure M-5b:** Fit of the high-frequency FAS for BSSA14 for the **M**6.0 and $R_x$ = 5, 10 and 20 km scenarios.

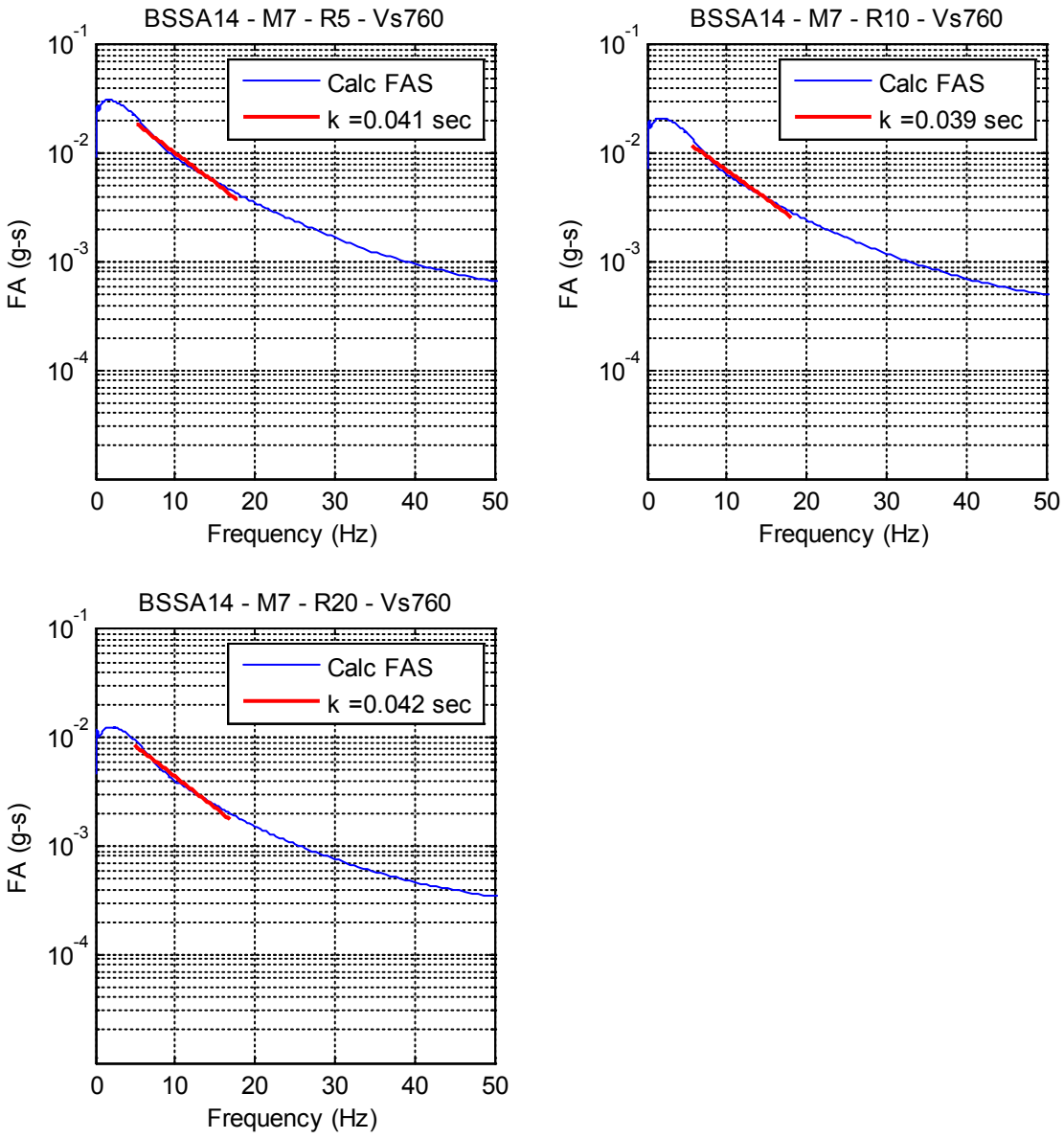



**Figure M-5c:** Fit of the high-frequency FAS for BSSA14 for the **M**7.0 and $R_x$ = 5, 10, and 20 km scenarios.

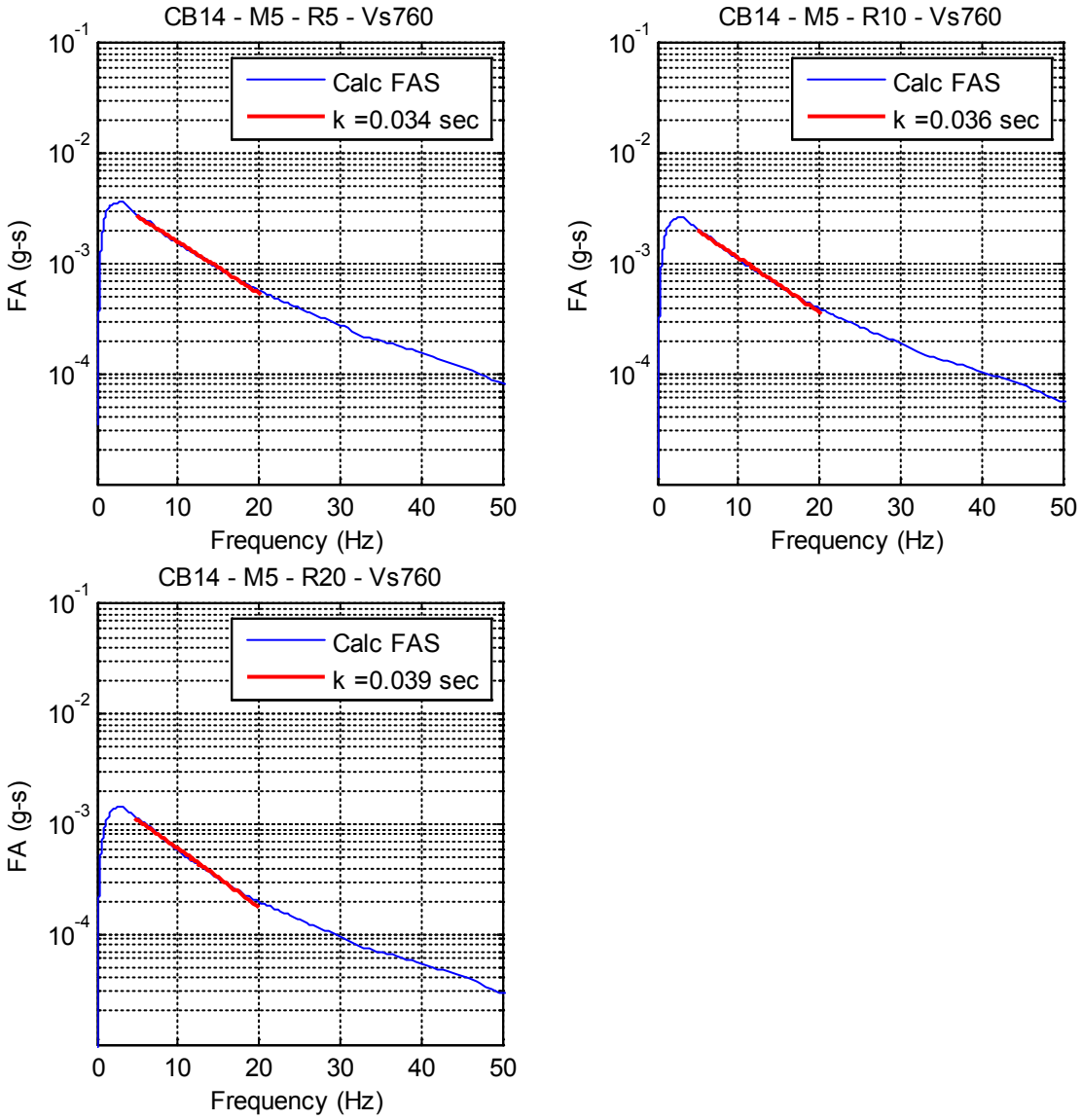



**Figure M-6a:** Fit of the high-frequency FAS for CB14 for the **M**5.0 and $R_x$ = 5, 10, and 20 km scenarios.

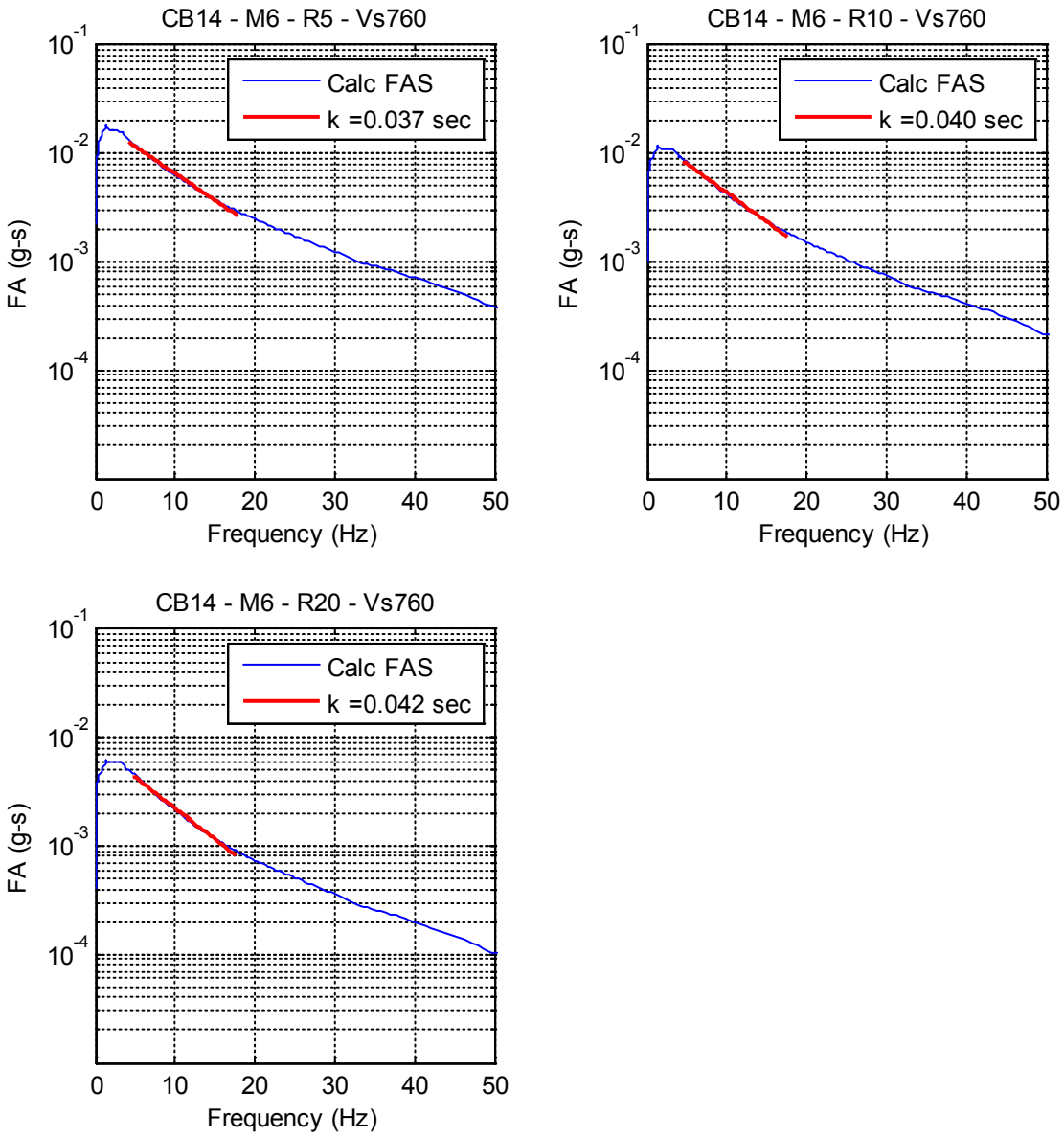



**Figure M-6b:** Fit of the high-frequency FAS for CB14 for the **M**6.0 and $R_x$ = 5, 10 and 20 km scenarios.

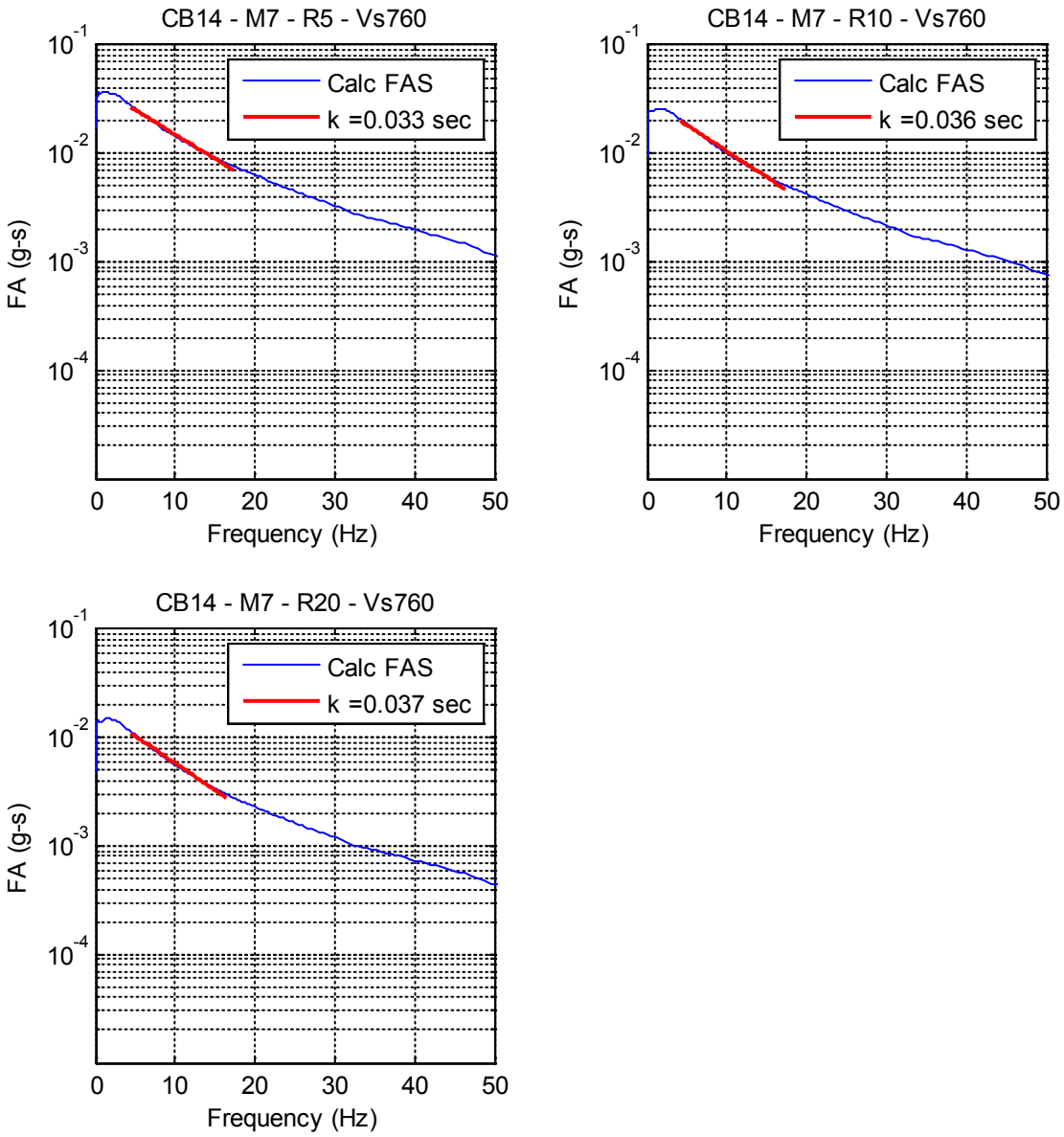



**Figure M-6c:** Fit of the high-frequency FAS for CB14 for the **M**7.0 and $R_x$ = 5, 10, and 20 km scenarios.

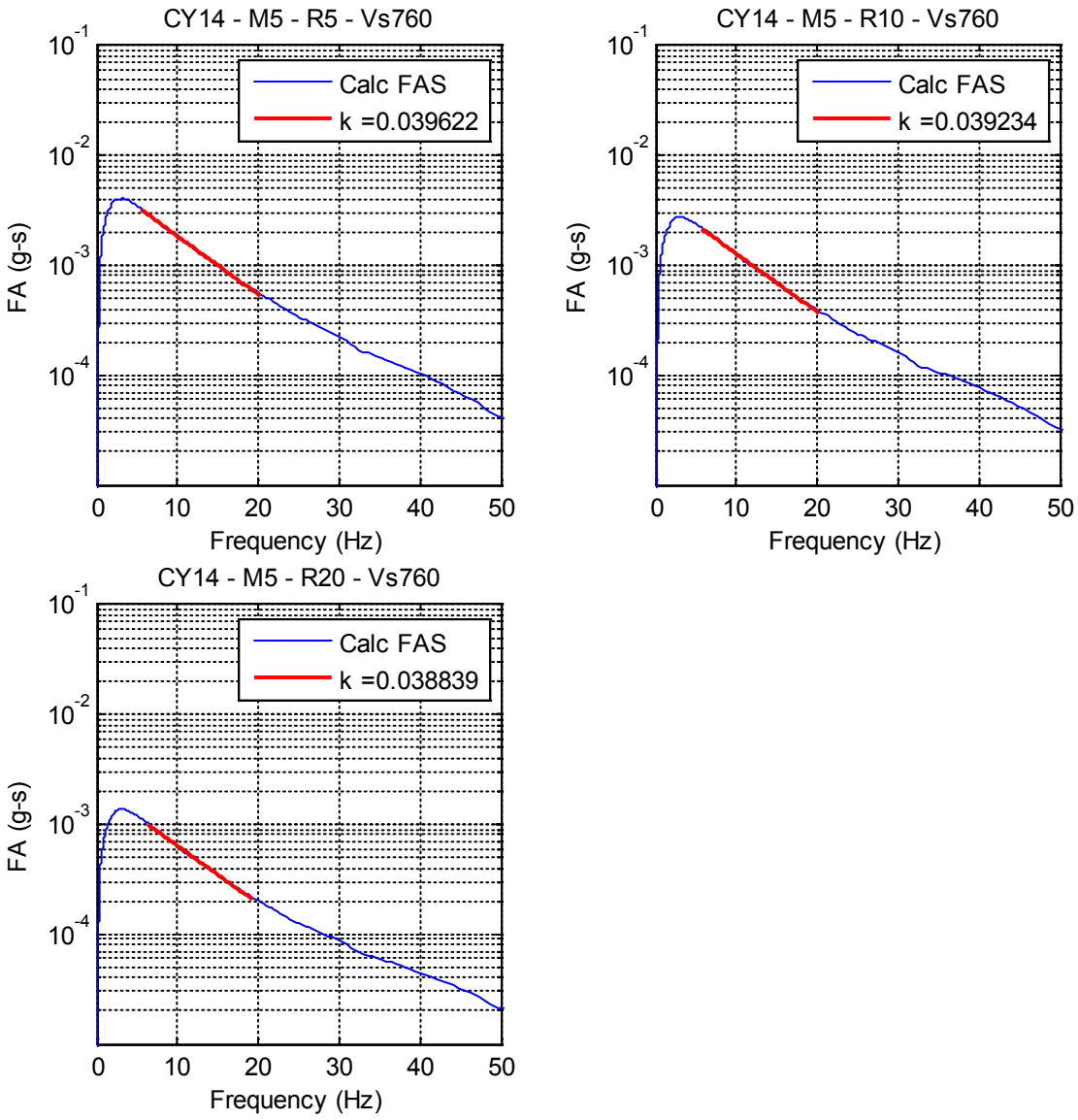



**Figure M-7a:** Fit of the high-frequency FAS for CY14 for the **M**5.0 and $R_x$ = 5, 10, and 20 km scenarios.

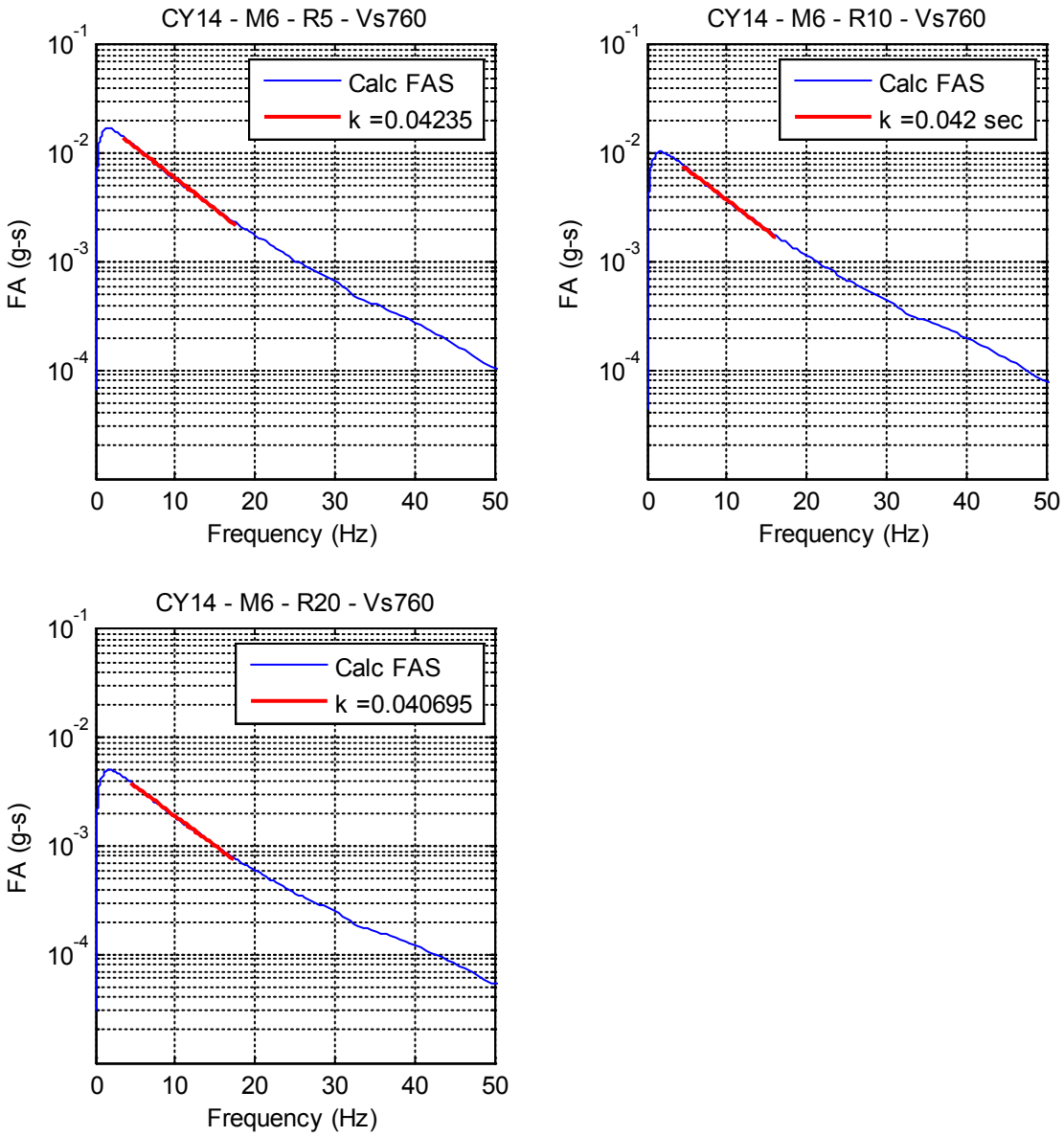



**Figure M-7b:** Fit of the high-frequency FAS for CY14 for the **M**6.0 and $R_x$ = 5, 10 and 20 km scenarios.

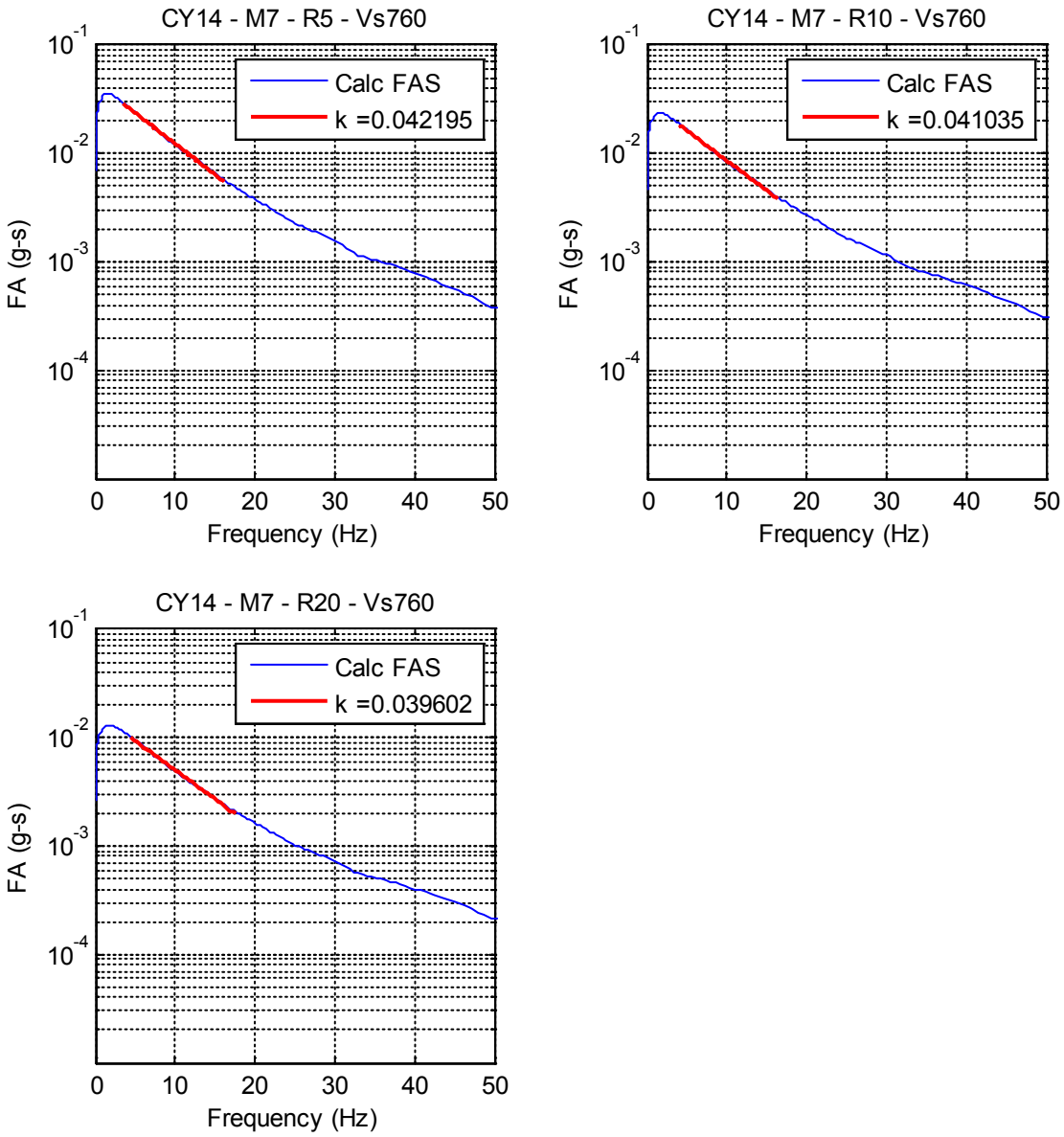



**Figure M-7c:** Fit of the high-frequency FAS for CY14 for the **M**7.0 and $R_x$ = 5, 10 and 20 km scenarios.

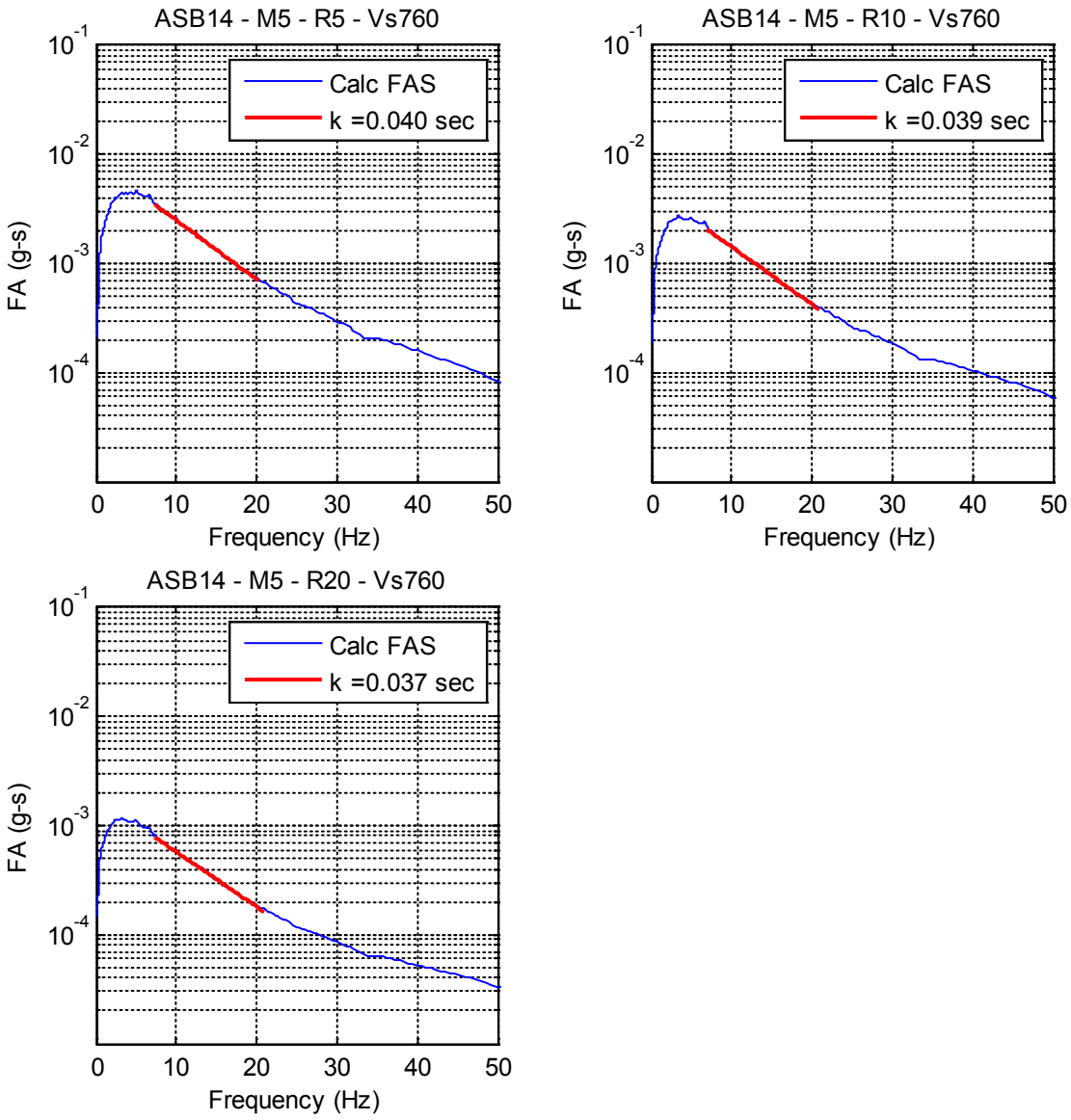



**Figure M-8a:** Fit of the high-frequency FAS for ASB14 for the **M**5.0 and $R_x$ = 5, 10, and 20 km scenarios.

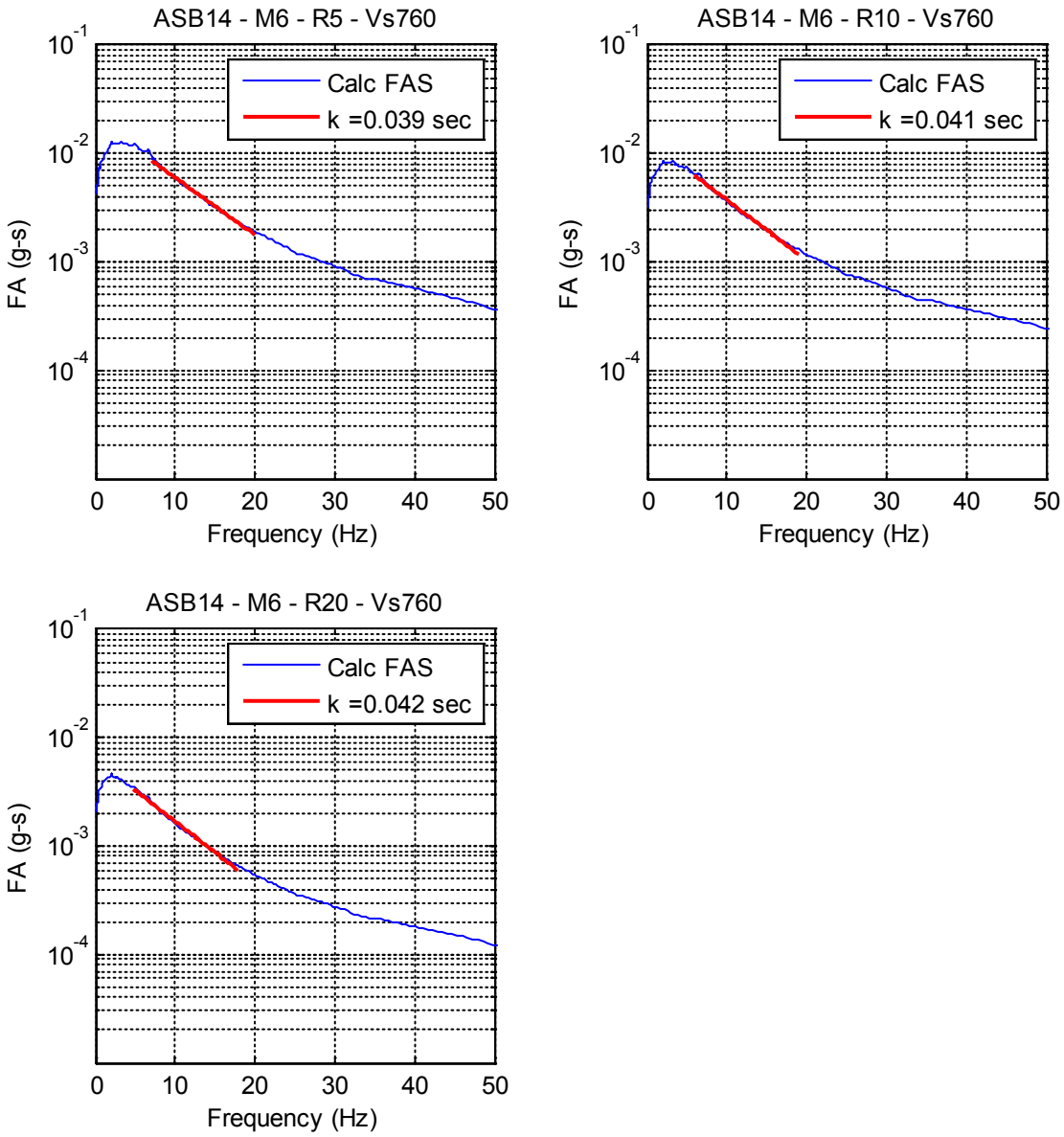



**Figure M-8b:** Fit of the high-frequency FAS for ASB14 for the **M**6.0 and $R_x$ = 5, 10 and 20 km scenarios.

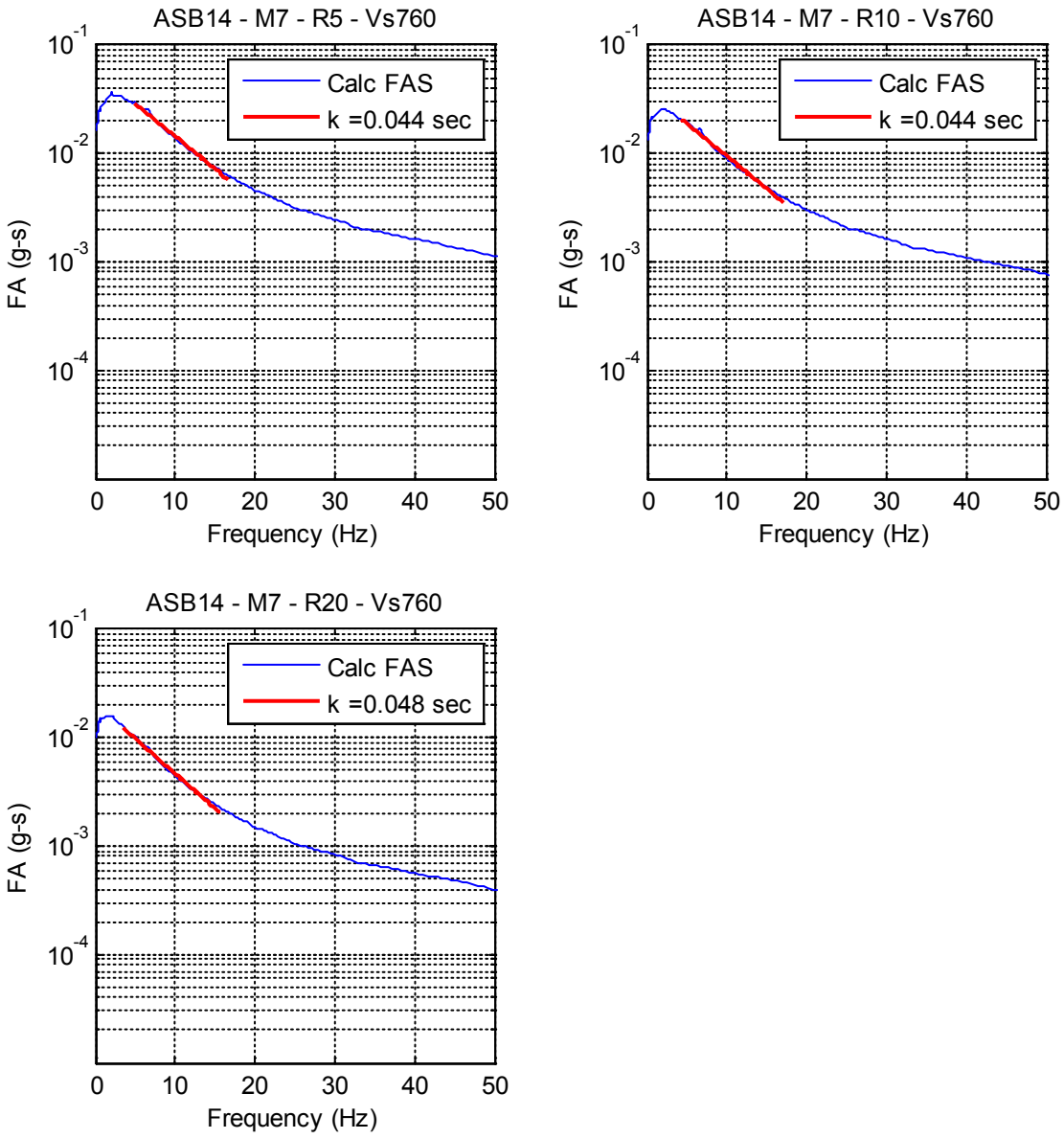



**Figure M-8c:** Fit of the high-frequency FAS for ASB14 for the **M**7.0 and $R_x$ = 5, 10 and 20 km scenarios.

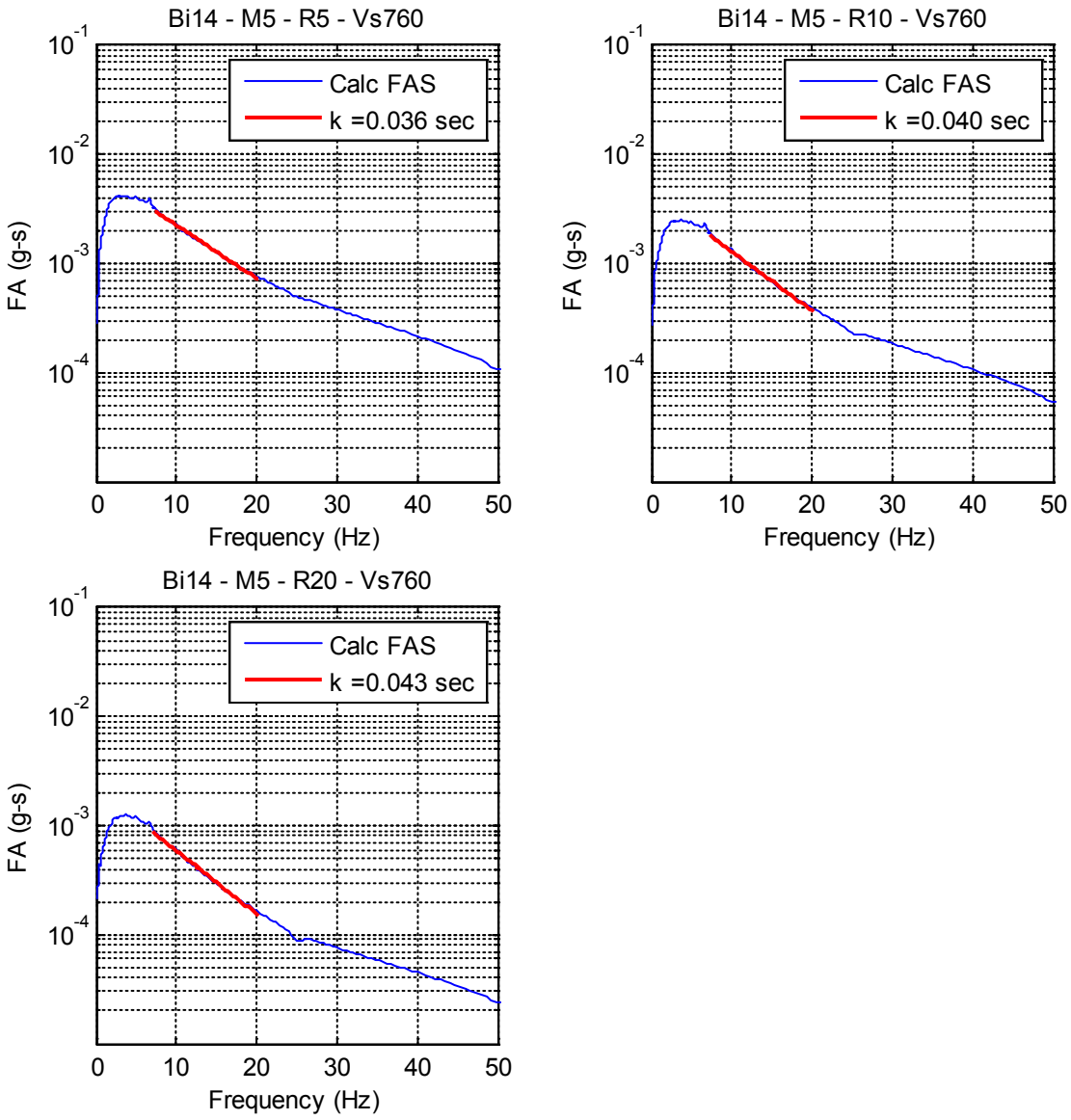



**Figure M-9a:** Fit of the high-frequency FAS for Bi14 for the **M**5.0 and $R_x$ = 5, 10, 20 km scenarios.

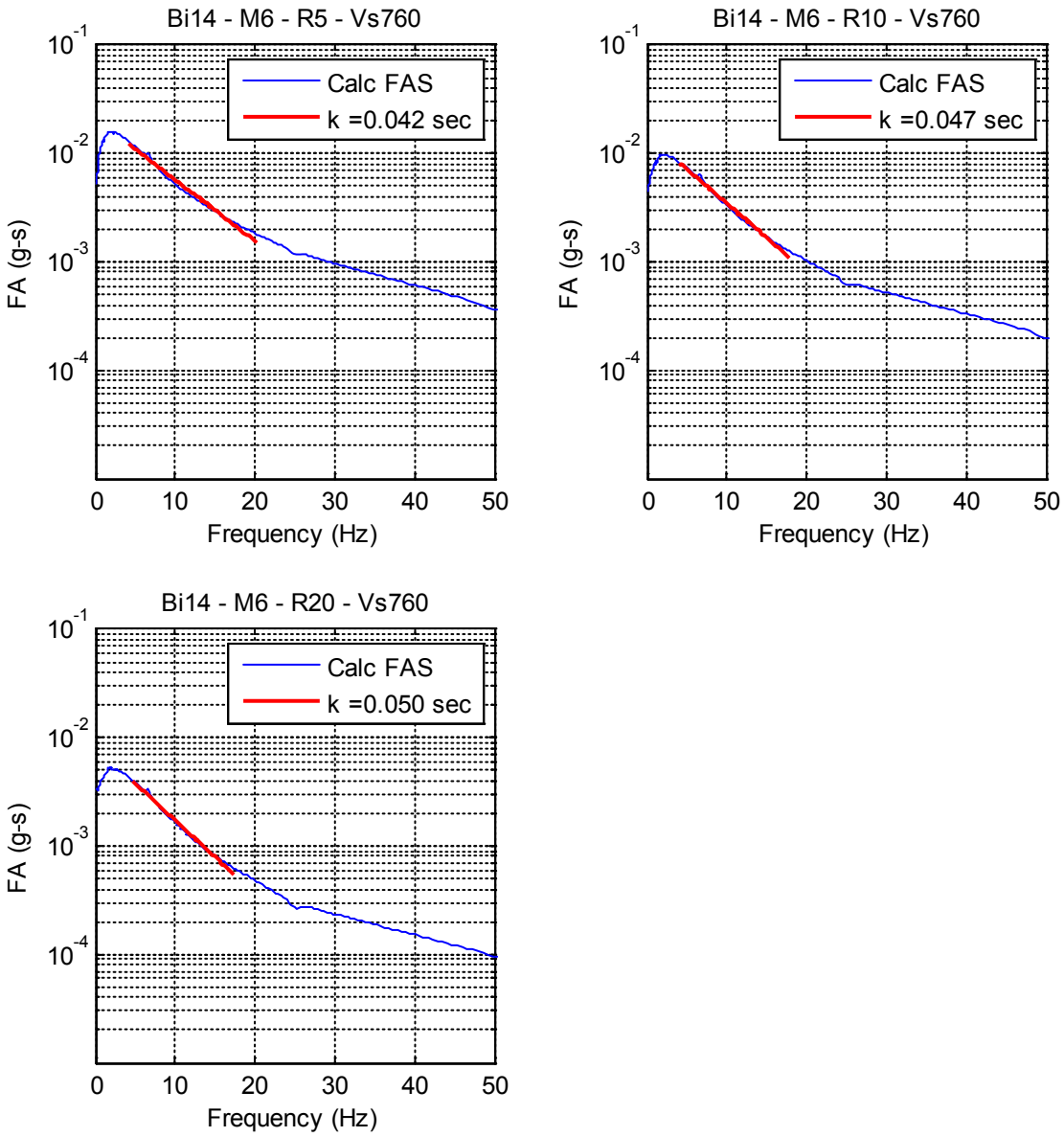



**Figure M-9b:** Fit of the high-frequency FAS for Bi14 for the **M**6.0 and $R_x$ = 5, 10 and 20 km scenarios.

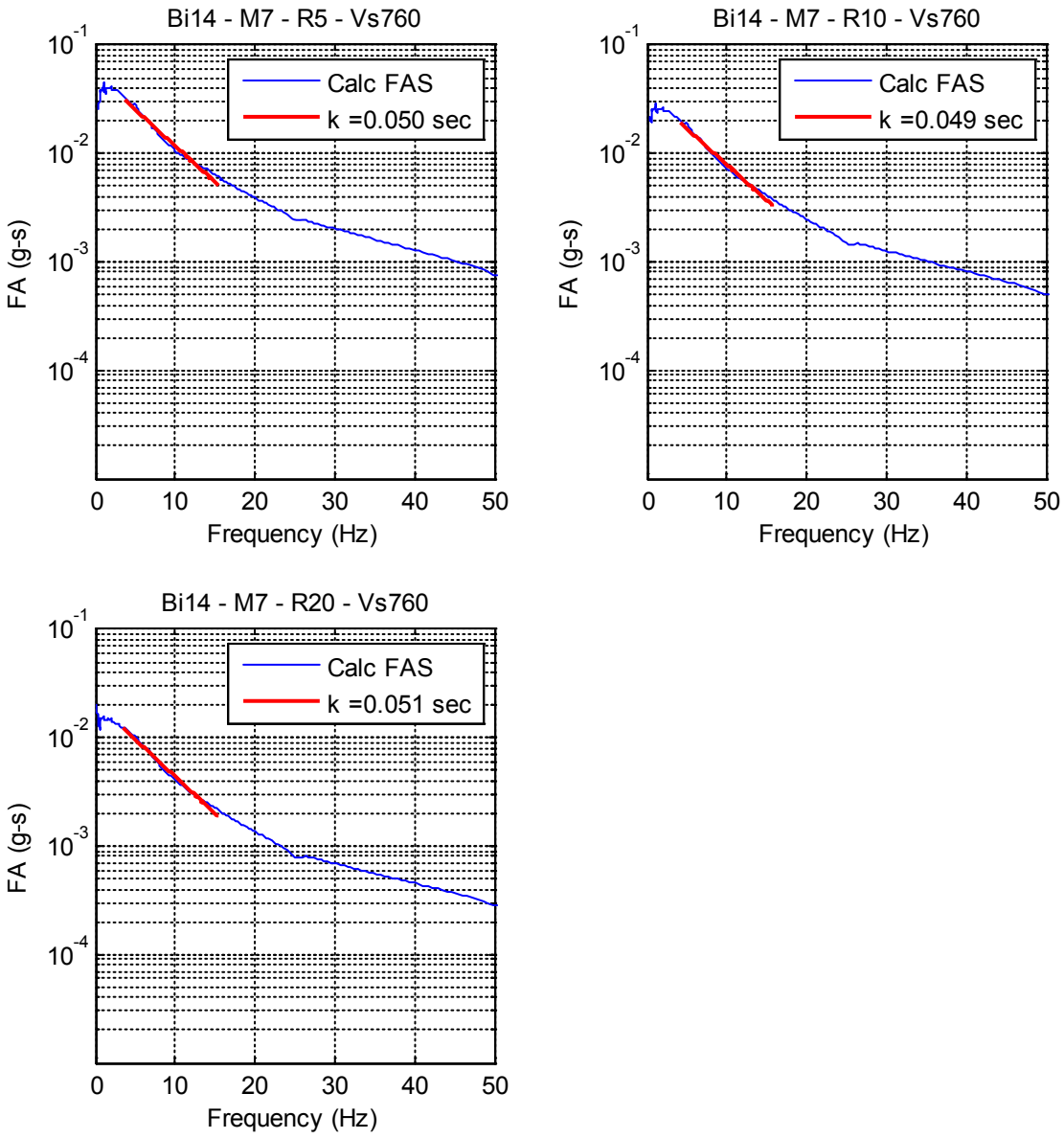



**Figure M-9c:** Fit of the high-frequency FAS for Bi14 for the **M**7.0 and $R_x$ = 5, 10 and 20 km scenarios.

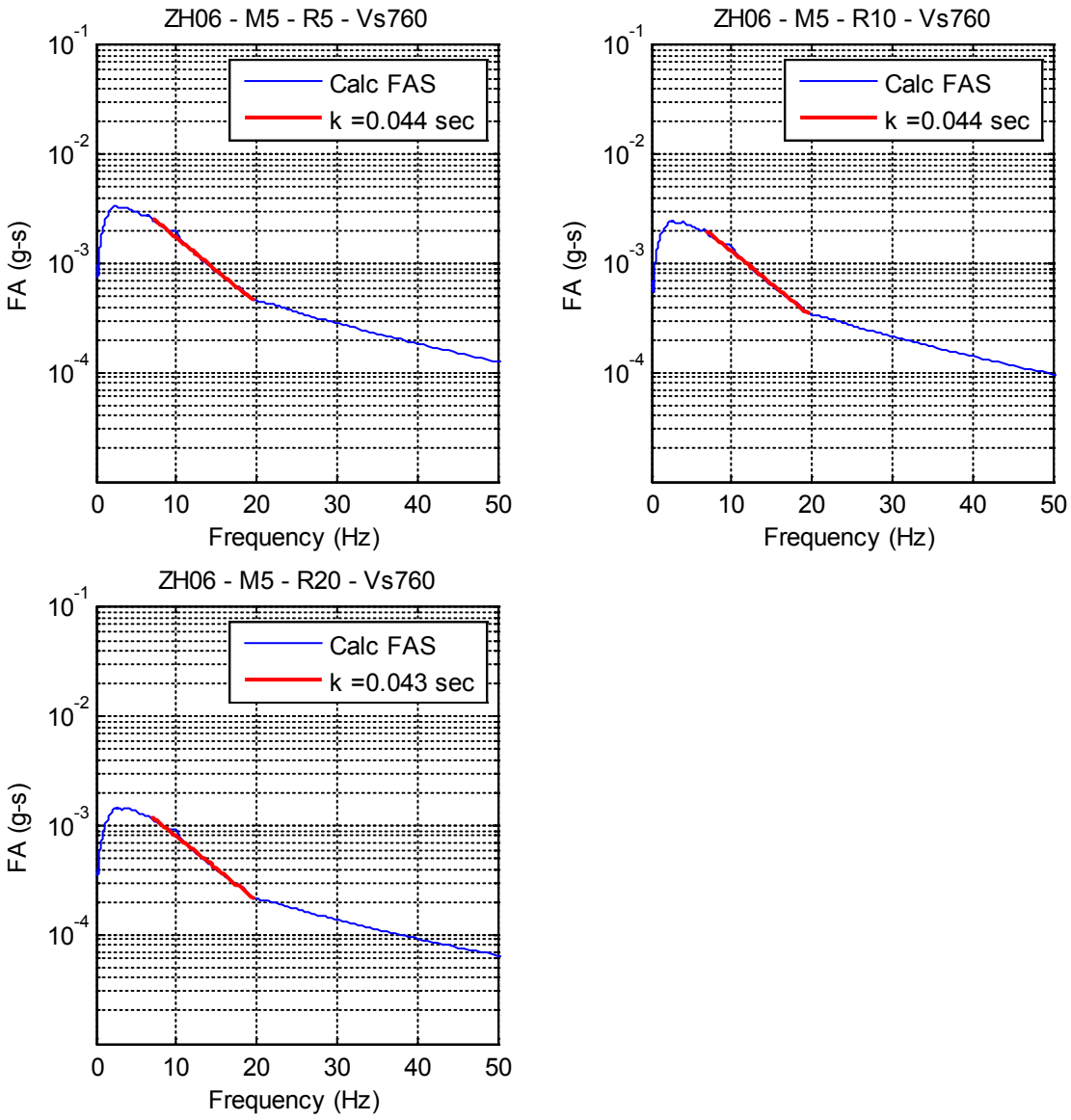



**Figure M-10a:** Fit of the high-frequency FAS for ZH06 for the **M**5.0 and $R_x$ = 5, 10, and 20 km scenarios.

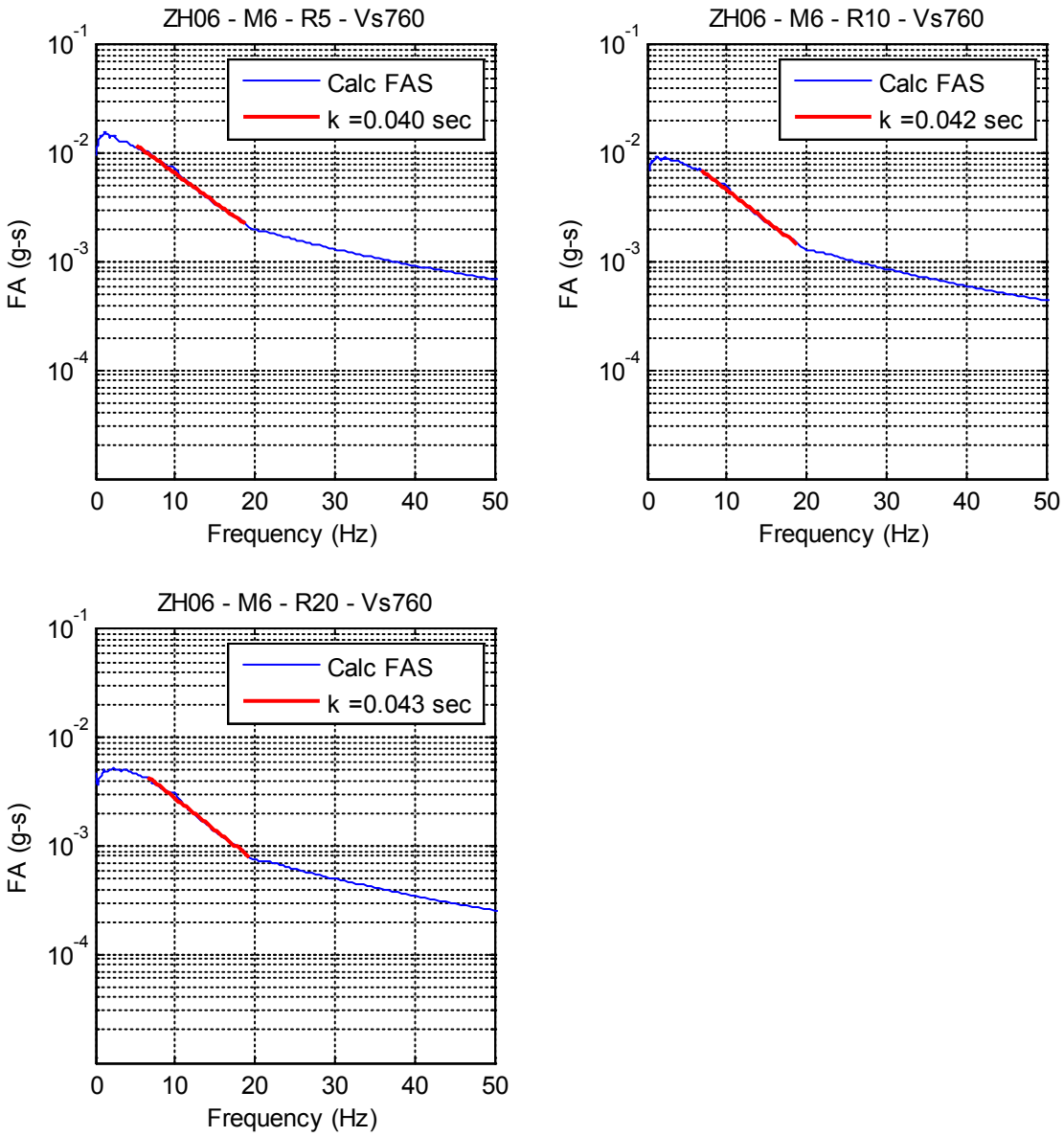



**Figure M-10b:** Fit of the high-frequency FAS for ZH14 for the **M**6.0 and $R_x$ = 5, 10 and 20 km scenarios.

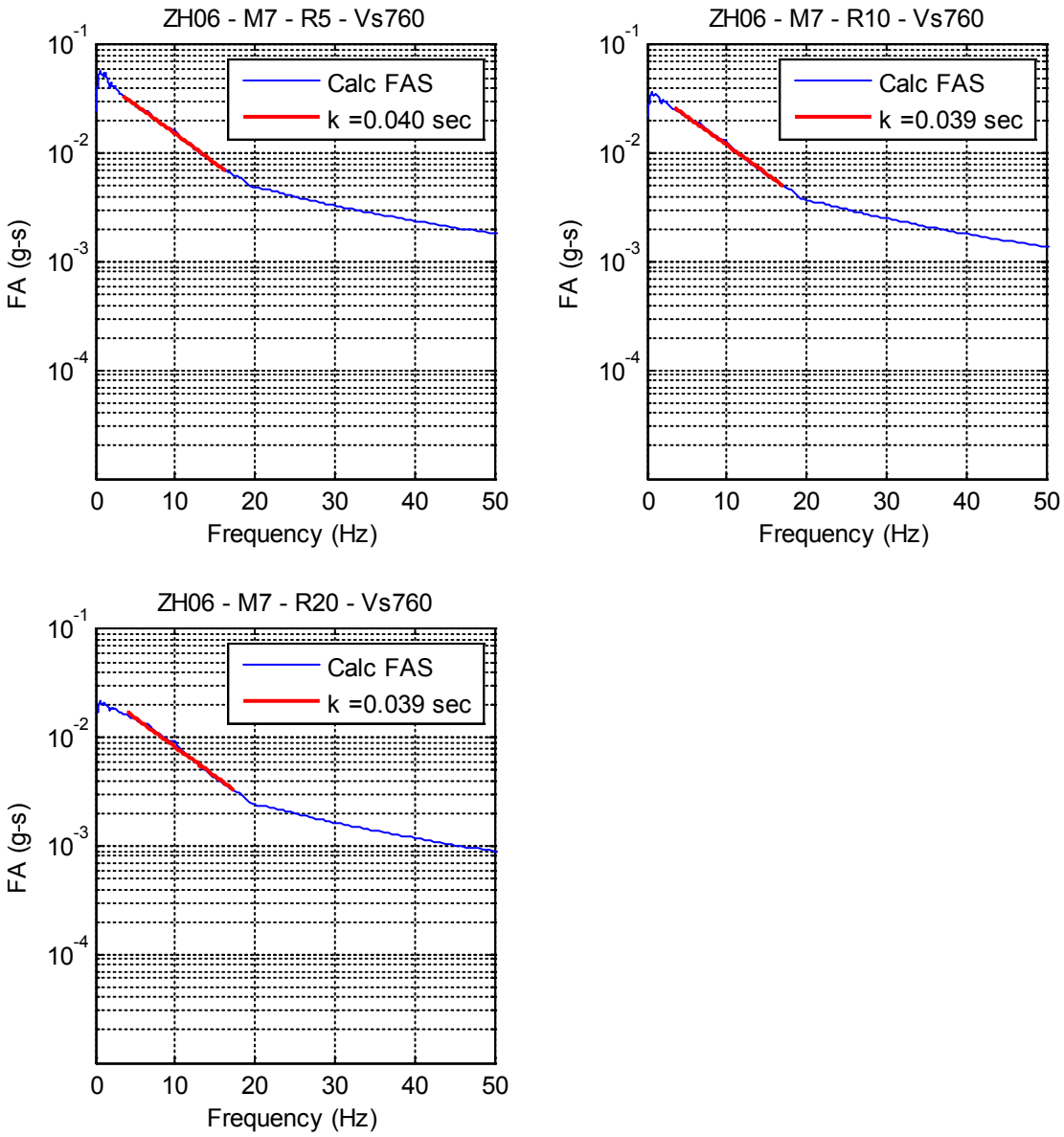



**Figure M-10c:** Fit of the high-frequency FAS for ZH06 for the **M**7.0 and $R_x$ = 5, 10 and 20 km scenarios.

## M.4 References

Abrahamson, N.A., Silva, W.J., and Kamai, R. (2014). Summary of the AKS14 Ground-Motion Relation for Active Crustal Regions, *Earthquake Spectra*, Vol. 30(3), 1025-1055, DOI: 10.1193/070913EQS198M.

Akkar, S., Sandikkaya, M.A., and Bommer, J.J. (2014a). Empirical ground-motion models for point- and extended-source crustal earthquake scenarios in Europe and the Middle East, *Bull. Earthquake Eng*., Vol. 12(1), 359–387, DOI 10.1007/s10518-013-9461-4.

Akkar, S., Sandikkaya, M.A., and Bommer, J.J. (2014b). Erratum to: Empirical ground-motion models for point- and extended-source crustal earthquake scenarios in Europe and the Middle East, *Bull. Earthquake Eng*., Vol. 12(1), 389-390, DOI 10.1007/s10518-013-9508-6.

Al Atik, L., Kottke, A., Abrahamson, N.A, and Hollenback, J. (2013). Kappa ($\kappa$) Scaling of Ground-Motion Prediction Equations Using an Inverse Random Vibration Theory Approach, *Bull. Seismol. Soc. Am.,* Vol. 14, 336-346. DOI: 10.1785/0120120200.

Anderson, J.G., and Hough, S.E. (1984). A model for the shape of the Fourier amplitude spectrum of acceleration at high frequencies, *Bull. Seismol. Soc. Am.,* Vol. 74, 1969-1993.

Bindi D., Massa M., Luzi L., Ameri G., Pacor F., Puglia R., and Augliera, P. (2014a). Pan-European Ground-Motion Prediction Equations for the Average Horizontal Component of PGA, PGV, and 5%-Damped PSA at Spectral Periods up to 3.0 s using the RESORCE dataset, *Bull. Earthquake Eng*., Vol. 12, 391–430, DOI 10.1007/s10518-013-9525-5.

Bindi D., Massa M., Luzi L., Ameri G., Pacor F., Puglia R., and Augliera, P. (2014b). Erratum to: Pan-European Ground-Motion Prediction Equations for the Average Horizontal Component of PGA, PGV, and 5%-Damped PSA at Spectral Periods up to 3.0 s using the RESORCE dataset, *Bull. Earthquake Eng*., Vol. 12, 431-448, DOI 10.1007/s10518-014-9589-x.

Boore, D.M. (2005). SMSIM--Fortran Programs for Simulating Ground Motions from Earthquakes: Version 2.3--A Revision of OFR 96-80-A, *U.S. Geological Survey Open-File Report*, 59 pp.

Boore, D.M., Stewart, J.P., Seyhan, E., and Atkinson, G.M. (2014). NGA-West 2 Equations for Predicting PGA, PGV, and 5%-Damped PSA for Shallow Crustal Earthquakes, *Earthquake Spectra*, Vol. 30(3), 1057-1085, DOI: 10.1193/070113EQS184M.

Campbell, K.W. (2009). Estimates of shear-wave Q and κ0 for unconsolidated and semiconsolidated sediments in Eastern North America, *Bull. Seismol. Soc. Am.*, Vol. 99(4), 2365−2392.

Campbell, K.W., Hashash, Y.M.-A., Kim, B., Kottke, A.R., Rathje, E., Silva, W.J., and Stewart, J.P. (2014) Reference-Rock Site Conditions for Central and Eastern North America: Part II - Attenuation (Kappa)

Definition, *PEER Report 2014/12* , Pacific Earthquake Engineering Research (PEER) Center, University of California, Berkeley, CA, August 2014, 54 pp.

Campbell, K. W. (2003). Prediction of strong ground motion using the hybrid empirical method and its use in the development of ground-motion (attenuation) relations in eastern North America, *Bull. Seismol. Soc. Am.*, Vol. 93, 1012-1033.

Campbell, K.W., and Bozorgnia, Y. (2014). NGA-West2 Ground Motion Model for the Average Horizontal Components of PGA, PGV, and 5%-Damped Linear Acceleration Response Spectra, *Earthquake Spectra*, Vol. 30(3), 1087-1115, DOI: 10.1193/062913EQS175M.

Chiou, B.S.-J., and Youngs, R.R. (2014). Update of the Chiou and Youngs NGA Model for the Average Horizontal Component of Peak Ground Motion and Response Spectra, *Earthquake Spectra*, Vol. 30(3), 1117-1153, DOI: 10.1193/072813EQS219M.

Hashash, Y.M.-A., Kottke, A.R., Stewart, J.P., Campbell, K.W., Kim, B., Moss, C., Nikolaoy, S., Rathje, E., and Silva, W.J. (2014) Reference Rock Site Condition for Central and Eastern North America, *Bull. Seismol. Soc. Am.*, Vol. 104(2), 684–701.

Kamai, R., Abrahamson, N.A., and Silva, W.J. (2013). Nonlinear Horizontal Site Response for the NGA-West2 Project, *PEER Report 2013/12*, Pacific Earthquake Engineering Research (PEER) Center, University of California, Berkeley, CA, May 2013, 70 pp.

Kottke, A.R., and Rathje, E.M. (2008). Technical manual for Strata, *PEER Report 2008/10*, Pacific Earthquake Engineering Research (PEER) Center, University of California, Berkeley, CA.

Purvance, M.D., and Anderson, J.G. (2003). A Comprehensive Study of the Observed Spectral Decay in Strong-Ground Accelerations Recorded in Guerrero, Mexico, *Bull. Seism. Soc. Am.*, Vol. 93, 600–611.

Van Houtte, C., Drouet, S., and Cotton, F. (2011). Analysis of the Origins of κ (kappa) to Compute Hard Rock to Rock Adjustment Factors for GMPEs, *Bull. Seism. Soc. Am.*, Vol. 101(6), 2926−2941.

Wells, D.L., and Coppersmith, K.J. (1994). New empirical relationships among magnitude, rupture length, rupture width, rupture area, and surface displacement, *Bull. Seism. Soc. Am.*, Vol. 84, 974-1002.

Zhao, J.X., Zhang, J., Asano, A., Ohno, Y., Oouchi, T., Takahashi, T., Ogawa, H., Irikura, K., Thio, H.K., Somerville, P.G., Fukushima, Y., and Fukushima, Y. (2006). Attenuation Relations of Strong Ground Motion in Japan Using Site Classification Based on Predominate Period, *Bull. Seism. Soc. Am*., Vol. 96, 898-913.

# APPENDIX N

# LONG PERIOD EXTRAPOLATION

## N.1 Introduction

The common-form models based on the Sammon's maps were developed for periods only up to 3 second because some of the original GMPEs used to develop the covariance structure were not defined for periods greater than 3 seconds. Although the long period ground motions are not a key issue for nuclear power plants, the ground-motion model should be applicable for periods up to 10 seconds for completeness. Therefore, the ground-motion models developed for the SWUS GMC Project need to extrapolate reasonably for the periods from 4 to 10 seconds, but a simple model is adequate without adding additional branches to the logic trees. This Appendix describes the extrapolation of the common-form models for periods from 4 to 10 seconds.

## N.2 Methodology

A simplified method is used to develop a simple scaling relation for estimating the long period pseudo spectral acceleration (PSA) values based on the PSA value at T = 3 seconds. The five NGA-West2 GMPEs are all defined for periods up 10 seconds. Using the five NGA-West2 models with equal weight, the ratio of the PSA(T) / PSA(T = 3 sec) is computed for strike-slip earthquakes for a range of magnitudes (**M**5 to **M**8.5) and a range of distances ($R_{RUP}$ = 3 to 60 km). The site condition is $V_{S30}$ = 760 m/s and the depth to top of rupture ($Z_{TOR}$) is computed using the Chiou and Youngs (2014) model for strike-slip earthquakes.

The PSA ratio for periods of T = 4, T = 5, T = 7.5, and T = 10 seconds are shown as functions of magnitude in Figure N-1. This figure shows that there is strong magnitude dependence to the PSA ratio but only a weak distance dependence. Because the spectral values at periods greater than 3 seconds are not critical for nuclear power plants, a simplified method is used to for the long period extrapolation based on the common-form model that captures the magnitude dependence of the PSA ratio.

The functional form used for the common-form models is given in Eq. (N-1).

$$Ln\left(SA_{BASE}(M,R_{RUP},Z_{TOR},F,T)\right) = a_0(T) - a_7^2(T)R_{RUP} + a_8^2(T)Z_{TOR} + a_9^2(T)F_{RV} + \left(a_4(T) + a_5(T)(M-5)\right)\ln\left(\sqrt{R_{RUP}^2 + a_6(T)}\right) + a_{10}(T)F_{NML} + \begin{cases} -a_1(T) + a_2(T)(M-5.5) & for\ M < 5.5 \\ a_1(T)(M-6.5) & for\ 5.5 \le M \le 6.5 \\ a_3(T)(M-6.5) & for\ M > 6.5 \end{cases} \quad \text{(Eq. N-1)}$$

The ratio of PSA at long periods to the PSA at T = 3 seconds is modeled using the magnitude scaling and the constant term from the common-form model so that the long-period model can be specified by just changing the coefficients of the common-form model for T = 3 seconds.

$$\ln\left(\frac{PSA(T)}{PSA(T=3)}\right) = \Delta a_0 + \begin{cases} -\Delta a_1(T) + \Delta a_2(T)(M-5.5) & for\ M < 5.5 \\ \Delta a_1(T)(M-6.5) & for\ 5.5 \le M \le 6.5 \\ \Delta a_3(T)(M-6.5) & for\ M > 6.5 \end{cases} \quad \text{(Eq. N-2)}$$

The resulting fit is shown in Figure N-1. The fitted model is close to the mean ratio for rupture distances between 15 and 30 km. It over-estimates the ratio for distances less than 15 km by less than 0.2 natural log units (about 20% in PSA), and over-estimates the ratio for distances greater than 30 km by less than 0.1 natural log units (about 10% in PSA). Because the PSA at periods greater than 3 seconds are not critical for nuclear power plants, this misfit to the distance scaling is acceptable.

The coefficients for the long-period common-form model are computed by adding the estimated $\Delta a_i$ terms listed in Table N-1 to the $a_i$(T = 3 sec) for the common-form model:

$$a_0(T) = \Delta a_0(T) + a_0(T = 3\text{sec})$$

$$a_1(T) = \Delta a_1(T) + a_1(T = 3\text{sec})$$

$$a_2(T) = \Delta a_2(T) + a_2(T = 3\text{sec})$$

$$a_3(T) = \Delta a_3(T) + a_3(T = 3\text{sec})$$

## N.3 References

Abrahamson, N.A., Silva, W.J., and Kamai, R. (2014). Summary of the AKS14 Ground-Motion Relation for Active Crustal Regions, *Earthquake Spectra*, Vol. 30(3), 1025-1055, DOI: 10.1193/070913EQS198M.

Boore, D.M., Stewart, J.P., Seyhan, E., and Atkinson, G.M. (2014). NGA-West 2 Equations for Predicting PGA, PGV, and 5%-Damped PSA for Shallow Crustal Earthquakes, *Earthquake Spectra*, Vol. 30(3), 1057-1085, DOI: 10.1193/070113EQS184M.

Campbell, K.W., and Bozorgnia, Y. (2014). NGA-West2 Ground Motion Model for the Average Horizontal Components of PGA, PGV, and 5%-Damped Linear Acceleration Response Spectra, *Earthquake Spectra*, Vol. 30(3), 1087-1115, DOI: 10.1193/062913EQS175M.

Chiou, B.S.-J., and Youngs, R.R. (2014). Update of the Chiou and Youngs NGA Model for the Average Horizontal Component of Peak Ground Motion and Response Spectra, *Earthquake Spectra*, Vol. 30(3), 1117-1153, DOI: 10.1193/072813EQS219M.

Idriss, I.M. (2014). An NGA-West2 Empirical Model for Estimating the Horizontal Spectral Values Generated by Shallow Crustal Earthquakes, *Earthquake Spectra*, Vol. 30(3), 1155-1177, DOI: 10.1193/070613EQS195M.

**Table N-1:** Adjustments to the coefficients at long period relative to the coefficients for T = 3 seconds.

| Period (sec) | $\Delta a_0$ | $\Delta a_1$ | $\Delta a_2$ | $\Delta a_3$ |
|---|---|---|---|---|
| 3 | 0 | 0 | 0 | 0 |
| 4 | -0.4018 | 0.1310 | 0.1007 | 0.1301 |
| 5 | -0.7060 | 0.2294 | 0.1969 | 0.2404 |
| 7.5 | -1.3314 | 0.4297 | 0.3100 | 0.4273 |
| 10 | -1.8588 | 0.5178 | 0.3668 | 0.5043 |

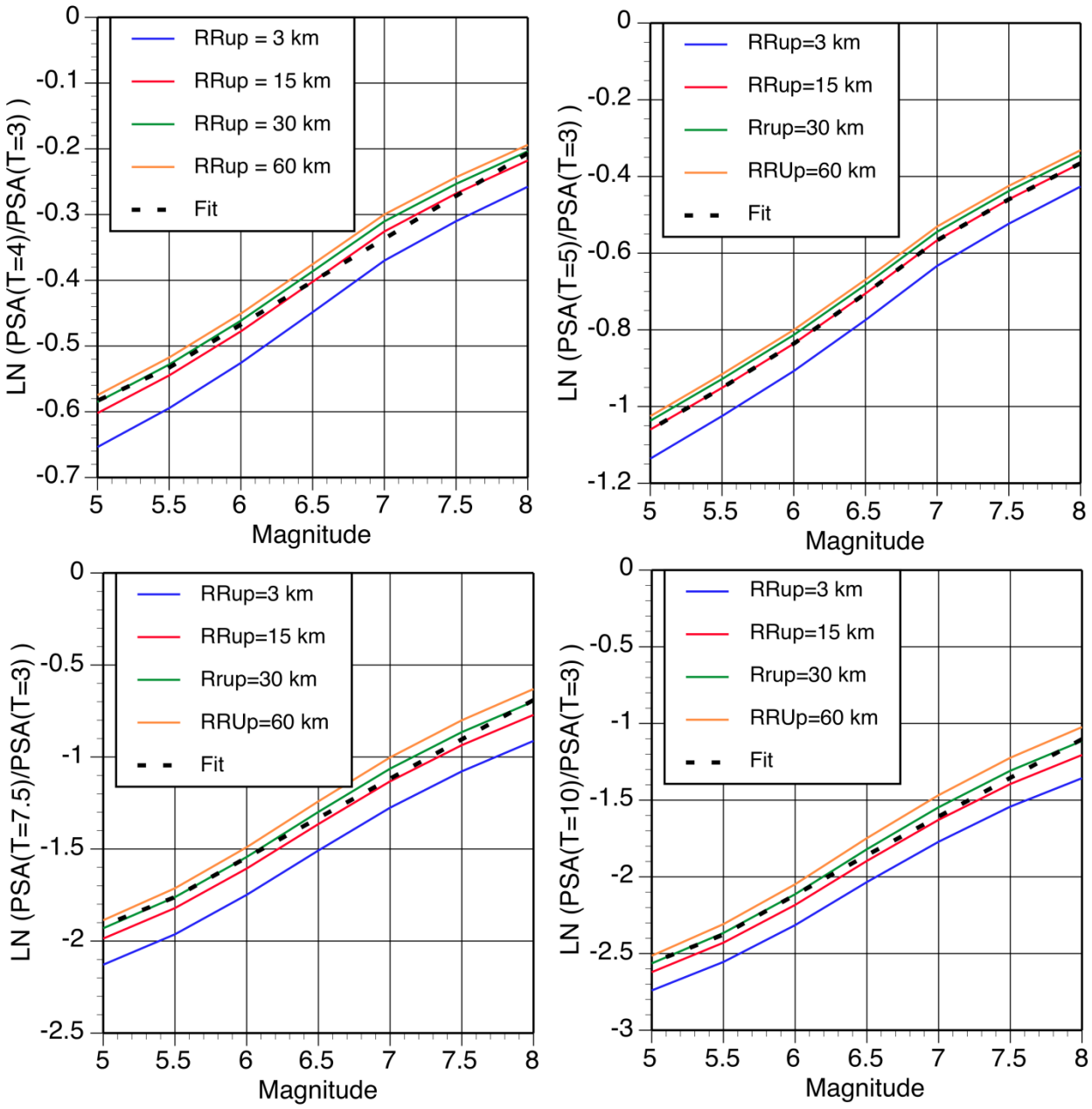



**Figure N-1:** Magnitude dependence of the long-period spectral ratio (relative to the T = 3 seconds PSA value) based on the five NGA-West2 GMPEs. The fit is shown by the dashed black curve.

# APPENDIX O

# COMPARISON OF HAZARD: ORIGINAL GMPES VERSUS COMMON-FORM BASED MODELS

## O.1 Introduction

The hazard sensitivity analyses performed as part of the hazard feedback used for the development of the GMC logic trees are presented in Chapter 14. A separate set of hazard sensitivities are presented in this Appendix. These sensitivities are based on the comparison between the individual candidate GMPE models considered in the development of the common-form models and the resulting representative suite of common-form models. Specifically, for DCPP, the suite of common-form models were developed for use in the hazard analysis for the closest seismic sources contribution the most to the seismic hazard, while the more distant seismic sources were modeled with the NGA-West2 GMPE models. For PVNGS, the suite of common-form models were developed only for the Greater Arizona seismic sources, while the more distant Region 1 and Regions 2&3 seismic sources were modeled with the NGA-West2 GMPE models.

For these sensitivities for DCPP, the same simplified seismic source model discussed and used in Chapter 14 is used for the results provided in this Appendix. This simplified seismic source model comprises the closest sources, which are the significant contributors to the overall hazard at the DCPP site. For PVNGS, a similar approach is used where a simplified seismic source model that contains the significant contributing seismic sources to the overall hazard at the PVNGS site are included. For these sensitivities for PVNGS, the same simplified seismic source model discussed and used in Chapter 14 is used for the results provided in this Appendix. These simplified source models are intended to capture the broad features of the controlling seismic sources in terms of magnitude, distance, and hanging-wall contributions to the hazard. They are not intended to represent the actual hazard level for DCPP and PVNGS.

Hazard curves were computed by the Nick Gregor for both sites using the PG&E PSHA program Haz43b (PG&E, 2014). For both the DCPP and PVNGS applications, hazard curves are presented in this Appendix for five spectral frequencies: PGA, 10, 5, 1, and 0.5 Hz. These results are all

based on an assumed $V_{S30}$ value of 760 m/sec. For all of these cases, the central value from the recommended total sigma model is used.

Additionally, for both applications, plots are included to show the fractiles curves (5th, 15th, 50th, 85th, and 95th fractiles) using the representative suite of common-form models and the candidate GMPEs with the Al Atik and Youngs (2014) epistemic uncertainty.

## O.2 Hazard for DCPP

For DCPP, the common functional-form model is based on the $R_{RUP}$ distance and for the foot-wall side of the rupture plane but with the inclusion of the suite of hanging-wall models (Sections 6.4.1.1 and 6.4.3). As part of the development of this common-form model, eight candidate GMPE models were analyzed:

- Akkar et al. (2014a, 2014b) – ASB14
- Abrahamson et al. (2014) – ASK14
- Boore et al. (2014) – BSSA14
- Campbell and Bozorgnia (2014) – CB14
- Chiou and Youngs (2014) – CY14
- Idriss (2014) – Id14
- Zhao et al. (2006) – ZH06
- Zhao and Lu (2011) – ZL11

For the representative suite of common-form models, there are a total of 23 models for PGA, 22 models for 10 Hz, 23 models for 5 Hz, 27 models for 1 Hz, and 27 models for 0.5 Hz.

Mean hazard curves are shown in Figures O.2-1a to O.2-5a for PGA and the spectral frequencies of 10, 5, 1 and 0.5 Hz, respectively. The hazard curves for the representative suite of common-form models are shown as grey lines, identified in the legend by their model ID number. Also shown in these figures are the weighted mean from the representative suite of common-form models and the individual hazard curves from the eight candidate GMPE models listed above. Additionally, a hazard curve is shown for the Graizer (2014) model, referred to as GK14. The GK14 model was not included for the common-form model development because of its unique distance scaling.

One reason for the differences in hazard between the candidate GMPEs and the representative suite of common-form models is the change in the HW models at low magnitudes (**M** < 6.5). As described in Section 6.3, the magnitude taper in the candidate GMPEs were removed. Therefore

HW effect from **M**5 and **M**6 is stronger in the common-form models than in the candidate GMPEs. To demonstrate the impact of this change in the hazard, one additional hazard curve is shown in Figure O.2-3a for a modified version of the ASK14 model in which the magnitude taper of the HW model was removed consistent with the approach used in the development of the common-form models. With this modification of the hanging-wall model, the hazard increases about 10%. Figure O.2-3c plots just the ASK14 and modified ASK14 for 5 Hz to make them easy to distinguish from the other curves. This difference is smaller than the change in the mean hazard between the representative suite of common-form models and the candidate GMPEs, so other factors (such as the weighting scheme) are responsible for most of the cause of the differences. Figures O.2-1b to O.2-5b are similar plots with respect of the previous ones, but with the representative suite of common-form model hazard curves not plotted.

Based on these plots, the representative suite of common-form models spans a greater range than the eight candidate GMPE models used in their development as well as the hazard curve for the GK14 model. For the higher spectral frequency cases (PGA, 10 and 5 Hz) and at the $10^{-4}$ AFE and lower, the mean hazard from the representative suite of common-form model plots at the upper range of the eight hazard curves from the published GMPE models, while at $10^{-3}$ AFE or higher, the mean hazard from the representative suite of common-form model plots within the middle of the range of the eight hazard curves from the published GMPE models.

For the lower spectral frequency cases (1 and 0.5 Hz), the hazard curves show a larger spread in their distribution than the higher spectral frequency cases both for the empirical GMPE models and the representative suite of common-form models. For the 1 and 0.5 Hz spectral frequency cases, the weighted mean of the representative suite of common-form model falls closer to the center of the distribution of the empirical hazard curves than for the PGA, 10 and 5 Hz spectral frequency cases. For the representative suite of common-form models, the selected models span the range of hazard curves computed based on the eight candidate GMPEs as well as the hazard curve associated to the GK14 model.

Figures O.2-6 to O.2-10 show the $5^{th}$, $15^{th}$, $50^{th}$, $85^{th}$ and $95^{th}$ fractiles curves for the five analyzed periods, respectively. The fractiles curves using the representative suite of common-form models are compared to the fractiles curves using the suite of candidate GMPEs with the Al Atik and Youngs (2014) additional epistemic uncertainty. To simplify the hazard calculation, the Al Atik and Youngs (2014) uncertainty for **M** ≥ 7 was applied to all magnitudes. The mean hazard curves for the representative suite of common-form models and the candidate GMPEs are also shown. Comparing the fractiles for the GMPEs and common-form models, at low probability levels the median hazard curves for the representative suite of common-form models are generally above the median hazard curves for the candidate GMPEs. The ranges of the $5^{th}$ to $95^{th}$ fractiles are similar but with the representative suite of common-form models shifted slightly to higher hazard. The range of the fractiles from the representative suite of common-form models

does not always bound the range from the candidate GMPEs at the 5$^{th}$ fractiles. This low range is not critical to the hazard. The differences can be attributed to two causes: the representative suite of common-form model includes the range of the distance and magnitude scaling that is not captured with a simple scale factor from the Al Atik and Youngs (2014) epistemic uncertainty, and the model weights depend on comparison of selected data subsets and not just on the equal weight given to each candidate GMPE. The weights are also set to sample the Sammon's map, so models that are very similar (redundant) are given lower weight than if equal weighting was applied to all candidate GMPEs.

The TI Team considers this as an improvement in the characterization of the uncertainty over the traditional method of applying weights to the GMPEs based on their data coverage and models' strengths and weaknesses.

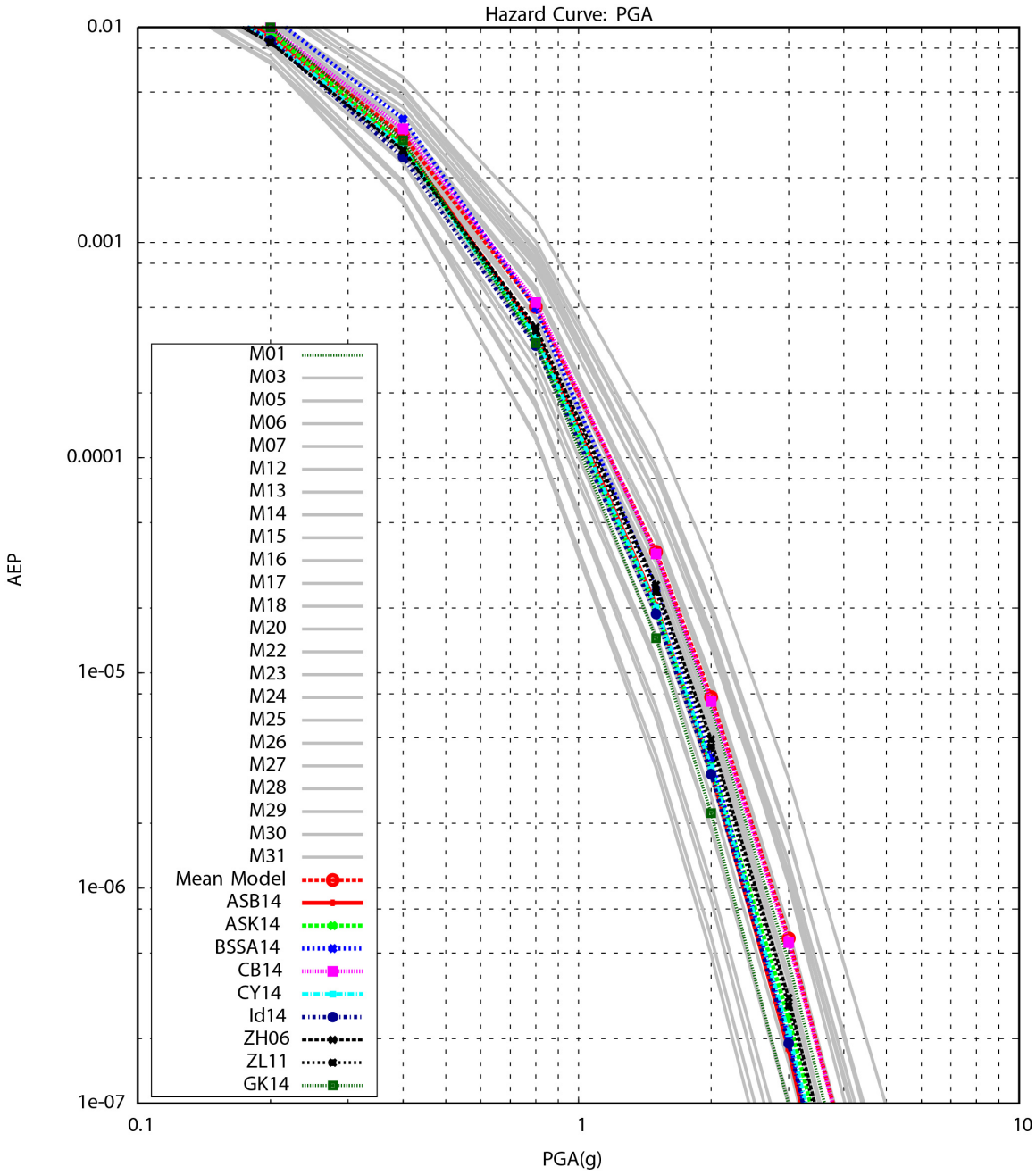



**Figure O.2-1a:** Comparison of PGA hazard curves using the representative suite of common-form models (grey lines), weighted mean of the representative suite of common-form models and the eight candidate empirical GMPE models. The hazard curve for the GK14 model is also shown.

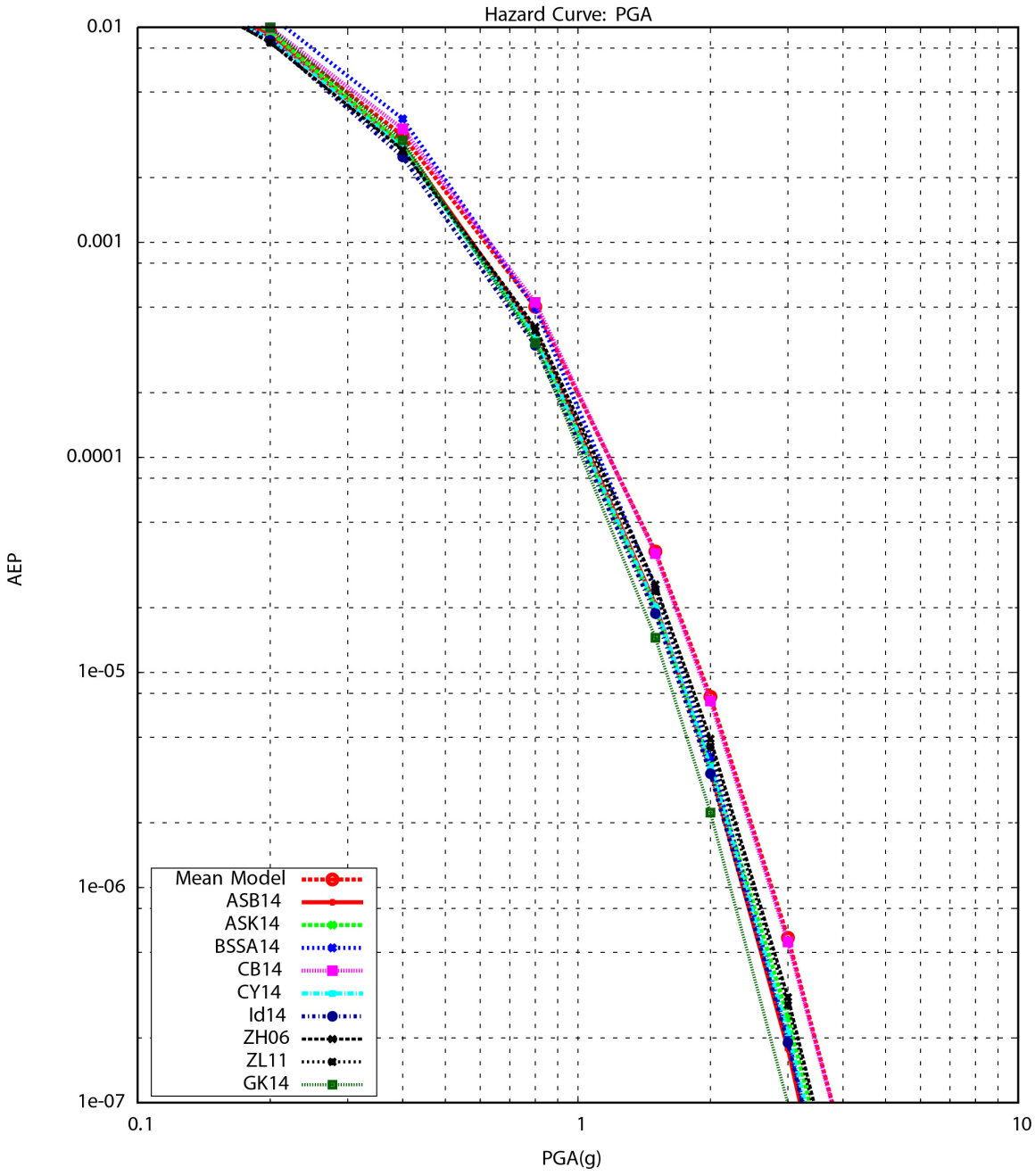



**Figure O.2-1b:** Comparison of PGA hazard curves using the weighted mean of the representative suite of common-form models and the eight candidate empirical GMPE models. The hazard curve for the GK14 model is also shown.

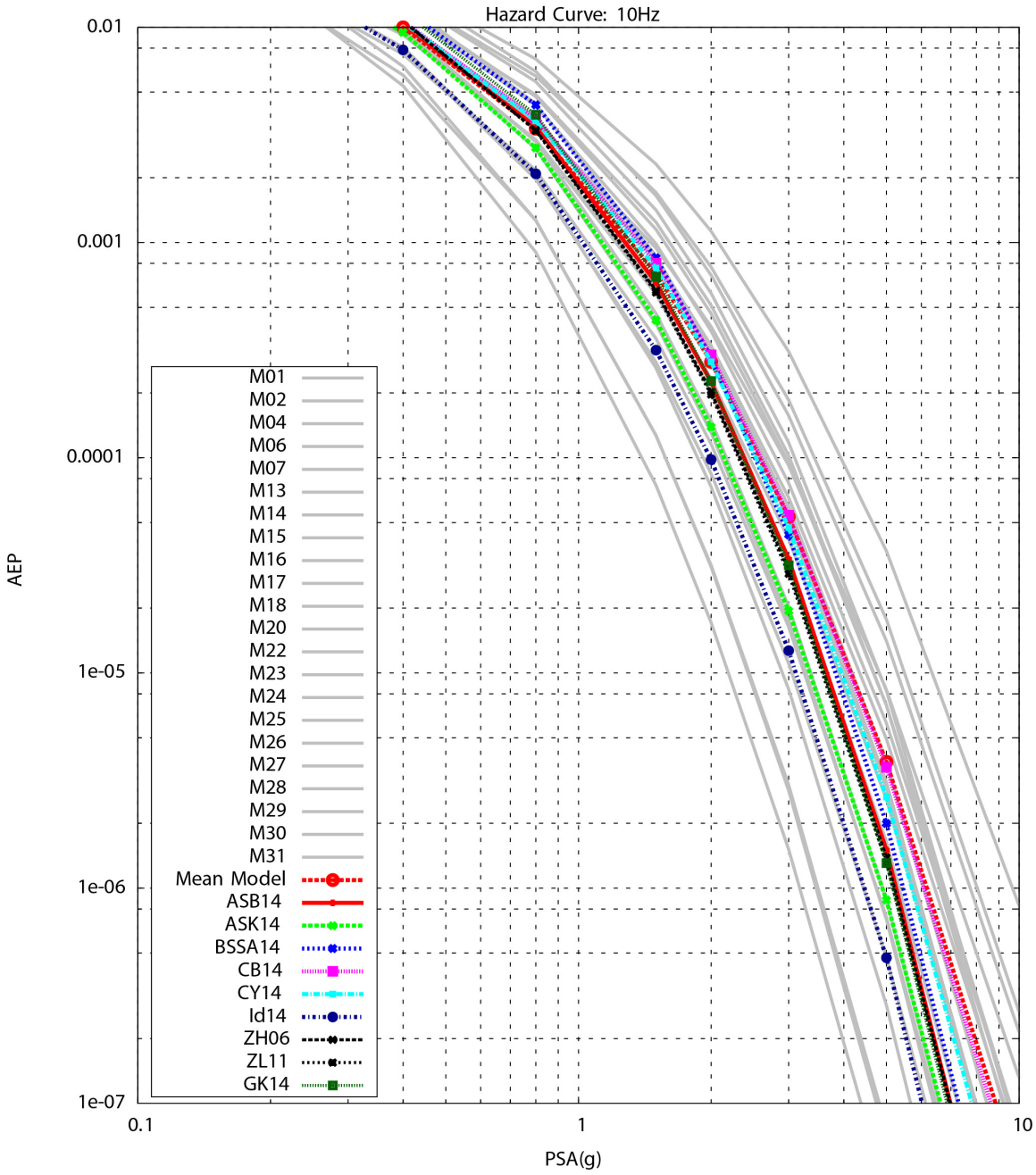



**Figure O.2-2a:** Comparison of 10 Hz spectral acceleration hazard curves using the representative suite of common-form models (grey lines), weighted mean of the representative suite of common-form models and the eight candidate empirical GMPE models. The hazard curve for the GK14 model is also shown.

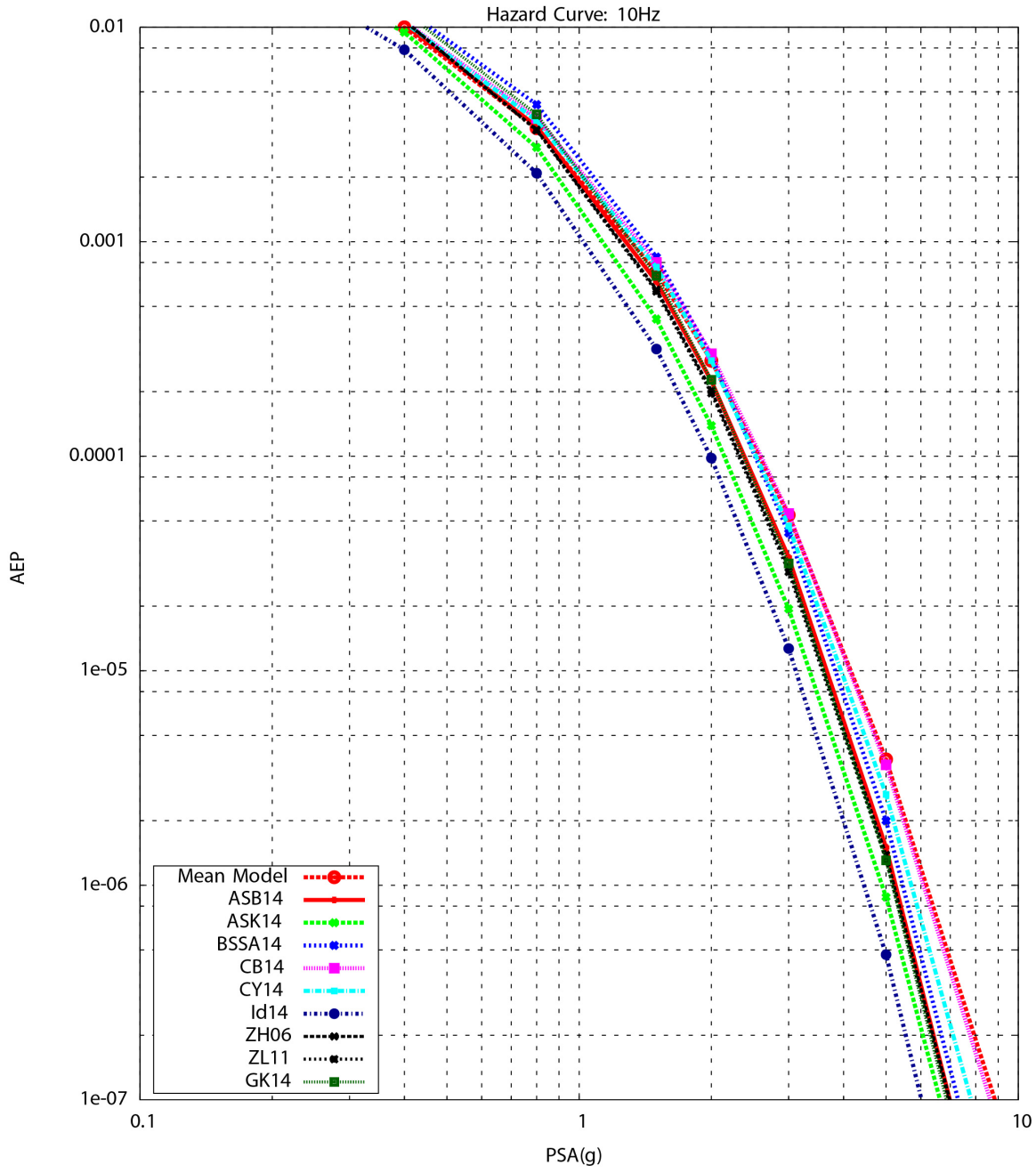



**Figure O.2-2b:** Comparison of 10 Hz spectral acceleration hazard curves using the weighted mean of the representative suite of common-form models and the eight candidate empirical GMPE models. The hazard curve for the GK14 model is also shown.

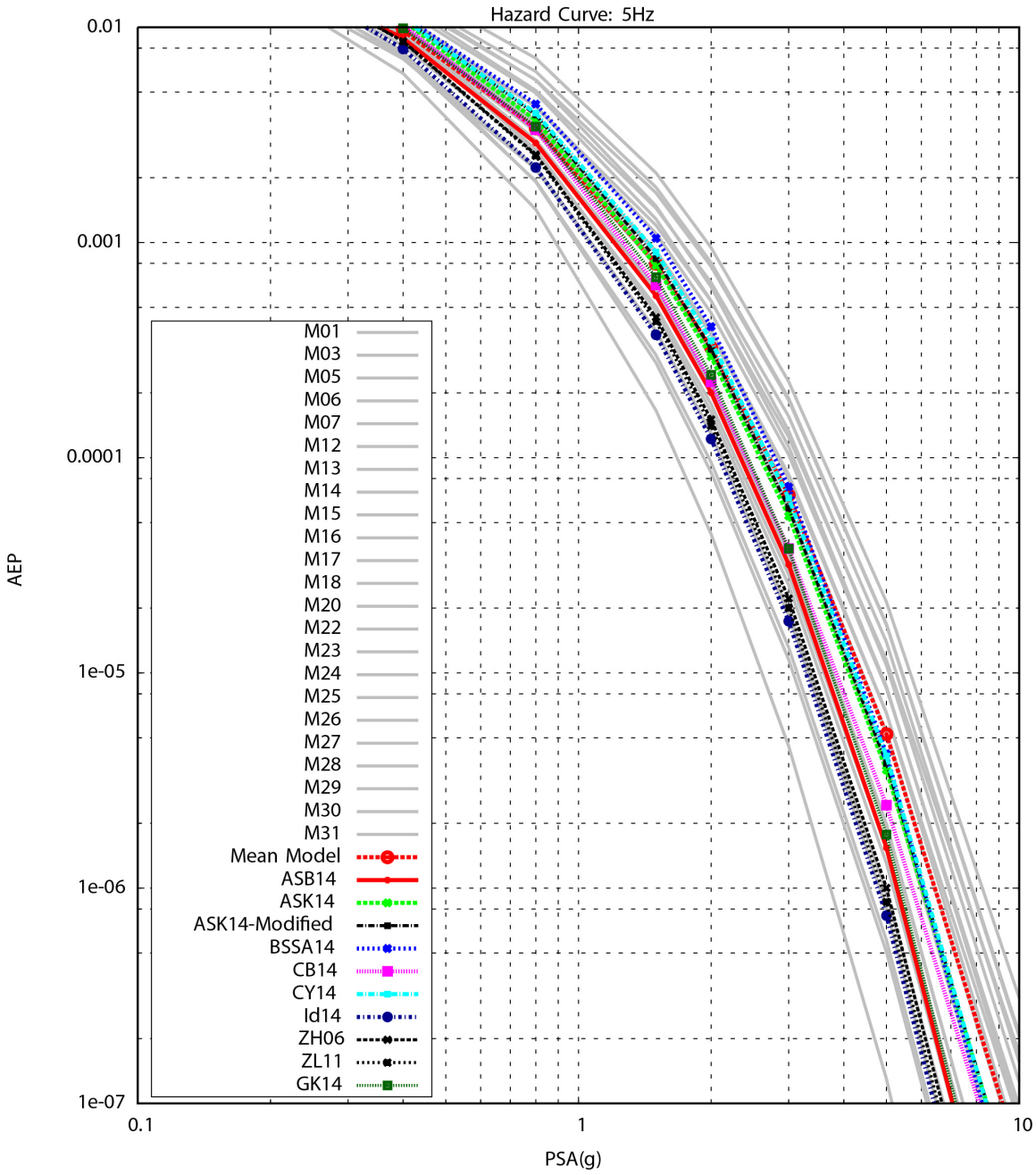



**Figure O.2-3a:** Comparison of 5 Hz spectral acceleration hazard curves using the representative suite of common-form models (grey lines), weighted mean of the representative suite of common-form models and the eight candidate empirical GMPE models. Also shown are the hazard curves for the ASK14 model modified for the hanging-wall scaling, and for the GK14 model.

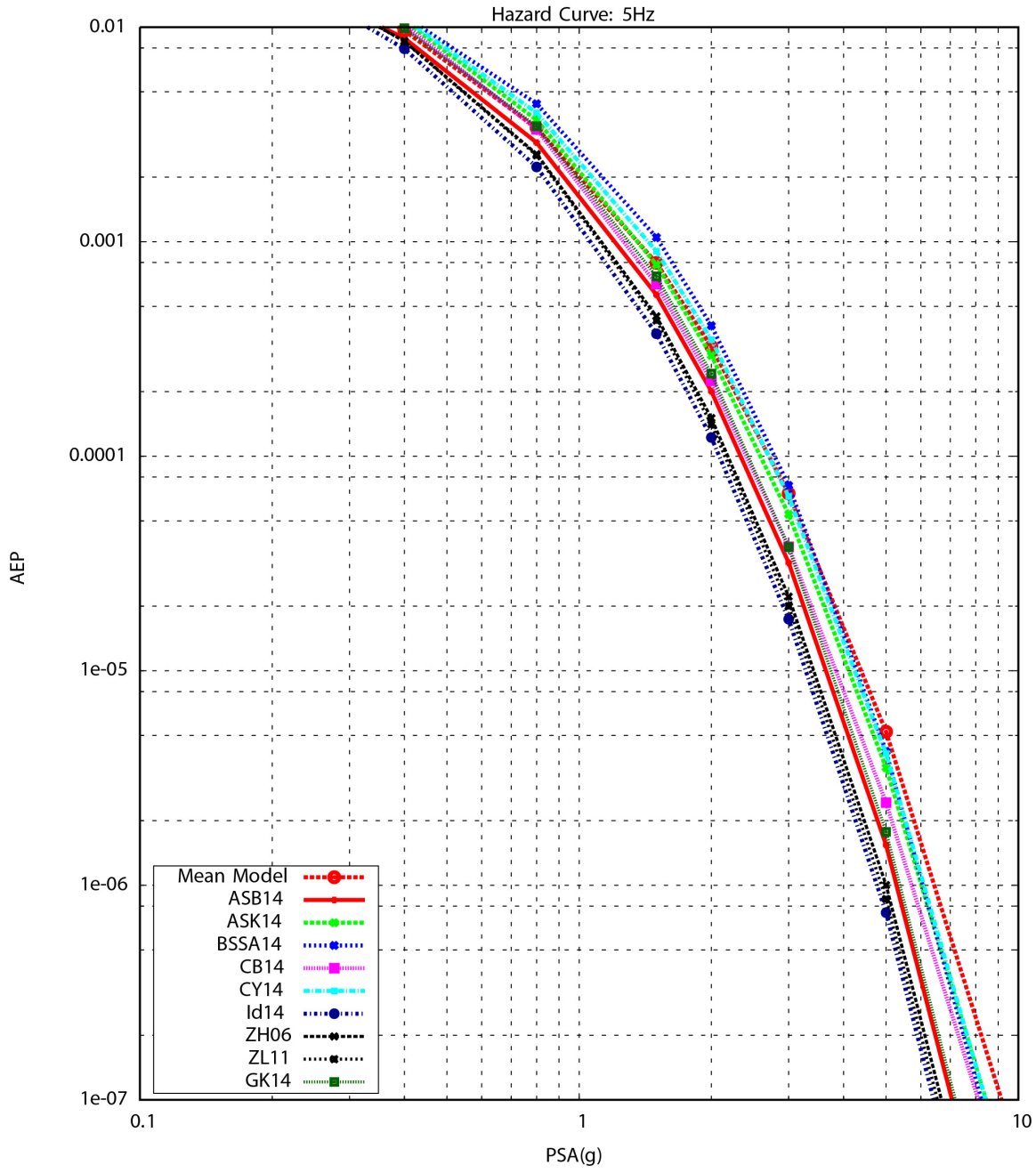



**Figure O.2-3b:** Comparison of 5 Hz spectral acceleration hazard curves using the weighted mean of the representative suite of common-form models and the eight candidate empirical GMPE models. The hazard curve for the GK14 model is also shown.

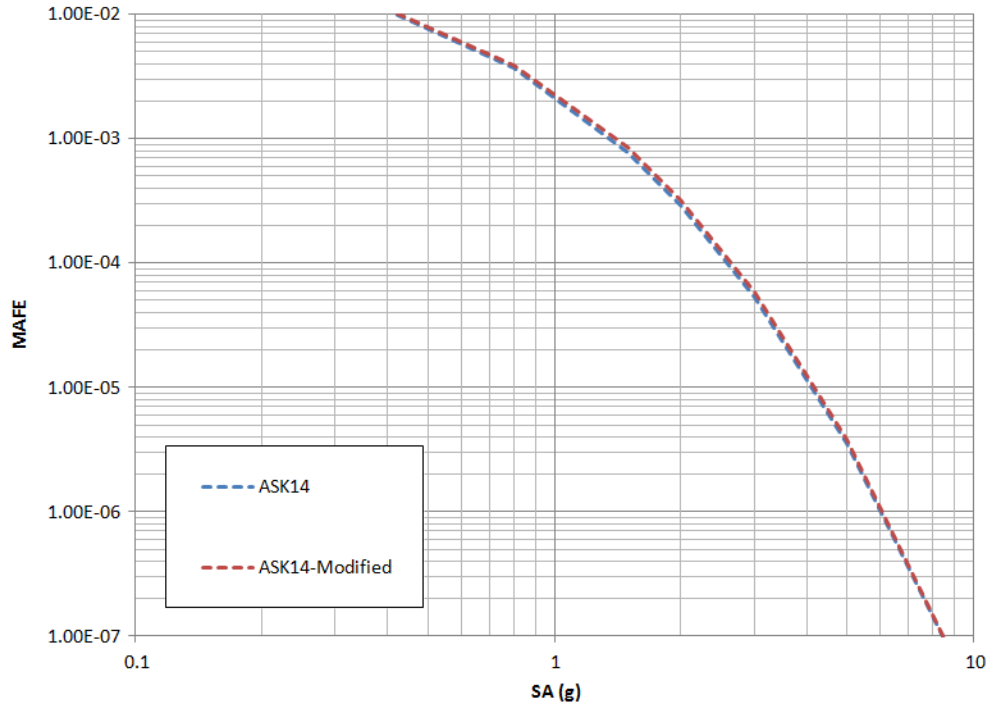



**Figure O.2-3c:** Comparison of 5 Hz spectral acceleration hazard curves using the ASK14 model and the ASK14 model modified to remove the magnitude taper of the HW model. Although the change in ground motion is small (on the order of 3%), the change in the resulting hazard is about 10% increase when using the ASK14 modified model.

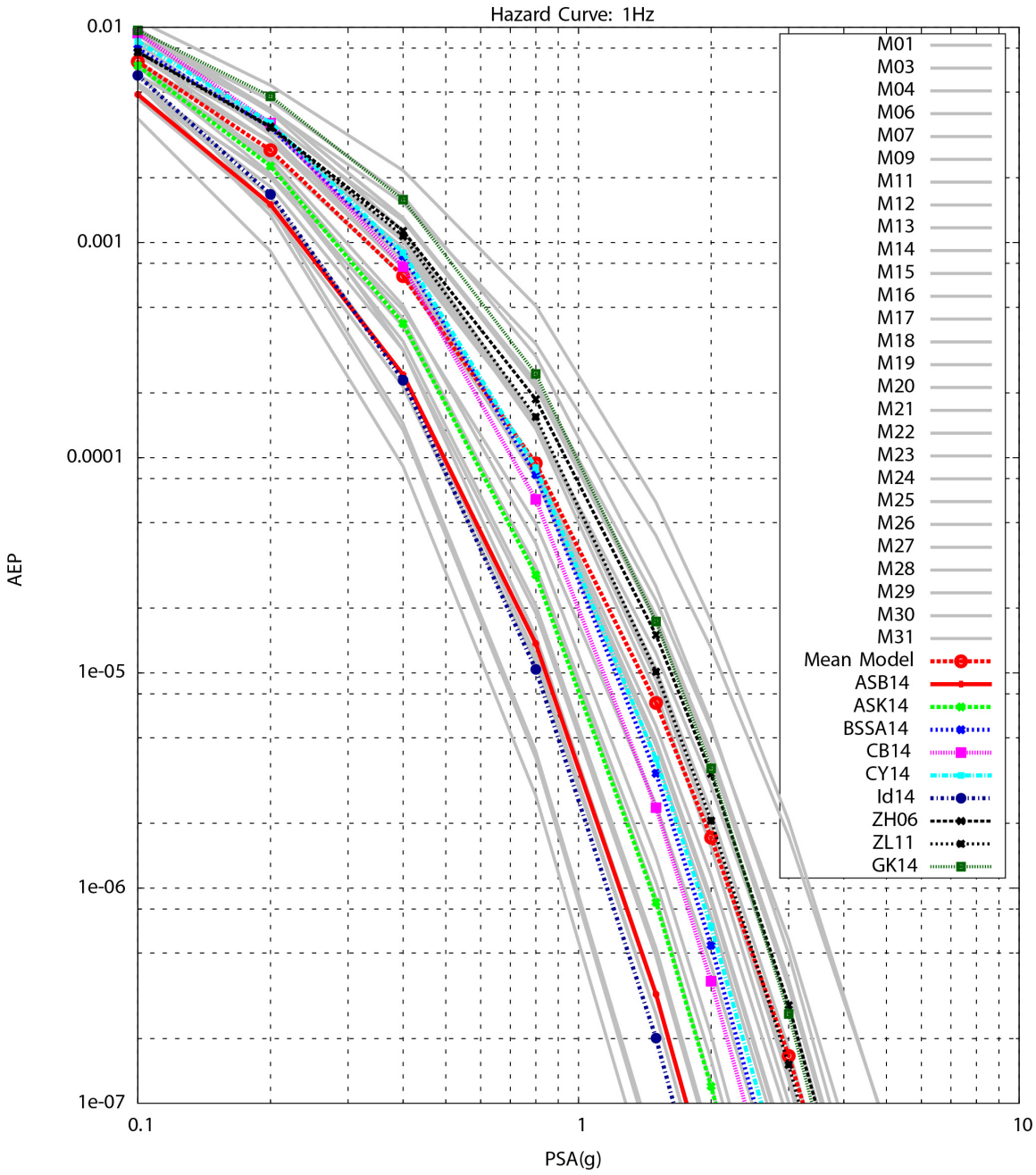



**Figure O.2-4a:** Comparison of 1 Hz spectral acceleration hazard curves using the representative suite of common-form models (grey lines), weighted mean of the representative suite of common-form models and the eight candidate empirical GMPE models. The hazard curve for the GK14 model is also shown.

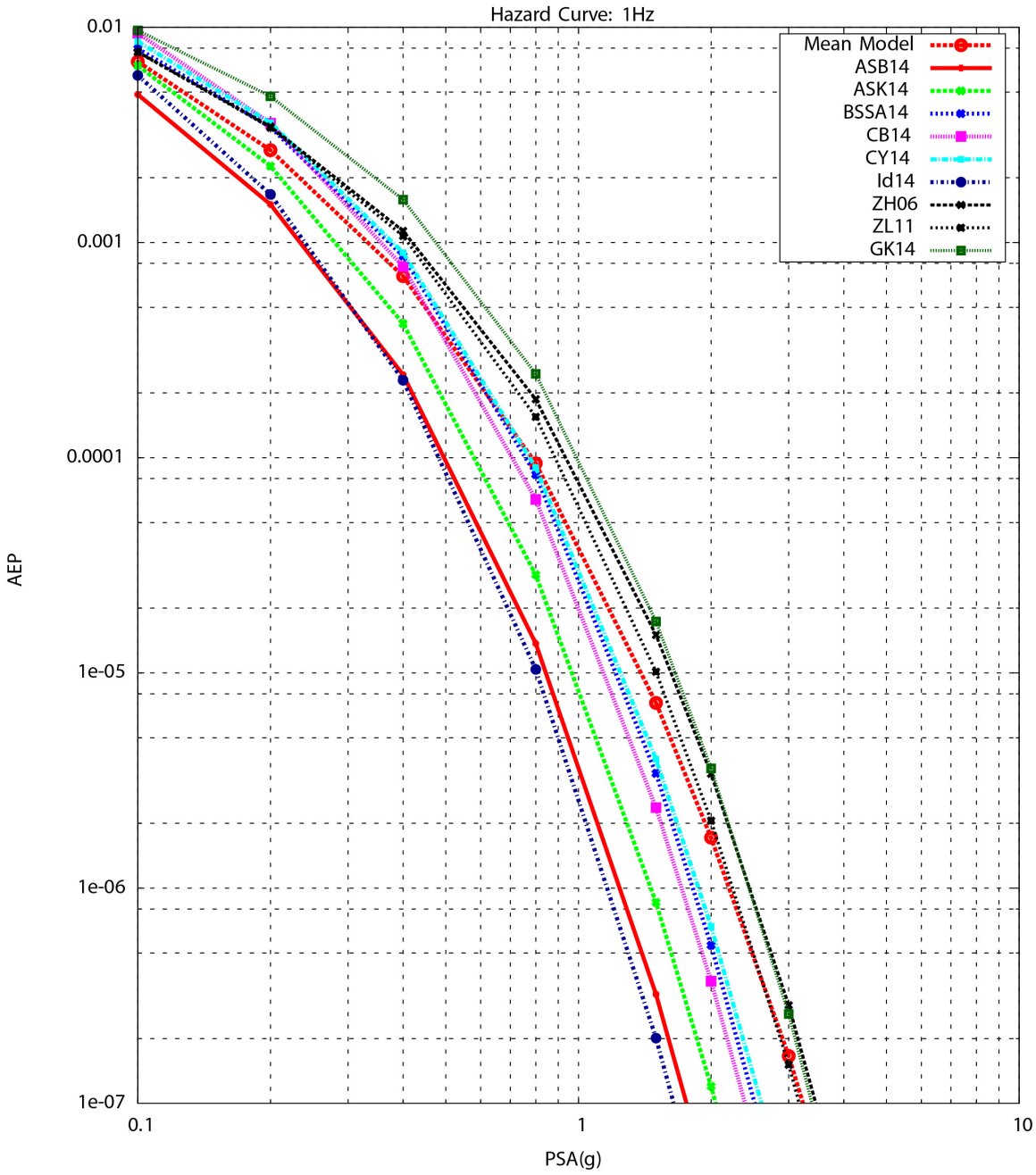



**Figure O.2-4b:** Comparison of 1 Hz spectral acceleration hazard curves using the weighted mean of the representative suite of common-form models and the eight candidate empirical GMPE models. The hazard curve for the GK14 model is also shown.

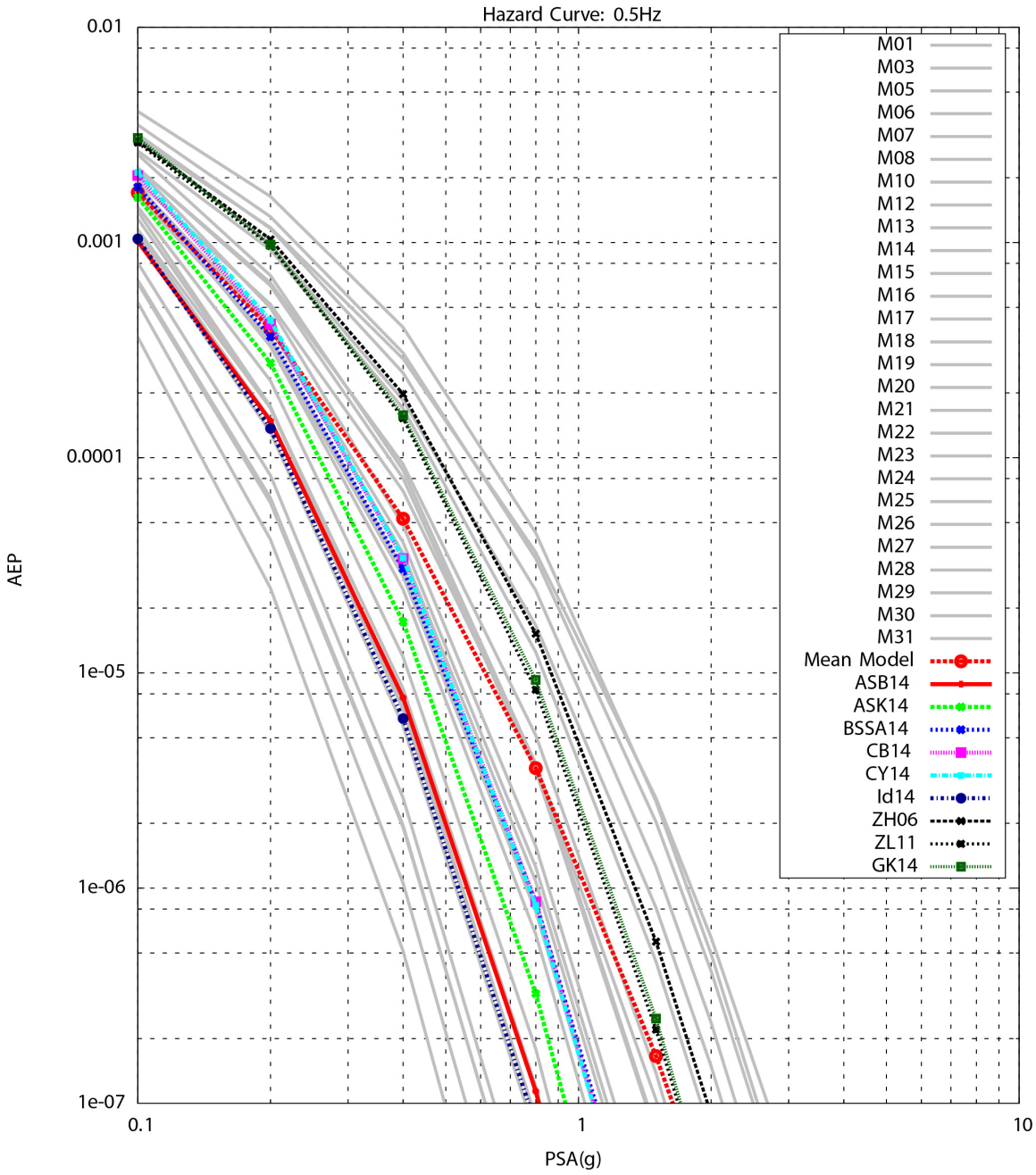



**Figure O.2-5a:** Comparison of 0.5 Hz spectral acceleration hazard curves using the representative suite of common-form models (grey lines), weighted mean of the representative suite of common-form models and the eight candidate empirical GMPE models. The hazard curve for the GK14 model is also shown.

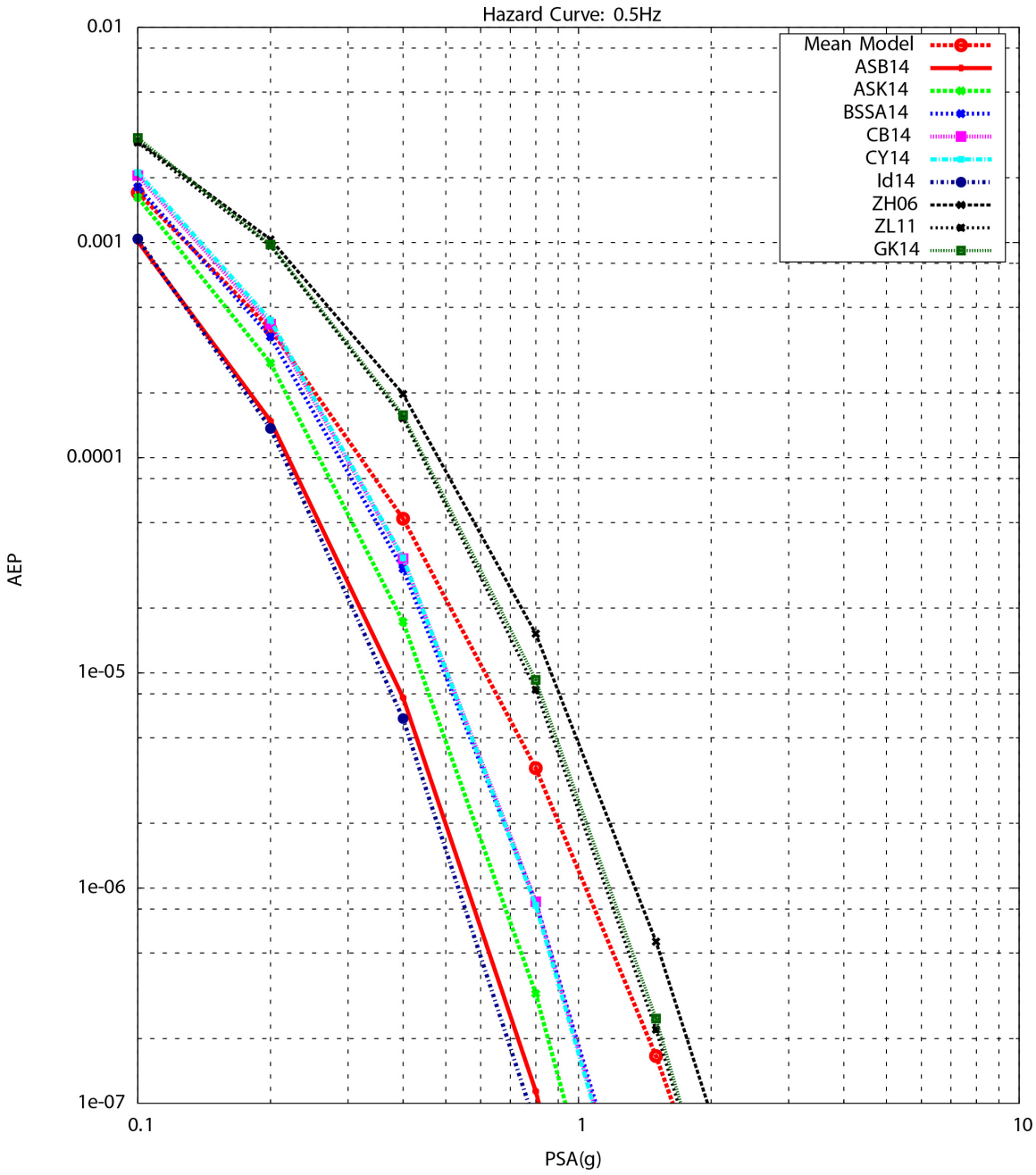



**Figure O.2-5b:** Comparison of 0.5 Hz spectral acceleration hazard curves using the weighted mean of the representative suite of common-form models and the eight candidate empirical GMPE models. The hazard curve for the GK14 model is also shown.

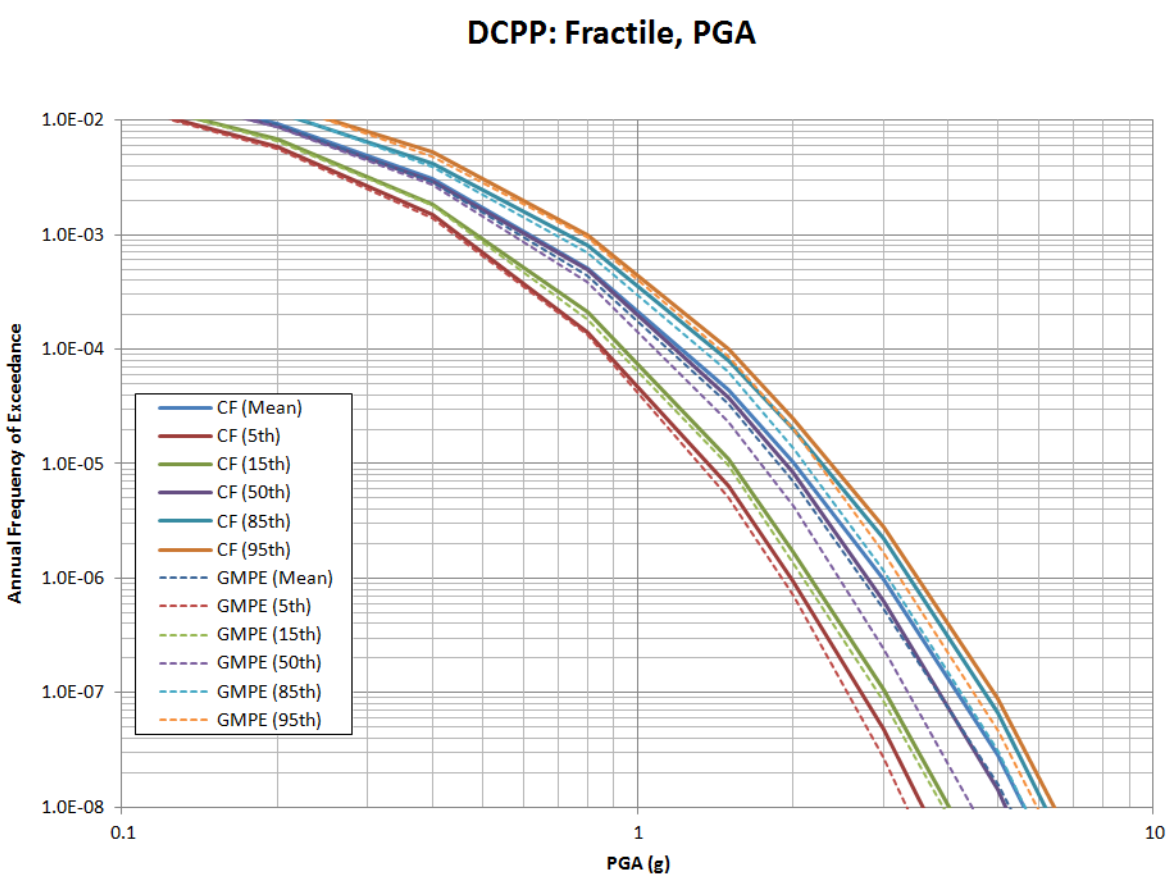



**Figure O.2-6:** Comparison of PGA fractiles curves for the 5th, 15th, 50th, 85th and 95th fractiles using the representative suite of common-form models (solid curves) and the candidate GMPEs with the Al Atik and Youngs (2014) additional epistemic uncertainty (dashed curves). The mean hazard curves for the representative suite of common-form models and the candidate GMPEs are also shown.

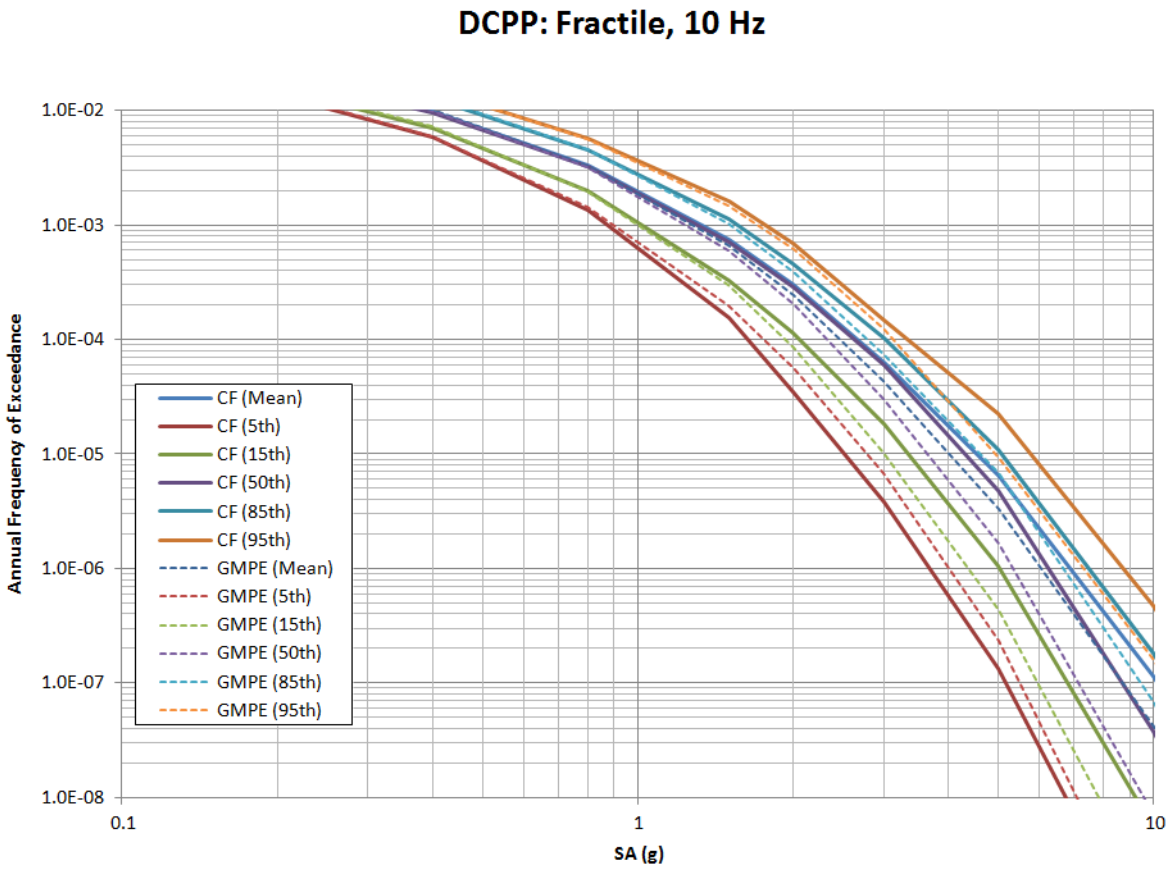



**Figure O.2-7:** Comparison of 10 Hz spectral frequency fractiles curves for the 5th, 15th, 50th, 85th and 95th fractiles using the representative suite of common-form models (solid curves) and the candidate GMPEs with the Al Atik and Youngs (2014) additional epistemic uncertainty (dashed curves). The mean hazard curves for the representative suite of common-form models and the candidate GMPEs are also shown.

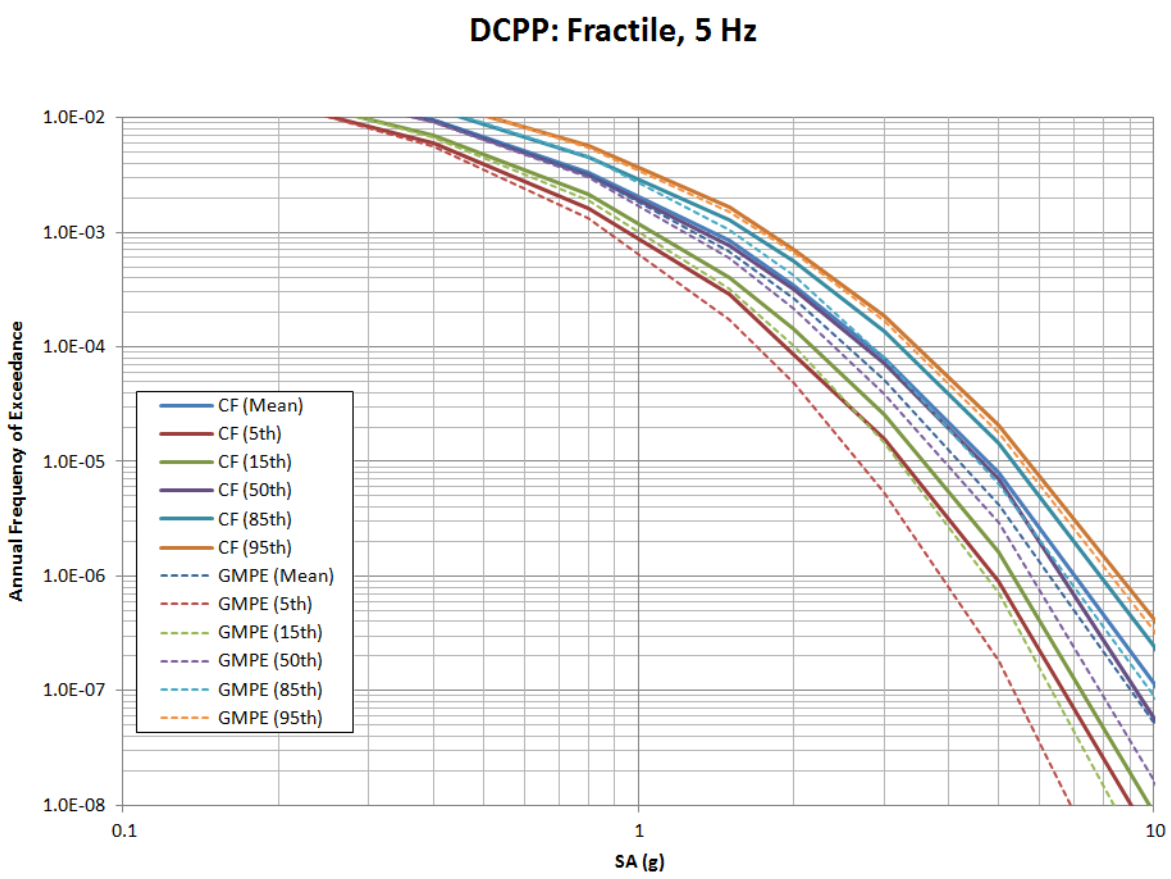



**Figure O.2-8:** Comparison of 5 Hz spectral frequency fractiles curves for the 5$^{th}$, 15$^{th}$, 50$^{th}$, 85$^{th}$ and 95$^{th}$ fractiles using the representative suite of common-form models (solid curves) and the candidate GMPEs with the Al Atik and Youngs (2014) additional epistemic uncertainty (dashed curves). The mean hazard curves for the representative suite of common-form models and the candidate GMPEs are also shown.

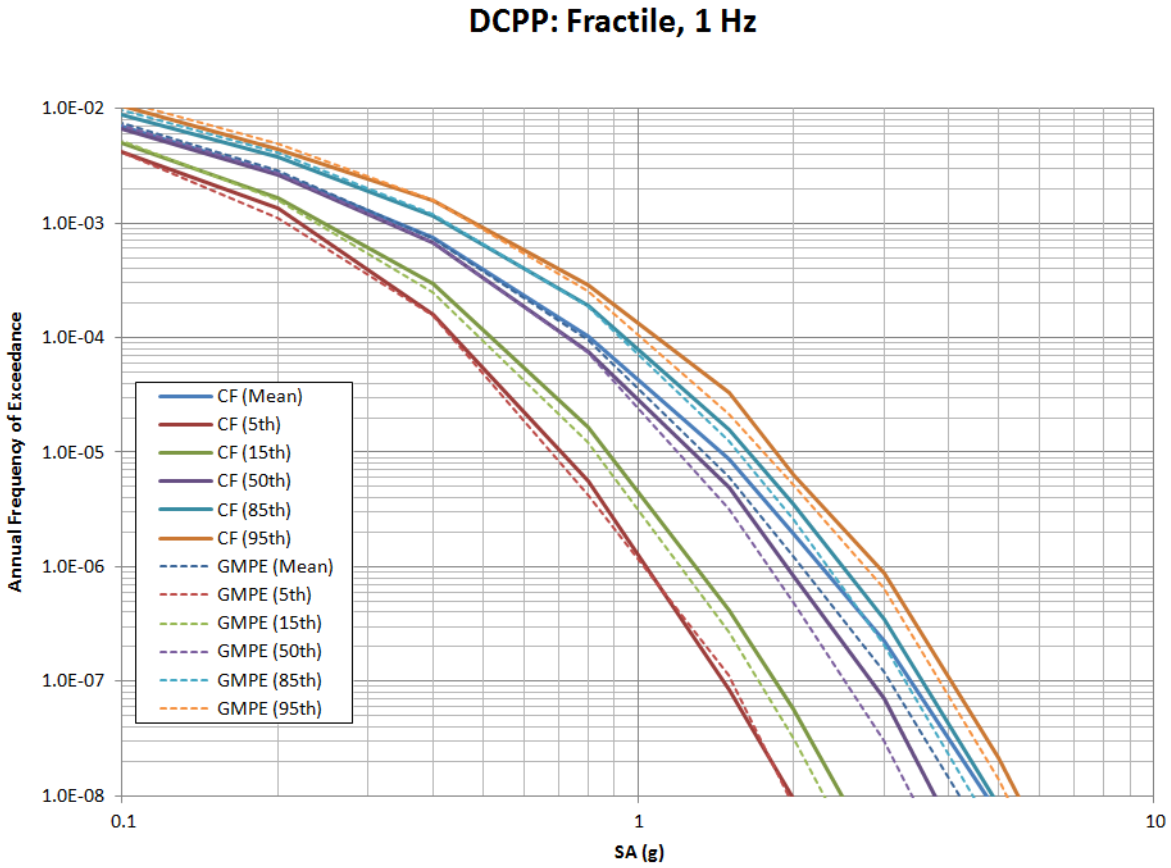



**Figure O.2-9:** Comparison of 1 Hz spectral frequency fractiles curves for the 5$^{th}$, 15$^{th}$, 50$^{th}$, 85$^{th}$ and 95$^{th}$ fractiles using the representative suite of common-form models (solid curves) and the candidate GMPEs with the Al Atik and Youngs (2014) additional epistemic uncertainty (dashed curves). The mean hazard curves for the representative suite of common-form models and the candidate GMPEs are also shown.

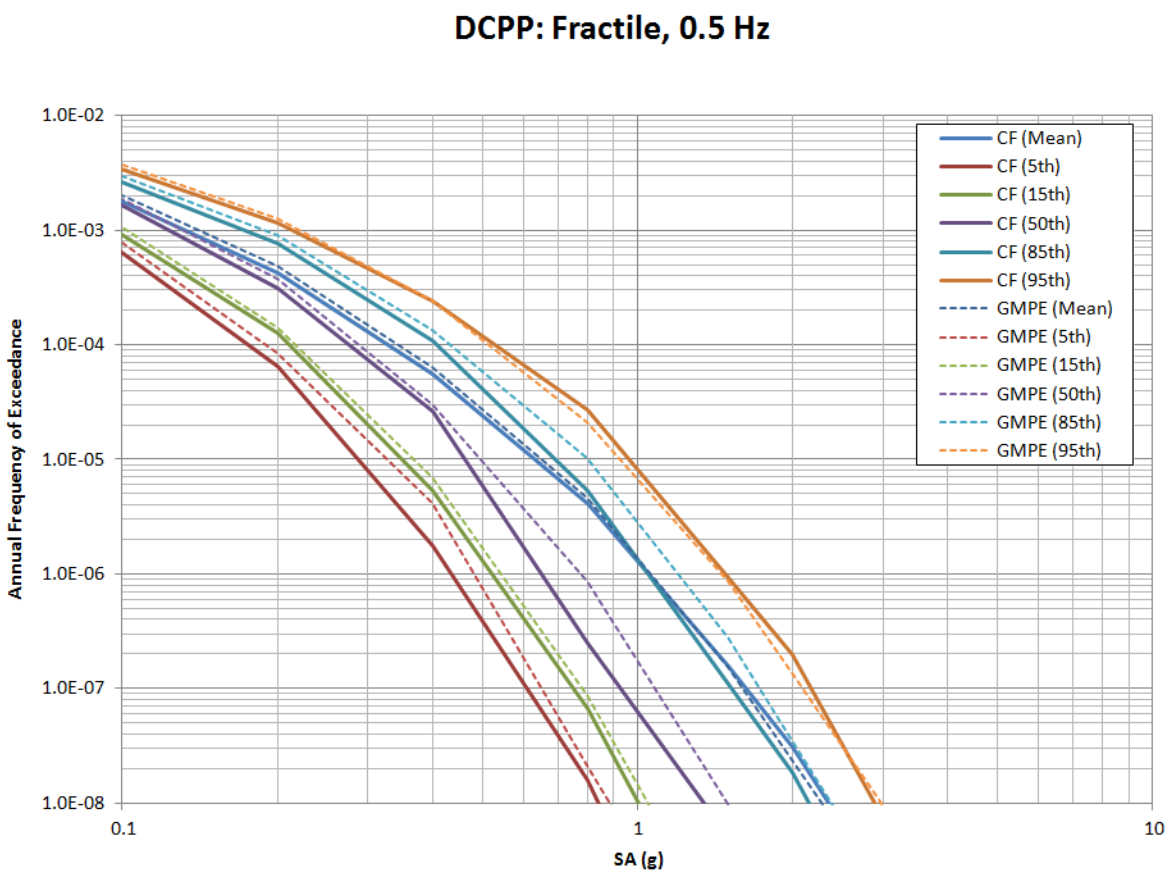



**Figure O.2-10:** Comparison of 0.5 Hz spectral frequency fractiles curves for the 5$^{th}$, 15$^{th}$, 50$^{th}$, 85$^{th}$ and 95$^{th}$ fractiles using the representative suite of common-form models (solid curves) and the candidate GMPEs with the Al Atik and Youngs (2014) additional epistemic uncertainty (dashed curves). The mean hazard curves for the representative suite of common-form models and the candidate GMPEs are also shown.

## O.3 Hazard for PVNGS

For PVNGS, the common functional form models are based on both the $R_{RUP}$ (Model A) and $R_{JB}$ (Model B) distance metrics with the $R_{RUP}$-based models also including the hanging-wall adjustments (Sections 6.4.1.2 and 6.4.3). For PVNGS, the common functional-form models are used to model the ground motions associated with the local Greater Arizona sources, while the suite of five NGA-West2 GMPE models are used in the hazard analysis for the distant seismic sources located in Southern California and Mexico (Regions 1 and 2&3). Both the common functional-form GMPE models and the NGA-West2 GMPEs are computed using an assumed $V_{S30}$ of 760 m/sec and the default additional parameters (e.g., $Z_1$ and $Z_{2.5}$) based on this assumed $V_{S30}$ value.

As part of the development of the common-form models (i.e., both Model A and Model B), six candidate GMPE models were analyzed:

- Akkar et al. (2014a, 2014b) – ASB14
- Abrahamson et al. (2014) – ASK14
- Bindi et al. (2014a, 2014b) – Bi14
- Boore et al. (2014) – BSSA14
- Campbell and Bozorgnia (2014) – CB14
- Chiou and Youngs (2014) – CY14

For the representative suite of common-form Model A, there are a total of 23 models for PGA, 24 models for 10 Hz, 21 models for 5 Hz, 21 models for 1 Hz, and 24 models for 0.5 Hz. For the representative suite of common-form Model B, there are a total of 23 models for PGA, 21 models for 10 Hz, 20 models for 5 Hz, 22 models for 1 Hz, and 23 selected models for 0.5 Hz.

For these sensitivity analyses, the comparison is between the representative suite of common-form models and the six candidate empirical models used in the development of the common-form models. For the hazard analysis, the GMPE associated with the Greater Arizona sources is varied and for the more distant Region 1 and Region 2&3 seismic sources, the hazard is computed using the BSSA14 NGA-West2 GMPE model. In the hazard curve comparison plots, the individual hazard curve from Regions 1 and 2&3 sources are also plotted. These seismic sources contribute 30 % or more to the total hazard for 0.5 Hz spectral frequency at PSA less than 0.3 g (annual hazard greater than $3x10^{-7}$).

The representative suite of common-form Model A and Model B hazard curves are shown in Figure O.3-1a to O.3-5a for PGA and the spectral frequencies of 10, 5, 1 and 0.5 Hz, respectively. The hazard curves for the representative suite of common-form Model A and Model B models are shown as grey lines, identified in the legend by their model ID numbers along with “MA” for

Model A and "MB" for the Model B cases. Also shown in these figures are the weighted mean from the representative suite of common-form for Model A, Model B, and combined Model A+B, the total contribution from Region 1 and Region 2&3, and the individual hazard curves from the six candidate GMPE models listed above. Additionally, in some of these figures, a hazard curve is shown for the Graizer (2014) model, referred to as GK14. The GK14 model was not included for the common-form model development because of its unique distance scaling. Figures O.3-1b to O.3-5b are similar plots with respect of the previous ones, but with the representative suite of common-form model hazard curves not plotted.

Based on these three plots, the selection of the representative suite of common-form models (i.e., combining the distribution range from both Model A and Model B) spans a greater range than the six candidate GMPE models used in their development. For the higher spectral frequency cases (PGA, 10 and 5 Hz), the mean hazard for the representative suite of common-form model falls within the central distribution of the six empirical GMPE models.

For the lower spectral frequency cases (1 and 0.5 Hz), these hazard curves show a larger spread in their distribution than the higher spectral frequency cases both for the candidate empirical GMPE models and the representative suite of common-form models. For the 1 and 0.5 Hz spectral frequency cases, the mean weighted representative suite of common-form model is close to the center of the distribution of the candidate GMPEs hazard curves. For the representative suite of common-form models, the selected models span the range of hazard curves computed based on the six candidate empirical GMPEs.

Another observation in these comparisons for the 1 and 0.5 Hz spectral frequency cases is the reduced range of the representative suite of common-form models for high hazard levels (i.e., low ground motions). This observation is a result of the significant contribution from the distant Region 1 and Region 2&3 seismic source to the total hazard curves for each individual model shown by the grey lines. The variation in the individual models is limited when comparing the total hazard curves by the contribution from these distant sources. For lower hazard levels (i.e., higher ground-motion values), this observation of the clustering of the individual models is not as strong, because the contribution from the Greater Arizona sources increases relative to the distant sources.

Figures O.3-6 to O.3-10 show the $5^{th}$, $15^{th}$, $50^{th}$, $85^{th}$ and $95^{th}$ fractiles curves for the five analyzed periods, respectively. The fractiles curves using the representative suite of common-form models (combining the weighted distribution range from both Model A and Model B) are compared to the fractiles curves using the candidate GMPEs with the Al Atik and Youngs (2014) additional epistemic uncertainty. To simplify the hazard calculation, the Al Atik and Youngs (2014) uncertainty for $\mathbf{M} \geq 7$ was applied to all magnitudes.

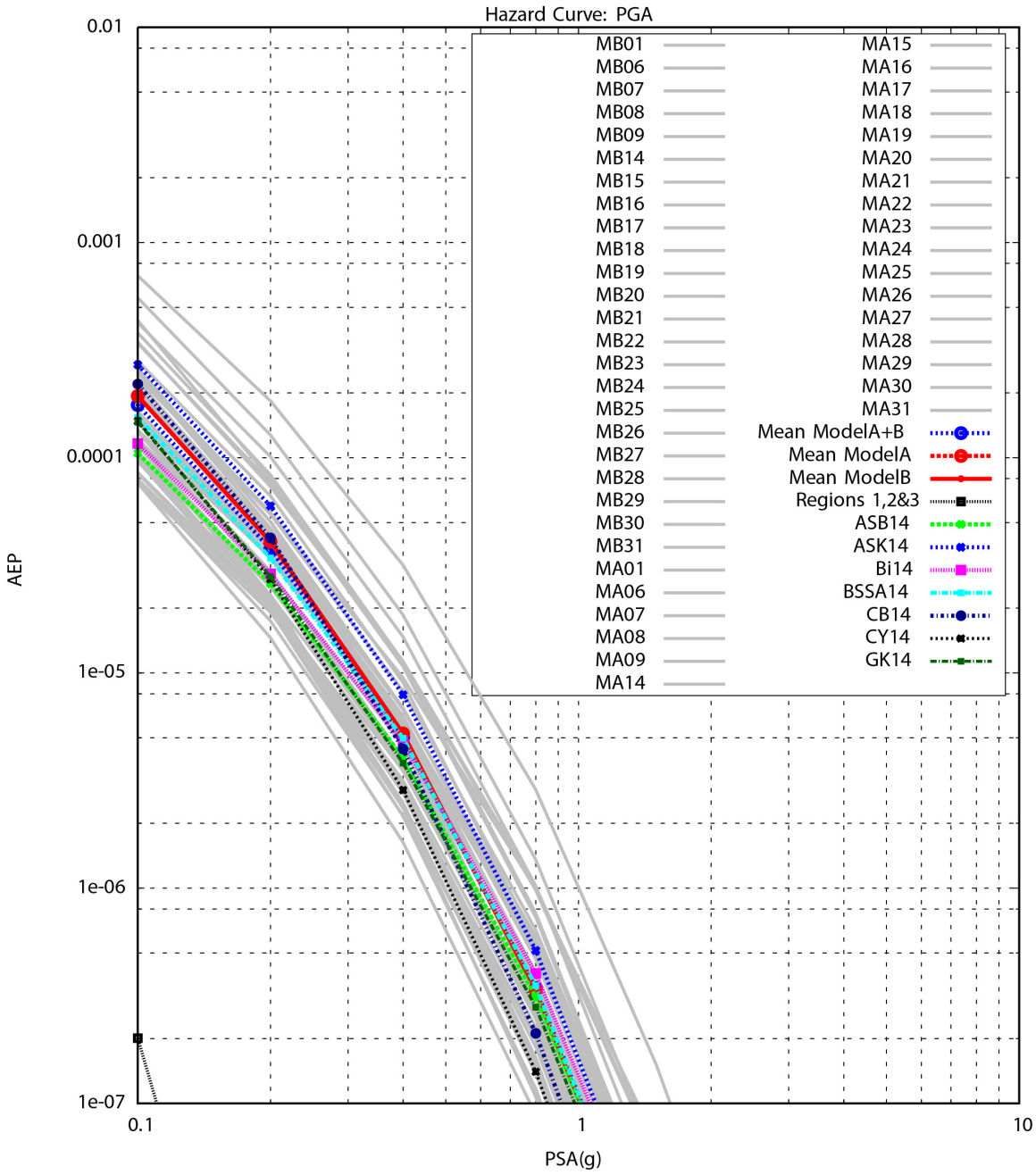



**Figure O.3-1a:** Comparison of PGA hazard curves using the representative suite of common-form for Model A and Model B models (grey lines), weighted mean of the representative suite of common-form models (Model A, Model B, and Model A+B), the contribution from the distant Region 1 and Region 2&3 sources, and the six candidate empirical GMPE models. The hazard curve for the GK14 model is also shown.

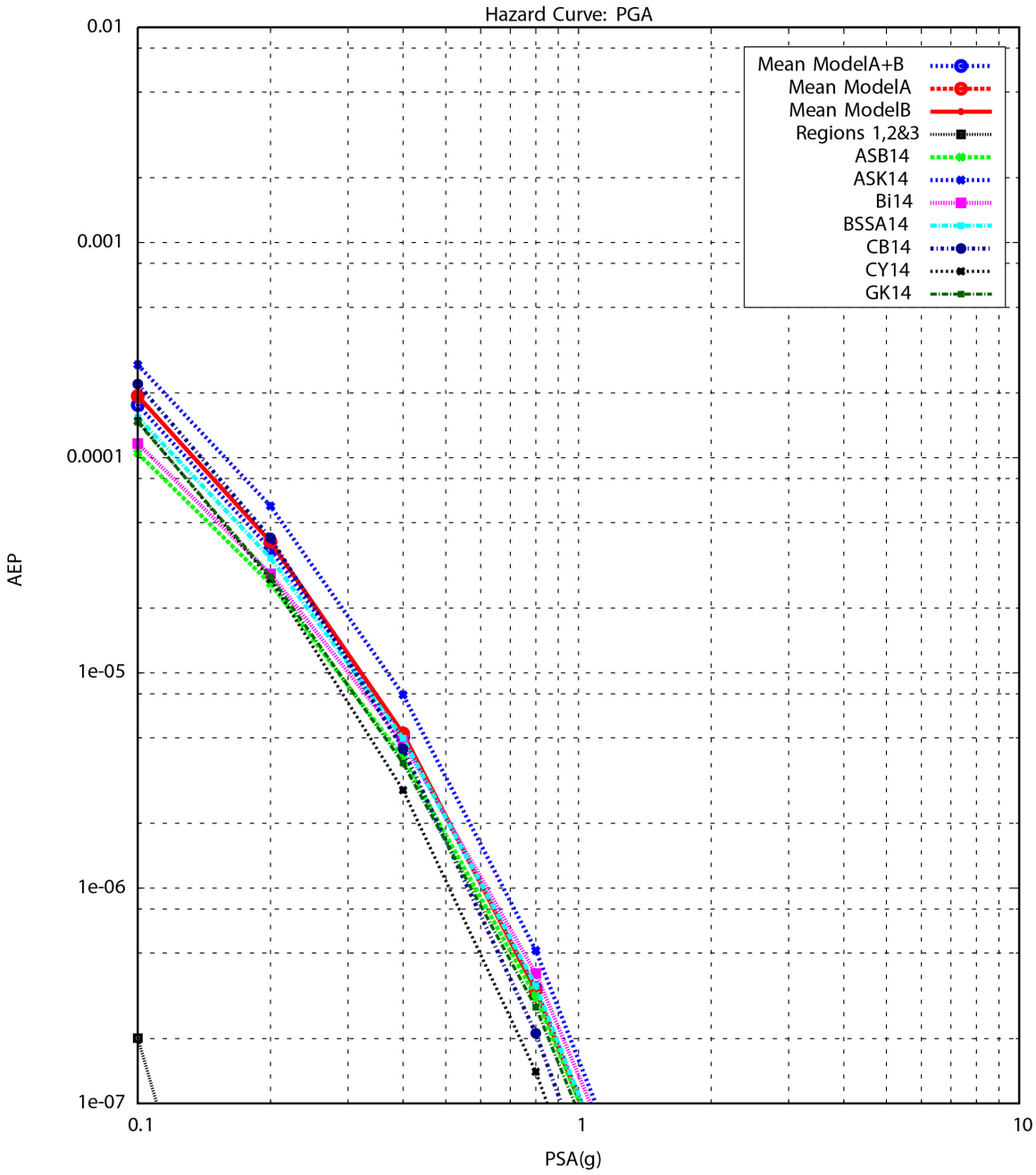



**Figure O.3-1b:** Comparison of PGA hazard curves using the weighted mean of the representative suite of common-form Model A+B, Model A, Model B models, and the six candidate empirical GMPE models. The hazard curve for the GK14 model is also shown.

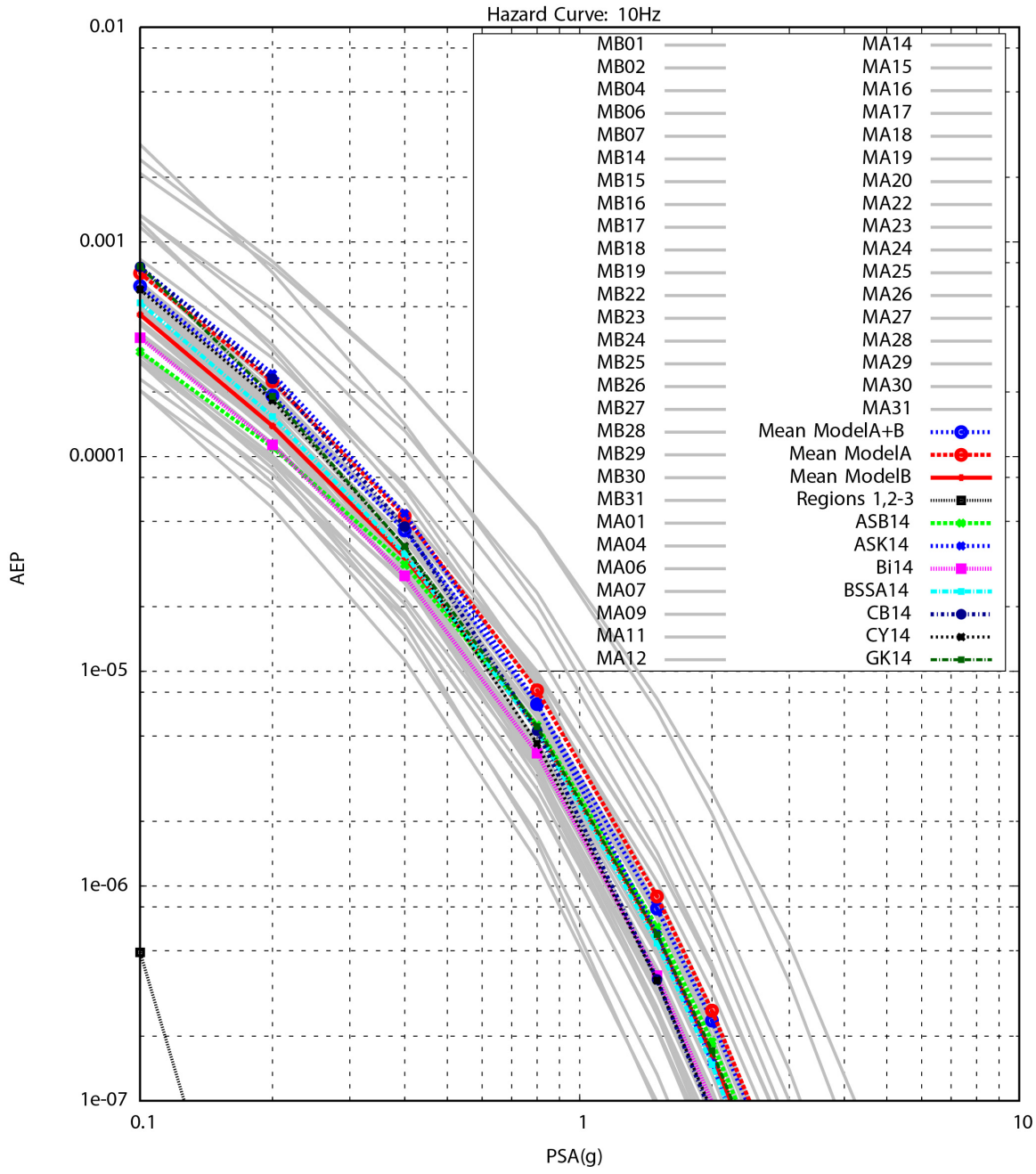



**Figure O.3-2a:** Comparison of 10 Hz spectral acceleration hazard curves using the representative suite of common-form for Model A and Model B models (grey lines), weighted mean of the representative suite of common-form models (Model A, Model B, and Model A+B), the contribution from the distant Region 1 and Region 2&3 sources, and the six candidate empirical GMPE models. The hazard curve for the GK14 model is also shown.

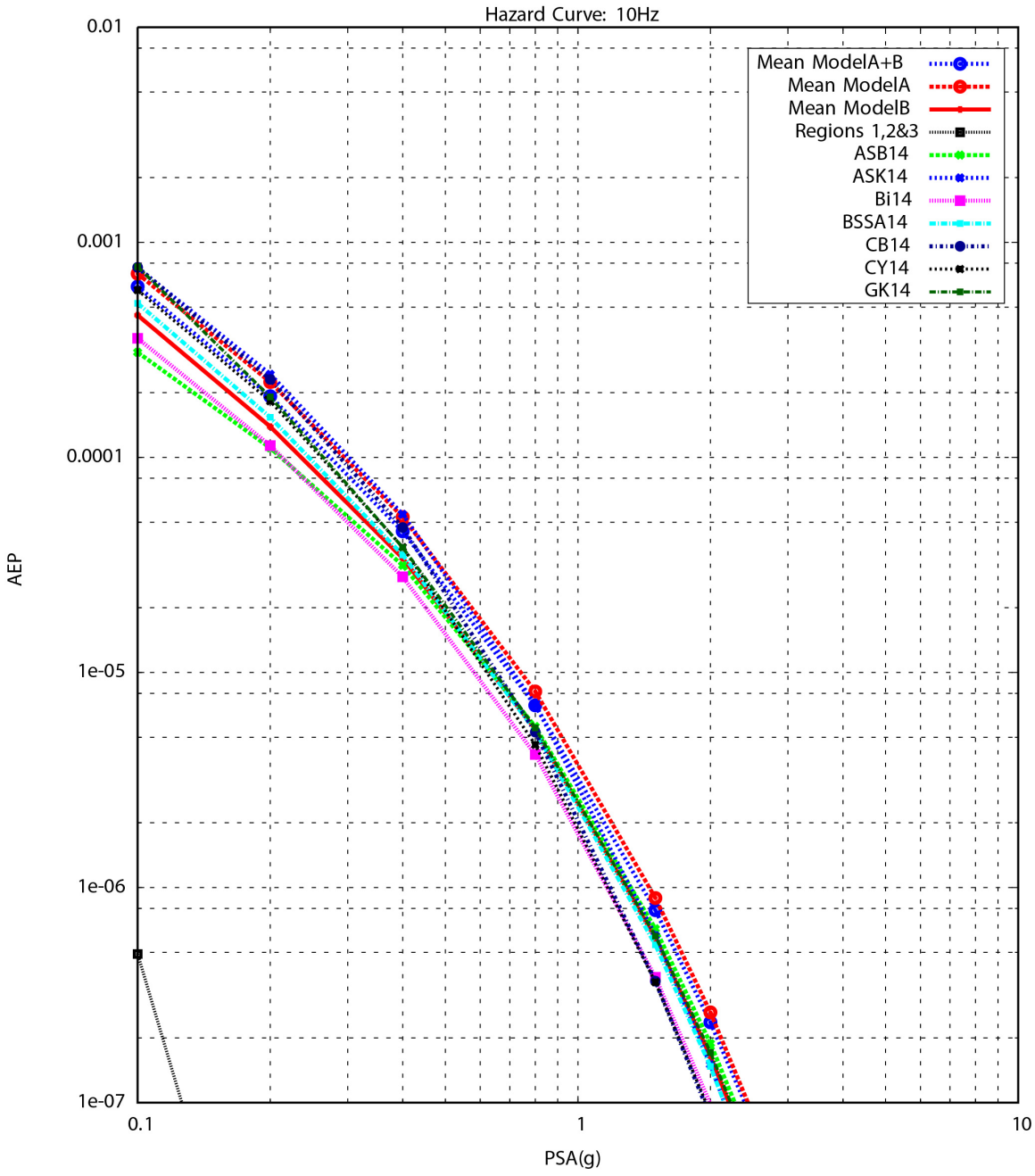



**Figure O.3-2b:** Comparison of 10 Hz spectral acceleration hazard curves using the weighted mean of the representative suite of common-form Model A+B, Model A, Model B models, and the six candidate empirical GMPE models. The hazard curve for the GK14 model is also shown.

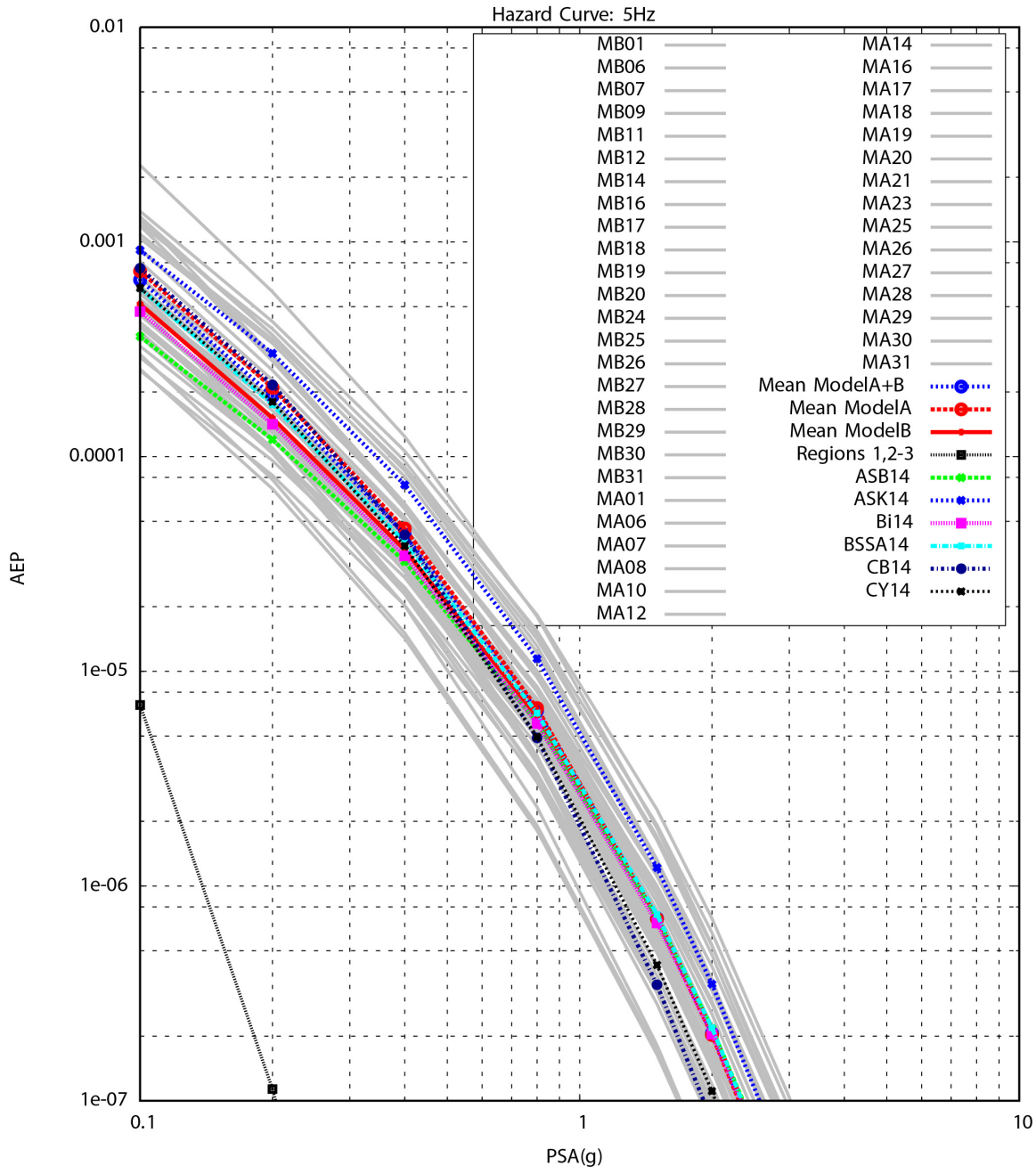



**Figure O.3-3a:** Comparison of 5 Hz spectral acceleration hazard curves using the representative suite of common-form for Model A and Model B models (grey lines), weighted mean of the representative suite of common-form models (Model A, Model B, and Model A+B), the contribution from the distant Region 1 and Region 2&3 sources, and the six candidate empirical GMPE models.

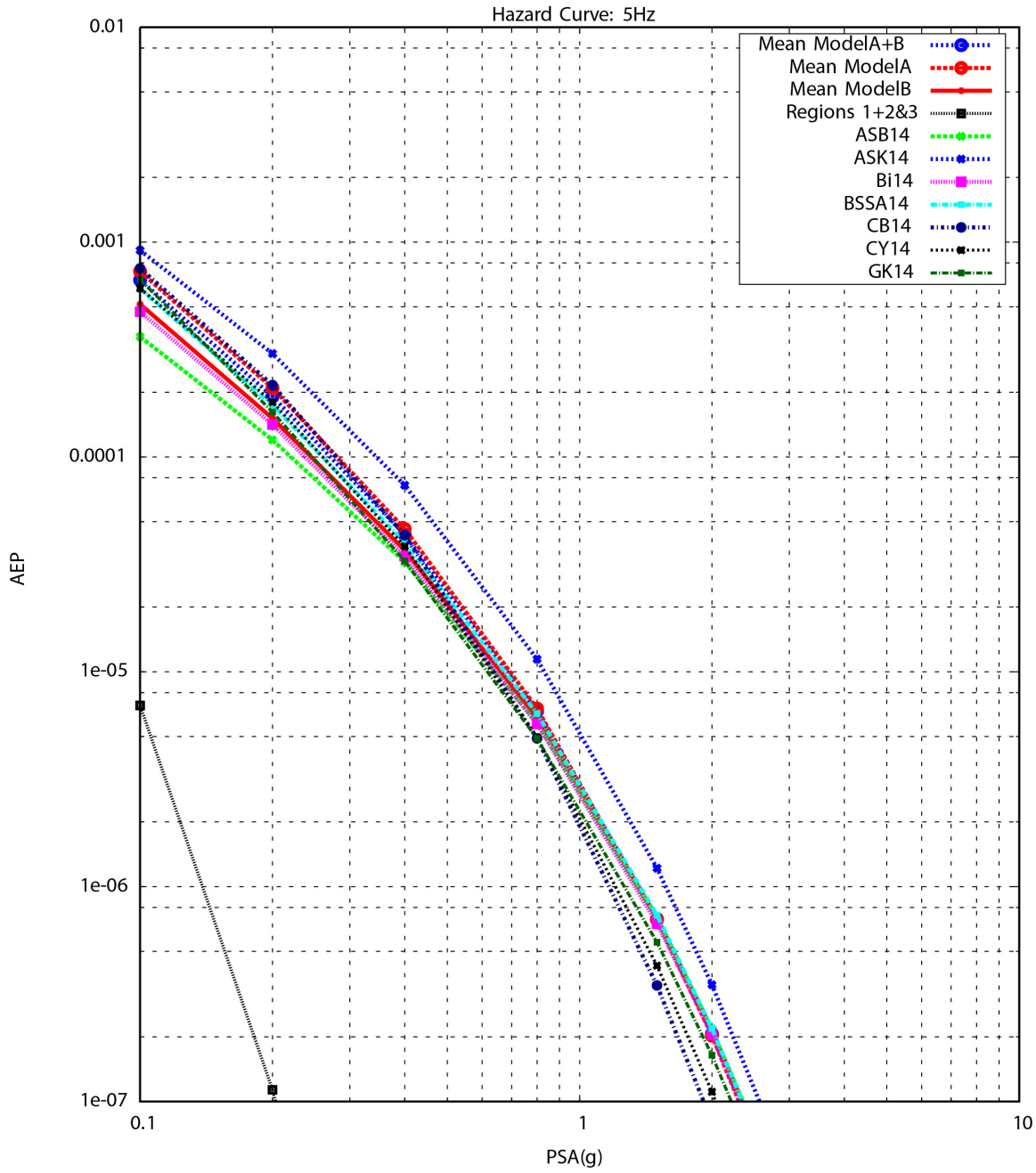



**Figure O.3-3b:** Comparison of 5 Hz spectral acceleration hazard curves using the weighted mean of the representative suite of common-form Model A+B, Model A, Model B models, and the six candidate empirical GMPE models. The hazard curve for the GK14 model is also shown.

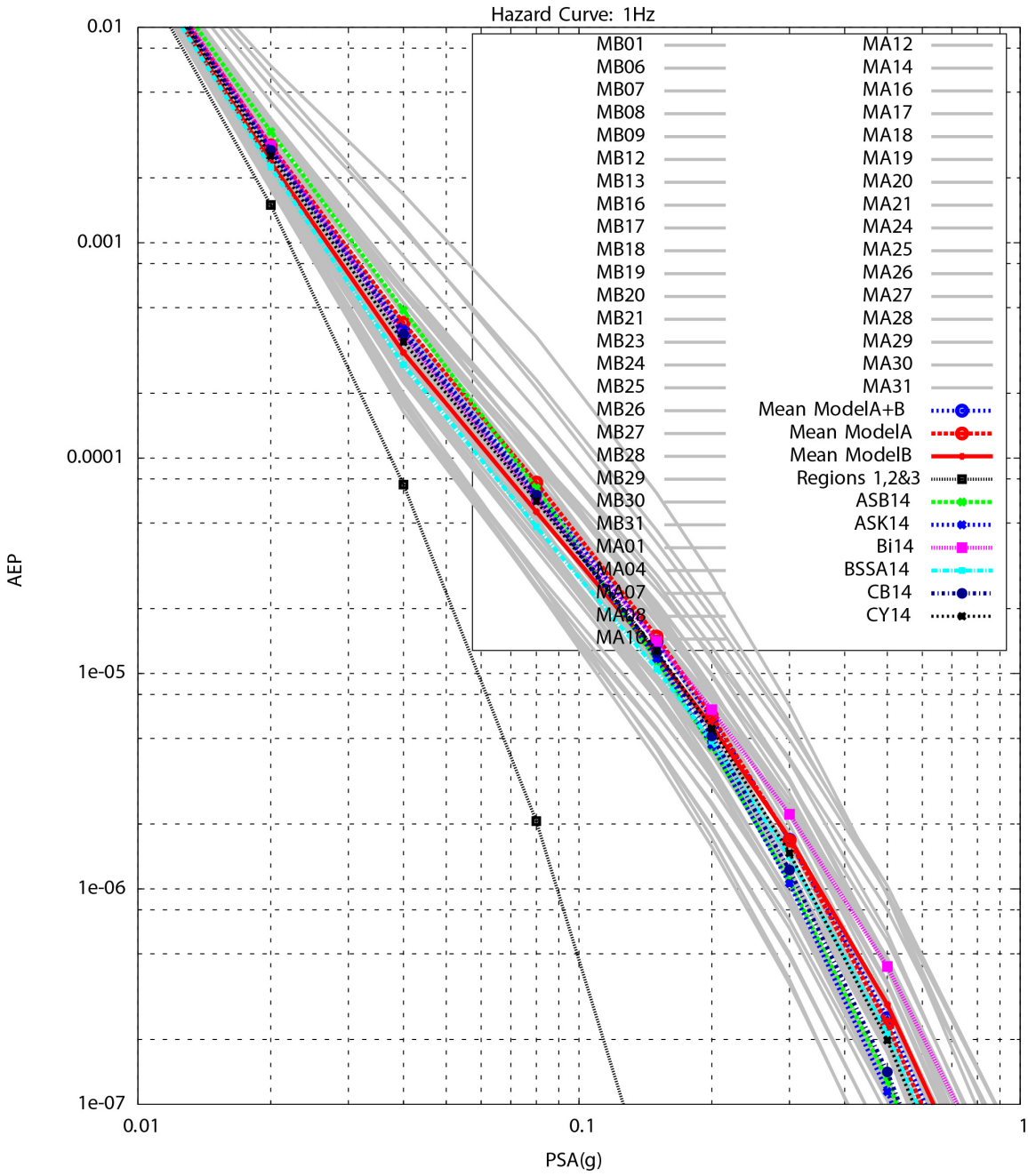



**Figure O.3-4a:** Comparison of 1 Hz spectral acceleration hazard curves using the representative suite of common-form for Model A and Model B models (grey lines), weighted mean of the representative suite of common-form models (Model A, Model B, and Model A+B), the contribution from the distant Region 1 and Region 2&3 sources, and the six candidate empirical GMPE models.

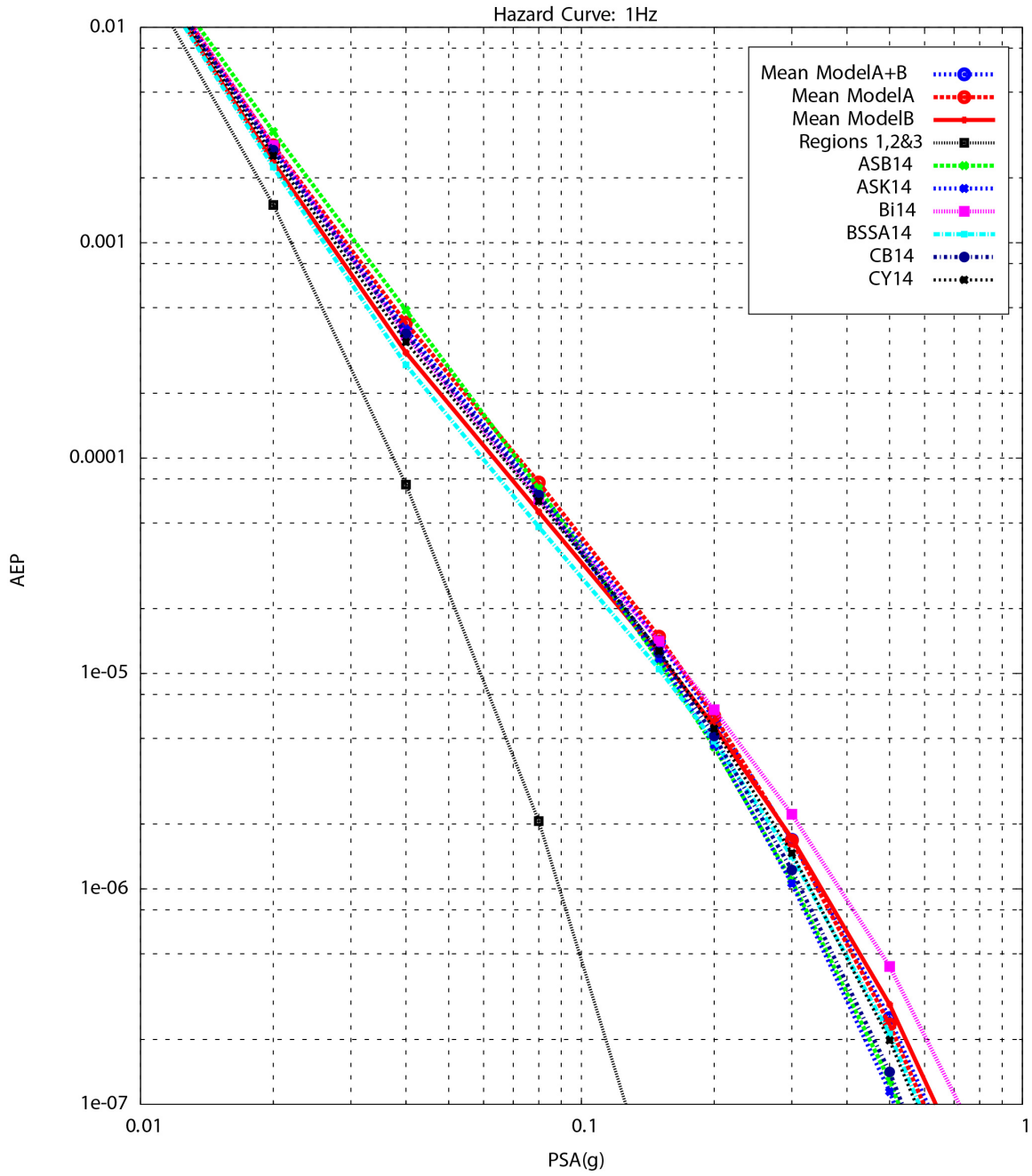



**Figure O.3-4b:** Comparison of 1 Hz spectral acceleration hazard curves using the weighted mean of the representative suite of common-form Model A+B, Model A, Model B models, and the six candidate empirical GMPE models.

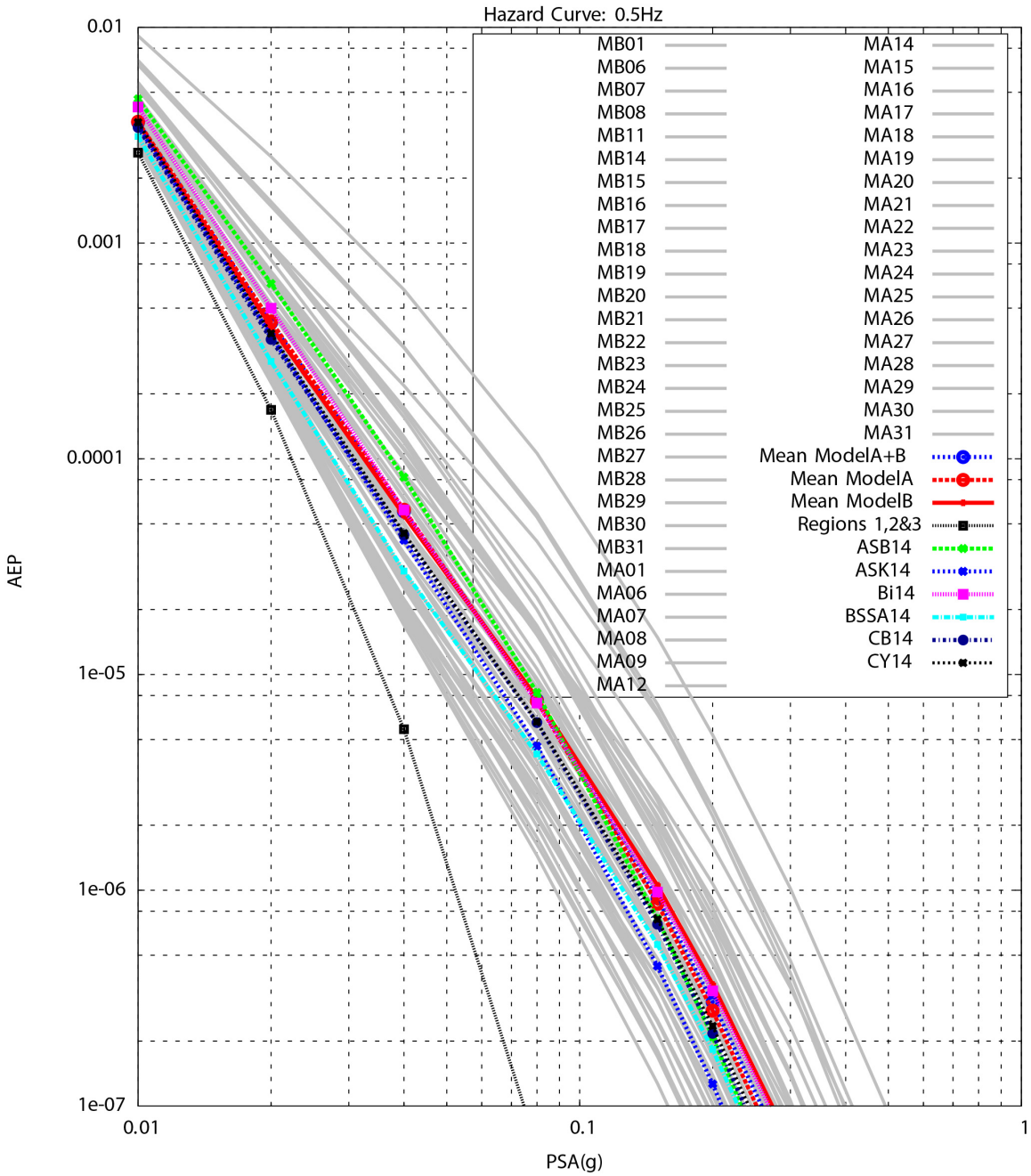



**Figure O.3-5a:** Comparison of 0.5 Hz spectral acceleration hazard curves using the representative suite of common-form for Model A and Model B models (grey lines), weighted mean of the representative suite of common-form models (Model A, Model B, and Model A+B), the contribution from the distant Region 1 and Region 2&3 sources, and the six candidate empirical GMPE models.

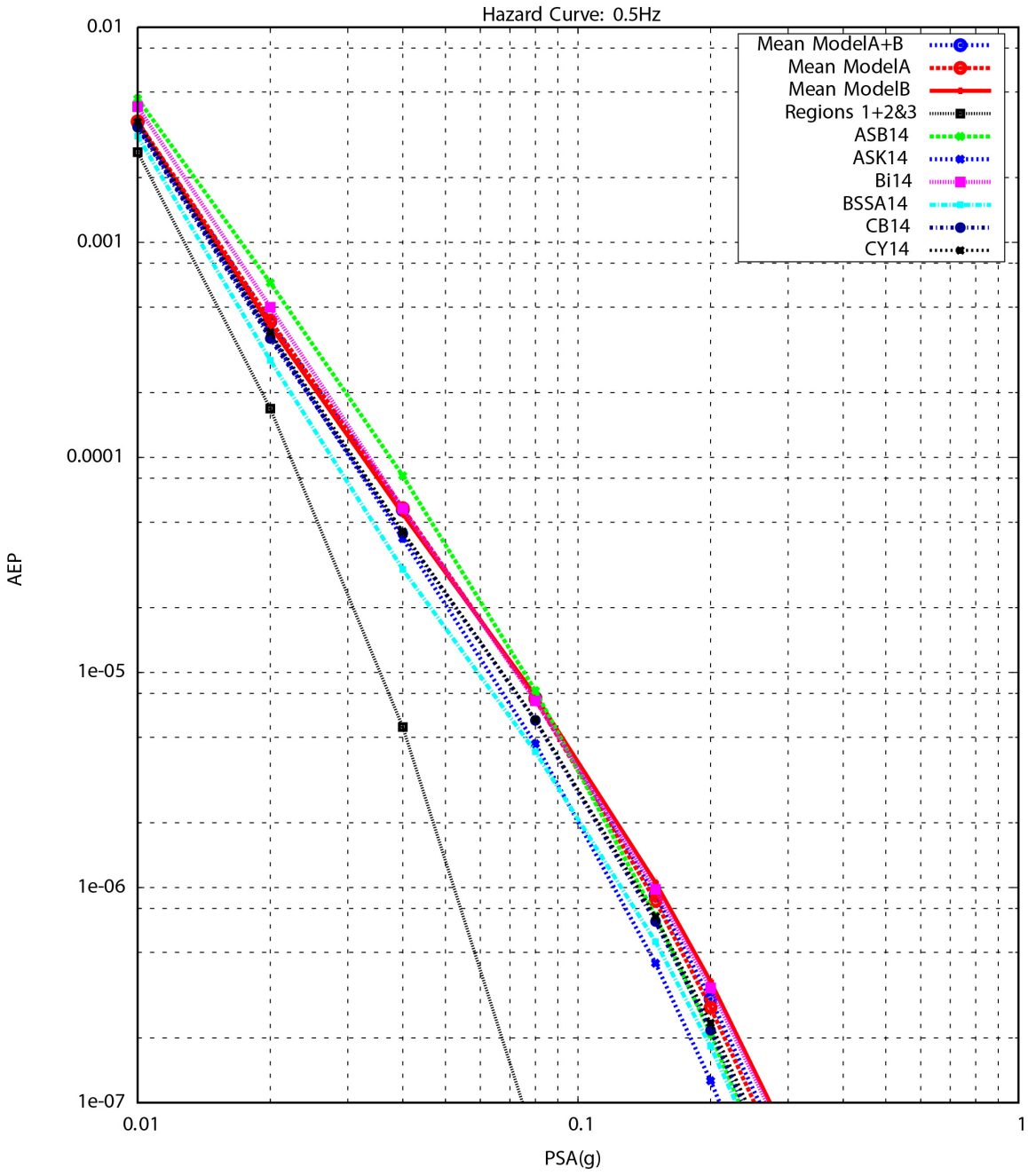



**Figure O.3-5b:** Comparison of 0.5 Hz spectral acceleration hazard curves using the weighted mean of the representative suite of common-form Model A+B, Model A, Model B models, and the six candidate empirical GMPE models.

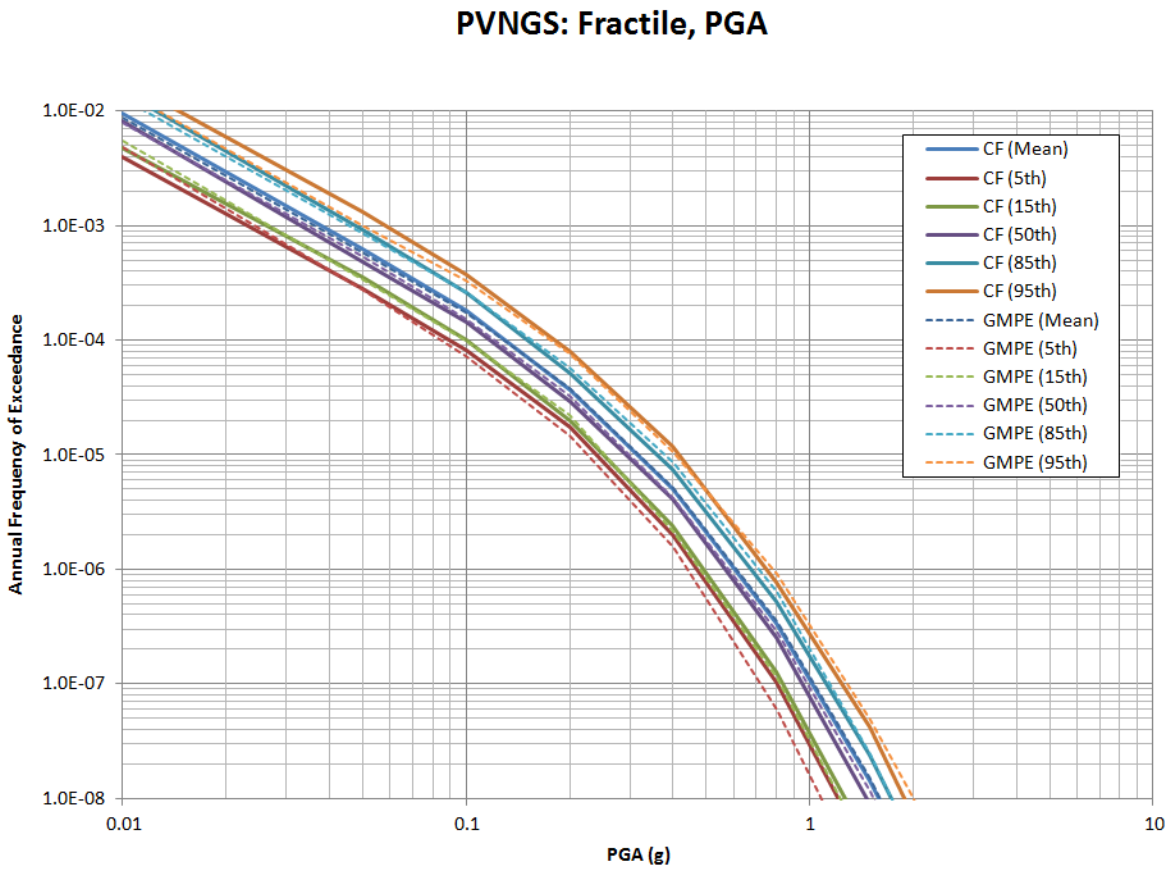



**Figure O.3-6:** Comparison of PGA fractiles curves for the 5th, 15th, 50th, 85th and 95th fractiles using the representative suite of common-form models (solid curves) and the candidate GMPEs with the Al Atik and Youngs (2014) additional epistemic uncertainty (dashed curves). The weighted mean hazard curves for the representative suite of common-form models and the candidate GMPEs are also shown.

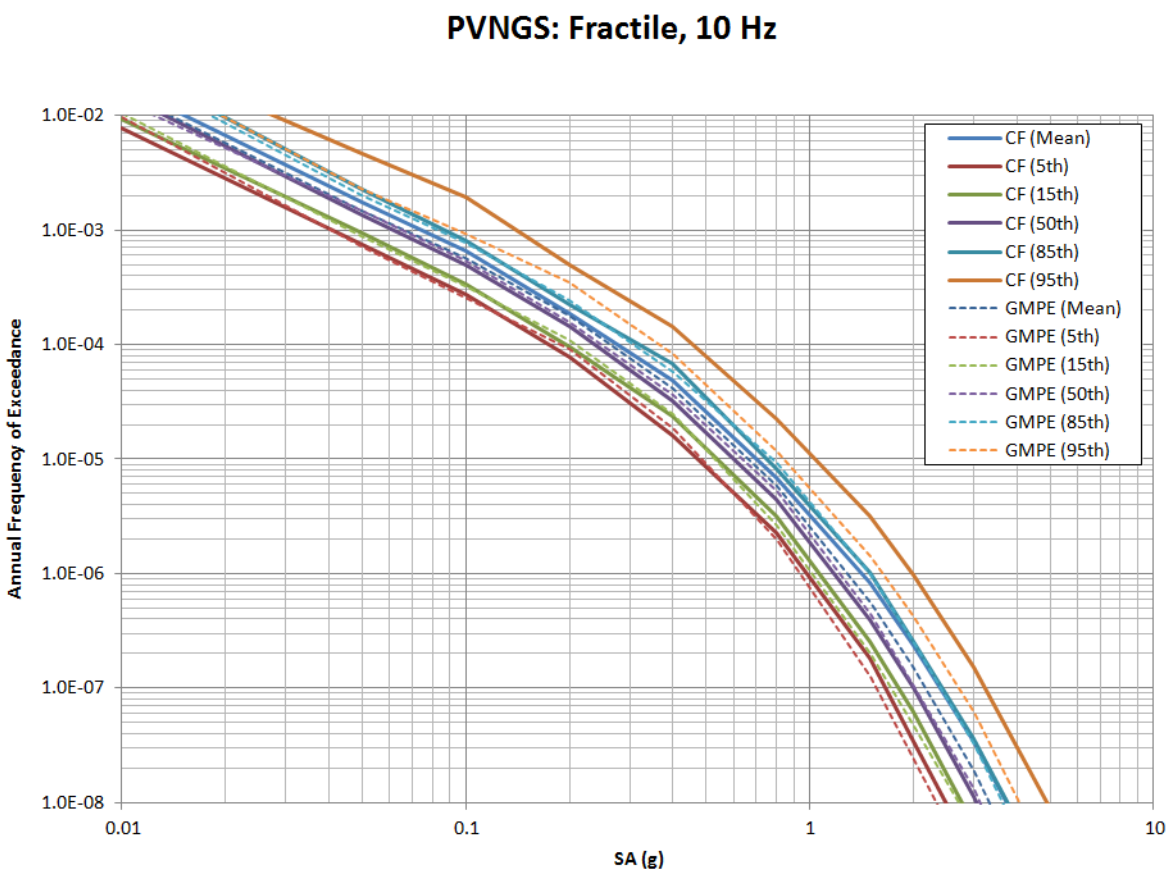



**Figure O.3-7:** Comparison of 10 Hz spectral acceleration fractiles curves for the 5$^{th}$, 15$^{th}$, 50$^{th}$, 85$^{th}$ and 95$^{th}$ fractiles using the representative suite of common-form models (solid curves) and the candidate GMPEs with the Al Atik and Youngs (2014) additional epistemic uncertainty (dashed curves). The weighted mean hazard curves for the representative suite of common-form models and the candidate GMPEs are also shown.

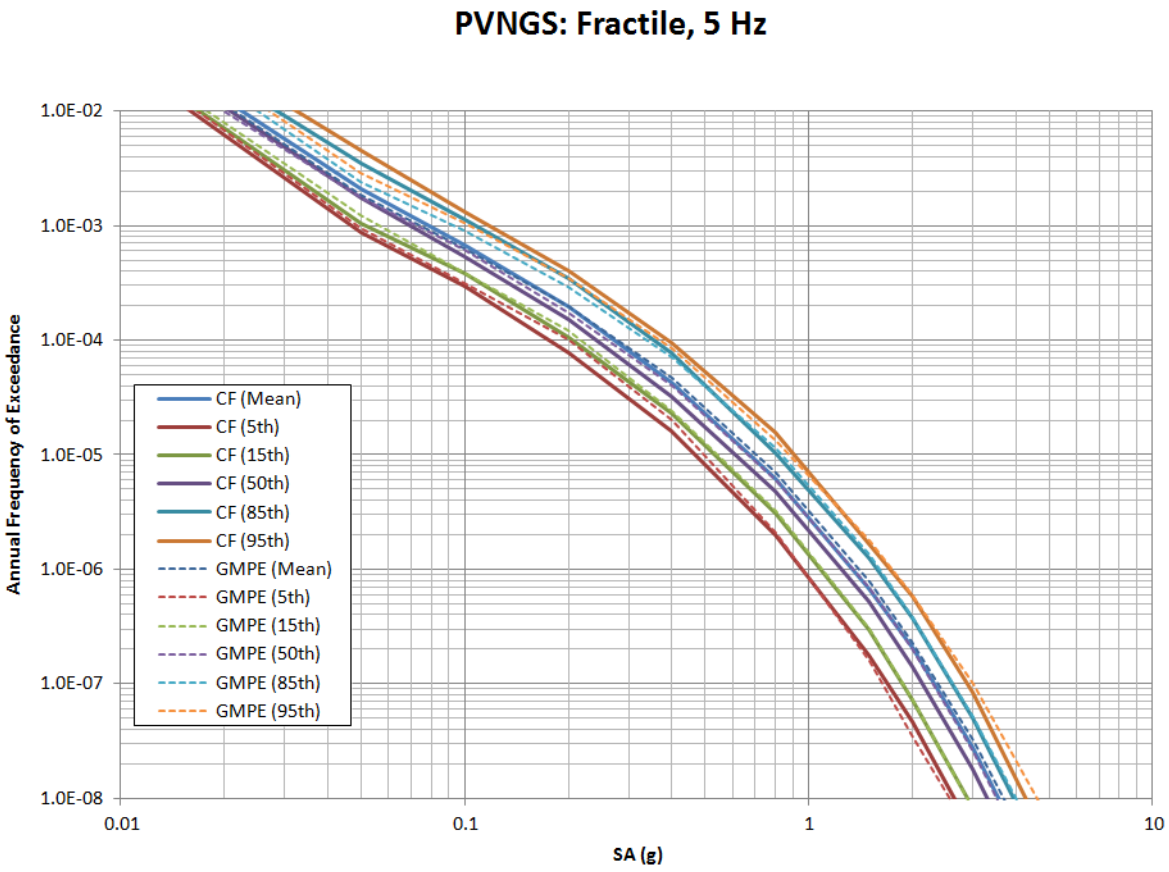



**Figure O.3-8:** Comparison of 5 Hz spectral acceleration fractiles curves for the 5$^{th}$, 15$^{th}$, 50$^{th}$, 85$^{th}$ and 95$^{th}$ fractiles using the representative suite of common-form models (solid curves) and the candidate GMPEs with the Al Atik and Youngs (2014) additional epistemic uncertainty (dashed curves). The weighted mean hazard curves for the representative suite of common-form models and the candidate GMPEs are also shown.

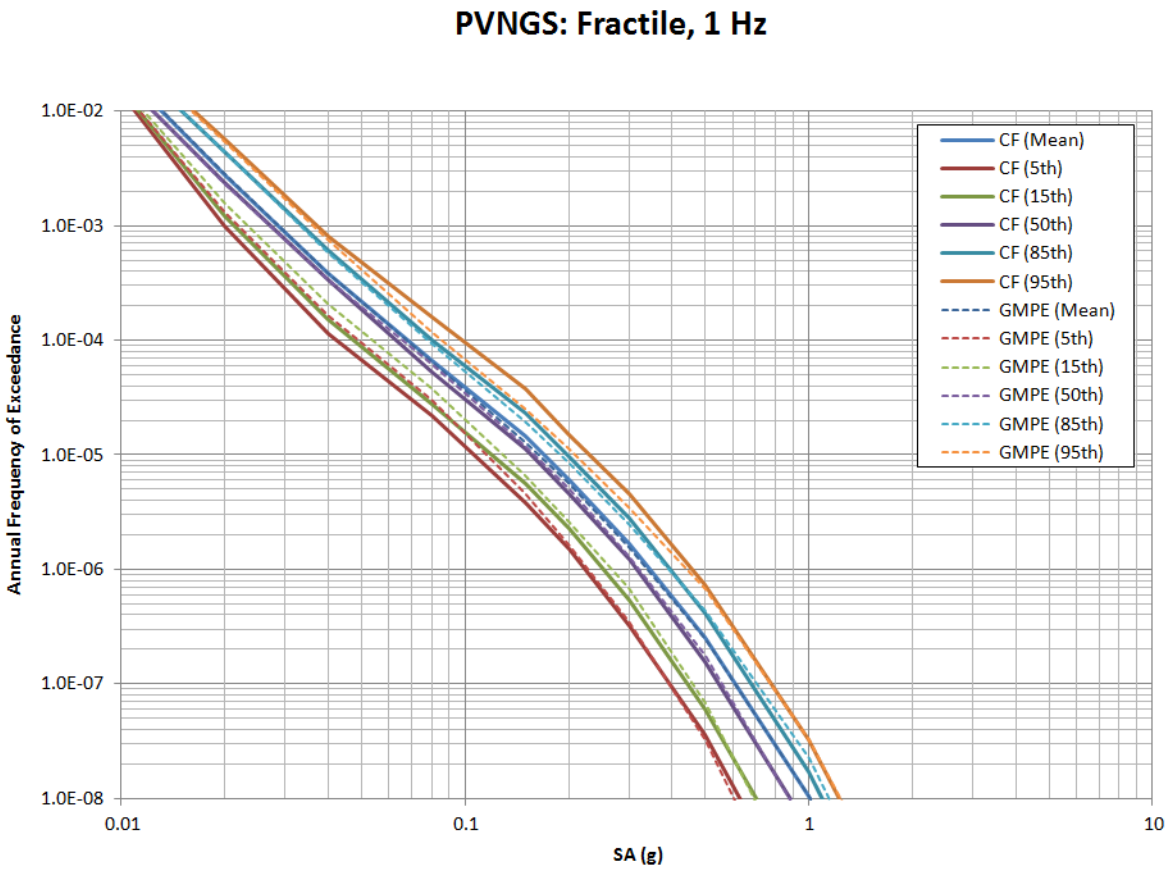



**Figure O.3-9:** Comparison of 1 Hz spectral acceleration fractiles curves for the 5$^{th}$, 15$^{th}$, 50$^{th}$, 85$^{th}$ and 95$^{th}$ fractiles using the representative suite of common-form models (solid curves) and the candidate GMPEs with the Al Atik and Youngs (2014) additional epistemic uncertainty (dashed curves). The weighted mean hazard curves for the representative suite of common-form models and the candidate GMPEs are also shown.

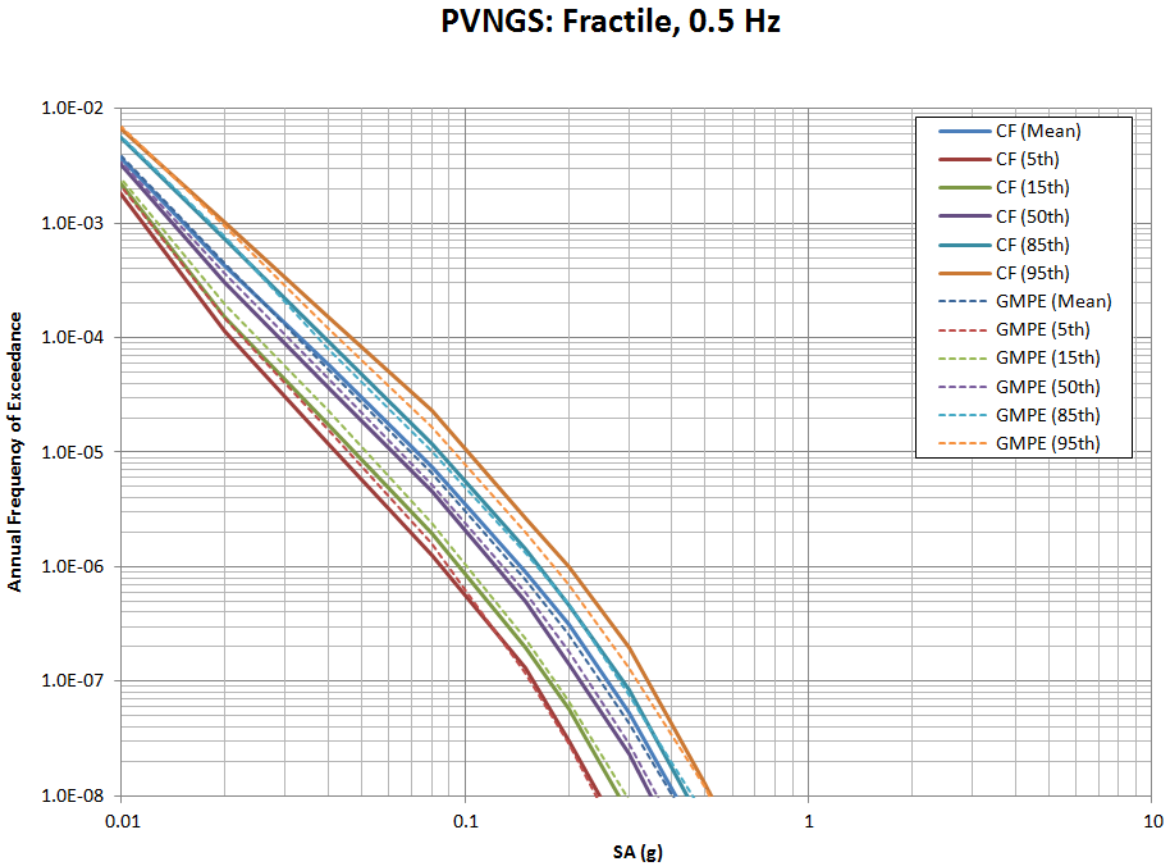



**Figure O.3-10:** Comparison of 0.5 Hz spectral acceleration fractiles curves for the 5th, 15th, 50th, 85th and 95th fractiles using the representative suite of common-form models (solid curves) and the candidate GMPEs with the Al Atik and Youngs (2014) additional epistemic uncertainty (dashed curves). The weighted mean hazard curves for the representative suite of common-form models and the candidate GMPEs are also shown.

## O.4 References

Abrahamson, N.A., Silva, W.J., and Kamai, R. (2014). Summary of the AKS14 Ground-Motion Relation for Active Crustal Regions, *Earthquake Spectra*, Vol. 30(3), 1025-1055, DOI: 10.1193/070913EQS198M

Akkar, S., Sandikkaya, M.A., and Bommer, J.J. (2014a). Empirical ground-motion models for point- and extended-source crustal earthquake scenarios in Europe and the Middle East, *Bull. Earthquake Eng.*, Vol. 12(1), 359-387, DOI: 10.1007/s10518-013-9461-4.

Akkar, S., Sandikkaya, M.A., and Bommer, J.J. (2014b). Erratum to: Empirical ground-motion models for point- and extended-source crustal earthquake scenarios in Europe and the Middle East, *Bull. Earthquake Eng.*, Vol. 12(1), 389-390, DOI: 10.1007/s10518-013-9508-6.

Bindi D., Massa M., Luzi L., Ameri G., Pacor F., Puglia R., and Augliera, P. (2014a). Pan-European Ground-Motion Prediction Equations for the Average Horizontal Component of PGA, PGV, and 5%-Damped PSA at Spectral Periods up to 3.0 s using the RESORCE dataset, *Bull. Earthquake Eng*., Vol. 12, 391-430, DOI: 10.1007/s10518-013-9525-5.

Bindi D., Massa M., Luzi L., Ameri G., Pacor F., Puglia R., and Augliera, P. (2014b). Erratum to: Pan-European Ground-Motion Prediction Equations for the Average Horizontal Component of PGA, PGV, and 5%-Damped PSA at Spectral Periods up to 3.0 s using the RESORCE dataset, *Bull. Earthquake Eng*., Vol. 12, 431-448, DOI: 10.1007/s10518-014-9589-x.

Boore, D.M., Stewart, J.P., Seyhan, E., and Atkinson, G.M. (2014). NGA-West 2 Equations for Predicting PGA, PGV, and 5%-Damped PSA for Shallow Crustal Earthquakes, *Earthquake Spectra*, Vol. 30(3), 1057-1085, DOI: 10.1193/070113EQS184M.

Campbell, K.W., and Bozorgnia, Y. (2014). NGA-West2 Ground Motion Model for the Average Horizontal Components of PGA, PGV, and 5%-Damped Linear Acceleration Response Spectra, *Earthquake Spectra*, Vol. 30(3), 1087-1115, DOI: 10.1193/062913EQS175M.

Chiou, B.S.-J., and Youngs, R.R. (2014). Update of the Chiou and Youngs NGA Model for the Average Horizontal Component of Peak Ground Motion and Response Spectra, *Earthquake Spectra*, Vol. 30(3), 1117-1153, DOI: 10.1193/072813EQS219M.

Graizer, V. (2014). Updated Graizer-Kalkan Ground-motion Prediction Equations for Western United States, *Proceedings for the 10th U.S. National Conference on Earthquake Engineering Frontiers of Earthquake Engineering*, July 21-25, 2014, Anchorage, Alaska, Paper ID 1097, 11 pp.

Idriss, I.M. (2014). An NGA-West2 Empirical Model for Estimating the Horizontal Spectral Values Generated by Shallow Crustal Earthquakes, *Earthquake* Spectra, Vol. 30(3), 1155-1177, DOI: 10.1193/070613EQS195M.

PG&E (2014). Probabilistic Seismic Hazard Analysis (PSHA) code, Haz43b. Fortran Computer Program.

Zhao, J.X., Zhang, J., Asano, A., Ohno, Y., Oouchi, T., Takahashi, T., Ogawa, H., Irikura, K., Thio, H.K., Somerville, P.G., Fukushima, Y., and Fukushima, Y. (2006). Attenuation Relations of

Strong Ground Motion in Japan Using Site Classification Based on Predominate Period, *Bull. Seism. Soc. Am*., Vol. 96, 898-913.

Zhao, J.X., and Lu, M. (2011). Magnitude-Scaling Rate in Ground-Motion Prediction Equations for Response Spectra from Large, Shallow Crustal Earthquakes, *Bull. Seism. Soc. Am*., Vol. 101, 2643-2661.

# APPENDIX P

# DISCRETIZATION OF CONTINUOS DISTRIBUTIONS FOR LOGIC TREE BRANCHES

## P.1 Chi-Square Distribution

The chi-square $(\chi^2)$ distribution describes the distribution of the sum of the squares of *k* independent normal random variables. Denoted as chi-squared with *k* degrees of freedom, $\chi_k^2$, the distribution has a mean of *k* and a variance of 2*k*. As described by many references (e.g. Ang and Tang, 2007), the sample variance of a normal distribution follows a scaled chi-square distribution. This suggests that the chi-square distribution is a natural choice to model the shape of the epistemic uncertainty distribution for the aleatory variance components. Coppersmith et al. (2014) proposed that the $\chi_k^2$ distribution shape be used to model the epistemic uncertainty in the variance components of ground motion by applying a scale factor *c* to scale the general chi-square distribution to match the mean and variance of the epistemic uncertainty distribution. Defining *Z* as a scaled chi-squared variable, $c\chi_k^2$, it follows that the scaled chi-square distribution has mean *ck* and variance $2c^2k$, as *c* is just a scalar multiplier.

Given the mean and variance of *Z*, *E*(*Z*) and *V*(*Z*), respectively, the parameters of the scaled chi-squared distribution are computed from the relationships:

$$E(Z) = ck \quad \text{and} \quad V(Z) = 2c^2k \qquad \text{(Eq. P-1a and b)}$$

The result is:

$$c = \frac{V(Z)}{2E(Z)} \quad \text{and} \quad k = \frac{2E(z)^2}{V(Z)} = 2CV(Z)^2 \qquad \text{(Eq. P-2a and b)}$$

where *CV*( ) is the coefficient of variation. As an example, Chapter 10 assessed the between-event aleatory variability, $\tau$, for **M**7 earthquakes applicable to the DCPP site to be 0.338 and the epistemic uncertainty in $\tau^2$ for **M**7 earthquakes is represented by a standard deviation of 0.045. Setting *Z* equal to $\tau^2$ yields *c* equal to 0.0089 and *k* equal to 12.9. Figure P-1 shows the resulting density function, *f*( ), and cumulative distribution function, *F*( ), for $\tau^2$.

For ease of implementation in PSHA, continuous distributions are represented discretely in a logic tree format. Keefer and Bodily (1983) proposed the extended Pearson-Tukey (EP-T) three point discrete approximation to a continuous distribution consisting of weight 0.63 on the median value and weights of 0.185 on the 5th and 95th percentiles. Because of the monotonic one-to-one relationship between $\tau^2$ and $\tau$, the cumulative distribution for $\tau^2$ and $\tau$ are equivalent such that:

$$F_{\tau}(\tau_i) = F_{\tau^2}\left(\tau_i^2\right) \qquad \text{(Eq. P-3)}$$

The percentiles of the distribution for $\tau$ are thus given by:

$$\tau(95\%) = \sqrt{c\chi_{2,k}^{-1}(0.95)},$$

$$\tau(50\%) = \sqrt{c\chi_{2,k}^{-1}(0.5)}, \text{ and } \tau(5\%) = \sqrt{c\chi_{2,k}^{-1}(0.05)} \qquad \text{(Eq. P-4 a, b, and c)}$$

where $\chi_{2,k}^{-1}(x)$ is the inverse of the chi-square distribution.

For use in this study, these weights are rounded to 0.6 on the 50th percentile and 0.2 on the 5th and 95th percentiles. The rounding is done to indicate the level of precision in the assessment (one significant figure instead of 3), and has little effect on the outcome, as the resulting variance is less than 10 percent larger using the rounded weights. Also, for nearly symmetric distributions, placement of the central weight on the mean versus the median makes only a small difference. In the example shown in Figure P-1, the difference between the mean and median of $\tau^2$ is about 5 percent, which would translate into a 3 percent difference in the mean of the 3-point discrete distribution. Transformation of the scaled chi-square distribution for $\tau^2$ into a distribution for $\tau$ results in less skewness, bringing the median and mean closer together. Thus, for most applications, mean estimates may be used for the central branch instead of medians with little impact on the results.

Similarly, the models for the central, high and low branches of the $\phi_{SS}$ logic trees are obtained by assuming that the variance of the site-corrected within-event residuals ($\phi_{SS}^2$) follows a scaled chi-square distribution with mean given by $\phi_{SS}^2$ and standard deviation given by SD($\phi_{SS}^2$). The derivation of the coefficient of variation of $\phi_{SS}$ (CV = 0.12) is described in Section 7.3.1. This CV was derived using the global dataset (Abrahamson et al., 2014 [ASK14] and Lin et al. (2011) data) for stations with a minimum of 10 recordings per site and was assumed to be applicable to all the derived $\phi_{SS}$ models due to the small number of stations with a minimum of 10 recordings per site in the magnitude and distance restricted datasets used to derive the $\phi_{SS}$ models. It is shown below that the CV of the variance of a normal distribution can be approximated as twice the CV of the standard deviation. Therefore, the high

and low branches of the $\phi_{SS}$ logic trees are calculated using equations (1) and (2) replacing $\tau^2$ with $\phi_{SS}^2$ where the SD( $\phi_{SS}^2$ ) is calculated using CV( $\phi_{SS}^2$ ) = 2* CV( $\phi_{SS}$ ) and CV( $\phi_{SS}$ ) is 0.12.

The models for the central, high and low branches of $\phi_{SP-R}$ are obtained by assuming that the variance of the path-corrected site-corrected within-event residuals ( $\phi_{SP-R}^2$ ) follows a scaled chi-square distribution with mean given by $\phi_{SP-R}^2$ and standard deviation given by SD( $\phi_{SP-R}^2$ ). The high and low branches of $\phi_{SP-R}$ are calculated according to equations 1 and 2 replacing $\tau^2$ with $\phi_{SP-R}^2$ where the

SD( $\phi_{SP-R}^2$ ) is calculated using CV( $\phi_{SP-R}^2$ ) = 2* CV( $\phi_{SP-R}$ ) and the CV( $\phi_{SP-R}$ ) is derived from the Arizona dataset as described in Section 7.4.2.

Finally, a discrete uncertainty distribution for total aleatory variability is developed in Chapter 13 using the same process. For the DCPP site, the computed values of *k* are in the range of 31 to 38 for **M**5 and 5.5 to 35 to 45 for **M**7. The values of *c* are in the range of 0.006 to 0.01. Similar ranges were obtained for the PVNGS site analyses.

## P.2 Derivation of the Coefficient of Variation of Variance

The sample variance ($s^2$) of a normal distribution follows a scaled chi-square distribution:

$$(n-1)\frac{s^2}{\sigma^2} \sim \chi_{n-1}^2 \qquad \text{(Eq. P-5)}$$

where n is the number of samples, $\sigma^2$ is the variance of the continuous distribution, and $\chi_{n-1}^2$ is a chi-square distribution with (n-1) degrees of freedom. The mean and the variance of $\chi_{n-1}^2$ are (n-1) and 2(n-1), respectively. The mean and variance of the sample variance ($s^2$) can therefore be written as:

$$E(s^2) = E\left(\frac{\sigma^2}{n-1}\chi_{n-1}^2\right) = \sigma^2 \qquad \text{(Eq. P-6)}$$

and

$$Var[s^2] = Var\left(\frac{\sigma^2}{n-1}\chi_{n-1}^2\right) = \frac{\sigma^4}{(n-1)^2}Var(\chi_{n-1}^2) = \frac{2\sigma^4}{n-1} \qquad \text{(Eq. P-7)}$$

The CV of $s^2$ can be written as:

$$CV[s^2] = \frac{SD[s^2]}{E(s^2)} = \frac{\sqrt{\frac{2\sigma^4}{n-1}}}{\sigma^2} = \sqrt{\frac{2}{n-1}}. \qquad \text{(Eq. P-8)}$$

Kenny and Keeping (1951) showed that the variance of the sample standard deviation of a normal distribution, Var[s], can be approximated as:

$$Var[s] \approx \frac{1}{2n}\sigma^2 \qquad \text{(Eq. P-9)}$$

and that the mean of s can be written as:

$$E(s) \approx b(n)\sigma \qquad \text{(Eq. P-10)}$$

where b(n) is a constant less than 1 and for large n, b(n) is close to 1.

The coefficient of variation of s can be written as:

$$CV[s] = \frac{SD[s]}{E(s)} = \frac{\sqrt{\frac{1}{2n}}\sigma}{b(n)\sigma} \approx \sqrt{\frac{1}{2n}} \approx \sqrt{\frac{1}{2(n-1)}} \qquad \text{(Eq. P-11)}$$

Therefore:

$$\frac{CV[s^2]}{CV[s]} = \frac{\sqrt{\frac{2}{n-1}}}{\sqrt{\frac{1}{2(n-1)}}} = 2. \qquad \text{(Eq. P-12)}$$

## P.3 Statistical Uncertainty in the Estimation of $\tau^2$

The assessment of the uncertainty in the between-event variance developed in Chapter 10 incorporates the statistical uncertainty in estimation of $\tau^2$ from data. This statistical uncertainty was assessed using the CY14 residuals. The maximum likelihood formulation for the mixed-effects regression model presented in Searle (1971) provides an explicit formulation for estimating the asymptotic covariance of the between-event and within-event variance terms:

$$V(\tau^2, \varphi^2) = 2\left(Trace\left[\Sigma^{-1}\frac{\partial\Sigma}{\partial\tau^2}\Sigma^{-1}\frac{\partial\Sigma}{\partial\varphi^2}\right]\right)^{-1} \qquad \text{(Eq. P-13)}$$

where Σ is the block-diagonal covariance matrix for the residuals. Eq. P-13 was used to compute the covariance of $\tau^2$ and $\phi^2$ from the CY14 residuals.

## P.4 References

Abrahamson, N.A., Silva, W.J., and Kamai, R. (2014). Summary of the AKS14 Ground-Motion Relation for Active Crustal Regions, *Earthquake Spectra*, Vol. 30(3), 1025-1055, DOI: 10.1193/070913EQS198M

Ang, A.H.-S., and Tang, W.H. (2007). *Probability Concepts in Engineering: Emphasis on Applications to Civil and Environmental Engineering (Vol. 1)*. John Wiley and Sons, New York, 409 pp.

Coppersmith, K.J., Bommer, J., Hanson, K., Coppersmith, R., Unruh, J.R., Wolf, L., Youngs, R., Al Atik, L., Rodriguez-Marek, A., Toro, G., and Montaldo-Falero, V. (2014). Hanford Sitewide Probabilistic Seismic Hazard Analysis, *PNNL-23361*, Pacific Northwest National Laboratory, Richland Washington.

Keefer, D.L., and Bodily, S. E. (1983). Three-point approximations for continuous random variables, *Management Science,* Vol. 29, 595-609.

Kenney, J.F., and Keeping, E.S. (1951). The Distribution of the Standard Deviation. §7.8 in Mathematics of Statistics, Pt. 2, 2nd ed. Princeton, NJ: Van Nostrand, 170-173, 1951.

Lin, P.-S., Chiou, B., Abrahamson, N., Walling, M., Lee, C.-T., and Cheng, C.-T. (2011). Repeatable source, site, and path effects on the standard deviation for empirical ground-motion prediction models, *Bull. Seismol. Soc. Am.,* Vol. 101(5), 2281-2295, DOI: 10.1785/012009031.

Searle, S. R. (1971). *Linear Models*, John Wiley and Sons, New York.

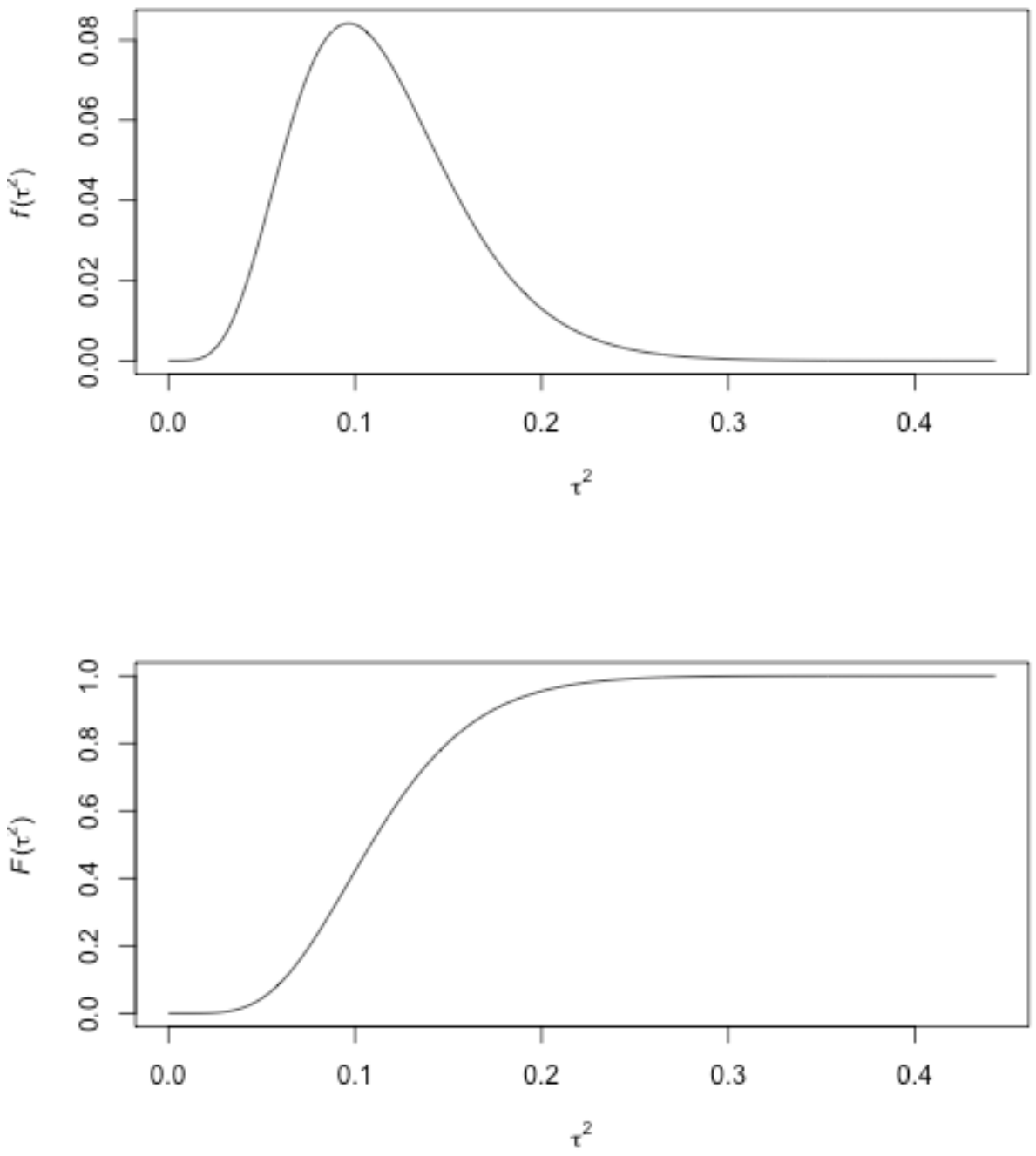



**Figure P-1:** Example density (top) and CDF (bottom) for $\tau^2$ .